

Solvent uptake as a tool for investigating polymer morphology

D. A. Blackadder* and P. I. Vincent

*Imperial Chemical Industries Limited, Plastics Division, Welwyn Garden City, Herts, UK
(Received 25 June 1973)*

Attention is drawn to the potential value of measurement of the rate of solvent uptake as a technique for following changes in the morphology of a polymer specimen, and for detecting small morphological differences between specimens. Examples of each use are described. The rate of sorption of carbon tetrachloride by polypropylene film is very sensitive to the slow changes associated with physical ageing in a specimen, and the effect of different cooling rates after heat treatment is easily observed. For a variety of samples of drawn poly(ethylene terephthalate) it appears that the sorption of benzene or 1,2-dichloroethane is dependent upon two distinct types of orientation in the film.

INTRODUCTION

The morphological examination of non-crystalline polymer, or of the non-crystalline regions in semi-crystalline polymer, is proving to be a matter of some difficulty. Techniques such as X-ray diffraction, differential scanning calorimetry, electron microscopy and density measurement, which can give information about the nature and proportion of crystallites, are notably uninformative concerning the detailed morphology of non-crystalline material. Voids and very small elements of partly ordered chains are particularly resistant to direct observation. Any technique which offers scope for measuring small morphological changes by means of a gross macroscopic property is therefore of particular interest. The sorption of organic liquids by polymer films is one such technique, the full potentialities of which have yet to be realized.

The study of the permeation of organic liquids and vapours through polymeric membranes has generated a considerable literature, but there has been little emphasis on the morphological implications of the results, especially where the permeant interacts with and modifies the permeate. The work of Michaels *et al.*¹⁻³, despite an inadequate model, paved the way for later attempts to interpret measurements of permeability, diffusion coefficients and solubilities in morphological terms. Illers⁴ made use of solvent sorption measurement in his work on the properties of poly(vinyl chloride) as modified by thermal treatment, and Ochiai *et al.*⁵ studied the equilibrium sorption of organic solvents by polypropylene. Blackadder and Keniry⁶⁻⁸ described a variety of experiments involving polyethylene membranes and organic permeants in the form of vapours and liquids. Kapur and Rogers⁹ have used the transport properties of permanent gases to investigate some features of ageing in quenched polypropylene film. These and other papers suggest that the time is ripe to

draw special attention to the importance of solvent sorption in morphological studies.

The starting point is the assertion that the initial rate of solvent sorption gives information of a qualitatively different kind to that obtainable from equilibrium sorption data at long times. The rate of sorption seems very likely to depend on the nature of the non-crystalline material in a given polymer sample as well as on its amount. At long times, however, the non-crystalline material might well become 'homogenized' by the swelling solvent so that the final uptake is directly related to the total amount of permanently swellable polymer.

The purpose of this short paper is to present some typical situations where solvent sorption techniques appear to provide a convenient means of: (a) distinguishing between morphologically different samples of the same polymer; and (b) following small morphological changes in a given sample.

EXPERIMENTAL

Materials

Polypropylene. An isotactic homopolymer was used, and film specimens were obtained by compression moulding at 220°C for 4 min. The films were either cooled slowly at about 0.7°C/min or quenched by rapid immersion in cold water. The crystallinities (kindly determined by Miss A. Turner-Jones using methods described previously¹⁰) were 64.5% and 56.0% respectively. These results indicate that the quenching was not of the fastest. The thickness was typically 0.5 mm.

Poly(ethylene terephthalate). Some experiments were based on commercial biaxially drawn and crystallized films (about 20 μm thick) from two different manufacturers. Other experiments involved a set of research samples which had been uniaxially drawn to various draw ratios in the range 1.0 to 4.5. All of these films had a thickness of about 170 μm.

* Permanent address: Department of Chemical Engineering, University of Cambridge, Cambridge CB2 3RA, UK.

Carbon tetrachloride, benzene and 1,2-dichloroethane of analytical reagent grade were used without further purification.

Procedure

Film strips 10 cm × 1 cm were convenient, and the average thickness of each strip was determined together with its weight. In a typical experiment a strip was immersed in solvent at 25°C, controlled by a thermostat to ±0.1°C. On removal from the solvent after an appropriate period of time the strip was quickly dabbed dry with tissue and its weight noted at intervals over a period of 4 min. Graphical extrapolation of the results then gave the weight of the film at the time of its withdrawal from the solvent. Specimens left in solvent for a week or longer appeared to reach or approach equilibrium. In some experiments with polypropylene the strips were dried out by prolonged exposure to vacuum, and the original weights were almost unchanged.

RESULTS AND DISCUSSION

Figure 1 shows that slow cooled and quenched samples of polypropylene film differ markedly with respect to the sorption of carbon tetrachloride at 25°C. It is convenient to plot the uptake as mass of solvent per unit dry weight of polymer, and the use of $(t)^{1/2}/l$ as abscissa eliminates the effect of variations in thickness from one strip to another where this would otherwise disturb the results. Here t is the time of immersion in seconds and l is the average thickness of the strip in mm. For films of highly uniform thickness t itself may be used for the plots. Figure 1 shows that the difference between the final uptakes (about 4:3) is not as large as the difference in the initial rate of uptake (about 2:1 as measured by the uptakes after 1 h, corresponding to $(t)^{1/2}/l = 120$). The detailed morphological implications of the results will be pursued in a later paper, but it certainly seems that if the final uptake is related to the total amount of swellable material the initial rate of

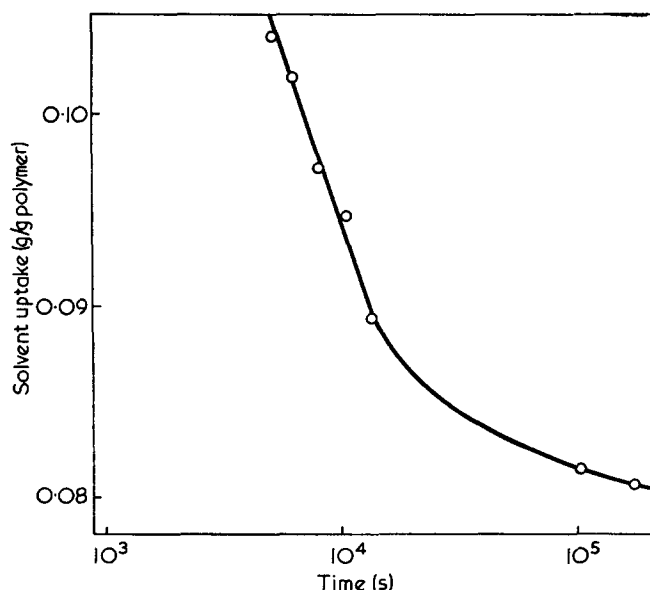


Figure 2 Ageing of quenched polypropylene film. Each specimen immersed in carbon tetrachloride at 25°C for 1 h

uptake is additionally dependent on the nature of this material.

It is becoming increasingly likely⁹ that the amount and nature of the non-crystalline material in polypropylene is closely related to the ageing processes observed in quenched samples of this polymer. The technique of solvent sorption is very appropriate as a tool to investigate such phenomena and one example follows. Instead of leaving strips of polymer in solvent for varying times, the procedure was to immerse strips of different ages for the same time and note the uptake. Ageing was thus reflected in the changing rate of uptake as measured by brief immersion. An immersion period of 1 h was suitable and this became an increasingly trivial fraction of the total age of the specimen as shown in Figure 2. The large change in rate of uptake with increasing age was easily measured with high precision. (The specimens shown in Figure 1 were sufficiently aged to be virtually unchanged during the relatively short time of the complete experiments represented there.)

Poly(ethylene terephthalate) is a different kind of polymer but is also susceptible to investigation by solvent sorption. Figure 3 shows the sorption of benzene at 25°C by the series of films which had been uniaxially drawn. These results may be tentatively interpreted on the basis of the infra-red measurements made by Heffelfinger and Schmidt¹¹ on a similar series of films. They showed that, between film as cast and film uniaxially drawn 2.0:1, there was a substantial change in the orientation of the molecular axes but relatively small changes in the other structural parameters they measured. This suggests that the initial rate of solvent uptake, as exemplified by the 1 h values in Figure 3, is strongly affected by axial orientation. On the other hand, the largest structural change found by Heffelfinger and Schmidt between draw ratios of 3.5 and 4 was the increasing perfection of orientation of the phenyl rings parallel to the film surface. This suggests that the final solvent concentration, exemplified by the 212 h results in Figure 3, is affected by the planar orientation of the phenyl rings rather than by the axial orientation.

Finally, Figure 4 shows the different sorption charac-

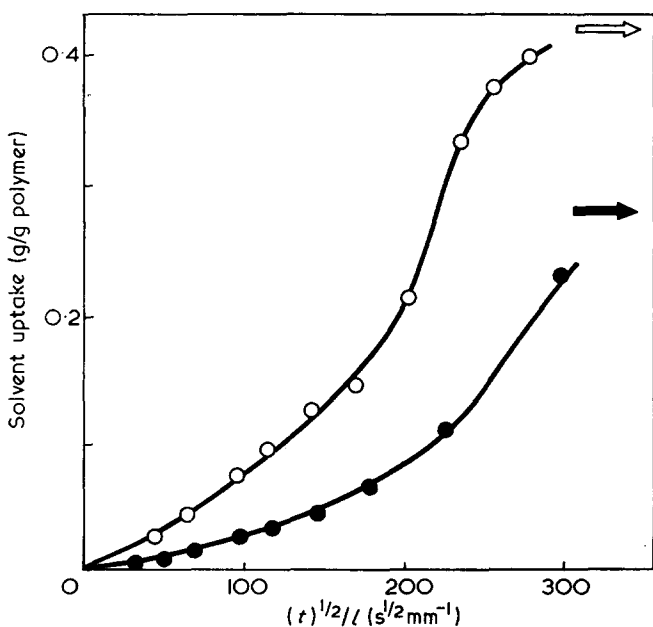


Figure 1 Sorption of carbon tetrachloride by polypropylene films at 25°C. ○, Quenched film; ●, film cooled at 0.7°C/min. Arrows indicate sorption after 2 days

teristics of the two commercial samples of poly(ethylene terephthalate) in 1,2-dichloroethane. (They did not absorb enough benzene for adequate sensitivity.) The samples were similar in density and in axial orientation but sample A was higher in concentration of *trans* isomer and also in planar orientation of the phenyl rings. Here again, it would seem that the sorption technique merits further development.

CONCLUSIONS

The study of the uptake of organic liquids appears to be a promising method of investigating polymer morphology, especially the morphology of non-crystalline regions. In addition, small and subtle changes brought about by thermal treatment of ageing can be followed.

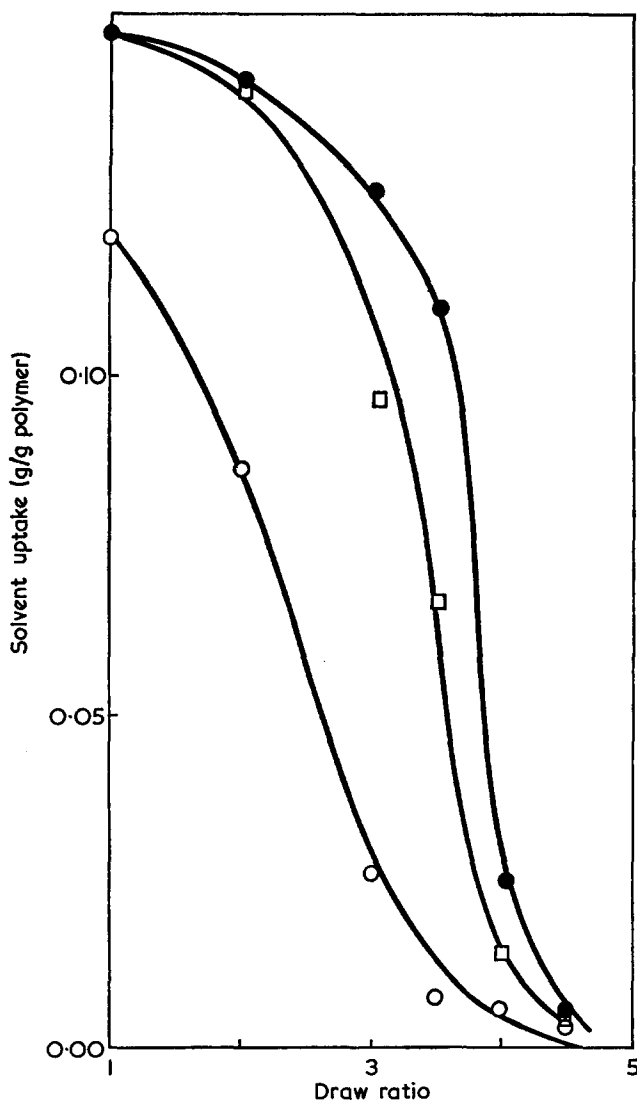


Figure 3 Sorption of benzene by poly(ethylene terephthalate) films at 25°C. Dependence of sorption on draw ratio for uniaxially drawn specimens. ○, Immersed for 1h; □, immersed for 65h; ●, immersed for 212h

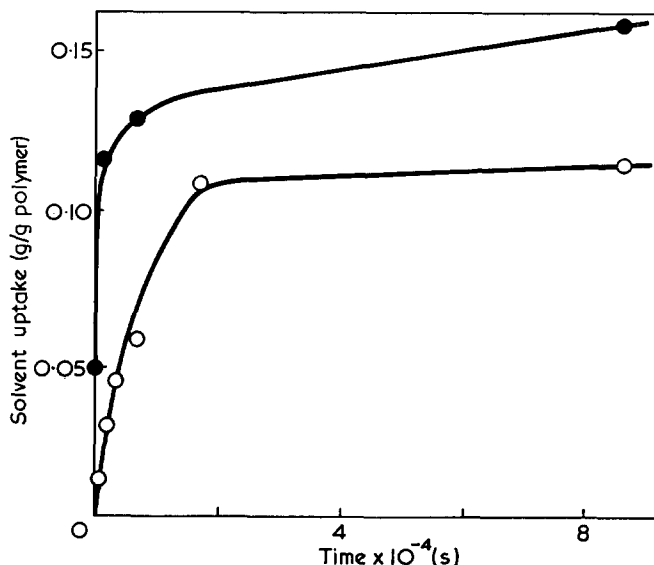


Figure 4 Sorption of 1,2-dichloroethane by biaxially drawn films of poly(ethylene terephthalate) at 25°C. ○, Sample A, density 1.3923g/cm³; ●, sample B, density 1.3940g/cm³

The technique is simple, requires no special apparatus, and can be made extremely precise. It enjoys the considerable advantage over many other techniques that small changes in morphology produce very large changes in sorption characteristics.

ACKNOWLEDGEMENTS

This work was carried out while one of us (D. A. B.) was on Sabbatical Leave from the University of Cambridge. Thanks are due to the Directors of Imperial Chemical Industries Limited, Plastics Division, for providing facilities for him in their Research Laboratories at Welwyn Garden City. The infra-red work of Mrs V. J. I. Zichy and the experimental assistance of Mr K. S. Beare are gratefully acknowledged.

REFERENCES

- 1 Michaels, A. S., Baddour, R. F., Bixler, H. J., and Choo, C. Y. *Ind. Eng. Chem. (Process Des. Develop.)* 1962, 1, 14
- 2 Baddour, R. F., Michaels, A. S., Bixler, H. J., de Filippi, R. P. and Barrie, J. A. *J. Appl. Polym. Sci.* 1964, 8, 897
- 3 Michaels, A. S., Vieth, W., Hoffman, A. S. and Alcalay, H. A. *J. Appl. Polym. Sci.* 1969, 13, 577
- 4 Illers, K. H. *Makromol. Chem.* 1969, 127, 1
- 5 Ochiai, H., Gekko, K. and Yamamura, H. *J. Polym. Sci. (A-2)* 1971, 9, 1629
- 6 Blackadder, D. A. and Keniry, J. S. *J. Appl. Polym. Sci.* 1972, 16, 1261
- 7 Blackadder, D. A. and Keniry, J. S. *J. Appl. Polym. Sci.* 1972, 16, 2141
- 8 Blackadder, D. A. and Keniry, J. S. *J. Appl. Polym. Sci.* 1973, 17, 351
- 9 Kapur, S. and Rogers, C. E. *J. Polym. Sci. (Polym. Phys.)* 1972, 10, 2107
- 10 Turner-Jones, A. *Polymer* 1971, 12, 487
- 11 Heffelfinger, C. J. and Schmidt, P. G. *J. Appl. Polym. Sci.* 1965, 9, 2661

Nuclear magnetic resonance studies of polydienes: 1. ^{13}C n.m.r. of 1,4-polybutadiene obtained by π -allyl nickel trifluoroacetate catalysts

F. Conti and A. Segre

Istituto di Chimica delle Macromolecole, Nucleo di Roma, c/o Istituto Chimico, Università di Roma, Roma, Italy

and P. Pini and L. Porri

Istituto di Chimica Organica Industriale, Università di Pisa, Pisa, Italy
(Received 16 July 1973)

^{13}C n.m.r. spectra of 1,4-polybutadienes catalysed by π -allyl Ni trifluoroacetate systems show *cis-trans* sequence distribution. The assignment of different peaks is obtained both by comparison with model compounds as well as by comparing samples with different *cis:trans* ratios. All the observed peaks are assigned in terms of triads of steric configuration and a quantitative analysis of triad content is possible. Information on the structure of the so-called 'equibinary' polybutadienes is also reported.

INTRODUCTION

Proton magnetic resonance has proved to be of great interest for the study of the microstructure of diolefin polymers. *cis*- and *trans*-1,4-Polybutadiene, and natural and synthetic *cis*- and *trans*-1,4-polyisoprene have been investigated by this method and accurate quantitative determinations of the *cis:trans* ratios and of the amount of minor structural units (1,2- or 3,4-) have been obtained¹⁻⁵.

However, it provides very little information on the distribution of the various isomeric structural units in the polymer chains⁶. ^{13}C nuclear magnetic resonance (n.m.r.) seems to be particularly attractive for investigating these microstructural features of diolefin polymers. Recently, Mochel has investigated by ^{13}C n.m.r. a *n*-BuLi catalysed polybutadiene and has reported data concerning the isomeric structural unit distribution in the polymer chains⁷.

We began a systematic study on the structure of various diolefin polymers obtained by transition metal catalysts. This paper reports the results of an investigation by ^{13}C n.m.r. of 1,4-polybutadienes obtained by π -allyl nickel trifluoroacetate, with or without additional ligands. Catalysts of this type are known⁸ to give polymers consisting almost exclusively of *cis*-1,4 and *trans*-1,4 units, in almost equal amounts, but scarce information is at present available concerning the distribution of the structural units in the polymer chains.

EXPERIMENTAL

All ^{13}C n.m.r. spectra were run on 12mm samples containing ~10% solutions (w/v) of polymer in 1,4-

dioxane (20% D_8 + 80% H_8). Experimental peak positions are reported in ppm from tetramethyl silane (TMS), used as an internal standard. The spectrometer used was a Varian XL 100 operating in the Fourier transform (FT) mode. The FT conditions were as follows:

Spectral width (Hz)	5000-1000
Acquisition time (sec)	0.8-2
Pulse width (μsec)	30-45
K transients	2000
Data length	8192-4096
Signal enhancement (sec)	0.40
FT length	8192-4096
Hertz/point	1.25-0.50

Polymer preparation

π -Allyl nickel trifluoroacetate, $\pi\text{-C}_3\text{H}_5\text{-Ni-OCOCF}_3$, and 2,6,10-dodecatriene-12-yl nickel trifluoroacetate, $\pi\text{-C}_{12}\text{H}_{19}\text{-Ni-OCOCF}_3$, used as polymerization catalysts, were prepared according to the methods reported in the literature^{9,10}. The polymerizations were carried out following the procedure already described¹¹. The percentages of *cis*-1,4, *trans*-1,4 and 1,2-units of the polybutadienes were determined by infra-red analysis, according to the method of Morero *et al.*¹², on polymer solutions in carbon disulphide, or on thin films prepared by evaporating polymer solutions in carbon disulphide. A Perkin-Elmer model 225 spectrophotometer was used. The polymerization conditions and the infra-red analysis of the polymers that have been subsequently investigated by ^{13}C nuclear magnetic resonance are summarized in Table 1.

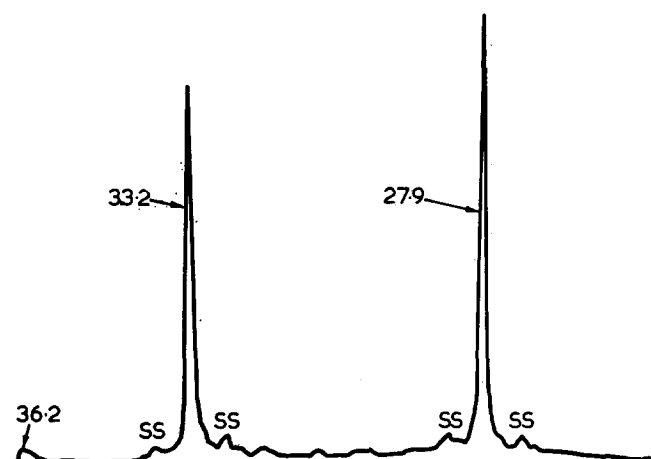
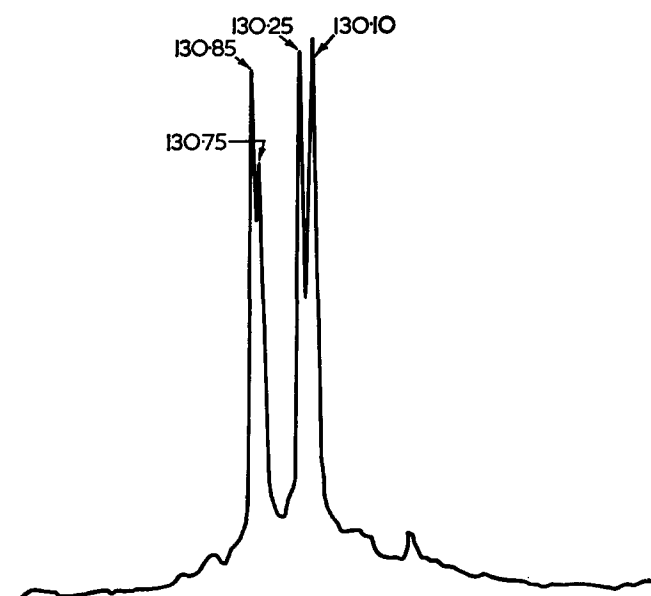
Table 1 Polymerization of butadiene by π -allyl nickel trifluoroacetate catalysts*

Run	Catalyst system†	Solvent	I.r. analysis of the polymers‡		
			% cis	% trans	% 1,2
1	π -C ₁₂ H ₁₉ -Ni-OCOCF ₃ + CF ₃ COOH	heptane	51	49	—
2	π -C ₁₂ H ₁₉ -Ni-OCOCF ₃ + CF ₃ COOH	heptane	51	49	—
3	π -C ₈ H ₅ -Ni-OCOCF ₃ + CF ₃ COOH	heptane	72	25	3
4	π -C ₈ H ₅ -Ni-OCOCF ₃ + CF ₃ COOH	heptane	55	45	—
5	π -C ₈ H ₅ -Ni-OCOCF ₃	benzene	57.5	38	4.5

* Polymerization temperature: runs 1, 2, 4—20°C; run 3, 55°C; run 5, 70°C

† CF₃COOH/nickel complex: 20

‡ Analyses were performed on the CH₃OH-insoluble polymers for runs 1, 2, 3, 5. Crude polymer from run 4 was extracted with methyl ethyl ketone (MEK) and i.r. analysis were performed on the residue to MEK extraction

Figure 1a Aliphatic range ¹³C n.m.r. spectrum of sample 2 (see Table 1)Figure 1b Vinylenic range ¹³C n.m.r. spectrum of sample 2 (see Table 1)

RESULTS AND DISCUSSION

Spectra relative to different 1,4-polybutadienes show peaks in two different regions as shown in Figures 1a and 1b for one of the samples. In the range of the aliphatic carbons two intense resonances, at 33.2 and 27.9 ppm respectively, are present in every spectrum. In some of the samples a few minor additional peaks are present. In the range of the vinylenic carbons, four main peaks (Figure 1b) at 130.85, 130.75, 130.25 and 130.10 ppm are always present, whose relative intensity is different for the various samples. A few minor peaks are also observable in some samples. On the basis of the data reported in previous papers^{7, 13, 14}, it is possible to assign the two peaks at 33.2 and 27.9 ppm respectively to the methylenic carbons directly bonded to a *trans* or a *cis* double bond. The minor multiplicity of the resonance peaks observed for the aliphatic carbons with respect to the vinylenic carbons, shows that the first ones are sensitive only to the configuration of the directly bonded double bond. This result is in full agreement with the conclusion of Roberts *et al.*¹³ for compounds which could be considered as models for our polymers. It is, however, in disagreement with the conclusions that Mochel⁷ derived from the study of a *n*-BuLi catalysed polybutadiene and of some model compounds (*cis*, *trans*, *trans*-1,5,9-cyclododecatriene; *cis*, *trans*-4,8-dodecadiene; 3,7-decadiene). Mochel's conclusions are that the effect of *cis* and *trans* structures of the adjacent unit is much more pronounced on the aliphatic carbons than on the olefinic carbons. It is to be noted, however, that Mochel does not take into account the peaks at 130.85 and 130.10 ppm, also present in the spectrum of the polybutadiene of his work. Furthermore, he uses as model compound *cis*, *trans*, *trans*-1,5,9-cyclododecatriene, although it has already been recognized that alkenes which include cyclic structures do not fit as well into the additivity rules¹³. With regard to the ¹³C n.m.r. spectrum of *cis*, *trans*-4,8-dodecadiene, it is possible to calculate the chemical shift of the various aliphatic carbons on the basis of the additivity coefficients, reported by Roberts *et al.*¹³, and by Grant and Paul¹⁵. Results of this calculation are reported in Table 2, together with experimental frequencies as obtained from the spectra of ref. 7. The calculated values are essentially in agreement with Mochel assignments, except for the inversion of the assignment of the signals due to C₃ and C₇. Our assignment is in agreement with the insensitivity of aliphatic ¹³C chemical shifts with regard to the configuration of double bonds in β position¹³. This insensitivity is also supported by the small chemical shift difference (0.14 ppm) of carbons in position 11 and 2

Table 2 Calculated and observed aliphatic carbon chemical shifts for *cis*, *trans*-4,8-dodecadiene

Carbon	Shift* (ppm)		Assignment as from ref. 7
	Calc.†	Exp.‡	
3	30.4	30.8	7
6	32.9	33.2	6
7	27.4	27.5	3
10	24.9	25.3	10

* From TMS

† According to refs 13 and 15

‡ From ref. 7

of *cis*, *trans*-4,8-dodecadiene¹⁶, and by the coincidence of the signals due to β aliphatic carbons in mixtures of *cis*- and *trans*-2-heptene and of *cis*- and *trans*-2-octene¹⁷.

A quantitative determination of the relative content of *cis* and *trans* units in 1,4-polybutadienes follows from the assignment of the main peaks at 33.2 and 27.9 ppm.

The assignment of the vinylic main peaks at 130.85, 130.75, 130.25, 130.10 ppm can be made on the basis of the results obtained from *trans*-1,4- and *cis*-1,4-polybutadiene¹⁴, as well as by considering the relative intensities of the peaks in our samples having different *cis:trans* ratios (Figure 2). The peak at 130.75 can be assigned to *ttt* sequences, while that at 130.25 can be assigned to *ccc* sequences. The equivalence by symmetry of the vinylic carbons of the central unit both in the *ccc* and in the *ttt* triads (Table 3) has already been pointed out¹⁴.

The *ctc* and *tct* triads have C_1 and C_2 equivalent by symmetry. Considering, as generally admitted, that there is an additivity of the neighbour's contribution, we attribute the peaks at 130.85 and 130.10 ppm to the *ctc* and *tct* triads respectively, being the most different from the already assigned *ccc* and *ttt* triads.

In the asymmetric triads *cct*, *tcc*, *ttc* and *ctt*, C_1 and C_2 are not equivalent. Let us consider, for instance, the *cct* triad in which C_1 is in a configurational situation with respect to its first neighbours similar to that of C_1 and C_2 of the *ccc* unit and in which C_2 is in a configurational situation with respect to its first neighbours, similar to that of C_1 and C_2 of the *tct* unit. It follows that the signals due to C_1 and C_2 of the *cct* sequences may have chemical shifts similar to the ones found for *ccc* and *tct* units respectively. Analogous considerations hold for the other asymmetric triads. The resultant assignment is summarized in Table 4.

Experimental data for the polybutadienes examined, based on the above assignments, are presented in Table 5. Samples 1 and 2 consist exclusively of *cis*-1,4- and *trans*-1,4 units, in a ratio very close to 1. This is in

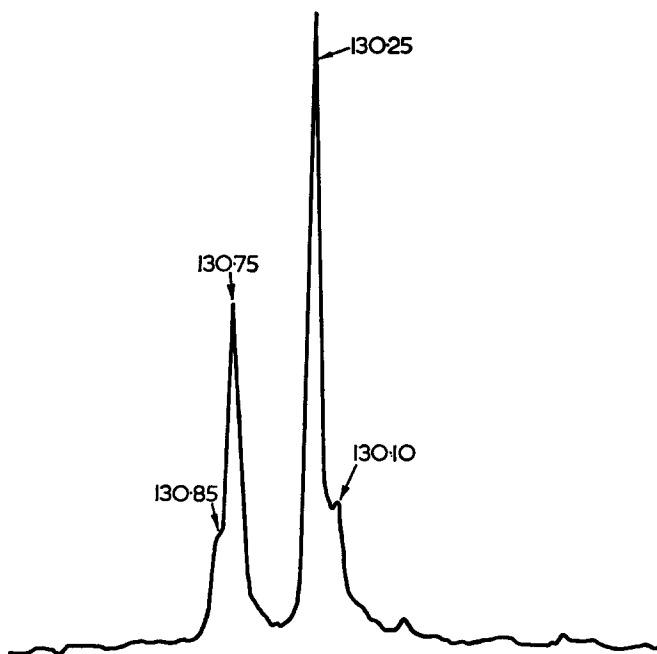


Figure 2 Vinylenic range ^{13}C n.m.r. spectrum of sample 5 (see Table 1)

Table 3 Triads of 1,4-polybutadienes

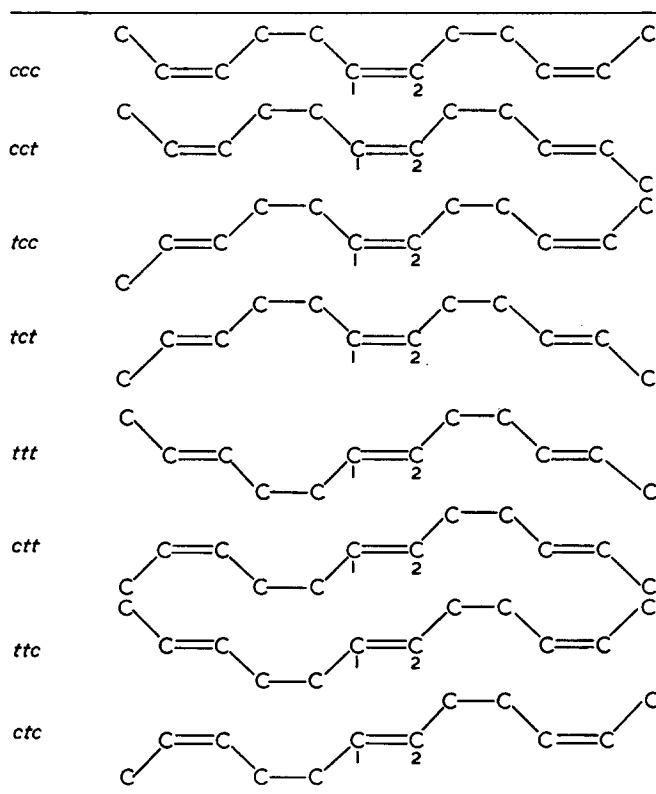


Table 4 Olefinic carbon chemical shift assignment for 1,4-polybutadienes

Exp. frequency (ppm from TMS)	Triad assignment
130.85	<i>ctc</i> <i>ttc</i> <i>ctt</i> $C_1, C_2 + C_2 + C_1$
130.75	<i>ttt</i> <i>ttc</i> <i>ctt</i> $C_1, C_2 + C_1 + C_2$
130.25	<i>ccc</i> <i>tcc</i> <i>cct</i> $C_1, C_2 + C_2 + C_1$
130.10	<i>tct</i> <i>tcc</i> <i>cct</i> $C_1, C_2 + C_1 + C_2$

full agreement with the data reported by Teyssié *et al.*⁸⁻¹¹, who defined these polymers as 'equibinary polybutadienes'.

With regard to the distribution of the *cis* and *trans* units in the polymer chains the ^{13}C n.m.r. spectra permit to exclude a regular distribution of the type *ctctctc*, since in that case only two peaks, at 130.85 and 130.10, should be present, with only very weak or absent peaks at 130.25 and 130.75.

In the spectrum of sample 1 (and to a lesser degree of sample 2) the four peaks in the olefinic region are almost of the same intensity. This finding could be rationalized on the basis that sequences of the type *ccttccttc* are present in that polymer. However, regularity bands have been found to be absent in the infra-red spectrum of the solid polymer, in the temperature range from -180° to $+100^\circ\text{C}$, and, in addition, no crystallinity has been detected by X-ray examination. This seems to indicate that sequences of the type *ccttccttc*, if present, are rather short. A distribution consisting of short

Table 5 Relative intensities of ^{13}C resonance peaks

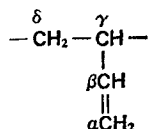
Sample	Vinyleneic ^{13}C resonances				Methyleneic ^{13}C resonances		1,2 units ^{13}C resonances			
	130·85 (ppm)	130·75 (ppm)	130·25 (ppm)	130·10 (ppm)	33·20 (ppm)	27·90 (ppm)	112·40 (ppm)	145·26 (ppm)	44·20 (ppm)	25·40 (ppm)
	$ctc + \frac{1}{2}ttc + \frac{1}{2}ctt$	$ttt + \frac{1}{2}ttc + \frac{1}{2}ctt$	$ccc + \frac{1}{2}tcc + \frac{1}{2}cct$	$tct + \frac{1}{2}tcc + \frac{1}{2}cct$	CH_2 <i>trans</i>	CH_2 <i>cis</i>	C_α	C_β	C_γ	C_δ
1	25·4	23·3	25·4	25·9	49	51	absent	absent	absent	absent
2	24·9	21·2	26·6	27·4	46	54	absent	absent	absent	absent
3	12·6	10·6	61·4	15·2	24	76	present	present	present	present
4	23·3	20·3	31·5	24·0	43	57	absent	absent	absent	absent
5	~9·0	28·2	51·5	~11·5	38	62	present	present	present	present

sequences *ccc* and *ttt*, interspersed by sequences *ctc* and *tct*, seems more probable, on the basis of the ^{13}C n.m.r. spectra as well as of the infra-red and X-ray examinations.

In the olefinic portion of the spectra of samples 3, 4 and 5 the peak at 130·25 is the most intense, which is indicative of a predominance of the *ccc*, *tcc* and *cct* triads in these polymers. This is consistent with the higher percentage of *cis* units in these polymers, in agreement with the infra-red analysis (Table 1).

As a conclusion we may say that the catalyst system $\pi\text{-C}_{12}\text{H}_{19}\text{-Ni-OCOCF}_3 + \text{CF}_3\text{COOH}$ (Table 1, runs 1 and 2) is able to give 'equibinary' polybutadienes, but these do not consist of regular sequences *ctctct*, as proposed in earlier studies⁸.

With regard to the peaks of minor intensity in the olefinic region of the spectra of some of the samples examined, those at 112·4 and 145·2 ppm (samples 3 and 5) can be attributed to C_α and C_β of the 1,2 units, in agreement with Mochel's assignment:



Analogously, some of the minor peaks in the region of the aliphatic carbons are most probably due to the methylene (C_δ) and methine (C_γ) carbons of the 1,2 units. Mochel tentatively assigned⁷ the peaks at 44·2 and 38·6 ppm present in the spectra of his polybutadienes to the methine carbons (C_γ) of the 1,2 units which are linked to *trans*-1,4 and *cis*-1,4 units, respectively. Similarly, the peaks at 30·7 and 25·4 ppm were assigned to the methylene carbon (C_δ) connected to a *trans* or a *cis* unit, respectively. Our findings do not seem fully in agreement with these assignments, since in one of our samples (sample 3) the peak at 38·6 ppm is missing. For this reason there is the possibility that C_γ and C_δ give only single peaks, at 44·2 and 25·4

respectively, independently of the stereochemistry of the next neighbour unit. As a consequence, the weak peaks at 38·6, 36·2, and 30·7 ppm present in the spectra of some samples, independently of the 1,2 unit content, might be due to satellites (^{13}C - ^{13}C couplings) or to possible crosslinks, or also to the presence of oligomers.

ACKNOWLEDGEMENTS

The financial support of the Consiglio Nazionale delle Ricerche is gratefully acknowledged. We thank Mr A. Seritti for the assistance in preparing the polymers. The authors are deeply indebted to Dr F. Werhly of Varian AG, Zug (Switzerland), for running the n.m.r. spectra.

REFERENCES

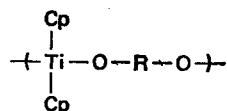
- Chen, H. Y. *Analyt. Chem.* 1962, **34**, 1134
- Chen, H. Y. *Analyt. Chem.* 1962, **34**, 1793
- Worsfold, D. J. and Bywater, S. *Can. J. Chem.* 1964, **42**, 2884
- Stehling, F. C. and Bartz, K. W. *Analyt. Chem.* 1966, **38**, 1467
- Chen, H. Y. *J. Polym. Sci. (B)* 1966, **4**, 891
- Bovey, F. A. 'High Resolution NMR of Macromolecules', Academic Press, New York, 1972, p 224
- Mochel, V. D. *J. Polym. Sci. (A-1)* 1972, **10**, 1009
- Dawans, F. and Teyssié, Ph. *Ind. Eng. Chem. (Prod. Res. Develop.)* 1971, **10**, 261 and references cited therein
- Dawans, F., Marechal, J. C. and Teyssié, Ph. *J. Organometal. Chem.* 1970, **21**, 259
- Durand, J. P. and Teyssié, Ph. *J. Polym. Sci. (C)* 1968, **6**, 299
- Durand, J. P., Dawans, F. and Teyssié, Ph. *J. Polym. Sci. (A-1)* 1970, **8**, 979
- Morero, D., Santambrogio, A., Porri, L. and Ciampelli, F. *Chim. Ind. (Milan)* 1959, **41**, 758
- Dorman, D. E., Jautelat, M. and Roberts, J. D. *J. Org. Chem.* 1971, **36**, 2557
- Duch, M. W. and Grant, D. M. *Macromolecules* 1970, **3**, 165
- Grant, D. M. and Paul, E. G. *J. Am. Chem. Soc.* 1964, **86**, 2984
- Mochel, V. D., Lawson, D. F. and Farrar, T. C. *J. Am. Chem. Soc.* 1962, **94**, 6202
- Le Roy Johnson, F. and Jankowsky, W. C. 'Carbon-13 NMR Spectroscopy', Wiley, New York, 1972

Tentative identification of reactive species in the interfacial and aqueous solution synthesis of titanium polymers*

Charles E. Carraher Jr. and Samuel T. Bajaht

Department of Chemistry, Vermillion, University of South Dakota, South Dakota 57069, USA
(Received 11 July 1973)

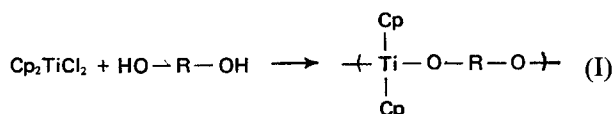
The active species in the synthesis of titanium polyethers of the following form



are tentatively identified as follows. Aqueous solution syntheses: $\text{Cp}_2\text{Ti}^{2+}$ and R-O^{\ominus} ; interfacial syntheses: Cp_2TiCl_2 and R-OH with reaction occurring near the interface or in the organic phase. The above is based on pH studies and on studies as a function of diol nature. For aqueous solution systems the yield increases with increase in pH whereas for interfacial systems the yield remains constant over the pH range 8.7 to 12.7. For aqueous syntheses polymer is formed in only systems employing aromatic diols whereas for interfacial systems polyethers are formed using both aliphatic and aromatic diols. Other results are cited and are consistent with this.

INTRODUCTION

Relatively little work has been reported on the synthesis of organometallic polymers partly owing to a lack of suitable preparative methods. We have reported the synthesis of titanium polyamines, polyesters and polythioethers¹⁻⁷. Recently we reported the synthesis of titanium polyethers of the form (I)⁵:



All the above syntheses have utilized the low temperature interfacial and solution condensation techniques avoiding or limiting undesirable thermally dependent reactions.

Much of our work is largely based on the simple Lewis acid (the metal moiety)-Lewis base (diamine, dithiol, etc.) concept. Even so the Lewis acids and bases can exist in several forms. Also several reaction sites are possible for interfacial syntheses. The present paper presents evidence aimed at tentatively identifying the active species of the metal and diol for both titanium polyether synthesis being effected by the solution and interfacial techniques as well as the site of polymerization for interfacial syntheses.

EXPERIMENTAL

Polymerization procedures are similar to those described in detail elsewhere³. Briefly, solutions of Cp_2TiCl_2 are added to stirred aqueous solutions containing diol and

any added base. For interfacial systems Cp_2TiCl_2 is contained in a water immiscible solvent whereas for aqueous solution systems Cp_2TiCl_2 is contained in water. The reaction apparatus is similar to that described elsewhere⁸. Essentially reaction occurs under rapidly stirred conditions in a 1 pint Kimax Emulsifying Mill jar placed on a Waring Blendor with a recorded rotor speed of 23 500 rev/min (no load). Solutions are added through a large mouthed funnel placed in a hole in the jar lid. Addition is rapid such that 100 ml of solution can be added in less than 3 sec. A second hole in the jar lid acts as a vent. Timing for each reaction is begun after the second phase has been introduced into the stirring jar. Syntheses employing hydroquinone or substituted hydroquinones were accomplished under a nitrogen atmosphere utilizing equipment described elsewhere⁸.

Polymer precipitates rapidly from the reaction jar as a tacky to 'powdery' solid. It is recovered using suction filtration, washed repeatedly with portions of water, and then transferred to a preweighed Petri dish for drying. After drying the Petri dish is weighed to determine product yield. The products vary in colour from yellow to dark orange. Some dry to give glasses from which strong, flexible films are formed when they are scraped from the Petri dish while others dry to give powdery solids. All can be ground to give powders which are electrostatic.

RESULTS AND DISCUSSION

While we have spent considerable effort in the synthesis of organometallic polymers, results aimed at describing the active species have been quite limited. This is mainly

* Portions of this paper are taken from the thesis of S.T.B.
† Present address: University of Ibadan, Ibadan, Nigeria.

due to the following: (a) rapidity of reaction—most reactions are complete within 60 sec; (b) complexity of reaction, reactive species and possible reaction pathways; (c) complexity of reaction system—rapidly stirred and for interfacial reactions the reaction system is heterophasic; (d) lack of prior similar and/or credulous research in analogous condensations; and (e) most of the organometallic products are insoluble in all solvents thus precluding determinations requiring solution of the products. The present polyethers follow this trend preventing the use of molecular weight as an index for study. Because of this, identification of the reactive species and reaction site(s) will necessarily be of a speculative nature.

The exact form of the aqueous solubilized Cp_2TiCl_2 is unknown. Various structures have been suggested which include $\text{Cp}_2\text{Ti}^{2+}$ and Cp_2TiOH^+ ⁹⁻¹¹. Probably aqueous solutions contain several species. Aqueous solutions are acidic, exhibiting a pH in the range of 1 to 2. This is indicative of the occurrence of hydrolysis which would favour the presence of species such as Cp_2TiOH^+ . A 0.08 M aqueous solution of Cp_2TiCl_2 gives a pH of 1.7. Assuming the two most prevalent species to be $\text{Cp}_2\text{Ti}^{2+}$ and Cp_2TiOH^+ , this would indicate the ratio of $\text{Cp}_2\text{Ti}^{2+}:\text{Cp}_2\text{TiOH}^+$ to be 3:1. At high pH values insoluble $\text{Cp}_2\text{Ti}(\text{OH})_2$ is formed. Aqueous solutions of Cp_2TiCl_2 can be evaporated to dryness to give Cp_2TiCl_2 quantitatively. Thus the formation of species such as $\text{Cp}_2\text{Ti}^{2+}$ and Cp_2TiOH^+ is reversible. Other characteristics of aqueous solutions of Cp_2TiCl_2 have already been described³⁻⁷. For simplicity, Cp_2TiCl_2 solubilized in water will be designated as $\text{Cp}_2\text{Ti}^{2+}$.

Synthesis of titanium polyethers was general for the interfacial syntheses but was effected with only aromatic diols using aqueous solution systems⁵. This suggests that the active form(s) of reactants is different for the two synthetic systems. The lack of polymer formation in aqueous solutions with aliphatic diols may be due to the difference in acidity between aromatic and aliphatic diols. For instance, hydroquinone is 99% mono-ionized at pH values >12 and over 99% di-ionized at pH values >13.8 (for hydroquinone $\text{p}K_{a_1}=10^{12}$ and $\text{p}K_{a_2}=12^{12}$). Aliphatic diols remain largely un-ionized even at a pH of 14 (for instance ethylene glycol has a $\text{p}K_{a_1}$ of 15.1¹³ and 1,3-dihydroxyacetone has a $\text{p}K_{a_1}$ of 13.5¹⁴). It is possible that polycondensation is only effected in aqueous solution with deprotonated diols whereas other criteria are critical for interfacial synthesis of titanium polyethers. The active aromatic diol species in analogous aqueous solutions has been identified to be the deprotonated diol¹⁵⁻¹⁷. The active aromatic diol species for aqueous solution polycondensation is probably also the ionized diol for the present system, in agreement with a lack of polymer formation where aliphatic diols are employed. If the interfacial syntheses involve the deprotonated diol then one should expect an increase in reaction rate with pH¹⁵. To evaluate this possibility, yield was studied as a function of pH utilizing buffered aqueous solutions for the solution condensation of Cp_2TiCl_2 with hydroquinone. Initially the molar ratio of buffer to hydroquinone was 2:1. It was not possible to control the pH of such systems. Variations greater than 2 pH units were experienced between the initial and final pH values. Buffering was effected when the ratio was increased to 6:1. Results appear in Table 1.

Table 1 Results as a function of pH for aqueous solution systems^a

Buffer pairs (amount)	Average pH ^b	Yield (%)
KCl (0.003M)	12.5	98
NaOH (0.0018M)		
Na_2HPO_4 (0.0012M)	11.3	30
NaOH (0.0009M)		
Na_3PO_4 (0.00072M)	10.6	12
Na_2HPO_4 (0.00138M)		
Na_2CO_3 (0.00072M)	9.8	3
NaHCO_3 (0.00138M)		

^a Reaction conditions: Cp_2TiCl_2 (0.00033M) in 25ml of H_2O added to rapidly stirred aqueous solutions containing hydroquinone (0.00033M) with added buffer at 25°C for a stirring time of 30 sec, 23 500 rev/min (no load) stirring time

^b The average pH is initial pH plus the final pH after the reaction divided by two. The pH difference in no instance was greater than 0.3pH unit

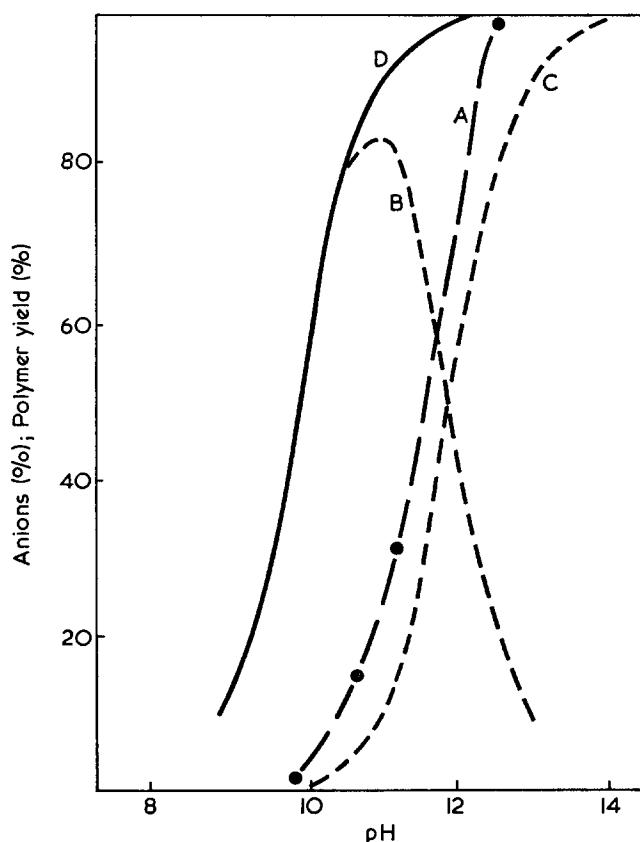


Figure 1 Plots of (A) variation of polymer yield with pH, taken from Table 1; (B) variation with pH of the percentage of total HQ present as mono-anions; (C) variation with pH of the percentage of total HQ present as di-anions; and (D) the sum of curves B and C

Figure 1 is a plot of percentage mono-ionized hydroquinone, di-ionized hydroquinone, sum of mono- and di-ionized hydroquinone and yield from Table 1. The plot of polymer yield resembles curves D and C and is consistent with the idea that the predominating active diol species in the aqueous solution condensations with Cp_2TiCl_2 is the deprotonated diol.

As noted above the active diol species for interfacial systems is probably different. The reaction of diols with acid halides occurs rapidly when the diol is in a deprotonated form¹⁶ although there are few studies

available on rates and mechanisms for this type of reaction in interfacial systems¹⁷.

Interfacial condensations utilizing buffered aqueous phases were conducted. Initially buffer solutions in the range 8.8 to 13 were used employing a 25-fold mole excess of buffer compared to diol and Cp_2TiCl_2 for interfacial systems. $\text{Cp}_2\text{Ti}(\text{OH})_2$ was produced and not the desired product. Israeli and ourselves have studied the hydrolysis of Cp_2TiCl_2 ^{18, 19}. Formation of $\text{Cp}_2\text{Ti}(\text{OH})_2$ in neutral or acidic solutions is slow, but is greatly accelerated in the presence of base. Presumably the large excess of buffer employed acted to accelerate the hydrolysis of Cp_2TiCl_2 at the exclusion of the desired ether formation. After further study, buffered systems were used where the amount of buffer was decreased representing a two-fold mole excess of buffer compared to diol and Cp_2TiCl_2 . Such systems eliminated detectable $\text{Cp}_2\text{Ti}(\text{OH})_2$ formation yet offered adequate pH control. Results appear in Table 2.

A similar pH profile study was made for the interfacial condensation of phenylphosphonic dichloride and hydroquinone where the active hydroquinone is believed to be the ion¹⁵. No product was formed below pH 9. Product yield increased with pH in a manner directly related to the increase in the amount of ionized hydroquinone. The obvious difference between the yield-pH relationship found for the reaction between phenylphosphonic dichloride and hydroquinone and the present system is consistent with the reactive species being different for the two systems.

Presumably then the active species for the interfacial condensation of Cp_2TiCl_2 with hydroquinone is the un-ionized hydroquinone. This might also imply that reaction occurs in the organic phase or near the interface since were the reaction to occur in the aqueous phase, one should expect reaction with the more active RO^\ominus to occur at the expense of the slower reaction with the un-ionized hydroquinone resulting in some pH-yield dependence similar to that observed for the reaction

Table 3 Results as a function of substituted hydroquinone

Diol	Yield (%)	
	Aqueous solution ^a	Interfacial ^b
Hydroquinone	1	46
Chlorohydroquinone	41	61
Tetrachlorohydroquinone	53	22
Methylhydroquinone	30	52
t-Butylhydroquinone	41	24
2,5-di-t-Butylhydroquinone	74	41
2,3-Dicyanohydroquinone	70	72

^a Reaction conditions; same as given in Table 1 except that Cp_2TiCl_2 is contained in 50 ml of water. Also 0.002 M of NaOH is used instead of the buffer combination

^b Same as given in Table 2, except 0.002 M of NaOH is used instead of the buffer combination

between phenylphosphonic dichloride and hydroquinone.

Further supporting evidence was sought by comparing the relative reactivity trends for interfacial and solution systems as a function of substituent(s) on the diol. Results appear in Table 3. Solubility, etc. trends were established and shown to be unimportant in determining the relative trends (Table 4). We can argue that if the reactive species in both systems is the same, then the orders of reactivity should be the same for both system types, the only difference being the presence of an organic layer which supplies a constant supply of organometallic reactant. That is, the active titanium species in both systems is the $\text{Cp}_2\text{Ti}^{2+}$ (the $\text{Cp}_2\text{Ti}^{2+}$ formed in the interfacial systems via migration from the organic layer to the aqueous layer with subsequent ionization). Further the active diol species would be either ROH or RO^\ominus with reaction occurring in the aqueous phase to permit the ionization of Cp_2TiCl_2 . The trends are dissimilar. Thus the reactive species are presumably not the same for the two types of systems.

Several observations are apparent from the trends listed in Table 4. The bottom three yields for the interfacial systems are found for the most sterically hindered diols indicating that steric hindrance is a critical factor in the interfacial systems. Steric hindrance appears to be much less important for the aqueous systems. This difference in priority is expected if the reactive titanium containing species are Cp_2TiCl_2 in interfacial systems and $\text{Cp}_2\text{Ti}^{2+}$ for aqueous solution systems. Reaction with Cp_2TiCl_2 probably occurs via a bimolecular transition state where steric considerations are important whereas reaction with $\text{Cp}_2\text{Ti}^{2+}$ occurs via a simple addition of the diol which involves less steric constraint. Second, the electronic nature of the diol appears to be of secondary importance in both the aqueous and interfacial systems.

While the direct identification of various reactive species has not yet been accomplished, the following results are consistent with the experimental results reported here. It is currently believed that the active species involved in the aqueous solution syntheses are the ionized diol and the solvated $\text{Cp}_2\text{Ti}^{2+}$ cation. The active species for the interfacial syntheses are believed to be un-ionized diol and un-ionized Cp_2TiCl_2 . Further, that the interfacial condensation occurs either quite near the interface or in the organic phase.

Table 2 Results as a function of pH for interfacial systems^a

Buffer pairs (amount)	Average pH ^b	Yield (%)	Solubility ^c (mol/l)	Distribution ratio ^d ($\text{CHCl}_3:\text{H}_2\text{O}$)
KCl (0.0004 M)	12.7	38	6.9	0.023
NaOH (0.0016 M)				
KCl (0.008 M)	12.6	33	6.6	0.020
NaOH (0.0012 M)				
Na_2HPO_4 (0.0012 M)	11.1	35	6.6	0.020
NaOH (0.0008 M)				
NaHCO_3 (0.00128 M)	9.3	35	6.5	0.023
Na_2CO_3 (0.00072 M)				
Na_2HPO_4 (0.0012 M)	8.7	36	6.4	0.020
NaHCO ₃ (0.0008 M)				

^a Reaction conditions: Cp_2TiCl_2 (0.001 M) in 50 ml CHCl_3 added to aqueous solutions containing hydroquinone (0.001 M) with added buffer (50 ml) at 25°C for a stirring time of 1 min at a stirring rate of 23 500 rev/min (no load)

^b The average pH is the initial pH of the solution plus the final pH of the aqueous layer after the reaction was run divided by two. The pH difference in no instance was greater than 0.5 pH unit

^c Solubility of hydroquinone in 10 ml of buffer solution at 25°C

^d Distribution ratio of 0.001 M of hydroquinone in 50 ml of CHCl_3 and 50 ml of buffer solution at 25°C

Table 4 Summary of solubility and reaction yield trends

Reaction order		O-H bond polarity ^{b,d}	Solubility in water (mol/l) ^c	Solubility in CHCl ₃ (mol/l) ^c	Distribution ratio of moles in CHCl ₃ ; moles in H ₂ O ^e
Aqueous solution systems ^a	Interfacial systems ^a				
2,5-di-t-Butylhydroquinone	Dicyanohydroquinone	Methylhydroquinone 2,5-di-t-Butylhydroquinone	t-Butylhydroquinone (0·13)	t-Butylhydroquinone (0·136)	64
Dicyanohydroquinone	Chlorohydroquinone		Chlorohydroquinone (0·11)	Chlorohydroquinone (0·102)	1·1
Tetrachlorohydroquinone	Methylhydroquinone	t-Butylhydroquinone	2,5-di-t-Butylhydroquinone (0·043)	2,5-di-t-Butylhydroquinone (0·0392)	7·1
Chlorohydroquinone	Hydroquinone	Hydroquinone	Methylhydroquinone (0·025)	Methylhydroquinone (0·025)	0·19
t-Butylhydroquinone	2,5-di-t-Butylhydroquinone	Chlorohydroquinone	Tetrachlorohydroquinone (0·012)	Tetrachlorohydroquinone (0·0122)	17
Methylhydroquinone	t-Butylhydroquinone	Tetrachlorohydroquinone	Hydroquinone (0·0040)	Hydroquinone (0·0091)	0·19
Hydroquinone	Tetrachlorohydroquinone	2,3-Dicyanohydroquinone	2,3-Dicyanohydroquinone (0·0031)	2,3-Dicyanohydroquinone (0·00125)	17

^a Taken from Table 3. Listed in order of yield, highest first

^b Based on Taft σ^* and Hammett σ meta, σ para values

^c At room temperature, 25°C

^d Listed in increasing order of O-H bond polarity

^e Determined using 0·001 M of diol, 50 ml CHCl₃ and 50 ml of H₂O to which 0·002 M NaOH had been added at 25°C. Order corresponds to listing in column 1

REFERENCES

- 1 Carraher, C. E. and Reimer, J. T. *Polymer* 1972, **13**, 153
- 2 Carraher, C. E. *Chem. Technol.* 1972, p 741
- 3 Carraher, C. E. and Nordin, R. *Makromol. Chem.* 1973, **164**, 87
- 4 Carraher, C. E. *Eur. Polym. J.* 1972, **8**, 215
- 5 Carraher, C. E. and Bajah, S. T. *Polymer* 1973, **14**, 42
- 6 Carraher, C. E. *Angew Makromol. Chem.* 1973, **28**, 145
- 7 Carraher, C. E. and Lessek, P. *Eur. Polym. J.* 1972, **8**, 1339
- 8 Carraher, C. E. *J. Chem. Educ.* 1969, **46**, 314
- 9 Andra, K. Z. *Chem.* 1967, **7**, 318
- 10 Calderazzo, F. *Organometal. Chem. Rev.* 1969, **B5**, 547
- 11 Doyle, G. and Tobias, R. *Inorg. Chem.* 1968, **7**, 2484
- 12 Abichandiain, C. and Jatkar, S. *J. Ind. Inst. Sci.* 1938, **21A**, 417
- 13 Long, F. and Ballinger, P. *J. Am. Chem. Soc.* 1968, **90**, 795
- 14 Carraher, C. E. *Dissert. Abstr.* 1968, **291**, 148-B
- 15 Millich, F. and Carraher, C. E. *J. Polym. Sci. (A-1)* 1969, **7**, 2669
- 16 Jaffe, H. *Chem. Rev.* 1953, **53**, 191
- 17 Morgan, P. 'Condensation Polymers: by Interfacial and Solution Methods,' John Wiley, New York, 1965
- 18 Israeli, Y. *Bull. Soc. Chim. Fr.* 1966, **3**, 837
- 19 Carraher, C. E. unpublished results

Composites formed by interstitial polymerization of vinyl monomers in polyurethane elastomers: 3. The role of graft copolymerization

G. Allen, M. J. Bowden* and G. Lewis†

Department of Chemistry, University of Manchester, Manchester M13 9PL, UK

and D. J. Blundell and G. M. Jeffs

*Imperial Chemical Industries Ltd, Corporate Laboratory,
The Heath, Runcorn, Cheshire WA7 4QE, UK*

(Received 22 May 1973)

The high impact strength of composites prepared by interstitial polymerization of methyl methacrylate (MMA) in polyurethane elastomer gels does not appear to involve graft copolymerization mechanisms for maximum efficiency in contrast with conventional rubber-modified thermoplastics. Chemical studies on 'model' systems coupled with solvent extraction measurements on the composite materials indicate that grafting does not take place. These conclusions were substantiated by dynamic mechanical results. Incorporation of poly(1,2-butadiene) into the backbone chain resulted in a marked drop in impact strength and although dynamic mechanical measurements suggest grafting occurs in this system, the lower impact strengths are probably due to the large upward shift in T_g of the corresponding elastomer.

INTRODUCTION

Conventional rubber-modified high-impact plastics consist, morphologically, of a continuous matrix of the glassy polymer in which are embedded a large number of rubbery inclusions¹⁻³. These composites can be formed by mechanical blending of preformed species, e.g. polybutadiene rubber with PVC³. An alternative method is polymerization of the vinyl monomer in the presence of a pre-formed rubber either in bulk, e.g. high-impact polystyrene (HIPS), or in emulsion as is usually done with the acrylonitrile-butadiene-styrene terpolymers (ABS)⁴.

The second method has been shown by analytical procedures⁵ to contain graft copolymer. Thermodynamic considerations^{6,7} suggest that the graft copolymer is located in the interphase region between the rubber and glassy phases where it may be thought of as improving adhesion between the phases. Where comparative studies have been carried out on such two-phase materials with and without grafting, it has been observed that samples prepared by grafting techniques are up to three times more efficient in promoting toughness than the same weight fraction of mechanically blended rubber^{8,9}. Thus, grafting of the rubber to the matrix is desirable for maximum toughness at low rubber contents.

In Part 1 we reported a novel method for obtaining high-impact cast plastics by the technique of interstitial

polymerization of a vinyl monomer, e.g. methyl methacrylate (MMA), in a polyurethane (PU) elastomer gel¹⁰. These materials have been shown to consist mainly of a continuous matrix of the elastomer with inclusions of poly(methyl methacrylate) (PMMA)¹¹. The question therefore arises whether grafting plays an important role in determining the properties of these materials.

There are reports in the literature^{12,13} that the polymerization of vinyl monomers in the presence of liquid polyether polyols leads to graft copolymers. Kuryla *et al.*¹⁴ reported their results on the polymerization of a series of vinyl compounds in the presence of excess polyether using azobisisobutyronitrile (AIBN) or benzoyl peroxide (BP) initiators. These workers claimed large percentages of grafted species although no exact figures were quoted. The products isolated after polymerization initiated with AIBN or BP were reported to be similar and they reported no evidence of improved grafting efficiency using BP as opposed to AIBN. This is contrary to other results, e.g. MMA/polyisoprene which has been shown to yield graft copolymer with BP but not AIBN¹⁵.

Beachall *et al.*¹⁶ grafted vinyl monomers to a pre-formed polyurethane but the method involved a two-step reaction via abstraction of a hydrogen atom from the urethane nitrogen with sodium hydride followed by reaction with an alkyl hydride, e.g. bromoethylacrylate, to yield a substituted urethane having a pendant ethyl acrylate group which could take part in subsequent vinyl polymerization.

* Present address: Bell Telephone Laboratories, Mountain Avenue, Murray Hill, NJ 07974, USA.

† Present address: Department of Physical Sciences, The Polytechnic, Wolverhampton WV1 1LY, UK.

In order to establish whether grafting is important in the composites prepared by interstitial polymerization we have relied on conventional extraction techniques coupled with studies on 'model' systems. We have also examined the effect on the mechanical and dynamic loss properties of composites in which telechelic hydroxy 1,2-polybutadiene was incorporated into the elastomer network to provide more potential grafting sites.

EXPERIMENTAL

Purification of materials

The purification of reagents was carried out as previously described¹⁰. Telechelic hydroxy 1,2-polybutadiene of molecular weight (*MW*) 2000 (PB-2000) (Nippon Soda Co. Ltd, Japan) was used as supplied.

Synthesis of 'model' compounds

(i) 50% w/w of MMA was mixed with 50% w/w of poly(oxypropylene glycol) of *MW* 2000 (PPG-2000) and 0.6% AIBN w/w was added. The contents were degassed and the mixture was given a normal curing cycle of 15 h at 50°C followed by 1 h at 90°C and 2 h at 120°C. An identical composite was prepared using 0.6% BP (samples A and B respectively).

(ii) 5% w/w of PB-2000 was dissolved in 95% MMA and 0.08% AIBN was added. The mixture was cured as in (i) (sample C).

(iii) A similar procedure to (ii) was carried out on a sample of pure PB-2000 (sample D).

(iv) A hydroxy-terminated prepolymer was synthesized by mixing 40 g PPG-2000 with 2.38 g of diphenylmethane 4,4'-diisocyanate (MDI). The mixture was warmed to 40°C and 0.04 g benzoyl chloride and 0.08 g dibutyltindilaurate (DBTL) were added. The reaction was exothermic rising to 90°C. It was allowed to cool back to 70°C and maintained at this temperature with vigorous stirring under N₂ for 2 h. On cooling to room temperature, a viscous liquid was obtained (sample E).

(v) 60% w/w of MMA was mixed with 40% w/w of the prepolymer and 0.6% w/w AIBN was added. The resultant mixture was cured as in (i). An identical composite was prepared using 0.6% BP (samples F and G respectively).

(vi) A low *MW* sample of PMMA was synthesized by refluxing 48 ml MMA, 75 ml toluene and 0.75 g BP for 2 h followed by precipitation into excess methanol. The filtered polymer was washed with methanol containing a few drops of HCl (to remove BP) and finally with water. The polymer was vacuum dried overnight at 55°C (sample H).

(vii) A linear polyurethane (PU) was synthesized by mixing 5.29 g MDI, with 40.71 g PPG-2000 and 0.5 g DBTL. The mixture was allowed to react overnight at room temperature followed by the cure cycle described in (i) (sample I).

Preparation of composites

Composites were prepared as described previously¹⁰ from MDI, PPG-2000 and OPG-3000 and MMA using the one-shot technique. In some cases, PPG-2000 was replaced by PB-2000. AIBN was used as the initiator although a few samples were produced with BP as the initiator.

Gel permeation chromatography (g.p.c.)

Measurements were made on a Waters Associate Instrument using the following conditions: injection time, 120 sec; flow rate, 1 ml/min; columns, 7 × 10⁵ to 5 × 10⁶ Å, 5 × 10⁴ to 1.5 × 10⁵ Å, 5 × 10³ to 1.5 × 10⁴ Å and 700 to 2000 Å; solvent, tetrahydrofuran (THF). The high molecular weight column was removed for the measurement of the prepolymer and an additional column, 100 to 350 Å, was placed at the end.

Extractions

Samples were extracted on a Soxhlet extraction apparatus using chloroform as the solvent. The extract was examined by infra-red (i.r.) and nuclear magnetic resonance (n.m.r.) techniques.

ATR infra-red spectra

The i.r. of a series of composites containing PB-2000 were measured by attenuated total internal reflection (ATR) techniques. The surfaces of the 45 mm × 15 mm were prepared with a Kent Mk II polishing machine. Spectra were calibrated by casting polymer mixtures containing known concentrations of PMMA (sample H), linear PU (sample I) and PB-2000 from chloroform solution. The solvent was flash-evaporated in an attempt to obtain a homogeneous film. The spectra contained reasonably well-defined peaks at 905 cm⁻¹ (characteristic of the —CH=CH₂ side groups in PB-2000) and 988 cm⁻¹ (characteristic of PMMA). Hydrogenation of PB-2000 led to the complete disappearance of the 905 cm⁻¹ peak. The calibrated mixtures contained 80% w/w PMMA with the remaining 20% containing linear PU and PB-2000 in proportions varying from 0 to 100% w/w PB-2000. The ratio of optical density at 905 cm⁻¹ to optical density at 988 cm⁻¹ (*R*₁) is plotted against percentage of PB-2000 in Figure 1. A smooth curve can be drawn through the points and hence by measuring *R*₁ for the insoluble composite samples, it was possible to make a reasonable estimate of the percentage of unreacted double bonds in the PU phase which contained PB-2000.

Mechanical measurements

The dynamic mechanical loss measurements were performed with a torsion pendulum as described previously¹¹. At temperatures above *T*_g, the moduli of the bulk PU samples were too low for measurements to be made.

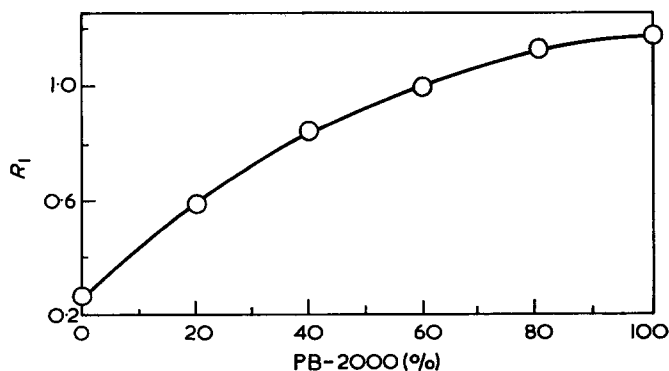


Figure 1 Ratio *R*₁ of optical densities at 905 cm⁻¹ and 988 cm⁻¹ plotted against PB-2000 (%) in the elastomer phase of a series of 80:20 PMMA/PU model mixtures

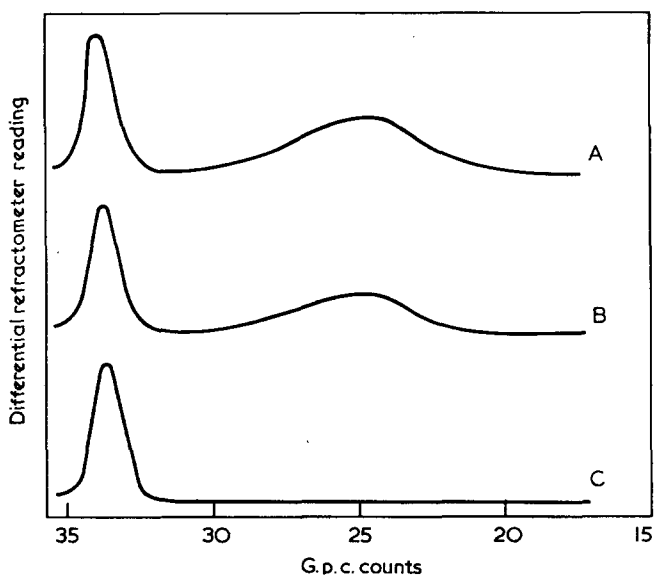


Figure 2 G.p.c. traces for a series of model composites: (A) sample A, (B) sample B, (C) 0.125% PPG-2000. Concentration of A and B in THF was 0.25%

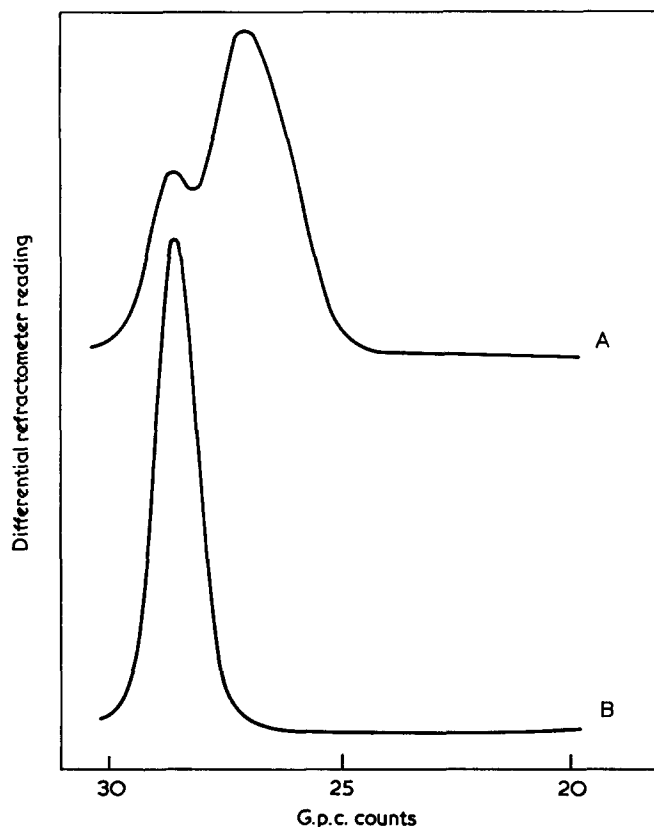


Figure 3 G.p.c. traces of (A) model prepolymer (sample E) and (B) pure PPG-2000

RESULTS AND DISCUSSION

Analysis of the g.p.c. chromatograph of both samples A and B [Figures 2(A) and 2(B)] shows that they consist of two well separated peaks. The first was very broad with a maximum at a count number of 23 and containing a low molecular weight tail extending down to 30 count numbers. The second was very sharp and centred at a count number of 33.5. The former peak was attributed to PMMA. The low molecular weight fraction could be reduced by decreasing the initiator concentration but

this increased the average molecular weight causing partial blockage of the column. The latter peak coincides with the position of a sample of pure PPG-2000 [Figure 2(C)] which is superimposable with the sharp peak on the composite when put through the column at an equivalent concentration.

The g.p.c. trace of the hydroxy-terminated prepolymer (sample E) is shown in Figure 3(A). It consists of two peaks, a somewhat broad peak centred at a count number of 27 and a sharp overlapping peak at 28.5. The latter coincides with the count number of pure PPG-2000 [Figure 3(B)]. This peak appears at a lower count number than the peak in Figure 2(C) because of the different column sequence.

Examination of the g.p.c. traces of samples F and G [Figures 4(A) and 4(B)] shows that the peaks of the prepolymer are not quite separated from the broad PMMA peak. The prepolymer peaks are unchanged in position or intensity and appear to be superimposable to within experimental accuracy with the peaks of the pure prepolymer at an equivalent concentration [Figure 4(C)]. It therefore appears that grafting does not take place on to either the polyether backbone chain or the urethane group under the conditions of composite formation. This is in contrast to the reported results of Kuryla *et al.*¹⁴.

Direct evidence for the lack of grafting has been obtained from extraction experiments on normal 80:20 PMMA/PU composites. The chloroform extract was evaporated to about 5–10 ml and the extract was precipitated into methanol. Examination of this extract by n.m.r. and i.r. showed it to consist entirely of PMMA homopolymer, the α -methyl peaks in the n.m.r. spectrum being typical for a free radical polymerization¹⁷. The methanol soluble fraction was evaporated and dried to constant weight. The extract was a viscous liquid which was identified by i.r. as a urethane linked polyether fraction. This must then represent the fraction of rubber not contributing to the elastomer network.

The amount of extractable PMMA depended on the dimension of the composite pieces being extracted. Three weeks extraction of samples from impact tests

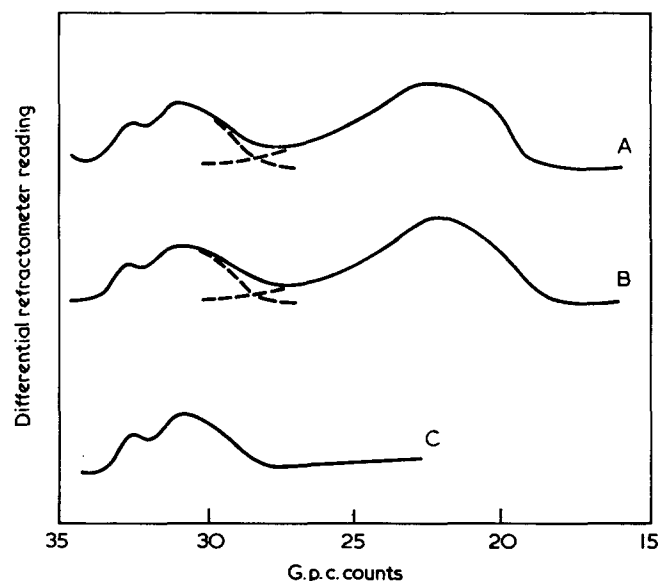


Figure 4 G.p.c. traces for a series of model composites: (A) sample F, (B) sample G, (C) 0.096% prepolymer solution. Concentration of F and G in THF was 0.25%

($\approx 25 \times 5 \times 3$ mm) only resulted in 10% PMMA as opposed to 55.8% for finely divided samples. On further two weeks extraction, the former figure rose to 20% and the latter to 65%, at which stage the experiment was abandoned. The result suggests that given long enough time, all the PMMA could be extracted since it is well known that it is difficult to extract a soluble polymer from a crosslinked matrix of a second polymer¹⁸. The amount of extractable elastomer was independent of particle size and indicated that 10–20% of the elastomer was not part of the network.

The possible effects of grafting were examined by incorporating into the polyurethane backbone chain a group, viz. poly(1,2-butadiene), to which MMA might be expected to graft. This was suggested by the fact that sample C was incompletely insoluble (in contrast to A and B) but that the g.p.c. chromatogram of sample D was identical with pure PB-2000 (Figure 5), indicating that intermolecular crosslinking of the polybutadiene did not occur under the prevailing conditions. Hence, the complete insolubility of C can only be interpreted as being due to crosslinking involving grafting of PMMA to the polybutadiene. The mechanical properties of a set of composites of composition 60:40 PMMA/PU in which the PU was prepared as described in Part 1¹⁰ but with PPG-2000 being selectively replaced by PB-2000 is shown in Table 1.

It is seen that replacing PPG-2000 with PB-2000 results in a marked decrease in notched impact strength. Since it was shown in Part 2 that impact strength is

Table 1 Variation of impact strength of a set of 60:40 PMMA/PU composites where the PU component contains varying proportions of PB-2000

Sample number	Composition of PU phase (w/w)			N/S (kJ/m ²)
	OPG-3000 (%)	PPG-2000 (%)	PB-2000 (%)	
1	25	75	0	25.4
2	25	60	15	23.1
3	25	45	30	20.1
4	25	30	45	19.9
5	25	15	60	16.5
6	25	0	75	11.8

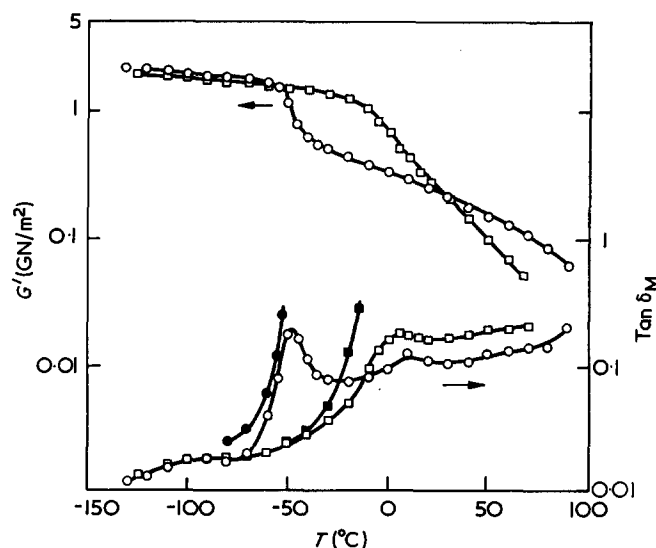


Figure 6 Variation of shear modulus (G') and loss tangent ($\tan \delta_M$) for: \circ , 60:40 PMMA/PU(25% OPG-3000/75% PPG-2000); \square , 60:40 PMMA/PU(25% OPG-3000/75% PB-2000); \bullet , PU(25% OPG-3000/75% PPG-2000); \blacksquare , PU(25% OPG-3000/75% PB-2000)

closely connected with the PU- α relaxation process¹¹, dynamic mechanical measurements might be expected to throw further light on this point.

Figure 6 shows the variation of G' and $\tan \delta_M$ with temperature for samples 1 and 6 in Table 1. The forms of the curves are similar to those described in Part 2, the dominant features being the peaks in $\tan \delta_M$ and fall in G' associated with the glass transition temperature (T_g) of the PU. However, the temperature at which this process occurs differs in the two cases. In the material containing PPG-2000 the loss peak is centred at -48°C and in the material containing PB-200 it is centred at $+6^\circ\text{C}$. In the former case the peak is well resolved and is accompanied by a discrete change in G' . The loss peak of the latter is comparatively broad and the change in G' is rather diffuse. This effect is exaggerated since the PU- α process almost coincides with the PMMA- β process. Also illustrated in Figure 6 are $\tan \delta_M$ plots for the respective bulk polyurethanes. The curve for the PU composed (w/w) of 25% OPG-3000 and 75% PPG-2000 rises quickly on approaching -50°C . Although the apparatus cannot follow the curve through the peak, the T_g can be presumed to lie in the range -52°C to -48°C . The PU composed of 25% OPG-3000 and 75% PB-2000 rises quickly near -15°C . Again the apparatus is unable to trace the peak. From the form of the curve, the T_g can be presumed to lie in the range -15°C to -10°C .

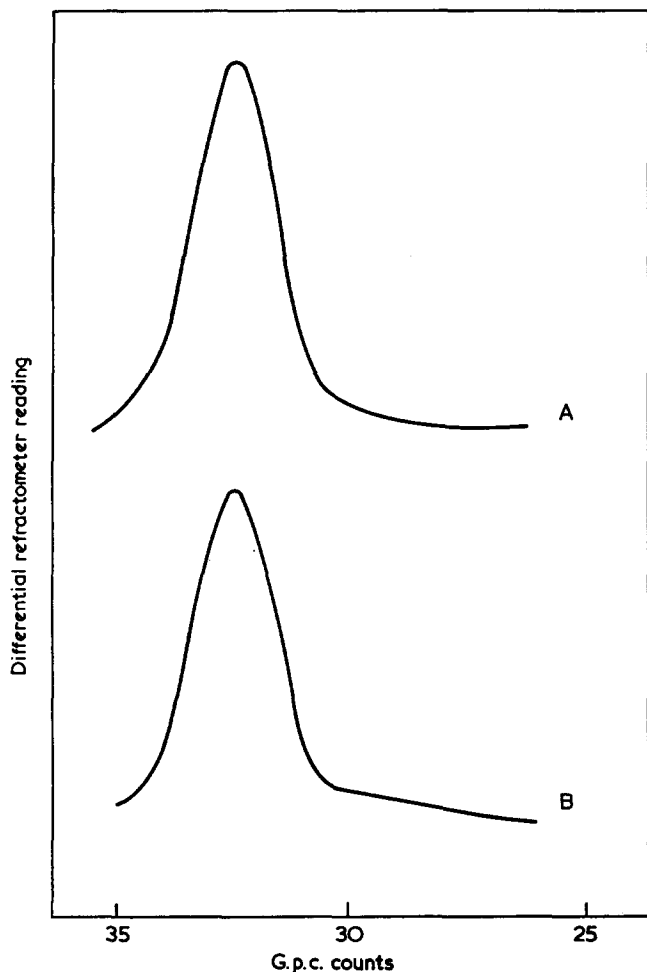


Figure 5 G.p.c. traces for (A) sample D and (B) PB-2000

The temperature of the PU- α or T_g process is substantially the same in the bulk PU containing PPG-2000 and in the corresponding composite. However, in materials containing PB-2000 the T_g of the PU in the composite is some 20°C higher than the corresponding bulk PU. This corresponds to hindrance of the PU- α process motion and would be interpreted as due to grafting of the MMA to the elastomer backbone. A similar effect was observed by Turley⁸ in studies of the effect of grafting in HIPS in which the T_g of the grafted rubber was some 10°C higher than the corresponding blended material. At the temperatures under consideration, the PMMA is immobile and would provide considerable hindrance to the PU chains bonded to it. The polyoxypropylene arms of the OPG-3000 component could undergo some motion at lower temperatures than the grafted PB-2000 sections and this spread of temperatures could result in the broad peak and diffuse change in G' .

In the PB-2000 containing materials where conditions favour grafting, the observed effects are indeed consistent with the presence of grafting. When a composite is prepared as described in Part 1¹⁰, the PU- α process occurs substantially at the same temperature as in bulk PU. Thus, on the basis of the above argument, there is no evidence of any grafting between the PU and PMMA phases thereby conforming with the conclusion drawn from extraction studies and studies on 'model' systems.

Figure 7 shows the temperature dependence of $\tan \delta_M$ and G' for each of the composites listed in Table 1. As discussed, the PU- α process of the first sample containing 75% w/w PPG-2000 occurs at -48°C and is characterized by a sharp peak in the $\tan \delta_M$ and a discrete change in G' . The intermediate materials in the series which contain PPG-2000 and PB-2000 in varying proportions show broad PU- α peaks which move upwards in temperature with increasing content of PB-2000 finally reaching a value of +6°C for 75% w/w PB-2000.

The curves for the material in which the PU consists (w/w) of 25% OPG-3000, 45% PPG-2000 and 30% PB-2000 are typical of the intermediate zone and the

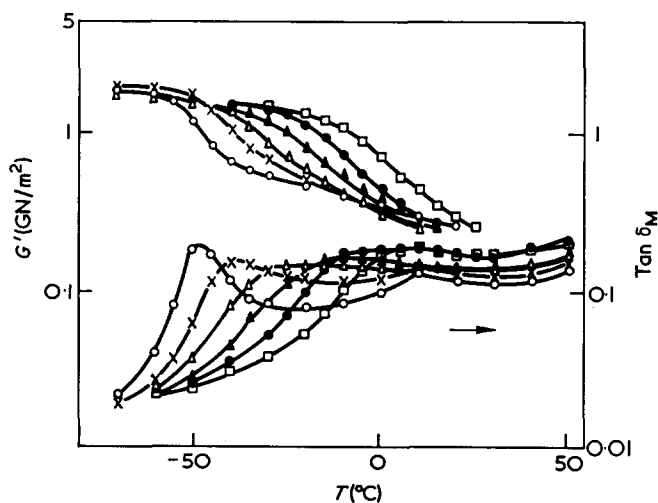


Figure 7 Variation of shear modulus (G') and loss tangent ($\tan \delta_M$) for a set of 60:40 PMMA/PU composites. The polyurethane consisted of 25% OPG-3000, the remaining fraction being: ○, 75% PPG-2000; ×, 60% PPG-2000/15% PB-2000; △, 45% PPG-2000/30% PB-2000; ▲, 30% PPG-2000/45% PB-2000; ●, 15% PPG-2000/60% PB-2000; □, 75% PB-2000

Table 2 ATR estimation of polybutadiene in the elastomer phase of the composite having unreacted double bonds

Sample number	K (%)	R_1	L (%)
1	9	0.481	13
2	22	0.650	25
3	44	0.934	52
4	66	1.120	80
5	66	0.986	58

peak in $\tan \delta_M$ extends from -25°C until it merges with the PMMA β -process at room temperature. The corresponding change in G' occurs over a similarly broad temperature range. Electron microscopy¹¹ suggested that the PB-2000 sequences were not uniformly distributed within the PU and was interpreted as due to a separation into regions rich in PPG-2000 and PB-2000 respectively. This could explain the observed broadness in the plots of $\tan \delta_M$ and G' against temperature with the regions rich in PPG-2000 undergoing motion at the lower temperature followed at higher temperatures by the grafted PB-2000 segments. This would tend to produce double peaks in $\tan \delta_M$ which might be observed as broad peaks of the form shown in Figure 7. Since the dynamic mechanical and 'model' composite studies suggest that grafting takes place in the polybutadiene chain, it should be possible to gain some insight into the mechanism from infra-red studies. There appear to be, *a priori*, three possible mechanisms¹⁹: (1) abstraction of the allylic hydrogen by the initiator radical to give a free radical site which can subsequently initiate polymerization; (2) addition of an initiator radical to the double bond; (3) chain transfer of the growing PMMA chain to the polybutadiene backbone.

Table 2 shows the ATR results for a series of 80:20 PMMA/PU composites containing known percentages (K) of PB-2000. The ratio R_1 of optical densities at 905 cm^{-1} and 988 cm^{-1} was measured and the percentage of double bonds (L) was calculated by reference to Figure 1.

This comparison can only be approximate in view of the errors involved in the measurements, viz. the homogeneity of the calibration film and the precise determination of R_1 for both calibrated samples and composites due to the peaks not being well-defined. It appears that the double bond concentration in the composite is overestimated since $L > K$ with the exception of sample 5 which was initiated by 0.24% BP in contrast to the others which were initiated with 0.08% AIBN. However, in spite of the errors in the measurement it would appear that grafting through the $-\text{CH}=\text{CH}_2$ group with AIBN initiation does not take place, i.e. (2) can be eliminated. (3) can also be eliminated in view of the low chain transfer constant of a growing PMMA chain¹⁹ suggesting that grafting takes place, by abstraction of the tertiary allylic hydrogen atom²⁰ thus providing a site for polymerization of MMA. In the case of initiation by BP, the ATR spectra indicate that mechanism (2) is also important, presumably as a result of the enhanced reactivity of the benzoyloxy radical.

CONCLUSIONS

Both chemical and dynamic mechanical evidence point to the fact that composites prepared by the method

described in Part 1 do not contain any grafted species. Unfortunately it has not proved possible to establish what effect grafting would have on the mechanical or morphological properties of these composites.

In view of the results of Part 2¹¹, the poor impact strength obtained when PB-2000 was incorporated in the backbone chain is probably associated with the large upward shift of the loss peak, i.e. T_g of the rubber phase from -48°C to $+6^\circ\text{C}$, although grafting does appear to take place in this system.

ACKNOWLEDGEMENTS

The authors wish to thank Mr D. Roy for carrying out the g.p.c. analyses.

One of us (M. J. B.) wishes to thank Imperial Chemical Industries and later the University of Queensland for the award of successive Post Doctoral Fellowships.

REFERENCES

- 1 Williams, R. J. and Hudson, R. W. *Polymer* 1967, **8**, 643
- 2 Kato, K. *Polym. Eng. Sci.* 1967, **7**, 38
- 3 Matsuo, M., Nozaki, C. and Jyo, E. *Polym. Eng. Sci.* 1969, **9**, 197
- 4 Fettes, E. M. and Mackay, W. N. *Appl. Polym. Symp.* 1968, **7**, 3
- 5 Gesner, B. D. *J. Polym. Sci. (A)* 1965, **3**, 3825
- 6 Molau, G. E. *J. Polym. Sci. (A)* 1965, **3**, 1267
- 7 Molau, G. E. *J. Polym. Sci. (A)* 1965, **3**, 4235
- 8 Turley, S. G. *J. Polym. Sci. (C)* 1963, **1**, 101
- 9 Bergen, R. L. *Appl. Polym. Symp.* 1968, **7**, 41
- 10 Allen, G., Bowden, M. J., Blundell, D. J., Hutchinson, F. G., Jeffs, G. M. and Vyvoda, J. *Polymer* 1973, **14**, 597
- 11 Allen, G., Bowden, M. J., Blundell, D. J., Jeffs, G. M., Vyvoda, J. and White, T. *Polymer* 1973, **14**, 604
- 12 Chem. Werke Huls AG, Ger. Pat. 1 132 724 (1962)
- 13 Kahrs, K. H. and Zimmerman, J. W. *Makromol. Chem.* 1962, **58**, 75
- 14 Kuryla, W. C., Critchfield, F. E., Platt, L. W. and Stamberger, P. *J. Cellular Plast.* 1966, **2**, 84
- 15 Allen, P. W., Ayrely, G., Moore, C. G. and Scanlon, J. *J. Polym. Sci.* 1959, **36**, 55
- 16 Beachall, H. C., Blumstein, R. and Peterson, J. C. *J. Polym. Sci. (C)* 1969, **22**, 569
- 17 Bovey, F. A. and Tiers, G. V. D. *J. Polym. Sci.* 1960, **44**, 173
- 18 Morton, M. and Healy, J. C. *Appl. Polym. Symp.* 1968, **7**, 155
- 19 Ceresa, R. J. 'Block and Graft Copolymers', Butterworths, London, 1962, Ch 2
- 20 van der Hoff, B. M. E. *Appl. Polym. Symp.* 1968, **7**, 21

Composites formed by interstitial polymerization of vinyl monomers in polyurethane elastomers:

4. Preparation, properties and structure of acrylonitrile and styrene based composites

G. Allen, M. J. Bowden* and G. Lewis†

Department of Chemistry, University of Manchester, Manchester M13 9PL, UK

and D. J. Blundell, G. M. Jeffs and J. Vyvoda

*Imperial Chemical Industries Ltd, Corporate Laboratory,
The Heath, Runcorn, Cheshire WA7 4QE, UK*

(Received 22 May 1973)

The preparation of composites by interstitial polymerization of acrylonitrile in a polyurethane and also of styrene in a polyurethane are described. The styrene composites are more difficult to prepare but the acrylonitrile composites are similar in ease of preparation, appearance and properties to that of the MMA composites described in Parts 1 and 2. The polymerization conditions, morphology, relaxation properties and impact strength for a series of composites of each kind are reported and compared with the corresponding MMA composites.

INTRODUCTION

Previous papers¹⁻³ in this series have dealt with the preparation, properties and structure of composites of high impact strength prepared by interstitially polymerizing methyl methacrylate (MMA) within a polyurethane (PU) gel. This paper describes an extension of this interstitial process in which the vinyl monomer is replaced by acrylonitrile and styrene with particular emphasis on polyacrylonitrile/polyurethane (PAN/PU) composites.

Briefly, the interstitial process involves first dissolving the PU precursors (i.e. polyols and diisocyanate) in the vinyl monomer. Next the PU component is gelled by using a selective catalyst that promotes the urethane reaction at room temperature. Finally, the vinyl monomer is polymerized at a higher temperature by free radical initiation. The basic process can, in principle, be extended to any polymer/elastomer combination providing the monomer can both dissolve the elastomer precursors and swell the gel, and providing the relation of the elastomer can be carried out independently of the polymerization of the monomer. Studies on the PMMA/PU system have shown that an inclusion of 20% PU can promote about a tenfold increase in impact resistance for about a 50% drop in modulus. It has been found that the morphology² consists essentially of near-spherical domains of the PMMA phase embedded

in a continuous matrix of the PU phase. Studies of the molecular relaxation processes² confirmed the existence of two distinct phases but also indicated some degree of interaction between phases. Factors that were found to have the most effect upon the properties or structure of the composites were: (i) overall ratio of PMMA/PU; (ii) molar ratio of isocyanate to hydroxyl groups; (iii) theoretical molecular weight \bar{M}_c between crosslinks in PU network; and (iv) time interval between gelation of the PU and subsequent polymerization of MMA.

Acrylonitrile fulfils the required conditions of compatibility which allows interstitial composites to be made with the same type of polyether urethane as was used in the PMMA study. Most of the PAN/PU composites discussed in this paper use a PU made by reacting near-stoichiometric amounts of diphenylmethane 4,4'-diisocyanate (MDI) with oxypropylated glycerol of molecular weight 3000 (OPG-3000); this gives a theoretical \bar{M}_c for the PU network of 2250 compared with the 4500 used in the majority of the work on the PMMA/PU system. The case of PAN is of particular interest in that unlike PMMA, it is insoluble in its monomer. This property is problematic in trying to produce good glassy solids of PAN by bulk polymerization. The polymerizing monomer soon becomes turbid and finally the polymer precipitates to give a compact aggregation of precipitated particles⁴. Shavit and co-workers^{5,6} discovered a process for obtaining clear samples by bulk polymerization which involved polymerization of monomer around the precipitated polymer particles at a slow enough rate to allow monomer to

* Present address: Bell Telephone Laboratories, Murray Hill, Mountain Avenue, NJ 07994, USA.

† Present address: Department of Physical Sciences, The Polytechnic, Wolverhampton WV1 1LY, UK.

diffuse into the voids. This process, later improved by Pellon *et al.*⁷ required several days in order to obtain transparent sheets, a typical cure cycle with *p*-toluenesulphonic acid in aqueous hydrogen peroxide initiator being 3 days at 20°C, 2 days at 23°C, 2 days at 29°C, 1 day at 35°C and 5 days at 40°C⁸. The process was further complicated by the continual addition of uncatalysed monomer to compensate for the shrinkage (~30%) on polymerization. Recent advances in this field^{8,9} have been concerned with moulding of the final product to give a clear sheet but, as yet, bulk polymerization has proved unsatisfactory as a commercial casting process. The final product is also very brittle¹⁰. The interstitial systems of PAN are therefore of additional interest as a means of easily producing strong castings by a bulk polymerization process which avoids the difficulties normally encountered with pure PAN.

Styrene is similar to MMA in that the polymer is soluble in the monomer and hence should give composites with similar characteristics to the PMMA interstitial system. However, it is difficult to take the monomer to 100% conversion without using conditions which might prove adverse to the final composite, such as a final cure at 160°C as is used in the commercial bulk polymerization of styrene¹¹. Attempts have therefore been made to complete the conversion of the monomer using γ -irradiation. Even so, it was difficult to obtain samples with reproducible mechanical properties. In this paper the work on the polystyrene/polyurethane (PS/PU) system is therefore only reported briefly and the results are included mainly to demonstrate the generalities of the interstitial process for vinyl monomers and to compare the relaxation properties.

EXPERIMENTAL

Purification of materials

All materials were purified, similarly to that described in Part 1¹. Styrene was fractionally distilled from CaH₂ (c.p. 65°C at 50 mmHg) and acrylonitrile (AN) was fractionally distilled at atmospheric pressure (c.p. 80°C at 760 mmHg). Since commercial AN contained about 7% water, it was carefully dried by refluxing for several hours over powdered CaH₂ followed by fractional distillation. The presence of water above trace amounts caused cloudiness to develop during gelation. Hence, it was essential that all materials were scrupulously dry. Azobisisobutyronitrile (AIBN) was used as supplied but benzoyl peroxide (BP) was purified by recrystallization from chloroform.

Preparation of samples

Composites were prepared by the one-shot technique described previously. The polymerization of AN is extremely exothermic which placed an upper limit of ~50°C for the initial polymerization temperature at the initiator concentrations used. A final cure of 2–4 h at 90°C was used to ensure complete polymerization.

A sample of pure PAN homopolymer was prepared by the method described by Shavit *et al.*⁵. Approximately 16 g of AN containing 0.04% AIBN were sealed into a glass tube (i.d. 10 mm) and polymerized for 24 h at 45°C with the tube half immersed in the bath. The temperature was then raised gradually to 80°C at which

Table 1 Effect of γ -irradiation on the properties of 70:30 PS/PU composites after initial thermal treatment with different initiators (BP: 4 days at 80°C; AIBN: 4 days at 60°C)

Dose (Mrad)	BP		AIBN	
	NIS (kJ/m ²)	G' (GN/m ²)	NIS (kJ/m ²)	G' (GN/m ²)
0.00	6.1	0.26	27.5	0.28
0.47	4.0	0.39	24.5	0.35
0.64	4.0	0.40	25.7	0.33
1.28	4.0	0.39	25.6	0.33
3.77	3.7	0.40	24.2	0.34

temperature the bottom half of the immersed sample was transformed into a yellow glassy transparent material. This was sectioned for mechanical testing.

Different polymerization conditions were used for PS/PU composites in an effort to obtain high conversion. AIBN was found to be unsuitable for curing at 120°C, owing to the formation of bubbles in the sample, presumably as a result of nitrogen gas liberated from the decomposing initiator or local 'hot spots' resulting in vaporization of the monomer. This problem did not occur using BP as the initiator, but the impact strength decreased after two days at 120°C and moduli were low. In addition, discoloration of the composite occurred at this temperature. An alternative technique was devised in which styrene was polymerized using conventional initiators (AIBN and BP) at comparatively low temperatures (60°C and 80°C respectively) and the cure was completed by γ -irradiation at room temperature. The total dose from the ⁶⁰Co source was measured by Avisco cellophane dosimetry. The results are shown in Table 1, where it can be seen that AIBN initiated samples have much higher impact strengths than BP initiated samples for little sacrifice in shear modulus. On the basis of Table 1, samples were prepared using 0.4% AIBN at 60°C for 4 days followed by a total dose of 1.3 Mrad.

Mechanical measurements

The mechanical measurements of shear modulus (*G'*) and notched impact strength (*NIS*) were carried out as previously described². All measurements were at room temperature (22–24°C).

Loss measurements

The measurement of the dynamic mechanical and dielectric loss characteristics were carried out as previously described².

Morphological measurements

Samples were sectioned with a microtome, shadowed and examined by electron microscopy as previously described². Owing to differences in cutting characteristics on sectioning, micrographs of PAN/PU composites were in general more difficult to analyse than the corresponding PMMA/PU composites. The accuracy of measurements of the mean chord intercept length \bar{L} across the domains was therefore lower, being typically about 25%.

RESULTS

Physical properties

The elastomer precursors gelled in solutions of both monomers to give clear gels. Providing thermal runaway

did not occur, the polymerization of AN in the gel posed no experimental difficulties. The variation in turbidity as polymerization proceeded was quite striking. The transmittance through the gel first decreased until the castings were opaque and then increased again as the conversion became complete. The final transmittance at room temperature of a typical 70% PAN sheet 3 mm thick at 590 nm wavelength was about 70–75%. In the few PS/PU samples examined the corresponding transmittance was no better than 40%. In the normal bulk polymerization of PAN, if no special precautions are taken, the final product is powdery and completely opaque owing to the gaps in the polymer aggregates. It was only when the method of Shavit *et al.* was used that the final polymer was a clear continuous solid. The bulk polymer produced by this method did not dissolve in dimethylformamide (DMF) but only swelled. The PAN/PU composites could only be swelled by 30%. This should be compared with the PMMA/PU systems which normally swell by as much as 1000%. All the PAN/PU composites cured at temperatures >90°C developed a yellow colour.

Morphology

Electron microscopy of PAN/PU and PS/PU composites gave similar results to the corresponding PMMA/PU composites. The micrographs were consistent with the interpretation of a morphology consisting to a first approximation of spherical domains of the vinyl polymer embedded in a continuous matrix of PU. Figure 1 shows a typical section from a 70:30 PAN/PU composite based on OPG-3000 polyol. The inclusions, about 100 nm across, were interpreted as the PAN domains. Similar micrographs were obtained from PS/PU composites. Several PAN/PU composites were examined to investigate the effect of the experimental parameters on the size of the inclusions.

The variation of \bar{L} with PAN/PU composition is shown in Table 2. The PU was prepared from 100% OPG-3000. The ranges of the other parameters investigated were: (i) theoretical \bar{M}_c from 950 to 4500; (ii) NCO/OH molar ratio from 0.9:1 to 1.2:1; (iii)

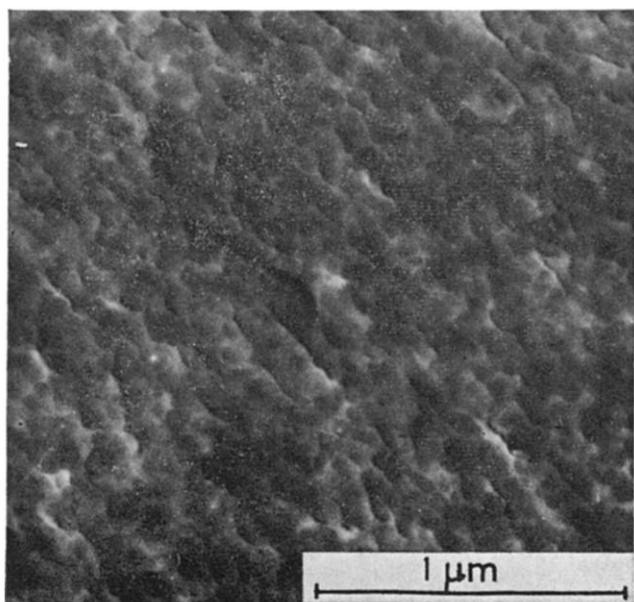


Figure 1 Electron micrograph of a section from a 70:30 PAN/PU composite based on OPG-3000 polyol

Table 2 Variation of domain size with proportion of PAN for a series of PAN/PU composites with \bar{M}_c 2250

PAN (%)	\bar{L} (nm)
80	90
70	65
60	50
50	40

Table 3 Variation of NIS and G' with PU \bar{M}_c for different polyvinyl inclusions (70:30 polyvinyl/PU)

\bar{M}_c	PMMA/PU		PS/PU		PAN/PU	
	NIS (kJ/m ²)	G' (GN/m ²)	NIS (kJ/m ²)	G' (GN/m ²)	NIS (kJ/m ²)	G' (GN/m ²)
4500	17.1	0.35	—	0.08	34.7	0.50
2250	13.0	0.41	26.0	0.34	26.2	0.52
1250	2.1	0.89	—	—	—	—
950	1.8	1.19	2.4	0.56	12.0	0.56

[AIBN] from 0.06% to 0.6%; and (iv) the effect of the time difference between gelation and polymerization. The effect of polymerization temperature was not investigated. The variation in the above four parameters was found to produce no significant change in domain size. Thus, within the ranges studied, neither the polymerization rate of the vinyl phase, as affected by the initiator concentration, nor the molecular structure of the gel network, as affected by the other parameters, appeared to affect the nucleation and growth of the glassy domains in PAN/PU composites.

Mechanical properties

The parameters involved in preparing PAN/PU composites of optimum mechanical properties have been fully investigated. The results are qualitatively the same as those for PMMA/PU composites but different values were necessary to ensure optimum properties, e.g. an NCO/OH molar ratio of 1.2:1 has been found to give the best and most reproducible properties.

For styrene a similar search for optimum properties was not made because of the difficulties of preparation.

The most marked property changes are observed by varying \bar{M}_c or composition as shown in Tables 3 and 4.

The NIS decreases and G' increases as \bar{M}_c is decreased or as the percentage of elastomer is decreased. The results for PAN/PU were more reproducible than those for PS/PU composites. The sample of PS/PU for $\bar{M}_c=4500$ was too rubbery for the NIS to be determined, while the PAN/PU with 10% elastomer was too brittle to notch.

Also shown in Tables 3 and 4 for the purpose of comparison are the NIS and G' of the PMMA/PU composites. The best combinations of modulus and impact strength are possessed by PAN/PU composites with PMMA/PU composites having medium toughness and moduli. PS/PU composites were often very tough but this was offset by low moduli, presumably owing to polymerization difficulties.

Relaxation measurements

Dynamic mechanical measurements. The dynamic mechanical properties of PAN/PU and PS/PU composites are

Table 4 Variation of NIS and G' with composition for different polyvinyl inclusions (PU \bar{M}_c 2250)

Composition polyvinyl/PU (%)	PMMA/PU		PS/PU		PAN/PU	
	NIS (kJ/m ²)	G' (GN/m ²)	NIS (kJ/m ²)	G' (GN/m ²)	NIS (kJ/m ²)	G' (GN/m ²)
90:10	1.5	1.15	—	—	—	1.15
80:20	2.4	0.76	23.0	0.44	11.7	0.91
70:30	13.0	0.50	26.0	0.34	26.2	0.52
60:40	23.2	0.27	38.7	0.16	27.0	0.22
50:50	42.5	0.14	—	0.08	31.0	0.09

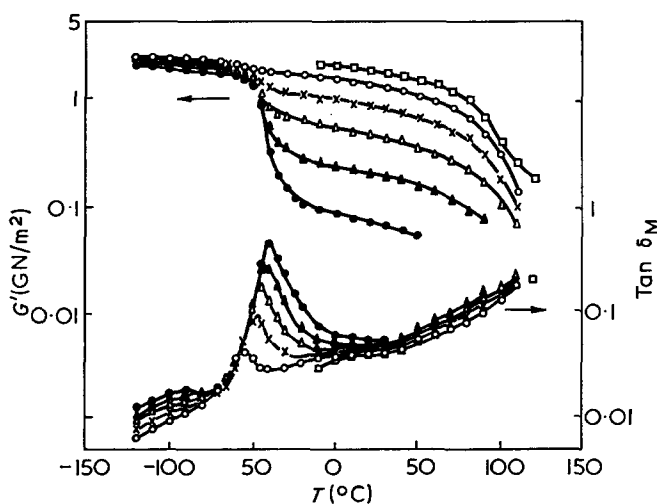


Figure 2 Shear modulus (G') and loss tangent ($\tan \delta_M$) as functions of temperature (T) for 100% PAN (\square) and for composites PAN/PU: \circ , 90:10; \times , 80:20; \triangle , 70:30; \blacktriangle , 60:40; \bullet , 50:50. PU $\bar{M}_c=2250$

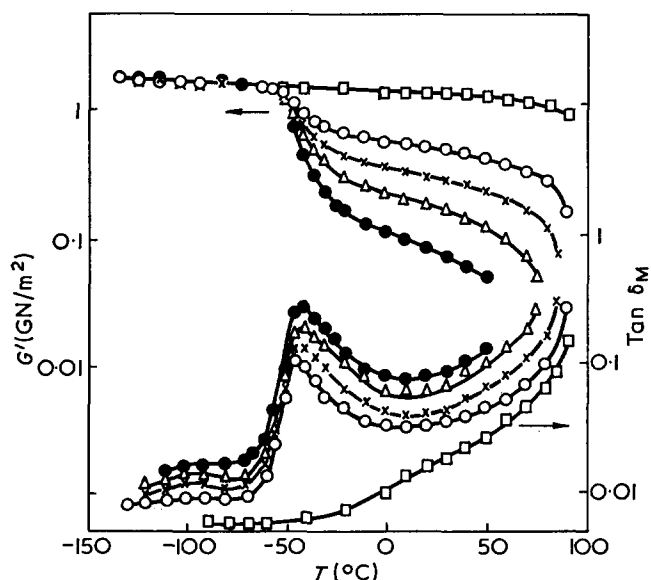


Figure 3 Shear modulus (G') and loss tangent ($\tan \delta_M$) as functions of temperature (T) for 100% PS (\square) and for composites PS/PU: \circ , 80:20; \times , 70:30; \triangle , 60:40; \bullet , 50:50. PU $\bar{M}_c=2250$

illustrated in Figures 2 and 3 where both shear modulus, G' , and loss tangent, $\tan \delta_M$, are plotted as functions of temperature for the vinyl homopolymers and for composites containing progressively increasing amounts of PU with \bar{M}_c 2250. Both sets of curves show a peak in $\tan \delta_M$ at low temperatures ($\sim -90^\circ\text{C}$); this is the PU- β relaxation process. The amplitude of this peak increases with increasing proportion of PU in the composites. This process is rather broad and shallow and consequently no significant drop in G' was observed.

Both sets of curves also show a much larger peak in $\tan \delta_M$ at higher temperatures (-50 to -40°C). The amplitude of this peak also increases with increasing proportion of PU in the composite and, in addition, the peaks move to higher temperatures. This peak is evidence of the α or glass transition process of the PU, and is accompanied by a large and discrete fall in G' .

In Figure 2 a rather insignificant loss process is observed as a plateau at about 10°C in the $\tan \delta_M$ curves. This process is most prominent in the case of the 100% PAN material and this is presumably the β -process of PAN. There is little change in G' through this process and no significant fall in G' is observed for PAN/PU composites until G' falls (and $\tan \delta_M$ increases) on approaching the α or glass transition process of PAN near 100°C . In Figure 3 the β -process¹² of PS is not very prominent and the loss curves above room temperature are dominated by a general increase in $\tan \delta$ merging with the α or glass transition process near 100°C . In this temperature range it is seen that there is an appreciable fall in G' .

The effect of varying \bar{M}_c on the dynamic mechanical properties of the composites is illustrated in Figures 4 and 5 where G' and $\tan \delta_M$ are plotted as functions of temperature for PU \bar{M}_c values of 4500 (only for PAN/PU), 2250, 1250 (only for PAN/PU) and 950. All the composites contained 70% of the respective polyvinyl.

For all the composites, the PU- β process is seen to have been relatively unaffected by the variation of \bar{M}_c . However, the positions of the PU- α peaks and the corresponding changes in G' are dependent upon \bar{M}_c and move to higher temperatures as \bar{M}_c decreases. Varying \bar{M}_c appears to have little effect on the peak shapes or amplitudes.

Comparison of dynamic mechanical properties in the three composite systems. Figure 6 shows the variation of G' and $\tan \delta_M$ with temperature for PMMA/PU, PS/PU and PAN/PU composites, each containing 70% of the respective polyvinyl and 30% of PU with \bar{M}_c 2250.

At higher temperatures the PMMA/PU composite displays a large PMMA- β loss peak and consequently G' drops quite quickly. The loss processes in the other composites are less active near room temperature and in these cases the fall in G' is less pronounced. Near 100°C all plots show evidence of the respective α -processes in the polyvinyls. The increase in $\tan \delta_M$ and the fall of G' in PAN/PU composites are less rapid than in the other two composites. These differences in behaviour are reflected by the temperatures at which the G' of the respective composites falls below the arbitrary 'softening level' of 0.1 GN/m^2 . For PMMA/PU, PS/PU

and PAN/PU the temperatures are 75, 82 and 102°C respectively.

Dielectric measurements and comparison with measurements on PMMA/PU composites. Figure 7 illustrates the variation of the dielectric loss tangent, $\tan \delta_D$, with temperature for PAN/PU and PS/PU composites together with the plot for a PMMA/PU composite. The measurements were made at 1 kHz and all samples contained (w/w) 40% of the respective vinyl polymer and 60% of PU with \bar{M}_c 4500. Measurements were also made over the frequency range from 60 Hz to 10 kHz.

At low temperatures the PU- β peaks appear at similar positions. The amplitude of this peak in the PS/PU composite falls below its level in the other materials. This is due to the very much lower dielectric loss in PS compared with the other vinyl polymers. The PU- α peaks of the three materials differ both in amplitude and in temperature. The PAN/PU composite possesses the largest amplitude PU- α peak which occurs at -30°C. In the PS/PU composite the peak is of smaller amplitude

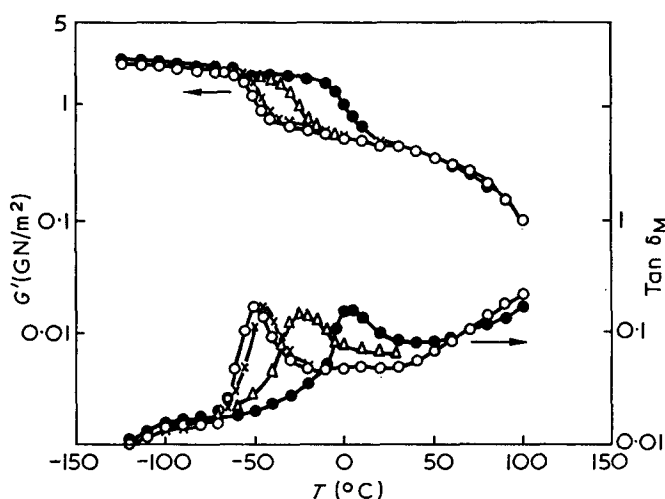


Figure 4 Shear modulus (G') and loss tangent ($\tan \delta_M$) as functions of temperature (T) for 70:30 PAN/PU composites. PU theoretical \bar{M}_c : \circ , 4500; \times , 2250; \triangle , 1250; \bullet , 950

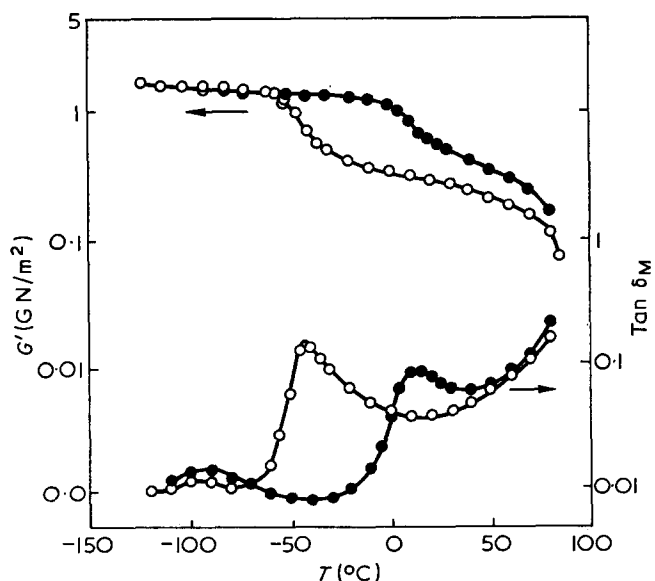


Figure 5 Shear modulus (G') and loss tangent ($\tan \delta_M$) as functions of temperature (T) for 70:30 PS/PU composites. PU theoretical \bar{M}_c : \circ , 2250; \bullet , 950

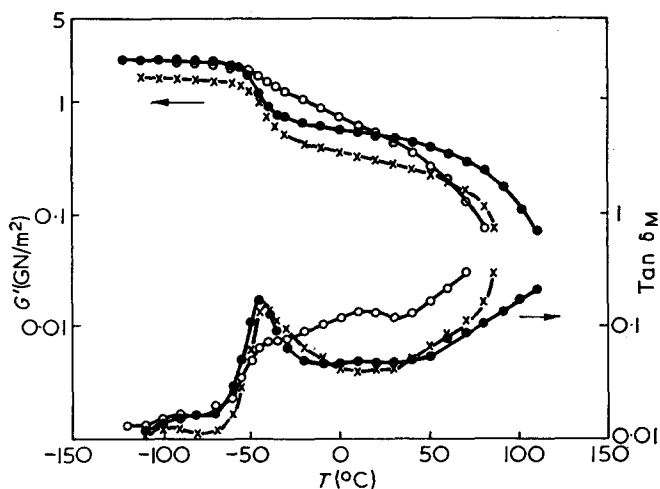


Figure 6 Comparison of dynamic mechanical properties of 70:30 PAN/PU (\bullet) and 70:30 PS/PU (\times) composites with 70:30 PMMA/PU (\circ) composite. PU \bar{M}_c =2250

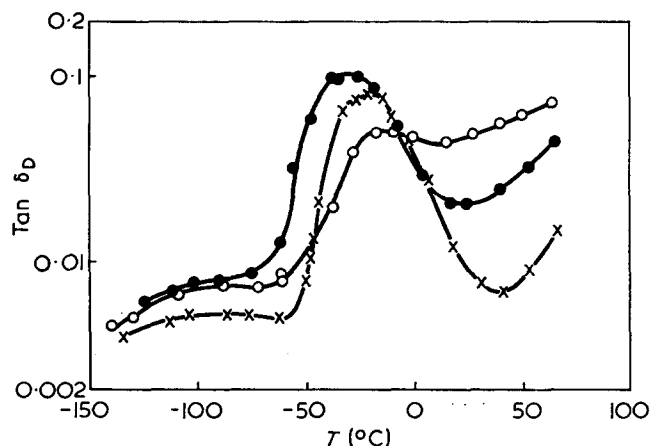


Figure 7 Dielectric loss tangent ($\tan \delta_D$) as a function of temperature (T) for: \bullet , 40:60 PAN/PU; \times , 40:60 PS/PU; \circ , 40:60 PMMA/PU. PU \bar{M}_c =4500

and occurs at -22°C and in the PMMA/PU composite the amplitude is further reduced and the peak occurs at -14°C.

At high temperatures, $\tan \delta_D$ drops to a low level in the PS/PU composite and in the PMMA/PU system $\tan \delta_D$ increases on approaching the β -process of PMMA which is centred at 80°C².

Temperature dependence of impact strength. The variation of toughness with temperature for PAN/PU composites is shown in Figure 8 where NIS is plotted for samples containing 70% of PAN and 30% (w/w) of PU with \bar{M}_c 2250 and 950. Both composites were brittle at low temperatures. The sample of higher \bar{M}_c begins to toughen near -50°C and the NIS increases rapidly to a value of 18 kJ/m² at -30°C above which temperature the increase is less rapid. The sample of lower \bar{M}_c begins to toughen at -10°C and the NIS increases quickly to 9 kJ/m² at 10°C and then increases less quickly.

Comparison of these results with those for a similar experiment (Part 2) with PMMA/PU composites shows that, for a given PU \bar{M}_c , the onset of toughening occurs at a lower temperature in PAN/PU than in PMMA/PU composites.

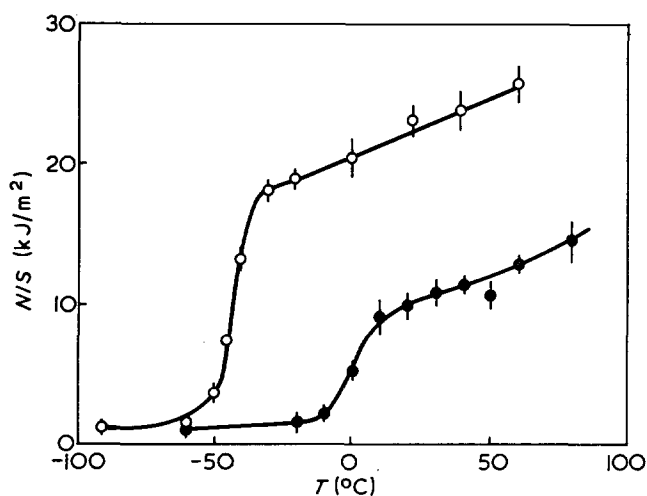


Figure 8 Charpy notched impact strength (N/S) as a function of temperature (T) for 70:30 PAN/PU composites of PU theoretical \bar{M}_c 2250 (○) and 950 (●)

DISCUSSION

Polymerization and morphology

The basic morphology consisting to a first approximation of polyvinyl domains embedded in a continuous PU matrix occurs in all the vinyl interstitial systems examined. Its occurrence appears to be independent of whether the polymer is insoluble in its monomer as with PAN or whether the polymer can be swollen by its own monomer as with MMA and styrene.

The variation of the domain size with the PAN/PU composition ratio is similar to that found in the PMMA system. However, for a given composition, the size of the PAN domains is relatively insensitive to the other experimental variables. This is surprising when compared with the PMMA/PU system where it was found that the domain size depended critically on those factors affecting the structure of PU gel, i.e. $[NCO]/[OH]$ ratio, \bar{M}_c and the period allowed between gelation and the beginning of vinyl polymerization. The non-dependence on the post-gelation period in the PAN case is probably a result of the induction time at 50°C being long enough for the PU gel to form completely before any appreciable AN polymerization. The choice of $[NCO]/[OH]$ and \bar{M}_c is expected to determine the structure of the PU at a molecular level. The difference in the effect of these parameters between the PMMA and PAN systems is perhaps related to the differences in solubility of the polymers in their respective monomers and hence to differences in the nucleation and growth of the polymer domains inside the gel. Another distinction between the two systems which may have important effects on the structure of the gel at the supramolecular level is the different swelling powers of AN and MMA inside the PU gel. For a given PU elastomer it has been found that the equilibrium uptake of AN in the elastomer is only about two-thirds that of MMA monomer. Consequently any microgel regions formed during the initial stages of gelation would be in a tighter conformation in AN than in MMA. Microsyneresis from the microgel regions would therefore be more likely to occur in AN and it is possible that the resulting inhomogeneities in the supramolecular structure might become insensitive to the details at a molecular level. This could explain the observed insensitivity to $[NCO]/[OH]$ and

\bar{M}_c without contradicting the general conclusion made in Part 2 that the domain size is governed by the tightness of the gel structure (mainly at a supramolecular level).

In some respects the polymerization process and turbidity changes in the PAN/PU composites are similar to the bulk polymerization of PAN. In both cases there is an initial increase in turbidity associated with the formation of PAN domains which are a consequence of the insolubility of the polymer in the suspending medium. In the bulk polymerization the medium is the liquid monomer which allows the free movement of the PAN domains. In the composite case where the medium is the PU gel swollen with monomer. Incompatibility is enhanced and the domains are restrained to the positions in the gel where they were originally nucleated. As polymerization proceeds the domains in the bulk polymerization diffuse until agglomeration and normal growth cause an opaque precipitate to form at the bottom of the reaction tube. If the polymerization is carried out normally at about 50°C, the gaps both within and between the agglomerates are usually never completely filled by polymer so that the final product is a white powdery solid. When, however, the method of Shavit *et al.* is used, where the diffusion and polymerization of AN inside the gaps is carefully controlled, the opaque region can be transformed into a clear, glassy solid. This final transformation is physically analogous to the final stages in the preparation of the composite in which the turbidity decreases to a level which depends on the domain size and the difference in refractive index between the PAN and PU phases¹². The comparison between the composite and the two cases of bulk polymerization shows that apart from its main purpose as an impact modifier, the PU plays an additional role in enabling good, strong solids to be obtained with comparative ease from the normally difficult polymerization of AN. The PU gel provides a uniformly nucleated system in which there are strong restraints on the movement and agglomeration of the PAN domains. This structure provides a ready diffusion path for supplying monomer to the growing domains, thus simulating the controlled conditions used by Shavit *et al.* in their bulk polymerization of AN.

The yellowing observed in composites cured at >90°C and also seen in the clear bulk polymerized PAN sample is probably due to conjugation resulting from the cyclization of the $C\equiv N$ bonds¹³. The insolubility of the bulk polymerized PAN sample in DMF indicates a slight crosslinking and agrees with previous findings¹⁴. The low swelling of the PAN/PU composites compared with the PMMA/PU system indicates that similar crosslinking phenomena occur in the PAN phase of the composites.

Relaxation phenomena

The frequency-temperature behaviour of the PU- β process is similar in all three composite systems. It was shown in Part 2 that wetting enhanced the $\tan \delta_M$ peaks and vacuum drying caused the process to disappear. For the three types of composite, the peak appears at the same temperature (-90°C at 1 Hz) regardless of the T_g of the PU. Most secondary relaxation phenomena arising from polymeric molecular reorientation occur at a temperature (T) related to T_g by $T/T_g \approx 0.7$ (in K)¹⁵. Hence, one can conclude that this process arises from

Table 5 Dielectric relaxation results from a set of 40:60 polyvinyl/PU composites

Composite	Temperature of maxima in $\tan \delta_D$ ($^{\circ}\text{C}$)			ΔH (kJ/mol)	Features of polyvinyl phase
	200Hz	1kHz	10kHz		
PMMA/PU	-20	-14	-11	151	bulky, polar side group
PS/PU	-27	-21	-15	130	bulky, non-polar side group
PAN/PU	-37	-30	-20	118	small, polar side group
Bulk PU	-34	-28	-15	101	

the relaxation of water molecules. These molecules are probably hydrogen-bonded to the PU chains.

Little evidence is seen of the β -process of PS in the PS/PU composite. This process is normally found at about 30°C for 1 Hz¹⁶. A small process has been observed (Figure 2) for PAN at about 10°C (1 Hz) but the peaks are insufficiently resolved to gain further information about this process. The β -process of PMMA has been discussed in Part 2 and elsewhere¹⁷.

The α -processes of the three vinyl polymers are similar in nature and occur at similar temperatures, 105°C , 100°C and 105°C for PMMA, PS and PAN respectively.

The major interest centres on the PU- α process in all three composites, as studied by both dynamic mechanical and dielectric techniques. The information concerning the behaviour of the α -process in PU when it is combined with various vinyl polymers to form the interstitial composites can be summarized as follows: (a) the temperature at which maxima in $\tan \delta$ (and particularly maxima in $\tan \delta_D$) occur and the apparent activation energies characteristic of the molecular motions responsible for the processes vary according to the manner set out in Table 5; (b) the forms of the curves of $\tan \delta_M$ versus temperature as the \bar{M}_c of the PU is varied in the different composites shows that the best resolved PU peaks occur in PAN/PU composites and that the least resolved peaks occur in PMMA/PU composites. The peaks in PS/PU composites fall into an intermediate category.

The only difference between the composite samples used for dielectric measurements was the different vinyl monomer used in the synthesis and it has been shown that the morphologies of all three composites are similar. The varying amounts of hindrance to the PU- α motion and the different activation energies associated with it can only arise from the presence of the different polyvinyls. The main differences in these polymers are listed in the right-hand column of Table 5, i.e. in the descriptions of the side groups. The side groups are immobile at the temperatures and frequencies listed. The greatest hindrance, highest activation energy and least resolved peaks are found in the PMMA/PU case where a bulky and highly polar side group is a feature of the vinyl polymer. Less hindrance, a lower activation energy and better peak resolution is found in the PS/PU case where the PS side group is still bulky, but is only slightly polar. The least hindrance, lowest of the three activation energies and the best resolved peaks are found in the PAN/PU case where the side group, although polar, is spatially insignificant. The results for the bulk PU might be misleading, although the activation energy follows the trend described above. It has been shown in Part 2 that bulk-prepared PU polymers have tighter networks than PU prepared in a solution of the vinyl

monomer. Thus the higher temperatures for the peaks in bulk PU compared with the PAN/PU system probably arise from differences in the tightness of the network.

For differences in such fine structures as side groups to be effective, the polyvinyl and PU must be in extremely close contact. The polymer chains of the different species must, in some instances, be adjacent. Since the polyvinyl inclusions give no indication of a fine structure, this intimate mixing probably occurs in the predominantly PU phase. This is further evidence of an interaction between the polyvinyl and the PU which was discussed in Part 2. There it was shown that the interaction is greater when the PMMA domains are small and the interphase area between the PMMA and the predominantly PU phase is large. This evidence indicates that the interaction occurs at, or near the interphase boundaries. The consequence of this is that the 'PU phase' has a higher modulus than that of bulk PU. This is further discussed in the next paper¹⁸.

Hindrance to the PU- α motion would also arise if the PU were in a state of tension or compression due to its environment in between the polyvinyl domains. However, this alone would not produce the systematically varying hindrance discussed above.

Aspects of toughening

The temperature at which the various dielectric loss peaks occur was discussed earlier. Comparison of Table 5 with plots of notched impact strength vs. temperature (Figure 8) shows that the onset of toughening and consequent impact strength at room temperature is related to the position of the α -peak of the PU, i.e. its T_g . The temperature of the onset of toughening coincides with the position of the PU- α process as measured dielectrically at about 1 kHz. Further evidence of this relation can be seen from a comparison of Figures 4 and 5 with the NIS data in Table 3. Similar observations have been made on conventional rubber modified plastics by several investigators^{19, 20}. The comparative lack of hindrance to the molecular motion responsible for the PU- α peak in PAN/PU composites results in toughening at a lower temperature than in PMMA/PU composites where hindrance to motion is much greater. Consequently, the larger PU- α peak in PAN/PU composites mirrors the higher impact strength at room temperature compared with PMMA/PU composites.

The increased toughening above 50°C in PMMA/PU composites where the PU has a \bar{M}_c of 4500 can be attributed to the onset of PMMA- β process (at 1 kHz). Although this process does not directly toughen the composite, the motion of the side group can be envisaged as removing the hindrance to the motion of the PU chains thus allowing them to become more mobile thereby contributing further to the toughening mechanism.

Referring again to *Figure 8* of this paper, the composite of PU with \bar{M}_c 950 does not become as tough as the composite of PU with \bar{M}_c 2250, even at elevated temperatures. Above its glass transition temperature a crosslinked polymer will not be as mobile as a non-crosslinked polymer and this mobility will vary directly with \bar{M}_c . Thus the PU in the composite of lower \bar{M}_c will be less mobile and less efficient at promoting the toughening mechanism than the composite whose PU phase is less tightly crosslinked. Although there is a relationship between the size of the PU- α peak and toughness, this does not necessarily imply that this loss process is responsible for the toughening effect. The loss peak simply reflects the molecular state of the elastomer and it could well be the case that the elastomer needs to be in a particular state to initiate energy absorption mechanisms. The extensive whitening of the fracture surface is similar to the phenomenon observed in conventional rubber modified systems where crazing in the glassy phase is probably the major energy dissipation mechanism²⁰. However, the whitening observed in the interstitial systems may have a different origin as a result of differences in morphology.

Design of interstitially polymerized composites and comparisons with other toughened systems

Analysis of relaxation properties coupled with the temperature dependence of impact strength allows certain conclusions to be made about the design of interstitially polymerized composites, particularly as far as toughness is concerned. The PU- α loss process has to be at sufficiently low temperature, i.e. below -40°C (1 Hz) for the material to be tough at room temperature. Furthermore a well resolved loss peak is necessary for efficient toughening.

The other important mechanical properties are a high modulus at room temperature and above and a high softening temperature. A consideration of *Figure 6* will illustrate many of the factors which affect these parameters. Considering, first, the curves for the PS/PU composite the modulus of PS is lower than that of the other polyvinyls and its T_g , at 100°C , is lower than those of PMMA (105°C) and PAN (105°C). These differences are reflected in the lower modulus at all temperatures and in the comparatively low softening temperature (as defined above) of 82°C .

Considering the PMMA/PU composite, the poorly resolved PU peak and consequently poor toughening is compensated by the small fall in G' through the process. This advantage is soon lost because of the presence of the PMMA- β process at room temperature resulting in a decrease in G' over a wide temperature range. This range is continued into the α -region and results in a low softening temperature of 75°C . Hence it is advantageous if the vinyl phase does not have such a secondary relaxation process thereby resulting in relatively high modulus at room temperature and above, and a high softening temperature.

The PAN/PU composite exhibits the best design features. The high modulus at low temperatures is followed by a discrete change through the PU- α process, the well defined peak in $\tan \delta_M$ at -45°C being a prerequisite for high toughness. From -30°C up to about 70°C the modulus only falls very slowly because of the insignificance of the polyvinyl β -process. This results

Table 6 Comparison of mechanical properties of interstitial composites with other rubber-modified materials

Type	Material or grade	NIS (kJ/m ²)	G' (GN/m ²)
Interstitial composites	80:20 PMMA/PU (\bar{M}_c 4500)	12.5	0.65
	70:30 PMMA/PU (\bar{M}_c 2250)	13.0	0.50
	80:20 PAN/PU (\bar{M}_c 2250)	11.7	0.91
	70:30 PAN/PU (\bar{M}_c 4500)	34.7	0.50
	70:30 PAN/PU (\bar{M}_c 2250)	26.2	0.52
Marbon ABS	Cyclolac G A	15.5	0.81
	Cyclolac X 27	8.0	1.04
	Cyclolac DM	6.3	0.98
	Cyclolac H	20.0	0.68
Dow HIPS	Styron 456	5.5	0.73
	Styron 492D	5.4	0.67
	Styron 9403	5.3	0.57

in a high modulus at room temperature. The slow fall in G' only begins to accelerate near T_g and a 'softening temperature' of 102°C is achieved.

Thus the important features for good mechanical properties are a polyvinyl or 'glassy' polymer with high modulus over a broad temperature range, no significant β -process and a high T_g . In addition, the rubbery material, in this case PU, should have its T_g below -40°C (1 Hz). Finally, the interaction between the two phases must be such that the PU- α process is not greatly hindered by the presence of the polyvinyl.

These considerations are merely those for optimum mechanical properties. Other considerations, such as the thermal and ultra-violet stability of the components, will also be important if a viable product is to be obtained. Unfortunately, both heat and ultra-violet stability of these composites are poor, as will be discussed in a later paper.

Finally, it is interesting to compare the mechanical properties of the interstitial composites discussed in this paper with other rubber-modified materials. The results are listed in *Table 6*. It can be seen that interstitially polymerized composites compare favourably with ABS and HIPS although other desirable properties such as ease of fabrication or optical clarity have not been considered.

CONCLUSIONS

The technique of interstitial polymerization in polyurethane elastomer gels has been shown to produce rubber-modified thermosets from a variety of polyvinyl glassy homopolymers. The monitoring of the toughness and stiffness of the composites has shown that the PAN/PU composites have the best combinations of properties. These are fully comparable to those of the better commercial rubber toughened plastics (ABS). The mechanical properties of PMMA/PU composites are nearly as good as those of PAN/PU composites and their optical clarity is superior. Owing to the difficulties described in this paper the mechanical properties of PS/PU systems are inferior to those of the other composites.

The morphology of the composites from PMMA, PAN and PS is similar each having a PU matrix filled with polyvinyl domains. To a first approximation the relaxation studies support this view. A closer examina-

tion of the relaxation results has shown that the molecules of the various polyvinyls and the PU are in close proximity and it is suggested that the predominantly PU phase contains polyvinyl chains, i.e. the 'PU phase' is composed in part of interpenetrating networks of polyvinyl and PU chains. The significance of this is further discussed in Part 5 of this series¹⁸.

ACKNOWLEDGEMENTS

One of us (M. J. B.) is grateful to Imperial Chemical Industries and later to the University of Queensland for the award of successive Post Doctoral Fellowships.

REFERENCES

- 1 Allen, G., Bowden, M. J., Blundell, D. J., Hutchinson, F. G., Jeffs, G. M. and Vyvoda, J. *Polymer* 1973, **14**, 597
- 2 Allen, G., Bowden, M. J., Blundell, D. J., Jeffs, G. M., Vyvoda, J. and White, T. *Polymer* 1973, **14**, 604
- 3 Allen, G., Bowden, M. J., Lewis, G., Blundell, D. J. and Jeffs, G. M. *Polymer* 1974, **15**, 13
- 4 Schildknecht, C. E. in 'Polymer Processes' (Ed. C. E. Schildknecht), Interscience, New York, 1956
- 5 Shavit, N. et al. *J. Polym. Sci. (A-1)* 1966, **4**, 2041
- 6 Oplatka, A., Konigsbuch, M. and Shavit, N. *J. Polym. Sci. (C)* 1967, **16**, 2795
- 7 Pellon, J. J., Smyth, N. M., Kugel, R. L. and Thomas, W. M. *J. Appl. Polym. Sci.* 1966, **10**, 421
- 8 Griffith, R. K. *J. Appl. Polym. Sci.* 1968, **12**, 1939
- 9 Griffith, R. K. and Zorska, R. *J. Appl. Polym. Sci.* 1969, **13**, 1159
- 10 Pellon, J. J. et al. *J. Appl. Polym. Sci.* 1966, **10**, 429
- 11 Rubens, L. C. and Boyer, R. F. in 'Styrene, its Polymers, Copolymers and Derivatives', (Eds R. H. Boundy and R. F. Boyer) Reinhold, New York, 1952, Ch 7
- 12 Blundell, D. J., Longman, G. W., Wignall, G. D., and Bowden M. J., *Polymer* 1974, **15**, 33
- 13 Friedlander, H. N., Peebles, L. H., Brandrup, J. and Kirby, J. R. *Macromolecules* 1968, **1**, 79
- 14 Shavit, N. and Konigsbuch, M. *J. Polym. Sci. (C)* 1967, **16**, 43
- 15 Matsuoka, S. and Ishida, Y. *J. Polym. Sci. (C)* 1966, **14**, 257
- 16 Illers, K. H. *Z. Elektrochem.* 1961, **65**, 679
- 17 Deutsch, K., Hoff, E. A. W. and Reddish, W. *J. Polym. Sci.* 1954, **13**, 565
- 18 Allen, G., Bowden, M. J., Todd, S. M., Blundell, D. J., Jeffs, G. M. and Davies, W. E. A. *Polymer* 1974, **15**, 28
- 19 Bucknall, C. B. and Street, D. G. *Soc. Chem. Ind. Monogr.* 26 1967, p 272
- 20 Matsuo, M., Ueda, A. and Kondo, Y. *Polym. Eng. Sci.* 1970, **10**, 253

Composites formed by interstitial polymerization of vinyl monomers in polyurethane elastomers: 5. Variation of modulus with composition

G. Allen, M. J. Bowden* and S. M. Todd

Department of Chemistry, University of Manchester, Manchester M13 9PL, UK

D. J. Blundell and G. M. Jeffs

*Imperial Chemical Industries Ltd, Corporate Laboratory,
The Heath, Runcorn, Cheshire WA7 4QE, UK*

and W. E. A. Davies

*Physics Department, University of Manchester, Manchester M13 9PL, UK
(Received 22 May 1973)*

Various theories which have been proposed for the shear modulus of two-phase composites are discussed in relation to their applicability to interstitial composites. The best fit to the experimental data is provided by a theory which considers particle-particle interactions. Non-interacting theories are found to be more suitable for model composites of pre-formed particles in a rubbery matrix. For the interstitial composites this is interpreted as evidence for molecular interactions between the two components in an interfacial layer.

INTRODUCTION

The first four papers in this series have covered the preparation^{1,4}, macroscopic physical properties^{1,4}, microscopic structure^{3,4} and molecular properties²⁻⁴ of polymeric composites which have been prepared according to the interstitial method. In this paper, we report some studies on the variation of shear modulus (G) with composition and how this variation compares with various theories which might be applicable to the situation. We will concentrate on composites of poly(methyl methacrylate) (PMMA) and polyurethane (PU) but will include some results of the variation of G with composition for composites of polyacrylonitrile (PAN) and PU.

Studies on the morphology² have shown that the composites of PMMA and PU have a structure consisting of roughly spherical PMMA domains in a mainly PU matrix. *Figure 1* shows a micrograph displaying the typical structure of a composite of 85:15 (w/w) PMMA/PU. The PMMA domains are about 300 nm across for this composition and their size decreases as the PMMA content decreases. Further studies^{2,4}, involving dynamic mechanical and dielectric relaxation techniques, whilst supporting the morphological evidence

of a two phase structure, have also indicated that there is some interaction between the two phases.

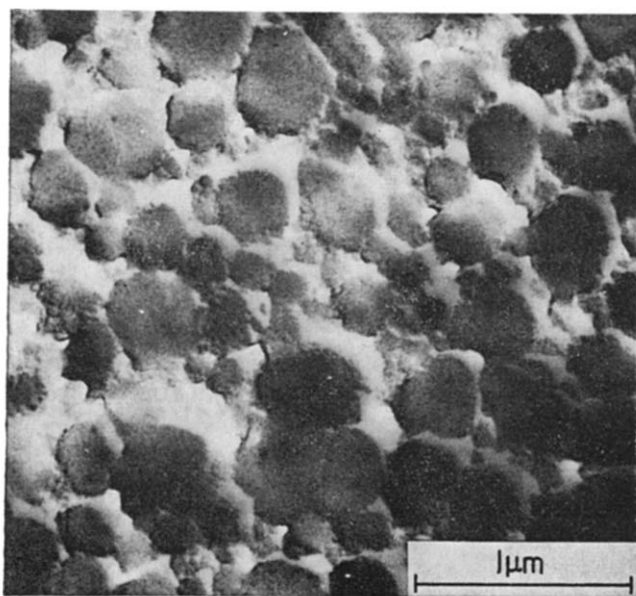


Figure 1 Transmission electron micrograph of 85:15 PMMA/PU composite

* Present address: Bell Telephone Laboratories, Mountain Avenue, Murray Hill, NJ 07974, USA.

The evidence of these studies is therefore, that to a first approximation, the composites are formed of spherical PMMA domains in a PU matrix. A second, and closer approximation, is that there is also some interaction between the phases.

THEORIES OF MODULI OF COMPOSITES

Many theories have been developed for the moduli of filled systems where one phase is in the form of spheres which are distributed in the second phase which is a continuous matrix. Neilson⁵ has listed and discussed many of the theories which are applicable to spherical fillers as well as those of more general shape. All theories assume that the adhesion between the two phases is perfect. Moreover, most theories assume that the inclusions are uniformly distributed within the matrix, the whole sample being macroscopically homogeneous and isotropic.

Many of the early theories have been based upon Einstein's⁶ relation for the viscosity:

$$\eta = \eta_1(1 + 2.5\phi_2) \quad (1)$$

of a suspension of rigid spherical bodies in a viscous fluid. η_1 is the viscosity of the fluid and ϕ_2 is the volume fraction of the spherical inclusions. Equation (1) can be adapted to the case of shear moduli by means of the relation⁷:

$$\frac{\eta}{\eta_1} = \frac{G}{G_1} \quad (2)$$

Hence

$$G = G_1(1 + 2.5\phi_2) \quad (3)$$

This relation is only valid as the volume fraction of the inclusion, ϕ_2 approaches zero. It will be noted that this expression only involves the modulus of the continuous phase and the volume fraction of the inclusions. Thus the modulus of the composite is independent of the modulus, G_2 , of the inclusions (if $G_2 \gg G_1$).

Smallwood⁷ and Guth⁸ have extended Einstein's theory to account for the reinforcement of rubber by carbon black. Their equation:

$$G = G_1(1 + 2.5\phi_2 + 14.1\phi_2^2) \quad (4)$$

predicts a higher degree of reinforcement than Einstein's equation. Their analysis takes into account solvation, i.e. the binding of the rubber by the carbon black. It is applicable over a wider range of concentrations than Einstein's equation.

Another development of Einstein's theory has been formulated by Mooney⁹. This analysis is partly empirical, and when expressed in terms of shear moduli rather than viscosities, yields the relation:

$$G = G_1 \exp\left(\frac{2.5\phi_2}{1 - k\phi_2}\right) \quad (5)$$

This equation takes into account the agglomeration or flocculation of the filler particles. Agglomerations of spheres might contain air spaces which would make the apparent volume of filler greater than the true volume of the filler. If the spheres were bound together the reinforcement would be larger than if the spheres were well dispersed. This is accounted for by the factor $1 - k\phi_2$ where k , the crowding factor, is defined as:

$$\frac{\text{apparent volume occupied by the filler}}{\text{true volume occupied by the filler}}$$

For the case of close packed spheres, all the same size, $k=1.35$, and for close packed spheres of infinite size distribution, $k=1$. Mooney's equation has been shown¹⁰ to account for the viscosity behaviour of suspensions in fluids up to volume fractions ϕ_2 of at least 0.5, k being adjusted in the range 1 to 2.

Kerner¹¹ has produced a theory for the elastic moduli of filled systems by considering the effect of hydrostatic compression and tension on a single, typical, filler particle. This theory, as with those mentioned previously, requires that the adhesion between the matrix and the filler particles be perfect, so that displacements are continuous across phase boundaries. Kerner's theory also requires the particles to be spherical in the mean. Kerner's theory also requires the particles to be spherical in the mean. When simplified to the case of one type of filler in the matrix, this theory yields the expression:

$$G = G_1 \left(\frac{\frac{\phi_1}{15(1-\sigma_1)} + \frac{\phi_2 G_2}{(7-5\sigma_1)G_1 + (8-10\sigma_1)G_2}}{\frac{\phi_1}{15(1-\sigma_1)} + \frac{\phi_2 G_1}{(7-5\sigma_1)G_1 + (8-10\sigma_1)G_2}} \right) \quad (6)$$

where σ_1 is Poisson's ratio of the matrix material. This expression involves the modulus, G_2 , of the filler material. If, as often occurs in practice, the filler is much more rigid than the matrix ($G_1 \ll G_2$) the expression simplifies to:

$$\left. \begin{aligned} G &= G_1 \left(1 + \frac{\phi_2}{\phi_1} \frac{1}{\beta_1} \right) \\ \text{where} \quad \beta_1 &= \frac{2(4-5\sigma_1)}{15(1-\sigma_1)} \end{aligned} \right\} \quad (7)$$

Hashin and Shtrikman¹² have formulated a theory which provides upper and lower bounds for any of the four elastic constants of two phase systems. This theory allows arbitrary phase geometry provided that the sample is macroscopically homogeneous and isotropic. For two phase composites the shear modulus G is bounded by:

$$G_1 + \frac{(G_2 - G_1)\phi_2}{1 + \beta_1\phi_1\left(\frac{G_2}{G_1} - 1\right)} \leq G \leq G_2 + \frac{(G_1 - G_2)\phi_1}{1 + \beta_2\phi_2\left(\frac{G_1}{G_2} - 1\right)} \quad (8)$$

provided $(\lambda_1 - \lambda_2)(G_1 - G_2) > 0$ where $\lambda = 2G\sigma/(1-2\sigma)$ and $\beta = 2(4-5\sigma)/15(1-\sigma)$ with appropriate subscripts. When $G_2 \gg G_1$ this expression simplifies to:

$$G_1 + \frac{\phi_2}{\phi_1} \frac{G_1}{\beta_1} \leq G \leq G_2 - \frac{\phi_1 G_2}{1 - \beta_2\phi_2} \quad (9)$$

The separation of these bounds is very dependent upon the relative magnitudes of G_1 and G_2 . These bounds, in fact, coincide with the two extreme cases accounted for by Kerner's theory.

More elementary bounds for any geometry are:

$$\begin{cases} G \leq G_1\phi_1 + G_2\phi_2 \\ G \geq \phi_1/G_1 + \phi_2/G_2 \end{cases}$$

These results are not used in this paper and are given only for completeness.

In an attempt to include domain-domain interactions, Budiansky¹³ assumed that an 'average' sphere of phase 2 is embedded directly in the effective medium. For bulk moduli $k_1=k_2=k=\infty$ his equation becomes:

$$\phi_2 = \frac{G_1 - G}{G(G_1 - G_2)} \left(\frac{3}{5}G + \frac{2}{5}G_2 \right) \quad (10)$$

This equation is unchanged by the replacements $\phi_2 \leftrightarrow \phi_1$, and $G_1 \leftrightarrow G_2$. It has been suggested¹⁴ that this equation should be used in geometries where phase 2 consists of spherical domains at low volume fractions, flocculation occurring as ϕ_2 is increased until continuity of phase 2 is reached at $\phi_2=0.4$. This phase inversion implies that phase 1 should lose its continuity at $\phi_2=0.6$.

Finally, Davies¹⁴ has proposed a new relation:

$$G^{1/5} = \phi_1 G_1^{1/5} + \phi_2 G_2^{1/5} \quad (11)$$

The derivation of this equation also considers domain-domain interactions and that $k_1=k_2=k$. This equation is obtained by assuming that two composites with moduli $G+\Delta G$ and $G-\Delta G$ respectively have been mixed to obtain a new composite with modulus G . It is suggested that equation (11) is best suited to morphologies which have continuity of both phases at all $0 < \phi_2 < 1$.

APPLICATION OF THE THEORIES TO COMPOSITES

Shear modulus measurements were performed on a series of PMMA/PU interstitial composites which had been prepared according to the method described in the first paper¹ of this series. The shear moduli were measured at low frequency (~1 Hz) by means of a torsion pendulum. Data were recorded for composites of composition varying from 90:10 PMMA/PU to 25:75 PMMA/PU and for a 100% PMMA sample. The measurement of the modulus of a wholly PU sample was performed with the aid of a simple low-friction stretching device. The strain employed was less

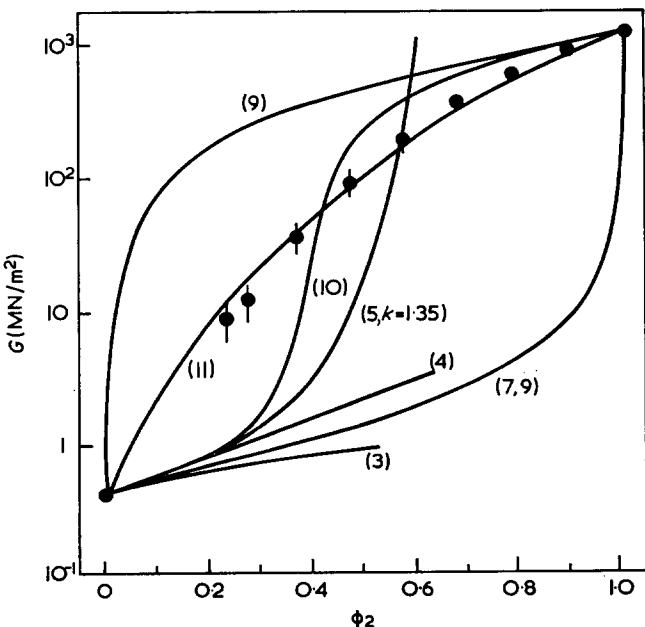


Figure 2 Log₁₀ (shear modulus), G as a function of volume fraction (ϕ_2) of PMMA for PMMA/PU interstitial composites. \blacklozenge are experimental points and numbers on theoretical curves refer to equations in the text

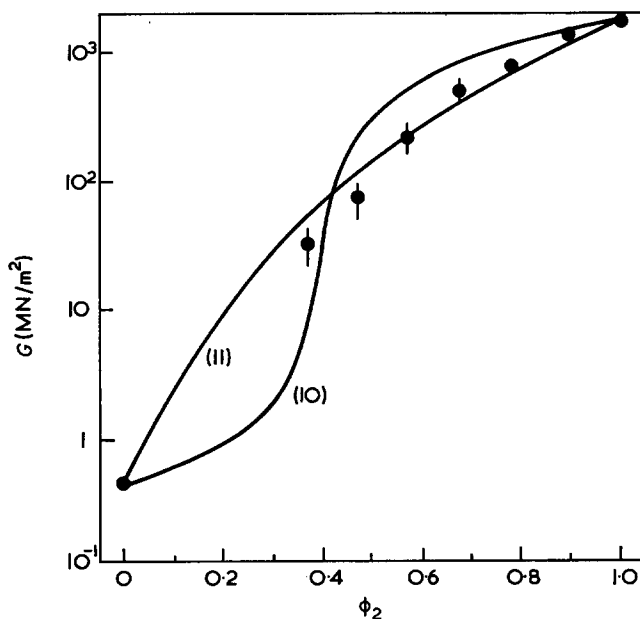


Figure 3 Log₁₀ (shear modulus), G as a function of volume fraction (ϕ_2) of PAN for PAN/PU interstitial composites. \blacklozenge are experimental points and numbers on theoretical curves refer to equations in the text

Table 1 Elastic constants of the two components of PMMA/PU interstitial composite

G_1	0.42 MN/m ²
G_2	1.47×10^3 MN/m ²
σ_1^{15}	0.499
σ_2^{16}	0.35

Table 2 Elastic constants of the components of the PAN/PU interstitial composite

G_1	0.42 MN/m ²
G_2	1.90×10^3 MN/m ²
σ_1	0.499
σ_2	0.35

than 1% and the Young's modulus, E , so obtained was converted to a shear modulus, G , by means of the relation:

$$G = \frac{E}{2(1 + \sigma)} \quad (12)$$

assuming Poisson's ratio, σ , for the PU of 0.499¹⁵.

The data are plotted in Figure 2 where $\log_{10} G$ is plotted against volume fraction. It is seen that the modulus of the composition falls away from the modulus of PMMA (1.47×10^3 MN/m²) as the proportion of PU is increased and approaches that of PU (0.42 MN/m²).

In order to test the applicability of these various theories for the prediction of the modulus behaviour of PMMA/PU composites the values of the various parameters have been used as set out in Table 1. The PU matrix is denoted by subscript 1 and the PMMA by subscript 2. The results of fitting these values into expressions (3)–(5), (7), (9)–(11) are plotted in Figure 2.

Comparable plots of expressions (10) and (11) are shown in Figure 3 together with experimental points for PAN/PU composites. The parameters used in plotting the expressions are listed in Table 2.

Table 3 Particle size of various grades of Diakon

Diakon grade	Size (μm)
DV400	10–30
MG101	270
MG102	600

To test the applicability of some of the theories discussed in the previous section to the case where definite preformed spherical filler particles are included in a continuous matrix, a series of model composites was prepared. The preformed spheres used were a range of PMMA particles (Diakon Moulding Powders, ICI Ltd) whose diameters were as shown in Table 3.

The matrix material was a PU composed of equal proportions of difunctional and trifunctional poly(oxypropylene) polyols of molecular weights 2000 and 3000 respectively (PPG-2000 and OPG-3000, ICI Ltd), reacted with hexamethylene diisocyanate. This diisocyanate was preferred to diphenylmethane 4,4'-diisocyanate, which was used in forming the interstitial composites, because it provided a longer gelation time which was found to be necessary for a thorough mixing in of the particles and the removal of air bubbles by degassing. Thick films (5mm) were cast over mercury and the curing of the PU was completed at room temperature. (The properties of the elastomer were unchanged if the curing were carried out at elevated temperatures.)

Model composites were prepared in this manner containing up to 45% (v/v) of PMMA particles. Figure 4 is a typical scanning electron micrograph of such a composite filled to 30% with spheres of the smallest size (DV400).

The modulus measurements were performed as described for bulk PU samples and the shear moduli were derived from the Young's moduli by means of equation (12). The results of these measurements are plotted in Figure 5 and it is seen that, within experimental

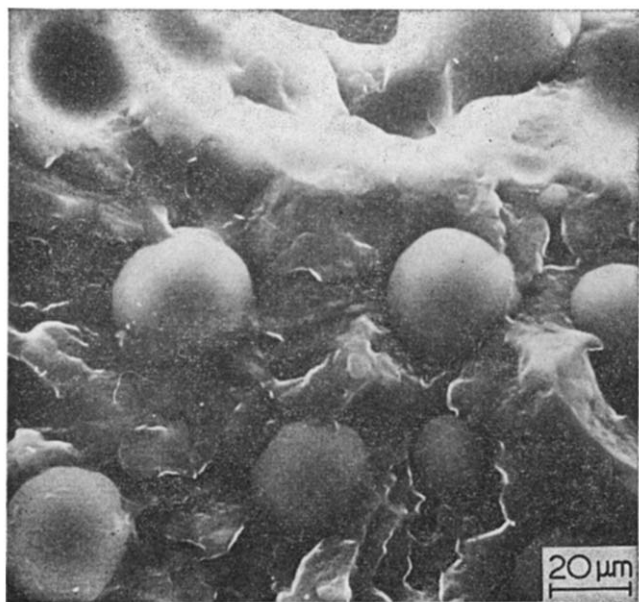


Figure 4 Scanning electron micrograph of a model composite consisting of PMMA particles (Diakon DV400) in a PU matrix

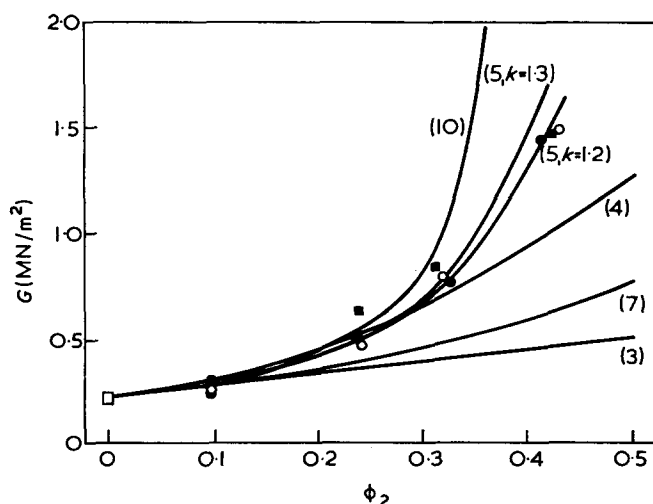


Figure 5 Shear modulus (G) as a function of volume fraction (ϕ_2) of PMMA particles in a PU matrix. \square , PU; \circ , Diakon DV400; \bullet , Diakon MG101; \blacksquare , Diakon MG102. Numbers on theoretical curves refer to equations in the text

error, equal reinforcement is obtained with filler particles of different sizes (within the available range). In Figure 5 are also plotted curves for expressions (3)–(5), (7) and (10) based upon the modulus of unfilled PU of 0.22 MN/m².

DISCUSSION

When the Einstein equation (3) and the Guth and Smallwood equation (4) are applied to the cases of the interstitial composites of PMMA/PU and PAN/PU the predicted moduli are too low at all volume fractions ϕ_2 . The Mooney equation (5) predicts moduli which are too low at low ϕ_2 and which increase too quickly at higher ϕ_2 . It can be seen that the bounds of the Hashin and Shtrikman theory (9) are too wide to be of any predictive value. This is to be expected since the ratio of moduli of the homopolymers (G_2/G_1) is of the order of 4×10^3 . However, the bounds do enclose the experimental points. Kerner's equation (7) predicts moduli which coincide with the lower bound of the Hashin and Shtrikman theory. If Kerner's theory is applied to the inverted case where PU spheres are embedded in a PMMA matrix then the predicted moduli are in agreement with the upper bound of Hashin and Shtrikman theory. There is relatively close agreement between the predictions of Kerner's theory as applied to the inverted situation and the experimental points for large ϕ_2 .

The Kerner and Hashin and Shtrikman equations correspond to the case where particle-particle interactions are absent. The Budiansky equation (10) and the Davies equation (11) are derived from theories which consider such interactions. The Budiansky equation appears to give too little interaction for $\phi_2 < 0.4$ and rather overestimates it for $\phi_2 > 0.4$. However, it is a distinct improvement on the no-interaction equations. The best fit to the experimental points measured for the interstitial composites is achieved by the Davies equation. It is remembered that this theory is supposedly best suited to materials where both phases are continuous and would therefore be thought to be least appropriate.

Considering now the case of composites formed of

definite PMMA spherical particles in a PU matrix, it is seen that the theories derived on a basis of no particle-particle interactions have variable degrees of success in predicting the experimental moduli. The Einstein and Kerner equations are successful only up to volume fractions, ϕ_2 , of 0.1. The Guth and Smallwood equation is suitable for volume fractions up to nearly 0.3. The closest fit is obtained with the Mooney equation where k , the crowding factor, is chosen to be 1.2. This denotes a situation where, typically, the particles of varying sizes are close-packed. The final curve in Figure 5, for the Budiansky equation, fits the experimental points for ϕ_2 up to nearly 0.3. At higher ϕ_2 this equation predicts moduli which are much higher than the experimental values.

It is seen that some of the theories derived on a basis of no particle-particle interactions are adequate in describing the variation of modulus with filler content when the filler is in the form of separate, preformed, spherical particles. The Mooney equation is particularly successful. An equation which is derived with consideration of such interactions is only successful at low ϕ_2 .

The theories which do not consider particle-particle interactions are inadequate to predict the variation of modulus of interstitial composites. More success is obtained by theories which take into account such interactions. The best fit is obtained by an equation which suggests continuity of both phases and it is remembered that Kerner's theory as applied to the case of a polyvinyl matrix is fairly successful at high ϕ_2 .

These indications of continuity in the polyvinyl are not directly supported by morphological studies. Deviations from the simple polyvinyl domain in a PU matrix (first approximation) model could occur in two situations. The relaxation studies^{2, 4} indicated that a measure of interaction is taking place between the polyvinyl and the PU. This interaction correlates with domain size and could be occurring through an intermingling of the molecules of the two species near the domain boundaries. This would have the effect of increasing the modulus of the rubber. Since the interdomain regions are quite narrow (5–20 nm) this effect could modify the behaviour of most of the PU. Another possibility is that molecules of PMMA connect one domain to another. It is not expected that there would be sufficient of these to bring the modulus of the PU near that of the polyvinyl and hence make the latter phase effectively

continuous. However, there could be sufficient polyvinyl links to appreciably stiffen the PU. Thus, although the domains and matrix may be chemically different, the local modulus between domains would be physically equivalent to a continuity of polyvinyl phase such as is envisaged in Davies' model.

CONCLUSIONS

In the prediction of the modulus of interstitially polymerized composites, the theories which consider particle-particle interactions are more successful than those which do not consider such interactions. The Davies theory is particularly successful. The theories which do not consider particle-particle interactions are more successful in predicting the moduli of composites of preformed spherical particles in a rubber matrix.

The success of the Davies equation supports relaxation studies and suggests interactions between PU and polyvinyl molecules in the interdomain regions.

ACKNOWLEDGEMENTS

One of us (M. J. B.) wishes to thank Imperial Chemical Industries and later the University of Queensland for the award of successive Post Doctoral Fellowships.

REFERENCES

- 1 Allen, G., Bowden, M. J., Blundell, D. J., Hutchinson, F. G., Jeffs, G. M. and Vyvoda, J. *Polymer* 1973, **14**, 597
- 2 Allen, G., Bowden, M. J., Blundell, D. J., Jeffs, G. M., Vyvoda, J and White, T. *Polymer* 1973, **14**, 604
- 3 Allen, G., Bowden, M. J., Lewis, G., Blundell, D. J. and Jeffs, G. M. *Polymer* 1974, **15**, 13
- 4 Allen, G., Bowden, M. J., Lewis, G., Blundell, D. J., Jeffs, G. M. and Vyvoda, J. *Polymer* 1974, **15**, 27
- 5 Neilson, L. E. *J. Compos. Mat.* 1967, **1**, 100
- 6 Einstein, A. *Ann. Phys.* 1905, **19**, 549
- 7 Smallwood, H. M. *J. Appl. Phys.* 1944, **15**, 758
- 8 Guth, E. *J. Appl. Phys.* 1945, **16**, 20
- 9 Mooney, M. J. *Colloid Sci.* 1951, **6**, 162
- 10 Eilers, H. *Kolloid Z.* 1941, **97**, 313
- 11 Kerner, E. H. *Proc. Phys. Soc.* 1956, **69**, 808
- 12 Hashin, Z. and Shtrikman, S. *J. Mech. Phys. Solids* 1963, **11**, 127
- 13 Budiansky, B. *J. Mech. Phys. Solids* 1965, **13**, 223
- 14 Davies, W. E. A. *J. Phys. (D)* 1971, **4**, 318
- 15 Allen, G., Bianchi, U. and Price, C. *Trans. Faraday Soc.* 1963, **59**, 2493
- 16 ICI Technical Information 'Perspex'

Composites formed by interstitial polymerization of vinyl monomers in polyurethane elastomers: 6. Low angle X-ray scattering and turbidity

D. J. Blundell, G. W. Longman and G. D. Wignall

*Imperial Chemical Industries Limited, Corporate Laboratory,
The Heath, Runcorn, Cheshire WA7 4QE, UK*

and M. J. Bowden*

*Department of Chemistry, University of Manchester, Manchester M13 9PL, UK
(Received 17 July 1973)*

Low angle X-ray scattering (LAXS) from an interstitially polymerized poly(methyl methacrylate)-polyurethane system has been analysed in terms of a model due to Debye to give the mean chord intercept lengths of the disperse phase (PMMA) and matrix (PU). The model was found to fit the scattering within the experimental errors and the results are in excellent agreement with the results of electron microscopy. A theoretical expression is derived relating the turbidity with (a) the difference in refractive indices between the polyvinyl and polyurethane phases, (b) the size of the two phase domain structure, and (c) the volume fraction of the phases. The expression has been tested experimentally. The domain sizes derived from the turbidity equation agree reasonably with those observed by LAXS and electron microscopy.

INTRODUCTION

This paper is concerned with the low angle X-ray scatter (LCXS) and turbidity of two phase interstitial composites and with their correlation with the morphology as revealed by the electron microscope (e.m.). The work has been carried out with composites made by interstitially polymerizing poly(methyl methacrylate) (PMMA) inside a gel of polyurethane (PU). Details of the preparation and properties of these samples have been given in Part 1¹ and their morphology has been described in Part 2².

In Part 2² it was shown that to a first approximation the final composite morphology consists of spherical domains of PMMA closely packed and embedded in a continuous matrix of PU. The domains cover a distribution of size in which the mean size depends on the PMMA/PU composition and on several other preparation details. Typically the domains are in the region between 50 and 500 nm diameter while the thickness of the PU between domains is about 10–30 nm. Visually, these composites appear clear or very slightly hazy depending on the domain size.

The LAXS from interstitial systems is continuous, showing no discrete maxima. Several methods of analysis of the scattering profile have been tried. The method which most successfully agreed with electron microscopic observation and which is therefore described here was

found to be that based on the approach of Debye *et al.*^{3,4} in which the geometry of the domain structure is represented by a spatial correlation function of exponential form. Apart from the constant of proportionality, the problem of describing the scattered radiation is the same for both light and X-rays, and is essentially a geometric diffraction problem which depends on the ratio of the size of the structural details to the wavelength of the radiation. The theory successfully used in the X-ray work was therefore extended to cover the optical turbidity. The experimental work used to test this theoretical relation involves the measurement of refractive indices and turbidity together with associated X-ray and electron microscopy results.

THEORY

Both low angle X-ray diffraction and light scattering from interstitial composites can be described generally by the theory first introduced by Debye and co-workers^{3,4}. For light scattering in particular, the same theoretical approach has been further generalized and examined more rigorously by Ross⁵.

For this theory it is necessary to describe the inhomogeneities associated with the domain structure by a spatial two point correlation function, $\gamma(r)$, defined by:

$$\gamma(r) = \frac{\langle \eta_A \eta_B \rangle}{\langle \eta^2 \rangle}$$

* Present address: Bell Telephone Laboratories Inc., Murray Hill, NJ 07974, USA.

In terms of visible light scattering, η_A and η_B are the local fluctuations from the mean dielectric constant at the points A and B which are a distance r apart. The quantity $\langle\eta_A\eta_B\rangle$ represents the average product for all pairs of points a distance r apart. $\langle\eta^2\rangle$ is the mean square deviation over all points. For low angle X-ray scattering η_A and η_B will be the corresponding fluctuations in electron density. In a given interstitial two phase composite, $\gamma(r)$ should be identical for both light and X-ray scattering.

For an isotropic composite the scattered intensity $i(h)$ per unit volume of scatterer is then given by:

$$\frac{i(h)}{I_0} = 4\pi K \langle\eta^2\rangle \int_{i=0}^{\infty} \gamma(r) r^2 \frac{\sin hr}{hr} dr \quad (1)$$

where $h = \frac{4\pi}{\lambda} \sin\theta$

λ = wavelength of radiation in medium,

2θ = total angle of scatter,

I_0 = incident radiation.

K is a proportionality factor which for scattering with unpolarized light is given by:

$$K = \frac{\pi^2}{\epsilon^4 \lambda^4 R^2} \frac{(1 + \cos^2\theta)}{2}$$

where R is the distance of observation from sample.

For LAXS, the factor K is effectively constant for all θ .

At the levels of turbidity and with the domain sizes encountered in most of the interstitial composites, equation (1) is rigorous. The problem is to determine the form of $\gamma(r)$ and relate it in a useful way to the structure of the composite. For a so-called 'random two phase structure', Debye *et al.*⁴ have shown that $\gamma(r)$ should take the form of a simple exponential form, $e^{-r/a}$, where a is a characteristic correlation length. Equation (1) then reduces to:

$$\frac{i(h)}{I_0} = \frac{8\pi K a^3 \langle\eta\rangle^2}{(1 + h^2 a^2)^2} \quad (2)$$

It is easy to test whether experimental observations of $i(h)$ follow the form of this equation since a plot of $i^{-1/2}$ vs. h^2 should give a straight line whose ratio of slope/intercept = a^2 . Alternatively one could plot $i^{-1/2}$ vs. θ^2 for the angles studied in the LAXS patterns as $\sin\theta \simeq \theta$.

Debye *et al.* also demonstrated for their random two phase model that the specific interphase surface per unit volume of composite, S_v , is given by:

$$S_v = \frac{4\phi(1-\phi)}{a}$$

where ϕ = volume fraction occupied by phase 1. However, quite generally for any two phase structure it can also be shown that⁶:

$$S_v = \frac{4\phi}{L_1}$$

where L_1 is the mean chord intercept length across continuous sequences of phase 1 when a straight line is drawn randomly through the structure. Thus it follows that:

$$L_1 = \frac{a}{1-\phi}$$

Similarly the mean chord intercept length of the matrix L_2 is given by:

$$L_2 = \frac{a}{\phi}$$

In favourable cases L_1 and L_2 can also be estimated directly from electron micrographs. Thus if the form of equation (2) is followed, it is in principle possible to compare the L obtained from a scattering experiment with the L from the electron microscopy.

Electron microscopy of interstitial composites reveals a structure where the major phase exists as spherical domains closely packed into a continuous matrix of the second minority phase. *A priori*, there is no reason why this structure should satisfy the requirements of Debye's random two phase structure. However, in the experimental work described in this paper it has been found that the LAXS patterns give straight line plots consistent with the form of equation (2). Furthermore it has been found that the values of L_1 and L_2 deduced from the ratio of slope/intercept of the plots were in close agreement with the values of L obtained from electron micrographs¹. The fact that there is both qualitative and quantitative agreement with equation (2) shows that in the realm of low angle X-rays the simple random two phase model is an apt one for these interstitial systems. This gives confidence in extending equation (2) to the corresponding light scattering phenomenon and in particular to the optical turbidity of the composites.

The turbidity τ is an intrinsic property of a material and is defined by the Lambert extinction law:

$$I = I_0 e^{-\tau x}$$

where x is the optical path difference in the medium. If it is assumed that the extinction is due entirely to scattering of light by the medium, τ can then be identified with the total fraction of light scattered per unit volume of the medium. Equation (2) can therefore be integrated over all scattering directions to give:

$$\tau = \frac{i_{\text{total}}}{I_0} = \frac{\pi}{2\lambda} \frac{\langle\eta^2\rangle}{\epsilon^2} B(y) \quad (3)$$

where $B(y) = \frac{(y^2+2)}{y} \left[\frac{y^2+2}{y^2+1} - \frac{2}{y^2} \ln(y^2+1) \right]$

and $y = \frac{4\pi a}{\lambda} = \frac{4\pi}{\lambda} L_1(1-\phi)$

For a simple two phase structure where one phase occupies a volume fraction ϕ , it can be shown that the mean square deviation in dielectric constant $\langle\eta^2\rangle$ is given by:

$$\langle\eta^2\rangle = (\Delta\epsilon)^2 \phi(1-\phi)$$

where $\Delta\epsilon$ is the difference in dielectric constant between the two phases. Since the dielectric constant ϵ is related to refractive index by $\epsilon = \eta^2$, equation (3) can be re-written as:

$$\tau = \frac{2\pi\phi(1-\phi)}{\lambda} \frac{(\Delta\eta)^2}{\eta^2} B(y) \quad (4)$$

EXPERIMENTAL

Low angle X-ray scattering

The LAXS patterns were obtained using a low angle camera designed by Kratky and coworkers⁷. Monochromatization of the scattering was achieved by means

of a dual filter technique⁸ in which the scattering on one half of the film is filtered through Ni foil and the scattering on the other half is filtered through Co foil. The thickness of the foils are adjusted so that the difference in intensities (monitored by a Joyce-Loebl microdensitometer) is due to the $\text{Cu}(K\alpha_1 - K\alpha_2)$ peak in the incident spectrum.

In principle one needs to know the angular distribution of intensity which would be produced when an incident beam from a point source is scattered from a point sample, through an angle 2θ , and detected by a point detector. In practice one uses a finite source and finite sample so that the experimental results represent an average over a finite range of scatter angles. The experimental curve must therefore be corrected for this 'smearing' effect produced by imperfect collimation, and a computer programme was used to accomplish 'de-smearing' of the experimental results. The programme was based upon the work of Chu and Tan Creti⁹.

Electron microscopy

Full details of the electron microscopy have been reported elsewhere². Briefly the samples were sectioned with an LKB ultramicrotome and shadowed with evaporated chromium in order to reveal the domain structure. In principle it is possible to measure statistically the mean chord intercept length of domains directly from the electron micrographs. However, since the exact positions of the domain boundaries are often difficult to resolve, an alternative method was used. Lines were drawn on the micrograph and a measurement was made of N_L which is the average number of domains that are cut per unit length of line. L_1 is then given by⁷:

$$L_1 = \frac{\phi}{N_L} \quad (5)$$

where ϕ = volume fraction occupied by the domains. In practice ϕ was calculated from the weight fraction of vinyl monomer used in making the composite and from the densities of pure PU and vinyl polymer by assuming a simple two phase structure.

Turbidity

The turbidities were determined from measurements of absorbance made with a Perkin-Elmer u.v. spectrometer at a wavelength of 589 nm.

The samples were ground to a thickness of about 3 mm and polished on both sides. A correction was made for reflections at the entry and exit surfaces of the sample by assuming that the fraction of light transmitted at each surface was $4n/(1+n)^2$ where n is the refractive index of the sample.

The turbidity results quoted in Table 1 relate to τ in the Lambert extinction law.

Table 1 Summary of turbidity results

Sample No.	Wt % PMMA	τ (cm ⁻¹)	L_1 from turbidity (nm)	L_1 from e.m. (nm)	L_1 from LAXS (nm)
1	90	0.68	360	500	390
2	85	0.66	200	280	210
3	80	0.42	112	114	135
4	75	0.33	77	80	85
5	80	0.78	150	170	
6	80	0.24	89	89	

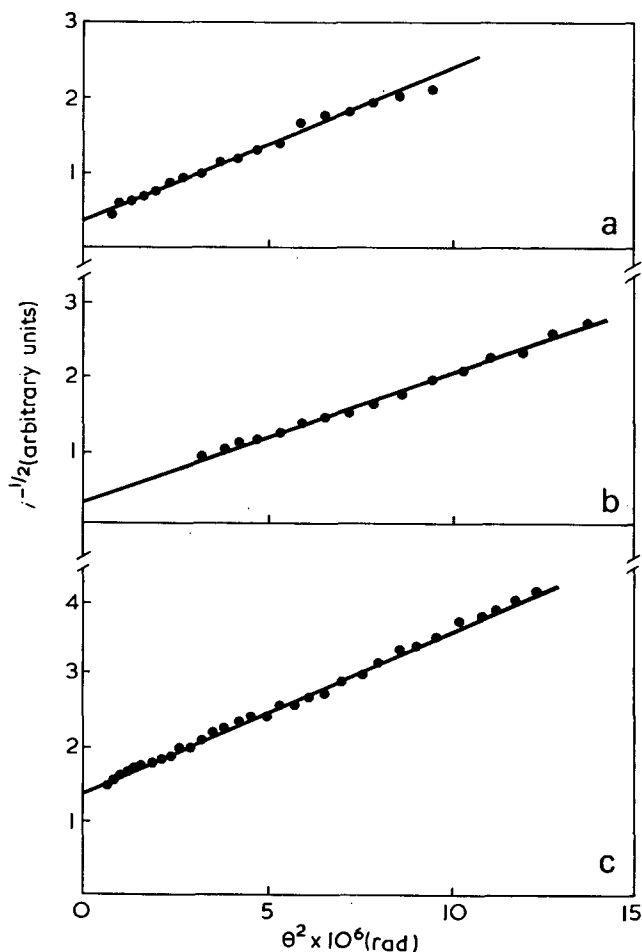


Figure 1 Debye plots of LAXS data for three different PMMA compositions: (a) 80%; (b) 60%; (c) 30%

The accuracy of the measured absorbance on the Perkin-Elmer instrument is not better than 0.005. However, the main disadvantage of the instrument for determining turbidity is that the beam is poorly collimated so that there is a systematic error from light scattered by the sample at very low angles.

The difference in refractive index of phases Δn in equation (4) was determined from the difference of the values measured for pure PMMA and PU samples at the 589.3 nm doublet of sodium using a thermostated Abbé refractometer operating at 20°C.

RESULTS AND DISCUSSION

For the LAXS measurements a series of interstitial composites of different PMMA/PU compositions was examined. Figure 1 shows three typical Debye plots of $i^{-1/2}$ vs. θ^2 . The plots are linear within experimental error, showing that the assumption of an exponential form of correlation function is reasonable. Figures 2 and 3 respectively show the results for all samples presented as mean chord intercept lengths L_1 of the PMMA (disperse) phase and L_2 the PU (matrix) phase calculated from the slopes of the Debye plots. Also shown on the same graphs are the estimates of L_1 and L_2 obtained by electron microscopy. Where a direct comparison is possible, the agreement between the individual pairs of L is good. Electron microscope results for the composites with low PMMA content could not be obtained, because of the difficulty in

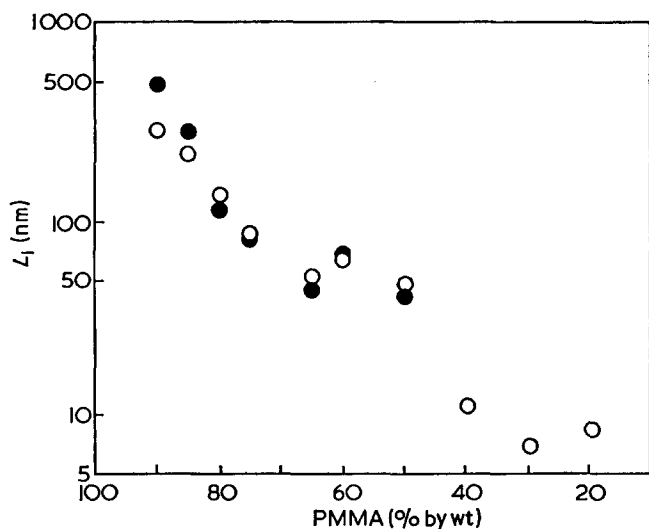


Figure 2 Plot of L_1 vs. PMMA composition. \circ , from LAXS data; \bullet , from electron micrographs

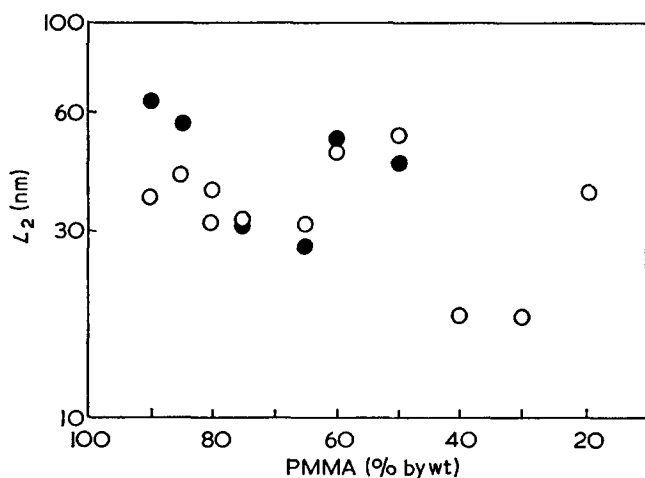


Figure 3 Plot of L_2 vs. PMMA composition. \circ , from LAXS data; \bullet , from electron micrographs

sectioning rubbery samples. The fluctuations from a smooth relation with PMMA composition, especially in L_2 , are probably due to slight variations in the preparation conditions of the samples.

The results of the turbidity measurements are shown in Table 1. The first few samples listed in Table 1 are for varying composition and are identical to those used

in the X-ray experiments. The last two samples containing 80% PMMA were prepared under other preparation conditions giving different size domain structures and turbidities. The difference in refractive index between PMMA and the PU was found to be 0.013 at 20°C for all the samples. The values of L_1 deduced from equation (5) is in good agreement with the corresponding values obtained from electron microscopy and LAXS.

These results demonstrate that the random two phase model of Debye *et al.* provides a good basis for describing both LAXS and light scattering from interstitial types of polymer composite. The applicability to LAXS is particularly convincing since apart from giving values of L_1 which agree well with e.m. observations, the shape of the scattering profiles agree qualitatively with that predicted from an exponential correlation function. The applicability to turbidity is more tenuous since no independent check has yet been made on the shape of the light scattering profile and the expressions for τ contain both L_1 and the functional form of $\gamma(r)$ as unknowns. Also whereas the LAXS have been made in the domain $h > 4 \times 10^5 \text{ cm}^{-1}$, light scattering and turbidity are associated with the angular domain defined by $h < 4 \times 10^5 \text{ cm}^{-1}$. Thus although the LAXS profiles are consistent with an exponential form for $\gamma(r)$, there is *a priori* no reason why the light scattering profile should not depart from them. Further work is therefore being carried out to check whether the light scattering profile follows the form of equation (2).

The success of the random two phase model in correlating the e.m. observations with the LAXS data suggests that it is well worth using the model as a trial for other two phase systems of similar structural size.

REFERENCES

- Allen, G., Bowden, M. J., Blundell, D. J., Hutchinson, F. G., Jeffs, G. M. and Vyvoda, J. *Polymer* 1973, **14**, 597
- Allen, G., Bowden, M. J., Blundell, D. J., Jeffs, G. M., Vyvoda, J. and White T. *Polymer* 1973, **14**, 604
- Debye, P. and Bueche, A. M. *J. Appl. Phys.* 1949, **20**, 518
- Debye, P., Anderson, Jr, H. R. and Brumberger, H. *J. Appl. Phys.* 1957, **28**, 679
- Ross, G. *Optica Acta* 1968, **15**, 451; 1969, **16**, 95
- Underwood, E. E. 'Quantitative Stereology', Addison-Wesley, Reading, Mass., 1970
- Kratky, O. and Skala, Z. *Z. Elektrochem.* 1958, **62**, 73
- Saules, J. A., Gordon, W. L. and Shaw, C. M. *Rev. Sci. Instrum.* 1956, **27**, 12
- Chu, B. and Tan Creti, D. M. *Acta Crystallog.* 1965, **18**, 1083

Image intensification and the electron microscopy of radiation sensitive polymers

Edwin L. Thomas* and Dieter G. Ast

Department of Materials Science and Engineering, Cornell University, Ithaca, NY 14850, USA

(Received 4 June 1973; revised 10 July 1973)

The role of image intensification in the electron microscopy of radiation sensitive polymers is analysed. It is shown that image intensification cannot improve the quality of the usual internal recording with electron image plates. The chief advantage of image intensification is the reduced radiation damage to the specimen during focusing and alignment. For bright-field microscopy, unaided focusing imparts an electron dose to the specimen which is approximately 9 times larger than the dose sustained during the subsequent recording. Image intensification reduces the radiation damage during focusing to an insignificant fraction of the unavoidable radiation damage which occurs during the exposure of the plate and improves the picture quality correspondingly. In the darkfield case the chief advantage of the image intensifier is the greatly improved yield of useful pictures rather than improved quality. Optimum working conditions, including optimum voltage, for radiation sensitive specimens are calculated. Experimental results on polyethylene single crystals confirm the analysis.

INTRODUCTION

Electron microscopy of crystalline polymers is limited by the degradation of the specimen in the electron beam. Electron beam damage can be reduced by the use of specimen cooling, low electron dose rates and higher acceleration potentials. However, lower electron dose rates and higher acceleration potentials make focusing difficult or impossible, require longer photographic exposures and may lead to specimen drift during exposure. Therefore, image intensification has been introduced in an attempt to extend beam sensitive specimen lifetime^{1,2}. Since one of us is engaged in an extended study of crystal defects³ in radiation sensitive polymers a systematic study of the recording process was undertaken.

FOCUSING

Focusing is a necessary step in the operation of the microscope but if carried out in the usual fashion introduces considerable radiation damage into the specimen[†]. The situation is improved if the focusing is done with the aid of an image intensification system.

Unaided focusing

The dark adapted eye requires a phosphor screen brightness of at least 1.5×10^{-2} ft Lambert for the

* Present address: Dept. of Chemical Engineering and Materials Science, University of Minnesota, Minneapolis, Minnesota 55455, USA.

† A possible method of circumventing the problem is to focus on an area which is then damaged, followed by translation to an adjacent undamaged area for subsequent recording. The chief drawback of this method is the low yield of useful pictures.

focusing of $100 \mu\text{m}$ wide Fresnel fringes⁴. The current density necessary to produce this minimum brightness is dependent on the microscope voltage, and the thickness of the phosphor screen. Resolution on the phosphor screen of 10 lines/mm is sufficient for focusing. The resolution of the recorded image is much higher (~ 50 lines/mm) because the focus control can be 'centred' by 'rocking' the focus and observing the phase shift of Fresnel fringes. It takes about a minute for an experienced operator to focus an image. Assuming that the thickness of the phosphor screen is matched to the operating voltage, the total electron dose for focusing can be calculated as a function of voltage. The results are summarized in *Table 1*. It can be seen that the dose at the screen plane is approximately 1×10^{-10} A sec/cm² for 60 kV and declines to roughly half this value at voltages above 200 kV.

Focusing with image intensification

The lower limit at which an ideal image intensification system can be used for focusing is limited by the statistical electron beam noise to about 1×10^{-14} A/cm²‡. This is a factor 100–200 lower than the current densities for unaided focusing, provided the image intensification does not introduce additional noise.

‡ This can be estimated as follows: a beam current of 1×10^{-14} A/cm² corresponds to 6×10^5 electrons/cm²/sec. We assume that the phosphor screen has a persistence time of about 1 sec. Resolution on the phosphor screen is approximately 10 lines/mm, or 4×10^4 picture elements/cm². During the integration period of the phosphor each picture element receives approximately 16 electrons. The statistical noise is given by $(16)^{1/2}$ and hence the signal to noise ratio is ≈ 4 . This is about the lower limit⁵ necessary to detect a signal in a noisy background.

Table 1 Current densities and doses for unaided focusing at 1.5×10^{-2} ft Lambert

Microscope voltage (keV)	Current density (screen plane) $\times 10^{12}$ (A/cm ²)	Total dose for 60 sec focusing (screen plane) $\times 10^{11}$ (A sec/cm ²)	Screen* resolution (lines/mm)	Screen mass thickness† (mg/cm ²)
60	1.75	10.5	11	9
100	1.25	7.5	8	21
200	1.15	6.9	5	44
1000‡	1.0	6.0	1	80

* From von Ardenne¹⁶† Optimized based on range of electrons in the phosphor at the particular voltage and light absorption by the phosphor¹⁶

‡ Usually, to improve resolution, a thinner than optimum screen is used for focusing. The total dose for focusing is correspondingly higher

Focusing with channeltron image intensifiers

Channeltron image intensifiers are devices which can intensify an electron image by a factor up to 10^5 . A channeltron plate consists of an array of $40 \mu\text{m}$ diameter single channel electron multipliers fused together in the shape of a disc. Electron multiplication is achieved by secondary emission of electrons from the semi-conducting material lining the inside walls of each channel. The output of the device is an (amplified) electron image which is converted to a photon image via proximity focusing of the electrons on a phosphor screen. The channeltron image intensifier introduces inherent additional noise into the image during the amplification process for two reasons: (a) every input electron does not enter into a channel (50% open area of channels); (b) there is a statistical spread in the output pulse of each channel. Further external noise can arise from secondary electrons and ions present in the microscope column which must be removed from the channelplate input⁷. The overall quantum detection efficiency (QDE) is about 0.25⁶. Thus, an image can be focused at approximately 25–50 times lower current densities than with a conventional system. Using commercially available microchannel plates⁷, a channeltron image intensifier system can be easily built for about \$2000.

Focusing with SEC image intensifiers

A variety of commercially available light image intensification systems can be employed in the electron microscope by converting the primary electron image into a photon image via a transmission phosphor screen. The photon image is then (fibre) optically coupled to the input of the image intensifier. Typical examples would be the RCA three stage cascade image intensifier or the Westinghouse one stage image intensifier followed by an SEC storage tube. The latter system has the advantage that the image can be further processed via standard television systems, as well as integrated over arbitrary periods of time. These commercially available systems have been developed to the point where they closely approach an ideal intensifier, e.g. no significant noise is introduced in the intensification process⁸. Disadvantages are the high cost of a complete system (about \$30 000) and the required magnetic shielding. The extra expense could be justified if the gain of a factor 4 in QDE is significant. Analysis of the microscope recording process will show that this is not the case.

RECORDING

An ideal recording device detects all incident electrons ($QDE=1$), has an overall noise level less than the noise level of the primary electron image, and has a resolution better than the fluctuations in the primary electron image. Various studies^{9,10} have shown that most commercially available electron image plates are essentially perfect recording devices for 60–100 kV electrons. That is, the quantum efficiency is approximately one* and the noise level in the recorded image (graininess) results from the statistical noise of the primary electron beam. At higher beam energies the QDE of commercially available electron microscope plates decreases (see Table 3) but could probably be improved by going to thicker emulsions and a higher silver halide/gelatin ratio. For optimum recording, the plate exposure dose should be $\approx 5 \times 10^7$ electron/cm²†, (e.g. 1×10^{-12} A/cm² for 10 sec). The corresponding photographic densities are 0.3–1.2 depending on development conditions. It is worth pointing out that the use of Tri-X plates for recording micrographs of radiation sensitive polymers¹¹ will actually lead to somewhat degraded images since the QDE of Tri-X for electrons is lower than for electron image plates due to a thinner emulsion and lower silver halide/gelatin ratio. Since the QDE of the electron image plate is approximately one, an image intensification system of quantum detection efficiency, QDE_{im} , needs to collect a factor $1/QDE_{im}$ more electrons to match the photographic quality of conventional recording. Thus there is no advantage to use a channeltron based image intensification system for individual plate recording. However, such a device is indispensable for recording a large number of short exposure images (ciné photography) for *in situ* kinetic studies. Even the best converter system cannot surpass the conventional recording with electron microscope plates. The sole drawback of internal plate recording is the somewhat increased microscope contamination. Ultra high vacuum, high resolution microscopes, employing image intensification with external recording are therefore being developed¹².

OPTIMUM MICROSCOPE OPERATION

Because polymer specimens undergo radiation damage, there is a limited information content available from a relatively undamaged specimen. Optimum information extraction is achieved if all information is transferred losslessly (e.g. with $QDE=1$) to the recording medium and if the information loss in the necessary, but unproductive, focusing step is negligible in comparison to the radiation damage which occurs during recording.

Optimum focusing

The ratio 'electrons used for focusing'/ 'electrons used for recording' (F/R) is a figure of merit for the efficiency of the information extraction from the microscope. This ratio depends strongly on the operation mode of the

* The situation for light is entirely different. It takes about 10 photons to render developable one grain, but one electron will render developable about 10 grains; the reason being that the particle energy in the latter case is approximately 10^4 times higher.

† The resolution of an electron image plate is of the order of 50 line pairs/mm, or 1×10^6 picture elements per cm². The above dose corresponds to 50 electrons per picture element. Signal to noise ratio is $50/(50)^{1/2}=7$.

Table 2 Ratio of electrons used for focusing/electrons used for recording (for various operational modes) (F/R)*

	Total dose (screen plane) (electrons/cm ²)	Focus in bright-field (BF)	Focus in dark-field (DF)	Focus in BF switch to DF	Focus in BF†, Re-adjust in DF
Standard EM	4.7×10^8	9.4	9.4	0.16	0.48
EM+MCP	1.5×10^7	0.30	0.30	0.01	0.03
EM+SEC	3.7×10^6	0.08	0.08	0.0002	0.0006

* Optimum recording at 5×10^7 electrons/cm² (see text) at 100 keV
 † For 110 reflection of polyethylene

microscope and the method used for focusing. A dark-field image can either be focused by focusing first the brightfield image followed by switching to the darkfield mode (in practice the beam has to be switched off between these two steps, to allow for dark adaption and 'dying' of the brightfield image on the phosphor screen) or by focusing the darkfield image directly.

We have calculated this ratio for a conventional electron microscope, one equipped with a channeltron image intensifier and finally for one equipped with an SEC based intensification system (Table 2).

It can be seen that during the minute it takes to find and focus a specimen in a conventionally equipped microscope, the crystal receives approximately enough electrons/cm² to record 9 brightfield micrographs.

The brightfield mode of operation is the most frequently used mode since many radiation sensitive materials (e.g. biological specimens, non-crystalline polymers) are amorphous. Image intensified focusing will therefore greatly improve the quality of the brightfield recording.

For the darkfield mode there seems to be little advantage in using an image intensifier if the focusing of the darkfield image is done in brightfield ($F/R=0.16$). It should be kept in mind that the calculations are based on the assumption that no further adjustment of the darkfield image is necessary. However, owing to the lack of contrast in the brightfield image and the need to focus on a convenient 'dirt particle' or crystal edge, the specimen frequently needs to be repositioned slightly in the darkfield mode, a process which requires approximately 10 sec with the current density at the specimen higher by a factor I_0/I_{hkl} . Under these conditions the figure of merit changes by a factor of 3 [ϕ_{focus} is now $\phi_{\text{focus}}^{\text{BF}} + \phi_{\text{adjust}}^{\text{DF}}$ (for 110 reflection of polyethylene)]. Experience shows in addition that the use of an intensifier for darkfield examination permits a much higher yield of informative darkfield micrographs since the operator has time to select interesting specimen areas and to systematically vary the diffraction condition with low current density on the specimen.

Returning to the brightfield case we see that the channeltron image intensification system will lower the ratio of 'focusing' over 'recording' electrons to about 0.3, and the SEC based system to approximately 0.1, i.e. either system will record practically all the information available from the specimen. However, a channeltron system will do it at a price one to two orders of magnitude lower than that of a SEC based system. Thus, unless further electronic processing of the image is desired (e.g. automatic particle counting, etc.) there is little advantage in the use of an SEC system.

Optimum recording for polymers

The visual appearance of a polymer specimen in the electron microscope is a strong function of its particular radiation damage mechanism and the total radiation exposure¹³. Electron beam damage to polymers occurs owing to the ionization of main chain atoms and subsequent crosslinking of chains and/or chain scission. In order to record micrographs which are nearly radiation damage artifact free, it is necessary to assess the damage as a function of dose. For crystalline polymers, such as polyethylene, one can monitor the diffracted beam intensity as a function of time. As radiation damage causes the polyethylene lattice to distort, the diffracted intensity drops off exponentially¹⁴. A sensitive way to assess radiation damage artifacts is to compare darkfield images of the crystal taken at different fractions of the crystal lifetime. For polyethylene, the darkfield image develops a 'textured'* appearance during irradiation and all diffraction contrast features become fainter and finally disappear altogether.

The 110 darkfield diffracted intensity from a crystal as a function of total incident dose is shown in Figure 1. The crystal lifetime τ , usually determined as the time it takes to change the diffraction pattern into an amorphous halo for a given incident beam intensity, corresponds approximately to the point on the diffracted intensity-electron dose curve at which the diffracted intensity no longer changes with increasing electron dose. We have determined that an unacceptable amount of artifact diffraction contrast in the dark-field image from radiation damage to the lattice occurs at about 60% of the crystal lifetime. The electron dose which can pass through the nearly undamaged (as determined from the darkfield contrast studies) specimen, $\phi_{\text{max}}^{\text{spec}}$, corresponding to 0.6τ is approximately 3×10^{16} electrons/cm² at 100 keV. The total diffracted intensity I_{hkl} , will be $\int_0^t J_{hkl}(t) dt$. The optimum electron dose for recording $\phi_{\text{opt}}^{\text{plate}}$ is set by the noise consideration and photographic plate density (e.g. 5×10^7 electrons/cm²). Thus there exists an optimum magnification at which a maximum of information is extracted from the nearly undamaged specimen. This magnification M is given by.

$$M = \left[\frac{\phi_{\text{max}}^{\text{spec}}}{I_0 \left[\frac{\phi_{\text{focus}}}{I_{000}} + \frac{\phi_{\text{opt}}^{\text{plate}}}{I_{hkl}} \right]} \right]^{1/2}$$

* Radiation damage in polyethylene is primarily from crosslinking. The strain fields from the crosslinks break the lattice up into small diffracting regions. This yields a fine black-and-white patchwork in the darkfield image.

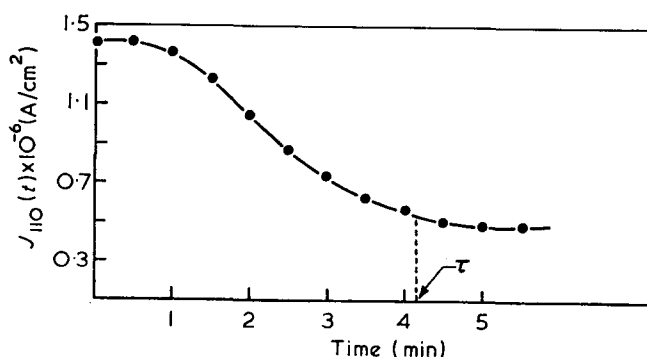


Figure 1 Typical 110 darkfield diffracted intensity from a polyethylene crystal as a function of dose. $J_0 = 4 \times 10^{-5} \text{ A/cm}^2$

where

I_0 = incident beam intensity,

I_{000} = brightfield intensity,

I_{hkl} = diffracted beam intensity,

$\phi_{\max}^{\text{spec}}$ = maximum electron dose in the specimen plane before extensive texturizing of darkfield image,

$\phi_{\text{opt}}^{\text{plate}}$ = optimum plate exposure,

ϕ_{focus} = minimum dose on phosphor screen, for brightfield focusing.

For polyethylene at 100 keV the optimum working magnification for brightfield is ($I_{000} \approx 0.5I_0$) $M \sim 14\,000\times$ and for a 110 darkfield ($I_{110} \approx 0.03I_0$) $M \sim 4000\times$. The specimen detail resolvable at a given magnification depends inversely on the contrast of the image. For a monolayer polyethylene crystal 120 \AA thick, brightfield contrast is about 40% while darkfield contrast is nearly 100%. Thus the two different modes of operation yield about the same resolved specimen detail.* If n photographs of an undamaged specimen are desired, then the working magnification must be lowered by a factor $n^{-1/2}$.

EXPERIMENTAL RESULTS

Figures 2 and 3 are brightfield micrographs of a polyethylene single crystal taken at $12\,500\times$ and 100 keV. Focusing and alignment were accomplished with a microchannelplate image intensifier. Several diffraction contrast features (bend contours, dislocations and Moiré fringes) are visible in Figure 2. Figure 3 was taken after 60 sec of further irradiation, which corresponds to the approximate total dose required for unaided focusing at this magnification. Contrast features in Figure 3 result chiefly from absorption contrast since all diffraction contrast features have by now faded owing to radiation damage. Although image intensification is thus very helpful for obtaining optimum photographs of a nearly

* The smallest detail which can be resolved in an undamaged crystal is of the order of 50 \AA based on photographic plate resolution of $\sim 50\text{ lp/mm}$.

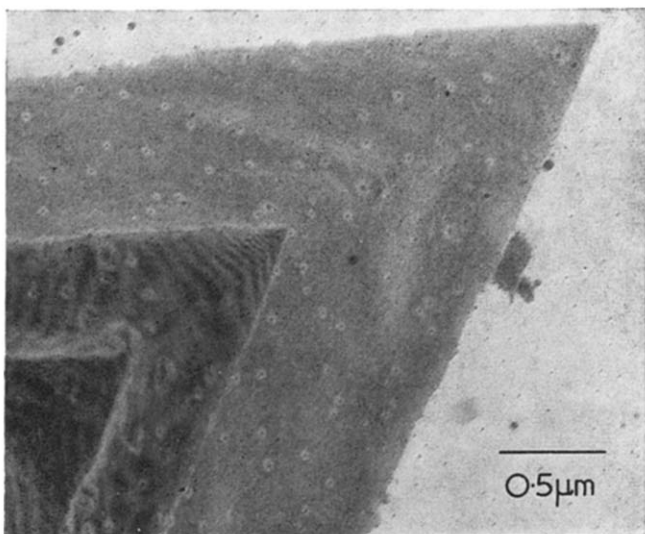


Figure 2 Brightfield micrograph of a polyethylene single crystal. Specimen current density $2.5 \times 10^{-4}\text{ A/cm}^2$, 10sec exposure

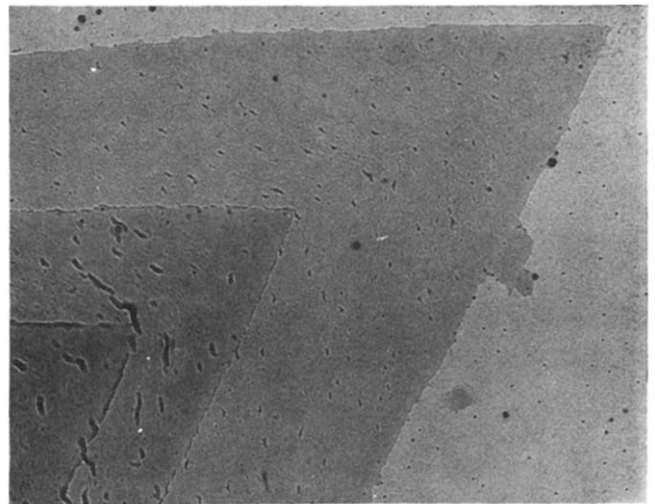


Figure 3 Brightfield micrograph of same area taken after another 60sec of irradiation. Specimen current density $2.5 \times 10^{-4}\text{ A/cm}^2$ 10sec exposure

undamaged crystal, such photographs are also (albeit somewhat more tediously because of the low yield of useful pictures) obtainable by focusing on an area which is damaged, followed by translation to an adjacent area to record an undamaged crystal.

Finally, we would like to comment on the optimum voltage for the electron microscopy of polymers which has been reported to be in the vicinity of 300 keV¹⁵. The observed specimen lifetime increases with increasing accelerating voltage, but the intensity of the diffracted beams (and hence the contrast) decreases (Table 3). Based on available experimental lifetime data for polyethylene we have calculated the total diffracted intensity as a function of voltage. It can be seen that the total diffracted intensity is practically independent of voltage.* Since the *QDE* of electron image plates in the region of 50–300 keV is practically a constant, there is no optimum recording voltage. However, in the absence of image intensification the electron dose required for focusing is a smaller fraction of the total specimen dose $\phi_{\max}^{\text{spec}}$ the higher the microscope operating voltage provided the image contrast is sufficient ($\geq 10\%$). Thus, for a conventionally equipped microscope, the optimum voltage for operation lies in the vicinity of the *QDE* ‘fall-off’ and with sufficient brightfield contrast, i.e. in the vicinity of 300 keV.

CONCLUSIONS

An analysis of the use of image intensification for the electron microscopy of radiation sensitive polymers leads to the following conclusions.

(1) The chief advantage of image intensification is the reduced radiation damage during focusing and aligning of the specimen. Image intensification will not improve the quality of recording.

(2) In the brightfield case, the radiation damage imparted to the specimen during focusing is large compared to the radiation damage occurring during subsequent recording. Thus image intensified focusing

* The reason is that the radiation damage and electron scattering are both being largely controlled by the electron-electron interaction.

Table 3 Diffracted intensity (kV)

Electron energy (keV)	2 beam BF contrast QDE	2 beam BF contrast		Theoretical $J_{110} \times 10^{6*}$ (A/cm ²)	Specimen lifetime, $\tau \dagger$ (sec)	$\int_0^{0.6\tau} J_{110}^*(t) dt \times 10^4$ (C/cm ²)	$\int_0^{0.6\tau} J_{110}^*(t) dt$ [$\int_0^{0.6\tau} J_{110}^*(t) dt$] ₁₀₀
		$I_0 - I_{000}$ I_0 (%)					
50	> 0.7	36		35.7	35	3.75	0.88
100	> 0.7	20		20.2	70	4.25	1.00
200	> 0.6	13		12.7	125	4.77	1.12
300		10		10.1	140	4.22	0.99
500		8		8.15	170	4.15	0.98
1000	> 0.23†	7		6.83	250	5.12	1.21

* Calculated from (the kinematical approximation at the Bragg condition)

$$J_{hkl}(kV) = J_0 \frac{(\lambda(kV))^2 |F(hkl, kV)|^2 t^2}{V_c^2}$$

where t = thickness = 120 Å, V_c = volume unit cell = 92.4 Å³ and J_0 = incident beam intensity at specimen = 1×10^{-4} A/cm²

† Exp data¹⁷ at $J_{spec} = 1 \times 10^{-4}$ A/cm²

will improve the quality (information content) of bright-field micrographs.

(3) Darkfield micrographs are usually recorded after the focusing has been done in brightfield conditions. In this case the radiation damage during focusing, even in the conventional microscope, is small compared to the radiation damage during recording. Hence, image intensified focusing will not improve the quality of the micrographs. However, it allows the operator to make further adjustments in the darkfield image before the actual recording. This, in general, increases the yield of informative and useful pictures.

(4) Optimum recording (i.e. information extraction) of crystalline polyethylene is achieved at a magnification of $\sim 14\,000\times$ for brightfield and $4000\times$ for darkfield and at an optimum working voltage of 300 keV.

(5) If image intensified focusing is used, the optimum working voltage is now a wide band between 50 and 300 keV.

ACKNOWLEDGEMENTS

We would like to thank Professor S. L. Sass for stimulating discussions. The comments of a referee are gratefully acknowledged. Financial support was received from

the National Science Foundation through the Materials Science Center at Cornell.

REFERENCES

- 1 Premsela, H. F. *Phillips Tech. Bull.* 1968
- 2 Thomas, E. L. and Danyluk, S. *J. Phys. (E)* 1971, **4**, 843
- 3 Thomas, E. L. and Sass, S. L. to be published
- 4 Agar, A. *Br. J. Appl. Phys.* 1957, **8**, 410
- 5 Zweig, H. J. *Photo Sci. Eng.* 1961, **5**, 142
- 6 Adams, J. J. *Electro-Opt. Systems Des.* 1969, **1**, 46
- 7 Thomas, E. L. and Ast, D. G. *J. Phys. (E)* 1973, **6**, 273
- 8 Herrmann, K. H., Krahl, D. and Rindfleish, V. *Siemens Forsch. Entwickl. Ber.* 1972, **1**, 167
- 9 Valentine, R. C. and Wrigley, N. G. *Nature* 1964, **203**, 713
- 10 Hamilton, J. F. and Marchant, J. C. *J. Opt. Soc. Am.* 1967, **57**, 232
- 11 Holland, V. F. and Lindenmeyer, P. H. *J. Appl. Phys.* 1965, **36**, 3049
- 12 Siegel, B. M. personal communication
- 13 Grubb, D. T., Keller, A. and Groves, G. W. *J. Mat. Sci.* 1972, **7**, 131
- 14 Grubb, D. T. and Groves, G. W. *Phil. Mag.* 1971, **24**, 815
- 15 Thomas, K. and Richardson, M. J. *Proc. Fifth Eur. Congr. Electron Microsc. Manchester* 1972, p 562
- 16 von Ardenne, M. 'Tabellen der Elektronenphysik Ionen-physik und Übermikroskopie', Deutscher Verlag Wissenschaften, Berlin, 1956
- 17 Thomas, L. E., Humphreys, C. J., Duff, W. A. and Grubb, D. T. *Radiat. Effects* 1970, **3**, 89

Transition and relaxation processes in ω -amino acid polyamides*

F. W. Lord

Research Department, Imperial Chemical Industries Ltd, Organics Division,
Blackley, Manchester M9 3DA, UK
(Received 23 July 1973)

Differential thermal analysis has been used to study the thermal transitions that occur on heating efficiently quenched samples of ω -amino acid polyamides. With 'even' amino acid polyamides (nylons-4, -6, -8, etc.) an endothermic type of transition was observed in the region of 30–40°C; this was followed immediately by an exothermic transition. No such transitions were observed with the 'odd' polyamides (nylons-5, -7, -11, etc.). From X-ray diffraction spectra and structural considerations, these transitions have been shown to be associated with the formation of hydrogen-bonded structures, that are possible with 'even' polyamides, but not with the 'odd' members. From a combination of differential thermal analysis, density and X-ray diffraction data, a new picture of the low temperature crystallization behaviour of this type of polyamide has emerged.

INTRODUCTION

Physical and mechanical properties of polymers are directly related to molecular mobility. In order to fabricate brittle or glassy polymers which have little or no molecular mobility, it is necessary to know the temperature range over which segments or groups acquire mobility. This temperature range, or transition, one of the most important, is known as the glass-rubber transition T_g and has been the subject of many publications. It is associated only with the amorphous phase and is shown by all amorphous and partly crystalline polymers. No new phases and no latent heat effects are associated with this transition, which is therefore a second-order process.

The glass-rubber transition, for practical purposes can be defined as the temperature or temperature range over which a sudden change in slope is observed in the curves of such thermodynamic properties as volume expansion or heat capacity, when plotted as a function of temperature. Many polymers show more than one second-order transition, but at the glass-rubber transition the change in properties is very large and the transition is therefore usually unambiguous.

Many values for the T_g of polyamides have been suggested¹⁻⁸: these range from -50°C to +80°C, the generally accepted value being 45°C–50°C. Polyamides, however, exhibit some properties at room temperature which are not consistent with the second quoted temperature range for T_g . They exhibit certain rubber-like properties at temperatures below 45°C, e.g. nylon-6 shows considerable creep behaviour at 20°C.

Some methods used for the determination of T_g (dilatometry, penetrometer methods, etc.) whilst possessing adequate accuracy and sensitivity provide insufficient control of the thermal treatment of the sample particu-

larly when this is a crystalline polymer. Nucleation and crystallization can occur between sample preparation and the start of the determination. The results obtained from low-temperature studies and described by Hartley *et al.*³ were undoubtedly obtained on crystalline material as a result of inefficient quenching.

Differential thermal analysis (d.t.a.), because of its high sensitivity and extremely small temperature requirements ensures better control of fusion and quenching. It was therefore used to study the thermal transitions occurring in a series of ω -amino acid polyamides. The use of differential thermal analysis methods for the determination of glass-rubber transitions has been described by Ke and Yoshimoto^{6, 9}.

EXPERIMENTAL

The thermal transitions were studied using the Du Pont 900 differential thermal analyser and its associated calorimeter cell. This cell was selected because it dispensed with the use of glass sample holders; the polymer samples were contained in small aluminium dishes. A further advantage is that the sample can readily be detached from the metal dish and used for subsequent tests such as density determinations, microscopic and X-ray examinations.

X-ray diffraction spectra were obtained with the Nonius horizontal version of the Guinier de Wolff focusing Powder Camera No. 1 operating at 35 kV and 20 mA using CuK α radiation with bent quartz crystal monochromator.

Density determinations were carried out in a carbon tetrachloride-toluene density gradient column operating at 25°C.

An amorphous sample is essential for the unambiguous determination of T_g . With crystalline polymers the sample must be melted at a temperature sufficiently high to

* Presented at the IUPAC International Symposium on Macromolecules, Aberdeen, September 1973.

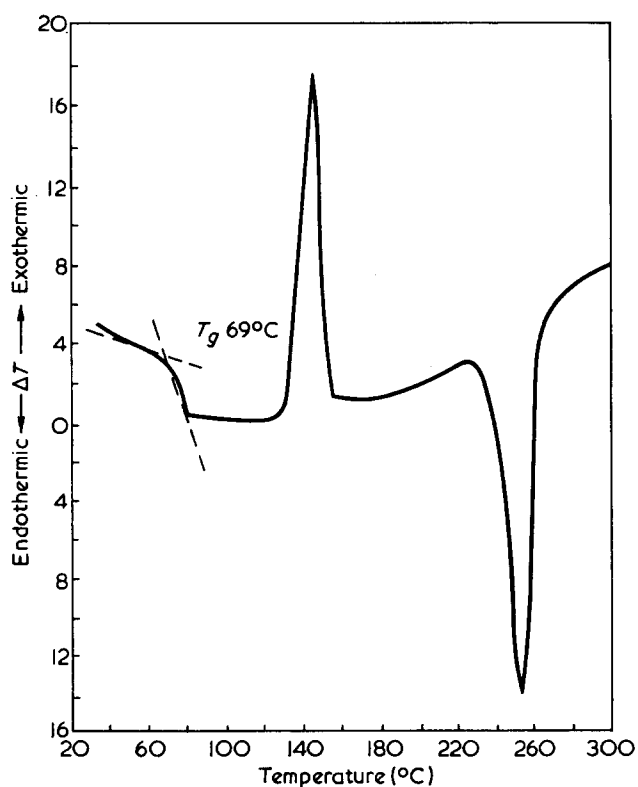


Figure 1 Thermogram of amorphous poly(ethylene terephthalate). Heating rate=20°C/min

destroy all previous thermal history and then be efficiently quenched. The quenching conditions should be such that nucleation effects occurring in the sample during the cooling process are minimized.

The suitability of the Du Pont apparatus for this type of work was illustrated by using amorphous poly(ethylene terephthalate) (PET) the thermogram of which is shown in Figure 1. The value of T_g for PET agreed well with data obtained by dilatometry and other techniques. The exotherm at 130°C is due to a low temperature crystallization process; this is also in good agreement with data from other techniques². The endotherm at 250°C represents the melting of the crystalline polymers.

Special precautions, however, are necessary in order to obtain an amorphous sample of a polyamide. A fusion temperature of at least 30°C above the crystalline melting point and extremely rapid quenching to liquid nitrogen temperatures are essential. A typical thermogram obtained with nylon-6 is shown in Figure 2.

In the case of nylon-6, the efficiency of the fusion and quenching operation can be assessed by measurement of the area under the exotherm (Figure 2). Unmelted, crystalline nylon-6 showed no exotherm, and a sample melted at a temperature just above the melting point prior to quenching showed only a small exotherm.

From the mass of sample used and the cell characteristics the value of ΔH for the exotherm can be calculated from:

$$H = \frac{EA\Delta T_s \cdot T_s}{M a} \quad (1)$$

where

E = cell calibration coefficient,

A = peak area,

ΔT_s = Y-axis sensitivity,

T_s = X-axis sensitivity,

M = mass of sample,

a = heating rate.

The effect of water on the transitions observed by d.t.a. has been investigated. Undried nylon-6 gave ΔH value of 6.2–6.5 cal/g (25.93–27.2 J/g). Samples dried for 16 h at 100°C and 1.0×10^{-4} mHg gave the same value. A rigorous drying treatment for 14 days at 1.0×10^{-4} mHg over P_2O_5 gave a slightly higher value of 6.7–7.0 cal/g (28.03–30.29 J/g). The main disadvantage of using undried polymer is that small bubbles, present in the samples after melting, make density determination unreliable. The sample after melting, however, is extremely sensitive to moisture and precautions must be adopted to minimize this effect.

The effect on ΔH of nucleation affects due to poor quenching or incomplete fusion is shown in Table 1.

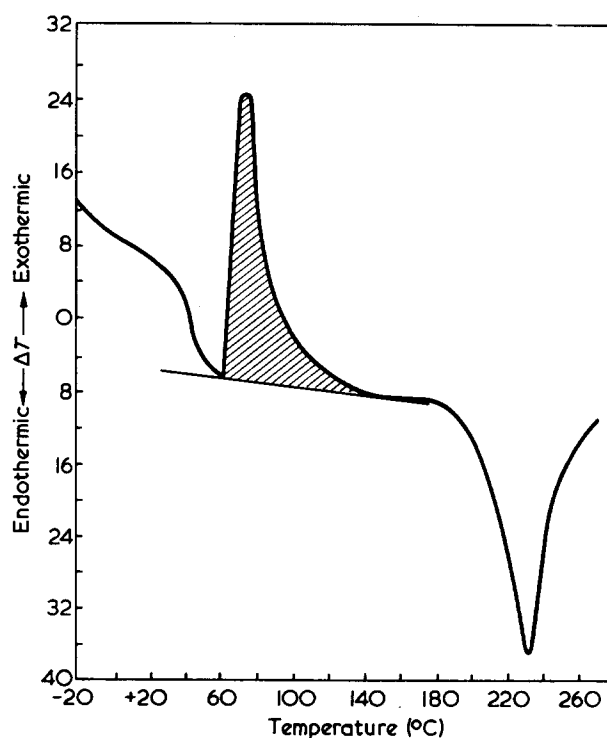


Figure 2 Thermogram of efficiently quenched nylon-6. Heating rate=20°C/min

Table 1 Effect of fusion temperature and quenching conditions on ΔH

Fusion temperature (°C)	Time of fusion (min)	Quench temperature (°C)	ΔH (cal/g)	ΔH (J/g)
300	5.0	-180	7.47	31.25
275	5.0	-180	7.10	29.7
275	5.0	-180	7.10	29.7
255	5.0	-180	6.50	27.20
255	5.0	-180	6.50	27.20
230	5.0	-180	6.13	25.65
225	5.0	-180	5.10	21.34
220	5.0	-180	0.94	3.81
255	15.0	-180	6.60	27.61
255	5.0	-180	6.40	26.78
255	2.0	-180	6.10	25.52
255	5.0	-100	3.20	13.39
255	5.0	-70	1.00	4.18
255	5.0	0	0	0

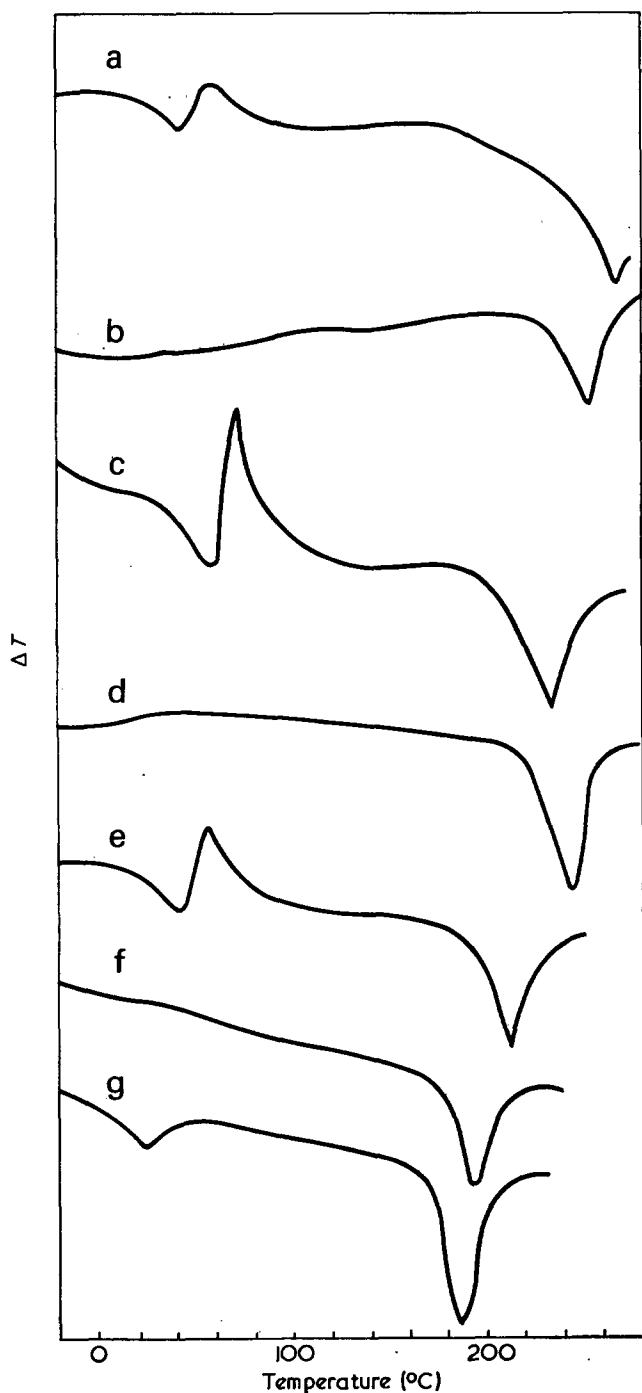


Figure 3 Thermogram of efficiently quenched amino acid polyamides. (a) Nylon-4; (b) nylon-5; (c) nylon-6; (d) nylon-7; (e) nylon-8; (f) nylon-11; (g) nylon-12

The mass of sample used in the above experiments was < 5.0 mg and the heating rate $20^{\circ}\text{C}/\text{min}$. The standard conditions adopted for all subsequent experiments using nylon-6 were a 2.0 mg sample, fusion conditions of 5 min at 255°C followed by liquid nitrogen quenching. Higher fusion temperatures whilst giving somewhat higher values of ΔH produced samples containing small bubbles together with some discoloration which made subsequent density and microscopic determinations difficult and uncertain.

Samples of nylon-6 fused at 255°C and quenched in liquid nitrogen showed no spherulitic structure when $10\ \mu\text{m}$ thick sections were examined at room temperature under a polarizing microscope. Moreover, no spherulites developed when the samples were held at 200°C for

30 min; at this temperature spherulites, if present, grow rapidly.

RESULTS

The thermograms obtained from a series of ω -amino acid polyamides presented an unexpected observation (Figure 3). All the 'even' polyamides, i.e. those containing an even number of carbon atoms in the chain, showed an endotherm-like transition at about 30°C followed immediately by an exotherm having a peak temperature of about 70°C . No such transitions were observed in any of the 'odd' polyamides examined.

The temperature of the endotherm-like transition corresponded to that observed by workers using other techniques and assumed by them to be the glass-transition. The absence of such a transition in the case of 'odd' polyamides demanded some explanation and the following hypothesis was advanced.

The transitions observed in this series of polyamides are associated with 'parallel' and 'anti-parallel' configurations well known in ω -amino acid polyamides and described by Slichter¹⁰. Polyamides in general tend to achieve structures containing the maximum molecular coupling. Molecules of 'even' amino acid polyamides being unsymmetrical can be arranged in two configurations: (1) where the atom sequence in polymer chains lying alongside each other is in the same direction. This is known as the 'parallel' form in which only 50% of hydrogen bonds are possible if there is a planar zig-zag and no chain distortion. The plane of the completed hydrogen bonds is tilted with reference to the molecular axis; (2) where the atom sequences in adjacent chains are in opposite directions, known as the 'anti-parallel' form, in which all hydrogen bonds are completed and the plane is normal to the molecular axis.

With 'odd' polyamides, e.g. nylon-7, hydrogen bonding is complete in both 'parallel' and 'anti-parallel' configurations. These structures are shown in Figure 4.

The association of the observed transitions in 'even' polyamides with hydrogen bonding was substantiated by examination of samples of iso-butyl substituted nylon-6. A glass transition was observed at temperatures between -60 and $+20^{\circ}\text{C}$, the actual temperature being dependent upon the degree of substitution. When the degree of substitution was high enough to hinder or prevent crystallization, no exotherm was observed on the thermogram.

In the light of these findings it was necessary to find a full explanation for the thermograms obtained with the 'even' and 'odd' polyamides.

If the thermogram of nylon-6 is interpreted in the same way as was done for Terylene, then the exotherm should be due to low temperature crystallization. This hypothesis was tested by obtaining X-ray diffraction spectra of samples of nylon-6 removed from the calorimeter cell after they had been raised to temperatures corresponding to different parts of the thermogram. The X-ray findings are shown in Table 2.

These results show that crystallization to the γ -form occurred after completion of the exothermic process and that no heat effects were detected associated with the change of the γ - to the α -form.

Similar experiments carried out on nylon-7 (in which no thermal transitions were observed) showed two fairly sharp reflections at all temperatures. The linear

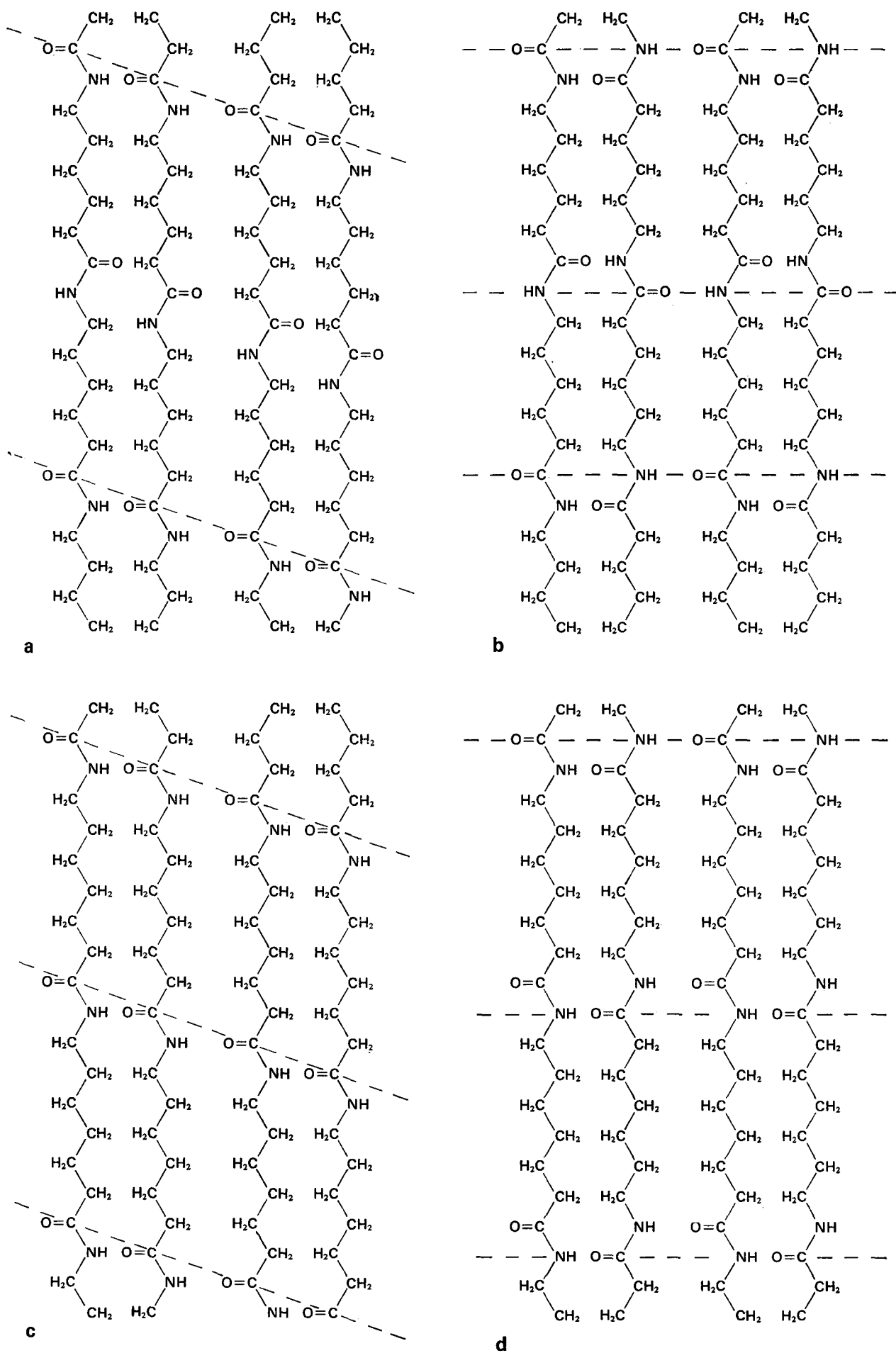


Figure 4 Parallel and anti-parallel forms of nylon-6 and nylon-7. (a) Nylon-6, parallel form; (b) nylon-6, anti-parallel form; (c) nylon-7, parallel form; (d) nylon-7, anti-parallel form

Table 2 X-ray spectra of nylon-6 removed from the calorimeter cell at different temperatures

Temperature of sample at time of removal (°C)	X-ray spectra	Comments
20	Broad halo	Temperature range covers passage through the transitions and completion of exothermic process
40		
60		
80		
90	Fairly sharp, single reflection	γ -form
100		
120		
140		
150	Mixture of single reflection of γ -form and double reflection of α -form	α -form increasing with increasing temperature
160		
170		
180		
190	Double reflection	α -form only
195		
200		

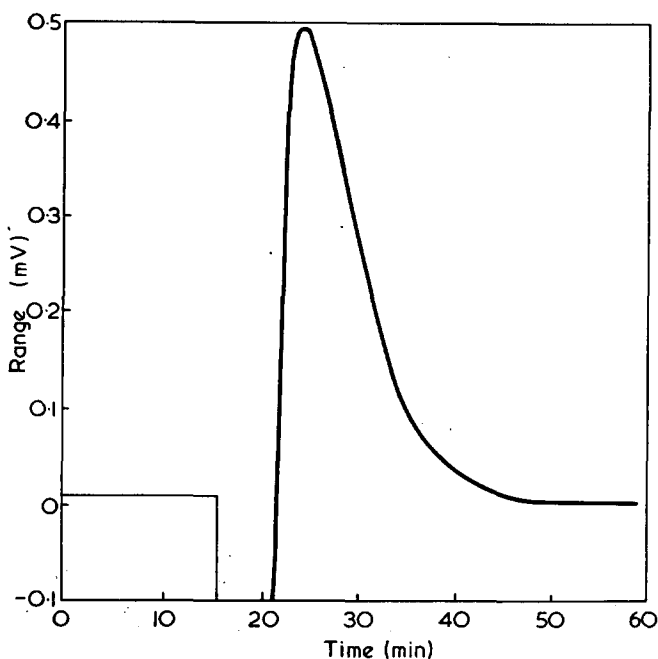


Figure 5 Isothermal 'crystallization' of nylon-6. Rate of crystallization at 55°C

separation between the two reflections increased slightly with increasing temperature.

Further evidence that the exotherm observed in 'even' polyamides was not entirely due to crystallization was obtained from attempts to measure isothermal rates of crystallization over the temperature range 25°–60°C.

2 mg of nylon-6 were fused for 5 min at 250°C, quenched in liquid nitrogen and then transferred to the calorimeter cell which had been pre-set to the desired isothermal temperature. As shown in Figure 5, a rapid exothermic process commenced even before the sample had achieved the steady isothermal state. This effect was observed at temperatures as low as 25°C.

It has already been shown that the value of ΔH (Table 1) is considerably reduced by the nucleation or crystallization processes which can result from slow cooling from the melt or from incomplete fusion. Changes in ΔH values should therefore be a measure of any changes affected in well quenched samples by annealing

at temperatures between 20°C and 60°C. The results are shown in Figure 6.

At the same time density determinations were carried out on annealed samples. The density-annealing time curves are shown in Figure 7. A broken curve of ΔH -annealing time measured at 55°C is included to illustrate the large change in ΔH that can occur with only a very small change in density.

X-ray diffraction spectra of annealed samples of nylon-6 measured in terms of the half-width of the single reflection gave similar curves to those obtained by ΔH determinations. The half-width-time curves are shown in Figure 8. Despite extremely long annealing times only a poorly ordered γ -form of nylon-6 was obtained.

DISCUSSION

The structures of ω -amino acid polyamides have been studied and reported by many workers¹⁰⁻²⁷. The changes in structure that occur on heating a quenched sample of nylon-6 to a temperature just below the melting point, together with the effect of orientation, have been described by Roldan and Kaufman¹⁹.

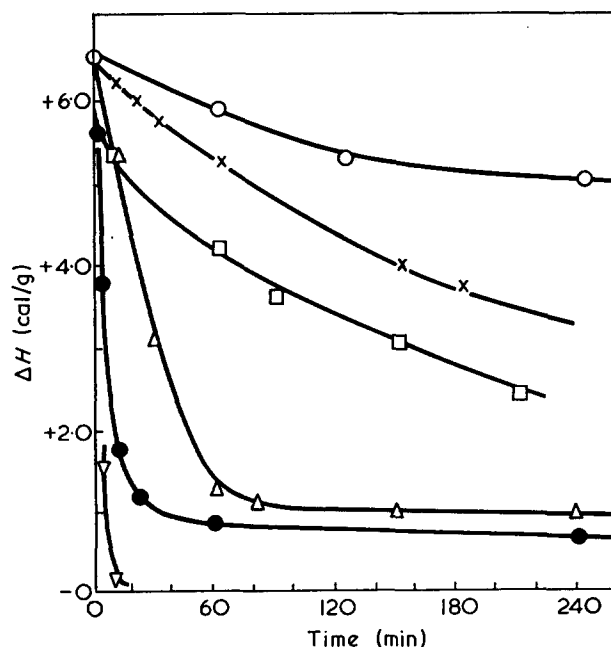


Figure 6 Effect of annealing conditions on ΔH of nylon-6. \circ , 20°C; \times , 40°C; \square , 45°C; \triangle , 50°C; \bullet , 55°C; ∇ , 60°C

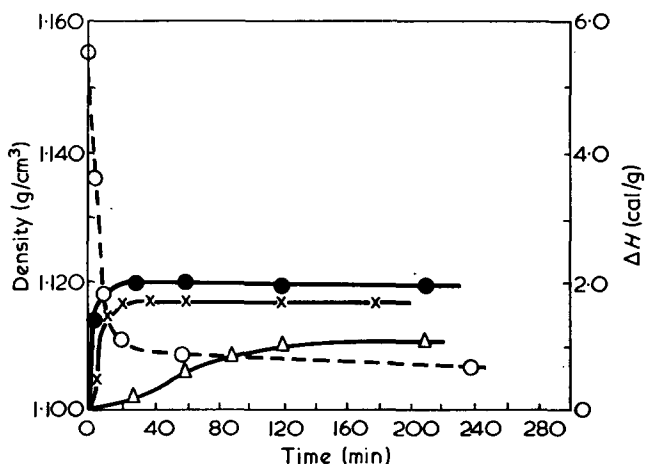


Figure 7 Effect of annealing conditions on density of nylon-6. \triangle , 45°C; \times , 55°C; \bullet , 60°C; \circ --- \circ , see text

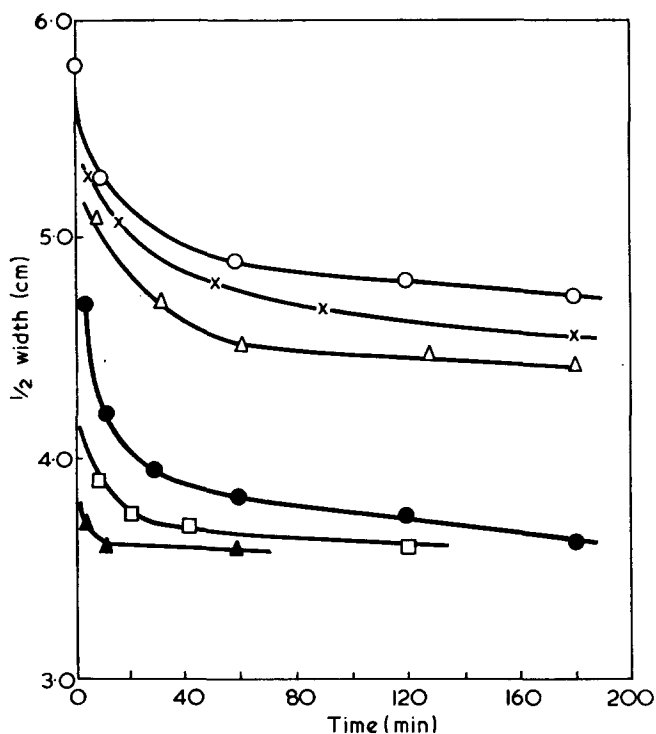


Figure 8 Effect of annealing conditions on X-ray diffraction spectra of nylon-6. \circ , 40°C; \times , 45°C; \triangle , 50°C; \bullet , 55°C; \square , 60°C; \blacktriangle , 70°C

Quenching of a nylon-6 melt results in a loosely packed amorphous structure (amorphous 1) showing on X-ray diffraction a broad halo of spacing 4.30 Å. On exposure to moisture or on warming, a denser amorphous form is produced (amorphous 2), which shows a halo of spacing 4.16 Å and density 1.084 g/cm³. On heating above the so-called T_g short range intermolecular order between chains develops without ordering along the length. The chains are assumed to be randomly twisted. Small elements comprised of groups of cylindrically shaped molecules having a unique spacing are formed giving a single reflection characteristic of a pseudo-hexagonal form of spacing 4.13 Å and density 1.155 g/cm³. Moderate orientation of the chains produces longitudinal order of the amide groups along the chain length resulting in a sharper X-ray diffraction spectra and producing a hexagonal form of spacing 4.10 Å and density 1.150 g/cm³ (β -hexagonal or γ -form). Stretching of this β -hexagonal form results in a transformation to a paracrystalline monoclinic form of spacing:

$$\begin{array}{l} d_{202+002} \quad 4.30-4.50 \text{ \AA} \quad \text{and density } 1.136-1.174 \text{ g/cm}^3 \\ d_{200} \quad 3.70-3.86 \text{ \AA} \end{array}$$

There is another form, that of the highly crystalline α -monoclinic form proposed by Bunn, of spacing:

$$\begin{array}{l} d_{202+002} \quad 4.40 \text{ \AA} \quad \text{and density } 1.225 \text{ g/cm}^3 \\ d_{200} \quad 3.70 \text{ \AA} \end{array}$$

From measurements of the spectra obtained on efficiently quenched nylon-6, structures can now be assigned to the polymer before and after the thermal transitions described in this report. These are given in Table 3.

Vogelso¹⁴ has shown that the γ or β -form of nylon-6 corresponds to a hexagonal structure in which all the chains lie in the same direction but a twist in the chain

enables all the hydrogen bonds to be made, i.e. a 'parallel' configuration. Heating at temperatures above 165°C resulted in the formation of the monoclinic α -form, an 'anti-parallel' structure in which the chains lie in opposite directions.

The X-ray diffraction spectra of a nylon-6 melt showed a broad halo of spacing 4.66 Å¹⁹. This indicated some structure in the melt, evidence of which has been provided by other techniques.

A model can now be proposed to explain the transitions observed in 'even' polyamides and the absence of such transitions in 'odd' polyamides.

If the structure known to persist in the melt consists of small regions of 'parallel' and 'anti-parallel' order and if the 'parallel' regions are fully extended, then this will result in unassociated -NH groups and these will be frozen into the structure on quenching.

On heating, a temperature will be reached at which the methylene sequences in any 'parallel' regions acquire sufficient mobility to twist and so enable hydrogen bonding to be completed. The temperature region at which the twisting of methylene sequences occurs is 40°-50°C and the resulting hydrogen bonding is responsible for part of the exotherm observed by d.t.a. Crystallization of the now fully hydrogen bonded 'parallel' regions to form the γ -form cannot occur to any high degree of perfection, partly because of the twist in the structure but mainly because of the constraints of neighbouring 'anti-parallel' regions. The poor degree of crystallinity is shown by X-ray diffraction and the low densities observed (1.120 g/cm³ at 25°C even after prolonged heating at 55°C compared with 1.150 g/cm³ at 25°C for the α -form). Further heating at higher temperature causes crystallization of the 'anti-parallel' regions and disruption of the chain extended 'parallel' form. This is consistent with X-ray diffraction data which show a steady increase of the α -form together with an equally steady decrease of the γ -form.

The existence of unassociated -NH groups in polyamides has never been reported; in fact many workers have concluded, from infra-red studies, that polyamides are always fully hydrogen bonded. However, the sample preparation itself and ingress of water into the sample always favours the completion of hydrogen bonds before the sample is subjected to infra-red examination.

The other 'even' polyamides present the same transitions as were observed with nylon-6 and it would be expected that they also possess two crystal forms. However, nylon-8 shows normally only the 'parallel' form, the 'anti-parallel' form being induced only by

Table 3 X-ray diffraction analysis of nylon-6 compared with published data

Sample	Literature spacing (Å)	Observed spacing (Å)	Structure
Quenched nylon-6	Halo 4.30	4.31	Amorphous 1
Quenched nylon-6 heated 2 h at 55°C	Sharp 4.13	4.11	Hexagonal α -form or γ -form
Quenched nylon-6 heated 16 h at 150°C	Sharp 4.10	4.10	Hexagonal β -form or γ -form
Quenched nylon-6 heated 10 min at 210°C	$d_{202+002}$ 4.30-4.50 d_{200} 3.70	4.36	Monoclinic α -form

drawing at temperatures near to the melting point. This is due to the increasing stability of the twist in the structure arising from the increase in $-\text{CH}_2$ sequence length. On this basis nylon-12 should be still more stable and in fact the 'anti-parallel' form of nylon-12 is at present unknown.

Nylon-7 and 'odd' polyamides in general have not been so extensively studied. As with nylon-6, both types of structure will persist in the melt and be frozen-in on quenching. Hydrogen bonding is complete in both 'parallel' and 'anti-parallel' regions, no twisting of the chains is required and no further hydrogen bonding is possible. Crystallization will, as a result be much faster. This is indicated by the absence of any transitions even after the severe quenching conditions.

It is now possible to propose a more reasonable explanation for the zig-zag in the melting point-methylene sequence length relation than the ones previously reported.

Nylon-6 has a lower melting point than nylon-7. As the methylene sequence length increases a reduction in melting point would be expected. Nylon-6 is known to favour the 'anti-parallel' form in which complete hydrogen bonding is achieved without distortion of the chains. It does not, however, achieve the maximum intermolecular coupling. Nylon-7, on the other hand, can achieve both requirements and hence has a higher melting point.

Nylons-8, -10 and above do not readily form 'anti-parallel' structure but exist in a poorly crystalline 'parallel' form in which a twist in the chains is necessary for complete hydrogen bonding. This results in lower melting points than the corresponding odd polyamides-9, -11, etc.

The low temperature crystallization processes occurring in well quenched nylon-6 do not agree with the data described by Hartley *et al.*³. It is certain that the mass of sample used in their work was far too large to be efficiently quenched. The density changes observed by them at -30°C were probably secondary effects resulting from crystallization which had occurred during the relatively slow cooling of the samples.

The present work now shows that molecular re-arrangement detectable by d.t.a. occurs at temperatures between 30°C and 70°C . This results in only a marginal change in density and no significant change in the X-ray spectra. Crystallization, as defined by X-ray diffraction, occurs only after these re-arrangements are completed, i.e. at temperatures over 80°C .

CONCLUSIONS

(1) The thermal transitions observed by d.t.a. on heating efficiently quenched 'even' ω -amino acid polyamides are due to the persistence of 'parallel' and 'anti-parallel' regions of order in the melt and in the quenched state. Similar considerations explain the absence of such transitions in 'odd' polyamides.

(2) The existence of a transition in the region of 40°C , reported in the literature as the T_g has been confirmed. The unexpected high value for this transition has been shown to be due to hydrogen bonded structures. The temperature of this transition has been reduced to -60°C by chemical substitution.

ACKNOWLEDGEMENT

The author wishes to thank Mr F. D. Hartley for helpful discussions during the preparation of this paper.

REFERENCES

- 1 Forster, M. J. *Text. Res. J.* 1968, p 474
- 2 Morgan, L. B. *J. Appl. Chem., Lond.* 1954, 4, 160
- 3 Hartley, F. D., Lord, F. W. and Morgan, L. B. *Ric. Scient.* 1955, 25A, 577
- 4 Rybnikan, F. *J. Polym. Sci.* 1958, 28, 633
- 5 Beaman, R. G. *J. Appl. Polym. Sci.* 1965, 9, 3949
- 6 Yoshimoto, T. and Miyagi, A. *J. Chem. Soc. Japan* 1966, 69, 1771
- 7 Gröbu, V., Versäumer, H., Winkler, F., Daive, G. and Schmidt, F. *Faserforsch. Textiltech.* 1967, 18, 27
- 8 Temin, S. C. *J. Appl. Polym. Sci.* 1965, 9, 471
- 9 Ke, B. 'Newameihords of Polymer Characterisation', Interscience, New York, 1964, pp 347-376
- 10 Kinoshita, Y. *Makromol. Chem.* 1959, 33, 1
- 11 Brill, R. *J. Prakt. Chem.* 1943, 161, 49
- 12 Slichter, W. P. *J. Polym. Sci.* 1959, 35, 77
- 13 Slichter, W. P. *J. Polym. Sci.* 1959, 36, 259
- 14 Vogelsong, D. C. and Pearce, E. M. *J. Polym. Sci.* 1960, 45, 546
- 15 Vogelsong, D. C. *J. Polym. Sci. (A)* 1963, 1, 1055
- 16 Geil, P. H. *J. Polym. Sci.* 1960, 44, 449
- 17 Holmes, D. R., Bunn, C. W. and Smith, D. J. *J. Polym. Sci.* 1955, 17, 159
- 18 Ogawa, M. T. *et. al. J. Polym. Sci. (B)* 1963, 1, 57
- 19 Roldan, L. G. and Kaufman, H. S. *J. Polym. Sci. (B)* 1963, 1, 603
- 20 Roldan, L. G., Rahl, F. and Paterson, A. R. 'Analysis and Fractionation of Polymers', Interscience, New York, 1965, p 145
- 21 Arimoto, M., Iohibashi, M., Hirai, M. and Chatari, Y. *J. Polym. Sci. (A)* 1965, 3, 317
- 22 Brill, R. *Z. Phys. Chem. (B)* 1943, 53, 61
- 23 Sandiman, I. and Keller, A. *J. Polym. Sci.* 1956, 19, 401
- 24 Rybuikan, F. and Burda, J. *Faserforsch. Textiltech.* 1961, 12, 324
- 25 Ruland, W. *Polymer* 1964, 5, 89
- 26 Arimoto, H. *J. Polym. Sci. (A)* 1964, 2, 2283
- 27 Little, K. *Br. J. Appl. Phys.* 1959, 10, 225

Structure and properties of polypivalolactone*

H. A. Oosterhof

Koninklijke/Shell-Laboratorium, PO Box 3003, Amsterdam, The Netherlands
(Received 30 July 1973)

Pivalolactone (α,α -dimethyl- β -propiolactone) can be polymerized to linear polyesters with widely different molecular weights. The polymer has a high degree of crystallinity and a high crystalline melting point. Several other basic properties of the polymer have been determined, such as molecular weight, glass-transition temperature, rheological characteristics, etc., and its possible use in the fibre and plastics field has been extensively investigated. It was found that the polymer, when adequately stabilized, has a high thermal stability and shows hardly any discoloration upon processing.

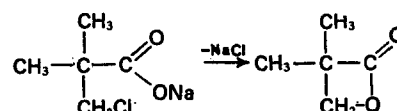
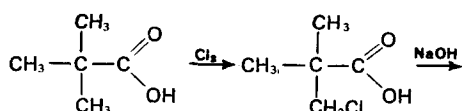
Ultimate products such as fibres and injection-moulded articles based on polypivalolactone have a high resistance to hydrolysis, heat and chemicals, and exhibit excellent weathering properties. A remarkable characteristic of the products is their high elastic recovery, in particular after annealing at high temperatures. Many of the observed properties can be explained by means of the molecular and crystalline structure of the polymer.

INTRODUCTION

Earlier investigations by Shell into the use of tertiary carboxylic acids ('versatic' acids) in the preparation of alkyd resins^{1,2} and paint latices^{3,4} showed that direct esterification of such acids was difficult owing to the steric hindrance caused by the branching at the α -carbon atom. However, this difficulty could be circumvented by causing the acid to react with epichlorhydrin and subjecting the resultant product to dehydrochlorination. The glycidyl ester thus obtained proved suitable for use in alkyd resins. Vinyl esters of the α -branched acids could readily be prepared via reaction with acetylene. The application of such esters in, for instance, vinyl acetate copolymer emulsions was found to lead to high-quality paint latices.

Although steric hindrance makes the esterification of such branched acids difficult, it imparts a remarkably good stability to the resultant ester⁵. The ultimate paint films exhibit a high resistance to alkali, weathering and discoloration.

The lowest molecular weight tertiary carboxylic acid is pivalic acid, which can be prepared from isobutylene, carbon monoxide and water. It can be converted via chlorination into hydroxypivalic acid, another potential base material for the preparation of polyesters. However, here too, steric hindrance impedes esterification to products of sufficiently high molecular weight. In this case, direct esterification can be avoided by preparing the corresponding lactone from monochloropivalic acid via ring closure with sodium hydroxide:



Owing to the highly strained ring system this lactone can be readily polymerized via ring opening, yielding the required high molecular weight linear polyester. Details on the polymerization of pivalolactone have been described in an earlier publication⁶.

The present paper discusses the basic properties of polypivalolactone and evaluates its usefulness for application in fibres and plastics.

BASIC PROPERTIES

Crystallinity

Pivalolactone can be polymerized to products with a wide range of molecular weights, from low molecular weight oligomers to polymers with molecular weights of several millions.

The very high degree of crystallinity of the polymer is related to the symmetrical arrangement of the repeating unit in the polymer chain, as is the case with, for example, polyethylene. This fact combined with infra-red data and the chemistry of the anionic polymerization process point to a high structural purity of the polymer.

The crystalline melting point of the polymer is about 245°C; its glass-transition temperature (T_g) is -10°C.

Extensive studies have been made of the crystalline structures occurring in polypivalolactone. A detailed description of this work will be made shortly.

Three crystalline modifications have been observed: (i) the α -modification, which is the main product crystallizing from the melt. In this modification the polymer chain has a helical structure with two monomer units per turn; (ii) the β -modification, which crystallizes in

* Presented as a Symposium Lecture at the IUPAC International Symposium on Macromolecules, Aberdeen, September 1973.

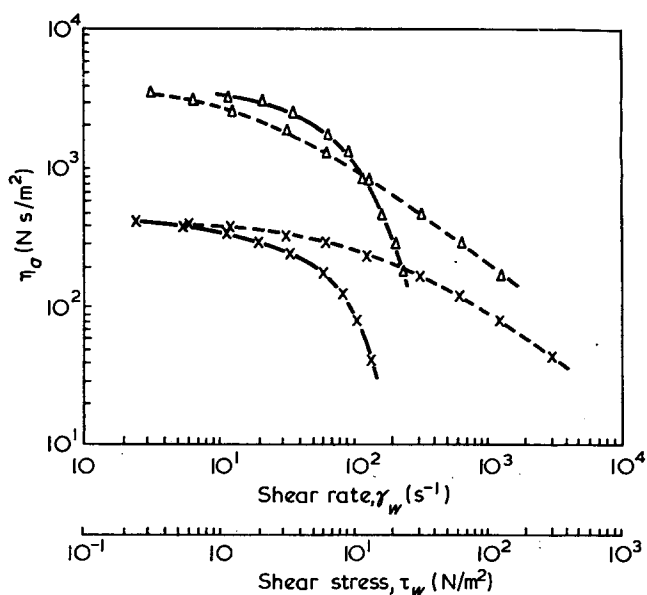


Figure 3 Influence of shear on melt viscosity of polypivalolactone at 260°C. Δ , LVN 1.7 (mol. wt. $\sim 300\,000$); \times , LVN 0.95 (mol. wt. $\sim 150\,000$). ---, shear rate (γ_w); —, shear stress (τ_w). $l_c/d_c=80.9$; $d_c=0.1257$ cm

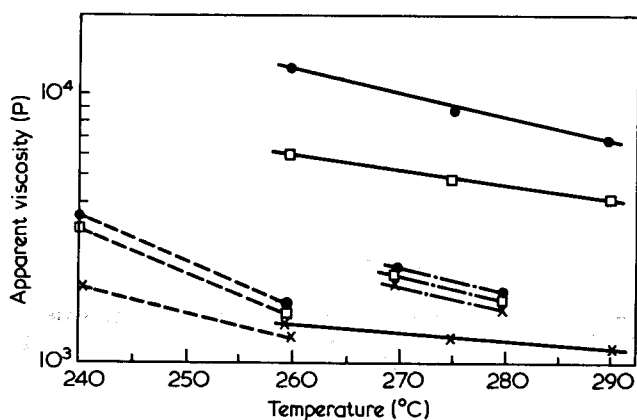


Figure 4 Apparent viscosities of polypivalolactone (LVN 1.3) (—), nylon-6 (---) and PET (.....). Capillary: entrance angle, 90°; $l_c/d_c=80.9$; $d_c=0.1257$ cm. Shear rate, $\dot{\gamma}$: \bullet , 10; \square , 100; \times , 1000 s^{-1}

above 200°C. They are mainly applied as synthetic fibres and to a lesser extent as films and plastics.

We have carried out an extensive investigation into the processing characteristics and ultimate properties of polypivalolactone in the above-mentioned fields of application.

Fibre processing and properties

Melt spinning and stretching. Polypivalolactone can be processed with the normal melt-spinning equipment. The temperature of extrusion is restricted on the one hand by the melting point of the polymer ($\sim 245^\circ\text{C}$) and on the other by its degradation (gas formation). In general, spinneret temperature of 260–300°C can be adopted. Care should be taken to avoid dead or hot spots in the spinning machine. As discussed before, prolonged heating of the polymer results not only in a decrease in \bar{M}_w , but also in decomposition of the polymer into carbon dioxide and isobutene. Such gas formation will give rise to strand breakage directly beneath the spinneret.

Because of the very high rate of crystallization the rate of cooling of the molten filaments plays an important role: the faster the cooling, the less pronounced spherulite formation will be. In a normal air atmosphere cooling can be improved by applying high linear speeds of spinning (Table 1 and Figure 5). It was further observed that higher spinning speeds lead to fibres with a higher degree of pre-orientation (shown by an increase in tenacity and a decrease in elongation). At low spinning speeds brittle fibres are produced which cannot be stretched afterwards.

Of course, the thickness of the filament also has a pronounced influence on the cooling rate. With air cooling unstretched fibres can be spun with a maximum thickness of 3.5–6 tex (after stretching ~ 1 –1.2 tex). At higher tex values the fibres become brittle and cannot be stretched to a higher degree of orientation.

The cooling rate can be considerably increased by applying a water quench. In this way completely or almost completely spherulite-free fibres can be obtained (Figure 6). This even holds for high filament thicknesses (investigated up to 12–14 tex). Compared to air-cooled fibres, the water-quenched ones have a very high degree of preorientation.

Table 1 Influence of winding speed on the properties of air-cooled polypivalolactone fibres

Winding speed (m/min)	200	300	1050
Number of holes/jet diameter (mm)	8/0.8	8/0.8	8/0.8
Production (cm^3/min)	2.0	3.2	8.9
Draw-down ratio	430	420	440
Titre (tex)	8.6	9.5	7.6
Tenacity (g/tex)	*	10.8	14.4
Elongation at break (%)	—	400	240
Stretch ratio	—	3.8	2.7
Stretch temperature ($^\circ\text{C}$)	—	195	195
Titre, tex (8 filaments)	—	2.5	2.9
Tenacity (g/tex)	—	27	37
Elongation at break (%)	—	28	27

* Impossible to determine; fibre was very brittle

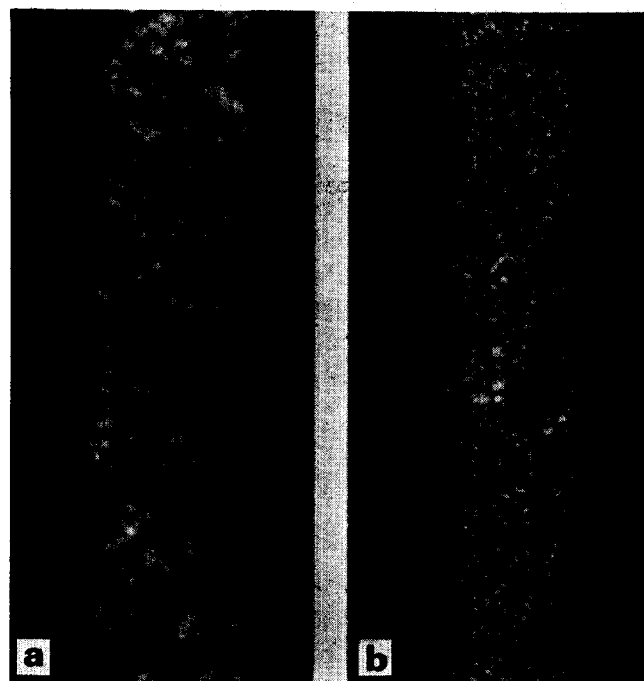


Figure 5 Influence of spinning speed on spherulite formation (air cooling). (a) 150 m/min; (b) 570 m/min

As discussed above the use of nucleating agents prevents the formation of large spherulites. However, it appears that even with rapid cooling in water many small spherulites are formed, which have an adverse effect on subsequent stretching (Figure 7).

The spun fibres can easily be oriented by stretching over hot plates or hot pins. The stretching temperature

can be varied from 20 to 210°C. At the lower temperatures, however, (20–50°C) some distortion occurs, resulting in fibres with a dull appearance. After adequate stretching the spherulites present in the original spun fibre disappear (Figure 8).

Fibre properties. From extensive laboratory spinning and stretching experiments the following picture emerges of the ultimate properties of polypivalolactone fibres.

(a) Mechanical properties. The tensile strength and modulus increase, as can be expected, with the level of orientation. Normal (one-step) stretching results in a maximum tenacity of 45–55 g/tex. By applying a two-step stretching procedure and annealing the fibre between the two stretching steps fibres can be obtained with a tenacity of 75–90 g/tex, a very high modulus (up to 1100 g/tex) and a low elongation at break (8–10%). Such fibres contain a very high proportion of the metastable γ -crystalline form (zig-zag structure). During heat treatment at elevated temperature (150–200°C), which is generally required to remove shrinkage, the γ -crystalline structure converts into the α -form. This conversion decreases the tenacity to 45–55 g/tex, the modulus to 350 g/tex and gives a 60–80% increase in elongation. This means that, although high-tenacity fibres with an interestingly high modulus can be prepared, they cannot be used in those applications in which an additional heat treatment is required.

One of the outstanding features of polypivalolactone fibres is their very high elastic recovery. It is important to note that the recovery remains at least on the same high level after removal of shrinkage by heat treatment in steam or dry air (Table 2).

The remarkable fact that these highly crystalline fibres can show such high elongations at relatively high tenacity

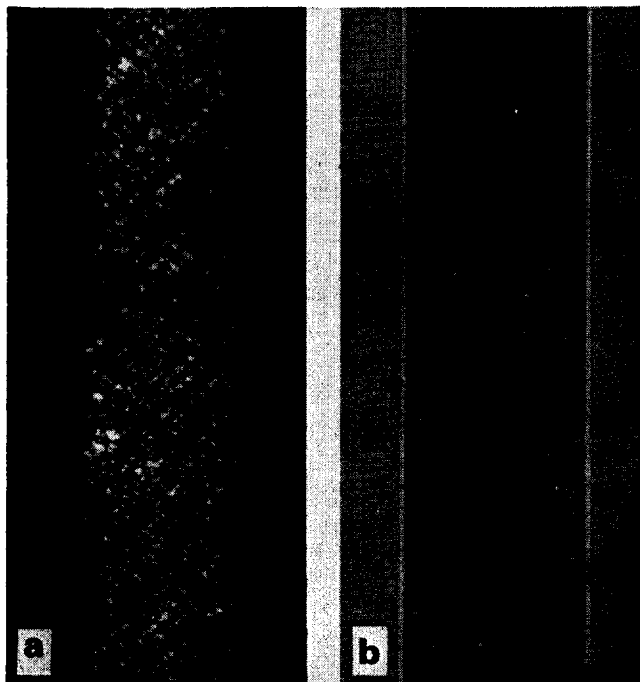


Figure 6 Influence of water quenching on spherulite formation. (a) 570 m/min (air cooled); (b) 260 m/min (water at 15°C cooled—water level 30 cm below spinneret)

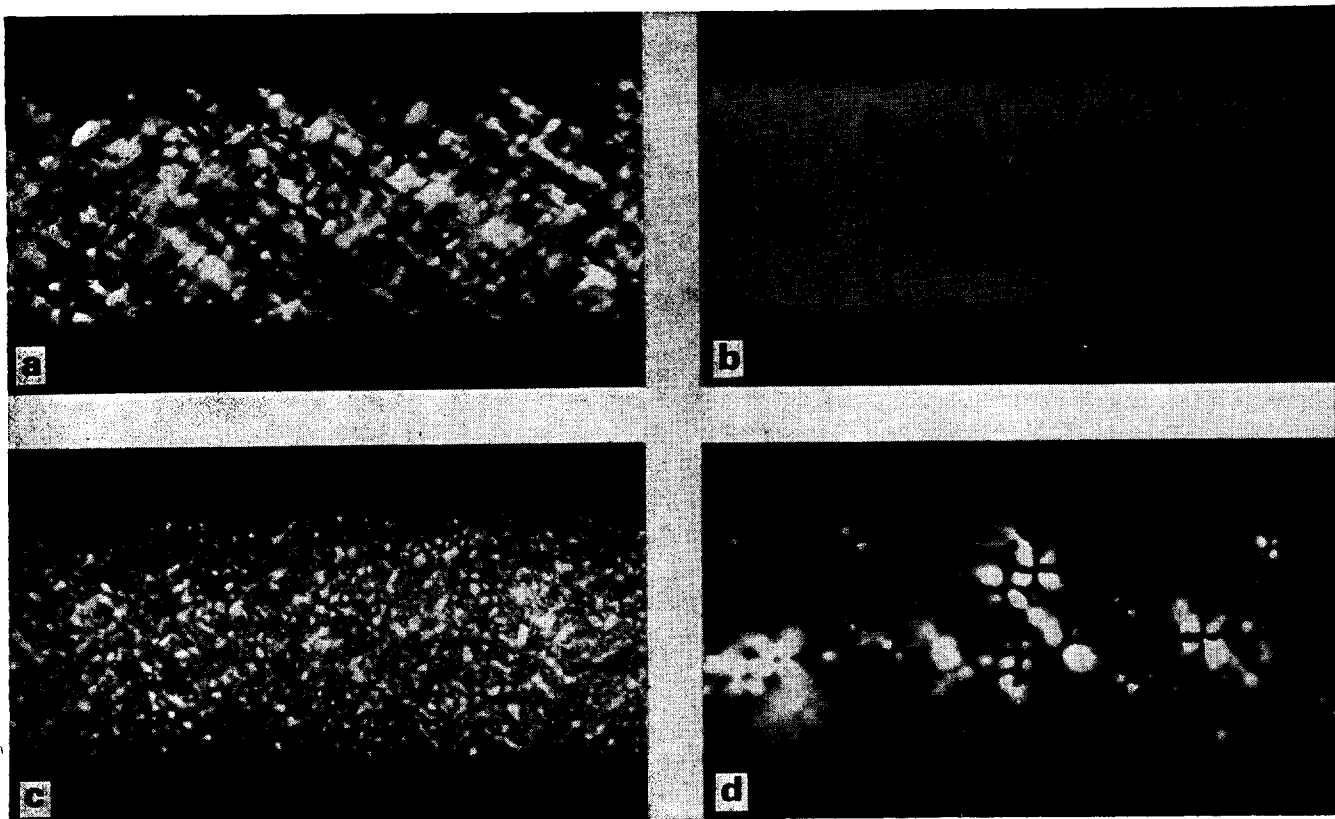


Figure 7 Influence of nucleation on spherulite formation. Water-quenched: (a) nucleated; (b) non-nucleated. Air cooled: (c) nucleated; (d) non-nucleated. Spinning conditions: jet size, 0.5 mm; spinning speed, 3.5 m/min; take-up speed, 260 m/min; titre, 24 den

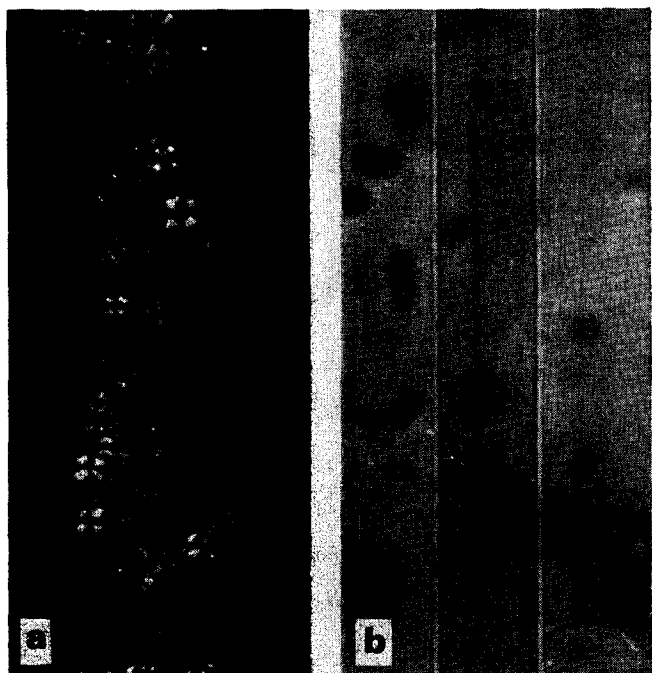


Figure 8 Polypivalolactone fibre (air cooled) (a) before and (b) after stretching. Stretching ratio: 2.5

Table 2 Influence of heat treatment on tensile recovery (%) and stress decay (%)

	Treatment		
	None	30 min at 126°C in steam	5 min at 180°C in air oven
Tensile recovery*:			
Polypivalolactone fibre	94	80	86
PET fibre	96	61	80
Nylon-6 fibre	97	60	54
Stress decay*:			
Polypivalolactone fibre	3.9	5.4	5.1
PET fibre	13.0	18.9	17.5
Nylon-6 fibre	11.5	23.6	—

* At 5% elongation; holding time 1 min

and moreover possess such good recovery properties has to be ascribed to the above-mentioned α - γ transformation.

(b) Chemical resistance. Polypivalolactone fibres have excellent resistance to acids, alkali, solvents, bleaching agents and detergents. Only a small change in tenacity is observed after 30 days' immersion at room temperature in 5% by wt. caustic soda in water. In this respect they are superior to PET fibres, which under the same conditions lose 50–60% of their original strength (Figure 9). The high alkali resistance of the polypivalolactone fibre is not surprising since esters derived from tertiary carboxylic acids are well known to resist saponification⁵.

(c) Weathering properties. Polypivalolactone fibres have a high resistance to weathering. After 18 months' outdoor exposure (45°, facing south) only a limited decrease in strength and elongation is observed (Figure 10). Here too, we believe that the resistance of this ester to hydrolysis contributes a great deal to the retention of the tensile properties.

(d) Whiteness and whiteness retention. The polymer powder is converted to nibs via extrusion at nearly 300°C, and subsequently melt spun at the same tempera-

ture to fibres. The resulting fibres nevertheless do not exhibit any significant discoloration. The colour retention after weathering for 18 months or after oven ageing at 100°C for 1000 h proved to be excellent. In this respect the polypivalolactone fibres are far superior to nylon fibres and even better than fibres derived from PET.

(e) Dyeability. Just as with PET fibres the polypivalolactone fibres can only be coloured with dyes that are applied from an aqueous dispersion. It was found that a number of disperse dyes normally used for PET fibres give good shades on polypivalolactone fibres on pressure dyeing at 125–130°C. However, the percentage of dye take-up from the bath is generally on the low side compared to that of PET. Good dyeability of the latter type of fibre can also be attained at 95–100°C by the use of carriers. (Carriers are generally solvents which assist the transport of dye from the dispersion to the fibre.) For polypivalolactone fibres no suitable carriers have been found. Apparently, the high degree of crystallinity has an adverse effect on the uptake of the dye molecules.

Plastics processing and properties

Processing. During preliminary compression and injection-moulding experiments with polypivalolactone it proved difficult to produce homogeneous articles. It was found that the irregularities in the articles were

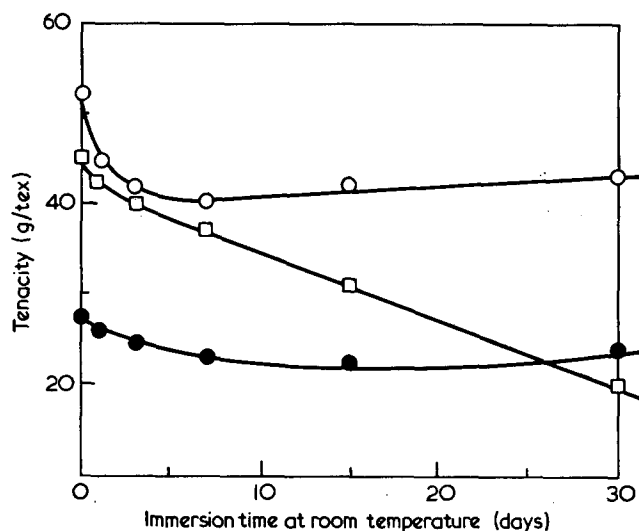


Figure 9 Alkali resistance of polypivalolactone-based fibres in 5% by wt. NaOH. ●, Polypivalolactone; ○, nylon-6; □, PET

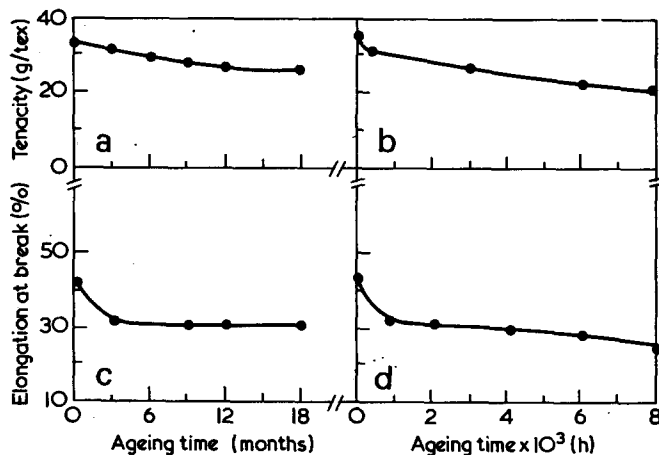


Figure 10 Influence of u.v. ageing on tenacity and elongation at break. (a) and (c), outdoor, unprotected; (b) and (d), Xenon tester

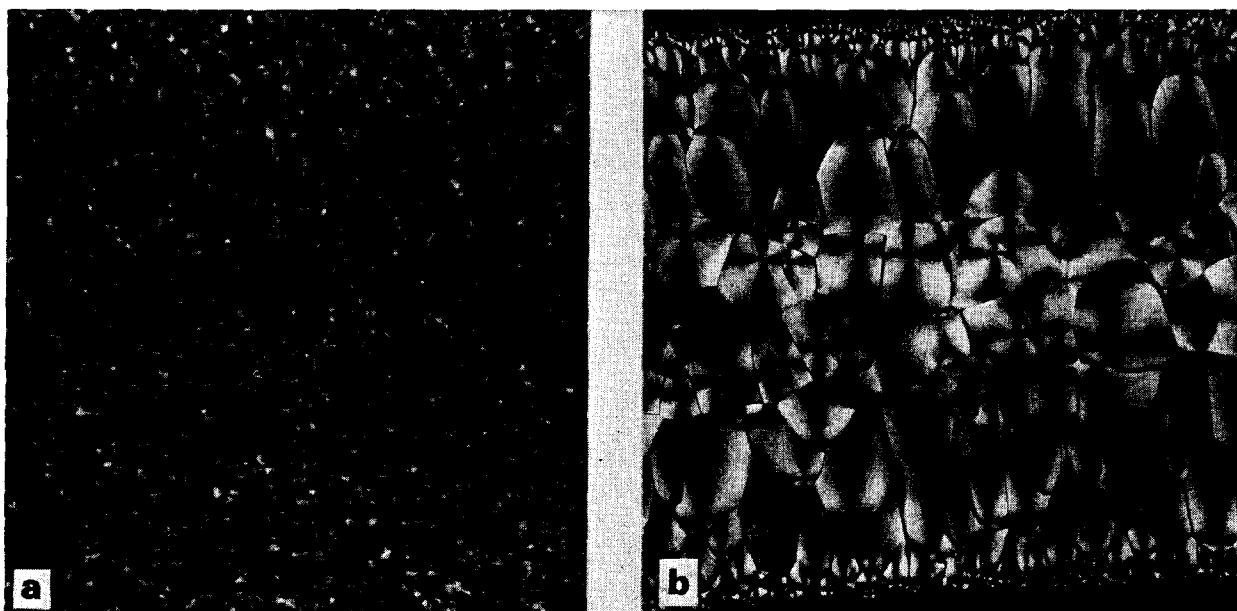


Figure 11 Influence of nucleation on spherulite size. (a) Polypivalolactone nucleated with 0.1 phr sodium α -naphthalenesulphonate; (b) non-nucleated polypivalolactone. Cross-section of quenched sheets; magnification 180 \times ; crossed polarizers

caused by the formation of large spherulites, which sometimes even led to initial cracks in the moulded article. A much more uniform pattern of crystallization can be obtained by the use of nucleating agents, for instance, with small amounts (0.1% by wt.) of the sodium salt of α -naphthalene-sulphonic acid (Figure 11).

Compounds containing a nucleating agent can be injection-moulded with the conventional types of injection-moulding machine at mass temperatures of 260–300°C. The mould temperatures can lie between room temperature and 150°C. The molecular weight can be varied between approximately 150 000 and 400 000. At lower molecular weights the products are too brittle, while at higher molecular weights the decrease in flow affects the processability.

Owing to its high degree of crystallinity polypivalolactone shows a relatively high mould shrinkage.

Properties. A survey of the typical properties of polypivalolactone is presented in Table 3. Particular features are its hardness, dimensional stability at elevated temperatures and high stresses, and its resistance to u.v. light, heat and chemicals.

(a) Influence of high-temperature annealing on mechanical properties. The combination of good dimensional and heat stability observed with polypivalolactone at elevated temperatures prompted us to make it the subject of a further investigation.

The mechanical properties of injection-moulded articles were determined before and after heating at different temperatures. It appeared that the products can safely be heated to a temperature of 220°C without showing any distortion of the polymer. The only effect is a further increase in crystallinity. It is remarkable, however, that even after short heating (5 min) at temperatures of 180–200°C a very distinct change in mechanical properties occurs (Figure 12 and Table 4). The elongation at break strongly increases, while moreover an improvement in impact strength is noted. The annealing step apparently removes the stresses in the material which are caused by the high degree of crystallinity. The finding that after

Table 3 Typical properties of polypivalolactone

Property	Value or rating
Specific gravity	1.18
Hardness, Shore D	85
Yield stress	38 MN/m ²
Yield strain	4–6%
G modulus (torsion pendulum at 1 Hz)	
at 20°C	1500 MN/m ²
at 200°C	300 MN/m ²
Vicat softening temperature	220°C
Heat distortion temperature (264 lbf/in ²)	180–200°C
Creep resistance (10 ⁴ h at 20°C at a stress of 20.6 MN/m ²)	0.8% (length increase)
Izod impact strength	4 kJ/m ²
Water absorption (24 h)	0.2%
Volume resistivity	
at 20°C	60 \times 10 ¹² cm
at 180°C	0.2 \times 10 ¹² cm
Chemical resistance (after 30 days immersion at room temp.) to:	
aliphatic hydrocarbons	excellent
aromatic hydrocarbons	very good
alcohols	excellent
ketones	excellent
alkali	stress corrosion
acetic acid	excellent

Table 4 Influence of annealing on some mechanical properties of polypivalolactone*

Property	Value
Yield stress	original 39 MN/m ²
	annealed 37 MN/m ²
Elongation at break	original 10%
	annealed 69%
Set after break	original 1.7%
	annealed 1.0%
Tensile impact strength	original 100 kJ/m ²
	annealed > 600 kJ/m ²
Charpy impact strength (notched)	original 3.4 kJ/m ²
	annealed 6.5 kJ/m ²
Charpy impact strength (unnotched)	original 4.6 kJ/m ²
	annealed 40 kJ/m ²

* Injection-moulded articles from polypivalolactone ($M_w \sim 250\ 000$)
Annealing conditions: 5 min at 200°C

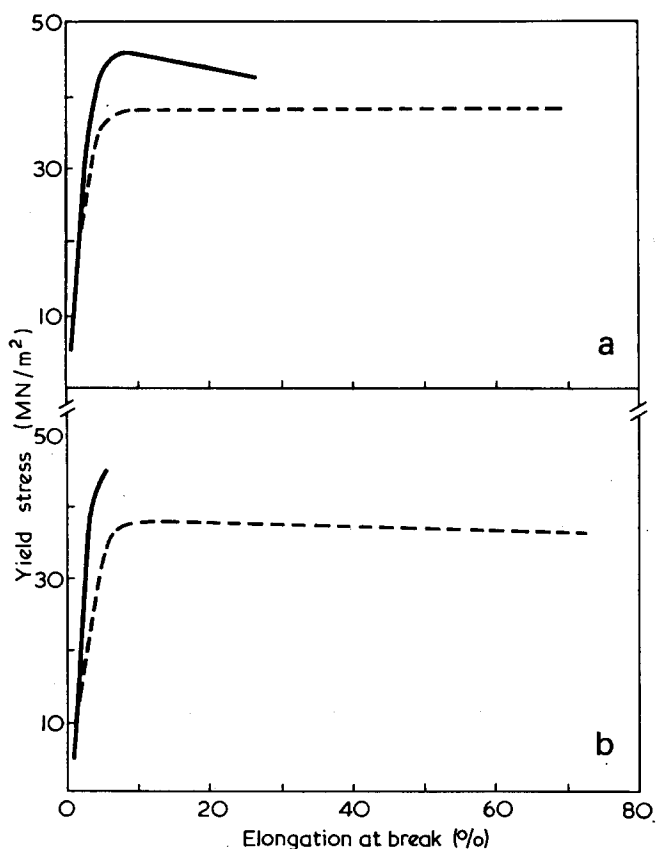


Figure 12 Influence of annealing on stress-strain behaviour of polypivalolactone. —, Original; ----, annealed. (a) Mol. wt. 350 000; (b) mol. wt. 150 000

annealing at 200°C this highly crystalline material produces a substance with an elongation at break of 70% and a very low set at break (the specimen reverts almost completely to its original dimension after breaking) must again be ascribed to the reversible crystalline transformations from the stable α -modification to the metastable γ -form upon elongation.

(b) Heat-ageing characteristics. As already stated before, articles based on polypivalolactone have an excellent dimensional stability at high temperatures. It was, therefore, of interest to study the effect of ageing on this property.

To this end injection-moulded dumbbells based on polypivalolactone stabilized with different types of

antioxidant were subjected to heat-ageing tests in air ovens at temperatures varying from 150–200°C. The polymer behaviour was checked by determining the change in tensile properties and molecular weight breakdown.

The maximum allowable residence time depends on the temperature adopted and on the type of antioxidant employed. Very good heat resistance is achieved with amine types of antioxidant such as phenyl- β -naphthylamine and phenyl-di(β -naphthylamine). Polypivalolactone samples stabilized with these types of antioxidant reach storage lives of up to 800 h at 200°C and of more than 5000 h at 150°C.

CONCLUSIONS

Our study has clearly shown that polypivalolactone is a polymer with a number of interesting properties. This had been confirmed by a further assessment of its merits as a base material for fibres and plastics by independent evaluations outside Shell. Yet, it is difficult to reach a final conclusion as regards the applicability of such a relatively new polymer in the existing field of fibres and engineering plastics. The costs of producing the monomer and polymer also play a dominant role and it is mainly such economic factors rather than technical considerations which have prevented the polymer from being commercially available at present.

ACKNOWLEDGEMENT

The author wishes to express his thanks to all his colleagues from the Amsterdam and Delft Shell Laboratories, who, with their enthusiasm and collaboration have helped to advance the knowledge of polypivalolactone to the present stage.

REFERENCES

- 1 Goppel, J. M., Bruin, P. and Zonsveld, J. J. *6th Fatigue Congr.* 1962, p 31
- 2 Vogelzang, E. J. W. *J. Oil Colour Chem. Ass.* 1963, **46**, 89
- 3 Bruin, P., Oosterhof, H. A., Vegter, G. C. and Vogelzang, E. J. W. *7th Fatigue Congr.* 1964, p 49
- 4 Oosterhof, H. A. *J. Oil Colour Chem. Ass.* 1965, **48**, 256
- 5 Herzberg, S. *6th Fatigue Congr.* 1962, p 319
- 6 Mayne, N. R. *Chem. Tech.* 1972, p 728

Note to the Editor

Preparation and properties of the poly(2-chlorocyanurate) of bisphenol A

G. Allen and A. G. De Boos*

Department of Chemistry, University of Manchester, Manchester M13 9PL, UK
(Received 30 May 1973; revised 3 August 1973)

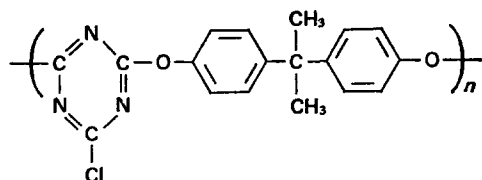
INTRODUCTION

In recent years interest has been shown in polymers containing *s*-triazine rings, particularly those based on cyanuric acid derivatives of bisphenols¹⁻⁷. These polymers are noted for their high transition temperatures and high thermal stabilities. Most of the latest work has been based on the poly(2-R-cyanurates) prepared by interfacial polycondensation of 2-R-4,6-dichloro-*s*-triazines with 2,2-bis(*p*-hydroxyphenyl) propane (bisphenol A). The preparative technique developed by Breed and Elliot³ used a chloroform-water interfacial system which was stirred for 10 min in a Waring Blendor. *s*-Collidine was used as acid acceptor. When the organic layer had been separated, the solvent was evaporated on a steam bath and the polymer was heated for 1 h. The heat treatment was essential for the production of high molecular weight polymers.

The technique developed by Nakamura *et al.*^{5,6} used a nitrobenzene-water interfacial system, sodium hydroxide as acid acceptor and a cationic emulsifying agent. The period of stirring was from 0.5 to 5 h at temperatures in the range 7-95°C depending on the nature of the substituent R. After decanting the aqueous phase, the reaction mixture was poured into an excess of acetone and the polymer was collected by filtration. Nakamura also modified this technique to include a two step addition of acid acceptor and made a cursory survey of some of the physical properties of the poly(2-R-cyanurates).

Sherliker⁷ developed a technique which used a chloroform-water system, sodium hydroxide as acid acceptor and a cationic emulsifying agent. A high speed emulsifier was employed and the emulsion was stirred for 4 min at room temperature. The merits of this method over previous recipes include the feasibility of larger scale preparations, shorter reaction times and lower temperatures.

The preparative technique used in this work was similar to that used by Sherliker. Some aspects of the solution properties, nucleophilic chemistry and physical properties of the poly(2-chlorocyanurate) of bisphenol A are reported.



* Present address: Division of Textile Industry, CSIRO, PO Box 21, Belmont, Victoria 3216, Australia.

PREPARATION

Purification of reagents

Cyanuric chloride (AR grade) and 2,2-bis(*p*-hydroxyphenyl) propane (bisphenol A) (AR grade) were recrystallized from petroleum ether (b.p. 80-100°C) and chlorobenzene respectively, dried and stored under vacuum. Cetyltrimethylammonium bromide and sodium hydroxide, both of reagent grade, were used as supplied. The solvents, tetrahydrofuran (THF) and benzene were distilled over calcium hydride immediately prior to use while other solvents were used as supplied.

Preparation of the poly(2-chlorocyanurate) of bisphenol A

A solution of the bisphenol (0.0201 mol), sodium hydroxide (0.0404 mol) and cetyltrimethylammonium bromide (0.5 g) in de-ionized water (200 ml) was agitated strongly in a high speed mixer (MSE atomix). A solution of cyanuric chloride (0.0200 mol) in chloroform (50 ml) was added rapidly and the stirring continued for 4 min. The mixture was transferred to a separating funnel and the organic phase was run into an excess of acetone from which the high molecular weight polymer precipitated. The polymer was separated, redissolved in chloroform, reprecipitated in petroleum ether and dried under vacuum. Polymer prepared by this method had a unimodal molecular weight distribution and had a reduced specific viscosity (1 g/dl in chloroform) of 1.03-1.35 which corresponded to an intrinsic viscosity of 0.75-1.00 dl/g. The polymer was isolated in a yield of 60-70%. Microanalysis yielded the results in Table 1. The infrared spectrum of a cast film, n.m.r. spectrum (in deuteriochloroform solution) and ultra-violet spectrum (in chloroform solution) of the polymer, shown in Figure 1, confirmed the expected structure.

The scale of preparation (0.02 M), which could be easily increased further, was greater than that of previous recipes⁶, the reaction time was shorter³, the temperature of the polycondensation was lower³, and no thermal after-treatment was required. Further, the polymer had a unimodal molecular weight distribution and the reduced specific viscosity was as high as, or higher than, that of polymers prepared by other methods. The

Table 1 Elemental analysis of the polymer

Element	Experimental	Theory
Carbon	63.3	63.7
Hydrogen	4.3	4.1
Nitrogen	12.0	12.4
Chlorine	10.0	10.4
Oxygen*	10.4	9.4

* By difference

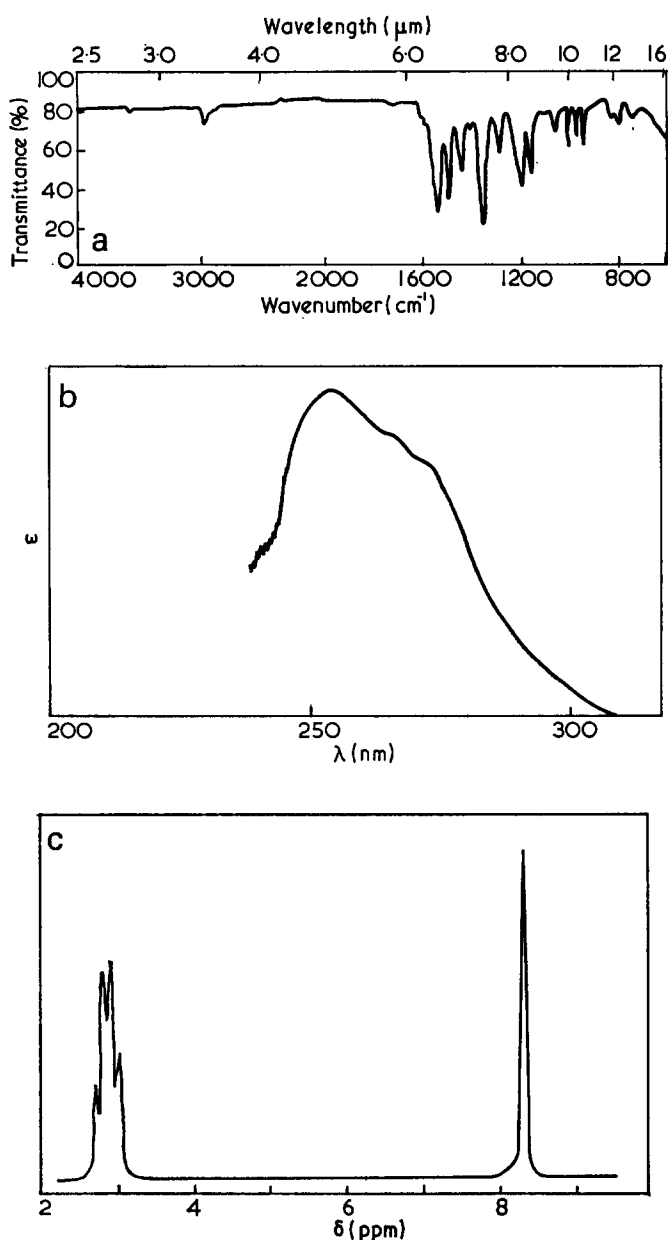


Figure 1 Spectra of PCC-bisphenol A. (a) Infra-red; (b) ultra-violet; (c) n.m.r.

technique is also applicable to other polycyanurates although optimum parameters for polycondensation would be expected to differ from polymer to polymer.

CHARACTERIZATION

A typical poly(2-chlorocyanurate), (PCC-bisphenol A), product was characterized using the normal methods. Osmometric measurements were made with a Melabs recording osmometer (Model CSM-2) using THF as solvent. The specific refractive index increments of the polymer in the various solvents were determined using a Brice-Phoenix differential refractometer, which had been previously calibrated with an aqueous sucrose solution. Light scattering studies were performed in a Sofica light scattering photometer, using monochromatic light ($\lambda = 546$ nm). Viscosity measurements were made at 25°C in a Desreux-Bischoff viscometer, the kinetic energy correction of which was negligible for the solvents used. Gel permeation chromatography (g.p.c.) was

performed in a Waters Associates Model 200 gel permeation chromatograph which had been previously calibrated with low dispersity linear polystyrene, using THF as solvent.

Results and Discussion

Although no comprehensive work has been published on the solution properties of poly(cyanurates) our results for PCC-bisphenol A, shown in Table 2, are in line with those previously published⁷.

In all cases M_w/M_n (g.p.c.) < M_w/M_n (true) and the difference exceeded experimental error. Further, the polymer did not fit on the universal calibration curve⁹ for the columns, the molecular weight average determined by g.p.c. being much lower than the true values. There was some evidence that PCC tended to 'adhere' to the columns even when the solution was rigorously filtered. This behaviour was attributed to the reactive acid chloride side groups, since similar behaviour has also been reported for other highly polar polymers, especially those with highly reactive pendant groups.

The Zimm¹⁰ plots for PCC-bisphenol A in THF and benzene were complex and the complexity of the angular dependence of the Rayleigh ratio did not allow any meaningful determination of radius of gyration to be made. Nevertheless, it was possible to determine the second virial coefficients of the two polymer-solvent systems. The correlation between the second virial coefficients for PCC-bisphenol A in THF obtained by light scattering and osmometry was good, considering the errors involved in their determination. THF was almost a θ solvent for the polymer at 25°C. The second virial coefficient in benzene was negative indicating that this solvent was a very poor solvent for the polymer. The low intrinsic viscosity of the polymer in benzene compared to that in the other solvents reinforced this conclusion. The high refractive index of the polymer, due to the aromatic groups in the polymer backbone, simplified light scattering work.

Table 2 Characterization of a typical poly(2-chlorocyanurate) of bisphenol A

Technique	Parameter	Solvent	Value
Viscometry	RV †	chloroform	1.03
	$[\eta]$	chloroform	0.75
		THF	0.64
		DMA	0.60
Light scattering	M_w	benzene	0.44
		THF	220 000
	A_2	benzene	180 000
		THF	0.23×10^{-4}
Osmometry	M_n	benzene	-3.3×10^{-4}
	A_2	THF	65 000
	M_w/M_n	THF	0.17×10^{-4}
Gel permeation chromatography	M_w/M_n	THF	2.2
U.v. spectroscopy	$E(254)$ (l/g)	chloroform	23.0
Differential refractometry	dn/dc (ml/g)	THF	0.189
		chloroform	0.156
		benzene	0.106
		<i>o</i> -dichlorobenzene	0.056
Gladstone-Dale plot	N_p/ρ^*		1.611
			1.08

* Density (g/ml)

† Reduced specific viscosity (at 1.0 g/dl)

NUCLEOPHILIC CHEMISTRY OF THE POLY(2-CHLOROCYANURATE) OF BISPHENOL A

While the thermal stability of PCC-bisphenol A is known to be high, several workers have reported that the long term chemical stability of the polymer in air is low⁵⁻⁷. Because degradation was thought to occur by a nucleophilic mechanism, and as no full investigation of this effect had been made, this aspect of the chemistry of the polymer was examined. Furthermore, it has been suggested⁷ that poly(2-R-cyanurates) can be prepared from PCC by a second condensation at the reactive chlorine atom. Consequently, a more extensive investigation of the nucleophilic chemistry of the polymer was made.

Experimental

To a solution of the polymer in anhydrous THF was added an equivalent of the appropriate nucleophilic reagent. Anhydrous sodium carbonate was used as acid acceptor when phenols were the nucleophile while triethylamine was used as acid acceptor in other cases. The mixture was stirred for one hour at room temperature, filtered and the polymer was precipitated by adding the mixture to an excess of petroleum ether. The effect of a series of reagents on PCC-bisphenol A is shown in Tables 3 and 4. To determine the cause of the long term degradation of the polymer, a sample was dissolved in chloroform, precipitated in methanol or petroleum ether and dried and stored under various conditions. The change in the intrinsic viscosity of the polymer was determined as a measure of degradation (Table 5). The stability of the polymer in organic solvent was determined by measuring the change in solution viscosity with time, shown in Figure 2.

Results and Discussion

Partial substitution of the acid chloride groups of PCC-bisphenol A by phenols was achieved with little degradation of the polymer. This is in contrast to

Table 3 Reactions of phenols with the poly(2-chlorocyanurate) of bisphenol A

Phenols	Intrinsic viscosity (dl/g)	Chlorine content (wt %)
—	0.62	10.0
phenol	0.62	8.3
p-hydroxybenzaldehyde	0.56	7.0
p-nitrophenol	0.56	7.6
p-chlorophenol	0.60	—
p-bromophenol	0.55	—

Table 4 Reaction of amines with the poly(2-chlorocyanurate) of bisphenol A

Amine	Intrinsic viscosity (dl/g)		Chlorine content (wt %)
	Chl	DMA	
—	0.36	0.29	10.0
butylamine	0.12	—	4.8
aniline	0.17	—	—
pyridine	—	0.08	—
ethanolamine	—	0.19	—

Table 5 Stability of the poly(2-chlorocyanurate) of bisphenol A

Precipitant	Intrinsic viscosity (dl/g)					
	Drying method			Storing method*		
	Air	Heat	Vacuum	Air	SG†	Vacuum
petroleum ether	0.81	0.77	0.80	0.45	0.79	0.80
methanol	0.66	0.63	0.44	—	—	—

Initial polymer $[\eta]=0.80$

* Sample stored for 30 days

† Sample stored over silica gel

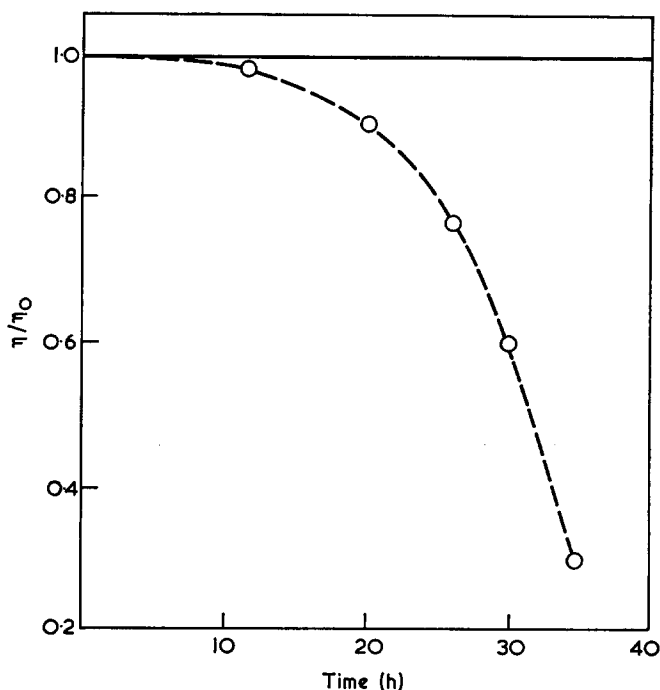


Figure 2 Degradation of PCC-bisphenol A in solution as measured by change in intrinsic viscosity. O, Chloroform; —, THF, dioxane, benzene

poly(2-chloro-4,6-N-phenyl-s-triazinyleneimide) which degraded when treated with phenol⁸. An increase in the temperature of reaction had no significant effect on the degree of substitution or extent of degradation. However, in the presence of amines nucleophilic substitution of the chlorine atom was accompanied by a large decrease in molecular weight of the polymer probably due to nucleophilic attack at the main chain ester links. Some of the partly substituted polymers were insoluble in chloroform and their intrinsic viscosities were measured in dimethyl acetamide. Extensive degradation of the polymer also occurred when the polymer was condensed with alcohols and sodium phenoxide, again probably a result of nucleophilic attack at the main chain ester links.

In the presence of difunctional nucleophilic species (bisphenols, diamines, water) crosslinking and subsequent gelation occurred. The crosslink formed by water was probably an ether link with properties similar to those of an anhydride.

These results suggest that attempts to prepare high molecular weight poly(2-R-cyanurates) from PCC by a second condensation reaction were likely to be unprofitable because of the relatively high reactivity of the main chain ether links which is enhanced by the activating effect of the chlorine substituent.

The long term stability of PCC-bisphenol A, in the absence of atmospheric moisture or other nucleophilic species, was high, both in solution and in the solid state (Table 5 and Figure 2). Degradation of solid PCC-bisphenol A occurred when either atmospheric moisture or alcohol were present. Similarly, degradation of the polymer in chloroform solution was probably a result of the action of the alcohol stabilizing agent. From these results it appeared that long term degradation was a result of simultaneous nucleophilic attack, by atmospheric moisture, on the ester and acid chloride groups in the polymer. Even though hydrolysis of 2-chloro-4,6-diphenoxy-s-triazine is a fairly slow reaction at room temperature, attack at relatively few ester links would have resulted in measurable degradation of the polymer.

PHYSICAL PROPERTIES

Examination of the physical properties of PCC-bisphenol A was made difficult by the intractability of the polymer. Attempts to mould PCC-bisphenol A at temperatures up to 200°C and for times exceeding 15 min in a 20 ton (20·321 Mg) hydraulic press were unsuccessful and moulded samples, suitable for physical testing could not be produced. Consequently physical testing was conducted either on the dried polymer in its precipitated form or on a thin film cast from THF on to a mercury surface and dried under vacuum at room temperature for 2 months. This film contained 7% w/w THF but attempts to remove the residual solvent using higher temperatures caused the film to 'blow out' and rendered it unsuitable for physical testing.

The transition temperatures of the polymer were determined by differential scanning calorimetry in a Dupont 900 Differential Thermal Analyser fitted with a DSC cell. A heating rate of 20°C/min was used and the polymer samples in the precipitated form were scanned from -100°C to 175°C. Only one transition, at 140°C, was observed which corresponded to the glass transition of the polymer. This value agreed with similar measurements made on related polymers by other workers^{6,7}. The thermal stability of the polymer was determined by thermogravimetric analysis in a nitrogen atmosphere using a simple thermobalance at a heating rate of 6°C/min. The thermogram indicated that the polymer was stable to nearly 400°C under these conditions.

The shear modulus of the solvent-cast film of the polymer was determined using a Weissenberg rheogoniometer. The shear modulus and dissipation factor were measured at 5°C intervals and the results are shown in Figure 3. The major mechanical transition that

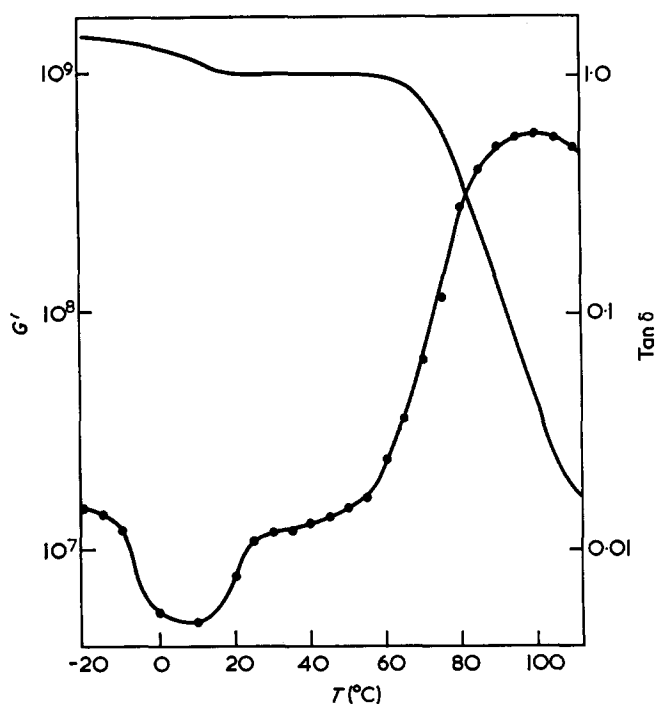


Figure 3 Effect of temperature on the shear modulus G' (—) and $\tan \delta$ (●) of a solvent cast film of PCC-bisphenol A

occurred at 100°C corresponded to the plasticized glass transition of the polymer but because of the presence of residual solvent, and in the absence of more information outside the scope of this work, no interpretation could be made of the secondary transitions.

ACKNOWLEDGEMENT

A. G. De B. is grateful to CSIRO for the award of a scholarship which enabled him to complete this work.

REFERENCES

- Picklesimer, L. and Saunders, T. *J. Polym. Sci. (A-1)* 1965, **3**, 2673
- Tamura, K., Nakagura, I. and Nakamura, Y. *Kogyo Kagaku Zasshi* 1965, **68**, 1626; *Chem. Abstr.* 1965, **63**, 18085
- Breed, L. and Elliot, R. *J. Polym. Sci. (A-1)* 1969, **7**, 2749
- Audebert, R. and Néel, J. *Bull. Soc. Chim. Fr.* 1970, **2B**, 606
- Seta, K., Tamura, K., Saito, Y. and Nakamura, Y. *Kogyo Kagaku Zasshi* 1967, **70**, 588, 784, 2066; *Chem. Abstr.* 1968, **68**, 40409, 50432, 115052
- Nakamura, Y., Mori, K., Tamura, K. and Saito, Y. *J. Polym. Sci. (A-1)* 1969, **7**, 3089
- Sherliker, F. *MSc Thesis* Manchester University, 1967
- Ehlers, G. and Ray, J. *J. Polym. Sci. (A-1)* 1964, **2**, 4989
- Grubisic, Z., Benoit, H. and Rempp, P. *J. Polym. Sci. (B)* 1967, **5**, 753
- Zimm, B. *J. Chem. Phys.* 1948, **16**, 1093, 1099

Letters

Energy transfer in illuminated PMMA

It has been known for a long time that γ -irradiation of poly(methyl methacrylate) (PMMA) produces degradation of the polymer. For every 61 eV of ionizing energy absorbed, there is a main chain break^{1,2}. However, when the polymer contains an aromatic as a solute, the amount of chain break is lowered⁷, owing to the protection by the solute on the polymer. For instance, PMMA containing 5% by wt of pyrene is completely protected from chain break by ionizing radiation³. Others such as *p*-terphenyl, xylene and benzene are also effective in this protective action. Wundrich⁴ attributed the inhibiting effect of pyrene and naphthalene on the degradation of γ -irradiated PMMA to energy transfer from the polymer to the aromatic solute. Aromatic amines added to PMMA are also instrumental in quenching degradation by γ -irradiation^{5,6}; the protection provided by the guest molecules on the host is explained by the transfer of electrons from the amines to the irradiated polymer, since the cation radicals of amines have been detected in the latter⁷.

Thin film samples of PMMA have been illuminated, using an Osram HBO 200W super high pressure mercury arc and a stable radical in the polymer was found at room temperature. The electron spin resonance (e.s.r.) spectrum of this 9-line radical is shown in *Figure 1*, similar to the e.s.r. spectrum observed in γ -irradiated PMMA⁸. This radical has been identified as the $-\text{CH}_2\text{C}(\text{CH}_3)\text{COOCH}_3$ species⁹. Since the effective shortest wavelength of the mercury lamp is 253.7 nm, corresponding to a 4.9 eV photon, it is clear that the radical is produced by polymer segments in the highly excited state following the adsorption of the u.v. light.

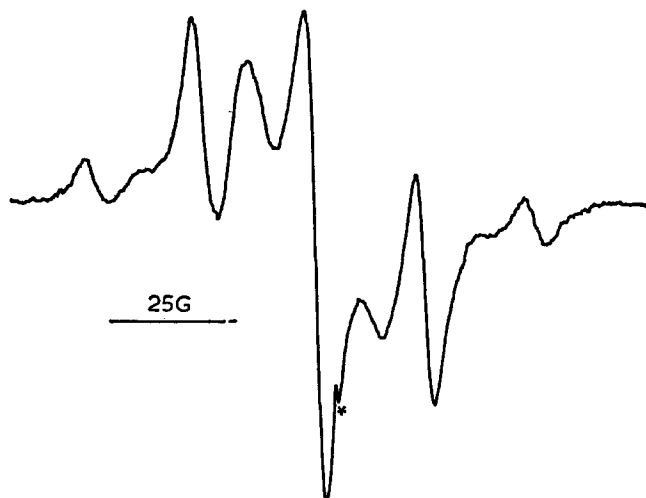


Figure 1 E.s.r. spectrum of u.v. irradiated poly(methyl methacrylate) film at room temperature. The 9-line signal is due to the radical $-\text{CH}_2\text{C}(\text{CH}_3)\text{COOCH}_3$. The small sharp line denoted by * is due to the quartz signal. The field strength increases from left to right

It appears, therefore, that the polymer is capable of transmitting the excitation along the polymer chain until it is localized at an appropriate site, at which a carbon-carbon bond dissociation results.

Evidence of excitation energy transfer in PMMA comes from the observation that polymer films containing various solutes exposed to u.v. light for the same length of time as the solute-free polymer contain the above radicals at concentrations much lower than those of the latter. For example, triphenylamine, triphenylphosphine or naphthalene, present separately in polymer samples as a guest molecule to the extent of 2-3 mol% (the monomer of the plastic is used as the molecular weight) will lower the radical concentration by 50%. Polymer films containing 8 mol% of any of the above three solutes have no radical signal within the sensitivity of the e.s.r. spectrometer.

Apparently the solute molecules act as energy sinks in the polymer. The excitation energy in the polymer (which may exist as excitons) is transmitted to the solute molecules, in preference to being localized in the polymer chains, thus resulting in decreased chain scission. The protective effect by the solute on the polymer is not due to a filter effect on the incident photons from the light source; this possibility is precluded by the work of Gardner *et al.*³. Neither is it likely that the observed lowerings of radicals in the solute-containing polymer are due to radical scavenging, since the mobility of the solute molecules is very limited, in view of the fact that the quenching effect persists even at liquid nitrogen temperature⁵. Other molecules used in the same manner are found to be ineffective as energy interceptors, viz. tetracyanoethylene (a very efficient electron scavenger) and brilliant green (a strongly absorbing dye) have no effect on the radical formation in the illuminated polymer.

The PMMA films, after exposure to the intense radiation from the mercury arc, acquire a light brown colour. When a piece of the irradiated film is observed in a Cary 14 spectrophotometer, a rather sharp band appears at 342.5 nm, as shown in *Figure 2*. It has not been ascertained whether this band is related to the radical spectrum shown in *Figure 1*.

The following is a brief description of the experimental procedure. The polymer, obtained from Borden Chemical Co., was dissolved in ethyl acetate and precipitated in cyclohexane. The dried, gummy polymer was redissolved in acetone. Thin films of the material were obtained by evaporating the acetone solution on a mercury surface very slowly. The films were then lifted from the mercury surface, cut to appropriate dimensions and rolled into cylinders and inserted into quartz tubings (about 9 mm o.d.) and evacuated overnight to a residual pressure of about 5×10^{-5} mmHg on a grease-free vacuum manifold. The quartz tubes were then flame-sealed, placed in an unsilvered quartz Dewar containing ice-water and photolysed by the Osram lamp located 6 in (~ 15 cm) away from the polymer sample. After irradiation, the

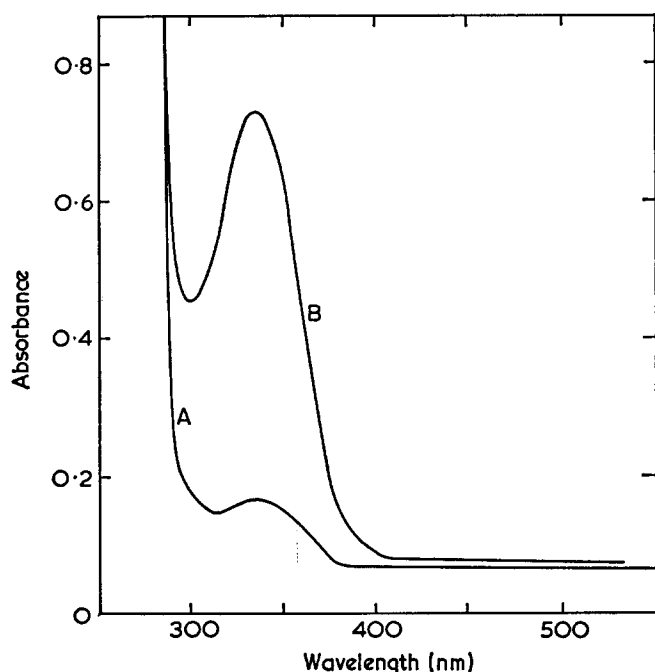


Figure 2 Optical spectrum of u.v. irradiated poly(methyl methacrylate) film. A, before irradiation; B, after 80 min of irradiation. The band maximum is at 342.5 nm

sample tube was inserted into the cavity of the Varian Associates 4500 e.s.r. spectrometer for radical detection. For optical work, a piece of the polymer film was cut to size and inserted into a special cell of 2 mm optical path (from Pyrocell Co.). After evacuation and illumination as described above, the optical spectrum was obtained in a Cary 14 spectrophotometer.

More detailed work on the kinetics of radical growth and decay and on the effects of various solutes on the radical species is being carried out.

P. K. Wong

Department of Chemistry,
Queensborough Community College,
City University of New York,
Bayside, NY 11364, USA, and
Brookhaven National Laboratory,
Upton, NY 11973, USA

(Received 9 October 1973)

References

- Alexander, P. and Charlesby, A. *Nature* 1954, 173, 578
- Alexander, P., Charlesby, A. and Ross, M. *Proc. R. Soc.* 1954, A223, 392
- Gardner, D. G. and Epstein, L. M. *J. Phys. Chem.* 1961, 34, 1653
- Wundrich, K. '3rd Tihany Symposium on Radiation Chemistry' (Eds J. Dobó and P. Hedvig), Akadémiai Kiadó, Budapest, 1972, Vol. 1, p 747
- Bagdasar'yan, Kh. S., Krongauz, V. A. and Kardash, N. S. *Pror. Akad. Sci. USSR (Chem. Ser.)* 1962, 144, 37a
- Milyutinskaya, R. I. and Bagdasar'yan, Kh. S. *Rum. J. Phys. Chem.* 1964, 38, 419
- Borovkova, L. Ya. and Bagdasar'yan, Kh. S. *High Energy Chem.* 1967, 1, 295
- Kaul, W. and Kevan, L. '3rd Tihany Symposium on Radiation Chemistry' (Eds J. Dobó and P. Hedvig), Akadémiai Kiadó, Budapest, 1972, Vol 1, p 919
- Iwasaki, M. and Sakai, Y. *J. Polym. Sci. (A)* 1969, 7, 1537

Quantitative morphological characterization of semi-crystalline PET

Introduction

In this report it is shown that semi-crystalline poly(ethylene terephthalate) (PET) samples with the same degree of crystallinity but different morphological structures are obtained by suitable crystallization and annealing treatments. The morphological structure of the samples is related to their mechanical properties.

Experimental

PET sheets supplied by Agfa-Gevaert, Antwerp, were thermally crystallized and annealed in an oven under vacuum. The volume crystallinity, X_v , was obtained from density measurements. Small-angle X-ray scattering (SAXS) measurements were made with a Kratky camera (slit collimation) and desmeared using a computer program kindly provided by Vonk¹. Mechanical measurements were performed with an Instron testing machine.

PET samples with similar degree of crystallinity were prepared in two different ways. Sample I was crystallized from the glassy state at 200°C; the other samples were crystallized at 100°C (samples II and III) and at room temperature in the presence of acetone (sample IV). They were heated in different ways to 200°C and annealed at this temperature for a certain time (see Table 1). The crystallinity of samples II, III and IV was measured after the annealing.

Results and Discussion

Morphological structure from SAXS. Desmeared SAXS curves of samples I to IV exhibit one maximum which shifts to greater angles from I to IV. The Tsvankin analysis² as modified by Buchanan³ was applied to the desmeared scattering curves; the morphological parameters are listed in Table 1. The experimental observed long period, d , decreases considerably from sample I to IV and the calculated values obtained for the mean long period, L , the average lamellar thickness, l , and the average thickness of the amorphous regions, a , follow the same trend. The linear crystallinities of these samples, k [$=l/(a+l)$], which corresponds to the one-dimensional alternation of crystalline and amorphous domains, are higher than the corresponding volume crystallinities, X_v . This suggests that part of the amorphous phase is outside the lamellar bundles. Indeed, k is not related to amorphous regions which do not form part of the regular alternating two phase structure².

It should be noted that in the temperature range between 100°C and 200°C, there is a gradual increase in X_v and k . The structural changes induced by thermal treatments of sample V depend on the heating rate (Table 1, samples II and III).

For sample III (slow heating) a decrease of the mean long period is observed, suggesting interlamellar crystallization (see evolution of L , k and a). In sample II (quickly heated) the mean periodicity is almost constant. However, the values of k and l increase while a decreases. Tentatively this is ascribed to intralamellar crystallization, i.e., incorporation of interlamellar amorphous chain segments into the existing lamellae. It is clear that during the heating process lamellar thickening

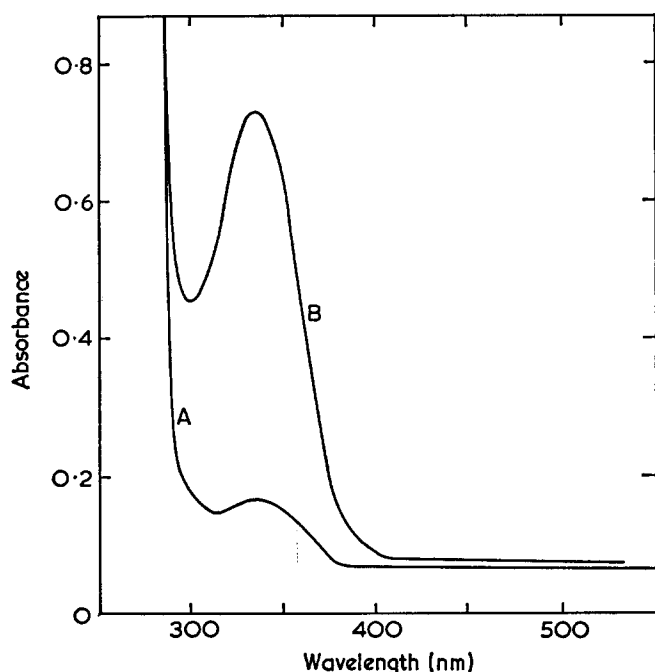


Figure 2 Optical spectrum of u.v. irradiated poly(methyl methacrylate) film. A, before irradiation; B, after 80 min of irradiation. The band maximum is at 342.5 nm

sample tube was inserted into the cavity of the Varian Associates 4500 e.s.r. spectrometer for radical detection. For optical work, a piece of the polymer film was cut to size and inserted into a special cell of 2 mm optical path (from Pyrocell Co.). After evacuation and illumination as described above, the optical spectrum was obtained in a Cary 14 spectrophotometer.

More detailed work on the kinetics of radical growth and decay and on the effects of various solutes on the radical species is being carried out.

P. K. Wong

Department of Chemistry,
Queensborough Community College,
City University of New York,
Bayside, NY 11364, USA, and
Brookhaven National Laboratory,
Upton, NY 11973, USA

(Received 9 October 1973)

References

- Alexander, P. and Charlesby, A. *Nature* 1954, 173, 578
- Alexander, P., Charlesby, A. and Ross, M. *Proc. R. Soc.* 1954, A223, 392
- Gardner, D. G. and Epstein, L. M. *J. Phys. Chem.* 1961, 34, 1653
- Wundrich, K. '3rd Tihany Symposium on Radiation Chemistry' (Eds J. Dobó and P. Hedvig), Akadémiai Kiadó, Budapest, 1972, Vol. 1, p 747
- Bagdasar'yan, Kh. S., Krongauz, V. A. and Kardash, N. S. *Pror. Akad. Sci. USSR (Chem. Ser.)* 1962, 144, 37a
- Milyutinskaya, R. I. and Bagdasar'yan, Kh. S. *Rum. J. Phys. Chem.* 1964, 38, 419
- Borovkova, L. Ya. and Bagdasar'yan, Kh. S. *High Energy Chem.* 1967, 1, 295
- Kaul, W. and Kevan, L. '3rd Tihany Symposium on Radiation Chemistry' (Eds J. Dobó and P. Hedvig), Akadémiai Kiadó, Budapest, 1972, Vol 1, p 919
- Iwasaki, M. and Sakai, Y. *J. Polym. Sci. (A)* 1969, 7, 1537

Quantitative morphological characterization of semi-crystalline PET

Introduction

In this report it is shown that semi-crystalline poly(ethylene terephthalate) (PET) samples with the same degree of crystallinity but different morphological structures are obtained by suitable crystallization and annealing treatments. The morphological structure of the samples is related to their mechanical properties.

Experimental

PET sheets supplied by Agfa-Gevaert, Antwerp, were thermally crystallized and annealed in an oven under vacuum. The volume crystallinity, X_v , was obtained from density measurements. Small-angle X-ray scattering (SAXS) measurements were made with a Kratky camera (slit collimation) and desmeared using a computer program kindly provided by Vonk¹. Mechanical measurements were performed with an Instron testing machine.

PET samples with similar degree of crystallinity were prepared in two different ways. Sample I was crystallized from the glassy state at 200°C; the other samples were crystallized at 100°C (samples II and III) and at room temperature in the presence of acetone (sample IV). They were heated in different ways to 200°C and annealed at this temperature for a certain time (see Table 1). The crystallinity of samples II, III and IV was measured after the annealing.

Results and Discussion

Morphological structure from SAXS. Desmeared SAXS curves of samples I to IV exhibit one maximum which shifts to greater angles from I to IV. The Tsvankin analysis² as modified by Buchanan³ was applied to the desmeared scattering curves; the morphological parameters are listed in Table 1. The experimental observed long period, d , decreases considerably from sample I to IV and the calculated values obtained for the mean long period, L , the average lamellar thickness, l , and the average thickness of the amorphous regions, a , follow the same trend. The linear crystallinities of these samples, $k [=l/(a+l)]$, which corresponds to the one-dimensional alternation of crystalline and amorphous domains, are higher than the corresponding volume crystallinities, X_v . This suggests that part of the amorphous phase is outside the lamellar bundles. Indeed, k is not related to amorphous regions which do not form part of the regular alternating two phase structure².

It should be noted that in the temperature range between 100°C and 200°C, there is a gradual increase in X_v and k . The structural changes induced by thermal treatments of sample V depend on the heating rate (Table 1, samples II and III).

For sample III (slow heating) a decrease of the mean long period is observed, suggesting interlamellar crystallization (see evolution of L , k and a). In sample II (quickly heated) the mean periodicity is almost constant. However, the values of k and l increase while a decreases. Tentatively this is ascribed to intralamellar crystallization, i.e., incorporation of interlamellar amorphous chain segments into the existing lamellae. It is clear that during the heating process lamellar thickening

Table 1 Morphological parameters of the PET samples*

Sample number	Sample history	Degree of cryst., X_V (%)	Observed long period, d (Å)	Mean long period, L (Å)	Average lamellar thickness, l (Å)	Average thickness of amorph. regions, a (Å)	Linear degree of cryst., k
I	200°C for 17h	54	128	144	72	72	0.50
II	(100°C for 17h; 29%) + (from 100 to 200°C very quickly) + (200°C for 17h)	53	103	110	63	47	0.57
III	(100°C for 17h; 29%) + (from 100 to 200°C at 4°C/h) + (200°C for 17h)	50	93	98	59	39	0.60
IV	(Acetone-induced cryst. at 25°C; 30%) + (from 25 to 200°C at 4°C/h) + (200°C for 17h)	51	84	87	54	33	0.62
V	100°C for 17h	29	96	115	50	65	0.44
VI	Acetone-induced cryst. at 25°C	30	68	72	42	30	0.57

* $\epsilon = 0.2$ (fractional thickness of transition zone)^{2,3}

$\beta/\alpha = 0.3$ (dispersion of crystallite sizes about the average)^{2,3}

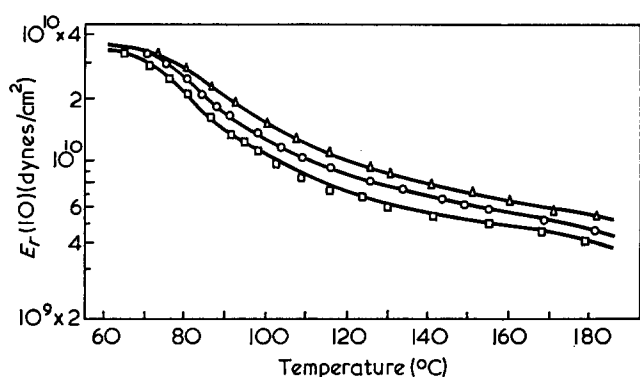


Figure 1 Modulus-temperature curves. □, Sample I; ○, sample II; △, sample IV

cannot be excluded⁴. The structural parameters for samples IV and VI are not yet understood; however, these samples are interesting with regard to their mechanical properties.

Viscoelastic properties. The morphological parameters (l and a) together with the arrangement of the chains within the amorphous domains determine the viscoelastic relaxation behaviour of the polymer⁹. This property is a sensitive tool in investigating the fine structure of the amorphous layers. The temperature dependence of the stress relaxation modulus after 10 sec, $E_r(10)$, is given in Figure 1. It is observed that the glass transition temperature, T_i , increases from sample I to IV. The annealed samples II, III, and IV exhibit a higher rubbery plateau than sample I: $E_{IV} > E_{III} > E_{II} > E_I$. For sample I isothermally crystallized at high temperature (200°C), only a small fraction of polymer segments is expected to be involved in interlamellar links within the relatively large interlamellar amorphous layers according to the theory of nucleation^{8, 10}.

More entanglements and tie molecules will occur in samples II and III as a consequence of the initial crystallization at low temperature (100°C). In these samples

with small amorphous layers, the segmental mobility of the amorphous material is reduced. This is reflected in an increase of T_i . The value of the rubbery modulus is determined by the arrangement of the chains within the amorphous regions but also by the volume concentration of the crystalline lamella acting simultaneously as physical crosslinks and filler particles. This picture can account for the observed results in Figure 1.

Besides their influence on the viscoelastic properties, the morphological changes also alter the melting behaviour of these samples. This, however, is beyond the scope of this paper and the results will be published elsewhere.

Acknowledgements

The authors are indebted to the Centrum voor Hoogpolymeren (IWONL, Agfa-Gevaert) (G.G.) and NFWO (HR) for equipment and research grants.

G. Groeninckx, H. Reynaers
and H. Berghmans

Universiteit te Leuven,
Laboratorium voor Macromoleculaire
en Organische Scheikunde,
3030 Heverlee, Belgium

(Received 10 October 1973; revised 22 October 1973)

References

- 1 Vonk, C. G. *J. Appl. Crystallog.* 1971, 4, 340
- 2 Tsvankin, D. Ya. *Polym. Sci. USSR* 1964, 6, 2304, 2310
- 3 Buchanan, D. R. *J. Polym. Sci. (A-2)* 1971, 9, 645
- 4 Holdsworth, P. J. and Turner-Jones, A. *Polymer* 1971, 12, 195
- 5 Roberts, R. C. *J. Polym. Sci. (B)* 1970, 8, 381
- 6 Sweet, G. E. and Bell, J. P. *J. Polym. Sci. (A-2)* 1972, 10, 1273
- 7 Overbergh, N., Berghmans, H. and Smets, G. *J. Polym. Sci. (C)* 1972, 38, 237
- 8 Hoffman, J. D. *SPE Trans.* 1964, 4, 1
- 9 Groeninckx, G., Berghmans, H., Smets, G. and Gryte, C. *Polymere* 1971 (Symp. Varna), 7
- 10 Hoffman, J. D., Williams, G. and Passaglia, E. *J. Polym. Sci. (C)* 1966, 14, 173

Book Reviews

Ring-forming polymerizations: Parts B1 and B2. Heterocyclic rings

R. J. Cotter and M. Matzner

Academic Press, New York, 1972. B1: 422 pp. \$34.50; B2: 568 pp. \$39.50

In these two volumes the authors complete their survey of polymerization systems in which cyclic units are formed to become integral parts of the polymer chain. Part A, published in 1969 dealt solely with carbocyclic and organometallic rings and the present work gives attention to heterocyclic unit formation. The treatment of this very extensive field follows that so well adopted in the earlier volume, both in the provision of critical reviews of the syntheses involved and in extensive tabulation where each individual polymer is listed together with available data on properties and relevant references.

The volumes are the result of a long and detailed study of the journal and patent literature and indicate the enormous amount of work which has gone into polymers of this type, work promoted to some considerable extent by the search for materials of high thermal resistance and enhanced physical and mechanical properties. Several such products are, of course, now commercially available. In the three chapters comprising Part 1 attention is given to polymers based on multibond reactions (e.g. poly Schiff's bases, carbodiimides) and to those with heterocyclic units containing two or three carbon atoms (oxa- and thiadiazoles, triazoles, imidazoles, triazines, etc.). Part 2 has four chapters covering heterocyclic units with four carbon atoms (polyimides, amido- and ester-imides, piperazine, acetals, ketals), intra/intermolecular reactions, polymerization of α,β -unsaturated aldehydes (acrolein polymers) and a miscellany of ring-forming reaction products ranging from polytetrazoles to polyferrocenes.

The work forms a worthwhile contribution to the bibliography of polymers. It has been meticulously and clearly presented and, thanks to the introduction of supplementary lists of references, includes literature published up to 1971. Subject and author indexes are given and the many tables relating to synthesis and properties are particularly useful. Printing and binding are of excellent standard.

Both volumes will be of considerable interest not only to those engaged primarily in polymer synthesis but indeed to organic chemists more generally, as well as to many of other disciplines who are concerned with polymer structure/property studies and specialized applications. The books will form a standard source for consultation and reference, and can be recommended to library shelves, but the prices quoted (\$75 in all), while being understandably high for a work of this nature, may place them out of reach for personal acquisition by many individuals.

R. J. W. Reynolds

Structure and properties of polymer films

Edited by R. W. Lenz and R. S. Stein

Plenum Press, New York, 1973, 345 pp. \$22.50

This is the first volume in a symposium series on Polymer Science and Technology and contains the edited proceedings of the Borden Award Symposium, Boston, April 1972. It contains eighteen papers by distinguished authors covering applications of light scattering (four papers), stress-optical phenomena, dichroism, interferometry, infra-red spectroscopy and X-ray analysis, together with studies on mechanical properties in relation to structure (five papers including one on the e.s.r. study of molecular fracture) and on the transport of fluids through polymer films (two papers).

The co-ordinating theme of this collection of research papers is, of course, polymer films, their structure and properties. 'Structure' here covers crystal structure and orientation, amorphous phase orientation and lamellar, fibrillar and spherulitic morphologies. Having said this, there is little further that can be added to integrate the scope and treatment of the subject matter, since, as in most

symposia, almost all the papers are devoted to specific research topics, materials or techniques. The inevitably disjointed result is offset by the consistently high standard of the work reported, and by the value of the collection as a means of bringing workers in the field up to date. It is thus to be recommended to those wishing to keep abreast of developments in the 'structure-property' field of solid polymers in general (i.e. not just films). It is clearly not intended to provide either a reference book or a textbook on the subject.

E. H. Andrews

Chemistry in space research

Edited by R. F. Landel and A. Rembaum

Elsevier, Amsterdam, 1972. Dfl, 653 pp. 133.00

In many respects this book is unique. It is the first attempt to present in one volume a survey of the principal areas of space research through chemistry. Chemistry has played an indispensable role in opening space to man and his instruments. Chemically powered rockets made possible man's departure from earth to the moon and the exploitation of high temperature ablative polymers assured his safe return through the intense heat of re-entry into the earth's atmosphere. To meet the demands of the extreme environmental conditions encountered in the space programme new materials had to be developed.

Under the conditions of outer and inner space, chemistry is very different from the chemistry we are familiar with in the terrestrial environment. In a very illuminating opening chapter, Libby reviews four general aspects of the space environment which have chemical significance—high pressure chemistry, radiation chemistry, high temperature chemistry and vacuum chemistry. High pressure chemistry is of relevance to studies of the matter inside planets. It is interesting to read of recent progress in the construction of a megabar (1 million atm) press. Such a facility would open up the science of planetary interiors to more direct laboratory attack. Radiation chemistry, which is essentially the chemistry of ions, concerns the chemical effects of solar radiation and cosmic rays. (Young contributes a separate chapter on chemistry in planetary atmospheres.) High temperature chemistry arises from the very high solar temperatures reaching into the chemistry of plasma. Vacuum chemistry relates to the chemical consequences of the extremely low population of molecules in interplanetary space, largely the chemistry of very clean surfaces devoid of air and other gases. Libby envisages the possibility of using space ships as chemical laboratories for the production of materials such as diamond by the evaporation of carbon. Atmospheric contamination of the surfaces has been held responsible for past failures and the hope is that the use of high vacuum of the levels available in outer space will lead to success.

As the Editors remark, 'space—vast, unexplored space—constitutes a problem and a mystery . . . By the mystery of space we mean the mystery of life'. The search for extraterrestrial life and the quest for clues to the origin of life as we know it on this earth have been strong motivating factors in space exploration. Three very stimulating chapters are devoted to Prebiological synthesis of organic compounds, Carbonaceous meteorites—possible sites of extraterrestrial life?, and terrestrial and extraterrestrial stable organic molecules.

Of most direct interest to readers of this journal are those chapters dealing with the various roles of polymeric materials in the space programme. The urgent need to extend the operating range of plastic materials to meet the extremely stringent environmental requirements spawned and spurred an intensive effort on the synthesis of high temperature polymers. In a comprehensive and authoritative chapter, Pezdirtz and Johnston review the techniques for evaluating thermal stability, new concepts and criteria for achieving thermal stability and some basic molecular structures which promote stability in polymers. Again, ablative polymers and composite materials are the foundation of re-entry. An excellent, in-depth treatment of the chemical aspects of ablation is provided by Ladacki. (In a book singularly free of errors, one misconception has crept in on p 298: the polymer Noryl is not produced from *o*-cresol but is a binary polymer of PPO and polystyrene.) The

Book Reviews

requirement for materials suitable for use in the cryogenic temperature range has stimulated the study of low-temperature relaxations in polymers. In his contribution, Shen aims at providing a basic understanding of low temperature mechanical behaviour of polymers on a molecular basis and correlating the relaxation processes with some of the molecular parameters.

Only about 0.1% of the mass leaving the earth on the Apollo flights to the moon returns with the astronauts, most of the remaining 99.9% is taken up by rocket systems and propellant mass. This observation serves to illustrate the vital role of the propulsion systems.

Chemical propulsion—solid propellants and liquid propellant rockets—and spacecraft sterilization are considered in detail in the last three chapters. A good deal of prominence is given to the use of special polymers for solid propellant binders and to the effects of sterilization methods on polymeric spacecraft components.

Chemists generally and polymer chemists in particular will find in this volume a wealth of information and much food for thought. The value of the book is enhanced because its authors look beyond the achievements of the first decade in space. By indicating the limitations of current knowledge, they point to useful areas for future chemical and polymer research. It is highly recommended.

J. Idris Jones

Block and graft copolymerization

Edited by R. J. Ceresa

Wiley, New York, 1973. 390 pp. £10

This is the first of two volumes of reviews of the preparation, properties and usage of block and graft copolymers. It is organized so as to juxtapose the views of chemists and technologists on selected topics. The present volume deals with copolymeric modifications of several natural polymers (starch, rubber, wool and silk) and with the wholly synthetic block copolymeric elastomers based on styrene and dienes. Contributors are: G. F. Fanta (starch); R. J. Ceresa, R. D. Pendle (natural rubber); K. Arai (wool and silk); W. L. Wasley (wool); L. J. Fetters, G. Holden (synthetic elastomers).

Within a given topic (starch, elastomers, wool), the reviews interrelate well and offer an unusually broad range of information. However, there is no unifying view and the collection (at £10) seems best suited to the institutional, rather than the individual, library.

C. Booth

Principles of plastics extrusion

J. A. Brydson and D. G. Peacock

Applied Science, London, 1973. 108 pp. £2.00

This paperback is essentially a simple teaching programme designed for students and industrial trainees who have little or no background in science or in the technology of polymers. Seven sections set out in simple form a series of short notes, diagrams, questions and answers concerning single and multiple screw machines, die design, and processes for extruded sections, monofil, film, and wire-covering. Factors associated with polymer properties and machine design and operation are related to basic principles. The book is a text teaching only the very elements of extrusion from a practical angle.

R. J. W. Reynolds

Biomaterials, medical devices and artificial organs

Volume 1, Number 1, 1973

Marcel Dekker, New York. \$35.00/vol.

A new journal to pull together doctors, engineers and chemists was inevitable. The editorial for the first issue states that at least 100 000 people live with artificial arteries and 45 000 with artificial heart valves, in the USA; a large figure, but Europe cannot be far behind.

Compared with 20 years ago when prostheses were inserted and removed soon afterwards with remarkable regularity, things certainly have changed. The new quarterly journal, 15 × 22 cm, is virtually a book of 240 pages; printed in black and white by the web-offset process, the contents are well laid out, reproduction of half-tone photographs excellent, and it is easy to read. The first issue contains 12 original articles and a fascinating 50-page review of orthoptic heart prostheses.

The quality of all papers is high and if the editor can maintain this standard—and precautions have been taken by having an editorial board of 54 distinguished names, surely the largest yet!—then the journal will have wide appeal for scientists and clinicians in many fields. Weight for weight it's expensive when compared with other journals, most of whom carry advertising. But then quality counts.

James Calnan

Conference Announcement

1974 Colston Symposium

Structures of fibrous biopolymers

Bristol University, 2–4 April 1974

The 1974 Colston Symposium on Structure of Fibrous Biopolymers will be held at the University of Bristol from 2 to 4 April 1974, under the auspices of the Colston Research Society. A number of invited speakers will cover aspects of the molecular architecture and properties of polysaccharides, collagen and related fibrous biopolymers. Further information may be obtained from the Conference Organizer: Dr E. D. T. Atkins, H. H. Wills Physics Laboratory, University of Bristol, Royal Fort, Tyndall Avenue, Bristol BS8 1TL, UK.

Conference Announcement

Plastics Processing

Aachen, W. Germany, 20–22 March 1974

The Institut für Kunststoffverarbeitung in Industrie und Handwerk is organizing its 7th Symposium on Plastics Processing from 20 March to 22 March 1974, in Aachen, West Germany. Among the various processing topics to be covered are: injection moulding; extrusion; material testing; designing; mechanical properties; reinforcement. Further details may be obtained from Professor Dr-Ing. G. Menges, Director, Institut für Kunststoffverarbeitung, 5100 Aachen, Pontstrasse 49, West Germany.

Book Reviews

Ring-forming polymerizations: Parts B1 and B2. Heterocyclic rings

R. J. Cotter and M. Matzner

Academic Press, New York, 1972. B1: 422 pp. \$34.50; B2: 568 pp. \$39.50

In these two volumes the authors complete their survey of polymerization systems in which cyclic units are formed to become integral parts of the polymer chain. Part A, published in 1969 dealt solely with carbocyclic and organometallic rings and the present work gives attention to heterocyclic unit formation. The treatment of this very extensive field follows that so well adopted in the earlier volume, both in the provision of critical reviews of the syntheses involved and in extensive tabulation where each individual polymer is listed together with available data on properties and relevant references.

The volumes are the result of a long and detailed study of the journal and patent literature and indicate the enormous amount of work which has gone into polymers of this type, work promoted to some considerable extent by the search for materials of high thermal resistance and enhanced physical and mechanical properties. Several such products are, of course, now commercially available. In the three chapters comprising Part 1 attention is given to polymers based on multibond reactions (e.g. poly Schiff's bases, carbodiimides) and to those with heterocyclic units containing two or three carbon atoms (oxa- and thiadiazoles, triazoles, imidazoles, triazines, etc.). Part 2 has four chapters covering heterocyclic units with four carbon atoms (polyimides, amido- and ester-imides, piperazine, acetals, ketals), intra/intermolecular reactions, polymerization of α,β -unsaturated aldehydes (acrolein polymers) and a miscellany of ring-forming reaction products ranging from polytetrazoles to polyferrocenes.

The work forms a worthwhile contribution to the bibliography of polymers. It has been meticulously and clearly presented and, thanks to the introduction of supplementary lists of references, includes literature published up to 1971. Subject and author indexes are given and the many tables relating to synthesis and properties are particularly useful. Printing and binding are of excellent standard.

Both volumes will be of considerable interest not only to those engaged primarily in polymer synthesis but indeed to organic chemists more generally, as well as to many of other disciplines who are concerned with polymer structure/property studies and specialized applications. The books will form a standard source for consultation and reference, and can be recommended to library shelves, but the prices quoted (\$75 in all), while being understandably high for a work of this nature, may place them out of reach for personal acquisition by many individuals.

R. J. W. Reynolds

Structure and properties of polymer films

Edited by R. W. Lenz and R. S. Stein

Plenum Press, New York, 1973, 345 pp. \$22.50

This is the first volume in a symposium series on Polymer Science and Technology and contains the edited proceedings of the Borden Award Symposium, Boston, April 1972. It contains eighteen papers by distinguished authors covering applications of light scattering (four papers), stress-optical phenomena, dichroism, interferometry, infra-red spectroscopy and X-ray analysis, together with studies on mechanical properties in relation to structure (five papers including one on the e.s.r. study of molecular fracture) and on the transport of fluids through polymer films (two papers).

The co-ordinating theme of this collection of research papers is, of course, polymer films, their structure and properties. 'Structure' here covers crystal structure and orientation, amorphous phase orientation and lamellar, fibrillar and spherulitic morphologies. Having said this, there is little further that can be added to integrate the scope and treatment of the subject matter, since, as in most

symposia, almost all the papers are devoted to specific research topics, materials or techniques. The inevitably disjointed result is offset by the consistently high standard of the work reported, and by the value of the collection as a means of bringing workers in the field up to date. It is thus to be recommended to those wishing to keep abreast of developments in the 'structure-property' field of solid polymers in general (i.e. not just films). It is clearly not intended to provide either a reference book or a textbook on the subject.

E. H. Andrews

Chemistry in space research

Edited by R. F. Landel and A. Rembaum

Elsevier, Amsterdam, 1972. Dfl, 653 pp. 133.00

In many respects this book is unique. It is the first attempt to present in one volume a survey of the principal areas of space research through chemistry. Chemistry has played an indispensable role in opening space to man and his instruments. Chemically powered rockets made possible man's departure from earth to the moon and the exploitation of high temperature ablative polymers assured his safe return through the intense heat of re-entry into the earth's atmosphere. To meet the demands of the extreme environmental conditions encountered in the space programme new materials had to be developed.

Under the conditions of outer and inner space, chemistry is very different from the chemistry we are familiar with in the terrestrial environment. In a very illuminating opening chapter, Libby reviews four general aspects of the space environment which have chemical significance—high pressure chemistry, radiation chemistry, high temperature chemistry and vacuum chemistry. High pressure chemistry is of relevance to studies of the matter inside planets. It is interesting to read of recent progress in the construction of a megabar (1 million atm) press. Such a facility would open up the science of planetary interiors to more direct laboratory attack. Radiation chemistry, which is essentially the chemistry of ions, concerns the chemical effects of solar radiation and cosmic rays. (Young contributes a separate chapter on chemistry in planetary atmospheres.) High temperature chemistry arises from the very high solar temperatures reaching into the chemistry of plasma. Vacuum chemistry relates to the chemical consequences of the extremely low population of molecules in interplanetary space, largely the chemistry of very clean surfaces devoid of air and other gases. Libby envisages the possibility of using space ships as chemical laboratories for the production of materials such as diamond by the evaporation of carbon. Atmospheric contamination of the surfaces has been held responsible for past failures and the hope is that the use of high vacuum of the levels available in outer space will lead to success.

As the Editors remark, 'space—vast, unexplored space—constitutes a problem and a mystery . . . By the mystery of space we mean the mystery of life'. The search for extraterrestrial life and the quest for clues to the origin of life as we know it on this earth have been strong motivating factors in space exploration. Three very stimulating chapters are devoted to Prebiological synthesis of organic compounds, Carbonaceous meteorites—possible sites of extraterrestrial life?, and terrestrial and extraterrestrial stable organic molecules.

Of most direct interest to readers of this journal are those chapters dealing with the various roles of polymeric materials in the space programme. The urgent need to extend the operating range of plastic materials to meet the extremely stringent environmental requirements spawned and spurred an intensive effort on the synthesis of high temperature polymers. In a comprehensive and authoritative chapter, Pezdirtz and Johnston review the techniques for evaluating thermal stability, new concepts and criteria for achieving thermal stability and some basic molecular structures which promote stability in polymers. Again, ablative polymers and composite materials are the foundation of re-entry. An excellent, in-depth treatment of the chemical aspects of ablation is provided by Ladacki. (In a book singularly free of errors, one misconception has crept in on p 298: the polymer Noryl is not produced from *o*-cresol but is a binary polymer of PPO and polystyrene.) The

Book Reviews

requirement for materials suitable for use in the cryogenic temperature range has stimulated the study of low-temperature relaxations in polymers. In his contribution, Shen aims at providing a basic understanding of low temperature mechanical behaviour of polymers on a molecular basis and correlating the relaxation processes with some of the molecular parameters.

Only about 0.1% of the mass leaving the earth on the Apollo flights to the moon returns with the astronauts, most of the remaining 99.9% is taken up by rocket systems and propellant mass. This observation serves to illustrate the vital role of the propulsion systems.

Chemical propulsion—solid propellants and liquid propellant rockets—and spacecraft sterilization are considered in detail in the last three chapters. A good deal of prominence is given to the use of special polymers for solid propellant binders and to the effects of sterilization methods on polymeric spacecraft components.

Chemists generally and polymer chemists in particular will find in this volume a wealth of information and much food for thought. The value of the book is enhanced because its authors look beyond the achievements of the first decade in space. By indicating the limitations of current knowledge, they point to useful areas for future chemical and polymer research. It is highly recommended.

J. Idris Jones

Block and graft copolymerization

Edited by R. J. Ceresa

Wiley, New York, 1973. 390 pp. £10

This is the first of two volumes of reviews of the preparation, properties and usage of block and graft copolymers. It is organized so as to juxtapose the views of chemists and technologists on selected topics. The present volume deals with copolymeric modifications of several natural polymers (starch, rubber, wool and silk) and with the wholly synthetic block copolymeric elastomers based on styrene and dienes. Contributors are: G. F. Fanta (starch); R. J. Ceresa, R. D. Pendle (natural rubber); K. Arai (wool and silk); W. L. Wasley (wool); L. J. Fetters, G. Holden (synthetic elastomers).

Within a given topic (starch, elastomers, wool), the reviews interrelate well and offer an unusually broad range of information. However, there is no unifying view and the collection (at £10) seems best suited to the institutional, rather than the individual, library.

C. Booth

Principles of plastics extrusion

J. A. Brydson and D. G. Peacock

Applied Science, London, 1973. 108 pp. £2.00

This paperback is essentially a simple teaching programme designed for students and industrial trainees who have little or no background in science or in the technology of polymers. Seven sections set out in simple form a series of short notes, diagrams, questions and answers concerning single and multiple screw machines, die design, and processes for extruded sections, monofil, film, and wire-covering. Factors associated with polymer properties and machine design and operation are related to basic principles. The book is a text teaching only the very elements of extrusion from a practical angle.

R. J. W. Reynolds

Biomaterials, medical devices and artificial organs

Volume 1, Number 1, 1973

Marcel Dekker, New York. \$35.00/vol.

A new journal to pull together doctors, engineers and chemists was inevitable. The editorial for the first issue states that at least 100 000 people live with artificial arteries and 45 000 with artificial heart valves, in the USA; a large figure, but Europe cannot be far behind.

Compared with 20 years ago when prostheses were inserted and removed soon afterwards with remarkable regularity, things certainly have changed. The new quarterly journal, 15 × 22 cm, is virtually a book of 240 pages; printed in black and white by the web-offset process, the contents are well laid out, reproduction of half-tone photographs excellent, and it is easy to read. The first issue contains 12 original articles and a fascinating 50-page review of orthoptic heart prostheses.

The quality of all papers is high and if the editor can maintain this standard—and precautions have been taken by having an editorial board of 54 distinguished names, surely the largest yet!—then the journal will have wide appeal for scientists and clinicians in many fields. Weight for weight it's expensive when compared with other journals, most of whom carry advertising. But then quality counts.

James Calnan

Conference Announcement

1974 Colston Symposium

Structures of fibrous biopolymers

Bristol University, 2–4 April 1974

The 1974 Colston Symposium on Structure of Fibrous Biopolymers will be held at the University of Bristol from 2 to 4 April 1974, under the auspices of the Colston Research Society. A number of invited speakers will cover aspects of the molecular architecture and properties of polysaccharides, collagen and related fibrous biopolymers. Further information may be obtained from the Conference Organizer: Dr E. D. T. Atkins, H. H. Wills Physics Laboratory, University of Bristol, Royal Fort, Tyndall Avenue, Bristol BS8 1TL, UK.

Conference Announcement

Plastics Processing

Aachen, W. Germany, 20–22 March 1974

The Institut für Kunststoffverarbeitung in Industrie und Handwerk is organizing its 7th Symposium on Plastics Processing from 20 March to 22 March 1974, in Aachen, West Germany. Among the various processing topics to be covered are: injection moulding; extrusion; material testing; designing; mechanical properties; reinforcement. Further details may be obtained from Professor Dr-Ing. G. Menges, Director, Institut für Kunststoffverarbeitung, 5100 Aachen, Pontstrasse 49, West Germany.

Temperature dependence of polymer chain dimensions in the polystyrene–cyclopentane system

N. Kuwahara, S. Saeki, S. Konno and M. Kaneko

Department of Polymer Science, Hokkaido University, Sapporo, Japan
(Received 6 July 1973)

The limiting viscosity number in polystyrene–cyclopentane system has been determined over the temperature range of θ_u to θ_l in which θ_u and θ_l are the θ or Flory temperature for the upper and lower critical solution temperatures. The temperature coefficient of unperturbed mean square end-to-end distance observed for the polystyrene ($M_w=20 \times 10^4$, $M_w/M_n < 1.06$ and $M_w=67 \times 10^4$, $M_w/M_n < 1.10$) in cyclopentane is negligibly small. The observed temperature dependence of the polymer chain dimension over the temperature range of $\theta_u=19.6^\circ$ to $\theta_l=154.2^\circ\text{C}$ shows a parabolic curve with a maximum in the neighbourhood of 90°C and is qualitatively interpreted by the free volume theory of polymer solution, which gives a new χ_1 -temperature function.

INTRODUCTION

In the polymer–solvent system phase separation occurs at the upper critical solution temperature (*UCST*) and lower critical solution temperature (*LCST*) which appears in the vicinity of the vapour–liquid critical temperature of the solvent^{1–9}. The existence of both *UCST* and *LCST* is a very common phenomenon in polymer solutions and the two types of cloud-point curves behave like mirror images across the temperature axis of the intermediate region of the *UCST* and *LCST*^{5–9}. The *UCST* is raised and *LCST* is lowered as the molecular weight of the polymer increases, thus shrinking the temperature region of complete miscibility of the polymer^{7–9}. The Patterson–Delmas theory of corresponding states^{10–12}, based on the Prigogine theory¹³, semi-quantitatively predicts the *UCST* and *LCST* through the new type of polymer–solvent interaction parameter χ_1 which takes account of free volume effects^{6–9}. Investigations of *UCST* and *LCST* in polymer solutions have supplied useful information and empirical parameters such as the number of external degrees of freedom of the solvent molecule^{6–9}.

It is well known that the limiting viscosity number $[\eta]$ gives us information on the polymer dimension in the solution. The limiting viscosity number at θ_l , like at θ_u ¹⁴, affords the unperturbed mean square end-to-end distance $\langle r_0^2 \rangle$ of the polymer¹⁵ in which θ_l and θ_u are the θ or Flory temperature for the lower and upper critical solution temperatures. It is of particular interest to observe the temperature dependence of the polymer dimension in solvent over the temperature range of θ_u to θ_l and also determine the temperature coefficient of unperturbed mean square end-to-end distance $\text{dln}\langle r_0^2 \rangle/\text{dT}$ of the polymer. The polystyrene–cyclopentane system was selected from the view point of the appearance of θ_u in the neighbourhood of room tem-

perature and θ_l at a temperature less than 160°C . In this temperature region thermal degradation of polystyrene is not appreciable. The values of θ_u and θ_l in the polystyrene–cyclopentane system described elsewhere⁹ were adopted in the present work.

EXPERIMENTAL

The Pressure Chemical Co. products, batch 1c ($M_w=20 \times 10^4$, $M_w/M_n < 1.06$) and batch 13a ($M_w=67 \times 10^4$, $M_w/M_n < 1.10$), were used as polystyrene samples. Cyclopentane was reagent grade and was further purified before use. Cyclopentane was dried over anhydrous potassium carbonate and fractionally distilled by use of a column of 100 cm length and 10 mm diameter packed with stainless-steel helices. Several solutions in cyclopentane were prepared for the viscosity measurements in the concentration range of 0.7 to 1.7 g/dl for sample 1c and 0.2 to 0.7 g/dl for sample 13a. All solutions were stirred with a magnetic stirrer for at least 24 h and then filtered directly into viscometers. The concentration of solutions was determined by evaporating a known volume to dryness and weighing the residue. The density of cyclopentane was determined with a flame-sealed pycnometer over the temperature range of θ_u to θ_l .

Viscosity measurements were carried out with flame-sealed viscometers of Ubbelohde type having negligible kinetic energy corrections. The viscometers were placed in a silicone oil bath controlled to $\pm 0.05^\circ\text{C}$. The thermal degradation of polystyrene in cyclopentane was minimized by flame sealing after keeping polystyrene solutions under dry nitrogen gas and was examined by reproducibility of the flow time of the solution at temperature lower than 50°C . The lowering of the flow time by the thermal degradation was estimated as less than 1%.

for sample 13a of $M_w=67 \times 10^4$ and negligible for sample 1c of $M_w=20 \times 10^4$.

RESULTS AND DISCUSSION

Viscosity data were treated by double extrapolation of η_{sp}/C and $(\ln\eta_{rel})/C$ against C to determine the limiting viscosity number, in which η_{sp} and η_{rel} are the specific and relative viscosity and C is the concentration (g/dl). The limiting viscosity number for the two samples, 1c and 13a, are plotted against temperature in Figure 1 over the temperature range of $\theta_u=19.6^\circ$ to $\theta_l=154.2^\circ\text{C}$. $[\eta]$ first increases and then pass through a maximum before decreasing as temperature increases from θ_u to θ_l . The expansion factor of viscosity α_η^3 is defined by:

$$\alpha_\eta^3 = [\eta]/[\eta]_\theta \quad (1)$$

in which $[\eta]_\theta$ is the limiting viscosity number at the θ temperature. The values of α_η^3 are plotted against temperature in Figure 2. α_η^3 increases steadily with increasing temperature in the range of temperature lower than 90°C and then decreases at higher temperatures than 90°C after attaining a maximum in the neighbourhood of 90°C . The maximum values of α_η^3 are 1.24 for sample 1c and 1.41 for sample 13a.

The constant K_θ is given by:

$$K_\theta = [\eta]_\theta / M^{1/2} = \Phi_0 \langle r_0^2 \rangle / M^{3/2} \quad (2)$$

in which M is the molecular weight of polymer and Φ_0 is a universal constant with the theoretical value of 2.87×10^{23} for non-draining flexible coil polymers¹⁶. The effect of polymer heterogeneity is negligibly small for our samples in estimating K_θ from $[\eta]_\theta$ and M_w . Values of $[\eta]_\theta$ and K_θ at θ_u and θ_l are listed in Table 1. Values of $d \ln \langle r_0^2 \rangle / dT$ given in the last column was calculated from:

$$d \ln \langle r_0^2 \rangle / dT = (2/3) d \ln K_\theta / dT \quad (3)$$

The $d \ln \langle r_0^2 \rangle / dT$ value obtained from the values of K_θ

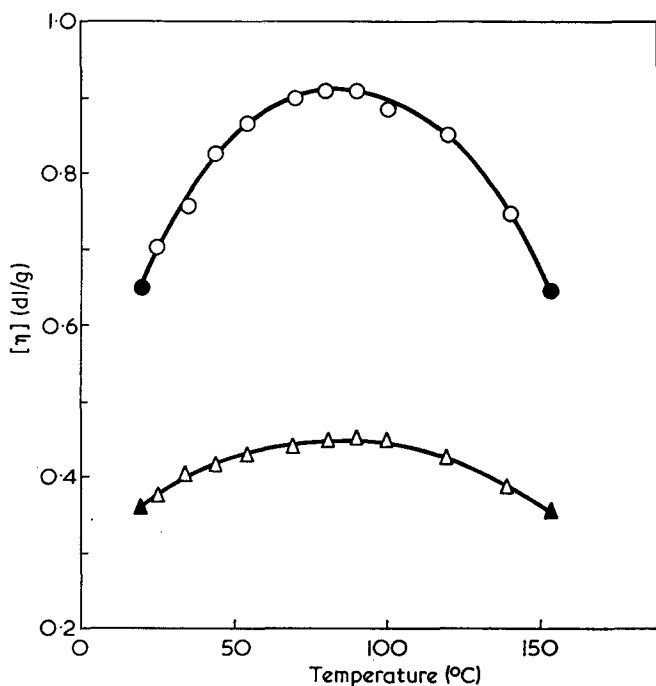


Figure 1 Limiting viscosity number vs. temperature plot for the polystyrene-cyclopentane system for samples 13a (O) and 1c (Δ). ● and ▲ indicate θ_u and θ_l

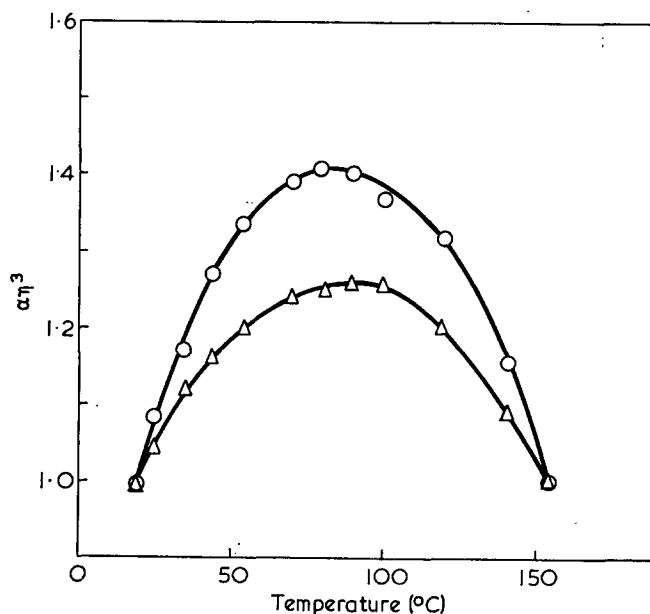


Figure 2 Expansion factor vs. temperature plot for the polystyrene-cyclopentane system for samples 13a (O) and 1c (Δ)

Table 1 Parameters obtained from viscosity for the polystyrene-cyclopentane system

	Sample 1c	Sample 13a
$M_w \times 10^{-4}$ (g mol wt)	20	67
M_w/M_n	1.06	1.10
$[\eta]_{\theta_u}$ (dl/g)	0.362 ± 0.004	0.650 ± 0.005
$[\eta]_{\theta_l}$ (dl/g)	0.355 ± 0.005	0.640 ± 0.010
$K_{\theta_u} \times 10^4$ (dl/g) \times (g mol wt) ^{-1/2}	8.09 ± 0.09	7.94 ± 0.06
$K_{\theta_l} \times 10^4$ (dl/g) \times (g mol wt) ^{-1/2}	7.94 ± 0.11	7.82 ± 0.12
$d \ln \langle r_0^2 \rangle / dT \times 10^3$ (deg ⁻¹)	-0.1	-0.1

corresponding to θ_u and θ_l is $-0.1 \times 10^{-3} \text{ deg}^{-1}$ which is zero within experimental error. It is to be compared with the value of $(0.44 \pm 0.2) \text{ deg}^{-1}$ obtained by the use of different θ solvents over the temperature range of 6.6° to 58.6°C ^{17, 18}.

The role of free volume or thermal expansion is of great importance in explaining the behaviour of polymer chain dimension over the temperature range of θ_u to θ_l . The temperature dependence of the polymer chain dimension must be interpreted through a new χ_1 parameter derived by taking account of the dissimilarities between the free volumes of the components.

The Patterson¹⁰⁻¹² and Flory theories¹⁹⁻²¹ of polymer solution thermodynamics lead to essentially the same expression²² for χ_1 as a function of temperature. The former gives:

$$\chi_1 = -(U_1/RT)v^2 + (C_{p,1}/2R)\tau^2 \quad (4)$$

The quantity $-U_1$ is the energy of vaporization of the solvent, $C_{p,1}$ is its configurational heat capacity, and R is the gas constant. The v^2 parameter is related to the cohesive energy and segment size of the solution components, while the τ parameter reflects the free volume change, which occurs in mixing the dense polymer with the relatively expanded solvent. The τ parameter is related to the characteristic temperature reduction parameter T_1^* of solvent (1) and polymer (2) by

$$\tau = 1 - T_1^*/T_2^* \quad (5)$$

Using the van der Waals model, equation (4) gives χ_1 at

the critical miscibility point. At zero pressure $\chi_1(\text{crit})$ is given as a function of the reduced volume \bar{V}_1 of the solvent by⁷:

$$\begin{aligned} \chi_1(\text{crit}) &= c_1\nu^2/(1-\bar{V}_1^{-1/3}) + c_1\tau^2/2[(4/3)\bar{V}_1^{-1/3}-1] \\ &= (1/2)(1+r^{-1/2})^2 \end{aligned} \quad (6)$$

where $3c_1$ is the number of external degrees of freedom of the solvent molecule, r is the ratio of molar volumes of the polymer and solvent and is taken to be independent of temperature. The reduced temperature \bar{T}_1 of the solvent is given by:

$$\bar{T}_1 = \bar{V}_1^{-1}(1-\bar{V}_1^{-1/3}) = T/T_1^* \quad (7)$$

The temperature dependence of χ_1 , which is of great importance in explaining the UCST and LCST of non-polar polymer solutions, for the polystyrene-cyclopentane system is given in Figure 3, in which the dependence of the $c_1\nu^2$ and $c_1\tau^2$ on temperature are also included. Values of χ_1 are calculated by the aid of equation (6) with the suitable molecular parameters such as $c_1\nu^2$ and $c_1\tau^2$, which are obtained from the experimental values of the UCST and LCST over the wide range of molecular weight of the polymer^{8,9}. The experimental values of $c_1\nu^2=0.022$ and $c_1\tau^2=0.100$ were adopted in calculating χ_1 . The shift of temperature by 27°C adopted for fitting the theoretical curve to the experimental points for the UCST and LCST in the polystyrene-cyclopentane system⁹ was also used for the estimations on the χ_1 values in Figure 3. χ_1 first decreases and then passes through a minimum in the neighbourhood of 95°C before increasing as temperature increases. The θ condition for the UCST and LCST are characterized by contributions of the two terms in equation (6) to $\chi_1(\text{crit})$ of 0.5. In the polystyrene-cyclopentane system the contributions of the ν^2 and τ^2 terms at θ_u are 0.285 and 0.215, while those of the ν^2 and τ^2 terms at θ_l are 0.155 and 0.345. At the minimum point of χ_1 in the neighbourhood of 95°C the τ^2 term is dominant compared to the ν^2 term.

The dimension of polystyrene in cyclopentane attains

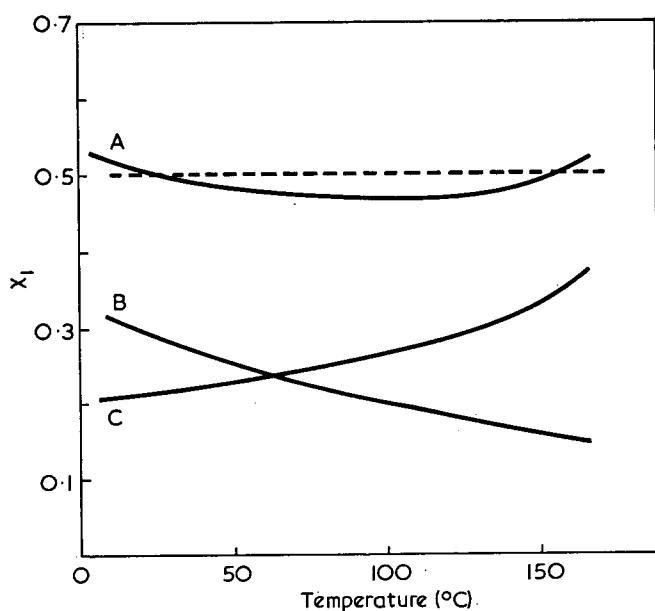


Figure 3 Interaction parameter (χ_1) vs. temperature (A), $c_1\nu^2$ vs. temperature (B) and $c_1\tau^2$ vs. temperature (C) plots for the polystyrene-cyclopentane system

a maximum at 90°C, while χ_1 shows a minimum at 95°C. It is of great importance that behaviour of the polymer chain dimension on temperature is in excellent agreement with that of χ_1 on temperature. There has been no consideration of a concentration dependence of the χ parameter^{7, 23-25} in determining the χ_1 value and θ temperatures. The flat shape of the cloud-point curves in the polystyrene-cyclopentane system indicates that there is some concentration dependence of the χ parameter⁷. Thus the temperature dependence of χ_1 would be somewhat different if it were taken into account, although the deviation from the present χ_1 behaviour is not so large.

In conclusion we emphasize that the effect of free volume or thermal expansion plays an important role in explaining the thermodynamic behaviour of non-polar polymer solutions. The behaviour of the polymer chain dimension over the temperature range of θ_u to θ_l is qualitatively described by the Patterson-Delmas theory of corresponding state and Flory model with the Flory-Huggins critical value of χ_1 .

ACKNOWLEDGEMENT

The authors thank the Ministry of Education in Japan for supporting them by a grant.

REFERENCES

- Freeman, P. I. and Rowlinson, J. S. *Polymer* 1960, 1, 20
- Delmas, G. and Patterson, D. *Int. Symp. Macromol. Chem., Toronto* 1968
- Allen, G. and Baker, C. H. *Polymer* 1965, 6, 181
- Liddell, A. H. and Swinton, F. L. *Discuss. Faraday Soc.* 1970, 49, 115
- Wolf, B. A., Breitenbach, J. W. and Senftl, H. *J. Polym. Sci. (C)* 1970, 31, 345
- Cowie, J. M. G., Maconnachie, A. and Ranson, R. J. *Macromolecules* 1971, 4, 57
- Siow, K. S., Delmas, G. and Patterson, D. *Macromolecules* 1972, 5, 29
- Saeki, S., Kuwahara, N., Konno, S. and Kaneko, M. *Macromolecules* 1973, 6, 246
- Saeki, S., Kuwahara, N., Konno, S. and Kaneko, M. *Macromolecules* 1973, 6, 589
- Patterson, D. and Delmas, G. *Trans. Faraday Soc.* 1969, 65, 708
- Patterson, D. *J. Polym. Sci. (C)* 1968, 16, 3379
- Patterson, D. and Bhattacharyya, S. N. *Polymer* 1965, 6, 455
- Prigogine, I., Belleman, A. and Mathot, V. 'The molecular theory of solutions', North Holland, Amsterdam and Interscience, New York, 1957
- Flory, P. J. 'Principles of polymer chemistry', Cornell University Press, Ithaca, 1953
- Delmas, G. and Patterson, D. *Polymer* 1966, 7, 513
- Kurata, M. and Stockmayer, W. H. *Fortschr. Hochpolym. Forsch.* 1963, 3, 196
- Orofino, T. A. and Ciferri, A. *J. Phys. Chem.* 1964, 68, 3136
- Flory, P. J. 'Statistical mechanics of chain molecules', John Wiley, New York, 1969
- Flory, P. J., Orwoll, R. A. and Vrij, A. *J. Am. Chem. Soc.* 1964, 86, 3507
- Flory, P. J., Orwoll, R. A. and Vrij, A. *J. Am. Chem. Soc.* 1964, 86, 3515
- Flory, P. J. *J. Am. Chem. Soc.* 1965, 87, 1833
- Biroš, J., Zeman, L. and Patterson, D. *Macromolecules* 1971, 4, 30
- Baker, C. H., Brown, W. B., Gee, G., Rowlinson, J. S., Stubble, D. and Yeadon, R. E. *Polymer* 1962, 3, 215
- Kuwahara, N., Oikawa, T. and Kaneko, M. *J. Chem. Phys.* 1968, 49, 4972
- Flory, P. J. and Höcker, H. *Trans. Faraday Soc.* 1971, 67, 2258

The far infra-red spectrum of crystalline polytetrafluoroethylene

G. W. Chantry, J. W. Fleming and Elisabeth A. Nicol

Division of Materials Applications, National Physical Laboratory, Teddington, Middlesex TW11 0LW, UK

H. A. Willis and M. E. A. Cudby

Imperial Chemical Industries Ltd, Plastics Division, Welwyn Garden City, Herts, UK

and F. J. Boerio

Department of Materials Science, University of Cincinnati, Ohio 45221, USA

(Received 8 June 1973; revised 4 October 1973)

The far infra-red spectrum of highly crystalline polytetrafluoroethylene has been shown to contain a new band near 33cm^{-1} , the band at 55cm^{-1} has been shown to be a close doublet and two further bands at 291 and 308cm^{-1} have been observed. These results strongly support the conclusions of Boerio and Koenig from Raman observations that the unit cell contains at least two molecular segments.

INTRODUCTION

Polytetrafluoroethylene (PTFE) has been extensively studied by a wide range of physical techniques. It is known to undergo a phase transition at 19°C , but the available X-ray data^{1,2} indicate that, both above and below this temperature, the unit cell contains only one molecular segment. The change at the transition temperature appears to be purely intramolecular and to involve a transformation from a molecular helix with 15 CF_2 groups in 7 turns to one with 13 CF_2 groups in 6 turns³.

Experimental investigations of the lattice dynamics of PTFE have not been common. There has been little advance in the mid-infra-red situation since the work of Liang and Krimm⁴ apart from the careful work of Brown⁵ who investigated the temperature and pressure dependence of the spectrum. The Raman spectrum was hardly known until the introduction of laser-Raman techniques but since then there have been the investigation by Peacock *et al.*⁶ and the series of investigations by Koenig and Boerio⁷ which have all yielded excellent spectra. The neutron spectrum is in principle the most powerful source of knowledge of the dispersion diagrams and there have been several valuable contributions here from La Garde *et al.*⁸, from Twistleton and White⁹ and most recently from Piseri *et al.*¹⁰. Numerous assignments have been published from time to time but the most recent, those of Boerio and Koenig¹¹ and of Piseri *et al.*¹⁰ are supported by normal coordinate calculations of the dispersion diagrams based on reliable force fields and for this reason they must be preferred. These two assignments are given in *Table 1* where the quoted wavenumber (cm^{-1}) is that of Boerio and Koenig and where the value of Piseri *et al.* is different it is presented in parentheses. Values calculated but not observed by the authors are indicated by an asterisk.

Table 1 Vibrational assignments for polytetrafluoroethylene

Branch	Description	A_1	A_2	E_1	E_2
B1	CF_2 symmetric stretch	1380	—	1298 (1207)	1347* (1384)*
B2	CF_2 asymmetric stretch	—	1210 (1450)	1242 (1298)	1215 (1449)*
B3	CC stretch	731	—	1150	741
B4	CF_2 rocking	—	638	552	676
B5	CF_2 wagging	—	516 (520)	332 (321)	524
B6	CF_2 'scissors'	387	—	277	385
B7	CF_2 twisting	291	—	203	308 (288)*
B8	Skeletal deformation (chain extension)	—	0	6* (31)*	140 (136)
B9	Skeletal deformation (chain twisting)	—	0	0	15* (20)

* See text

It will be seen from *Table 1* that there are some significant differences between the two assignments. The work of Piseri *et al.* was mostly on the 15_7 helix above 19°C whereas that of Boerio and Koenig involved both types of helix. However, this difference is unlikely to be the cause of the discrepancy since the available evidence is that the vibrational frequencies of the two types of helix are closely similar.

At temperatures much below 19°C , the lines in the Raman spectrum show splittings¹² and the far infra-red spectrum develops a sharp set of absorption bands¹³. These phenomena can only arise from the effects of interchain forces but there is some disagreement as to what the outcome of these forces will be. Boerio and Koenig¹² interpreted their Raman splittings as correlation splittings arising from a unit cell containing more than one segment. Chantry *et al.*¹³ supported this view and interpreted their far infra-red spectrum

as the predicted lattice spectrum. Piseri and his colleagues¹⁰, however, reject this view and are of the opinion that the relaxation of the helical selection rules, due to the effect of the neighbouring chains, is sufficient to account for the much enriched spectrum. Clearly more work is required especially in the far infra-red to resolve the dispute. We have therefore carefully observed the far infra-red spectrum from 6 to 400 cm⁻¹ to see whether weak features can be detected additional to those already known and also to determine whether the 200 cm⁻¹ E_1 intense mode shows an observable splitting.

THEORY

The symmetries of infinite helices can be described in terms of line groups¹⁴ and the spectral activity in terms of a line factor group which is D_{15} for the high temperature phase and D_{13} for the low temperature phase. These dihedral groups have modes divided as follows:

$$D_{15} \Gamma_Q = 4A_1 + 5A_2 + 9(E_1 + E_2 + E_3 + E_4 + E_5 + E_6 + E_7) \quad (1)$$

$$D_{13} \Gamma_Q = 4A_1 + 5A_2 + 9(E_1 + E_2 + E_3 + E_4 + E_5 + E_6) \quad (2)$$

The spectral activity is confined to A_1 (Raman polarized), A_2 (infra-red), E_1 (Raman depolarized plus infra-red) and E_2 (Raman depolarized). Four of these modes (two of which form a doubly degenerate pair) have necessarily zero frequency since they correspond to either rigid translations or rigid rotations, so the final listing of active modes is:

$$\Gamma_a = 4A_1 + 3A_2 + 8E_1 + 9E_2 \quad (3)$$

A similar result can be obtained¹⁵ by considering the dispersion diagrams for the nine basic modes (i.e. 3 for each of the three atoms of a CF₂ group) in which frequency as ordinate is plotted against phase angle, between the motions of adjacent CF₂ groups, as abscissa. This yields nine curves (B1–B9) which are uniquely defined within the reduced Brillouin zone 0–180°. The equivalent of the familiar $\Delta k=0$ ¹⁶ selection rule is that the phase angle should be simply related to the screw angle of the helix and therefore spectral activity in the case of the 15₇ helix occurs for $\theta=0^\circ$ (A_1 and A_2), $\theta=168^\circ$ (E_1) and $\theta=360^\circ-2 \times 168^\circ=24^\circ$ (E_2). The intersections of the vertical ordinates $\theta=0$, $\theta=168^\circ$ and $\theta=24^\circ$ with the nine branches therefore define the possible infra-red or Raman bands. For the case of the 13₆ helix, the angle is 166° and spectral activity will occur at $\theta=0$, $\theta=166^\circ$ and $\theta=28^\circ$. The evidence from neutron diffraction¹⁰ is that the form of the dispersion curves does not alter much as the molecule goes through the phase transition and since the helix angles are so similar, the vibrational frequencies, as observed in the infra-red and Raman spectra will be very similar. This has been confirmed experimentally¹⁵.

It is worth pointing out that the neutron workers often quote the abscissa of their dispersion diagrams in terms of the wave vector $q_c=2\pi/c$ where c is a unit cell dimension. In terms of this, the equivalents of our spectroscopic nomenclature are A_1 , $q_c=0$; E_1 , $q_c=0.4666$; E_2 , $q_c=0.0666$; E_3 , $q_c=0.4$; E_4 , $q_c=0.1333$; E_5 , $q_c=0.3333$; E_6 , $q_c=0.2$; E_7 , $q_c=0.2666$. The q_c values are altered in proportion for the 13₆ case. Because the phase angle (24° for 15₇, 28° for 13₆) is so small,

the higher frequency E_2 modes tend to be close in frequency to the corresponding A modes. The curves B8 and B9 necessarily pass through the origin, for if θ is zero, the motions would be z-axis translation and z-axis rotation respectively.

It is not possible, of course, to observe the spectra of conformationally ordered, isolated macromolecules for even if one could observe gas-phase spectra or dilute-solution spectra, the conformational order, which is present in the crystal would be lost. For this reason, nearly all polymer spectra are observed in the solid, and preferably the crystalline, phase. The specimen may be a continuous sample of the polymer or else may be made of small particles thereof dispersed in a transparent matrix but in either case one has to consider how the ideal selection rules worked out for an isolated helix will be modified in the real solid where interchain forces will be significant. If the solid polymer is crystalline, the effects are well understood but if it is amorphous they are much less so. A crystalline polymer will show to first order a spectrum similar to that expected for the isolated macromolecule but to second order there will be correlation splittings if the unit cell contains more than one molecular segment and there will be a lattice spectrum in the far infra-red. If the unit cell does contain more than one segment the lattice spectrum may have several lines, depending on the unit cell symmetry, but if there is only one segment per unit cell, there will be only one line in the lattice spectrum, that corresponding to the z-axis rigid rotation mode.

The assignment discrepancies mentioned earlier are fortunately not very important as far as the present study is concerned for they occur mostly for wavenumbers in excess of 1000 cm⁻¹ and the only point of difference in the far infra-red concerns the E_2 intersection of B7. Piseri *et al.*¹⁰ find it impossible from the shape of their B7 curve for the E_2 intersection to have a frequency greater than that of the A_1 intersection and they point out that Boerio and Koenig only observed a line at 308 cm⁻¹ in the Raman spectrum for very low temperatures—far below the 19°C transition. It is possible therefore that the line at 308 is the E_2 intersection of B7 for the 13₆ helix and that the corresponding line for the 15₇ helix has not so far been observed.

EXPERIMENTAL

Our observations were made with an RIIC lamellar grating interferometer coupled to a Putley indium antimonide detector for the 6 to 40 cm⁻¹ region and with an NPL–Grubb Parsons modular cube interferometer with Golay cell detector for the higher frequency region. The highly crystalline pre-form powder was cold pressed into discs of suitable thickness or else dispersed in a cold pressed polyethylene disc when the thickness required of the pure material would have been too small to be practical. Some of our experimental results are shown in Figures 1–5. At higher resolution (0.5 cm⁻¹) the 55 cm⁻¹ feature is partly resolved into a stronger component at 53.5 cm⁻¹ and a weaker feature at 56.7 cm⁻¹. The error bars in the Figures show the maximum variation of α between four independent runs. The ‘noise’ on any individual run is very much less. Small features whose heights are less than the error bars may nevertheless therefore be well observed and characterized.

RESULTS AND DISCUSSION

The proposed crystal structure of Boerio and Koenig¹² predicts five lattice modes; three of which are translational in character and two rotational. This characterization cannot be absolute in the absence of a centre of symmetry but may well be a good approximation in practice. Our previous results¹³ revealed four lattice bands at 46, 55, 70 and 85 cm⁻¹ and the new band (see Figure 2) 30 cm⁻¹ at room temperature, 33.5 cm⁻¹ at 120 K, could be the missing fifth lattice band. However, this band unlike its higher frequency counterparts is observable at room temperature and does not show any large change of intensity as the specimen is cooled and because of this behaviour, an assignment to the E_1 intersection of B8 (calculated by Piseri *et al.* to be 31 cm⁻¹) is quite plausible. The band does, however, shift upwards in frequency as the temperature is lowered, a form of behaviour usually regarded as an indication that the band in question arises from an external mode. However, it has been shown¹⁷ that in many cases, bands arising from internal modes nevertheless show shifts in frequency as the temperature is altered. An explanation for this may be found in the strong coupling which must exist between external modes and internal modes of the same symmetry and closely similar frequencies. In this connection, it is interesting to note that Brandli and Sievers¹⁸ have published, more-or-less in passing, a far infra-red spectrum of PTFE at 4.2 K. These authors do not comment on the spectrum or advance any

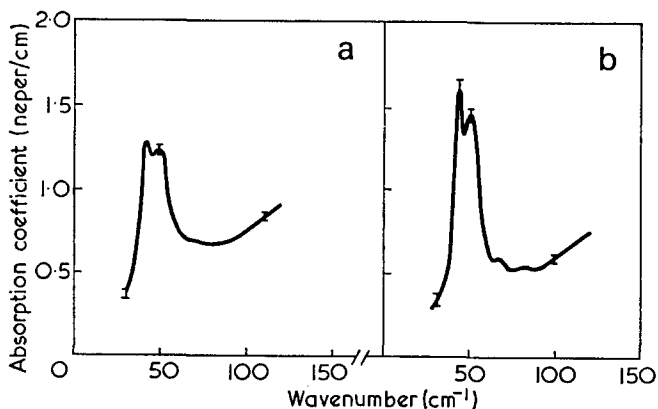


Figure 1 Low wavenumber absorption spectra of crystalline PTFE at (a) ice/water and (b) at dry ice/acetone temperatures; resolution 4 cm⁻¹

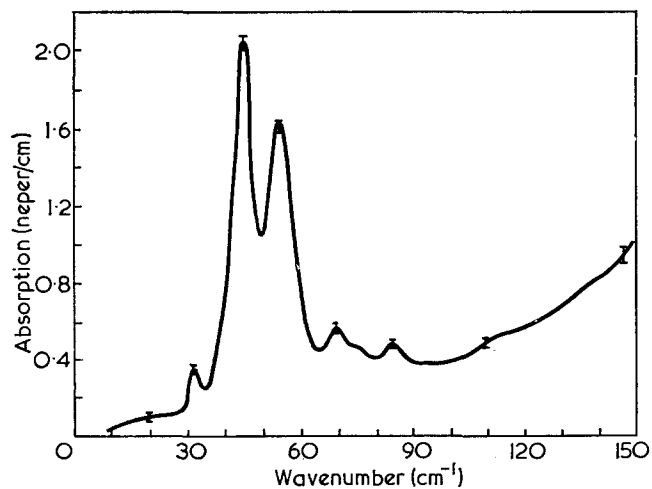


Figure 2 Low wavenumber absorption spectrum of crystalline PTFE at liquid nitrogen temperature; resolution 4 cm⁻¹

explanation for it, but they do observe a line at 33.5 cm⁻¹ which is undoubtedly the same one that we have observed. The fact that there is a large blue-shift in going from room temperature to liquid nitrogen temperature and then virtually none in going down further to liquid helium temperature, is rather reminiscent of the behaviour of the B_{1u} lattice band of polyethylene. However, the balance of the evidence favours the assignment of this band to the E_1 intersection of the B8 branch especially since this particular branch is the one most well characterized by the neutron work¹⁰.

This assignment then leaves us with five lines which can now very naturally be ascribed to the expected five line lattice spectrum. The splitting of the 55 cm⁻¹ line into two components has also been observed by Johnson and Rabolt¹⁹ and it is very clearly resolved in the helium temperature spectrum of Brandli and Sievers¹⁸. We suggest that the persistence of the band near 50 cm⁻¹ above 19°C (see Fig. 1 of ref 16) can be explained as follows. At temperatures above 19°C, there is only one molecular segment per unit cell and therefore there will be only one lattice mode, that corresponding to the z-axis rotation of the free molecule. The 50 cm⁻¹ feature is ascribed to this. As the temperature is lowered through the 19°C transition this band shifts towards 55 cm⁻¹ (see Figure 1) and is split into two components by the in-phase and out-of-phase coupling which must occur in the unit cell of the low temperature phase. The three lines at 46, 70 and 85 cm⁻¹ would then be the three translational lattice modes.

Two alternative theories have been advanced to account for the Raman splittings and the far infra-red line spectrum. Piseri and his colleagues suggest¹⁰ that they arise from the activation of the E_3 , E_4 , E_5 and E_6 intersections by the lowered site symmetry due to interchain forces and Zerbi has suggested²⁰ conformational disorder as an explanation. However, both these theories have features which make them unlikely. First, if the Raman splittings arise from the effects of lowered site symmetry it would be most unlikely that the two components would have roughly equal intensities yet Boerio and Koenig¹² find just this for all three bands that show an observable splitting. If, on the other hand, the splitting arises from correlation effects in a unit cell which contains more than one segment it would be most surprising if the intensities were not roughly equal. Secondly, the calculated values¹⁰ of the E_3 , E_4 , E_5 and E_6 intersections of B8 and B9 do not coincide with any observed features. Thus all the intersections of the B9 branch must lie below 35 cm⁻¹ and the low frequency intersections of B8 ($E_3=95$ cm⁻¹, $E_2=140$ cm⁻¹, $E_5=158$ cm⁻¹) occur in featureless regions of the spectrum. The conformational disorder theory is unattractive because the effects are only seen at low temperatures and experience of the infra-red spectra of disordered materials shows them to be diffuse with intense 'liquid-lattice' type absorption bands. Behaviour of this type can be seen for sintered materials in ref 13 and it is clear from the spectra shown there that the far infra-red lines cannot owe their origin to conformational disorder. If they did, the lines would be far more intense for the sintered than for the unsintered material, whereas the observed lines are slightly weaker in the sintered specimen. Our highly crystalline material is conformationally highly ordered and at liquid nitrogen temperatures is one of the most transparent materials

known in the interband regions. For these reasons we consider the two-segment unit cell theory to be the more attractive and now go on to discuss the higher frequency infra-red spectrum in terms of it.

The 203 cm^{-1} band of several specimens of PTFE, fabricated in several ways and all studied to a resolution of 1 cm^{-1} at a specimen temperature of 130 K have been observed repeatedly. In no case was any splitting observed. This is in contradistinction to the Raman observations of Boerio and Koenig¹² on the higher frequency bands where correlation splitting was observed. However, the splitting of this particular band should be small since it arises from a nearly pure CF_2 twisting motion and it may be beyond present techniques even for helium specimen temperatures.

The 300 cm^{-1} region of the spectrum is shown in Figures 3 and 4 and the temperature dependence of the absorption is shown in Figure 5. The weak feature at 278 cm^{-1} is coincident with the Raman band at 277 cm^{-1} which has been assigned (see Table I) to the E_1 intersection of B6. The occurrence of strong features at 293 and 311 cm^{-1} is more interesting since these probably correspond to the $291 (A_1)$ and $308 (E_2)$ Raman bands, which are of course forbidden in the infra-red. That we observe these forbidden bands both above and below the transition temperature (292 K) presents an enigma. The data of Figure 5 can be most simply interpreted as indicating that the halfwidths of all three components fall monotonically as the temperature is reduced. The change from a 15 to 13 CF_2 group helix as remarked

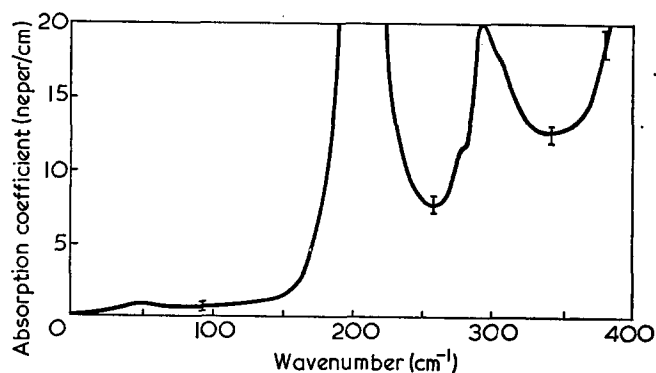


Figure 3 Far infra-red absorption spectrum of crystalline PTFE at room temperature; resolution 4 cm^{-1}

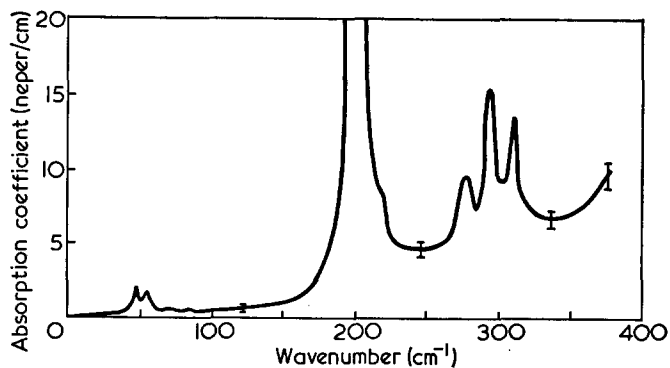


Figure 4 Far infra-red absorption spectrum of crystalline PTFE at liquid nitrogen temperature; resolution 4 cm^{-1}

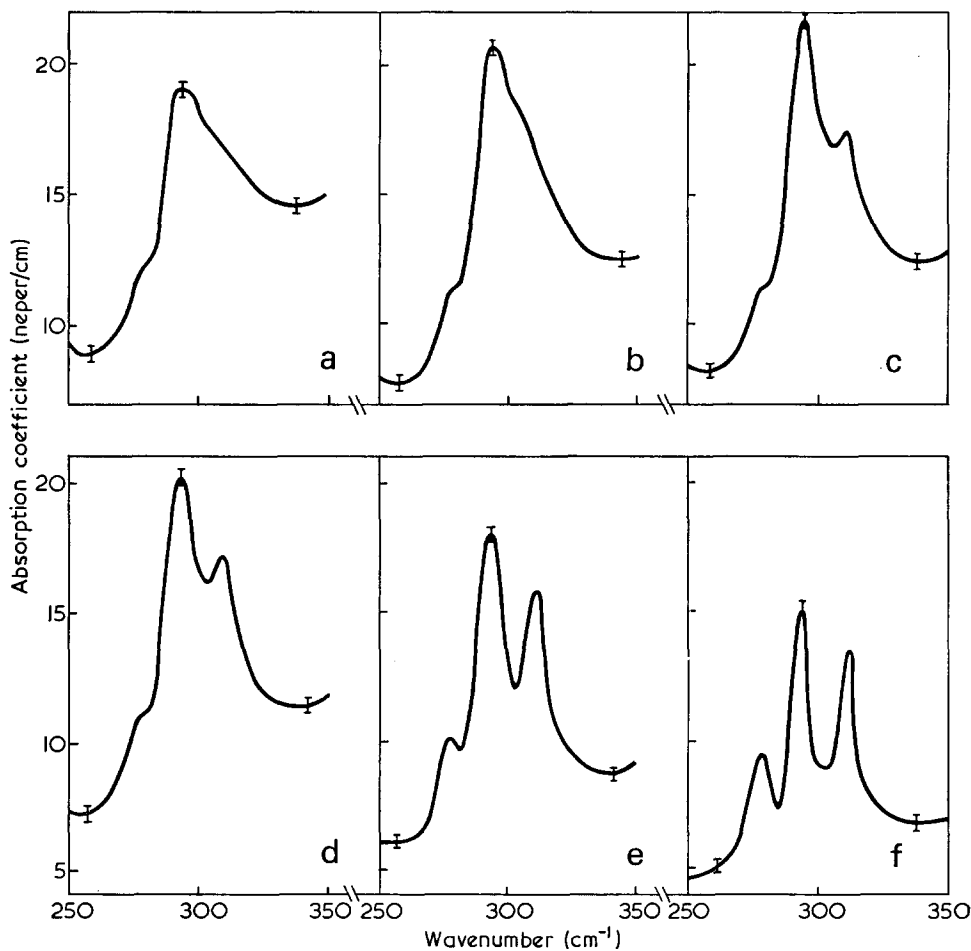


Figure 5 Variation with temperature of the absorption of crystalline PTFE in the 300 cm^{-1} region; resolution 4 cm^{-1} . (a) 313 K ; (b) 288 K ; (c) 283 K ; (d) 273 K ; (e) 213 K ; (f) 113 K

earlier makes very little difference to the vibrational frequencies¹⁵ so this transformation is unlikely to show any obvious effects in the spectrum. However, the 203 cm⁻¹ band (i.e. the E_1 intersection of B7) is inherently very intense ($\alpha_{\text{max}}=200$ neper/cm)²¹ so any mechanism which would make its A_1 and E_2 counterparts weakly allowed would make them readily observable. For the low temperature phase, an obvious mechanism would be the lowered effective symmetry due to the presence of two segments per unit cell. For the high temperature phase, Zerbi's idea²⁰ of conformational disorder, brought about by the large amplitude thermal motions, is attractive. This concept is also of value in interpreting the X-ray data. These two mechanisms may be, of course, only different facets of one phenomenon. The X-ray data tend to give a time-averaged picture of the ensemble whereas the infra-red activity is governed by the instantaneous molecular configurations. An ensemble which is basically one segment per unit cell but with each segment subject to large random perturbations could appear instantaneously to be a melange of crystallites with varying numbers of segments per unit cell. As the temperature falls, the instantaneous picture comes more and more, on the large scale, to resemble the static picture. We may thus certainly interpret our low temperature data as further evidence that the unit cell contains more than one molecular segment. The occurrence of the forbidden features at high temperatures may then be ascribed to the effects of thermally induced conformational disorder.

REFERENCES

- 1 Krimm, S. *Fortschr. Hochpolym. Forsch.* 1960, **2**, 51
- 2 Kilian, H. G. *Kolloid-Z.* 1962, **185**, 13
- 3 Clark, E. S. and Muus, L. T. *Z. Kristallog.* 1962, **117**, 119
- 4 Liang, C. Y. and Krimm, S. *J. Chem. Phys.* 1956, **25**, 563
- 5 Brown, R. G. *J. Chem. Phys.* 1961, **40**, 2900
- 6 Peacock, C. J., Hendra, P. J., Willis, H. A. and Cudby, M. E. A. *J. Chem. Soc. (A)* 1970, p 2943
- 7 Koenig, J. L. and Boerio, F. J. *J. Chem. Phys.* 1969, **50**, 2823
- 8 La Garde, V., Prask, H. and Trevino, S. *Discuss. Faraday Soc.* 1969, **48**, 15
- 9 Twistleton, J. F. and White, J. W. *Polymer* 1972, **13**, 40
- 10 Piseri, L., Powell, B. M. and Dolling, G. *J. Chem. Phys.* 1973, **58**, 158
- 11 Boerio, F. J. and Koenig, J. L. *J. Chem. Phys.* 1970, **52**, 4826
- 12 Boerio, F. J. and Koenig, J. L. *J. Chem. Phys.* 1971, **54**, 3667
- 13 Chantry, G. W., Fleming, J. W., Nicol, E. A., Willis, H. A. and Cudby, M. E. A. *Chem. Phys. Lett.* 1972, **16**, 141
- 14 Zbinden, R. 'Infrared Spectroscopy of High Polymers', Academic Press, New York and London, 1964
- 15 Hannon, M. J., Boerio, F. J. and Koenig, J. L. *J. Chem. Phys.* 1969, **50**, 2829
- 16 Chantry, G. W. 'Submillimetre Spectroscopy', Academic Press, London and New York, 1971
- 17 Chantry, G. W., Fleming, J. W., Cook, R. J., Moss, D. G., Nicol, E. A., Willis, H. A. and Cudby, M. E. A. *Infrared Phys.* 1973, **13**, 157
- 18 Brandli, G. and Sievers, A. *J. Phys. Rev. (B)* 1972, **5**, 3550
- 19 Johnson, K. W. and Rabolt, J. F. *J. Chem. Phys.* 1973, **58**, 4536
- 20 Zerbi, G. personal communication; Zerbi, G. and Sacchi, M. *Macromolecules* 1973, **6**, 692; Masetti, G., Cabassi, F., Morelli, G. and Zerbi, G. *Macromolecules* 1973, **6**, 700
- 21 Chamberlain, J. and Gebbie, H. A. *Appl. Optics* 1966, **5**, 393

Electron spin resonance studies of spin-labelled polymers: Part 6. End-labelled poly(methyl methacrylate)

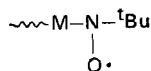
A. T. Bullock, G. G. Cameron and J. M. Elsom

*Department of Chemistry, University of Aberdeen, Old Aberdeen, AB9 2UE, UK
(Received 15 June 1973; revised 10 September 1973)*

The anionic synthesis of poly(methyl methacrylate) (PMMA) carrying a nitroxide spin-label at the chain end is described. With *n*-butyl lithium as initiator it is necessary to polymerize at -70°C and add the labelling agent, 2-methyl-2-nitrosopropane, to the active polymer anion at the same temperature. At higher temperatures initiator attack at the ester groups yields spin-labelled side chains. The correlation time for rotational diffusion of an end-labelled PMMA sample is 2.8×10^{-10} sec which is shorter than that from fluorescence depolarization studies. The probable reasons for this discrepancy are discussed.

INTRODUCTION

The technique of spin-labelling with nitroxide radicals has recently been employed to obtain information on the motions of synthetic macromolecules both in the solid and in dilute solution. The method involves attaching a suitable stable nitroxide group to some point on the polymer molecule. This is followed by a line-width analysis of the electron spin resonance (e.s.r.) spectrum of the labelled polymer to evaluate τ_c , the correlation time for rotational diffusion of the nitroxide radical. τ_c reflects the mobility of the polymer chain in the neighbourhood of the radical. Most of our studies¹⁻⁴ so far have been concerned with polymers labelled randomly at specific points within the main chain. Other workers have studied polyesters, polyamides⁵ and polyethers⁶ labelled at chain ends and it has recently been shown⁷ that a number of end-labelled addition polymers can be prepared by reacting 'living' polymeric anions with 2-methyl-2-nitrosopropane (MNP). The radical end groups from this synthesis should have the structure:



With poly(methyl methacrylate) (PMMA), however, difficulties in preparing an authentic end-labelled specimen by this route have been encountered^{7, 8}.

A considerable body of evidence on the free radical polymerization of MMA indicates that termination is diffusion controlled⁹⁻¹². In thermodynamically 'good' solvents segmental rotation appears to be the diffusion-controlling process but segment density also affects the termination reaction so that in 'poor' solvents radical-radical termination is hindered by the tightly coiled configuration of the macroradicals¹³. There is, therefore, particular interest in obtaining end-labelled samples of this polymer since the e.s.r. spectra could yield, in a

more direct manner than hitherto, information concerning the mobility of segments near the chain ends. Preliminary experiments along these lines suggest⁸ that the spin-labelling technique can improve our understanding of the factors affecting termination in radical polymerization and supplement existing data from dielectric relaxation and fluorescence depolarization studies.

In this communication we describe the preparation and characterization of an end-labelled PMMA. Our observations on this synthesis also have some relevance to the mechanism of anionic polymerization of MMA.

EXPERIMENTAL

Tetrahydrofuran (THF) was freed from moisture and peroxides by refluxing over sodium wire. It was then distilled and the central cut of the distillate was collected and stored over sodium.

MMA was distilled under reduced pressure, dried over calcium hydride and stored in a cold-room.

All polymerizations were performed under vacuum using *n*-butyl or fluorenyl lithium as initiator. *n*-Butyl lithium (0.3 M) in *n*-hexane or toluene was freshly prepared before each polymerization by reaction of *n*-butyl chloride and lithium metal.

MNP was prepared as before¹⁴.

n-BuLi in hexane (20 ml) was introduced by syringe through a serum cap into the reaction vessel which was then evacuated. Degassed THF (20 ml) was distilled in from a reservoir containing a little freshly formed green naphthyl sodium. The reaction vessel was then immersed in methanol/solid CO₂ coolant, the contents were stirred vigorously and 4 ml of pure degassed MMA were added slowly by distillation. After the required reaction time the system was 'killed' by adding 0.25 g MNP in THF solution stored in a side arm of the reaction vessel.

Fluorenyl lithium was prepared by adding *n*-BuLi in toluene (5 ml) to 1.0 g fluorene in the reaction vessel. THF (60 ml) was then added as above, the vessel was brought up to room temperature and the contents were stirred for 1 h to ensure that all the BuLi had been converted to 9-fluorenyl lithium. Thereafter the procedure above was followed.

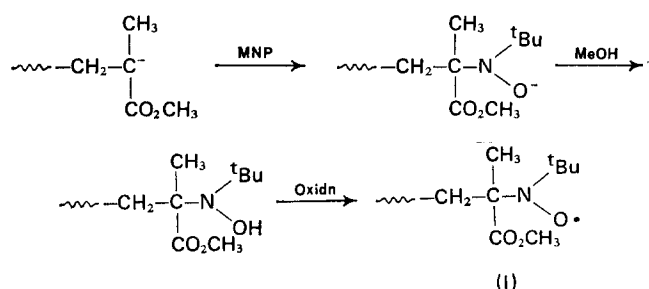
With both initiators the system was killed by MNP at varying temperatures between -70°C and room temperature.

The polymers were isolated by pouring the THF solutions into cold methanol, and purified by repeated precipitation in methanol from chloroform solution. Before the final precipitation the polymer solution was shaken with silver oxide to ensure complete oxidation of any hydroxylamine to nitroxide. The polymers were dried under vacuum at room temperature.

E.s.r. spectra were recorded at room temperature from 5% (w/v) solutions in toluene using a Decca X3 spectrometer. Field measurements were made with a Systron-Donner 3193 Digital Gaussmeter and isotropic *g* values were measured by comparison with the spectrum of Frémy's salt¹⁵ for which $g = 2.00554 \pm 0.00001$.

RESULTS AND DISCUSSION

Ideally MNP should react with the living carbanion of PMMA to produce the nitroxide (I) as follows:



The structure of (I) predicts a three-line e.s.r. spectrum due to interaction of the unpaired electron with the ^{14}N nucleus. *Figure 1a* shows such a spectrum for which $g = 2.00587 \pm 0.00006$ and $a_{\text{N}} = 41.91 \pm 0.16$ MHz. With BuLi as initiator this pattern was observed only when polymerization and termination were conducted at -70°C . If the reaction vessel was allowed to reach room temperature, held there for approximately 10 min then killed with MNP the polymer gave a six-line e.s.r. spectrum—a triplet of doublets (*Figure 1b*) with the same *g* value as *Figure 1a* and $a_{\text{N}} = 38.83 \pm 0.22$ MHz. The doublet splitting is due to a single proton, $a_{\text{H}} = 6.04 \pm 0.11$ MHz. Unlike the three-line spectrum the six-line spectrum was not easily reproduced.

At 0°C or after short times at room temperature, the product polymer gave a seven-line spectrum—a superposition of *Figures 1a* and *1b* in which the outermost lines of the two spectra overlapped exactly. It was tentatively suggested⁸ that *Figure 1b* is the spectrum of radical (II):

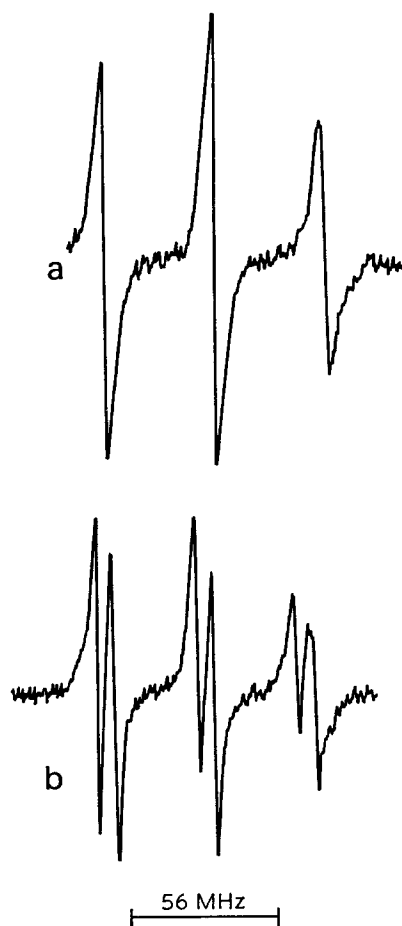
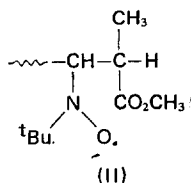


Figure 1 (a) E.s.r. spectrum of end-labelled PMMA (I) polymerized anionically with *n*-BuLi in THF and 'killed' with MNP at -70°C ; (b) six-line e.s.r. spectrum of labelled PMMA polymerized at -70°C as in (a) and 'killed' with MNP after 10 min at room temperature

following rearrangement of the PMMA anion. This explanation can be attacked on energetic grounds and is now untenable because: (i) fluorenyl lithium yielded a polymer with a three-line spectrum at all termination temperatures; and (ii) deuterated MMA ($\text{CD}_2=\text{C}(\text{CH}_3)\text{CO}_2\text{CH}_3$) behaves exactly as normal MMA¹⁶. The radical giving rise to *Figure 1b* has not been identified but it probably arises from attack of BuLi at the ester side groups. This suggestion is supported by the observations that preformed PMMA reacts with BuLi and MNP to give a product with an e.s.r. spectrum identical to *Figure 1b*, and that fluorenyl lithium is a much 'cleaner' initiator for MMA than BuLi.

The most important point in this communication, however, is that under the right reaction conditions a PMMA sample carrying an end-label of structure (I) can be produced. The resulting e.s.r. spectrum (*Figure 1a*) shows a dependence of line-width upon m_{N} , the ^{14}N magnetic quantum number. This permits evaluation of τ_c . For illustrative purposes we quote one value here, viz. $\tau_c = 2.8 \times 10^{-10}$ sec¹⁷. This figure pertains to a polymer ($\bar{M}_v = 80\,000$) in ethyl acetate solution (5%) at 25°C and is about two orders of magnitude longer than τ_c for rotation of a small nitroxide radical in a low viscosity solvent. Fluorescence depolarization studies¹⁸ gave a larger value for τ_c , viz. 54×10^{-10} sec for PMMA carrying dichlorofluorescein groups at the chain ends. Apart from the unreliability of the steady-state de-

polarization technique¹⁸, two factors which control the rotational mobilities of the fluorescent and spin-labels should be kept in mind when considering this discrepancy. These are the facility of segmental reorientation of the monomer units adjacent to the label and the contribution arising from the viscous drag exerted by the solvent on the label. At present we cannot comment on the relative weights of these contributions but the fluorescence measurements were carried out in dimethyl formamide which is appreciably more viscous than ethyl acetate. Also, the hydrodynamic radius of the dichlorofluorescein label is larger than that of the spin-label. Both effects will give rise to higher values of τ_c from the fluorescence measurements. A study of the effect of temperature and solvent viscosity on τ_c should help to clarify the situation.

ACKNOWLEDGEMENT

We are grateful to the Science Research Council for an equipment grant.

REFERENCES

- 1 Bullock, A. T., Butterworth, J. H. and Cameron, G. G. *Eur. Polym. J.* 1971, 7, 445

- 2 Bullock, A. T., Cameron, G. G. and Smith, P. M. *J. Phys. Chem.* 1973, 77, 1635
- 3 Bullock, A. T., Cameron, G. G. and Smith, P. M. *J. Polym. Sci. (A-2)* 1973, 11, 1263
- 4 Bullock, A. T., Cameron, G. G. and Smith, P. M. *Polymer* 1972, 13, 89
- 5 Törmälä, P., Silvennoinen, K. and Lindberg, J. J. *Acta Chem. Scand.* 1971, 25, 19
- 6 Törmälä, P. *et al. Acta Chem. Scand.* 1970, 24, 3066
- 7 Forrester, A. R. and Hepburn, S. P. *J. Chem. Soc. (C)* 1971, p 701
- 8 Bullock, A. T., Butterworth, J. H., Cameron, G. G. and Elsom, J. M. *Prepr. IUPAC Conf. Chemical Transformations of Polymers, Bratislava* 1971, p 21
- 9 North, A. M. and Reed, G. A. *Trans. Faraday Soc.* 1961, 57, 859; North, A. M. *Makromol. Chem.* 1965, 83, 15
- 10 Bamford, C. H. and Brumby, S. *ibid.* 1967, 105, 122
- 11 Schulz, G. V. and Fischer, J. P. *ibid.* 1967, 107, 253
- 12 Burnett, G. M., Cameron, G. G. and Zafar, M. M. *Eur. Polym. J.* 1970, 6, 823
- 13 Cameron, G. G. and Cameron, J. *Polymer* 1973, 14, 107
- 14 Calder, A., Forrester, A. R. and Hepburn, S. P. *Org. Syn.* in press
- 15 Kerr, C. M. L. *PhD Thesis* University of Aberdeen, 1970
- 16 Bullock, A. T., Cameron, G. G. and Elsom, J. M. unpublished work
- 17 Bullock, A. T., Cameron, G. G. and Krajewski, V. to be published
- 18 North, A. M. and Soutar, I. *JCS Faraday Trans. I* 1972, 68, 1101

Measurements of anisotropic light scattering: application to the determination of the difference $H_h - H_v$ for $\theta = \pi/2$

Jean-Claude Ravey, Paul Mazon and Yves Sere

Laboratoire de Biophysique, Université de Nancy I, 54037 Nancy Cedex, France
(Received 20 July 1973; revised 3 September 1973)

By improving the performance of a photogoniometer, a technique for the accurate determination of various light scattering components has been developed. An original adaptation of the method is the measurement of $(H_h - H_v)_{90^\circ} / (H_v)_{90^\circ}$, the value of which is dependent only on the scattering particles shape. A few examples are presented.

INTRODUCTION

A series of theoretical papers has been recently devoted to light scattering by anisotropic particles¹⁻³. Using the Rayleigh-Debye approximation, the depolarized intensities have been specially considered. These intensities are generally weak, and their precise measurement necessitates high performances from the light scattering photometer used. The present paper deals with simple improvements made on a standard Sofica photometer, which permits such precision, and successful checking of some original features of previous theoretical work.

EXPERIMENTAL

Apparatus

Measurements were made on a Sofica photogoniometer (PGD)⁴ (type 42 000: the variations of the intensity of the incident light are compensated by using a reference phototube), the performance of which was improved by the following modifications (see Figure 1): (i) the initial polarizer (Polaroid HN32) is replaced by an easily removable Glazebrook's prism, G_1 , which

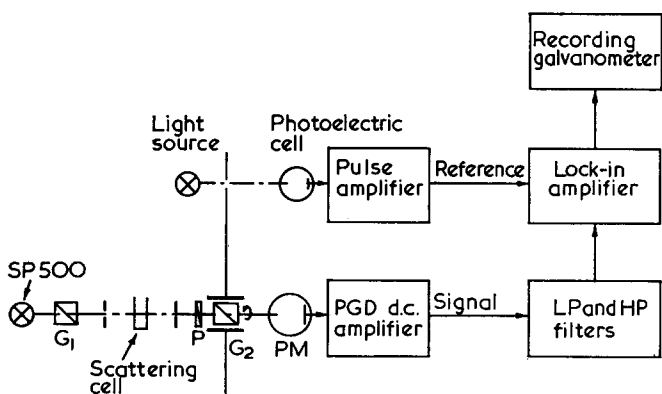


Figure 1 Experimental arrangement showing optical and electronic assemblies. SP500, initial light source; G_1 , Glazebrook prism; P, polaroid; G_2 , Glazebrook prism; PM, photomultiplier; LP, HP, low and high pass filters

may be orientated from the top of the PGD plate, with a precision of 0.1° ; (ii) a second Glazebrook's prism, G_2 , is placed just in front of the photomultiplier (PM). It is movable round its axis and it is driven by a synchronous micromotor at the constant rate of $N = \omega/2\pi$ rev/sec. According to the chosen type of measurement, G_2 will act as an analyser or a modulator; (iii) a removable polaroid P (type HN 32) may be set on the scattered beam in front of G_2 ; (iv) the galvanometer and damping circuits of the Sofica instrument are disconnected and the signal which is received from the direct current amplifier of the PGD is put into a lock-in amplifier (Tekelec TE 9000) acting on the $2N$ frequency. In addition high pass (HP) and low pass (LP) filters are used. The synchronization between the modulator and the detector is effected by means of an optical system including a photoelectric cell (LF 1 A) connected to a logical output amplifier (statiphot S 5201 S Cometa); (v) the device is completed by a recording galvanometer. We used the initial light source SP500, though its spectrum is modulated to a frequency of 100 Hz, since it is supplied by a 50 Hz a.c. voltage; it is sufficient to choose low enough frequencies for the modulation (below 10 Hz for example). The optical parts of the apparatus were adjusted with great care; the divergence of the incident and scattered beams was reduced by using additional sets of diaphragms. High optical quality cells (Sofica) were also used.

Such a device enables us to get very accurate measurements of the various light scattering components V_v , H_v , V_h , H_h and their differences.

H_v measurements

The incident and scattered beams are respectively vertically (G_1) and horizontally (P) polarized. The transmitted scattered light intensity is $(H_v/2)(1 + \cos 2\omega t)$. $\frac{1}{2}H_v$ is then modulated to the $2N$ frequency; the recorded output signal of the lock-in amplifier will then be the effective value $[1/2(2)^{1/2}]H_v$. The determination of other light scattering components will be recorded in the same manner.

$H_h - H_v$ measurements: an original adaptation of the device

The polaroid P is removed and the incident beam is horizontally polarized. The transmitted intensity after G_2 is then:

$$H_h \cos^2 \omega t + H_v \sin^2 \omega t = \frac{H_h - V_h}{2} \cos 2\omega t + \frac{H_h + V_h}{2}$$

$(H_h - V_h)/[2(2)^{1/2}]$ will then be recorded.

When Krishnan's reciprocity relation is valid, i.e. for unoriented scattering particles, or when the orientation of the particles has a cylindrical symmetry round preferential directions which are the axes of the reference frame built on the exterior and interior bisectors of the scattering angle θ , $H_v = V_h$. This measurement is carried out for $\theta = \pi/2$. As was theoretically shown by Ravey², the study of the ratio $R = [(H_h - H_v)/H_v]_{90^\circ}$ is a very sure way of ascertaining the scattering particle shape (prolate or oblate ellipsoid), for any optical anisotropy value of δ provided that $\delta \neq 0$. Characteristic examples of this determination are shown below.

$H_h - V_v$ measurements

G_1 and P being removed, the transmitted intensity after G_2 is $(H_h + H_v) \cos^2 \omega t + (V_v + V_h) \sin^2 \omega t$, and finally $[1/2(2)^{1/2}](H_h - V_v)$ is recorded on the galvanometer. This difference depends on both optical anisotropy and particle shape; the results of this study related to very anisotropic and anisodiametric particles will be presented elsewhere.

RESULTS AND DISCUSSION

Performance of the apparatus

By studying the light scattered by various organic liquids, it was first experimentally verified that the following relations hold within 1%:

$$H_v(\theta) = V_h(\theta)$$

$$I(\theta) = I(\pi - \theta)$$

Exhaustive measurements were thus performed with benzene. In Table 1, it is shown that H_v is constant within 0.3% and that the measurements are quite symmetrical, as they must be for benzene. The relation $H_h = V_v \cos^2 \theta + H_v \sin^2 \theta$, i.e. $H_h - H_v = (V_v - H_v) \cos^2 \theta$ which holds for small anisotropic molecules, is also verified; in Figure 2 the experimental variations of this function of θ (the variations of the scattering volume are taken into account by the term $\sin \theta$) are plotted.

Table 1 Angular dependence of H_v for benzene

θ	H_v
30	760
37.5	752
45	756
60	753
75	754
90	755
105	754
120	753
135	756
142.5	752
150	760

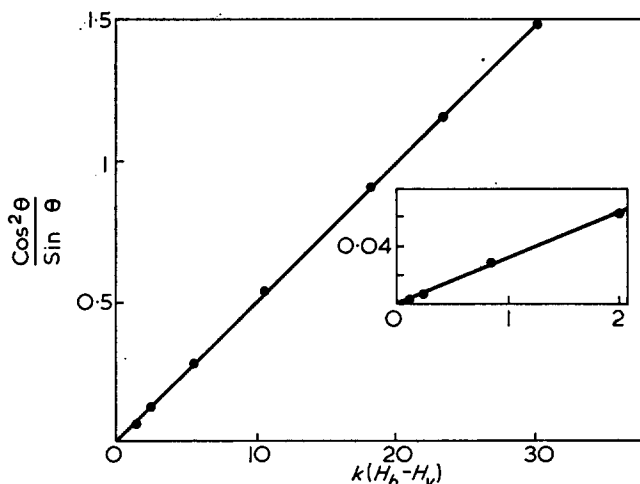


Figure 2 $H_h - H_v$ plot of experimental results for benzene

A deviation from the proportionality to $\cos^2 \theta$, probably due to imperfect optics, takes place for θ values between 87° and 93° . For these angles, the scattered intensity corresponds to about one-hundredth of the H_v intensity scattered by benzene at $\theta = 90^\circ$ [$H_v^B(90^\circ)$].

If suspensions of very small and/or slightly anisotropic particles are studied, it will be necessary to take into account these small deviations, by writing:

$$(H_h - H_v)_{\text{particles}} = (H_h - H_v)_{\text{suspension}} - (H_h - H_v)_{\text{solvent}}, \text{ for } \theta = 90^\circ.$$

The response of the photomultiplier has also been tested for different states of light polarization. By using our dynamic method, the relative difference $\Delta I/I$ of the response for vertical and horizontal polarization has been measured; it has been found that:

$$\frac{\Delta I}{I} \simeq 7\% \text{ for an R106 photomultiplier (Fica)}$$

$$\text{and } \frac{\Delta I}{I} \simeq 0.3\% \text{ for the original RCA-1 P 28}$$

which is thus good enough for all our measurements.

Principle of the measurements of $H_h - H_v$

In order to obtain results which are independent of the optical anisotropy of the scattering particles, the ratio R , as previously defined, has been studied.

We must separately evaluate the absolute values of $(H_h - H_v)_{90^\circ}$ and $(H_v)_{90^\circ}$. For this purpose, benzene is used as a reference. The evaluation of the difference $(H_h - H_v)_{90^\circ}$ is carried out as follows. Let A be the value in arbitrary units of $(H_h - H_v)_{90^\circ}$ for the solution studied. The solution is replaced by benzene, and the scattering angle θ_1 corresponding to the galvanometer deviation B is sought so that A and B have magnitudes of the same order. The quantity of interest will then be:

$$(H_h - H_v)_{90^\circ} = \frac{1 - \rho_v \cos^2 \theta_1}{1 + 3\rho_v \sin^2 \theta_1} \frac{A}{B} R_{90^\circ}^B$$

where $R_{90^\circ}^B$ represents the Rayleigh's ratio for benzene, $\theta = 90^\circ$, and ρ_v is the depolarization ratio of benzene ($\rho_v = H_v/V_v \simeq 0.277$). It is also derived that for $(H_v)_{90^\circ}$:

$$(H_v)_{90^\circ} = \frac{\rho_v}{1 + 3\rho_v} \frac{A'}{B'} R_{90^\circ}^B$$

where A' (solution) and B' (benzene) are the measured

values of H_v for $\theta = \pi/2$. Using the Rayleigh-Gans approximation, it has been shown² that if the scattering particle dimension is less than a critical value (about λ), R must be negative for an elongated particle and *vice versa* (it must be positive for a flat one). For spheroids the first terms of the series expansion of R are:

$$R = -\frac{X^2}{14} \frac{\omega}{\omega+3} \left(1 + \frac{X^2}{14} \frac{1-2\omega}{\omega+3} + \dots \right)$$

where $\omega = p^2 - 1$,

p = ellipticity of the spheroid,

$X = 4\pi\rho/\lambda$,

ρ = radius of gyration of the particle.

The actual theoretical curves are shown in Figure 3. The exact expressions for R are rather complicated and can be found in previous papers^{1, 2}.

Results: study of R

Single crystals of PEO-PS copolymer. Poly(ethylene oxide) (PEO)-polystyrene (PS) single crystals were prepared by B. Lotz (Centre de Recherches sur les Macromolécules, Strasbourg). As shown in the electron micrograph (Figure 4), they are quite monodisperse (Figure 4), and their average size is about $0.6 \mu\text{m}$ (their thickness is about 150 \AA). For such thin platelets, the theoretical value of R must be nearly equal to $+7.5^2$. It was found that $R = 5 \pm 1$. The agreement is satisfactory, given the rather low precision of the $H_v(90^\circ)$ measurement; the value of the component H_v scattered by the single crystals is less than one-fifth of the intensity scattered by the solvent in which they are in suspension (*p*-xylene).

Tobacco mosaic virus (TMV). Different TMV preparations were supplied by Miss Lebeurier (Institut de Botanique, Strasbourg). Most aqueous suspensions were rather polydisperse. By means of differential centrifugations, it was possible to obtain various TMV fractions, which have enabled us to carry out light scattering measurements on rods of various length, L . Both green and violet incident lights have also been used. The results of this study are presented in Figure 5; it may be seen that the experimental points are in close agreement

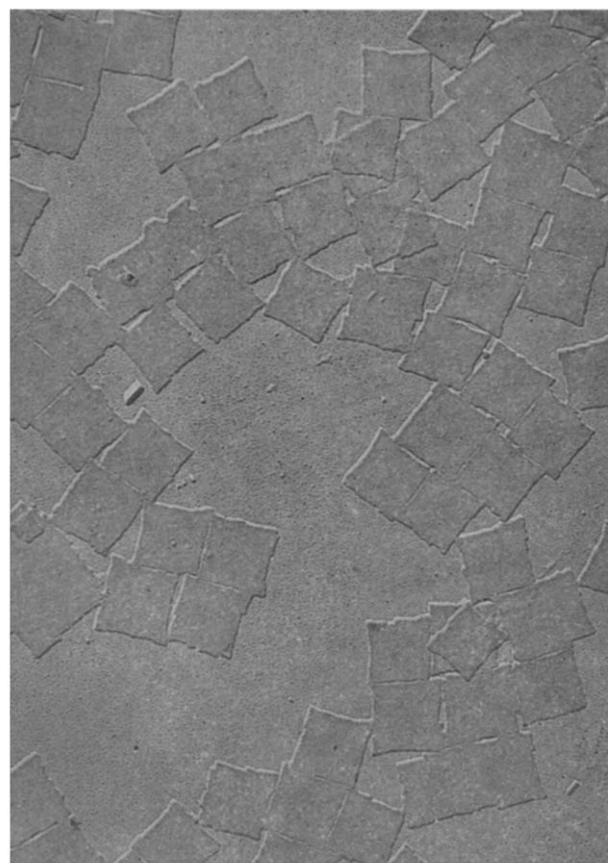


Figure 4 Electron micrograph of the PEO-PS monocystals (from B. Lotz)

with the theoretical curve. For example, the following interesting result has been derived from the best TMV preparation (it has been found by a classical light scattering experiment that L/λ is about $2/3$): at $\lambda_0 = 5460 \text{ \AA}$, $R = -6\%$ while at $\lambda_0 = 4360 \text{ \AA}$, $R = +8\%$. Changing the wavelength of the incident light leads to a positive value of R as predicted by the theory for such rods.

It is worth noting that the experimental and theoretical results are in fairly good agreement although the measured intensities are very small. The experimental accuracy lies between 10 and 20%, according to the values of L .

Aqueous suspensions of bentonite. Bentonite is a clay mineral⁵, the particles of which consist of stacks of sheets; thus, the scattering particles in water are thought to behave roughly like very oblate particles. The study of R would then provide a convenient means for the determination of the actual shape of the bentonite particles in aqueous suspensions.

These suspensions were dialysed and fractionated by successive centrifugations. Then we obtained roughly monodisperse products; from classical light scattering measurements, the 'diameter' D of these particles was found to be:

$$0.7 < \frac{D}{\lambda} < 0.8 \quad \text{or} \quad X \approx 3$$

Depending on the concentration of the suspensions, experimental values of R between $+40\%$ and 80% were found. The theoretical values of R relative to spheroids of the above dimension, the ellipticities p of which are between $\frac{1}{2}$ and 0, vary between $+50\%$ and $+100\%$. It may be noted that for prolate spheroids ($p > 2$) of

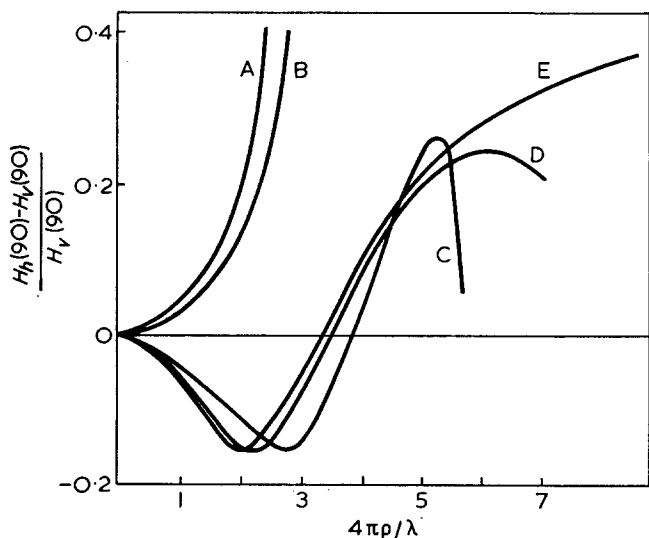


Figure 3 Theoretical variations of R for spheroids of various ellipticities, p . A, $p = \frac{1}{4}$; B, $p = \frac{1}{2}$; C, $p = 2$; D, $p = 3$; E, $p = 4$

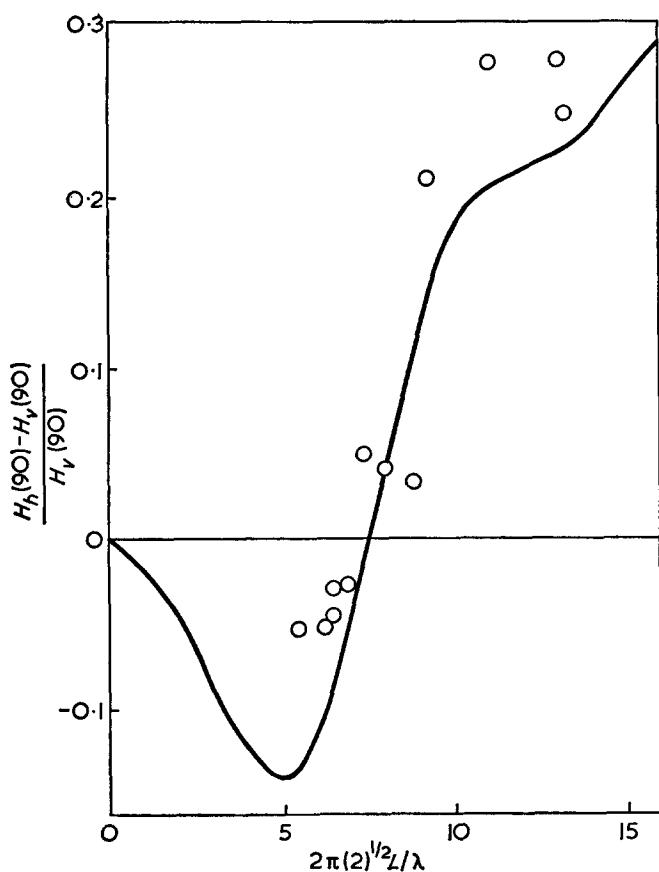


Figure 5 Theoretical (—) and experimental (○) variations of R for TMV fractions

the same dimension, R would have small negative values. Thus, by means of this new technique, it is shown that the colloidal aggregates of bentonite are flattened particles.

CONCLUSIONS

The potential of this new scattering technique as a tool for determining particle shape in a solution is clear from the above results. The method requires neither the knowledge of the optical anisotropy of the particles, nor the utilization of an orientation field force. This is also applicable to absorbing particles (another interesting example of this study related to particles of carbon black will be presented elsewhere). The experimental conditions for the measurements are rather difficult since the scattering volume is minimum for $\theta = \pi/2$ and the measurements are not made on a single intensity but on the difference of two weak intensities of comparable magnitude. Under these conditions, fairly good agreement between experimental and theoretical results is noteworthy.

REFERENCES

- 1 Ravey, J. C. *Eur. Polym. J.* 1972, **8**, 937
- 2 Ravey, J. C. *Eur. Polym. J.* 1973, **9**, 47
- 3 Ravey, J. C. *Eur. Polym. J.* 1973, **9**, 57
- 4 Wippler, C. and Scheibling, G. *J. Chim. Phys.* 1954, **51**, 201
- 5 Hofmann, U., Endell, K. and Wilm, D. *Z. Kristallogr.* 1933, **A85**, 340
- 6 Lotz, B., Kovacs, A. J., Bassett, G. A. and Keller, A. *Kolloid Z. Z. Polym.* 1966, **209**, 115

Morphology of cold-drawn high-density polyethylene fibres

W. G. Harland, M. M. Khadr and R. H. Peters

Department of Polymer and Fibre Science, University of Manchester Institute of Science and Technology, Manchester M60 1QD, UK

(Received 11 June 1973; revised 22 August 1973)

Drawn fibres of high-density polyethylene, and their crystalline residues obtained by nitric acid digestion of the amorphous phase, exhibit single- or double-peaked melting endotherms depending on the degree of crystallinity of the fibre, the draw ratio and, in the case of some of the crystalline residues, whether or not they have been melted once or twice. The melting behaviour of the drawn fibres and their crystalline residues has been accounted for in terms of the rupture of a fraction of the original lamellar structure and the growth of a new crystalline structure.

INTRODUCTION

There is a considerable amount of evidence to show that the process of cold drawing high-density polyethylene (HDPE) involves rupture of the original lamellar structure and the formation of a new crystalline microfibrillar structure¹⁻⁵. At some intermediate stage of drawing at least two different crystalline entities must co-exist and they would be expected to have different melting points; nevertheless drawn HDPE products with two or more melting points have not been reported. However, Meinel *et al.*^{3,6} have observed that the crystalline residues obtained from drawn HDPE film by removing the amorphous fraction with nitric acid yield endotherms with twin peaks when melted a second time; furthermore, the position on the temperature axis of one of the twin peaks was observed to change markedly as drawing proceeded. Twin melting peaks were not observed with undrawn and drawn parent films, with crystalline residues from undrawn film, or with crystalline residues from drawn film after a first melting.

Meinel and Peterlin attributed the low-temperature peak (*LTP*) to the presence of lamellae which had had their folds cut by the nitric acid treatment, and the high temperature peak (*HTP*) to the melting of a crystalline entity formed from tie molecules which had survived the nitric acid treatment. They argued that initially these two components of differing low molecular weight would constitute a molecular mixture and as such exhibit a single melting point, but would separate by a process of fractional crystallization during solidification after melting, and when remelted would exhibit separate melting points.

The validity of these arguments is dependent on tie molecules surviving the nitric acid treatment, for which the evidence is slender. Meinel and Peterlin⁶ considered that to a first approximation the elastic modulus of the acid-treated films should be proportional to the number of tie molecules. They claimed that for as long as the modulus could be measured, namely for up to 8 h

treatment with acid, the value was practically unchanged. After further acid treatment the specimens were too brittle to make measurements with. This evidence is not satisfactory in that their data show a decrease in modulus of 13% and, more significantly still, show that after 8 h treatment the weight loss was only 5 or 6% whereas the samples whose melting endotherms were under consideration were derived from film that had received 50 h acid treatment and suffered a weight loss equal to its amorphous content (about 25%).

The investigations of Meinel *et al.*^{3,6} were confined to two moulded samples of HDPE film, one of which had been slowly cooled and the other quench cooled to yield isotropic products of 75 and 68% crystallinity respectively. The absence of twin melting points in the endotherms of drawn film and uncertainty as to the identity of the two crystalline fractions giving rise to twin peaks in the melting endotherms of the crystalline residues, prompted the authors of this paper to conduct a similar investigation with samples of HDPE in a lower but overlapping range of initial degree of crystallinity, and with samples also differing in initial degree of orientation. Since these two parameters are difficult to vary with films the necessary samples were obtained by extrusion as fibres. It has been found that a fibre containing about 60% crystalline material (hereafter designated 60-fibre) gives, after drawing, a twin-peaked melting endotherm, while fibres of 67.5 and 70% crystallinity (67.5-fibre and 70-fibre) yield only single peaks. The crystalline residues derived from the 60-fibre (60-residues) yield twin peaks when melted or remelted, whereas the 67.5 and 70 residues have endotherms with twin peaks only when remelted. At very high draw ratios all fibres and crystalline residues have a single melting point. In addition to studying melting behaviour, the degree of crystallinity of the fibres and the molecular weight of the crystalline residues have been measured at various draw ratios.

The discovery that HDPE of lower degree of crystallinity than that used by Meinel *et al.*^{3,6} yields cold-

drawn products which have melting endotherms with twin peaks, and that the crystalline residues derived from these products exhibit endotherms with corresponding twin peaks during melting and remelting, has simplified the identification of the crystalline fractions responsible for the twin-peak phenomenon. Arguments are put forward to show that in the initial stages of drawing they are the torn-off blocks of folded chains and the original lamellae; the former constituting the *LTP* and the latter the *HTP*. As drawing proceeds both components undergo modification and the changes in melting characteristics of both fibres and residues are consistent with partial destruction of the original lamellae and formation of a new crystalline structure. While the conclusions as to the identity and origins of the crystalline fractions differ from those of Meinel and Peterlin⁶ they are in qualitative agreement with the accepted mechanism of deformation and with models proposed for the crystalline fibrillar structure of oriented polyethylene¹⁻⁵.

Notwithstanding the above conclusions, consideration has also been given to the possibility that the presence of twin melting points in endotherms obtained when crystalline residues are melted a second time is connected with the presence of buried chain folds in lamellae. It is possible that fractional crystallization would occur during solidification after a first melting and the endotherm of remelting would have multiple peaks corresponding to multiple traverses of the lamellae. However, twin melting peaks are not observed in undrawn HDPE or their corresponding crystalline residues, although Ward and Williams⁷ have obtained gel permeation chromatograms with multiple peaks from such residues. When the residues of drawn HDPE are investigated multiple peaks in melting endotherms are formed but not in gel permeation chromatograms. The two phenomena appear to be mutually exclusive.

EXPERIMENTAL

Polymer

Commercial HDPE (Code No. 65.045) was supplied by Shell Plastics Laboratory, Carrington. It had a viscosity-average molecular weight of 6.0×10^4 and a melt flow index of 4.5 g/10 min at 190°C.

Fibres

Fibres were extruded at 200°C from a rod-type spinning unit. The output rate was kept constant, but the wind-up velocity and the distance below the spinneret at which the fibres were quench-cooled in water was varied. Variation of these two parameters provided fibres of different degree of crystallinity and different birefringence as shown in *Table 2*.

Drawing procedure

Filaments (2 cm lengths) were drawn at 23°C and 0.5 cm/min on an Instron machine. Samples were drawn to their natural draw ratio and to draw ratios of 10, 15 and 20. The natural draw ratio was calculated as the ratio of the cross-sectional area of fibre in the relaxed state before and after drawing.

Oxidation with nitric acid

Samples of drawn and undrawn fibres were treated with 95% nitric acid at 80°C for 50 h. The residues were

Table 1 Crystalline content (%) from ΔH and nitric acid digestion

Draw ratio	70-fibre		60-fibre ($\Delta n=0.0016$)		60-fibre ($\Delta n=0.012$)	
	ΔH	HNO ₃	ΔH	HNO ₃	ΔH	HNO ₃
Undrawn	71	71	60	62	60	61
10	74	75	77	76	74	74
15	75	75	79	78	75	75
20	76	76	80	80	76	75
25	77	76	81	81	—	—

washed in water until free from acid, extracted with hot acetone for 4 h, and dried *in vacuo* at 60°C to constant weight. The main requirement of the nitric acid treatment is that it should be adequate to remove all the amorphous phase from a variety of fibres which differ in crystallinity and orientation. *Table 1* compares degree of crystallinity calculated from heat of fusion with percentage weight of residual material. The two sets of figures are very similar and, since those derived from residual weight are inflated slightly by the presence of terminal carboxyl groups, it follows that the duration of acid treatment was more than adequate.

Molecular weight of crystalline residues

Intrinsic viscosities were determined from decalin solutions at 120°C and viscosity-average molecular weights were calculated from the expression⁸:

$$[\eta] = 2.76 \times 10^{-4} (\bar{M}_v)^{0.78}$$

Values at different draw ratios are given in *Table 2*. Owing to the presence of buried and uncut chain folds the molecular weights give only a rough indication of fold length.

Melting endotherms

The endotherms were determined with a Perkin-Elmer differential calorimeter Model DSC-1. Samples of known weight (3–4 mg), were heated in dry nitrogen (18 ml/min) at a rate of 8°C/min. In the case of crystalline residues heating was continued to 10°C above the melting point and the sample was cooled in the instrument at 8°C/min. The thermogram for remelting was obtained from the newly crystallized sample with the same rate of heating as before. Percentage crystallinities were derived from heats of fusion and a value for crystalline polyethylene of 66 cal/g.

RESULTS AND DISCUSSION

Fibres

From a wide variety of experimental methods an impressive amount of evidence has been accumulated to show that cold drawing HDPE involves rupture of the original lamellar structure and the formation of crystalline microfibrils from small blocks of folded chains¹⁻⁵. The derivation by Meinel and Peterlin¹ of a differential work density curve from a true stress-strain curve is particularly informative since it clearly demonstrates the existence of two more or less simultaneous deformation mechanisms—destruction of the original lamellar structure and deformation of the new structure. It was proposed that the second process occurs by longitudinal slip of microfibrils which are

Table 2 Properties of fibres and crystalline residues

Draw ratio	70-fibre: (280) ^a (9.2) ^b (19.5) ^c (0.60) ^d			67.5-fibre: (260) ^a (6.8) ^b		
	Crystallinity ^e (%)	Δn^f	MW of residues	Crystallinity (%)	Δn	MW of residues
Undrawn	70.8	0.0015	1360	67.5	0.0018	1160
10	74.0	0.016	1500	75.2	0.029	1480
15	75.2	0.022	1540	76.8	0.039	1560
20	75.9	0.025	1610	77.9	0.040	1670
Rupture	77.9	—	—	—	—	—

Draw ratio	60-fibre(low Δn): (220) ^a (5.1) ^b (22.1) ^c (0.24) ^d			60-fibre(high Δn): (45) ^a (2.6) ^b (21.2) ^c (0.30) ^d		
	Crystallinity ^e (%)	Δn^f	MW of residues	Crystallinity (%)	Δn	MW of residues
Undrawn	60.4	0.0016	1000	60.0	0.012	1100
10	77.0	0.035	1640	74.0	0.032	1540
15	79.1	0.050	1740	74.8	0.044	1670
20	80.2	0.051	1750	76.0	0.046	1720
Rupture	81.3	—	—	80.2	—	—

^a Filament denier (g/9000m)

^b Natural draw ratio

^c Ultimate strength based on final denier (g/denier)

^d Ratio of nominal tenacities at yield and rupture

^e Derived from heats of fusion

^f Measured with a polarizing microscope and a calibrated quartz-wedge compensator

connected together by relatively few tie molecules. To this interpretation of the drawing process must be added changes which occur in total crystalline content and in fold length (Table 2). Nevertheless, it is not at variance with the established concepts to suggest that during drawing, segmental and molecular mobility are so enhanced that increases in degree of crystallinity and fold length may readily occur. The data in Table 2 suggest that the increase in crystallinity is largely accounted for by the increase in fold length. It is anticipated that increases in fold length may occur both in the remainder of the original lamellae and in the smaller blocks of folded chains. It should, however, be easier for fold length increases to occur in the latter since the co-operative movement of a smaller number of folds will be required.

The melting behaviour of the fibres and their crystalline residues must be related to morphological changes accompanying drawing. The melting endotherms of 60-fibres at their natural draw ratios (Figure 1) clearly show that a new crystalline species of lower melting point is being created. In order to explain the lower melting point it must be assumed that the size of the crystal units are less than in the original lamellae such that the surface free energy contribution to melting is increased, and/or the fold length has decreased. Estimates of crystal dimensions from the line broadening of wide-angle X-ray scattering, and calculations of crystal-thickness from the long period obtained by small-angle X-ray scattering show that both changes may occur during drawing⁹. The fraction of lower melting point is, therefore, identified with torn-off blocks from the original lamellae, and the fraction of higher melting point with the original lamellae.

As drawing proceeds both peak temperatures increase but that of the LTP increases the more rapidly (Figure 1). These changes are a reversal of those occurring in the initial stages of drawing and may be attributed to a differential rate of fold growth and aggregation of small crystals into larger units (fibrils) with a lower surface free energy. Owing to lack of resolution of the two peaks it is not clear whether the whole or only a part of the original lamellar structure is destroyed by drawing.

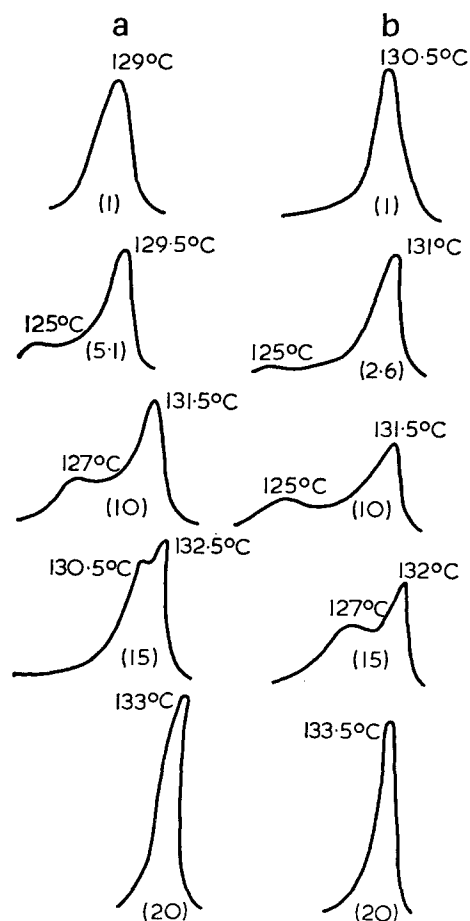


Figure 1 Melting endotherms of 60-fibres at draw ratios shown in parentheses. Δn undrawn state: (a) 0.0016; (b) 0.012. Peak temperatures indicated

Meinel and Peterlin¹ are of the opinion that with HDPE film destruction is complete at a draw ratio of about 10, but the fact that the height of the HTP is maintained up to draw ratios of at least 15 suggests otherwise for fibres. This view is supported by evidence derived from the endotherms of the crystalline residues which is discussed later.

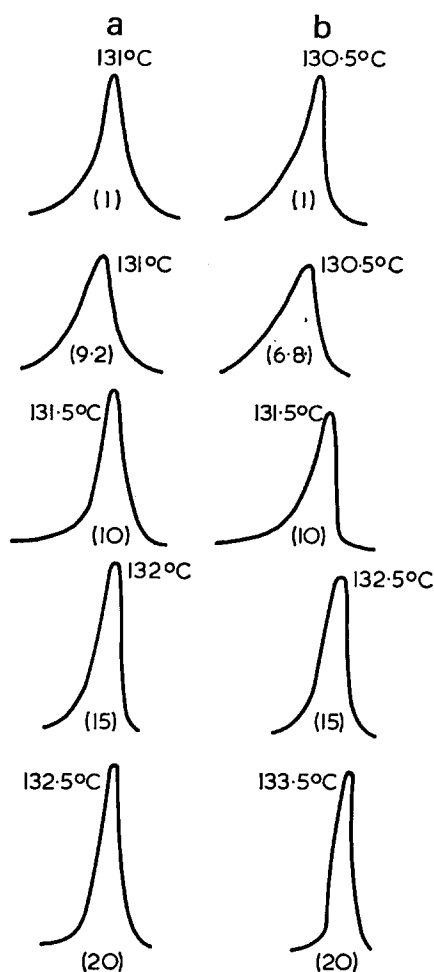


Figure 2 Melting endotherms of (a) 70-fibres and (b) 67.5-fibres at drawn ratios shown in parentheses. Δn undrawn state: (a) 0.0015; (b) 0.0018. Peak temperatures indicated

Drawn fibres of 67.5 and 70% crystallinity do not appear to have two melting points (Figure 2). Since there is no reason to suspect that a different deformation mechanism applies, the possibility that twin melting points exist at extents of deformation less than the natural draw ratio must be examined. There is no reason to expect equivalent structural changes to occur at equal extents of deformation in materials with different natural draw ratios. This situation arises first because drawing takes place in two stages—drawing to the natural draw ratio at a neck followed by uniform extension of the material which has already been drawn to its natural draw ratio, and secondly, because the rate of deformation, and hence the intensity of deformation, is enormously greater when drawing is proceeding at a neck. Thus at equal draw ratios different extents of morphological change are to be expected in 67.5-, 70-, and 60-fibres of low and high orientation, which have draw ratios of 9.2, 6.8, 5.1 and 2.6 respectively. In particular the significant morphological changes which give rise to twin melting endotherms appear at lower extents of deformation the higher the natural draw ratio. Furthermore, close inspection of Figure 2 shows evidence for the previous existence of twin melting peaks by the fact that the endotherms are wider for fibres at their natural draw ratio than they are for fibres in the undrawn state or at a draw ratio of 10. Between the undrawn state and the natural draw ratio

the widths of the peaks at half height increase from 1.5 to 2.1°C and 1.5 to 3.7°C for 70- and 67.5-fibres respectively. Thus there is no reason to suppose that the morphology and melting behaviour of the drawn versions of the fibres of relatively high crystallinity are in any way anomalous.

At high extents of drawing (Figures 1 and 2) only a single melting peak is observed for all fibres regardless of their original degree of crystallinity and orientation, which is consistent with the formation of a homogeneous fibrillar structure. It is interesting but not surprising that at ultimate elongation the fibres have the same melting point ($135^\circ \pm 0.5^\circ\text{C}$), a similar degree of crystallinity, and a similar tensile strength (Table 2). It is possible that if a much lower rate of drawing had been used differences would be even less.

Crystalline residues

Having established the identity of the two crystalline fractions responsible for the twin melting peaks of fibres, it is necessary to consider their relation to the melting endotherms of residues. By comparing Figures 1, 2 and 3 it may be seen that in terms of the existence of single or twin melting peaks at equal draw ratios, and after the first melting of the residues, the residues and fibres are strictly comparable. However, where twin peaks exist in fibres and residues there is a noticeable difference in the degree of resolution of the two peaks.

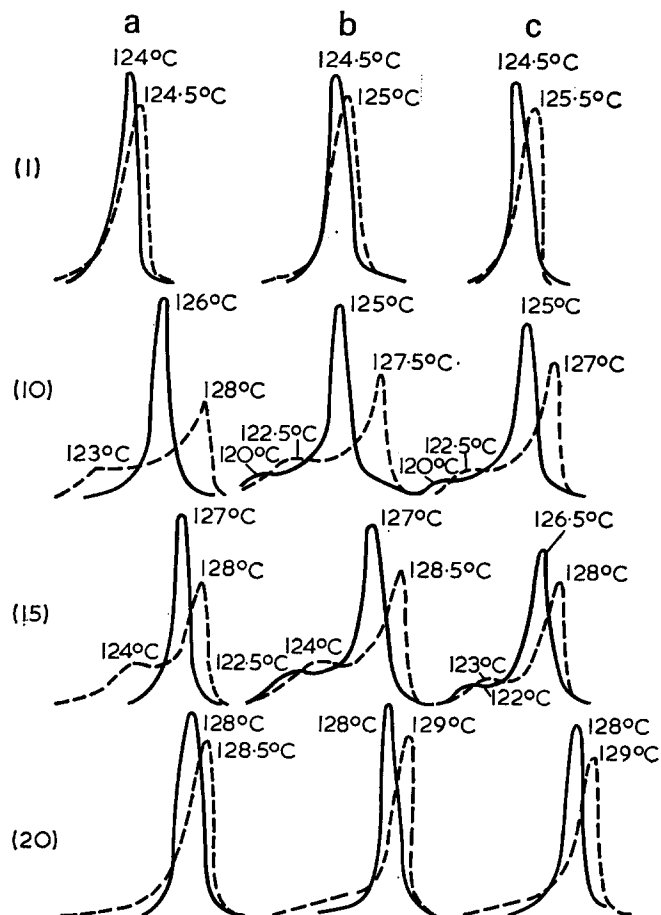


Figure 3 Melting endotherms of (a) 70-residues, (b) and (c) 60-residues. —, First melt; ---, second melt. Δn of undrawn parent fibre: (a) 0.0015; (b) 0.0016; (c) 0.012. Draw ratios of parent fibres shown in parentheses. Peak temperatures indicated

The resolution is far better at higher draw ratios in the residues than in the fibres. Such differences of detail are possibly the result of changes in morphology occurring during the course of heating fibre samples to determine their melting endotherms. In this connection Hosemann *et al.*^{10, 11} have commented on the susceptibility of the crystals of drawn fibre to thicken and give rise to a higher melting point practically independent of the original crystal thickness. In principle such changes cannot occur in the residues and it is concluded that the melting endotherms of the residues give a more realistic picture of the fibre morphology.

The first- and second-melting endotherms of the 60-residues are slightly different. After first melting and solidification both peak temperatures increase by about 2°C, the area of the *LTP* increases at the expense of the *HTP*, and the degree of crystallinity also falls by up to 5% as observed by Meinel and Peterlin⁶. These changes undoubtedly result from a more effective fractionation of the molecules during recrystallization and indicate that, while the two crystalline fractions produced by the drawing process have different melting points largely owing to differences of fold length in the fibres, differences in overall crystallite size also exist. It would appear that the first-melting endotherms of the residues give the best indication of the morphological changes brought about by drawing, but unfortunately, the relative peak areas cannot be resolved accurately. A rough visual estimate would suggest that about 30% of the lamellar structure of the 60-fibres has been degraded and about 20% in the case of the 60-fibre of higher initial orientation.

The endotherms of the 70-residues are more difficult to interpret; a single peak is obtained from the first melting and a double peak from the second melting. Identical behaviour has been described by Meinel and Peterlin⁶ for residues derived from drawn HDPE film. Their explanation, which has already been given in the introduction, is feasible if, as they claim, tie molecules and molecules derived from oxidized lamellae are involved in a fractional crystallization process during solidification following the first melting. Since this claim cannot be valid for 60-residues, which have double-peaked endotherms when first melted, and since there is no reason to suspect any radical difference between drawing 60, 67.5, and 70-fibres, their explanation is of doubtful validity. While the experimental data from this investigation offer no explanation for the phenomenon, it should be noted that geometrical differences between crystals give rise to different surface free energy contributions to melting and hence two crystalline fractions of different thickness may melt at the same temperature. Such an occurrence would, however, be fortuitous. Fortunately for present purposes an explanation is not essential.

The absence of twin melting peaks for 70-fibres (*Figure 2*) and for the first melting of 70-residue (*Figure 3*) makes estimation of the fraction of lamellar structure degraded during drawing difficult. Judged from a comparison of endotherms obtained during the second melting of 60 and 70-residues there does not appear to be any significant difference. However, these endotherms are not a reliable guide and if, as claimed by Meinel and Peterlin¹, HDPE with a crystalline content of more than 70% becomes less crystalline at extents of drawing below the natural draw ratio while polymer of less

than 70% crystallinity shows only an increase, it is a reasonable deduction that the fraction of lamellae degraded in the 70-fibres is somewhat greater than for the 60-fibres. Certainly there is no evidence for complete destruction of lamellar structure in fibres as has been suggested for drawn HDPE film.

According to Meinel and Peterlin¹ the destruction of the original lamellar structure is nearly completed at a draw ratio of about 10, and further deformation proceeds largely by longitudinal slip of newly formed microfibrils that are believed to be attached to one another by a small number of tie molecules which transverse quasi-amorphous boundary layers. While this mechanism may be consistent with the negligible changes which occur between draw ratios of 10 and 15 it does not assist in explaining the disappearance of the *LTP* at draw ratios between 15 and 20, which was not observed in the work of Meinel and Peterlin⁶ on drawn films. Another significant difference between the two investigations is that rupture of the films occurred at nominal stresses less than the yield stress, whereas rupture of the fibres occurred at nominal stresses appreciably greater than the yield stress (*Table 2*). The different behaviour of the fibres suggests that in their case a more coherent fibrillar structure is developed and undergoes further deformation by slipping of constituent blocks of folded chains until lateral cohesive strength is improved to the point where it equals that of the fibrils, or that of interfibrillar tie molecules, and the fibre ruptures. Such a mechanism would destroy the identity of the original crystalline blocks used to build the fibrils, and hence the crystalline phase would exhibit a single melting point.

The experimental data and deductions also have a bearing on the investigations of Ward and Williams⁷ into the distribution of buried chain folds in the lamellar structure of cold-drawn bulk polyethylene. Using gel permeation chromatography to elucidate the distribution of chain lengths in crystalline residues, they detected multiple peaks corresponding to multiple chain traverses in lamellae derived from branched polymer, but obtained a single broad distribution from residues of linear polyethylene. Since the twin melting peaks discussed in this paper have been attributed to the creation of two crystalline fractions of different thickness, it is interesting to question why they were not detected in the investigation of Ward and Williams. The reason is almost certainly because the residues of both fractions contain buried chain folds and hence have distributions of chain lengths which when combined overlap to produce a single-peaked broad distribution. The same concept also serves to explain the observation of Meinel and Peterlin⁶ that annealing residues just below their melting point removes the *LTP* and leaves a broad low-temperature tail in the endotherm; annealing would eliminate the chain folding and produce an imperfect chain-extended structure with a broad melting range.

Since the present work contains evidence that the extent of lamellar degradation incurred by drawing is less for 60-fibres than 70-fibres, it is probably much less still or even negligibly small, for cold-drawn branched polyethylene with a crystalline content of less than 50% and a much higher compliance. Therefore, the crystalline residues from cold-drawn low-density polymer and undrawn HDPE should have a distribution of molecular weight unconfounded with that of the crystals of a

second fraction of significantly different dimensions, as in fact observed by Ward and Williams⁷.

Ward and Williams concluded that the absence of multiple peaks in the crystalline residues of cold-drawn HDPE was the result of large fluctuations in crystal thickness⁷. It will be noted that the above explanation only differs in detail; it has been pursued to make it abundantly clear that twin peaks in melting endotherms do not have the same origin as the multiple peaks in the gel permeation chromatograms.

CONCLUSIONS

The appearance and disappearance of twin peaks in the melting endotherms of cold-drawn fibres of HDPE and in the melting endotherms of the corresponding residues obtained by removal of the amorphous phase by oxidation with nitric acid is consistent with a mechanism of drawing which involves degradation of a fraction of the original lamellar structure and the formation of a microfibrillar crystalline structure. The two crystalline fractions giving rise to the twin melting peaks are the

original lamellae and torn-off blocks of folded chains. In a fibre of 70% crystallinity and low orientation the extent of lamellar degradation is not more than about 40% and is less for fibres of lower crystallinity and higher orientation.

REFERENCES

- 1 Meinel, G. and Peterlin, A. *J. Polym. Sci. (A-2)* 1971, **9**, 67
- 2 Peterlin, A. in 'Man-Made Fibres' (Eds H. Mark, S. M. Atlas and C. Cernia), Interscience, New York, 1967, Vol 1, pp 283-340
- 3 Meinel, G., Morosoff, N. and Peterlin, A. *J. Polym. Sci. (A-2)* 1970, **8**, 1723
- 4 Hosemann, R. *J. Appl. Phys.* 1963, **34**, 25
- 5 Takayanagi, M., Imada, K. and Kajiyama, T. *J. Polym. Sci. (C)* 1966, **1**, 263
- 6 Meinel, G. and Peterlin, A. *J. Polym. Sci. (A-2)* 1968, **6**, 587
- 7 Ward, I. M. and Williams, T. *J. Macromol. Sci. (B)* 1971, **5**, 693
- 8 Duch, E. and Kuchler, B. *J. Electrochem. Soc.* 1956, **60**, 218
- 9 Glenz, W. and Peterlin, A. *J. Polym. Sci. (A-2)* 1971, **9**, 1243
- 10 Wilke, W., Vogel, W. and Hosemann, R. *Kolloid-Z. Z. Polym.* 1967, **237**, 317
- 11 Hosemann, R. and Wilke, W. *Makromol. Chem.* 1968, **118**, 230

Ziegler–Natta catalysis: 6. Effect of electron donors on the course of polymerization

D. R. Burfield

Department of Chemistry, University of Malaya, Kuala Lumpur, Malaysia

and P. J. T. Tait

Department of Chemistry, University of Manchester Institute of Science and Technology, Manchester M60 1QD, UK

(Received 23 July 1973; revised 4 September 1973)

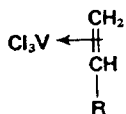
The activating effect of triethylamine in the VCl_3/AlR_3 system has been explained in terms of a previously proposed kinetic scheme. Activation is observed at low amine concentrations and is thought to occur by removal of adsorbed aluminium alkyl species from the catalyst surface. Deactivation occurs at higher donor concentrations and is believed to be due to competitive adsorption of donor with monomer. These proposals are consistent with the rate, molecular weight and polymer tacticity findings of other workers in Ziegler–Natta systems where the donor is capable of interaction with both the transition metal and metal alkyl components.

INTRODUCTION

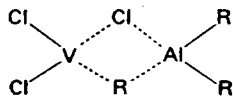
In the previous papers in this series^{1–5} the kinetics of the catalyst system VCl_3/AlR_3 for the polymerization of 4-methylpentene-1 have been described and interpreted in terms of a kinetic scheme in which propagation is considered to occur between an alkylated vanadium species and adsorbed monomer*. The effect of triethylamine on the course of polymerization is now reported, and the results are discussed in relation to the previously proposed scheme.

* The term adsorption, in this present study, has been used in the sense of chemisorption of species on to the catalyst surface, i.e. where chemical bonding of some description is involved. Thus only those species which are capable of a specific interaction with the active site are considered as adsorbed, any physisorption will be much weaker and is neglected.

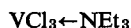
Thus the monomer is adsorbed through formation of a π -donor complex, e.g.



Aluminium alkyl species are adsorbed through bridge structures such as:



whereas triethylamine forms a strong σ -donor complex, e.g.



However, species such as Al_2R_6 , and $AlR_3 \cdot NEt_3$ are not considered to have any coordinating capacity, and thus will not be adsorbed. Monomeric adsorption is supported by Caunt^{3,2} and in the present system chain transfer with adsorbed monomeric metal alkyl has been demonstrated⁴.

The effect of electron donors in Ziegler–Natta polymerization has been extensively investigated and comprehensively reviewed^{6–9}. Electron donors are found to activate or deactivate the polymerization depending on the nature of the catalyst system and donor, and on the experimental conditions employed. Unambiguous interpretation of results is, however, often difficult as the donor may assume various roles in the polymerization. Thus in most systems, electron donors are capable of interaction with both the transition metal halide and the metal alkyl component. Boor¹⁰, in his extensive work on donor interactions, claims to circumvent this difficulty by the use of $ZnEt_2$ which he states is a weak acceptor and does not coordinate with donors. Boor thus interprets his findings on the basis of interaction with the transition metal alone. However, several complexes of zinc alkyls with donors such as ethers, tertiary amines, and pyridine have been reported¹¹, and although less stable than their aluminium analogues, are by no means completely dissociated in hydrocarbon solvents. Apart from this complication, correlation of Boor's results with the more conventional aluminium alkyl activated systems is not as straightforward as it might appear. Keii *et al.*¹² have shown that the activities of the $TiCl_3/AlEt_3$ and $TiCl_3/ZnEt_2$ catalyst systems for the polymerization of propylene are very different, and have gone as far as to suggest the presence of two types of active centre. Whether or not their conclusion is justified, it is clear from Boor's own work¹⁰ that the activity of the $AlEt_3$ based system is a factor of $100 \times$ greater than the comparable $ZnEt_2$ system. Whatever the reason for this difference in activity, the effect of interaction of the donor with the transition metal component may well be different, at least quantitatively in both cases.

In the present study the effect of a strong donor, triethylamine, which is capable of complex formation with both the transition metal and aluminium alkyl was investigated. The experiments were, however, designed so as to vary the extent of the interaction of the donor with the catalyst components in an attempt to distinguish the relative importance of both complex formation with the transition metal and complex formation with the aluminium alkyl.

EXPERIMENTAL

Reagents

Details of catalysts, and solvents have already been published².

4-Methylpentene-1 (4-MP-1). The monomer was kindly supplied by BP Chemicals Ltd, Sunbury, in a 99.6% pure state and was purified as previously described².

Triethylamine (Et₃N). This reagent was dried by refluxing over KOH and purified by subsequent fractionation. The fraction boiling at 89.0°C at 1 atmosphere ($\equiv 101.325 \text{ kN/m}^2$) was collected and stored over fresh KOH pellets under nitrogen in the dry box.

Bis(triethylamine) vanadium trichloride. This complex was prepared by a method analogous to that used by Fowles *et al.*¹³ for the preparation of bis(trimethylamine) vanadium trichloride. Vanadium trichloride was refluxed with a 12M excess of triethylamine for 5 h under nitrogen. The product, which was insoluble in Et₃N, was filtered off under an inert atmosphere, and evacuated for 10 h at 10⁻² mmHg to remove excess Et₃N. Elemental analysis of the dark brown product corresponded to a formula of VCl₃.O.42Et₃N, showing that only partial complex formation had been achieved.

Polymerization procedure

Polymerizations were carried out in a manner previously described². The order of addition of reaction components was, however, varied as indicated in the results section. Addition of triethylamine during the course of polymerization was accomplished by utilizing a specially constructed dilatometer with a side arm containing an ampoule of Et₃N sealed under vacuum. Benzene was used as solvent throughout this study.

RESULTS AND DISCUSSION

Effect of order of addition of Et₃N on course and rate of polymerization

Since the triethylamine can interact with both of the catalyst components, as well as with the alkylated sites, the order of addition of transition metal halide, aluminium alkyl, monomer, and Et₃N is likely to be important. The effect of varying the order of addition on the steady state rate of polymerization under standard conditions is shown in Table 1. As can be seen the triethylamine was added in three distinct orders which proved to be of significance, viz.:

VCl₃/Et₃N/4-MP-1/benzene/Al(iBu)₃ Order A

VCl₃/4-MP-1/Et₃N/benzene/Al(iBu)₃ Order B

VCl₃/4-MP-1/Al(iBu)₃/benzene/Et₃N Order C

It is immediately apparent that under these conditions Et₃N has an activating effect, and that the order of addition is important.

The course of polymerization in the presence of amine (orders A and B) is shown in Figure 1, and is seen to be analogous to that of the control polymerization, i.e. there is an initial settling period which is followed by a region during which the polymerization rate, corrected for decrease in monomer concentration, remains constant up to at least 55% conversion.

Rather surprisingly the key order of addition for catalyst activation is between monomer and amine rather than between aluminium alkyl and amine as might have been expected. Thus the rates of polymerization for orders B and C, where monomer was added prior to amine, are almost double that of order A, where amine was added first. Furthermore, the polymerization activity is almost identical for orders B and C where the order of addition of amine and metal alkyl was

Table 1 Effect of order of addition of components on rate of polymerization
[4-MP-1]=2.00 mol/l; [VCl₃]=18.5 mmol/l; [Al(iBu)₃]=37.0 mmol/l; [Et₃N]=18.5 mmol/l (except for control runs); temperature=30°C

Order of addition		$R_p/[VCl_3]$ (mol/l min [VCl ₃])
Control*	VCl ₃ /Al(iBu) ₃ /Benzene/4-MP-1	0.271
Control	VCl ₃ /4-MP-1/Benzene/Al(iBu) ₃	0.274
A	VCl ₃ /Et ₃ N/4-MP-1/Benzene/Al(iBu) ₃	0.292
B	VCl ₃ /4-MP-1/Et ₃ N/Benzene/Al(iBu) ₃	0.468
C	VCl ₃ /4-MP-1/Al(iBu) ₃ /Benzene/Et ₃ N	0.467

* Catalyst components aged for 30 min at 30°C and the monomer distilled in

N.B. As used throughout this paper, R_p refers to the steady state rate of polymerization corrected for depletion in monomer concentration

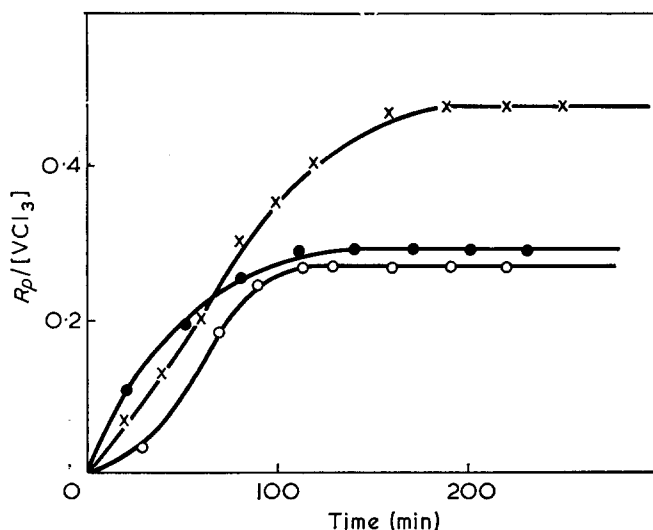


Figure 1 Dependence of rate of polymerization on addition of Et₃N. [4-MP-1]=2.00 mol/l; [VCl₃]=18.5 mmol/l; [Al(iBu)₃]=37.0 mmol/l; temperature = 30°C. ○, Control polymerization: [Et₃N]=18.5 mmol/l; ●, order of addition A; ×, order of addition B

varied, the monomer having been added beforehand. These observations seem to suggest that there must be some specific interaction between the monomer and VCl_3 surface which is a prerequisite to active site formation. This preliminary monomer interaction, and consequently the number of active centres formed, would be expected to be reduced in the case of prior Et_3N addition, as this donor is known to be strongly adsorbed⁷.

The importance of the order of addition of catalyst components in 3-component catalyst systems has already been noted. Hence Vesely *et al.*¹⁴ show that the deactivating effect of H_2O on the catalyst system $TiCl_3/AlEt_3$ for the polymerization of propylene is most pronounced when the H_2O is allowed to interact preferentially with the $TiCl_3$. This interaction leads to both rate lowering and an increased settling period. Chirkov *et al.*¹⁵ whilst reporting somewhat different findings for the same system again show that the order of addition of catalyst components is critical. (The results of Keii *et al.*¹⁶ with $SeOCl_2$ as donor are analogous to those of Vesely *et al.*)

The order of addition of monomer and $Al(iBu)_3$ in the absence of additive is seen to be unimportant as far as the overall rate is concerned, which suggests that $Al(iBu)_3$ is neither irreversibly nor very strongly adsorbed at sites used for monomer coordination, and is in keeping with previous results⁴ where the adsorption constant (K_A) for $Al(iBu)_3$ on VCl_3 was found to be 5.12 l/mol at $30^\circ C$.

In 2-component catalyst systems little attention has been paid to the pretreatment of the transition metal component with monomer, probably because metal alkyl is usually added first to scavenge impurities. A notable exception is the study by Keii *et al.*¹⁷, which, in contradistinction to the present study, demonstrated that higher rates could be obtained by the addition of propylene to $TiCl_3$ prior to the introduction of $AlEt_3$. (It is noteworthy that $AlEt_3$ is very much more strongly adsorbed than $Al(iBu)_3$ ⁴, and it is probable that the order of addition of monomer and aluminium alkyl is consequently critical, as is the case with strong donors such as Et_3N .) The kinetics of the polymerization in the initial region were also changed, the rate being first order with respect to monomer in the former case but becoming second order when $AlEt_3$ was added first. The importance of monomer in active site formation was also shown by their observation that the removal of supernatant $AlEt_3$ from the catalyst system had little effect on the rate, providing that monomer had been introduced beforehand. Further, it has been shown that the number of active centres in the present system is reduced at low monomer concentrations⁴. All these findings, together with those of McCarty *et al.*¹⁸ and Overberger *et al.*¹⁹, emphasize the importance of monomer in active site formation, which will be discussed further in a subsequent publication²⁰.

Effect of variation of $[Et_3N]$ on rate of polymerization

The effect of variation of donor concentration on the rate of polymerization was examined over a limited range for both orders of addition A and B. The results are summarized in Table 2.

In the case where Et_3N is added prior to the monomer (order A) the polymerization rate was reduced when $[Et_3N]:[Al(iBu)_3]=0.25$. This reduction was followed by slight activation as the ratio is increased to 0.5.

Table 2 Dependence of rate of polymerization on triethylamine concentration
[4-MP-1]=2.00 mol/l; $[VCl_3]=18.5$ mmol/l; $[Al(iBu)_3]=37.0$ mmol/l; temperature= $30^\circ C$

Order of addition	$[Et_3N]$ (mmol/l)	$\frac{[Et_3N]}{[Al(iBu)_3]}$	$R_p/[VCl_3]$ (mol/l min $[VCl_3]$)
A	9.3	0.25	0.240
A	18.5	0.50	0.292
A	37.0	1.00	0.00023
B	9.3	0.25	0.423
B	18.5	0.50	0.468
B	27.8	0.75	0.684
Control	—	—	0.271

These findings are somewhat analogous to those of Boor¹⁰ for the system $ZnEt_2/TiCl_3/Et_3N$ /propylene (in this order of addition), where amine is added prior to monomer introduction. At equimolar proportions of Et_3N and $Al(iBu)_3$ the steady state rate is, however, reduced by a factor of 1000. This result is comparable to the findings of other workers, in systems where strong amine coordination with the metal alkyl occurs, who observe no, or very slow, polymerization when the amine is present in excess of the metal alkyl concentration^{14, 21-24}, but is in contrast to the results of Boor¹⁰ for $ZnEt_2$, which indicated that catalytic activity was maintained even in the presence of excess donor. The decrease in rate is thus most likely associated with complex formation of the aluminium alkyl which is complete in the presence of excess amine²⁵. It seems likely that alkylation of the transition metal is dependent on the presence of uncomplexed monomeric metal alkyl, which is likely to be the case with the $ZnEt_2$ catalyst even in the presence of excess amine, since the zinc donor complexes are weaker than the analogous aluminium compounds.

Polymerization in the presence of equimolar proportions of Et_3N and $Al(iBu)_3$ is quite distinct from that previously described, as is shown in Figure 2. The polymerization rate increases to a maximum within 2 h and subsequently decreases over the next 200 h by a factor of about 12, after which the reaction continues at a slow but constant rate for at least a further 600 h. At the same time it was observed that the supernatant liquid, when the stirrer was stopped and the catalyst allowed to settle, was a light brown colour as distinct from colourless which is usually the case. This is suggestive of the formation of soluble vanadium species in the reaction mixture. It consequently seemed possible that the complex form of the rate curve might be due to the presence of two distinct systems, viz. a heterogeneous polymerization of steady rate and a homogeneous polymerization of decaying rate. Detailed analysis of the rate curve supports this hypothesis.

The kinetics of a related soluble catalyst system have been studied²⁶ and a rapid decrease in the rate of polymerization as a function of time was observed. The rate curve was found to fit equations of the form:

$$R_0/R_t = C_0 k_a t + 1 \quad (1)$$

and

$$\ln([M]_0/[M]_t) = (k_p/k_a) \ln(k_a C_0 t + 1) \quad (2)$$

where R_0 and R_t are the rates of the polymerization at $t=0$ and $t=t$ respectively, k_a is the second order decay

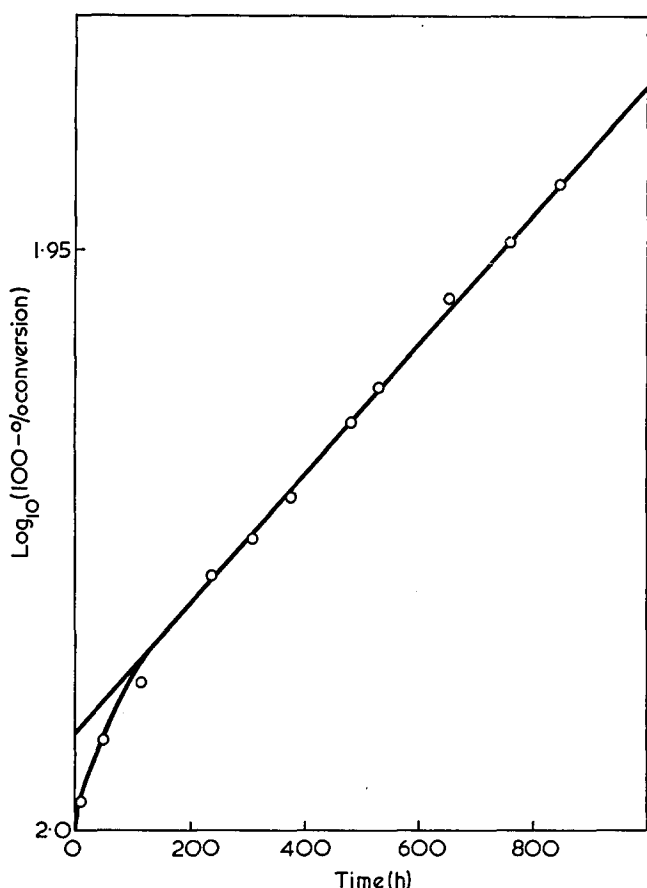


Figure 2 Plot of $\log_{10}(100-\% \text{ conversion})$ versus time. $[4\text{-MP-1}] = 2.00 \text{ mol/l}$; $[\text{VCl}_3] = 18.5 \text{ mmol/l}$; $[\text{Al}(\text{iBu})_3] = 37.0 \text{ mmol/l}$; $[\text{NEt}_3] = 37.0 \text{ mmol/l}$; order of addition A; temperature = 30°C

constant, k_p is the propagation rate constant, and C_0 is the active centre concentration.

In the present case the overall rate of polymerization, at time t is given by:

$$R_t(\text{total}) = R_t(\text{homogeneous}) + R_t(\text{heterogeneous}) \quad (3)$$

In order to separate these two terms it is necessary to assume that the rate of the heterogeneous polymerization reaches a constant value within 2 h (as is normally the case) and is equal in magnitude to the final steady state rate, which was reached after 200 h, when the rate of the homogeneous polymerization is assumed to have decayed to zero.

Plots of $(R_0/R_t) - 1$ vs. time and $\log M_0/M_t$ vs. $\log(k_d C_0 t + 1)$ are shown in Figures 3 and 4 respectively, and are seen to be linear with slopes of $3.98 \times 10^{-3} \text{ min}^{-1}$ and 4.50×10^{-3} which correspond to a value of $k_p C_0 = 1.80 \times 10^{-5} \text{ min}^{-1}$. It is not, however, possible using the present data to separate the k_p and C_0 terms.

It should be emphasized that this phenomenon of a decaying rate, and coloration of the reaction mixture is not observed at 30°C in the absence of additive, or in the presence of additive where the molar ratio of $[\text{NEt}_3]:[\text{Al}(\text{iBu})_3]$ is less than one. (Deactivation has been observed at higher temperatures in the absence of additive but does not follow second order kinetics.) Consequently it is considered that soluble vanadium species are only formed in the presence of excess amine, since at lower concentrations most of the amine will be used up in complex formation of the aluminium alkyl and little extensive interaction with the VCl_3 surface will occur.

This polymerization is also of interest because it demonstrates that after the initial rate decay, the rate of the heterogeneous polymerization remains constant over an extended period (600 h).

For order B the steady state rate is seen to be increased significantly, even at low amine concentrations, when compared with that of the control experiment. This is in contrast to the behaviour obtained for order A, where the steady state rate is initially reduced. This difference in behaviour between orders A and B again emphasizes the importance of the monomer-transition metal interaction. The lower rates for the order of addition A is thought to be due to a reduction in the number of active centres when the amine is added prior to the monomer. The significance of the rate activation is discussed later in this paper. It is believed that the same mechanism of activation is operative in both systems but that this is not so apparent for order A, as the rate is simultaneously lowered by reduction of active site concentration.

Polymerization activity of $\text{VCl}_3 \cdot 0.42\text{NEt}_3$ complex

The amine complex was found to be completely inactive (less than $2 \times 10^{-3}\%$ conversion in 50 h) for the polymerization of 4-MP-1 in the absence of metal alkyl at both 30 and 60°C in contrast to the metal alkyl free (MAF) systems reported by Boor. In the presence of $\text{Al}(\text{iBu})_3$ polymerization occurs, the course of which (Figure 5) is analogous to that found in the system (order A) where equimolar proportions of amine

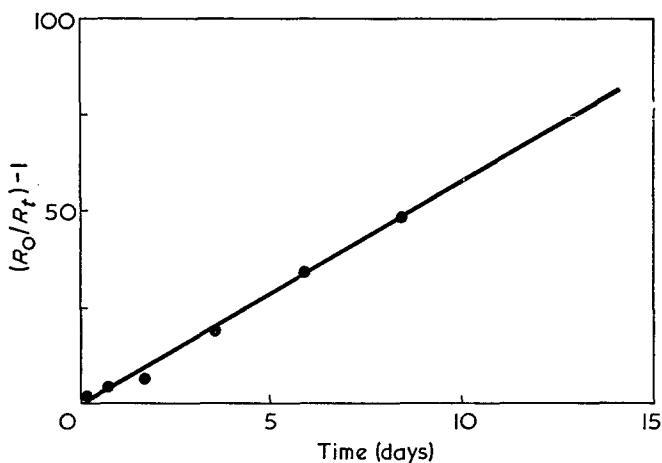


Figure 3 Plot of $(R_0/R_t) - 1$ versus time. Experimental conditions as for Figure 2

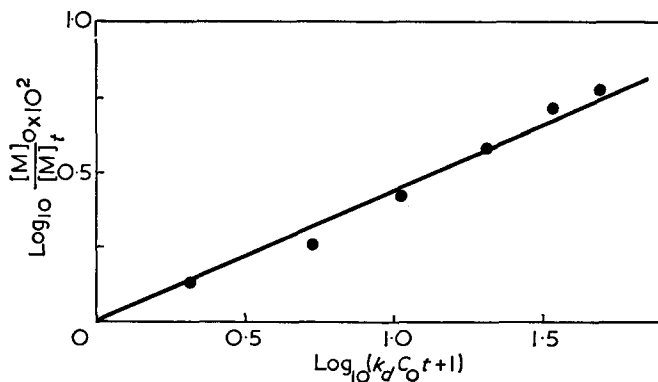


Figure 4 Plot of $\log_{10}([M]_0/[M]_t)$ versus $\log_{10}(k_d C_0 t + 1)$. Experimental conditions as for Figure 2

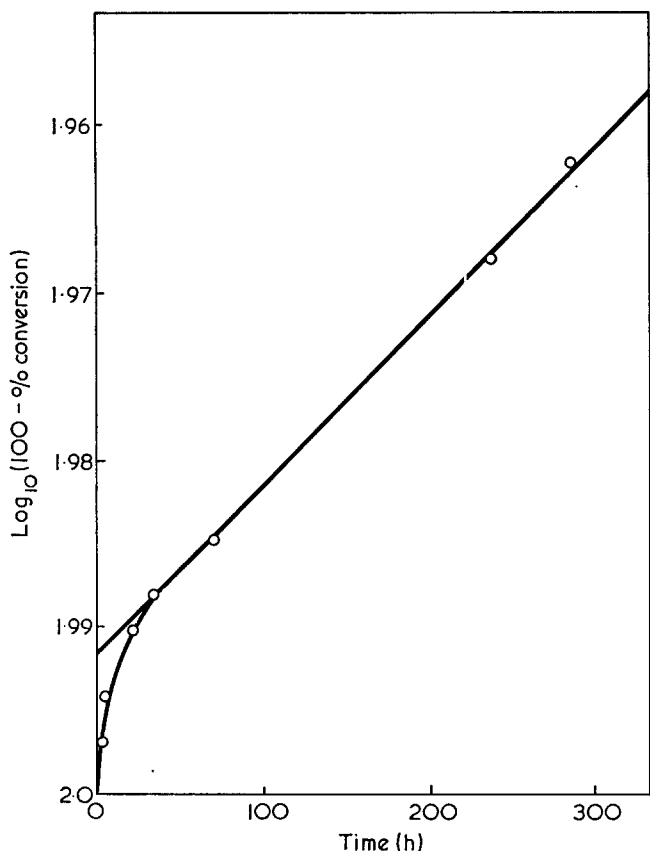


Figure 5 Plot of $\log_{10}(100-\% \text{ conversion})$ versus time for amine complex. $[4\text{-MP-1}] = 2.0 \text{ mol/l}$; $[\text{VCl}_3 \cdot 0.42\text{NEt}_3] = 30.0 \text{ mmol/l}$; $[\text{Al}(\text{iBu})_3] = 37.0 \text{ mmol/l}$; temperature = 30°C

and metal alkyl were used. Thus the initial rate decreases by a factor of about 11 to a steady rate, the value of which ($2.5 \times 10^{-4} \text{ mol/lmin} [\text{VCl}_3]$) was the same as that obtained in the former case within experimental error.

Chirkov *et al.*²⁷ similarly showed that the complex $\text{TiCl}_3 \cdot 0.42\text{Et}_2\text{NH}$ was an active catalyst for the polymerization of propylene in the presence of excess AlEt_3 . It was less active at 30°C than the unmodified system, and the overall activation energy was much higher at 23 kcal/mol (96.1 kJ/mol) compared with 11.6 kcal/mol (48.5 kJ/mol) for TiCl_3 alone. They concluded that the complex was fully stable and that the amine was not removed from the surface by interaction with the AlEt_3 since the rate remained constant throughout the course of the polymerization. Their findings, however, are not completely conclusive as it is possible that removal of amine could occur very rapidly during the mixing of the catalyst components and before the onset of polymerization. (Such a rapid equilibrium is demonstrated in the following section.)

The present results suggest that where extensive interaction occurs between Et_3N and VCl_3 the effect is to deactivate rather than activate the catalyst, either by blocking the sites for monomer coordination or by prevention of active centre formation or both. It is believed that excess metal alkyl must be present to ensure removal of the amine from the surface, followed by subsequent alkylation to give an active system.

Effect of Et_3N addition during polymerization on rate of polymerization

Triethylamine was added to the reaction mixture during the course of polymerization after the attainment

of a steady rate, and therefore after attainment of a constant number of active centres (Figure 6). The effect of the addition of varying amounts of Et_3N is shown in Figure 7.

It can be seen that the rate activation is similar in magnitude to that observed when amine is added at the onset of polymerization (order B). Therefore it seems likely that the basic action of the amine is the same in both cases. However, in this case of activation the new steady state rate is achieved rapidly within about 3–4 min of the addition, whereas (for order B) initial site formation and chain initiation is complete only after about 100 min. Since this amine activation is a much faster process than the initial formation of sites active in polymerization, it is unlikely that these processes are identical. Consequently, these findings are not compatible with the proposals that activation is due to an increase in the number of active centres caused by further breakdown of the crystal lattice^{7, 24, 28, 29}, or by

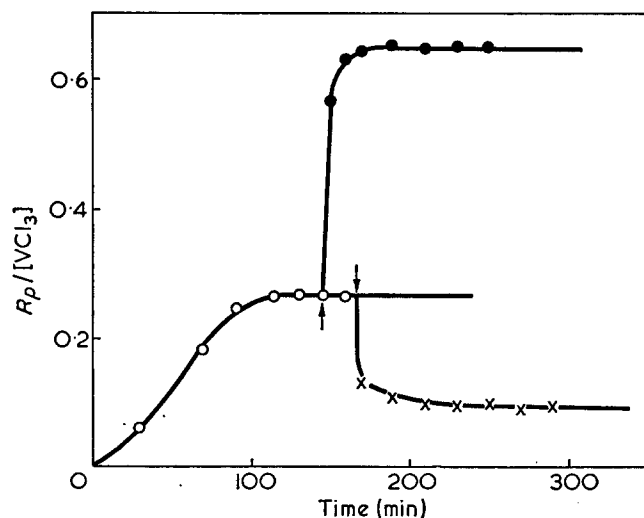


Figure 6 Effect of amine additions during course of polymerization. $[4\text{-MP-1}] = 2.00 \text{ mol/l}$; $[\text{VCl}_3] = 18.5 \text{ mmol/l}$; $[\text{Al}(\text{iBu})_3] = 37.0 \text{ mmol/l}$; temperature = 30°C . \circ , Control polymerization. Polymerization after addition of triethylamine: \bullet , $[\text{NEt}_3] = 18.5 \text{ mmol/l}$; \times , $[\text{NEt}_3] = 34.3 \text{ mmol/l}$. \downarrow denotes addition of donor

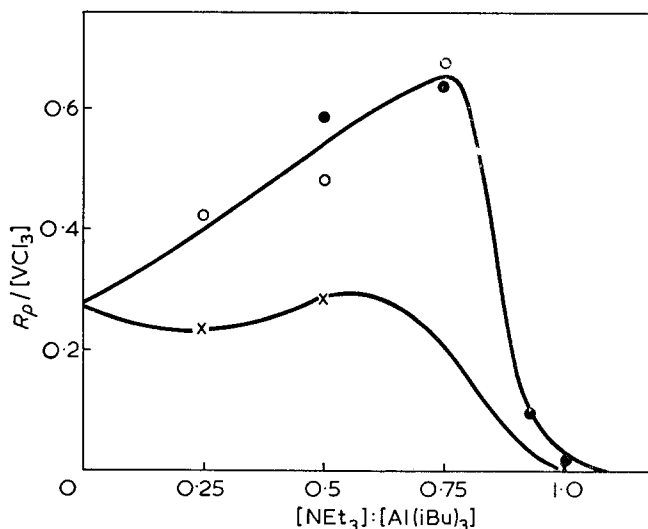


Figure 7 Plot of $R_p/[\text{VCl}_3]$ versus $[\text{NEt}_3]:[\text{Al}(\text{iBu})_3]$ ratio for different orders of addition of donor. $[4\text{-MP-1}] = 2.00 \text{ mol/l}$; $[\text{VCl}_3] = 18.5 \text{ mmol/l}$; $[\text{Al}(\text{iBu})_3] = 37.0 \text{ mmol/l}$; temperature = 30°C . \times , Order of addition A; \circ , order of addition B; \bullet , donor added during polymerization

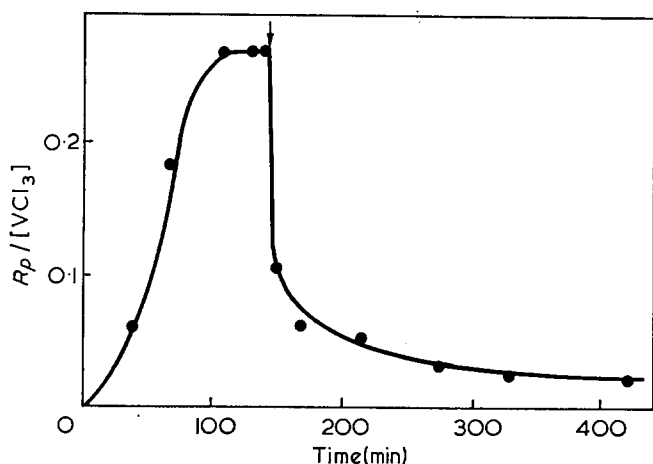


Figure 8 Plot of $R_p/[VCl_3]$ versus time. [4-MP-1]=2.00 mol/l; $[VCl_3]=18.5$ mmol/l; $[Al(iBu)_3]=37.0$ mmol/l; $[NEt_3]=37.0$ mmol/l; temperature=30°C. ↓ denotes addition of triethylamine

Table 3 Dependence of rate of polymerization on triethylamine added during the course of polymerization [4-MP-1]=2.00 mol/l; $[VCl_3]=18.5$ mmol/l; $[Al(iBu)_3]=37.0$ mmol/l; temperature=30°C

$R_p/[VCl_3]$	[Et ₃ N] (mmol/l)	[Et ₃ N]		R_p^* [VCl ₃]	R_p^\dagger [VCl ₃]
		[Al(iBu) ₃]	[VCl ₃]		
0.270	18.5	0.50	—	—	0.558
0.270	27.8	0.75	—	—	0.641
0.270	34.3	0.93	—	—	0.102
0.270	37.0	1.00	0.0443	—	—
0.270	56.0	1.50	0.00735	—	—
0.270	74.0	2.00	0.00413	—	—
0.270	93.0	2.50	0.00273	—	—

* Rate measured 120 min after addition of Et₃N

† Steady state rate after addition of Et₃N

increased site forming capacity of the metal alkyl in the presence of amine^{22, 23}.

At $[Et_3N]:[Al(iBu)_3] \geq 1$, the rate of polymerization is immediately reduced when amine is added during the course of polymerization (Figure 8). This initial rapid rate reduction is followed by a further slow deactivation analogous to that observed for order A when equimolar proportions of amine and metal alkyl were used. Therefore in the presence of excess amine it appears that extensive interaction with the VCl_3 surface must occur leading to solubilization of part of the propagating active sites. It was not possible to measure accurately the final steady state rate due to the very low activity of these polymerizations, but the polymerization rate 210 min after the amine addition is recorded in Table 3. The final steady state rate was approximately $\times 7$ lower than this recorded rate, and was reached after about 200 h.

It has already been proposed¹ that the polymerization is governed by adsorption equilibria, and typically that the overall rate of polymerization (R_p) is given by:

$$R_p = k_p \theta_M C_0 \quad (4)$$

where θ_M is given by:

$$\theta_M = \frac{K_M[M]}{1 + K_M[M] + K_A[A] + K_D[D]} \quad (5)$$

in the presence of an additive D, assuming that only monomeric species are adsorbed. The addition of donors

capable of interaction with either or both of the catalytic components will affect the value of θ_M , the actual magnitude of the effect being governed by the various equilibria present.

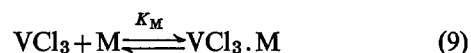
In order to quantitatively account for both the activating and deactivating effects of Et₃N in the present system, it is necessary to consider the interactions and the equilibrium reactions which may be involved. Tertiary amines are known to form strong complexes with aluminium alkyls^{30, 31} and thus the following equilibrium reaction may be important:



The 'free' uncomplexed NEt_3 can also be adsorbed on to the VCl_3 surface:



$Al(iBu)_3$ and monomer can similarly be adsorbed:



Hence, θ_M will be given by equation (5).

As the surface area of the VCl_3 used in this study is low (2.3 m²/g), complete coverage by any one component requires only about 10^{-3} mol of component/mol VCl_3 , and consequently the bulk concentration of any component will be little changed by adsorption and hence any such change may be neglected.

When the metal alkyl is in excess of the Et₃N, then there will be little free Et₃N. In addition, the concentration of free metal alkyl will be reduced, as will its adsorption on to VCl_3 . Hence the value of θ_M will increase and activation will be observed.

On the other hand, when amine is in excess, although the $K_A[A]$ term will be largely removed from the denominator of θ_M , free amine is now present and will be strongly adsorbed and equation (5) becomes:

$$\theta_M = \frac{K_M[M]}{1 + K_M[M] + K_D[D]_F} \quad (10)$$

and deactivation is predicted. Combining equation (10) with equation (4) yields:

$$R_p = \frac{k_p C_0 K_M [M]}{1 + K_M [M] + K_D [D]_F} \quad (11)$$

where $[D]_F$ is the concentration of free uncomplexed amine. Assuming that the metal alkyl is fully complexed it is possible to write:

$$[D]_F = [D]_{total} - [A] \quad (12)$$

Inverting equation (11) gives rise to:

$$1/R_p = \frac{1 + K_M[M] + K_D[D]_F}{k_p C_0 K_M [M]} \quad (13)$$

If $k_p C_0$ remains constant as $[D]$ is varied, a plot of $1/R_p$ versus $[D]$ should therefore be linear with positive intercept. Certainly the value of $k_p C_0$ is different from that observed when $[NEt_3]:[Al(iBu)_3] < 1$ as rate decay is observed and solubilization of active sites has been postulated. However, it is felt that within this particular set of polymerizations, at a constant reaction time (in this case 210 min), $k_p C_0$ may be taken to be constant.

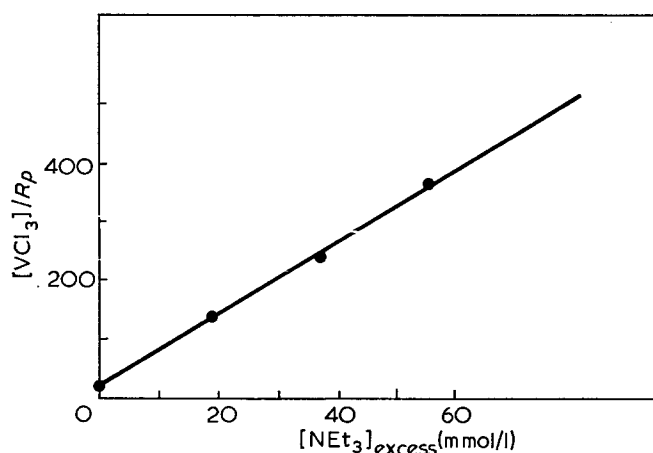


Figure 9 Plot of $[VCl_3]/R_p$ versus $[NEt_3]_{\text{excess}}$. $[4\text{-MP-1}] = 2.00$ mol/l; $[VCl_3] = 18.5$ mmol/l; $[Al(iBu)_3] = 37.0$ mmol/l; temperature = 30°C

This assumption seems to be justified by the linear plot obtained (Figure 9).

From the ratio of slope/intercept, and using a previously determined value⁴ of K_M , a value of $K_D = 360$ l/mol is found*. The triethylamine is seen to be very strongly adsorbed compared to $Al(iBu)_3$ ($K_A = 5.2$ l/mol). Thus the very marked deactivation observed when the amine concentration is slightly increased from 27.8 to 34.3 mmol/l is predictable, as a small concentration of free amine will have a large effect. Figure 7 is somewhat analogous to a titration curve. The equivalence point is, however, nearer to 33 than 37 mmol/l, as should be the case. This discrepancy is probably due to a combination of factors leading to a reduction in the $Al(iBu)_3$ concentration; consumption in alkylation and scavenging reactions, dissociation of the amine-metal alkyl complex, initial purity of the $Al(iBu)_3$, and experimental errors in measurement of the amine and metal alkyl concentrations.

The postulate that metal alkyl is reversibly adsorbed on to the transition metal surface, and that the polymerization rate is governed by such adsorption equilibria has also been demonstrated by Caunt³² and Kern *et al.*³³, who have shown that in the polymerization of propylene by the catalyst system $TiCl_3/AlEt_2Cl$, the addition of $AlEtCl_2$ during the course of polymerization has a rate lowering effect identical to that obtained when $AlEtCl_2$ is present in the initial catalyst mixture. The rate decrease is found to be readily reversed by addition of further $AlEt_2Cl$ or $AlEt_3$. It appears therefore that the rate lowering is explicable in terms of adsorption equilibria rather than in terms of changes in numbers of active centres. Caunt has concluded that $AlEtCl_2$ acts as an inhibitor by adsorption on to the catalyst surface, a proposal which is consistent with our present proposals.

In addition, however, $AlEt_2Cl$ (activator) may also be considered to be an inhibitor, since it too will be adsorbed, albeit less strongly than $AlEtCl_2$ and this adsorption will lead to a consequent reduction in θ_M . It can be shown that this hypothesis is in keeping with the results obtained by Caunt³². For provided that

* It should be noted that the K_M , K_A and K_D values quoted in this series are calculated with respect to factors affected by adsorption at the active centre. Consequently, the values so obtained may not be the same as those relating to adsorption on unreacted VCl_3 crystal surfaces.

the $TiCl_3/AlEt_2Cl$ /propylene system can also be described in terms of the adsorption equilibria established for the $VCl_3/Al(iBu)_3/4\text{-MP-1}$ system, θ_M is now given by:

$$\theta_M = \frac{K_M[M]}{1 + K_M[M] + K'_A[AlEt_2Cl] + K''_A[AlEtCl_2]} \quad (14)$$

Caunt has shown that in the presence of excess activator his polymerization data are consistent with the equation:

$$[AlEtCl_2] \approx K \frac{[Al_2Et_2Cl_4]}{[Al_2Et_4Cl_2]^{1/2}} \quad (15)$$

and also that:

$$[AlEt_2Cl] = K_1[Al_2Et_4Cl_2]^{1/2} \quad (16)$$

Therefore from equations (4), (14), (15) and (16):

$$\frac{1}{R_p} = \frac{1}{k_p C_0} \times \left[\frac{1 + K_M[M] + K'_A K_1^{1/2} [Al_2Et_4Cl_2]^{1/2} + \frac{K''_A K [Al_2Et_2Cl_4]}{[Al_2Et_4Cl_2]^{1/2}}}{K_M[M]} \right] \quad (17)$$

Hence if $[Al_2Et_4Cl_2]$ is kept constant, and $[Al_2Et_2Cl_4]$ is varied, a plot of $1/R_p$ versus $[Al_2Et_2Cl_4]$ should be linear with a positive intercept. Using the initial rate data of Caunt³² the plot in Figure 10 is obtained, which is in excellent agreement with the above derivation. Unfortunately, the dependence on $[AlEt_2Cl]$ cannot be tested with the data available in the above reference.

Kern *et al.*³³ have shown that the relative rates in the polymerization of propylene with the catalyst systems $TiCl_3/AlEt_xCl_{(3-x)}$ is as follows: $AlEt_3 : AlEt_2Cl :$

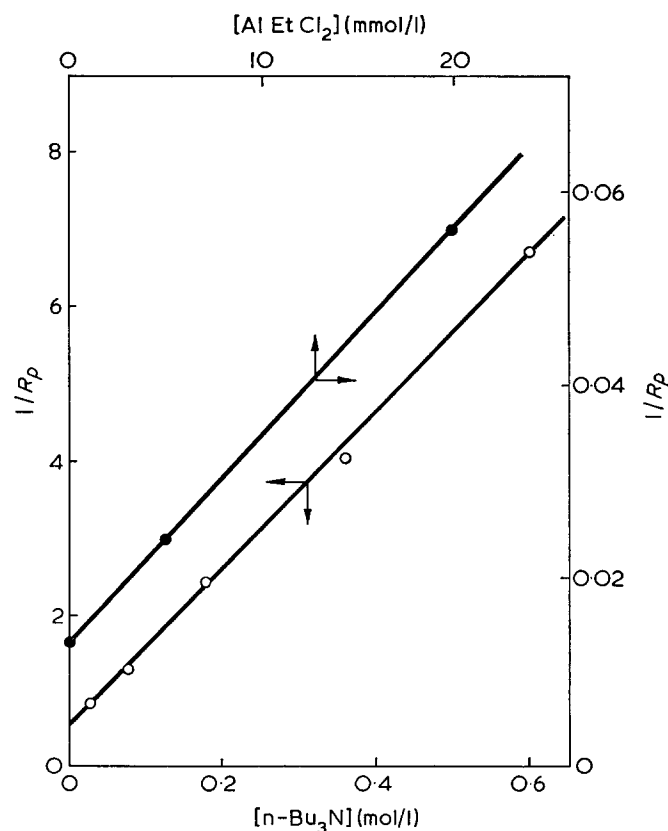


Figure 10 Langmuir plots. ●, Data from Caunt (Fig. 1); ○, data from Boor (Fig. 2)

$\text{Al}_2\text{Et}_3\text{Cl}_3:\text{AlEtCl}_2=100:12:3:0$. This order may in part be due to differences in alkylating ability but probably it largely reflects the relative strengths of adsorption of the aluminium alkyls.

That the effect of donors in the ZnEt_2 system is different from the $\text{AlR}_x\text{Cl}_{(3-x)}$ systems is to be expected, since even when excess donor is used, considerable free ZnEt_2 is still present in solution, and alkylation can still readily occur. The rate would, however, be reduced through competitive adsorption. An initial deactivation is in fact observed¹⁰, but this is followed by a subsequent activation, giving rates, up to a Et_3N concentration of 0.15 mol/l, which were slightly higher than the initial rate. At higher concentrations still the rate again decreases until it is almost negligible at $[\text{Et}_3\text{N}]=4.5$ mol/l.

The initial deactivation at low amine concentrations is comparable to that observed in the present study in the case where amine was added prior to monomer. This is thought to be due to a reduction in the number of active centres, which is effectively the same as Boor's interpretation¹⁰, except that Boor considers that the less stereoregulating sites are preferentially removed.

The subsequent activation as the donor concentration is increased is explained by Boor¹⁰ in terms of higher activity of the remaining sites (increased k_p) and/or an increase in the number of active sites. There is no supporting evidence for the proposal that activation occurs by an increase in activity of the polymerization centres. However, the possibility that additional active centres are formed must be allowed, since Boor³⁴ has shown that propylene can be polymerized by metal alkyl free (MAF) systems. Comparison of the activities of the MAF and ZnEt_2 catalyst systems reveal that they are of similar magnitude, as is shown in Table 4. Thus it seems possible that in the presence of Et_3N additional sites are formed by a mechanism analogous to that in the MAF systems. The ZnEt_2 could aid such site formation, and further increase the rate, by acting as a scavenger for impurities.

It is also conceivable that activation may take place by a mechanism similar to that proposed for the aluminium alkyl based system, e.g., removal of zinc alkyl species from the catalyst surface. This mechanism is likely to be much less effective for the zinc based systems as the donor complexation is weaker. Nevertheless the effect could be significant, especially if the zinc alkyl species are strongly adsorbed.

The deactivation observed at higher amine concentrations, which is also found in MAF system³⁴, may be explained in terms of competitive adsorption of amine with monomer. Thus using the data obtained by Boor³⁴ a plot of $1/R_p$ versus $[(\text{nBu})_3\text{N}]$ can be plotted

Table 4 Comparison of propylene polymerization rate in MAF and ZnEt_2 activated systems

Catalyst	Rate ($\frac{\text{g polymer}}{\text{g cat} \times \text{h} \times \text{g C}_3\text{H}_6}$)	Reference
$\text{TiCl}_3 \cdot \text{AA}/(\text{nBu})_3\text{N}$	0.0248*	Boor ³⁴
$\text{TiCl}_3 \cdot \text{AA}/(\text{nBu})_3\text{N}/\text{H}_2$	0.27†	
$\gamma\text{-Al}_x\text{Ti}_y\text{Cl}_z-160/\text{ZnEt}_2$	0.18	Boor ¹⁰

* Rate corrected to a temperature of 50°C using a value of $E_a=17.4$ kcal/mol (72.7 kJ/mol) deduced from ref. 33

† Rate similarly corrected using $E_a=12.1$ kcal/mol (50.6 kJ/mol)

Table 5 Effect of variation of aluminium alkyl on rate activation [4-MP-1]=2.00 mol/l; $[\text{AlR}_3]=37.0$ mmol/l; $[\text{VCl}_3]=18.5$ mmol/l; $[\text{Et}_3\text{N}]=18.5$ mmol/l; temperature=30°C

Aluminium alkyl	$R_p/[\text{VCl}_3]^*$ (mol/l min $[\text{VCl}_3]$)	$R_p/[\text{VCl}_3]^\dagger$ (mol/l min $[\text{VCl}_3]$)	Activation (%)
AlEt_3	0.241	0.580	140
$\text{Al}(\text{iBu})_3$	0.270	0.467	73
$\text{Al}(\text{nBu})_3$	0.185	0.238	29
$\text{Al}(\text{nDec})_3$	0.078	0.097	24

* Control polymerization

† With Et_3N present (order B)

Table 6 Comparison of actual and predicted rate activation [4-MP-1]=2.00 mol/l; $[\text{AlR}_3]=37.0$ mmol/l; $[\text{VCl}_3]=18.5$ mmol/l; temperature=30°C

AlR_3	θ_M	θ_M^*	Activation (%)	
			Predicted	Observed
AlEt_3	0.137	0.247	80	140
$\text{Al}(\text{iBu})_3$	0.216	0.247	14	73
$\text{Al}(\text{nBu})_3$	0.225	0.247	10	29
$\text{Al}(\text{nDec})_3$	0.227†	0.247	8	24

* θ_M in the presence of added Et_3N , assuming adsorbed metal alkyl removed by complexation

† Estimated

and is shown in Figure 10. An excellent linear plot is obtained consistent with the above proposals.

Effect of variation of aluminium alkyl on rate activation

The rate of polymerization in the presence of Et_3N , was determined with AlEt_3 , $\text{Al}(\text{nBu})_3$ and $\text{Al}(\text{nDec})_3$ using order of addition B. The results are summarized in Table 5. It is immediately apparent that the magnitude of the activating effect varies with the aluminium alkyl employed. The order of decreasing effectiveness being the same as the order of decreasing strength of adsorption, e.g. $\text{AlEt}_3 > \text{Al}(\text{iBu})_3 > \text{Al}(\text{nBu})_3 > \text{Al}(\text{nDec})_3$. This is expected if the activating effect is due to removal of adsorbed aluminium alkyl species from the catalyst surface. The activation cannot be explained in terms of increasing the catalyst activity (k_p), by adsorption of the donor at, or adjacent to, the active site, as it has been previously shown³ that the propagation rate constant (k_p) is independent of the nature of the aluminium alkyl. Any increase in k_p should consequently be the same in each case, which is clearly not observed here.

From a knowledge of values of K_M and K_A previously determined⁴ it is possible to calculate the rate activation based on removal of aluminium alkyl species from the catalyst surface. Comparison of the calculated and experimental activation is made in Table 6. Although the metal alkyls are placed in the right order, the calculated values are in every case low compared to the experimental values. This discrepancy is thought to be outside the limits of experimental error, and may be due to the adsorption of aluminium chloroalkyl species which have been neglected in the above calculations. Thus during the initial active centre formation reactions AlR_2Cl will be formed by chloroalkyl exchange reactions and thus is likely to be more strongly adsorbed than AlR_3 , as already discussed. θ_M will consequently be increased by more than the predicted value by removal of these additional 'inhibitors'.

Effect of [VCl₃] on rate activation

If the discrepancy between the predicted and observed rate activation is due to the presence of aluminium chloroalkyl species, then it would be expected that the rate activation, at constant metal alkyl concentration, would be dependent on the concentration of VCl₃, since $[Al(iBu)_2Cl] \propto [VCl_3]$ in these experiments.

Experiments were conducted varying the [VCl₃] and adding Et₃N after a steady state rate had been achieved. The results are recorded in Table 7. It is immediately apparent that the rate activation increases with the concentration of VCl₃. This strongly suggests that aluminium chloroalkyl species are present and that the equation for θ_M should be modified to:

$$\theta_M = \frac{K_M[M]}{1 + K_M[M] + K_A[A] + K'_A[A']} \quad (18)$$

where $A' = Al(iBu)_2Cl$.

These results are also significant in that the value of $R_p/[VCl_3]$, after addition of amine, is constant irrespective of the initial $[Al(iBu)_3]:[VCl_3]$ ratio (Figure 11). This is of considerable interest as it may explain the well documented increase in rate of polymerization in Ziegler–Natta systems as the metal alkyl to transition metal ratio is increased up to a value of about 2:1. This is usually interpreted as being caused by an increase in active centre concentration due to more extensive alkylation of the catalyst surface. These results, however, seem to indicate that the increase in rate is due to removal of aluminium chloroalkyl species rather than an increase in the number of active centres.

Table 7 Effect of concentration of vanadium trichloride on rate activation
[4-MP-1]=2.00 mol/l; [Al(iBu)₃]=37.0 mmol/l; temperature=30°C

[VCl ₃]	$R_p/[VCl_3]^*$ (mol/l min [VCl ₃])	$R_p/[VCl_3]^\dagger$ (mol/l min [VCl ₃])	Activation (%)
3.63	0.341	0.685	101
18.5	0.270	0.641	134
44.9	0.208	0.689	174

* Before addition of amine

† After addition of amine [Et₃N]=27.8 mmol/l

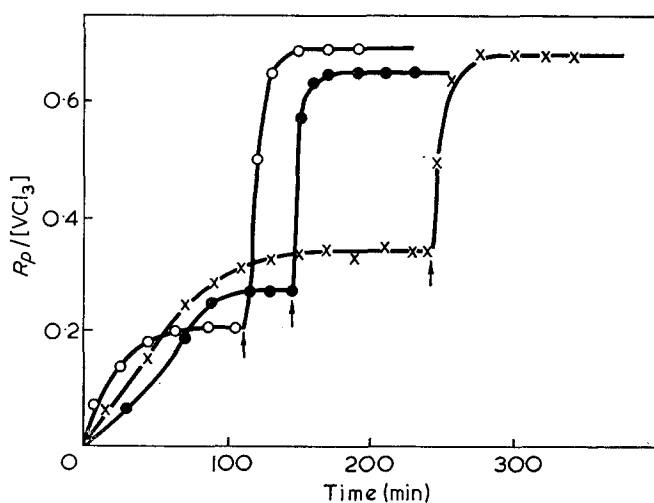


Figure 11 Variation of rate activation with [VCl₃]. [4-MP-1]=2.00 mol/l; [Al(iBu)₃]=37.0 mmol/l; [NEt₃]=27.8 mmol/l; temperature=30°C. [VCl₃]: ×, 3.63 mmol/l; ●, 18.5 mmol/l; ○, 44.9 mmol/l. ↓ denotes addition of donor

Table 8 Comparison of the rate of polymerization and number of active centres in the control and modified systems

[4-MP-1]=2.0 mol/l; [VCl₃]=18.5 mmol/l; [Al(iBu)₃]=37.0 mmol/l; temperature=30°C

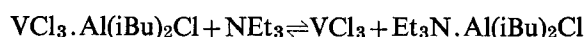
	$R_p/[VCl_3]$ (mol/l min [VCl ₃])	$C_0 \times 10^4$ (mol/mol VCl ₃)
Control system	0.270	3.8 ± 0.4
Modified system*	0.684	4.6 ± 0.5

* [NEt₃]=27.8 mmol/l (order B)

Equilibrium reactions such as:



and



may be envisaged. Thus the initial alkylation reaction may well be complete even at low metal alkyl concentrations. Higher concentrations are necessary, however, to remove the aluminium chloroalkyl species from the catalyst surface.

Number of active centres in donor modified system

It has been suggested in this paper that the rate activation observed on addition of Et₃N, is due to removal of adsorbed aluminium alkyl species from the sites for monomer coordination rather than an increase in number of active centres. In order to confirm this the number of active centres in the modified system was determined by the tritium quench technique already described³.

Preliminary results are shown in Table 8. It is immediately apparent that, whereas the steady state rate for the donor modified system is over 150% higher, the number of active centres is only marginally higher and is in fact constant within the limits of experimental error. This clearly confirms the proposal that donor activation occurs by modification of the adsorption equilibrium rather than an increase in active centres.

In addition these results help to distinguish between two possible hypothetical models for the polymerization system: (i) the adsorbed species, monomer and alkyl, could be considered as mobile on the surface and that a dynamic situation is achieved so that polymer chains could appear at all the possible centres. The momentary proximity of an alkyl molecule at any given centre would hold up temporarily the propagation of a polymer chain at that centre—all centres would nevertheless carry polymer molecules; (ii) the alkyl when adsorbed would remain in position for periods of time longer than the mean growth time for a polymer molecule. In this case polymer could only be attached to centres where the alkyl was absent.

The above results, together with the kinetic results presented earlier which demonstrated that the addition of triethylamine during the course of the polymerization brought about a very rapid activation are considered to strongly favour the first hypothesis.

Effect of donors on the molecular weight and isotacticity of polymer

Although the effect of donors on the molecular weight and isotacticity of the polymer have not yet

been investigated in this present study, it is informative to examine the present proposals in the light of the findings of other workers. The addition of donors, such as tertiary amines, to a variety of catalytic systems is found, without exception, to increase the molecular weight of the polymer by a factor of between 1.5 and 4^{10, 14, 23, 27, 35-39}. It has been previously shown^{4, 5} that chain transfer occurs with adsorbed metal alkyl and consequently the addition of donors would be expected to reduce the rate of chain transfer as the concentration of adsorbed metal alkyl would be reduced by complexation or competitive adsorption. Calculations on the system $VCl_3/AlEt_3/4-MP-1$, using the molecular data previously presented⁵, indicate that the molecular weight would be expected to increase by a factor of 2-3, which is similar to the values reported for the $TiCl_3/AlEt_3$ /propylene system of 1.5-3^{36, 38}. The isotactic content of the polymer has also been found to increase in the presence of added donors^{10, 16, 22, 37}. The effect of donors in the $TiCl_3/ZnEt_2$ /propylene system has been explained by Boor¹⁰ on the basis that donors preferentially coordinate with, and thus remove, less stereospecific sites. Keii *et al.*¹⁶, on the other hand, present evidence to show that in the $TiCl_3/AlEt_3$ /propylene system increased stereospecificity can be explained in terms of a decrease in the concentration of adsorbed metal alkyl leading to less extensive reduction of the catalyst. They conclude that the stereospecificity of the catalyst is largely governed by the reducing ability of the metal alkyl and is not directly influenced by the donor.

The latter explanation is consistent with the proposals in this study.

It is noteworthy that the form of the curves of change in molecular weight and isotacticity *versus* donor concentration are shown to be exactly analogous¹⁰. This may mean that the factors affecting the molecular weight and isotacticity are the same, which is again consistent with the explanation that donors alter the concentration of adsorbed metal alkyl, upon which both the molecular weight and tacticity are dependent. Although removal of less stereospecific sites could explain the increase in isotactic content, there seems no reason why these sites should yield higher molecular weight polymer, especially if transfer with metal alkyl is the predominant regulation step as would be expected in the $ZnEt_2$ based systems.

REFERENCES

- Burfield, D. R., McKenzie, I. D. and Tait, P. J. T. *Polymer* 1972, 13, 302
- McKenzie, I. D., Tait, P. J. T. and Burfield, D. R. *Polymer* 1972, 13, 307
- Burfield, D. R. and Tait, P. J. T. *Polymer* 1972, 13, 315
- Burfield, D. R., Tait, P. J. T. and McKenzie, I. D. *Polymer* 1972, 13, 321
- McKenzie, I. D. and Tait, P. J. T. *Polymer* 1972, 13, 510
- Reich, L. and Schindler, A. 'Polymerization by Organometallic Compounds', Interscience, New York, 1966
- Boor, J. Jr. *Macromol. Rev.* 1967, 2, 115
- Jordan, D. C. 'The Stereochemistry of Macromolecules', (Ed. A. D. Ketley), Marcel Dekker, New York, 1967, Ch 1
- Hoeg, H. 'The Stereochemistry of Macromolecules', (Ed. A. D. Ketley), Marcel Dekker, New York, 1967, Ch 2
- Boor, J. Jr. *J. Polym. Sci. (A)* 1965, 3, 995
- Coates, G. E., Green, M. L. H. and Wade, K. 'Organometallic Compounds', Methuen, London, 3rd Edn, 1967, Vol 1, p 132
- Soga, K. and Keii, T. *J. Polym. Sci. (A-1)* 1966, 4, 2429
- Clark, R. J. H. 'The Chemistry of Titanium and Vanadium', Elsevier, Amsterdam, 1968, p 106
- Vesely, K., Ambroz, J., Vilim, R. and Hamrik, O. *J. Polym. Sci.* 1961, 55, 25
- Mezhikovskii, S. M., Kissin, Yu. V. and Chirkov, N. M. *Vysokomol. Soedin. (A)* 1967, 9, 2006
- Soga, K., Takano, Y., Go, S. and Keii, T. *J. Polym. Sci. (A-1)* 1967, 5, 2815
- Keii, T., Soga, K. and Saiki, N. *J. Polym. Sci. (C)* 1967, 16, 1507
- McCarty, W. H. and Parravano, G. *J. Polym. Sci. (A)* 1965, 3, 4029
- Overberger, C. G. and Jarovitzky, P. A. *J. Polym. Sci. (C)* 1963, 4, 37
- Burfield, D. R. and Tait, P. J. T. to be published
- Zambelli, A., Dipietro, J. and Gatti, G. *J. Polym. Sci. (A)* 1963, 1, 403
- McConnell, R. L. *et al. J. Polym. Sci. (A)* 1965, 3, 2135
- Coover, H. W. Jr. and Joyner, F. B. *J. Polym. Sci. (A)* 1965, 3, 2407
- Cooper, W., Eaves, D. E., Owen, G. D. T. and Vaughan, G. *J. Polym. Sci. (C)* 1964, 4, 211
- Razuvaev, G. A. and Graevskii, A. I. *Dokl. Akad. Nauk. SSSR* 1959, 128, 309
- Haszeldine, R. N., Hyde, T. G. and Tait, P. J. T. *Polymer* 1973, 14, 224
- Pirogov, O. N. and Chirkov, N. M. *Vysokomol. Soedin.* 1965, 7, 491
- Minsker, K. S. and Bykovskii, V. K. *Vysokomol. Soedin.* 1960, 2, 535
- Ambroz, J. and Hamrik, O. *Coll. Czech. Chem. Commun.* 1963, 28, 2550
- Davidson, N. and Brown, H. C. *J. Am. Chem. Soc.* 1942, 64, 316
- 'Handbook of Organometallic Compounds', (Eds N. Hagihara, M. Kumada and R. Okawara), Benjamin, New York, 1968, p 164
- Caunt, A. D. *J. Polym. Sci. (C)* 1963, 4, 49
- Schnecko, H., Reinmoller, M., Weirauch, K. and Kern, W. *J. Polym. Sci. (C)* 1963, 4, 71
- Boor, J. *J. Polym. Sci. (A-1)* 1971, 9, 617
- Milovskaya, Ye. B. and Dolgopol'skaya, T. I. *Vysokomol. Soedin.* 1962, 4, 145
- Razuvaev, G. A., Minsker, K. S., Fedoseeva, G. T. and Bykhovskii, V. K. *Vysokomol. Soedin.* 1960, 2, 404
- Boor, J. and Short, G. A. *J. Polym. Sci. (B)* 1971, 9, 235
- Razuvaev, G. A., Minsker, K. S., Fedoseeva, G. T. and Savel'er, L. A. *Vysokomol. Soedin.* 1959, 1, 1961
- Razuvaev, G. A., Minsker, K. S., Chernovskaya, R. P. and Burlakova, G. I. *Vysokomol. Soedin.* 1965, 7, 39

Phase structure of solution cast films of α -methylstyrene/butadiene/styrene block copolymers*

G. S. Fielding-Russell and P. S. Pillai

Research Division, Goodyear Tire & Rubber Company, Akron, Ohio 44316, USA
(Received 6 July 1973)

The phase structure of solvent cast films of α -methylstyrene/butadiene/styrene of differing compositions was investigated using physical methods. Both dynamic mechanical and differential scanning calorimetry measurements exhibited a single high temperature transition at 150°C. The transition has been shown to originate from a composite domain of the two glassy end blocks. Light scattering measurements showed that these domains varied in size from 0.35 to 0.40 μm and that they are randomly arranged within the butadiene matrix. The results are compared with the results of similar studies of ABA systems.

INTRODUCTION

Studies on the physical properties of thermoelastic elastomers of the type ABA, i.e., two-component triblock copolymers, where A is a glassy polymer (often styrene) and B is a rubbery polymer (often butadiene or isoprene) are well documented¹⁻⁵. The properties of such polymers may be conveniently altered, and therefore tailored, not only by selective block copolymerization, but also by varying block composition, block molecular weights, and casting solvent. A further method of altering the physical properties of the triblock system without necessarily changing the molecular weights and the rubber to glassy polymer ratio, and hence perhaps not drastically affecting processability, is to replace one end block with a third polymer to form a three component ABC triblock copolymer. C is usually a rigid amorphous⁶ or crystalline⁷ polymer, which may or may not be compatible with A, with its major transition temperature (T_g or T_M) different from that of A.

In this paper the results of an investigation into the phase structure of three solution cast α -methylstyrene/butadiene/styrene (α -MS/B/S) copolymers that contain different block compositions are reported. The techniques used include light scattering, electron microscopy, mechanical and thermal methods.

EXPERIMENTAL

Materials

The polymers used in this study were prepared in these laboratories by R. E. Cunningham. Their compositions and block molecular weights are listed in Table 1⁸. The butadiene microstructure is reported as 44% *trans*-1,4-, 36% *cis*-1,4-, and 8% vinyl for all samples used⁸. Reagent grade benzene was used to prepare 5wt% polymer solutions from which clear sheets, of convenient thickness, were cast using either

Table 1 Details of the composition and molecular weights of the three triblock copolymers used

Sample	Component (%)			Block mol wt $\times 10^{-3}$		
	α -MS	B	S	α -MS	B	S
1	29	43	28	35	55	35
2	17	53	30	25	63	37
3	23	60	17	30	90	30

glass or Teflon moulds. The cast sheets were dried, stored under vacuum prior to use, and found to be relatively strain free if the rate of solvent evaporation was kept low.

Apparatus

A schematic diagram of the light scattering apparatus is shown in Figure 1. It is sufficient to note here that a He-Ne laser ($\lambda=6328 \text{ \AA}$) was used as the light source. The intensity of scattered radiation was measured as a function of angle as previously reported⁹. Electron micrographs of the OsO₄ stained samples were obtained using an RCA EMU3 transmission electron microscope. Dynamic mechanical data, on cast samples with the approximate dimensions 5.0 \times 0.5 \times 0.1 cm, were taken over the limited frequency range of 1 to 10³ Hz using a RheoVibron instrument equipped with a modified Imass temperature chamber. An Instron Universal tester was used to obtain the tensile stress-strain data of ring samples cut from the cast sheets. The speed of tensile testing was 50.8 cm/min and the strain $\epsilon (=1-\lambda)$ was calculated from the equation¹⁰:

$$(1-\lambda) = 2\Delta L/\pi p + (h_0/p)(\lambda)^{-1/2} \quad (1)$$

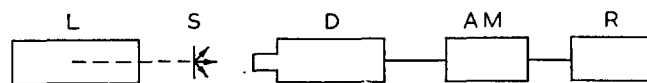


Figure 1 Schematic diagram of the light scattering apparatus: L, laser; S, sample; D, detector; AM, amplifier; R, recorder

* Presented at a meeting of the Polymer Division, American Chemical Society, Detroit, Michigan, May 1-4, 1973.

where ΔL , p and h_0 are the Instron crosshead separation, the initial ring circumference and the sample thickness respectively. Equation (1) takes into account the twist of the sample during extension. Differential scanning calorimetry (d.s.c.) thermograms were obtained using a Perkin-Elmer 1B unit at a scan speed of 20°C/min.

RESULTS AND DISCUSSION

The light scattering data were analysed via the Debye-Bueche expression¹¹, relating the scattered intensity I to the scattering angle θ :

$$I = KV\bar{\eta}^2\pi^{3/2}a^3\exp[-4\pi^2\sin^2(\theta/2)a^2/\lambda^2] \quad (2)$$

where K is a constant and $\bar{\eta}^2$, a and λ are the mean square fluctuation of the dielectric constant, the mean size of the scattering domain and the wavelength respectively. A plot of the logarithm of I as a function of $\sin^2(\theta/2)$ should therefore yield linear regions the slopes of which are characteristic of the sizes of the scattering domains. Figure 2 shows such plots for the three polymers used in this study; in all cases two linear regions are shown. The characteristic mean dimensions a_1 and a_2 , which are listed for each sample in Table 2, may be respectively taken as the sizes of the scattering domain and the interdomain separation distance. From the nature of the intensity versus $\sin^2(\theta/2)$ plots it appears that the domains are spherical, reasonably monodispersed and randomly distributed.

Electron micrographs of the three samples, shown in Figure 3 at a magnification of 30 000 \times , indicate a two phase structure and tend to confirm the light scattering observations of monodispersion and randomness.

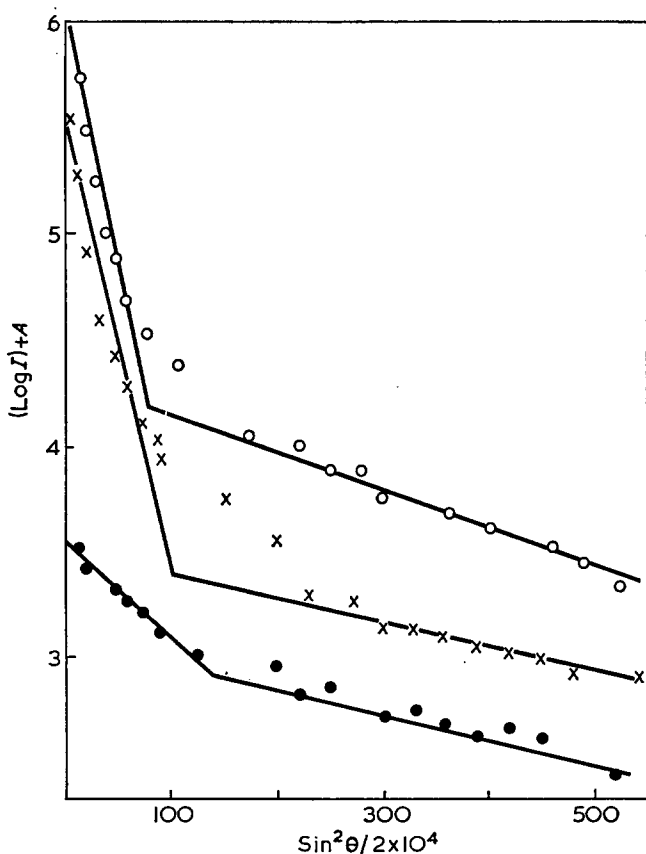


Figure 2 Log intensity as a function of scattering angle. A is an arbitrary separation factor. O, $A=0$; x, $A=0$; ●, $A=-1$

Table 2 Characteristic dimensions from light scattering

Sample	a_1 (μm)	a_2 (μm)
1	0.40	1.20
2	0.39	1.33
3	0.35	0.66

Limited frequency dynamic mechanical data (Young's modulus E' and the loss tangent $\tan \delta$) are plotted in Figure 4 as a function of temperature for each of the three samples. Only two relaxation processes, as defined by maxima in $\tan \delta$ and corresponding decreases in E' , are given. A low temperature process is centred around -60°C (110 Hz) and a single high temperature process is centred around 150°C .

The low temperature process is associated with the butadiene glass-rubber transition T_g since the $\tan \delta$ peak heights and the modulus step heights both vary with the butadiene content. The relatively high temperature location of the butadiene transition reflects a certain amount of phase mixing and also the multiplicity of structure of the butadiene component. (T_g values of the butadiene homopolymers are listed as follows¹²: *cis*-1,4-, -102°C ; *trans*-1,4-, -83°C ; and the vinyl structure as -4°C .)

The single high temperature process, which is also evident in the d.s.c thermograms shown in Figure 5, falls in the temperature region of 150°C which is intermediate between the T_g values of the glassy end block homopolymers; polystyrene and poly(α -methylstyrene) are respectively listed at 100°C ¹² and 180°C ¹³⁻¹⁵. Using the empirical equation¹⁶:

$$V_1B_1(T_g - T_{g_1}) + V_2B_2(T_g - T_{g_2}) = 0 \quad (3)$$

where the subscripts refer to the two components and B is a constant, which is taken to be the same for these polymers, and V is the volume fraction, an effective T_g is calculated in the range of 140 – 148°C . Therefore, the high temperature transition is attributed to a composite phase formed by the mixing of the glassy end blocks.

It is also apparent that this mixed glassy phase forms the scattering domain, previously characterized by the mean dimension a_1 , since the sum of the percentage of end blocks when raised to the one-third power is directly proportional to the domain size, viz.:

$$(40)^{1/3} \cdot (47)^{1/3} \cdot (57)^{1/3} = 0.35^* : 0.38^* : 0.41^* \\ \approx 0.35 : 0.39 : 0.40$$

where * indicates reduced values standardized with respect to the first dimension.

Thus taking the information gained from the various physical measurements a model for these solution cast copolymers may be constructed. It consists of a two phase system, similar to that shown by the various ABA triblock copolymers, namely SBS^{17, 18}, SIS¹⁹ and ISI¹⁹, which also show single low and high temperature loss peaks at around the T_g values of the components, where the mixed spherical domains containing α -MS and S are randomly dispersed in a butadiene matrix. The glassy domains appear to be inter-connected in much the same way as has been postulated for certain solution cast SBS block copolymers¹⁸, because on straining the

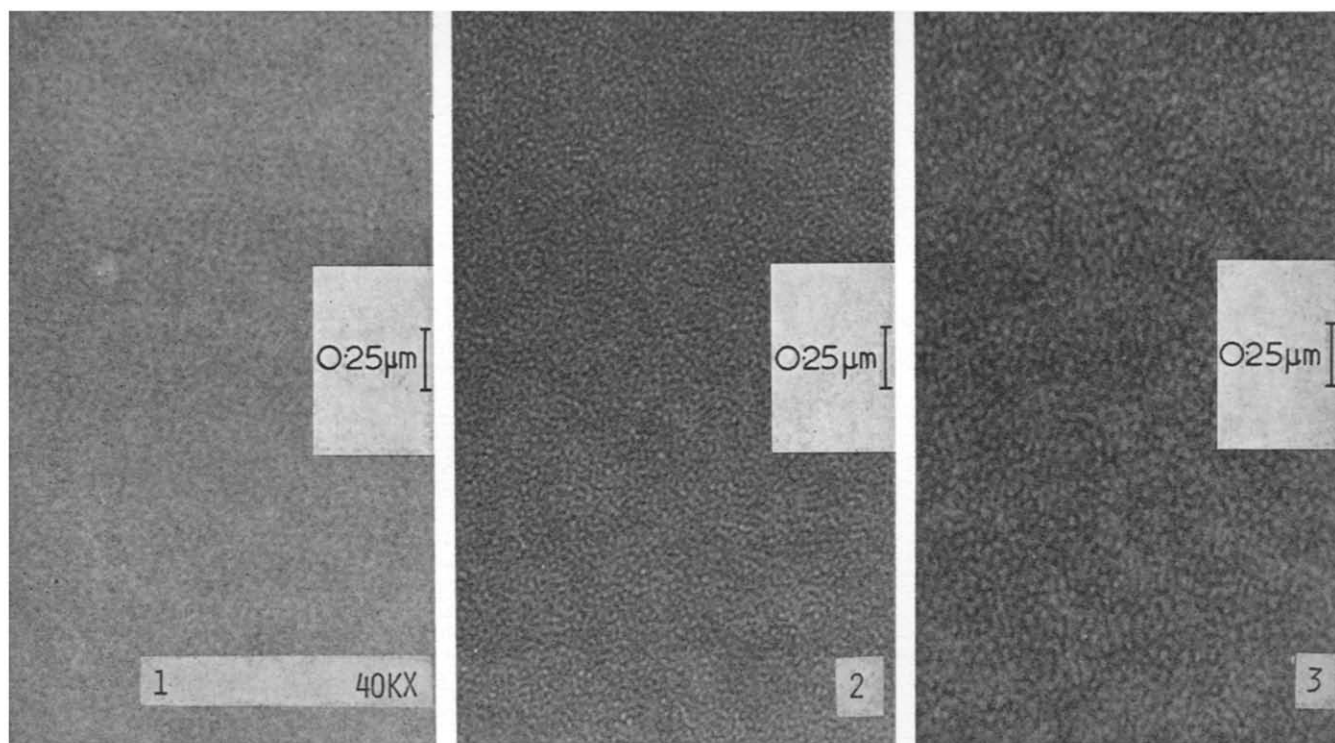


Figure 3 Electron micrographs of three samples at 30 000 \times magnification

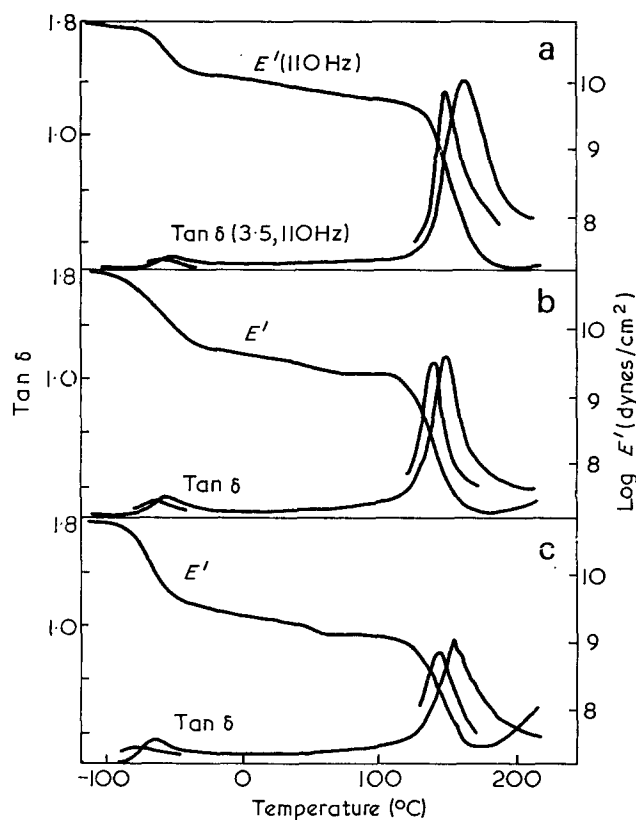


Figure 4 Dynamic mechanical properties at 3.5 and 110 Hz as a function of temperature. (a) Sample 1; (b) sample 2; (c) sample 3

polymers exhibit a definite plastic yield at low strains (Figure 6).

Although polymers are generally considered incompatible, it was found in the present study that the two glassy components gave a single composite phase which formed the scattering domain. Baer¹⁵ studied block copolymers of α -MS/S/ α -MS and S/ α -MS/S and found

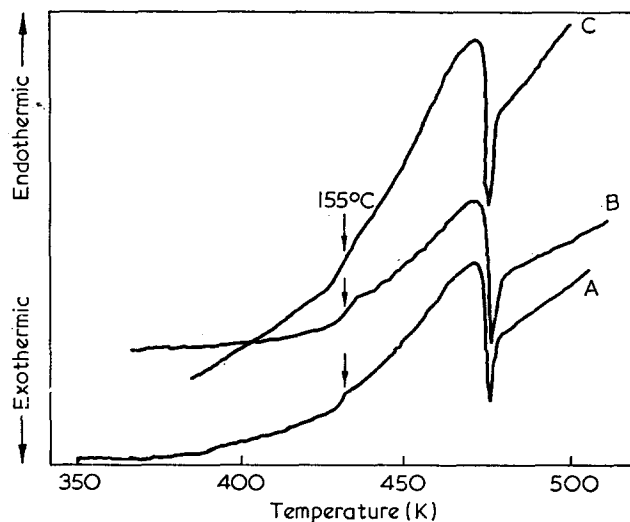


Figure 5 D.s.c. thermograms in the high temperature region. A, Sample 1; B, sample 2; C, sample 3

a single phase system characterized by a loss peak at around 150°C. However, physical mixtures of polystyrene and poly(α -methylstyrene) yield two mechanical loss peaks¹⁵, at the respective T_g values, showing their incompatibility. Mixing of the glassy components to form the mixed domains and the interconnectivity of these domains may be due, in the present case, to the relative insolubility of the glassy components, when compared to butadiene, in the casting solvent. Thus, in the solution state the polystyrene and poly(α -methylstyrene) may tend to aggregate into mixed but interconnected spherical domains which remain dispersed in the butadiene matrix upon solvent evaporation.

CONCLUSION

Benzene cast films of α -MS/B/S triblock copolymers exhibit a two phase structure. A composite domain

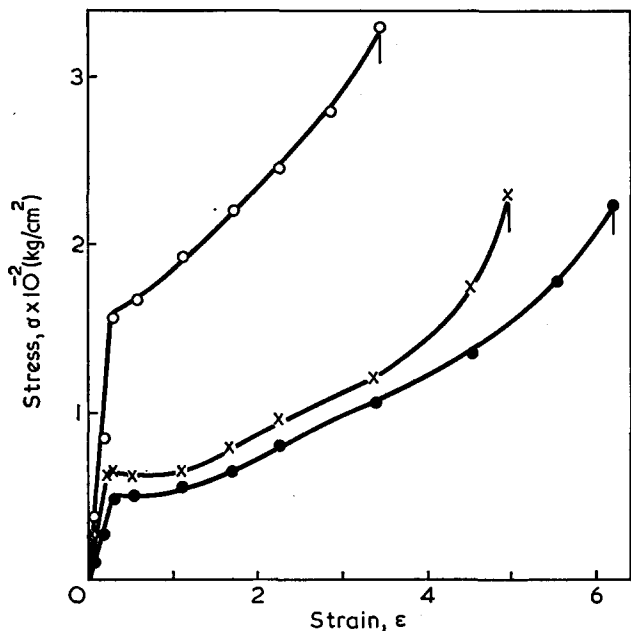


Figure 6 Stress-strain curves at 25°C. ○, Sample 1; ×, sample 2; ●, sample 3

of the glassy end blocks is randomly dispersed in the rubbery matrix.

ACKNOWLEDGEMENTS

The authors would like to thank Dr R. E. Cunningham for preparing the polymers, Professor A. N. Gent,

University of Akron, and Dr D. I. Livingston for their helpful discussion and Messrs J. E. Alchier and J. D. Strang for their assistance in the experimental work. Contribution No. 506.

REFERENCES

- 1 Beecher, J. F., Marker, L., Bradford, R. D. and Aggarwal, S. L. *J. Polym. Sci. (C)* 1971, **26**, 169
- 2 Brunwin, D. M., Fischer, E. and Henderson, J. F. *J. Polym. Sci. (C)* 1969, **26**, 135
- 3 Smith, T. L. and Dickie, R. A. *J. Polym. Sci. (C)* 1969, **26**, 163
- 4 Hendus, H., Illers, K-H. and Rapte, E. *Kolloid-Z. Z. Polym.* 1967, **216-217**, 110
- 5 Keller, A., Pedemonte, E. and Willmouth, F. W. *Kolloid-Z. Z. Polym.* 1970, **238**, 25
- 6 Morton, M. *Adv. Chem. Ser.* 1971, **99**, 31
- 7 Estes, G. M., Cooper, S. L. and Tobolsky, A. V. *J. Macromol. Sci. (C)* 1970, **4**, 313
- 8 Cunningham, R. E. personal communication
- 9 Pillai, P. S., Livingston, D. I. and Strang, J. D. *Rubber Chem. Technol.* 1972, **45**, 241
- 10 Livingston, D. I. and Fitzhugh, R. L. personal communication
- 11 Debye, P. and Bueche, A. M. *J. Appl. Phys.* 1947, **20**, 518
- 12 Lee, W. A. and Knight, G. J. 'Polymer Handbook' (Eds J. Brandrup and E. A. Immergut), Interscience, New York, 1966
- 13 Barb, W. G. *J. Polym. Sci.* 1959, **37**, 515
- 14 Boyer, R. F. *Rubber Chem. Technol.* 1963, **36**, 1303
- 15 Baer, M. *J. Polym. Sci. (A)* 1964, **2**, 417
- 16 Wood, L. A. *J. Polym. Sci.* 1958, **28**, 317
- 17 Miyamoto, T., Kodama, K. and Shibayana, K. *J. Polym. Sci. (A-2)* 1970, **8**, 2095
- 18 Fielding-Russell, G. S. *Rubber Chem. Technol.* 1972, **45**, 252
- 19 Robinson, R. A. and White, E. F. T. 'Block Polymers', Plenum Press, New York, 1970

Fracture properties of thermosets

A. D. S. Diggwa*

Engineering Group, Rubber and Plastics Research Association of Great Britain,
Shawbury, Shrewsbury SY4 4NR, UK

(Received 18 July 1973; revised 29 August 1973)

Fracture surface energy (*FSE*) measurements using a cleavage technique gave values of 42 J/m² for the polyester, 80 J/m² for the epoxide and 310 J/m² for a rubber-modified epoxide with standard errors of 6 J/m², 5 J/m² and 10 J/m² respectively. A modified method of calculation was introduced to accommodate the considerable within-sample variability of *FSE* of some samples. The effect of water on unmodified thermosets tested was examined and found to be relatively small.

INTRODUCTION

Weichers¹ used the double cantilever fracture energy test for a highly crosslinked material (an epoxide resin). The method was originally developed by Berry² for thermoplastic materials. A similar method has now been used to study the properties (dry and wet) of a further epoxide resin and a polyester resin. Both of these resins were used previously in a study of the creep of glass reinforced thermosets by Diggwa and Norman³. They showed that most of their categorized micro-failures were initiated very early in the creep curve and most significantly appeared in the resin or resin/interface regions—some were initiated in the 'elastic part' of the creep curve. The investigation was essentially an attempt to quantify and categorize the various types of micro-damage and associate them with the various parts of the so elucidated creep curve.

Both unreinforced materials presented new difficulties in the preparation of the testpieces and in the variability of the product, so that modified methods of specimen preparation and results interpretation had to be developed for the *FSE* work presented here. The increased product variability in the case of the epoxide material used was probably due to the harsh cure schedule, which was made so in an attempt to elevate the glass transition temperature of the epoxide.

An attempt was made to vary the resin stiffness to detect whether this had any effect on the fracture energy. However, the readily available methods of changing stiffness also gave comparable changes in both strength and ultimate elongation. Therefore their *FSE* was not measured.

Additional tests were also carried out (dry only) on some rubber modified epoxide resins. All the material formulations are given in *Table 1*, where all the additions are given in parts (by wt) per hundred resin (phr).

EXPERIMENTAL

Casting of samples

For the epoxide samples the mould, as shown in *Figure 1*, essentially consisted of a sheet of butyl rubber

gasket (6.35 mm thick cut into the shape shown) clamped between glass plates (340 mm × 195 mm × 6.35 mm) lined with a sheet of poly(ethylene terephthalate) (PET) 127 μm thick. The assembled mould was held in a vertical position to receive the resin mixture. To aid release of the cured samples from the mould and butyl rubber gasket, a PTFE spray was applied before mould assembly.

Table 1 Material formulation

	Epoxide	McGarry type modified epoxide	T1*	T2*	Poly-ester
Resin Epikote 828	100	100	100	100	
Hardener Epikure NMA	95		95	95	
Accelerator BDMA	0.5		0.5		
Hardener DMP30		4		4	
CTBN		10	10	10	
Resin Beetle 4128					100
MEKP					1
Cobalt naphthenate					0.5
Initial cure or gel (h/°C)	4/100 3/180	19/80 2/120	19/80 2/120	19/80 2/120	2/25 3/80

* See text

DMP30=tri(dimethylaminomethyl) phenol

MEKP=methyl ethyl ketone peroxide

BDMA=benzyl dimethylamine

CTBN=carboxyl-terminated butadiene-acrylonitrile

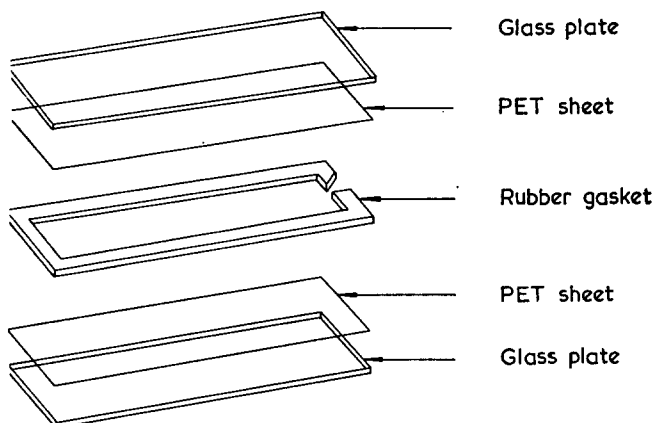


Figure 1 The mould

* Present address: Moulding Materials Research Dept, Turner Bros. Asbestos Ltd, PO Box 40, Rochdale, Lancs, UK.

When polyester samples were prepared using PET liners, undulating surfaces were obtained although there was no adhesion. The application of a silicone mould release spray was found to give adequate release without the use of PET and PTFE spray.

By precipitation in epoxide resins of an elastomeric second phase, namely, carboxyl-terminated butadiene-acrylonitrile (CTBN) rubber, McGarry⁴ found three-fold improvement in fracture energy. It was decided to produce a similar material and study the production technique and results.

After a close examination of the preparation technique and numerous disappointments, an acceptable method was devised. Essentially the method consisted of: (1) moulds were assembled as shown in Figure 1; (2) weighed quantities of resin and rubber were separately heated to about 80°C and exposed to a hard vacuum to remove microbubbles and impurities such as water; (3) the appropriate amounts of resin and rubber were thoroughly mixed together, introducing as few bubbles as possible. Vigorous mechanical stirring was avoided as it resulted in bubbles in the cured sample. The mixture, which now appeared cloudy, was heated to about 80°C until the two components were well mixed with each other. When the cloudiness disappeared, a hard vacuum was applied; (4) when all the visible bubbles had been removed the mixture was removed from the evacuation chamber and cooled to about 55°C; (5) using a 50 ml pipette the appropriate amount of hardener (DMP 30) was introduced below the surface of the mixture and the mixture was stirred rapidly and thoroughly; (6) the mixture was then poured into the moulds which were already heated to 100°C. The initial gelation followed within several minutes of the introduction of the hardener.

A typical distribution of the rubber particles in a cured sample are shown in Appendix II (Figure 7). Figure 8 shows an irregular particle.

To assess the importance of DMP 30 in the final precipitation of the rubber particles in the two phase material produced by McGarry⁴, the following samples were also prepared: T1—the first epoxide formulation given in Table 1 with 10 parts of CTBN per 100 parts of resin added; and T2—the first epoxide formulation given in Table 1 but with the BDMA replaced by 4 parts of DMP 30 per 100 parts of resin and 10 parts of CTBN per 100 parts of resin.

It should, however, be noted that direct mixing of CTBN with epoxide at room temperature will not give a sufficiently reactive mixture for curing with the first cure system (Table 1) for optimum properties of the cured samples. A pre-reaction technique is necessary.

A batch of samples (M6), of the best rubber modified formulation, was made in the form of a single sheet using the same moulding techniques. The mould was 350 mm × 350 mm thereby making it large enough for cutting six samples.

Curing and machining of samples

The samples were cured in an oven using the schedule shown in Table 1. At the end of the cure cycle the samples were cooled slowly (not more than say 20°C/h) and removed from the moulds at room temperature.

The samples were machined to 50 mm × 280 mm using a routing tool. Two longitudinal grooves were machined (to give the cross-section shown in Figure 2) by means

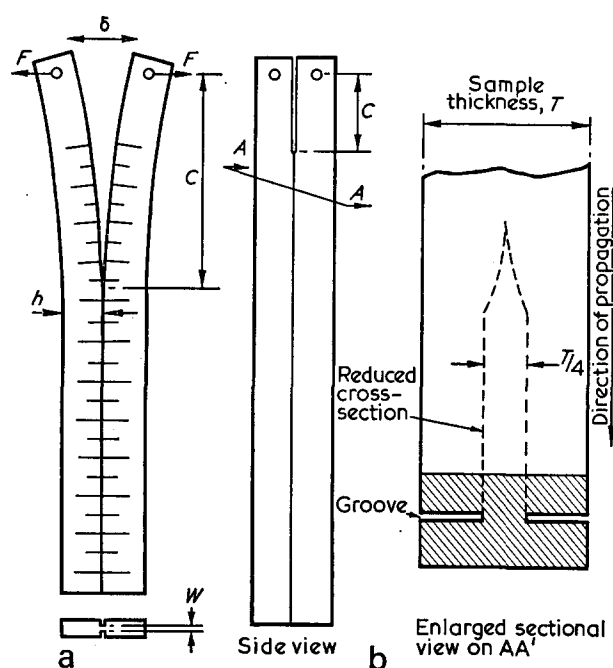


Figure 2 Machined sample. (a) Under load; (b) showing fish tail

of a high precision circular saw with a blade 50.8 mm diameter and 0.13 mm thick.

With the initial polyester samples the resulting fracture surface had erratic undulations. Reduction of the sample thickness between the grooves from one-third to one-quarter of the sample thickness led to a smooth fracture surface. Although with epoxide samples no visible difference in quality was observed, the groove depth used for polyester samples was adopted for consistency.

Also it was observed that the quality of the fracture surface was critically dependent upon the method of crack initiation and the initiating fish tail so the latter was made very acute as shown in Figure 2b. Finally, a series of reference lines, at 1 cm intervals, were engraved on the sample as shown in Figure 2a.

The rubber modified epoxides were not translucent and the position of the crack tip could not be seen by looking into the groove width of 0.138 mm. This was rectified by using a circular saw blade of 3.2 mm thickness for machining the groove.

Measurement of fracture surface energy

Conditioning of samples. The properties of polyester samples change significantly during the first 10 days or so after moulding. Therefore all samples were rested for at least 12 days before machining. During this period the samples were maintained at room temperature, in a dry and dark place.

Samples to be tested in a wet environmental condition were left totally immersed in distilled water at 30°C for 12 days after conditioning. This immersion period was a compromised minimum (see Appendix I). Initially a batch of samples was tested in air with water injected at the crack tip prior to each crack jump. The water was injected with the aid of a micro-pipette fitted with a hypodermic needle. Care was taken not to introduce stress during injection. A second batch of samples was tested while they were immersed in distilled water at room temperature.

All measurements of fracture surface energy (*FSE*) were carried out at room temperature.

Method of testing. Initial tests on the unmodified epoxide and polyester samples were made using the torsional test described by Outwater and Gerry⁵. However, fewer jumps (points on the graph) were obtained for each specimen and the fracture surface was very erratically undulating. The cleavage method was found to be superior in all these respects and was therefore adopted.

Essentially the apparatus consisted of an Instron Universal Bench Model testing machine. The samples were machined as described above and set up in the Instron in a horizontal position held by pins of 3 mm diameter inserted into the holes seen in *Figure 2*. The sample was loaded at a constant crosshead speed of 0.4 mm/min and when the crack jumped the crosshead was immediately reversed. The maximum load, crosshead deflection and the crack tip position was recorded relative to the nearest reference line by means of a cathetometer. After relaxation of the sample for at least 15 min after each loading cycle all subsequent fracturing modes were carried out at a crosshead speed of 4 mm/min following the above procedure. (At the end of each loading the sample was relaxed for at least three times the amount of time taken to reach the load required to make the crack jump.)

Treatment of results. The empirical relation to represent the behaviour of the beams in cleavage by Berry² is $F = (\phi C^{-\nu})\delta$, where F is the force and δ is the separation of the two halves of a beam at which a crack of length C is about to move (see *Figure 2a*). ϕ and ν are arbitrary constants. A plot of $\log [F/\delta]$ against $\log C$ gives an estimation of ν .

For the crack to be stable, Berry² further showed that $\gamma = (F\delta/WC) \cdot (\nu/4)$ where γ is the fracture surface energy, and W is the crack width. Wiechers¹ plotted $F\delta/W$ against C and used the slope thus obtained with the estimated value of ν to calculate γ . It was found in the current investigations that very erratic values were obtained at values of crack length less than 80 mm or greater than 200 mm, and these results were ignored in the calculations of ν and γ . (The assumptions made in the theory become invalid when either the crack length is short or the remaining uncracked length is short.) With some samples, however, the scatter was still considerable between these limits. *Figures 3* and *4* show one of the best and one of the worst respectively.

In the worst cases the scatter of the results was such that the 95% confidence limits for the slope of $F\delta/W$ against C were very wide. The method of calculation used by Wiechers¹ was therefore changed to make use of the fact that the theory predicts that $F\delta/W$ should be proportional to C and not merely linearly related to C . Wiechers¹ found a linear relationship which did not quite go through the origin, but was very close to it (the scatter of the points about the line having been small for their material). It was therefore concluded that it was more meaningful to calculate the value of $F\delta/WC$ for each point on the graph and to use the individual values of this to compute the mean and the 95% confidence limits.

Broutman⁶ showed theoretically that ν should vary with crack length and beam height (see *Figure 5*), taking into account the contribution of the deflections due to bending, shear and end rotation of the beam. It can be

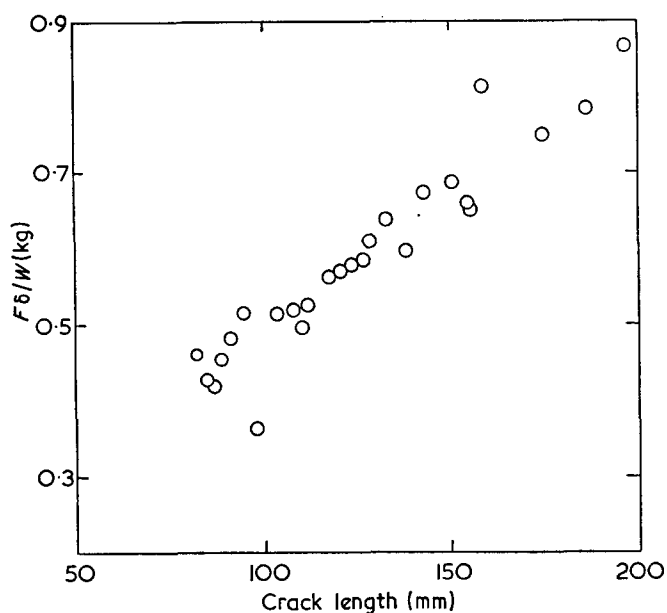


Figure 3 Example of low scatter in sample K3

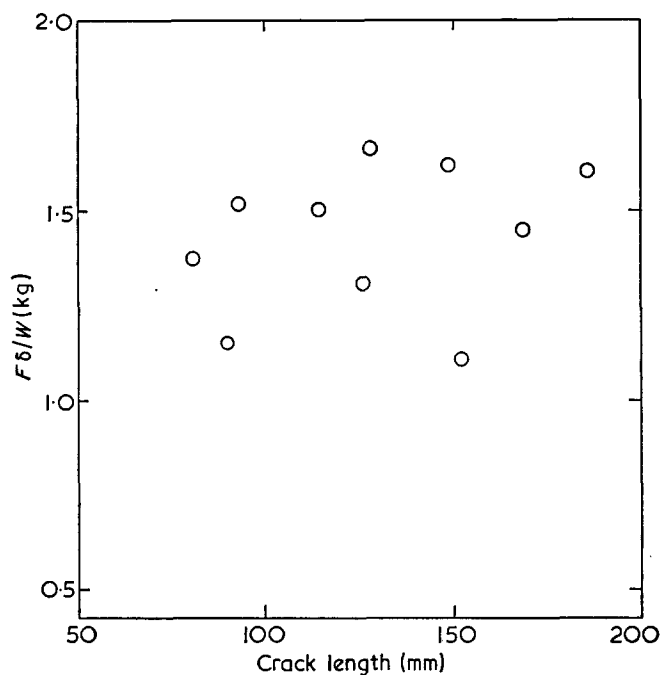


Figure 4 Example of very high scatter in sample L3

estimated from *Figure 5* that for a beam height of 25 mm and crack lengths of 80 to 200 mm the value of ν varies from about 2.4 to 2.8 giving an average of 2.6. Broutman then used his individual values of ν to calculate *FSE* and took the average value of *FSE*.

Although, in this work, individual values of ν for each value of C have not been calculated, an effective average value of ν has been used. This is adequate in view of the material.

There are thus three methods of calculation for *FSE*: (i) Berry²—using the average experimental value of ν with the slope of $F\delta/W$ against C ; (ii) Broutman⁶—using the individually calculated theoretical values of ν for each point and the slope of $F\delta/W$ against C ; and (iii) as in this report—using the average experimental value of ν and the average of the individual values of $F\delta/WC$.

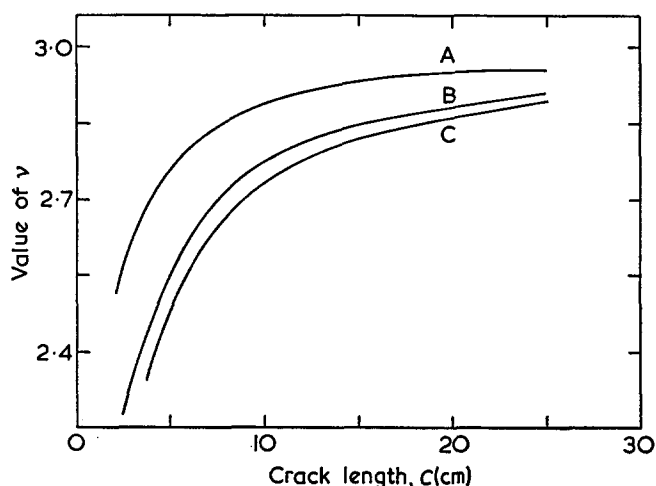


Figure 5 Values of ν for different crack lengths and dimensions, h (see Figure 2a). A, $h=6.35$ mm; B, $h=12.7$ mm; C, $h=15.24$ mm

Table 2 Values of FSE for dry and wet epoxide and polyester materials
All values of FSE are quoted in J/m^2

Batch	Tested dry	Immersion period			Average error
		12 days water injected	12 days surface dried	70 days water injected	
Polyester:					
H	56	66	—	—	21
K	31	34	28	—	4
P	30	45	29	37	3
Column mean	39	48	28	37	—
Epoxide:					
J	87	126	59	—	12
L	62	—	69	—	13
M	66	87	59	—	7
N	91	79	73	98	17
O	77	85	76	82	9
Column mean	77	94	67	90	—

Applying these three methods to Broutman's results we obtain the following FSE values: (a) $205 J/m^2$; (b) $238 J/m^2$ with a standard error of $12 J/m^2$; (c) $215 J/m^2$.

These values should not be compared with those obtained from the work in this paper since the material used by Broutman was different.

RESULTS AND DISCUSSION

Effect of water on resins

The fracture surface energies (FSE) for the unmodified epoxide and polyester resins were measured and are shown in Table 2. The row corresponding to a particular letter contains samples from one batch of mixed compound. The first column of figures shows the dry FSE values. The values quoted in the second column of figures refer to samples which were conditioned by 12 days immersion in water and tested with water injected at the crack tip before each jump. The next column gives the results of samples which were conditioned as those above, but were surface dried by blotting the surface with tissue paper immediately before testing. Finally results are shown for a few samples that were

immersed in water for 70 days and then tested as those in the second column.

The 95% confidence limits for the estimation of the result for each sample were calculated. The deviations of these limits from their respective means were averaged and are given as 'average error' in the last column. The scatter of results which would be expected for the various samples in one batch (if tested under the same conditions) was greater than would be anticipated from the 'average error' quoted, since the latter takes no account of variation between samples. Sample L tested under wet conditions was omitted because its very erratic results meant that the mean value was useless.

Table 3 shows values of FSE in the first column, as in Table 2, but the second column gives values of samples that were immersed in water for 12 days and tested while totally immersed during test.

Table 4 is a consolidated form of the results showing percentage changes in FSE from the corresponding 'dry' values of each batch of mixed compound.

The dry samples give average FSE values of $42 \pm 6 J/m^2$ for the polyester and $80 \pm 5 J/m^2$ for the epoxide.

Weichers¹ showed that FSE of epoxide varies with

Table 3 FSE values of samples tested dry and totally immersed in water
All values of FSE are quoted in J/m^2

Batch	Tested dry	12 days immersion (totally immersed during test)		Average error
Polyester:				
R	36	32	2	2
S	54	53	12	12
Column mean	45	42	—	—
Epoxide:				
T	95	81	21	21
U	80	72	11	11
Column mean	87	76	—	—

Table 4 Changes in FSE shown as a percentage of the dry value

Batch	FSE dry (J/m^2)	Immersion period			Average error ($\pm\%$)
		12 days water injected (%)	12 days surface dried (%)	70 days water injected (%)	
H	56	+18	—	—	38
K	31	+10	-10	—	13
P	30	+50	-3	+23	12
Column mean	39	+25	-7	+23	—
J	87	+45	-32	—	14
L	62	—	+11	—	21
M	66	+32	-11	—	11
N	91	-13	-20	+8	19
O	77	+10	-1	+7	13
Column mean	77	+18	-11	+7	—

Batch	FSE dry (J/m^2)	12 days immersion (totally immersed during test) (%)		Average error ($\pm\%$)
R	36	-11	7	7
S	54	-2	22	22
Column mean	45	-6	—	—
T	95	-15	22	22
U	80	-10	14	14
Column mean	87	-13	—	—

cure temperature and that a minimum value of *FSE* is obtained at a curing temperature of about 140°C (for 24h). Furthermore a reduction in cure time from 24h to 8h (with a cure temperature of 120°C) gives a linear increase in *FSE*. The epoxide material used in this work was cured at a higher temperature of 180°C but for 3h. In accordance with his observation a higher value of *FSE* than obtained by Weichers at 155°C was obtained.

Although the changes produced by water immersion were in most cases insignificant relative to the 'average error' (Tables 3, 4 and 5) there was a trend that suggests that the injection of, and immersion in, water during test increases and decreases the value of *FSE* respectively. The changes in all cases are not more than 50%.

The absorption of water appeared to decrease the *FSE*, as seen from the results on samples which were surface dried. When the water was injected the *FSE* was increased and this effect must be assumed to be related to the presence of water at the surface. It might be thought that this effect results from an alteration in the true surface energy changes occurring on cracking, but it was several orders of magnitude too large. No obvious explanation could be found and further work would be required to confirm the effect and to elucidate the mechanism. The results for the totally immersed samples were similar to those for the surface dried samples. This cannot be explained unless it is assumed that injection produces a more intimate contact between water and the crack tip.

Rubber modified epoxide

With the rubber modified epoxides it was noted that the visible quality of the fracture surface was changed by the mode of the crack initiation, i.e. the fish tail and the speed of initiation. No visible difference was observed on: (a) changing the crack width from a half to a quarter of sample thickness; (b) changing the groove width from 0.13mm to 3.2mm; and (c) using crosshead speeds (loading rates) after initiation of 0.4, 1 and 4mm/min.

Table 5 shows values of *FSE* for rubber modified epoxides. The mix details of the other additives are given in Table 1. Samples M3 to M6 (the suffixes indicate different batches) were materials as described by McGarry which includes DMP 30 as the sole curing agent. Samples T1 contain the same curing agents as in the unmodified epoxide material. The curing agents in samples T2 were the same as those in the unmodified material with BDMA replaced by DMP 30 (this is the same as NMA added to the McGarry material).

The addition of the rubber to the unmodified material doubled the *FSE* (see T1). The use of DMP 30 in place of the other curing agent doubled the *FSE* (see T2).

Table 5 *FSE* of rubber modified epoxide resins

Batch	Mean batch <i>FSE</i> (J/m ²)	Standard deviation
M3	260	29
M4	330	45
M6	310	25
T1	160	22
T2	210	20

The McGarry type material showed a fourfold improvement in *FSE* compared with the unmodified material. The average *FSE* of the McGarry type material was 310 ± 10 J/m². Hence comparing M3-6 with T2 showed that the inclusion of NMA while assisting the production by lowering the viscosity, limited the improvement that could be obtained by using the rubber.

The between-batch variability of the M3-6 sample was similar to that for unmodified resins. Although the standard deviation of the samples M6 (cut from one sheet) was lower than that for M3 and M4 it was not significantly so.

CONCLUSIONS

(1) The fracture surface energy for the dry tested samples was 42J/m² for the polyester and 80J/m² for the epoxide with standard errors of 6J/m² and 5J/m² respectively.

(2) Water absorbed by the resin in 12 days at 30°C tends to reduce the fracture surface energy, although the average decrease for the epoxide was only about 10%. The decrease for the polyester was about half that for the epoxide.

(3) The presence of water around the sample during test, after an immersion period of 12 days at 30°C, tends to reduce the fracture surface energy, although the average decrease for the epoxide was only about 10%. The decrease for the polyester was about half that for the epoxide.

(4) Under certain circumstances, if free water was in contact at the beginning of the fracture mode with the previously soaked sample, the values of fracture surface energy tended to increase. The average change was about 20%.

(5) The best rubber modified materials tested showed an increase in fracture surface energy of about four compared with the unmodified material.

(6) The modifications given in this paper were necessary to improve the test method. The use of a wide groove on the rubber modified samples did not lead to wandering of the crack within the useful region of the crack length.

ACKNOWLEDGEMENTS

The author is grateful to the Army Department of the Ministry of Defence for their support for the work described. Thanks are also extended to Mr D. I. James of RAPRA for carrying out the electron microscopy.

REFERENCES

- Weichers, W. *MSc Thesis* Loughborough University, 1969
- Berry, J. P. *J. Appl. Phys.* 1963, **34**, 62
- Diggwa, A. D. S. and Norman, R. H. *Plastics and Polymers* 1972, **40**, 263
- McGarry, F. J. *IUPAC Conf., Toronto* 1968, **2**, Sect. A9.4, p 5
- Outwater, J. O. and Gerry, D. J. *Mod. Plast.* 1967, **44**, 156
- Broutman, L. J. *et al. Ill. Inst. Technol. Tech. Rep. AD 698567* 1969 (Aug.)

APPENDIX I

Water absorption check

In order to assess whether 12 days immersion was adequate to produce substantial saturation a number of sections of epoxide and polyester were immersed in

distilled water at 30°C over an extensive period. In order to approximate the water absorption at the bottom of the groove of the FSE sample, sheet samples were produced 1.5 mm thick and were machined down to sections approximately 20 mm square. Their flat surfaces were slightly ground to resemble the machine surface of the groove. Periodically weight measurements were taken and Figure 6 shows the percentage water absorption with time of immersion.

The water absorption of the polyester samples changes only slowly after 12 days immersion. However, to

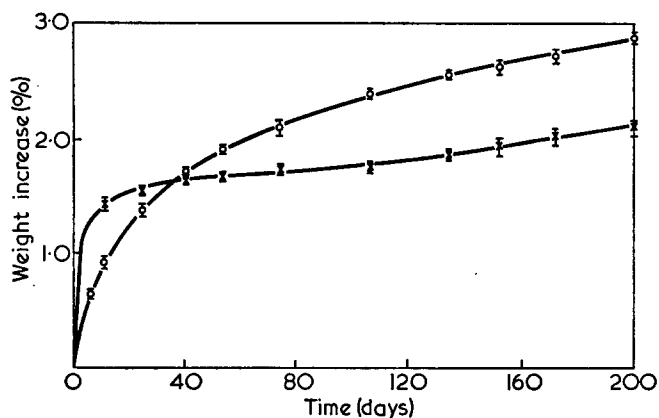


Figure 6 Water absorption curves. ○, Epoxide; ×, polyester

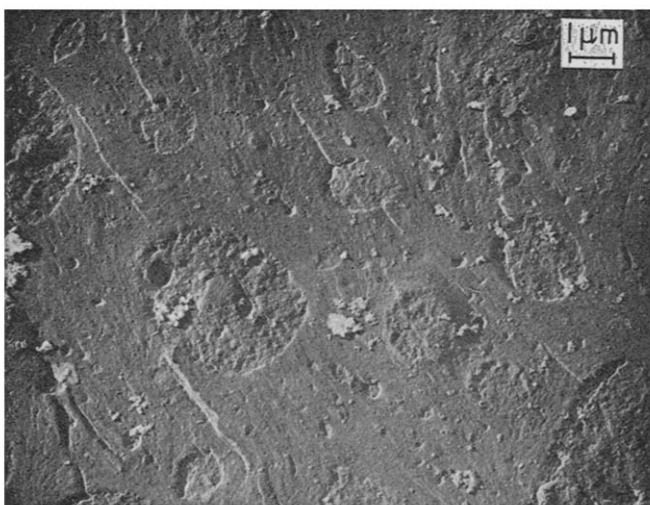


Figure 7 Electron micrograph of rubber modified epoxide material showing the typical distribution of rubber particles

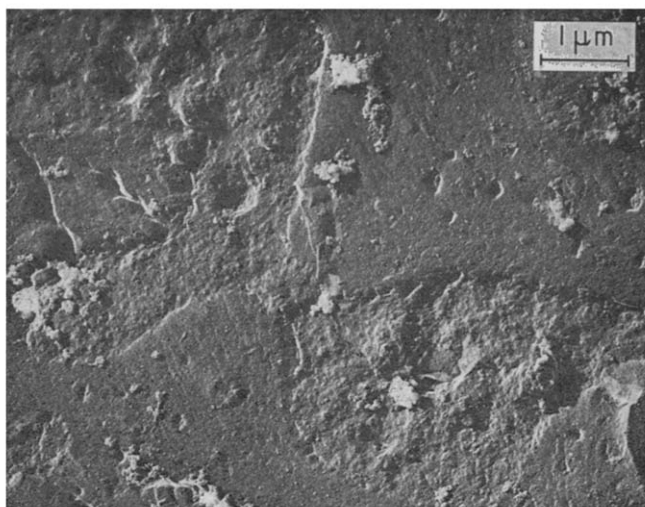


Figure 8 Electron micrograph of an irregular particle in rubber modified epoxide

achieve a similar condition with the epoxide samples about 100 days would be required and this was impractical. Nevertheless after 12 days immersion the epoxide samples reached about 40% of the 200 day figure and this should be sufficient to at least observe whether water has any effect.

APPENDIX II

Electron microscopy of rubber modified material

Specimens were cut from the McGarry⁴ type material and an unsuccessful attempt was made to produce a section suitable for transmission electron microscopy. Difficulty was encountered in staining the specimens as a few days immersion in osmic acid gave insufficient staining. Even long term immersion (four weeks) gave poor absorption and upon sectioning, using an ultramicrotome, all the sections obtained were badly fractured or shattered.

A replica was then made and assessed using standard techniques, of the fracture surface in the region where the crack tip came to rest during the fracture mode of the test. Figure 7 shows a typical distribution of rubber particles of the order of 1 μm diameter. It is reasonable to assume that this reinforced epoxide material is basically similar to that used by McGarry⁴. The type of irregular particle, about 7 μm in length shown in Figure 8 was found to be exceptional. It can also be seen in these Figures that a series of directional fractures (or crazes) run within and between particles.

A correlation of Young's modulus with yield stress in oriented poly(vinyl chloride)

F. F. Rawson and J. G. Rider

*Department of Physics, University of Surrey, Guildford, Surrey, UK
(Received 14 September 1973)*

The variations of tensile and compressive yield stresses and of Young's modulus of oriented poly(vinyl chloride) sheet with direction and with degree of orientation, represented by birefringence, are shown. Young's modulus was calculated from elastic stiffness constants measured by an ultrasonic pulse method at 5MHz with estimated strain and strain rate amplitudes of 2×10^{-5} and 100 s^{-1} . Yield strains were about 5×10^{-2} measured at strain rates of about $2 \times 10^{-2} \text{ s}^{-1}$. Although the measuring conditions were so different there was found to be a close correlation between tensile yield stress and Young's modulus, the two quantities being connected by a simple linear relationship, as direction of measurement and degree of orientation were varied. Compressive yield stress did not correlate with Young's modulus, and changed little with direction or degree of orientation by comparison with tensile yield stress. The empirical linear relationship between tensile yield stress and Young's modulus, difficult to account for theoretically, might form the basis of a method for determining tensile yield stress ultrasonically.

INTRODUCTION

Several authors have suggested that there is a correlation between the changes in tensile yield stress and Young's modulus which take place when a thermoplastic polymer is oriented¹⁻⁵. The present paper discusses the existence of such a correlation in oriented poly(vinyl chloride) (PVC), a polymer not considered in refs 1 to 4. Two points of difference between the present work and that cited above are first, that consideration is given not only to tensile but also to compressive yield stress, and secondly that Young's modulus was determined from elastic stiffness constants measured at 5MHz by an ultrasonic pulse method, rather than from the load-extension curve or by a low frequency resonance method.

EXPERIMENTAL

Young's modulus and compressive yield stress were measured on 5.5mm thick Darvic (ICI Ltd) sheet. Comparatively few tensile yield stress measurements could be obtained from this material because of premature fracture. For this reason use is also made of tensile yield stress data which had already been obtained on thinner sheet of other grades, namely 0.5mm thick Vybak (Bakelite Ltd) sheet and 1mm Cobex (Bakelite-Xylonite Ltd) sheet.

The sheets were oriented by drawing in a tensile testing machine at an elevated temperature and holding at constant length while cooling to room temperature. The Darvic and Cobex were drawn at 80°C, while some Vybak was drawn at 71°C and some at 90°C. Elastic stiffness constants, tensile and compressive yield stresses and optical birefringence were all measured at room temperature. Some of these measurements have been reported elsewhere in other contexts and the methods of measurement described⁶⁻⁸.

One point about the measurements which is relevant here is that the yield stresses on one hand and the elastic constants on the other were measured at widely different strains and strain rates. Yield strains were typically about 5×10^{-2} and yield stresses were measured at strain rates of about $2 \times 10^{-2} \text{ s}^{-1}$. Young's modulus values were derived from stiffness constants measured by means of stress pulses in which the frequency was 5MHz, the strain amplitude, estimated from the power in the pulses, was about 2×10^{-5} , and the strain rate was about 100 s^{-1} . Furthermore, while yield stresses in tension and compression were measured separately, the Young's modulus values represent some average of tensile and compressive behaviour about a mean zero stress.

The complications of making use of results from three different drawing temperatures and three different grades of PVC were overcome by using birefringence rather than draw ratio as a measure of the degree of orientation in the material, and by normalizing all yield stresses by dividing the yield stresses for a given grade by the yield stress of that grade in the unoriented state to give the quantity referred to hereafter as the yield stress ratio.

RESULTS

Tensile yield stress

For a given degree of orientation the tensile yield stress varied with direction in the plane of the sheet in the characteristic manner shown in *Figure 1*. The angle plotted, λ , is that between the direction in which the material was drawn to orient it (the draw direction) and the direction in which the tensile yield stress was subsequently measured. The experimental values in *Figure 1* were obtained on Vybak of birefringence 3.56×10^{-3}

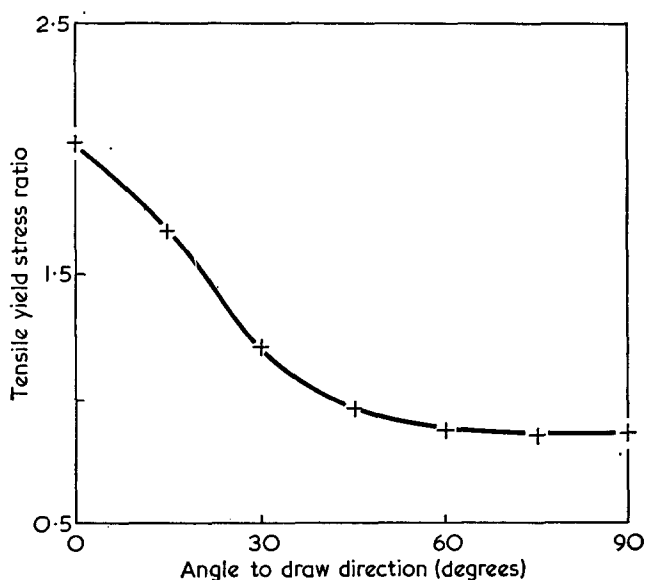


Figure 1 Variation with direction of the ratio of the tensile yield stress of oriented PVC to that of the unoriented material. This example is Vybak oriented by drawing at 71°C to a residual birefringence of 3.56×10^{-3}

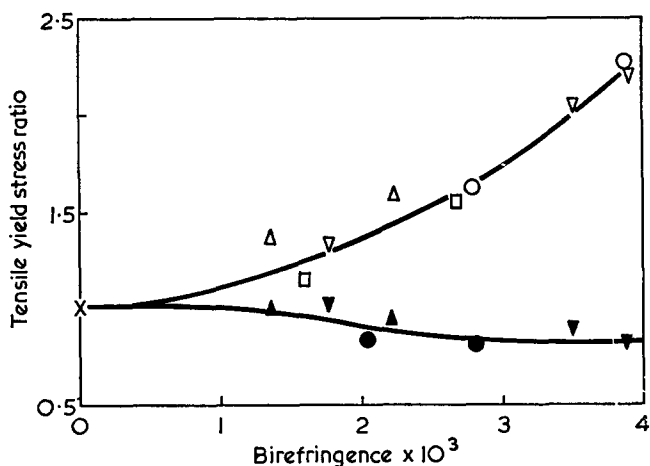


Figure 2 Variation with degree of orientation, indicated by birefringence, of the ratio of the tensile yield stress of oriented PVC to that of the unoriented material, for directions parallel to $\lambda=0^\circ$ and at right-angles to $\lambda=90^\circ$, the orientation direction. The materials, orienting draw temperature and direction are indicated as follows:

Material	Draw temperature (°C)	Symbol	
		$\lambda=0^\circ$	$\lambda=90^\circ$
Darvic	80	□	■
Cobex	80	○	●
Vybak	71	▽	▼
Vybak	90	△	▲

which had been drawn at 71°C; the shape of the curve is typical.

The variation of tensile yield stress with degree of orientation is shown in Figure 2, in which the yield stress ratios parallel to and at right-angles to the draw direction ($\lambda=0^\circ$ and $\lambda=90^\circ$) are plotted against birefringence. The graph includes measurements made on Darvic and Cobex drawn at 80°C, and Vybak drawn at 71°C and 90°C. For clarity, yield stress ratios at intermediate angles are not shown in this Figure; as Figure 1 indicates they fall between the lines for $\lambda=0^\circ$ and $\lambda=90^\circ$.

Compressive yield stress

The corresponding graphs for compressive yield stress ratios are given in Figure 3 (Darvic, birefringence 3.63×10^{-3}) which typifies the variation with direction, and in Figure 4 (Darvic) which shows the variation at $\lambda=0^\circ$ and $\lambda=90^\circ$ with birefringence. (The normalization process conceals the fact that in the unoriented material the compressive yield stress was about 19% higher than the tensile yield stress⁷.)

Young's modulus

The Young's modulus values were calculated from the stiffness constants measured by Rawson and Rider⁸ on the Darvic sheet using a 5 MHz ultrasonic pulse technique. The oriented sheet was found to be elastically isotropic about the draw direction. Thus there were five independent elastic constants for any given state of orientation, and Young's modulus in a direction making

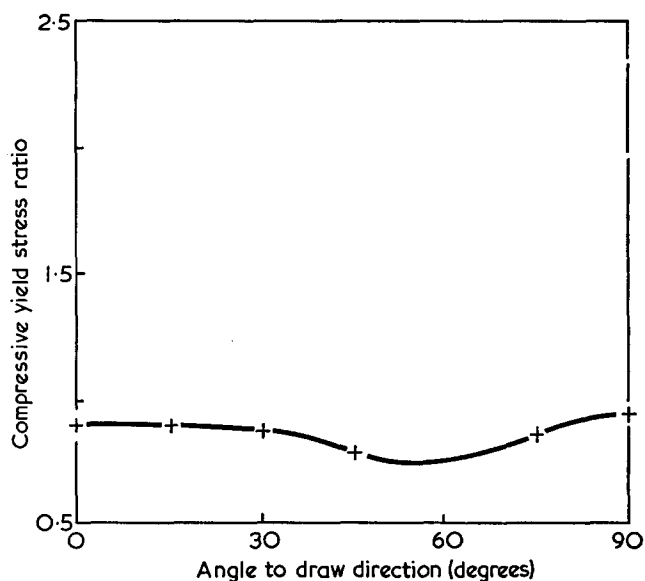


Figure 3 Variation with direction of the ratio of the compressive yield stress of oriented PVC to that of the unoriented material. This example is Darvic oriented by drawing at 80°C to a residual birefringence of 3.63×10^{-3}

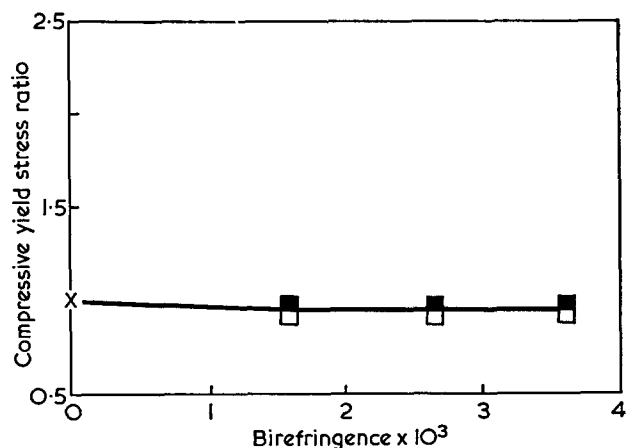


Figure 4 Variation with degree of orientation, indicated by birefringence, of the ratio of the compressive yield stress of oriented PVC to that of the unoriented material, for directions parallel to $\lambda=0^\circ$ (□), and at right angles to $\lambda=90^\circ$ (■), the orientation direction. The material was Darvic oriented by drawing at 80°C to the residual birefringence shown

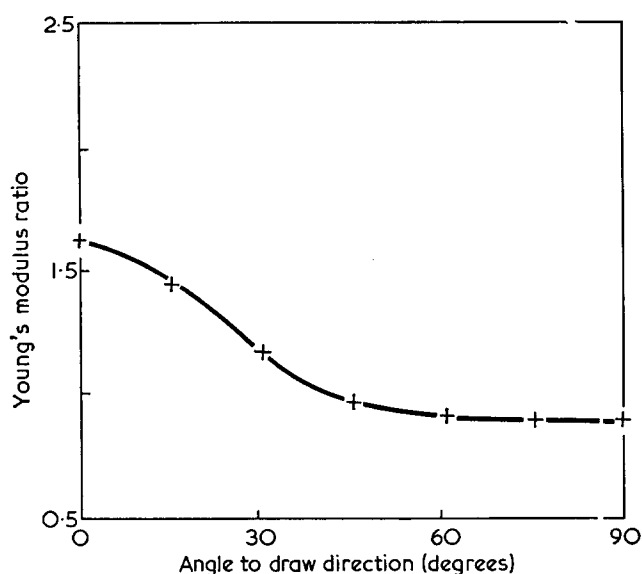


Figure 5 Variation with direction of the ratio of the ultrasonically determined Young's modulus of oriented PVC to that of the unoriented material. This example is Darvic oriented by drawing at 80°C to a residual birefringence of 3.63×10^{-3}

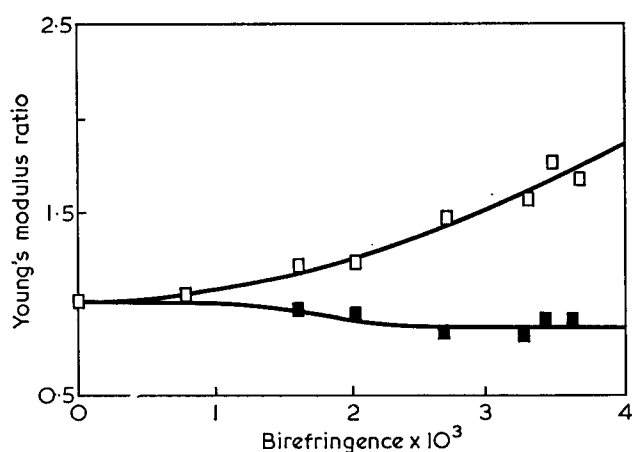


Figure 6 Variation with degree of orientation, indicated by birefringence, of the ratio of the ultrasonically determined Young's modulus of oriented PVC to that of the unoriented material, for directions parallel to $\lambda=0^\circ$ (\square), and at right-angles to $\lambda=90^\circ$ (\blacksquare), the orientation direction. The material was Darvic oriented by drawing at 80°C to the residual birefringence shown

angle λ with the draw direction was given by:

$$E_\lambda = [s_{11}\sin^4\lambda + s_{33}\cos^4\lambda + (2s_{13} + s_{44})\sin^2\lambda\cos^2\lambda]^{-1}$$

where s_{11} etc. are the compliance constants, which were calculated from the measured stiffness constants c_{11} etc.⁹; axis 3 is along the draw direction.

As with the yield stresses, the Young's modulus values have been normalized by division by the value for the unoriented material and the results are illustrated in the same way as the yield stresses. Figure 5 shows the variation of Young's modulus ratio with direction for a given degree of orientation (birefringence 3.63×10^{-3}) and Figure 6 shows the variation of Young's modulus ratios parallel to and at right-angles to the draw direction with birefringence. Young's modulus ratios for intermediate angles fall between the two lines in Figure 6.

CORRELATION BETWEEN YIELD STRESS AND YOUNG'S MODULUS

The procedures of normalizing the yield stresses and using birefringence as a parameter to indicate degree of orientation have been successful in bringing together the tensile yield stress data from the different materials and drawing temperatures (Figure 2) and establishing clearly the pattern of behaviour. The tensile yield stress in the direction of molecular orientation (the draw direction) rose steeply compared with the slight fall and levelling-off at right-angles to the orientation direction as the degree of molecular alignment increased.

Marked differences in behaviour between tensile and compressive yield stresses can be seen by comparing Figures 1 and 3 and Figures 2 and 4. The variations of compressive yield stress both with direction and with degree of orientation were small. Compressive yield stress at right-angles to the orientation direction was slightly higher than in the orientation direction and there was a minimum value in the region of about 45°–60° to the orientation direction. With increasing degree of orientation the compressive yield stress in all directions fell below the value for the unoriented state. Similar results of measurements in the orientation direction on polypropylene have been reported by Duckett *et al.*¹⁰.

The behaviour of Young's modulus clearly paralleled that of the tensile yield stress but not that of the compressive yield stress, as Figures 1 to 6 show. The close similarity in behaviour between Young's modulus and tensile yield stress is brought out in Figure 7 in which the tensile yield stress ratio is plotted against the Young's modulus ratio using smoothed values read from the curves in Figures 2 and 6 for $\lambda=0^\circ$ and $\lambda=90^\circ$ at the same set of birefringence values and from the curves in Figures 1 and 5 for intermediate values of λ for a birefringence of 3.6×10^{-3} (considering the actual values

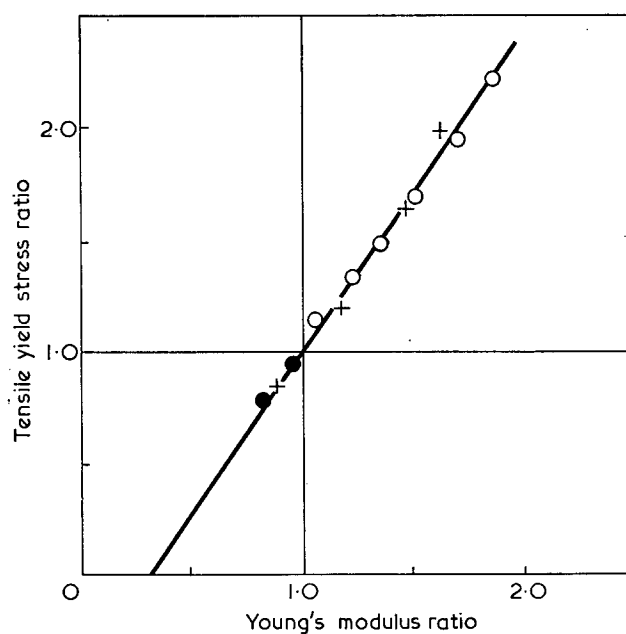


Figure 7 Tensile yield stress ratio plotted against ultrasonically determined Young's modulus ratio. Source of data: +, for a range of directions, birefringence 3.6×10^{-3} , Figures 1 and 5; o, for a range of birefringence, parallel to the orientation direction, upper curves of Figures 2 and 6; •, for a range of birefringence, at right-angles to the orientation direction, lower curves of Figures 2 and 6

of 3.56×10^{-3} and 3.63×10^{-3} to be the same). All the points lie close to a common straight line, thus emphasizing the close correlation of the tensile yield stress and Young's modulus ratios. This empirical result can be written:

$$\frac{\sigma_\lambda - \sigma_u}{\sigma_u} = 1.45 \frac{(E_\lambda - E_u)}{E_u} \quad (1)$$

Here, σ denotes the tensile yield stress and E the Young's modulus. Subscript λ indicates that the quantity is measured in the oriented material at angle λ to the draw direction and subscript u refers to the unoriented material. The equation holds for all values of λ .

There was no such general correlation between compressive yield stress and Young's modulus. Although, as Figures 4 and 6 show, compressive yield stress and Young's modulus at 90° to the orientation direction behaved in the same way in that both decreased slightly with increasing orientation, such similarity in behaviour did not extend to other directions, the difference being most marked in the orientation direction.

DISCUSSION

The results show that the effects of orientation on Young's modulus and tensile yield stress were closely correlated although the two quantities were measured under widely different conditions, whereas the effect on compressive yield stress did not correlate. Robertson¹ has given a theory providing a relationship between yield stress and elastic constants based on the hypothesis that yield takes place at a specified state of strain irrespective of the degree of orientation. There are two difficulties in applying his theory to these results. First, the elastic constants in the theory are those appropriate to the conditions in which the yield stress is measured, whereas in these experiments this condition did not hold. Secondly, no allowance is made in the theory for

the observed difference in yield stress in tension and compression, a difference which has been shown^{7, 10} to arise from two sources, the effect of the mean normal stress and the effect of orientation. What has to be explained here is why the Young's modulus correlates with the tensile yield stress and not the compressive.

Because of these difficulties it does not seem possible at present to give a satisfactory explanation for the empirically determined equation (1). Nevertheless this equation may provide the basis for a method of determining the tensile yield stresses of oriented PVC (and perhaps other thermoplastics) from ultrasonic elastic constant measurements which might in some circumstances be advantageous.

ACKNOWLEDGEMENTS

The authors wish to thank the Science Research Council and the Department of Trade and Industry for financial assistance with various parts of the work.

REFERENCES

- 1 Robertson, R. E. *Rep. No. 64-RL-(3580 C)*, General Electric Research Laboratory, Schenectady, NY, 1964
- 2 Vincent, P. I. 'The Encyclopaedia of Polymer Science and Technology', John Wiley, New York, 1967, Vol 7, p 292
- 3 Allison, S. W. and Ward, I. M. *Br. J. Appl. Phys.* 1967, **18**, 1151
- 4 Bridle, C., Buckley, A. and Scanlan, J. *J. Mater. Sci.* 1968, **3**, 622
- 5 Hargreaves E. *PhD Thesis*, University of Surrey, 1970
- 6 Rider, J. G. and Hargreaves, E. *J. Polym. Sci. (A-2)* 1969, **7**, 829
- 7 Rawson, F. F. and Rider, J. G. *J. Polym. Sci. (C)* 1971, **33**, 87
- 8 Rawson, F. F. and Rider, J. G. *J. Phys. (D: Appl. Phys.)* 1974, **7**, 41
- 9 Nye, J. F. 'Physical Properties of Crystals', Clarendon Press, Oxford, 1957
- 10 Duckett, R. A., Ward, I. M. and Zihlif, A. M. *J. Mater. Sci.* 1972, **7**, 480

Impact strength and mechanical losses in thermoplastics*

P. I. Vincent

Imperial Chemical Industries Limited, Plastics Division, Welwyn Garden City, Herts, UK
(Received 7 September 1973)

Statistical analysis of results on twenty different thermoplastics shows that there is an inverse correlation between impact strength and dynamic modulus. However, at best, this correlation only accounts for about two-thirds of the variance in impact strength. It is less satisfactory for composites than for pure polymers and it does not account for other secondary factors such as the embrittling effect of bulky side groups and reduction in molecular weight.

Some of the residual variance may be accounted for by an additional direct influence of mechanical losses on impact strength. Impact tests on some polymers over a wide temperature range have shown pronounced peaks in *brittle* impact strength close to peaks in loss tangent.

INTRODUCTION

Many authors¹⁻¹⁸ have considered the possibility that there is some relation between the short-term toughness of thermoplastics, as judged by their impact strengths or by their brittle points, and their moduli and loss processes determined by dynamic mechanical experiments. The significance of this line of study is that it helps in the explanation and understanding of observed trends in toughness; more is known about the influences of chemical constitution and secondary factors on dynamic mechanical properties than about their influences on toughness. If a trend in impact strength is inversely correlated with a trend in dynamic modulus, it implies that the change in impact behaviour is caused by a change in molecular or segmental mobility. Conversely, if there is a trend in impact strength, without a related trend in dynamic mechanical properties, it indicates that the cause is a change in the severity of structural defects or in some other factor which does not affect molecular mobility.

The main purposes of this paper are to consider how far the effects of chemical constitution on toughness can be accounted for by the inverse correlation between impact strength and dynamic modulus, and to present some evidence relating peaks in *brittle* impact strength to relaxation processes.

CORRELATION OF TOUGHNESS WITH MODULUS

The evidence for some relation between toughness and loss processes has been reviewed by Oberst³, Boyer¹⁴ and Heijboer¹⁵. To obtain further quantitative detail, statistical analyses were performed on results which had been obtained on the twenty thermoplastics which are listed and classified in *Table 1*. The following five mechanical tests were used.

* Presented as a Symposium Lecture at the IUPAC International Symposium on Macromolecules, Aberdeen, September 1973.

1. The impact behaviour was assessed using Charpy-type impact tests, with various notch tip radii¹⁹. For the preliminary analyses, the results were taken every 10°C from -20°C to +60°C. It was found that better correlations were obtained by using the four-fold classification described by Vincent¹⁹ than by using the actual values of impact strengths. The following nomenclature will be used in this paper: $IS(UN)$ = impact strength of unnotched specimens; $IS(x)$ = impact strength of specimens with notch tip radius x mm; $IS(VS)$ = impact strength with very sharp notches; class 1—specimens break even when unnotched, $IS(UN) < 40$ kJ/m²; class 2—no break unnotched or $IS(UN) > 40$ kJ/m², $IS(2) < 20$ kJ/m²; class 3— $IS(2) > 20$ kJ/m² or no complete break, $IS(1/4) < 10$ kJ/m²; class 4— $IS(1/4) > 10$ kJ/m² or no complete break. The class numbers 1-4 were used for impact strength rating in the statistical analyses; 1.5, 2.5 and 3.5 were used for borderline cases, giving a seven point scale.

2. The real part of the dynamic Young's modulus in flexure (E') was obtained from the vibrating reed apparatus described by Robinson²⁰. The frequency range covered was approximately 100-300 Hz (in this apparatus it varies with the modulus).

3. The yield stress (σ_Y) was obtained from tensile tests as described by Vincent²¹ at an extension speed of 0.5 in/min (0.21 mm/s). Occasionally, when σ_Y could not be measured in tension, because of supervening brittle fracture, it was estimated using compression tests.

4. The tensile yield stress in static fatigue was obtained at +20°C by the method described by Gotham²². The values at 10², 10⁴ and 10⁶ s were used for analysis.

5. The flexural strength in dynamic fatigue was obtained at +20°C/0.5 Hz by the method described by Gotham²³. Again the values at 10², 10⁴ and 10⁶ s were used.

The matrix of correlation coefficients between the various test methods was obtained from the assembled

results. There is little doubt of the statistical significance of the correlations quoted below. Typically, a correlation coefficient of ± 0.70 is significant at the 0.1% level and one of ± 0.60 at the 1.0% level.

The stress needed to cause failure in dynamic fatigue after 100s correlated highly with the static fatigue stress at the same time (0.97). The corresponding correlation for 10⁴s was much poorer (0.68) and after 10⁶s the correlation between dynamic and static fatigue was not significant even at the 5% level. Furthermore, there was no significant correlation between impact behaviour and dynamic fatigue. It can be deduced that additional considerations are needed to account for the effects of chemical constitution on fracture under cyclic stressing. Fatigue will not be considered further in this paper; the 'toughness' discussed is only that observed in fast or short-term tests.

With due allowance for the difference in effective testing rate, E' and σ_Y were well correlated (0.81 to 0.94) so it is clearly likely that, if there is an inverse correlation between impact strength rating (ISR) and E' , there will also be one between ISR and σ_Y . This proved to be true but the correlations between ISR and E' were better than those between ISR and σ_Y , between ISR and $1/E'$ or between ISR and $1/\sigma_Y$. Figure 1 is a graph of the correlation coefficient between ISR and E' plotted against the difference between the temperatures at which the two measurements were made. It can be judged from the graph that the best correlations were obtained when the dynamic modulus was measured somewhat below the temperature of the impact strength rating. For the remainder of the analysis, ISR at temperature T was compared with E' at $(T-10)^\circ\text{C}$. In Figure 1, the correlation coefficients under these conditions lie from -0.69 to -0.80 . Thus it seems that there is a statistically significant inverse correlation between modulus and impact strength but that 36 to 50% of the variance in impact strength rating is not accounted for by changes in dynamic modulus.

Various changes were made in an attempt to refine and explore this correlation further: (1) some additional results were included, outside the previously selected temperature range. Table 1 lists the total temperature ranges of impact strength rating used for the various

Table 1 Thermoplastics used for statistical analysis

Material	Temperature range ($^\circ\text{C}$)	Code No.	Abbreviation
Non-crystalline polymers:			
Poly(methyl methacrylate) sheet	-130 to +80	1	PMMA
Poly(vinyl chloride) sheet	-130 to +60		
Polysulphone of bisphenol A	-20 to +60		
Poly(2,6-dimethyl-1,4-phenylene ether)	-20 to +60	2	PPO
Polycarbonate of bisphenol A	-20 to +60	3	PC
Non-crystalline composites:			
ABS	-20 to +60		
Two modified acrylics	-20 to +60		
Crystalline polymers:			
Low density polyethylene	-30 to +60		
High density polyethylene	-20 to +70	5	HDPE
Polypropylene (injection moulding)	-20 to +60	6	
Polypropylene (extrusion)	-20 to +60		
Two propylene-ethylene polymers	-20 to +60		
4-Methyl pentene-1 polymer	-20 to +60	7	P4MP
Oxymethylene polymer	-20 to +80		
Poly(ethylene terephthalate)	-20 to +70		
Polytetrafluoroethylene sheet	-20 to +70	8	PTFE
Nylon-6,6 (dry)	-80 to +70		
Glass-filled nylon-6,6 (dry)	-20 to +80	9	

All injection moulded except where otherwise indicated

materials; (2) the results on the glass-filled nylon were excluded because some of them were clearly discrepant on the high modulus-high impact strength side; (3) the results on the 4-methyl pentene-1 polymer (P4MP) were excluded because they were totally discrepant on the low modulus-low impact strength side; (4) values of E' above 5.5 and below 1.0 GN/m² were omitted because it was obvious that the relation became non-linear if these ranges were included.

These restrictions left 133 pairs of results on the 18 remaining materials. For these results, the correlation coefficient between ISR and E' was -0.80 so that 64% of the variance in impact strength was accounted for. Figure 2 is a diagram in which ISR is plotted against E' . It shows the calculated regression line (broken) and a band lying half a rating point above and below the regression line. The band is extended to high and low moduli and then defines a zig-zag region within which 65% of the results lie. Thus one can conclude that there is a correlation, permitting some prediction of impact behaviour from dynamic modulus, but that it is only a partial correlation and that there are significant deviations. Some of these deviations may be explained by considering secondary factors, other than dynamic modulus; their influences are discussed below.

SECONDARY FACTORS

The main difficulty in relating impact behaviour to chemical constitution is that there are many secondary factors which have substantial influences on impact strength. Some of these secondary factors may explain deviations from the general correlation between impact strength rating and dynamic modulus. Eleven points have been plotted in Figure 2 to represent the largest deviations of the most discrepant materials. For two materials, two points of each have been plotted, to

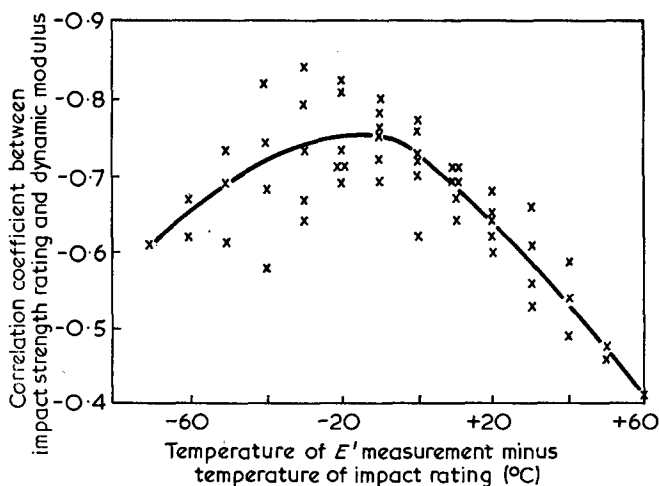


Figure 1 Correlation coefficient between impact strength rating and dynamic modulus as a function of the difference between the temperatures of measurement. The correlation appears best if the modulus is taken about 10°C below the temperature of the impact strength rating

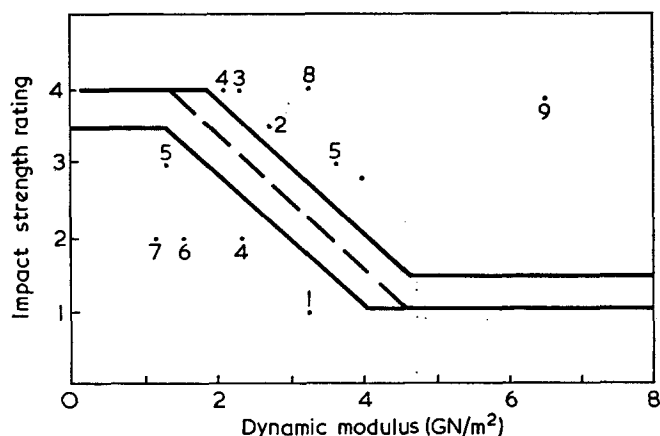


Figure 2 Correlation between impact strength rating and dynamic modulus. ----, regression equation; —, defines a band which contains 65% of the results. Points represent the most deviant results of the most discrepant materials. Code numbers refer to Table 1

represent deviations on both the high and low sides of the band. The code numbers, adjacent to the points, refer to Table 1.

The most discrepant material was the glass-filled nylon (code 9) between +60°C and +80°C. It seems likely that the substantial improvement in its impact behaviour between +50°C and +80°C is caused by the increased mobility of molecular segments on passing through the α process (the nomenclature for the various loss processes mentioned in this paper follows that of McCrum *et al.*²⁴). The dynamic modulus falls on passing through the α process but only to 6.5 GN/m² at +70°C. This shows that the effect on the impact strength of a high modulus caused by the presence of glass fibres differs from the effect of a high modulus caused by rigid molecules. One should not expect glass-filled or similar materials to be in the same correlation band as unfilled polymers.

The two points coded 4 in Figure 2 refer to the non-crystalline composites. It is true that addition of rubbery particles does both decrease the modulus and improve the impact strength but the quantitative agreement is poor; only about a third of the results for the three composites lie in the band. It seems best to conclude that these composites, like glass-filled nylon, need special consideration and do not fit simply into the pattern shown by the pure polymers.

Heijboer¹⁵ reported significant deviations from a correlation between the brittle point of unnotched specimens and the temperature of pronounced damping peaks. It was shown²⁵ that some of these deviations may be explained by the reduction in critical tensile strength with increasing molecular cross-sectional area; in particular, polymers with bulky side groups tend to be more brittle than would be expected from their dynamic mechanical properties. In the same way, bulky side groups can account for the low impact rating of PMMA at +80°C (code 1 in Figure 2) and of P4MP between -20°C and +60°C (e.g. code 7).

The results on the extrusion grade of polypropylene all lie inside the correlation band but most of the results on the injection moulding grade lie low (e.g. code 6 in Figure 2). This is probably a consequence of the well-known sensitivity of crystalline polymers to changes in molecular weight and in fabrication conditions.

If the results on these materials are omitted, 96 pairs of results remain; the correlation is improved and 77% of the results lie inside the band. Table 2 lists the four materials which are still discrepant, on the high side.

After examination of the evidence presented in the next section, a suggestion will be made why these particular materials should have relatively high impact strength rating for their moduli.

PEAKS IN BRITTLE IMPACT STRENGTH

Vincent¹⁹ gave reasons for believing that it is useful, for prediction of service performance, to measure impact strength as a function of test temperature on specimens with different notch tip radii. After making such measurements, on a wide range of thermoplastics, it is clear that the largest and most important change of impact strength with temperature occurs over the relatively narrow range of temperature where the type of fracture changes between brittle and ductile—the brittle point. Under some conditions this brittle point is close to a relaxation process but this is not invariably true.

For unnotched specimens, the brittle point may be formally defined as the temperature at which the brittle strength (σ_B)=the yield stress (σ_Y). σ_B is much less sensitive than σ_Y to changes in temperature and is not affected by dynamic loss peaks. Because of the correlation between E' and σ_Y , a reduction in E' shows up as a reduction in σ_Y and therefore, for constant σ_B , to a movement of the brittle point to lower temperatures and an improvement in the impact behaviour.

To some extent, this formal approach can be carried over to notched specimens, defining the brittle point as the temperature at which the brittle fracture energy (W_B)=the energy to yield (W_Y). Provided that W_B is not sensitive to changes in temperature or to the presence of loss peaks, the same procedure can be adopted. A reduction in E' shows up as a reduction in W_Y , movement of the brittle point down in temperature and an improvement in impact behaviour. This fits satisfactorily with the observed general inverse correlation between E' and impact strength rating.

Sometimes, however, W_B is not independent of temperature or of the presence of loss peaks; this complicates the formal approach and leads to exceptions from the general correlation. Careful selection of the notch tip radius may be needed to demonstrate peaks in W_B associated with peaks in the dynamic losses. If the notch is too blunt, the specimens become tough in the region of the loss process and the peak is only observable as a slight bump on the low temperature side of the steeply rising impact strength curve. If the notch is too sharp, the peak in W_B may not appear.

The first example considered will be a polysulphone (Union Carbide P 1700). The losses and the impact

Table 2 Thermoplastics with good impact behaviour relative to their dynamic moduli

Material	Temperature range of discrepancy (°C)	Code number
PTFE	-10 to +20	8
HDPE	-20 to +10	5
PC	-20 to +60	3
PPO	-30 to +20	2

behaviour of this polymer both depend in a very complicated way on the moulding conditions, heat treatment, storage times and water content and on interactions between these variables. As shown by Heijboer²⁶, its glass transition lies between 150°C and 200°C and it has a prominent β process around -100°C at 1 Hz. There is also another process, between the β process and the glass transition, which can be as large as the β process but which is particularly sensitive, both in amplitude and in temperature, to changes in the variables listed above. It can be suppressed completely by slow cooling or by suitable heat treatments. Because of this type of variability it is essential, when comparing impact behaviour and loss processes, to ensure that the specimens for the two experiments are in the same state and are stressed in the same direction. Figure 3b shows an impact strength as a function of test temperature under the following conditions: injection moulded discs, edge gated; specimens cut and stressed perpendicular to the flow direction; notch tip radius, 1 mm; 30 days in laboratory atmosphere before test; otherwise, as described in ref. 19. Figure 3a shows $\tan \delta$ as a function of temperature, for a specimen from the same sample, in the vibrating reed dynamic mechanical test. The β process has its peak at -65°C; this is a higher temperature than in Heijboer's test, presumably because of the higher frequency (220 Hz).

The marked similarity of the two peaks in Figure 3 is good evidence for some relation between the two properties. Either the impact strength is directly dependent on the mechanical losses or both are affected by the same changes in segmental mobility. It is important

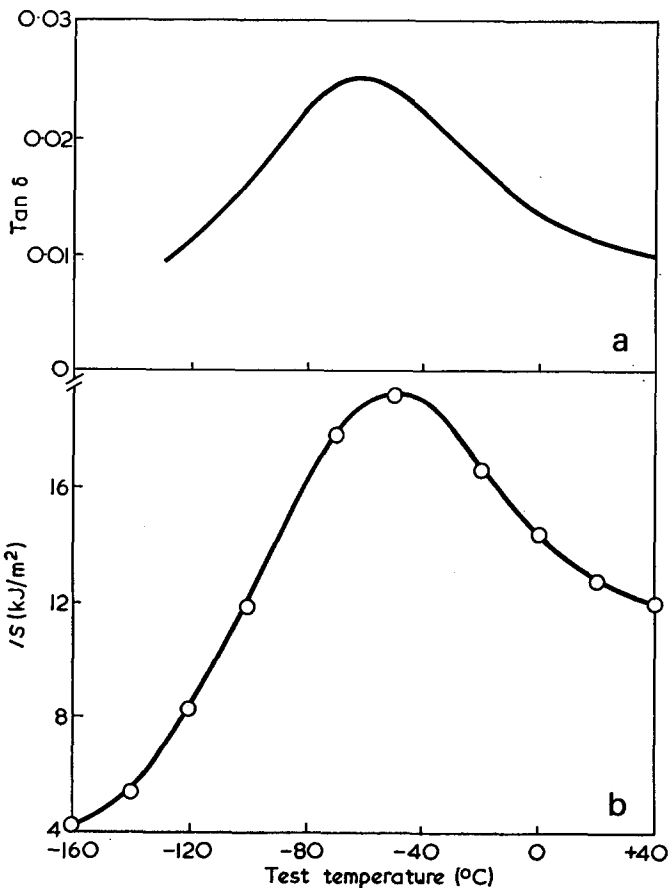


Figure 3 Effect of test temperature on a sample of the polysulphone of bisphenol A. (a) $\tan \delta$; (b) brittle impact strength with 1 mm radius notches

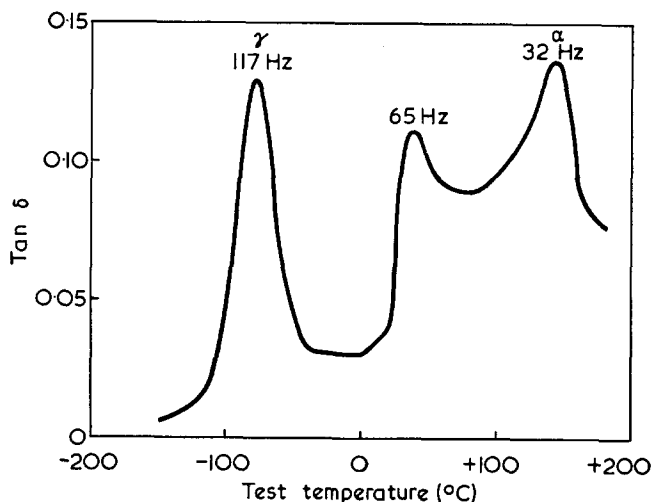


Figure 4 Effect of test temperature on $\tan \delta$ for a sample of PTFE. The frequencies at the peaks were as marked. The α and γ peaks are named following ref. 24

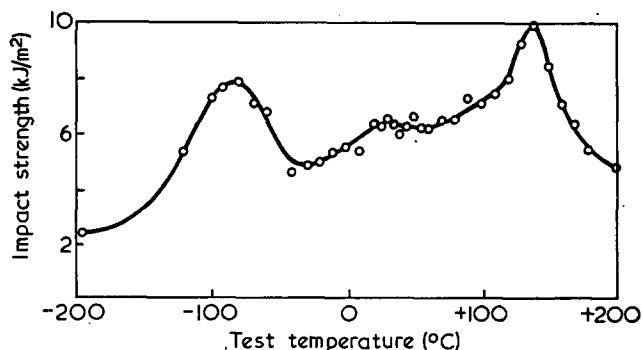


Figure 5 Effect of test temperature on impact strength with very sharp notches for a sample of PTFE similar to that of Figure 4

to emphasize that all the fractures represented in Figure 3b were brittle; the increasing impact strength between -160°C and -50°C is not a brittle-ductile transition. The decrease in impact strength between -50°C and +40°C is particularly significant; because it is accompanied by a decrease in E' , it cannot be expected to fit the general inverse correlation between E' and ISR . It is also worth noting that the peak in $\tan \delta$ occurs about 15°C below the peak in $IS(1)$. This supports the trend shown in Figure 1 in suggesting that the effective frequency of the impact test is higher than 200 Hz.

The second example is a PTFE (ICI Plastics Division Fluon G 163). The curve of $\tan \delta$ as a function of temperature from the vibrating reed experiment is shown in Figure 4 and is reasonably similar to the curve found in torsion at 1 Hz by McCrum²⁴ for a PTFE sample of 48% crystallinity. Impact strength, on specimens which were very sharply notched with razor blades, is shown as a function of temperature in Figure 5. It must again be emphasized that all the fractures appeared brittle; there is no question of a brittle-ductile transition. The similarity between the impact strength and $\tan \delta$ curves is even more striking than with the polysulphone and again there are regions where the impact strength is decreasing where the modulus is decreasing (-85°C to -30°C and +140°C to +200°C). It is also of interest to note that the α and γ processes, which are assigned to motion in the disordered regions of the polymer²⁴, appear more prominently in Figure 5 than the crystal disordering transitions in the room temperature region.

The third example is a polycarbonate of bisphenol A (Bayer Makrolon E). Figure 6a gives $\tan \delta$ as a function of temperature showing the prominent, high amplitude β process at -70°C . Figure 6b shows two curves of impact strength against temperature (1/4 mm notch tip radius and very sharp notches). Again, all the fractures represented were brittle and with very sharp notches the impact behaviour remained brittle up to $+140^\circ\text{C}$. $IS(VS)$ is constant between -100 and $+60^\circ\text{C}$ and is apparently not affected by the β process. In contrast, $IS(1/4)$ nearly doubled between -100 and -40°C , presumably because of the presence and influence of the β process. Between -40 and 0°C , $IS(1/4)$ sweeps up even more rapidly towards the very high (ductile) fracture energy at $+20^\circ\text{C}$. It is difficult to resist the conclusion that the good impact behaviour with 1/4 mm radius notches at $+20^\circ\text{C}$ is a consequence of the dependence of W_B on the β process. Most workers in this field have felt that there was a connection between the good impact behaviour of polycarbonate and its large β process. In particular, Turley¹³ showed that PC has a peak in dart drop impact strength near -50°C .

Figures 7a and 7b show $\tan \delta$ and $IS(1/4)$ as functions of test temperature for a sample of poly(2,6-dimethylene-1,4-phenylene ether) (General Electric PPO C-1001). As usual, all the fractures were brittle. The bump in $IS(1/4)$ between 0 and $+80^\circ\text{C}$ is probably associated with the bumps in $\tan \delta$ observed over a similar temperature range. The $\tan \delta$ curve differs somewhat from the two $\tan \delta$ curves given by Heijboer^{15, 26}; probably his samples were more slowly cooled.

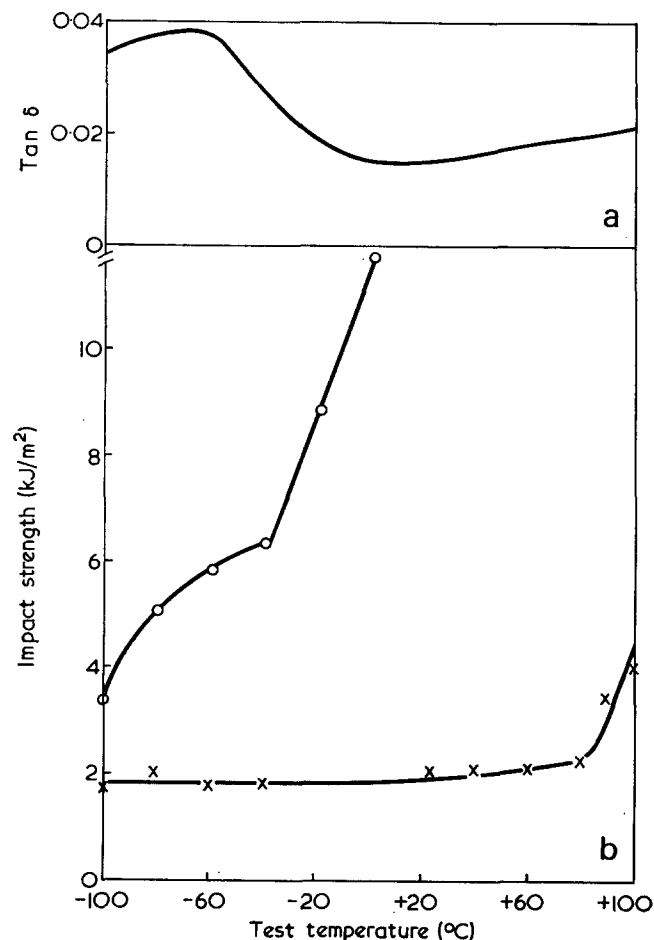


Figure 6 Effect of test temperature on a sample of the polycarbonate of bisphenol A. (a) $\tan \delta$; (b) brittle impact strength with 1/4 mm radius notches (O) and very sharp notches (x)

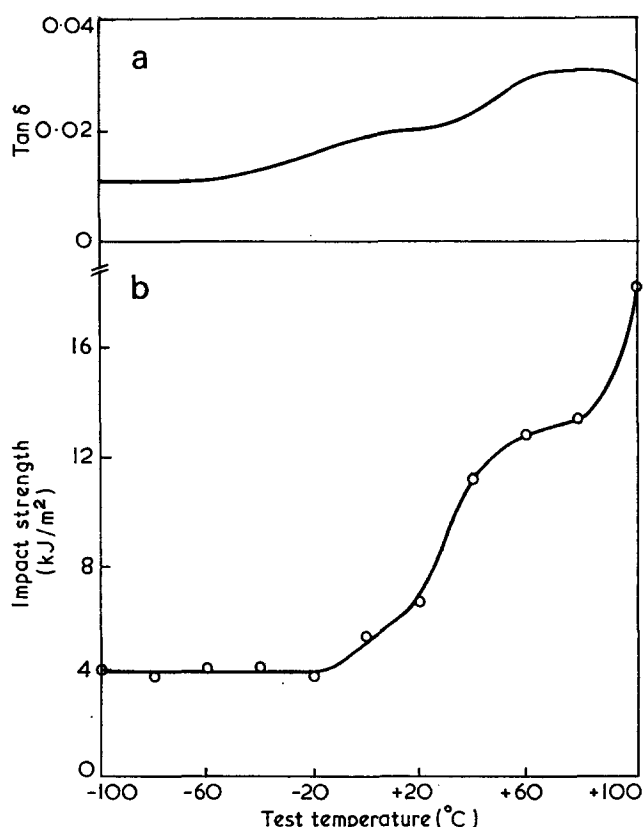


Figure 7 Effect of test temperature on a sample of poly(2,6-dimethyl-1,4-phenylene ether). (a) $\tan \delta$; (b) brittle impact strength with 1/4 mm radius notches

Figures 8a and 8b show $\tan \delta$ and $IS(1/4)$ as functions of test temperature for a sample of polyoxymethylene (du Pont Delrin 150). All the fractures were brittle and there is a peak in impact strength in the brittle region but the peak does not coincide with the peak in $\tan \delta$ at $-50^\circ\text{C}/300\text{Hz}$. In this example, it seems more true to suggest that the rise in $IS(1/4)$ from 2.5kJ/m^2 at -100°C to 6.9kJ/m^2 at -20°C coincides with the γ process. Park²⁷ investigated an oxymethylene copolymer by means of high speed tensile tests on unnotched specimens. He located the brittle-ductile transition at -40°C and found an improvement in ductility near the β process (smaller peak in Figure 8a).

In 1960, Staverman and Heijboer⁷ published a graph showing good agreement between the impact strength of polypropylene (in kg cm/cm^2) and its compliance (in $10^{-11}\text{cm}^2/\text{dyne}$) between -20 and $+40^\circ\text{C}$. That is, as the compliance increases on warming through the β process, the impact strength increases in a very similar way. Figure 9 shows the same plot, in the same units, for a sample of polyethylene (ICI Plastics Division Alkathene Q 4011, specimen density 0.9370Mg/m^3) from -60 to $+50^\circ\text{C}$. The parallelism between the two properties seems too striking to be fortuitous. On the other hand, Figure 10 shows the same plot for a sample of higher density polyethylene (Chemische Werke Hüls Vestolen A 120, specimen density 0.9535Mg/m^3). Here there is no agreement between the two properties; above the peak at -20°C , $IS(1/4)$ falls while the compliance rises. Once again, the simple correlation between impact strength and modulus is disturbed by the influence of the β process on the brittle impact strength.

In the face of this evidence, there cannot be any

serious doubt that it is possible to observe pronounced peaks in toughness closely related to peaks in the mechanical losses. These peaks disturb the simple inverse correlation between impact strength and modulus. It seems particularly significant that all the four polymers listed in Table 2 as being discrepant on the high side have peaks in W_B near a prominent loss process when tested with notches of 1/4 mm radius or sharper.

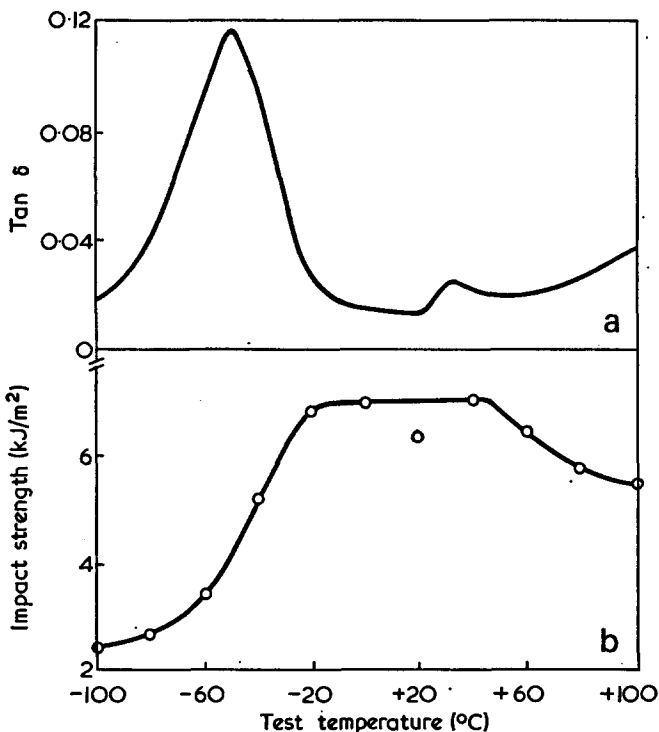


Figure 8 Effect of test temperature on a sample of polyoxymethylene. (a) $\tan \delta$; (b) brittle impact strength with 1/4 mm radius notches

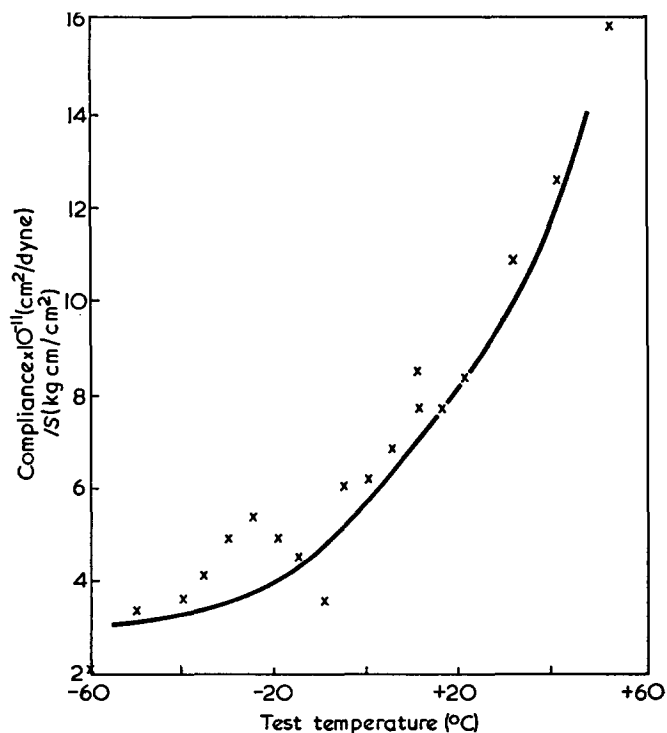


Figure 9 Effect of test temperature on a sample of medium density polyethylene. x, Brittle impact strength with 1/4 mm radius notches; —, compliance

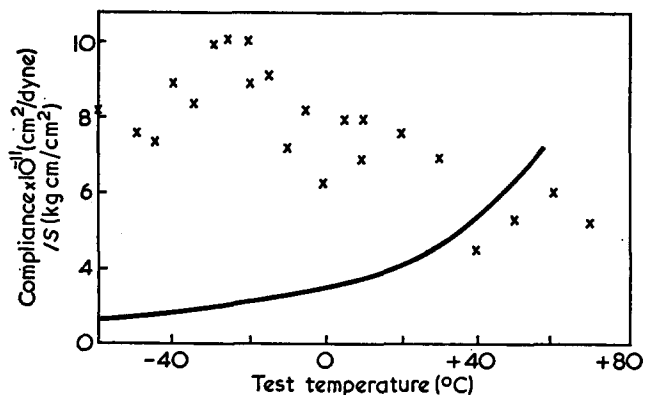


Figure 10 Effect of test temperature on a sample of higher density polyethylene. x, Brittle impact strength with 1/4 mm radius notches; —, compliance

CONCLUSIONS

The short-term toughness of thermoplastics is affected by changes in molecular mobility in two quite distinct ways. In the first place, up to 64% of the variance in impact strength can be accounted for by the variance in dynamic modulus. Some of the residual variance is caused by changes in secondary factors, such as additives, bulky side groups and molecular weight. But finally, some polymers have peaks in the impact strength of notched specimens which are directly related to peaks in mechanical losses.

ACKNOWLEDGEMENTS

Thanks for their contributions to this work are due to L. G. Calvete, E. A. Cole, C. M. R. Dunn, K. V. Gotham and P. R. Shearer.

REFERENCES

- 1 Boyer, R. F. and Spencer, R. S. 'Advances in colloid science', Interscience, New York, 1946, Vol II
- 2 Reed, M. C. *J. Polym. Sci.* 1947, 2, 115
- 3 Haward, R. N. 'The strength of plastics and glass', Cleaver-Hume, London, 1949
- 4 Hoff, E. A. W. and Turner, S. *ASTM Bull.* 1957, 225, 58
- 5 Webber, A. C. *ASTM Bull.* 1958, 227, 40
- 6 Vincent, P. I. *Polymer* 1960, 1, 425
- 7 Staverman, A. J. and Heijboer, J. *Kunststoffe* 1960, 50, 23
- 8 Oberst, H. *Kunststoffe* 1963, 53, 4
- 9 Staverman, A. J. *Proc. R. Soc. (A)* 1964, 282, 115
- 10 Retting, W. *Kolloid Z.* 1966, 210, 54
- 11 Retting, W. *Kolloid Z.* 1966, 213, 69
- 12 Wada, Y. and Kasohara, T. *J. Appl. Polym. Sci.* 1967, 11, 1661
- 13 Turley, S. G. *Polymer Prepr.* 1967, 8 (2), 1524
- 14 Boyer, R. F. *Polym. Eng. Sci.* 1968, 8, 161
- 15 Heijboer, J. *J. Polym. Sci. (C)* 1968, 16 (7), 3755
- 16 Retting, W. *Eur. Polym. J.* 1970, 6, 853
- 17 Oberst, H. and Retting, W. *J. Macromol. Sci. (B)* 1971, 5, 559
- 18 Roe, J. M. and Baer, E. *Int. J. Polym. Mat.* 1972, 1, 133
- 19 Vincent, P. I. 'Impact tests and service performance of thermoplastics', Plastics Institute, London, 1971, p 26
- 20 Robinson, D. W. *J. Sci. Instrum.* 1955, 32, 2
- 21 Vincent, P. I. 'Encyclopedia of polymer science and technology' (Ed. Bikales *et al.*) Wiley, New York, 1967, Vol 7, p 292
- 22 Gotham, K. V. *Plastics and Polymers* 1972, 40, 59
- 23 Gotham, K. V. *Plastics and Polymers* 1969, 37, 309
- 24 McCrum, N. G., Read, B. E. and Williams, G. 'Anelastic and dielectric effects in polymeric solids', Wiley, London, 1967
- 25 Vincent, P. I. *Polymer* 1972, 13, 558
- 26 Heijboer, J. *Br. Polym. J.* 1969, 1, 3
- 27 Park, I. K. *Makromol. Chem.* 1968, 118, 375

Notes to the Editor

Microphase separation in a graft copolymer

C. Price, R. Singleton and D. Woods

*Department of Chemistry, University of Manchester, Manchester M13 9PL, UK
(Received 10 August 1973)*

Numerous studies have been reported of microphase separation in block copolymers¹. For block copolymers having a well defined primary structure (e.g. AB, ABA, ABABA type copolymers) it has been found that microphase separation can lead to ordered arrays of regular domains²⁻⁵. Three main types of domain have been found; spheres, cylinders and lamellae⁶. The compositional order in which these usually occur is shown in *Table 1*. In the case of solvent cast specimens of AB and ABA type copolymers the nature and regularity of the domain morphologies obtained have been shown to depend on such factors as the block lengths and overall composition of the copolymer, polymer solvent interactions, the degree of incompatibility of the two polymer components, the casting temperature and the rate of evaporation of the solvent^{7, 8}.

To date, relatively little work has been reported on the two-phase morphologies of graft copolymers. Intuitively, one might expect that with these more complex systems the type of microphase separation obtained would be less distinct and the resulting morphology far less regular than that observed for the types of system cited above. In this note, however, we present evidence which shows that under certain conditions graft copolymers can also exhibit the regular two-phase structures normally associated with simple block copolymers. The system investigated was a copolymer formed by grafting polyisoprene chains onto a polystyrene backbone.

EXPERIMENTAL AND RESULTS

Preparation and characterization of the graft copolymer

Details of the method of preparation and characterization of the sample (designated 1G1) are to be found elsewhere⁹. Briefly, the graft copolymer was synthesized by adding poly(isoprenyl lithium) ($M_n = 12\,500$) to chloromethylated polystyrene ($M_n = 190\,000$) having a narrow molecular weight distribution. The sample studied was one of a series of fractions isolated from the reaction mixture by liquid-liquid separation. In carrying out the latter, successive quantities of methanol were added to a 1% solution in a 1:1 (v/v)

mixture of toluene and heptane. The two liquid phases obtained after each addition were equilibrated using the usual heating and cooling cycles and then separated by syphoning off the dilute phase. Fractions were isolated by freeze-drying.

The number-average molecular weight and apparent weight-average molecular weight (in tetrahydrofuran) of the selected fraction were 5.5×10^5 and 6.5×10^5 respectively. U.v. spectroscopy carried out on chloroform solutions gave the wt% polystyrene in the fraction to be 29.2. Gel permeation chromatography was used to check that traces of homopolymer had been effectively removed from the sample.

Electron microscopy

Electron micrographs of specimens were obtained using an AEI EM6G electron microscope operated at an accelerating voltage of 100 kV. Specimens were prepared by spraying dispersions of the graft copolymer (0.2% by wt concentration) in hexane onto mounted carbon films. After the solution had been allowed to evaporate the specimen was stained using osmium tetroxide vapour, which selectively reacts with the olefinic bonds of the polyisoprene chains.

An electron micrograph of the graft copolymer is shown in *Figure 1*. In spite of the complex chain geometry of the copolymer regular hexagonal arrays of 'circular' domains are observed. Light regions indicate polystyrene and dark regions polyisoprene. Thus the morphology consists of polystyrene domains in a matrix of

Table 1 Effect of composition on the domain morphology of AB type block copolymers

	Domains	Matrix
100% A	B spheres	A
	B rods	A
	A and B lamellae	
	A rods	B
100% B	A spheres	B

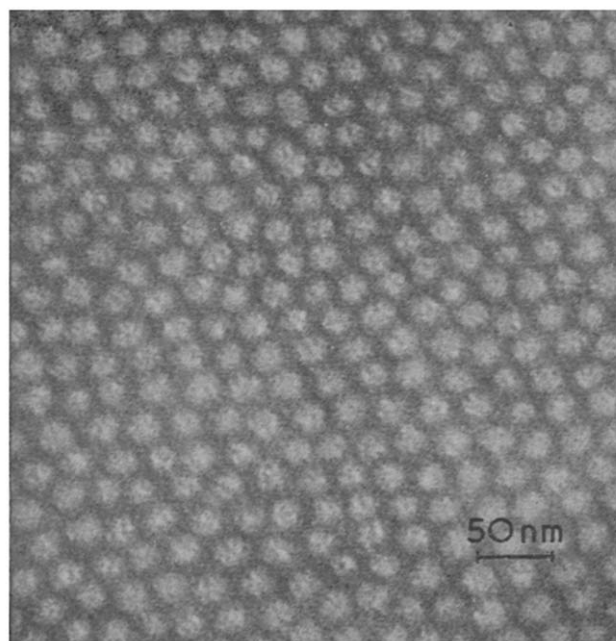


Figure 1 Electron micrograph of graft copolymer 1G1

Table 2 Measured number-average domain diameter and interdomain distance of the two copolymers

Sample	Type	<i>D</i> (nm)	<i>d</i> _{int} (nm)	Vol % of polystyrene		
				From e.m. assuming spheres	From e.m. assuming cylinders	From chemical composition
1G1	graft	17.5	25.0	25.4	44.6	26.4
1D1	block	13.0	25.0	10.4	24.6	22.4

D = domain diameter; *d*_{int} = interdomain distance; e.m. = electron microscopy

polyisoprene. The variation in contrast within domain 'areas' is a reproducible feature and will be referred to later.

The measured number-average domain diameter and interdomain distance (i.e. nearest distance between centres) are given in *Table 2*. The average value reported for the domain diameter must be treated as slightly arbitrary, however, because of the somewhat diffuse nature of the two-phase boundaries.

If we assume there is complete phase separation of the two components, the volume fraction of polystyrene may be calculated by two independent methods. In the first instance we can obtain it from a knowledge of the chemical composition of the polymer chain, and secondly from measured area fractions assuming a particular domain structure (i.e. either spheres or cylinders). From such a comparison, given in *Table 2*, we conclude the polystyrene domains are approximately spherical in shape. If we also assume that the density of the polystyrene domains is the same as that of polystyrene homopolymer, it can be calculated that each domain should contain ~9 backbone chains.

An electron micrograph of a specimen of a polystyrene-*b*-polyisoprene (AB type) block copolymer taken in a similar way to that of the graft copolymer is given in *Figure 2* for the purpose of comparison. For the block copolymer (designated 1D1) the number-average molecular weights of the polystyrene block and overall polymer were 13 000 and 51 000 respectively, whilst u.v. spectroscopy gave the wt% polystyrene to be 25.2. A surface area analysis of the electron micrograph shown in *Figure 2* suggests the 'circular' domains in this case are polystyrene cylinders viewed end on (see *Table 2*).

As reported previously¹⁰ on preparing specimens of the graft copolymer by casting from benzene solution (i.e. in a good solvent for both components), quite distinct phase separation was also observed but the morphology was much more irregular than that observed in the present study. In contrast, as is well known from numerous reports in the literature, polystyrene-*b*-polyisoprene block copolymers readily give highly ordered domain morphologies when cast from benzene solution.

Low-angle X-ray diffraction

A low-angle X-ray study was made on the graft copolymer using a Rigaku Denki low-angle X-ray camera. Specimens in sheet form (approximately 1 mm thick) were prepared by casting from hexane. The specimen gave a single sharp peak at a Bragg spacing of 18.1 nm. On heating at 120°C the peak remained well defined but shifted to lower angles. After heating

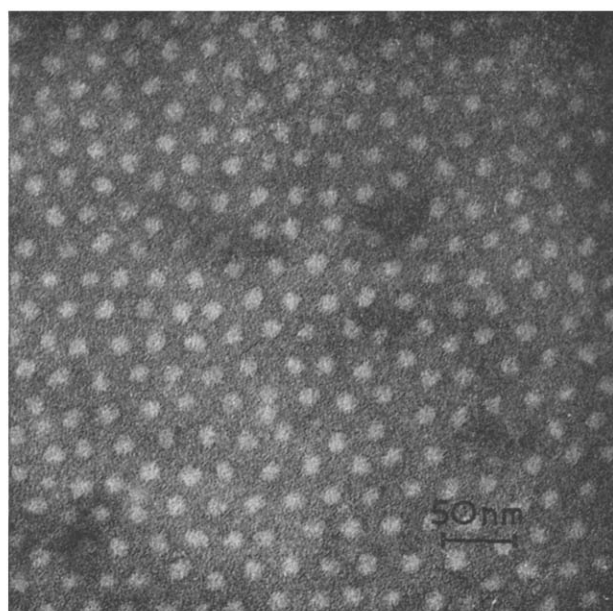


Figure 2 Electron micrograph of block copolymer 1D1

for 72 h the position of the peak remained constant at a Bragg spacing of 23.4 nm. If it is assumed we have face centred cubic packing of spherical polystyrene domains in a polyisoprene matrix then the nearest neighbour interdomain distance is estimated to be 28.5 nm. This value is in satisfactory agreement with that obtained from electron microscopy.

The method by which the graft copolymer was synthesized would essentially lead to a random spacing of polyisoprene chains along the polystyrene backbone. This structural feature might be expected to hinder the complete separation of the two phases. The assumption of complete separation made earlier may therefore be a gross oversimplification. The diffuse nature of the domain boundaries and the structural features observed within these regions (present in *Figure 1* but not in *Figure 2*) are probably a reflection of the packing difficulties involved in the case of the graft copolymer.

ACKNOWLEDGEMENTS

We thank the Science Research Council for the award of a CAPS Studentship for D. W. and for an ACS Studentship for R. S. We also thank Esso Chemicals Research Centre, Abingdon, for their general co-operation on the project carried out by D. W.

REFERENCES

- 1 'Block Copolymers' (Eds D. C. Allport and W. H. Janes), Applied Science, London, 1973
- 2 Matsuo, M. *Japan Plastics* 1968, **19**, 6
- 3 Lewis, P. R. and Price, C. *Nature* 1969, **223**, 494
- 4 Dlugosz, J. *et al. Kolloid-Z.* 1970, **242**, 1126
- 5 Kämpf, G., Krömer, H. and Hoffmann, M. *J. Macromol. Sci.* 1972, **B6**, 167
- 6 Matsuo, M., Sagal, S. and Asai, H. *Polymer* 1969, **10**, 79
- 7 Inoue, T., Soen, T., Hashimoto, T. and Kawai, H. 'Block Polymers' (Ed. S. L. Aggarwal), Plenum Press, New York, 1970, pp 53-78
- 8 Lewis, P. R. and Price, C. *Polymer* 1972, **13**, 20
- 9 Price, C. and Woods, D. *Polymer* 1973, **14**, 82
- 10 Price, C., Lally, T. P., Watson, A. G., Woods, D. and Chow, M. T. *Br. Polym. J.* 1972, **4**, 413

Effect of addition of graft copolymer on the microstructure and impact strength of PS/LDPE blends

W. M. Barentsen, D. Heikens and P. Piet

Laboratory of Polymer Technology, Eindhoven University of Technology, PO Box 513, Eindhoven, The Netherlands
(Received 4 June 1973)

Graft copolymers prepared by Friedel-Crafts alkylation of the aromatic rings in polystyrene (PS) with the olefinic groups in low density polyethylene (LDPE) are found to be emulsifiers in mechanical blends of PS and LDPE. Moreover, this copolymer acts as an adhesive between the two homopolymers.

The graft copolymers were prepared by the method described by Carrick¹. The reaction was started by adding $AlCl_3$ to a 5% solution of a 3:2 blend of PS (Styron 666E, Dow) and LDPE (Stamylan 1510, DSM) in cyclohexane. The reaction was stopped after 3 min reaction time by adding isopropyl alcohol. The remaining free PS and LDPE were removed from the graft copolymer by extraction of the reaction mixture with ethyl acetate and n-heptane. The PS content of the copolymer was 47% by vol. as determined by infra-red

measurements. It was concluded from the proposed reaction scheme and the observed resistance to flow at high temperatures that the copolymer contained very high molecular weight material.

It was concluded from microscopic examination that if the content of one of the polymers in PS/LDPE blends is less than 40%, this polymer forms the dispersed phase. Blends of PS, LDPE and graft copolymer were prepared on a laboratory mill at 195°C. The amount of added copolymer was 0, 5 and 30% of the dispersed polymer. The graft copolymer was first melt blended with the polymer that will form the dispersed phase. The mixture was added to the matrix polymer. All blends were compression moulded at 200°C to unnotched strips for Dynstat impact strength measurements (DIN 53 453).

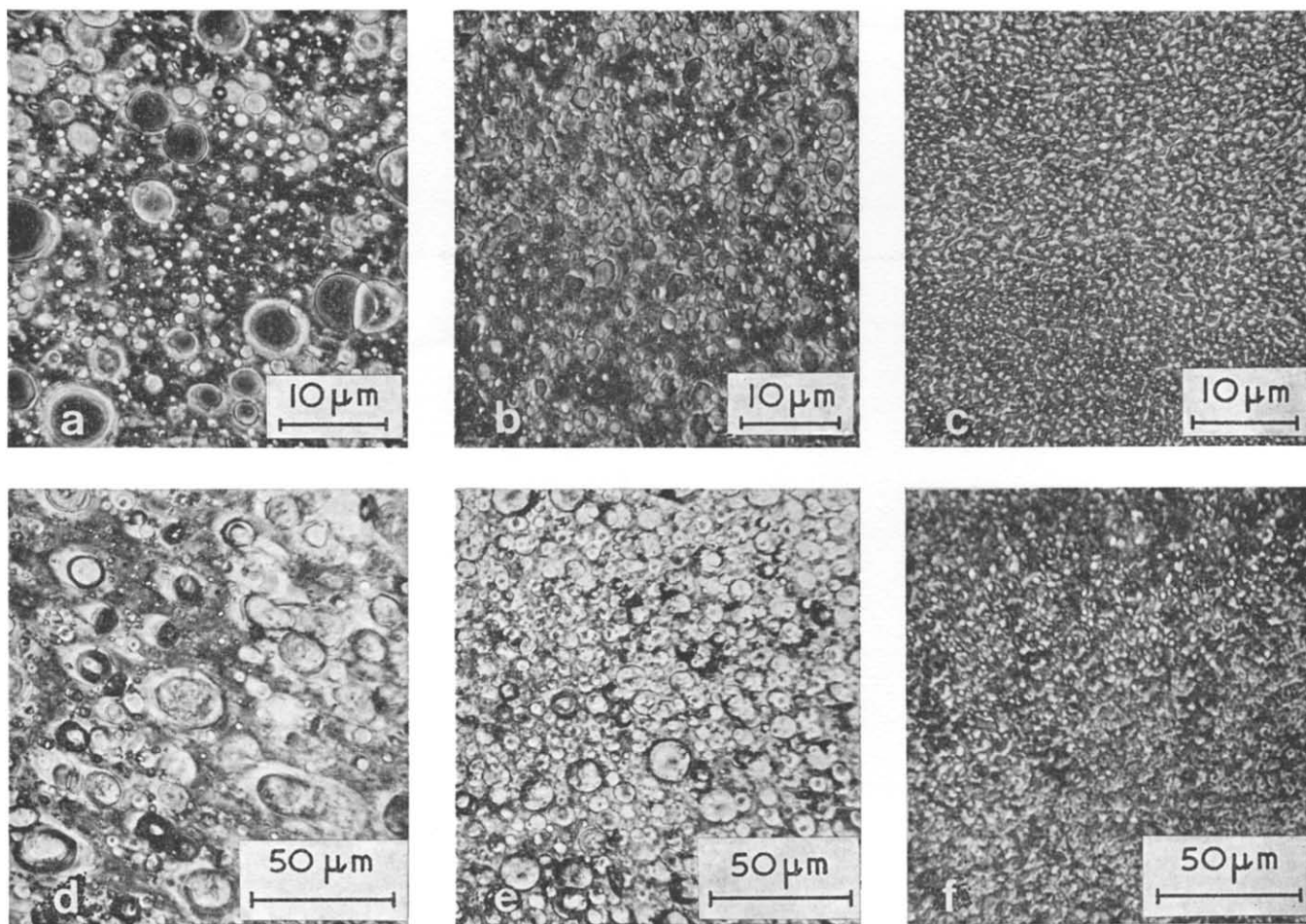


Figure 1 Phase contrast microscopy of PS/LDPE blends. (a) 75 : 25 PS/LDPE; (b) 75 : 25 : 1·25 PS/LDPE/copolymer; (c) 75 : 25 : 7·5 PS/LDPE/copolymer; (d) 25 : 75 PS/LDPE; (e) 25 : 1·25 : 75 PS/copolymer/LDPE; (f) 25 : 7·5 : 75 PS/copolymer/LDPE

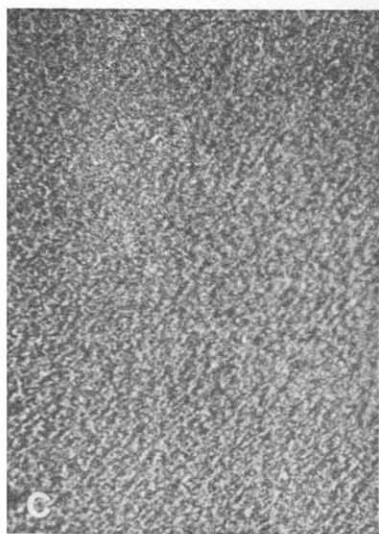
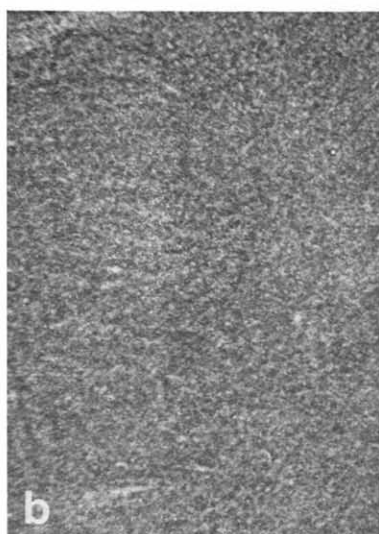
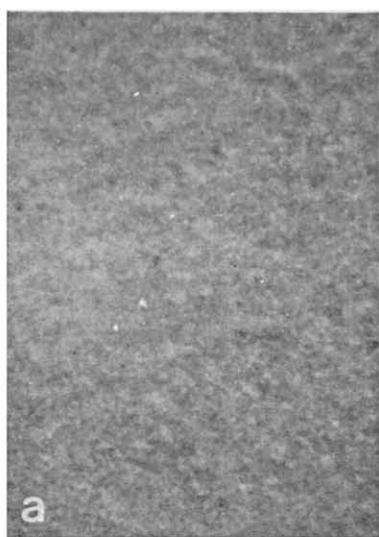


Figure 2 Phase contrast microscopy of (a) pure graft copolymer; (b) 75:25 LDPE/graft copolymer; and (c) 75:25 PS/graft copolymer

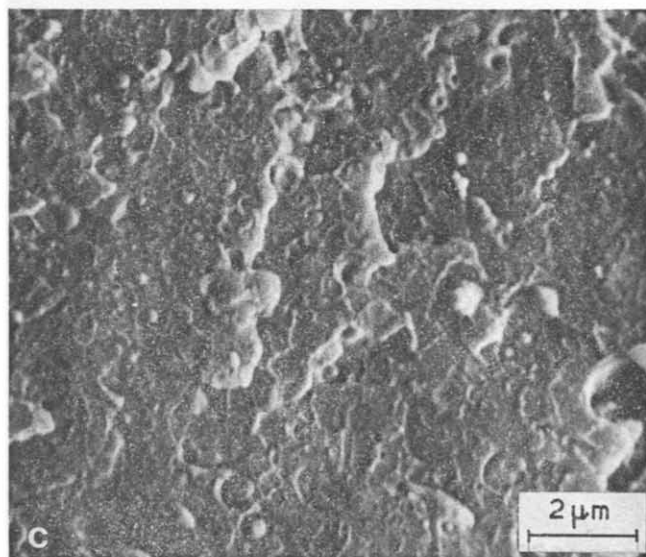
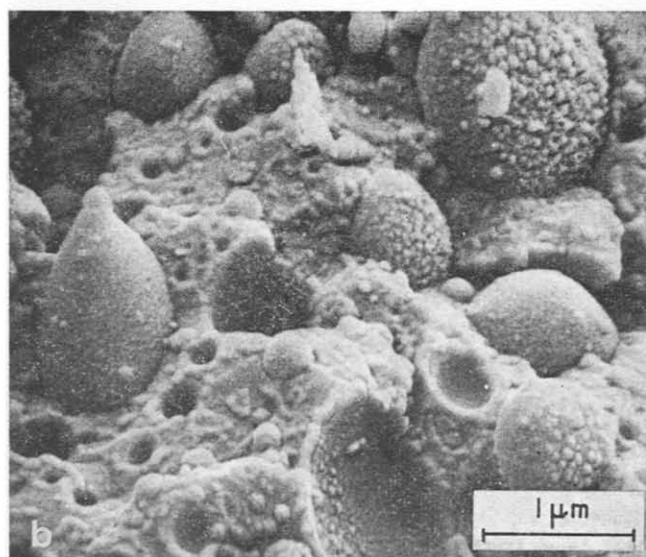
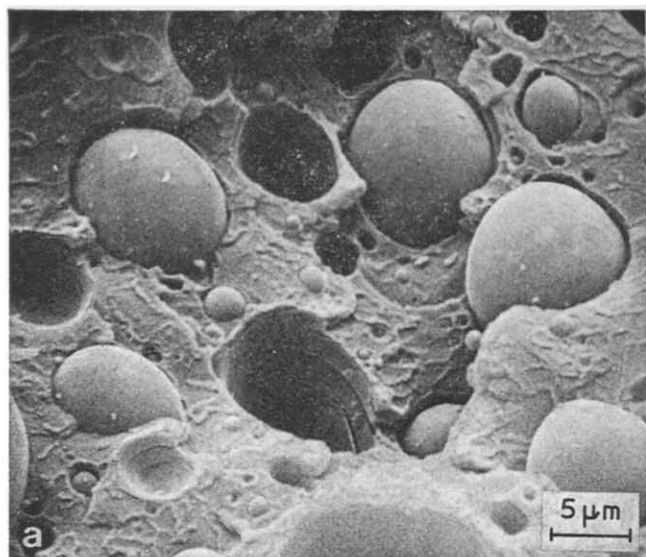


Figure 3 Electron scanning microscopy of fracture surfaces. (a) 75:25 PS/LDPE; (b) 75:25:1.25 PS/LDPE/copolymer; (c) 75:25:7.5 PS/LDPE/copolymer

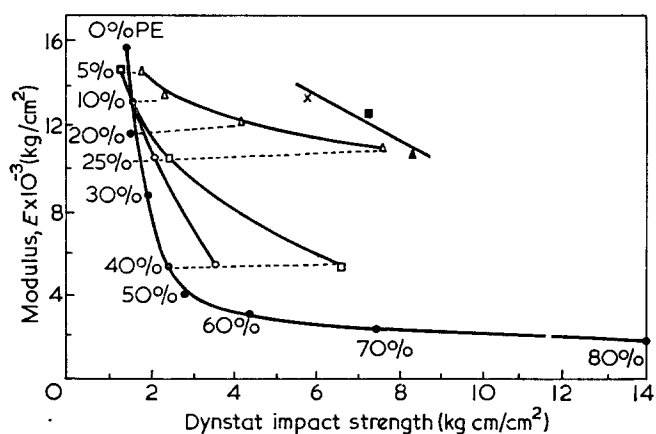


Figure 4 Young's modulus and impact strength of PS/LDPE/graft copolymer blends. ●, PS/LDPE blends; ○, blends of PS and LDPE with 5% copolymer relative to the amount of dispersed polymer added; □, blends of PS and LDPE with 30% copolymer relative to the amount of dispersed polymer added; △, blends of PS and graft copolymer (47% PS). ×, Polystyrol 475 (BASF); ■, Styron 453 (Dow); ▲, Styron 456 (Dow)

The effect of copolymer addition on the microstructure of the blends can be seen in the phase contrast micrographs in Figure 1. In the dispersed phase or the matrix no traces of the graft copolymer can be observed.

Figure 2 shows that the graft copolymer does not dissolve in either homopolymer. It was concluded from these observations that the copolymer concentrates at the interface in the blends of homopolymers. Electron scanning micrographs of fracture surfaces of PS/graft copolymer and LDPE/graft copolymer blends suggest that the graft copolymer adheres to both polymers. This was confirmed by peel test measurements. Tensile tests on blends indicated that the strength increases as the amount of copolymer increases. Clearly, the low strength interface of PS and LDPE is reinforced by the copolymer that forms an adhering layer between the homopolymers².

The decrease of particle size of the dispersed polymer upon adding the graft copolymer was substantiated by electron scanning microscopy of fracture surfaces. Figure 3 shows fracture surfaces of 75:25 PS/LDPE blends with increasing amounts of copolymer. The

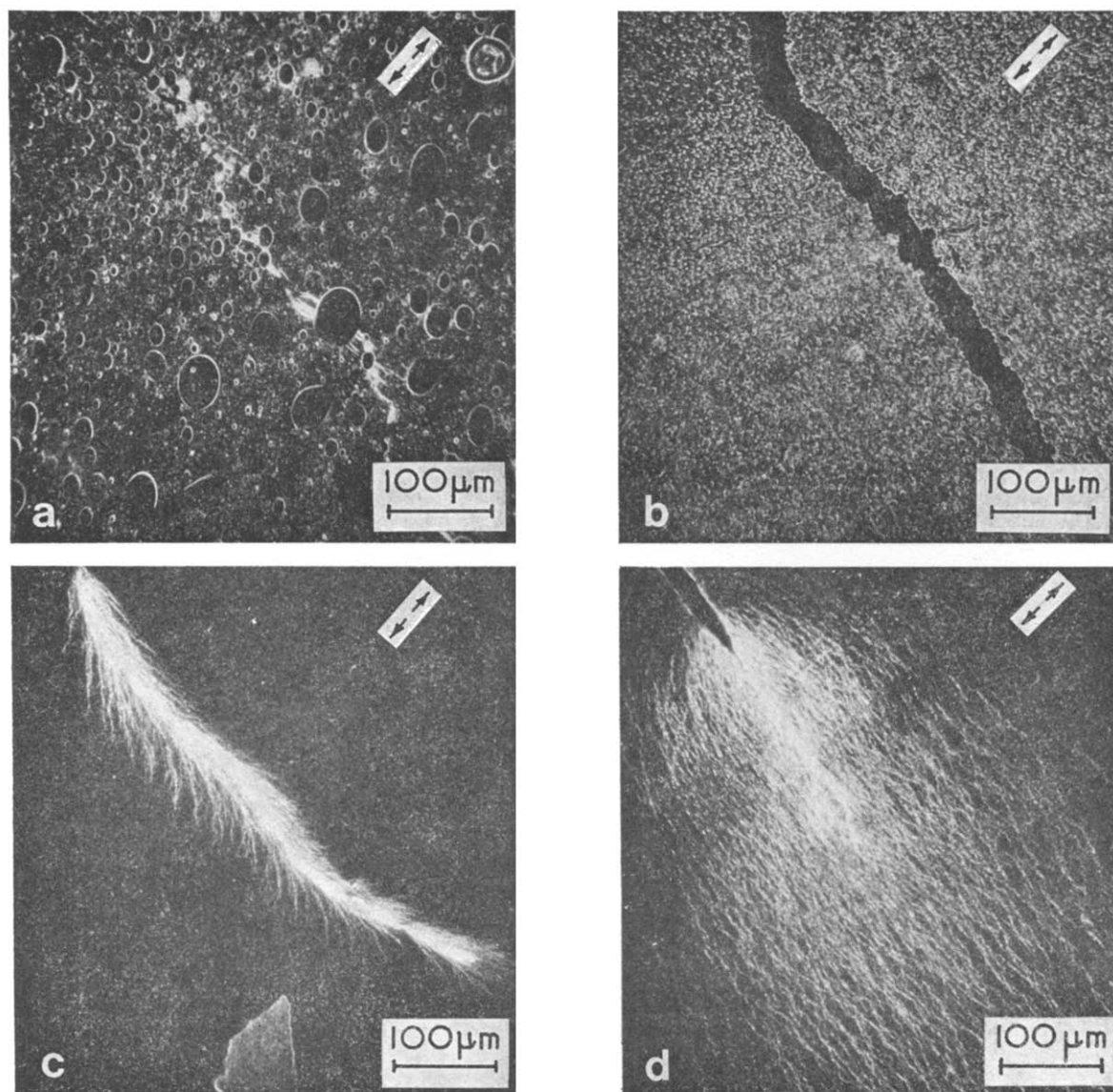


Figure 5 Dark field phase contrast microscopy of blends. Arrows refer to the direction of stretching. (a) 75:25 PS/LDPE; (b) 75:25:1.25 PS/LDPE/graft copolymer; (c) 75:25 PS/graft copolymer; (d) Styron 453 (Dow)

micrographs show a high degree of resemblance to those published by Haward and Mann of ABS fracture surfaces³. The hemispherical bumps that become visible on the disperse polymer particles as well as in the holes from which the particles were extracted, consist of graft copolymer. The amount of the surface irregularities was estimated. It agreed well with the amount of graft copolymer in the blend. This supports the validity of the concept that the bilaterally adhering graft copolymer reinforces the interface.

The data of the impact strength measurements are given in *Figure 4*. The best results are obtained with blends of PS and pure graft copolymer. Impact strength and modulus of these blends can be made comparable to those of commercially available impact polystyrenes.

The increase in impact strength can be correlated to craze forming in the blends. This is demonstrated in *Figure 5*. Thin sections of the blends were given a small cut with a razor blade and stretched before mounting on microscope slides. The adopted method was essen-

tially the same as described by Bucknall and Smith⁴. Only the blend of PS and graft copolymer exhibits craze formation comparable to impact PS. Evidently, uncrosslinked LDPE cannot prevent crack initiation in the crazes in PS (*Figure 5a*) even if it adheres to PS by the graft copolymer layer at the interface (*Figure 5b*). In blends of PS and graft copolymer, the latter forms a bridge between the crack sides with increasing resistance to deformation upon stretching due to the very high molecular weight content. This is a response to deformation which is also found for the crosslinked rubbery phase in impact polystyrenes.

REFERENCES

- 1 Carrick, W. L. *J. Polym. Sci. (A-1)* 1970, **8**, 215
- 2 Barentsen, W. M. *Thesis* Eindhoven University of Technology, 1972
- 3 Haward, R. N. and Mann, J. *Proc. R. Soc. (A)* 1964, **282**, 120
- 4 Bucknall, C. B. and Smith, R. R. *Polymer* 1965, **6**, 437

Letters

Comments on paper: 'Steady flow and dynamic viscoelastic properties of branched polyethylene'

(J. J. Labaig, Ph. Monge and J. Bednarick, *Polymer* 1973, 14, 384-386)

When a viscoelastic medium is subjected to an alternating shear stress T , the strain S also varies periodically with time and so does the rate of strain dS/dt . In general, however, S may lag behind in phase relative to T . To describe this situation, one may thus introduce two frequency dependent complex quantities:

$$G^*(j\omega) = \frac{\text{stress}}{\text{strain}} = \frac{T}{S} \quad (1)$$

$$\eta^*(j\omega) = \frac{\text{stress}}{\text{rate of strain}} = \frac{T}{j\omega S} \quad (2)$$

It is convenient to define a complex compliance:

$$J^*(j\omega) = \frac{1}{G^*} = \frac{1}{j\omega\eta^*} \quad (3)$$

This approaches the limiting compliance J_∞ as the frequency of the applied stress rises, whereas the complex viscosity equation:

$$\eta^*(j\omega) = \frac{\eta_0}{1 + (j\omega\tau_0)^{1-h}} \quad (4)$$

which is proposed by Labaig, Monge and Bednarick¹ (LMB) would result in $J_\infty = 0$.

It is interesting to extend the application of Cole-Cole analysis² to the viscoelastic properties of liquids. This can be done as a consequence of the viscoelastic-dielectric analogy, which makes current correspond to the rate of strain and voltage to stress.

Although the LMB expression (equation 4) may be used as an empirical equation to describe the complex viscosity over a limited frequency range, it should not be used in the determination of the distribution function of the relaxation times for the following reasons: (1) the Cole-Cole expression is established for the dielectric constant which is the ratio electric displacement/applied electric field. It is therefore reasonable to apply the same analysis to the corresponding quantity in the mechanical system, which is the shear compliance (=shear strain/shear stress) and not to the shear viscosity; (2) equation (4) leads to the prediction of unlimited shear modulus, which is physically unreasonable; (3) the relaxation spectrum derived from equation (4) is not terminated at large relaxation times. The lack of a large time termination results in an infinite term for the recoverable creep compliance, which is physically unacceptable.

It is useful to give a brief review of the present state of knowledge on viscoelastic relaxation under periodic

shear. Barlow *et al.*³, Barlow and Lamb⁴, have shown that, for pure liquids, the complex compliance can be represented by:

$$J^*(j\omega) = J_\infty \left[1 + \frac{1}{j\omega\tau_m} \right] + \frac{2J_\infty}{(j\omega\tau_m)^{1/2}} \quad (5)$$

where τ_m is the 'Maxwell relaxation time' equal to ηJ_∞ where η is the steady-flow shear viscosity. This equation has been derived theoretically on the basis of a defect-diffusion model⁵ and has very well correlated the data obtained in the relaxation region by variation of pressure and temperature⁶. A modification of equation (5) was found to be a satisfactory means of representing data obtained for liquid mixtures⁷:

$$J^*(j\omega) = J_\infty \left[1 + \frac{1}{j\omega\tau_m} \right] + \frac{2KJ_\infty}{(j\omega\tau_m)^{1/2}} \quad (6)$$

This equation gives an adequate description of the viscoelastic behaviour of castor oil⁸ which has been determined as a function of pressure and temperature. Subsequently, Barlow and Erginsav⁹ have shown that equation (6) does not completely describe the viscoelastic relaxation, and a better representation is given by:

$$J^*(j\omega) = J_\infty \left[1 + \frac{1}{j\omega\tau_m} \right] + \frac{J_r}{(1 + j\omega\tau_r)^\beta} \quad (7)$$

where τ_r is a retardation time parameter, J_r is the retardational compliance and β is a numerical factor, $0 < \beta < 1$. The second term in equation (7) follows the empirical equation used by Davidson and Cole¹⁰ in their analysis of dielectric relaxation of supercooled liquids. In the analysis of the viscoelastic data, β is found to be close to a value of 0.5, in which case the second term in equation (7), can be written as $J_r(j\omega\tau_r)^{-1/2}$, which is of similar form to the second term of equation (6), namely $2KJ_\infty(j\omega\tau_m)^{-1/2}$. It is important to make a note that the retardation time τ_r is the terminal time in the long time end of the relaxation spectrum. Investigations into polymers are in progress in this laboratory and the data obtained under atmospheric pressure as well as under high pressures can be represented by the viscoelastic analogy of the Davidson-Cole equation for dielectric relaxation, equation (7).

Because of the relation between J^* and η^* in equation (3) the compliance J^* defined by equation (7) will result in an expression for complex viscosity:

$$\eta^*(j\omega) = \frac{\eta}{1 + j\omega\tau_m + \frac{j\omega\tau_m J_r / J_\infty}{(1 + j\omega\tau_r)^\beta}} \quad (8)$$

For the case where $1 \ll \omega\tau_r$, equation (8) can be written as:

$$\eta^*(j\omega) = \frac{\eta}{1 + j\omega\tau_m + (j\omega\tau_r)^{1-\beta}}, \quad \tau = \left(\frac{\tau_m J_r}{J_\infty \tau_r^\beta} \right)^{1/(1-\beta)} \quad (9)$$

which is equivalent to equations (5) and (6) if $\beta = 0.5$.

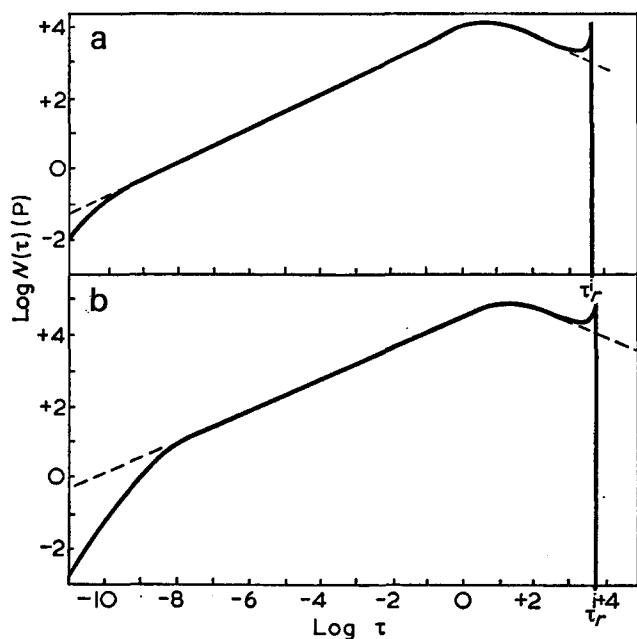


Figure 1 Distribution function of the logarithm of the relaxation times against the logarithm of the relaxation times. (a) LMB sample A group I; (b) LMB sample G group II. —, determined from equation (8); ---, determined from equation (4)

In addition, if $\omega\tau_m$ is very small compared with unity and $\omega\tau_m \ll (\omega\tau)^{1-\beta}$, one can write

$$\eta^*(j\omega) = \frac{\eta}{1 + (j\omega\tau)^{1-\beta}} \quad (10)$$

which is identical with equation (4) with $\eta = \eta_0$, $\tau = \tau_0$ and $\beta = h$. If the first condition $1 \ll \omega\tau_r$ was met in the work of LMB for the case of branched polyethylene, the second condition is valid for the frequencies employed in their work. However, equation (10) should not be assumed to be valid at the low frequency side where the first condition $1 \ll \omega\tau_r$ would not hold, as well as at the high frequency end where the second conditions $\omega\tau \ll 1$ and $\omega\tau_m \ll (\omega\tau)^{1-\beta}$ will fail.

In Figure 1, the distribution functions which are determined from equation (8) are shown along with those which are determined by LMB. Extension of the LMB spectra into the time zone below 10^{-4} sec are determined from equation (4). Sample A is chosen because the parameter h is 0.5 for this sample. Sample G is chosen because h has largest deviation from 0.5 and is 0.55 for this sample. The value of τ_r is chosen as 5000 sec which alters the value of τ_0 by less than 10% which is the specified uncertainty in the determination of τ_0 . A value of 10^{-10} cm²/dyne, is taken as a typical value of J_∞ at a temperature of 100°C above the glass transition temperature for various liquids including polymers.

The spectra which are shown as solid lines are determined from equation (8), the viscoelastic analogy of the Davidson-Cole expression for dielectric relaxation. The depression in the shorter time distribution is due to the second term $j\omega\tau_m$ in the denominator of equation (8) which corresponds to the first term J_∞ in equation (7) and leads to a finite shear modulus, which is physically reasonable. The termination of spectrum at τ_r results in a finite term for the recoverable creep compliance, which is physically acceptable.

The peak at the right hand end of the spectrum is generally known as the plateau zone in spectrum for high molecular weight polymers and attributed to the entanglement couplings¹¹.

Min Gon Kim

Dept. of Electronics and Electrical Engineering,
University of Glasgow,
Glasgow G12 8QQ, UK
(Received 2 November 1973)

References

- 1 Labaig, J. J., Monge, Ph. and Bednarick, J. *Polymer* 1973, **14**, 384
- 2 Cole, K. S. and Cole, R. H. *J. Chem. Phys.* 1941, **9**, 341
- 3 Barlow, A. J., Erginsav, A. and Lamb, J. *Proc. R. Soc. (A)* 1967, **298**, 481; 1969, **309**, 473
- 4 Barlow, A. J. and Lamb, J. *Discuss. Faraday Soc.* 1967, **43**, 223
- 5 Phillips, M. C., Barlow, A. J. and Lamb, J. *Proc. R. Soc. (A)* 1972, **329**, 193
- 6 Barlow, A. J., Harrison, G., Irving, J. B., Kim, M. G., Lamb, J. and Pursley, W. C. *Proc. R. Soc. (A)* 1973, **327**, 403
- 7 Barlow, A. J., Erginsav, A. and Lamb, J. *Proc. R. Soc. (A)* 1969, **309**, 473
- 8 Barlow, A. J., Harrison, G., Kim, M. G. and Lamb, J. *JCS Faraday Trans. II* 1973, **69**, 1446
- 9 Barlow, A. J. and Erginsav, A. *Proc. R. Soc. (A)* 1972, **327**, 175
- 10 Davidson, D. W. and Cole, R. H. *J. Chem. Phys.* 1951, **19**, 1484
- 11 Ferry, J. D. 'Viscoelastic Properties of Polymers', John Wiley, New York, 1961

On the mechanism of motions of nitroxyl radicals in polymers

Short range segmental motions of polymers have been studied extensively by the spin-labelling method¹⁻⁴. However, only a few comments have been made on the mechanism by which segmental motions of polymers are experienced by radicals. Thus Cameron *et al.*⁴ found that correlation times (τ) of spin-labels in polystyrene are in good accord with relaxation times for the δ -relaxation in polystyrene.

Results of our recent report³ indicate that τ of free and covalently esterified nitroxyl radicals in solid poly(ethylene glycol) (PEG) reaches a constant value when the molecular weight of PEG is ≥ 15000 . This indicates the short chain nature of molecular motion experienced by radicals.

The temperature dependence of the rotational frequency values ($f = 1/2\pi\tau$)⁵ of free and bonded nitroxyl radicals in amorphous PEG ($\bar{M}_n = 22000$) are given in Figure 1. Figure 1 also gives β - and γ -relaxation frequencies of some dielectric^{6,7} and mechanical⁸ relaxation measurements.

From Figure 1 it can be seen that the rotational frequencies of free radicals are in linear correlation with the dielectric low temperature γ -relaxation frequencies. This relaxation is caused by local rotations of short main chain segments⁹. It can also be seen that rotations of bonded radicals are shifted to lower frequency values. Similar shifts to lower frequencies are also observed in the case of spin-labelled polystyrene⁴

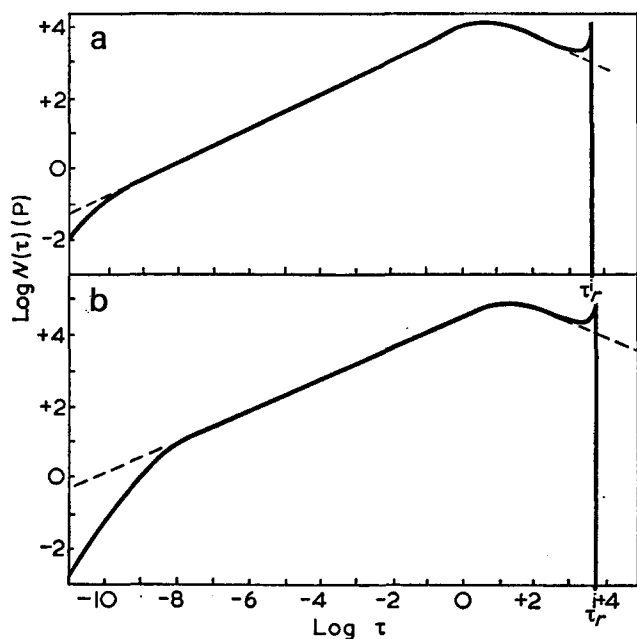


Figure 1 Distribution function of the logarithm of the relaxation times against the logarithm of the relaxation times. (a) LMB sample A group I; (b) LMB sample G group II. —, determined from equation (8); ---, determined from equation (4)

In addition, if $\omega\tau_m$ is very small compared with unity and $\omega\tau_m \ll (\omega\tau)^{1-\beta}$, one can write

$$\eta^*(j\omega) = \frac{\eta}{1 + (j\omega\tau)^{1-\beta}} \quad (10)$$

which is identical with equation (4) with $\eta = \eta_0$, $\tau = \tau_0$ and $\beta = h$. If the first condition $1 \ll \omega\tau_r$ was met in the work of LMB for the case of branched polyethylene, the second condition is valid for the frequencies employed in their work. However, equation (10) should not be assumed to be valid at the low frequency side where the first condition $1 \ll \omega\tau_r$ would not hold, as well as at the high frequency end where the second conditions $\omega\tau \ll 1$ and $\omega\tau_m \ll (\omega\tau)^{1-\beta}$ will fail.

In Figure 1, the distribution functions which are determined from equation (8) are shown along with those which are determined by LMB. Extension of the LMB spectra into the time zone below 10^{-4} sec are determined from equation (4). Sample A is chosen because the parameter h is 0.5 for this sample. Sample G is chosen because h has largest deviation from 0.5 and is 0.55 for this sample. The value of τ_r is chosen as 5000 sec which alters the value of τ_0 by less than 10% which is the specified uncertainty in the determination of τ_0 . A value of 10^{-10} cm²/dyne, is taken as a typical value of J_∞ at a temperature of 100°C above the glass transition temperature for various liquids including polymers.

The spectra which are shown as solid lines are determined from equation (8), the viscoelastic analogy of the Davidson-Cole expression for dielectric relaxation. The depression in the shorter time distribution is due to the second term $j\omega\tau_m$ in the denominator of equation (8) which corresponds to the first term J_∞ in equation (7) and leads to a finite shear modulus, which is physically reasonable. The termination of spectrum at τ_r results in a finite term for the recoverable creep compliance, which is physically acceptable.

The peak at the right hand end of the spectrum is generally known as the plateau zone in spectrum for high molecular weight polymers and attributed to the entanglement couplings¹¹.

Min Gon Kim

Dept. of Electronics and Electrical Engineering,
University of Glasgow,
Glasgow G12 8QQ, UK
(Received 2 November 1973)

References

- 1 Labaig, J. J., Monge, Ph. and Bednarick, J. *Polymer* 1973, 14, 384
- 2 Cole, K. S. and Cole, R. H. *J. Chem. Phys.* 1941, 9, 341
- 3 Barlow, A. J., Erginsav, A. and Lamb, J. *Proc. R. Soc. (A)* 1967, 298, 481; 1969, 309, 473
- 4 Barlow, A. J. and Lamb, J. *Discuss. Faraday Soc.* 1967, 43, 223
- 5 Phillips, M. C., Barlow, A. J. and Lamb, J. *Proc. R. Soc. (A)* 1972, 329, 193
- 6 Barlow, A. J., Harrison, G., Irving, J. B., Kim, M. G., Lamb, J. and Pursley, W. C. *Proc. R. Soc. (A)* 1973, 327, 403
- 7 Barlow, A. J., Erginsav, A. and Lamb, J. *Proc. R. Soc. (A)* 1969, 309, 473
- 8 Barlow, A. J., Harrison, G., Kim, M. G. and Lamb, J. *JCS Faraday Trans. II* 1973, 69, 1446
- 9 Barlow, A. J. and Erginsav, A. *Proc. R. Soc. (A)* 1972, 327, 175
- 10 Davidson, D. W. and Cole, R. H. *J. Chem. Phys.* 1951, 19, 1484
- 11 Ferry, J. D. 'Viscoelastic Properties of Polymers', John Wiley, New York, 1961

On the mechanism of motions of nitroxyl radicals in polymers

Short range segmental motions of polymers have been studied extensively by the spin-labelling method¹⁻⁴. However, only a few comments have been made on the mechanism by which segmental motions of polymers are experienced by radicals. Thus Cameron *et al.*⁴ found that correlation times (τ) of spin-labels in polystyrene are in good accord with relaxation times for the δ -relaxation in polystyrene.

Results of our recent report³ indicate that τ of free and covalently esterified nitroxyl radicals in solid poly(ethylene glycol) (PEG) reaches a constant value when the molecular weight of PEG is ≥ 15000 . This indicates the short chain nature of molecular motion experienced by radicals.

The temperature dependence of the rotational frequency values ($f = 1/2\pi\tau$)⁵ of free and bonded nitroxyl radicals in amorphous PEG ($\bar{M}_n = 22000$) are given in Figure 1. Figure 1 also gives β - and γ -relaxation frequencies of some dielectric^{6,7} and mechanical⁸ relaxation measurements.

From Figure 1 it can be seen that the rotational frequencies of free radicals are in linear correlation with the dielectric low temperature γ -relaxation frequencies. This relaxation is caused by local rotations of short main chain segments⁹. It can also be seen that rotations of bonded radicals are shifted to lower frequency values. Similar shifts to lower frequencies are also observed in the case of spin-labelled polystyrene⁴

Structural aspects of soda-cellulose II

The basic molecular repeat of natural cellulose, or cellulose I, was established by Meyer and Misch¹ in 1937 and it is now generally accepted that cellulose I has a monoclinic unit cell containing two chain segments. The general features of the X-ray fibre diffraction pattern and the fibre repeat of 1.03 ± 0.01 nm are consistent with a two-fold helical conformation which has an axial rise per glucose moiety of 0.515 nm.

Cellulose I under the action of sodium hydroxide undergoes a series of changes eventually forming cellulose II, a process of considerable industrial importance in the manufacture of mercerized cotton (for a recent review see Warwicker *et al.*²). Cellulose II may be regarded as a 'swollen' form of cellulose I, the fibre repeat remaining essentially constant. During the swelling process an intermediate crystalline phase can be obtained, known as soda-cellulose II, which contains both sodium and hydroxyl ions in the crystalline lattice. It is with this distinct solid-state phase that we have been concerned.

The X-ray fibre diffraction pattern obtained from soda-cellulose II is shown in *Figure 1*. The reflections index on a hexagonal unit cell with $a = 1.00 \pm 0.02$ nm and c (fibre axis) = 1.51 ± 0.02 nm, and with meridional reflections occurring on every third layer line. The simplest interpretation of this pattern is that each residue rotates, about successive glycosidic bonds, in response to the ionic environment to form a three-fold helix repeating in a distance of 1.51 nm. In fact Meyer *et al.*³ in 1939 originally suggested this interpretation. More recently Warwicker and Wright⁴ preferred to interpret this 1.51 nm fibre repeat in terms of sheets of cellulose molecules (where the molecular chains are two-fold helices similar to that for natural cellulose) which stagger relative to each other by units of one-third the fibre repeat distance. We wish to consider the soda-cellulose II data in somewhat more detail in an attempt to resolve the conformation of the molecular chains.

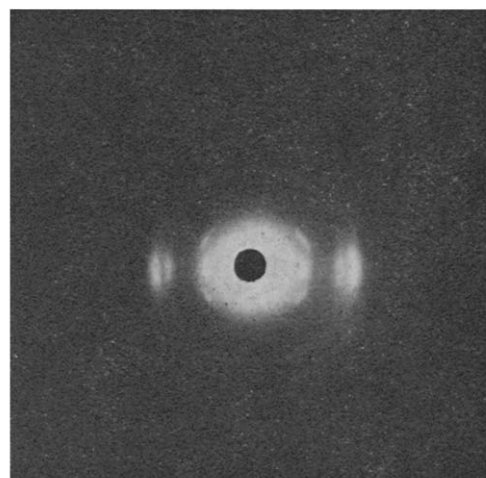


Figure 1 X-ray fibre diffraction pattern obtained from soda-cellulose II. The fibre axis is vertical and the reflections index on a hexagonal unit cell. Meridional reflections occur on the third and sixth layer lines only

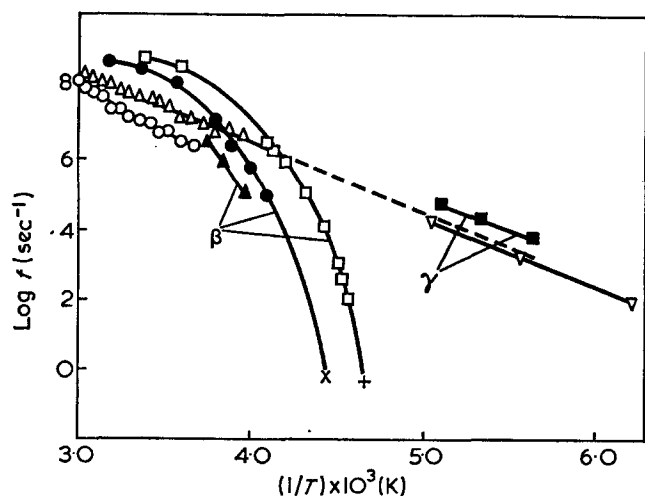


Figure 1 Log f against $1/T$ for PEG. Dielectric^{6,7}: \square , melt crystallized, \bar{M}_w 2.8×10^6 ; \bullet , melt crystallized, \bar{M}_w 2.8×10^5 ; \blacktriangle , melt crystallized, \bar{M}_w 3×10^4 ; ∇ , melt crystallized; \blacksquare , solution crystallized. Mechanical⁸: $+$, moulded annealed, \bar{M}_w 2.8×10^6 ; \times , moulded, annealed, \bar{M}_w 2.8×10^5 . Electron spin resonance⁹: Δ , solution crystallized, \bar{M}_n 2.2×10^4 (free radicals); \circ , solution crystallized, \bar{M}_n 2.2×10^4 (bonded radicals)

and nylon-6,¹⁰ where rotations of bonded radicals are in good accord with γ -relaxation frequencies.

These experimental observations show that free radicals experience the short range relaxations in polymers in a quite straightforward manner. Thus, the covalent bonding of radicals to the polymer backbone causes a small shift to lower frequencies as compared to the values of corresponding dielectric and mechanical relaxation measurements. It seems evident that this shift is caused by the slightly restricted rotation around the covalent bond^{3,10}.

Acknowledgement

The author thanks Prof. J. J. Lindberg and H. Lättilä for their valuable aid.

P. Törmälä

Department of Wood and Polymer Chemistry,
University of Helsinki, Helsinki, Finland
(Received 12 November 1973)

References

- 1 Wasserman, A. M., Buchachenko, A. L., Kovarskii, A. L. and Neiman, M. B. *Eur. Polym. J.* 1969, **5**, 473
- 2 Bullock, A. T., Cameron, G. G. and Smith, P. M. *J. Phys. Chem.* 1973, **77**, 1635
- 3 Törmälä, P., Lättilä, H. and Lindberg, J. J. *Polymer* 1973, **14**, 481
- 4 Bullock, A. T., Cameron, G. G. and Smith, P. M. *J. Polym. Sci. (A-2)* 1973, **11**, 1263
- 5 Gutowsky, H. S. and Pake, G. E. *J. Chem. Phys.* 1950, **18**, 162
- 6 Connor, T. M., Read, B. E. and Williams, G. *J. Appl. Chem.* 1964, **14**, 74
- 7 Ishida, Y., Matsuo, M. and Takayanagi, M. *J. Polym. Sci. (B)* 1965, **3**, 321
- 8 Read, B. E. *Polymer* 1962, **3**, 529
- 9 Yamafuji, K. and Ishida, Y., *Kolloid-Z. Z. Polym.* 1962, **183**, 15
- 10 Törmälä, P. *Thesis* Univ. Helsinki, 1973

Structural aspects of soda-cellulose II

The basic molecular repeat of natural cellulose, or cellulose I, was established by Meyer and Misch¹ in 1937 and it is now generally accepted that cellulose I has a monoclinic unit cell containing two chain segments. The general features of the X-ray fibre diffraction pattern and the fibre repeat of 1.03 ± 0.01 nm are consistent with a two-fold helical conformation which has an axial rise per glucose moiety of 0.515 nm.

Cellulose I under the action of sodium hydroxide undergoes a series of changes eventually forming cellulose II, a process of considerable industrial importance in the manufacture of mercerized cotton (for a recent review see Warwicker *et al.*²). Cellulose II may be regarded as a 'swollen' form of cellulose I, the fibre repeat remaining essentially constant. During the swelling process an intermediate crystalline phase can be obtained, known as soda-cellulose II, which contains both sodium and hydroxyl ions in the crystalline lattice. It is with this distinct solid-state phase that we have been concerned.

The X-ray fibre diffraction pattern obtained from soda-cellulose II is shown in *Figure 1*. The reflections index on a hexagonal unit cell with $a = 1.00 \pm 0.02$ nm and c (fibre axis) = 1.51 ± 0.02 nm, and with meridional reflections occurring on every third layer line. The simplest interpretation of this pattern is that each residue rotates, about successive glycosidic bonds, in response to the ionic environment to form a three-fold helix repeating in a distance of 1.51 nm. In fact Meyer *et al.*³ in 1939 originally suggested this interpretation. More recently Warwicker and Wright⁴ preferred to interpret this 1.51 nm fibre repeat in terms of sheets of cellulose molecules (where the molecular chains are two-fold helices similar to that for natural cellulose) which stagger relative to each other by units of one-third the fibre repeat distance. We wish to consider the soda-cellulose II data in somewhat more detail in an attempt to resolve the conformation of the molecular chains.

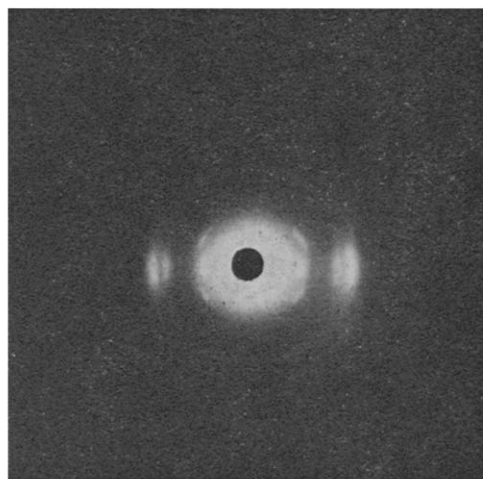


Figure 1 X-ray fibre diffraction pattern obtained from soda-cellulose II. The fibre axis is vertical and the reflections index on a hexagonal unit cell. Meridional reflections occur on the third and sixth layer lines only

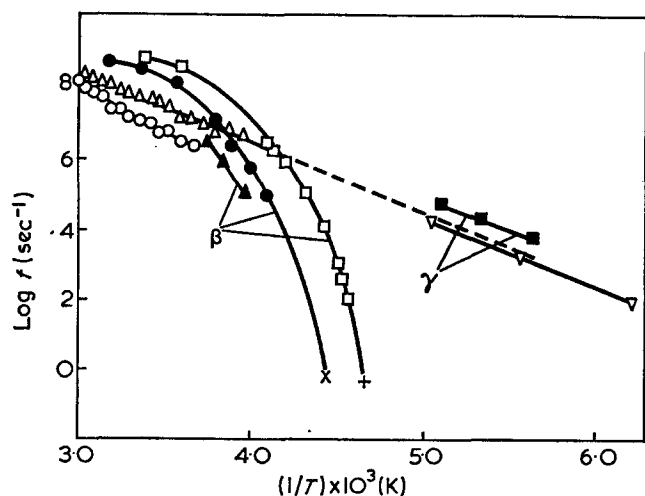


Figure 1 Log f against $1/T$ for PEG. Dielectric^{6,7}: \square , melt crystallized, \bar{M}_w 2.8×10^6 ; \bullet , melt crystallized, \bar{M}_w 2.8×10^5 ; \blacktriangle , melt crystallized, \bar{M}_w 3×10^4 ; ∇ , melt crystallized; \blacksquare , solution crystallized. Mechanical⁸: $+$, moulded annealed, \bar{M}_w 2.8×10^6 ; \times , moulded, annealed, \bar{M}_w 2.8×10^5 . Electron spin resonance⁹: Δ , solution crystallized, \bar{M}_n 2.2×10^4 (free radicals); \circ , solution crystallized, \bar{M}_n 2.2×10^4 (bonded radicals)

and nylon-6,¹⁰ where rotations of bonded radicals are in good accord with γ -relaxation frequencies.

These experimental observations show that free radicals experience the short range relaxations in polymers in a quite straightforward manner. Thus, the covalent bonding of radicals to the polymer backbone causes a small shift to lower frequencies as compared to the values of corresponding dielectric and mechanical relaxation measurements. It seems evident that this shift is caused by the slightly restricted rotation around the covalent bond^{3, 10}.

Acknowledgement

The author thanks Prof. J. J. Lindberg and H. Lättilä for their valuable aid.

P. Törmälä

Department of Wood and Polymer Chemistry,
University of Helsinki, Helsinki, Finland
(Received 12 November 1973)

References

- 1 Wasserman, A. M., Buchachenko, A. L., Kovarskii, A. L. and Neiman, M. B. *Eur. Polym. J.* 1969, **5**, 473
- 2 Bullock, A. T., Cameron, G. G. and Smith, P. M. *J. Phys. Chem.* 1973, **77**, 1635
- 3 Törmälä, P., Lättilä, H. and Lindberg, J. J. *Polymer* 1973, **14**, 481
- 4 Bullock, A. T., Cameron, G. G. and Smith, P. M. *J. Polym. Sci. (A-2)* 1973, **11**, 1263
- 5 Gutowsky, H. S. and Pake, G. E. *J. Chem. Phys.* 1950, **18**, 162
- 6 Connor, T. M., Read, B. E. and Williams, G. *J. Appl. Chem.* 1964, **14**, 74
- 7 Ishida, Y., Matsuo, M. and Takayanagi, M. *J. Polym. Sci. (B)* 1965, **3**, 321
- 8 Read, B. E. *Polymer* 1962, **3**, 529
- 9 Yamafuji, K. and Ishida, Y., *Kolloid-Z. Z. Polym.* 1962, **183**, 15
- 10 Törmälä, P. *Thesis* Univ. Helsinki, 1973

Specimens of soda-cellulose II were prepared from Ramie by the method of Schramek and Succolowsky⁵. In their paper the authors distinguish two forms, soda-cellulose II and IIh; the latter form displaying a single crystallographic phase, and thus, more correctly designated 'soda-cellulose II'. This nomenclature is used throughout this letter.

All the X-ray photographs were taken with nickel-filtered $\text{CuK}\alpha$ radiation with a flat film camera. The intensities were measured with a Joyce-Loebl Mk III c microdensitometer and standard corrections were made⁶.

The measured bulk density of soda-cellulose II is consistent with a unit cell containing six monomer units together with six sodium ions, six hydroxyl ions and at least six water molecules. The fibre repeat of 1.51 nm corresponds to three monomer units and therefore there are two chains running through the unit cell. Soda-cellulose II has many features in common with the molecular chain conformation and structure of β , 1→4 linked xylan hydrate⁶. Thus, on the basis of this refined xylan structure together with results from conformational analysis^{7,8}, we assert that the soda-cellulose II chains are left-handed helices. Cellulose chain coordinates incorporating a three-fold screw axis ($n = -3$) and with an axial advance per monomer (h) of 0.503 nm, $(\phi, \psi) = (30.4^\circ, 41.8^\circ)^*$ were derived.

Molecular chains were packed as a function of chain rotation, chain translation and side group rotation. 95% of the generated structures could be eliminated on steric grounds⁹, and of the two allowed regions,

* The conformation with $(\phi, \psi) = (0^\circ, 0^\circ)$ is chosen as the one in which the C(1)-H(1) bond is *cis* to the O-C(4') bond and the C(4')-H(4') bond is *cis* to the C(1)-O bond.

Table 1 Intensity measurements for soda-cellulose II

<i>hkl</i>	Spacing (nm)	Intensity*	
		Calc.	Obs.
300	0.289	vw	vw
301	0.284	w	w
200	0.433	s	vs
201	0.416	w	w
202	0.376	vw	w
203	0.328	w	w
204	0.285	w	w
120	0.327	vw	vw
121	0.320	w	w
122	0.300	m	m
100	0.866	s	w
101	0.751	w	w
102	0.569	vw	w
103	0.335	vw	vw
104	0.346	vw	vw
110	0.500	s	s
111	0.475	vw	w
112	0.417	m	w
113	0.355	vw	w
114	0.301	w	w

* vw=very weak, w=weak, m=medium, s=strong, vs=very strong

Comparison of the calculated and observed intensities for all observed reflections for the sterically allowed model. The only major discrepancy, in the (100) reflection intensity, is a consequence of ignoring the sodium and hydroxyl ions in the vacant position when calculating intensities. The (100) reflection is the most affected by the absence

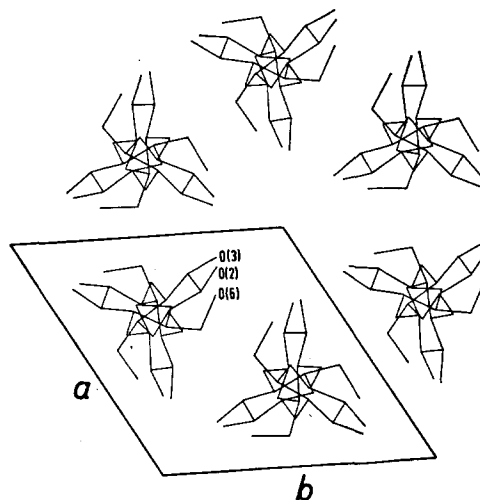


Figure 2 Projection of proposed structure for soda-cellulose II down the fibre axis. Each chain is a three-fold helix and packs in the manner shown with six chains surrounding the hole containing sodium, and hydroxyl ions together with water molecules. Note that the O(2) and O(3) atoms point towards the central hole. The chains are shown in an anti-parallel arrangement but parallel chains are equally possible in the present analysis

Table 2 Fractional coordinates for the proposed model for soda-cellulose II

Atom	X_f	Y_f	Z_f
C(1)	0.317	0.720	0.595
C(2)	0.321	0.765	0.548
C(3)	0.166	0.717	0.465
C(4)	0.273	0.689	0.407
C(5)	0.349	0.615	0.460
C(6)	0.469	0.595	0.409
O(1)	0.613	0.734	0.405
O(2)	0.402	0.807	0.667
O(3)	0.145	0.821	0.605
O(5)	0.109	0.799	0.418
O(6)	0.420	0.704	0.587

The fractional coordinates are given for one asymmetric unit of the cellulose chain

only one yielded an acceptable intensity agreement (see Table 1).

A projection of the proposed structure, viewed along the fibre axis, and calculated using polysaccharide chains only, is illustrated in Figure 2. The fractional coordinates for this model are given in Table 2. It will be observed that the O(2) and O(3) atoms of each cellulose residue point towards the postulated position for the missing ions. This volume, surrounded by hydrophilic groups, would be expected to contain the water molecules which, in addition to the sodium and hydroxyl ions, would organize themselves around the three-fold symmetry axis.

The chain packing and Fourier transform calculations of the proposed model are in general agreement with the observed intensity distribution supporting our contention that the molecular chains have a three-fold helical conformation, and therefore pack naturally in a trigonal array. Only when the ion positions have been defined more precisely can the chain polarity problem be broached.

Acknowledgements

We thank the Science Research Council for support.

P. M. Whitaker, I. A. Nieduszynski
and E. D. T. Atkins

H. H. Wills Physics Laboratory,
University of Bristol,
Bristol BS8 1TL, UK
(Received 16 November 1973)

References

- 1 Meyer, K. H. and Misch, L. *Helv. Chim. Acta* 1937, **20**, 232
- 2 Warwicker, J. O., Jeffries, R., Colbran, R. L. and Robinson, R. N. *Shirley Inst. Pamphlet No. 93* 1966
- 3 Meyer, K. H., Misch, L. and Badenhuizen, N. P. *Helv. Chim. Acta* 1939, **22**, 59
- 4 Warwicker, J. O. and Wright, A. C. *J. Appl. Polym. Sci.* 1967, **11**, 659
- 5 Schramek, W. and Succolowsky, O. *Kolloid-Z.* 1937, **80**, 129
- 6 Nieduszynski, I. A. and Marchessault, R. H. *Biopolymers* 1972, **11**, 1335
- 7 Rees, D. A. and Skerrett, R. J. *Carbohydr. Res.* 1968, **7**, 334
- 8 Sundararajan, P. R. and Rao, V. S. R. *Biopolymers* 1970, **9**, 1235
- 9 Ramachandran, G. N., Ramakrishnan, C. and Sasisekharan, V. *J. Mol. Biol.* 1963, **7**, 95

Solvent resistant membranes

Recently we have been concerned with the characterization of a series of copolymers involving acrylonitrile and vinyl-sulphone compounds. These copolymers were prepared by the mutual irradiation technique in which the two monomers were present in aqueous solution. A complete account of the work will be presented in due course. Here we wish to draw attention to problems which arose during the determination of number-average molecular weights by membrane osmometry.

Solvents for polyacrylonitrile and its copolymers are not commonplace. Usually one is restricted to *N,N*-dimethylformamide (DMF) and dimethylsulphoxide (DMSO). Membranes used in conjunction with these solvents are required to be highly solvent resistant and, ideally, should show little change with prolonged use.

For this section of the polyacrylonitrile characterization we used a Hewlett-Packard Series 500 Membrane Osmometer. 'Solvent resistant' membranes (type 0-8), specified by the manufacturer as being suitable for solutions of polymers in *N,N*-dimethylformamide for up to three weeks, were assessed for overall performance. Invariably these membranes began to break up after only two days in the solvent and were thus discarded.

Attention was then placed on the possibility of using modified cellulose membranes having a low degree of substitution. Here we were fortunate in our choice. Hydroxyethylcellulose film, having a degree of substitution of approximately 0.4, was chosen. As supplied by the manufacturer, this film was coated with a nitrocellulose lacquer which was completely removed before use. This was achieved by swabbing with cotton wool soaked in methylene chloride. The film was then soaked in fresh methylene chloride for several minutes to get rid of the last traces of the surface coating. It was found to be imperative that the film be kept flat during these operations since the swollen film is easily creased and is then of no use as a membrane. The film was then

dried in a vacuum desiccator to remove the methylene chloride.

The film was conditioned by soaking in water for a few minutes, then in 50:50 DMF/water for at least 4 h and finally in 100% DMF until required. A minimum of 4 h was placed on this final stage.

Membranes made in this way have a useful life of many weeks. In fact the upper lifetime limit is unknown as membranes, placed in DMF four months ago, are still intact. Hence no absolute figures regarding the stability of these membranes to DMF can be quoted. Subsequently other films were tried, none being as satisfactory as hydroxyethylcellulose. The main difficulty arises from the length of time taken for the polymer solution/membrane/solvent system to achieve dynamic equilibrium. One case in point is regenerated cellulose film, which although moderately unaffected by DMF took hours to reach an equilibrium condition which, even then, was not altogether reproducible.

Although inconvenient under any conditions, the long time taken to achieve equilibrium is critical with solvents such as DMF owing to their uptake of atmospheric moisture. In many cases this can result in precipitation of the polymer from solution. With the hydroxyethylcellulose membranes described above, equilibrium was achieved usually within 20 min.

In order to evaluate the performance of these membranes in molecular weight determinations by osmometry, trials were carried out using a standard sample of polystyrene. The characteristics of the standard sample, with regard to \bar{M}_n were previously obtained by osmometry in toluene and dioxane using Hewlett-Packard type 0-8, solvent resistant membranes. Values for \bar{M}_w for the standard were determined by light scattering with dioxane and toluene as solvents. On measurement of the \bar{M}_n of the standard by osmometry, using the hydroxyethylcellulose membranes recommended above and DMF as solvent, agreement was satisfactory, being within $\pm 3\%$.

Expansion of the study to include solutions of polyacrylonitrile and solutions of copolymers containing polyacrylonitrile enabled their number-average molecular weights to be determined with considerable consistency, even with values as low as $\bar{M}_n = 25\,000$.

We intend to widen the range of solvents in which hydroxyethylcellulose membranes can be used to include solvents such as dioxane, tetrahydrofuran, dimethylsulphoxide etc. We are confident that hydroxyethyl membranes have provided a solution to the question of obtaining membranes which are resistant to DMF. Further evaluation is being carried out regarding the nature of the stability of the hydroxyethylcellulose membranes and also the question of possible solute leakage when low molecular weights ($< 15\,000$) are used.

Acknowledgements

We are indebted to Transparent Paper Ltd for supplying samples of hydroxyethylcellulose film and regenerated cellulose film. We are also grateful to the Perkin Bequest for providing one of us (N. S. B.) with financial support.

N. S. Batty and J. T. Guthrie

Department of Colour Chemistry and Dyeing,
University of Leeds, Leeds LS2 9JT, UK
(Received 2 November 1973; revised 23 November 1973)

Acknowledgements

We thank the Science Research Council for support.

P. M. Whitaker, I. A. Nieduszynski
and E. D. T. Atkins

H. H. Wills Physics Laboratory,
University of Bristol,
Bristol BS8 1TL, UK
(Received 16 November 1973)

References

- 1 Meyer, K. H. and Misch, L. *Helv. Chim. Acta* 1937, **20**, 232
- 2 Warwicker, J. O., Jeffries, R., Colbran, R. L. and Robinson, R. N. *Shirley Inst. Pamphlet No. 93* 1966
- 3 Meyer, K. H., Misch, L. and Badenhuizen, N. P. *Helv. Chim. Acta* 1939, **22**, 59
- 4 Warwicker, J. O. and Wright, A. C. *J. Appl. Polym. Sci.* 1967, **11**, 659
- 5 Schramek, W. and Succolowsky, O. *Kolloid-Z.* 1937, **80**, 129
- 6 Nieduszynski, I. A. and Marchessault, R. H. *Biopolymers* 1972, **11**, 1335
- 7 Rees, D. A. and Skerrett, R. J. *Carbohydr. Res.* 1968, **7**, 334
- 8 Sundararajan, P. R. and Rao, V. S. R. *Biopolymers* 1970, **9**, 1235
- 9 Ramachandran, G. N., Ramakrishnan, C. and Sasisekharan, V. *J. Mol. Biol.* 1963, **7**, 95

Solvent resistant membranes

Recently we have been concerned with the characterization of a series of copolymers involving acrylonitrile and vinyl-sulphone compounds. These copolymers were prepared by the mutual irradiation technique in which the two monomers were present in aqueous solution. A complete account of the work will be presented in due course. Here we wish to draw attention to problems which arose during the determination of number-average molecular weights by membrane osmometry.

Solvents for polyacrylonitrile and its copolymers are not commonplace. Usually one is restricted to *N,N*-dimethylformamide (DMF) and dimethylsulphoxide (DMSO). Membranes used in conjunction with these solvents are required to be highly solvent resistant and, ideally, should show little change with prolonged use.

For this section of the polyacrylonitrile characterization we used a Hewlett-Packard Series 500 Membrane Osmometer. 'Solvent resistant' membranes (type 0-8), specified by the manufacturer as being suitable for solutions of polymers in *N,N*-dimethylformamide for up to three weeks, were assessed for overall performance. Invariably these membranes began to break up after only two days in the solvent and were thus discarded.

Attention was then placed on the possibility of using modified cellulose membranes having a low degree of substitution. Here we were fortunate in our choice. Hydroxyethylcellulose film, having a degree of substitution of approximately 0.4, was chosen. As supplied by the manufacturer, this film was coated with a nitrocellulose lacquer which was completely removed before use. This was achieved by swabbing with cotton wool soaked in methylene chloride. The film was then soaked in fresh methylene chloride for several minutes to get rid of the last traces of the surface coating. It was found to be imperative that the film be kept flat during these operations since the swollen film is easily creased and is then of no use as a membrane. The film was then

dried in a vacuum desiccator to remove the methylene chloride.

The film was conditioned by soaking in water for a few minutes, then in 50:50 DMF/water for at least 4 h and finally in 100% DMF until required. A minimum of 4 h was placed on this final stage.

Membranes made in this way have a useful life of many weeks. In fact the upper lifetime limit is unknown as membranes, placed in DMF four months ago, are still intact. Hence no absolute figures regarding the stability of these membranes to DMF can be quoted. Subsequently other films were tried, none being as satisfactory as hydroxyethylcellulose. The main difficulty arises from the length of time taken for the polymer solution/membrane/solvent system to achieve dynamic equilibrium. One case in point is regenerated cellulose film, which although moderately unaffected by DMF took hours to reach an equilibrium condition which, even then, was not altogether reproducible.

Although inconvenient under any conditions, the long time taken to achieve equilibrium is critical with solvents such as DMF owing to their uptake of atmospheric moisture. In many cases this can result in precipitation of the polymer from solution. With the hydroxyethylcellulose membranes described above, equilibrium was achieved usually within 20 min.

In order to evaluate the performance of these membranes in molecular weight determinations by osmometry, trials were carried out using a standard sample of polystyrene. The characteristics of the standard sample, with regard to \bar{M}_n were previously obtained by osmometry in toluene and dioxane using Hewlett-Packard type 0-8, solvent resistant membranes. Values for \bar{M}_w for the standard were determined by light scattering with dioxane and toluene as solvents. On measurement of the \bar{M}_n of the standard by osmometry, using the hydroxyethylcellulose membranes recommended above and DMF as solvent, agreement was satisfactory, being within $\pm 3\%$.

Expansion of the study to include solutions of polyacrylonitrile and solutions of copolymers containing polyacrylonitrile enabled their number-average molecular weights to be determined with considerable consistency, even with values as low as $\bar{M}_n = 25\ 000$.

We intend to widen the range of solvents in which hydroxyethylcellulose membranes can be used to include solvents such as dioxane, tetrahydrofuran, dimethylsulphoxide etc. We are confident that hydroxyethyl membranes have provided a solution to the question of obtaining membranes which are resistant to DMF. Further evaluation is being carried out regarding the nature of the stability of the hydroxyethylcellulose membranes and also the question of possible solute leakage when low molecular weights ($< 15\ 000$) are used.

Acknowledgements

We are indebted to Transparent Paper Ltd for supplying samples of hydroxyethylcellulose film and regenerated cellulose film. We are also grateful to the Perkin Bequest for providing one of us (N. S. B.) with financial support.

N. S. Batty and J. T. Guthrie

Department of Colour Chemistry and Dyeing,
University of Leeds, Leeds LS2 9JT, UK
(Received 2 November 1973; revised 23 November 1973)

Book Reviews

Radiation chemistry of macromolecules

Edited by Malcolm Dole

Academic Press, New York, 1973. Vol 1: \$23.00; Vol 2: \$25.00

In the editorial preface, Professor Dole announces that his aim has been to produce a comprehensive review of macromolecular radiation chemistry with emphasis placed mainly on the period since the earlier books of Charlesby (1960) and Chapiro (1962). Moreover, he asserts that the size of the work testifies to the advances made in the field since the early sixties. Quantity there is certainly—almost 800 pages divided into two volumes which may be roughly described as: volume 1, for beginners; volume 2, for specialists.

Background science forms the bulk of volume 1 to which ten authors contribute fourteen chapters. Eleven of these deal with the essential principles of radiation physics, charge mobility and trapping, excitation migration, polymer properties, etc. upon which an appreciation of the phenomenological material of the subject depends. As a result, professional scientists having little prior knowledge of the speciality, but who require a high-level introduction to the principles and practices, now have their needs met in one up-to-date volume. A group of ten chapters, collected under the sub-title 'Fundamental processes and theory', is made up briefly of: Early processes, Energy transfer, Thermoluminescence, Free radical theory, Molecular mobility in polymers, Solid state reaction theory, Electrical conductivity—theory and practice, Trapped electron studies, and Statistical theories of crosslinking. Together with a chapter on Experimental techniques, this group forms an excellent underlying foundation for a modern study, and non-specialists will applaud the contributors for spending some little time with the 'nuts and bolts'—conceptual as well as practical.

The final two chapters of volume 1 and the whole of volume 2 are concerned with radiation effects in synthetic and natural polymers. Fourteen authors provide nineteen chapters, each devoted to reviewing one polymer or a related group. Individual consideration is given to the common vinyl polymers—polyethylene (volume 1), polypropylene, poly(propylene oxide), poly(vinyl chloride), poly(vinyl acetate), polystyrene and poly(methyl methacrylate). Of the non-vinyl types, poly(ethylene terephthalate) and polyoxymethylene merit individual treatment, whereas other non-vinyls—polyamides, polysiloxanes, fluoropolymers and elasto-

mers—are accorded group consideration. Four chapters are devoted to the radiolytic modification of physical properties and state of synthetics, and the final chapter deals with macromolecules of biological interest—nucleic acids, proteins and polysaccharides.

The impression left by reading these volumes in numerical order is anti-climactic. The modern approach of the introductory volume engenders an expectancy about the content of the second part which remains essentially unrequited. The clue to understanding the anomaly is contained in the chronological distribution in the reference lists appended to each chapter. It is significant that of the nineteen specialist chapters, fourteen have 75% of their citations before 1968. This forces the conclusion that in the six years prior to the publication of these volumes, interest in macromolecular systems has declined. The outstanding exception is in the area of Biological molecules: of 170 references cited by Dr Myers, 87 are post-1968. This growing disinterest in synthetics must be viewed in the light of the continuing upsurge in effort and reward in the parent fields of polymer science and small molecule radiation chemistry. In the latter particularly, the intense activity of the past ten years or so has effected a transformation in the thinking about mechanisms of radiolysis. There is now universal acceptance of the important roles played by electrons, positive holes, and molecular excited states in the primary processes which lead eventually to stable products via free radicals. The introductory material in volume 1 puts over these concepts admirably, but only glimpses appear in the specialist reviews; that the radiation chemistry of some (not all) polymeric systems can be discussed in 1973 without reference to ionization or excitation is unbelievable.

Macromolecular radiation chemistry clearly needs new directions. The wider application of the modern experimental techniques which have proved so successful in breaking the free radical stranglehold in the low molecular weight field is now a timely requirement of the macromolecular exponents, as also is some diversion away from the well trodden paths into investigation of the materials of today. This field is too important to lie fallow; hopefully these volumes will provide stimulus for new efforts.

M. A. J. Rodgers

Fluoropolymers

RAPRA Data Handbook, compiled by W. A. Lee and R. A. Rutherford

Rubber and Plastics Research Association, Shawbury, 1973. 113 Sheets. £10 (£7.50 to RAPRA members)

For many years personnel of the Materials Department of RAE Farnborough have been concerned with the synthesis and properties of novel polymers, and with their collaboration RAPRA propose to issue a comprehensive handbook listing information on the transition behaviour of polymers. This will take the form of a series of loose-leaf data sheets and the present volume forms the first of these, covering fluorocarbon polymers based on a carbon-carbon chain, the fluorine atoms occurring in this main chain or in substituent groups.

The 113 sheets, covering 90 fluoropolymers, contain data on T_g and T_m and other transition points, relevant sample preparations, thermal history, methods of measurement, and results, together with the appropriate references. This information is clearly set out, readily accessible and is provided with an index.

An introductory chapter discusses transitions in polymers, their determination, interpretation and practical significance, and lists 125 general references.

For those interested in the thermal behaviour of polymers, either from a scientific or technical point of view, the handbook will prove to be a most useful compilation and provide a valuable reference source leading to much saving in time and effort in literature searching. It is well produced in a robust binding that will withstand the hard wear which it is likely to receive. One looks forward to the publication of further sections in this series.

R. J. W. Reynolds

Conference Announcement

Polymerization in Ordered Systems

Midland, Michigan, 19–23 August 1974

The Midland Macromolecular Institute will sponsor an international Symposium on 'Polymerization in ordered systems' to be held from August 19 to 23, 1974 in Midland, Michigan. The Symposium will consist of both invited and contributed papers. The invited papers will offer critical reviews on polymerization of micelles, mesophases, mono- and multi-layers, and monomer crystals. Contributed papers are solicited. For further information write to: Symposium Secretary, Midland Macromolecular Institute, 1910 West St Andrews Drive, Midland, Michigan 48640, USA.

Studies of crystalline forms of nylon-6 by X-ray and i.r. spectrophotometry

B. D'Alò, G. Coppola and B. Pallesi

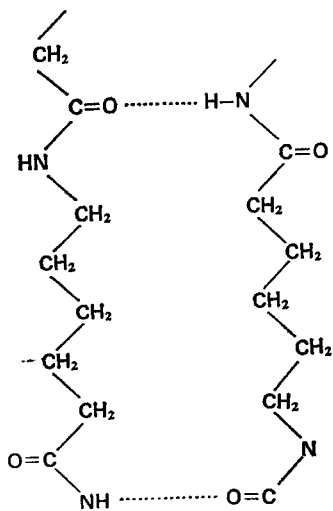
*Snia Viscosa, Centro Sperimentale 'F. Marinotti', 20031 Cesano Maderno, Milano, Italy
(Received 5 March 1973; revised 9 October 1973)*

The crystalline forms, α and γ , of two different polyamide fibres (nylon-6) were examined by X-ray diffraction and infra-red spectroscopy. The first type of fibre (α) was left one week with 5% of water before being drawn and it represents the α crystalline stable form. The second type of fibre was spun and drawn at the same time between two thermo-regulated rolls with a draw ratio of 3.8. This last fibre has the γ (unstable) crystalline form. By changing the temperature of the draw rolls, the $\gamma \rightarrow \alpha$ transformation has been studied. Increasing the draw roll temperature causes a decrease in γ .

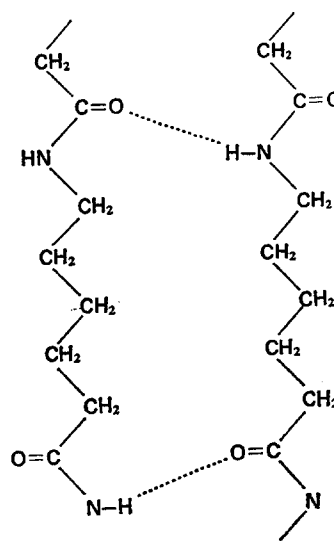
INTRODUCTION

The crystalline forms of nylon-6 after thermal and mechanical treatment have been examined by several authors¹⁻⁸. They found the following forms: amorphous 1, amorphous 2, γ -pseudo hexagonal, β -hexagonal, α -paracrystalline and α -Bunn¹. Our studies concern the α stable form and γ unstable form.

It has been demonstrated that the polyamide unit cell contains fully extended planar zig-zag chains, where adjacent macromolecules are joined by hydrogen bonds of the amido groups ($-\text{C}(\text{O})-\text{NH}-$). The shifting of the hydrogen bonds generates different crystalline forms, e.g. the α form which is characterized by sheets of antiparallel chains^{2,4}:



and the γ form with parallel chains^{4,7,8}:



In this latter one we can see the deformation of the hydrogen bond.

Samples consisted of two different types of nylon-6 fibres obtained in a laboratory plant: (i) normal nylon-6, obtained from a cold roll and left one week with about 5% of water before being drawn; (ii) special nylon-6, spun and drawn at the same time between two thermo-regulated rolls, slow and fast, with a draw ratio of 3.8. This sample also contains 3-5% of water. The 'normal nylon' had the α form, which shows two X-ray diffraction peaks at $20.3-20.7^\circ$ and at $23.35-23.9^\circ$. The second type of fibre, 'special nylon-6', had a predominance of the γ form, that gives a diffraction peak at $21.3-21.5^\circ$. By means of mechanical and thermal treatments the γ unstable form turns into the α stable form.

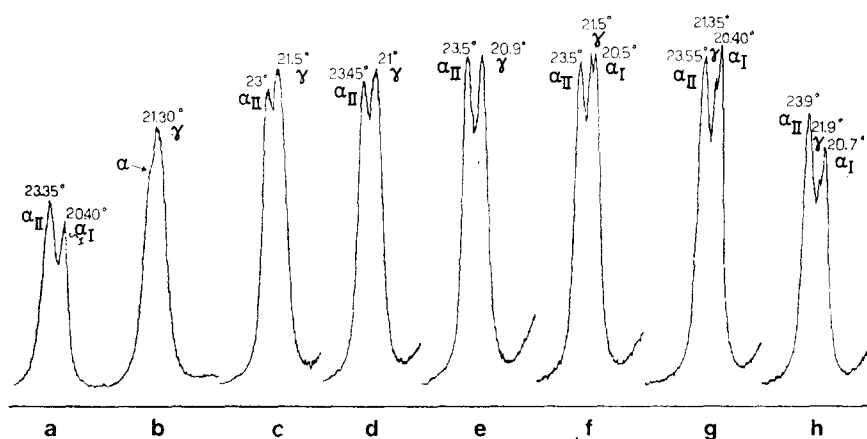


Figure 1 X-ray diffraction patterns of (a) 'normal nylon-6' and (b)-(h) 'special nylon-6' slow rolled at room temperature and fast rolled at: (b) 150°; (c) 170°; (d) 182°; (e) 193°; (f) 195°; (g) 201°; (h) 205°C

EXPERIMENTAL AND RESULTS

The X-ray diffraction patterns were obtained with a Philips diffractometer model PW 1010 with nickel-filtered $\text{CuK}\alpha$ radiation. The conditions of the X-ray scattering were as follows: 36 kV; 16 mA; Geiger tension, 1650 V; slits: divergence, 1°; receiving, 0.1°; diff., 1°. As already outlined, our 'normal nylon' has two diffraction peaks that belong to the α stable form. We will call these peaks α_{I} and α_{II} , in agreement with Roldan¹ who gives the diffraction peaks of α_{I} at 20.5° and α_{II} at 23.7–23.9°. Our corresponding values are 20.3–20.7° and 23.35–23.9° (Figure 1a). The X-ray photograph of this type of fibre shows diffraction spots only along the equatorial line, characteristic of the α form^{4,5} (Figure 2a). The distances between the diffraction sheets obtained from values of θ angle are: $d_{\alpha_{\text{I}}}=4.35$; $d_{\alpha_{\text{II}}}=3.83$. These values also agree with published data for α .

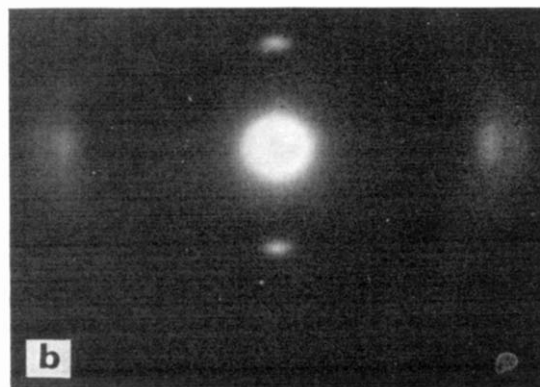


Figure 2 X-ray photographs of (a) 'normal nylon-6' and (b) and (c) 'special nylon-6' slow rolled at room temperature and fast rolled at: (b) 150°; (c) 195°C

Table 1 Observations on X-ray diffraction patterns of 'special nylon-6' fibres slow rolled at room temperature and fast rolled at temperatures from 150°C to 205°C

Fast roll temp. (°C)	Comments
150	Strong diffraction peak at 21.3° that belongs to the γ form (Figure 1b). Figure 2b shows clear spots on the meridional line (γ form) and unfocused spots on the equatorial line (α form), which indicate that there is prevalence of γ and that α has not been completely eliminated. A shoulder at $2\theta=23^\circ$ indicates presence of α_{II} form
170	The γ peak at 21.5° and a second peak at about 23° indicates an increase of α_{II} form (Figure 1c)
182	The γ peak is shifted to 21° while α_{II} appears at 23.45° (Figure 1d)
193	The angle shifting becomes more evident. Now we have γ at 20.9° and α_{II} at 23.5°. This shows the $\gamma \rightarrow \alpha$ transformation with temperature treatment. In fact the values lead to 20.3–20.7 for α_{I} , and 23.35–23.9 for α_{II} (Figure 1e)
195	The peak that appeared at 20.9° separates into a double peak at 21.5° (γ) and at 20.5° (α_{I}). This could be a transition temperature (Figure 1f). The X-ray photograph shows clear spots both on the equatorial line (α) and on the meridional line (γ) (Figure 2c)
201	The γ form has almost disappeared, while the α_{I} and α_{II} peaks are at 20.4° and 23.55° respectively. The peak of α_{I} is higher than α_{II} , probably due to the influence of γ on it (Figure 1g)
205	A very light peak corresponding to γ at 21.9°, while α_{I} and α_{II} appear at 20.7° and 23.9° respectively (Figure 1h)

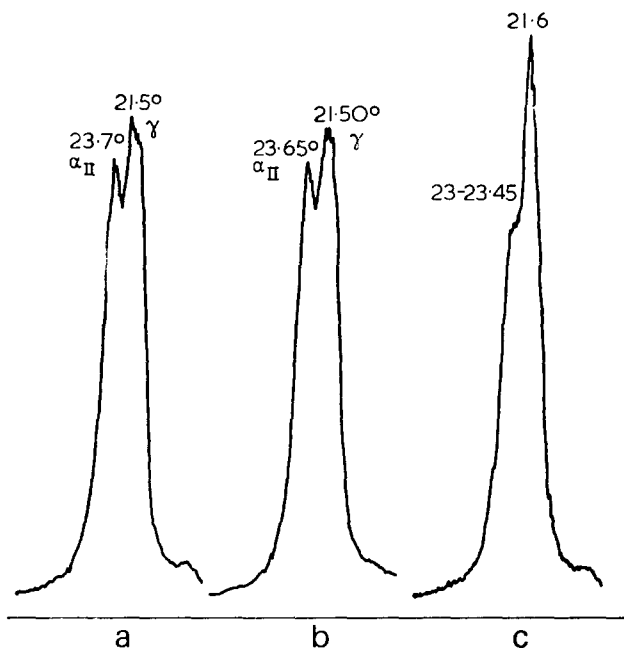


Figure 3 X-ray diffraction patterns of 'special nylon-6' fast rolled at 185°C and slow rolled at: (a) 50°; (b) 80°; (c) 100°C

Table 2 Observations on X-ray diffractions of 'special nylon-6' fibres fast rolled at 185°C and slow rolled at 50°C or 100°C

Slow roll temp. (°C)	Comments
50	This sample is similar to the sample of Figure 1d. Both the diffraction peaks of γ at 21.5° and α_{II} at 23.7° (Figure 3a and 3b) are seen
100	Similar to the sample in Figure 1b. Marked predominance of γ at 21.6°. The α form appears only as a light shoulder on the γ peak (Figure 3c)

On the other type of fibre, 'special nylon-6' several thermal treatments have been carried out by changing the temperature of the draw rolls. The X-ray diffraction patterns are shown in Figures 1b to 1h and observations are mentioned in Table 1. X-ray photographs for fibres fast rolled at 150°C and 195°C are given in Figures 2b and 2c.

In a further series of measurements we changed the temperature of the slow roll and kept the fast roll constant at 185°C. It can be seen from the results (Figure 3 and Table 2) that thermal treatments are responsible for transformations on the nylon crystalline structure. In the case of the slow roll temperature at 100°C and fast roll temperature at 185°C, the γ form originates from a reduction in drawing tension, probably due to the fact that the temperature of the fibre on the slow roll is above the glass transition temperature.

By leaving a sample for 6 h in boiling water, it is possible to transform the γ form into the α form.

INFRA-RED SPECTROPHOTOMETRY

It is possible to recognize the α and γ form by infra-red spectrophotometry, since α gives a sharp absorption peak at 690 cm^{-1} while γ gives it at 975 cm^{-1} . From the spectrum of 'normal nylon' (Figure 4) we notice the absorption at 690 cm^{-1} which is less marked than the spectrum of the 'special nylon-6' (Figure 5). We also observed an absorption at 975 cm^{-1} corresponding to

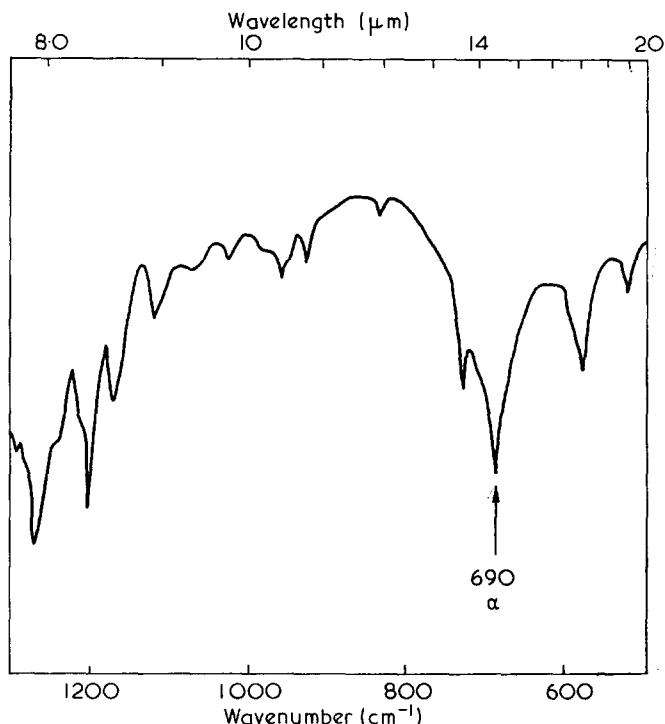


Figure 4 Infra-red spectrum of 'normal nylon-6'

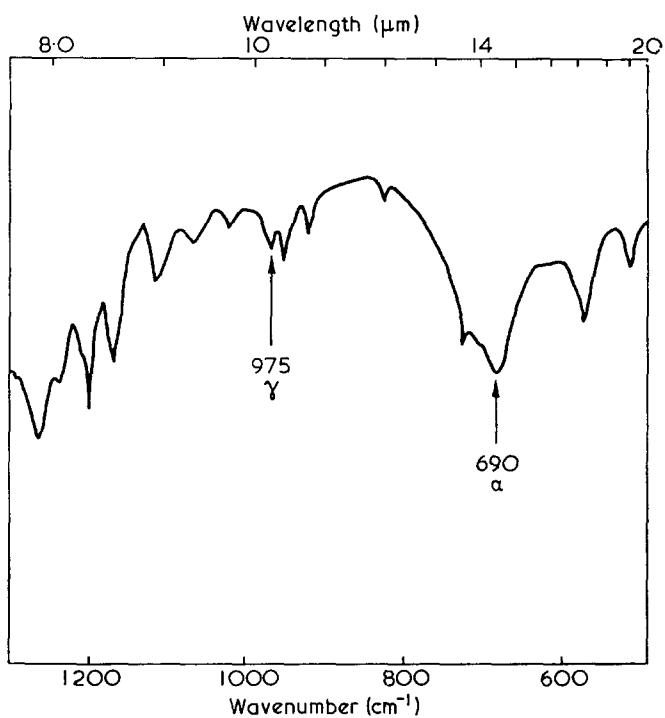


Figure 5 Infra-red spectrum of 'special nylon-6'

the γ form. These results agree with the X-ray diffraction patterns and photographs. All the samples examined were films obtained from formic acid solutions.

REFERENCES

- 1 Roldan, L. G., et al. *J. Polym. Sci. (C)* 1965, 8, 145
- 2 Holmes, D. R., et al. *J. Polym. Sci.* 1955, 17, 159
- 3 Sandeman, I. and Keller, A. *J. Polym. Sci.* 1956, 19, 401
- 4 Kinoshita, Y. *Makromol. Chem.* 1959, 33, 1
- 5 Kinoshita, Y. *Makromol. Chem.* 1959, 33, 21
- 6 Hosemann, R. *Polymer* 1962, 3, 349
- 7 Bradbury, E. M., Brown, L., Elliott, A. and Parry, D. A. D. *Polymer* 1965, 6, 465
- 8 Arimoto, H. *J. Polym. Sci. (A)* 1964, 2, 2283

Synthesis of cellulosic graft copolymers and their analysis by ultra-violet and infra-red spectroscopy

James T. Guthrie and Zia Haq

*Department of Colour Chemistry, University of Leeds, Leeds LS2 9JT, UK
(Received 10 August 1973; revised 30 October 1973)*

Two types of graft copolymer were prepared by irradiating regenerated cellulose and hydroxyethylcellulose, both in film form, in the presence of styrene. Dioxane was used as solvent for the styrene and water as swelling agent for the substrate. The rate and extent of grafting was investigated gravimetrically and through ultra-violet and infra-red spectroscopy. Spectroscopic techniques are shown to be valuable aids in kinetic studies of grafting reactions under otherwise difficult conditions. Excellent correlation between gravimetric and spectroscopic analysis occurs. Grafting to regenerated cellulose exhibits steady state kinetics whereas anomalies exist in grafting to hydroxyethylcellulose film. Such anomalies are explained in terms of the changing nature of the grafting medium.

INTRODUCTION

Studies of grafting to cellulose and cellulose derivatives are legion¹. In most cases grafting rates are obtained by gravimetric procedures which can give rise to error. Prime among these is the ease of moisture uptake by the ungrafted samples, which renders weighing difficult unless carried out under constant temperature and humidity conditions. Secondly, there exists, with cellulosic films, the possibility of film loss through handling procedures which could render a complete experiment useless. The technique presented obviates the use of gravimetry once the relationship between gravimetric and spectroscopic techniques has been established. Ultra-violet (u.v.) spectroscopic techniques, though more sensitive, are of limited application. The use of infra-red (i.r.) spectroscopy opens up a wide range of monomer-substrate graft copolymerization systems hitherto dependent on gravimetric methods as the main means of elucidation.

Although this study is limited to the kinetics of grafting to cellulose films, the technique may be applied to a wide variety of copolymer systems. Further work along these lines is continuing in this Department.

Much work has been carried out on spectroscopic investigations of vinyl monomers. However, studies of homopolymers and copolymers are scarce. In general the majority of investigations of polymers have been aimed at spectral interpretation with minimum interest being shown in the applied aspects of the technique^{2,3}.

In this work, graft copolymers were prepared using the heterogeneous mutual irradiation technique^{4,5}. Two substrates were studied, namely regenerated cellulose and hydroxyethylcellulose (D.S. 0.4–0.5). Styrene was used as the monomer throughout.

EXPERIMENTAL

Materials

All solvents and monomers were purified using standard techniques. Triply distilled water was used throughout.

Regenerated cellulose and hydroxyethylcellulose films used in this study were supplied by Transparent Paper Ltd, Bury, Lancashire. Purification of these films prior to grafting was carried out using the method outlined in a previous paper⁵.

Grafting procedure

Since extensive details of the grafting technique have been given elsewhere^{4,5} only an outline will now be presented. Grafting of the monomer to film took place in evacuated sealed ampoules at 18–21°C using the ⁶⁰Co γ -irradiation facility located in the School of Chemistry at this University. A dose rate of 0.37×10^{-2} W/kg was employed. Dosimetry was by means of Frické solutions made up according to standard procedures. Post-irradiation grafting procedures were as described by Guthrie *et al.*⁵ and will not be expanded here except to state that great care was taken to ensure complete removal of occluded homopolymer from the film. No attempt was made to condition films to standard relative humidities either before or after grafting, since initial experiments were found to give inconsistent results. Instead, all samples were dried to constant weight. The extent of grafting was determined both gravimetrically and spectroscopically.

Spectroscopic analysis

Grafted samples were presented in film form for infra-red (Perkin-Elmer Infra-red Spectrophotometer Model 157G) and ultra-violet (Unicam SP800A Ultraviolet Spectrophotometer) spectroscopic analysis. The ungrafted film was taken as standard reference in both cases. For u.v. spectroscopy, the instrument was zero adjusted using the ungrafted film in both the reference and sample beams. Multiple checks were made on film thickness consistency. It was found that reproducibility of film thickness for a wide variety of industrially produced films was excellent. Non-uniform film thickness is a serious drawback to using the methods outlined. However, industrially produced

substrates carry a high degree of thickness control which is difficult to achieve in small-scale operations. Spectra were examined in detail to ascertain those locations giving absorptions useful for quantitative interpretations. For u.v. spectroscopy (Figure 1) absorption at 271 nm was taken as the reference point. Evidence of complete removal of ungrafted styrene is shown by the lack of absorption at 282 and 291 nm. In the case of i.r. spectroscopy (Figure 2), isolation of a suitable absorption band is more difficult. Ideally, the most useful situation arises when absorption occurs free from interference. Suitable examples are the $\text{—C}\equiv\text{N}$ group absorption from polyacrylonitrile¹¹ or the C=O absorption from polyesters. However, using the absorption at 750 cm^{-1} of the polystyrene spectrum we have been able to use i.r. spectroscopy with a high degree of sensitivity. Other possibilities exist in the polystyrene spectrum but these are less satisfactory from a quantitative standpoint. Measurements of extent of absorption were taken from peak areas at 750 m^{-1} and not from peak heights. In some cases standardization of a baseline was necessary, but this does not introduce too serious an error.

RESULTS

Regenerated cellulose/polystyrene copolymers

Samples of varying extents of graft polymerization were analysed spectroscopically after gravimetric methods had been applied. Figure 3 represents the correlation between percentage grafting on initial film weight against (a) absorbance and (b) area under the absorption peak in i.r. spectroscopy. (Four films were taken and the average is shown.) The accuracy of the calibration curve was then checked using samples of unknown extents of grafting but known initial film weights. The extent of grafting was

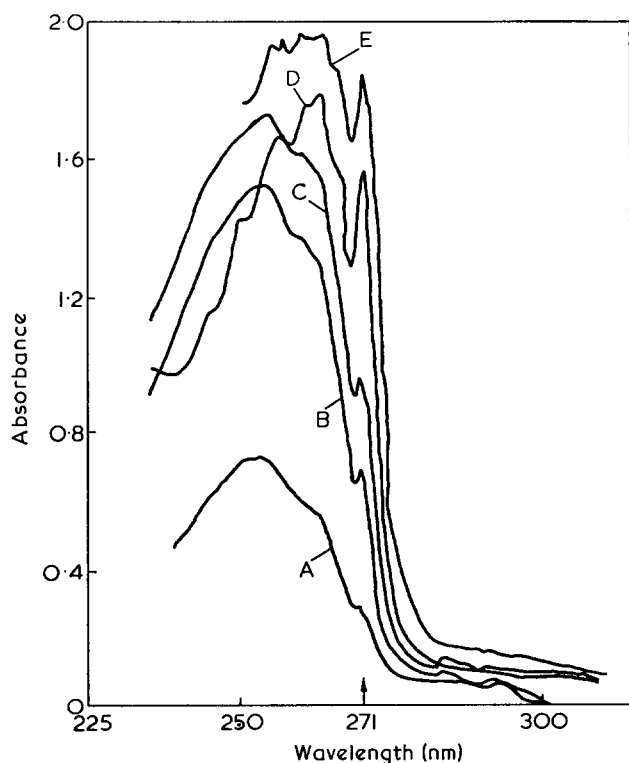


Figure 1 U.v. spectra of samples of hydroxyethylcellulose/polystyrene graft copolymers. Variation of absorbance with extent of grafting (G) (λ_{max} at 271 nm). A, 3.5%G; B, 8.5%G; C, 18.5%G; D, 20.0%G; E, 42.8%G

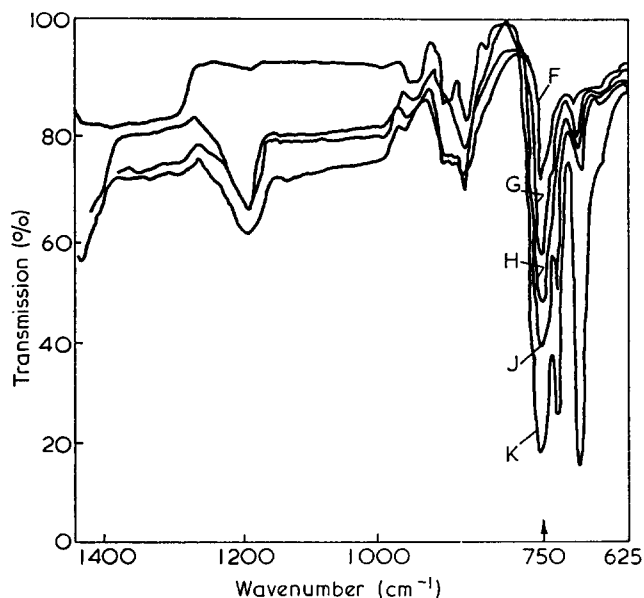


Figure 2 Section of i.r. spectrum of regenerated cellulose/polystyrene copolymers (absorption at 750 cm^{-1}). F, 17%G; G, 20.3%G; H, 30.0%G; J, 42.8%G; K, 52.0%G

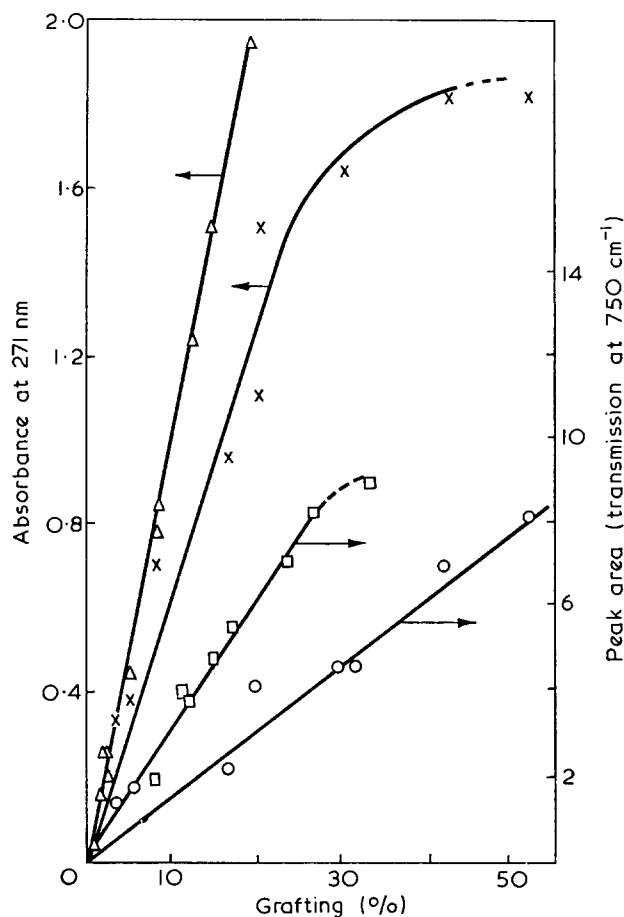


Figure 3 Correlation between spectroscopic data and extent of grafting. x, u.v. spectroscopy with hydroxyethylcellulose substrate; o, i.r. spectroscopy with hydroxyethylcellulose substrate; Δ, u.v. spectroscopy with regenerated cellulose substrate; □, i.r. spectroscopy with regenerated cellulose substrate

obtained gravimetrically afterwards. At low percentage grafting the degree of compatibility is excellent, but at high conversions is less so. This is due to the concentration of polystyrene graft exceeding the limit of the instruments. In the range 0–20% (u.v.) and 0–30% (i.r.) grafting, both u.v. and i.r. spectroscopy are seen to

correlate well with the gravimetric method. Duplicate analyses demonstrate that spectroscopic methods exhibit greater reproducibility in the specified range than gravimetric methods. Typical u.v. spectra are shown in *Figure 1*. Note that samples in this survey came from a wide variety of backgrounds, differing both in irradiation intensity and in the initial monomer concentration. Hence the only constants in the polymerization programme were the film thickness and the concentration of water in the grafting medium (2%). This type of calibration should be useful for many types of cellulose/polystyrene copolymer, irrespective of their mode of preparation.

Hydroxyethylcellulose/polystyrene copolymers

The investigation of the applicability of spectroscopic techniques to grafting studies was expanded to cover the kinetics of grafting styrene to hydroxyethylcellulose film (D.S. 0.4 to 0.5). Spectroscopic data were obtained in a manner similar to the previous study of grafting to regenerated cellulose. The calibration curve was obtained using mixtures of hydroxyethylcellulose film in 20:78:2 styrene/dioxane/water. Solutions were made up on a percentage by volume basis. The monomer dependence of the grafting reaction was studied in detail. A check against the method was made by studying the process gravimetrically. In order to study the effect of substrate form on the grafting process hydroxyethylcellulose powder (equivalent weight to the film form) was included in each reaction ampoule. It was hoped that differences in polymer macrostructure would be exhibited in differences in grafting behaviour. Such information could prove useful in ascertaining the inherent physical weaknesses of hydroxyethylcellulose films relative to regenerated cellulose produced from the cellulose xanthation process. However, it has been shown that both sample forms exhibit similar grafting behaviour.

DISCUSSION

Many studies of grafting reactions involving cellulose as substrate have been carried out and those cited are examples. Interest has been shown by Dilli and Garnett⁶⁻¹³, Huang *et al.*^{14, 15}, Arthur *et al.*¹⁶⁻²⁰ and Stannett *et al.*²¹. Almost without exception high radiation dose rates and total doses have been employed. Thus the extent of grafting has been considerable. This facilitates monitoring by gravimetric techniques. In instances involving low extents of grafting, gravimetry is not a satisfactory method owing to errors arising from technique and presentation, which become more important at low extents of grafting. Spectroscopy was considered as a viable alternative to gravimetric procedures.

Spectroscopic studies of polymers have received relatively little attention in the past. Where interest has been shown, the main emphasis has concerned the optical properties of the polymer in question and not the application of the technique to characterization. Several extensive publications²² have led to an understanding of the optical rotatory dispersion and absorption spectrum of synthetic polymers. Vala and Rice²³ have suggested a test of the theory of hypochromism of the 260 nm absorption band of polystyrene together with the effects of solvents on the magnitude of such hypochromism. Evidence is given suggesting that retention of local structure occurs when isotactic polystyrene passes from a crystalline phase into solution.

Ultra-violet spectroscopy has been used in the determination of low concentrations of styrene in a variety of situations. McGovern *et al.*²⁴ used the technique in the determination of residual styrene in polystyrene. Guthrie *et al.*²⁵ found that an extension of this work provided a means of acquiring detailed information concerning the grafting of styrene to cellulose. Imrišova and Máryska²⁶ employed infra-red spectral analysis in a study of cotton/polystyrene copolymers prepared using the pre-irradiation technique. The degree of grafting was determined from the absorption at 700 cm⁻¹. A similar study, involving cellulose-acrylonitrile, has also been carried out by these authors²⁷. In view of the nature of the substrate, the method employed by these authors was experimentally complex. Difficulties in the quantitative determination of the polystyrene content of the copolymer were assigned to interference by the characteristic absorption bands of cotton in the polystyrene absorption bands. At low frequencies, the absorption by cotton is minimal which provides for reasonable accuracy. Simionescu and Rusan²⁸ employed i.r. spectroscopy in their study of the synthesis of copolymers of polysaccharides by anionic mechanisms, where the presence of grafted reactive groups on the polymer backbone was unambiguously proven.

In their spectroscopic studies of cellulose/polystyrene copolymers prepared by the pre-irradiation technique, Imrišova and Máryska obtained a linear correlation between the extent of grafting and change in the absorption band intensity at 700 cm⁻¹. This band arises from the deformation vibration of the —CH— group of the monosubstituted benzene ring. We feel that the absorption band at 750 cm⁻¹ is a more useful monitor of the grafting process for two fundamental reasons: its greater freedom from interference of absorbance by the substrate; and its applicability over a more extended range of grafting. However, in both instances linear correlations are observed. Direct comparisons are not possible since different methods of sample presentation were used. These authors used the KBr disc method whilst we examined the grafted films in their entirety.

From the results obtained in this study certain features are worthy of comment:

(1) The technique is useful only for relatively low extents of grafting, thus for hydroxyethylcellulose/polystyrene copolymers (u.v., 0-25%; i.r., 0-50%) and for regenerated cellulose-polystyrene copolymers (u.v., 0-18%; i.r., 0-30%). Within this range considerable accuracy of measurement is available. Above the upper levels quoted, the concentration of polystyrene in the copolymer renders the technique useless.

(2) At low extents of grafting a level of reproducibility, greater than available using gravimetric techniques, is available. This was demonstrated by irradiating several samples under identical conditions and for the same total dose. Whilst reproducibility in spectral determinations was achieved, the level of coherence using gravimetry was less satisfactory.

(3) Use of methods based on spectroscopy depends on the substrate being graft copolymerized. One might expect the extent of absorption to be dependent only on the primary absorbing species, i.e. polystyrene. However, differences in sensitivity arise when comparing the results obtained using the two substrates. Saturation occurs at a much lower extent of grafting using regenerated cellulose than it does with hydroxyethylcellulose as substrate. This indicates that less of the initial energy is reaching the

detecting system in the latter case. The most probable explanation lies in the differences in crystallinity of the samples. Thus light scattering or energy dissipation is taking place from the hydroxyethylcellulose film owing to its increased regularity of structure relative to the regenerated cellulose and thus less light energy reaches the detector. This does not, however, negate the use of the technique provided calibration for each substrate takes place.

(4) The absorption bands at $850\text{--}900\text{cm}^{-1}$ (Figure 2) are highly confused owing to interference from the substrate. This indicates the difficulties of selection of those absorptions, due to the graft, which are free from interference from the substrate. Bands at 750 and 700cm^{-1} are seen to be suitable choices, though the one at 750cm^{-1} is considered to be the more useful.

The kinetics of grafting to hydroxyethylcellulose film is of interest for various reasons. Films of low degree of substitution have been used in the packaging industry for many years. However, their application has been limited owing to inherent structural weaknesses arising from the low level of flexibility of the cast film. Considerable interest has been shown recently in the use of substituted cellulose as membranes for a variety of purposes^{29,30}. Indeed work is being carried out in this Department along these lines. Hydroxyethylcellulose of low D.S. has been shown to have many desirable characteristics. Hence we are interested in expanding the scope of its use by modification through grafting. The kinetics of grafting to cellulose, using styrene, has recently been clarified by Guthrie *et al.*^{4,5} by extending work carried out by Odian *et al.*^{31,32}. Grafting was shown to be dependent on the first power of the monomer concentration and the square root of the radiation intensity. Here we are interested in the monomer dependence of grafting to hydroxyethylcellulose and a similar approach is made.

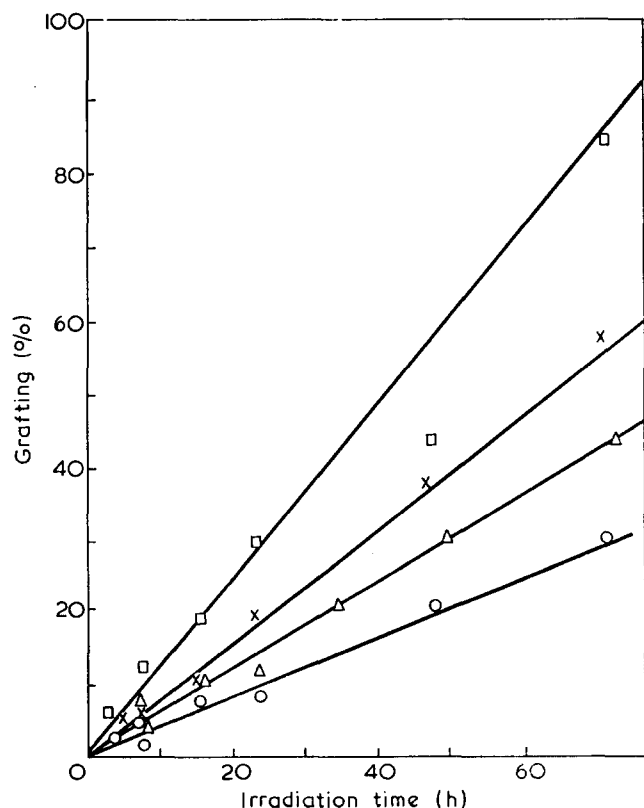


Figure 4 Variation of extent of grafting with irradiation time for different bulk monomer concentrations. \circ , 10%; \triangle , 20%; \times , 30%; \square , 40%

Figure 4 shows the dependence, on the monomer concentration of the bulk medium, of the grafting reaction. In the range of grafting studies, linear relationships are observed. At high conversions acceleration in the rate of grafting is a general feature indicating the presence of viscosity of Trommsdorf effects. Grafting was found to be dependent on monomer to the power 0.82, i.e., less than the value of unity demanded by steady state conditions and observed by other workers^{4,5,31,32}. Note that grafting was again followed both spectroscopically and gravimetrically. The difference in the dependence of the rate of grafting on the monomer concentration may be explained in terms of the mode of expression of the monomer concentration. This work uses the monomer concentration of the bulk medium as the parameter, whereas in a previous study of grafting to cellulose we chose the concentration of monomer in the film as the valid factor. Hence we have direct evidence that the two modes of expression of monomer concentration are not synonymous. Moreover, we see that the concentration of monomer within the film does not vary linearly with the bulk monomer concentration. This fact had been observed in swelling studies on regenerated cellulose film and is endorsed here. We feel that the most satisfactory method of expressing monomer concentrations is as concentration of monomer in the swollen film.

We have seen that spectroscopy provides a useful means of studying the kinetics of copolymerization reactions under specialized circumstances. The technique may be expanded to cover a wide range of substrates and monomers. Heterogeneous graft copolymerization reactions are noted to be extremely complex in view of the changing nature of the substrate both prior to and during grafting.

REFERENCES

- 1 Krassig, H. A. and Stannett, V. *Adv. Polym. Sci.* 1965, **4**, 111
- 2 Crompton, T. R. and Myers, L. W. *Eur. Polym. J.* 1968, **4**, 355
- 3 Bright, K., *et al. Chem. Ind.* 1965, p 610
- 4 Guthrie, J. T., Huglin, M. B. and Phillips, G. O. *J. Polym. Sci. (C)* 1972, **37**, 205
- 5 *Idem*, *Appl. Polym. Sci.* 1972, **16**, 1017
- 6 Dilli, S. and Garnett, J. L. *J. Polym. Sci. (A-1)* 1966, **4**, 2323
- 7 Dilli, S. and Garnett, J. L. *J. Appl. Polym. Sci.* 1967, **11**, 839
- 8 Dilli, S. and Garnett, J. L. *J. Appl. Polym. Sci.* 1967, **11**, 859
- 9 Dilli, S. and Garnett, J. L. *Aust. J. Chem.* 1968, **21**, 397
- 10 Dilli, S. and Garnett, J. L. *Aust. J. Chem.* 1968, **21**, 1827
- 11 Dilli, S., Ernst, I. T. and Garnett, J. L. *ibid.* 1967, **20**, 911
- 12 Dilli, S. and Garnett, J. L. *Aust. J. Chem.* 1970, **23**, 1163
- 13 Dilli, S. and Garnett, J. L. *Aust. J. Chem.* 1970, **23**, 1767
- 14 Huang, R. Y-M., *et al. J. Polym. Sci. (A)* 1963, **1**, 1257
- 15 Huang, R. Y-M. and Rapson, W. H. *J. Polym. Sci. (C)* 1963, **2**, 169
- 16 Arthur, J. C. Jr. and Daigle, D. J. *Text. Res. J.* 1964, **34**, 653
- 17 Arthur, J. C. Jr. *Adv. Chem. Ser.* 1969, **91**, 574
- 18 Arthur, J. C. Jr. *J. Macromol. Sci. (A)* 1970, **4**, 1057
- 19 Arthur, J. C. Jr. and Blouin, F. A. *Am. Dyest. Rep.* 1962, **51**, 1024
- 20 *Idem*, *J. Appl. Polym. Sci.* 1964, **8**, 2813
- 21 Kesting, R. E. and Stannett, V. *Makromol. Chem.* 1962, **55**, 1
- 22 Moffat, W. J. *Chem. Phys.* 1956, **25**, 467
- 23 Vala, M. T. Jr. and Rice, S. A. *J. Chem. Phys.* 1963, **39**, 2348
- 24 McGovern, J. J., *et al. Analyt. Chem.* 1948, **20**, 312
- 25 Guthrie, J. T., *Angew. Makomol. Chem.* 1970, **13**, 199
- 26 Imrišova, D. and Máryska, S. *J. Appl. Polym. Sci.* 1968, **12**, 2007
- 27 Imrišova, D. and Máryska, S. *J. Appl. Polym. Sci.* 1967, **11**, 901
- 28 Simionescu, C. I. and Rusan, V. *J. Polym. Sci. (C)* 1972, **37**, 173
- 29 Dilli, S., *et al. J. Polym. Sci. (C)* 1972, **37**, 291
- 30 Hopfenberg, H. B. *et al. 'Membranes from Cellulose and Cellulose Derivatives'* (Ed. A. F. Turbak), Wiley-Interscience, New York, 1970, pp 139-155
- 31 Odian, G., *et al. J. Polym. Sci.* 1961, **55**, 663
- 32 Odian, G., *et al. J. Polym. Sci. (A)* 1963, **1**, 639

Organized structures in amorphous styrene/*cis*-1,4-isoprene block copolymers: low angle X-ray scattering and electron microscopy*

R. Mayer

Centre de Biophysique Moléculaire, CNRS, 45045-Orléans-Cedex, France
(Received 23 July 1973; revised 1 October 1973)

It is shown that amorphous styrene/*cis*-1,4-isoprene block copolymers form organized structures in concentrated solutions as well as in the solid state. The effects of the nature and the concentration of the solvent, the composition of the copolymer and the temperature on the parameters determined by low angle X-ray scattering and electron microscopy are discussed. It is observed that, independent of the nature or concentration of the solvent, a given block copolymer exhibits only one ordered structure which may be lamellar or hexagonal.

INTRODUCTION

In recent years there has been considerable interest in heterophase polymer systems with regard to fundamental aspects and to enhanced physical properties. For copolymers, the nature and arrangement of the blocks in the molecule are most important in determining structure and properties.

It has been shown by low angle X-ray scattering that block copolymers exhibit organized structures under proper conditions of concentration in different solvents. When at least one block of the copolymer is crystallizable, three types of structure have been found: lamellar, hexagonal and cubic¹⁻⁴. It has been shown later that a crystallizable block is not necessary in the molecule for forming organized structures and that such organization is a general property of all block copolymers, which is related to the incompatibility of the two components and to their heterosolubility⁵⁻¹³.

The present paper describes the organized structures formed by styrene/*cis*-1,4-isoprene block copolymers (PS-PI), both blocks of which are amorphous and non-polar. The copolymers were prepared anionically and completely characterized in dilute solution. The influence of the solvent, the temperature, the concentration and composition of the copolymer on the nature and parameters of the structures are studied by low angle X-ray scattering. Moreover, since polyisoprene blocks can be stained preferentially, direct imaging of the structures by electron microscopy is closely combined with the X-ray scattering data.

EXPERIMENTAL

Preparation of the block copolymers

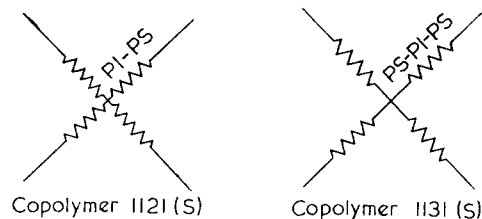
AB and ABA block copolymers of styrene and isoprene were synthesized by an anionic polymerization

* This work was performed in partial fulfilment of the requirements for the 'Grade de Docteur ès-Sciences Physiques' (University Louis Pasteur, Strasbourg, March 1971).

technique¹⁴. All polymerizations were carried out in a non-polar solvent (toluene), at room temperature, with *s*-butyllithium as catalyst, in order to have only *cis*-1,4 addition in the isoprene block. An all-glass sealed vessel equipped with break-seals was used. This apparatus was especially well suited for the preparation of a series of AB copolymers with the same first block A. After complete polymerization of the styrene (monomer A), the solution containing 'living' polystyryllithium anions was poured into several flasks, each equipped with an ampoule containing a different known quantity of prepurified isoprene (monomer B).

ABA block copolymers were prepared in the same manner, by adding styrene monomer to the solution of living AB copolymer. Symmetrical ABA block copolymers may also be prepared by using a dilithium catalyst but polyisoprene blocks with pure *cis*-1,4 form cannot be obtained in this manner.

Star copolymers with four identical branches, each one made from a block copolymer were also prepared. Following the method of Altares *et al.*¹⁵, the living ends of the AB and ABA copolymers were killed with 1,2,4,5-tetra(chloromethyl)benzene. The copolymers thus obtained may be schematized as:



Characterization of the block copolymers

The weight-average molecular weights of the blocks A, AB and ABA were determined by light scattering for all copolymers. The apparent molecular weight thus obtained must be close to the true values owing to the low spread of composition of the samples ($\bar{M}_w/\bar{M}_n < 1.1$). Number-

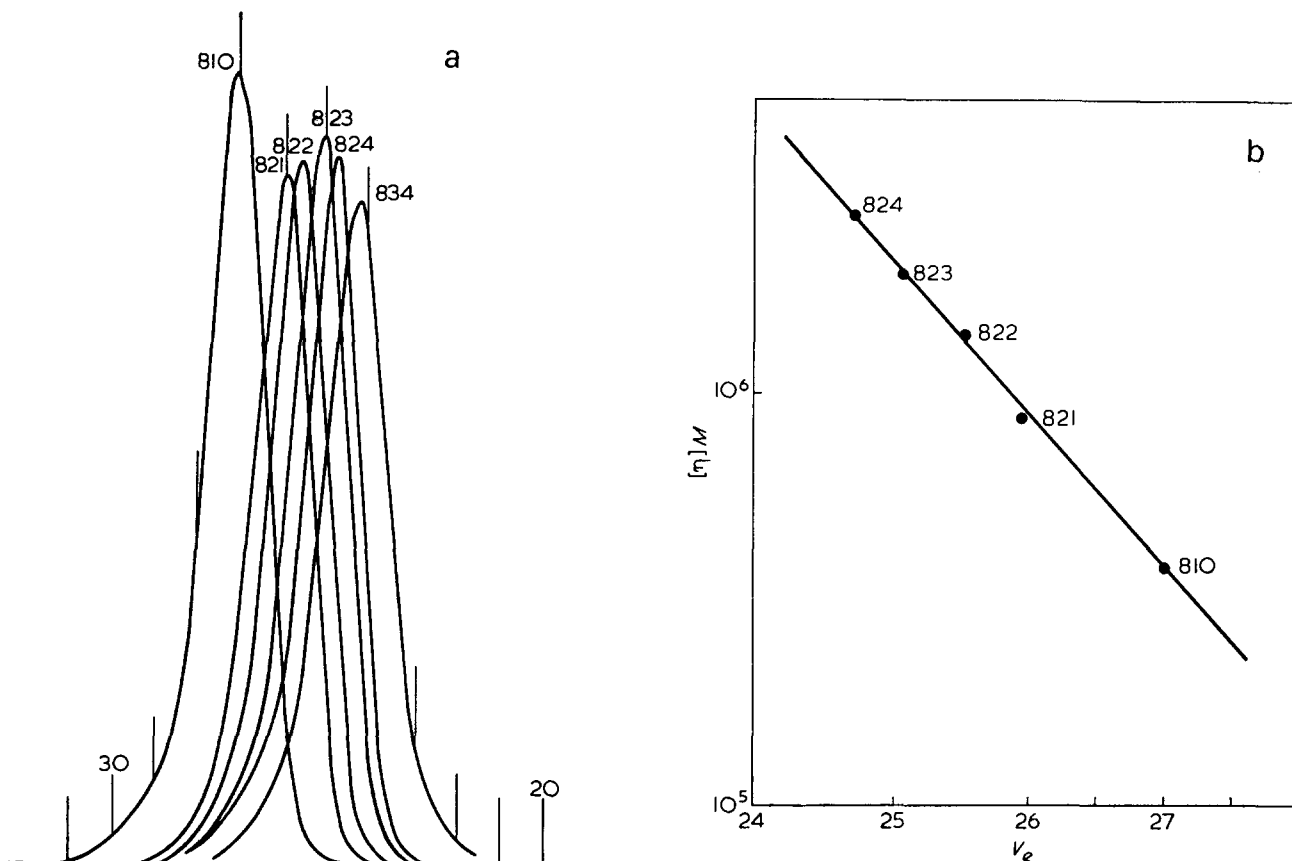


Figure 1 (a) Gel permeation chromatograms of homopolystyrene 810 and copolymers 821, 822, 823 and 824; (b) relation between the hydrodynamic volume and the elution volume of these block copolymers

average molecular weights were determined in toluene at 30°C, using a Mechrolab 501 membrane osmometer. Gel permeation chromatograms (g.p.c.) were obtained with a Waters 200 instrument, using tetrahydrofuran. The g.p.c. traces, shown in Figure 1, indicate a low polydispersity for a series of block copolymers with the same first block of polystyrene ($\bar{M}_{w(810)} = 23\,000$) and the absence of homopolystyrene. The linear relation between the hydrodynamic volume, $\log[\eta] \cdot M$, and the elution volume, V_e ¹⁶, was also observed to be valid for block copolymers. Intrinsic viscosities were measured in tetrahydrofuran at 25°C, using a Ubbelohde viscometer. The styrene contents of the copolymers and the microstructure of the isoprene blocks were established, using nuclear magnetic resonance combined with infra-red spectroscopy. The *cis*-1,4 content of polyisoprene was always more than 90%; thus 3,4 addition takes place only to a small extent.

The molecular characteristics and specimen codes for the linear and star block copolymers are collected in Tables 1 and 2 respectively.

X-ray scattering

When sufficient molecular uniformity of the copolymers is achieved, a fully periodic structure may be obtained, in which the repeating elements are not atoms but submicroscopic particles. Thus, spheres give rise to cubic lattices, cylinders arrange themselves in a two-dimensional hexagonal lattice while lamellae form an equidistant arrangement of parallel lamellae of infinite lateral extension. The scale of the observed periodicity (several hundred Å) calls for X-ray scattering at low angles. However, X-ray patterns yield only the main structural

parameters, i.e. the total thickness of the lamella or the distance between the axes of the cylinders. Determination of the structure and calculation of all its parameters may be obtained from the observed spacings and the composition of the system, if it is assumed that the values for the respective specific volumes hold for the finely dispersed state¹⁷. In these calculations it is necessary to know the distribution factor of the solvent between the two phases. This coefficient is quite difficult to evaluate and, until now, it was assumed as a first approximation that the solvent was exclusively located in one phase of the system. Recently Terrisse¹⁸ has shown that this assumption is unreasonable and he measured, by X-ray scattering, some of these coefficients for oriented styrene-isoprene block copolymers. As most of the distribution factors for the solvents we have used are unknown, only the values of the main structural parameters and the detailed structure corresponding to the 'dry' copolymer, after complete evaporation of the solvent, are reported here.

We used a Guinier camera¹⁹, operating in vacuum and equipped with a high temperature attachment. Monochromatic $\text{CuK}\alpha_1$ radiation ($\lambda = 0.1541\text{ nm}$) was used.

Samples were prepared by dissolution of a known quantity of copolymer in a small excess of solvent. After complete homogenization, the desired copolymer concentration was reached by slow evaporation of the solvent and the 'gel' was then put in a closed cell.

Electron microscopy

With styrene-isoprene block copolymers it is possible to stain preferentially the polyisoprene blocks²⁰ and to

Table 1 Characterization data of the linear block copolymers

Copolymer	Weight-average molecular weight			Molecular weight of the copolymer		[η] _{THF} (ml/g)	PS (%)
	1st block (PS)	2nd block (PI)	3rd block (PS)	\bar{M}_w	\bar{M}_n		
210	12 600			12 600	—	10.3	
220	12 600	6 000		18 600	—	18.1	68
310	46 900			46 900	—	25.9	
320	46 900	17 000		63 900	—	43.5	73
410	62 000			62 000	—	30.9	
420	62 000	70 000		132 000	—	86.4	47
430	62 000	70 000	70 000	202 000	—	112.2	75
610	8 700			8 700	—	—	
620	8 700	6 000		14 700	—	—	59
630	8 700	6 000	7 000	21 700	—	—	72
810	23 000			23 000	—	16.4	
821	23 000	8 000		31 000	—	27.5	74
822	23 000	17 500		40 500	36 900	34.1	57
823	23 000	21 000		44 000	46 000	42.7	52
824	23 000	28 000		51 000	52 600	51.4	45
834	23 000	28 000	33 000	84 000	78 600	63.4	67
910	30 000			30 000	30 000	19.8	
921	30 000	17 500		47 500	47 000	36.6	63
922	30 000	39 000		69 000	70 000	57.5	43
923	30 000	60 000		90 000	70 000	58.0	33
931	30 000	60 000	29 000	119 000	102 000	65.8	49
932	30 000	60 000	52 000	142 000	132 000	74.0	58

Table 2 Characterization data of the star copolymers

Copolymer	Weight-average molecular weight			Molecular weight of the copolymer		PS (%)
	1st block (PS)	2nd block (PI)	3rd block (PS)	\bar{M}_w	\bar{M}_n	
1110	29 000			29 000		100
1121	29 000	7 000		36 000		81
1121(S)					110 000	81
1122	29 000	34 000		63 000		47
1122(S)					185 000	47
1123	29 000	20 000		49 000		60
1123(S)					145 000	60
1131	29 000	20 000	28 000	77 000		74
1131(S)					220 000	74

directly examine the phase structure of the system by transmission electron microscopy. This situation is unique in structure studies, in that the image of the structures can be directly compared to the results of X-ray scattering. The main difference between these two techniques lies in the fact that electron microscopy requires special sample preparation while X-ray scattering does not. The latter may be applied in particular to liquid or swollen systems. The structure of solutions of block copolymers is only amenable to electron microscopy investigation if the solutions can be transformed into solid samples of identical structure, which can then be treated by the usual methods. This was done by using a polymerizable solvent, the subsequent polymerization of which left the microphase structure unaltered. In addition, this procedure made it possible to observe, by electron microscopy, how the mesomorphic structure disappears when the solvent concentration gradually increases^{21, 22}.

In order to compare the results obtained by both techniques, the samples for electron microscopy were prepared in three different ways: (i) by heating the block copolymer, under high vacuum, to temperatures between 200° and 300°C; (ii) by slow and complete evaporation of the solvent of the gel used for X-ray scattering; (iii) by hardening the gel prepared in a monomeric solvent, such

as styrene or methyl methacrylate, by a radical polymerization of this solvent at 60°C with traces of benzoyl peroxide.

Solvent casting has been mainly used for thin film preparation; it was nevertheless found that the resulting morphology depends strongly on the method of film preparation. For this reason ultrathin sections of the organized systems rather than films of copolymer were examined. The samples were sectioned with a cryo-ultramicrotome. Liquid nitrogen was used to cool the specimen holder and the knife support, insulated from ambient air, at about -100°C. This temperature, 20° lower than the glass transition of *cis*-1,4-polyisoprene, was necessary to avoid deformation during cutting and to obtain sufficiently thin sections (500 to 800 Å).

The sections were placed on grids and, to enhance contrast, the grids were suspended above a 1% aqueous osmium tetroxide solution in a closed container for about 1 h. Since OsO₄ selectively reacts with the olefinic bonds of polyisoprene, dark regions indicate polyisoprene and light regions polystyrene.

A Philips EM 300 electron microscope, operated at an accelerating voltage of 100 kV, was used. Micrographs were taken at magnifications of 20 000 for lamellar structures, and 50 000 for cylindrical structures.

RESULTS

Structural determination

Three types of structure (lamellar, hexagonal and cubic) have been found in concentrated solutions of block copolymers. These structures are now well known; only the lamellar and hexagonal structures, which we have found, will be considered here.

Lamellar structure. The reciprocal spacings of consecutive orders of the lamellar structure are in the ratio 1:2:3:4:5. The sharply defined reflections observed on the X-ray patterns indicate that the periodic structure extends over domains large in comparison to the thickness of the lamellae. This structure consists of a set of plane and parallel lamellae of infinite lateral extension where each lamella results from the superposition of two layers: one formed by the styrene blocks, the other by the isoprene blocks. The solvent will swell one layer more than the other. The structural parameters are:

- d = total thickness of a lamella ($d = d_s + d_I$), which is calculated directly from the spacing values;
- d_s = thickness of the layer containing the polystyrene blocks;
- d_I = thickness of the layer containing the polyisoprene blocks;
- S = specific area defined as the mean cross-sectional area available for a molecule at the phase boundary.

Hexagonal structure. The reciprocal spacing ratios 1:(3)^{1/2}:(4)^{1/2}:(7)^{1/2} correspond to a regular hexagonal arrangement of parallel cylinders of infinite length. These cylinders consist of the shortest blocks of the copolymer and are separated from each other by the other blocks. The solvent will swell one phase more than the other but the distribution factor may differ from that of the lamellar structure since the hexagonal structure appears only in copolymers with very dissymmetrical blocks, as will be seen later. The structural parameters are:

- D = distance between the axes of two neighbouring cylinders, which is calculated from the spacing values;
- R = radius of the cylinders;
- S = specific area defined as before.

Low angle X-ray scattering

Organized structures obtained with concentrated solutions of styrene/*cis*-1,4-isoprene block copolymers were investigated by low angle X-ray scattering. Influence of solvent, temperature, concentration and composition of the copolymer on the structural parameters was examined.

Influence of nature of the solvent. Lamellar structures were found for most of the two block styrene/*cis*-1,4-isoprene copolymers in concentrated solutions in different solvents. This type of structure appears for a copolymer concentration higher than 60% and remains in the 'dry' copolymer, after complete evaporation of the solvent. Within experimental errors, the nature of the solvent does not seem to influence the structural parameters, as illustrated in Figure 2 for copolymer 822.

With monomeric solvents such as styrene or methyl methacrylate no periodic structures were found with the linear block copolymers. This behaviour is unusual, but

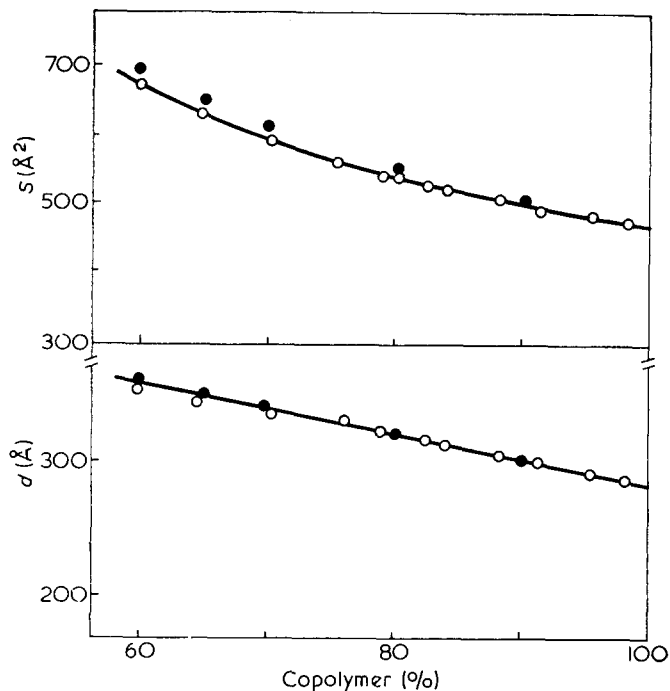


Figure 2 Variation of the structural parameters of the lamellar structure against copolymer concentration for the systems copolymer 822/toluene (○) and copolymer 822/acetone (●)

may be explained if one considers that these two solvents have no particular selectivity for either blocks.

Hexagonal structures were found only with copolymer 220 ($M_{PS}=12\,000$, $M_{PI}=6000$) and copolymer 1121 ($M_{PS}=29\,000$, $M_{PI}=7000$) in solvents such as acetone or toluene. These structures appear for copolymer concentrations higher than 70% and remain in the dry copolymer. As for the lamellar structures, the nature of the solvent has no apparent effect on the structural parameters.

Influence of concentration on structural parameters. On varying the copolymer concentration, styrene/*cis*-1,4-isoprene block copolymers exhibit only one type of structure. This behaviour is similar to that observed with styrene/butadiene copolymers²², but differs from that observed with styrene/2- or 4-vinylpyridine block copolymers²³ which may organize themselves successively in cubic, hexagonal and lamellar structures with increasing copolymer concentration.

Variations of the total thickness d of a lamella and of the specific area S of the system copolymer 822 ($M_{PS}=23\,000$, $M_{PI}=17\,500$)/acetone (or toluene) with copolymer concentration are shown in Figure 2. The lamellar structure appears for a copolymer concentration higher than 60% and remains after complete evaporation of the solvent. The structural parameters for the dry copolymer are identical to those obtained with the same copolymer after heating under vacuum to temperatures between 200° and 300°C. Therefore, this structure may be considered as thermodynamically stable. For copolymer concentrations lower than 60%, an isotropic solution is formed and no hexagonal or cubic structure was found in the transition region between the lamellar structure and the aggregates.

As shown in Figure 2, the variation of the structural parameters is monotonous. When the copolymer concentration of the system increases, the total thickness d of a lamella decreases from 355 Å for a gel of 60% copolymer

to 286 Å for the dry copolymer; the specific area S decreases simultaneously. After complete evaporation of the solvent, the thickness of the styrene layer is $d_S = 153$ Å and the thickness of the isoprene layer is $d_I = 133$ Å.

A hexagonal structure was only observed for samples 220 and 1121 in different solvents such as acetone or toluene, for copolymer concentrations higher than 70%. It remains in the dry copolymer, after complete evaporation of the solvent, and its parameters are identical to those of the pure copolymer after heating under vacuum above 200°C. For these two copolymers the hexagonal structure observed seems thus to be thermodynamically stable. Further, no lamellar structure for the solid copolymer nor cubic structure in the transition region between cylinders and aggregates were observed.

The variations of the structural parameters D and S of the system copolymer 220/acetone against copolymer concentration are shown in Figure 3. Assuming that the cylinders contain the polyisoprene blocks (as evidenced by electron microscopy, see later) the diameter of the cylinders in the dry copolymer is 108 Å.

Influence of copolymer composition on structural parameters. The influence of the copolymer composition (i.e. the effect of the length of each block) on the structural parameters was studied with several copolymers, one block of which remains unchanged.

In Table 3 the structural parameters d , d_S and d_I of the lamellar structure of different dry copolymers are compared. Samples 821, 822, 823 and 824 have the same polystyrene block while samples 822, 921 and 320 have the same polyisoprene block. When the length of one block is held constant, while the other is increased, the thickness of the layer containing the first block remains constant whereas the thickness of the other layer increases linearly in the range of the molecular weights considered.

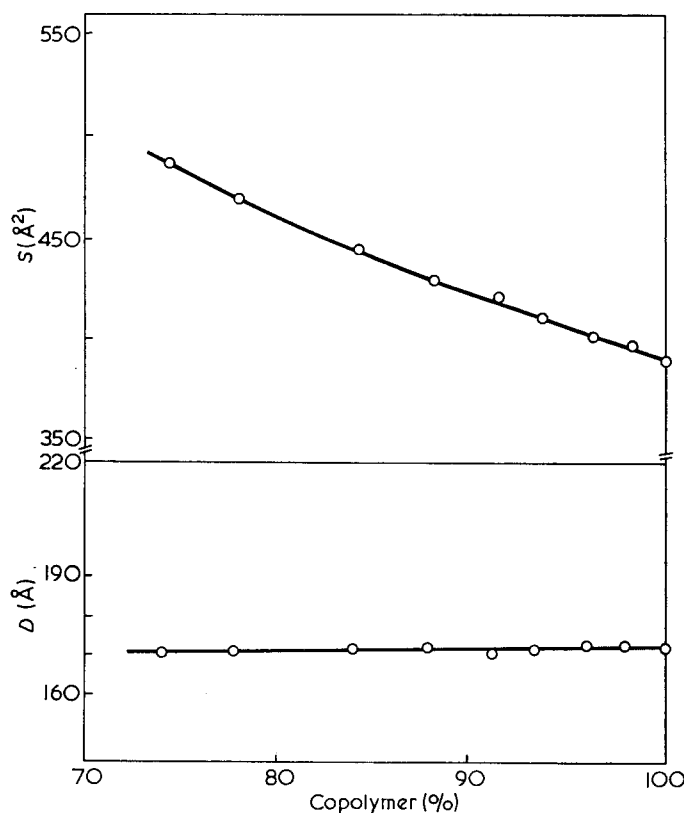


Figure 3 Variation of the structural parameters of the hexagonal structure for the system copolymer 220/acetone

Table 3 Structural parameters of dry copolymers—influence of the length of one block when the other remains unchanged

Copolymer	Molecular weight		Structural parameters			
	PS	PI	d (Å)	d_S (Å)	d_I (Å)	S (Å ²)
821	23 000	8 000	218	156	62	462
822	23 000	17 500	286	153	133	470
823	23 000	21 000	314	154	160	470
824	23 000	28 000	364	152	213	472
822	23 000	17 500	286	153	133	470
921	30 000	17 500	340	206	134	466
320	46 900	17 000	448	317	131	464
			R (Å)	D (Å)	S (Å ²)	
220	12 000	6 000	54	175	395	
1121	29 000	7 000	64	272	390	

Our observations on styrene/*cis*-1,4-isoprene block copolymers in different solvents indicate that hexagonal structures only occur when the copolymer contains less than 30% of one block. However, copolymers 320 ($M_{PS} = 46\,900$, $M_{PI} = 17\,000$) and 821 ($M_{PS} = 23\,000$, $M_{PI} = 8000$), which have a polyisoprene content of only 26%, exhibit a lamellar structure. Possibly the molecular weight of the shortest block also plays an important role, and must be lower than about 7000 as is the case for copolymers 220 and 1121.

When a copolymer contains two highly unequal blocks it appears that the type of structure of the copolymer is determined primarily by the length of the shortest one. As long as the two blocks remain incompatible, it would be of interest to extend the study to samples of which one block has a very low molecular weight to see if they form cubic structures. This has not yet been done owing to difficulty in preparing such monodisperse low molecular weight blocks.

The polyisoprene blocks of copolymers 220 and 1121 have approximately the same length. It is then possible to examine the effect of the length of the polystyrene blocks on the structural parameters of the hexagonal structure observed in acetone. It appears in Table 3 that, for these two dry copolymers, the radius of the cylinders of polyisoprene is similar while the distance D between the cylinder axes increases with the length of the polystyrene blocks.

Influence of temperature on structural parameters. The effect of the temperature on the domain dimensions of lamellar and hexagonal structures was studied between 25 and 100°C on several systems. In this temperature range no structural changes were observed; furthermore, within experimental errors, the structural parameters remain constant.

This result agrees with those of Grosius *et al.*²⁴ for styrene/vinylpyridine block copolymers and of Brown *et al.*²⁵ for styrene/butadiene/styrene block copolymers. Nevertheless, it must be noted that Terrisse¹⁸ observed a decrease in the structural parameters of oriented samples of styrene/isoprene block copolymers at temperature higher than 100°C.

Organized structures of three block and star block copolymers. For styrene/*cis*-1,4-isoprene/styrene three block copolymers, the central block was always *cis*-1,4-polyisoprene. Of the copolymers prepared, only sample 1131 ($M_{PS} = 29\,000$, $M_{PI} = 20\,000$, $M_{PS} = 28\,000$) exhibited an organized structure. A lamellar structure was

observed for copolymer concentrations higher than 60%. If we compare the structural parameters, in the dry state, of the three block copolymer 1131 to those of the two block copolymer 823 which has a similar length of the polyisoprene block it appears that the thickness d_1 of the polyisoprene layer is much lower for copolymer 1131 than for copolymer 823 (103 Å and 160 Å respectively).

Since among the three block copolymers prepared only sample 1131 exhibits an organized structure it seems that this type of copolymer may exhibit mesomorphic structures only if the central block is flanked by two blocks of the same length. This observation agrees with the results of Vanzo *et al.*⁷ on styrene/butadiene/styrene copolymers which is also in line with the fact that most of the three block copolymers studied so far, exhibiting ordered structures, were prepared with a bifunctional initiator.

To increase the order of the molecular structure, star copolymers with four branches were prepared, each branch being itself a styrene/*cis*-1,4-isoprene block copolymer. As soon as the copolymer concentration exceeds 60% an organized structure is observed in different solvents such as acetone or toluene. In Table 4 the structural parameters of the star copolymers and the corresponding linear block copolymer which constitutes the branches of the star are compared in the dry state, after evaporation of the solvent. When the branch is a two block copolymer it appears that the star has the same structure as the branch alone. Provided that the overall composition remains the same [as in cases 1121/1121 (S) and 1122/1122 (S)] the magnitude of the structural parameters is not significantly affected by the change in chain geometry from a conventional block copolymer to a star block copolymer. This somewhat surprising result was also observed by Price *et al.*²⁶ for star copolymers with two, three and four branches, each branch itself being a styrene/isoprene block copolymer. However, for the case where the branch of the star is a three block copolymer [sample 1131 (S)], which by itself exhibits a lamellar structure, the star copolymer has a hexagonal structure.

Table 4 Structural parameters of the star copolymers and of the corresponding linear block copolymer at the dry state

Copolymer	Type of structure	Structural parameters
1121	Hexagonal	$D=272$ $R=64$ $S=390$
1121(S)	Hexagonal	$D=275$ $R=65$ $S=385$
1122	Lamellar	$d=498$ $d_S=235$ $d_1=263$ $S=462$
1122(S)	Lamellar	$d=496$ $d_S=235$ $d_1=263$ $S=462$
1131	Lamellar	$d=371$ $d_S=268$ $d_1=103$ $S=346$
1131(S)	Hexagonal	$D=307$ $R=85$ $S=416$

The mesomorphic structures of the star copolymers seem to be very stable. The structural parameters for the dry copolymer are identical to those obtained with the same copolymer after heating to 300°C under vacuum. Indeed, while no organized structures are observed when styrene or methyl methacrylate are used as solvents for the linear two or three block copolymers, the star copolymers exhibit ordered structures in these two solvents; furthermore the structural parameters are the same as those obtained with the other solvents such as acetone or toluene.

After hardening the gels by a subsequent radical polymerization of these monomeric solvents, the micro-phase structure appears unaltered, and the structural parameters are not appreciably modified by the shrinking of the system during polymerization. It is now possible to observe these hardened organized structures by electron microscopy. Further, this procedure makes it possible to follow the progressive disappearance of the mesomorphic structures with increasing swelling of the system.

Electron microscopy

With styrene/isoprene block copolymers, structural studies by low angle X-ray scattering can be closely compared with the images obtained by electron microscopy.

Lamellar structure. Figures 4a to 4c clearly reveal the lamellar structure of copolymer 320. The solid samples were prepared from gels, by evaporation of the solvents (acetone, butyl acetate or isoprene), and were sectioned at room temperature. The sections were cut in a direction perpendicular to the plane of the alternating layers of polystyrene (light) and polyisoprene (dark).

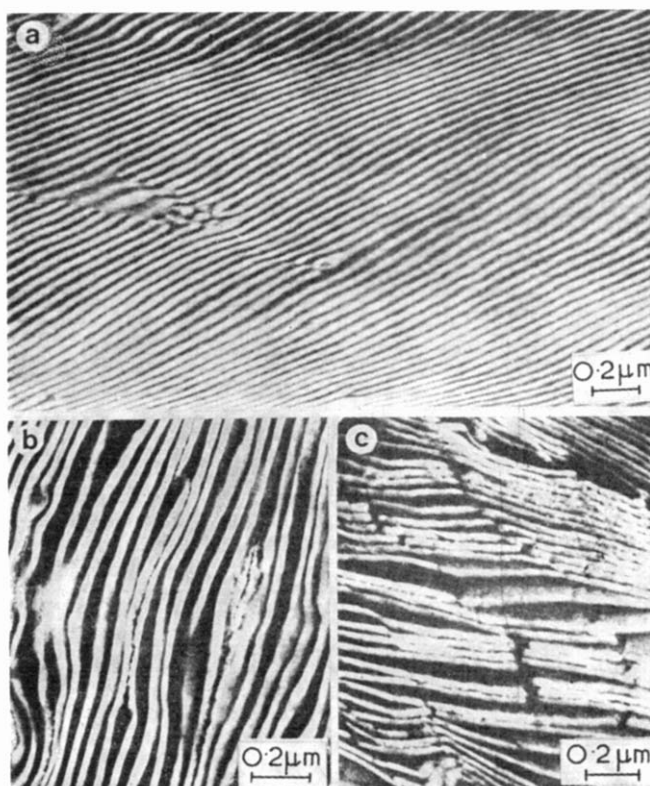


Figure 4 Lamellar structures in ultrathin sections of copolymer 320 cut at room temperature. Dry copolymer obtained by complete evaporation of the solvent of gels in: (a) acetone; (b) butyl acetate; (c) isoprene

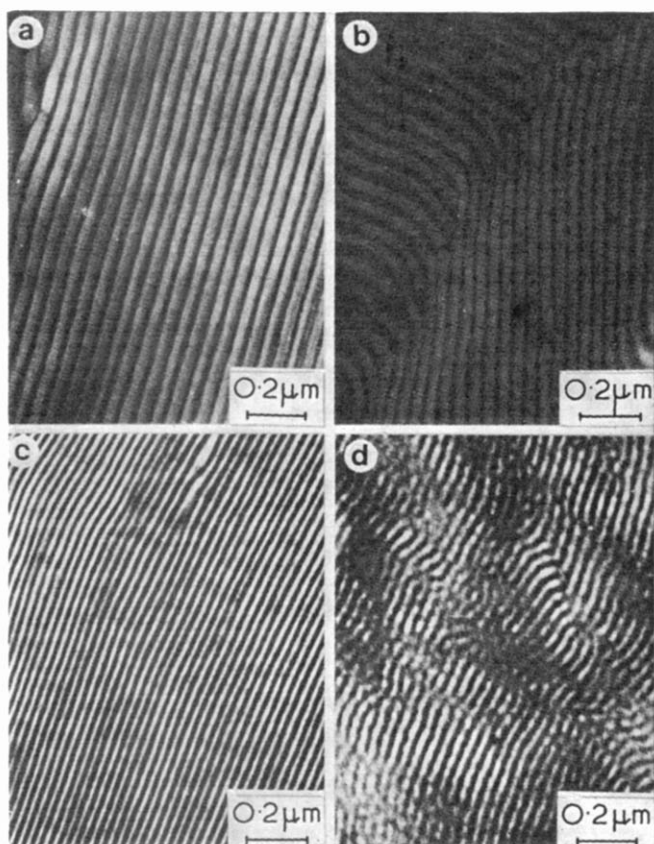


Figure 5 Lamellar structures in ultrathin sections of heated copolymers, cut at low temperature (-100°C). (a) and (b) copolymer 320; (c) copolymer 822; (d) copolymer 824

The electron micrographs in Figures 5a to 5d represent pure copolymers 320, 822 and 824, heated to 280°C under vacuum, and cut at low temperature (-100°C).

As indicated by X-ray scattering, these micrographs reveal that the lamellar structure exists in the heated and in the dried block copolymer and that long range order extends over several microns. Comparing the two sets of micrographs, it appears that cutting at temperatures below the lowest glass temperature of each block of the copolymer is necessary to avoid distortion. With copolymers of high polystyrene content, it is possible to cut at room temperature, but even so, the periodic structure appears deformed. Indeed, while the thickness of the polystyrene layers (light) remains about constant, that of the polyisoprene layers (dark) appears irregular. This is due to the rubbery polyisoprene layers distortion during ultramicrotomy. This has been observed by Vanzo²⁷ and Hendus *et al.*⁶ for surface replicas of thin films or sections when one phase projects beyond the other.

In these micrographs of lamellar structures, only the ratio between the thicknesses of polystyrene and polyisoprene layers is independent of the angle between the plane of cutting and that of the lamellae. Thus the structural parameters must be measured on electron micrographs from sections cut exactly perpendicular to the plane of the lamellae.

In Table 5 structural parameters of the dry copolymers 320, 822 and 824 obtained by low angle X-ray scattering and electron microscopy are compared. It appears that both qualitative and quantitative correspondence between direct observation of sections and X-ray scattering patterns have been achieved.

Hexagonal structure. This arrangement of dark spots of polyisoprene in a light matrix of polystyrene is clearly visible in the micrographs of Figure 6. These ordered structures, which extend over several microns, were obtained with copolymer 1121 after heating to 200°C under vacuum. The ultra-thin sections shown in Figure 6a and 6b were cut respectively at room temperature and at

Table 5 Comparison of the structural parameters found by electron microscopy and X-ray scattering for the lamellar structure

Copolymer	Total thickness of the lamella (\AA)	
	Electron microscopy	X-ray scattering
320	460	448
822	300	286
824	360	364

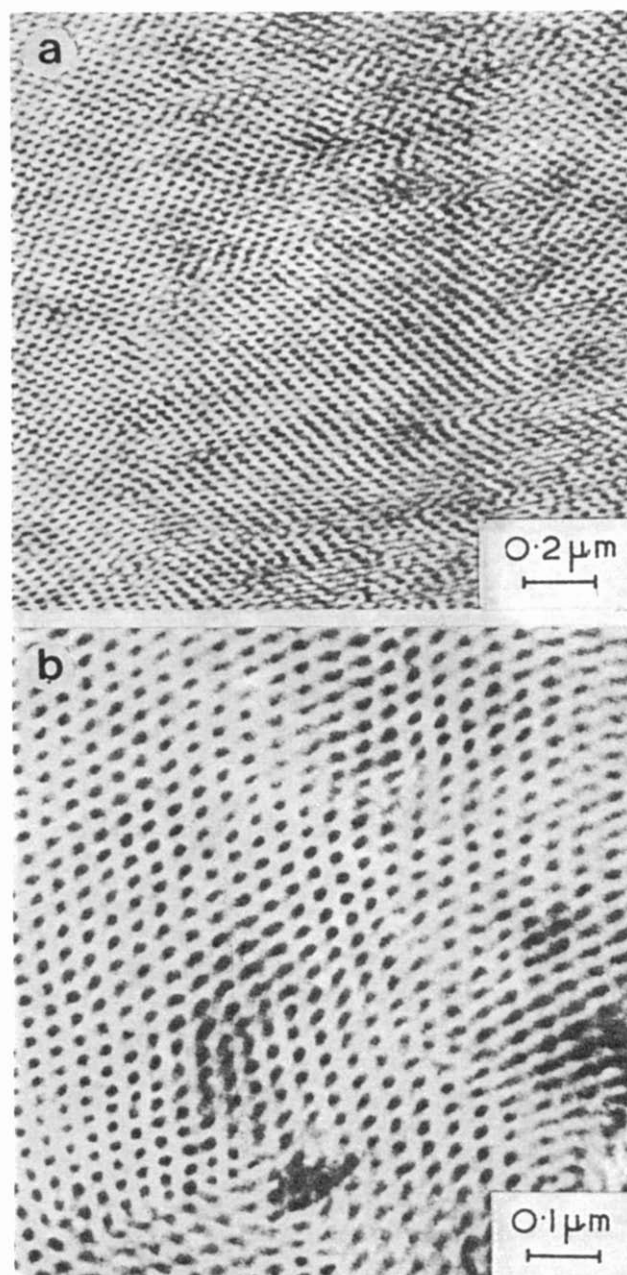


Figure 6 Hexagonal structures in ultrathin sections of copolymer 1121. (a) Cut at room temperature; (b) cut at low temperature (-100°C)

-100°C. The definite advantage in using cryo-ultramicrotomy for styrene/isoprene/*cis*-1,4-isoprene copolymers is again evident.

The distinct black circles correspond to polyisoprene cylinders which are perpendicular to the plane of observation, whereas the somewhat elongated spots correspond to cylinders which are inclined. However, by using a goniometer stage it is possible to tilt the sections so that the cylinders are perpendicular to the observation plane, and to confirm the proposed hexagonal arrangement. The real nature of hexagonal arrangement is, however, more clearly established when it is possible to study oriented structures¹².

The distance between the axes of two neighbouring cylinders and their diameters can be measured on the electron micrographs. Agreement with X-ray results is achieved to within experimental error. For the dry copolymer 1121, for example, the measured *D* values are 285 Å by electron microscopy and 272 Å by X-ray scattering.

Microphase separation without organization. Since no organized structures were observed when styrene or methyl methacrylate were used as solvents with linear AB or ABA copolymers it is of interest to examine the texture of these systems by electron microscopy (Figure 7). Figure 7a shows the texture of copolymer 834 after complete evaporation of the solvent. A microphase separation but no periodicity is observed as was suggested by the X-ray results. Figures 7b to 7d show the texture of various samples after polymerization of the monomeric solvent (respectively copolymers 320 and 921 in methyl methacrylate and 824 in styrene). In the range of copolymer concentrations where organized structures usually appear, a microphase separation may be observed, again with no periodicity (Figure 7b: 73% of copolymer

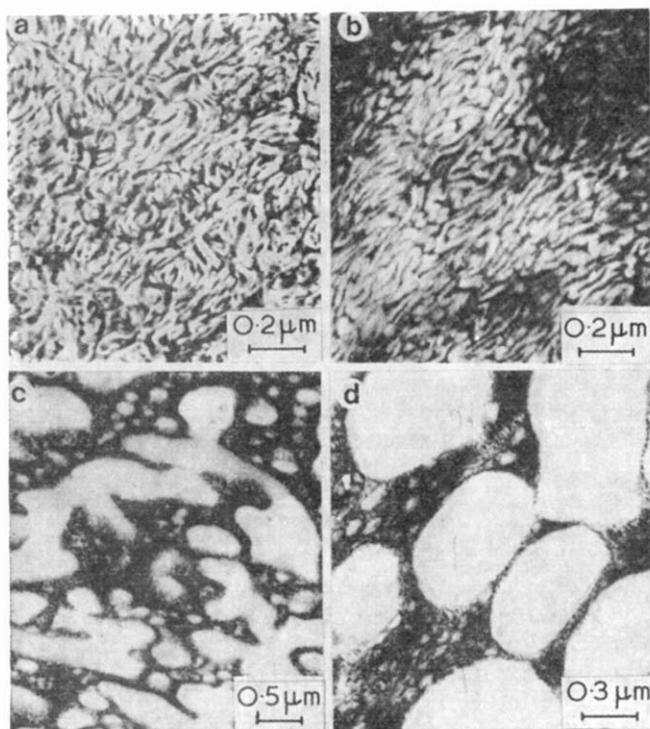


Figure 7 Microphase separation without organization in ultrathin sections of: (a) dry copolymer 834, (b) solution of 73% copolymer 320 in polymerized methyl methacrylate; (c) solution of 30% copolymer 921 in polymerized methyl methacrylate; (d) solution of 20% copolymer 824 in polymerized styrene

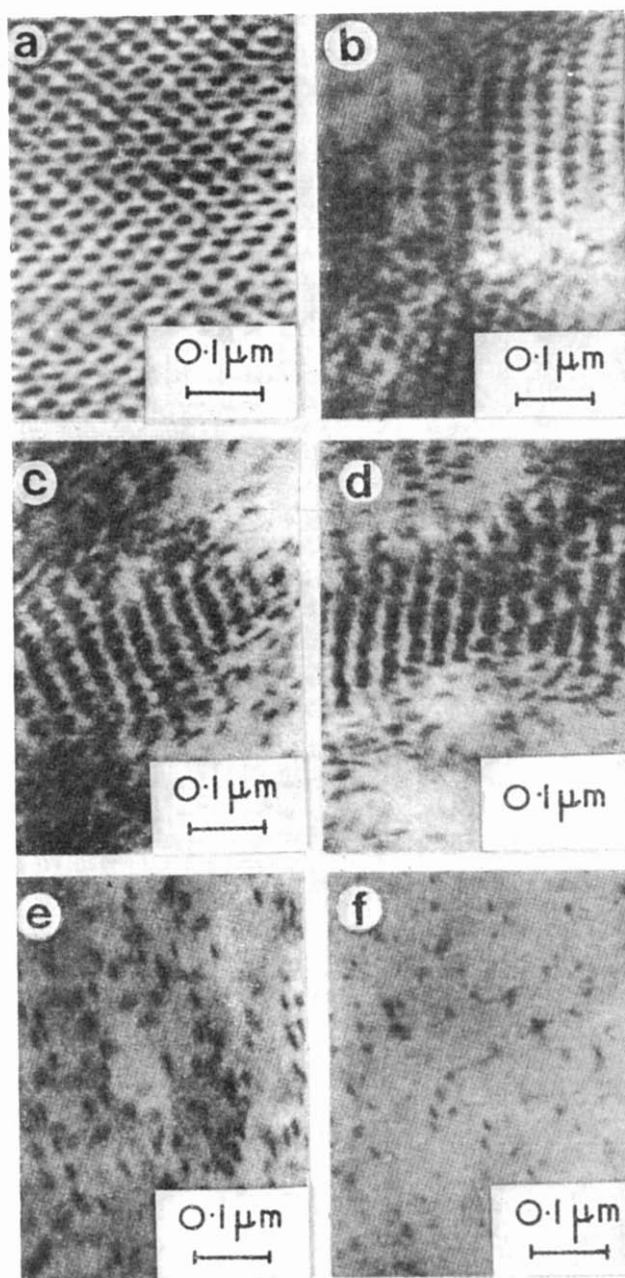


Figure 8 Progressive dislocation of the hexagonal structure of copolymer 1121(S) in a polymerized solution of styrene: (a) 80%; (b) 50%; (c) 40%; (d) 30%; (e) 15%; (f) 5% of copolymer

320 in methyl methacrylate). For lower copolymer concentrations, one can see a random suspension of droplets of polymerized solvent in a matrix of copolymer (Figures 7c and 7d). It appears that chains of polymerized solvent segregate from the copolymer chains during polymerization to form particles of homopolymer. Nevertheless some polystyrene blocks of the copolymer may be present in these droplets, but cannot be detected by our staining technique.

Organized structures of star copolymers. These exhibit organized structures in monomeric solvents, such as styrene or methyl methacrylate, even when their two block constituents do not form organized structures by themselves in these solvents. This is not completely surprising since star copolymers, as sample 1121(S), may be considered as the intersection of two symmetrical three block copolymers at their centres.

Electron microscopic examination of the gels hardened by polymerization of the monomeric solvent also agrees well with X-ray results. For copolymer concentrations higher than 60%, lamellar and hexagonal structures were observed for copolymers 1122 (S) and 1121 (S) respectively, and measured parameters are in good agreement with those found by X-ray scattering.

Furthermore, it is possible to observe how these mesomorphic structures are progressively destroyed when copolymer concentration of the system becomes lower than 60%. Figures 8a to 8f show clearly that the copolymer 1121 (S) has only one type of structure whose organization gradually disappears as the copolymer concentration decreases. Disordered regions already exist for a copolymer concentration of 50% (Figure 8b). When this concentration falls to 20%, only some islands of organized structure remain, which are surrounded by micelles of polyisoprene. This behaviour was also observed for this copolymer in methyl methacrylate and for copolymer 1131 (S) in styrene and in methyl methacrylate.

CONCLUSIONS

Styrene/*cis*-1,4-isoprene block copolymers, which are made of two amorphous and non-polar blocks, give rise to organized structures in concentrated solutions as well as in the solid state. The formation of such structures is a general property of block copolymers which results from the incompatibility of the two components and their heterosolubility. It seems, however, that the chemical nature of the blocks may play a role in the formation of given structures. Thus, the behaviour of the styrene/*cis*-1,4-isoprene copolymers, which exhibit only a single type of regular structure in all the range of copolymer concentrations may be due to the presence of two amorphous and non-polar blocks whose interactions are only weakly sensitive to the swelling of the system. In opposition, copolymers, in which one block is crystallizable or which have intermolecular hydrogen bonding, may adopt various structures, depending generally upon the nature of the solvent and its concentration.

Styrene/isoprene block copolymers are an ideal system for structure studies as direct imaging of the structures by transmission electron microscopy and low angle X-ray scattering analysis can be closely combined. While electron microscopy requires special sample preparation and is therefore limited to bulk polymers or hardened gels, X-ray scattering can be applied to all samples and especially to swollen systems. Furthermore, diffraction, by its averaging nature, can be more representative of the sample as a whole.

We have investigated how the mesomorphic structure varies with the following parameters: nature and concentration of the solvent, composition of the block copolymer, and temperature. It seems that the nature of the solvent does not significantly affect the magnitude of the main structural parameters. When the solvent concentration of the system increases, the variation of the structural parameters is monotonic over the range of concentration for which the copolymer exhibits an organized structure. In particular we could not detect any transition from one type of structure to another. Most of our styrene/*cis*-1,4-isoprene block copolymers have a lamellar structure. Hexagonal structures are observed only when the copolymer contains less than 30% of one block. Nevertheless a further condition is necessary: the molecular

weight of these blocks must be low (for these copolymers lower than about 7000). It would be interesting to study samples with monodisperse blocks of very low molecular weight in order to see if they are able to adopt a cubic structure.

In order to observe directly, by electron microscopy, one phase in a matrix composed of the other, sufficient contrast between the two phases was created by selectively staining the polyisoprene blocks. Results obtained by this technique agree qualitatively and quantitatively with X-ray analysis. Electron microscopy is not only a complementary technique to low angle X-ray scattering but moreover, when copolymer solutions can be transformed into an equivalent solid sample by polymerization of the selective monomeric solvent used, it is possible to observe how these mesomorphic structures disappear when the solvent content of the system increases.

ACKNOWLEDGEMENTS

The author wishes to express his gratitude to Professor Ch. Sadron and to Professor H. Benoit (Centre de Recherches sur les Macromolécules, Strasbourg) for the interest they have shown during the development of this work and for stimulating discussions, Dr A. Skoulios and Dr B. Lotz (Centre de Recherches sur les Macromolécules, Strasbourg), for helpful criticism of the manuscript, Dr B. Gallot, for help with low angle X-ray scattering, and Dr J Escaig (Laboratoire de Microscopie Electronique Appliquée à la Biologie, Paris), for help with electron microscopy.

REFERENCES

- Skoulios, A., Finaz, G. and Parrod, J. *C. R. Acad. Sci.* 1960, **251**, 739
- Skoulios, A. and Finaz, G. *J. Chim. Phys.* 1962, **59**, 473
- Tsouladze, G. and Skoulios, A. *J. Chim. Phys.* 1963, **60**, 626
- Franta, E., Skoulios, A., Rempp, P. and Benoit, H. *Makromol. Chem.* 1965, **87**, 271
- Gallot, B., Mayer, R. and Sadron, Ch. *C. R. Acad. Sci. (C)* 1966, **263**, 42
- Hendus, H., Illers, K. H. and Ropte, E. *Kolloid-Z. Z. Polym.* 1967, **216**, 110
- Bradford, E. B. and Vanzo, E. *J. Polym. Sci. (A-1)* 1968, **6**, 1661
- Inoue, T., Soen, T. and Kawai, H. *J. Polym. Sci. (B)* 1968, **6**, 75
- Matsuo, M., Sagae, S. and Asai, H. *Polymer* 1968, **9**, 425; 1969, **10**, 79
- Lewis, P. R. and Price, C. *Nature* 1969, **223**, 494
- Keller, A., Pedemonte, E. and Willmouth, F. M. *Kolloid-Z. Z. Polym.* 1970, **238**, 385
- Dlugosz, J., Keller, A. and Pedemonte, E. *Kolloid-Z. Z. Polym.* 1970, **242**, 1125
- Kämpf, G., Hoffmann, M. and Krömer, H. *Ber. Bunsenges. Phys. Chem.* 1970, **74**, 851
- Szwarc, M. 'Carbanions, living polymers and electron transfer process', Interscience, New York, 1968
- Altares, T., Wyman, D. P., Allen, V. R. and Meyersen, K. *J. Polym. Sci. (A)* 1965, **3**, 4131
- Grubisic, Z., Rempp, P. and Benoit, H. *J. Polym. Sci. (B)* 1967, **5**, 753
- Luzzati, V., Mustacchi, H. and Skoulios, A. *Acta Crystallog.* 1960, **13**, 660
- Terrisse, J. *Thesis* University of Strasbourg, 1973
- Baro, R. and Luzzati, V. *J. Phys. Radium* 1961, **22**, 186A
- Kato, K. *J. Polym. Sci. (B)* 1966, **4**, 35
- Rossi, J. *Thesis* University of Orleans, 1971
- Douy, A. and Gallot, B. *Mol. Cryst. Liq. Cryst.* 1971, **14**, 191
- Grosius, P., Gallot, Y. and Skoulios, A. *Makromol. Chem.* 1969, **127**, 94; 1970, **132**, 35
- Grosius, P., Gallot, Y. and Skoulios, A. *C. R. Acad. Sci. (C)* 1970, **270**, 1381
- Brown, D. S., Fulcher, K. U. and Wetton, R. E. *J. Polym. Sci. (B)* 1970, **8**, 659
- Price, C., Lally, T. P., Wason, A. G., Woods, D. and Chow, M. T. *Br. Polym. J.* 1972, **4**, 413
- Vanzo, E. *J. Polym. Sci. (A-1)* 1966, **4**, 1727

Investigation of orientation phenomena in drawn films of poly[(±)-β-aminobutyric acid]

H. W. Siesler

Department of Chemistry including Biochemistry, University of the Witwatersrand, Johannesburg, South Africa
(Received 11 July 1973; revised 29 October 1973)

Orientation data of drawn films of poly[(±)-β-aminobutyric acid] (structural unit $[-NH-CHCH_3-CH_2-CO-]_n$), are derived from the infra-red dichroism of the N-H stretching vibration and wide angle X-ray diffraction measurements. In combination with accessibility data from deuteration experiments, these parameters are used to examine the applicability of two-phase polymer models for uniaxial orientation to the investigated polymer.

INTRODUCTION

One of the most important methods for measuring orientation in polymers, makes use of polarized infra-red (i.r.) radiation¹. The effect of orientation on a particular absorption band in the i.r. spectrum of a polymer is characterized by the dichroic ratio, R :

$$R = A_{\parallel} / A_{\perp} \quad (1)$$

where A_{\parallel} and A_{\perp} are the measured absorbances with radiation polarized parallel and perpendicular to the draw direction, respectively.

Various polymer models for uniaxial or fibre-type orientation, are discussed in the literature, relating the dichroic ratio R to the orientation of the chain molecules causing the absorption²⁻⁴. The simplest model introduces an orientation factor f , defined by assuming a fraction f of the polymer to be perfectly oriented in the direction of stretch, while the remaining fraction $1-f$ is completely unoriented. The dichroic ratio R is then given by⁵:

$$R = \frac{f \cos^2 \alpha + \frac{1}{3}(1-f)}{\frac{1}{2}f \sin^2 \alpha + \frac{1}{3}(1-f)} \quad (2)$$

where α is the angle between the transition moment of the absorbing group and the chain axis of the polymer molecule. Equation (2) may be put into a different form:

$$f = \frac{(R-1)(R_0+2)}{(R_0-1)(R+2)} \quad (3)$$

Here R is the measured dichroic ratio of the investigated band and R_0 is given by:

$$R_0 = 2 \cot^2 \alpha \quad (4)$$

In general, separate orientation functions f can be derived from equation (3) for the crystalline and amorphous phase of the polymer by evaluating the dichroic effects of absorption bands peculiar to these regions. If the i.r. dichroic measurements refer to the whole polymer, equation (2) or preferably equation (6) (see below) may be used to characterize orientation.

The orientation function f can also be expressed in terms of $\langle \cos^2 \beta \rangle$, where β is the angle between the draw direction and the chain axis⁶:

$$f = (3 \langle \cos^2 \beta \rangle - 1) / 2 \quad (5)$$

Hence if the direction of the transition moment with respect to the chain axis is known, the average orientation of the chain segments can be determined from the dichroic ratio.

Some polymeric materials are best defined by a model containing a fraction f in which all chains make an angle β with the direction of stretch while the remaining fraction $1-f$ is unoriented. For such a polymer the dichroic ratio R is given by⁷:

$$R = \frac{f \cos^2 \alpha + \frac{2 \sin^2 \beta}{2 - 3 \sin^2 \beta} + \frac{1}{3}(1-f)}{\frac{1}{2}f \sin^2 \alpha + \frac{2 \sin^2 \beta}{2 - 3 \sin^2 \beta} + \frac{1}{3}(1-f)} \quad (6)$$

where α is the inclination of the transition moment to the molecular axis. As the angle β can be evaluated from X-ray diffraction measurements, f can be calculated from the dichroic ratios of samples stretched to various extents, if α is known.

An approximate degree of crystallinity can be derived from deuteration experiments. N-H groups in chains involved in crystalline regions are less exposed to substitution than are those in amorphous regions. Thus, a measurement of the degree of deuteration gives information on the amorphous content and can be correlated with the fraction $1-f$ of unoriented polymer.

Another instrumental technique for the characterization of orientation in polymers is wide angle X-ray diffraction. With increasing orientation in a semi-crystalline polymer the rings in the X-ray diffraction pattern of the unoriented sample degenerate into arcs. The more perfect the orientation, the narrower are these arcs. Thus, their widths give an indication of the dispersion of the orientations in the polymer. A combination of i.r. dichroism and X-ray diffraction measurements on the same specimen is probably the best method

of characterizing orientation in polymers. The equatorial reflections of the X-ray diffraction pattern, may be photometered to determine the angle with the equator at which the intensity falls to half-value. This angle can be equated with the average angle of disorientation β in equation (6).

EXPERIMENTAL

Synthesis, chemical and physical properties of poly(β-amides) have been discussed by Bestian⁸. The unit cell of the investigated polymer was found⁹ to belong to the orthorhombic system with identity periods: $a=10.9\text{Å}$, $b=9.6\text{Å}$ and c (chain axis) $=4.8\text{Å}$. Films ($\sim 10\ \mu\text{m}$ thick) of optical inactive, atactic poly[(±)-β-aminobutyric acid] ($\bar{M}_w \approx 250\ 000$) were cast from HCOOH solutions (1.2 g/100 ml) on roughened glass plates, in order to avoid interference fringes in the i.r. spectra. The films were damped with water and drawn at room temperature (25°C) with draw ratios $\lambda=l/l_0$ in the range of 1 to 6. The films were dried at 50°C for 48 h in vacuum while being held in position in the stretching jig. Specimens for the i.r. dichroism and wide angle X-ray measurements were cut from the central portions, between the neck positions.

The i.r. spectra were run with a Perkin-Elmer double-beam grating spectrophotometer (model 325), with a wire grid polarizer in the path of the recombined light beam. For the dichroic measurements, the film was

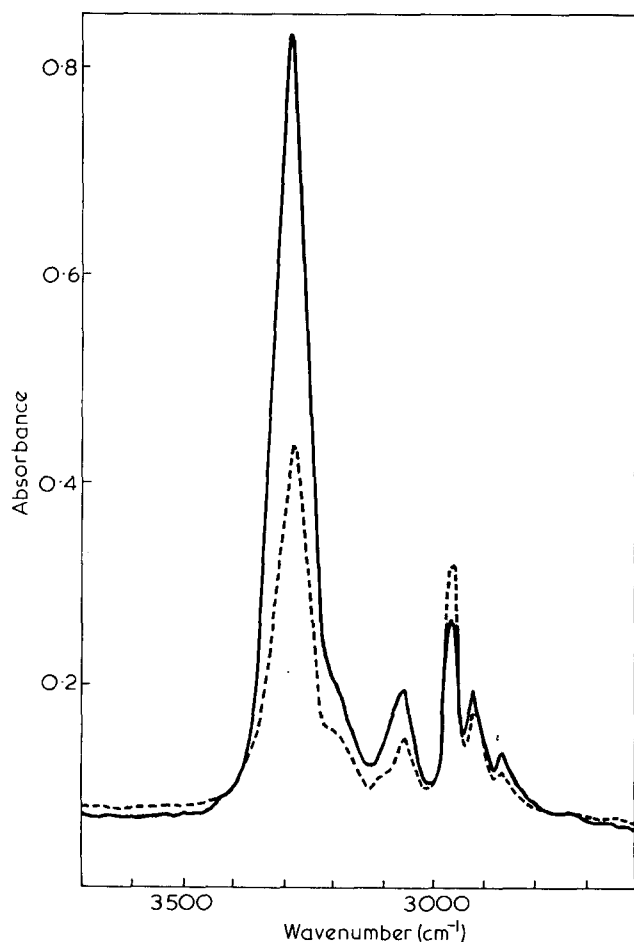


Figure 1 Infra-red spectra of drawn poly[(±)-β-aminobutyric acid] ($\lambda=5$), using polarized light perpendicular (—) and parallel (---) to the draw direction

placed in the sample beam with the stretch axis at 45° to the entrance slit of the monochromator, and the polarizer rotated to bring the electric vector of the polarized light parallel and perpendicular to the draw direction. This inclination of the stretch-axis minimizes the effect of machine polarization. Typical i.r. spectra (Figure 1) in the wavenumber region 2600–3700 cm^{-1} of drawn ($\lambda=5$) poly[(±)-β-aminobutyric acid], using radiation polarized parallel and perpendicular to the draw direction illustrate the σ -dichroism of the N–H stretching vibration at 3285 cm^{-1} . For the evaluation of the absorbance, the peak area applying the baseline method, was used, after separating the N–H absorption band from the neighbouring bands with a curve resolver.

In the deuteration experiment, specimens with different draw ratios were exposed to D₂O vapour¹⁰ and the percentage intensity decrease of the N–H band was measured and related to the amorphous fraction $1-f$ of the polymer. The H–D isotope exchange results in the partial replacement of the N–H band at 3285 cm^{-1} by two bands at 2480 cm^{-1} and 2420 cm^{-1} .

Transmission X-ray diffraction photographs were taken on the same specimens as used for i.r. dichroism measurements and the equatorial reflections of the 200 and 120 planes were photometered on a microdensitometer for the evaluation of the average angle of disorientation β . Figure 2 shows the diffraction patterns of the unoriented, and two drawn ($\lambda=3$ and 6) films of poly[(±)-β-aminobutyric acid]. The contraction of the equatorial reflections with increasing draw ratio is clearly visible.

RESULTS AND DISCUSSION

By wide angle X-ray measurements and i.r. experiments using a polymer film tilted with respect to the light beam, it was established that in the case of drawn poly[(±)-β-aminobutyric acid] there is rotational symmetry around the draw direction. Therefore the formulae for uniaxially deformed samples can be used for the evaluation of the i.r. spectra.

Deuteration experiments on samples with draw ratios $\lambda=1-6$ showed that the percentage of accessible regions remained approximately constant in all samples varying randomly between 30 and 40%. Thus, it was assumed that no remarkable crystallinity changes took place as a result of the drawing process.

To determine the degree of orientation, the dichroic ratio of the N–H stretching vibration was measured as a function of the draw ratio. Figure 3 shows, that the dichroic ratio R decreases linearly with λ , tailing off at higher draw ratios.

In general, the N–H stretching vibration will be practically confined to an oscillation of the hydrogen atom in the bond direction. Thus, the associated transition moment will not deviate remarkably from the N–H bond direction, which is approximately perpendicular to the chain axis⁹. Therefore, f was calculated from equation (3), with the measured dichroic ratios, assuming α between 85° and 90°, and listed in Table 1. No agreement with the experimental values of f , derived from the deuteration experiments, was found. From wide angle X-ray investigations on drawn specimens ($\lambda=2.25-6$), the average angle of disorientation β was evaluated as mentioned above (Table 2). These results imply a con-

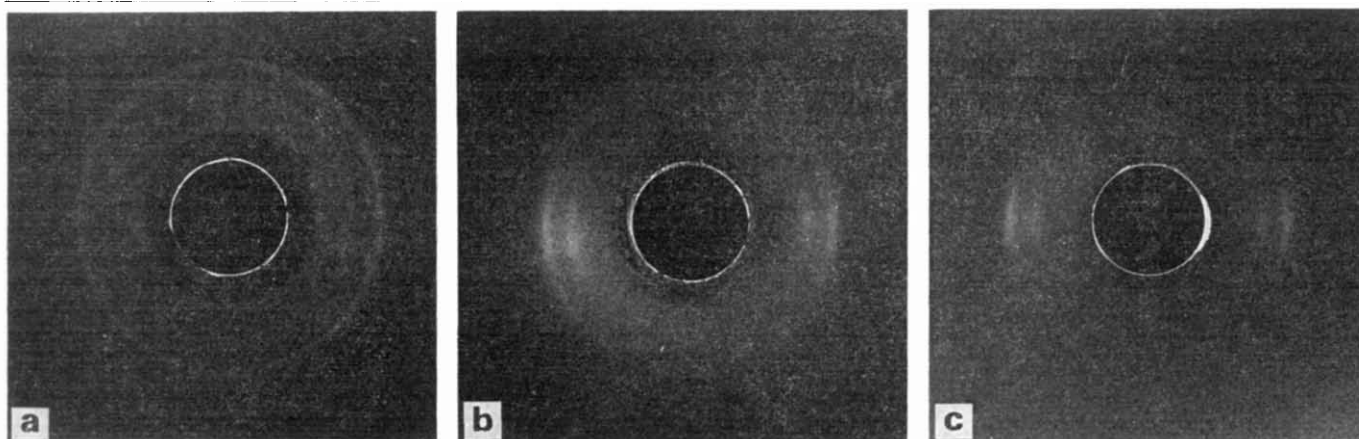


Figure 2 Wide-angle X-ray diffraction patterns of drawn films of poly[(±)-β-aminobutyric acid]. (a) $\lambda=1$; (b) $\lambda=3$; (c) $\lambda=6$

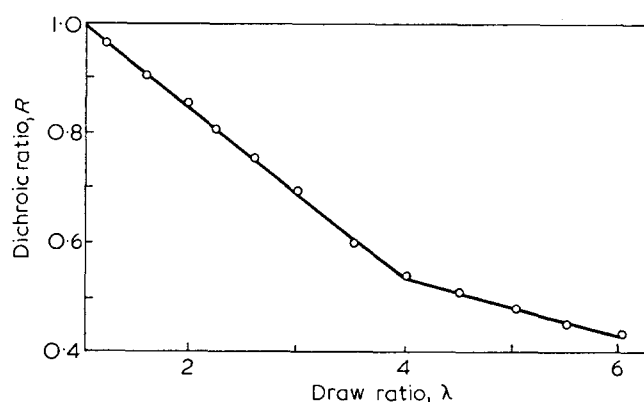


Figure 3 Dichroic ratio R versus draw ratio λ for the N-H stretching vibration at 3285 cm^{-1}

Table 1 Comparison of calculated (eqn 3) and experimental orientation functions f for different draw ratios λ

λ	R	f_{calc}	f_{exp}
1	1	0	~ 0.65
2	0.85	0.11	~ 0.65
3	0.69	0.23	~ 0.65
4	0.53	0.38	~ 0.65
5	0.47	0.43	~ 0.65
6	0.42	0.48	~ 0.65

Table 2 Average angle of disorientation β and calculated (eqn 6) and experimental orientation functions f for different draw ratios λ

λ	R	$\beta(\pm 1^\circ)$	f_{calc}	f_{exp}
2.25	0.80	41	0.65	~ 0.65
3	0.69	34	0.65	~ 0.65
4	0.53	24	0.63	~ 0.65
5	0.47	20	0.62	~ 0.65
6	0.42	17	0.63	~ 0.65

Table 3 Dichroic ratio R and calculated angle α (eqn 6) of the amide I band at 1645 cm^{-1} for different draw ratios λ

λ	$R_{\text{N-H}}$	$R_{\text{amide I}}$	$\alpha_{\text{amide I}}$ (degrees)
2.25	0.80	0.84	75
3	0.69	0.76	73
4	0.53	0.60	75
5	0.47	0.53	76
6	0.42	0.48	77

siderable alignment of the chains in the crystalline region with increasing draw ratio, as β decreases from $54^\circ 44'$ (for random orientation) to 17° for the highest drawn sample ($\lambda=6$). With these β values and α between 85° and 90° , f was calculated with the aid of the expanded equation (6) and listed in Table 2. Agreement between calculated and experimental values of f was good over the whole range of investigated draw ratios.

Additionally, the σ -dichroism of the amide I band at 1645 cm^{-1} was investigated. In Table 3, the dichroic ratios R for specimens of different draw ratios are listed together with the R values of the N-H stretching vibration, which were found to be 5–10% lower. Though the absorption of the amide I band is generally attributed to the C=O stretching vibration, the transition moment of this vibration is displaced from the bond direction because of mechanical interaction of the C=O and C-N stretching vibration, and an additional oscillating dipole moment in the N-O direction in the resonance structure of the amide group⁵. From equation (6) α was calculated with the known values of β and f for the dichroic ratios of the amide I band and found to be approximately 75° . This reveals that the transition moment of the amide I band is displaced for $\sim 15^\circ$ from the C=O bond direction, which is nearly perpendicular to the chain axis of the investigated polymer.

ACKNOWLEDGEMENTS

The author is indebted to Dr F. R. L. Schöning (Department of Physics, University of the Witwatersrand) for his help in connection with X-ray work and to Dr H. Bestian and Dr E. Schmidt (Farbwerke Hoechst AG, Frankfurt am Main, West Germany) for the supply of polymer sample and useful information.

REFERENCES

- Zbinden, R. 'Infrared spectroscopy of high polymers', Academic Press, New York, 1964, Ch V
- Fraser, R. D. B. *J. Chem. Phys.* 1956, **24**, 89
- Fraser, R. D. B. *J. Chem. Phys.* 1958, **28**, 1113
- Beer, M. *Proc. R. Soc. (A)* 1956, **236**, 136
- Fraser, R. D. B. *J. Chem. Phys.* 1953, **21**, 1511
- Hermans, P. H. 'Contributions to the physics of cellulose fibres', Elsevier, Amsterdam, 1946, p 138
- Elliott, A. 'Infrared spectra and structure of organic long-chain polymers', Arnold, London, 1969, pp 68, 86
- Bestian, H. *Angew. Chem.* 1968, **80**, 304
- Schmidt, E., *Angew. Makromol. Chem.* 1970, **14**, 185
- Grass, F., Siesler, H. and Krässig, H. *Melliand Textilber.* 1971, **52**, 1001

Ductile fracture of rigid poly(vinyl chloride)

P. L. Cornes and R. N. Haward

*Plastic Materials Laboratory, Centre for Materials Science, University of Birmingham,
PO Box 363, Birmingham B15 2TT, UK
(Received 28 August 1973)*

The fracture processes which take place in rigid poly(vinyl chloride) have been investigated. Under tension, crazes are formed and when necking occurs they pass almost unaltered through the neck. The crazes have the fibrillar structure generally observed with other plastics. After necking, fracture occurs either by the propagation of a crack from the edge of the test-piece or by the formation of a diamond-shaped cavity which initiates from a surface craze. The characteristic form of the diamond-shaped cavity appears to be controlled by the yield behaviour of the deformed polymer. At low temperatures (-40°C) it is possible to apply the methods of fracture mechanics to notched specimens and a value of $1.05 \times 10^{-3} \text{ MN/m}$ is obtained for the energy of formation of a new surface in un-drawn material.

INTRODUCTION

The brittle fracture of plastics has been extensively studied and a number of theoretical treatments have been developed. Most of these derive from the original theory of Griffith¹, who used the calculations of Inglis² to relate the strain energy released during the propagation of a crack to the energy required for crack growth. The actual stress required to initiate fracture can then be related to the size of the smallest crack or flaw in the material. When no artificial crack is introduced, the strength may be related to 'intrinsic flaws' assumed to be present. More recently, the structures of crazes have also been studied and the intrinsic flaw in the plastic appears to be generated from the prior formation of a craze³. In any case it has been shown, both by Kambour⁴ and by Murray and Hull⁵ that cavities can form within a craze, which at a critical stage can propagate as a crack. The process of crack growth according to this mechanism is now fairly well understood, and measurements of the energy of crack propagation have been reported by several workers^{6,7}.

Much progress has also been reported in determining the structure of crazes, especially in the case of polystyrene, and detailed accounts may be found in two recent reviews^{8,9}. Examples of this work include that of Kambour and Holik¹⁰ who show that polystyrene crazes consist of two interconnected networks, one of voids, and one of polymer fibrils, each approximately estimated at 200 \AA in diameter. Also, Beahan *et al.*¹¹ were able to observe even finer strands of material between the larger fibrils. Thus the occurrence of crazes in a number of plastic materials has been clearly demonstrated and their detailed structure determined. In the case of poly(vinyl chloride), however, the existence of crazes and their role in the fracture process remains uncertain. For example, Gotham¹² and Vincent¹³ refer to crazing in rigid poly(vinyl chloride) while Kambour¹⁴ failed to find any evidence of pre-crack craze formation.

Poly(vinyl chloride) is also an example of a plastic material which characteristically exhibits a large deformation or necking process in tension¹⁵ before fracture takes place. Much less is known about the processes of fracture under these conditions or of the role, if any, of crazes in the process. We may, however, note that Spurr and Niegish¹⁶ reported that in polycarbonate, which also generally necks before fracture, crazes form which survive the necking process almost unchanged. At later stages of the process they observed that some of the crazes opened to form diamond-shaped pits.

Doubt also exists as to the possibility of crazes growing in highly extended material. For example, Sauer and Hsiao¹⁷ reported that orientation causes the diminution and gradual disappearance of crazing, while Haward *et al.*¹⁸ using injection moulded test-pieces of polystyrene found the crazes did not readily propagate in a direction perpendicular to orientation.

Thus it can be concluded that the processes which determine the initiation and propagation of fractures in rigid but extendable plastics are not yet known. As an example of such materials, rigid poly(vinyl chloride) (PVC) sheet was selected for study.

EXPERIMENTAL

Material

The material used was commercial, rigid poly(vinyl chloride) sheet, Darvic Clear 025 (ICI Ltd). It has a Fikentscher *K* value of 55 and no added plasticizer, but does contain small amounts ($< 5\% \text{ w/w}$) of stabilizers, lubricants and pigments. It has a relative density of 1.39 and a glass transition temperature measured with a differential scanning calorimeter (at $10^{\circ}\text{C}/\text{min}$) of 67°C .

Tensile measurements

Strips of material were cut from 1 mm and 2 mm thick sheets and made into dumbbell-shaped test-pieces

using a routing machine. The jig used resulted in a dumb-bell with a parallel length of 6 cm and width 8 mm. Alternatively, strips of material 1 cm wide were tested directly. All tests were made in a controlled environment of $23 \pm 1^\circ\text{C}$ and $50 \pm 5\%$ relative humidity unless otherwise stated. Tests were performed in simple uniaxial tension using an Instron tensile testing machine (floor model) equipped with environmental chamber and controls.

Microscopic study of fracture phenomena

Test-pieces were studied by a variety of optical microscopic techniques and, after uniformly coating with gold-palladium, by scanning electron microscopy.

Samples were prepared for transmission electron microscopy using a Reichert OMU2 ultramicrotome with glass knife. Working below room temperature was found to be unnecessary. Samples were mounted on wooden supports in such a way that the crazes ran at an angle to the cutting direction, thus ensuring that crazes were easily distinguished from cutting and fold lines. A light carbon coating on the sample was found very effective in reducing beam damage.

RESULTS AND DISCUSSION

When a tensile stress was applied to notched samples of rigid PVC at a low temperature (-40°C), brittle fracture took place and the results could be treated by the methods of fracture mechanics. At normal temperatures, visible crazes first appeared on the surface of the test-piece, and then as the stress was increased necking and extension of the test-piece took place, followed by a rupture within the necked region of the specimen. The details of these processes will now be described.

Formation of crazes

As stated above, under a tensile stress, samples of PVC showed marked crazing which set in before necking of the test-piece took place, thus confirming the work of Gotham¹² and Vincent¹³. The crazes could in some cases be seen by the naked eye, but in all cases they were visible under the microscope at low magnification. Although the crazes seen in this way had all the characteristic features of crazes, as seen in other plastics (e.g. polystyrene), observations of this sort do not, of course, confirm that their structure is the same. We therefore set out to study their constitution in the optical microscope at high magnifications and by electron microscopy. However, very little information on the nature of the crazes could be obtained by scanning electron microscopy, possibly because the outer surface was closed by a skin of polymer.

Optical micrographs were obtained at low magnifications (Figure 1a) and at magnifications of up to $1500\times$ using axially reflected light as shown in Figure 2. Although the structures observed appeared to be just beyond the resolving power of the optical microscope, Figure 2 gives an indication of fibrillar connections within the crazes suggesting that they do in fact have a similar structure to that observed with other materials. Confirmation of the structure was then obtained by transmission electron microscopy as shown in Figure 3. This shows a microtomed craze cross-section from outside the necked region which clearly has a structure similar to that of other crazes⁹. Close examination

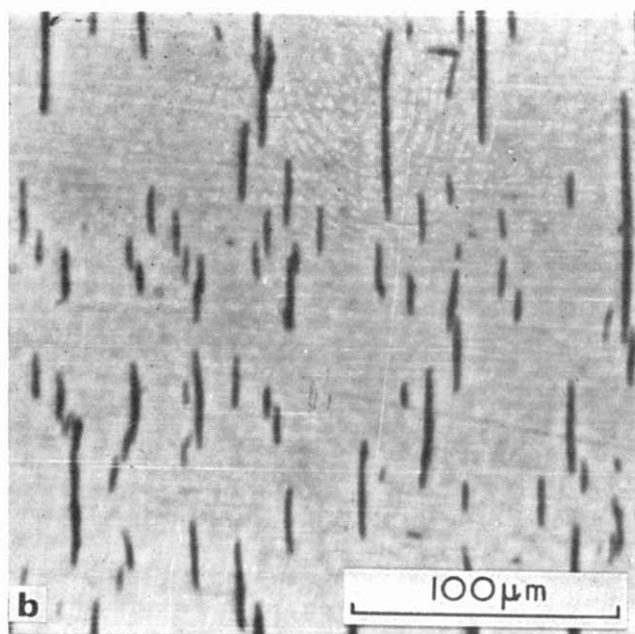
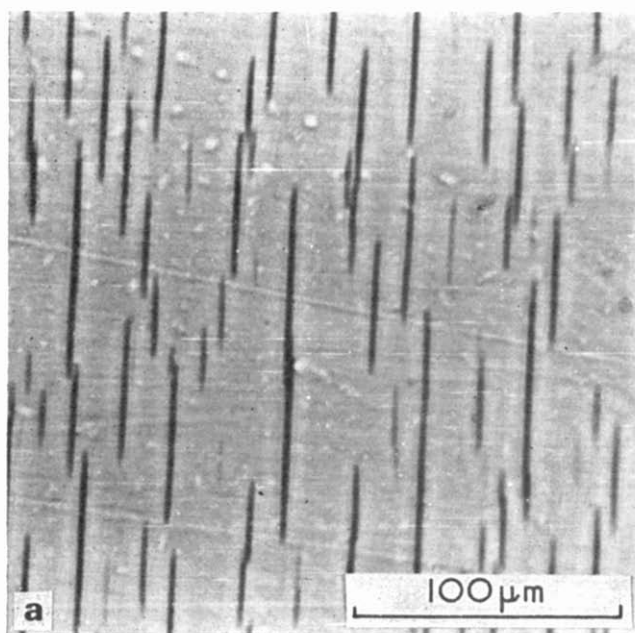


Figure 1 Transmitted light micrograph of craze in PVC (a) before yielding and (b) within the yielded region

reveals the presence of finer strands of material linking the main fibrils. A number of problems were encountered in obtaining this electron micrograph since, as reported by Beahan *et al.*¹¹ it was difficult to resolve the craze structure after microtoming. Thus, so far only a few electron micrographs have been obtained, all of them from parts of the test-piece where no necking has occurred.

Previous work^{8,9} with other materials showed that the ease of craze formation depends on several factors, including temperature, strain rate and the condition of the specimen. For poly(vinyl chloride) it was found that the maximum size and frequency of crazes occurs around 40°C and that above 60°C crazes were absent. The value of strain rate up to $5.6 \times 10^{-3} \text{ s}^{-1}$ made little difference to craze formation although there was a tendency towards larger crazes at lower strain rates.

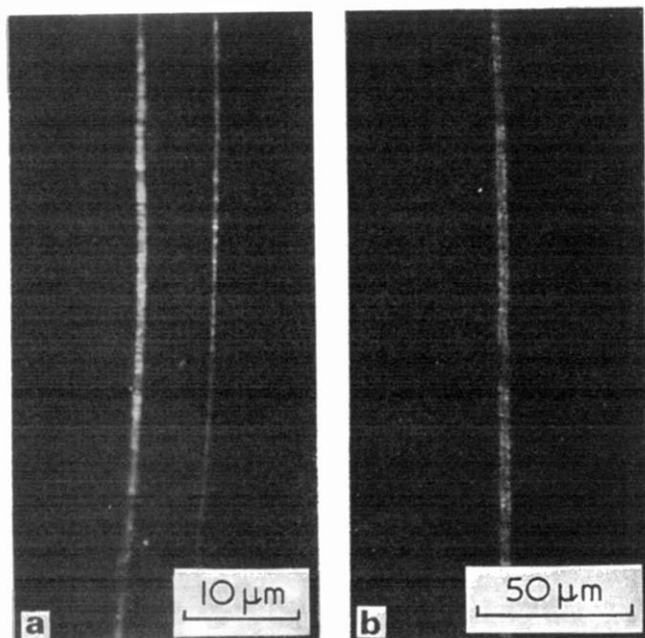


Figure 2 Axially reflected light micrograph of craze (a) prior to yielding and (b) within the necked region. The lower magnification in (b) corresponds to a widening of the craze

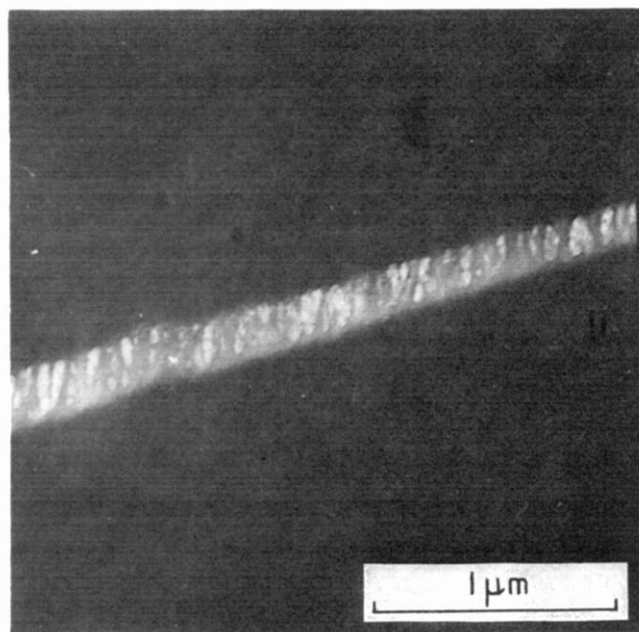


Figure 3 Electron micrograph of PVC craze prior to yielding

On the other hand, the size and number of crazes was markedly affected by the condition of the sample surface. Fingering of the specimen produced a large number of crazes, and scratching with emery paper led to very large crazes. If the sample was kept perfectly clean after the removal of the protective paper supplied by the manufacturer, then small crazes, only visible under the optical microscope, were produced.

Nearly all crazes started at the surface of the material but a few internal crazes were also seen which, however, always appeared to be initiated by extraneous particles of impurity.

Necking of crazed samples

From the above it will be clear that the application of stresses, below the yield stress, to PVC test-pieces

leads to the formation of surface crazes. The tensile test may then be continued until yielding takes place with the formation of a neck, followed ultimately by fracture. Under these conditions, it is possible to observe the movement of the crazes and the changes which occur as necking takes place. In practice, we found, as did Spurr and Niegish with polycarbonate¹⁶ that the crazes passed through the neck almost unchanged. Thus the crazes in the necked portion are not markedly different from the crazes in the undeformed material, as shown in Figure 1b. However, they do not necessarily remain perpendicular to the applied tensile stress while they pass through the neck, especially when the neck is initially formed as an angled shear band. They may be bent or distorted in a similar way to those shown in Figure 5 (see later).

By examining the positions of bench marks and crazes in different parts of the material, we find that the permanent strain of the necked part of the test-piece was 1.2 and that the distance between particular crazes increased in exactly the same ratio. The length of the crazes, however, did not diminish in proportion to the width reduction of the test-piece and the crazes generally appeared to widen during necking as indicated in Figure 2b.

Measurement of crack propagation energy at low temperatures

At room temperature, PVC does not show brittle fracture and when notches are introduced substantial¹⁹ yielding occurs at the notch before fracture takes place. In order to study brittle fracture, it was necessary to use single edge notched specimens at -40°C , when conventional results relating the fracture stress (σ_c) to the notch length, a , were obtained.

In all cases the stress-strain curves of the notched specimens up to the advent of fracture were non-linear so that the results could be treated in two different ways to give different results for the quantities concerned, viz:

(I) Using the methods of linear fracture mechanics, which derive ultimately from the theories of Griffiths, we obtain: $K_c = \sigma_c Y(a)^{1/2}$ where K_c is a critical stress intensity factor, σ_c the stress at fracture, Y a finite width correction factor²⁰ and a the initial crack length.

A graph of σ_c against $1/[Y(a)^{1/2}]$ would be expected to give a straight line of gradient K_c passing through the origin. In our experiments, the line curves over at short crack lengths (Figure 4) but a value of K_c may be obtained from the first part of the line. The surface energy for the growth of unit length of the crack G_c is then defined as $G_c = K_c^2/E = 2\gamma$ where γ is the energy required for the formation of unit area of a new surface, and E the Young's modulus was taken as $4.2 \times 10^3 \text{ MN/m}^2$. From our line we obtained $G_c = 2.1 \times 10^{-3} \text{ MN/m}$ ($\gamma = 1.05 \times 10^{-3} \text{ MN/m}$) which compares with a similar value of $G_c = 2.45 \times 10^{-3} \text{ MN/m}$ obtained by Williams²¹ from three notch-bend tests at the same temperature. However, this good agreement must be treated with caution since our results (Figure 4) are not fully linear.

* This was obtained from ICI Technical Service Note D106 (2nd Edn) and the values were confirmed from our own measurements of tangent modulus. A 1% secant modulus would have been significantly lower, leading to a somewhat higher value of γ .

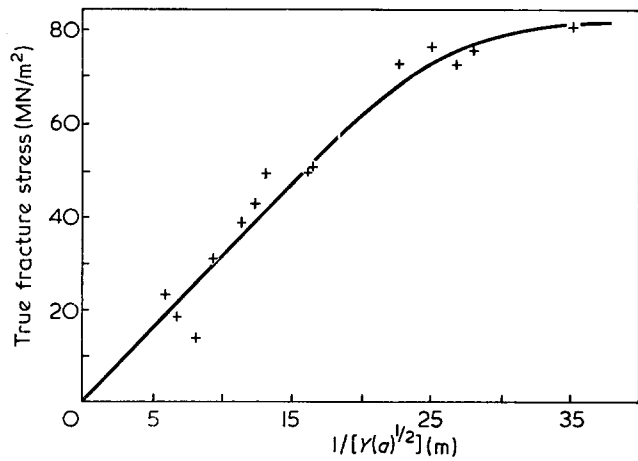


Figure 4 Graph of fracture stress against reciprocal corrected crack length for rigid PVC at -40°C

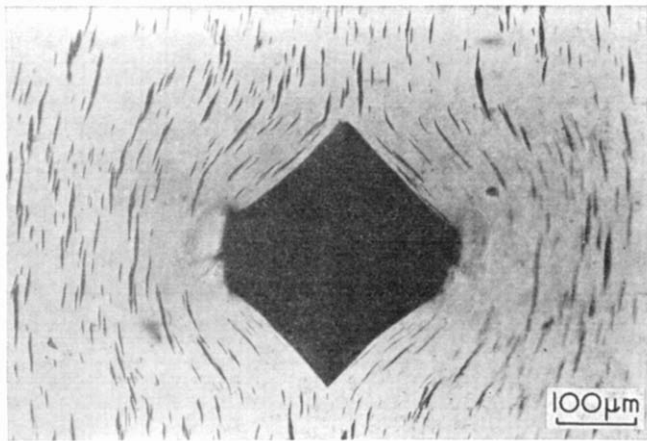


Figure 5 Transmitted light micrograph of a diamond cavity in yielded PVC showing deformed crazes

(II) An alternative method of treatment uses an equation developed by Andrews²² from work by Rivlin and Thomas²³. A tearing energy T is defined according to the equation: $T = W_c Y^2 a$. W_c is the critical stored energy density in the bulk material at fracture. In using this relation the areas under the stress-strain curves are used, and since the curves are not linear the results obtained are not equivalent to those given by the previous treatment. In fact, however, the graph of $(W_c)^{1/2}$ against $1/[Y(a)^{1/2}]$ behaves in a similar way to Figure 4 with curvature at low values of a . From the initial linear part of the relation we get $T = 2.1 \times 10^{-3} \text{ MN/m}$. If the material was perfectly elastic we would expect to obtain $T = \gamma$.

Attempts to apply either of these two treatments to the oriented polymer after necking failed since the points obtained showed excessive scatter and did not appear to give a line through the origin. We may note that Vincent²⁴ also found difficulty in applying these procedures to the case of oriented poly(ethylene terephthalate).

Fracture of necked material

After the material has necked a new mechanism of fracture from crazes is observed. Examination of samples of PVC which have necked and fractured reveals under the microscope, large diamond-shaped cavities ('diamonds') within the drawn material (Figure 5). These cavities all have a characteristic shape, with two blunt

edges normal to the drawing direction, and two pointed extremities which tear across the specimen at right angles to the applied tensile stress. This latter point has been verified by observing directly in the microscope the growth of cavities under the influence of an applied tensile stress and means that the diamond cavity is propagating by tearing across the direction of orientation of the drawn material. Crazes surrounding a diamond follow the contours of the cavity, indicating the way in which the material deformed. The nature of this deformation is determined by the presence of the four shear bands which radiate from each end of the straight edges of the cavity (Figure 6). When the edges of the sample are examined, V-shaped notches resembling the pointed, propagating part of the diamond cavity are observed (Figure 7). The bottom of both types of cavity has an irregular furrowed appearance which shows up quite clearly in the scanning electron microscope (Figure 8). This appearance seems to be caused by the tearing apart of material during growth of the diamond, since depressions on one side of the cavity can be linked with protrusions on the other. The bottom surface has a

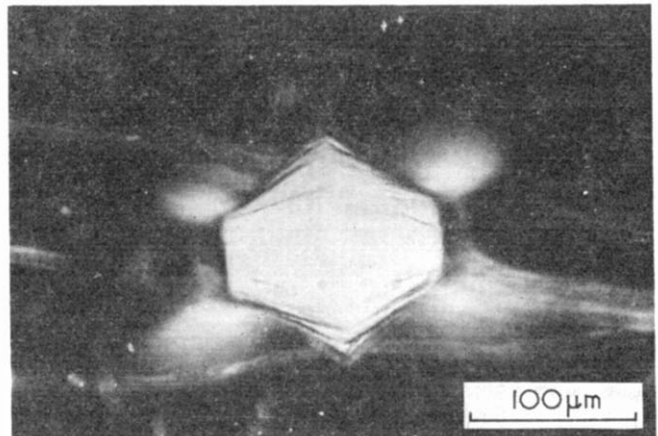


Figure 6 Reflected light micrograph of a diamond cavity showing yielded bands

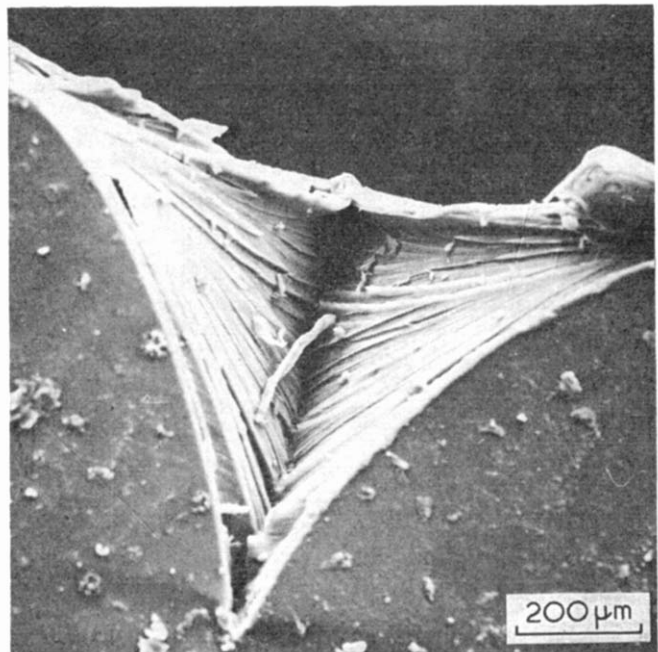


Figure 7 Scanning electron micrograph showing the beginning of fracture from an edge of the specimen in yielded PVC

number of pointed, leaf-like ridges which run at right angles to the original line of fracture.

Observations of many fractures has led to the conclusion that the diamond cavities are initiated by a craze. For example, *Figure 9* shows optical micrographs of the formation of a diamond in a craze. A diamond

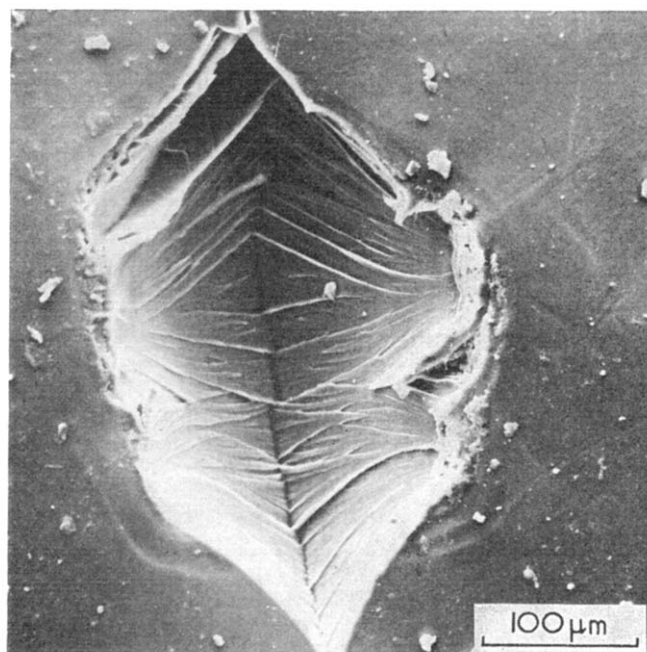


Figure 8 Scanning electron micrograph of a diamond cavity in yielded PVC showing the appearance of the bottom surface

is initiated within the matrix of the craze, and then grows by tearing of the craze material at the pointed tips of the diamond. At the same time the diamond expands outwards, beyond the boundaries of the craze into the surrounding oriented material. It is at this last point that the mechanism differs from that observed in a brittle fracture. Hull⁵ reports the formation of cavities in polystyrene which propagate by tearing the craze matrix, and somewhat similar formations in methacrylate have been reported by Lednicky and Pelzbauer²⁵. However, in these cases the size of the cavity is limited to the thickness of the craze, and eventually the cavity gives rise to a crack, leading to brittle fracture. In the case of a ductile fracture, the diamond grows to a thickness many times that of the craze. The initiation of the diamond cavity within the craze may well be by the mechanism described by Hull for polystyrene, that is voids developing around inhomogeneities in the craze matrix. The cavity then grows in size until the initiating craze is completely absorbed within the diamond. It seems that once a diamond has formed, crazes are not essential for further growth, and cavities have been found in material with no other crazes in close proximity. *Figure 10* shows the various stages of diamond growth from the widening of crazes to the formation of the cavity outside the craze boundary.

Since a diamond is initiated by the pulling apart of the craze matrix, then craze remnants would be expected along the edges of the cavity. *Figure 11* is a scanning micrograph showing such an edge on which the structure is reminiscent of a broken craze, although these features appear to be significantly larger than the craze fibrils observed in the electron micrograph (*Figure 3*).

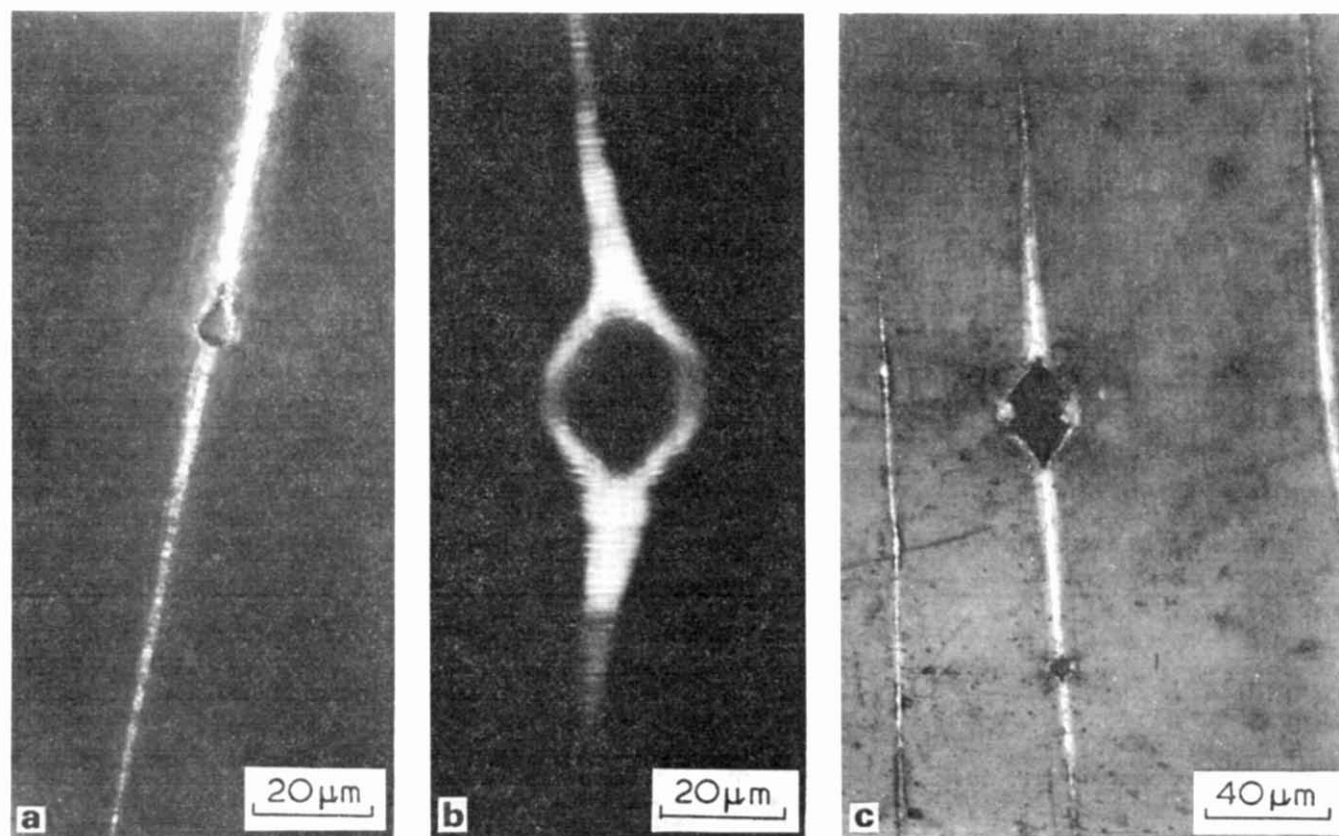


Figure 9 Axially reflected light micrograph of a cavity (a) beginning to grow within a craze, (b) expanding within a craze and (c) growing outside the boundaries of the craze. Possible craze remnants are visible in (c) on either side of the cavity. A smaller cavity is seen further along the craze

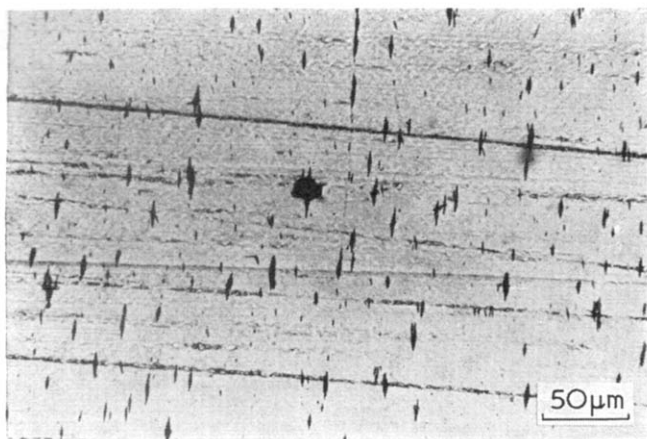


Figure 10 Transmitted light micrograph of the surface of a yielded PVC specimen, showing the stages in diamond formation

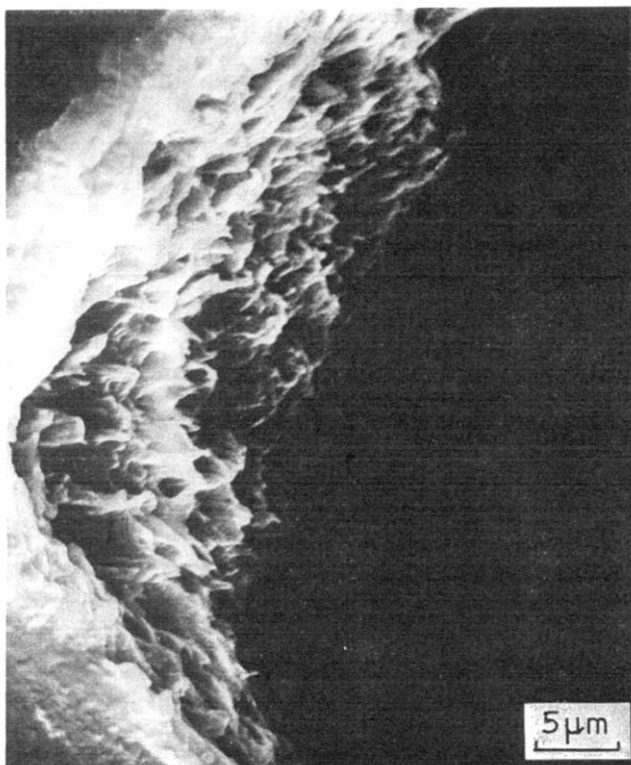


Figure 11 Scanning electron micrograph showing possible craze remnants

On rare occasions diamonds were found in which the point of the cavity did not follow the line of the craze (Figure 12). This is surprising since both crazes and cavities propagate normal to the direction of maximum tensile stress. Probably the alignment of the craze is not always exact after bulk deformation of the material has taken place.

According to these observations we find that a craze first develops a cavity, which may well be similar to cavities developed under the conditions of brittle fracture. Once formed, however, they grow quite differently. We ascribe this difference in growth to the specific properties of the strained polymer, in which shear deformations most easily occur along angled shear bands.

Once a diamond-shaped cavity has formed it continues growing slowly in the manner indicated until the local stress becomes high enough for rapid catastrophic

failure to occur. When the whole fracture surface of a test-piece is examined, two typical cases are found to occur (Figure 13). The first type has a smooth area starting in one corner and spreading out until it suddenly changes to a rougher type of surface. This smooth area which shows the characteristic structure visible inside a diamond (Figure 9) is interpreted as being associated with a slow tearing while the more coarse surface is associated with rapid fracture. This type of fracture surface results from initiation by an edge diamond. The second type of fracture surface has been reported in the literature²⁵. It consists of a small semi-circular area which we associate with the slow growth of a diamond, surrounded by a more coarse area from rapid failure. This process is illustrated in Figure 14. The fact that the smooth area arising from diamond fracture is semi-circular suggests that the lateral cross-section is disc-shaped. Further, it should be noted that both types of surface contain depressions, either at the edge or at the focal point of the hemisphere. The other half of the fractured specimen is similar so that the two halves do not match up. This unusual situation is attributed to the shapes of the diamond or half-diamond which initiate fracture.

CONCLUSIONS

It has been shown that under the influence of an applied tensile stress, crazes are produced in rigid PVC. Further, these crazes appear to retain their form after the gross plastic deformation inherent in the necking process. A new mechanism of post yield fracture is presented which consists of the following stages: (i) crazes are produced which pass over into the necked region. Further elongation of the neck results in a widening of the crazes; (ii) cavities are initiated within the craze and propagate initially within the craze matrix; (iii) the cavities grow in size and take on a diamond-shaped appearance, with two flattened edges and two pointed extremities. Growth is by tearing at the pointed zones

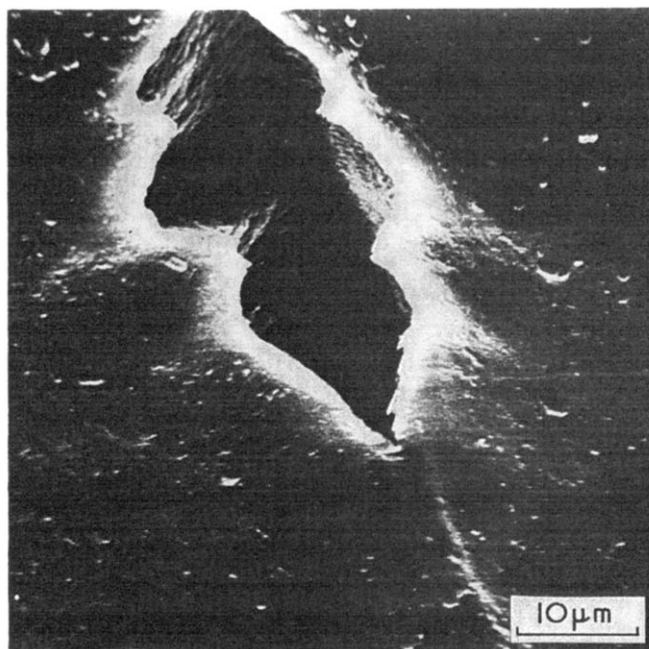


Figure 12 Scanning electron micrograph of a diamond cavity propagating away from the line of the craze

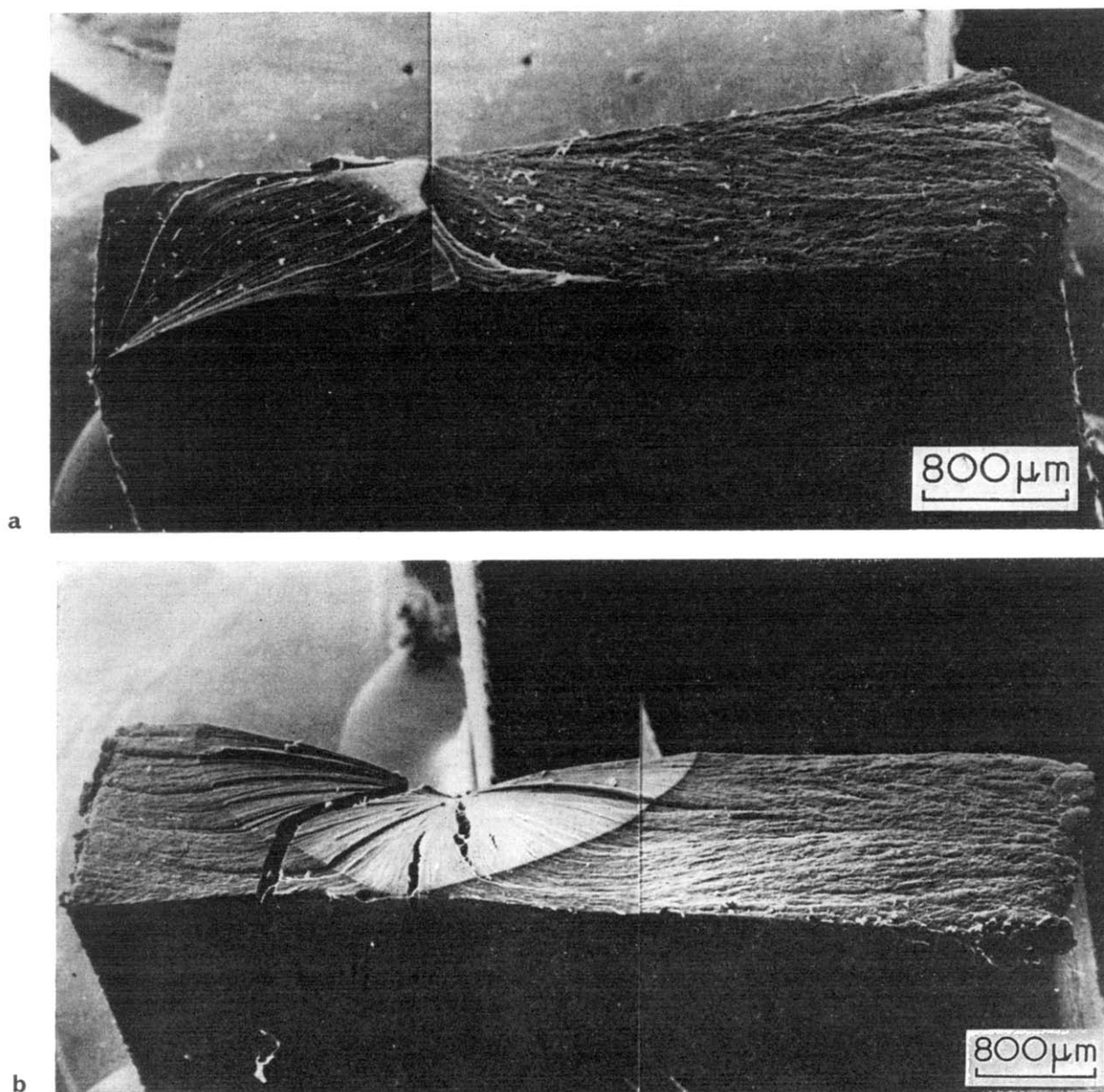


Figure 13 Scanning electron micrograph of the fracture surface resulting from (a) an edge failure and (b) failure of a diamond cavity initiated on the face of the test-piece

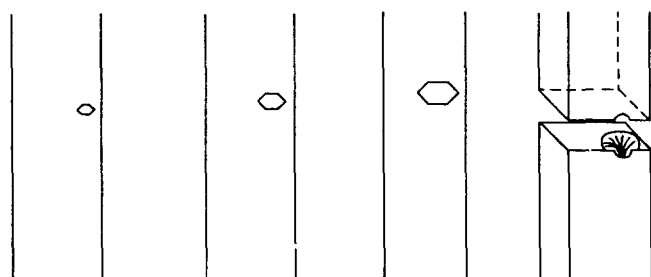


Figure 14 Diagrammatic representation of the production of a typical fracture surface from failure of a 'diamond'

perpendicular to the tensile stress and across the direction of polymer orientation in the specimen. It is not limited by the boundaries of the craze; (iv) the cavities continue to grow in size, completely engulfing the original craze, until local stresses become sufficiently high to cause rapid, catastrophic failure; (v) a characteristic fracture surface is obtained on which the area of slow growth of the cavity is easily distinguished; (vi) alternatively,

the whole process can start from the edge of the specimen, when a second characteristic fracture surface results.

ACKNOWLEDGEMENTS

P. L. C. wishes to thank Shell Research Limited for financial support, and Mr R. Marriott for assistance in experimental work. We would also like to thank Professor Hull and coworkers (University of Liverpool) for helpful discussion in the field of electron microscopy, and the Material Science Groups at Queen Mary College and Imperial College (University of London) for much helpful advice.

REFERENCES

- 1 Griffith, A. A. *Phil. Trans. R. Soc.* 1921, **A221**, 163
- 2 Inglis, C. E. *Trans. Inst. Nav. Archit.* 1913, **55**, 219
- 3 Berry, J. P. *J. Polym. Sci.* 1961, **50**, 313
- 4 Kambour, R. P. *J. Polym. Sci. (A-2)* 1966, **4**, 349

Ductile fracture of rigid PVC: P. L. Cornes and R. N. Haward

- 5 Hull, D. and Murray, J. *Polymer* 1969, **10**, 451
- 6 Berry, J. P. 'Fracture Processes in Polymeric Solids' (Ed. B. Rosen), Interscience, New York, 1964, p 221
- 7 Andrews, E. H. 'Physics of Glassy Polymers' (Ed. R. N. Haward), Applied Science, London, 1973, p 405
- 8 Rabinowitz, S. and Beardmore, P. CRC Critical Reviews in Macromolecular Science, Jan. 1972
- 9 Kambour, R. P. *J. Polym. Sci. (D)* to be published.
- 10 Kambour, R. P. and Holik, A. S. *J. Polym. Sci. (A-2)* 1969, **7**, 1393
- 11 Beahan, P., Bevis, M. and Hull, D. *Phil. Mag.* 1971, **24**, 1267
- 12 Gotham, K. V. *Plastics and Polymers* 1969, **37**, 309
- 13 Vincent, P. I. 'Encyclopaedia of Polymer Science and Technology', Wiley, New York, 1967, Vol 7, p 332
- 14 Kambour, R. P. *J. Polym. Sci. (A-2)* 1966, **4**, 17
- 15 Haward, R. N. 'Physics of Glassy Polymers', Applied Science, London, 1973, Ch VI
- 16 Spurr, O. K. and Niegish, W. D. *J. Appl. Polym. Sci.* 1962, **6**, 585
- 17 Sauer, J. A. and Hsiao, C. C. *Trans. Am. Soc. Mech. Eng.* 1953, **75**, 895
- 18 Haward, R. N. *et al. Proc. 2nd Int. Conf. Fracture, Brighton* 1969, Paper 45, p 517
- 19 Mills, N. J. *Conf. Yield, Deformation and Fracture of Polymers, Cambridge*, 1973, Paper 6, Plastics Institute, London
- 20 Brown, W. F. and Strawley, J. E. *ASTM Spec. Tech. Publ. No. 410* 1966, p 12
- 21 Williams, J. G., Radon, J. C. and Turner, C. E. *Polym. Eng. Sci.* 1968, p 130
- 22 Andrews, E. H. 'Fracture in Polymers', Oliver and Boyd, Edinburgh, 1968, p 124
- 23 Rivlin, R. S. and Thomas, A. G. *J. Polym. Sci.* 1953, **10**, 291
- 24 Vincent, P. I. *Polymer* 1971, **12**, 534
- 25 Lednicky, F. and Pelzbauer, Z. *J. Polym. Sci. (C)* 1972, **33**, 375
- 26 Berry, J. P. 'Fracture Processes in Polymeric Solids' (Ed. B. Rosen), Interscience, New York, 1964, p 256

Permeability of a series of alcohols through poly(γ -methyl-D-glutamate)

A. Takizawa, T. Hamada, H. Okada, S. Imai and S. Kadota

Department of Fiber and Polymer Technology, Nagoya Institute of Technology,
Nagoya 466, Japan
(Received 3 July 1973; revised 11 September 1973)

To elucidate the permeation mechanism in polypeptide membranes, permeation of a series of alcohols through poly(γ -methyl-D-glutamate) is studied. Breaks occur at the second order transition temperature in the Arrhenius plots of the diffusion coefficient and so it is concluded that the diffusion of small molecular substances in polypeptide occurs through the side-chain region between helices. These contain local coarse areas which contribute to the diffusion as effective holes without requiring vigorous molecular motion. The diffusion coefficient decreases systematically with increase of molecular size of penetrant.

INTRODUCTION

In order to investigate the relation between the sorption and diffusion of small molecular substances and the unique higher order structure of synthetic polypeptides, the authors elucidated¹ that: (i) the permeability of water vapour through poly(γ -methyl-D-glutamate) was as high as the order of $10^{-6} \text{ cm}^3 \text{ cm}^{-1} \text{ sec}^{-1} \text{ cmHg}^{-1}$ at 25°C , although the polymer itself had a low affinity to water; (ii) high permeability of the poly(methyl-glutamate) was due to the high diffusion coefficient; (iii) the polymer had a second order transition point at 28°C using dilatometry, which was related to the molecular motion of the side-chains; and (iv) the Arrhenius plot of the diffusion coefficient of CO_2 showed an inflection at 28°C though that of water vapour showed no clear inflection. This indicated that the diffusion of small molecular substances takes place where the volume expansion is promoted by the molecular motion of side-chains, namely at the apertures between the helices.

In the present paper, for the purpose of elucidating the above permeation mechanism in more detail, the permeation of a series of alcohols (methyl, ethyl, isopropyl and t-butyl alcohols, which are different in molecular size) through the poly(γ -methyl-D-glutamate) (PMDG) is studied.

EXPERIMENTAL

Materials

Poly(γ -methyl-D-glutamate) (PMDG) supplied by Ajinomoto K. K. (Japan) was obtained by the polymerization of *N*-carboxy amino acid anhydride. The viscosity-average degree of polymerization was 1150 as determined by the intrinsic viscosity in dichloroacetic acid solution at 25°C . PMDG membranes are prepared by dissolving the 5% polymer in the mixed solvent of

dichloroethane-perchloroethylene-toluene (7:2:1) and by air-drying a thin layer of the above solution on a glass plate, and finally vacuum drying at 50°C for a day. The density of the membrane was 1.302 g/cm^3 , and the thickness $0.07\text{--}0.16 \text{ mm}$. The membranes were confirmed to have α -helical structures by infra-red absorption spectra². Each alcohol used as the penetrant was of extra pure grade.

Permeation and sorption experiments

Permeation measurements were made using Rouse's apparatus³. Accordingly the pressure of the lower pressure side of the membrane is always zero. The amount permeated $Q(t)$ is expressed by the volume at the standard state per unit area of the membrane (cm^3/cm^2). An example of the permeation curve [$Q(t)$ vs. time, t] is shown in Figure 1 for the PMDG-methyl alcohol system. The linear portion of the permeation

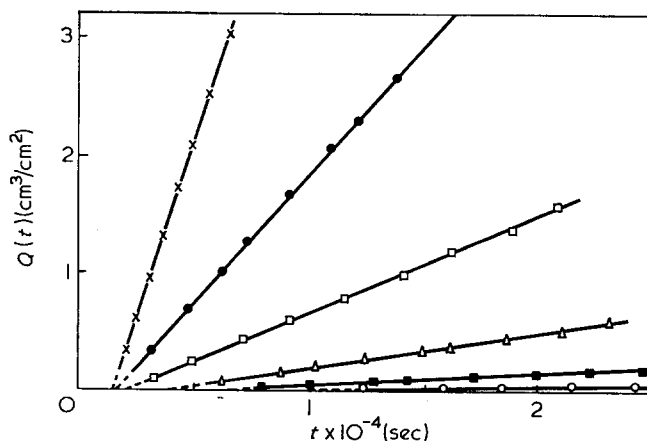


Figure 1 Permeation curves (amount permeated $Q(t)$ vs. time t) of PMDG-methyl alcohol system. Applied pressure (cmHg): \circ , 1.28; \blacksquare , 2.96; \triangle , 5.36; \square , 7.11; \bullet , 9.33; \times , 11.53. The membrane thickness is 0.16 mm

curve corresponds to the stationary state of permeation, from whose slope the permeation coefficient \bar{P} [$\text{cm}^3 \text{cm}/(\text{cm}^2 \text{sec cmHg})$] = the slope \times membrane thickness/applied pressure] is determined. Dividing \bar{P} by the solubility coefficient S [$\text{cm}^3/(\text{cm}^3 \text{cmHg})$] of penetrant to the polymer, the stationary state diffusion coefficient \bar{D} is obtained. S is determined from the sorption isotherms described later. The intercept of the extrapolation of the above linear portion of the permeation curve with the time axis corresponds to the time lag θ , from which the non-steady state diffusion coefficient \bar{D}_θ ($\bar{D}_\theta = (\text{membrane thickness})^2/6\theta$) is calculated. Bars on the P and D denote the concentration averages.

The pressure of the higher pressure side of the membrane is set up by controlling the temperature of the alcohol filled flask, which is connected to the higher pressure side of the membrane in the vacuum system and so the pressure corresponds to the saturated vapour pressure of the alcohol at that temperature.

The sorption measurement for alcohol vapours is performed by the gravimetric method using the usual quartz spiral balance⁴.

Both the permeation and sorption measurements were carried out at 25°C unless otherwise stated.

RESULTS AND DISCUSSION

Sphere like alcohols were desirable as penetrants; so non-linear alcohols were used.

The sorption isotherms of various alcohols obtained by sorption experiment are shown in Figure 2. The sorption amount (ordinate) is expressed in cm^3/cm^3 which is directly related to the number of molecules sorbed. The larger the molecular weight of the alcohol, the less number of molecules are sorbed. The amount sorbed divided by vapour pressure ($\text{cm}^3/\text{cm}^3 \text{cmHg}$) corresponds to the solubility coefficient S .

The permeability coefficient \bar{P} obtained from the stationary state permeation is plotted against the relative vapour pressure of the alcohol in Figure 3. The larger the molecular size of the alcohol, the lower is the permeability. Stationary diffusion coefficient \bar{D} obtained by dividing \bar{P} by S is shown in Figure 4. The diffusion coefficient depends markedly on the molecular size. Non-steady state diffusion coefficient, \bar{D}_θ calculated from time lag θ is plotted in Figure 5. Although the

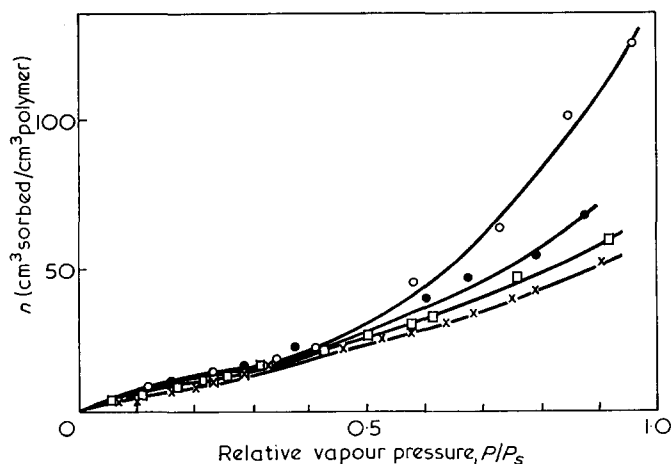


Figure 2 Sorption isotherms (amount sorbed n vs. relative vapour pressure P/P_s) of PMDG-alcohol systems: ○, methyl alcohol; ●, ethyl alcohol; □, isopropyl alcohol; ×, t-butyl alcohol

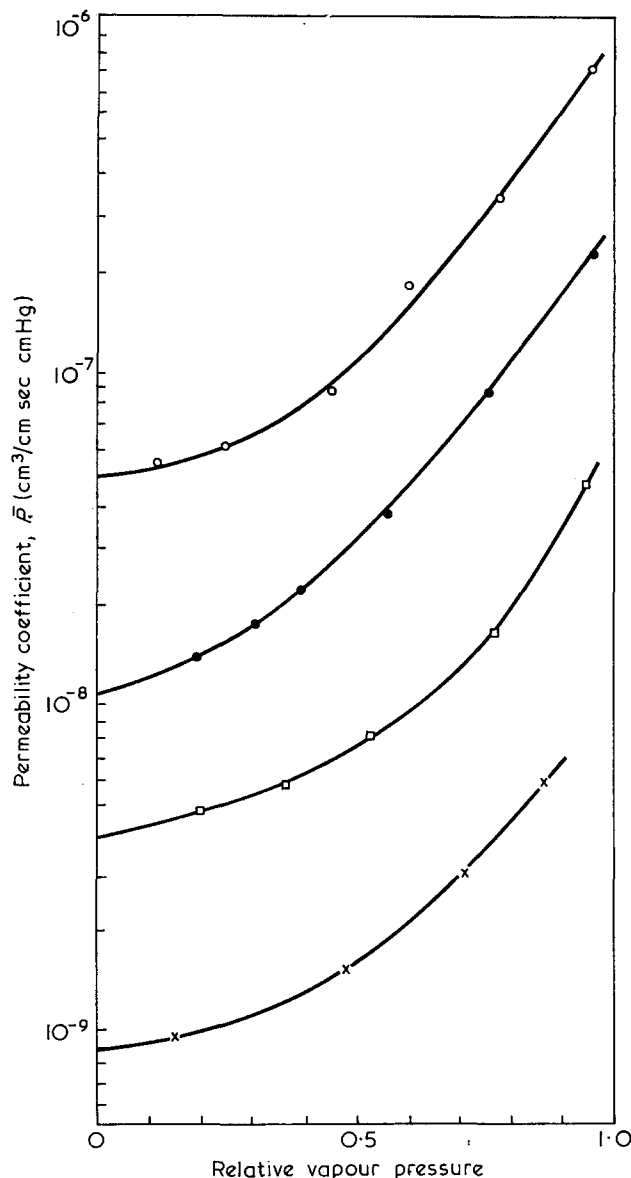


Figure 3 Relation between permeability constant \bar{P} at 25°C and applied relative vapour pressure of alcohols: ○, methyl alcohol; ●, ethyl alcohol; □, isopropyl alcohol; ×, t-butyl alcohol

difference among the \bar{D}_θ values of various alcohols is similar to the case of \bar{D} values, the absolute values of \bar{D} and \bar{D}_θ are different under the same conditions. This is true at zero penetrant concentration, which shows that the diffusion process of the PMDG-alcohol systems is of the non-Fickian type. In other words the process does not satisfy the Fickian conditions that the surface concentration of the membrane is always constant, or that the diffusion coefficient is not time dependent⁵. The fact that the experiments are performed at 25°C which is 3°C lower than the second order transition temperature 28°C of PMDG may contribute to the non-Fickian behaviour.

From Figure 4, diffusion coefficient $D(C)$ is calculated as a function of concentration C of penetrant in polymer using the relation:

$$\bar{D} = (1/C_1) \int_0^{C_1} D(C) dC$$

and the numerical differentiation of the $\bar{D}C_1$ vs. C_1 relationship. The result is shown in Figure 6. The plasticization effect of the penetrant is evident for all of the alcohols.

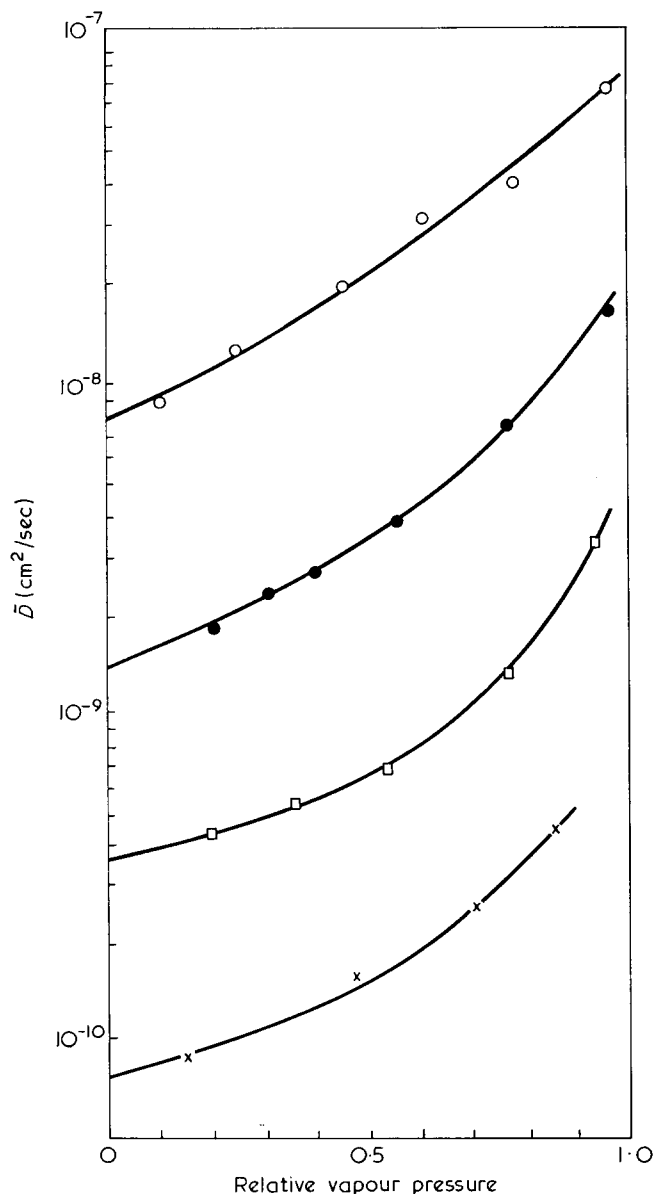


Figure 4 Relation between steady state diffusion coefficient \bar{D} at 25°C and applied relative vapour pressure of alcohol. For legend see Figure 3

The \bar{D}_0 obtained by the extrapolation of the diffusion coefficient \bar{D} or $D(C)$ to zero penetrant concentration is plotted against the molecular size (diameter) of the penetrant in Figure 7. In this case, the molecular size is calculated from the liquid density at 25°C assuming the closest packing. For each unit step in the diffusion of a penetrant molecule 'holes' which are larger than the penetrant molecule, are required near the penetrant molecules. The probability of finding larger holes decreases exponentially with the hole size⁶; this explains the present results.

Next, the temperature dependency of the permeation behaviour of PMDG-alcohol systems was studied. As described previously, the second order transition point of the polymer is 28°C, and this reflects the motion of side-chain, which is confirmed by the viscoelastic measurements⁷ and broadline n.m.r. observation⁸. The experiments were performed in a narrow temperature range of 20–35°C, which includes the above transition temperature. Since the temperature dependency of the sorption amount at the same relative vapour

pressure may almost be neglected¹, the relative vapour pressure is maintained constant, keeping the concentration of the penetrant in the polymer at about 0.11 g/g. Although the comparison of the diffusion coefficients should be done with \bar{D}_0 at each temperature, the experiments have been carried out for simplicity at the same concentration which causes the same degree of plasticization. The Arrhenius plot of $\log \bar{D}$ vs. $1/T$ is shown in Figure 8. As the molecular size of alcohol increases, the inflection becomes significant near the transition temperature. In a previous paper¹, it was reported that in the case of water the inflection was not clear. When the size of the penetrant molecule is small compared to the local pore size in the polymer, diffusion occurs by means of the molecular motion of small constitutive units below the transition temperature. Thus, the segmental motion which accompanies the change of volume expansion coefficient does not seriously affect the diffusional jump frequency. On the other hand, when the size of penetrant molecule is nearly equal or larger

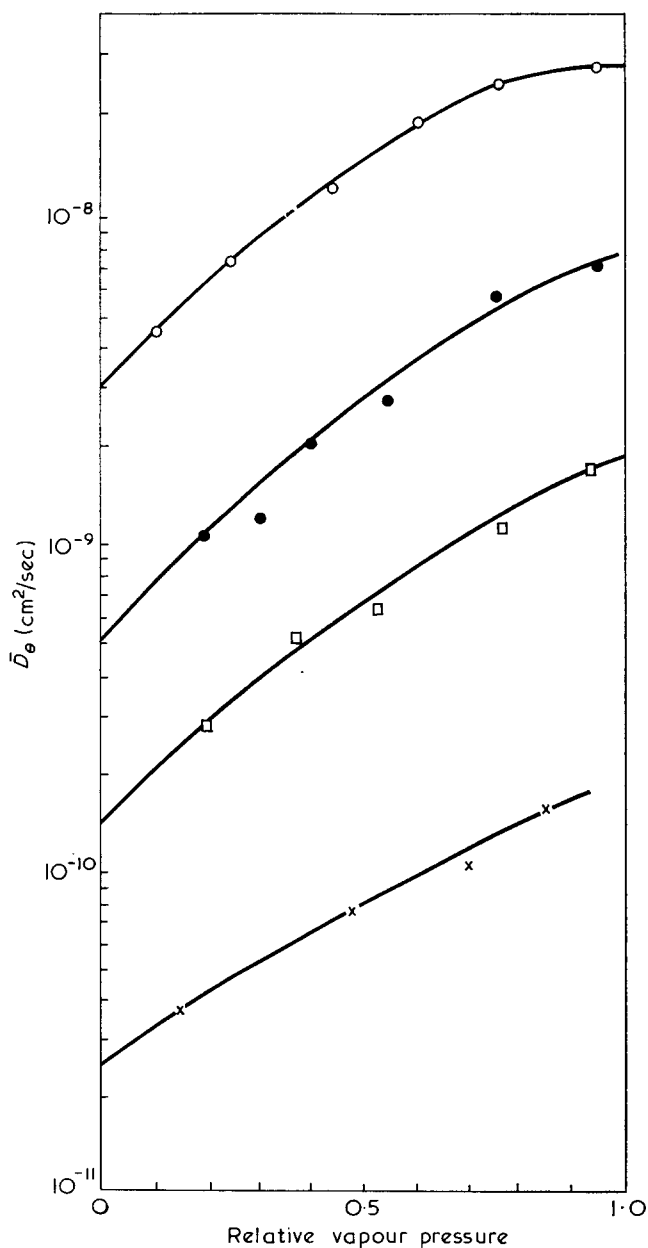


Figure 5 Relation between non-steady state diffusion coefficient \bar{D}_0 at 25°C and applied relative vapour pressure of alcohol. For legend see Figure 3

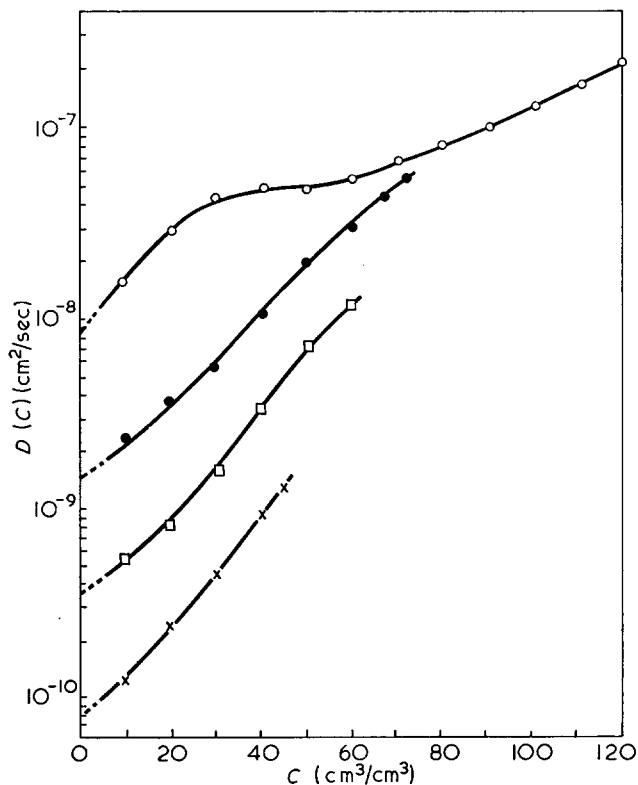


Figure 6 Concentration dependence of diffusion coefficient $D(C)$. For legend see Figure 3

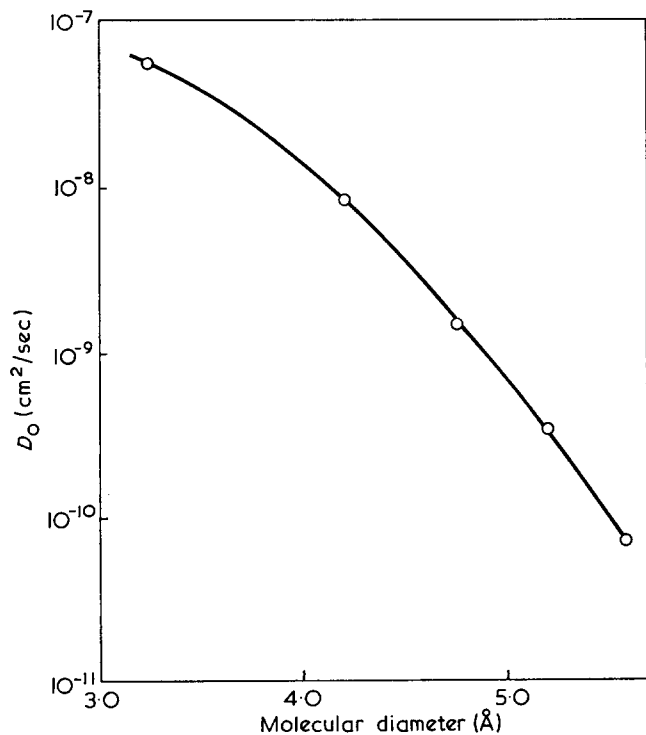


Figure 7 Extrapolated diffusion coefficient \bar{D}_0 vs. molecular diameter of penetrant. The point of the lowest molecular diameter corresponds to water¹

than the local pore size, diffusion of penetrant requires cooperative motion of the segmental motion and is affected markedly by the transition phenomena which accompanies the volume expansion change. This behaviour is similar to that reported for the diffusion coefficient of water in poly(methyl methacrylate) which shows an inflection at 65°C though other gases do not

show it at the same temperature⁹.

As the diffusion phenomena before the change of volume expansion occurs is interesting, the activation energy is calculated from the Arrhenius plot below the transition temperature. The result is shown in Figure 9 against the diameter of the penetrant molecule. The

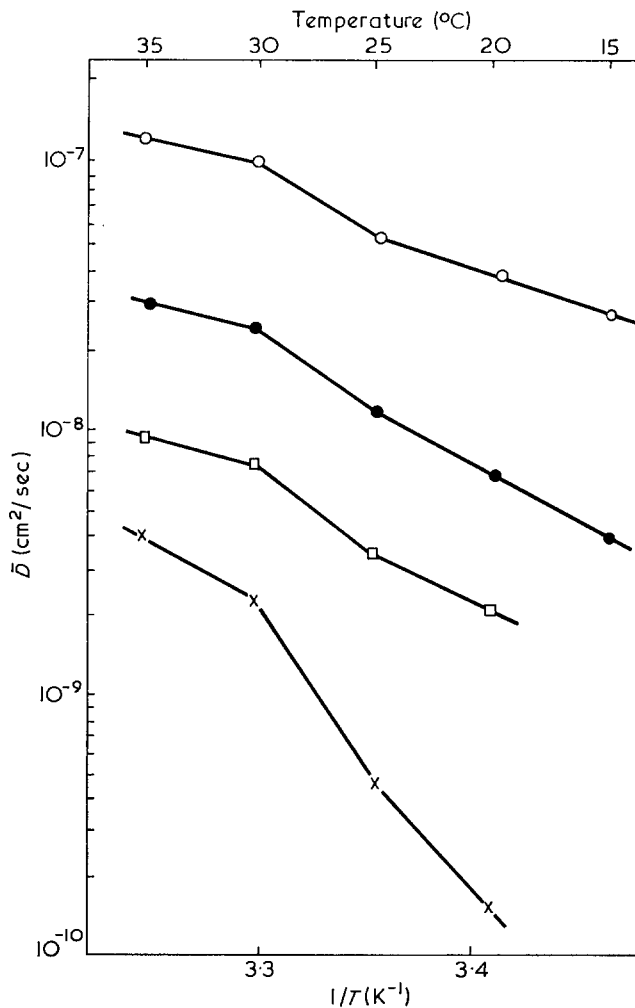


Figure 8 Temperature dependence of the diffusion coefficient of alcohol in PMDG (Arrhenius plot). \circ , Methyl alcohol; \blacksquare , ethyl alcohol; \square , isopropyl alcohol; \times , t-butyl alcohol

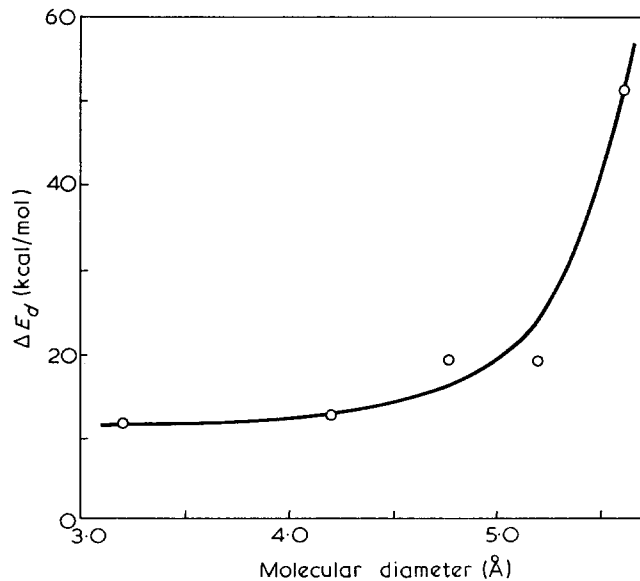


Figure 9 Activation energy of diffusion ΔE_d vs. molecular diameter of penetrant

activation energy ΔE_a increases considerably for t-butanol, which means molecular motion of the polymer equivalent to the large activation energy is necessary for diffusion of t-butanol. It is noted that ΔE_a of water is 11 kcal/mol and is smaller than 20 kcal/mol of usual polymers.

Even though the diffusion coefficients correspond to polymers containing 0.11 g penetrant/g of polymer the inflection point of the Arrhenius plot is almost the same as the second order transition point of the dry polymer. It has been reported that the side chain dispersion of poly(n-alkyl methacrylate) is less affected by penetrant than the glass transition temperature¹⁰. Since the transition temperature of 28°C is also related to the molecular motion of side-chain in the PMDG-alcohol systems, this could explain why the inflection and the transition point are at the same temperature. This indicates that the penetrant molecules diffuse through the region of side-chains between the helices.

ACKNOWLEDGEMENTS

The authors gratefully acknowledge the support of the Japanese Ministry of Education for the Science Research Grant (No. 747056 in 1972). We also express our thanks to Ajinomoto K.K. for supplying the samples.

REFERENCES

- 1 Takizawa, A., et al. *Kobunshi Kagaku* 1971, **28**, 751
- 2 Masuda, Y. *Kobunshi Kagaku* 1963, **20**, 34
- 3 Rouse, R. E. *J. Am. Chem. Soc.* 1947, **60**, 1068
- 4 Takizawa, A. and Ishikawa, K. *J. Polym. Sci. (A-1)* 1968, **6**, 475
- 5 Fujita, H. 'Diffusion in Polymers' (Eds J. Crank and G. S. Park), Academic Press, London, 1968, p 76
- 6 Bueche, F. 'Physical Properties of Polymers', Interscience, New York, 1962, p 86
- 7 Saba, R. G., Sauer, J. A. and Woodward, A. E. *J. Polym. Sci. (A-1)* 1963, **1**, 1483
- 8 Hikichi, K. *J. Phys. Soc. Japan* 1964, **19**, 2169
- 9 Stannett, V. and Williams, J. L. *J. Polym. Sci. (C)* 1965, **10**, 45
- 10 Shen, M. C. and Strong, J. D. *J. Appl. Phys.* 1967, **38**, 4197

Copolymerization and oligomerization by transition metal catalysts*

Junji Furukawa

*Department of Synthetic Chemistry, Kyoto University, Kyoto 606, Japan
(Received 13 September 1973)*

Alternating copolymerization of diolefins and olefins is possible by controlling the coordination site and the coordination ability with alkylvanadium halide as catalyst prepared at extremely low temperature. Alternating structure of the isoprene-propylene copolymer is established by nuclear magnetic resonance spectroscopy and ozonolysis analysis and the alternating addition of isoprene at the 4,1-position and of propylene at the α,β -position is proposed. The model reaction indicates that the π -allylvanadium bond prefers propylene, whereas the ethylvanadium bond prefers butadiene. However, the selectivity is lowered with bulky α -olefins. Acetylene is also copolymerized with nickel catalyst to give random copolymers possessing active methylene groups available for drying oil. Controlling the amount and acidity of the protic component added to Ni^0 , cyclo-, or linear oligomers of butadiene and the 1,3-1,2 adduct of butadiene are prepared selectively. Also, the addition of amine or alcohol to butadiene is successful. The reaction occurs through a π -allyl nickel intermediate and the reaction is extended to π -allyl exchange reactions.

INTRODUCTION

The discovery of Ziegler-Natta catalysts enabled the polymerization of ethylene, α -olefin and diolefin to give highly stereoregular polymers. However, the copolymerization of these monomers is not always successful. Only ethylene and propylene are copolymerized but the alternating tendency seems to be not so high as that of radical copolymerization. The Ziegler-Natta polymerization proceeds through so-called coordinate ionic polymerization, in which the coordination of monomers is very important as well as the polymerization ability. Diolefins seem to be very different from olefins in coordination ability, but we have succeeded in the copolymerization of butadiene and propylene or ethylene by adjusting the number of coordination sites. This idea is also extended to the copolymerization of acetylene with diolefins and olefins. In relation to the coordination and reaction ability of transition metal catalysts the oligomerization by nickel catalyst is discussed.

DIOLEFIN-OLEFIN COPOLYMERIZATION

Furukawa and coworkers have reported an alternating copolymerization of butadiene with propylene or ethylene by means of a special Ziegler catalyst prepared at extremely low temperature unlike conventional catalysts activated by ageing above room temperature¹⁻⁵.

The catalyst consisting of vanadium-alkylaluminium possesses divalent vanadium and exists in a dimeric form with a halogen bridge, which enables dissociation

followed by alternating coordination of butadiene and propylene⁴.

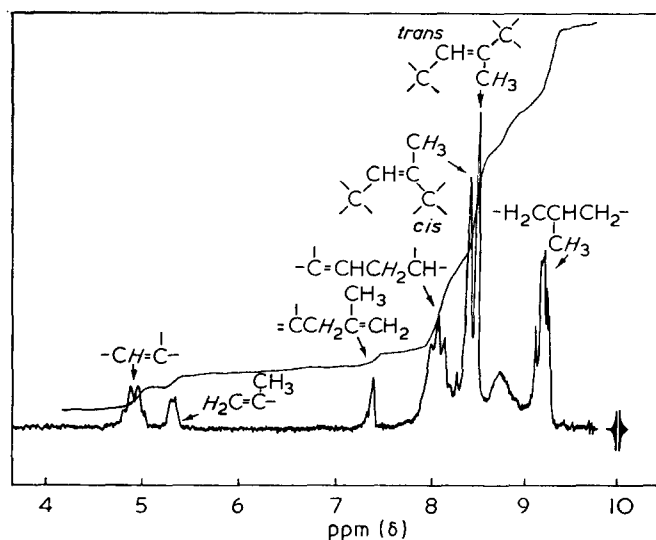
The alternating structure of a butadiene-propylene copolymer was established by 220 MHz nuclear magnetic resonance (n.m.r.) spectroscopy and ozonolysis analysis⁶. Further details were obtained from an alternating copolymer of isoprene and propylene⁷. The results are summarized in *Table 1*. The main product is 4-methyl-5-acetyl pentanal (80.1% in composition of ozonolysis product) arising from the alternating sequence of isoprene and propylene. The structure suggests that the copolymerization takes place at the 4,1-position of isoprene and the α,β -position of propylene. Formation of a considerable amount (7%) of acetylacetone is attributed to the product from the polymer terminal, since the sample subjected to analysis is a semi-solid polymer of low molecular weight. It indicates also alternating structure and that the end group is a propylene unit. The termination occurs at the propylene terminal by a hydrogen transfer. Propylene is incorporated into polymers by anionic polymerization, because the addition to propylene takes place at its α -carbon atom. The presence of levulinic aldehyde and succinodialdehyde (11% in total) indicates the existence of a small amount of isoprene block. This means that the alternating degree of isoprene-propylene copolymer is somewhat lower than that of butadiene-propylene copolymer since the ozonolysis product of the latter copolymer possesses only 0.3% succinic acid, but adipic acid is obtained in 88% yield.

In addition to the above product the isoprene-propylene copolymer yielded 3.7% 3-methylhexanal arising from an isoprene-propylene-isoprene sequence in which the head-to-tail structure of isoprene is dis-

* Presented as a Symposium Lecture at the IUPAC International Symposium on Macromolecules, Aberdeen, September 1973.

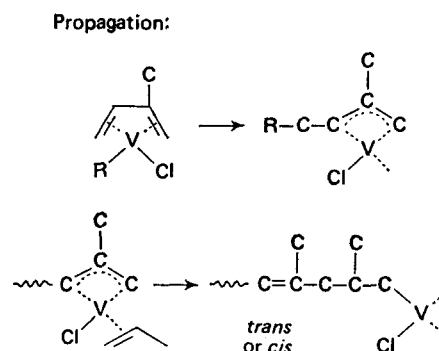
Table 1 Products of ozonolysis of isoprene-propylene copolymer

Alternating sequence:	
$\text{C}-\text{C}(\text{C})=\text{C}(\text{C})-\text{C}(\text{C})-\text{C}(\text{C})-\text{C}(\text{C})=\text{C}(\text{C})-\text{C}(\text{C})$ (80.1%) 4-Me-5-acetyl pentanal	$\text{C}-\text{C}(\text{C})=\text{C}(\text{C})-\text{C}(\text{C})-\text{C}(\text{C})=\text{C}(\text{C})$ (7%) Acetylacetone
$\text{C}-\text{C}(\text{C})=\text{C}(\text{C})-\text{C}(\text{C})-\text{C}(\text{C})-\text{C}(\text{C})=\text{C}(\text{C})-\text{C}(\text{C})$ (0%) 3-Me-5-acetyl pentanal	$\text{C}-\text{C}(\text{C})=\text{C}(\text{C})-\text{C}(\text{C})-\text{C}(\text{C})-\text{C}(\text{C})-\text{C}(\text{C})=\text{C}(\text{C})-\text{C}(\text{C})$ (3.7%) 3-Me-hexanal
Block sequence:	
$\text{C}-\text{C}(\text{C})=\text{C}(\text{C})-\text{C}(\text{C})-\text{C}(\text{C})-\text{C}(\text{C})=\text{C}(\text{C})-\text{C}(\text{C})$ (7.35%) Levulinic aldehyde	$\text{C}-\text{C}(\text{C})=\text{C}(\text{C})-\text{C}(\text{C})-\text{C}(\text{C})-\text{C}(\text{C})-\text{C}(\text{C})=\text{C}(\text{C})-\text{C}(\text{C})$ (3.35%) Succinodialdehyde

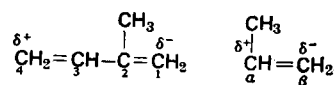
Figure 1 100 MHz n.m.r. spectrum of isoprene-propylene alternating copolymer in CDCl_3

turbed. Another isomer, 3-methyl-5-acetyl pentanal was not present.

The copolymer was also subjected to 100 MHz n.m.r. analysis. Figure 1 indicates the presence of a methylene at 5.3τ of an isopropenyl terminal, which is not from isoprene terminal, because of its singlet nature of n.m.r. at 7.36τ . These results lead us to the conclusion that a coordinate anionic polymerization proceeds through an alternating coordination of isoprene and propylene as proposed previously⁵. The coordination of monomers is controlled by the structure of the terminal unit of polymer so that the catalyst linking with the propylene terminal provides two available coordination sites for the bidentate coordination of isoprene and the catalyst linked with isoprene unit provides only one site for the unidentate coordination of propylene, since the terminal isoprene unit exists in a π -allyl form and two coordination sites are occupied.

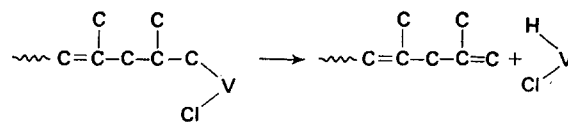


Ozonolysis data suggest that the methyl groups of the isoprene unit and propylene unit are located at the penultimate carbon atom and this fact is compatible with the mechanism of anionic polymerization and that of minimized steric hindrance in the terminal unit:

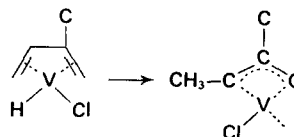


The existence of an isopropenyl end group also indicates the occurrence of a hydrogen transfer at the propylene terminal and initiation by a vanadium hydride formed by hydrogen transfer.

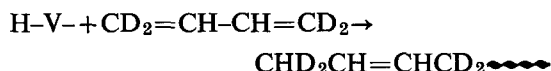
Termination:



Initiation:



Indeed, in the case of the copolymerization of 1,4-d₄-butadiene with propylene, the hydride reacts with butadiene to initiate the polymerization; formation of the CHD₂ group is confirmed by n.m.r.:



The alternating coordination was shown by gas chromatography of the reaction products of a mixture of propylene and butadiene with vanadium catalyst possessing an ethyl group and a π -allyl group.

In the system VOAcac₂-Et₃Al-allyl bromide the product of its reaction with a mixture of propylene and butadiene yielded mainly allyl group products and propylene (Table 2). In addition, a considerable amount of pentane and 2-methylbutane were obtained which may come from the reaction of the allyl group and ethyl group. Therefore, the catalyst possesses both the ethyl group and the allyl group. In fact, the reaction with propylene also yields the same product. Moreover, the catalyst itself gives the reaction product of allyl and ethyl groups. In any case there is no product expected from the reaction of an allyl group with butadiene. On the other hand, the catalyst composed of VOAcac₂-Et₃Al-Et₂AlCl yields 1-hexene and 2-hexene in the reaction with a mixture of propylene and butadiene. The catalyst also gives hexene in the reaction with butadiene but not in the reaction with propylene. In the latter case the reaction product of the ethyl group and propylene was formed. Accordingly, the allyl group reacts exclusively with propylene, but the ethyl group reacts mainly with butadiene and also reacts with propylene if propylene exists in excess.

The less selectivity of the ethyl or hydride group is reflected on the co-oligomerization by the same catalyst in the presence of an excess amount of propylene. From a 25:1 propylene-isoprene mixture a cotrimer of propylene-isoprene-propylene is obtained in a good yield of 68% based on isoprene monomer together with its isomer in 11% and the alternating copolymer in 21% yield. This fact indicates that in the presence of an excess of propylene the vanadium hydride as well as ethyl vanadium reacts with propylene instead of isoprene to initiate the reaction, but the second unit is always isoprene. The selectivity in the reaction with propylene is assumed to be in the order: π -allyl > methallyl > ethyl \cong H.

Table 2 Analyses of hydrocarbons produced by the reaction of monomers with VOAcac₂-based catalyst

		Pentane	2-Me-butane	4-Me-1-pentene	Hexene
VOAcac ₂ Et ₃ Al Allyl Br	—	Et-Allyl 0.30	Et-PP —	PP-Allyl —	PP-Allyl —
	PP 20	0.38	0.15	0.03	0.18
	BD 20	0.04	—	—	0.07
	PP+BD 20+20	0.13	0.09	0.01	0.22
VOAcac ₂ Et ₃ Al Et ₂ AlCl	—	Et-PP 0.11	Et-PP 0.16	—	Et-BD —
	PP 20	—	—	—	—
	BD 20	—	—	—	0.12
	PP+BD 20+20	—	0.08	—	0.23

VOAcac₂, 1 mmol; Et₃Al, 5 mmol; Et₂AlCl, 5 mmol; allyl bromide, 10 mmol

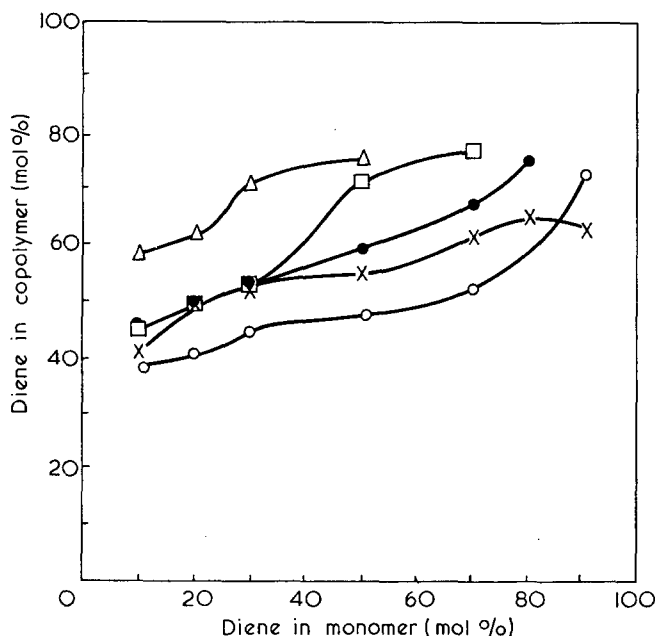


Figure 2 Copolymer composition curves as a function of monomer feed. Δ , BD-3MB; \square , BD-4MP; \bullet , BD-Bu; \circ , IP-Pr; \times , BD-Pr (Hirai, R. et al. *J. Polym. Sci. (A-1)* 1972, 10, 681)

Table 3 Effect of donor substances on the formation of alternating and homo-oligomers

Oligomer	Catalyst* without donor	Catalyst Pφ ₃ † or pyridine
PP/IP/PP	2.8	trace
IP/IP	28.0	30.0
IP/IP/IP	16.0	17.0

* VOAcac₂ + Et₃Al + Et₂AlCl (1:3:3)
† Triphenylphosphine

In relation to the selectivity the copolymerizations with other olefins such as 1-butene, 3-methyl-1-butene and 4-methyl-1-pentene were investigated. The copolymer composition curves shown in Figure 2 indicate that the bulky group, especially the branched alkyl group, disturbs the alternating tendency. Isobutene does not copolymerize by this sort of catalyst. The order of alternation is in the order: ethylene \geq propylene > 1-butene > 4-methyl-1-pentene > 3-methyl-1-butene > isobutene, and butadiene > isoprene.

It is also noticed that some homo-oligomers are produced besides the co-oligomers in the copolymerization with the same catalyst, i.e. VOAcac₂-Et₃Al-Et₂AlCl (1:3:3) as shown in Table 3. The formation of isoprene dimer and trimer may not be associated with alternating co-oligomerization or alternating copolymerization since the addition of an electron-donor ligand such as triphenyl phosphine or pyridine retards the formation of the cotrimer and copolymer but not that of homo-oligomer. This fact suggests that the active species for the alternating addition possesses an additional site for coordination which is vulnerable towards the attack of donor ligands.

COPOLYMERIZATION OF BUTADIENE WITH ACETYLENE

The copolymerization of acetylene seems to be of particular interest since the coordination ability of acetylene may be different from olefins and diolefins

and the copolymer, if prepared, may possess an active methylene group neighbouring two double bonds. However, there have been no scientific reports on this problem. Some patents described the formation of acetylene-diolefin copolymers but they were a black powder or a sparingly soluble solid and were assumed to be an acetylene homopolymer or a highly crosslinked copolymer. At the same time as the author's work a patent for the copolymer of methylacetylene and butadiene appeared from Kawasaki *et al.* in which a vanadium catalyst similar to that for propylene-butadiene alternating copolymerization was used and the copolymer possessed a 1:1 composition and the alternating structure was claimed. In the author's work a large variety of catalyst systems were examined but the product was always a black sparingly soluble powder.

However, an excellent catalyst was found⁸ in a nickel complex which yielded a completely soluble pale yellow semi-solid or a liquid polymer. This contained an active methylene unit arising from the alternating acetylene-butadiene sequence as shown in Figure 3 which indicates the presence of an active methylene n.m.r. absorption at 2.8δ but also that of a methylene of the butadiene-butadiene diad at 2.12δ. Chemical analyses also indicate the incorporation of acetylene but its amount is arbitrary. It was also found that the amount of alternating sequence parallels the amount of acetylene incorporated. The population of acetylene diad (F_{AA}), alternating diad (F_{AB}) and butadiene diad (F_{BB}) agrees with the result from the calculation for the random copolymerization as shown in Table 4.

By using a standard catalyst of Ninaphthenate- Et_2AlCl (3 mmol:15 mmol) several kinds of diene such as butadiene, isoprene, chloroprene, and 2,3-dimethylbutadiene (0.39 mol) were copolymerized with acetylene (0.12 mol) at 30°C for 3 h. The results are summarized in Table 5.

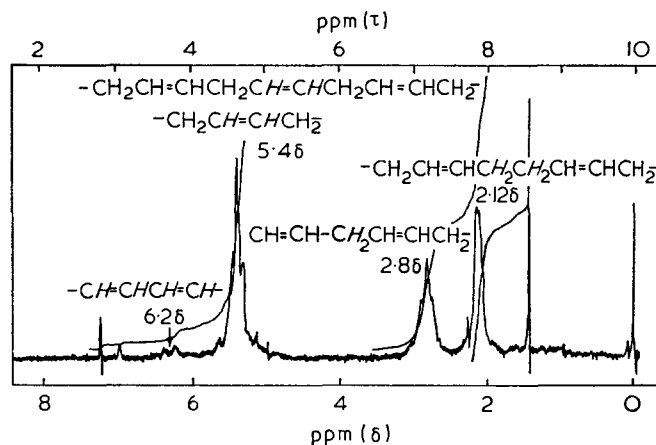


Figure 3 100 MHz n.m.r. spectrum of acetylene-butadiene copolymer

Table 4 Population of diads

Composition of A	N.m.r.			Random assumption		
	F_{AA}	F_{AB}	F_{BB}	F_{AA}	F_{AB}	F_{BB}
0.180	0.035	0.290	0.675	0.032	0.295	0.673
0.296	0.111	0.370	0.519	0.088	0.417	0.495
0.323	0.128	0.391	0.481	0.104	0.437	0.459
0.382	0.115	0.537	0.348	0.146	0.472	0.382
0.441	0.189	0.505	0.306	0.195	0.493	0.312

Table 5 Copolymerization of acetylene and dienes

Diene	Yield (g)	CHCl_3 soluble			
		(g)	A*	$[\eta]$	Microstructure
Butadiene	24.11	21.99	0.218	0.10	<i>cis</i> , 81.3; <i>trans</i> , 11.5; 1,2-, 7.2
Isoprene	11.80	9.54	0.439	0.10	<i>cis</i> , 92.9; 3,4-, 7.1
Chloroprene	1.10	0.85	0.410	0.18	<i>trans</i> , 100
2,3-Dimethylbutadiene	5.33	4.17	0.623	0.12	<i>trans</i> , 100

Conditions: toluene, 70 ml; Et_2AlCl , 15 mmol; Ni naphthenate, 3 mmol; diene, 0.39 mol; acetylene, 0.12 mol; catalyst reaction, 30°C, 10 min; polymerization, 30°C for 3 h

* Content of acetylene

The products were copolymers of acetylene with dienes. The microstructure of the diene unit is *cis* both for butadiene and isoprene, whereas that both for chloroprene and 2,3-dimethylbutadiene is *trans*. The copolymer possesses active methylene groups and therefore is very sensitive towards crosslinking. The copolymer with a controlled amount of active methylene group can be stored if some antioxidant is added, but is capable of crosslinking on exposure to air. Cobalt naphthenate is useful as a hardening catalyst. The active methylene group is also easily metallized by lithium. Consequently, the material seems to be versatile for paint, vulcanizing plasticizers and as a starting material for graft or star polymers.

OLIGOMERIZATION AND POLYMERIZATION

In relation to the polymerization by transition metal catalysts, the oligomerization of butadiene is interesting, since the mode of oligomerization is also associated with the coordination ability and the reactivity of the catalyst. A variety of cyclo-oligomers as well as linear oligomers are known in the literature. In addition to these the author has reported previously the preparation of methylenevinylcyclopentane (MVCP) by some nickel catalysts; i.e., a 1,3-1,2 coaddition product of butadiene⁹. The mechanism of the formation of cyclodimer and cyclotrimer was established by Bogdanović *et al.*¹⁰, but those of linear dimers and 2-methylenevinylcyclopentane were not completely elucidated.

Cyclo-oligomers are prepared by Ni^0 catalysts, whereas linear ones are also formed by transition metal catalysts other than nickel, e.g., cobalt, or iron catalysts, and MVCP by Ni^I . The author has found that the oligomers of butadiene can be prepared selectively by nickel catalysts whose catalytic activity is controlled by the addition of a protic acid or protic solvent. A Ni^0 catalyst such as $\text{Ni}[\text{P}(\text{OEt})_3]_4$ is capable of cyclo-oligomerization of butadiene in hydrocarbon solvents such as benzene to give cyclo-octadiene or vinylcyclohexene as reported by Bogdanović *et al.*¹⁰.

Furukawa found that the regulation of reactivity in oligomerization is also possible by adjusting acid strength and acidity with use of weak protic solvent, strong protic acid or their mixture. In this way cyclodimer, linear dimer or MVCP were prepared relatively preferentially as summarized in Table 6¹¹. Use of inorganic acids such as sulphuric acid or perchloric acid results in the 1,4-*trans*-polymerization, which is assumed to be characteristic of the catalyst composed of Ni^0 -protic

Table 6 Dimerization and polymerization of butadiene with Ni[P(OEt)₃]₄

Protic medium	52	25		trans-PBD
Benzene	52	25		
C ₂ H ₅ OH		88		
C ₂ H ₅ OH-CF ₃ COOH	10	23	50	
CH ₃ OH-CF ₃ COOH				80
ⁱ PrOH-H ₂ SO ₄				100
ⁱ PrOH-HClO ₄				100

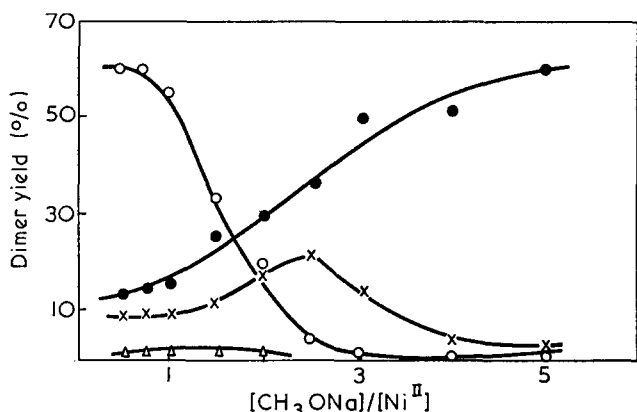


Figure 4 Effect of [CH₃ONa] on the dimerization of butadiene at 80°C. ○, MVCP; ●, 2,4,6-OT; ×, 1,3,6-OT; △, 1,3,7-OT. Conditions: [NiBr₂·(n-Bu₃P)₂], 0.3 mmol; [butadiene]=25 mmol

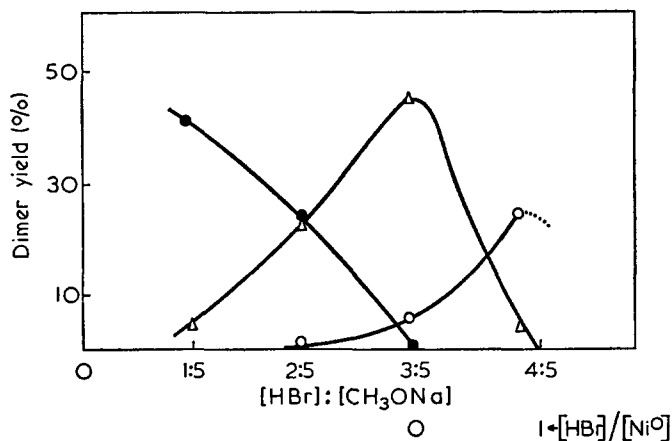


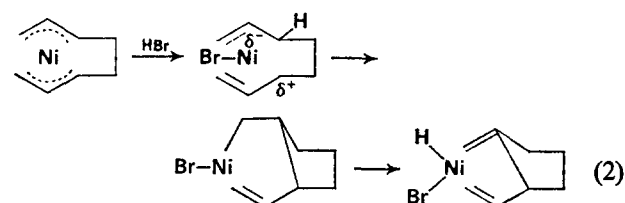
Figure 5 Effect of [HBr] on the dimerization of butadiene at 80°C. ●, 2,4,6-OT; △, 1,3,7-OT; ○, MVCP. Conditions: [NiBr₂·(n-Bu₃P)₂], 0.3 mmol; [CH₃ONa], 1.5 mmol; [butadiene]=20 mmol

acid-electron donor¹². When the phosphine complex of nickel bromide is reacted with sodium methoxide the reaction product possesses catalytic activity for the oligomerization; octatriene (OT) and MVCP are formed according to the amount of sodium methoxide added as illustrated in Figure 4. The addition of 1 mol of methoxide favours the formation of MVCP whereas further addition favours that of OT. It is supposed that the reaction of nickel salt with sodium methoxide or sodium borohydride is expressed as follows:

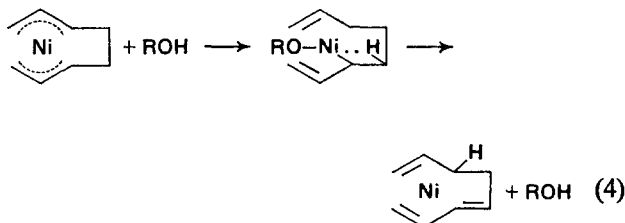
$NiBr_2L_2 + CH_3ONa \rightarrow Ni^0L_2 + HBr + HCHO + NaBr$
Consequently, partly reduced nickel system (Ni⁰ and HBr) may be an active catalyst for MVCP formation and further reduced nickel system for OT. The reduction

is reversible since the further reduced nickel system thus prepared alters its reactivity by the addition of hydrogen bromide¹³. As illustrated in Figure 5, the addition of 3/5 mol HBr with respect to methoxide gives the catalyst for OT and further addition that for MVCP. These observations lead to the conclusion that the active species for the cyclo-oligomer such as cyclo-octadiene and vinylcyclohexene is Ni⁰ whereas that for linear dimer is Ni⁰ combined with alcohol and that for MVCP is Ni⁰ combined with hydrogen bromide. Since all kinds of oligomers require the coupling of butadiene at the first stage, Ni⁰ is a common active species which gives bis- π -allyl nickel.

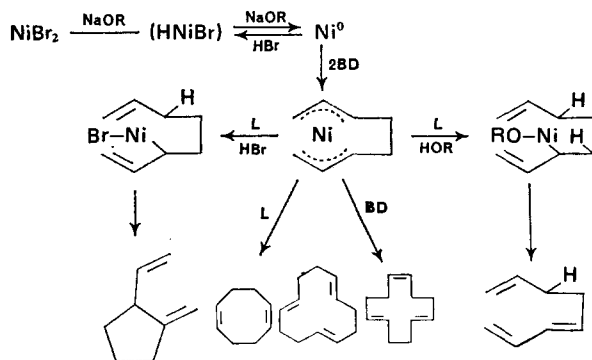
In benzene it decomposes to give cyclodimer, whereas in alcohol linear dimers and in alcohol-acid mixture MVCP. The mechanism of these reactions may be interpreted by the intramolecular hydrogen transfer for OT and by the intramolecular insertion of a double bond to nickel-carbon for MVCP:



Reactions (2) and (3) involve the formation and decomposition of HNiBr and the formation of such type of complex has already been confirmed by n.m.r.¹⁴. In reaction (1) the hydrogen transfer may be facilitated by a hydride of HNiOR as an intermediate:

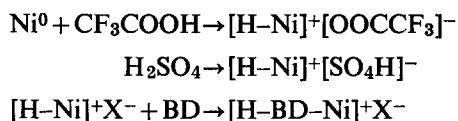


In summary, the following reaction scheme is presented in which the mode of reaction is controlled by the acidity and acid strength of protic reagent or the stability of an intermediate hydride complex.

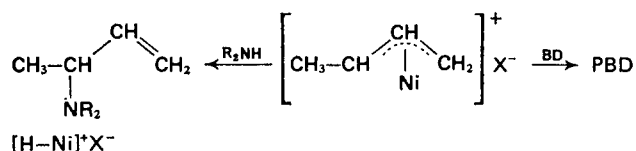


Weak acid or protic solvent may form a very unstable hydride which can exist transiently in the hydrogen

transfer process, whereas acid of medium acid strength forms a relatively stable hydride which protonates bis- π -allyl nickel. As a result the remaining Ni-C bond is polarized and subjected to the further insertion of the remaining double bond. If a stronger acid is used Ni⁰ is converted to HNiX, X being Br, CF₃COO etc., and the dimerization of butadiene is retarded. Instead, the insertion of butadiene to the H-Ni bond takes place to give the π -allyl nickel complex:



The latter complex possesses a highly polarized π -allyl capable of the further insertion of butadiene (BD) to the Ni-C bond to give polybutadiene.



If the preparation of the π -allyl complex is carried out in protic solvents such as alcohol, thiol or amine, the corresponding ether, thioether or imine is obtained in good yield as shown in Table 7. The reaction takes place smoothly above room temperature with good selectivity.

A similar reaction of butadiene with amine without acid was already reported by Baker *et al.*¹⁵, Rose¹⁶ and Furukawa *et al.*¹⁷, but the product is a mixture of butadiene oligomers and amine adducts of butadiene dimer as well as butadiene monomer. The effect of added acid is very pronounced for enhanced selectivity. The reaction is assumed to take place between π -allyl nickel or nickel hydride and free amine, and consequently there exists a suitable amount of acid for

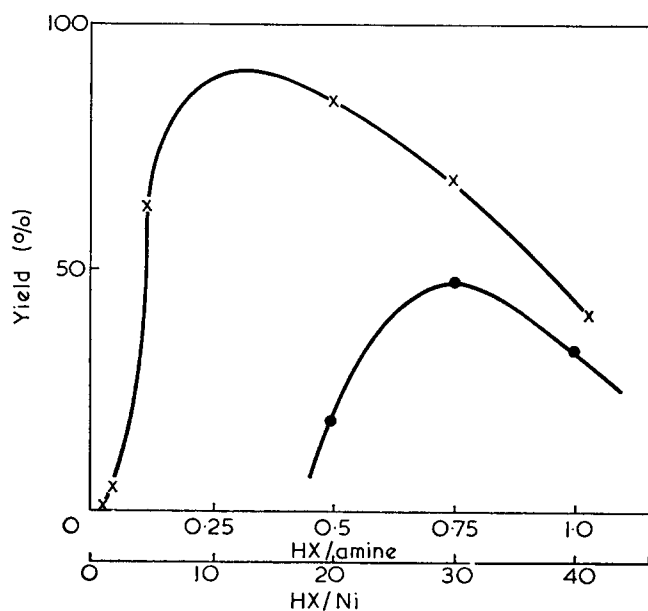
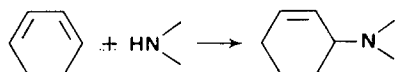


Figure 6 Effect of CF₃COOH on the reaction of 1,3-cyclohexadiene by Ni[P(OEt)₃]₄ at 80°C.



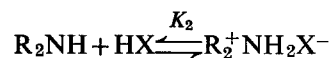
x, Morpholine; ●, piperidine

Table 7 Reaction of diene with amines and thiols

Diene	RH	Products	Yield (%)
			77
	n-PrNH ₂		70
			10
			75
			20
			57
			66
	t-BuSH		70
			19
	n-PrSH		40
			6

80°C 20-40 h

maximum yield according to the basicity of amine employed as expected from the following reaction:



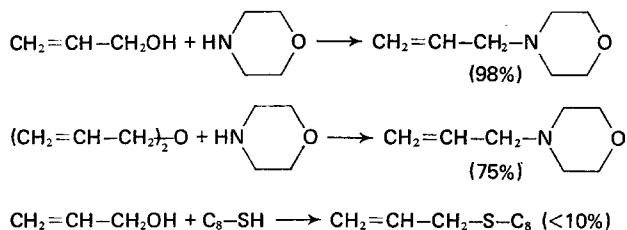
$$\text{Rate} = k[\text{HNiX}][\text{R}_2\text{NH}]$$

$$\text{Maximum yield at } \frac{[\text{HX}]}{[\text{R}_2\text{NH}]} = \frac{1}{1 + (K_1/K_2)^{1/2}}$$

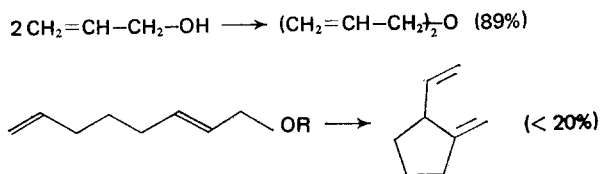
Here, the zero-valent nickel as well as amine is regarded as a basic reagent and the protonation occurs with basic material. The maximum yield will be obtained at a concentration of acid added to amine depending on equilibrium constants K_1 and K_2 for nickel and amine,

respectively. Figure 6 indicates the result of the action of cyclohexadiene with morpholine or piperidine in accord with the above mechanism¹⁸.

The above reaction proceeds through a π -allyl nickel halide compound and accordingly, the compound with some leaving group at the allylic position will be able to react with basic reagents by Ni⁰ catalyst through a π -allyl nickel intermediate. Thus, the allyl transfer reaction will be realized¹⁹. Indeed, not only allyl halide but also allyl alcohol, and even diallyl ether can exchange allyl groups with morpholine as well as thiol.



Without basic reagents, diallyl ether or MVCP are formed from allyl alcohol and octadienyl ether, respectively.



CONCLUSION

It is possible to control the coordination site and/or the valence state of transition metals and conduct polymerization, copolymerization as well as oligomerization. Versatile synthetic reactions are also developed.

ACKNOWLEDGEMENTS

This work was done with the cooperation of Drs J. Kiji, E. Kobayashi, S. Tsuruki, K. Yamamoto, and E. Sasakawa.

REFERENCES

- 1 Furukawa, J., Hirai, R. and Nakaniwa, M. *J. Polym. Sci. (B)* 1969, **7**, 671
- 2 Kawasaki, A., Maruyama, I., Taniguchi, M., Hirai, R. and Furukawa, J. *ibid.* 1969, **7**, 613
- 3 Furukawa, J., Amano, H. and Hirai, R. *J. Polym. Sci. (A-1)* 1972, **10**, 681
- 4 Furukawa, J. and Hirai, R. *ibid.* 1972, **10**, 2139
- 5 Furukawa, J. *Angew. Makromol. Chem.* 1972, **23**, 189
- 6 Kawasaki, A. *et al. Prepr. 27th Autumn Meet. Japan Chem. Soc.* 1972, **2**, 20
- 7 Furukawa, J., Tsuruki, S. and Kiji, J. *Prepr. 28th Spring Meet. Japan Chem. Soc.* 1973, **4**, 2080; *J. Polym. Sci. (Chem. Edn)* in press
- 8 Furukawa, J., Kobayashi, E. and Kawagoe, T. *Prepr. 28th Spring Meet. Japan Chem. Soc.* 1973, **4**, 2081; *J. Polym. Sci. (B)* 1973, **11**, in press
- 9 Kiji, J., Masui, K. and Furukawa, J. *Tetrahedron Lett.* 1970, p 2561; *Bull. Chem. Soc. Japan* 1971, **44**, 1956
- 10 Bogdanović, B., Heimbach, P., Kröner, M. and Wilke, G. *Ann. Chem.* 1969, **727**, 143
- 11 Furukawa, J., Kiji, J., Konishi, T., Yamamoto, K., Mitani, S. and Yoshikawa, S. *Makromol. Chem.* 1973, **174**, 65
- 12 Durand, J. P., Dawans, F. and Teysse, Ph. *J. Polym. Sci. (A-1)* 1970, **8**, 979
- 13 Kiji, J., Yamamoto, K., Mitani, S., Yoshikawa, S. and Furukawa, J. *Bull. Chem. Soc. Japan* 1973, **46**, 1791
- 14 Tolman, C. A. *J. Am. Chem. Soc.* 1970, **92**, 6785
- 15 Baker, R., Halliday, D. E. and Smith, T. N. *Chem. Commun.* 1971, p 1583; Baker, R., Cook, A. H. and Smith, T. N. *Tetrahedron Lett.* 1973, p 503
- 16 Rose, D. *Tetrahedron Lett.* 1972, p 4197
- 17 Furukawa, J., Kiji, J., Mitani, S., Yoshikawa, S., Yamamoto, K. and Sasakawa, E. *Chem. Lett.* 1972, p 1211
- 18 Kiji, J., Yamamoto, K., Sasakawa, E. and Furukawa, J. *21st Symp. Organometal. Chem. Japan*, 1973
- 19 Furukawa, J., Kiji, J., Yamamoto, K. and Tōjō, T. *Tetrahedron* 1973, p 3149

Highly active polymerization catalysts of long life derived from σ - and π -bonded transition metal alkyl compounds*

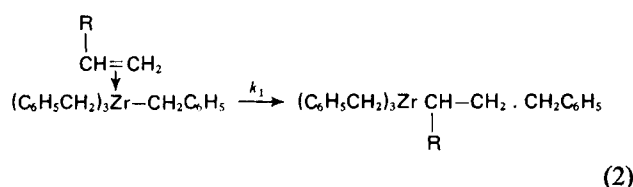
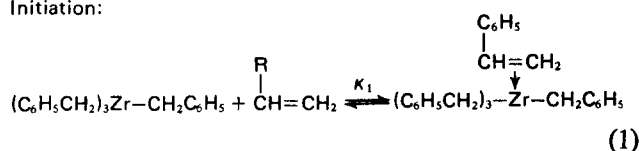
D. G. H. Ballard, E. Jones, R. J. Wyatt, R. T. Murray
and P. A. Robinson

Imperial Chemical Industries Limited, Corporate Laboratory,
The Heath, Runcorn, Cheshire WA7 4QE, UK
(Received 10 September 1973)

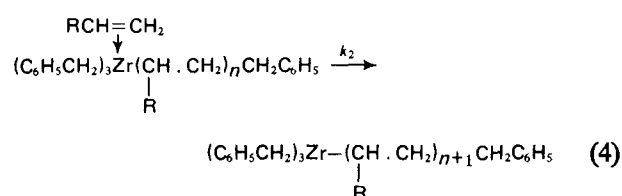
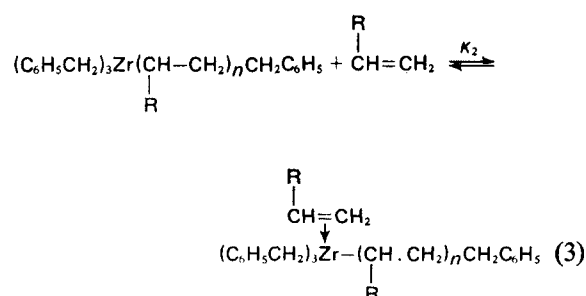
TRANSITION METAL ALKYL CATALYSTS

We have described the behaviour of transition metal allyl¹, benzyl² and silanylmethyl³ compounds as homogeneous catalysts for the polymerization of vinyl monomers and olefins. In general they are inferior catalysts because of the slowness of the initiation steps^{3,4}, and the loss of propagating centres as a result of dimerization reactions. The homogeneous system studied in depth by our research group is the polymerization of styrene by $Zr(\text{benzyl})_4$ which illustrates some of the features of polymerizations initiated by transition metal alkyl compounds. The process is concisely described by the following reactions.

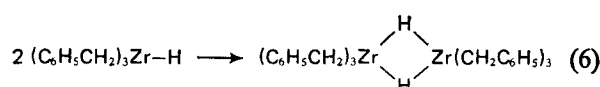
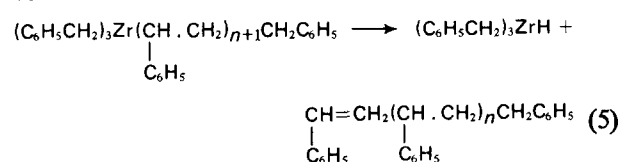
Initiation:



Propagation:



Termination:



Even where the re-alkylation of the transition metal hydrides is possible, dimerization reactions similar to reaction (6) take place. In the above system less than 1% of the available transition metal centres are employed because of the slowness of reactions (1) and (2). An additional termination reaction to (5) has been identified giving an unreactive species in which the polymer chain is still attached to the metal.

We have made a detailed study of the relationship between the structure of transition metal alkyls and their ability to polymerize olefins and vinyl monomers, and have identified two basic groups of interest for polymerization purposes. These are the π -complexes of which the transition metal allyl compounds of Ti, Zr, Hf, Cr, V are the only ones active, and the σ -complexes of the same metals where the ligands can be $-CH_2\text{Aryl}$, $-CH_2\text{Si}(\text{CH}_3)_3$, $-CH_2\text{C}(\text{CH}_3)_3$, etc.^{3,6}

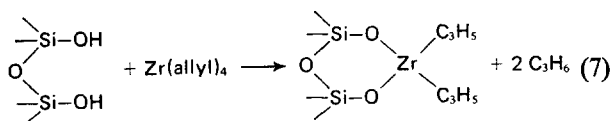
Experiments have shown⁶ that only certain types of anionic ligands derived from strong acids activate transition metal alkyl compounds for polymerization. It has also been shown that it is necessary to prevent migration of transition metal centres so as to inhibit

* Presented as a Symposium Lecture at the IUPAC International Symposium on Macromolecules, Aberdeen, September 1973.

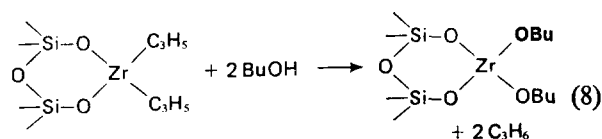
metal-metal interactions which deactivate. Both of these requirements can be met by using the strongly acidic -OH groups on the surface and alumina. These, on reaction with transition metal alkyls were found to give highly active polymerization catalysts of long lifetime⁵. In this paper the mechanism of polymerization of styrene and ethylene initiated by these catalysts is discussed.

NATURE OF THE CATALYSTS

The surface of silica and alumina freed from physically adsorbed water contain acidic OH groups which will react with transition metal alkyls. These reactions can be followed in the infra-red⁶. It has been found that transition metal alkyl compounds can react with the OH groups in more than one way and the product obtained depends on several factors. For example, Zr(allyl)₄ reacts with silica pre-dried at 200°C to give two molecules of propene per metal atom utilizing in the course of this process two OH groups per metal atom. The chemistry of the process is accurately described by the equation:

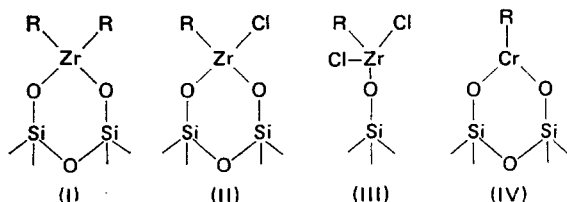


The structure for the transition metal centre is confirmed by measuring the amount of propene produced on reaction of (I) with n-butanol:



We have observed similar reactions with Zr(CH₂C₆H₅)₄, Zr[CH₂Si(CH₃)₃]₄, Zr[CH₂OCH₃]₄ etc. and also silica can be replaced by alumina and other matrices, giving transition metal centres with structures related to (I) in which the organic ligands are CH₂C₆H₅, CH₂Si(CH₃)₃, etc.

If some of the hydrocarbyl ligands in Ti, Zr or Hf alkyls are replaced by halogen atoms, transition metal centres of type (II) and (III) are obtained:



Zr(allyl)₃Cl gives primarily but not exclusively a centre of type (II) since only two molecules of propene per Zr atom are evolved on reaction with silica, and halogen compounds are not found in the solvent or in the gas. The compound SiO₂/Zr(allyl)₃Cl gives one molecule of propene per zirconium atom with excess butanol, and one molecule of HCl per zirconium atom on reaction with excess benzoic acid solution. The structure of (III)

was determined in a similar manner. Chromium allyl gives a transition metal centre with structure (IV).

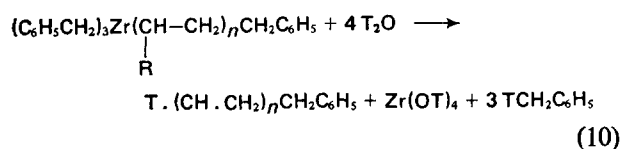
It is evident from the structures of the transition metal centres (I), (II) and (IV) that the distribution of -OH groups on the surface is not random but that a significant number of -OH groups occur in pairs. This implies that on 200°C dried silica the transition metal centres are approximately 10 Å apart.

KINETICS OF THE POLYMERIZATION OF STYRENE

A study has recently been made of the polymerization of styrene by Zr(benzyl)₄ under homogeneous conditions and the kinetics of the process adequately defined⁴. The rate of polymerization is accurately represented by the simple equation:

$$R_p = k_2 K_2 \sum_1^{\infty} [D_n] \cdot [M]_0 \quad (9)$$

where K_2 is the equilibrium constant for process (3), and like K_1 is less than unity⁷, and k_2 the velocity constant for the insertion reaction (4); $[M]_0$ is the initial or stationary monomer concentration and $[D_n]$ is the concentration of growing polymer chains of degree of polymerization n (equation 3), and $\sum_1^{\infty} [D_n]$ is the total concentration of such chains. In the homogeneous model the quantity $\sum_1^{\infty} [D_n]$ can be calculated in terms of the velocity and equilibrium constants and is directly measurable using radiochemical techniques. Hydrolysis of the reaction mixture with tritium oxide results in all chains attached to Zr atoms acquiring a radioactive tritium atom thus:



Counting of tritium atoms in the purified polymer gives the stationary concentration of polymer chains attached to metal atoms from which the quantity $\sum_1^{\infty} [D_n]$ can be obtained. In our studies of the heterogeneous systems, therefore, we have used equation (9) to determine values of $k_2 K_2$ from rate measurements and values of $\sum_1^{\infty} [D_n]$. In the heterogeneous systems D_n corresponds to (VII) ($n \geq 0$), and is not related in any known way to the number of Zr atoms initially added.

Figure 1 shows typical changes in polymerization rate, R , with time obtained for the polymerization of

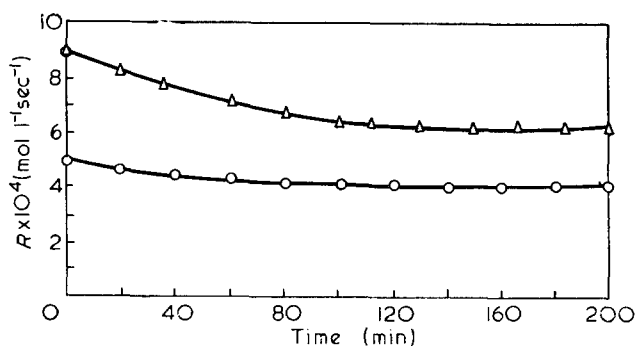


Figure 1 Polymerization of ethylene by Zr(benzyl)₄/Al₂O₃ in toluene. Initial catalyst concentration $[C]_0 = 1.5 \times 10^{-4}$ Zr atoms/l. Pressure 4 atm; equal partial pressures of ethylene and hydrogen. Δ, 40°C; ○, 25°C

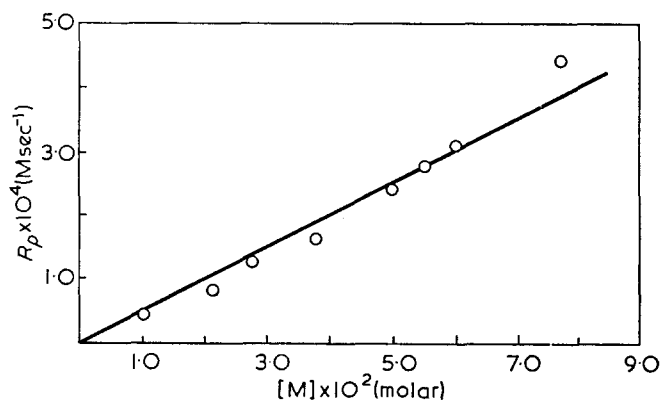


Figure 2 Dependence of rate on monomer concentration for the polymerization of ethylene at 80°C in toluene. $[C]_0 = 4.5 \times 10^{-4}$ Zr atoms/l

Table 1 Studies of the polymerization of styrene and ethylene using $Zr(\text{benzyl})_4/Al_2O_3$

$[M]_0$ (M)	$[C]_0$ (M)	$\frac{\sum_1^{\infty} [D_n]}{1} \times 10^5$ (M)	$\frac{[C]_0}{\sum_1^{\infty} [D_n]}$	Temp. (°C)	$R \times 10^5$ (M sec ⁻¹)	$\frac{R \times 10^5}{[M]_0}$ (sec ⁻¹)	$k_2 K_2$ (M ⁻¹ sec ⁻¹)
Styrene:							
0.5	0.01	—	—	30	0.56	1.12	—
1.0	0.01	0.4	2500	30	0.9	0.9	2.2
2.0	0.01	0.6	1670	30	2.5	1.25	2.1
Ethylene:							
0.055	(4.5×10^{-5})	0.0225	200	80	27.0	492	21 800

Table 2 Polymerization of styrene at 30°C in toluene, $[C] = 10^{-2}$ M

$[M]_0$	Conversion (%)	$M_n \times 10^{-6}$	$R \times 10^5$ (M sec ⁻¹)	$\frac{\sum_1^{\infty} [D_n] \times 10^{-5}}{1}$ [M]
2.0	2.7	1.8	2.5	0.30
	4.3	1.8	2.5	0.60
	7.4	1.6	2.5	0.70
1.0	8.2	2.0	2.5	0.60
	4.1	0.8	0.9	0.3
	8.8	0.7	0.9	0.4
	11.3	0.6	0.9	0.6

ethylene using $Zr(\text{benzyl})_4/Al_2O_3$ catalysts. These steady rates can be maintained over long periods provided mass transfer problems do not interfere. The dependence of rate on monomer concentration is given in Figure 2 and is seen to be, over the range of concentrations studied, accurately first order. A similar result is obtained for the polymerization of styrene with a fourfold change in the concentration of monomer, and is shown in Table 1. We may conclude, therefore, that equation (9) describes reasonably the change in rate with monomer concentration.

Measurements of $\sum_1^{\infty} [D_n]$ have been carried out in the case of styrene and ethylene systems and the results are summarized in Tables 1 and 2. A notable feature is that this quantity is small and that only one atom of Zr in about 10^2 is used at any one time in polymer growth, which is comparable in order of magnitude (10^2 – 10^3) with the homogeneous model. The closeness of the styrene and ethylene values for $\sum_1^{\infty} [D_n]$, particularly since the latter polymerizes 10 000

times faster, suggests that the measurements are independent of rates and type of monomer. Values of $\sum_1^{\infty} [D_n]$ in Table 2 show that the number of propagating centres remains more or less constant with conversion suggesting that all chains attached to metal atoms are actively growing. This was not the case with the homogeneous system studied⁴.

MOLECULAR WEIGHTS AND END GROUP MEASUREMENTS

In the absence of transfer agent molecular weights of the polymers formed tend to be very high, chain termination does occur, however, principally by β -hydrogen abstraction. Molecular weights are independent of conversion as shown by the data for polystyrenes made with these catalysts and summarized in Table 2. It is also evident from Table 2 that the molecular weight is markedly dependent on the monomer concentration. This was also observed in the homogeneous polymerization of styrene by $Zr(\text{benzyl})_4$.

Direct evidence of the insertion between the zirconium–metal bond was obtained from work with catalysts prepared from $Zr(^{14}CH_2C_6H_5)_4$ and is summarized in Table 3. It will be seen that the amount of polymer derived from the initial insertion reaction remains stationary but the proportion of the total declines as the amount of polymer originating from the re-alkylated Zr–H centres (equation 16) becomes more important. The latter centres are responsible for the conversion of the majority of monomer to polymer in the ethylene system and the initiation stage is even less important.

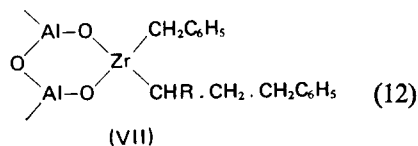
It is not possible to measure the very high molecular weights of polyethylene prepared with these catalysts in the absence of hydrogen. In the presence of the latter the value of M_n obtained are sensitive to both the concentration of ethylene and hydrogen. The data obtained are summarized in Table 4 and plotted in Figure 3 in the manner suggested by equation (30). This gives a very good straight line over a wide range of hydrogen and ethylene concentrations.

Table 3 Polymerization of styrene by $Zr[^{14}CH_2C_6H_5]_4/Al_2O_3$ in toluene at 30°C; $[M]_0 = 1.0$ M; $[C]_0 = 1.0 \times 10^{-2}$ M

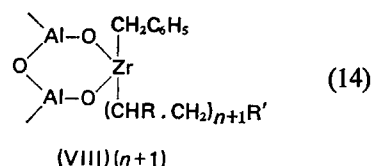
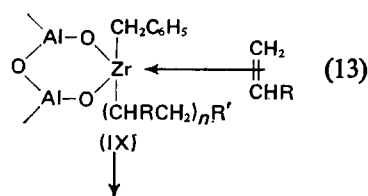
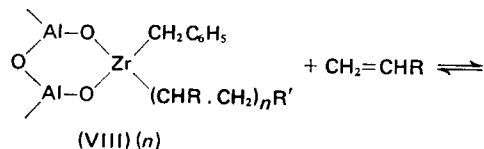
Conversion (%)	$M_n \times 10^6$	Concentration of ¹⁴ C polymer $\times 10^5$ (M)	Fraction of total of ¹⁴ C polymer chains (%)
6.8	0.53	0.35	34
14.7	0.64	0.39	18

Table 4 Molecular weights of polyethylenes prepared in the presence of hydrogen at 80°C in toluene, $[C]_0 = 4.5 \times 10^{-5}$ M⁻¹

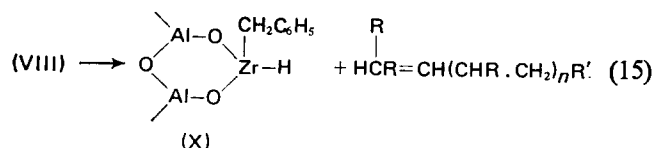
$[H_2]$ $\times 10^3$ (M)	$[C_2H_4]$ $\times 10^2$ (M)	\bar{M}_n
2.25	2.1	14 200
5.03	3.8	13 400
9.00	5.0	12 400
12.50	6.0	11 400
16.25	7.0	10 600
20.00	7.7	9 000
23.25	8.4	8 000



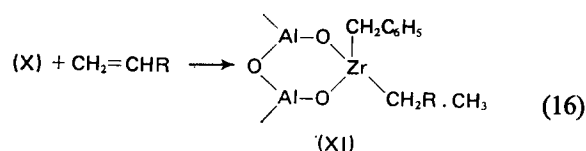
Insertion of the monomer between the benzyl group and metal atom gives (VII). Repetition of this process (equations 13 and 14) gives high molecular weight polymers. A generalized reaction scheme can be written as follows:



An important method of molecular weight control is the β -hydrogen abstraction process:



Re-alkylation of (X) reactivates the propagating centre,



and repetition of reactions (13) and (14) gives a new polymer chain (VIII) where R' is now CH₂R·CH₃

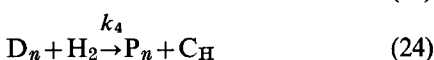
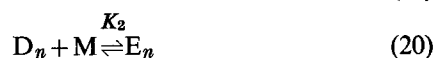
An important difference between the homogeneous and heterogeneous transition metal alkyl compounds is that the hydride species (X) is an active centre and re-alkylates readily whereas species such as [C₆H₅CH₂]₃Zr·H are inactive in solution as a result of dimerization⁴ (equation 6).

In the polymerization of ethylene hydrogen can be used as a transfer agent giving the hydride (X) and a saturated polymer molecule:



In analysing the kinetics of the process it is worth noting that the initiation reactions (11) and (12) together with re-alkylation of the hydride (16) consume relatively little monomer compared to the growth reactions (13)

and (14). The analysis is then as follows:



C_A is (V) or (XI); E...E_n are species (VI) and (IX); D₁-D_n represent (VII) and (VIII); P_n is a polymer molecule derived from process (15) or (17); C_H is (X).

The following relations can be written:

$$[\text{E}] = K_1[\text{C}_A][\text{M}] \quad (26)$$

$$[\text{E}_n] = K_2[\text{D}_n][\text{M}] \quad (27)$$

and if K₂ is independent of *n*, it follows:

$$\sum_1^\infty [\text{E}_n] = K_2 \sum_1^\infty [\text{D}_n][\text{M}] \quad (28)$$

$$[\text{C}_A]_0 = \sum_1^\infty [\text{D}_n] + \sum_1^\infty [\text{E}_n] + [\text{C}_A] + [\text{C}_H] \quad (29)$$

The rate of polymerization gives equation (9):

$$R = -(\text{d}[\text{M}]/\text{d}t) = k_2 \sum_1^\infty [\text{E}_n] = K_2 k_2 \sum_1^\infty [\text{D}_n][\text{M}]$$

In the homogeneous system $\sum_1^\infty [\text{D}_n]$ can be computed from the concentrations of Zr(benzyl)₄ and styrene but this is not possible in this case since we cannot calculate the number of propagating Zr atoms located on the terminal position of the stacks of lamellae shown in *Figure 5*. It is therefore necessary to use the tritium oxide quenching procedure to measure $\sum_1^\infty [\text{D}_n]$ direct. The product $K_2 k_2$, determined from the ratio $R/[\text{M}] \sum_1^\infty [\text{D}_n]$, will tend to be too small by an amount related to difference in concentration of monomer around the growing polymer tip and that close to the catalyst site within the tip. The values of $K_2 k_2$ quoted in *Tables 1* and *2* must therefore be regarded as minimum values.

The number-average degree of polymerization is given by the relationship:

$$\bar{P}_n = \frac{K_2 k_2 \sum_1^\infty [\text{D}_n][\text{M}]_0}{k_3 \sum_1^\infty [\text{D}_n] \cdot [\text{H}_2] + k_4 \sum_1^\infty [\text{D}_n]}$$

$$\bar{P}_n = \frac{K_2 k_2 [\text{M}]_0}{k_3 [\text{H}_2] + k_4} \quad (30)$$

In the absence of hydrogen $\bar{P}_n = (K_2 k_2 / k_4)[\text{M}]_0$, i.e. there should be a marked dependence of molecular weight on monomer concentration. The limited amount of information in *Table 2* supports this statement. It has also been found that hydrogen modifies the molecular weight during the polymerization of ethylene.

Equation (30) predicts that a plot of $[\text{M}]_0/\bar{P}_n$ against

$[H_2]$ will be a straight line with slope k_3/k_2K_2 and intercept k_4/k_2K_2 . A typical plot is shown in Figure 3 using the data in Table 4. The intercept is very small and hardly detectable on the scale, confirming that $k_3 \ll k_4$, which is consistent with the observation that in the absence of hydrogen very high molecular polymers are obtained. Allowing for this fact the agreement between equation (30) and Figure 3 is very good, and we derive from it $k_4 = 1.25 \times 10^{-2} k_2 K_2$ and $k_3 \leq 1.5 \times 10^{-5} k_2 K_2$.

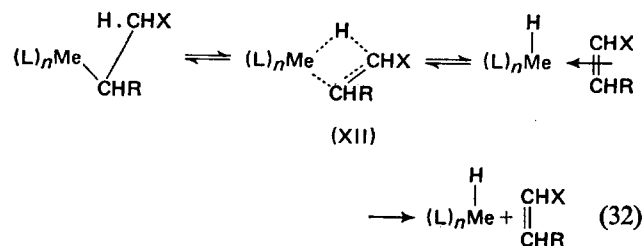
MECHANISM OF POLYMERIZATION

Recently an analysis of the common features of homogeneous processes involving an organometallic reaction site has been carried out⁹. It has been adduced that the chemistry is dominated by two processes, namely, β -hydrogen abstraction and olefin insertion. Also, since essentially the same fundamental reactions occur with Al^{III} , Ti^{IV} , Zr^{IV} , Hf^{IV} (no d electrons) as well as with metals such as Pd, Pt, Co (rich in d electrons), it is concluded that the nature of the metal is not critical provided it is sufficiently electron deficient to form an olefin complex by overlap of S orbitals of the metal with the π -orbitals of the olefin. Thus in the case of Zr and Hf silylmethyl, for example, the equilibrium with ethylene at 28°C gives the value of $K \approx 0.02 M^{-1}$. Therefore, the amount of complex present in the polymerization process is relatively small but this does not prevent high molecular weight ($> 10^6$) polymers being formed⁶.

Supporting this view is the close similarity between transition metal alkyl chemistry and aluminium alkyl chemistry. For example, aluminium alkyls like their transition metal counterparts, form a complex with amines, ethers, etc. and presumably with olefins, olefin insertion and β -hydrogen abstraction forming an $\equiv Al-H$ group are well-established features of the chemistry. It is also a well established feature that olefin insertion between the $\equiv Al-H$ bond and β -hydrogen abstraction are part of an equilibrium process. Thus 1Bu_3Al readily forms isobutene and ${}^1Bu_2Al-H$ at 120–150°C; these recombine at 60–70°C. The overall process has been written¹⁰:



Since olefin insertion between the metal hydride bond and β -hydrogen abstraction are part of an equilibrium process, they will have a common transition state. The latter process gives important information on the structure of this intermediate since the products formed suggest only one reaction pathway, namely:

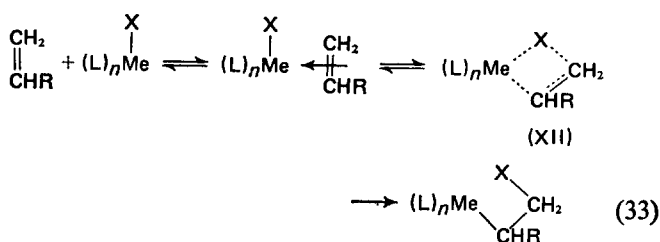


The olefin insertion reaction is the reverse of process (32) and we generalize it to include metal alkyls $(L)_nMeX$

Table 5 Bimolecular rate constants for the polymerization by various mechanisms

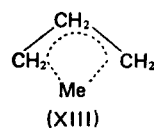
	Temp. (°C)	k_p or k_2K_2 ($M^{-1} sec^{-1}$)
Styrene:		
Radical	25	27 ¹²
Anionic	25	$\sim 55\,000$ ¹³
Zr(benzyl) ₄ /Al ₂ O ₃	25	20
Ethylene:		
Zr(benzyl) ₄ /Al ₂ O ₃	80	21 800

as well as metal hydrides $(L)_nMe.H$, as shown below:



In equations (32) and (33), $R=H$, alkyl, aryl; $X=H$, $-(CHR.CH_2)_nR'$ $n \geq 0$; Me is a transition metal, Ti, Zr, Cr, etc., or an electron-deficient metal such as Al. L can be any of the following ligands, $CH_2Si(CH_3)_3$, $CH_2C_6H_5$, allyl, $Al-O^-$, $Si-O^-$, halogen, etc.

The quadripolar transition state (XII) is probably structurally similar to the π -allyl compounds¹¹ in which the type of bonding is illustrated by (XIII). A species of this type has been described by Egger¹⁴ for the elimination of isobutylene from aluminium triisobutyl.



In (XIII) all carbon atoms are the same distance from the metal atom and the plane of the carbon atoms is nearly perpendicular to that of the metal.

Finally, it is interesting to compare the data obtained with these catalysts with radical and anionic propagation processes. Comparable data are summarized in Table 5. It is evident that propagation rates for transition metal alkyl catalysts are at the higher end of the three types and similar to the polymerization of free anions in solution.

REFERENCES

- Ballard, D. G. H., *et al. J. Chem. Soc. (B)* 1968, p 1168
- Ballard, D. G. H. and van Lienden, P. W. *Makromol. Chem.* 1972, **154**, 177
- Ballard, D. G. H. *XXIII Int. Congr. Pure Appl. Chem., Boston* 1971, Special Lectures, Vol 6, p 219
- Ballard, D. G. H., *et al. Makromol. Chem.* 1973, **165**, 173
- Ballard, D. G. H., Jones, E., Pioli, A. J. P., Robinson, P. A. and Wyatt, R. J. Br. Pat. Appln 40416/69 and 404171/69
- Ballard, D. G. H. *Adv. Catal.* 1973, **23**, 263
- Ballard, D. G. H., *et al.* unpublished results
- Grubb, D. T., *et al. J. Mat. Sci.* 1972, **7**, 131, 822
- Ballard, D. G. H. *Chem. Brit.* 1974, **10**, 20
- Coates, G. E., Green, M. L. H. and Wade, K. 'Organometallic Compounds', Methuen, London, 1967, Vol 1
- Deetrich, H. and Uttech, R. *Z. Naturwiss.* 1963, **50**, 613; *Z. Kristallog.* 1965, **122**, 60
- Matheson, M. S., *et al. J. Am. Chem. Soc.* 1951, **73**, 1700
- Worsfold, D. J. and Bywater, S. *J. Phys. Chem.* 1966, **70**, 162
- Egger, K. W. *J. Am. Chem. Soc.* 1969, **91**, 2867

Elastomeric block polymers from ethylene sulphide*

W. Cooper, P. T. Hale and J. S. Walker

*Research Centre, Dunlop Ltd, Kingsbury Road, Birmingham B24 9QT, UK
(Received 14 September 1973)*

Block polymers of ethylene sulphide with butadiene, isoprene and styrene have been prepared by anionic synthesis, and their properties have been examined. The ABA polymers from ethylene sulphide and isoprene are elastomers with good thermal stability but unless of low molecular weight are difficult to process except at high temperatures, when they are prone to degradation. ABC block polymers from styrene, isoprene or butadiene and ethylene sulphide are strong resilient elastomers with improved thermal stability compared with the conventional styrene/butadiene block polymers. Good properties are obtained with small amounts (2–4%) of low molecular weight (~ 4000), highly crystalline poly(ethylene sulphide) blocks. X-ray, differential scanning calorimetry, and gel permeation chromatography data show the ethylene sulphide blocks to be anisotropic, extended-chain crystallites which aggregate large numbers of the attached diene/styrene chains. These aggregates persist at temperatures above the softening point of the polystyrene domains, and in solution. The polymers possess unusual flow characteristics which are not well understood. Electron micrographs of stained, cast or microtomed films show the elastomers to have a two-phase morphology. It has not been possible to identify the structure of the small poly(ethylene sulphide) domains. The ABC polymers can be oil extended and compounded with carbon black. Vulcanizates using accelerated sulphur systems have good physical properties.

INTRODUCTION

An interesting and important characteristic of block and graft copolymers is the tendency for the individual polymer segments to aggregate together in the bulk polymer in separate zones or domains, the morphology being dependent on the nature, shape, size and distribution of the domains¹.

Some of the more important block polymers are composed of elastomeric and plastic segments and display the properties of crosslinked elastomers over a limited range of operating temperatures². Above the softening point of the plastic component the polymer behaves as a viscoelastic fluid, albeit with flow properties significantly different from either of the homopolymers of equivalent molecular weight³.

It is apparent that judged as elastomers, since the network stability is maintained by physical bonds, the retention of useful properties will be at temperatures below the softening point of the plastic domains. In practice, this is from 30 to 50°C, depending on the composition of the block polymer. As the polymers must be processed and shaped at temperatures well above the softening point, and as most elastomers are subject to severe thermal and oxidative degradation at temperatures greatly above 200°C, an upper limit to the serviceability of a thermoplastic elastomer will be in the region of 150°C. In principle, the two groups of

elastomers with outstanding resistance to high temperature, namely the silicones and the fluorocarbons, could be employed as the elastomeric segments and so raise the operating temperature range to $\sim 200^\circ\text{C}$. The cost of these polymers, however, and limitations in the polymerization processes which can be employed for the preparation of block polymers in high purity has eliminated such compositions from consideration, at least for large volume applications.

Further restrictions result from the fact that for reasonable physical properties the elastomeric segment must be flanked by hard segments either as ABA compositions or in multiblock sequences and there are a relatively limited number of monomers readily available which have suitable polymerization properties, particularly the absence of chain transfer and termination reactions for block copolymerization. As would be expected for the development of satisfactory properties, segment molecular weight and composition must be controlled with some precision. Block polymers commercially available are based on butadiene and styrene⁴ and polymerization techniques permit excellent control over composition and purity. The polymers have good physical properties at ambient temperatures but the relatively low softening point of the polystyrene block restricts the use of these polymers, which are usually compounded with oil to facilitate processing, to temperatures only a little above 50°C. α -Methylstyrene has been used instead of styrene, with an improvement of about 20°C in network stability with good physical

* Presented as a Symposium Lecture at the IUPAC International Symposium on Macromolecules, Aberdeen, September 1973.

properties⁵, but these polymers have not achieved commercial significance. Some recently introduced thermo-plastic elastomers which contain a higher melting point plastic segment have reasonable dimensional stabilities at temperatures up to 125–150°C⁶. Their compositions have not been disclosed but they appear to be either block or graft polymers of isotactic polypropylene with an essentially saturated ethylene/propylene type elastomer.

Condensation processes in general permit more ready control over the structure and composition of the block polymer and here it is possible to take advantage of the relatively high melting points of the polyester and polyamide plastics and the reasonably stable elastomeric polyester and polyether segments. Thermoplastic polyurethane elastomers have service temperatures up to 100°C⁷, and multiblock polyether-ester [polytetrahydrofuran-poly(butylene glycol terephthalate)] elastomers have comparable or greater network stability⁸.

The alkylene sulphides polymerize by anionic mechanisms, chain transfer and termination are of minor significance and the propagating thiolate ion is relatively stable and not unduly sensitive to the presence of impurities such as oxygen or moisture⁹. It should thus be possible to prepare block copolymers with conjugated dienes or styrene with adequate control of block size and without formation of homopolymer.

Of the alkylene sulphide polymers, poly(ethylene sulphide) (PES) is of interest in this context since it is a strong, chemically resistant, high melting point plastic. However, it has a relatively small temperature interval between melting point (195–210°C) and the onset of thermal decomposition (230–250°C), and severe loss of strength occurs on high temperature ageing in air, and has not achieved industrial importance¹⁰. These shortcomings were not thought to be quite so significant in elastomeric compositions which would not be subjected to prolonged high temperature ageing and its melting point is such that networks of good thermal stability should be obtained while processing would be at temperatures still below the limit for hydrocarbon-based elastomers. They should thus approach the ultimate in network stability for polymers based on cheap polydiene elastomeric segments. There are reports in the literature of the anionic synthesis of elastomeric block polymers from ethylene sulphide and propylene sulphide¹¹ and

the latter monomer has provided the elastomeric segment in copolymers with styrene and α -methylstyrene¹². An interesting feature of the ethylene sulphide polymers is that the reinforcing and crosslinking domain is a highly crystalline entity rather than an amorphous plastic.

EXPERIMENTAL

ABA—poly(isoprene-*b*-ethylene sulphide) (ES/I/ES)

These polymers were prepared using sodium or lithium naphthalene as initiator. In the first group of polymers the isoprene was polymerized in tetrahydrofuran containing the appropriate amount of initiator at –30°C and the ethylene sulphide, carefully purified and dried, was added to the active polydiene solution with vigorous stirring. The temperature was allowed to rise to 20°C and left overnight to complete the polymerization, the solution being converted to a firm gel. Polymer yields, overall, ranged from 75 to 100%. In some instances the ethylene sulphide was added slowly in small increments until sufficient had been added to form a gel. This was possible because of the very rapid rate of polymerization of ethylene sulphide in tetrahydrofuran at ambient temperatures.

The gel was readily reduced to a fine crumb which was washed with methanol and dried either under vacuum or on mill rolls at 160°C with addition of 1–2% of Flectol H as an antioxidant. *Table 1* gives details of a number of ES/I/ES polymers prepared in this way. They contain a central block with 75% 3,4-/25% 1,2-microstructure. Blocks of high 1,4-structure (70–80% 1,4-structure in the case of isoprene) were prepared by changing the solvent from THF to hexane after completion of the initiation reaction. After polymerization of the diene the hexane was replaced by tetrahydrofuran, followed by addition of ethylene sulphide to form the block polymer. Examples of polymers made by this technique are given in *Table 2*.

Some physical properties of ES/I/ES polymers are given in *Table 3*. The effect of the structure of the centre block on rebound resilience is shown in *Figure 1*. *Figure 2* shows stress-strain curves for some of the polymers, *Figure 3* illustrates typical stress relaxation data, and *Figure 4* shows thermal transitions using differential thermal analysis (d.t.a.) and differential scanning calorimetry (d.s.c.).

Table 1 Preparation of ES/I/ES block polymers

Exp. No	Li naphthalene (mmol)	Isoprene (g)	Ethylene sulphide (g)	Polymer yield (%)	Ethylene sulphide in polymer (%)	\bar{M}_n ES/I blocks (calc.)	Mol. wt I block (extracted)†
IS46	5.14	25.1	3.1*	—	8.8	300/ 4 900	M_v 6 200
IS47	5.27	38.7	5.2*	75	12.0	495/ 7 350	M_v 9 500
IS48	2.19	30.5	9.3*	75	20.9	2 130/ 14 000	M_v 8 900
IS49	2.35	23.5	11.2*	75	40.2	2 390/ 10 000	—
IS50	4.96	39.8	11.0*	80	22.8	1 100/ 8 000	—
IS52	9.8	73	9.4	~100	10.4	480/ 7 450	—
IS53	4.93	49	9.8	—	14.7	995/ 9 950	\bar{M}_w 12 800 \bar{M}_n 11 200

* Ethylene sulphide added incrementally

† \bar{M}_v from viscosity, \bar{M}_w and \bar{M}_n from g.p.c.

Table 2 Preparation of high 1,4-microstructure ES/I/ES block polymers

Exp. No.	Li naphthalene (mmol)	Hexane (ml)	Isoprene (g)	Ethylene sulphide (g)	Ethylene sulphide (% in polymer)	Polymer yield (%)	T_g ($^{\circ}\text{C}$)
CP9	3.2	200	41.1	5.7	14.4	88	-30
CP10	3.0	250	44.3	7.9	6.1	87	-31
CP11	2.2	250	53	9.4	7.4	61	-35
CP21	1.48	500	92	23.3	20.2	45	-48
CP24	1.35	500	115	22.8	13.1	71	-53

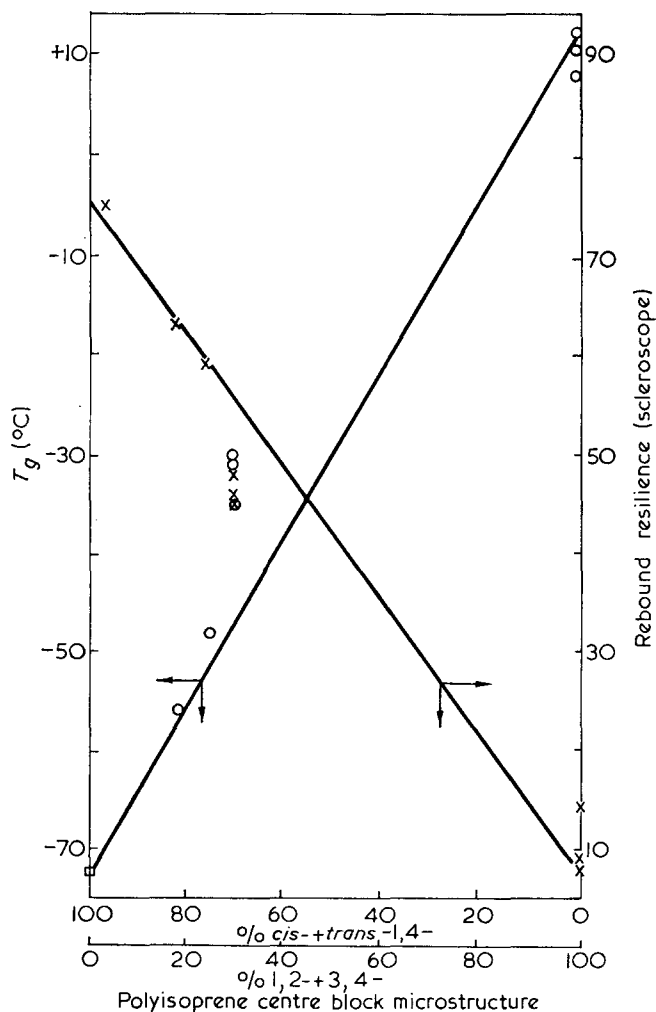


Figure 1 Glass transition temperature (O) and rebound resilience (x) and polyisoprene structure in ES/I/ES block polymers

ABC—poly(styrene-*b*-diene-*b*-ethylene sulphide) (S/I or B/ES)

These polymers were made by sequential polymerization of the three monomers using *n*-butyllithium–anisole as initiator. Small samples were prepared in conventional vacuum line equipment and larger samples in stirred stainless-steel vessels.

Cyclohexane was the preferred solvent for the synthesis of the A and AB blocks and THF was added for polymerization of the ethylene sulphide. The following method was found suitable.

A carefully dried and nitrogen purged reactor was charged with cyclohexane and styrene and anisole–*n*-butyllithium. The temperature was raised to 55–58 $^{\circ}\text{C}$ for ~ 5 h and then reduced to $\sim 30^{\circ}\text{C}$ when half of the

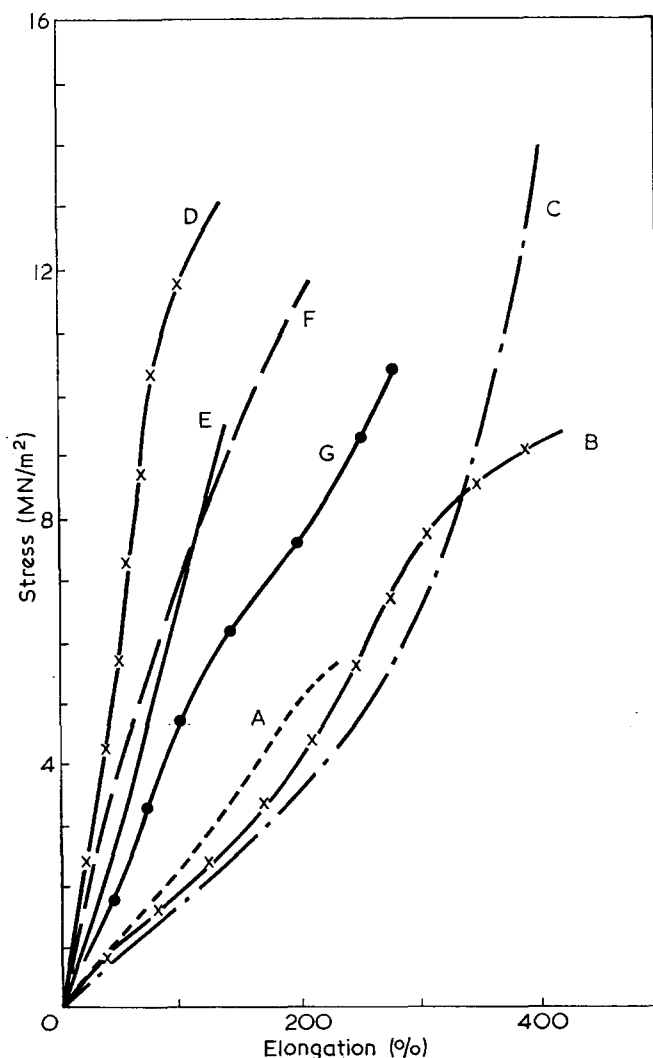
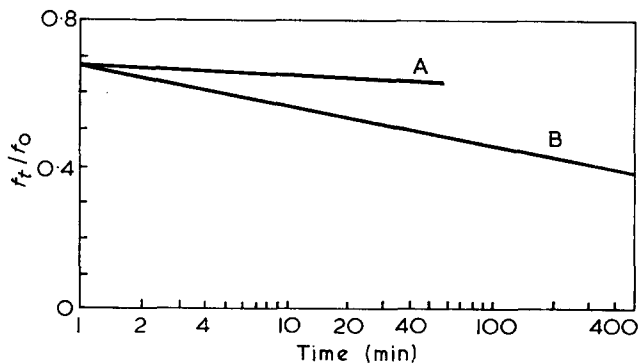


Figure 2 Stress-strain curves of ES/I/ES block polymers. Compositions are given in Table 1. A, IS46; B, IS47; C, IS48; D, IS49; E, IS50; F, IS53; G, IS52

Figure 3 Stress relaxation of ES/I/ES block polymers at 22 $^{\circ}\text{C}$. A: 100% extension; 10.4% ES; \bar{M}_n (I block), 7450. B: 85% extension; 16.2% ES; \bar{M}_n (I block), 545 000

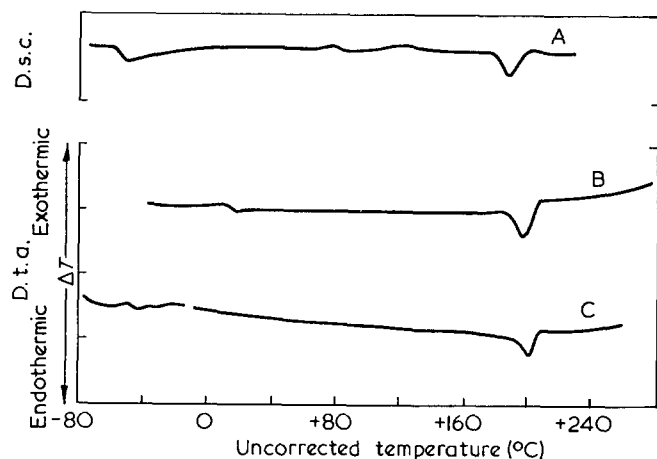


Figure 4 Thermal transitions in S/I/ES and ES/I/ES polymers. A: 3.6% ES; T_m (corr.), 186°C; 90% 1,4-structure in I block of S/I/ES. B: 16.2% ES; T_m (corr.), 195°C; 0% 1,4-structure in I block of ES/I/ES. C: 13.1% ES; T_m (corr.), 198°C; 70% 1,4-structure in I block of ES/I/ES

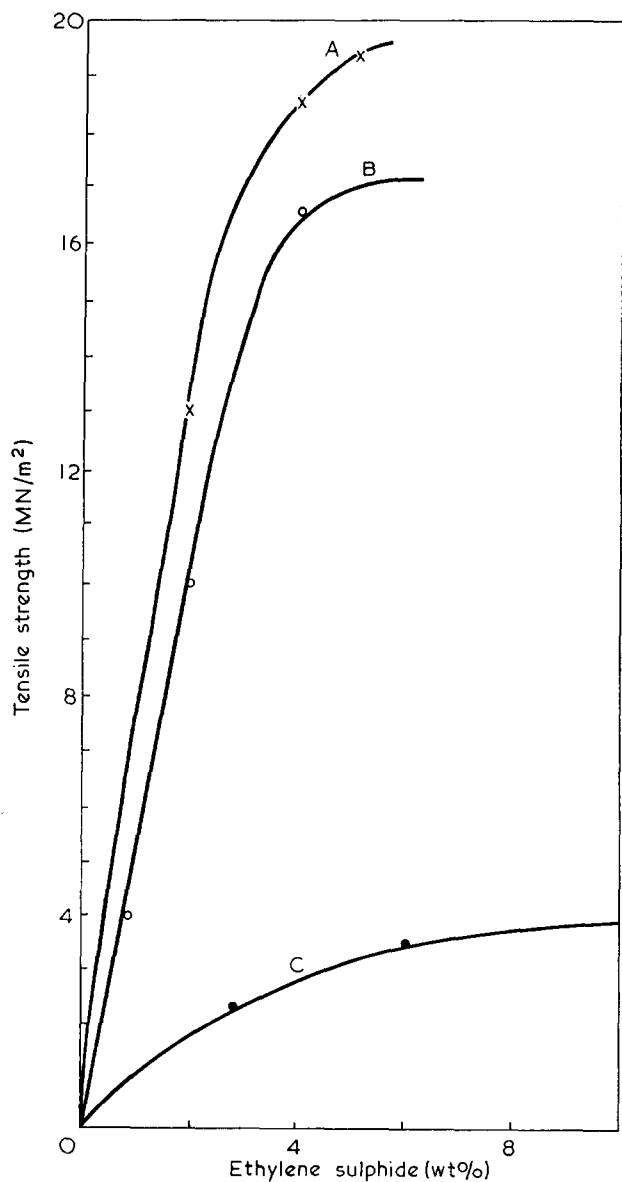


Figure 5 Tensile strength vs. ES content in S/I/ES block polymers. $\bar{M}_n \times 10^{-3}$ (I block): A, 150; B, 100; C, 35

isoprene was added and the temperature was raised to 55–58°C. The remainder of the isoprene was added and the temperature was maintained at 55–58°C for 6–8 h to complete the polymerization. After cooling to ~30°C the ethylene sulphide was added, followed by THF, the mixture was stirred for 90 min and then left for 20–72 h at 30°C. The polymer was isolated by the addition of an equal volume of isopropanol and milling to dryness of the precipitate on hot mill rolls with the addition of 1–2% Flectol H.

Table 4 gives preparative details on several of these polymers and their properties are illustrated in Figures 5–12 and Tables 5 and 6.

Figure 5 shows the dependence of tensile strength on ethylene sulphide content and Figure 6 the effect on tensile modulus. In Figure 7 the effect of PES molecular weight on strength is illustrated. The gel permeation chromatography (g.p.c.) elution curves for typical S/I/ES polymers, exhibiting the peaks for the S, S/I and S/I/ES species are given in Figure 8. Figure 9 illustrates the dependence of tensile modulus and torsional modulus on styrene content, and Figure 10 shows torsional modulus–temperature curves for polymers with isoprene and butadiene as centre blocks. Figure 11 shows stress relaxation data of typical terpolymers, while Figure 12 shows the flow viscosity dependence on shear rate.

Table 5 gives characterization and physical properties of S/I/ES polymers, and Table 6 gives details of the preparation and properties of S/B/ES polymers.

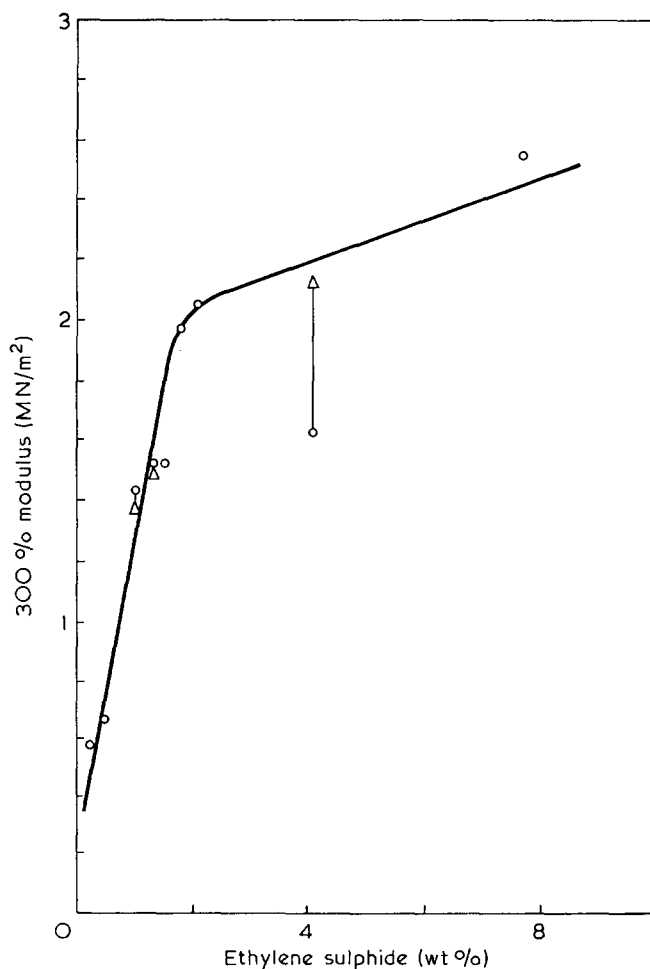


Figure 6 300% tensile modulus vs. ES content in S/I/ES block polymers. O, As prepared; Δ, annealed at 80°C for 24 h or extracted with boiling cyclohexane for 24 h

AB—poly(isoprene-b-ethylene sulphide)

These polymers were made essentially by the same process as the terpolymers. Typical properties are shown in Table 7. Viscosity–shear rate curves for linear polybutadiene and block polyisoprene–ethylene sulphide polymers are shown in Figure 13.

DISCUSSION

The ABA type ethylene sulphide block polymers can be

produced with a high level of purity. They form networks which are stable up to 150°C and retain moderate mechanical properties up to 100°C. The stress relaxation properties at room temperature are good (Figure 3), although there is a rapid short-period relaxation. The processing temperature of these polymers is such that they are prone to degradation and consequent stickiness*. A further difficulty is that the diene centre block is high in 3,4-structure unless a three-stage preparative

* For easy moulding low molecular weights were necessary.

Table 3 Physical properties of ES/I/ES block polymers

Sample*	Moulding temp.† (°C)	Modulus (MN/m ²)		Tensile strength (MN/m ²)		Elongation at break (%)	Resilience (rebound) (%)	Tension set (%)
		100%	300%	22°C	100°C			
IS46	160	2.1	—	5.5	1.5	230	6	6 at 200%
IS47	175	1.9	7.3	9.3	1.7	420	19	7 at 200%
IS48	205	1.7	6.4	14.0	2.2	400	17	15 at 300%
IS49	170	11.5	—	13.0	2.1	140	25	—
IS50	180	6.4	—	9.3	1.6	140	—	—
IS52	180	4.6	—	10.2	—	280	—	—
IS53	190	6.6	—	11.5	—	205	—	—
CP9	225	—	—	4.4	—	650	45	—
CP10	225	—	—	6.3	—	780	46	—
CP11	225	—	—	2.0	—	700	—	—
CP21	225	—	—	0.9	—	800	59	—
CP24	225	—	—	low	—	—	63	—

* IS46–IS53: isoprene (75% 3,4-/25% 1,2-microstructure); CP9–CP24: isoprene (70–82% 1,4-microstructure)

† Good mouldings obtained at or about 170°C with the polymers IS46–IS53. The polymers CP9–CP24 were of much higher molecular weight and moulding was accompanied by slight degradation

Table 4 Preparation of S/I/ES block polymers

Exp. No.	Cyclohexane (ml)	Styrene (g), polymerization time (h) at 55°C	Isoprene (g), polymerization time (h) at 57°C	Ethylene sulphide* (g)	Anisole (ml), n-BuLi (mmol)	THF (ml)	Polymer composition (wt %) calc. (found)		
							S	I	ES
807	8500	490	1800	110	12.5	2200	20.4	75.0	4.6
		4.25	10		31.2		(19.1)	(77.1)	(3.8)
809	8300	449	1790	101	11.3	2100	19.2	76.5	4.3
		4.5	10		28.2		(20.4)	(75.6)	(4.0)
816	9000	650	1800	100	11.3	2250	25.5	70.6	3.9
		4	10		28.2		(23.8)	(72.4)	(3.8)

* Polymerization for 90 min at 35–38°C after addition of THF, solution allowed to stand for 80 h before isolation

Table 5 Properties of S/I/ES block polymers

Exp. No.	Block molecular weights	Polymer yield (%)	Modulus 100%, modulus 300%, tensile strength (MN/m ²), elongation at break (%)		Heat of fusion of ES block (J/g ES)	Tension set (%) at 100% and 200% strain	Hardness (BSD) (°), triposometer resilience at 22°C
			100%	300%			
806	S 26 800	96	0.7		113.0	2.5	30
	I 121 600		1.1			6	
	ES 5 500		12.6				
	$\bar{M}_w/\bar{M}_n=1.28$ (S/I block)		1280				
807	S 23 700	98.7	0.8		135.8	3	36.5
	I 143 200		1.3				
	ES 6 300		15.3				
			1300				
809	S 22 500	97.5	1.1		119.1	3.5	36.5
	I 143 600		1.4			6.5	
	ES 6 900		15.3				
	$\bar{M}_w/\bar{M}_n=1.10$ (S/I block)		1110				
816	S 20 900	97.3	1.2		138.8	4	51.0
	I 85 500		2.1			6	
	ES 4 400		19.8				
	$\bar{M}_w/\bar{M}_n=1.39$ (S/I block)		1040				

Table 6 Preparation and properties of S/B/ES block polymers

Exp. No.	60:40 Benzene/n-hexane (ml), n-BuLi (mmol), anisole (ml)		Styrene (g)	Butadiene (g)	ES (g)	THF (ml), polymer yield (%)	Conversion of ES (%)	Polymerization time (h) and temp. (°C)
	Block molecular weights							
T83	250	1.48 0.5	11.1	46.2	3.3	70 ~100	94	70 22°
T86	250	1.48 0.5	20.8	46.5	3.3	70 ~100	88	120 22°
T87	250	1.48 0.5	11.8	36.5	3.3	60 ~100	80	120 22°
T83	S 13 000 B 74 600 ES 4 700 $\overline{M}_w/\overline{M}_n=1.02$ (S/I block)	-90	82.8	8.7 800	1.5, 1.7, 2.0	57 72	5 12	
T86	S 15 000 B 61 530 ES 3 420 $\overline{M}_w/\overline{M}_n=1.15$ (S/I block)	-89	147.7	25.3 800	2.8, 3.8, 5.1	75 51	6 9	
T87	S 14 100 B 44 630 ES 3 270 $\overline{M}_w/\overline{M}_n=1.17$ (S/I block)	-89	133.9	12.0 710	2.2, 2.6, 3.3	68 64	6 11	

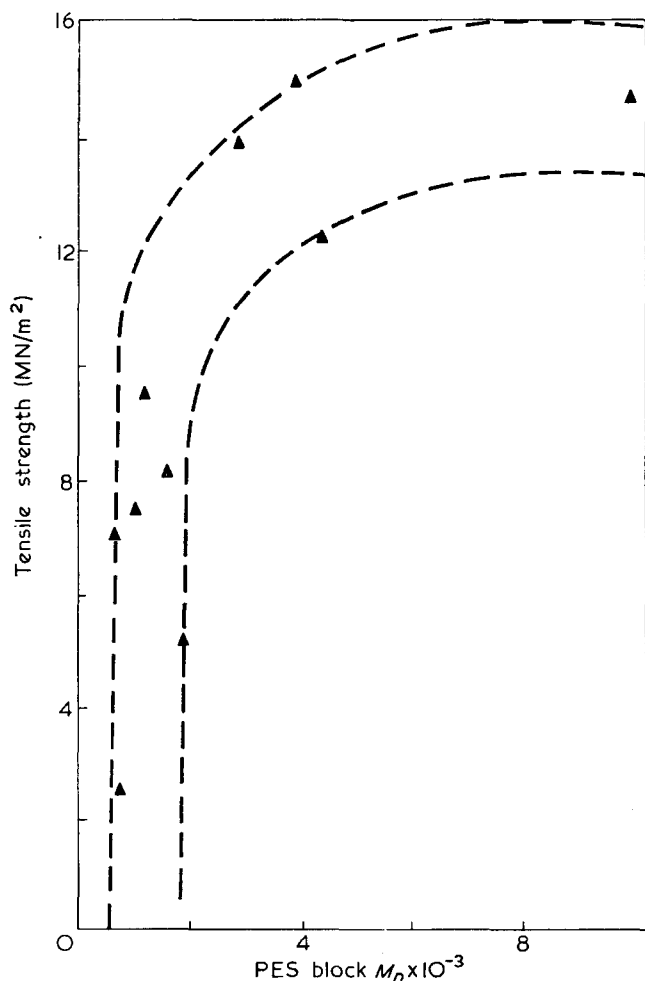


Figure 7 Tensile strength vs. molecular weight of ES block in S/I/ES block polymers

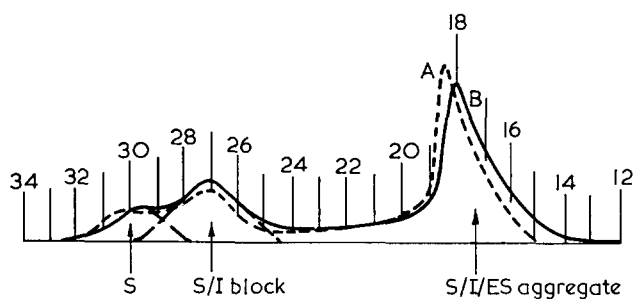


Figure 8 G.p.c. elution curves for S/I/ES block polymers (THF solvent). Numerals refer to g.p.c. count numbers. A: 100% solubility; 2.2% ES. B: 83% solubility; 3.8% ES

procedure is used. (Attempts to prepare the diene bis-anions and polymerize the ethylene sulphide in pure hydrocarbon media proved unsuccessful because of solubility problems which resulted in large amounts of predominantly AB polymer, and because of the basicity of the ethylene sulphide anion the polymers could not be prepared by sequential polymerization.) Those polymers containing the diene in the 1,4-form had greatly improved low temperature properties and resilience (Figure 1). Strengths, however, were lower and did not exceed 7 MN/m² in the best obtained. It is noteworthy here that high temperature network stability is not necessarily associated with high strength, but whether this is the result of the intrinsic properties of the material or from imperfections in the polymer network is not certain. The intractable nature of PES makes it difficult to establish whether any free homopolymer is present and the block polymers themselves are insoluble in all common solvents. The ethylene sulphide blocks are present in crystalline domains, as shown by d.t.a. and X-ray studies. Elastomers containing

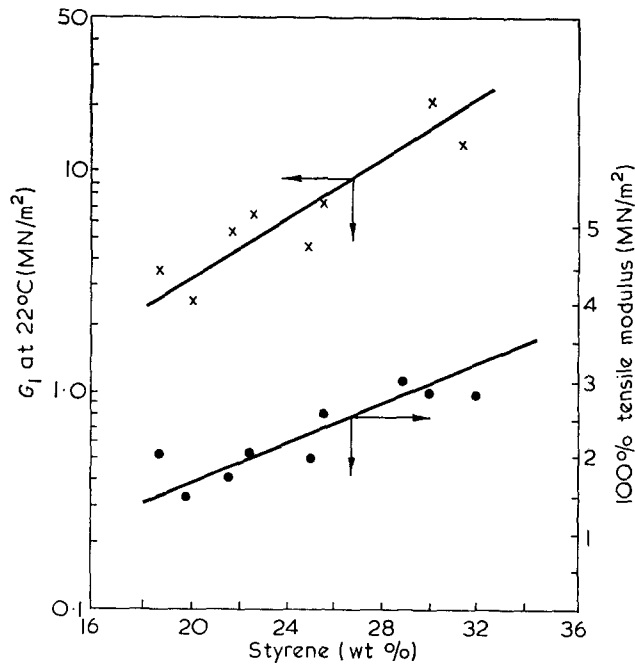


Figure 9 Effect of styrene content on storage modulus (x) and 100% tensile modulus (●) of S/I/ES block polymers

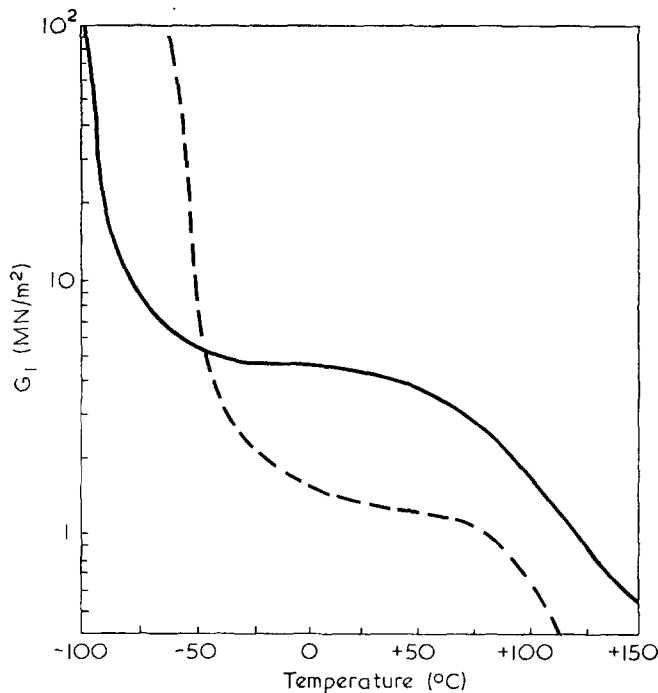


Figure 10 Torsional modulus vs. temperature curves for S/B/ES (—) and S/I/ES (---) block polymers

less than 20% of ethylene sulphide are transparent and the crystallites are extremely small. At higher concentrations (20–40%) opaque polymers are formed, but it is possible in these instances that free PES may be present.

The styrene-*b*-diene-*b*-ethylene sulphide terpolymers are of particular interest in that high strength elastomers are obtained with small amounts (2–4%) of PES, and a relatively stable network results from ethylene sulphide molecular weights of only 2000; the styrene segments required are comparable in molecular weight to those in the well-known S/B/S types.

The stress-strain curves show no sign of a yield

point at low strains and the polymers are of low modulus and are highly resilient, with good recovery from high extensions. Polymers with reasonable physical properties are obtained with ~15% styrene, considerably less than that necessary for S/I/S triblock polymers. This shows that it is the molecular weight of the polystyrene segment

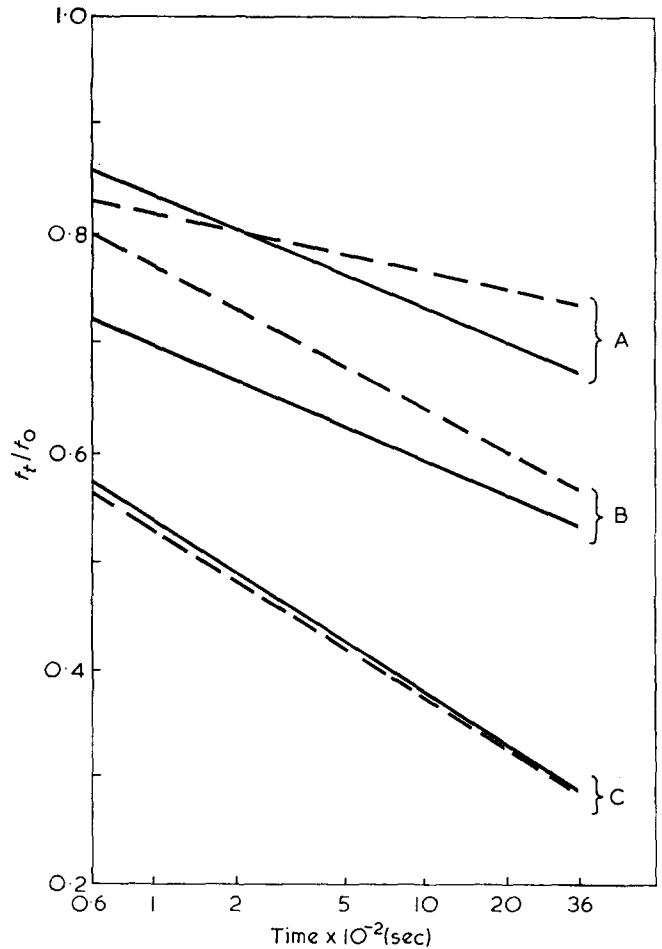


Figure 11 Stress relaxation (100% extension) of block polymers: —, S/B/ES; ---, S/I/ES. A, 22°C; B, 50°C; C, 80°C

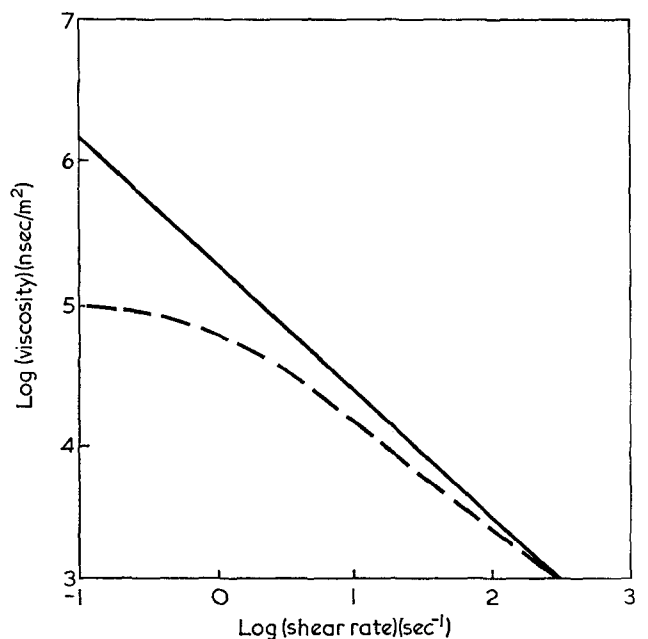


Figure 12 Bulk viscosity at 170°C vs. shear rate curves of block polymers: —, S/B/ES (2.2% ES); ---, S/I/ES (5.0% ES)

Table 7 Preparation and properties of I/ES block polymers

Exp. No.	ES (%)	$\bar{M}_w \times 10^{-5}$ for B block	Purity (% block polymer)	PPI*	Polymerization	
1	2.0	1.76	75	0.47	Cyclohexane	1.5 l
2	2.6	1.19	78	1.84	n-BuLi	0.16 g
3	2.9	1.10	72	1.93	Anisole	2.0 ml
4	4.5	1.20	70	0.47	Isoprene	300 ml
5	8.5	2.28	75	11.1	Ethylene sulphide THF	Variable 400 ml
24-48 h at 40-45°C						
Exp. No.	Modulus at 100% (MN/m ²)	Tensile strength (MN/m ²)	Elongation at break (%)	Vulcanization		
1	0.48	2.63	300	Polymer	100	
2	0.85	1.69	400	Sulphur	1.5	
3	0.77	2.41	350	CBS	0.7	
4	0.80	3.43	440	Zinc oxide	5.0	
5	0.76	4.22	700	Stearic acid	2.0	
50 min at 140°C						

* Processing pressure index—the pressure drop ($N/m^2 \times 10^5$) required to extrude the polymer through a die of length 0.800 cm and of diameter 0.2096 cm at a rate of $1.144 \times 10^{-9} m^3/sec$ at 150°C

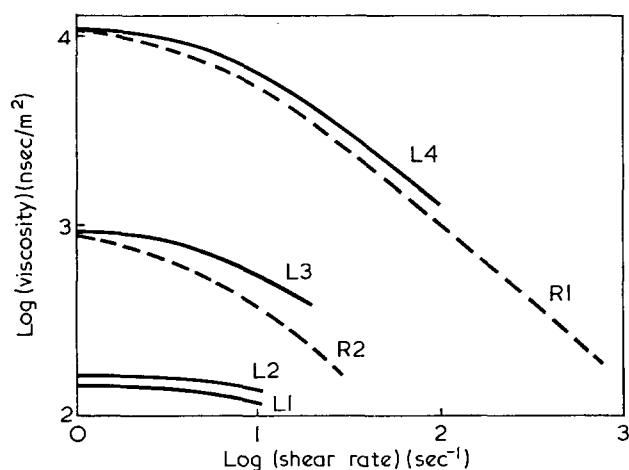


Figure 13 Bulk viscosity at 150°C vs. shear rate for linear (—) polyisoprene and radial (---) isoprene/ethylene sulphide polymers. L1, $\bar{M}_w 119 \times 10^3$; L2, $\bar{M}_w 137 \times 10^3$; L3, $\bar{M}_w 182 \times 10^3$; L4, $\bar{M}_w 433 \times 10^3$. R1 (prepared from L1), 2.6% ES; R2 (prepared from L2), 2.6% ES

rather than the stoichiometry which is important in building up the network, although the increase in strength with polystyrene content (Figure 9) is evidence for reinforcement conferred by the hard phase. Thus the S/I/ES polymers are of interest in that for a given molecular weight elastomeric segment considerably larger polystyrene blocks can be attached with retention of rubbery properties.

The low molecular weights of the ethylene sulphide blocks (3000-4000) for optimum properties show that a mechanically stable crystallite requires less material than an amorphous plastic domain. From estimates of peak broadening of the 4.2 Å reflection of the PES crystallites (using zinc oxide as reference standard) a typical polymer containing 4.6% ethylene sulphide was estimated to have average domain sizes of 100-150 Å. The crystallites are evidently anisotropic in shape since, on stretching, the X-ray diffraction pattern shows reversible changes in the relative intensities of the two principal scattering peaks at $2\theta = 21.1^\circ$ and 24.9° in the stressed and unstressed state as a function of stress and strain (Figure 14). Estimates of the anisotropy ratio

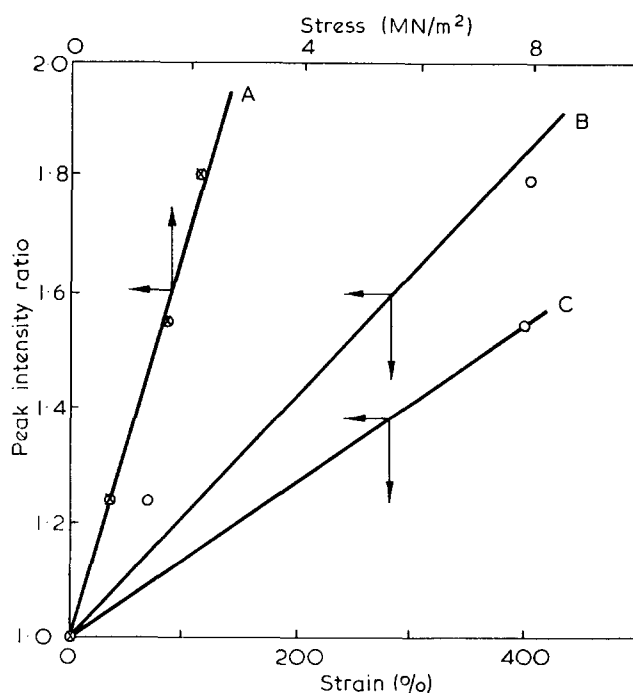


Figure 14 Dependence of X-ray scattering ratio ($2\theta_{21.1^\circ}/2\theta_{24.9^\circ}$) on stress and strain in S/I/ES block polymers. A, 4.6, 3.56% ES; B, 4.6% ES; C, 3.56% ES

vary from 1.3 to 4.2 increasing, as would be expected, with increasing molecular weight of the ethylene sulphide block. From this it is inferred that extended chain crystallites, extensively studied by Wunderlich *et al.*¹³, are produced. In contrast moulded ES/I/ES block polymers have X-ray patterns unaffected by strain, and it is presumed that spherical crystallites are present. This is almost certainly due to the high processing temperatures required for the latter, since the X-ray spectra of S/I/ES polymers which have been heated above the melting point of the ethylene sulphide block likewise show no strain effect.

These estimates of crystallite size correspond to numbers of PES domains of the order of $0.5-1.0 \times 10^{16}/cm^3$ and 450-1000 molecules/aggregate.

This estimate is confirmed by molecular weight

determinations on the fraction of polymer which dissolves in solvents such as benzene or cyclohexane. From the g.p.c. measurements molecular weights are extremely high—up to 5×10^7 . Taking into account the molecular weights of S/I blocks, in the region of 10^5 , and ethylene sulphide blocks ranging from 2000 to 4000, up to 400 chains are linked by each PES crystallite. The somewhat lower value compared with that estimated from X-ray data may be explained by the fact that only a portion—presumably smaller aggregates containing less PES—of the block polymer is soluble.

From the X-ray and d.s.c. data the PES segments exist in relatively pure crystallites and from the stoichiometry they will possess about one-fifth of the volume of polystyrene domains, which presumably form a separate phase. Network formation should be efficient since each elastomeric segment must pass from a PES crystallite to a polystyrene domain.

Electron photomicrographs of films cast from solution and stained with OsO_4 show an irregular two-phase structure (Figure 15) apparently an interpenetrating network produced by disordered lamellae with layer thicknesses in the region of $0.025\text{--}0.05\ \mu\text{m}$, the polydiene layers being the thicker. Lengths of the plastic zones are greater by a factor of about ten. The darker circular regions of $\sim 0.1\ \mu\text{m}$ are possibly thicker sections from polymer aggregates. Satisfactory photomicrographs could not be obtained from moulded polymer but so far as it was possible to judge from the photographs the morphology was similar. A replica taken from a torn surface of the rubber likewise showed an interpenetrating network (Figure 16). It was not possible to distinguish the polystyrene and poly(ethylene sulphide) domains.

To see whether there was any preferred orientation in the structure, a milled sheet of S/I/ES elastomer (Sample 816) was pressed in a mould and test samples cut in two directions at right angles. Stress-strain properties are shown in Figure 17 and show small but probably significant differences; the samples cut in



Figure 15 S/I/ES polymer cast from benzene stained with OsO_4 ($\times 45\ 000$)



Figure 16 Replica of torn surface of S/I/ES polymer ($\times 90\ 000$)

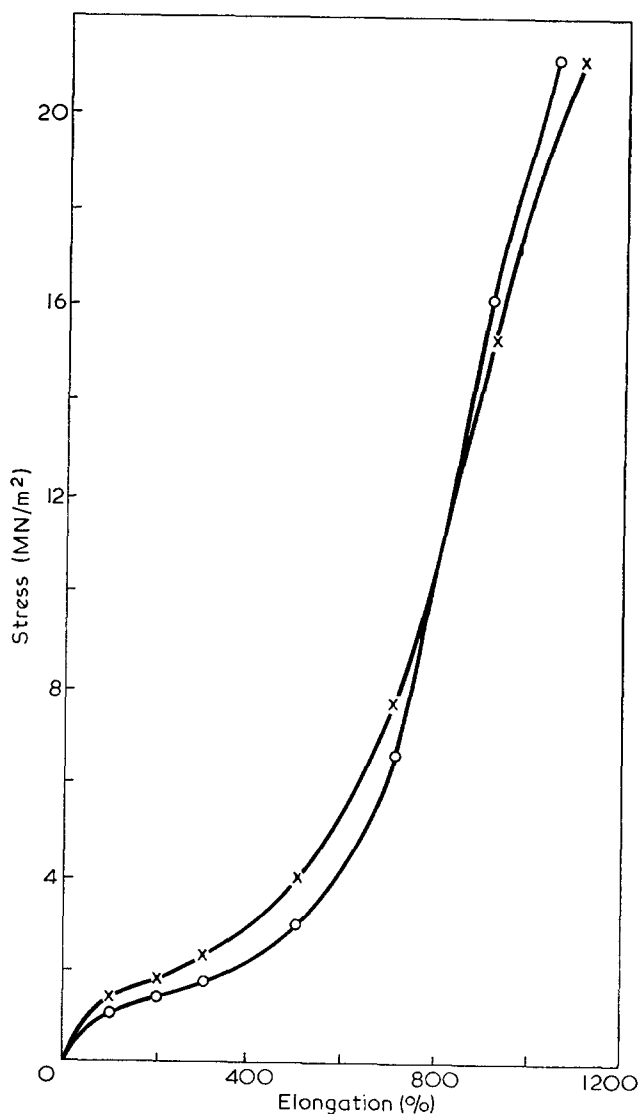


Figure 17 Tensile properties of S/I/ES polymer from test samples cut at right-angles from moulded sheet. O, Direction of mill rotation; x, lateral to direction of mill rotation

the direction of mill rotation have slightly lower modulus.

The stress relaxation data (Figure 11) show that at temperatures above about 80°C the network relaxes rapidly, the result of softening of the polystyrene segments, while the poly(ethylene sulphide) crystallites remain intact up to nearly 200°C (Figure 4).

Superficially it is surprising that elastomers containing such high molecular weight aggregates can readily be processed, although, in fact, it has long been known that polymers containing substantial amounts of microgel process well¹⁴. Furthermore, comparable rheological properties were found with isoprene or butadiene/ethylene sulphide block polymers. These, as would be expected, do not behave as crosslinked elastomers at ambient temperatures and are similar in properties to conventional uncrosslinked rubbers. As can be seen from Figure 18 flow properties (at 150°C) change only slightly with increase in the number of branches (calculated from g.p.c. data) attached to the crystallite. It seems unlikely that the polyethylene sulphide crystallites will break down at temperatures 30–40°C below their melting point and, therefore, the reason why the polymers should behave in this way is not obvious.

The block polymers were not pure and contained quantities of polystyrene and S/I block polymer (Table 8 and Figure 8). It is possible that these were acting as plasticizers, since it has been observed that polystyrene in a S/B/ES block polymer considerably improves processability. Attempts were made to obtain substantial quantities of pure S/I/ES polymer but these were not very successful since, although the polymers are not completely soluble in common solvents, those which dissolve the S/I block polymer also take into solution substantial amounts of the S/I/ES polymer.

Another possibility is that the flow units under shear are particulate, formed by internal fractures in the elastomer, and that above a certain molecular weight the shear strength reaches a constant value. Quite

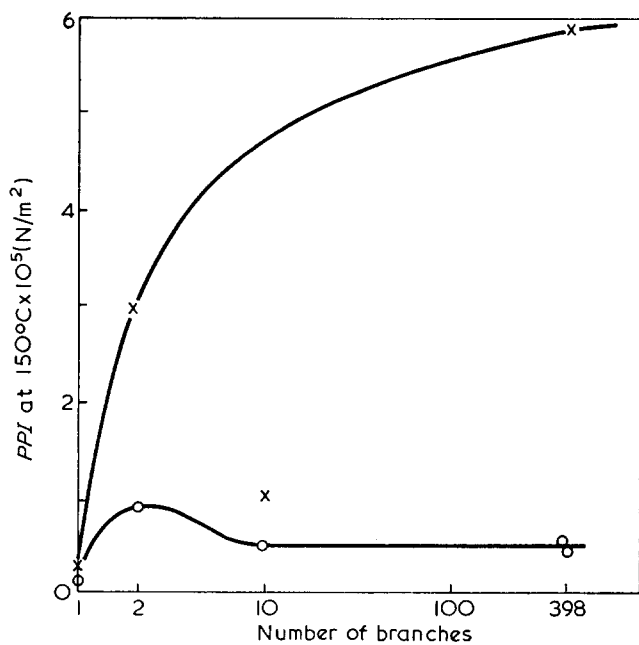


Figure 18 Effect of branch length and number on processing properties of B/ES radial polymers. \times , \bar{M}_w 190×10^3 ; \circ , \bar{M}_w 120×10^3 . Ordinate units are defined in footnote to Table 7

Table 8 Composition of S/I/ES block polymers*

Sample	S	S/I (% wt)	S/I/ES
1	5.2	25.8	69.0
2	8.2	21.6	71.2
3	7.3	21.0	71.7
4	2.9	16.7	80.4
5	5.3	14.1	79.7

* Fractionation using benzene/methanol. Composition calculated from C, H and S contents. The results were in good agreement with compositions calculated from g.p.c. peak heights, both on whole polymers and fractions

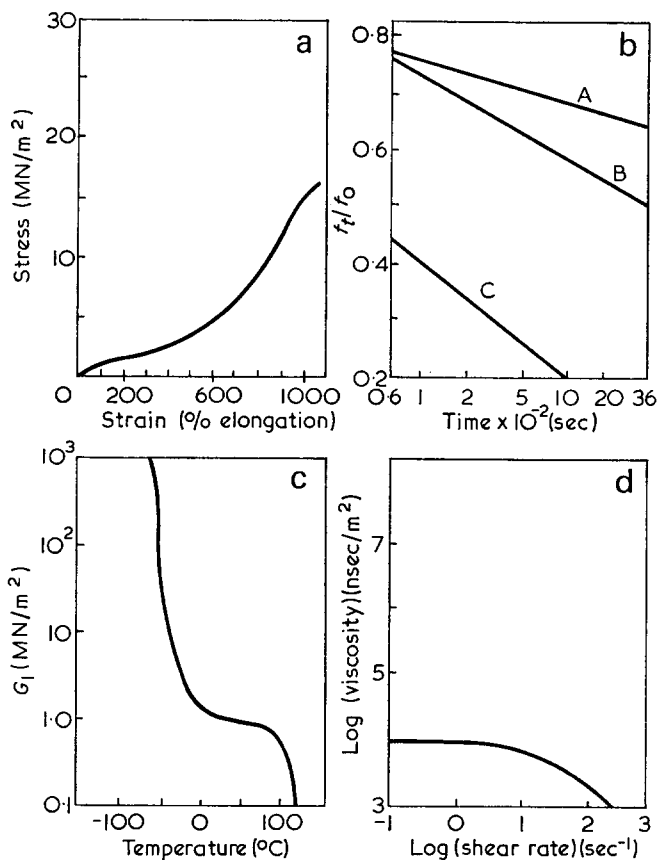


Figure 19 Properties of S/I/DVB (23:76:1) block polymer. (a) Stress-strain; (b) stress relaxation (100% extension): A, 22°C; B, 50°C; C, 80°C; (c) torsional modulus vs. temperature; (d) viscosity at 170°C vs. shear rate

obviously on such limited evidence this proposal is very tentative, but it is not inconsistent with a flow theory proposed by Mooney some years ago¹⁵. Mooney suggested that substantial polymer elements were involved in polymer flow and their sizes were calculated to be in the range $1-30 \times 10^{-4}$ cm.

As the amount of polymer even in the smallest of these will contain many molecular aggregates the flow processes do not involve individual aggregates. It is conceivable, however that internal fracture surfaces occur more readily in highly branched polymers than in linear polymers. A detailed study of the flow processes of highly purified radial polymers would be necessary to elucidate the mechanisms.

To eliminate the possibility that breakdown of the PES crystallite was the explanation for the flow charac-

teristics, polymers were prepared using a covalently crosslinked poly(divinyl benzene) (PDVB) domain as an alternative to the PES crystallite. In these there would be no reason to expect that the crosslinked plastic domains would soften at processing temperatures. Figure 19 shows stress-strain, torsional modulus, stress relaxation and flow properties of an S/I/DVB block terpolymer, which are very similar to those of the corresponding ethylene sulphide polymers*.

These DVB polymers are not so highly ramified as the S/I/ES types. It was found that the relative rates of initiation and propagation of divinyl benzene impose a practical limit of about 10–20 chains per aggregate, broadly in agreement with the results of Worsfold *et al.* for styrene–DVB block polymers¹⁶. It is considered

* To maintain stability on storage and during processing it was necessary to hydrogenate the residual double bonds in the DVB kernel.

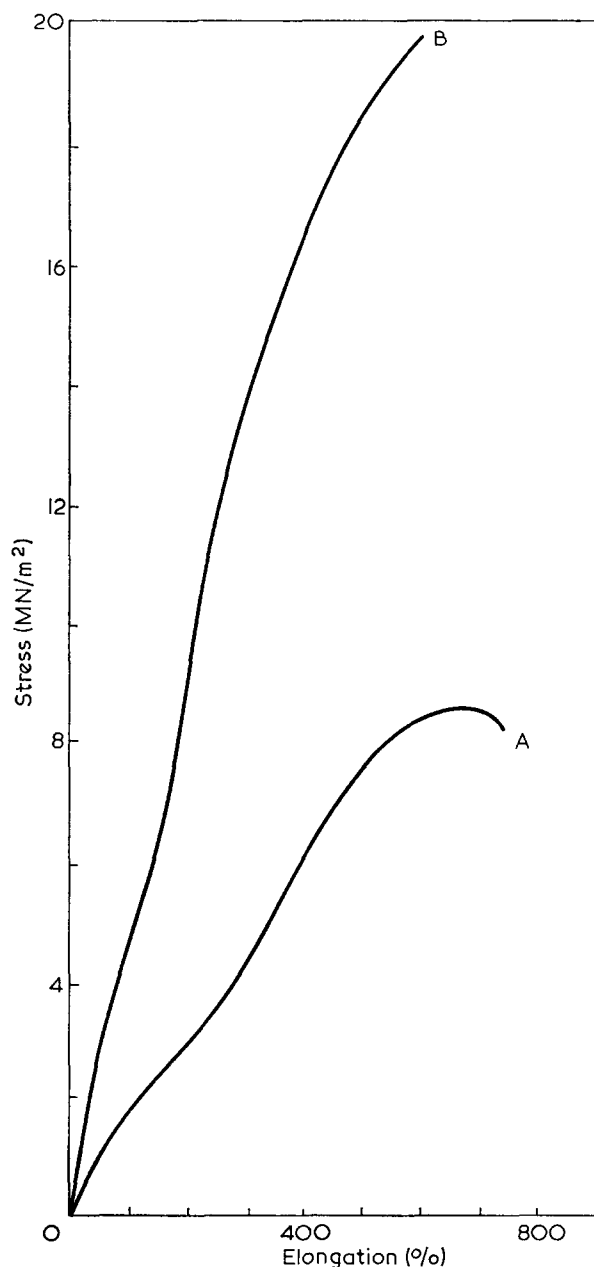


Figure 20 Compounded S/I/ES (26:70:4) block polymer properties. A, 50 phr HAF black and 50 phr Circosol oil 4240; B, A + 0.5 phr Santocure, 3 phr sulphur, 5 phr ZnO, 3 phr stearic acid and 1 phr Nonox HFN vulcanized for 55 min at 134°C

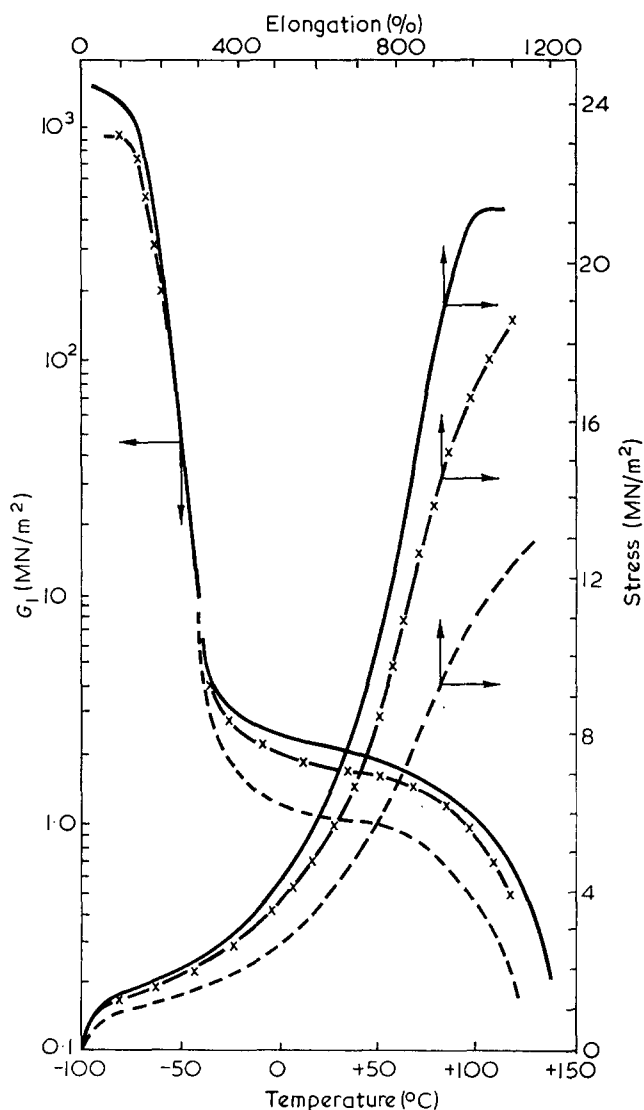


Figure 21 Effect of oil on stress-strain and torsional modulus vs. temperature curves of S/I/ES (26:70:4) block polymer. —, No oil; x, 5 phr Circosol oil 4240; ----, 15 phr Circosol oil 4240

that, notwithstanding the differences in aggregate complexity, the correspondence in properties between the ethylene sulphide and the DVB block polymers in terms of strength, network stability and flow properties show this to be a consequence of their radial structures.

The curves in Figure 18 show the flow properties to be very sensitive to the length of the chains comprising the branches. However, too great a weight should not be placed on data which relate to polymers of variable purity and composition. To illustrate this the data on two polymers of comparable branch lengths and ethylene sulphide contents are shown in Figure 13. The linear polymers from which they were derived have the expected flow characteristics but the radial polymers are different. The explanation is clearly concerned with purity of the aggregated polymer since the higher viscosity polymer (R1) was less soluble in tetrahydrofuran than the other (R2); the solubilities were respectively 22% and 77%. The shear dependence of the radial polymers is such that at high shear rates their viscosities more closely approach those of the linear polymers from which they were prepared.

A feature of these block polymers is that they can be

readily compounded with carbon black and oil and, after vulcanization, give high strength elastomers. Figures 20 and 21 show the effect of oil and black on the stress-strain curves of a typical S/I/ES block polymer and the effect of vulcanization.

CONCLUSIONS

Ethylene sulphide is a very suitable monomer for the preparation of elastomeric block polymers. The ABA types have good temperature stability but are difficult to process without some oxidative degradation. However, with care it is possible to press or injection mould the elastomers into complex shapes without degradation. The styrene/diene/ethylene sulphide polymers are more difficult to prepare but easier to process. They have superior strength and elongation but obviously a significantly reduced operating temperature range.

REFERENCES

- 1 Dawkins, J. V. 'Block Copolymers' (Eds D. C. Allport and W. H. Janes), Applied Science, London, 1973, Ch 8A
- 2 Bailey, J. J., Bishop, E. T., Hendricks, W., Holden, G. and Legge, N. R. *Rubber Age* 1966, **98**, 69
- 3 Holden, G., Bishop, E. T. and Legge, N. R. *J. Polym. Sci. (C)* 1969, **26**, 37
- 4 Shell Int. Res. Br. Pat. 1 028 388; 1 020 709
- 5 Fetters, L. J. and Morton, M. *Macromolecules* 1969, **2**, 453
- 6 Uniroyal TPR, *Rubber & Plastics News* 1973 (9 April), p 4 (paper to SPE meeting, Montreal, May 7-10 1973)
- 7 Williams, B. L., Weissbein, L. and Singh, A. *Rubber Age* 1958, **100** (7), 57
- 8 Brown, M. and Witsiepe, W. K. Paper to 100th Meeting ACS Division of Rubber Chemistry, Cleveland, Oct. 12-17, 1971
- 9 Cooper, W. *Br. Polym. J.* 1971, **3**, 28
- 10 Adamek, S., MacKillop, D. and Schnecko, H. *J. Appl. Polym. Sci.* 1972, **16**, 2511
- 11 MacKillop, D. A. *J. Polym. Sci. (B)* 1970, **8**, 199
- 12 Morton, M., Kammereck, R. F. and Fetters, L. J. *Br. Polym. J.* 1971, **3**, 120
- 13 Wunderlich, B. *Angew. Chem. (Int. Edn)* 1968, **7**, 912
- 14 'Polysar Handbook', Polysar, Sarnia, Ontario, 1960, pp 656-731
- 15 Mooney, M. and Wolstenholme, W. E. *Rubber Chem. Technol.* 1955, **28**, 488; Mooney, M. *Rubber Chem. Technol.* 1957, **30**, 460; 1964, **37**, 503
- 16 Worsfold, D. J., Zillion, J. G. and Rempp, P. *Can. J. Chem.* 1969, **47**, 3379

Evidence for aggregation of polystyrene in solution from magneto-optic birefringence

The optical birefringence Δn induced by an applied magnetic field B is termed the Majorana¹ effect when found in colloidal suspensions, and the Cotton-Mouton² effect in gases, liquids and solutions of small molecules. In both effects the birefringence is due to the partial preferential alignment of optically anisotropic colloid particles or molecules against the disorientating forces of Brownian motion. While the Cotton-Mouton birefringence is always proportional to B^2 , the Majorana birefringence may depend on B non-quadratically and complete particle alignment (saturation) may occur provided the particles and applied field are large enough. Examples of non-quadratic behaviour with rigid particles have been found by Mehta³ and Desai *et al.*⁴ in colloidal suspensions of bentonite and ferrite respectively.

According to the theory of Stuart and Peterlin⁵ the response of a flexible polymer chain to an applied magnetic field is a partial preferential orientation of short diamagnetically anisotropic segments of the chain. Thus a B^2 dependence of Δn , and very short orientational relaxation times (10^{-9} – 10^{-11} sec) would be expected, as found in solutions of small molecules.

This letter reports non-quadratic and time dependent behaviour of the birefringence induced by magnetic fields in solutions of the flexible chain polymer polystyrene dissolved in benzene and cyclohexanone. It is the first report of such observations as far as the author is aware, although a similarly long time dependence of permittivity has been cited by Brown and Shaw⁶ in liquid crystalline phases of small molecules and Sobajima⁷ has found time dependent n.m.r. spectra in a magnetic field of the liquid crystalline phase of the rigid rod polymer poly(γ -benzyl-L-glutamate) in methylene chloride solution.

The apparatus used here consisted of a Newport type electromagnet (0–2 T) with a 200 mm polarimeter tube holding the solution between the pole pieces. The birefringence was measured at room temperature using a Hg lamp, filter and collimator, with a polarizer, quarter-wave plate and analyser used as a Senarmont compensator, at a wavelength of 546 nm.

The polystyrene was a commercial sample with a weight average of 3×10^5 . Figure 1 shows the birefringence and its concentration dependence in cyclohexanone. Some solutions showed quadratic behaviour until they had experienced the applied field for several minutes, e.g. 0.83% in Figure 1. The apparent negative slope of the lower concentrations at high fields is explicable as the difference in sign of the solvent and solute birefringence. Solvent-corrected curves (broken line), obtained by subtracting the birefringence of the pure solvent, are seen to have positive slopes in all cases. The curves shown in Figure 1 refer to the solutions in their equilibrium state,

and neither time lapses of several days nor cycling of the magnetic field produced any deviation from the original curves.

In benzene solution, marked time dependent behaviour was observed. This produced non-quadratic hysteresis curves as shown in Figure 2. Its other effect was to cause a noticeable time delay of the birefringence in following any changes in field. Most noticeable were the birefringence lags when the field had been switched off from some value at which the birefringence had been previously steady at Δn_0 . Figure 3 shows the decay of birefringence after the solution had been at some time at 0.5 T at which a steady birefringence Δn_0 had been reached and also $\ln_e |\Delta n(t)|$ plotted with time t . Assuming that $\Delta n(t) = \Delta n_0 e^{-t/\tau}$ defines a relaxation time τ , the slope of the logarithmic plot gives about 19 sec for τ . Similar long relaxation times were found for other solutions in benzene.

An interpretation of the above results for polystyrene is to propose the existence of optically and diamagnetically anisotropic polymer chain aggregates in solution which are much larger than single polymer molecules. Assuming

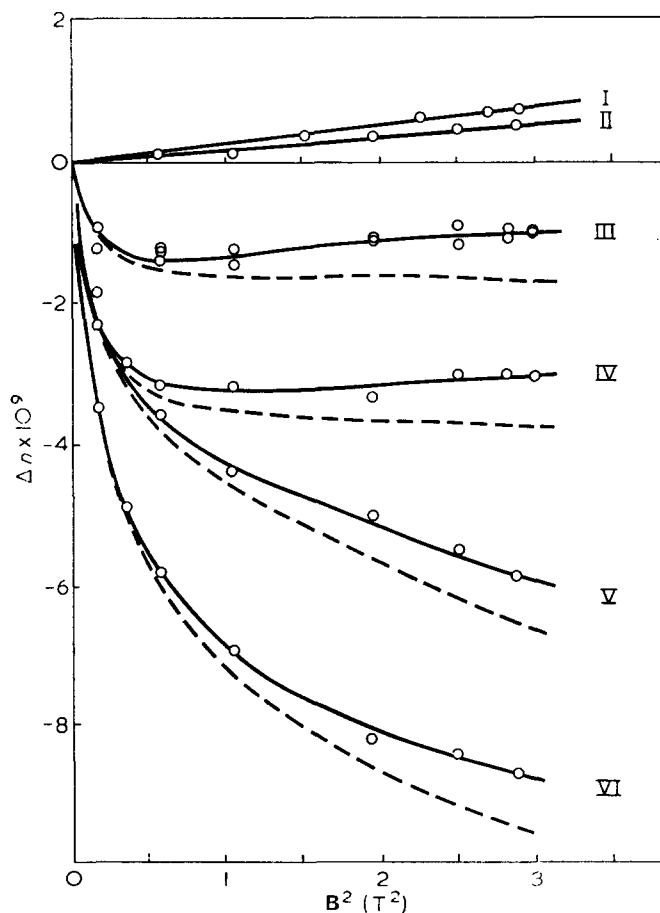


Figure 1 Quadratic and non-quadratic magnetic birefringence of solvent and solutions. I, Pure cyclohexanone; II, 0.83%; III, 0.42%; IV, 0.83%; V, 1.63%; VI, 2.75% polystyrene. Broken curves (---) are solvent corrected using curve I and represent the birefringence of the polystyrene only

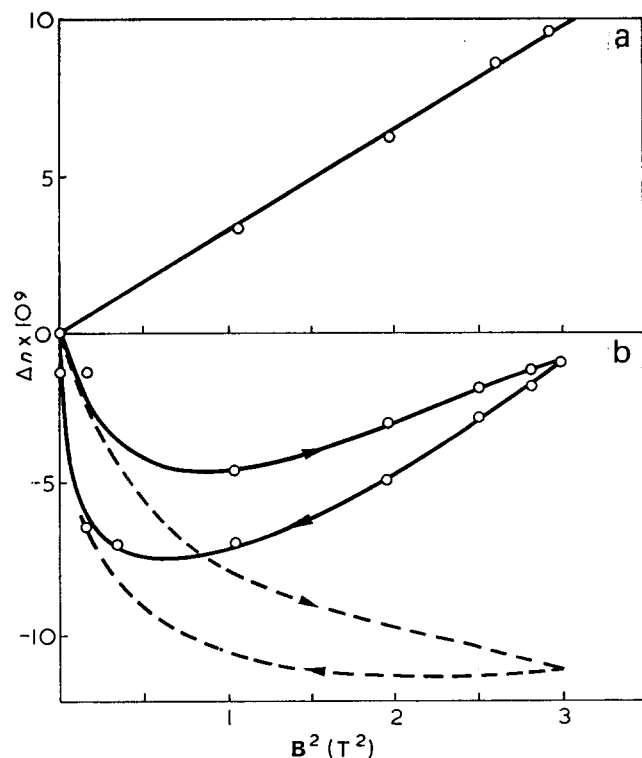


Figure 2 (a) Magnetic birefringence of pure benzene. (b) Birefringence hysteresis of 2.1% polystyrene solution in benzene (—) and solvent corrected solution data using the line for pure benzene in (a) (----). The arrows show the direction of time increasing

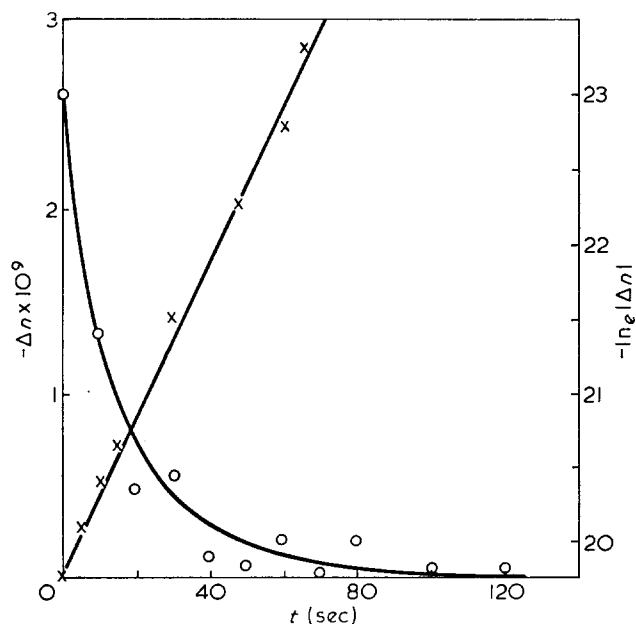


Figure 3 Decay of birefringence with time (○) after removal of magnetic field. Right hand (×) ordinate shows a logarithmic plot of the decay using smoothed data from the curve drawn through the circles. Solvent=benzene; solute=2.1% polystyrene with mol.wt. 3×10^5

the aggregates to be rigid ellipsoids of revolution the birefringence decay theory of O'Konski *et al.*⁸ shows that $\tau \approx \eta V/kT$ where η is the solvent viscosity, kT the thermal energy and V the equivalent spherical volume of the ellipsoid. Putting $\tau = 19$ sec as found, gives $120 \times 10^{-18} \text{ m}^3$ for V and an equivalent radius of about $4 \mu\text{m}$. This aggregate size corresponds to an aggregate of many million single polymer molecules. Similar aggregation has been

proposed by Tager *et al.*⁹ to explain light scattering anomalies of polystyrene in solution.

For all solutions the solute birefringence was negative, implying parallel major optical polarizability and diamagnetic susceptibility axes of the aggregate. The Kerr effect theory of Shah¹⁰ relates the anisotropy of optical and zero-frequency polarizability to the negative birefringence induced in a dilute rigid particle suspension by an applied electric field. Replacing electrical fields and susceptibilities by their magnetic analogues, Shah's theory suggests that:

$$\Delta n = -K \left(1 - \frac{3kT}{|\chi_3 - \chi_1| B^2} \right) \quad (1)$$

where $|\chi_3 - \chi_1|$ is the magnitude of the diamagnetic anisotropy of the particles and K is a function of the particle concentration, optical anisotropy and refractive index.

Equation (1) is only valid when the degree of orientation is approaching saturation and the birefringence is markedly non-quadratic, defined by $|\chi_3 - \chi_1| B^2 > 20kT$. This condition is estimated here to hold over most of the applied field range judged by the non-linearity of the birefringence curves. Thus graphs of Δn plotted with B^{-2} should be linear with (slope)/(intercept) = $-3kT/|\chi_3 - \chi_1|$. Figure 4 shows the variation of Δn with B^{-2} for solvent cyclohexanone. The lower concentrations are seen to fit Shah's theory closely, with straight lines for values of B^2 between 0.125 and 3 T². The higher concentrations diverge from the B^{-2} dependence. This may be due to interaction between the orientating aggregates of which Shah's theory takes no account. $|\chi_3 - \chi_1|$ may be calculated from (slope)/(intercept) = $-3kT/|\chi_3 - \chi_1|$ to be 25×10^{-20} and $19 \times 10^{-20} \text{ J T}^{-2}$ for 0.42% and 0.833% solutions respectively.

Aggregate size can be estimated from volume V and $|\chi_3 - \chi_1|$ as follows. If the density of the aggregate is assumed to be that of the solid polymer and $V = 120 \times 10^{-18} \text{ m}^3$ then the average aggregate mass is about 10^{-14} kg . Taking the polymer molecular weight to

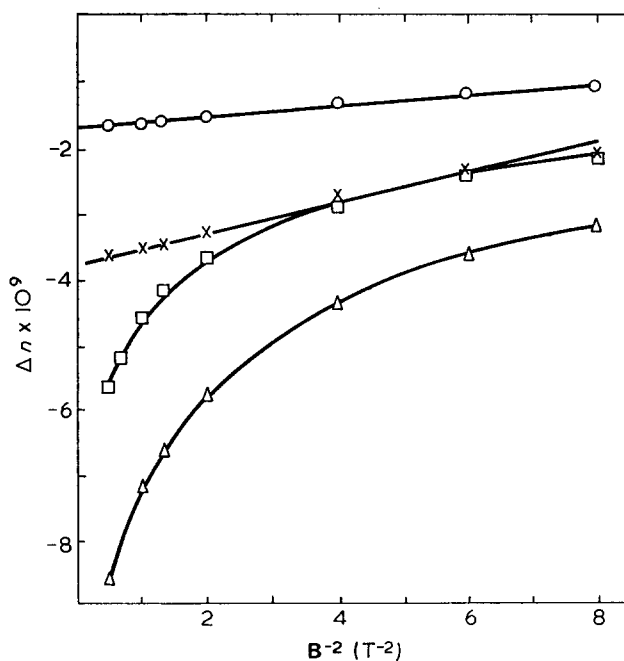


Figure 4 Birefringence versus B^{-2} for polystyrene of mol.wt. 3×10^5 dissolved in cyclohexanone. ○, 0.42%; ×, 0.833%; □, 1.65%; △, 2.75%

be 3×10^5 thus gives about 3×10^4 polymer molecules per aggregate.

Bothner-By and Pople¹¹ give $5.97 \times 10^{-4} \text{ JT}^{-2} \text{ mol}^{-1}$ for the diamagnetic anisotropy of a benzene ring, or about 10^{-24} JT^{-2} per molecule. Compared with the benzene ring anisotropy, bond anisotropies in the polystyrene monomer unit may be neglected as they are typically only $0.1 \times 10^{-4} \text{ JT}^{-2} \text{ mol}^{-1}$. Thus assuming the aggregate diamagnetic anisotropy is due only to the benzene rings and putting $|\chi_3 - \chi_1| = 20 \times 10^{-20} \text{ JT}^{-2}$ gives about 10^5 polymer molecules per aggregate.

The agreement between different estimations of aggregate size and the agreement between Shah's theory and experiment at low concentrations supports the proposal of polymer chain aggregation for polystyrene in cyclohexanone and benzene, the aggregate size being between 10^4 and 10^5 polymer molecules.

G. H. Meeten

Physics Department,
Sir John Cass School of Science and Technology,
Jewry Street, London EC3N 2EY, UK
(Received 14 November 1973)

References

- 1 Majorana, Q. C. R. *Acad. Sci.* 1902, **135**, 159
- 2 Cotton, A. and Mouton, M. C. R. *Acad. Sci.* 1905, **141**, 317
- 3 Mehta, R. V. *J. Colloid Interface Sci.* 1973, **42**, 165
- 4 Desai, J. N., Naik, Y. G., Mehta, R. V. and Dave, M. J. *Indian J. Pure Appl. Phys.* 1969, **7**, 534
- 5 Stuart, H. A. and Peterlin, A. *J. Polym. Sci.* 1950, **5**, 551
- 6 Brown, G. H. and Shaw, W. G. *Chem. Rev.* 1957, **57**, 1049
- 7 Sobajima, S. *J. Phys. Soc. Japan* 1967, **23**, 1070
- 8 O'Konski, C. T., Yoshioka, K. and Ortung, W. H. *J. Phys. Chem.* 1959, **63**, 1558
- 9 Tager, A. A., Andreyeva, V. M. and Yevsina, Ye. M. *Macromol. Sci. USSR* 1964, **6**, 2107
- 10 Shah, M. J. *J. Phys. Chem.* 1963, **67**, 2215
- 11 Bothner-By, A. A. and Pople, J. A. *A. Rev. Phys. Chem.* 1965, **16**, 43

Diagnosis of graft copolymers by adhesion analysis

Difficulty has long existed for research workers in selecting methods which would differentiate between a physical blend of two polymers and their corresponding graft copolymer. We wish to report the use of an adhesion analysis technique based on differential swelling to identify the presence of a graft copolymer. It is well known that reinforcing fillers restrict the swelling of elastomeric vulcanizates. Several attempts have been made to analyse this behaviour, one of the most elegant being that of Kraus¹. This analysis assumes that in the case of particulate reinforcing filler there exists some form of adhesion at the filler-polymer interface which results in bond localized resistance to swelling on immersion in organic solvents known to swell the unfilled vulcanized elastomer. At a distance from this interface, no restriction is offered to swelling, the behaviour corresponding to an unfilled (gum) vulcanizate. Based on these assumptions, Kraus showed that for a reinforcing (i.e. adhering) filler-polymer system:

$$\frac{V_{r0}}{V_r} = 1 - [3C(1 - V_{r0}^{1/3}) + V_{r0} - 1] \frac{\phi}{1 - \phi} \quad (1)$$

where V_r is the volume fraction of polymer in swollen polymer phase for a filled vulcanizate,

V_{r0} is the same quantity for the corresponding unfilled (gum) vulcanizate,

ϕ is the volume fraction of filler component in the filler-polymer system,

C is a parameter related to the filler but independent of ϕ and V_{r0} .

For the case of a non-reinforcing (hence non-bonding) filler-polymer system the corresponding expression is:

$$\frac{V_{r0}}{V_r} = 1 + (1 - V_{r0}) \frac{\phi}{1 - \phi} \quad (2)$$

The validity of this treatment has been questioned by some sources². However, Zapp³ recently showed that this treatment could be used at least as a diagnostic technique to demonstrate filler-polymer adhesion, since the linear relation predicted for a plot of V_{r0}/V_r against $\phi/(1 - \phi)$ from equations (1) and (2) could result in a negative slope for the reinforcing case but a positive slope for the non-reinforcing case. Kraus had presented some experimental evidence to prove this point which was confirmed by Zapp. We felt that the same arguments could be extended to diagnose graft copolymer formation. Since the components of a graft copolymer are chemically bonded, greater adhesion between the components could be expected in comparison with a physical blend of the same components. If a solvent which swells one component of a suspected graft while being relatively inert towards the other could be found, it resembles the case of a filler-polymer system and hence Kraus' analysis could be applied.

To test this technique we chose a graft copolymer system which has been previously investigated in detail, namely natural rubber (NR)/methyl methacrylate (MMA). Work at the Natural Rubber Producers' Research Association (NRPRA), confirmed subsequently⁵, has shown that for the polymerization of MMA monomer in the presence of NR, efficiency of graft copolymer formation with benzoyl peroxide (Bz_2O_2) as initiator is much higher than if azobisisobutyronitrile (AZBN) is used. Gross products of different composition having NR as the major component (i.e. PMMA treated as a filler in the NR matrix) were prepared by polymerizing MMA monomer in the presence of toluene solutions of NR using Bz_2O_2 and AZBN as initiators. The gross products thus obtained were vulcanized using a non-reverting semi-efficient type of sulphur curing system and the vulcanizates were subjected to equilibrium swelling in hexane (hexane swells NR but is inert to PMMA). V_{r0}/V_r values for the different NR/PMMA compositions have been plotted against $\phi/(1 - \phi)$ values. For comparison purposes, results from NR-HAF black (reinforcing) and SBR-clay (non-reinforcing) elastomers were also investigated. The C values for equation (1), calculated from gradients and V_{r0} values are as follows: NR-MMA (Bz_2O_2 initiated), 1.25; NR-MMA (AZBN initiated), 1.04; NR-HAF black, 1.53.

In his treatment, Kraus did not define the exact nature of the parameter C , but from experimental evidence concluded that it would be abnormally low for a filler-polymer system with low adhesion (non-

be 3×10^5 thus gives about 3×10^4 polymer molecules per aggregate.

Bothner-By and Pople¹¹ give $5.97 \times 10^{-4} \text{ JT}^{-2} \text{ mol}^{-1}$ for the diamagnetic anisotropy of a benzene ring, or about 10^{-24} JT^{-2} per molecule. Compared with the benzene ring anisotropy, bond anisotropies in the polystyrene monomer unit may be neglected as they are typically only $0.1 \times 10^{-4} \text{ JT}^{-2} \text{ mol}^{-1}$. Thus assuming the aggregate diamagnetic anisotropy is due only to the benzene rings and putting $|\chi_3 - \chi_1| = 20 \times 10^{-20} \text{ JT}^{-2}$ gives about 10^5 polymer molecules per aggregate.

The agreement between different estimations of aggregate size and the agreement between Shah's theory and experiment at low concentrations supports the proposal of polymer chain aggregation for polystyrene in cyclohexanone and benzene, the aggregate size being between 10^4 and 10^5 polymer molecules.

G. H. Meeten

Physics Department,
Sir John Cass School of Science and Technology,
Jewry Street, London EC3N 2EY, UK
(Received 14 November 1973)

References

- 1 Majorana, Q. C. R. *Acad. Sci.* 1902, **135**, 159
- 2 Cotton, A. and Mouton, M. C. R. *Acad. Sci.* 1905, **141**, 317
- 3 Mehta, R. V. *J. Colloid Interface Sci.* 1973, **42**, 165
- 4 Desai, J. N., Naik, Y. G., Mehta, R. V. and Dave, M. J. *Indian J. Pure Appl. Phys.* 1969, **7**, 534
- 5 Stuart, H. A. and Peterlin, A. *J. Polym. Sci.* 1950, **5**, 551
- 6 Brown, G. H. and Shaw, W. G. *Chem. Rev.* 1957, **57**, 1049
- 7 Sobajima, S. *J. Phys. Soc. Japan* 1967, **23**, 1070
- 8 O'Konski, C. T., Yoshioka, K. and Ortung, W. H. *J. Phys. Chem.* 1959, **63**, 1558
- 9 Tager, A. A., Andreyeva, V. M. and Yevsina, Ye. M. *Macromol. Sci. USSR* 1964, **6**, 2107
- 10 Shah, M. J. *J. Phys. Chem.* 1963, **67**, 2215
- 11 Bothner-By, A. A. and Pople, J. A. *A. Rev. Phys. Chem.* 1965, **16**, 43

Diagnosis of graft copolymers by adhesion analysis

Difficulty has long existed for research workers in selecting methods which would differentiate between a physical blend of two polymers and their corresponding graft copolymer. We wish to report the use of an adhesion analysis technique based on differential swelling to identify the presence of a graft copolymer. It is well known that reinforcing fillers restrict the swelling of elastomeric vulcanizates. Several attempts have been made to analyse this behaviour, one of the most elegant being that of Kraus¹. This analysis assumes that in the case of particulate reinforcing filler there exists some form of adhesion at the filler-polymer interface which results in bond localized resistance to swelling on immersion in organic solvents known to swell the unfilled vulcanized elastomer. At a distance from this interface, no restriction is offered to swelling, the behaviour corresponding to an unfilled (gum) vulcanizate. Based on these assumptions, Kraus showed that for a reinforcing (i.e. adhering) filler-polymer system:

$$\frac{V_{r0}}{V_r} = 1 - [3C(1 - V_{r0}^{1/3}) + V_{r0} - 1] \frac{\phi}{1 - \phi} \quad (1)$$

where V_r is the volume fraction of polymer in swollen polymer phase for a filled vulcanizate,

V_{r0} is the same quantity for the corresponding unfilled (gum) vulcanizate,

ϕ is the volume fraction of filler component in the filler-polymer system,

C is a parameter related to the filler but independent of ϕ and V_{r0} .

For the case of a non-reinforcing (hence non-bonding) filler-polymer system the corresponding expression is:

$$\frac{V_{r0}}{V_r} = 1 + (1 - V_{r0}) \frac{\phi}{1 - \phi} \quad (2)$$

The validity of this treatment has been questioned by some sources². However, Zapp³ recently showed that this treatment could be used at least as a diagnostic technique to demonstrate filler-polymer adhesion, since the linear relation predicted for a plot of V_{r0}/V_r against $\phi/(1 - \phi)$ from equations (1) and (2) could result in a negative slope for the reinforcing case but a positive slope for the non-reinforcing case. Kraus had presented some experimental evidence to prove this point which was confirmed by Zapp. We felt that the same arguments could be extended to diagnose graft copolymer formation. Since the components of a graft copolymer are chemically bonded, greater adhesion between the components could be expected in comparison with a physical blend of the same components. If a solvent which swells one component of a suspected graft while being relatively inert towards the other could be found, it resembles the case of a filler-polymer system and hence Kraus' analysis could be applied.

To test this technique we chose a graft copolymer system which has been previously investigated in detail, namely natural rubber (NR)/methyl methacrylate (MMA). Work at the Natural Rubber Producers' Research Association (NR/PRA), confirmed subsequently⁵, has shown that for the polymerization of MMA monomer in the presence of NR, efficiency of graft copolymer formation with benzoyl peroxide (Bz_2O_2) as initiator is much higher than if azobisisobutyronitrile (AZBN) is used. Gross products of different composition having NR as the major component (i.e. PMMA treated as a filler in the NR matrix) were prepared by polymerizing MMA monomer in the presence of toluene solutions of NR using Bz_2O_2 and AZBN as initiators. The gross products thus obtained were vulcanized using a non-reverting semi-efficient type of sulphur curing system and the vulcanizates were subjected to equilibrium swelling in hexane (hexane swells NR but is inert to PMMA). V_{r0}/V_r values for the different NR/PMMA compositions have been plotted against $\phi/(1 - \phi)$ values. For comparison purposes, results from NR-HAF black (reinforcing) and SBR-clay (non-reinforcing) elastomers were also investigated. The C values for equation (1), calculated from gradients and V_{r0} values are as follows: NR-MMA (Bz_2O_2 initiated), 1.25; NR-MMA (AZBN initiated), 1.04; NR-HAF black, 1.53.

In his treatment, Kraus did not define the exact nature of the parameter C , but from experimental evidence concluded that it would be abnormally low for a filler-polymer system with low adhesion (non-

reinforcing). For example, graphitized, hence non-adhering, and fine thermal low adhering, carbon blacks were shown by Kraus to have C values of 0.77 and 0.92 respectively. Our C values for the two NR-MMA systems (AZBN and Bz_2O_2 initiated) appear to indicate adhesion although it must be noted that the C value for the Bz_2O_2 initiated system is about 20% higher than that for the AZBN initiated system. This seems to be in accordance with the higher grafting efficiency of the Bz_2O_2 initiated system. This apparent adhesion in a system where grafting efficiency has been reported to be low is probably the result of micelle formation. Several reports in the literature reveal that small amounts of graft copolymer are sufficient to homogenize and increase the compatibility of a physical blend. Differential swelling measurements thus appear to be capable of diagnosing the effect on bulk properties of a blend exerted by small amounts of graft copolymer.

We are at present applying this technique to binary elastomeric systems formed by polymerization of cyclic ethers in the presence of polydienes, detailed results of which will be published in the future⁶.

Acknowledgement

The authors are pleased to acknowledge the considerable interest and advice of Professor R. J. W. Reynolds in furthering this work.

L. P. Mendis and C. Hepburn

*Institute of Polymer Technology,
Loughborough University of Technology,
Loughborough, Leics LE11 3TU, UK
(Received 3 December 1973)*

References

- 1 Kraus, G. J. *Appl. Polym. Sci.* 1963, 7, 861
- 2 Porter, M. *Rubber Chem. Technol.* 1967, 40, 866
- 3 Zapp, R. L. *Adv. Chem. Ser.* 1971, 99, Ch 6
- 4 Allen, P. W. 'Chemistry and Physics of Rubber-like Substances', (Ed. L. Bateman), Maclaren, London, 1963, Ch 5
- 5 Ghosh, P. and Sengupta, P. K. *J. Appl. Polym. Sci.* 1967, 11, 1603
- 6 Hepburn, C., Mendis, L. P. and Reynolds, R. J. W. *IUPAC Macromol. Symp., Aberdeen 1973*, paper F5

ERRATUM

'Nuclear magnetic resonance studies of polydienes: 1. ¹³C n.m.r. of 1,4-polybutadiene by π -allyl nickel trifluoroacetate catalysts' by F. Conti, A. Segre, P. Pini and L. Porri, *Polymer* 1974, 15, 5-8.

Page 5, Authors' names:
for P. Pini, read D. Pini

The senior author apologizes for this oversight.

ENERGY POLICY

the economics and planning of energy

third issue • December 1973

Energy in the USA — the future —

" we are well on the way towards expanding domestic production of oil, and with additional Government initiative, we could move within a decade to a more comfortable balance in our energy supplies"

William E. Simon, who is now the head of the new US Federal Energy Administration, writing on changes in investment and balance of payments in the December issue. A companion article by Professor Stephen McDonald of the University of Texas at Austin examines future patterns of supply and demand.

In the same issue:

The impact of the motor car on oil reserves by Gerald Leach; The future growth of nuclear power: Part 2. Choices and obstacles, by A.J. Surrey; A survey of the market for nuclear power in developing countries by O.B. Falls; Beauty and the beast: the siting dilemma in New York State by Alvin Kaufman

Other sections

- News
- Conference reports
- Forthcoming conferences
- Book reviews and announcements
- Publications received

ENERGY POLICY is

International: covering the resources and capabilities of particular countries and regions and the increasing interdependence of their needs:

Integrative: including coal, oil, gas, nuclear, hydro and alternative energy sources:

Interdisciplinary: drawing together studies by technologists with those of economists, geographers, environmentalists and political scientists.

One-year subscription (four issues) £14.00 (\$ 36.00)

Published quarterly in March, June, September, December, commencing with June 1973 issue.

For full details apply to:
IPC Science and Technology Press Limited (Dept AD.EP9E)
IPC House, 32 High Street, Guildford, Surrey, England.
Telephone Guildford (0483) 71661

reinforcing). For example, graphitized, hence non-adhering, and fine thermal low adhering, carbon blacks were shown by Kraus to have C values of 0.77 and 0.92 respectively. Our C values for the two NR-MMA systems (AZBN and Bz_2O_2 initiated) appear to indicate adhesion although it must be noted that the C value for the Bz_2O_2 initiated system is about 20% higher than that for the AZBN initiated system. This seems to be in accordance with the higher grafting efficiency of the Bz_2O_2 initiated system. This apparent adhesion in a system where grafting efficiency has been reported to be low is probably the result of micelle formation. Several reports in the literature reveal that small amounts of graft copolymer are sufficient to homogenize and increase the compatibility of a physical blend. Differential swelling measurements thus appear to be capable of diagnosing the effect on bulk properties of a blend exerted by small amounts of graft copolymer.

We are at present applying this technique to binary elastomeric systems formed by polymerization of cyclic ethers in the presence of polydienes, detailed results of which will be published in the future⁶.

Acknowledgement

The authors are pleased to acknowledge the considerable interest and advice of Professor R. J. W. Reynolds in furthering this work.

L. P. Mendis and C. Hepburn

*Institute of Polymer Technology,
Loughborough University of Technology,
Loughborough, Leics LE11 3TU, UK
(Received 3 December 1973)*

References

- 1 Kraus, G. J. *Appl. Polym. Sci.* 1963, 7, 861
- 2 Porter, M. *Rubber Chem. Technol.* 1967, 40, 866
- 3 Zapp, R. L. *Adv. Chem. Ser.* 1971, 99, Ch 6
- 4 Allen, P. W. 'Chemistry and Physics of Rubber-like Substances', (Ed. L. Bateman), Maclaren, London, 1963, Ch 5
- 5 Ghosh, P. and Sengupta, P. K. *J. Appl. Polym. Sci.* 1967, 11, 1603
- 6 Hepburn, C., Mendis, L. P. and Reynolds, R. J. W. *IUPAC Macromol. Symp., Aberdeen 1973*, paper F5

ERRATUM

'Nuclear magnetic resonance studies of polydienes: 1. ¹³C n.m.r. of 1,4-polybutadiene by π -allyl nickel trifluoroacetate catalysts' by F. Conti, A. Segre, P. Pini and L. Porri, *Polymer* 1974, 15, 5-8.

Page 5, Authors' names:
for P. Pini, read D. Pini

The senior author apologizes for this oversight.

ENERGY POLICY

the economics and planning of energy

third issue • December 1973

Energy in the USA — the future —

" we are well on the way towards expanding domestic production of oil, and with additional Government initiative, we could move within a decade to a more comfortable balance in our energy supplies"

William E. Simon, who is now the head of the new US Federal Energy Administration, writing on changes in investment and balance of payments in the December issue. A companion article by Professor Stephen McDonald of the University of Texas at Austin examines future patterns of supply and demand.

In the same issue:

The impact of the motor car on oil reserves by Gerald Leach; The future growth of nuclear power: Part 2. Choices and obstacles, by A.J. Surrey; A survey of the market for nuclear power in developing countries by O.B. Falls; Beauty and the beast: the siting dilemma in New York State by Alvin Kaufman

Other sections

- News**
- Conference reports**
- Forthcoming conferences**
- Book reviews and announcements**
- Publications received**

ENERGY POLICY is

International: covering the resources and capabilities of particular countries and regions and the increasing interdependence of their needs:

Integrative: including coal, oil, gas, nuclear, hydro and alternative energy sources:

Interdisciplinary: drawing together studies by technologists with those of economists, geographers, environmentalists and political scientists.

One-year subscription (four issues) £14.00 (\$ 36.00)

Published quarterly in March, June, September, December, commencing with June 1973 issue.

For full details apply to:
IPC Science and Technology Press Limited (Dept AD.EP9E)
IPC House, 32 High Street, Guildford, Surrey, England.
Telephone Guildford (0483) 71661

Book Reviews

Advances in polymer science and engineering

Edited by K. D. Pae, D. R. Morrow and Yu Chen
Plenum Press, New York, 1973, 350 pp. \$19.50

This book is a compendium of eighteen papers presented to a Symposium held at Rutgers University on 26 and 27 October 1972, in honour of Professor J. A. Sauer's sixtieth birthday. As would be expected, the papers cover a wide range of topics on the structure and mechanical behaviour of polymers, reflecting Professor Sauer's own broad interests. The papers on structure include an excellent summary by Peterlin of the morphological changes occurring during the drawing of crystalline polymers and a very substantial article on the interpretation of small angle X-ray diffraction from crystalline polymers by Burmester and Geil. There are three papers concerned with single crystals, including one by Professor Sauer and his coworkers on surface morphology and deformation of polypropylene single crystals.

The papers on mechanical properties cover an even wider range. Experimental studies of linear polyethylene, ABA type block copolymers, polycarbonate, wood and poly(ethylene terephthalate) concentrate primarily on low strain dynamic mechanical behaviour, usually in conjunction with other techniques such as dielectric relaxation or sorption characteristics. There are also papers on higher strain behaviour, including an interesting study of the influence of pressure on polychlorotrifluoroethylene, a theoretical development in non-linear viscoelasticity, and discussion of the structure of tie molecules. A final group of papers on melt rheology, includes consideration of structural factors which influence the flow behaviour of low density polyethylene and ethylene-acrylic acid copolymers, and a theoretical treatment of die swell by Yu Chen.

These papers are of a uniformly high standard, and present a wide range of material, most of which is of very recent origin. The book can therefore be recommended as providing a reliable account of the present state of the art in this area of research.

I. M. Ward

Reclaiming rubber and other polymers

J. A. Szilard

Noyes Data Corporation, Park Ridge, New Jersey, 1973, 310 pp. \$36.00

This book contains a detailed summary of some 125 US patent specifications published between 1955 and 1972. Its major purpose is to describe the number of technical possibilities available which may open up profitable areas for research and development in the reclaiming of rubber and other polymers.

Although in the foreword it is stated that many of the patents are being used commercially, there is, not unexpectedly, no indication of which these are. This book does not, therefore, meet a requirement for one to which reference may be made for information on industrially important polymer reclaiming processes.

Almost since the beginning of the industry, with the discovery of vulcanization about 135 years ago, scrap rubber has been re-used as a compounding ingredient with new rubber, either as a finely ground dust or as a chemically and/or thermally devulcanized or depolymerized plastic material. The reviewer prefers to confine the terms 'reclaim' and 'reclaimed rubber' to the latter as, indeed, such authorities as J. M. Ball have done in their publications. It is to be regretted that the preparation and uses of ground scrap vulcanized rubber and reclaimed rubber are not separately assembled in the three long chapters, which constitute considerably more than half the text, on the technology, the additives and the uses of reclaimed rubber.

The range of processes described is wide, covering such matters as the elimination of fibres from unvulcanized rubber scrap, the

pelletizing of reclaimed rubber and oxidative distillation. The 'additives' chapter reports on chemicals to aid the degradation and plasticization of the product, and on the use of other polymers to bind ground scrap. The term 'uses' of reclaimed rubber has similarly been widely interpreted to the extent that description of a barrier to prevent the staining of the white sidewall of a tyre by a carcass compound containing reclaimed rubber is included.

The remaining nine chapters deal with polyesters, polyurethanes, polystyrenes, polyamides, polysiloxanes, polyolefins, fluorocarbons, polyvinyls and miscellaneous polymers; five of them cover less than five patents. The objective in the majority of these patents, concerned with plastics polymers, is to recover the polymer, prepolymer or monomer from association with filler and pigment, from fibres, metal or a second polymer in waste material or scrap components. Reclaiming is again interpreted very broadly and processes based on chemical and physical methods are included. Elastomers based on silicones, fluorocarbon and nitroso polymers, which one might expect to find in the first three chapters covering rubbers, are included in the respective chapters alongside plastics.

The author is to be congratulated on producing interesting and readable accounts from the legally phrased patent specifications and the book is certainly an idea-promoting publication. Adequate, informative and clear line drawings of equipment and processes and tables of recipes and properties add much to the value of the book. The only indexes are to inventors, companies and patent numbers; a subject index, or subtitling in the contents list, would have made the book easier to use for reference.

C. M. Blow

Condensation monomers

Edited by J. K. Stille and T. W. Campbell

Wiley-Interscience, New York, 1973, 745 pp. £18.50

The compilation of this multi-author work, which forms Vol 27 of the Wiley-Interscience High Polymers series, was begun in 1967 initially under the editorship of the late T. W. Campbell (to whom it is dedicated) and subsequently of J. K. Stille, another noted American worker in synthetic polymer chemistry.

The book describes the synthesis, utility and general properties of intermediates useful for the preparation of linear condensation polymers. Questions of semantics arise at the outset since these intermediates, in general, are strictly not 'monomers' but co-reactants; furthermore, the term 'condensation polymers' extends by common usage to important groups of substances, e.g. polyurethanes and certain nylons, which are not made in practice, by polycondensation methods. The editors have therefore wisely, if unsystematically, extended the scope of their book to include diisocyanates and some other non-condensant precursors of polar and/or crystalline polymers. Attention is drawn to another recently published book, Frisch's 'Cyclic Monomers' (Vol 26 of the High Polymers series), which has been planned in parallel with the present work and includes further classes of starting materials for 'condensation' polymers.

The larger part of the Stille-Campbell book is devoted to the principal aliphatic 'monomers' (dicarboxylic acids, hydroxy acids, diamines, diols and bischloroformates); aromatic 'monomers' (dicarboxylic acids and their derivatives, diamines, bisphenols and their chloroformates); and diisocyanates. Accounts are also given of carbonyl and thiocarbonyl monomers, and of the tetra-functional precursors of the newer polyheterocyclic materials. For each series the main emphasis is placed on surveying and describing methods of synthesis, especially on the laboratory scale and often with full experimental detail, followed by summary accounts of physical properties, analytical procedures, relevant storage and toxicological data, and concise discussions of the use of the materials in polymerization. More than 3500 literature references are included.

Mild criticism must be made of the arbitrariness of selection at various points. Chapters 1 and 4, for example, describe aliphatic dicarboxylic and hydroxycarboxylic acids, virtually irrespective of their specific utility as condensants, and hence including many substances of minimum interest as 'monomers'. Industrial processes are treated only sketchily and little attempt is made to present a critical comparison of the various large-scale routes and procedures available for intermediates manufacture. Surprisingly, the important family of amino acids is not considered, and other significant omissions concerned the phenol precursors of aromatic polyethers; trimesic acid; the diphenyl- and diphenoxyalkane dicarboxylic acids; the biscarbamoyl chlorides; the methyladipic acids, and the difunctional trimethyl hexamethylene compounds, all of which have acquired considerable interest as condensants in recent years.

There has been some laxity in proof-reading. The many errors noted included various mis-spellings of the names 'Qiana' and 'Henkel' and (on pp 105 and 509) certain difficulties with 'formyl' and 'phthaloyl'. On p 303, Dickson (the co-inventor of Terylene) is misnamed. The pagination of pp 437-8 was unfortunately transposed in the review copy, and it is to be hoped that users of the analytical method on p 457 will not maintain their water condensers at 250°C! Spectra of the more important substances could usefully have been included, as could an author index.

The book is not a work of theory, nor one designed to offer new insights into the subject. Its value is as a compendium of facts and methods, particularly for laboratory use. As such, despite some limitations and blemishes, it can be recommended to research workers seeking help in planning the synthesis of novel condensation polymers.

I. Goodman

Water soluble polymers

Edited by N. M. Bikales

Plenum Press, New York, 1973, 424 pp. \$23.00

In recent years water soluble polymers have been attracting increasing attention because of their usefulness in industrial and environmental applications. The most notable properties of these polymers is their ability to flocculate suspended solids and this has led to important applications in sewage treatment and paper making technology (drainage and retention aids). Other important applications include the so-called secondary recovery of petroleum from oil fields, the reduction of turbulent friction of fluids and as a component of water based finished and coatings. This book, which is based on papers presented to a symposium held by the American Chemical Society in August 1972, provides an important and valuable review of the above topics and also a number of papers on the synthesis and characterization of water soluble polymers. The industrial manufacture of one of the most important

of these polymers, polyacrylamide, is described in detail. The description of many new polymers and their synthesis is discussed in six papers. The section on Characterization (six papers) includes the description of the methods of exclusion chromatography, sedimentation equilibrium, viscoelastic properties together with an account of the biological activity of these polymers.

The papers as a whole provide a thorough examination of this new and important area of polymer science and application.

C. E. H. Brown

High-modulus wholly aromatic fibres

Edited by W. B. Black and J. Preston

Marcel Dekker, New York, 1973. \$22.50

The search for fibres having improved strength, modulus and high-temperature performance compared with conventional materials for use as reinforcing agents and in other specialized applications is of the greatest industrial importance. The publication of a book devoted to one particular class of materials which show great promise is, therefore, welcome, even though it is based on the proceedings of a conference at which the contributors, with one exception, were from a single company, and some of the contributions have previously been published elsewhere. Actually, although the editors in their preface apologize for the restricted sources of the contributions, this is in fact an advantage from the reader's point of view, for it gives to the whole a unity of aim and general cohesion which is all too often lacking in collective works of this kind.

The contributions are arranged in three main sections, concerned respectively with: (a) the chemistry involved in the preparation of aromatic fibres, mainly of the polyamide-hydrazide type; (b) the characterization of the morphology and physical properties of a representative type of fibre; and (c) applications to composites, tyre cords, etc.

The materials examined have values of tenacity of the order of 500 g/denier, combined with sufficiently high values of extensibility (~4% or more) to give them considerable advantages over their principal competitors (glass, carbon fibres, etc.). It is surprising (to the reviewer) to see how far the technical development and scientific assessment of this class of materials has advanced. Of particular interest are the frequent allusions to the calculated values of elastic modulus, inspired by the original work of H. Mark, work which at the time must surely have been regarded as of purely academic interest, but which is now seen to have quite direct practical relevance.

The book is well produced, and will be held in considerable esteem by both academic and industrial workers in the field of synthetic polymers and fibres.

L. R. G. Treloar

Conference Announcement

Rubber and Rubber Elasticity

UMIST, Manchester, 27 and 28 March 1974

The Fifth Biennial Manchester Polymer Symposium on Rubber and Rubber Elasticity has been organized at UMIST on 27 and 28 March 1974 to mark the retirement of Professor L. R. G. Treloar from his Chair of Polymer and Fibre Science in the Institute. Recent developments in the chemistry and physics of elastomers will be presented by distinguished workers from USA, Japan and UK. Applications for registration should be made as soon as possible to The Registrar, University of Manchester Institute of Science and Technology (UMIST), PO Box 88, Manchester M60 1QD, UK.

Conference Announcement

State of order in amorphous polymers

Sorrento, Naples, Italy, 1-3 May 1974

The 2nd Europhysics Conference of the Section of Macromolecular Physics (of the European Physical Society, Division of the Physics of Condensed Matter), originally scheduled to take place in October 1973 at Naples, will now be held from 1 to 3 May 1974 at Sorrento, near Naples. A full programme of both invited and contributed papers on the State of Order in Amorphous Polymers has been arranged. Further details may be obtained from Professor Paolo Corradini, Istituto Chimico, Via Mezzocannone 4, 80134 Napoli, Italy.

Book Reviews

Advances in polymer science and engineering

Edited by K. D. Pae, D. R. Morrow and Yu Chen
Plenum Press, New York, 1973, 350 pp. \$19.50

This book is a compendium of eighteen papers presented to a Symposium held at Rutgers University on 26 and 27 October 1972, in honour of Professor J. A. Sauer's sixtieth birthday. As would be expected, the papers cover a wide range of topics on the structure and mechanical behaviour of polymers, reflecting Professor Sauer's own broad interests. The papers on structure include an excellent summary by Peterlin of the morphological changes occurring during the drawing of crystalline polymers and a very substantial article on the interpretation of small angle X-ray diffraction from crystalline polymers by Burmester and Geil. There are three papers concerned with single crystals, including one by Professor Sauer and his coworkers on surface morphology and deformation of polypropylene single crystals.

The papers on mechanical properties cover an even wider range. Experimental studies of linear polyethylene, ABA type block copolymers, polycarbonate, wood and poly(ethylene terephthalate) concentrate primarily on low strain dynamic mechanical behaviour, usually in conjunction with other techniques such as dielectric relaxation or sorption characteristics. There are also papers on higher strain behaviour, including an interesting study of the influence of pressure on polychlorotrifluoroethylene, a theoretical development in non-linear viscoelasticity, and discussion of the structure of tie molecules. A final group of papers on melt rheology, includes consideration of structural factors which influence the flow behaviour of low density polyethylene and ethylene-acrylic acid copolymers, and a theoretical treatment of die swell by Yu Chen.

These papers are of a uniformly high standard, and present a wide range of material, most of which is of very recent origin. The book can therefore be recommended as providing a reliable account of the present state of the art in this area of research.

I. M. Ward

Reclaiming rubber and other polymers

J. A. Szilard

Noyes Data Corporation, Park Ridge, New Jersey, 1973, 310 pp. \$36.00

This book contains a detailed summary of some 125 US patent specifications published between 1955 and 1972. Its major purpose is to describe the number of technical possibilities available which may open up profitable areas for research and development in the reclaiming of rubber and other polymers.

Although in the foreword it is stated that many of the patents are being used commercially, there is, not unexpectedly, no indication of which these are. This book does not, therefore, meet a requirement for one to which reference may be made for information on industrially important polymer reclaiming processes.

Almost since the beginning of the industry, with the discovery of vulcanization about 135 years ago, scrap rubber has been re-used as a compounding ingredient with new rubber, either as a finely ground dust or as a chemically and/or thermally devulcanized or depolymerized plastic material. The reviewer prefers to confine the terms 'reclaim' and 'reclaimed rubber' to the latter as, indeed, such authorities as J. M. Ball have done in their publications. It is to be regretted that the preparation and uses of ground scrap vulcanized rubber and reclaimed rubber are not separately assembled in the three long chapters, which constitute considerably more than half the text, on the technology, the additives and the uses of reclaimed rubber.

The range of processes described is wide, covering such matters as the elimination of fibres from unvulcanized rubber scrap, the

pelletizing of reclaimed rubber and oxidative distillation. The 'additives' chapter reports on chemicals to aid the degradation and plasticization of the product, and on the use of other polymers to bind ground scrap. The term 'uses' of reclaimed rubber has similarly been widely interpreted to the extent that description of a barrier to prevent the staining of the white sidewall of a tyre by a carcass compound containing reclaimed rubber is included.

The remaining nine chapters deal with polyesters, polyurethanes, polystyrenes, polyamides, polysiloxanes, polyolefins, fluorocarbons, polyvinyls and miscellaneous polymers; five of them cover less than five patents. The objective in the majority of these patents, concerned with plastics polymers, is to recover the polymer, prepolymer or monomer from association with filler and pigment, from fibres, metal or a second polymer in waste material or scrap components. Reclaiming is again interpreted very broadly and processes based on chemical and physical methods are included. Elastomers based on silicones, fluorocarbon and nitroso polymers, which one might expect to find in the first three chapters covering rubbers, are included in the respective chapters alongside plastics.

The author is to be congratulated on producing interesting and readable accounts from the legally phrased patent specifications and the book is certainly an idea-promoting publication. Adequate, informative and clear line drawings of equipment and processes and tables of recipes and properties add much to the value of the book. The only indexes are to inventors, companies and patent numbers; a subject index, or subtitling in the contents list, would have made the book easier to use for reference.

C. M. Blow

Condensation monomers

Edited by J. K. Stille and T. W. Campbell

Wiley-Interscience, New York, 1973, 745 pp. £18.50

The compilation of this multi-author work, which forms Vol 27 of the Wiley-Interscience High Polymers series, was begun in 1967 initially under the editorship of the late T. W. Campbell (to whom it is dedicated) and subsequently of J. K. Stille, another noted American worker in synthetic polymer chemistry.

The book describes the synthesis, utility and general properties of intermediates useful for the preparation of linear condensation polymers. Questions of semantics arise at the outset since these intermediates, in general, are strictly not 'monomers' but co-reactants; furthermore, the term 'condensation polymers' extends by common usage to important groups of substances, e.g. polyurethanes and certain nylons, which are not made in practice, by polycondensation methods. The editors have therefore wisely, if unsystematically, extended the scope of their book to include diisocyanates and some other non-condensant precursors of polar and/or crystalline polymers. Attention is drawn to another recently published book, Frisch's 'Cyclic Monomers' (Vol 26 of the High Polymers series), which has been planned in parallel with the present work and includes further classes of starting materials for 'condensation' polymers.

The larger part of the Stille-Campbell book is devoted to the principal aliphatic 'monomers' (dicarboxylic acids, hydroxy acids, diamines, diols and bischloroformates); aromatic 'monomers' (dicarboxylic acids and their derivatives, diamines, bisphenols and their chloroformates); and diisocyanates. Accounts are also given of carbonyl and thiocarbonyl monomers, and of the tetra-functional precursors of the newer polyheterocyclic materials. For each series the main emphasis is placed on surveying and describing methods of synthesis, especially on the laboratory scale and often with full experimental detail, followed by summary accounts of physical properties, analytical procedures, relevant storage and toxicological data, and concise discussions of the use of the materials in polymerization. More than 3500 literature references are included.

Mild criticism must be made of the arbitrariness of selection at various points. Chapters 1 and 4, for example, describe aliphatic dicarboxylic and hydroxycarboxylic acids, virtually irrespective of their specific utility as condensants, and hence including many substances of minimum interest as 'monomers'. Industrial processes are treated only sketchily and little attempt is made to present a critical comparison of the various large-scale routes and procedures available for intermediates manufacture. Surprisingly, the important family of amino acids is not considered, and other significant omissions concerned the phenol precursors of aromatic polyethers; trimesic acid; the diphenyl- and diphenoxyalkane dicarboxylic acids; the biscarbamoyl chlorides; the methyladipic acids, and the difunctional trimethyl hexamethylene compounds, all of which have acquired considerable interest as condensants in recent years.

There has been some laxity in proof-reading. The many errors noted included various mis-spellings of the names 'Qiana' and 'Henkel' and (on pp 105 and 509) certain difficulties with 'formyl' and 'phthaloyl'. On p 303, Dickson (the co-inventor of Terylene) is misnamed. The pagination of pp 437-8 was unfortunately transposed in the review copy, and it is to be hoped that users of the analytical method on p 457 will not maintain their water condensers at 250°C! Spectra of the more important substances could usefully have been included, as could an author index.

The book is not a work of theory, nor one designed to offer new insights into the subject. Its value is as a compendium of facts and methods, particularly for laboratory use. As such, despite some limitations and blemishes, it can be recommended to research workers seeking help in planning the synthesis of novel condensation polymers.

I. Goodman

Water soluble polymers

Edited by N. M. Bikales

Plenum Press, New York, 1973, 424 pp. \$23.00

In recent years water soluble polymers have been attracting increasing attention because of their usefulness in industrial and environmental applications. The most notable properties of these polymers is their ability to flocculate suspended solids and this has led to important applications in sewage treatment and paper making technology (drainage and retention aids). Other important applications include the so-called secondary recovery of petroleum from oil fields, the reduction of turbulent friction of fluids and as a component of water based finished and coatings. This book, which is based on papers presented to a symposium held by the American Chemical Society in August 1972, provides an important and valuable review of the above topics and also a number of papers on the synthesis and characterization of water soluble polymers. The industrial manufacture of one of the most important

of these polymers, polyacrylamide, is described in detail. The description of many new polymers and their synthesis is discussed in six papers. The section on Characterization (six papers) includes the description of the methods of exclusion chromatography, sedimentation equilibrium, viscoelastic properties together with an account of the biological activity of these polymers.

The papers as a whole provide a thorough examination of this new and important area of polymer science and application.

C. E. H. Brown

High-modulus wholly aromatic fibres

Edited by W. B. Black and J. Preston

Marcel Dekker, New York, 1973. \$22.50

The search for fibres having improved strength, modulus and high-temperature performance compared with conventional materials for use as reinforcing agents and in other specialized applications is of the greatest industrial importance. The publication of a book devoted to one particular class of materials which show great promise is, therefore, welcome, even though it is based on the proceedings of a conference at which the contributors, with one exception, were from a single company, and some of the contributions have previously been published elsewhere. Actually, although the editors in their preface apologize for the restricted sources of the contributions, this is in fact an advantage from the reader's point of view, for it gives to the whole a unity of aim and general cohesion which is all too often lacking in collective works of this kind.

The contributions are arranged in three main sections, concerned respectively with: (a) the chemistry involved in the preparation of aromatic fibres, mainly of the polyamide-hydrazide type; (b) the characterization of the morphology and physical properties of a representative type of fibre; and (c) applications to composites, tyre cords, etc.

The materials examined have values of tenacity of the order of 500 g/denier, combined with sufficiently high values of extensibility (~4% or more) to give them considerable advantages over their principal competitors (glass, carbon fibres, etc.). It is surprising (to the reviewer) to see how far the technical development and scientific assessment of this class of materials has advanced. Of particular interest are the frequent allusions to the calculated values of elastic modulus, inspired by the original work of H. Mark, work which at the time must surely have been regarded as of purely academic interest, but which is now seen to have quite direct practical relevance.

The book is well produced, and will be held in considerable esteem by both academic and industrial workers in the field of synthetic polymers and fibres.

L. R. G. Treloar

Conference Announcement

Rubber and Rubber Elasticity

UMIST, Manchester, 27 and 28 March 1974

The Fifth Biennial Manchester Polymer Symposium on Rubber and Rubber Elasticity has been organized at UMIST on 27 and 28 March 1974 to mark the retirement of Professor L. R. G. Treloar from his Chair of Polymer and Fibre Science in the Institute. Recent developments in the chemistry and physics of elastomers will be presented by distinguished workers from USA, Japan and UK. Applications for registration should be made as soon as possible to The Registrar, University of Manchester Institute of Science and Technology (UMIST), PO Box 88, Manchester M60 1QD, UK.

Conference Announcement

State of order in amorphous polymers

Sorrento, Naples, Italy, 1-3 May 1974

The 2nd Europhysics Conference of the Section of Macromolecular Physics (of the European Physical Society, Division of the Physics of Condensed Matter), originally scheduled to take place in October 1973 at Naples, will now be held from 1 to 3 May 1974 at Sorrento, near Naples. A full programme of both invited and contributed papers on the State of Order in Amorphous Polymers has been arranged. Further details may be obtained from Professor Paolo Corradini, Istituto Chimico, Via Mezzocannone 4, 80134 Napoli, Italy.

Effects of crosslink density and length on the number of intramolecular crosslinks (defects) introduced into a rubbery network

Alan E. Tonelli

Bell Laboratories, Murray Hill, New Jersey 07974, USA
(Received 1 June 1973; revised 31 July 1973)

Estimates are presented for the effects of the crosslink density, or the molecular weight of polymer chains between crosslinks, and the length of crosslinks, or crosslinking agents, upon the expected ratio of internal or intramolecular (possibly elastically ineffective) to external or intermolecular (elastically effective) crosslinks introduced in rubber networks crosslinked in both the dry and dissolved states. Model calculations are performed on *cis*-1,4-polyisoprene with the following results: (i) in rubber networks formed by crosslinking in the dry state, the number of possibly inactive, intramolecular crosslinks introduced is negligibly small; and (ii) the relative number of intramolecular crosslinks introduced may become appreciable for those networks formed by lightly crosslinking low molecular weight rubber molecules in solutions, where the volume fraction of rubber present is small, using initiators that produce short crosslinks.

INTRODUCTION

The accompanying sketch (Figure 1) illustrates portions of a crosslinked rubber possessing various network defects (after Flory¹). An entanglement of crosslinked chains (b) can be considered¹ as elastically effective as a chemical crosslink. On the other hand, the defects illustrated in (c) and (d) are not effective in contributing to the modulus of the network. The decrease in the modulus produced by the elastically ineffective chain segments AD and BC shown in (d), both of which are attached to the network at one end only, has been successfully accounted for¹ in terms of the molecular

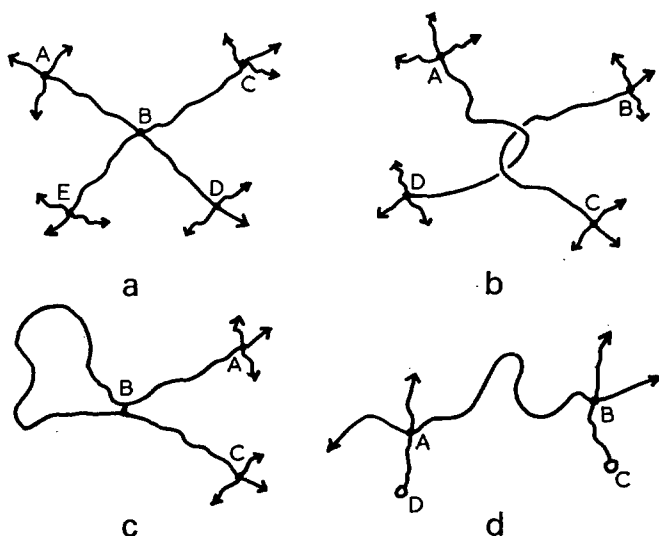


Figure 1 Portions of a crosslinked rubber with various network defects (after Flory¹). (a) Perfect; (b) entanglement; (c) intramolecular crosslink; (d) chain ends. ●, Crosslink; ○, chain end

weight of the rubber before crosslinking. Correction for the presence of chain ends becomes negligible for high initial molecular weights and high degrees of crosslinking.

In a similar manner, the chain loop in (c) formed by the internal, or intramolecular crosslink at B contributes nothing to the elasticity of the network, aside from possibly shortening the effective length of the elastically active chain segment from A to C to the extent that it no longer behaves in a Gaussian fashion¹⁻³. It therefore becomes important to be able to estimate the relative frequency of occurrence of elastically ineffective, internal or intramolecular crosslinks, such as B in (c), relative to those external or intermolecular crosslinks, such as B in (a), which bear the stress in a strained rubber network. Just such an estimate is presented here.

ESTIMATION OF THE RELATIVE NUMBER OF INTRAMOLECULAR CROSSLINKS

A polymer molecule in the amorphous bulk state may be considered⁴ as a spherical cloud of segments distributed in a Gaussian manner* about its centre of gravity. The size of the domain pervaded by the cloud of segments can be characterized by the mean-square radius of gyration^{3, 4} $\langle s^2 \rangle_0$ of the polymer chain. Consequently, a typical polymer chain only physically occupies a small fraction ($\sim 1\%$) of the volume influenced by its segments.

* Flory and Fisk, using the even moments of the radius of gyration calculated by Fixman (see ref 3, Ch VIII), have demonstrated that the distribution of radii of gyration in a long polymer chain is narrowed in comparison to a Gaussian distribution.

Keeping this picture of a polymer chain in the amorphous bulk in mind, we ask the following question: what is the likelihood of finding two segments of the same polymer chain separated by a distance equal to the length of a crosslink relative to a pair of segments belonging to different chains? If we approximate the disposition of polymer segments belonging to the same chain as being uniformly distributed over its spherical domain of influence, then the relative frequency of occurrence of intramolecular crosslinks, i.e. the ratio of intra- to inter-molecular crosslinks, is estimated to be the ratio of the molecular (MOL) to the sphere of influence (SOI) volumes of a polymer chain.

In a dry polymer sample the amount of volume physically occupied by a single chain is:

$$V_{\text{MOL}} = \frac{M \times 10^{24}}{\rho N_A} (\text{\AA}^3) \quad (1)$$

where M is the molecular weight, ρ is the density in g/cm^3 and N_A is Avogadro's number. On the other hand, the amount of volume actually pervaded or influenced by a single chain can be obtained from:

$$V_{\text{SOI}} = \frac{4\pi}{3} (\langle s_n^2 \rangle_0)^{3/2} \quad (2)$$

where $\langle s_n^2 \rangle_0$ is the unperturbed mean-square radius of gyration of a polymer chain of n bonds.

For *cis*-1,4-polyisoprene^{3, 5}, $V_{\text{MOL}} = 31n$ and $V_{\text{SOI}} = 23 \cdot 3n^{3/2}$, both expressed in \AA^3 . Consequently, the ratio of the molecular to the sphere of influence volumes for synthetic rubber is:

$$R_V \equiv V_{\text{MOL}}/V_{\text{SOI}} = 1 \cdot 33n^{-1/2} \quad (3)$$

and we equate this volume ratio with the relative frequency of occurrence of intramolecular crosslinks, i.e., the ratio of internal to external crosslinks. This ratio is presented as a function of chain length in *Table 1*.

DISCUSSION

It is clear from *Table 1* that the assumption of a uniform distribution of segments of the same chain in its sphere of influence volume leads to the prediction that the relative frequency of occurrence of intramolecular crosslinks should increase with an increase in degree of crosslinking due to the concomitant decrease in the average length of the chains between crosslinks. As the degree of crosslinking increases, the length and

molecular weight of the chains between crosslinks decrease resulting in larger values of R_V .

On the other hand, a uniform distribution of segments belonging to the same polymer chain results in the independence of the relative number of intramolecular crosslinks formed and the length of the crosslinking agent*. Consideration of the more realistic Gaussian-like distribution³ of segments within each polymer chain's sphere of influence permits a qualitative accounting of the effect of crosslink length upon the frequency of forming intramolecular crosslinks.

The segment density in each polymer chain's sphere of influence is greatest at the centre and decreases continuously with the distance from the centre. If one end of a crosslink is attached to a segment of a chain near its centre of gravity, then clearly the other end of the crosslink is most likely to find another segment of the same chain at short rather than long distances away from the first segment, hence short crosslink lengths favour the formation of intramolecular crosslinks near the centre of gravity. Near the surface of the cloud of segments, crosslinks of short length also favour the production of intramolecular crosslinks, because they are less likely than long crosslinks to extend beyond the segment cloud surface where only intermolecular crosslinks will be formed. Based on these qualitative observations, it appears that crosslinking agents of short length tend to favour the introduction of intramolecular crosslinks in a rubbery network.

From *Table 1* it is apparent that only for short *cis*-1,4-polyisoprene chains with molecular weights ($M = 17n$) less than $\sim 20\,000$ does the ratio of intra- to inter-molecular crosslinks introduced in a dry network exceed a few per cent¹. Division by the volume fraction of rubber present in solution serves to convert the calculated ratios of internal to external crosslinks presented in *Table 1* for rubbers crosslinked in the dry state to those appropriate to networks formed in solution.

Networks lightly crosslinked in solutions where the volume fraction of rubber present is less than 0.5 may possess a significant fraction of intramolecular crosslinks^{1, 8} which may not contribute to the elasticity of the network, especially if the length of the crosslinks, as obtains in peroxide and radiation initiated crosslinking, is short. In fact, the polymer loops formed by intramolecular crosslinks may act as an internally generated diluent in dry networks formed by crosslinking in relatively dilute solution, thereby reducing⁹⁻¹¹ the departures from the kinetic or statistical theory of rubber elasticity^{1, 2} which are often observed^{2, 12} in networks crosslinked in the dry state.

The conclusion that the introduction of intramolecular crosslinks may have a negligible effect upon the elastic properties of a rubbery network formed in the dry state is further strengthened by the observation that the loop produced by an intramolecular crosslink is very likely to be involved in an elastically effective

Table 1 Ratio R_V of molecular to sphere of influence volume calculated as a function of chain length (n = number of backbone bonds) for *cis*-1,4-polyisoprene

n	R_V	n	R_V
100	0.133	4 000	0.021
200	0.095	5 000	0.019
300	0.078	6 000	0.017
400	0.067	7 000	0.016
500	0.059	8 000	0.015
600	0.055	9 000	0.014
700	0.050	10 000	0.013
800	0.047	20 000	0.009
900	0.044	30 000	0.008
1000	0.042	40 000	0.007
2000	0.030	50 000	0.006
3000	0.025	60 000	0.005

* The shortest possible crosslink in rubber is the length of a C-C bond (1.54 \AA) obtained⁶ when the crosslinking is initiated by peroxides or by exposure to radiation in the form of an electron beam. Crosslinking⁷ with typical bisazodicarboxylic esters and bithiolacids leads to the longest crosslinks of ~ 20 - 25 \AA in length. Sulphur vulcanization produces⁶ crosslinks of intermediate length which depend on the time of cure but usually are in the range 4.0-8.0 \AA .

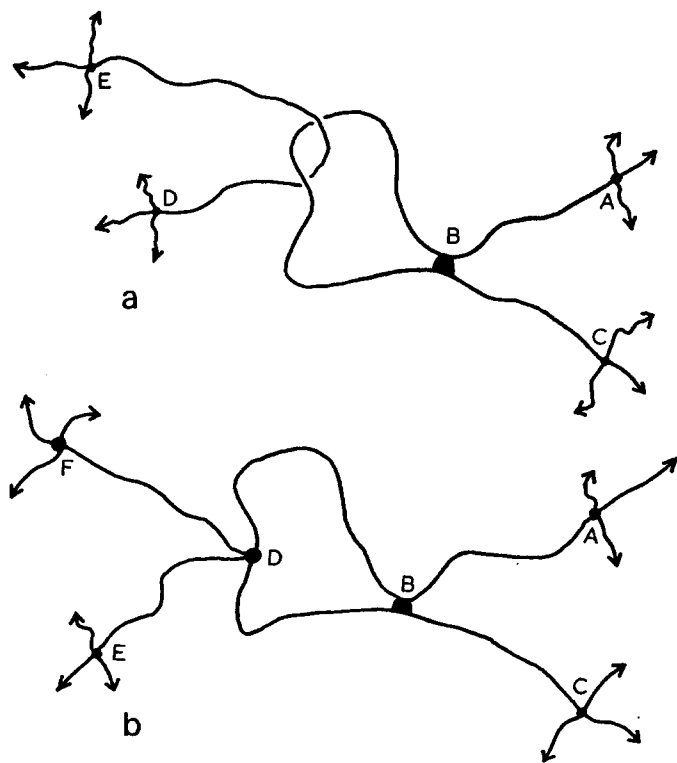


Figure 2 Intramolecular crosslinking showing (a) loop entanglement and (b) loop crosslink

entanglement or crosslinked to an elastically active portion of the network¹³ (see Figure 2). Such entanglements and crosslinks involving the internally cross-

linked chain loop are less likely to occur in those networks lightly crosslinked in solution. Consequently, the introduction of intramolecular crosslinks may still have an appreciable effect (reduction of modulus) upon the elastic properties of those rubbery networks formed in relatively dilute solution.

ACKNOWLEDGEMENT

Valuable conversations with Dr F. A. Bovey and Dr E. Helfand are most appreciated.

REFERENCES

- 1 Flory, P. J. *Chem. Rev.* 1944, **35**, 51
- 2 Treloar, L. R. G. 'The Physics of Rubber Elasticity', Oxford University Press, London, 1958, Ch III-VII
- 3 Flory, P. J. 'Statistical Mechanics of Chain Molecules', Interscience, New York, 1969, Ch I, V and VIII
- 4 Flory, P. J. 'Principles of Polymer Chemistry', Cornell University Press, Ithaca, 1953, Ch XII and XIV
- 5 Lewis, G. O. 'Physical Constants of Linear Homopolymers', Springer-Verlag, New York, 1968
- 6 Bateman, L., Moore, C. G., Porter, M. and Saville, B. in 'The Chemistry and Physics of Rubber-Like Substances', (Ed. L. Bateman), John Wiley, New York, 1963, Ch 15
- 7 Flory, P. J., Rabjohn, N. and Shaffer, M. C. *J. Polym. Sci.* 1949, **4**, 225
- 8 Flory, P. J. *Ind. Eng. Chem.* 1946, **38**, 417
- 9 Mark, J. E. *J. Am. Chem. Soc.* 1970, **92**, 7252
- 10 Price, C., Allen, G., de Candia, F., Kirkham, M. C. and Subramaniam, A. *Polymer* 1970, **11**, 486
- 11 de Candia, F., Amelino, L. and Price, C. *J. Polym. Sci. (A-2)* 1972, **10**, 975
- 12 Mark, J. E. and Flory, P. J. *J. Appl. Phys.* 1966, **37**, 4635
- 13 Tonelli, A. E. and Helfand, E. *Macromolecules* in press

Macromolecular properties of heparin in dilute solution: 1. Application of various hydrodynamic models in 0.5 M NaCl, pH 2.5

S. S. Stivala* and J. Ehrlich†

Department of Chemistry and Chemical Engineering, Stevens Institute of Technology,
Hoboken, NJ 07030, USA

(Received 25 June 1973; revised 3 December 1973)

Bovine heparin was fractionated according to molecular weight by fractional precipitation utilizing a method described previously. The solution data from sedimentation analysis, intrinsic viscosities and partial specific volumes at pH 2.5 and in 0.5 M NaCl were treated according to the Mandelkern and Flory theory for random coil in calculating the constant β . It was found that the calculated β values for all the fractions were in close agreement with the theoretical value. Based on this observation, the solution data were then treated in light of various hydrodynamic theories for linear polymers to calculate various dimensional and other physical parameters, e.g., $(\bar{r}^2)^{1/2}$, α (expansion factor), A_2 . In comparing $(\bar{r}^2)^{1/2}$ of a fraction to that calculated from the experimental value of $(\bar{s}^2)^{1/2}$ obtained from low angle X-ray scattering for a comparable molecular weight sample, it was found that heparin in solution with suppressed charges may best be described as approximating the closely related models of Debye and Bueche, Flory and Fox, or Kuhn and Kuhn.

INTRODUCTION

Heparin, a glycosaminoglycan found in high concentration in the liver, lung, and spleen, is important pharmacologically as a blood anticoagulant. The chemistry and pharmacology of heparin has been recently reviewed by Ehrlich and Stivala¹. Owing to its high negative charge, it exhibits in aqueous solution typical polyelectrolyte²⁻⁴ behaviour. Therefore, physico-chemical measurements are sensitive to changes in pH and ionic strength^{2, 4-6}. Heparin has been shown to be polydispersed with molecular weights ranging from 6000 to 20 000^{2, 4, 7}. Laurent⁷, and Stivala *et al.*^{2, 4} have demonstrated that the anticoagulant activity of heparin increases with increasing molecular weight, based on discrete fractions obtained from the fractionation of bovine heparin. On the other hand, Barlow *et al.*⁵ and Braswell⁸ reported that there is no relation between biological activity and molecular weight, based on unfractionated heparin obtained from various sources. The effect of polydispersity on biological activity was not considered by these workers.

It has been suggested that the blood anticoagulant activity of heparin is related to: (a) structural features, e.g., degree of sulphation⁹⁻¹¹, degree of dissociation⁶; and (b) molecular shape and size^{6, 9, 12, 13}. These factors appear to be related to biological activity by virtue of their importance in the ion-binding capacity of heparin⁶. Lasker and Stivala², based on dilute solution studies

of heparin, suggested that heparin can exhibit flexibility thus approximating a wormlike coil. Based on dye-stacking techniques, Stone¹⁴ suggested that heparin behaves like the helical polypeptides. Stivala *et al.*¹⁵, using low angle X-ray scattering, reported that heparin in water can be described as a Gaussian coil molecule.

This paper aims to ascribe a hydrodynamic model of heparin in 0.5 M NaCl at pH 2.5, which was not previously reported, from data obtained by Lasker and Stivala² from viscosity and sedimentation analysis. Accordingly, various dilute solution theories, based on numerous models, were invoked in eliciting a reasonable model with corresponding dimensional parameters. A subsequent paper¹⁶ will discuss hydrodynamic properties of fractionated heparin as a function of pH, ionic strength and desulphation.

EXPERIMENTAL

Materials

Pure commercial bovine lung sodium heparin with an anticoagulant activity of 125 IU/mg was supplied by Organon Inc., West Orange, NJ.

Methods

Fractionation of heparin, including sedimentation analysis, partial specific volume, and viscosity measurements were described in an earlier paper by Lasker and Stivala². The Schlieren peaks from sedimentation velocity experiments of the fractions were sharp, narrow and non-skewed. Further, the peaks showed no evidence

* To whom inquiries should be addressed.

† Present address: Department of Oral Biology, New Jersey Dental School, College of Medicine and Dentistry of New Jersey, Jersey City, New Jersey, USA.

of other components. Therefore, it can be assumed that the fractions have narrow molecular weight distributions. Additionally, the ratio \bar{M}_w/\bar{M}_n for unfractionated heparin was calculated, from fractionated data^{2,4} and measured \bar{M}_w was obtained by sedimentation analysis of the fractions, using the expression $\bar{M}_n = 1/\sum(w_i/M_i)$ where M_i is weight fraction of fraction i . The ratio was found to range from 1.05 to 1.15 for several fractionations. Various dimensional parameters were calculated from experimental data and dilute solution theories using the data reported by Lasker and Stivala². The experimental conditions in this work were such that negative charges were suppressed and heparin did not exhibit its normal polyelectrolyte behaviour (pH 2.5 and ionic strength of 0.5 M NaCl).

THEORY AND HYDRODYNAMIC MODELS

Numerous theories and equations have been proposed for linear, non-charged macromolecules relating various physical parameters to different hydrodynamic models, e.g., spheres, ellipsoids of revolution, rods, random coils. Heparin is a negatively charged polyelectrolyte but nevertheless, if sufficient positive ions are added to the medium it will exhibit non-charged properties. The theories and equations which were applied to the heparin fractions in assessing a hydrodynamic model from experimental data are briefly summarized below (but is not intended to be a critical review).

Svedberg¹⁷ related molecular weight, M , with sedimentation coefficient, S^0 , and diffusion coefficient, D^0 , for any particle with the following equation:

$$M = RTS^0/D^0(1 - \bar{v}\rho) \quad (1)$$

where the superscript refers to extrapolation to infinite dilution, \bar{v} is the partial specific volume of the particle, ρ is the density of the solvent, T is the absolute temperature and R is the gas constant.

According to Mark and Houwink^{18,19}, the molecular weight is related to the intrinsic viscosity, $[\eta]$, and the sedimentation coefficient by the equations:

$$[\eta] = KM^a \quad (2)$$

and

$$S^0 = K'M^{a'} \quad (2a)$$

where a and a' are exponents related to the shape of the particle.

Volume parameters, such as the effective volume, V_e , of a particle, and the shape factor, ν , may be expressed²⁰ by:

$$[\eta] = N(V_e/M)\nu \quad (3)$$

and

$$\nu = [\eta]/\bar{v} \quad (4)$$

where N is Avogadro's number, and $[\eta]$ is in dl/g. Combining equations (3) and (4) leads to the following expression for effective volume:

$$V_e = M\bar{v}/N \quad (4a)$$

The frictional coefficient, f , of any particle can be expressed as²¹:

$$f = kT/D^0 \quad (5)$$

where k is the Boltzmann constant. The frictional coefficient of an equivalent sphere, f_0 , was given by Stokes²² as:

$$f_0 = 6\pi\eta_0 \left[\frac{3\bar{v}M}{4\pi N} \right]^{1/3} \quad (6)$$

where η_0 is the solvent viscosity, and by Svedberg¹⁷:

$$f_0 = \frac{M^{1/3} \times 8.43 \times 10^{14}}{N} \quad (6a)$$

for the particle in water at 20°C. The frictional ratio, f/f_0 , can be calculated from the following Svedberg relations assuming that the solvation is negligible:

$$f/f_0 = \frac{1.19 \times 10^{-15} M^{2/3} (1 - \bar{v}\rho)}{S_{20,w}^0 \bar{v}^{1/3}} \quad (7)$$

and

$$f/f_0 = \frac{f}{(162\pi^2)^{1/3} V_e^{1/3} \eta_0} \quad (8)$$

The frictional ratios could also be obtained from the individual values of f and f_0 (equations 4–6).

The theoretical relations between the particle asymmetry (axial ratio) p , and $[\eta]$ was calculated by Simha²³ for an assumed prolate ellipsoid model as:

$$[\eta] = \frac{\bar{v}}{10} \left[\frac{p^2}{15(\ln 2p - 1.5)} + \frac{p^2}{5(\ln 2p - 0.5)} + 14/15 \right] \quad (9)$$

This equation assumes that the particles are rigid and impermeable to solvent. Also, if the initial linear portion of a Perrin²⁴ plot of axial ratios versus frictional ratios is selected, and a best line fit is made of this portion, then axial ratios can be related to frictional ratios directly.

The following models were proposed for linear, flexible chains in dilute solutions.

Debye and Bueche

Debye and Bueche²⁵ suggested that the polymer coil be treated as a porous sphere consisting of uniformly resisting points which represent the monomer units in the chain. The root mean square end-to-end distance $(\bar{r}^2)^{1/2}$, may be obtained from:

$$(\bar{r}^2)^{1/2} = \frac{1}{0.92} \left(\frac{\sigma}{N\pi\psi(\sigma)} \right)^{1/3} ([\eta]M)^{1/3} \quad (10)$$

where $[\eta]$ is in ml/g, σ is the shielding ratio and $\psi(\sigma)$ is a tabulated function of the shielding ratio, or from:

$$(\bar{r}^2)^{1/2} = \frac{(1 - \bar{v}\rho)M}{6\pi N(0.527)\eta_0 S^0 \psi(\sigma)} \quad (11)$$

Another relation for obtaining $(\bar{r}^2)^{1/2}$ is

$$(\bar{r}^2)^{1/2} = 2R_s/1.054 \quad (12)$$

where R_s , the radius of a bead, is given by:

$$[\eta] = \frac{(4\pi/3)NR_s^3\psi(\sigma)}{M} \quad (12a)$$

An alternate method of obtaining $(\bar{r}^2)^{1/2}$, reported by Debye²⁶, is

$$(\bar{r}^2)^{1/2} = \left(\frac{3600\eta_0 S^0 [\eta]}{1 - \bar{v}\rho} \right)^{1/2} \quad (13)$$

where σ approaches zero for the case of the free draining coil. Further, the root mean square radius of gyration, $(\bar{s}^2)^{1/2}$, was given by²⁵:

$$(\bar{s}^2)^{1/2} = \left(\frac{M_0[\eta]}{R_s 3/2\pi} \right)^{1/2} \quad (14)$$

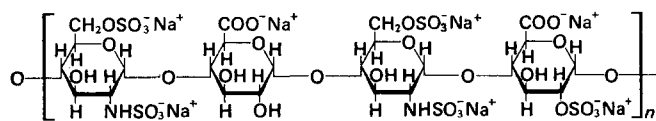
where R_g may be obtained from equation (12) and M_0 represents the molecular weight of the monomer unit (the bead). As in equation (12) σ approaches zero for the case of a free draining coil.

Kirkwood and Riseman

The Kirkwood and Riseman theory²⁷ is derived on the basis of a model consisting of a string of beads arranged to give a random coil. By taking into account the hydrodynamic interaction of the monomer units and the hindered flow through the coil, they obtained for the effective bond length, b , of the molecule:

$$b^3 = \frac{6M_0(6\pi^3)^{1/2}[\eta]}{N\pi^3 Z^{1/2}} \left(\frac{1}{xF(x)} \right) \quad (15)$$

where $[\eta]$ is in ml/g, Z is the degree of polymerization, and $xF(x)$ is a tabulated function determined from the Mark-Houwink relation. The value of M_0 used in our calculation of the heparin fractions was based on a repeating tetrasaccharide unit of Jaques²⁸ with the counter-ions included in the structure, as shown below:



Using Miyake's theory²⁹ for a translational diffusion constant, it is possible to obtain b from:

$$b = \frac{0.196kT}{Z^{1/2}\eta_0 D^0} \quad (16)$$

The value of b is a measure of the flexibility of the molecule, which may be used to obtain the root mean square end-to-end distance from the Kirkwood and Riseman²⁷ equation:

$$(\bar{r}^2)^{1/2} = bZ^{1/2} \quad (17)$$

and the root mean square radius of gyration, $(\bar{S}^2)^{1/2}$, from:

$$(\bar{S}^2)^{1/2} = \left(\frac{Zb^2}{6} \right)^{1/2} \quad (18)$$

Additionally, from this theory, $(\bar{r}^2)^{1/2}$ can be calculated from:

$$(\bar{r}^2)^{1/2} = \left(\frac{[\eta]M}{(\pi/6)^{3/2}N/100xF(x)} \right)^{1/3} \quad (19)$$

where here $[\eta]$ is in dl/g.

Peterlin

Peterlin³⁰ presented a coil that is purely statistical and is composed of chain elements so selected that each element is oriented independently of each other. He gave several alternate equations for calculating $(\bar{r}^2)^{1/2}$, thus:

$$(\bar{r}^2)^{1/2} = 1.01 \times 10^{-23} \cot \alpha M^{1/2} \quad (20)$$

where $\tan \alpha$ is the slope of an $[S^0]$ versus $M^{1/2}$ plot,

$$(\bar{r}^2)^{1/2} = 3.25 \times 10^{-25} \cot \alpha^* M^{1/2} \quad (21)$$

where $\tan \alpha^*$ is the slope of an $[S^0]$ versus $M^{1/2}$ plot, and

$$[S^0] = \frac{S^0 \eta_0}{1 - \bar{v}\rho} \quad (21a)$$

Also:

$$(\bar{r}^2)^{1/2} = \frac{1.62 \times 10^{-2} M}{[S^0](1-b')} \quad (22)$$

where b' is obtained from:

$$[F] = \frac{Nf}{\eta_0} = K_2 M^{b'} \quad (22a)$$

and $[F]$ is the intrinsic frictional coefficient. In addition, $(\bar{r}^2)^{1/2}$ can be obtained from:

$$(\bar{r}^2)^{1/2} = 1.52 \times 10^{-8} (100 \cot \alpha') M^{1/2} \quad (23)$$

where $\tan \alpha'$ is the slope of the $M/[\eta]$ versus $M^{1/2}$ plot, and $[\eta]$ is in dl/g. Peterlin showed that $(\bar{r}^2)^{1/2}$ can be calculated from:

$$(\bar{r}^2)^{1/2} = 1.21 \times 10^{-8} \left(\frac{[\eta]M}{1-a} \right)^{1/3} \quad (24)$$

where a is the Mark-Houwink exponent and $[\eta]$ is in ml/g.

Flory and Fox

In contrast to the other theories, the assumption was made by Flory and Fox³¹ that the distribution of end-to-end distances remains Gaussian even in good solvents where the coil undergoes a uniform expansion due to the excluded volume effect. The $(\bar{r}^2)^{1/2}$ was expressed as:

$$(\bar{r}^2)^{1/2} = \left(\frac{M[\eta]}{\phi} \right)^{1/3} \quad (25)$$

where ϕ is a proportionality constant and was assumed to have the value of 2.1×10^{21} for all of our calculations, and $[\eta]$ is in dl/g. The unperturbed root mean square end-to-end distance, $(\bar{r}_0^2)^{1/2}$, is given as:

$$K_\theta = \phi \left(\frac{\bar{r}_0^2}{M} \right)^{3/2} \quad (26)$$

where K_θ is obtained from the intercepts of various linear equations given later. Accordingly, it is possible to calculate the expansion or swelling coefficient, α , by the equation:

$$\alpha = \frac{(\bar{r}^2)^{1/2}}{(\bar{r}_0^2)^{1/2}} \quad (27)$$

or from:

$$[\eta] = \phi \left(\frac{\bar{r}_0^2}{M} \right)^{3/2} M^{1/2} \alpha^3 \quad (28)$$

Kurata and coworkers^{32, 33} showed that the expansion of a polymer chain which is close to the θ point (critical miscibility temperature for infinite molecular weight chain), occurs mostly at the outside of the sphere rather than at the centre. If the assumption is made that the system is close to the θ point, values of α can also be calculated from:

$$[\eta] = \phi \left(\frac{\bar{r}_0^2}{M} \right)^{3/2} M^{1/2} \alpha^{2.43} \quad (29)$$

Ptitsyn and Birshtein

Ptitsyn and Birshtein³⁴ related the frictional coefficient, F , to $(\bar{r}^2)^{1/2}$ by the relation:

$$F = P(\bar{h}^2)^{1/2} \eta_0 \quad (30)$$

where $P = 5.2$ for linear Gaussian chains, and $(\bar{h}^2)^{1/2}$ is the same as $(\bar{r}^2)^{1/2}$. Additionally:

$$(\bar{s}^2)^{1/2} = \left(\frac{\bar{h}^2}{6}\right)^{1/2} \quad (31)$$

Kuhn and Kuhn

These investigators³⁵⁻³⁷ considered the polymer molecules to be made up of statistically independent segments of length, A_m , which are freely jointed to each other. They presented the following equations for the determination of $(\bar{r}^2)^{1/2}$:

$$S_0 = \frac{M_0(1-\bar{v}\rho)}{Nb_0\eta_0} \left[-0.03 + 0.16 \log\left(\frac{A_m}{d_h}\right) + 0.136 \left(\frac{Zb_0}{A_m}\right)^{1/2} \right] \quad (32)$$

and

$$[\eta] = \frac{Nb_0^2 A_m}{100M_0} \left(\frac{0.43Z}{-1.6 + 2.3 \log\left(\frac{A_m}{d_h}\right) + \left(\frac{Zb_0}{A_m}\right)^{1/2}} \right) \quad (32a)$$

where b_0 is the length of a monomeric unit and d_h is the hydrodynamic thickness of the monomeric unit. Accordingly, A_m may be calculated from the following equation, based on a cellulosic model, for heparin:

$$A_m = \frac{(\bar{r}_0^2)^{1/2}}{21.2Z} \quad (33)$$

and, therefore:

$$(\bar{r}^2)^{1/2} = (A_m b_0 Z)^{1/2} \quad (33a)$$

Mandelkern and Flory

The theory of Mandelkern and Flory³⁸ is based on the assumptions of Flory and Fox³¹. The distributions of segments in the polymer coil is considered to be Gaussian, with the coil undergoing uniform expansion due to solvent effect. The sedimentation coefficient is related to $(\bar{r}^2)^{1/2}$ by:

$$S^0 = \frac{M(1-\bar{v}\rho)}{P\eta_0 N (\bar{r}^2)^{1/2}} \quad (34)$$

where P is a universal constant analogous to ϕ in equation (25), and is independent of the polymer-solvent system, having the value of 5.1. From this the following were obtained:

$$\phi^{1/3} P^{-1} = \frac{NS^0 [\eta]^{1/3} \eta_0}{M^{2/3} (1-\bar{v}\rho)} \quad (35)$$

$$\phi^{1/3} P^{-1} = \frac{D^0 [\eta]^{1/3} M^{1/3} \eta_0}{RT} \quad (35a)$$

$$\phi^{1/3} P^{-1} = \frac{N^{1/3} F_v^{1/3}}{(16200\pi^2)^{1/3}} \quad (35b)$$

where

$$F = f_0/f \quad (35c)$$

Scheraga and Mandelkern³⁹ set $\phi^{1/3} P^{-1} = \beta$, and tabulated values of β as a function of axial ratios for ellipsoids of revolution. The value of β for a random coil should approach 2.5×10^6 . Also, a Flory constant, F' , is obtained from:

$$F' = \frac{([\eta]M)^{1/3} \eta_0 D}{T} \quad (36)$$

which should be independent of molecular weight.

Determination of K_θ

A series of equations follows which permit the calculation of the unperturbed root mean square end-to-end distance $(\bar{r}_0^2)^{1/2}$ using equation (26), and K_θ , which may be obtained from among the following equations.

(a) The equation of Flory-Fox-Shaefgen³¹ is:

$$\frac{[\eta]^{2/3}}{M^{1/3}} = K_\theta^{2/3} + K_\theta^{5/3} C_T \frac{M}{[\eta]} \quad (37)$$

where C_T is a constant giving the relation between α and the excluded volume. Here and in all following equations $[\eta]$ is in dl/g.

(b) The following equation was given by Inagaki *et al.*⁴⁰:

$$\frac{[\eta]^{4/5}}{M^{2/5}} = 0.786 K_\theta^{4/5} + 0.950 K_\theta^{7/5} M^{1/3} \quad (38)$$

(c) The relation proposed by Kurata and Stockmayer⁴¹ was:

$$\frac{[\eta]^{2/3}}{M^{1/3}} = K_\theta^{2/3} + 0.363 \frac{\phi_0 B g(\alpha) M^{2/3}}{[\eta]^{1/3}} \quad (39)$$

(d) Stockmayer and Fixman⁴² reported the following equation:

$$\frac{[\eta]}{M^{1/2}} = K_\theta + 0.51 \phi_0 B M^{1/2} \quad (40)$$

(e) According to Shanbhag⁴³, the relation presented by Ptitsyn and Eizner⁴⁴ can be written in the following form:

$$\frac{[\eta]^{2/3}}{M^{1/3}} = 0.786 \frac{\phi(\epsilon)}{\phi_0} K_\theta^{2/3} + 0.950 (0.33B)^{2/3} [\phi(\epsilon)^{2/3} M^{1/3}] \quad (41)$$

where:

$$\phi(\epsilon) = \phi_0 (1 - 2.63\epsilon + 2.86\epsilon^2) \quad (41a)$$

and ϵ can be calculated from the exponent in the Mark-Houwink relation:

$$\epsilon = \frac{2a-1}{3} \quad (41b)$$

(f) The equation given by Berry⁴⁵ is:

$$\frac{[\eta]}{M^{1/2}} = K_\theta^{1/2} + 0.035 \frac{K_\theta^{5/2}}{\phi_0} + \frac{BM}{[\eta]} \quad (42)$$

Additional parameter

Benoit. According to Benoit⁴⁶, the root mean square end-to-end distance of a freely jointed cellulosic chain $(\bar{r}_f)^{1/2}$ is related to the degree of polymerization, Z by:

$$(\bar{r}_f^2)^{1/2} = 7.90Z^{1/2} \quad (43)$$

from which a steric factor, σ , may be calculated from:

$$\sigma = \frac{\bar{r}_0^2}{\bar{r}_f^2} \quad (44)$$

It is also possible to calculate a contour length, L , from:

$$L = 21.2Z \quad (45)$$

where 21.2 is the length of a cellulose tetrasaccharide unit, in Å.

Eliezer and Hayman. In the *trans*-1,4-polysaccharides.

Eliezer and Hayman⁴⁷ used the following relation in obtaining $(\bar{r}_g^2)^{1/2}$

$$(\bar{r}_g^2)^{1/2} = 7.75Z^{1/2} \quad (46)$$

Orofino and Flory. The second virial coefficient, A_2 , was related to the expansion factor, α , by Orofino and Flory⁴⁸ by the equations:

$$A_2 = (32)^{1/2} \pi N [\eta] \ln[1 + 0.885(\alpha^2 - 1)] \quad (47)$$

$$A_2 = 16\pi N (\bar{r}_g^2)^{3/2} \ln[1 + 0.885(\alpha^2 - 1)] \quad (48)$$

RESULTS AND DISCUSSION

Table 1 summarizes various physical parameters obtained from sedimentation analysis and viscosity measurements. M_1 represents molecular weights reported by Lasker and Stivala² which were obtained from sedimentation equilibrium. M_2 represents a molecular weight calculated from equation (35). It is interesting

Table 1 Experimental data and calculated parameters of fractionated bovine heparin in 0.5 M NaCl, pH 2.5

Physical parameter	Heparin fractions					Equation number
	61	55	47	45	41	
M_1^a	5540	7500	11 340	11 900	13 970	
M_2	4871	5873	9 036		11 753	35
$[\eta]^b$ (dl/g)	0.079	0.099	0.138	0.144	0.163	
$S^0 \times 10^{13}$ (sec)	1.38	1.45	1.73		1.95	
Z	4.61	6.25	9.44	9.91	11.6	
$V_e \times 10^{20}$ (cm ³ /molecule)	0.427	0.578	0.874	0.917	1.09	4a
$\nu \times 10^{-2}$	0.170	0.213	0.291	0.310	0.351	4
$[S^0] \times 10^{15}$	2.78	2.92	3.48		3.92	21a
$D^0 \times 10^7$ (cm ² /sec)	11.5	8.93	7.08		6.45	1
f (Å)	3.52	4.53	5.74		6.27	5
f_0^c (Å)	2.25	2.49	2.70	2.90	3.06	6, 6a
f/f_0^c	1.72	2.00	2.24		2.25	5-8
ρ^c	11.5	16.8	22.4	17.5	23.5	9, Perrin plot

a Calculated from the measured molecular weight (M_1) and the molecular weight of the monomer unit (M_0)

b Experimental value obtained from ref. 2

c Averaged values from the various equations indicated

to note that the calculated molecular weights, M_2 , using $\beta = 2.5 \times 10^6$ for a random coil, agree reasonably with those obtained directly from experiment, M_1 . Table 1 also shows experimental data of S^0 and $[\eta]$ reported by Lasker and Stivala. Using these data, the present authors calculated Z , V_e , ν , $[S^0]$, D^0 , f , f_0 , (f/f_0) and p , from the various equations contained in the section on theory and hydrodynamic models. All of these parameters, with the exception of D^0 , increase with increasing molecular weight as expected. The calculated values of f/f_0 and p may indicate deviation from spherical symmetry. However, not much more can be said about these values since the amount of bound water, if any, is not known for heparin.

Table 2 summarizes calculated parameters using the various hydrodynamic models based on linear flexible chains. Thus, it is to be noted that b , R_s , $(\bar{r}_g^2)^{1/2}$, L increase, whereas A_m decreases with increasing molecular weight as expected. The data tend to show that A_2 and σ appear to be independent of molecular weight in the range examined. The Flory constant, F' , for the heparin fractions is independent of molecular weight in accordance with the Mandelkern and Flory³⁸ theory. Further, β calculated from the Mandelkern-Flory equations (35) and (35a) for the heparin fractions is constant and agrees reasonably well, within experimental error, with the theoretical value of 2.5×10^6 for the random coil model. Recently, Ehrlich¹³ obtained values of β closer to this theoretical value. Accordingly, this tends to support the premise that heparin under the conditions examined, where charges are suppressed, can best be described as a Gaussian coil. Additionally, the concept of flexibility of heparin in 0.5 M NaCl at pH 2.5 was substantiated by the relation between $[\eta]$ and M and $[\eta]$ and S^0 . Lasker and Stivala obtained values of a of 0.8, see equation (2), and a value of a' of 0.44 using equation (2a). A value of 0.8 in the Mark-Houwink relationship is near the upper limit for the random coil. Theory⁴⁹ predicts that for a compact coil $S^0 \sim M^{1/3}$, while for a free-draining coil $S^0 \sim M^0$. For flexible polymers S^0 should vary as $M^{1/2}$ in a poor solvent and roughly as $M^{0.45}$ in a better solvent⁵⁰.

Table 2 Hydrodynamic parameters from various hydrodynamic models, for fractionated bovine heparin in 0.5 M NaCl, pH 2.5

Hydrodynamic parameter	Heparin fractions					Equation number	Hydrodynamic model
	61	55	47	45	41		
b^* (Å)	32.0	34.0	35.2	36.2	35.3	15, 16	Kirkwood and Riseman; Miyake
R_s (Å)	35.1	41.9	53.7	55.4	60.9	12a	Debye and Bueche
A_m (Å)	0.425	0.369	0.297	0.296	0.261	33	Kuhn and Kuhn
$(\bar{r}_g^2)^{1/2*}$ (Å)	70.7	86.1	109	114	120	10-13, 17, 19-25, 30, 33a, 34	Debye and Bueche; Kirkwood and Riseman; Peterlin, Flory and Fox; Ptitsyn and Birshtein; Kuhn and Kuhn; Mandelkern and Flory
$(\bar{r}_g^2)^{1/2*}$ (Å)	41.6	48.9	59.5	62.1	64.3	26, 37-42	Flory and Fox; Flory, Fox and Shaefgen; Inagaki, Suzuki and Kurata; Kurata and Stockmayer; Stockmayer and Fixman; Ptitsyn and Eizner; Berry
α^*	1.56	1.59	1.66	1.66	1.67	27-29	Flory and Fox; Kurata
$(\bar{r}_g^2)^{1/2*}$ (Å)	16.8	19.6	24.1	24.6	26.7	43, 46	Benoit, Eliezer and Hayman
σ	2.47	2.50	2.47	2.52	2.41	44	Benoit
L^* (Å)	97.8	132	200	210	247	45	Benoit
$(\bar{s}^2)^{1/2*}$ (Å)	22.6	31.2	39.9	38.6	43.6	14, 18, 31	Debye and Bueche; Kirkwood and Riseman; Ptitsyn and Birshtein
$\beta^* \times 10^{-6}$	2.31	2.13	2.14		2.24	35	Mandelkern and Flory
F' (erg/degree)	0.316	0.293	0.297		0.357	36	Mandelkern and Flory
$A_2^* \times 10^2$	0.219	0.212	0.213	0.215	0.40	47, 48	Orofino and Flory

* These are averaged values

Table 3 Root mean square end-to-end distance (\AA) calculated from various hydrodynamic models for fractionated bovine heparin in 0.5 M NaCl, pH 2.5

Heparin fractions					Equation number	Hydrodynamic model
61	55	47	45	41		
52.2	65.9	84.4	87.0	95.7	10	Debye and Bueche
66.7	79.5	101	106	116	12	Debye and Bueche
83.3	107	136		148	11	Debye and Bueche
88.9	102	132		116	13	Debye
72.4	86.3	111	115	125	15, 17	Kirkwood and Riseman
72.4	86.3	111	114	125	19	Kirkwood and Riseman
64.9	83.7	106		116	16, 17	Miyake; Kirkwood and Riseman
70.9	84.5	108	112	123	24	Peterlin
86.0	111	140		154	22	Peterlin
74.5	86.7	107	109	118	23	Peterlin
57.0	66.3	81.6		90.5	20	Peterlin
91.1	106	130		145	21	Peterlin
59.3	70.7	90.7	93.5	103	25	Flory and Fox
76.9	89.5	110	92.7	122	32a, 33, 33a	Kuhn and Kuhn
63.2	73.6	90.5	92.7	122	32, 33, 33a	Kuhn and Kuhn
64.9	83.6	106		114	34	Mandelkern and Flory
63.7	81.9	104		114	30	Ptitsyn and Birshtein
Av. 70.7	86.1	109	114	120		

It is interesting to note that Yuan *et al.*⁵¹ proposed a semi-empirical relation between η_{sp}/c and concentration, c , as

$$\eta_{sp}/c = [\eta]_{\infty} [1 + k/(c)^{1/2}] \quad (49)$$

where $[\eta]_{\infty}$ is the shielded intrinsic viscosity obtained by extrapolating η_{sp}/c vs. $1/(c)^{1/2}$ to infinite concentration, and k is an interaction parameter independent of the dielectric constant of the solvent. They showed that k can be expressed as:

$$k \approx 5.22(P/l^2)^{1/2} \quad (50)$$

where P is the molecular weight divided by the length in \AA and l is the equivalent freely jointed segment length when the backbone of the polyion is represented by a Gaussian coil of N segments. Yuan and Stivala⁵² studied the viscosity of heparin as a function of dielectric constant using equation (49) and found that the data conformed to this equation.

In view of the above experimental and theoretical evidence in support of a Gaussian coil, radii of gyration, perturbed and unperturbed end-to-end distances, and expansion factors, α , were calculated from the various hydrodynamic theories for linear flexible chains. The values of these parameters are shown in Table 2 as averaged values from the equations indicated in the Table. As expected these values increase with increasing molecular weight.

Based on the model of a Gaussian coil, as substantiated by the data, end-to-end distances were calculated for the heparin fractions from the various hydrodynamic theories as shown in Table 3. Stivala *et al.*¹⁵, using low-angle X-ray scattering, obtained a radius of gyration of 35.9 \AA for a heparin fraction of molecular weight 12 600. For a molecular weight of 11 900 an average value of the radius of gyration was calculated to be 38.6 \AA (Table 2). This value is in reasonable agreement with that obtained experimentally by low-angle X-ray scattering for a comparable molecular weight, thus substantiating the concept of a Gaussian coil. Using the relationship of equation (31), a value of $(\bar{r}^2)^{1/2}$ of 87.9 \AA was calculated from the radius of gyration obtained experimentally by Stivala *et al.* This value for a com-

parable molecular weight appears to agree with the $(\bar{r}^2)^{1/2}$ of the Debye and Bueche, Flory and Fox, and Kuhn and Kuhn theories.

From earlier work by Stivala, Ehrlich, Lasker and coworkers and as further substantiated by the treatment in this paper, it would appear that heparin in solution can be best described as a Gaussian coil when charges are suppressed.

ACKNOWLEDGEMENTS

The authors are grateful to Organon, Inc. for their generous supply of sodium heparin. This work was supported in part by National Institutes of Health grant, No. HE-5943 and Public Health Service Fellowship (J. E.), No. F3-HE-29, 038-03.

REFERENCES

- Ehrlich, J. E. and Stivala, S. S. *J. Pharm. Sci.* 1973, **62**, 517
- Lasker, S. E. and Stivala, S. S. *Arch. Biochem. Biophys.* 1966, **115**, 360
- Liberti, P. A. and Stivala, S. S. *J. Polym. Sci. (B)* 1966, **4**, 137
- Liberti, P. A. and Stivala, S. S. *Arch. Biochem. Biophys.* 1967, **119**, 510
- Barlow, G. H., Sanderson, N. D. and McNeill, G. H. *Arch. Biochem. Biophys.* 1961, **84**, 518
- Stivala, S. S. and Liberti, P. A. *Arch. Biochem. Biophys.* 1967, **122**, 40
- Laurent, T. L. *Arch. Biochem. Biophys.* 1961, **92**, 224
- Braswell, E. *Biochim. Biophys. Acta* 1968, **158**, 103
- Brimacombe, J. S. and Webber, J. M. 'Mucopolysaccharides', Elsevier, New York, 1964
- Wolfrom, M. L. and Karabinos, J. U. *J. Am. Chem. Soc.* 1948, **67**, 679
- Stivala, S. S., Yuan, L., Ehrlich, J. and Liberti, P. A. *Arch. Biochem. Biophys.* 1967, **122**, 32
- Jensen, R., Snellman, O. and Sylvén, B. *J. Biol. Chem.* 1948, **174**, 265
- Ehrlich, J. *PhD Dissertation* Stevens Institute of Technology, 1971
- Stone, A. L. *Biopolymers* 1964, **2**, 315
- Stivala, S. S., Herbst, M., Kratky, O. and Pilz, T. *Arch. Biochem. Biophys.* 1968, **127**, 795
- Ehrlich, J. and Stivala, S. S. *Polymer* 1974, **15**, 204
- Svedberg, T. and Pedersen, K. O. 'The Ultracentrifuge', Clarendon Press, Oxford, 1940, pp 5, 40

- 18 Mark, H. 'Der Feste Koerper Hinzl', Springer-Verlag, Leipzig, 1938
- 19 Houwink, R. *J. Prakt. Chem.* 1940, **157**, 15
- 20 Scheraga, H. A. 'Protein Structure', Academic Press, New York, 1967, pp 5-30
- 21 Einstein, A., *Ann. Phys.* 1905, **17**, 549; 1906, **19**, 371
- 22 Stokes, G. G. *Trans. Cambridge Phil. Soc.* 1856, **9**(2), 148
- 23 Simha, R. *J. Phys. Chem.* 1940, **44**, 25
- 24 Perrin, F. *J. Phys. Radium* 1936, **7**(7), 1
- 25 Debye, P. and Bueche, A. M. *J. Chem. Phys.* 1948, **16**, 573
- 26 Debye, P. *J. Chem. Phys.* 1946, **14**, 636
- 27 Kirkwood, J. G. and Riseman, J. J. *J. Chem. Phys.* 1948, **16**, 565; 1955, **23**, 213
- 28 Jaques, L. B. *Progr. Med. Chem.* 1967, **5**, 139
- 29 Miyake, A. *Int. Symp. Macromol. Chem., Kyoto* 1966
- 30 Peterlin, A. *J. Polym. Sci.* 1950, **5**, 473
- 31 Flory, P. J. and Fox, T. G. *J. Am. Chem. Soc.* 1951, **73**, 1904, 1915
- 32 Kurata, M. *et al. J. Chem. Phys.* 1958, **28**, 785
- 33 Kurata, M. and Yamakawa, H. *J. Chem. Phys.* 1958, **29**, 311
- 34 Ptitsyn, O. B. and Birshtein, T. M. 'Conformations of Macromolecules', Interscience, New York, 1969, p 9
- 35 Kuhn, H. and Kuhn, W. *J. Chem. Phys.* 1948, **16**, 838
- 36 Kuhn, H. and Kuhn, W. *J. Colloid Sci.* 1950, **5**, 331
- 37 Kuhn, H. and Kuhn, W. *J. Polym. Sci.* 1950, **5**, 519; 1952, **9**, 1
- 38 Mandelkern, L. and Flory, P. J. *J. Chem. Phys.* 1952, **20**, 212
- 39 Scheraga, H. A. and Mandelkern, L. *J. Am. Chem. Soc.* 1953, **75**, 179
- 40 Inagaki, H., Suzuki, H. and Kurata, M. *J. Polym. Sci. (A-1)* 1966, **4**, 409
- 41 Kurata, M. and Stockmayer, W. H. *Fortsch. Hochpolym. Forsch.* 1963, **3**, 196
- 42 Stockmayer, W. H. and Fixman, M. *J. Polym. Sci. (C)* 1963, **1**, 137
- 43 Shanbhag, V. P. *Arkiv. Kemi* 1968, **29**(14), 139
- 44 Ptitsyn, O. B. and Eizner, Y. E. *Soviet Phys-Tech. Phys.* 1960, **4**, 1020
- 45 Berry, G. B. *J. Chem. Phys.* 1966, **44**, 4550; 1967, **46**, 1338
- 46 Benoit, H. *J. Polym. Sci.* 1958, **3**, 376
- 47 Eliezer, I. and Hayman, H. J. G. *J. Polym. Sci.* 1957, **23**, 287
- 48 Orofino, T. A. and Flory, P. J. *J. Chem. Phys.* 1957, **26**, 1067
- 49 Kuhn, W. and Kuhn, H. *Helv. Chim. Acta* 1943, **26**, 1394
- 50 Tanford, C. 'Physical Chemistry of Macromolecules', Wiley, New York, 1961, p 382
- 51 Yuan, L., Dougherty, T. J. and Stivala, S. S. *J. Polym. Sci. (A-2)* 1972, **10**, 171
- 52 Yuan, L. and Stivala, S. S. *Biopolymers* 1972, **11**, 2079

Macromolecular properties of heparin in dilute solution: 2. Dimensional parameters as a function of pH, ionic strength and desulphation

J. Ehrlich* and S. S. Stivala†

Department of Chemistry and Chemical Engineering, Stevens Institute of Technology, Hoboken, NJ 07030, USA

(Received 25 June 1973; revised 3 December 1973)

A bovine heparin fraction was examined by sedimentation analysis and intrinsic viscosity measurements as a function of ionic strength in the range of 0.1 to 1.0 M, and at pH 2.5 and 6.0. The following experimental parameters were obtained: M , $S_{20,w}^0$, $D_{20,w}^0$, \bar{v} , and $[\eta]$. Other physical parameters were calculated based on a random coil model (supported by the theory of Mandelkern and Flory) e.g., $(\bar{r}^2)^{1/2}$, $(\bar{S}^2)^{1/2}$. Similar studies were made on a heparin sample as a function of desulphation as resulting from graded mild hydrolysis. Since desulphation is accompanied by decreasing anticoagulant activity of heparin, the latter was correlated with various calculated and measured physical parameters. Significantly $(\bar{r}^2)^{1/2}$ decreases with decreased desulphation and therefore decreased biological activity.

INTRODUCTION

The preceding paper¹ treated solution data of heparin, obtained from sedimentation analysis and intrinsic viscosities measured in 0.5 M NaCl at pH 2.5, in light of various dilute solution theories of linear polymers. In the present paper, heparin was fractionated into a series of fractions of varying molecular weights. A given fraction was experimentally examined for variation in partial specific volume, \bar{v} , molecular weight, M , sedimentation coefficient, S^0 , $S_{20,w}^0$, diffusion constant, D^0 , $D_{20,w}^0$, and intrinsic viscosity, $[\eta]$, as a function of pH and ionic strength. Additionally, heparin samples were subjected to mild graded hydrolysis for obtaining aliquots of heparin having varying degrees of sulphation. Since desulphation results in loss of blood anticoagulant activity, then in effect, hydrodynamic behaviour can also be examined in terms of the latter. This paper aims to treat the solution data obtained in this work in terms of various hydrodynamic models in a similar manner as discussed in our earlier paper¹.

EXPERIMENTAL

Materials

Pure commercial bovine lung sodium heparin with a biological activity of 164 USP units/mg was supplied by Organon Inc., West Orange, NJ. It was fractionated according to molecular weights and was denoted by the A series.

Water used for all preparations and measurements

* Present address: Department of Oral Biology, New Jersey Dental School, College of Medicine and Dentistry of New Jersey, Jersey City, New Jersey, USA.

† To whom reprint requests should be addressed.

was distilled, then passed through a Culligan de-ionizing column.

The alcohol used for the fractionation was absolute ethanol (USP, N.F.).

Sodium chloride was ACS certified for biological work, batch S-671 (Fischer) and was used to make up the stock solutions of different ionic strengths.

Sephadex G-25 (Pharmacia), was utilized as a column packing material for desalination, in recovery of samples.

Bioassay

Samples were dried over P₂O₅ for a minimum of 48 h prior to analyses. Blood anticoagulant activities were determined according to the USP XVI method, by the South Mountain Laboratories, Maplewood, NJ.

Chemical analyses of heparin samples were performed by Schwarzkopf Microanalytical Laboratory, Woodside, NY.

Viscosity

Viscosity measurements were made in a No. 50 semimicro Cannon-Ubbelohde dilution viscometer. A water constant temperature bath was used for temperature control. Flow times were determined within 0.2 sec by means of a stop watch. Kinetic energy and shear corrections were not deemed necessary because of long efflux times and low molecular weights of the samples. The viscometer was filled with dichromate cleaning solution for 24 h before each determination, then rinsed with de-ionized water, then with tetrahydrofuran (reagent grade) and dried with pure nitrogen. All solvents were filtered through a 0.22 μ m millipore filter prior to use.

The viscometer was calibrated with benzene (reagent grade) for the determination of the viscosity of the saline-aqueous solvents.

Heparin was dried at constant evacuation over P_2O_5 (Baker) for 48 h and used immediately to make up 1% solutions, which were run without delay. No density correction was considered necessary since densities of solution and solvent were close together. Calculations of the intrinsic viscosity were done by means of a Fortran Computer Program using linear regression.

Fractionation of heparin (A series)

The fractionation of heparin into various molecular weight fractions was accomplished by fractional solution with a non-solvent (absolute ethanol). 22 g of heparin (Lot No. 21075, Organon) were added to 700 ml of absolute ethanol and then water to make up a volume of 1 litre. The resulting precipitate was mixed with a magnetic stirrer at 20°C for 12 h. The supernatant was removed and flash evaporated to a small volume. Absolute ethanol was then added to the latter supernatant and the resulting precipitate was removed by centrifugation and freeze-dried. This was labelled fraction 1.

The above procedure was repeated for each fraction by dissolving the initial precipitate with less absolute ethanol and more water each time until no more heparin could be removed from the supernatant. Eleven fractions were obtained by this procedure. Fraction 6 was used in the ionic strength and pH studies.

Nuclear magnetic resonance (n.m.r.)

N.m.r. spectra of heparin (unfractionated Lot No. 21075) were obtained from a Varian Associates n.m.r. spectrometer model A60A. Solutions of approximately 10% heparin in D_2O (99.8% Stohler isotope chemicals) were prepared. After magnetically stirring in a sealed weighing bottle for 24 h, the solution was freeze-dried for 48 h, then redissolved in D_2O . This procedure was repeated six times before a spectrum could be obtained that did not exhibit a large obscuring DOH peak.

The spectra compared favourably with those of Jaques *et al.*², Inoue and Inoue³ and Perlin *et al.*⁴ for pure heparin. The absence of a signal in the region of 8τ also indicates that there is no acetyl group present from dermatan sulphate as a contaminant.

Partial specific volumes

Density measurements of solvents and solutions were made by means of a Cahn RG Electrobalance equipped with a weigh-below stand, density cell, wire suspension and glass plummet. Constant temperature at 20°C ($\pm 0.001^\circ C$) was attained with a thermostatically controlled water bath and a Branwell circulator. Readings were recorded on a 1 mV Minneapolis-Honeywell recorder.

The procedure used was essentially that of Cahn⁵ and Elgert and Cammann⁶ with the following modification: the suspended plummet was weighed in the various media to get the necessary information from the weight of plummet + pigtail + metal tab and submerged wire rather than weighing also the suspension wire with plummet removed.

Ultracentrifugation

Preparation of solutions. Solutions were prepared by dissolving approximately 40 mg of heparin in 2.5 ml of saline solvent with pH either adjusted or unadjusted. The solutions were dialysed in cellulose bags at 4°C

against 250 ml of solvent under magnetic stirring for 24 h, then the dialysate was discarded and the solution was again dialysed against 250 ml of fresh solvent. Dilutions were made up with the dialysate as solvent. Quantities of solutions of different concentrations were sufficient for sedimentation velocity, equilibrium and diffusion measurements. In most cases six concentrations were used for each determination.

Determination of initial concentrations. Initial concentration runs were made in a Spinco Model E Analytical Ultracentrifuge which had been aligned essentially by the procedure of Gropper³⁹ with an An-D rotor at a speed of 5227 rev/min, at room temperature, with the Schlieren analyser set at 90°. A double sector, capillary type synthetic boundary, interference cell with Epon centrepieces was employed. Solvent (dialysate) was placed on the left side and solution on the right side. A photograph was taken on a Kodak 11-G spectrographic plate as soon as the boundary was formed and from this the fractional number of fringes was estimated. Then the fringes were allowed to spread and the number of integral fringes was counted using a Nikon comparator equipped with a micrometers. The same concentrations were used for sedimentation velocity, equilibrium and diffusion determinations.

Sedimentation velocity. The method for determining the sedimentation coefficients, S^0 in the ultracentrifuge was given by Ehrlich *et al.*⁷. The relationship between S^0 and concentration, c , is:

$$1/S = 1/S^0(1 + k_s c) \quad (1)$$

Correction of the observed sedimentation coefficient, S_{obs}^0 to the standard state that the material would have in water at 20°C, $S_{20,w}$ was obtained through the relation:

$$S_{20,w} = S_{obs}^0 \left(\frac{\eta}{\eta_0} \right) \left(\frac{1 - \bar{v}\rho_{20,w}}{1 - v\rho_{20}} \right) \quad (2)$$

where η/η_0 is the relative viscosity of the solvent to that of water, \bar{v} is the partial specific volume of heparin in the solvent at 20°C, and $\rho_{20,w}$ and ρ_{20} are the densities of water and solvent at 20°C, respectively.

Sedimentation equilibrium. The method for determining the molecular weights by sedimentation equilibrium in the ultracentrifuge was given by Ehrlich *et al.*⁸.

A standard sample of ribonuclease (Worthington No. 21 196) in phosphate buffer, at pH 7.65, with reported molecular weight of 13 683, was run and the molecular weight was experimentally determined as 13 901, for purpose of procedural check.

Diffusion. The method for determining the diffusion coefficients in the ultracentrifuge was given by Ehrlich *et al.*⁹. The diffusion coefficient referred to water at 20°C ($D_{20,w}$) was calculated from:

$$D_{20,w} = D_{obs}^0 \left(\frac{\eta}{\eta_0} \right) \quad (3)$$

where D_{obs}^0 is the observed diffusion coefficient. This equation was used merely to correct the solvent to pure water, since all measurements were conducted at 20°C.

Deactivation

Hydrolysis. Mild acid hydrolysis of heparin was carried out by a modification of the procedure of Helbert and Marini¹⁰. Two slightly different methods were used for the hydrolysis.

Method I (L series). In the L series, three high molecular weight fractions of Lot No. 210791 (Organon) from fractionation, series A, weighing about 8 g, were dissolved in several ml of water. The solution was slowly passed through an ion exchange column, IR-120 (hydrogen form) to convert sodium heparinate to heparinic acid. The column was eluted with cold distilled water until no more heparin was detected with toluidine blue. 100 ml of eluate were removed as a 'zero time' aliquot (L-00), and immediately refrigerated at 5°C. The remainder of the eluate was placed in a constant temperature bath at 57°C, and aliquots were removed every 1.5 h over a total period of 6 h and then after 24 and 48 h of hydrolysis. The reaction was stopped immediately by placing the aliquot in an ice bath. Part of each aliquot was passed through an IRA-400 column (hydroxyl form) to remove hydrolysed sulphate groups, titrated with 0.1 N NaOH to pH 12 and back-titrated with 0.1 N HCl to the equivalence point. The remaining portion of the aliquot was first titrated with 0.1 N NaOH to pH 12, back-titrated with 0.1 N HCl to the equivalence point, and then passed through an IRA-400 column (hydroxyl form). The two parts of each aliquot were then combined and the NaCl resulting from the back-titration was removed by reprecipitation in absolute alcohol, and the heparin was removed by freeze-drying.

Method II (F series). The hydrolysis was performed with unfractionated heparin (ABO) of Lot No. 22419 with resulting samples designated as the F series. 20 g were dissolved in distilled water and slowly passed through an IR-120 (hydrogen form) ion-exchange column and the column was eluted with 2 l of cold distilled water until no more heparin appeared in the eluate. This eluate was then divided into 10 portions. One portion was then divided in two parts (FOC and FOA2) and refrigerated. The remaining nine flasks were placed into a constant temperature bath at 57°C and the flasks were removed after the following times: 0.5, 1.0, 2.0, 2.5, 4.3, 5.8, 9.0, 48.0, 200.0 h, and were labelled F1 to F9 respectively. Half of the amount of each flask was then passed through an IRA-400 (hydroxyl form) ion-exchange column. The eluates were adjusted to neutral pH and called the F-A series. The remaining half in each flask was first titrated to equivalence with 0.1 N NaOH, then passed through an IRA-400 (hydroxyl form) ion-exchange column. This was now designated as the F-C series. The solutions from the F-A and F-C series were separately passed through a G-25 Sephadex column to remove any excess NaOH. They were then suspended in air in cellulose bags to reduce their volumes and finally freeze-dried.

All measurements for the various aliquots of the different parameters were made at 0.5 M NaCl and unadjusted pH. The intrinsic viscosity of FOA-2 and F-9A were also measured in water.

Computers. The computers employed during the course of the study were the IBM 1620-(11), the IBM 360/40, and the PDP-10 (Digital Equipment Corp.).

RESULTS AND DISCUSSION

Effect of ionic strength

The results of our study of the effect of ionic strength on the sedimentation coefficient, S^0 and $S_{20,w}^0$, of unfractionated heparin are shown in Table 1. With the exception of 0.035 ionic strength there is a gradual

Table 1 Effect of ionic strength on the sedimentation coefficient of unfractionated heparin

NaCl ionic strength (M)	$S^0 \times 10^{13}$ (sec)	$S_{20,w}^0 \times 10^{13}$ (sec)
0.03	2.04	
0.035	2.19	
0.050	2.08	
0.10	2.12	2.14
0.20	2.16	
0.40	2.24	2.35

increase in S^0 from 2.04 to 2.24 S with increased ionic strength. The sedimentation coefficient corrected to water at 20°C, $S_{20,w}^0$, shows a more pronounced increase because the viscosity and density effects of the solvent have been eliminated. With fractionated heparin (Table 2), the variation of S^0 shows no definite trend because of the aforementioned effects, but $S_{20,w}^0$ increases up to 0.4 M NaCl, then levels off. The result is similar to that obtained by Barlow *et al.*¹¹. However, their work was performed on unfractionated heparin at one particular concentration since they accepted the premise of Patat and Elias¹² that heparin shows no concentration dependence on the sedimentation coefficient. Our results, in addition to those of Creeth and Record¹³, Laurent¹⁴, and Lasker and Stivala¹⁵ indicate concentration dependence. However, as indicated by the k_s values, this dependence decreases as the ionic strength is raised to 1.0 M NaCl.

Table 2 summarizes additional physical parameters. The molecular weight is independent of ionic strength. There is close agreement in molecular weight values as obtained by sedimentation equilibrium and from diffusion-sedimentation velocity measurements from the Svedberg equation (equation (1) of ref 1), and from viscosity-sedimentation velocity measurements using the Mandelkern and Flory equation (equation (35) of ref 1).

The partial specific volume, \bar{v} , shows no change with ionic strength up to 0.5 M, then from 0.5 to 1.0 M it increases from 0.454 to 0.470 ml/g. It is possible that the electrostriction effect is balanced by a small excluded volume until the ionic strength becomes large enough to increase the excluded volume by reduction of the repulsive forces. Gagen¹⁶ found a similar effect with ovalbumin. The partial molar volume, \bar{V} , and the effective volume, V_e , show variation but no definite trend since these parameters vary with molecular weight (see Table 2).

The intrinsic viscosity was obtained by the methods of Huggins¹⁷, Mead and Fuoss¹⁸, and Schulz and Blaschke¹⁹. The plots were all linear and the values of $[\eta]$ are in close agreement. The Huggins intrinsic viscosity decreases from 0.173 to 0.128 dl/g for an increase in ionic strength from 0.1 M to 1.0 M NaCl. The trend is the same as that reported by Liberti and Stivala²⁰ for fractionated heparin in 0.01 M to 0.50 M NaCl. The Huggins constant, k , also shows an appreciable increase from 1.26 to 3.24. This increase was likewise encountered by Liberti and Stivala²⁰. According to the findings of Shanbhag²¹, k is dependent in some complicated way on the solvent, the size of the polymer chain, the temperature and the heterogeneity of the sample. The unusual behaviour of the constant here might be attributed to relative variations in total ionic strength which results as the concentration of the polyelectrolyte decreases since the dilutions were not

Table 2 Effect of ionic strength of unhydrolysed heparin fraction 6 at pH 2.5 on various physical parameters

Property	0.1 M NaCl	0.3 M NaCl	0.4 M NaCl	0.5 M NaCl	1.0 M NaCl	Equation No.*
M	13 578	12 942	11 284	11 751	12 598	
M_1	12 225	12 315	12 530	12 645	12 503	35
M_2				11 733		1
\bar{v} (ml/g)	0.454	0.454	0.454	0.454	0.470	
$V_e \times 10^{20}$ (cm ³ /molecule)	1.02	0.969	0.845	0.880		4a
\bar{V} (l/mol)	6.16	5.88	5.12	5.34	5.92	
$[\eta]_1$ (dl/g)	0.173	0.170	0.161	0.136	0.128	Huggins
$[\eta]_2$ (dl/g)	0.168	0.170	0.161	0.137	0.126	Mead-Fuoss
$[\eta]_3$ (dl/g)	0.168	0.170	0.161	0.138	0.127	Schulz-Blaschke
k	1.26	0.668	0.503	2.89	3.24	Huggins
ν	38.1	37.4	35.5	30.0	26.6	4
$S^0 \times 10^{13}$ (sec)	2.11	2.09	2.34	2.18	2.06	
$S_{20,w}^0 \times 10^{13}$ (sec)	2.13	2.15	2.35	2.30	2.33	2
k_s (dl/g)	0.689	0.288	0.457	0.524	0.461	1
$[S^0] \times 10^{15}$	3.95	4.00	4.33	4.30	4.51	2, 2a
$D_{20,w}^0 \times 10^7$ (cm ² /sec)				8.38		
$D^0 \times 10^7$ (cm ² /sec)	6.95	7.25	8.96	8.40	7.77	1
$D_{20,w}^0$ (cm ² /sec)	7.00	7.39	9.26	8.72	8.47	1, 4a
f (g/sec)	5.79	5.49	4.30	4.99	4.86	4a, 5
f_0 (g/sec)	3.02	2.94	2.80	2.88	3.01	6, 6a
(f/f_0)	2.23	2.15	1.78	1.86	1.81	(5-8)
ρ	24.0	21.1	16.1	16.4	15.2	Perrin plot, 9
$\beta \times 10^{-6}$	2.33	2.43	2.85	2.56	2.57	35a, b, c
$(\bar{r}^2)^{1/2}$ (Å)	111	105	83.9	88.1	91.6	30, 34
$(\bar{s}^2)^{1/2}$ (Å)	44.8	42.2	33.9	35.6	37.0	31

* These equation numbers refer to those in ref 1

made isoionically. The intrinsic viscosity change can be explained on the basis of the effect of solvent on the solute, e.g., the chain becomes more compact (lower hydrodynamic volume) as the ionic strength increases. Recently, Yuan and Stivala²² reported the effect of dielectric constant on the viscosity of heparin. They found that the shielded intrinsic viscosity, $[\eta]_\infty$ (condition under which charges are swamped), increased linearly with increasing dielectric constant of the solvent.

Plots of D^0 and $D_{20,w}^0$ versus concentration were linear and showed definite concentration dependence. The calculated values in 0.5 M NaCl are in good agreement with the experimental data (Table 2). The diffusion coefficients, $D_{20,w}^0$ do not follow the usual decrease with ionic strength as reported by Flaig and Beutelspacher²³ and Suzuki *et al.*²⁴ with other polyelectrolytes, but increase, within experimental error, with ionic strength up to 0.4 M. The frictional coefficients, f , f_0 , frictional ratio, f/f_0 , and the axial ratio, ρ , generally decrease with increasing ionic strength to 0.4 M, then tend to remain fairly constant. In calculating the axial ratios, the amount of solvation was assumed to be zero, since the amount of bound water to heparin is not known.

The values of β^{25} seem to be independent of the ionic strength but approach the 2.5×10^6 value which can indicate that heparin can be described as a flexible random coil when charges are swamped.

The root mean square end-to-end distance, $(\bar{r}^2)^{1/2}$, and the root mean square radius of gyration, $(\bar{s}^2)^{1/2}$, decrease with increased ionic strength. This may indicate a less extended coil and increased flexibility of the molecule with a decrease in the magnitude of the chain length²⁶. These values were calculated from various hydrodynamic models for linear chains (see Table 2). In an earlier paper¹, the authors invoked the model of a Gaussian coil to best describe heparin in saline solution, where charges are swamped.

Heparin in water with its high charge density behaves as a typical polyelectrolyte. Most of the parameters

are ionic strength dependent. At low ionic strength, the concentration of byions is less than that of the counterions, hence the chain is more extended. This is the primary charge effect and its decrease is exceptionally pronounced on the sedimentation coefficient, causing it to increase when the concentration of byions becomes equal to and finally greater than the counter-ion concentration. The chain is then no longer extended but tends to coil. Since heparin has about 7 negative charges per tetrasaccharide repeating unit, it is likely that the primary charge effect is strong. Addition of byions results in a lower field strength. It is clear that as the electric field strength is lowered, and therefore intramolecular repulsions between charges on the chain become weaker, the heparin chain may undergo a change in shape offering less frictional resistance to its transport as is the case with albumin²⁷.

The secondary charge effect should present no special problem in the present system since the sedimentation rates of Na^+ and Cl^- of the solvent are very close together²⁸.

Effect of pH

The sedimentation coefficient parameters (Table 3), S^0 , $S_{20,w}^0$, $[S^0]$, and k_s , increase at higher pH. These results are in accord with those reported for S^0 of heparin by Creeth and Record¹³. However, the lower value of $D_{20,w}^0$ at pH 2.5 is not consistent with theoretical considerations, since at lower pH the chain should be less extended due to diminished negative charges. This discrepancy might exist because the values of the diffusion constants here are calculated ones, involving the molecular weights, which could vary for merely experimental reasons. The other parameters that follow from the diffusion coefficients such as frictional coefficients, f , f_0 , frictional ratios, f/f_0 , and axial ratios, ρ , likewise are higher at the lower pH, contrary to expectation.

The partial specific volume, \bar{v} , and partial molar volume, \bar{V} , show an increase with increased pH. The value of \bar{v} at pH 2.5 (0.464 ml/g) agrees closely with

the value of 0.470 ml/g of Lasker and Stivala¹⁵. The partial specific volume should increase with less electrostriction as indicated by Charlwood²⁹ in investigations on the gelatins and ovalbumins. In the case of heparin, part of the electrostriction is eliminated by decreasing the pH and therefore the partial specific volume should increase, as experienced. The effective volume, V_e , also increases with lower pH.

The intrinsic viscosity (Table 3) at pH 6 is lower than at pH 2.5 for solutions of ionic strength of 0.5. Stivala and Liberti³⁰, on the other hand, observed increasing $[\eta]$ up to about pH 3.5-4.0 with no further increase in $[\eta]$ up to pH 7, at a given ionic strength. The results of these workers appear reasonable since the chain is more extended at the higher pH, where the competition of the carboxyl groups for H^+ is diminished.

The value of β does not change appreciably with pH but remains close to 2.5×10^6 which again supports the concept of a random coil.

The root mean square end-to-end distance, $(\bar{r}^2)^{1/2}$, and root mean square radius of gyration, $(\bar{s}^2)^{1/2}$, increase at lower pH. Again, here the expectation would be that these would tend to go in the opposite direction.

In summary, the general effect of lowering the pH of the environment of heparin is that the ionization of the carboxyl groups is suppressed. Titration studies

of heparinic acid¹⁰ have indicated that all sulphate groups are titrated below pH 3 and the carboxyl groups between pH 3 and 7. Stivala and Liberti³⁰ additionally found that decreasing the pH results in decreased copper binding since the competition is greater for the negative sites. Also, the extension of the chain should decrease, since repulsion due to charged groups is decreased.

Effect of mild hydrolysis

The biological activity of both fractionated (L series) and unfractionated (F series) of heparin show the sharpest drop after approximately 1.5 h of hydrolysis, and after 9 h almost no activity remains (see Tables 4 and 5).

The chemical analysis shown in Table 4 reveals that hydrolysis results essentially in the loss of sulphur from sulphate groups with the sharpest drop occurring after 9 h. Lasker and Stivala¹⁵ experienced no decrease in the sulphur content even after 7 h of hydrolysis. This was probably because the detached sulphate was not removed from the sample as was the case in the present procedure. The data of Braswell³¹ gave the same indications as the latter investigators and probably for the same reason. However, Stivala *et al.*³², subsequently showed that sulphate groups were cleaved upon hydrolysis, with loss of up to 130 units of anticoagulant activity for the heparin sample. They removed the detached sulphate by an ion-exchange column.

The drop in molecular weight accompanying hydrolysis mainly reflects desulphation rather than depolymerization^{15, 32-34}. There is good agreement, in most instances, among the molecular weights obtained by sedimentation equilibrium, by sedimentation velocity and intrinsic viscosity²⁵, and by sedimentation velocity and diffusion measurements²⁵.

The partial specific volume, \bar{v} , increases with hydrolysis time in both series (see Tables 6 and 7). This could be due to decrease in electrostriction with loss in charged sulphate groups. The partial molar volume, \bar{V} , and the effective volume, V_e , decrease due to their dependence on molecular weight.

The intrinsic viscosity in 0.5 M NaCl, and the shape factor, ν , decrease and the Huggins constant, k , increases with hydrolysis time for both series (see Tables 6 and 7). The change in $[\eta]$ appears to be more pronounced with heparin in water. The Liberti-Stivala³⁵ constant, K_{LS} is an interaction parameter dependent on the solute-solvent system. The observed difference in K_{LS} (Table 7) upon hydrolysis of heparin reflects desulphation.

The sedimentation coefficients, S^0 , $S_{20,w}^0$ and the intrinsic sedimentation coefficient, $[S^0]$, decrease with hydrolysis time (see Tables 6 and 7). Parallel studies on

Table 3 Effect of pH on various parameters of heparin fraction 6 at constant ionic strength (0.5 M NaCl)

Property	pH 6	pH 2.5	Equation No.*
M	11 751	12 582	
M_1	12 645	11 855	35
M_2	11 733		1
$V_e \times 10^{20}$ (cm ³ /molecule)	0.880	0.976	4a
\bar{v} (ml/g)	0.454	0.464	
\bar{V} (l/mol)	5.34	5.84	
$[\eta]_1$ (dl/g)	0.136	0.151	Huggins
$[\eta]_2$ (dl/g)	0.137	0.151	Mead and Fuoss
$[\eta]_3$ (dl/g)	0.137	0.151	Schulz and Blaschke
k	2.89	0.877	Huggins
ν	30.0	30.7	4
$S^0 \times 10^{13}$ (sec)	2.18	2.01	
$S_{20,w}^0 \times 10^{13}$ (sec)	2.30	2.23	2
k_s (dl/g)	0.524	0.148	1
$[S^0] \times 10^{15}$	4.30	4.05	2, 2a
$D_{20,w}^0 \times 10^7$ (cm ² /sec)	8.72	8.05	1, 3
f (g/sec)	4.99	5.14	4a, 5
f_0 (g/sec)	2.88	2.95	6, 6a
(f/f_0) (Å)	1.86	1.95	(5-8)
p	16.4	18.4	Perrin plot, 9
$(\bar{r}^2)^{1/2}$ (Å)	88.1	98.8	30, 34
$(\bar{s}^2)^{1/2}$ (Å)	35.6	40.5	31
$\beta \times 10^{-6}$	2.56	2.46	35a, b, c

* These equation numbers refer to those in ref 1

Table 4 Chemical analysis and biological assay of L series hydrolysates

Sample	Hydrolysis time (h)	Carbon (%)	Nitrogen (%)	Hydrogen (%)	Sulphur (%)	Ash (%)	Biological activity (USP units/mg)
L-00	—	23.50	2.24	4.82	11.43	32.83	164
L-0	0	23.48	2.88	4.87	11.40	33.74	164
L-1	1.50						98
L-2	3.00	24.45	2.53	4.77	10.83	31.83	34.8
L-3	4.75						13.4
L-4	6.30	23.34	2.80	4.83	10.05	29.12	8.5
L-5	7.10						13.3
L-6	9.00	25.89	2.61	4.76	10.31	30.07	5
L-7	32.00	23.97	2.38	5.16	8.80	24.16	0
L-8	48.00	24.93	2.88	4.96	7.67	23.68	0

unfractionated heparin by Stivala *et al.*³² showed the same effect. The investigations of Braswell³¹ also indicate a decrease of sedimentation coefficient with hydrolysis. The results of Jensen *et al.*³⁴ on the inactivation of heparin to 44% activity with warm dilute acetic acid, however, demonstrates an increase in $S_{20,w}$ from 2.07 to 2.70S. A reduction of sedimentation coefficient would seem more reasonable owing to decrease of molecular weight and the possibility of subtle changes in shape and dimensions resulting from desulphation.

The diffusion coefficient increases and the frictional coefficients, frictional ratios and axial ratios decrease with deactivation (see *Tables 6* and *7*). Jensen and colleagues³⁴ also found that the frictional ratios decrease with deactivation. Likewise, Stivala *et al.*³² reported a decrease in axial ratios with hydrolysis. These parameters express the departure from ideal spherical shape and are intended to describe the hydrodynamic rather than the actual shape, since the degree of hydration may contribute to the frictional ratio and thus to the axial ratio.

The value of β is unaffected within experimental error, upon desulphation (see *Tables 6* and *7*). This supports the premise that heparin, at varying degrees of sulphation, may be described as a random coil,

since the values of β are in close agreement with the theoretical value. Therefore, these hydrolysed samples were treated in light of various hydrodynamic models in obtaining the dimensional parameters of $(\bar{r}^2)^{1/2}$, $(\bar{s}^2)^{1/2}$, including other physical parameters. Since anticoagulant activity is associated with degree of sulphation of heparin, the dimensional parameters can also be correlated with biological activity. As noted in *Tables 4-7*, $(\bar{r}^2)^{1/2}$ decreases with increasing desulphation; hence, with decrease in anticoagulant activity. As sulphate groups are removed, the charges are diminishing and therefore end-to-end distance should diminish as the chain becomes more compact. The effect of size on biological activity was effectively demonstrated from binding studies by Stivala and Liberti³⁰.

It is interesting to note that even though there was a difference in path used for hydrolysis in the F-A and F-C series, the results are similar except for a more pronounced decrease in molecular weight and increase in diffusion coefficient in the F-A series. Additionally, hydrolysis of fractionated heparin (L series) produced parallel results.

In summary, hydrolysis of heparin results in loss of sulphate groups, and accordingly, decrease of repulsive charges. The drop in molecular weight essentially reflects desulphation but not depolymerization. The partial specific volume increases with desulphation probably because of the decrease in repulsive charges which leads to less electrostriction and a larger volume. The sedimentation coefficient and intrinsic viscosity decrease because of the reduction in molecular weight and/or a change in size to a form offering less friction. Likewise, the diffusion coefficient increases due to less frictional resistance with decreased extension of the chain. This is reflected in the decreased frictional coefficients, frictional ratios and axial ratios, which may indicate the tendency to form a more compact molecule. A similar phenomenon is seen with the root mean square end-to-end distance and radius of gyration for

Table 5 Biological activity of F series hydrolysates

Sample	Hydrolysis time (h)	Activity (USP units/mg)	
		A series	C series
F-0	0	168	165
F-1	0.6	145	157
F-2	1.0	114	141
F-3	2.0	121	50
F-4	2.5	84	85
F-5	4.25	30	75
F-6	5.8	16	10.4
F-7	9.00	5	5
F-8	48.00	0	0
F-9	200.00	0	0

Table 6 Effect of hydrolysis time on various parameters for the L series measured in 0.5 M NaCl and pH 6 (unadjusted)

Property	L-00	L-3	L-5	L-6	L-8	Equation No.*
M	16 605	15 204	12 895	12 973	11 523	
M_1	15 352	13 638	13 088	12 757	10 854	35
M_2	16 926	15 491	13 240	13 246	11 760	1
\bar{v} (ml/g)	0.453	0.480	0.480	0.486	0.479	
\bar{V} (l/mol)	7.52	7.30	6.19	6.31	5.52	
$V_e \times 10^{20}$ (cm ³ /molecule)	1.24	1.20	1.02	1.04	0.911	4a
$[\eta]_1$ (dl/g)	0.183	0.162	0.155	0.149	0.140	Huggins
$[\eta]_2$ (dl/g)	0.183	0.163	0.156	0.151	0.145	Mead and Fuoss
$[\eta]_3$ (dl/g)	0.184	0.165	0.157	0.155	0.151	Schulz and Blaschke
k	1.48	2.20	2.69	3.89	6.23	Huggins
ν	40.4	33.7	32.3	30.7	29.4	4
$S^0 \times 10^{13}$ (sec)	2.29	2.09	2.07	2.03	1.89	
$S_{20,w}^0 \times 10^{13}$ (sec)	2.43	2.27	2.20	2.16	2.01	2 (in this paper)
k_s (dl/g)	0.402	0.439	0.375	0.437	0.456	1 (in this paper)
$[S^0] \times 10^{15}$	4.52	4.35	4.29	4.27	3.91	21a
$D_{20,w}^0 \times 10^7$ (cm ² /sec)	6.26	6.38	7.43	6.93	8.12	3 (in this paper)
$D_{20,w}^0 \times 10^7$ (cm ² /sec)	6.49	6.99	7.95	7.87	8.14	1
f (g/sec)	6.42	6.12	5.30	5.49	5.08	5
f_0 (g/sec)	3.23	3.16	2.99	3.00	2.88	6, 6a
(f/f_0)	2.27	2.16	1.96	2.02	1.93	(5-8)
ρ	25.1	22.1	18.6	19.3	17.6	Perrin plot, 9
$(\bar{r}^2)^{1/2}$ (Å)	119	113	96.9	97.9	94.0	30, 34
$(\bar{s}^2)^{1/2}$ (Å)	47.9	45.6	39.2	39.6	38.4	31
$\beta \times 10^{-6}$	2.37	2.32	2.50	2.41	2.39	35a, b, c

* These equation numbers refer to those in ref 1

Table 7 Effect of hydrolysis time on various parameters for the F-A and F-C series measured in 0.5 M NaCl and pH 6 (unadjusted)

Property	FOC	F-9C	FOA-2	F-5A	F-9A	Equation No.*
M	13 860	11 696	13 839	13 273	9 128	
M_1	14 345	11 310	13 480	13 118	10 560	35
M_2	13 655					1
\bar{v}	0.439	0.484	0.458	0.481	0.471	
\bar{V} (l/mol)	6.085	5.661	6.338	6.371	4.299	
$V_a \times 10^{20}$ (cm ³ /molecule)	1.004	0.934	1.046	1.051	0.709	4a
$[\eta]_1$ (dl/g)	0.193	0.167	0.190	0.182	0.155	Huggins
$[\eta]_2$ (dl/g)	0.193	0.170	0.189	0.182	0.157	Mead and Fuoss
$[\eta]_3$ (dl/g)	0.194	0.167	0.189	0.181	0.160	Schulz and Blaschke
$[\eta]_{H_2O}$ (dl/g)			22.6		1.51	Stivala and Liberti
k	0.368	1.164	0.206	0.420	2.069	Huggins
k_{LS}			0.466		0.498	Stivala and Liberti
ν	44.0	34.5	41.5	37.9	32.9	4
$S^0 \times 10^{13}$ (sec)	2.21	1.81	2.06	1.96	1.87	
$S_{0,w}^0 \times 10^{13}$ (sec)	2.36	1.97	2.23	2.12	2.03	2 (in this paper)
k_s (dl/g)	5.02	0.434	0.134	0.254	0.514	1 (in this paper)
$[S^0] \times 10^{15}$	4.24	3.80	4.09	4.07	3.81	21a
$D_{20,w}^0 \times 10^7$ (cm ² /sec)	7.65				10.16	3 (in this paper)
$D_{20,w}^0 \times 10^7$ (cm ² /sec)	7.40	7.93	7.25	7.47	10.23	1
f (g/sec)	5.52	5.18	5.68	5.49	4.09	4a, 5
f_0 (g/sec)	3.02	2.90	3.04	3.02	2.66	6, 6a
(f/f_0)	2.05	1.99	2.11	2.01	1.69	(5-8)
p	22.0	19.5	22.6	20.4	14.2	Perrin plot, 9
$(\bar{r}^2)^{1/2}$ (Å)	105	99.3	109	105	78.2	30, 34
$(\bar{s}^2)^{1/2}$ (Å)	42.6	40.2	44.1	42.5	31.1	31
$\beta \times 10^{-6}$	2.63	2.50	2.47	2.53	2.87	35a, b, c

* These equation numbers refer to those in ref. 1

the same preceding reason. Most importantly, heparin under the conditions described approximates a Gaussian coil and its anticoagulant activity is due not only to the presence of its negative groups but also to size. Additionally, it should be mentioned that β of about 2.5×10^6 for a random coil can show experimental values of axial ratios 15–20³⁶ which is in the range of this work. Under such circumstances, support for the Gaussian coil may be obtained from the values of $k_s/[\eta]$ (see equation 1). Values of $k_s/[\eta]$ below 1.5 indicate asymmetry^{37, 38}. In this work values of this ratio were above 1.5, thus substantiating spherical symmetry. This lends further support for the Gaussian coil model.

ACKNOWLEDGEMENTS

The authors are grateful to Organon Inc. for the generous supply of sodium heparin. This work was supported, in part, by the National Institutes of Health grant HE-5943 and Public Health Service Fellowship (J. E.) No. F3-HE-29,038-03.

REFERENCES

- Stivala, S. S. and Ehrlich, J. *Polymer* 1974, **15**, 197
- Jaques, L. B., Kavanagh, L. W., Mazurek, M. and Perlin, A. S. *Biochem. Biophys. Res. Commun.* 1966, **24**, 447
- Inoue, S. and Inoue, Y. *Biochem. Biophys. Res. Commun.* 1966, **23**, 513
- Perlin, A. S., Mazurek, M., Jaques, L. B. and Kavanagh, L. W. *Carbohydr. Res.* 1968, **7**, 369
- Cahn, L. Instruction Manual for Model RG and Density Cell, Cahn Instrument Co., Paramount, Calif.
- Elgert, K. F. and Cammann, K. *Z. Analyt. Chem.* 1967, **226**, 193
- Ehrlich, J., Weiner, P. and Stivala, S. S. *J. Macromol. Sci. (A)* 1967, **1**, 1127
- Ehrlich, J., Liddle, D. and Stivala, S. S. *US CFSTI* 1969, AD-695009
- Ehrlich, J., Wonica, D. and Stivala, S. S. 'PDP-10 Applications in Science', Digital Equipment Corp., 1972, Vol 2, p 162
- Helbert, J. R. and Marini, M. A. *Biochemistry* 1967, **2**, 1101
- Barlow, G. H., Sanderson, N. D. and McNeill, P. D. *Arch. Biochem. Biophys.* 1961, **84**, 518
- Patat, F. and Elias, H. G. *Naturwissenschaften* 1957, **46**, 322
- Creeth, J. M. and Record, B. R. *Biochem. J.* 1952, **52**, 30
- Laurent, T. C. *Arch. Biochem. Biophys.* 1961, **92**, 224
- Lasker, S. E. and Stivala, S. S. *ibid.* 1966, **115**, 360
- Gagen, W. L. *Biochemistry* 1966, **5**, 2552
- Huggins, M. L. *J. Am. Chem. Soc.* 1942, **64**, 2716
- Mead, D. F. and Fuoss, R. M. *J. Am. Chem. Soc.* 1942, **64**, 277
- Schulz, G. V. and Blaschke, F. *J. Prakt. Chem.* 1941, **158**, 130
- Liberti, P. A. and Stivala, S. S. *Arch. Biochem. Biophys.* 1967, **119**, 510
- Shanbhag, V. P. *Arkiv. Kemi* 1968, **29**, 1
- Yuan, L. and Stivala, S. S. *Biopolymers* 1972, **11**, 2079
- Flaig, W. and Beutelspacher, H. *Proc. 2nd Symp. Isotop. Radiat. Soil Org. Matter Stud.* 1968, p 23
- Suzuki, Y., Noda, I. and Nagasawa, M. *J. Phys. Chem.* 1967, **71**, 200
- Mandelkern, L. and Flory, P. J. *J. Chem. Phys.* 1952, **20**, 212
- Cowie, J. M. G. *Makromol. Chem.* 1961, **52**, 230
- Harrington, W. F., Johnson, P. and Ottewill, R. H. *Biochem. J.* 1956, **62**, 569
- Pedersen, E. O. *J. Phys. Chem.* 1958, **62**, 1282
- Charlwood, P. A. *J. Am. Chem. Soc.* 1957, **79**, 776
- Stivala, S. S. and Liberti, P. A. *Arch. Biochem. Biophys.* 1967, **122**, 40
- Braswell, E. *Biochim. Biophys. Acta* 1968, **158**, 103
- Stivala, S. S., Yuan, L., Ehrlich, J. and Liberti, P. A. *Arch. Biochem. Biophys.* 1967, **122**, 32
- Yuan, L. *Doctoral Dissertation* Stevens Institute of Technology, 1970
- Jensen, R. *et al. J. Biol. Chem.* 1948, **174**, 265
- Liberti, P. A. and Stivala, S. S. *J. Polym. Sci. (B)* 1966, **4**, 137
- Scheraga, H. A. and Mandelkern, L. *J. Am. Chem. Soc.* 1953, **75**, 179
- Wales, M. and Van Holde, R. E. *J. Polym. Sci.* 1954, **14**, 81
- Creeth, J. M. and Knight, C. G. *Biochim. Biophys. Acta* 1965, **102**, 549
- Gropper, L. *Analyt. Biochem.* 1964, **7**, 401.

Formation of supermolecular structure in thin polymer films*

M. Kryszewski, A. Gałęski, W. Jabłoński and S. Sapięha

*Centre of Molecular and Macromolecular Studies, Polish Academy of Sciences,
Łódź, Poland*

(Received 14 September 1973)

The morphological structure of thin glow discharge films of thickness 100Å – $6\mu\text{m}$ was investigated. The layers have well developed nodular surface structure and spherulitic structures in bulk. The size of the structure elements increases with the increase of support temperature and decreases with the increase of discharge current density and frequency. Investigations of spatial arrangement of spherulites show that spherulites exist only in the vicinity of the gold layer used as support while the upper layer is shown to be amorphous. The spherulites are built of radially arranged fibrils of about 5000Å in diameter. It is shown that crystallization of spherulites takes place during the polymerization process.

INTRODUCTION

Thin polymer films obtained by the method of glow discharge in vapours of different monomers show very interesting properties from the point of view of their application in electronics and as coatings. For this reason much attention was paid to the methods and mechanism of their formation and characteristics of their electrical properties. Less attention has been paid until now to their supermolecular structure, it being often assumed that they are typically amorphous. Our previous investigations have shown, however, that such layers have definite morphological structures which depend on the pertaining conditions rather than on the kind of monomer. Thin films obtained by glow discharge in benzene show hemispherical structures of the nodular type on the surface and spherulitic structures in bulk^{1, 2}. In the layers of thicknesses over 800Å , nodules of 500Å in diameter and 250Å high were found, while in layers over 8000Å thick spherulites were observed. The number of spherulites in unit volume increased with an increase of layer thickness.

The mechanism of formation of the structure in films of such thickness is not fully known. Because of this attention was given to the dependence of the formation of nodular structure on the parameters of the polymerization process. The formation and spatial arrangement of spherulites in polymers obtained by glow discharge is also discussed.

Investigations of dielectric breakdown effects in thin glow discharge polymer films using self-healing techniques show that breakdown channels also contain material of nodular structure³. Thus it seems reasonable to compare the results of structural investigations of fresh films with the investigations of the structure of breakdown channels in self-healing breakdown since during the breakdown process and the process of polymer formation the conditions are similar.

* Presented at the IUPAC International Symposium on Macromolecules, Aberdeen, September 1973.

EXPERIMENTAL

Thin layers for these investigations were obtained by glow discharge in benzene vapours at 1 mmHg pressure^{1, 4, 5}. Discharge current density in the polymerization process was changed from 0.8 to 4.8mA/cm^2 and the frequency in the range 2 – 200kHz . The layers obtained in these conditions were 100Å to $6\mu\text{m}$ thick. The layers were prepared on a glass support covered with a thin layer of vacuum deposited gold. The support temperature was regulated using suitable thermostatic equipment.

In the investigations of the inside of the breakdown channel, layers about 2500Å thick were used. To ensure self-healing breakdowns with incomplete destruction of the inside of the breakdown channel, thin vacuum deposited gold electrodes were used. The breakdown energy was limited to 1×10^{-5} to $5 \times 10^{-3}\text{J}^3$.

Investigations of the morphological structure of thin films were carried out with a Tesla BS 242 E electron microscope using the replication technique and with a polarizing microscope. Electron diffraction experiments were also carried out with an electron microscope.

RESULTS

The size and the shape of the morphological structures on the surface of thin glow discharge layers depend on three basic parameters of the polymerization process: the density and the frequency of the discharge current and the support temperature, as well as the thickness of the deposited layer.

Effect of the discharge current density

The current density is a dynamic parameter characterizing the state of plasma in the discharge process. It may also cause a rise in the support temperature which, as is well known, results in an increase in size and aggregation of nodules. However, for short discharge times (about 1 – 5sec) this dynamic factor can be neglected.

It was found that with an increase of discharge current density from 0.8 to 4.8 mA/cm² average globule diameter decreased from 1200 Å to 400 Å. Microphotographs illustrating the above effect are presented in Figures 1a-1c.

Effect of the frequency of discharge current

It was found that the size of structures on the surface layer decreases with an increase in discharge frequency. Typical electron micrographs of the surface layers obtained at different frequencies varying from 2 to 200 kHz at constant discharge current density and a support temperature of 25°C are presented in Figures 1d-1f. With an increase of frequency from 2 to 200 kHz the magnitude of the surface nodules decreases from 1100 Å to 200 Å. The decrease of nodule diameter with increase of frequency is independent of the support temperature. The layers obtained at much lower frequency of discharge, i.e. 50 Hz, have non-uniform surfaces and are characterized by cracked areas not adhering to the support. In view of that, microscopic investigation of the surface layers obtained at this frequency was not advisable.

Effect of the support temperature

The results of the investigations into the effect of the support temperature at constant discharge current density and frequency show that the size of the structures increases with an increase in support temperature.

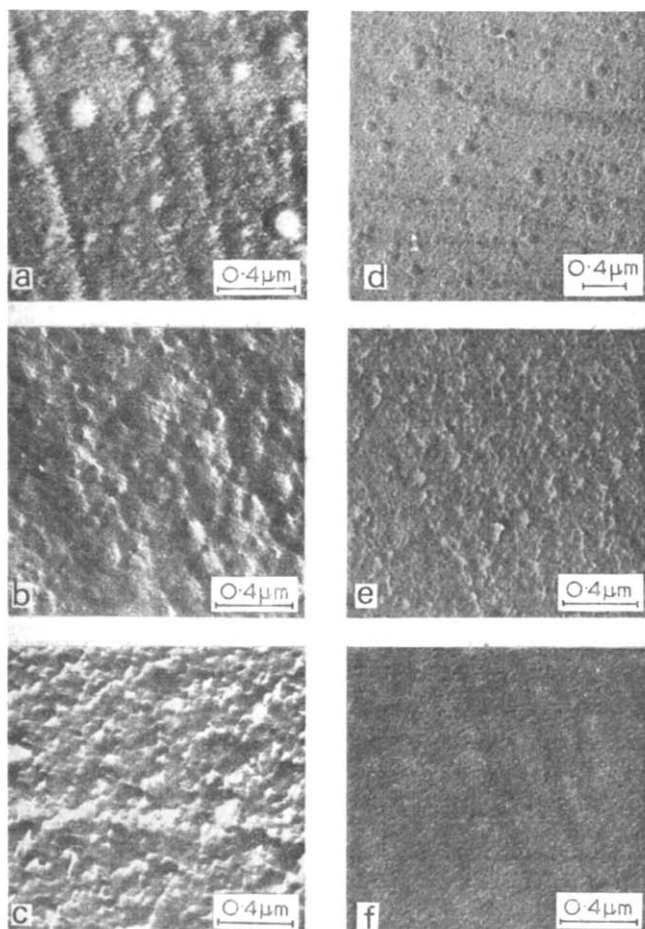


Figure 1 Influence of glow discharge current density (a, b, c) and current frequency (d, e, f) on the size of structure elements in glow discharge films obtained from benzene. (a) 0.8 mA/cm²; (b) 2.4 mA/cm²; (c) 4.8 mA/cm²; (d) 2 kHz; (e) 10 kHz; (f) 80 kHz

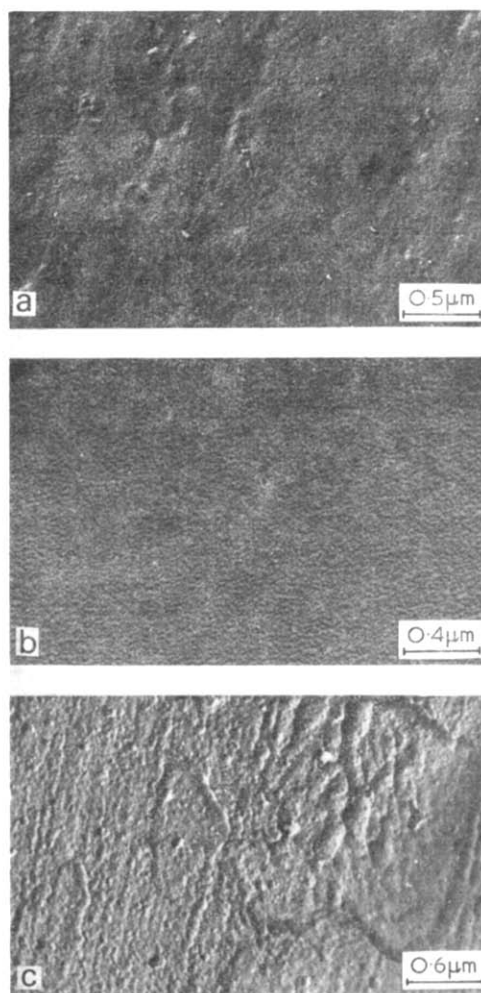


Figure 2 Surface of glow discharge films obtained from benzene at different support temperatures. (a) 20°C; (b) 50°C; (c) 75°C

This regularity was observed for all sets of layers. Figures 2a, 2b and 2c show microphotographs of the layers obtained at support temperatures of 30°C, 50°C and 75°C respectively, and at a frequency of 10 kHz and discharge current density of 2 mA/cm². At support temperatures higher than 70°C aggregation of these surface structure elements was observed (Figure 2c). Figure 2c also shows that aggregation of structure elements occurs first of all on the support fissures.

Globular structures in breakdown channels

It was found that in channels of self-healing breakdowns globular structures similar to those found on fresh glow discharge polymer layers are observed (Figure 3)³. The size of the globules formed in both cases was similar to and was about 1000 Å.

Etching of the layers

In order to establish whether the structure of the material forming globules is different from the material of the remaining area of the film, thin layers of polybenzene were subjected to ionic etching in an atmosphere of krypton. The current density used was 7 μA/cm², the discharge frequency was 5.8 MHz, the krypton pressure was 6.0 × 10⁻² mmHg, etching time was changed and the energy of the krypton ions calculated using equations given by Lochte-Holtgreven⁶ was 7.05 eV.

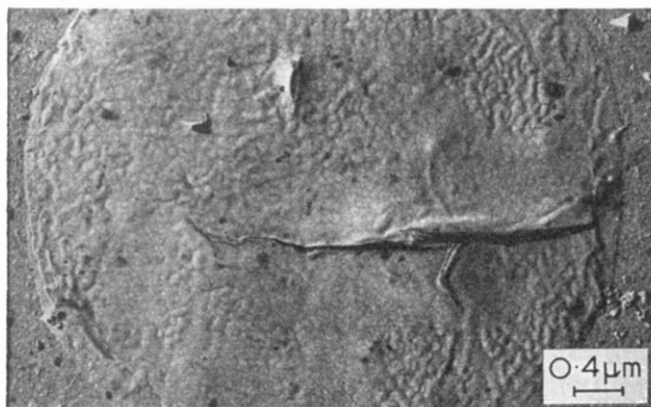


Figure 3 Structures on interior of breakdown channel in glow discharge films obtained from benzene. Thickness of layer 2500 Å

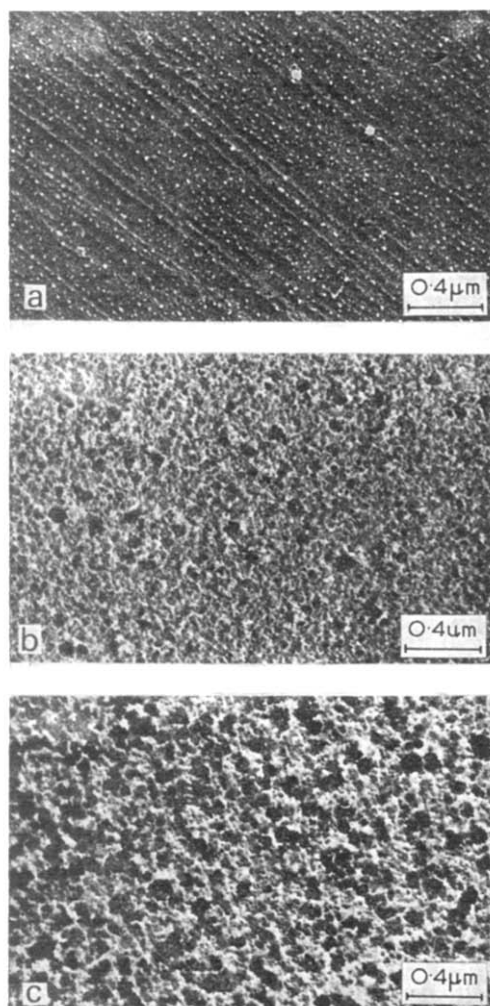


Figure 4 Surface of glow discharge film from benzene etched in krypton atmosphere after different etching times. (a) Non-etched; (b) etched 120s; (c) etched 240s

Figures 4b and 4c show the fragments of the layer presented in Figure 4a for two etching times. The microphotographs show different stages of exposing of the bulk structure of the layer. It can be seen that the layer is not etched uniformly and the highest etching rate characterizes the interglobular material. This property is responsible for the relative increase in globule size, especially their height in the course of layer etching.

It can be concluded from the above, that the globule material is more crosslinked compared with interglobular areas.

Spherulitic structures

Microscopic observations show that in polybenzene layers of thicknesses over 8000 Å spherulites may arise now and then. With electron microscopy it was found that the spherulites are flat, built of radially arranged fibrils about 5000 Å wide and up to several microns long.

In this work the results of investigations into the structure of glow discharge polybenzene layer containing spherulites at different depths are reported. The separation of the layer was achieved by tearing away the surface layer of the film with a drop of aqueous poly(acrylic acid) solution on it, which is characterized by strong adhesion to the surface of the layer after evaporation of water. As a result of microscope measurements the surface layer contains no spherulites and no anisotropies at all while all the spherulites are situated deeper, close to the gold layer. Separated in the above way the upper layer of the film shows only diffusional diffraction of electrons while after contrasting with Pt/Pd alloy one can see in the electron microscope a relief of the spherulites remaining close to the gold layer. In the lower part of the film undamaged spherulites were observed, and after removing the gold electrode, electron microscope investigations were carried out. Electron diffraction pattern of this layer shows three, relatively wide diffraction rings with diffused edges (Figure 5a). This result indicates the existence of a crystalline arrangement in spherulites. It is not possible to attribute precisely any definite size of the unit cell to the above arrangement.

The diffraction pattern indicates a strongly defected, mosaic-like lattice. The above conclusion arises from strongly diffused diffraction rings, not found in other cases. The pattern is not affected by the support material which is illustrated by the diffraction pattern of thin gold layer showing sharp and distinct diffraction rings even of relatively high order (Figure 5b). To estimate the structure of thin layers measurements of small angle light scattering were carried out. The apparatus described earlier⁷ was used. The results obtained are presented in Figures 6a, 6b, 6c and 6d. Scattering patterns obtained for samples without immersion show a relatively wide diffraction ring for scattering angle equal to 3°55'. For smaller angles the light scattered comes from larger elements of the inner structure. The H_v and V_v patterns obtained for samples with immersion do not show any diffraction ring and the scattering pattern is typical of large spherulites.

Comparing the scattering patterns obtained for samples with and without immersion it can be concluded that on the surface of glow discharge film obtained from benzene there exist relatively large (2 to 3 μm), hemispherical structures. In bulk specimens, however, one can find relatively well organized spherulites of average size about 6 μm (for layers 2 μm thick) (Figure 6d).

DISCUSSION

On the basis of presented experimental results one can formulate some suggestions regarding the mechanism of formation of supermolecular structure in thin layers

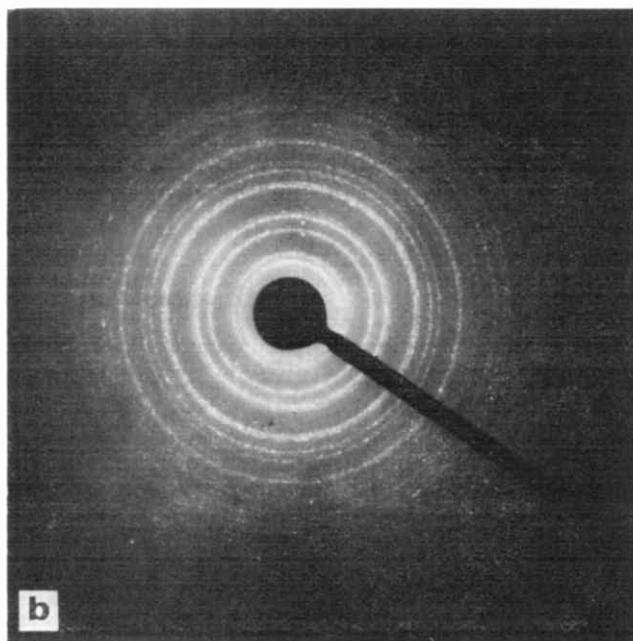
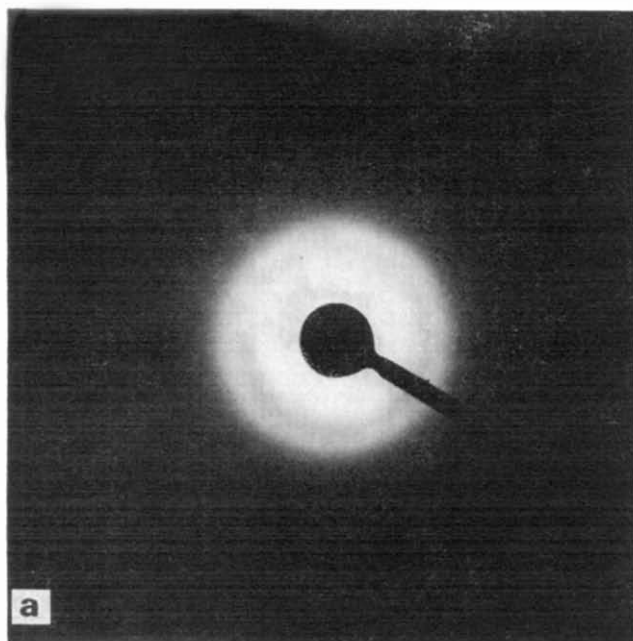


Figure 5 (a) Electron diffraction pattern of glow discharge films from benzene (part of the layer close to gold support); (b) electron diffraction pattern of gold layer used as film support

obtained by a glow discharge method. The globular structure depends on the conditions of the polymerization process. At constant pressure of monomer vapours the size of the structures found on the surface layer decreases with increase of discharge current density and frequency, while an increase of support temperature results in an increase of the size of globular structures.

The mechanism of formation of supermolecular structure in thin glow discharge films responsible for formation of globular and spherulitic structure is now discussed.

Globular structures

The dependence of globule size on temperature mentioned above indicates that the globular structure observed on the surface layer is formed as a result of

condensation of radicals or ionized monomer molecules on the support. A similar hypothesis was given by Häfer *et al.*² on the basis of investigations arising from glow discharge layers of tetramethylsilane, styrene and benzene. The dependence of the size of these structures on the support temperature agree with the general rule, according to which supermolecular structures growing as a result of condensation can reach greater size at higher temperatures as their growth rate is then smaller.

The mechanism of growth of supermolecular structure on the bottom of breakdown channel is in general similar to one of surface layer formation from the plasma during glow discharge in monomer vapours. As a result of high power density reaching in breakdown process values as high as 10^9 W/cm^2 ^{3,8} the macromolecules of the original layer are broken into ionized fragments and form a microcloudlet of plasma. The plasma might condensate in this case in a similar way as in the process of layer formation from ionized monomer during glow discharge, but in the former case the condensation takes place not on the surface of the metal electrode, but on the support covered with fragments of the original layer. The greater size of the globules in this case can be explained by unknown but certainly high temperature of the support resulting from dielectric breakdown. Similarly the formation of globules of greater size occurs at higher temperatures of the support as in the process of polymerization (Figure 2). In this case the deposition of the layer occurs after finishing of breakdown process, while in the case of polymerization the layer is formed during electric current flow.

Spherulitic structures

As a result of investigations of arrangement of flat spherulitic structures in the bulk of the layer, it was found that they are placed close to the metal surface. One can conclude from the above that in the first stage of polymerization slightly crosslinked polymer is formed,

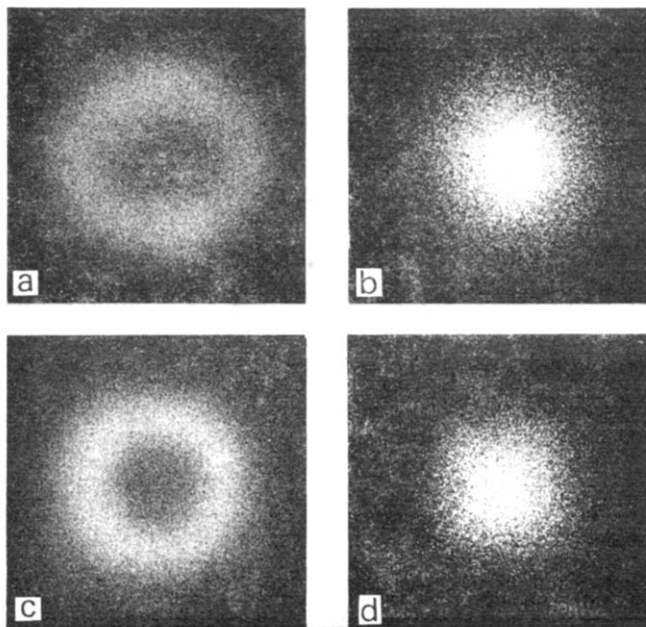


Figure 6 V_V (a, b) and H_V (c, d) small angle light scattering patterns for thin glow discharge layer from benzene. (a) and (c) without immersion; (b) and (d) with immersion

capable of crystallization in spherulitic structures. The lack of larger amounts of microcrystalline material not organized into supermolecular structures as well as the formation of spherulites along fissures of the support¹ indicates the heterogeneous character of nucleation. The fibrils, of which the spherulites are built up, are crystalline with a statistically varying intermolecular distance in the lattice. It appears that they are formed by molecules which slightly differ in their structure.

Hemispherical structures observed on the surface of relatively thick layers are found only above spherulites, because the light scattering pattern, in the form of a ring, is not observed in areas where no spherulites exist. This fact leads us to conclude that crystallization of the

material in the form of spherulites takes place already during the polymerization process.

REFERENCES

- 1 Kryszewski, M. *Pure Appl. Chem.* 1972, **31**, 21
- 2 Häfer, D., Tiller, H. J. and Meyer, K. *Plast. Kaut.* 1972, **5**, 354
- 3 Sapięha, S., Jabłoński, W. and Kryszewski, M. *Elect. Compon. Technol.* in press
- 4 Gregor, L. V. *IBM J. Res. Develop.* 1968, **12**, 140
- 5 Mearns, A. M. *Thin Solid Films* 1969, **3**, 201
- 6 Lochte-Holtgreven, W. 'Plasma diagnostics', North-Holland, Amsterdam, 1968
- 7 Kryszewski, M., Gałęski, A., Pakuła, T. and Szyldhabel, R. *Polimery* 1971, **16**, 8
- 8 Klein, N. *Adv. Electr. Electr. Phys.* 1969, **26**, 364

Participation of Lewis base on vinyl chloride polymerization with $\text{Al}(\text{C}_2\text{H}_5)_3/\text{CCl}_4$ catalyst system

Akira Akimoto

Central Research Laboratory, Toyo Soda Manufacturing Co. Ltd, Yamaguchi-ken, Japan
(Received 26 September 1973)

The polymerization of vinyl chloride has been investigated using an $\text{Al}(\text{C}_2\text{H}_5)_3/\text{CCl}_4$ catalyst system in the presence of various Lewis bases. Effective Lewis bases are γ -butyrolactone, diglyme and diethylenetriamine which are multidentate. The rate of polymerization is dependent not only on the basicity of the Lewis base used but also on a coordination number of one. The latter is the predominant factor. For the effect of polymeric amines, a tentative hypothesis is discussed.

INTRODUCTION

Polymerization of vinyl chloride initiated by organoaluminium compounds, which, unlike the known Ziegler-Natta processes, proceeds via a free-radical mechanism, is of great interest. The $\text{Al}(\text{C}_2\text{H}_5)_3/\text{CCl}_4$ ^{1, 2}, $\text{Al}(\text{C}_2\text{H}_5)_3/\text{Lewis base}/\text{CCl}_4$ ³ and $\text{Al}(\text{C}_2\text{H}_5)_3/\text{CuCl}/\text{CCl}_4$ catalyst systems⁴ are known to initiate the free-radical polymerization of vinyl chloride. These systems are significant especially in respect of the polymerization catalyst behaviour of the organometallic compound.

In recent years systems based on aluminium alkyls and acyl peroxides have been used to initiate the polymerization of vinyl chloride⁵. The effective polymerization of vinyl chloride with this catalyst system could be carried out in the presence of the complexing agent—ester, ether and nitrile⁶. The role of complexing agent is characteristic. This was also found for the vinyl chloride polymerization with $\text{Al}(\text{C}_2\text{H}_5)_3/\text{Lewis base}/\text{CCl}_4$ catalyst system³.

In this paper the participation of the Lewis base is dealt with in the vinyl chloride polymerization with $\text{Al}(\text{C}_2\text{H}_5)_3/\text{CCl}_4$ catalyst system in greater detail. Some features of this catalyst system are discussed.

EXPERIMENTAL

Reagents

Vinyl chloride monomer (Toyo Soda Manufacturing Co. Ltd) was dried and purified by passing it through a column containing calcium chloride and then one containing phosphorus pentoxide.

Benzene was purified by the usual methods and distilled over calcium hydride. The middle fraction was then stored with sodium wire in a dry box.

Lewis bases were refined according to the conventional methods⁷.

Triethylaluminium (Texas Alkyls Inc.) was redistilled under reduced pressure and nitrogen atmosphere. 1 mol/l stock solution of $\text{Al}(\text{C}_2\text{H}_5)_3$ in anhydrous benzene was prepared prior to use.

Carbon tetrachloride was washed with concentrated sulphuric acid, then with water, and distilled before the polymerization.

Polymerization procedure

The polymerization was carried out in a sealed glass tube, which was shaken in a water bath maintained at a given temperature. After the glass tube had been evacuated, vinyl chloride was distilled into a glass tube, kept below -78°C , in which was the required amount of the catalyst $\text{Al}(\text{C}_2\text{H}_5)_3$, Lewis base, carbon tetrachloride and solvent.

After a definite time, the polymerization mixture was poured into a large amount of methanol containing hydrochloric acid.

I.r. spectra of $\text{Al}(\text{C}_2\text{H}_5)_3$ complex

Infra-red spectra were taken using a sealed cell of potassium bromide to protect the organoaluminium compound from moisture and air.

RESULTS AND DISCUSSION

Vinyl chloride was polymerized with the $\text{Al}(\text{C}_2\text{H}_5)_3/\text{CCl}_4$ catalyst system in the presence of various Lewis bases at 40°C . *Figure 1* presents the relation between the yield of poly(vinyl chloride) (PVC) and the electron donating power ($\Delta\nu_D$) of the Lewis base⁸. The results in *Figure 1* indicate that the yield of PVC first rose, then passed through a maximum with an increase in the $\Delta\nu_D$ values. The rate of polymerization of vinyl chloride was increased by using Lewis bases which had $\Delta\nu_D$ values from about 60 to about 110. γ -Butyrolactone was the most effective complexing agent of all those studied, and β -propiolactone was more effective than methyl acetate regardless of their $\Delta\nu_D$ value.

It is interesting to note that cyclic esters such as γ -butyrolactone and β -propiolactone are more effective Lewis bases than linear aliphatic esters which have

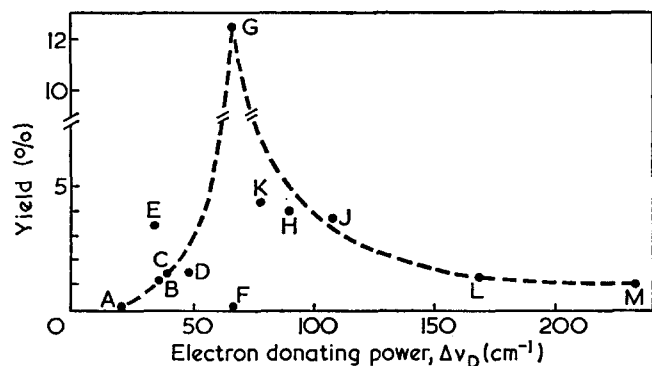


Figure 1 Polymer yield vs. electron-donating power. Vinyl chloride, 5 ml; C_6H_6 , 5 ml; $\text{Al}(\text{C}_2\text{H}_5)_3$, 1 mol% on monomer; catalyst ratio $\text{Al}(\text{C}_2\text{H}_5)_3/\text{CCl}_4/\text{Lewis base}=1:1:1$; polymerization at 40°C for 20 h. A, Vinyl acetate; B, methyl acetate; C, ethyl acetate; D, acetonitrile; E, β -propiolactone; F, cyclohexanone; G, γ -butyrolactone; H, THF; J, DMF; K, ethyl ether; L, pyridine; M, ethylamine

the same number of carbon atoms, such as ethyl acetate and methyl acetate.

Infra-red spectra of the mixture of $\text{Al}(\text{C}_2\text{H}_5)_3$ and Lewis base were studied to clarify the effect of γ -butyrolactone, and also to check which oxygen atom of the ester group takes part in the complexing interaction. Comparing the spectra of $\text{Al}(\text{C}_2\text{H}_5)_3/\gamma$ -butyrolactone and $\text{Al}(\text{C}_2\text{H}_5)_3/\text{ethyl acetate}$ complexes with those of the corresponding free γ -butyrolactone and ethyl acetate, it follows that in the presence of $\text{Al}(\text{C}_2\text{H}_5)_3$ the carbonyl oxygen absorption band of γ -butyrolactone is shifted towards low frequencies (1721 cm^{-1}) from the single band of the corresponding free γ -butyrolactone (1795 cm^{-1}).

The carbonyl oxygen absorption band of γ -butyrolactone is shifted towards lower frequencies (1665 cm^{-1}) in the SnCl_4/γ -butyrolactone complex⁹. The carbonyl oxygen absorption band in the infra-red spectra of $\text{Al}(\text{C}_2\text{H}_5)_3/\text{ethyl acetate}$ complex is split into two bands, one of which corresponds to the carbonyl oxygen of the free ethyl acetate (1752 cm^{-1}), the other corresponding to the carbonyl oxygen of the ethyl acetate in the complex of $\text{Al}(\text{C}_2\text{H}_5)_3$ (1678 cm^{-1}). The results obtained lead to the conclusion that the complexing between $\text{Al}(\text{C}_2\text{H}_5)_3$ and γ -butyrolactone occurs both with the carbonyl oxygen and with the ether oxygen, and the one between $\text{Al}(\text{C}_2\text{H}_5)_3$ and ethyl acetate occurs only with the carbonyl oxygen. It seems likely that these structural differences of complexes reflect the activity of the polymerization catalysts.

In Table 1 are shown the results of polymerizing vinyl chloride with $\text{Al}(\text{C}_2\text{H}_5)_3/\text{CCl}_4$ catalyst in the presence of various esters. The effect of esters on catalytic activity permits some assessment to be given of the electronic nature of esters. Table 2 shows the Taft polar constants of substituents present in the ester. A correlation was found to exist between the Taft induction constants (σ^*)¹⁰ and the catalytic activity shown by the relative rate (Figure 2). As shown in Figure 2, the relative rate became smaller, as σ^* became larger. However, the influence of substituent in the ester is small. γ -Butyrolactone is the most effective Lewis base and the different complexing seems to cause the high catalytic activity. Table 3 presents the results of polymerizing vinyl chloride with $\text{Al}(\text{C}_2\text{H}_5)_3/\text{CCl}_4$ catalyst in the presence of Lewis bases that are able to

behave as multidentate ligands. In the presence of multidentate Lewis bases the yield of PVC is always higher than in the presence of the corresponding monodentate Lewis base. In particular, when diethylenetriamine is used as a multidentate Lewis base, the increase in the yield of PVC is significant.

For the effect of polymeric amines some reasons are considered. It has been reported that an amine-alkyl halide combination is a very active catalyst system for free radical polymerization of vinyl monomers¹²⁻¹⁴. Then, the effect of order of mixing was studied to

Table 1 Effect of various esters on polymerization of vinyl chloride with $\text{Al}(\text{C}_2\text{H}_5)_3/\text{CCl}_4$ system^a

No.	Ester	Yield (%)	Relative rate
4	Methyl acetate	4.60	1.00
2	Ethyl acetate	5.70	1.24
3	Butyl acetate	5.66	1.23
1	Ethyl propionate	5.90	1.28
8	Methyl cyanoacetate	0.37	0.08
6	Methyl benzoate	3.08	0.67
5	Ethyl benzoate	4.20	0.91
7	Methyl chloroacetate	1.84	0.40

^a Vinyl chloride, 5 ml; C_6H_6 , 5 ml; $\text{Al}(\text{C}_2\text{H}_5)_3$, 1 mol% on monomer; catalyst ratio $\text{Al}(\text{C}_2\text{H}_5)_3/\text{CCl}_4/\text{ester}=1:1:1$; polymerization at 40°C for 40 h

Table 2 Taft polar constants of substituents present in RCOOR'

R	R'	σ_R	$\sigma_{R'}$	$\sigma^* = \sigma_R + \sigma_{R'}$
CH_3	CH_3	0.00	0.00	0.00
CH_3	C_2H_5	0.00	-0.10	-0.10
CH_3	$n\text{-C}_4\text{H}_9$	0.00	-0.13	-0.13
$n\text{-C}_8\text{H}_{17}$	C_2H_5	-0.12	-0.10	-0.22
$\text{CH}_2(\text{CN})$	CH_3	+1.30	0.00	+1.30
C_6H_5	CH_3	+0.60	0.00	+0.60
C_6H_5	C_2H_5	+0.60	-0.10	+0.50
CH_2Cl	CH_3	+1.05	0.00	+1.05

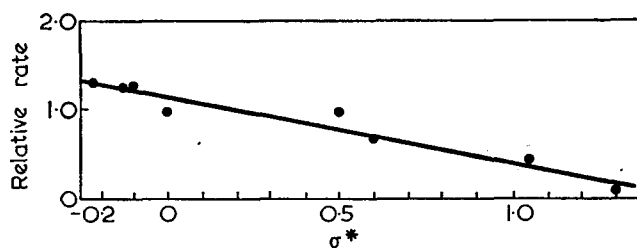


Figure 2 Relative rate as function of the Taft polar constants σ^* of substituents present in RCOOR' compounds

Table 3 Effect of multidentate ligand Lewis bases on polymerization of vinyl chloride with $\text{Al}(\text{C}_2\text{H}_5)_3/\text{CCl}_4$ system^a

No.	Lewis base	Yield (%)	\bar{P}_n^b
9	$\text{H}_2\text{NCH}_2\text{CH}_2\text{NHCH}_2\text{CH}_2\text{NH}_2$	38.0	450
10	$\text{CH}_3\text{CH}_2\text{NH}_2$	4.1	420
11	$\text{CH}_3\text{OCH}_2\text{CH}_2\text{OCH}_2\text{CH}_2\text{OCH}_3$	9.6	490
12	$\text{CH}_3\text{CH}_2\text{OCH}_2\text{CH}_3$	5.1	450

^a Vinyl chloride, 5 ml; C_6H_6 , 5 ml; $\text{Al}(\text{C}_2\text{H}_5)_3$, 1 mol% on monomer; catalyst ratio $\text{Al}(\text{C}_2\text{H}_5)_3/\text{CCl}_4/\text{Lewis base}=1:1:1$; polymerization at 40°C for 40 h

^b By measurement on dilute nitrobenzene solution at 30°C . \bar{P}_n was calculated using the following equation: $\bar{P}_n = 500(\text{antilog}[\eta]/0.168 - 1)^{11}$

Table 4 Order of mixing and catalyst activity on vinyl chloride polymerization^a

No.	Order of mixing	Yield (%)
9	Amine ← CCl_4 ← $\text{Al}(\text{C}_2\text{H}_5)_3$	38.0
13	$\text{CCl}_4/\text{amine}$ ← $\text{Al}(\text{C}_2\text{H}_5)_3$ ^b	37.4
14	Amine/ $\text{Al}(\text{C}_2\text{H}_5)_3$ ← CCl_4 ^c	37.6
23	Amine ← CCl_4	0.0

^a Vinyl chloride, 5 ml; C_6H_6 , 5 ml; $\text{Al}(\text{C}_2\text{H}_5)_3$, 1 mol% on monomer; catalyst ratio $\text{Al}(\text{C}_2\text{H}_5)_3/\text{CCl}_4/\text{diethylenetriamine}=1:1:1$; polymerization at 40°C for 40 h

^b CCl_4 and amine were premixed at room temperature and then $\text{Al}(\text{C}_2\text{H}_5)_3$ was added

^c Amine and $\text{Al}(\text{C}_2\text{H}_5)_3$ were premixed at room temperature and then CCl_4 was added

Table 5 Effect of various amines on polymerization of vinyl chloride with $\text{Al}(\text{C}_2\text{H}_5)_3/\text{CCl}_4$ system^a

No.	Amine	Yield (%)	\bar{P}_n ^b
9	Diethylenetriamine	38.0	450
15	Triethylenetetramine	31.2	470
16	Tetraethylenepentamine	33.2	460
10	Ethylamine	4.1	420
17	2-Ethylhexylamine	2.0	—
18	Stearylamine	2.1	—
19	Ethylenediamine	0.6	—
20	<i>N,N,N',N'</i> -tetramethylethylenediamine	trace	—
22	—	1.6	—

^a Vinyl chloride, 5 ml; C_6H_6 , 5 ml; $\text{Al}(\text{C}_2\text{H}_5)_3$, 1 mol% on monomer; catalyst ratio $\text{Al}(\text{C}_2\text{H}_5)_3/\text{CCl}_4/\text{amine}=1:1:1$; polymerization at 40°C for 40 h

^b By measurement on dilute nitrobenzene solution at 30°C. \bar{P}_n was calculated by using the following equation: $\bar{P}_n=500(\text{antilog } [\eta]/0.168-1)$ ¹¹

elucidate the high catalytic activity in the presence of diethylenetriamine (Table 4). In Table 4, amine, CCl_4 , and $\text{Al}(\text{C}_2\text{H}_5)_3$ were added in this order in a glass tube for No. 9. For No. 13, CCl_4 and amine were premixed at room temperature and then $\text{Al}(\text{C}_2\text{H}_5)_3$ was added. For No. 14, amine and $\text{Al}(\text{C}_2\text{H}_5)_3$ were premixed at room temperature and then CCl_4 was added. The yield of PVC was constant in spite of any order of mixing. Therefore, charge transfer interaction etc. between amine and CCl_4 does not contribute to the initiation reaction of polymerization. Furthermore this is well supported by the fact that amine- CCl_4 cannot initiate the polymerization of vinyl chloride in the absence of $\text{Al}(\text{C}_2\text{H}_5)_3$. The effect of diethylenetriamine seems to be due to complexing between amine and $\text{Al}(\text{C}_2\text{H}_5)_3$.

It has been found that complexing the Cr^{2+} ion with ligands such as ethylenediamine greatly enhances its ability to reduce even primary alkyl halides to alkanes¹⁵. On polymerization of vinyl chloride catalysed by ethanolamine and CCl_4 , any trace metal can play a significant part in the initiation of the polymerization¹⁶. Ultimately in this case the formation of a complex with multidentate ligands is assumed to be responsible for the changes in the catalytic activity.

Table 5 presents the results of vinyl chloride polymerization with $\text{Al}(\text{C}_2\text{H}_5)_3/\text{CCl}_4$ in the presence of various amines. Diethylenetriamine, triethylenetetramine and tetraethylenepentamine are effective Lewis bases, and monodentate amines (such as ethylamine, 2-ethylhexylamine and stearylamine) are not effective ones.

Among these polymeric amines, ethylenediamine and *N,N,N',N'*-tetramethylethylenediamine do not initiate the polymerization of vinyl chloride at all.

In alkylaluminium chemistry, alkylaluminium forms only a tetradentate 1:1 complex with excess amine having a monodentate ligand. However, it is evident that alkylaluminium forms a pentadentate complex with a rigid bidentate amine such as dipyriddy¹⁷⁻¹⁹. A pentadentate aluminium complex with amine is known to be the most effective catalyst in the anionic polymerization of methyl methacrylate.

Therefore it is likely that the catalytic activity is dependent on the type of aluminium-amine complex.

Polymeric amines seem to form pentadentate complexes according to their structural characteristic. This complex is the most effective. However, ethylenediamine and *N,N,N',N'*-tetramethylethylenediamine, although bidentate bases, form tetradentate complexes by their flexible main chain. Tetradentate complexes seem to have lower activity.

ACKNOWLEDGEMENTS

The author is grateful to Dr Y. Kosaka and Mr S. Imura for valuable discussions.

REFERENCES

- Minsker, K. S., Sangalov, Yu. A. and Razuwayev, G. A. *J. Polym. Sci. (C)* 1967, **16**, 1489
- Razuwayev, G. A., Sangalov, Yu. A., Minsker, K. S. and Kovaleva, N. V. *Polym. Sci. USSR* 1965, **7**, 597
- Breslow, D. S., Christman, D. L., Espy, H. N. and Lukach, C. A. *J. Appl. Polym. Sci.* 1967, **11**, 73
- Kawai, W., Ogawa, M. and Ichihashi, T. *J. Polym. Sci. (A-1)* 1970, **8**, 3033
- Milovskaya, E. B., Zhuravleva, T. G. and Zamoiskaya, L. W. *J. Polym. Sci. (C)* 1967, **16**, 899
- Milovskaya, E. B., Kopp, E. L., Mikhailicheva, O. S., Denisov, V. M. and Koltsov, A. I. *Polymer* 1972, **13**, 288
- Weisberger, A. 'Organic Solvents', Interscience, New York, 1955, Vol VII
- Kagiya, T., Sumida, Y. and Inoue, T. *Bull. Chem. Soc. Japan* 1968, **41**, 767
- Ito, K., Inoue, T. and Yamashita, Y. *Makromol. Chem.* 1970, **139**, 153
- Taft, R. W. *J. Am. Chem. Soc.* 1953, **75**, 4231
- Sakurada, I., Matuda, J., Shiotani, S. and Kawasaki, A. *Kogyo Kagaku Zasshi* 1958, **61**, 1362
- Furukawa, J., Tsuruta, T. and Fueno, T. *J. Polym. Sci.* 1955, **15**, 594
- Chapiro, A. and Hardy, G. *J. Chem. Phys.* 1962, **59**, 993
- Imoto, M., Takemoto, K. and Azuma, K. *Makromol. Chem.* 1968, **114**, 210
- Kochi, J. and Mocadlo, P. *J. Am. Chem. Soc.* 1966, **88**, 4094
- Imoto, M. and Takemoto, K. *Makromol. Chem.* 1969, **125**, 294
- Thiele, K. H., Müller, H. K. and Brüser, W. *Z. Anorg. Allgem. Chem.* 1966, **345**, 194
- Thiele, K. H. and Brüser, W. *ibid.* 1966, **348**, 179
- Thiele, K. H. and Brüser, W. *ibid.* 1967, **349**, 33

Viscometric studies on chlorinated polyethylenes in dilute solution

Takanori Saito and Kinya Yamaguchi

Central Research Laboratory, Showa Denko Co., Ohta-ku, Tokyo, Japan
(Received 13 July 1973; revised 5 October 1973)

High density polyethylene (PE) was fractionated by the column elution technique and the fractions had molecular weight distribution, $M_w/M_n=1.2-1.3$ and degree of polymerization, n , ranging from 357 to 14 600. These PE fractions were used as parent polymers of chlorinated PE(CPE). CPE samples were prepared by solution chlorination in tetrachloroethane at 120°C. Results of osmometry on the CPE indicated that neither scission nor crosslinking of CPE molecules take place during the chlorination. Solution viscosities of CPE samples varying in chlorine content, x from ~ 10 to 60% w/w were measured in *o*-dichlorobenzene (ODCB) at 135°C. Those of parent PE and whole polymers of poly(vinyl chloride) (PVC) were also included in the measurements. The corresponding constants of the Mark-Houwink-Sakurada equation have been determined as a function of x . Unperturbed dimensions and parameters bearing upon the excluded volume effect have been estimated from the Stockmayer-Fixman plot and the recent theory on polymer solutions. It was found that an increase in x of CPE leads to a decrease in the intrinsic viscosity of CPE prepared from the same parent PE. This trend has been attributed to a decreasing ratio of the effective hydrodynamic volume in the unperturbed state to the molecular weight of CPE with increase in x , because the excluded volume parameter changes only slightly regardless of x in the present CPE-ODCB system. Unperturbed dimensions of CPE and PVC have been discussed briefly, and those of CPE having ultimate x and some fluoropolymers have been compared with each other. The molecular dimensions of CPE samples reflect their random sequence distribution of chlorines as well as both x and n , and those of polar polymers are affected by the species of polar groups.

INTRODUCTION

Some studies on the structure and properties of chlorinated polyethylene (CPE) have been made by several investigators since the work by Thompson *et al.*¹ and Oakes *et al.*² in the 1940s. Emphasis has been, however, mostly placed upon elucidating a correlation of some properties and/or the structure of CPE with chlorinating conditions. Little attention has been given to the solution properties of CPE, particularly the influence of molecular weight as well as chlorine content on various properties. This paper is mainly concerned with a facile method to estimate the molecular weight and molecular dimensions of CPE from the data of solution viscosity.

The relationship between molecular weight, M , and intrinsic viscosity $[\eta]$ for polymers can be generally represented by the Mark-Houwink-Sakurada empirical equation:

$$[\eta] = K_m M^a \quad (1)$$

where K_m and a are constants depending on species of polymers, operating temperature and, especially in the case of polar polymers, solvents^{3a, b}. On the other hand, $[\eta]$ is theoretically given by Kurata and Yamakawa⁴ introducing the excluded volume effect on the basis of the Kirkwood-Riseman theory⁵ as:

$$[\eta] = \Phi_0 \langle r^2 \rangle_0^{3/2} M^{-1} f(z) = [\eta]_\theta f(z) \quad (2)$$

where Φ_0 , $\langle r^2 \rangle_0$, z and $[\eta]_\theta$ are Flory's universal constant, the mean square end-to-end distance in the unperturbed state, the excluded volume parameter and the intrinsic viscosity in the unperturbed state, respectively. The function $f(z)$ is increasing with z , and $f(0)$ is equal to unity as given by:

$$f(z) = 1 + C_1 z - \dots \quad (3)$$

where C_1 is a constant whose value was found to be 1.55 by Kurata and Yamakawa⁴, 1.80 by Fixman⁶, and 1.06 by Yamakawa and Tanaka⁷. Comparing equation (1) with equation (2), it is evident that the constants K_m and a in equation (1) depend on the molecular dimension in dilute solutions. The molecular dimensions are greatly affected by the interactions between chain elements of long chain molecules⁸, and those of the stereoregular polymer and copolymers will be in particular affected by factors such as tacticities, compositions and the sequence distribution of chemical units through intramolecular interactions⁹ as well as the polymer-solvent interaction. The influence of the species of polar groups on molecular dimensions has been studied for halogenated polystyrenes^{10a, b}.

Since CPE can be regarded as a kind of random polar copolymer^{11, 12}, it is expected that its intrinsic viscosity and the molecular dimension depend on both the chlorine content and the degree of polymerization

of the skeletal chain. The solution viscosity of CPE prepared by chlorinating the fractionated samples of high density polyethylene (PE) and that of poly(vinyl chloride) (PVC) as a reference were measured.

EXPERIMENTAL

Preparation of polymers

Thirteen PE fractions were obtained by fractionating a commercial high density PE (Sholex 6000C) by means of the large-scale column elution technique at 125°C with mixed solvents of xylene and butyl cellosolve according to the method of Saeda *et al.*¹³. It had been ascertained that this technique gave fractions whose molecular weight distribution M_w/M_n was in the range of ~ 1.2 to 1.3 for high density PE¹³. Five PE samples of the viscosity-average molecular weight M_v ranging from 1.0×10^4 to 41.0×10^4 were chosen as the parent polymers of CPE.

Chlorinating reactions of those PE fractions and whole polymer of high density PE (Sholex 3520) were carried out in tetrachloroethane at 120°C. A 5 l flask charged with 3 g PE and 3 l solvent, the contents of which were agitated by a vibromixer, was flushed with N₂ at the rate of 20 l/h. When the reaction temperature reached 120°C, N₂ was stopped and chlorine gas was passed through the solution at the rate of 25.5 l/h. Several CPE samples varying in chlorine content, x , from ~ 10 to 60% w/w were made from each PE sample by changing the reaction time. The relationship between x and the reaction time is shown in Figure 1. A previous study¹⁴ showed that the distribution of chlorines among different CPE chains may be regarded as very close to monodispersed distribution under conditions such as low concentration of the polymer and sufficient mixing. CPE samples were precipitated with ~ 18 l of methanol. Evaporation of the solvent showed that all of the CPE was precipitated. Then, if neither scission nor crosslinking of CPE chains occurred during the chlorination, the molecular weight distribution of CPE can be assumed to be almost equal to that of original PE fractions, viz., $M_w/M_n = \sim 1.2-1.3$. CPE samples were purified by

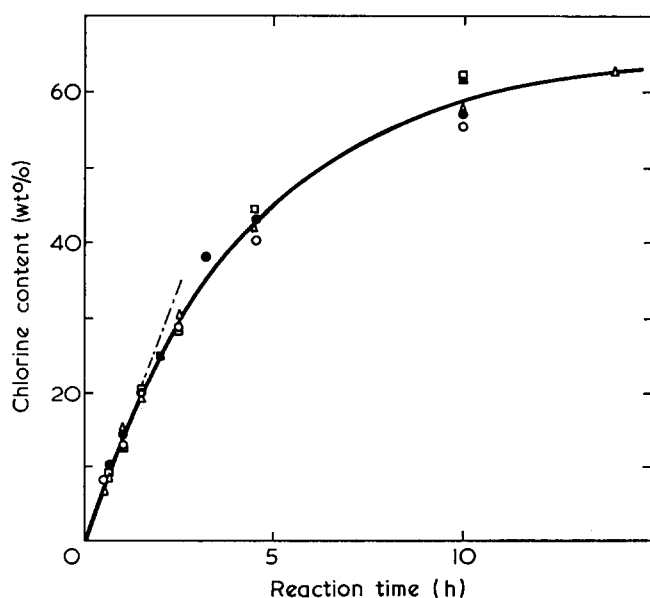


Figure 1 Mean chlorine content of CPE vs. reaction time of the chlorination in the solution of tetrachloroethane at 120°C. $M_v \times 10^{-4}$ of parent PE: ○, 1; △, 1.73; □, 3.81; ●, 8.66; ■, 41.0

extraction with methanol for 8–10 h and dried in a vacuum drier at 50°C for 4–5 days. The chlorine content of CPE was determined by the method of Kinoshita *et al.*¹⁵.

Five samples of PVC were prepared from the tetrahydrofuran solution of $\sim 1\%$ w/w of commercial PVC such as S9008, S901, S903 (Kureha Chem. Co.) and KR800, KR900 (Mitsubishi Monsanto Co.) by precipitation with methanol. The molecular weight of those PVC samples purified were determined by viscometry in tetrahydrofuran at 30°C using the relation¹⁶:

$$[\eta] = 2.19 \times 10^{-3} M^{0.54} \quad (4)$$

Viscometric measurements

Measurements of solution viscosities in purified *o*-dichlorobenzene (ODCB) were made in a capillary viscometer of the Cannon–Fenske type at 135°C. Anti-oxidants, i.e. dialuryl-thio-dipropionate (0.571% w/v), 2,6-di-*t*-butyl-*p*-cresol (BHT) (0.286% w/v), tetrakis[methylene-3-(3',5'-di-*t*-butyl-4'-hydroxyphenyl)propionate]methane (0.143% w/v) and a thermal stabilizer, mercapto-organotin compound (KS 41 by Kyodo Chem. Co.) (1.0% v/v) were added to the solvent. Densities of the ODCB containing antioxidants and a thermal stabilizer were observed to be 1.302 and 1.175 g/ml at 20°C and 135°C, respectively. Solutions for viscosity measurements were made by heating and shaking the polymer–solvent mixture (concentration of the polymer $\sim 0.1-0.5$ g/dl at 20°C) in a glass ampoule at $\sim 145^\circ\text{C}$ for 2 h. No correction for the kinetic energy was made with viscosity measurement. Intrinsic viscosities were determined in terms of the Huggins equation:

$$\eta_{sp}/C = [\eta] + k'[\eta]^2 C \quad (5)$$

where η_{sp} , C and k' are the specific viscosity, concentration of the solution in g/dl corrected to 135°C and the Huggins constant, respectively. Solution viscosities of the parent PE in decalin (containing 0.1% w/v BHT) at 135°C were also measured. Densities of this solvent were 0.8869 and 0.7897 g/ml at 20°C and 135°C, respectively. The molecular weight–intrinsic viscosity relation based on the light scattering measurements¹⁷,

$$[\eta] = 6.2 \times 10^{-4} M^{0.7} \quad (6)$$

was used to determine the molecular weight of the parent PE of CPE.

Osmotic measurements

Osmotic pressure was determined at 80°C in monochlorobenzene using a Hewlett–Packard High Speed Membrane Osmometer Model 502 and a gel cellophane membrane (Mechrolab Type 0–8). Before use the membrane had been treated successively for 24 h each with distilled water, ethanol, isopropanol, toluene and finally monochlorobenzene. The concentration of the solution free from additives ranged from 0.1 to 0.8 g/dl. The density of the solvent was observed to be 1.110 and 1.040 g/ml at 20°C and 80°C, respectively. The results were analysed by the following equation:

$$\pi/C = RT(1/M_n + A_2 C) \quad (7)$$

where π , C , R , T , M_n , and A_2 are osmotic pressure, corrected concentration of the solution at 80°C, the gas constant, the absolute temperature, the number-

average molecular weight and the second virial coefficient, respectively. Equilibrium was established in the osmometer within ~ 20 sec and the equilibrium state continued at least for 3 min even in the case of the CPE prepared from whole polymer of PE. The osmotic pressure at 30 sec was used in analysis of the results.

RESULTS

Influence of chlorinating reaction on polymerization degree of skeletal chain

The molecular weight of the CPE having chlorine content x , $(M)_x$ can be calculated from:

$$(M)_0 = (M)_x(1-x) \quad (8)$$

where x is given as weight fraction of chlorine and $(M)_0$ is the molecular weight of the parent PE of the same degree of polymerization. This equation is generally valid for M_w , M_n or M_v . Results of $(M_n)_x$ and A_2 by osmometry and $(M_n)_0$ estimated from equation (8) are listed in Table 1. Calculated values of $(M_n)_0$ of each CPE prepared from whole polymer of the PE were substantially constant. The average value of $(M_n)_0$ was 3.37×10^4 , which was close to M_n of the parent PE, i.e. 2.89×10^4 determined by the quantitative analysis of the vinyl end-groups with the aid of i.r. spectroscopy¹⁸. These results indicate that 'neither scission nor cross-linking of CPE chains occur during the chlorination', and that the degree of polymerization of parent PE is unchanged in the course of chlorinating. The molecular weight of CPE may therefore be calculated from that of parent PE using transformed equation (8). Values of M_v determined by equation (6) and the degree of polymerization, n , estimated from M_v of the parent PE fractions are summarized in Table 2.

Table 1 Results of osmometry for CPE samples in monochlorobenzene at 80°C

x^a (%w/w)	$(M_n)_x^b \times 10^{-4}$	$(M_n)_0^c \times 10^{-4}$	$A_2^d \times 10^5$
18.8	4.08	3.31	1.57
24.4	4.34	3.30	1.67
34.0	5.12	3.38	1.67
43.2	6.06	3.45	1.39
52.2	7.15	3.42	1.04

^a Mean chlorine content of CPE by chemical analysis¹⁵

^b Molecular weight of CPE observed

^c Molecular weight calculated for the case of zero chlorine content according to equation (8)

^d Second virial coefficient in $\text{mol cm}^3 \text{g}^{-2}$

Table 2 Molecular weight (M_v) and degree of polymerization (n) of parent polyethylene of CPE

Sample code	$M_v^a \times 10^{-4}$	$n \times 10^{-3}$
A	1.00	0.357
B	1.73	0.618
C	3.81	1.36
D	8.66	3.09
E	41.0	14.6

^a Viscosity-average molecular weight determined by equation (6)

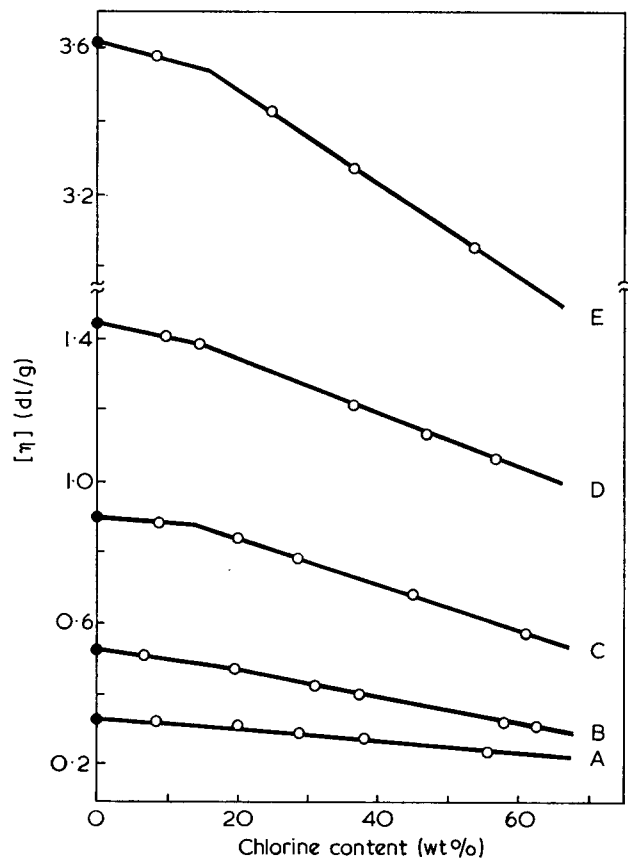


Figure 2 Intrinsic viscosity $[\eta]$ in *o*-dichlorobenzene at 135°C as a function of mean chlorine content. ●, Parent PE; ○, CPE. A-E are sample codes of parent PE as listed in Table 2

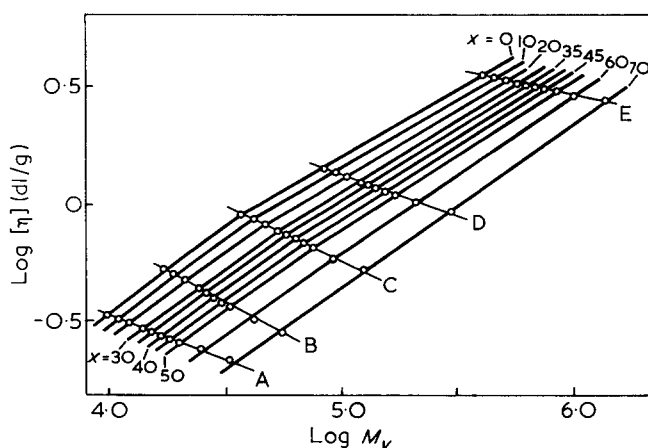


Figure 3 Log-log plot of intrinsic viscosity $[\eta]$ and viscosity-average molecular weight M_v . A-E are sample codes of parent PE as in Table 2, and x denotes mean chlorine content in %w/w

Relationship between molecular weight, intrinsic viscosity and chlorine content

The dependence of $[\eta]$ on x at the same n is shown in Figure 2. The relation between $[\eta]$ and x appears to be linear for a wide range of x . The values of $[\eta]$ of CPE varying in x and n , which can be read off Figure 2 with accuracy, are listed in Table 3. The value of $(M_v)_x$ determined by equations (6) and (8), being not far from the weight-average one^{3a}, are henceforth denoted as M in estimating molecular dimensions of CPE and PE.

The constant a in equation (1) was determined from the slope in the plot of $\log [\eta]$ against $\log M_v$ as shown in Figure 3. All the lines depicted showed a break point

Table 3 Intrinsic viscosity, $[\eta]$ in *o*-dichlorobenzene at 135°C, molecular weight, M , degree of polymerization, n and $[\eta]/M^{1/2}$ of polyethylene, CPE and poly(vinyl chloride)

Samples	x^a (%w/w)	$[\eta]^b$ (dl/g)	$M^c \times 10^{-4}$	$n \times 10^{-3}$	$([\eta]/M^{1/2}) \times 10^3$
PE	0	0.391d	1.00	0.357	3.91
		0.573d	1.73	0.618	4.34
		0.996d	3.81	1.36	5.11
		1.770d	8.66	3.09	6.02
		5.254d	41.0	14.6	8.21
PE	0	0.335	1.00	0.357	3.35
		0.530	1.73	0.618	4.02
		0.913	3.81	1.36	4.68
		1.440	8.66	3.09	4.90
		3.610	41.0	14.6	5.64
CPE	10	0.323	1.11	0.357	3.08
		0.503	1.92	0.618	3.62
		0.885	4.23	1.36	4.30
		1.407	9.62	3.09	4.54
		3.561	45.6	14.6	5.28
CPE	20	0.315	1.25	0.357	2.81
		0.473	2.16	0.618	3.22
		0.835	4.76	1.36	3.83
		1.335	10.8	3.09	4.06
		3.483	51.3	14.6	4.87
CPE	30	0.295	1.43	0.357	2.46
		0.435	2.47	0.618	2.77
		0.775	5.44	1.36	3.33
		1.257	12.4	3.09	3.57
		3.353	58.5	14.6	4.38
CPE	40	0.275	1.67	0.357	2.13
		0.398	2.88	0.618	2.34
		0.713	6.35	1.36	2.83
		1.183	14.4	3.09	3.12
		3.223	68.3	14.6	3.90
CPE	50	0.255	2.00	0.357	1.81
		0.365	3.46	0.618	1.96
		0.650	7.62	1.36	2.36
		1.105	17.3	3.09	2.66
		3.092	82.0	14.6	3.41
CPE	60	0.235	2.50	0.357	1.49
		0.322	4.32	0.618	1.55
		0.588	9.52	1.36	1.90
		1.030	21.7	3.09	2.21
		2.960	102.5	14.6	2.93
CPE	70	0.215	3.33	0.357	1.18
		0.283	5.76	0.618	1.18
		0.525	12.7	1.36	1.48
		0.953	28.8	3.09	1.78
		2.827	136.5	14.6	2.42
PVC	56.8	0.485	4.71	0.753	2.24
		0.575	7.46	1.194	2.11
		0.680	10.2	1.638	2.13
		0.890	18.4	2.937	2.07
		1.032	23.7	3.792	2.12

^a Mean chlorine content

^b Values of $[\eta]$ were read off Figure 2

^c Molecular weight of CPE was estimated from equation (8), and those of PE and PVC were determined by viscometry using equations (6) and (4), respectively

^d Measured in decalin at 135°C

at n of 1360 with the slope of the line greater at n above 1360. Two sets of a and K_m were then obtained for the range of n as in Table 4. The evaluation of critical value of n can be made according to equations (9) and (10) which are formulations of the relation between $[\eta]$ and x of CPE having $n=1360$ in Figure 2.

$$[\eta] = -61.7x + 0.957 \quad (x \geq 0.125) \quad (9)$$

$$[\eta] = -15.0x + 0.900 \quad (x < 0.125) \quad (10)$$

Accordingly M_v of CPE can be estimated from the relation of equation (1) with the above values of K_m

and a , or it can be simply determined graphically in terms of the plot of $[\eta]$ against M_v .

Parameters of short and long range interactions

The short-range interaction parameter K and the long-range interaction parameter B are given by the modified Stockmayer-Fixman theory^{19, 20} with $[\eta]$ in good solvent and molecular weight M , viz.,

$$[\eta]/M^{1/2} = pK + q\Phi_0 BM^{1/2} \quad (11)$$

where Φ_0 is Flory's universal constant being assumed to be 2.5×10^{21} for intrinsic viscosities in dl/g^{20, 21}. According to Tanaka *et al.*²⁰, p and q in equation (11) are given to be

$$p = 1.00 \text{ and } q = 0.346 \quad (0 < \alpha_\eta^3 < 1.6) \quad (12)$$

$$p = 1.05 \text{ and } q = 0.287 \quad (0 < \alpha_\eta^3 < 2.5) \quad (13)$$

where α_η^3 is the viscosity-radius expansion factor. If $[\eta]$ were defined by equation (2), α_η^3 is written as:

$$\alpha_\eta^3 = [\eta]/[\eta]_\theta = f(z) \quad (14)$$

or

$$\alpha_\eta^3 = [\eta]/KM^{1/2} \quad (15)$$

each being defined by comparing equation (2) with the empirical theory of Flory and Fox²². The Stockmayer-Fixman plots according to equation (11) using data in Table 3 are shown in Figure 4. The parameters B and

Table 4 K_m and a in the equation $[\eta] = K_m M a$

x^a (%w/w)	$n^b \geq 1.36 \times 10^3$		$n < 1.36 \times 10^3$	
	$K_m \times 10^4$	a	$K_m \times 10^4$	a
0	21.2	0.576	3.61	0.744
10	17.4	0.585	3.51	0.744
20	13.6	0.596	3.40	0.725
30	9.38	0.616	3.12	0.717
35	7.60	0.627	2.90	0.714
40	6.36	0.635	2.68	0.713
45	5.17	0.644	2.47	0.711
50	4.03	0.657	2.45	0.700
60	2.33	0.684	2.08	0.694
70	1.35	0.704	1.35	0.704

^a Mean chlorine content

^b Degree of polymerization

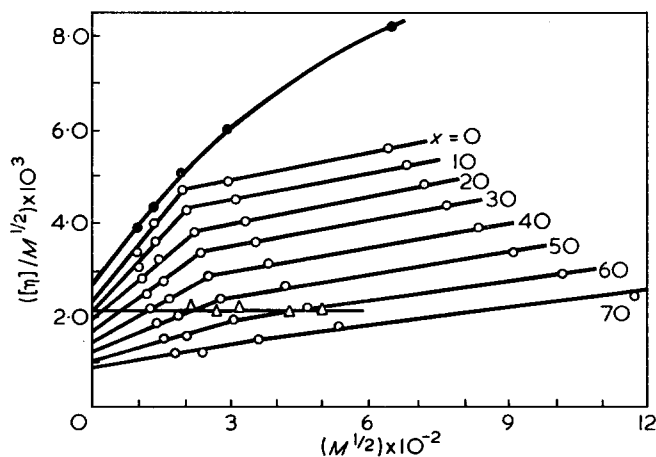


Figure 4 Stockmayer-Fixman plots of parent PE, CPE and PVC. ●, PE in decalin at 135°C; ▲, PVC in *o*-dichlorobenzene at 135°C; ○, PE and CPE in *o*-dichlorobenzene at 135°C, and x denotes mean chlorine content in %w/w

K were determined from the initial slope and the intercept of the plot corresponding to the region of n below 1360, respectively. Since most values of α_n^3 , roughly estimated from equations (15) and (11) with $p=1.00$, were above the range of 1.6, p and q were assumed to be 1.05 and 0.287, respectively as given in equation (13).

The mean square end-to-end distance in the unperturbed state $\langle r^2 \rangle_0$ was calculated from values of K and M using:

$$\langle r^2 \rangle_0 = MA^2 \quad (16)$$

and

$$A^2 = (K/\Phi_0)^{2/3} \quad (17)$$

where A is the short-range interaction parameter independent of the size of the statistical segment. Results for the short-range interaction are listed in Table 5. A plot of $\langle r^2 \rangle_0/M (=A^2)$ against x is shown in Figure 5, which indicates that $\langle r^2 \rangle_0/M$ decreases immediately with increasing x . Then $\langle r^2 \rangle_0/M$ of CPE having 85.5% w/w of chlorine, which may be compared to polytetrachloroethylene (PTCE) and which cannot be obtained by any chlorinating reaction of PE^{11,14} or PVC²³, was deduced to be $0.378 \times 10^{-16} \text{ cm}^2 \text{ mol g}^{-1}$ from linear extrapolation of the line in Figure 5. The effective bond length, l , i.e., $(\langle r^2 \rangle_0/n)^{1/2}$ of PTCE was calculated to be 7.92 Å from equation (16). The list of l values of related polymers are shown in Table 6.

Table 5 Short-range interaction parameters K , A^2 and unperturbed dimension per monomeric unit $(\langle r^2 \rangle_0/n)^{1/2}$ of PE, CPE and PVC in *o*-dichlorobenzene at 135°C

Samples	x^a (% w/w)	$K \times 10^3$	$A^2 \times 10^{16}$ ($\text{cm}^2 \text{ mol g}^{-1}$)	$(\langle r^2 \rangle_0/n)^{1/2}$ (Å)
PE	0	2.50 ^b	1.00 ^b	5.29 ^b
PE	0	2.19	0.916	5.06
CPE	10	1.95	0.847	5.13
	20	1.76	0.791	5.26
	30	1.52	0.718	5.36
	40	1.33	0.657	5.54
	50	1.16	0.599	5.80
	60	1.00	0.543	6.16
	70	0.828	0.479	6.68
PVC	56.8	2.03	0.870	7.37

^a Mean chlorine content
^b In decalin at 135°C

The binary-cluster integral for a pair of segments β was calculated from the value of B and M as

$$\beta = m^2 B \quad (18)$$

and

$$m = M/n \quad (19)$$

where m is the molecular weight per monomeric unit. Results of B and β are listed in Table 7.

The excluded volume parameter, z , was also determined using the two interaction parameters A , B and M by the equation:

$$z = 0.330BA^{-3}M^{1/2} \quad (20)$$

Results of α_n^3 estimated from equation (15) and those of z from equation (20) are summarized in Tables 8 and 9, respectively.

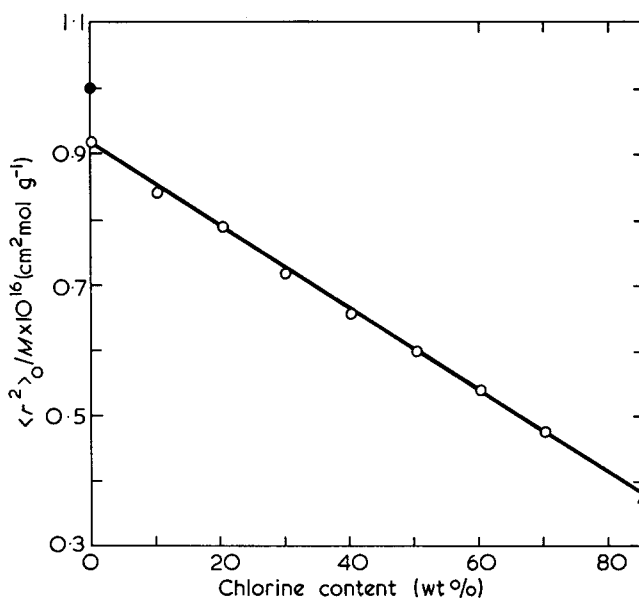


Figure 5 Mean square end-to-end distance per molecular weight as a function of mean chlorine content. ●, PE in decalin at 135°C; ○, PE and CPE in *o*-dichlorobenzene at 135°C; ▲, extrapolated value of PTCE

Table 6 Unperturbed dimension of linear polymer molecules

Polymer	Solvent	Temp. (°C)	$(\langle r^2 \rangle_0/M)^{1/2} \times 10^3$ (Å mol ^{1/2} g ^{-1/2})	$(\langle r^2 \rangle_0/n)^{1/2}$ (Å)
PE	α -chloronaphthalene tetralin, <i>p</i> -xylene	~100	950 ± 40 ^b	5.03 ± 0.21
PE	bis-2-ethylhexyladipate	145	940 ± 40 ²⁵	4.97 ± 0.21
PE	bis-2-ethylhexyladipate	140	1070 ²⁴	5.66
PE	decalin	135		5.29
PE	<i>o</i> -dichlorobenzene	135		5.06
CPE ^a	<i>o</i> -dichlorobenzene	135		6.03
PVC	benzyl alcohol	155.4	820 ²⁶	6.49
PVC	cyclohexane, tetrahydrofuran	~25	720 ± 30 ^b	5.70 ± 0.24
PVC	<i>o</i> -dichlorobenzene	135		7.37
PCTFE	2,5-dichlorobenzotrifluoride	130	580 ± 15 ^b	6.26 ± 0.16
PTFE	(calculation ²⁹)	327		8.2 ± 2.2 ^c
PTFE		135		9.0 ± 2.8 ^d
PTCE ^b	<i>o</i> -dichlorobenzene	135		7.92

^a Mean chlorine content is 56.8% w/w, and unperturbed dimension was read off Figure 6

^b Unperturbed dimension of PTCE was estimated from Figure 5 through equation (16)

^c Calculated from the characteristic ratio, $\langle r^2 \rangle_0/nb^2 = 30 \pm 15^{29}$ with bond length, $b = 1.54 \text{ Å}^{30}$

^d Estimated from the temperature coefficient of $\langle r^2 \rangle_0$, $\text{dln} \langle r^2 \rangle_0/\text{dT}$ of $-(0.9 \pm 0.5) \times 10^{-3} (\text{deg}^{-1})^{29}$

Table 7 Polymer-solvent interaction parameter B and binary cluster integral per monomeric unit, β of PE, CPE and PVC in *o*-dichlorobenzene at 135°C

Sample	x^a (% w/w)	$B \times 10^{26}$ (cm ³)	$\beta \times 10^{23}$ (cm ³)	$\beta_a b \times 10^{23}$ (cm ³)
PE	0	1.77 ^c	1.39 ^c	0 ^c
PE	0	1.70	1.32	0
CPE	10	1.53	1.48	0.16
	20	1.25	1.53	0.21
	30	1.05	1.67	0.35
	40	0.794	1.72	0.40
	50	0.585	1.83	0.51
	60	0.390	1.91	0.59
	70	0.250	2.18	0.86
PVC	56.8	0.0	0.0	-1.32

^a Mean chlorine content

^b Excess dipolar contribution estimated from equation (21) by assuming the non-polar dipolar contribution to be 1.32×10^{-23} cm³

^c In decalin at 135°C

Table 8 Cubic viscosity-radius expansion factor α_v^3 of PE, CPE and PVC in *o*-dichlorobenzene at 135°C

Sample	x^a (% w/w)	Degree of polymerization				
		357	618	1360	3090	14 600
PE	0	1.56 ^b	1.74 ^b	2.04 ^b	2.41 ^b	3.28 ^b
PE	0	1.53	1.84	2.14	2.24	2.58
CPE	10	1.58	1.86	2.21	2.33	2.71
	20	1.60	1.83	2.18	2.31	2.77
	30	1.62	1.82	2.19	2.35	2.88
	40	1.60	1.76	2.13	2.35	2.93
	50	1.56	1.69	2.03	2.29	2.94
	60	1.49	1.55	1.90	2.21	2.93
	70	1.43	1.43	1.79	2.15	2.92
PVC	56.8	1.10	1.04	1.05	1.02	1.04

^a Mean chlorine content

^b In decalin at 135°C

Table 9 Excluded volume parameter, z of PE, CPE and PVC in *o*-dichlorobenzene at 135°C

Sample	x^a (% w/w)	Degree of polymerization				
		357	618	1360	3090	14 600
PE	0	0.584 ^b	0.771 ^b	1.14 ^b	1.72 ^b	3.74 ^b
PE	0	0.639	0.843	1.25	1.88	4.09
CPE	10	0.678	0.898	1.33	2.00	4.36
	20	0.656	0.861	1.28	1.93	4.19
	30	0.682	0.892	1.32	2.00	4.34
	40	0.636	0.838	1.24	1.87	4.07
	50	0.588	0.776	1.15	1.73	3.78
	60	0.509	0.669	0.995	1.50	3.26
	70	0.453	0.598	0.886	1.34	2.91
PVC	56.8	0.0	0.0	0.0	0.0	0.0

^a Mean chlorine content

^b In decalin at 135°C

DISCUSSION

Unperturbed end-to-end distances

A dependence of the effective bond length l of CPE and related polymers on x is shown in Figure 6. The value of l of PE in ODCB at 135°C is slightly less than in decalin at 135°C; both are close to reported values of l for PE at 100°C⁸, at 140°C²⁴, and at 145°C²⁵. This fact suggests that an uncertainty on values of l due to few experimental results used in our analysis is no

significant, hence values of l derived from viscometric data may be regarded as reliable.

Figure 6 gives some information for influences of polar groups on l . Firstly, l increases exponentially with increase in x . This may result from the increase in potential barrier of the internal rotation as well as increase in bond angles arising from an introduction of bulky chlorines. Second, from comparing l of PVC, viz. 7.37 Å obtained in this work and 6.49 Å at 155.4°C in benzyl alcohol²⁶ with 6.03 Å of CPE having x of 56.8% w/w, it was found that the l of CPE is smaller than that of PVC ($x=56.8\%$ w/w) although l of PVC obtained by this work deviates considerably from the reported values in various solvents (Table 6 and Figure 6). It appears that l of polar polymers containing chlorine seems to be affected by the sequence distribution of chlorines.

The CPE chain consists of substantially random sequence distribution of chlorines and contains chemical units such as $-(CH_2)_n$ ($n \geq 2$) and at x above 40% w/w, $-(CHCl-CH_2-CCl_2-CH_2)_n-CHCl-$ which are quite different from the sequence of PVC^{11,12}. The symmetry of the chemical units such as $-(CH_2)_n$ and $-CH_2-CCl_2-CH_2-$ will make internal rotation of the CPE chain easier than the unit of $-(CHCl-CH_2)_n$ in the PVC chain. The dipole moment, resulting mainly from the short-range interaction²⁷, of CPE is also smaller than that of PVC^{2,28}. It is clear from comparing l and the dipole moment of CPE with those of PVC that the short-range interaction along the overall chain of CPE

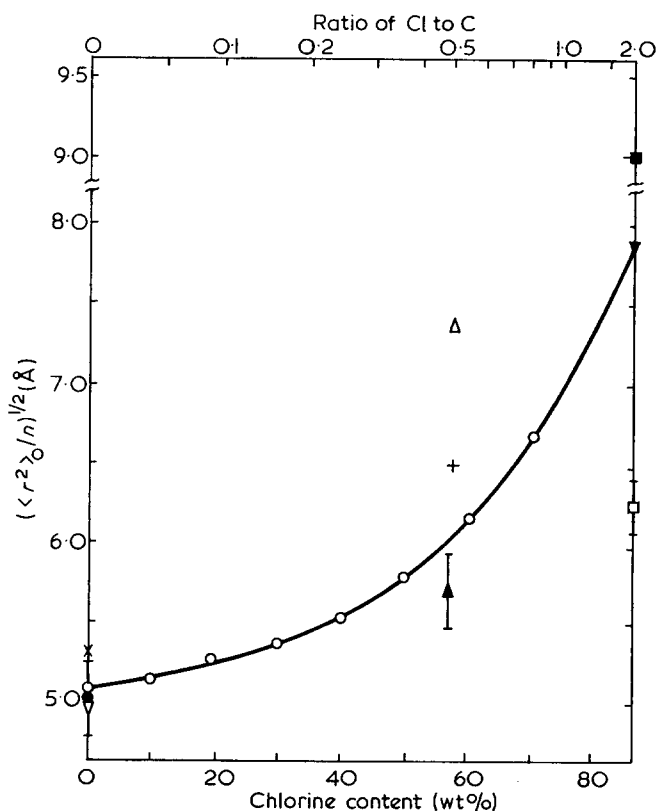


Figure 6 Unperturbed dimension per degree of polymerization of CPE and related polymers as a function of mean chlorine content. x, PE in decalin at 135°C; ●, PE at ~100°C; ▽, PE in bis-2-ethylhexyladipate at 145°C; △, PVC in *o*-dichlorobenzene at 135°C; +, PVC in benzyl alcohol at 155.4°C; ▲, PVC at ~25°C; ■, PTFE at 135°C calculated from reported values on the characteristic ratio and the temperature coefficient of $\langle r^2 \rangle_0$ ²⁹; ▼, PTCE estimated from an extrapolation as shown in Figure 5; □, PCTFE in 2,5-dichlorobenzotrifluoride at 130°C⁸

is less than that of PVC owing to the random sequence distribution of chlorines in the chain of CPE.

Comparison of l of polymers containing chlorines with those of fluoropolymers shows the influence of polar species on l . Bates *et al.*²⁹ calculated the characteristic ratio $\langle r^2 \rangle_0 / nb^2$ (b = bond length) at 600K and the temperature coefficient of $\langle r^2 \rangle_0$, $d \ln \langle r^2 \rangle_0 / dT$ for polytetrafluoroethylene (PTFE) to be 30 ± 15 and $-(0.9 \pm 0.5) \times 10^{-3} \text{ deg}^{-1}$, respectively, and l of PTFE was deduced by assuming $b = 1.54 \text{ \AA}$ after Miyazawa³⁰ to be $\sim 8.2 \pm 2.2 \text{ \AA}$ at 327°C and $\sim 9.0 \pm 2.8 \text{ \AA}$ at 135°C (Table 6). The value of l of PTCE is 7.92 \AA at 135°C and l of polychlorotrifluoroethylene (PCTFE) is $6.26 \pm 0.16 \text{ \AA}$ at 130°C in 2,5-dichlorobenzotrifluoride⁸. Since all of those polymers may be regarded as perhalogenated PE, values of l plotted at the position of ultimate x , i.e., 85.5% w/w in Figure 6 suggest that l of PTFE is the largest, and smallest for PCTFE.

Excluded volume effect

The polymer-solvent interaction parameter B independent of the choice of segmental size decreases with increase in x , whilst the binary cluster integral for a pair of segments β increases against x as shown in Figure 7. The segment used was a monomeric unit as assumed homopolymers possess structurally similar backbones^{10a}. Though it was shown by Utracki^{3b} using the theory of Yamakawa *et al.*³¹ that interactions in dilute solution of PVC depend in particular on the nature of the solvent, the long-range interaction in the present CPE-ODCB system represented by parameter

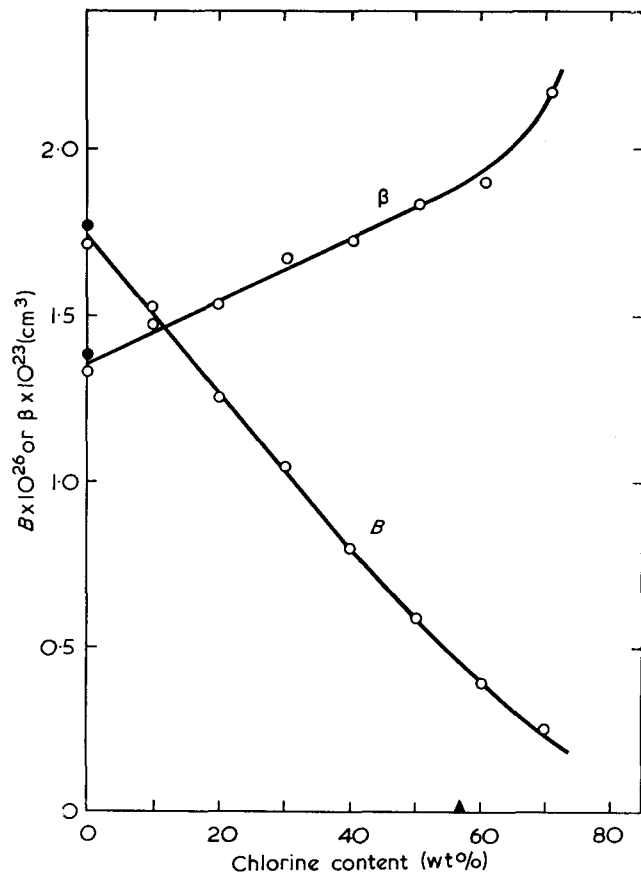


Figure 7 Polymer-solvent interaction parameter, B and the binary cluster integral per monomeric unit, β as a function of mean chlorine content. ●, PE in decalin at 135°C ; ○, PE and CPE in *o*-dichlorobenzene at 135°C ; ▲, PVC in *o*-dichlorobenzene at 135°C

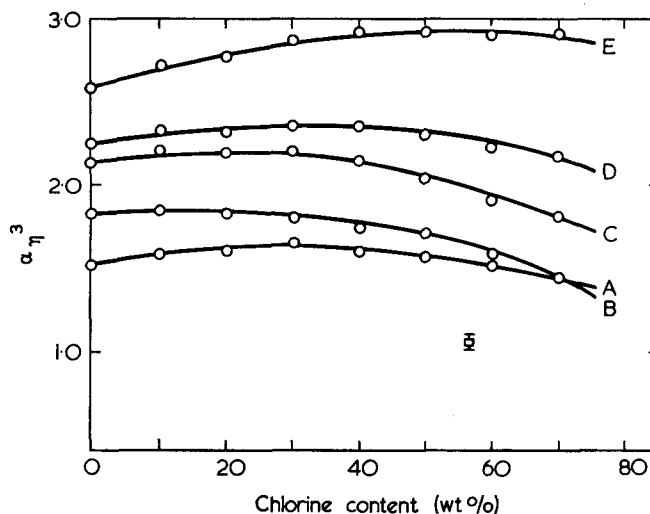


Figure 8 Cubic viscosity-radius expansion factor, α_z^3 in *o*-dichlorobenzene at 135°C as a function of mean chlorine content. ○, PE and CPE; □, PVC; A-E are sample codes of parent PE as in Table 2

B becomes stronger as the chlorine content, viz. the concentration of the polar group, increases.

Yamakawa *et al.*³¹ express β as:

$$\beta = \beta_0 + \beta_e \quad (21)$$

where β_0 and β_e are the non-polar and the excess dipolar contributions, respectively. Assuming β_0 of CPE and PVC to be equivalent to β_0 of PE, i.e. 13.2 \AA^3 , values of β_e of these polymers estimated from equation (21) are listed in Table 7. In the case of *p*-halogenated polystyrenes, β is reduced by introducing chlorines or bromines and β_e has a negative value^{10a}. But since β of CPE is larger than that of PE, the values of β_e for the CPE are positive. These trends of β and positive β_e contradict the theory of Yamakawa *et al.*³¹ and the work of Noguchi *et al.*^{10a}. The values β and β_e of polar polymers seemed to be affected not only by the nature of the solvent^{3b} but also by polar groups through the dipole-dipole interaction among polymer segments and solvent molecules.

The long-range interaction parameter B and β of PVC unfractionated is zero in ODCB solution at 135°C , and this implies that PVC is in the unperturbed state, and β_e of PVC was estimated to be -13.2 \AA^3 . On the other hand, β and β_e of CPE having the same x as that of PVC were deduced to be 19.2 \AA^3 and 5.9 \AA^3 , respectively, from Figure 7. On the basis of theoretical equation on β_e given by Yamakawa *et al.*³¹, the above trend for β_e of CPE and PVC seems to arise from smaller dipole moment^{2, 28} and polarizability of CPE owing to random sequence distribution of chlorines in the CPE chain.

Information on the long-range interaction of CPE in ODCB solution was also obtained from consideration of the dependence of the expansion factor α_z^3 and the excluded volume parameter z on the chlorine content (Figures 8 and 9). In contrast α_z^3 of CPE varies from ~ 1.4 to 3.0 with degree of polymerization, α_z^3 of PVC is ~ 1.05 being almost equal to unity independently of the molecular weight. Though α_z^3 vs. x of CPE shows a maximum, similar to the dependence of the second virial coefficient A_2 on x obtained by osmometry (Table 1), the change of α_z^3 with the variation of x is small for constant n . The chlorine content dependence of z also

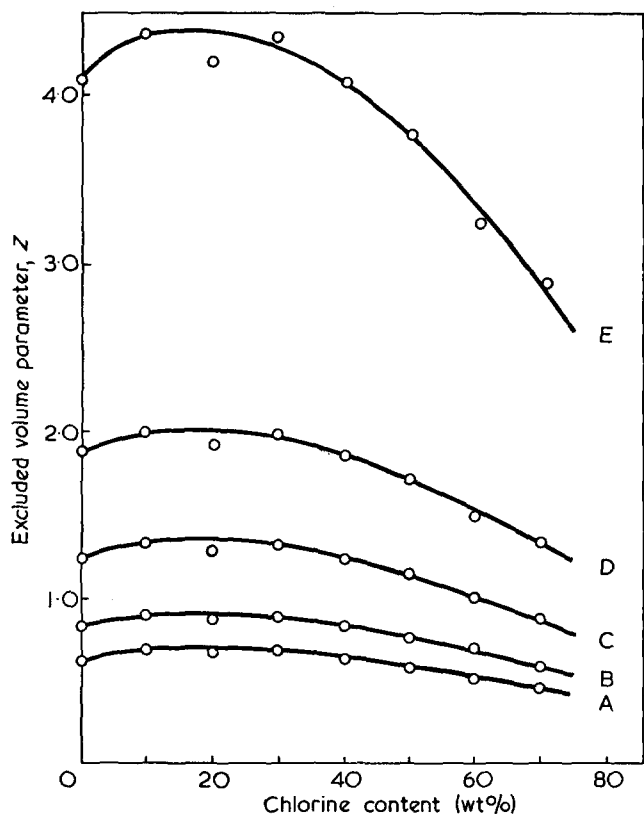


Figure 9 Excluded volume parameter of PE and CPE in *o*-dichlorobenzene at 135°C as a function of mean chlorine content. A-E are sample codes of parent PE as in Table 2

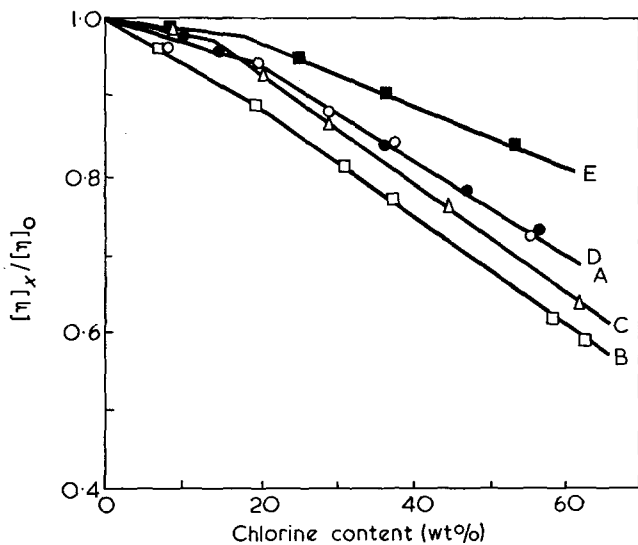


Figure 10 Ratio of intrinsic viscosity of CPE having chlorine content x , $[\eta]_x$, to that of parent PE, $[\eta]_0$ vs. mean chlorine content. A-E are sample codes of parent PE as in Table 2

shows a maximum at $\sim 20\%$ w/w of x for any values of n , and z decreases slightly in the region of x above 20% w/w with increase in x as shown in Figure 9. These results are discussed below.

Chlorine content dependence of intrinsic viscosity and interactions in dilute solution

As shown in Figure 2, $[\eta]$ of CPE shows a tendency to decrease linearly with increasing x . The ratio of $[\eta]$ of CPE to that of PE, $[\eta]_x/[\eta]_0$ plotted against x (Figure 10) also shows the above trend. The ratio of $[\eta]_x/[\eta]_0$

is somewhat affected by n , but it decreases considerably with increase in x , although slopes of all lines in Figure 10 change slightly in the vicinity of $15\text{--}20\%$ w/w of x .

According to equation (2), $[\eta]$ is proportional to the product of $\langle r^2 \rangle^{3/2}/M$ and $f(z)$ defined by equation (3) or α_z^3 by equations (14) or (15). As stated in the previous section, both z and α_z^3 vary only slightly with x so that the decrease of $[\eta]$ with x is mainly due to decreasing $\langle r^2 \rangle_0^{3/2}/M$ with increase in x .

A change of the slope in plots of $[\eta]$ or $[\eta]_x/[\eta]_0$ vs. x in addition to an existence of a maximum in x -dependence of z also shows that both the short-range and the long-range interactions in the CPE-ODCB system vary appreciably with x at $\sim 20\%$ w/w of x . In the chain of CPE above x of 20% w/w, long-methylene sequences $-(\text{CH}_2)_n$ ($n \geq 30$) are unlikely and the mean sequence number of methylenes at x of 20% w/w is $\sim 8\text{--}9$ as shown in previous papers^{11,12}. The calculations of Jernigan *et al.*³² and Abe *et al.*³³ indicated that the end group of the chain influences the conformation of internal bonds up to 4 units. The bonds of $-\text{CH}_2-\text{CH}_2-$ in the sequence such as $-\text{CHCl}-(\text{CH}_2)_n-\text{CHCl}-$ ($n \leq 9$) seems to show different conformations from those of internal bonds in the long-methylene sequence beyond the fourth from the differing unit due to the influence of $-\text{CHCl}-$ units. Thus above x of 20% w/w, the conformation of most bonds such as $-\text{CH}_2-\text{CH}_2-$ in the chain of CPE may be restrained by the unit of $-\text{CHCl}-$, and will differ from those in the chain of CPE below x of 20% w/w.

The sequence distribution of chlorines thus affects not only the intramolecular interaction but also the intermolecular one through the restraint of the conformation which cause the number of contacts among polymer segments and the solvents to change^{3a}. As a result, the dependence of $[\eta]$ and z on x in the CPE-ODCB system seems to change in the vicinity of x at 20% w/w. The unperturbed dimension and β of CPE also seems to differ from those of PVC due to unlike sequence distribution of chlorines in both polymer chains.

ACKNOWLEDGEMENT

The authors are grateful to Drs S. Saeda and T. Hama for their valuable suggestions and fruitful discussions in the course of this study.

REFERENCES

- Thompson, H. W. and Torkington, P. *Trans. Faraday Soc.* 1945, **41**, 246
- Oakes, W. G. and Richards, R. B. *Trans. Faraday Soc.* 1946, **42A**, 197
- 3a Dondos, A. and Benoit, H. *Macromolecules* 1971, **4**, 279
- 3b Utracki, L. A. *Polymer J.* 1972, **3**, 551
- Kurata, M. and Yamakawa, H. *J. Chem. Phys.* 1958, **29**, 311
- Kirkwood, J. G. and Riseman, J. *J. Chem. Phys.* 1948, **16**, 565
- Fixman, M. *J. Chem. Phys.* 1966, **45**, 785, 793
- Yamakawa, H. and Tanaka, G. *J. Chem. Phys.* 1971, **55**, 3188
- Kurata, M. and Stockmayer, W. H. *Fortschr. Hochpolym. Forsch.* 1963, **3**, 196
- Flory, P. J. 'Statistical Mechanics of Chain Molecules', Interscience, New York, 1969, pp 117 and 229
- 10a Noguchi, Y., Aoki, A., Tanaka, G. and Yamakawa, H. *J. Chem. Phys.* 1970, **52**, 2651
- 10b Matsuo, K. and Stockmayer, W. H. *J. Polym. Sci. (Polym. Phys.)* 1973, **11**, 43
- Saito, T., Matsumura, Y. and Hayashi, S. *Polymer J.* 1970, **1**, 639

- 12 Saito, T. and Matsumura, Y. *Polymer J.* 1973, **4**, 124
- 13 Saeda, S., Suzuki, T. and Yamaguchi, K. *Zairyo* 1971, **20**, 621
- 14 Saito, T., Yamaguchi, K. and Hayashi, S. *Kobunshi Kagaku* 1972, **29**, 78, 83
- 15 Kinoshita, M. and Hozumi, K. *Bunseki Kagaku* 1965, **14**, 352
- 16 Kobayashi, T. *Bull. Chem. Soc. Japan* 1962, **35**, 726
- 17 Chiang, R. *J. Polym. Sci.* 1959, **36**, 91
- 18 Smith, D. C. *Ind. Eng. Chem.* 1956, **48**, 1161
- 19 Stockmayer, W. H. and Fixman, M. *J. Polym. Sci. (C)* 1963, **1**, 137
- 20 Tanaka, G., Imai, S. and Yamakawa, H. *J. Chem. Phys.* 1970, **52**, 2639
- 21 Brandrup, J. and Immergut, E. H. 'Polymer Handbook', Interscience, New York, 1966, Ch IV, p IV-1
- 22 Flory, P. J. and Fox, Jr T. G. *J. Am. Chem. Soc.* 1951, **73**, 1904
- 23 Pham, Q. T. and Berticat, P. *Eur. Polym. J.* 1968, **4**, 265
- 24 Flory, P. J., Ciferri, A. and Chiang, R. *J. Am. Chem. Soc.* 1961, **83**, 1023
- 25 Kotera, A., Matsuda, H. and Wada, A. *Prepr. Soc. Polym. Sci. Japan 13th Polym. Symp., Tokyo* 1964, p 13
- 26 Sato, M., Koshiishi, Y. and Asahina, A. *J. Polym. Sci. (B)* 1963, **1**, 233
- 27 Birstein, T. M. and Ptitsyn, O. B. 'Conformations of Macromolecules', Interscience, New York, 1966, Ch 1
- 28 Sasabe, H. and Saito, S. *Prepr. Soc. Polym. Sci. Japan 15th Polym. Symp., Osaka* 1966, p 137
- 29 Bates, T. W. and Stockmayer, W. H. *Macromolecules* 1968, **1**, 17
- 30 Miyazawa, T. *J. Polym. Sci.* 1961, **55**, 215
- 31 Yamakawa, H., Rice, S. A., Corneliussen, R. and Kotin, L. *J. Chem. Phys.* 1963, **38**, 1759
- 32 Jernigan, R. L. and Flory, P. J. *J. Chem. Phys.* 1969, **50**, 4165
- 33 Abe, A., Matsumura, Y. and Moriguchi, T. *Prepr. Soc. Polym. Sci. Japan 19th Polym. Symp., Kyoto* 1970, p 567

Determination of the molecular weight and hydrodynamic dimensions of micelles formed from a block copolymer

C. Price, J. D. G. McAdam, T. P. Lally and D. Woods

*Department of Chemistry, University of Manchester, Manchester M13 9PL, UK
(Received 25 October 1973)*

An investigation has been made of micelle formation by a polystyrene–polyisoprene two-block copolymer in *n*-decane. For the sample studied the number-average molecular weights of the polystyrene block and overall copolymer chain were 13 000 and 51 000 respectively. Light-scattering studies in *n*-decane were made within the temperature range 25–65°C. Conventional light scattering was used to obtain weight-average molecular weights; at 25°C, M_w of the micelles was $1.73 \pm 0.14 \times 10^6$. Translational diffusion coefficients were determined from Rayleigh linewidth measurements; the micelles were found to have a hydrodynamic radius of 19.6 nm at 25°C. Intrinsic viscosities were determined for the copolymer in *n*-decane and methyl cyclohexane within the temperature range –20° to 75°C. Finally, data obtained earlier in an electron microscopy study of freeze-etched specimens were compared with the results obtained in the present study.

INTRODUCTION

In recent years much interest has been shown in the effect of solvent selectivity on the solution properties of block and graft copolymers^{1–8}. If a copolymer in either of these categories is dispersed in a medium which is a non-solvent for one of the polymer components and a good solvent for the other, monomolecular or multimolecular micelles may be formed. In the simplest situation such micelles will consist of a compact core of the least soluble polymer component surrounded by a flexible fringe formed by the other polymer component. If the core is non-crystalline it will be necessarily somewhat swollen. In the present contribution we report an investigation of multimolecular micelle formation by a polystyrene–polyisoprene two-block copolymer in *n*-decane. The two main techniques used in the work were conventional Rayleigh light scattering and Rayleigh light-scattering spectroscopy. Measurements of intrinsic viscosities were also made to provide additional information.

EXPERIMENTAL

Material

The polystyrene–polyisoprene two-block copolymer, which was designated sample 1DI for reference, was prepared by step-wise anionic polymerization in benzene solution using *n*-butyl lithium as the primary initiator. Details concerning the method of synthesis, fractionation and structural characterization have been described elsewhere^{9, 10}. The number-average molecular weights of the polystyrene block and overall copolymer were 13 000 and 51 000 respectively, and the wt % polystyrene in the product as determined by u.v. spectro-

scopy was 25.2. Gel permeation chromatography was used to check the homogeneity of the sample.

Conventional light scattering

Measurements were made using a Sofica instrument. Polymer solutions and solvents were clarified either by centrifugation for 2 h at 2×10^4 rev/min in a No. 30 rotor of a Spinco Model L preparative ultracentrifuge or by filtration through solvent inert Millipore filters having a pore size of 0.45×10^3 nm. Light scattering measurements were made with light of wavelength 546 nm at 11 angles from 30° to 150°. The instrument was calibrated using benzene for which the Rayleigh ratio is known over a range of temperature¹¹.

The light scattered from a dilute polymer solution may be expressed in the general form¹²:

$$\left(\frac{Kc}{R_\theta}\right) = \frac{1}{M_w P(\theta)} + 2A_2c + 3A_3c^2 + \dots \quad (1a)$$

where K is an optical constant for the particular system in question, c the concentration, R_θ the difference between the Rayleigh ratio of the solution and that of the pure solvent, M_w the weight-average molecular weight, $P(\theta)$ the particle scattering function which equals 1 at $\theta=0$, and A_2 and A_3 are the second and third virial coefficients. For homopolymers the weight-average molecular weight can be obtained in a straightforward manner by carrying out a double extrapolation of the data to zero angle and zero concentration, since from equation (1a):

$$\left(\frac{Kc}{R_\theta}\right)_{\substack{c=0 \\ \theta=0}} = \frac{1}{M_w} \quad (1b)$$

In the case of copolymers that are heterogeneous in chemical composition, equation (1b) yields an apparent molecular weight (M_{app}) rather than a true weight-average molecular weight. The problem has been treated by Stockmayer *et al.*¹³ and Bushuk and Benoit¹⁴. Using the notation of the latter:

$$M_{app} = M_w + 2[(\nu_A - \nu_B)/\nu]P + [(\nu_A - \nu_B)/\nu]^2 Q \quad (2)$$

where ν , ν_A and ν_B are the refractive index increments for the copolymer and two homopolymers respectively and:

$$P = \frac{\sum_i w_i M_i (x_i - x)}{\sum_i w_i}$$

and

$$Q = \frac{\sum_i w_i M_i (x_i - x)^2}{\sum_i w_i}$$

where x is the weight fraction of component A in the overall copolymer and x_i characterizes the particular composition of the i th molecule. If the copolymer is homogeneous in composition, or alternatively if $\nu_A = \nu_B$ so that as far as light scattering is concerned the copolymer behaves as a homopolymer, then $M_{app} = M_w$. For the present study, in view of the controlled synthetic methods and fractionation procedures used in obtaining the copolymer sample, application of equation (1b) can be taken as providing a reliable measure of the weight-average molecular weight, regardless of the refractive index of the solvent.

Refractive index increments

These were measured for the copolymer solutions at each temperature studied by light scattering using a Brice-Phoenix differential refractometer calibrated in the recommended manner.

Light-scattering spectroscopy

Translational diffusion coefficients of the polymer in solution were determined from Rayleigh linewidths using a correlation technique¹⁵. The molecular centre-of-mass motion causes a range of quasi-elastic frequency shifts in the scattered light whose linewidth is characteristic of the ensemble average motion of the particle. Details of the apparatus are to be found fully described elsewhere¹⁶. Briefly the spectrometer resolves the optical linewidth of the scattered light by homodyne light-beating and the photomultiplier photocurrent from the detected scattered light is analysed with an autocorrelation function computer. A 60 mW helium-neon laser (Spectra-Physics model 125) was used as the monochromatic light source and a Hewlett-Packard model 3721 A correlator was used to analyse the photocurrent signal.

For particles small compared with the wavelength of light the autocorrelation function is exponential with a time constant τ_c given by¹⁷:

$$\tau_c = (2K_1^2 D_c)^{-1} \quad (3)$$

where $K_1 (= 4\pi n \sin(\theta/2)/\lambda_0)$ is the scattering wave-vector in a medium of refractive index n for an incident light wave of wavelength λ_0 and scattering angle θ . The translational diffusion coefficient was obtained from a least squares computer fitting of the observed exponential function.

Solutions studied by this technique were clarified in the manner described for conventional light scattering.

Intrinsic viscosities

Flow times were measured in a modified Desreux-Bischoff viscometer. Measurements were made for at least four concentrations and plots of η_{sp}/c versus c and $\ln \eta_r/c$ versus c were extrapolated to zero concentration to obtain $[\eta]$.

RESULTS AND DISCUSSION

Conventional light-scattering measurements

Determinations of R_θ as a function of concentration and angle for copolymer 1D1 in n-decane were made at four temperatures (25°, 45°, 55° and 65°C). Over the range of interest n-decane is a non-solvent for polystyrene, but a relatively good solvent for polyisoprene. In Figure 1 values of (Kc/R_θ) extrapolated to zero angle are plotted against the concentration. It is important to note that at all four temperatures (Kc/R_θ) showed only a very small dependence on angle. For this reason it was not possible to use the angular dissymmetry to determine the dimensions of the particle in solution.

Determinations of R_θ were also made on the copolymer in chloroform, cyclohexane, tetrahydrofuran and 1-chloropropane at a single temperature (25°C). Values of M_w obtained by extrapolating (Kc/R_θ) to zero concentration and angle are given in Table 1. The copolymer would be expected to form true molecular solutions in all four solvents. The satisfactory agreement between the values supports the claim that for the

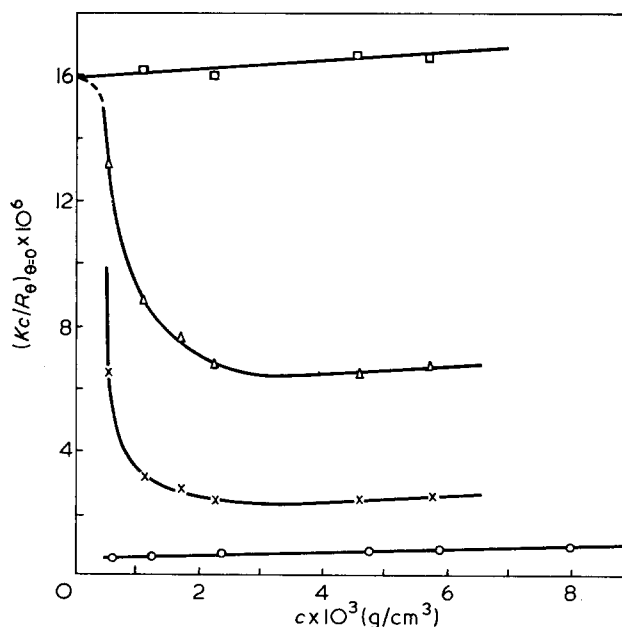


Figure 1 Plot of $(Kc/R_\theta)_{\theta=0}$ versus concentration for copolymer 1D1 in n-decane at 25°C (○), 45°C (×), 55°C (△) and 65°C (□). (At 25°C, two other points were obtained which could not be fitted conveniently on the plot: $c = 1.179 \times 10^{-2}$ g/cm³, $Kc/R_\theta = 1.40 \times 10^{-6}$ and $c = 1.919 \times 10^{-2}$ g/cm³, $Kc/R_\theta = 1.73 \times 10^{-6}$.)

Table 1 Values of M_{app} determined in different solvents at 25°C

Solvent	$M_{app} \times 10^{-4}$
chloroform	6.5
cyclohexane	6.6
tetrahydrofuran	6.2
1-chloropropane	5.7

polymer system under investigation observed values of M_w are not subject to compositional heterogeneity effects.

Let us now consider the data plotted in Figure 1. At 65°C the plot of $(Kc/R_\theta)_{\theta=0}$ versus c is approximately linear over the range investigated, and the intercept at $c=0$ gives a value for M_w ($=62\,900$), which is in good agreement with values given in Table 1. We conclude from this that at 65°C in dilute n-decane solution the copolymer molecules do not aggregate into micelles. At 55° and 45°C plots are obtained which turn sharply upwards at lower concentrations. The shape of these suggests that an equilibrium is established between individual polymer coils and multimolecular micelles. At 25°C the plots remain linear in the limiting region down to the lowest concentration which was investigated. This suggests that the equilibrium is predominantly in favour of micelles at 25°C. If we assume that at 25°C over the lower concentration range studied the molecular weight of the micelles is independent of concentration and that any very small concentration of unaggregated chains has a negligible effect on the scattering data, then M_w can be obtained in the usual way from the intercept,

$$\left(\frac{Kc}{R_\theta}\right)_{c=0, \theta=0}$$

This gives a value of M_w for the micelles of $(1.73 \pm 0.14) \times 10^6$.

Intrinsic viscosity measurements

In Figure 2, the intrinsic viscosity, $[\eta]$, of the copolymer in n-decane is plotted as a function of temperature. The sharp step in the plot is a reflection of the coil/multimolecular micelle transition. For the purpose of comparison values are also given for the copolymer in a solvent, methyl cyclohexane, in which multimolecular micelles do not form over the temperature range of interest. In Figure 3 values of η_{sp}/c are plotted as a function of temperature. The data show a transition in the same region as those in Figure 2.

Translational diffusion coefficients

In Figure 4, values of D_c for the copolymer 1D1 in n-decane ($c = 1.03 \times 10^{-2} \text{ g/cm}^3$) are plotted as a function

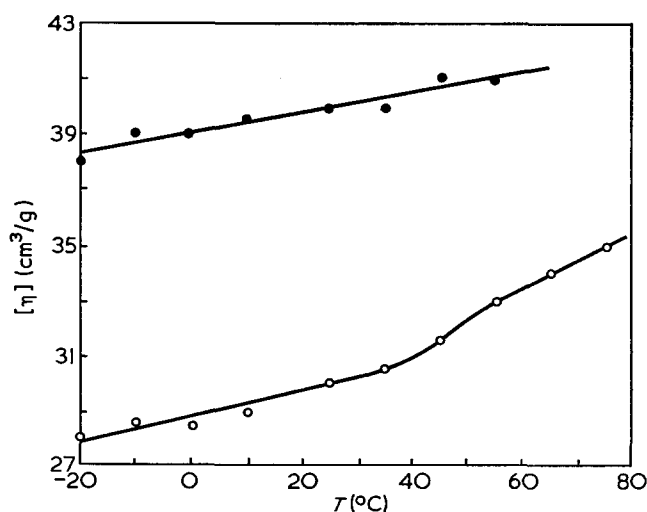


Figure 2 Dependence of intrinsic viscosity on temperature for copolymer 1D1 in n-decane (O), and copolymer 1D1 in methyl cyclohexane (●)

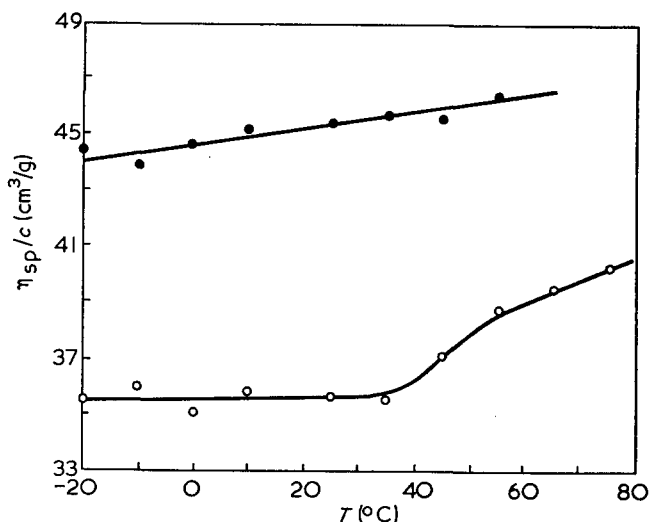


Figure 3 Dependence of η_{sp}/c on temperature for copolymer 1D1 in n-decane at $c = 0.649 \times 10^{-2} \text{ g/cm}^3$ (O), and copolymer 1D1 in methyl cyclohexane at $c = 0.747 \times 10^{-2} \text{ g/cm}^3$ (●)

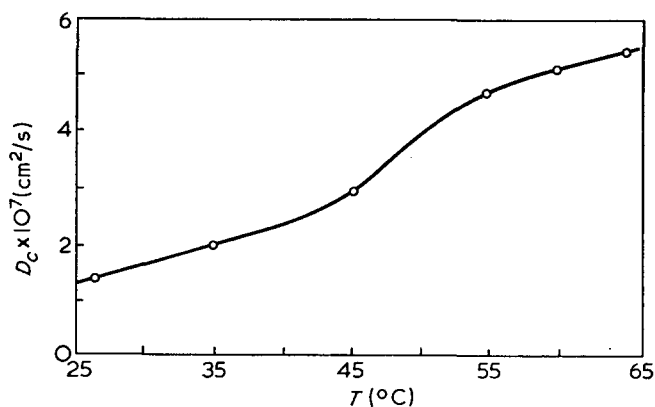


Figure 4 Dependence of the translational diffusion coefficient of copolymer 1D1 in n-decane on temperature ($c = 1.032 \times 10^{-2} \text{ g/cm}^3$)

of temperature. Each of the plotted points is an average value of D_c calculated from a number of runs at several different angles; a typical plot of linewidth (τ^{-1}) versus $2K_1^2$ is shown in Figure 5. In agreement with the viscosity and light-scattering data the results in Figure 4 show a distinct transition. At 25°C values of D_c were measured at a series of concentrations below 1.1% concentration. The plot was linear with almost zero slope and on extrapolation to infinite dilution gave a value of $D_0 = (1.31 \pm 0.04) \times 10^{-7} \text{ cm}^2/\text{sec}$.

If we represent the micelles by hydrodynamically equivalent spheres then¹⁸:

$$D_0 = \frac{kT}{6\pi\eta R_d} \quad (4)$$

and

$$[\eta] = \left(\frac{10\pi}{3}\right) \cdot \frac{R_\eta^3 N_0}{M} \quad (5)$$

where k is Boltzmann's constant, N_0 Avogadro's number, η the viscosity of the solvent, T the absolute temperature, and R_d and R_η are the radii of spheres which are equivalent to the micelles in translational diffusion and intrinsic viscosity respectively. By combining equations

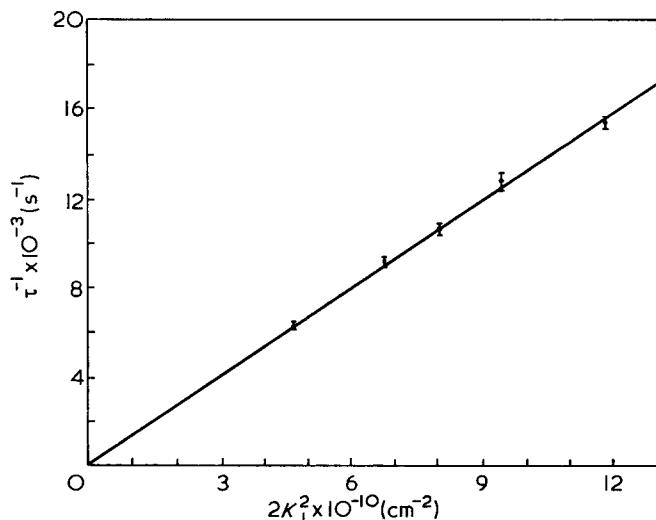


Figure 5 Plot of linewidth (τ^{-1}) versus $2K_1^2$

(4) and (5), an expression for the molecular weight is obtained^{19, 20}:

$$M = \frac{k^3 N_0}{64 \cdot 8 \pi^2} \cdot \left(\frac{T^3}{\eta^3} \right) \left(\frac{R_\eta}{R_d} \right)^3 \cdot \frac{1}{[\eta] D_0^3} \quad (6)$$

Data obtained for linear flexible coils by Tsvetkov and Klenin give R_η/R_d ratios in the range 1.1 to 1.3 depending on the nature of the solvent²⁰. For compact structures such as the copolymer micelles we can expect R_η/R_d to lie in the range 1.0 to 1.1. We have chosen the intermediate value of $R_\eta/R_d = 1.05$ which we believe is unlikely to be in error by more than $\pm 5\%$ for this parameter. Substituting the data for copolymer 1DI in n-decane at 25°C into equation (6) we obtain a value for the molecular weight of the micelles of $(1.82 \pm 0.24) \times 10^6$ which is in very good agreement with the value obtained from conventional light scattering. It should be noted, however, that equation (6) will yield a somewhat complex molecular weight average. We have not concerned ourselves with this point in the present study because there is good evidence that the multimolecular micelles formed by well-defined simple block copolymers are approximately monodisperse in size²¹. On substituting the value for D_0 at 25°C into equation (4) we obtain a value for the hydrodynamic radius (R_d) of 19.6 nm.

In the present contribution we have only considered results obtained for a single copolymer/solvent system. It is hoped that detailed investigations currently under way on a series of block and graft copolymers will enable us to assess in a thorough manner the general usefulness of equation (6) in the study of micellar solutions.

Comparison with results obtained by electron microscopy

In a recent publication²¹ we outlined a new method for studying the presence of micellar aggregates in solutions of block and graft copolymers. Specimens for examination in the electron microscope were prepared using a freeze-etching/replication technique. One of the samples studied was the block copolymer 1DI. Technical white oil, which is a 'non-solvent' for polystyrene, was taken as the dispersion medium. It was chosen because its relatively high viscosity facilitated the specimen preparation procedure. (N.B. Technical white oil contains a mixture of saturated aliphatic hydrocarbons.)

The micrographs obtained for 1DI showed an array of spherical micelles approximately monodisperse in size.

From the results it was possible to tentatively estimate the average molecular weight of the micelles. In order to do this, however, it was necessary to assume that the polymer coils collapsed upon themselves during the specimen preparation stage and assumed a density similar to the bulk state. Whilst the assumption was found to be valid for the case of a sample of homopolystyrene (dissolved in a mixture of toluene and technical white oil) no independent evidence could be offered at the time to check the molecular weights obtained for the copolymer micelles. Since n-decane could be expected to solvate the copolymer in a similar manner to technical white oil, it is useful at this stage to compare the present results with those obtained previously by the electron microscopy technique. The density of the copolymer in the collapsed micelle was taken to be that of the bulk copolymer at the replication temperature [$\rho(-90^\circ\text{C}) = 1.003 \text{ g/cm}^3$]. Hence $M = (\text{volume of collapsed micelle}) \times N_0 \times \rho = (2.78 \pm 0.83) \times 10^6$. (N.B. The density used in the original paper for the collapsed copolymer was slightly lower than the value given here; the original value was obtained by a rather elaborate extrapolative method which we now know to be unreliable.)

The value obtained for the micelle molecular weight by electron microscopy is somewhat higher than the values $[(1.73 \pm 0.14) \times 10^6$ and $(1.82 \pm 0.24) \times 10^6]$ given by the other two methods. It should be stressed, however, that the electron microscopy value corresponds to micelles formed in technical white oil rather than n-decane. There is also an uncertainty associated with the electron microscopy value which stems from the freeze-etching technique used. In the specimen preparation procedure a small sample of solution is first shock-cooled, and then its surface is microtomed, etched and replicated. It is difficult to determine in practice the exact solution temperature to which the observed micelles correspond. In any event, this temperature will be lower than 25°C.

ACKNOWLEDGEMENTS

Funding for these studies has been provided by the Science Research Council. We should like to thank Drs T. A. King and A. Knox for experimental assistance with the Rayleigh linewidth measurements and Esso Chemical Research Centre, Abingdon, for general assistance given to D. W.

REFERENCES

- 1 Gallot, Y., Leng, M., Benoit, H. and Rempp, P. *J. Chim. Phys.* 1962, **59**, 1093
- 2 Gallot, Y., Franta, E., Rempp, P. and Benoit, H. *J. Polym. Sci. (C)* 1963, **4**, 473
- 3 Krause, S. *J. Phys. Chem.* 1964, **68**, 1948
- 4 Schlick, S. and Levy, M. *J. Phys. Chem.* 1960, **64**, 883
- 5 Ye Bresler, S., Pyrkov, L. M., Ya Frenkel, S., Laius, P. A. and Klenin, S. I. *Vysokomol. Soedin.* 1962, **4**, 250
- 6 Molau, G. E. and Wittbrodt, V. M. *Macromolecules* 1968, **1**, 260
- 7 Dawkins, J. V. 'Block Copolymers' (Eds D. C. Allport and W. H. Janes), Applied Science, London, 1973, Ch 9
- 8 Price, C. and Woods, D. *Polymer* 1973, **14**, 82
- 9 Price, C., Lally, T. P., Watson, A. G., Woods, D. and Chow, M. T. *Br. Polym. J.* 1972, **4**, 413
- 10 Price, C., Watson, A. G. and Chow, M. T. *Polymer* 1972, **13**, 333

Molecular weight and hydrodynamic dimensions of micelles from a block copolymer: C. Price et al.

- 11 Ehl, J., Loucheux, C., Reiss, C. and Benoit, H. *Makromol. Chem.* 1964, **75**, 35
- 12 Zimm, B. H. *J. Chem. Phys.* 1948, **16**, 1093, 1099
- 13 Stockmayer, W. H., Moore, L. D., Fixman, M. and Epstein, B. N. *J. Polym. Sci.* 1955, **16**, 517
- 14 Bushuk, W. and Benoit, H. *Can. J. Chem.* 1958, **36**, 1616
- 15 Cummins, H. Z. and Swinney, H. L. *Progr. Optics*, 1970, **8**, 134
- 16 Knox, A. *PhD Thesis* University of Manchester, 1972
- 17 Pecora, R. *J. Chem. Phys.* 1964, **40**, 1604
- 18 Debye, P. and Beuche, A. M. *J. Chem. Phys.* 1948, **16**, 573
- 19 Morawetz, H. 'Macromolecules in Solution', Interscience, New York, 1965, Ch VI
- 20 Tsvetkov, V. N. and Klenin, S. I. *J. Polym. Sci.* 1958, **30**, 187
- 21 Price, C. and Woods, D. *Eur. Polym. J.* 1973, **9**, 827

Preparation of ultra-high modulus linear polyethylenes; effect of molecular weight and molecular weight distribution on drawing behaviour and mechanical properties

G. Capaccio and I. M. Ward

*Department of Physics, University of Leeds, Leeds LS2 9JT, UK
(Received 27 March 1973; revised 30 May 1973)*

A systematic investigation of the effect of molecular weight and molecular weight distribution on the cold drawing behaviour of linear polyethylene has been undertaken. In the molecular weight range studied, the natural draw ratio was very sensitive to the morphology of the initial material; spectacular effects on the natural draw ratio were observed provided that an optimum initial morphology was achieved. These effects can be related to both molecular weight and molecular weight distribution.

The extensional modulus and melting behaviour of the drawn material was also examined. To a first approximation the extensional modulus related to the natural draw ratio, and at very high draw ratios (~ 30) extremely high extensional moduli (~ 700 kbar) were obtained. The structure and properties of the drawn material did, however, also depend on the molecular weight and molecular weight distribution. In particular, when certain molecular weight requirements were satisfied, the oriented samples showed the presence of extended chain material. It does, however, appear that although differences in molecular weight and molecular weight distribution give rise to differences in extensional moduli, the presence of extended chain crystallization *per se* is not a necessary requirement for the production of high modulus material.

INTRODUCTION

A number of values have been proposed for the Young's modulus of fully aligned linear polyethylene (LPE) on the basis of theoretical calculations and various experimental determinations of the crystalline stiffness^{1, 2}. All these estimates, although far from being in good agreement amongst themselves, indicate that a Young's modulus of at least 2 Mbar should be expected for a completely oriented sample. This value is several orders of magnitude higher than is usually achieved^{3, 4} by cold drawing conventional LPE to a typical draw ratio (λ) of about 9–10. There is therefore considerable interest in attempting to obtain higher draw ratios and hence higher moduli, and also in exploring the structural factors which prevent the theoretical moduli from being achieved. In a previous publication⁵ the effect of molecular weight has been studied using a number of samples having different number-average molecular weights (\bar{M}_n) as well as different weight-average molecular weights (\bar{M}_w). The results, due to the particular selection of samples available, could not be considered conclusive; nevertheless they indicated a dependence of draw ratio on molecular weight and suggested that there was a good correlation between the Young's modulus and the draw ratio achieved.

The present paper discusses: (a) the effect of molecular weight on the morphology of the initial material and

hence on the draw ratio and final modulus; and (b) the formation of extended chain crystals in drawn samples as a function of molecular weight and draw ratio. Furthermore we present a new material, in the form of a highly oriented film, which exhibits the highest unidirectional modulus ever obtained at room temperature for LPE, and almost in the range predicted for fully aligned chains.*

EXPERIMENTAL

The materials used were four commercial grades of Rigidex (BP Chemicals) LPE homopolymer and the gel permeation chromatographic (g.p.c.) molecular weight data in *Table 1* were kindly supplied by Mr J. M. Squire, BP Research & Development Dept., Grangemouth Division, Grangemouth, UK.

Sheets 0.05–0.07 cm thick were obtained by compression moulding pellets of polymer at 160°C between copper plates. Some sheets were immediately quenched in cold water while others were slowly cooled, at a rate of 7–9°C/min, to a temperature T_q (measured either inside the sheet or on the surface of the copper plates) and then quenched in cold water.

The density of the isotropic sheets was measured at

* G. Capaccio and I. M. Ward, Br. Pat. Appln. 10746/73 (filed 6 March 1973).

Table 1 G.p.c. molecular weight data of LPE samples used

Sample No.	Rigidex grade	Batch No.	\bar{M}_n	\bar{M}_w
1	9	BL 9022	6 060	126 600
2	50	9099	6 180	101 450
3	25	6050/1	12 950	98 800
4	140-60	2H31/A/278	13 350	67 800

23°C in a density gradient column using either isopropyl alcohol and diethyleneglycol or isopropyl alcohol and water as solvents. The mass fraction of the crystalline phase (α_m) as a function of the sample density (ρ), the density of the crystalline phase (ρ_c) and the density of the amorphous phase (ρ_a) was calculated from the equation:

$$\alpha_m = [(\rho - \rho_a)/(\rho_c - \rho_a)] \frac{\rho_c}{\rho}$$

assuming a value of 1.000 g/cm³ for ρ_c and a value in the range 0.855–0.870 g/cm³ for ρ_a ⁶⁻⁸.

Dumbbell samples of dimensions 2 cm × 0.2 cm were cut and drawn on an Instron Tensile Testing machine at 75°C at a draw speed of 10 cm/min for 60–90 sec. Only sample 2 had to be drawn at a speed of 1 cm/min to attain $\lambda=30$. The draw ratio was measured from marks on the surface of the undrawn samples spaced at intervals of 0.2 or 0.1 cm. In general at very high draw ratio (>25) only 30–50% of the drawn segment showed a homogeneous draw.

The melting curves were measured on a Du Pont Thermal Analyzer with a Du Pont DSC cell and operated in a differential scanning calorimetry (d.s.c.) heat mode. Untreated aluminium pans were used. The temperature was measured by chromel/alumel thermocouples and corrected in accordance with the Du Pont manual. The experiment was carried out in an atmosphere of nitrogen at normal pressure and the gas flow was (1–3) × 10³ cm³/min. The samples were heated up at a rate of 5°C/min from a starting temperature of 90°C.

The room temperature Young's modulus was measured by a dead-loading creep experiment⁹, taking the 10 sec response at stresses (σ) corresponding to strains (ϵ) below 0.01.

RESULTS AND DISCUSSION

Pre-treatment

The cooling pattern of the four samples, under the same conditions, is very similar and the cooling curves do not show any appreciable differences; as an example, the curve for sample 4 is plotted in Figure 1.

All the samples show a phase transition in the region 120–123°C which is associated with the main part of the primary crystallization of the polymer. The temperature range in which this occurs is in good agreement with predictions obtained by comparing the molecular weight distribution of the samples and their rate of cooling with the crystallization rate data published for LPE fractions isothermally crystallized at high supercooling^{10, 11}. One therefore expects to obtain a polymer of low crystalline fraction α_m at temperatures higher than 123°C whereas at lower temperatures the crystalline fraction should be much higher and keep increasing slowly with decreasing temperature owing to further crystallization.

If a few samples are now taken along this cooling path and quenched in cold water the morphology of the quenched material will be directly related to the morphology at the final temperature on the slow cooling path and will therefore be a function of the temperature T_q at which the slow cooling process has been suddenly stopped. As a consequence we would expect to obtain significant variations in α_m for different values of T_q . Figure 2 and Table 2 show very well the extent of these variations.

All four samples when quenched at $T_q=160^\circ\text{C}$ show a low α_m and this value should be quite typical for any sample quenched at a temperature higher than the observed crystallization temperature. For $T_q=110^\circ\text{C}$ a dramatic increase in α_m is observed; the crystallization process has, at this stage, involved most of the molecules available, and the differences between different samples

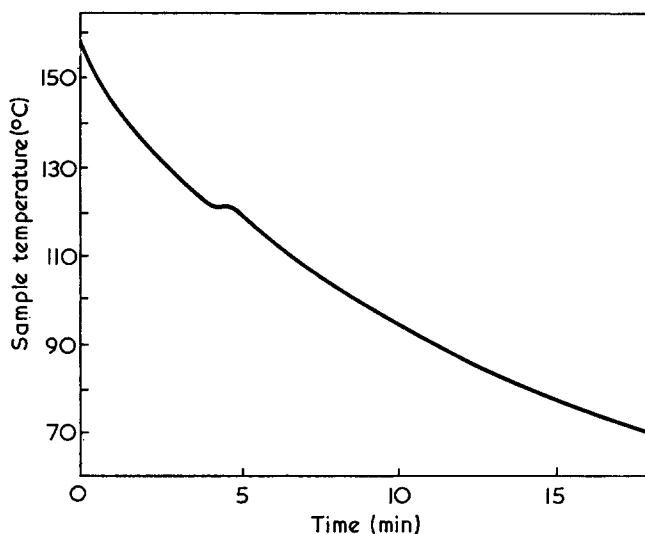


Figure 1 Cooling curve of an isotropic film of sample 4 compression moulded at 160°C

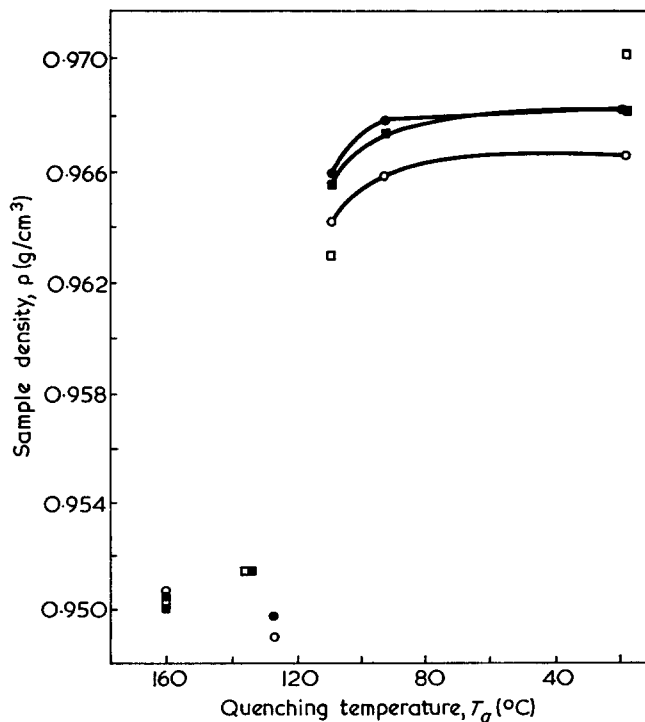


Figure 2 Density ρ of the isotropic samples as a function of the quenching temperature T_q . □, Sample 1; ■, Sample 2; ○, sample 3; ●, sample 4

Table 2 Crystalline mass fraction α_m as a function of T_q for different samples. Values calculated for $\rho_a=0.855\text{g/cm}^3$ (bottom) and $\rho_a=0.870\text{g/cm}^3$ (top)

T_q (°C)	Sample No.			
	1	2	3	4
160	0.67	0.66	0.65	0.65
	0.71	0.70	0.69	0.69
110	0.74	0.76	0.75	0.76
	0.77	0.79	0.78	0.79
20	0.79	0.78	0.77	0.78
	0.82	0.81	0.80	0.81

can then be related, in a qualitative manner, to the differences in molecular weight.

Previous work has shown the effect of molecular weight on both the crystallization rate^{10,11} and the equilibrium crystallinity¹². The crystallization rate vs. molecular weight curve for isothermally crystallized LPE fractions at high supercooling, for example 121°C, goes through a maximum¹¹ at a molecular weight of about 2×10^4 and is asymmetric, being very sharp on the very low molecular weight side and fairly smooth on the high molecular weight side. On the other hand, the equilibrium crystallinity is constant at low molecular weights, but falls off monotonically¹² at molecular weights greater than about 10^4 . Although these results were obtained for fractionated polymers, there are indications that in unfractionated polymer fractionation occurs during crystallization¹³, and so it would be expected that they would still be of relevance to the present investigation.

In our experiments the effect of crystallization rate is probably predominant. However, the results can be interpreted either in terms of kinetic effects alone or of a combination of kinetic effects and equilibrium crystallinity. Thus, sample 1 with its long very high molecular weight tail as well as very low molecular weight tail in the molecular weight distribution curve has the lowest α_m . Sample 2, on the other hand, with the same \bar{M}_n but a narrower distribution exhibits a relatively higher α_m .

Sample 3, with a higher \bar{M}_n but with \bar{M}_w fairly close to that of sample 2, has a lower value of α_m than the latter because of its molecular weight distribution which is shifted as a whole towards higher molecular weight. Sample 4 if compared with sample 3, of almost identical \bar{M}_n , shows the expected increase of α_m for a narrower molecular weight distribution and reaches the value measured for sample 2. The equivalence of samples 2 and 4 can therefore be attributed to the combination of effects acting on two opposite directions; first, the narrowing of the molecular weight distribution, which reduces the proportions of both very low and very high molecular weight material and secondly, the overall shift of the molecular weight distribution towards higher \bar{M}_n .

When slowly cooled down to room temperature ($T_q=20^\circ\text{C}$), a very small increase in α_m is observed in samples 2, 3 and 4, whilst sample 1 reaches a value higher than the others. This unusual behaviour can be attributed to the continuous crystallization, even at very low temperatures, of very low molecular weight molecules⁷ which are present in substantial quantity in this sample of low \bar{M}_n and very broad molecular weight distribution.

Drawing behaviour

The drawing behaviour of these samples supports this interpretation of the initial morphology and a close analysis of the variation of the yield stress (σ_y) and draw ratio with T_q provides more information on the possible morphological features of some of the samples.

The yield stress data do not show any dramatic dependence on molecular weight and molecular weight distribution. The σ_y values for all four samples are fairly close and are only a function of T_q . As an example of the trends and fluctuations the values of the yield stress for samples 3 and 4 are shown in Figure 3. An initial increase of over 50% is observed in the region $T_q=130\text{--}110^\circ\text{C}$ after which the yield stress levels off and no temperature dependence is detectable below 110°C .

The initially low value of the yield stress at high quenching temperatures may be related to the more compliant behaviour of samples of low crystallinity. The development of further crystallization, at and just below the observed crystallization temperature, is likely to produce a net increase in the stiffness of the material which can account for the observed increase of the yield stress. This reaches a maximum value at $T_q=110^\circ\text{C}$ when presumably an optimum morphology has been achieved. In fact, the yield stress might be expected to reflect the presence of two conflicting effects; the increase in crystallinity which results in a stiffening of the structure and a segregation process, by which non-crystallized low molecular weight molecules are more and more segregated at the spherulite boundaries. In principle, therefore, the ultimate stage should be represented by a very weak structure in which large spherulites are well separated by highly compliant low molecular weight material. According to this picture the plot of σ_y vs. T_q should go through a maximum which is not observed in our results but which has been found in other polymers¹⁴.

It does, however, appear that more complex effects are seen in the strain hardening behaviour, as revealed by the pattern of draw ratio with quenching temperature. In particular, the draw ratio shows a maximum value (λ_{max}) as a function of quenching temperature at $T_q=110^\circ\text{C}$ for samples 2, 3 and 4, whereas for sample 1 the draw ratio remains constant for $T_q < 110^\circ\text{C}$.

In Figure 4 the average values of several determinations

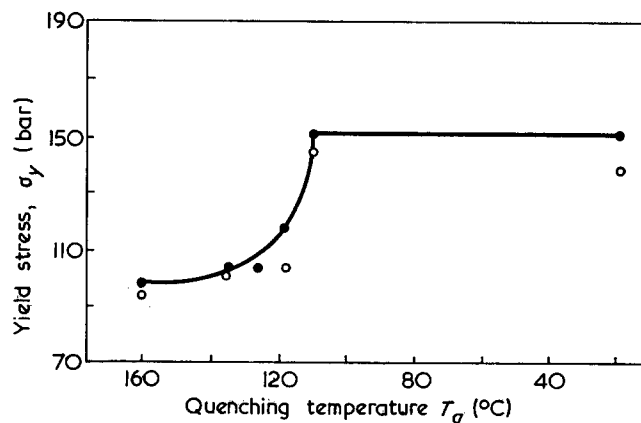


Figure 3 Yield stress σ_y as a function of quenching temperature T_q for samples 3 (○) and 4 (●) drawn at 75°C at a draw speed of 10cm/min

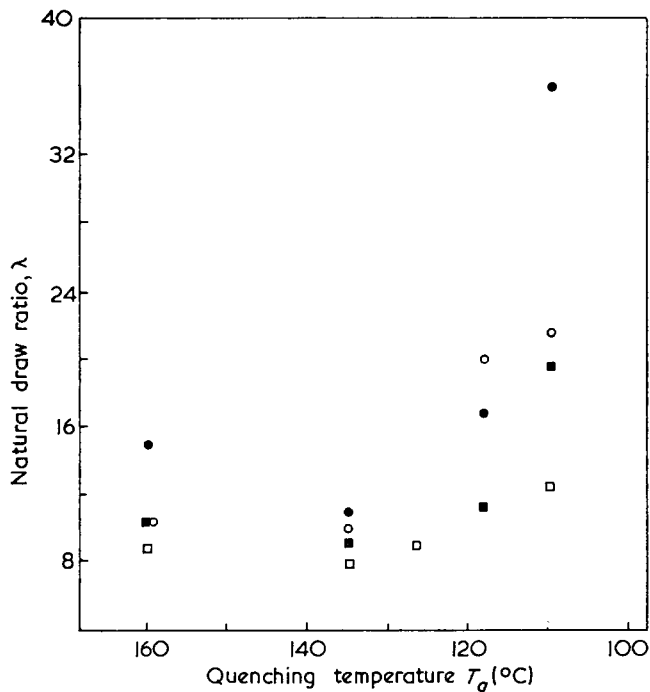


Figure 4 Variation of draw ratio λ with quenching temperature T_q for samples drawn at 75°C at a draw speed of 10cm/min. □, Sample 1; ■, sample 2; ○, sample 3; ●, sample 4

of the draw ratio are shown for the four samples as a function of the quenching temperature in the temperature range 160–110°C. The results for $T_q < 110^\circ\text{C}$, which are not shown in the Figure, showed much greater scatter, but except for sample 1, they consistently indicated that the draw ratio reached a value which is intermediate between λ_{max} and the draw ratio for $T_q = 160^\circ\text{C}$.

These results also clearly show for the first time the effect of molecular weight and molecular weight distribution on the draw ratio. A sharper maximum in the draw ratio as a function of quenching temperature appears to be characteristic of the samples with higher \bar{M}_n , i.e. samples 3 and 4. At the same time, by comparing samples 1 and 2 with samples 3 and 4, we can see that there is a spectacular effect of \bar{M}_w . At a given value of \bar{M}_n , a substantial increase in draw ratio is always obtained by narrowing the molecular weight distribution i.e. by reducing \bar{M}_w .

At high draw ratios there is an excellent correlation between draw ratio and the crystallinity of the undrawn material, the highest draw ratios having the highest crystallinity. This suggests that both are, to some extent, dependent on the same parameter—the concentration of very high molecular weight material. This view is supported by the behaviour of sample 1, which has the highest \bar{M}_w , and would therefore be expected to possess many interlamellar tie molecules^{15, 16}. This sample shows no change in draw ratio for quenching temperatures below 110°C.

However, very high molecular weight material can be only partly responsible for these effects. The presence of a maximum in the draw ratio for the other three samples (2, 3 and 4) suggests that other factors, such as the extent of segregation and the nature of the material segregated during the slow cooling of the isotropic sheet, also play a significant role in the plastic deformation process.

Thermal analysis

A preliminary investigation of the texture of the drawn samples has been carried out by examining their melting behaviour (Figures 5 and 6). Samples 1 and 2

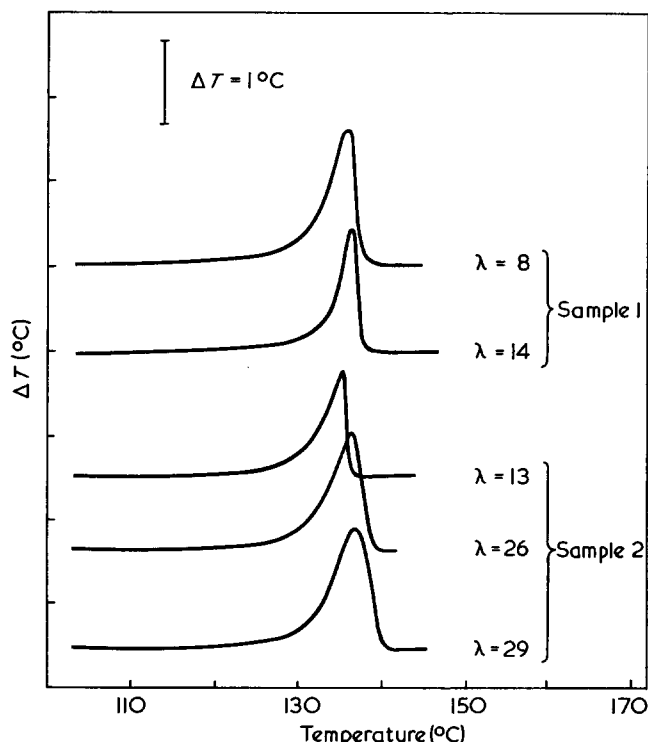


Figure 5 D.s.c. traces for samples 1 and 2 at different draw ratios λ

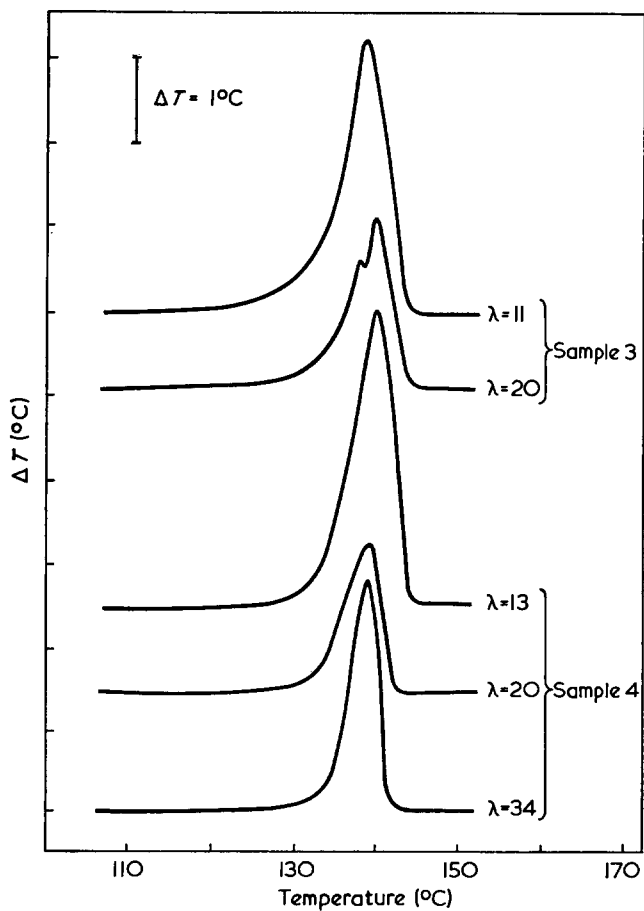


Figure 6 D.s.c. traces for samples 3 and 4 at different draw ratios λ

show an increase in the melting temperature T_m ($T_m \approx 133^\circ\text{C}$ for the isotropic material) with increasing draw ratio. At its highest attainable draw ratio sample 2 melted at $\sim 137^\circ\text{C}$. Much more remarkable behaviour is shown by samples 3 and 4 even at lower draw ratio. Sample 4 always shows a melting peak at 138.5°C whereas sample 3 gives a single peak at 137.5°C at $\lambda=11$ which splits into a double peak at $\lambda=20$ with a substantial fraction melting at 138.5°C . This shows that the plastic deformation of samples 3 and 4 has produced crystalline material with a crystallite thickness greater than $\sim 1500 \text{ \AA}$ ^{17, 18}, conventionally termed extended chain crystals.

The fact that only samples 3 and 4 exhibit this peculiar behaviour suggests that the formation of extended chain material is related to a critical molecular weight range, i.e. a critical value of \bar{M}_n . For very narrow molecular weight distributions (sample 4) the result becomes completely independent of the initial morphology and draw ratio. With a broader molecular weight distribution, as obtained with sample 3, the phenomenon occurs only partially and only at high draw ratio. It appears therefore that extended chain samples of LPE can be easily prepared by cold drawing provided that polymers of suitable molecular weight and molecular weight distribution are chosen. The present results do not rule out the possibility that even at values of \bar{M}_n which are lower or higher than $\sim 13\,000$ the same

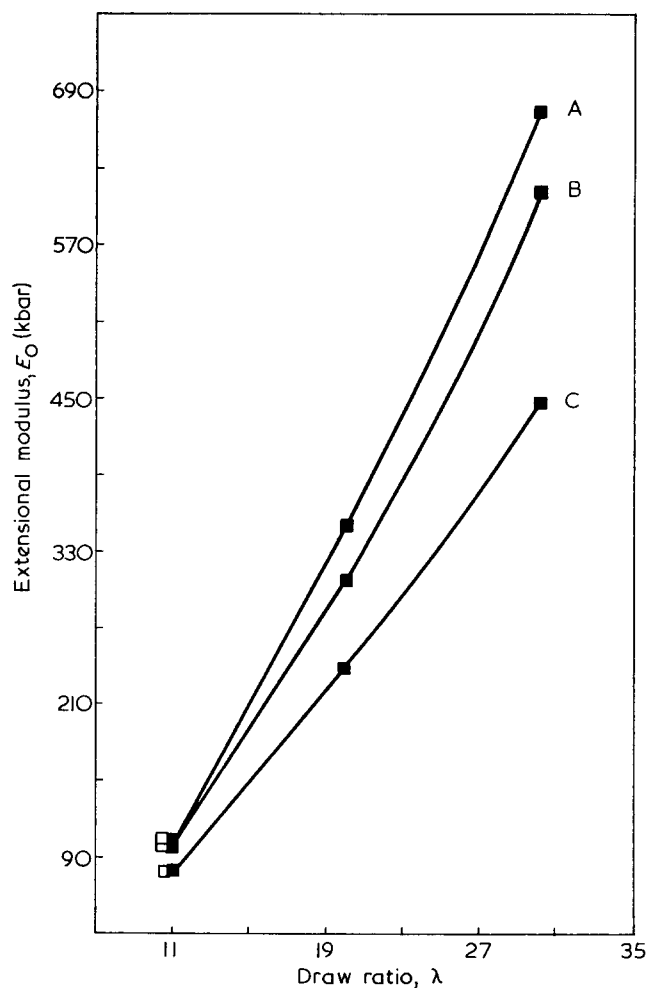


Figure 7 Young's modulus, calculated from the 10sec isochronal stress-strain curves, as a function of draw ratio λ , at various strains, for samples 1 (\square) and 2 (\blacksquare). A, $\epsilon=0.001$; B, $\epsilon=0.002$; C, $\epsilon=0.005$

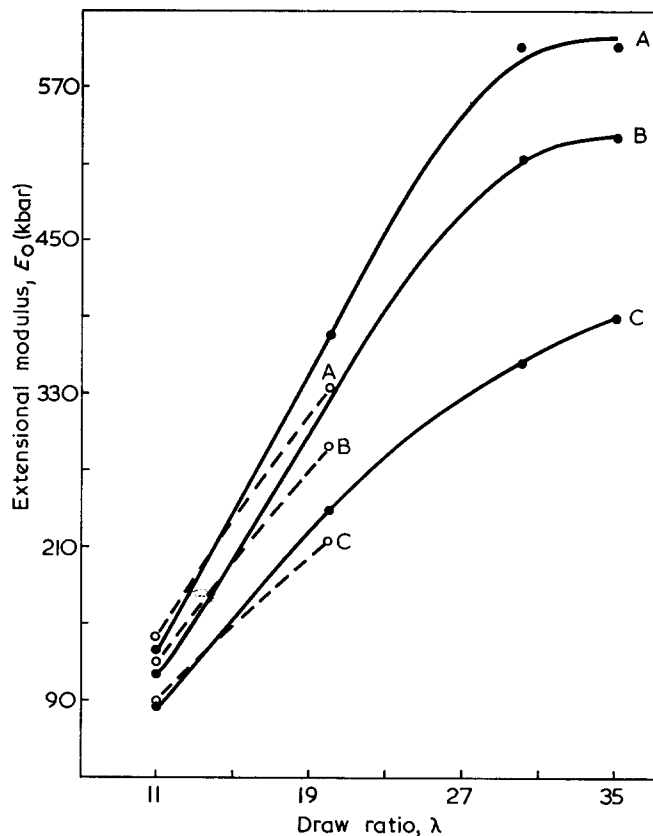


Figure 8 Young's modulus, calculated from the 10sec isochronal stress-strain curves, as a function of draw ratio λ , at various strains, for samples 3 (\circ) and 4 (\bullet). A, $\epsilon=0.001$; B, $\epsilon=0.002$; C, $\epsilon=0.005$

effect may be obtained with an appropriately matched molecular weight distribution.

We are aware that this particular aspect of the problem requires further detailed discussion and will present a more extensive study in a future paper.

Mechanical properties

The room temperature creep behaviour was studied for each sample. From the creep response, the 10sec isochronal stress-strain curves were constructed, so that values of the Young's modulus could be obtained for various strains. The results are shown in Figures 7 and 8 as a function of sample draw ratio.

A complete comparison cannot be obtained from the results shown in Figure 7 because sample 1 could be drawn only to a relatively low draw ratio. However, taking the results shown in Figures 7 and 8 overall, it is clear that the modulus is, to a first approximation, related only to draw ratio, at least for $\lambda < 30$. This result is consistent with that obtained previously at a lower range of draw ratios and moduli⁵. It is possible that results shown in Figure 8 may be indicative of a small effect due to molecular weight at draw ratio 20.

The results show also that the achievement of high modulus does not necessarily require the presence of extended chain crystals. This result is consistent with the view that the non-crystalline phase is likely to give the major contribution to the overall compliance. It is therefore reasonable to expect that the macroscopic deformation would not be affected by any change in the crystalline structure, as distinct from the fraction of crystalline material or the degree of molecular

orientation. On this view the concentration of fully extended chains in the non-crystalline regions is mainly responsible for the stiffness of the polymer, i.e. oriented tie molecules. It is also possible that extended chain crystals could play a similar role to oriented extended chain tie molecules in contributing to the overall stiffness.

It would appear that there are also some molecular weight effects on the modulus. Sample 2 at a draw ratio of 30 has a higher modulus than sample 4 at the same draw ratio. This suggests that the presence of high molecular weight molecules is important, because although sample 4 has a higher \bar{M}_n value than sample 2, it has a narrower molecular weight distribution. The flattening of the modulus/draw ratio plot for sample 4 supports the view that the amount of high molecular weight material may in the limit determine the highest modulus attainable.

Orientation studies by wide angle X-ray and broad line nuclear magnetic resonance methods are presently being carried out in an attempt to resolve some of these problems and will be reported very soon.

CONCLUSIONS

The present study has clearly shown the effect of initial morphology and molecular weight on the cold drawing behaviour and mechanical properties of LPE.

The results presented indicate that, under the experimental conditions adopted, an optimum morphology must be obtained to achieve very high deformation ratios.

We suggest that the extent of nucleation in the crystallization process, crystallite growth and segregation of low molecular weight material are all likely to influence the critical morphology. All these parameters are molecular weight dependent. In this investigation the effects of \bar{M}_n and the ratio \bar{M}_w/\bar{M}_n have been clearly demonstrated with respect to their influence on draw ratio and final modulus.

A highly oriented material of very high stiffness (Young's modulus > 600 kbar) has been prepared. It appears that the presence of extended chain crystals, formed during the cold drawing process, is not directly relevant to the value of the extensional modulus achieved.

ACKNOWLEDGEMENTS

We wish to thank Mr J. D. Mellor for his assistance in the preparation of the samples, and Dr F. Jones, Department of Colour Chemistry, Leeds University for generously undertaking the thermograms. We also wish to acknowledge that one of us (G. C.) was supported by the Science Research Council.

REFERENCES

- 1 Frank, F. C. *Proc. R. Soc. (A)* 1970, **319**, 127
- 2 Holliday, L. and White, J. W. *Pure Appl. Chem.* 1971, **26**, 545
- 3 Meinel, G. and Peterlin, A. *J. Polym. Sci. (A-2)* 1968, **6**, 587
- 4 Gupta, V. B. and Ward, I. M. *J. Macromol. Sci.* 1968, **B2**, 89
- 5 Andrews, J. M. and Ward, I. M. *J. Mat. Sci.* 1970, **5**, 411
- 6 Glenz, W., Morosoff, J. and Peterlin, A. *J. Polym. Sci. (B)* 1971, **9**, 211
- 7 Chiang, R. and Flory, P. J. *J. Am. Chem. Soc.* 1961, **83**, 2857
- 8 Okada, T. and Mandelkern, L. *J. Polym. Sci. (A-2)* 1967, **5**, 239
- 9 Gupta, V. B. and Ward, I. M. *J. Macromol. Sci.* 1967, **B1**, 373
- 10 Mandelkern, L., Fatou, J. M. G. and Ohno, K. *J. Polym. Sci. (B)* 1968, **6**, 615
- 11 Fatou, J. M. G. and Barrales Rienda, J. M. *J. Polym. Sci. (A-2)* 1969, **7**, 1755
- 12 Fatou, J. G. and Mandelkern, L. *J. Phys. Chem.* 1965, **69**, 2, 417
- 13 Anderson, F. R. *J. Polym. Sci. (C)* 1963, **3**, 123
- 14 Way, J. L. and Atkinson, J. R. *Plastics and Polymers* in press
- 15 Mandelkern, L. *J. Polym. Sci. (C)* 1967, **18**, 51
- 16 Steidl, J. and Pelzbauer, Z. *J. Polym. Sci. (C)* 1972, **38**
- 17 Meinel, G., Morosoff, M. and Peterlin, A. *J. Polym. Sci. (A-2)* 1970, **8**, 1723
- 18 Bassett, D. C. personal communication

Conversion of work of deformation to heat in polymers

P. Zoller and H. Bont

*Kunststofflabor, Neu-Technikum Buchs, CH-9470 Buchs, Switzerland
(Received 30 July 1973; revised 3 December 1973)*

The time dependence of the conversion of mechanical work of deformation to heat in polymers is investigated using viscoelastic models. The deformation chosen is a constant strain rate, $\dot{\epsilon}_0$, in tension for $t \leq t_0$ and a constant strain $\epsilon_0 = \dot{\epsilon}_0 t_0$ for $t \geq t_0$. For a simple Maxwell model with only one relaxation time, τ , the ratio of heat produced to work done ('conversion fraction') is calculated as a function of time for different values of t_0/τ . At $t = t_0$ the conversion fraction is high only when $\tau \ll t_0$. For a continuous Maxwell model with a distribution of relaxation times $H(\tau)$ we obtain the result that the conversion fraction is near 100% at $t = t_0$ if $H(\tau)$ is not peaked strongly in the region $\tau > 0.1t_0$ but extends with reasonable values into the region $\tau < 0.1t_0$. A formula is given which allows the calculation of the conversion fraction at $t = t_0$ from the distribution of relaxation times $H(\tau)$.

INTRODUCTION

It is well known that polymers in states ranging from the glassy or crystalline states at low temperatures to polymer melts have mechanical properties intermediate between those of Hookean elastic solids and ideal viscous fluids. Manifestations of this more complicated behaviour of polymers are, e.g., the existence of creep, stress relaxation, melt elasticity etc. The phenomenological theory of linear viscoelasticity¹ is a suitable framework for describing the observed phenomena.

One consequence of viscoelasticity is the fact that energy is dissipated (converted to heat) whenever a viscoelastic body is deformed. In a Hookean solid all work of deformation is stored as potential energy; in an ideal viscous fluid all work is converted to heat instantaneously. Here, too, the behaviour of a viscoelastic body is intermediate between the limiting cases: some work is stored as potential energy, some is dissipated, and the fraction which is dissipated can be an explicit function of time. The most familiar examples of this behaviour are the experiments involving periodic (sinusoidal) deformations of a polymer. In such experiments a loss angle is determined as the phase angle between stress and strain, and the tangent of the phase angle is proportional to the ratio of energy dissipated in one cycle to the maximum energy stored in one cycle. Under the usual conditions of the experiment the absolute magnitude of the energy dissipated is too small to affect the temperature of the sample appreciably, especially since the sample will also exchange heat with its surroundings. However, under conditions of ultrasonic welding (very high frequencies) the temperature rise is sufficient to melt and weld polymer samples.

In a number of other experiments a temperature rise is more apparent, especially in situations involving large strains, such as stretching of films for orientation,

tensile testing etc. In such experiments the amount of heat generated can be a nuisance because it destroys the assumption of constant sample temperature.

One can go one step further and propose to use the energy dissipated whenever a viscoelastic body is deformed to plasticize the material without any additional sources of heat. In this way one would hope, starting from 'cold' material, to reach temperatures sufficient for further processing (such as bottle blowing, injection moulding etc). Such a process would become interesting if it heated up a polymer either faster or more uniformly than conventional means of heating. Both these advantages are claimed for a process developed by Menges and coworkers². A slug of non-molten polymer is extruded with great force through a narrow die. The observed temperature rise is due to the conversion of mechanical work of extrusion to heat (plus some friction between polymer and extrusion barrel). The temperature uniformity claimed by Menges is questioned by Schenkel³ on the basis of non-uniformity of stresses and deformations in the extrusion die. The other claim is that the polymer is heated 'within fractions of a second'. The purpose of this paper is to shed some light on the mechanism of this work to heat conversion process, especially the speed with which such a conversion can take place. We do this first on the basis of a simple Maxwell model (spring and dashpot in series) with a single relaxation time, τ . We then extend the results to the discussion of a continuous Maxwell model with a distribution of relaxation times $H(\tau)$. We realize, of course, that the process described by Menges² does not belong to the framework of linear viscoelasticity because of the large strains involved. Nevertheless, we believe that the discussion of these models will provide some guidance for the discussion of the work to heat conversion mechanisms in the real processes.

THEORY FOR THE SIMPLE MAXWELL MODEL

Considering the simple Maxwell model of a viscoelastic body, the differential equation connecting stress, $\sigma(t)$ and strain, $\epsilon(t)$ in tension is given by:

$$\frac{1}{\eta}\sigma + \frac{1}{G}\dot{\sigma} = \dot{\epsilon} \tag{1}$$

η and G are the two parameters of the model. η/G has the dimension of a time and is called the relaxation time τ . By choice we have written the differential equation for stress and strain in tension. It could just as well have been written for a shear stress and a shear strain without changing the further course of the development.

It is well known that a Maxwell viscoelastic body, characterized by equation (1), can be represented by an ideal spring and an ideal dashpot in series. Let $\epsilon_1(t)$ denote the strain of the spring, $\epsilon_2(t)$ the strain of the dashpot. In the spring the stress $\sigma(t)$ is proportional to the strain $\epsilon_1(t)$:

$$\sigma(t) = G\epsilon_1(t) \tag{2}$$

In the dashpot the stress $\sigma(t)$ is proportional to the time rate of change of the strain $\epsilon_2(t)$:

$$\sigma(t) = \eta\dot{\epsilon}_2(t) \tag{3}$$

The stress is the same in both elements because the elements are in series, and the total strain $\epsilon(t)$ of the Maxwell element is $\epsilon(t) = \epsilon_1(t) + \epsilon_2(t)$. Using this to combine equations (2) and (3) yields equation (1).

This model is subjected to the strain history given in Figure 1. Starting from $t = 0$ the sample is strained with a constant strain rate $\dot{\epsilon}_0$ until a total strain ϵ_0 is reached. This occurs at $t = t_0 = \epsilon_0/\dot{\epsilon}_0$. For $t \geq t_0$ the strain is kept constant. This process was chosen because of its analogy with tensile testing, an experiment on which tests for the theoretical ideas developed here can most conveniently be made.

The differential equation (1) can be solved explicitly for the strain history of Figure 1, giving the stress as a function of time:

$$t \leq t_0: \sigma(t) = \eta\dot{\epsilon}_0[1 - \exp(-t/\tau)] \tag{4}$$

$$t \geq t_0: \sigma(t) = \eta\dot{\epsilon}_0[\exp(-\{t - t_0\}/\tau) - \exp(-t/\tau)] \tag{5}$$

When the Maxwell body is deformed, mechanical work is done on the spring and on the dashpot. The work done on the spring is stored as potential energy, the work done on the dashpot is dissipated as heat. We will proceed to calculate the work $W_M(t)$ done in deforming the whole Maxwell model and the work $W_D(t)$ done

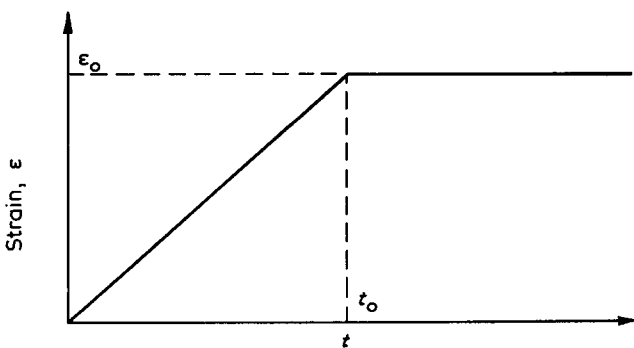


Figure 1 Strain, ϵ as a function of time

in deforming the dashpot alone from time zero up to time t . The ratio $W_D(t)/W_M(t)$ is (as a function of time t) the fraction of the total work done up to time t which has been converted to heat at time t .

The general expression for work done (per unit volume) when a sample is stretched according to the strain function $\epsilon(t)$ from time t_1 to time t_2 is given by:

$$W_{12} = \int_{t_1}^{t_2} \sigma(t')\dot{\epsilon}(t')dt' \tag{6}$$

This expression is applied to the Maxwell model as a whole, by substituting the strain history of Figure 1 and the stress of equations (4) and (5):

$$t \leq t_0: W_M(t) = \eta\dot{\epsilon}_0^2[t + \tau\exp(-t/\tau) - \tau] \tag{7}$$

$$t \geq t_0: W_M(t) = W_M(t_0) = \text{constant} \tag{8}$$

Applied to the dashpot alone equation (6) yields:

$$W_D(t) = \int_0^t \sigma(t')\dot{\epsilon}_2(t')dt' = \frac{1}{\eta} \int_0^t \sigma^2(t')dt' \tag{9}$$

(where we have made use of equation 3). Carrying out the integration with the stress of equations (4) and (5) yields:

$$t \leq t_0:$$

$$W_D(t) = \eta\dot{\epsilon}_0^2[t + \tau\{2 - 0.5\exp(-t/\tau)\}\exp(-t/\tau) - 1.5\tau] \tag{10}$$

$$t \geq t_0:$$

$$W_D(t) =$$

$$\eta\dot{\epsilon}_0^2[t_0 + \tau\exp(-t_0/\tau) - \tau - 0.5\tau\exp\{-2(t - t_0)/\tau\} + \tau\exp\{-(2t - t_0)/\tau\} - 0.5\tau\exp(-2t/\tau)] \tag{11}$$

The work to heat conversion percentages $C_r(t) = 100W_D(t)/W_M(t)$ thus become:

$$t \leq t_0:$$

$$C_r(t) = 100 \left[1 - \frac{0.5\exp(-2t/\tau) - \exp(-t/\tau) + 0.5}{t/\tau + \exp(-t/\tau) - 1} \right] \tag{12}$$

$$t \geq t_0:$$

$$C_r(t) = 100 \left[1 - \frac{\{0.5 + 0.5\exp(2t_0/\tau) - \exp(t_0/\tau)\}\exp(-2t/\tau)}{t_0/\tau + \exp(-t_0/\tau) - 1} \right] \tag{13}$$

Note that in equations (12) and (13) the parameters η and G of the model enter only through their ratio $\tau = \eta/G$, and the process parameters ϵ_0 and $\dot{\epsilon}_0$ only through their ratio $\epsilon_0/\dot{\epsilon}_0 = t_0$. Moreover, the times t and t_0 enter only through their ratios to the relaxation time τ : t/τ and t_0/τ . Accordingly we have evaluated $C_r(t)$ as a function of the reduced time t/τ with t_0/τ as a parameter. The resulting family of curves is given in Figure 2.

DISCUSSION OF THE SIMPLE MAXWELL MODEL

After a sufficiently long time all work done in stretching the Maxwell model is converted to heat, irrespective of the relaxation time, τ . This is intuitively clear: even after one has stopped stretching the Maxwell model as a whole the strain in the dashpot is increasing at the expense of the strain in the spring, keeping the total

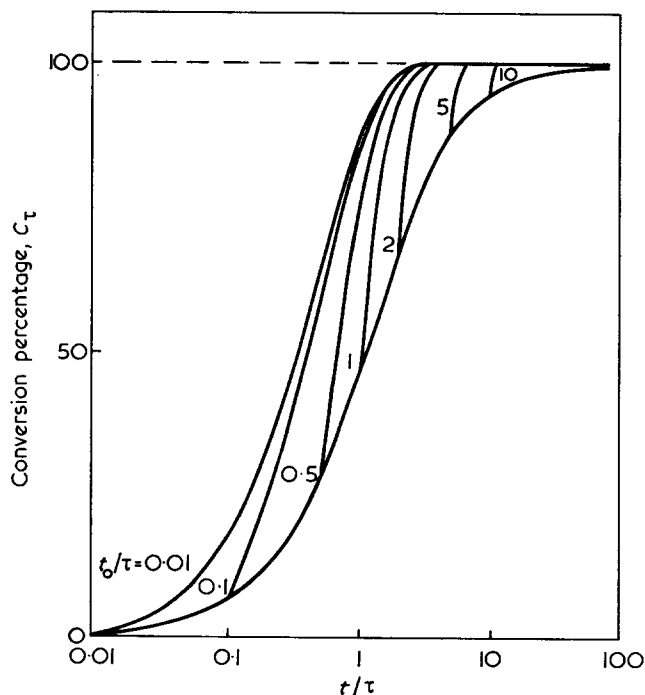


Figure 2 Plot of the conversion percentage $C_\tau(t)$ according to equations (12) and (13) as a function of reduced time t/τ with t_0/τ as a parameter

Table 1 $C_\tau(t_0)$ and $t(90\%)$ as a function of t_0/τ

t_0/τ	$C_\tau(t_0)$	$t(90\%)/t_0$
0.01	0.7%	116
0.1	6.4%	12.5
0.5	27.3%	3.2
1	45.6%	1.85
2	67.1%	1.35
5	87.7%	1.02
10	94.4%	0.6

strain constant. A changing strain in the dashpot means energy dissipation. Eventually the stress will decay to zero (spring unstretched), i.e. all the energy stored in the extended spring has been used to stretch the dashpot and is dissipated to heat in the process.

Of special interest is the energy conversion percentage $C_\tau(t_0)$ at the termination of stretching. This time t_0 is, after all, the time at which one would like to process the sample further. $C_\tau(t_0)$ is a strong function of the ratio t_0/τ of the stretching time t_0 to the relaxation time τ . If $t_0 \ll \tau$ only a small fraction of the work of stretching has been converted to heat at $t = t_0$; however, if, say, $t_0 > 10\tau$ the conversion is essentially complete at $t = t_0$. Table 1 gives some values of $C_\tau(t_0)$ as a function of t_0/τ . After the completion of stretching, the conversion of work to heat continues, with the detailed time dependence to be taken out of Figure 2. Table 1 also gives values for $t(90\%)$ (expressed in units of stretching time t_0), which is the time at which 90% of the work of stretching has been converted to heat

EXTENSION TO A CONTINUOUS MAXWELL MODEL

The simple Maxwell model with a single relaxation time does not describe adequately real polymeric materials. One therefore introduces a continuous

Maxwell model, consisting of an infinite series of simple Maxwell models with different relaxation times in parallel to one another⁴. The model is usually completed by a spring in parallel to all the component models. This spring, however, needs to be introduced only for crosslinked materials, such as elastomers and thermosetting resins. It is therefore disregarded here. The infinite series of Maxwell models is described by a distribution of relaxation times $H(\tau)$ ⁴. This characteristic function (with the dimension of a modulus) can be determined for each material (as time consuming as this might be) from viscoelastic data such as creep and stress relaxation experiments, forced vibrations, torsional oscillations etc. The various approximations used for the determination of $H(\tau)$ are discussed in the literature⁵.

In stretching the continuous Maxwell model all component models (being in parallel) are subjected to the same strain programme as the total model (Figure 1). For the component models with relaxation times in the interval $(\tau, \tau + d\tau)$ equations (12) and (13) for the conversion percentages are therefore still valid. To obtain a conversion factor for the model as a whole one also needs to know how the work of stretching is distributed among the components of the continuous Maxwell model. This information is contained in $H(\tau)$. We will proceed to calculate the conversion percentage for the continuous Maxwell model at $t = t_0$.

Let $dA(\tau)$ denote the work required to stretch the elements with relaxation times τ in the interval $(\tau, \tau + d\tau)$ from $t = 0$ to $t = t_0$ according to the strain programme of Figure 1. This work is given by equation (7) evaluated at $t = t_0$ when the constant η is replaced by $H(\tau)d\tau$:

$$dA(\tau) = H(\tau) \epsilon_0^2 [t_0 + \tau \exp(-t_0/\tau) - \tau] d\tau \quad (14)$$

The work to heat conversion percentage at $t = t_0$ for the continuous Maxwell model is then given by:

$$K(t_0) = \frac{\int C_\tau(t_0) dA(\tau)}{\int dA(\tau)} \quad (15)$$

in which the integrations are extended over all relaxation times τ from 0 to ∞ , and where $C_\tau(t_0)$ is the conversion percentage at $t = t_0$ of the simple Maxwell model with relaxation time τ (given by equation 12). Evaluating $K(t_0)$ yields [changing the integration variable from τ to $\log(\tau/t_0)$]:

$$K(t_0) = 100 \left[1 - \frac{\int_{-\infty}^{+\infty} H(\tau) f_1(\tau/t_0) d\log(\tau/t_0)}{\int_{-\infty}^{+\infty} H(\tau) f_2(\tau/t_0) d\log(\tau/t_0)} \right] \quad (16)$$

with:

$$f_1(\tau/t_0) = (\tau/t_0) [0.5 \exp(-2t_0/\tau) - \exp(-t_0/\tau) + 0.5]$$

$$f_2(\tau/t_0) = [1 + (\tau/t_0) \exp(-t_0/\tau) - (\tau/t_0)]$$

For any material with a known relaxation time spectrum $H(\tau)$ these integrals may be evaluated numerically and the conversion factor obtained. To help with this evaluation we have also calculated values of f_1 and f_2 over a wide range of values of $\log(\tau/t_0)$ in Table 2.

In many cases a detailed integration may not be necessary. By inspection of Table 2 one finds that f_1 and f_2 have comparable values only for $\tau/t_0 > 0.1$. For $\tau/t_0 < 0.1$ f_1 is much smaller than f_2 . Therefore, if $H(\tau)$

Table 2 f_1 and f_2 defined in equation (16) as a function of τ/t_0

τ/t_0	f_1	f_2
10^{-4}	0.5×10^{-4}	1
10^{-3}	0.5×10^{-3}	0.999
10^{-2}	0.5×10^{-2}	0.99
5×10^{-2}	0.025	0.95
10^{-1}	0.05	0.90
0.5	0.19	0.57
1	0.20	0.37
5	0.082	0.093
10^1	4.52×10^{-2}	4.83×10^{-2}
10^2	4.95×10^{-3}	4.98×10^{-3}
10^3	5×10^{-4}	5×10^{-4}
10^4	5×10^{-5}	5×10^{-5}

is not peaked very strongly in the region $\tau > t_0/10$, but continues with reasonably large values into the region $\tau < t_0/10$, the numerator of equation (16) will be much smaller than the denominator, giving a conversion percentage close to 100%. For conversion 'within fractions of a second' (say, $t_0 = 1/10$ sec) this would

require a large $H(\tau)$ for $\tau < 0.01$ sec. Such relaxation time distributions are found e.g. for polyethylene and isotactic polystyrene for temperatures around 25°C. $H(\tau)$ for these materials changes by less than a factor of five for 10^{-9} sec $< \tau < 10^4$ sec. For these materials the conversion of mechanical work of deformation is indeed very fast.

ACKNOWLEDGEMENT

We would like to thank R. Preisig and M. Spirig for doing the numerical calculations.

REFERENCES

- 1 Flügge, W. 'Viscoelasticity', Blaisdell, Waltham, Mass., 1967
- 2 Menges, G., Dalhoff, W. and Mohren, P. *Kunststoffe* 1970, 60, 85
- 3 Schenkel, G. *Kunststofftechnik* 1973, 12, 1
- 4 Lenk, R. S. 'Plastics Rheology', Maclaren, London, 1968
- 5 Sharma, M. G. in 'Testing of Polymers' (Ed. J. V. Schmitz), Interscience, New York, 1965, Vol 1, Ch 4
- 6 Oberst, H. and Bohn, L. *Rheol. Acta* 1961, 1, 608

Characterization of the thermomechanical behaviour of polymers: non-isothermal creep deflection processes*

A. Pavan, M. Rink, G. Blundo and F. Danusso

*Industrial Chemistry Department, Macromolecular Chemistry and Materials Section,
Polytechnic Institute, Milan, Italy
(Received 6 August 1973; revised 1 November 1973)*

A non-isothermal creep process of a thermorheologically simple polymer is considered. For such a material, if the results of isothermal creep experiments are known, the creep compliance can be calculated as a function of time for any given thermal history by a suitable method. The results of creep deflection measurements on a sample of commercial polystyrene are reported. The data isothermally obtained at different temperatures are determined so as to obtain the master curve of the compliance as a function of time and the shift factor as a function of temperature. As an example, the above method is applied to predict the course of a laboratory test which is commonly used to determine the heat deflection temperature of thermoplastic polymers. The experimental results agree satisfactorily with the predicted values.

INTRODUCTION

The end uses of polymeric materials often involve variations of temperature with time, concomitant with the action of (varying or constant) mechanical stresses. On the other hand, in research laboratories these materials are usually studied isothermally, at different (constant) temperatures. Since the viscoelastic functions depend on the particular 'thermomechanical history' followed during a transformation, the data obtained from isothermal experiments cannot supply directly the value of a viscoelastic function at a certain time of a non-isothermal transformation. However, when the material is linearly viscoelastic and thermorheologically simple¹, the thermomechanical behaviour of the material during a non-isothermal transformation can be predicted from isothermal experimental data by means of a suitable method.

For a technological characterization of polymeric materials, non-isothermal tests which follow simple, standard temperature histories are also in use. For evaluating the heat dimensional stability or the maximum use temperature of rigid thermoplastics, one normally resorts, for instance, to the heat deflection temperature (*HDT*) test. This test, usually carried out according to an ASTM standard method², corresponds to a non-isothermal flexural creep experiment, where the temperature is increased at a constant rate of 2°C/min. This test is rather simple and quick, but it provides only conventional information.

This paper reports the results of a series of isothermal flexural creep experiments, at different temperatures, on

samples of a commercial polystyrene and shows how a suitable method can be used in order to obtain the deformation of the specimen as a function of time for any particular thermal history. As an example, the method has been applied to describe the course of the experiment for determining the *HDT*, as specified by the ASTM standard method.

In practice, for design problems, the same method can be used to predict the course of the deformation under load for a specific thermal history, to be compared with the permissible value of the deformation.

EXPERIMENTAL

Material

A commercial sample of atactic polystyrene was used. The intrinsic viscosity ($0.70 \times 10^2 \text{ cm}^3/\text{g}$) measured in toluene at 30°C corresponds to a viscosity-average molecular weight $M_v = 177\,000$, according to the equation reported by Danusso and Moraglio³.

The polymer was compression moulded at 140°C, and the test specimens were annealed for 2 h at 80°C and then slowly cooled (0.2°C/min) to room temperature in order to reduce the frozen-in thermal stresses.

Apparatus

Flexural creep measurements were carried out using a commercial instrument (CEAST, Turin) built according to the ASTM specification for testing the heat deflection temperature².

In order to measure the deflection with greater precision and to make continuous recordings, the deflection measurement device of the commercial unit was slightly

* Presented in part at the 2nd Meeting of the Italian Society of Rheology, Siena, Italy, 10-12 May 1972.

modified: the mechanical dial gauge connected to the loading rod was replaced with an inductive transducer, whose signal could be detected by an appropriate measuring bridge and then recorded.

In order to find the loading rod position corresponding to zero deformation, the upper surface of the test specimens was coated with conductive paint, so that the contact of the metallic loading rod with the specimen could be detected by an ohmmeter.

Temperature of the specimen

The specimen was immersed in a mineral oil thermostating bath as specified in the ASTM method. Before each isothermal experiment the specimen was kept in the bath for 30 min in order to reach thermal equilibrium.

During the non-isothermal experiment, the temperature of the thermostating oil was increased at a constant rate of 2°C/min (starting from 27°C) according to the ASTM specification.

In a test conducted under the same conditions, the temperature in the core of the polymer specimen was measured by means of a thermocouple and recorded throughout the experiment. At the same time the temperature of the thermostating medium was measured and recorded. Soon after the experiment was commenced a constant temperature difference of 3°C was observed between the core of the specimen and the heat transfer medium.

To take this temperature gradient into account, we have found the temperature that a sham specimen under conditions of uniform temperature ought to have in order to deform exactly as the actual specimen. By solving the heat-transfer problem for the given boundary conditions (assuming that the temperature gradient with respect to time is constant throughout the specimen and that the temperature gradient with respect to space coordinates is constant with time), we have determined the temperature profile on the specimen's cross-section. The thermal conductivity of amorphous polystyrene was taken from ref 4. Assuming the temperature dependence of the tensile modulus to be approximately linear within the small temperature difference covered on the specimen cross-section, we have calculated the flexural deformation of the specimen for the corresponding modulus distribution on the specimen's cross-section. By assuming that the deformation of the sham specimen under uniform temperature conditions is equal to the deformation of the actual specimen, the temperature of the former was finally estimated to be 1.2°C higher than the temperature in the core of the latter, i.e. 1.8°C lower than the temperature of the bath. Considering the precision of our determinations, we have thus associated to the values of our viscoelastic functions a temperature value 2°C lower than the temperature of the bath. Therefore, the temperature history $T = T(t)$ followed by the specimen in the varying temperature experiment was assumed to be

$$T(^{\circ}\text{C}) = 25 + 2t(\text{min}) \tag{1}$$

Evaluation of the compliance

At high temperature it was observed that the contact edges of the supports and of the piece by which load is applied produce some indentation on the specimen surface, giving a slight (positive) contribution to the

vertical displacement of the loading rod. This contribution was measured in separate tests by preventing the specimen from deflecting, and it was subtracted from the measured displacement of the loading rod.

In the non-isothermal experiment, the measured displacement had to be corrected also for the (negative) contribution given by the thermal expansion of the polymer; this was calculated from the dilatometric data quoted in ref 5.

From the displacement of the loading rod measured as a function of time t and corrected as stated above, the tensile compliance or creep function $D(t)$ was calculated by the relation⁶:

$$D(t) \equiv \frac{\epsilon(t)}{\sigma} = b \frac{f(t)}{P} \tag{2}$$

- where $\epsilon(t)$ = tensile strain (cm/cm),
- σ = tensile stress (kg/cm²),
- b = form factor (cm),
- $f(t)$ = corrected displacement of the loading rod, equal to the deflection of the midpoint of the beam (cm),
- P = load (kg).

Equation (2) holds for the hypothesis of small deformations and stress-strain proportionality. In our experiments the largest tensile strain was 5×10^{-3} , while the linearity of viscoelastic behaviour was checked with a series of additional creep experiments under different loads. *Figure 1* shows an example of these tests which prove that linearity is met even at the maximum fibre stress ($\sigma = 18.5 \text{ kg/cm}^2$) adopted in our experiments.

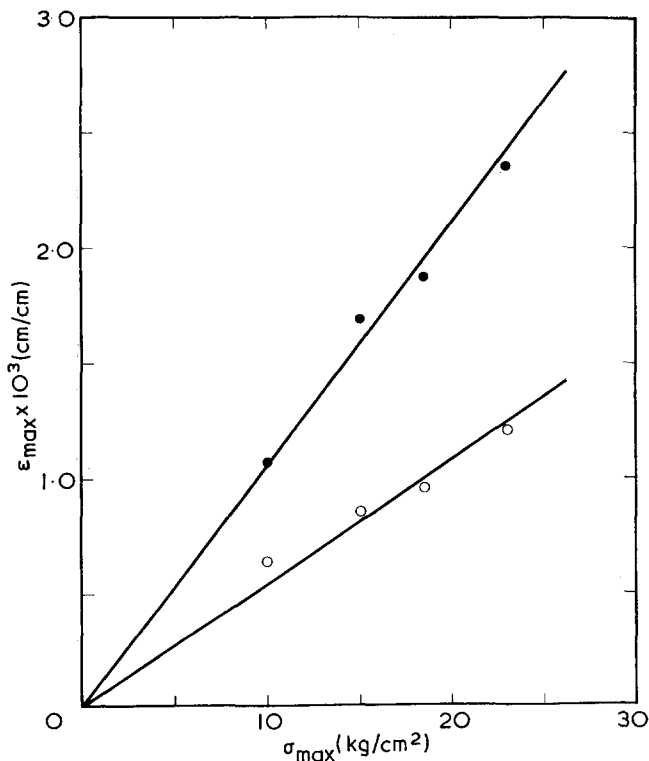


Figure 1 Linearity of viscoelastic behaviour. Example of isochronous tensile stress-tensile strain plots obtained from several isothermal creep experiments under different loads at 71°C. ○, $t = 100 \text{ sec}$; ●, $t = 1000 \text{ sec}$. Stress and strain evaluated at the midpoint of the external fibres, where they are maximum

RESULTS

Experimental data

Figure 2 shows the isothermal creep compliance $D_T(t)$ measured as a function of time t at six different temperatures T ranging from 27 to 80°C, i.e. over the same temperature span covered by the non-isothermal experiment (see later). Only experimental points starting from 0.5 sec are reported; measurements taken at shorter times tended to be erratic owing to inertial effects of the creep apparatus.

The form of the curves of the creep compliance plotted against the logarithmic time in Figure 2 is characteristic of the initial part of the viscoelastic transition from glasslike to rubberlike consistency.

The experimental compliance $D(t)$ relative to the non-isothermal creep experiment where the temperature was varied according to equation (1), is plotted in Figure 7. The deflection of the test bar was measured up to the specific value prefixed by the ASTM standard method. The corresponding temperature of the heating medium (heat deflection temperature at 18.5 kg/cm²) was 79°C, which corresponds to a temperature of 77°C for the sham specimen at uniform temperature (see experimental section).

Isothermal data elaboration

The results of the isothermal experiments have been treated following the reduced variables procedure suggested by the time-temperature equivalence principle. The reduced isothermal curves that resulted were superposable, within the precision limits of the whole determination, into a single 'master curve' of the compliance. This fact is assumed as evidence of the applicability of the time-temperature equivalence principle, i.e. the material can be considered as thermorheologically simple.

Following Ferry⁷ and McCrum and Morris⁸, in the time region of the transition zone near the glassy zone, the existence of an approximately asymptotic limiting value of the compliance should be taken into account;

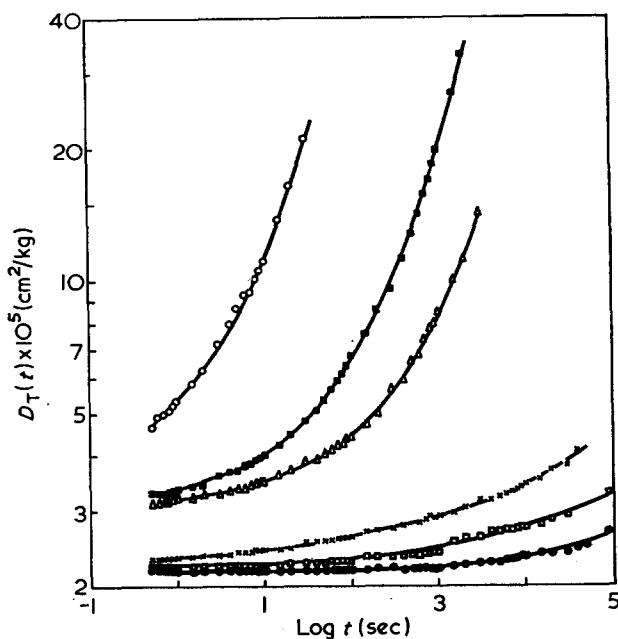


Figure 2 Isothermal creep compliance $D_T(t)$, measured at six different temperatures versus logarithmic time. ●, 27°C; □, 39.5°C; ×, 49°C; △, 71°C; ■, 74.5°C; ○, 80°C

for this each (isothermal) compliance $D_T(t)$ should be reduced into a corresponding (isothermal) compliance $D_{T_0}^p(t)$ as follows:

$$D_{T_0}^p(t) = \frac{T\rho}{T_0\rho_0} [D_T(t) - D_T(0)] + D_{T_0}(0) \quad (3)$$

Here ρ and ρ_0 are the polymer densities at the absolute temperature T and reference temperature T_0 respectively, while $D_T(0)$ and $D_{T_0}(0)$ are the values at T and T_0 of the glasslike compliance, which can be defined as the limiting value of the experimental compliance at zero time.

The isothermal curves $D_T^p(t)$ can then be superposed into a single master curve $D_{T_0}(t)$ if one reduces the time coordinate as follows:

$$D_{T_0}(t) = D_{T_0}^p(a_T^{T_0} \cdot t) \quad (4)$$

where $a_T^{T_0}$ is the shift factor of the isothermal curve $D_T^p(t)$ with respect to the reference curve $D_{T_0}(t)$.

To perform the reduction indicated by equation (3) one needs to know the value $D_T(0)$ for each temperature T . As can be seen in Figure 2, at the lowest temperature (27°C) the compliance remains practically constant, equal to $2.18 \times 10^{-5} \text{ kg}^{-1} \text{ cm}^2$, over a large time interval, so that we can assume $D_{27^\circ\text{C}}(0)$ equal to this value.

At higher temperatures, however, the experimental data would have to be extrapolated to obtain the asymptotic value. On the other hand, we can perform the whole reduction in the following alternative way.

Combining equations (3) and (4) we obtain:

$$D_{T_0}(\log t) = \frac{T\rho}{T_0\rho_0} D_T(\log t + X_T^{T_0}) + Y_T^{T_0} \quad (5)$$

where

$$X_T^{T_0} \equiv \log a_T^{T_0} \quad (6)$$

$$Y_T^{T_0} \equiv D_{T_0}(0) - \frac{T\rho}{T_0\rho_0} D_T(0) \quad (7)$$

From equation (5), we see that the master curve $D_{T_0}(\log t)$ can be obtained by multiplying each isothermal compliance $D_T(\log t)$ by the respective factor $T\rho/T_0\rho_0$, and translating the corrected isothermal curves along both axes of a semi-logarithmic plot, so as to obtain the best superposition.

The two shifts correspond quantitatively to $X_T^{T_0}$ and $Y_T^{T_0}$. The values of $a_T^{T_0}$ and $D_T(0)$ are thus determined by the empirical shifts at each temperature through equations (6) and (7).

The factor $T\rho/T_0\rho_0$ was calculated from the known value of the density of atactic polystyrene at each temperature⁵.

The resultant master curve at $T_0 = 27^\circ\text{C}$ is shown in Figure 3 (where only for sake of clearness it is plotted in a double logarithmic diagram). Figures 4 and 5 show the values of $a_T^{27^\circ\text{C}}$ and $D_T(0)$ obtained as functions of temperature.

With regard to Figure 4, it is well known¹ that in the transition region from glasslike to rubberlike consistency the shift factor $a_T^{T_0}$ most generally obeys the Williams-Landel-Ferry equation. In the glassy region on the other hand, when other viscoelastic mechanisms are present, $a_T^{T_0}$ often follows an equation of the Arrhenius form⁸. The results shown in Figure 4, however, do not fit satisfactorily either of these two equations. We are led to suppose that the region covered by our

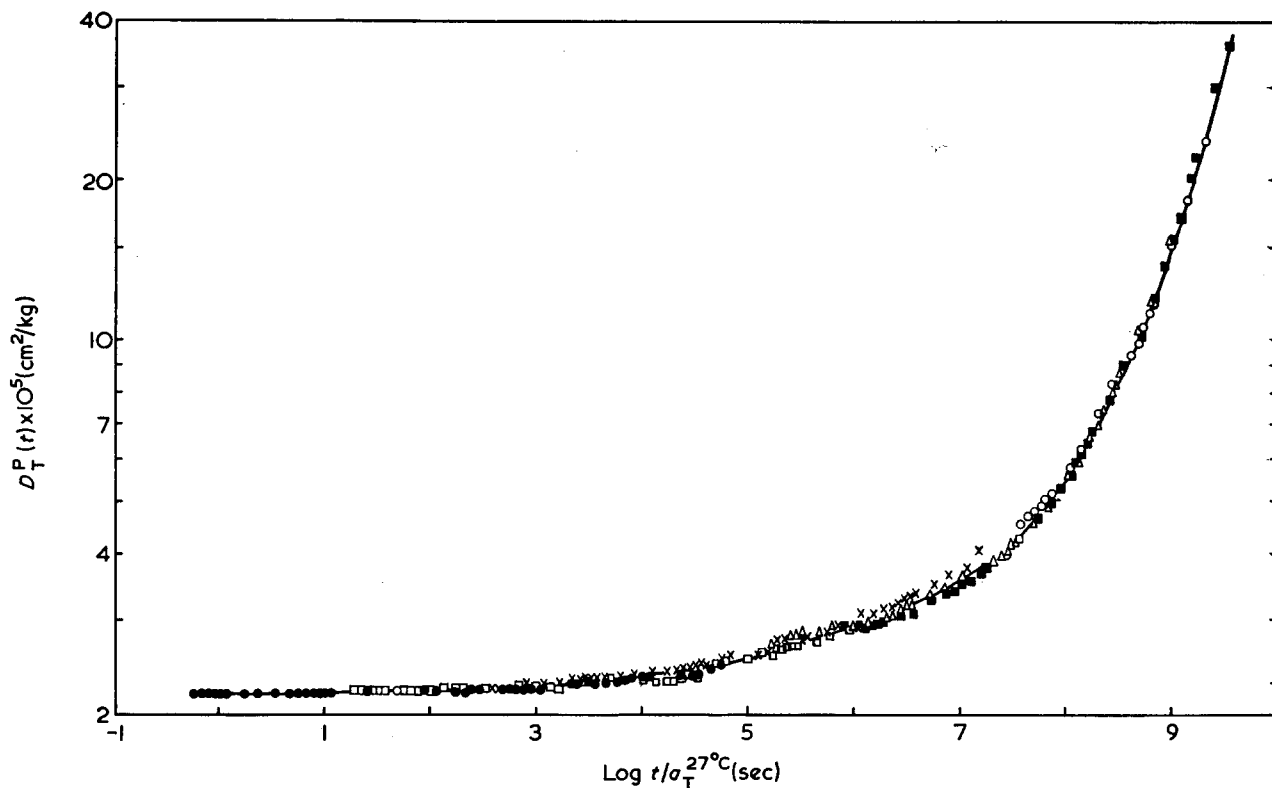


Figure 3 Composite master curve of the isothermal creep compliance. Reference temperature $T_0=27^\circ\text{C}$. Symbols as in Figure 2

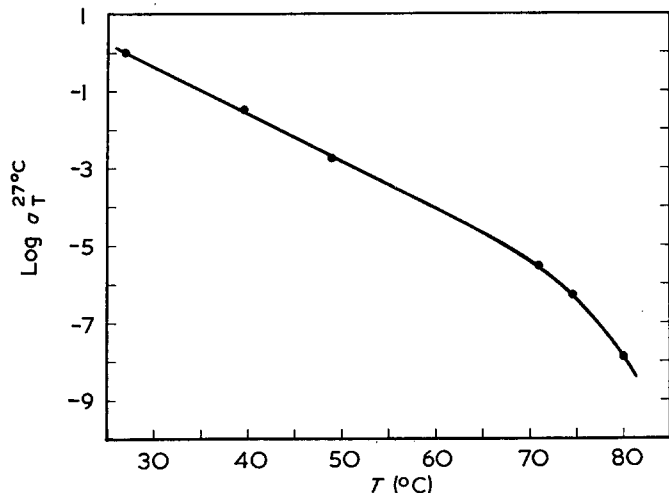


Figure 4 Temperature dependence of the shift factor $a_T^{27^\circ\text{C}}$

experiments is characterized by more than one viscoelastic mechanism^{9a}. Some scattering of the experimental points in the central part of the master curve in Figure 3 could also be attributed to the presence of a secondary transition^{9b}.

With reference to Figure 5, the almost linear increase of $D_T(0)$ with increasing temperature is in agreement with the results of other authors¹⁰⁻¹².

Calculation of the compliance in non-isothermal experiments

The thermorheological problem of the stress-strain analysis when the temperature varies from point to point and with time, has been dealt with by Morland and Lee¹³ for the case of homogeneous, isotropic, linearly viscoelastic and thermorheologically simple materials.

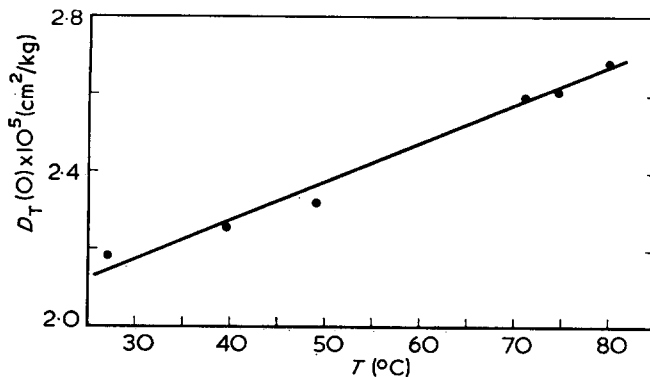


Figure 5 Temperature dependence of the glasslike compliance $D_T(0)$

Adapting their treatment to the present case of creep experiments at varying temperature in the transition region near the glassy zone, the method for evaluating the non-isothermal creep function can be formulated as follows.

Defining a 'reduced time' ξ as:

$$\xi(t, T) = \frac{t}{a_T^p} \tag{8}$$

the relationship of equivalence between isothermal compliances can be written:

$$D_T^p(t) = D_{T_0}(\xi) \tag{9}$$

In the case of a non-isothermal process, with the temperature describing a thermal history $T=T(t)$, Morland and Lee¹³ consider that every elementary retardation (or relaxation) process is accelerated or retarded by the same factor a_T^p —varying with time through T —regardless of the kind of thermal history followed. It is thus possible to define a 'fictitious time' ξ such that:

$$D^p(t) = D_{T_0}(\xi) \tag{10}$$

where $D^p(t)$ is the non-isothermal reduced compliance.

The fictitious time, unlike the reduced time defined by equation (8), is now a functional of the thermal history $T(t)$ given by:

$$\xi(t) = \int_0^t [a_T^p(t')]^{-1} dt' \quad (11)$$

Therefore, if we have one isothermal curve $D_{T_0}(t)$ and we know the shift factor a_T^p as a function of temperature T , for any given thermal history $T = T(t)$ the corresponding (reduced) compliance can be determined by means of equations (10) and (11).

To do that, the reciprocal of $a_T^{27^\circ\text{C}}$ was plotted against the experimental time t corresponding to each temperature T as in equation (1), and graphically integrated to produce the function $\xi(t)$ shown in Figure 6. Once obtained the relationship between the real time t of the non-isothermal experiment and the fictitious time ξ in the corresponding isothermal experiment at T_0 , the non-isothermal (reduced) compliance $D^p(t)$ is determined through equation (10). The actual non-isothermal compliance $D(t)$ can then be obtained from $D^p(t)$ by reversing equation (3):

$$D(t) = \frac{T_0 \rho_0}{T(t) \rho} [D^p(t) - D_{T_0}(0)] + D_{T(t)}(0) \quad (12)$$

where the temperature T and therefore also the density ρ and the glasslike compliance $D_T(0)$ are now varying with time. The appropriate values of $D_T(0)$ were deduced from Figure 5 by interpolation.

The so-calculated function $D(t)$ fits satisfactorily the

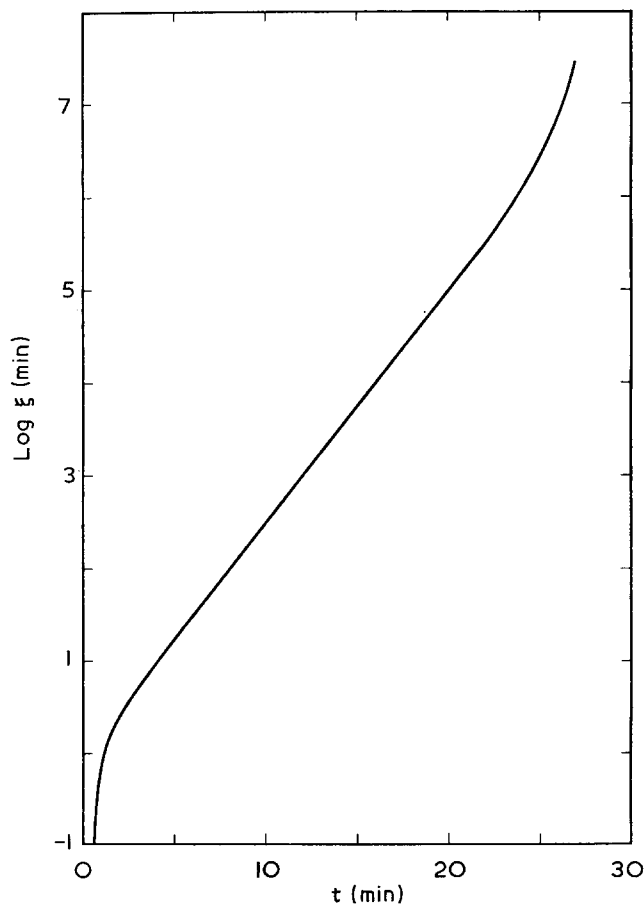


Figure 6 Fictitious time, ξ in the isothermal experiment at $T_0 = 27^\circ\text{C}$, as function of the real time t in the non-isothermal creep experiment (see text)

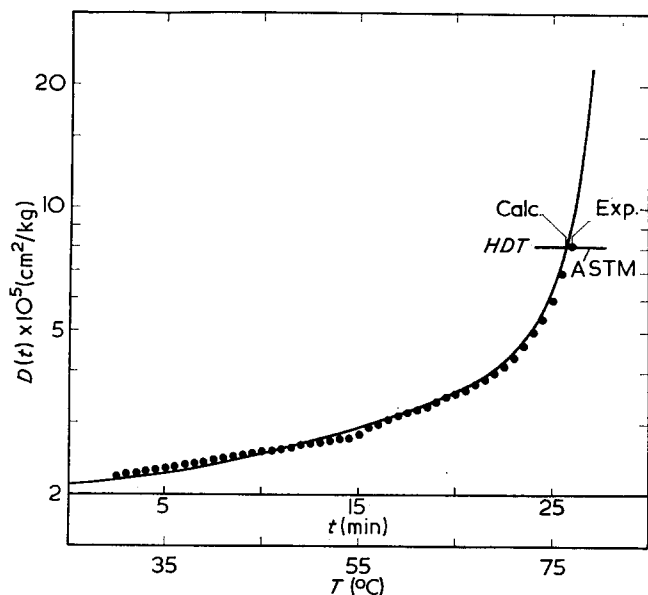


Figure 7 Experimental (points) and calculated (—) compliance in the non-isothermal creep experiment (see text) versus time, t or temperature, T

experimentally recorded compliance (Figure 7). In this Figure we have also indicated the experimental and calculated temperatures reached by the polymer specimen when its deflection matched the value prescribed in the standard test for determining the heat deflection temperature (HDT). The two temperatures differ less than 1°C . In Figure 7 we have also shown the temperature correspondingly reached by the oil bath, which is taken as heat deflection temperature by the ASTM standard method².

ACKNOWLEDGEMENTS

This work was carried out with the partial support of ANIC, SpA, San Donato Milanese and the National Research Council, Rome.

REFERENCES

- 1 Ferry, J. D. 'Viscoelastic Properties of Polymers', 2nd edn, Wiley, New York, 1970, Ch 11
- 2 Method D 648-56 (revised D 648-72), Am. Soc. Test. Mat., Philadelphia
- 3 Danusso, F. and Moraglio, G. *J. Polym. Sci.* 1957, **24**, 161
- 4 Boundy, R. H. and Boyer, R. F. (Eds) 'Styrene, Its Polymers, Copolymers and Derivatives', Reinhold, New York, 1952
- 5 Danusso, F., Moraglio, G., Ghiglia, W., Motta, L. and Talamini, G. *Chim. Ind. (Milan)* 1959, **41**, 748
- 6 Ferry, J. D. *ibid.* 1959, **41**, 25, 171
- 7 Ferry, J. D., *ibid.* 1959, **41**, 301
- 8 McCrum, N. G. and Morris, E. L. *Proc. R. Soc.* 1964, **A281**, 258; see also McCrum, N. G., Read, B. E. and Williams, G. 'Anelastic and Dielectric Effects in Polymeric Solids', Wiley, New York, 1967, p 127 *et seq.*
- 9a For several references, see McCrum, N. G., Read, B. E. and Williams, G. 'Anelastic and Dielectric Effects in Polymeric Solids', Wiley, New York, 1967, p 409 *et seq.*
- 9b Child, W. C., Jr. and Ferry, J. D. *J. Colloid Sci.*, 1957, **12**, 327
- 10 Barlow, A. J., Lamb, J., Matheson, A. J., Padmini, P. R. K. L. and Richter, J. *Proc. R. Soc.* 1967, **A298**, 467
- 11 Barlow, A. J., Erginsav, A. and Lamb, J. *Proc. R. Soc.* 1967, **A298**, 481
- 12 Lamb, J. *6th Int. Congr. Rheology, Lyon* 1972
- 13 Morland, L. W. and Lee, E. H. *Trans. Soc. Rheol.* 1960, **4**, 233; see also Christensen, R. M. 'Theory of Viscoelasticity', Academic Press, New York, 1971, p 103

Note to the Editor

Effect of end-groups on the motions of free nitroxyl radicals in poly(ethylene glycol)

P. Törmälä and J. Tulikoura

Department of Wood and Polymer Chemistry, University of Helsinki, Helsinki, Finland
(Received 22 October 1973)

INTRODUCTION

In a recent report¹ we suggested that several structural factors (e.g. the free volume, the crystallinity, the chain packing and the end-groups) may affect the rotational relaxations of nitroxyl radicals in poly(ethylene glycol) (PEG). In this note the end-group effect is studied by comparing the rotations of radicals in PEG with hydroxyl and acetoxy end-groups. On the basis of these comparisons some conclusions are drawn concerning the structure of the amorphous phase in partly crystalline PEG.

EXPERIMENTAL

Materials

PEG with hydroxyl end-groups (A) was of commercial origin (Fluka) with molecular weight=1500. It was purified by dissolving in absolute ethanol, by precipitation with diethyl ether and by drying in vacuum.

PEG with acetoxy end groups (B) was prepared by dissolving 20 g of polymer (A) in 100 ml of freshly distilled acetic anhydride and adding 0.5 ml of pyridine to this solution. The mixture was boiled under reflux for several hours. The unreacted acetic anhydride was distilled off, the polymer was precipitated by cold ether, sintered and dried. The crude polymer was purified by dissolution and precipitation using chloroform and ether, respectively. The treatment was repeated seven times. The degree of esterification was determined by boiling a small amount of polymer B in 10% NaOH solution under reflux for several hours. The solution was acidified by 10% H₂SO₄ and the acetic acid was distilled and neutralized by 0.1 N NaOH. The consumption of NaOH indicated that the esterification of PEG was practically complete (>99%). This was verified also by infra-red spectroscopy in inspecting the ester carbonyl stretching at 1740 cm⁻¹.

The spin probe radical 3-carbamoyl-2,2,5,5-tetramethylpyrroline-1-oxyl was prepared by the method of Rozantsev². Minute amounts (~300 ppm) of radicals were incorporated into polymers by dissolving the samples into chloroform and evaporating the solvent¹. The samples for electron spin resonance (e.s.r.) measurements were treated in a high vacuum (2.5 × 10⁻³ mmHg) and sealed under dynamic vacuum. Before the e.s.r. measurement every sample was immersed for 5 min in an oil bath whose temperature was 6°C above the melting point of the polymer. The samples were then cooled to 24°C.

Methods

The e.s.r. spectra were measured using a Varian E-4 X-band spectrometer equipped with a Varian E-257 variable temperature accessory. The temperature calibration was made by an iron/constantan thermocouple with an accuracy of ±2K. The used modulation amplitude was 0.25 G and the microwave power was 1 mW.

A Perkin-Elmer differential scanning calorimeter (1B) was used for the measurements of the melting points.

The number-average molecular weights (\bar{M}_n) and the molecular weight distributions (\bar{M}_w/\bar{M}_n) of the polymers A and B were determined by vapour pressure osmometry and by gel permeation chromatography as was reported earlier¹.

RESULTS AND DISCUSSION

Molecular characteristics (\bar{M}_n , \bar{M}_w/\bar{M}_n), melting points (T_m) and heats of fusion (ΔH_m) of the polymers are given in Table 1. The e.s.r. spectra of radicals in polymers A and B corresponded to those of radicals in isotropic environments. The rotations of radicals were characterized by the rotational relaxation time (τ). It was calculated from the anisotropies of the linewidths in the e.s.r. spectra by the methods reported earlier¹. In Figure 1 the $-\ln \tau$ values are given as a function of $1/T$. The open symbols express the τ values calculated on the basis of the theory of rapid rotations³ and the solid symbols give those calculated according to the theory of slow rotations⁴.

Figure 1 supports our earlier suggestion that the rotation of radicals is a phase-dependent process. If the results obtained from Figure 1 are compared with our earlier studies using 3-methoxy-carbonyl-2,2,5,5-tetramethylpyrroline-1-oxyl it is evident that the change of —OCH₃ group to —NH₂ in the side group of the pyrroline ring has practically no effect on the shape of $1/T$ vs. $-\ln \tau$ plot¹. Four rotational relaxation regions can be seen in the case of polymer A. They are numbered as in our earlier report¹: I=the liquid region, II=the

Table 1 Molecular characteristics (\bar{M}_n , \bar{M}_w/\bar{M}_n), melting points (T_m) and heats of fusion (ΔH_m) of poly(ethylene glycol)

End-groups of polymer	\bar{M}_n	\bar{M}_w/\bar{M}_n	T_m (K)	ΔH_m (J/g)
-OH	1450±100	1.28	317.0±0.5	190
-OCOCH ₃	1650±100	1.23	318.0±0.5	210

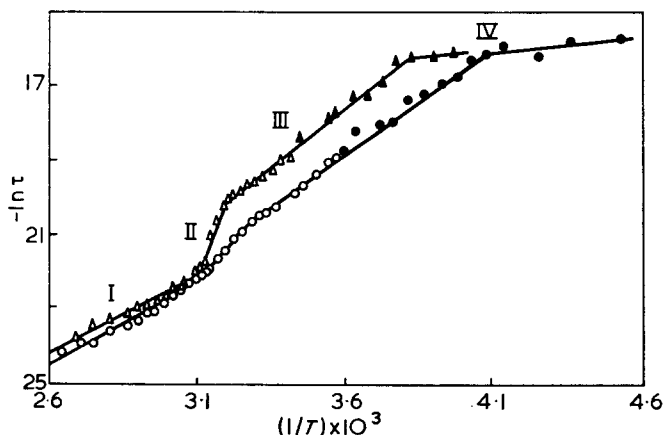


Figure 1 $1/T$ against $-\ln \tau$ plots of hydroxy- (Δ) and acetoxy (\circ)-ended PEG

Table 2 Rotational activation energies (E_a) of nitroxyl radicals in poly(ethylene glycol) (relaxation regions I-IV)

End-groups of polymer	E_a^I (kJ)	E_a^{II} (kJ)	E_a^{III} (kJ)	E_a^{IV} (kJ)
-OH	34	180	52	8
-OCOCH ₃	37	65	47	6

melting region, III=the solid region, and IV=the restricted solid region. In polymer B the melting region (II) is almost continuing in the solid region (III). The plot of the experimental points is not completely linear, but a slightly curved line covering regions II and III fits best with experimental results. However, to compare the results with those of polymer A linearity was assumed at both ends of the curve. The rotational activation energies calculated from the slopes of the plots in each temperature region are given in Table 2.

Booth *et al.*^{5,6} reported a decrease in T_m of PEG as a consequence of the esterification of its end-groups. From Table 1 such a trend cannot be deduced. The melting points of polymers A and B are practically identical. This fact is explained by the differences in the molecular characteristics of the polymers A and B. \bar{M}_n of polymer B is higher than that of polymer A and the molecular weight distribution of polymer B is also somewhat narrower than that of polymer A. It is evident that during the purification of polymer B some fractionation of molecules has occurred. Earlier studies indicated that T_m of low molecular weight PEG is strongly dependent on \bar{M}_n of the sample⁷. It can be seen from Fig. 1 of ref. 7 that T_m of PEG with \bar{M}_n 1650 is 324K. This indicates that the esterification of the end-groups decreases T_m 6K, which agrees well with the results of Booth *et al.*^{5,6}. Evidently the change of the polar hydroxyl end-groups to the more lipophilic acetoxy groups increases the solubility of low molecular weight PEG in ether.

Figure 1 shows that esterification affects markedly the rotational relaxations of nitroxyl radicals in PEG. In the acetoxy-ended PEG (B) the rotations of radicals at a certain temperature above T_g , are increased in relaxation regions I, II and III if they are compared to rotations in hydroxy-ended PEG (A) although the molecular homogeneity of polymer B is higher. Earlier studies have shown that the small molecular PEGs are highly crystalline^{1,6}. If the probe radicals should be

distributed evenly in the polymer the e.s.r. spectrum would be mainly caused by radicals in the crystalline phase. In this case the esterification of end-groups would not facilitate the rotations of radicals because most of the radicals should be located in the intact crystalline phase. Ashman and Booth⁶ have also shown that the esterification does not affect markedly the lamellar spacing of the polymers. Consequently it is reasonable to assume that radicals are predominantly confined to the amorphous phase. This is in accordance with the results of Kovarskii *et al.*⁸ for the lateral diffusion of nitroxyl radicals in partly crystalline polymers. We conclude that the facilitation of short range motion in the lamellar interphase after esterification is caused by the elimination of hydroxy-hydroxy⁶ and hydroxy-nitroxyl⁹ hydrogen bonds.

In the polymer melt (region I) where no separate amorphous and crystalline phases exist τ of radicals in polymer A, and E_a values are almost equal. Physically it seems realistic to assume that in the melt radicals are distributed statistically in the polymer. In this case they experience mostly the environment of rotating chain segments and the effect of end-groups is of minor importance.

In the transition region (II) an anomalously high E_a value (180 kJ) in polymer A is observed as was also found earlier¹. It is evident that this value has no significance in terms of an actual activation energy. Rather, it evidences the fact that different molecular mechanisms are dominant above and below the transition, and E_a is a measure of the differences between these two states. Region II is the temperature range in which the transition between the statistical melt and the non-statistical partly crystalline solid state occurs. The high E_a value in polymer A indicates that the amorphous interphase in the solid state differs considerably from the melt. It is evident that this effect is caused by the hydroxyl end-groups. When the crystallization occurs strains are induced in the amorphous phase and their discharge is hindered by hydrogen bond formation. The esterification of hydroxyl groups eliminates the possibility of this kind of intermolecular bond formation and therefore the strains maintained by —OH groups can discharge. The structural changes in the melting region (II) are in this case small which can be seen as a small E_a^{II} value (65 kJ/mol) of polymer B. We think that these results are in accordance with the results of Booth *et al.*^{5,6} that the end interfacial energy (σ_e) increases when the hydroxy-ends of PEG are replaced by chloro-, phenoxy- or acetoxy-ends. The exchange of hydroxy- to acetoxy-groups can be treated also as a self-plasticization process, which loosens the structure in the phase boundary¹⁰.

It must be pointed out that Porter and Boyd¹¹ did not find a transition region by dielectric loss measurements near the melting point of high molecular weight PEG. The amount of end-groups in high molecular weight PEG (Carbowax) is negligible; therefore hydrogen bond formation via hydroxyl groups is almost eliminated. It is also probable that intermolecular strains are experienced by bulky nitroxyl radicals in a different way than by dipoles.

In polymer B E_a^{III} and E_a^I differ from each other less than those in polymer A. This is in accordance with the view that when the end-group effect is absent the

Note to the Editor

motions in the amorphous polymer are of the same nature as those in the melt¹¹.

At moderately low temperatures there can be seen a kind of freezing-in of the amorphous phase at 262K and at 242K in PEG with hydroxyl and acetoxyl end-groups, respectively. We can conclude that these temperatures represent the outset of some segmental motion in the amorphous phase and that hydroxyl end-groups hinder the activation of this process. E_a^{IV} values prove that these are not the usual glass transition temperatures (T_g) because E_a below T_g is very low (~ 2 kJ/mol)¹². However, these temperatures are near the upper glass transition [$T_g(U)$] of PEG (250K)¹³.

ACKNOWLEDGEMENTS

One of the authors (P.T.) wishes to thank the Academy of Finland, the Foundation of Neste Oy and the University of Helsinki for financial aid.

REFERENCES

- 1 Törmälä, P., Lättilä, H. and Lindberg, J. J. *Polymer* 1973, **14**, 481
- 2 Rozantsev, E. G. and Krinitskaya, L. A. *Tetrahedron* 1965, **21**, 491
- 3 Waggoner, A. S., Griffith, O. H. and Christensen, C. R. *Proc. Nat. Acad. Sci. US* 1967, **57**, 1198
- 4 Shimshick, E. J. and McConnell, H. M. *Biochem. Biophys. Res. Commun.* 1972, **46**, 321
- 5 Booth, C., Bruce, J. M. and Buggy, M. *Polymer* 1972, **13**, 475
- 6 Ashman, P. C. and Booth, C. *Polymer* 1973, **14**, 300
- 7 Törmälä, P. and Savolainen, A. *Acta Chem. Scand.* 1973, **27**, 1430
- 8 Kovarskii, A. L., Wasserman, A. M. and Buchachenko, A. L. *J. Magn. Reson.* 1972, **7**, 225
- 9 Morishima, I., Endo, K. and Yonezawa, T. *Chem. Phys. Lett.* 1971, **9**, 143
- 10 Ueberreiter, K. in 'Plasticization and Plasticizer Processes', (Ed. N. A. J. Platzer), American Chemical Society, Washington, D.C., 1965, p 35
- 11 Porter, C. H. and Boyd, R. H. *Macromolecules* 1971, **4**, 589
- 12 Törmälä, P. *Eur. Polym. J.* in press
- 13 Boyer, R. F. *Plastics and Polymers* 1973, **41**, 71

Letters

Crack stability in PMMA

Introduction

It has been shown previously^{1,2} that crack growth in poly(methyl methacrylate) (PMMA) can be described in terms of a fixed crack opening displacement (u) criterion. If a fixed yield strain (e_y) is assumed¹ the stress intensity factor, K_c for crack growth may be expressed in terms of the modulus (E) as:

$$K_c^2 = EG_c = Eu\sigma_y = ue_y E^2 \quad (1)$$

i.e.

$$K_c = (ue_y)^{1/2} E \quad (2)$$

where σ_y is the yield stress and G_c is the strain energy release rate at fracture. For a viscoelastic material where the degree of time dependence is not large E may be taken as a time dependent quantity. The crack tip region may be modelled by a Dugdale line plastic zone as shown in *Figure 1*. The crack opening displacement is given in equation (1) and the length Δ is:

$$\Delta = \frac{\pi}{8} \frac{K^2}{\sigma_y^2} = \frac{\pi}{8e_y^2} \left(\frac{K}{E} \right)^2 \quad (3)$$

The time scale appropriate to the crack zone may be derived by considering the strain rate in the region of the crack tip and is^{1,3}:

$$t = \left(\frac{8}{\pi^2} \right) \frac{\Delta}{\dot{a}} \quad (4)$$

The time dependence of E can be represented by a power law form:

$$E = E_0 t^{-n} \quad (5)$$

where E_0 is the unit time modulus. n is not constant and tends to zero at both short and long times and may be expressed in terms of the loss factor $\tan \delta$. For small n an approximate relationship may be derived by approximating sinusoidal loading to a ramp and is:

$$\tan \delta = \frac{4}{\pi} \left(\frac{2^n - 1}{1 + n} \right)$$

which approximates to:

$$\tan \delta = 0.88n \quad (6)$$

For quite a range of times, however, n does not vary greatly and useful results may be obtained by assuming

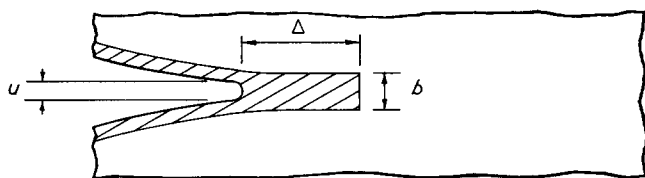


Figure 1 Dugdale line zone at the crack tip

it to be constant. Combining equations (2), (3), (4) and (5) gives:

$$K_c = (ue_y)^{1/2} \left(\frac{\pi e_y}{u} \right)^n \cdot E_0 \dot{a}^n \quad (7)$$

and clearly K_c increases with increasing \dot{a} giving inherently stable crack growth. At the extremes of time, of course, $n \rightarrow 0$ so that the result tends to the usual Griffith type of instability for an elastic material. It has been observed, however, that cracks become unstable at moderate crack speeds (10 mm/s) when n is still significant (~ 0.06). This crack speed is temperature sensitive and two explanations have been proffered. One⁴ proposes that instability occurs at a $\tan \delta$ (and therefore n) peak. This seems unlikely since a maximum n would result in the most stable system since stability is dependent on n and not its derivative.

Isothermal-adiabatic transition

An earlier suggestion⁵⁻⁷ was that the temperature generated at the tip of the running crack could reach a sufficient magnitude to cause local softening with a consequent drop in E , and hence K_c , leading to instability. The particular speed would depend on the thermal conductivity of the material and a useful approximation may be obtained by regarding the crack tip plastic zone as an embedded strip of width b (see *Figure 1*) in which heat is generated at a fixed rate^{5,8}. The adiabatic temperature rise $\Delta \tilde{T}$ is given by the energy dissipated per unit area, G_c , the density ρ and the specific heat c such that:

$$\Delta \tilde{T} = \frac{G_c}{\rho c b} = \frac{e_y E u}{\rho c \cdot b} \quad (8)$$

The temperature rise at the centre of the zone is⁸:

$$\Delta T = \Delta \tilde{T} \left[1 - 4i^2 \operatorname{erfc} \left(\frac{b^2}{16\kappa t} \right)^{1/2} \right] \quad (9)$$

where $\kappa = k/\rho c$, k is the thermal conductivity and t is the time to reach ΔT . Since b is expected to be small this may be approximated to give:

$$\Delta T = \frac{ue_y E}{(\pi \rho c k)^{1/2}} \cdot \frac{1}{(t)^{1/2}} = \frac{(ue_y)^{1/2} e_y E (\dot{a})^{1/2}}{(\rho c k)^{1/2}} \quad (10)$$

It should be noted that this result is for $b \rightarrow 0$ so that $\Delta \tilde{T} \rightarrow \infty$ and the result will give an upper bound to the temperature rise. An estimate may be made of the effect of b by retaining a further term in equation (9) to give:

$$\Delta T = ue_y E \left[\frac{1}{(\pi \rho c k)^{1/2} (t)^{1/2}} - \frac{b}{8\kappa t} \right] \quad (11)$$

In addition ρ , c , k and E are assumed to be constant so that the result will only be useful for small values of ΔT and n .

In previous analyses^{5,6,9} some estimate has been made for ΔT in equation (10) and a crack speed deduced from t so that the critical speed is independent of the

temperature. However, this procedure may be considerably improved by expressing the change in E with temperature by means of the Arrhenius equation so that equation (5) becomes:

$$E = E_0 t^{-n} \exp \left[\frac{nH}{R} \left(\frac{1}{T} - \frac{1}{T_0} \right) \right] \quad (12)$$

where T_0 is the original temperature, R is the gas constant and H is the activation energy. The expression for K_c now becomes:

$$K_c = (ue_y)^{1/2} \left(\frac{\pi e_y}{u} \right)^n E_0 \dot{a}^n \exp \left[\frac{nH}{R} \left(\frac{1}{T} - \frac{1}{T_0} \right) \right] \quad (13)$$

and the instability condition may be found from $dK_c/d\dot{a} = 0$. This is:

$$\frac{dT}{d\dot{a}} = \frac{RT^2}{H\dot{a}} \quad (14)$$

and from equation (10) $dT/d\dot{a}$ may be determined for this case:

i.e.

$$\frac{dT}{d\dot{a}} = \frac{(ue_y)^{1/2} e_y E}{(\rho c k)^{1/2}} \frac{1}{2(\dot{a})^{1/2}} \quad (15)$$

Combining equations (14) and (15) gives the result:

$$\frac{2R}{H} \cdot T^2 = \frac{(ue_y)^{1/2} e_y E}{(\rho c k)^{1/2}} (\dot{a})^{1/2} = \bar{T} - T_0 \quad (16)$$

and solving for the temperature, \bar{T} , at the critical condition gives:

$$\bar{T} = \frac{H}{4R} \left[1 - \left(1 - \frac{8R}{H} \cdot T_0 \right)^{1/2} \right] \quad (17)$$

The critical crack speed may be derived from equation (16) using \bar{T} from equation (17) giving \dot{a}_c as a function of T_0 . E is, in fact, a function of crack speed but is assumed constant in deriving equation (9). As a first approximation, therefore, an average value will be taken and since the variations of E are not large ($n \sim 0.06$) this is not expected to introduce a significant error.

Data for PMMA

Some precise experiments have been performed on PMMA at a wide range of temperatures to determine K_c versus \dot{a} curves using the double torsion method³.

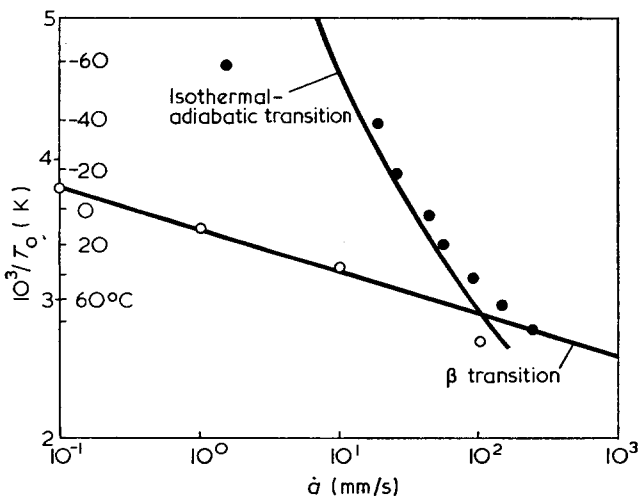


Figure 2 Crack speeds at instability in PMMA. ●, Crack speed instability; ○, maximum n

Table 1 Temperature rises and crack speeds at instability

T_0 (°C)	$\bar{T} - T_0$ (°C)	\dot{a}_c (mm/s)	Experimental \dot{a}_c (mm/s)
80	29.2	126.4	240
60	25.7	92.4	140
40	22.5	66.5	85
20	19.5	46.8	50
0	16.8	32.4	40
-20	14.3	21.7	24
-40	12.0	14.0	17
-60	9.9	8.8	1.4

By measuring n from the curves an estimate of the temperature for peak n at each crack speed may be determined. The points are shown in Figure 2 together with a line drawn with the slope for the β transition in PMMA¹⁰ ($H/R \sim 10^4$ K). The peaks follow this transition as expected since K_c is proportional to E but the instability crack speeds at each temperature do not. The prediction of the isothermal-adiabatic theory was computed using the following values for PMMA:

$$\frac{H}{R} = 10^4 \text{K}; e_y = 0.06; u = 1.6 \mu\text{m}^1 \cdot \text{s}^3; E = 2900 \text{MN/m}^2; \rho = 1.2 \text{g/cm}^3; k = 5 \times 10^{-5} \text{cal/cm}^\circ\text{C s}$$

Since $\bar{T} - T_0$ is not large (see Table 1) a refinement was added to include the linear variation of c with temperature such that: $c = 1.2 \times 10^{-3} T_0 \text{ cal/}^\circ\text{C g}$ (T_0 in K). The values of \dot{a}_c are given in Table 1 and are also shown in Figure 2 indicating very close agreement with the experimental points for instability crack speeds. The theoretical line gives lower crack speeds as expected since ΔT is an upper bound and the difference would indicate a value of b of about 10^{-4} m.

The agreement at -60°C is not good and this probably arises from changes in n and H at the lower instability speeds and no stable growth could be achieved below -60°C . A more refined version of the theory would be required to predict this effect but it is felt that the agreement is sufficiently close over the rest of the points to confirm the nature of the instability.

J. G. Williams and G. P. Marshall

Department of Mechanical Engineering,
Imperial College of Science and Technology,
Exhibition Road, London SW7 2BX, UK
(Received 24 January 1974)

References

- Williams, J. G. *Int. J. Fract. Mech.* 1972, 8, 393
- Williams, J. G. and Marshall, G. P. *Proc. R. Soc.* submitted
- Williams, J. G. and Marshall, G. P. to be published
- Johnson, F. A. and Radon, J. C. *Eng. Fract. Mech.* 1972, 4, 555
- Kambour, R. P. and Barker, R. E. Jr. *J. Polym. Sci. (A-2)* 1966, 4, 359
- Williams, J. G. *Appl. Mat. Res.* 1965 (April) p 104
- Williams, J. G., Radon, J. C. and Turner, C. E. *Polym. Eng. Sci.* 1968 (April) p 130
- Carslaw, H. S. and Jaeger, J. G. 'Conduction of Heat in Solids', 2nd Edn, Oxford University Press, 1959
- Levy, N. and Rice, J. R. 'Physics of Plasticity and Fracture', MIT Press, Cambridge, Mass., 1969-70
- McCrum, N. G., Read, B. E. and Williams, G. 'Anelastic and dielectric effects in polymeric solids', John Wiley, New York, 1967

Measurement of dynamic rheological properties using the principle of externally shifted and restored resonance

When dynamic viscoelastic properties are measured at applied frequencies which encompass the resonant frequency of the measuring system complicated graphical¹ or iteration techniques² are often required to solve the resulting equations of motion. It is possible to circumvent these difficulties by using an apparatus in which the resonant frequency can be altered³, and making measurements only at these frequencies. However, owing to the practical difficulties associated with the construction of such an apparatus, measurements are normally made at frequencies well away from the resonant frequency to allow the use of simple analytical expressions².

By using an electrical feed-back system we have been able to construct a simple apparatus with which it is possible to shift the resonant frequency, and to restore the system to resonance at any arbitrary frequency within the range over which resonance can be shifted. The resulting expressions for viscoelastic parameters are very simple. We have used this principle to construct a sensitive surface rheometer, to investigate the ageing processes in films of the hydrocolloid gum *Acacia senegal* at the water-air and water-oil interface⁴.

The rheometer consists of three connected systems: system I is a moving coil galvanometer movement driven by the oscillator section of a JM1600 Digital Transfer Analyser (Solatron Ltd); system II is a platinum du Nuoy ring attached to the galvanometer movement and immersed parallel in the surface of an ageing solution of the gum *Acacia*. The amplitude of motion of the moving combination of systems I and II is measured using a proximity gauge (Graham and White Instruments). System III is a calibrated potentiometer feeding part of the output voltage signal of the proximity gauge back into the input to the galvanometer. A block diagram of the apparatus is shown in *Figure 1*.

With the present apparatus it was found that resonant frequency could be shifted from its unperturbed value of 2.96 Hz over the range 1.60 to 30.35 Hz. When using the method of restored resonance the feed-back voltage is adjusted until there is a phase angle of 90° between the vector representing the driving force and the vector representing the amplitude of physical movement of system I, as measured on the DTFA.

The equation of motion of the rheometer is:

$$I \frac{d^2\theta}{dt^2} + \phi \frac{d\theta}{dt} + k\theta = T \quad (1)$$

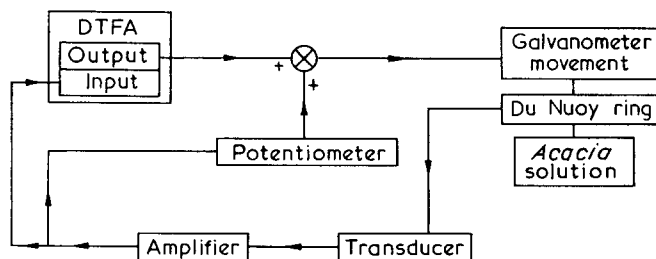


Figure 1 Block diagram of the microsurface rheometer showing the positive feed-back loop

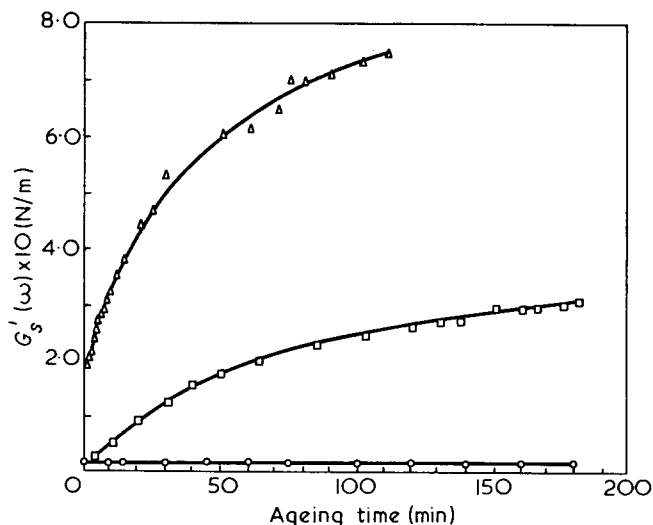


Figure 2 Effect of concentration of *Acacia senegal* on the ageing profile at the water-air interface. Resonance restored to 4.0 Hz. ○, 0.1% w/w; □, 1% w/w; △, 10% w/w

where θ is the angle turned through by the movement, t is time, ϕ the total friction, k the total restoring torque, T the driving torque and I the moment of inertia. From equation (1) it may be shown that $G'_s(\omega)$, the in-phase component of the surface shear modulus at frequency ω , is given by:

$$G'_s(\omega) = x \cdot \frac{c_f}{g_f} \quad (\text{N/m}) \quad (2)$$

where x is the fraction of the full potentiometer value required to restore the system to resonance at frequency ω , g_f is a geometrical factor, and c_f is a calibration constant. In the present apparatus:

$$g_f = 4\pi \left(\frac{1}{R_1^2} - \frac{1}{R_2^2} \right) \quad (3)$$

where R_1 is the radius of the du Nuoy ring and R_2 is the radius of the cylindrical vessel, and

$$c_f = c_g \cdot c_p \quad (4)$$

where c_g is the driven sensitivity of the galvanometer coil (99.83×10^3 dyne cm/A) and c_p is the sensitivity of the proximity gauge (131.84 V/rad).

Typical results using this apparatus to investigate the effect of gum concentration on the ageing of *Acacia* films at the water-air interface are shown in *Figure 2*. Previous work using a former design of macrosurface rheometer indicated only a slight effect of concentration on the ageing process, and it was found that up to 1 h was required before the aged film had sufficient solid properties to be detected^{5,6}. The results obtained with the present apparatus show that the film, in fact, starts to age immediately it is formed, and that the ageing profile is concentration dependent. The ageing process can be interpreted in terms of the theory of anisotropy as proposed by Warburton^{5,7}.

The present apparatus has also been used to monitor the crosslinking of interfacial films of sodium alginate with calcium ions, and to observe the effect of the enzyme hyaluronidase on the D-glucuronic acid residues in *Acacia*.

Although the use of this feed-back system has, at the present moment, been restricted to an oscillatory surface

Letters

rheometer, there is no reason why it should not be applied to such systems as a forcibly driven torsion pendulum and a Weissenberg rheogoniometer, thus making the analysis of experimental data much simpler than existing methods.

Acknowledgements

One of the authors (M. S.) acknowledges the receipt of a Postdoctoral Fellowship from The School of Pharmacy, University of London.

M. Sherriff and B. Warburton

Department of Pharmaceutics, The School of Pharmacy,
University of London, Brunswick Square,
London WC1N 1AX, UK

(Received 4 February 1974)

References

- 1 Roscoe, R. *Rheol. Acta* 1969, 8, 195
- 2 Walters, K. and Kemp, R. A. *ibid.* 1967, 7, 1
- 3 Birnboim, M. H. and Ferry, J. D. *J. Appl. Phys.* 1961, 32, 307
- 4 Sherriff, M. and Warburton, B. Br. Pat. (provisional specification) No. 54861 (27 November, 1973)
- 5 Warburton, B. *PhD Thesis* London University, 1973
- 6 Shotton, E., Wibberley, K., Warburton, B., Davis, S. S. and Finlay, P. L. *Rheol. Acta* 1971, 10, 142
- 7 Warburton, B. *J. Texture Stud.* 1970, 1, 370

An improved etch method for electron microscopy of ABS Polymers

Etching and sectioning are complementary techniques for studying microstructure in polymers. Sectioning is the preferred method for studying details of fine structure, but suffers from the disadvantage that cutting tends to compress and distort the structure. Etch methods can overcome this difficulty, and are therefore particularly valuable in studying rubber particle shape, and hence orientation, in rubber-modified plastics^{1, 2}. Etch methods also have some advantages in studying crazing and shear band formation in these materials¹.

The etch techniques used for two-phase polymers include gas-discharge etching³, solvent-etching⁴, acid-etching¹, and alkaline hydrolysis⁵. Chemical methods are preferable to solvent-etching, which tends to cause distortion of the specimen, especially when molecular orientation is present.

The applications of an acid etch method were described in a previous paper¹. Specimens of acrylonitrile-butadiene-styrene (ABS), high impact polystyrene (HIPS), and HIPS/poly(2,6-dimethyl-1,4-phenylene oxide)(PPO) blend were microtomed to produce flat surfaces, which were etched with a solution consisting of 400 ml H₂SO₄, 130 ml H₃PO₄, 125 ml H₂O, and 20 g CrO₃. This solution attacks the unsaturated rubber component preferentially, revealing details of rubber particle size, shape, and distribution. Strained regions in the matrix are also attacked, so that crazes and shear bands can be observed.

Although this method gives good results with HIPS and HIPS/PPO blends, it is unsatisfactory for ABS polymers, especially emulsion grades¹. The etch is not sufficiently selective, so that the matrix is also etched.

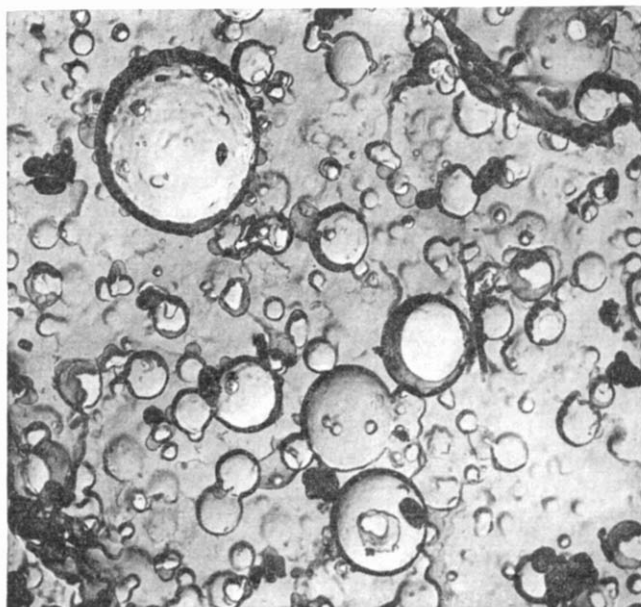


Figure 1 Carbon replica of etched ABS fracture surface. Transmission electron micrograph. Magnification $\times 15\,000$

Furthermore, ultramicrotoming of ABS polymers often causes distortion of rubber particle shape, not only in the microtomed section, but also in the surface from which it was cut.

Recent work at this laboratory has shown that these problems can be overcome by the following procedure: (a) fracturing the specimen at liquid nitrogen temperatures; (b) etching the fracture surface at 40°C with concentrated aqueous CrO₃ solution; (c) single-stage replication with carbon, followed by transmission electron microscopy; or (d) metallizing, followed by scanning electron microscopy.

Optimum etching conditions depend upon the level of molecular orientation and the composition of the ABS. At 40°C, a typical compression-moulded specimen requires 5 min in 10 M CrO₃, or 2 days in 5 M CrO₃. A highly oriented specimen would need only half as long, as mechano-chemical effects cause faster etching. Most ABS polymers contain a high volume fraction of small rubber particles, so that the layer of matrix material separating neighbouring particles is very thin in places. Etching times should therefore be kept to a minimum, to avoid the formation of interconnecting channels.

In order to prepare replicas, the specimens were first carbon-coated and metal-shadowed in the usual way, and then immersed in methyl ethyl ketone (MEK). The replica became detached from the etched surface, and was transferred, after washing in MEK and distilled water, to a bath containing the chromic-phosphoric acid mixture described above, at 70°C. This solution removed chemically the last traces of ABS adhering to the carbon film.

Figure 1 is a typical electron micrograph prepared, as described above, from a piece of commercial grey extruded sheet. The replica clearly shows the sizes, shapes, and distribution of the rubber particles. Particles of TiO₂ pigment can also be seen as opaque objects approximately 0.2 μm across.

Acknowledgement

The authors thank the Materials Quality Assurance

Letters

rheometer, there is no reason why it should not be applied to such systems as a forcibly driven torsion pendulum and a Weissenberg rheogoniometer, thus making the analysis of experimental data much simpler than existing methods.

Acknowledgements

One of the authors (M. S.) acknowledges the receipt of a Postdoctoral Fellowship from The School of Pharmacy, University of London.

M. Sherriff and B. Warburton

Department of Pharmaceutics, The School of Pharmacy,
University of London, Brunswick Square,
London WC1N 1AX, UK

(Received 4 February 1974)

References

- 1 Roscoe, R. *Rheol. Acta* 1969, 8, 195
- 2 Walters, K. and Kemp, R. A. *ibid.* 1967, 7, 1
- 3 Birnboim, M. H. and Ferry, J. D. *J. Appl. Phys.* 1961, 32, 307
- 4 Sherriff, M. and Warburton, B. Br. Pat. (provisional specification) No. 54861 (27 November, 1973)
- 5 Warburton, B. *PhD Thesis* London University, 1973
- 6 Shotton, E., Wibberley, K., Warburton, B., Davis, S. S. and Finlay, P. L. *Rheol. Acta* 1971, 10, 142
- 7 Warburton, B. *J. Texture Stud.* 1970, 1, 370

An improved etch method for electron microscopy of ABS Polymers

Etching and sectioning are complementary techniques for studying microstructure in polymers. Sectioning is the preferred method for studying details of fine structure, but suffers from the disadvantage that cutting tends to compress and distort the structure. Etch methods can overcome this difficulty, and are therefore particularly valuable in studying rubber particle shape, and hence orientation, in rubber-modified plastics^{1, 2}. Etch methods also have some advantages in studying crazing and shear band formation in these materials¹.

The etch techniques used for two-phase polymers include gas-discharge etching³, solvent-etching⁴, acid-etching¹, and alkaline hydrolysis⁵. Chemical methods are preferable to solvent-etching, which tends to cause distortion of the specimen, especially when molecular orientation is present.

The applications of an acid etch method were described in a previous paper¹. Specimens of acrylonitrile-butadiene-styrene (ABS), high impact polystyrene (HIPS), and HIPS/poly(2,6-dimethyl-1,4-phenylene oxide)(PPO) blend were microtomed to produce flat surfaces, which were etched with a solution consisting of 400 ml H₂SO₄, 130 ml H₃PO₄, 125 ml H₂O, and 20 g CrO₃. This solution attacks the unsaturated rubber component preferentially, revealing details of rubber particle size, shape, and distribution. Strained regions in the matrix are also attacked, so that crazes and shear bands can be observed.

Although this method gives good results with HIPS and HIPS/PPO blends, it is unsatisfactory for ABS polymers, especially emulsion grades¹. The etch is not sufficiently selective, so that the matrix is also etched.

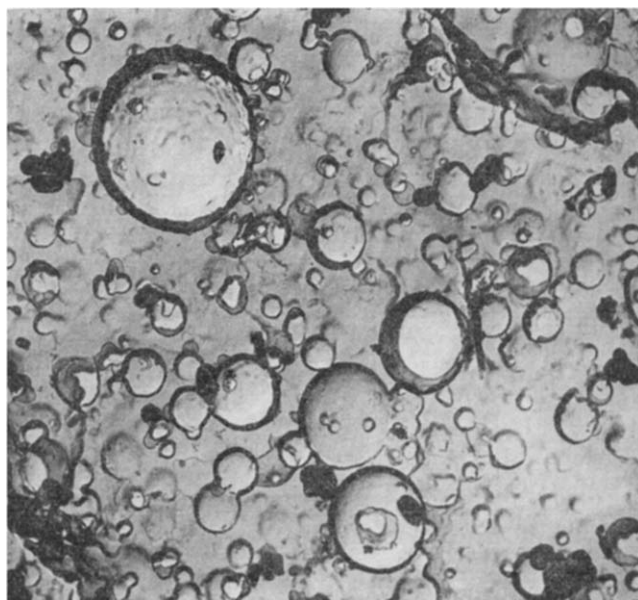


Figure 1 Carbon replica of etched ABS fracture surface. Transmission electron micrograph. Magnification $\times 15\,000$

Furthermore, ultramicrotoming of ABS polymers often causes distortion of rubber particle shape, not only in the microtomed section, but also in the surface from which it was cut.

Recent work at this laboratory has shown that these problems can be overcome by the following procedure: (a) fracturing the specimen at liquid nitrogen temperatures; (b) etching the fracture surface at 40°C with concentrated aqueous CrO₃ solution; (c) single-stage replication with carbon, followed by transmission electron microscopy; or (d) metallizing, followed by scanning electron microscopy.

Optimum etching conditions depend upon the level of molecular orientation and the composition of the ABS. At 40°C, a typical compression-moulded specimen requires 5 min in 10 M CrO₃, or 2 days in 5 M CrO₃. A highly oriented specimen would need only half as long, as mechano-chemical effects cause faster etching. Most ABS polymers contain a high volume fraction of small rubber particles, so that the layer of matrix material separating neighbouring particles is very thin in places. Etching times should therefore be kept to a minimum, to avoid the formation of interconnecting channels.

In order to prepare replicas, the specimens were first carbon-coated and metal-shadowed in the usual way, and then immersed in methyl ethyl ketone (MEK). The replica became detached from the etched surface, and was transferred, after washing in MEK and distilled water, to a bath containing the chromic-phosphoric acid mixture described above, at 70°C. This solution removed chemically the last traces of ABS adhering to the carbon film.

Figure 1 is a typical electron micrograph prepared, as described above, from a piece of commercial grey extruded sheet. The replica clearly shows the sizes, shapes, and distribution of the rubber particles. Particles of TiO₂ pigment can also be seen as opaque objects approximately 0.2 μm across.

Acknowledgement

The authors thank the Materials Quality Assurance

Directorate, Ministry of Defence, for their support of this work.

C. B. Bucknall and I. C. Drinkwater

Department of Materials, Cranfield Institute of Technology,
Cranfield, Bedford, UK

(Received 6 February 1974)

References

- 1 Bucknall, C. B., Drinkwater, I. C. and Keast, W. E. *Polymer* 1972, **13**, 115
- 2 Evans, L. J., Bucknall, C. B. and Hall, M. M. *Plastics and Polymers* 1971, **39**, 118
- 3 Spit, B. J. *Polymer* 1963, **4**, 109
- 4 Keskkula, H. and Traylor, P. A. *J. Appl. Polym. Sci.* 1967, **11**, 2361
- 5 Eastmond, G. C. and Smith, E. G. *Polymer* 1973, **14**, 509

Book Reviews

Progress in polymer science Japan, Vol 4

Edited by K. Imahori and Y. Iwakura

Kodansha Ltd, Tokyo and Halstead Press, New York,
1973, 278 pp. £7.00

This is a volume in yet another of the 'Progress in' type series of book which have expanded the volume of the scientific literature and drained the financial resources of libraries in recent years. While many people might doubt the value of such volumes, this particular series has a potentially useful and specific role to play.

The Society of Polymer Science, Japan has about 10 000 members in universities and industry, representing a massive effort in the polymer field. Inevitably this effort has produced a vast literature much of which is published in Japanese, either in journals or conference proceedings. Japanese scientists will tell you that most of the good work is published in English eventually, sometimes three years after its appearance in Japanese. A significant fraction of the papers appear in the English language literature published in Japan, including research bulletins of individual universities. These volumes suffer from a limited circulation and readership and are not well-known. Consequently, a large proportion of the literature is, at least temporarily, lost to the Western reader. It is the stated purpose of these volumes to rectify this situation by having Japanese authors review specific and important aspects of Japanese polymer research. If the editors succeed in attaining their objective we should have access to a coherent, rather than the present fragmentary, picture of polymer science in Japan.

Volume 4 of this series contains five articles, the authors of which concentrate on research carried out in their own laboratories. The first article, by Yoda *et al.* of Toray Industries, discusses the preparation of thermally stable polymers. The materials described contain heterocyclic ring structures and are produced by 'cyclo-polycondensation reactions' (polycondensation and subsequent ring closure). Particular emphasis is placed on polymerizations in poly(phosphoric acid) solutions. Some practical details relating to characterization, properties and preparation, including the preparation of tractable materials in the intermediate stages, are presented. In the second article, Iwakura *et al.* review the chemistry of pseudoxazolones and describe a number of new polymerizations and copolymerizations involving these monomers. The article by Okawara and coworkers outlines synthetic routes to a wide variety of polymers carrying reactive functional groups, prepared mainly by reactions on preformed polymers. Some applications of the functional polymers are described. This article contains a particularly high proportion of references (>50%) to original Japanese language publications and conference proceedings.

Kawai and coworkers describe their contribution to the study of multicomponent polymers. They discuss experimental observations and theoretical considerations relating to microphase separation in AB and ABA block copolymers and blends of those polymers with homopolymers of the constituent monomers. Microphase separation in poly(methyl acrylate)-polystyrene graft copolymers

is also discussed. Finally, Hatano and Nozawa consider the use of polypeptide-metal complexes as models for metalloenzymes, concentrating on the characterization of poly(L-lysine)-Cu(II) complexes and commenting on the reactivity of the complexes.

The standard of English in the volume and the overall presentation are very good. Although the individual articles are commendable, in view of their diversity it cannot be expected that any one individual will have special interest in more than one contribution. On this basis, the price per page of information is very high and is high even for background availability in libraries. Surely, to achieve their worthwhile objective of improving western awareness of Japanese polymer science the publishers should consider methods of providing more value for money in future volumes?

G. C. Eastmond

Injection moulding—theory and practice

Irvin I. Rubin

John Wiley, New York, 1973, 672 pp. £12.50

An up-to-date book which brings together the many aspects of plastics injection moulding in one volume has been long overdue. If only for this reason it is a useful reference book which is further augmented by extensive bibliographies. Thus either the layman, the polymer technologist or the engineer will gain something of value from the contents. The most important feature of the treatment are the straightforward explanations of the influence on processability and properties of mouldings of melt rheology and polymer structure. For once a serious attempt has been made to marry scientific principles to the practical situation revealing that the 'art' of moulding is logically explicable. The moulder can only benefit from such an understanding. This approach could have been carried further but Mr Rubin has fallen into the trap of including unhelpful complexities on the one hand and unnecessary trivia on the other. Explanations of molecular weight calculations and too detailed an account of chemical structure seem as much out of place in this context as does the usual stuff on examples of mouldings. More on part design, mould design and process control would have been more profitable and less on electrical and hydraulic mechanisms. The check list on correcting moulding faults contrasts with the earlier understanding of melt flow behaviour and its usefulness is overstated.

For once the diagrams are mostly clear and uncomplicated but there are numerous irritating printing errors throughout the text which do nothing to help the author's somewhat staccato style. All pertinent English language publications have not been included as claimed on the dust cover. Regrettably, none of the many foreign language papers are mentioned.

R. R. Whisson

Concise guide to biomedical polymers

C. C. Thomas, Springfield, Illinois, 1973, \$14.75

The clinician of today has at his disposal an increasing array of machines and devices to assist in his treatment of patients. Much of the equipment incorporates plastics or rubbers in a variety of forms. A whole new technology is evolving around these biomedical polymers and this book presents a useful guide to the selection of a material for a particular purpose. Information is provided on the physical and mechanical properties of those polymer systems which have been examined for medical use and due attention is given to those disadvantages which preclude the use of a polymer either totally or partly from consideration. Much of the content is concerned with the practical aspects of working with plastic and rubber compositions and ranges from compounding and moulding to machining and finishing. The surgeon and bioengineer will find the information supplied in this text and supplemented from the additional references cited, of use in narrowing the choice of materials and in gaining an understanding of the fabrication techniques required for the production of a medical device. The importance attached to the use of medical grade materials in medical work is stressed and the list of trade names and sources of medical polymers is a most worthwhile inclusion, coupled with details of appropriate sterilization techniques which have to take into account the possibility of chemical reaction or degradation occurring during such treatments.

Directorate, Ministry of Defence, for their support of this work.

C. B. Bucknall and I. C. Drinkwater

Department of Materials, Cranfield Institute of Technology,
Cranfield, Bedford, UK

(Received 6 February 1974)

References

- 1 Bucknall, C. B., Drinkwater, I. C. and Keast, W. E. *Polymer* 1972, **13**, 115
- 2 Evans, L. J., Bucknall, C. B. and Hall, M. M. *Plastics and Polymers* 1971, **39**, 118
- 3 Spit, B. J. *Polymer* 1963, **4**, 109
- 4 Keskkula, H. and Traylor, P. A. *J. Appl. Polym. Sci.* 1967, **11**, 2361
- 5 Eastmond, G. C. and Smith, E. G. *Polymer* 1973, **14**, 509

Book Reviews

Progress in polymer science Japan, Vol 4

Edited by K. Imahori and Y. Iwakura

Kodansha Ltd, Tokyo and Halstead Press, New York,
1973, 278 pp. £7.00

This is a volume in yet another of the 'Progress in' type series of book which have expanded the volume of the scientific literature and drained the financial resources of libraries in recent years. While many people might doubt the value of such volumes, this particular series has a potentially useful and specific role to play.

The Society of Polymer Science, Japan has about 10 000 members in universities and industry, representing a massive effort in the polymer field. Inevitably this effort has produced a vast literature much of which is published in Japanese, either in journals or conference proceedings. Japanese scientists will tell you that most of the good work is published in English eventually, sometimes three years after its appearance in Japanese. A significant fraction of the papers appear in the English language literature published in Japan, including research bulletins of individual universities. These volumes suffer from a limited circulation and readership and are not well-known. Consequently, a large proportion of the literature is, at least temporarily, lost to the Western reader. It is the stated purpose of these volumes to rectify this situation by having Japanese authors review specific and important aspects of Japanese polymer research. If the editors succeed in attaining their objective we should have access to a coherent, rather than the present fragmentary, picture of polymer science in Japan.

Volume 4 of this series contains five articles, the authors of which concentrate on research carried out in their own laboratories. The first article, by Yoda *et al.* of Toray Industries, discusses the preparation of thermally stable polymers. The materials described contain heterocyclic ring structures and are produced by 'cyclo-polycondensation reactions' (polycondensation and subsequent ring closure). Particular emphasis is placed on polymerizations in poly(phosphoric acid) solutions. Some practical details relating to characterization, properties and preparation, including the preparation of tractable materials in the intermediate stages, are presented. In the second article, Iwakura *et al.* review the chemistry of pseudoxazolones and describe a number of new polymerizations and copolymerizations involving these monomers. The article by Okawara and coworkers outlines synthetic routes to a wide variety of polymers carrying reactive functional groups, prepared mainly by reactions on preformed polymers. Some applications of the functional polymers are described. This article contains a particularly high proportion of references (>50%) to original Japanese language publications and conference proceedings.

Kawai and coworkers describe their contribution to the study of multicomponent polymers. They discuss experimental observations and theoretical considerations relating to microphase separation in AB and ABA block copolymers and blends of those polymers with homopolymers of the constituent monomers. Microphase separation in poly(methyl acrylate)-polystyrene graft copolymers

is also discussed. Finally, Hatano and Nozawa consider the use of polypeptide-metal complexes as models for metalloenzymes, concentrating on the characterization of poly(L-lysine)-Cu(II) complexes and commenting on the reactivity of the complexes.

The standard of English in the volume and the overall presentation are very good. Although the individual articles are commendable, in view of their diversity it cannot be expected that any one individual will have special interest in more than one contribution. On this basis, the price per page of information is very high and is high even for background availability in libraries. Surely, to achieve their worthwhile objective of improving western awareness of Japanese polymer science the publishers should consider methods of providing more value for money in future volumes?

G. C. Eastmond

Injection moulding—theory and practice

Irvin I. Rubin

John Wiley, New York, 1973, 672 pp. £12.50

An up-to-date book which brings together the many aspects of plastics injection moulding in one volume has been long overdue. If only for this reason it is a useful reference book which is further augmented by extensive bibliographies. Thus either the layman, the polymer technologist or the engineer will gain something of value from the contents. The most important feature of the treatment are the straightforward explanations of the influence on processability and properties of mouldings of melt rheology and polymer structure. For once a serious attempt has been made to marry scientific principles to the practical situation revealing that the 'art' of moulding is logically explicable. The moulder can only benefit from such an understanding. This approach could have been carried further but Mr Rubin has fallen into the trap of including unhelpful complexities on the one hand and unnecessary trivia on the other. Explanations of molecular weight calculations and too detailed an account of chemical structure seem as much out of place in this context as does the usual stuff on examples of mouldings. More on part design, mould design and process control would have been more profitable and less on electrical and hydraulic mechanisms. The check list on correcting moulding faults contrasts with the earlier understanding of melt flow behaviour and its usefulness is overstated.

For once the diagrams are mostly clear and uncomplicated but there are numerous irritating printing errors throughout the text which do nothing to help the author's somewhat staccato style. All pertinent English language publications have not been included as claimed on the dust cover. Regrettably, none of the many foreign language papers are mentioned.

R. R. Whisson

Concise guide to biomedical polymers

C. C. Thomas, Springfield, Illinois, 1973, \$14.75

The clinician of today has at his disposal an increasing array of machines and devices to assist in his treatment of patients. Much of the equipment incorporates plastics or rubbers in a variety of forms. A whole new technology is evolving around these biomedical polymers and this book presents a useful guide to the selection of a material for a particular purpose. Information is provided on the physical and mechanical properties of those polymer systems which have been examined for medical use and due attention is given to those disadvantages which preclude the use of a polymer either totally or partly from consideration. Much of the content is concerned with the practical aspects of working with plastic and rubber compositions and ranges from compounding and moulding to machining and finishing. The surgeon and bioengineer will find the information supplied in this text and supplemented from the additional references cited, of use in narrowing the choice of materials and in gaining an understanding of the fabrication techniques required for the production of a medical device. The importance attached to the use of medical grade materials in medical work is stressed and the list of trade names and sources of medical polymers is a most worthwhile inclusion, coupled with details of appropriate sterilization techniques which have to take into account the possibility of chemical reaction or degradation occurring during such treatments.

Despite the very widespread medical use of plastics and rubbers, it is still most necessary to proceed with extreme caution, particularly so with materials and devices for implant within the body. Arising from the diversity of purpose and the variation in properties and composition of polymers there are no standard test methods laid down for evaluating an implant prior to use. As a result the author confines himself to listing those test methods evolved for evaluating industrial grade polymers along with brief accounts of the biological testing of particular materials for particular purposes. One anticipates that this first edition will prove to be the forerunner of more comprehensive treatises in which more guidance will be offered for a reliable evaluation of biocompatibility.

The information contained in this guide, as a whole, is well laid out and accessible. For its price this book will serve as a useful reference work for both surgeons and bioengineers and should serve to remind implantable-device fabricators that their designs must operate within the limits of the mechanical properties of their material of choice while performing the required biological function.

T. Gilchrist

Peptides 1971

Edited by H. Nesvadba

North-Holland, Amsterdam, 1973, 428 pp. Dfl 80.00

The European Peptide Symposia, though transient in themselves, provide a forum for the rapid dissemination and appraisal of research findings and thereby exert a lasting influence on the development of peptide chemistry. When one compares the contents of this volume with those of the Chemical Society Specialist Periodical Reports, it is apparent that most of the work discussed at the Symposium appeared subsequently in regular journals; inevitably, nearly all of the main contributions were reported elsewhere before these proceedings became available. In these circumstances, speculation about the value of the symposium report as opposed to the symposium itself may not seem out of place.

Yet the report is a valuable addition to the literature. It is an historic account of an important occasion which, together with sister volumes covering previous symposia, constitutes a unique record of the achievements and disappointments of modern peptide chemistry; its section headings and plenary lectures highlight the problems of the moment and provide pointers to the future; and its individual papers, couched in more discursive terms than journals permit, provide stimulating reading.

Thus, conventional methods of peptide synthesis only occupies a quarter of the present volume whereas, not so long ago, this

topic would have been of major concern. This is an indication of the progress of recent years, whilst the emphasis on mechanisms is indicative of the manner in which further advances are likely to be made. Solid phase synthesis, as befits its achievements and potential, now takes nearly as much space as conventional techniques. At the same time, a new pre-occupation with theoretical considerations reflects the probability that desired improvements of solid phase methods demand detailed investigations into the basic chemistry involved. Purification, isolation and characterization of peptides has also matured into a separate section, whilst perhaps as a measure of the success achieved in these various areas and in recognition of the ultimate problem, conformation and biological activity has become the largest section.

It is a tribute to the quality of this production that all peptide chemists will wish to acquire this volume for their libraries. Many more personal copies would be sold except for the price, although regrettably, in these days, this is hardly excessive for such a production.

H. D. Law

Poly(vinyl alcohol) properties and applications

Edited by C. A. Finch

John Wiley, London and New York, 1973, 622 pp. £14.00

Impetus for poly(vinyl alcohol) research and commercial exploitation has arisen very largely from the Japanese interest in the polymer as a textile fibre during the last two decades. Even though the editor of this book has specifically excluded considerations of poly(vinyl alcohol) as a textile fibre (and also medical applications) two-thirds of this book on poly(vinyl alcohol) has been written by Japanese workers. This is one of the strengths of the work since in many cases it is the first time that much useful information about poly(vinyl alcohol) that was only previously obtainable in Japanese has appeared in the English language.

Although much of the material is concerned with the industrial uses of poly(vinyl alcohol) (PVAL) a balance between technology and fundamental science is maintained throughout. The book deals mainly with the copolymer resulting from the incomplete hydrolysis of poly(vinyl acetate) (PVAC) but other materials including essentially pure PVAL are also considered.

After a rapid survey of production statistics in the introduction (C. A. Finch) and an intriguing historical chapter (Heinz Winkler), a very informative and detailed chapter on the properties of the polymer such as solubility, viscosity and surface tension, that are important in the industrial applications (K. Toyoshima) is included. Five chapters then follow on PVAL formation dealing with both basic principles of PVAC production, its conversion to PVAL, the production of PVAL and modified poly(vinyl alcohols) from other polymers and copolymers (K. Noro). A chapter on the thermal properties (Robert K. Tubbs and Ting Kai Wu) is followed by ones on the chemical properties and on the stereochemistry of the polymer (C. A. Finch). Two chapters deal extensively with the application of PVAL in warp sizing (Kaname Tsunemitsu and Hasuhumi Murakami). The next four chapters are concerned with the properties of PVAL films, the reactions of PVAL with clays, the application of PVAL in adhesives and the acetalization of PVAL (K. Toyoshima). The use of PVAL in emulsion polymerization (E. V. Gulbekian and G. E. J. Reynolds), the photosensitized reactions of PVAL used in printing technology and other applications (B. Duncalf and S. S. Dunn) and PVAL in optical films (Howard C. Haas) are considered next. Two final chapters deal with moulded products from PVAL and other miscellaneous applications (K. Toyoshima). The book is completed by two appendixes dealing with compatibility and with the preparation of solutions (K. Toyoshima) and one appendix outlining analytical methods (C. A. Finch).

Even though fourteen authors have been involved in the writing of this book, there is relatively little overlap between the 21 chapters, and the editor has succeeded in welding these into a readable English treatise. The book is well produced with many useful figures and tables. It must now be regarded as the source book on poly(vinyl alcohol) and at the price of 2.2p per page it can be regarded as a good buy for most organizations concerned with the production or use of poly(vinyl alcohol).

G. S. Park

Conference Announcement
**IUPAC International Symposium on
Macromolecules (SIM)**

Rio de Janeiro, Brazil, 26-31 July 1974

An IUPAC sponsored International Symposium on Macromolecules will be held in the Hotel Nacional, Rio de Janeiro, Brazil from 26 to 31 July 1974. The symposium will cover the following main topics: (1) solution and bulk properties of polymers; (2) polymer characterization methods; (3) homo- and co-polymerization reactions; (4) photopolymerization; (5) chemical reactions on macromolecules; (6) evaluation of polymer properties; (7) advances in polymer technology; (8) natural polymers—reactions and technology; (9) advances in biopolymers and their synthetic models. Further details about registration, social events and the full programme may be obtained from the General Coordinator, Professor E. B. Mano, Academia Brasileira de Ciências, Caixa Postal 229, 20.000 Rio de Janeiro, GB, Brazil.

Directorate, Ministry of Defence, for their support of this work.

C. B. Bucknall and I. C. Drinkwater

Department of Materials, Cranfield Institute of Technology,
Cranfield, Bedford, UK

(Received 6 February 1974)

References

- 1 Bucknall, C. B., Drinkwater, I. C. and Keast, W. E. *Polymer* 1972, **13**, 115
- 2 Evans, L. J., Bucknall, C. B. and Hall, M. M. *Plastics and Polymers* 1971, **39**, 118
- 3 Spit, B. J. *Polymer* 1963, **4**, 109
- 4 Keskkula, H. and Traylor, P. A. *J. Appl. Polym. Sci.* 1967, **11**, 2361
- 5 Eastmond, G. C. and Smith, E. G. *Polymer* 1973, **14**, 509

Book Reviews

Progress in polymer science Japan, Vol 4

Edited by K. Imahori and Y. Iwakura

Kodansha Ltd, Tokyo and Halstead Press, New York,
1973, 278 pp. £7.00

This is a volume in yet another of the 'Progress in' type series of book which have expanded the volume of the scientific literature and drained the financial resources of libraries in recent years. While many people might doubt the value of such volumes, this particular series has a potentially useful and specific role to play.

The Society of Polymer Science, Japan has about 10 000 members in universities and industry, representing a massive effort in the polymer field. Inevitably this effort has produced a vast literature much of which is published in Japanese, either in journals or conference proceedings. Japanese scientists will tell you that most of the good work is published in English eventually, sometimes three years after its appearance in Japanese. A significant fraction of the papers appear in the English language literature published in Japan, including research bulletins of individual universities. These volumes suffer from a limited circulation and readership and are not well-known. Consequently, a large proportion of the literature is, at least temporarily, lost to the Western reader. It is the stated purpose of these volumes to rectify this situation by having Japanese authors review specific and important aspects of Japanese polymer research. If the editors succeed in attaining their objective we should have access to a coherent, rather than the present fragmentary, picture of polymer science in Japan.

Volume 4 of this series contains five articles, the authors of which concentrate on research carried out in their own laboratories. The first article, by Yoda *et al.* of Toray Industries, discusses the preparation of thermally stable polymers. The materials described contain heterocyclic ring structures and are produced by 'cyclo-polycondensation reactions' (polycondensation and subsequent ring closure). Particular emphasis is placed on polymerizations in poly(phosphoric acid) solutions. Some practical details relating to characterization, properties and preparation, including the preparation of tractable materials in the intermediate stages, are presented. In the second article, Iwakura *et al.* review the chemistry of pseudoxazolones and describe a number of new polymerizations and copolymerizations involving these monomers. The article by Okawara and coworkers outlines synthetic routes to a wide variety of polymers carrying reactive functional groups, prepared mainly by reactions on preformed polymers. Some applications of the functional polymers are described. This article contains a particularly high proportion of references (>50%) to original Japanese language publications and conference proceedings.

Kawai and coworkers describe their contribution to the study of multicomponent polymers. They discuss experimental observations and theoretical considerations relating to microphase separation in AB and ABA block copolymers and blends of those polymers with homopolymers of the constituent monomers. Microphase separation in poly(methyl acrylate)-polystyrene graft copolymers

is also discussed. Finally, Hatano and Nozawa consider the use of polypeptide-metal complexes as models for metalloenzymes, concentrating on the characterization of poly(L-lysine)-Cu(II) complexes and commenting on the reactivity of the complexes.

The standard of English in the volume and the overall presentation are very good. Although the individual articles are commendable, in view of their diversity it cannot be expected that any one individual will have special interest in more than one contribution. On this basis, the price per page of information is very high and is high even for background availability in libraries. Surely, to achieve their worthwhile objective of improving western awareness of Japanese polymer science the publishers should consider methods of providing more value for money in future volumes?

G. C. Eastmond

Injection moulding—theory and practice

Irvin I. Rubin

John Wiley, New York, 1973, 672 pp. £12.50

An up-to-date book which brings together the many aspects of plastics injection moulding in one volume has been long overdue. If only for this reason it is a useful reference book which is further augmented by extensive bibliographies. Thus either the layman, the polymer technologist or the engineer will gain something of value from the contents. The most important feature of the treatment are the straightforward explanations of the influence on processability and properties of mouldings of melt rheology and polymer structure. For once a serious attempt has been made to marry scientific principles to the practical situation revealing that the 'art' of moulding is logically explicable. The moulder can only benefit from such an understanding. This approach could have been carried further but Mr Rubin has fallen into the trap of including unhelpful complexities on the one hand and unnecessary trivia on the other. Explanations of molecular weight calculations and too detailed an account of chemical structure seem as much out of place in this context as does the usual stuff on examples of mouldings. More on part design, mould design and process control would have been more profitable and less on electrical and hydraulic mechanisms. The check list on correcting moulding faults contrasts with the earlier understanding of melt flow behaviour and its usefulness is overstated.

For once the diagrams are mostly clear and uncomplicated but there are numerous irritating printing errors throughout the text which do nothing to help the author's somewhat staccato style. All pertinent English language publications have not been included as claimed on the dust cover. Regrettably, none of the many foreign language papers are mentioned.

R. R. Whisson

Concise guide to biomedical polymers

C. C. Thomas, Springfield, Illinois, 1973, \$14.75

The clinician of today has at his disposal an increasing array of machines and devices to assist in his treatment of patients. Much of the equipment incorporates plastics or rubbers in a variety of forms. A whole new technology is evolving around these biomedical polymers and this book presents a useful guide to the selection of a material for a particular purpose. Information is provided on the physical and mechanical properties of those polymer systems which have been examined for medical use and due attention is given to those disadvantages which preclude the use of a polymer either totally or partly from consideration. Much of the content is concerned with the practical aspects of working with plastic and rubber compositions and ranges from compounding and moulding to machining and finishing. The surgeon and bioengineer will find the information supplied in this text and supplemented from the additional references cited, of use in narrowing the choice of materials and in gaining an understanding of the fabrication techniques required for the production of a medical device. The importance attached to the use of medical grade materials in medical work is stressed and the list of trade names and sources of medical polymers is a most worthwhile inclusion, coupled with details of appropriate sterilization techniques which have to take into account the possibility of chemical reaction or degradation occurring during such treatments.

Despite the very widespread medical use of plastics and rubbers, it is still most necessary to proceed with extreme caution, particularly so with materials and devices for implant within the body. Arising from the diversity of purpose and the variation in properties and composition of polymers there are no standard test methods laid down for evaluating an implant prior to use. As a result the author confines himself to listing those test methods evolved for evaluating industrial grade polymers along with brief accounts of the biological testing of particular materials for particular purposes. One anticipates that this first edition will prove to be the forerunner of more comprehensive treatises in which more guidance will be offered for a reliable evaluation of biocompatibility.

The information contained in this guide, as a whole, is well laid out and accessible. For its price this book will serve as a useful reference work for both surgeons and bioengineers and should serve to remind implantable-device fabricators that their designs must operate within the limits of the mechanical properties of their material of choice while performing the required biological function.

T. Gilchrist

Peptides 1971

Edited by H. Nesvadba

North-Holland, Amsterdam, 1973, 428 pp. Dfl 80.00

The European Peptide Symposia, though transient in themselves, provide a forum for the rapid dissemination and appraisal of research findings and thereby exert a lasting influence on the development of peptide chemistry. When one compares the contents of this volume with those of the Chemical Society Specialist Periodical Reports, it is apparent that most of the work discussed at the Symposium appeared subsequently in regular journals; inevitably, nearly all of the main contributions were reported elsewhere before these proceedings became available. In these circumstances, speculation about the value of the symposium report as opposed to the symposium itself may not seem out of place.

Yet the report is a valuable addition to the literature. It is an historic account of an important occasion which, together with sister volumes covering previous symposia, constitutes a unique record of the achievements and disappointments of modern peptide chemistry; its section headings and plenary lectures highlight the problems of the moment and provide pointers to the future; and its individual papers, couched in more discursive terms than journals permit, provide stimulating reading.

Thus, conventional methods of peptide synthesis only occupies a quarter of the present volume whereas, not so long ago, this

topic would have been of major concern. This is an indication of the progress of recent years, whilst the emphasis on mechanisms is indicative of the manner in which further advances are likely to be made. Solid phase synthesis, as befits its achievements and potential, now takes nearly as much space as conventional techniques. At the same time, a new pre-occupation with theoretical considerations reflects the probability that desired improvements of solid phase methods demand detailed investigations into the basic chemistry involved. Purification, isolation and characterization of peptides has also matured into a separate section, whilst perhaps as a measure of the success achieved in these various areas and in recognition of the ultimate problem, conformation and biological activity has become the largest section.

It is a tribute to the quality of this production that all peptide chemists will wish to acquire this volume for their libraries. Many more personal copies would be sold except for the price, although regrettably, in these days, this is hardly excessive for such a production.

H. D. Law

Poly(vinyl alcohol) properties and applications

Edited by C. A. Finch

John Wiley, London and New York, 1973, 622 pp. £14.00

Impetus for poly(vinyl alcohol) research and commercial exploitation has arisen very largely from the Japanese interest in the polymer as a textile fibre during the last two decades. Even though the editor of this book has specifically excluded considerations of poly(vinyl alcohol) as a textile fibre (and also medical applications) two-thirds of this book on poly(vinyl alcohol) has been written by Japanese workers. This is one of the strengths of the work since in many cases it is the first time that much useful information about poly(vinyl alcohol) that was only previously obtainable in Japanese has appeared in the English language.

Although much of the material is concerned with the industrial uses of poly(vinyl alcohol) (PVAL) a balance between technology and fundamental science is maintained throughout. The book deals mainly with the copolymer resulting from the incomplete hydrolysis of poly(vinyl acetate) (PVAC) but other materials including essentially pure PVAL are also considered.

After a rapid survey of production statistics in the introduction (C. A. Finch) and an intriguing historical chapter (Heinz Winkler), a very informative and detailed chapter on the properties of the polymer such as solubility, viscosity and surface tension, that are important in the industrial applications (K. Toyoshima) is included. Five chapters then follow on PVAL formation dealing with both basic principles of PVAC production, its conversion to PVAL, the production of PVAL and modified poly(vinyl alcohols) from other polymers and copolymers (K. Noro). A chapter on the thermal properties (Robert K. Tubbs and Ting Kai Wu) is followed by ones on the chemical properties and on the stereochemistry of the polymer (C. A. Finch). Two chapters deal extensively with the application of PVAL in warp sizing (Kaname Tsunemitsu and Hasuhumi Murakami). The next four chapters are concerned with the properties of PVAL films, the reactions of PVAL with clays, the application of PVAL in adhesives and the acetalization of PVAL (K. Toyoshima). The use of PVAL in emulsion polymerization (E. V. Gulbekian and G. E. J. Reynolds), the photosensitized reactions of PVAL used in printing technology and other applications (B. Duncalf and S. S. Dunn) and PVAL in optical films (Howard C. Haas) are considered next. Two final chapters deal with moulded products from PVAL and other miscellaneous applications (K. Toyoshima). The book is completed by two appendixes dealing with compatibility and with the preparation of solutions (K. Toyoshima) and one appendix outlining analytical methods (C. A. Finch).

Even though fourteen authors have been involved in the writing of this book, there is relatively little overlap between the 21 chapters, and the editor has succeeded in welding these into a readable English treatise. The book is well produced with many useful figures and tables. It must now be regarded as the source book on poly(vinyl alcohol) and at the price of 2.2p per page it can be regarded as a good buy for most organizations concerned with the production or use of poly(vinyl alcohol).

G. S. Park

Conference Announcement

IUPAC International Symposium on Macromolecules (SIM)

Rio de Janeiro, Brazil, 26-31 July 1974

An IUPAC sponsored International Symposium on Macromolecules will be held in the Hotel Nacional, Rio de Janeiro, Brazil from 26 to 31 July 1974. The symposium will cover the following main topics: (1) solution and bulk properties of polymers; (2) polymer characterization methods; (3) homo- and co-polymerization reactions; (4) photopolymerization; (5) chemical reactions on macromolecules; (6) evaluation of polymer properties; (7) advances in polymer technology; (8) natural polymers—reactions and technology; (9) advances in biopolymers and their synthetic models. Further details about registration, social events and the full programme may be obtained from the General Coordinator, Professor E. B. Mano, Academia Brasileira de Ciências, Caixa Postal 229, 20.000 Rio de Janeiro, GB, Brazil.

The Physics of Polymers

This issue of POLYMER includes 7 representative papers that were presented at the Biennial Conference of the Polymer Physics Group of the Institute of Physics, held at RMC Shrivenham from 19 to 21 September 1973. To underline the value and breadth of the Conference, we invited Professor I. M. Ward (Chairman, Polymer Physics Group) to highlight some of the main features from papers presented at Shrivenham but not published in this special issue of POLYMER:

The Conference opened with several papers on the statistics of chain molecules by Professors M. Gordon (University of Essex) and C. Domb (King's College, London). The basis of the chain statistics used in dilute solution and rubber elasticity theory has become so enshrined in the folklore of polymer physicists that it is very appropriate indeed, particularly as new experimental techniques become available, for the presuppositions and approximations of these theories to be very closely scrutinized.

The problem of order in polymers is another subject with many facets. Dr P. J. Hendra (University of Southampton) described the use of Raman spectroscopy to study order in polybutadienes and polyisoprenes, Dr V. J. McBrierty (Trinity College, Dublin) presented an account of pulsed n.m.r. studies of block copolymers, and Dr B. W. Delf (University College, Cardiff) discussed the application of small angle X-ray scattering to the measurement of the spatial distribution of ions in carboxylic rubbers.

The session on crystalline polymers opened with 3 papers on radiation effects. Miss Hilary Jenkins (University of Bristol) presented an account of the extensive evidence obtained by Professor Keller's group for preferential crosslinking in the fold regions of polyethylene. The next 2 papers dealt with the effects of radiation on mechanical behaviour [stress relaxation studies by M. Crook (Polytechnic of the South Bank) and D. Evans (Rutherford Laboratory)] and electron and optical behaviour [Professor A. Charlesby (RMC Shrivenham)]. Although radiation effects are perhaps of limited value in their own right with regard to polymers, they do provide an entry to an understanding of their structure and properties.

Dr D. C. Bassett (University of Reading) then explained his recent views on chain-extended crystallization of polyethylene, the most important point being the proposal that a new intermediate phase is essential for crystallization of this form from the melt at high pressures. Accounts were given of the structure of rolled polyoxymethylene sheets by N. J. Mills (University of Birmingham) and biaxially oriented PTFE by Dr P. B. Bowden (University of Cambridge). In both cases, interpretation of the results was given in terms of classical ideas of crystal plasticity.

The final session was devoted to molecular properties and started with Dr B. R. Jennings' (Brunel University) account of electric birefringence studies of polymer solutions. This technique promises to give new insight into changes in orientation and conformation when molecules in solution are subjected to an electric field. The next two papers, on birefringence and thermoelasticity of swollen elastomers by Professor A. N. Gent (Akron University, USA) and on flow birefringence of polycarbonate solutions by Dr G. H. Meeten (City of London Polytechnic), were along more familiar lines. In both cases a detailed quantitative treatment was possible and very interesting molecular information was obtained from careful experiments at a phenomenological level.

A paper by J. Maxfield (University of Manchester) described an investigation using Raman spectroscopy of rotational isomerism in polydimethylsiloxane where the data were interpreted on the basis of the recent Flory theories of rubber elasticity.

The last paper was given by Dr E. G. Wilson (Queen Mary College, London) and described a whole range of experiments which provide information on the electronic band structure of the polyethylene chain. Solid state polymer physics is a comparatively unexplored area, which could be of both fundamental and technological importance.

In summary, this was yet another excellent Shrivenham Conference. It is of particular interest to note the way in which the subject of polymer physics has diversified over the years, and that it shows no signs as yet of the arid formalism which can affect some branches of science as they become well established.

Phase transition in a polymer chain in dilute solution*

C. Domb

Wheatstone Physics Laboratory, King's College, Strand, London WC2, UK
(Received 12 October 1973)

Some general theoretical arguments are advanced to help in an understanding of the behaviour of a single molecular chain with intramolecular forces of van der Waals type. Analogy with a fluid suggests that as $N \rightarrow \infty$ a first-order phase transition takes place at a unique condensation temperature and this defines a unique θ -temperature. However, for finite N the transition becomes rounded and hence the θ -temperature is dependent on N . Instead of a θ -temperature one should now talk of a θ -region, an idea already put forward by Mazur *et al.* from an analysis of Monte Carlo data. Evidence for this pattern of behaviour is adduced from a lattice model of a self-avoiding walk with near-neighbour attractive forces using ideas which have proved useful in critical phenomena. Attention is drawn to a ferroelectric model which shows some similarities in behaviour.

One of the central problems in the theory of a polymer chain in dilute solution is the effect of intramolecular forces on the shape and size of the chain. The intramolecular forces are usually assumed to be of van der Waals type consisting of a hard core repulsion and longer range attraction. In fact the problem is mathematically similar to the condensation of a gas of molecules with van der Waals forces, but the existence of the chain imposes restrictions in the configurational space of the molecules; for a system of N molecules the $3N$ degrees of freedom are reduced to $(2N+1)$. There are many parallels between the two problems, and the aim of the present paper is to use our well established knowledge of the behaviour of a condensing gas to help in an understanding of the behaviour of the chain.

We may first expect that at sufficiently high temperatures the repulsive forces will dominate in the 'gaseous' phase, whereas at sufficiently low temperatures the attractive forces will dominate giving rise to a 'condensation'. At some intermediate temperature a balance can be achieved between repulsive and attractive forces; for a fluid this is the Boyle temperature, T_B at which the second virial coefficient vanishes, and the behaviour of the fluid approximates to an ideal gas; for a chain Flory¹ introduced the term θ -point to characterize the corresponding temperature at which the polymer approximates to a chain of random segments.

For a polymer chain particular interest centres on the mean square end-to-end distance $\langle R_N^2 \rangle$ measured by the expansion factor over a random chain:

$$\alpha^2 = \langle R_N^2 \rangle / N \quad (1)$$

and the mean square radius of gyration $\langle S_N^2 \rangle$. To estimate how these quantities depend on the length, N

and temperature, T above the θ -temperature most theoretical treatments^{2,4} have made use of a model in which the intramolecular forces are replaced by a pseudo-potential $w\delta(\mathbf{R}_{ij})$. Here $\mathbf{R}_{ij} = \mathbf{R}_i - \mathbf{R}_j$, \mathbf{R}_i and \mathbf{R}_j being the positions in space of the $(i+1)$ th and $(j+1)$ th molecules; $\delta(\mathbf{R})$ is the three-dimensional Dirac δ function and w is the second virial coefficient for the intramolecular potential, $V(r)$:

$$-w = \int [1 - \exp -\beta V(r)] dr \quad (2)$$

Such a pseudo-potential takes account of binary collisions correctly but not ternary and higher order collisions.

Even the pseudo-potential problem cannot be treated exactly and a large number of different approximations have been developed, the best known of which is the Flory formula²:

$$\alpha^5 - \alpha^3 = \frac{3(3)^{1/2}}{2} z \quad [z = -(3/2\pi b^2)^{3/2} w N^{1/2}] \quad (3)$$

where b^2 is the mean square length of a unit of the chain. Flory's argument is 'mean-field' in character; nevertheless, a recent numerical calculation³ based on experience gained with the Ising model has suggested the following.

(A) The exponent corresponding to asymptotic behaviour:

$$\alpha^2 \sim A(w) N^{1/5} \quad (4)$$

is correct.

(B) Equation (3) provides a reasonable approximation to the behaviour of α^2 for values of N and w of interest.

For the pseudo-potential model when w becomes positive the chain collapses very rapidly to zero for all N ⁴. When w is negative equation (4) is always satisfied asymptotically, but for small w the asymptotic equation becomes valid only for correspondingly large N . The nature of the transition is depicted in *Figure 1*, the θ -temperature, T_p being unique and independent of N

* Presented at the van der Waals Centenary Conference, Amsterdam, August 1973 and at the Polymer Physics Group (Institute of Physics) Biennial Conference, Shrivvenham, September 1973.

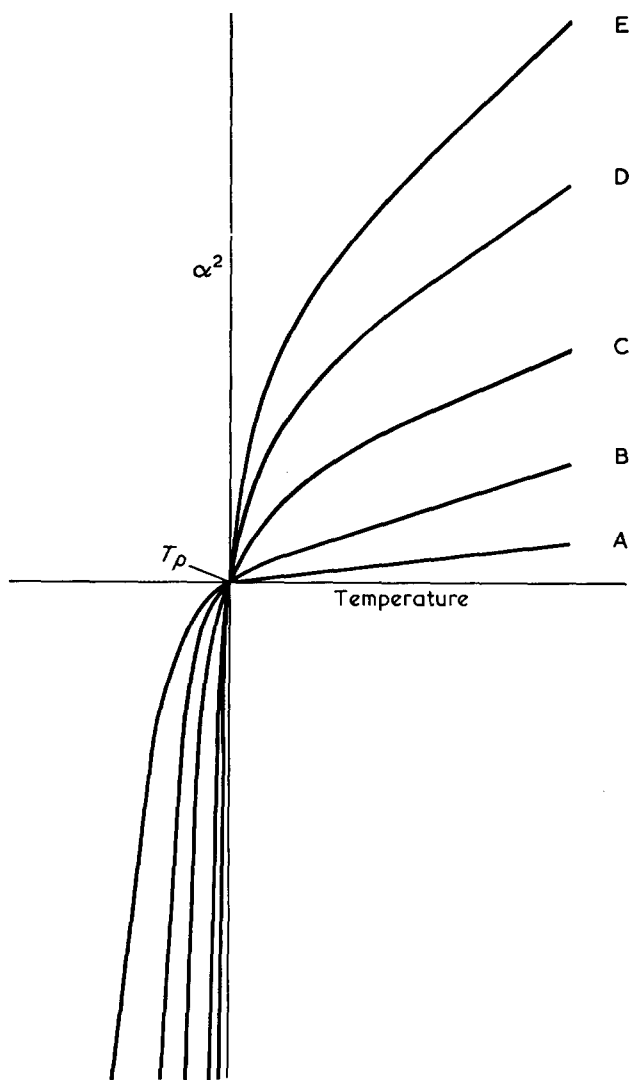


Figure 1 Expansion factor of a polymer chain in the pseudo-potential model. A, $N=10$; B, $N=100$; C, $N=1000$; D, $N=7800$; E, $N=32\ 500$

This behaviour is exactly paralleled by a condensing fluid in the pseudo-potential model which collapses to zero volume at the Boyle temperature, T_B .

However, for a fluid we know what happens when we take the finite hard core into account properly. Even though detailed calculations are prohibitively difficult, experiment and lattice model and Monte Carlo calculations confirm that nothing dramatic takes place at T_B , but there is a temperature T_t below T_B at which a first order transition occurs. Lifshitz has argued⁵ that the same behaviour is to be expected for a polymer chain, and we shall shortly adduce evidence in favour of this from a lattice model. We first investigate the expected behaviour of α^2 in the transition region in the case of a first order transition.

We know that a discontinuous phase transition occurs only in the limit of very large N for which Figure 2 depicts the idealized behaviour. For the 'gaseous' phase we assume that equation (4) holds as for the pseudo-potential model; for the 'condensed' phase the chain has folded up and we have instead:

$$\alpha^2 \approx N^{-1/3} \quad (5)$$

If we cool the system from a temperature $T > T_t$, when we reach the transition temperature T_t the condensed

phase starts to separate out, and the temperature remains at T_t until the chain has condensed completely. At some point during this transition $\langle R_N^2 \rangle$ and $\langle S_N^2 \rangle$ pass through their random chain values, and likewise higher moments $\langle R_N^4 \rangle$, $\langle R_N^6 \rangle$, ... Thus for very large N there is a unique θ -temperature equal to T_t , at which $\langle R_N^2 \rangle$, $\langle S_N^2 \rangle$ and all moments pass through their random chain values; however, the detailed character of the chain is very different from a random coil.

For finite N we expect a smoothing of the discontinuities and a broadening of the transition region as N decreases; Figure 3 depicts the form we might expect α^2 to take as a function of temperature for different values of N . There are several points worthy of note. First, the θ -temperature $T_\theta(N)$ defined by $\alpha^2=1$ is no longer unique but depends on N ; as $N \rightarrow \infty$, $T_\theta(N) \rightarrow T_t$ but because of the complication caused by the intersection of the $\alpha^2(N)$ curves, the convergence may be non-monotonic. Likewise for a given T in the transition region the behaviour of α^2 as a function of N may first drop to a minimum and then rise monotonically.

Since T_θ depends on N it is clear that $\langle S_N^2 \rangle$ which represents a weighted average of $\langle R_n^2 \rangle$ for different n will achieve its random chain value at a different temperature $T'_\theta(N)$. Similarly one would expect curves corresponding to other moments $\langle R_N^{2g} \rangle$ each to give rise to its own temperature $T^{(g)}_\theta(N)$. However, as $N \rightarrow \infty$ all of these θ -temperatures should tend to the same value T_t . We are therefore presented with a picture of a ' θ -region' for finite N tending to a unique θ -temperature as $N \rightarrow \infty$. The existence of a θ -region rather than a single θ -temperature is one of the important conclusions of recent Monte Carlo work⁹.

We shall now indicate how the above general picture can be examined in numerical detail for a lattice model. We consider the model first introduced by Orr⁶ of a self-avoiding walk with an attractive interaction J between nearest neighbours. Monte Carlo studies for this model were initiated by Wall and Mazur⁷ and Wall

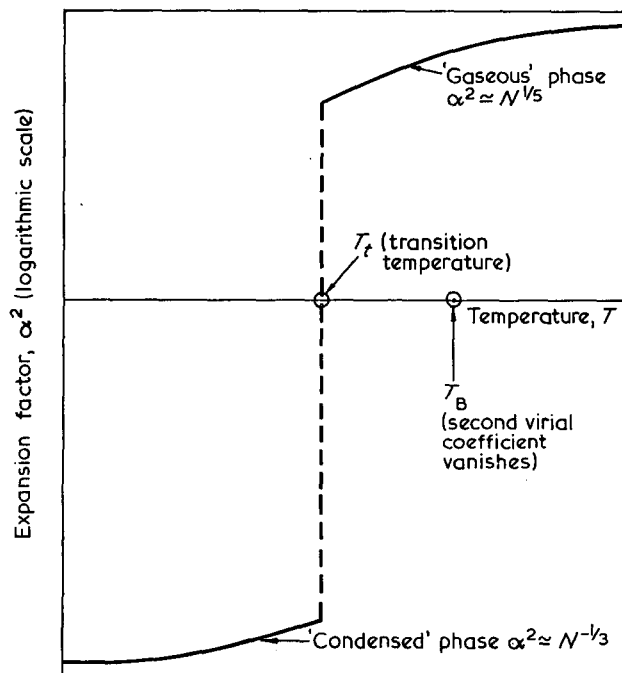


Figure 2 Schematic behaviour of long chain (by analogy with a condensing gas)

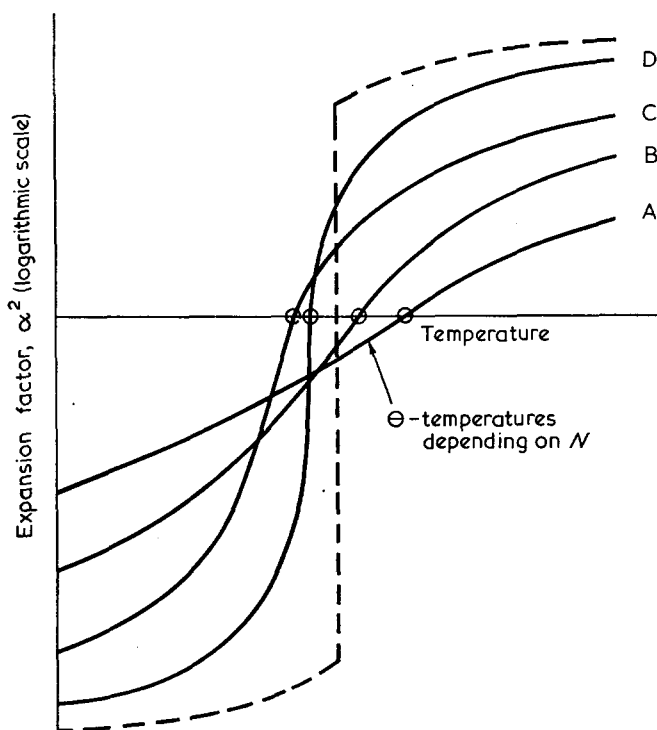


Figure 3 Schematic behaviour of finite chains. A, $N=10$; B, $N=10^2$; C, $N=10^3$; D, $N=10^4$

*et al.*⁸ and have been greatly extended recently for the s.c. and f.c.c. lattices by Mazur and McCrackin⁹ and McCrackin *et al.*¹⁰. Exact enumerations for short chains were made by Orr himself for the s.q. and s.c. lattices⁶, and these were extended by Fisher and Hiley¹¹ and by Domb *et al.*¹². Very recently exact enumerations for the f.c.c. lattice have been made by Rapaport¹³.

Our own interpretation of the data differs from those given previously in one important respect. Both the Monte Carlo and exact enumerations assumed that when an attractive force is introduced into a self-avoiding walk the asymptotic formula for α^2 becomes

$$\alpha^2 \approx N^\epsilon \quad (6)$$

Here the exponent ϵ is a function of J/kT , which varies continuously from the value $1/5$ given by equation (4) to the value $-1/3$ corresponding to condensation. Based on the smoothness postulate¹⁴ and the pseudo-potential model³ we assume instead that for $T > T_t$ ϵ remains equal to $1/5$, and for $T < T_t$ it remains equal to $-1/3$. However, in the critical region $T \sim T_t$ the asymptotic behaviour will not be attained until N becomes very large. We are thus assuming that the values of ϵ to which exact enumerations and Monte Carlo data have been fitted apply only to a limited range of N and are not true asymptotic formulae.

There is one piece of direct evidence to support the above picture. Some years ago P. G. Watson discovered a star-triangle relation between the honeycomb and kagomé lattices in two dimensions in which a polymer chain with a purely repulsive interaction on the honeycomb lattice transforms into one with an attractive interaction on the kagomé lattice. The transformation does not involve any change of exponent. (This work is to be published shortly.)

To obtain more insight into the nature of condensation we refer back to Orr's discussion of the configurations of the lowest energy state of the model.

A typical such configuration is shown in Figure 4 and Orr pointed out that there was a finite entropy S_0 associated with this energy state which he estimated as $k \ln 1.4$ for the s.q. lattice and $k \ln 1.9$ for the s.c. lattice. In fact this entropy is closely related to the entropy of ice and the KDP model of a ferroelectric for which an exact solution has been obtained by Lieb¹⁵ for the s.q. lattice. The latter problem corresponds to the same vertex configurations as in Figure 4 without the condition of a single continuous chain (i.e. allowing closed loops). Thus the entropy of ice for any lattice provides an upper limit to S_0 above.

For the KDP problem an electric field is introduced which associates an energy with certain vertex configurations. This singles out one lowest energy state, and the system remains frozen in this state until a finite temperature T_t , and then undergoes a first order phase transition. The 'frozen in' argument can be made rigorous¹⁶ so as to establish the existence of a first order transition for the s.c. lattice, for example, for which no exact solution exists.

In the polymer chain problem the energy arises from the interaction of neighbouring vertex configurations and the entropy of the lowest energy state is no longer resolved by the introduction of this interaction. There are nevertheless qualitative indications of a similar 'frozen in' type of behaviour at low temperatures suggesting the same type of first order transition as above. The free energy of the system is illustrated diagrammatically in Figure 5, T_t corresponding to the intersection of the free energies of the 'gaseous' and 'condensed' phases. We may note incidentally an alternative definition of a θ -temperature^{10,11} as the temperature at which the free energy is exactly equal to that of a random chain. The latter corresponds to the broken line through the origin in Figure 5, and we can see no reason why the intersection of this line with the solid curves should coincide with T_t .

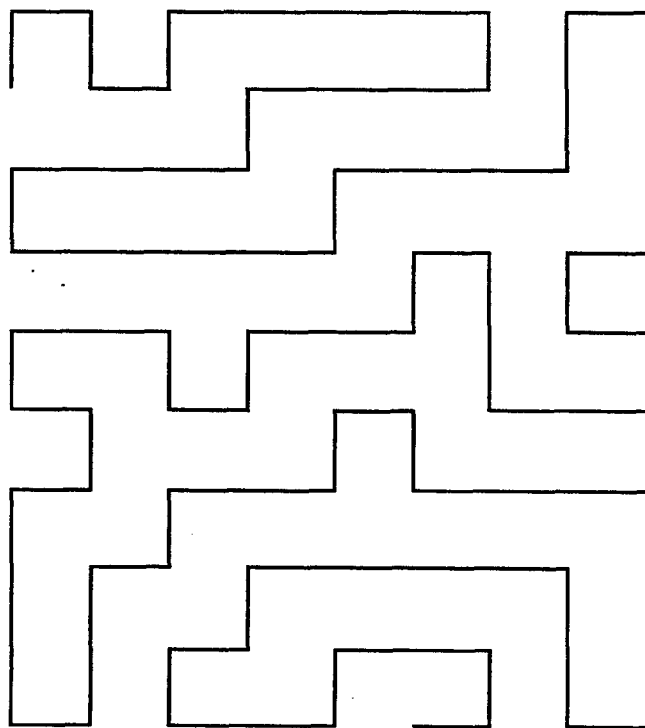


Figure 4 Typical condensed configuration on s.q. lattice (after Orr, 1947)

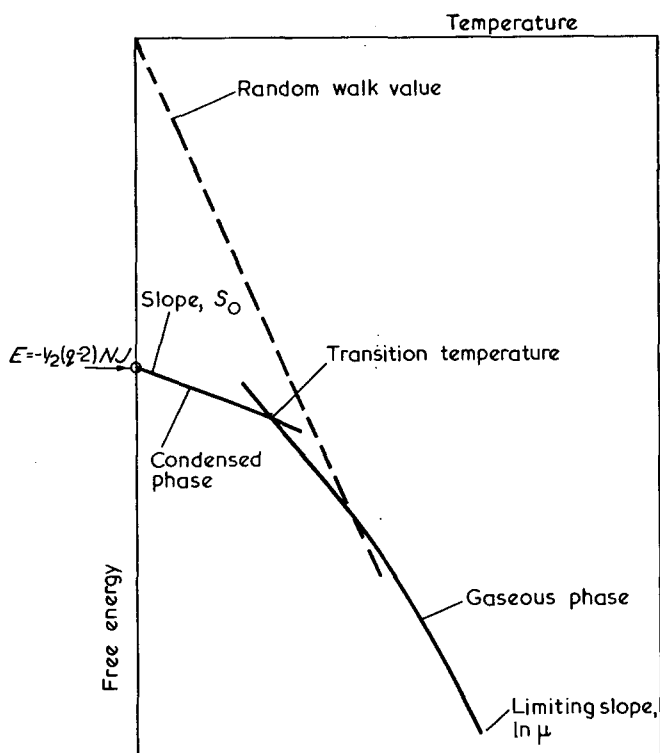


Figure 5 Free energy of two phases of a chain

Although the above discussion has been largely qualitative it has provided a framework for the numerical estimation of relevant parameters for a lattice model from exact enumerations and Monte Carlo data. These estimates will be discussed in a separate publication.

ACKNOWLEDGEMENTS

The author is grateful to Professor S. F. Edwards for several illuminating discussions, and to Professor E. H. Lieb for helpful correspondence. He is indebted to Dr J. Mazur for making his Monte Carlo results available before publication. Many of the suggestions in the paper resulted from a study of these Monte Carlo enumerations. This work was supported in part by the US Department of the Army through its European Research Office.

REFERENCES

- 1 Flory, P. J. 'Principles of Polymer Chemistry', Cornell University Press, Ithaca, 1953
- 2 see Yamakawa, H. 'Modern Theory of Polymer Solutions', Harper and Row, New York, 1971, Ch 3
- 3 Domb, C., Barrett, A. J. and Lax, M. *J. Phys. (A)* 1973, **6**, L82
- 4 Edwards, S. F. in 'Critical Phenomena', 1966 (Eds M. S. Green and J. V. Sengers), *Nat. Bur. Stand. Miscell. Publ.* 273 p 225
- 5 Lifshitz, I. M. *Soviet Physics JETP* 1969 **28**, 280 (*Zh. Eksp. Teor. Fiz.* 1968, **55**, 2408)
- 6 Orr, W. J. C. *Trans. Faraday Soc.* 1947, **43**, 12
- 7 Wall, F. T. and Mazur, J. *Ann. NY Acad. Sci.* 1961, **89**, 573
- 8 Wall, F. T., Windwer, S. and Gans, P. J. *J. Chem. Phys.* 1963, **38**, 2220
- 9 Mazur, J. and McCrackin, F. L. *J. Chem. Phys.* 1968, **49**, 648
- 10 McCrackin, F. L., Mazur, J. and Guttman, C. M. *Macromolecules* 1973, **6**, 85
- 11 Fisher, M. E. and Hiley, B. J. *J. Chem. Phys.* 1961, **34**, 1253
- 12 Domb, C., Gillis, J. and Wilmers, G. unpublished data (1963)
- 13 Rapaport, D. C. *Macromolecules* in press
- 14 Griffiths, R. B. *Phys. Rev. Lett.* 1970, **24**, 1479
- 15 Lieb, E. H. and Wu, F. Y. in 'Phase Transitions and Critical Phenomena' (Eds. C. Domb and M. S. Green), Academic Press, London, 1972, Vol 1, Ch 8
- 16 Nagle, J. *Comm. Math. Phys.* 1969, **13**, 62

The polyuronides: their molecular architecture*

E. D. T. Atkins, D. H. Isaac, I. A. Nieduszynski, C. F. Phelps†
and J. K. Sheehan

*H. H. Wills Physics Laboratory, University of Bristol, Bristol BS8 1TL, UK
(Received 6 December 1973; revised 30 January 1974)*

The polyuronides (uronic acid containing polymers) are considered for the first time as a coherent group. Until now the dearth of X-ray diffraction data resulted in many questions of polyuronic structure and conformation remaining unasked. The recent success in crystallizing the polyuronides is illustrated with X-ray diffraction patterns of hyaluronic acid, dermatan and chondroitin sulphates, heparan sulphate and heparin. The influence of the chemical structure, the glycosidic linkages and the charged substituents on the molecular conformations is considered together with the marked association with water which these molecules display. Computer-drawn projections of plausible molecular conformations are shown.

INTRODUCTION

It is only now that we can speak in molecular terms of a collection of disparate polymers whose identifying characteristic is the presence of a uronic acid moiety as a component of their structure. These occur ubiquitously in both the plant and animal kingdoms, uniquely as extracellular components. Their diversity is astonishing: thus pectin is the intercellular adhesive in plants, some seaweeds utilize alginate polymers as structural matrices and bacterial capsules may contain polyuronic components in their protective coating. In the animal kingdom, these uronic acid containing polymers (polyuronides) are of even greater versatility. All are of mesenchymal origin and are specific components of the connective tissue of the animal. Various forms of these polyuronides occur: hyaluronate occurs largely in articular joints, the vitreous humour of the eye and in Wharton's jelly of the umbilical cord, whilst the chondroitin sulphates figure extensively in structural tissues such as cartilage and blood vessels, and heparin occurs as packets of polymeric material in mast cells¹⁻⁴.

It may therefore be asked, what conditions the physiological behaviour and function of the polymer? Is there a significant reason for the deployment of so many species containing uronic acid, and further is there an interpretable design in the way in which each polyuronic is 'selected' for its particular role?

One means of investigating this area is to obtain detailed information on the molecular architecture of these polymers and thereby to attempt a reconciliation of such resultant structures with their functions.

Until recently little was known of the molecular conformation of the polyuronides. A considerable amount of chemical and biochemical data existed which favoured linear unbranched biopolymers with

relatively simple covalent structure. Large regions of the plant polyuronides were thought to be composed of monosaccharide repeating units while many of the animal connective tissue polyuronides appeared to be based on a disaccharide, or a tetrasaccharide repeating sequence. One would therefore expect some ordered arrangements at a molecular level and X-ray diffraction patterns should produce valuable structural information. Some early success in obtaining X-ray fibre diagrams was reported for the plant polyuronides sodium pectate by Palmer and Hartzog⁵ and alginic acid by Astbury⁶. By contrast the other connective tissue polyuronides remained almost unexplored until 1971 (however, see refs 7 and 8). The crystallization of these polymers as oriented films and fibres^{9, 10} was the critical development which enabled X-ray photographs of exceptional quality to be produced (*Figure 1*)¹¹⁻¹⁹.

X-RAY DIFFRACTION

Many gross parameters such as particle shape, size and chain flexibility together with polymer-polymer and polymer-solvent interactions can be elicited from solution studies. These data are all bulk values corresponding to the distribution of configurational states in the polymer. Clearly a technique which would delineate detailed molecular configurations and interactions would be most desirable. X-ray diffraction is just such a technique. The dimensional characteristics of the diffraction pattern reveal such parameters as the axial repeats along the chain and lateral periodicities between chains. An examination of the distribution of the intensities of the diffraction spots gives an indication of general features of the structure such as whether there are single or multi-strand helices. Ancillary information from bulk density determination and from model building using computer predictions as well as space filling constructions limits the permissible structures. Ultimately the use of all the intensity data in a high resolution X-ray photograph will define the precise

* Presented at the Polymer Physics Group (Institute of Physics) Biennial Conference, Shrivenham, September 1973.

† Department of Biochemistry, The Medical School, University of Bristol, University Walk, Bristol BS8 1TD, UK.

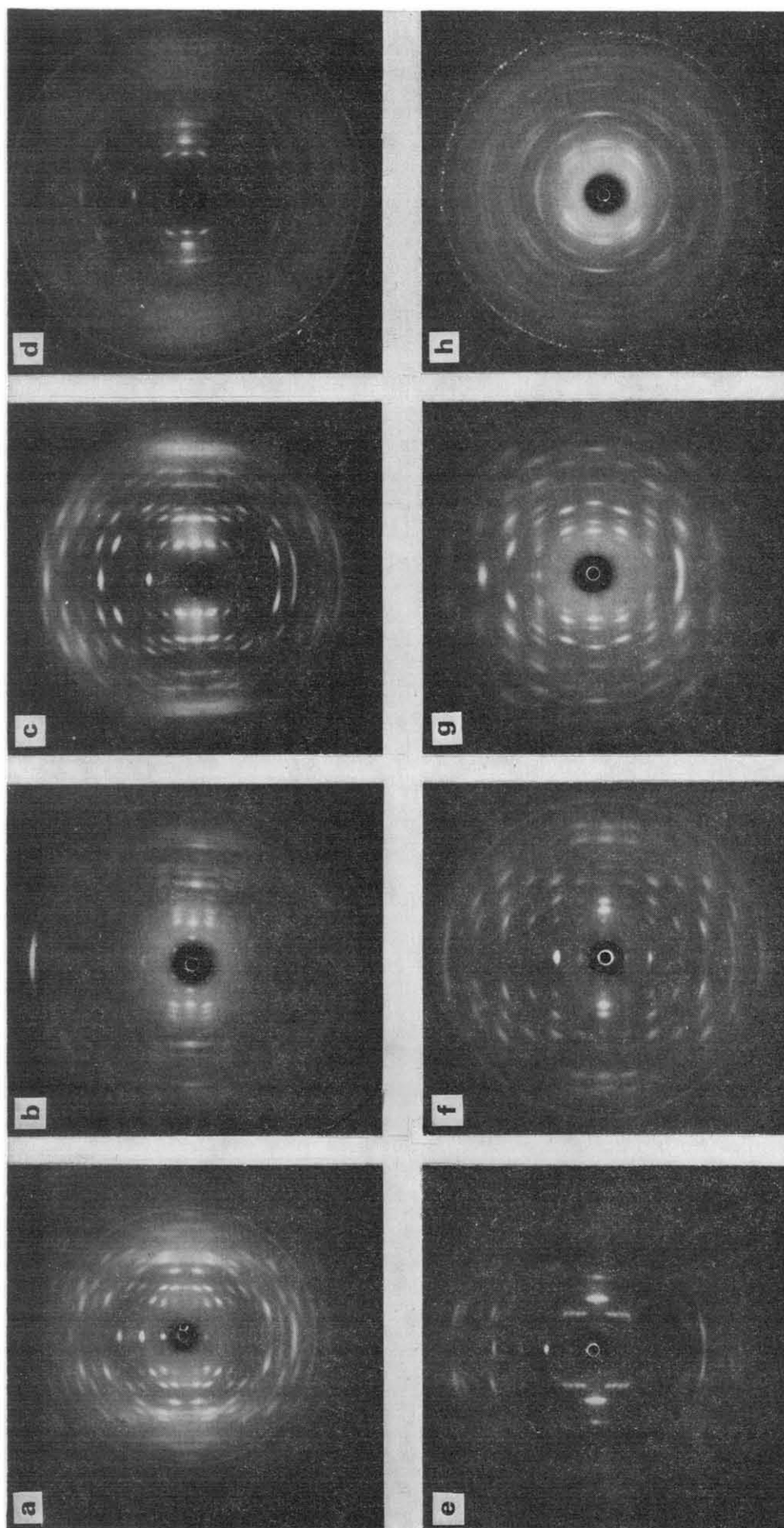


Figure 1 X-ray fibre diffraction patterns obtained from oriented films of the polyuronates. (a) Potassium hyaluronate: the reflections index on an orthorhombic unit cell with $a=1.10 \pm 0.01$ nm, $b=0.99 \pm 0.01$ nm, and c (fibre axis) $=3.30 \pm 0.03$ nm. The structure is interpreted as two antiparallel helices intertwining to form a double-stranded molecule¹⁶ (see Figure 4c). (b) Sodium hyaluronate: the reflections index on a large orthorhombic unit cell with $a=1.17 \pm 0.01$ nm, $b=3.42 \pm 0.03$ nm, and c (fibre axis) $=2.85 \pm 0.03$ nm. The helical conformation is three-fold (see Figure 4a) similar to the hexagonal forms reported previously^{10,11}. It often occurs as mixed phase with the double helix structure and may be useful in the understanding of the relationship between double and single helix conformation. (c) Chondroitin-4-sulphate, sodium salt form: this pattern is interpreted as a three-fold helical conformation (see Figure 5a) packing in a hexagonal unit cell with $a=1.45 \pm 0.01$ nm and c (fibre axis) $=2.88 \pm 0.03$ nm. On lowering of the pH to 2.5 the conformation relaxes into a two-fold helix¹⁴. (d) Sodium salt of chondroitin-6-sulphate: again the X-ray pattern clearly indicated a three-fold helical conformation (see Figure 5b) but the original indexing of the two-dimensional packing lattice proved ambiguous¹². Closer inspection shows it consists of a mixture of two separate phases; a three-fold helical conformation packing hexagonally together with some type of eight-fold conformation packing tetragonally¹⁹. (e) Sodium salt of dermatan sulphate: this X-ray pattern has a very large layer line spacing of 7.44 nm^{-3} . The pattern may be interpreted as a helix with eight disaccharide units repeating in three complete turns¹⁶. See computer drawn conformation in Figure 6a. (f) On lowering the pH of the sample which gives the X-ray pattern 1(e) a three-fold helix is obtained (see Figure 6b), which on annealing relaxes into this two-fold conformation. The projected axial rise per disaccharide of 0.97 ± 0.01 nm rules out the 1C chair for the L-iduronic acid moiety¹⁸. (g) Calcium salt of heparan sulphate: the X-ray pattern displays a layer line spacing of 1.68 nm, a significant reduction from the 1.86 nm repeat found for the sodium salt form¹³. The reflections index on an orthorhombic unit cell with $a=1.27 \pm 0.01$ nm, $b=1.70 \pm 0.02$ nm, and c (fibre axis) $=1.68 \pm 0.02$ nm. (h) Heparin, sodium salt form: the unit cell is triclinic so that the $00l$ reflections lie off the meridian. The chain periodicity of 1.65 nm corresponds to a tetrasaccharide repeat¹⁵. The broadening of the non-equatorial reflections is a function of the limited length of the molecule (~ 10 tetrasaccharide repeats). A full structure determination of this pattern is not yet completed and so the conformations given in Table 1 must still be regarded as tentative. A model with all $1ax \rightarrow 4eq$ glycosidic linkages may, however, be ruled out¹⁵

conformation and the types of interactions between chains and their environments.

MOLECULAR CONFORMATION

This paper is concerned with a study of the polyuronic structures. These may be discussed in two ways: (a) the various classes of polyuronic can be compared, and (b) each single polymer may be examined for the variety of structural modes it displays. In this last respect, the conformations of a biopolymer are determined by both intra- and inter-molecular interactions, the former resulting from the backbone geometry and the number and nature of the linkages, and the latter from such environmental constraints as the presence of adjacent chains, the nature of the counterion, and the effect of water. One other major influence on the conformation adopted is the presence of charge which affects both the intra- and inter-molecular forces.

Glycosidic linkage rules

The effect of linkages on polyuronic geometry may be investigated in the alginates which comprise block copolymers of D-mannuronate (M) and L-gulonate (G) and the combination $(-M-G)_n$ ²⁰ (see Table 1). The freedom of rotation about the two bonds at each linkage may be computed²¹⁻²⁴ and investigations show that for those linkages occurring in the polyuronides (i.e. 1→4 and 1→3) there is only one stereochemically allowed region, which comprises a maximum of 10% of the total conformations. The more complicated polyuronides are restricted further by large substituent side groups. Thus, some mean conformation will be energetically favourable, and for 1eq→4eq* linkages this mean is close to a two-fold helix²⁵ which distributes the substituents of successive residues on alternate sides of the chain axis (syndiotactic). However, the charges attendant on ionization form an electrostatic environment, which modulates the mean backbone conformation. Thus poly(mannuronic acid) is a two-fold helix which on formation of the monovalent salt converts into a three-fold left-handed helix (Figures 2, 3a and 3b). Since the linkages are close to and nearly parallel with the chain axis, the angular distribution of side groups may be varied with little change in the projected axial periodicity. Thus, balance between charge distribution and backbone flexibility is a controlling influence on polyuronic behaviour.

D-Mannuronic acid exists in the C1 chair form but its C(5) invert, L-gulononic acid, flips into the 1C chair²⁶ since its large axial carboxyl group would clash with the axial C(2) hydroxyl group. All axial groups become equatorial and *vice versa*, resulting in a different polymer shape: poly(L-gulononic acid) becomes diaxially 1→4 linked (1ax→4ax) as shown in Figure 3c. It is of interest that this change from mannuronate to guluronate appears to occur biologically at the polymer level²⁷. Interestingly, the two-fold disposition²⁸ of side groups in poly-(gulonic acid) is unperturbed by conversion to the monovalent salt forms²⁹ since the pronounced zig-zag

shape of the polymer (seen in Figure 3c) allows counterions to pack conveniently without conformational change. Three-fold guluronate conformations are sterically permissible, and the chemically homologous sodium pectate (1ax→4ax sodium polygalacturonate) is a three-fold helix⁵. From these findings we may formulate an initial hypothesis. Polysaccharides adopt a mean conformation where the substituent groups are distributed on alternate sides of the backbone. In polyuronides the previous requirement is compounded by the need to dispose the charges incorporated in a symmetrically uniform manner over the surface of the cylinder to minimize the electrostatic repulsion. It is profitable to examine this hypothesis with respect to the connective tissue polyuronides. The glycosidic linkages of hyaluronic acid are typical of a number of the polydisaccharide connective tissue polyuronides being alternately (1eq→4eq) and (1eq→3eq)^{32, 33}. The covalent disaccharide repeat consists of alternating *N*-acetylglucosamine and glucuronic acid as shown in Table 1. What is the reason for alternating 1eq→3eq and 1eq→4eq glycosidic linkages? Certainly such sequential alternative bond attachment is biosynthetically expensive. That a linkage system occurs for a whole group of polyuronides argues for some general principle. The linkage hypothesis offers an explanation.

If all the glycosidic linkages were 1eq→4eq, successive residues would rotate through approximately 180° about the chain axis. Let us designate this a type I linkage. Passage from one uronic acid residue to the next would involve two rotations bringing successive uronic residues into a similar disposition along the chain. This model contradicts our hypothesis. If every alternate linkage has approximately zero rotation (a type II linkage) then successive disaccharide repeats are oriented equally about the chain axis. The 1eq→3eq bond has precisely this property of being a dummy linkage for these polydisaccharides.

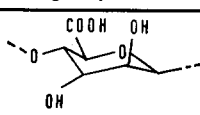
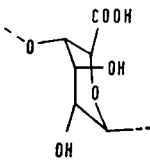
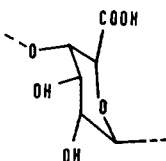
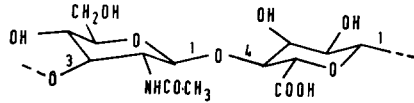
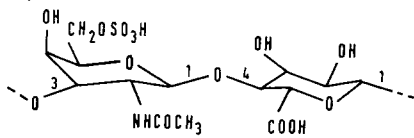
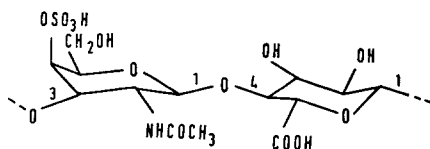
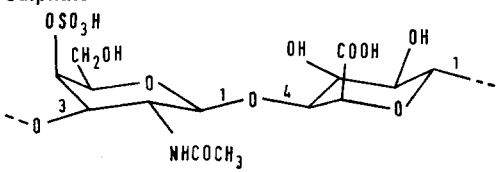
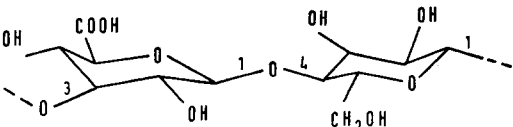
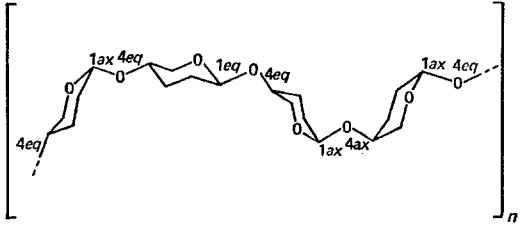
Geometrical framework of connective tissue polyuronides

Reference to Table 1 shows how hyaluronic acid is the parent molecule to which the other connective tissue polyuronides are chemically related. It is then meaningful to study the great variety of conformations deduced from the experimental data shown in Figures 3-6. The free acid, as predicted in the previous section has a two-fold screw axis and on forming univalent salts, three-fold (Figure 4a) and even four-fold forms (Figure 4b) are displayed. In addition Figure 4c represents a structure with a reduced axial periodicity which is best interpretable as a double helix. Of these forms the prevalence of the three-fold conformation is indicated by its occurrence in three distinct crystalline lattices in the sodium salt alone.

The proposed models shown in Figures 3-6 obey certain constraints derived from the X-ray diffraction pattern together with certain stereochemical criteria. First, the projected axial covalent repeat (*h*) and the number of repeat units per turn of helix (*n*) places an overall constraint on each particular model. Secondly, we have chosen left-handed helices since they appear more probable on stereochemical examination. This assumption, however, does not weaken any of the arguments presented in this report. Thirdly, the torsional angles ϕ and ψ for both the 1→4 and 1→3 glycosidic linkages, for the two-fold conformation, have been

* The symbols 'eq' and 'ax' are abbreviations for *equatorial* and *axial* dispositions of bonds which lie approximately in the plane and perpendicular to the plane of the sugar ring respectively (see ref 30 for a more detailed definition).

Table 1 Details of the polyuronides under consideration

Polyuronic acid	Chemical and structural repeating sequences	Probable chair conformation ^c	Glycosidic linkages	Typical occurrence
Polymonosaccharides: poly(D-mannuronic acid)	D-mannuronic acid 	C1	1eq→4eq	Cell wall tissue of brown algae
poly(L-guluronic acid)	L-guluronic acid 	1C	1ax→4ax	Intercellular region of brown algae
pectin	esterified D-galacturonic acid 	C1	1ax→4ax	Intercellular adhesive in fruit
Polydisaccharides: hyaluronic acid	<i>N</i> -acetylglucosamine D-glucuronic acid 	both C1	1eq→4eq alternating with 1eq→3eq	Vitreous humour of the eye, human umbilical cord, synovial fluid
chondroitin-6-sulphate (chondroitin sulphate C or D)	<i>N</i> -acetylgalactosamine 6-sulphate D-glucuronic acid 	both C1	1eq→4eq alternating with 1eq→3eq	Intercellular matrix in cartilage
chondroitin-4-sulphate (chondroitin sulphate A)	<i>N</i> -acetylgalactosamine 4-sulphate D-glucuronic acid 	both C1	1eq→4eq alternating with 1eq→3eq	Intercellular matrix in cartilage
dermatan sulphate (chondroitin sulphate B)	<i>N</i> -acetylgalactosamine 4-sulphate L-iduronic acid 	both C1	1eq→4eq alternating with 1eq→3eq	Intercellular matrix in skin
pneumococcus ^a type III	glucuronic acid glucose 	both C1	1eq→4eq alternating with 1eq→3eq	Gelatinous envelope covering pneumococcus bacteria
Polytetrasaccharides: heparin ^b (one of three possible structures ¹⁵)	sulphated <i>N</i> -acetylglucosamine D-glucuronic acid sulphated <i>N</i> -acetylglucosamine L-iduronic acid 	C1 and 1C	1ax→4eq, 1eq→4eq, 1ax→4ax, 1ax→4eq	Liver tissue
heparan sulphate	Similar to heparin but usually with only one sulphated group per tetrasaccharide repeat	C1 and 1C	similar to heparin	Human aorta

Footnotes—see page 267

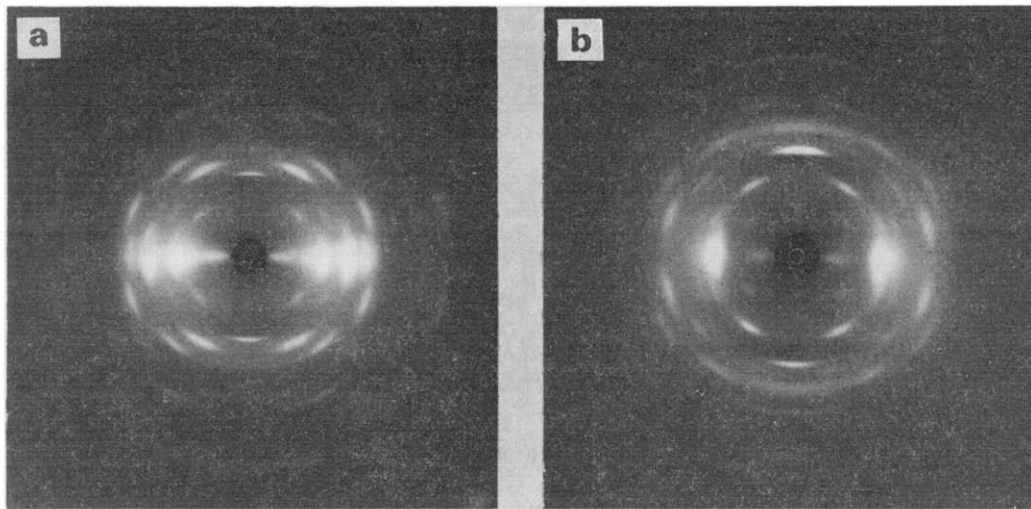


Figure 2 X-ray fibre diffraction photographs. (a) Poly(mannuronic acid): the reflections index on an orthorhombic unit cell with $a=0.76$ nm, $b=0.86$ nm and c (fibre axis)= 1.04 nm. The pattern is interpreted as a two-fold helix with the D-mannuronic acid units in the C1 chair conformation. (b) Sodium poly(D-mannuronate): here there has been an increase in the fibre repeat from 1.04 nm to 1.51 nm with meridional reflections occurring on every third layer line. The pattern clearly indicates a three-fold helical conformation

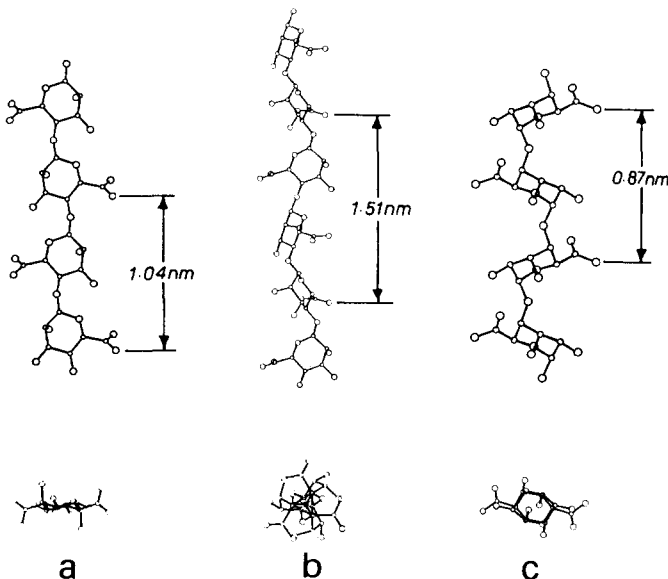


Figure 3 Computer drawn chain conformation of: (a) the two-fold poly(mannuronic acid) helix, in directions perpendicular and parallel to the chain axis; and (b) corresponding projections for the three-fold sodium salt form. [This change from two-fold to three-fold, on formation of the univalent salt is noticed in a number of polyuronides and may be regarded as typical behaviour of a $1e_q \rightarrow 4e_q$ glycosidic linkage.] (c) The two-fold poly(guluronic acid) helix, in directions perpendicular and parallel to the chain axis. Note the pronounced zig-zag shape of the polymer, the clefts providing sites for divalent cations such as calcium. The interaction between the guluronic acid segments in the alginate polymer provide the junction points in the polymeric gel

chosen close to the centre of the stereochemical allowed region. In deriving the three-fold and four-fold conformations the major part of the rotation is about the $1 \rightarrow 4$ glycosidic linkage. In the case of the double helix conformation an additional rotation has been allowed

about the $1 \rightarrow 3$ glycosidic linkage in order to reduce the value of h to the observed lower value. All the models have been checked for short contacts and found to be stereochemically feasible.

Application of structure refinement procedures based on least squares methodology might possibly enable more accurate structures to be formulated. However, this is by no means a proven technique and would necessarily have to take full account of the large volumes occupied by organized water within the crystal lattice.

We can suggest that the modifications to the hyaluronic acid geometrical framework³⁴ necessary to achieve the other mammalian connective tissue polyuronides are fourfold: (a) change of linkage between hexosamine and uronic acid moiety; (b) change of *N*-acetylhexosamine; (c) polymer level inversion of glucuronic \rightarrow iduronic acid; (d) polymer level sulphation.

Chondroitin-4-sulphate possesses a chemical structure³⁵ which departs from that of hyaluronate in only two respects, namely points (b) and (d) above and is a simple analogue in which to observe conformational changes engendered by these modifications. Such work as exists shows both two and three-fold conformations with the same helical parameters as observed for hyaluronate, though the unit cell dimensions increase commensurately with the importation of a sulphate ester group¹⁴.

Chondroitin-6-sulphate and dermatan sulphate are close relatives of chondroitin-4-sulphate, differing respectively in the position of sulphate ester and in the nature of the hexuronic acid moiety [type (c) modification]³⁶. These polymers also present similar three-fold helices (Figure 5) and, interestingly, all the chondroitin and dermatan sulphates give unit cell dimensions which are very closely related. This indicates that the gross features of the structure are not predicated solely by the position of the sulphate groups and suggest that

Footnotes to Table 1:

^a X-ray fibre diffraction patterns obtained from this material supplied by Professor M. Heidelberger clearly indicate a three-fold helical conformation although the axial rise per disaccharide is in the range 0.91 to 0.95 nm (E. D. T. Atkins, unpublished results)

^b The structure proposed is one of a number of possibilities which are compatible with the tetrasaccharide repeat of 1.59 nm¹⁵

^c As determined by X-ray fibre diffraction of solid state preparations

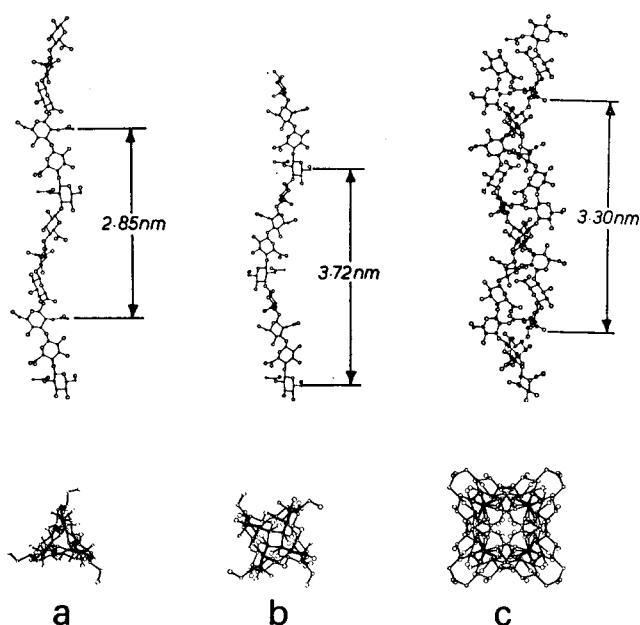


Figure 4 Computer drawn chain conformations of: (a) the three-fold helical conformation for sodium hyaluronate. This conformation has been observed to pack in a number of two-dimensional modes, e.g. two hexagonal lattices with $a=1.17\text{nm}$ and 1.87nm respectively have been reported¹¹ together with the rectangular mode shown in *Figure 1b*. The projection down the chain axis (bottom) is on a different scale; (b) the four-fold helical conformation for potassium hyaluronate. The published X-ray pattern¹⁷ has many features in common with that shown in *Figure 1a* but the layer line repeat of 3.72nm , i.e. 0.42nm greater than in *Figure 1a* enables the possibility of two chains intertwining to be ruled out on stereochemical packing criteria; (c) two antiparallel hyaluronate chains (see *Figure 1a*) intertwining to form a double helix¹⁶. The individual chains are four-fold helices similar to that shown in *Figure 4b* but compressed axially from a repeat of 3.72nm to 3.30nm . This allows the chains to intertwine^{16,17}. Note that the carboxyl groups are buried in the centre of the molecule. Double helix formation is thought to be the basic mechanism of gel formation³¹

water may influence the ordering of these molecules. Chondroitin-6-sulphate and dermatan sulphate display forms that have a crystallographic tetrasaccharide repeat which indicates differences in ionic environment of otherwise identical disaccharide units.

The formal similarity in C(5) inversion between glucuronic and iduronic acid in these connective tissue polymers is reminiscent of the mannuronic and guluronic acid transition which resulted in chair inversion. The C1 conformation for L-iduronic acid disposes the large carboxyl group in the energetically unfavoured axial position³⁶. It is possible, therefore, that L-iduronic acid in dermatan sulphate might be in the alternative 1C form, but the axial periodicities from X-ray evidence eliminate this possibility, at least for two of the three observed conformations (*Figure 6b*)¹⁸.

The most complicated chemical structures in the connective tissue polyuronides are those of heparan sulphate and heparin which, however, are still encompassed within the framework and modifications outlined above^{1, 37-39}. Their covalent structures are incompletely established but are believed to be related and may be described as an alternative sequence of glucuronic or iduronic acid moieties with interspaced hexosamine units. Heparan sulphate is probably a block copolymer with parts of the chains principally *N*-sulphated and others *N*-acetylated, and with variable sulphate content.

Heparin has a high ratio of five sulphates to four saccharide residues, the sulphates occurring in *N*-sulphate, *O*-sulphate and 6-sulphate configurations. The glycosidic linkages are all thought to be 1→4 in contrast to the hyaluronates and chondroitins.

Several forms of heparan sulphate have been crystallized. X-ray photographs (*Figure 1g*) show axial periodicities which are consistent with a tetrasaccharide repeat¹³. The measured periodicities exclude an uniquely α , 1→4 linkage system since they exceed the maximum extension obtainable for such a polysaccharide. Chemical evidence from the well studied and cognate polymer, heparin, indicates the presence of β -linkages, and an attractive model which conforms with the axial periodicities, and complies with linkage rules, would be one composed of alternating α and β linkages. Conformational flexibility is still evidenced in heparan sulphate by the crystallization of a calcium salt with a sufficiently decreased axial periodicity to suggest a double helical structure (see *Figure 1g*).

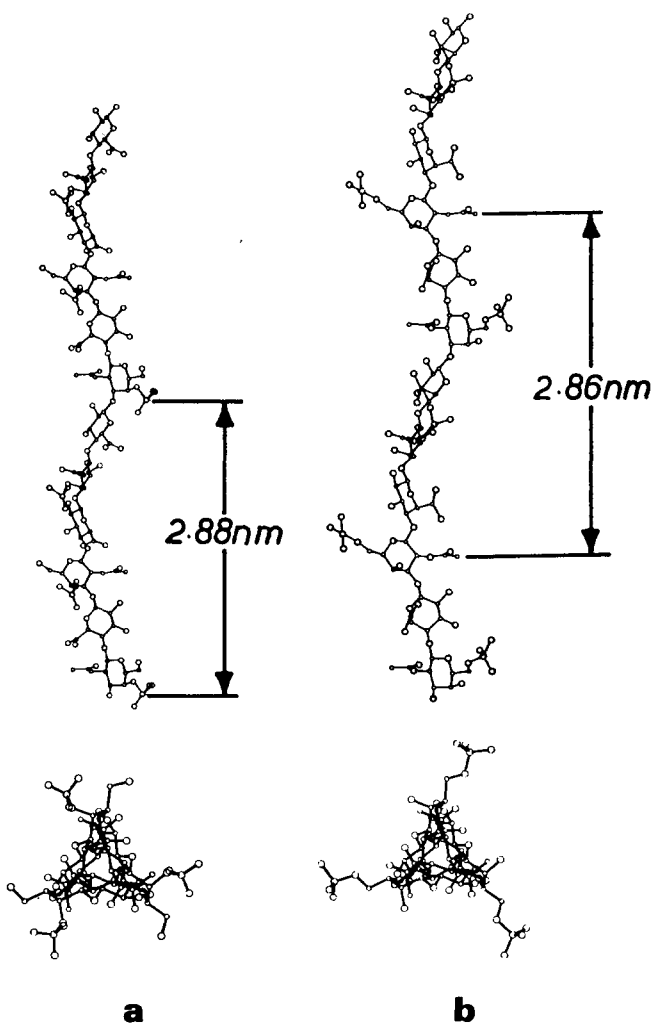


Figure 5 Computer drawn projections of the three-fold helical conformations obtained from: (a) chondroitin-4-sulphate: the X-ray pattern is shown in *Figure 1c*. The layer line repeat of 2.88nm is a little higher than that found for the hyaluronates. Comparison with the projection, as viewed down the helix axis of sodium hyaluronate (*Figure 4a*) shows that the sulphate in the axial 4-position is relatively close to the helix axis; (b) chondroitin-6-sulphate: this conformation is deduced from the X-ray pattern shown in *Figure 1d*. Note how the sulphate groups in the 6-position extend well beyond the normal periphery of the molecule

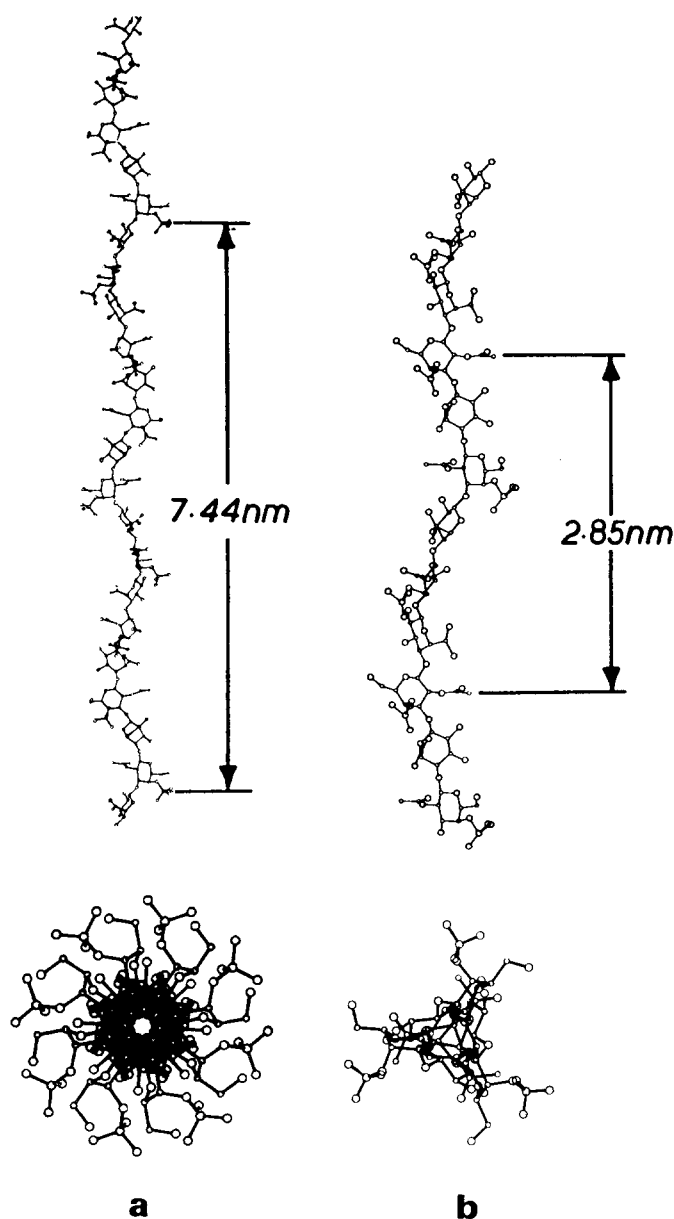


Figure 6 Computer drawn chain conformations of: (a) an 8/-3 helix (eight disaccharide units in three left-handed turns) of dermatan sulphate. Projections both perpendicular to, and down the helix axis are shown on different scales. This conformation has been proposed¹⁸ to explain the X-ray diffraction pattern shown in *Figure 1e*. An 8/-3 helix may be thought of as a 2.67/-1 helix and occurs between a two-fold and a three-fold helix; (b) a three-fold helix of dermatan sulphate which can be formed¹⁸ from the helix shown in *Figure 6a*

The X-ray pattern (*Figure 1h*) of the sodium salt of heparin is consistent with one chain comprising a tetrasaccharide repeat unit passing through the unit cell. The material crystallizes in the fibrous form despite its low molecular weight, and the X-ray evidence indicates a polymer length of only 16 nm equivalent to 10 structural units. The axial periodicity, although less than that observed for heparan sulphates still excludes an all α -linked model. In heparin, the iduronic acid becomes C(2) *O*-sulphated. We have previously indicated that this acid component of dermatan sulphate in the solid state is in the C1 conformation. The axial periodicity in heparin, however, suggests that iduronic acid in this polymer may well be in the 1C form. Could it be that the process of sulphation at C(2) triggers a change in the chair and chain conformation?

CHARGE

The carboxyl groups of the polyuronides are located by definition only on C(5) of the pyranose ring. Sulphate ester groups are introduced in a variety of positions after polymerization is completed. Both groups require complicated biochemical enzymatic mechanisms for their incorporation into the carbohydrate backbone and prompt the question why these particular charges are needed. At present all we can document is their nature and relative positions.

The radial distances of the carboxyl groups in these polymers are rarely more than 0.3 nm from the helix axis but are clearly dependent on the conformation adopted. The double-helical form of hyaluronic acid appears to bury its carboxyl groups within the interior of the molecule effectively suppressing the polyelectrolyte character of the molecule. The radial distances of the outermost oxygens in the sulphate ester groups are about 0.6 nm for chondroitin-4-sulphate and dermatan sulphate and 0.8 nm for chondroitin-6-sulphate. Thus, the sulphate ester groups are perimetric charges and must play a dominant role in chain-chain interactions.

Do sulphate ester groups interact with carboxyl groups? The fact that there is a homologous series of three-fold hyaluronates, chondroitin-4-sulphates, dermatan sulphates and chondroitin-6-sulphates suggests that the sulphate ester groups do not perturb the conformation by virtue of any interaction (either steric or electrostatic) with the carboxyl groups.

The carboxyl groups have only a small degree of conformational freedom because of both the torsional potential energy barriers about the C(5)-C(6) bond and because of van der Waals repulsions with atoms of the sugar ring. By contrast the sulphate ester groups are better able to dispose themselves to optimize interactions with their counterions—this being particularly so for chondroitin-6-sulphate which has an extra bond to provide rotational freedom.

So far charge has been considered in isolation, but preliminary results suggest that the influence of the counterion in conditioning the type of structure generated may be considerable. In particular, the valency and ion size may be ultimate determinants in effecting single to multi-strand conversions.

We have seen that there is great backbone flexibility in hyaluronic acid and its salts. The increasing incorporation of large charged groups, results in a compromise between chain flexibility and polyanionic character.

WATER

Hydrodynamic data have provided ample groundwork to indicate the importance of water in these polymer systems. So far our attention has been directed to the molecular conformation derivable from a small proportion of the X-ray diffraction data. Unit cells dimensions extractable from all the spacings, offer a bulk representation of the water content associated with these polymers.

An examination of volumes of the unit cells of all available polysaccharide structures shows that the molar volume contributions of the constituent groups are additive (see *Table 2*). This is a well recognized principle in structural chemistry (see for example Bondi⁴⁰). If the number of saccharide residues per unit cell is known

Table 2 Molar volume contributions of substituent groups in crystalline polysaccharide structures

Group	Molar volume component (nm ³)
Pyranose residue ^a	0.165 ± 0.005
-O.CO.CH ₃ ^{b,c}	0.068 ± 0.003
-NH.CO.CH ₃ ^{b,d}	0.067 ± 0.003
-O.SO ₃ ^{b,e} (anhydrous)	0.065 ± 0.010
H ₂ O ^e (crystalline)	0.025 ± 0.005

^a Volume contribution to polymer of a pyranose residue with principally equatorial substituents. Evaluated from the unit cell dimensions of the various modifications of cellulose, mannan and amylose⁴¹

^b Volume to be added when such a group replaces an -OH group on the pyranose ring

^c Evaluated from unit cell dimensions of cellulose triacetate⁴²

^d Evaluated from unit cell dimensions of chitin⁴¹

^e Adapted from ref 43

Table 3 Water content of certain crystalline polyuronides as derived from published results¹¹⁻¹⁸

Material	Calculated 'dry' volume/disaccharide (nm ³)	Observed volume/disaccharide (nm ³)	No. of water molecules/disaccharide
Hyaluronic acid	0.400	0.403-0.582	0-7
Heparan sulphate	0.420 ^a	0.593	7
Chondroitin-4-sulphate	0.465	0.656-0.865	8-16
Dermatan sulphate	0.465	0.707-0.818	10-14
Chondroitin-6-sulphate	0.465	0.847-0.931	15-19
Heparin	0.500 ^a	0.894	16

^a Calculated on the basis of the sulphate content of material used in this investigation

then it is possible to quantitate their molar content (see Table 3).

The *uncharged* polyuronide structures contain little or no water in the solid state. However, water is always incorporated when the carboxyl groups are ionized (the very low pK_a value of the sulphate ester group precludes its occurrence in the uncharged state). The water associated with the charged polyuronide structures may be categorized as anion hydrate, cation hydrate and as water required to fill space.

We can relate one or two water molecules with each carboxyl group and at least six water molecules per sulphate ester group. In general the three-fold helical conformations have high water contents. There are certain constant features of all the sodium hyaluronate trigonal lattices which indicate the presence of water structure. These are: the intensities of the meridional reflections; and the inference, in all these structures, of a lattice site of constant dimensions which does not contain polymer. This indicates an organized water structure. In contrast the double helical form of hyaluronic acid can be readily dehydrated to zero water content which is consistent with the buried carboxyl groups.

CONCLUSIONS

Few of the questions broached in the introduction to this article have been even partly answered. What has been achieved is that for the first time the sufficiency of information permits the polyuronides to be discussed

as a coherent group in terms of their molecular architecture. We have seen how the chemical linkage conditions a backbone flexibility susceptible to the linkage rules, which allows even distribution of bulky substituents. With the creation of charge and its concomitant importation of electrostatic energy there is a perturbation of the potential energy surface towards a new stable conformation of the chain. Additionally, charge directs interchain relationships either by the nature of the counterion or by the position of the polyanion substituent group. Externally water constitutes the universal environment and the structures of these polymers are controlled by the organization of interstitial water.

Certain principles have emerged therefore which require for their further confirmation a study of chemically modified polyuronides. Thus, for instance, the functions of *N*-acetyl, carboxyl and sulphate groups may become clearer by studying differences between normal and chemically modified molecules. In this way we may understand why hyaluronic acid is never sulphated and why heparin contains such an abundance of positional substituents.

Detailed structure determinations should illuminate ionic environments and the nature of chain-chain and chain-water interactions. They should also elucidate the incompletely formulated chemical structures of heparan sulphate and heparin. There is thus an urgent need for hydrodynamic measurements on the solution properties of these polymer systems, to unravel the meaning of interaction parameters and to extend where possible the solid-state findings into the realms of dilute solutions. Likewise the promise now exists that other carbohydrate oligomeric structures will succumb to X-ray diffraction techniques even if heterodisperse.

Whereas in the past, the determination of structure of other biopolymers has bred the belief that in this detailed examination is the function apparent, it is worth a final caution that although the polyuronides are structural polymers, the secret of their function does not reside directly in this term but rather, in the way that this structure may control the external environment.

REFERENCES

- Bettelheim, F. A. in 'Biological Polyelectrolytes' (Ed. A. Veis), Marcel Dekker, New York, 1970
- 'Chemistry and Molecular Biology of the Intercellular Matrix' (Ed. E. A. Balazs), Vol II, Academic Press, London and New York, 1970
- Jeanloz, R. W. in 'The Carbohydrates' (Eds W. W. Pigman and D. Horton), Academic Press, New York, 1970, p 589
- Mathews, M. B. in 'The Connective Tissue' (Eds B. M. Wagner and D. E. Smith), Williams and Wilkins, Baltimore, 1967, p 304
- Palmer, K. J. and Hartzog, M. B. *J. Am. Chem. Soc.* 1945, **67**, 2122
- Astbury, W. T. *Nature* 1945, **155**, 667
- Bettelheim, F. A. *Nature* 1958, **182**, 1301
- Bettelheim, F. A. *Biochim. Biophys. Acta* 1964, **83**, 350
- Atkins, E. D. T. and Mackie, W. *Biopolymers* 1972, **11**, 1685
- Atkins, E. D. T. and Sheehan, J. K. *Biochem. J.* 1971, **125**, 92; *Nature (New Biol.)* 1972, **235**, 253
- Atkins, E. D. T., Phelps, C. F. and Sheehan, J. K. *Biochem. J.* 1972, **128**, 1255
- Atkins, E. D. T., Gaussen, R., Isaac, D. H., Nandanwar, V. and Sheehan, J. K. *J. Polym. Sci. (B)* 1972, **10**, 863
- Atkins, E. D. T. and Laurent, T. C. *Biochem. J.* 1973, **133**, 603
- Isaac, D. H. and Atkins, E. D. T. *Nature (New Biol.)* 1973, **244**, 252

- 15 Nieduszynski, I. A. and Atkins, E. D. T. *Biochem. J.* 1973, **135**, 729
- 16 Dea, I. C. M. *et al. Science* 1973, **179**, 560
- 17 Atkins, E. D. T. and Sheehan, J. K. *Science* 1973, **179**, 562
- 18 Atkins, E. D. T. and Isaac, D. H. *J. Mol. Biol.* 1973, **80**, 773
- 19 Arnott, S., Guss, J. M., Hukins, D. W. L. and Mathews, M. B. *Science* 1973, **180**, 743
- 20 Haug, A., Larson, B. and Smidsrød, U. *Acta Chem. Scand.* 1966, **20**, 183
- 21 Ramachandran, G. N., Ramakrishnan, C. and Sasisakaran, V. in 'Aspects of Protein Structure' (Ed. G. N. Ramachandran), Academic Press, New York, 1963, p 121
- 22 Rao, V. S. R., Sundararajan, R. R., Ramakrishnan, C. and Ramachandran, G. N. in 'Conformation of Biopolymers', Academic Press, New York, 1967, Vol 11, p 721
- 23 Rees, D. A. and Skerrett, R. J. *Carbohyd. Res.* 1968, **7**, 334
- 24 Rees, D. A. *J. Chem. Soc. (B)* 1969, p 217
- 25 Sathyanarayana, B. K. and Rao, V. S. R. *Biopolymers* 1971, **10**, 1605
- 26 Atkins, E. D. T., Mackie, W., Parker, K. D. and Smolko, E. E. *J. Polym. Sci. (B)* 1971, **9**, 311; Atkins, E. D. T., Nieduszynski, I. A., Mackie, W., Parker, K. D. and Smolko, E. E. *Biopolymers* 1973, **12**, 1865
- 27 Haug, A. and Larsen, B. *Carbohyd. Res.* 1971, **17**, 345
- 28 Whittington, S. *Biopolymers* 1971, **10**, 1481
- 29 Mackie, W. *Biochem. J.* 1971, **125**, 89
- 30 Sundaralingham, M. *Biopolymers* 1968, **6**, 189
- 31 Rees, D. A. *Biochem. J.* 1972, **126**, 257
- 32 Muir, H. *Am. J. Med.* 1969, **47**, 673
- 33 Brimacombe, J. S. and Webber, J. M. 'Mucopolysaccharides: Chemical Structure, Distribution and Isolation', Elsevier, Amsterdam, 1964
- 34 Laurent, T. C. in 'Chemistry and Molecular Biology of the Intercellular Matrix' (Ed. E. A. Balazs), Academic Press, London and New York, 1970, Vol II, p 703
- 35 Roden, L. *ibid.* p 797
- 36 Fransson, L.-Å. *ibid.* p 823
- 37 Lindahl, U. *ibid.* p 943
- 38 Cifonelli, J. A. and Dorfman, A. *Biochem. Biophys. Res. Commun.* 1962, **7**, 41
- 39 Helting, T. and Lindahl, U. *J. Biol. Chem.* 1971, **246**, 5442
- 40 Bondi, A. *J. Phys. Chem.* 1964, **68**, 441
- 41 Marchessault, R. H. and Sarko, A. *Adv. Carbohyd. Chem.* 1967, **22**, 421
- 42 Dulmage, W. J. *J. Polym. Sci.* 1957, **26**, 277
- 43 'Handbook of Chemistry and Physics', 51st edn, Chemical Rubber Co., pp B217-218

Effect of molecular weight on the morphology of melt-crystallized PTFE and the occurrence of row-nucleated crystallization*

M. J. Gall

Wilkinson Sword (Research) Ltd, Colnbrook, Slough SL3 0HA, UK
(Received 27 November 1973; revised 22 January 1974)

The crystallites obtained from the crystallization of the melt of as-polymerized, dispersion grade polytetrafluoroethylene (PTFE) samples in the form of thin films ($\sim 1 \mu\text{m}$) differ in size depending on the molecular weight of the polymer and its thermal history. The production of large crystallites is favoured by slow cooling rates, high maximum melt temperatures and low molecular weight polymer. Subjecting thin, crystallized PTFE films on blade edges to cutting leaves a very thin ($\sim 10 \text{ nm}$) oriented film of polymer, which can melt to recrystallize in a row-nucleated form. Reduction of the molecular weight of the PTFE lowers the tendency to adopt this form.

INTRODUCTION

The commercial product of the emulsion polymerization of tetrafluoroethylene (TFE) yields 'dispersion' grades of PTFE in the form of submicron, oval particles suspended in water¹⁻³. Depending on the manufacturer and his process the number-average molecular weight, M_n , is estimated to be in the range 5-10 million. In the dispersion particles the polymer exists in a highly crystalline state, usually greater than 95% crystalline by weight. On the basis of electron diffraction studies²⁻⁴ it is thought that the particles are made up from single crystal units, possibly with the PTFE molecules in an extended-chain form³. Also dependent on the polymerization process is the appearance of thin rod-like forms, typically $0.05 \times 2 \mu\text{m}$, where the PTFE molecules are aligned parallel to the rod long axis.

The rapid melting and crystallization of particles containing highly organized arrays of polymer molecules is of interest in the case of PTFE since the high melt viscosity of this polymer^{1,2} can inhibit the total loss of structure on melting.

Any structure retained in the melt will clearly affect subsequent crystallization and morphology. It is known from optical depolarization measurements² that after high molecular weight PTFE is melted a small amount of order persists in the melt for long periods of time, even when the sample is held at a high temperature; for example, traces of order were still present in a melt of 'granular' PTFE (a grade of somewhat higher molecular weight than most dispersion grades) after 5 h at 375°C. The effect of rapid melting and crystallization on as-polymerized dispersion PTFE and samples of lower molecular weight polymer are reported in this paper.

* Presented at the Polymer Physics Group (Institute of Physics) Biennial Conference, Shrivenham, September 1973.

EXPERIMENTAL

Preparation of lower molecular weight PTFE samples by γ -irradiation

In the presence of a radical scavenger, such as oxygen, γ -irradiation reduces the molecular weight of PTFE^{5,6} since chain scission is the predominant reaction over branching and the production of unsaturation. By controlling the amount of available oxygen and the radiation dose the reduction in molecular weight can be quite selective.

If the concentration of available oxygen is low the radicals generated by the irradiation of highly crystalline material can recombine due to the cage effect. This

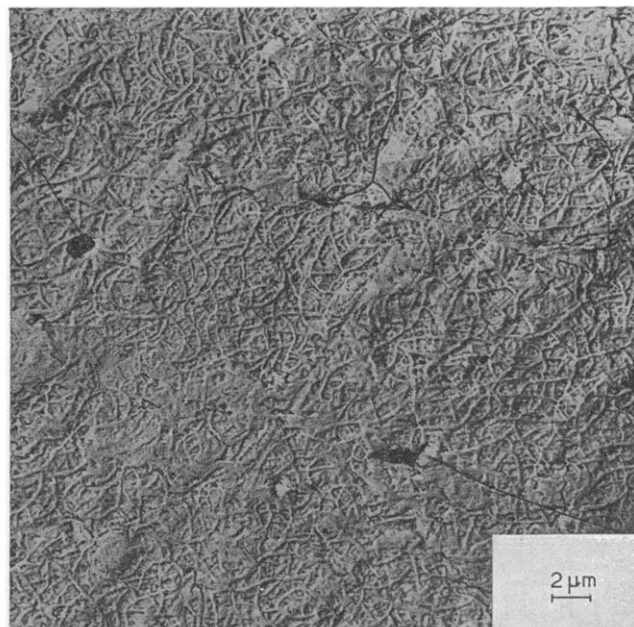


Figure 1 PTFE ($M_n \sim 8 \times 10^6$) after cycle to 440°C at 12°C/min, cooling at 24°C/min

method of irradiation of PTFE dispersion particles possesses the advantage owing to the small particle size that the availability of oxygen to the polymer throughout is not as uneven as would be the case with larger particles. PTFE dispersions with and without oxygen bubbling through them were subjected to γ -irradiation from a ^{60}Co source at the UK Atomic Energy Laboratories, Harwell at doses of from 1 to 20 Mrad. The molecular weight of the resulting products was estimated by a standard specific gravity method using known samples supplied as calibrants.

Preparation of micron-thick films of PTFE

The films were prepared by spraying commercial and irradiated dispersions on to razor blade edges so as to give a layer 1–2 μm thick of dispersion particles.

The aqueous dispersions employed were GP1 (ICD), Teflon 30N (Du Pont) and Halon D6000 (Allied Chemical

Corp.) and the non-aqueous telomer dispersion Vydax 1000 (Du Pont). For the sake of consistency the results reported in this paper refer to PTFE on a metal substrate of 20–40 nm of chromium on stainless steel, although very similar behaviour was observed on a variety of other substrates, e.g. stainless and carbon steels. The blades coated with PTFE dispersion were heated in a 3:1 hydrogen–nitrogen gas mixture ambient to a pre-arranged temperature above the melting point, which can be taken⁷ as about 340°C for as-polymerized high molecular weight PTFE at heating rates in the region of 10°C/min. The nitrogen in the ambient gas is inert to PTFE and the hydrogen component provides effective heat transfer although it should be remembered that reaction between hydrogen and PTFE⁸ becomes effective above 450°C. All commercial dispersions contain around 5%, relative to the PTFE content, of wetting agents. It is stated² that these are removed during heating up to

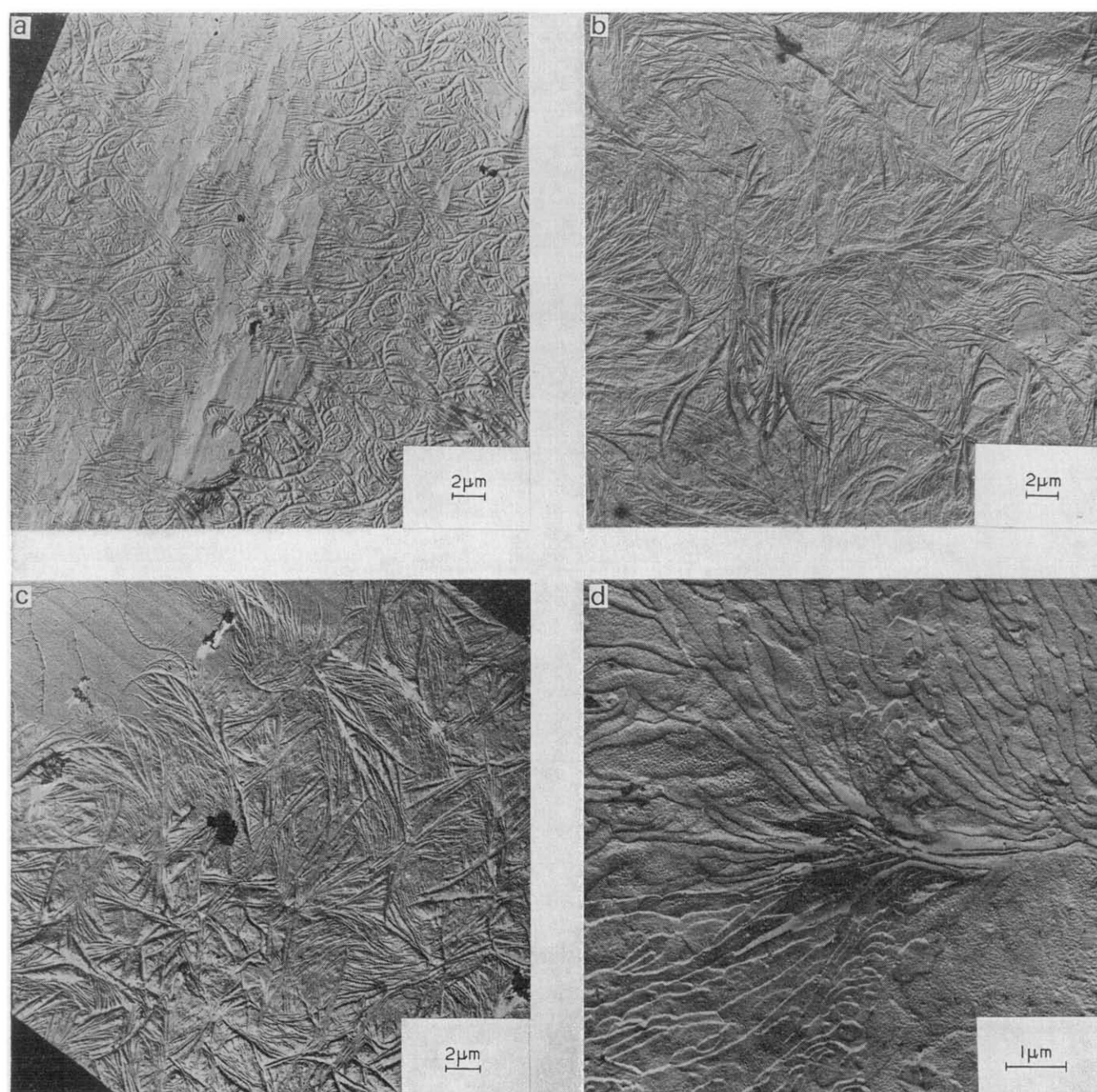


Figure 2 PTFE after cycle to 400°C at 12°C/min, cooling at 24°C/min. (a) $M_n \sim 3 \times 10^5$; (b) $M_n \sim 10^5$; (c) $M_n \sim 5 \times 10^4$; (d) $M_n \sim 2 \times 10^4$

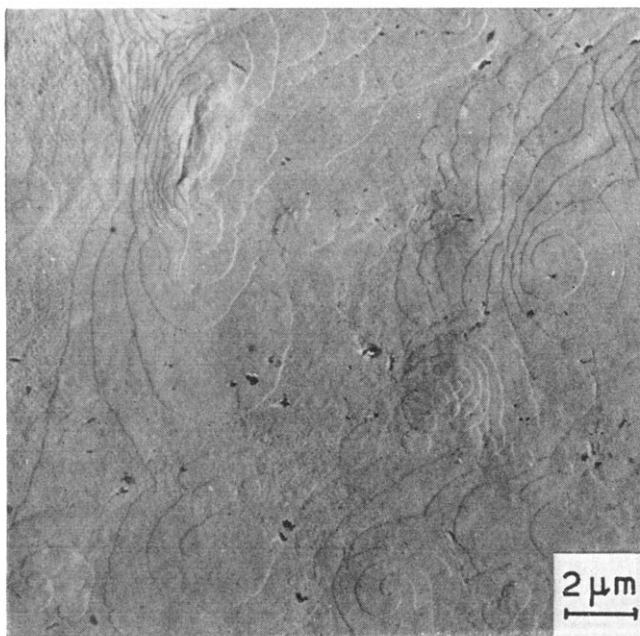


Figure 3 PTFE ($M_n \sim 2 \times 10^4$) after the same cycle as samples illustrated in Figure 2

300°C, i.e. before the PTFE begins to melt.

The PTFE melts were cooled at a variety of rates to give continuous films of maximum thickness $\sim 1 \mu\text{m}$.

Electron microscopy

Electron micrographs were obtained after replication of the top surface, i.e. that remote from the substrate, of the PTFE film by a standard two-stage replication method⁹, using polystyrene and carbon replicas. These micrographs were obtained using a Metropolitan Vickers EM6 microscope. Scanning electron micrographs were obtained using a Cambridge Stereoscan.

RESULTS

In the case of thin films at very fast heating and cooling rates the original particulate form of the film degrades and small lamellae can be distinguished. With PTFE of molecular weight $\sim 8 \times 10^6$ taken to 400°C at 80°C/min and cooled at 100°C/min lamellae of typical dimensions $0.1 \times 0.4 \mu\text{m}$ long are found. At slower heating and cooling rates, around 10°C/min, the lamellae are distinct and larger, typical dimensions being $0.25 \times 1.25 \mu\text{m}$ long when the same type of PTFE is taken to a maximum temperature of 400°C. They resemble the crystallites grown from PTFE dispersion particles on a glass substrate¹⁰. Like the familiar fracture surface replicas^{1,2} the lamellae show at high magnification striations perpendicular to their long dimension. At very slow cooling rates, around 0.08°C/min, Mellilo and Wunderlich¹¹ have grown lamellae, typically $1.5 \times 20 \mu\text{m}$ long, radially disposed so as to form spherulitic structures.

By raising the maximum temperature of the molten film while also keeping the heating and cooling rates high it is found that the crystallites elongate and grow in the form of fibrils (Figure 1) without thickening to a great extent. With a maximum temperature of 440°C and heating and cooling rates around 12°C/min typical lamellar dimensions are $0.35 \times 5 \mu\text{m}$ long. If the maximum temperature is taken much higher spherulitic forms can

be observed. These are probably formed by polymer which has been thermally degraded or which has reacted with the hydrogen content of the gas atmosphere.

The progressive reduction of molecular weight has a series of effects on the morphology of films formed in the same thermal cycle, which comprised a maximum temperature of 400°C with heating and cooling rates around 12°C/min and 24°C/min respectively.

In the first case (Figure 2a: PTFE of $M_n \sim 330\,000$) the tendency to form fibrils is apparent. As the molecular weight is reduced still further the tendency is for lamellae to stack parallel to the substrate (Figures 2b–2d) and to form sheaves. Figure 2d is an example of the low molecular weight telomer Vydax 1000 ($M_n \sim 25\,000$), which forms very similar structures to those reported for polyoxymethylene⁴. A further similarity is that spiral growths can be formed (Figure 3) with the PTFE, analogous to those found after the thermal degradation of high molecular weight polymer¹², where electron diffraction studies¹³ have shown the molecules oriented normal to the substrate surface.

Very thin films of PTFE

When high molecular weight PTFE is slid on a variety of substrates at room temperature at rates around 1 mm/sec and a normal load of 10 N, a thin film ($\sim 5 \text{ nm}$), oriented in the direction of sliding is deposited¹⁴. A similar event occurs when a PTFE coated razor blade cuts into material such as hair, nylon fibres or cellulose in the form of a paper pad at room temperature at speeds between 0.2 and 100 mm/sec, but in this case a thin film ($\sim 10 \text{ nm}$) is left on the blade. The molecular orientation is parallel to the direction of cutting¹³. In addition to this, as Figure 4 shows, fibrils are formed in the peeling process. This is reminiscent of the observations of O'Leary and Geil¹⁵, who reported the formation of fibrils with diameters of the order of 50 nm containing oriented polymer upon the abrasion, fracture and peeling of high molecular weight PTFE.

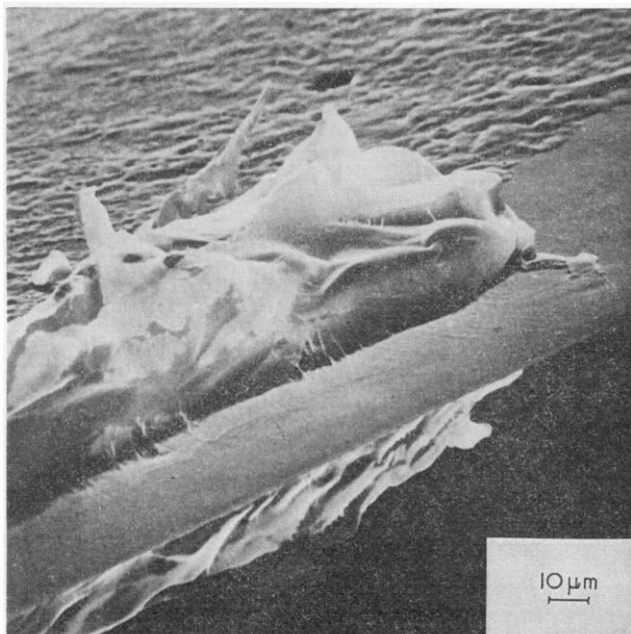


Figure 4 Scanning electron micrograph of a razor blade after cutting into a cellulose pad at room temperature at about 1 cm/sec

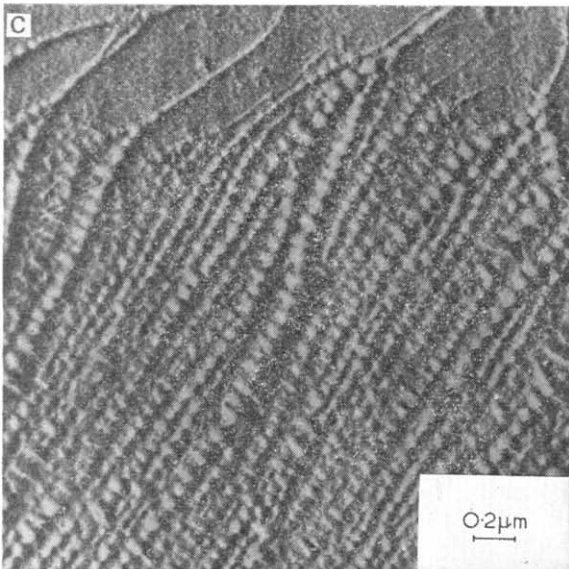
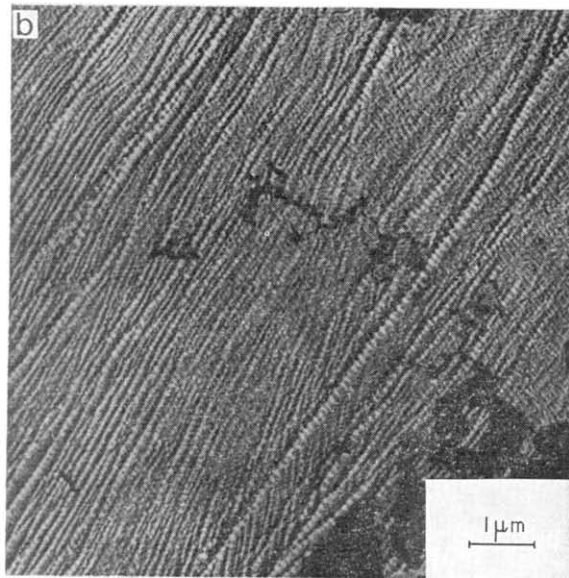
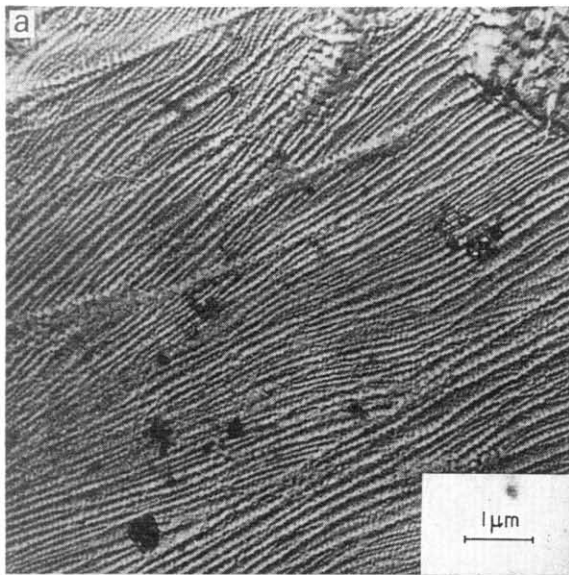


Figure 5 (a) Very thin film of PTFE ($M_n \sim 8 \times 10^6$) after cycle to 400°C at 12°C/min and cooling at 23°C/min. Unpeeled film at top right-hand corner. (b) Different area of the same sample as in (a). (c) Fibrils going across bare blade and through a region of very thin film of PTFE ($M_n \sim 8 \times 10^6$) after the same thermal cycle as the sample in (a)

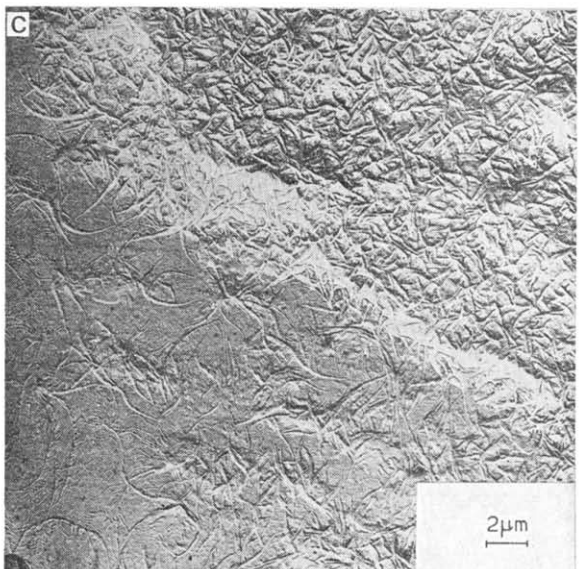
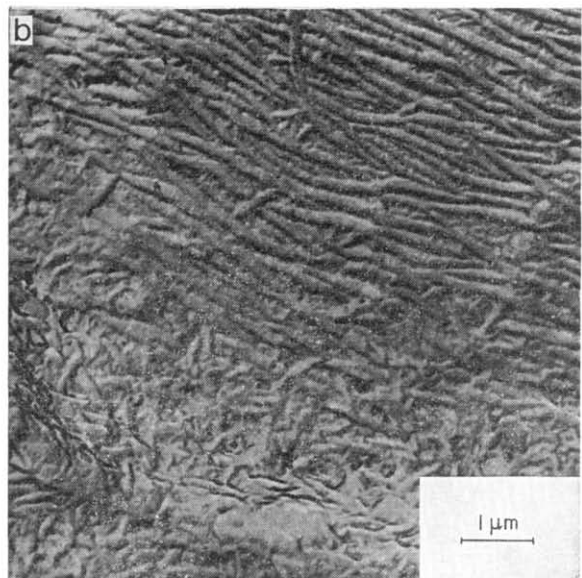
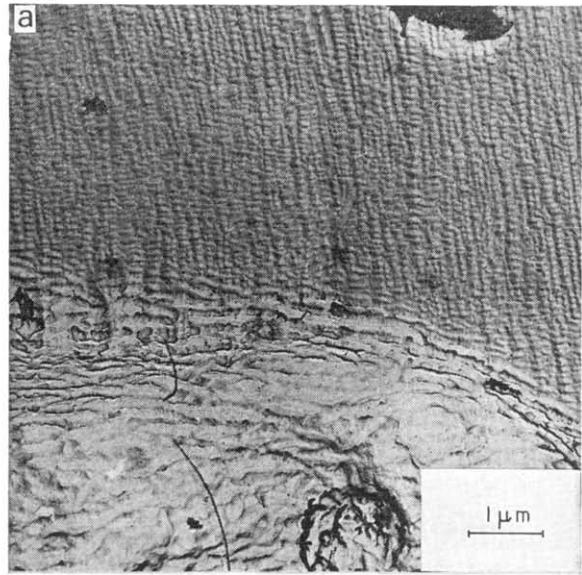


Figure 6 (a) Very thin film of PTFE ($M_n \sim 5 \times 10^6$) after cycle to 400°C at 12°C/min and cooling at 24°C/min. Unpeeled film at bottom of micrograph. (b) Very thin film of PTFE ($M_n \sim 10^6$) after the same cycle as in (a). Unpeeled film at bottom of micrograph. (c) Very thin film of PTFE ($M_n \sim 5 \times 10^5$) after the same cycle as in (a). Unpeeled film on the right of the micrograph

Subjecting a thin oriented film on a blade edge to rapid melting and crystallization shows interesting features. The bulk, i.e. unpeeled, polymer changes slightly in that the crystallites become somewhat thicker, but in the very thin film region the fibrils can be clearly discerned and they have overgrowths of crystallites (Figures 5a and 5b). These row-nucleated crystallites vary in size depending on their location, presumably owing to the variation of fibril density and availability of PTFE in the very thin film, whose thickness is not constant because of inhomogeneities in the substrate and cutting operation. In regions where fibrils pass through very thin film the ordering effect can be observed (Figure 5c).

The dimensions of the overgrowth crystallite is also governed by the thermal cycle from melting to the completion of freezing. Owing to the difference in size of crystallite overgrowth on different fibrils it is difficult to make rigorous comparisons between row-nucleated crystallites produced in different cycles. However, as an indication, it seems that for given heating and cooling rates the size is not greatly affected by an increase in maximum temperature, e.g. on samples which had been taken to 335°C and 400°C at heating and cooling rates of around 12°C/min the long dimension was approximately doubled. This may be contrasted with the effect of reduced cooling rate, e.g. cycles up to 400°C (at 12°C/min) with cooling at 23°C/min and 5°C/min produced crystallites about one-quarter as long in the first case compared with the second. In all cases the short dimension does not appear to be very sensitive to thermal cycle.

The effect of reducing molecular weight is also important. A thin film is found on cutting but the peeling process is progressively less well defined and fibrils are not discerned. Putting these films through the same rapid heating and cooling cycle yields morphologies strongly dependent on molecular weight. These are demonstrated in Figures 6a-6c, where it may be seen that as the molecular weight reaches below the five million range the central fibrils are less easily discernible and the overgrowths larger. Below molecular weights of one million the row-nucleated appearance is lost.

DISCUSSION

The crystalline morphology produced by the rapid melting and freezing of as-polymerized PTFE is for a given cycle strongly molecular weight dependent. The difference in viscosity between samples as temperature falls is largely responsible for this. For a given high molecular weight polymer the viscosity at any given temperature is the same, but slower cooling rates allow the time for larger crystallites to grow. An increase in the maximum temperature, for a given heating and cooling rate and molecular weight of PTFE, also produces longer crystallites. Since high molecular weight as-polymerized PTFE is known⁷ to superheat at the heating rates employed in this study it may be expected that in high temperature cycles the polymer is allowed to disorder itself further and fewer aggregations are left to act as crystallite nuclei during the solidification process. If the molecular weight is reduced then the degree of superheating under comparable thermal conditions is less, as is the melt viscosity, and consequently larger crystallites can be formed. At the lower

molecular weights a competing process to crystallite extension, namely spiral growth, can be seen to be progressively favoured. In the cases studied here these growths may be nucleated at the substrate surface. Irrespective of how the spiral growths are nucleated they can grow without the processes of secondary nucleation which crystallite extension requires. It has been calculated¹⁶ and demonstrated for fractionated polyethylenes¹⁷ that a low molecular weight species, i.e. one with a degree of polymerization less than 10^3 , crystallizes more slowly than those of medium degree, say 10^3 - 10^4 , at a given supercooling. Very high molecular weight species under comparable conditions crystallize more slowly owing to their increased melt viscosity. For the lower molecular weight species the free energy of nucleus formation is higher and this effect is marked at low supercoolings. For this reason it would not be surprising if the formation of features such as spiral growths were found with low molecular weight PTFE.

When thin oriented films of high molecular weight PTFE are rapidly melted and cooled it is to be expected that the superheating phenomena do not permit a large amount of destruction of order in the regions making up features such as fibrils. During cooling, these ordered regions provide nucleation sites for the overgrowth crystallites. An interesting observation was made by Mellilo and Wunderlich¹¹ who took high molecular weight PTFE samples with well characterized striations on lamellae making up a fracture surface and heated them to just below the melting point, followed by immediate cooling. They observed 'ripple decoration' on the striations which they interpreted as the formation of shallow chain-folded crystals on the striations. The diminution of the row-nucleated phenomenon after a given thermal treatment with decreasing molecular weight may be due to the lessening tendency to form fibrils in the peeling process coupled with the reduction of superheating effects and melt viscosity.

ACKNOWLEDGEMENTS

The aid of Mr H. Simon in the preparation of thin film samples and of Miss S. Hide in the making of surface replicas is gratefully acknowledged.

REFERENCES

- 1 Sperati, C. A. and Starkweather, H. W. *Fortsch. Hochpolym. Forsch.* 1961, **2**, 465
- 2 Sherratt, S. 'Encyclopedia of Chemical Technology', Wiley, New York, 1966, Vol 9, p 805
- 3 Rahl, F. J. *et al. J. Polym. Sci. (A-2)* 1972, **10**, 1337
- 4 Geil, P. H. 'Polymer Single Crystals', Wiley, New York, 1953, Vol 5
- 5 Charlesby, A. 'Atomic Radiation and Polymers', Pergamon Press, New York, 1960
- 6 Pinkerton, D. M. and Thompson, K. R. L. *J. Polym. Sci. (A-2)* 1972, **10**, 473
- 7 Hellmuth, E. *et al. Appl. Polym. Symp.* 1966, **2**, 101
- 8 Michaelson, J. D. and Wall, L. A. *J. Nat. Bur. Stand. Res.* 1957, **58**, 327
- 9 Bradley, D. E. 'Techniques for Electron Microscopy' (Ed. D. H. Kay), Blackwell, Oxford, 1965, p 119
- 10 Symons, N. K. *J. Polym. Sci.* 1963, **1**, 2843
- 11 Mellilo, L. and Wunderlich, B. *Kolloid-Z.* 1972, **250**, 417
- 12 Bunn, C. W., *et al. J. Polym. Sci.* 1958, **28**, 365
- 13 Symons, N. K. *J. 25th EMSA Meet., Chicago* 1967
- 14 Pooley, C. M. and Tabor, D. *Proc. R. Soc. (A)* 1972, **329**, 251
- 15 O'Leary, K. and Geil, P. H. *J. Appl. Phys.* 1967, **38**, 4169
- 16 Mandelkern, L. *et al. J. Phys. Chem.* 1965, **69**, 956
- 17 Mandelkern, L. *et al. J. Polym. Sci. (B)* 1968, **6**, 615

Shrinkage and chain folding in drawn poly(ethylene terephthalate) fibres*

M. P. W. Wilson

ICI Fibres, Hookstone Road, Harrogate, Yorkshire HG2 8QN, UK
(Received 9 July 1973; revised 4 October 1973)

By using an improved infra-red (i.r.) technique in a comparative study of the structural changes accompanying relatively slow shrinkage in an oven and rapid shrinkage in a hot air tube, the role of chain folding in the shrinkage of drawn poly(ethylene terephthalate) (PET) fibres has been established. It has been shown that the overall shrinkage process involves a rapid initial stage, which is associated with disorientation in the amorphous regions and is essentially responsible for the fibre length change. This is followed, if time permits, by a crystallization stage. Chain folding, as detected by i.r. spectroscopy, is associated with the later crystallization stage. Because chain folding occurs after the fibre length change it cannot be said that there is a unique, or cause and effect, relationship between chain folding and shrinkage. This picture of the shrinkage process satisfactorily combines the rubber elasticity type of approach to shrinkage with the later folded chain models. The load-extension behaviour, strength, modulus, and birefringence of yarns shrunk both in air and in oil are discussed in terms of the overall picture.

INTRODUCTION

In the simplest molecular picture thermal shrinkage of an oriented poly(ethylene terephthalate) (PET) fibre is seen as a rubber-like contraction^{1, 2}. The production of a PET fibre is taken to involve a high degree of molecular orientation along the fibre axis. To some extent this orientation may be locked in by crystallites, but in the non-crystalline regions the orientation is preserved by freezing it in when the fibre is cooled to room temperature. If the fibre is subsequently heated so as to 'unfreeze' the non-crystalline regions, then these regions become rubbery; there is a general disorientation as relatively straight molecules assume statistically more probable, and shorter, end-to-end distances, and the fibre shrinks. In short, the oriented fibre contains regions which behave as frozen stretched rubbers; thermal shrinkage is the rubber-like contraction which occurs when these regions are unfrozen. More recently Dismore and Statton³, in order to explain the large increase in low angle X-ray intensity accompanying shrinkage in nylon-6,6, suggested that shrinkage involved chain folding. In fact they found that the shrinkage of yarns during heating appeared to be governed by the number of folds which were introduced. Subsequently Statton *et al.*⁴, relying on the assignment by Koenig and Hannon⁵ of the 988 cm⁻¹ absorption in the infra-red (i.r.) spectrum to the folded chain configuration, have confirmed that chain folding occurs during the shrinkage of drawn PET above 200°C. They suggest that their results verify the close relationship, perhaps even cause and effect, between chain folding and

shrinkage. In other studies of chain folding and shrinkage in PET, Dumbleton^{6, 7} has suggested that chain folding is the basic mechanism of shrinkage in air. The additional shrinkage in oil is due to disorientation in the amorphous regions. Prevorsek and Sibilja⁸ tentatively concluded that samples having a large degree of regular chain folding are in general more ductile than those in which regular chain folding is low.

In the present work the mechanical and physical changes associated with shrinkage in air and oil have been studied and related to changes in i.r. fold band intensities. Whereas all of the workers mentioned above studied yarns which were heated for at least 1 min (except possibly Prevorsek and Sibilja who do not give experimental details), in this work an equal emphasis has been placed on yarns which have been shrunk in much shorter times (< 1 s). As a result, a more comprehensive picture of shrinkage has emerged. Essentially it is shown that there is not a cause and effect relationship between chain folding and shrinkage in PET. Rather the shrinkage (i.e. the length change) of PET fibres involves a disorientation in the non-crystalline regions. Regular chain folding is associated with a subsequent crystallization stage, which need not involve any fibre length change, and which occurs only if time is available and temperature conditions are right.

EXPERIMENTAL

In this work commercial grade PET yarns drawn ~3.5 times over a hot roller were used throughout. 167 dtex yarns with normal amounts of delustrant were used in the experiments involving oil and air oven shrinkages only (*Figures 2-9*). In order to obtain better i.r. spectra 74 dtex yarns with much less delustrant were used in

* Presented at the Polymer Physics Group (Institute of Physics) Biennial Conference, Shrivenham, September 1973.

the (subsequent) experiments when slow and rapid shrinkages were compared.

Rapid shrinkage of the yarns was effected by passing yarns from one roller, through a tube containing hot air, to a slower roller. In two sets of experiments the yarn temperatures on leaving the hot air tube were 150°C and 235°C. These temperatures were measured using a Cambridge Consultants infra-red pyrometer. The residence time of the yarn in the tube was 0.2 s. Yarns were also shrunk as skeins with no restraining load for 10 min in an air oven and for 1 min in an oil bath. These were the conditions used by Dumbleton⁷ and were sufficient to give maximum shrinkage. After immersion in oil samples were quenched and washed in carbon tetrachloride and then in a laboratory surfactant RBS 25. Control experiments showed that this washing procedure was satisfactory in so much as it eliminated any effects of residual oil on density measurements. Shrinkages were calculated according to the formula:

$$S = \frac{\text{initial length} - \text{final length}}{\text{initial length}} \times 100\%$$

In the case of the rapid shrinkages, initial and final lengths were proportional to the speeds of the rollers.

Yarns treated in air and in oil 'at constant length' were wound on to formers. This prevented shrinkage and hindered expansion, if any.

Density measurements were made in a calcium nitrate density column.

Infra-red spectra were obtained from fibre grids mounted in a Beckman IR 12 spectrometer. The grids were carefully prepared by winding yarns directly on to KBr plates with a precision winder, at a pitch at which a single close packed layer of filaments was formed on the KBr plate. The KBr plates were mounted as windows in formers which could be held both in the winder and in the spectrometer. Details are shown in Figure 1. This technique has the advantage that there is no chance of sample preparation altering microstructure.

Tensile properties were derived from data obtained on an Instron tensile testing machine. The 200 mm samples were strained at 100%/min.

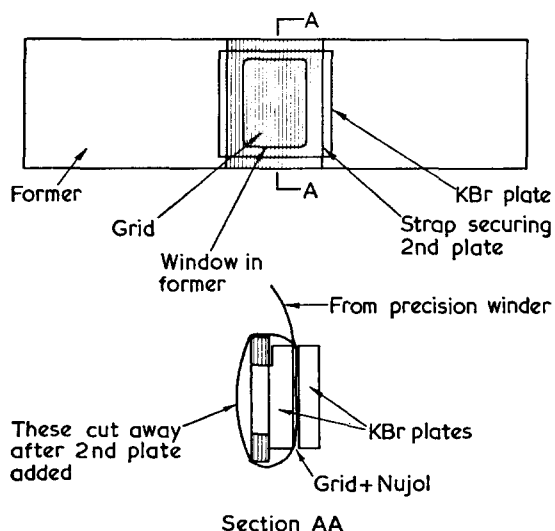


Figure 1 Fibre grid. The grid was wound on to the left-hand KBr plate of section AA. When the grid was complete the second plate was added and the unwanted fibres cut away

RESULTS

Yarns shrunk for 10 min in air and 1 min in oil

These results are summarized in Figures 2-9. Figure 2 shows that at shrinkage temperatures above 100°C the amount of shrinkage in oil was greater than the amount in air. The progressive increase in shrinkage with temperature was accompanied by a corresponding progressive decrease in overall orientation, as measured by birefringence, only at temperatures up to 100°C (Figure 3). Thereafter there was no further net disorientation in air. In oil further disorientation occurred above 200°C. For comparison, data showing the effect on birefringence of heat treatment at constant length for 1 min in oil are also given in Figure 3. Infra-red spectra of yarns shrunk in air at 96°C and above (Figure 4) show evidence of an absorption at 988 cm⁻¹, corresponding to chain folding⁵. The absorption becomes more pronounced with increasing temperature. As

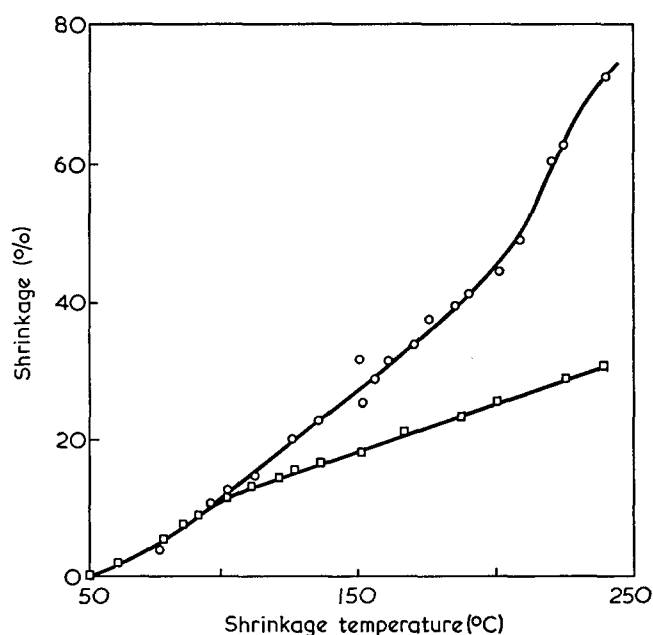


Figure 2 Shrinkage versus shrinkage temperature. □, Shrinkage after 10 min in air oven; ○, shrinkage after 1 min in oil

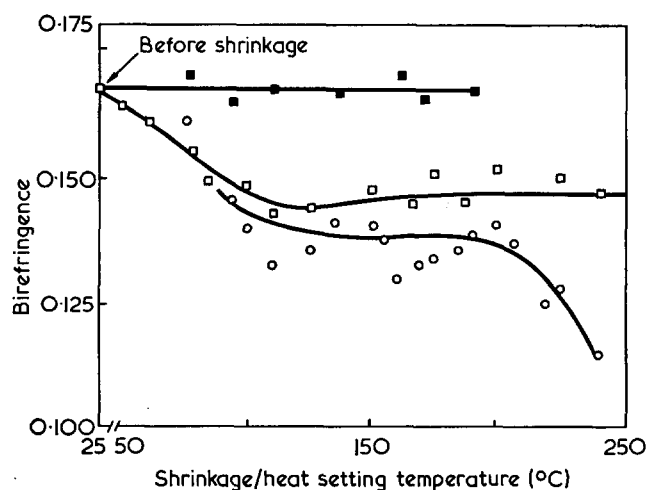


Figure 3 Birefringence after shrinkage and heat setting at constant length versus shrinkage/heat setting temperature. ■, Heated in oil at constant length; ○, shrunk in oil; □, shrunk in air

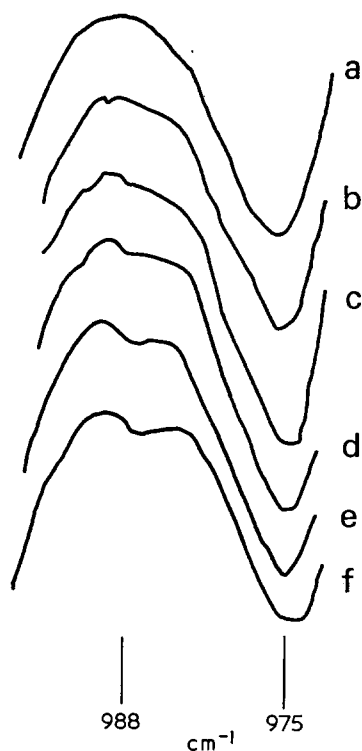


Figure 4 Infra-red spectra of yarn shrunk for 10 min in an air oven at 85°C (a), 92°C (b), 96°C (c), 110°C (d), 125°C (e) and 150°C (f)

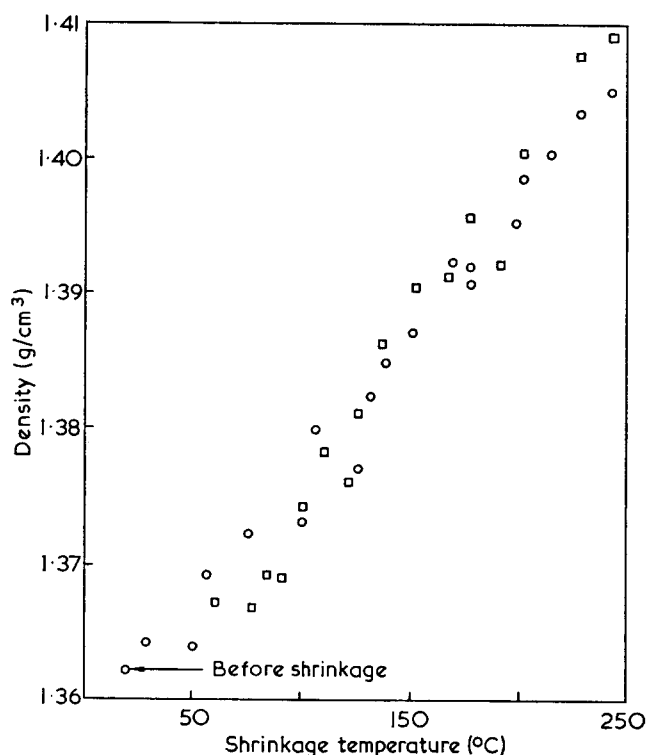


Figure 5 Density after shrinkage versus shrinkage temperature. □, Shrunk in air oven; ○, shrunk in oil bath

might be expected, the overall crystallinities of these yarns, as indicated by their densities, were a function of shrinkage temperature rather than the amount of shrinkage (Figure 5).

Some mechanical properties were considerably affected by shrinkage. For example, the shapes of load-extension curves were markedly altered by the introduction of a

progressively more pronounced yield at low strains. Surprisingly, yield loads, as defined in Figure 6, varied little with amount or temperature of shrinkage. Initial moduli were reduced by shrinkage. Figures 7 and 8 show that this reduction was determined more by the amount of shrinkage than by the shrinkage temperature. Breaking loads were markedly affected by shrinkage only at temperatures above 200°C (Figure 9). Even after very different amounts of shrinkage, the breaking loads of yarns shrunk in air and oil at 240°C were very similar.

Yarns shrunk in 0.2 s in hot air tubes

Infra-red spectra of yarns shrunk in about 0.2 s by from 0 to 33% through a hot air tube, yarn exit temperature 235°C, are shown in Figure 10, together with the spectra of two yarns redrawn after being shrunk by

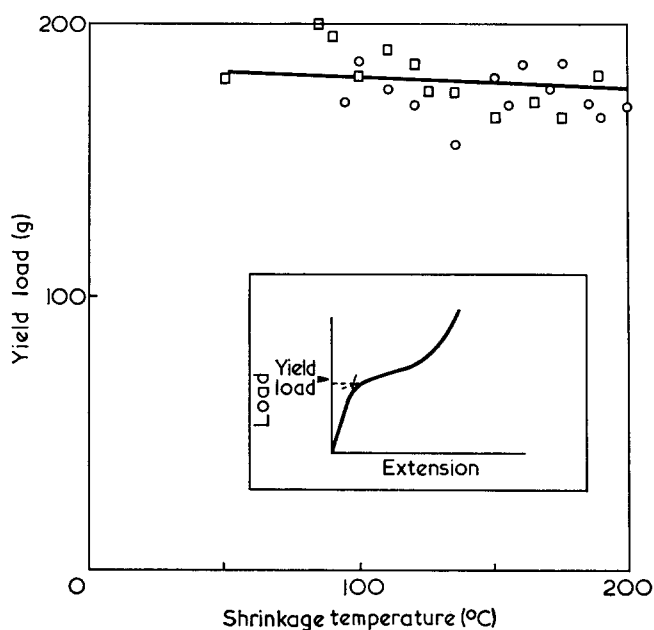


Figure 6 Yield loads for yarns shrunk in air (□) and oil (○)

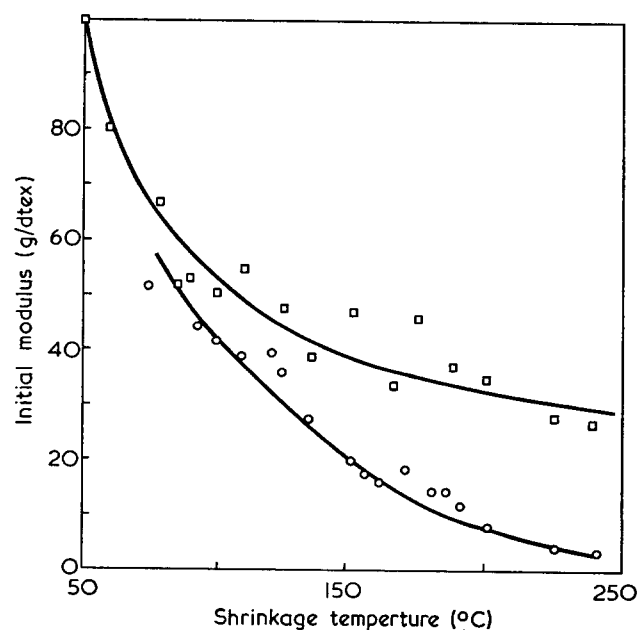


Figure 7 Initial modulus after shrinkage versus shrinkage temperature. □, After shrinkage in air; ○, after shrinkage in oil

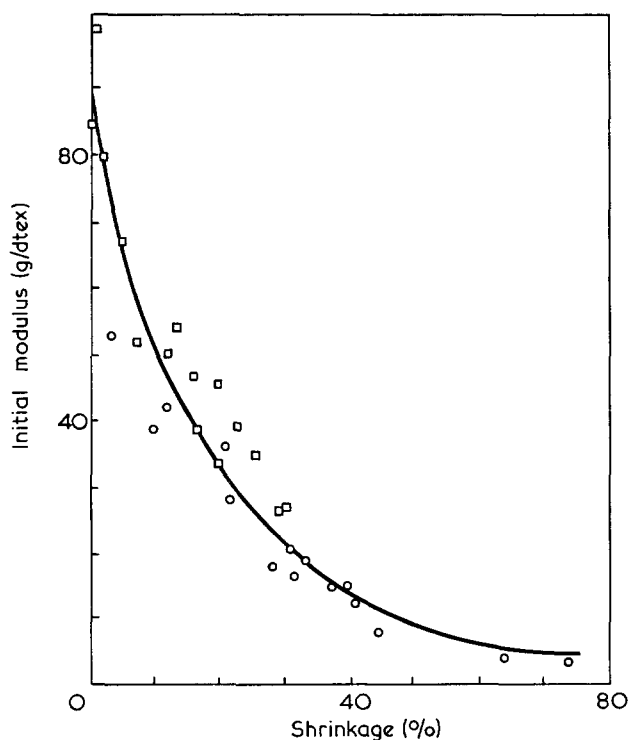


Figure 8 Initial modulus after shrinkage versus shrinkage. □, after shrinkage in air; ○, after shrinkage in oil

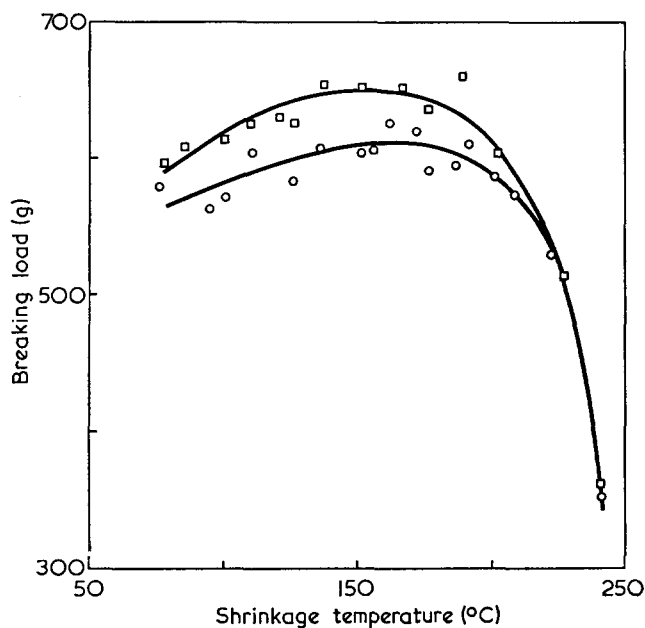


Figure 9 Breaking load after shrinkage versus shrinkage temperature. □, After shrinkage in air; ○, after shrinkage in oil

33%. A progressive intensification of the 988 cm^{-1} folded chain absorption with increasing shrinkage (Figures 10b-e) and a reversal of this trend on redrawing (Figures 10e-g) can be clearly seen. Note that Figure 10g refers to yarn shrunk by 33% and then redrawn cold $1.54\times$, i.e. redrawn approximately to its original length. Figure 10g can be seen to be very similar to Figure 10b which refers to a yarn subjected to very nearly the same heat treatment and which has suffered the same (zero) net length change. Figure 11 refers to heat treatments at 150°C , where molecular movements are slower than at 235°C . The marked difference at 988 cm^{-1} between Figures 11b and c shows clearly that

different amounts of folded chain structures can arise even when a given amount of shrinkage occurs on heating a yarn to a given final temperature. It is also seen that if the yarn of Figure 11c is held at constant length in an air oven at 150°C for 10 min, so that overall it has been shrunk by the same amount and been held at the final temperature for the same length of time as the yarn of Figure 11b, then the resulting yarn has a spectrum (Figure 11d), which is similar to spectrum Figure 11b.

Density and birefringence data relating to the yarns of Figures 10 and 11 are summarized in Figure 12. Changes brought about by free shrinkage, heat setting at constant length, and by redrawing are set out. Again, in terms of the changes occurring, a 10 min shrinkage in an oven at 150°C is seen to be about equivalent to the rapid hot air tube shrinkage plus the constant length heat treatment. The overall molecular disorientation occurring during the oven shrinkage, as indicated by the fall in birefringence, is seen as the sum of a larger fall during the rapid shrinkage in the hot air tube, followed by a rise during the heat setting stage. The density results show that the major part of the increase in crystallinity occurred during this later stage which, as shown above, was also responsible for a marked development of the 988 cm^{-1} absorption in the i.r. spectrum.

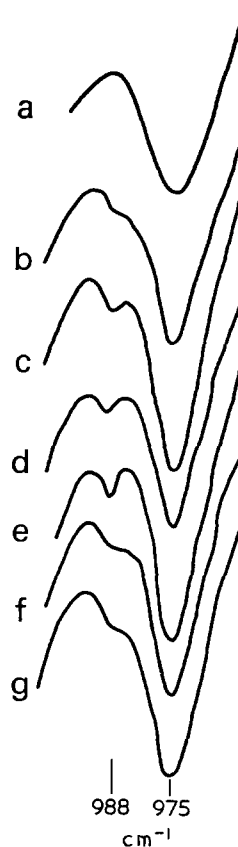


Figure 10 Infra-red spectra of yarns shrunk in hot air tube; yarn exit temperature 235°C . (a) Drawn yarn; (b) drawn yarn passed through hot air tube, shrinkage 0%; (c) as (b), allowed shrinkage 10%; (d) as (b), allowed shrinkage 20%; (e) as (b), allowed shrinkage 33%; (f) as (e), then redrawn $1.5:1$; (g) as (e), then redrawn $1.54:1$

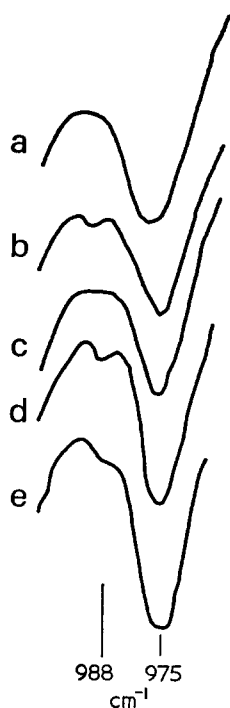


Figure 11 Infra-red spectra of yarns heat treated at 150°C. (a) Drawn yarn; (b) drawn yarn shrunk 17% in an air oven at 150°C for 10 min; (c) drawn yarn shrunk 17.5% in a hot air tube, yarn exit temperature 150°C; (d) as (c), then heat set at constant length for 10 min at 150°C; (e) drawn yarn heat set at constant length for 10 min at 150°C

It can be seen from Figure 12 that densities fell when shrunk yarns were redrawn. Redrawing also removed the yields introduced into load-extension curves by both oven and more rapid shrinkage.

DISCUSSION

Comparison of the i.r. spectra, densities and birefringences relating to yarn shrunk for 10 min at 150°C with those relating to yarn shrunk within 1 s in a hot air tube at the same temperature suggests that shrinkage in an oven is approximately equivalent to a rapid shrinkage plus a heat setting at constant length. The major part of the chain folding, as detected by i.r. spectroscopy, is not connected with the fibre length change during the rapid shrinkage, but with the subsequent crystallization stage, during which no shrinkage occurred. Clearly the amount of shrinkage, i.e. fibre length change, is not uniquely related to the amount of chain folding, nor can it be said that there is a cause and effect relationship between chain folding and shrinkage, because to a large extent shrinkage can precede detectable chain folding. Therefore, from the i.r. results, some process other than chain folding must be responsible for the shrinkage.

It is now suggested that the results presented above are consistent with the view that the basic shrinkage mechanism which is responsible for the fibre length change is a rapid rubber-like contraction, associated with disorientation in the amorphous phase. That disorientation will be followed by a crystallization

stage, during which the formation of i.r. detectable folded chain structures will be favoured, only if sufficient time is allowed. The amount of time required will depend on the crystallization temperature which, for a given time and fibre length change, will also determine the number of detectable folded chains. The folded chain structures may be more or less completely new, formed by taking up some slack in the disoriented amorphous regions and associated with a change from an extended chain to a folded chain fibre structure; or they may simply result from the perfection of lamellar or other structures present in a distorted form in the drawn yarn. Of course, it is not suggested that in shrinkage processes no crystallization occurs before all amorphous disorientation is complete. In practice the rate of heating will determine the extent to which crystallization at one temperature will overlap the process of amorphous disorientation at a higher temperature.

On this basis there is no need to postulate different mechanisms for the different amounts of shrinkage occurring in oil and air. Rather we can follow Bosley²: in general more amorphous disorientation and hence more shrinkage will occur after rapid heating in oil because more shrinkage inhibiting crystals, with a wider range of melting temperatures, will be melted at once. This will only be true at temperatures where the envisaged process of crystallite melting followed by recrystallization is significant. Our results suggest that this is at above 100°C.

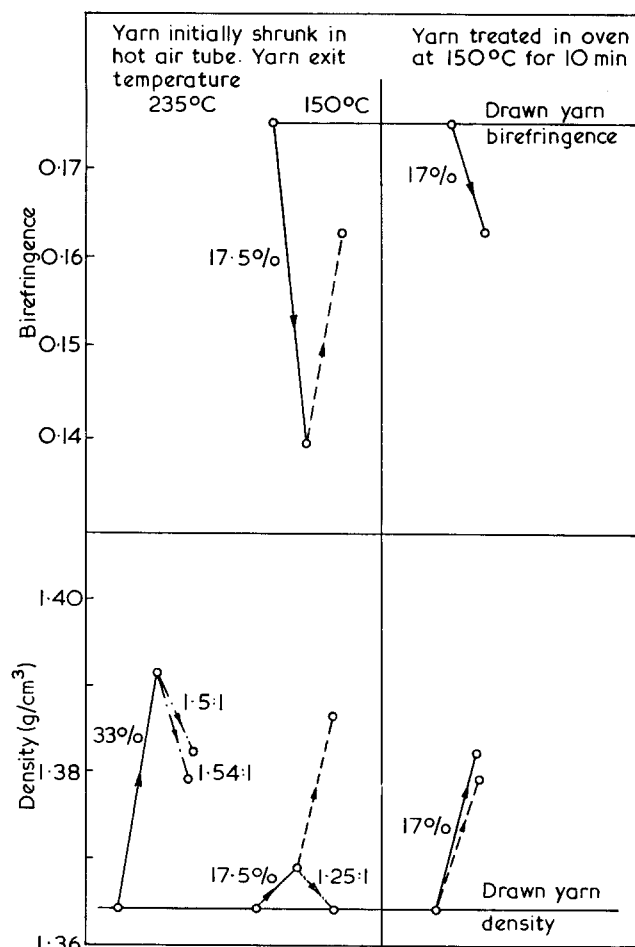


Figure 12 Densities and birefringence of yarns of Figures 10 and 11. —, Yarn shrunk for $n\%$; ---, yarn heat set at constant length at 150°C for 10 min; - · - ·, yarn redrawn after shrinkage, draw ratio $m:1$

The observation that the fall in modulus after oven and oil shrinkage correlated with the amount of shrinkage, rather than with shrinkage temperature, is consistent with the view that tensile modulus is determined by elements in the amorphous regions, the progressive disorientation of which produces both increasing shrinkage and decreasing modulus. The degree of crystallinity, which in these longer time shrinkages depended on shrinkage temperature (Figure 5) obviously only had a minor effect on modulus. (In fact crystallization of rapidly shrunk yarn will produce a small increase in modulus.)

The observed fall in birefringence after rapid shrinkage in a hot air tube is the expected accompaniment to the disorientation producing that shrinkage. Now it has been seen that the subsequent crystallization stage is associated with a rise in birefringence (Figure 12) which, it is suggested, occurs as molecules in the amorphous region crystallize on pre-existing more highly oriented crystallites. (Dumbleton^{6,7} has shown that in both drawn and shrunk PET filaments the crystalline orientation is higher than the amorphous orientation.) The birefringence *versus* shrinkage curves for the oven and oil shrunk yarns (Figure 3) reflect this compound nature of the shrinkage process. At temperatures up to 100°C similar falls in air and oil birefringence reflect similar amounts of shrinkage and amorphous disorientation. Above this temperature further falls are offset by the rises accompanying crystallization. The lower net birefringence in oil reflects the higher shrinkage and greater initial amorphous disorientation.

Many of the changes which accompanied shrinkage, such as those in load-extension curves, density and infra-red absorption at 988 cm⁻¹ were at least partly reversed by cold redrawing. Such redrawing will occur during a tensile test to determine breaking load. The fact that breaking loads (*not* stresses) of oven shrunk yarns were little affected by shrinkages at temperatures below 200°C suggests that the structural features which determined the breaking loads of the original drawn yarn were recovered during tensile tests of the shrunk yarns. There is evidence of chain folding below 200°C, and so chain folding *per se* does not reduce breaking loads. In fact breaking loads decrease for shrinkages above 200°C, irrespective of medium or amount of shrinkage. Now the shrinkage temperature determined the level of crystallinity (Figure 5). This suggests that above a certain level of crystallinity the shrunk yarn is set to an extent at which it is no longer possible to recover the desired structural features of the original drawn yarn. In connection with redrawing it should also be noted that contrary to earlier suggestions⁸, a larger degree of chain folding does not necessarily correspond to an increased yarn ductility. For example comparison of a yarn shrunk 17% at 150°C with a yarn shrunk 10% at 235°C showed that the former had less regular chain folding (compare Figures 10c and 11c), but a higher ductility (38% extension to break compared with 28%).

It is not yet possible confidently to relate the yield behaviour of shrunk PET yarns to structure. It may well be, as Duckett⁹ suggests, that yielding is not associated

with any meaningful elastic-plastic transition: rather it is a viscoelastic property, in this case of the disordered regions produced during shrinkage, which is a continuous development of mechanisms operative from the lowest stresses. On the other hand, the fact that the yield load (*not* stress) for the oven shrunk yarns varied little with the amount or temperature of shrinkage might suggest that the yield process was associated with the break up of specific structures, e.g. folded chain crystals, created during the overall shrinkage process. The 988 cm⁻¹ absorption is, of course, much reduced, as is fibre density, when shrunk yarns are redrawn and the yield removed. However, marked yielding still occurred in the yarn relaxed quickly at 150°C which exhibited little or no absorption at 988 cm⁻¹; but it could be argued that the yield is then associated with the break-up of imperfect undetectable or relatively few undetected folds. Further elucidation of the yield mechanism in such yarns is required.

CONCLUSION

In this work we have studied the structural and other changes associated with the shrinkage of drawn PET fibres. This has involved the use of an improved i.r. technique. It has been shown that the overall shrinkage process involves a rapid initial stage, which is associated with disorientation in the amorphous regions and is essentially responsible for the fibre length change. This is followed, if time permits, by a crystallization stage. Chain folding, as detected by i.r. spectroscopy, is associated with the later crystallization stage. Because chain folding occurs after the fibre length change it cannot be said that there is a unique, or cause and effect, relationship between chain folding and shrinkage.

This picture of the shrinkage process satisfactorily combines the rubber elasticity type of approach to shrinkage with the later folded chain models.

ACKNOWLEDGEMENTS

Much of the experimental work described was carried out by Mr M. Rowsby. The author also thanks Mr G. Ogilvie for his help with infra-red spectroscopy and ICI Fibres for permission to publish.

REFERENCES

- 1 Pinnock, P. R. and Ward, I. M. *Trans. Faraday Soc.* 1966, **62**, 1308
- 2 Bosley, D. E. *J. Polym. Sci. (C)* 1967, **20**, 77
- 3 Dismore, P. F. and Statton, W. O. *J. Polym. Sci. (C)* 1966, **13**, 133
- 4 Statton, W. O., Koenig, J. L. and Hannon, M. *J. Appl. Phys.* 1970, **41**, 4290
- 5 Koenig, J. L. and Hannon, M. *J. Macromol. Sci. (B)* 1967, **1**, 199
- 6 Dumbleton, J. H. *J. Polym. Sci. (A-2)* 1969, **7**, 667
- 7 Dumbleton, J. H. *Polymer* 1969, **10**, 539
- 8 Prevorsek, D. C. and Sibilja, J. P. *J. Macromol. Sci. (B)* 1971, **5**, 617
- 9 Duckett, R. A. Conference on Testing of Polymers for Service, Institute of Physics, London, 1972, Paper 3

The crystallization of oriented poly(ethylene terephthalate)*

F. S. Smith and R. D. Steward

ICI Fibres, Hookstone Road, Harrogate, Yorkshire HG2 8QN, UK
(Received 15 May 1973; revised 26 June 1973)

The rate of crystallization of oriented poly(ethylene terephthalate) has been measured at 100°, 120° and 150°C using carefully prepared amorphous fibre samples. The samples were held to length during crystallization so that shrinkage did not occur, and the course of crystallization was followed by measuring the changes in density and boiling water shrinkage of the samples. The results show that the rate of crystallization is strongly dependent on the degree of orientation. Nucleation and initial growth of crystallites occur in times of the order of milliseconds at 120°C in samples of birefringence 0.08 compared with times of several minutes in isotropic material. It was found that crystallization in oriented material cannot be described by the Avrami equation.

INTRODUCTION

Molecular orientation in a polymer sample affects the rate of crystallization and Keller *et al.*¹ found that even slight distortion of their samples of poly(ethylene terephthalate) (PET) altered the kinetics appreciably. Although several other investigators have determined the rate of crystallization in PET²⁻⁸, only Spruiell *et al.*⁸ have considered the effect of orientation, and they allowed their samples to shrink during crystallization with consequent disorientation of the amorphous regions. In the work reported here, we have measured the rate of crystallization in oriented samples which were held so that disorientation could not occur during the crystallization process.

EXPERIMENTAL

For this investigation we needed non-crystalline samples with different, well-defined degrees of orientation. We achieved this by making the samples in the form of fibres, which could be oriented without crystallizing using a carefully controlled drawing process. Commercial grade poly(ethylene terephthalate) containing 0.5% TiO₂ was extruded through fine holes in a die at a temperature of 295°C, the resulting fibres being quenched rapidly to room temperature. The melt was held at 295°C for 10 min prior to extrusion to ensure that there were no nuclei remaining from previous crystallizations¹. The fibres made in this way had a diameter of about 45 μm, a density of 1.340 g/cm³, and X-ray diffraction showed no crystallinity. By drawing these fibres isothermally in water at about 50°C samples were made with higher orientation, whilst still preserving the non-crystalline nature of the material. The orientation was characterized by measuring the fibre

birefringence, that is the difference in refractive index along and across the fibre axis.

Since crystallization in oriented material is very much faster than in the isotropic state, it was necessary to hold the samples at the chosen crystallization temperature for only brief periods in order to measure the rate at which crystallization proceeded. This was done by passing the fibres continuously through a heating bath containing glycerol at the required temperature, and then into a cold water quench, a system of rollers being used so that the fibres were held at constant length throughout the process. Well defined heat treatment times as short as a few milliseconds could be achieved. Measurements made with an infra-red pyrometer showed that the fibres attained the temperature of the hot glycerol in less than 7 ms.

MEASUREMENTS OF CRYSTALLINITY

Classically, crystallinity is associated with the ability of a material to diffract X-rays in discrete directions. In order to do this, there must exist regions of almost perfect order extending over a range of at least 20–30 Å⁹, and well crystallized polymer samples are in fact sufficiently ordered to show discrete diffraction of X-rays. Other measures of crystallinity are often used when dealing with polymers, notably density and infra-red absorption at certain wavelengths. It is found that these measures of crystallinity are not consistent with each other when applied to PET, because in this polymer, as in many others, a completely crystalline structure is never achieved, and each method of measurement is affected differently by the size and perfection of the crystalline regions. Thus there is no unique measure of crystallinity in polymers.

However, the industrial importance of crystallinity in oriented polymers lies not in the way it changes the X-ray diffraction or the density, but in the stability

* Presented at the Polymer Physics Group (Institute of Physics) Biennial Conference, Shrivenham, September 1973.

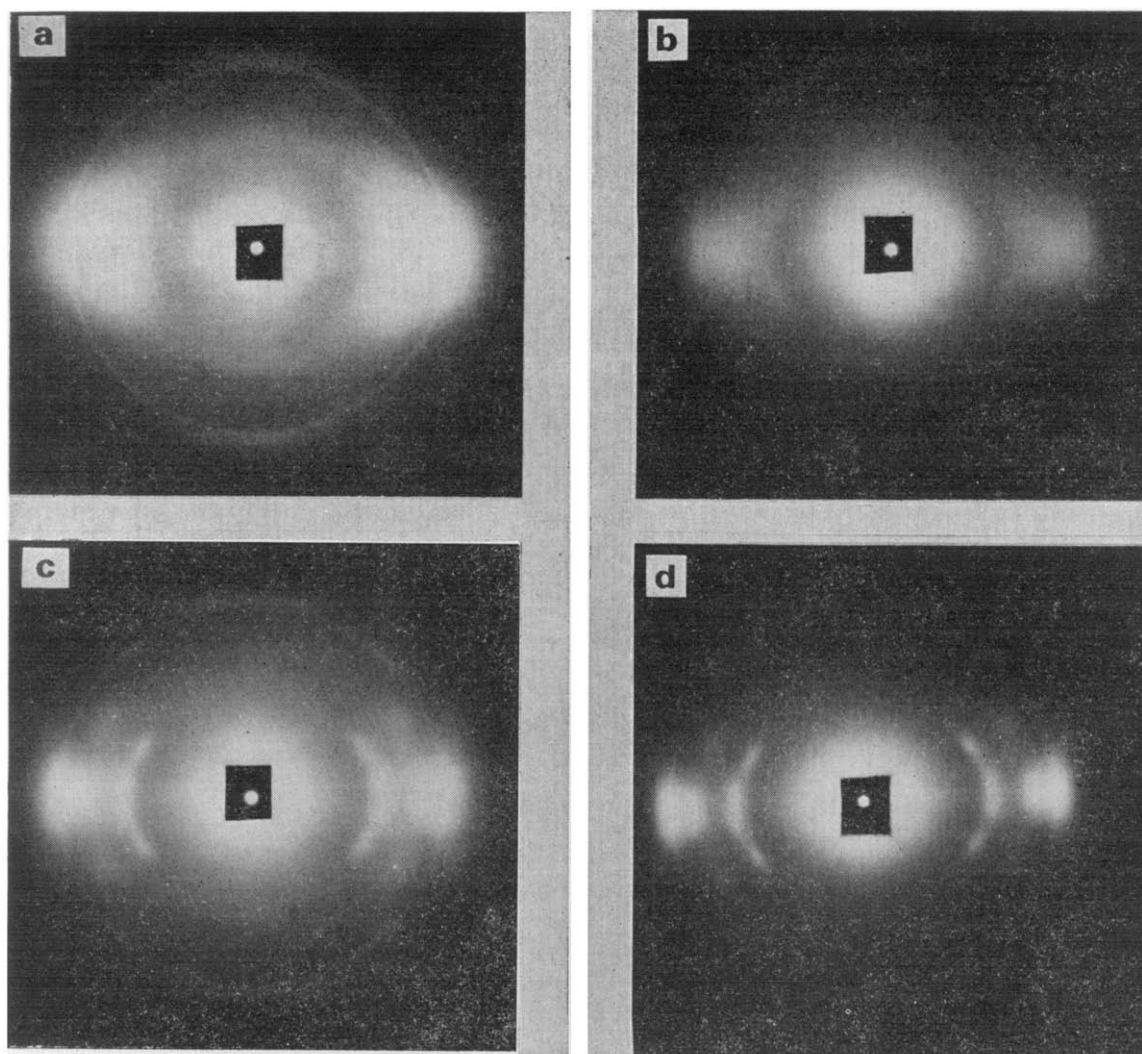


Figure 1 X-ray diffraction photographs of PET fibres crystallized at constant length at 120°C. Crystallization time: (a) 0; (b) 10 ms; (c) 50 ms; (d) 300 ms. Shrinkage in boiling water: (a) 35%; (b) 15%; (c) 8%; (d) 5%

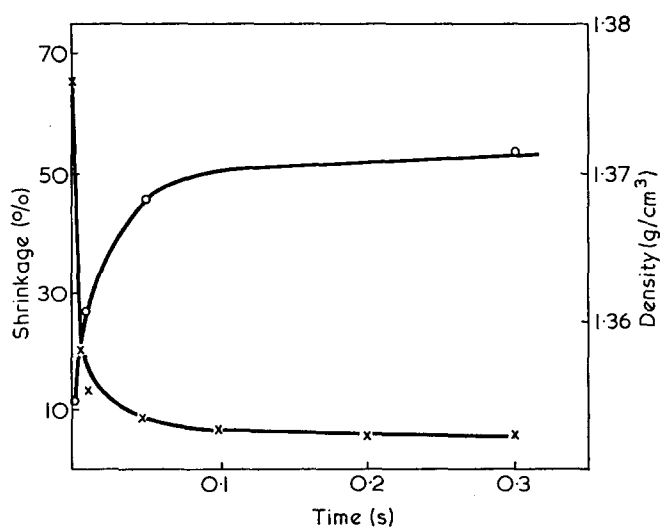


Figure 2 Change in shrinkage and density of PET fibres, \bar{M}_n 21 000, birefringence 0.08, crystallized at constant length at 120°C. x, Shrinkage; o, density

which it confers on the oriented structure. When crystallization occurs, segments of the polymer molecules arrange themselves in a regular array which is a lower energy state than the random configuration, the net energy change appearing as heat. Bond rotation cannot

occur in the crystalline regions, so fully crystalline polymers do not disorient or shrink when heated above the glass transition temperature. This essential effect of crystallinity can often be detected long before the conditions are met for discrete X-ray diffraction. For example, Figure 1 shows X-ray diffraction photographs of fibres which have been crystallized for different times at 120°C. The shrinkage of the fibres in boiling water is also listed. It can be seen that whereas considerable changes in shrinkage occur within 10 ms, discrete diffraction spots become apparent only after about 50 ms, and the major reduction in shrinkage has occurred long before a fully crystalline X-ray pattern is achieved. On the other hand, the density, which is also widely used as a measure of crystallinity in polymers, follows the shrinkage changes quite closely (Figure 2).

In this work we were concerned with the practical effects of crystallinity in oriented material. We therefore followed the course of crystallization by making measurements of the shrinkage in boiling water of samples which had been subject to heating for different lengths of time. An initially unoriented PET fibre will shrink back to its unstretched length from extensions as high as 200% if no crystallization occurs during stretching. On the other hand, a fully crystalline fibre cannot disorient or shrink, and so for a given orientation, the shrinkage observed may be used as a measure of the

degree of crystallinity. The shrinkage change achieved after a given time at the crystallization temperature can be expressed as a fraction θ of the total possible change, defined by:

$$\theta = \frac{S_I - S}{S_I - S_\infty}$$

where S is the shrinkage measured after crystallizing for a time t , S_I is the initial shrinkage in the absence of crystallization and S_∞ is the shrinkage after very long time at the crystallization temperature. In practice S_∞ is not zero since 100% crystallinity is never attained and in this work we used the value obtained after 1 h at the crystallization temperature.

RESULTS

The course of crystallization in samples which had different degrees of orientation is shown in Figure 3. The large effect of orientation is apparent. The sample with the lowest orientation (birefringence value 0.005) showed a definite induction time before crystallization started, as is found in unoriented material. However, even at this level of orientation the time scale was greatly reduced compared with isotropic material, and with increasing orientation the half time for crystallization was rapidly reduced still further (Table 1).

The rate of crystallization was increased by raising the temperature as shown in Figure 4. At temperatures above 150°C crystallization was too rapid to permit measurement by this method. The effect of molecular weight on crystallization in highly oriented samples is shown in Figure 5. Increasing molecular weight reduced the rate of crystallization, as has been found for isotropic material^{1,7}.

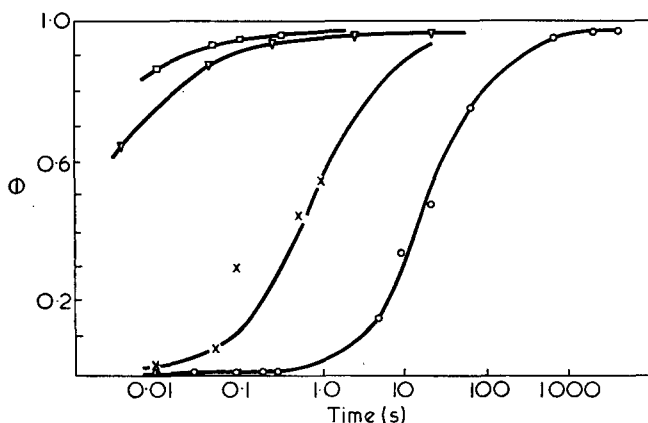


Figure 3 Crystallization of PET of M_n 21 000 at 120°C. Birefringence values: ○, 0.005; ×, 0.027; ▽, 0.08; □, 0.15

Table 1 Crystallization of poly-(ethylene terephthalate)
 $M_n=21\ 000$; $T_c=120^\circ\text{C}$

Birefringence	Half-time(s)
0	660*
0.005	20
0.027	0.7
0.080	<0.01

* Determined by d.t.a. on bulk sample of the polymer

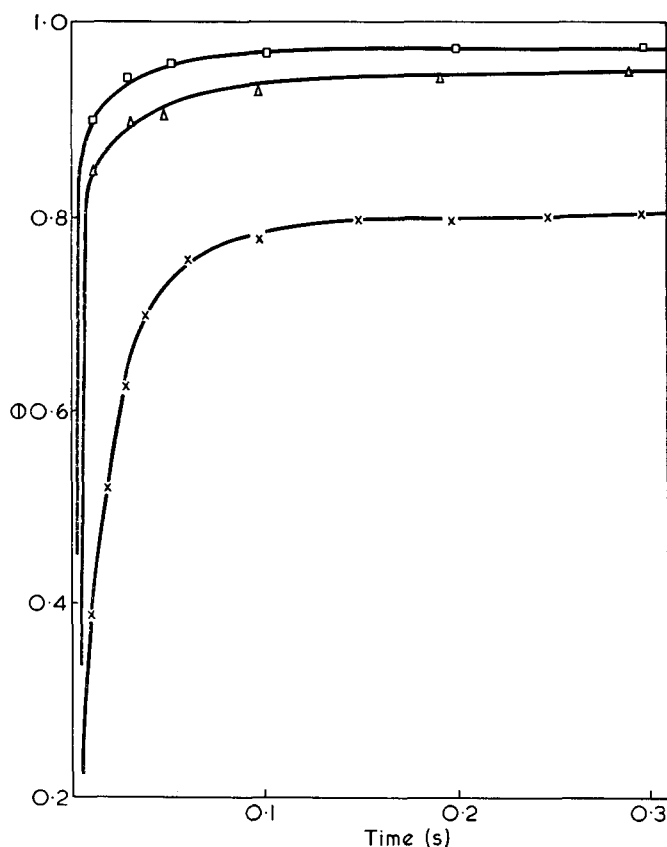


Figure 4 Crystallization of PET of M_n 21 000. Birefringence 0.08, at different temperatures: ×, 100°C; △, 120°C; □, 150°C

DISCUSSION

Crystallization in polymeric materials is usually described in terms of a nucleation and growth model¹⁰. It is assumed that nuclei of ordered material are formed as a result of thermal fluctuations, and that some of these nuclei grow by the addition of more material to form crystallites. The course of crystallization is determined, therefore, by both the rate of nucleation and the subsequent rate of growth of crystals on these nuclei. The results we have obtained show that the nucleation and initial growth of crystallites is an extremely rapid process in oriented PET, occurring in times of the order of milliseconds for samples of birefringence 0.08, compared with minutes in unoriented material. The shape of the crystallization curves indicates that the main effect of orientation is to reduce the induction or nucleation time as was also found by Spruiell *et al.*⁸. Mechanical orientation of the molecules assists the production of nuclei by bringing molecular segments into favourable juxtaposition, leading to a reduction in the configurational entropy change needed for nucleus formation¹¹. However, it should be noted that strain *per se* does not produce crystallization as is sometimes implied by the use of the term 'strain crystallization', though it greatly increases the rate at which crystallization proceeds at any given temperature. The rates of crystallization which we have found in oriented specimens are much greater than those observed by Spruiell *et al.*⁸ because our samples were not allowed to relax during crystallization. The shrinkages observed by Spruiell *et al.* during annealing indicate considerable disorientation in the amorphous regions, which would greatly reduce the rate of crystallization.

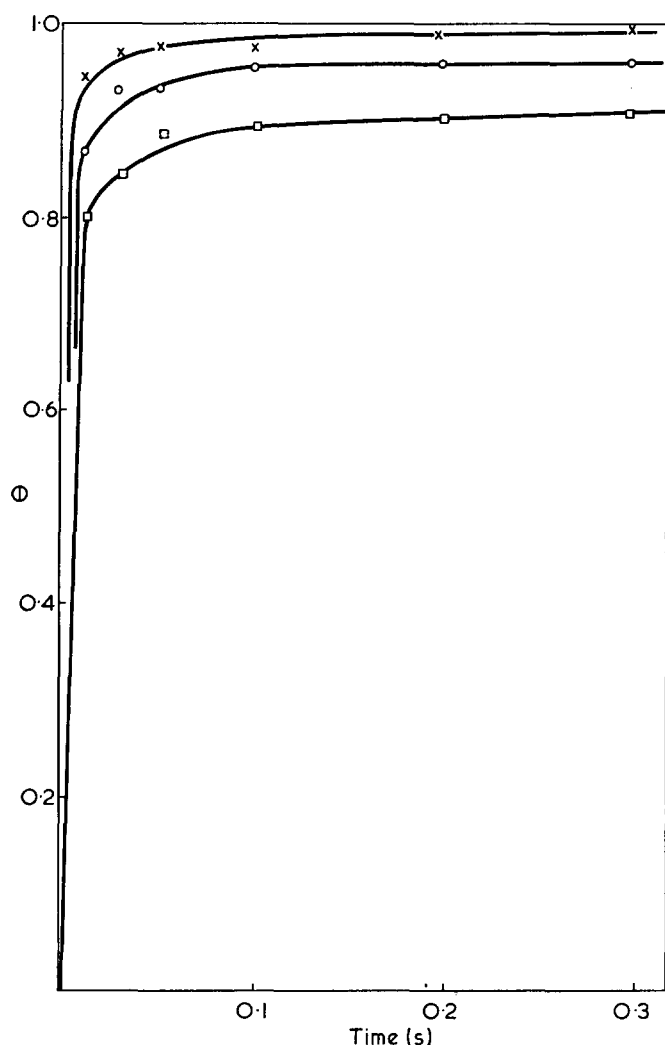


Figure 5 Crystallization of PET. Birefringence 0.15, at 120°C. x, $\bar{M}_n=12\,800$; o, $\bar{M}_n=21\,000$; □, $\bar{M}_n=32\,000$

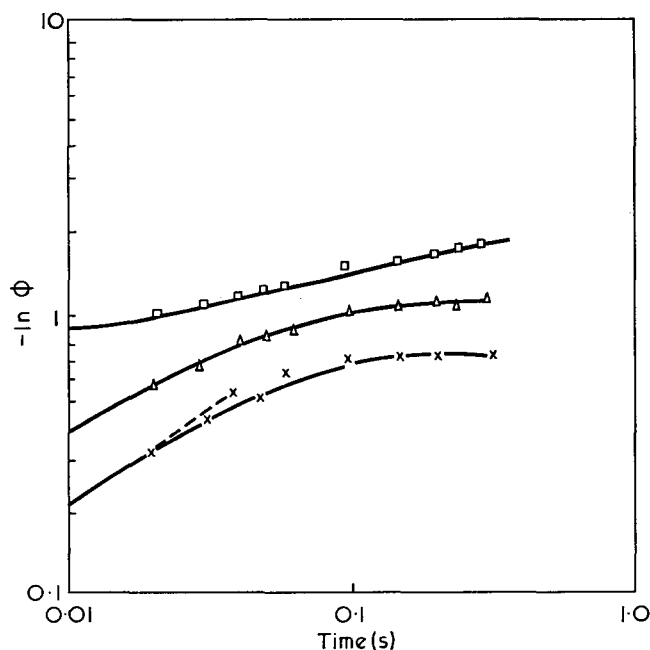


Figure 6 Avrami plots for samples $\bar{M}_n=21\,000$ crystallized at 100°C. Birefringence values: x, 0.08; △, 0.15; □, 0.18. ----, $n=0.7$

The course of crystallization in many materials can be described by the Avrami equation:

$$\phi = \exp(-kt^n)$$

where ϕ is the volume fraction of uncrystallized material at time t , and k and n are constants. Hartley *et al.*¹² using carefully prepared strain-free amorphous samples showed that for PET this equation applied with values for n of 2 at temperatures up to 160°C, corresponding to fibrillar crystalline growth and 4 at 240°C where fibrillar spherulitic growth occurred. Other investigators have obtained values for n which are not in accord with these results, and in many cases are fractional and not integers are required by the Avrami theory²⁻⁷. The Avrami equation may be expected to hold in the initial stages of the crystallization before the conditions assumed by the theory break down because of impingement of one crystalline region on another and the increasing concentration of non-crystallizable matter in the amorphous regions. However, a plot of $\log(-\ln \phi)$ against $\log t$ for the fibre samples crystallized at 100°C showed that n had already fallen below 1 at the shortest times and was continuing to fall (Figure 6). For fibres crystallized at higher temperatures, the value of n fell even more rapidly. Thus the Avrami equation cannot be used to describe the course of crystallization in oriented PET and it seems quite likely that the departures from Avrami behaviour found by some workers in nominally isotropic material were the result of adventitious orientation caused by strain in the sample.

CONCLUSIONS

The rate of crystallization in PET is strongly dependent on the degree of orientation. Isotropic samples used for measurement of crystallization kinetics must therefore be prepared with great care so that unknown strains are avoided, and the degree of orientation of oriented samples must be well defined and shrinkage prevented during the crystallization process if the results are to be meaningful. Crystallization in oriented specimens does not follow the simple Avrami theory, and departures from Avrami behaviour could be a sensitive indicator of adventitious strain in nominally isotropic samples.

ACKNOWLEDGEMENT

Some of the experimental work was carried out by Mrs S. Stone as part of the industrial training phase of a Bradford University degree course.

REFERENCES

- 1 Keller, A., Lester, G. R. and Morgan, L. B. *Phil. Trans. R. Soc.* 1954, A247, 1
- 2 Cobbs, W. H. and Burton, R. L. *J. Polym. Sci.* 1953, 10, 275
- 3 Mayhan, K. G., James, W. J. and Bosch, W. J. *Appl. Polym. Sci.* 1965, 9, 3605
- 4 Mitsuishi, Y. and Ikeda, M. *J. Polym. Sci. (A-2)* 1966, 4, 283
- 5 Miller, B. *J. Appl. Polym. Sci.* 1967, 11, 2343
- 6 Fielding-Russell, G. S. and Pillai, P. S. *Makromol. Chem.* 1970, 135, 263
- 7 Turska, E. and Przygocki, W. *Faserforsch. Textiltech.* 1964, 15, 561
- 8 Spruiell, J. E., McCord, D. E. and Beuerlein, R. A. *Trans. Soc. Rheol.* 1972, 16, 535
- 9 Bonart, R. *Kolloid Z.* 1966, 213, 1
- 10 Turnbull, D. and Fisher, J. C. *J. Chem. Phys.* 1949, 17, 71
- 11 Andrews, E. H. *Proc. R. Soc.* 1964, A277, 562
- 12 Hartley, F. D., Lord, F. W. and Morgan, L. B. *Phil. Trans. R. Soc.* 1954, A247, 23

A study of the orientations of fluorescent molecules incorporated in uniaxially oriented poly(ethylene terephthalate) tapes*

J. H. Nobbs, D. I. Bower and I. M. Ward

Department of Physics, University of Leeds, Leeds LS2 9JT, UK

and D. Patterson

Department of Colour Chemistry and Dyeing, University of Leeds, Leeds LS2 9JT, UK

(Received 22 November 1973; revised 8 February 1974)

The theory of the polarized fluorescence from fluorescent molecules incorporated in an oriented solid polymer is developed for a very general model of the optical behaviour of the molecules and it is concluded that any observed intensity can be expressed in terms of the components of a fourth rank tensor. Only twelve of these components are independent for samples of orthotropic symmetry and only six for samples of uniaxial symmetry. The effects of the birefringence of the polymer and the significant polarization-dependent absorption of the exciting light on the observed intensities are considered. The results of the analysis are presented for the uniaxial case in a form which allows values of $\overline{\cos^2\theta}$ and $\overline{\cos^4\theta}$ to be calculated from the experimental measurements of intensity. θ is the angle between the unique axis in the polymer and a unique axis in a fluorescent molecule and the bars denote the averages over the sample. The theory has been applied to molecules of a stilbene derivative (VPBO) incorporated at concentrations of 50–200 ppm in poly(ethylene terephthalate) (PET) of low crystallinity. It is concluded that the unique axes of the VPBO molecules are more highly oriented than the PET chains, but the two distributions of orientations appear to be uniquely related over the range of drawing temperatures (65–90°C) and draw ratios (1–5.85) used.

INTRODUCTION

There is considerable interest in developing methods for determining molecular orientation in 'amorphous' polymers and in the non-crystalline regions of crystalline polymers. It is often difficult to apply spectroscopic techniques, such as nuclear magnetic resonance and infra-red spectroscopy, because these may require a detailed knowledge of the polymer conformation, which is not available for the disordered regions. One method which circumvents such difficulties involves the incorporation into the polymer of dye molecules whose orientation is then determined. Previous work by two of the present authors¹, has shown the value of measuring the optical dichroism of dyestuffs incorporated in polyester fibres. The orientation parameters obtained from the optical dichroism were examined in conjunction with birefringence and X-ray diffraction measurements to provide a structural understanding of the drawing and hot water shrinkage of these fibres.

For a uniaxial sample the optical dichroism determines $\overline{\cos^2\theta_A}$, the average value of $\cos^2\theta_A$, where θ_A is the angle between the symmetry axis of the sample and the absorption axis of a dye molecule. If the orientation of the dye molecule relative to the surrounding polymer

molecules is known, then the corresponding value of $\overline{\cos^2\theta_p}$, where θ_p is the angle between the symmetry axis of the sample and a polymer molecule, can be derived. The optical dichroism method provides information related to $\overline{\cos^2\theta_p}$ only and it is important to develop methods which also provide information about $\overline{\cos^4\theta_p}$. Not only do such data define the distribution of molecular orientations more closely, but they are also of direct value in understanding the relationship between the anisotropy of mechanical properties and molecular orientation². The polarized fluorescence of suitable organic molecules incorporated in the polymer offers the means to obtain such information, in a parallel experiment to the measurement of optical dichroism. The use of this technique was first reported by Nishijima³ and has subsequently been the subject of several theoretical and experimental publications^{4–12}. In most of the experimental studies so far reported, however, the information about the orientation distribution has been presented in terms of a single parameter, usually related in a complex way to $\overline{\cos^2\theta}$ and $\overline{\cos^4\theta}$, where θ measures the orientation of a unique axis in the fluorescent molecule, and some of the information available has been discarded. It has therefore not been possible to compare the information quantitatively with that obtained from, for instance, birefringence or optical dichroism measurements. In addition, the effects on the

* Presented at the Polymer Physics Group (Institute of Physics) Biennial Conference, Shrivenham, September 1973.

fluorescence intensity of the birefringence of the sample and the progressive absorption of the exciting light as it travels through the sample have not been properly accounted for.

For these reasons we feel that the potentialities of the fluorescence method have not been fully realized. We have therefore redeveloped the theory, incorporating the effects of birefringence and of absorption into the analysis, and have written the results for the uniaxial case in such a way that values of $\overline{\cos^2\theta}$ and $\overline{\cos^4\theta}$ can be extracted directly from experimental measurements. The theoretical treatment and the experiments have been restricted to cases where the incident light enters and the observed fluorescent light leaves the polymer sample normal to its surface, since it was felt that until the method had been thoroughly proved in this simple situation its extension to fibres was unjustified.

In this paper we describe measurements of the intensity of the polarized fluorescence of an optical brightening agent, which is a stilbene derivative, incorporated in oriented tapes of poly(ethylene terephthalate) (PET). For a series of specimens produced in a variety of ways, the value of $\overline{\cos^2\theta}$ obtained from polarized fluorescence measurements is compared with that obtained from optical dichroism measurements and with the birefringence. It is concluded that reliable numerical information about the orientation of the fluorescent molecules can be obtained using the approach described in this paper.

In a subsequent paper the preparation of the samples will be described in more detail and the relationships between the orientations of the fluorescent molecules and those of the polymer molecules will be discussed in the light of results of orientation measurements by other techniques, together with the implications that the values of $\overline{\cos^2\theta_p}$ and $\overline{\cos^4\theta_p}$ have for understanding the drawing mechanism of PET.

THEORY

Introduction

A fluorescent molecule will absorb light of a particular wavelength, λ , if λ is within the absorption band of the molecule and if there is a component of the light polarized so that its electric vector is parallel to the absorption axis, **A**, of the molecule. A short time later it will emit light of a longer wavelength from an oscillating dipole μ which is parallel to the emission axis **B**, of the molecule. **A** and **B** can be regarded as unit vectors which may or may not be identical. The rates of absorption and emission of energy are proportional to the incident light intensity and to intrinsic properties of the molecule.

It is easy to write down the intensity of the fluorescence from a single isolated fluorescent molecule. Let the exciting light be plane-polarized with electric vector **E** and let the fluorescent light be observed after passing through a perfect analyser which transmits only light polarized with electric vector parallel to a vector **T'**. The observed intensity will be proportional to $\cos^2\Delta_1\cos^2\Delta_2$ where Δ_1 is the angle between **E** and **A** and Δ_2 is the angle between **T'** and **B**.

The complete problem is to calculate the total fluorescent intensity from a sample consisting of an array of fluorescent molecules dispersed in a solid polymer. This will depend on the orientations of the fluorescent

molecules, the birefringence of the sample and the rate of absorption of the exciting light by the sample. The problem involves, therefore, transformations between systems of coordinates on each fluorescent molecule and a system of coordinates fixed within the sample. Such transformations can be simply made by representing the electric vector of the light as a column matrix (E_i) and multiplying this by the appropriate rotation matrix.

Since the emission is incoherent we can treat each fluorescent molecule independently and add the resulting fluorescent light intensities to find the total intensity emitted by the array. To avoid the complication from refraction of the light at the sample surfaces we shall assume that the incident plane-polarized monochromatic light enters the sample, and the observed fluorescent light leaves the sample, normal to its surface. We shall neglect, initially, the effects of the birefringence and absorption and they will be considered in a separate section.

Development for orthotropic symmetry

In the treatment that follows we neglect the partial reflection of the incident and fluorescent radiations at the surfaces of the sample and also the difference between the local and macroscopic electric fields within the sample. These are considered in the Appendix.

The polymer sample is assumed to have at least the statistical symmetry described by three mutually perpendicular 2-fold rotation axes (orthotropic symmetry). A right-handed set of axes $O-X_1X_2X_3$ is chosen parallel to these three axes. For a uniaxial sample OX_3 is chosen parallel to the unique axis. Each fluorescent molecule is assumed to have a unique axis **M** fixed within it and these unique axes are assumed to have a distribution of orientations which is related to that of the polymer chains and so has the symmetry of the sample. The precise nature of this relationship will be discussed in a later paper and we shall now consider only how the distribution of orientations of the unique axes **M** with respect to $O-X_1X_2X_3$ determines the observed intensities and what information can be deduced about the distribution from the intensities.

The polar and azimuthal angles of the vector **M** for a typical fluorescent molecule are θ and ϕ with respect to $O-X_1X_2X_3$. A set of axes $O-x_1x_2x_3$ is chosen fixed within the molecule so that Ox_3 is parallel to **M**. The polar coordinates of the absorption axis **A** with respect to this set of axes are α and β and the polar coordinates of the emission axis **B** are α' and β' (Figure 1). An angle ϵ is defined to be the difference between the azimuthal angles of the emission and absorption axes:

$$\epsilon = \beta' - \beta \quad (1)$$

It will be necessary to make specific assumptions about ϵ later, but for the moment no restrictions on it are implied.

If the electric vector **E** of the incident light has polar coordinates γ , η in the $O-X_1X_2X_3$ frame it may be represented in matrix form by:

$$(E_i) = \begin{pmatrix} E \sin\gamma \cos\eta \\ E \sin\gamma \sin\eta \\ E \cos\gamma \end{pmatrix} \quad (2)$$

where $E = E^0 \exp(i\omega t)$.

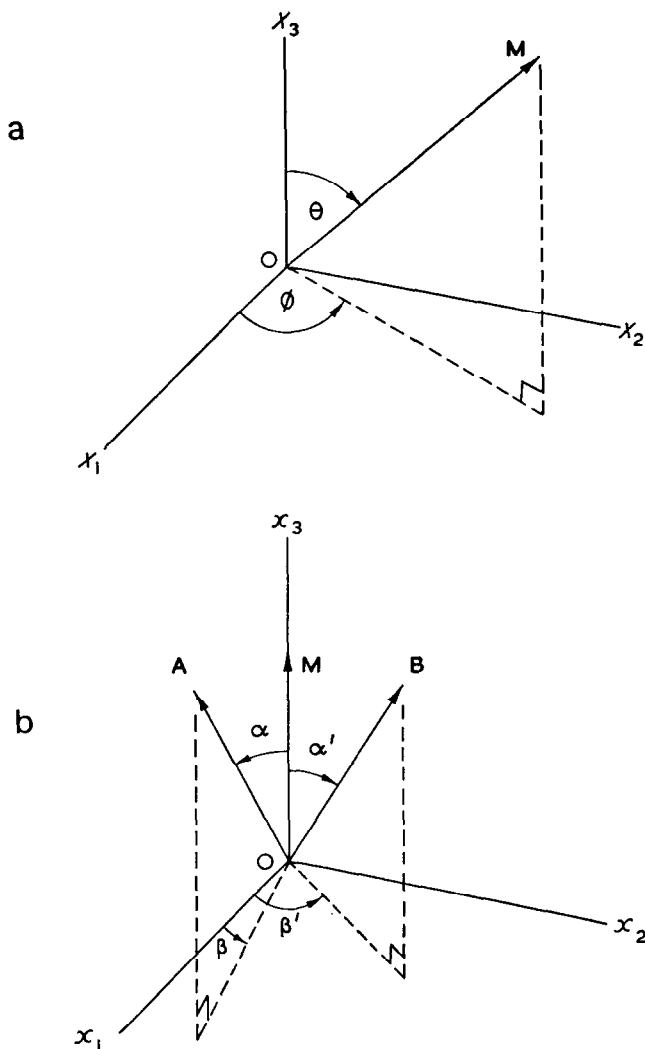


Figure 1 (a) Orientation of unique axis, **M**, of a fluorescent molecule with respect to symmetry axes, $O-X_1X_2X_3$, of sample. (b) Orientation of absorption and emission axes, **A** and **B**, respectively, with respect to axes $O-X_1X_2X_3$ fixed in fluorescent molecule

If we define (T_i) by:

$$(T_i) = \begin{pmatrix} \sin\gamma\cos\eta \\ \sin\gamma\sin\eta \\ \cos\gamma \end{pmatrix} \quad (3)$$

then

$$(E_i) = (T_i)E \quad (4)$$

To find the component, E_A , of the electric vector along the absorption axis, **A**, of the fluorescent molecule we take the scalar product of (E_i) and (A_i) . To do this they must first be referred to the same set of axes. In the frame $O-X_1X_2X_3$, (A_i) is given by:

$$(A_i) = \begin{pmatrix} \sin\alpha\cos\beta \\ \sin\alpha\sin\beta \\ \cos\alpha \end{pmatrix} \quad (5)$$

(E_i) may be referred to $O-X_1X_2X_3$ by using the transformation matrix (O_{ij}) which relates quantities expressed with respect to $O-X_1X_2X_3$ to those expressed with respect to $O-X_1X_2X_3$.

Thus

$$E_A = A_i O_{ij} T_j E \quad (6)$$

where we use the Einstein repeated subscript convention for summation.

Since $O-X_1X_2X_3$ can be imagined to be brought from initial coincidence with $O-X_1X_2X_3$ into its actual orientation by successive rotations of ϕ about OX_3 , θ about Ox_2 and ψ about Ox_3 , (O_{ij}) is given explicitly by:

$$(O_{ij}) = \begin{pmatrix} \cos\theta\cos\phi\cos\psi - \sin\phi\sin\psi & \cos\theta\sin\phi\cos\psi + \sin\theta\cos\psi & -\sin\theta\cos\psi \\ -\cos\theta\cos\phi\sin\psi - \sin\phi\cos\psi & -\cos\theta\sin\phi\sin\psi + \cos\phi\cos\psi & \sin\theta\sin\psi \\ \sin\theta\cos\phi & \sin\theta\sin\phi & \cos\theta \end{pmatrix} \quad (7)$$

The rate of absorption of the light, I_A , is proportional to the product of E_A and its complex conjugate, E_A^*

$$I_A = CE_A E_A^* \quad (8)$$

or

$$I_A = C |A_i O_{ij} T_j E|^2 \quad (9)$$

where C is a constant.

In a similar way, the equations that refer to the light emitted by the fluorescent molecule can also be expressed either in terms of the matrix or the repeated subscript notation.

The fluorescent molecule emits light from an oscillating dipole $\mu = \mu B$, parallel to the emission axis **B**. μ^2 is proportional to I_A , since the intensity emitted is proportional to that absorbed.

In the $O-X_1X_2X_3$ frame:

$$(B_i) = \begin{pmatrix} \cos\beta'\sin\alpha' \\ \sin\beta'\sin\alpha' \\ \cos\alpha' \end{pmatrix} \quad (10)$$

so that in the $O-X_1X_2X_3$ frame μ is given by:

$$\mu_i = \mu O'_{ij} B_j \quad (11)$$

where (O'_{ij}) is the transpose of (O_{ij}) .

If the analyser is assumed perfect, so that it transmits only light with electric vector parallel to the unit vector **T'** which has polar coordinates γ' , η' with respect to $O-X_1X_2X_3$, then the transmitted electric vector has magnitude $E_{T'}$ proportional to the scalar product of **T'** and μ . The transmitted intensity, ΔI , is proportional to the product of this quantity and its complex conjugate. Hence:

$$\Delta I \propto \mu^2 |T'_i O'_{ij} B_j|^2 = G' |A_i O_{ij} T_j E|^2 |T'_p O'_{pq} B_q|^2 \quad (12)$$

where G' is a constant and ΔI is the intensity due to a single fluorescent molecule.

The total intensity detected is found by summing equation (12) over all the N fluorescent molecules under observation, so that:

$$I = G \langle |A_i O_{ij} T_j|^2 |T'_p O'_{pq} B_q|^2 \rangle_{av} \quad (13)$$

where $G = |E|^2 G' N$.

Equation (13) may be written:

$$I = G \langle A_i A_l B_q B_t \rangle \langle O_{ij} O_{lm} O'_{pq} O'_{st} \rangle T_j T_m T'_p T'_s \quad (14)$$

since the quantities in the angled brackets are assumed to be independent of each other. (O'_{ij}) is merely the transpose of (O_{ij}) and equation (14) thus becomes:

$$I = G \langle A_i A_l B_q B_t \rangle \langle O_{ij} O_{lm} O_{qp} O_{ts} \rangle T_j T_m T'_p T'_s \quad (15)$$

Performing the sum over all values of i, l, q and t leads to:

$$I = F_{j m p s} T_j T_m T'_p T'_s \quad (16)$$

where

$$F_{j m p s} = G \langle A_i A_l B_q B_t \rangle \langle O_{ij} O_{lm} O_{qp} O_{ts} \rangle \quad (17)$$

The intensity is now expressed as a sum of the products of pairs of terms. One term of each pair, $F_{j m p s}$, may be regarded as a component of a fourth rank tensor [$F_{j m p s}$] and depends (apart from the constant G) only on the properties of the specimen; the other, $T_j T_m T_p T_s'$, depends only on the polarization vectors of the polarizer and analyser.

If we now take into account the orthotropic symmetry of the specimen the number of non-zero terms in the sum over j, m, p , and s in equation (16) reduces from 81 to 21. The elements O_{ij} for $j=1, 2, 3$ may be regarded as components of a unit vector, parallel to the Ox_i axis. Since the specimen has orthotropic symmetry, the quantities $\langle O_{ij} O_{lm} O_{qp} O_{ts} \rangle$ must be invariant under the rotations represented by:

$$\begin{pmatrix} 1 & 0 & 0 \\ 0 & -1 & 0 \\ 0 & 0 & -1 \end{pmatrix}, \begin{pmatrix} -1 & 0 & 0 \\ 0 & 1 & 0 \\ 0 & 0 & -1 \end{pmatrix}, \begin{pmatrix} -1 & 0 & 0 \\ 0 & -1 & 0 \\ 0 & 0 & 1 \end{pmatrix}$$

applied to the $O-X_1 X_2 X_3$ axes. Each O_{ij} transforms into $-O_{ij}$ under two of these rotations and into $+O_{ij}$ under the other, according to the value of j . Thus if any of j, m, p or s occurs only once in $\langle O_{ij} O_{lm} O_{qp} O_{ts} \rangle$, this average must be zero. There are thus only 21 possible non-zero terms in the summation given in equation (16), nine terms with $j=m$ and $p=s$ and twelve terms with either $j=p$ and $m=s$ or $j=s$ and $m=p$. These twelve form three groups of four equal terms, each group having the same pair of subscripts j and m . There is thus a total of twelve independent terms on the right hand side of equation (16), nine terms of the form $F_{j j p p} T_j T_j T_p T_p'$ and three of the form $F_{j p j p} T_j T_p T_j T_p'$. The corresponding twelve components of $F_{j m p s}$, and only these, determine the intensity of the fluorescence for all possible combinations of polarization directions of incident and observed scattered light.

The nine components of the form $F_{j j p p}$ correspond to the nine intensities $I_{j p}$ defined by Desper and Kimura⁴. Each of these components can be measured directly. When the polarization vectors of the polarizer and analyser are parallel to axes of the $O-X_1 X_2 X_3$ frame, one of the quantities $T_j T_j T_p T_p'$ is unity and all the other quantities $T_j T_m T_p T_s'$ are zero. The intensity measured is therefore the value of the corresponding component $F_{j j p p}$. The determination of the components $F_{j p j p}$ requires measurements in which both polarization vectors are inclined to the axes of the $O-X_1 X_2 X_3$ frame.

Each component $F_{j m p s}$ is the product of a constant G and two other terms. The first of these, $\langle A_i A_l B_q B_t \rangle$, depends only on the properties of the fluorescent molecules and the second, $\langle O_{ij} O_{lm} O_{qp} O_{ts} \rangle$, depends only on functions of θ, ϕ and ψ averaged over the distribution of orientations; it is these averages that we wish to determine.

Each of the twelve components $F_{j m p s}$ depends, in the most general case, on a large number of unknown quantities. A great simplification is made by assuming that the fluorescent molecules have no preferred orientation around their Ox_3 axes and that if every fluorescent molecule is rotated through 180° around any axis normal to Ox_3 the distribution of orientations remains unchanged. These assumptions appear to be reasonable for a long thin fluorescent molecule which does not

bind chemically to the polymer chains. The Ox_3 axis would then be expected to be the geometric long axis of the molecule.

Making these assumptions is equivalent to setting $\psi=0$ in equation (7) and regarding β and β' as random, whilst retaining the relationship given by equation (1) between them. This leads to a reduction of the number of unknown quantities to eleven. These are five averages of functions of θ and ϕ , the unknown constant G and the quantities $\overline{\cos^2 \alpha}, \overline{\cos^2 \alpha'}, \overline{\cos^2 \alpha \cos^2 \alpha'}, \overline{\cos^2 \epsilon \sin^2 \alpha \sin^2 \alpha'}$ and $\overline{\cos \epsilon \sin 2\alpha \sin 2\alpha'}$. The number of independent components $F_{j m p s}$ is correspondingly reduced to eleven, since the following relationship now holds:

$$(F_{1122} - F_{2211}) + (F_{2233} - F_{3322}) + (F_{3311} - F_{1133}) = 0 \quad (18)$$

In principle the eleven independent $F_{j m p s}$ could be used to evaluate the eleven unknown quantities unless $\overline{\cos^2 \alpha} = \overline{\cos^2 \alpha'}$, when each of the differences in equation (18) is individually zero. It may be noted that if $\alpha = \alpha' = 0$ the results of the present treatment are equivalent to those of Bower¹¹. If α and α' are non-zero and ϵ is assumed to be random, then the treatment is equivalent to one given by Kimura *et al.*⁵, although they disregard the components $F_{j p j p}$.

We now consider how the determination of the components $F_{j m p s}$ is affected by the birefringence of the polymer sample and the attenuation of the exciting light as it passes through the sample and after that we turn to a detailed consideration of how information about the distribution of orientations may be obtained by means of measurements on uniaxial samples, for which the number of unknown quantities is further reduced.

Birefringence and absorption

The effect of the optical anisotropy of a polymer on the propagation of light through it is in general quite complex. It is relatively simple only if the light propagates along one of the symmetry axes Ox_1, Ox_2 or Ox_3 . Since it is possible, at least in principle, to determine all the required components $F_{j m p s}$ from measurements in which both the exciting and fluorescent light propagate along the same axis Ox_i , we shall consider the effects of birefringence and absorption only for such measurements.

If the symmetry axes normal to the direction of propagation are Ox_j and Ox_p , the non-zero components of the electric field of the exciting light are ET_j and ET_p as it enters the specimen. When the wave corresponding to the component ET_j has travelled a distance x into the sample the electric field is $ET_j \exp(-i\omega x n_j/c - x\alpha_j/2)$, where n_j and α_j are the refractive index and linear absorption coefficient, respectively, for exciting light of frequency ω polarized parallel to Ox_j . Similarly, light which is emitted by a fluorescent molecule at distance x within the sample and subsequently propagates in the same direction as the exciting light will have an electric field component in the Ox_p direction proportional to $\mu_p \exp[-i\omega'(d-x)n_p'/c - (d-x)\alpha_p'/2]$ when it reaches the surface of the sample, at distance d from the first surface. The primed quantities refer to the fluorescent light. A fraction T_p' of this will be transmitted by the analyser. We see that, for the arrangement considered, equation (16) must be modified to:

$$I = F_{j m p s}^2 T_j T_m T_p T_s' \quad (19)$$

where

$$F_{j m p s} = R_{j m p s} F_{j m p s} \quad (20)$$

with

$$R_{j m p s} = \langle \exp[-i\omega x(n_j - n_m)/c - i\omega'(d-x)(n'_p - n'_s)/c - x(\alpha_j + \alpha_m)/2 - (d-x)(\alpha'_p + \alpha'_s)/2] \rangle \quad (21)$$

The average is taken over all values of x and we have assumed a homogeneous distribution of fluorescent molecules throughout the thickness of the sample.

In the present work the specimens were almost completely transparent to the fluorescent light. When this is true we can write:

$$R_{j j p p} = (1/d) \int_0^d \exp(-\alpha_j x) dx \\ = [1 - \exp(-\alpha_j d)] / (\alpha_j d) \quad (22)$$

The quantity $\alpha_j d$ is simply the optical density, D_j , of the specimen for incident light polarized parallel to OX_j and can easily be determined, so that $R_{j j p p}$ may be regarded as known.

The quantities $R_{j p j p}$ are complex but equation (19) shows that the intensities determined must always depend on $F_{j p j p}^c$:

$$\text{where } F_{j p j p}^c = F_{j p j p}^c + F_{j p p j}^c + F_{p j p j}^c + F_{p j j p}^c \\ = F_{j p j p}^c (R_{j p j p} + R_{j p p j} + R_{p j p j} + R_{p j j p}) \quad (23)$$

The quantity in parenthesis is real and we call it $R'_{j p j p}$. $R'_{j p j p}$ can only be calculated if $(n_j - n_m)d$ and $(n'_p - n'_s)d$ are accurately known. Determination of $(n_j - n_m)d$ would require accurate measurements of refractive index at the wavelength of the ultra-violet exciting light and this quantity, and hence $R'_{j p j p}$, must usually be regarded as unknown. In the limit of very high birefringence ($d\Delta n \gg \lambda$), $R'_{j p j p}$ is zero and in the limit of very low birefringence ($d\Delta n \ll \lambda$) it has the value:

$$8\{1 - \exp[-(\alpha_j + \alpha_p)d/2]\} / [(\alpha_j + \alpha_p)d] \quad (24)$$

Uniaxial symmetry

For a sample of uniaxial symmetry each component $F_{j m p s}$ must be invariant under rotation through any arbitrary angle around the OX_3 axis, which is chosen to be parallel to the unique axis of the specimen. This reduces the number of independent components to six and the corresponding quantities $F_{j m p s}^c$ may be shown to be given by:

$$F_{1111}^c = F_{2222}^c = GR_{1111}(A_0 \overline{\cos^4 \theta} + A_1 \overline{\cos^2 \theta} + A_2) \quad (25a)$$

$$F_{3333}^c = 8GR_{3333}(A_3 \overline{\cos^4 \theta} + A_4 \overline{\cos^2 \theta} + A_5) \quad (25b)$$

$$F_{2233}^c = F_{1133}^c = 4GR_{2233}(A_6 \overline{\cos^4 \theta} + A_7 \overline{\cos^2 \theta} + A_8) \quad (25c)$$

$$F_{3322}^c = F_{3311}^c = 4GR_{3322}(A_9 \overline{\cos^4 \theta} + A_{10} \overline{\cos^2 \theta} + A_{11}) \quad (25d)$$

$$F_{2323}^c = F_{1313}^c = 4GR_{2323}'(A_{12} \overline{\cos^4 \theta} + A_{13} \overline{\cos^2 \theta} + A_{14}) \quad (25e)$$

$$F_{1122}^c = F_{2211}^c = GR_{1122}(A_{15} \overline{\cos^4 \theta} + A_{16} \overline{\cos^2 \theta} + A_{17}) \quad (25f)$$

In addition, the following relationship holds:

$$2F_{1212} = F_{1111} - F_{1122} \quad (26)$$

The eighteen coefficients A_0 to A_{17} depend only on the following averages: $\overline{\cos^2 \alpha}$, $\overline{\cos^2 \alpha'}$, $\overline{\cos^2 \alpha \cos^2 \alpha'}$, $\overline{\cos^2 \epsilon \sin^2 \alpha \sin^2 \alpha'}$, $\overline{\cos \epsilon \sin 2\alpha \sin 2\alpha'}$. Since R'_{2323} cannot be accurately calculated or obtained from the results of a separate experiment, the six equations (25) contain nine unknown quantities and cannot be solved. It is necessary, therefore, to make some further assumptions. We therefore assume that if α and α' are not the same for every

Table 1 Coefficients of equation (27)

$\chi = \overline{\cos^2 \epsilon}$					
A	D	K	L	M	N
A_0	$3+6\chi$	$-15-6\chi$		$51+6\chi$	-12
A_1	$2+4\chi$	$6-4\chi$		$-62+4\chi$	8
A_2	$3+6\chi$	$1-6\chi$		$19+6\chi$	4
A_3	$1+2\chi$	$-5-2\chi$		$17+2\chi$	-4
A_4	$-2-4\chi$	$6+4\chi$		$-10-4\chi$	4
A_5	$1+2\chi$	$-1-2\chi$		$1+2\chi$	
A_6	$-1-2\chi$	$5+2\chi$		$-17-2\chi$	4
A_7	$-2+4\chi$	-4χ	-6	$10+4\chi$	-4
A_8	$3-2\chi$	$-1+2\chi$	2	$-1-2\chi$	
A_9	$-1-2\chi$	$5+2\chi$		$-17-2\chi$	4
A_{10}	$-2+4\chi$	-4χ	6	$10+4\chi$	-4
A_{11}	$3-2\chi$	$-1+2\chi$	-2	$-1-2\chi$	
A_{12}	$-1-2\chi$	$5+2\chi$		$-17-2\chi$	4
A_{13}	2	-6		18	-3
A_{14}	$-1+2\chi$	$1-2\chi$		$-1+2\chi$	1
A_{15}	$1+2\chi$	$-5-2\chi$		$17+2\chi$	-4
A_{16}	$22-20\chi$	$-30+20\chi$		$22-20\chi$	8
A_{17}	$1+2\chi$	$11-2\chi$		$-15+2\chi$	-4

fluorescent molecule the distribution of values is sufficiently narrow that some effective mean values can be used, so that the unknown quantities that depend on the properties of the fluorescent molecules but not on their orientations become α , α' , $\overline{\cos^2 \epsilon}$, $\overline{\cos \epsilon}$.

The forms of the coefficients A_0 to A_{17} which result when this assumption is made are given by Table 1. If A represents one of the coefficients then:

$$A = D + K(\overline{\cos^2 \alpha} + \overline{\cos^2 \alpha'}) + L(\overline{\cos^2 \alpha} - \overline{\cos^2 \alpha'}) + \\ M \overline{\cos^2 \alpha \cos^2 \alpha'} + N \overline{\cos \epsilon \sin 2\alpha \sin 2\alpha'} \quad (27)$$

If $\overline{\cos^2 \epsilon}$ and $\overline{\cos \epsilon}$ are fixed, the six equations (25) contain six unknowns and can be solved. Various models will be discussed in the section on data analysis in which different values are given to $\overline{\cos^2 \epsilon}$ and $\overline{\cos \epsilon}$.

In the experiments to be described, the quantities $F_{j m p s}^c$ were determined in the following way. The exciting light and observed fluorescent light travelled parallel to the OX_1 axis of the specimen and the polarization vectors of the polarizer and analyser were either parallel or crossed. The specimen was rotated about the OX_1 axis so that OX_3 made a variable angle γ with the polarization vector of the incident light. By inserting the appropriate expressions for T_i and T_i' in terms of γ into equations (19) the observed intensities are found to be given by:

$$I_{\parallel}(\gamma) = B_0 + B_1 \cos 2\gamma + B_2 \cos 4\gamma \quad (28a)$$

$$I_{\perp}(\gamma) = B_3 + B_4 \cos 2\gamma + B_5 \cos 4\gamma \quad (28b)$$

where subscripts \parallel and \perp signify parallel and crossed polarizer and analyser respectively and:

$$B_0 = (3F_{3333}^c + 3F_{2222}^c + F_{3322}^c + F_{2233}^c + F_{2323}^c) / 8 \quad (29a)$$

$$B_1 = (F_{3333}^c - F_{2222}^c) / 2 \quad (29b)$$

$$B_2 = (F_{3333}^c + F_{2222}^c - F_{3322}^c - F_{2233}^c - F_{2323}^c) / 8 \quad (29c)$$

$$B_3 = (F_{3333}^c + F_{2222}^c + 3F_{3322}^c + 3F_{2233}^c - F_{2323}^c) / 8 \quad (29d)$$

$$B_4 = (F_{3322}^c - F_{2233}^c) / 2 \quad (29e)$$

$$B_5 = -B_2 \quad (29f)$$

The six coefficients B_0 to B_5 can be obtained by fitting equations (28) to the measured intensities for a large number of values of γ . For the experiments to be described a small systematic difference was found between B_5 and $-B_2$ and a possible explanation for

this is given in the Appendix. Once B_0 to B_4 are known equations (29) can be used to determine the five quantities F_{jpp}^c on the left of equations (25a) to (25e). This procedure is preferable to determining the five quantities directly, using only measurements with $\gamma=0, \pi/4$ or $\pi/2$, since in this way much more data can be used in the determination and the theory can be tested more fully. F_{1122}^c does not occur in the equations for the intensities for the experimental arrangement used in the present work and, since there are six unknown quantities to be determined, it is necessary to obtain one more equation relating them. This may be done by considering a random sample.

Random orientation

For a specimen in which the molecules are randomly oriented there are only two independent intensities, I_{\parallel} and I_{\perp} :

$$I_{\parallel} = F_{1111}^c = F_{2222}^c = F_{3333}^c \quad (30a)$$

$$I_{\perp} = F_{jjpp}^c \text{ for } j \neq p \quad (30b)$$

Also, for random orientation:

$$R_{jjjj} = R_{jjpp} = R_{pppp} \quad (31)$$

for all j and p .

By setting $\overline{\cos^2\theta} = 1/5$ and $\overline{\cos^2\theta'} = 1/3$ in equations (25a) and (25c) we obtain the following equation:

$$R = I_{\parallel}/I_{\perp} = (1 + 2\overline{\cos^2\alpha'}) / (2 - \overline{\cos^2\alpha''}) \quad (32)$$

where

$$\overline{\cos^2\alpha''} = \chi(1 - \overline{\cos^2\alpha} - \overline{\cos^2\alpha'}) + (1 + \chi)\overline{\cos^2\alpha}\overline{\cos^2\alpha'} + \zeta/2 \quad (33)$$

with $\chi = \overline{\cos^2\epsilon}$ and $\zeta = \overline{\cos^2\epsilon} \sin 2\alpha \sin 2\alpha'$. $\overline{\cos^2\alpha''}$ is simply the average of the cosine of the angle between the absorption and emission axes of the fluorescent molecule.

Equation (32) is the extra equation required for determining the unknown quantities. The method used for solving the equations is described later.

Optical dichroism

The quantity $\overline{\cos^2\theta_A}$, where θ_A is the angle between the absorption direction of the fluorescent molecule and the draw direction, can be determined from optical dichroism measurements¹. For uniaxial symmetry:

$$\overline{\cos^2\theta_A} = \frac{D_3}{D_3 + 2D_2} \quad (34)$$

where D_3 is the optical density for incident light polarized parallel to the draw direction and D_2 is the optical density for light polarized normal to the draw direction. The same quantity can be deduced from the fluorescence results using the equation:

$$\overline{\cos^2\theta_A} = (1/2)[(3\overline{\cos^2\alpha} - 1)\overline{\cos^2\theta} + 1 - \overline{\cos^2\alpha}] \quad (35)$$

It is possible, therefore, to compare directly the values of $\overline{\cos^2\theta_A}$ obtained from fluorescence measurements and optical dichroism measurements.

Although it is not clear from equation (35), the value of $\overline{\cos^2\theta_A}$ obtained from the fluorescence measurements should be independent of the choice of values for $\overline{\cos^2\epsilon}$ and $\overline{\cos^2\alpha}$ because ϵ is not defined if only absorption is considered. If it were possible to determine F_{1122} experimentally then $\overline{\cos^2\theta_A}$ could be determined directly from

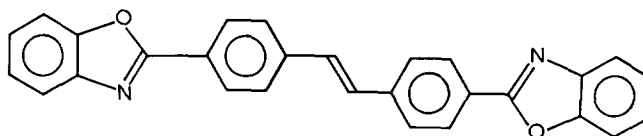
the equation:

$$\overline{\cos^2\theta_A} = \frac{F_{3333} + 2F_{3322}}{F_{3333} + 2(F_{1111} + F_{1122} + F_{3322} + F_{2233})} \quad (36)$$

EXPERIMENTAL

Specimen preparation

The photostable compound 4,4'-(dibenzoxazolyl) stilbene (VPBO)* was used as the fluorescent additive. Its structure is shown below:



This compound has an absorption band in the region of the intense 365 nm ultra-violet line in the mercury arc spectrum, and it fluoresces in the region 400 nm to 550 nm. The molecule is long and thin, and it has a high quantum efficiency of fluorescence.

Different amounts of the compound were mixed with bis(2-hydroxyethyl terephthalate) so that, after polycondensation, a series of batches of PET were formed containing the compound at a concentration of 200, 150, 100 or 50 ppm by weight. The mixtures were then melt spun in the form of thin tapes with cross-section approximately 1.5×10^{-3} m by 1.0×10^{-4} m. The number-average molecular weight \overline{M}_n was estimated from intrinsic viscosity measurements to be 2.3×10^4 . The samples were subsequently oriented by drawing around a smooth stationary 'pin' to draw ratios in the range 1 to 6. The 'pin' was heated to temperatures in the range 65–90°C and was located between feed and wind-up rollers rotating at different rates. Table 2 shows the draw ratios, drawing temperatures and other data for individual samples. Random samples were produced by annealing as-spun samples at 70°C in water until no

* Some authors use the name 2,2'-(vinylendi-*p*-phenylene)bis-benzoxazole and it is convenient to use the abbreviation based on this name.

Table 2 Specification of PET samples

Sample	Draw temp. (°C)	Draw ratio	Refractive indices at 551 nm			Density (g/cm ³)	Conc. VPBO (ppm)
			n_3	n_2	n_0		
1	—	1	1.583	1.583	1.583	1.338	200
2	80	1.38	1.590	1.577	1.581	1.338	200
3	80	1.87	1.602	1.572	1.582	1.338	200
4	80	2.00	1.603	1.570	1.581	1.338	200
5	80	2.19	1.608	1.570	1.582	1.339	200
6a	80	2.54	1.630	1.561	1.581	1.342	200
7	80	2.66	1.625	1.563	1.582	1.340	200
8	80	3.16	1.647	1.555	1.580	1.347	200
9	80	3.78	1.669	1.549	1.575	1.362	200
10	80	4.40	1.707	1.533	1.573	1.367	200
11	80	5.10	1.716	1.544	1.584	1.366	200
12	80	5.85	1.717	1.528	1.578	1.370	200
13	65	2.66	1.669	1.548	1.582	1.347	150
14	70	2.66	1.639	1.558	1.581	1.344	150
15	75	2.66	1.632	1.561	1.583	1.339	150
16	80	2.66	1.625	1.563	1.582	1.340	150
17	85	2.66	1.620	1.565	1.580	1.343	150
18	90	2.66	1.617	1.569	1.585	1.338	150

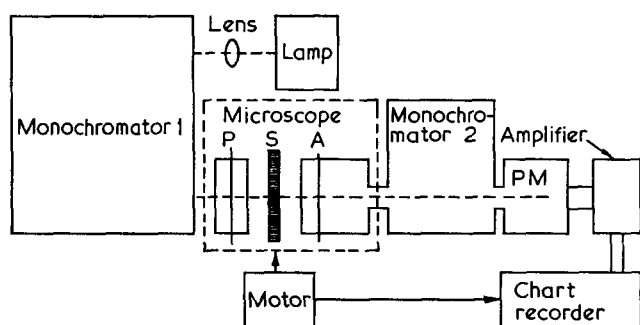


Figure 2 Block diagram of fluorescence apparatus

orientation could be detected by birefringence and polarized fluorescence measurements. (Before annealing the birefringence was <0.001 .)

X-ray photographs showed that the drawn specimens were of low crystallinity and the low values of the densities, which were determined by means of a density-gradient column and are shown in Table 2, support this conclusion.

Measurement of fluorescence intensity

The polarized fluorescence was measured using apparatus constructed from commercially available equipment. A block diagram is shown in Figure 2. Light from a 250 W mercury arc lamp was focused by a quartz lens onto the entrance slit of a Hilger Monospek 600 grating monochromator. The light emerging from the exit slit passed through an auxiliary lens and Nicol prism polarizer and an image of the slit was formed in the first focal plane of the substage condenser of a Vickers M 41 microscope. The sample, mounted on a microscope slide, was held on the microscope stage which could be rotated by a small motor. Light from each point of the slit passed as a collimated beam through the sample and the largest angle made by any such beam with the normal to the sample surface was about 2° .

The fluorescent light from the sample was collected by the microscope objective, passed through an analyser and was then either viewed with an eyepiece fitted with an ultra-violet (u.v.) filter or focused onto the entrance slit of a small Hilger and Watts (D292) monochromator. An EMI 9502S photomultiplier tube measured the intensity of the light that emerged from the exit slit of this monochromator. The signal from the photomultiplier was amplified and recorded on a Servoscribe chart recorder.

When the first monochromator was set to transmit the u.v. exciting line at 365 nm it also transmitted some stray light at other wavelengths. Since the fluorescent light was observed in the propagation direction of the incident u.v. light it was possible for the stray light to be detected by the photomultiplier. Its intensity was greatest at the wavelengths 436 nm and 405 nm which correspond to two other lines in the mercury arc spectrum. For fluorescence measurements made at these wavelengths a correction for this stray light was made. Most of the fluorescence measurements were made at the wavelength 469 nm and the intensity of the stray light at this wavelength was 0.5% of the minimum signal intensity.

The sensitivity of the detection system depended on the polarization of the light incident on the entrance

slit of the second monochromator. The relative sensitivity to the two polarizations used was measured throughout the fluorescence spectrum for a particular slit width by observing light from an incandescent lamp which was polarized, either parallel or perpendicular to the slit, by the analyser. All polarized fluorescence measurements were made using the same slit width.

The emission spectrum of the fluorescent molecules in the random tape sample of PET when it was illuminated with light of wavelength 365 nm consisted of three overlapping peaks, two of them of similar magnitude at 415 nm and 438 nm, and a smaller one at 469 nm. The value of the ratio R (see equation 32) for a random sample was measured and found to be constant throughout the fluorescence spectrum within experimental error, implying that $\overline{\cos^2\alpha}$ does not change. Table 3 contains these results and Figure 3 shows the emission spectrum. In view of the constancy of $\overline{\cos^2\alpha}$ it was considered unnecessary to determine the intensity of fluorescence at more than one selected narrow wavelength region when studying oriented specimens.

In the theory it was assumed that the incident and collected fluorescent light propagate along the normal to the specimen surface. It was possible to satisfy this condition closely only for the incident light. A cone of fluorescent light was collected whose semi-angle depended on the numerical aperture of the objective. Measurements were made of the ratio R on a random sample for a series of objectives of different numerical aperture. Table 4 gives the results. The change of R with numerical aperture was small, showing that the effect of divergence on the polarization of the fluorescent light could be neglected. As an additional check some of the measurements on oriented specimens were also made using several different objectives and the results were always

Table 3 Ratio R for various emission wavelengths and sample temperatures

T (K)	λ (nm)				
	405	425	436	450	469
290	2.26	2.31	2.31	2.28	2.24
81	2.27	2.24	2.29	2.27	2.31

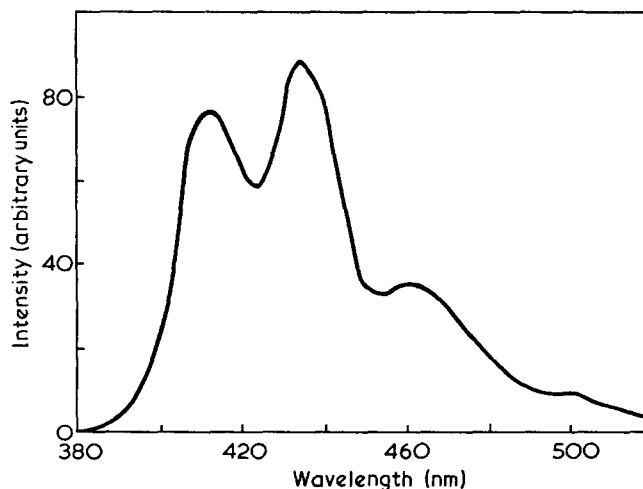


Figure 3 Emission spectrum of VPBO in PET

Table 4 Ratio R for various values of numerical aperture (at 469 nm)

Numerical aperture	R
0.70	2.27
0.50	2.33
0.25	2.24
0.12	2.24

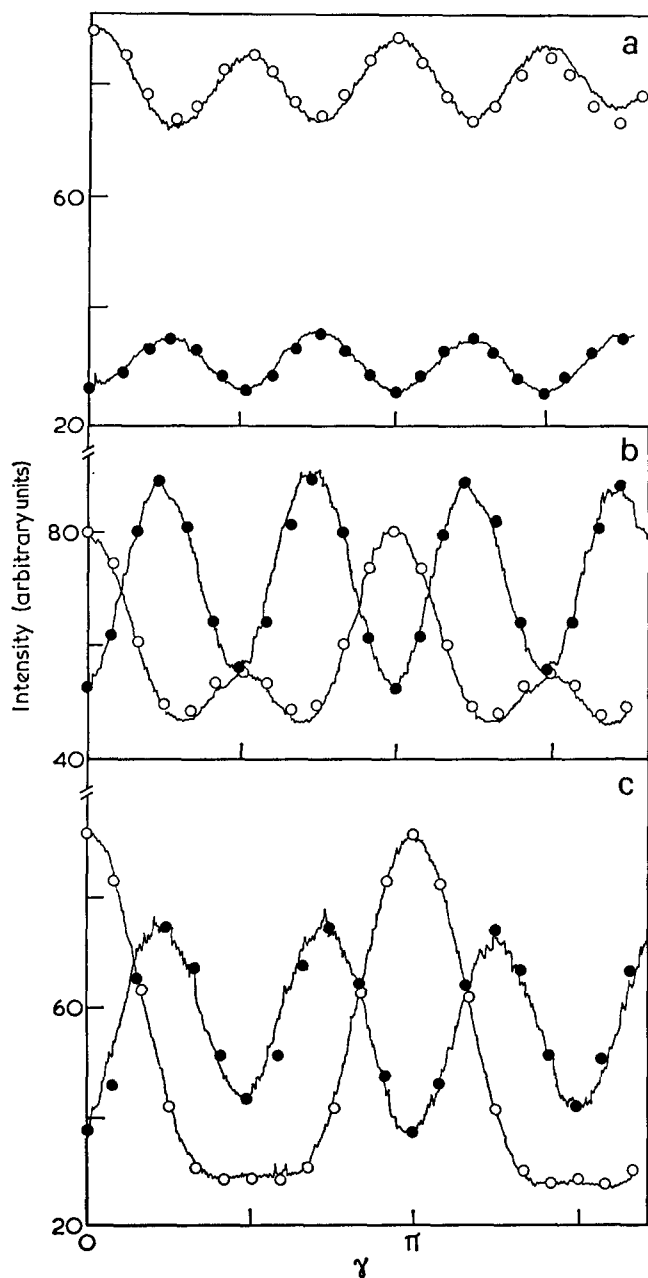


Figure 4 Fluorescence intensity as function of angle, γ , of rotation of specimen about OX_1 . (a) Specimen 1; (b) specimen 2; (c) specimen 5. Points are calculated from fits to equations (28). \circ , Polarizer and analyser parallel; \bullet , polarizer and analyser crossed. (See also text)

the same within experimental error. Because the oriented specimens are birefringent the effective angle of the collection cone depends on the polarization vector. The effect of this on the observed intensities is considered in the Appendix.

The measurements of fluorescence intensity as a function of γ were made by rotating the sample on the

microscope stage at a constant rate and recording the intensity under conditions of either crossed or parallel polarizers. The chart recorder and microscope stage drives were coupled together. Typical results are shown in Figure 4.

Other measurements

The polarized fluorescence apparatus was modified for measuring the optical dichroism of the samples and determining the quantities R_{jjpp} by placing two pinholes in the optical path. The first pinhole was placed before the substage condenser of the microscope so that its image was focused by the condenser into the plane of the sample. The microscope objective was replaced by the second pinhole so that only parallel rays of plane polarized u.v. light that had passed normally through the sample entered the detection system. The sample was again mounted on a microscope slide but it was found necessary to immerse the sample in a liquid of similar refractive index to reduce light loss by scattering and reflection at the sample surfaces. Omission of this precaution gives serious errors in the determination of the absorption coefficients; its effects on the fluorescence measurements are discussed in the Appendix.

The refractive indices of the samples for light polarized parallel to the draw direction, n_3 , and normal to it, n_2 , were measured by means of an image-splitting interference microscope. Each sample was immersed in a standard refractive index liquid whose index was very close to the particular index of the sample being measured and the difference between the indices (which was always <0.004) was determined by counting interference fringes. The assumption that the specimens were uniaxially oriented was checked by using the equation:

$$\frac{n_0^2 - 1}{n_0^2 + 2} = \frac{\rho_0}{3\rho} \left(\frac{n_1^2 - 1}{n_1^2 + 2} + \frac{n_2^2 - 1}{n_2^2 + 2} + \frac{n_3^2 - 1}{n_3^2 + 2} \right) \quad (37)$$

and the assumption $n_1 = n_2$ to calculate for each specimen the refractive index n_0 of the isotropic material. The values of n_0 , which are shown in Table 2, were found to be constant within experimental error. Equation (37), in which ρ and ρ_0 are the densities of the sample and the isotropic material, respectively, may be derived by applying the Lorentz-Lorenz equation¹³ to the first order invariant of the polarizability tensor of the chain segments.

Data analysis

Before the fluorescence data can be analysed, a model for the optical behaviour of the fluorescent molecule must be assumed so that the values of $\overline{\cos^2 \epsilon}$ and $\overline{\cos \epsilon}$ are defined. We shall quote results for two models.

$$\text{Model 1} \quad \epsilon \text{ random; } \overline{\cos^2 \epsilon} = \frac{1}{2}, \quad \overline{\cos \epsilon} = 0$$

$$\text{Model 2} \quad \epsilon = \pi; \quad \overline{\cos^2 \epsilon} = 1, \quad \overline{\cos \epsilon} = -1$$

It was found that the values of $\overline{\cos^2 \theta}$ and $\overline{\cos^4 \theta}$ lay between those obtained for models 1 and 2 for any other choices of $\overline{\cos^2 \epsilon}$ and $\overline{\cos \epsilon}$ that gave mathematically allowable values for all specimens.

The directly measured fluorescence intensities were first corrected for the differential polarization sensitivity of the detection system and for stray light. Certain other possible corrections were considered but not applied and these are discussed in the Appendix. The data

were next treated in the following way. A least squares fit of equations (28) was made to the intensity variations to obtain the coefficients B_0 to B_5 . Equations (29) were then solved to obtain F_{2222}^c , F_{3333}^c , F_{2233}^c and F_{3322}^c and the following ratios were calculated:

$$\frac{F_{3333}^c - F_{2222}^c}{F_{3333}^c + F_{2222}^c}, \frac{F_{3333}^c + F_{2233}^c + F_{3322}^c}{F_{3333}^c + F_{2222}^c}, \frac{F_{2233}^c - F_{3322}^c}{F_{3333}^c + F_{2222}^c}$$

The unknown constant G was thus eliminated and the three ratios could be expressed, using equations (25), in terms of the remaining unknown quantities α , α' , $\overline{\cos^2\theta}$, $\overline{\cos^4\theta}$ and the known values R_{jpp} .

A value for $(\cos^2\alpha' - \cos^2\alpha)$ was assumed and, using the ratio R determined for a random sample, $\cos^2\alpha$ and $\cos^2\alpha'$ were calculated from equation (33). Values of $\overline{\cos^2\theta}$ and $\overline{\cos^4\theta}$ were then calculated from the first two ratios above and the third ratio was used to recalculate $(\cos^2\alpha' - \cos^2\alpha)$. Unless this value differed from the starting value by less than 1×10^{-5} the calculations were repeated, substituting the new value for that originally assumed. The iteration was continued (using a PDP8E digital computer) until this condition was satisfied.

RESULTS

Table 5 contains values of the ratio R for a set of random samples each containing a different concentration of the fluorescent molecules. The ratio is the same within experimental error for all concentrations, which shows that resonant energy transfer between non-parallel molecules does not occur. The overall average value of R is 2.27 ± 0.02 , corresponding to a value of $\overline{\cos^2\alpha''} = 0.83 \pm 0.01$ and a mean angle $\alpha'' = 24^\circ$.

Table 5 Ratio R for various concentrations of VPBO (at 469nm)

VPBO (ppm)	R
200	2.24
150	2.28
100	2.21
50	2.24

Table 6 Orientation parameters and values of α and α' for models 1 and 2

Sample	$n_3 - n_2$	Model 1				Model 2			
		$\overline{\cos^2\theta}$	$\overline{\cos^4\theta}$	α (degrees)	α' (degrees)	$\overline{\cos^2\theta}$	$\overline{\cos^4\theta}$	α (degrees)	α' (degrees)
1	0.000	0.333	0.200	18	18	0.333	0.200	12	12
2	0.013	0.396	0.258	12	21	0.392	0.254	6	18
3	0.030	0.508	0.353	16	19	0.495	0.341	10	14
4	0.033	0.575	0.444	18	17	0.557	0.420	13	11
5	0.038	0.556	0.423	18	17	0.539	0.401	13	11
6a	0.069	0.720	0.605	18	18	0.691	0.563	12	12
7	0.062	0.679	0.557	18	18	0.653	0.521	12	12
8	0.092	0.853	0.814	17	18	0.814	0.743	11	13
9	0.120	0.926	0.890	18	17	0.881	0.812	13	11
10	0.174	0.968	0.957	18	17	0.920	0.869	13	11
11	0.172	0.949	0.919	19	16	0.903	0.838	13	11
12	0.189	0.960	0.938	18	17	0.913	0.853	13	11
13	0.121	0.903	0.853	18	17	0.859	0.779	12	12
14	0.081	0.801	0.707	18	17	0.765	0.653	12	12
15	0.071	0.776	0.673	19	16	0.743	0.624	14	10
16	0.062	0.738	0.625	19	16	0.708	0.583	14	10
17	0.055	0.701	0.599	18	17	0.674	0.557	13	11
18	0.048	0.627	0.499	19	16	0.605	0.470	14	11

Figure 4 shows some intensity variations as recorded by the chart recorder. The plotted points are calculated from the least squares fits to equations (28). The open circles denote parallel polarizers and the solid circles crossed polarizers. The sample used in Figure 4a, sample 1, had not been drawn and any orientation present must have arisen during the melt spinning stage of sample preparation. The two curves in this Figure have the same scale and zero level. Figures 4b and 4c refer to samples 2 and 5, which were drawn at 80°C to draw ratios 1.38 and 2.19, respectively. The two curves in each Figure have the same zero level, but the intensities shown for the crossed polarizers should be multiplied by 0.54.

The values of $\overline{\cos^2\theta}$, $\overline{\cos^4\theta}$, α , α' and the birefringence $n_3 - n_2$ are given in Table 6. The values of $\overline{\cos^2\theta}$ and $\overline{\cos^4\theta}$ obtained for model 1 are greater than those for model 2, except for a random sample where they agree. Table 7 gives the values of $\overline{\cos^2\theta_A}$ calculated from the fluorescence data using equation (35) together with the corresponding values of $\overline{\cos^2\theta_A}$ measured by optical dichroism. The value of $\overline{\cos^2\theta_A}$ derived from the fluorescence data is independent of the choice of model. Figure 5 is a plot of $\overline{\cos^2\theta_A}$ measured by optical dichroism against the corresponding value measured by polarized fluorescence. It is linear with a gradient of 1.04 ± 0.02 . Table 8 contains values of $\overline{\cos^2\theta_A}$ measured by the two different methods and the ratio of the absorption terms R_{2222} and R_{3333} for a series of specimens drawn at the same temperature (80°C) to the same draw ratio (2.54) but containing different concentrations of the fluorescent molecules. Tables 7 and 8 and Figure 5 show that the values of $\overline{\cos^2\theta_A}$ measured by the two methods agree, within experimental error, over a wide range of orientations and are independent of the concentration of fluorescent molecules.

Figure 6 shows a plot of $\overline{\cos^2\theta_A}$ determined from the fluorescence measurements against the birefringence $n_3 - n_2$. If the birefringence corresponding to complete orientation of the polymer chains ($\cos^2\theta_p = 1$) is taken as 0.235 ± 0.01 , as suggested by the work of Kashiwagi *et al.*¹⁴ and Purvis *et al.*¹⁵, the value of $\overline{\cos^2\theta_A}$ corresponding to complete orientation of the chains is 0.91 ± 0.01 .

Table 7 $\overline{\cos^2\theta_A}$ from fluorescence and optical dichroism

Sample	n_3-n_2	$\overline{\cos^2\theta_A}$	
		Fluor.	Opt. dich.
1	0.000	0.33	0.33
2	0.013	0.39	0.35
3	0.030	0.49	0.49
4	0.033	0.54	0.53
5	0.038	0.52	0.53
6a	0.069	0.67	0.68
7	0.062	0.63	0.66
8	0.092	0.79	0.77
9	0.120	0.84	0.80
10	0.174	0.87	0.83
11	0.172	0.85	—
12	0.189	0.87	—
13	0.121	0.82	0.82
14	0.081	0.74	0.72
15	0.071	0.71	0.70
16	0.062	0.67	0.68
17	0.055	0.66	0.63
18	0.048	0.58	0.57

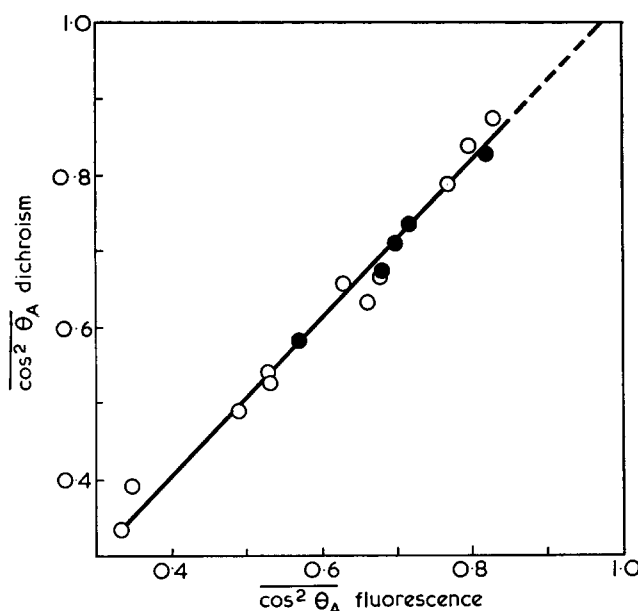


Figure 5 $\overline{\cos^2\theta_A}$ determined by fluorescence and dichroism. O, Samples 1 to 12; ●, samples 13 to 18

Table 8 Absorption correction for various concentrations of VPBO

Sample	n_3-n_2	$\overline{\cos^2\theta_A}$		VPBO conc. (ppm)	$\frac{R_{2222}}{R_{3333}}$
		Fluor.	Opt. dich.		
6a	0.069	0.67	0.67	200	1.25
6b	0.069	0.67	0.68	150	1.21
6c	0.069	0.67	0.67	100	1.15
6d	0.070	0.68	0.67	50	1.06

By assuming that complete alignment of the chains also produces complete alignment of the unique axes, \mathbf{M} , of the fluorescent molecules ($\overline{\cos^2\theta} = 1$), we can conclude that this value is equal to $\cos^2\alpha$. The corresponding value of α , $17.5^\circ \pm 1^\circ$, is in good agreement with the values obtained using model 1 (Table 6). We shall, therefore, not consider the results for other models any further.

Figure 7 is a plot of $\overline{\cos^2\theta}$ against the birefringence of the sample. The points for the series 1 to 12 drawn at 80°C and those for the series 13 to 18 drawn at different temperatures to draw ratio 2.66 lie on the same curve, suggesting that there is a unique relationship between $\overline{\cos^2\theta}$ and birefringence for PET samples of low crystallinity.

DISCUSSION

Orientations of fluorescent molecules

The agreement, within experimental error, of the values of $\overline{\cos^2\theta_A}$ measured by polarized fluorescence and the corresponding values measured by optical dichroism, which is a simpler technique both theoretically and

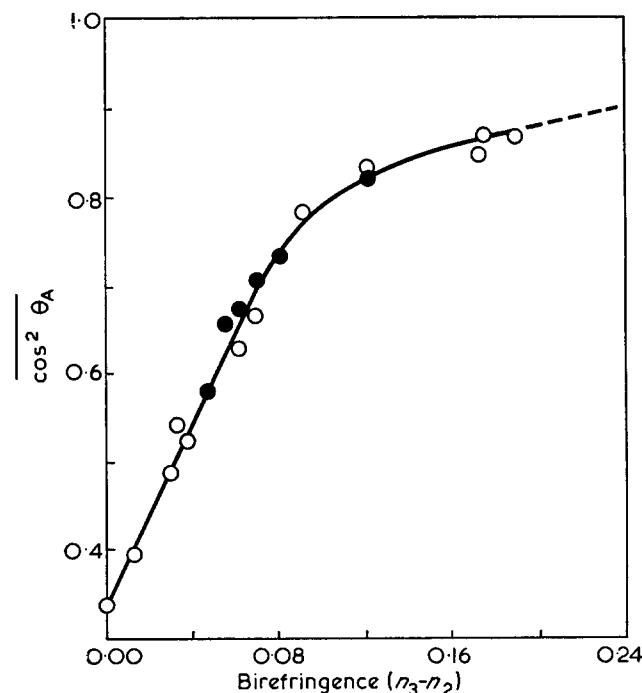


Figure 6 $\overline{\cos^2\theta_A}$ determined by fluorescence plotted against the birefringence (n_3-n_2). O, Samples 1 to 12; ●, samples 13 to 18

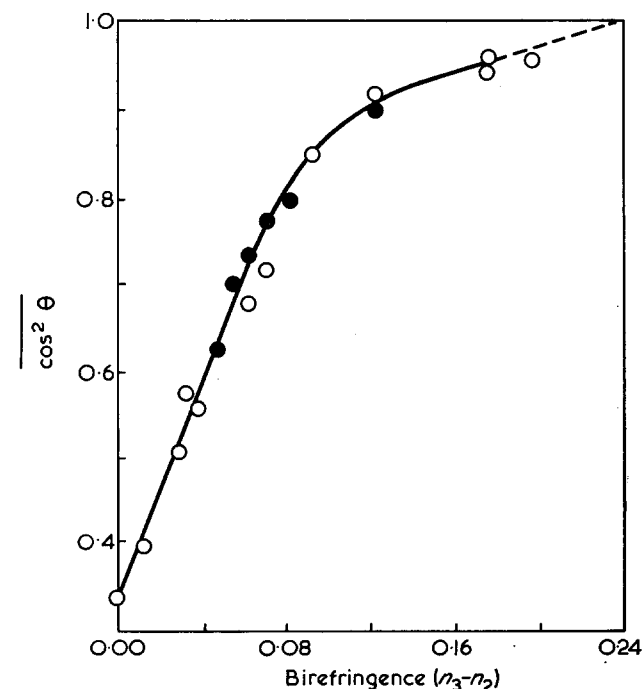


Figure 7 $\overline{\cos^2\theta}$ plotted against the birefringence (n_3-n_2). O, Samples 1 to 12; ●, samples 13 to 18

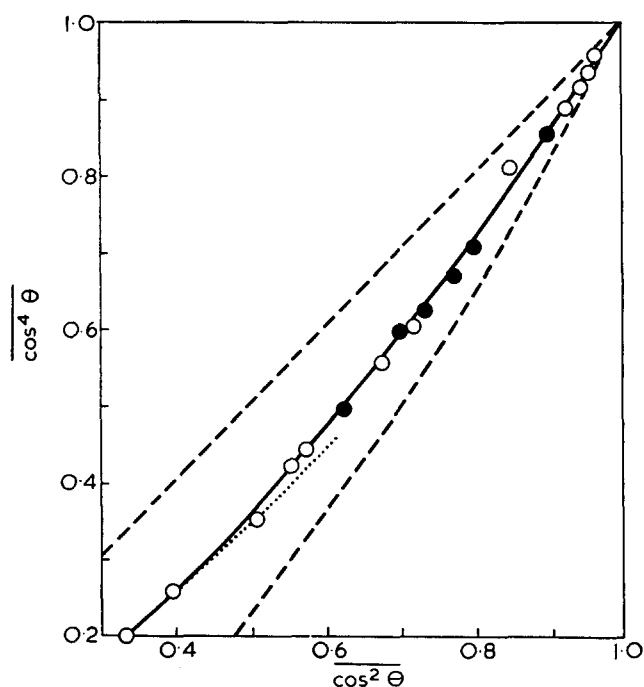


Figure 8 $\overline{\cos^4\theta}$ plotted against $\overline{\cos^2\theta}$. \circ , samples 1 to 12; \bullet , samples 13 to 18. ----, $\overline{\cos^4\theta} = \overline{\cos^2\theta}$ and $\overline{\cos^4\theta} = (\overline{\cos^2\theta})^2$; —, pseudo-affine deformation model; ·····, affine rubber deformation model

experimentally, strongly suggests that the method developed in the present paper for determining $\overline{\cos^2\theta}$ and $\overline{\cos^4\theta}$ for fluorescent molecules incorporated in an oriented polymer is a valid one. Unfortunately no values of $\overline{\cos^4\theta}$ for the fluorescent molecules determined by a different method are available for comparison.

To show that the values of $\overline{\cos^4\theta}$ obtained using model 1 are reasonable they have been plotted against the corresponding values of $\overline{\cos^2\theta}$ in Figure 8. The two broken lines represent the bounds of possible corresponding values which may be specified on purely mathematical grounds. The upper line represents $\overline{\cos^4\theta} = \overline{\cos^2\theta}$ and this clearly gives an upper bound to the value of $\overline{\cos^4\theta}$ for a given $\overline{\cos^2\theta}$, since every $\cos^4\theta$ is less than or equal to the corresponding $\cos^2\theta$. Any point on this boundary line corresponds to a distribution of orientations such that a fraction $\overline{\cos^2\theta}$ of the molecules have their axes exactly parallel to the draw direction and the remainder have their axes in the plane normal to this direction. The lower line represents $\overline{\cos^4\theta} = (\overline{\cos^2\theta})^2$ and Schwartz's inequality shows that this gives a lower bound to the value of $\overline{\cos^4\theta}$ for a given $\overline{\cos^2\theta}$. Any point on this boundary line corresponds to a distribution of orientations with all molecules having their axes on a cone of angle θ_c such that $\cos^2\theta_c = \overline{\cos^2\theta}$.

It is clear that any real distribution of orientations is likely to be fairly different from either of these extremes unless it is produced in a rather special way, so that points lying somewhere near the middle of the allowed region would be expected for the present experiments, and this expectation is confirmed. The solid and dotted lines in Figure 8 show the relationships between $\overline{\cos^4\theta_p}$ and $\overline{\cos^2\theta_p}$ predicted on the basis of the pseudo-affine deformation scheme¹⁶ and the affine rubber deformation scheme¹⁷, respectively, for the polymer. The closeness of the points to these lines may be to some extent fortuitous since, as discussed below, the fluorescent molecules do not simply lie parallel to the polymer

chains. It does, however, indicate that the values of $\overline{\cos^2\theta}$ and $\overline{\cos^4\theta}$ correspond to a distribution of orientations that is reasonable on physical grounds.

The theory of polymer birefringence^{2, 18} indicates that to a first approximation the birefringence should be linearly related to $\overline{\cos^2\theta_p}$, with $\overline{\cos^2\theta_p} = 1/3$ for zero birefringence and $\overline{\cos^2\theta_p} = 1$ for a maximum value of the birefringence, which we have already assumed to be 0.235 ± 0.01 for PET. Figure 7 indicates that although $\overline{\cos^2\theta}$ for the fluorescent molecules is probably uniquely related to the birefringence, and hence to $\overline{\cos^2\theta_p}$, the fluorescent molecules are always more highly oriented than the polymer chains. We shall defer detailed consideration of the relationship between the two distributions of orientations to a subsequent publication in which the present results will be compared with those obtained from infra-red and laser-Raman studies of molecular orientation in PET. We wish to simply comment here that two possible explanations of the higher orientation are either that each fluorescent molecule takes up the average orientation of the surrounding polymer chains or that the fluorescent molecules align themselves preferentially with the longer straight segments of polymer chain, which are probably on average those which are more closely aligned with the draw direction.

Optical behaviour of fluorescent molecules

In this paper we have assumed that the deviation of the observed value of R from 3 for a random sample occurs because α or α' is non-zero and we have obtained, on the basis of model 1, a value $17.5^\circ \pm 1.5^\circ$ for α and α' which is independent of the degree of orientation of the sample and of the concentration of the fluorescent molecules. Kimura *et al.*⁵ have shown that the deviation can also be explained in terms of thermal rotation of the fluorescent molecules. We have made measurements on a random sample at liquid nitrogen temperature and Table 3 shows that we obtained the same value of R at this temperature as obtained at room temperature. Since poly(ethylene terephthalate) is below its β relaxation at liquid nitrogen temperature, but above it at room temperature¹⁹, different values of R might have been expected if the deviation of R from 3 is primarily due to thermal motions.

For model 1 the assumptions made about the absorption and emission axes of the fluorescent molecule are similar to those made by Kimura *et al.* in one of their models, where they assume that the absorption and emission axes each have cylindrically symmetric distributions about a common principal axis. With the present model it is not necessary, however, to assume that each fluorescent molecule has a distribution of absorption and emission axes. It is sufficient to assume that although there may be fixed emission and absorption axes in each molecule the angle ϵ is random for the assembly of molecules considered together. A possible explanation for this is that there is a distribution of rotational isomeric states among the fluorescent molecules arising from rotations about the single bonds which occurred when the sample was in the molten state and which were subsequently frozen in.

Birefringence and absorption

Some authors have attempted to deduce the general nature of a distribution of orientations directly from the

form of the angular dependence of the fluorescence intensity. This is not always possible, since we have shown that the angular dependence is not determined only by the values of $\overline{\cos^2\theta}$ and $\overline{\cos^4\theta}$ which characterize the distribution of orientations of the fluorescent molecules. The effects of birefringence and absorption can drastically change the observed angular dependence. For example, the angular dependence produced by the as-spun sample shown in Figure 4a might at first sight be interpreted as arising from a distribution of orientations of the fluorescent molecules in which their unique axes show preferential alignment both parallel and perpendicular to the draw direction. We interpret it as arising from a simple uniaxial distribution of orientations with preferential alignment only parallel to the draw direction in a sample of very low birefringence. The coefficients B_2 and B_5 of equations (28) are determined for this sample essentially by its birefringence and thickness. (For a truly random sample $B_1=B_2=B_4=B_5=0$.) Figures 4a and 4b should be interpreted as showing minima in the intensity $I_{\parallel}(\gamma)$ for $\gamma \sim \pi/4$ rather than maxima for $\gamma = \pi/2$. For more highly oriented specimens the minimum disappears, but the angular dependence is still different from that for vanishingly small birefringence.

The only information that the angular dependences of $I_{\parallel}(\gamma)$ and $I_{\perp}(\gamma)$ contain about the distribution of orientations for a uniaxial sample is the values of $\overline{\cos^2\theta}$ and $\overline{\cos^4\theta}$, and all the information needed for calculating these quantities is contained in the value R for a random sample and the four intensities $I_{\parallel}(0)$, $I_{\parallel}(\pi/2)$, $I_{\perp}(0)$ and $I_{\perp}(\pi/2)$ for the oriented sample. These four intensities are independent of the birefringence but not of the effects of dichroic absorption. An effect of the latter can be seen in Figures 4b and 4c, where the observed intensities $I_{\perp}(0)$ and $I_{\perp}(\pi/2)$ are unequal. After correcting for absorption they become equal, although this is only because α and α' are equal. Table 8 shows that even with a modest degree of orientation a correction for absorption must be made if a significant systematic error in the results is to be avoided.

We conclude that the theoretical treatments that neglect birefringence and absorption are not adequate. The effects of birefringence have previously been considered by Seki²⁰, Onogi and Nishijima²¹ and Bower¹¹, but it was not explicitly shown in these treatments that for uniaxial symmetry the birefringence correction can be determined from the observed fluorescence intensities or eliminated when determining the orientation parameters. For orthotropic samples it will usually be necessary to make measurements in such a way that corrections for birefringence are required.

CONCLUSIONS

The experimental and theoretical results of the present work show that it is possible to determine two numbers, $\overline{\cos^2\theta}$ and $\overline{\cos^4\theta}$, which characterize the distribution of orientations of the unique axes of fluorescent molecules dispersed within a uniaxially oriented solid polymer from suitable measurements of the intensity of the polarized fluorescence. If the absorption of the incident radiation by the fluorescent molecules is not very small, then incorrect results will be obtained if the difference in absorption for different polarization directions of the

exciting light is not taken into account. If measurements are made with the polarization vectors of either the exciting or observed fluorescent radiations not parallel to symmetry axes of the specimen, then it is also necessary to correct for the birefringence of the specimen.

For the particular fluorescent molecule-polymer system used in the experimental work the distribution of orientations of the fluorescent molecules is not the same as the distribution of orientations of chain axes, as often suggested or implied in earlier work, but appears to be uniquely related to that distribution over a wide range of drawing temperatures and draw ratios. If the relationship is indeed unique and if it can subsequently be confirmed that the fluorescent molecules do not enter the crystallites of a crystalline polymer, then the fluorescence method will be capable of characterizing the orientation of the non-crystalline regions of such a polymer and will thus be of great use in understanding the role that these regions play in determining the macroscopic properties of solid polymers. We therefore propose now to study the fluorescence from crystalline samples of PET containing the same fluorescent probes as well as the changes produced in the polarized fluorescence of non-crystalline samples by shrinkage.

ACKNOWLEDGEMENTS

This research was undertaken as part of a research project financed by the Science Research Council, and J.H.N. also holds an SRC CAPS studentship. We are indebted to ICI Ltd, Fibres Division, Harrogate as the industrial sponsor, and wish to thank Dr H. Brody and Dr M. P. Wilson for their advice and assistance.

REFERENCES

- 1 Patterson, D. and Ward, I. M. *Trans. Faraday Soc.* 1957, **53**, 1516
- 2 Ward, I. M. *Proc. Phys. Soc.* 1962, **80**, 1176
- 3 Nishijima, Y., Onogi, Y. and Asai, T. *J. Polym. Sci. (C)* 1966, **15**, 237
- 4 Desper, C. R. and Kimura, I. *J. Appl. Phys.* 1967, **38**, 4225
- 5 Kimura, I., Kagiya, M., Nomura, S. and Kawai, H. *J. Polym. Sci. (A-2)* 1969, **7**, 709
- 6 Nishijima, Y. and Asai, T. *Rep. Prog. Polym. Phys. Japan* 1969, **12**, 429
- 7 McGraw, G. E. *J. Polym. Sci. (A-2)* 1970, **8**, 1323
- 8 Nishijima, Y. *J. Polym. Sci. (C)* 1970, **31**, 353
- 9 Roe, R.-J. *J. Polym. Sci. (A-2)* 1970, **8**, 1187
- 10 Weill, G. and Hornick, C. *Biopolymers* 1971, **10**, 2029
- 11 Bower, D. I. *J. Polym. Sci. (Polym. Phys.)* 1972, **10**, 2135
- 12 Badley, R. A., Martin, W. G. and Schneider, H. *Biochemistry* 1973, **12**, 268
- 13 Born, M. and Wolf, E. 'Principles of Optics', Pergamon Press, Oxford, 4th Edn, 1970, Ch 2
- 14 Kashiwagi, M., Cunningham, A., Manuel, A. J. and Ward, I. M. *Polymer*, 1973, **14**, 111
- 15 Purvis, J., Bower, D. I. and Ward, I. M. *Polymer* 1973, **14**, 398
- 16 Ward, I. M. 'Mechanical Properties of Solid Polymers', Wiley, London, 1971, p 258
- 17 Roe, R.-J. and Krigbaum, W. R. *J. Appl. Phys.* 1964, **35**, 2215
- 18 Hermans, P. H. 'Physics and Chemistry of Cellulose Fibres', Elsevier, New York, 1949, Part 2, Ch 4
- 19 McCrum, N. G., Read, B. E. and Williams, G. 'Anelastic and Dielectric Effects in Polymeric Solids', Wiley, London, 1967, Ch 13
- 20 Seki, J. *Sen-i Gakkaishi* 1969, **25**, 16
- 21 Onogi, Y. and Nishijima, Y. *Rep. Prog. Polym. Phys. Japan* 1971, **14**, 533, 537, 541

APPENDIX

In the theory section we neglected, for simplicity, various corrections to the observed intensities that must be considered when the birefringence of the sample is high and which are, unlike the absorption and birefringence corrections considered there, independent of the thickness of the sample. For many polymers these corrections will not be important, but the birefringence of PET is sufficiently high that their effects on the results of the experiments presented in this paper must be considered.

In the simple theory, no account was taken of the following: (a) partial reflection of the incident light at the surface of the sample; (b) the effect of the medium on the absorption cross-section of the fluorescent molecules; (c) the effect of the medium on the emission probability of the fluorescent molecules; and (d) the effect of the refractive index of the medium on the solid angle of the cone of observed scattered light within the medium. Since these effects all depend on the refractive index of the medium they will depend on the polarization of the incident and observed scattered radiations, and all measured intensities should be corrected for them. We now consider the corrections in turn and consider for simplicity only the effects on components of the form F_{jpp}^c .

In the equations n is the refractive index of the medium surrounding the sample and n_i is the refractive index for light polarized parallel to the OX_i axis. We neglect dispersion since we shall eventually be concerned only with differences of refractive index from that of the isotropic material and these differences will show much smaller dispersion than the refractive indices themselves.

(a) The intensity transmission coefficient, t_j , for light with polarization vector parallel to OX_j incident normally on the sample is given by:

$$t_j = 4nn_j/(n + n_j)^2$$

(b) Dexter (*Solid State Phys.* 1958, 6, 353) has considered the effective absorption cross-section for an atomic system embedded in a cubic or isotropic dielectric of refractive index μ and concludes that it will be given approximately by the value that it would have outside the medium multiplied by $(2 + \mu^2)^2/(9\mu)$. We shall assume that this factor is approximately correct for the fluorescent molecule in the anisotropic polymer sample, provided that the refractive index appropriate to the polarization vector of the incident light is inserted instead of μ .

(c) Dexter concludes that the emission probability for an atomic system embedded in the dielectric is increased by the factor $\mu(2 + \mu^2)^2/9$ over its value outside the medium. We shall assume that this factor can be applied for a fluorescent molecule in the anisotropic polymer, provided the appropriate refractive index is substituted.

(d) Since the samples are very thin compared with the working distances of the microscope objectives used, the solid angle of the cone of light collected by a given objective from an elementary volume in the sample depends only on the properties of the objective and the medium between it and the sample, provided that this cone angle, Ω_0 , is measured outside the sample. The solid angle, Ω , measured inside the sample is then $n^2\Omega_0/n_p^2$ for fluorescent light polarized parallel to OX_p .

The intensity observed when the incident and observed fluorescent radiations are polarized parallel to OX_j and

OX_p , respectively, should thus be divided by the factor:

$$\frac{(n_j^2 + 2)(n_p^2 + 2)^2}{(n_j + n)^2 n_p} \quad (\text{A1})$$

to obtain the quantity F_{jpp}^c for substitution into equations (25). (An unimportant numerical constant has been omitted, since only ratios of the components F_{jpp}^c are significant.)

If we write $n_i = n_0 + \Delta n_i$ where n_0 is the refractive index for an isotropic sample, and assume that $n = 1$, then for small values of Δn_i (again neglecting an unimportant constant) the correction factor, g , is given by:

$$g = 1 + a\Delta n_j + b\Delta n_p \quad (\text{A2})$$

where

$$a = 4n_0/(n_0^2 + 2) - 2/(1 + n_0) \quad (\text{A3a})$$

$$b = 4n_0/(n_0^2 + 2) - 1/n_0 \quad (\text{A3b})$$

For PET, $n_0 = 1.582$ and thus $a = 0.63$ and $b = 0.77$.

We estimate the effect of the correction on the values of $\overline{\cos^2\theta}$ and $\overline{\cos^4\theta}$ by considering the forms taken by equations (25a) to (25d) when $\alpha = \alpha' = 0$ and corrections for absorption are negligible. Including the correction given by equation (A2) they are:

$$F_{1111}^c = (3/8)k(1 - 2\overline{\cos^2\theta} + \overline{\cos^4\theta})[1 + (a + b)\Delta n_1] \quad (\text{A4a})$$

$$F_{3333}^c = k\overline{\cos^4\theta}[1 + (a + b)\Delta n_3] \quad (\text{A4b})$$

$$F_{1133}^c = \frac{1}{2}k(\overline{\cos^2\theta} - \overline{\cos^4\theta})[1 + a\Delta n_1 + b\Delta n_3] \quad (\text{A4c})$$

$$F_{3311}^c = \frac{1}{2}k(\overline{\cos^2\theta} - \overline{\cos^4\theta})[1 + a\Delta n_3 + b\Delta n_1] \quad (\text{A4d})$$

where k is a constant.

In the method of calculation used in this paper F_{1133}^c and F_{3311}^c are added together in determining $\overline{\cos^2\theta}$ and $\overline{\cos^4\theta}$. We can thus replace equations (A4c) and (A4d) by:

$$F_{1133}^c = \frac{1}{2}k(\overline{\cos^2\theta} - \overline{\cos^4\theta})[1 + \frac{1}{2}(a + b)(\Delta n_1 + \Delta n_3)] \quad (\text{A4e})$$

We see that the corrections to F_{1111}^c , F_{3333}^c and F_{1133}^c , and hence also to $\overline{\cos^2\theta}$ and $\overline{\cos^4\theta}$, depend only on $(a + b)$. The corrections to $\overline{\cos^2\theta}$ and $\overline{\cos^4\theta}$ will also depend only on $(a + b)$, to a first approximation, when the more general forms of equations (25) are used.

Solution of equations (A4a), (A4b) and (A4e) for $a + b = 0$ gives:

$$\overline{\cos^2\theta} = (6F_{1133}^c + 3F_{3333}^c)/(3F_{3333}^c + 12F_{1133}^c + 8F_{1111}^c) \quad (\text{A5a})$$

$$\overline{\cos^4\theta} = 3F_{3333}^c/(3F_{3333}^c + 12F_{1133}^c + 8F_{1111}^c) \quad (\text{A5b})$$

It is now easy to calculate the change produced in $\overline{\cos^2\theta}$ and $\overline{\cos^4\theta}$ for any value of $(a + b)$ provided that the corresponding refractive indices are known. Table 9 shows the uncorrected and corrected values for four sets of $\overline{\cos^2\theta}$ and $\overline{\cos^4\theta}$ lying on the pseudo-affine deformation curve shown in Figure 8. The values of Δn_j are estimated from the data in Tables 2 and 6 and

Table 9 Estimated corrections to $\overline{\cos^2\theta}$ and $\overline{\cos^4\theta}$

Uncorrected		Corrected		Δn_1	Δn_3
$\overline{\cos^2\theta}$	$\overline{\cos^4\theta}$	$\overline{\cos^2\theta}$	$\overline{\cos^4\theta}$		
0.395	0.250	0.392	0.248	-0.005	0.007
0.555	0.420	0.545	0.410	-0.013	0.025
0.801	0.720	0.787	0.703	-0.025	0.056
0.968	0.956	0.960	0.946	-0.050	0.124

$(a+b)$ is taken as 1.4. It is seen that the largest corrections are smaller than the scatter of points in *Figures 7 and 8*. Similar results are obtained if the full forms of equations (25) are used and the theoretical values of a and b are inserted.

Since equation (A2) has been derived by making several assumptions and approximations it is necessary to ask whether the corrections estimated in this way are at all reliable. Whatever the detailed theory may be, it seems reasonable to expect the correction to be approximately of the form given by equation (A2) and it is thus only the values of a and b which are in serious doubt. Fortunately, it is possible to estimate $(a+b)$ directly from the experimental data.

If equations (29) are rewritten taking into account the

corrections considered in this Appendix it is found that equation (29f) may be replaced approximately by:

$$B_5 + B_2 = (a+b)(B_0 + B_1 + B_2)\Delta n_3/4 \quad (\text{A6})$$

The data show that B_5 is systematically different from $-B_2$ and equation (A6) allows an estimate of $(a+b)$ to be made from this difference. The value obtained, 0.7 ± 0.2 , is half that estimated theoretically and this suggests that the corrections to be made to $\overline{\cos^2\theta}$ and $\overline{\cos^4\theta}$ are certainly not significant compared with experimental error. The values quoted in the results section are therefore those calculated without the correction.

Similar considerations show that the corrections to the optical dichroism results are negligible.

Conformation of polycarbonate by flow and magnetic birefringence*

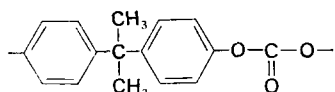
J. V. Champion, R. A. Desson and G. H. Meeten

Department of Physics, Sir John Cass School of Science and Technology,
City of London Polytechnic, London EC3N 2EY, UK
(Received 17 December 1973; revised 31 January 1974)

Solutions of polycarbonate in chloroform and tetrahydrofuran have been used to make measurements of flow birefringence, magnetic birefringence and viscosity. The results are used with standard theories of the two effects to derive optical and magnetic polarizability anisotropies of the polymer's statistical segment. These anisotropies are then used to determine the average mutual orientation of the phenyl rings in the chain and the average number of monomer units per statistical segment.

INTRODUCTION

The linear polycarbonate poly[2,2-propane bis(4-phenylcarbonate)] consists of phenyl rings connected by C and O-C-O atoms. The monomer unit is shown below:



Previous experimental measurements of the mean square end-to-end distance \bar{s}^2 have been made using viscometric¹ and light scattering² methods in various solvents. The values so obtained of \bar{s}^2/M , where M is the polymer molecular weight, indicate that polycarbonate has a chain of moderate flexibility, being less flexible than poly(vinyl acetate) or poly(methyl methacrylate)³. Measurements using the above techniques only give information about the long range order of the polymer chain since, for example, \bar{s}^2 is independent of the phenyl ring orientation in polycarbonate. Short range information extending over a few monomer units may be derived from the anisotropy of electrical or magnetic polarizability of the chain. From this information the mutual orientation of the phenyl rings along the chain may be estimated. The technique of flow birefringence (Maxwell effect) is capable of measuring the electrical polarizability anisotropy of a statistical segment of the chain at optical frequencies. This may be termed the optical polarizability which will differ slightly from the static field polarizability due to dispersion. The technique of magnetic birefringence (Cotton-Mouton effect) is capable of measuring the product of the segmental optical and magnetic polarizability anisotropies, from which the magnetic polarizability can be evaluated using the flow birefringence value of optical polarizability. The use of reliably known bond or group optical or magnetic polarizability anisotropies then enables the monomer unit's optical or magnetic polarizability anisotropy to be calculated for various models of the segment. Comparison between these calculated seg-

mental anisotropies and those measured then indicates the short range phenyl ring mutual orientation.

MATERIALS

The polycarbonate was supplied by RAPRA from the Polymer Supply and Characterization Centre through the SRC scheme. It had their code number PCI. This was an unfractionated commercial sample and the properties as given by RAPRA were $M_w=25\ 000$ (light scattering), $M_w=27\ 000$ (g.p.c.), $M_n=8500$ (g.p.c.). The intrinsic viscosity in chloroform solution at 25°C was measured by us, and using the equation⁴ $[\eta]=1.12 \times 10^{-7} M_v^{0.82}$ gave a viscosity average molecular weight $M_v=26\ 000$.

Fractionated samples were obtained by precipitation from chloroform solution using methanol. Fractions redissolved in chloroform were used for intrinsic viscosity measurements, giving molecular weights for seven fractions of 4, 10, 17.5, 20, 21, 25.5 and 30.5×10^3 . Chloroform solutions of both fractionated and unfractionated polycarbonate with concentrations up to $100\ \text{kg/m}^3$ were used for all subsequent measurements. Some flow birefringence and viscosity measurements were made using unfractionated material dissolved in tetrahydrofuran.

FLOW BIREFRINGENCE

Apparatus and procedure

The flow birefringence machine was a coaxial cylinder pair with the outer cylinder being the rotor and the inner cylinder the stator. It was designed to enable high velocity gradients to be attained, without turbulence, for high and low viscosity solvents and solutions. Typical usable velocity gradients were $30\ 000\ \text{s}^{-1}$. Figure 1 shows a section of the machine which was made from stainless steel. The design of similar machines has been previously discussed⁵. Troublesome reflections of light from the metallic intercylinder gap, producing phase differences and thus errors in the measured birefringence of the sheared liquid, have been reduced by coating the inside of the rotor and outside of the stator with a thin layer

* Presented at the Polymer Physics Group (Institute of Physics) Biennial Conference, Shrivenham, September 1973.

of matt black resin reinforced Teflon. The diameters of the coated rotor and stator were 19.063 mm and 18.536 mm respectively, giving a gap width of 0.263 mm. The stator length was 76.20 mm. All measurements were made at $25 \pm 0.2^\circ\text{C}$.

The measurement of the phase difference δ induced in the sheared liquid is accomplished by mounting the flow birefringence machine in an optical system, shown in Figure 2. The birefringence $\Delta n = \lambda\delta/2\pi L$ where λ is

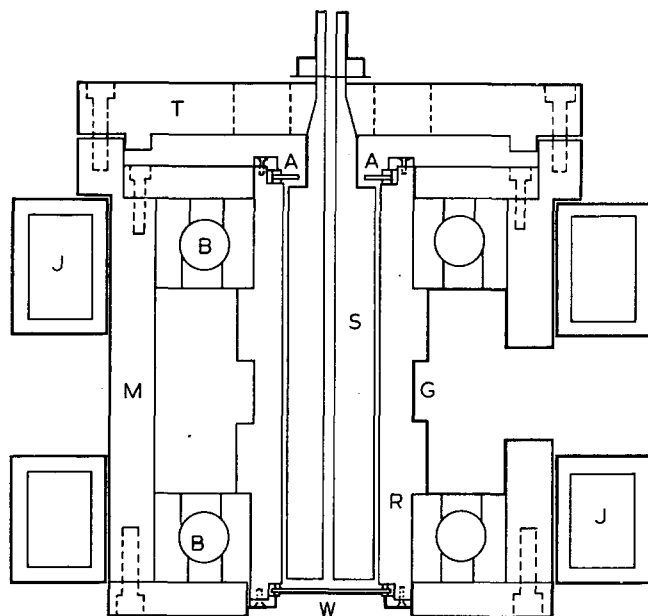


Figure 1 Flow birefringence machine. G, Groove for driver motor belt; R, rotor; S, stator; B, angular contact ball bearings; T, top plate holding stator; J, water jackets for temperature control; A, annular window revolving with rotor; W, circular window revolving with rotor; M, main body of machine

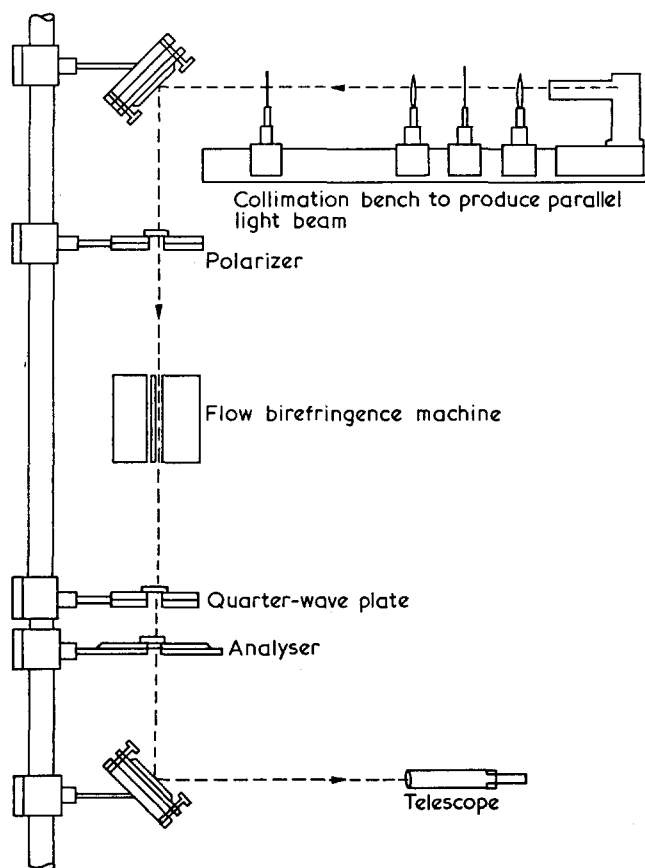


Figure 2 Flow birefringence machine in its optical bench

the wavelength of the light used (546.1 nm), L is the stator length and δ was measured by using the quarter-wave plate and analyser as a Senarmont compensator, the end-point being determined visually. Shearing times less than 10s were used in order to minimize viscous heating and consequent light beam refraction and reflection in the intercylinder gap. The temperature of the solution was measured by a calibrated thermocouple in contact with the solution in the axial hole of the stator. To measure the angle of isocline χ , the quarter-wave plate was removed and the polarizer crossed for extinction with the analyser. The birefringent liquid then caused a visible cross of isocline in the telescope when focused on the bottom of the intercylinder gap. A divided circle attached to the telescope eyepiece was arranged to rotate double cross-hairs in the eyepiece focal plane. These cross-hairs could be rotated to follow any motion of the cross of isocline and thus any change of χ with velocity gradient. Tests with liquids for which χ was known to be 45° served to establish the 45° position on the telescope divided circle. Owing to the cylindrical geometry of the sheared solution, the velocity gradient G is not constant over the gap. In this work, G was taken to be the shear rate in the centre of the intercylinder gap given by $\omega_2 R_2 / (R_2 - R_1)$ where ω_2 , R_2 and R_1 are the rotor angular velocity, rotor radius and stator radius respectively. The fractional change in G across the intercylinder gap was about $1\frac{1}{2}\%$, this being less than typical experimental error. The rotor speed was measured by an electromagnetic pick-up and calibrated with a stroboscope.

Results

Over the ranges of molecular weights, concentrations and shear rates used, it was found that: (a) the angle of isocline was constant at 45° to within the measurement error of about $\pm 0.5^\circ$; and (b) the birefringence was linearly proportional to the velocity gradient. It follows from (b) above that the Maxwell constant $M = \Delta n/G$ was a function only of concentration and molecular weight. For each solution M was measured by taking the least squares fitted slope of a Δn versus G graph with about 12 points, each point being the mean of 2 or more Δn determinations at the same value of G . Table 1 shows the results for the Maxwell constant as a function of molecular weight and concentration, in the solvents chloroform and tetrahydrofuran.

VISCOSITY

The solution viscosity was measured over a range of shear rates, concentration and molecular weights. The flow birefringence machine was adapted to form a viscometer by hanging a stator inside the rotor on a phosphor-bronze torsion wire. This arrangement proved self-centring for all shear rates used. The torque on the stator was measured by means of the angular motion of the torsion wire as indicated by a small mirror attached to the lower end of the wire, and a galvanometer lamp and scale. Liquids of known viscosity were used to calibrate the apparatus at $25 \pm 0.2^\circ\text{C}$, the temperature of all measurements. The viscosity, η , calculated from shear stress S by $\eta = S/G$, was found for chloroform and tetrahydrofuran solutions to be independent of G for all concentrations and molecular weights used. The results are shown in Table 1.

Table 1 Maxwell constant and excess viscosity of polycarbonate solutions

Solvent	Polymer conc. c_2 (kg/m ³)	$M_v \times 10^{-3}$	Maxwell constant, $M \times 10^{12}$ (s)	Excess viscosity, $\eta \times 10^3$ (Pa s)
CHCl ₃	0	—	1.6, 1.2	0
CHCl ₃	9.98	30.5	6.7, 7.0	0.42
CHCl ₃	10.05	26.0	5.1	0.35
CHCl ₃	12.05	4.0	1.2, 1.8	0.21
CHCl ₃	14.98	26.0	6.28	0.68
CHCl ₃	18.25	10.0	5.3	0.37
CHCl ₃	19.92	26.0	14.5	1.00
CHCl ₃	20.10	26.0	10.7	0.80
CHCl ₃	20.12	25.5	13.5, 13.9	0.96
CHCl ₃	20.20	21.0	9.1, 9.7	0.83
CHCl ₃	20.25	20.5	11.7	0.74
CHCl ₃	20.57	17.5	7.5	0.63
CHCl ₃	29.78	26.0	24.3	1.98
CHCl ₃	29.96	26.0	20.4	1.60
CHCl ₃	34.92	26.0	29.6	2.02
CHCl ₃	40.0	26.0	36.7	2.82
CHCl ₃	50.0	26.0	63.3	5.03
CHCl ₃	50.03	26.0	49.8	4.70
CHCl ₃	59.55	26.0	76.6	5.56
CHCl ₃	69.85	26.0	95.8	9.13
CHCl ₃	80.12	26.0	133	14.35
CHCl ₃	100.0	26.0	301.3	29.18
CHCl ₃	100.1	26.0	230.6	28.11
THF	0	—	0	0
THF	10.18	26.0	3.3	0.34
THF	18.49	26.0	10.02, 10.45	0.75
THF	42.62	26.0	31.2	2.51
THF	48.07	26.0	37.7	3.52

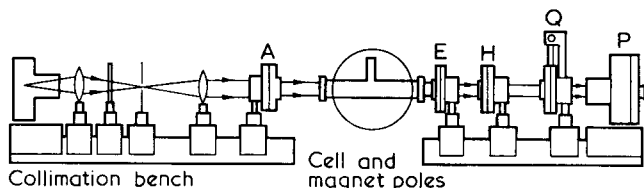


Figure 3 Magnetic birefringence apparatus. A, Glan-Thompson prism polarizer; E, aperture; H, half-shade; Q, quarter-wave plate; P, prism analyser and telescope. The cell length was 200 mm and minimum measurable phase difference about 0.06 mrad

MAGNETIC BIREFRINGENCE

Apparatus and procedure

The solution was contained in a cell between the poles of a Newport type E electromagnet. Figure 3 shows the general arrangement of components. Linearly polarized light incident upon the cell at 90° to the magnetic field, and polarized at ±45° to both the principal refractive indices and the magnetic field, emerges elliptically polarized. The phase difference between the principal vibrations of this ellipse was measured using a Senarmont compensator as for the flow birefringence but with the addition of a half shade device to improve the sensitivity of the compensator. The half shade was a thin glass slip with a polished 90° edge which covered half the beam emerging from the cell. About 0.2 mrad of phase was introduced into this half of the beam from the strain birefringence of the slip caused by the tension of a spring. The telescope was focused on the division of the field of view made by the polished edge of the slip and the analyser prism rotated until the halves of the field of view were of equal intensity. Analyser setting errors were typically ±0.06 mrad of phase

compared with about 1 mrad of phase induced by the solution in the magnetic field. The magnetic field was variable between 0–2 T and was calibrated using liquids of known Cotton–Mouton constants. The cell temperature was uncontrolled and took on the laboratory temperature, 23 ± 1°C. Unlike viscosity and hence flow birefringence, magnetic birefringence is not strongly temperature dependent.

Results

Within experimental error the induced birefringence was linearly proportional to the square of the applied field. This is the normal Cotton–Mouton effect which is quadratically dependent on the applied field, owing to the very low degree of preferential orientation of the diamagnetically and optically anisotropic segments of the polymer. For each solution a graph of birefringence versus B^2 was plotted, where B is the magnetic induction. The slope of this graph was then used to derive the Cotton–Mouton constant $C = \Delta n / \lambda B^2$, where λ is the free space wavelength of the light. C was found to be dependent only on the solution concentration as shown in Figure 4, in which points representing solutions of different molecular weight lie on the same line within experimental error.

DISCUSSION

Flow birefringence

Peterlin⁶ has given an equation relating the polymer solution excess Maxwell constant ($M - M_0$) to the excess viscosity of the solution, $\eta - \eta_0$, where M_0 is the solvent Maxwell constant and η_0 is the solvent viscosity. Peterlin's theory considered the flow birefringence to arise from the preferential orientation of optically anisotropic polymer molecules. Lodge⁷, starting from the polymer solution regarded as an entangled network subject to the forces set up by viscous flow, has deduced exactly the same equation. Both equations can be written:

$$(M - M_0) \sin 2\chi = \frac{(n^2 + 2)^2}{45kT\epsilon_0 n} (\alpha_1 - \alpha_2)_s (\eta - \eta_0) \quad (1)$$

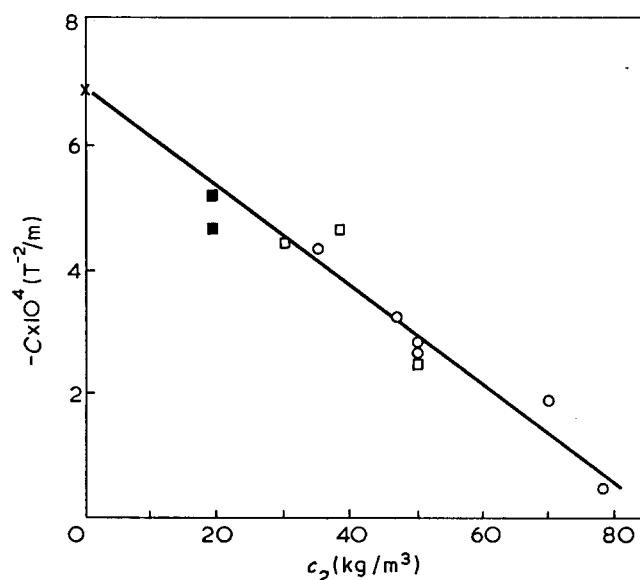


Figure 4 Cotton–Mouton constant of polycarbonate solution versus polycarbonate concentration. ○, Unfractionated, $M_v=26\,000$; □, fractionated, $M_v=25\,500$; ■, fractionated, $M_v=17\,500$; ×, pure chloroform

where n is the solution refractive index, k is Boltzmann's constant, ϵ_0 is the permittivity of free space and T the absolute temperature. The quantity $(\alpha_1 - \alpha_2)_s$ is the intrinsic optical anisotropy of the polymer chain's statistical segment. This segment is the length of chain over which it is effectively rigid. The molecular weight dependence of equation (1) is only valid if there is no anisotropy contributions due to macroform anisotropy⁸. This is an internal field anisotropy arising from the non-spherical shape of the whole polymer chain, when the mean refractive indices of the chain and solvent differ. It is generally molecular weight dependent⁸.

The relation between the angle of isocline χ and other parameters has also been given by Peterlin⁶ as:

$$\tan 2\chi = \frac{RTc}{MG(\eta - \eta_0)} \quad (2)$$

where c is the polymer concentration and R the gas constant. Our results support equations (1) and (2) in the sense that M and χ are independent of G as predicted by equation (1), and $\chi = 45^\circ \pm 0.5^\circ$ by experiment, whereas $\chi = 44.5^\circ$ as predicted by equation (2) using maximum experimental values of M , G and $(\eta - \eta_0)/c$.

Figure 5 shows a graph of $\log(M - M_0)$ versus $\log(\eta - \eta_0)$. The points on this graph represent measurements made using various concentrations of unfractionated and fractionated polymer in chloroform solution, and various concentrations of unfractionated polymer in tetrahydrofuran solution. Thus a single line represents all solutions which were measured, within the experimental error which on average is about $\pm 10\%$ in M , but rising to $\pm 30\%$ for the smallest Maxwell constants. Errors in $\eta - \eta_0$ were of a few per cent, negligible compared to errors in M .

In order to derive a value for the intrinsic anisotropy of a segment, which is solely determined by the conformation of the optically anisotropic bonds and chemical groups within the segment, it is necessary to account

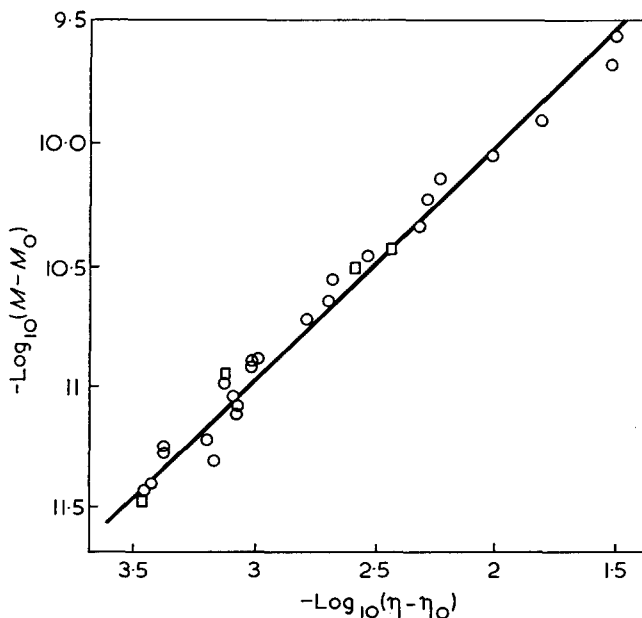


Figure 5 $\log_{10}(M - M_0)$ versus $\log_{10}(\eta - \eta_0)$ for polycarbonate solutions. Units of M are s, units of η are Pa s. \circ , All molecular weight fractions (10 000–30 000) and concentrations (0–100 kg/m³) dissolved in chloroform; \square , unfractionated polycarbonate ($M_v = 26 000$) dissolved in tetrahydrofuran

for the other contributions to $(\alpha_1 - \alpha_2)_s$ which may be present. These are: (i) the macroform anisotropy; (ii) specific solvation of orientated anisotropic solvent molecules onto the chain⁹; and (iii) the microform anisotropy.

(i) Any macroform anisotropy is linearly proportional to the molecular weight of the polymer⁸. Since the points representing different molecular weight fractions lie on a single line in Figure 5, there is no significant molecular weight dependence of $(\alpha_1 - \alpha_2)_s$ and hence no macroform anisotropy.

(ii) The low solvent optical anisotropy and the similarity between experimental results using two different solvents as shown in Figure 5 shows that there is negligible solvent effect for polycarbonate in both solvents used.

(iii) The microform anisotropy is due to the optical interaction between nearby segments, where one segment experiences the anisotropic field due to the anisotropic optical polarization of neighbouring segments⁸. This anisotropy contribution is always positive and adds to the intrinsic anisotropy. According to Tsvetkov¹⁰, the microform anisotropy contribution in flexible chain polymers never exceeds about 1/5 of the macroform anisotropy, owing to the random angular relationships between neighbouring segments along the chain. Since it has been shown above that the macroform anisotropy is very small, the microform anisotropy also will be regarded as negligible.

If micro- and macro-form anisotropy contributions are negligible, equation (1) with the data from Figure 5 gives the segmental anisotropy $(\alpha_1 - \alpha_2)_s = 16.3 \times 10^{-40} \text{ C}^2 \text{ m}^2 \text{ J}^{-1}$. In equation (1), $\sin 2\chi$ has been assumed to be unity, since even if $\chi = 44.5^\circ$ in reality rather than 45° , $\sin 2\chi$ is unity within 0.02%.

Magnetic birefringence

If a magnetic field is applied to a polymer chain having diamagnetically anisotropic segments, slight segmental re-orientation occurs in order to minimize the free energy of interaction between the segments and the applied field. This re-orientation is opposed by thermal motion, and if each segment is optically anisotropic, magnetic birefringence is set up in the polymer chain solution. The polymer chain may thus be regarded as an ensemble of rotationally independent segments, which was first shown by Stuart and Peterlin¹¹ who considered a polymer chain interacting with an electric and a magnetic field.

The Cotton-Mouton constant of the polymer is defined as $C_2^* = \Delta n_2 / \lambda B^2$ where Δn_2 is the magnetically induced birefringence of the polymer and B the magnetic induction, and Stuart and Peterlin's theory gives:

$$\frac{C_2^*}{c_2} = \frac{100(n^2 + 2)^2 N_A (\alpha_1 - \alpha_2)_s (\chi_1 - \chi_2)_s}{27n\lambda kT \epsilon_0 M_s} \quad (3)$$

c_2 is the concentration, N_A is Avogadro's number, M_s the segmental molecular weight and $(\chi_1 - \chi_2)_s$ the diamagnetic anisotropy of a segment. Other symbols are as for equation (1). In the case of segments in solution where the solvent birefringence is not negligible it may be assumed that interaction between different polymer chains is absent at low solute concentrations, and the observed birefringence is the sum of the birefringences of the two components weighted according to their respective number densities. It then follows that:

$$C_2^* = \frac{dC}{dc_2} + \left(1 - \frac{d\rho}{dc_2}\right) \frac{C}{\rho_1} - \frac{C_1(3n_1^2 - 2)}{n_1(n_1^2 + 2)} \frac{dn}{dc_2}$$

where C and ρ are the Cotton-Mouton constant and the density of the solution respectively, and c_2 the polymer concentration expressed as kg of polymer per m^3 of solution. C_1 and ρ_1 are the Cotton-Mouton constant and density of the pure solvent, chloroform, being $-0.77 \times 10^{-3} m^2 T^{-2} kg^{-1}$ and $1475 kg/m^3$ respectively. The value of $d\rho/dc_2$ was found to be -0.11 and using $dC/dc_2 = 6.77 \times 10^{-6} m^2 T^{-2} kg^{-1}$ from Figure 4, the segmental quantity $(\alpha_1 - \alpha_2)_s(\chi_1 - \chi_2)_s/M_s = 4.68 \times 10^{-69} C^2 m^2 T^{-2}$.

Chain conformation

The optical and diamagnetic polarizabilities of chemical bonds are generally a factor of 10 or more smaller than the corresponding quantities for the phenyl group or free benzene ring^{12, 13}. This is due to the presence of mobile π electrons in the phenyl group, which may be regarded as ring currents in the plane of the benzene ring. Thus to a first approximation we neglect the contribution by other bonds in the monomer unit to $(\alpha_1 - \alpha_2)_s$ and $(\chi_1 - \chi_2)_s$, compared with the phenyl groups' contributions. A suitable model of a statistical segment is then a number of phenyl rings having axes of rotation about a line drawn through each ring's *para* carbon atoms. Examination of molecular models shows that these axes make tetrahedral angles with adjacent axes, and that they are coplanar if the segment's conformation is as a part of a fully extended chain. Space-filling molecular models indicate that there is some rotational freedom of each ring around its *para* carbon atom axis. Thus the general segment may be considered to have n monomer units, each phenyl ring with its normal at an average angle ϕ to the plane containing the *para* carbon atom axes. Using this model segment, $(\alpha_1 - \alpha_2)_s = n(\alpha_r - \alpha_l)\overline{\cos^2\phi}$ and $(\chi_1 - \chi_2)_s = n(\chi_r - \chi_l)\overline{\cos^2\phi}$, where subscripts l and r refer to directions parallel and perpendicular respectively to the normal of the phenyl ring. Putting $M_s = nM_0$, where M_0 is the monomer unit molecular weight (246) and using the measured values of $(\alpha_1 - \alpha_2)_s$ and $(\alpha_1 - \alpha_2)_s(\chi_1 - \chi_2)_s/M_s$ above, values of $\overline{\cos^2\phi} = 0.73$ and $n = 3.5$ result, where $(\alpha_r - \alpha_l) = 6.25 \times 10^{-40} C^2 m^2 J^{-1}$ and $(\chi_r - \chi_l) = 0.99 \times 10^{-27} J T^2$ have been used^{12, 13}.

The value of $\overline{\cos^2\phi}$ gives information about the mutual orientation of the phenyl rings, and although its magnitude alone does not unambiguously predict the monomer unit conformation, certain conformations are eliminated from consideration. Thus the conformation resulting from X-ray measurements¹⁴, in which the ring normals are coplanar, yields $\overline{\cos^2\phi} = 0$, while the other extreme conformation in which the ring planes are coplanar yields $\overline{\cos^2\phi} = 1$. A possible conformation, not excluded by steric considerations, is an alternation of ϕ between 0° and 90° for successive rings along the chain. This gives $\overline{\cos^2\phi} = 0.5$. A random orientation of the rings along the chain also gives $\overline{\cos^2\phi} = 0.5$, but since owing to steric hindrances many values of ϕ are unlikely, a truly random orientation is also unlikely. The observed value, $\overline{\cos^2\phi} = 0.73$, is thus indicative of an approximate 90° alternation of the rings along the chain, with a tendency towards coplanarity of the ring planes. The value of n implies that there are on

average 3.5 monomer units per statistical segment.

The value of n derived here is comparable with the same parameter calculated from chain dimensions estimated using light scattering and viscometric methods. This parameter is given by s^2/s_f^2 where s^2 is the mean square end-to-end distance of the chain in chloroform solution and s_f^2 is the same quantity assuming free rotation is possible for monomer units around the valence bonds by which the monomer units are linked. In chloroform, which is not a θ -solvent, $s^2 = \alpha^2 s_0^2$, where s_0^2 is the unperturbed end-to-end distance which exists in a θ -solvent and α is the swelling or expansion factor of the chain in chloroform. Thus $\alpha^2 s_0^2/s_f^2$ is the parameter to be compared with n . The two available estimates^{1, 2} of s_0^2/s_f^2 agree closely at 1.82 and 1.69 respectively. Published values of α vary according to whether the Flory-Fox or Kurata-Yamakawa equations are used to relate the intrinsic viscosity $[\eta]$ to α . The former, used by Moore and Uddin¹ gives $\alpha^3 = [\eta]/[\eta]_\theta$ and yields experimental values for chloroform solution in the range $\alpha = 1.04$ to 1.17 , increasing slightly with molecular weight, for the molecular weight range used here. The latter, used by Sitaramaiah¹⁵, gives $\alpha^{2.43} = [\eta]/[\eta]_\theta$ and yields experimental values in the range $\alpha = 1.25$ to 1.41 . Thus, from light scattering and viscometric data, n falls in the range 1.83 to 3.6 compared with 3.5 derived from flow birefringence and magnetic birefringence measurements.

CONCLUSION

The two techniques described above, flow birefringence and magnetic birefringence, give information about the short range order of the polymer chain. When used to study polycarbonate solutions, estimates of the mutual orientations of the phenyl rings and the number of monomer units per segment are possible. The quantity $\overline{\cos^2\phi}$ has a value which entirely eliminates the possibilities of solution state conformations where (i) the planes of the phenyl rings are coplanar, and (ii) the normals to the planes of the phenyl rings are coplanar, as in solid polycarbonate. The measured value of 0.73 for $\overline{\cos^2\phi}$ thus suggests an approximate 90° alternation between the orientations of successive rings along the chain. The quantity n lies in the range of estimates made using conventional viscometric and light scattering methods, thus confirming the general validity of the flow and magnetic birefringence techniques.

REFERENCES

- 1 Moore, W. B. and Uddin, M. A. *Eur. Polym. J.* 1970, **6**, 121
- 2 Berry, G. C. et al. *J. Polym. Sci.* 1967, **5**, 1
- 3 Moore, W. R. and Uddin, M. A. *Eur. Polym. J.* 1967, **3**, 673
- 4 Moore, W. R. and Uddin, M. A. *Eur. Polym. J.* 1969, **6**, 185
- 5 Champion, J. V. *Proc. Phys. Soc.* 1960, **75**, 421
- 6 Peterlin, A. *J. Polym. Sci.* 1954, **12**, 45
- 7 Lodge, A. S. *Nature* 1955, **176**, 838
- 8 Tsvetkov, V. N. *J. Polym. Sci.* 1957, **23**, 151
- 9 Frisman, E. V. and Dadivanyan, A. K. *ibid.* 1967, **16**, 1001
- 10 Tsvetkov, V. N. 'Newer methods of polymer characterisation' (Ed. B. Ke), Interscience, New York, 1964
- 11 Stuart, H. A. and Peterlin, A. *J. Polym. Sci.* 1950, **5**, 551
- 12 Le Fevre, R. J. W. *Adv. Phys. Org. Chem.* 1965, **3**, 1
- 13 Bothner-By, A. A. and Pople, J. A. *A. Rev. Phys. Chem.* 1965, **16**, 43
- 14 Prietzschk, A. *Kolloid-Z.* 1958, **156**, 8
- 15 Sitaramaiah, G. *J. Polym. Sci.* 1965, **3**, 2743

Effects of chain defects on the thermal behaviour of polyethylene

E. Martuscelli and M. Pracella

Laboratorio di Ricerche su Tecnologia dei Polimeri e Reologia, CNR, 80072 Arco Felice, Napoli, Italy

(Received 4 June 1973; revised 31 October 1973)

The annealing behaviour and thermodynamics of fusion of mats of solution-grown single crystals of ethylene-propylene and ethylene/1-butene crystallizable random copolymers are examined in comparison with linear polyethylene crystallized from the melt and from dilute solution. Correlation of quantities such as long spacing, annealing temperature, and apparent enthalpy of fusion, leads to the conclusion that the single crystal aggregates are involved in a morphological transformation during the process of annealing. The long spacing and the annealing temperature corresponding to this transformation decrease with the degree of constitutional defects present in the polyethylenic chain (percentage of propylene or 1-butene comonomeric units). Data in the plots of melting temperatures *versus* the reciprocal of the long spacing can be represented by straight lines. The thermodynamic equilibrium melting temperature T_m° and the surface free energy σ_e have been determined. Both T_m° and σ_e depend upon the number of constitutional defects in the chain. In the case of ethylene-propylene random copolymers σ_e increases drastically with the percentage of CH_3 side groups. A completely opposite effect is observed in the case of ethylene/1-butene random copolymers; here decrease in σ_e with the percentage of CH_3CH_2 side groups is observed. Both classes of polymers show a lowering in T_m° with the number of side groups, though this effect is much more pronounced in the ethylene-propylene copolymers. The apparent enthalpy of fusion of annealed single crystal aggregates is not in linear relation with the reciprocal of the long spacing and with the corresponding melting temperature. Some consideration on the distribution of the defects in the crystals is also reported.

INTRODUCTION

The chain defects in a linear macromolecule may be classified as 'constitutional', 'configurational' and 'chain ends'.

Constitutional defects take place when some units of chemical constitution different from the fundamental repetitive one are statistically distributed along the macromolecule.

Configurational defects. In this case, statistically distributed along the macromolecule, there are repetitive units with a configuration different from that of the repetitive unit characterizing the stereoregularity of the chain.

Chain ends. Because of the molecular weight distribution the lengths of linear synthetic macromolecules are never uniform, and in consequence when a crystallizable polymer is allowed to crystallize the terminal groups cannot all be in a regular register as is the case of linear uniform normal paraffins.

The succession of repeat units with different conformations, along the main chain, give rise to *conformational* chain defects. The latter are equilibrium chain defects and their number and nature depend mainly on temperature. The morphological, thermodynamic,

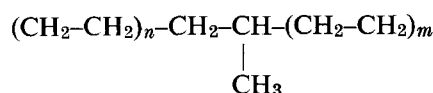
mechanical and technological characteristics of polymeric materials depend on the number and nature of the chain defects. In the case of semi-crystalline polymers the chain defects can to some extent be incorporated in the crystalline part as defects or present in the amorphous regions (probably on the surface in polymer single crystals). Thus many of the more important properties of semi-crystalline polymers depend on the distribution of the chain defects between crystalline and amorphous regions.

In previous papers the influence of the number of the configurational and constitutional defects on the above-mentioned properties have been studied in the case of *trans*-polyalkenamers¹ and ethylene-carbon monoxide copolymers². For *trans*-polyalkenamers, the configurational defects consist of repetitive units with a carbon-carbon double bond in a *cis* configuration. For ethylene-carbon monoxide copolymers, the C=O groups, statistically distributed along the polyethylene chain, may be considered as constitutional defects. In this paper, influence of the 'constitutional' defects on the thermal behaviour of aggregates of single crystals of polyethylene is examined, using samples of polyethylenes branched by methyl and ethyl groups statistically distributed along the chain. Such polymers are

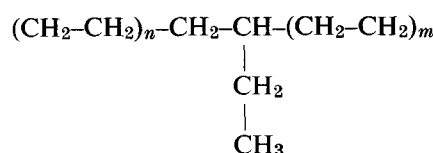
obtained by copolymerizing ethylene with propylene and 1-butene. The introduction, during copolymerization, of propylenic and butenic units gives rise to the formation of constitutional defects in the polyethylenic chain; such defects, due to the kind of polymerization kinetics, are statistically distributed along the macromolecule.

The structure of the examined copolymers are schematized below.

Ethylene-propylene copolymers:



Ethylene/1-butene copolymers:



The results obtained by studying the annealing behaviour of aggregates of single crystals of a series of linear polymers, with different chemical constitution, allowed us to conclude that, during such a process, the materials undergo a morphological transformation characterized by a well defined pair of values of long spacing and annealing temperature^{1, 2}.

In the present paper such phenomena are systematically analysed for linear polyethylene and for a series of ethylene-propylene and ethylene/1-butene copolymers with a different content of side groups. The aim is to explain in general the annealing process mechanism and the kind of morphological transformation which takes place, and moreover, to examine also the influence of the number and of the nature of chain defects in the process.

Fusion of aggregates of annealed single crystals of ethylene-propylene and ethylene/1-butene statistical copolymers is complicated by the fact that, owing to the thickening of crystals and therefore to the increase in long spacing, a certain number of side groups is incorporated as a defect in the crystalline lattice. Consequently, the thermodynamic parameters of fusion of the above-mentioned materials and also the ones characterizing the fold surface, will depend on the number of side groups in the polyethylene chain and their hindrance. An aim of the present work therefore was to also look for a correlation between apparent enthalpy of fusion and melting point with annealing temperature

and long spacing, and to analyse the effect of constitutional defects on such quantities. Moreover, we sought to determine for each sample the surface free energy of fold and the equilibrium thermodynamic melting temperature. Correlating such thermodynamic data with the number of side groups can give information on the disorder state of the fold surface and the preference some side groups may have in settling on or away from the crystal surface.

EXPERIMENTAL

As starting materials, two series of random ethylene-propylene (EP) and ethylene/1-butene (EB) copolymers, with different amounts of chain branching, were used in this study, together with a sample of linear polyethylene (Marlex 6009) (LPE).

All these materials were crystallized from dilute xylene solution using the self-seeding techniques³ or other standard procedures. The numbering and some of the bulk properties of the polymer samples with the corresponding crystallization conditions are reported in Table 1. In agreement with the finding of Holdsworth and Keller⁴, the crystals of the copolymers are of the lamellar type, similar to the chain-folded crystals of LPE but less regularly developed. Mats, obtained by slow filtration of the suspensions, displayed the features of the chain-folded crystal aggregates.

Discrete small-angle X-ray reflections, in the form of arcs centred on the meridian, are obtained when the X-ray beam is parallel to the plane of the mats. The long spacing, L , of the crystal aggregates was calculated from the position of these reflections by using the Bragg relation. The small-angle X-ray patterns were recorded at room temperature by means of a pinhole collimated Rigaku-Denki camera.

Melting behaviour of the mats of EP and EB copolymers and of LPE was investigated using a Perkin-Elmer differential scanning calorimeter (d.s.c.). The apparent enthalpy of fusion, ΔH_f^* , was computed from the areas under the endothermic melting peak. This area was integrated and expressed in cal/g using a calibration factor determined from melting a known weight of indium under the same conditions. A value of 6.8 cal/g was taken for the heat of fusion of the indium. According to this method the fusion heats are measured within ± 2 cal/g. The calorimeter was calibrated in the appropriate temperature range, at the scanning speed to be used, using substances with standard melting points. The peak maximum temperatures were assumed to correspond to the melting temperatures of the samples.

Table 1 Numbering and some of the bulk properties of the ethylene-propylene (EP), ethylene/1-butene (EB) copolymers and of linear polyethylene (LPE) with the corresponding crystallization conditions

Samples	Number of branches per 1000 C atoms	Molecular weight or I.V.	Source of the samples	Solvent	Concentration (% w/w)	Apparent dissolution temperature, T_D (°C)	Seeding temperature, T_s (°C)	Crystallization temperature, T_c (°C)	Melting temperature, T_m (°C)	Apparent enthalpy of fusion, ΔH_f^* (cal/g)	Long spacing, L (Å)
EP1	36.8	510 000	Du Pont	Xylene	0.35	57	60.0	30.0	102	20	115
EP2	25.5	225 000	Du Pont	Xylene	0.35	66	69.0	45.0	108.5	27	114
EP3	4.7	I.V.=8	Hercules	Xylene	0.05	99	101.0	75.5	133.5	43	136
EP4	2.9	I.V.=1.5	Hercules	Xylene	0.05	100-103	107.0	80.0	129	47	127
EB1	36.5		Hercules	Xylene	0.05	91-93		71.0	127	27	129
EB2	10.7		Hercules	Xylene	0.05	96-98	100.0	75.0	123	33	129
LPE	0		Marlex 6009	Xylene	0.05	99-101	103.0	85.0	129	50	147

These could be measured with a precision of $\pm 0.5^\circ\text{C}$. All samples were run through at a heating rate of $16^\circ\text{C}/\text{min}$. The long spacing, L , the apparent enthalpy of fusion, ΔH_f^* , the melting temperature, T_m , of the unannealed mats of the EP and EB copolymers and of LPE are reported in Table 1.

Small pieces of the single crystal aggregates, wrapped in aluminium foil, were annealed at the desired temperature for 24 h by placing them in identical thin-walled test tubes in a constant temperature oil bath.

RESULTS AND DISCUSSION

Variation of long spacing with annealing temperature

In Figures 1 and 2 the long spacing, L of single crystal mats of copolymers EP, EB and of linear polyethylene is plotted against the annealing temperature, T_A . On the

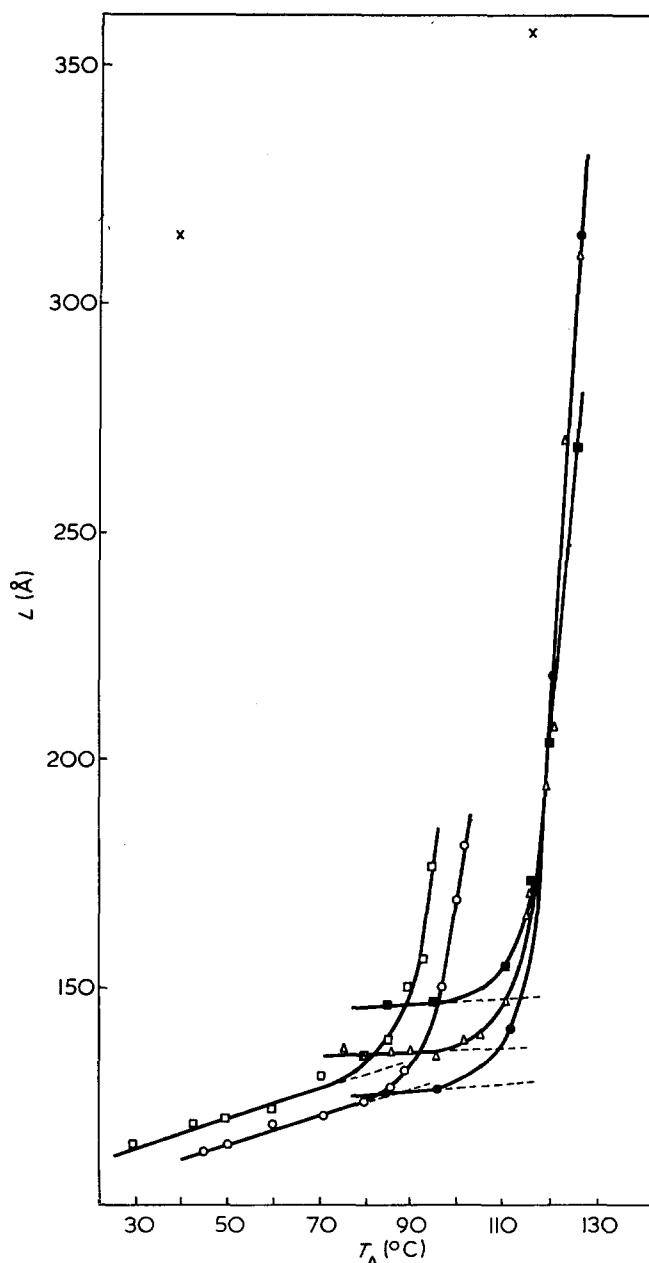


Figure 1 Long spacing, L of single crystal mats of copolymers ethylene-propylene (EP) and of linear polyethylene (LPE) as function of the annealing temperature, T_A . \square , EP1; \circ , EP2; \triangle , EP3; \bullet , EP4; \blacksquare , LPE (single crystals); \times , LPE (bulk)

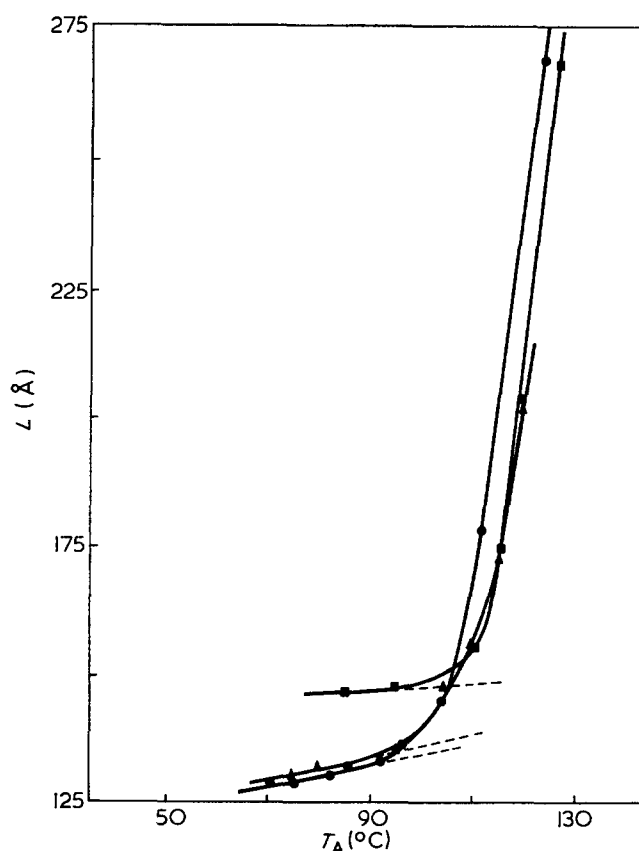


Figure 2 Long spacing, L of single crystal mats of copolymers ethylene/1-butene (EB) and of linear polyethylene (LPE) as function of the annealing temperature, T_A . \bullet , EB1; \blacktriangle , EB2; \blacksquare , LPE (single crystals)

basis of these curves, it becomes clear that in each case long spacing increases as annealing temperature increases; the lamella thickness would seem to be restricted, during annealing, owing to branching. The long spacing versus annealing temperature curves can be divided into two regions: a low annealing temperature one, with a comparatively slow long spacing variation rate and the other at higher annealing temperature, with a much more pronounced slope. The first region is called region I, the second region II.

In Figures 3 and 4 we represent the variation with polymer chain branching number of long spacings, L^T , and annealing temperature, T_A^T corresponding, in the L - T_A curves, to the transition between region I and region II. The branching number is defined as the number of CH_3 or C_2H_5 side groups per 1000 carbon atoms in the backbone. The values of L^T and T_A^T were calculated, both for methyl-branched and ethyl-branched samples, on the basis of the graphs shown in Figures 1 and 2, in two different ways: (a) from long spacing and annealing temperature values relative to the deflection point; (b) from long spacing and annealing temperature values corresponding to the intersection point of the straight line extrapolated from the parts of the curve corresponding to region II and region I, respectively (Figures 1 and 2).

In both EP and EB copolymers the transformation annealing temperature, T_A^T , seems to decrease in a linear way as the percentage of side-chain groups decreases. A more complicated trend is instead observed for the transition long spacing, L^T . In both classes of polymers under examination, the L^T value, starting from the

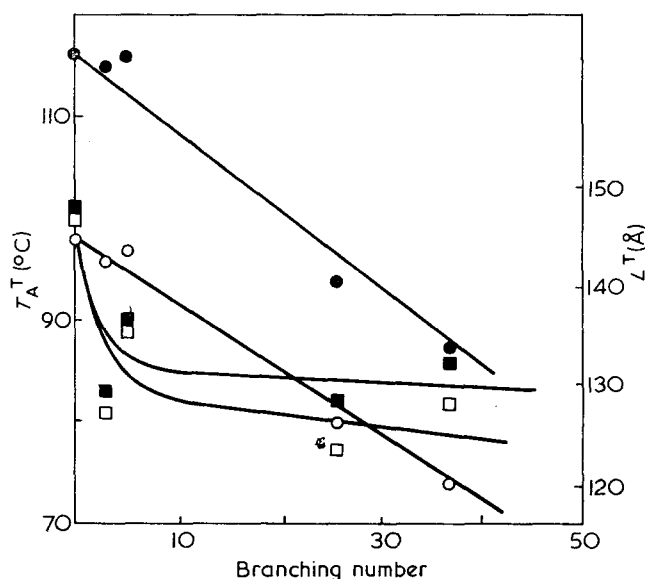


Figure 3 Long spacing, L^T and annealing temperature, T_A^T of transition as function of the number of side groups in the chain for ethylene-propylene (EP) copolymers. \circ , T_A^T from the deflection point; \square , L^T from the deflection point; \bullet , T_A^T from the intersection point; \blacksquare , L^T from the intersection point

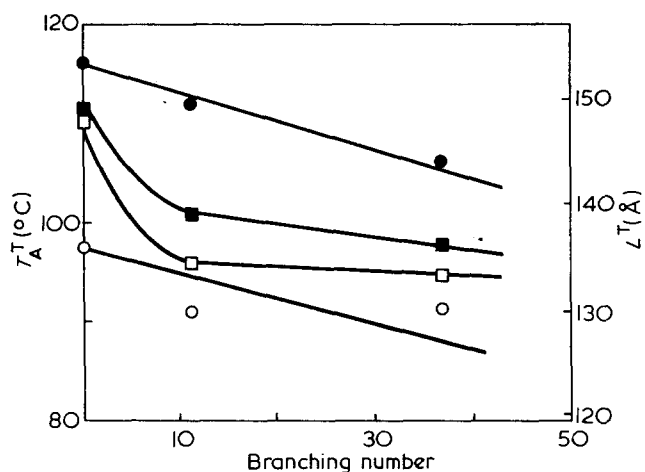


Figure 4 Long spacing, L^T and annealing temperature, T_A^T of transition as function of the number of side groups in the chain for ethylene/1-butene (EB) copolymers. \circ , T_A^T from the deflection point; \square , L^T from the deflection point; \bullet , T_A^T from the intersection point; \blacksquare , L^T from the intersection point

value corresponding to the linear polyethylene, sharply decreases assuming then a value, which seems to be almost independent of the number of side groups. It is interesting to observe that the percentage lowering in the transition long spacing, is about the same (13–15%) for both EP1 and EB1 samples, where percentage of side groups are approximately equal.

Variation of the apparent enthalpy of fusion with annealing temperature and long spacing

In Figures 5, 6, 7 and 8 values of the apparent enthalpy of fusion, ΔH_f^* of single crystal mats of EP, EB copolymers and of linear polyethylene against annealing temperature, T_A and long spacing, L respectively, are reported. The dependence of the apparent enthalpy of

fusion from T_A and L is analogous for each sample examined, the crystals of which have been obtained by crystallization from dilute solutions. All curves (for T_A and L low values) show an increasing ΔH_f^* trend, passing through a more or less determinate maximum, and they then begin to decrease with a slope reversal.

In Table 2, the values of the annealing temperature and of the long spacing, corresponding to the maxima in $\Delta H_f^* \rightarrow T_A$ and $\Delta H_f^* \rightarrow L$ curves (called T_A^T and L^T), are reported and compared with the values obtained from $L \rightarrow T_A$ curves. The trend is the same even if a certain discrepancy among values is found. The origin of such a discrepancy is not yet clear, but it can be due to values (L^T and T_A^T) which derive from different physical quantities, obtained by completely different techniques.

Besides quantity discrepancy, it is important to underline that a certain correlation is possible between L^T , T_A^T and the number of branches in the polyethylene chain. It must be mentioned, however, that owing to the shape of $\Delta H_f^* \rightarrow L/T_A$ curves, the uncertainty in determining L^T and T_A^T is rather high. In fact in this case, for some of the curves, maxima are indeed very flat. An anomalous trend may be found in the apparent enthalpy of fusion of linear polyethylene, which has been isothermally crystallized from the melt at 41°C. Here the apparent enthalpy of fusion monotonically increases with the increase of annealing temperature, and no maximum is found. Roe and Bair⁵ starting

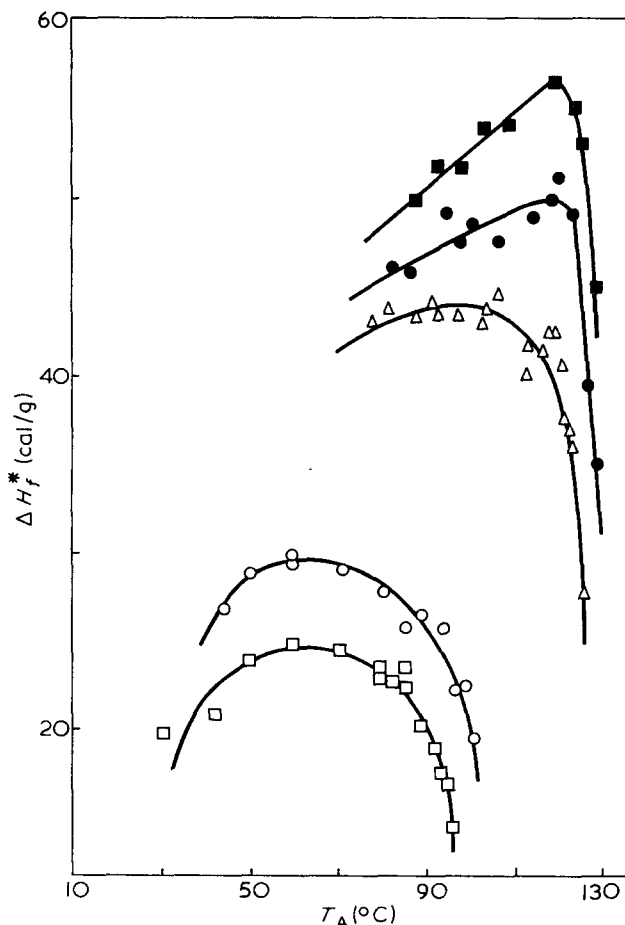


Figure 5 Apparent enthalpy of fusion, ΔH_f^* as function of the annealing temperature for single crystal mats of EP copolymers and of linear polyethylene (LPE). \square , EP1; \circ , EP2; \triangle , EP3; \bullet , EP4; \blacksquare , LPE (single crystals)

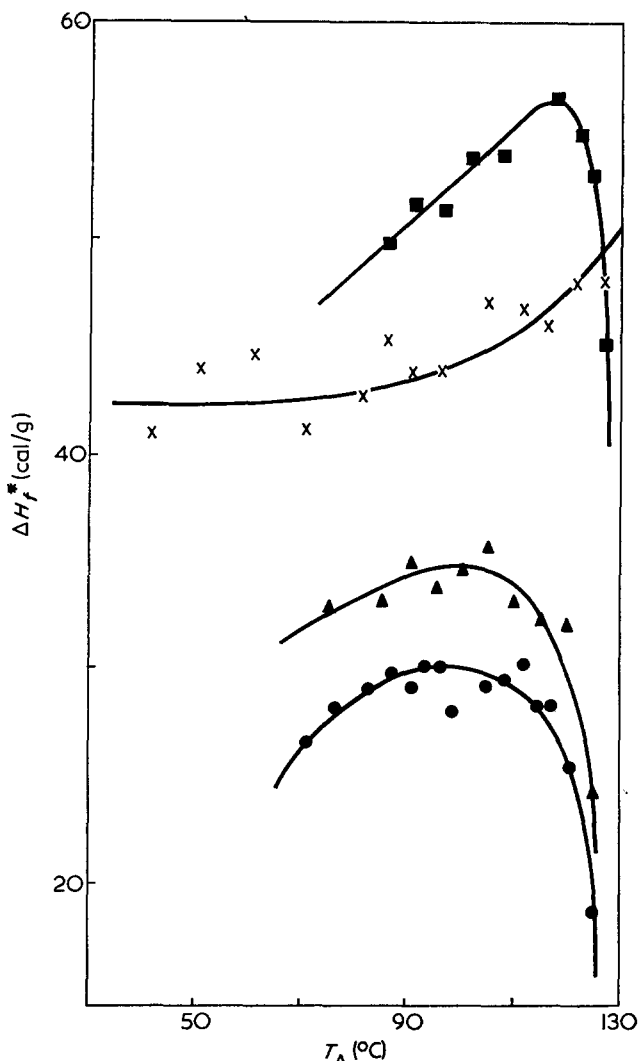


Figure 6 Apparent enthalpy of fusion, ΔH_f^* as function of the annealing temperature for single crystal mats of EB copolymers and of linear polyethylene (LPE). For comparison the ΔH_f^* of melt crystallized LPE is also reported. ●, EB1; ▲, EB2; ■, LPE (single crystals); ×, LPE (bulk)

Table 2 Comparison between the critical values of long spacing, L^T and of annealing temperature, T_A^c obtained from the curves $L \rightarrow T_A$ (Figures 1 and 2) and $\Delta H_f^* \rightarrow T_A/L$ (Figures 5-8)

Sample	From curves $L \rightarrow T_A$				From curves $\Delta H_f^* \rightarrow T_A/L$	
	T_A^c (°C)		L^T (Å)		T_A^c (°C)	L^T (Å)
	a	b	a	b		
EP1	88	74	134	130	63	125
EP2	94	80	130	125	64	120
EP3	116	97	138	137	98	140
EP4	115	96	131	129	115	145
EB1	107	92	136	133	100	133
EB2	112	91	139	134	104	143
LPE	116	98	149	148	116	165

a From the intersection point (see text)
 b From the deflection point (see text)

from strictly thermodynamic considerations, derived the following equation:

$$\Delta H_f^* = \Delta H_f - \frac{2q_e}{L} \quad (1)$$

which provides for the linear behaviour of ΔH_f^* with $1/L$ by correlating the values for the apparent enthalpy

of fusion, thermodynamic enthalpy of fusion, surface crystal enthalpy, q_e and long spacing. Equation (1) was verified experimentally by these authors for single crystals of linear polyethylene obtained from several solvents at various crystallization temperatures. Only one of the samples examined referred to annealed polyethylene single crystal aggregates. However, equation (1) seems not to be verified during the annealing of single crystal aggregates of linear polyethylene and of EP and EB copolymers (see Figures 7 and 8) at least not in the entire long spacing interval examined.

A linear relationship between ΔH_f^* and $1/L$ was also found by Quinn and Mandelkern⁶ in the case of solution grown single crystals of polyethylene.

Calculation of the equilibrium thermodynamic temperature of fusion and the surface folding free energy

Figures 9, 10 and 11 report the fusion temperatures of single crystal mats of copolymers EP, EB and linear polyethylene as a function of the annealing temperature,

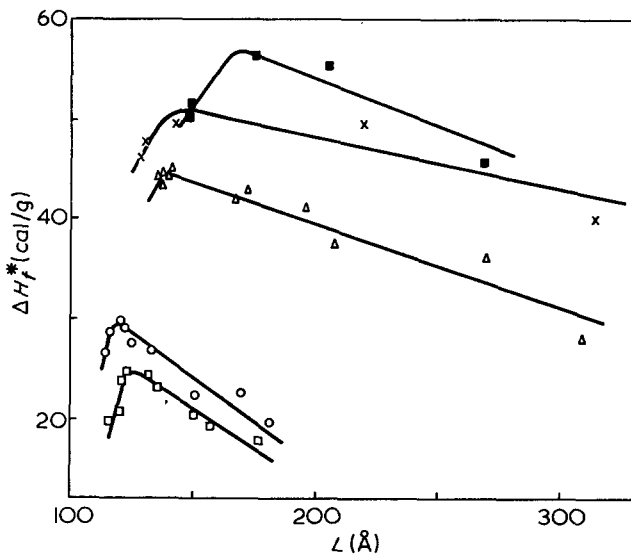


Figure 7 Apparent enthalpy of fusion, ΔH_f^* as function of the long spacing, L for annealed single crystal aggregates of EP copolymers and of linear polyethylene (LPE). □, EP1; ○, EP2; △, EP3; ×, EP4; ■, LPE (single crystals)

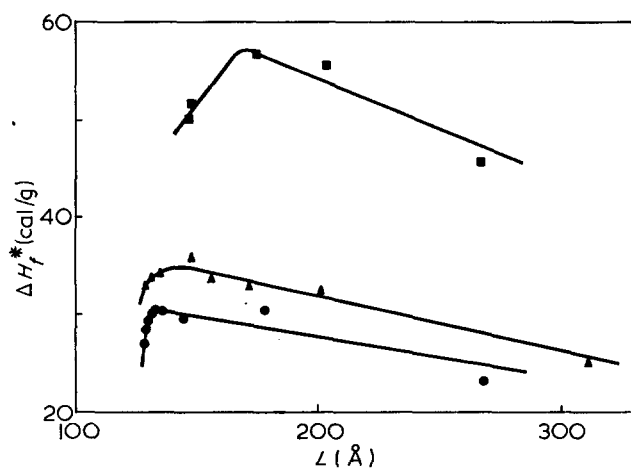


Figure 8 Apparent enthalpy of fusion, ΔH_f^* as function of the long spacing, L for annealed single crystal aggregates of EB copolymers and of linear polyethylene (LPE). ●, EB1; ▲, EB2; ■, LPE (single crystals)

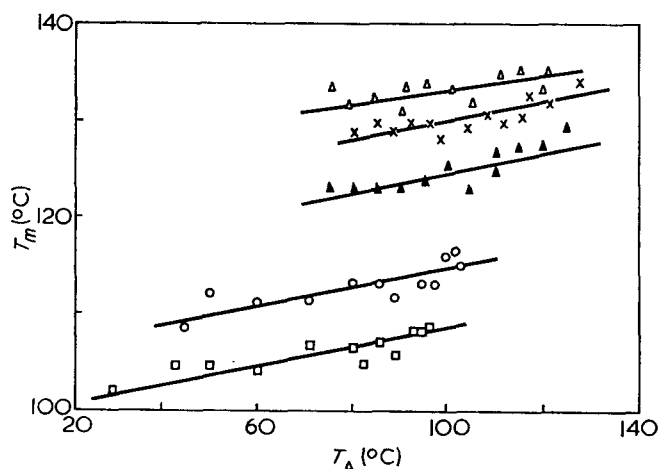


Figure 9 Melting temperature, T_m as function of the annealing temperature, T_A for single crystal aggregates of EP and EB copolymers. \square , EP1; \circ , EP2; \triangle , EP3; \times , EP4; \blacktriangle , EB2

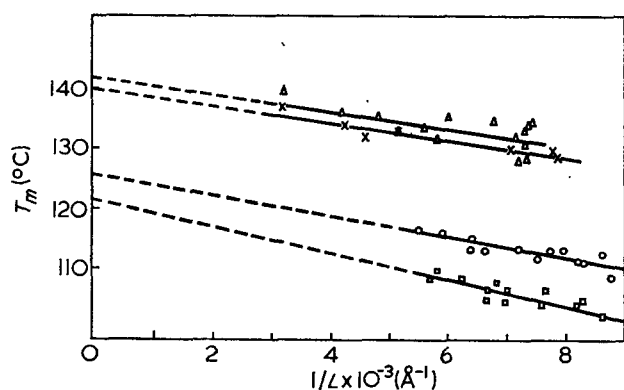


Figure 10 Melting temperature, T_m as function of the reciprocal of the long spacing, $1/L$ for annealed single crystal aggregates of EP copolymers. \square , EP1; \circ , EP2; \triangle , EP3; \times , EP4

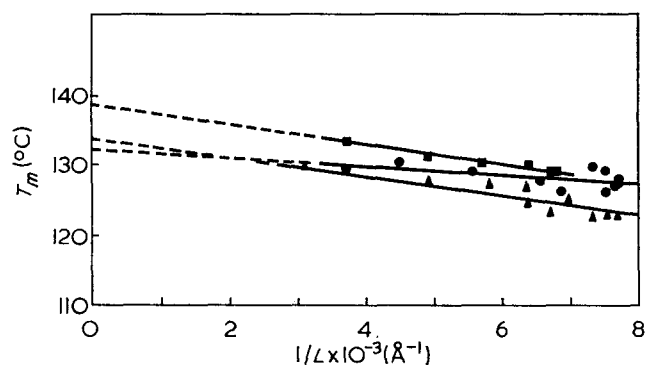


Figure 11 Melting temperature T_m as function of the reciprocal of the long spacing, $1/L$ for annealed single crystal aggregates of EB copolymers and of linear polyethylene (LPE). \bullet , EB1; \blacktriangle , EB2; \blacksquare , LPE (single crystals)

T_A and the reciprocal of the long spacing, $1/L$, respectively. We observe a linear trend in the fusion temperature for all samples examined, increasing when reported as a function of T_A and decreasing when reported as a function of $1/L$.

These results lead us to consider applicable and valid the Hoffman⁷ expression that provides for a linear trend in the fusion temperature with $1/L$ correlating these two quantities according to:

$$T_m = T_m^\circ - 2 \frac{T_m^\circ \sigma_e}{\Delta H_f} \frac{1}{L} \quad (2)$$

where T_m° is the equilibrium thermodynamic temperature of fusion (the fusion temperature of a crystal of infinite thickness), σ_e is the surface free energy of folding, and ΔH_f the thermodynamic enthalpy of fusion. Applying this relation to the experimental data reported in Figures 10 and 11, it is possible to find T_m° by extrapolation to $1/L=0$ and, in addition, to find the surface free energy of folding from the slope of the straight line, given the thermodynamic enthalpy of fusion.

At this point we should make some general observations concerning the value to assign to ΔH_f in equation (2) for each copolymer sample.

(1) Assuming that equation (2) is correct, the fact that T_m varies in a linear manner is a strong indication that ΔH_f does not change during the thickening phenomenon following the annealing process.

(2) The enthalpy of fusion for EP and EB copolymers depends upon the number of ramifications, decreasing drastically as the latter increases. Wilchinsky and Ver Strate⁸ have calculated this variation for a series of EP copolymers having widely varying percentages of ethylene as a ratio of the apparent enthalpy of fusion and the degree of crystallinity determined by X-ray and density measurements. In Table 3 we report the average values of ΔH_f for the compositions corresponding to the copolymers examined obtained by interpolation of curves $\Delta H_f \rightarrow \%CH_3$ based on data from Wilchinsky and Ver Strate. It is interesting to note that the values for ΔH_f reported in the Table are experimental and do not take into consideration theoretical assumptions regarding whether or not the comonomeric units are included in the crystalline lattice.

(3) Alternatively, by means of Wunderlich and Dole's equation⁹:

$$\Delta H_f = 55.9 + 0.1942 T_m^\circ - 7.2 \times 10^{-4} (T_m^\circ)^2 \quad (3)$$

it is possible to obtain values for the thermodynamic enthalpy of fusion, correct only for differences in the equilibrium temperature of fusion of the copolymers examined by us. As we have already mentioned, the values for T_m° are obtained by extrapolation to $1/L=0$ of the experimental curves reported in Figures 10 and 11. In this case no correction was made for the presence of copolymer units. We should note that ΔH_f calculated on the basis of Wunderlich and Dole's equation proves to be almost equal ($\Delta H_f \approx 69$ cal/g) for all samples examined, whether EP or EB.

In Figures 12 and 13 the surface free energies of folding calculated using equation (2) with the values for thermodynamic enthalpy, which appear in Table 3 and

Table 3 Thermodynamic enthalpy of fusion, equilibrium melting point and surface free energy of single crystal aggregates of EP and EB copolymers and LPE

Sample	ΔH_f^a (cal/g)	ΔH_f^b (cal/g)	T_m° (°C)	σ_e^a (erg/cm ²)	σ_e^b (erg/cm ²)
EP1	57.0	68.87	122	219	264
EP2	58.5	68.94	126	174	206
EP3	62.5	68.96	142	131	145
EP4	63.0	68.98	140	130	143
EB1	—	68.99	133	—	74
EB2	—	68.99	134	—	146
LPE	63.5	68.98	139	143	155

^a ΔH_f from interpolation of the data of Wilchinsky and Ver Strate⁸
^b ΔH_f using the Wunderlich and Dole equation⁹

the thermodynamic temperature of fusion, are reported as a function of the percentage of ramifications for EP and EB copolymers, respectively. In the case of EP copolymers, σ_e decreases slightly at first for low values of the number of branchings, and then increases drastically.

The behaviour of σ_e is always similar whether we use the values for ΔH_f obtained from Wilshinsky's data or whether we adopt Wunderlich and Dole's values. In fact, the corresponding curves show parallel trends. In the first case, the values for σ_e (Figure 12) are consistently lower than they are in the second (for linear polyethylene $\sigma_e=155$ and 143 erg/cm² while for EP1 $\sigma_e=265$ and 219 erg/cm²). We observe a totally different trend when σ_e of EB copolymers is reported as a function of the percentage of branchings. In this case, σ_e decreases significantly ($\sigma_e=155$ erg/cm² for linear polyethylene and $\sigma_e=75$ erg/cm² for EB1).

In the case of EP copolymers, the values for T_m° decrease in an apparently linear manner as the percentage of branchings increases, moving from a value of 139°C for polyethylene to 121°C for EP1. For EB copolymers, the lateral groups seem to have only a

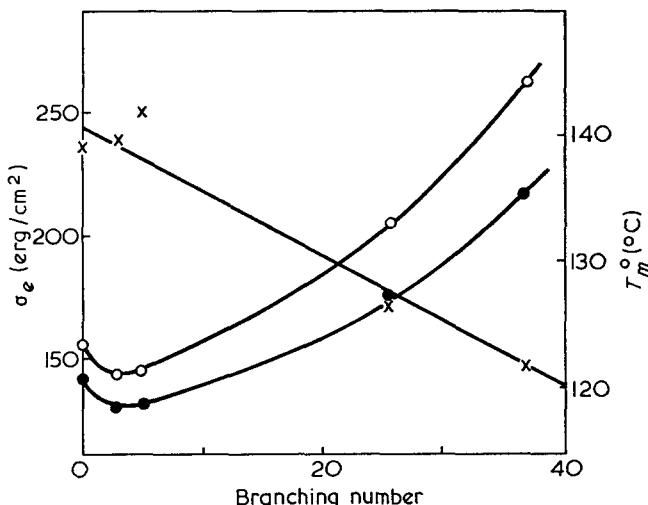


Figure 12 Equilibrium melting point, T_m° (x) and surface free energy, σ_e (O, ●) as function of the number of methyl side groups for EP copolymers

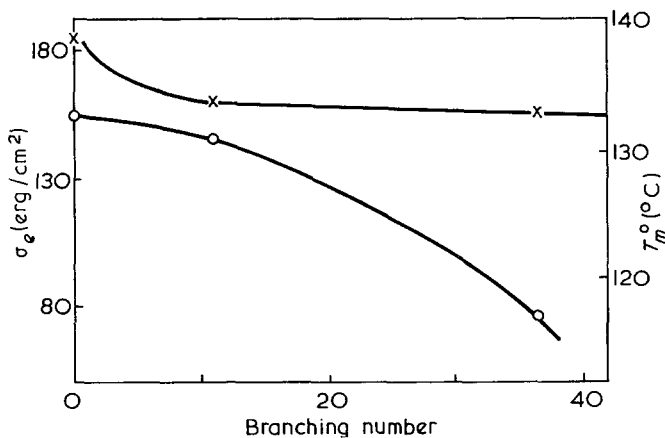


Figure 13 Equilibrium melting point, T_m° (x) and surface free energy, σ_e (O) as function of the number of ethyl side groups for EB copolymers

slight negative influence on the T_m° values which pass from 139°C for polyethylene to 133°C for EB1.

Assuming, on the basis of the above, that the thermodynamic enthalpy of fusion remains constant during annealing then the overall crystallinity $X_c = \Delta H_f^\circ / \Delta H_f$ should present the same trend as ΔH_f° if reported vs. the melting temperature. From the trends of the curves of Figures 7, 8, 10 and 11 we conclude that increasing the melting temperature (and thus L) the overall crystallinity of annealed single crystal aggregates first increases, reaches a maximum value, and then drastically drops.

CONCLUSIONS

The results reported and illustrated here, along with others which we have published previously, permit us to discuss and draw some conclusions concerning: (a) the general behaviour of polymeric material which undergoes annealing; and (b) the effect of constitutional and configurational types of chain defects on the morphological and thermodynamic characteristics of polymer crystals.

The behaviour of semi-crystalline polymers to annealing is a much debated topic, especially regarding the thickening mechanism of crystals during such processes. The increase in long spacing in semi-crystalline polymers, due to annealing, is interpreted by two different theories or mechanisms: (i) the thickening process takes place by a special mechanism of 'sliding diffusion' which allows for movement of complete molecular sequences within the crystalline lattice¹⁰. For such a mechanism, a high mobility of the chains in the crystal is, of course, foreseen; (ii) long spacing increase comes from a complete¹¹ or partial¹² fusion phenomenon of crystals and a subsequent recrystallization of the melted material at annealing temperature. Wide experimental evidence in favour of both mechanisms (i) and (ii) are reported in the literature¹³.

The annealing behaviour of aggregates of single crystals of linear polyethylene and of EP and EB copolymers turns out to be similar to the one observed by Martuscelli and coworkers for *trans*-polyalkenamers and polyketones^{1, 2}. Such behaviour can be interpreted assuming that, during the annealing process, at the critical long spacing and annealing temperature, the material which in all the cases examined is formed by aggregates of lamellar single crystals, undergoes a morphologic transformation of the kind illustrated schematically in Figure 14. It is likely that at annealing temperatures below T_A^* the lamella thickening occurs largely by a sliding diffusion mechanism. In such temperature intervals the corresponding increase in the apparent enthalpy of fusion, and therefore in crystallinity, is perhaps due to better packing conditions of lamellae in the same mat (Figure 14a). Moreover, eventual defects in the lattice can be eliminated owing to the diffusion phenomenon and chain refolding.

Above the critical annealing temperature, the mechanism (ii), which predicts a partial fusion of crystallites and a subsequent recrystallization, may prevail over mechanism (i). In conclusion, this process brings an interpenetration of the elementary lamellae forming the starting mat (Figure 14b). The lamellae lose their individuality and the material assumes a morphology

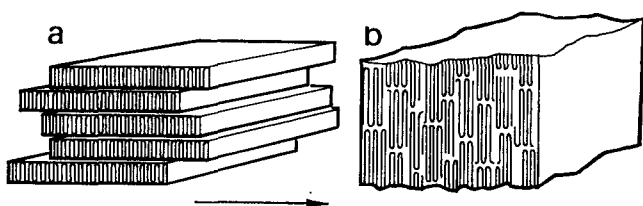


Figure 14 Schematic representation of the type of morphological transformation in the single crystal aggregate at the critical annealing temperature, T_A^* . (a) Below T_A^* the system shows the starting morphology of single crystal aggregates; (b) above T_A^* a complicated morphology is obtained and the lamellae lose their individuality (see text)

that is similar to the one obtained for polymers crystallized from the melt.

As observed experimentally in all the examined samples, such a process of partial fusion and recrystallization is followed by a more or less pronounced decrease in the fusion apparent enthalpy and therefore in the total crystallinity of the material. In the case of polyethylene crystallized from the melt, the apparent enthalpy of fusion, and hence the crystallinity, do not present maxima or discontinuities when they are reported as a function of annealing temperature and long spacing, but increase with them. These results are noteworthy insofar as they permit us to conclude that the initial morphological state drastically influences the way in which polymeric material reacts to thermal treatments such as annealing. It is also interesting to note that the physical and thermodynamic parameters which are brought about in single crystal aggregates during annealing are characteristic of single lamellae only when the annealing temperatures in question are lower than the transformation temperatures. All parameters, whether physical or thermodynamic, detected in annealed material at temperatures higher than those of transformation cannot be considered characteristic of the initial individual lamellae. In fact, at such annealing temperatures, the lamellae have already lost their individuality following the fusion and recrystallization processes. For example, the long spacing found at such temperatures does not represent the thickness of the single crystal annealed at those temperatures, but rather a periodicity which corresponds physically to an average fluctuation of the electronic density in the material which, following transformation takes on the morphology shown in Figure 14b.

Polymers of different chemical natures (*trans*-polyalkenamers, linear polyethylene, ethylene/ α -olefin copolymers, polyketones) qualitatively show the same morphological transformation phenomenon when the corresponding single crystal aggregates undergo annealing. Such behaviour at annealing can, in our opinion, be considered characteristic of all polymeric materials that are in the morphological starting state of lamellar single crystal mats.

As far as point (ii) is concerned, the following observations and considerations are noteworthy.

(1) The morphology of the single crystals of EP and EB copolymers depends upon the percentage of the side groups. With increase in these, the external form of the crystals moves continuously away from that of linear polyethylene (lozenge) until it takes on indefinite and complicated forms (e.g. ovoid) with irregular, indented edges. However, the crystals are lamellar in

up to at least 3.7% of branchings, i.e. they are composed of molecules folded at the surface. This is in agreement with the findings of Holdsworth and Keller¹⁴.

(2) The long spacing, L^T and the annealing temperature, T_A^T which characterize the transformation during annealing of the single polymer crystal aggregates decrease as the number of constitutional and configurational defects increase. In fact, we find this interdependence in the case of EP and EB copolymers in which the percentage of side groups is a measure of the constitutional defects. In the case of *trans*-polyalkenamers, the percentage of *cis* double bonds furnishes a standard for the number of configurational defects present in the macromolecular chains.

(3) Apparent enthalpy of fusion, ΔH_f^* values for samples of single crystals of EP and EB copolymers decrease as the percentage of branchings increases when compared on the basis of equal T_A (see Figures 5 and 6) and equal L (see Figures 7 and 8). This is true throughout the entire interval of annealing temperatures and long spacings examined experimentally.

(4) For EP copolymers, the thermodynamic temperature of fusion, T_m , decreases as the percentage of side groups (and hence constitutional defects) increases. In the case of *trans*-polyalkenamers, T_m^0 decreases as the *cis* double bonds increase (increase of configurational defects). For EB copolymers, the effect of the percentage of side groups on T_m is very slight. In fact, EB1 (36.5 C₂H₅ per 1000 C) and EB2 (10.7 C₂H₅ per 1000 C) have practically the same T_m value (133°C and 134°C, respectively). These values are comparable with the value found for linear polyethylene (139°C).

(5) In the case of EP copolymers, the surface free energy of folding, σ_e , significantly increases as the percentage of lateral methyl groups present in the polymer chain grows. From the equation:

$$\sigma_e = q_e - Ts_e \quad (4)$$

we deduce that a relative increase of σ_e can be due either to an increase of surface enthalpy of folding, q_e , or to a decrease of the surface entropy of folding, s_e . The fact that the glass transition temperature, T_g , of the branched polyethylene is higher than that of linear polyethylene¹⁵ leads us to believe that the mobility of the polymer chains, and with it s_e in equation (4), probably decrease as the number of branchings increases. At this stage we are not able to draw any conclusions about the interdependence of q_e on the number of branchings. The effect caused by the ethyl groups is a large reduction in the value of σ_e which passes from 155 erg/cm² for linear polyethylene to 74 erg/cm² for EB1 (37 C₂H₅ per 1000 C). In this case as well, it is difficult to establish which of the two terms in equation (4) causes the lowering of σ_e . The ethyl groups are probably expelled from the lattice in numbers relatively larger than those of the methyl groups (this would also explain the low decrease in T_m^0 for EB copolymers) causing the formation of loops on the crystal surfaces bringing a high entropy value, s_e , which would off-set the corresponding increase in the value of q_e . These results would seem to indicate a far more disorderly crystal surface for EB copolymers than for EP copolymers.

(6) The validity of equation (2) throughout the range of annealing temperatures and long spacings explored and thus the linear dependence of T_m on $1/L$ leads us

to the conclusion that the ratio $\sigma_e/\Delta H_f$ remains constant during the process of annealing of single crystal aggregates of EP, EB and LPE. This result is a strong indication that the average distribution of side groups between disordered and crystalline regions is not dependent on the annealing temperature, long spacing and crystallinity.

REFERENCES

- 1 Martuscelli, E. and Vittoria, V. *Polymer* 1972, **13**, 360; Facioni, E. and Martuscelli, E. *J. Polym. Sci. (B)* 1972, **10**, 423
- 2 Alfonso, G. C., Fiorina, L., Martuscelli, E., Pedemonte, E. and Russo, S. *Polymer* 1973, **14**, 373
- 3 Blundell, D. J., Keller, A. and Kovacs, A. J. *J. Polym. Sci. (B)* 1966, **4**, 481
- 4 Holdsworth, P. J. and Keller, A. *J. Polym. Sci. (B)* 1967, **5**, 605
- 5 Roe, R. J. and Bair, H. E. *Macromolecules* 1970, **3**, 454
- 6 Quinn, T. A. and Mandelkern, L. *J. Am. Chem. Soc.* 1958, **80**, 3178
- 7 Hoffman, J. D. *SPE Trans.* 1964, **4**, 315
- 8 Ver Strate, G. and Wilchinsky, Z. W. *J. Polym. Sci. (A-2)* 1971, **9**, 127
- 9 Dole, M. *J. Polym. Sci. (C)* 1967, **18**, 57
- 10 Reneker, D. H. *J. Polym. Sci.* 1962, **59**, 539; Peterlin, A. *J. Polym. Sci. (B)* 1963, **1**, 279; Dreyfus, P. and Keller, A. *J. Polym. Sci. (B)* 1970, **8**, 253
- 11 Kawai, T. *Kolloid-Z. Z. Polym.* 1965, **201**, 104
- 12 Fisher, E. W. *8th IUPAC Microsymp., Prague* 1971
- 13 Statton, W. O. and Geil, P. H. *J. Appl. Polym. Sci.* 1960, **3**, 357; Keller, A. *Polymer* 1962, **3**, 393; Fisher, E. W. *Angew. Chem.* 1962, **74**, 551
- 14 Holdsworth, P. J. and Keller, A. *J. Polym. Sci. (B)* 1967, **5**, 605
- 15 Fisher, E. W. and Kloos, F. *J. Polym. Sci. (B)* 1970, **8**, 685

Gelation in the reactions of aliphatic di-isocyanates with triols*

W. Hopkins, R. H. Peters and R. F. T. Stepto

Department of Polymer and Fibre Science, University of Manchester Institute of Science and Technology, PO Box 88, Manchester M60 1QD, UK
(Received 24 October 1973; revised 23 November 1973)

Gelation in reactions of Niox triols with hexamethylene and decamethylene di-isocyanates has been studied. The gel points occur at extents of reaction in excess of those predicted by Flory-Stockmayer theory. The excess, intramolecular reaction increases with dilution and with decreases in the molecular weights of the reactants. Kilb's theory of gelation does not explain the results, but a semi-quantitative explanation is found in terms of a combination of Frisch's and Kilb's theories. In this, λ , the intramolecular branching parameter of Frisch, is given by the equation $\lambda = \text{const.} \nu^{-3/2} (\text{OH}_0 + \text{NCO}_0)^{-1}$, with ν the number of bonds in the smallest ring which can form.

INTRODUCTION

The occurrence of gelation in non-linear polymerizations is well known, and the basic explanation of the gel point as the point of incipient network formation has been well established by the work of Flory and of Stockmayer¹. However, in polycondensations the extents of reaction of functional groups at the gel point are rarely those predicted by simple theory. Given the equal reactivity of like functional groups, this is due to the occurrence of intramolecular reaction.

Previous studies²⁻⁷ have shown that intramolecular reaction increases with the dilution of a reaction mixture. By measuring gel points in reactions of aliphatic di-isocyanates and triols the present study seeks to elucidate further the dependence of the gel point on dilution, and on the chain lengths of reactants, and to this end Frisch's⁸ and Kilb's⁹ theories of gelation are applied to the data.

EXPERIMENTAL

The reactants chosen were similar to those used in a previous investigation⁶. Two di-isocyanates and three triols were used and the solvent was nitrobenzene. Reactions were carried out at 80°C and were catalysed by triethylene diamine (TED).

Materials

Hexamethylene di-isocyanate (HDI) was kindly supplied by ICI Dyestuffs Division and by Mobay Chemical Company. Purification was by careful fractional distillation under reduced pressure, as previously described¹⁰ (MW 168.2, theory 168.2).

Decamethylene di-isocyanate (DDI) was prepared by phosgenation of decamethylene diamine, and subsequent heating of the diamino-chloride formed¹¹. The product was purified as for HDI, and the fraction with b.p.

* Details of the experimental results presented in this paper are available on request to R. F. T. S.

122°–130°C at 1.5–3.0 mmHg was accepted (MW 226, theory 224).

Triols were the Niox triols LHT 240, LHT 112, LG56 manufactured by Union Carbide Corporation, being propylene oxide adducts of 1,2,6-hexane triol (LHT 240, LHT 112) and of glycerol (LG56). They were dried by azeotropic distillation with benzene¹⁰, and their molecular weights were determined by quantitative acetylation of the hydroxyl groups¹². In order to obtain reproducible results, the acetylation was allowed to take place over 2 h rather than the 1 h recommended. This was presumably because the majority of the hydroxyl groups were secondary¹³. The molecular weights determined were LHT 240, 711 ± 2 ; LHT 112, 1590 ± 1 ; LG56, 2927 ± 2 .

TED was manufactured by Koch-Light Laboratories. It was titrated with HCl (MW 224.2, theory 224.2).

Nitrobenzene was purified by steam distillation and subsequent distillation.

Gelation procedure

The apparatus and experimental procedure have been described in detail elsewhere⁶. Briefly, samples were withdrawn at intervals from a reaction mixture contained in a sealed flask, and were titrated for isocyanate groups remaining. The gel time was noted as that time at which the reaction mixture climbed the mechanical stirrer. The reactions were found to follow second-order kinetics, and in a given reaction the extents of reaction at gelation were determined by extrapolation of the linear second-order kinetic plot to the gel time, together with knowledge of the initial concentrations.

RESULTS AND DISCUSSION

Flory-Stockmayer theory and equal reactivity

The gel point results are presented in *Figure 1* where the reciprocal of the product of the critical extents of reaction at gelation, $(\rho_{\text{OH}}\rho_{\text{NCO}})^{-1}$ is plotted *versus* the

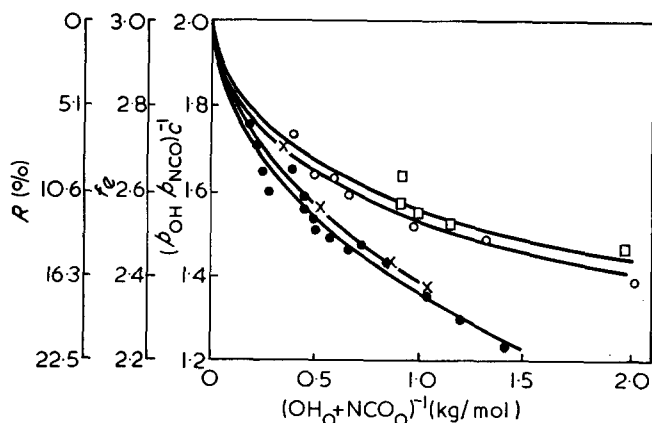


Figure 1 $(p_{OH}p_{NCO})_e^{-1}$ versus $(OH_0 + NCO_0)^{-1}$. The alternative ordinates, f_e and R , are discussed in the text. ●, System 1, LHT 240+HDI, $\nu=36$; ×, system 2, LHT 240+DDI, $\nu=40$; ○, system 3, LHT 112+HDI, $\nu=66$; □, system 4, LG 56+HDI, $\nu=112$

initial dilution of reactive groups, $(OH_0 + NCO_0)^{-1}$. The other ordinates shown will be discussed shortly.

For the present systems the Flory-Stockmayer theory¹ gives:

$$\alpha_c^{-1} = f - 1 \quad (1)$$

where $\alpha_c = (p_{OH}p_{NCO})_e$, and f is the functionality of the branched reactant. However, the predicted value of 2 for $(p_{OH}p_{NCO})_e^{-1}$ is obtained only in the limit of zero dilution of reactive groups. In this limit only intermolecular reaction can occur. As expected²⁻⁷, α_c^{-1} decreases, that is the extents of reaction at gel increase, as the reactants are diluted. In this respect it may be noted that the initial concentrations used in the present experiments ranged from bulk to about 15% w/w of reactants.

The attainment of the Flory-Stockmayer limit at zero dilution is indicative not only of the absence of ring formation but also of the equal reactivity of like functional groups. Equal reactivity was further confirmed by the fact that the present catalysed reactions followed second order kinetics. The effects of unequal reactivity may have been observed because of a small proportion (probably less than 1%¹³) of the hydroxyl groups of the triols being primary rather than secondary. Obviously, to within the sensitivity of the analytical techniques employed, the hydroxyl groups may be considered as all secondary.

The difference in the reactivities of primary and secondary hydroxyl groups *ab initio* may be considered as an intrinsic unequal reactivity. An induced unequal reactivity may arise when the reaction of the first group of a reactant affects the reactivity of the other group or groups still to react. (This is the so-called first-shell substitution effect of Gordon and coworkers¹⁴.) Induced unequal reactivity was not expected nor were its effects observed with the present di-isocyanates and triols, presumably because their functional groups were separated by sufficiently large numbers of bonds. For the triols, the number-average values for the numbers of bonds between hydroxyl groups were: LHT 240, 25; LHT 112, 55; LG56, 101. In contrast, it was found¹⁵ that the catalysed reaction of trimethylol propane and HDI showed deviations from second order kinetics which corresponded to the rate constant for the reaction of the first hydroxyl group on a trimethylol propane molecule being approximately twice that for the reaction

of the others. The details of this kinetic analysis will be reported elsewhere. For the present it is noted that such an induced unequal reactivity, due presumably to steric hindrance, should also occur with trimethylol ethane. However, no account was taken of it in a previously reported gelation study using this molecule³.

Qualitative discussion of intramolecular reaction

In Figure 1 the right-hand ordinate given, $(p_{OH}p_{NCO})_e^{-1}$ or α_c^{-1} , is the simplest to use in a quantitative interpretation of results. However, the other ordinates, f_e and R , are perhaps more immediate in their physical significance.

f_e is the effective functionality of the triol, and is defined by:

$$f_e - 1 = \alpha_c^{-1}$$

Thus when $\alpha_c^{-1} = 2$, $f_e = 3$. Such an effective functionality has been used¹⁶ to describe delayed gelation due to induced unequal reactivity and intramolecular reaction. Here, the variation of f_e with dilution is solely the result of intramolecular reaction.

R is the % of ring reaction at gelation, and is defined in cases where the initial ratio of isocyanate to hydroxyl groups, r , is equal to unity. It is given by:

$$R = 100\{1 - [(f-1)\alpha_c]^{-1/2}\} \%$$

Here, $(f-1)^{-1/2}$ equals the extent of reaction at gelation of hydroxyl or isocyanate groups, assuming no ring formation (equation 1).

The use of the three ordinates may be illustrated by reference to system 1. Here, the initial concentrations ranged from 17% w/w monomers to bulk, α_c^{-1} ranges from 1.23 to 1.76, f_e from 2.23 to 2.76, and R from 21.6% to 6.2%. In subsequent discussion α_c^{-1} will be used.

It was reported previously⁶ that the amount of intramolecular reaction depended systematically on the initial ratio of reactive groups, r . Most of the results presented here refer to reactions with $r=1$, and no detailed investigation of the effect of r was undertaken. Hence, in Figure 1 single curves are drawn through the four sets of points, although some of the scatter present will be due to the secondary dependence of α_c^{-1} upon r .

The decrease in α_c^{-1} with dilution apparent in the curves in Figure 1 is in accord with the expected increase in intramolecular reaction with dilution. In addition, at a given dilution the amount of intramolecular reaction increases as ν , the number of bonds in the smallest ring which can form, decreases. The values of ν given for the various pairs of reactants are the number-average values of the number of bonds between the isocyanate group and one of the hydroxyl groups of a dimer.

The Jacobson-Stockmayer theory¹⁷ of ring formation in linear equilibrium polycondensates shows that P_{ab} , the mutual concentration of the two reactive groups of one molecule, is given by the expression:

$$P_{ab} = \left(\frac{3}{2\pi\nu b^2} \right)^{3/2} \text{ functional groups per unit volume}$$

This expression assumes that the chain, having ν bonds each of effective bond length b , obeys Gaussian statistics, so that the mean-square end-to-end distance, $\langle r_0^2 \rangle$, is equal to νb^2 . In general ring formation increases as P_{ab} increases. Whilst the present non-linear non-equi-

librium polycondensations cannot be explained by the Jacobson-Stockmayer theory, the observed increase in intramolecular reaction with decrease in ν is in agreement with the mechanism of ring-chain competition proposed by these authors.

The chain structures of the polymers formed from the various pairs of reactants and, therefore, their effective bond lengths, b , will be different. The representation of ν as the parameter determining ring formation at a given dilution assumes that variations in b are of secondary importance, and from the relative positions of the curves in *Figure 1*, ν appears to be the important parameter.

Application of Frisch's and Kilb's theories

A quantitative interpretation of the results may be attempted in terms of Frisch's⁸ and Kilb's⁹ theories of gelation. According to Frisch's theory:

$$\alpha_c^{-1} = (f-1)[1 - (1-\alpha_c)\lambda] \quad (2)$$

where λ is an intramolecular branching parameter. When $\lambda=0$ the Flory-Stockmayer equation is obtained. Kilb's theory gives essentially:

$$\alpha_c^{-1} = (f-1)(1-\lambda') \quad (3)$$

where λ' is also an intramolecular branching parameter.

Both theories apply to reactions with only small numbers of rings. However, by rearrangement of equation (2), to an explicit expression for α_c in terms of λ , one obtains:

$$\alpha_c = -\frac{(1-\lambda)}{2\lambda} \pm \frac{(1-\lambda)}{2\lambda} \left(1 + \frac{4\lambda}{(f-1)(1-\lambda)^2}\right)^{1/2} \quad (4)$$

Expansion of the binomial and retention of only the first two terms gives:

$$\alpha_c^{-1} = (f-1)(1-\lambda) \quad (5)$$

for small λ . Thus for extremely small numbers of rings λ and λ' are identical, and Frisch's expression includes and extends the range of λ' covered by Kilb's expression.

A distinction between the two theories is that Kilb expresses λ' in molecular terms, whereas Frisch introduces λ purely as a statistical parameter. However, the preceding equivalence of equations (3) and (5) enables λ and λ' to be equated, at least approximately, and to be interpreted in the terms proposed by Kilb. According to these λ' is: (i) directly proportional to the dilution of the reaction mixture, although a precise definition of dilution is not given, and (ii) for a given value of b , directly proportional to $\nu^{-3/2}$.

If the reciprocal of the initial concentration of reactive groups is taken to represent the dilution of the reaction system, the curves in *Figure 1* may be viewed as a test of Kilb's theory. That is, assuming

$$\lambda' = \frac{\text{const.}}{\nu^{3/2}(\text{OH}_0 + \text{NCO}_0)} \quad (6)$$

one should, according to equation (3), obtain linear plots in *Figure 1*. It is apparent that such plots are not obtained, and the following interpretation of the data according to Frisch's theory indicates that this is because the data lie outside the range of α_c covered by Kilb's theory.

To test Frisch's theory equation (2) may be rearranged

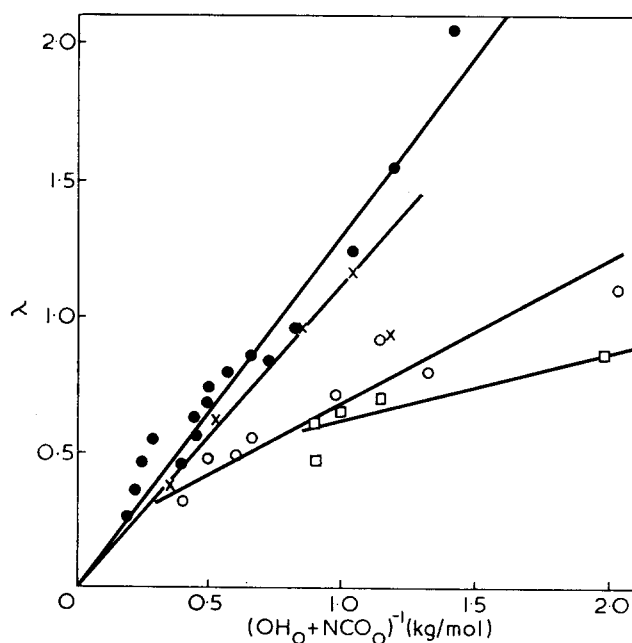


Figure 2 λ versus $(\text{OH}_0 + \text{NCO}_0)^{-1}$. Symbols are the same as for *Figure 1*

so that λ is derived from the experimental values of α_c , i.e.

$$\lambda = \frac{\alpha_c(f-1) - 1}{(1-\alpha_c)\alpha_c(f-1)} \quad (7)$$

If λ is equated to λ' and interpreted according to equation (6) then plots of λ versus $(\text{OH}_0 + \text{NCO}_0)^{-1}$ should be linear and pass through the origin. Such plots are illustrated in *Figure 2* where, in accordance with equation (6), lines with slopes in proportion to $\nu^{-3/2}$ have been drawn through the data. The lines for systems 1 and 2 follow the behaviour predicted by equations (6) and (7), with λ directly proportional to dilution and to $\nu^{-3/2}$. For systems 3 and 4, the lines of the required slopes through the data points do not extrapolate to the origin. In cognisance of the fact that λ must be zero when $\alpha_c^{-1} = f-1$, it is apparent that on the basis of the lines drawn for systems 1 and 2 the data for systems 3 and 4 show deviations from what may be termed Frisch-Kilb behaviour, as defined by equations (6) and (7). The neglect of the previously mentioned dependence of α_c^{-1} upon r , and of variations in b with chain structure may well be responsible for this.

The deviations may also be due to approximations inherent in the very bases of the theories as applied to non-equilibrium polymerizations. The theories attempt to represent the ring-chain competition in terms of single parameters, λ and λ' , which are constant throughout the course of a reaction. However, the concentration of groups external to a given molecule, and which can react intermolecularly with that molecule, must decrease as the reaction proceeds. The present interpretation of λ and λ' according to equation (6) assumes that the 'external' concentrations presented to a given molecule may be replaced by some average value which is directly proportional to the initial concentration of functional groups. This assumption, which is the simplest to make, has still to be justified.

In conclusion, it appears that the dependence of α_c on dilution is approximately explicable in terms of Frisch's theory, provided that λ is interpreted in terms

proposed by Kilb, and dilution is taken as the initial dilution with respect to functional groups. Previously⁶, apparent agreement with Kilb's expression had been found, with α_c^{-1} varying linearly with $(\text{OH}_0 + \text{NCO}_0)^{-1}$. The results reported then covered α_c^{-1} values only in the range $1.3 < \alpha_c < 1.5$. Over such a limited range, curvature, such as that present in the plots in *Figure 1*, was not apparent.

REFERENCES

- 1 Flory, P. J. 'Principles of Polymer Chemistry', Cornell Univ. Press, Ithaca, 1953, Ch IX
- 2 Stockmayer, W. H. and Weil, L. L., quoted in 'Advancing Fronts in Chemistry', (Ed. S. B. Twiss), Reinhold, New York, 1945, Ch 6
- 3 Price, F. P., Gibbs, J. H. and Zimm, B. H. *J. Phys. Chem.* 1958, **62**, 972
- 4 Price, F. P. *J. Phys. Chem.* 1958, **62**, 977
- 5 Zimm, B. H., Price, F. P. and Bianchi, J. P. *J. Phys. Chem.* 1958, **62**, 979
- 6 Peters, R. H. and Stepto, R. F. T. *SCI Monogr.* 20 1965, p 157
- 7 Bates, R. F. and Howard, G. J. *J. Polym. Sci. (C)* 1967, **16**, 921
- 8 Frisch, H. L. *128th Meet. Am. Chem. Soc. Minneapolis* 1955
- 9 Kilb, R. W. *J. Phys. Chem.* 1958, **62**, 969
- 10 Greenshields, J. N., Peters, R. H. and Stepto, R. F. T. *J. Chem. Soc.* 1964, p 5101
- 11 Pinner, S. H. *Plastics (London)* 1947, **11**, 206
- 12 Sorenson, W. R. and Campbell, T. W. 'Preparative Methods of Polymer Chemistry', Interscience, New York, 1961, p 134
- 13 Hanna, J. G. and Siggia, S. J. *J. Polym. Sci.* 1962, **56**, 297
- 14 Gordon, M. and Scantlebury, G. R. *Trans. Faraday Soc.* 1963, **60**, 604
- 15 Hopkins, W. *PhD Thesis* University of Manchester, 1967
- 16 Fogiel, A. W. *Macromolecules* 1969, **2**, 581
- 17 Jacobson, H. and Stockmayer, W. H. *J. Chem. Phys.* 1950, **18**, 1600

Effect of polymer microstructure on methyl group torsional vibrations

G. Allen, C. J. Wright and J. S. Higgins

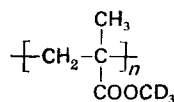
Department of Chemistry, University of Manchester, Manchester M13 9PL, UK
(Received 9 October 1973; revised 19 November 1973)

Fundamental torsional frequencies of methyl groups have been measured with neutron incoherent inelastic scattering for isotactic poly(methyl methacrylate)-COOCD₃, and heterotactic, syndiotactic and head-to-head isomers of poly(α -methylstyrene). The measurements confirm that the spectrum of isotactic PMMA differs considerably from the syndiotactic polymer in the region of the fundamental vibration, but no difference is found for the two stereoregular forms of poly(α -methylstyrene). However, the torsional frequency of the methyl group in the head-to-head configuration of α -methylstyrene lies at lower wavenumbers than that observed in the head-to-tail.

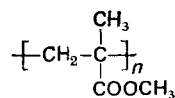
INTRODUCTION

Studies of fundamental torsional frequencies of methyl groups in small molecules show that the torsional frequency, and hence the barrier to internal rotation of the methyl group, is sensitive to the nature of the neighbouring substituents. In polymer molecules, the influence not only of the chemical nature of the neighbouring groups, but also the stereoregularity and the possibility of head-to-head, tail-to-tail as well as head-to-tail placings must be considered. In poly(methyl methacrylate) (PMMA) for example, it is well known that the relaxation phenomenon associated with the α -methyl group is influenced¹ by the stereoregular character of the polymer, and in a previous paper² we tentatively showed that this difference was also reflected in the methyl group torsional frequencies observed for these different configurations.

In this paper we show how the neutron incoherent inelastic scattering (n.i.i.s.) spectrum of poly(α -methylstyrene) is influenced by chain configurations as exhibited in heterotactic and syndiotactic head-to-tail samples and a sample containing a high proportion of head-to-head units. In addition the n.i.i.s. spectrum of isotactic



has been studied to complement previous work on isotactic



and to provide a more precise value for the α -CH₃ torsion frequency which had previously been deduced by subtracting the overlapping -OCH₃ torsion from the spectrum.

Neutron incoherent inelastic scattering spectroscopy

is the preferred technique for this work because: (a) the corresponding infra-red and Raman bands are extremely weak and are overlapped by skeletal modes of similar intensity; (b) the n.i.i.s. vibrational band intensities are proportional to the mean square amplitude of displacement in the normal mode; and (c) the n.i.i.s. cross-section for protons is large compared with the cross-sections of other nuclei. Factors (b) and (c) combine to give the expectation that the -CH₃ torsions will be the most intense bands in the n.i.i.s. spectra of these polymers and furthermore selective deuteration can be used to confirm assignments or to simplify spectra.

EXPERIMENTAL

Spectra

N.i.i.s. spectra were obtained using the 6H time-of-flight spectrometer³ at AERE, Harwell. Raw data were corrected by the procedures previously described² and finally presented as $\rho(\omega)$ spectra, where $\rho(\omega)$ is the hydrogen-amplitude-weighted frequency distribution:

$$\rho(\omega) = \omega \hbar \lim_{Q \rightarrow 0} \left| \frac{\exp(\hbar\omega/2k_B T)}{Q^2} \frac{\hbar}{b^2} \frac{\mathbf{k}_0 \cdot \boldsymbol{\tau}^3}{\mathbf{k} \cdot m} \frac{\partial^2 \sigma}{\partial \Omega \partial \tau} \right|$$

In this expression $\partial^2 \sigma / \partial \Omega \partial \tau$, the parameter determined by experiment, is the double differential cross-section with respect to neutron time-of-flight, τ and solid angle Ω into which the neutron is scattered. b is the scattering length of the atom of mass m , \mathbf{k}_0 and \mathbf{k} are respectively the incident and scattered neutron wave vectors and Q is the momentum transferred to the neutron in the scattering event.

The expression for $\rho(\omega)$ emphasizes the suitability of the n.i.i.s. technique for the study of torsional frequencies. Not only is $\rho(\omega)$ large for normal modes of this type but ω is small (200–300 cm⁻¹) resulting in a relatively large value of $\partial^2 \sigma / \partial \Omega \partial \tau$ to be measured.

Samples were examined in the form of 5 cm square thin films approximately 0.2 mm thick.

Materials

High molecular weight specimens of isotactic poly-(methyl methacrylate)-COOCD₃ and syndiotactic poly-(α -methylstyrene) were prepared from the appropriate monomers using methods reported in the literature⁴⁻⁶. Tacticities were determined by ¹H n.m.r. spectroscopy using solutions in CDCl₃^{4,7} at 22°C. From the α -CH₃ resonances the following results were obtained:

	% iso	% hetero	% syndio
Isotactic PMMA	75	12	13
Syndiotactic poly(α -methylstyrene)	0	10	90
Heterotactic poly(α -methylstyrene)	20	51	29

The sample of heterotactic poly(α -methylstyrene) was supplied by Dr D. J. Worsfold.

A sample of head-to-head poly(α -methylstyrene) was supplied by Dr D. H. Richards; evidence for its predominantly head-to-head character⁸ was found by n.m.r. spectroscopy. The molecular weight ($\eta_{sp}=0.127$, 1% solution in THF at 25°C) was of the order of $\bar{M}_v \sim 10\,000$.

RESULTS

Poly(methyl methacrylate)

In Figure 1 the frequency distribution functions for syndiotactic² and isotactic poly(methyl methacrylate)-COOCD₃ are compared. Since the CD₃ torsional band is weak, the most prominent vibrational band in each spectrum is the fundamental torsional frequency of the α -CH₃ group. The torsional band is centred at 360 cm⁻¹ in the syndiotactic stereoisomer but it shifts to 300 cm⁻¹ in the isotactic polymer. The breadth of the band in the former is probably connected with its lower stereochemical purity, which would also account for its shoulder at 300 cm⁻¹.

Previously² we estimated the α -methyl group torsional frequency in the isotactic isomer to be 250 cm⁻¹ by

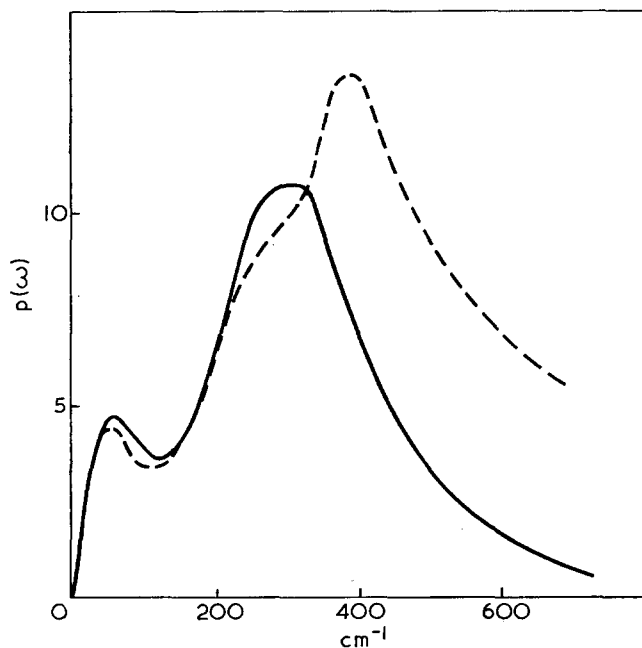


Figure 1 Frequency distribution functions of isotactic (—) and syndiotactic (---) poly(α -methyl methacrylate)

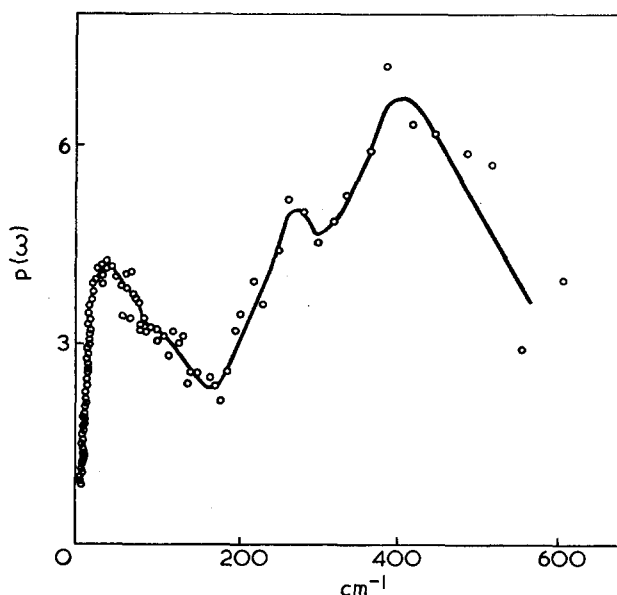


Figure 2 Frequency distribution function of syndiotactic and heterotactic poly(α -methylstyrene)

subtracting an overlapping -OCH₃ torsional band obtained from the n.i.s. spectrum of poly(α -chloro methacrylate). The present value of 300 cm⁻¹ must be considered more reliable since it is a direct observation.

In consequence the values of the torsion frequency ν_{tor} and ' V_3 neutrons' the 3-fold barrier calculated from this frequency, which were listed in Tables 1 and 2 of ref 2, must be revised. In the Table below the revised values are shown together with E_a obtained⁹ from relaxation measurements. From these relaxation data, assuming that proton tunnelling occurs², ' V_3 n.m.r.' can be calculated. The agreement between ' V_3 n.m.r.' and V_3 neutrons is now better than it was in ref 2.

α -CH ₃ group in HMMA	ν_{tor} (cm ⁻¹)	V_3 neutrons (kJ/mol)	E_a (kJ/mol)	V_3 n.m.r. (kJ/mol)
Syndiotactic	360 ± 10	33	23-35	30
Isotactic	300 ± 10	23	16	22.6

Poly(alpha-methylstyrene)

Figure 2 shows the frequency distribution function for syndiotactic and heterotactic poly(α -methylstyrene). The function is the same for both isomers and the most intense peak, again assigned to the methyl torsion frequency on account of its intensity, is centred at 380 cm⁻¹. In the spectrum of the head-to-head polymer shown in Figure 3¹⁰, the torsional peak is at a lower frequency, 300 cm⁻¹.

α -CH ₃ group in poly(α -methylstyrene)	ν_{tor} (cm ⁻¹)	V_3 neutrons (kJ/mol)
Syndiotactic/heterotactic	380 ± 10	37
Head-to-head	300 ± 10	23

The weaker peak in the head-to-tail poly(α -methylstyrene) spectrum at 260 cm⁻¹ may arise from the polystyrene skeleton of the molecule, since results on polystyrene¹¹ (which is always predominantly head-to-tail) show that there is a band of similar intensity at 240 cm⁻¹. Even if fortuitously there is a peak of similar intensity in the same spectral region for the head-to-head isomer it would be buried in the wing of the CH₃

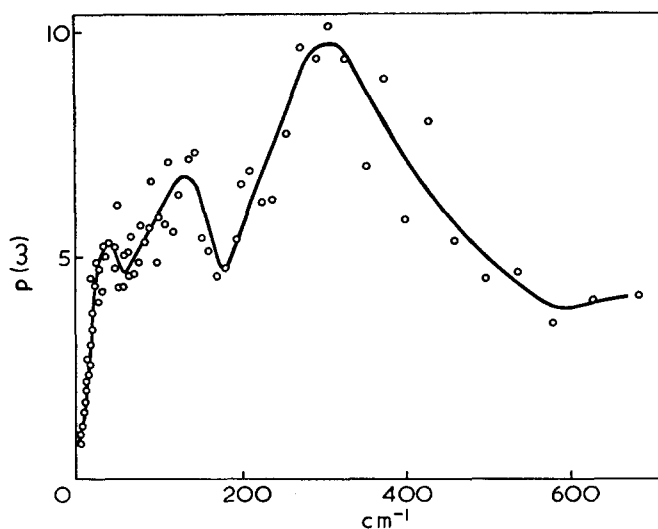


Figure 3 The frequency distribution function of head-to-head poly(α -methylstyrene)

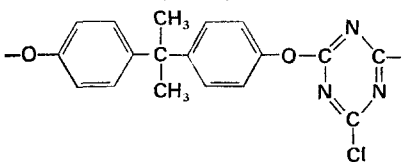
torsional band since the latter lies at lower frequency than in the head-to-tail isomer.

CH_3 torsion in other polymers

In Table 1 are recorded the torsional frequencies of methyl groups in differing chemical environments so that the effects of chemical and stereochemical environments may be contrasted. All the values of V_3 have been calculated assuming a threefold cosine potential function.

The most important caveat with respect to these values of V_3 is that they assume that the methyl group rotation is not coupled with other normal modes of the polymer molecule. This and other assumptions underlying the calculation of V_3 have been discussed earlier.

Table 1 Torsional frequencies and potential barriers for methyl groups in polymers

Polymer	cm^{-1}	V_3 neutrons (kJ/mol)
Vinyl ether (O- CH_3)	100	2.5
Dimethyl siloxane	165	6.9
Propylene oxide	228	13
-P(CH_3) ₂ =N-	240	15
4-Methyl pentene-1	240	15
Isotactic PMMA (α - CH_3)	300	23
	~300	~23
Isobutene	305	24
Syndiotactic PMMA	360	33

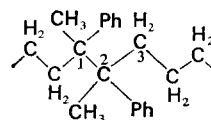
DISCUSSION

The α -methyl torsion in PMMA shows a pronounced shift to lower frequency when the chain configuration is changed from syndio- to iso-tactic. There are no similar shifts reported for stereoisomers of small molecules and the origin of the shift in PMMA is not immediately obvious.

We have studied poly(α -methylstyrene) and find that a similar shift probably does not occur. Unfortunately

our evidence is not as decisive as it should be because the sample with the highest degree of isotacticity contained only 20% of isotactic placements. The shoulder at 260 cm^{-1} is equally prominent in both syndio- and hetero-tactic forms. However, a shift to lower wavenumbers of the α -methyl torsion, similar in magnitude to that observed in PMMA isomers, is observed between the head-to-tail and head-to-head structural isomers of poly(α -methylstyrene). At first sight the most sterically hindered form (head-to-head) has the lower torsional frequency and hence the lower barrier to internal rotation, V_3 .

In a previous paper we suggest that intramolecular forces control the magnitudes of V_3 . It is unlikely that 1-2 non-bonded repulsions are primarily responsible otherwise the head-to-head isomer would have the largest barrier. A more likely explanation is that steric hindrance in the head-to-head isomer forces the 1-2 bond almost exclusively into a *trans*-conformation:



Thus the predominant interactions are $-C-CH_3 \dots H-C-$ and $-C-Ph \dots H-C-$ in this isomer. In the head-to-tail form there are no such configurations of extreme steric hindrance and so $-C-CH_3 \dots CH_3-C-$ and $C-CH_3 \dots Ph-C-$ repulsions are likely to occur more frequently in the conformations adopted by the chain in the amorphous states, thus contributing to a higher barrier to rotation of the α - CH_3 group. Qualitatively, at least, this could explain the observed torsional frequencies.

Structural evidence^{1,2} on syndio- and iso-tactic forms of PMMA suggests that the local conformations likely to prevail in isotactic triads will be related to the 3/1 chain helix and over similar short distances in syndiotactic chains a planar zig-zag structure is more probable. Simple models show that in this case the non-bonded repulsions in the isotactic form will be predominantly $-C-CH_3 \dots$ ester group and in the syndiotactic form they will be $-C-CH_3 \dots CH_3-C-$. The shift of the α - CH_3 torsion to higher wavenumbers is then in the same direction as the difference observed for head-to-head and head-to-tail poly(α -methylstyrene). It should be noted, however, that this argument would suggest that the isotactic form of poly(α -methylstyrene) *should* have a low torsional frequency. We have mentioned earlier that no such shift is detected in a partly isotactic specimen and unfortunately the polymer has not yet been prepared with a high degree of isotactic purity.

Theoretical analysis of methyl group torsion in PMMA

In principle the different values for the methyl group torsion in syndio- and iso-tactic PMMA can be accounted for in terms of non-bonded repulsions which influence the barriers to internal rotation of the methyl groups. Unfortunately there are too many unknown bond angles, bond distances and repulsion potentials for the calculation to be attempted with certainty, but we have tried to show that with reasonable assumptions the difference between the two forms of PMMA can be accounted for on this basis.

Calculations of the barrier to rotation of the α - CH_3 group for the 5/1 helical conformation of the isotactic

polymer¹³ and the two preferred conformations for syndiotactic vinyl chains¹⁴, (*tt*) (*gg*) and (*tt*) (*tt*) have been carried out which agree with experiment in that the barrier to rotation in isotactic PMMA is less than that in either of the two syndiotactic forms.

The barrier has been represented by a function of the form:

$$V(\theta) = \frac{V_0}{2}(1 + \cos 3\theta) + \sum_{ij} V(r_{ij})$$

where $V(r_{ij})$ is the pair potential between a pair of atoms ij . The potentials used have been the C...H and H...H functions due to Williams¹⁵ which have been tested against enthalpies of sublimation, geometries and elastic moduli of alkanes. The O...H potential used has not been so rigorously tested¹⁶, but as our calculations only attempt to display relative barriers we believe that this is not of prime importance. V_0 was taken as 8.4 kJ/mol¹⁷.

The bond distances and angles used for isotactic PMMA were those found by X-ray diffraction¹³. The angle of torsion about the bonds CH₃-C-CO-O found in the same paper by a minimum energy calculation, led to a value of the barrier which was much too high, 564 kJ/mol. An assumed value for this angle of -5° was chosen for our calculation since this led to a minimum value for the barrier. The same bond lengths and bond angles, apart from the chain torsion angles, were used for calculations of the syndiotactic isomer.

The barriers found for the three polymers are: isotactic PMMA, 54 kJ/mol; syndiotactic PMMA (*tt*) (*gg*), 138 kJ/mol; syndiotactic PMMA (*tt*) (*tt*), 88 kJ/mol.

All values are 3-4 times higher than the experimental values, which is not too surprising in view of the assumptions made, but nevertheless V_3 for the isotactic form is consistently less than for the syndiotactic forms in agreement with our observations.

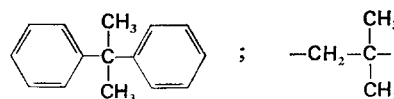
Shifts in torsional frequencies due to chemical structure

So far this paper has been concerned with shifts in methyl group torsions arising from geometrical isomerism. Table 1 lists torsional frequencies and values of V_3 obtained for a series of methyl groups in different chemical environments. In each case the torsional frequency does not shift appreciably on dissolution of the polymer.

It is clear from these results that the influence of chemical structural change is wider ranging than simple changes in local geometry in geometrical isomers. Unfortunately the theoretical analysis of non-bonded repulsions in stereoisomers is, as we have seen, a formidable problem. It is quite impossible at this stage to

account for electronic effects arising from changes in the chemical nature of the structure as well.

The results in Table 1 taken together with corresponding relaxation studies of methyl group motion do underline the predominant influence of intramolecular effects on bulk relaxation phenomena associated with CH₃ groups. Generally loss phenomena such as maxima in dielectric and mechanical loss spectra and minima in n.m.r. spin-lattice relaxation time-temperature plots occur at very low temperatures and have low activation energies for O-CH₃ groups. This is paralleled by a low torsional frequency. Methyl groups attached directly to main chains have loss phenomena in a higher temperature range and also higher activation energies, and this is paralleled by increased torsional frequencies, e.g. -Si(CH₃)₂O-, -CH₂CH(CH₃)O-. Methyl groups in sterically hindered environments, e.g.



tend to have simultaneously high values for the temperature of maximum loss, the activation energy of the process and a high torsional frequency.

REFERENCES

- Connor, T. M. and Hartland, A. *Phys. Lett.* 1966, **23**, 662
- Higgins, J. S., Allen, G. and Brier, P. N. *Polymer* 1972, **13**, 157
- Bunce, L. J., Harris, D. C. E. and Stirling, G. C. *UKAEA Rep.* 126246 1970
- Liu, K. J. *J. Polym. Sci. (A-2)* 1967, **5**, 699
- Bovey, F. A. and Tiers, G. V. D. *J. Polym. Sci.* 1960, **44**, 173
- Cowie, J. M. G. and Bywater, S. *J. Polym. Sci. (A-2)* 1968, **6**, 499
- Brownstein, S., Bywater, S. and Worsfold, D. J. *Makromol. Chem.* 1961, **48**, 127; Elgert, K. F., Seiler, E., Puschendorf, G., Ziemann, W. and Cantow, H.-J. *Makromol. Chem.* 1971, **144**, 73
- Richards, D. H. and Scilly, N. F. *Chem. Commun.* 1968, p 1515
- Stejskal, E. O. and Gutowsky, H. S. *J. Chem. Phys.* 1958, **28**, 388
- Pearce, D. A. *Thesis* Oxford University, 1971
- Allen, G. and Wright, C. J. unpublished work
- Schneider, B., Stoker, J., Dirlekov, S. and Mihailov, M. *Macromolecules* 1971, **4**, 715
- Tadokoro, H., Chatani, Y., Kusanagi, H. and Yokoyama, M. *Macromolecules* 1970, **3**, 441
- Flory, P. J. 'Statistical Mechanics of Chain Molecules', John Wiley, New York, 1969, p 217
- Williams, D. E. *J. Chem. Phys.* 1967, **47**, 4680
- Scott, R. A. and Scheraga, H. A. *J. Chem. Phys.* 1966, **45**, 2011
- Scott R. A. and Scheraga, H. A. *J. Chem. Phys.* 1966, **44**, 3054

Note to the Editor

Comment on the paper:

'Introduction of hydroxymethyl groups into polystyrene and styrene' by C. H. Bamford and H. Lindsay (*Polymer* 1973, 14, 330-332)

J. Štamberg, O. Wichterle and D. Doskocilova
Institute of Macromolecular Chemistry, Czechoslovak Academy of Sciences, 162 06 Prague 6, Czechoslovakia
(Received 5 November 1973)

Reactive polymers (PX) may be obtained from the monomer M either by a polymeric (M→P→PX) or a monomeric (M→MX→PX) route. However, quite frequently the same type of reaction cannot be used in both cases for introducing the group X.

In 1953, Wichterle and Černý tried to chloromethylate monomeric styrene instead of polystyrene. The reaction proceeded with a good yield of the monochloromethylated product, C₉H₉Cl, and was described in a patent¹ where the question to which of the four nucleophilic sites of the styrene molecule the chloromethyl group became attached was not discussed. However, the same authors found later that chloromethylation occurred exclusively in the side chain, and that cinnamyl chloride (CC), and not styrene chloromethylated in the ring, was the main reaction product². We were therefore surprised to find that Bamford and Lindsay³, on the contrary, assigned this product exclusively as 4-vinylbenzyl chloride (4-VBC).

The boiling points of CC and VBC are comparatively close, and the values given in the literature cover a considerable range, so that they cannot be used to determine the structure of the product. The refractive index was measured in an earlier paper only² (n_D^{20} 1.5783) and seems to be similar to that of Ar-VBC (n_D^{25} 1.5743⁴, 1.5725^{5,6}) rather than CC (n_D^{25} 1.5802⁷, 1.5807⁸; n_D^{20} 1.5830⁹, 1.5851¹⁰). To identify the product, Wichterle and Černý² prepared a number of cinnamyl derivatives, among them also an alcohol and an acetate which Bamford and Lindsay³ describe as *p*-vinylbenzyl derivatives. The great similarity between physical properties of both types of compounds and the large scatter of values given in the literature make it difficult to decide about the structure of the product. Nor does the phenylurethane prepared by Bamford and Lindsay from an alcohol elucidate the chemical structure of chloromethylated styrene, since its melting point (93–94°C) lies between the values for the cinnamyl (91–91.5°C¹¹, 90–91.5°C¹², 90–92°C¹³) and Ar-vinylbenzyl (95–96°C¹⁴) derivative.

In order to determine the real structure of the product of chloromethylation, we repeated its preparation and identification. The reaction of styrene with formaldehyde and hydrogen chloride^{1,2} was carried out under reflux (80–100°C); the product was distilled and analysed by gas chromatography. With Apiezon L, only a single peak was obtained (besides a low amount of more volatile impurities); the polar phase (Silicone Gum Rubber XE-60, Hewlett-Packard) allowed the determination of two compounds in comparable amounts.

They were separated on a preparative chromatograph (fractions 1 and 2) and identified.

From the mass spectra, molecular peaks 152 (fraction 1) and 188 (fraction 2) and the chemical formulae C₉H₉Cl (calc. 23.23% Cl) and C₉H₁₀Cl₂ (calc. 37.50% Cl) were determined, i.e. the formula of fraction 2 differed from that of fraction 1 by one additional HCl. The results of elemental analysis were 23.39% Cl (fraction 1) and 37.14% Cl (fraction 2). In both cases the infra-red spectra exhibited bands corresponding to monosubstitution at the aromatic ring (708 cm⁻¹ and 1750–2000 cm⁻¹). In the spectrum of fraction 2 the bands of the double bond, 975 cm⁻¹ and 1670 cm⁻¹, were missing; their disappearance was accompanied by a relative increase in absorption in the region of 2800 cm⁻¹ to 3000 cm⁻¹ corresponding to a higher content of CH bonds with saturated carbon atoms than with unsaturated or aromatic carbon atoms.

Convincing data on the structure were found in the n.m.r. spectra (Figure 1). For fraction 1 the results were: 4.13 ppm, doublet 6.7 Hz, intensity 2H (–CH₂Cl); 6.4 ppm, multiplet, 2H (–CH=CH–); 7.3 ppm, multiplet, 7.2H (aromatic); plus a number of very weak bands between 1 and 6 ppm whose total intensity amounts to about 25% of the whole intensity of non-aromatic bands of the main component. The chemical shifts and relative intensities correspond to the structure of the main component given by the formula of cinnamyl chloride. This structure is corroborated in particular by the pattern of the multiplet at 6.4 ppm having the form of an AB quartet with J_{AB} = 15.5 Hz corresponding to two olefinic protons in the *trans* position. One component of this quartet is further split into triplets with coupling constant of 6.7 Hz, equivalent to the spacing of the doublet at 4.13 ppm. This spacing obviously corresponds to the coupling of the olefinic proton in position 2 with the CH₂Cl group.

The structure of Ar-vinylbenzyl chloride is ruled out, since ClCH₂–φ cannot give a doublet, and CH₂=CH–φ would give two doublets with a spacing of ~15 and ~11 Hz. CH₂=CH–φ cannot be hidden in the aromatic band as pointed out by Bamford and Lindsay³, because it gives four lines with a maximum spacing of ~25 Hz.

The apparently non-stoichiometric ratio of the intensity of aromatic hydrogen atoms to the other hydrogen atoms of the main component is clearly due to the content of impurities the aromatic bands of which absorb in the same place while the other bands are scattered over a wide frequency range.

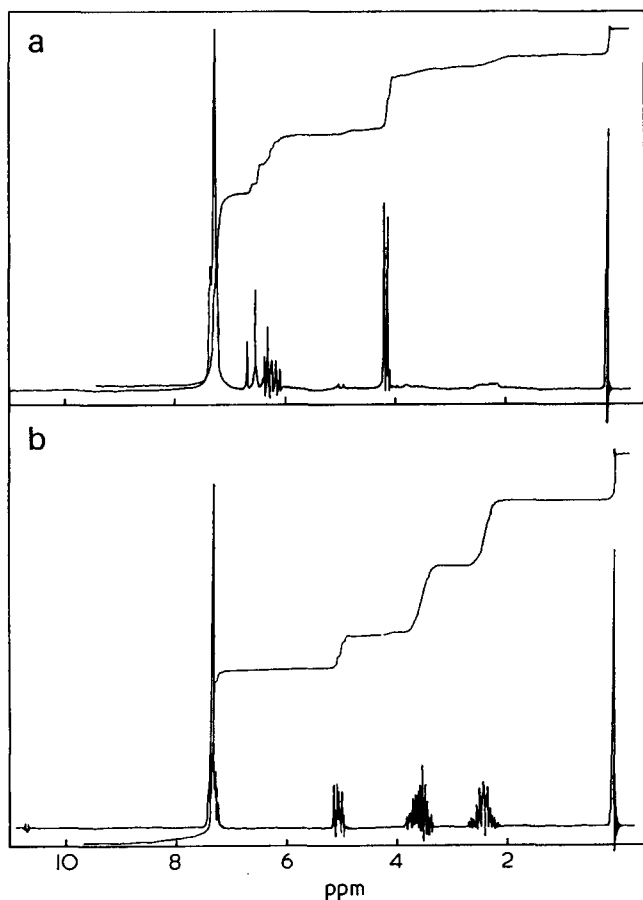


Figure 1 N.m.r. spectra of 10%w/v solutions in CCl_4 with internal HMDS, JEOL-PS-100, 100MHz. (a) Fraction 1; (b) fraction 2

The spectrum of fraction 2 contains the multiplet 2.4 ppm, intensity 2H ($-\text{C}-\text{CH}_2-\text{C}-$), multiplet 3.5 ppm, 2H ($-\text{CH}_2\text{Cl}$), multiplet 5.05 ppm, 1H ($\phi-\text{CHCl}-\text{C}$), multiplet 7.33 ppm, 5H (aromatic). The

chemical shifts, forms of multiplets (especially 5.05 ppm) and relative intensities correspond to 1-phenyl-1,3-dichloropropane.

It may be summarized, in conclusion, that the reaction of styrene with formaldehyde and hydrogen chloride does not give rise to 4-vinylbenzyl chloride, but to cinnamyl chloride, along with 1-phenyl-1,3-dichloropropane owing to a consecutive addition of hydrogen chloride. A similar finding was obtained not only for chloromethylation, but also for propionylation catalysed with aluminium chloride. While polystyrene yielded poly(4-propionylstyrene), monomeric styrene gave rise to styryl ethyl ketone¹⁵. It appears that in many cases the polymer analogous transformation is an effective alternative suitable for the synthesis of reactive polymers.

REFERENCES

- 1 Wichterle, O. and Černý, J. Czech. Pat. 83 721 (1955); *Chem. Abstr.* 1956, **50**, 5738h
- 2 Wichterle, O. and Černý, J. *Collect. Czech. Chem. Commun.* 1955, **20**, 1288
- 3 Bamford, C. H. and Lindsay, H. *Polymer* 1973, **14**, 330
- 4 Hoffenberg, D. S. U.S. Pat. 2 981 758 (1961); *Chem. Abstr.* 1961, **55**, 25 859c
- 5 Arcus, C. L. and Salomons, N. S. *J. Chem. Soc.* 1962, p 1515
- 6 Morris, L. R., Mock, R. A., Marshall, C. A. and Howe, J. H. *J. Am. Chem. Soc.* 1959, **81**, 377
- 7 Hatch, L. F. and Alexander, H. E. *J. Am. Chem. Soc.* 1950, **72**, 5643
- 8 Goebel, H. L. and Wenzke, H. H. *J. Am. Chem. Soc.* 1938, **60**, 697
- 9 Carroll, M. F. *J. Chem. Soc.* 1940, p 1266
- 10 Martin, H. and Trinh, N. Q. *C. R. Acad. Sci.* 1949, **228**, 688
- 11 Pauly, H., Schmidt, H. and Böhme, E. *Chem. Ber.* 1924, **57**, 1329
- 12 Schimmel & Co. *Geschäftsbericht* 1910 (April); *Chem. Zentr.* 1910, **I**, 1720
- 13 Palmer, C. S. and Adams, R. *J. Am. Chem. Soc.* 1922, **44**, 1380
- 14 Abramo, J. G. and Chapin, E. C. *J. Org. Chem.* 1961, **26**, 2671
- 15 Štamberg, J. *Thesis*, Prague, 1958

Conference Announcement

IUPAC XXIII International Symposium on Macromolecules

Madrid, Spain, 15-20 September 1974

The XXIII IUPAC International Symposium on Macromolecules will be held at Palacio de Congresos, Avenida del Generalísimo, Madrid (Spain) from 15 to 20 September 1974.

The Scientific Programme will consist of four main topics; (1) new developments in polymerization; (2) chemical modifications and reactions of polymers; (3) properties of amorphous and crystalline polymers; (4) influence of structure on technical properties.

There will be six Main Lectures and over 30 Invited and Symposium Lectures in addition to

numerous short communications. Discussion of three IUPAC Working Party reports is also planned.

The registration fees of 5000 ptas for active delegates, 1500 ptas for ladies and 2000 ptas for students should be sent with the registration form by 30 May 1974 to Prof. J. G. Fatou, General Secretary, IUPAC International Symposium on Macromolecules, Juan de la Cierva 3, Madrid-6, Spain, from whom further details about accommodation etc. (Circular 3) are obtainable.

Some observations on the colloidal behaviour of block copolymers

Introduction

The formation of multimolecular micelles by block copolymers in the presence of a selectively bad solvent for one of the polymer components is well known¹. A micelle may be considered to consist of a compact swollen core of the insoluble polymer component, surrounded by a protective flexible fringe of the soluble polymer component which maintains the system in the colloidal state. Recently, we reported² a detailed study of micelle formation by a polystyrene-polyisoprene two-block copolymer [$\bar{M}_n(\text{total})=51\,000$, $\bar{M}_n(\text{polystyrene block})=13\,000$]. In n-decane at 25°C, the copolymer forms stable multimolecular micelles [$\bar{M}_w=1.7 \times 10^6$] which we believe are spherical in shape. On heating, the concentration of micelles falls and at 65°C the measured molecular weight corresponds to that expected for unassociated chains. The transition from a solution containing predominantly micelles to one in which the chains are molecularly dispersed occurs over a range of temperature (~20 degrees). One method of interpreting such results would be to introduce an equilibrium model similar to that first used by Jones and Berry³ to describe the properties of soap solutions.

The behaviour reported for the polystyrene-polyisoprene copolymer in n-decane is fairly typical of that for many block copolymers in selectively bad solvents. In a current study of micelle formation by block copolymers, however, we have observed quite a different type of behaviour. A preliminary account of the results is presented in this letter. The work is concerned with a polystyrene-polybutadiene-polystyrene three-block copolymer in ethyl acetate.

Experimental and Results

The polystyrene-polybutadiene-polystyrene copolymer, designated TR-41-1469, was kindly supplied by the Shell Chemical Company, together with relevant information concerning the method of synthesis and basic characterization data; the copolymer had been specially prepared for the purpose of research. The method of synthesis had involved sequential anionic polymerization in a hydrocarbon solvent. A small amount (about 0.3% vol of the total solution) of tetrahydrofuran had been added to the reaction mixture at the end of the butadiene polymerization in order to keep the molecular weight distribution of the final polystyrene block as narrow as possible. The average molecular weights of the three blocks were given as 13 600 (polystyrene), 69 800 (polybutadiene) and 14 500 (polystyrene), and the polybutadiene microstructure as 41% (*cis*-1,4-), 50% (*trans*-1,4-) and 9% (1,2-).

Light scattering measurements were made on dilute solutions of the copolymer in ethyl acetate using a Sofica instrument at a wavelength of 546 nm. Solutions

were clarified by filtration through Millipore filters (pore size 0.45×10^3 nm). Measurements were made at a series of concentrations and angles. For copolymers polydisperse in composition, light scattering^{4,5} gives an apparent molecular weight, \bar{M}_{app} , rather than a real weight-average molecular weight, \bar{M}_w . With the present copolymer system, however, the composition is sufficiently homogeneous to take $\bar{M}_w \approx \bar{M}_{\text{app}}$. The method used to evaluate the data for micellar solutions was similar to that discussed previously² and basically involved the double extrapolation of the quantity (Kc/R_θ) to zero angle and zero concentration as for homopolymers⁶.

At 25°C, the observed apparent average molecular weight of the copolymer particles in ethyl acetate was very high (1.2×10^7) but the apparent mean-square radius of gyration $\langle S_{\text{app}}^2 \rangle^{1/2}$ was only 35 nm. The results indicate the presence of multimolecular micelles at 25°C; they are probably spherical in shape and in view of the nature of the solvent contain a core consisting of polybutadiene blocks. On raising the temperature there was a slight decrease in the observed molecular weight for the first part of the range covered. Then on further heating a temperature was reached for each solution at which the dissymmetry ratio, $I_{45^\circ}/I_{135^\circ}$ (= reduced intensity at 45°/reduced intensity at 135°) underwent a very large increase. Visual observation in laboratory light showed that at the transition temperature the system changed from a clear solution (with the expected bluish cast) to one which was cloudy white. A typical plot of dissymmetry ratio *versus* temperature, for $c=0.160 \times 10^{-2}$ g/cm³, is shown in Figure 1. Figure 2 shows the dependence of the 'cloud point' on concentration.

On heating somewhat further all the solutions became clear again, and at 65°C the observed molecular weight ($\bar{M}_{\text{app}}=10.1 \times 10^4$) corresponded to that expected for

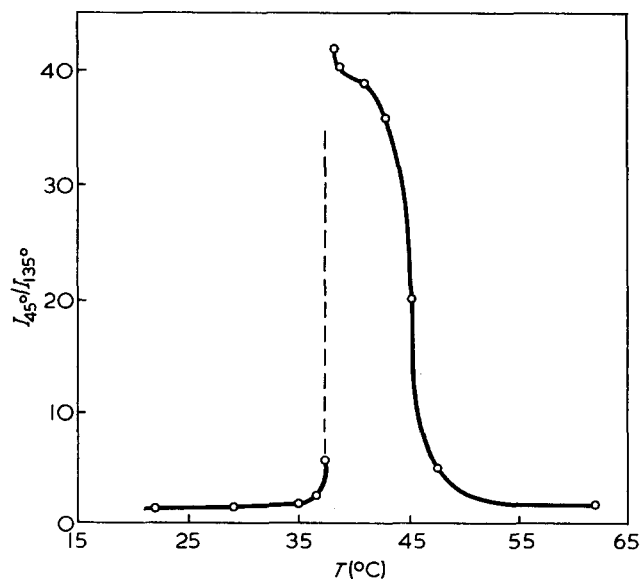


Figure 1 Plot of dissymmetry ratio *versus* temperature for copolymer TR-41-1469 in ethyl acetate ($c=0.160 \times 10^{-2}$ g/cm³)

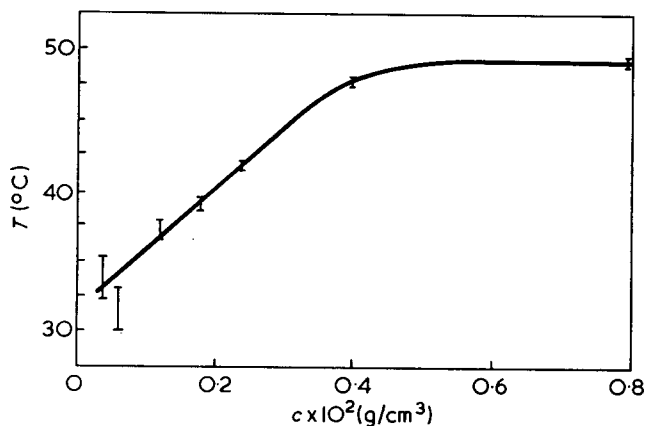


Figure 2 Dependence of 'cloud point' on concentration for copolymer TR-41-1469 in ethyl acetate

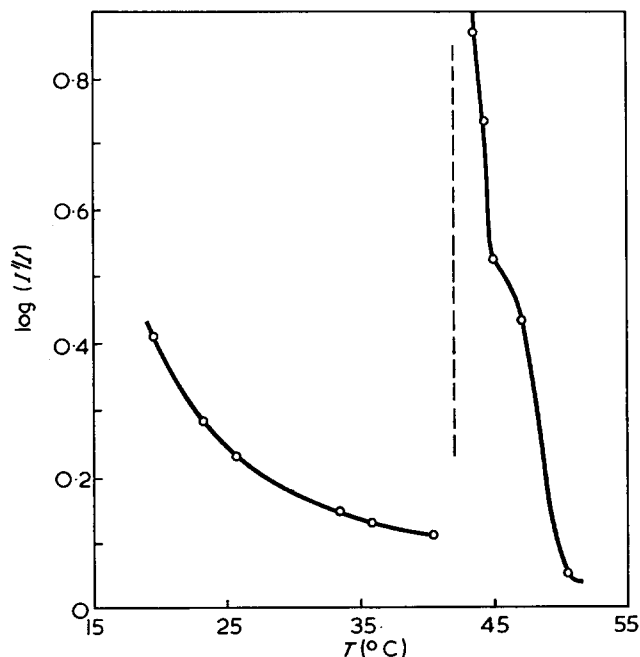


Figure 3 Plot of absorbance versus temperature for copolymer TR-41-1469 in ethyl acetate ($c=0.250 \times 10^{-2} \text{ g/cm}^3$)

the unassociated copolymer. This change from a cloudy solution to a clear solution occurred over a range of temperature, and was much more gradual than the onset of cloudiness which occurred at lower temperatures. The variation in the dissymmetry ratio is again shown in Figure 1; values are omitted from the middle portion of the range because they were too high to measure with our instrument. The solutions could be heated quite slowly through the cloudy region without precipitation. If the solutions, however, were allowed to stand for 24 h in parts of the cloudy region (e.g. at 44°C for $c=0.254 \times 10^{-2} \text{ g/cm}^3$) then precipitation of a gel phase occurred. This quickly entered the solution again either on heating or cooling. For a given concentration, precipitation only occurred over a narrow range of temperature.

In addition to measuring the intensity of light scattered, we have also made transmittance studies using a Perkin-Elmer 402 ultra-violet/visible spectrometer. A typical plot of $\log(I'/I)$ versus temperature is shown in Figure 3 ($c=0.250 \times 10^{-2} \text{ g/cm}^3$ and $\lambda=400 \text{ nm}$); I and I' are the transmitted intensities for the

solution and pure solvent respectively. The results are in accord with those obtained by light scattering.

All the changes we have reported are quite reversible; whether the temperature is being raised or lowered the lower transition is always sharp and the upper one gradual.

A limited number of measurements have been made on a polystyrene-polybutadiene-polystyrene copolymer having a similar structure and overall composition to copolymer TR-41-1469, but having a lower overall molecular weight (i.e. a copolymer in which all the block lengths are shorter). With this copolymer the 'cloud points' and related effects were all shifted to lower temperatures.

At this stage we do not wish to put forward a thermodynamic or molecular explanation of the observed changes. There are several interesting possibilities which we are currently investigating in our laboratory. We intend to report a complete account of the work at some later date.

Acknowledgements

We thank the SRC for the award of a studentship to T. P. L. and for support of our general programme of research on block copolymers. We thank the Shell Chemical Company for the supply of the copolymer sample, TR-41-1469.

T. P. Lally and C. Price

Department of Chemistry, University of Manchester,
Manchester M13 9PL, UK
(Received 21 January 1974)

References

- 1 Molau, G. E. in 'Block Polymers' (Ed. S. L. Aggarwal), Plenum Press, New York, 1970, p 79
- 2 Price, C., McAdam, J. D. G., Lally, T. P. and Woods, D. *Polymer* 1974, 15, 228
- 3 Jones, E. R. and Berry, C. R. *Phil. Mag.* 1927, 4, 841
- 4 Stockmayer, W. H., Moore, L. P., Fixman, M. and Epstein, B. N. *J. Polym. Sci.*, 1955, 16, 517
- 5 Bushuk, E. and Benoit, H. *Can. J. Chem.* 1958, 36, 1616
- 6 Zimm, B. H. *J. Chem. Phys.* 1948, 16, 1093, 1099

Variation of molecular weight averages during polycondensation

The variation of the different molecular weight averages throughout the course of a polycondensation reaction has been the subject of considerable study. For the important case of a linear polycondensation where the reacting species consistently conform to a 'most probable' distribution of molecular weights, the relevant equations are well known¹. The common molecular weight averages are then interrelated by equations such as:

$$\bar{M}_w/\bar{M}_n = (1 + p) \quad (1)$$

$$\bar{M}_z/\bar{M}_n = (1 + 4p + p^2)/(1 + p) \quad (2)$$

where the parameter p is in general defined by:

$$M_0/\bar{M}_n = (1 - p) \quad (3)$$

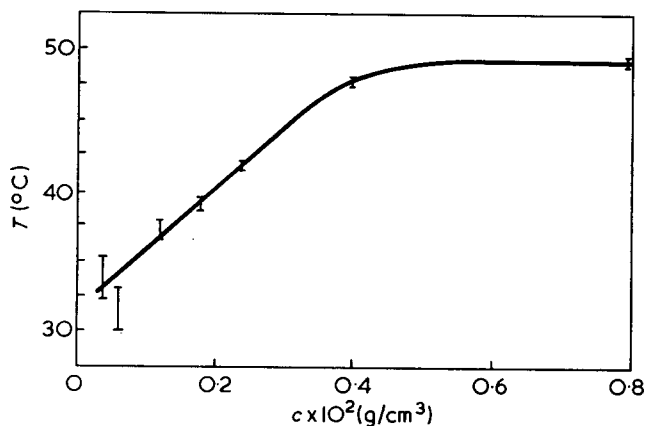


Figure 2 Dependence of 'cloud point' on concentration for copolymer TR-41-1469 in ethyl acetate

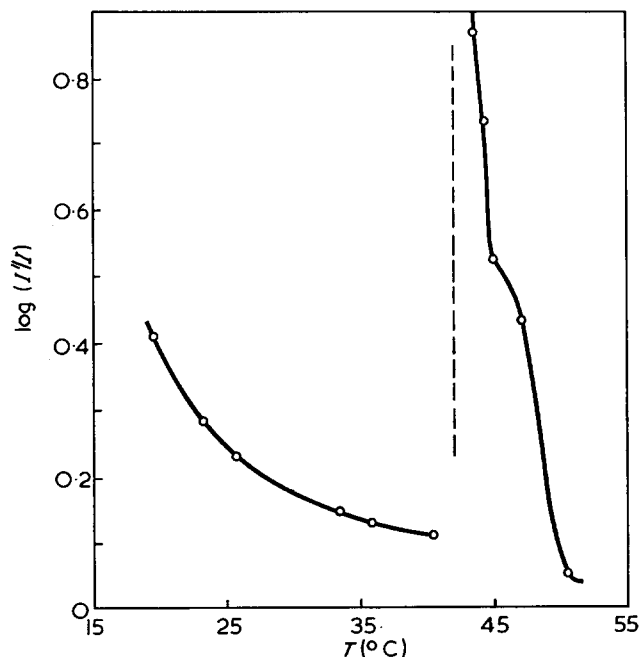


Figure 3 Plot of absorbance versus temperature for copolymer TR-41-1469 in ethyl acetate ($c=0.250 \times 10^{-2} \text{ g/cm}^3$)

the unassociated copolymer. This change from a cloudy solution to a clear solution occurred over a range of temperature, and was much more gradual than the onset of cloudiness which occurred at lower temperatures. The variation in the dissymmetry ratio is again shown in Figure 1; values are omitted from the middle portion of the range because they were too high to measure with our instrument. The solutions could be heated quite slowly through the cloudy region without precipitation. If the solutions, however, were allowed to stand for 24 h in parts of the cloudy region (e.g. at 44°C for $c=0.254 \times 10^{-2} \text{ g/cm}^3$) then precipitation of a gel phase occurred. This quickly entered the solution again either on heating or cooling. For a given concentration, precipitation only occurred over a narrow range of temperature.

In addition to measuring the intensity of light scattered, we have also made transmittance studies using a Perkin-Elmer 402 ultra-violet/visible spectrometer. A typical plot of $\log(I'/I)$ versus temperature is shown in Figure 3 ($c=0.250 \times 10^{-2} \text{ g/cm}^3$ and $\lambda=400 \text{ nm}$); I and I' are the transmitted intensities for the

solution and pure solvent respectively. The results are in accord with those obtained by light scattering.

All the changes we have reported are quite reversible; whether the temperature is being raised or lowered the lower transition is always sharp and the upper one gradual.

A limited number of measurements have been made on a polystyrene-polybutadiene-polystyrene copolymer having a similar structure and overall composition to copolymer TR-41-1469, but having a lower overall molecular weight (i.e. a copolymer in which all the block lengths are shorter). With this copolymer the 'cloud points' and related effects were all shifted to lower temperatures.

At this stage we do not wish to put forward a thermodynamic or molecular explanation of the observed changes. There are several interesting possibilities which we are currently investigating in our laboratory. We intend to report a complete account of the work at some later date.

Acknowledgements

We thank the SRC for the award of a studentship to T. P. L. and for support of our general programme of research on block copolymers. We thank the Shell Chemical Company for the supply of the copolymer sample, TR-41-1469.

T. P. Lally and C. Price

Department of Chemistry, University of Manchester,
Manchester M13 9PL, UK
(Received 21 January 1974)

References

- 1 Molau, G. E. in 'Block Polymers' (Ed. S. L. Aggarwal), Plenum Press, New York, 1970, p 79
- 2 Price, C., McAdam, J. D. G., Lally, T. P. and Woods, D. *Polymer* 1974, 15, 228
- 3 Jones, E. R. and Berry, C. R. *Phil. Mag.* 1927, 4, 841
- 4 Stockmayer, W. H., Moore, L. P., Fixman, M. and Epstein, B. N. *J. Polym. Sci.*, 1955, 16, 517
- 5 Bushuk, E. and Benoit, H. *Can. J. Chem.* 1958, 36, 1616
- 6 Zimm, B. H. *J. Chem. Phys.* 1948, 16, 1093, 1099

Variation of molecular weight averages during polycondensation

The variation of the different molecular weight averages throughout the course of a polycondensation reaction has been the subject of considerable study. For the important case of a linear polycondensation where the reacting species consistently conform to a 'most probable' distribution of molecular weights, the relevant equations are well known¹. The common molecular weight averages are then interrelated by equations such as:

$$\bar{M}_w/\bar{M}_n = (1 + p) \quad (1)$$

$$\bar{M}_z/\bar{M}_n = (1 + 4p + p^2)/(1 + p) \quad (2)$$

where the parameter p is in general defined by:

$$M_0/\bar{M}_n = (1 - p) \quad (3)$$

M_0 being the mean monomeric weight. In certain circumstances, p may be considered as the fractional extent of reaction of one of the functional groups.

It is not widely recognized, however, that there exist other relations, of comparable simplicity but greater generality, that offer a valid description of the progress of a linear polycondensation even where the initial and subsequent molecular weight distributions may not be of the most probable type. The straightforward arguments required for their derivation will be illustrated for the case of the weight-average.

Consider initially a polycondensate of Flory's type (i), that is, derived from a monomer A-B¹. The mole fraction of chains of molecular weight M_i present in this sample will be denoted n_i , where $i = 1, 2, \dots$. Let further intermolecular condensation occur, to give a small increase δp in the parameter p . It follows from equation (3) that as a result of this reaction the total number of molecules will be reduced by a fraction $\delta p/(1-p)$. If, then, δp is taken to be sufficiently small for the condensation to consist exclusively in the coupling of original chains, without subsequent reaction of the molecules so produced, the number fraction of the original molecules which have reacted must be given by:

$$f = 2\delta p/(1-p) = 2\delta\bar{M}_n/\bar{M}_n \quad (4)$$

where $\delta\bar{M}_n$ is the accompanying increase in \bar{M}_n .

According to the principle of equal reactivity, the probability that a molecule has been selected for reaction will not depend upon its chain length. It follows that the molecular weight distribution of the unreacted material will be identical to that of the initial sample. The parameter f , defined above as the *number* fraction of the original molecules to have reacted, therefore assumes additional significance. For it will also represent the number or weight fraction of the original chains of any particular molecular weight to have coupled and thence the *weight* fraction of the entire sample to have reacted. After the reaction, therefore, the polymer may be considered as a composite of two parts: a weight fraction $(1-f)$ with the initial molecular weight distribution, and a weight fraction f with a new distribution, that resulting from random coupling of the original molecules.

Consider now the combination of chains of molecular weight M_i and M_j , to give molecules of weight $(M_i + M_j)$. (Neglecting the mass of any condensation byproduct.) The products of this reaction will appear in the newly generated polymer as a mole fraction $2n_i n_j$, if the original chains were of different molecular weight ($i \neq j$), but only n_i^2 , if the combination was between identical species ($i = j$); for it is necessary to take into account the relative number of distinguishable configurations available to a pair of molecules undergoing either class of reaction. The selected method of calculation must embrace this distinction: however, rather than explicitly employ mole fractions in these differing forms, it is found more convenient to regard them as the elements of the double summation:

$$\sum_{i=1}^{\infty} \sum_{j=1}^{\infty} n_i n_j = 1 \quad (5)$$

in which all elements with $i \neq j$ are automatically subject to the required duplication.

Adopting this formalism, the weight-average molecular weight of the reacted polymer may be written as:

$$\bar{M}_w = \frac{\sum_{i=1}^{\infty} \sum_{j=1}^{\infty} n_i n_j (M_i + M_j)^2}{\sum_{i=1}^{\infty} \sum_{j=1}^{\infty} n_i n_j (M_i + M_j)} \quad (6)$$

or:

$$\bar{M}_w = \frac{\sum_{i=1}^{\infty} n_i \left(M^2 \sum_{j=1}^{\infty} n_j + 2M_i \sum_{j=1}^{\infty} n_j M_j + \sum_{j=1}^{\infty} n_j M_j^2 \right)}{\sum_{i=1}^{\infty} n_i \left(M_i \sum_{j=1}^{\infty} n_j + \sum_{j=1}^{\infty} n_j M_j \right)} \quad (7)$$

Equation (7) contains terms that correspond to the standard expressions for the molecular weight averages of the original sample, and appropriate substitution gives:

$$\bar{M}_w = \sum_{i=1}^{\infty} n_i (M^2 + 2M_i \bar{M}_n + \bar{M}_n \bar{M}_w) / \sum_{i=1}^{\infty} n_i (M_i + \bar{M}_n) \quad (8)$$

This in turn may be reduced to:

$$\bar{M}_w = (\bar{M}_w + \bar{M}_n) \quad (9)$$

The weight-average molecular weight for the entire sample is found by suitable combination of those for the randomly coupled weight fraction f , and the unchanged residue $(1-f)$. It is:

$$(1-f)\bar{M}_w + f\bar{M}_w$$

From this, the increase $\delta\bar{M}_w$ in \bar{M}_w which accompanies the increase δp in p is found to be:

$$\delta\bar{M}_w = f\bar{M}_n \quad (10)$$

Finally, combination of equations (10) and (4) gives the simple result:

$$\frac{d\bar{M}_w}{d\bar{M}_n} = 2 \quad (11)$$

in the limit $\delta p \rightarrow 0$.

This result is fully compatible with equation (1), from which it may be obtained directly, by differentiation. Unlike the earlier relation, however, equation (11) is derived without the assumption of a most probable distribution of molecular weights. Thus it is equally applicable to the polycondensation of genuinely monomeric reactants, and to the further polymerization of samples of higher molecular weight, but indeterminate distribution, obtained by some prior procedure. (It is supposed here that this further polymerization is not accompanied by bond-interchange reactions, to which no regard has been given in the foregoing discussion.)

For polycondensations of Flory's type (ii), that is, between monomers A-A and B-B, the derivation of equation (11) is complicated by the necessity to distinguish between chains bearing different combinations of end-groups: nonetheless, it is valid, at least to the extent that these various species may be considered to possess identical molecular weight distributions. Likewise, it may be applied to cases where A-A and B-B are themselves polymeric, provided that they exhibit closely coincident distributions. Indeed, even when this requirement is not met, it will still be possible to use equation (11) as a good approximation if the molecular weight of one component is negligible compared to that of the other: for example, the extreme case of chain extension by means of a monomeric bifunctional

linking agent will be accurately described by this relation.

The variation of the higher molecular weight averages may be examined similarly. The relations so obtained differ from that for the weight-average, however, in that they contain terms that depend upon the form of the molecular weight distribution. For the z -average, for instance:

$$\frac{d\bar{M}_z}{d\bar{M}_n} = 2 \left[3 - \left(\frac{\bar{M}_z}{\bar{M}_w} \right) \right] \quad (12)$$

which subsumes equation (2) for the special case of a most probable distribution.

The viscosity-average molecular weight, \bar{M}_v , is also frequently of interest. Unfortunately, the coefficient $d\bar{M}_v/d\bar{M}_n$ is not generally accessible by the method outlined above. The equation analogous to (6) has the numerator:

$$\sum_{i=1}^{\infty} \sum_{j=1}^{\infty} n_i n_j (M_i + M_j)^{1+a}$$

where a is the Mark-Houwink exponent. This double summation bears no clear relation to the common molecular weight averages, and cannot be evaluated without reference to a particular distribution. The simplest case, that of a monodisperse material, is of immediate interest; it may readily be shown that:

$$\frac{d\bar{M}_v}{d\bar{M}_n} = \frac{2(2^a - 1)}{a} = \beta \quad (13)$$

By other arguments, Schaeffgen and Flory² demonstrated that for a random polycondensation:

$$\left(\frac{\bar{M}_v}{\bar{M}_n} \right) = C\alpha \quad (14)$$

where α is the familiar function:

$$\alpha = [(1+a)\Gamma(1+a)]^{1/a} \quad (15)$$

and C is given by:

$$C = \frac{(1-p)}{-\log_e p} \left[\frac{(1-p)}{-\log_e p} \frac{21}{p} \right]^{1/a} \quad (16)$$

provided that p is not so low that certain underlying approximations become inapplicable. In the limit of high molecular weight, C approaches unity, and then the increase in \bar{M}_v is described by:

$$\frac{d\bar{M}_v}{d\bar{M}_n} = \alpha \quad (17)$$

For the values of the exponent a encountered in practice, α will be slightly greater than β . For example, at $a=0.5$, $\alpha=1.77$, $\beta=1.66$; both functions converge on 2 as $a \rightarrow 1$. It is evident that during the random polycondensation of a pure monomer, $d\bar{M}_v/d\bar{M}_n$ must progressively rise from the initial value β towards the

limiting value α . This transition may be examined quantitatively, by employing a computer to evaluate the required double summations for a series of model distributions of the most probable type. These calculations have shown that there is a roughly linear correspondence between the increase in $d\bar{M}_v/d\bar{M}_n$ and the growth of the ratio \bar{M}_w/\bar{M}_n . To a good approximation, therefore:

$$\frac{d\bar{M}_v}{d\bar{M}_n} = \alpha - \left[2 - \left(\frac{\bar{M}_w}{\bar{M}_n} \right) \right] (\alpha - \beta) \quad (18)$$

Departures from equation (18) never exceed 2% at $a=0.5$, and diminish further as a approaches unity. Moreover, the numerical similarity of α and β ensures that even equation (17) is an adequate approximation over most of the polymerization. Indeed, this simple equation gives results very close to those of equation (14), within the limitations imposed by the approximations inherent in the latter.

Analogy with equations (11) and (12) might suggest that the applicability of equation (18) extends beyond the case of a most probable distribution. This possibility has been investigated by computer calculations on a wide variety of molecular weight distributions. For distributions with $\bar{M}_w/\bar{M}_n < 2$, such calculations indicate that the approximate equation (18) enjoys a generality comparable to that of the preceding relations. In particular, it applies at least as well to distributions typical of narrow fractions, as to distributions of the most probable type. For cases with $\bar{M}_w/\bar{M}_n > 2$, however, the results of equation (18) are somewhat less reliable.

It is apparent that the empirical equations (17) and (18) are merely approximations to a more general function; which, however, reduces exactly to equation (11) for the special case of $a=1$. It would be of interest if the precise form of this general relationship could be established by other means.

Acknowledgement

Thanks are due to Dr C. Booth for many helpful discussions on this subject.

D. R. Cooper

Department of Chemistry,
University of Manchester,
Manchester M13 9PL, UK

(Received 2 January 1974; revised 7 March 1974)

References

- 1 Flory, P. J. 'Principles of Polymer Chemistry', Cornell University Press, Ithaca, 1953
- 2 Schaeffgen, J. R. and Flory, P. J. *J. Am. Chem. Soc.* 1948, **70**, 2709

Circular dichroism and magnetic circular dichroism of the haemin-poly(L-lysine) complex system

Seigo Yamamoto, Tsunenori Nozawa and Masahiro Hatano

*Chemical Research Institute of Non-Aqueous Solutions, Tohoku University, Sendai, Japan
(Received 20 June 1973; revised 2 January 1974)*

Circular dichroism (c.d.) and magnetic circular dichroism (m.c.d.) of the haemin-poly(L-lysine) (PLL) complex system in water were examined in the Soret and Q region with variation of pH. C.d. bands were induced in the Soret region and their magnitudes rose with increase in the helix content of PLL. M.c.d. also showed a nearly similar trend. At pH 10.7 where PLL has the α -helix conformation, one negative and one positive c.d. band centred at around 25.5 and $24.0 \times 10^3 \text{ cm}^{-1}$ respectively, were observed in the Soret region. The wavenumbers of these two c.d. bands nearly correspond with each of the m.c.d. bands in this region. At pH 8.7 where PLL has a random coil form, we could not detect any c.d. band in the Soret region. The m.c.d. spectrum was very small at pH 8.7 in comparison with that at pH 10.7. The m.c.d. in the Q region indicates that the haemin in its PLL complex exists in both a low spin and a high spin form at pH 10.7. From these experimental results, the m.c.d. character of the bound haemin as well as its electronic structure are discussed.

INTRODUCTION

Since haemin-poly(L-lysine) (PLL) complexes are considered as a model for haemichromes of biological origin, the haemin-PLL complexes have previously been investigated by measurements of absorption spectrum, optical rotatory dispersion and paramagnetic properties¹⁻⁵. Blauer and his collaborators prepared the PLL complex and investigated its nature extensively, on the basis of the absorption spectra and the paramagnetic properties¹⁻⁵. The Cotton effect of the haemin-PLL complex was observed and related to the helix structure of PLL by Stryer⁶. As a similar system, the poly(L-histidine)-haemin system was studied with circular dichroism (c.d.) by Beychok⁷.

Although the structure of the haemin-PLL complex has been partly clarified by Blauer *et al.*¹⁻³, the electronic states of bound haemin have not been fully discussed yet. Since magnetic circular dichroism (m.c.d.) has been found to be one of the most sensitive optical techniques for studying the electronic state⁸, we investigated the m.c.d. of the haemin-PLL with its c.d., and both its structure and electronic state are discussed.

EXPERIMENTAL

Materials

Poly(L-lysine.HBr) (PLL.HBr) was prepared by the conventional method⁹. An average degree of polymerization (*DP*) of this sample was 920. Ferrihaeme chloride (haemin) was obtained from Daiichi Pure Chemicals Co. Ltd.

Complex formation

The haemin-PLL complexes were prepared by Blauer's method³. The pH of the mixed solution was brought to the desired pH by addition of 0.1 N NaOH or 0.1 N HCl. The final lysyl residue concentration of PLL in the solution was 5.4×10^{-3} M, and that of haemin was 3.6×10^{-5} M. The lysyl residue to haemin molar ratio was kept at 150.

Measurements

The c.d. and m.c.d. measurements were carried out with a Jasco Model J-20A spectropolarimeter with or without a 12.5×10^3 G electric magnet. The intensity of c.d. and m.c.d. are expressed by the molar ellipticity $[\theta]$ or $[\theta]_M$ with the unit of degree cm^2/dmol or degree $\text{cm}^2/\text{dmol G}$ respectively. The haemin concentration is used for the calculation of $[\theta]$ or $[\theta]_M$ except for $[\theta]$ at $45.0 \times 10^3 \text{ cm}^{-1}$. The absorption spectra were measured with a Hitachi Model EPS-3T spectrometer. The pH measurements of the solutions were made with a Toa Denpa Kogyo Model HM-8 pH meter.

The titration vessel was continuously purged with nitrogen during the pH titration in order to exclude the effect of CO_2 . All measurements were taken at room temperature.

RESULTS AND DISCUSSION

C.d. spectra of the haemin-PLL complex

Figure 1 shows the c.d. spectra in the Soret region of the haemin-PLL complex in aqueous solution at

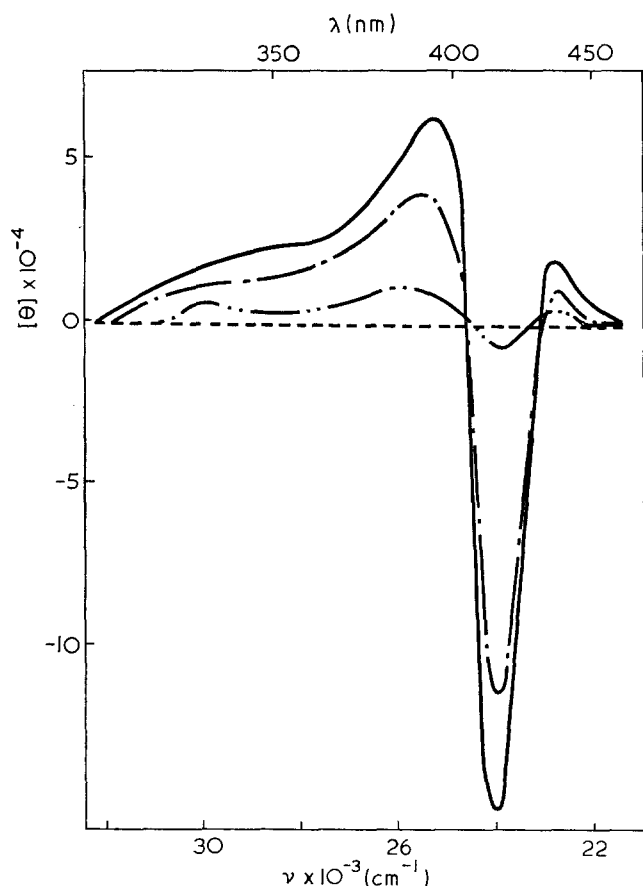


Figure 1 Soret c.d. spectra of haemin-PLL complex as a function of pH. The ratio of the lysyl residue concentration (R) to the molar concentration of haemin (H) is 150 and $H=3.6 \times 10^{-5}$ M. —, pH 10.7; ---, pH 9.9; - · - ·, pH 9.6; · · · ·, pH 8.7

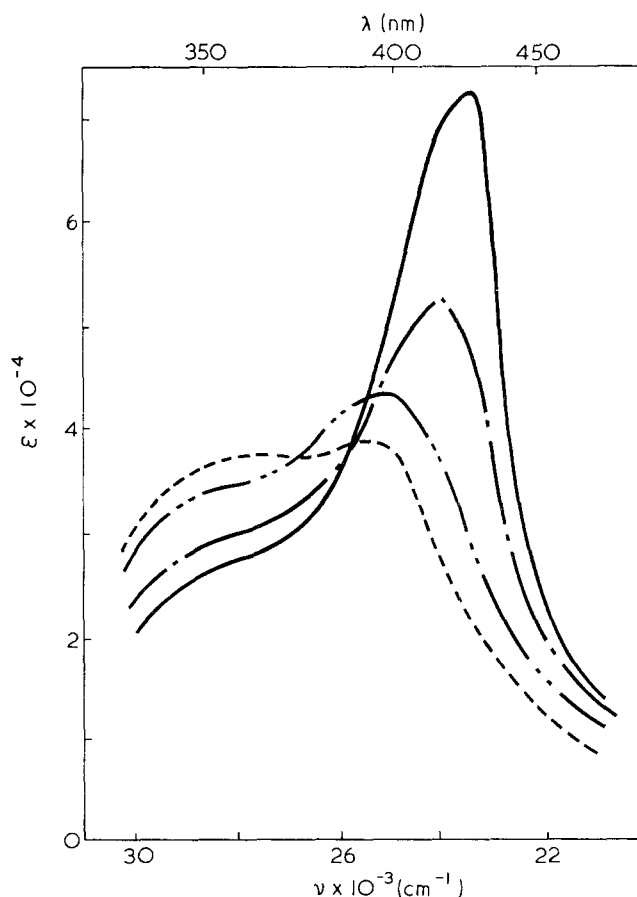


Figure 3 Soret absorption spectra of haemin-PLL complex as a function of pH. The molar extinction coefficient ϵ is calculated for the haemin molar concentration (H). ($R/H=150$; $H=3.6 \times 10^{-5}$ M.) —, pH 10.7; ---, pH 9.9; - · - ·, pH 9.6; · · · ·, pH 8.7

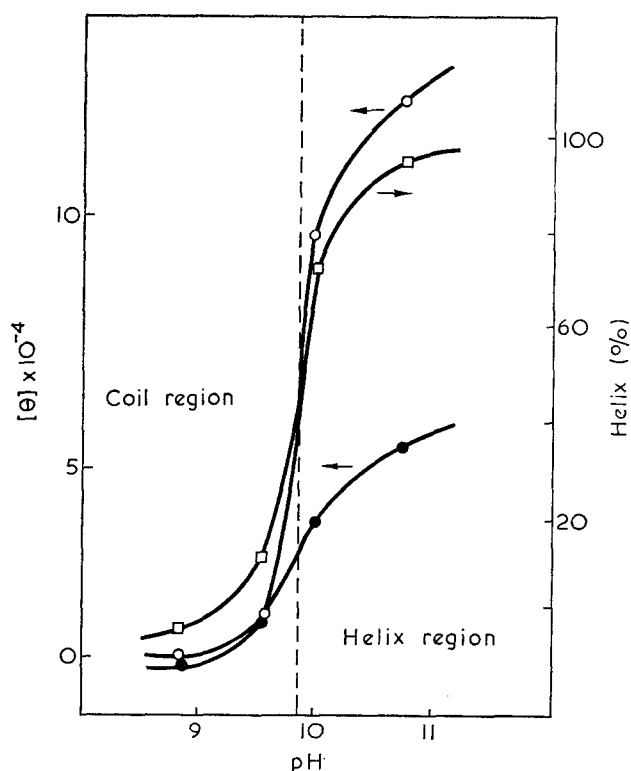


Figure 2 pH dependence of the magnitude of the induced c.d. bands at 25.5 and $24.0 \times 10^3 \text{ cm}^{-1}$ and % helix of haemin-PLL complex. Values of % helix are calculated with the assumption that $[\theta]$ at $45.0 \times 10^3 \text{ cm}^{-1}$ is $30\,000 \text{ degree cm}^2/\text{dmol}$ for 100% helix. ●, $[\theta]$ at $25.5 \times 10^3 \text{ cm}^{-1}$; ○, $[\theta]$ at $24.0 \times 10^3 \text{ cm}^{-1}$; □, the % helix

various pH values. At pH 10.7 there are two c.d. bands of opposite signs with the negative one at the lower wavenumber. The two c.d. bands centred at around 25.5 and $24.0 \times 10^3 \text{ cm}^{-1}$ become weak with decreasing pH value. At pH 8.7, the two c.d. bands were no longer detectable within experimental error. The magnitudes $[\theta]$ of the two c.d. bands varied with the pH value as shown in Figure 2. The solid and open circles represent the variation in the magnitudes of the induced c.d. bands at 25.5 and $24.0 \times 10^3 \text{ cm}^{-1}$ respectively. In this Figure, the open square represents the variation in the magnitude of the c.d. band at $45.0 \times 10^3 \text{ cm}^{-1}$ as a function of pH, which corresponds to the helix content of PLL in the system. The α -helix contents were calculated with the assumption that $[\theta]=30\,000$ for 100% helix⁹ and are shown in Figure 2. It should be mentioned that PLL in the haemin-PLL complex shows a helix-coil transition in the same pH range as that of PLL itself in aqueous solution⁹.

Figure 2 indicates that these two c.d. bands are induced only in the helix region of PLL. As is evident from the mechanism of helix-coil transition⁹, PLL in the complex should keep the helix form in the pH region where the amino groups in the side chains deprotonate and coordinate to the haemin iron. Therefore, the induced c.d. should have its origin in the fixation of the haemin in the close vicinity of the helical polypeptide by the ligation of the amino group to the haemin iron.

Absorption spectra of the haemin-PLL complex

Figure 3 shows the absorption spectra of the haemin-PLL complex at several pH values. The spectral feature is in accordance with that reported by Blauer *et al.*^{1,3}. The absorption spectra at pH 10.7 show a typical haemichrome spectra^{1,3}. The lack of isosbesticity in Figure 3, especially at pH 9.6 can be attributed to the presence of some intermediate complex species, one of which is probably the haemin with one amino ligand.

M.c.d. spectra of the haemin-PLL complex

Figure 4 shows the m.c.d. spectra in the Soret region of the haemin-PLL complex. The magnitude of the m.c.d. band at pH 10.7 increased by a factor of 10-20 in comparison with those at pH 8.7. Since some haemichromes with nitrogen bases, such as pyridine and imidazole, exhibit m.c.d. with similar shape and magnitude in the Soret region (Figure 5), the large magnitudes of the m.c.d. bands centred at 24 and $25 \times 10^3 \text{ cm}^{-1}$ are also indicative of the formation of a haemichrome as suggested by the absorption spectra.

In the Q band region the haemin-PLL exhibited some rather complex m.c.d. spectra both at pH 10.7 and at pH 8.7 (Figures 6 and 7); however, it can be interpreted by comparison with the following m.c.d. of the pyridine-haemin complex.

The pyridine-haemin complex showed a time variation in the m.c.d. (Figure 8). Curve (A) is the m.c.d. of the haemin in the absence of pyridine. In these conditions,

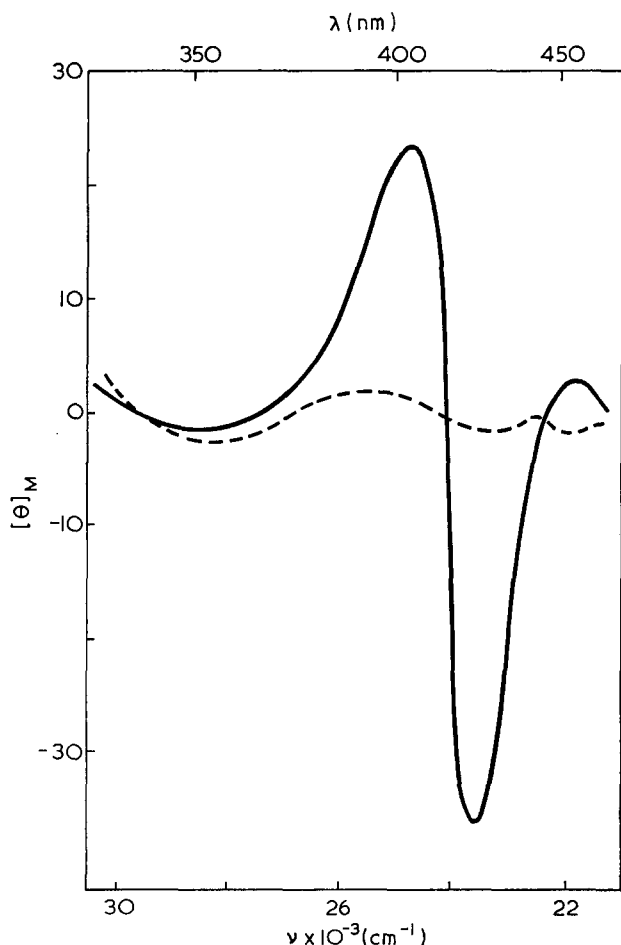


Figure 4 Soret m.c.d. spectra of haemin-PLL complex. (R/H=150; H=3.6 x 10⁻⁹ M.) —, pH 10.7; ---, pH 8.7

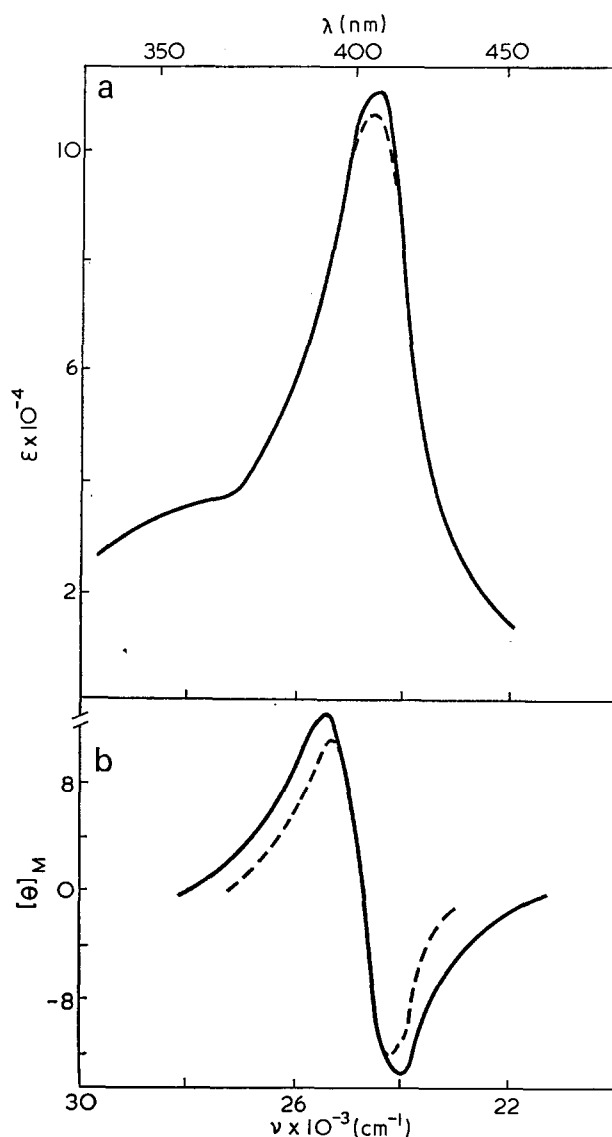


Figure 5 (a) Absorption and (b) magnetic circular dichroism spectra of haemin with imidazole (—) and pyridine (---) at pH 10.0 (H=1 x 10⁻⁴ M; [imidazole]=1 M; [pyridine]=1 M)

Blauer *et al.* reported that the haemin forms a high spin dimer⁴. Hence, curve (A) should be a m.c.d. for a high spin type haemin. The m.c.d. long enough after an addition of pyridine is the typical low spin type m.c.d. for haemichrome with two pyridines. Therefore the m.c.d. changes with time from (A) to (D) is considered to correspond to haemichrome formation from the hemin dimer.

From the fact that the m.c.d. for the haemin-PLL at pH 10.7 is similar to that for the haemin-pyridine complex (B), the m.c.d. in the Q region therefore suggests that the haemin-PLL complex at this pH has both high and low spin type haemins. Free haemin dimer and/or haemin with only one amino nitrogen may be the high spin type. The low spin type will correspond to the haemin bound to PLL with two amino nitrogens.

When we compare the m.c.d. for the free haemin (Figure 8) with that for the haemin complex with PLL at pH 8.7 (Figure 9) in the Q region, we find that they are similar to each other except in the high wavenumber region ($18-22 \times 10^3 \text{ cm}^{-1}$) where the charge transfer bands make a simple comparison difficult.

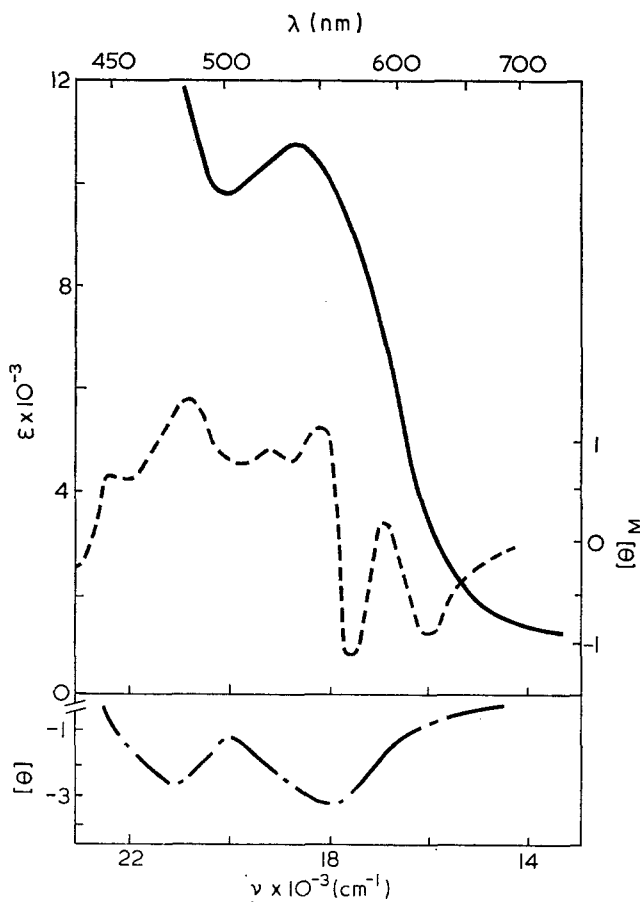


Figure 6 Absorption (—) and magnetic circular dichroism (---) and circular dichroism (---) spectra of haemin-PLL complex at pH 10.7. (R/H=150; H=3.6 × 10⁻⁵M)

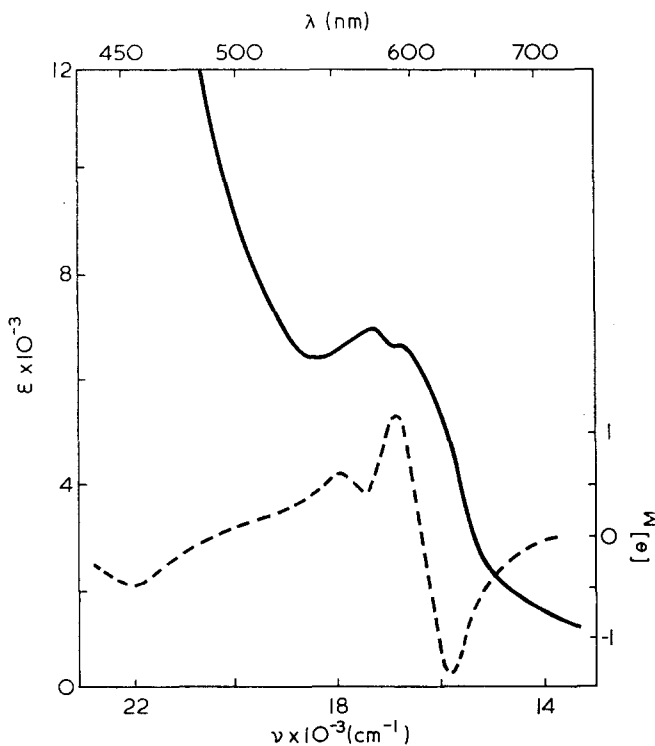


Figure 7 Absorption (—) and magnetic circular dichroism (---) spectra of haemin-PLL complex at pH 8.7. (R/H=150; H=3.6 × 10⁻⁵M)

The haemin in the presence of PLL forms the 'green complex' at pH 8.7^{1,3}. It has the effective magnetic moment μ_{eff} of 2.7 Bohr magneton (1 Bohr magneton = $9.273 \times 10^{-24} \text{ A m}^2$) which corresponds to a fairly low spin type haemin. Blauer and his coworkers attributed

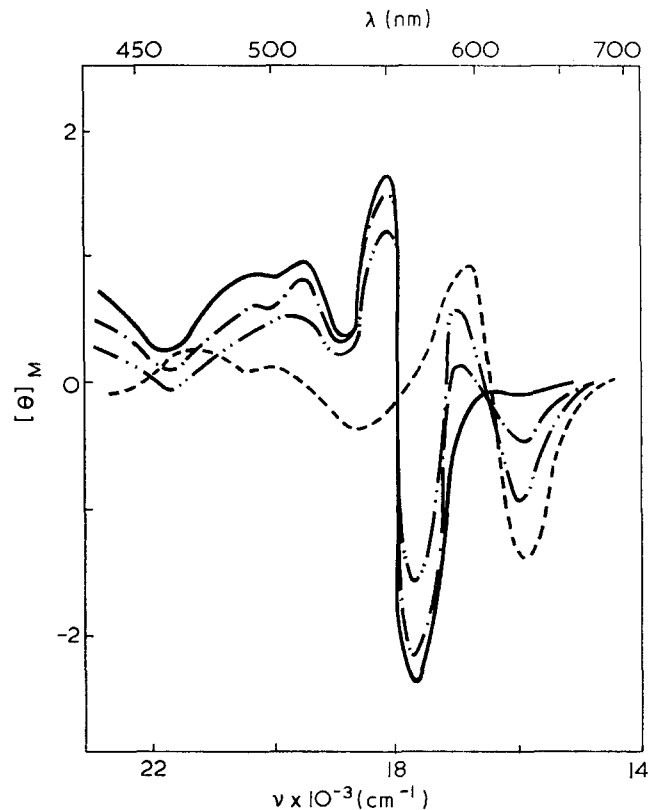


Figure 8 Time dependent magnetic circular dichroism spectra for haemin-pyridine system at pH 10. [Pyridine]/H=10³; H=1 × 10⁻⁴M. ---, Pyridine free (A); -.-., with pyridine at 3h after addition (B); ---, with pyridine at 6h after addition (C); —, with pyridine at 9h after addition (D)

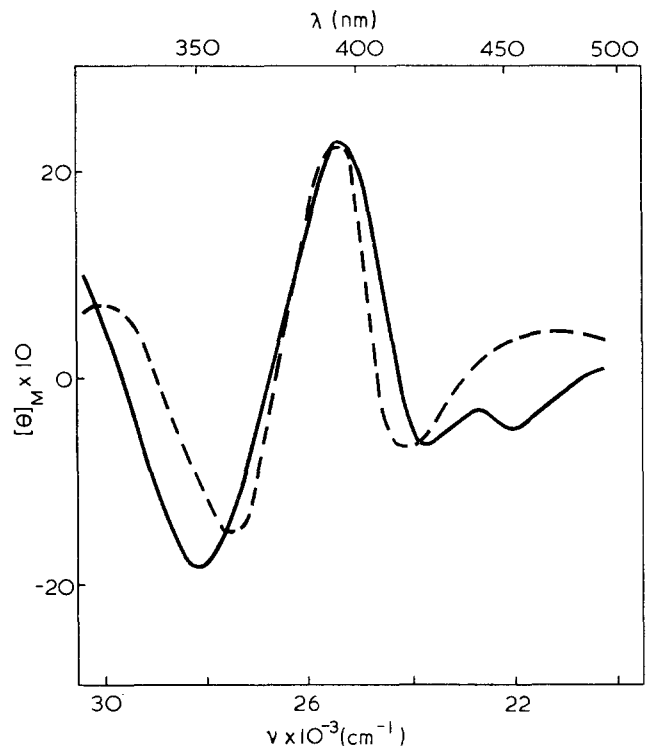


Figure 9 Magnetic circular dichroism of haemin-PLL complex and free haemin. —, Haemin-PLL (R/H=150; H=3.6 × 10⁻⁵M, pH 8.7); ---, haemin (H=1 × 10⁻⁴M, pH 10.0)

it to the formation of a micellar aggregate of the haemin itself. In the absence of PLL the haemin has μ_{eff} of high spin type (5.1–5.8 Bohr magneton).

In the Soret region the m.c.d. for the free haemin resembles fairly well that for the haemin-PLL at pH

8·7. This fact suggests that in spite of the low value of the magnetic susceptibility, the green complex has a very similar electronic state to that for the haemin without PLL (the high spin type). This means that the apparent low value of the magnetic moment for the green complex does not indicate a monomeric unit of a low spin haemin which show the very intense m.c.d. in the Soret region. Instead, it suggests that there exists some magnetic haeme-haeme interactions which make the μ_{eff} value as low as that for a low spin type haemin.

CONCLUSION

The direct relationship between the induced c.d. band magnitudes and the α -helix contents was shown for the haemin-PLL complex in an aqueous solution. The m.c.d. spectra for the haemin-PLL complex were

explained from the established nature of the haemin and its complexes, and were used to elucidate the structure and electronic state of the haemin-PLL complex.

REFERENCES

- 1 Blauer, G. *Nature* 1961, **189**, 396
- 2 Blauer, G. and Ehrenberg, A. *Acta Chem. Scand.* 1963, **17**, 8
- 3 Blauer, G. *Biochim. Biophys. Acta* 1964, **79**, 547
- 4 Blauer, G. and Ehrenberg, A. *ibid.* 1966, **122**, 496
- 5 Blauer, G. and Zvilichousky, B. *ibid.* 1970, **221**, 442
- 6 Stryer, L. *ibid.* 1261, **54**, 397
- 7 Beychok, S. 'Poly- α -amino acids', (Ed. G. D. Fasman), Marcel Dekker, New York, 1967, p 499
- 8 (a) Buckingham, A. D. and Stephens, P. J. *A. Rev. Phys. Chem.* 1966, **17**, 399
(b) Schatz, P. N. and McCaffery, A. J. *Q. Rev. Chem. Soc.* 1969, **23**, 552
- 9 Hatano, M. and Yoneyama, M. *J. Am. Chem. Soc.* 1970, **92**, 1392

Studies on the thermal degradation of phosphorus containing polymers: 7. Thermal degradation of phosphorylated poly(vinyl alcohol)

Norihiro Inagaki, Kiyoshi Tomiha and Kakuji Katsuura

Department of Industrial Chemistry, Faculty of Engineering, Shizuoka University, Hamamatsu 432, Japan
(Received 8 October 1973; revised 5 November 1973)

The thermal degradation of phosphorylated poly(vinyl alcohol) was investigated using thermogravimetric analysis, infra-red spectroscopy and gas chromatography. The introduction of phosphoric acid groups changed the course of the thermal degradation of the polymer. The dehydration was accelerated and the scission of the polymer chain was inhibited. The *cis*- β -elimination mechanism of the phosphorus ester group was proposed for the accelerated dehydration.

INTRODUCTION

During the study of the thermal degradation of cellulose phosphate, it was found that the phosphorus ester group changed the course of the thermal degradation process and that the efficiency of inflammability depended on the chemical structure of the phosphorus ester group¹⁻³.

Phosphorylated poly(vinyl alcohol) (PVA) has ion exchange properties⁴. Studies on phosphorylated PVA have been devoted to the subject of its preparation⁵⁻⁹ and ion exchange properties⁴. Few reports have been made on the thermal degradation of phosphorylated PVA¹⁰.

In order to confirm the relationship between fundamental flammability characteristics of phosphorus containing polymer and its thermal degradation, the thermal degradation of phosphorylated PVA was investigated. The effect of the phosphorus ester group on the thermal degradation of PVA is also discussed.

EXPERIMENTAL

Material

Completely hydrolysed PVA (acetyl content was less than 0.1 mol %) was used. The molecular weight of the polymer was found to be 61.6×10^3 by viscosity measurements.

Four phosphorylated PVA (P-PVA) samples were prepared according to a previous method⁹ having a different phosphorus content in the range of 1.00–13.51 wt % (Table I).

Thermogravimetry and differential thermal analysis (d.t.a.)

A Shinku-Riko DGC-3 Thermogravimetric Analyser and a Shinku-Riko 1500 Differential Thermal Analyser were used. Samples were ground to a fine powder (80

mesh), and pyrolysed at various heating rates between 0.65 and 4.5°C/min in vacuum (10^{-3} mmHg). The apparent activation energy of the degradation was estimated by Ozawa's method¹¹.

Analysis of degradation product

A sample (1 g) was placed in a Pyrex tube connected to a liquid nitrogen trap and then was pyrolysed at a prescribed temperature for 1 h in vacuum. The residue in the Pyrex tube and condensates in the trap were obtained as decomposition products.

The infra-red spectrum of the residue was examined as a KBr disc using a Nihon-Bunko Spectrophotometer model IR-S.

When the liquid nitrogen was removed, the condensates separated into two layers; a water layer and an oil layer. These two fractions were analysed separately by gas chromatography. A separation column (4 mm i.d. \times 4 m) containing 25 wt % of Carbowax 4000 coated on C-22 (30–60 mesh) was used. The column temperature was 100°C and the flow rate of carrier gas (He) was maintained at 50 ml/min. The degradation products were identified by comparison with the retention data of known substances.

RESULTS AND DISCUSSION

Thermogravimetry

The thermogravimetric analysis (t.g.a.) curves in Figure 1 show that weight loss begins at a lower temperature in P-PVC than in PVA. There was a thermally pseudo-stable stage within the temperature range 250–350°C, which was not observed in the case of PVA. P-PVA yielded a greater amount of residue than PVA. With an increase in phosphorus content, the threshold temperature for pyrolysis decreased and the amount

of the residue increased. Laszkiewicz¹⁰ found a similar effect when phosphorus acid groups were introduced to side chains of PVA. He suggested that the phosphorus acid groups in PVA acted as an initiator for the dehydration and as an inhibitor for the degradation of the polymer. However, the initiation or inhibition mechanism has not yet been discussed.

In order to confirm the effect of phosphoric acid groups on the thermal degradation of PVA, the values of the apparent activation energy were estimated. These values are summarized in Table 1.

Recently, Kabilov *et al.*¹² have reported that the thermal reactions of PVA were dehydration and unsaturated chain-scission for which activation energies were 37 ± 2 and 46 ± 2 kcal/mol, respectively. In this experiment, it was found that the thermal degradation of PVA proceeded in three stages for which the activation energies were 35.9, 43.5 and 73.5 kcal/mol. The d.t.a. curve also indicates the three stage degradation processes (Figure 2); the peaks are an endotherm at 235°C (melting), an exotherm at 310°C, an endotherm at 340°C and an exotherm at 415°C. However, the basic reason for this difference could not be ascertained.

When phosphoric acid groups were introduced to side chains of PVA, there was a marked change in activation energy, namely the value for both the first stage and the second stage reactions decreased and the value for the third stage reaction increased. These values for the respective stages were independent of phosphorus content.

From the detailed discussion on t.g.a. curves, it appears that the introduction of phosphoric acid groups changed the course of the thermal degradation of PVA.

Infra-red spectrum of residue

The infra-red (i.r.) spectra of PVA and P-PVA degraded at various temperatures, are shown in Figures 3

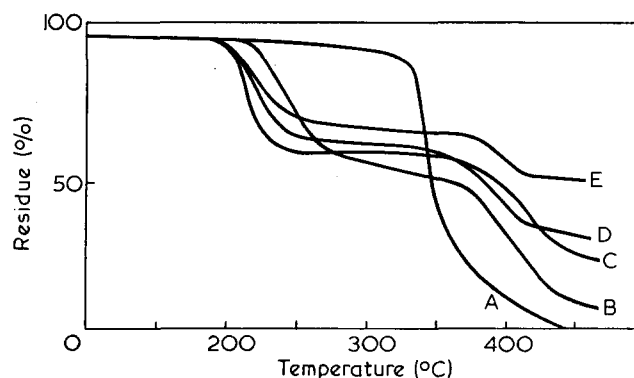


Figure 1 T.g.a. curves for PVA and P-PVA. A, PVA; B, P-PVA 1; C, P-PVA 2; D, P-PVA 3; E, P-PVA 4

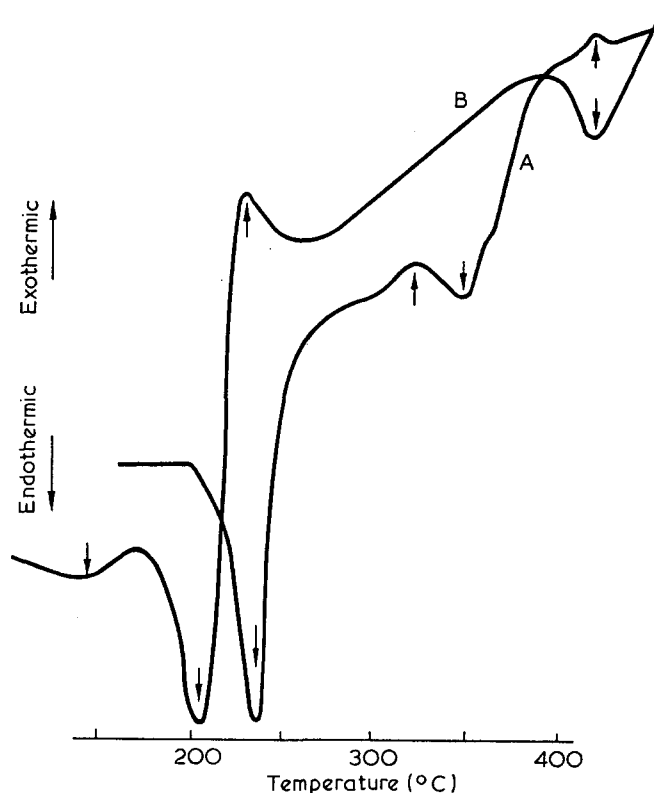


Figure 2 D.t.a. curves for PVA and P-PVA. A, PVA; B, P-PVA 2

and 4, respectively. The change in the i.r. spectrum of PVA on heating was identical with the results given by others^{13, 14}; in the first stage degradation, the band at 1620 cm^{-1} , attributed to the C=C group, was observed and the intensity of the absorption of OH and CH_2 groups decreased. In the third stage, the band at 1600 cm^{-1} , attributed to the conjugated C=C group, appeared and the absorption bands of OH and CH_2 groups became less intense.

After phosphorylation, four absorption bands at 1700 , 1400 , 1200 and 1000 cm^{-1} attributed to C=O, NH_4^+ , P=O and P-O-C groups respectively, appeared and the crystalline band at 1146 cm^{-1} disappeared. This appearance of the absorption band at 1700 cm^{-1} indicates that chain-scission (equation 1) or oxidation (equation 2) took place during phosphorylation.

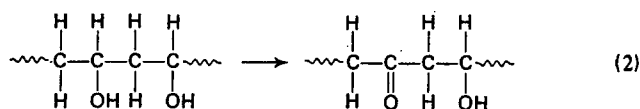
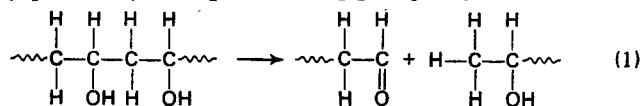


Table 1 Thermogravimetry of phosphorylated poly(vinyl alcohol)

Sample No.	Preparation* reaction time (min)	Phosphorus content (%)	Threshold temperature (°C)	Residue (%)	Activation energy (kcal/mol)		
					1st stage	2nd stage	3rd stage
PVA		0	230	1.5	35.9	43.5	73.5
P-PVA 1	5	1.00	180	12.8	25.0	30.0	82.4
P-PVA 2	20	4.27	140	28.6	18.0	30.4	88.5
P-PVA 3	60	7.61	130	34.6	18.0	28.9	84.9
P-PVA 4	100	13.51	126	56.2	18.9	29.8	86.9

* Reaction conditions: PVA, 22g; phosphoric acid, 24.5g; urea, 60g; trimethylamine, 125ml; dimethyl formamide, 375ml; reaction temperature=150°C

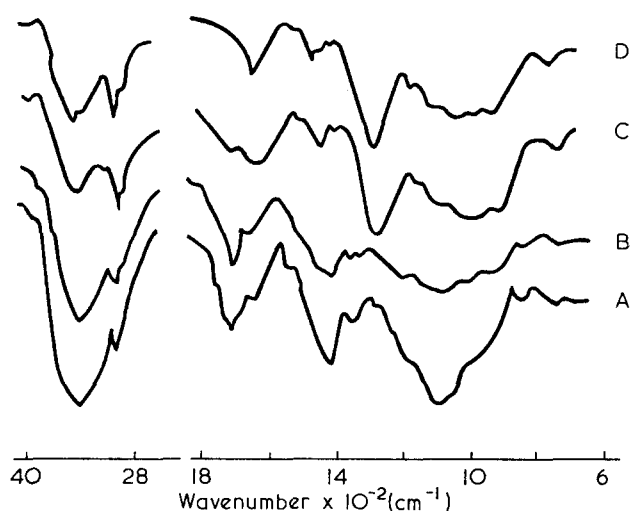


Figure 3 I.r. spectra for PVA residue. A, Original; B, degraded until the first stage reaction; C, degraded until the second stage reaction; D, degraded until the third stage reaction

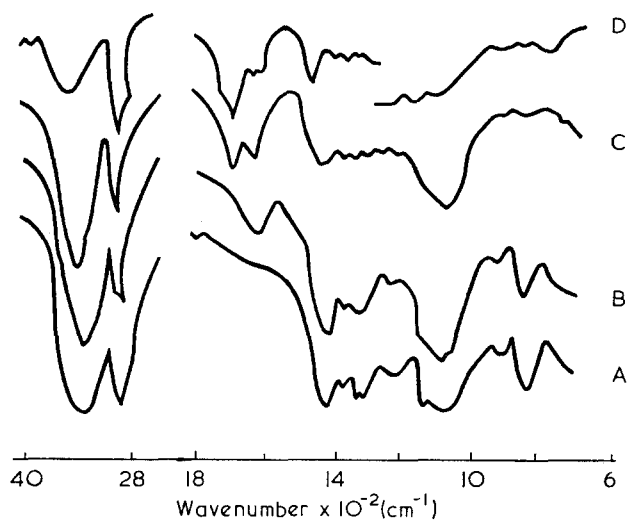
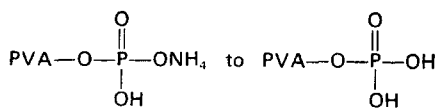


Figure 4 I.r. spectra for P-PVA residue. A, Original; B, degraded until the first stage reaction; C, degraded until the second stage reaction; D, degraded until the third stage reaction

The changes in the i.r. spectrum of P-PVA on heating were as follows; in the first stage reaction, the OH band at 3350 cm^{-1} became weak in absorbance and a new band at 1620 cm^{-1} ($\text{C}=\text{C}$) was observed. In the second stage, the band at 1400 cm^{-1} (NH_4^+) disappeared and the absorption band at 3350 cm^{-1} (OH) and 1700 cm^{-1} ($\text{C}=\text{O}$) became less intense. The $\text{P}=\text{O}$ band at 1200 cm^{-1} shifted to 1250 cm^{-1} at the same time. This fact indicates that the chemical structure of the phosphoryl group in PVA changes from



A similar change of the phosphoryl group has been reported during the degradation of cellulose phosphate¹ and phosphonate².

Further the new band at 740 cm^{-1} attributed to *cis* $\text{C}=\text{C}$ group appeared. In the third stage, there was no

change in the i.r. spectrum except for the disappearance of the carbonyl band at 1700 cm^{-1} .

These results suggest that the major thermal reaction of P-PVA is similar to that of PVA except that the formation of the double bond group occurs at a lower temperature (by 100°C) and that the formation of the carbonyl group is small.

Analysis of volatile products

The analysis of the i.r. spectrum of the residue could not satisfactorily reveal the effect of the phosphoric acid group on the thermal reaction of PVA; hence the volatile products were analysed. The quantitative data determined by peak areas on the gas chromatogram are represented in Table 2.

Studies on the major decomposition products of PVA have been made^{13, 15, 16} and agree with the results reported here.

However, on pyrolysis of P-PVA, a small amount of an oil layer fraction containing aldehydes was formed. Thus the major volatile product was water and the formation of crotonaldehyde and acetaldehyde, which were major products from PVA, was small. This fact indicates that the dehydration is accelerated and the scission of the polymer chain is inhibited. The lack of the formation of carbonyl groups in the residue of P-PVA gives strong support to this assumption.

Assumption of accelerated dehydration mechanism

In view of pyrolysis of organophosphorus esters¹⁷⁻¹⁹ which give a quantitative amount of olefin and phosphoric acid, the reaction mechanism for the accelerated dehydration was proposed to be as follows.

(1) The *cis*- β -elimination of the phosphorus ester group occurs:

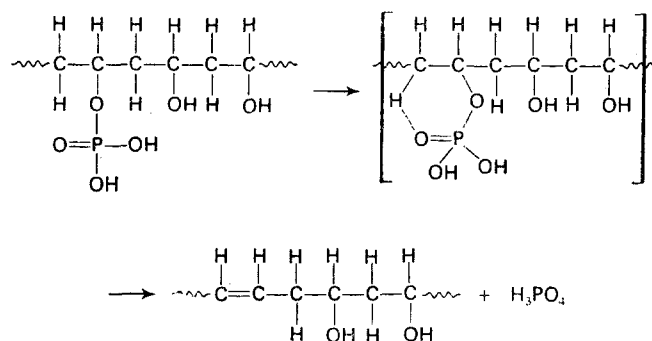
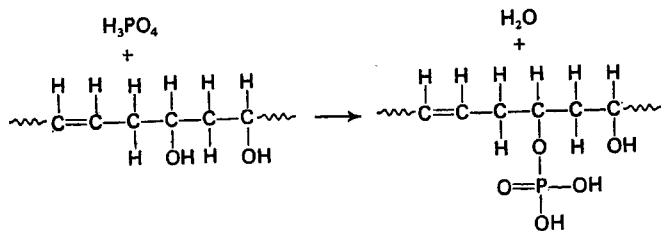


Table 2 Composition (%) of volatile products of PVA and P-PVA

Compound	PVA (1g)		P-PVA (1g)	
	Oil layer (240 mg)	Water layer (400 mg)	Oil layer (30 mg)	Water layer (150 mg)
Methyl crotonate	1.5	trace	49.6	3.9
Acetaldehyde	25.6	37.1	2.0	0.2
Formaldehyde	5.6	6.3	0.1	
Ethyl acetate	0.9			
Ethanol	1.7	10.5		
Benzene	0.4			
Water	0.8	46.1	48.3	95.9
Crotonaldehyde	58.6			
Unknown	5.0			

(2) Esterification of the removed phosphoric acid with hydroxyl group in PVA:



REFERENCES

- 1 Inagaki, N. and Katsuura, K. *Kogyo Kagaku Zasshi* 1971, **74**, 982
- 2 Inagaki, N., Kawarabayashi, S. and Katsuura, K. *Kogyo Kagaku Zasshi* 1971, **74**, 1411
- 3 Inagaki, N. and Katsuura, K. *Kogyo Kagaku Zasshi* 1971, **59**, 1899
- 4 Egawa, H. and Motori, Y. *Kogyo Kagaku Zasshi* 1956, **59**, 479
- 5 Katsuura, K. and Yamame, T. *Sen-i Gakkaishi* 1968, **24**, 378
- 6 Carraher, C. E. and Torre, L. *J. Polym. Sci. (A-1)* 1971, **9**, 975
- 7 Laszkiewicz, B. *J. Macromol. Sci. (A)* 1971, **5**, 421
- 8 Nifant'ev, E. E., Fedorov, S. G. and Fursenko, I. V. *Chem. Abstr.* 1972, **77**, 115189a
- 9 Katsuura, K., Inagaki, N. and Sakurai, S. *Nippon Kagaku Kaishi* 1972, **1972**, 1305
- 10 Laszkiewicz, B. *J. Appl. Polym. Sci.* 1971, **15**, 437
- 11 Ozawa, T. *Bull. Chem. Soc. Japan* 1965, **38**, 1881
- 12 Kabilov, Z. A., Mavlyanov, A. M. and Muiov, T. M. *Chem. Abstr.* 1972, **77**, 62474f
- 13 Yamaguchi, K. and Amagasa, M. *Kobunshi Kagaku*, 1961, **18**, 645
- 14 Marupov, R., Kalontorov, I. Ya. and Konovalova, G. I. *Chem. Abstr.* 1968, **69**, 19878p
- 15 Nima, H., Tanaka, H. and Ainnai, Z. *Kobunshi Kagaku* 1957, **14**, 528
- 16 Tsuchiya, Y. and Sumi, K. *J. Polym. Sci. (A-1)* 1969, **7**, 3151
- 17 Higgins, C. E. and Baldwin, W. H. *J. Org. Chem.* 1965, **30**, 3173
- 18 Canavan, A. E., Dowden, B. F. and Eaborn, C. *J. Chem. Soc.* 1962, p 331
- 19 Baumgarten, H. E. and Setterquist, R. A. *J. Am. Chem. Soc.* 1957, **79**, 2605

Poly(squaryl amides)

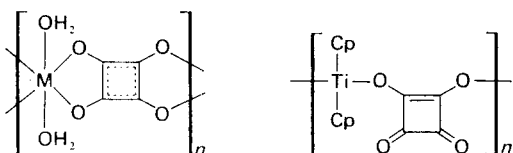
Eberhard W. Neuse and Brian R. Green

Department of Chemistry, University of the Witwatersrand, Johannesburg, South Africa
(Received 20 August 1973)

The solution polycondensation of squaric acid with *p*-phenylenediamine in selected protic, aprotic or strongly acidic solvents furnishes linear polyamide structures possessing units with 1,2- as well as those with 1,3-orientation of the substituent links on the four-membered ring system. The relative occurrence of these two unit types as assessed by infra-red spectroscopy depends on the basicity of the medium, the extent of 1,2-orientation decreasing with increasing solvent basicity. The same type of polyamide results from a solution polycondensation of the diamine with diethyl squarate. These findings, contradicting earlier results of other workers, are in accord with more recent non-polymeric squaric acid amidation studies. A reference polyamide with maximum content of units possessing the 1,2-substituent orientation is synthesized from *p*-phenylenediamine and squaryl dichloride under low temperature solution polymerization conditions. Polymer inherent viscosities range from about 10 to 30 ml/g, highest values being obtained under conditions of homogeneous polymerization.

INTRODUCTION

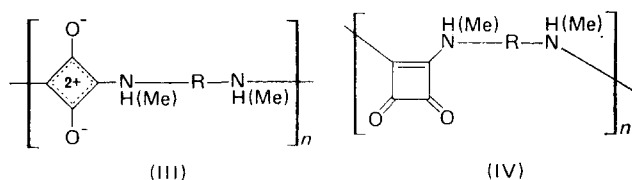
The four-membered ring system of squaric acid (1,2-dihydroxycyclobutene-3,4-dione) has only recently become of interest as a constituent segment in macromolecular compounds. West and Niu¹, for example, prepared divalent metal complexes of squaric acid, for which they proposed the polymeric structure (I), and Doyle and Tobias² obtained a compound believed to be II from titanocene diperchlorate and squarate ion.



(I) (M = Mg²⁺, Mn²⁺ etc.) (II) (Cp = π -cyclopentadienyl)

The first polyamides derived from squaric acid were described by Gauger and Manecke^{3,4}. Condensing squaric acid with difunctional amines, these workers achieved polymerization by use of solution or melt techniques and, on the basis of infra-red (i.r.) spectroscopic evidence, ascribed structures (III) to the resulting polymeric products. In the same study, the diethyl ester of squaric acid (1,2-diethoxycyclobutene-3,4-dione), when allowed to react with difunctional amines in boiling *N,N*-dimethylformamide (DMF) solution, gave polyamides assigned structure (IV). Since the earlier literature covering squaric acid chemistry commonly accepted that reaction of squaryl esters with (primary or secondary) amines would lead only to 1,2-diamides (1,2-diaminocyclobutene-3,4-diones)³⁻⁹, whereas the analogous amidation of the free acid would give exclusively the 1,3-disubstituted isomers (1,3-diaminocyclobutenediylum 2,4-diolates)^{3,4,10-14}, the cited polyamide study^{3,4} did not, at the time of publication, present unexpected results with regard to the substituent orientation of the

four-membered ring. More recently, however, it was demonstrated that the concept of sole 1,2-orientation of the substituents in amidation reactions of squaryl esters, and of exclusive 1,3-orientation in corresponding amidations of squaric acid itself, can no longer be supported. Hünig and Pütter¹⁵, for example, observed 1,3-diamide formation from squaryl esters and certain weakly basic amines, and extensive work in our laboratory has shown¹⁶ that even the more strongly basic aniline reacts with squaryl esters to give not exclusively the 1,2-dianilino-cyclobutenedione, as previously reported, but rather an isomer mixture composed of both the 1,2- and 1,3-dianilino derivatives, albeit with the former as the predominant species. Likewise, and again in contrast to earlier work, reaction of the free acid with aniline yields mixtures of both isomers, the 1,3-diamide generally representing the prevalent product in this reaction¹⁷.



(R = 1,4-phenylene, 4,4'-biphenylene, oligomethylene)

In the light of these recent developments in the non-polymeric chemistry of squaric acid, the assignments of structure (III) to the polyamides formed under the Gauger-Manecke conditions^{3,4} from squaric acid, and of IV to those formed from squaryl esters, must be viewed as oversimplifications. One would rather predict copolymer structures in either case comprising in the backbone the units of both III and IV in variable proportions. In order to clarify this question of substituent orientation, we have re-investigated the polyamidation

molecular weights resulted from use of the PPA medium, which not only acts as an excellent condensing agent, but offers the additional advantage of solvating the products by virtue of its phosphorylating action on the secondary amino groups, so as to prevent inhomogeneity of the reaction mixture and premature precipitation of the growing polyamide chains. Experiment 5, although not necessarily optimized, furnished the highest molecular weight. The preceding experiment, employing lower reactant concentration, gave a lower viscosity value despite longer heating periods and, ultimately, a higher temperature. A further increase of reactant concentration beyond that employed in experiment 5, on the other hand, failed to produce higher polymer viscosities in spite of additional heating periods at further elevated temperatures (experiment 6). The relatively low viscosity values attained even in PPA despite homogeneous polymerization conditions are likely to be due to an imbalance in reactant stoichiometry caused by side reactions with the medium. Self-condensation of certain amines in PPA at higher temperatures has been observed in Marvel's laboratory*²¹; in the present case, a related reaction could account for a reduced amino group concentration in the PPA solution. Blocking of amino groups might also result from salt formation with PPA. The propensity of PPA for undergoing formation of stable salts with strongly basic diamines even at elevated temperatures is well known^{22, 23}. For such salt formation, however, to have an effective bearing on the availability of amine reactants for polycondensation, equilibrium polymerization conditions would be a prerequisite, as only these would allow a fraction of the stoichiometric quantity of amine to be rendered unavail-

* These authors employed aromatic bis-*o*-diamines, and polycondensation (with loss of ammonia) accordingly led to phenazine heterocycles. Although in the present case the energetic driving force of ring formation is not given, the first step of Marvel's reaction, formation of a -NH- bridge, is feasible, as 'blank' reactions involving *p*-phenylenediamine have shown.

able for polymerization; practical irreversibility of the polycondensation, on the other hand, should result in complete consumption of all amino groups (originally present in proper stoichiometry) by continuous removal from the amine-PPA equilibrium. In addition to imbalances due to an amino group deficiency, the possibility of side reactions of the medium with the squaric acid component, either through (reversible) formation of mixed anhydrides or through (irreversible) ring-opening steps, cannot be discounted. These questions all require further investigation.

The i.r. spectra of the polyamides exhibit the typical cyclobutenediylum diolate absorption^{12, 18, 24, 25} in the vicinity of 1600 cm⁻¹, partly merging with a strong band due to a phenylene ring deformation mode near 1550 cm⁻¹, and in addition show in weak to moderate intensity the two carbonyl stretching bands near 1785 and 1675 cm⁻¹ characteristic of the cyclobutene-3,4-dione system²⁶. This indicates that the polymers comprise not merely the units of V possessing 1,3-orientation of the substituents on the four-membered ring, but also the units of VII containing the 1,2-disubstituted cyclobutenedione system. Hence, the copolymer structure VI indeed holds for all polymers including the products obtained under the experimental conditions of the earlier investigation^{3, 4} (experiment 1), for which exclusive 1,3-orientation according to structure V had been assumed.* That the observed two cyclobutenedione carbonyl stretching bands truly reflect an intrinsic content of units A and not just the presence of low molecular weight impurities, intermediary adduct structures³, or squaric acid end groups of the cyclobutene-3,4-dione type, was ascertained by further rigorous washing

* Very weak i.r. carbonyl absorption at 1700-1800 cm⁻¹ was observed by the quoted authors³ in polymers obtained by self condensation of *p*-aminoanilinosquaric acid in boiling glycerol. This was explained as an end-group effect, although the possibility of statistical incorporation of 1,2-type units was indicated by the authors.

Table 1 Polycondensations of certain 1,2-disubstituted cyclobutenediones with *p*-phenylenediamine

Exp. No.	Substrate ^a	Solvent ^b	Substrate conc. (mol/l)	Time (h)	Temperature (°C)	Polymer yield (%)	Inherent viscosity ^c (ml/g)	Analysis (found) (%) ^d		
								C	H	N
1e	squaric acid	glycerol	0.25	0.17	278	91.5	15.8	62.77	3.81	13.92
2	squaric acid	glycerol/Py (2:1 by vol)	0.16	3/0.5f	140/200	98.8	11.9	63.05	3.63	14.18
3	squaric acid	NMP (+5% LiCl)	0.09	4	186	61.3g	9.7			
4	squaric acid	PPA	0.17	20/2.5	160/220h	92.5	17.1	62.90	4.01	13.55
5	squaric acid	PPA	0.67	15	165h	96.8	29.1	61.18	3.58	13.83
6	squaric acid	PPA	1.00i	16/16/8	105/130/150i	96.0	22.0			
7	squaric acid	PPA/TFA (9:1 by vol)	0.67	1.5/16	105/165	98.2	29.5	62.61	4.10	13.91
8j	diethyl squarate	DMF	0.06	2.5	146	57.8	7.7	61.84	4.30	14.29
9	squaryl dichloride	NMP(+2.5% LiCl)/Py(18:1 by vol)	0.32	1.0/1.0/0.25	0/23/40	97.7	29.3k	62.29	3.55	12.76

a Substrate and diamine conc. equimolar throughout

b Py=pyridine; NMP=*N*-methylpyrrolidone; PPA=polyphosphoric acid; TFA=trifluoroacetic acid, DMF=*N,N*-dimethylformamide

c 0.5% (w/v) at 30°C in 98% H₂SO₄; determined on reprecipitated samples (similar results on crude polymers)

d Mean values of duplicate determinations on reprecipitated samples. Calcd for (C₁₀H₈N₂O₂)_n: C, 64.51%; H, 3.25%; N, 15.05%

e Experimental conditions essentially as described in ref 3, except that 40 min were required for partial solvent removal by distillation

f After 3h at reflux (140°C), 17% of solvent distilled off, and heating continued for 0.5h at reflux (200°C). See Experimental for these and subsequent time-temperature data

g Yield of first fraction precipitating during reaction. Additional 36.8% of second fraction precipitated with water (η_{inh} 7.3 ml/g)

h 0.25h heat-up period from 25°C to 160°C and 165°C respectively

i 6h heat-up period from 25° to 105°C. Following completion of 150°C treatment, mixture was diluted with PPA to substrate conc. of 0.67 mol/l and heating continued for 16h at 165°C

k Experimental conditions from ref 3

Interfacial polycondensation in CHCl₃/H₂O-pyridine (0.7M substrate) gave 46% yield of polyamide with η_{inh} 7.1 ml/g

of the polymers with hot pyridine and DMF, by additional heat treatments (12h at 130°C *in vacuo* or 1h in refluxing glycerol), and by a post-condensation with excess *p*-phenylenediamine either in glycerol (2.5h at 278°C) or in PPA (6h at 160°C); in no instance were we able to observe a significant decrease in intensity, let alone complete disappearance, of the two carbonyl bands.

In order to arrive at a more quantitative measure of the contents of units A with 1,2-substituent orientation in the polyamides studied, we determined the ratio of the absorbance of the *asym* carbonyl stretching peak (preferred over the *sym* band because of the latter's partial overlap with the broad cyclobutenediylum diolate absorption band) to that of the out-of-plane phenyl-ring C-H deformation band near 825 cm⁻¹ (Table 2). In an effort to derive from these data an absolute unit-A content, an attempt was made to correlate the values so obtained with the corresponding ratios determined for such 1,2-disubstituted cyclobutenedione model compounds as 1,2-bis(*p*-methoxyanilino)cyclobutene-3,4-dione, 1,2-bis[*p*-(diethylamino)anilino]cyclobutene-3,4-dione, and 1-anilino-2-[*p*-(diethylamino)anilino]cyclobutene-3,4-dione. However, for reasons of excessive scattering of the A_{1785}/A_{825} values determined for the model compounds, these attempts failed to produce consistent results. We therefore restricted our efforts towards calculating the fraction of units A in the backbone relative to a reference polyamide prepared from squaryl dichloride and *p*-phenylenediamine by low temperature solution polymerization (experiment 9) considered to be predominantly of the type VII (see below). The fractions obtained on this basis are listed in the fifth column of Table 2.

Notwithstanding the considerable uncertainty with which the tabulated values are afflicted, a distinct increase is noticed in the unit A contents on going from experiment 3 to experiment 1 and further to

Table 2 Infra-red spectral data of polyamides VIa

Polymer from exp.	$\nu_{C=O}(asym)$ (cm ⁻¹)	$\nu_{C=O}(sym)^b$ (cm ⁻¹)	Absorbance ratio ^c A_{1785}/A_{825}	Fraction of units A in backbone ^d
1	1781	1675 ^e	0.43 ^f	0.20
2	1780	1675 ^e	0.15	0.07
3	1782	1670 ^e	0.26	0.12
4	1785	1675	1.00	0.47
5	1785	1674	1.05	0.49
6	1785	1667	1.65	0.77
7	1787	1672	1.75	0.82
8	1780	1666	0.48	0.22
9	1787	1670	2.14	1.00

a Spectra taken on KBr pellets. Error limits: $\nu_{C=O}(asym) \pm 2$ cm⁻¹; $\nu_{C=O}(sym) \pm 3$ cm⁻¹

b Broad shoulder on high-frequency side of superposed C=C stretching, phenyl ring deformation and cyclobutenediylum diolate absorption in 1550–1650 cm⁻¹ range. Additional, indistinct shoulder in all spectra at 1682–1689 cm⁻¹

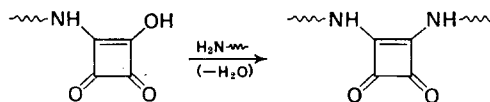
c Absorbance, $A = \log(I_0/I)$, determined by baseline method^{30, 31} as average of three measurements

d Value from preceding column divided by 2.14 (absorbance ratio for polymer of experiment 9); estimated uncertainty ± 0.05 (< 0.45); ± 0.08 (> 0.50)

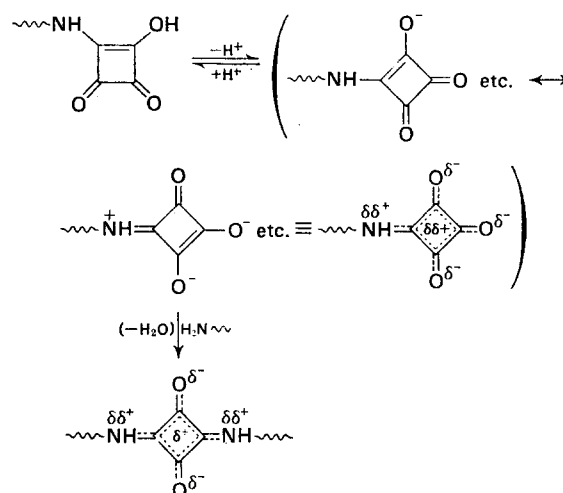
e Almost completely merged with 1550–1650 cm⁻¹ absorption

f A ratio of 0.37 was found for a polyamide obtained as in experiment 1 except that after addition of another 10 mol% *p*-phenylenediamine refluxing was continued for 2.5h

experiments 4–6, conducted in *N*-methylpyrrolidone, glycerol and PPA, respectively. This trend accords with recent unpublished findings in our laboratory indicating that basic reaction media in squaric acid amidations are conducive to 1,3-orientation of the amino substituents on the four-membered ring. In an essentially neutral medium, squaric acid, either *per se* or as an end group on a growing chain, will be present in both the undissociated and the dissociated states. While vinylogous substitution on the undissociated acid species will produce 1,2-diamides (H₂N— = *p*-phenylenediamine or NH₂-terminated chain):



the squarate anion resulting from ionization will preferentially be attacked by the nucleophile at C₃, yielding the 1,3-diamide isomers:



Hence, both substituent orientations will occur, the latter generally prevailing on account of the high degree of ionization experienced by the strongly acidic substrate*. This case is represented by experiment 1. The prevalence of 1,3-orientation will be enhanced even more in a basic medium, which shifts the ionization equilibrium of the acid substrate farther to the right and so causes an increase in squarate ion concentration. Experiment 3 exemplifies this situation. An acidic solvent, on the other hand, in which the substrate's ionization is repressed, will produce the undissociated species in increased concentration, thus enhancing 1,2-orientation. The PPA used in experiments 4–6 is representative of such a medium.

In order to test this trend further, an experiment was conducted in a PPA/trifluoroacetic acid medium (experiment 7). The enhanced acidity of this solvent system, as expected, entailed a population of 1,2-oriented units in the polymer more than four times as large as found in the product of experiment 1. The increased absorbance ratio A_{1785}/A_{825} (Table 2) reflects this situation. Conversely, a polycondensation run performed substantially as in experiment 1 except that pyridine was added for increased substrate ionization (experiment 2), furnished a polyamide for which the significantly reduced $\nu_{C=O}$

* For squaric acid, an early report²⁷ quoted 1 and 2.2 for the pK_a values of the first and second ionization steps; later authors²⁸ found 1.5 and 2.93 respectively. For phenylsquaric acid, 1-hydroxy-2-phenylcyclobutene-3,4-dione, pK_a was determined²⁹ as 0.37 ± 0.04 .

intensities suggest a structure with the proportion of units A decreased to almost one-third of that in the polyamide of experiment 1. The extremely small residual carbonyl band intensities in this polymer show clearly, however, that even under the conditions of enhanced ionization the polymer structure merely approaches, but cannot strictly be ascribed to, the idealized structure V exhibiting a purely 1,3-oriented substituent pattern.

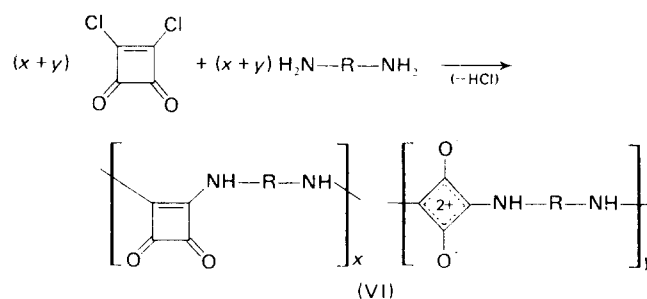
Polycondensation of *p*-phenylenediamine with diethyl squarate

The condensation of the diamine with diethyl squarate in refluxing DMF (experiment 8), carried out precisely under the experimental conditions described by the previous authors³, furnished a low molecular weight polyamide identical in appearance, solubility and elemental composition with the polymers derived from the free acid. The i.r. spectrum reveals a copolymer structure (VI) comprising both 1,2- and 1,3-type substituent orientation (Scheme 1), which, in contrast to the earlier assumption^{3,4} of exclusive composition according to VII, is in agreement with the more recently established findings^{15,16} in squaryl ester amidation chemistry. The moderate content of units A in the chain (Table 2) in fact suggests a backbone structure not substantially different from that of the polyamide formed from the free acid in glycerol (experiment 1).

Polycondensation of *p*-phenylenediamine with squaryl dichloride

The two reactants, *p*-phenylenediamine and squaryl dichloride (1,2-dichlorocyclobutene-3,4-dione), were allowed to condense in equimolar quantities under both interfacial and low temperature solution polymerization conditions. Best results with respect to high molecular weights were obtained in a solution polymerization run that was conducted in *N*-methylpyrrolidone solvent (containing 2.5% lithium chloride) in the presence of pyridine as a hydrogen chloride acceptor (experiment 9). Under the same conditions, the non-polymeric model reaction of squaryl dichloride with 2 mol aniline gives 75% of the 1,2-diamide, yet little more than 2% of the 1,3-isomer (unpublished results), the Schotten-Baumann conditions in this reaction allowing for extremely rapid vinyllogous substitution at C₂. It appears reasonable to conclude from the results of the model reaction that the conditions of experiment 9 accordingly lead to the nearly exclusive formation of units A in the polymer and so result in a polyamide structure closely approaching, albeit not entirely matching, the pure 1,2-substituent pattern of VII. Although the high absorbance ratio A_{1785}/A_{825} (2:14; see Table 2) would seem to bear out this inference, confirmation must await an absolute determination of the unit-A content with the aid of an independent technique*. All that can, at this stage, be derived from the spectroscopic evidence is a justification

for use of this polyamide as a reference compound of structure VI with the maximum x/y ratio experimentally attainable (Scheme 2).



Scheme 2 (R = 1,4-phenylene)

The polymer, on account of its high percentage of units with 1,2-substituent orientation, exhibits considerably better solubility characteristics than those shown by polyamides with higher unit-B contents; it dissolves, for example, in the *N*-methylpyrrolidone/LiCl system, which is a virtual non-solvent for the polymers of experiments 1-8. This behaviour is in accord with the solubility properties of non-polymeric 1,2- and 1,3-diamides of squaric acid, the more polar, mesoionic 1,3-derivatives generally showing poorer solubility in organic solvents than do the 1,2-isomers.

We are currently investigating the effect of the ratio x/y in the various types of VI on the X-ray photoelectron and electronic absorption spectra in an attempt to establish differences, if any, in the net charges on the N atoms and, hence, in the extent of electronic delocalization expected along the polymer chains.

EXPERIMENTAL*

Glassware was over-dried (flamed in experiment 9) and flushed with dried nitrogen after assembly. All solvents were degassed at 90-100°C by means of a nitrogen stream, and the amide solvents were pre-dried by refluxing over calcium hydride (DMF for experiment 8 by passing through Linde molecular sieves, type 4A), followed by distillation under reduced pressure and collection under nitrogen. Trifluoroacetic acid and polyphosphoric acid (82% P₂O₅), both reagent grade, were used as received. All reactions were conducted under moisture protection; LiCl and reagents were pre-dried over P₂O₅ *in vacuo*. Squaric acid (Chemische Werke Hüls AG) was used as received. *p*-Phenylenediamine, commercial grade, was sublimed at 90°C at 0.05 mmHg (m.p. 140-141°C).

Diethylsquarate (1,2-diethoxycyclobutene-3,4-dione)^{7,16} and *squaryl dichloride* (1,2-dichlorocyclobutene-3,4-dione)³² were prepared by literature methods.

1,2-Bis(p-methoxyanilino)cyclobutene-3,4-dione was synthesized from squaric acid (0.8 M) and *p*-anisidine

* Measurement of the C 1s or N 1s binding energies by photoelectron spectroscopy would seem to suggest itself as a potential analytical approach to this problem. Preliminary results indicate, however, that the charge densities on the two types of nitrogen in cases A and B are not sufficiently different to allow reasonable band separation with currently available instrument resolving power.

* Melting points, uncorrected, taken in sealed capillaries. Viscosities determined with Cannon-Fenske viscometers (kinetic energy corrections neglected). I.r. spectra (KBr pellets) taken on Perkin-Elmer Model 521 spectrometer; absorbance, $A = \log(I_0/I)$, determined by the baseline method^{30,31} (I_0 = intensity of incident beam, I = intensity of transmitted beam). Elemental analyses by Mr P. Jwili of this Department (samples removed from Abderhalden drying apparatus immediately prior to weighing).

(1.6 M) in refluxing (2 h) DMF containing 10 M aqueous hydrochloric acid (15:1 by vol) and was separated by fractional crystallization of the reaction product from DMF by a previously described technique¹⁶; the compound, constituting the more soluble isomer, was collected in 35% yield [greyish-white needles, m.p. 322–323°C with decomp. (from DMF)] in addition to the less soluble 1,3-isomer [20%, bright yellow (from dimethylsulphoxide), infusible below 330°C]. In a similar fashion, 1,2-bis[*p*-(diethylamino)anilino]cyclobutene-3,4-dione was prepared in 12% yield from diethyl squarate (0.4 M) and *p*-amino-*N,N*-diethylaniline (0.8 M) in dry DMF (2.2 h at reflux); the compound forms bright-yellow needles, m.p. 270–273°C with decomp. (from methanol). The less soluble, orange 1,3-isomer (12%; infusible below 330°C) could not be recrystallized because of decomposition in most solvents at the high dissolution temperatures required. For preparation of 1-anilino-2-[*p*-(diethylamino)anilino]cyclobutene-3,4-dione the equimolar mixture (0.25 M each) of 1-anilino-2-hydroxycyclobutene-3,4-dione¹³ and *p*-amino-*N,N*-diethylaniline (HCl salt) was heated (2 h at reflux) in DMF containing 10 M aqueous hydrochloric acid (20:1 by vol). Fractional crystallization from DMF¹⁶ produced the pale-yellow compound in 28% yield [m.p. 251–253°C with decomp. (from DMF/ethylene glycol)] in addition to the yellow, less soluble 1,3-isomer (17%, decomp. ~320°C). All three 1,2-substituted model compounds described gave satisfactory elemental analyses and exhibited $\nu_{C=O}$ (*asym*) at 1785–1792 and $\nu_{C=O}$ (*sym*) at 1655–1670 cm⁻¹.

Polycondensation of *p*-phenylenediamine with squaric acid

In glycerol (experiments 1 and 2). In experiment 1, 1.14 g (10.0 mmol) of squaric acid and 1.08 g (10.0 mmol) of *p*-phenylenediamine were allowed to react in 40 ml of refluxing glycerol. Reaction and work-up conditions were those of the earlier work^{3, 4}, except that 40 (instead of 10) min were required for the prescribed removal of 10 ml of the solvent by distillation at atmospheric pressure*. The yield of dried polyamide was 1.70 g (91.5%). The dark brown polymer, infusible below 350°C, was readily soluble in 98% sulphuric acid and fluoro-sulphonic acid, slightly so in formic acid, and practically insoluble in *N*-methylpyrrolidone (containing 5% LiCl), DMF, *m*-cresol, acetonitrile and other aprotic solvents.

A 0.25 g sample was dissolved in 50 ml of 98% H₂SO₄, and the filtered solution was dropwise stirred into 200 ml of ice water. The precipitated polymer was washed thoroughly with water, 0.5 M NaHCO₃ solution, 0.1 M aqueous hydrochloric acid and, again, water and was dried for four days at 100°C and 0.1 mmHg (yield 0.21 g). This precipitated product had the appearance and solubility properties shown by the crude polymer*, and

no significant changes in i.r. spectrum and elemental analyses were apparent.

In experiment 2, 0.57 g (5.0 mmol) of squaric acid and 0.54 g (5.0 mmol) of *p*-phenylenediamine were allowed to react for 3 h in a refluxing solvent mixture consisting of 20 ml of glycerol and 10 ml of pyridine (solvent temperature 140°C) under a blanket of nitrogen and light protection. The mixture gradually turned dark red in colour, and product precipitated from solution. Following the removal of 5 ml of solvent (containing some of the water of condensation) by distillation over a period of 10 min, refluxing of the reaction mixture (solvent temperature 200°C) was continued for another 0.5 h. Work-up as described³ gave 0.91 g (98.8%) of polyamide. Reprecipitation as in the preceding experiment produced polymer identical in appearance and solubility characteristics with the previous product. Use of methanol as the precipitant did not change properties or analytical results.

In *N*-methylpyrrolidone (experiment 3). The combined solutions of 0.50 g (4.45 mmol) of squaric acid in 25 ml of methylpyrrolidone (containing 1.25 g of LiCl) and of 0.48 g (4.45 mmol) of *p*-phenylenediamine in 25 ml of the same solvent were maintained for 4 h at reflux under N₂ and light protection. The solution, initially yellow, turned dark red, and a major portion of product precipitated as the condensation proceeded. The polymer fraction filtered off from the cooled mixture was thoroughly washed with methylpyrrolidone, water and methanol and was dried for 4 days at 100°C and 0.1 mmHg, to give 0.50 g (61.3%) of polyamide identical in appearance and solubility behaviour with the products obtained in glycerol.

A second polymer fraction was collected from the mother liquor by precipitation with 150 ml of water. The dark brown polymer, separated, washed and dried as above (0.30 g, 36.8%), retained partial solubility in methylpyrrolidone/LiCl.

For analytical purposes, a sample of the first fraction was reprecipitated as before.

In polyphosphoric acid (experiments 4–7). All condensations in PPA medium were performed by heating, under N₂ and light protection, the stirred solution of reactants in PPA (experiments 4–6) or PPA/trifluoroacetic acid (9:1 by vol; experiment 7) under the conditions of concentration, time, and temperature listed in Table 1. (Temperatures given are those of the heating bath in these experiments.) For example, in experiment 6 a 16 h heating period at 105°C (6 h required to raise temperature from 25° to 105°C) was followed by 16 h at 130°C and 8 h at 150°C, the substrate concentration being 1.0 M; after dilution of the viscous solution to 0.62 M (substrate) with additional PPA, stirring was continued for another 16 h at 165°C, at which point the solution nearly gelled. The homogeneous, dark reddish-brown solution in each experiment was poured slowly, with rapid stirring, into the five-fold volume of ice water. The precipitated product was separated by filtration, washed with water, 0.5 M NaHCO₃ solution,

* This point deserves emphasis because such extended heating, while not affecting the *x/y* ratio in the polymer, could possibly result in some molecular weight increase. The inherent viscosity measured on this polyamide (Table 1) thus probably represents an upper limit, being higher than would have been obtained by strict adherence to the literature conditions.

* These results are at variance with the literature³, in which almost colourless polyamides are reported to arise by reprecipitation of the crude, coloured polymers from sulphuric acid solution (by water) or from formic acid solution (by DMF). We were unable to duplicate these findings, the colour (and electronic spectra) of our polymers remaining unchanged upon reprecipitation.

0.1 M aqueous hydrochloric acid and again water and was dried as in preceding experiments. Yields of the polyamides so obtained are given in Table 1. All polymers were reprecipitated as before.

Polycondensation of p-phenylenediamine with diethyl squarate (experiment 8)

Following the prescribed³ procedure, the combined solutions of 1.27 g (7.50 mmol) of diethyl squarate in 15 ml of DMF and of 0.81 g (7.50 mmol) of *p*-phenylenediamine in 135 ml of the same solvent were allowed to reflux for 2.5 h under N₂. Polymer precipitated from the solution during this period. After removal of 110 ml of DMF by distillation, the polyamide was worked up as described³ [yield 0.80 g (57.8%)]. Reprecipitation gave dark brown polymer with the same solubility characteristics as exhibited by the products derived from free squaric acid.

Polycondensation of p-phenylenediamine with squaryl dichloride (experiment 9)

The solution of 0.96 g (6.36 mmol) of squaryl dichloride in 10 ml methylpyrrolidone (containing 0.25 g of LiCl) was added dropwise over 15 min to a stirred solution of 0.685 g (6.36 mmol) of *p*-phenylenediamine in 10 ml of the same solvent at 0°C under N₂. After the addition of 1.12 ml of pyridine, the solution was stirred for 1 h at 0°C, followed by 1 h at 23°C and 15 min at 40°C under N₂ and light protection. The polymer, remaining in solution throughout, was precipitated by 100 ml of aqueous methanol (1:1). The product, separated by filtration and washed with water and methanol, was dried as before. 1.14 g (97.7%) of reddish black polyamide was obtained, which was soluble in 98% sulphuric acid and fluorosulphonic acid and also dissolved slowly in methylpyrrolidone containing 5% LiCl. No changes in properties were observed on reprecipitation from sulphuric acid or methylpyrrolidone solutions.

ACKNOWLEDGEMENTS

Support of this work by the Council for Scientific and Industrial Research is gratefully acknowledged. One of us (B. R. G.) thanks the National Institute for Metallurgy for a scholarship grant.

REFERENCES

- West, R. and Niu, H. Y. *J. Am. Chem. Soc.* 1963, **85**, 2589
- Doyle, G. and Tobias, R. S. *Inorg. Chem.* 1968, **7**, 2484
- Manecke, G. and Gauger, J. *Makromol. Chem.* 1969, **125**, 231
- Gauger, J. and Manecke, G. *Prepr. Int. Symp. Macromol. Chem.* 1969, **1**, 31; *Angew. Chem. (Int. Edn)* 1969, **8**, 898
- Maahs, G. and Hegenberg, P. DBP Anm. C36340 IVb/120 (1965); DOS 1518660 (1969)
- Maahs, G. and Hegenberg, P. *Angew. Chem. (Int. Edn)* 1966, **5**, 888
- Cohen, S. and Cohen, S. G. *J. Am. Chem. Soc.* 1966, **88**, 1533
- Seitz, G. and Morck, H. *Synthesis* 1971, p 146
- Griffiths, G. R., Rowe, M. D. and Webb, G. A. *J. Mol. Struct.* 1971, **8**, 363
- Sprenger, H.-E. DBP Anm. C41650 IVb/120 (1967); DOS 1618211 (1971)
- Manecke, G. and Gauger, J. *Tetrahedron Lett.* 1967, p 3509; 1968, p 1139
- Sprenger, H.-E. and Ziegenbein, W. *Angew. Chem. (Int. Edn)* 1968, **7**, 530
- Gauger, J. and Manecke, G. *Chem. Ber.* 1970, **103**, 2696
- Gauger, J. and Manecke, G. *Chem. Ber.* 1970, **103**, 3553
- Hünig, S. and Pütter, H. *Angew. Chem. (Int. Edn)* 1972, **11**, 431
- Neuse, E. W. and Green, B. R. *Liebigs Ann. Chem.* 1973, p 619
- Neuse, E. W. and Green, B. R. *Liebigs Ann. Chem.* 1973, p 633
- Treibs, A. and Jacob, K. *Liebigs Ann. Chem.* 1966, **699**, 153
- Sprenger, H.-E. and Ziegenbein, W. *Angew. Chem. (Int. Edn)* 1967, **6**, 553
- Green, B. R. and Neuse, E. W. *Polymer* 1973, **14**, 230
- Marvel, C. S. and Fabbro, D. U.S. Pat. 3 598 766 (10 Aug 1971); Banihashemi, A. and Marvel, C. S. *Iran. J. Sci. Technol.* 1972, **2**, 203.
- Kurihara, M. and Yoda, N. *Makromol. Chem.* 1967, **107**, 112
- Kurihara, M., Saito, H., Nukada, K. and Yoda, N. *J. Polym. Sci. (A-1)* 1969, **7**, 2897
- Treibs, A. and Jacob, K. *Angew. Chem. (Int. Edn)* 1965, **4**, 694
- Treibs, A. Jacob, K. and Tribollet, R. *Liebigs Ann. Chem.* 1970, **741**, 101
- Baglin, F. G. and Rose, C. B. *Spectrochim. Acta* 1970, **26A**, 2293
- Cohen, S., Lacher, J. R. and Park, J. D. *J. Am. Chem. Soc.* 1959, **81**, 3840
- Broser, W. and Seekamp, M. *Tetrahedron. Lett.* 1966, p 6337
- Smutny, E. J., Caserio, M. C. and Roberts, J. D. *J. Am. Chem. Soc.* 1960, **82**, 1793
- Rao, C. N. R. 'Chemical Applications of Infrared Spectroscopy', Academic Press, New York, 1963, Ch XI
- Henniker, J. C. 'Infrared Spectrometry of Industrial Polymers', Academic Press, New York, 1967, Ch 7
- De Selms, R. C., Fox, C. J. and Riordan, R. C. *Tetrahedron Lett.* 1970, p 781

Dilute solution behaviour of polymers near the phase separation temperature

Carla Cuniberti and Umberto Bianchi

*Istituto di Chimica Industriale dell'Università di Genova, 16132 Genova, Italy
(Received 24 September 1973; revised 10 December 1973)*

Light scattering and viscosity measurements performed in the temperature range between the θ -point and the temperature of phase separation with dilute solutions of polystyrene in cyclohexane and poly(acrylic acid) in dioxane have indicated a different mechanism of precipitation in the two systems. While polystyrene molecules give rise to progressively growing clusters the poly(acrylic acid) coils assume compact forms before precipitating. Phase separation is achieved in the former case by extensive clustering, in the latter by particle coalescence. The dimensions that the compact form of the poly(acrylic acid) molecule can reach before precipitation sets in correspond to a solid-like density inside the molecular domain. From the experimental data the temperatures characteristic for cluster formation (T_c) and for coil to globule transition (T_g) have been obtained.

INTRODUCTION

The average coil dimensions of a real chain in dilute solution approach the ideal behaviour of the random coil whenever the environment makes polymer segment-segment contacts more favourable compared to segment-solvent contacts; the more compact conformations acquire a higher statistical weight and this compensates exactly the excluded volume effects in theta-solvents.

In a given system below the θ -temperature the attractive forces between polymer segments predominate and polymer-polymer contacts can increase by two different mechanisms: the contraction of the individual coils or the interpenetration of different coils. If a single chain were present in the solution, it should collapse to a rather dense form when the net attraction between its parts becomes sufficiently large¹. In a solution of given concentration, however, coil contraction and aggregation should be competitive processes and phase separation could then occur by coalescence of either the collapsed coils or the aggregates.

It has been shown² that in polymer solutions, at the critical concentration, extensive order sets in before reaching the critical temperature, while at the same time the average coil size is reduced with respect to the unperturbed dimensions.

In dilute solutions, where isolated coils may be assumed to exist in ideal conditions, the lowering of the temperature below the θ -point gives rise at first to a shrinkage of the coil volume, followed by precipitation³. To our knowledge no detailed studies of the molecular status of polymers in dilute solutions in the precipitation conditions have been reported.

Since, presumably, the prevailing of one mechanism of precipitation or of the other is determined by the strength of the attractive forces between different parts of the chain, two polymers differing in the chemical character of their side groups have been chosen.

Here the results of light scattering and viscosity measurements performed between the θ -temperature and the precipitation point are presented for polystyrene in cyclohexane and for poly(acrylic acid) in 1,4-dioxane.

The θ -temperatures for the two systems are respectively⁴ 34.5°C and 30°C. However, while polystyrene-cyclohexane solutions give rise to phase separation by cooling, poly(acrylic acid) in dioxane presents a lower critical solution temperature as a consequence of the strong interactions of the carboxylic groups on the chain and the oxygen atoms of the solvent molecules.

The forces acting between the pendent phenyl groups in polystyrene are much weaker than those between the carboxyls in poly(acrylic acid) and noticeable differences in behaviour can be presumed to occur when polymer-polymer contacts become highly favoured.

EXPERIMENTAL

The polystyrene (PS) sample employed in this study was one of the standard 'monodisperse' polymers supplied by Pressure Chemical. The sample was purified by precipitating it out of a dilute benzene solution with an excess of methanol.

Poly(acrylic acid) (PAA) was obtained by solution polymerization in methyl ethyl ketone at 60°C with benzoyl peroxide as initiator. Fractionation of the polymer was carried out by a standard precipitation technique with methanol as the solvent and ether as the non-solvent. The fraction chosen for investigation was further purified by precipitation of a dilute aqueous solution with sulphuric acid. After dialysis against conductance water the polymer was recovered by lyophilization.

Reagent grade cyclohexane (CH) and 1,4-dioxane (DO) were dried over sodium and carefully distilled. Analysis by gas chromatography showed that no impurities were present in appreciable amounts.

Stock solutions containing about the same number of chain molecules per unit volume were prepared for the two polymer-solvent systems.

The light scattering measurements were carried out with a Sofica Model 42M photometer in the available angular range 30–150°, using unpolarized light of wavelength 564 and 435 nm.

The temperature of the cell bath was maintained with the aid of an external circulating thermostat. However, a control within $\pm 0.01^\circ\text{C}$ could not be achieved for a long time. Solutions studied for time effects were therefore kept in a separate bath and transferred to the photometer only at the desired moment.

Viscosities were measured in an Ostwald dilution viscometer. Temperature correction to the concentration values were calculated according to standard literature data for densities and thermal expansion coefficients of the solvents⁴.

Phase separation tests by visual inspection were carried out in sealed tubes kept overnight in a thermostated bath.

Data characteristic of the two polymers at their theta-temperatures are reported in Table 1. Radius of gyration and molecular weight were calculated from light scattering data by using literature values⁴ of the refractive index increments ($dn/dc = 0.107$ for PS-CH and $dn/dc = 0.088$ for PAA-DO).

RESULTS AND DISCUSSION

The inverse of the excess scattering at 90°, $(\Delta I(90))^{-1}$, and the dissymmetry ratio, Z , for PS-CH and PAA-DO

Table 1 Characteristics of samples

Sample	$M_w \times 10^{-5}$	$\langle r^2 \rangle_0^{1/2}$ (Å)	$[\eta]_\theta$ (dl/g)
PS	4.23	470	0.550
PAA	2.84	410	0.600

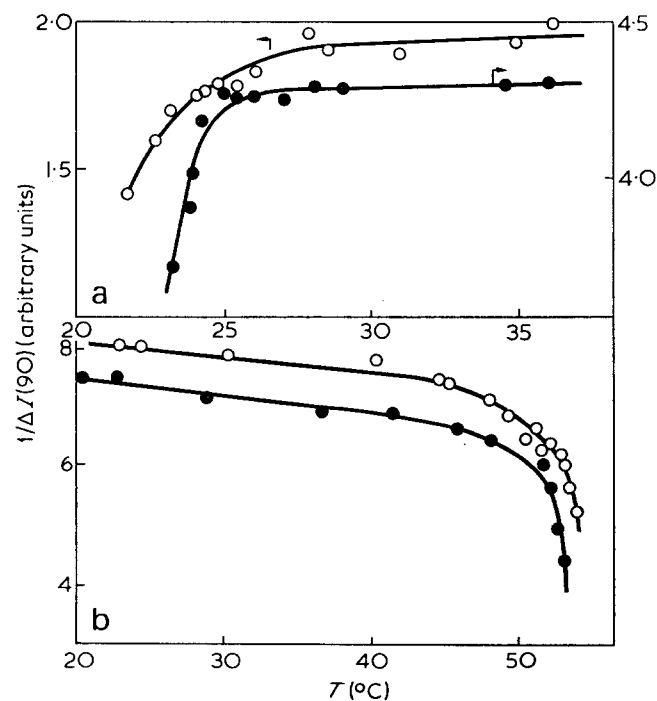


Figure 1a $(\Delta I(90))^{-1}$ vs. temperature for polystyrene in cyclohexane ($C = 1 \times 10^3$ g/cm³). \circ , $\lambda_0 = 546$ nm; \bullet , $\lambda_0 = 436$ nm
 Figure 1b $(\Delta I(90))^{-1}$ vs. temperature for poly(acrylic acid) in dioxane ($\lambda_0 = 546$ nm). \circ , $C = 6.5 \times 10^{-4}$; \bullet , $C = 7.4 \times 10^{-4}$ g/cm³

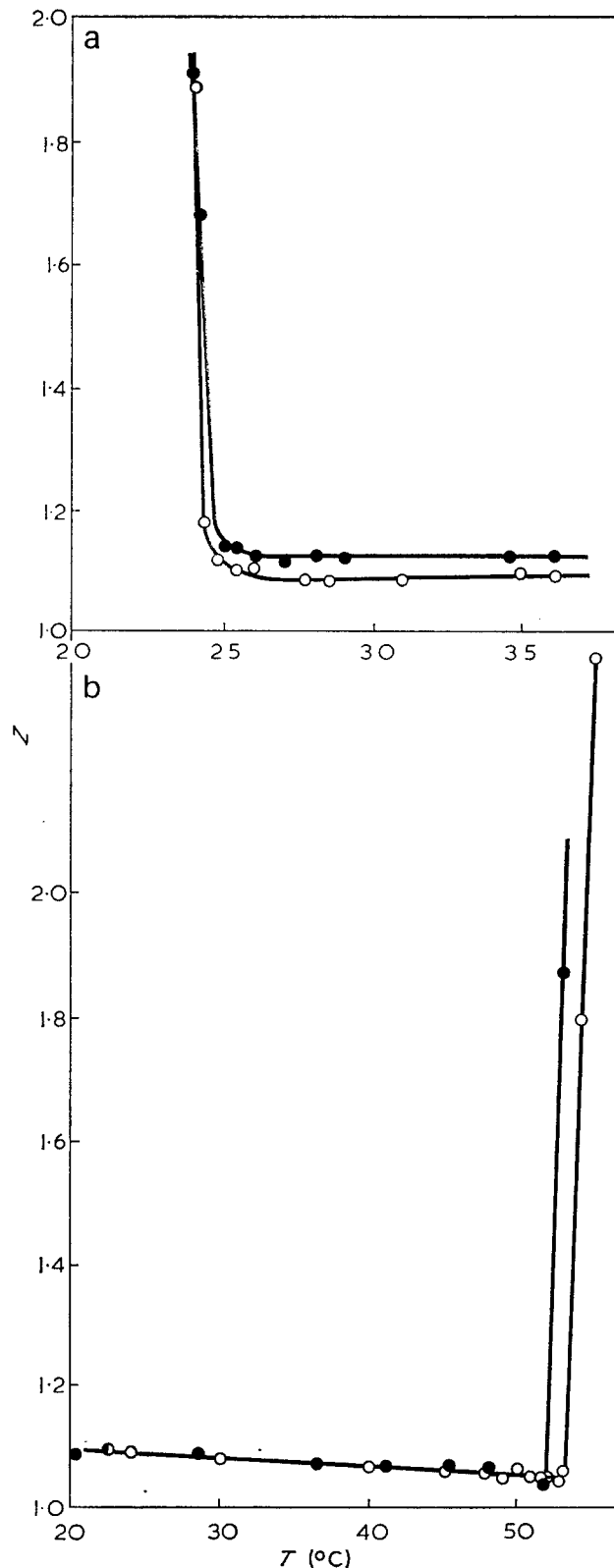


Figure 2a Dissymmetry ratio, Z , vs. temperature for polystyrene in cyclohexane (symbols as in Figure 1a)

Figure 2b Dissymmetry ratio, Z , vs. temperature for poly(acrylic acid) in dioxane (symbols as in Figure 1b)

plotted against the temperature and covering the range from just above the θ point down/up to the precipitation point are shown in Figures 1a and 1b and 2a and 2b respectively. By extrapolating the two linear parts of the curves representing the systems before and after the occurrence of the phase separation the precipitation points of the different solutions can be estimated. In

Table 2 Precipitation points of the solutions by different techniques

System	$C \times 10^4$ (g/cm ³)	λ_0 (nm)	T_p ($\Delta I(90^\circ)$) (°C)	T_p (Z) (°C)	T_p (V.I.) (°C)
PS-CH	10	546	24.3	24.4	23.1
	10	436	24.5	24.7	—
PAA-DO	7.4	546	51.7	52.2	53.4
	6.5	546	52.6	53.2	54.3
	3.7	546	—	—	65.6

Table 2 such values are shown together with the cloud points determined by visual inspection.

We attribute the delay in the visually determined precipitation points to the difficulty of detecting the initial opalescence for such dilute solutions; moreover, the dissymmetry ratio being a property much more sensitive to any change occurring in the solutions, we assume the values of the $T_p(Z)$ as the true points of phase separation.

It can be observed that PS-CH solutions show a slight wavelength dependence of the T_p so determined. The difference is, however, so small that it can be attributed to the experimental inaccuracy of the extrapolation performed.

The theory of light scattering of dilute polymer solutions relates the excess scattered intensity in a given direction to the molecular parameters of the solute and the molecular interactions by the relation³:

$$\frac{Kc}{R(\theta)} = \frac{1}{MP(\theta)} + 2A_2C \quad (1)$$

By introducing the usual $P(\theta)^{-1}$ expression it can be also written in the form:

$$\frac{1}{R(\theta)} = \frac{1}{KcM} \left[(1 + 2A_2Mc) + \frac{16\pi^2 n^2 \langle s^2 \rangle \sin^2 \theta}{3\lambda_0^2} \right] \quad (2)$$

At constant concentration equation (2) is linear in $\sin^2 \theta/2$ as long as the molecular weight and the polydispersity of the solute are not too high.

In order to get information about the temperature dependence of the mean square radius of gyration, $\langle s^2 \rangle$, one can avoid measuring the refractive index increment contained in K , by making use of the ratio between the slope and the intercept of equation (2):

$$\frac{S}{I} = \frac{16\pi^2 n^2 \langle s^2 \rangle}{3\lambda_0^2 (1 + 2A_2Mc)} \quad (3)$$

The temperature dependent factors in equation (3) are, besides $\langle s^2 \rangle$, the refractive index n , the concentration c and the second virial coefficient A_2 .

In PS-CH solutions, where phase separation is accomplished by lowering the temperature, the ratio $n^2/(1 + 2A_2Mc)$ increases in going from θ down to T_p . It is more difficult to forecast its behaviour for PAA in dioxane, where the precipitation is achieved by heating, since both n and c decrease in this case while A_2 assumes increasingly negative values, but certainly its contribution to the dependence of the ratio of equation (3) on temperature will be smaller than in the previous case.

Some typical plots from which S and I have been obtained are shown in Figures 3 and 4.

In PS-CH solutions a progressive downward curvature at small angles develops at temperatures higher than the cloud point. This happens in a temperature range

much wider ($\approx 4^\circ\text{C}$) than in the experiments performed at the critical concentration⁵ ($\approx 0.2^\circ\text{C}$). Moreover, such behaviour starts to show up at a temperature which happens to be near the critical temperature for the sample employed ($\approx 27^\circ\text{C}^*$). It seems reasonable to infer that the extensive ordering of the solutions that takes place at the critical concentration in the vicinity of the critical temperature results, in dilute solutions, in the formation of metastable clusters or molecular

* The value of 27°C for the critical temperature has been interpolated from the plot T_{crit} versus molecular weight⁶.

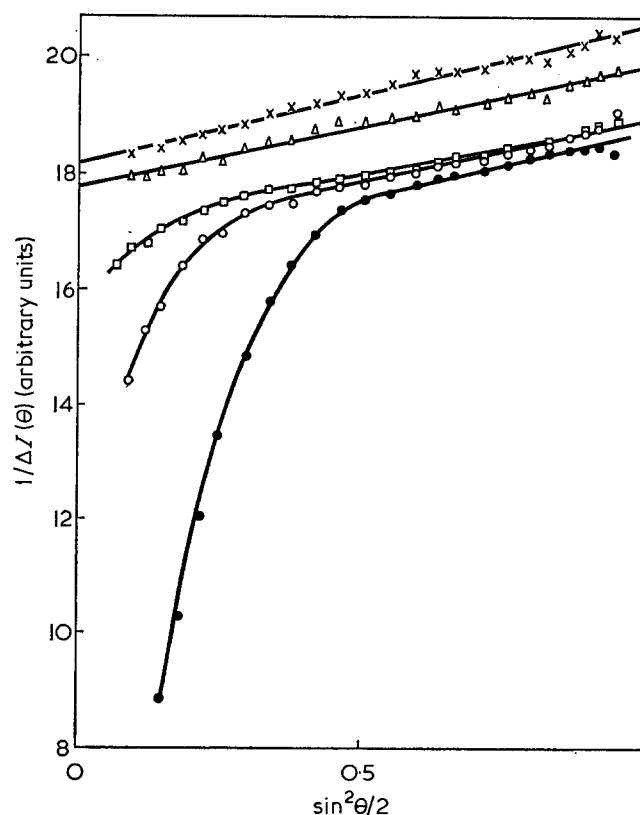


Figure 3 $(\Delta I(\theta))^{-1}$ against $\sin^2 \theta/2$ for polystyrene in cyclohexane, ($C=1 \times 10^{-3}$ g/cm³, $\lambda_0=546$ nm) at different temperatures: \times , 34.8° ; Δ , 27.7° ; \square , 24.8° ; \circ , 24.35° ; \bullet , 24.0°C

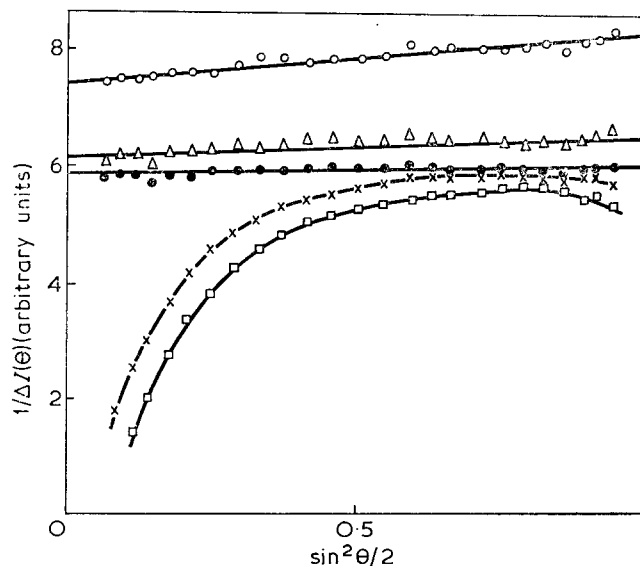


Figure 4 $(\Delta I(\theta))^{-1}$ against $\sin^2 \theta/2$ for poly(acrylic acid) in dioxane ($C=6.5 \times 10^{-4}$ g/cm³, $\lambda_0=546$ nm) at various temperatures: \circ , 30.0° ; Δ , 50.3° ; \bullet , 53.0° ; \times , 53.4° ; \square , 54.0°C

aggregates to which appropriate molecular weights and sizes can be attributed. The low polydispersity of the sample, as well as some considerations on the behaviour of the system PAA-DO made below, encourage us to attribute the behaviour found experimentally more to the intermolecular condensation process described above than to the precipitation of the highest molecular weight fractions.

The ratio S/I for PS-CH is plotted against temperature in Figure 5. For the plots of Figure 3 showing the downward curvature at low angles the initial part has been considered significant in obtaining S and I . However, the rather large value of the minimum angle at which our measurements could be performed (30°) does not enable us to obtain correct extrapolations of the curves. The values of S/I in these cases have no quantitatively meaningful significance beyond the fact that the large increase before precipitation can be used to indicate the temperature characteristic of cluster formation as the point obtained by the intersection of the linear portions of the curve of Figure 5. This temperature is $T_c = 26.6^\circ\text{C}$, independently of the wavelength employed.

In PAA-DO solutions the plots of the inverse scattering intensity against $\sin^2\theta/2$ do not show any sign of downward curvature before the precipitation point. The two curved plots in Figure 4 refer in fact to the already phase separated solutions. The temperature dependence of the ratio S/I for such a system is shown in Figure 6. The slight decrease up to about 45°C is well accounted for by a coil contraction that slightly overpasses the factor $n^2/(1+2A_2Mc)$, while the much larger variation in the range from 45°C up to the precipitation point can only be due to the collapse of the coil to a more compact form. This collapse presumably takes place when the polymer concentration inside the coil volume reaches a value that makes a large number of carboxylic groups belonging to distant parts of the chain to approach within the distance for hydrogen bonding while the solvation of the same groups by the dioxane molecules becomes highly disfavoured.

That a different mechanism underlies phase separation in the two systems studied is further enhanced by the significant time effect characterizing the precipitation of PAA in dioxane. Figure 7 shows how the dissymmetry ratio changes with time at temperatures close to the precipitation point. As already pointed out, the location of this point on the temperature scale is quite precisely

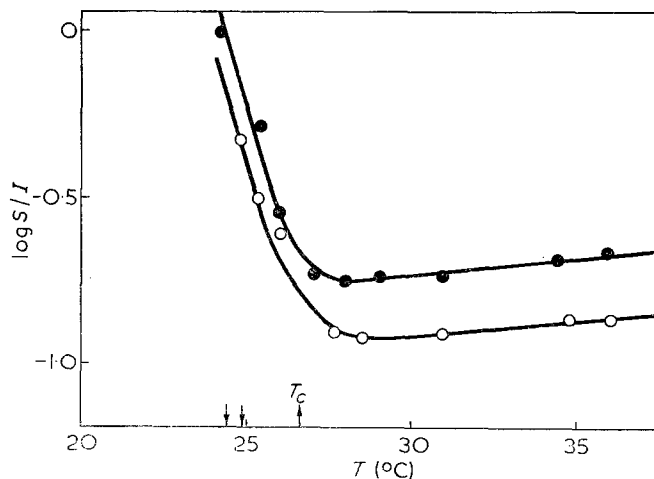


Figure 5 Ratio S/I plotted against temperature for PS in CH (symbols as in Figure 1a); $\downarrow\downarrow$ indicates precipitation points

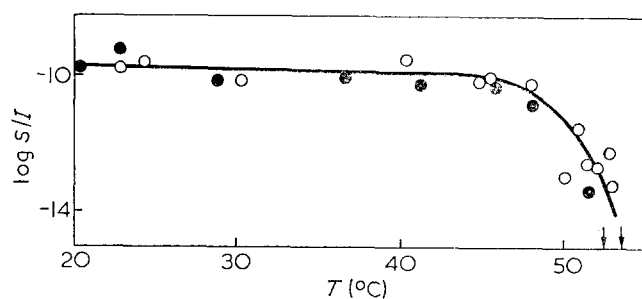


Figure 6 Ratio S/I plotted against temperature for PAA in DO (symbols as in Figure 1b); $\downarrow\downarrow$ indicates the precipitation points

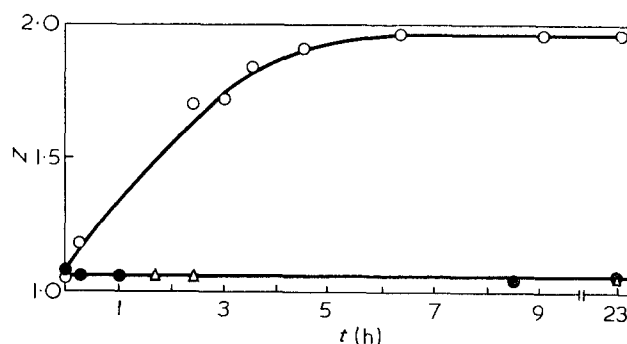


Figure 7 Dissymmetry ratio, Z , vs. time for poly(acrylic acid) in dioxane in the vicinity of and at the precipitation point: Δ , 52.9° ; \bullet , 53.0° ; \circ , 53.4°C

detected by observing the variation of Z in equilibrium conditions (Table 2); alternatively it could be defined by the temperature at which the time effect shown in Figure 7 starts to show up (53.4°C).

The large extent of time (about 6 h) necessary to achieve complete precipitation is reminiscent of the coalescence of particles in dispersions⁷. No analogous time effect was detected in PS-CH solutions in the region where the dissymmetry ratio starts to increase. Since the polydispersity of the PAA sample, though certainly higher than for the polystyrene used in these experiments, does not apparently interfere in the described mechanism of precipitation, we take it as a proof that the different behaviour of PS in cyclohexane underlies an aggregation phenomenon prior to precipitation more than a polydispersity effect.

In order to obtain further evidence of the difference existing between the two systems, viscosity measurements were also performed and are shown in Figure 8.

In the system PS-CH, η_{sp}/c behaves linearly down to the precipitation point either for a solution of the same concentration as the one employed in the light scattering studies and for a concentration one half of that. For PAA-DO a large decrease starts to show up at about 40°C for both the solutions employed. In the more dilute solution, in which the cloud point detected by visual inspection is moved up to 65.6°C , this behaviour is strongly enhanced. The small value of the concentration employed and the undetectable influence of the concentration on η_{sp}/c enable us to assume $\eta_{sp}/c \approx [\eta]$ so that any change induced by the temperature on the specific viscosity reflects directly the size variation of the dissolved coils. In Figure 9 the ratio of the mean square radius of gyration to its value at the theta point, as calculated by the viscosity values, is plotted against the temperature.

The temperature coefficient of the coil dimensions at the θ point is 2.5×10^{-3} while it reaches a value about

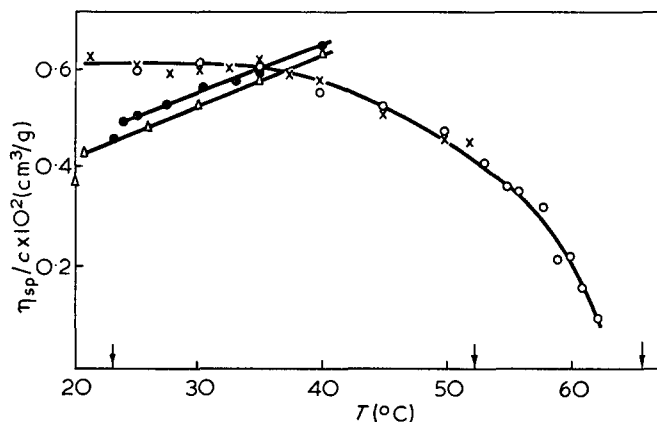


Figure 8 η_{sp}/c against temperature for polystyrene in cyclohexane (\bullet , $C=10 \times 10^{-4}$; Δ , 5×10^{-4} g/cm³) and poly(acrylic acid) in dioxane (\times , $C=7.4 \times 10^{-4}$; \circ , $C=3.7 \times 10^{-4}$ g/cm³)

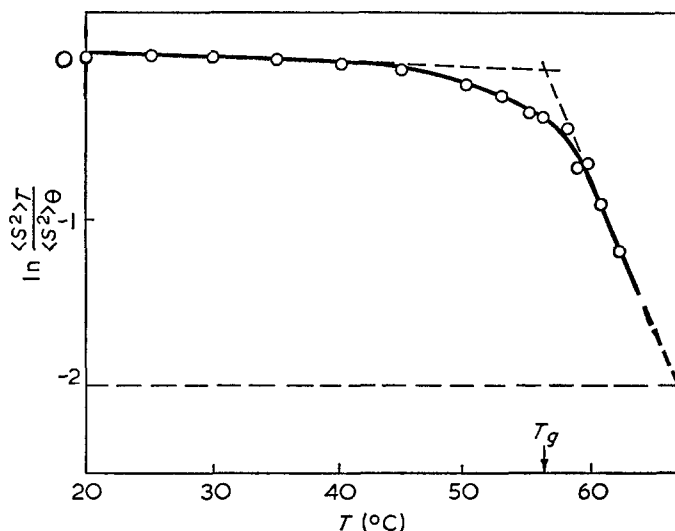


Figure 9 Plot of the ratio $\langle S^2 \rangle_T / \langle S^2 \rangle_\theta$ against temperature for poly(acrylic acid) in dioxane

one hundred times larger in the pre-precipitation range. The broken horizontal line in Figure 9 represents the ratio $\langle s^2 \rangle_T / \langle s^2 \rangle_\theta$ of the completely collapsed coil calculated assuming a spherical particle with the density of the solid polymer and the molecular weight and mean square radius of gyration given in Table 1.

The line passing through the points in the pre-precipitation region points to this value at the precipitation temperature.

While it is not our intention to affirm that the molecule does effectively acquire the density of the solid we think that the behaviour shown in Figure 9 stresses the degree of compactness reached by the 'coil' before phase separation. This intramolecular condensation can take place simply as a consequence of the attraction forces between carboxylic groups. Compact globules in synthetic polymers usually involve aqueous solutions⁸ where water structure and hydrophobic bonds seem to play a major role with respect to groups interactions⁹.

Hydrogen bonding between carboxylic groups is highly disfavoured in dioxane¹⁰, where they strongly interact with the solvent. As a consequence of this, strong polymer-solvent interaction PAA in dioxane shows the phenomenon of the inverse solubility. The carboxyl-dioxane bonds are weakened by increasing the temperature and the coil undergoes a progressive contraction as predicted by the thermodynamics of polymer solutions.

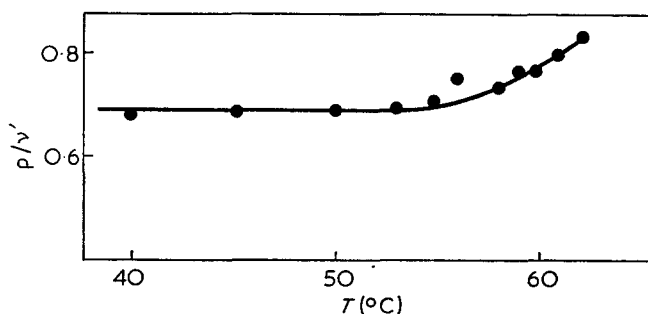


Figure 10 Change of the average size of the closed loops induced by the temperature in the poly(acrylic acid) coil

The probability that two reacting groups on the chain become associated is inversely related to the coil size, and a point can be reached where the intramolecular phase transition from the state of statistical coil to the compact globular state takes place. This point can be tentatively evaluated from Figure 9 by the intersection of the two straight lines, which gives $T_g = 56.5^\circ\text{C}$.

By choosing a model that represents the chain as a linear sequence of closed loops alternating with linear parts¹¹, the ratio $(1-\rho) = ([\eta]_T / [\eta]_\theta)^{2/3}$ represents the average fraction of segments which are in the linear sections. Moreover, it is possible to predict what decrease of the intrinsic viscosity is to be expected when interacting groups on the chain are statistically involved in stable association¹².

$$\frac{[\eta]_\theta - [\eta]_T}{[\eta]_\theta} = \frac{\nu 2^{1/2}}{N_m} = \nu' \quad (4)$$

where ν is the number of rings which have been formed on average in each macromolecule and N_m is the number of statistical chain elements. In the limit of a constant N_m the ratio ρ/ν' represents the mean ring size. In Figure 10 this ratio is plotted against the temperature starting from 40°C (i.e. from the point that limits the end of the linear behaviour in Figure 9), which may be taken as the temperature at which closed loops start to be formed. Within the approximation of this model one can conclude that the mean ring size remains constant up to approximately 55°C , while its increase at higher temperature should be attributed to the association of groups belonging predominantly to segments far apart along the chain.

ACKNOWLEDGEMENTS

The research upon which this paper is based was supported by the Consiglio Nazionale delle Ricerche, Italia, under contract No. 72/71.01761.03/115.3836.

REFERENCES

- 1 Ptitsyn, O. B., *et al. J. Polym. Sci. (C)* 1968, **16**, 3509
- 2 Debye, P., *et al. J. Chem. Phys.* 1960, **32**, 933; 1960, **33**, 1746
- 3 Flory, P. J. 'Principles of Polymer Chemistry', Cornell Univ. Press, Ithaca, 1953
- 4 Brandrup, J. and Immergut, E. H. 'Polymer Handbook', John Wiley, New York, 1966
- 5 McIntyre, D., *et al. J. Chem. Phys.* 1966, **37**, 3059
- 6 Utacki, L. and Simha, R. *J. Phys. Chem.* 1963, **67**, 1052
- 7 Lips, A., *et al. Trans. Faraday Soc.* 1971, **67**, 2979
- 8 Leyte, J. C. and Mandel, M. *J. Polym. Sci. (A)* 1964, **2**, 1879
- 9 Nemethy, G., *et al. Biopolymers* 1963, **1**, 255
- 10 Allen, G. and Caldin, E. F. *Q. Rev.* 1953, **7**, 255
- 11 Priel, Z. and Silderberg, A. *J. Polym. Sci. (A-2)* 1970, **8**, 689
- 12 Khun, W. and Balmer, G. *J. Polym. Sci.* 1962, **57**, 311

Crystallization studies of isotactic polystyrene

B. C. Edwards and P. J. Phillips

*Department of Materials, Queen Mary College, London E1 4NS, UK
(Received 9 November 1973; revised 17 January 1974)*

The kinetics of lamellar crystallization in thin films of isotactic polystyrene have been determined using transmission electron microscopy. The morphological changes accompanying crystallization have also been investigated as a function of solvent, supercooling and strain prior to crystallization. Crystallization temperatures have been attained by both cooling from the melt and warming from the glass. Similar growth rates were obtained in both cases. The nucleation density of spherulites is difficult to control when warming from the glass but does depend on the solvent used in preparing the thin film. The rate of lamellar growth follows a 'bell' shaped curve *versus* crystallization temperature and the kinetics were analysed using the secondary nucleation theory of Hoffman and Lauritzen. The end surface free energy, σ_e , of the lamellar crystals was determined using the variation of lamellar thickness with supercooling.

INTRODUCTION

The crystallization kinetics of polymers are commonly studied using microscopic measurements on bulk material. Techniques such as calorimetry, X-ray diffraction and thermal analysis are employed from which the degree of conversion to a new phase is obtained. These methods yield no knowledge of the fundamental physical processes involved in the nucleation and growth. A more definitive treatment of the kinetics is obtained using thin film optical microscopy which enables spherulitic growth rates to be measured. It is well established¹ that the growth of a spherulite is a co-operative process involving growth of lamellar crystals, diffusional segregation of molecular species and nucleation of new lamellar crystals. Hence, the optical measurement of spherulitic growth rate may not equal the actual growth rate of individual lamellar crystals. Direct measurements of the rate of lamellar growth were first made by Andrews *et al.*² on stained films of *cis*-polyisoprene.

In this work the thin film technique has been extended to a linear polymer which is not a member of the polyene family. The electron microscope methods adopted provide the necessary resolution for simultaneous measurement of growth rate and lamellar thickness as a function of crystallization temperature. From these measurements the parameters governing growth may be determined. Isotactic polystyrene (iPS) was chosen for this study because of its low rate of crystallization which allows quenching to the glassy state without appreciable crystallization occurring. It is therefore possible to determine the parameters governing the lamellar crystallization from the glass as well as from the melt. One further objective was to show that the results of investigations on natural rubber are equally applicable to 'non-rubbery' polymers.

EXPERIMENTAL

Materials

Isotactic polystyrene ($M_v = 2.1 \times 10^6$) was supplied by the Dow Chemical Company. Prior to use the powder

was extracted for 24h using methyl ethyl ketone in a Soxhlet tube, in order to remove atactic material, and then dried.

Preparation of thin films

Homogenized solutions (2% by wt) of the polymer were prepared using benzene, xylene or dichlorobenzene. Thin films (80–100 nm) were cast from the solutions onto water, ethylene glycol or mica surfaces, the thickness being judged by the interference colours. The films were then either: (a) crystallized from the glass at a predetermined temperature in a silicone oil bath, or (b) crystallized from the melt after a prior heat treatment of 30 min at 250°C.

The effect of strain prior to crystallization was investigated by applying known extension ratios to polymer films cast onto ethylene glycol at temperatures above the glass transition temperature (90°C). The extension was applied by separation of parallel needles placed in contact with its upper surface, as described by Andrews³. Results obtained confirm that high strains were retained by this method, presumably because of the very high molecular weight.

Electron microscope studies were carried out using a JEM 7 microscope operated at 100 kV.

RESULTS AND DISCUSSION

Morphology

Representative electron micrographs of the morphologies obtained by crystallization from the glass and the melt are shown in *Figures 1a* and *b* respectively. Spherulites formed on crystallizing from the glassy state are nucleated in very high densities and are evenly distributed throughout the film. Crystallization from the melt results in spherulites which are randomly distributed and a low nucleation density is obtained. The morphologies present in *Figure 1* represent different stages of spherulitic growth.

The initial stage of growth of a spherulite is the formation of a single lamella crystal as shown in

Figure 2. The growth of this crystal perturbs the surrounding melt so as to facilitate the nucleation of further lamellar crystals and a 'sheaf-like' bundle of lamellae is formed, as discussed later. A significant observation of the present investigation was that in unstrained films the lamellar crystals usually nucleate in the 'edge-on' orientation. This orientation is normally associated with strained films and hence it seems likely that nucleation occurs at points of stress concentration or localized strain. A similar effect was observed in thin films of natural rubber by Owen⁴. In certain areas, (A, Figure 2) crystals nucleated in the 'side-on' position

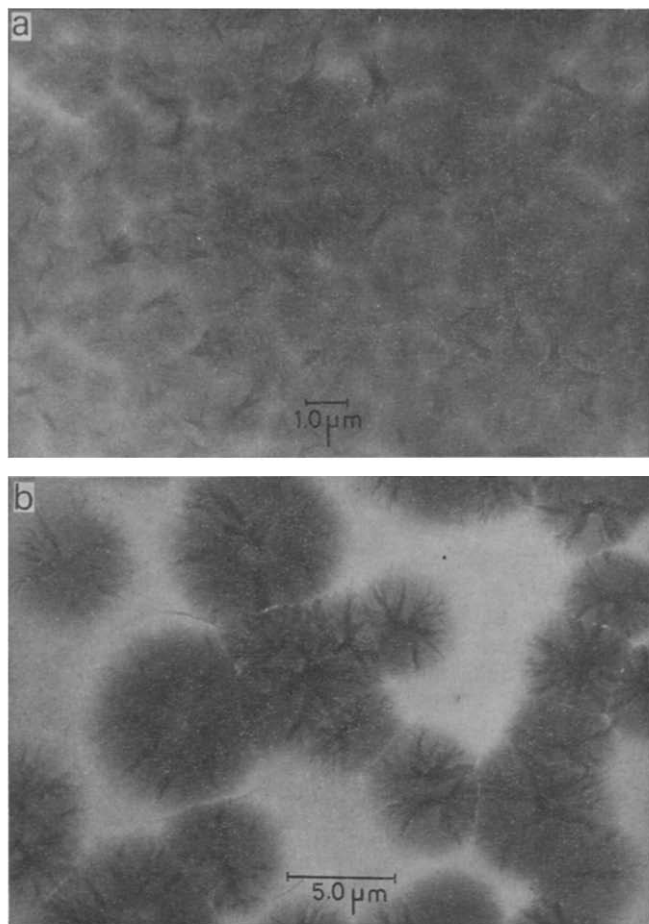


Figure 1 Specimens crystallized from (a) the glass and (b) the melt at 200°C for 60 min

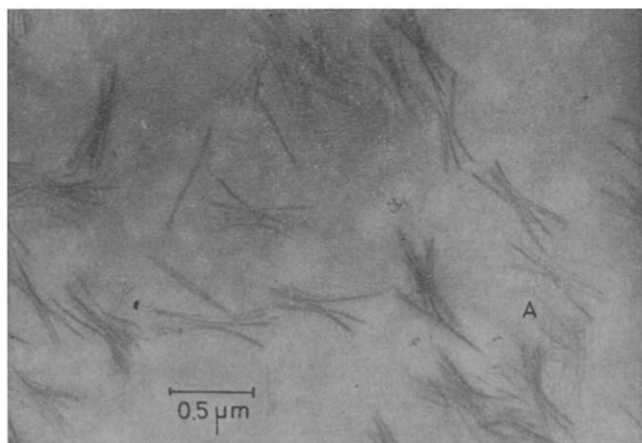


Figure 2 Specimen crystallized from the glass at 180°C for 1 min

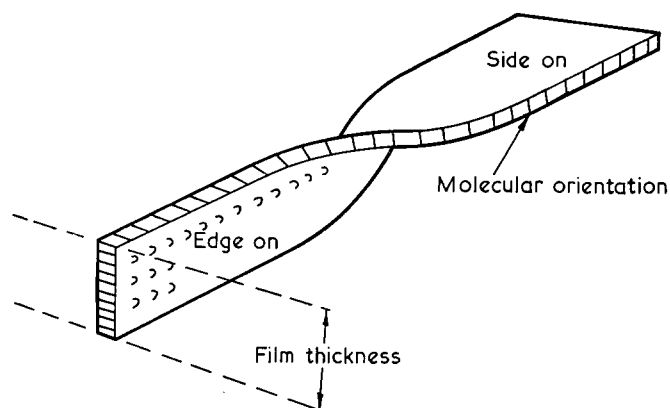


Figure 3 Diagrammatic representation of the 'side-on' and 'edge-on' orientations of the lamellar crystals, with respect to the electron beam

are present. A diagrammatic representation of the 'side-on' and 'edge-on' orientations is shown in Figure 3.

The space filling mechanism of spherulitic growth is often referred to as 'branching'¹. However, an inspection of high resolution micrographs (Figure 2) shows that no physical branching of the lamellae is involved but instead a new lamella crystal is nucleated some distance (up to 40nm) away from a growing lamella. Similar observations have been reported in stained films of natural rubber⁴ and gutta percha¹⁵ and the description of 'spawning' used by Owen will be adopted here.

The 'branch-like' appearance of spherulites in some micrographs of this paper, e.g. Figure 1b, is due to the heating effect of the electron beam producing deformation of the lamellar crystals. Figures 4a and b are micrographs obtained by: (a) focusing on an adjacent area and photographing using a low beam intensity and long exposure time, and (b) focusing on the area itself, the micrograph being taken 30 sec after the impingement of the electron beam. Irradiation by the electron beam produces deformation of the lamellar crystals and loss of resolution. Polystyrene is known to be highly resistant to radiation damage in the amorphous phase⁵ and the crystalline phase is expected to be even more resistant by comparison with polyethylene. The observed effects are probably thermal caused by different coefficients of expansion of the amorphous and crystalline phases; however, other effects cannot be ruled out. Similar observations of the deformation of structure have been reported by Andrews⁶ for the electron irradiation of natural rubber where, however, crosslinking is the predominant product of irradiation.

Spawning of new lamellar crystals is probably a general feature of all high molecular weight crystallizing polymers (this work) and lightly crosslinked^{4, 15} crystallizing polymers and is a fundamental process of spherulitic growth. The growth of a spherulite from its inception as a single lamellar crystal can be described as a spawning phenomenon. It is important to emphasize at this point that the observation of spawning is critically dependent upon the lamellar orientation in the film and that thin film electron microscopy is ideally suited to study this phenomenon since nucleation of lamellar crystals usually occurs in the 'edge-on' orientation.

Spawning may be explained⁴ as resulting from entanglements in the melt. As molecules are 'reeled in' to the

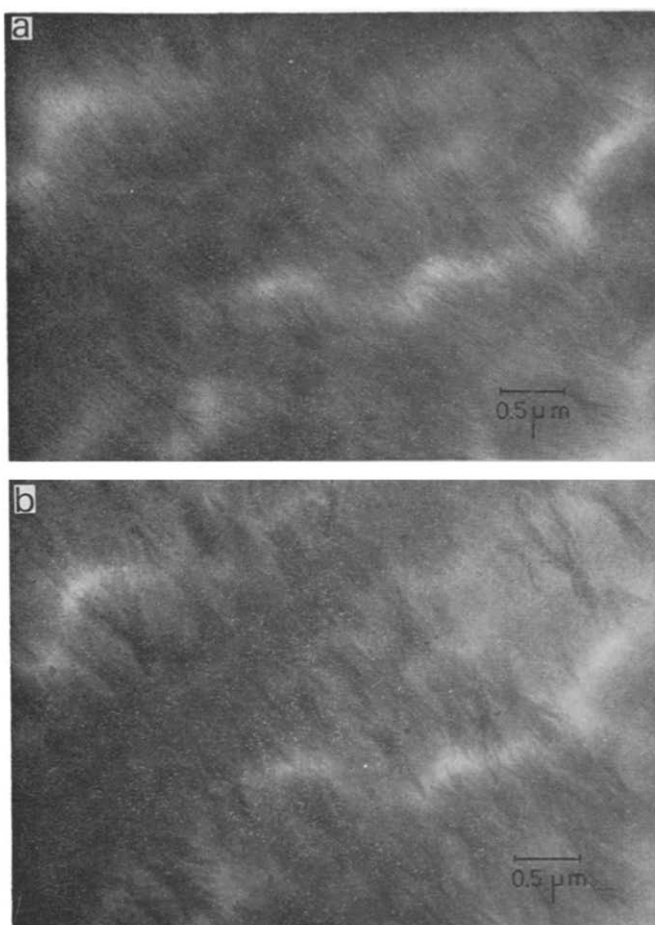


Figure 4 (a) Area photographed immediately after focusing on an adjacent area, taken using low beam intensity; (b) same area as (a) but photographed after 30 sec in the beam, with increased beam intensity

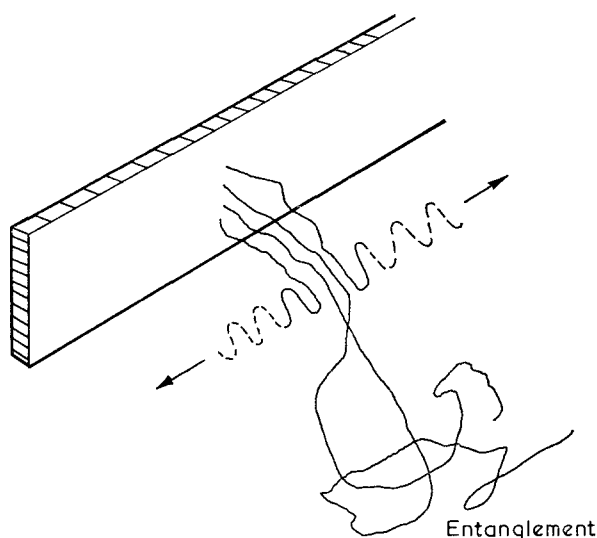


Figure 5 Schematic representation of the spawning of new lamellar crystals

growth front of a lamellar crystal, entanglements cause neighbouring molecules to become aligned in a direction normal to the parent lamella. These molecules can then act as nucleating sites for new lamellar crystals, as shown diagrammatically in Figure 5. The different stages of spherulitic growth are shown in Figure 6. The curved profile of the spawned crystals may be due to a concentration gradient of crystallizable material¹.

The non-crystallized region between the spawned and the parent crystal may be considered as a segregation of non-crystallizable species which have been rejected during crystallization. A related feature is the presence of non-crystallizable material between impinging spherulites. This may be explained as due to the segregation of low molecular weight species, which possess sufficient mobility in the melt to diffuse away radially in advance of the growing spherulite¹. This segregation may also explain the breakdown of the linear lamellar growth rate at long times as shown in Figure 7. As the spherulites approach impingement the growth rate decreases owing to increasing impurity concentration at the growth front.

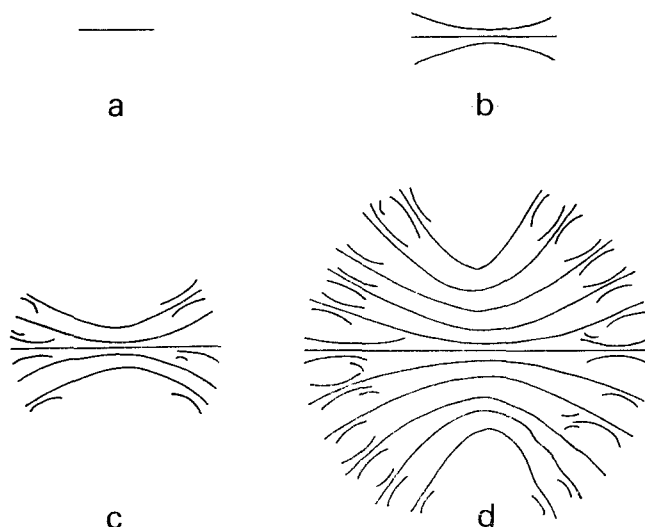


Figure 6 Schematic representation of the different stages of spherulitic growth, as viewed using thin film electron microscopy. (a) Single lamellar crystal; (b) spawning of new lamellar crystals; (c), (d) formation of radial spherulite by spawning mechanism

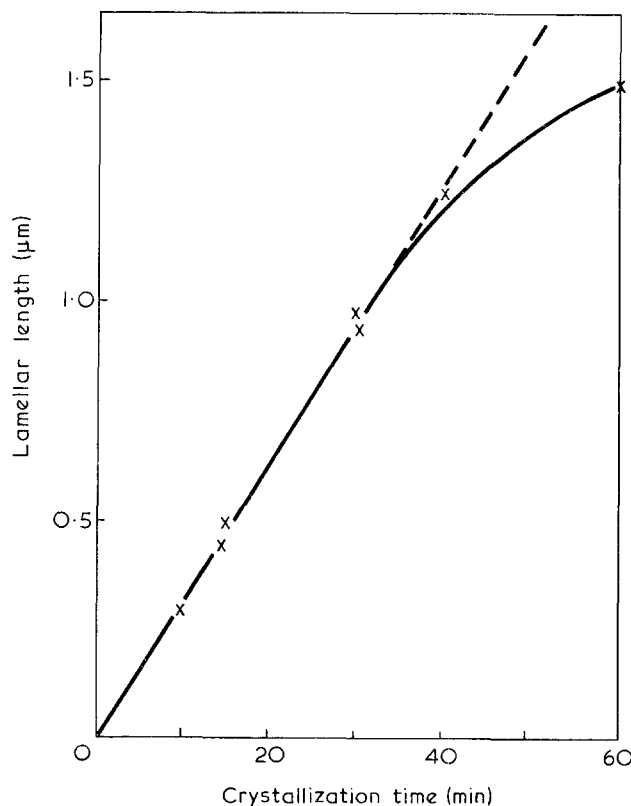


Figure 7 Lamellar growth rate at 140°C on crystallizing from the glassy state

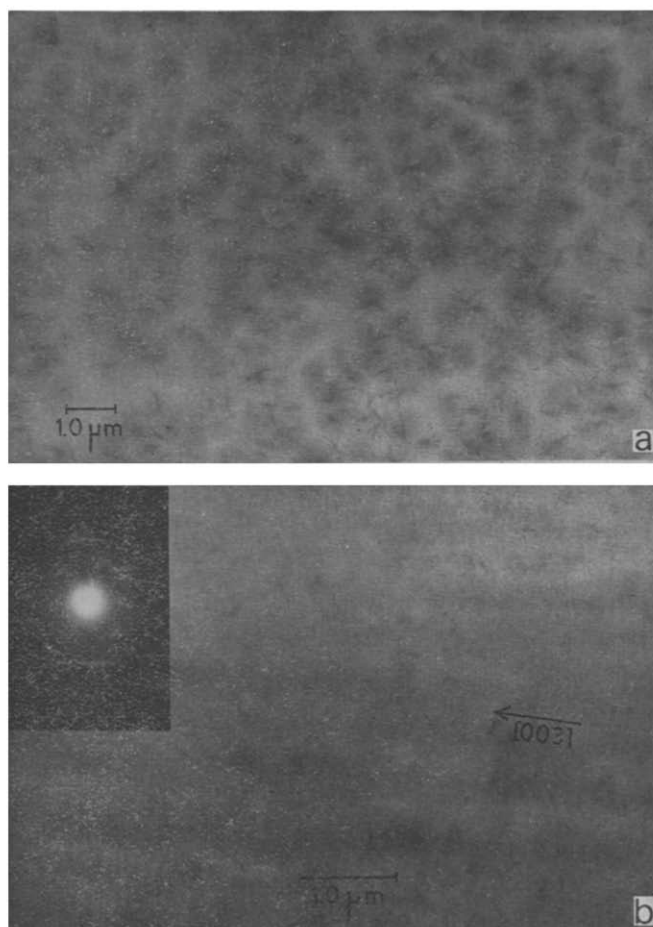


Figure 8 Specimen strained to (a) 100% and (b) 200% extension prior to crystallization at 140°C for 15 min

Pre-straining of the films results in the production of aligned row nucleated structures similar to those reported by Andrews³ for natural rubber. Figure 8a is a micrograph of a film strained 100% prior to crystallization. Row nucleated lamellar crystals are present with an 'edge-on' orientation normal to the strain direction. On increasing the strain to 200% prior to crystallization (Figure 8b) the density of lamellar crystals increases. The selected area diffraction pattern is a fibre pattern with the *c*-axis aligned parallel to the strain direction. The nature of strain induced crystallization will be discussed in detail in a future publication.

Kinetics of crystallization

Primary nucleation. The differences in the nucleation densities of films crystallized from the glass and from the melt were described in the previous section. The nucleation density of spherulites in films crystallized from the glass is independent of crystallization temperature over the range studied but somewhat surprisingly is dependent on the solvent from which the film was cast, the results are shown in Table 1.

The difference in nucleation density of films cast at room temperature does not appear to be caused by residual solvent as evacuation for 24 h prior to crystallization had no effect. This effect could be due to differing amorphous densities, structures or strains caused by different rates of solvent evaporation.

Casting the film onto a substrate above the glass transition temperature had the effect of reducing the nucleation density. These results are given in Table 1.

In the case of iPS-benzene solutions, the substrate was at a temperature above the boiling point of benzene and hence more disorder would be expected in the thin film.

Lamellar growth rates. Lamellar growth rates were determined as a function of crystallization temperature. The growth rate was difficult to determine using benzene as a solvent, as impingement of the spherulites occurred after short crystallization times (e.g. 20 min at 140°C; 5 min at 180°C). Casting above the glass transition temperature onto ethylene glycol had the desirable effect of reducing the nucleation density and hence, the growth rate could be determined over a longer time period. No difference in the growth rate was found by casting above or below the glass transition temperature although the nucleation density was significantly

Table 1 Nucleation densities of spherulites crystallized from the glass

Condition	Nucleation density of spherulites cast at 21°C × 10 ⁻¹² (m ⁻²)	Nucleation density of spherulites cast at 120°C × 10 ⁻¹² (m ⁻²)
iPS-benzene	~2.0	1.1-1.6
iPS-xylene	~1.9	0.2
iPS-dichlorobenzene	~0.40	0.90

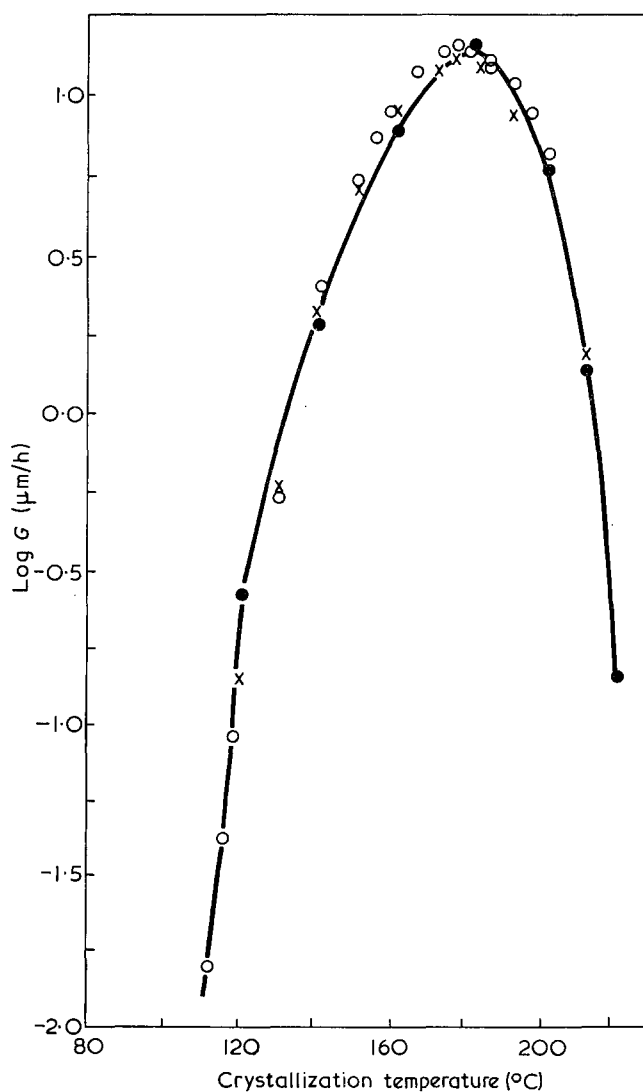


Figure 9 Graph of log growth rate, *G* vs. crystallization temperature. ●, Present study; ×, Boon *et al.*⁷; ○, Suzuki and Kovacs⁸

affected. Similarly, the solvent used had no influence on the growth rate but affected the nucleation density.

A plot of the log radial growth rate *versus* crystallization temperature for samples crystallized from the glass is shown in Figure 9, together with the growth rates for samples crystallized from the melt obtained using optical microscopy by Boon *et al.*⁷ and Suzuki and Kovacs⁸.

The general features of the log *G* *versus* *T* graph suggest that the lamellar growth rate obeys the Hoffman-Lauritzen⁹ secondary nucleation theory which may be expressed as:

$$G = G_0 \exp\left\{\frac{-\Delta F^*}{RT}\right\} \exp\left\{\frac{-4b_0\sigma\sigma_e T_m}{kT\Delta H_f \Delta T}\right\} \quad (1)$$

where b_0 is the monomolecular thickness, σ and σ_e are the side and end interfacial energies respectively between the nucleus and the melt, ΔH_f is the heat of fusion per unit volume, T_m is the equilibrium melting point and ΔT is the supercooling.

Hoffman and Weeks¹⁰ equated the transport term ΔF^* to the activation energy for viscous flow, which has a temperature dependence derived from the WLF equation of:

$$\Delta F^* = \Delta F_{WLF} = \frac{C_1 T}{C_2 + T - T_g} \quad (2)$$

where C_1 and C_2 are constants generally made equal to 17.24 kJ/mol and 51.6K respectively; T_g is the glass transition temperature. Substituting in equation (1) we obtain:

$$\log G + \frac{\Delta F_{WLF}}{2.303 RT} = \log G_0 - \frac{4b_0\sigma\sigma_e T_m}{2.303kT\Delta H_f \Delta T} \quad (3)$$

To ascertain if the lamellar growth rate of iPS can be described using the above approximation, the quantity $\log G + (\Delta F_{WLF}/2.303RT)$ is plotted against $T_m/T\Delta T$. If the growth rate can be described by equation (3) then the plot is a straight line with a slope of $-(4b_0\sigma\sigma_e/2.303k\Delta H_f)$. Such a plot is shown in Figure 10. With $C_2 = 51.6\text{K}$ it was not possible to fit the growth rate data to the above equation. However, if C_2 is chosen to be 81K, as found by calorimetry measurements¹¹, a reasonable straight line is obtained. From the slope of the line, with $b_0 = 0.55\text{ nm}$, $\Delta H = 91.1 \times 10^6\text{ J/m}^3$, $\sigma\sigma_e$ was calculated to be $153.0 \times 10^{-6}\text{ J}^2/\text{m}^4$, by taking b_0 as the distance between adjacent molecular layers in the [110] direction. This plot yields a value of $4.7 \times 10^8\text{ }\mu\text{m/h}$ for G_0 .

Using the plot suggested by Suzuki and Kovacs⁸, $\log G + (345.2/T - T_\infty)$ *versus* $T_m/T\Delta T$, with $T_\infty = 333.5\text{K}$, $T_m = 515.2\text{K}$; an approximate linear relationship was obtained from which a value of $\sigma\sigma_e = 140 \times 10^{-6}\text{ J}^2/\text{m}^4$ was obtained; however, the data do not fit this plot at high and low values of ΔT as well they do the Hoffman-Weeks equation.

The lamellar growth rates of specimens crystallized from the melt were found to be in good agreement with those obtained from the glassy state. This indicates that the growth rate is independent of the thermal history and depends only on the crystallization temperature. A similar result has been found by Magill¹² using optical microscopy, for poly(tetramethyl-*p*-silphenylene) siloxane.

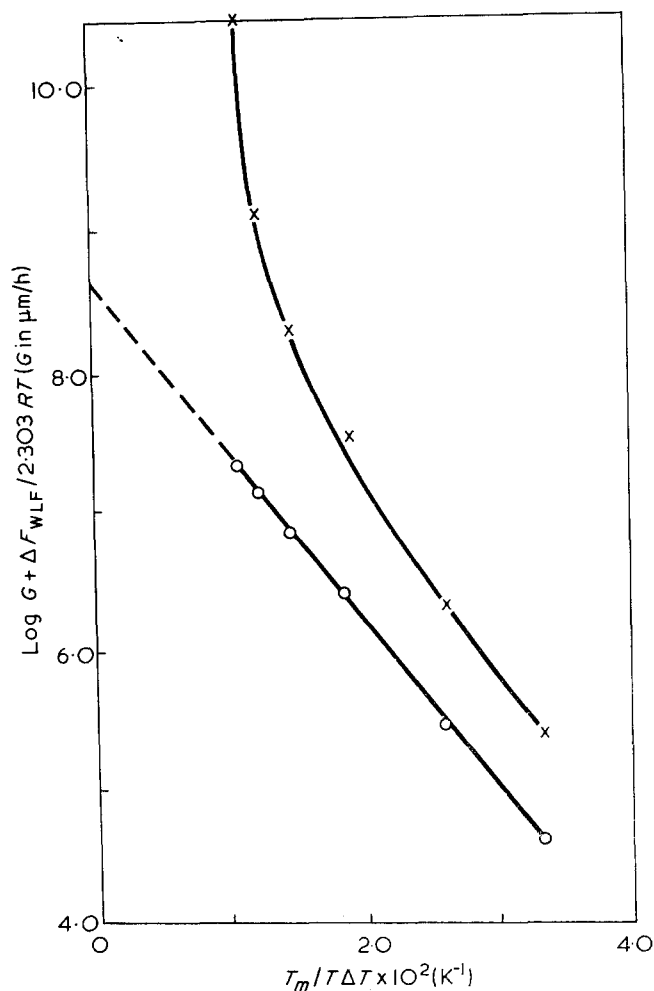


Figure 10 Graph of $\log G + \Delta F_{WLF}/2.303RT$ versus $T_m/T\Delta T$. \times , $C_2 = 51.6\text{K}$; \circ , $C_2 = 81.0\text{K}$

Lamellar thickness. One of the predictions of secondary nucleation theory is that lamellar thickness, l , should be inversely proportional to the supercooling. This has now been shown to be the case for a number of polymers including natural rubber² and polyethylene¹³. The variation of lamellar thickness of isotactic polystyrene with reciprocal supercooling is shown in Figure 11 together with the variation of X-ray long period by Blais and Manley¹⁴.

A value of σ_e of $28.8 \times 10^{-3}\text{ J/m}^2$ has been calculated from the slope using the equation $l = 2\sigma_e T_m / \Delta H \Delta T$ and values of $T_m = 515.2\text{K}$ and $\Delta H = 91.1 \times 10^6\text{ J/m}^3$.

Combining this value with the earlier derived values of the product $\sigma\sigma_e$, values of 5.3×10^{-3} and $4.9 \times 10^{-3}\text{ J/m}^2$ have been calculated for σ . (Values of σ_e of 32.0×10^{-3} and $26.6 \times 10^{-3}\text{ J/m}^2$ were obtained by Suzuki and Kovacs assuming $\sigma = 4.16 \times 10^{-3}$ and $5.0 \times 10^{-3}\text{ J/m}^2$ respectively).

It is useful to compare these values of σ and σ_e with the values for other polymeric systems (Table 2). It is important to emphasize that the values of σ_e quoted in this Table were calculated from the measured lamellar thickness, using transmission electron microscopy^{2, 15} or from X-ray long period¹⁶. These values of σ and σ_e are based on experimental measurements and do not rely on any empirical formulation of σ .

An approximately linear relationship between σ and σ_e was found (Figure 12) with the ratio σ_e/σ equal to 5.8 ± 0.8 . The values for natural rubber calculated were for (110) and (120) growth faces.

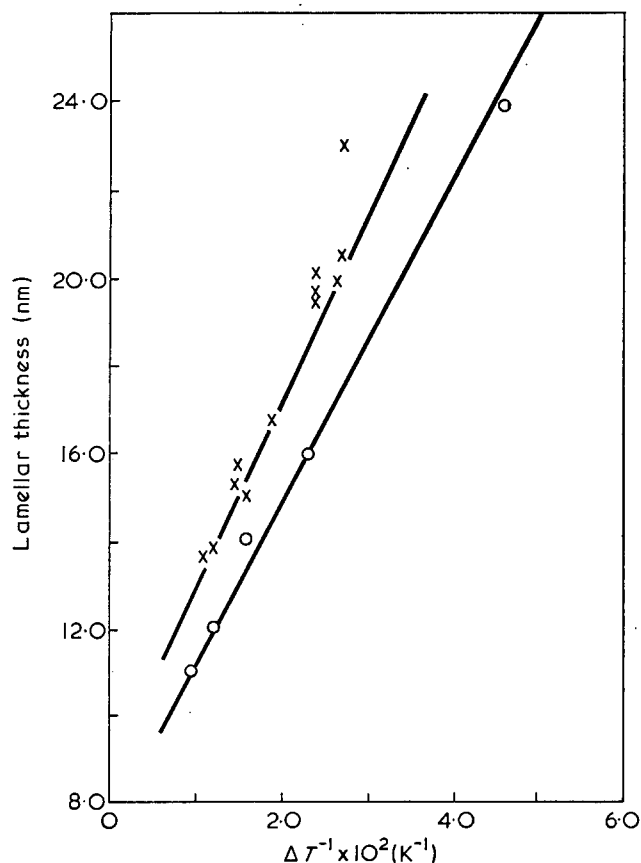


Figure 11 Graph of lamellar thickness vs. reciprocal supercooling. x, long period of Blais and Manley¹⁴; o, present study

Table 2 Surface free energies obtained from investigations of growth rates and lamellar thicknesses

Polymer	$\sigma\sigma_e \times 10^6$ (J ² /m ⁴)	$\sigma_e \times 10^8$ (J/m ²)	$\sigma \times 10^8$ (J/m ²)	$A_0 \times 10^{20}$ (m ²)	$q \times 10^{20}$ (J/mol-fold)
Isotactic polystyrene	153	28.8	5.3	70.5	3.32
(present study)	140	28.8	4.9	70.5	3.37
Natural rubber ²	300	35.2	8.5	27.69	1.48
assuming (120) growth face	251	35.2	7.13	27.69	1.55
Gutta percha ¹⁵ :					
low melting form	247	43.5	7.0	20.15	1.47
high melting form	492	58.0	9.7	23.59	2.27
Polyethylene ¹⁶	540	0.06	0.009	18.3	1.86

The value of the surface free energy σ_e of a folded chain nucleus is related to the work required to form a fold¹⁷.

$$\sigma_e = \sigma_{e0} + \frac{q}{2A_0}$$

where q is the work required to form a fold, A_0 is the cross-sectional area of the polymer molecule and σ_{e0} is the contribution to σ_e due to factors other than folding. To a reasonable approximation σ_{e0} can be equated to σ .

$$\therefore \frac{\sigma_e}{\sigma} = 1 + \frac{q}{2A_0\sigma} \quad (4)$$

Values of q obtained using this relationship are shown in Table 2. q contains an important contribution from the internal rotational potential of atoms or groups in the loop and the trends obtained are consistent with the trends in the molecular structure. The values of q

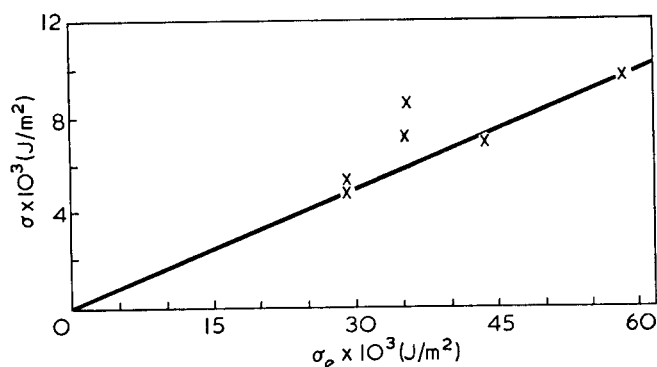


Figure 12 Graph of surface free energy σ versus end surface free energy σ_e

of natural rubber and gutta percha (low melting form) are lower than that for polyethylene presumably owing to a less constrained system resulting from a larger number of bonds in the loop. The high value of q is obtained for iPS due to the steric hindrance of the phenyl groups causing a highly constrained system. Assuming the same number of monomer units/fold (i.e. 2) for both crystal structures of gutta percha, the high melting form (HMF) has the larger value of q because the larger value of a_0 produces a more constrained chain, where a_0 is the monomolecular width. (Gutta percha LMF: $a_0 = 0.426$ nm, $b_0 = 0.437$ nm; HMF: $a_0 = 0.479$ nm, $b_0 = 0.493$ nm.)

From the above analysis it may be inferred that $q/2A_0\sigma$ is nearly constant and equal to 4.8 ± 0.8 . This in itself is not unreasonable since the factors ($q/2A_0$) and σ will both be determined by the molecular structure of the chain involved. Since all of the polymers considered are non-polar the properties determining these parameters will be those of simple van der Waal's forces and steric hindrance. To a first approximation it is, therefore, possible to obtain a value for σ_e from kinetic data by substituting $\sigma_e^2/5.8$ for $\sigma\sigma_e$ in the Hoffman-Lauritzen expression.

ACKNOWLEDGEMENTS

We are grateful to Professor E. H. Andrews for many valuable discussions and to the SRC for support through a Research Grant.

REFERENCES

- Keith, H. D. and Padden, F. J. Jr *J. Appl. Phys.* 1964, **35**, 1270
- Andrews, E. H., et al. *Proc. R. Soc. (A)* 1971, **324**, 79
- Andrews, E. H. *Proc. R. Soc. (A)* 1964, **277**, 562
- Owen, P. J. *PhD Thesis* University of London, 1970
- Charlesby, A. 'Atomic Radiation and Polymers', Pergamon, New York, 1960
- Andrews, E. H. *Proc. R. Soc. (A)* 1962, **270**, 232
- Boon, J., et al. *J. Polym. Sci. (A-2)* 1968, **6**, 1791
- Suzuki, T. and Kovacs, A. J. *Polym. J.* 1970, **1**, 82
- Lauritzen, J. I. and Hoffman, J. D. *J. Res. Nat. Bur. Stand.* 1960, **64A**, 1
- Hoffman, J. D. and Weeks, J. J. *J. Chem. Phys.* 1962, **37**, 1723
- Karasz, F. E., et al. *J. Phys. Chem.* 1965, **69**, 2657
- Magill, J. H. *J. Appl. Phys.* 1964, **35**, 3249
- Kavesh, S. and Schultz, J. M. *J. Polym. Sci. (A-2)* 1971, **9**, 85
- Blais, J. J. B. P. and Manley, R. St John. *J. Macromol. Sci. (B)* 1967, **1**, 525
- Ong Eng Long, *PhD Thesis*, University of London, 1973
- Gornick, F. and Hoffman, J. D. *Ind. Eng. Chem.* 1966, **58**, 41
- Hoffman, J. D. and Lauritzen, J. I. Jr *J. Res. Nat. Bur. Stand.* 1961, **65A**, 297

High temperature vulcanization of elastomers:

2. Network structures in conventional sulphenamido-sulphur natural rubber vulcanizates

C. T. Loo

*Institute of Polymer Technology, Loughborough University of Technology,
Loughborough, Leics LE11 3TU, UK
(Received 30 October 1973; revised 4 December 1973)*

A natural rubber (NR) gum mix with a conventional *N*-cyclohexyl-2-benzothiazylsulphenamide (CBS) accelerated sulphur system (0.5:2.5 CBS/S) was vulcanized at temperatures from 140°C to 200°C. The influence of cure temperature on (a) the chemical crosslink density, (b) the distribution of crosslink types, (c) the extent of sulphidic main-chain modifications, and (d) the zinc sulphide formation was investigated. Results show that elevated cure temperatures produce a network with a lower crosslink density, in particular a lower polysulphidic crosslink density. The formation of intramolecular sulphidic groups and zinc sulphide increases with increasing temperatures. The possibility of chain scission during vulcanization was examined by a quantitative analysis of the sol-gel data. Less than 1 site of scission per 100 crosslinked isoprene units was established in the temperature range of 140–200°C. The network results can be satisfactorily correlated with the physical properties of a tyre tread mix of NR as reported in Part 1. Mechanistic interpretations are made to account for the network results.

INTRODUCTION

In Part 1¹, results were reported to show that high vulcanization temperatures (for example 180–200°C) produce vulcanizates with inferior physical properties. This work suggested a more fundamental study of the network structures formed at various vulcanization temperatures.

It is now well established that the network structures present in an accelerated-sulphur vulcanizate^{2,3} can be schematically represented as in *Figure 1*. They include chemical crosslinks of various sulphur ranks (mono-, di-, and poly-sulphide crosslinks), intramolecular sulphidic groups (cyclic sulphides, pendent sulphidic

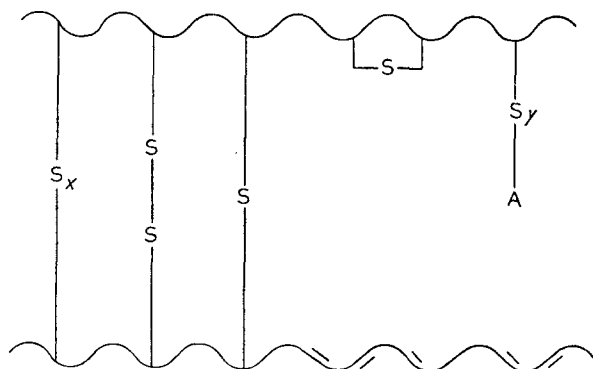


Figure 1 Structures in an accelerated sulphur vulcanizate of natural rubber. S, sulphur atom; A, accelerator residue. $x \geq 3$; $y \geq 1$

groups terminated by an accelerator fragment) and conjugated unsaturation. However, these network features were generally determined for vulcanizates prepared at a conventional temperature of 140°C, and thus the network features of vulcanizates cured at a higher temperature than 140°C are scarcely understood. This paper reports the findings of the influence of cure temperature (140–200°C) and times on the network structures of natural rubber vulcanizates in terms of: (i) the chemical crosslink density; (ii) the distribution of crosslink types; (iii) the extent of main-chain modifications by intramolecular sulphidic groups; and (iv) any main-chain scission occurring during vulcanization in the case of a conventional *N*-cyclohexyl-2-benzothiazylsulphenamide (CBS) accelerated sulphur system (0.5 part CBS/2.5 parts sulphur by wt).

Chain scission during vulcanization

In many network investigations, main-chain scission during vulcanization has been assumed to be negligible. Because of the high temperatures used for vulcanization in the present work, it was considered essential to attempt a quantitative estimation of chain scission as this might account for the inferior properties of the vulcanizates. The methods used to estimate chain scission during network formation are the analysis of sol-gel data⁴⁻⁶, stress relaxation⁷ and the use of the empirical relationship between the crosslink density and the onset of finite extensibility in the Mooney-Rivlin

plot of equilibrium stress-strain data⁸. The stress relaxation method which involves the use of the 'two-network' theory has been stated to be deficient^{7, 9, 10}. Chain scission results estimated from the onset of finite extensibility should be taken with reservation because of the need for exceedingly precise stress-strain data³. Sol-gel analysis is more reliable, and has been successfully applied by different authors^{4, 6, 11, 12}. In this paper, estimation of chain scission obtained using the sol-gel method and also some data for the onset of finite extensibility are reported.

EXPERIMENTAL

Preparation of vulcanizates

The natural rubber gum mix (Table 1) was prepared by the standard procedure on a two-roll mill at 70–80°C to attain a Wallace Rapid plasticity (100°C, 1 cm platen; BS 1673, Part 3, 1969) of 20. The mix was vulcanized in a steam-heated press for various times at a range of temperatures (140–200°C ± 0.5°C) to produce sheets 150 × 150 × 1 mm. Mouldings were cooled rapidly in water at the end of the curing cycle.

Determination of (\bar{M}_n) of the uncured rubber in the mix

The \bar{M}_n value of the rubber hydrocarbon component in the mix was determined from the limiting viscosity number, $[\eta]_{\text{toluene}}(\text{dl/g})$ at 25°C by means of the relationships¹³:

$$[\eta]_{\text{toluene}} = 1.076[\eta]_{\text{benzene}} - 0.15$$

and

$$[\eta]_{\text{benzene}} = 2.29 \times 10^{-7} \bar{M}_n^{1.33}$$

Determination of chemical crosslink density

The density of chemical crosslink was estimated from the value of the elastic constant, C_1 , using the Mullins relationship¹⁴ which was established to account for the contributions of chain ends and physical entanglements in the natural rubber vulcanizates:

$$C_{1, \text{RH}} = [\rho RT (2M_{c, \text{chem}})^{-1} + 0.78 \times 10^6] \times (1 - 2.3M_{c, \text{chem}} \bar{M}_n^{-1}) \text{ dyne/cm}^2$$

where ρ is the vulcanizate density, R is the gas constant, T is the absolute temperature, \bar{M}_n is the initial molecular weight of rubber hydrocarbon in the mix. $[2M_{c, \text{chem}}]^{-1}$ is the density of chemical crosslink, and is reported as number of gmol/g rubber hydrocarbon (gmol/g RH).

Table 1 Mix formulation and molecular weight (\bar{M}_n)

Parts by weight	
Natural rubber (SMR 5)	100
Zinc oxide	5
Stearic acid	1
Antioxidant (Flectol H) ^a	2
N-cyclohexyl-2-benzothiazylsulphenamide	0.5
Sulphur	2.5
Wallace Rapid plasticity (100°C, 1 cm platen)	20
$[\eta]_{\text{toluene}}$ of rubber hydrocarbon component of mix at 25°C (dl/g)	2.93
$\bar{M}_n \times 10^{-5}$ of rubber hydrocarbon component of mix	2.14

^a Polymerized 1,2-dihydro-2,2,4-trimethylquinoline

$C_{1, \text{RH}}$, the elastic constant pertinent to the rubber hydrocarbon in the vulcanizate, was calculated from the measured value of C_1 with due allowance for the stiffening effect of non-reinforcing fillers and for the diluent effect of soluble extra-network materials in the network¹⁵.

Stress-strain measurement. The C_1 value was determined, via the Mooney-Rivlin plot, from the equilibrium stress-strain data obtained on the dry unextracted vulcanizate:

$$f/2A_0(\lambda - \lambda^{-2}) = C_1 + \lambda^{-1}C_2$$

where f is the force to extend a testpiece of unstrained cross-sectional area, A_0 ; λ is the extension ratio; and C_1 and C_2 are elastic constants. The extension ratio, λ^* , at which the Mooney-Rivlin plot departs from linearity by 2.5% of C_1 , was also measured for vulcanizates prepared at 160°C and 200°C.

In order to obtain a reliable C_1 value, a special apparatus was constructed to measure accurately the force produced in the testpiece held at a series of pre-determined extensions, allowing 90 sec for stress relaxation at each extension. This C_1 apparatus is a modification of the modulus tester described in BS 1673: Part A4 (1955), using a testpiece of similar shape but of 5 mm width and 1 mm thick.

Description of C_1 apparatus. The C_1 apparatus (Figure 2) consists of a triple beam balance (A) with sliding weights (B) and a dial weight application system (C) (Ohaus Dial-O-Gram model) capable of applying a maximum load of 1600 g and sensitive to ± 0.1 g.

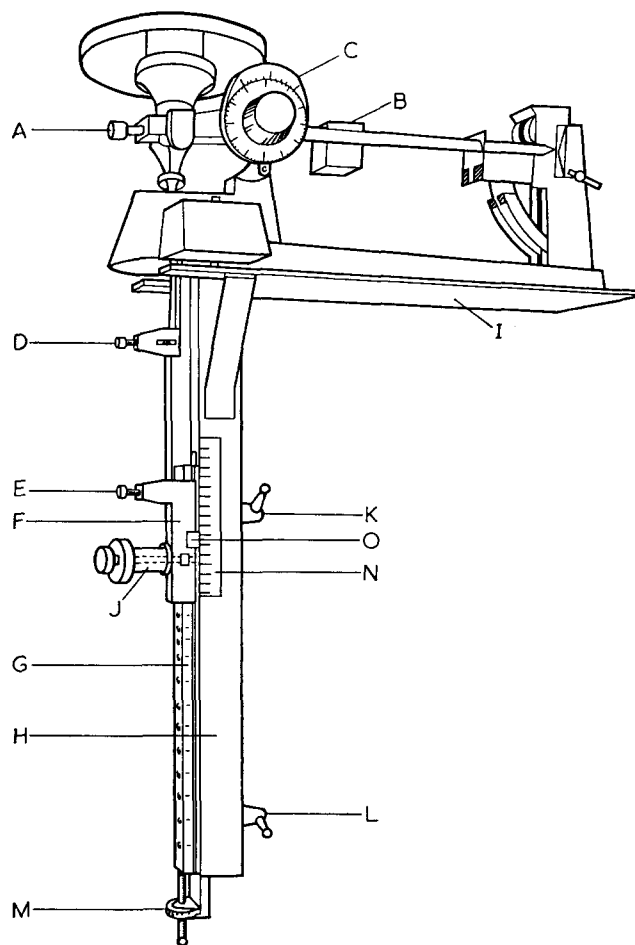


Figure 2 Construction of the elastic constant (C_1) apparatus

An upper grip (D) is attached to the underside of the balance pan by an extension rod. The lower grip (E) is incorporated in a slider (F) moving vertically along a rectangular column (G) clamped to a vertical channel member (H) which is fixed to the base of the balance (I). Both the specimen grips have screw operated jaws to hold the testpiece securely at each end. The column (G) is drilled at spaced intervals to accommodate a locating pin (J) forming part of the slider. This arrangement enables a series of predetermined extensions ($1 < \lambda < 3.5$), which were accurately calibrated using a cathetometer, to be applied to the rubber specimen. On releasing clamps K and L, the vertical position of the drilled column together with that of the lower grip can be precisely adjusted by a screw-thread operated control (M) situated at the bottom of the column. The extent of this movement can be obtained from the precision scale (N) and the indicator (O) fixed to the channel member and the slider respectively. This latter arrangement allows accurate determination of stress-strain data at very small extensions which can be used to extrapolate the specimen length (nominally 105 mm), between the grips, at zero strain.

Determination of the concentration of each crosslink type

The concentrations of three crosslink types (mono-sulphidic S_1 , disulphidic S_2 and polysulphidic S_x) were estimated from determinations of chemical crosslink densities of vulcanizates before and after treatment with thiol-amine chemical probes¹⁶ which specifically break particular crosslink types. Treatment of vulcanizates with propane-2-thiol (0.4 M) and piperidine (0.4 M) in *n*-heptane solution at room temperature for 2 h cleaves the polysulphidic crosslinks in the network. To cleave both di- and poly-sulphidic crosslinks, leaving monosulphidic crosslinks intact, the vulcanizates are treated with a solution of *n*-hexanethiol (1.0 M) in piperidine at 25°C for 48 h. Assuming that the carbon-carbon crosslink is absent in the network, concentrations of mono-, di- and poly-sulphidic crosslinks can be arrived at. The experimental methods used were, in detail, those described by Campbell and Saville¹⁷.

Determination of the E , E' and F values

The crosslinking efficiency of sulphur, E , is defined as the number of sulphur atoms combined in the vulcanizate network per chemical crosslink present. F is the number of sulphide ions (principally as zinc sulphide) in the network per chemical crosslink present:

$$E = [S_c]/[2M_{c, \text{chem}}]^{-1}$$

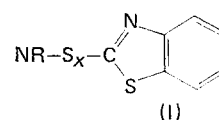
and

$$F = [S^{2-}]/[2M_{c, \text{chem}}]^{-1}$$

$[S_c]$ is the g atoms of sulphur combined in the network/ g RH whereas $[S^{2-}]$ is the g ions of sulphide sulphur present in the network/ g RH¹⁵. E' is the E value of the network after treatment with triphenylphosphine (Ph_3P) which merely reduces the rank of the sulphur in the crosslinks as well as that in the pendent sulphidic groups to 1 or 2¹⁸. The experiment of treating vulcanizates with triphenylphosphine was carried out at 80°C for 96 h *in vacuo* as described by Saville and Watson³.

The E value can be interpreted as a measure of overall structural complexity of a sulphur-vulcanized network,

i.e. the lower the E value, the more efficiently is the sulphur utilized in crosslink formation. The significance of E' is that $E' - 1$ (or 2) is a direct measure of sulphur combined in the main-chain modifications such as the cyclic sulphidic groups and pendent sulphidic groups existing as:



where $x \geq 1$

Chemical analysis of the sulphur content

The vulcanizates were extracted with hot azeotropic solvents (chloroform/methanol/acetone) for 96 h in the dark in an atmosphere of nitrogen. The chemically combined sulphur in the network, $[S_c]$, was determined as the difference between the total sulphur content present in the extracted vulcanizate (i.e. $[S_c] + [S^{2-}]$) and the content of sulphide sulphur, $[S^{2-}]$, present in the same vulcanizate.

The total sulphur content was determined by the Schöniger method of combusting the extracted vulcanizate (about 0.02 g) between platinum electrodes in oxygen. The sulphur dioxide produced was absorbed by hydrogen peroxide, and the sulphate ions were quantitatively titrated with barium perchlorate¹⁹.

Sulphide sulphur was measured iodometrically from the formation of cadmium sulphide as described in BS 903: Part B10 (1958).

Determinations of the sol and gel fractions

The vulcanizates were extracted with hot acetone in the dark for 3 days, and dried to constant weight *in vacuo* at room temperature. Weighed samples of extracted vulcanizates (about 1 g) were continuously extracted with cold benzene in the dark, for 8–10 days, the benzene being renewed three times during this period. After benzene extraction, samples were dried to constant weight *in vacuo*. The sol fraction (S) was then estimated from the loss in weight during benzene extraction. Sol determinations were made in duplicate.

The gel fraction⁴ (q , fraction of sites at which crosslinking has occurred) was calculated from $[2M_{c, \text{chem}}]^{-1}$ estimated from the stress-strain measurement. The application of the Mullins calibration in estimating the density of chemical crosslink assumes no chain scission during vulcanization. Bristow has pointed out that the error in the calculated value of q caused by not correcting for chain scission would be negligible provided the scission is not large ($< 2\%$ scission)⁶.

RESULTS AND DISCUSSION

Chemical crosslink density

The results of $[2M_{c, \text{chem}}]^{-1}$ for the NR mix with a conventional CBS/accelerated sulphur system vulcanized for various times at 140–200°C are plotted in Figure 3. These plots reveal clearly that the maximum density of chemical crosslinks in the network falls substantially, and the rate of subsequent reduction in crosslink density increases as the vulcanization temperature is raised from 140°C to 200°C. In other words, the conventional cure system as widely used in tyre tread compounds suffers serious reversion, in terms of the density of chemical

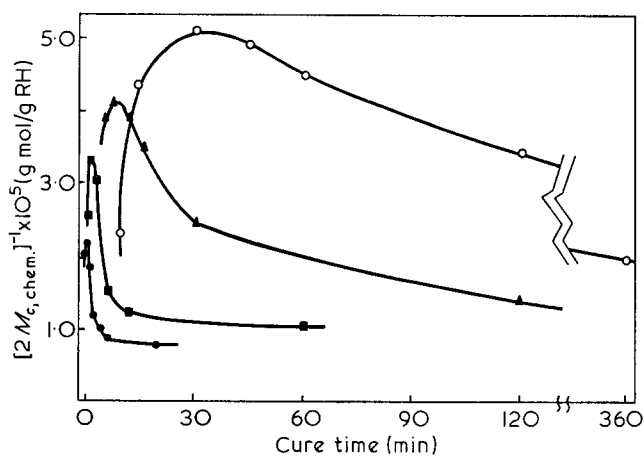


Figure 3 Influence of vulcanization temperature and time on the crosslink density for the conventional cure system (Table 1). \circ , 140°C; \blacktriangle , 160°C; \blacksquare , 180°C; \bullet , 200°C

crosslink, during high temperature vulcanization, as well as on prolonged curing at 140°C. These findings agree well with those previously reported^{20, 21}.

Distribution of mono-, di- and poly-sulphidic crosslinks

To understand better the above results for chemical crosslink density, it is highly desirable to examine at various cure times how the vulcanization temperature influences the concentration of each crosslink type. Figures 4-7 summarize the results of this investigation. They show that the crosslinks formed initially in the network during vulcanization at 140-200°C are polysulphidic. On prolonged vulcanization, these polysulphidic crosslinks disappear while a higher proportion of mono- and di-sulphidic crosslinks is formed in the network. This conclusion is consistent with the reactions of model olefins with sulphur additives² and the reported work on network characterization of vulcanizates cured at 140°C²².

The four Figures (Figures 4-7) for the four vulcanization temperatures 140°C, 160°C, 180°C, 200°C further show that the reduction in the chemical crosslink density with increasing temperature is due to a considerable drop in the number of polysulphidic crosslinks and to a moderate drop in the number of disulphidic crosslinks. At all four temperatures, the concentration of monosulphidic crosslinks builds up slowly to about 1 g mol/g RH on prolonged cure. These results will be further discussed mechanistically alongside additional results reported below. As expected from the order of bond energy, these results suggest that the order of decreasing thermal stability of the crosslink types is: $S_1 > S_2 > S_x$. It is to be expected, therefore, that a vulcanization system which produces monosulphidic crosslinks in the network in greater quantity and more rapidly such as the efficient vulcanization system^{23, 24} will resist thermal degradation better during high temperature vulcanization.

Crosslinking efficiencies of sulphur

Table 2 shows the influence of vulcanization temperature on the values of E and E' at various times. At 140°C, E varies from 10 at undercure to 27 at overcure, indicating that the present cure system is inefficient in crosslink formation. The high E' values (4-25) together with the high E values establish that a considerable

amount of network combined sulphur is wasted in forming intramolecular sulphidic groups (43% for the 15 min cure increasing to 93% for the 360 min cure). The calculated values of % $[S_c]$ removed by triphenylphosphine treatment reveal clearly that a large amount

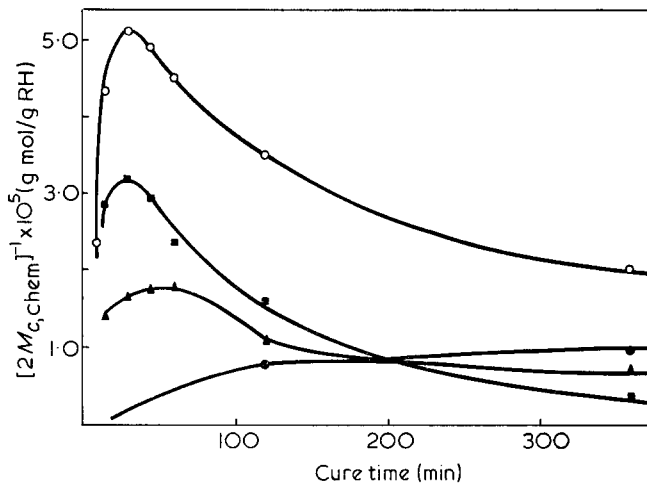


Figure 4 Distribution of crosslink types as a function of cure time at 140°C for the conventional cure system (Table 1). \circ , Total crosslinks; \bullet , monosulphidic crosslinks; \blacktriangle , disulphidic crosslinks; \blacksquare , polysulphidic crosslinks

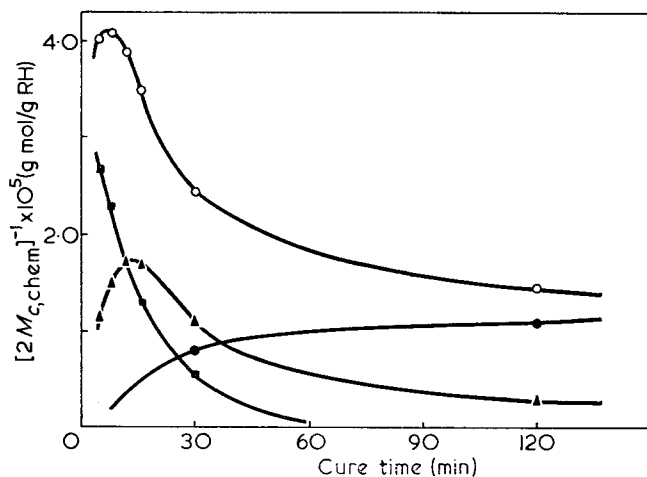


Figure 5 Distribution of crosslink types as a function of cure time at 160°C for the conventional cure system (Table 1). \circ , Total crosslinks; \bullet , monosulphidic crosslinks; \blacktriangle , disulphidic crosslinks; \blacksquare , polysulphidic crosslinks

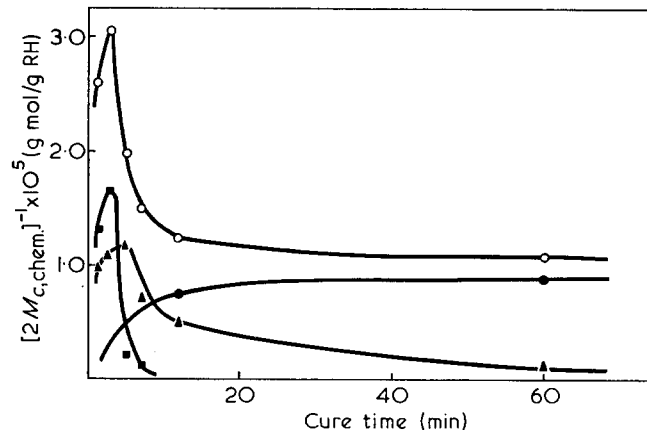


Figure 6 Distribution of crosslink types as a function of cure time at 180°C for the conventional cure system (Table 1). \circ , Total crosslinks; \bullet , monosulphidic crosslinks; \blacktriangle , disulphidic crosslinks; \blacksquare , polysulphidic crosslinks

of network combined sulphur exists initially as polysulphidic crosslinks as the results of the analysis for crosslink types show. The presence of sulphur in the pendent groups (I) cannot contribute much to the $[S_c]$ values since the total sulphur content (i.e. $[S_c] + [S^{2-}]$) measured does not exceed 8.05×10^{-4} g atoms/g RH which is equivalent to 2.5 g of sulphur/100 g of natural rubber.

As vulcanization temperatures are raised from 140°C, values of E and E' increase, especially at long cure times. This result means that the extent of sulphur-containing main-chain modifications increases with increasing curing temperatures. These main-chain modifications probably exist as a minor proportion of pendent

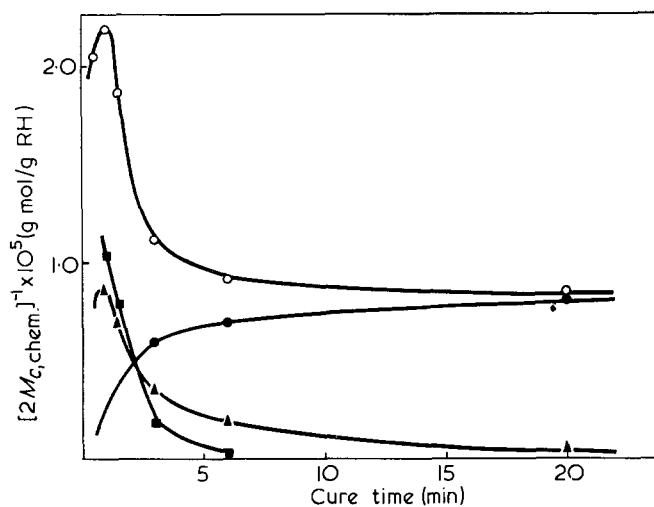


Figure 7 Distribution of crosslink types as a function of cure time at 200°C for the conventional cure system (Table 1). ○, Total crosslinks; ●, monosulphidic crosslinks; ▲, disulphidic crosslinks; ■, polysulphidic crosslinks

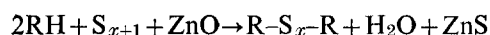
Table 2 Chemical characterization of vulcanizate networks

Vulcanization time (min)	$C_1, RH \times 10^{-5}$ (N/m ²)	$[2M_{c,chem}]^{-1} \times 10^5$ (g mol/g RH)	Network combined sulphur $\times 10^4$ (g atoms/g RH)		Sulphur efficiencies (atoms/chemical crosslink)		% $[S_c]$ removed by Ph_3P treatment	$[S^{2-}]$ sulphide sulphur $\times 10^4$ (g atoms/g RH)	F (sulphide ions/chemical crosslink)
			$[S_c]$, before Ph_3P treatment	$[S_c]$, after Ph_3P treatment	E	E'			
At 140°C:									
15	1.55	4.35	4.29	1.86	9.9	4.3	57	1.00	2.3
30	1.73	5.10	5.47	3.15	10.7	6.2	42	1.50	2.9
45	1.67	4.90	5.79	—	11.8	—	—	1.54	3.1
120	1.34	3.50	5.54	4.72	15.8	13.5	15	1.97	5.6
360	0.92	2.00	5.40	5.04	27.0	25.2	7	2.22	11.1
At 160°C:									
5	1.47	4.03	4.43	2.04	11.0	6.0	45	1.22	3.0
8	1.49	4.10	5.61	3.00	13.7	7.3	47	1.54	3.8
12	1.45	3.90	5.83	3.75	15.0	9.6	36	1.64	4.2
30	1.06	2.45	5.61	5.47	22.9	22.3	5	2.11	8.6
120	0.72	1.45	5.47	5.44	37.7	37.5	1	2.32	16.0
At 180°C:									
2	1.29	3.30	5.33	3.36	16.2	10.2	37	1.43	4.3
3	1.22	3.05	5.51	3.65	18.1	12.0	34	1.72	5.6
5	0.92	2.00	6.15	5.44	30.8	27.2	12	1.93	9.7
60	0.55	1.08	5.44	5.40	50.4	50.0	1	2.25	20.8
At 200°C:									
2	0.60	1.20	5.83	4.72	48.5	39.3	19	1.61	13.4
3	0.57	1.12	5.90	5.01	52.7	44.7	15	1.79	16.0
20	0.41	0.85	5.22	4.79	61.4	56.4	8	2.22	26.1

groups terminated with accelerator residues, and a major proportion of cyclic monosulphidic groups which latter are formed intramolecularly by the reactions of polysulphidic sulphur with the double bond in the rubber chain²⁵. Further, the increase in cyclic sulphur formation could be accompanied by an increase in the conjugated triene content^{2, 26}.

Formation of sulphide sulphur during vulcanization

The formation of sulphide sulphur during vulcanization has been investigated by many authors^{2, 27-29} whose conclusions can be briefly summarized as follows: (a) under conditions for efficient crosslinking, the formation of sulphide sulphur is closely associated with the formation of a crosslink. In this case, the ratio of sulphide ions to crosslinks (F value) approaches unity:



(b) under conditions where crosslinking is inefficient, and on prolonged vulcanization, the formation of sulphide sulphur is additionally related to: the extent of crosslink decomposition; the reaction of sulphur with zinc salts of accelerator; and the reaction of zinc oxide or zinc soap with hydrogen sulphide which could be produced thermally by sulphur-sulphenamide or sulphur-amine reactions.

Table 2 shows the results of the effect of increasing vulcanization temperatures (140–200°C) on the formation of sulphide sulphur. The F values are high (> 1), reflecting the inefficiency of the present cure system in crosslink formation. Increasing the vulcanization temperature brings an increase in the F values especially on extended cure. This suggests that more zinc sulphide was produced at the expense of crosslink decomposition. In view of the low concentration of CBS accelerator

Table 3. Sol-gel data for vulcanizates prepared at 140–200°C

Vulcanization time (min)	Sol		Gel	
	Wt %	$S + S^{1/2}$	$[2M_{c,chem}]^{-1} \times 10^5$ (g mol/g RH)	$q^{-1} \times 10^{-2}$
At 140°C:				
15	0.233	0.0497	4.35	1.69
30	0.205	0.0473	5.10	1.44
60	0.259	0.0535	4.50	1.63
120	0.386	0.0660	3.50	2.10
360	1.072	0.1142	2.00	3.68
At 160°C:				
5	0.242	0.0526	4.03	1.82
8	0.227	0.0499	4.10	1.79
16	0.445	0.0712	3.50	2.10
30	0.724	0.0924	2.45	2.99
120	2.218	0.1708	1.45	5.05
At 180°C:				
1.5	0.608	0.0842	2.60	2.82
2	0.436	0.0704	3.30	2.23
5	1.046	0.1128	2.00	3.68
12	2.745	0.1932	1.25	5.88
60	3.814	0.2334	1.08	6.80
At 200°C:				
1	1.010	0.1106	2.18	3.37
1.5	1.239	0.1237	1.87	3.92
2	2.637	0.1888	1.20	6.13
4	3.848	0.2347	1.05	6.99
20	4.869	0.2694	0.85	8.62

used, the formation of sulphide sulphur by the reaction of sulphur with the zinc salt of accelerator and by the reaction of zinc compounds with hydrogen sulphide is of less importance.

Main-chain scission during vulcanization

The determinations of the sol and gel fractions for vulcanizates prepared at 140–200°C for various times are recorded in Table 3. To measure the extent of chain-scission during vulcanization, the sol-gel data were analysed using the relationship established by Charlesby and Pinner⁴:

$$S + S^{1/2} = pq^{-1} + (q\bar{y}_n)^{-1}$$

where S is the sol fraction, p and q are the fractions of sites at which random scission and crosslinking have occurred respectively, and \bar{y}_n is the number-average chain length of an uncured polymer having a random chain length distribution. Crosslinking and chain-scission are expected to be random during vulcanization. The chain length distribution, in the case of the present NR mix which has been milled to a limiting viscosity number of 2.93 dl/g, should be close to random because it has been shown that the NR mixes milled to a viscosity in the range $1.5 < |\eta| < 4.0$ dl/g possess a random distribution with very small deviation³⁰. These facts justify plotting the sol-gel data as $S + S^{1/2}$ against q^{-1} to give a linear line of slope \bar{y}_n^{-1} and intercept pq^{-1} (ratio of scission/crosslinking).

Figure 8 is the Charlesby-Pinner plot of the sol-gel data given in Table 3. A linear fit to all the data proves that there is negligible dependence of the ratio of scission/crosslinking on cure temperature in the range 140–200°C. The linear equation derived from the application of the least squares principle is:

$$S + S^{1/2} = -0.0024 + 3.26 \times 10^{-4} q^{-1}$$

A value for pq^{-1} of -0.0024 , which is not very different from zero, suggests that there is no chain scission during vulcanization at 140–200°C. This proves the validity of the assumption used in the Mullins calibration. A further statistical analysis of the plotted data shows that pq^{-1} is less than 0.0083 at 90% confidence limit. This means that less than one random chain scission has occurred for every hundred crosslinks formed in the network. As a check on the accuracy of the plot (Figure 8), the value of \bar{M}_n , computed from the slope of the line, is 2.09×10^5 which is very close to the \bar{M}_n value of 2.14×10^5 obtained using the solution viscosity method¹³. The sol content in the benzene extract was also recovered by freeze drying, and examination of its infra-red spectrum showed that it was, indeed, the hydrocarbon of natural rubber.

Table 4 records the change of C_1 values with λ^* values of vulcanizates prepared at 160°C and 200°C. According to the empirical relationship between C_1 and λ^* established by Mullins⁸, C_1 depends on both crosslink density and the molecular weight of the primary rubber chain, while λ^* varies with crosslink density but is independent of the initial molecular weight. Results

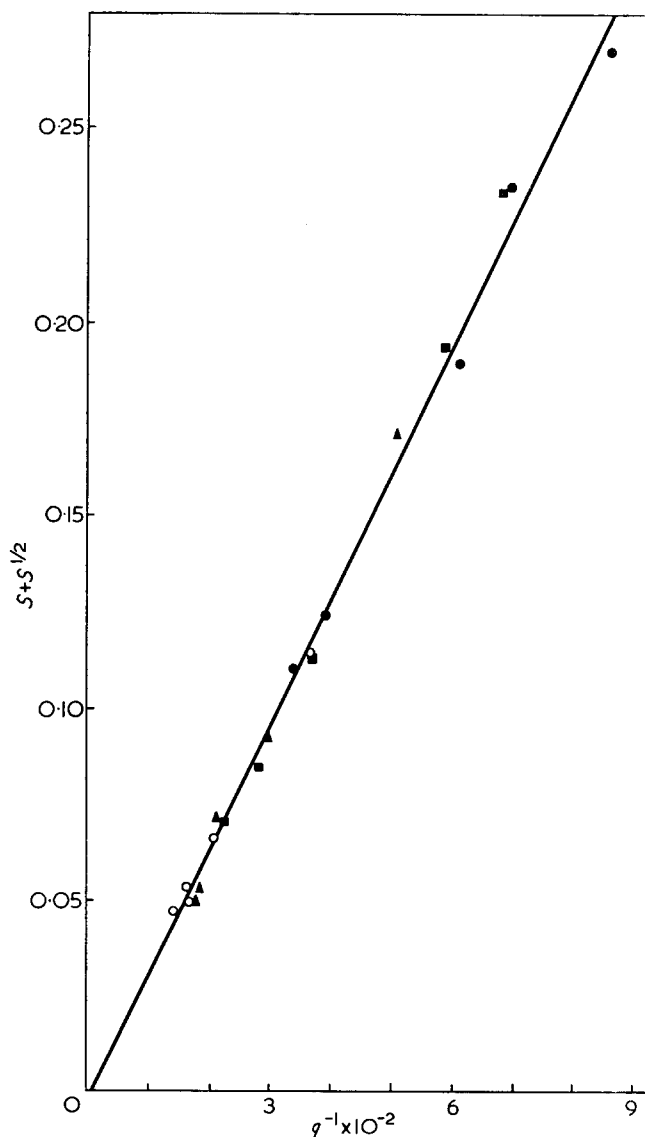


Figure 8 Plot of $S + S^{1/2}$ versus q^{-1} for natural rubber vulcanized with a conventional cure system (Table 1), at 140°C–200°C. ○, 140°C; ▲, 160°C; ■, 180°C; ●, 200°C

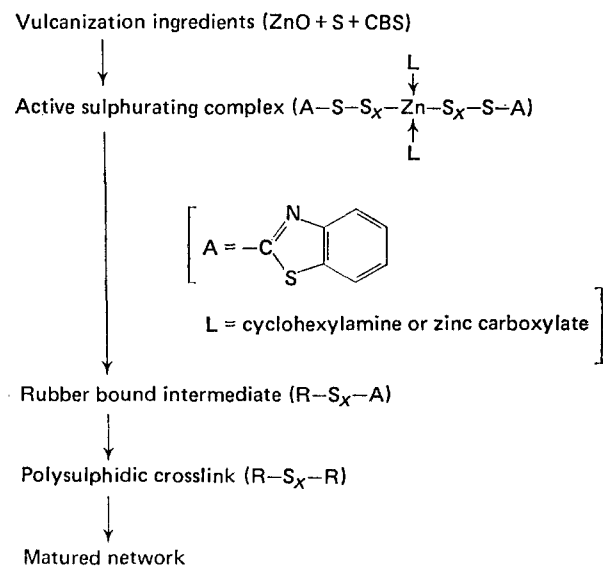
Table 4 Values of C_1 and λ^* for vulcanizates prepared at 160°C and 200°C

Vulcanization time (min)	$C_1 \times 10^{-5}$ (N/m ²)	λ^*
At 160°C:		
5	1.42	2.89
8	1.44	2.74
12	1.40	2.78
16	1.30	2.79
30	1.03	2.82
120	0.70	3.17
At 200°C:		
1	0.95	2.94
1.5	0.85	2.98
3	0.56	3.03
4	0.50	3.13
6	0.44	3.18
220	0.39	3.23

(Table 4) show that λ^* increases as C_1 decreases when the vulcanization temperature is raised from 160°C to 200°C. This indicates that there is no reduction in the molecular weight of the rubber chains as vulcanization temperatures are increased. This same conclusion was reached by Porter²⁰. Therefore, the result inferred from the values of λ^* and C_1 appears to support the conclusion found from the sol-gel analysis.

Mechanistic interpretations

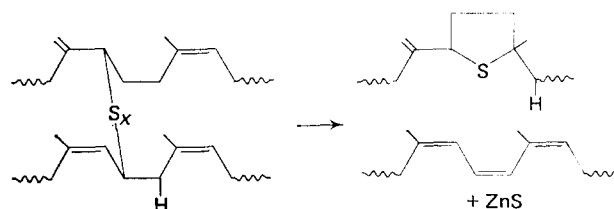
The mechanism of sulphur vulcanization is extremely complex, and has been extensively studied and reviewed^{2, 31}. To ease the present discussion, the important stages in the course of a sulphenamide-accelerated sulphur vulcanization may be briefly summarized as follows³¹:



The active sulphurating complex is the zinc mercaptide coordinated with ligands (L) which render it more soluble in rubber. The rubber bound intermediate is the crosslink precursor. The polysulphidic crosslink formed initially undergoes maturation consisting of three competitive reactions, namely, desulphuration, decomposition and interchange of sulphur bonds. The relative rates of these maturing reactions are governed

by the structure of the crosslink termini, the concentration of active sulphurating complex, and the temperature of vulcanization.

Effect of cure temperature on maturing reactions. In the present system, the low concentration of the sulphurating complex of zinc mercaptide promotes formation of polysulphidic crosslinks predominantly at the carbon atom α -methylene to the double bond of the rubber macromolecule². Such polysulphidic crosslinks can only desulphurate slowly, thus rendering the crosslinks very susceptible to thermal decomposition at high cure temperatures. This leads to the formation of cyclic sulphides, conjugated dienes and trienes and zinc sulphide:

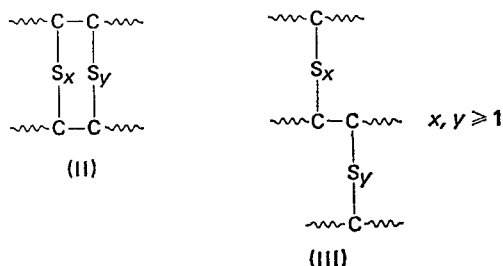


Interchange of polysulphidic crosslinks is catalysed by zinc mercaptide and its complexes. Reactions between these complexes and model crosslinks at 50–140°C have shown that interchange at 140°C is less effective than that occurring at lower temperatures³². This result suggests that interchange during maturation at the elevated cure temperature (above 140°C) would be less effective, resulting in polysulphidic crosslinks of higher sulphur ranks. Since thermal instability increases with the number of sulphur atoms in the crosslink, such polysulphidic crosslinks would also be more prone to thermal destruction.

These maturing reactions certainly play an important role in the influence of cure temperature on: (i) the chemical crosslink density (Figure 3); (ii) the concentrations of different crosslink types (Figures 4–7); and (iii) the extent of main-chain modifications (Table 2). However, in view of the much lower density of chemical crosslinks at the higher cure temperatures, it is unlikely that this is the sole explanation. It may be that fewer polysulphidic crosslinks are initially formed at the higher cure temperatures owing to fewer effective sulphurating complexes or fewer polysulphidic pendent groups (I) being available.

Effect of curing temperature on crosslinking intermediates, prior to crosslink formation. At high cure temperature, it is possible that the sulphurating complexes of zinc mercaptide possess a reduced intrinsic activity as they remain partly dissociated³². Although the cyclohexylamine complex of zinc mercaptide has recently been reported to be stable up to 160°C³³, temperatures in the neighbourhood of 200°C may decompose part of these sulphurating complexes into some unreactive products. In consequence, some sulphur may react directly with the rubber chain without any formation of crosslink. It is of particular interest that the reaction of sulphur with olefin at temperatures above 140°C favours the intramolecular sulphuration and dehydrogenation³⁴. Another consequence is that some of the polysulphidic crosslinks formed at higher cure

temperatures may exist as *vicinal* crosslinks as in (II) and (III) which act physically as a single crosslink:



Pendent accelerator groups of polysulphidic character can be expected to undergo desulphuration, decomposition and interchange in the presence of sulphurating complexes of zinc mercaptide. While interchange between this rubber bound intermediate and zinc perthiomercaptide (formed from zinc mercaptide) could lead to crosslink formation, desulphuration and decomposition could be the predominant reactions at high cure temperatures.

A combination of these postulated mechanisms and the maturation of crosslinks could adequately account for the lower crosslink density, and the higher E , E' and F values obtained at higher cure temperatures.

Comparison with an unaccelerated sulphur vulcanization. Table 2 shows that at the high temperature of 200°C, about 48 to 61 sulphur atoms are combined in the network to form one chemical crosslink. The fact that these E values are as high as those of an unaccelerated sulphur system^{35, 36} suggests that the mechanism of an unaccelerated sulphur vulcanization may become operative at high cure temperatures. However, the known characteristics of an unaccelerated sulphur vulcanization cannot rationalize the following aspects of the present network results. First, the crosslink density of an unaccelerated sulphur vulcanizate of NR has been found to increase with increasing cure temperatures (140°C, 150°C and 160°C)³⁷. This is clearly contrary to the results shown in Figure 3. Second, it has been established that, in the case of an unaccelerated sulphur vulcanization, chain scission occurs during the vulcanization, and the extent of scission increases with increasing cure time³⁵. These findings are inconsistent with the results as shown in Figure 8. Third, the rate of vulcanization for an unaccelerated sulphur vulcanization is exceedingly slow, and it is unlikely that it will effectively compete with the much faster rate of an accelerated vulcanization, as observed experimentally.

Correlation of network structure and properties

The network results obtained for the present gum mix can be correlated with the physical properties of the filled NR mix, having a similar cure system, reported in Part 1. This correlation is justified as Porter^{38, 39} has shown that the presence of carbon black alters the crosslinking efficiency of sulphur and network structure only slightly.

Part 1 showed that elevated cure temperatures reduce the tensile strength, tear strength and resilience of NR vulcanizates. It is now clear that this lower level of properties can be attributed to a lower level of chemical crosslinks in the vulcanizates, in particular a lower number of polysulphidic crosslinks, and also to extensive main-chain modification which inhibits strain-induced

crystallization. The sol-gel results show that this lower level of properties is not due to any chain scission during high temperature vulcanization.

In the case of the present cure system, vulcanizate networks produced at elevated temperatures and after long cure times consist of a major proportion of mono-sulphidic crosslinks (Figures 6 and 7) and a highly modified main-chain structure. It is worth noting that such network arrangement gave good resistance to flex fatigue as previously reported in Part 1. This unexpected finding has been recently confirmed by Bristow and Tiller⁴⁰ and by Blackman and McCall²⁶. They have shown that the unaged fatigue life of such networks equals that of a network consisting of a high proportion of polysulphidic crosslinks (about 70%) and some degree of main-chain modification ($E' = 7$) as encountered in the conventional sulphenamamide-accelerated system cured at 140°C.

The effect of cure temperatures on the microstructure of rubber chains, particularly the *cis-trans* isomerized groups, has not been investigated in this paper. Recently, evidence has been obtained from infra-red analysis that *cis-trans* isomerism and polymer cyclization also occurred during vulcanization at high temperatures²¹. It is well known that the strength of vulcanizates can drop sharply if substantial *cis-trans* isomerized groups have been formed in the vulcanizate networks⁴¹. The irregularity caused by the presence of these undesirable microstructures in the network produced during high temperature vulcanization can evidently bring about a much lower level of physical properties.

CONCLUSIONS

Increasing the cure temperature from 140°C to 200°C causes a reduction in the crosslink density, particularly the density of polysulphidic crosslinks. At elevated cure temperatures, a high proportion of network-combined sulphur is wasted in forming intramolecular sulphidic groups and an increased amount of zinc sulphide is simultaneously produced. The extent of chain scission in the vulcanization at 140–200°C was found to be negligible. These network results correlate well with the inferior physical properties in high temperature vulcanizates reported in Part 1. The mechanistic interpretations reveal that the maturing reactions of the polysulphidic crosslinks, formed at the initial stage of crosslinking, cannot satisfactorily account for all the network results. It is suggested that the influence of high cure temperatures on the thermal stability and reactivity of the various crosslinking intermediates, formed prior to crosslink formation, is important.

To counteract the reversion at high temperature vulcanization, it is suggested that a formulation must be chosen such that the polysulphidic crosslinks formed initially can desulphurate rapidly into a thermally stable network. This is not the case for the cure system reported here (Table 1). A sufficient number of crosslinks with a relatively low extent of main-chain modification must also be present in the final vulcanizates as will be shown in a subsequent paper.

ACKNOWLEDGEMENTS

The author is grateful to Dr C. M. Blow for his useful advice and guidance. His thanks are due to Drs D. S.

Campbell, M. Porter, B. K. Tidd, D. Barnard and G. M. Bristow (MRPRA) for their assistance and stimulating discussions, and to Mr G. L. Colter (Dunlop Limited, Tyre Technical Headquarters, Birmingham) for helping in the sulphur analyses. Acknowledgement is also made to Professor R. J. W. Reynolds for his interest and for granting facilities to carry out this work, and to Mr C. Lines for constructing the C₁ apparatus. The author also thanks the Malayan Rubber Fund Board for awarding a scholarship.

REFERENCES

- 1 Blow, C. M. and Loo, C. T. *J. Inst. Rubber Ind.* 1973, **7**, 205
- 2 Bateman, L., Moore, C. G., Porter, M. and Saville, B. 'The Chemistry and Physics of Rubber-like Substances', (Ed. L. Bateman), Maclaren, London, 1963, Ch 15
- 3 Saville, B. and Watson, A. A. *Rubber Chem. Technol.* 1967, **40**, 100
- 4 Charlesby, A. and Pinner, S. H. *Proc. R. Soc. (A)* 1959, **249**, 367
- 5 Scott, K. W. *J. Polym. Sci.* 1962, **58**, 517
- 6 Bristow, G. M. *J. Appl. Polym. Sci.* 1963, **7**, 1023
- 7 Moore, C. G. and Scalan, J. *J. Polym. Sci.* 1960, **43**, 23
- 8 Mullins, L. *J. Appl. Polym. Sci.* 1959, **2**, 257
- 9 Thomas, D. K. *Polymer* 1966, **7**, 125; *Rubber Chem. Technol.* 1967, **40**, 621
- 10 Calderon, N. and Scott, K. W. *J. Polym. Sci. (A)* 1965, **3**, 551
- 11 Bristow, G. M. *J. Appl. Polym. Sci.* 1964, **8**, 1619
- 12 Bristow, G. M. *J. Appl. Polym. Sci.* 1965, **9**, 3255
- 13 Bristow, G. M. and Wistall, B. J. *J. Appl. Polym. Sci.* 1965, **9**, 495
- 14 Mullins, L. *J. Appl. Polym. Sci.* 1959, **2**, 1
- 15 Bristow, G. M. and Porter, M. *J. Appl. Polym. Sci.* 1967, **11**, 2215
- 16 Campbell, D. S. *J. Appl. Polym. Sci.* 1969, **13**, 1201
- 17 Campbell, D. S. and Saville, B. *Proc. Int. Rubber Conf., Brighton* 1967, p 1
- 18 Moore, C. G. and Trego, B. R. *J. Appl. Polym. Sci.* 1964, **8**, 1957
- 19 White, D. C. *Mikrochim. Acta* 1962, **5**, 807
- 20 Porter, M., Skinner, T. D. and Wheelans, M. A. *J. Appl. Polym. Sci.* 1967, **11**, 2271
- 21 Polyak, M. A., Cernyak, N. B., Zakharov, N. D. and Kostyukina, G. I. *Int. Symp. Isoprene Rubber, Moscow* 1972
- 22 Campbell, D. S. *J. Appl. Polym. Sci.* 1970, **14**, 1409
- 23 Skinner, T. D. and Watson, A. A. *Rubber Age* 1967, **99**, 76
- 24 Russell, R. M., Skinner, T. D. and Watson, A. A. *Rubber Age* 1967, **99**, 69
- 25 Dogadkin, B. A., Shumanov, L. A. and Tutorsky, I. A. *Polymer* 1968, **9**, 413
- 26 Blackman, E. J. and McCall, E. B. *Rubber Chem. Technol.* 1970, **43**, 651
- 27 Barton, B. C. *J. Polym. Sci.* 1955, **18**, 559
- 28 Bhatnagar, S. K. and Banerjee, S. *J. Inst. Rubber Ind.* 1968, **2**, 177; *Rubber Chem. Technol.* 1969, **42**, 1366
- 29 Porter, M. *J. Appl. Polym. Sci.* 1967, **2**, 2255
- 30 Bristow, G. M. *J. Polym. Sci. (A)* 1963, **1**, 2261
- 31 Porter, M. 'The Chemistry of Sulfides', (Ed. A. V. Tobolsky), Interscience, New York, 1968, p 165
- 32 Milligan, B. *Rubber Chem. Technol.* 1966, **39**, 1115
- 33 Geiling, I. R. *Rubber Chem. Technol.* 1973, **46**, 524
- 34 Porter, M. in 'Mechanisms of Reactions of Sulphur Compounds' (Ed. N. Kharasch), Intra-Science Research Foundation, California, 1968, Vol 3, p 145
- 35 Moore, C. G., Mullins, L. and Swift, P. McL. *J. Appl. Polym. Sci.* 1961, **5**, 293
- 36 Moore, C. G. and Trego, B. R. *J. Appl. Polym. Sci.* 1961, **5**, 299
- 37 Chakravarty, P. K., Chatterjee, P. K. and Sicar, A. K. *J. Appl. Polym. Sci.* 1965, **9**, 1395
- 38 Porter, M. *Rubber Chem. Technol.* 1967, **40**, 866
- 39 Porter, M., *Kautsch. Gummi* 1969, **22**, 419
- 40 Bristow, G. M. and Tiller, R. F. *Kautsch. Gummi* 1970, **23**, 55
- 41 Cunneen, J. I. and Higgins, G. M. C. 'The Chemistry and Physics of Rubber-like Substances', (Ed. L. Bateman), Maclaren, London, 1963, p 36

Preparation and moduli of model polymer networks

D. J. Walsh, G. Allen and G. Ballard

Department of Chemistry, University of Manchester, Manchester M13 9PL, UK
(Received 1 August 1973; revised 30 November 1973)

Polystyrene containing a small number of randomly spaced *p*-substituted secondary amine groups has been prepared. This polymer has been crosslinked in solution at concentrations in the range 5–20%, by hexamethylene diisocyanate, to form gels. The moduli of these gels were measured and the results compared to theoretical predictions from rubber elasticity theory. The dependence of the moduli on the concentration at which crosslinking takes place has been explained in terms of chemical crosslinks, closed loops and entanglements. The results support a value for the ideal modulus of nkT , where n is the number of crosslinks per cm^3 .

INTRODUCTION

The kinetic theory of rubber elasticity leads to a general expression for the free energy change on deformation of a network of the form:

$$\Delta F_{el} = A \left(\frac{\nu}{2} \right) kT (\lambda_x^2 + \lambda_y^2 + \lambda_z^2 - 3) - B\nu kT \ln \lambda_x \lambda_y \lambda_z \quad (1)$$

where ν is the number of elastically effective network chains (which in an ideal network is equal to the total number of chains due to the absence of defects),

k is the Boltzmann constant,

T is the absolute temperature,

$\lambda_x \lambda_y \lambda_z$ are the deformation ratios in each direction specified by the x , y and z axis, and

A and B are constants.

The theories of Flory and Wall^{1–4} sum over all the chains in the network before and after deformation and result in a specific form of equation (1) with $A=1$ and $B=\frac{1}{2}$. On the other hand, James and Guth^{5–8} sum over all crosslink positions and consider the effect of a gradual, rather than an instantaneous crosslinking process. Their version of equation (1) gives a value of A which is dependent on the crosslinking process, and for the non-instantaneous crosslinking of existing polymer chains $A \sim \frac{1}{2}$ and $B=0$. (N.B. This is worked out on the assumption that every site on the chain is available for crosslinking.) In practice the logarithmic term in equation (1) is only significant when deformation of the network is accompanied by a change in volume. Although dilation occurs in most deformation processes the change is only appreciable in swelling experiments.

Edwards⁹ considers the network to be an infinitely long polymer molecule, the entropy of which is limited by the crosslinks which are put in theoretically as Δ functions. The crosslinks are considered to be random and 'free to slide along the chains' and then frozen in position. Unlike James and Guth, Edwards does not assume any crosslinking process; however, the result which he gets for the free energy of deformation is

consistent with the result obtained by James and Guth, with $A=\frac{1}{2}$.

Taking $A=\frac{1}{2}$ and $B=0$, equation (1) becomes:

$$\Delta F = \frac{1}{2} G (\lambda_x^2 + \lambda_y^2 + \lambda_z^2 - 3) \quad (2)$$

which for simple elongation gives for the stress:

$$f/A_0 = G(\lambda - \lambda^{-2}) \quad (2a)$$

where G is the modulus of elasticity given by:

$$G = \frac{\nu}{2} kT = nkT \quad (3)$$

where n is the effective number of crosslinks per unit volume.

The theory of Flory and Wall produces, for an ideal polymer network, a value of G :

$$G = 2nkT \quad (4)$$

Real polymer networks have defects. Three commonly considered network defects are: (i) unreacted functionalities and free chain ends; (ii) closed loops; (iii) entanglements¹⁰. These defects are considered in detail by Prins¹¹.

Two major problems arise when attempts are made to test the relations derived from statistical theories. These relate: (a) to the shape of the stress/strain curve, and (b) to the quantitative prediction of G .

Real polymer networks do not obey equation 2(a) over an appreciable range of extension ratios ($\sim \lambda_x = 1 \rightarrow 2$). Thus Mooney¹² added an extra term to equation (2) and this becomes:

$$\Delta F = C_1 (\lambda_x^2 + \lambda_y^2 + \lambda_z^2 - 3) + C_2 \left(\frac{1}{\lambda_x^2} + \frac{1}{\lambda_y^2} + \frac{1}{\lambda_z^2} - 3 \right) \quad (5)$$

Unfortunately this modified equation only slightly extends the range of applicability beyond that of equation (2). Measurements made on swollen rubbers show that the C_2 term becomes less important and the network becomes more ideal as the degree of swelling increases^{13, 14}.

So far it has not proved possible to predict quantitatively a value of G owing to the uncertainties in estimating the number of effective crosslinks introduced into the network. Early experiments were carried out using sulphur vulcanized natural rubber¹⁵. Unfortunately the number of crosslinks is not precisely known because the number of sulphur atoms per crosslink can vary. To overcome this problem an attempt was made to refer the measurements back to the gel point where two crosslinks are present on each chain¹⁶, but this procedure does not account for network defects.

Special note should be taken of closed loop network defects. These will be more likely to be formed when chain segments which are close to each other are available for crosslinking^{17, 18} and are thus more likely to be formed in very dilute solution^{17, 19}. Attempts have been made to prepare model networks by crosslinking various polymers at reactive sites in solution^{20, 21}. In all these instances, however, many or all of the polymer segments have reactive sites. Unfortunately these conditions are conducive to the formation of a large number of closed loops and consequently the effective number of network chains is uncertain.

In this paper we report the preparation of networks with complete, or virtually complete, intermolecular crosslinking of a small number of prechosen sites on polymer chains in solution. The polymers used in this work are identical to those used in previous experiments on the preparation of intramolecular crosslinked chains in very dilute solution²².

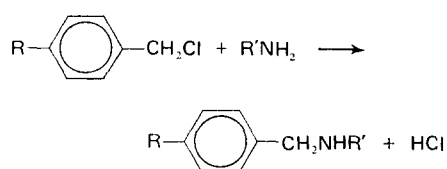
PREPARATION

Preparation and characterization of substituted polystyrene

(a) Polystyrene was chloromethylated to the required degree of substitution²³.

Polystyrene (25 g of the desired molecular weight and distribution) was dissolved in carbon tetrachloride (400 ml) and the solution was cooled in an ice bath to 0°C. Chlorodimethyl ether (100 ml) at 0°C and anhydrous stannic chloride (2 ml) were added. (Chlorodimethyl ether is toxic and possibly carcinogenic and hence should be treated with great care.) The mixture was stirred and stood at 0°C for 25 min. A mixture of dioxane (90 ml) and water (10 ml) was added to stop the reaction followed by 25% of concentrated hydrochloric acid (100 ml) to extract the stannic chloride. The mixture was shaken and then poured into a separating funnel. The lower organic layer was run slowly, with stirring, into a ten times excess of methanol in order to precipitate the polymer. The polymer was filtered off, dried, dissolved in chloroform (500 ml), reprecipitated, filtered and dried to yield a fluffy white product with about 1% of the styrene units chloromethylated (90–100% yield).

(b) The chloromethylated polystyrene was then reacted with a primary amine to convert the chloromethyl sites into secondary amine groups²².



Chloromethylated polystyrene (25 g) was dissolved in tetrahydrofuran (250 ml) and *n*-butylamine (250 ml) was

added. This mixture was allowed to stand at room temperature for three days. The solution was then precipitated into methanol, reprecipitated from chloroform into methanol and dried under high vacuum to yield a fluffy white product.

(c) The aminated polystyrene was reacted with 1-fluoro-2,4-dinitrobenzene and the degree of substitution was determined from the ultra-violet spectra of the product.

Aminated polystyrene (1 g) was dissolved in carbon tetrachloride (20 ml), triethylamine (0.5 ml) and 1-fluoro-2,4-dinitrobenzene (0.2 ml) were added and the mixture stood overnight. The polymer was precipitated into methanol, reprecipitated twice from chloroform into methanol and dried to yield a fluffy yellow product.

Measurements were made using solutions of the product in chloroform in cells of 10 mm thickness, on a Unicam SP800 spectrophotometer. The absorption at 376 nm was studied and the extinction coefficient was determined by ultra-violet studies on solutions of the product of 1-fluoro-2,4-dinitrobenzene with an excess of *n*-ethyl benzylamine in chloroform to be $1.68 \times 10^7 \text{ cm}^2/\text{mol}$. The method was also checked against other methods outlined in another paper²².

Network formation

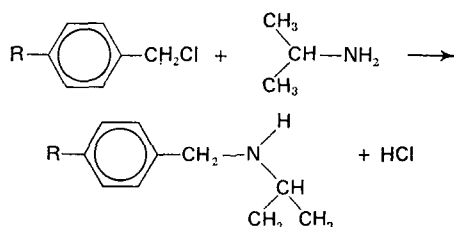
The aminated polymer was dissolved in tetralin (dried over calcium hydride) at 20°C. A concentration was chosen to give a final concentration in the useful range of between 5 and 25% and a total volume of about 150 ml.

To the solution was added a known quantity of hexamethylene diisocyanate (redistilled under reduced pressure), calculated to be 5% less than the stoichiometrically required quantity, dissolved in a little tetralin. A small correction to the amount of diisocyanate used owing to incomplete transfer could be made by weighing the flask (usually a 10 ml volumetric flask) empty, and after transfer. The solution was quickly stirred and poured into the required mould where gelation took place. The mixture reached its gel point in a time between 10 sec and 5 min, depending on degree of substitution etc. and was allowed to stand at least 30 min for the reaction to complete before it was tested.

The mould was typically a 3.5 in (88.9 mm) diameter crystallizing dish. The concentration limits were set by experimental considerations because at low concentrations a continuous network of sufficient strength to test was not formed, and at high concentration the reaction was too fast and the solution too viscous to allow efficient mixing before gelation.

Networks were made over as wide a range of concentration as possible. In order to prepare high concentration networks it was essential to have long gel times and low initial solution viscosities. This was easier to obtain with low molecular weight polymers of low degree of substitution. The disadvantage was that such polymers have a large correction due to free chain ends. An optimum polystyrene was found in the range supplied by Pressure Chemical Co. having $\bar{M}_w = 110\,000$ and \bar{M}_w/\bar{M}_n less than 1.06. At low concentrations it was possible to use polystyrene of higher molecular weight (Shell, H. R. Nibbs, $\bar{M}_w = 240\,000$) because the reaction was slower, and the viscosity of the solution was not a problem. The size of the chain end correction depends on \bar{M}_n , but the viscosity depends on \bar{M}_v , which approximates to \bar{M}_w .

It was possible, by putting different amine groups onto the polystyrene chain, to alter the rate of reaction with isocyanates to give longer mixing times. With the isopropylamine adduct:



the gel time was increased by a factor of 10 relative to *n*-butylamine substituent.

Owing to the slower rate of the amination reaction it was necessary to reflux the solution for three days. The completion of reaction was shown by the disappearance of the chloromethyl (CH_2Cl) absorption at 1266 cm^{-1} from the infra-red spectrum of the polymer. Reaction of the isopropylamine adduct with 1-fluoro-2,4-dinitrobenzene was greatly impeded, presumably owing to steric factors. Therefore analysis was always carried out on the *n*-butylamine adduct prepared from the same chloromethylated polymer.

Use of hydroxyl-containing polymers or use of blocked diisocyanates such as the diphenyl ether of methylene diphenyl diisocyanate were not favoured because the rates of reaction were extremely slow at room temperature, elevated temperatures were not desirable due to possible syneresis on cooling the gel, and competitive reactions with adventitious water would become more critical.

Efficiency of reaction

The number of unreacted isocyanate groups remaining in the gel after completion of the reaction was measured using a ^{14}C labelling technique.

After a sample of the gel had been prepared and mechanically tested, a 10 g sample was broken into small pieces and placed in a stoppered vessel. Dry tetralin (10 ml) and $^{14}\text{CH}_3\text{OH}$ (1 ml of a suitable activity) were added to label the residual isocyanate with $^{14}\text{CH}_3$ groups. To ensure completion of reaction with the methanol the mixture was left to stand for one week. The gel was then washed by standing in a large excess of solvent, the solvent being changed each day. The solvents used in turn on alternate days were heptane, benzene containing 5% methanol and methyl ethyl ketone; about 10 series of washing were required to produce a constant value. The sample was then dried under high vacuum, swollen in benzene and redried.

Into sample bottles were placed: (a) 0.1 g of purified and dried gel, 1 ml of toluene, 7 ml of scintillation 'cocktail'; (b) 0.1 g of pure polystyrene, 1 ml of a 0.1% solution of the ^{14}C methanol in toluene, 1 ml of 'cocktail'; (c) 0.1 g of pure polystyrene, 1 ml of toluene, 7 ml of 'cocktail'. The 'cocktail' consisted of a solution of 3/10% diphenyl oxazole (PPO) and 3/100% 1,4-bis(5-phenyloxazol-2-yl)-benzene (POPOP) in xylene. The solutions were counted on a Packard Liquid Scintillation Spectrometer Model 3320. The efficiency of counting was about 73% in each case, despite the fact that one contained lumps of swollen gel. A direct comparison of counts was used to calculate the number of reacted groups in the gel.

From the result the number of free isocyanate groups in the gel was calculated to be 7% of the original diisocyanate added to form the gel. This measurement was made in two cases only (at 7½ and 10% concentration), and 7% of groups were found in each case. This therefore represents a possible systematic error of 7% in the results. All the results in *Table 1 et seq.* have been corrected by this factor.

MEASUREMENT OF MODULI

Introduction

Many standard methods for the measurement of moduli are not easily applicable to our gels because: (a) the gels are rather weak and tend to crack or break when subjected to large deformations; (b) the gels have a much lower modulus than dry rubber networks; and (c) it is virtually impossible to clamp or stick the samples onto anything so that they may be pulled or twisted.

The method finally chosen was indentation by a rigid sphere, which forms the basis of a measurement commonly used in the rubber industry to evaluate Young's modulus. The method and apparatus used were similar to those used by Waters²⁴.

The problem of evaporation of solvent from the gel surface was reduced to negligible proportions by using tetralin (b.p. 170°C).

Theory

The theoretical solution to the problem of the pressure distribution between two spherical bodies in contact was first given by Hertz²⁶. This has been applied to the particular problem of the relationship between indentation, applied load and ball size for a rigid sphere pressed into a plane elastic medium. The solution is based on the assumption that the medium is semi-infinite in extent, i.e. that the boundaries of the medium are stress free except over the area of contact with the rigid sphere.

For a rigid sphere of radius R indenting into a semi-infinite elastic medium of modulus G , the indentation d produced by a force P is shown to be:

$$d = \frac{KP^{2/3}}{(3G)^{2/3}R^{1/3}}$$

where

$$K = \left(\frac{81}{256}\right)^{1/3}$$

Hence

$$G = \frac{3.P}{16d^{3/2}R^{1/2}}$$

Waters²⁴ has extended this to the case of an infinite sheet of finite thickness t , and a correction can be made by introducing a factor depending on R , G , t and P . The samples used in this work were generally of sufficient thickness ($\sim 3\text{ cm}$) that this factor could be neglected; however, a correction was used when it was likely to exceed 1% of the measured value. The correction is smaller if the bottom surface of the sample is free to slip. The samples prepared in this work had a fixed lower boundary, and attempts to lubricate the lower boundary did not produce complete freedom of movement. Hence the corrections used were those calculated for a fixed lower boundary.

At higher deformations the force-extension curves sometimes showed slight curvature (see *Figure 1*). This could be due to the result of finite thickness or due to the assumption of Hookean behaviour in the above equations. It is perhaps worth pointing out that the actual strains involved in the method are relatively small (up to 3%) when the sphere is indented to a depth of its radius. This arises because the strain is taken up over the surface of the gel and not restricted to the area over which the indenter makes contact.

Apparatus

The apparatus²⁴ was constructed by modifying a dial gauge (jewelled movement, calibrated in 0.002 mm). The main spring and the return spring on the rack and pinion gearing were removed, hence the operating column was free to move. A load platform was fixed to one end of the operating column, and the anvil on the other end was replaced by a piece of aluminium rod having a conical depression to act as a seat for the indenting sphere. The gauge was rigidly fixed to the arm of a comparator bench. On to the arm of the comparator bench, near to the gauge, was fixed an electrically operated buzzer. The action of the buzzer during the measurements had the effect of reducing the friction in the gauge mechanism.

Experimental

Indentations were measured relative to the upper surface of the sample. The dial gauge reading for zero indentation was found by allowing the indenter to rest on a glass microscope slide, of known thickness, pressed on to the surface of the sample. When weights were placed on the loading platform while the glass slide was in position, very little indentation resulted, but a small correction could be applied (*vide infra*) to take account of the indentation caused by the weight of the operating column alone on the slide.

A value of the indentation d of the ball bearing into the gel, was found for each of a series of loads. The results were not time dependent, probably owing to the short relaxation times in a swollen gel. Measurements were also taken during deloading and the indentations were found to be reversible. A typical plot of P against $d^{3/2}$ is shown in *Figure 1*.

As drawn, the intercept on the Y axis represents the weight of the operating column, platform and ball

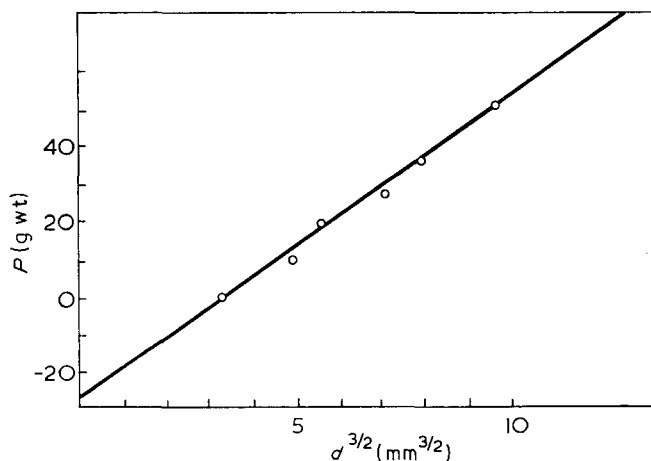


Figure 1 Example of a plot of load against (indentation)^{3/2} for one sample of gel

bearing indenter, which was found to be 28 ± 1 g in every case. This was checked by suspending the gauge over the pan of a direct reading balance, actuating the vibrator and measuring the weight. In all cases a ball bearing of 5.09 mm radius was used. In practice this gave the most conveniently measurable values of d .

It is very important that the sphere should be free to slide on the surface of the gel and should not stick to the surface during indentation. Lubricating the surface with water, or soapy water, and using spheres made of glass and polytetrafluoroethylene, were methods tried to ensure that surface effects were not serious, but no significant differences in the value of G were found.

The assumption made that the gel could be treated as an infinite sheet was checked by preparing samples in a special mould which consisted of a cylinder, at one end of which was a ground glass flanged joint resting on a ground glass cover plate as a base. A sample was prepared in the mould and G determined. The sample was then separated from the sides of the cylinder using a spatula and removed from it, still attached to and standing on the glass cover plate; G was again determined. No significant difference was found in the two values of G . An infinite sheet should give a value of G intermediate between the cases of fixed and free boundaries. Thus no significant correction to the direct measurements of G was required.

RESULTS AND CALCULATIONS

For an ideal network prepared by crosslinking existing polymer chains, n , the number of effective crosslinks per cm^3 is given by:

$$n = \frac{N_0}{2} \cdot K \cdot \frac{c}{100} \left(\frac{1}{104N + 85} \right) \quad (6)$$

where N_0 is Avogadro's number,

c is the concentration of polymer in g/dl,

N is the mean number of monomer units between crosslinks, and

K is a corrective factor for the number of crosslinks required to join the chains into an infinite network given by:

$$K = 1 - \frac{2 \times 104 \times N}{\bar{M}_n}$$

with \bar{M}_n the number-average molecular weight of the original polymer.

For the polystyrene sample of wide molecular weight distribution the value of \bar{M}_n determined by osmometry was used in the foregoing equation. In practice this will be larger than the true value of \bar{M}_n because the membrane is permeable to the species of lower molecular weight. However, there is a high probability that very small species contain no reactive groups and thus need not be counted in the correction factor. Overall the maximum uncertainty which will be introduced by this procedure is only 2%. In the use of polymers with narrow molecular weight distribution the problem does not arise.

The estimated statistical error in n is $\pm 3\%$; however, this does not include the systematic error arising from the inefficiency of the crosslinking reaction.

The results for the samples prepared are given in *Table 1*; in all cases the results have been corrected by 7% to allow for incomplete crosslinking.

Table 1 Properties of polystyrene gel

Sample	Polymer	Units between reactive groups, N_g	Units between crosslinks, N	Concentration modulus			
				%v/v	G (g/mm ²)	nkT (g/mm ²)	Modulus $\frac{nkT}{nkT}$
1	A	65	76	5.0	0.271	0.71	0.38
2	A	65	76	7.5	0.571	1.07	0.53
3	A	62	71	5.0	0.35	0.78	0.45
4	A	62	71	7.5	0.654	1.16	0.56
5	C	60	68	12.5	1.20	1.67	0.72
6	B	66	75	17.5	2.07	2.32	0.89
7	B	66	75	20.0	2.73	2.64	1.03
8	A	79	93	5.0	0.27	0.65	0.42
9	A	79	93	10.0	0.82	1.30	0.63
10	A	78	89	5.0	0.23	0.66	0.35
11	A	78	89	7.5	0.54	0.99	0.55
12	A	76	86	5.5	0.31	0.74	0.42
13	A	76	86	7.0	0.40	0.95	0.43
14	B	71	81	16.0	1.42	1.93	0.74
15	B	17	81	20.0	2.70	2.41	1.12

A is polymer of \overline{M}_w 240 000, $\overline{M}_w/\overline{M}_n > 1.6$ reacted with n-butylamine

B is polymer of \overline{M}_w 110 000, $\overline{M}_w/\overline{M}_n$ 1.06 reacted with isopropylamine

C is polymer of \overline{M}_w 70 000, $\overline{M}_w/\overline{M}_n$ 1.06 reacted with n-butylamine

The error in the measured modulus estimated from the graphs of P against $d^{3/2}$, was $\pm 5\%$.

INTERPRETATION OF RESULTS

Chemical aspects

The n-butylaminomethylated polystyrene contains a small number of reactive sites distributed at random along the length of the polymer chain. A network with a known number of crosslinks is formed in solution by the almost complete crosslinking of these sites.

The formation of a network by the reaction of a diisocyanate with the amine-containing polymer can be expected to go to completion as far as the steric restrictions of the network allow; this is inferred from the short time-to-gelation and hence fast reaction rate. Steric limitations were reduced by using a 5% less-than-stoichiometric amount of diisocyanate. It was found, however, that 7% of this reduced amount of diisocyanate added did not react and this has been taken into account in presenting the results.

A factor which must be considered is the possibility of hydrogen bonding between the substituted urea groups in the crosslinks. These would have the effect of increasing the modulus of the network. Such hydrogen bonds were considered unlikely because (a) of the distance apart of urea groups in the network and (b) the use of an aromatic solvent tends to suppress hydrogen bonding²⁵. One type of hydrogen bond which is possible is one between urea groups on the same crosslink. This is sterically possible but it would not affect the modulus of the network to any appreciable degree.

Comparison with theory

The results in Table 1 have been used to calculate a parameter, measured modulus/ nkT , for each sample of gel, where n is calculated from equation (1). For an ideal network this will be equal to $2A$, where A is the unknown front factor suggested in the various theories. Because our networks are made and tested at the same concentration, as long as the concentration is sufficiently

high for the chains to approximate to their unperturbed dimensions, it is not necessary to include a correction factor for changes in chain conformations.

In Figure 2 this quantity has been plotted against the concentration. Because the samples have been prepared with various values of N_g (the number of chain units between reactive sites) and hence N (the average number of chain units between crosslinks), the results are presented in two groups with $N_g = 75 \pm 4$ and $N_g = 63 \pm 3$ respectively.

If we assume that all the reacted diisocyanate leads quantitatively to crosslink formation, the divergence of the measured values of modulus from any theoretical prediction must be explained in terms of closed loops which reduce the modulus at low concentrations, and entanglements which increase the modulus at high concentrations.

The dependence of modulus on concentration may arise from a combination of these effects. Closed loops

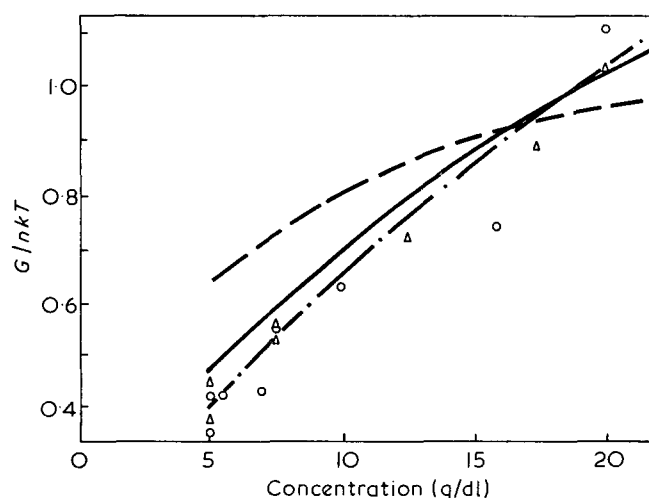


Figure 2 Plots of modulus/ nkT against concentration. ---, Plot of $G/nkT = 1 + 0.25 - [8/(8+c)]$; —, plot of $G/nkT = 1 + 0.015c - [8/(8+c)]$; - · - · -, plot of $G/nkT = 1 + 0.02c - [12/(12+c)]$. Δ , Samples with $N_g = 63 \pm 3$; \circ , sample with $N_g = 75 \pm 4$

reduce the value of the quotient modulus/ nkT by a quantity which is shown in the Appendix to be of the form $K'/(K'+c)$. The effect of entanglements is more open to question and we shall discuss two possibilities.

(1) Edwards²⁶ has predicted that the effect of entanglements on modulus is proportional to c^2 , and this has been verified for swollen, uncrosslinked natural rubber in measurements of the dynamic modulus²⁷. Since n is proportional to c , the effect of entanglements on modulus/ nkT will thus be proportional to c . Combining this with the effect of closed loops this gives a resultant of the form:

$$\frac{\text{modulus}}{nkT} = 1 + Kc - \frac{K'}{K'+c} \quad (8)$$

assuming $A = \frac{1}{2}$.

Taking the value of K' , estimated in the Appendix, this becomes:

$$\frac{\text{modulus}}{nkT} = 1 + Kc - \frac{8}{8+c} \quad (8)$$

K has been assigned the value of 0.015. This is not an unreasonable value as it represents a contribution of entanglements to the modulus of the same order as those found for uncrosslinked rubbers²⁷. In *Figure 2* the solid line represents a plot of modulus/ nkT against concentration as predicted by this equation.

(2) An alternative estimate of the effect of entanglements is obtained by adopting the assumption frequently made for polymer solutions that the molecular weight between entanglements is constant²⁸. One can show that the contribution to the modulus of physical entanglements is then given by:

$$G = \frac{ApRT}{M_e}$$

where p is the density of network chains,

R is the gas constant,

T is the absolute temperature,

M_e is the molecular weight between entanglements,

A is the front factor in the equation for deformation of a network, being 1 (Flory and Wall) or $\frac{1}{2}$ (James and Guth) according to the theory considered.

Using $A = \frac{1}{2}$ and a value of $M_e = 35\,000$ ^{28, 29} for polystyrene one can show that for our networks this represents a constant contribution to modulus/ nkT of 0.25.

We now get a resulting equation:

$$\frac{\text{modulus}}{nkT} = 1 + Kc - \frac{K'}{K'+c} \quad (9)$$

and substituting our values for the constants:

$$\frac{\text{modulus}}{nkT} = 1 + 0.25 + \frac{8}{8+c} \quad (10)$$

In *Figure 2* the broken line represents a plot of modulus/ nkT against concentration as predicted by this equation.

It is clear from *Figure 2* that neither of the equations fits the experimental results very closely. It is possible to fit equation (7) (but not equation (9)) by treating the constants as adjustable parameters. The broken line in *Figure 2* was calculated by putting $K = 0.02$, $K' = 12$.

CONCLUSIONS

Any conclusions must, at this stage, be tentative. It is evident from the scatter of results in *Figure 2* that the results are subject to experimental error. A systematic error in the chemistry of the network is perhaps a more probable source of the discrepancy between theory and experiment than a genuine value of $K' = 12$. It should be pointed out that we have throughout assumed the chains to have their unperturbed dimensions which may lead to errors at low concentrations.

Notwithstanding this, we believe that our results are more consistent with a c^2 dependence of entanglements rather than with the assumption of a constant average molecular weight between physical entanglements.

The main purpose of our investigation was to obtain evidence regarding the value of A . It is possible to explain the results we have obtained in terms of a value of $A = \frac{1}{2}$. We cannot, on the basis of our results, demonstrate that the value is actually $\frac{1}{2}$ but it would be very difficult to explain the results on the basis of a value very far from $\frac{1}{2}$, and almost impossible to explain them in terms of the alternative value of 1.

A possible, but unlikely, interpretation of *Figure 2*, obtained by direct extrapolation is that the quotient, modulus/ nkT , will reach the value of 2 required by Wall and Flory at a gel concentration of about 50%, the implication being that network formation is not complete until this polymer concentration is reached. The fact that the crosslinking reaction is 93% complete in the concentration range in which we have worked, and the estimations we have made of closed loop formation, argue strongly against this interpretation. We believe that the curve in *Figure 2* arises from an interplay of the three effects already discussed for a network which is substantially complete. So far attempts to work at higher concentrations have failed because of the excessive speed of crosslinking and the difficulty of mixing reactive components into a viscous solution.

Further work in progress in our laboratories into this system and into others where, by reacting together two polymers containing different reactive groups, excluding the possibility of a simple closed loop from one chain to itself, should give a more definitive answer to the value of the modulus, and the relative importance of network defects in crosslinked polymers.

ACKNOWLEDGEMENT

The authors are extremely grateful to Professor S. F. Edwards for many helpful discussions.

REFERENCES

- 1 Flory, P. J. 'Principles of Polymer Chemistry', Cornell University Press, Ithaca, 1953
- 2 Flory, P. J. *J. Chem. Phys.* 1950, **18**, 108, 112
- 3 Wall, F. T. and Flory, P. J. *J. Chem. Phys.* 1951, **19**, 1435
- 4 Wall, F. T. *J. Chem. Phys.* 1943, **11**, 527
- 5 James, H. M. *J. Chem. Phys.* 1947, **15**, 651
- 6 James, H. M. and Guth, E. *J. Chem. Phys.* 1947, **15**, 669
- 7 James, H. M. and Guth, E. *J. Chem. Phys.* 1953, **21**, 1039
- 8 Guth, E. *J. Polym. Sci. (C)* 1966, **12**, 89
- 9 Edwards, S. F. and Freed, K. F. *J. Phys. (C. Solid St. Phys.)* 1970, **3**, 739, 750, 760
- 10 Flory, P. J. *Chem. Rev.* 1944, **35**, 51
- 11 Dusek, K. and Prins, W. *Adv. Polym. Sci.* 1969, **6**, 1
- 12 Mooney, R. S. *J. Appl. Phys.* 1940, **11**, 582

- 13 Gee, G. *Trans. Faraday Soc.* 1946, **42**, 585
- 14 Price, C., Allen, G., de Candia, F., Kirkham, M. C. and Subramaniam, A. *Polymer* 1970, **11**, 486
- 15 Gee, G. *J. Polym. Sci.* 1947, **2**, 451
- 16 Flory, P. J., *Ind. Eng. Chem.* 1946, **38**, 417
- 17 Kuhn, W. *Kolloid Z.* 1934, **68**, 2
- 18 Jacobson, H. and Stockmayer, W. H. *J. Chem. Phys.* 1930, **18**, 1600
- 19 Kuhn, W. and Mayer, H. *Makromol. Chem.* 1955, **18/19**, 239
- 20 Mukherji, B. and Prins, W. *J. Polym. Sci. (A)*, 1964, **2**, 4367
- 21 Rizke, A. M. and Prins, W. *J. Polym. Sci.* 1962, **59**, 171
- 22 Allen, G., Burgess, J., Edwards, S. F. and Walsh, D. J. *Proc. R. Soc. (A)* 1973, **334**, 453, 465, 477
- 23 Allares, T., Jr., Wyman, D. P., Allen, V. R. and Mayerson, K. *J. Polym. Sci. (A)* 1965, **3**, 4131
- 24 Waters, N. E. *Br. J. Appl. Phys.* 1965, **16**, 557
- 25 Allen, G., Watkinson, J. G. and Webb, K. H. *Spectrochim. Acta* 1966, **22**, 807
- 26 Edwards, S. F. in 'Amorphous Materials', (Eds E. W. Douglas and E. Bryan), Wiley, New York, 1972, p 279
- 27 Yoshimura, N. *PhD Thesis* Victoria University of Manchester, 1969
- 28 Porter, R. S., McKnight, W. J. and Johnson, J. F. *Rubber Chem. Technol.* 1968, **41**, 1
- 29 Williams, M. L. *J. Appl. Phys.* 1958, **29**, 1395
- 30 Flory, P. J. 'Statistical Mechanics of Chain Molecules', Interscience, New York, 1969

APPENDIX

Probability of closed loop formation during crosslinking in solution

For a chain containing n links of length l , with one end fixed at the origin, the probability that the other end is in a box of sides dx , dy , dz at distances x , y , z along each Cartesian coordinate is given by:

$$W(xyz)dx dy dz = \left(\frac{\beta}{\pi^{1/2}}\right)^3 \exp[-\beta^2(x^2 + y^2 + z^2)] dx dy dz$$

where

$$\beta = \left(\frac{3}{2nl^2}\right)^{1/2}$$

Hence, in the region where the two chain ends are near together and x , y and z are all small, the probability that one end is in a volume dV near to the other end is^{17, 18}:

$$W(dV) = \left(\frac{3}{2nl^2\pi}\right)^{3/2} dV$$

In order to calculate the relative probabilities of closed loop formation and crosslinks from one chain to another, it is assumed that the relative probabilities of reaction of each site are dependent only on the concentrations of the other reacting groups in its vicinity.

For a real polymer molecule it is necessary to take account of fixed bond angles and barriers to rotation;

this is done by multiplying nl^2 in the above equations by the characteristic ratio, which for polystyrene is 10^{-230} .

Take, for example, a polystyrene chain containing reactive groups with an average number of styrene units between the groups $N_g=65$; to simplify the calculation we assume that they are equally spaced along the chain. Choosing any reactive site and taking $n=130$ and $l=1.54 \text{ \AA}$, the probability that one of its two neighbouring sites is in a volume dV near to it is:

$$W(dV)_{\text{loop}} = 2 \left(\frac{3}{2 \times 130 \times 1.54^2 \times 10^{-2} \times \pi} \right)^{3/2} dV \\ = 3.74 \times 10^{-6} dV$$

If the concentration of polymer in solution is c (g/dl) then the probability that a group attached to another macromolecule is in a volume dV (\AA^3) is:

$$W(dV)_{\text{crosslink}} = \frac{cN_0 10^{-26} \cdot dV}{(65 \times 104 + 85)} \\ = c \times 0.876 \times dV$$

Hence the fraction of simple closed loops formed

$$= \frac{W(dV)_{\text{loop}}}{W(dV)_{\text{crosslink}} + W(dV)_{\text{loop}}} \\ = \frac{3.74 \times 10^{-6}}{3.74 \times 10^{-6} + c \times 0.876 \times 10^{-6}} \approx \frac{4}{4+c}$$

Various inadequacies in this treatment are: (a) the reactive sites have been taken as equal distances apart when in fact they are randomly distributed. In our system this could increase the effect by up to 50%; (b) closed loop formation between two chains has not been estimated. The average loop formed will be twice as large as a simple closed loop and the probability will therefore be 1/2 to 3/2 of that of simple closed loops, i.e. it would increase the effect by 36%; (c) networks were formed in tetralin which is not a theta solvent, thus the chain will be more extended and closed loops will be less favoured. This effect will operate in the opposite direction to (a) and (b). The dimensions of the chain are concentration dependent becoming nearer the unperturbed dimensions at high concentrations; this error will therefore be higher at lower concentrations.

If we include the errors (a) and (b) in our estimate the fraction of closed loops formed becomes $8/(8+c)$. The other error is difficult to estimate but should not be important above 10% concentration.

Because of these inadequacies this calculation can only be considered as a rough guide but it is unlikely to be out by a large factor, and certainly not by more than a factor of 2.

Solvent-swelling of vulcanizates reinforced by fibrillar fillers*

Zvi Rigbi and Nissim Sabatov

Department of Mechanics, Technion-Israel Institute of Technology, Haifa, Israel
(Received 12 October 1973; revised 19 December 1973)

Two models are proposed for vulcanizates reinforced by fibrillar fillers. These are then analysed for swelling behaviour by considering the swelling of a cylinder of elastomer surrounding an individual fibre and firmly attached to it. A complex of such cylinders in a laminated geometry is then studied. Graphs are given which may be used to study the swelling of rubberized cord.

INTRODUCTION

The mechanics of the restraint of swelling in solvents of elastomers bonded to substrates has been studied in general terms by Scanlan¹, and in greater detail in the case of bonded plates by Thomas and Southern². One of us³ has extended this analysis to the case of a spherical shell of vulcanized elastomers bonded to a rigid sphere, and has attempted to apply the results to a system of spheres dispersed in a matrix of vulcanizate.

The model chosen previously approximates a true carbon black elastomer system only very poorly. It is known that only the very coarsest blacks tend to disperse as separate particles, and finer blacks disperse as clumps and chains of widely different dimensions and geometries. Accordingly, we propose in this paper to study other models including one in which the vulcanizate is composed of layers of parallel inextensible cords, each layer disposed with the cords at a given angle to those in the contiguous layers. Such a geometry is also similar to that found in tyre construction, and the discussion which follows may be helpful in studying some tyre phenomena. In this model, the smallest complete element is one in which a tube of vulcanized elastomer is bonded on its inner surface to a rigid core. A second model has unidirectional fibres randomly dispersed in the mass.

SWELLING OF AN ELASTOMERIC TUBE BOUND TO AN INEXTENSIBLE CORD

Figure 1 shows a section taken through a typical element under consideration, and our approach to the solution. In (a), we have the bonded element before swelling. Following immersion, we assume that the tubular part swells freely in all directions as in (b). The swelling will proceed until the volume ratio of dry rubber in the swollen matrix reaches the value v_{20} , which is governed

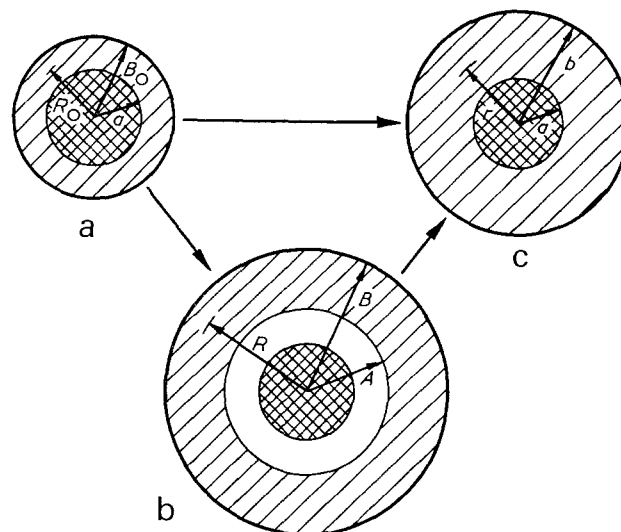


Figure 1 Scheme for the calculation of restrained swelling. (a) Unswollen composite; (b) freely swollen shell; (c) restrained swelling

by Flory's equation⁴:

$$\frac{RT}{V_1} \left[\ln(1 - v_{20}) + v_{20} + \mu v_{20}^2 + \frac{\gamma V_1}{M_c} \left(v_{20}^{1/3} - \frac{v_{20}}{2} \right) \right] = 0 \quad (1)$$

(see Nomenclature). The swollen tube is then simultaneously compressed longitudinally and a traction is applied to its inner surface to bring it in contact with the circumference of the cord, as in (c). The stresses and subsequent pressure arising in every elementary volume of swollen rubber in (c) are then exactly as they would be were the tube allowed to swell while being restrained, that is, in going directly from situation (a) to situation (c).

Writing subscripts 0 for the situation in (b), and l , r and t for the longitudinal, radial and circumferential (tangential) direction respectively, we see that the longitudinal extension ratio is given by:

$$\lambda_l = v_{20}^{1/3} \quad (2)$$

* Presented at the CNRS International Symposium on Elastomer Reinforcement, Obernai, France, September 1973.

The elastic problem can be solved with the help of a strain-energy function, a possible form for which has been given for a considerable range of the third invariant of the extension ratios $I_3 = \lambda_1^2 \lambda_2^2 \lambda_3^2$ as⁵:

$$W = C_{dry} v_2^{1/3} (I_1 - 3) - L(I_3 - 1) \quad (3)$$

where it can be shown that:

$$L/RT = (\gamma/2M_c) v_{20}^{1/3}$$

from which it is possible to deduce the function relating the principal stresses acting in the matrix to the principal extension ratios by⁶:

$$\begin{aligned} \sigma_i &= \lambda_i^2 \phi + \lambda_i^2 (\lambda_j^2 + \lambda_k^2) \theta + Q \\ \phi &= \frac{2}{(I_3)^{1/2}} \frac{\partial W}{\partial I_1} \quad \theta = \frac{2}{(I_3)^{1/2}} \frac{\partial W}{\partial I_2} \\ Q &= 2(I_3)^{1/2} \frac{\partial W}{\partial I_3} \end{aligned} \quad (4)$$

It is of some importance to note that the derivative of the strain-energy function with respect to the third invariant of the extension ratios is clearly defined, unlike the situation arising in incompressible materials.

The value of C_{dry} has been given by Treloar⁷ as $\gamma RT/2M_c$ and, by definition, $I_3 = (v_{20}/v_2)^2$. Substituting these values in equation (4) above, we obtain the three principal stresses as:

$$\frac{\sigma_r}{RT} = \frac{\gamma}{M_c} \left(\frac{v_{20}^{1/3}}{v_2^{2/3}} \frac{1}{\lambda_i^2} - \frac{v_{20}^{4/3}}{v_2} \right) \quad (5a)$$

$$\frac{\sigma_t}{RT} = \frac{\gamma}{M_c} \left(\frac{v_{20}^{4/3}}{v_2} \lambda_i^2 - \frac{v_{20}^{4/3}}{v_2} \right) \quad (5b)$$

$$\frac{\sigma_l}{RT} = \frac{\gamma}{M_c} \left(\frac{v_{20}^{4/3}}{v_2} - \frac{v_{20}^{4/3}}{v_2} \right) \quad (5c)$$

The stress tensor at any given point for which the principal stresses are given may be split into a deviatoric component, which is of no interest for the present discussion, and an isotropic component, the trace of which is equal to three times the pressure acting at that point. This pressure is, in turn, related to the swelling through Flory's equation, giving:

$$\begin{aligned} \frac{P}{RT} &= \frac{\gamma}{3M_c} \frac{v_{20}^{4/3}}{v_2} \left[\frac{v_{20}^{4/3}}{v_2^2} \frac{1}{\lambda_i^2} + \lambda_i^2 + v_{20}^{2/3} - 3 \frac{v_{20}^{7/3}}{v_2} \right] \\ &= -\frac{1}{V_1} \left[\ln(1 - v_2) + v_2 + \mu v_2^2 + \frac{\gamma V_1}{M_c} \left(v_2^{1/3} - \frac{v_2}{2} \right) \right] \end{aligned} \quad (6)$$

Equation (6) may be solved for λ_i in terms of v_2 , and use of equation (5) will then give the principal stresses as functions of either of the principal extension ratios λ . λ_i is constant throughout, as stated previously. There is no difficulty involved in solving these problems on a small computer, and we have in fact plotted Figures 2 and 3 from values calculated on a Wang 700/702 model.

It must be pointed out that we have selected a number of values of M_c computed from equation (1) for a set of values of v_{20} within a frequently observed range for the system SBR/benzene. The interaction constant for this system was taken as $\mu = 0.37$, and although it is known that it changes with v_2 , this variation was not taken into account.

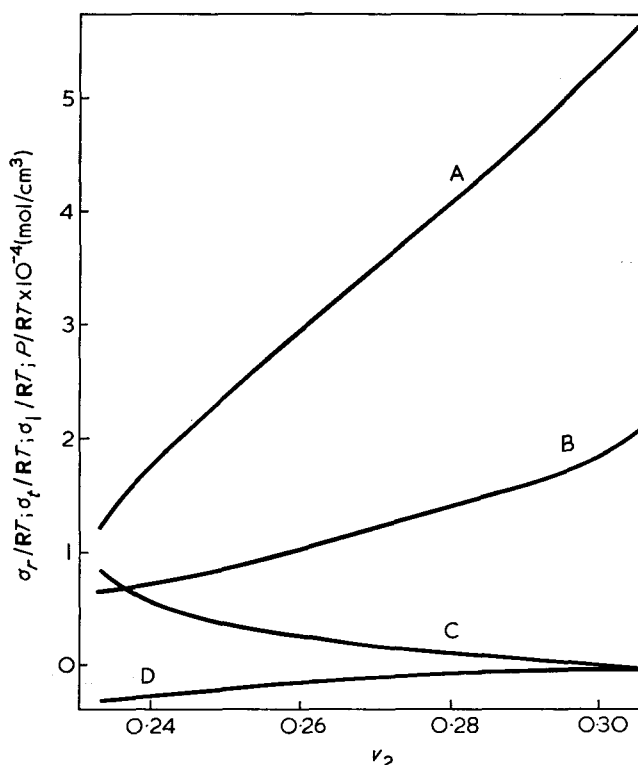


Figure 2 Principal stresses and mean pressure in restrained shell as a function of dry rubber content of the swollen gel. A, σ_r/RT ; B, P/RT ; C, σ_t/RT ; D, σ_l/RT . $M_c = 6133$; $v_{20} = 0.18$; $V_1 = 87$

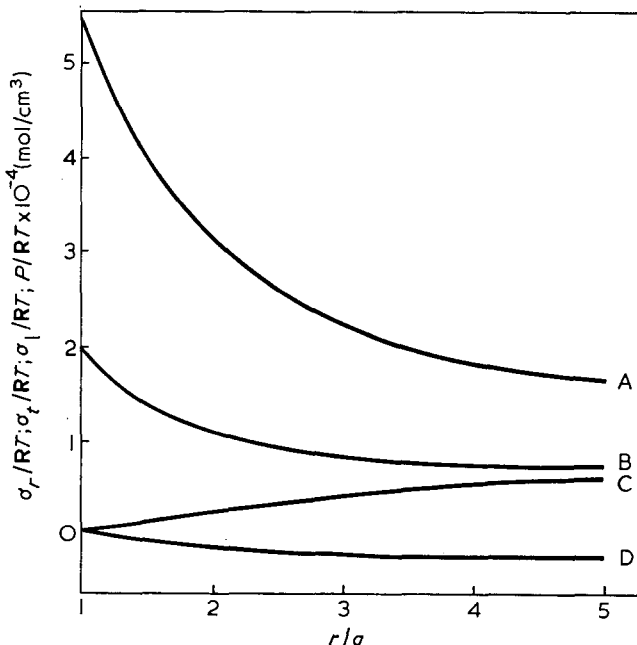


Figure 3 Principal stresses and mean pressure in restrained shell as a function of radial distance. A, σ_r/RT ; B, P/RT ; C, σ_t/RT ; D, σ_l/RT . $M_c = 6133$; $v_{20} = 0.18$; $V_1 = 87$

We cannot accept the simple equation given by Corey *et al.*⁸ (their eqn. 1c) as representing the true state of affairs in an elastomer whose swelling is restrained in a single direction. This equation completely disregards the effect of hydrostatic pressure resulting from the restraint on the swelling.

The relations obtained as graphs are not sufficient to determine the stresses or extension ratios at any

given point in the matrix. To find these, we recollect that equilibrium in a cylindrical system requires:

$$\frac{d\sigma_r}{dr} = \frac{\sigma_t - \sigma_r}{r} \quad (7)$$

from which we may write:

$$\frac{d\sigma_r}{dr} \cdot \frac{dr}{d\lambda_t} = \frac{d\sigma_r}{d\lambda_t} = \frac{\sigma_t - \sigma_r}{r} \cdot \frac{dr}{d\lambda_t} = \frac{\sigma_t - \sigma_r}{r} \cdot \frac{dr}{d(r/R)} \quad (8)$$

But from equation (5a):

$$\frac{d\sigma_r}{d\lambda_t} = -\frac{2\gamma RT}{M_c} \frac{v_2^{1/3}}{v_2^{2/3}} \frac{1}{\lambda_t^3} \quad (9)$$

hence

$$r \frac{d(r/R)}{dr} = \frac{\lambda_t}{2} - \frac{v_2^2}{2v_2^{4/3}} \lambda_t^5 \quad (10)$$

or, remembering that $\lambda_t = r/R$, we can integrate to give:

$$\ln \frac{r}{a} = \int_{v_2^{1/3}}^{r/R} \frac{d(r/R)}{r - \frac{v_2^2}{2R} \left(\frac{r}{R}\right)^5} \quad (11)$$

Since v_2 is a function of the pressure and through it, of r , the integral can only be evaluated numerically. If it is now remembered that R_0 , R and r are the radii determining the position of the same point in the elastomeric tube before swelling, after free swell and on restrained swelling, and that

$$R = R_0 v_{20}^{-1/3} \quad (12)$$

we can plot *Figure 4*, showing the relation between the (dimensionless) radii r/R_0 and R_0/a . Every point in an infinitely thick cylinder would be restrained by the bond to the fibre. However, at radii larger than a given value, the difference between the swelling of a restrained and a circumferentially unrestrained cylinder is so slight as to be negligible. We arbitrarily limit the radius of restrained swelling to regions where v_{20}/v_2 is less than 98%. This radius is defined as R_{01} . Our cal-

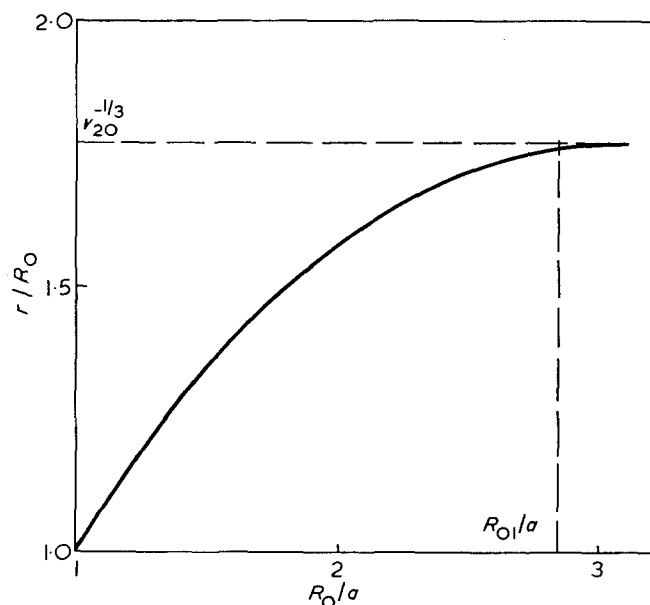


Figure 4 Swollen radius as a function of initial radius. $M_c=6133$; $v_{20}=0.18$; $V_1=87$

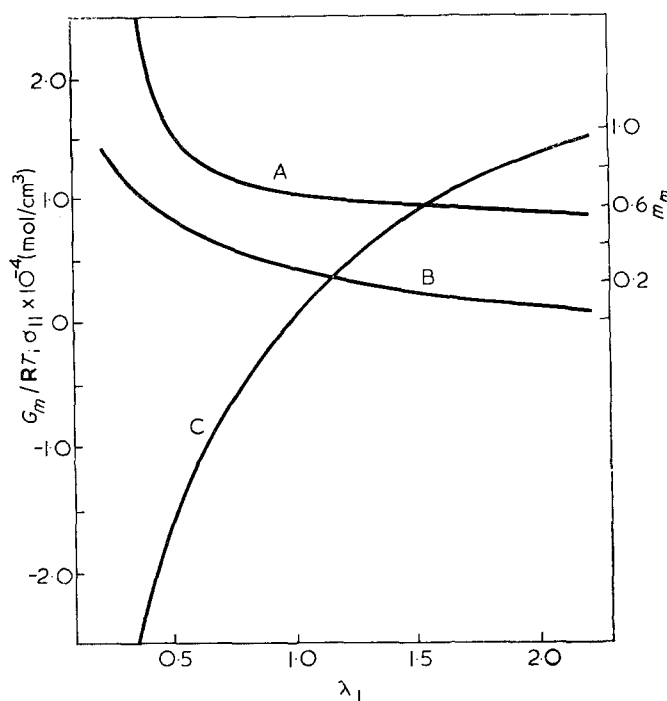


Figure 5 Stress-extension ratio curves for swollen elastomer, and some of its elastic constants. A, G_m/RT ; B, m_m ; C, σ_{11}/RT . $M_c=6133$; $v_{20}=0.18$; $V_1=87$

culations show that R_{01}/a is of the order of 2.4 for filled rubbers and 2.8 for a gum compound. We shall use the value of 2.8 in the following developments.

ELASTIC CONSTANTS OF A SWOLLEN VULCANIZATE

In the following sections, we shall require material constants for the matrix which correspond to the modulus of elasticity and Poisson's ratio in infinitesimal elasticity theory. Of course, there is no real equivalent to these in the behaviour of highly elastic rubber-like materials, particularly when the added complication of solvent imbibition is considered. Nevertheless, theory allows us to construct stress-elongation ratio curves for the swollen matrix material, and approximations to these curves around the calculated elongation ratio at zero external stress may be given in the form of straight lines. In this way, the 'elastic constants' can be defined. This has been presented by us elsewhere⁹, and the curves are shown in *Figure 5* as functions of extension ratio. Making use of the results described above, we have plotted the values of Young's modulus, Poisson's ratio, and the shear modulus as functions of the unswollen radius. We shall require these values for further computations.

The curves shown in *Figure 5*, it must be noted, were calculated for a pure gum compound with a given average value of M_c . This is, in fact, the description of the rubber vulcanizate which would fill the space between the fibres of a fibrillar filler. Where a structure such as tyre cord is considered, the curves should correspond to the highly complex rubber compound used as cushion-gum. Studies¹⁰ which may provide some basis for theoretical stress-elongation ratio curves of solvent-swollen black-filled rubbers have been published, but the experimental determination of such curves and the justification and refinement of the theory used must still be undertaken.

Fibrillar models

Our first model has been very briefly described above. We now define this model more accurately: (i) the fibres are substantially straight and of very high aspect ratio such that it may be considered infinite; (ii) they are dispersed within a matrix in layers or laminae of equal thickness, all fibres in a lamina being parallel; (iii) the model is further simplified by concentrating all fibres in a central plane in which they lie at equal distances from each other; (v) the laminae are placed over each other with the fibres in alternate laminae parallel. Figure 6 shows the laminae and the stacked structure.

Because the fibres are numerous and because their diameter is small compared to the thickness of the lamina, we may assume the geometry before and after swelling to appear as in Figure 7, with the areas of

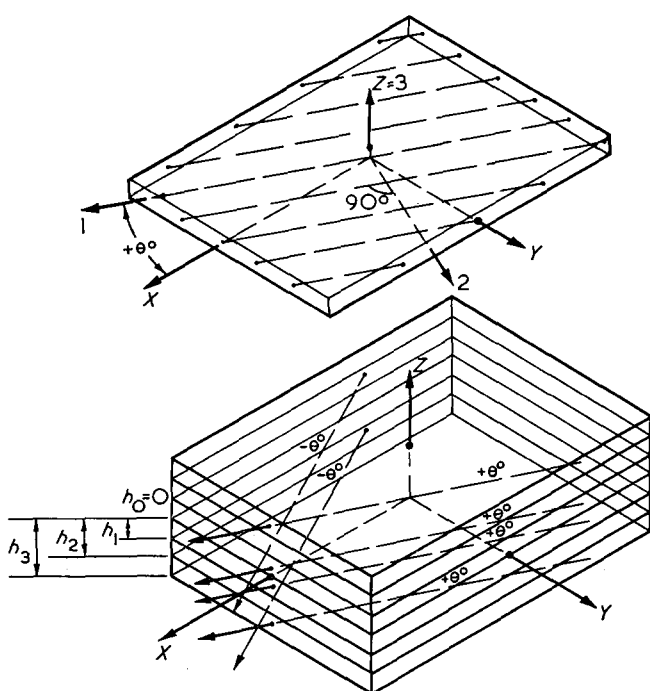


Figure 6 Single lamina and stacked structure showing principal directions of fibres (1, 2, 3) and of structure (X, Y, Z)

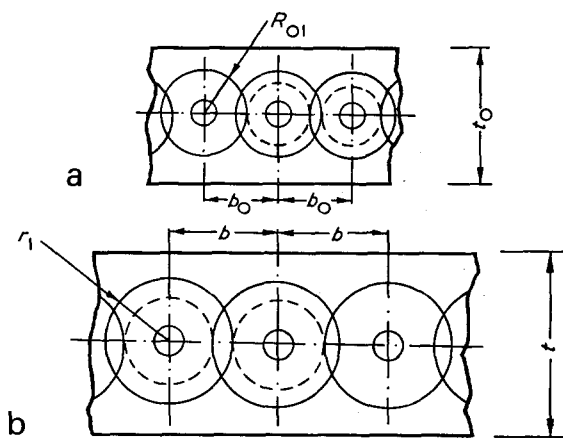


Figure 7 Section of reinforced lamina. (a) Before swelling; (b) after swelling

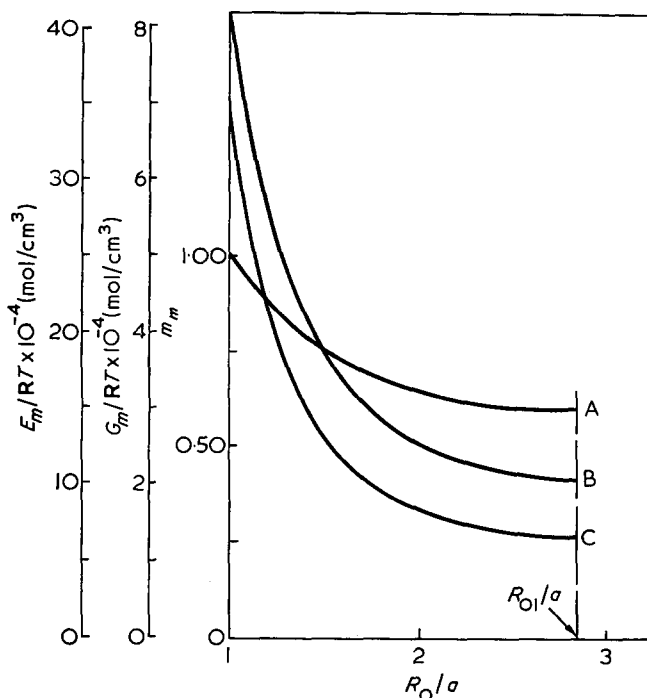


Figure 8 Pointwise equivalent elastic constants in shell restrained by fibre. A, m_m ; B, G_m/RT ; C, E_m/RT . $M_c=6133$; $\nu_{20}=0.18$; $\nu_1=87$

influence of the fibres overlapping. Swelling across the fibres (direction 2) is therefore hindered along the central plane, the influence diminishing towards the outer surfaces until it substantially vanishes at a distance of 2.8 radii from the central plane. The degree of swelling in direction 2 can only be estimated making use of doubtful assumptions but provided the thickness t_0 is of the order of $2R_{01}$, this is not likely to be very different from the averaged linear swelling over the distance (b_0-2a) . The swelling in direction 3 is similarly averaged over the distance $2(R_{01}-a)$.

Taking for a numerical example the values $b_0=2.5a$, $R_{01}=2.8a$, $t_0=5.6a$, and using Figure 4 we have $b \approx 3.7a$, $t=9.69a$. We may now calculate three anisotropic swelling coefficients, which are similar in function to the three products of the anisotropic coefficients of expansion by temperature rise. These are:

$$\begin{aligned} \alpha_1 &= 0 \\ \alpha_2 &= b/b_0 - 1 = 0.48 \\ \alpha_3 &= t/t_0 - 1 = 0.73 \end{aligned} \tag{13}$$

The total swelling ratio of the lamina is $\Delta V/V_0=1.46$ as compared to the swelling of an unreinforced material which should be $(\nu_{20}^{-1}-1)c_m=3.425$, or a restraint of about 57.6%.

For other distributions, elastomers and swelling solvents, we are able to calculate other swelling ratios.

As the proportion of solvent in the restrained swollen elastomer varies from point to point, it is necessary to calculate mean values of the elastic constants. Pointwise constants were first calculated from values of ν_2 as a function of R_0/a and these are given in Figure 8. The curves for E_m and m_m were then integrated up to R_{01}/a , and \bar{G}_m calculated using the usual elastic formula. The results are shown in Figure 9.

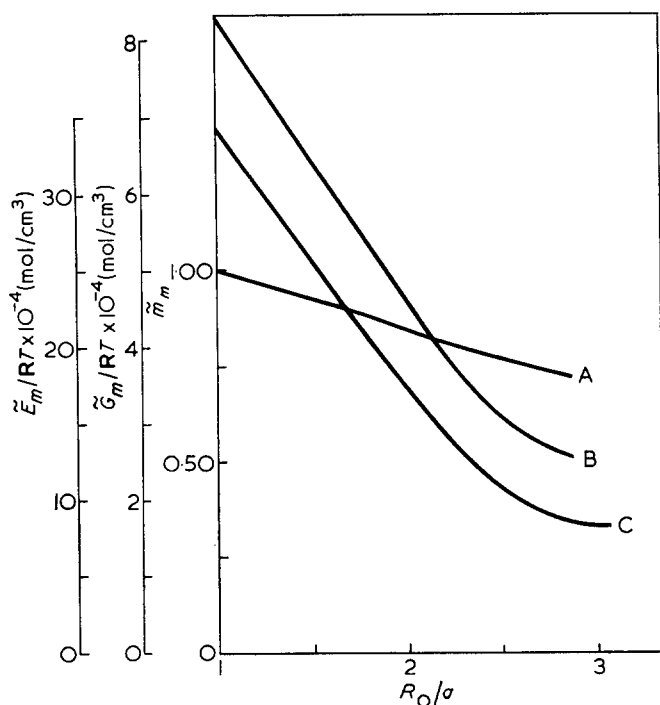


Figure 9 Equivalent elastic constants in restrained shell integrated up to radius indicated. A, \tilde{m}_m ; B, \tilde{G}_m/RT ; C, \tilde{E}_m/RT

We are now in a position to calculate the elastic constants of a lamina, and to this end we use the expressions derived by Halpin and Tsai¹¹:

$$E_{11} = E_m c_m + E_f c_f \quad (14)$$

$$E_{22} = E_m \frac{1 + 2c_f[(E_f - E_m)/(E_f + 2E_m)]}{1 - c_f[(E_f - E_m)/(E_f + 2E_m)]} \quad (15)$$

$$m_{12} = c_f m_f + c_m m_m \quad (16)$$

$$m_{21} = m_{12} E_{22} / E_{11} \quad (17)$$

$$G_{12} = G_m \frac{1 + c_f[(G_f - G_m)/(G_f + G_m)]}{1 - c_f[(G_f - G_m)/(G_f + G_m)]} \quad (18)$$

Using these expressions for the distribution given previously, we calculate $c_m = 0.775$, $c_f = 0.225$, and from Figure 9, $\tilde{E}_m = 8.75 \times 10^{-4} \text{ mol/cm}^3$, $\tilde{G}_m = 1.75 \times 10^{-4} \text{ mol/cm}^3$, $\tilde{m}_m = 0.73$. For the fibres, we assume values pertaining to nylon-6,6, $E_f = 0.445 \text{ mol/cm}^3$ and $m_f = 0.37$, giving $G_f = 0.1625 \text{ mol/cm}^3$. The values derived are then:

$$E_{11} = 0.100803 \text{ mol/cm}^3$$

$$E_{22} = 0.002943 \text{ mol/cm}^3$$

$$G_{12} = 0.000276 \text{ mol/cm}^3$$

$$m_{12} = 0.6659$$

$$m_{21} = 0.1944$$

While we have no test results on experimental fibre-reinforced elastomers of the nature described, it is of interest to note that one of us¹² has applied this method to the study of various types of tyre-cord frictioned with three types of cushion gum, and has obtained very substantial agreement between theory and experiment.

We may also apply the results obtained to study the swelling of the second model, which may be described as a random distribution of parallel fibres within a

matrix, using a method very similar to that given for a distribution of spheres in ref 10. There is little point in describing the details of this here. The model would be expected to describe fairly closely the behaviour of a CA type of block copolymer morphology as described e.g. by Mieras and Wilson¹³.

Swelling of laminated construction

When the laminae described above are combined in a symmetrical composite as shown in Figure 6, it is possible to determine the effective values of the elastic constants in the principal directions as the result of dispositions at various angles. Some results are shown in Figure 10, but attempts to correlate these with swelling studies have failed. We believe that this is due to difficulty of taking shear coupling effects between the layers, such effects being traditionally ignored in the many studies of more rigid laminates.

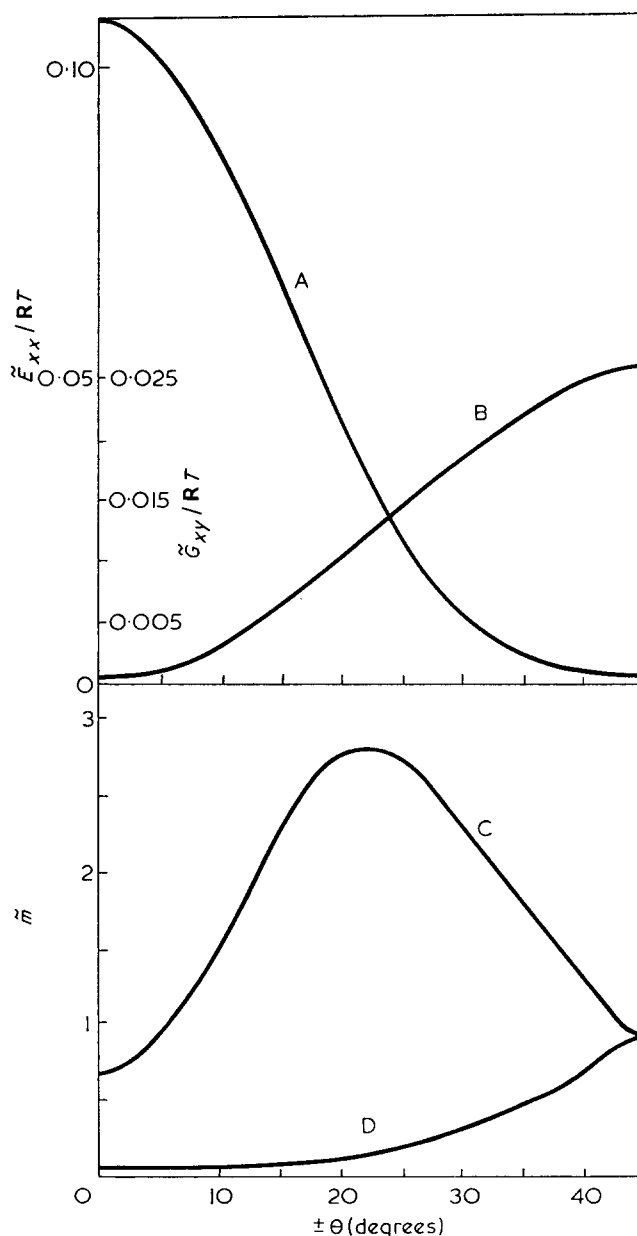


Figure 10 Theoretical elastic behaviour of a swollen laminated fibrillar structure as a function of the angle $\pm\theta$. A, E_{xx}/RT ; B, G_{xy}/RT ; C, \tilde{m}_{xy} ; D, \tilde{m}_{yx}

NOMENCLATURE

a	radius of fibre
c_f	volume fraction of fibrous filler
C_{dry}	elastic constant for dry elastomer
E	modulus of elasticity in tension
G	modulus of elasticity in shear
I_1, I_3	invariants of extension ratio tensor
m	Poisson's ratio
M_c	average molecular weight between crosslinks
p	pressure
r	radial distance from centre of fibre to point in swollen restrained tube (see <i>Figure 1</i>)
R	value of r for swollen unrestrained tube
R_0	value of R for unswollen tube
RT	thermodynamic constant
v_2	volume ratio of dry elastomer in swollen gel
v_{20}	value of v_2 at $p = 0$
V_1	molar volume of solvent
W	strain energy function for swollen elastomer
α	anisotropic swelling coefficients
γ	density of dry elastomer
λ	principal extension ratios
μ	solvent-elastomer interaction coefficient
σ	true stress

Subscripts

i, j, k selected orthogonal directions

f	filler
m	matrix
l, r, t	longitudinal, radial and tangential directions of tube
1, 2, 3	directions in laminate

REFERENCES

- 1 Scanlan, J. *Rev. Gen. Caoutch. Plast.* 1964, **41**, 514
- 2 Southern, E. and Thomas, A. H. *J. Polym. Sci. (A)* 1965, **3**, 641
- 3 Rigbi, Z. *Rev. Gen. Caoutch. Plast.* 1970, **47**, 1143
- 4 Flory, P. J. 'Principles of Polymer Chemistry', Cornell Univ. Press, Ithaca, 1953
- 5 Rigbi, Z. *Int. J. Eng. Sci.* 1969, **7**, 1163
- 6 Hart-Smith L. J. and Crisp, J. D. C. *Int. J. Eng. Sci.* 1967, **5**, 1
- 7 Treloar, L. R. G. 'The Physics of Rubber Elasticity', Oxford Univ. Press, 1958, Ch 7
- 8 Coran, A. Y., Boustany, K. and Hamed, P. *J. Appl. Polym. Sci.* 1971, **15**, 2471
- 9 Rigbi, Z. *Int. J. Polym. Mat.*, in press
- 10 Rigbi, Z. *J. Appl. Polym. Sci.* 1968, **12**, 2736
- 11 Halpin, J. C. and Tsai, S. W. 'Environmental Factors in Composite Materials Design', AFML-TR423, 1967
- 12 Sabatov, N. *MSc Thesis Technion—Israel Institute of Technology*, 1973
- 13 Mieras, H. J. M. A. and Wilson, E. A. *J. Inst. Rubber Ind.* 1973, **7**, 72

Mechanical properties of oriented polymers*

I. M. Ward

*Department of Physics, University of Leeds, Leeds LS2 9JT, UK
(Received 30 October 1973)*

The anisotropic mechanical behaviour of oriented polymers at low strains is discussed. In the case of amorphous polymers and polymers of low crystallinity, attempts to interpret the anisotropy in terms of an aggregate model are reviewed. This is followed by an account of recent work on the measurement of all the elastic constants for polymer films of orthorhombic symmetry. After a brief discussion of cold drawn crystalline polymers, where very high Young's moduli can be obtained, the behaviour of annealed oriented polymers is considered. It appears that the latter can be understood in terms of a composite solid model, combining the early notions of Takayanagi with more recent ideas of interlamellar shear.

INTRODUCTION

This paper attempts to present a fairly general account of the physical aspects of the mechanical anisotropy of polymers at low strains. For the purposes of the discussion, linear elastic or linear viscoelastic behaviour will be assumed, accepting that even at very low strains (<0.5%) the behaviour in some cases may very well show significant non-linearity.

Much of the initial stimulus to the interpretation of low strain mechanical anisotropy in polymers came from two models: (1) the re-orienting element aggregate model^{1, 2}; and (2) the Takayanagi composite model³. These two models were originally proposed for polymer systems with very different characteristics. The aggregate model was first suggested for poly(ethylene terephthalate) (PET) in the glassy state¹, whereas the Takayanagi model gave a good explanation of the high temperature relaxation behaviour of highly annealed oriented linear polyethylene³. Branched polyethylene (i.e. low density polyethylene) subsequently appeared to occupy an intermediate position. In its cold drawn oriented state the mechanical anisotropy could be given an adequate semi-phenomenological explanation in terms of the aggregate model^{2, 4, 5}. Cold drawn and annealed samples, on the other hand, were better explained on a composite model approach^{6, 7}.

Much of the definitive research on mechanical anisotropy in polymers has been carried out on these three polymers: poly(ethylene terephthalate), linear polyethylene and branched low density polyethylene. Many of the quantitative ideas are therefore still based on elaborations of the earliest work. However, it is intended to indicate where several other polymers come into the picture, although information concerning them is usually less extensive.

THE AGGREGATE MODEL

The aggregate model arose from the observation that

in PET, overall molecular orientation, including particularly the orientation of the non-crystalline regions^{1, 8}, rather than crystallinity, appears to influence the mechanical anisotropy. It is important to recall that this model was conceived before the impact of chain-folded crystallization, and that it was proposed for the non-crystalline or comparatively poorly crystalline situation of PET.

The problems with the application of the aggregate model were two-fold. First, it was necessary to know *all* the elastic constants, which led to a considerable amount of complicated experimental physics. Secondly, measures of the molecular orientation were required which at that time were not available. This led to the adoption of theoretical schemes to predict the distribution of molecular orientation, and hence the required orientation functions for the theory.

These two aspects will be discussed in turn. As indicated, the aggregate model appears applicable to polymers of low crystallinity or preferably non-crystallizing polymers. Apart from PET, it was subsequently applied with success by Hennig⁹ to poly(vinyl chloride) (PVC), and by Kausch to PET, poly(methyl methacrylate) (PMMA), PVC and polyacrylonitrile^{10, 11}. An unsatisfactory feature has been the prediction of the molecular orientation on the basis of a theoretical scheme. Moreover, the scheme which fits the results well is one in which the polymer is regarded as an aggregate of transversely isotropic units, whose axes rotate towards the draw direction in the same way as lines joining pairs of points in the macroscopic body, which deforms uniaxially at constant volume. This assumes that the units rotate like needles in Plasticine†, and leaves unanswered questions regarding the connectivity of the molecular chains, etc. This scheme (which has been termed pseudo-affine¹², to distinguish it from the affine deformation scheme of rubber elasticity) works remarkably well for PET¹², as shown in *Figure 1*

* Presented as a Symposium Lecture at the IUPAC International Symposium on Macromolecules, Aberdeen, September 1973.

† I am indebted to Professor F. C. Frank for this graphic description.

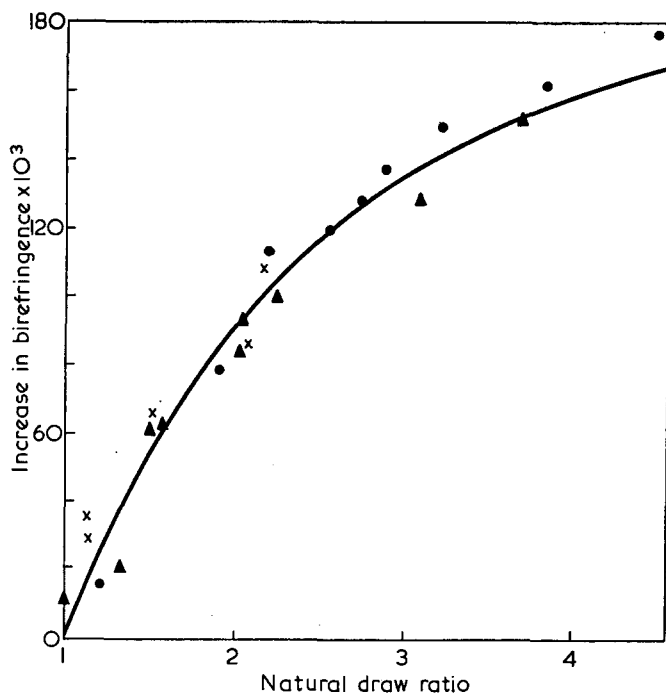


Figure 1 Variation in birefringence with natural draw ratio for PET fibres. \times , \bullet , Δ , experimental data for drawing at -20 , $+24$ and 62°C respectively; —, theoretical curve based on pseudo-affine deformation scheme

Table 1 Comparison of calculated values for Young's modulus ($\times 10^9 \text{N/m}^2$) with measured values Y_E for a range of natural draw ratios (NDR) and initial birefringences Δn^{13}

NDR	$\Delta n \times 10^{-3}$	Reuss bound Y_R	Voigt bound Y_V	Measured Y_E	$\frac{2Y_E}{Y_R + Y_V}$
1.25	67.8	1.81	6.76	4.94	1.15
1.59	46.0	1.93	7.58	5.35	1.12
1.92	28.0	1.98	7.94	5.58	1.12
2.36	13.1	2.14	8.48	6.28	1.18
2.52	9.52	2.22	8.62	6.09	1.12
2.64	5.43	2.24	8.70	6.27	1.15
3.19	3.52	2.68	9.62	7.02	1.14
3.99	1.37	3.31	10.55	7.85	1.13

and Table 1, and according to Hennig⁹, very well for PVC. There have, however, been few attempts to check its validity directly, because of the paucity of methods for determining orientation in amorphous polymers. At Leeds University we have recently developed several spectroscopic techniques in an attempt to resolve these problems, and some of the relevant results obtained will now be discussed.

The aggregate model requires values for the orientation functions $\overline{\cos^2\theta}$ and $\overline{\cos^4\theta}$, where θ is the angle which the unique axis of an anisotropic unit makes with the draw direction and $\overline{\cos^2\theta}$ and $\overline{\cos^4\theta}$ are the average values of $\cos^2\theta$ and $\cos^4\theta$ respectively for the aggregate. In the early work, values of $\overline{\cos^2\theta}$ calculated from the pseudo-affine deformation scheme were used, first to predict the optical birefringence, as a guide to the likely success of the calculations, and then combined with values of $\overline{\cos^4\theta}$ calculated on the same basis, to predict the mechanical anisotropy.

In some cases an effective draw ratio might be used, which is equivalent to taking a value of $\overline{\cos^2\theta}$ from the

birefringence data and then assuming a value for $\overline{\cos^4\theta}$ which was consistent with the pseudo-affine orientation distribution. Our recent spectroscopic measurements of $\overline{\cos^2\theta}$ and $\overline{\cos^4\theta}$ provide an understanding of the success of this early work.

Figure 2 shows the correspondence between laser-Raman spectroscopic values¹⁴ of $\overline{\cos^2\theta}$ and $\overline{\cos^4\theta}$ for the chain orientation in uniaxially oriented PET film, compared with the relationship between these quantities predicted by the affine and the pseudo-affine deformation schemes respectively. The reasonable agreement of the measured $\overline{\cos^2\theta}$ and $\overline{\cos^4\theta}$ values with the pseudo-affine deformation scheme for a variety of specimens, taken in conjunction with infra-red spectroscopic measures¹⁵ of $\overline{\cos^2\theta}$, confirm that the previous theoretical treatments were indeed justified.

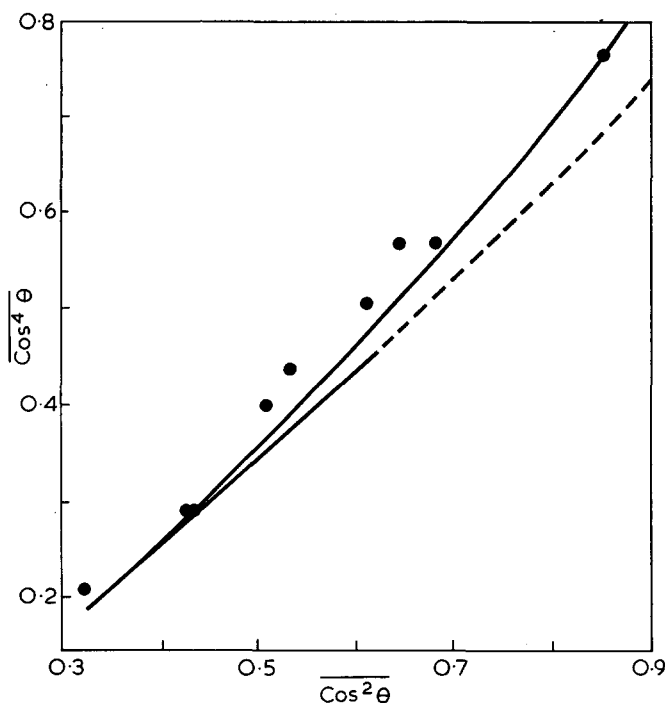


Figure 2 Comparison of $\overline{\cos^4\theta}$ and $\overline{\cos^2\theta}$ obtained for a series of uniaxially oriented PET films using polarized Raman scattering. ---, Predicted relationship according to the affine rubber elasticity model; —, pseudo-affine deformation scheme

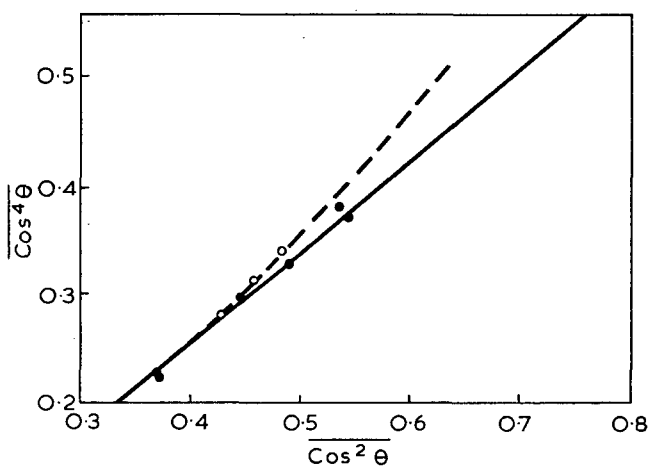


Figure 3 Comparison of $\overline{\cos^4\theta}$ and $\overline{\cos^2\theta}$ obtained for oriented PVC (\circ) and oriented PMMA (\bullet). Curves show predicted relationship according to the affine rubber elasticity model (---) and the pseudo-affine deformation scheme (—)

Broad line nuclear magnetic resonance has also been of considerable value in this respect. Figure 3 shows the values of $\overline{\cos^2\theta}$ versus $\overline{\cos^4\theta}$ obtained using this technique for oriented PMMA¹⁶ and PVC¹⁷. It is to be noted that PVC appears to follow the pseudo-affine deformation scheme, in accord with Hennig's previous work, whereas PMMA is closer to the affine deformation scheme.

Figure 4 shows the mechanical anisotropy of PMMA and it can be seen that as in PET, the experimental results fall very close to half way between the Reuss and Voigt bounds, i.e. the bounds obtained by averaging compliances and stiffnesses respectively on the aggregate model.

The second feature which the aggregate model highlighted was the necessity of determining all the elastic constants. For the purposes of this discussion it is most convenient to define the elastic behaviour by the generalized Hooke's law relating strains e_p to stresses σ_q by the compliance constants matrix S_{pq} . The compliance constants then relate to the strains observed in simple loading situations. For a fibre or uniaxially oriented film there are five independent elastic constants (Figure 5). For a one-way drawn polymer film with orthorhombic symmetry there are nine independent elastic constants (Figure 6). We will consider in detail mechanical anisotropy in PET where all five constants for highly oriented fibre monofilaments have been determined and, more recently, all nine constants for a highly oriented one-way drawn film.

In the fibre, the Young's modulus elastic constant S_{33} , the torsional modulus constant S_{44} , and the axial Poisson's ratio constant S_{13} can be measured by straightforward methods. The transverse elastic constant S_{11} and its associated Poisson's ratio constant S_{12} are less

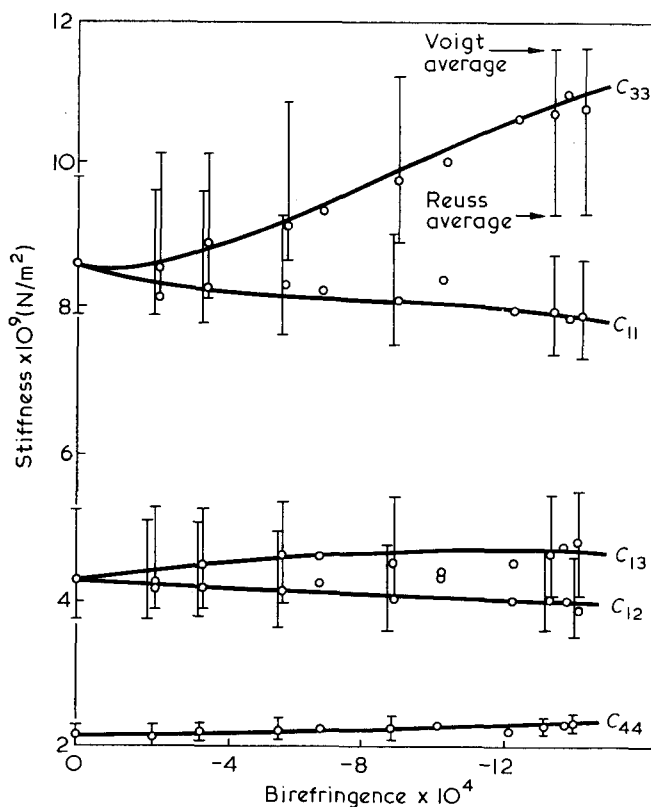


Figure 4 Stiffness constants of PMMA as a function of birefringence in a series of uniaxially oriented samples

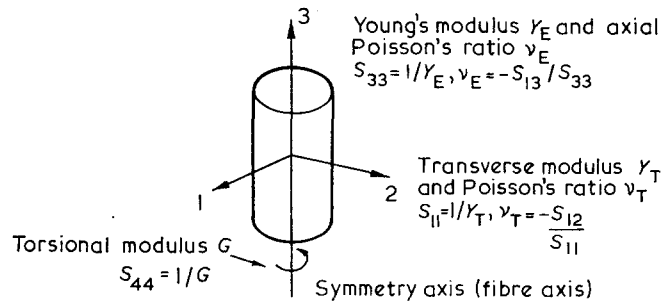


Figure 5 The five independent compliance constants for fibre symmetry

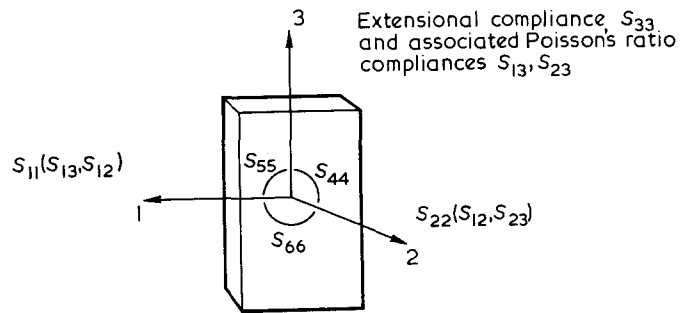


Figure 6 The nine independent compliance constants for film of orthorhombic symmetry. S_{44} , S_{55} , S_{66} are shear compliances for shear in 23, 13 and 12 planes respectively

straightforward, but have been determined by transverse compression of fibre monofilaments. The width of the contact zone and the diametrical expansion of the monofilament relate primarily to the elastic constants S_{11} and S_{12} . In these measurements the monofilament is compressed on the stage of an optical microscope under conditions of plane strain. (For details see refs 18 and 19.)

In the case of orthorhombic films, several new techniques had to be devised. Only two of the elastic constants, those corresponding to Young's moduli in the plane of the film, i.e. S_{11} and S_{33} , could be measured easily. The third extensional compliance S_{22} was measured by compression of the film in a carefully designed compression apparatus²⁰. By comparing results for two plane strain situations (compression of thin strips cut parallel to the 1 and 3 directions respectively) and a small square section sample, S_{22} could be determined, providing that the relevant Poisson's ratio constants are known independently.

The Poisson's ratio constant S_{13} corresponds to a contraction in the 1 direction when the film is loaded in the 3 direction. This was measured by the distortion of an electron microscope grid printed on the surface of the sample²¹. The Poisson's ratio constants S_{12} and S_{23} correspond to changes in thickness caused by loading the film in the 1 and 3 directions respectively. We have determined these constants by an interferometric technique²². The optical path length alters owing to changes in refractive index as well as macroscopic changes in dimension when the sample is loaded. It has been shown that the changes in refractive index are less important than the dimensional changes, but this still leads to a measure of uncertainty in the final results. The value of the constant S_{12} has also been confirmed by a direct transducer method where the change of

thickness of the film under load was determined²³. This direct method is, however, not feasible for determining S_{23} which is a much smaller quantity. Fortunately, we will see that it is the order of magnitude of the elastic constants which is of real significance, and that errors even up to 20% in the constant S_{12} can be tolerated if we only seek a physical understanding.

Finally, there are the shear compliances S_{44} , S_{55} and S_{66} . For these compliances a compound torsion system was used²⁴, which allowed variable weights to be added in the axial direction, so that extrapolation to zero axial stress could be carried out. Only S_{55} , corresponding to shear in the plane of the film, is comparatively easy to determine. Two values are obtained; from narrow strips twisted around the 1 and 3 directions respectively. The torsion of very narrow strips with different aspect ratios, then gives extrapolation curves for S_{44} and S_{66} ²⁵.

The measured elastic constants for a film and two fibres of different orientation are shown in Table 2. There are several features worthy of note. In the first place there is the very large anisotropy of elastic constants, and they fall into 3 groups. First, the extensional compliance S_{33} is the smallest, and this is expected because it may involve distortion of bonds in the molecular chain. Secondly, the film shear compliances S_{44} and S_{66} for shear of planes parallel to the plane of the film are the largest compliances. We believe that this relates to the planar orientation of the film. The 100 planes, planes of maximum electron density, are preferentially oriented in the plane of the film, and it is reasonable to postulate the analogy with graphitic structures, where van der Waals forces are largely responsible for the cohesion of the graphitic plane sheets.

Thirdly, the compliances S_{11} , S_{12} and S_{55} , which relate to distortions in the plane of the sheet, occupy an intermediate position. It is possible to speculate that these compliances involve changes in molecular conformation, i.e. bond rotations as well as dispersion forces.

In the second place, the comparison between film and fibres is of interest. In both cases we can compare the predicted bounds for the isotropic compliance constants, based on the aggregate model, with the experimental values. This comparison is shown in Table 3(a), and we see that the experimental values fall convincingly between the bounds. We can also make an approximate calculation of the fibre elastic constants

Table 2 Compliance constants (10^{-10} m²/N) for oriented PET of orthorhombic film and two fibres

	Orthorhombic film	Fibres	
		A	B
S_{11}	4.4	8.9	16.1
S_{22}	6.14		
S_{33}	0.58	1.1	0.71
S_{44}	26.2	13.6	13.6
S_{55}	5.88		
S_{66}	27.7		
S_{12}	3.3	-3.9	-5.8
S_{13}	-0.19	-0.47	-0.31
S_{23}	-0.40		

Table 3 Comparison of calculated and measured compliance constants (10^{-10} m²/N) for isotropic PET and PET fibres based on the film data

(a) Isotropic polymer					
	Experimental	Calculated bounds from film data		Calculated bounds from fibre data	
		Reuss	Voigt	Reuss	Voigt
S_{33}	4.4	5.8	2.1	10.4	3
S_{44}	11	16.2	5.6	25	7.6
(b) Fibres					
	Experimental		Approximate calculation undertaken by randomizing film data		
	A	B	Reuss	Voigt	
S_{11}	8.9	16.1	6.7	6.2	
S_{12}	-3.9	-5.8	-4.6	-4.2	
S_{13}	-0.47	-0.31	-0.30	-0.28	
S_{33}	1.1	0.71	0.58	0.58	
S_{44}	13.6	13.6	16.0	9.6	

from the film data, by averaging the film constants in the plane normal to the film draw direction. On the aggregate model this calculation involves several independent sets of equations. In particular, the shear compliance S_{44} for the 'equivalent fibre' relates only to the S_{44} and S_{55} compliances of the film, and the S_{13} compliance for the fibre relates only to the S_{13} and S_{23} compliances for the film. From Table 3(b) it can be seen that the predicted bounds for the fibre are in the correct range, the result being very good in the case of the S_{44} compliance. The comparison is less good for the S_{12} compliance, and quite incorrect for the S_{11} compliance. This result suggests that the compression measurement of the S_{11} fibre constant may be in error, possibly owing to a different surface structure in the fibre which has so far eluded detection by structural techniques.

CRYSTALLINE POLYMERS

These detailed studies of the aggregate model confirm that geometrical rearrangement of the structure can account very well for the pattern of anisotropy in a glassy polymer of comparatively low crystallinity. It is more surprising that such a model would work well for low density polyethylene where complex morphological changes occur as drawing. However, it has been very clearly demonstrated how this pattern of anisotropy arises both with regard to the non-affine orientation distribution^{5, 26, 27} and the minimum in Young's modulus which is associated with a unique relaxation process, the *c*-shear relaxation^{5, 28, 29}. This topic has been extensively discussed in previous publications and will not be considered further here. The aggregate model certainly does not work for high density polyethylene and polypropylene, where the isotropic elastic constants are significantly outside the predicted bounds, and it probably does not work for nylon-6,6 (Table 4). There are increases in stiffness on orientation in these polymers which are not related to geometrical rearrangements but to profound structural changes, as would be expected from morphological studies, such as those carried out

by Peterlin and his colleagues³⁰. In polypropylene, it was concluded³¹ that geometrical rearrangements were probably adequate to explain the development of mechanical anisotropy for low and intermediate states of orientation, but this assumption breaks down for high orientation. It was even speculatively suggested³¹ that the point of breakdown might correspond to the point at which the lamellae are broken up, and this suggestion appears to receive confirmation from the more recent ideas of Peterlin on deformation in a very similar polymer, high density polyethylene³⁰. Another polymer where the aggregate model proves quite inadequate is nylon-6. Recent work³² has shown that the mechanical anisotropy shows considerable complexity, which can be attributed to structural changes occurring during the drawing process.

The development of mechanical anisotropy in crystalline polymers is therefore particularly rewarding with regard to the insight which it may provide on the rela-

Table 4 Comparison of calculated and measured extensional and torsional compliances ($\times 10^{10} \text{m}^2/\text{N}$) for unoriented polymers (ref 12, p 256)

	Extensional compliance S_{33}			Torsional compliance S_{44}		
	Calculated			Calculated		
	Reuss	Voigt	Measured	Reuss	Voigt	Measured
	High-density polyethylene	10	2.1	17	30	6
Polypropylene	7.7	3.8	14	23	11	2.7
Nylon-6,6	6.6	5.2	4.8	17	13	12

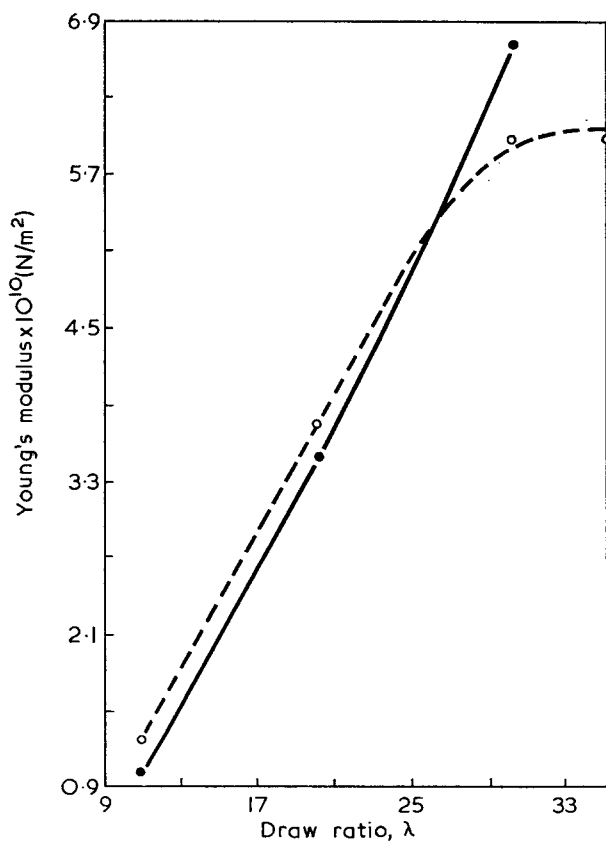


Figure 7 Variation of Young's modulus with draw ratio for high density polyethylenes. ●—●, $\bar{M}_n=6180$ and $\bar{M}_w=101450$; ○---○, $\bar{M}_n=13350$ and $\bar{M}_w=67800$

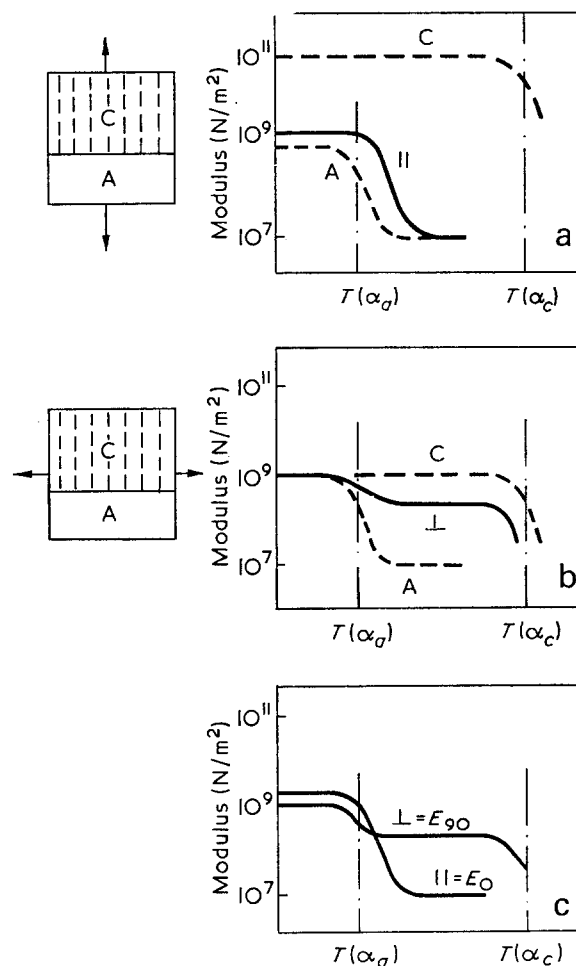


Figure 8 Schematic representation of change in modulus E with temperature on the Takayanagi model for (a) the || and (b) the \perp situations corresponding to E_0 and E_{90} respectively. Calculations assume amorphous relaxation at temperature $T(\alpha_a)$ and crystalline relaxation at temperature $T(\alpha_c)$ and (c) shows combined results. C, Crystalline phase; A, amorphous phase (after Takayanagi *et al.*)

tionship between structure and properties when these materials are deformed to high molecular orientation. An interesting example of the extreme situation which can occur is illustrated by the cold drawing of high density polyethylene³³ and is shown in *Figure 7*. At very high draw ratios the Young's modulus reaches $\sim 7 \times 10^{10} \text{N/m}^2$ which is about one-third of the theoretical modulus for perfectly oriented polyethylene. Such high draw involves drastic changes in structure, and may even lead to an appreciable increase in the melting point owing to the production of extended chain crystallites³³. This is an area of considerable importance technologically as well as being of some scientific interest.

THE TAKAYANAGI COMPOSITE MODEL

At the other extreme from the amorphous oriented polymers, are the cold drawn and annealed polymers. In this case the key initial work was carried out by Takayanagi, who found the unusual result that the modulus along the draw direction became less than that perpendicular to the draw direction at temperatures above the major relaxation transition. He interpreted this result in terms of his well known model (*Figure 8*) where the amorphous material, whose modulus falls

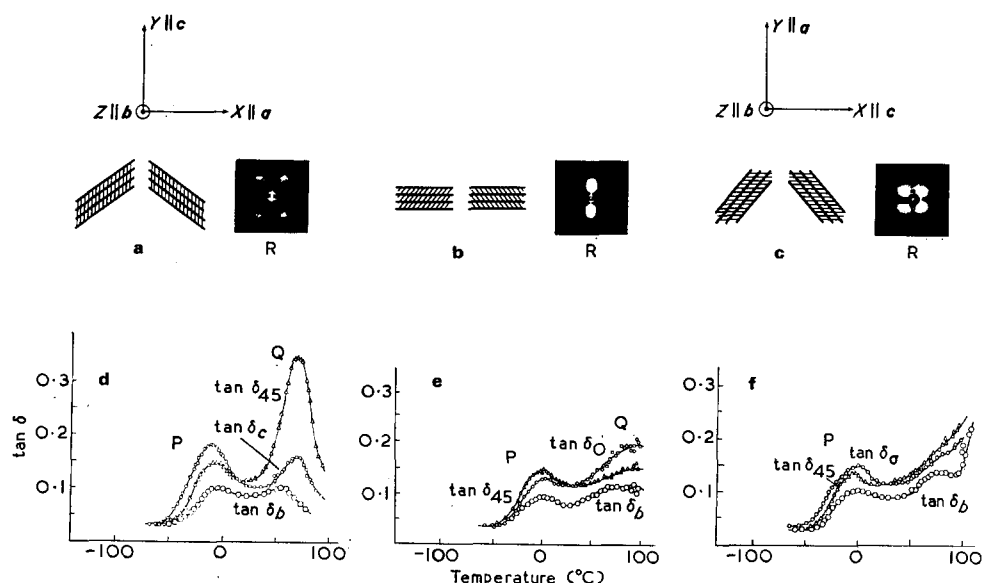


Figure 9 Schematic structure diagrams and mechanical loss spectra. (a) and (d): for *b-c* sheet; (b) and (e): for parallel lamellae sheet; (c) and (f): for *a-b* sheet. P, interlamellar shear process; Q, *c*-shear process; R, low angle X-ray diagram, beam along Z

above the major relaxation, is in series with the crystalline material for the draw direction situation, and in parallel for the perpendicular situation. This composite solid model is an excellent starting point for understanding the mechanical anisotropy of oriented crystalline polymers, provided that they are sufficiently annealed for substantial relaxation of the interlamellar material to have occurred. The Takayanagi model does, however, need to be converted to a three-dimensional model. In theoretical terms this means that shear strains as well as extensional strains must be considered. In physical terms it is the shear strains which are of predominant importance, and this in turn leads to a recognition that the orientation of the lamellae is the critical factor in determining the patterns of mechanical anisotropy.

This aspect has been demonstrated very clearly by comparative studies of specially oriented sheets of low density polyethylene. Schematic structure diagrams and mechanical loss spectra for three sheets, each possessing structure of particular simplicity, are shown in Figure 9. The '*b-c* sheet' in Figure 9a gives a wide angle X-ray diffraction pattern showing that the *b* and *c* axes of the crystalline regions lie in the plane of the sheet. Low angle X-ray diffraction results show that the lamellae are arranged with their normals inclined at about 40° to the direction of the *c* axis. The '*a-b*' sheet shown in Figure 9c has a similar lamellar texture, but the *a* and *b* axes now lie in the plane of the sheet and the *c* axis normal to this direction. Finally, there is the 'parallel lamellae sheet' of Figure 9b where the lamellar planes are now normal to the initial draw direction in the sheet (i.e. the *c*-axis direction of the '*b-c* sheet') and the *c* axes make an appreciable angle with that direction.

Figures 9d, e and f show the dynamic mechanical loss spectra for thin strips cut from these sheets in the indicated directions, the experiments being carried out in bending at approximately constant frequency over a range of temperatures. There are two relaxation processes P, the interlamellar shear process, and Q the *c*-shear relaxation process. Examination of the results for these sheets shows that the loss spectra are exactly

consistent with this interpretation, the interlamellar shear process showing maximum loss for situations where the resolved shear stress parallel to the lamellar planes is a maximum, and the *c*-shear relaxation showing maximum loss when the resolved shear stress is parallel to the mean direction of the *c*-axes. (For a more detailed discussion see refs 28, 29 and 34.) Exactly comparable results were obtained for the variation of extensional moduli with temperature³⁵, and similar cross over points were observed to those first shown by Takayanagi for high density polyethylene. The interpretation is consistent with the original ideas of Takayanagi, but introduces the orientation of the lamellar planes as a key factor, and the more precise definition of the relaxation process in sub-macroscopic terms as 'interlamellar shear'.

The next step was to combine these ideas to give a quantitative interpretation of the anisotropy of both losses and moduli. Before proceeding with this, it appeared desirable to examine how the mechanical anisotropy was reflected at a molecular level. Dielectric relaxation measurements were therefore undertaken³⁶ on sheets similar to the *b-c* and *a-b* sheets described above, on low density polyethylene samples which had previously been subjected to a small amount of oxidation so that carbonyl groups could be incorporated into the polyethylene chain. It was found that the *c*-shear process showed the dielectric anisotropy expected for a relaxation involving rotation of the chain around its axis, i.e. consistent with the process proposed by Hoffman *et al.*³⁷ for this relaxation, where there is rotation of the chain through 90° together with its simultaneous translation along its axis. The interlamellar shear relaxation, on the other hand, showed no dielectric anisotropy, confirming that the mechanical anisotropy is not molecular in origin but arises entirely from the morphological structure and the anisotropic arrangement of lamellae. With these results in mind, it was possible to set up a simple model⁶ for the anisotropy of $\tan \delta$ for the interlamellar shear relaxation (conventionally called the β -relaxation) of low density polyethylene and the similar relaxation in high density polyethylene (which is con-

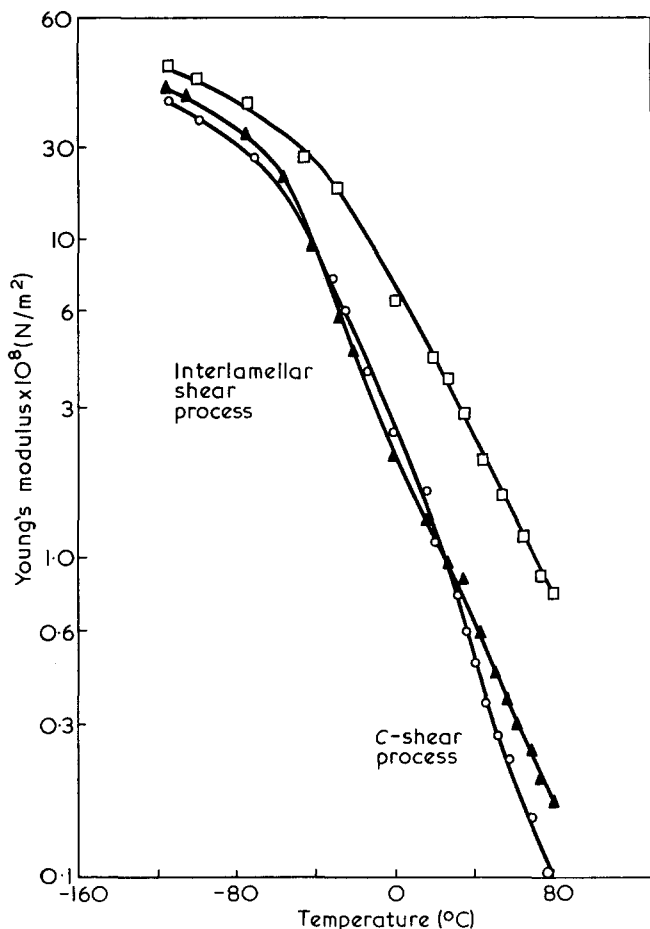


Figure 10 Young's modulus for parallel lamellae low density polyethylene sheet. \circ , E_0 normal to lamellar planes; \square , E_b parallel to lamellar planes and to b axis; \blacktriangle , E_{45} at an angle of 45° with these directions in plane of sheet

ventionally called the α -relaxation). It is assumed that there are no constraints to shear in the plane of the lamellae so that the motion of the lamellae is in the direction for which the shear stress is a maximum. This simple assumption makes the mathematical treatment very straightforward so that the loss anisotropy relates to the quantity $\cos^2\gamma\sin^2\gamma$ where γ is the angle between the applied stress direction and a lamellar plane normal. The calculated anisotropy agreed well with the experimental results, and this has recently been confirmed by Buckley and McCrum³⁸ for high density polyethylene sheets with orthorhombic symmetry.

Following the success of this simple model for the loss anisotropy, it appeared worthwhile to attempt to explain the anisotropy of moduli on a similar basis. Figure 10 shows the 10 sec Young's modulus data for the parallel lamellae low density polyethylene sheet. Two points are worthy of note. First, there are two crossover points in the modulus curves; one at about -40°C corresponding to the onset of interlamellar shear and another at about $+20^\circ\text{C}$ when the c -shear relaxation is the predominant process. These results are, of course, exactly consistent with the loss data of Figure 9e. Secondly, the modulus in the direction normal to the lamellar planes (E_0) does fall appreciably owing to the interlamellar shear relaxation. This led to the proposal⁷ that *pure* shear occurs as well as *simple* shear and that the increase in compliance due to both

types of shear must be added to explain the anisotropy in a range where interlamellar shear is the predominant process, i.e. near to room temperature. This composite model was very successful in explaining the modulus anisotropy to the parallel lamellae sheet at room temperature and for the a - b sheet, i.e. for situations where the c -shear relaxation does not contribute. More recent studies, which include creep measurements in torsion as well as extension³⁹, suggest that the situation is basically as proposed in this earlier work, and that all the results can be explained in terms of the sum of contributions from the two relaxation processes.

Finally, it may be asked how relevant these ideas of interlamellar shear and the composite model are to other polymers. In polypropylene⁴⁰, which is a polymer very similar in mechanical properties to high density polyethylene, the pattern of mechanical anisotropy could be attributed to the onset of interlamellar shear at temperatures above the β -relaxation in highly annealed samples. This then allowed the α -relaxation to show the loss anisotropy predicted by the simple model for an interlamellar shear loss process discussed above. Hot-drawn and hydrostatically extruded materials, on the other hand, did not show clear interlamellar shear, in spite of their distinct lamellar texture, as revealed by low angle X-ray diffraction. This suggests the importance of tie molecules and intercrystalline material in determining the mechanical properties. It is a result entirely consistent with the other work on low density and high density polyethylene, where intensive annealing is required to allow the interlamellar shear process. Infrared measurements have clearly shown how annealing removes most of the orientation of the non-crystalline material³⁵.

In PET, a combined study of mechanical and dielectric relaxation in oriented samples⁴¹, showed that the mechanical anisotropy of the α -relaxation contrasted with the isotropy of the dielectric α -process, as had been found for the β -relaxation in low density polyethylene. The pattern of mechanical anisotropy for the α -relaxation again suggested an interlamellar shear mechanism, but the simple continuity of stress model for interlamellar shear did not give a quantitative fit to the data. It was concluded that a more detailed model is required, taking into account both the orientation of the lamellae and the detailed nature of the stress and strain continuity. Such a model requires more detailed information on both mechanical properties and structure, and this is now being sought. It is interesting to note that in a sense this brings us back to the Takayanagi model where the stress and strain continuity problem is dealt with in terms of the relative proportions of crystalline and non-crystalline material and the degree of series and parallel coupling.

CONCLUSIONS

To conclude, this account of mechanical anisotropy in polymers suggests that the subject can be conveniently discussed under three main headings, although, of course, this is bound to be an arbitrary division in many cases.

(1) Amorphous polymers and polymers of low crystallinity can be considered in the light of the aggregate model and continuum ideas for molecular orientation on drawing. We might perhaps speculate that these

are systems where fringed micelle rather than chain folding morphologies predominate.

(2) Cold drawn highly crystalline polymers at high draw, where the pulling out of chain folds, to give many tie molecules or even extended chain crystallites, should be considered in a separate category. It seems likely that the composite solid approach, including the analogy with fibre reinforcement, will be relevant here.

(3) Oriented, highly annealed crystalline polymers can be understood in terms of the theories of composite solids, particularly in the situation where interlamellar shear is the predominant deformation process.

Finally, it may be remarked that there is a clear need to devise and undertake methods for measuring anisotropic mechanical behaviour in detail, so that theoretical models for the behaviour may be tested more stringently. Moreover, although our understanding of the mechanical properties of polymers is only as good as our understanding of their structure, this is not a unidirectional process, and there is much to be gained in structural understanding from detailed studies of mechanical behaviour.

REFERENCES

- 1 Ward, I. M. *Text. Res. J.* 1961, **31**, 650
- 2 Ward, I. M. *Proc. Phys. Soc.* 1962, **80**, 1176
- 3 Takayanagi, M., Imada, K. and Kagiya, J. *J. Polym. Sci. (C)* 1966, **15**, 263
- 4 Gupta, V. B. and Ward, I. M. *J. Macromol. Sci. (B)* 1967, **1**, 373
- 5 Stachurski, Z. H. and Ward, I. M. *J. Macromol. Sci. (B)* 1969, **3**, 427
- 6 Davies, G. R., Owen, A. J., Ward, I. M. and Gupta, V. B. *J. Macromol. Sci. (B)* 1972, **6**, 215
- 7 Owen, A. J. and Ward, I. M. *J. Mater. Sci.* 1971, **6**, 485
- 8 Pinnock, P. R. and Ward, I. M. *Proc. Phys. Soc.* 1963, **81**, 260
- 9 Hennig, J. *J. Polym. Sci. (C)* 1967, **16**, 2751
- 10 Kausch-Blecken von Schmeling, H. H. *Kolloid-Z.* 1970, **237**, 251
- 11 Kausch-Blecken von Schmeling, H. H. *Kolloid-Z.* 1969, **234**, 1148
- 12 Ward, I. M. 'Mechanical Properties of Solid Polymers', Wiley, London, 1971, p 258
- 13 Allison, S. W. and Ward, I. M. *Br. J. Appl. Phys.* 1967, **18**, 1151
- 14 Purvis, J., Bower, D. I. and Ward, I. M. *Polymer* 1973, **14**, 398
- 15 Cunningham, A., Ward, I. M., Willis, H. A. and Zichy, V. L. *Polymer* 1974, **15**, in press
- 16 Kashiwagi, M., Folkes, M. J. and Ward, I. M. *Polymer* 1971, **12**, 697
- 17 Kashiwagi, M. and Ward, I. M. *Polymer* 1972, **13**, 145
- 18 Hadley, D. W., Ward, I. M. and Ward, J. *Proc. R. Soc. (A)* 1965, **285**, 275
- 19 Pinnock, P. R., Ward, I. M. and Wolf, J. M. *Proc. R. Soc. (A)* 1966, **291**, 267
- 20 Cunningham, A. and Ward, I. M. to be published
- 21 Ladizesky, N. H. and Ward, I. M. *J. Macromol. Sci. (B)* 1971, **5**, 661
- 22 Cunningham, A. and Ward, I. M. to be published
- 23 Croll, S. G. and Duckett, R. A. to be published
- 24 Ladizesky, N. H. and Ward, I. M. *J. Macromol. Sci. (B)* 1971, **5**, 745
- 25 Ladizesky, N. H. and Ward, I. M. *J. Mater. Sci.* 1973, **8**, 980
- 26 Gupta, V. B., Keller, A. and Ward, I. M. *J. Macromol. Sci. (B)* 1968, **2**, 139
- 27 McBrierty, V. J. and Ward, I. M. *Br. J. Appl. Phys. (J. Phys.: D)* 1968, (Ser. 2), **1**, 1529
- 28 Stachurski, Z. H. and Ward, I. M. *J. Polym. Sci. (A-2)* 1968, **6**, 1817
- 29 Stachurski, Z. H. and Ward, I. M. *J. Macromol. Sci. (B)* 1969, **3**, 445
- 30 Peterlin, A. *J. Polym. Sci. (C)* 1965, **9**, 61
- 31 Pinnock, P. R. and Ward, I. M. *Br. J. Appl. Phys.* 1966, **17**, 575
- 32 Owen, A. J. and Ward, I. M. *J. Macromol. Sci. (B)* 1973, **7**, 279
- 33 Capaccio, G. and Ward, I. M. *Nature (Phys. Sci.)* 1973, **243**, 143
- 34 Ward, I. M. *Phys. Bull.* 1970, **21**, 71
- 35 Gupta, V. B. and Ward, I. M. *J. Macromol. Sci. (B)* 1968, **2**, 89
- 36 Davies, G. R. and Ward, I. M. *J. Polym. Sci. (B)* 1969, **7**, 353
- 37 Hoffman, J. D., Williams, G. and Passaglia, E. A. *J. Polym. Sci. (C)* 1966, **14**, 173
- 38 Buckley, C. P. and McCrum, N. G. *J. Mater. Sci.* 1973, **8**, 928
- 39 Ladizesky, N. H. and Ward, I. M. *J. Macromol. Sci. (B)* 1974, **9**, 565
- 40 Owen, A. J. and Ward, I. M. *J. Macromol. Sci. (B)* 1973, **7**, 417
- 41 Davies, G. R. and Ward, I. M. *J. Polym. Sci. (A-2)* 1972, **10**, 1153

Synthesis and polymerizability of 5-methyl-2-vinyliminobibenzyl and 10-ethyl-2-vinylphenothiazine

P. Hyde, L. J. Kricka*, A. Ledwith and K. C. Smith

*Dept. of Inorganic, Physical and Industrial Chemistry, University of Liverpool, PO Box 147, Liverpool L69 3BX, UK
(Received 29 January 1974)*

INTRODUCTION

Ring vinylation of condensed heteroaromatic molecules has not been extensively investigated mainly owing to the inadequacy of available synthetic vinylation procedures. The principal routes by which a C-vinyl group may be introduced at a ring position are dehydration, pyrolysis, dehydrohalogenation, and reductive dehydration of the appropriate α - or β -hydroxyethyl, acyloxyethyl, β -haloethyl¹, and acetyl derivatives², severally. Also the Hoffman elimination reaction, and the Wittig reaction have been employed to generate a vinyl group from a β -*N,N*-dialkylaminoethyl and a formyl derivative, respectively³.

We wish to report the synthesis and polymerizability of the new vinyl monomers, 5-methyl-2-vinyliminobibenzyl (II) and 10-ethyl-2-vinylphenothiazine (VII). Our interest in these ring systems stems from their electron donor properties and from the possible exploitation of polymers and copolymers based on these ring systems as antioxidants, as light sensitive materials for photoreproduction, and for the synthesis of pharmacologically active copolymers.

5-Methyl-2-vinyliminobibenzyl was prepared by the reaction of 2-formyl-5-methyliminobibenzyl (I) with methyldiene triphenylphosphorane. Formylation of 5-methyliminobibenzyl was achieved at room temperature using phosphorus oxychloride/*N,N*-dimethylformamide. Friedel-Crafts acetylation of 10-acetylphenothiazine (III) using aluminium trichloride as catalyst produced 2,10-diacetylphenothiazine (IV)⁴. Hydrolysis of the latter by alcoholic potassium hydroxide afforded 2-acetylphenothiazine (V)⁴ which upon alkylation⁵ with thallium (I) ethoxide/ethyl iodide gave 10-ethyl-2-

acetylphenothiazine (VI) in moderate yield. Reductive dehydration of VI with aluminium isopropoxide-active alumina afforded 10-ethyl-2-vinylphenothiazine (VII). Previously 2-vinylphenothiazine has been prepared in low yield from 2-(1-hydroxyethyl)phenothiazine by dehydration using activated alumina⁷.

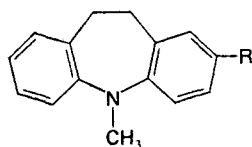
EXPERIMENTAL AND MONOMER SYNTHESIS

¹H n.m.r. spectra were measured at 60 MHz for solutions in deuteriochloroform with tetramethylsilane as internal standard. I.r. spectra were recorded for Nujol mulls. Mass spectra were measured by the Physico-Chemical Measurements Unit, Harwell. Alumina for chromatography was Brockmann Grade 1 neutral (BDH).

5-Methyl-iminobibenzyl, m.p. 106–107°C (lit.⁸ 107–108°C), 10-acetylphenothiazine, m.p. 197–199°C (lit.⁴ 197–197.5) and 2-acetylphenothiazine, m.p. 190–191°C (lit.⁴ 187–188°C; lit.⁹ 193°C) were prepared as outlined in the literature. 2,10-Diacetylphenothiazine was prepared by the method of Cauquil and Casadevall⁹ and was converted to 2-acetylphenothiazine⁴ without further purification. 2-Formyl-5-methyliminobibenzyl (78%), m.p. 90–92°C (lit.¹⁰ 90–93°C; lit.¹¹ 94–95°C), ν_{\max} 1690, 1680 (C=O), 1600 br, 1490, 1325, 1210, 1105, 820 and 765 cm⁻¹. *m/e* 237 (*M*⁺, 100%), 238 (*M*+1, 19), 236 (19), 223 (16), 222 (*M*-Me, 95), 194 (11), 193 (18) and 192 (11), *M*^{*} 208 (237→222), was prepared by stirring together 5-methyliminobibenzyl, phosphoryl chloride and *N,N*-dimethylformamide at room temperature¹².

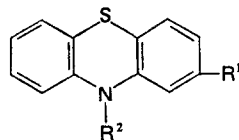
5-Methyl-2-vinyliminobibenzyl

A solution of *n*-butyllithium (21%) in hexane was added by means of a syringe to a stirred suspension of triphenylmethyl phosphonium bromide (10.0 g) in tetrahydrofuran (100 ml) under nitrogen. The orange coloured homogeneous solution was stirred at room temperature for 2 h, and then a solution of 2-formyl-5-methyliminobibenzyl (7.1 g) in tetrahydrofuran (75 ml) was added dropwise during 0.25 h, after which the mixture was refluxed for 2 h. Addition of the cooled reaction mixture to hexane (400 ml) precipitated triphenylphosphine oxide. This was removed by filtration and the filtrate evaporated to afford a yellow oil which crystallized upon standing. The crude product (4.7 g) was chromatographed on a column of neutral alumina (~200 g) made up in petroleum ether. Elution with petroleum ether (b.p. 30–40°C) afforded 5-methyl-2-



(I) R = CHO

(II) R = CH=CH₂



(III) R¹ = H; R² = Ac

(IV) R¹ = R² = Ac

(V) R¹ = Ac; R² = H

(VI) R¹ = Ac; R² = Et

(VII) R¹ = CH=CH₂; R² = Et

* Present address: Dept. of Clinical Chemistry, Queen Elizabeth Hospital, University of Birmingham, Birmingham B15 2TJ, UK.

vinyliminobibenzyl (3.2 g, 45%), m.p. 69–70°C. Found: M^+ 235.1362; C, 86.6%; H, 7.3%; N, 6.1%. $C_{17}H_{17}N$ requires: M^+ 235.1361; C, 86.8%; H, 7.3%; N, 6.0%. ν_{\max} 1625 (CH=CH₂), 1600, 1490 br, 1325, 1265, 1103, 1090, 895, 825, and 750 cm⁻¹. τ [CDCl₃] 2.70–3.20 (7H, m, ArH), 3.40 and 3.75 (1H, two *d*, J_{vic} 10 Hz, *vic* olefinic proton), 4.32 and 4.60 (1H, two *d*, J_{gem} 2 Hz, *trans*, *gem* olefinic proton), 4.85 and 5.05 (1 H, two *d*, *cis*, *gem* olefinic proton), 6.75 (3H, s, NMe) and 6.92 (4H, s, ArCH₂). M/e 235 (M^+ , 100%), 236 ($M+1$, 17), 234 (17), 221 (10), 220 ($M-Me$, 65) and 219 (12). M^* 206 (235→220).

2-Acetyl-10-ethylphenothiazine

2-Acetylphenothiazine (24.1 g, 0.1 mol) was dissolved in 200 ml of dry ether and sufficient *N,N*-dimethylformamide to complete solution. After stirring for 5 min at 30°C, thallium (I) ethoxide (24.9 g, 0.1 mol) was added and the solution was stirred for 3/4 h. Ethyl iodide (17.0 g) was added slowly and after stirring for 1 h at 30°C and 24 h at room temperature, thallium (I) iodide was filtered off. Evaporation of the filtrate yielded a viscous solution which was poured into water and extracted with chloroform. The combined extracts were washed with water and dried (MgSO₄). Evaporation afforded an oil which after recrystallization from absolute ethanol (charcoal) yielded 2-acetyl-10-ethylphenothiazine (15.3 g, 57%) as yellow needles, m.p. 86–88°C. Found: C, 71.5%; H, 5.6%; N, 5.1%; O, 5.8%; S, 11.9%. $C_{16}H_{15}NOS$ requires: C, 71.3%; H, 5.6%; N, 5.2%; O, 5.9%; S, 11.9%. ν_{\max} 1675 (C=O), 1590, 1285, 1225, 1130, 1110, 915, 900, 820, and 750 cm⁻¹. τ [CDCl₃] 7.50–6.70 (7H, m, ArH), 3.84 (2H, q, J 7 Hz, CH₂.Me), 2.47 (3H, s, COMe) and 1.33 (3H, t, J 7 Hz, Me). M/e 269/271 (M^+ 56.5/3.6%), 270 ($M+1$, 11.3), 254/256 ($M-Me$, 14.1/1.0), 255 ($M+1-Me$, 2.8), 240/242 ($M-Et$, 100/5.3), 241 ($M+1-Et$, 15.4), 197/199 (240-COMe, 25.7/2.8), 198 (5.3), M^* 239.8 (269→254), 214.1 (269→240), 161.7 (240→197).

10-Ethyl-2-vinylphenothiazine

A mixture of 2-acetyl-10-ethylphenothiazine (8.6 g), aluminium isopropoxide (25 g), aluminium oxide (10 g) in nitrogen-flushed xylene (250 ml) was refluxed for 5 h, during which time the acetone formed was distilled from the reaction mixture. The volume of solution was reduced to 100 ml. After cooling, the reaction mixture was poured into water and was then extracted with dichloromethane. The combined extracts were washed with water and dried (MgSO₄). Evaporation afforded a yellow oil which after recrystallization from propan-2-ol (charcoal) yielded 10-ethyl-2-vinylphenothiazine (4.5 g, 55%) as pale yellow needles, m.p. 99–101°C. Found: M^+ 253.0922; C, 76.0%; H, 6.0%; N, 5.7%; S, 12.5%. $C_{16}H_{15}N^3S$ requires: M^+ 253.0925; C, 75.8%; H, 6.0%; N, 5.5%; S, 12.7%. ν_{\max} 1625 (wk), 1580, 1555, 1280, 1260, 1230, 990, 910, 880, 825, 755, 735 and 710 cm⁻¹. τ [CDCl₃] 7.30–6.42 (7H, m, ArH and an olefinic proton), 5.82 and 5.52 (1H, two *d*, J_{gem} 1.5 Hz, *trans*, *gem* olefinic proton), 5.30 and 5.12 (1H, two *d*, *cis*, *gem* olefinic proton), 3.94 (2H, q, J 7 Hz, CH₂.Me) and 1.42 (3H, t, J 7 Hz, Me). M/e 255/253 (M^+ , 7%/59), 256/254 ($M+1$, 2/10), 238 ($M-Me$, 13), 226/224 ($M-Et$, 13/100), M^* 223.0 (253→238), 198.5 (253→224).

Polymerizability of *N*-ethyl-2-vinylphenothiazine (NE2VP)

Typically a vacuum degassed benzene solution containing AIBN ($6.1 \times 10^{-3}M$) and NE2VP (0.79 M) gave a 83% yield of homopolymer on precipitation into methanol after 20 h at 70°C. The polymer had $\bar{M}_n = 62\ 000$. After only 2 h at 70°C a similar reaction mixture gave a 28% yield of the same polymer. Related experiments in which NE2VP was the minor component in monomer mixtures with styrene showed that radical copolymerization with the latter monomer was conveniently effected. On the other hand, attempted radical copolymerizations with maleic anhydride were unsuccessful and yielded only a pink coloured low molecular weight product (possibly a 1:1 adduct).

All attempts to induce cationic polymerization by reaction with tropylium hexachloroantimonate¹³ in dichloromethane failed.

The reactions between *n*-butyllithium and NE2VP in tetrahydrofuran in a dry nitrogen atmosphere at room temperature were characterized by immediate formation of a red-purple propagating anion. Polymers were obtained (80–90% yields) by precipitation into methanol with \bar{M}_n in the range 10 000–30 000.

Polymerizability of *N*-methyl-2-vinyliminobibenzyl (NM2VB)

Free radical homopolymerization of vacuum degassed benzene solutions of NM2VB were readily achieved by thermal initiation with AIBN at 70°C. Similarly free radical copolymerizations with styrene and alternating copolymerization with maleic anhydride were easily accomplished. In the latter case a characteristic charge transfer spectrum, obtained on mixing the monomers in benzene, gradually faded during polymerization to give, ultimately, a white polymer on precipitation into methanol–petroleum ether mixture.

Cationic homopolymerization was accomplished¹³ by reaction of monomer with tropylium hexachloroantimonate in dichloromethane at 0°C. Essentially quantitative yields of polymer were obtained on precipitation into methanol having \bar{M}_n 60 000.

In a manner similar to that observed for NE2VP, reactions of NM2VB with *n*-butyllithium in THF gave rise to red coloured propagating anions and essentially quantitative conversion of monomer to polymer, $\bar{M}_n = 20\ 000$ –40 000.

It is worth noting that free radical homopolymers were usually much less soluble than corresponding materials prepared by cationic or anionic processes, possibly indicating some degree of branching or cross-linking in radical polymerization via the reactive benzylic hydrogens.

CONCLUSIONS

Synthesis of the two ring vinylated heteroaromatic molecules NE2VP and NM2VB affords convenient methods for incorporation of useful electron donor nuclei in a range of new homopolymers and copolymers. It is interesting that the phenothiazine monomer can be polymerized by free radical mechanisms because of the well known antioxidant and radical chain inhibition characteristics of phenothiazine and its derivatives¹⁴.

The ring vinylated iminobibenzyl derivative behaves, as would be expected, like a typical substituted styrene

although the high reactivity and apparent stability of the propagating anion is worthy of comment. Conceivably non-planarity of the iminobibenzyl nucleus¹⁵ reduces the normal conjugative anion de-stabilizing effect of *p*-amino substituents.

Homopolymers of both NE2VP and NM2VB exhibited melting behaviour similar to that of vinylated carbazole derivatives² with complete softening occurring in the region 200–250°C.

ACKNOWLEDGEMENTS

We are grateful to SRC for a Research Assistantship (L. J. K.) and a research studentship (K. C. S.).

REFERENCES

- Oediger, H., Moller, F. and Eiter, K. *Synthesis* 1972, p 591
- Hyde, P., Kricka, L. J. and Ledwith, A. *Polymer* 1973, **14**, 124

- Takemoto, K. *J. Macromol. Sci. (C)* 1970, **5**, 29
- Gorlach, G. A. and Dykhanov, N. N. *Med. Prom. SSSR* 1959, **13** (4), 35–40; *Chem. Abstr.* 1959, **53**, 20066a
- Kricka, L. J. and Ledwith, A. *JCS Perkin I* 1972, p 2292
- Lopatinskii, V. P. and Sirotkina, E. E. *Metod. Poluch. Khim, Reakt. Prep.* 1964, **11**, 40; *Chem. Abstr.* 1966, **65**, 2203
- Kamogawa, H., Larkin, J. M., Tsei, K. and Cassidy, H. G. *J. Polym. Sci. (A)* 1964, **2**, 3603
- Huisgen, R., Laschtuvka, E. and Bayerlein, F. *Chem. Ber.* 1960, **93**, 392
- Cauquil, G. and Casadevall, A. *Bull. Soc. Chim. Fr.* 1955, p 768
- Fitz, K. and Sallmann, A. Ger. Pat. 1 910 291 (1969); *Chem. Abstr.* 1970, **72**, 43496v
- Porai-Koshits, B. A., Ya. Kvitko, I. and Favorskii, O. V. *Zh. Org. Khim.* 1965, **1**, 1516
- Burghardt, L., Reckziegel, E. and Wahl, O. Ger. Pat. 950 617 (1956); *Chem. Abstr.* 1960, **54**, 16241a
- Bowyer, P. M., Ledwith, A. and Sherrington, D. C. *Polymer* 1971, **12**, 509
- Scott, G. 'Atmospheric Oxidation and Antioxidants'. Elsevier, Amsterdam, 1965
- Abraham, R. J., Kricka, L. J. and Ledwith, A. *Chem. Commun.* 1973, p 282

Light-scattering study of micelle formation by polystyrene-*g*-polyisoprene graft copolymers

C. Price and D. Woods

Department of Chemistry, University of Manchester, Manchester M13 9PL, UK
(Received 8 January 1974)

INTRODUCTION

A short while ago we reported a study of the effect of temperature on the intrinsic viscosities of a number of polystyrene-*g*-polyisoprene graft copolymer fractions¹. Measurements were made in two solvents, *n*-decane and methyl cyclohexane. Some of the results are shown in *Figure 1*. In methyl cyclohexane two steep regions X and Z, separated by a short shallow extension, Y, were observed. At 0°C, methyl cyclohexane is a very poor solvent for polystyrene ($\theta \approx 74^\circ\text{C}$), but is still a relatively good solvent for polyisoprene. We tentatively suggested therefore that the well defined decrease in $[\eta]$ over the region designated Z was associated with an intramolecular phase separation leading to a species having a compact, but swollen polystyrene core, surrounded by a flexible polyisoprene fringe, and that the lower transition region, designated X, was associated with the formation of intermolecular micelles.

Only a single transition was observed for the graft copolymers in *n*-decane. This was believed to be due to the formation of intermolecular micelles on cooling. Because of stability problems, however, it was only possible to work up to $\sim 120^\circ\text{C}$. It is just feasible that a second transition region occurs above 120°C since *n*-decane is a much poorer solvent for polystyrene than methyl cyclohexane.

In this short contribution we present data obtained in a light-scattering study of the graft copolymers. The results enable us to test some of the tentative arguments put forward in the original paper.

EXPERIMENTAL

Graft copolymers

The graft copolymers were prepared by adding poly(isoprenyl lithium) ($\bar{M}_n = 12\,500$) to chloromethylated polystyrene ($\bar{M}_n = 190\,000$). Liquid-liquid separation was used to remove uncoupled homopolymer. Details of the preparation, fractionation and characterization of the samples are to be found elsewhere¹. A summary of the relevant characterization data is provided in *Table 1*.

Light-scattering measurements

Measurements were made using a Sofica instrument. Polymer solutions and solvents were clarified either by centrifugation for 2 h at 2×10^4 rev/min in a No. 30

Table 1 Characterization data on the graft copolymers

Sample	$M_n^a \times 10^{-5}$	Wt % polystyrene ^b	$M_{app}^c \times 10^{-5}$	$\langle S_w^2 \rangle^{1/2d}$ (nm)	M_{app}/M_n
1G1	5.5	29.2	6.5	116	1.18
1G2	4.9	34.9	5.4	90	1.10
1G3	4.2	38.1	5.1	84	1.21

^a Number-average molecular weights determined by osmometry using toluene as solvent

^b Wt % polystyrene by u.v. spectroscopy

^c and ^d Apparent weight-average molecular weights (M_{app}) and apparent mean-square radii of gyration $\langle S_w^2 \rangle^{1/2}$ determined from light-scattering measurements in tetrahydrofuran solutions

although the high reactivity and apparent stability of the propagating anion is worthy of comment. Conceivably non-planarity of the iminobibenzyl nucleus¹⁵ reduces the normal conjugative anion de-stabilizing effect of *p*-amino substituents.

Homopolymers of both NE2VP and NM2VB exhibited melting behaviour similar to that of vinylated carbazole derivatives² with complete softening occurring in the region 200–250°C.

ACKNOWLEDGEMENTS

We are grateful to SRC for a Research Assistantship (L. J. K.) and a research studentship (K. C. S.).

REFERENCES

- Oediger, H., Moller, F. and Eiter, K. *Synthesis* 1972, p 591
- Hyde, P., Kricka, L. J. and Ledwith, A. *Polymer* 1973, **14**, 124

- Takemoto, K. *J. Macromol. Sci. (C)* 1970, **5**, 29
- Gorlach, G. A. and Dykhanov, N. N. *Med. Prom. SSSR* 1959, **13** (4), 35–40; *Chem. Abstr.* 1959, **53**, 20066a
- Kricka, L. J. and Ledwith, A. *JCS Perkin I* 1972, p 2292
- Lopatinskii, V. P. and Sirotkina, E. E. *Metod. Poluch. Khim, Reakt. Prep.* 1964, **11**, 40; *Chem. Abstr.* 1966, **65**, 2203
- Kamogawa, H., Larkin, J. M., Tsei, K. and Cassidy, H. G. *J. Polym. Sci. (A)* 1964, **2**, 3603
- Huisgen, R., Laschtuvka, E. and Bayerlein, F. *Chem. Ber.* 1960, **93**, 392
- Cauquil, G. and Casadevall, A. *Bull. Soc. Chim. Fr.* 1955, p 768
- Fitzzi, K. and Sallmann, A. Ger. Pat. 1 910 291 (1969); *Chem. Abstr.* 1970, **72**, 43496v
- Porai-Koshits, B. A., Ya. Kvitko, I. and Favorskii, O. V. *Zh. Org. Khim.* 1965, **1**, 1516
- Burghardt, L., Reckziegel, E. and Wahl, O. Ger. Pat. 950 617 (1956); *Chem. Abstr.* 1960, **54**, 16241a
- Bowyer, P. M., Ledwith, A. and Sherrington, D. C. *Polymer* 1971, **12**, 509
- Scott, G. 'Atmospheric Oxidation and Antioxidants'. Elsevier, Amsterdam, 1965
- Abraham, R. J., Kricka, L. J. and Ledwith, A. *Chem. Commun.* 1973, p 282

Light-scattering study of micelle formation by polystyrene-*g*-polyisoprene graft copolymers

C. Price and D. Woods

Department of Chemistry, University of Manchester, Manchester M13 9PL, UK
(Received 8 January 1974)

INTRODUCTION

A short while ago we reported a study of the effect of temperature on the intrinsic viscosities of a number of polystyrene-*g*-polyisoprene graft copolymer fractions¹. Measurements were made in two solvents, *n*-decane and methyl cyclohexane. Some of the results are shown in *Figure 1*. In methyl cyclohexane two steep regions X and Z, separated by a short shallow extension, Y, were observed. At 0°C, methyl cyclohexane is a very poor solvent for polystyrene ($\theta \approx 74^\circ\text{C}$), but is still a relatively good solvent for polyisoprene. We tentatively suggested therefore that the well defined decrease in $[\eta]$ over the region designated Z was associated with an intramolecular phase separation leading to a species having a compact, but swollen polystyrene core, surrounded by a flexible polyisoprene fringe, and that the lower transition region, designated X, was associated with the formation of intermolecular micelles.

Only a single transition was observed for the graft copolymers in *n*-decane. This was believed to be due to the formation of intermolecular micelles on cooling. Because of stability problems, however, it was only possible to work up to $\sim 120^\circ\text{C}$. It is just feasible that a second transition region occurs above 120°C since *n*-decane is a much poorer solvent for polystyrene than methyl cyclohexane.

In this short contribution we present data obtained in a light-scattering study of the graft copolymers. The results enable us to test some of the tentative arguments put forward in the original paper.

EXPERIMENTAL

Graft copolymers

The graft copolymers were prepared by adding poly(isoprenyl lithium) ($\bar{M}_n = 12\,500$) to chloromethylated polystyrene ($\bar{M}_n = 190\,000$). Liquid-liquid separation was used to remove uncoupled homopolymer. Details of the preparation, fractionation and characterization of the samples are to be found elsewhere¹. A summary of the relevant characterization data is provided in *Table 1*.

Light-scattering measurements

Measurements were made using a Sofica instrument. Polymer solutions and solvents were clarified either by centrifugation for 2 h at 2×10^4 rev/min in a No. 30

Table 1 Characterization data on the graft copolymers

Sample	$M_n^a \times 10^{-5}$	Wt % polystyrene ^b	$M_{app}^c \times 10^{-5}$	$\langle S_w^2 \rangle^{1/2d}$ (nm)	M_{app}/M_n
1G1	5.5	29.2	6.5	116	1.18
1G2	4.9	34.9	5.4	90	1.10
1G3	4.2	38.1	5.1	84	1.21

^a Number-average molecular weights determined by osmometry using toluene as solvent

^b Wt % polystyrene by u.v. spectroscopy

^c and ^d Apparent weight-average molecular weights (M_{app}) and apparent mean-square radii of gyration $\langle S_w^2 \rangle^{1/2}$ determined from light-scattering measurements in tetrahydrofuran solutions

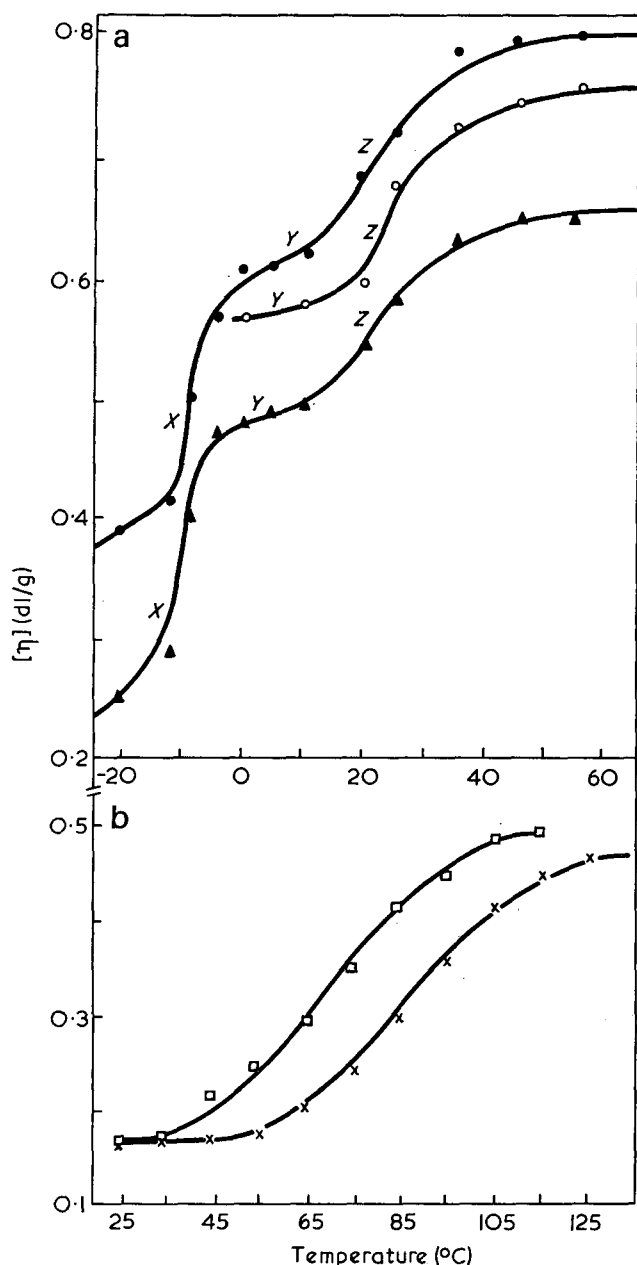


Figure 1 Plots of $[\eta]$ versus temperature for (a) the graft copolymers 1G1 (●), 1G2 (○) and 1G3 (▲) in methyl cyclohexane and (b) the graft copolymers 1G1 (□) and 1G3 (×) in n-decane

rotor of a Spinco Model L preparative ultracentrifuge or by filtration through solvent inert Millipore filters having a pore size of 0.45×10^3 nm. Light-scattering measurements were made with light of wavelength 546 nm at 11 angles from 30° to 150° . The instrument was calibrated using benzene for which the Rayleigh ratio is known over a range of temperature².

The light scattered from a dilute polymer solution at low angles may be expressed in the general form³:

$$\frac{Kc}{R_\theta} = \frac{1}{M_w} \left[1 + \left(\frac{16\pi^2}{3\lambda^2} \right) \langle S^2 \rangle_z \sin^2 \left(\frac{\theta}{2} \right) \right] + 2A_2c + 3A_3c^2 + \dots \quad (1a)$$

where K is an optical constant for the particular system in question, c the concentration, R_θ the difference between the Rayleigh ratio of the solution and that of the pure solvent, M_w the weight-average molecular weight, $\langle S^2 \rangle_z$ the z -average mean-square radius of

gyration, θ the scattering angle, λ the wavelength of light in the medium, and A_2 and A_3 are the second and third virial coefficients. For homopolymers the weight-average molecular weight can be obtained in a straightforward manner by carrying out a double extrapolation of the data to zero angle and zero concentration, since from equation (1a):

$$\left(\frac{Kc}{R_\theta} \right)_{c=0} = \frac{1}{M_w} \quad (1b)$$

In the case of copolymers that are heterogeneous in chemical composition, equation (1b) yields an apparent molecular weight (M_{app}), (the value of which varies with the refractive index of the solvent) rather than a real weight-average molecular weight^{4, 5}. For the present study, in view of the carefully controlled synthetic method and fraction scheme used in obtaining the copolymer samples, the M_{app} can be expected to be fairly close to M_w regardless of the refractive index of the solvent. Supporting evidence for this claim is provided by values of M_{app} determined for sample 1G2 in four different solvents (see Table 2). All the values lie fairly close to each other, and are not too different from the measured value of $M_n (=4.9 \times 10^5)$. Since $M_n < M_w$ (real), we can reasonably assume that $M_{app} \approx M_w$.

In the case of a homopolymer the z -average mean-square radius of gyration may be calculated from the limiting slope of the plot (Kc/R_θ) versus $\sin^2 \theta/2$. For a copolymer, this procedure yields an apparent radius of gyration $\langle S_*^2 \rangle^{1/2}$ even when the chains are homogeneous in chemical composition^{6, 7}.

$$\langle S_*^2 \rangle = y \langle S_A^2 \rangle + (1-y) \langle S_B^2 \rangle + y(1-y)l^2$$

where $\langle S_A^2 \rangle$ and $\langle S_B^2 \rangle$ are the mean-square radii of gyration of the A and B components about their centres of gravity G_A and G_B respectively, l^2 is the mean-square of the distance $G_A G_B$ separating the two centres of gravity, and $y = W_A \cdot \nu_A / \nu$; W_A is the weight fraction of the A component, and ν_A and ν are the refractive index increments of the A component and the total copolymer respectively. For a graft copolymer containing sufficient number of short grafted chains, $l^2 = 0$ for a true solution, and $\langle S_A^2 \rangle = \langle S_B^2 \rangle = \langle S_*^2 \rangle$; in this case $\langle S_*^2 \rangle = \langle S^2 \rangle_z$ (the real z -average radius of gyration). If the graft copolymer forms micelles having symmetrical structures, so that $G_A = G_B$, then again $l^2 = 0$, but $\langle S_A^2 \rangle \neq \langle S_B^2 \rangle$ and $\langle S_*^2 \rangle \neq \langle S^2 \rangle_z$.

Refractive index increments

These were measured for the copolymer solutions at each temperature studied by light scattering using a Brice-Phoenix differential refractometer calibrated in the recommended manner.

Table 2 Effect of solvent in the apparent molecular weight of sample 1G2

Solvent	$M_{app} \times 10^{-5}$
Chloroform	5.7
Cyclohexane	5.6
Tetrahydrofuran	5.4
1-Chloropropane	5.5

Table 3 Light-scattering data for copolymer 1G1

T (°C)	$M_{app} \times 10^{-6}$	$\langle S_{*}^2 \rangle^{1/2}$ (nm)	R_{η} (nm)
n-decane:			
25	5.8	26.8	24.8
35	4.1	27.6	22.3
45	2.3	27.1	19.9
55	1.9	29.1	19.3
65	1.7	36.1	19.8
75	1.6	42.5	20.8
85	1.4	46.5	21.2
methyl cyclohexane:			
15	0.75	61	19.8
25	0.69	61	19.9
30	0.70	62	20.3
35	0.68	63	20.4
40	0.71	66	20.8
50	0.72	70	20.9
60	0.68	71	20.6

Table 4 Light-scattering data for copolymers 1G2 and 1G3

T (°C)	$M_{app} \times 10^{-6}$	$\langle S_{*}^2 \rangle^{1/2}$ (nm)	R_{η} (nm)
1G2 in methyl cyclohexane:			
15	1.03	55	21.3
25	0.74	59	19.9
30	0.75	60	20.3
35	0.74	59	20.4
40	0.78	65	20.9
50	0.73	67	20.6
65	0.69	69	20.3
1G3 in n-decane:			
25	9.8	29.1	29.5
35	9.1	30.0	29.1
45	7.6	30.3	27.4
55	6.3	30.2	26.0
65	5.0	34.8	25.1
75	3.6	38.2	24.1
85	2.1	42.1	21.5

RESULTS AND DISCUSSION

Determinations of R_{θ} as a function of concentration and angle were made for copolymer 1G1 in n-decane and methyl cyclohexane over a range of temperatures. Following the usual procedure values of Kc/R_{θ} were plotted against $\sin^2\theta/2 + kc$ (where k is an arbitrary constant). The plots were conventional in shape⁸ and with both solvents $(Kc/R_{\theta})_{\theta=0}$ versus c remained linear down to the lowest concentration for each temperature studied. Values of M_{app} and $\langle S_{*}^2 \rangle^{1/2}$ obtained from the plots are given in Table 3.

For copolymer 1G1 in n-decane the molecular weight results indicate the presence of intermolecular micelles, the average number of molecules per micelle increasing with decreasing temperature. Also as the molecular weight ($M_{app} \approx M_w$) increases $\langle S_{*}^2 \rangle^{1/2}$ decreases. Whilst the latter is only the apparent radius of gyration, we estimate that for micelles formed from 1G1 in n-decane, its value will not depart from the real value by more than -6%. Thus as the temperature is lowered the data clearly indicate that the micelles become more

compact. This result suggests that at the lower temperatures the degree of segregation of the two polymer components is greatly increased, leading to micelles with very compact, well-defined cores (e.g. consisting say of 20% volume fraction of polystyrene in n-decane).

If we represent the micelles by hydrodynamically equivalent spheres then⁹:

$$[\eta] = \frac{10\pi}{3} \frac{R_{\eta}^3 N_0}{M} \quad (3)$$

where N_0 is Avogadro's number, and R_{η} is the radius of impermeable spheres that are equivalent to the micelles in intrinsic viscosity. (The equivalent radius of gyration for a solid sphere S_{η} would equal $0.775 R_{\eta}$.) Values of R_{η} calculated from equation (3) are listed in Table 3; no attempt was made to correct for polydispersity. The average hydrodynamic dimensions are seen to remain remarkably constant throughout the range of temperature studied, and in agreement with the suggestion that the micelles become more compact at the lower temperatures the observed values of $\langle S_{*}^2 \rangle^{1/2}$ and S_{η} become closer.

In methyl cyclohexane the molecular weight of 1G1 ($M_{app} \approx M_w$) remains approximately constant over the range 15–60°C having an average value of 7.0×10^5 . The latter agrees, within experimental error, with the value obtained in tetrahydrofuran and indicates that the molecules remain virtually unaggregated over the range covered by light scattering. This result is consistent with our earlier suggestion that the sharp decrease in $[\eta]$ over the range marked Z (Figure 1) is due to the formation of intramolecular micelles. The transition is accompanied by a decrease in $\langle S_{*}^2 \rangle^{1/2}$; in this case the values of $\langle S_{*}^2 \rangle^{1/2}$ and $\langle S_z^2 \rangle^{1/2}$ should lie well within experimental error. The magnitude of $\langle S_{*}^2 \rangle^{1/2}$, however, remains high even at the lowest temperatures studied. We conclude therefore on the basis of the present evidence that the intramolecular micelles must have fairly open structures, in which the two polymer components are perhaps only partly segregated.

Light-scattering measurements at a series of temperatures were made also on copolymer 1G3 in n-decane and on 1G2 in methyl cyclohexane. The results, which are listed in Table 4, show in general similar trends to those discussed for sample 1G1. There are some minor differences however, which are worthy of mention. At a given temperature in n-decane, the average number of molecules per micelle is greater for 1G3 than 1G1. This difference might have been predicted since the average length of polystyrene backbone chain between polyisoprene grafts is greater for 1G3 than 1G1. At the lowest temperature investigated, 15°C, the data show that copolymer 1G2 in methyl cyclohexane has started to form intermolecular micelles. It would have been interesting to follow this behaviour into the temperature regions marked X and Y in Figure 1, but unfortunately it was not possible to work down to lower temperatures with the equipment available.

ACKNOWLEDGEMENTS

We thank the Science Research Council for the award of a CAPS Studentship for D. W. We also thank Esso Chemicals Research Centre, Abingdon, for their help and co-operation on the project carried out by D. W.

REFERENCES

- 1 Price, C. and Woods, D. *Polymer* 1973, **14**, 82
- 2 Ehl, J., Loucheux, C., Reiss, C. and Benoit, H. *Makromol. Chem.* 1964, **75**, 35
- 3 Zimm, B. H. *J. Chem. Phys.* 1948, **16**, 1093, 1099
- 4 Stockmayer, W. H., Moore, L. D., Fixman, M. and Epstein, B. N. *J. Polym. Sci.* 1955, **16**, 517

- 5 Bushuk, W. and Benoit, H. *Can. J. Chem.* 1958, **36**, 1616
- 6 Leng, M. and Benoit, H. *J. Chim. Phys.* 1961, **58**, 480
- 7 Cordier, P. *J. Chim. Phys.* 1966, **63**, 1158
- 8 Evans, J. M. in 'Light Scattering from Polymer Solutions', (Ed. M. B. Huglin), Academic Press, London, 1972, Ch 5
- 9 Debye, P. and Beuche, A. M. *J. Chem. Phys.* 1948, **16**, 573

Investigations on oxidative polymerization of 1-naphthol using Cu^I-pyridine initiator system

R. N. Mukherjea and A. K. Bandyopadhyay

Process Engineering and Technology Section, Chemical Engineering Department, Jadavpur University, Calcutta-700032, India

(Received 2 January 1974; revised 11 March 1974)

INTRODUCTION

Earlier investigations on oxidative polymerization leading to the formation of poly(phenylene ethers), having high thermal stability have been done mostly with substituted phenols¹⁻³. We are presently studying the application of the same technique to substituted binuclear aromatics in order to obtain polymers having enhanced thermostability, which may be expected due to the increased aromaticity in the polymer backbone.

We wish to report here the polymerization of 1-naphthol using cuprous chloride-pyridine initiator system.

EXPERIMENTAL

Materials

Analytical grade solvents were taken and were used without further purification. 1-Naphthol was re-crystallized and vacuum dried prior to polymerization. Cuprous chloride was freshly prepared using standard methods.

Polymerization procedure

A measured amount of cuprous chloride was added, under a continuous stream of oxygen, to a mixture of nitrobenzene and pyridine kept at 40°C in a three-necked flask; 1-naphthol was then added in portions to this initiator system, with vigorous stirring. A thick viscous mass was obtained after about 20 min reaction time. It was diluted with chloroform and the polymer was precipitated by pouring into acidified methanol. The crude polymer was purified by dissolving in chloroform and reprecipitating from acidified methanol three times, washing finally with acidified methanol and drying in vacuum at 40°C.

RESULTS AND DISCUSSION

Polymer samples of different molecular weights ranging from 10 000 to 25 000 were prepared by varying the monomer : initiator ratio. Light scattering was used for molecular weight determination. Thermogravimetric analysis of two polymer samples having molecular weight 24 500 and 15 000, respectively, showed complete decomposition at 400°C of the latter, while the former

had only 15% weight loss at 500°C. The increased thermal stability of the higher molecular weight polymer, obtained by reducing the initiator concentration, may be explained by increased crosslinking in the polymer backbone.

Acid and alkali resistance of thin polymer films was studied according to standard methods⁴. The polymer was found to possess excellent acid resistance while the alkali resistance was not satisfactory.

Mechanism of polymerization

Endres and Kirstek have discussed the mechanism of polymerization of disubstituted phenols using CuCl-pyridine initiator system and have suggested the intermediate formation of a copper-amine complex followed by transfer of electrons from oxygen to copper and the consequent formation of phenoxy radicals, leading to the coupling of the free phenoxy radicals to give poly(phenylene ethers).

We believe that in a similar manner naphthoxy radicals are formed which finally leads to C-O-C coupling. Although it may appear that the reaction of free phenoxy as well as free naphthoxy radicals is principally C-C coupling actually C-O-C compounds are formed which may in all probability be due to the formation of a Cu-amine complex which remains bound to the catalyst.

Infra-red spectra of the polymer samples taken in Nujol film also indicated the presence of C-O-C linkage at 1350 cm⁻¹ (aromatic ether) and a hump at 1425 cm⁻¹ probably for aromatic -OH.

ACKNOWLEDGEMENTS

Grateful acknowledgement is due to the Indian Institute of Experimental Medicine, Calcutta for the i.r. spectral analysis and also to the University Grants Commission, India for a fellowship to one of the authors (A. B.).

REFERENCES

- 1 Hay, A. S., Blanchard, H. S., Endres, G. F. and Eustance, W. *J. Am. Chem. Soc.* 1959, **81**, 6336
- 2 General Electric Co., U.S. Pat. 3 306 874 (1967)
- 3 Blanchard, H. S., Frikbeiner, H. L. and Russell, C. A. *J. Polym. Sci.* 1962, **58**, 469
- 4 Indian Standard Specification No. IS-101 (1950)
- 5 Endres, G. F. and Kristek, J. *J. Polym. Sci.* 1962, **58**, 593

REFERENCES

- 1 Price, C. and Woods, D. *Polymer* 1973, **14**, 82
- 2 Ehl, J., Loucheux, C., Reiss, C. and Benoit, H. *Makromol. Chem.* 1964, **75**, 35
- 3 Zimm, B. H. *J. Chem. Phys.* 1948, **16**, 1093, 1099
- 4 Stockmayer, W. H., Moore, L. D., Fixman, M. and Epstein, B. N. *J. Polym. Sci.* 1955, **16**, 517

- 5 Bushuk, W. and Benoit, H. *Can. J. Chem.* 1958, **36**, 1616
- 6 Leng, M. and Benoit, H. *J. Chim. Phys.* 1961, **58**, 480
- 7 Cordier, P. *J. Chim. Phys.* 1966, **63**, 1158
- 8 Evans, J. M. in 'Light Scattering from Polymer Solutions', (Ed. M. B. Huglin), Academic Press, London, 1972, Ch 5
- 9 Debye, P. and Beuche, A. M. *J. Chem. Phys.* 1948, **16**, 573

Investigations on oxidative polymerization of 1-naphthol using Cu^I-pyridine initiator system

R. N. Mukherjea and A. K. Bandyopadhyay

Process Engineering and Technology Section, Chemical Engineering Department, Jadavpur University, Calcutta-700032, India

(Received 2 January 1974; revised 11 March 1974)

INTRODUCTION

Earlier investigations on oxidative polymerization leading to the formation of poly(phenylene ethers), having high thermal stability have been done mostly with substituted phenols¹⁻³. We are presently studying the application of the same technique to substituted binuclear aromatics in order to obtain polymers having enhanced thermostability, which may be expected due to the increased aromaticity in the polymer backbone.

We wish to report here the polymerization of 1-naphthol using cuprous chloride-pyridine initiator system.

EXPERIMENTAL

Materials

Analytical grade solvents were taken and were used without further purification. 1-Naphthol was re-crystallized and vacuum dried prior to polymerization. Cuprous chloride was freshly prepared using standard methods.

Polymerization procedure

A measured amount of cuprous chloride was added, under a continuous stream of oxygen, to a mixture of nitrobenzene and pyridine kept at 40°C in a three-necked flask; 1-naphthol was then added in portions to this initiator system, with vigorous stirring. A thick viscous mass was obtained after about 20 min reaction time. It was diluted with chloroform and the polymer was precipitated by pouring into acidified methanol. The crude polymer was purified by dissolving in chloroform and reprecipitating from acidified methanol three times, washing finally with acidified methanol and drying in vacuum at 40°C.

RESULTS AND DISCUSSION

Polymer samples of different molecular weights ranging from 10 000 to 25 000 were prepared by varying the monomer : initiator ratio. Light scattering was used for molecular weight determination. Thermogravimetric analysis of two polymer samples having molecular weight 24 500 and 15 000, respectively, showed complete decomposition at 400°C of the latter, while the former

had only 15% weight loss at 500°C. The increased thermal stability of the higher molecular weight polymer, obtained by reducing the initiator concentration, may be explained by increased crosslinking in the polymer backbone.

Acid and alkali resistance of thin polymer films was studied according to standard methods⁴. The polymer was found to possess excellent acid resistance while the alkali resistance was not satisfactory.

Mechanism of polymerization

Endres and Kirstek have discussed the mechanism of polymerization of disubstituted phenols using CuCl-pyridine initiator system and have suggested the intermediate formation of a copper-amine complex followed by transfer of electrons from oxygen to copper and the consequent formation of phenoxy radicals, leading to the coupling of the free phenoxy radicals to give poly(phenylene ethers).

We believe that in a similar manner naphthoxy radicals are formed which finally leads to C-O-C coupling. Although it may appear that the reaction of free phenoxy as well as free naphthoxy radicals is principally C-C coupling actually C-O-C compounds are formed which may in all probability be due to the formation of a Cu-amine complex which remains bound to the catalyst.

Infra-red spectra of the polymer samples taken in Nujol film also indicated the presence of C-O-C linkage at 1350 cm⁻¹ (aromatic ether) and a hump at 1425 cm⁻¹ probably for aromatic -OH.

ACKNOWLEDGEMENTS

Grateful acknowledgement is due to the Indian Institute of Experimental Medicine, Calcutta for the i.r. spectral analysis and also to the University Grants Commission, India for a fellowship to one of the authors (A. B.).

REFERENCES

- 1 Hay, A. S., Blanchard, H. S., Endres, G. F. and Eustance, W. *J. Am. Chem. Soc.* 1959, **81**, 6336
- 2 General Electric Co., U.S. Pat. 3 306 874 (1967)
- 3 Blanchard, H. S., Frikbeiner, H. L. and Russell, C. A. *J. Polym. Sci.* 1962, **58**, 469
- 4 Indian Standard Specification No. IS-101 (1950)
- 5 Endres, G. F. and Kristek, J. *J. Polym. Sci.* 1962, **58**, 593

Some solution properties of poly(*trans*-2,5-dimethylpiperazine-3,4-thiofurazan amide)

P. Manaresi, F. Pilati and B. Fortunato

Università di Bologna, Istituto Chimico della Facoltà di Ingegneria, Bologna, Italy
(Received 19 November 1973; revised 3 December 1973)

INTRODUCTION

Recently the application of polyamides from *trans*-2,5-dimethylpiperazine for high flux membranes employed on water desalination by reverse osmosis processes was described^{1, 2}.

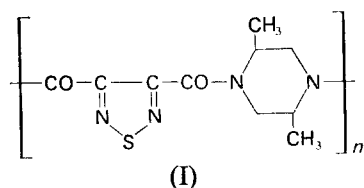
Although solution properties of these polymers may have a great importance for the membrane preparation, very few data have been published on this subject.

This paper is concerned with some solution properties of poly(*trans*-2,5-dimethylpiperazine-3,4-thiofurazan amide) (*t*-2,5-DMPip-TFZ), which is one of the most interesting among these materials².

EXPERIMENTAL

Fractionation

The polymer, *t*-2,5-DMPip-TFZ (I):



supplied from Montedison SpA, had an intrinsic viscosity of 3.70 (in chloroform at 30°C), and was fractionated by fractional precipitation at 32 ± 0.1°C in a thermostated vessel, following the literature methods³. Chloroform was the solvent and acetone or petroleum ether were the non-solvents. A 2.14 g polymer sample was dissolved in 300 ml of a 5:1 by vol mixture of chloroform-acetone, and gradually precipitated with acetone into 6 fractions. Subsequent fractions, up to a total of 9 fractions, were obtained with petroleum ether as non-solvent. The first fraction was refractionated (using acetone as non-solvent) into 5 fractions. Precipitate recovery was troublesome because of adhesion of the polymer to the glass, and so it was necessary to transfer the supernatant solution to another identical thermostated vessel, and dissolve the precipitate in the first vessel with chloroform. Fractions were recovered, after partial evaporation of the solvent under vacuum, by precipitation with a large volume of petroleum ether and drying to constant weight *in vacuo* at 65°C.

Osmometry

The number-average molecular weights (\bar{M}_n) of some polymer fractions were determined at 30°C in chloroform, with a Mechrolab Model 502 high-speed membrane osmometer.

Non-aqueous Schleicher and Schuell Type 0-8 membranes were used. Data were taken at four or five different concentrations and graphical extrapolations were made of π/c versus c plots to zero concentration.

Viscosity

All viscosity measurements were made in chloroform at 30 ± 0.05°C. Solvent time of the viscometer was 150 sec. Data were taken at four or five different concentrations (between 0.07 and 0.6 g/dl) and the intrinsic viscosities were evaluated by graphical extrapolation of η_{sp}/c versus η_{sp} , following the Schulze and Blaschke equation⁴ instead of the Huggins equation, as proposed by Ibrahim⁵.

RESULTS AND DISCUSSION

The experimental results are collected in Table 1. The intrinsic viscosity/number-average molecular weight relationship was established by plotting data of viscosity against number-average molecular weight on log-log coordinates. The following relationship was obtained by the least-squares method:

$$[\eta] = 8.0 \times 10^{-3} \bar{M}_n^{0.46} \quad (1)$$

The value of the exponent on the Mark-Houwink relation is slightly less than the minimum theoretical Flory-Fox value of 0.5, characteristic of tight coils in a θ solvent. Chloroform is a very poor solvent for *t*-2,5-DMPip-TFZ, probably because of strong intrachain polar interactions, and the solution at 30°C is to be considered in a metastable state.

The cumulative weight fractions $C(M_i)$ of Table 1 were calculated according to the standard Schulz procedure⁶. The data were found to fit well enough the empirical distribution functions of Tung⁷:

$$W(M) = yz \exp(-yM^z) M^{z-1} \quad (2)$$

$$I(M) = \int_0^M W(M) dM = 1 - [\exp(-yM^z)] \quad (3)$$

Table 1 Fractionation, viscometric and osmometric results for poly(*trans*-2,5-dimethylpiperazine-3,4-thiofurazan amide)

Fraction No.	Weight (mg)	Weight fraction, W_i	Cumulative fraction, $C(M_i)$	$[\eta]$ (dl/g)	$\bar{M}_n \times 10^{-3}$ (obs.)	$\bar{M}_n \times 10^{-3}$ (eqn. 1)
1	163	0.0808	0.0404	< 0.100	—	< 1.0
2	60	0.0297	0.0956	0.280	—	2.2
3	40	0.0198	0.1204	0.370	—	4.2
4	71	0.0352	0.1479	0.535	—	9.2
5	254	0.1260	0.2285	0.905	39	30.0
6	294	0.1456	0.3643	1.530	78	94.0
7	151	0.0750	0.4746	2.055	174	174.0
8	60	0.0297	0.5269	2.325	—	229.0
9	101	0.0502	0.5669	3.200	—	468.0
10	161	0.0796	0.6318	4.300	—	881.0
11	174	0.0860	0.7146	5.500	1740	1510.0
12	141	0.0697	0.7924	7.025	—	2630.0
13	348	0.1725	0.8273	7.575	—	3090.0
2018						
(94.3% rec.)						
Unfractionated polymer				3.70	51	631.0

were y and z are adjustable parameters. The y and z values, calculated according to the Tung procedure, are 0.004 21 and 0.403, respectively. Figure 1 shows the integral and differential experimental distributions; curves are calculated from equations (2) and (3).

These results show the very broad molecular weight distribution of *t*-2,5-DMPip-TFZ, ranging from oligo-

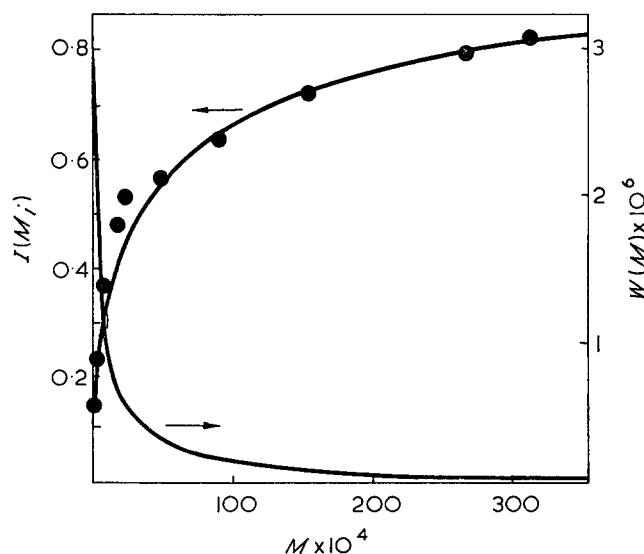


Figure 1 Integral (●) and differential (—) molecular weight distributions for poly(*trans*-2,5-dimethylpiperazine-3,4-thiofurazan amide)

mers ($\bar{M}_n < 1000$) to very high molecular weight fractions ($\bar{M}_n > 1\,000\,000$). The ratio \bar{M}_w/\bar{M}_n calculated from the fractionation data (excluding the first oligomeric fraction from the calculus) is about 25. It is reasonable to infer that such broad distribution is connected with the method of interfacial polycondensation employed⁸.

ACKNOWLEDGEMENTS

We thank Professor L. Credali and Dr G. P. Guidetti (Montedison SpA, Centro Ricerche, Ferrara) for kindly providing the polymer and for many suggestions, and Professor P. Chiorboli for encouraging this work.

This work was supported by Consiglio Nazionale delle Ricerche, Rome.

REFERENCES

- 1 Credali, L., Chiolle, A. and Parrini, P. *Polymer* 1972, **13**, 503
- 2 Credali, L., Chiolle, A. and Parrini, P. *4th Int. Symp. Fresh Water from the Sea, Heidelberg* 1973, p 95
- 3 Cantow, M. J. R. 'Polymer fractionation', Academic Press, New York, 1967
- 4 Schulz, G. V. and Blaschke, F. J. *Prakt. Chem.* 1941, **158**, 130
- 5 Ibrahim, F. W. J. *Polym. Sci. (A)* 1965, **3**, 469
- 6 Schulz, G. V. *Z. Phys. Chem.* 1940, **B47**, 155
- 7 Tung, L. M. J. *Polym. Sci.* 1956, **20**, 495
- 8 Morgan, P. V. 'Condensation polymers: by interfacial and solution methods', Interscience, New York, 1965

Letters

Dependence of fracture surface energy of PMMA on molecular weight

Berry has reported that the dependence of the fracture surface energy (γ) of poly(methyl methacrylate) PMMA on molecular weight, M , can be represented by the equation $\gamma = A - BM^{-1}$, where A and B are arbitrary constants. By extrapolation of experimental data obtained for values of M in the range $(0.9 \text{ to } 60) \times 10^5$ he concluded that γ should become zero for $M = 2.5 \times 10^4$ but stated that, 'in view of the uncertain validity of that extrapolation, it would clearly be desirable to determine directly the fracture surface energy and other ultimate properties of samples with molecular weights extending down to the critical value'¹. It is most difficult to prepare specimens of such low molecular weight which would be suitable for measurements of tensile fracture. However, in the present work, this is achieved by controlled degradation effected by exposure of PMMA specimens to high energy radiation².

Rectangular bars ($6.7 \times 2.2 \times 0.25$ cm) were cut at random from commercially available sheets of Plexiglas G (Rohm and Haas Co.). This polymer is made from methyl methacrylate without inclusion of other monomers or plasticizers. A slot, 0.22 or 0.44 cm deep, was cut in the middle of each bar using a circular saw 0.016 cm

thick. Sharp cracks were avoided to prevent the likelihood of crack propagation due to internal pressure build-up during subsequent irradiation. The bars were heated for 5 h at 90°C to relieve any internal stress.

In order to reduce the molecular weight of the PMMA, the slotted bars were exposed in air to ⁶⁰Co γ -rays at a dose rate of 2.1 Mrad/h. Irradiation also results in the formation of gas³. By reference to the complete absence of foaming in samples heated above the glass transition temperature, 100°C, it was judged that the bars were free of gas several months after irradiation.

Outgassed bars were tested in tension on an Instron machine at a crosshead separation of 0.1 cm/min. Bars which had been given high doses of radiation were very brittle and lap joints had to be bonded to their ends in order to grip them without fracture.

Limiting viscosity numbers $[\eta]$ were determined in benzene at 25°C. Viscosity average molecular weights, M_v , were calculated from the Mark-Houwink equation $[\eta] = KM^\alpha$, using $K = 5.5 \times 10^{-5}$ dl/g and $\alpha = 0.764$.

Values of fracture surface energy, γ , were calculated from Griffith's equation, for the case of plane strain⁵:

$$\sigma = \left[\frac{2E\gamma}{\pi c(1-\nu^2)} \right]^{1/2} \quad (1)$$

σ is the stress at fracture, referred to the initial load bearing cross-section; ν is Poisson's ratio (0.32); and c the crack length, as defined by the depth of the slot.

were y and z are adjustable parameters. The y and z values, calculated according to the Tung procedure, are 0.004 21 and 0.403, respectively. Figure 1 shows the integral and differential experimental distributions; curves are calculated from equations (2) and (3).

These results show the very broad molecular weight distribution of *t*-2,5-DMPip-TFZ, ranging from oligo-

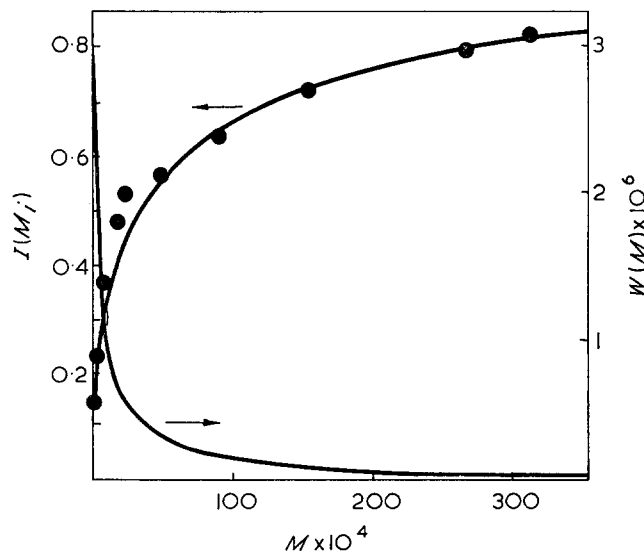


Figure 1 Integral (●) and differential (—) molecular weight distributions for poly(*trans*-2,5-dimethylpiperazine-3,4-thiofurazan amide)

mers ($\bar{M}_n < 1000$) to very high molecular weight fractions ($\bar{M}_n > 1\,000\,000$). The ratio \bar{M}_w/\bar{M}_n calculated from the fractionation data (excluding the first oligomeric fraction from the calculus) is about 25. It is reasonable to infer that such broad distribution is connected with the method of interfacial polycondensation employed⁸.

ACKNOWLEDGEMENTS

We thank Professor L. Credali and Dr G. P. Guidetti (Montedison SpA, Centro Ricerche, Ferrara) for kindly providing the polymer and for many suggestions, and Professor P. Chiorboli for encouraging this work.

This work was supported by Consiglio Nazionale delle Ricerche, Rome.

REFERENCES

- 1 Credali, L., Chiolle, A. and Parrini, P. *Polymer* 1972, **13**, 503
- 2 Credali, L., Chiolle, A. and Parrini, P. *4th Int. Symp. Fresh Water from the Sea, Heidelberg* 1973, p 95
- 3 Cantow, M. J. R. 'Polymer fractionation', Academic Press, New York, 1967
- 4 Schulz, G. V. and Blaschke, F. J. *Prakt. Chem.* 1941, **158**, 130
- 5 Ibrahim, F. W. J. *Polym. Sci. (A)* 1965, **3**, 469
- 6 Schulz, G. V. *Z. Phys. Chem.* 1940, **B47**, 155
- 7 Tung, L. M. J. *Polym. Sci.* 1956, **20**, 495
- 8 Morgan, P. V. 'Condensation polymers: by interfacial and solution methods', Interscience, New York, 1965

Letters

Dependence of fracture surface energy of PMMA on molecular weight

Berry has reported that the dependence of the fracture surface energy (γ) of poly(methyl methacrylate) PMMA on molecular weight, M , can be represented by the equation $\gamma = A - BM^{-1}$, where A and B are arbitrary constants. By extrapolation of experimental data obtained for values of M in the range $(0.9 \text{ to } 60) \times 10^5$ he concluded that γ should become zero for $M = 2.5 \times 10^4$ but stated that, 'in view of the uncertain validity of that extrapolation, it would clearly be desirable to determine directly the fracture surface energy and other ultimate properties of samples with molecular weights extending down to the critical value'¹. It is most difficult to prepare specimens of such low molecular weight which would be suitable for measurements of tensile fracture. However, in the present work, this is achieved by controlled degradation effected by exposure of PMMA specimens to high energy radiation².

Rectangular bars ($6.7 \times 2.2 \times 0.25$ cm) were cut at random from commercially available sheets of Plexiglas G (Rohm and Haas Co.). This polymer is made from methyl methacrylate without inclusion of other monomers or plasticizers. A slot, 0.22 or 0.44 cm deep, was cut in the middle of each bar using a circular saw 0.016 cm

thick. Sharp cracks were avoided to prevent the likelihood of crack propagation due to internal pressure build-up during subsequent irradiation. The bars were heated for 5 h at 90°C to relieve any internal stress.

In order to reduce the molecular weight of the PMMA, the slotted bars were exposed in air to ⁶⁰Co γ -rays at a dose rate of 2.1 Mrad/h. Irradiation also results in the formation of gas³. By reference to the complete absence of foaming in samples heated above the glass transition temperature, 100°C, it was judged that the bars were free of gas several months after irradiation.

Outgassed bars were tested in tension on an Instron machine at a crosshead separation of 0.1 cm/min. Bars which had been given high doses of radiation were very brittle and lap joints had to be bonded to their ends in order to grip them without fracture.

Limiting viscosity numbers $[\eta]$ were determined in benzene at 25°C. Viscosity average molecular weights, M_v , were calculated from the Mark-Houwink equation $[\eta] = KM^\alpha$, using $K = 5.5 \times 10^{-5}$ dl/g and $\alpha = 0.764$.

Values of fracture surface energy, γ , were calculated from Griffith's equation, for the case of plane strain⁵:

$$\sigma = \left[\frac{2E\gamma}{\pi c(1-\nu^2)} \right]^{1/2} \quad (1)$$

σ is the stress at fracture, referred to the initial load bearing cross-section; ν is Poisson's ratio (0.32); and c the crack length, as defined by the depth of the slot.

A tensile modulus of elasticity, E , was estimated from a three-point bending experiment to be 3.8×10^{10} dyne/cm². This value was not significantly changed by irradiation. This latter finding is in agreement with a report by Sisman and Bopp that the slope of tensile stress-strain curves remains constant after exposure of PMMA to high energy radiation. In this respect, it should be noted that Berry reported that his samples of PMMA generally gave lower values of E with decrease in molecular weight.

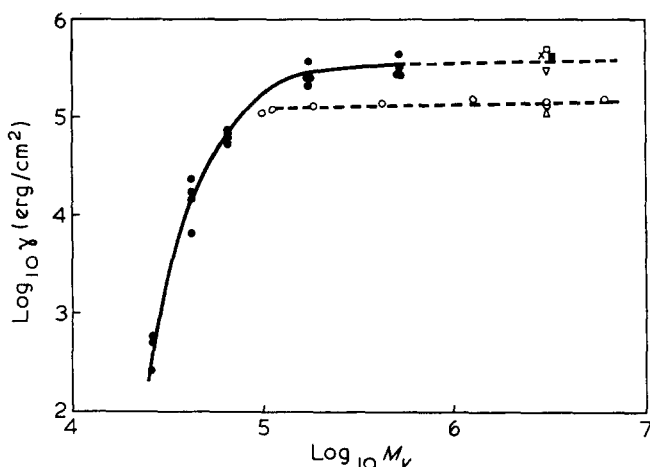


Figure 1 Dependence of fracture surface energy, γ , on viscosity average molecular weight, M_v

Symbol	Investigators	PMMA designation	Test method
□	Benbow and Roesler ⁷	Perspex	Wedge splitting
×	Irwin and Kies ⁸	Plexiglas II	Central notch
■	Svensson ⁹	Perspex	Wedge splitting
▽	Berry ⁹	Plexiglas II	Tensile test
○	Berry ¹	Plexiglas II	Cleavage test
△	Broutman and McGarry ¹¹	Plexiglas II	Cleavage test
●	Present work	Plexiglas G	Tensile test

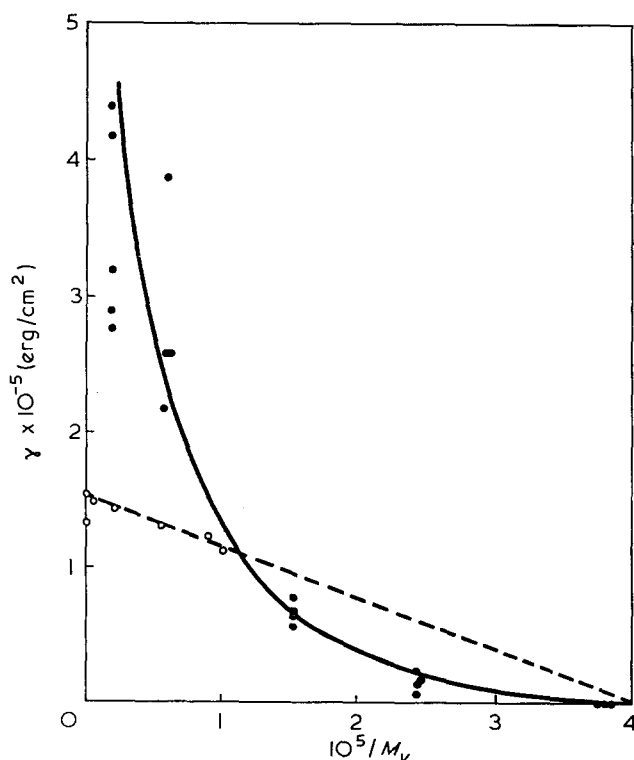


Figure 2 Dependence of γ on reciprocal of M_v

A plot of $\log_{10}\gamma$ vs. $\log_{10}M_v$ is given in Figure 1 along with data reported for PMMA by previous investigators. In Figure 2 Berry's data, stated to be reproducible to within 5%, are replotted in the form γ vs. M_v^{-1} for comparison with equation (2), in which A and B represent arbitrary constants:

$$\gamma = A - BM_v^{-1} \quad (2)$$

It will be seen that the present results agree with Berry's prediction that γ 'should become zero for a polymer of molecular weight 25 000'. More precisely, the results show that at the lowest molecular weight studied ($M_v = 25\,000$), γ has a low value of 450 erg/cm². Berry⁹ actually calculated a theoretical value for brittle fracture of 450 erg/cm² but this exact correspondence is judged to be fortuitous.

Despite the agreement reported above it should be noted that the validity of Berry's extrapolation depends on the validity of equation (2) down to low values of M_v . However, the present experimental data are not consistent with equation (2) (Figure 2). Instead the trend is similar, qualitatively, to Vincent's data on the relationship between the flexural strength of PMMA at -196°C and the reciprocal of number average molecular weight¹².

The present data may be criticized with respect to details concerning the geometry of the sample, the crack, and the precise form of the Griffith equation used. Nevertheless the results are important in providing a wide range of data, previously unavailable for any polymer, by showing how γ varies over three orders of magnitude with molecular weight. In order to make a more direct comparison with Berry's results, double cantilever beam specimens are currently being irradiated. Because of their massive size, however, a delay of one year before testing is anticipated to ensure that the gaseous products escape.

Acknowledgement

This investigation was supported by NIH research grant number DE-02668 from the National Institute of Dental Research and by NIH grant number RR-05333 from the Division of Research Facilities and Resources.

R. P. Kusy and D. T. Turner

Dental Research Center,
University of North Carolina at Chapel Hill,
Chapel Hill, N.C. 27514, USA

(Received 26 March 1974)

References

- Berry, J. P. *J. Polym. Sci. (A)* 1964, 2, 4069
- Sisman, O. and Bopp, C. D. *ORNL* 1951, p 928
- Charlesby, A. 'Atomic Radiation and Polymers', Pergamon Press, London, 1960, Ch 18
- Cantow, H. J. and Schulz, G. V. *Z. Phys. Chem. (N.F.)* 1954, 2, 117
- Griffith, A. A. *Phil. Trans. R. Soc.* 1921, A221, 163
- Irwin, G. R. and Kies, J. A. *Welding J. Res. Suppl.* 1952, 31, 955; 1954, 33, 1935
- Benbow, J. J. and Roesler, F. C. *Proc. Phys. Soc.* 1957, 70B, 201
- Svensson, N. L. *Proc. Phys. Soc.* 1961, 77, 876
- Berry, J. P. *J. Polym. Sci.* 1961, 50, 107
- Berry, J. P. *J. Polym. Sci.* 1961, 50, 313
- Broutman, L. J. and McGarry, F. J. *J. Appl. Polym. Sci.* 1965, 9, 589
- Vincent, P. I. *Polymer* 1960, 1, 425

Electro-optical properties of nucleic acids and nucleoproteins: 6. Reversal of the birefringence sign for sonicated DNA at low fields

Native DNA displays a negative electric and flow birefringence, the origin of which has been discussed by Takashima¹. It results from the preferential orientation of the base planes perpendicularly to the helix axis.

In the course of our study of the effect of sonication on the electro-optical properties of DNA and nucleohistone^{2,3} we observed reversals of the birefringence sign at low fields for sonicated DNA, concomitantly with the appearance of particular shapes of the photocurrent signals (Figure 1). The nucleohistone never showed this behaviour.

Similar low field deformations of the electro-optical signals have been reported for various macromolecules and colloidal particles⁴⁻¹⁰ in given conditions of pH, concentration and solvent. Association, dissociation, polymerization or aggregation processes⁸⁻¹⁰, and the existence of particular molecular structures⁵ have been invoked to explain these observations. Recently, Schweitzer and Jennings¹¹, and Brown and Jennings¹² have considered that such photocurrent signals may be due to molecular associations related to counter-ion effects because they seem to predominantly occur in con-

ducting media under rectangular electric fields and disappear in pulsed sinusoidal fields.

The necessary checks were made to ensure that the behaviour observed with sonicated DNA was not due to an artefact, and did not originate from a contribution of the solvent. The shape of the photocurrent pulses was perfectly reproducible and did not show any alteration during the application of several electric pulses (5 to 10) to the same sample; thus, this particular behaviour does not arise from a degradation or denaturation effect caused by the electric field.

The effect has been observed for all the DNA preparations, provided that the sonication time exceeded 3 min, i.e. for molecular weights smaller than 6.5×10^5 . DNA samples from calf thymus and *Micrococcus lysodeikticus*, sonicated in a citrate buffer showed similar behaviour, as well as DNA extracted from sonicated nucleohistone by gel filtration on a Sepharose 4B column, using 2 M NaCl as eluant (the DNA solutions were always exhaustively dialysed against a 1 mM NaCl solution before every electro-optical measurement).

The increase of the DNA concentration of the solutions greatly enhanced the amplitude of the positive birefringence contribution.

Discussion

There is no reason to carry out the analysis of the field strength dependence of the electric birefringence in the present case considering one single molecular entity holding a transverse dipole moment. Although this assumption would account for the reversal of the birefringence sign, it could not explain, however, the appearance of a transient in the field-free relaxation.

Complex mechanisms can be invoked to explain the particular behaviour observed, including the orientation of subunits into the macromolecular chain, or the presence of two distinct molecular entities independently oriented in the electric field. The latter hypothesis, which seems to us the most probable, can account for the shape of the signals and for the reversal of the birefringence sign (Figure 2). The component with negative birefringence, $\Delta n(-)$, would be oriented by a pure induced-dipole mechanism and would correspond to single sonicated DNA molecules; it is the smallest oriented entity (relaxation time = $40 \mu\text{s}$, i.e. a molecular length of about 1500 \AA for a rigid rod). The component with positive birefringence, $\Delta n(+)$, would have an appreciable contribution of a longitudinal permanent dipole moment to its orientation and would arise from some kind of aggregate; it is the longest oriented entity (relaxation time = $280 \mu\text{s}$, i.e. a molecular length of about 3000 \AA). Its orientation reaches saturation at a relatively low field (1.5 kV/cm). A fitting of the birefringence curve for this latter component, taking a value of $\beta^2/2\gamma = 0.5$ yielded values of the polarizability $\Delta\alpha = 7.5 \times 10^{-14} \text{ cm}^3$ ($8.3 \times 10^{-30} \text{ F m}^2$) and of the longitudinal permanent dipole $\mu_3 = 3.2 \times 10^4 \text{ D}$ ($1.1 \times 10^{-25} \text{ C m}$). The polarizability value is two orders of magnitude higher than that of the entity with negative birefringence³.

The main problem is to understand what is the nature of the entity with positive birefringence and why sonicated nucleohistone does not display this behaviour. The important influence of the concentration naturally suggests the occurrence of an aggregation process.

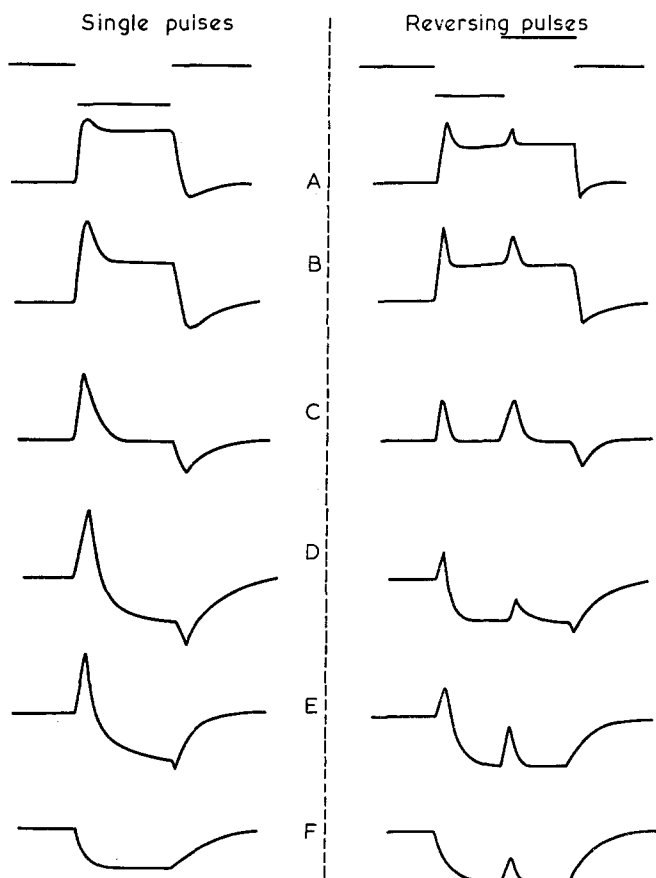


Figure 1 Particular electro-optical behaviour observed at low field strengths with DNA sonicated for 5 min or more. The field strength is decreasing from A (2.5 kV/cm) to F (0.2 kV/cm)

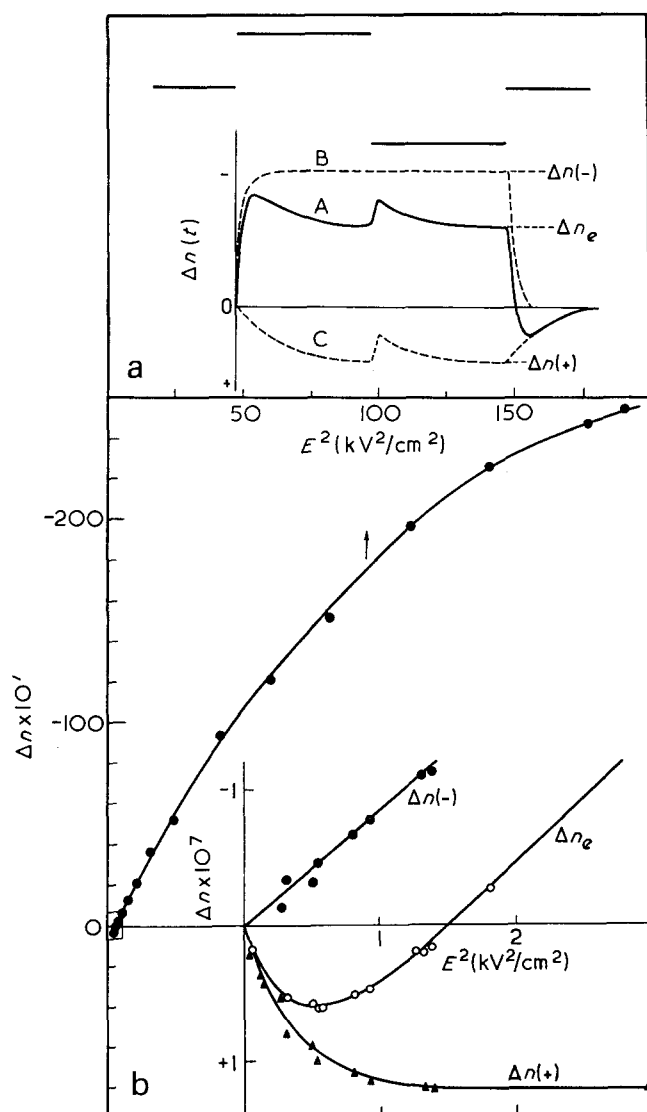


Figure 2 Analysis of the birefringence of sonicated DNA, considering the orientation of two distinct entities. (a) Typical decomposition of an electro-optical signal; (b) field strength dependence of the birefringence; the insert gives the enlarged part of the curve at low field strengths and its analysis in terms of two contributions. Δn_e , steady-state birefringence; $\Delta n(-)$ and $\Delta n(+)$, negative and positive contributions to the steady-state birefringence

However, until now, we have been unable to find any evidence for the presence of such aggregates by gel filtration, ultracentrifugation or filtration through Millipore filters ($0.45 \mu\text{m}$ pore size). It must be kept in mind that this entity will remain very difficult to identify since its contribution to the total optical anisotropy does not exceed about 2%.

Although we cannot exclude the possibility that a small percentage of RNA-like structure⁵ could be present in the sonicated DNA samples, this should not produce the observed changes with concentration. A superhelical arrangement could also be imagined. However, it is known to occur preferentially in nucleohistone and only at very high concentrations.

The interest of this study lies in the fact that many polyelectrolytes appear to show similar behaviour and that it should be useful to understand if it reflects some common features of the ionic atmosphere polarization

mechanisms. Further studies are in progress to clarify the problem.

Acknowledgements

The authors are grateful to Professor V. Desreux for helpful discussions, and to the Fonds National de la Recherche Fondamentale Collective for financial support.

One of us (P. C.) is indebted to the Fonds National de la Recherche Scientifique for a fellowship. The award of a fellowship by the Administration Générale de la Coopération au Développement (Belgique) to one of us (J. A. B.) is gratefully acknowledged.

P. Colson, C. Houssier and E. Fredericq

Laboratoire de Chimie Physique,
Université de Liège, B-4000 Liège, Belgium

and J. A. Bertolotto

On leave from:

Department of Physical Chemistry,
National University of Rosario, Rosario, Santa Fé, Argentina

(Received 14 March 1974)

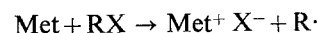
References

- 1 Takashima, S. *Biopolymers* 1968, **6**, 1437
- 2 Colson, P. *Thesis* University of Liège, 1972
- 3 Colson, P., Houssier, C. and Fredericq, E. *Biochim. Biophys. Acta* 1974, **340**, 244
- 4 O'Konski, C. T. and Zimm, B. H. *Science* 1950, **111**, 113
- 5 Golub, E. I. and Nazarenko, V. G. *Biophys. J.* 1967, **7**, 13
- 6 Haschemeyer, A. E. V. and Tinoco, I. Jr. *Biochemistry* 1962, **1**, 996
- 7 Haschemeyer, A. E. V. *Biochemistry* 1963, **2**, 851
- 8 Kobayasi, S., Asai, H. and Oosawa, F. *Biochim. Biophys. Acta* 1964, **88**, 528
- 9 Jennings, B. R., Brown, B. L. and Plummer, H. J. *Colloid Interface Sci.* 1970, **32**, 606
- 10 Matsumoto, M., Watanabe, H. and Yoshioka, K. *Biopolymers* 1972, **11**, 1711
- 11 Schweitzer, J. and Jennings, B. R. *J. Phys. (D: Appl. Phys.)* 1972, **5**, 297
- 12 Brown, B. L. and Jennings, B. R. *J. Colloid Interface Sci.* 1973, **43**, 170

Polymerization of vinylferrocene in chloroform

Introduction

The polymerization of vinyl monomers by metallocenes^{1,2}, metal carbonyls³ and metal acetylacetonates⁴ in the presence of halogenated and oxygenated solvents is generally accepted to occur by a free radical mechanism. The radicals which initiate the polymerization reaction are generated as a result of an electron transfer reaction between the metal nucleus (Met) and the solvent and the reaction can be depicted as:



Vinylferrocene^{5,6} like its parent compound ferrocene⁷, is decomposed in halogenated solvents, the decomposition

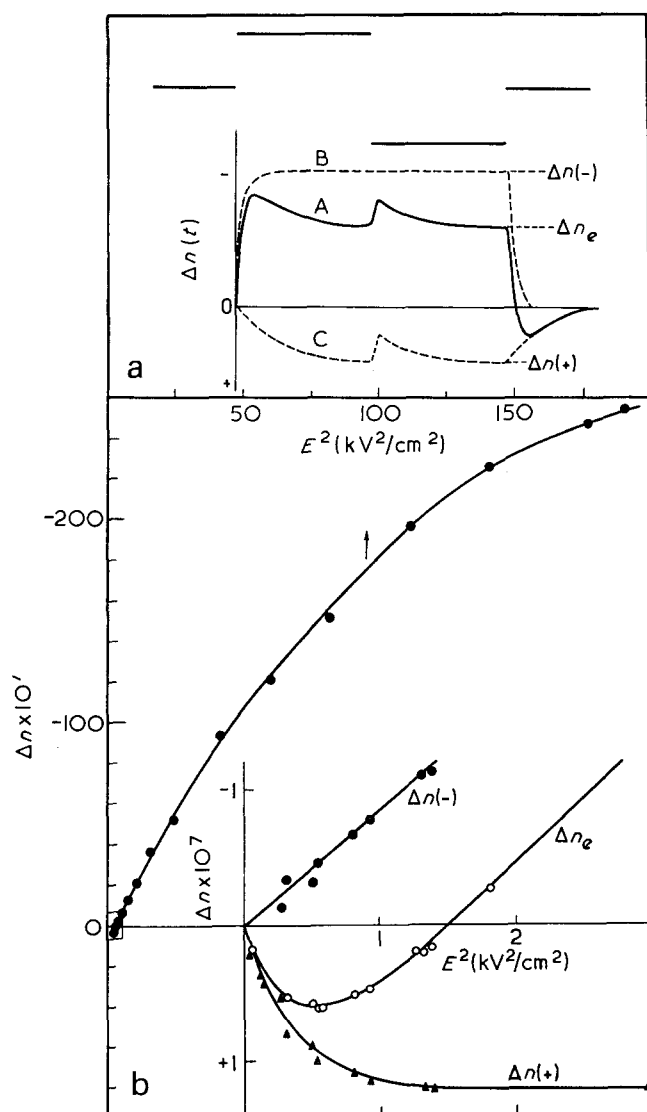


Figure 2 Analysis of the birefringence of sonicated DNA, considering the orientation of two distinct entities. (a) Typical decomposition of an electro-optical signal; (b) field strength dependence of the birefringence; the insert gives the enlarged part of the curve at low field strengths and its analysis in terms of two contributions. Δn_e , steady-state birefringence; $\Delta n(-)$ and $\Delta n(+)$, negative and positive contributions to the steady-state birefringence

However, until now, we have been unable to find any evidence for the presence of such aggregates by gel filtration, ultracentrifugation or filtration through Millipore filters ($0.45 \mu\text{m}$ pore size). It must be kept in mind that this entity will remain very difficult to identify since its contribution to the total optical anisotropy does not exceed about 2%.

Although we cannot exclude the possibility that a small percentage of RNA-like structure⁵ could be present in the sonicated DNA samples, this should not produce the observed changes with concentration. A superhelical arrangement could also be imagined. However, it is known to occur preferentially in nucleohistone and only at very high concentrations.

The interest of this study lies in the fact that many polyelectrolytes appear to show similar behaviour and that it should be useful to understand if it reflects some common features of the ionic atmosphere polarization

mechanisms. Further studies are in progress to clarify the problem.

Acknowledgements

The authors are grateful to Professor V. Desreux for helpful discussions, and to the Fonds National de la Recherche Fondamentale Collective for financial support.

One of us (P. C.) is indebted to the Fonds National de la Recherche Scientifique for a fellowship. The award of a fellowship by the Administration Générale de la Coopération au Développement (Belgique) to one of us (J. A. B.) is gratefully acknowledged.

P. Colson, C. Houssier and E. Fredericq

Laboratoire de Chimie Physique,
Université de Liège, B-4000 Liège, Belgium

and J. A. Bertolotto

On leave from:

Department of Physical Chemistry,
National University of Rosario, Rosario, Santa Fé, Argentina

(Received 14 March 1974)

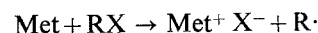
References

- 1 Takashima, S. *Biopolymers* 1968, **6**, 1437
- 2 Colson, P. *Thesis* University of Liège, 1972
- 3 Colson, P., Houssier, C. and Fredericq, E. *Biochim. Biophys. Acta* 1974, **340**, 244
- 4 O'Konski, C. T. and Zimm, B. H. *Science* 1950, **111**, 113
- 5 Golub, E. I. and Nazarenko, V. G. *Biophys. J.* 1967, **7**, 13
- 6 Haschemeyer, A. E. V. and Tinoco, I. Jr. *Biochemistry* 1962, **1**, 996
- 7 Haschemeyer, A. E. V. *Biochemistry* 1963, **2**, 851
- 8 Kobayasi, S., Asai, H. and Oosawa, F. *Biochim. Biophys. Acta* 1964, **88**, 528
- 9 Jennings, B. R., Brown, B. L. and Plummer, H. J. *Colloid Interface Sci.* 1970, **32**, 606
- 10 Matsumoto, M., Watanabe, H. and Yoshioka, K. *Biopolymers* 1972, **11**, 1711
- 11 Schweitzer, J. and Jennings, B. R. *J. Phys. (D: Appl. Phys.)* 1972, **5**, 297
- 12 Brown, B. L. and Jennings, B. R. *J. Colloid Interface Sci.* 1973, **43**, 170

Polymerization of vinylferrocene in chloroform

Introduction

The polymerization of vinyl monomers by metallocenes^{1,2}, metal carbonyls³ and metal acetylacetonates⁴ in the presence of halogenated and oxygenated solvents is generally accepted to occur by a free radical mechanism. The radicals which initiate the polymerization reaction are generated as a result of an electron transfer reaction between the metal nucleus (Met) and the solvent and the reaction can be depicted as:



Vinylferrocene^{5,6} like its parent compound ferrocene⁷, is decomposed in halogenated solvents, the decomposition

probably being induced by an initial electron transfer process with resulting formation of free radicals. Since vinylferrocene is readily polymerized by free radicals⁸⁻¹² this monomer may initiate its own polymerization in solvents which promote electron transfer reactions. Vinyl ferrocene does not polymerize at 60°C, in the absence of added initiator, in solvents such as benzene and toluene, which do not react with the ferrocene nucleus to produce free radicals. Accordingly, the polymerization of vinylferrocene in chloroform at 60°C has been studied and been found to proceed in the absence of any added free radical initiator.

Experimental

Vinylferrocene was purified by sublimation at 30°C and 0.1 mmHg (m.p. 52.5–53.5°C, lit. value¹³ 52–53.5°C). Gas chromatography (Pye Unicam 101, Carbowax column at 150°C), confirmed the purity of the monomer. Analar chloroform was dried over Linde molecular sieves (3A) and distilled under reduced pressure prior to use. Polymerizations were carried out in sealed glass vessels, after degassing the reactants by three successive freeze–pump–thaw cycles at 10⁻⁴ mmHg. Other reactions were also attempted after simply passing oxygen-free nitrogen over the frozen reactants before sealing the vessels. The reactants were heated for seven days at 60°C and then precipitated into Analar methanol. Polymers were only obtained from experiments conducted *in vacuo*. The polymers were redissolved in chloroform, precipitated into methanol, collected on a sintered glass crucible (porosity 3) washed with methanol and dried to constant weight at 30°C and 0.1 mmHg. After precipitation and filtration of the polymer the filtrate was evaporated and yielded only negligible amounts of unreacted vinylferrocene.

The polymers were characterized by elemental analysis, infra-red (i.r.) and ultra-violet (u.v.) spectroscopy. Number-average molecular weights were determined by vapour pressure osmometry in benzene and the molecular weight distribution was examined by gel permeation chromatography.

Table 1 Homopolymerization of vinylferrocene in chloroform and benzene at 60°C

Initial monomer concentration (mol/dm ³)	Solvent	Initiator concentration × 10 ² (mol/dm ³)	Conversion (%)	Iron (%)	Chlorine (%)	\bar{M}_n^b
1	CHCl ₃	—	30	23.1, 23.4	0.84	1 140
4	CHCl ₃	—	77	24.0, 24.1	0.54	1 200
4c	CHCl ₃	—	0	—	0.08	—
4	CHCl ₃	—	0	—	0.10	—
1	benzene	1.0 ^d	15	26.2, 26.1	0.01	5 800
4	benzene	1.0	2	26.4, 26.3	—	5 600
4	benzene	1.0	25	25.2, 25.4	—	12 800

a 2,2'-Azobisisobutyronitrile used to initiate polymerization in benzene

b Number-average molecular weight determined by vapour pressure osmometry in benzene at 37°C

c Nitrogen passed over frozen reactants before sealing. Small amounts of oxygen therefore remain in the reaction vessels

d Polymerization did not occur in benzene solution at 60°C in the absence of added AIBN

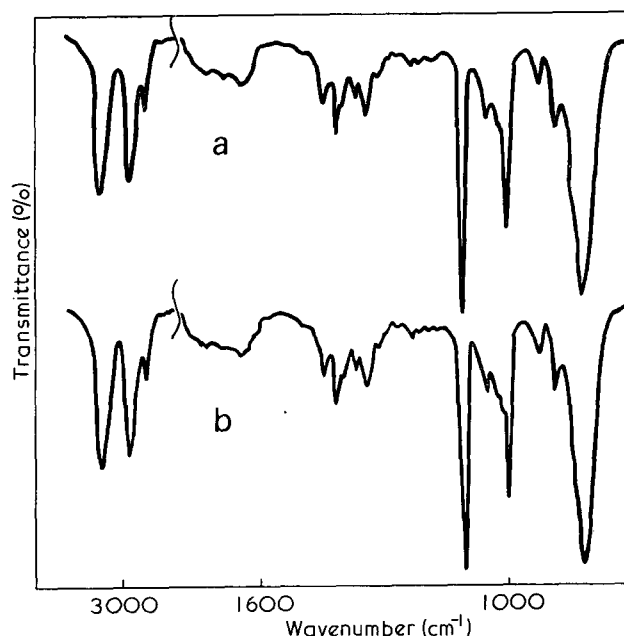


Figure 1 Infra-red spectra of polyvinylferrocene; films cast from benzene. (a) Prepared at 60°C in benzene with 1.0×10^{-2} mol/dm³ AIBN; (b) prepared at 60°C in chloroform, no added initiator

To investigate the presence of chlorine in the polymers prepared in chloroform, they were irradiated for 1 min in the pneumatic tube facility of the HERALD reactor (AWRE, Aldermaston, at a thermal neutron flux of 4×10^{12} neutron cm⁻² s⁻¹. The 37.5 min ³⁸Cl activity was measured using a high resolution Ge(Li) detector.

Results and Discussion

The results of the polymerization of vinylferrocene in chloroform are recorded in Table 1, together with those of polymerizations initiated by 2,2'-azobisisobutyronitrile (AIBN) in benzene. Polyvinylferrocene obtained from reactions in chloroform with the initial monomer concentration $[M]_0 = 4.0$ mol/dm³ were yellow powders whereas those obtained from reactions with $[M]_0 = 1.0$ mol/dm³ were coloured green. The green polymer showed an absorption at 635 nm, characteristic of the ferricenium species, which indicated that the polymer contained oxidized ferrocene units¹⁴. These could be reduced with ascorbic acid to give a yellow polymer which did not contain this longwave absorption.

Polymerization did not occur in the presence of oxygen and the monomer was decomposed to a brown ionic solid.

The purified polymers obtained from chloroform had identical i.r. spectra to those obtained by free radical initiation in benzene, which suggests that a similar mechanism is operative in both polymerizations. Some typical spectra are shown in Figure 1.

The u.v. and visible spectrum of polyvinylferrocene prepared in chloroform is the same as that of polyvinylferrocene obtained by free radical initiation in benzene. Typical absorption maxima and extinction coefficients are recorded in Table 2. The characteristic ferrocene absorptions near 330 nm and 450 nm appear in both. The lower extinction coefficients for the repeat unit of the polymers obtained from chloroform are in accord with their lower iron contents.

All the polymer samples show a similar electron spin resonance signal which consists of a broad line of width ~ 600 G and a g value equal to 2.06. This signal has been ascribed to the presence of a high spin Fe(III) complex in polyvinylferrocene prepared by radical initiation in benzene¹². It has been suggested that the complex is formed as a result of a termination reaction which involves an electron transfer from the ferrocene nucleus to the growing polymer chain radical. The presence of a paramagnetic species in polyvinylferrocene prepared in chloroform suggests that a similar free radical mechanism is also operative in this polymerization.

In agreement with results of other workers^{11,14,15} all the polymers have low molecular weights and the molecular weight distributions are broad and often appear binodal. These results suggest that transfer reactions are significant in radical polymerizations of vinylferrocene. In accordance with this suggestion the transfer constant to monomer has been estimated to be $\sim 8 \times 10^{-3}$ for vinylferrocene polymerized by free radicals in benzene¹⁶. In this system transfer to solvent was found to be negligible.

The very low molecular weights of polyvinylferrocene prepared in chloroform suggest that transfer to this solvent is more important. This is to be expected because of the high transfer activity of the monomer¹⁶ and chloroform¹⁷ in radical polymerizations.

The presence of chlorine in polyvinylferrocene prepared in chloroform was confirmed by neutron activation

analysis. A typical graph of the γ spectrum is shown in Figure 2. The two major ^{38}Cl peaks are well defined. ^{56}Mn and ^{24}Na peaks are also present in the polymers.

From the above discussion it seems apparent that the polymerization of vinylferrocene in chloroform has occurred by a free radical mechanism. Radical polymerization of suitable olefinic ferrocene derivatives in halogenated solvents is not unexpected since the ferrocene nucleus is oxidized in these solvents with the resulting formation of free radicals. The effects of oxygen on the polymerization reaction further supports a radical mechanism for the polymerization reaction.

The chlorine content in the polymers is too low for initiation by a radical species containing chlorine. For example even one chlorine atom per chain would result in a chlorine content of $\sim 3\%$ w/w in a polymer of molecular weight 1200. When the high transfer activity of the system is considered it seems more probable that chlorine is introduced into the polymers as a result of transfer reactions. This view is supported by the higher chlorine contents in polyvinylferrocene prepared in a high concentration of chloroform.

If chlorine is not present in the initiating radical it suggests that the polymerization has been initiated by a hydrogen radical. Since chloroform is readily decomposed to give a stable $-\text{CCl}_3$ anion¹⁸ and ferrocene is readily oxidized in chloroform⁵⁻⁷, the following reaction scheme can be suggested to account for the polymerization of vinylferrocene in chloroform:

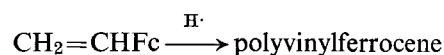
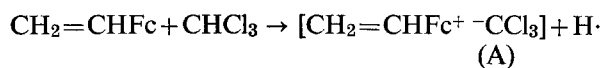


Table 2 Ultra-violet spectra of polyvinylferrocene in chloroform

Initial monomer concentration (mol/dm ³)	λ_{max} (nm)	ϵ (dm ³ mol ⁻¹ cm ⁻¹)
1.0a	330; 450	54; 81
4.0a	330; 450	55; 71
1.0b	330; 446	88; 99
2.0b	330; 446	86; 96

a Polymerized in chloroform; no added initiator
b Polymerized in benzene with 1.0×10^{-2} mol/dm³ AIBN

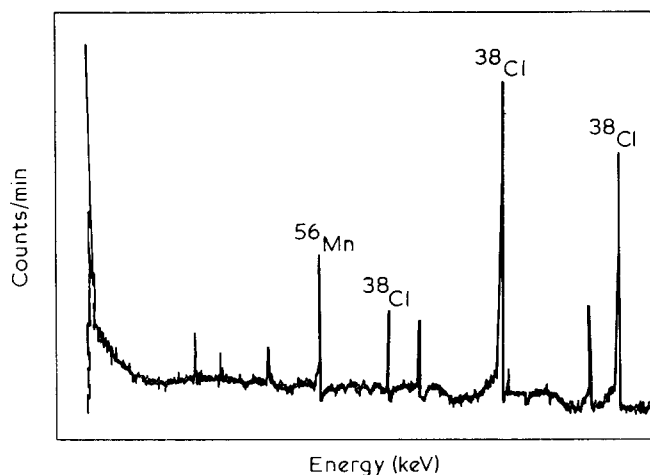


Figure 2 γ spectrum of polyvinylferrocene after irradiation for 1 min in the HERALD reactor. Polymer sample prepared at 60°C in chloroform, no added initiator

where Fc denotes the ferrocenyl group $\text{C}_{10}\text{H}_9\text{Fe}$.

The presence of the ferricenium species, A, in the polymerization reaction is supported by the fact that the colour of the reactants changed from dark red to green. The ferricenium species is very reactive towards free radicals, undergoing ring substitution^{19,20}, and will therefore act as a radical scavenger. However, radical addition to the olefinic double bond must still occur, presumably because of the lower activation energy for this reaction compared with ring substitution, although substitution reactions cannot be precluded.

Although a green polymer was obtained in reactions with a high mole fraction of chloroform, it is unlikely that species (A) has been polymerized. It is more probable that the green colour has resulted because of oxidation of the polyvinylferrocene formed initially. Thus, yellow solutions of polyvinylferrocene in carbon tetrachloride have been observed to turn green and precipitate a green ionic species¹⁵. Similar results have been found in chloroform in the present study.

A recent kinetic study of the radical initiated polymerization of vinylferrocene in benzene has shown that the termination step is monomolecular¹². Thus, the rate of polymerization at 60°C in benzene is related to the mean monomer and initiator concentration by the expression $R_p = k[\bar{M}]^{1.1}[\bar{I}_n]^{1.1}$ where k is a composite constant.

Self-initiation in solvents which promote electron transfer from the nucleus seems to be another unusual feature of this monomer.

More detailed kinetic studies of the polymerization of vinylferrocene in a range of solvents are in progress to elucidate the precise mechanisms operating in the polymerization reactions of vinylferrocene.

Acknowledgement

We are grateful to G. C. Goode, Atomic Weapons Research Establishment, Aldermaston, for carrying out activation analysis of polyvinylferrocene.

Maurice H. George

Department of Chemistry, Imperial College of Science and Technology, London, SW7 2AY, UK

and Gerard F. Hayes

Rocket Propulsion Establishment, Westcott, Nr Aylesbury, Buckinghamshire HP18 ONZ, UK

(Received 7 February 1974)

References

- 1 Kaeriyama, K. *Polymer* 1971, **12**, 422
- 2 Bamford, C. H. and Finch, C. A. *Naturforsch.* 1962, **176**, 500
- 3 Bamford, C. H. *et al. Trans. Faraday Soc.* 1963, **59**, 118, 540, 548; 1964, **60**, 751, 1432; 1965, **61**, 1459; 1966, **62**, 2531, 2544
- 4 Riches, Von K. M. *Makromol. Chem.* 1967, **103**, 175
- 5 Rausch, M. D. and Siegal, A. *J. Organometal. Chem.* 1968, **11**, 317
- 6 Simionescu, Cr., *et al. Makromol. Chem.* 1973, **163**, 59
- 7 Rosenblum, M. 'Chemistry of the Iron Group Metallocenes', Part I, Wiley, New York, 1965, p 42
- 8 Arimoto, F. S. and Haven, Jr., A. C. *J. Am. Chem. Soc.* 1955, **77**, 6295
- 9 Fitzgerald, W. P. *Dissert. Abstr.* 1964, **24**, 2687
- 10 Baldwin, M. G. and Johnson, K. E. *J. Polym. Sci. (A-1)* 1967, **5**, 2091
- 11 Lai, J. C., Rounsfell, T. and Pittman, Jr., C. U. *J. Polym. Sci. (A-1)* 1971, **9**, 651
- 12 George, M. H. and Hayes, G. F. *J. Polym. Sci. (B)* 1973, **11**, 471
- 13 Horspool, W. M. and Sutherland, R. G. *Can. J. Chem.* 1968, **46**, 3453
- 14 Aso, C., Kunitake, T. and Nakashima, T. *Makromol. Chem.* 1969, **124**, 232
- 15 Sasaki, Y., Walker, L. L., Hurst, E. L. and Pittman, Jr., C. U. *J. Polym. Sci. (A-1)* 1973, **11**, 1213
- 16 Hayes, G. F. and George M. H. in preparation
- 17 Gregg, R. A. and Mayo, F. R. *J. Am. Chem. Soc.* 1953, **75**, 3530
- 18 Walling, C. 'Free Radicals in Solution', Wiley, New York, 1957, p 158
- 19 Beckwith, A. L. J. and Leydon, R. J. *Tetrahedron Lett.* 1963, **6**, 385
- 20 Little, W. F., Lynn, K. N. and Williams, R. J. *J. Am. Chem. Soc.* 1963, **85**, 3055
- 21 Golding, R. M. and Orgel, L. E. *J. Chem. Soc.* 1962, p 363

Book Review

Block copolymers

Edited by D. C. Allport and W. H. Janes

Applied Science, London, 1973, 620 pp. £12.00

This is a carefully planned review of the 'state-of-art' in block copolymer chemistry and technology up to the beginning of 1972. With the recent burst of interest in block and segmented copolymers as novel elastomers, adhesives and emulsifying/stabilizing agents, this book is indeed timely. The contributors in addition to the editors themselves are: J. H. Atherton, J. V. Dawkins, T. G. Heggs, A. A. Mahajer and J. B. Plumb, all of whom at the time of writing were with ICI Ltd. This latter fact must count a little against the book in that one would have expected authors from Shell and Du Pont in particular to have contributed some inside know-how. To be fair to the present authors, however, they have done an excellent job in reading between the lines in patent and manufacturers' specifications and have put forward shrewd guesses as to what is really happening. Certainly I found the book very revealing in the detail it contains of the chemistry and technology of commercial products. The coverage and discussion of the patent literature is particularly thorough and useful and presumably owes much to the delving of the technical intelligence sections at ICI. Patent references are given at the end of each chapter together with the normal journal references.

The chapters written by the separate contributors range in topics from radical polymerization methods for end-capping, through condensation and ionic methods of block copolymer production to property-structure relationships, with existing technology included as appropriate. It is indeed difficult to find an existing route to blocky structures which is not covered in this book, but the authors are a little reserved in predicting or suggesting new approaches. I found the chapters on Ziegler catalyst systems for block polymerization (Heggs), isocyanate chemistry and technology (Allport and Mahajer) and siloxane block copolymers (Plumb and Atherton) particularly interesting and the general reviews of property/structure/composition relationships (Dawkins) also very useful.

The book is solidly packed with useful information and references which generously give it the status of the major source book on block copolymer chemistry. If looking for criticism of the subject matter I would say that radical reactions are given rather too much prominence for their importance whilst cationic reactions deserve more attention in view of their relatively unexploited potential.

In the introduction the editors suggest a systematic nomenclature scheme for block copolymers. The common styrene-butadiene-styrene three block would be represented as $ABApoly(M_1-b-M_2)$, where ABA shows the block sequence order. A more complex system would be $ABpoly(M_1-b-(M_2-g-[M_1-alt-M_2]))$ and if the reader can decipher this the system will work.

The book is very free of trivial errors, clearly printed and illustrated and well bound in a hard-back version, which at £12 represents good value for money. This book is more than a library curiosity and should be on the shelf of any research and development scientist concerned with the problems of producing new property polymers from existing monomers.

R. E. Wetton

More detailed kinetic studies of the polymerization of vinylferrocene in a range of solvents are in progress to elucidate the precise mechanisms operating in the polymerization reactions of vinylferrocene.

Acknowledgement

We are grateful to G. C. Goode, Atomic Weapons Research Establishment, Aldermaston, for carrying out activation analysis of polyvinylferrocene.

Maurice H. George

Department of Chemistry, Imperial College of Science and Technology, London, SW7 2AY, UK

and Gerard F. Hayes

Rocket Propulsion Establishment, Westcott, Nr Aylesbury, Buckinghamshire HP18 0NZ, UK

(Received 7 February 1974)

References

- 1 Kaeriyama, K. *Polymer* 1971, **12**, 422
- 2 Bamford, C. H. and Finch, C. A. *Naturforsch.* 1962, **176**, 500
- 3 Bamford, C. H. *et al. Trans. Faraday Soc.* 1963, **59**, 118, 540, 548; 1964, **60**, 751, 1432; 1965, **61**, 1459; 1966, **62**, 2531, 2544
- 4 Riches, Von K. M. *Makromol. Chem.* 1967, **103**, 175
- 5 Rausch, M. D. and Siegal, A. *J. Organometal. Chem.* 1968, **11**, 317
- 6 Simionescu, Cr., *et al. Makromol. Chem.* 1973, **163**, 59
- 7 Rosenblum, M. 'Chemistry of the Iron Group Metallocenes', Part I, Wiley, New York, 1965, p 42
- 8 Arimoto, F. S. and Haven, Jr., A. C. *J. Am. Chem. Soc.* 1955, **77**, 6295
- 9 Fitzgerald, W. P. *Dissert. Abstr.* 1964, **24**, 2687
- 10 Baldwin, M. G. and Johnson, K. E. *J. Polym. Sci. (A-1)* 1967, **5**, 2091
- 11 Lai, J. C., Rounsfell, T. and Pittman, Jr., C. U. *J. Polym. Sci. (A-1)* 1971, **9**, 651
- 12 George, M. H. and Hayes, G. F. *J. Polym. Sci. (B)* 1973, **11**, 471
- 13 Horspool, W. M. and Sutherland, R. G. *Can. J. Chem.* 1968, **46**, 3453
- 14 Aso, C., Kunitake, T. and Nakashima, T. *Makromol. Chem.* 1969, **124**, 232
- 15 Sasaki, Y., Walker, L. L., Hurst, E. L. and Pittman, Jr., C. U. *J. Polym. Sci. (A-1)* 1973, **11**, 1213
- 16 Hayes, G. F. and George M. H. in preparation
- 17 Gregg, R. A. and Mayo, F. R. *J. Am. Chem. Soc.* 1953, **75**, 3530
- 18 Walling, C. 'Free Radicals in Solution', Wiley, New York, 1957, p 158
- 19 Beckwith, A. L. J. and Leydon, R. J. *Tetrahedron Lett.* 1963, **6**, 385
- 20 Little, W. F., Lynn, K. N. and Williams, R. J. *J. Am. Chem. Soc.* 1963, **85**, 3055
- 21 Golding, R. M. and Orgel, L. E. *J. Chem. Soc.* 1962, p 363

Book Review

Block copolymers

Edited by D. C. Allport and W. H. Janes

Applied Science, London, 1973, 620 pp. £12.00

This is a carefully planned review of the 'state-of-art' in block copolymer chemistry and technology up to the beginning of 1972. With the recent burst of interest in block and segmented copolymers as novel elastomers, adhesives and emulsifying/stabilizing agents, this book is indeed timely. The contributors in addition to the editors themselves are: J. H. Atherton, J. V. Dawkins, T. G. Heggs, A. A. Mahajer and J. B. Plumb, all of whom at the time of writing were with ICI Ltd. This latter fact must count a little against the book in that one would have expected authors from Shell and Du Pont in particular to have contributed some inside know-how. To be fair to the present authors, however, they have done an excellent job in reading between the lines in patent and manufacturers' specifications and have put forward shrewd guesses as to what is really happening. Certainly I found the book very revealing in the detail it contains of the chemistry and technology of commercial products. The coverage and discussion of the patent literature is particularly thorough and useful and presumably owes much to the delving of the technical intelligence sections at ICI. Patent references are given at the end of each chapter together with the normal journal references.

The chapters written by the separate contributors range in topics from radical polymerization methods for end-capping, through condensation and ionic methods of block copolymer production to property-structure relationships, with existing technology included as appropriate. It is indeed difficult to find an existing route to blocky structures which is not covered in this book, but the authors are a little reserved in predicting or suggesting new approaches. I found the chapters on Ziegler catalyst systems for block polymerization (Heggs), isocyanate chemistry and technology (Allport and Mahajer) and siloxane block copolymers (Plumb and Atherton) particularly interesting and the general reviews of property/structure/composition relationships (Dawkins) also very useful.

The book is solidly packed with useful information and references which generously give it the status of the major source book on block copolymer chemistry. If looking for criticism of the subject matter I would say that radical reactions are given rather too much prominence for their importance whilst cationic reactions deserve more attention in view of their relatively unexploited potential.

In the introduction the editors suggest a systematic nomenclature scheme for block copolymers. The common styrene-butadiene-styrene three block would be represented as $ABA_{poly}(M_1-b-M_2)$, where ABA shows the block sequence order. A more complex system would be $AB_{poly}(M_1-b-(M_2-g-[M_1-alt-M_2]))$ and if the reader can decipher this the system will work.

The book is very free of trivial errors, clearly printed and illustrated and well bound in a hard-back version, which at £12 represents good value for money. This book is more than a library curiosity and should be on the shelf of any research and development scientist concerned with the problems of producing new property polymers from existing monomers.

R. E. Wetton

Crystallization kinetics of polyacrylonitrile: single crystal growth rate and thermodynamic considerations

R. M. Gohil, K. C. Patel and R. D. Patel

Department of Chemistry, Sardar Patel University, Vallabh Vidyanagar 388120, Gujarat, India
(Received 16 February 1973; revised 18 December 1973)

Single crystals of polyacrylonitrile (PAN) were grown by the film formation method. Lamellar thickness was measured at different crystallization temperatures. Growth rates of single crystals were measured in a wide range of temperatures. It was possible to fit the experimental data in the WLF equation by substituting $C_2=130$. Concentration dependence of growth rate has been examined. Thermodynamic calculations were carried out and various parameters were evaluated which were compared with the data of other polymers. The present study indicates that PAN is a stiff chain molecule.

INTRODUCTION

Generally the crystallization kinetics of polymers have been studied by measuring the growth rate of spherulites in a narrow temperature range just below the melting point. However, little work has been reported on the kinetics of crystallization of single crystals of polymers from solution. This may be mainly due to the narrow range of temperatures over which crystallization can be carried out by conventional methods and the experimental difficulty in measuring the single crystal dimensions after certain time intervals.

Holland and Lindenmeyer¹ showed that the growth rate of single crystals of polyethylene (PE) varied from $1.6 \mu\text{m}/\text{day}$ at 92°C to $0.2 \mu\text{m}/\text{sec}$ at 80°C . A strong negative temperature coefficient was observed and they found that the temperature dependence of initial growth rate agreed with the theoretical prediction and also the reported $\sigma\sigma_e = 700 (\text{erg}/\text{cm}^2)^2$. Bundell and Keller² repeated Holland and Lindenmeyer's experiment with seeded crystals and additionally found that at a given crystallization temperature, growth rate, G , was proportional to the solution concentration raised to the one-third power. Johnsen and Lehman³ have shown that the initial crystallization rate was proportional to the concentration raised to a power that increases from 0.24 to 0.44 depending on crystallization temperature. Nardini and Price⁴ have studied by optical microscopy, the growth rate of poly(ethylene oxide) (PEO) pseudo-dendrite in xylene-cyclohexane mixed solvent and showed exponential temperature dependence of growth rate. The same relation was obeyed by melt crystallized polymer indicating that the surface terms in exponent were similar in both cases. Recently, growth rate of polyacrylonitrile (PAN) single and multilayered crystals from dilute solutions have been measured at 100°C by Klement and Geil⁵ using the technique described by Holland and Lindenmeyer¹.

The film formation method^{6,7} for the growth of single crystals from solution provides a suitable technique for the study of crystallization kinetics of single crystals. Growth rate of single crystals of PE and cellulose triacetate were measured by this method⁸. PAN crystallizes rather slowly and hence it is possible to study kinetics of growth of single crystals over a wide range of temperatures. In this work crystallization kinetics of PAN single crystals have been reported at temperatures varying from 105° to 160°C .

EXPERIMENTAL

Polyacrylonitrile was prepared by cerium (IV) ion redox system⁹. The viscosity average molecular weight was found to be 6.68×10^5 . Propylene carbonate was used as the crystallization solvent and was purified by the method of Chiang *et al.*¹⁰. Crystals were grown on a glass slide according to the method developed in this laboratory^{6,7}. Growth rates of single crystals were measured after suitable time intervals by measuring the length of the crystal along the a axis. Generally about 7% size variation was observed. The thickness of the platelets was determined from electron micrographs by measuring the shadow length and shadow angle. In order to obtain the best possible average, a large number of individual measurements were made at each crystallization temperature⁷. The thickness could be measured with an accuracy of 15 \AA .

For electron microscopic observations, the glass slide on which the polymer crystals were grown, was placed in vacuum evaporator, coated with carbon and shadowed with chromium at a desired angle. The replica could be detached from the glass support by flotation on a water surface. The electron microscopy study was carried out on a Carl-Zeiss model EF-4.

RESULTS AND DISCUSSION

Crystal thickness

Since the discovery of folded chain crystals¹¹, several suggestions have been advanced to explain the cause of regularity of chain foldings. The thermodynamic theory was developed by Peterlin, Fischer and Reinhold¹²⁻¹⁵ while the kinetic theory was developed independently by Price¹⁶, Lauritzen and Hoffman^{17, 18} and Frank and Tosi¹⁹. According to the first theory, the fold period is determined thermodynamically corresponding to a minimum in the free-energy density of the crystals at the crystallization temperature. It explains some aspects of crystallization of PE from dilute solution, but does not seem to apply to crystallization from the melt. The kinetic theory can be applied to crystallization from both solution and melt. Both the theories succeeded in accounting for the observed dependency of fold length on temperature. Equilibrium theory failed to explain the dependence of solvent on lamellar thickness. However, fold length of solution grown single crystal depends on the temperature of crystallization and therefore, one may conclude that chain folded polymer crystallization generally follows the kinetic mechanism.

According to the kinetic theory, Hoffman and Lauritzen^{17, 18} developed the following relation:

$$l^* = \frac{2\sigma_e T_m^0}{\Delta H_u \Delta T} + \frac{kT}{b_0 \sigma} \quad (1)$$

where l^* is the height of lamella, σ_e and σ are the free energies per unit area of fold surface and lateral surface respectively, k is the Boltzmann constant and b_0 is the thickness of crystal volume, *i.e.*, the centre to centre distance between the chains. ΔH_u is the heat of fusion per unit volume of crystal and ΔT is the degree of supercooling ($T_m^0 - T_c$), T_m^0 and T_c being equilibrium melting point and crystallization temperatures.

The term $(2\sigma_e T_m^0 / \Delta H_u \Delta T)$ is considerably larger than $(kT/b_0\sigma)$ at the crystallization temperature of interest. Hence, a principal variation of l^* with temperature is mainly a result of the factor $1/\Delta T$. Thus, l^* increases as T_c increases. So, equation (1) can be experimentally verified by constructing and fitting crystal thickness data for certain values of σ_e and T_m^0 as suggested by Holland and Lindenmeyer¹. The results of lamellar thickness at different crystallization temperatures are shown in Figure 1(A). For finding out the best possible curve which fits with these experimental results, several curves are drawn for different values of T_m^0 and σ_e , and the curve which passes through a point of maximum crystallization temperature is selected. Figure 1(B) shows the best fit for $T_m^0 = 325^\circ\text{C}$ and $\sigma_e = 198 \text{ erg/cm}^2$. The value of σ_e is high compared to that calculated by the other method¹⁰. Hence, the validity of this equation seems to be doubtful. This may be due to the fact that the second term $kT/b_0\sigma$ in equation (1) is not considered in the above treatment.

If it is assumed²⁰ that $T = T^0$, one obtains:

$$\left(\frac{kT}{b_0\sigma}\right)_{\text{max}} = \left(\frac{kT_m^0}{b_0\sigma}\right) \quad (2)$$

Substituting for $b_0 = 5.09 \text{ \AA}$ and $\sigma = 5.13 \text{ erg/cm}^2$ (value derived later), one obtains:

$$\left(\frac{kT_m^0}{b_0\sigma}\right) = 22 \text{ \AA}$$

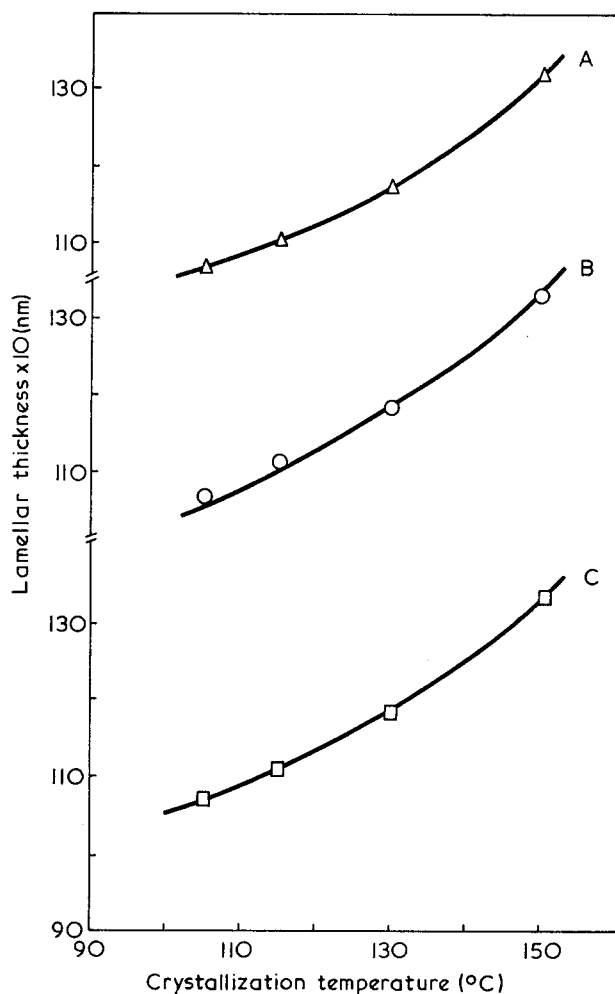


Figure 1 Lamellar thickness vs. isothermal crystallization temperature. \circ , $T_m^0 = 325^\circ\text{C}$; $\sigma_e = 198 \text{ erg/cm}^2$. \square , $T_m^0 = 310^\circ\text{C}$; $\sigma_e = 153 \text{ erg/cm}^2$

Since the value of the second term is not small compared to the value of l and is beyond limits of experimental error, the second term was included in constructing the theoretical curves. The best fit of theoretical line shown in Figure 1(C) gives the value of $T^0 = 310^\circ\text{C}$ and $\sigma_e = 153 \text{ erg/cm}^2$. Still the value of σ_e obtained by this relation is higher than those obtained for other polymers (Table 1). Hence, the value of σ_e was determined by the other method. Kinetic study can also throw some light on the value of σ_e .

Growth rate

The crystallization of synthetic high polymers and kinetics of morphology are most satisfactorily explained by nucleation controlled growth mechanism¹⁶⁻¹⁸. The development of spherulitic structure in bulk leads to the following expression for growth rate:

$$G = G_0 \exp\left(-\frac{\Delta F^*}{kT}\right) \exp\left(-\frac{\Delta \phi^*}{kT}\right) \quad (3)$$

where

ΔF^* = energy barrier to transport a material across the liquid crystal interface,

$\Delta \phi^*$ = work required to form a nucleus of critical size, and

G_0 = constant.

With appropriate modification^{21, 22}, equation (3) can be obtained in the form of equation (4) for two-dimensional surface nucleation:

$$G = G_0 \exp\left\{-\frac{C_1}{R(C_2 + T_c - T_g)}\right\} \exp\left\{-\frac{4b_0(\sigma\sigma_e)T_m^0}{\Delta H_u k T_c (\Delta T)}\right\} \quad (4)$$

where R is the gas constant, T_g is the glass transition temperature and C_1 and C_2 are constants. Equation (4) can be applied to calculate interfacial energies of a number of polymer crystals grown from melt. Nardini and Price⁴ showed that the same law was obeyed for PEO for solution and melt crystallized polymer which indicated that the surface energy terms in the exponent were similar in both the cases. Hence as with PE²² an attempt was made to use the same law of melt crystallized polymer to the solution grown crystals.

In the present investigation, growth rates of single crystals are measured at different temperatures from solution of 0.06% concentration. The length along the long axis of several single crystals with no overgrowth is measured at each crystallization temperature. On plotting the length of the single crystal against crystallization time, straight lines passing through the origin for all the values of T_c except 105°C are obtained. Results are shown in Figure 2. Growth rates, G are measured from this plot by taking the slope of the lines.

The procedure of Hoffman¹⁸ is adopted to check whether the growth rate of PAN single crystals can be described by equation (4) or not. This equation can be

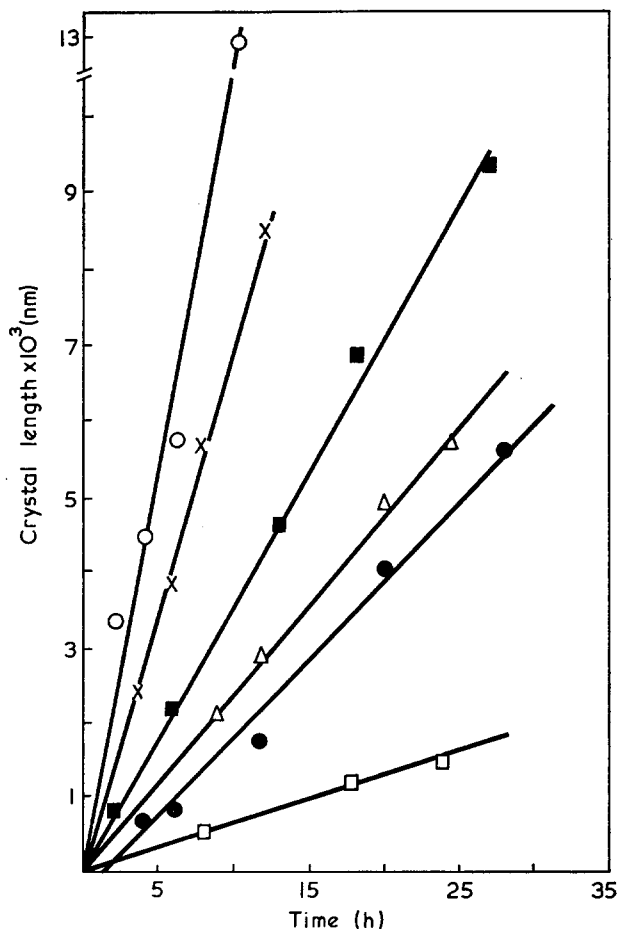


Figure 2 Crystal length vs. time for various crystallization temperatures: ●, 105°C; △, 115°C; ■, 130°C; ×, 140°C; ○, 150°C; □, 160°C

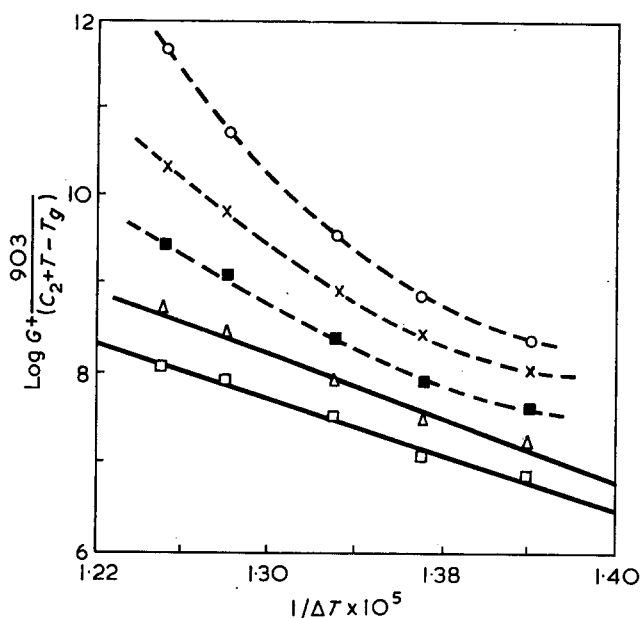


Figure 3 Plots of $\log G + [903/(C_2 + T - T_g)]$ vs. $[1/(\Delta T)]$ for different values of C_2 : ○, 80; ×, 100; ■, 110; △, 120; □, 130

written as:

$$\log G + \left(\frac{C_1}{2.303R(C_2 + T_c - T_g)}\right) = \log G_0 - \left(\frac{4b_0(\sigma\sigma_e)T_m^0}{2.303\Delta H_u k T_c (\Delta T)}\right) \quad (5)$$

Substituting the value of $C_1 = 4120$ cal/mol, $C_2 = 51.6$ K, $T_g = 377$ K and $T_m^0 = 590$ K, in equation (5), one obtains:

$$\log G + \left(\frac{903}{(T - 325.4)}\right) = \log G_0 - \left(\frac{1.02 \times 10^3(\sigma\sigma_e)}{\Delta H_u k T_c (590 - T_c)}\right) \quad (6)$$

By plotting the left hand side of equation (6) against $1/T(590 - T_c)$ no linear relationship is observed. Therefore, the left hand side of equation (6) is plotted as a function of $1/\Delta T$ for five different values of C_2 in Figure 3. The line corresponding to $C_2 = 130$ gives best agreement with theory. The slope of this line gives $\sigma\sigma_e = 669$ (erg/cm²)².

From the various reports²¹⁻²⁵, it is seen that the value of C_2 in the WLF equation varies from polymer to polymer. A study on poly(tetramethyl-*p*-silphenylene) siloxane²³ gives $C_2 = 90$ K, while in the case of nylon-6²⁴, $C_2 = 130$ K. The constant C_2 determined by relaxation measurement shows a little variation for different polymers²⁵. However, C_2 calculated from growth rate study deviates considerably from 51.6K and therefore the value of $C_2 = 130$ for PAN is not unjustifiable.

The extrapolation of the line having $C_2 = 130$ K gives $\log G_0 = 13.94$. Substituting the value of $C_2 = 130$ and G_0 in equation (4), one gets:

$$G = 8.7 \times 10^{13} \exp\left[-\frac{2.06 \times 10^3}{(T - 247)}\right] \exp\left[-\frac{12.3 \times 10^5}{T(590 - T_c)}\right] \quad (7)$$

The theoretical curve has been plotted according to equation (7) and is shown in Figure 4. The graph also shows that there is good agreement between experimental results and equation (7). As it is difficult to measure growth rate from 0.06% solution of PAN above 150°C, the growth rate is measured from 0.25% solution at

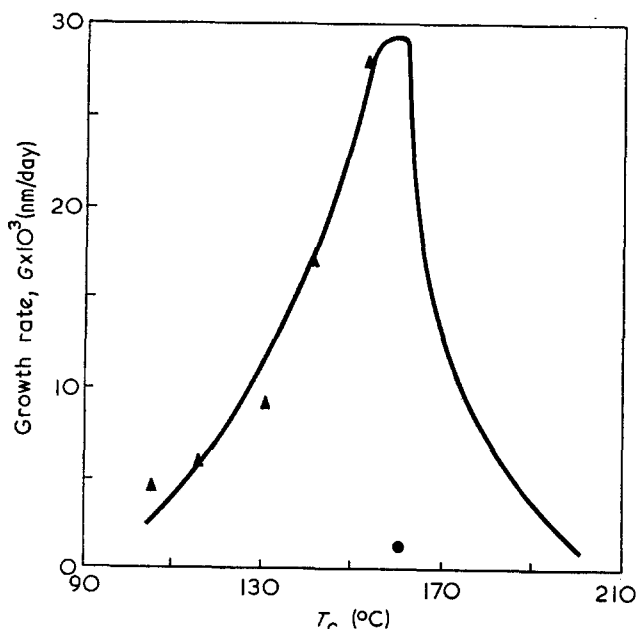


Figure 4 Growth rate G vs. crystallization temperature. \blacktriangle , Experimental values; —, theoretical curve according to equation (7); \bullet , point showing growth rate from 0.25% solution

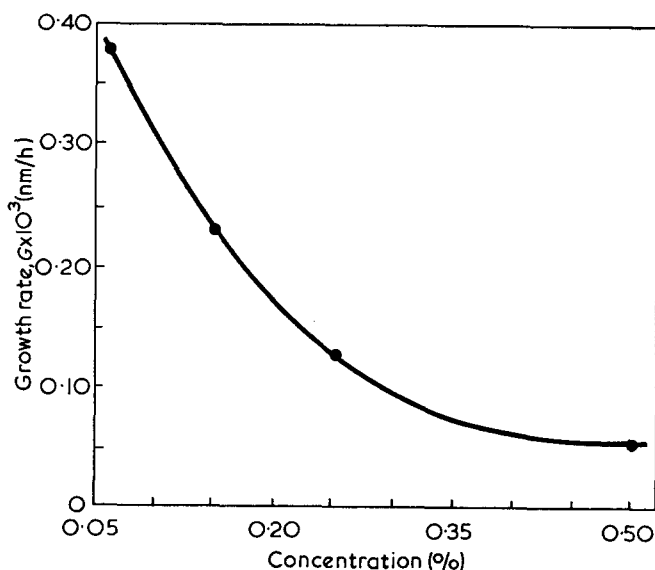


Figure 5 Growth rate as a function of concentration at 130°C

160°C. This point lies well below the theoretical value which clearly shows the decrease in growth rate above 150°C. This may be due to the increase in concentration. It is observed while studying the effect of concentration on growth rate at 130°C that the growth rate falls appreciably (Figure 5) with increase in concentration. This shows an inverse dependence compared to that observed from the self-seeded technique^{2, 26} which may be due to the inherent nature of the method adopted.

The growth rate increases with temperature up to a particular temperature and then decreases with increase in temperature according to the double exponential form of equation (7). This type of behaviour has been quantitatively confirmed in melt crystallization studies on nylon-6²⁷, natural rubber²⁸ and isotactic polystyrene^{29, 30}. Such behaviour is not observed in the case of PE because the polymer crystallizes so rapidly

that it apparently cannot be quenched in the molten state to a temperature anywhere near T_g .

The value of G_{max} , from the theoretical curve shown in Figure 4 comes out to be 0.02 $\mu\text{m}/\text{min}$. This value is very low compared to those of many other polymers where G_{max} is determined by measuring the growth rates of spherulite²⁹. For example G_{max} for PE³ is 5000 $\mu\text{m}/\text{min}$ while that of polycarbonate³² is 0.01 $\mu\text{m}/\text{min}$. However, G_{max} of PAN is nearly equal to that of polycarbonate and it is likely that the lower G_{max} may be due either to the polar CN group attached to the backbone of PAN or the growth rate of single crystals may be different from that of spherulite.

Growth rate parameters

In the previous section, the product $\sigma\sigma_e$ was calculated from equation (6) by using $b_0 = 5.09 \text{ \AA}$ which was calculated from unit cell dimensions. $\Delta H = 24 \text{ cal/g}$ was determined previously using the Flory diluent method³²:

$$\sigma\sigma_e = 669 \text{ (erg/cm}^2\text{)}^2 \quad (8)$$

But the value of σ_e obtained from thickness data is 153 erg/cm^2 . Therefore one obtains a value of $\sigma = 4.4 \text{ erg/cm}^2$ from equation (8).

Hoffman and Weeks²¹ pointed out that rough approximation to σ can be estimated from the Thomas-Steveley³⁴ relation, which assumes that the work necessary to form a surface is proportional to the heat of fusion. The proportionality is:

$$\alpha = \frac{\sigma}{b_0 \Delta H_u} \quad (9)$$

where α is a constant for materials of similar nature. It varies from 0.086 to 0.1 for chain containing crystals and 0.3 to 0.4 for simple molecular crystals consisting of approximately spherical molecules.

Using $\alpha = 0.1$ and $b_0 = 5.09 \text{ \AA}$, the value obtained for $\sigma = 5.1 \text{ erg/cm}^2$. Substituting this value of σ in equation (8), one obtains $\sigma_e = 151 \text{ erg/cm}^2$. The value of σ_e found from thickness data is 153 erg/cm^2 . The values of σ_e obtained by both methods are in good agreement.

The work, q , required to form a chain fold is given by:

$$q = 2A_0\sigma_e \quad (10)$$

where $A_0 = a_0b_0$, the cross-sectional area of chain.

Substituting the value of $\sigma_e = 151 \text{ erg/cm}^2$ and $A_0 = 30.54 \times 10^{-16} \text{ cm}^2$ in equation (10), one obtains $q = 13.27 \text{ kcal/mol}$ of folds.

Much of the work of folding may be attributed to the fact that certain segments in the fold will be in elevated intramolecular rotational energy states. Thus the work of chain folding is a measure of the 'stiffness' of polymer chain. For the polymer of ordinary stiffness, a value of q between 1 and 10 kcal/mol of folds, is to be anticipated. The value of q for PAN, is more than 10 kcal/mol of fold. It suggests that PAN consists of stiff chains. This is also supported by other evidence.

The value of σ_e and q of various polymers are given for comparison in Table 1; σ_e and q obtained from present investigation are considerably higher than those for many organic polymers. However, in the case of selenium³⁵ a very high value of q equal to 49.4 kcal/mol of folds was observed. Recently from thickness data,

Table 1 Summary of surface energy value for PAN and various other polymers

Polymer	$\sigma\sigma_e$ (from G) (erg ² /cm ⁴)	σ_e (erg/cm ²)	q (kcal/ mol of folds)	σ (erg/cm ²)	
				from $\sigma\sigma_e$	from Thomas- Staveley relation
Polyethylene ¹⁸	540	57	3.0	11.2	10
Polyoxy- methylene ³⁷	267	8.2	1.5		7.3
Polychlorotri- fluoroethylene ¹⁸	168	40.3	4.2	4.25	5.0
Polystyrene ³⁷	356	43.7	4.9		8.2
Polystyrene ²⁹	96	13.3	2.8		7.2
Polyisoprene ³⁷	122	11.8	1.2		10.3
Polypropylene ³⁷	1590	124	9.7		12.8
Selenium ²⁰	3180	337	19.2	9.5	13.8
PAN (present study)	669	151	13.2	4.4	5.1

Crystal²⁰ found that $q = 19.2$ kcal/mol of folds of selenium. Still this value is sufficiently higher than that for many organic polymers studied. The higher value of q for these polymers suggests that they consist of quite stiff chains.

Krigbaum and Tokita³³ have measured ΔH_u and ΔS of melting of PAN by using the Flory diluent method and found $T_m^0 = 317^\circ\text{C}$, $\Delta H = 1.25$ kcal/mol and $\Delta S_u = 2.1$ e.u. Both heat and entropy of fusion are low and this value of ΔH_u is close to that observed for poly(vinyl tetrafluoroacetate) and very much lower than that observed for polyethylene. These data also suggest that PAN consists of stiff chains with weak interchain forces.

Another measure of chain stiffness is obtained from the measurements of unperturbed chain dimension or Porodo-Kratky persistence length. Krigbaum³⁶ has estimated these values for a number of polymers including PAN which also suggests that PAN chains are relatively stiff compared to those of many other organic polymers. This is considered to be a consequence of the highly polar nature of the neighbouring CN groups along the chain.

The value of σ_e obtained from melting point and step height measurements¹⁰ is 45 erg/cm² while that determined by kinetic study comes out to be 151 erg/cm². Thus there is a large difference between the two values of σ_e . Even large differences of about 305 erg/cm² was observed²⁰ between the values of σ_e of selenium obtained by these methods. It seems that this unexpected large variation may lie in the inherent nature of the methods employed.

ACKNOWLEDGEMENT

One of us (R. M. G.) is grateful to UGC for providing a fellowship.

REFERENCES

- Holland, V. F. and Lindenmeyer, P. H. *J. Polym. Sci.* 1962, **57**, 589
- Blundell, D. J. and Keller, A. *J. Polym. Sci. (B)* 1968, **6**, 433
- Johnsen, U. and Lehman, J. *Kolloid-Z. Z. Polym.* 1969, **230**, 317
- Nardini, M. J. and Price, F. P. *J. Phys. Chem. Solids* 1967, **28**, 395
- Klement, J. J. and Geil, P. H. *J. Polym. Sci. (A-2)* 1968, **6**, 1381
- Patel, G. N. and Patel, R. D. *J. Polym. Sci. (A-2)* 1970, **8**, 47
- Gohil, R. M., Patel, K. C. and Patel, R. D. *Angew. Makromol. Chem.* 1972, **25**, 83
- Patel, G. N. *PhD Thesis* Sardar Patel University (1970)
- Mino, G. and Kaizerman, S. *J. Polym. Sci.* 1958, **31**, 242
- Chiang, R., Rodes, J. H. and Holland, V. F. *J. Polym. Sci. (A)* 1965, **3**, 479
- Keller, A. *Phil. Mag.* 1957, **2**, 1171
- Fischer, E. W. *Z. Naturforsch.* 1969, **14a**, 584
- Peterlin, A. and Fischer, E. W. *Z. Phys.* 1960, **159**, 272
- Peterlin, A., Fischer, E. W. and Reinhold, C. *J. Chem. Phys.* 1962, **37**, 1403
- Peterlin, A. and Reinhold, C. *J. Polym. Sci. (A)* 1965, **3**, 2801
- Price, F. P. *J. Polym. Sci.* 1960, **42**, 49; *J. Chem. Phys.* 1961, **35**, 1884
- Lauritzen, J. I. and Hoffman, J. D. *J. Res. Nat. Bur. Stand.* 1960, **64A**, 73
- Hoffman, J. D. *SPE Trans.* 1964, **4**, 315
- Frank, F. C. and Tosi, M. *Proc. R. Soc. (A)* 1961, **263**, 323
- Crystal, R. G. *J. Polym. Sci. (A-2)* 1970, **8**, 1755
- Hoffman, J. D. and Weeks, J. J. *J. Chem. Phys.* 1962, **37**, 1723
- Gornic, F. and Hoffman, J. D. *Ind. Eng. Chem.* 1966, **58**, 41
- Magill, J. H. *J. Appl. Phys.* 1964, **35**, 3249
- Magill, J. H. *Polymer* 1965, **6**, 367
- Williams, M. L., Landel, R. F. and Ferry, J. D. *J. Am. Chem. Soc.* 1955, **77**, 3701
- Cooper, M. and Manley, R. St. J. *J. Polym. Sci. (B)* 1973, **11**, 363
- Magill, J. H. *Polymer* 1962, **3**, 655
- Wood, L. A. and Bekkedahl, N. *J. Appl. Phys.* 1946, **171**, 362
- Boon, J., Challa, G. and Van Kreveton, D. W. *J. Polym. Sci. (A-2)* 1968, **6**, 1791
- Hay, J. N. *J. Polym. Sci. (A)* 1965, **3**, 433
- Price, F. P. *J. Phys. Chem.* 1960, **64**, 169
- Falkai, B. V. and Rellensmann, W. *Makromol. Chem.* 1964, **75**, 112
- Krigbaum, W. R. and Tokita, N. *J. Polym. Sci.* 1960, **43**, 467
- Thomas, D. G. and Staveley, L. A. K. *J. Chem. Soc.* 1952, p 4569
- Brewer, L. in 'Electron Structure and Alloy Chemistry of Transition Elements', (Ed. P. A. Beck), Interscience, New York, 1963, p 222
- Krigbaum, W. R. *J. Polym. Sci.* 1958, **28**, 213
- Blais, J. J. B. P. and Manley, R. St. J. *J. Macromol. Sci. (B)* 1967, **1**, 525

Effect of chemical structure on crystallization rates and melting of polymers: 2. Aliphatic polyesters

Marianne Gilbert* and F. J. Hybart†

Department of Chemistry, The University of Aston in Birmingham, Birmingham B4 7ET, UK
(Received 12 December 1973; revised 28 January 1974)

Crystallization rates have been measured by thermal analysis for two aliphatic polyesters. The value of the method for such measurements is assessed. Some observations are made on the melting behaviour and crystallization mechanisms of these polymers. X-ray measurements have been used to obtain the chain repeat distances. Glass transition temperatures have been measured for a series of linear polyesters, and the effect of changes of chemical structure on temperature transitions and crystallization is discussed in detail for the series.

INTRODUCTION

The work previously reported¹ has been extended to include crystallization rate measurements for two aliphatic polyesters, to study the effect of increasing chain flexibility. The polyesters chosen were poly(tetramethylene adipate) and poly(hexamethylene adipate), since the repeat distances of these were reasonably similar to those of the corresponding polyterephthalates already studied. Glass transition temperatures have also been measured for the series of seven linear polyesters, and results obtained for the series are discussed further.

EXPERIMENTAL

Materials

The aliphatic polyesters (Table 1) were prepared by heating dimethyl adipate with the appropriate glycol (using a molar ratio of 1:1.1) and 0.1% of butyl titanate catalyst for 2 h at 150–180°C under nitrogen. During this stage methanol was evolved. The pressure was slowly reduced to 0.2 mmHg (1 mmHg = 133.322 N/m²), while the temperature was increased as shown. The reaction was completed by heating for at least 4 h at

the higher temperature. The polyesters formed were precipitated from chloroform solution by adding methanol. Some of the lower molecular weight material was removed from the sample since it remained in solution. Number-average molecular weights of the precipitated polymers were measured in chloroform at 25°C using a Mechrolab Model 502 high speed osmometer².

Thermal analysis

Crystallization rates for both polymers were measured (Table 2) using a Du Pont thermal analyser fitted with a d.s.c. cell, as described previously¹. Samples were melted for 20 min at temperatures 25°C above their melting temperatures prior to crystallization.

Melting thermograms were also obtained for rapidly crystallized and slowly crystallized samples of each polymer, using a heating rate of 5°C/min. Heats of fusion were calculated from each trace.

Glass transition temperatures were measured (at the Institute of Polymer Technology, Loughborough University of Technology) for the complete series of seven polyesters using a Du Pont thermal analyser fitted with a thermomechanical analyser (t.m.a.) attachment. A chip of each polymer was melted, then the molten polymer was pressed into a small disc (~6 mm diam. × 0.5 mm thick), which was quenched in liquid nitrogen. The prepared disc was transferred to the t.m.a. apparatus previously cooled to below -120°C with liquid

* Present address: Institute of Polymer Technology, Loughborough University of Technology, Loughborough, Leics LE11 3TU, UK.

† Present address: Glamorgan Polytechnic, Llantwit Road, Treforest, Pontypridd, Glamorganshire CF37 1DL, UK.

Table 1 Preparation of the polyesters

Polymer	Repeat unit	Notation	\bar{M}_n	Polymerization temperature (°C)	
				Stage 1	Stage 2
Poly(tetramethylene adipate)	-O(CH ₂) ₄ OOC(CH ₂) ₄ CO-	46	14 700	150	250
Poly(hexamethylene adipate)	-O(CH ₂) ₆ OOC(CH ₂) ₄ CO-	66	16 500	170	220

nitrogen. The sample probe was loaded with a weight of 10 g and the t.m.a. trace from -120°C recorded, using a heating rate of $5^{\circ}\text{C}/\text{min}$. The temperature at which the probe first started to penetrate into the polymer was taken to be the glass transition temperature, T_g . The melting and quenching treatment was used to reduce crystallinity in the polymers to the lowest possible level.

Dilatometry

In order to compare crystallization rates obtained by differential thermal analysis (d.t.a.) and dilatometry for a polymer with highly temperature dependent crystallization rates, the latter method, described previously^{1,3}, was also used to measure crystallization rates for a low molecular weight sample of poly(hexamethylene adipate) ($\bar{M}_n = 5000$).

X-ray measurements

X-ray powder photographs were taken of the precipitated polymers, and drawn samples were prepared so that fibre diagrams could also be obtained.

Microscopy

A hot stage microscope fitted with crossed polaroids was used to measure the melting temperatures of slowly crystallized samples of each polyester, which were heated at $0.5^{\circ}\text{C}/\text{min}$. Spherulite growth rates were measured for the poly(tetramethylene adipate). It was necessary to increase the pre-melting temperature to 95°C to reduce the nucleation density sufficiently for such measurements to be made. For poly(hexamethylene adipate) the nucleation density was too high even if severe melting conditions were used.

RESULTS

Crystallization rates

Crystallization half-times obtained by the thermal analysis method for the two polyesters are listed in Table 2. As in ref 1, a computer program was used to calculate the Avrami integer n , from the Avrami equation expressed as follows:

$$n = t \frac{dA_t}{dt} \left/ \left[(A_{\infty} - A_t) \log_e \left(\frac{A_{\infty}}{A_{\infty} - A_t} \right) \right] \right.$$

where A_t and A_{∞} are the areas under the exothermic crystallization peak at time t , and at the end of crystallization respectively.

The program also assessed whether n was constant within the limits of ± 0.2 for the major part of the crystallization. For poly(tetramethylene adipate) a value of 3 was obtained when the values calculated at each temperature were averaged. This value was used to calculate the crystallization rate constant K from the equation:

$$K = \log_e 2 (t_{1/2})^{-n}$$

where $t_{1/2}$ is the crystallization half-time. For poly(hexamethylene adipate) constant values of n were not obtained. Conventional Avrami plots showed a change in slope, representing a lower value of n during the later part of the crystallization (Figure 1). Since n varied K was not calculated in this case.

Table 2 Crystallization data for aliphatic polyesters obtained by d.t.a.

Polymer	Crystallization temperature ($^{\circ}\text{C}$)	Crystallization half-time (sec)	n	K (sec^{-n})	G ($\mu\text{m}/\text{sec}$)
46	41.8	448	3.0	7.71×10^{-9}	—
	43.3	954		7.98×10^{-10}	—
	44.5	1614		1.65×10^{-10}	—
	44.6	1470		2.18×10^{-10}	—
	45.5	2196		6.54×10^{-11}	—
	46.8	3312		1.91×10^{-11}	0.0167
	47.2	—		—	0.0133
	47.7	4734		6.53×10^{-12}	—
	48.2	—		—	0.0103
	48.7	—		—	0.0085
	49.7	—		—	0.0050
66	49.9	384	n variable	—	—
	50.7	708		—	—
	51.5	1854		—	—
	51.8	3036		—	—
	52.3	4092		—	—
	53.0	8820		—	—

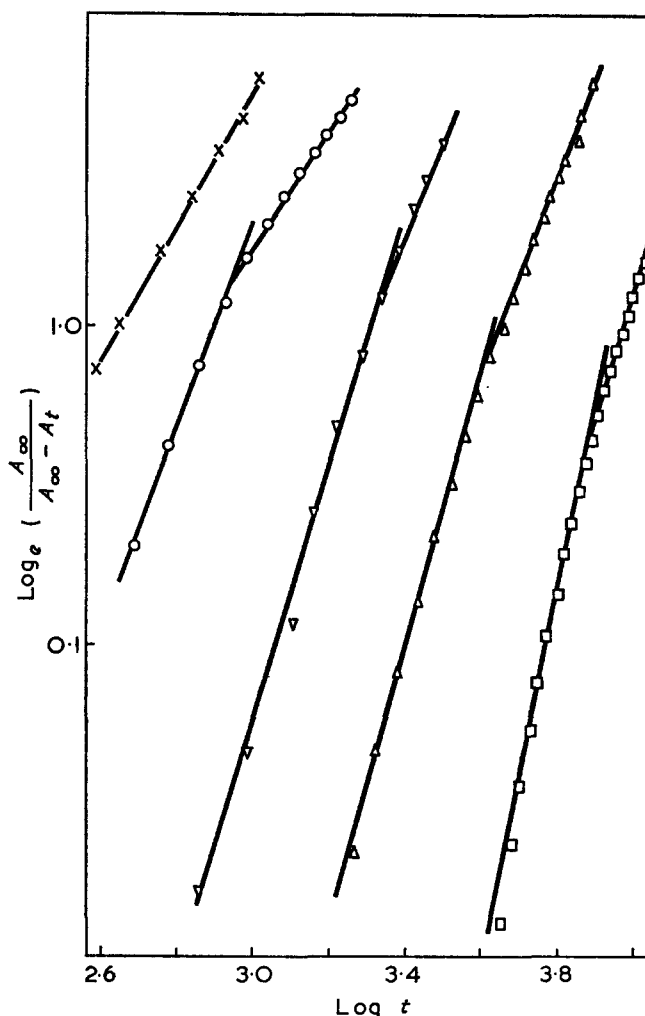


Figure 1 Avrami plots for poly(hexamethylene adipate). \times , 49.9°C ; \circ , 50.7°C ; ∇ , 51.5°C ; Δ , 52.3°C ; \square , 53.9°C

Crystallization half-times for the two aliphatic polyesters are plotted against ΔT , the extent of supercooling, in Figure 2. ($\Delta T = T_m - T$, where T_m is the melting temperature shown in Table 4 and T is the crystallization

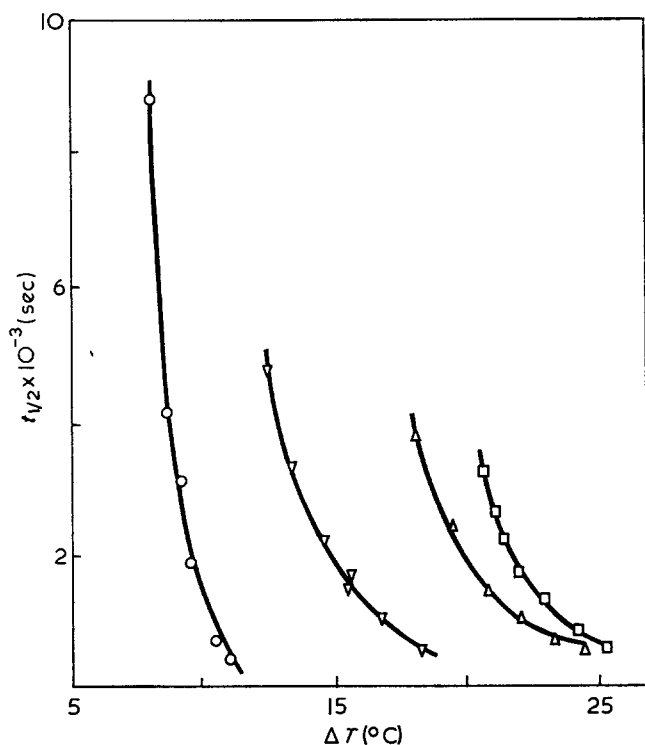


Figure 2 Crystallization half-times for polyesters. \circ , 66; ∇ , 46; \triangle , 6T; \square , 4T

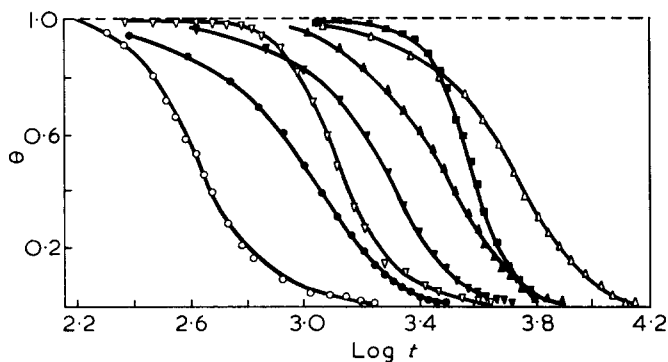


Figure 3 Crystallization isotherms for poly(hexamethylene adipate) by d.t.a. and dilatometry. D.t.a.: \bullet , 50.0°C; ∇ , 50.7°C; \blacktriangle , 51.2°C; \blacksquare , 51.5°C. Dilatometry: \circ , 50.0°C; ∇ , 51.0°C; \triangle , 52.0°C

Table 3 Heats of fusion of aliphatic polyesters

Poly- ester	Slowly crystallized samples ^a			Rapidly crystallized samples ^b	
	ΔH (J/g)	D.t.a. peak temperature (°C)	Crystallization temperature (°C)	ΔH (J/g)	D.t.a. peak temperatures (°C)
46	50.5	62	51	51.0	54, 58
66	63.5	62	53	60.2	62

^a Before fusion samples were crystallized for 16h at temperatures shown

^b These samples were crystallized rapidly during natural cooling in the d.s.c. cell

temperature.) For purposes of comparison, crystallization half-times for poly(tetramethylene terephthalate) and poly(hexamethylene terephthalate), obtained previously¹, are included.

Spherulite growth rates, G for the 46 polyester are also listed in Table 2.

Crystallization isotherms obtained by the d.t.a. method and dilatometry for the low molecular weight sample of poly(hexamethylene adipate) are shown in Figure 3. θ , the fraction of amorphous material is plotted against $\log t$.

Heats of fusion

Heats of fusion for the two aliphatic polyesters are listed in Table 3. These results showed that the different sample treatments did not significantly change the degree of crystallinity of the polymers as measured by this method. However, the additional peak observed in the thermogram [Figure 4(B)] of the more rapidly crystallized sample of poly(tetramethylene adipate) suggests that its crystalline nature is not identical to that of the more slowly crystallized material [Figure 4(E)].

Further experiments using the 46 polyester showed that the melting trace obtained depended on temperature and time of crystallization. If the sample was quenched in ice water a broad endotherm with a peak at 59°C was obtained [Figure 4(A)]. When the polyester was allowed to crystallize more slowly two peaks were observed below 59°C [Figure 4(B)–(D)]. As the crystal-

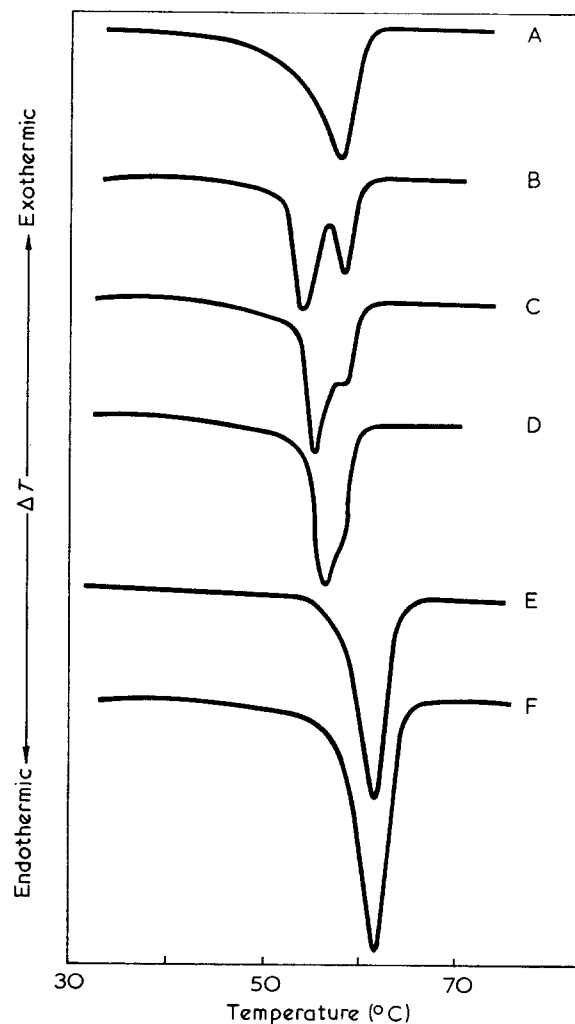


Figure 4 Melting traces for polyesters. A, 46, quenched in ice-water; B, 46, crystallized by cooling in d.s.c. cell; C, as B but held at room temp. 24 h before reheating; D, as B but held at room temp. 65 h before reheating; E, 46, crystallized at 51°C for 16 h; F, 66, crystallized by cooling in d.s.c. cell

Table 4 Transitions and crystallization data of linear polyesters

Polyester	Notation	Glass transition temperature (°C)	Melting temperature (°C)	ΔT_{40} (°C)
Poly(tetramethylene adipate)	46	-59	60	14
Poly(hexamethylene adipate)	66	-73	61	9
Poly(ethylene terephthalate)	2T	+72	276	38
Poly(tetramethylene terephthalate)	4T	+23	234	21
Poly(pentamethylene terephthalate)	5T	+8	142	49
Poly(hexamethylene terephthalate)	6T	-8	156	19
Poly(tetramethylene isophthalate)	4I	+24	150	—

lization time was increased the lower temperature peak increased in size and shifted to a higher temperature suggesting an increase in crystallite perfection or size. Similar observations were made using a hot stage microscope.

For poly(hexamethylene adipate), only one melting peak was obtained whatever crystallization conditions were used [Figure 4(F)], although the peak temperature increased when crystallization was slow.

Transition temperatures and crystallizability of polyesters

Glass transition temperatures for all seven polyesters studied are listed in Table 4 together with the melting temperatures.

To compare the crystallization behaviour of the polyesters, the degree of supercooling, ΔT_{40} corresponding to a crystallization half-time of 40 min is listed for each polymer. [For poly(tetramethylene isophthalate) the minimum value of $t_{1/2}$ obtained was about 210 min.]

X-ray diffraction results

Line positions and relative intensities on the X-ray powder type photographs were similar to one another, and also to those reported for poly(ethylene adipate)⁴. Identity periods obtained from fibre diagrams in the orientation direction of the polymer were 1.37 nm and 1.62 nm for the 46 and 66 polyesters respectively, compared to the repeat distances calculated for planar zig-zag chains of 1.482 nm and 1.734 nm.

DISCUSSION

Methods of crystallization rate measurement

The apparently different crystallization behaviour observed by dilatometry and d.t.a. for poly(hexamethylene adipate) was attributed to its very high temperature dependence of crystallization. It was considered that the larger sample (100–200 mg) used for dilatometry was not at a uniform temperature throughout, so that different parts of the sample were crystallizing at different rates at a given time. This effect would be reduced considerably with the 10–20 mg sample used for the d.t.a. method. While the crystallization isotherms obtained at different temperatures by d.t.a. were superimposable on one another, as is normally observed, those obtained by dilatometry varied in shape. Thus

the d.t.a. method was considered more suitable for measuring fairly rapid crystallization rates of polymers having a high temperature coefficient of crystallization. For poly(tetramethylene terephthalate), which has less temperature dependent crystallization behaviour, the two methods of measurement gave similar results¹.

Crystallization behaviour of poly(tetramethylene adipate) and poly(hexamethylene adipate)

In Figure 2 the crystallization rates of these two aliphatic polyesters are compared with the corresponding terephthalates studied previously¹. The aliphatic polyesters crystallize much more readily. Evidence suggests that this effect, previously observed when rates for the two terephthalates shown were compared, is due to increased chain flexibility. Even small changes in flexibility appear significant; poly(hexamethylene adipate) crystallizes more rapidly than poly(tetramethylene adipate), probably owing to the lower concentration of O—C(=O)— groups in the former polymer. These groups have been shown to be 'stiffer', i.e. to require more energy for rotation than —CH₂—CH₂— bonds⁵. Spherulite growth rates were also measurable for poly(tetramethylene adipate) at a lower degree of supercooling than for poly(tetramethylene terephthalate).

Although the Avrami treatment of polymer crystallization cannot usually determine the crystallization mechanism unequivocally, it may be used to detect differences in behaviour. Such differences were observed for the two aliphatic polyesters. For poly(tetramethylene adipate), an Avrami value of 3 coupled with heterogeneous nucleation (indicated by spherulite growth experiments, as all spherulites in the field of view were of the same size), suggested an unrestricted three dimensional growth of spherulites. For poly(hexamethylene adipate), n was variable, and approached 2 during the latter stages of crystallization. This observation could be related to very high nucleation density for this polymer, which made spherulite growth measurements impossible and seems likely to restrict three dimensional growth. The change of slope of the Avrami plots was observed after about 80% of the crystallization had occurred, and did not appear to be temperature dependent. It is suggested that spherulite growth became severely restricted at this stage.

Double melting endotherms

The different melting behaviour observed by d.t.a. for the two aliphatic polyesters also suggested different crystallization behaviour. The formation of lower melting species by a slower crystallization, as observed for poly(tetramethylene adipate) (comparing Figure 4(A) with Figure 4(B)–(D)], has been reported for many polymers, including poly(ethylene terephthalate)^{6–8}.

In this work, additional observations were made by hot stage microscopy. A thin film of poly(tetramethylene adipate) was crystallized slowly at 48°C for a period of 16 h. Large irregular spherulites were produced in an amorphous matrix. On removing the film from the hot plate, the amorphous material also crystallized as a highly birefringent mass, in which no distinct spherulites were detectable. On reheating the film, it was found that the large spherulites melted 1–2°C below the quenched material, which melted at 61°C. This result is analogous to that obtained by d.t.a. On subsequent

cooling the material which had been quenched crystallized first, probably owing to a large number of residual nuclei in this region. As cooling continued small spherulites developed within the outline of the original large ones.

These results suggest that the double peaks obtained by d.t.a. reflect morphology differences in the sample in this case, rather than changes which occur during heating in the cell, as suggested for poly(ethylene terephthalate)⁷. The microscope observations show that different melting temperatures can be correlated with different types of spherulitic material. However, it would be expected that larger spherulites obtained by slow crystallization would melt at a higher temperature. Furthermore, the material initially excluded from spherulites would be expected to be more irregular and contain more impurities so would not intuitively be expected to have a higher melting temperature. Thus it appears that an explanation must consider differences in the nature of the crystallites themselves. Explanations of this type have previously been proposed by Bell and Dumbleton⁸ and Roberts⁶ although their conclusions differ considerably. Further investigations are necessary to draw more detailed conclusions from the present work; it appears that hot-stage microscopy is a useful approach.

The lack of similar behaviour for poly(hexamethylene adipate) is probably due to the larger number of nuclei present in this sample.

Crystallinity and crystal structures

By measuring areas of melting endotherms, some estimation of the degree of crystallinity of the polyesters could be made from the heats of fusion. The similar amount of crystallinity achieved by different crystallization conditions was not observed for the analogous polyterephthalates. For the aromatic polyesters a higher degree of crystallinity was achieved for the more slowly crystallized samples¹. The difference between the two systems will be due to the greater ability of the aliphatic polyesters to crystallize, such that the maximum attainable degree of crystallinity is achieved even after relatively rapid cooling. Heats of fusion, ΔH^* , for 100% crystalline poly(decamethylene adipate) and poly(decamethylene terephthalate) have been reported⁹, and have very similar values. Assuming similar ΔH^* values for 66 and 6T, and 46 and 4T polyesters (ΔH^* values for the terephthalates are listed in ref 1), the degree of crystallinity attainable in the aliphatic polyesters is between 30 and 40%. The crystal structures of the poly(tetramethylene adipate) and poly(hexamethylene adipate) were shown by wide angle X-ray diffraction experiments to be similar to one another, and to other aliphatic polyesters having an even number of carbon atoms in both the acid and glycol units. In each case the measured repeat distance was 0.11 nm less than that calculated for a planar zig-zag chain containing one glycol and one acid unit. Similar results obtained for other aliphatic polyesters⁴ have been attributed to a slight distortion of the ester group from the planar zig-zag structure.

EFFECT OF CHEMICAL STRUCTURE ON CRYSTALLINITY AND TRANSITION TEMPERATURES

Melting temperatures

The effect of polymer structure on melting temperature has been frequently discussed. However, some

of the detailed measurements made in this work justify further comment.

Lowered melting points for polyesters containing an odd number of carbon atoms in either the glycol or acid unit of the chain have been frequently observed. The effect is demonstrated by the melting point of 142°C for poly(pentamethylene terephthalate). It is suggested that this lowering is due to distortion of the chain from a planar zig-zag form in the crystalline state. This distortion would be expected to make chain packing more difficult, hence reduce cohesion between chains, ΔH^* and therefore T_m .

Conix and Van Kerpel¹⁰ attributed the higher entropy of fusion observed for polyisophthalates than for the corresponding polyterephthalates to a greater degree of configurational freedom achieved on melting. In the case of the 4I polyester this may now be explained by the greater volume change observed on melting, compared with the 4T polyester. Kirshenbaum⁹ discusses the calculation of the entropy of fusion, which is made up of ΔS_{exp} representing the change of entropy associated with an increase in volume, and $(\Delta S_c)_v$ the change in entropy due to the increase in the number of conformations a macromolecule can assume on passing from the solid to the liquid state. From the method given by Kirshenbaum $(\Delta S_c)_v$ for 4T would be expected to be equal to, or greater than, that for 4I. Thus the larger entropy of fusion for 4I must be due to a larger volume change on melting. The volume contraction on crystallizing this polymer was actually found by dilatometry to be less (0.03–0.04 cm³/g) than that for the 4T polyester (0.05 cm³/g). However, while the crystallinity of the 4T polyester was about 40%, measurement of heats of fusion suggested that the crystallinity of 4I was 15% or less¹. Thus estimation of volume contractions on crystallizing (equivalent to volume change on melting) for a 100% crystalline polymer in each case shows this volume change to be almost twice as large for the 4I polyester. It can be visualized that the more bulky chain occupies more space than that of the 4T polyester, when not packed in a regular structure.

Glass transition temperatures

In the series of polymers considered chain flexibility was the main factor determining T_g values. Owing to its lower concentration of stiffer ester groups poly(hexamethylene adipate) has a lower T_g than poly(tetramethylene adipate) (Table 4).

For the aromatic polyesters T_g decreased steadily as the number of CH₂ groups in the glycol increased (Figure 5). The 5T polymer did not show anomalous behaviour in this case, confirming that its low melting temperature was due to crystal structure and chain irregularity. Chain regularity does not itself affect T_g . It is interesting to note that 4T and 4I polyesters have very similar glass transition temperatures. Again flexibility of chain constituents appears to be the predominant factor; their arrangement seems less important.

It is often considered that T_m and T_g are changed in the same way by any structural modification, and can only be modified separately by copolymerization. These results show that by the introduction of structural irregularities, it is possible to reduce T_m considerably, while reducing T_g by only a small amount.

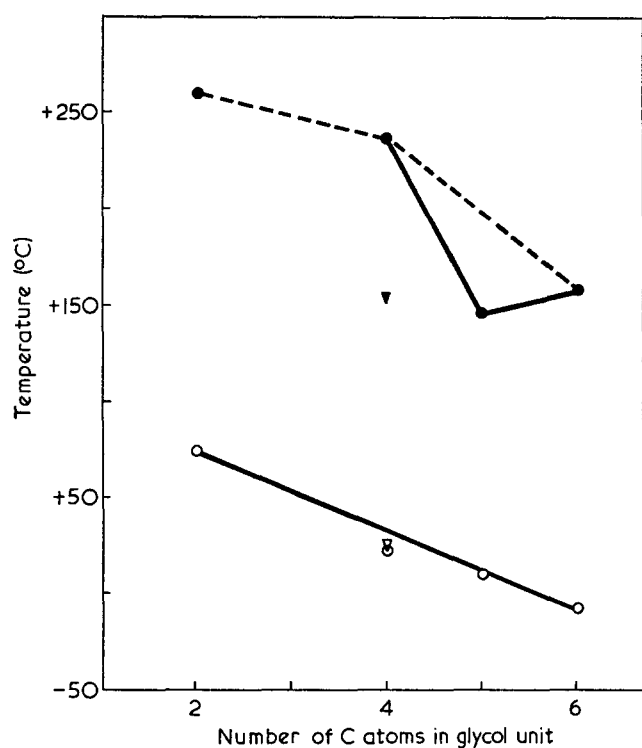


Figure 5 Transition temperatures for aromatic polyesters. ●, T_m for terephthalate esters; ▼, T_m for isophthalate ester; ○, T_g for terephthalate esters; ▽, T_g for isophthalate ester

Crystallization of polyesters

Crystallization rates may be compared by using values for ΔT_{40} (Table 4), a low value of this parameter corresponding to a readily crystallizing polymer. Where spherulite growth rates were measurable, they were found to be in the same order, i.e. $46 > 4T > 5T > 4I$. A comparison of results shows that, as expected, chain flexibility facilitates crystallization. All results, except for those obtained for poly(pentamethylene terephthalate) [and poly(tetramethylene isophthalate)] may be explained on this basis. If, however, flexibility were the only factor 5T would be expected to have behaviour intermediate between 4T and 6T polyesters. All other polyesters in the series were shown to have a slightly distorted planar zig-zag structure; the repeat distance of 1.22 nm observed for poly(pentamethylene terephthalate) suggested severe distortion of such a structure; the observed repeat distance could occur if the glycol chain twisted through 180° , but further work would be required to support this suggestion. However, deviations from a planar zig-zag structure have already been reported for aliphatic polyesters containing an odd number methylene units in the glycol¹¹. Meares¹² has suggested that the observed repeat distance, shorter than the extended planar zig-zag configuration for the polyesters could be explained by assuming two *gauche* linkages in each glycol residue, probably in alternate bonds. For a pentamethylene glycol unit three *gauche* linkages could occur in the same way. This would allow the glycol chain to twist through 180° , and a repeat distance similar to that observed could be obtained.

Thus it appears that crystal structure is another factor affecting crystallization rates. It is reasonable

that crystallization will be slower if chain twisting occurs.

4T and 6T polyesters crystallize much more readily than 2T. In view of the importance of chain flexibility, this may be because the flexible unit is longer than the rigid unit in the former polymers. In poly(ethylene terephthalate), the rigid benzene ring unit is longer than that of the flexible glycol.

The very slow crystallization of the 4I polymer is attributed to the difficulty in packing the bulky isophthalic acid group. It can be concluded that for the polymers studied: (a) chain flexibility increases crystallization rates; (b) an irregularly shaped chain crystallizes slowly; (c) crystallization rates depend to a lesser extent on crystal structure.

No obvious relationships were obtained between crystallization mechanism (for example, the Avrami number n , which depends on the type of nucleation and growth), and chemical structure. Any differences in nucleation appeared to be due to sample preparation and thermal history rather than structure.

A final comment concerns the observed degrees of crystallinity obtained from heat of fusion measurements. For carefully annealed samples, values of 62%, 39%, 38% and 13% were obtained for 2T, 4T, 6T and 4I polyesters respectively. A possible explanation for the higher crystallinity of 2T could be its shorter repeat unit. It is likely that greater difficulty is experienced in aligning longer repeat units as crystallization proceeds due to chain entanglement. This is supported by the values of 30–40% estimated for the 46 and 66 polyesters, which also have longer repeat distances. These results suggest that the maximum crystallization rate of a polymer, and the maximum degree of crystallinity available are not necessarily related, and may be modified independently. The low levels of crystallinity obtained for the less regular poly(tetramethylene isophthalate), and estimated for poly(pentamethylene terephthalate) (20%) may be expected. In addition the observed repeat distance (2.60 nm) for the 4I polyester is particularly long.

ACKNOWLEDGEMENT

We are grateful to the Science Research Council for the award of a Research Studentship to M. G.

REFERENCES

- Gilbert, M. and Hybart, F. J. *Polymer* 1972, **13**, 327
- Gilbert, M. and Hybart, F. J. *J. Polym. Sci. (A-1)* 1971, **9**, 227
- Hybart, F. J. and Pepper, B. J. *Appl. Polym. Sci.* 1967, **13**, 2643
- Fuller, C. S. and Frosch, J. J. *Phys. Chem.* 1939, **43**, 323
- Zavaglia, E. A. and Billmeyer, Jr, F. W. *J. Paint Technol. Eng. Offic. Dig.* 1964, **36**, 221
- Roberts, R. C. *Polymer* 1969, **10**, 117
- Holdsworth, P. J. and Turner Jones, A. *Polymer* 1971, **12**, 195
- Bell, J. P. and Dumbleton, J. H. *J. Polym. Sci. (A-2)* 1969, **7**, 1033
- Kirshenbaum, I. *J. Polym. Sci. (A)* 1965, **3**, 1869
- Conix, A. and Van Kerpel, R. *J. Polym. Sci.* 1959, **40**, 521
- Fuller, C. S., Frosch, C. J. and Paper, N. R. *J. Am. Chem. Soc.* 1942, **64**, 154
- Meares, P. 'Polymers: structure and bulk properties', Van Nostrand, New York, 1965

Eutectic crystallization of pseudo binary systems of polyethylene and high melting diluents

P. Smith and A. J. Pennings

Laboratory of Polymer Chemistry, State University of Groningen, Groningen, The Netherlands
(Received 16 October 1973)

The crystallization and melting behaviour of the pseudo binary systems of heterodisperse polyethylene and the high melting diluents 1,2,4,5-tetrachlorobenzene and hexamethylbenzene have been studied by differential scanning calorimetry and microscopy. Using the Flory-Huggins theory the equilibrium phase diagram of polyethylene/1,2,4,5-tetrachlorobenzene was calculated for $\chi=0.37$, which gave a eutectic temperature of 135°C for a polyethylene volume fraction of 0.51. The experimentally determined eutectic points were found to depend strongly on the crystallization circumstances; the lowest value for the eutectic temperature for the system polyethylene/1,2,4,5-tetrachlorobenzene was 106°C. A large degree of supercooling was required for the eutectic crystallization, indicating that the nucleation of the low molecular components is markedly hampered by the polymer molecules. If only crystals of the diluent are formed the morphology is needle-like. A spherulitic texture develops under eutectic conditions. By sublimation of the solid diluent from the pseudo binary mixtures a cellular polymeric material of a unique texture and morphology is produced.

INTRODUCTION

Eutectic crystallization from molten binary mixtures of low molecular weight organic and inorganic compounds has been the subject of many investigations. In inorganic chemistry it is a well known method for growing composites *in situ*^{1,2}, which have unique physical and mechanical properties. Eutectic crystallization of organic compounds for instance has been examined to obtain information about the mechanism of this kind of solidification³.

So far little attention has been paid to the occurrence of eutectics in polymeric systems. A eutectic-type minimum in the melting temperature-composition diagrams for copolyesters and copolyamides has been reported⁴⁻⁷ and crystalline copolymers in general have been regarded as pseudo eutectic systems⁸. Although the melting point depression of organic solvents due to a crystallizable polymeric solute has been described⁹ and the melting point depression of polyethylene by the solid diluent phenanthrene has been measured by means of differential thermal analysis (d.t.a.)¹⁰, the eutectic crystallization of such systems has not been dealt with.

The present paper reports a study of this subject which was undertaken to gain some understanding of growing composites *in situ* in polymeric systems and of the interaction between polymer molecules and crystallizable additives. The phase diagrams of two pseudo binary systems of unfractionated linear polyethylene and the diluents 1,2,4,5-tetrachlorobenzene and hexamethylbenzene were examined by means of differential scanning calorimetry (d.s.c.) in order to establish the eutectic temperature and composition.

Microscopic observations have been made of the simultaneous crystallization of the components and of the structure formation of the growing composites at polymer concentrations different from the eutectic one. Scanning electron micrographs display the structure of the cellular polymeric material that remains after removal of the solid diluent from the binary mixture.

THEORY

The eutectic temperature and composition of a binary system consisting of a polymer and a low molecular weight component can be assessed by determining the intersection of the two curves describing the melting temperature-composition relation. Clearly, the calculation of the eutectic condition applies only to the state of equilibrium between the polymer solution and the two pure solid phases. Particularly in the case of a polymeric system this state of stable equilibrium may not be attained. Nevertheless a eutectic point defined as the temperature and composition at which the components crystallize simultaneously may be observed experimentally and a comparison with the theoretical conditions provides information about the kinetics involved in this mode of solidification.

The melting temperature-composition relations for both components can be derived from the thermodynamic equation:

$$R \ln a = \Delta H \left[\frac{1}{T_m^0} - \frac{1}{T_m} \right] - \Delta c_p \ln \frac{T_m}{T_m^0} - \Delta c_p T_m^0 \left[\frac{1}{T_m^0} - \frac{1}{T_m} \right] \quad (1)$$

expressing the activity, a , of either of the components in the mixture as a function of temperature T_m at which the corresponding solid phase is in equilibrium with

the solution. Δc_p is the difference between the molar heat capacity of the solid and the partial molar heat capacity of the same component in solution. ΔH is the molar heat of fusion at the thermodynamic equilibrium melting temperature T_m^0 of the pure components, and R is the gas constant.

For the activity of the diluent, a_1 , the well known Flory-Huggins¹¹ equation may be employed:

$$R \ln a_1 = R [\ln(\phi_1) + (1 - 1/x)(1 - \phi_1) + \chi(1 - \phi_1)^2] \quad (2)$$

where ϕ_1 is the volume fraction of diluent, x the ratio of the molar volume of polymer and diluent, χ is the interaction parameter which may depend on concentration and temperature. This expression combined with equation (1) yields the melting point curve for the diluent.

The liquidus curve for the polymeric component is derived from equation (1) and the following relation in which the activity of the polymer is expressed per mole of structural units, a_u ,

$$R \ln a_u = R \left(\frac{V_u}{V_1} \right) \left[\ln(1 - \phi_1) \frac{1}{x} - (1 - 1/x)\phi_1 + \chi\phi_1^2 \right] \quad (3)$$

where V_u and V_1 are the molar volumes of the structural unit of the polymer and the solvent respectively. If the various thermodynamic quantities for the polymer-diluent system are known, the eutectic point may be found by a graphical solution of the pair of solubility equations. In general one may find that not all appropriate thermodynamic information is available and it might be desirable to dispose of a first approximation indicating the most pertinent requirements for the occurrence of a eutectic. If the eutectic temperature is not too far below the melting temperatures of the pure components, the temperature dependence of the heats of fusion may be neglected. This amounts to omitting the Δc_p terms. Further simplification is obtained by cancelling terms containing $1/x$ which is justified for very high molecular weight polymers. The liquidus curves for the two components are then given by:

$$\frac{1}{T_{m,1}} - \frac{1}{T_{m,1}^0} = -\frac{R}{\Delta H_1} [\ln \phi_1 - \phi_1 + 1 + \chi(1 - \phi_1)^2] \quad (4)$$

$$\frac{1}{T_{m,2}} - \frac{1}{T_{m,2}^0} = -\frac{R}{\Delta H_u} \frac{V_u}{V_1} [-\phi_1 + \chi\phi_1^2] \quad (5)$$

where the subscripts 1 and 2 refer to diluent and polymer species respectively and ΔH_u is the heat of fusion per mole of structural units of the polymer. A simple relationship for the eutectic composition, ϕ_1^e , is only found for a system that is characterized by $\chi=0$ and $(\Delta H_1 V_u)/(\Delta H_u V_1)=1$.

At the eutectic temperature T_m^e , which is then equal to $T_{m,2}$ and $T_{m,1}$, the latter can be eliminated from equations (4) and (5) resulting in:

$$\phi_1^e = \exp \left[\frac{\Delta H_1}{R} \left(\frac{1}{T_{m,1}^0} - \frac{1}{T_{m,2}^0} \right) - 1 \right] \quad (6)$$

This relation indicates that a eutectic point may be found experimentally if the melting temperature of the diluent does not differ substantially from that of the polymer. In the case where the melting point of the diluent is low compared to that of the polymer, the eutectic composition may be located close to the diluent

ordinate, as is observed for the system *p*-xylene/normal paraffin C₃₂ having an eutectic at 99.6% w/w of diluent¹². For polymers with a relatively low melting temperature the eutectic may occur according to equation (6) near the polymer ordinate of the phase diagram. For the present study low molecular weight compounds were selected, having melting temperatures close to that of linear polyethylene, so that the major thermodynamic requirement for observing the simultaneous crystallization of polymer and diluent is satisfied. It should be remarked that the above considerations only apply to a binary system, whereas the unfractionated polymer solvent system explored in this study actually consists of a large number of components.

However, it is to be expected that the effects arising from the multitude of polymer components such as fractionation¹² is by far overruled by the kinetic factors which govern the crystallization of polymers. Although we are dealing with a multi-component system experimentally it may not be distinguishable from a binary one and for this reason it is referred to as pseudo binary.

EXPERIMENTAL

The polyethylene used throughout this study was Marlex 6009 having the following molecular characteristics: intrinsic viscosity of 2.04 dl/g as determined in decalin at 135°C; $M_n=8 \times 10^3$ as obtained by ebulliometry and $M_w=13 \times 10^4$ as determined by light scattering in α -chloronaphthalene at 125°C. The solvents with the high melting temperatures were hexamethylbenzene ($T_m=166.5^\circ\text{C}$) and 1,2,4,5-tetrachlorobenzene ($T_m=141.5^\circ\text{C}$), which was purified by recrystallization from petroleum ether. The polymer solutions of about 5 mg were prepared by heating various mixtures of the components in liquid sealed aluminium pans at 200°C for 30 min in a differential scanning calorimeter (Perkin Elmer DSC-model 1B). This instrument was calibrated according to standard procedures. Microscopic investigations proved that the dissolving time of 30 min was long enough to give a homogeneous melt.

Microscopic studies were made using a Leitz polarizing microscope which was equipped with a Mettler temperature regulated hot stage, model FP 52.

The scanning electron microscopic observations were made using a Jeol instrument.

RESULTS

Determination of phase diagrams and eutectics

The eutectic points of the pseudo binary systems of polyethylene with 1,2,4,5-tetrachlorobenzene and hexamethylbenzene were assessed by determining the intersection of the solubility curves using d.s.c. After preparing homogeneous melts at 200°C the samples were quenched to 81°C. The major portion of the material crystallized rapidly during this cooling process. It is to be expected that in this manner rather small crystals are formed which should dissolve quickly in the heating experiment. Subsequently the samples were heated at a rate of 8°C/min. The melting curves obtained for various polyethylene/tetrachlorobenzene compositions are shown in Figure 1. It should be remarked that most of the thermograms, except those for the pure components and for a polymer volume fraction of 0.8, exhibit two melting peaks. The position of the low temperature

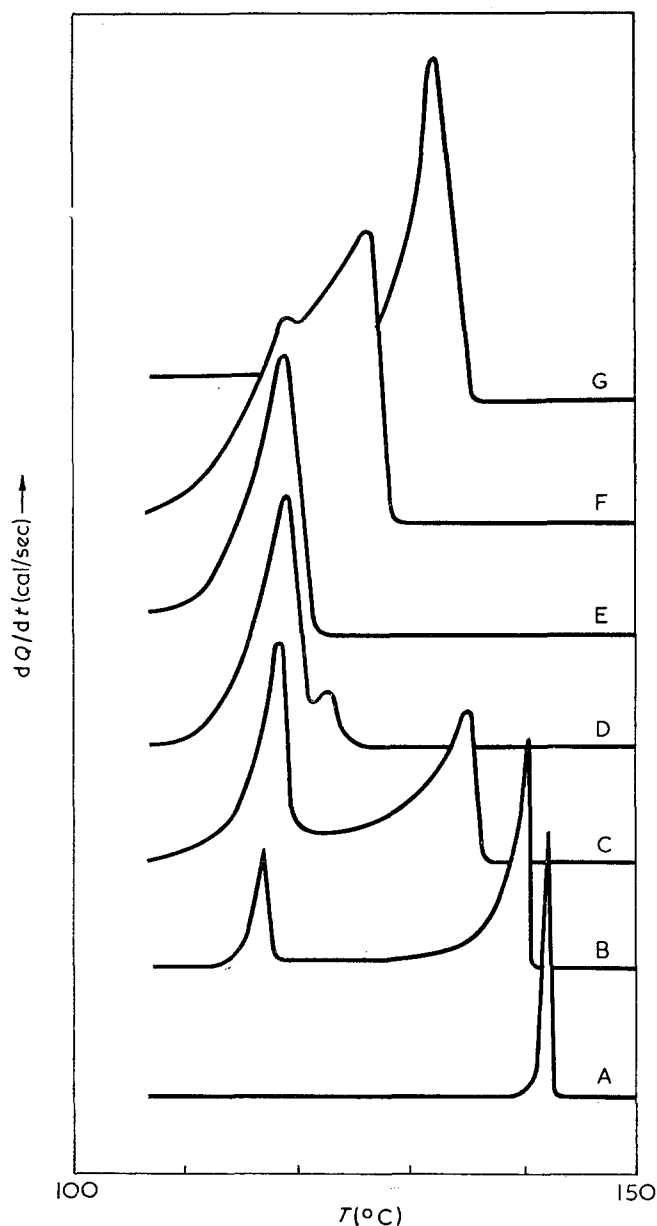


Figure 1 D.s.c.-melting thermograms of various mixtures of linear polyethylene and 1,2,4,5-tetrachlorobenzene. The samples were quenched to 81°C. Polyethylene volume fractions: A, 0; B, 0.2; C, 0.4; D, 0.7; E, 0.8; F, 0.9; G, 1.0

peak at 115°C appears to be independent of the overall polymer concentration and is therefore likely to be attributed to the melting of the eutectic composition. The peak at higher temperatures is due to the dissolution of an excess of either the pure polymer or the pure diluent crystals in the polymer solution. Before the construction of the phase diagram it was checked whether the melting process of the eutectic and the pure solids in the polymer solutions of other compositions were dependent on the heating rate. Figure 2 illustrates that in a scan speed range from 2°C/min to 36°C/min the effect of the heating on the peak temperature is of the order of 2°C. These temperatures were corrected for the temperature lag observed in melting the tin standard at various scan speeds. From these data it is inferred that no significant retardation occurs in the melting process of these quenched samples.

The extrapolated end melting temperatures and the peak temperature of the eutectic melting, both for zero

scan speed, were employed to construct the phase diagram for polyethylene/1,2,4,5-tetrachlorobenzene as illustrated in Figure 3 (the broken lines). For the quenched samples the eutectic temperature is found at 115°C and the eutectic composition at a polymer volume fraction of 0.79.

It would be interesting to compare these experimental conditions for the eutectic point with those calculated for thermodynamic equilibrium of the polymer solution and the ideal solids.

For this particular case the eutectic point was assessed by a graphical solution of the two solubility equations

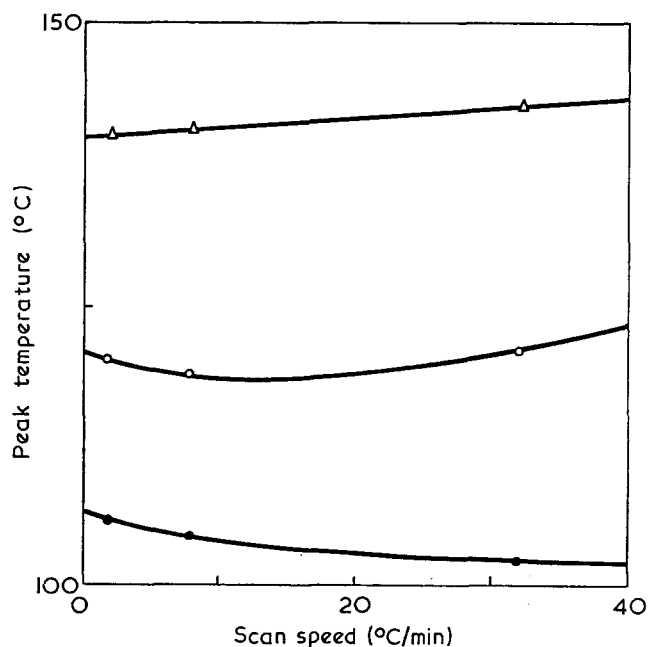


Figure 2 Effect of heating rate on the melting temperatures of the systems polyethylene/1,2,4,5-tetrachlorobenzene (O) and polyethylene/hexamethylbenzene (Δ) and the influence of the cooling rate on the crystallization temperatures of the system polyethylene/1,2,4,5-tetrachlorobenzene (●)

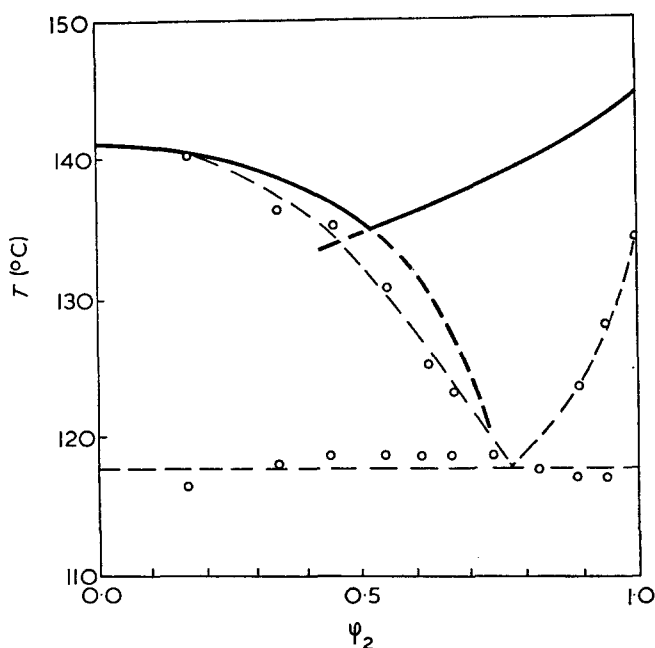


Figure 3 Phase diagram of the pseudo binary system linear polyethylene/1,2,4,5-tetrachlorobenzene. —, Calculated using equations (4) and (5), with $\chi=0.37$. O, Melting temperatures of samples quenched to 81°C

(4) and (5) using the following values for the various parameters.

The melting temperature of ideal polyethylene crystals is 145.5°C and the heat of fusion per mole of units $\Delta H_u = 980$ cal/mol. The melting temperature of 1,2,4,5-tetrachlorobenzene is 141.5°C and the molar heat of fusion $\Delta H_1 = 5.8 \times 10^3$ cal/mol, as determined by d.s.c. using hexamethylbenzene as references¹³. The Flory-Huggins parameter $\chi = 0.37$ was derived from cryometric data¹⁴. For the thermodynamic equilibrium condition a eutectic temperature of 135°C and a polyethylene volume fraction of 0.51 are estimated. A comparison of the two phase diagrams in Figure 3 shows that the experimentally determined liquidus curve for tetrachlorobenzene is in close accord with the theoretical curve and that the large discrepancy between the theoretical and experimental eutectic temperature is due to the low dissolution temperatures of the metastable polyethylene crystals. As a result of that there is a temperature region of 20°C in which pure tetrachlorobenzene is in metastable equilibrium with the polyethylene solution.

The strong influence of the experimental condition on the eutectic point is further demonstrated by Figure 4, in which the temperature (extrapolated onset) for spontaneous crystallization by cooling the melts at a rate of $2^{\circ}\text{C}/\text{min}$, is plotted against the composition. For these cooling curves a eutectic temperature as low as 106°C is found at a polymer volume fraction of 0.73. A eutectic temperature of 122°C is observed for end melting temperature from thermograms that were measured after quenching the melts to a temperature of 105°C and subsequent crystallization for a period of 45 min. These data plotted in Figure 4 reveal that there is no change in melting temperature of the tetra-

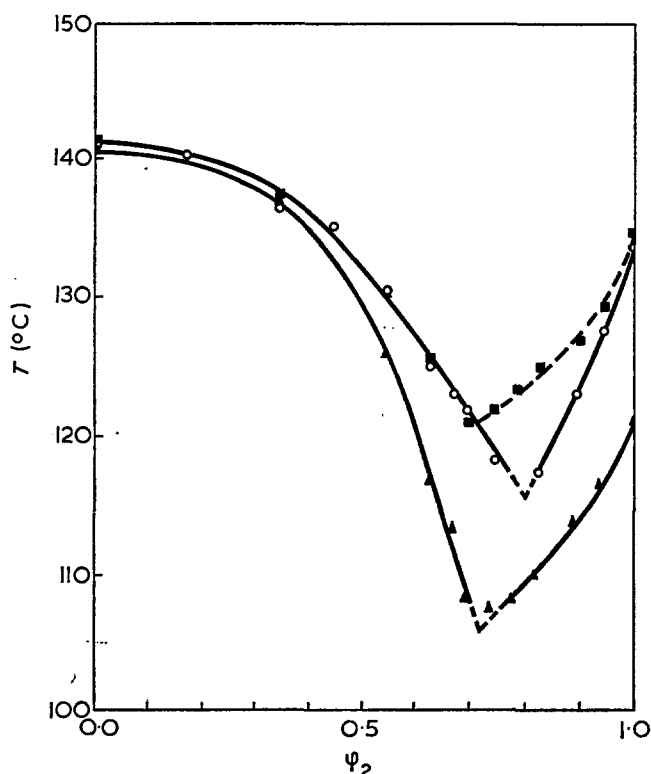


Figure 4 Phase diagram of the pseudo binary system linear polyethylene/1,2,4,5-tetrachlorobenzene. \circ , Melting temperatures of samples quenched to 81°C ; \blacksquare , melting temperatures of samples quenched to 105°C ; \blacktriangle , crystallization temperatures

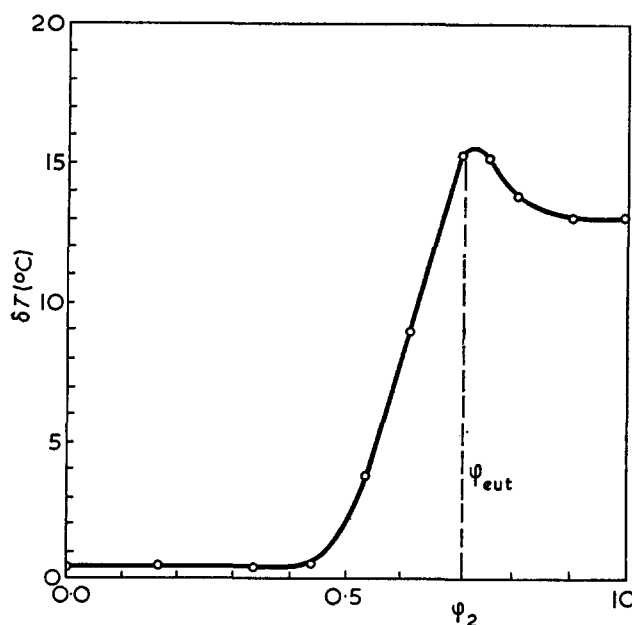


Figure 5 Experimentally determined supercooling, δT , required for crystallization in the system polyethylene/1,2,4,5-tetrachlorobenzene as function of the polymer volume fraction, ϕ_2

chlorobenzene crystals, whereas that of the polymer crystals has increased substantially.

The kinetic factors involved in the solidification of the component of this polymer system is most clearly illustrated by plotting against concentration the experimental supercooling defined as the difference between the peak temperature of the melting thermogram and that of the corresponding peak in the crystallization thermogram (Figure 5). Up to a polymer volume fraction of 0.5 the experimental supercooling for crystallization of tetrachlorobenzene from the polyethylene solutions amounts only to 0.5°C but for the eutectic crystallization a maximum supercooling of 15.5°C is needed. The latter even exceeds the undercooling of 13°C required for the spontaneous crystallization of polyethylene. From these data it is to be expected that the degree of crystallinity of the polyethylene fraction in the crystallized eutectic material is lower than in pure polyethylene, also quenched to 81°C . Indeed we calculated from the d.s.c. thermograms a reduction of the degree of crystallinity from 64% for pure polyethylene to 48% for the polyethylene in the eutectic mixture. Both samples were quenched to 81°C and then heated up in the d.s.c. It should be noted that also an experimental supercooling of 15.5°C for the eutectic crystallization of all mixtures investigated is required. This means that the eutectic crystallization was not promoted by the presence of any of the solid components.

Finally, the phase diagram of the system polyethylene/hexamethylbenzene needs some description (Figure 6). This diagram was also derived from the end melting temperatures of thermograms obtained by heating mixtures that were previously quenched to 81°C . The eutectic point is located at 122°C and at a polyethylene volume fraction of 0.73. At a temperature of 110.6°C a solid-solid phase transition occurs in hexamethylbenzene¹⁵, which appears to be independent of the polymer concentration. This may be regarded as evidence for the formation of a pure solid phase. Another peculiar feature of this system is that the hexamethylbenzene

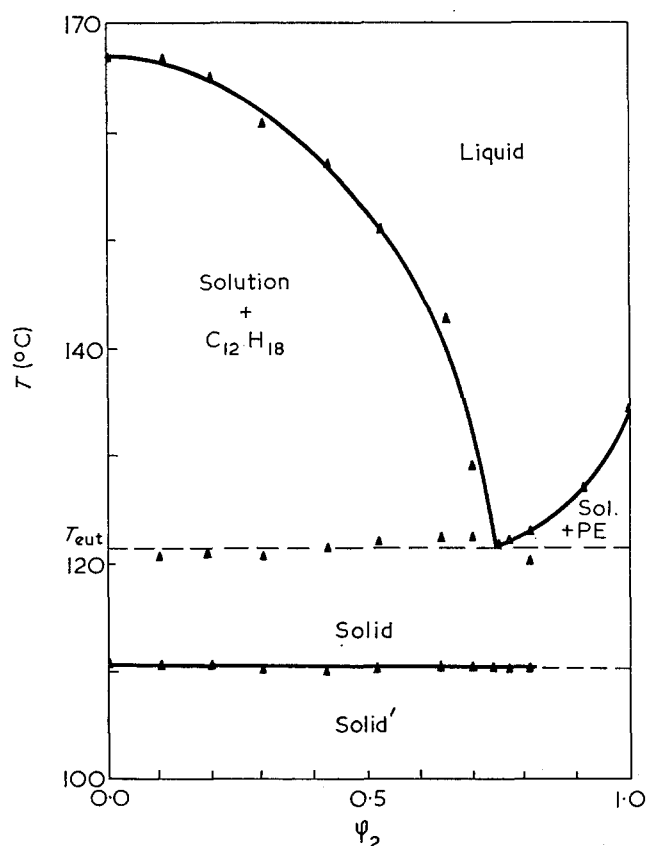


Figure 6 Phase diagram of the pseudo binary system polyethylene/hexamethylbenzene. Samples were quenched to 81°C



Figure 7 Photomicrograph of pure 1,2,4,5-tetrachlorobenzene crystals; magnification 20 diameters

liquidus may be described by equation (4) for a value of the Flory-Huggins parameter χ of -0.5 .

Morphology

This section deals with the most conspicuous phenomena of the crystallization and melting of the binary systems observed in the polarizing microscope. A typical example of a photomicrograph of the birefringent 1,2,4,5-tetrachlorobenzene crystals is shown in Figure 7. The habit of the diluent crystals grown in polymer solution (the volume fraction of polymer was 0.2) at 136°C is that of truncated needles, as shown in Figure 8. When the sample was heated and recrystallized the truncated needles appeared at different location.

Evidently this observation seems to justify the conclusion that at the temperature of 200°C a homogeneous melt is formed. Further cooling of the whiskerlike tetrachlorobenzene crystals surrounded by the polymer solution results in lateral growth until the eutectic composition is reached. At this point the remaining melt crystallize instantaneously (Figure 9a). An overall picture of the same sample at 25°C is given in the photomicrograph of Figure 9b exhibiting clearly the influence of the polyethylene on the crystallization of the diluent. The crystals are ramified during growth in the viscous

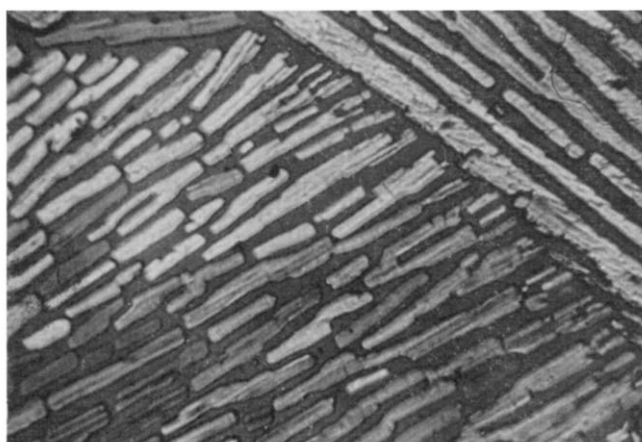


Figure 8 Photomicrograph of 1,2,4,5-tetrachlorobenzene crystals grown from a 20% v/v solution of polyethylene in 1,2,4,5-tetrachlorobenzene, at 136°C; magnification 46 diameters

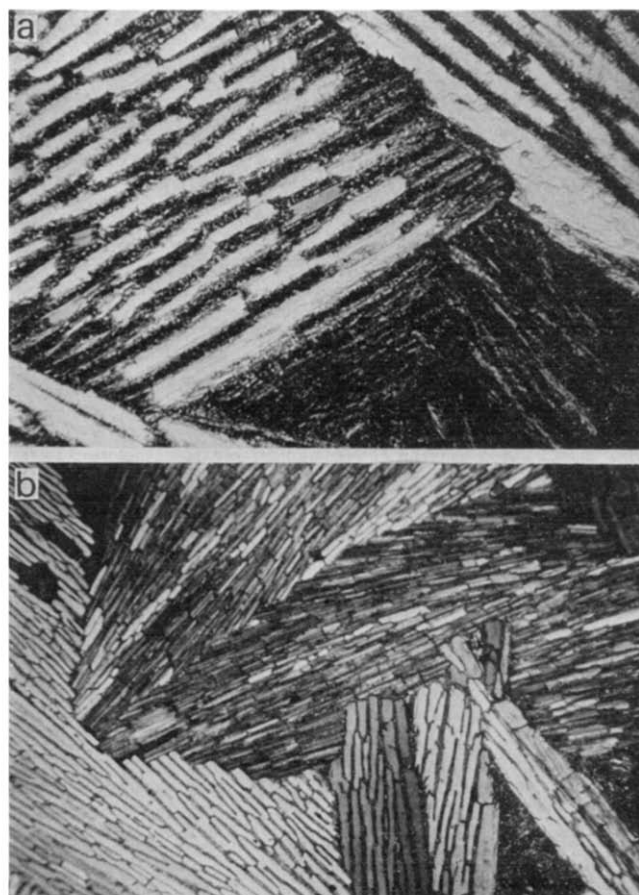


Figure 9 Photomicrographs of the solid formed by cooling a 20% v/v solution of polyethylene in 1,2,4,5-tetrachlorobenzene. Magnification: (a) 46 diameters; (b) 20 diameters.

melt after having acquired a length of roughly 0.03 cm. During the very rapid growth of the crystals the melt at the growth front become rich in polyethylene and this gives rise to the ramification of the crystals. In fact this phenomenon is well known in eutectic crystallization of inorganic materials and actually underlies the branching that is noticed in spherulitic growth in crystallization of polymers from a pure melt¹⁶.

The eutectic melt of the present polymer-diluent systems crystallize spherulitically as demonstrated by the microphotograph of *Figure 10*. This transition in morphology from needles to spherulites has also been observed in binary system of low molecular weight n-paraffins¹⁷.

So far the photomicrographs presented were taken from the system polyethylene/1,2,4,5-tetrachlorobenzene.

The second system under investigation, polyethylene/hexamethylbenzene, exhibited similar pictures under corresponding conditions, except that the hexamethylbenzene crystals with needle-shape habit displayed frequently a cleavage as indicated in *Figure 11*.

Finally, some interesting features need to be described of the polyethylene crystals that remained after removing the solid tetrachlorobenzene by sublimation.

Scanning electron micrographs of the cellular polyethylene crystallized from a polymer-diluent mixture of a polyethylene volume fraction of 0.6 are shown in



Figure 10 Photomicrograph of the spherulitic structures developed during simultaneous growth of polyethylene and 1,2,4,5-tetrachlorobenzene, at 105°C; magnification 46 diameters

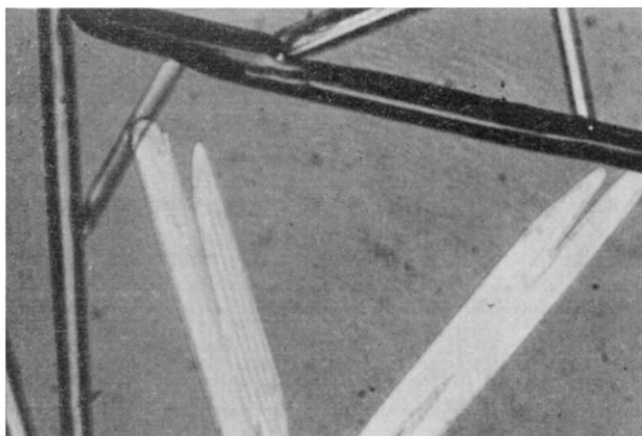


Figure 11 Photomicrograph of hexamethylbenzene crystals grown from a 20% v/v solution of polyethylene in hexamethylbenzene, at 155°C; magnification 230 diameters

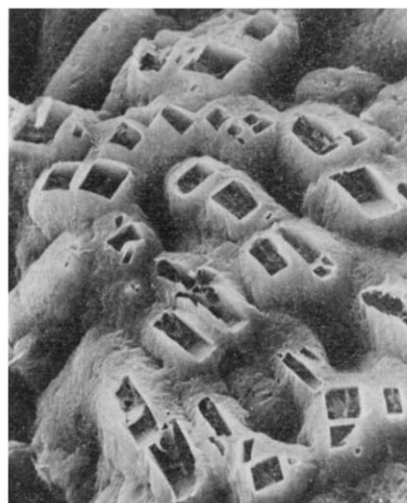


Figure 12 Scanning electron micrograph of a polyethylene surface displaying the cellular structure after sublimation of solid 1,2,4,5-tetrachlorobenzene. Polyethylene volume fraction 0.5; magnification 533 diameters

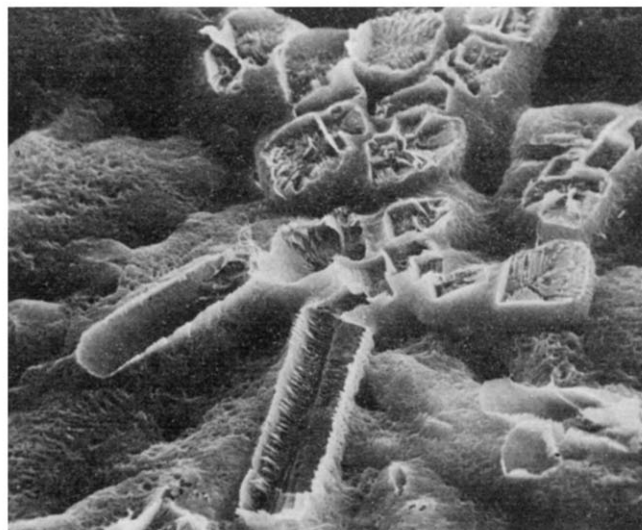


Figure 13 Scanning electron micrograph of the coarse and fine structure of cellular polyethylene due to the sublimation of the 1,2,4,5-tetrachlorobenzene needles and eutectic crystals; magnification 666 diameters

Figures 12 and 13. The spongelike material exhibits rectangular and quadratic holes, which were created by sublimation of tetrachlorobenzene crystals of corresponding morphology. In addition to the large holes, very small pores can be discerned, which originate from the eutectic crystallization.

DISCUSSION

The Flory-Huggins theory of the freezing point depression in concentrated polymer solutions predicts a eutectic point if the melting temperature of the diluent is close to that of the polymer. This stipulation is particularly pertinent for polymer-diluent systems whose phase diagrams are characterized by rather flat liquidus curves. This depends on the heat of fusion and the polymer diluent interaction. The polymer diluent systems described in this paper clearly demonstrate

that a eutectic point may be found experimentally at a temperature and composition that deviate markedly from those predicted for thermodynamic equilibrium. As a result of the large thermodynamic barriers for nucleation and growth of polymer crystals the polymer solution has to be supercooled more extensively in order to observe the simultaneous crystallization. Near the eutectic point in the polyethylene/tetrachlorobenzene system also the nucleation of the diluent appears to be hampered by the presence of the polymer molecules. These two factors account for the extreme supercooling of 15.5°C for the spontaneous eutectic crystallization, at a cooling rate of 2°C/min.

Microscopic studies disclose that the habit of the diluent crystals is needlelike. In fact, at the initial stage of the crystallization of the diluent, a large number of very thin needles are observed which subsequently grow laterally and they do not increase much in length. This growth process points at a poisoning effect of certain growth faces by the polymer molecules. That polymer molecules may poison crystal faces is known for instance in the case of the NaCl whisker growth from aqueous solution to which poly(vinyl alcohol) has been added¹⁸. The adsorption of polymer molecules on the crystal faces is likely to retard the nucleation and growth. The preferential growth in one direction leading to the needles has an additional implication, namely the accumulation of polymeric chains in the growth front. If the growth is very rapid, it might involve considerable strain in the polymer chains and it can be visualized that for polymeric systems with long relaxation times diluent growth may cause considerable deformation of the polymer coils¹⁹, which even may lead to chain fracture.

The transition from needle shape crystal growth to purely spherulitic growth when the eutectic point has been reached is similar to what happens in inorganic systems. However, in these systems composite growth *in situ* is achieved by conducting the crystallization experiment in a temperature gradient. This results then in unidirectional growth, as shown by several investi-

gators^{20, 21}. For the morphology of the products as function of the growth rate, mathematical relations are given in the literature^{22, 23}.

It is clear that the study of eutectic crystallization in polymeric systems is still in an embryonic stage in particular as far as the investigation of the morphology is concerned. Preliminary experiments in our laboratory indicate that the application of a temperature gradient results in unidirectional growth. Further work on the morphology of these crystals as well as on that of the cellular polymer material that is left after removal of the solid diluent from the eutectic by sublimation will be reported in future publications.

REFERENCES

- 1 Hunt, D. J. and Jackson, K. A. *Trans. Metall. Soc. AIME* 1966, **236**, 843
- 2 Kerr, H. W. and Winegard, W. C. *J. Metals* 1966, **18**, 563
- 3 Rastogi, R. P. and Bassi, P. S. *J. Phys. Chem.* 1964, **68**, 2398
- 4 Edgar, O. B. and Ellery, E. *J. Chem. Soc.* 1952, **3**, 2633
- 5 Sønnerskog, S. *Acta Chem. Scand.* 1956, **10**, 113
- 6 Izard, E. F. *J. Polym. Sci.* 1952, **8**, 503
- 7 Mandelkern, L. 'Crystallization of Polymers', McGraw-Hill, New York, 1964, p 88
- 8 Kilian, H. G. *Kolloid-Z. Z. Polym.* 1965, **202**, 97
- 9 Orthmann, H. J. and Ueberreiter, K. *Z. Elektrochem.* 1957, **61**, 107
- 10 Ke, B. *J. Polym. Sci.* 1961, **50**, 79
- 11 Flory, P. J. 'Principles of Polymer Chemistry', Cornell Univ. Press, London, 1971, pp 512 and 568
- 12 Pennings, A. J. *Proc. Conf. Charact. Macromol. Struct. Warrenton, Va* (1967 (April 5-7), p 233
- 13 Spaght, M. E., Benson Thomas, S. and Parks, G. S. *J. Phys. Chem.* 1932, **36**, 882
- 14 Pennings, A. J. unpublished results
- 15 Schniepp, O. *J. Chem. Phys.* 1959, **30**, 48
- 16 Keith, H. D. and Padden, F. J. *J. Appl. Phys.* 1964, **35**, 1270
- 17 Holder, G. A. *J. Macromol. Sci. (A-4)* 1970, **5**, 1049
- 18 Webb, W. W. *J. Appl. Phys.* 1960, **31**, 1, 194
- 19 Kuhn, W., Peterli, E. and Majer, H. *Z. Elektrochem.* 1958, **62**, 297
- 20 Carpay, F. M. A. *Acta Metallurgica* 1970, **18**, 747
- 21 Tiller, W. A. *J. Appl. Phys.* 1963, **34**, 3615
- 22 Albers, W. *Chem. Weekblad* 1969, **29**, 22
- 23 Chadwick, G. A. 'Progress in Materials Science', Pergamon Press, Oxford, 1965, Vol 12, p 99

Equilibrium ring concentrations and the statistical conformations of polymer chains: Part 12. Cyclics in molten and solid nylon-6

J. M. Andrews, F. R. Jones and J. A. Semlyen

Department of Chemistry, University of York, Heslington, York YO1 5DD, UK
(Received 2 January 1974)

The molar cyclization equilibrium constants K_x for cyclics $[\text{NH}(\text{CH}_2)_5\text{CO}]_x$ with $x=1-6$ were measured for an undiluted melt equilibrate of nylon-6 at 525K using gel permeation chromatography as the principal analytical technique. They were compared with the corresponding theoretical values calculated by the Jacobson and Stockmayer theory using the rotational isomeric state model of Flory and Williams to describe the statistical conformations of the corresponding open chain molecules. Ring-chain equilibration reactions were carried out on samples of nylon-6 at a temperature 46K below the melting point of the polymer. Polymers were prepared at 459K over periods of more than 30 days by (i) heating nylon-6 containing 11.5% w/w cyclic oligomers, (ii) heating nylon-6 containing no cyclic oligomers, (iii) polymerizing ϵ -caprolactam alone. These polymers were all found to contain ~2% w/w cyclics $[\text{NH}(\text{CH}_2)_5\text{CO}]$ with $x=1-6$. However, although the concentrations of the larger cyclic oligomers were identical within experimental error in the samples prepared by (i) and (ii), they were strikingly different from those in the sample prepared by (iii). These differences in cyclic concentrations are discussed in terms of the structures of the solid polymers at the equilibration temperature.

INTRODUCTION

A number of experimental and theoretical investigations have been concerned with elucidating the relationship between the concentrations of cyclics in polymeric systems undergoing ring-chain equilibration reactions and the statistical conformations of the corresponding open chain molecules¹. These investigations have established that the characterization of the distribution of cyclic molecules in polymeric equilibrates may be used to probe the structures of polymeric melts as well as dilute and concentrated polymer solutions.

This paper describes an extension of the equilibrium cyclic concentration method to the study of the conformations of chain molecules in a polymer *in the solid state*. The concentrations of cyclics have been measured for samples of nylon-6 prepared by heating the solid polymer and by polymerizing ϵ -caprolactam below the melting point of the polymer. These concentrations are compared with those found in nylon-6 prepared by a ring-chain equilibration reaction in the melt.

There have been many studies of the preparation and properties of nylon-6 and its cyclic and linear oligomers, and these have provided a foundation for the investigations to be described. They include descriptions of preparations of the polymer²⁻⁵ as well as methods for separating and identifying its cyclic oligomers⁶⁻¹¹.

EXPERIMENTAL

Polymerization reactions

The following procedure was adopted for the polymerization reactions. The monomeric cyclic ϵ -capro-

lactam was freshly distilled *in vacuo* into a previously weighed glass ampoule and 6-aminohexanoic acid was added at a concentration of 0.11 mol/kg. This gave an effective water concentration of 0.2% w/w. The molten ϵ -caprolactam was degassed under high vacuum and the ampoule was sealed. Polymerization was carried out by heating the ampoule in an oven maintained at the required temperature. After the required polymerization time, the reaction was quenched by cooling the ampoule. The latter was broken open and the polymeric product was obtained as a hard, white, opaque material. This was turned to small, fine shavings on a lathe prior to the extraction of cyclic oligomers.

Ring-chain interconversion reactions in the solid polymer

The following procedure was adopted for equilibration reactions in the solid polymer. Fine shavings of the polymer were loaded into a glass ampoule, which was then evacuated and sealed. The ampoule and its contents were maintained at the required temperature for the specified period of time. It was then cooled to room temperature, broken open and the shavings were removed.

Extraction of oligomers

Cyclic, and any linear, oligomers were extracted from shavings of nylon-6 by adding approximately twenty times their weight of freshly distilled Analar grade methanol and refluxing for 48 h. The hot methanol was then decanted off and removed on a rotary evaporator to leave a residue containing cyclic oligomers. Two such

extractions were found to remove effectively all of the cyclics $[\text{NH}(\text{CH}_2)_5\text{CO}]_x$ with $x=1-6$.

Removal of cyclic monomer from the oligomeric extracts

Up to 70% w/w of the combined oligomeric extracts consisted of cyclic monomer and this was removed quantitatively before analysing the residue of cyclic oligomers by gel permeation chromatography. A molecular distillation apparatus functioning under vacuum at 373K was set up and found to be effective for the quantitative removal of cyclic monomer from oligomeric mixtures.

Gas-liquid chromatography (g.l.c.) of cyclic monomer and dimer

A Pye Unicam (Series 104) gas-liquid chromatograph fitted with a heated dual-flame ionization detector was used for the quantitative analysis of cyclic monomer $\text{NH}(\text{CH}_2)_5\text{CO}$ and dimer $[\text{NH}(\text{CH}_2)_5\text{CO}]_2$. The chromatograph was fitted with sample and reference columns 1.2m in length and 4mm i.d. and nitrogen was used as the carrier gas at a flow rate of ~ 45 ml/min. The columns were packed with Embacel, which had been treated with hexamethyldisilazane by the method of Bohemen *et al.*¹², and then coated with 4% w/w of stationary phase OV-1 (supplied by the Field Instrument Company). Cyclic oligomers were dissolved in *m*-cresol at concentrations of 10–20% w/w and 2 μ l samples were injected through a serum cap using a microlitre syringe. In a typical analysis, the oven temperature was increased from 298 K at the rate of 2 K/min. Cyclic monomer, dimer and trimer eluted as increasingly symmetric peaks at 382, 492 and 554 K respectively. Samples of cyclic monomer, cyclic dimer and mixtures of cyclic oligomers were used to calibrate the gas-liquid chromatograph for detector response against molecular weight. Under the conditions of the analysis, there was no detectable decomposition of the cyclic oligomers.

Gel permeation chromatography (g.p.c.) of cyclic oligomers

Cyclic extracts were analysed by g.p.c. using a 4.5m column of i.d. 9mm packed with Sephadex G25 of nominal pore size 20–80 μ m (supplied by Pharmacia Ltd) and fitted at its output with a Waters model R4 Differential Refractometer. Samples were analysed at room temperature using 50% v/v glacial acetic acid in water as the solvent. Samples of monomer, dimer and mixtures of cyclic oligomers were used to calibrate the instrument for both elution volume and detector response as functions of molecular weight. Each cyclic oligomer was assumed to give a peak of Gaussian form and overlapping peaks were apportioned between different cyclics on this basis.

Molecular weight measurements of linear polymers

Following the removal of cyclic oligomers, the residual polymers were dried for 8 h at 373 K under a pressure of 1 mmHg. Their molecular weights were determined by both amino end group analysis (assuming that each molecule contains one amino end group) and by measurements of relative viscosities according to the procedure recommended by Matthes¹³.

RESULTS AND DISCUSSION

Experimental and theoretical cyclic concentrations in molten nylon-6

Although several groups of workers have described analytical investigations of the concentrations of cyclic oligomers in samples of nylon-6 prepared by ring-chain equilibration reactions in the melt^{8, 14–19}, no precise values for the concentrations of cyclic dimer, trimer or hexamer in such samples have been reported. Consequently, before investigating changes in the concentrations of ring molecules in samples of solid nylon-6 resulting from heating the polymer below its melting point, molar cyclization equilibrium constants for the cyclics $[\text{NH}(\text{CH}_2)_5\text{CO}]_x$ with $x=1-6$ were measured for a melt equilibrate.

A ring-chain equilibration reaction was carried out by heating 250 g ϵ -caprolactam (together with 6-amino-hexanoic acid at a concentration of 0.11 mol/kg) at 525 K. Although equilibrium should be reached in ~ 30 h under these conditions³, the reaction was allowed to proceed for 14 days before quenching by cooling to room temperature. The hard, white polymer was turned to fine shavings on a lathe. Cyclic oligomers were extracted from 100 g of the shavings by applying the extraction procedure described above and monomeric ϵ -caprolactam was sublimed from the extracted material to leave a mixture consisting primarily of the cyclics $[\text{NH}(\text{CH}_2)_5\text{CO}]_x$ from dimer to hexamer*. A gel permeation chromatogram of this mixture is shown in Figure 1. The number-average molecular weight \bar{M}_n of the cyclic oligomer-free polymer was found to be 1.60×10^4 by viscometric measurements and 1.55×10^4 by amino end-group analysis. Although the ring-chain equilibration reaction was allowed to proceed for 14 days, no traces of side-products could be detected by g.l.c. or g.p.c.

Now, the equilibrium between x -meric cyclics M_x and linear chains in molten nylon-6 may be represented as follows:



where M symbolizes a monomeric unit $\text{NH}(\text{CH}_2)_5\text{CO}$. Gel permeation chromatographic tracings of the polymeric product were in agreement with the expectation²⁰ that there should be a most probable distribution of

* The concentrations of monomer and dimer in the oligomeric extracts were determined by g.l.c. and found to be in good agreement with the gravimetrically determined monomer concentration and the dimer concentration found by g.p.c. The concentrations of larger cyclics were measured by g.p.c. alone.

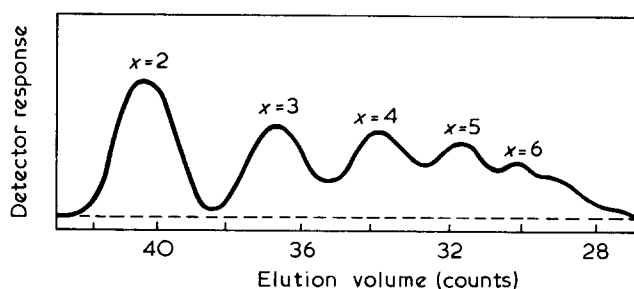


Figure 1 Gel permeation chromatogram of cyclics $[\text{NH}(\text{CH}_2)_5\text{CO}]_x$ with $x=2-6$ obtained from nylon-6 prepared by ring-chain equilibration in the melt at 525 K (see text)

chain lengths in the acyclic portion of the polymer. Hence the molar cyclization equilibrium constants K_x for cyclics formed by the forward step of equation (1) were calculated from the extent of reaction p of functional groups in the acyclic part of the polymer by the relation:

$$K_x = [M_x]/p^x \quad (2)$$

The factor p was obtained from the number-average molecular weight \bar{M}_n using the equation²¹:

$$p = 1 - M_0/\bar{M}_n \quad (3)$$

where M_0 is the weight of a monomeric unit. For the melt equilibrate, K_x values calculated by equations (2) and (3) are approximately equal to the concentrations $[M_x]$ of the cyclic oligomers. The difference is greatest for the cyclic hexamer, but even for that it amounts to only ~4%.

The molar cyclization equilibrium constants K_x (in mol/l) for cyclics $[\text{NH}(\text{CH}_2)_5\text{CO}]_x$ (with $x=1-6$) in molten nylon-6 at 525 K are shown in Figure 2. They were calculated from the weights of cyclics found in the equilibrate by assuming the density of the melt to be the literature value⁶ of 0.93 g/ml. The K_x values for the monomer, tetramer and pentamer were found to be in close agreement with the results of Spoor and Zahn⁸.

In Figure 2, the experimental molar cyclization equilibrium constants are compared with theoretical values calculated as described in a previous paper²². The latter were obtained using the Jacobson and Stockmayer cyclization theory^{23, 24} by assuming that oligomeric chains of nylon-6 obey the Gaussian expression for the probability that they will intramolecularly cyclize, and using the Flory and Williams²⁵ rotational isomeric state model to describe their average conformations. Chains in nylon-6 were assumed to be unperturbed by excluded volume effects and to have

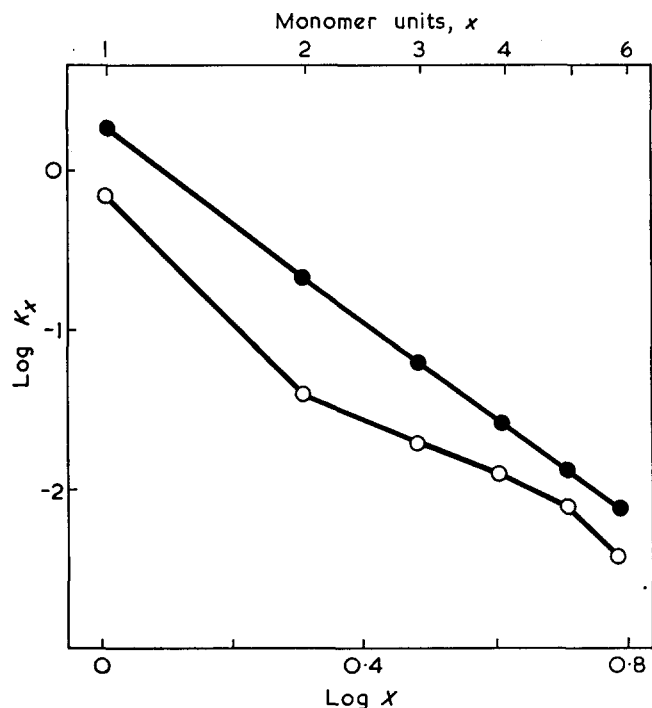


Figure 2 Experimental molar cyclization equilibrium constants K_x (in mol/l) for cyclics M_x in the melt at 525 K (O) are plotted as log K_x against log x . They are compared with theoretical values calculated by equation (4) which assumes that the corresponding open chain molecules obey Gaussian statistics (●)

similar end-to-end distances $\langle r_x^2 \rangle_0$ to those measured under θ -point conditions. The calculations take account of the effect of chain length and temperature on the dimensions of the unperturbed chains and relate K_x to $\langle r_x^2 \rangle_0$ as follows:

$$K_x = (3/2\pi \langle r_x^2 \rangle_0)^{3/2} (1/N_A x) \quad (4)$$

where N_A is the Avogadro constant.

It is not the purpose of this paper to make a detailed comparison of experimental molar cyclization equilibrium constants for cyclics in molten nylon-6 and those predicted theoretically using the rotational isomeric state theory of linear macromolecules. However, it is noted that since the uncertainties in the experimental K_x values for the cyclics from monomer to pentamer are believed to be less than $\pm 10\%$, the differences between the experimental and the corresponding theoretical values for K_4 , K_5 and K_6 are significant. The experimental K_4 , K_5 , K_6 values are lower than the calculated values by factors of 2, 1.7 and 2 respectively, and these differences are considerably larger than those found for cyclics of similar size in polydimethylsiloxane²⁶ and poly-(2,2,7,7-tetramethyl-1-oxa-2,7-disilacycloheptane)²⁷ melt equilibrates.

Cyclic concentrations in samples of solid nylon-6

The following experiments were carried out in order to investigate changes in the cyclic concentrations of samples of nylon-6 resulting from ring-chain equilibration reactions at temperatures below the melting point of the polymer (which is 505 K²⁸).

(i) Fine, small shavings of the polymer (with $\bar{M}_n = 1.6 \times 10^4$ and containing 11.5% w/w extractable oligomers), prepared by the ring-chain equilibration reaction described above, were heated in an evacuated ampoule at 459 K for 32 days. The polymer was cooled to room temperature and the shavings were found to be hard and brittle. The polymer had $\bar{M}_n = 2.1 \times 10^4$ (by viscometry) and 2.5×10^4 (by amino end-group analysis). It contained 1.8% w/w extractable oligomers. Individual cyclic concentrations in the polymer in mol/kg are plotted in Figure 3. They are compared with the corresponding concentrations in the melt equilibrate.

(ii) Oligomer-free shavings of the polymer obtained by (i) were dried *in vacuo* and heated in an evacuated ampoule at 459 K for 34 days, before cooling to room temperature. The resulting polymer was found to have $\bar{M}_n = 2.4 \times 10^4$ (by viscometry) and 3.3×10^4 (by amino end-group analysis). It contained 1.9% w/w extractable oligomers. The concentrations of individual cyclics in this polymer are plotted in Figure 3.

(iii) A sample of nylon-6 was prepared by polymerizing ϵ -caprolactam at 459 K. The contents of the ampoule were liquid initially, but set completely solid within two days. After a further 34 days, the reaction was quenched by cooling to room temperature. The polymer had $\bar{M}_n = 5.2 \times 10^4$ (by viscometry) and 6.3×10^4 (by amino end-group analysis). It contained 2.1% w/w extractable oligomers. The concentrations of individual cyclics in the polymer are plotted in Figure 4. They are compared with the corresponding concentrations in the melt equilibrate.

In confirmation of the conclusions of other workers^{28, 29}, the results presented in Figures 3 and 4 show that thermodynamic equilibria between monomeric ϵ -caprolactam and polymeric nylon-6 can be set up in

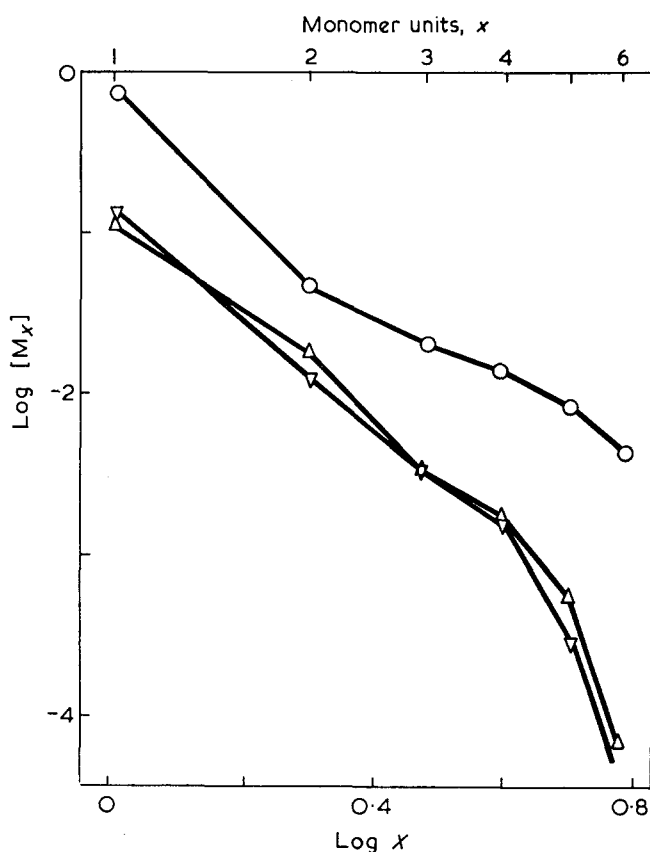


Figure 3 Concentrations of cyclics M_x (in mol/kg) in samples of nylon-6 prepared (i) by heating a melt polymerized sample in the solid state at 459 K for 32 days (Δ) and (ii) by heating a cyclic-free polymer in the solid state at 459 K for 34 days (∇). These values are compared with cyclic concentrations in a polymer prepared by ring-chain equilibration in the melt at 525 K (\circ)

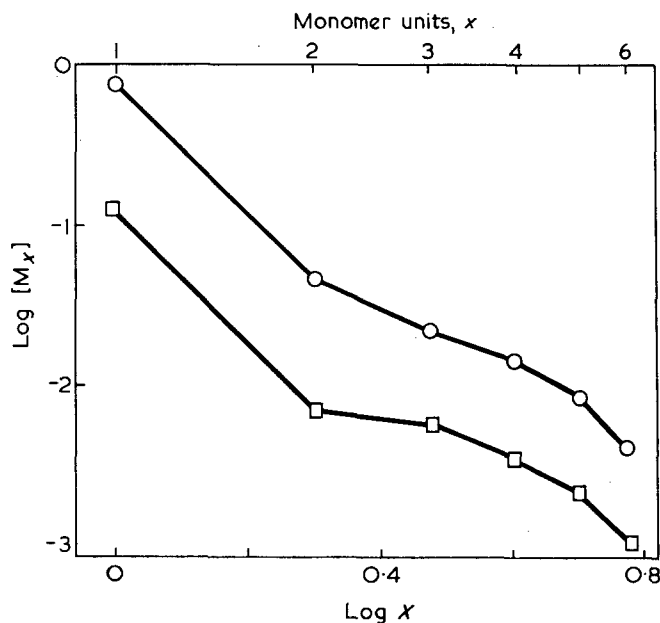


Figure 4 Concentrations of cyclics M_x (in mol/kg) in a sample of nylon-6 prepared by (iii) polymerizing ϵ -caprolactam at 459 K and heating for a total of 36 days (\square). These values are compared with cyclic concentrations in a polymer prepared by ring-chain equilibration in the melt at 525 K (\circ)

the solid polymer at temperatures well below its melting point. The same equilibrium monomer concentration (within experimental error) is obtained at 459 K starting with (i) polymer containing 8.2% w/w monomer, (ii)

polymer containing no monomer and (iii) monomer alone.

The concentrations of cyclic oligomers (with $x=3-6$) in the nylon-6 prepared by (iii) are lower by factors of about four than the corresponding values for polymer equilibrated in the melt (see Figure 4). Following Wichterle²⁸, these differences can be interpreted in terms of a polymer structure at 459 K consisting of about 80% crystalline regions (which are free of cyclic oligomers) together with about 20% amorphous regions—the latter containing rings in thermodynamic equilibrium with chains, which adopt similar random-coil conformations to those in the molten polymer.

It is noted, however, that if the concentrations of cyclic oligomers in the nylon-6 samples obtained by heating the solid polymers containing (i) 11.5% w/w cyclic oligomers and (ii) no cyclic oligomers are interpreted in similar terms, i.e., polymer structures consisting mainly of cyclic-free crystalline regions together with amorphous regions containing the cyclic oligomers, then chains in these latter regions must either be of limited length or they must fail to obey Gaussian statistics, or both. In fact, the high concentrations of cyclic monomer and dimer together with the rapid fall-off in cyclic concentrations with ring size in these solid polymers (see Figure 3) suggest that the average lengths of chain molecules in the amorphous regions of the polymers prepared by (i) and (ii) are far shorter than those in the amorphous regions of the polymer prepared by (iii).

It is well established that chains in crystalline regions of solid polymers including nylon-6 may have different average conformations depending on the method of preparation (see, for example, refs 30–33). Evidently the structures of the samples of nylon-6 prepared by (i) and (ii) are similar, although both are very different from that of the polymer of higher molecular weight prepared by the polymerization with crystallization reaction (iii). Furthermore, the studies described here have shown that although chemical ring-chain equilibria can be set up in different samples of nylon-6 some 46 K below the melting point of the polymer, the effect of maintaining the samples at 459 K over periods of many days does not result in the re-arrangement of the conformations of the chain molecules to produce similar polymer structures.

ACKNOWLEDGEMENTS

We are indebted to the Courtaulds' Educational Trust Fund for a Research Scholarship (to J. M. A.) and to the Science Research Council for a Research Fellowship (to F. R. J.). We thank Dr J. M. Evans of the Rubber and Plastics Research Association, Shawbury, Shrewsbury and also the Research Department of Courtaulds Limited, Spondon, Derby for molecular weight measurements.

REFERENCES

- Parts 1–11 of this series published in *Polymer* (1969–73): Semlyen, J. A. and Wright, P. V. *Polymer* 1969, **10**, 543; Semlyen, J. A. and Walker, G. R. *Polymer* 1969, **10**, 597; Wright, P. V. and Semlyen, J. A. *Polymer* 1970, **11**, 462; Walker, G. R. and Semlyen, J. A. *Polymer* 1970, **11**, 472; Beevers, M. S. and Semlyen, J. A. *Polymer* 1971, **12**, 373;

- Semlyen, J. A. *Polymer* 1971, **12**, 383;
Andrews, J. M. and Semlyen, J. A. *Polymer* 1972, **13**, 142;
Beevers, M. S. and Semlyen, J. A. *Polymer* 1972, **13**, 385;
Cooper, D. R. and Semlyen, J. A. *Polymer* 1972, **13**, 414;
Beevers, M. S. and Semlyen, J. A. *Polymer* 1972, **13**, 523;
Cooper, D. R. and Semlyen, J. A. *Polymer* 1973, **14**, 185
- 2 Hermans, P. H. *J. Appl. Chem.* 1955, **5**, 493
3 Reimscheussel, H. K. *J. Polym. Sci.* 1959, **41**, 457
4 Wichterle, O., Sittler, E. and Cefelin, P. *Coll. Czech. Chem. Commun.* 1959, **24**, 2356
5 Macchi, E. M., Morosoff, N. and Morawetz, H. *J. Polym. Sci. (A-1)* 1968, **6**, 2033
6 van Velden, P. F. et al. *Recueil* 1955, **74**, 1376
7 Hermans, P. H. *Recueil* 1953, **72**, 798
8 Spoor, H. and Zahn, H. *Z. Analyt. Chem.* 1959, **168**, 190
9 Kusch, P. and Zahn, H. *Angew. Chem.* 1965, **4**, 696
10 Mori, S. and Takeuchi, T. *J. Chromatog.* 1970, **49**, 230
11 Mulder, J. L. and Buytenhys, F. A. *J. Chromatog.* 1970, **51**, 459
12 Bohemen, J., Langer, S. H., Perrett, R. H. and Purnell, J. J. *J. Chem. Soc.* 1960, p 2444
13 Matthes, A. *Makromol. Chem.* 1950, **5**, 165
14 Zahn, H., Kunde, J. and Heidemann, G. *Makromol. Chem.* 1961, **43**, 220
15 Rothe, I. and Rothe, M. *Chem. Ber.* 1955, **88**, 284
16 Rothe, M. *J. Polym. Sci.* 1958, **30**, 227
17 Zahn, H. and Gleitsman, G. B. *Angew. Chem.* 1963, **75**, 772
18 Zahn, H. *Z. Ges. Textil. Ind.* 1964, **66**, 928
- 19 Katorzhnov, N. D. *Khim. Volokna* 1966, **1**, 3
20 Sbrolli, W. in 'Man-Made Fibres: Science and Technology', (Eds H. F. Mark, S. M. Atlas and E. Cernia), Interscience, New York, 1968, Vol II
21 Flory, P. J. 'Principles of Polymer Chemistry', Cornell Univ. Press, Ithaca, 1953
22 Semlyen, J. A. and Walker, G. R. *Polymer* 1969, **10**, 597
23 Jacobson, H. and Stockmayer, W. H. *J. Chem. Phys.* 1950, **18**, 1600
24 Flory, P. J. and Semlyen, J. A. *J. Am. Chem. Soc.* 1966, **88**, 3209
25 Flory, P. J. and Williams, A. D. *J. Polym. Sci. (A-2)* 1967, **5**, 399
26 Semlyen, J. A. and Wright, P. V. *Polymer* 1969, **10**, 543
27 Beevers, M. S. and Semlyen, J. A. *Polymer* 1972, **13**, 523
28 Wichterle, O., Sebenda, J. and Kralicek, J. *Fortschr. Hochpolym. Forsch.* 1961, **2**, 578; Wichterle, O. *Makromol. Chem.* 1960, **35**, 174
29 Tomka, J., Sebenda, J. and Wichterle, O. *J. Polym. Sci. (C)* 1967, **16**, 53
30 Wunderlich, B. and Liberti, F. *Bull. Am. Phys. Soc.* 1966, **11**, 248
31 Liberti, F. and Wunderlich, B. *J. Polym. Sci. (A-2)* 1968, **6**, 833
32 Wunderlich, B. 'Macromolecular Physics', Academic Press, New York, 1973, Vol 1
33 Dreyfuss, P. and Keller, A. *J. Macromol. Sci. (B)* 1970, **4**, 811

Dose kinetics of u.v. excited thermoluminescence in polyethylene

H. J. Wintle

Department of Physics, Queen's University, Kingston, Ontario, Canada
(Received 26 November 1973)

A model is developed to account for the observed maximum in thermoluminescence output with increasing u.v. dose. By postulating the destruction of ionized centres at a rate proportional to the dose rate, and allowing for the destruction of the un-ionized but excited centres by a separate bimolecular reaction, excellent fits to the experimental data are obtained and a discrepancy present in the original interpretation is removed. It is suggested that the bimolecular reaction is diffusion controlled, with the diffusion coefficient D of the migrating species being of the order of 10^{-9} cm²/sec.

INTRODUCTION

In a study of thermoluminescence of polyethylene irradiated by ultra-violet (u.v.) light, Charlesby and Partridge¹ noted a build up and subsequent decay of the light output as the dose was increased. They ascribed this behaviour to the competition between ionization of the luminescent centres (carbonyl groups) and their destruction, with the latter process dominant at large doses. The authors proposed a simple kinetic model to account for their data, and in outline this is undoubtedly correct, but they found that the rate constant for destruction was apparently independent of dose rate in isothermal studies, yet a function of prior dose rate when annealing methods were employed. They were unable to account for this discrepancy.

The loss of carbonyl groups could be an important factor in photodegradation mechanisms, which are not yet well understood². In addition, the thermoluminescence yield under γ -irradiation exhibits a low dose effect³, while the trapped electron yield⁴ and possibly certain trapped ion yields⁴⁻⁶ show maxima at about 0.5 Mrad and have largely vanished at about 1 Mrad. The u.v. experiments cannot be immediately compared with this work since the energy deposition required for peak thermoluminescence output is an order of magnitude higher, though the efficiency (or G value) is liable to be lower. Nevertheless, the similarity in behaviour suggests a common origin for these effects. It is therefore necessary to have accurate models for each process before comparisons can be made. In this paper we show that a modification of the original model for u.v. excited thermoluminescence fits the experimental results, removes the discrepancy remarked on above, and gives a more satisfactory account of the physical processes involved.

ORIGINAL MODEL

We first set out the equations used by Charlesby and Partridge¹. The rate of ionization of carbonyl groups

was proportional to the square of the dose rate because a two-step process was involved, and it was written as:

$$(dN_i/dt)_i = Cr^2(N - N_i) \quad (1)$$

where N_i is the concentration of ionized luminescence centres, C is a constant, r the dose rate, N the concentration of carbonyl groups (both ionized and un-ionized) at time t . The destruction of carbonyl groups was found to be a second order process, such that:

$$(dN/dt)_a = -krN^2 \quad (2)$$

where k is the appropriate rate constant. It followed that the ionized centres were destroyed at a rate:

$$(dN_i/dt)_a = -krNN_i \quad (3)$$

Combination of these equations gives a linear first order differential equation with asymptotic solutions:

$$N_i = CrN_0D \quad (D \text{ small}) \quad (4)$$

$$N_i = 1/kD \quad (D \text{ large}) \quad (5)$$

where $D = rt$ is the dose and N_0 is the initial concentration of carbonyl groups. The general solution was shown to fit the luminescent output data with a constant value of k .

A direct verification of equation (2) was made by irradiating to a dose D , annealing out the ionized centres, applying a small measuring dose D_m at the same dose rate and measuring the resulting light output. The N_0 for this test dose is in fact simply the carbonyl concentration N remaining after dose D . This experiment led to the result that $k \propto r$, and so was inconsistent with the previous results.

One variation suggested by Charlesby and Partridge was that the carbonyl groups were more likely to react in the excited state, so that the whole of the second-order disappearance should perhaps be ascribed to the reaction:

$$(dN_i/dt)_a = -krN_i^2 \quad (6)$$

They did not solve the set of equations (1), (2) and (6) but argued that the use of the linearized form equation (3) instead of equation (6) was adequate since at low doses N_i is small, while at high doses exhaustion occurs and $N_i \simeq N$. In fact, the combination of equations (1), (2) and (6) leads to a Riccati equation for N_i which can be solved by standard methods^{7,8}, and excellent fits to the data can be made. Despite the latitude afforded by the three adjustable parameters, k , N_0 and C , it has not proved possible to simultaneously select constant values for the last two and also have $k \propto r$ as demanded by the annealing experiments. The basic inconsistency therefore remains, confirming a surmise made by the original authors.

REVISED MODEL

There are two difficulties associated with the model outlined in the previous section. The first is that equation (1) does not properly reflect the fact that ionization takes place from an intermediate excited state, probably a triplet state, with concentration N_T . The lifetime τ of this state is approximately 2 sec while the irradiations extend over much longer periods. We therefore expect there to be a quasi-equilibrium set up between the excited state concentration and the ground state concentration N_G .

We have:

$$N_T/\tau = C_1 r N_G \quad (7)$$

where C_1 is the rate constant. We expect $N_T \ll N_G$. Further excitation of the excited state leads to ionization with a rate constant C_2 :

$$(dN_i/dt)_i = C_2 r N_T$$

Combining these two equations yields:

$$(dN_i/dt)_i = C r^2 N_G \quad (8)$$

where $C = C_1 C_2 \tau$ is a joint constant. This equation replaces equation (1) and differs from it only in that both triplet and ionized centres are subtracted from N .

The second difficulty with the original model is that while experimentally the carbonyl groups in the ground state vanish by second order kinetics, and probably by a bimolecular process as shown variously in equations (2), (3) and (6), all three of them imply an apparent three-body collision between two centres and a photon which is unlikely to occur. Indeed, if we incorporate the experimental result that $k \propto r$ from the annealing experiments, the situation becomes even worse. A concomitant difficulty is that it is not clear exactly how the destruction of ionized centres as described by equation (6), used in the calculation of N_i and thus in the calculation of luminescence output, leads back to equation (2) which describes the observed loss of carbonyl groups in the ground state. Another problem arises in the use of equation (5) in order to obtain a linearized solution. If the mechanism of ionization does involve an intermediate state, as seems entirely likely from the initial kinetics, then it is unlikely that the condition $N \simeq N_i$ will be satisfied even at high doses, and the use of the linearized solution is invalid even though good fits are obtained to the experimental data. The present proposal is that the loss of carbonyl groups is due to a bimolecular reaction among the excited species, but without explicit dependence upon the dose rate

that is given incorporated in equation (6). We have:

$$(dN_T/dt)_a = -l N_T^2 \quad (9)$$

where l is the rate constant. It is proper to substitute the quasi-equilibrium condition in on the right hand side, to obtain:

$$(dN_T/dt)_a = -l C_1^2 \tau^2 r^2 N_G^2$$

On the left hand side, we see that the loss of an excited centre will be shared between the excited level and the ground state in the ratio $N_T : N_G$. Thus, if $N_T \ll N_G$, then $(dN_T/dt)_a \simeq (dN_G/dt)_a$, so that finally

$$(dN_G/dt)_a = -m r^2 N_G^2 \quad (10)$$

where m is another rate constant. We note in passing that it need not in fact be the triplet state that is involved, since any excited level which is maintained in quasi-equilibrium and which vanishes by bimolecular recombination will lead to a result having the form of equation (10). We see that this mechanism automatically accounts for the annealing result, since by comparing equation (2) with equation (10) we see that $k = m r$ and is thus proportional to dose rate.

The reduction of N_G leads to a reduction in the ionization rate $(dN_i/dt)_i$, but it does not lead to a diminution of N_i . Therefore, we must allow for destruction of the ionized centres, and we assume that they are neutralized at a rate which is proportional to the dose rate, with a rate constant β :

$$(dN_i/dt)_a = -\beta r N_i \quad (11)$$

There is now no connection between the destruction of ground state centres and ionized centres as was necessarily the case before. A diagram of the transitions involved is shown in *Figure 1*. The fate of the ionized centres which are destroyed is left unspecified. They might return to the ground state, but this contribution is ignored since in the present model, the ionization is regarded as a perturbation of the dynamic equilibrium maintained in the GST system.

Integration of equation (10) gives:

$$\frac{1}{N_G} = \frac{1}{N_0} + m r D$$

and combination of equations (8) and (11) yields:

$$(dN_i/dt) = -\beta r N_i + C r^2 N_0 / (1 + m r N_0 D) \quad (12)$$

The solution of equation (12) is:

$$N_i = (C/m) \exp(-\beta D) \exp(-\beta/mrN_0) \int_1^x z^{-1} \exp(\beta z/mrN_0) dz \quad (13)$$

$$x = 1 + m r N_0 D$$

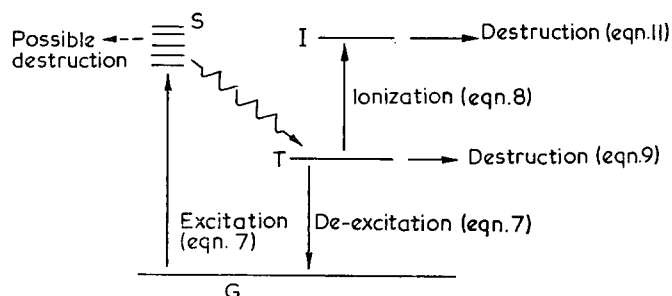


Figure 1 Model of a luminescence centre showing excitation from the ground state G to the singlet manifold S, intersystem crossing to the first triplet state T and de-excitation. Ionization to the ionized state I occurs from T.

Formally this solution can be written in terms of the tabulated function $Ei(x)^9$, and the asymptotic limits are:

$$N_i = (C/m)(x-1) = CrN_0D \quad (D \text{ small}) \quad (14)$$

$$N_i = C/m\beta D \quad (D \text{ large}) \quad (15)$$

These limiting forms should be compared with equations (4) and (5). A convenient computational method is to ignore the tabulated function and to change the variable by the substitution:

$$\exp[\beta(z-1)/mrN_0] = w$$

whence

$$N_i = (C/m)\exp(-\beta D) \int_1^{\exp(\beta D)} dw / (\beta/mrN_0 + \ln w) \quad (16)$$

The integral is now in a form that is readily evaluated by quadrature. The results plotted in *Figure 2* are typical. The two disposable parameters β and mN_0 are sufficient to define the position of the peak on the dose scale, and the shape of the peak. The parameter C/m defines the origin of the vertical scale. Since the experimentally observed quantity is the number of photons emitted, and this is less than the number of ionized luminescent centres owing to non-radiative transitions during the heating cycle, there is no way in which C/m can be evaluated and only relative values are of importance.

DISCUSSION

The curves shown in *Figure 2* provide a fit which is exact, within experimental accuracy, to the data given in Fig. 3 of ref 1. The values needed for this fit are:

$$\beta = 4 \times 10^{-18} \text{ cm}^2 \text{ photon}^{-1}$$

$$mN_0 = 1 \times 10^{-35} \text{ cm}^4 \text{ sec photon}^{-2}$$

and the experimental dose rates are 1.0, 2.8 and 6.2×10^{16} photons $\text{cm}^{-2} \text{ sec}^{-1}$. A check on the validity of the present model is to see if the values of β and mN_0 are

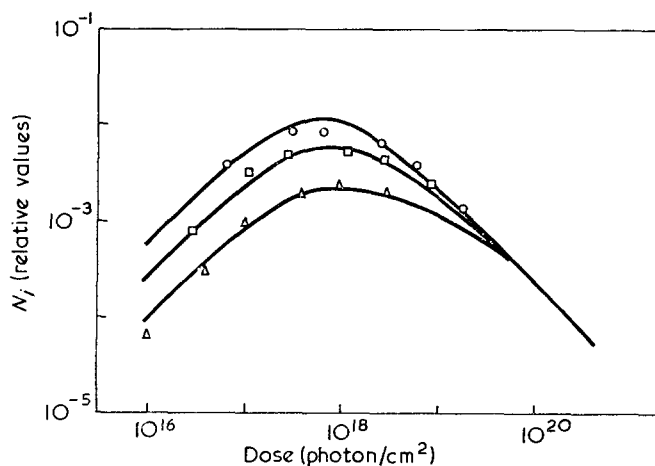


Figure 2 Curves showing the number of ionized centres versus total dose, calculated from equation (16). The parameters employed are given in the text. The points are experimental results for luminescent output¹, scaled up by a constant multiplier (reproduced from Charlesby, A. and Partridge, R. H. *Proc. R. Soc. (A)* 1965, **283**, 329 by permission of the Royal Society, London)

reasonable. For simplicity, we ignore the complication that the absorption depth is about one-seventh of the sample thickness. The parameter β is simply the cross-section for photon capture by an ionized luminescence centre. The physical cross-section of a carbonyl group is of the order of $4 \times 10^{-16} \text{ cm}^2$, so the value of β suggests a probability of 0.01 for the destruction interaction to occur. While there are no other figures available for comparison purposes, this seems to be a plausible one.

The parameter m is given by $m = IC_1^2\tau^2$. If the triplet state is involved in the destruction of luminescence centres, then $\tau \approx 2 \text{ sec}$, while if an excited singlet is implicated then the appropriate lifetime will be considerably less. The concentration N_0 of aldehydic carbonyl groups¹⁰ is not known, though it must exceed 10^{14} cm^{-3} and is probably much larger¹. For the sake of argument, we adopt an arbitrary figure of 10^{16} cm^{-3} . The cross-section for triplet formation is also uncertain, but a value comparable to β seems reasonable, and we set $C_1 = 10^{-18} \text{ cm}^2$. With these values we obtain $l = 10^{-16} \text{ cm}^3/\text{sec}$. The destruction reaction is probably controlled by the diffusion of some fragment of an excited carbonyl group to another excited carbonyl group, so we surmise that $l = 4\pi bD$, where b is a capture radius of order 10^{-8} cm and D is the diffusion coefficient. We thus find $D \approx 10^{-9} \text{ cm}^2/\text{sec}$. A smaller value of τ leads to a larger value of D , and so does a small value of N_0 . Hence, while there is considerable uncertainty in the absolute value of D , it is of the right order for diffusion of small molecules in low density polyethylene^{11,12}, so the mechanism suggested is certainly feasible.

One question which arises naturally out of this work is whether it is related to the apparently similar 'low dose effect' observed after γ -excitation³, and discussed theoretically in a recent review¹³. The luminescent molecules are relatively stable under γ -irradiation¹⁴, at least for doses in the 1 Mrad range. Presumably the γ energy is uniformly deposited, and transferred by the exciton mechanism¹⁵ to give direct ionization in a single step process, while the u.v. light is preferentially absorbed at the luminescent sites and this gives rise to an enhanced damage rate, despite the bimolecular kinetics. Thus there is a qualitative difference between the effects of the two methods of excitation.

One mechanism suggested for the reduction of luminescent centres under u.v. illumination was the production of alkyl radicals by a two quantum process¹. This mechanism does not seem to account for the observed bimolecular nature of the destruction reaction. The alkyl radicals formed do act as efficient electron traps, but the number formed at the maximum u.v. exposure employed was equal to the number formed by 0.17 Mrad of γ -radiation. This is well below the dose at which they provide important competition for other traps in the γ -excited thermoluminescence. Consequently, their effect has been ignored in the present context. It follows from these arguments that beyond common qualitative features, there is no connection between the u.v. dose kinetics and the low dose effect observed after γ -irradiation^{3,13}.

We have therefore been able to account for the observed thermoluminescence yield under u.v. excitation, including the dose rate dependence of the output at low doses, the shape and position of the peaks of the yield curves, and the destruction of the luminescent

centres at a rate proportional to the square of the dose rate. We have thus resolved the difficulty noted by the original authors. We suggest that the destruction reaction is diffusion controlled, and from the rate constant we have deduced a diffusion coefficient which corresponds with known values for the drift of small molecules. The chemical mechanism cannot be deduced from the work and requires further study.

ACKNOWLEDGEMENTS

The author wishes to thank the National Research Council of Canada for their financial support of this project, and Dr K. E. Russell for helpful discussion.

REFERENCES

- 1 Charlesby, A. and Partridge, R. H. *Proc. R. Soc. (A)* 1965, **283**, 329
- 2 Cicchetti, O. *Adv. Polym. Sci.* 1970, **7**, 70

- 3 Boustead, I. *Proc. R. Soc. (A)* 1970, **318**, 459
- 4 Campbell, D. J. *Polym. Sci. (B)* 1970, **8**, 313
- 5 Partridge, R. H. *J. Chem. Phys.* 1970, **52**, 1277
- 6 Keyser, R. M., Tsuji, K. and Williams, F. 'The Radiation Chemistry of Macromolecules', (Ed. M. Dole), Academic Press, New York, 1972, Vol 1, pp 145-191
- 7 Ince, E. L. 'Ordinary Differential Equations', Dover, New York, 1953, p 23
- 8 Kamke, E. 'Differentialgleichungen', 3rd Edn, Chelsea, New York, 1948, p 21
- 9 Abramowitz, M. and Stegun, I. A. 'Handbook of Mathematical Functions', National Bureau of Standards, Washington, 1964
- 10 Charlesby, A. and Partridge, R. H. *Proc. R. Soc. (A)* 1965, **283**, 312
- 11 Yasuda, H. and Stannett, V. J. *Polym. Sci.* 1962, **57**, 907
- 12 Paul, D. R. and DiBenedetto, A. T. *J. Polym. Sci. (C)* 1965, **10**, 17
- 13 Partridge, R. H. 'The Radiation Chemistry of Macromolecules', (Ed. M. Dole), Academic Press, New York, 1972, Vol 1, pp 193-222
- 14 Charlesby, A. and Partridge, R. H. *Proc. R. Soc. (A)* 1963, **271**, 170
- 15 Partridge, R. H. *J. Chem. Phys.* 1970, **52**, 2485

Solution properties and unperturbed dimensions of poly(vinylidene fluoride)

G. J. Welch*

Department of Chemistry, University of Manchester, Manchester M13 9PL, UK
(Received 29 May 1973; revised 5 February 1974)

A commercial sample of poly(vinylidene fluoride) (PVF₂) was fractionated and characterized. The following relationships were found: $(\eta) = 1.93 \times 10^{-4} M^{0.677}$ (in dimethylacetamide at 25°C); $(\eta) = 2.13 \times 10^{-4} M^{0.62}$ (in acetophenone at 85°C); $(\eta) = 6.86 \times 10^{-4} M^{0.50}$ (in benzophenone at 190°C), leading to a value of the steric factor: $\sigma = (\langle r^2 \rangle_0 / \langle r^2 \rangle_{0f}) = 1.66 \pm 0.05$, which is in agreement with the crystalline properties of the polymer. The concept of $M(\eta)$ as a universal parameter for g.p.c. calibration was valid for PVF₂ in dimethylacetamide.

INTRODUCTION

Poly(vinylidene fluoride) (PVF₂) is a semi-crystalline, thermoplastic material which is resistant to thermal degradation. In the polymerization of vinylidene fluoride approximately 5% of the monomer units are added in a reverse sense¹, so that the material is essentially a copolymer. Most studies of PVF₂ have been directed towards the elucidation of its crystal structure^{2,3}. It can exist in at least two crystal forms at room temperature and pressure. The most stable is the α -form in which the polymer molecules occur as 2₁ helices in the tg^+tg^- configuration³. In the β -form the chains assume the *trans*-planar configuration.

These features of the structure and properties of poly(vinylidene fluoride) led to an investigation of the solution properties and crystallization⁴ of this polymer. This paper describes the fractionation, characterization and viscometric measurement made on a commercial sample of poly(vinylidene fluoride) supplied by Pennsalt Chemicals as Kynar Resin Grade 301.

EXPERIMENTAL

Fractionation

The Kynar resin was fractionated by fractional precipitation between 136 and 158°C using acetophenone as solvent and *o*-dichlorobenzene as non-solvent. The proportion of reversed units in each fraction was calculated from the ¹⁹F n.m.r. spectrum of that fraction¹ measured with a 60 MHz Perkin-Elmer R10 instrument. There was no trend of heterogeneity with molecular weight, the mean proportion of reverse units being 0.057 ± 0.006 . The melting point of each fraction was determined under identical conditions using a microscope hot stage thermostated to $\pm 0.02^\circ\text{C}$ ⁴. The fractions, which were crystallized *in situ* at 136°C, all melted in the region $162 \pm 2^\circ\text{C}$.

* Present address: Unilever Research Ltd, Port Sunlight, Wirral, Cheshire L62 4XN, UK.

Light scattering measurements

The solvent used was acetophenone which dissolved the polymer only above 60°C. Solutions and solvent were clarified by ultracentrifugation in a Beckman model L ultracentrifuge at 65°C. Light scattering measurements were performed immediately using a Sofica instrument thermostated at 85°C. The results are shown in Table 1.

A Brice-Phoenix differential refractometer (thermostated to $\pm 0.1^\circ\text{C}$) was used to measure the dn/dc . The value obtained ($0.078 \pm 0.002 \text{ cm}^3/\text{g}$) was independent of temperature between 60°C and 80°C.

Viscometry

Dilute solution viscosities were determined with a Desreux-Bischoff viscometer⁵ for which shear and kinetic energy corrections were negligible. The solvents used were dimethylacetamide (DMA) at 25.0°C, acetophenone at 85.0°C and benzophenone between 150°C and 190°C. Concentrations were calculated for benzophenone solutions using standard density data⁶. Measurements were also made on polystyrene in DMA and dimethylformamide (DMF) at 25.0°C. The results are recorded in Tables 2 and 3.

Gel permeation chromatography (g.p.c.)

G.p.c. was used to estimate the polydispersity of each fraction in order to correct the viscosity and light scattering data. No calibration was available for PVF₂ so it was necessary to derive one. The procedure used⁷ was essentially one of trial and error. A series of possible calibration curves were used to analyse the g.p.c. data until one was found which gave the least difference between M_w calculated from g.p.c. and M_w actually measured by light scattering. This was taken as the calibration curve for PVF₂ and used to calculate the M_z , M_w and M_n values shown in Table 1. In no case is the difference between M_w for g.p.c. and light scattering greater than 12%.

The instrument used was a Waters Associates Inc

Table 1 Light scattering and g.p.c. data for PVF₂ fractions

Fraction	Light scattering (in acetophenone at 85°C)					G.p.c. data		
	$M_w \times 10^{-5}$	$\langle r^2 \rangle_z^{1/2} \times 10^8$ (cm)	$\langle r^2 \rangle_w^{1/2} \times 10^8$ (cm)	$\Phi \times 10^{-21}$	$A_2 \times 10^4$ (cm ³ g ⁻² mol)	$M_z \times 10^{-5}$	$M_w \times 10^{-5}$	$M_n \times 10^{-5}$
1.1	39.4	3110			0.0			
1.2	33.7	2760	1950	1.04	0.3	50.6	32.8	15.3
1.3	6.9	1490	960	0.67	1.3	13.9	6.3	1.9
2.1	20.2	2030	1650	0.81	0.0	28.5	19.0	9.4
2.2	11.2	1950	1300	0.61	1.0	23.8	11.0	3.6
2.3	10.8	1540	1150	0.84	5.9	22.2	12.1	5.1
2.4	6.7	1400	950	0.61	2.8	14.8	6.9	3.0
2.5	4.5	950	800	0.55	2.2	6.1	4.3	2.7
2.6	2.8				2.2		2.9	1.9
2.7	1.8				7.6		1.7	0.98
2.8	(0.90) ^a						0.80	0.59
2.9	(0.34) ^a						0.34	0.21

^a From the viscosity/molecular weight relationship for PVF₂ in DMA

 Table 2 Intrinsic viscosity data for PVF₂ in DMA, benzophenone and acetophenone

Fraction	$M_w \times 10^{-5}$	[η] (dl/g) in DMA at		[η] (dl/g) in benzophenone at					[η] (dl/g) in acetophenone at 85°C
		25°C	155°C	160°C	170°C	180°C	190°C		
1.1	39.4	5.64							
1.2	33.7	4.80							2.29
1.3	6.9	1.67	0.46	0.46	0.48	0.48	0.50		0.85
2.1	20.2	3.54							1.80
2.2	11.2	2.39	0.56	0.57	0.60	0.63	0.66		1.22
2.3	10.8	2.33	0.57	0.58	0.61	0.63	0.66		
2.4	6.7	1.74	0.48	0.49	0.50	0.51	0.52		0.78
2.5	4.5	1.29	0.38	0.39	0.39	0.40	0.41		0.62
2.6	2.8	0.94	0.31	0.32	0.33	0.34	0.35		
2.7	1.8	0.68	0.26	0.27	0.27	0.27	0.27		0.40
2.8		0.43							
2.9		0.22							

Table 3 Viscosity data for polystyrene samples in DMA and DMF at 25.0°C

Producer	Nominal mol. wt	Intrinsic viscosity (dl/g)		M_v
		DMA	DMF	
Pressure Chem	51 000	0.26	0.21	48 000
BDH		0.48	0.40	136 000
Pressure Chem	160 000	0.49	0.41	145 000
BDH		0.79	0.63	290 000

model 200 GPC equipped with five columns packed with Styragel. The column pore sizes were from 10⁶ to 10² Å. The eluent was DMA and the flow rate was 1 ml/min. Measurements⁸ were also made on polystyrene standards ($M_w/M_n < 1.06$).

RESULTS AND DISCUSSION

Viscosity/molecular weight relationships for PVF₂

The g.p.c. data in Table 1 indicate that the PVF₂ fractions are still fairly broad so that the effect of polydispersity must be considered. Kurata and Stockmayer⁹ showed that under θ conditions the Mark-Houwink relationship for a polydisperse fraction is:

$$(\eta) = q_w K_0 (M_w)^{0.5}$$

where $q_w = \Gamma(h+1.5)/[(h+1)^{0.5}\Gamma(h+1)]$ and h is $(M_w/M_n - 1)^{-1}$. In a good solvent q_w overcorrects.

Applying this treatment to the data in DMA at 25.0°C gives:

$$\text{corrected } (\eta) = 2.01 \times 10^{-4} M^{0.675}$$

$$\text{uncorrected } (\eta) = 1.93 \times 10^{-4} M^{0.677}$$

These relationships are nearly identical which shows that even with broad fractions the effect of heterogeneity is small when values of M_w are used instead of M_v ⁹. The corrected relationships in the other solvents are:

$$\text{acetophenone at 85°C } (\eta) = 2.13 \times 10^{-4} M^{0.620}$$

$$\text{benzophenone at 155°C } (\eta) = 15.2 \times 10^{-4} M^{0.43}$$

$$\text{benzophenone at 160°C } (\eta) = 13.6 \times 10^{-4} M^{0.44}$$

$$\text{benzophenone at 170°C } (\eta) = 9.62 \times 10^{-4} M^{0.47}$$

$$\text{benzophenone at 180°C } (\eta) = 7.54 \times 10^{-4} M^{0.49}$$

$$\text{benzophenone at 190°C } (\eta) = 6.86 \times 10^{-4} M^{0.50}$$

The Mark-Houwink plots for PVF₂ in DMA, acetophenone, and benzophenone at 190°C are shown in Figure 1. The value of the Mark-Houwink exponent indicates that 190°C is the θ temperature of the PVF₂/benzophenone system. At temperatures below 190°C the exponent assumes values less than 0.50. This has been observed for a small number of other polymer-solvent systems^{10, 11}.

This procedure for identifying the θ temperature is not very accurate but the value of 190°C is probably correct to $\pm 10^\circ\text{C}$. The value of K_0 from the θ point relationship is thus $K_0 = 6.9(\pm 0.1) \times 10^{-4}$ dl/g.

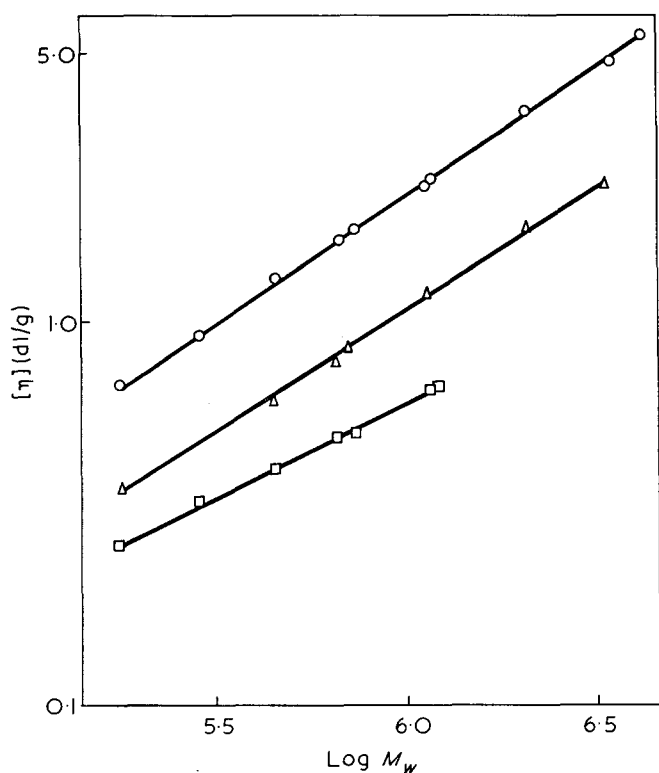


Figure 1 Intrinsic viscosity/molecular weight plots for PVF₂ in DMA at 25°C (O), in acetophenone at 85°C (Δ), and in benzophenone at 190°C (□)

θ point relationship for PVF₂

Various equations such as those of Stockmayer and Fixman¹², Berry¹³, and Flory *et al.*¹⁴ have been proposed for the determination of K_0 by viscosity measurements in a good solvent. These equations must be treated with caution since their theoretical and experimental basis is uncertain. Application to the PVF₂ viscosity data gave the following results.

Benzophenone. All three treatments gave linear plots at each temperature. The mean value of K_0 was $6.9 (\pm 0.1) \times 10^{-4}$ dl/g.

Acetophenone. The data in acetophenone yielded plots which curved slightly at high molecular weight. The intercepts gave (SF¹²) $K_0 = 6.9 (\pm 0.2) \times 10^{-4}$ dl/g, (B¹³) $K_0 = 6.8 (\pm 0.3) \times 10^{-4}$ dl/g and (FFS¹⁴) $K_0 = 5.9 (\pm 0.5) \times 10^{-4}$ dl/g. These are in satisfactory agreement with the θ point value of $6.9 (\pm 0.1) \times 10^{-4}$ dl/g except for the FFS¹⁴ plot which underestimates K_0 by about 15%.

DMA. For this solvent all the equations break down completely and curves are obtained from which no reliable intercepts can be derived.

Unperturbed dimensions of PVF₂

The Flory-Fox relationship¹⁴:

$$K_0 = \Phi_0 \langle r^2 \rangle_0 / M^{3/2}$$

has been confirmed both experimentally and theoretically for a number of polymer/ θ solvent systems¹⁵. The value of Φ recommended by Flory¹⁵ for θ point measurements is $2.6 (\pm 0.1) \times 10^{21}$ which agrees with recent experimental^{13, 16} and theoretical work¹⁷. Using this value and $K_0 = 6.9 (\pm 0.1) \times 10^{-4}$ gives $\langle r^2 \rangle_0 / M =$

$4.1 (\pm 0.2) \times 10^{-17}$ cm² for the unperturbed dimensions of the PVF₂ molecules. The steric factor (σ) is then $\langle r^2 \rangle_0 / \langle r^2 \rangle_{\text{of}} = 1.66 \pm 0.05$ where $\langle r^2 \rangle_{\text{of}}$ is the value for the freely rotating chain model with tetrahedral bond angles.

Flory and Mark¹⁵ have used the rotational isomeric state approximation to calculate the unperturbed dimensions of the polyoxymethylene (POM) chain for a range of configuration energies. The calculation is formally identical to that for the PVF₂ chain after correcting for the different bond lengths between the backbone atoms in the two polymers. PVF₂ occurs in two forms at room temperature. The α -form has a tg^+tg^- configuration and the slightly less stable β -form has a *trans*-planar configuration. The energy of the tg configuration is hence slightly greater than that of the tt configuration—say within the range 0 to 1 kcal/mol. The energy of the hindered g^+g^- configuration will be greater than 2 kcal/mol so that the steric factor (σ) must lie in the range 1.65–1.75¹⁵. The measured value of 1.66 is therefore in very good agreement with the crystalline properties of PVF₂.

Gel permeation chromatography

The g.p.c. calibration for PVF₂ was constructed from the g.p.c. and light scattering data by a process of trial and error. This method is tedious but reliable since fraction overlap ensures that any one point on the calibration curve is the mean of several estimates. From the calibration curve and the viscosity/molecular weight relationship for PVF₂ in DMA the universal calibration of Grubisic *et al.*¹⁸ was calculated. This is shown in Figure 2.

The viscosity data in Table 3 gives $(\eta) = 2.8 \times 10^{-4} M^{0.630}$ for the polystyrene/DMA system in the molecular weight range 51 000 to 300 000. Molecular weights were calculated from the viscosity relationship¹⁹ for polystyrene in DMF: $(\eta) = 3.18 \times 10^{-4} M^{0.603}$. The points in Figure 2 are for narrow polystyrene standards run on the same g.p.c. columns as the PVF₂. There is close correspondence between the polystyrene and PVF₂ universal calibration plots.

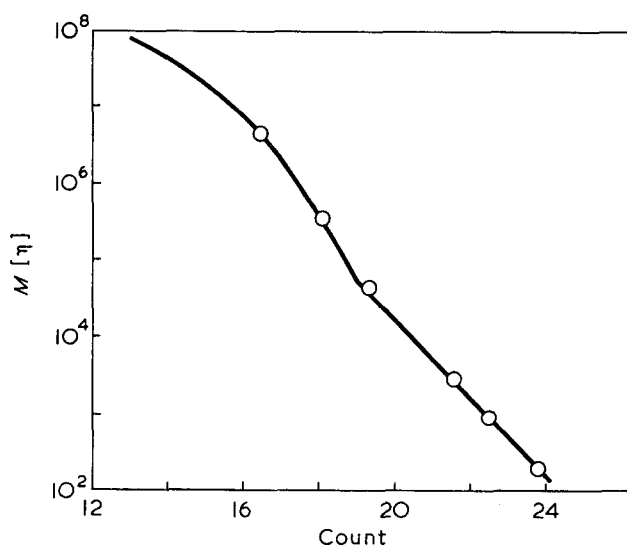


Figure 2 Universal g.p.c. calibration plot for PVF₂ (—) and polystyrene (O)

ACKNOWLEDGEMENTS

The author wishes to thank Mr E. Ambler, Organics Division, ICI Ltd for use of a Waters 200 GPC and for providing the polystyrene results quoted in this paper, Professor G. Allen, Chemistry Department, University of Manchester for invaluable help and discussion, and the Science Research Council for a grant to support this work.

REFERENCES

- 1 Wilson, C. H. and Santee, E. R. *J. Polym. Sci. (C)* 1965, **8**, 97
- 2 Lando, J. B., Olf, H. G. and Peterlin, A. *J. Polym. Sci. (A-2)* 1966, **4**, 941
- 3 Doll, W. W. and Lando, J. B. *J. Macromol. Sci. (B)* 1970, **4**, 309
- 4 Welch, G. J. and Miller, R. L. to be published
- 5 Desreux, V. and Bischoff, J. *Bull. Soc. Chim. Belg.* 1950, **59**, 93
- 6 Timmermans, J. 'Physical Chemical Constants of Pure Organic Compounds', Elsevier, New York, 1950
- 7 Ross, G. and Frolen, L. *J. Res. Nat. Bur. Stand. (A)* 1972, **76**, 163
- 8 Ambler, E. personal communication
- 9 Kurata, M. and Stockmayer, W. H. *Fortschr. Hochpolym. Forsch.* 1963, **3**, 196
- 10 Fee, J. G., Port, W. S. and Witnauer, L. P. *J. Polym. Sci.* 1958, **33**, 95
- 11 Kinsinger, J. B. and Hughes, R. E. *J. Phys. Chem.* 1963, **67**, 1922
- 12 Stockmayer, W. H. and Fixman, M. *J. Polym. Sci. (C)* 1963, **1**, 137
- 13 Berry, G. C. *J. Chem. Phys.* 1967, **46**, 1338
- 14 Flory, P. J. and Fox, T. G. *J. Am. Chem. Soc.* 1951, **73**, 1904
- 15 Flory, P. J. 'Statistical Mechanics of Chain Molecules', Interscience, New York, 1969
- 16 McIntyre, D., Wims, A., Williams, L. C. and Mandelkern, L. *J. Phys. Chem.* 1962, **66**, 1932
- 17 Pyun, C. W. and Fixman, M. *J. Chem. Phys.* 1966, **44**, 2107
- 18 Grubisic, Z., Rempp, R. and Benoit, H. *J. Polym. Sci. (B)* 1967, **5**, 753
- 19 Tsimpris, C. W., Suryanarayanan, B. and Mayhan, K. G. *J. Polym. Sci. (A-2)* 1972, **10**, 1837

Segmental orientation studies of block copolymers: 2. Non-hydrogen bonded polyurethanes

A. E. Allegrezza Jr*, R. W. Seymour†, H. N. Ng and S. L. Cooper‡

*Department of Chemical Engineering, University of Wisconsin, Madison, Wisconsin 53706, USA
(Received 5 November 1973)*

Uniaxial orientation of a series of polyurethane block copolymers of well characterized segmental molecular weight distribution has been studied by differential infra-red dichroism. These materials contain hard blocks incorporating piperazine units which have no possibility for hydrogen bonding. The soft segments orient into the direction of stretch at all strains but relax towards a random configuration when the load is removed. Hard segment orientation is transverse to the stretch direction at low strains, turning into the direction of stretch at higher strains. At the higher strains the hard segment orientation relaxes very little when the load is removed.

Compared to hydrogen bonding polyurethanes the polyurethanes of this study showed higher hard segment orientability and strain hysteresis. This may be partly attributed to the reduced strength of the intersegment bonding and more crystalline nature of the hard segment in the piperazine extended polymers. Segment polydispersity appears to have only a secondary influence on the sub-failure properties studied in this investigation.

INTRODUCTION

The first paper¹ in this series reported on the orientation behaviour of a group of hydrogen bonding polyether- and polyester-urethanes of varying composition. In this paper, the orientation behaviour of a series of specifically designed segmented polyurethanes of well characterized segmental molecular weight distribution (*MWD*) is studied by infra-red (i.r.) dichroism. These materials contain a hard segment of piperazine extended with the bischloroformate of 1,4-butane diol and thus have no possibility for hydrogen bonding.

Infra-red dichroism allows the study of the orientation of a particular molecular moiety during deformation of a polymer sample. These experiments may be done on samples undergoing large dynamic deformations, at various temperatures, or under various creep and stress relaxation conditions. From such studies, an understanding of the deformation process and its relationship to molecular parameters may be gained.

Linear segmented polyurethanes belong to the class of block copolymers known as thermoplastic elastomers. These materials have many of the properties of filled,

crosslinked elastomers at use temperatures, but may be processed as thermoplastics at elevated temperatures. The blocks of the major component are fluidlike at use temperature while the minor component is glassy or semi-crystalline and acts as a filler particle and multifunctional crosslink.

A segmented polyurethane has the general structure $(AB)_n$, where A and B are the hard and soft segments. They are usually made by the reaction of a polyether or polyester macroglycol (soft segment) of molecular weight less than 5000 with an aromatic diisocyanate, such as diphenylmethane diisocyanate (MDI). The hard segment content is adjusted by the addition of excess diisocyanate, balanced by a short chain diamine or diol. To prevent any covalent crosslinking, the stoichiometry and reaction conditions must be carefully controlled.

The interesting properties of the thermoplastic elastomers are due to the microphase separation of the dissimilar blocks which produces regions of high hard segment concentration, called domains². The domains act as solid filler and as tie-down points for the soft segment blocks. In the vinyl-diene ABA triblock copolymers produced by anionic methods the polymer architecture can be carefully controlled. It has been shown that the morphology, which changes with variations in composition, molecular weight, and method of sample preparation, controls polymer physical pro-

* Present address: Fabric Research Lab., Dedham, Massachusetts, USA.

† Present Address: Tennessee Eastman Co., Kingsport, Tennessee, USA.

‡ To whom correspondence should be addressed.

properties to a large extent^{3,4}. In the polyurethane block copolymers the relationship of polymer structure to domain morphology and thereby physical properties is made more complex by the broad segmental *MWD* and the hydrogen bonding capability of the hard segments. Although it is known that *MWD* affects the physical properties of homopolymers and copolymers, systematic studies of this effect on block copolymers have been lacking. Morton and coworkers^{5,6} have published some data for ABA vinyl-diene block copolymers indicating that an increase in the polydispersity of either the mid- or end-blocks decreases the tensile strength. Recently, a paper on the properties of the polyurethanes of the present study⁷ showed that copolymers with a narrow hard segment *MWD* exhibited better microphase separation and had higher modulus in the rubbery plateau region.

There is also substantial hydrogen bonding in conventional polyurethanes. While the major factor determining the properties of the segmented polyurethanes is their domain structure⁸, hydrogen bonding is a complicating consideration in any study of these polymers.

The object of this study was to gain a further understanding of the orientation mechanisms of block copolymers and the manner in which orientation is affected by composition, segmental *MWD* and intermolecular bonding. The copolymers used in this work were prepared by a carefully designed reaction sequence that produced polyurethanes having controlled hard segment molecular weight and *MWD*. These variables could therefore be systematically studied. A detailed description of these copolymers and their synthesis has been published elsewhere⁹. The hard segment formed from piperazine and 1,4-butanediol bischloroformate contains no hydrogen bonding donor. The behaviour of these copolymers can therefore be compared to that of hydrogen bonding polyurethanes in order to obtain an idea of the effect of hydrogen bonding on orientation.

Previous studies of polyurethane orientation

Using X-ray diffraction methods, Bonart^{10,11} and coworkers studied the orientation behaviour of polyurethanes and polyurea urethanes. They found that the soft segments oriented into the direction of stretch, with strain-induced crystallization occurring at about 150% strain.

Hard segment orientation was found to depend on whether the hard segment domain was partly crystalline or ordered in a paracrystalline state. The former was found in copolymers with longer average hard segment lengths. The paracrystalline segments were found to orient transverse to the stretch direction at strains below 200%. At higher strains the hard segments became oriented into the stretch direction with increasing strain. This behaviour was explained by a model where the hard segment lamellae orient as a whole into the stretch direction at low strains. At higher strains, they break up and the hard segments themselves orient into the stretch direction. Soft segment 'force strands' cause the hard segment lamellae to be rotated and oriented into the stretch direction. The more crystalline hard segment domains apparently

behave differently than the paracrystalline domains, and are described as acting more as inert filler. It was found that the hard segment orientation remained transverse in crystalline copolymers even at high elongations.

Kimura *et al.*¹² developed a similar model based on infra-red dichroism, X-ray diffraction and small angle light scattering. They concluded that the partly crystalline domains become disordered and oriented into the stretch direction at higher strains, although the superstructure of the crystallinity (spherulites) remains.

Estes¹³ studied a series of polyester and polyether urethanes of soft segment molecular weight 1000 containing no hard segment crystallinity. Upon stretching, both soft and hard segments oriented into the stretch direction. The soft segments relaxed almost completely when the load was removed, while the hard segment orientation recovered only slightly. No transverse hard segment orientation was found using infra-red dichroism.

Recently, Seymour¹ studied the orientation behaviour of polyester and polyether polyurethanes and found that the hard segment orientation mechanism was primarily a function of hard segment length. Three mechanisms were found, depending on whether the hard segment domains were interlocking, and whether or not they were partly crystalline. A lower limit of composition at which interlocking of the hard segments occurs was found. This composition is approximately 24% w/w MDI for 1000 molecular weight macroglycol soft segments. Polyurethanes with a composition above this limit retain their hard segment orientation after the load is removed. The interlocking morphology is due to a three dimensional connectivity of the hard segment lamellar like structure. This strongly hinders hard segment motion. Model calculations of this concept are presented elsewhere¹⁴.

For polyurethanes with 28–38% MDI, the hard segment orientation was found to lie in two bands, depending upon whether or not the hard segment domains were semi-crystalline. Polyurethanes with partly crystalline hard segment domains had a much lower average orientation than those with non-crystalline domains. This effect was ascribed to the transverse (negative) orientation of the hard segments in partly crystalline domains. It was also found that after a step increase in strain the orientation of the hard segments increased with time, while the soft segment orientation decreased. It was concluded that the decrease in the soft segment orientation was a result of the randomization of those segments due to an entropy driven stress relaxation. As the soft segments relax, they exert a tension on the hard segments causing them to increase their orientation.

Previous investigations have shown that the orientation behaviour of the two types of segments are quite different. Soft segment orientation is little affected by composition or molecular weight. Hard segment orientation, on the other hand, is controlled by hard segment molecular weight through its effect on domain size and crystallinity. It is to be expected that other block copolymers will behave in a generally similar manner, although differences in domain structure due to differences in polymer type and intermolecular bonding will play a large part in their orientation behaviour.

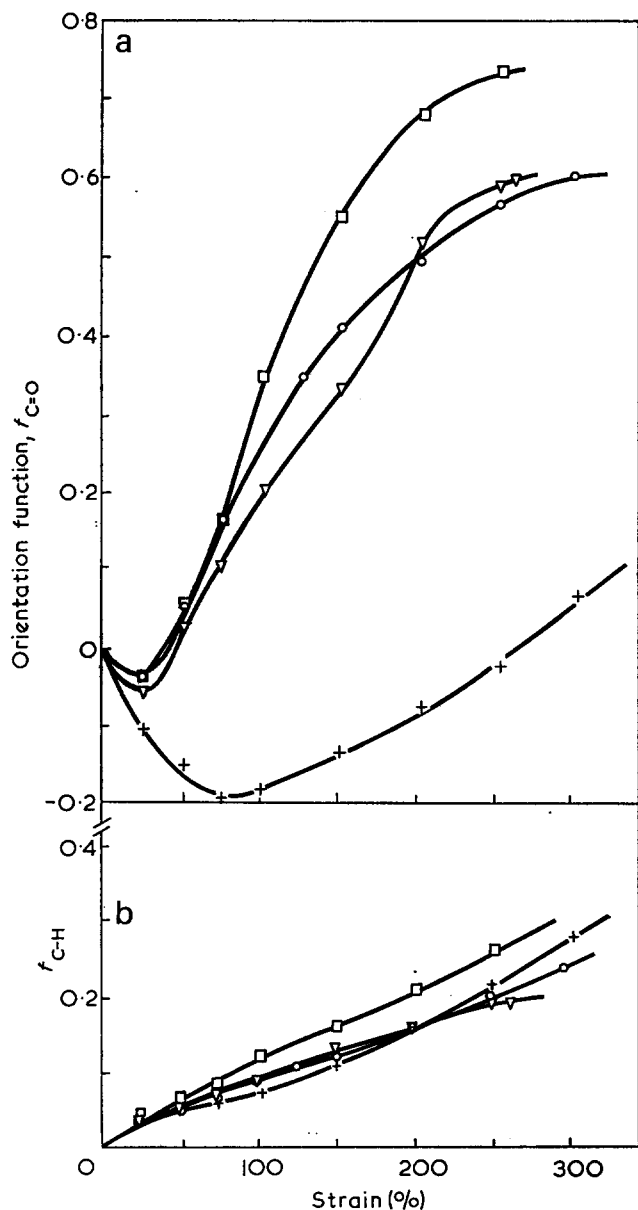


Figure 1 Orientation function vs. strain of control samples. (a) Hard segment; (b) soft segment. \square , BN2-3; ∇ , BN1-2; \circ , BB1-2; +, BB2-3

orientation function values may arise from orientation of lamellar domains as a whole into the stretch direction. This aligns the hard segments perpendicular to the stretch direction. Polyester and polyether polyurethanes show negative orientation only for copolymers having partly crystalline hard segment domains¹.

Wide angle X-ray diffraction and d.s.c. studies^{9, 15} have shown that the hard segment domains of the piperazine based copolymers are more crystalline than those of comparable MDI based copolymers. It is felt that the negative f values are manifestations of the orientation of the partly crystalline domains.

Another major difference in the orientation behaviour of these polymers compared to hydrogen bonded polyurethanes is the much higher level of hard segment orientation observed at the higher strain levels. For the latter, f values were never higher than 0.4, while ultimate f values for most of the piperazine polyurethanes were greater than 0.7.

The lack of hydrogen bonding in the piperazine copolymers may be significant in allowing higher hard

segment orientation. The non-hydrogen bonded hard segment domains are more easily disrupted than the hydrogen bonded polyurethanes, yet the system may be reinforced by a greater tendency to crystallize at high strains. Thus, the piperazine segments, unhindered by interchain hydrogen bonds and by strong inter-domain interactions, show a greater orientability than the hydrogen bonding MDI segments.

The soft segment orientation of these polymers is low and comparable to that in hydrogen bonded polymers. Since the soft segments are above their T_g and melting point, they tend to relax toward a random configuration after stress is applied. The soft segment f values for the 2-3 series are somewhat higher than for materials with 1000 molecular weight polyether. This may be due to a longer relaxation time for the higher molecular weight segments. Stress induced crystallization may also be a factor influencing orientability of the longer soft segments. However, there is not a large

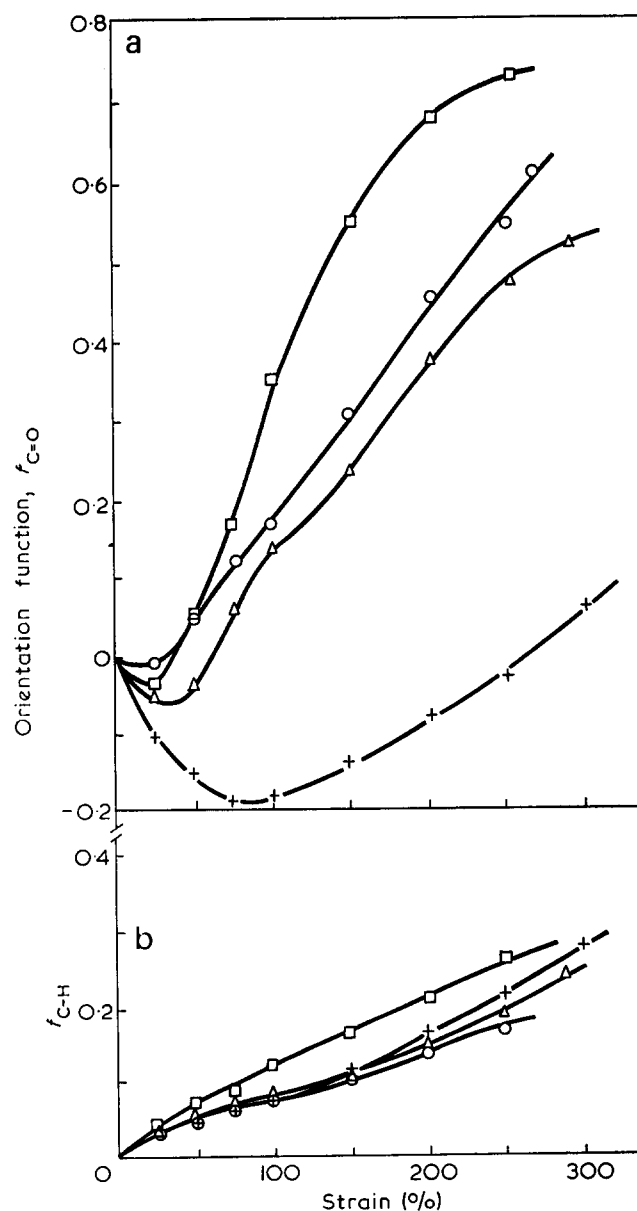


Figure 2 Orientation function vs. strain of control samples. (a) Hard segment; (b) soft segment. \square , BN2-3; \circ , BN1-4; Δ , BB1-4; +, BB2-3

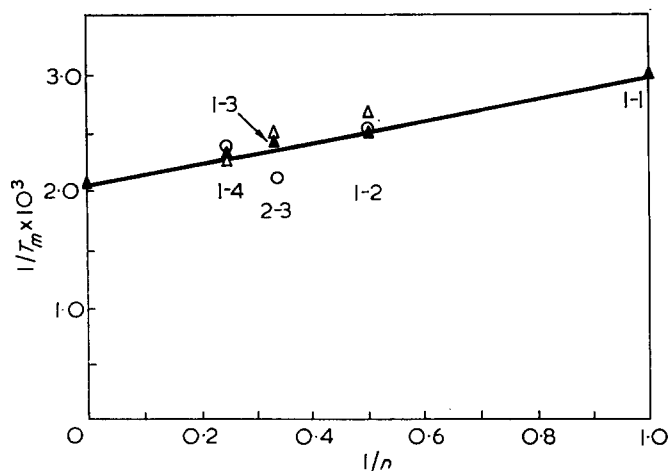


Figure 3 Effect of hard segment size on melting temperature. \circ , BB series, broad MWD; \triangle , BN series, narrow hard segment MWD; \blacktriangle , data of ref 9

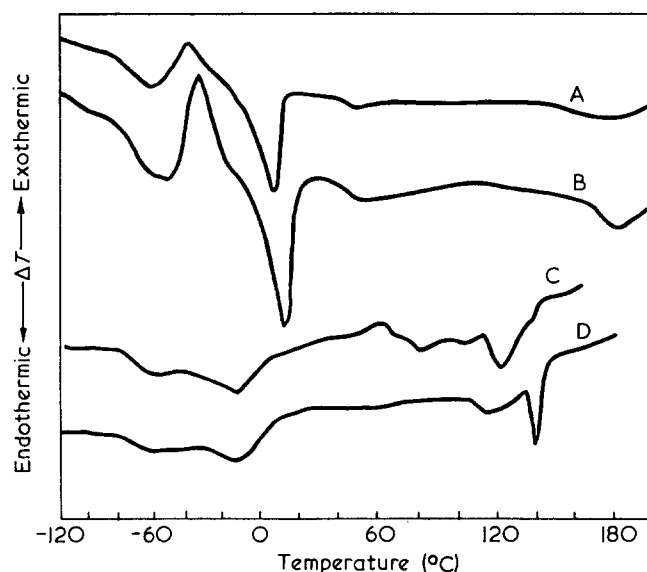


Figure 4 Effect of annealing on d.s.c. curves of BB2-3 and BN2-3. A, BB2-3 control; B, BB2-3 annealed at 160°C for 6h; C, BN2-3 control; D, BN2-3 annealed at 160°C for 6h

effect of composition and block length on the orientation of the soft segments.

There is little difference between the hard segment orientation function curves for the 1-2 and 1-4 series, as seen in Figures 1 and 2, although the BN polymers have somewhat higher values than the respective BB polymers. The BN2-3 curve takes on higher values at strains $>100\%$. This would appear to be due to the higher soft segment molecular weight as this is the major structural difference among these five polymers. The BB2-3 curve differs greatly from the others, showing negative orientation up to a strain of 250%.

At the present time, a complete explanation cannot be given for the anomalous behaviour of BB2-3. However, other data tend to indicate that the hard segment of this polymer may have an unusual size distribution. Figure 3 shows a correlation of d.s.c. melting points vs. $1/n$, where n is the hard block (average) length. Except for BB2-3, all fall on the correlation line. Using the correlation curve and the d.s.c. melting temperature, a value of $n=6-7$ is found for BB2-3,

much higher than the value of $n=3$ calculated from stoichiometry.

The reason the hard segment average length does not agree with that calculated may be in the method of polymerization. BB2-3 was polymerized using piperazine end capped macroglycols, whereas the other polymers were polymerized from chloroformate capped macroglycols. In effect, BB2-3 was polymerized using a two-step method, while the other copolymers were synthesized by a one-step method. For example, simple chain extension of the capped BB2-3 prepolymer would give a hard segment containing two piperazine units while in the case of the other copolymers, simple chain extensions would give only one piperazine unit. It is also probable that during the prepolymer step in the production of BB2-3 some chain extension of the soft segments occurred. This would raise the overall soft segment molecular weight and therefore cause the hard segment molecular weight to be higher than expected. Thus the anomalous physical properties of BB2-3 suggest that the different synthetic methods used resulted in an unexpected hard segment MWD, with particularly short and long sequences present.

The d.s.c. thermograms of BB2-3 also show a large endotherm at 8°C, indicative of soft segment crystallinity (Figure 4). A similar, but much smaller endotherm is seen at approximately -10°C for BN2-3. No soft segment endotherm is seen for the other copolymers

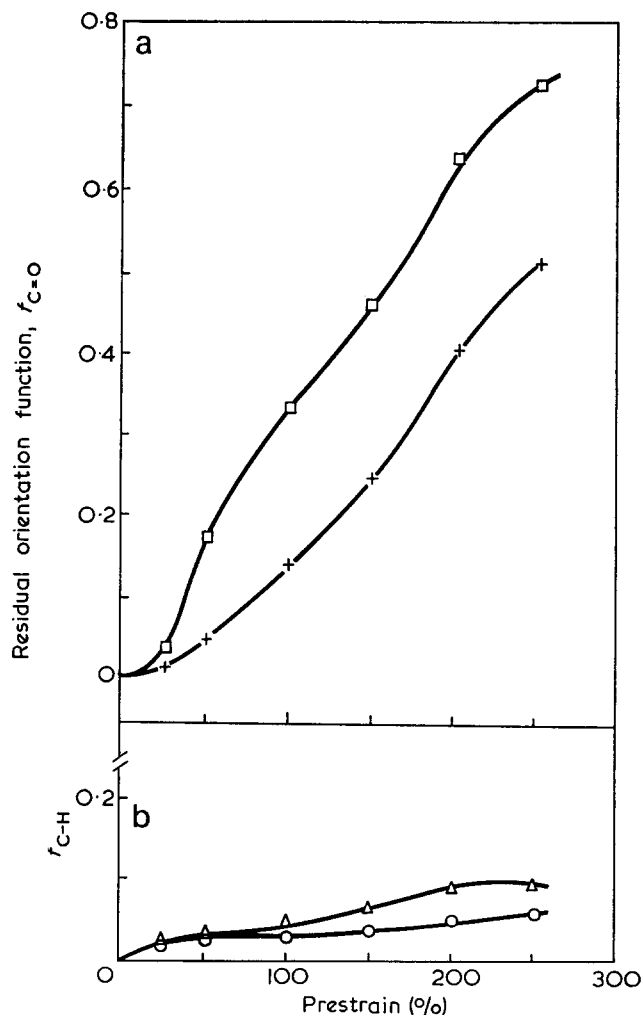


Figure 5 Residual orientations of BB1-2 (+, \circ) and BN1-2 (\square , \triangle) as a function of prestrain. (a) Hard segment; (b) soft segment

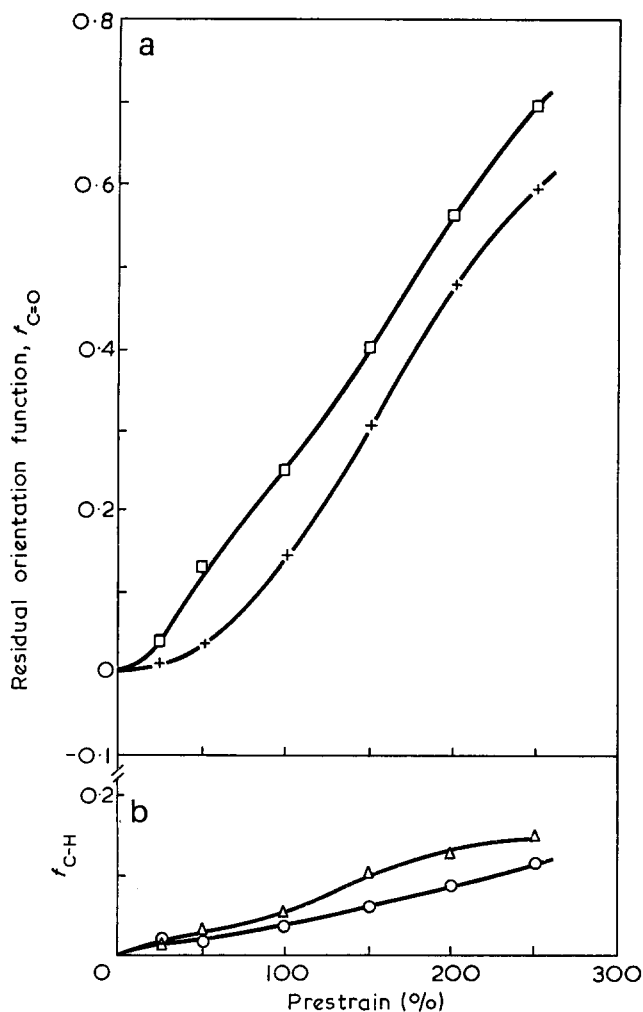


Figure 6 Residual orientations of BB1-4 (+, ○) and BN1-4 (□, △) as a function of prestrain. (a) Hard segment; (b) soft segment

of this paper, indicating a lack of soft segment crystallization in the unstretched materials.

Residual orientation

Figures 5, 6 and 7 show residual orientation function values plotted vs. prestrain. The results are analogous to those for hydrogen-bonded polyurethanes¹, showing high residual hard segment orientation and little residual orientation for the soft segments. In fact, at the higher strains, the control and residual hard segment orientation curves are comparable, indicating very little hard segment relaxation.

Except for BB2-3, the hard segment residual orientation curves do not show negative orientation at low prestrains. Apparently the orientation of the partly crystalline hard domains is largely reversible, and residual orientation is contributed primarily by the positively orienting amorphous segments.

It is interesting to note that there is a greater differentiation between the corresponding BN and BB residual hard segment curves than was observed for the control. This is also evident, though to a lesser extent, in the soft segments. Based on the results of dynamic mechanical testing⁷, it was suggested that the hard segment domain morphology of the BN series has a higher degree of microphase separation than those of the BB series. This is due to the lack of low molecular weight hard segments in the BN copolymers and their monodisperse

nature. It is reasonable to expect that hard segments not incorporated into domains, such as those at a diffuse domain boundary or surrounded by soft segments would relax considerably after elongation, thereby lowering the average orientation.

Orientation hysteresis

Figures 8 and 9 show the orientation hysteresis curves of BB 1-4 and BN 1-4, which are typical results for the piperazine copolymers. Each succeeding orientation function curve passes through a minimum at about the maximum strain of the preceding run. Also, the first point of each run is at a higher f value than the last point of the preceding run. The samples did not return to zero strain because of creep. Finally, a curve drawn through the last point of each run conforms very closely to the control curve, indicating that the orientation at any strain is not affected by a lesser prestrain.

These curves can be explained by considering two types of orienting hard segment species. One is the highly ordered, partly crystalline hard segment domain; the other, an ordered, but not crystalline, hard segment domain. When a uniaxial load is applied, the partly crystalline domains orient as a whole with their long dimension parallel to the direction of stretching. The hard segments that make up the lamellar domain are ordered perpendicular to the long dimension of the domain and accordingly take up a transverse orientation. This results in a negative segmental orientation function. Also, this transverse orientation appears to

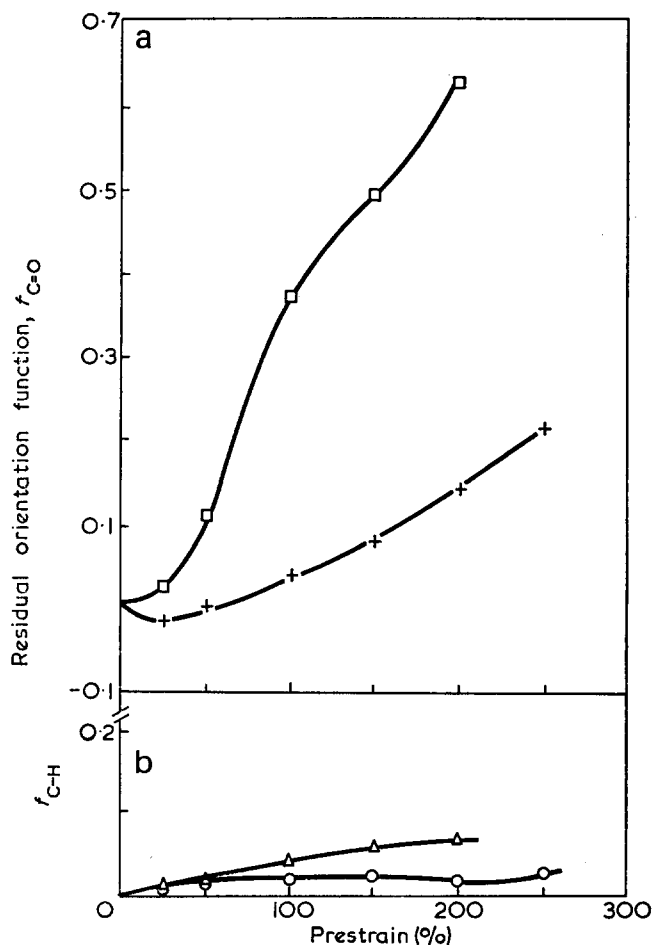


Figure 7 Residual orientations of BB2-3 (+, ○) and BN2-3 (□, △) as a function of prestrain. (a) Hard segment; (b) soft segment

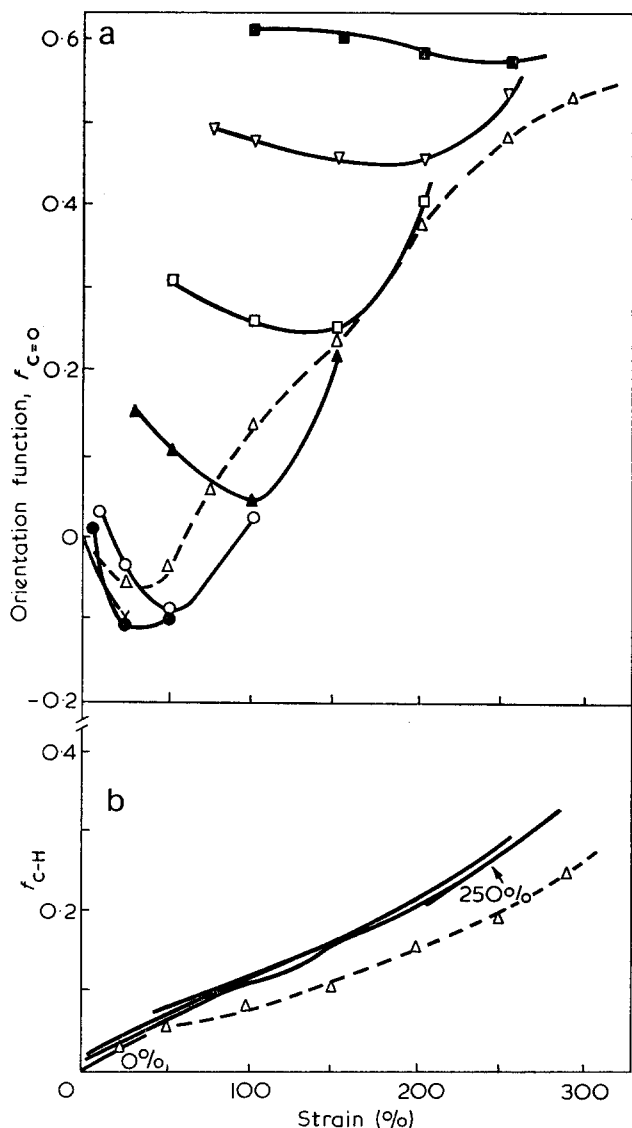


Figure 8 Orientation hysteresis of BB1-4 as a function of strain. (a) Hard segment; (b) soft segment. ----, Control. Prestrain: ×, 0%; ●, 25%; ○, 50%; ▲, 100%; □, 150%; ▽, 200%; ■, 250%

be reversible when the applied load is removed. For the non-crystalline domains, and presumably some of the crystalline domains, the applied stress causes a shearing force which disrupts the structure and orients the hard segments into the stretch direction. At higher elongations, this component outweighs the transverse orientation of the crystalline domains and a positive orientation function is obtained.

Two prominent features of the hysteresis can be explained by recourse to this model. The observation that the hard segment orientation function is higher at the beginning of each hysteresis cycle than it was at the highest strain of the previous run may be explained by the relaxation of the negatively oriented crystalline hard segments to a more random orientation. Upon subsequent stretching, the long axes of the highly ordered domains are again oriented as a whole into the strain direction causing a negative contribution to the hard segment orientation. Few, if any, positively orienting hard segments respond until the highest strain of the previous cycle is reached. Therefore, the f value decreases until that strain is reached. Above the previous strain level more of the less ordered hard segments are oriented

causing the f value to increase with increasing strain. This accounts for the minimum seen at the maximum strain of the previous run.

It is also of interest to compare the orientation hysteresis curves of the piperazine based copolymers with those of some MDI based polyurethanes. Figures 10 and 11 show these curves for two polyether polyurethanes, ET-38-1 and ET-38-2, which have 38% w/w MDI content and soft segment molecular weights of 1000 and 2000 respectively. The ET-38-2 polymer has been found to have partly crystalline hard segment domains, whereas no crystallinity is found in unannealed ET-38-1.

In neither of these two polyether urethanes does the 'dip' at the maximum strain of the previous run appear as strongly as in the piperazine copolymers. Also, the first point of each run lies at a lower f value than the final point of the previous run. This is thought to be

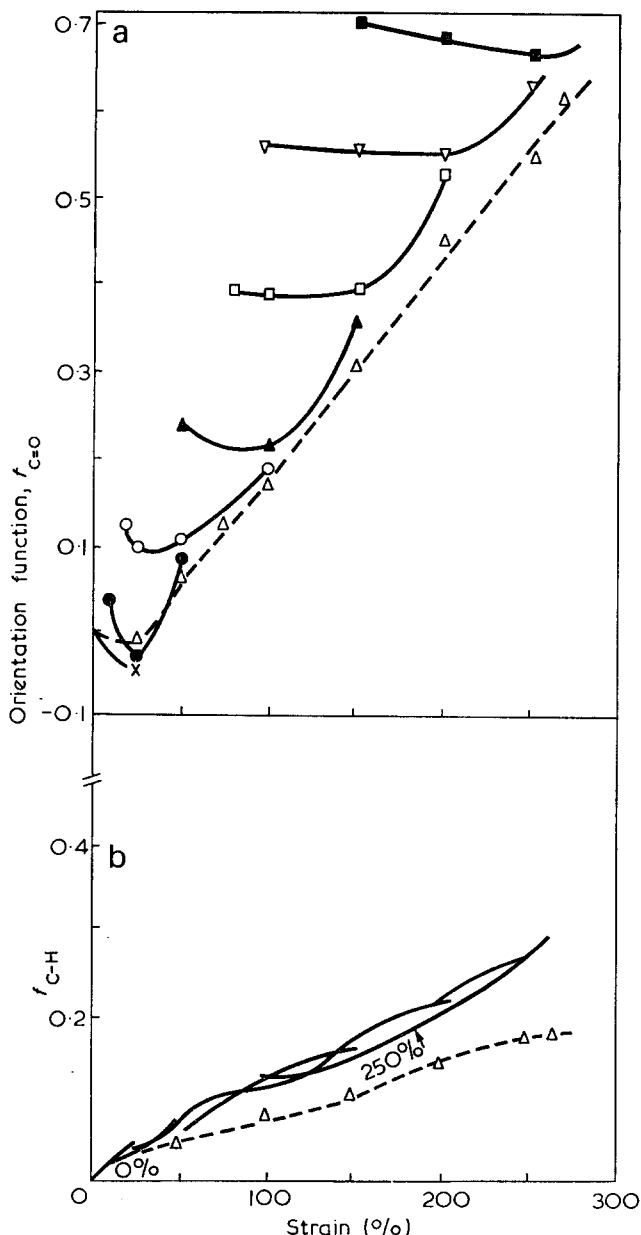


Figure 9 Orientation hysteresis of BN1-4 as a function of strain. (a) Hard segment; (b) soft segment. ----, Control. Prestrain: ×, 0%; ●, 25%; ○, 50%; ▲, 100%; □, 150%; ▽, 200%; ■, 250%

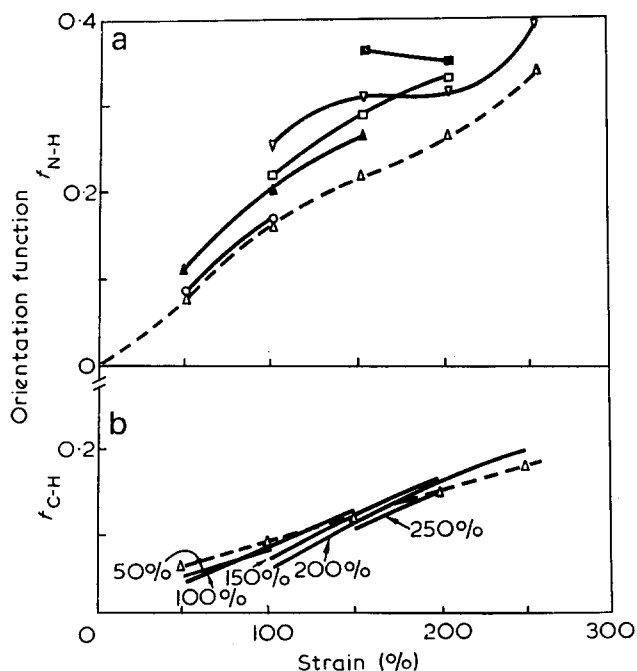


Figure 10 Orientation hysteresis for hydrogen bonded polyurethane ET-38-1 as a function of strain. (a) Hard segment; (b) soft segment. ----, Control. Prestrain: \circ , 50%; \blacktriangle , 100%; \square , 150%; ∇ , 200%; \blacksquare , 250%

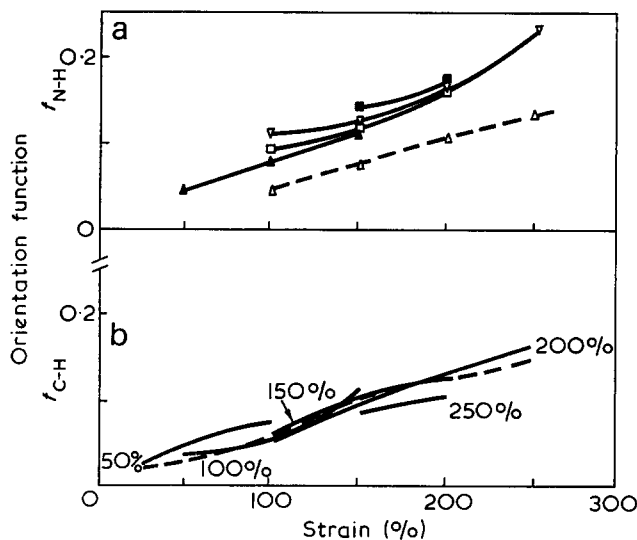


Figure 11 Orientation hysteresis for hydrogen bonded polyurethane ET-38-2 as a function of strain. (a) Hard segment; (b) soft segment. ----, Control. Prestrain: \blacktriangle , 100%; \square , 150%; ∇ , 200%; \blacksquare , 250%

due to the overall lower degree of crystallinity of these copolymers as compared to the piperazine based copolymers.

CONCLUSIONS

The i.r. dichroism results show that after elongation, the soft segments tend towards a random configuration while the overall hard segment orientation for these compositions does not relax. Hysteresis experiments do suggest, however, that orientation of crystalline hard segment domains is reversible so long as the domains are not disrupted by the strain. Hard segments in more poorly ordered domains orient into the stretch direction and do not relax extensively when the stress is removed. Furthermore, the overall hard segment orientation is dependent upon the maximum strain reached by the sample, and is not affected by lesser prestrains. It also appears that narrowing the hard segment *MWD* causes more hard segment orientation to be retained.

Compared to hydrogen bonding polyurethanes, these materials show generally higher levels of hard segment orientation. Some differences are also seen in the response of the two types of polyurethanes to the hysteresis experiment, which is attributed to a generally lower level of crystallinity in the hydrogen bonding materials. However, a large amount of hard segment orientational hysteresis is observed for both classes, which is thought to be due to the disruption of an interconnected lamellar hard segment morphology.

ACKNOWLEDGEMENTS

The authors wish to thank Dr L. L. Harrell, Jr of E. I. duPont de Nemours Co. for supplying us with the polymers described in this work. We are also grateful to the National Science Foundation for support of this research through Grant GH-31747.

REFERENCES

- 1 Seymour, R. W., Allegrezza, A. E. and Cooper, S. L. *Macromolecules* 1973, **6**, 896
- 2 Estes, G. M., Cooper, S. L. and Tobolsky, A. V. *J. Macromol. Sci. (C)* 1970, **4**, 169
- 3 *J. Polym. Sci. (C)* 1969, **26**
- 4 'Block Copolymers', (Eds D. C. Allport and W. H. Janes), John Wiley, New York, 1973
- 5 Morton, M. *Adv. Chem. Ser.* 1971, **99**, 490
- 6 Strauss, G. R. *PhD Thesis* University of Akron, 1970
- 7 Ng, H. N., Allegrezza, A. E., Seymour, R. W. and Cooper, S. L. *Polymer* 1973, **14**, 255
- 8 Seymour, R. W. and Cooper, S. L. *Macromolecules* 1973, **6**, 48
- 9 Harrell, Jr., L. L. *Macromolecules* 1969, **2**, 607
- 10 Bonart, R. *J. Macromol. Sci. (B)* 1968, **2**, 115
- 11 Bonart, R., Morbitzer, L. and Hentze, G. *J. Macromol. Sci. (B)* 1969, **3**, 337
- 12 Kimura, I., Ishihara, H., Ono, H., Yoshihara, N. and Kawai, H. *XXIII IUPAC Prepr.* 1971, p 525
- 13 Estes, G. M., Seymour, R. W. and Cooper, S. L. *Macromolecules* 1971, **4**, 452
- 14 Seymour, R. W. and Cooper, S. L. *J. Polym. Sci. (C)* in press
- 15 Samuels, S. L. and Wilkes, G. L. personal communication

Thermal crazing phenomena in epoxy resins

P. S. Theocaris, S. A. Paipetis and J. M. Tsangaris

*Department of Mechanics, National Technical University of Athens, Athens 147, Greece
(Received 1 November 1973)*

Hot-setting epoxy systems, consisting of a bisphenol A diglycidyl ether resin cured with phthalic anhydride and dibutyl phthalate as plasticizing agent (mainly for photoelastic applications), exhibit crazing phenomena when processed at moderately high temperatures. Chemical analysis and i.r. spectroscopy reveal that crazing is due to rejection of dibutyl phthalate from the surface layers of the specimens. The same phenomenon appears with triethylenetetramine (TETA)-cured cold-setting systems, where dibutyl phthalate undergoes transamidification with TETA before rejection.

INTRODUCTION

Crazing in polymers occurs under various conditions. A well known case is stress crazing of poly(methyl methacrylate) (PMMA), polycarbonate and associated materials¹⁻³ appearing in the form of fine hairlines when the latter are subjected to mechanical load higher than a certain limit for a sufficiently long time. Stress crazing is considerably accelerated by etching of the surface of the specimen with organic solvents such as alcohol, acetone, carbon tetrachloride or chloroform. Thermal crazing often appears with polymers in the case of extreme quenching⁴, by application of liquid nitrogen (-195°C). In all cases, crazes appear to follow principal stress patterns.

The particular case of thermal crazing dealt with in the present paper, concerns a class of photoelastic materials, based on a DGEBA epoxy resin*. The latter can combine with phthalic anhydride (PA) as curing agent, when a hot-setting system results, or with triethylenetetramine (TETA), leading to a cold-setting system. Both systems are generally suitable for photoelastic applications. However, hot-setting systems should be preferred for large castings associated with three-dimensional problems. In this case, usually applicable plasticizers, such as polysulphides cannot be used, and other plasticizing agents or diluents should be sought. Such an agent is dibutyl phthalate (DBP), which is a non-reactive diluent, providing plasticizing action by acting at the side chains of the macromolecule and decreasing the crosslinking density.

However, plasticized hot-setting systems with DBP proportions higher than 18%, developed surface crazing when subjected to moderately high temperatures ($130-140^{\circ}\text{C}$) for a few hours. This phenomenon⁵ possesses all common characteristics of the associated phenomena, such as crazes following principal stress patterns, high sensitivity towards stress gradients, and consequently it is more pronounced with rough surfaces, etc. (Figure

1). In addition, it was observed that surface hardness was increasing, while crazing was developing, and the material was becoming brittle. This led to the conclusion that the phenomenon should be attributed to rejection of the plasticizing agent by the surface layers of the material at the aforementioned temperature.

The object of the present work was the complete investigation of the phenomenon by means of chemical analysis and infra-red (i.r.) spectroscopy, in order to detect any molecular changes possibly leading to crazing. The investigation was extended also to cold-setting systems.

In this paper, any particular system will be designated by three successive numbers, of which the first is always 100 and refers to the basic resin or prepolymer, the second the percentage of plasticizer and the third the percentage of curing agent. Letters C or H denote cold-setting (curing agent TETA) or hot-setting (curing agent PA) systems respectively.

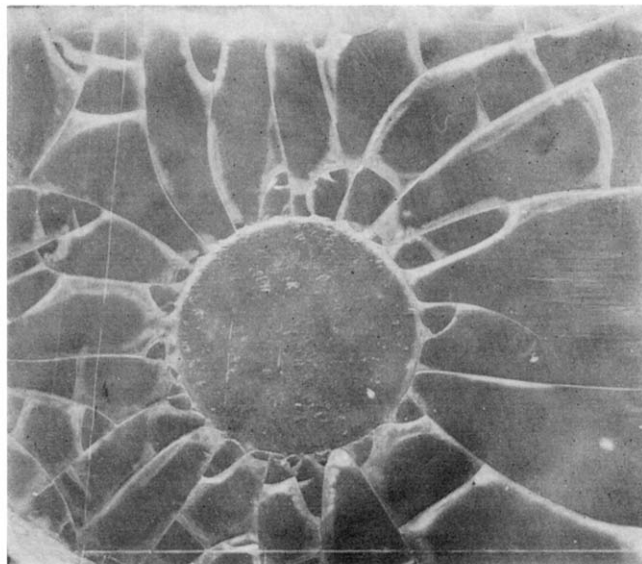


Figure 1 Crazed surface of a cross-section through a composite system consisting of spherical H 100-0-40 inclusion in a H 100-30-40 matrix

* Diglycidyl ether of bisphenol A, with epoxy equivalent 185-192 and viscosity of about 15 000 cP at 25°C , commercially available as Epikote 828 (Shell Co.).

Table 1 Compositions of the prepared specimens

Cold-setting system DGEBA-DBP-TETA	Hot-setting system DGEBA-DBP-PA
C 100-10-8	H 100-0-40
C 100-20-8	H 100-20-40
C 100-30-8	H 100-30-40
C 100-30-15	H 100-0-50
	H 100-20-50
	H 100-30-50

EXPERIMENTAL

Preparation of specimens

Two series of specimens were prepared, one corresponding to a cold-setting and the other to a hot-setting system. The exact compositions appear in Table 1.

The preparation for each system was carried out as follows.

For the cold-setting system, prepolymer, curing agent and plasticizer were mixed together at a temperature slightly higher than ambient (about 30-35°C) and after

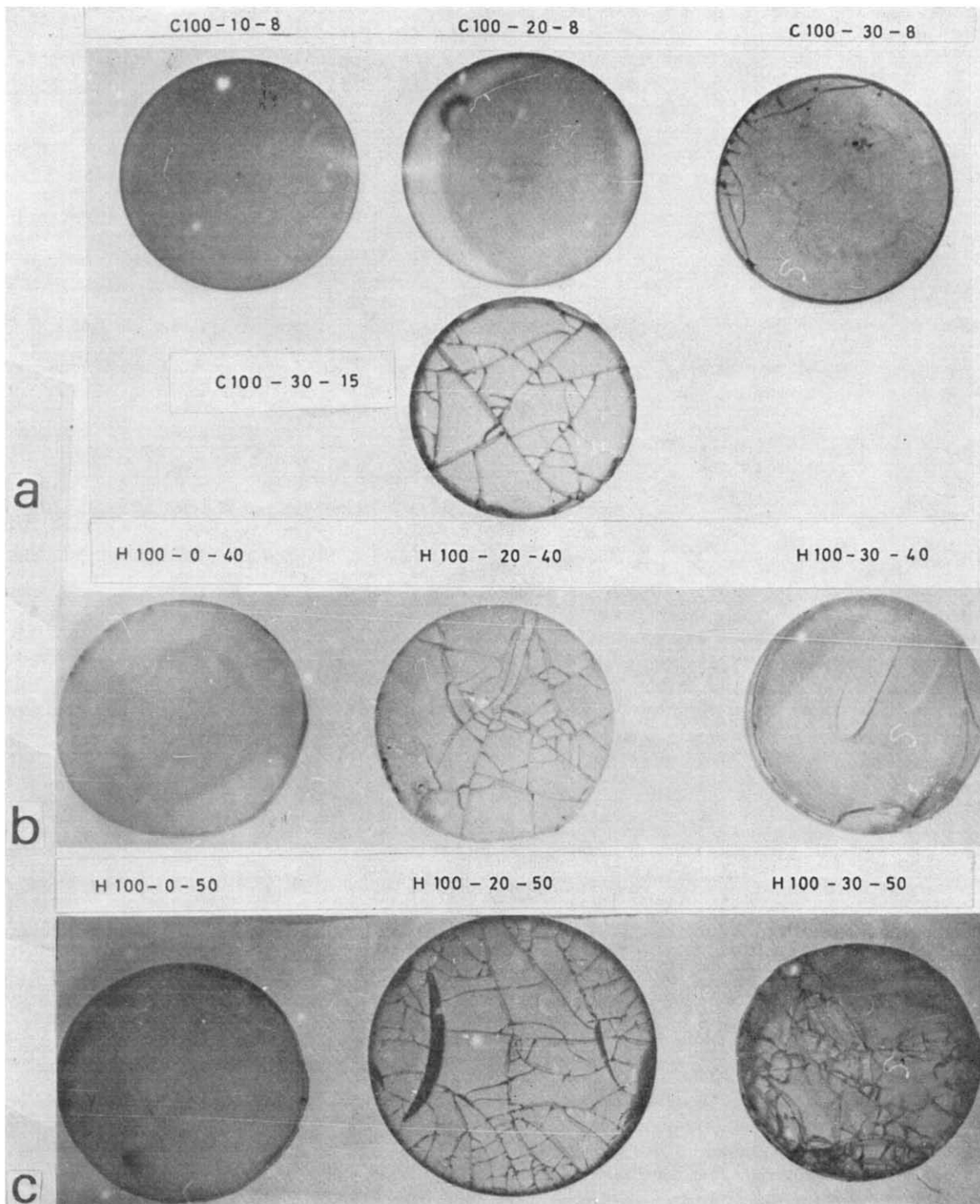


Figure 2 Crazed specimens: (a) cold-setting system; (b) hot-setting system with 40% PA (in the case of the H 100-30-40 specimen, a surface layer about 2mm thick was separated from the rest of the material); (c) hot-setting system with 50% PA

stirring, the mixture was put in a vacuum chamber for thorough degassing. The mixture was then cast into a mould, where it was left to set for about 24 h at ambient temperature. The casting was then removed from the mould and subjected to a curing procedure in an oven, consisting of a temperature rise of 5°C/h up to 100°C; the temperature was then maintained constant at 100°C for about 3 days and finally was lowered to ambient at a rate of 1°C/h. The castings were in disc form, about 80 mm diameter and 25 mm thick. After complete curing, they were split into two discs of average thickness 10 mm each by a saw-band, and the surfaces thus produced were finely machined on a lathe. One of the two pieces of each specimen was subsequently subjected to higher temperature to produce crazing.

For the hot-setting system, the prepolymer was initially heated up to 130–140°C where the curing agent (phthalic anhydride in platelet form) was easily dissolved. The plasticizer was then added and the whole mixture was cast, after proper stirring, into the mould, which was subsequently put into an oven at 110°C for about 8 days. The temperature was then lowered to ambient at 1°C/h. The casting was removed from the mould, and two identical specimens were produced, in the manner already described. Again, one of two pieces of each material was subjected to a thermal cycle up to the crazing temperature.

The latter procedure requires that the specimens remain at a temperature of 135°C for about 8 h. As expected, the necessary time for the crazes to develop varies from specimen to specimen and it is longer for less plasticized materials. On the contrary, with highly plasticized specimens crazes develop within 1 h and gradually turn to deep cracks.

Non-plasticized specimens did not develop any crazes. However, they were included in the present work in order to detect possible molecular changes due to processing at higher temperature. Also, two series of hot-setting specimens were produced (Figure 2), with 40% and 50% PA respectively, to investigate the effect of percentage curing agent.

Preparation of samples for chemical analysis and i.r. spectroscopy

As mentioned above, each specimen was split into two pieces, of which one was processed at high temperature, in order to develop crazing, while the other remained unprocessed. From the surface of each piece, samples in the form of filings were taken from a depth of 1 mm by means of a drill. Contaminating oils or other impurities were extracted from each sample in a Soxhlet apparatus by using alcohol and ether as solvents. The duration of extraction with alcohol was 2 h, and with ether 1 h. The samples were subsequently dried in high vacuum over CaCl₂. Samples thus purified were analysed for carbon and hydrogen, and the results of the analysis are presented in Table 2.

For the i.r. investigation the samples were further subjected to grinding to produce very fine powder. This difficult task was carried out by repeated use of quartz mortars and grinding mills. The powder thus produced was subjected to screening in standard sieves, to obtain uniformity of the grinding fineness and then it was purified again and dried in vacuum.

In the sequence, exactly 40 mg of powder were suspended in Nujol. The suspension was subjected to further

Table 2 Results of chemical analysis on samples taken from non-processed and from processed (crazed) specimens

Material	Non-processed specimens		Processed specimens	
	Carbon (%)	Hydrogen (%)	Carbon (%)	Hydrogen (%)
C 100-10-8	70.63	7.14	69.83	7.76
C 100-20-8	71.04	7.16	70.09	6.86
C 100-30-8	70.48	7.59	69.28	7.76
C 100-30-15	68.70	7.84	69.87	7.15
H 100-0-40	71.77	6.15	70.93	6.17
H 100-20-40	70.73	6.00	70.44	6.03
H 100-30-40	70.96	8.19	69.79	6.11
H 100-0-50	71.01	6.01	70.31	5.91
H 100-20-50	70.20	6.12	70.50	5.99
H 100-30-50	70.52	6.17	70.24	5.95

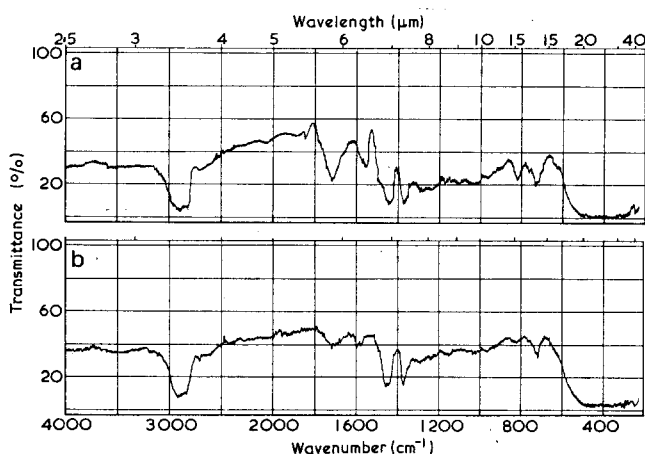


Figure 3 i.r. spectra for (a) unprocessed and (b) processed H 100-0-40 samples

grinding by a small agate mortar. From this final product mulls were produced, and the i.r. spectra were taken on a Perkin-Elmer 521 i.r. spectrophotometer.

The technique of obtaining i.r. spectra by means of potassium bromide pellets was not satisfactorily applicable in the present case.

RESULTS

The unprocessed H 100-0-40 sample compared to the processed one, exhibits a significant intensity diminution of the 1720 cm⁻¹ band owing to the carbonyl C=O stretching vibration (Figure 3). This band clearly stems from the carbonyl group of PA, since no DBP was contained in the unplasticized polymer. No other significant difference between the two was observed.

The unprocessed H 100-20-40 and H 100-30-40, compared to the processed ones, exhibit only a slight intensity diminution of the 1720 cm⁻¹ band. In this case the latter is due to the carbonyl stretching vibration of both PA and DBP.

Since Nujol possesses -CH₂- vibrations there was no possibility of drawing any conclusions concerning -CH₂- vibrations of processed and unprocessed samples.

The unprocessed H 100-0-50 exhibits a significant intensity diminution of the 1720 cm⁻¹ band compared with the processed one (Figure 4) as in the case of H 100-0-40 samples. Both H 100-20-50 (Figure 5) and H 100-30-50 processed samples exhibit slight diminution

of the 1720 cm^{-1} band, compared to the unprocessed ones. No other significant changes were observed, except in the $-\text{CH}_2-$ bands, from where no information can be obtained owing to the absorption of Nujol.

Unprocessed C 100-10-8, C 100-20-8 and C 100-30-8 samples compared to the processed ones, exhibit a slight diminution of the intensity of the 1720 cm^{-1} band, owing to the $\text{C}=\text{O}$ stretching vibration of DBP.

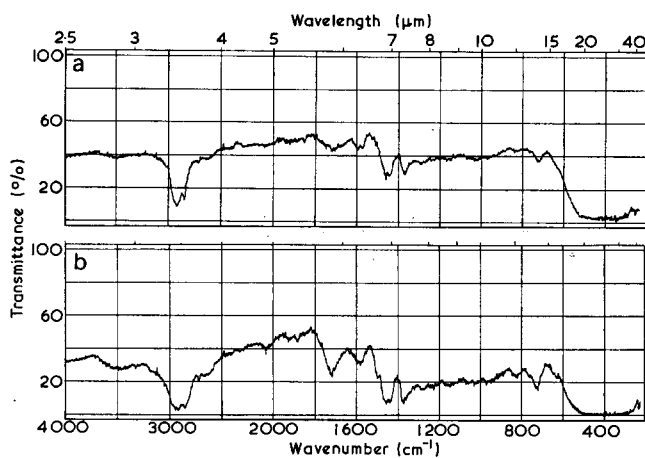


Figure 4 I.r. spectra for (a) unprocessed and (b) processed H 100-0-50 samples

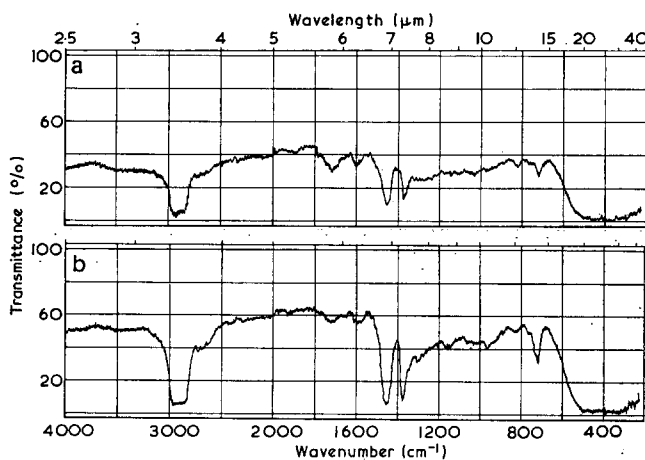


Figure 5 I.r. spectra for (a) unprocessed and (b) processed H 100-20-50 samples

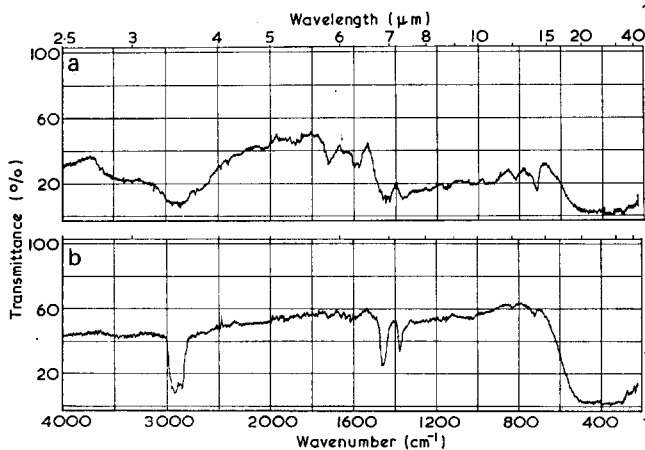


Figure 6 I.r. spectra for (a) unprocessed and (b) processed C 100-30-15 samples

Table 3 Carbonyl i.r. band vibration (1720 cm^{-1})

Material	Wavenumber (cm^{-1})		Integrated area before processing (cm^2)	Integrated area after processing (cm^2)	Area ratio
	From	to			
H 100-0-40	1640	1800	10.45	3.35	0.32
H 100-20-40	1650	1790	4.19	3.22	0.77
H 100-30-40	1650	1790	3.87	2.06	0.53
H 100-0-50	1650	1770	5.03	1.64	0.33
H 100-20-50	1660	1770	2.37	1.44	0.61
H 100-30-50	1670	1790	3.03	1.13	0.37
C 100-10-8	1680	1750	1.22	1.03	0.84
C 100-20-8	1670	1750	1.81	1.42	0.77
C 100-30-8	1700	1770	0.45	0.39	0.84
C 100-30-15	1670	1750	2.35	0.45	0.19

An interesting and dramatic change occurs in the i.r. spectrum of the processed C 100-30-15 sample (Figure 6). Apart from a significant diminution of the 1725 cm^{-1} carbonyl band, changes are observed in the region 2700 to 3700 cm^{-1} and also from 1550 to 1650 cm^{-1} .

As expected, N-H stretch vibrations of the primary amine and the secondary amine groups are located in the region 3000 to 3300 cm^{-1} . The aromatic C-H stretch band lies in the lower region around 2800 to 3000 cm^{-1} .

In the unprocessed sample a broad band appears with a shoulder at 3400 cm^{-1} . In the spectrum no sufficient resolution can be obtained, to detect peaks indicating separately the secondary N-H groups due to the NH asymmetric and NH symmetric stretch. All these bands overlap in the spectrum of unprocessed C 100-30-15 sample owing to the $-\text{NH}_2$ and NH groups of TETA. The 1600 and 1575 cm^{-1} medium intensity bands are probably due either to N-H in-plane bending vibration or to primary and secondary amine groups of TETA.

In the processed sample, the broad absorption between 3350 and 3000 cm^{-1} almost disappears, and the remaining peaks at 2920 and 2850 cm^{-1} are due to the aromatic $-\text{C}-\text{H}$ stretch. Also, 1600 and 1575 cm^{-1} bands owing to N-H bending vibrations disappear.

For reasons of comparison between intensities of the $\text{C}=\text{O}$ band at 1720 cm^{-1} of processed and unprocessed samples, the respective integrated areas under this band were measured and their ratio was evaluated, as reported in Table 3.

For obtaining the i.r. spectra, the same amount of material was accurately used for processed and unprocessed samples, and instrumental conditions were carefully maintained constant, such as the same narrow slit. However, it was extremely difficult to obtain repeatable extinction coefficients^{6,7}. Another difficulty arises, as plasticized polymer samples are two-component mixtures as far as $\text{C}=\text{O}$ stretching vibration due to PA and DBP is concerned. The main source of undetermined error in the present i.r. investigation stems from the uncertainty as far as the uniform distribution of polymer in the Nujol suspension in the layer between the i.r. cell windows is concerned.

DISCUSSION AND CONCLUSIONS

Unplasticized specimens (H 100-0-40 and H 100-0-50) did not develop any crazing. However, from the comparison of the i.r. spectra it can be concluded that a portion of PA was rejected during thermal processing. On the other hand, it is known that PA-cured resins

exhibit weight loss at higher temperature, generally proportional to the duration of processing⁸. This fact was attributed to possible splitting of the incompletely reacted anhydride and its subsequent volatilization. The present i.r. investigation completely supports this explanation. A comprehensive account of the chemical reactions involved in such a procedure has been given previously^{9,10}. Improved mechanical properties of processed specimens are due to the higher degree of polymerization thus produced.

With plasticized hot-setting specimens, as already stated, DBP with its long side chains inhibits cross-linking and consequently it prevents PA from evolving. Therefore, with increasing temperature, DBP is evolved, and crazing occurs. Crazing phenomena are more intense with increasing DBP percentage, as more non-reactive diluent has to be expelled. In this case C=O vibration in the i.r. spectra is due to DBP rejection. As indicated in *Table 3*, the ratio of integrated areas of processed and unprocessed specimens is decreasing with increasing DBP.

Crazing phenomena also appear with cold-setting systems. However, in *Table 3* it can be seen that the above ratios for TETA-cured resin, i.e. the amount of DBP evolved, is not proportional to its original percentage, but it actually depends on the TETA percentage. This probably indicates that DBP undergoes transamidification with TETA and then is expelled. This becomes very clear with C 100-30-15, where processed samples give i.r. spectra from which NH₂

vibrations are lacking, and most of the DBP was rejected, while highly crazed surfaces were produced.

ACKNOWLEDGEMENTS

The authors appreciate the assistance of Dr C. Mantzos of National Hellenic Research Foundation, in carrying out the carbon-hydrogen microanalysis and of Mr N. Mimicos and Miss P. Georgogala of Nuclear Research Centre 'Democritus' in obtaining the i.r. spectra. The research contained in this paper was partly supported by NATO Grant No. 558 (Scientific Affairs Division). The authors express their gratitude to this Agency.

REFERENCES

- 1 'Handbook of Experimental Stress Analysis' (Ed. Hetényi, M.) Wiley, New York, 1950, pp 641-643
- 2 Kambour, R. P. *J. Polym. Sci. (A-2)* 1965, **3**, 1713; 1966, **4**, 17, 349, 359
- 3 Narisawa, I. *J. Polym. Sci. (A-2)* 1972, **10**, 1789
- 4 Racké, H. H. and Fett, T. *Materialprüfung* 1971, **13**, 37
- 5 Theocaris, P. S. and Paipetis, S. A. *Fibre Sci. Technol.* 1974, **7**, 33
- 6 Kössler, I. in 'Characterization of Polymers' (Ed. Bikalas, N. M.), Wiley, New York, 1971, pp 125-148
- 7 Henniker, J. C. 'Infrared Spectrometry of Industrial Polymers', Academic Press, New York, 1967
- 8 Fisch, W., Hofman, W. and Koskikallio, J. *J. Appl. Chem.* 1956, **6**, 429
- 9 Lee, H. and Neville, K. 'Handbook of Epoxy Resins', McGraw-Hill, New York, 1967, p 21
- 10 'Epikote Resins for Electrical Castings', Technical Bulletin RES/EPX/301, Shell Chemicals, p 7

Solid-state extrusion of isotactic polypropylene through a tapered die: 2. Structure and some properties of extrudates

K. Nakamura*, K. Imada and M. Takayanagi

*Department of Applied Chemistry, Faculty of Engineering, Kyushu University, Fukuoka, Japan
(Received 19 July 1973; revised 8 February 1974)*

The structure and some properties of the solid-state extrudates of isotactic polypropylene (PP) were examined. The crystal modifications of the PP extrudates differed as the extrusion temperature changed. The formation of smectic crystals was observed in the samples extruded at temperatures below 70°C, while the monoclinic modification was predominant above 70°C. The crystal orientation factor, f_c , increased with increasing extrusion ratio (ER) and reached 0.988 when ER was 6.3, which was considered to be an upper limit of ER of PP extrusion. The mechanical properties and the thermal shrinkage of the extrudates were also examined. From these measurements the PP extrudates were considered to have structures similar to the drawn PP.

INTRODUCTION

In recent years we have investigated the plastic deformation and the solid-state extrusion of crystalline polymers under high pressures, and reported the work in a number of papers¹⁻⁶. Before being applied to polymeric materials, solid-state extrusion had been developed as one of the cold working processes for metals. The theoretical background of metal extrusion has been well established^{7,8} and many metals are now extruded successfully on a large scale. The solid-state extrusion of polymeric materials has been investigated recently⁹ and difficulties are apparent. Polymeric materials are quite different from metals in that the molecules are long and orient easily during deformation. At this stage then, it is important to clarify how the molecular orientation and strain hardening affect practical processing.

In previous papers we have reported the process of solid-state extrusion of high density polyethylene (HDPE)¹⁻³, blend systems of HDPE and n-paraffin⁴, isotactic polypropylene (PP)⁵ and nylon-6^{1,2}, from the viewpoint of the theory of deformation of plastic materials, and we proposed an equation to predict the extrusion pressure from tensile data^{3,5}. We have also examined the crystal orientation, superstructure and some properties of HDPE extrudates extruded at high temperatures (80–110°C)⁶. The properties and the structure of HDPE extrudates, which have excellent transparency in appearance and excellent thermal shrinkage characteristics, are shown to resemble those of HDPE drawn samples annealed with free ends after having been stretched.

In the present paper, the crystal modification, crystal orientation, mechanical properties and thermal shrinkage of the PP extrudates are considered.

EXPERIMENTAL

Material

PP resin used in the solid-state extrusion was a commercial grade of isotactic polypropylene, Noblen D501 (Sumitomo Chemical Co.). The viscosity-average molecular weight, \overline{M}_v , of the resin was 4.7×10^5 and the melt index (MI) was 0.46. Billets of 10 mm diameter were prepared by melting the PP pellets at 200°C in a mould placed in a conventional hydraulic press, and cooled slowly to room temperature in the mould under pressure. The billets thus formed were then turned into cylindrical rods on a lathe. The density of the billets was about 0.904 g/cm³ at 25°C.

Extrusion method

Figure 1 shows the extrusion device comprising a piston-cylinder system similar to that reported previously⁵. Tapered dies had half angle α of 25° and an inlet radius R of 5 mm. By using dies of various outlet radii as listed in Table I, the extrusion ratio (ER) was altered. Extrusion ratio, ER , is defined as the ratio of the cross-sectional areas of the entrance, (πR^2), and the exit, (πr^2), of the die, i.e. $ER = (R/r)^2$. Deformation ratio, DR , is also defined, for the samples which show the 'spring back' or die swell phenomenon at the die exit, as the ratio of the cross-sectional areas of the original billet, (πR^2), and that of the extrudate, ($\pi r'^2$), i.e. $DR = (R/r')^2$. The value of DR is usually smaller than ER by the factor of $(r/r')^2$. Die swell ratio is expressed by $(r' - r)/r$. Extrusion temperatures, T_e , covered

* On leave from the Central Research Laboratory of Sumitomo Chemical Industries Co. Ltd.

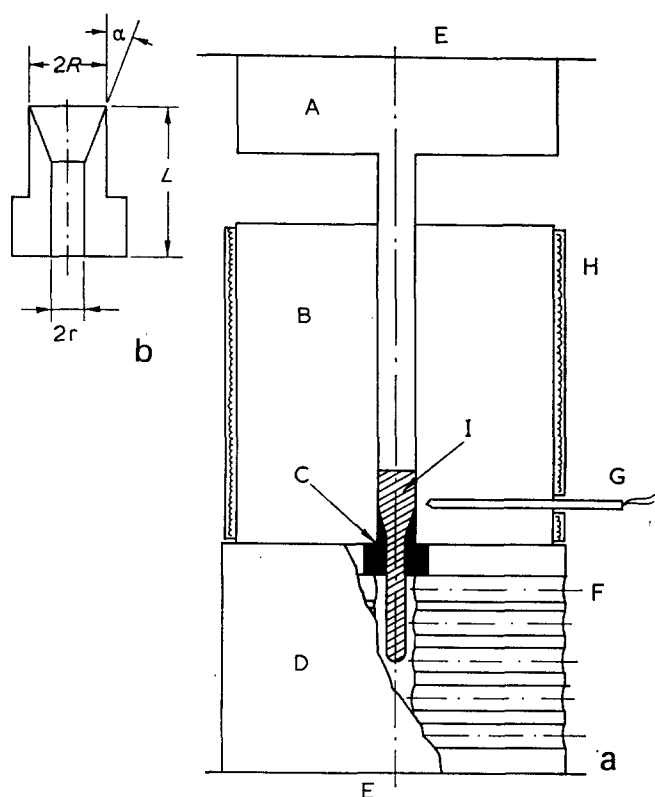


Figure 1 Extrusion device. (a) Piston cylinder; (b) vertical section of the die. A, Piston; B, cylinder; C, die; D, support; E, plate of press; F, eye hole; G, thermocouple; H, heater; I, material

Table 1 Outlet diameter and extrusion ratio of the dies used

Outlet diameter (mm)	Extrusion ratio
7.0	2.0
6.0	2.8
5.0	4.0
4.8	4.3
4.5	4.9
4.2	5.7
4.0	6.3
3.5	8.2

a range of 40 to 150°C and was controlled manually within an accuracy of 1°C. Extrusion was conducted after preheating for 1 h, putting the billet in the extrusion device at a prescribed temperature. Extrusion rate was also controlled manually between 5 to 10 mm/min. Structure and properties of the extrudates were ascertained not to be affected by extrusion rate in this range.

Structure analysis

For the analyses of the crystal modifications and crystal orientation of the PP extrudates, the wide angle X-ray scattering (WAXS) intensity was measured at room temperature by using a fibre specimen holder and a Geiger-Müller counter. Ni-filtered CuK α radiation with a point collimation system was used. Samples for X-ray measurements were sheets of 0.5 to 1.0 mm thickness cut from the extrudates including their central axes. In the cases of HDPE⁶, axis symmetric orientation of the *a* axis of the orthorhombic unit cell along the radial directions of the extrudate were observed. Williams¹⁰ reported that from measurements of birefringence the structure of

hydrostatically extruded isotactic polypropylene was isotropic with reference to the cross-section directions. This was not applied to our extrudates, but instead, testpieces cut out from the extrudates including their central axes were always used. The orientation factor, f_c of the *c* axis of the PP monoclinic crystal in the extrusion direction was evaluated from the intensity distribution of (110) and (040) planes along azimuthal angle and by using Wilchinskii's equation¹¹. The orientation factor f_β of the *b* axis was determined directly from the intensity distribution of (040) plane and f'_α of the *a** axis was determined by using the following equation based on the orthogonality between the *a**-, *b*- and *c*-axes:

$$f'_\alpha + f_\beta + f_c = 0$$

The fracture surface of the extrudate was observed with a scanning electron microscope (SEM). Small angle X-ray scattering (SAXS) photographs were taken at room temperature by using a small angle camera.

Measurement of the properties of extrudates

The stress-strain curves of the extrudates at room temperature ($\sim 23^\circ\text{C}$) were obtained by using a Tensilon UTM-III (Toyo-Baldwin Co.). Samples for testing were flat sheets 0.5 mm thick and 2 mm wide, cut out from the extrudate including its central axis. The initial distance between the crossheads of the testing machine was 20 mm and the extension rate was 5 mm/min. The measurements of the dynamic modulus of the extrudates were made by using a Rheovibron DDV-II at room temperature at 110 Hz. These mechanical properties were measured along the extrusion direction.

The thermal shrinkage of the extrudates was measured by using a Rheovibron. The samples used were sheets of about 0.5 mm thick and 0.8 mm wide. By separating a specimen holder so as to maintain a small constant tension of about 10^5 N/m^2 and heating the specimen at the rate of $1.5^\circ\text{C}/\text{min}$, the thermal shrinkage of the extrudate was measured as the change of the distance between specimen holders.

RESULTS AND DISCUSSION

Extrusion behaviour

Table 2 lists the extrusion pressure under typical extrusion conditions. The upper limit of ER was 6.3 in the range of extrusion temperatures of 70 to 150°C. At ER of 8.2 cracks appeared in the extrudate and stable extrusion could not be attained. At T_e of 40°C extrusion under higher ER values, such as 6.3, was not conducted because of the limit of the strength of the apparatus. According to Williams¹⁰ the upper limit of DR of hydrostatically conducted PP extrusion at 100°C was 5. He obtained extrudates of higher DR by further drawing of the extruded samples. We examined the extrusion of lower molecular weight PP resin Noblen W101 ($\bar{M}_v = 2.7 \times 10^5$, $MI = 7.90$, Sumitomo Chemical Co.), of which limiting ER was also 6.3.

Table 2 shows that the extrusion pressure increases with decreasing extrusion temperature and with increasing ER. As we reported previously, the extrusion pressure P can be estimated by the following equation from the tensile data of the polymer¹⁻⁵:

$$P = (1 + \mu \cot \alpha) \int_0^{2 \ln(R/r)} Y(\epsilon) \cdot \exp(\epsilon \mu \cot \alpha) d\epsilon$$

Table 2 Extrusion pressure, die swell and deformation ratio under typical extrusion conditions

T_e (°C)	ER	Pressure $\times 10^7$ (N/m ²)	Die swell (%)	DR
40	2.0	7.7	11.1	1.6
40	2.8	12.3	11.7	2.2
40	4.0	20.7	12.0	3.2
70	2.0	2.6	10.1	1.7
70	2.8	5.1	11.2	2.2
70	4.0	8.8	11.0	3.2
70	6.3	37.0	8.5	5.3
100	2.0	2.0	10.7	1.7
100	2.8	2.4	10.0	2.3
100	4.0	5.1	8.0	3.4
100	6.3	23.0	7.5	5.4
130	2.0	2.0	9.3	1.7
130	2.8	2.0	8.3	2.4
130	4.0	2.6	9.0	3.4
130	4.9	4.1	10.0	4.1
130	6.3	11.5	7.5	5.4

$$\text{Die swell} = (r' - r)/r$$

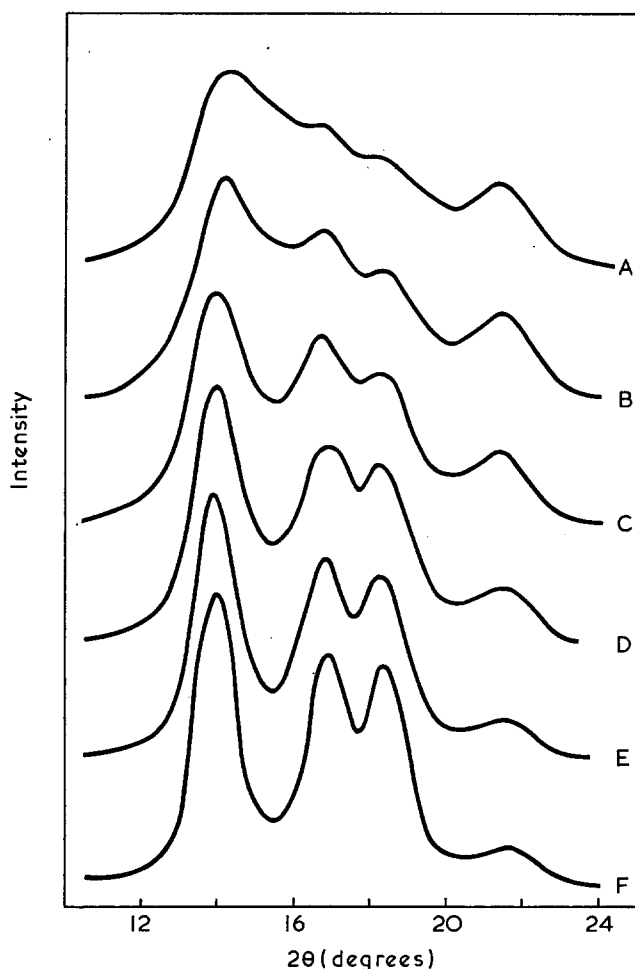


Figure 2 Equatorial diffraction curves of samples extruded at various temperatures under ER of 4.0. T_e : A, 40°; B, 55°; C, 70°; D, 85°; E, 100°; F, 130°C

where μ is a frictional coefficient between the material and the die wall and $Y(\epsilon)$ is the yield stress or deformation resistance of the material as a function of the strain ϵ . In the case of PP a reasonable value of extrusion pressure could be obtained by assuming the value of μ to be 0.30⁵.

In contrast to the HDPE extrusion, die swell occurred at the exit of the die and the diameters of the extrudates

became larger than the outlet diameter of the die. Thus DR is to be expressed as the ratio, $(R/r)^2$, of the cross-sectional areas of the material before and after the deformation by using r' , a radius of the extrudate, instead of the extrusion ratio $ER = (R/r)^2$. Table 2 lists the die swell and the DR of the extrudates. From preliminary experiments die swell was found to be affected by the molecular weights of the resins and the moulding conditions of the billets. Generally speaking, die swell increases with increasing molecular weight and with increasing annealing temperature of the billet.

Structural analysis of the extrudates

Figure 2 shows the equatorial WAXS profiles of the samples extruded at T_e of 40 to 130°C under ER of 4.0. WAXS profiles of the samples extruded above 85°C showed characteristic features of the monoclinic crystals of PP, while the samples obtained at lower temperatures gave very broad peak profile. The peak maximum of the sample extruded at 40°C locates at $2\theta = 14.4^\circ$, which differs from the correct peak position of (110) reflection of monoclinic crystal ($2\theta = 14.1^\circ$). WAXS observations on original billets are characteristic of monoclinic crystals, so the transition of the crystal structure is considered to occur during low temperature extrusion process.

It is well known that the monoclinic crystals of PP are converted into smectic ones which have broad ($hk0$) peak at $2\theta = 15.3^\circ$ by uniaxial drawing at low temperatures^{12, 13}. Natta¹⁴ has shown that the oriented smectic structure can be formed by drawing the quenched PP sheet below 70°C. From these results of drawn PP it is reasonable to consider that the broadening and the peak shift of the WAXS profiles of the samples obtained at extrusion temperatures below 70°C are due to the partial transition of the monoclinic crystals to smectic ones. The WAXS profile of the sample extruded at 40°C, as shown in Figure 2, resembles that of the overlap of diffraction intensity curves¹⁵ for films composed of the monoclinic crystals and quenched films composed of the smectic crystals.

Figure 3 shows the orientation factors of a^* -, b - and c -axes of monoclinic crystal of PP extrudates of various deformation ratios extruded at 130°C. The orientation factor f_e increases with increasing DR and reached 0.988 at DR of 5.4, which indicates that the molecular chains in the crystal orient along the extrusion direction almost completely. Figure 4 shows the SCEM photograph of the fracture surface of this highly deformed extrudate. In this SCEM image many fibrils are observed to run along the extrusion direction, which corresponds to the excellent c -axis orientation of the sample. In those samples a^* - and b -axes orient perpendicular to the extrusion direction as a foregone consequence of the c -axis orientation. However, the orientation of the a^* -axis in the plane perpendicular to the extrusion direction is not equal to that of the b axis but slower than that of the b -axis. Such tendency of the orientation had been also found in drawn PP¹⁵. The lag of the a^* axis orientation may probably be caused by the fact that the a^* axis orients along extrusion direction in the early stages of the deformations. The a^* axis orientation was positively observed in the sample drawn at high temperature¹⁶. The same a^* axis orientation was also observed in the extrudate from the billet annealed at

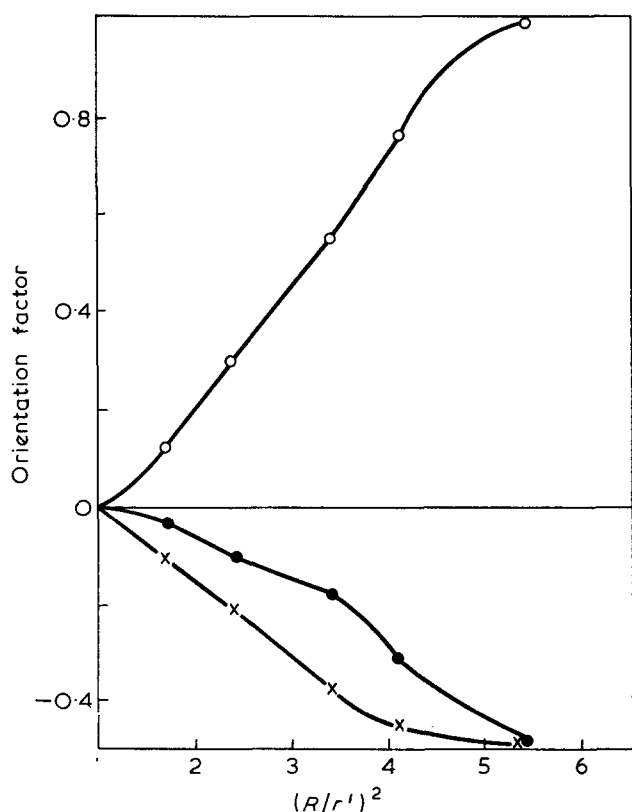


Figure 3 Orientation factor of samples extruded at 130°C. ○, f_{α} ; ●, f'_{α} ; ×, f_{β}

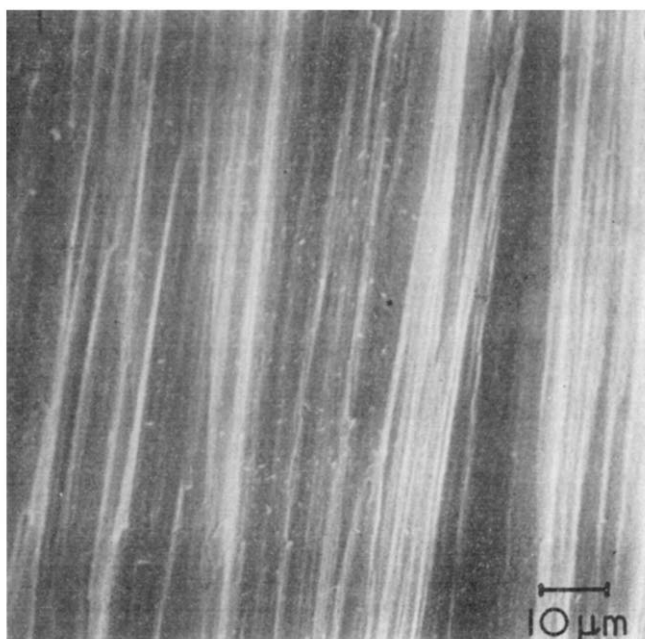


Figure 4 Scanning electron micrograph of the fracture surface of the sample extruded at 130°C at deformation ratio of 5.4

160°C for 2 h. The orientation factor f'_{α} of the samples extruded at 130°C at DR of 1.4 and 1.9 from annealed billets were positive at 0.030 and 0.049, respectively. This shows that a^* axis orientation along the extrusion direction really occurs in the early stages of the extrusion.

Figure 5 gives the SAXS photograph of the extrudate of DR=5.4 obtained at 130°C. This photograph exhibits a streak along the equator and weak ones where the centres lie on the meridian. These features resemble those of drawn samples. The long period calculated

from the meridional scattering gives 196 Å. According to Baltá-Calleja and Peterlin¹⁷ the long period of PP drawn at 130°C is about 200 Å, along the stretched direction. This value corresponds to that of the extrudate. The long periods of the extrudates obtained by extrusions at 100 and 150°C also correspond to those of the samples drawn at 100 and 150°C, respectively.

The results described above concerning the crystal modification, crystal orientation and the SAXS of the extrudates of PP agree with those of drawn PP. The structure of the PP extrudate is quite similar to that of the drawn PP. Such similarity of the structure observed between the extrudate and the drawn sample make it possible to estimate the extrusion pressure on the basis of the tensile data, as reported previously^{3, 5}.

Mechanical properties

Figure 6 shows nominal stress vs. nominal strain curves of the original sample and the extrudates extruded



Figure 5 SAXS photograph of the sample extruded at 130°C at deformation ratio of 5.4

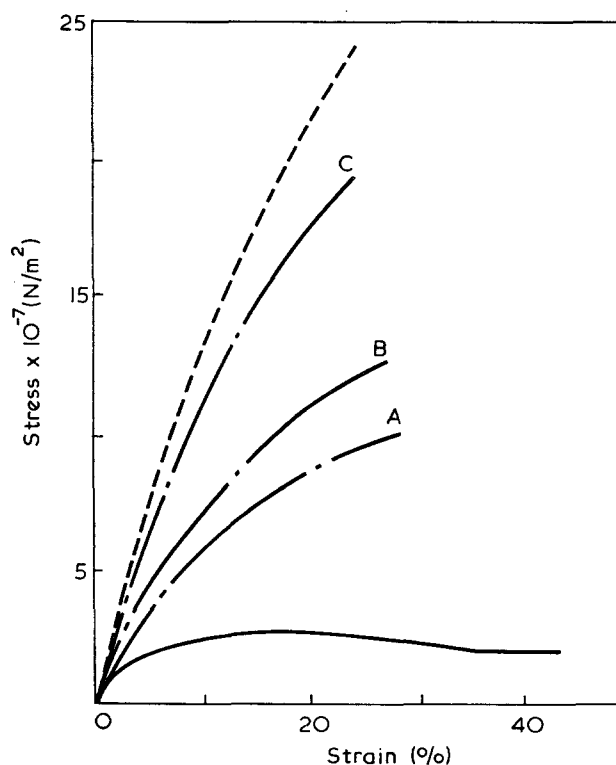


Figure 6 Stress-strain curves of undeformed sample (—), three samples extruded at 130°C (— · —) under deformation ratios of 3.4 (A), 4.1 (B), and 5.4 (C), and a sample drawn to a draw ratio of 6.2 (---)

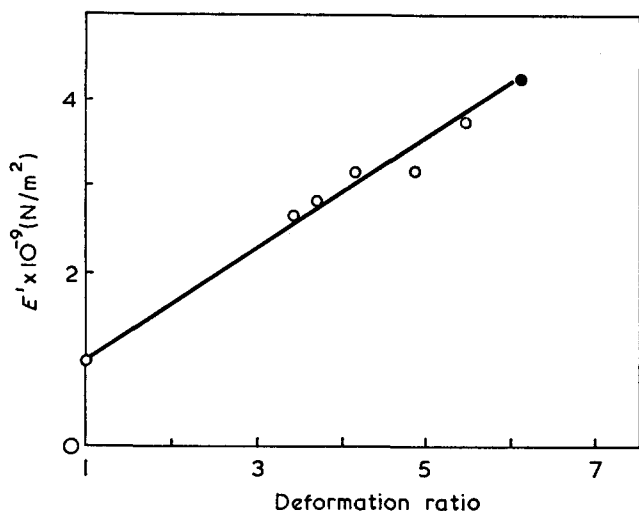


Figure 7 Dynamic modulus of the extrudates and drawn sample (●) measured at 110Hz

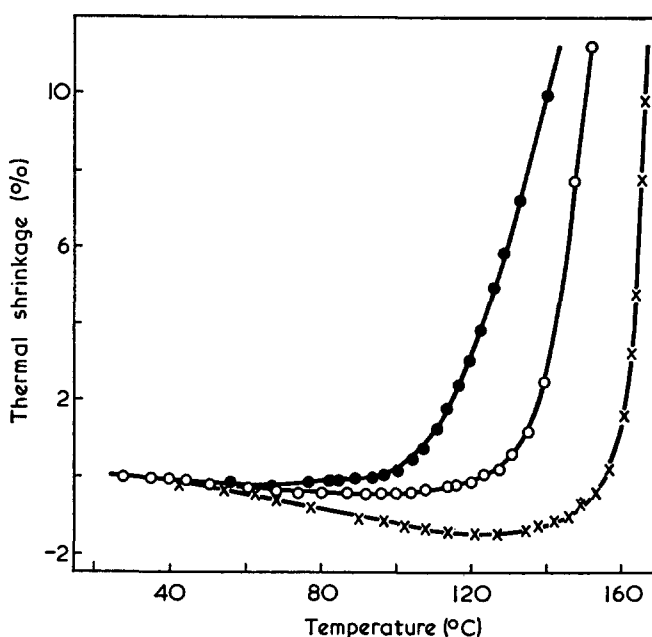


Figure 8 Thermal shrinkage of the sample extruded at 100° (●), 130° (○) and 150°C (x) under extrusion ratio of 6.3

at 130°C under various deformation ratios. For comparison, a curve of the sample drawn to a draw ratio of 6.2 at 130°C is also presented as a broken line in Figure 6. The mechanical properties of PP are observed to be improved by solid-state extrusion. Figure 7 presents dynamic modulus, E' , at 110 Hz of the same samples as those used in the stress-strain measurements. The modulus, E' , increases linearly with increasing extrusion ratio. The curve can be extrapolated to the point of the drawn sample (solid circle). Thus the mechanical properties of the extrudate and the drawn sample are the same when they are compared at the same values of the deformation ratio and the draw ratio.

Thermal shrinkage

Figure 8 shows the thermal shrinkage of the samples extruded at 100, 130 and 150°C at ER of 6.3. Although the length of each extrudate increases in the early

stages of heating owing to thermal expansion, shrinkage occurs at high temperatures. The temperatures at which shrinkage begins are about 100, 130 and 150°C for the samples extruded at 100, 130 and 150°C, respectively. We also examined the thermal shrinkage of the samples extruded at 130°C at different ER. The thermal behaviour was almost the same as shown in Figure 8 for other samples of different ER. Thus PP extrudates are found to shrink at about the temperatures at which the extrusions were conducted. As reported previously⁶, HDPE extrudate has high dimensional stability up to 120°C when it has been extruded at the temperatures above 100°C, while PP extrudates shrink considerably above the extrusion temperatures. To obtain a PP extrudate having high thermal stability, it is necessary to conduct the extrusion at the temperatures as high as would be encountered after the processing.

CONCLUSIONS

- (1) The upper limit of the extrusion ratio in the solid-state extrusion of PP was $(R/r)^2 = 6.3$ in the temperature range of 70° to 150°C. At higher extrusion ratio cracks were produced in the extrudate.
- (2) The crystal structure of the PP extrudates was affected by the extrusion temperature. Smectic crystals were formed in the samples extruded below 70°C, while on the extrudates prepared at higher temperatures the monoclinic crystals were observed predominantly.
- (3) The crystal orientation increased with increasing deformation ratio and the orientation factor reached 0.988 at the limiting extrusion ratio, $(R/r)^2 = 6.3$.
- (4) Mechanical properties of PP were improved by solid-state extrusion in comparison with the original unoriented samples. The extent of improvement was about the same as observed in drawn sample.
- (5) Thermal shrinkage of PP extrudates was observed to begin at about extrusion temperatures and seemed to be independent of the degree of deformation.

REFERENCES

- 1 Imada, K., Kondo, Y., Kanekiyo, K. and Takayanagi, M. *Rep. Progr. Polym. Phys. Japan* 1971, 14, 393
- 2 Imada, K., Kondo, Y., Kanekiyo, K. and Takayanagi, M. *Proc. 1971 Int. Conf. Mech. Behavior Mater.* 1972, 3, 476
- 3 Imada, K. and Takayanagi, M. *Int. J. Polym. Mater.* 1973, 2, 89
- 4 Maruyama, S., Imada, K. and Takayanagi, M. *Int. J. Polym. Mater.* 1973, 2, 105
- 5 Nakamura, K., Imada, K. and Takayanagi, M. *Int. J. Polym. Mater.* 1972, 2, 71
- 6 Imada, K., Yamamoto, T., Shigematsu, K. and Takayanagi, M. *J. Mater. Sci.* 1971, 6, 537
- 7 Hill, R. 'The Mathematical Theory of Plasticity', Clarendon Press, Oxford, 1950
- 8 Avitzur, B. 'Metal Forming Process and Analysis', McGraw-Hill, New York, 1968
- 9 Buckley, A. and Long, H. A. *Polym. Eng. Sci.* 1969, 9, 115
- 10 Williams, T. *J. Mater. Sci.* 1973, 8, 59
- 11 Wilchinskii, Z. W. *J. Appl. Polym. Sci.* 1963, 7, 923
- 12 Sobue, H. and Tabata, I. *J. Appl. Polym. Sci.* 1959, 2, 66
- 13 Takahara, H. and Kawai, H. *Rep. Progr. Polym. Phys. Japan* 1967, 10, 277
- 14 Natta, G. *Makromol. Chem.* 1960, 35, 94
- 15 Takahar, H., Kawai, H. and Yamada, T. *Sen-i Gakkaishi* 1967, 23, 102; 1968, 24, 219
- 16 Awaya, H. *Nippon Kagaku Kaishi* 1961, 82, 1575
- 17 Baltá-Calleja, F. J. and Peterlin, A. *J. Macromol. Sci. (B)* 1970, 4, 519

Thermal history and mechanical properties

C. M. R. Dunn and S. Turner

*Imperial Chemical Industries Ltd, Plastics Division, Welwyn Garden City, Herts, UK
(Received 11 December 1973; revised 5 February 1974)*

An account is given of three separate experiments in which the creep modulus and the recovery after creep are shown to be strongly affected by the thermal history. The tensile creep modulus of several amorphous plastics in their glassy state increases with storage time; the recovery after creep can be very much worse than normal under some quite ordinary operating conditions; the modulus in flexure of polypropylene at 20°C is remarkably sensitive to minor thermal treatment (e.g. quenching to 0°C after a short period at 40°C). The results, including those on the polypropylene, are all consistent with the concept of slow molecular re-ordering leading to a state of lower free volume. The implications for materials evaluation programmes are discussed.

INTRODUCTION

It has been known for many years that some of the mechanical and physical properties of thermoplastics are affected by the rate at which the sample has been cooled from the processing temperature or from some temperature at which it has been annealed or 'heat treated'. Large effects were observed in crystalline plastics and most were easily associated with observable changes in the crystallinity or the crystalline texture. Similar changes have been seen in the mechanical properties of glassy amorphous plastics but without concomitant changes in any observable structure parameter. McLoughlin and Tobolsky¹ observed that the stress relaxation of poly(methyl methacrylate) (PMMA) at high temperatures was affected in this way, and they suggested that the more rapidly cooled specimens had a larger free volume and hence easier mechanisms for stress relaxation. Earlier experiments by Alfrey *et al.*² showed that the volume of a sample used for dilatometry depended on the rate of cooling. Similarly, Turner³ published creep results for poly(vinyl chloride) (PVC) at 60°C showing extremely large changes induced by conditioning periods at 60°C prior to the creep experiments. The differences at low values of elapsed time were fairly modest, though significant, but the differences after long periods of creep were very large indeed, and this has since been verified for other plastics.

These findings for PMMA and PVC had important practical ramifications in relation to creep and relaxation experiments on glassy amorphous plastics, because if a sample changes during prolonged storage at some test temperature it will also change during a prolonged experiment at that temperature and the observed creep strain (or relaxation stress) will be compounded of the general viscoelastic response and the effects of the thermal conditioning. It is now known also that significant changes in property can occur in some polymers even at 20°C. Thus, the thermal history plays a fundamental part in determining the viscoelastic behaviour, in the sense that it is inescapably imposed during the processing of a sample and during subsequent

service. At the very least it has to be regarded as an important parameter in experiments of long duration.

This paper falls naturally into three parts. The first describes the 'ageing' phenomenon, i.e. the changes induced by thermal treatment, as observed in glassy amorphous plastics; the second contains some new results that clearly arise as a consequence of ageing and a discussion of their significance; the third section extends the study of crystalline plastics.

AGEING IN GLASSY AMORPHOUS PLASTICS

The study of creep in PVC at 60°C showed that the results are very sensitive to the duration of storage at that temperature prior to the creep test. The changes were progressive, and could be obliterated by rapid cooling from a temperature close to that of the glass-rubber transition³. All the facts are consistent with the concept of changes in free volume due to thermal history. The obvious implication is that all creep tests on glassy amorphous plastics will be subject to storage effects, and ever since these first results it has been our practice to monitor the changes occurring during storage prior to and during tests of long duration. A convenient measure of the effect is the change in short-term modulus, and in our case the particular choice was the 100 sec creep modulus at 0.002 strain. Some typical results are given in *Table 1*.

From our many results, only a few of which are given in the *Table*, it is clear that the effect is common to all glassy amorphous plastics. Our data for some polymers are probably unique in that they extend over storage periods of several years, and even then they do not suggest an equilibrium state. A sample of PMMA that had been stored for 3 years at 100°C has provided an example of even greater change than those tabulated above. *Table 2* shows a threefold increase of modulus at 100°C compared with a control and a nearly complete reversion to the original value after rapid cooling from 150°C. This reversion is evidence against the possible contention that the changes were due to crosslinking,

Table 1 100sec tensile creep modulus at 0.002 strain

Polymer and temperature	Storage time	Modulus (GN/m ²)
PVC at 60°C	1½ h	1.60
	19 h	1.82
	43 h	2.04
	20 days	2.31
	2430 days	2.70
Noryl* at 80°C	1 h	1.78
	1 day	1.95
	7 days	2.04
	14 days	2.10
	28 days	2.15
PMMA at 60°C	½ h	2.08
	22½ h	2.28
	71 h	2.31
	13 days	2.36
	70 days	2.56

* Noryl is a commercial blend of PPO and polystyrene

Table 2 100sec tensile creep modulus at 100°C and 0.002 strain

Specimen history	Modulus (GN/m ²) at 100°C	Relative density at 23°C
3 years at 100°C	2.05	1.1868
Control: 3 years at 20°C, then 1 h at 100°C	0.77	1.1852
3 years at 100°C, 1 h at 150°C followed by rapid cooling to 20°C then 1 h at 100°C	0.95	1.1862

loss of monomer or other irreversible process. The densities, measured at 23°C, support an explanation in terms of reduced free volume caused by storage at 100°C.

The picture that emerges, not surprisingly, is that as the conditioning temperature is increased towards that of the glass-rubber transition, the increase in modulus becomes more rapid and larger. On this basis one would expect the modulus of PVC to rise only very slowly during storage at room temperature; experiment confirms this, for example, a modulus of 3.2 GN/m² about 3 months after fabrication was 3.35 GN/m² after 15 months and 3.45 GN/m² after about 3½ years. Poly(ether sulphone) at room temperature, much further below its transition temperature, suffers no detectable change in modulus over a period of two years.

The changes in overall creep behaviour caused by thermal conditioning are much more complicated than the change in short-time modulus discussed in the preceding section. The typical data plotted in Figure 1 show that the differences between conditioned and unconditioned specimens are more pronounced at larger values of elapsed time. This is probably a genuine effect, though the picture is complicated by continuing changes in the state of all the specimens as the experiments proceed. Under these conditions each creep curve is to some extent ambiguous in that it is not the strain response function for a specific material state, i.e. the viscoelastic parameters of the system are not constant. The observed strain response becomes a close approximation to a genuinely characteristic viscoelastic function if the conditioning period is long compared

with the creep duration, but the results may be unrealistic in that the sample state will be rather different from that commonly found in service. The creep curves of crystalline plastics are generally changed in a regular and simple manner by an annealing treatment so that the results from tests carried out on well annealed, and therefore stable, samples can be converted via empirical rules⁴ into curves representing more realistic states. There is no corresponding technique for glassy amorphous plastics, nor is there an overriding thermal treatment producing a molecular state and/or mechanical behaviour that is virtually stable over a wide range of test temperatures, such as there is for crystalline plastics. 'Thermal conditioning' of glassy amorphous plastics gives a state that is specific only to that regime.

EFFECT OF AGEING ON VISCOELASTIC RECOVERY

It is clear that creep data for glassy amorphous plastics near to their limiting service temperature are difficult to interpret, particularly when the elapsed times are long. It is even more difficult to translate the results into meaningful statements about serviceability. In view of the evidence that changes occur in the molecular state during a prolonged test under these conditions, it is perhaps not surprising that some recent experiments have shown that the recovery behaviour after creep is radically different from what is observed at lower temperatures and in well annealed crystalline plastics*.

The recovery behaviour of crystalline plastics mostly follows a regular and simple pattern when the data are plotted as 'fractional recovered strain' vs. log 'reduced time'. These two quantities facilitate the presentation and manipulation of recovery data⁵. They are defined as follows:

$$\text{Fractional recovered strain} = \frac{\text{strain recovered}}{\text{maximum creep strain}}$$

$$\text{Reduced time} = \frac{\text{recovery time}}{\text{preceding creep time}}$$

Glassy amorphous plastics show a similar simplicity, though with slightly different characteristics, under

* The recovery of crystalline plastics after creep of very long duration is sometimes similar in some respects to that reported here for glassy amorphous plastics, but for simplicity the details are omitted.

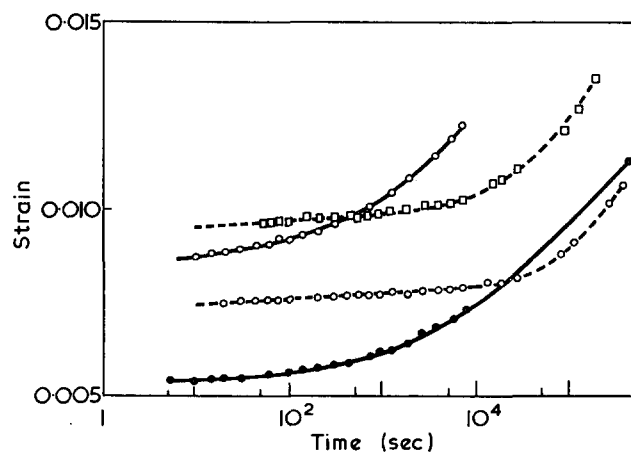


Figure 1 Effect of thermal conditioning on tensile creep of poly(ether sulphone) at 150°C. —, Unconditioned; ---, conditioned at 150°C for 12 days prior to creep. ●, 12.5; ○, 20; □, 25 MN/m²

some conditions, i.e. at temperatures well below that of the glass-rubber transition and when the creep duration is fairly short. The important feature within the present context has been that, at long times (reduced time greater than unity and often greater than ten) all the creep strain disappears (i.e. fractional recovered strain tends to unity), but it became increasingly clear during our experiments on glassy amorphous plastics, that the recovery was sometimes inferior to what had become accepted as typical of plastics, and this view was overwhelmingly confirmed by recent studies of the recovery characteristics of poly(ether sulphone) at 150°C⁶. It could be inferred from the experimental results that the ageing process during creep was affecting the subsequent recovery but there was little direct evidence because of interaction with other important variables such as the creep duration and the final creep strain. However, direct confirmation comes from a recent series of experiments in which the conditioning period prior to creep was varied while the other important quantities were held approximately constant or varied in a controlled manner. The material was a PVC pipe compound (based on a polymer of ICI *k* value 60 ($M_w \approx 140\,000$), the test temperature was 60°C, the specimens were stored at that temperature for either 1 h or 1 day before the creep period began, and the load was removed when the creep strain reached 0.01. In order that the other important variable, creep duration, should not vary widely despite the change in creep resistance caused by the different conditioning periods, the creep stresses had to be chosen with both care and inspiration but the results (Figure 2) clearly demonstrate the effect of conditioning. A comparison of curve (4) with curve (3) and curve (6) with curve (5) indicates that the longer a specimen is conditioned prior to the creep the better

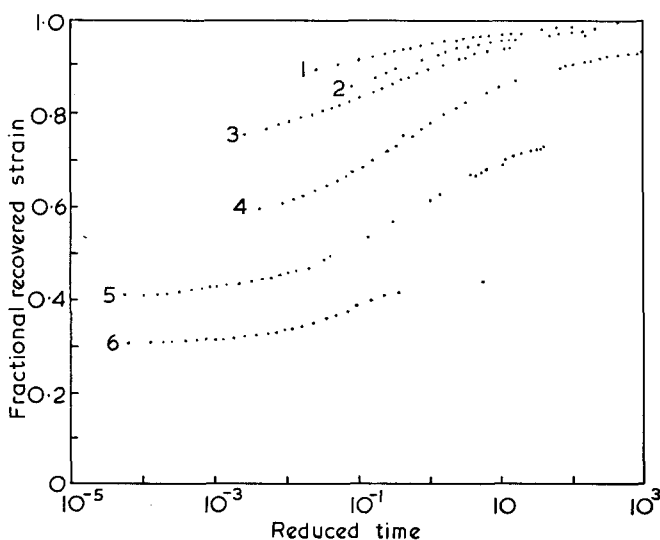


Figure 2 Recovery of PVC after creep at 60°C. Recovery is suppressed if ageing occurs during creep.

Curve	Storage time (h)	Creep duration (sec)
1	23	2×10^2
2	1	0.6×10^2
3	24	1.8×10^3
4	1	1.2×10^3
5	24	8.9×10^4
6	1	7.65×10^4

the subsequent recovery. Curves (1), (3) and (5) taken together and curves (2), (4) and (6) taken together show that ageing during the creep period (and also during the subsequent recovery) depresses the retraction and leaves more residual strain. The longer duration of creep in itself would depress the curves only slightly⁵; it would not give recovery curves that suggest a large final residual strain.

The probable explanation of these results is that an ageing process occurring simultaneously with the creep constantly changes or redefines the ground state of the polymer, effectively destroying the viscoelastic memory that would guarantee full recovery after removal of the force. The importance of this conclusion is the new limitation it imposes on the phenomenological theories of non-linear viscoelasticity. Such theories normally assume that the material remains unchanged in nature throughout its lifetime and the evaluation of the critical functions depends strongly on the observed responses to simple changes of stress such as total removal. Results such as those described here would make the recommended manipulations meaningless and the prospect is therefore one of additional levels of complication being introduced into the equations.

AGEING IN POLYPROPYLENE

It has generally been assumed that crystallinity is the dominant factor governing the mechanical properties of polyolefins and their sensitivity, to thermal history. However, there are some phenomena which, though possibly explicable within the framework of crystallinity concepts, may be regarded as manifestations of free volume changes. It has been known for some time, for instance, that the modulus and density of polypropylenes are differently related for changes induced by storage at room temperature and changes induced by annealing at high temperatures⁴, and it is tempting to speculate that the changes in this polymer due to storage at 20°C are more closely related to the effect observed in glassy amorphous plastics than to anything directly attributable to changes in crystallinity. There is support for this view in the results of some recent experiments on a sample of homopolymer in the form of injection moulded ASTM Type 1 tensile bars. The 100 sec Young's modulus at 20°C, was measured at intervals on specimens machined from the bars and tested in flexure by a 3-point bending technique. The attainable accuracy of the method is $\pm 0.5\%$ ⁷. There are two advantages of a flexure method; it is particularly sensitive to the properties of the skin layers (and hence to the effect of quenching) and the strain in the specimen can be so restricted that the test can be repeated indefinitely without deleterious consequences. It is therefore an ideal method for the monitoring of a progressive change in modulus.

Figure 3a shows the effect on the modulus at room temperature of re-heating specimens to temperatures in the range 40–100°C for 40 min and then quenching them in iced water. At the beginning of the experiments the modulus of the specimens lay in the range 1.65–1.75 GN/m². The treatment reduced this modulus, the effect being easily observable even when the annealing temperature was only 40°C but becoming more pronounced as the annealing temperature was increased to 100°C. The modulus increased with storage at 20°C, reaching its original starting value after 100–1000 h.

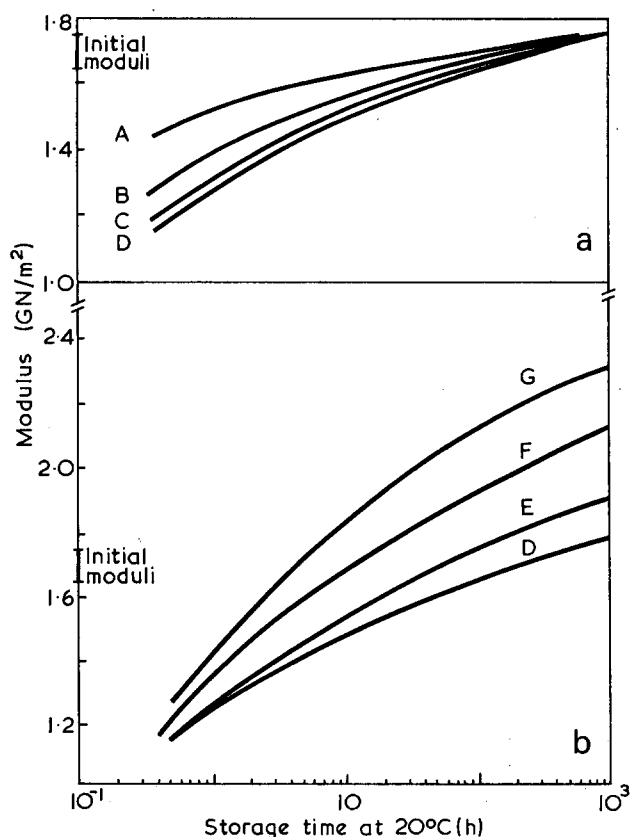


Figure 3 Increase of modulus (in flexure, at 100sec, 20°C) after quenching from following temperatures into water at 0°C: A, 40°C; B, 60°C; C, 80°C; D, 100°C; E, 120°C; F, 140°C; G, 150°C. Specimens held at temperature for 40 min. Results suggest further crystallization when temperature is higher than 100°C

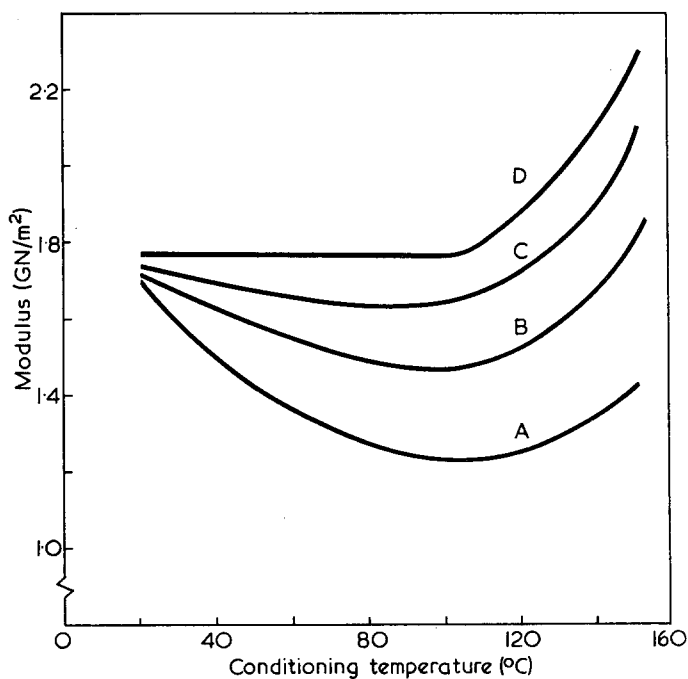


Figure 4 Cross-sections from Figure 3. Storage times: A, 1h; B, 10h; C, 100h; D, 1000h. 100°C is most effective temperature for reduction of modulus

Figure 3b is a similar graph showing the rather different effect observed when the treatment temperature was higher. The initial reduction was again observed though to a smaller degree for the higher annealing temperatures. When the treatment temperature was in the range 120–150°C, the storage effect at +20°C

eventually took the modulus to a higher value than that of the starting material. It seems likely that this behaviour was a consequence of an increase in crystallinity, because the 150°C treatment increased the density from 0.9034 to 0.9086*.

Cross-plots of these figures show clearly (Figure 4) that 100°C is the most effective treatment temperature for reducing the modulus. Presumably the reduction would be greater for higher treatment temperatures were it not for a superposed stiffening caused by the formation of more crystals.

A compression moulded specimen of the same type of homopolymer which had been stored at room temperature for five years was subjected to the same treatment, 40 min at 100°C followed by quenching, and suffered a modulus decrease from 1.71 GN/m² to 1.08 GN/m² (36 min after quenching). The modulus subsequently increased and had reached 1.65 GN/m² after 1000 h. Similarly, experiments on a sample of low density polyethylene showed that the 20°C modulus was reduced by 40 min treatment at either 40°C or 100°C, followed by quenching in iced water. Again the modulus increased with subsequent storage at 20°C.

DISCUSSION

This paper has presented three rather distinct sets of observations with two features in common. One is that slow changes occur in the modulus and creep behaviour of all the plastics studied, both glassy amorphous and crystalline, during prolonged storage. The other is that an explanation for all the results can be found in terms of changing free volume. It can be argued, of course, that the effects of thermal history on the modulus of polypropylene, and on the other polymers, are caused by the development of crystalline structure at a level lower than the limits of discrimination of current apparatus. As a sequel to the experiments reported here, structure studies could have been carried out to explore the possibilities, but a strong disincentive to such a course is the universality of ageing effects. If one were to interpret the behaviour of polypropylene in specific structural terms, it would be illogical not to seek a separate explanation for each of the many polymers in which similar effects have been observed. It seems clear that the effects are manifest through some general characteristic of polymer networks and free volume could be the common concept. An increase in 'amorphous order' is one route to reduced free volume and since, in the limit, amorphous order and crystallinity may be synonymous a final resolution of what is happening within the network may be unimportant.

At the purely phenomenological level, the manifestations of ageing do not conform to simple patterns and cannot be assessed by simple test programmes. The reason is that the ageing process is governed by the same segmental motions and energy barriers that govern the creep and the relaxation processes, so that molecular rearrangement towards a state of greater amorphous order is an inevitable hidden feature of any long duration mechanical test. It is already customary for a delay to be imposed between the processing of a

* N.B. Initially this increase in density was accompanied by a decrease in modulus. Many results of a similar nature, but in a different context, have been obtained on polyethylenes.

sample and the testing, but there is a limit to what delay can be tolerated and proper equilibrium is seldom attained before a test is started. In consequence, the experimental results are never a unique viscoelastic response, though of course they are a very close approximation in many cases. The recovery data are more prone to distortion than the creep data because of the combined effects of the preceding creep and the ageing process; in particular, the observable residual strain is a theoretically meaningless quantity because the original state of zero strain has been obliterated. In practice it may be immaterial whether a residual strain arises from a purely viscoelastic process or as a consequence of ageing, but the distinction should be identified and preserved in any theoretical developments. Such precautions do not appear to feature in the current theories seeking to provide superposition rules for non-linear viscoelastic materials under varying stress, and it is probably more than coincidental that those theories are much more successful in their predictions of the response to an increase of stress than in their predictions of the response to a decrease of stress.

ACKNOWLEDGEMENTS

The authors are indebted to C. Toates, who was responsible for the majority of the experiments on which this paper is based. They also had several helpful discussions with P. I. Vincent who has observed analogous ageing effects in totally different experiments, with P. L. Clegg and with E. A. Cole.

REFERENCES

- 1 McLoughlin, J. R. and Tobolsky, A. V. *J. Polym. Sci.* 1951, **7**, 658
- 2 Alfrey, T., Goldfinger, G. and Mark, H. *J. Appl. Phys.* 1943, **14**, 700
- 3 Turner, S. *Br. Plast.* 1964, **37**, 682
- 4 Turner, S. *Plastics and Polymers* 1970, **38**, 282
- 5 Turner, S. 'Testing of Polymers', (Ed. W. E. Brown), Interscience, New York, 1969, Vol 4, Ch 1
- 6 Gotham, K. V. and Turner, S. *Polymer* 1974, **15**, in press
- 7 Dunn, C. M. R. and Turner, S. *Plastics and Polymers* 1972, **40**, 26

Preparation and properties of poly(arylene ether sulphones)*

J. B. Rose

Imperial Chemical Industries Ltd, Plastics Division, Welwyn Garden City, Herts, UK
(Received 2 November 1973)

INTRODUCTION

The poly(arylene ether sulphones) form a family of thermoplastic polymers, some of which have been accepted for continual use under stress at temperatures in excess of 150°C and this paper summarizes the technical background to the development of these materials. The search for plastics of this type led naturally to polymers composed of linked aromatic rings as high thermal and oxidative stability would be expected from polymers of this structure. The linking groups must play a crucial part in determining properties for they control the flexibility of the polymer chain and determine the overall polarity of the macromolecule. Thus, to obtain the properties required these links should be selected such that good stability is retained and the polymer backbone is sufficiently flexible to show thermoplasticity below the decomposition temperature, but well above 150°C. This conclusion is reached without undue difficulty and the real problem

has been to devise synthetic methods for linking aromatic nuclei with sufficient versatility and freedom from side reactions to effect the synthesis of a wide range of high molecular weight polymers, in the hope that some of these would show the properties required. The sulphone linkage was a natural choice for investigation as the stability of diaryl sulphones was well known, but it appears that a polymer chain consisting only of phenylene rings linked via sulphone groups, i.e. poly(phenylene sulphone), is too rigid to show thermoplasticity. Fortunately, the synthetic procedures that were devised for preparing high polymers containing aryl sulphone linkages as the main structural feature led inevitably to the inclusion of other more flexible chain bonds, particularly the ether linkage, and attention became concentrated on the poly(arylene ether sulphones).

Routes to poly(ether sulphones) were discovered independently, and almost simultaneously, in the laboratories of 3M Corporation¹ and of Union Carbide Corporation² in the USA and in the Plastics Division of ICI³ in the UK. All three companies now market different polysulphone plastics and the structures of these materials are shown in Table 1 where they are

* Presented as a Symposium Lecture at the IUPAC International Symposium on Macromolecules, Aberdeen, September 1973.

Table 1 Available poly(ether sulphones)

Product	Polymer repeat unit(s)	Softening behaviour
		m.p. > 500°C with decomp.
Astrel 360 (3M)	and	T_g 285°C; injection moulds in special machines
Poly(ether sulphone) 720P (ICI Ltd)	first unit predominates: and	T_g 250°C; injection moulds with difficulty in conventional equipment
Poly(ether sulphone) 200 P (ICI)	second unit predominates:	T_g 230°C; injection moulds in conventional equipment
Udel Polysulfone (Union Carbide)		T_g 190°C; injection moulds in conventional equipment

compared with poly(phenylene sulphone). Poly(phenylene sulphone) decomposes before melting⁴ and the introduction of inter-ring linkages other than $-\text{SO}_2-$ is necessary to obtain thermoplasticity. This is achieved in the commercial products predominantly by the introduction of aryl ether linkages and as the proportion of these linkages is increased there is a progressive reduction in T_g and a corresponding increase in thermoplasticity.

This paper describes the two main synthetic routes to poly(arylene ether sulphones), examines briefly how polymer structure depends on the synthesis employed, and then considers polymer properties in relation to structure.

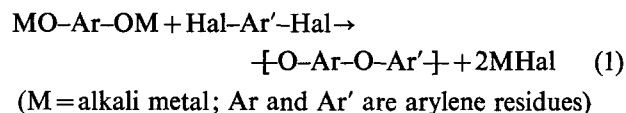
SYNTHETIC PROCEDURES

A priori, there are two possibilities for synthesizing the poly(ether sulphones): either a polyether synthesis could be used to join up aryl sulphone intermediates with ether linkages, or a polysulphonylation process employed to link up aryl ethers. In practice either method can be used and will give polymers of high molecular weight provided that the intermediates are selected within certain structural limitations and the reaction conditions are closely controlled. The methods are quite different chemically and are complimentary in that polymer structures made by one route cannot

usually be made by the other although some structures can be made by either process.

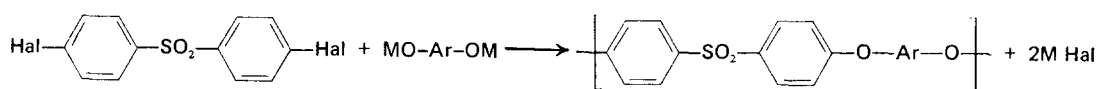
Polyetherification

A polyether synthesis according to equation (1) was described first² by Johnson and Farnham of Union Carbide Corporation. In this process:



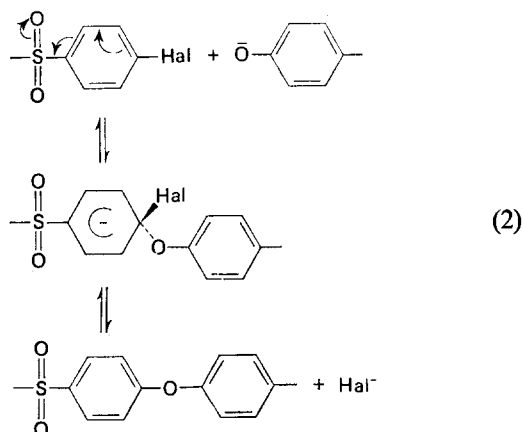
ether bonds are formed via displacement of halogen by phenoxide anions with removal of the halogen as alkali metal halide and to obtain poly(ether sulphones) one or both of the arylene residues must contain the sulphone group. In fact the sulphone group is an essential constituent of the dihalide, as it plays a vital part in the reaction by activating the halogens to attack by the phenoxides. Aromatic halides which do not contain powerful electron withdrawing groups such as sulphone are unreactive and in the absence of such groups the reaction is not suitable for the synthesis of high polymers⁵. The substitution reactions of activated aromatic halides have been widely studied using non-polymeric systems so that the reaction mechanism is well understood. It is accepted that reactions of this type proceed via an intermediate complex⁶ and that the sulphone group

Table 2 Polycondensation of 4,4'-dihalodiphenylsulphones with bisphenoxides¹¹

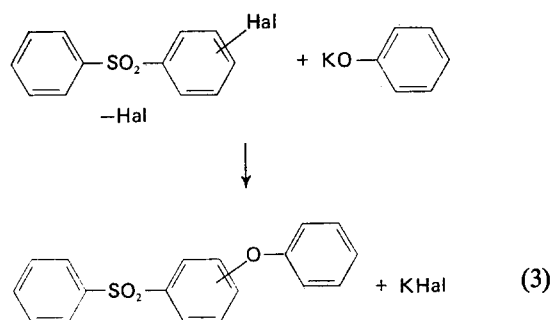


Hal in dihalide	Bisphenoxide	Reaction conditions			Polymer RV
		Solvent	Temp. (°C)	Time (h)	
F		DMSO	25-145	0.5	0.94
Cl		DMSO	135	4.0	0.71
Cl		DMSO	130	3.0	0.50
Cl		DMSO	165	4.0	0.70
Cl		DMSO	165	10.0	0.50
Cl		DMSO	165	10.0	0.30
Cl		Sulpholane	235	6.0	0.97

acts to stabilize the complex by accepting negative charge from the ring⁷:



Electron withdrawal towards sulphone is highly effective when the halogen is positioned *ortho* or *para* to sulphone, but not when in the *meta*-orientation, and attack on *o*-halogen is likely to be subject to steric hindrance. Thus, halogen reactivities would be expected to decrease in the order *para* > *ortho* > *meta* and these effects are quite large as indicated by the rate constants given below for the model reactions (3)⁸. In practice, the *m*-halides are useless for polymer synthesis, it is difficult to obtain polymers of high molecular weight using *o*-chlorides, while high polymers are readily obtained using the *p*-chlorides. In this respect the fluorides are better than the corresponding chlorides, but are too expensive for commercial use.



	<i>p</i> -F	<i>p</i> -Cl	<i>o</i> -Cl	<i>m</i> -Cl
$10^5 \times k_2$	~ 300 000	3024	100	10
(1 mol ⁻¹ sec ⁻¹ for reaction in dimethyl sulphoxide at 120°C)				

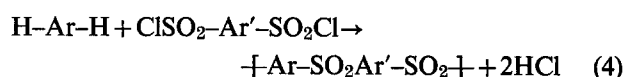
Thus, the *p*-chlorophenylsulphones are the reagents of choice for the polyether synthesis, and it is fortunate that sulphonylation of chlorobenzene gives high yields of *p*-chlorophenylsulphonyl derivatives, rather than the *o*- or *m*-isomers⁹. An example of this is 4,4'-dichlorodiphenyl sulphone which can be obtained in 80–90% yield from chlorobenzene¹⁰. This compound is an important intermediate and examples of its use for the synthesis of poly(ether sulphones) are given in Table 2. The polycondensations listed in Table 2 were performed in dimethyl sulphoxide or sulfolane and the use of these dipolar aprotic solvents is an important feature of the process. These solvents dissolve both the reactants and the polymers, and their use to enhance the rates of substitution reactions of this general type is well known¹².

In this series of polymers a reduced solution viscosity, $RV \geq 0.40$ is required to obtain useful mechanical properties, and this can be attained with a wide range of bisphenoxides, so that this synthesis can be used to give a wide range of potentially useful polymers.

Both of the functional groups required for the polyether synthesis can be included in a single polycondensation intermediate as shown in Table 3. These intermediates polycondense rapidly on melting¹³ and polymers of very high molecular weight can be obtained using the more reactive intermediates such as potassium 4-(4-fluorophenylsulphonyl)phenoxide. Polymers with solution viscosities > 0.4 were obtained from all of the *p*-halogenophenylsulphonyl derivatives, but it was much more difficult to do this with the *o*-halogeno compounds.

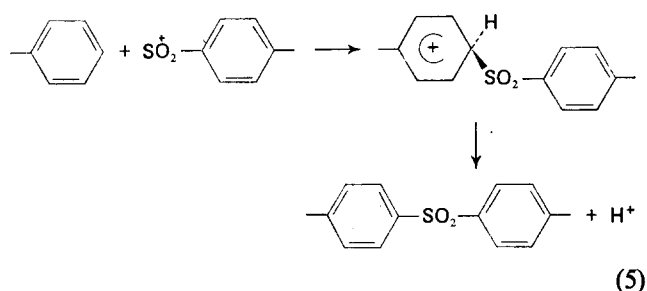
Polysulphonylation

The second important route to poly(aryl sulphones) is a polysulphonylation process (equation 4) in which sulphone linkages are formed by reaction of arylsulphonyl chlorides with aromatic nuclei:



This is a typical electrophilic aromatic substitution in which the aromatic substrate is attacked by some form of the arylsulphonylium cation and hydrogen displaced as a proton. The attacking reagent is formed by interaction of the sulphonyl chloride with a Friedel-Crafts catalyst which should be selected from FeCl₃, SbCl₅ or InCl₃ as with these halides only catalytic quantities are required, in contrast to the equimolar quantities usually recommended for Friedel-Crafts condensations with acid halides. This is important as it eliminates side reactions and helps considerably with the problem of catalyst removal from the polymers. (See ref 14 for a more complete discussion and for the primary references.)

Sulphonylation proceeds through a transition state of the type shown in equation (5):



in which the electron deficient reagent becomes bonded to the ring, and it is important that the ability of the ring to provide an electron pair for bond formation is not reduced by electron withdrawing substituents. Thus, ArH₂ can be diphenyl, diphenyl ether or naphthalene but not benzophenone or diphenyl sulphone. Further the substrate cannot be a single benzene ring as this would become deactivated by attachment of one sulphone group in the first polycondensation step and further chain growth would then be prevented.

Polysulphonylation can be carried out either in the melt or in solution and both functional groups can

Table 3 Melt polycondensation of halogenophenylsulphonyl phenoxides¹³

Halogenophenoxide	Polycondensation conditions		Polymer RV
	Temp. (°C)	Time (h)	
	280	1	3.0
	280	3	0.39
	280	0.5	1.0
	300	0.5	0.1
	300	0.25	2.3
	310	1	0.54

Table 4 Polysulphonylation with monosulphonyl chlorides in solution¹

Sulphonyl chloride	Solvent*	Reaction conditions			Polymer RV
		[FeCl ₃] (wt %)	Temp. (°C)	Time (h)	
	A	0.6	120	4	0.57
	B	0.08	170-190	6	0.59
	C	0.10	160-230	20	0.20
	B	0.08	140-220	15	0.57
	B	0.10	130-210	20	0.22
	B	0.13	150-200	20	0.20

* A=nitrobenzene, B=dimethylsulphone, C=chlorinated biphenyl

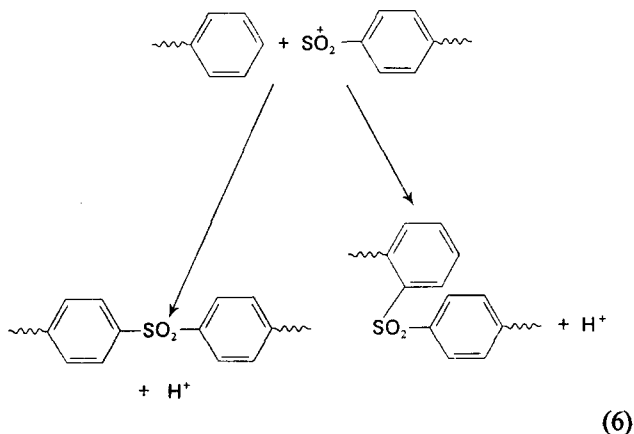
be built into a single intermediate as indicated in Table 4.

EFFECTS OF SYNTHESIS ON STRUCTURE

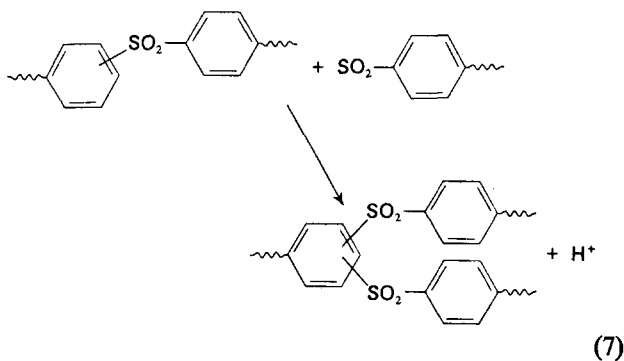
The main structural features of polymers made by either of the routes described above are determined by

the structures of the polymer intermediates employed, but certain significant variations can appear as a consequence of the polycondensation chemistry. In the polyether synthesis, equation (2), there is no problem, as ether bonds form where halogen is displaced and the structure of the polymer is determined by the structures of the intermediates from which it is made. However,

with polysulphonylation the situation is more complex as the sulphonyl chloride can, in principle, attack to form a sulphone bond either *o*, *m* or *p* to the other ring linkage. In practice, the synthesis only works when the polymer intermediates are selected such that sulphonylation occurs at a ring activated to electrophilic substitution so that the orientation of this substitution should be substantially *o/p* with little or no reaction at the *m* position:



A further complication is that chain branching via disulphonylation (equation 7) of a single ring is possible, and although this will occur far less readily than chain extension by monosulphonylation, as sulphone is a deactivating group, we do have evidence that in some systems a significant degree of chain branching can occur in this way¹⁵.



Structure of poly(ether sulphones) made by polysulphonylation

We have used n.m.r.¹⁶ to examine the structures of the poly(ether sulphones) with the same empirical structure produced by ether synthesis and by sulphonylation and some of these data are shown in Figures 1 and 2.

The polymer made by ether synthesis from potassium 4-(4-chlorophenyl sulphonyl) phenoxide should have an all *para*- structure and this is confirmed by its n.m.r. spectrum. This spectrum (Figure 1) shows only two resonance bands each being split to a doublet, just as expected of the all *para*- structure. This structure contains only two non-equivalent protons, hence only two resonance bands, and as the protons are *ortho* to each other both bands are split to doublets with the characteristic spin coupling constant of 8 Hz.

Polymer made by polysulphonylation from 4-phenoxybenzenesulphonyl chloride (Figure 1) gave virtually the same spectrum, indicating an all *para*- structure, and

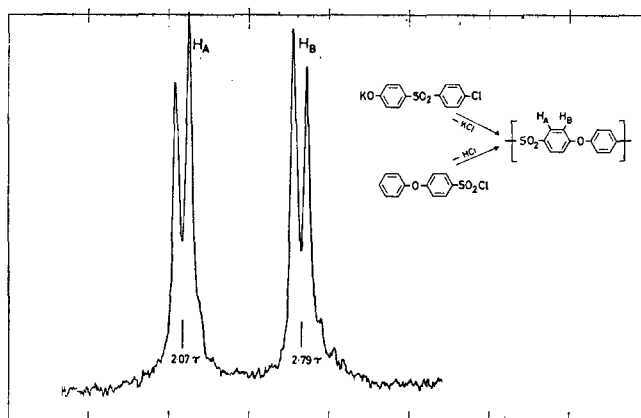


Figure 1 N.m.r. spectrum of 'all *para*' polymers

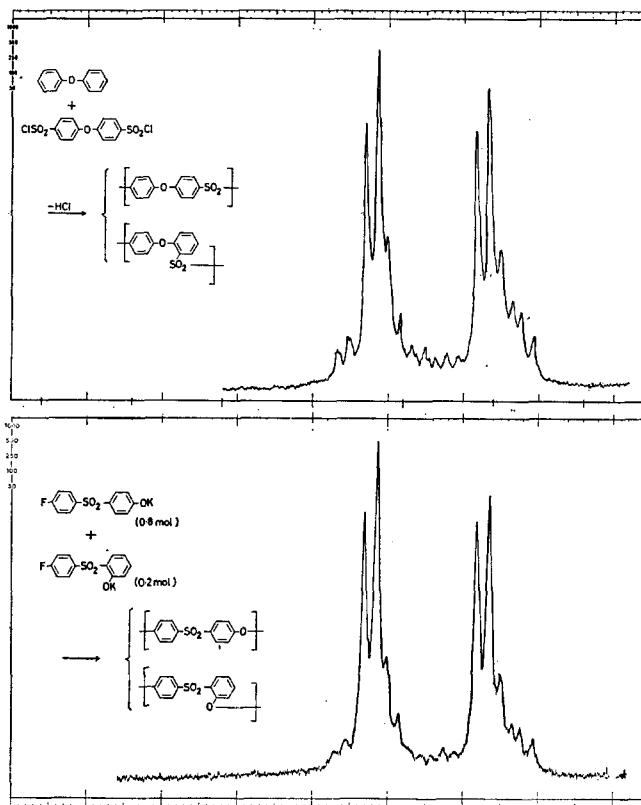


Figure 2 N.m.r. spectrum of *ortho/para* copolymers

this is at first sight rather surprising. However, on further examination it is seen that in this polycondensation sulphonyl chloride groups must always attack diphenyl ether residues attached to sulphonyl chloride or sulphone groups, and we have suggested¹⁶ that it is the electron withdrawing effect of the $-SO_2-$ group acting on the ether linkage that directs sulphonylation away from the *o*-positions, so that the orientation of sulphonylation is virtually all *para*.

We also examined the polymer from a two component polysulphonylation and obtained a rather different spectrum (Figure 2); the symmetry of the two doublets is disturbed and additional peaks appear on the high field side of the main resonance bands. This spectrum was recorded some years ago and at that time a study of non-polymeric model compounds indicated that the differences between this spectrum and that for the all *para*- polymers were due to the presence of some *o/p*-repeat units, inserted into a predominantly all *para*-

structure. This is as would be expected theoretically, for in this polycondensation half of the sulphone linkages are formed by monosulphonylation of diphenyl ether where, in the absence of sulphonyl substituents, a fairly normal *o/p*-substitution ratio is obtained leading to polymer containing a significant proportion of *o/p*-repeat units. Since that work was done we have polymerized mixtures of isomeric potassium 4-fluorophenylsulphonyl phenoxides to obtain polymers of unequivocal structure and the spectrum for the polymer made with 20% of the *o/p*-intermediate is almost identical with that for the polysulphonylation product. Thus, the original interpretation of the spectrum is confirmed and polymer from the polysulphonylation in Figure 2 contains ~20% of *o/p*-repeats.

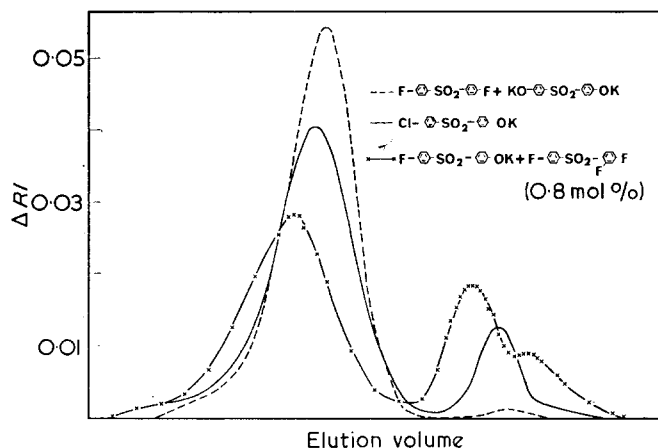


Figure 3 G.p.c. for poly(diphenylene ether sulphone)

Branching in the polyether synthesis

As far as we know polyetherification proceeds without complications due to orientation in the chain extension reaction and there is no obvious mechanism available for chain branching. However, we have obtained data from gel permeation chromatography (g.p.c.) which suggest that, in certain circumstances, branching can occur. Some of this information is shown in Figure 3, which gives g.p.c. molecular weight distribution curves for poly(ether sulphones) made in three different ways.

Polymer from the difluoride/bisphenoxide system shows only the symmetrical molecular weight distribution curve expected for a polycondensate. However, the product from polycondensation of the chlorophenoxide shows the symmetrical distribution peak and also an additional peak at the high molecular weight end of the chromatogram. Approximate calibration of the g.p.c. shows that whereas the maximum of the symmetrical peak corresponds to a molecular weight of ~30 000, the position of the second peak corresponds to a molecular weight greater than 10^6 , which is unlikely for a linear polycondensate. We suspect that this peak may be due to branched polymer and this appears likely as a polymer branched deliberately by including 0.8 mol% of a trifluoride in the polycondensation recipe shows a large peak at the high molecular weight end. The peak attributed to branched material is much more apparent in the chlorophenoxide polymer than in that from the difluoride plus bisphenoxide system where the average reactivity of the halogen function is much higher. Thus, branching may be due to a side reaction of the phenoxide ends, which would be more

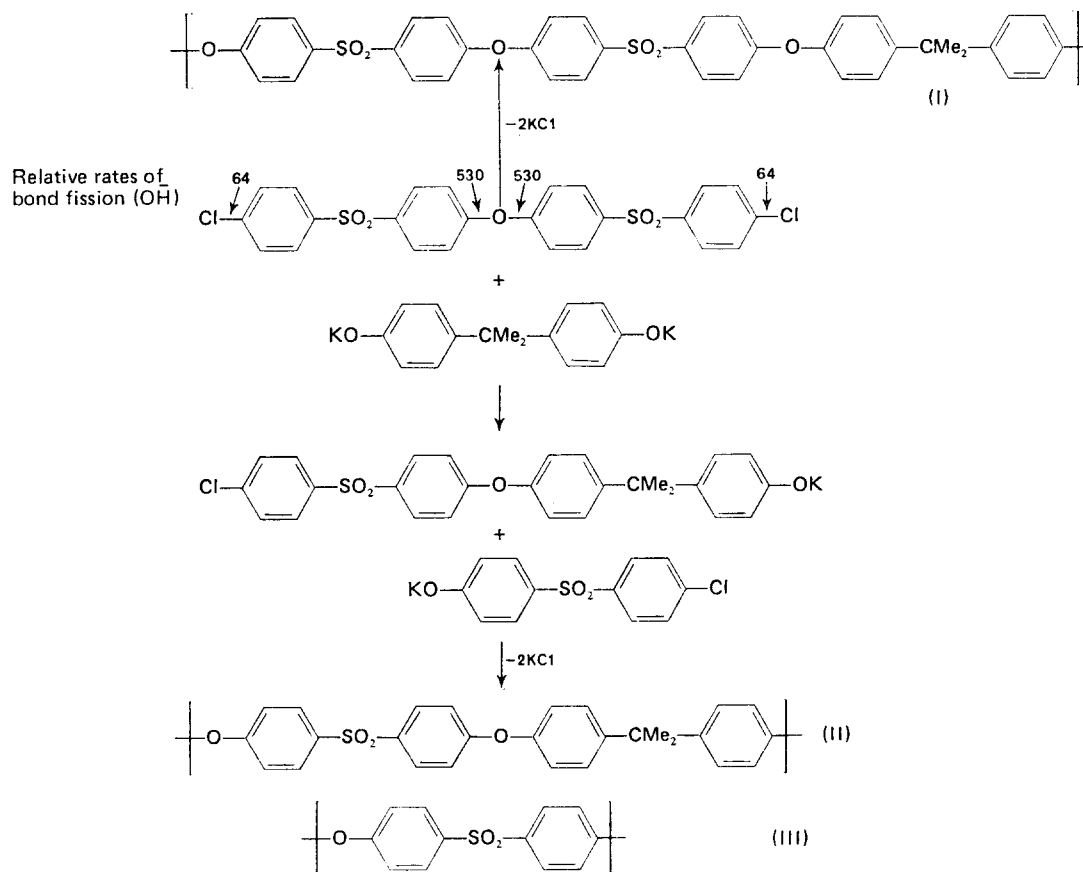


Figure 4 Ether fission during polycondensation

important in the system of lower halogen activity, and may occur by displacement of hydrogen from the ring as hydride ion. However, the extent of branching is small and does not appear to affect the bulk properties of the polymer.

Changes in repeat unit sequence due to ether interchange

Changes in polymer structure from that expected by simple polycondensation of the polymer intermediates will also occur if these contain activated ether linkages. Ether linkages between benzene nuclei are usually stable to attack by phenoxides, but when these links are activated by sulphone substituents they become labile under polycondensation conditions. In fact some kinetic data we have obtained^{8, 17} indicate that these ether linkages are likely to be about as reactive as the corresponding chlorides. Figure 4 shows relative rates of bond fission by OH for 4,4'-bis(4-chlorophenyl sulphonyl)diphenyl ether and although the relative reactivities with phenoxide would probably be different to some extent it is clear that ether fission must be taken into account when using this intermediate. Thus, polycondensation of this dichloride and bisphenate A¹⁸ will not give a polymer with the regularly repeating structure(I) but a much more random structure containing runs of repeat units II and III as well.

So far as we know chain linking and ether fission are the only processes introducing structural irregularities that can occur during the polyether synthesis and both can be avoided by appropriate choice of polycondensa-

tion system. Thus, polymers of unequivocal structure can be obtained by polyether synthesis and most of the polymer properties reported below were measured on polymers prepared in this way.

POLYMER PROPERTIES

Chemical stability

As a class, poly(aryl ether sulphones) are very stable chemically, and taking the ICI series of polymers as an example we find excellent stability to acids and alkalis and remarkable stability to oxidation. However, the high oxidative stability arises from the polymers' aromaticity and is easily spoiled by introducing aliphatic groups into the polymer repeat units. Thus, thin films of poly(ether sulphone) (III) were not embrittled, and were only slightly discoloured, by heating in air at 225°C for 170 days, whereas a polymer of comparable glass transition temperature (IV) which contained isopropylidene groups introduced via bisphenol A, darkened after 10 days becoming black and very brittle after 44 days.

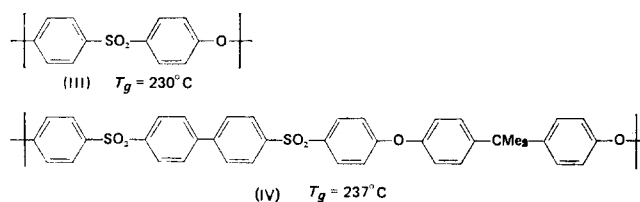


Table 5 Glass transition temperatures for poly(ether sulphones)^{11, 13, 19}

Polymer repeat unit	T_g (°C)
	180(R=H)-220(R=Ph)
	230
	225
	230
	250
	265
	280
	290
	360

Softening behaviour

Most poly(aryl ether sulphones) are amorphous materials and although a few are crystalline 'as made' or can be induced to crystallize by solvent treatment, we have not yet found one which will crystallize from the melt. Thus, the softening behaviour of these polymers is determined by their glass transition temperatures and these vary over a wide range, depending on repeat-unit as shown in Table 5.

Polymers from dichlorodiphenyl sulphone and simple bisphenols have T_g in the range 180–220°C depending on the bulk of the substituents on the central carbon atom and T_g can be pushed up a further 10 degrees by using even more bulky substituents. Further increase in T_g from 230° up to nearly 300°C is obtained from wholly aromatic systems linked only with sulphone and ether linkages. A fairly wide range of such polymers has been made, but at present it appears that copolymers consisting of diphenyl ether and di- or ter-phenyl residues linked through the *p*-positions by sulphone groups provide the best means of obtaining useful thermo-plastic materials with T_g in this range. Even higher T_g values can be obtained with condensed ring systems linked only by sulphone.

Mechanical properties

As a class the poly(aryl ether sulphones) show the high moduli expected of glassy polymers containing polar groups and as they have high glass transition temperatures they retain much of this rigidity at elevated temperatures. Unlike many glassy polymers certain poly(aryl ether sulphones) are tough under impact conditions at temperatures from T_g to -80°C . More remarkably, these tough polymers show a quite outstanding resistance to creep, that is to say they maintain resistance to an applied stress for long periods of time,

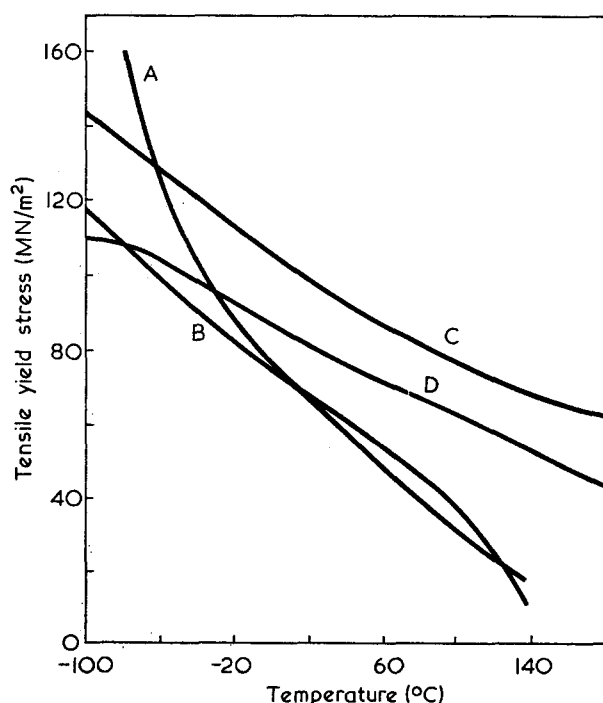


Figure 5 Tensile yield stress vs. temperature curves for poly(ether sulphone). A, Acetal copolymer; B, polycarbonate; C, poly(ether sulphone); D, Udel polysulfone

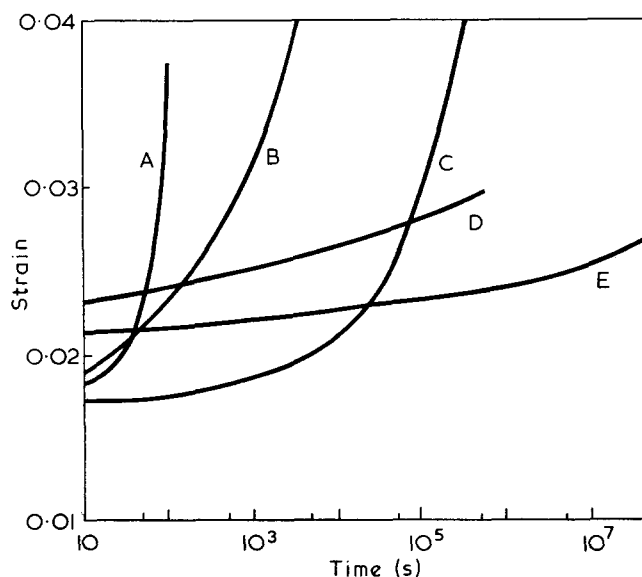
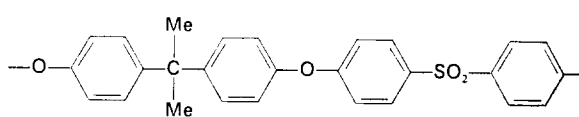
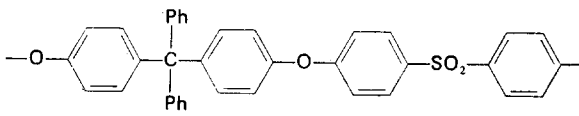
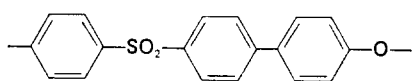
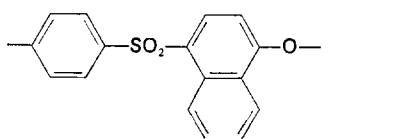
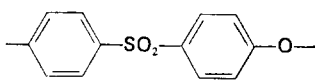
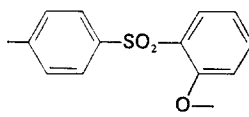
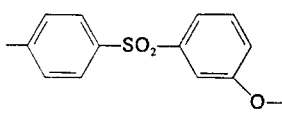


Figure 6 Tensile creep at 20°C and 50MN/m². A, Unplasticized PVC; B, PMMA; C, nylon-6,6; D, Udel polysulfone; E, poly(ether sulphone)

both at 20°C and at elevated temperatures. Figure 5 shows tensile yield stress as a function of temperature for two polysulphones compared with polycarbonate and an acetal copolymer, and demonstrates how the polysulphones retain strength at high temperature. Resistance to creep at room temperature is illustrated in Figure 6, which shows % strain *versus* time in tension for a series of thermoplastics. The poly(ether sulphones) show resistance to creep of a quite different order to the other materials and poly(ether sulphone) in this test is superior to any other unfilled thermoplastic tested in our laboratories.

The good mechanical properties shown by certain poly(ether sulphones) depends on their toughness and this is very dependent on structure, being easily spoilt by the inclusion of bulky side groups or by departing substantially from the all *para*-orientation of the groups forming the links between aromatic rings (Table 6). The effect of deviation from the all *p*-structure is very marked, and is discernible when a small proportion of the all *para*-repeat units are replaced by *o/p*-ones (Figure 7). Figure 7 shows the results of impact tests performed on a series of copoly(ether sulphones) in which the proportion of *o/p*-repeat units varied from 0 to 50%. The all *para*-homopolymer is a tough material, specimens of which do not break in a Charpy²¹ type test unless they are notched to make the test more severe. However, the copolymers become increasingly more brittle as the proportion of *o/p*-repeat units is increased, and are brittle unnotched if the proportions of these units is 20% or more. This effect was first noticed when testing poly(ether sulphones) prepared by the polysulphonylation reactions shown in Figures 1 and 2; the virtually 'all *para*' polymer made from the monosulphonyl chloride gave specimens which required notching before they would break whereas polymer from the disulphonyl chloride/diphenyl ether system gave specimens which were brittle unnotched. The data in Figure 7 show that the presence of ~20% of *o/p*-repeats is sufficient to account for this marked

Table 6 Effect of structure on toughness^{11,13}

Structure	Impact behaviour
	Tough
	Brittle
	Tough
	Brittle
	Tough
	Brittle
	Brittle

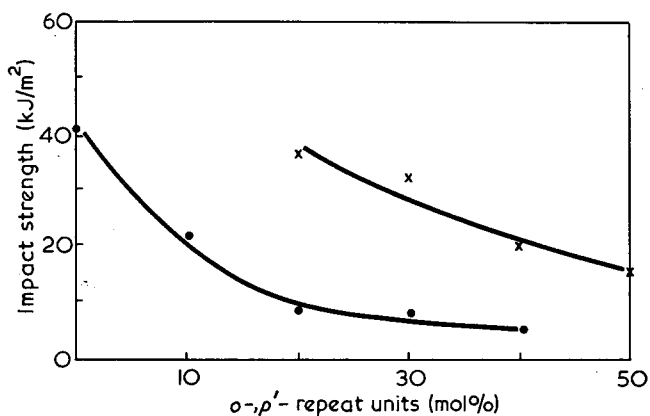


Figure 7 Impact strength of *p/p'*-homopolymers and of copolymers containing some *o,p'*-repeat units. ●, 2mm notch; x, unnotched

change in toughness, but the presence of branched chains in the product from the disulphonyl chloride/diphenyl ether system¹⁵ could be a contributing factor. Copolymers containing 50% of *o/p* repeats have a low impact strength and break before yielding in a tensile test at any temperature up to T_g ; this behaviour is in marked contrast with that of the 'all *para*' homopolymer which yields in tensile tests at all temperatures from T_g down to -80°C .

The brittleness shown by the 50% *o/p*-copolymer ruins its performance in a creep test conducted at 150°C (Figure 8) where the specimen fails in a brittle fashion after 1 h, before it has had time to creep.

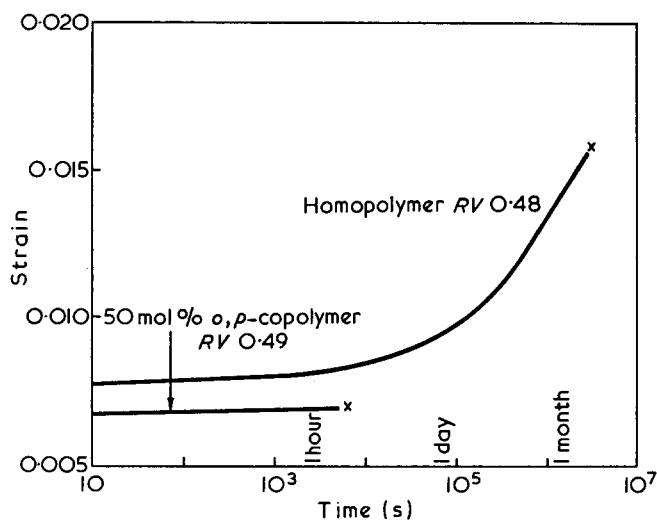
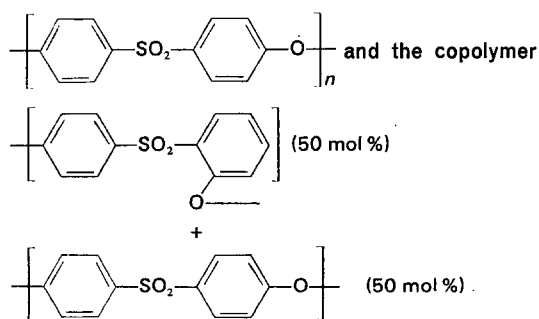


Figure 8 Creep in tension for the homopolymer



Temperature = 150°C ; stress = 20MN/m^2 ; x = point where sample fails

CONCLUSION

The general picture we now have is that the poly(ether sulphones) are a family of polymers from which a range of tough thermoplastics can be selected for use under continuous stress in the temperature range 150–250°C. This represents a considerable advance in the performance of thermoplastics when used continuously in air under stress. In this respect the best unfilled thermoplastics previously available were the polycarbonates, with an upper temperature limit of 125°C. The improvement in temperature performance provided by the poly(ether sulphones) is very substantial and it can now be seen that this advance has, like so many others, been accomplished by taking advantage of a fortunate sequence of technical events. Thus, in the first place, the synthetic routes to poly(aryl sulphones) lead naturally to the incorporation of flexible chain links, especially the ether linkage, without which these polymers would not have sufficient thermoplasticity. Secondly, the synthetic chemistry naturally provides polymer intermediates with *para* oriented functional groups. Thirdly, it is with these *p*-intermediates that the polycondensations go well to give polymers in which the *p*-substitution pattern is maintained. Finally, and perhaps most fortunately, it is the all *p*-polymers which show the best mechanical properties.

REFERENCES

- 1 Vogel, H. A. Br. Pat. 1 060 546 (April 1963)
- 2 Farnham, A. G. and Johnson, R. N. Br. Pat. 1 078 234 (July 1973)
- 3 Jones, M. E. B. Br. Pat. 1 016 245 (November 1962)
- 4 Inventa AG Br. Pat. 1 234 008 (July 1965)
- 5 Jennings, B. E., Jones, M. E. B. and Rose, J. B. *J. Polym. Sci. (C)* 1967, 16, 715
- 6 Sykes, P. A. 'A guidebook to Mechanism in Organic Chemistry', Longmans, London, 1961, p 120
- 7 Heppolletti, R. L. and Miller, J. *J. Chem. Soc.* 1956, p 2329
- 8 Newton, A. B. and Rose, J. B. *Polymer* 1972, 13, 465
- 9 Suter, C. M. 'The Organic Chemistry of Sulfur', John Wiley, New York, 1944, p 675
- 10 Bucourt, R., Mathiew, J. and Joly, R. *Rec. Trav. Chem.* 1959, 78, 527
- 11 Johnson, R. N., Farnham, A. G., Glendenning, R. A., Hall, W. F. and Merriam, C. N. *J. Polym. Sci. (A-1)* 1967, 5, 2375
- 12 Parker, A. J. *Q. Rev. Chem. Soc.* 1962, 16, 163
- 13 Unpublished ICI work
- 14 Rose, J. B. *Chem. Ind.* 1968, p 461
- 15 Cudby, M. E. A., Feasey, R. G., Gaskin, S., Kendal, V. and Rose, J. B. *Polymer* 1968, 9, 265
- 16 Cudby, M. E. A., Feasey, R. G., Jennings, B. E., Jones, M. E. B. and Rose, J. B. *Polymer* 1965, 6, 589
- 17 Attwood, T. E., Newton, A. B. and Rose, J. B. *Br. Polym. J.* 1972, 4, 391
- 18 Br. Pat. 1 294 982
- 19 Vogel, H. A. *J. Polym. Sci. (A-1)* 1970, 8, 2035
- 20 Gotham, K. and Turner, S. *31st ANTEC* 1973 (May)
- 21 Vincent, P. I. 'Impact Tests and the Service Performance of Plastics', Plastics Institute, London, 1971, p 8

Letters

G.p.c.: rapid thin layer characterization of aqueous gel networks using dyed protein standards

In seeking new matrices for the aqueous gel permeation chromatography (g.p.c.) of high molecular weight solutes, we wished to evaluate a number of crosslinked poly(acryloyl morpholine) networks prepared by bead polymerization at different monomer dilutions and varying monomer to crosslinker ratios. To have done this by conventional column techniques would have been a formidable task necessitating gradation of the gel beads by aqueous elutriation, column packing and tedious, sequential elution of standards. Consequently, we resorted to thin layer g.p.c. This also permitted investigation of gels too soft for column use.

There are two obstacles to the characterization of gel networks by thin layer g.p.c. The first is the difficulty in following the migration of standards during the actual development of the thin layer plate. The second is the difficulty in relating migration data to the Wheaton and Baumann¹ absolute distribution coefficient, K_a (i.e. to the fraction of the solvent accessible internal gel volume which is available to a given chromatographic standard).

We have overcome the former problem by using as standards a series of dyed globular proteins. The dyeing procedure applied was an adaption of that used by Dudman and Bishop² for polysaccharides. To a 2% solution (5 cm³) of each protein was added an aliquot (2 cm³) of a freshly prepared, 5% aqueous solution of Procion Brilliant Orange (Dylon International Ltd). After 5 min an aliquot (2 cm³) of 10% sodium chloride was added followed, after a further 30 min, by an aliquot (1 cm³) of 1% sodium carbonate solution. The mixture was left overnight to allow excess dye to hydrolyse. After centrifugation, the solutions of dyed protein were suitable for immediate use in g.p.c. calibration. Removal of excess hydrolysed dye was unnecessary since this is retarded strongly in comparison to the standards. The globular proteins dyed are listed in *Table 1*.

In general suspension polymerization conditions were selected such that the poly(acryloyl morpholine) gel beads to be evaluated had a diameter of less than 40 μ m in water. For thin layer g.p.c., the beads were equilibrated directly with a solution of 500 mM NaCl in 50 mM phosphate buffer (pH 8.65) and a slurry of suitable consistency was spread onto 20 \times 20 cm glass plates. These were placed in a thin layer g.p.c. apparatus (Pharmacia Ltd) and left to stand overnight. Then the standards were injected into the gel and the apparatus was inclined to effect development. A suspension of dyed cells of *Escherichia coli* (ATCC 11303) (Sigma Ltd) or a solution of a dyed sample of dextran 2000 (Sigma Ltd) was used to record the migration distance (d_0) of solutes totally excluded from the gel matrix. The thin layer g.p.c. of dyed dextrans has been reported by Aspinnall and Miller^{3,4}. Except in the case of total exclusion, these solutes are unsuitable for use as thin layer g.p.c. standards owing to their polydispersity.

Table 1 Proteins dyed for use as thin layer g.p.c. standards

Protein dyed	Molecular weight	Supplier	Type or grade	Catalogue number
Insulin	(6 000) ^a 12 000 ^b	Sigma	Bovine	I 5500
Ribonuclease A	13 600 27 200 ^b 40 800 ^c	Sigma Sigma Sigma	Bovine type IA	R4875
Chymotrypsinogen A	25 000	Sigma	Bovine type II	C4879
Ovalbumin	45 000 90 000 ^b	Sigma	Grade V	A5503
Transferrin	67 000 134 000 ^b	Calbiochem	Grade B	616396
Serum albumin	67 000 134 000 ^b 201 000 ^c	Sigma	Bovine	A4378
Fibrinogen	335 000	Sigma	Type I	F4000
Urease	490 000	P L Bio-chemicals	—	0634
β -Galactosidase	520 000	Sigma	Bovine grade III	G1875
Thyroglobulin	670 000	Sigma	Bovine type I	T001

^a Monomeric insulin is not apparent in dyed sample

^b Indicates dimer

^c Indicates trimer

To calculate the migration distance (d_s) of a zone of solvent molecules able to penetrate the gel at random, it was necessary to use T₂O elution data. It was assumed that the migration rate of H₂O and T₂O would be the same. The latter was detected by extracting bands of gel with water and measuring the radioactivity by liquid scintillation counting. For convenience, T₂O was chromatographed on separate plates together with dyed dextran 2000 as excluded standard. This enabled the zone migration distance for the solvent to be expressed as a fraction of d_0 and enabled d_s to be calculated simply for other plates of the same gel.

Providing d_0 and d_s are evaluated, the problem of relating the zone migration distance (d_c) for a given chromatographic standard to its absolute distribution coefficient K_a may be resolved.

For a totally excluded solute we may write:

$$d_0 = \frac{V}{V'} \quad (1)$$

where V' is the volume of solvent external to the gel per cm zone of plate and V is the volume of solvent displaced from the plate during development. Similarly, the zone migration distances of the solvent and chromatographic standard may be expressed:

$$d_s = \frac{V}{V' + v_s} \quad (2)$$

and

$$d_c = \frac{V}{V' + v_c} \quad (3)$$

where v_s and v_c are the internal gel volumes per cm zone of plate accessible to the solvent molecules and chromatographic standard respectively.

Using equation (1) to eliminate V from equations (2) and (3) we may obtain:

$$v_s = V' \left(\frac{d_0 - d_s}{d_s} \right) \quad (4)$$

and

$$v_c = V' \left(\frac{d_0 - d_c}{d_c} \right) \quad (5)$$

Since the Wheaton and Baumann distribution coefficient, K_d , can be expressed:

$$K_d = \frac{v_c}{v_s} \quad (6)$$

then, by combining equations (4), (5) and (6) we may write:

$$K_d = \frac{d_s(d_0 - d_c)}{d_c(d_0 - d_s)} \quad (7)$$

A relationship between zone migration data and K_d values is essential in order to obtain the logarithm molecular weight *versus* K_d plots necessary to obtain complete information on the range and distribution of pore sizes within a gel network. A typical example of such a plot is presented in *Figure 1*.

We believe that the simple methods described in this report are of importance, not only in the specific context of g.p.c., but also from the point of view of the rapid characterization of any polymer network which undergoes gelation in water. Using the coloured protein standards, it is easy to follow the course of chromatographic development and to obtain ideal chromatograms at the first attempt. With conventional standards this is not the case because the course of development can only be ascertained retrospectively using staining techniques. Pre-dyed protein standards have an additional advantage in that an exceptionally clear, permanent

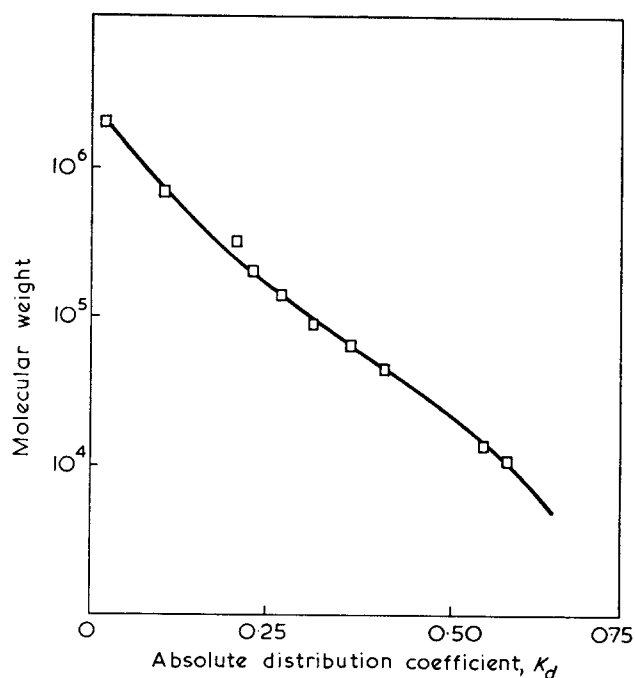


Figure 1 Characteristic logarithm molecular weight *versus* K_d relationship obtained by thin layer g.p.c. with dyed protein standards on a poly(acryloyl morpholine) network. The monomer to crosslinker ratio employed in preparing the network was 4:1 and the water regain $7.5 \text{ cm}^3/\text{g}$

record of a developed plate may be obtained simply by contacting a sheet of Whatman No. 1 chromatography paper with the gel surface.

The thin layer approach has been applied by us to evaluate new poly(acryloyl morpholine) networks in which the ratio of monomer to crosslinker varied from 200:1 to 5:1 and the nominal water content of the gel network varied from 2.5 to $15.0 \text{ cm}^3/\text{g}$. The anticipated increase in exclusion limit with polymerization volume was observed but, surprisingly, we found the exclusion limit to be relatively insensitive to diminution of crosslinker concentration. Maximum exclusion limits were observed when large amounts of crosslinker were employed. A full account of these gel networks will be reported shortly.

R. Epton, S. R. Holding and J. V. McLaren

Department of Physical Sciences,
Wolverhampton Polytechnic,
Wolverhampton WV1 1LY, UK
(Received 6 April 1974)

References

- 1 Wheaton, R. M. and Baumann, W. C. *Ann. NY Acad. Sci.* 1953, **57**, 159
- 2 Dudman, W. F. and Bishop, C. T. *Can. J. Chem.* 1968, **46**, 3079
- 3 Miller, J. N. *J. Chromatog.* 1972, **74**, 355
- 4 Aspinall, P. T. and Miller, J. N. *Analyt. Biochem.* 1973, **53**, 509

Reactivities towards the benzoyloxy radical of some conjugated dienes

The reactivities of various monomers towards the benzoyloxy radical have been compared¹; the study has now been extended to include some conjugated dienes. The procedure involved copolymerizations with styrene and the use of labelled benzoyl peroxide so that comparisons could be made between the numbers of benzoyloxy and phenyl end-groups in the copolymers. Copolymerizations have been used previously² in studies of this type but mainly to obtain information about unsaturated substances, e.g. maleic anhydride³, which do not readily engage in homopolymerization but which take part in copolymerizations; in the present case, copolymerizations were used to minimize problems associated with the production of insoluble polymers during the radical polymerizations of dienes.

The velocity constant for dissociation of $\text{C}_6\text{H}_5\text{CO}_2\text{O}$ to $\text{C}_6\text{H}_5\cdot$ and CO_2 is taken as k_1 , and those for the additions of $\text{C}_6\text{H}_5\text{CO}_2\text{O}$ to monomer-1 and monomer-2 as k'_2 and k'' . A fraction x , given by (number of benzoyloxy end-groups in a sample of copolymer)/(sum of numbers of benzoyloxy and phenyl end-groups), is related² to the concentrations of the monomers during the copolymerization thus:

$$x/(1-x)(M') = k'_2/k_1 + k''(M'')/k_1(M')$$

End-group analyses give values of x and so, from experiments in which (M') and (M'') are varied, the values of k_2 for the monomers can be compared.

Using equation (1) to eliminate V from equations (2) and (3) we may obtain:

$$v_s = V' \left(\frac{d_0 - d_s}{d_s} \right) \quad (4)$$

and

$$v_c = V' \left(\frac{d_0 - d_c}{d_c} \right) \quad (5)$$

Since the Wheaton and Baumann distribution coefficient, K_d , can be expressed:

$$K_d = \frac{v_c}{v_s} \quad (6)$$

then, by combining equations (4), (5) and (6) we may write:

$$K_d = \frac{d_s(d_0 - d_c)}{d_c(d_0 - d_s)} \quad (7)$$

A relationship between zone migration data and K_d values is essential in order to obtain the logarithm molecular weight *versus* K_d plots necessary to obtain complete information on the range and distribution of pore sizes within a gel network. A typical example of such a plot is presented in *Figure 1*.

We believe that the simple methods described in this report are of importance, not only in the specific context of g.p.c., but also from the point of view of the rapid characterization of any polymer network which undergoes gelation in water. Using the coloured protein standards, it is easy to follow the course of chromatographic development and to obtain ideal chromatograms at the first attempt. With conventional standards this is not the case because the course of development can only be ascertained retrospectively using staining techniques. Pre-dyed protein standards have an additional advantage in that an exceptionally clear, permanent

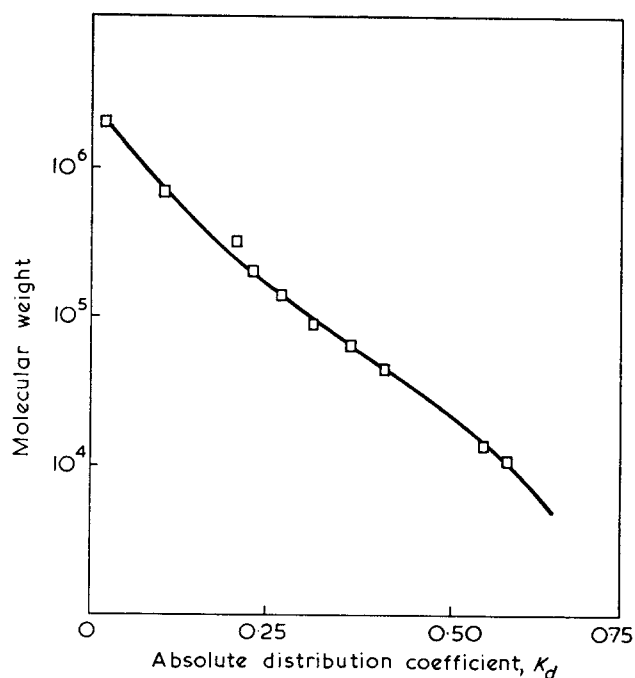


Figure 1 Characteristic logarithm molecular weight *versus* K_d relationship obtained by thin layer g.p.c. with dyed protein standards on a poly(acryloyl morpholine) network. The monomer to crosslinker ratio employed in preparing the network was 4:1 and the water regain $7.5 \text{ cm}^3/\text{g}$

record of a developed plate may be obtained simply by contacting a sheet of Whatman No. 1 chromatography paper with the gel surface.

The thin layer approach has been applied by us to evaluate new poly(acryloyl morpholine) networks in which the ratio of monomer to crosslinker varied from 200:1 to 5:1 and the nominal water content of the gel network varied from 2.5 to $15.0 \text{ cm}^3/\text{g}$. The anticipated increase in exclusion limit with polymerization volume was observed but, surprisingly, we found the exclusion limit to be relatively insensitive to diminution of crosslinker concentration. Maximum exclusion limits were observed when large amounts of crosslinker were employed. A full account of these gel networks will be reported shortly.

R. Epton, S. R. Holding and J. V. McLaren

Department of Physical Sciences,
Wolverhampton Polytechnic,
Wolverhampton WV1 1LY, UK
(Received 6 April 1974)

References

- 1 Wheaton, R. M. and Baumann, W. C. *Ann. NY Acad. Sci.* 1953, **57**, 159
- 2 Dudman, W. F. and Bishop, C. T. *Can. J. Chem.* 1968, **46**, 3079
- 3 Miller, J. N. *J. Chromatog.* 1972, **74**, 355
- 4 Aspinall, P. T. and Miller, J. N. *Analyt. Biochem.* 1973, **53**, 509

Reactivities towards the benzoyloxy radical of some conjugated dienes

The reactivities of various monomers towards the benzoyloxy radical have been compared¹; the study has now been extended to include some conjugated dienes. The procedure involved copolymerizations with styrene and the use of labelled benzoyl peroxide so that comparisons could be made between the numbers of benzoyloxy and phenyl end-groups in the copolymers. Copolymerizations have been used previously² in studies of this type but mainly to obtain information about unsaturated substances, e.g. maleic anhydride³, which do not readily engage in homopolymerization but which take part in copolymerizations; in the present case, copolymerizations were used to minimize problems associated with the production of insoluble polymers during the radical polymerizations of dienes.

The velocity constant for dissociation of $\text{C}_6\text{H}_5\text{CO}_2\text{O}$ to $\text{C}_6\text{H}_5\cdot$ and CO_2 is taken as k_1 , and those for the additions of $\text{C}_6\text{H}_5\text{CO}_2\text{O}$ to monomer-1 and monomer-2 as k'_2 and k'' . A fraction x , given by (number of benzoyloxy end-groups in a sample of copolymer)/(sum of numbers of benzoyloxy and phenyl end-groups), is related² to the concentrations of the monomers during the copolymerization thus:

$$x/(1-x)(M') = k'_2/k_1 + k''(M'')/k_1(M')$$

End-group analyses give values of x and so, from experiments in which (M') and (M'') are varied, the values of k_2 for the monomers can be compared.

The specific activity of a copolymer prepared using ^3H -benzoyl peroxide is proportional to the sum of the numbers of benzoyloxy and phenyl end-groups in a particular weight of copolymer; the specific activity after detachment by hydrolysis of the ester groups is proportional to the corresponding number of phenyl end-groups, provided that the hydrolysis has no other effect on the composition of the copolymer, so that:

$$x/(1-x) = (S_B - S_A)/S_A$$

where S_B and S_A = specific activities of a copolymer before and after hydrolysis respectively.

Polymerizations were performed at 60°C in sealed dilatometers completely free from air, with benzene as diluent; conversions were limited to 5%. The sample of ^3H -peroxide had a specific activity of $\sim 60 \mu\text{Ci/g}$. Copolymers were purified by repeated precipitation and finally dried in vacuum. Copolymers were subjected to alkaline hydrolysis⁴ and then purified. Materials were assayed by scintillation counting in solution⁵.

Stringent tests confirmed that, during the hydrolysis of copolymers, detachment of ester end-groups was complete, that there was no loss of tritium from the copolymers by exchange reactions, and that there was no significant change in the overall compositions of the copolymers.

Table 1 shows a typical set of results. From the slopes of the lines in Figure 1, the values of k_2/k_1 for butadiene, isoprene, 2,3-dimethylbutadiene and chloroprene are

Table 1 Copolymerization of isoprene and styrene at 60°C using ^3H -benzoyl peroxide as initiator

[Isoprene] (mol/l)	[Styrene] (mol/l)	Count rate (counts/sec/mg) for copolymer		$x/(1-x)$
		Before hydrolysis	After hydrolysis	
3.0	3.0	5.56	0.38	13.63
3.0	2.0	8.30	0.60	12.83
3.0	1.5	10.00	0.75	12.33
3.0	1.0	11.20	0.98	10.43
2.0	3.0	5.75	0.41	13.02
1.0	3.0	6.57	0.60	9.95

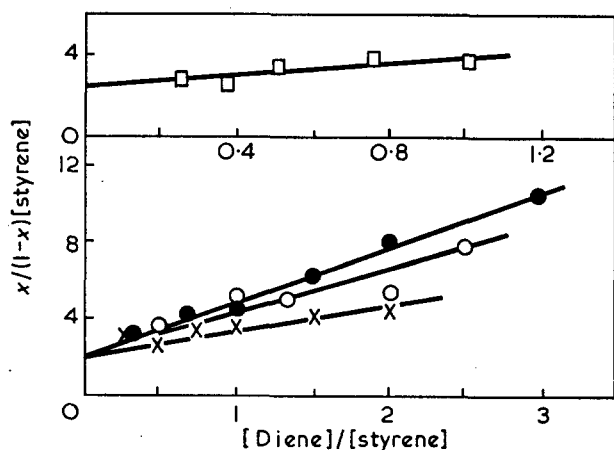


Figure 1 Plots of $x/(1-x)[\text{styrene}]$ vs. $[\text{diene}]/[\text{styrene}]$, where x is as defined in the text, for copolymerizations at 60°C with benzene as diluent and ^3H -benzoyl peroxide as initiator. \circ , Butadiene; \bullet , isoprene; \times , 2,3-dimethylbutadiene; \square , chloroprene

2.0, 2.6, 1.1 and 1.7 l/mol respectively; for each system, the intercept gives 2.5 l/mol for k_2/k_1 for styrene, in agreement with previous results⁶. The relative reactivities of styrene, butadiene, isoprene, 2,3-dimethylbutadiene and chloroprene towards the benzoyloxy radical at 60°C are therefore 1.00, 0.80, 1.04, 0.44 and 0.68 respectively.

Previous comparisons of unsaturated substances in their reactions with the benzoyloxy radical indicated the great importance of polar effects in the reactions of this radical; it was demonstrated⁷ that there is a general correlation between the reactivity of a monomer towards this radical and the value of e for the monomer as deduced from the results of copolymerizations. The accepted values of e for butadiene, isoprene and styrene are comparable and so it is reasonable that these monomers should have fairly similar reactivities towards the benzoyloxy radical. Detailed consideration of the result for 2,3-dimethylbutadiene and chloroprene must await more reliable values of e for these monomers.

Acknowledgement

P. K. S. thanks the Royal Society for a Commonwealth Award.

J. C. Bevington

Department of Chemistry,
University of Lancaster,
Lancaster LA1 4YA, UK

and P. K. SenGupta

On leave from:

Department of Applied Chemistry,
University of Calcutta,
Calcutta, India

(Received 5 April 1974)

References

- 1 Bevington, J. C. 'Radical Polymerization', Academic Press, London, 1961, p 41
- 2 Allen, J. K. and Bevington, J. C. *Trans. Faraday Soc.* 1960, **56**, 1762
- 3 Bevington, J. C. and Johnson, M. *Eur. Polym. J.* 1966, **2**, 185
- 4 Bevington, J. C. and Brooks, C. S. *J. Polym. Sci.*, 1956, **22**, 257
- 5 Bevington, J. C. and Jemmett, J. A. L. *JCS Faraday Trans. I* 1973, **69**, 1866
- 6 Bevington, J. C. *Proc. R. Soc. (A)* 1957, **239**, 420
- 7 Bevington, J. C., Harris, D. O. and Johnson, M. *Eur. Polym. J.* 1965, **1**, 235

Dilatometric study of monovalent counter-ion association with polymethacrylate

The existence of 'site binding', the specific association between counter-ions and the fixed ionic groups of macro-ion, is still the subject of much controversy¹⁻³. We report here a dilatometric study which may be taken as indicating the association states of alkali metal and tetraalkylammonium (TAA) salts of poly-(methacrylic acid) (PMA) in aqueous solution.

Volume changes associated with the protonation of three alkali metal (Li, Na and Cs) and three TAA

The specific activity of a copolymer prepared using ^3H -benzoyl peroxide is proportional to the sum of the numbers of benzoyloxy and phenyl end-groups in a particular weight of copolymer; the specific activity after detachment by hydrolysis of the ester groups is proportional to the corresponding number of phenyl end-groups, provided that the hydrolysis has no other effect on the composition of the copolymer, so that:

$$x/(1-x) = (S_B - S_A)/S_A$$

where S_B and S_A = specific activities of a copolymer before and after hydrolysis respectively.

Polymerizations were performed at 60°C in sealed dilatometers completely free from air, with benzene as diluent; conversions were limited to 5%. The sample of ^3H -peroxide had a specific activity of $\sim 60 \mu\text{Ci/g}$. Copolymers were purified by repeated precipitation and finally dried in vacuum. Copolymers were subjected to alkaline hydrolysis⁴ and then purified. Materials were assayed by scintillation counting in solution⁵.

Stringent tests confirmed that, during the hydrolysis of copolymers, detachment of ester end-groups was complete, that there was no loss of tritium from the copolymers by exchange reactions, and that there was no significant change in the overall compositions of the copolymers.

Table 1 shows a typical set of results. From the slopes of the lines in Figure 1, the values of k_2/k_1 for butadiene, isoprene, 2,3-dimethylbutadiene and chloroprene are

Table 1 Copolymerization of isoprene and styrene at 60°C using ^3H -benzoyl peroxide as initiator

[Isoprene] (mol/l)	[Styrene] (mol/l)	Count rate (counts/sec/mg) for copolymer		$x/(1-x)$
		Before hydrolysis	After hydrolysis	
3.0	3.0	5.56	0.38	13.63
3.0	2.0	8.30	0.60	12.83
3.0	1.5	10.00	0.75	12.33
3.0	1.0	11.20	0.98	10.43
2.0	3.0	5.75	0.41	13.02
1.0	3.0	6.57	0.60	9.95

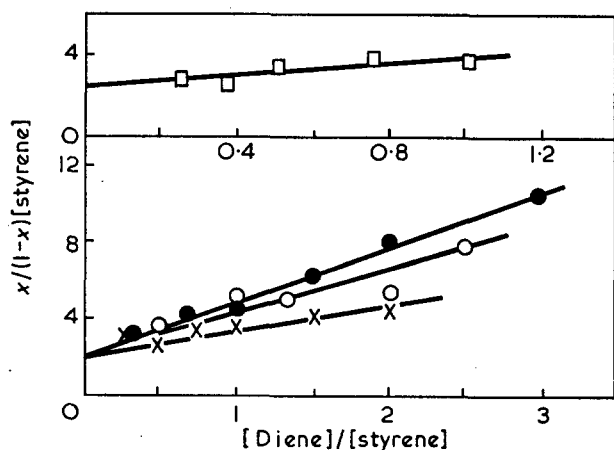


Figure 1 Plots of $x/(1-x)[\text{styrene}]$ vs. $[\text{diene}]/[\text{styrene}]$, where x is as defined in the text, for copolymerizations at 60°C with benzene as diluent and ^3H -benzoyl peroxide as initiator. \circ , Butadiene; \bullet , isoprene; \times , 2,3-dimethylbutadiene; \square , chloroprene

2.0, 2.6, 1.1 and 1.7 l/mol respectively; for each system, the intercept gives 2.5 l/mol for k_2/k_1 for styrene, in agreement with previous results⁶. The relative reactivities of styrene, butadiene, isoprene, 2,3-dimethylbutadiene and chloroprene towards the benzoyloxy radical at 60°C are therefore 1.00, 0.80, 1.04, 0.44 and 0.68 respectively.

Previous comparisons of unsaturated substances in their reactions with the benzoyloxy radical indicated the great importance of polar effects in the reactions of this radical; it was demonstrated⁷ that there is a general correlation between the reactivity of a monomer towards this radical and the value of e for the monomer as deduced from the results of copolymerizations. The accepted values of e for butadiene, isoprene and styrene are comparable and so it is reasonable that these monomers should have fairly similar reactivities towards the benzoyloxy radical. Detailed consideration of the result for 2,3-dimethylbutadiene and chloroprene must await more reliable values of e for these monomers.

Acknowledgement

P. K. S. thanks the Royal Society for a Commonwealth Award.

J. C. Bevington

Department of Chemistry,
University of Lancaster,
Lancaster LA1 4YA, UK

and P. K. SenGupta

On leave from:

Department of Applied Chemistry,
University of Calcutta,
Calcutta, India

(Received 5 April 1974)

References

- Bevington, J. C. 'Radical Polymerization', Academic Press, London, 1961, p 41
- Allen, J. K. and Bevington, J. C. *Trans. Faraday Soc.* 1960, **56**, 1762
- Bevington, J. C. and Johnson, M. *Eur. Polym. J.* 1966, **2**, 185
- Bevington, J. C. and Brooks, C. S. *J. Polym. Sci.*, 1956, **22**, 257
- Bevington, J. C. and Jemmett, J. A. L. *JCS Faraday Trans. I* 1973, **69**, 1866
- Bevington, J. C. *Proc. R. Soc. (A)* 1957, **239**, 420
- Bevington, J. C., Harris, D. O. and Johnson, M. *Eur. Polym. J.* 1965, **1**, 235

Dilatometric study of monovalent counter-ion association with polymethacrylate

The existence of 'site binding', the specific association between counter-ions and the fixed ionic groups of macro-ion, is still the subject of much controversy¹⁻³. We report here a dilatometric study which may be taken as indicating the association states of alkali metal and tetraalkylammonium (TAA) salts of poly(methacrylic acid) (PMA) in aqueous solution.

Volume changes associated with the protonation of three alkali metal (Li, Na and Cs) and three TAA

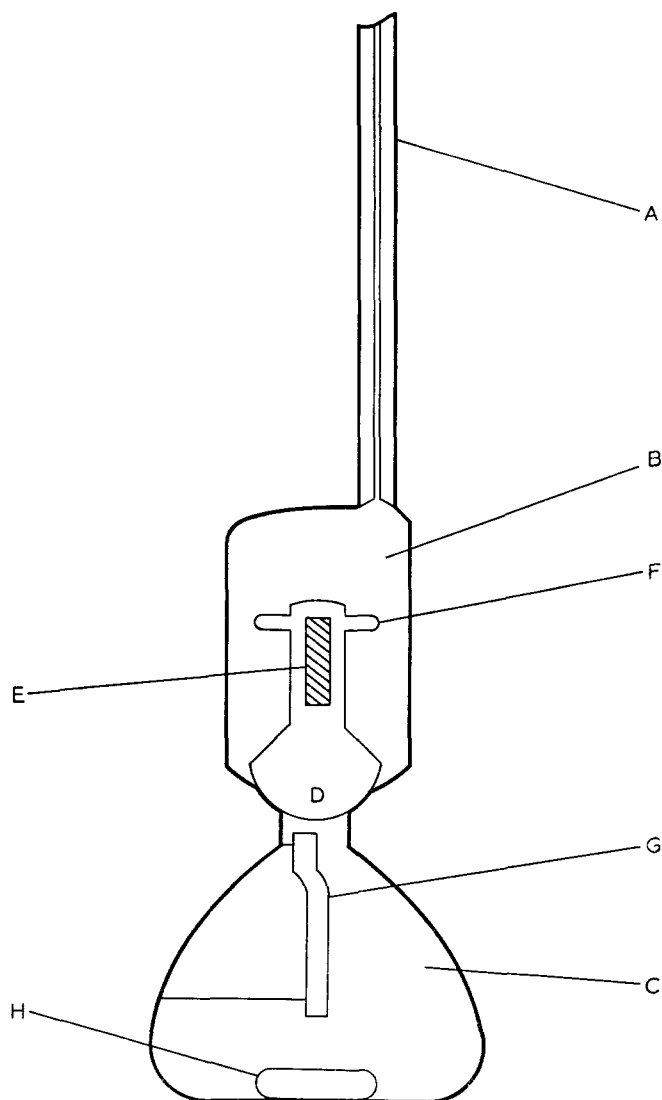


Figure 1 The circulation dilatometer. A, 1 mm precision bore tubing; B, upper compartment (20.31 ml); C, lower compartment (41.44 ml); D, ground glass ball stopper operated by a ring magnet from outside; E, magnetic bar in D; F, supporting glass nail; G, glass tubing channel; H, magnetic stirrer

(methyl, n-propyl and n-butyl) (TMA, TPA and TBA) salts of atactic PMA ($M_w = 1.43 \times 10^5$) have been measured at $25.00 \pm 0.001^\circ\text{C}$ using a simple dilatometer (Figure 1) which can be read to $0.04 \mu\text{l}$. Reproducibility of the volume change for an acid-base reaction was found within the limit of the reading against the observed change, $3.42 \mu\text{l}$. Aqueous solutions of a polymer salt (lower) and HCl (upper) in each compartment were mixed by opening the stopper and repeating the rotation of the stirrer for 2 min and the volume change was read at the capillary menisci. It is shown by the experiments given in Table 1 that this type of dilatometer is useful when the mixing solutions should not contact with any fluid like kerosene⁴.

The volume changes observed on mixing hydrochloric acid with the three TAA PMA solutions are exemplified in Figure 2. The differential molar volume change, $\Delta\bar{V}$, is obtained as the slope of the curves². Because the slopes appeared changing intricately with α , $\Delta\bar{V}$ was calculated as the difference of the two successive ΔV 's divided by the corresponding n_{H^+} difference. Figure 3 and Table 1 show $\Delta\bar{V}$ for the six PMA salts. For Na and TBA salts, Ikegami⁵ has given some explanations

on the volume increases in terms of the contributions of the hydrophobic substituent and the conformational transformation of the polymer. The finding that $\Delta\bar{V}$ values for the three alkali metal salts are essentially identical (within $\pm 3\%$)* over the entire range of α seems revealing. It was also found that $\Delta\bar{V}$ for KPMA and RbPMA are 19.8 and 19.9 ml in the α range 0.8 to 1.0, in agreement with the other alkali metal salts. A straightforward interpretation of this consistency would be that the primary hydrations of the alkali metal counter-ions have little to do with the protonation process of the macro-ion. This implies that before and

* In Table 1, it is found that $\Delta\bar{V}$ for LiPMA is somewhat larger than other alkali metal salts in a certain α range. This might be an indication of the outer-sphere association of this particular salt.

Table 1 Differential molar volume change (ml/mol) on protonation of carboxylates*†

Acid formed	Cation							
	Li	Na	K	Rb	Cs	TMA	TPA	TBA
Acetic		11.0				11.1		11.1
Pivalic	17.1	17.1 (16.9)			17.0	17.5		18.1 (18.7)
Glutaric								
A		12.1				12.1		12.1
B		13.1				13.3		14.8
PMA	20.6	19.7	19.8	19.9	19.9	26.2	27.3	28.8

* Measurements for mono- and di-carboxylates were done under the same concentrations as described in Figure 2 except that monocarboxylates at $\alpha = 0.85$ were used. Mean values in the α range 0.4 to 0.7 for monocarboxylates, 0.1 to 0.4 (A) and 0.7 to 0.95 (B) for glutarates, and 0.8 to 1.0 for PMA salts, are listed. Deviations are within $\pm 2\%$ for PMA salts and 1% for others † Numbers in parentheses are the values obtained in the presence of 0.0500 mol/l of the chloride salts of the relevant cations

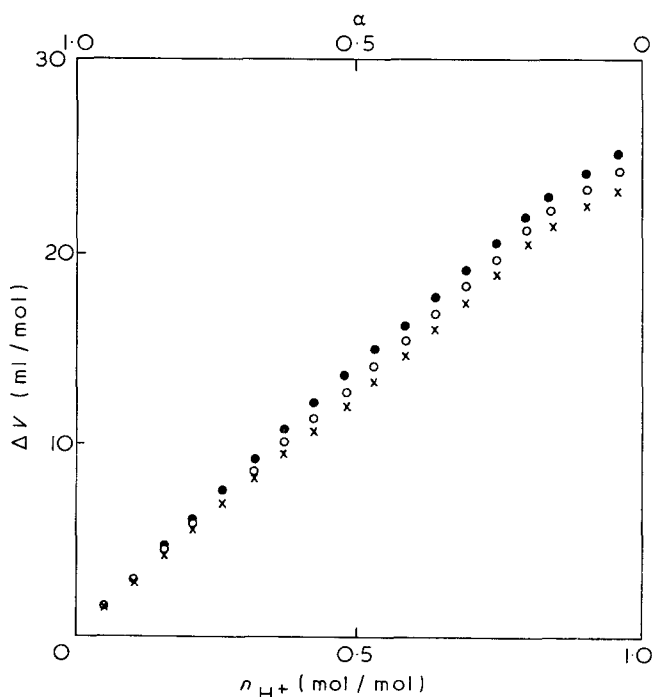


Figure 2 Volume change on protonation of PMA salts. x, TMA PMA; o, TPA PMA; ●, TBA PMA. α , degree of neutralization²; n_{H^+} , mol of reacted hydrogen ion/mol of the PMA salt. The PMA salts in 0.0460 mol/l in C of the dilatometer were mixed with aqueous HCl in B in the presence of 0.0100 mol/l of the chloride salts of the relevant cations

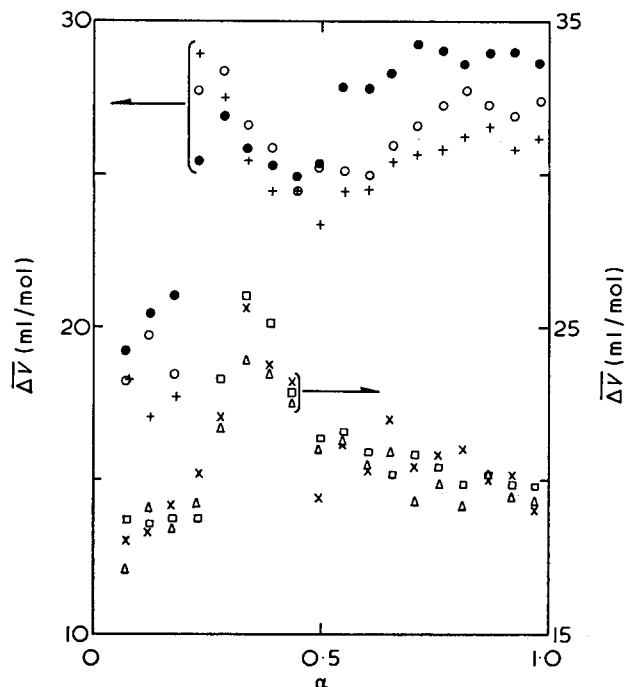


Figure 3 Differential molar volume change on protonation of PMA salts. +, TMA PMA; ○, TPA PMA; ●, TBA PMA; ×, Li PMA; △, Na PMA; □, Cs PMA

after the protonation reaction, the immediate surroundings of the counter-ions are not perturbed by the presence of the macro-ion or the chloride and *vice versa*. The possibility may be excluded, therefore, that these counter-ions interact with the respective charges on the macro-ion to such an extent as the primary hydration sheaths of pairing ions are shared^{6, 7}. With the three TAA salts, $\overline{\Delta V}$ was found quite dependent on the counter-ion species, in a way that the larger cation gives the larger volume increase, in the α range > 0.5 .

To find the origin of this TAA specificity, volume changes on the protonation of TAA and alkali metal salts of some mono- and di-carboxylic acids were measured. Table 1 summarizes the results, which show: (i) with the larger hydrocarbons on the carboxylate anion or on TAA cation, the volume increase becomes larger; (ii) this tendency is magnified when protonation occurs at the glutarate dianion; and (iii) alkali metals have no effect on $\overline{\Delta V}$. These observations lead us to the understanding that each TAA cation does exert specific influence on the protonation process of the carboxylate anions including PMA. The following experiments show that volume contraction occurs due to the interaction between TBA cation and pivalate anion. $\overline{\Delta V}$ at the mixing of 0.0460 mol/l of pivalic acid in C of the dilatometer with 0.700 equivalents of NaOH and TBAOH in B were 4.8 and 4.3 ml/mol, respectively*. The smaller increase in the latter indicates the volume contraction accompanying the formation of TBA pivalate. It is suggested therefore that the interaction between the hydrophobic ions of opposite sign, association, is responsible for the observed volume effect on the protonation of TAA carboxylates. This point of view is supported by the enhanced volume increase on the protonation of TBA pivalate in the concentrated TBA chloride solution (Table 1).

* The observed values were corrected for $\overline{\Delta V}$'s on the dilution of NaOH and TBAOH, -0.3 and +0.4 ml, at the experimental concentration.

Tondre and Zana⁸ have reported that the apparent molal volume of polyacrylate anion at infinite dilution is smaller for TMA salt than any of the alkali metal salts. Taking the volumes of relevant cations from Millero's compilation⁹, the molal volumes attributable to the same anion were calculated from Ise and Okubo's data¹⁰ assuming additivity. For Li, Na and K salts, the volumes are 39.4 ± 0.2 ml, while for TMA, TEA (ethyl), TPA and TBA salts, they are 33.8, 34.3, 41.0 and 31.1 ml, respectively. Again, the volume contraction of the TAA salts seems beyond experimental uncertainty except TPA. All of these discussions suggest that in aqueous solution, alkali metal salts of PMA do not associate to an extent that the primary hydrations of respective ions are perturbed and in contrast, TAA salts are under an interaction leading to the volume contraction.

J. Komiyama, Y. Takeda, M. Ando
and T. Iijima

Department of Polymer Science,
Tokyo Institute of Technology,
Tokyo, 152, Japan
(Received 16 April 1974)

References

- 1 Conway, B. E. *J. Macromol. Sci. (C)* 1972, 6, 113
- 2 Begala, A. J. and Strauss, U. P. *J. Phys. Chem.* 1972, 76, 254; Strauss, U. P. and Leung, Y. P. *J. Am. Chem. Soc.* 1965, 87, 1456
- 3 Ise, N. *Adv. Polym. Sci.* 1971, 7, 536
- 4 Kauzmann, W., Bodansky, A. and Rasper, J. *J. Am. Chem. Soc.* 1962, 84, 1777
- 5 Ikegami, A. *Biopolymers* 1971, 6, 431
- 6 Conway, B. E. 'Physical Chemistry: An Advanced Treatise', (Ed. H. Eyring), Academic Press, New York, 1970, Vol IXA, p 1
- 7 Spiro, T. G., Revesz, A. and Lee, J. *J. Am. Chem. Soc.* 1968, 90, 4000
- 8 Tondre, C. and Zana, R. *J. Phys. Chem.* 1972, 76, 3451
- 9 Millero, F. J. 'Water and Aqueous Solutions', (Ed. R. A. Horne), Wiley-Interscience, New York, 1970, p 533
- 10 Ise, N. and Okubo, T. *J. Am. Chem. Soc.* 1968, 90, 4527

Conference Announcement

Electro-optical Properties of Macromolecular Solutions

Liège, Belgium, 22-25 September 1974

The main concern of the meeting will be with any optical property of macromolecular solutions which is perturbed by the action of an electric field. Typical effects would be Kerr effect, electric dichroism, light scattering, optical activity, electrochromism, laser effects etc. Theoretical and experimental studies on rotational diffusion and the particular electro-optic characteristics of specific materials (e.g. liquid crystals), will be included.

Interested personnel are asked to write to Dr C. Houssier, Laboratoire de Chimie Physique, Université de Liège au Sart-Tilman, B-4000 Liège, Belgium, who with Professor E. Fredericq (Liège) and Dr B. R. Jennings (Brunel University, UK) is organizing the meeting.

Book Reviews

Mechanical testing of plastics

S. Turner

Iliffe Books, London, 1973, 180 pp. £5.00

'A good test carried out roughly is almost invariably more effective than a bad test carried out well.' These two concluding lines of Mr Turner's book effectively epitomize some of the sentiments underlying a very readable and well-presented treatise which must by no means be taken at the face value of its title. It is not a practical manual where one can find detail on equipment and experimental techniques: for these it would be better to go directly to such publications as BS 2782:1970 of the British Standards Institute or the 'Handbook of Plastics Test Methods' of Ives, Mead and Riley (see *Polymer* 1972, 13, 597). Rather it is, as the dust cover and preface suggest, an exposition of the philosophy of physical testing and an attempt to bridge the gap between research papers and published standards. The subject is approached by careful attention to the fundamental principles involved and amplified by discussion based on and with reference to specialist papers and standard works on test methods.

Many workers approach the testing of plastics in a hearty, enthusiastic manner, but often with little thought to those factors which may have a profound influence on their results from the points of view of both accuracy and interpretation. The teaching of the book will counteract this. Following brief introductory chapters on the growth of test methods and the significance of experimental results, there is a detailed discussion on the generalities of mechanical testing, attention being paid to mathematical representation of linear systems and the limitations of time, geometry and apparatus, in order that a rational system might be evolved.

Two chapters deal with deformation where sinusoidal and step excitation methods are employed, followed by two further chapters on strength tests, short term and long term, so that there is ample cover for measurements associated with tensile, elongation, recovery, creep, relaxation, flexure, impact, and static and dynamic fatigue data. The final chapter very properly deals with the test sample itself: polymer characteristics, preparation, conditioning. Three appendixes on probability, tests of significance and the fitting of curves have special appeal to the non-expert who has to deal mathematically with experimental data. Each chapter has many references to research papers and reviews and related bibliography.

The book, which is one of the monographs commissioned by the Plastics Institute in recent years, will be of interest to all engaged in plastics testing and who use data on the mechanical behaviour of polymers, as well as to many others who are associated with testing in theory and practice. It is well produced, well indexed and available at a reasonable price.

R. J. W. Reynolds

Processing for adhesives bonded structures

Edited by M. J. Bodnar

Applied Polymer Symposia No 19, Interscience, New York, 1972, 496 pp. £7.25

This book is a collection of 35 papers given at a symposium sponsored by the Picatinny Arsenal but only the first 14 papers may be said properly to reflect the title of the book. The first paper indeed presents a valuable review of the problems of process control and the effects of the variables which processing may introduce with the necessary emphasis on surface treatment of substrates and the need to control the time after treatment and before bonding. Other useful papers deal with the need for surface priming, treatment with siloxanes and methods of examining surfaces.

The organizers have succumbed to the temptations to accept all papers offered for the symposium and then to print them in the proceedings in a largely unedited form. This has resulted in a general conglomerate of papers on adhesives and adhesion in a very wide sense much of which is simply trade literature produced for advertising and customer service.

The book cannot be recommended solely on the value of a

few papers. Libraries who feel they ought to maintain running sets of this series are ill served by publishers producing an inflated volume, replete with unnecessary and uninformative photographs which have doubtless added to the cost of this volume and therefore to the difficulties of libraries and librarians.

Lest this be taken as the sour remarks of a non-contributor, the following points are taken from a very long list of shortcomings many of which must be blamed on the editor or on the publishers who have not issued to him a sufficient stock of blue pencils. A form of presentation, indeed subject matter generally, which might make for good and useful technical discussion is neither appropriate nor desirable on the printed page. Colloquialisms, trade names, unidentified initials occur throughout.

Fourteen blocks of photographs are used in the second paper showing parts of Apollo spacecraft. They probably enlivened and pointed the lecture; they convey little if anything to the reader. The same applied to the 'flight' picture on page 247. But the few graphs in the second paper are photographic reproductions of graph paper—a form which no respectable journal would tolerate. The next paper is set, as is all the text, in one of the usual founts, yet reproduces the tables photographically from a typewritten script but with footnotes set in the heavier fount. Paper 6 has used a typewriter to produce a list of 19 chemical formulae for Table 1 and this has been reduced photographically almost to the point of illegibility. If the money spent on blocks for photographs had been saved by their editorial elimination, as they should have been, the publishers would have afforded properly to set the necessary tables. A comparison of Tables I and II on pages 391–392 shows two different methods, type and typewriter immediately following one another. Have the editor and publisher no pride?

Nor are technical matters free from this casual presentation. Page 267 deals with shop environment and its influence on bonded structure with reference to a commercial adhesive whose chemical type is not even mentioned. The paper commencing on page 231 seems to be the transcript of a tape with the lecturer shooting rhetorical questions at an audience. Page 303, in the midst of photographs of US car manufacture, contains a phrase at least relevant to the subject matter. It reads, 'If required, this surface is wiped with a clean cloth saturated with a solvent . . .'. Fancy paying \$18 for this advice!

One last infelicity; page 417 refers to ' . . . curing the bond at 200°F cracked the crystals on cooling to 10°C whilst room temperature cures could safely be cooled to -43°'. Study of the paper shows this mixture of scales to be intended and the -43° to be Celsius; or is it?

W. C. Wake

IUPAC Macromolecular Chemistry

Volume 8

Butterworths, London, 1973, 459 pp. £18.00

In a book review some years ago (*Polymer* 1970, 11, 390) Professor A. M. North was driven to pose the polemic question 'Is this a *book* or a *journal*?' The circumstances attached to the present volume are similar in some respects. It comprises the plenary and main lectures delivered at the IUPAC International Symposium on Macromolecules in Helsinki, July 1972. By tradition such articles appear in journal form as a supplement to *Pure and Applied Chemistry*. The volume under review is described as being a supplement, but is actually a very highly priced hard backed edition. Discreet enquiry has revealed that the answer to the opening question is 'both' in this case. Thus, for regular subscribers to *Pure and Applied Chemistry* the volume is issued as a journal; otherwise one is obliged to purchase it as a more expensive book. Publishers' mores are difficult to fathom, but must be accepted for what they are if a book is one to command serious attention, which this certainly is.

The subdivision of the symposium into the following distinct groups will not be immediately obvious to the reader from the wholly random arrangement of the twenty-three articles: Polymerization and copolymerization reactions; Solution properties

Book Reviews

and characterization; Bulk properties; Degradation and decomposition; and Polysaccharides and derivatives. About a third of the chapters fall within the first group, whilst there are only two articles devoted to polysaccharides. These are 'Polysaccharides as models for stereoregular polymers' (E. Husemann) which inevitably involves some discussion of solution properties and morphology of trisubstituted cellulose derivatives, and 'New methods in structural polysaccharide chemistry' (B. Lindberg) in which modern techniques are used to analyse the fragments from partial hydrolysis and different specific degradations of unmodified and chemically modified polysaccharides. All the articles are fundamental in nature and this is true no less of the lucid chapter on 'Weathering of polyolefins' despite the suggestively applied tone of the title. A brief comment on disposal problems ends this chapter and, in view of current hysteria, Winslow's final sentence deserves a wider readership, viz.: 'Accelerated weathering of films would undoubtedly lessen the volume of litter, but the ultimate solution to plastic pollution lies in education since litter is more of a people problem than a materials problem'.

The contributions maintain a remarkably uniform level of presentation. Perhaps more significant is the fact that each is a really up-to-date review of the field instead of a thinly disguised forum for presenting the author's detailed personal research data (as is often the case). In two instances readers will be able to regard the articles as continued progress reports, since rather related contributions (by Flory and by Vinogradov) were made to the IUPAC Leiden Symposium in 1970 and have already been published in this series. The authorship is international, but English is used throughout. The printing, production and reproduction of diagrams are faultless and the number of places where symbols on graphs are undefined is too small to warrant listing here. No author or subject index is provided, but this does not seem a serious omission in a volume essentially without a unified theme. All libraries are recommended to obtain this book. The average polymer chemist, being only human, will not care to purchase a volume only a very small fraction of which is within his sphere of comprehension. Polymer chemists of exceptional breadth of interest are rare and may well be exemplified by the contributors themselves; but then they will probably possess their own free copies.

M. B. Huglin

Stress analysis of polymers

J. G. Williams

Longman, Harlow, 1973, 276 pp. £6.50

Although the title might imply that the subject is confined to polymers, this book is a more general treatment of stress analysis in viscoelastic materials. The usual engineering texts on 'Strength of materials' are largely confined to Hookean elastic time-independent behaviour, while at least one author has developed an extensive treatment for elastic perfectly plastic materials, i.e. elastic up to a yield point and thereafter strain at constant stress. This represents about the limit of the conventional treatment; more advanced and more realistic assumptions for polymers have tended to be treated either highly theoretically or for special cases.

The first section of this book provides a basic text, developing equations for stress and strain including non-linearity, viscoelasticity, anisotropy, and time dependence with special attention to approximations applicable to polymers such as large strain deformations at constant volume. The mathematics are kept simple, at some cost of brevity, but this is probably preferable for the majority of practical designers.

The second section, comprising nearly half the book, applies these equations to specific geometries, especially bending of beams, plates and struts and loading of axi-symmetric cylinders and membranes. The solutions are presented in simple algebraic form, requiring only material property data for numerical calculation; in several cases digital computation is desirable. It seems that an undue proportion of this section is devoted to linear elastic properties and the corrections to simple theories of bending and thin shells to take account of shear deflections, transverse restraints, e.g. wide beams, and large deflections. Among these are rather scattered references to non-linearity and viscoelastic behaviour,

but the reviewer found it difficult to follow the logic of the assumptions made in individual cases. It would perhaps have been helpful to concentrate on derivation of equations for non-linear stress/strain and rubber elasticity assumptions and compare results with those from linear/small strain and elastic perfectly plastic assumptions in practical conditions where the differences are significant.

The final shorter section discusses stress concentrations, mainly concerned with testing, and would seem to be justified as indicating how the effects of discontinuities and incipient flaws may be included in stress analysis for viscoelastic materials.

Although there are numerous references in the text to polymer properties, no actual data are given for comparison with the idealizations used. So while this book is directed to stress analysis rather than property data, little indication is given of the polymers, temperatures, strains, and times for which a particular idealization, and the equations derived from it, are a reasonable approximation. Some of the general statements on polymer properties also seem open to question: on p 55 it is stated 'Polymers above their glass transition temperature exhibit rubber-like properties in that they are essentially elastic up to strains of several hundreds of per cent'. Insofar as this is true of linear polymers, it also involves long recovery times. On pp 64 and 150, 'However, most polymers in the glassy state do undergo a process which can be equated with yielding' and 'Most polymers below their glass transition temperature can be described approximately as elastic perfectly plastic materials'. These hardly apply to polystyrene and PMMA without toughening, while rubbers and polyolefins are not usually used in this state.

The book is well laid out and sectionalized with concise index and bibliography. The nomenclature is clear and consistent, but should perhaps have been listed for reference. The production, including diagrams is extremely good. This book is an important step in advancing the analytical design of time-dependent viscoelastic materials by providing the basic equations and some derivations for specific geometries, but further consideration is needed of the applicability to commercial polymers.

M. J. Stevens

Nylon plastics

Edited by M. I. Kohan

Wiley-Interscience, London and New York, 1973,
£19.50

This book is one in the series of Society of Plastics Engineers monographs. It is claimed on the fly sheet that it is the first complete text on nylon plastics with well referenced coverage of nylon technology from monomer synthesis to end use application. It therefore attempts to provide information and references to information for all those concerned with nylon plastics technology. Intentionally it does not attempt to discuss fibre technology though there is a great deal of nylon science which will be valuable to the nylon fibre technologist.

There are 19 contributors including the editor, 16 of whom come from the DuPont Company. The book therefore represents a great deal of the publishable knowledge on nylon plastics from that company which of course first introduced us to the material following the work of Wallace Carothers. The cover is very wide from molecular weight distribution, thermal degradation, crystallization kinetics to injection moulding, quality control, design and economic considerations. There must be something for everyone with an interest in nylon, except perhaps the commercial people since only 12 pages out of 650 are devoted to economics. There is even a table listing the suppliers of nylon plastics and compositions but unfortunately this is restricted to the USA.

I recommend this book unreservedly. It contains an enormous amount of information and there appears to be little duplication between chapters written by different authors. It is reasonably up-to-date containing 1972 and 1971 references (and even a few from 1973) though most are from the 1960s. It is easy to read, the illustrations and diagrams are numerous and clear. It is a must for the book shelves of the library of any concern having any interest at all in nylon plastics. Though expensive it must be worth it. In my view the claim on the fly sheet is substantiated.

F. J. Hybart

Book Reviews

Mechanical testing of plastics

S. Turner

Iliffe Books, London, 1973, 180 pp. £5.00

'A good test carried out roughly is almost invariably more effective than a bad test carried out well.' These two concluding lines of Mr Turner's book effectively epitomize some of the sentiments underlying a very readable and well-presented treatise which must by no means be taken at the face value of its title. It is not a practical manual where one can find detail on equipment and experimental techniques: for these it would be better to go directly to such publications as BS 2782:1970 of the British Standards Institute or the 'Handbook of Plastics Test Methods' of Ives, Mead and Riley (see *Polymer* 1972, 13, 597). Rather it is, as the dust cover and preface suggest, an exposition of the philosophy of physical testing and an attempt to bridge the gap between research papers and published standards. The subject is approached by careful attention to the fundamental principles involved and amplified by discussion based on and with reference to specialist papers and standard works on test methods.

Many workers approach the testing of plastics in a hearty, enthusiastic manner, but often with little thought to those factors which may have a profound influence on their results from the points of view of both accuracy and interpretation. The teaching of the book will counteract this. Following brief introductory chapters on the growth of test methods and the significance of experimental results, there is a detailed discussion on the generalities of mechanical testing, attention being paid to mathematical representation of linear systems and the limitations of time, geometry and apparatus, in order that a rational system might be evolved.

Two chapters deal with deformation where sinusoidal and step excitation methods are employed, followed by two further chapters on strength tests, short term and long term, so that there is ample cover for measurements associated with tensile, elongation, recovery, creep, relaxation, flexure, impact, and static and dynamic fatigue data. The final chapter very properly deals with the test sample itself: polymer characteristics, preparation, conditioning. Three appendixes on probability, tests of significance and the fitting of curves have special appeal to the non-expert who has to deal mathematically with experimental data. Each chapter has many references to research papers and reviews and related bibliography.

The book, which is one of the monographs commissioned by the Plastics Institute in recent years, will be of interest to all engaged in plastics testing and who use data on the mechanical behaviour of polymers, as well as to many others who are associated with testing in theory and practice. It is well produced, well indexed and available at a reasonable price.

R. J. W. Reynolds

Processing for adhesives bonded structures

Edited by M. J. Bodnar

Applied Polymer Symposia No 19, Interscience, New York, 1972, 496 pp. £7.25

This book is a collection of 35 papers given at a symposium sponsored by the Picatinny Arsenal but only the first 14 papers may be said properly to reflect the title of the book. The first paper indeed presents a valuable review of the problems of process control and the effects of the variables which processing may introduce with the necessary emphasis on surface treatment of substrates and the need to control the time after treatment and before bonding. Other useful papers deal with the need for surface priming, treatment with siloxanes and methods of examining surfaces.

The organizers have succumbed to the temptations to accept all papers offered for the symposium and then to print them in the proceedings in a largely unedited form. This has resulted in a general conglomerate of papers on adhesives and adhesion in a very wide sense much of which is simply trade literature produced for advertising and customer service.

The book cannot be recommended solely on the value of a

few papers. Libraries who feel they ought to maintain running sets of this series are ill served by publishers producing an inflated volume, replete with unnecessary and uninformative photographs which have doubtless added to the cost of this volume and therefore to the difficulties of libraries and librarians.

Lest this be taken as the sour remarks of a non-contributor, the following points are taken from a very long list of shortcomings many of which must be blamed on the editor or on the publishers who have not issued to him a sufficient stock of blue pencils. A form of presentation, indeed subject matter generally, which might make for good and useful technical discussion is neither appropriate nor desirable on the printed page. Colloquialisms, trade names, unidentified initials occur throughout.

Fourteen blocks of photographs are used in the second paper showing parts of Apollo spacecraft. They probably enlivened and pointed the lecture; they convey little if anything to the reader. The same applied to the 'flight' picture on page 247. But the few graphs in the second paper are photographic reproductions of graph paper—a form which no respectable journal would tolerate. The next paper is set, as is all the text, in one of the usual founts, yet reproduces the tables photographically from a typewritten script but with footnotes set in the heavier fount. Paper 6 has used a typewriter to produce a list of 19 chemical formulae for Table 1 and this has been reduced photographically almost to the point of illegibility. If the money spent on blocks for photographs had been saved by their editorial elimination, as they should have been, the publishers would have afforded properly to set the necessary tables. A comparison of Tables I and II on pages 391–392 shows two different methods, type and typewriter immediately following one another. Have the editor and publisher no pride?

Nor are technical matters free from this casual presentation. Page 267 deals with shop environment and its influence on bonded structure with reference to a commercial adhesive whose chemical type is not even mentioned. The paper commencing on page 231 seems to be the transcript of a tape with the lecturer shooting rhetorical questions at an audience. Page 303, in the midst of photographs of US car manufacture, contains a phrase at least relevant to the subject matter. It reads, 'If required, this surface is wiped with a clean cloth saturated with a solvent . . .'. Fancy paying \$18 for this advice!

One last infelicity; page 417 refers to ' . . . curing the bond at 200°F cracked the crystals on cooling to 10°C whilst room temperature cures could safely be cooled to -43°'. Study of the paper shows this mixture of scales to be intended and the -43° to be Celsius; or is it?

W. C. Wake

IUPAC Macromolecular Chemistry

Volume 8

Butterworths, London, 1973, 459 pp. £18.00

In a book review some years ago (*Polymer* 1970, 11, 390) Professor A. M. North was driven to pose the polemic question 'Is this a *book* or a *journal*?' The circumstances attached to the present volume are similar in some respects. It comprises the plenary and main lectures delivered at the IUPAC International Symposium on Macromolecules in Helsinki, July 1972. By tradition such articles appear in journal form as a supplement to *Pure and Applied Chemistry*. The volume under review is described as being a supplement, but is actually a very highly priced hard backed edition. Discreet enquiry has revealed that the answer to the opening question is 'both' in this case. Thus, for regular subscribers to *Pure and Applied Chemistry* the volume is issued as a journal; otherwise one is obliged to purchase it as a more expensive book. Publishers' mores are difficult to fathom, but must be accepted for what they are if a book is one to command serious attention, which this certainly is.

The subdivision of the symposium into the following distinct groups will not be immediately obvious to the reader from the wholly random arrangement of the twenty-three articles: Polymerization and copolymerization reactions; Solution properties

Book Reviews

and characterization; Bulk properties; Degradation and decomposition; and Polysaccharides and derivatives. About a third of the chapters fall within the first group, whilst there are only two articles devoted to polysaccharides. These are 'Polysaccharides as models for stereoregular polymers' (E. Husemann) which inevitably involves some discussion of solution properties and morphology of trisubstituted cellulose derivatives, and 'New methods in structural polysaccharide chemistry' (B. Lindberg) in which modern techniques are used to analyse the fragments from partial hydrolysis and different specific degradations of unmodified and chemically modified polysaccharides. All the articles are fundamental in nature and this is true no less of the lucid chapter on 'Weathering of polyolefins' despite the suggestively applied tone of the title. A brief comment on disposal problems ends this chapter and, in view of current hysteria, Winslow's final sentence deserves a wider readership, viz.: 'Accelerated weathering of films would undoubtedly lessen the volume of litter, but the ultimate solution to plastic pollution lies in education since litter is more of a people problem than a materials problem'.

The contributions maintain a remarkably uniform level of presentation. Perhaps more significant is the fact that each is a really up-to-date review of the field instead of a thinly disguised forum for presenting the author's detailed personal research data (as is often the case). In two instances readers will be able to regard the articles as continued progress reports, since rather related contributions (by Flory and by Vinogradov) were made to the IUPAC Leiden Symposium in 1970 and have already been published in this series. The authorship is international, but English is used throughout. The printing, production and reproduction of diagrams are faultless and the number of places where symbols on graphs are undefined is too small to warrant listing here. No author or subject index is provided, but this does not seem a serious omission in a volume essentially without a unified theme. All libraries are recommended to obtain this book. The average polymer chemist, being only human, will not care to purchase a volume only a very small fraction of which is within his sphere of comprehension. Polymer chemists of exceptional breadth of interest are rare and may well be exemplified by the contributors themselves; but then they will probably possess their own free copies.

M. B. Huglin

Stress analysis of polymers

J. G. Williams

Longman, Harlow, 1973, 276 pp. £6.50

Although the title might imply that the subject is confined to polymers, this book is a more general treatment of stress analysis in viscoelastic materials. The usual engineering texts on 'Strength of materials' are largely confined to Hookean elastic time-independent behaviour, while at least one author has developed an extensive treatment for elastic perfectly plastic materials, i.e. elastic up to a yield point and thereafter strain at constant stress. This represents about the limit of the conventional treatment; more advanced and more realistic assumptions for polymers have tended to be treated either highly theoretically or for special cases.

The first section of this book provides a basic text, developing equations for stress and strain including non-linearity, viscoelasticity, anisotropy, and time dependence with special attention to approximations applicable to polymers such as large strain deformations at constant volume. The mathematics are kept simple, at some cost of brevity, but this is probably preferable for the majority of practical designers.

The second section, comprising nearly half the book, applies these equations to specific geometries, especially bending of beams, plates and struts and loading of axi-symmetric cylinders and membranes. The solutions are presented in simple algebraic form, requiring only material property data for numerical calculation; in several cases digital computation is desirable. It seems that an undue proportion of this section is devoted to linear elastic properties and the corrections to simple theories of bending and thin shells to take account of shear deflections, transverse restraints, e.g. wide beams, and large deflections. Among these are rather scattered references to non-linearity and viscoelastic behaviour,

but the reviewer found it difficult to follow the logic of the assumptions made in individual cases. It would perhaps have been helpful to concentrate on derivation of equations for non-linear stress/strain and rubber elasticity assumptions and compare results with those from linear/small strain and elastic perfectly plastic assumptions in practical conditions where the differences are significant.

The final shorter section discusses stress concentrations, mainly concerned with testing, and would seem to be justified as indicating how the effects of discontinuities and incipient flaws may be included in stress analysis for viscoelastic materials.

Although there are numerous references in the text to polymer properties, no actual data are given for comparison with the idealizations used. So while this book is directed to stress analysis rather than property data, little indication is given of the polymers, temperatures, strains, and times for which a particular idealization, and the equations derived from it, are a reasonable approximation. Some of the general statements on polymer properties also seem open to question: on p 55 it is stated 'Polymers above their glass transition temperature exhibit rubber-like properties in that they are essentially elastic up to strains of several hundreds of per cent'. Insofar as this is true of linear polymers, it also involves long recovery times. On pp 64 and 150, 'However, most polymers in the glassy state do undergo a process which can be equated with yielding' and 'Most polymers below their glass transition temperature can be described approximately as elastic perfectly plastic materials'. These hardly apply to polystyrene and PMMA without toughening, while rubbers and polyolefins are not usually used in this state.

The book is well laid out and sectionalized with concise index and bibliography. The nomenclature is clear and consistent, but should perhaps have been listed for reference. The production, including diagrams is extremely good. This book is an important step in advancing the analytical design of time-dependent viscoelastic materials by providing the basic equations and some derivations for specific geometries, but further consideration is needed of the applicability to commercial polymers.

M. J. Stevens

Nylon plastics

Edited by M. I. Kohan

Wiley-Interscience, London and New York, 1973,

£19.50

This book is one in the series of Society of Plastics Engineers monographs. It is claimed on the fly sheet that it is the first complete text on nylon plastics with well referenced coverage of nylon technology from monomer synthesis to end use application. It therefore attempts to provide information and references to information for all those concerned with nylon plastics technology. Intentionally it does not attempt to discuss fibre technology though there is a great deal of nylon science which will be valuable to the nylon fibre technologist.

There are 19 contributors including the editor, 16 of whom come from the DuPont Company. The book therefore represents a great deal of the publishable knowledge on nylon plastics from that company which of course first introduced us to the material following the work of Wallace Carothers. The cover is very wide from molecular weight distribution, thermal degradation, crystallization kinetics to injection moulding, quality control, design and economic considerations. There must be something for everyone with an interest in nylon, except perhaps the commercial people since only 12 pages out of 650 are devoted to economics. There is even a table listing the suppliers of nylon plastics and compositions but unfortunately this is restricted to the USA.

I recommend this book unreservedly. It contains an enormous amount of information and there appears to be little duplication between chapters written by different authors. It is reasonably up-to-date containing 1972 and 1971 references (and even a few from 1973) though most are from the 1960s. It is easy to read, the illustrations and diagrams are numerous and clear. It is a must for the book shelves of the library of any concern having any interest at all in nylon plastics. Though expensive it must be worth it. In my view the claim on the fly sheet is substantiated.

F. J. Hybart

N.m.r. of random copolymers of benzyl-L-aspartate with *o*- and *p*-nitrobenzyl-L-aspartate

Marie-H. Loucheux-Lefebvre, A. Forchioni* and Catherine Duflot

Laboratoire de Chimie Macromoléculaire, Université des Sciences et Techniques de Lille,
BP 36, 59650 Villeneuve d'Asq, France
(Received 5 November 1973; revised 3 December 1973)

The *p*- and *o*-substitution of the benzene ring of poly(β -benzyl-L-aspartate) (PBLA) with a nitro group induces a reversal of the helix sense in the PBLA. Therefore, two series of random copolymers of benzyl-L-aspartate with *o*- and *p*-nitrobenzyl-L-aspartate were prepared in order to study the left-handed \rightarrow right-handed α -helix transition. The conformational behaviour has been studied by nuclear magnetic resonance spectroscopy and the left-handed \rightarrow right-handed α -helix transition has been observed from the α -CH shift, from CDCl₃ solutions. Moreover, for each copolymer, the α -helix \rightarrow coil transition was also studied in CDCl₃/trifluoroacetic acid mixtures. In this case, the transition can be observed from the α -CH shift and from the splitting of the β -CH₂ resonance in the α -helical form also.

INTRODUCTION

The conformations of ester derivatives of poly(L-aspartic acid) have been shown to be dependent on the nature of the side chains. Thus, polymers from aliphatic L-aspartates with short side chains, e.g. methyl, were found to be left-handed α -helical^{1, 2} while the polymers with longer side chains, e.g. ethyl, n-butyl, n-propyl and isopropyl, assumed a right-handed α -helical conformation². Moreover, whereas poly(β -benzyl-L-aspartate) was shown to adopt a left-handed α -helical form^{3, 4}, it has been shown that *p*- and *o*-substitution of the benzene ring with a nitro group induces a reversal of the helix sense to the right-handed α -helical form⁵⁻⁷ while the *m*-nitro derivative remains in the left-handed α -helical form⁷. Therefore, in the case of left-handed α -helical form of poly(β -benzyl-L-aspartate), it is possible to induce a transition to the right-handed conformation by the addition of residues which have a preference to adopt a right-handed α -helix. Indeed, the left-handed \rightarrow right-handed α -helix transition was observed using circular dichroism and infra-red spectrometry on copolymers of β -benzyl-L-aspartate respectively with *o*- and *p*-nitro- β -benzyl-L-aspartate⁷.

Since many different nuclei in a molecule can be studied independently by high resolution nuclear magnetic resonance (n.m.r.) spectroscopy, we have used this technique to observe the main chain and side chain protons in order to obtain information about the secondary structure and mobility of the backbone and side chains under various conditions.

It is well known that the chemical shift of the α -CH is characteristic of the secondary structure. In particular from a study of copolymers containing β -benzyl-L-aspartate, Bradbury *et al.*⁸ have shown that the chemical

shift of the aspartate α -CH peak is situated at 4.30 ppm for the left-handed α -helix, 4.40 ppm for the right-handed α -helix and at 4.85 ppm for the random coil. As the side chains make an important contribution to the stabilities of the various conformations of polypeptides in solution⁹ the α -helix \rightarrow random coil transition as a function of solvent composition has also been studied on these copolymers.

The work presented in this paper extends the study of random copolymers of β -benzyl-L-aspartate with β -*o*- and β -*p*-nitrobenzyl-L-aspartate by 250 MHz n.m.r., in deuterated chloroform (CDCl₃)/trifluoroacetic acid (TFA) mixtures.

EXPERIMENTAL

Polymers

The copolymers were prepared by polymerization of the *N*-carboxyamino acid anhydrides (NCA) of β -benzyl-L-aspartate and *o*- and *p*- β -nitrobenzyl-L-aspartate¹⁰. Both anhydrides used in the synthesis were dissolved in nitrobenzene/dimethylformamide (DMF) mixtures for the *ortho* derivatives and in CHCl₃/DMF mixtures or pure DMF for the *para* derivatives. Triethylamine in 1% benzene solutions was used to initiate the polymerization; the molar ratio of anhydride to initiator was 35. The polymerizations were allowed to proceed for three days at 30°C and the polymer was precipitated with methanol, filtered, triticated under methanol or ether, filtered and dried at 40°C under vacuum.

The mol% nitro residue content for each of the copolymers was determined from their elemental analysis[†]. The amount of nitrobenzyl groups was also estimated from the measurement of the molar absorption

* Service de Chimie-Physique, Centre d'Etudes Nucléaires de Saclay, BP 2, 91190 Gif-sur-Yvette, France.

† Elemental analyses were carried out by P. Calmé, Centre de Recherches sur les Macromolécules, CNRS, Strasbourg.

Table 1 Starting quantities, yields and NO₂ content for copolymers of β-benzyl-L-aspartate (LAB) and β-o-nitrobenzyl-L-aspartate (LAoNB). Molar ratio of the total anhydride to initiator is always 35

LAB (mg)	NCA (mmol)	LAoNB (mg)	NCA (mmol)	Polymerization solvent		Yield (mg)	'Theoretical' amount of NO ₂ (%)	Determined amount of NO ₂ (%)			Adopted amount of NO ₂ (%)
				Nitro- benzene (ml)	DMF (ml)			From u.v.	From elemental analysis		
									C	N	
769	3.08	114	0.39	16	4	540	11	13	16	11	13
763	3.06	300	1.02	20	5	630	25	28	29	19	28
791	3.18	450	1.53	25	6	720	32	38	34	21	38
321	1.29	538	1.83	16	4	400	58	57	62	55	57
533	2.1	1467	5.00	40	10	1500	73	63	73	64	64

Table 2 Starting quantities, yields and NO₂ content for copolymers of β-benzyl-L-aspartate (LAB) and β-p-nitrobenzyl-L-aspartate (LApNB). Molar ratio of the total anhydride to initiator is always 35

LAB (mg)	NCA (mmol)	LApNB (mg)	NCA (mmol)	Polymerization solvent		Yield (mg)	'Theoretical' amount of NO ₂ (%)	Determined amount of NO ₂ (%)			Adopted amount of NO ₂ (%)
				CHCl ₃ (ml)	DMF (ml)			From u.v.	From elemental analysis		
									C	N	
2482	9.9	517	1.7	70	50	1710	15	15	20	13	15
1331	5.3	500	1.6	45	25	950	24	26	33	30	26
1992	8.0	1008	3.4	0	50	1750	29	28	35	28	28
1834	7.3	1166	4.0	0	50	1840	35	42	41	42	42
895	3.59	680	1.97	0	50	1000	36	48	44	45	46
1083	4.3	1917	6.5	0	50	1930	60	67	70	65	67

at 270 nm. At this wavelength, where the peptide bond absorption is negligible, the aspartates in solution in hexafluoroisopropanol have the following absorbances: $\epsilon_{270}=200$ for the β-benzyl-L-aspartate; $\epsilon_{270}=5500$ and $\epsilon_{270}=10\ 200$ for the *o*- and the *p*-β-nitrobenzyl-L-aspartates respectively.

Tables 1 and 2 summarize the conditions of polymerization and give the mol% nitro residue for each copolymer.

The molecular weights of the polymers have not been checked, but by comparison with those already prepared by the same method¹⁰ it is correct to assume that their molecular weight is not larger than 50 000.

Solvents

Deuteriochloroform, CDCl₃, of greater than 99.5% isotopic purity was obtained from CEA (Service des Molécules Marquées). Trifluoroacetic acid (TFA) was purchased from Aldrich Chemical Co.

Apparatus

Spectra were recorded on a Thomson-CAMECA 250 MHz spectrometer.

Solutions at about 7% w/v were made up in deuteriochloroform containing tetramethylsilane (TMS) as internal standard. The study was carried out at room temperature.

RESULTS AND DISCUSSION

A series of spectra at 250 MHz was obtained from two sets of the copolymers. The spectra were recorded in

CDCl₃/TFA solutions. Below a concentration of 1% (v/v) of TFA in CDCl₃, the linewidths are very broad, probably because the helix is too rigid and the mobility of the resonating protons is too low. In particular, the line corresponding to the helical NH proton is so large that it is not possible to observe it on the spectra. Moreover, the lines corresponding to the nitro aromatic protons are observed in this region also and sometimes overlap with the NH proton line. Therefore, the NH proton line has never been used even if the polymer adopts a random conformation.

The copolymers become insoluble in CDCl₃ when the percentage of nitro derivatives in the copolymers is about 45% for the *para* derivative and 65% for the *ortho* derivative.

Copolymers of β-benzyl-L-aspartate and β-p-nitrobenzyl-L-aspartate

Main chain protons. Figures 1-3 show the spectra obtained from three copolymers containing 15, 28 and 42% of the *p*-nitro derivative. At very low TFA concentrations, where the copolymer adopts a helical conformation one can observe that the position of the α-CH peak is changing with the composition of copolymers; it is at 4.32, 4.35 and 4.40 ppm for 15%, 28% and 42% respectively of nitro derivative with a slight apparent move towards low field accompanying the narrowing upon TFA addition. From Bradbury's values these chemical shifts correspond to a right-handed α-helix for the 42% nitro copolymer and a left-handed α-helix for the 15% nitro copolymer. These results are in good agreement with the circular dichroism

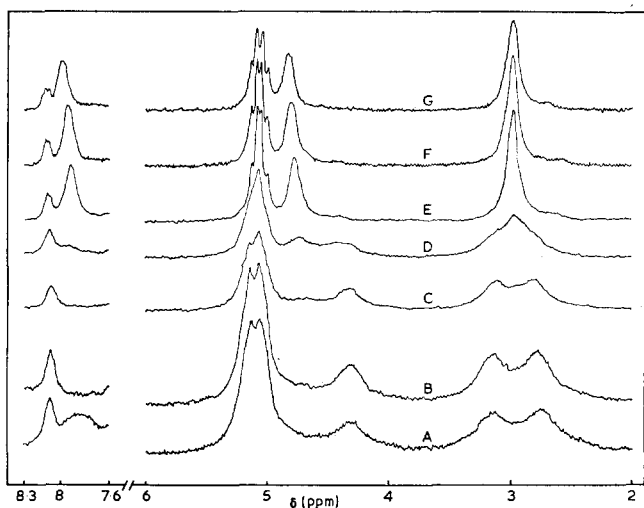


Figure 1 250MHz spectra of copoly(85% benzyl-L-aspartate/15% *p*-nitrobenzyl-L-aspartate) in CDCl_3/TFA . % TFA: A, 0.46; B, 0.67; C, 1.09; D, 1.44; E, 2.09; F, 2.38; G, 18.70

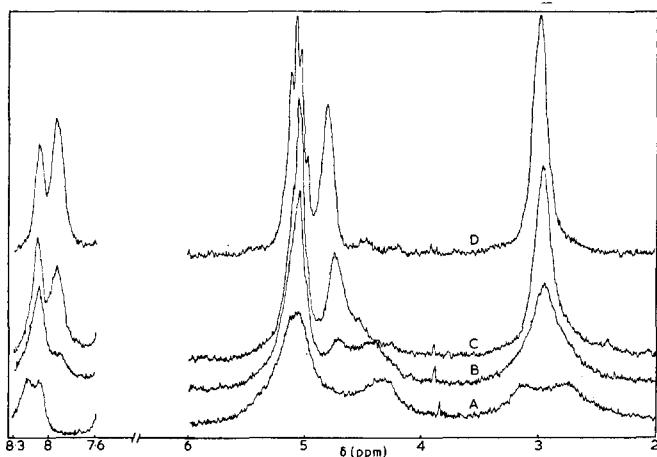


Figure 2 250MHz spectra of copoly(72% benzyl-L-aspartate/28% *p*-nitrobenzyl-L-aspartate) in CDCl_3/TFA . % TFA: A, 1.11; B, 2.28; C, 2.60; D, 3.43

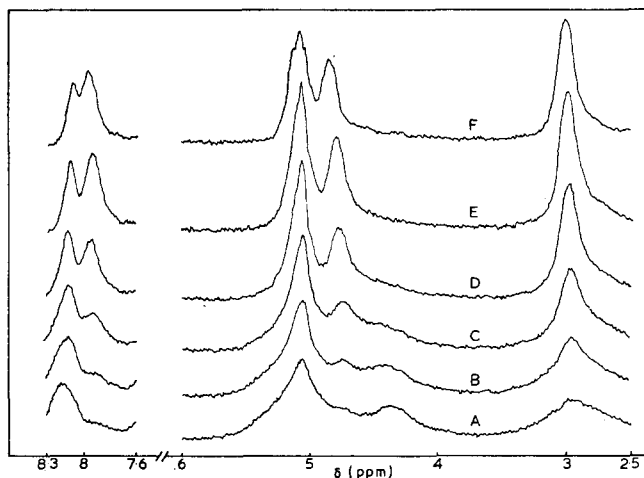


Figure 3 250MHz spectra of copoly(58% benzyl-L-aspartate/42% *p*-nitrobenzyl-L-aspartate) in CDCl_3/TFA . % TFA: A, 0.91; B, 1.30; C, 1.67; D, 2.00; E, 2.31; F, 4.12

(c.d.) measurements⁷. These c.d. measurements have shown that the left-handed \rightarrow right-handed α -helix transition takes place for a concentration of *p*-nitrobenzyl aspartate in the copolymer between 25 and 30%. In particular the 28% nitro copolymer is characterized by

a zero value of $[\theta]_{222}^{11}$; this means that this copolymer is either in random coil form or in 50:50 left-handed: right-handed α -helical form. Since the n.m.r. α -CH peak is observed at 4.35 ppm we must admit that this copolymer adopts a secondary structure formed by two equal amounts of left-handed and right-handed α -helix.

When more TFA is added the signal splits into two peaks for a concentration in TFA between 1 and 1.5%. This so called 'double peak' phenomenon concerning the α proton of the main chain in the range of the helix-coil transition has been the subject of much debate. To date Ullman's theory¹² seems to be the most satisfactory to explain the appearance of this 'double peak'. This theory assumes that there is a rapid interconversion between helix and coil states but the existence of two peaks arises from two factors: (i) the difference in helicity of the amino acid residues near the ends of the chain by comparison with the amino acid residues nearer the middle of the chain; and (ii) the polydispersity in molecular weight. The polydispersity of polymers is not known but their molecular weights are small. This is in good agreement with the appearance of a double peak, even if we admit the existence of a rapid interconversion of two different states. The chemical shifts of the α -CH proton plotted against TFA contents are given in Figure 4. The sharp variation downfield would mean that the helix-coil transition is very cooperative in this case. One can observe that in the transition range where the double peak phenomenon is observed the low field peak is moving further downfield while the position of the other remains the same. The first peak would be due mainly to the molecules of copolymers where both α -helix and random coil forms are present in rapid interconversion, the second one would be due to the higher molecular weight macromolecules which do not yet adopt a random coil structure.

In order to correlate the stabilities of the helical residues in the copolymers as a function of solvent composition, the chemical shifts of the α -CH proton

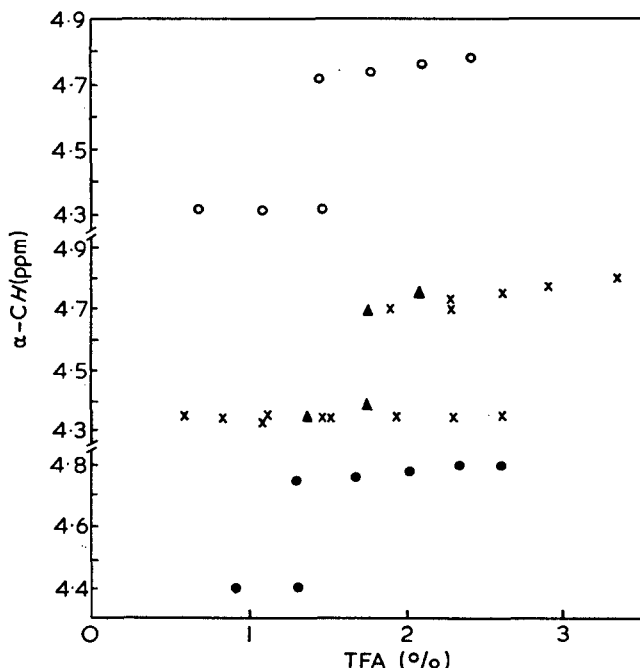


Figure 4 N.m.r. α -CH peak positions in CDCl_3/TFA mixtures of copoly(benzyl-L-aspartate/*p*-nitrobenzyl-L-aspartate). \circ , 15%; \blacktriangle , 26%; \times , 28%; \bullet , 42% nitro derivative

have been plotted against TFA contents (Figure 4). Although the chemical shift differences between the conformations are dependent on solvent, it has been assumed that the variation of α -CH chemical shifts for polyaspartates in CDCl_3 /TFA mixtures is mainly due to the helix-coil transition¹³. For copolymers containing 15% and 40% of nitrobenzyl derivative the transition midpoints of each copolymer are located approximately at the same value of the TFA content, i.e. about 1.4%. This value is the same as that obtained under the same conditions for poly(β -benzyl-L-aspartate) but it is different to those found in the literature: either 2%¹⁷ or 3%⁸. Since the molecular weights of our polymers and copolymers are unknown, this discrepancy may be due to the fact that the molecular weights of polymer studied are different. Therefore, it is not possible to conclude if the transition midpoint is affected by the introduction of nitro group or not.

Side chain protons. According to the calculations of Scheraga et al.¹⁴ the helix sense of poly(aspartate esters) depends on the conformation adopted by the side chains. A study has therefore been made on the spectra of the side chain protons when the copolymers adopt either a left-handed or a right-handed α -helix.

The aromatic ring protons peaks appear at 7.25 ppm with another line appearing at 8.21 ppm which can be attributed to the *ortho* protons of the nitro aromatic ring from the relative area of the signals in the series of copolymers. The linewidth is always very narrow, even in pure CDCl_3 , and their position does not change when TFA is added. This indicates that the rotation of aromatic ring is relatively free, which implies no regular structure of the aromatic nuclei when the polymer adopts a helical structure. However, the spectra from the benzyl CH_2 and the β - CH_2 protons provide more interesting information on the side chains. The benzyl CH_2 resonance centred at 5.08 ppm is an AB quartet and indeed when the polymers are fully random coil a well resolved quartet is observed. When the copolymer adopts a helical form the spectra seem dependent on the sense of the helix; for example, in the case of the 15% nitro copolymer which adopts a left-handed α -helix the benzyl CH_2 peak splits with $\Delta = 0.08$ ppm; this splitting is not observed with the 42% nitro copolymer, i.e. when the copolymer adopts a right-handed helical structure; owing to the fact that the benzyl CH_2 line is broad when the polymer adopts a helical conformation it is not possible to affirm that such a splitting exists or not. Indeed, Bradbury et al. have also studied polymers in which β -benzyl-L-aspartate adopts a right-handed α -helix conformation, that is a copoly(β -benzyl-L-aspartate-co-10% L-alanine) and in this case they have also observed the splitting of the benzyl CH_2 line.

It is interesting to compare these results with those obtained from the spectra of the β - CH_2 protons. The β - CH_2 line centred at 2.87 ppm is the A_2 part of the A_2X system where X is α -CH. When the polymers adopt a fully random coil conformation, only one peak centred at 2.87 ppm is observed. When the copolymer adopts a left-handed α -helical form (15% nitro copolymer), the β - CH_2 line splits and the difference in chemical shift is $\Delta \sim 0.37$, a similar value already observed for poly(β -benzyl-L-aspartate) in CDCl_3 solutions^{8, 15}. Although this shift difference is very sensitive to conformational changes, it is impossible to make interpretation on structural terms based on Δ values alone. When the

polymer adopts a conformation in right-handed α -helix the splitting of β - CH_2 resonance is not observed. As in the case of benzyl CH_2 , the lines are very broad and it is very difficult to distinguish if splitting exists or not.

Copolymers of β -benzyl-L-aspartate and β -o-nitrobenzyl-L-aspartate

Very similar observations have been made with copolymers with the difference that the left-handed \rightarrow right-handed α -helix transition of copolymers (β -benzyl-L-aspartate, β -nitrobenzyl-L-aspartate) is observed in using the circular dichroism for a concentration of about 55% of *ortho* derivative whereas it is observed for a concentration of 25–30% for *para* derivative^{7, 11}.

Main chain protons. The spectra corresponding to copolymers containing 13%, 28%, 38% and 57% of nitro derivative have been recorded. The chemical shift of α -CH for each copolymer in helical form is respectively 4.30, 4.31, 4.32 and 4.36 ppm. Since the chemical shift of α -CH is located at 4.40 and 4.30 ppm for a right-handed and a left-handed α -helix respectively, we have assumed that the left- and right-handed α -helical structures coexist and calculated their percentage (Table 3). Because of the accuracy of 0.01 ppm on the values of the chemical shifts, the helical composition of copolymer will be known with a precision of $\pm 10\%$. From these compositions we have calculated the values that the ellipticity at 222 nm should have for each copolymer (Table 3). These calculated values are compatible with the experimental ones. Therefore, we think that the copoly(β -benzyl-L-aspartate/ β -o-nitrobenzyl-L-aspartate) are made of both left-handed and right-handed α -helices.

When TFA is added to the CDCl_3 solutions, the α -CH resonance is shifted downfield and the linewidth decreases. When the copolymers adopt a fully random coil form, the chemical shift of α -CH has the expected value, 4.85 ppm. In the helix \rightarrow coil transition range, the peaks are broad and for this reason the 'double peak' phenomenon is more difficult to observe than in the case of *para* derivatives. Yet, it seems that it is much closer to a 'double peak' phenomenon than to a 'single shifting peak'.

This observation should be in good agreement with the fact that the right-handed α -helix of *ortho* derivatives is less stable than the right-handed α -helix of *para* derivatives; the probability of obtaining, in CDCl_3 /TFA solutions, some macromolecules containing only the helical conformation is very small.

The chemical shift of the α -CH resonance against the TFA concentration has been plotted (Figure 5); the sharp variation of α -CH shift downfield is in good

Table 3 Percentage of left-handed (LH) and right-handed (RH) α -helices in the copoly(β -benzyl-L-aspartate/ β -o-nitrobenzyl-L-aspartate) determined from the chemical shift of the α -CH resonance. $[\theta]_{222} = \pm 35\,000 \text{ deg cm}^2 \text{ dmol}^{-1}$ for 100% α -helical structure

NO ₂ (%)	δ α -CH (ppm)	RH (%)	LH (%)	$[\theta]_{222}$ (deg cm ² dmol ⁻¹)	
				Calculated	Experi- mental
13	4.30		100 \pm 10	35 000 \pm 3 500	28 000
28	4.31	10 \pm 10	90 \pm 10	28 000 \pm 7 000	26 000
38	4.32	20 \pm 10	80 \pm 10	21 000 \pm 7 000	28 000
57	4.36	60 \pm 10	40 \pm 10	-7 000 \pm 7 000	2 000

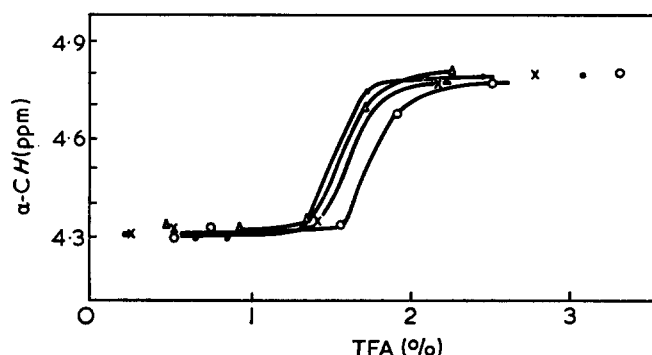


Figure 5 N.m.r. α -CH peak positions in CDCl_3/TFA mixtures of copoly(benzyl-L-aspartate/o-nitrobenzyl-L-aspartate). ●, 13%; ×, 28; ○, 38%; △, 57% nitro derivative

agreement with a cooperative phenomenon for the helix coil transition. The stability of each copolymer studied as a function of the solvent composition has been observed. This stability is approximately independent of the ratio of nitrobenzyl derivative in the copolymer. The midpoint of the transition is found at approximately 1.7% TFA, i.e. the stability of left-handed α -helix of poly(β -benzyl-L-aspartate) is the same as the right-handed α -helix of poly(β -nitrobenzyl-L-aspartate) in CDCl_3/TFA mixtures.

Side chain protons. The resonance centred at 7.25 ppm is due to aromatic protons. If the copolymer adopts either a helical structure or a random coil this band is always narrow. Two other bands due to the side chain protons are present in this region of the spectra: one at 7.56 ppm and the other at 7.92 ppm. The first one should come from the *meta* proton and the second one from the *ortho* proton of the nitro derivative aromatic ring. This assumption is in good agreement with the intensity of these bands, checked by weighing the areas and by taking the resonance band at 7.25 ppm as a reference.

For the benzyl CH_2 there are two resonance bands, one centred at 5.05 ppm, i.e. the same frequency as the one of the *para* derivative and another band located at 5.45 ppm. For the same polymer, these two bands are narrower when the polymer adopts a random coil conformation, but no variation in chemical shifts is observed in the transition range. The intensity of the 5.45 ppm band increases with the percentage of nitro derivative in the copolymer. Therefore we think that the 5.05 ppm band is from non-nitrated side chains whilst the 5.45 ppm band is from nitrated side chains.

For all *ortho* nitro copolymers studied, the β - CH_2 resonance is centred at 2.89 ppm and the line splits, with $\Delta \sim 0.35$ ppm when the polymer adopts a helical structure. Unfortunately, the copolymers adopt the left-handed α -helical conformation; i.e. it is not possible

to assume from this result if the splitting is observed only when the α -helix adopts a left-handed sense.

CONCLUSIONS

This work demonstrates the important point that when poly(β -benzyl-L-aspartate) is nitrated to change the helix sense from left hand to right hand, there is a corresponding change in the α -CH shift. The dependence of chemical shift of the backbone protons α -CH on the helix sense allows us to confirm the δ CH values attributed to the left- and right-handed α -helices. Moreover the left-handed \rightarrow right-handed α -helix and α -helix \rightarrow random coil transitions have been studied.

It is interesting to observe that although the modification of poly(β -benzyl-L-aspartate) is not considerable and far from the backbone the α -CH shift is a reliable indicator to the helix sense.

The side chain protons resonance do not allow further information on the degree of side chain immobilization to be obtained. But in the transition range, the α -helix \rightarrow random coil transition can be observed from these chemical shifts; the lines are more narrow when the polymer adopts a random coil conformation and their splitting, especially from β - CH_2 is due to the existence of an α -helix.

REFERENCES

- 1 Goodman, M., Boardman, F. and Litowsky, L. *J. Am. Chem. Soc.* 1963, **85**, 2491
- 2 Bradbury, E. M., Carpenter, B. G. and Goldman, H. *Biopolymers* 1968, **6**, 837
- 3 Karlson, R. H., Norland, K. S., Fasman, G. D. and Blout, E. R. *J. Am. Chem. Soc.* 1960, **82**, 2268
- 4 Bradbury, E. M., Downie, A. R., Elliott, A. and Hanby, W. E. *Proc. R. Soc.* 1960, **A259**, 110
- 5 Goodman, M., Felix, A. M., Deber, C. M., Branse, A. M. and Schwartz, G. *Biopolymers* 1963, **1**, 371
- 6 Hashimoto, M. and Aritomi, J. *Bull. Chem. Soc. Japan* 1966, **39**, 2707
- 7 Aragão, J. B. and Loucheux, M. H. *J. Chim. Phys.* 1971, **11-12**, 1578
- 8 Bradbury, E. M., Carpenter, B. G., Crane-Robinson, C. and Goldman, H. *Macromolecules* 1971, **4**, 557
- 9 Lotan, N., Berger, A. and Katchalski, E. *A. Rev. Biochem.* 1972, **41**, 869
- 10 Aragão, J. B. and Loucheux, M. H. *Bull. Soc. Chim. France* 1971, **12**, 4387
- 11 Duflot-Dewaele, C. *Thesis* University of Lille, 1973
- 12 Ullman, R. *Biopolymers* 1970, **9**, 471
- 13 Bradbury, E. M., Crane-Robinson, C., Paolillo, L. and Temussi, P. *Polymer* 1973, **14**, 303
- 14 Yan, J. F., Vanderkooi, G. and Scheraga, H. A. *J. Chem. Phys.* 1968, **49**, 2713
- 15 Bradbury, E. M., Carpenter, B. G., Crane-Robinson, C. and Goldman, H. *Nature* 1970, **225**, 64
- 16 Goodman, M., Toda, F. and Ueyama, N. *Proc. Nat. Acad. Sci. USA* 1973, **70**, 331
- 17 Bovey, F. A. *Pure Appl. Chem.* 1968, **16**, 417

Simulation of kinetic analysis on terpolymerization of styrene/butyl methacrylate/methacrylic acid system

E. Tsuchida, J. Aoyagi, K. Shinzo and I. Shinohara

*Department of Polymer Chemistry, Waseda University, Tokyo 160, Japan
(Received 10 July 1973; revised 19 February 1974)*

The simultaneous differential equations which connected the copolymerization kinetics of the component reaction in the multi-copolymerization system with the changing rate of the concentration of each monomer and radical, the concentration and the molecular weight of the polymer obtained are analysed in a number of ways. The distribution of the components and the degree of polymerization are also simulated. The styrene/butyl methacrylate/methacrylic acid terpolymerization system, using carbon tetrachloride as solvent and benzoyl peroxide as initiator, was chosen. The simulation model which satisfied the experimental values of the concentration of the multiple components in the system, the composition and molecular weight distribution and the number of chlorine atoms introduced into the copolymer ends is established. When the time interval changed, the effects on the distribution of the composition in copolymers and the distribution of the degree of polymerization were also calculated.

INTRODUCTION

The simulation model of a copolymerization reaction and given reaction conditions were estimated by the authors. The polymerization process means the change in composition of the system, the concentrations of the active agents, the amounts of produced polymers, their structures, molecular weights, the distribution of degree of polymerization, composition distribution and their variations with time.

In the reaction of oligostyrene formation, an equation model was set up, taking into account the molecular weight distribution, and the rate constants were estimated for the chain termination reactions which had been previously unknown¹⁻⁶. The distribution of degree of polymerization and composition for n -dimensional copolymers were theoretically calculated by the Markov probability theory⁷. In the course of the copolymerization reaction, the composition of produced polymers can be obtained by numerically integrating the differential composition equations of polydimensional copolymerization.

In this report a simulation model was built and examined with which we could estimate not only the composition of n -dimensional copolymers, but also the copolymerization rate, molecular weight, the probability of termination by recombination, and the content of termination agent which was introduced to the polymer ends through initiation and chain transfer reactions. As the next step, by using this analytical method, the ternary copolymerization of styrene/butyl methacrylate/methacrylic acid in carbon tetrachloride and benzoyl peroxide initiator was studied⁸.

EXPERIMENTAL

Copolymerization reaction

Three-dimensional copolymerization of styrene (S), butyl methacrylate (BMA), and methacrylic acid (MAA) was carried out in carbon tetrachloride with benzoyl peroxide initiator.

The calculated amount of monomers, initiator, and solvent, which were purified in the conventional way, were charged in a polymerization tube. The tube was flashed with nitrogen and sealed under vacuum. The polymerization was carried out by swirling the tube at 60°C in a constant temperature bath for a definite time. The copolymers formed were concentrated under reduced pressure when necessary and were precipitated in a large excess of petroleum ether. The purification by the precipitation was carried out twice more and the products were dried under vacuum.

Analysis of the formed copolymers

The composition of the copolymers was determined by elemental analysis, infra-red absorption spectroscopy, and titration in a non-aqueous solvent.

In infra-red absorption spectrum analysis, the styrene content was determined from the intensity ratio of specific absorptions of δ_{CH} at 699 cm^{-1} and $\nu_{\text{C=O}}$ at 1735 cm^{-1} .

Methacrylic acid content was determined by the non-aqueous medium titration: acetone solution of the copolymer was titrated with methanol solution of sodium ethoxide in the presence of thymolblue indicator.

The number-average molecular weight was obtained

Table 1 Rate constants of component reaction

		Propagation $\times 10^{-2}$ (l/mol sec):	
k_d	$1.36 \times 10^{-6} \text{ sec}^{-1}$	k_{paa}	6.66*
k_o	376 l/mol sec	k_{pab}	8.48*
Initiation (l/mol sec):		k_{pac}	39.0*
k_{oa}	376*	k_{pba}	40.8*
k_{ob}	708*	k_{pbb}	36.5
k_{oc}	1960*	k_{pbc}	103
k_{osa}	21.1*	k_{pca}	135*
k_{osb}	0.211*	k_{pcb}	73.3*
k_{osc}	0.211*	k_{pcc}	101*
Transfer (l/mol sec):		Termination $\times 10^{-7}$ (l/mol sec):	
k_{fas}	5.77*	k_{taa}	7.20
k_{fbs}	2.14*	k_{tbb}	1.70
k_{fcs}	2.55*	k_{tcc}	3.91*
		k_{tab}	50.0*
		k_{tbc}	25.0*
		k_{tca}	3.91*
		k_{tss}	8.00

by vapour pressure osmometry (v.p.o.) using acetone as solvent.

Chlorine content of the polymer ends was determined by halogen analysis.

Component reaction rate constant

Some of the component reaction rate constants which were employed in the calculation had been reported as the actual measured values, but others were unknown. These unknown rate constants were assumed from the values of the analogous reactions. It appears that these assumed rate constants do not satisfy all of the actual copolymerization rate curves. Therefore, the reported measured values were varied, and a new rate constant was obtained by modifying them within a reasonable range. The calculation curve was prepared and examined by using the new constant and the unknown rate constant. The optimum combination of the rate constants (*) are obtained by studying the variation of those calculation curves. These (optimum) values are listed in Table 1.

SIMULATION MODEL

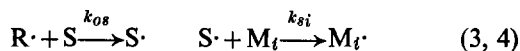
Reaction scheme of multiradical polymerization and the rate of reaction

The elementary reaction of multiradical polymerization in a solvent can be expressed by the following equations.

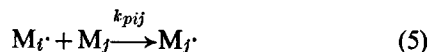
Decomposition of initiator:



Initiation:



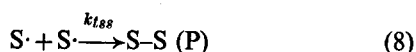
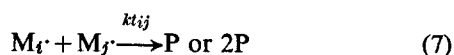
Propagation:



Chain transfer:



Termination:



where R-R represents an initiator, S transfer agent, M_i i -monomer, $M_i\cdot$ a polymer growing with polymer chains ending in M_i type radicals (we simplify the polymer radical and write as $M_i\cdot$ in this paper), P a polymer, S-S coupling products from transfer agents. $i, j = 1, 2, \dots, n$.

The rate of change of each radical concentration is given by:

$$d(R-R)/dt = -k_d(R-R) \quad (9)$$

$$dR\cdot/dt = 2k_d(R-R) - \left(\sum_{i=1}^n k_{oi}M_i + k_{os}S \right) R\cdot \quad (10)$$

$$dM_1\cdot/dt = M_1 \left(k_{o1}R\cdot + k_{s1}S\cdot + \sum_{i \neq 1}^n k_{pi1}M_i\cdot \right) - \left(2k_{t11}M_1\cdot + \sum_{i \neq 1}^n k_{ti1}M_i\cdot \right) M_1\cdot - \left(\sum_{i \neq 1}^n k_{pi1}M_i + k_{f1s}S \right) M_1\cdot \quad (11)$$

$$dM_2\cdot/dt = M_2 \left(k_{o2}R\cdot + k_{s2}S\cdot - \sum_{i \neq 2}^n k_{pi2}M_i\cdot \right) - \left(2k_{t22}M_2\cdot + \sum_{i \neq 2}^n k_{ti2}M_i\cdot \right) M_2\cdot - \left(\sum_{i \neq 2}^n k_{pi2}M_i + k_{f2s}S \right) M_2\cdot \quad (12)$$

$$dM_n\cdot/dt = M_n \left(k_{on}R\cdot + k_{sn}S\cdot + \sum_{i \neq n}^{n-1} k_{pin}M_i\cdot \right) - \left(2k_{tnn}M_n\cdot + \sum_{i=1}^{n-1} k_{tin}M_i\cdot \right) M_n\cdot - \left(\sum_{i=1}^{n-1} k_{pin}M_i + k_{fn}s \right) M_n\cdot \quad (13)$$

$$dS\cdot/dt = S \left(k_{os}R\cdot + \sum_{i=1}^n k_{fis}M_i\cdot \right) - \left(\sum_{i=1}^n k_{si}M_i + 2k_{tss}S\cdot \right) S \quad (14)$$

The rate of change of each monomer concentration is:

$$dM_1/dt = -M_1 \left(k_{o1}R\cdot + \sum_{i=1}^n k_{pi1}M_i\cdot + k_{s1}S\cdot \right) \quad (15)$$

$$dM_2/dt = -M_2 \left(k_{o2}R\cdot + \sum_{i=1}^n k_{pi2}M_i\cdot + k_{s2}S\cdot \right) \quad (16)$$

$$dM_n/dt = -M_n \left(k_{on}R\cdot + \sum_{i=1}^n k_{pin}M_i\cdot + k_{sn}S\cdot \right) \quad (17)$$

$$dS/dt = -S \left(\sum_{i=1}^n k_{fis}M_i\cdot + k_{os}R\cdot \right) \quad (18)$$

If the simultaneous differential equations mentioned above are given the initial value (the value for $t=0$), the concentration of individual components can be obtained as a function of time.

Average molecular weight

The average molecular weight of copolymer can be expressed as follows:

$$M_w = \int \left\{ \sum_{i=1}^n M_i (dM_{wi}/dt) + M_{wr} (dR_f/dt) + M_{ws} (dS_f/dt) \right\} dt / \int (dP/dt) dt \quad (19)$$

where

M_i = the molecular weight of i -monomer unit,

M_{wr} = the molecular weight of initiator fragments introduced in the polymer,

M_{ws} = the molecular weight of transfer agent fragments introduced in the polymer,

dR_f/dt = the rate of introducing initiator fragments into the polymer ends,

dS_f/dt = the rate of introducing transfer agent fragments into the polymer ends,

dM_i/dt = the rate of introducing M_i -monomer fragments into the polymers,

dP/dt = the rate of formation of polymers, namely,

$$dR_f/dt = \sum_{i=1}^n k_{oi} M_i R \quad (20)$$

$$dS_f/dt = \sum_{i=1}^n k_{fis} M_i S + \sum_{i=1}^n k_{si} M_i S \quad (21)$$

Rate of formation of polymer

When a parameter e which indicates part of recombination during termination, is introduced, the rate of formation of polymer, dP/dt , can be written as:

$$dP/dt = S \sum_{i=1}^n k_{fis} M_i + (2-e) \sum_{i=1}^n k_{tij} M_i M_j \quad (22)$$

Numerical solution of the system of differential equations

Assuming $(R-R)_0$ as an initial value, the concentration of the initiator $(R-R)$ can be deduced from equation (9) as follows:

$$(R-R) = (R-R)_0 \exp(-kat) \quad (23)$$

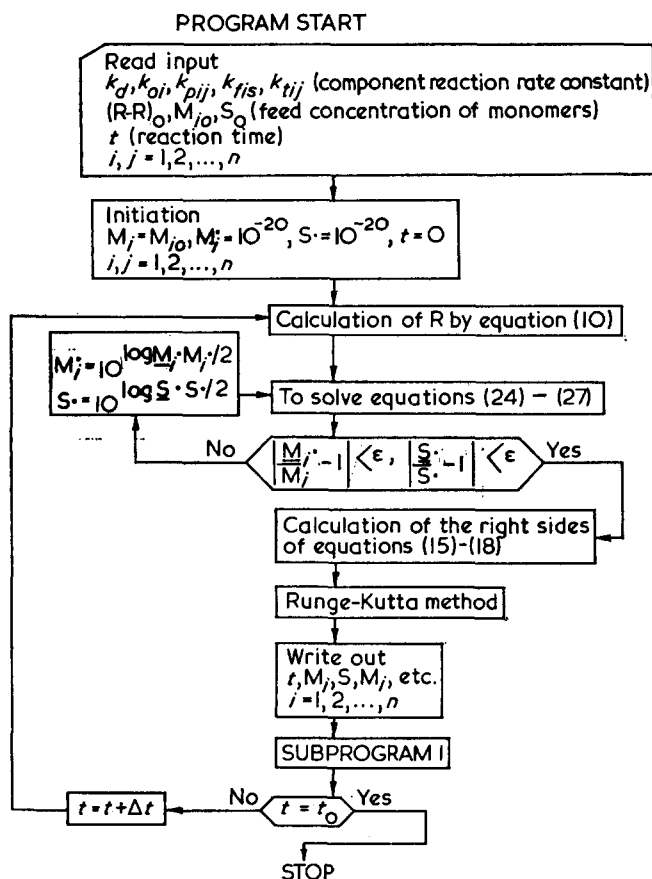


Figure 1 Main program flow chart. (Numerical solution of the system of differential equations)

In the stationary state of the reaction, the differential terms of the radical concentration in equations (9)–(14) are extremely small compared to those in equations (15)–(18). When the numerical calculation is carried out with 10^{-4} – 10^2 sec of integration interval, the differential terms in equations (9)–(14) can be neglected. This treatment corresponds to the so-called 'stationary assumption of radical concentration'.

According to a previous report¹, the numerical integration with 10^{-4} – 10^{-3} sec of the interval shows that the radical concentration reaches the stationary state in 1–2 sec after the start of the polymerization. Therefore, when the right hand side of equations (9)–(14) equals zero, the system of $(n+1)$ dimensional second-order equations (24)–(28) can be deduced concerning radical concentrations: M_1, M_2, \dots, M_n, S .

$$\left(2k_{t11}M_1 + \sum_{i \neq 1}^n k_{t1i}M_i + \sum k_{p1i}M_i + k_{f1s}S \right) M_1 - k_{p21}M_1M_2 - k_{p31}M_1M_3 - \dots - k_{pn1}M_1M_n - k_{s1}M_1S = k_{o1}M_1R \quad (24)$$

$$-k_{p12}M_2M_1 + \left(2k_{t22}M_2 + \sum_{i \neq 2}^n k_{t2i}M_i + \sum k_{p2i}M_i + k_{f2s}S \right) M_2 - k_{p32}M_2M_3 - \dots - k_{pn2}M_2M_n - k_{s2}M_2S = k_{o2}M_2R \quad (25)$$

$$-k_{pn1}M_nM_1 - k_{pn2}M_nM_2 - \dots - k_{pn(n-1)}M_nM_{(n-1)} + \left(2k_{tnn}M_n + \sum_{i \neq n}^n k_{tn(n-1)}M_{(n-1)} + \sum k_{pni}M_i + k_{fns}S \right) M_n - k_{sn}M_nS = k_{on}M_nR \quad (26)$$

$$-k_{f1s}SM_1 - k_{f2s}SM_2 - \dots - k_{fns}SM_n + \left(\sum k_{osi}M_i + 2k_{tss}S \right) S = k_{os}SR \quad (27)$$

Similarly, from equation (10), we can obtain:

$$R = 2fk_d(R-R)_0 \exp(-kat) / \left(\sum k_{oi}M_i + k_{os}S \right) \quad (28)$$

These systems of equations are numerically solved by the following method.

When M_1, M_2, \dots, M_n, S in parentheses in equations (24)–(27) are expressed by $\underline{M}_1, \underline{M}_2, \dots, \underline{M}_n, \underline{S}$ and these values are assumed, equations (24)–(27) can be reduced to a system of first-order equations, which can be easily solved.

By comparing the obtained solution with the initially assumed values, $\underline{M}_1, \underline{M}_2, \dots, \underline{M}_n, \underline{S}$ could be repeated until:

$$M_1 \simeq \underline{M}_1; M_2 \simeq \underline{M}_2; \dots; M_n \simeq \underline{M}_n; S \simeq \underline{S}$$

When the solution of the first-order equation is equal to the modified values, then it is the solution of the system of $(n+1)$ dimensional second-order equation.

Equations (15)–(22) are numerically integrated by the Runge-Kutta method, employing the values of the radical concentration: $M_1, M_2, \dots, M_n, S, R$, the values obtained by the repeated calculation described above.

Figure 1 shows the flow chart of the above calculation.

Distribution of the degree of polymerization and of the composition

Frensdorf et al.⁷ proved that the distribution of the degree of polymerization and of the composition of the formed polymers can be expressed by applying the Markov probability process theory, taking into account one molecular termination reaction only. By using the concentration of each radical component which is formed by the numerical solution of the differential equations described above, the authors have examined the solution method in which not only one molecular termination reaction but also the recombination reactions are incorporated, and have tried to apply this method to the calculation of the degree of polymerization distribution and the composition distribution for the general polydimensional copolymers.

Degree of polymerization distribution. The probability words necessary for calculation are defined as follows.

The probability that an initiation reaction will occur with *i* monomers, *I_i* is:

$$I_i = (k_{st}S \cdot + k_{ot}R \cdot) / \sum_{i=1}^n (k_{st}S \cdot + k_{ot}R \cdot) \quad (29)$$

The probability that *M_j* monomer will happen to be added to *M_i*· is:

$$P_{ij} = k_{pij}M_j / \alpha \quad (30)$$

where

$$\alpha = \sum_{j=1}^n k_{pij}M_j + k_{fij}S + \sum_{j=1}^n (k_{taij}M_j + k_{trij}M_j) \quad (31)$$

The probability that *M_i*· transferred to a solvent molecule is:

$$T_{fi} = k_{fis}S / \alpha \quad (32)$$

The probability that *M_i*· terminates by disproportionation is:

$$T_{di} = \sum_{j=1}^n k_{daij}M_j / \alpha \quad (33)$$

The probability that *M_i*· terminates by combination is:

$$T_{ri} = \sum_{j=1}^n k_{trij}M_j / \alpha \quad (34)$$

There is a relationship between probabilities mentioned above, as follows:

$$\sum_{i=1}^n I_i = 1, \quad \sum_{i=1}^n (P_{ij} + T_{fi} + T_{di} + T_{ri}) = 1 \quad (35)$$

Transitive matrix and multiplication of matrices. We denote the matrix *P* which has a transitive matrix *P_{ij}* at the *i*th row and *j*th column as follows:

$$P = \begin{pmatrix} P_{11}, & P_{12}, & \dots, & P_{1n} \\ P_{21}, & P_{22}, & \dots, & P_{2n} \\ \dots & \dots & \dots & \dots \\ P_{n1}, & P_{n2}, & \dots, & P_{nn} \end{pmatrix} \quad (36)$$

We denote the matrix obtained *P* to the *z*th power by *P^z* and element with *i* row, *j* column of *P^z* by *P^z(i, j)*. For example:

$$P^2(2, 1) = P_{21}P_{11} + P_{22}P_{21} + P_{23}P_{31} + \dots + P_{2n}P_{n1} \quad (37)$$

Equation (37) shows the probability of forming trimer radical fragments in which the first monomer unit of polymer is *M₂* and the end monomer unit of polymer is *M₁*.

Definition and calculation of degree of polymerization distribution. We define the probability of forming

polymers which have degree of polymerization *z*, degree of polymerization distribution *F(z)*, as:

$$F(z) = \sum_j \sum_i I_i P^{z-1}(i, j) (T_{fj} + T_{dj}) + \sum_{z=z_A+z_B} \sum_i \sum_j \sum_{i'} \sum_{j'} I_i P^{z_A-1}(i, j) T_{rj} I_{i'} P^{z_B-1}(i', j') T_{rj'} \quad (38)$$

Here, $\sum_{z=z_A+z_B}$ shows to sum over all combinations of integers given as *z_A + z_B = z*.

The first term of the above equation shows the probability that copolymers of degree of polymerization, *z* will be formed by termination by both transfer and disproportionation, and the second term shows the probability that copolymers of degree of polymerization, *z* will be formed by termination of combining *z_A*-units-mer with *z_B*-units-mer.

The calculating procedure is given as [here, the degree of polymerization distribution of *z* (=1~300) is calculated]: (1) calculate each transitive probability by equations (29)–(35); (2) calculate according to the determinant *P* (*z*=1~300); (3) calculate *F(z)* by equation (38) at suitable intervals of *z*. The flow chart of the calculating procedure mentioned above is given in Figure 2.

Definition and calculation of compositional distribution.

We denote the following equation *E(s, z)* to calculate the probability of forming polymer chains which have *k* units of *M_i*-monomer, namely, a polymer, of composition distribution:

$$E(s, z) = \sum_i \sum_j I_s(i) P_s^{z-1}(i, j) \quad (39)$$

Here, *I_s* is the vector which the element of *i*th column times *s* and *P_s* is the matrix which the element of *i*th column times *s*. They are defined as:

$$I_s = (I_1, I_2, \dots, sI_1, \dots, I_n)$$

$$P_s = \begin{pmatrix} P_{11}, & P_{12}, & \dots, & sP_{11}, & \dots, & P_{1n} \\ P_{21}, & P_{22}, & \dots, & sP_{21}, & \dots, & P_{2n} \\ \dots & \dots & \dots & \dots & \dots & \dots \\ P_{n1}, & P_{n2}, & \dots, & sP_{n1}, & \dots, & P_{nn} \end{pmatrix}$$

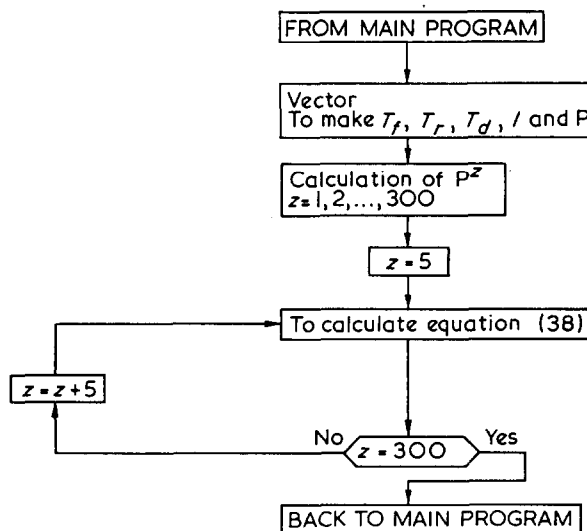


Figure 2 Flow chart of subprogram 1. (Calculation of degree of polymerization distribution)

$P_s^z(i, j)$ shows the cell in the i th row and j th column of the matrix P_s^z which is the z th power of the matrix P_s . $E(s, z)$ is the z th power expression of S . The coefficient of S^k indicates the probability of the formation of the polymer chain in which k M_i -monomers are present in the z -mer.

Since the i th column of equations (40) and (41) is multiplied at every transfer of the active end to the monomer M_i , k (=the power of S) indicates the number of M_i -monomers. The calculation of the compositional distribution is carried out in the following way. Here, the compositional distribution of the 100-mer is calculated as the typical one of this copolymerization.

Initiation

1. Take up a specified monomer n .
2. Prepare a matrix composed of n rows and z columns: $SFA(n, z)$, in order to get the probability of the formation of the polymer chain having k monomers of that species in the z -mer.

Calculation of CSK

3. The vector product $I_s \times P_s^z$ has as its cell $(z+1)$ th order polynomial expression of S . The cell of i th column which is the coefficient of S^k is expressed by $CSK(i, K+1)$.

Calculation of SCSK

4. Calculate the following equation to get the probability that the polymer chains having k units of n -monomer of that species in the z -mer are formed.

$$SCSK(n, K) = \sum_i CSK(i, K) \quad K=1, 2, \dots, z$$
5. Calculate about other monomers according to the same procedure as 1-4 and normalized.
6. Calculate the probability of the formation of the polymer having the special copolymer composition as the product of $SCSK(n, k)$ and the result obtained shows as a graph.

The flow chart mentioned above is shown in Figure 3, where, n is an order, n is the appointed monomer, m is the counter index of multiplication, k is the number of the appointed monomer unite in z -mer, CSK is the cell of i th column which is the coefficient of S , CSK is the convenient matrix to calculate CSK , $SCSK$ is the coefficient of S itself, z is the degree of polymerization and PPS is the probability of forming polymer having specific composition.

RESULTS AND DISCUSSION

The copolymerization reaction of S/BMA/MA system was carried out in carbon tetrachloride and the results obtained were examined by using the analytical process described above. The copolymerization curves obtained from experimental data and from calculation data are shown in Figure 4. Both curves are in accordance with each other.

e , the parameter which shows the recombination ratio to the total termination reaction, was determined so that the calculation results of number-average molecular weight could be identical with the experimental data. From Figure 5, $e=0.8$.

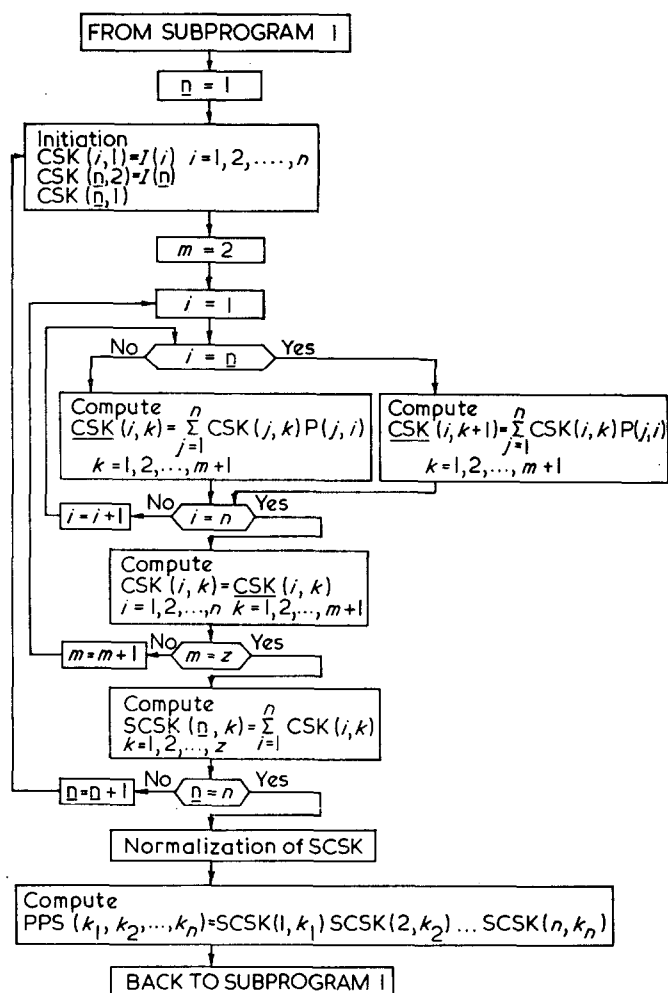


Figure 3 Flow chart of subprogram 2. (Calculation of compositional distribution)

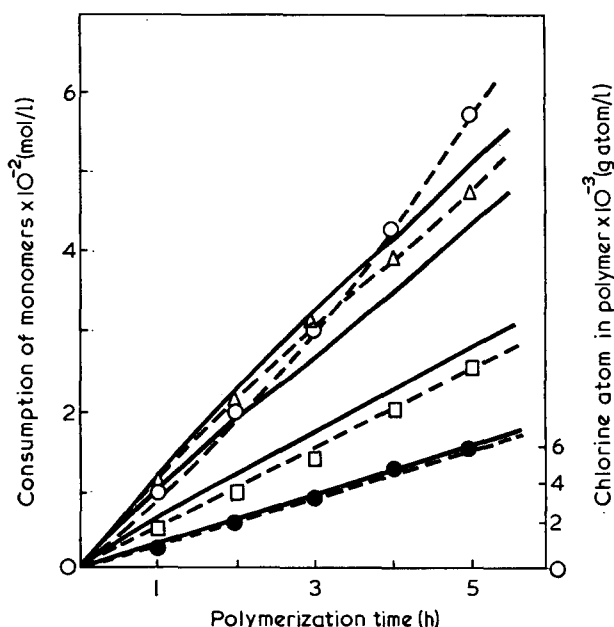


Figure 4 Results of the simulations between the amount of monomer consumption and the amount of chlorine atoms introduced into polymers. \circ , Styrene; Δ , n-butyl methacrylate; \square , methacrylic acid; \bullet , chlorine. —, Calculated values; ---, experimental values

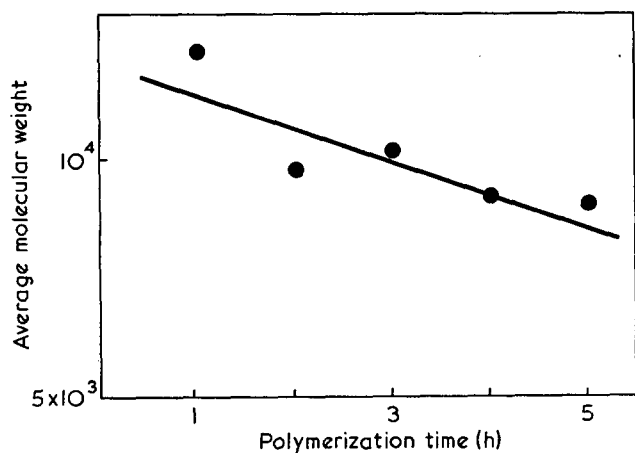


Figure 5 Results of the simulations of the relation between the average molecular weight and the time of polymerization, t . —, Experimental values; ●, calculated values

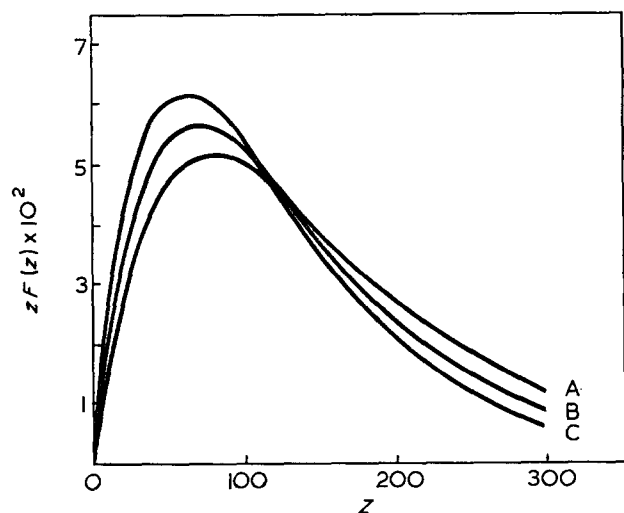


Figure 6 Results of the simulations of the distribution curves of degree of polymerization, Z obtained from kinetic analysis. Polymerization times: A, 1 h; B, 7 h; C, 13 h

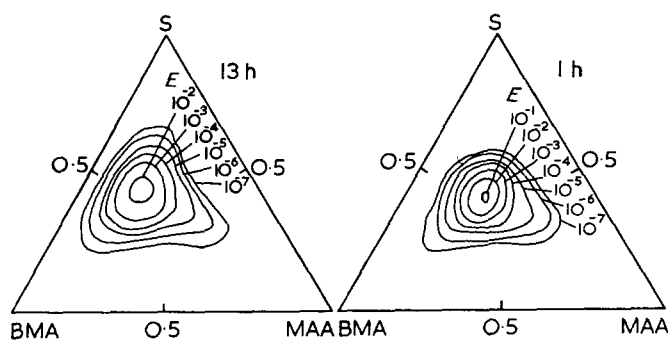


Figure 7 Results of the simulations of the relation between the compositional distribution and the time of polymerization, t . S, styrene; BMA, butyl methacrylate; MAA, methacrylic acid

By combining the calculation program of degree of polymerization distribution and of composition distribution, with the numerical analysis program of the differential equations of the reaction system, and by analysing them, the variation of the degree of polymerization distribution and of composition distribution against time could be obtained by calculation.

The distribution of degree of polymerization is shown in Figure 6. When the polymerization time increases, the distribution moves to the lower degree of polymerization range. This fact can be explained as follows.

As the polymerization proceeds, the composition of the polymerization system changes, $[S]/[M]$ (the ratio of solvent to monomer) increases, and lower molecular weight polymers are formed more easily by chain transfer reactions. The composition distribution of a copolymer whose degree of polymerization is 100, was calculated and it was taken up as the average composition distribution of the copolymers formed in this system. Figure 7 shows the composition distribution of the copolymers formed in 1 h and in 13 h. The composition of the copolymers is drawn on the triangle coordinates and the composition distribution is represented by the equal partition rate line.

Since the partition rate E below 10^{-3} could be neglected, we can conclude that the copolymer composition of this system is distributed within 10% range of each component from the centre of average composition. The composition distribution has a tendency to disperse as the polymerization proceeds.

ACKNOWLEDGEMENT

The authors are grateful to Dr Setsuo Mimashi (Computer Department, Mitsui-Toatsu Chemicals Inc.) for many calculations and helpful discussions during this work.

REFERENCES

- 1 Tsuchida, E. and Mimashi, S. *J. Polym. Sci. (A)* 1965, 3, 1401
- 2 Mimashi, S. and Tsuchida, E. *Kogyo Kagaku Zasshi* 1968, 71, 52
- 3 Tsuchida, E., Yao, Y., Kitamura, K. and Shinohara, I. *J. Polym. Sci. (A-1)* 1972, 10, 3605
- 4 Tsuchida, E., Kitamura, K. and Shinohara, I. *J. Polym. Sci. (A-1)* 1972, 10, 3639
- 5 Tsuchida, E., Mishima, K., Kitamura, K., Shinohara, I. and Mimashi, S. *J. Polym. Sci. (A-1)* 1972, 10, 3615
- 6 Tsuchida, E., Mishima, K., Kitamura, K. and Shinohara, I. *J. Polym. Sci. (A-1)* 1972, 10, 3627
- 7 Frensdorf, H. K. and Parisher, R. *J. Chem. Phys.* 1963, 39, 2303
- 8 *A. Meet. Soc. Polym. Sci. Japan*, Tokyo May 21, 1968

Influence of the polymerization temperature on the reactivity of 3-methyl- and 4-methylstyrenes in cationic polymerization

F. Visse and E. Marechal

*Institut National Supérieur de Chimie Industrielle de Rouen, 76130 Mont-Saint-Aignan, France
(Received 2 January 1974)*

The variations with respect to temperature of the reactivities of 3-methyl- and 4-methylstyrenes in cationic polymerization have been studied by determination of their reactivity ratios with styrene.

Former studies on the influence of experimental conditions on the reactivity of 4-methylstyrene have been made by Tobolsky^{1, 2} and Furukawa³. It does not appear that similar studies have been done with 3-methylstyrene.

In this paper the index 1 is relative to the methylated derivative and the index 2 to styrene; the reactivity ratios have been obtained by the differential method⁴.

Preliminary trials run at 5°C with the initiator and monomer concentrations which will be specified subsequently, have shown that the variation between r_2 and the nature of solvent is very small, r_1 is more dependent on this parameter and its value is maximum when methylene chloride is the solvent. The solvent used here was methylene chloride previously distilled, refluxed for 48 h in the presence of H₂SO₄ redistilled a second time and dried on 4 Å molecular sieve. The initiator was TiCl₄ (0.001 mol/l) and the total concentration of monomers was 0.05 mol/l. The variations of r_1 and r_2 with respect to the polymerization temperature θ are given in Table 1 for 3-methylstyrene and in Table 2 for 4-methylstyrene.

It has been impossible to determine r_1 and r_2 for temperatures above -5°C because a preliminary copolymerization study, run with the same molar fraction of each monomer, has shown that above -5°C the copolymer yield was negligible.

The variation, with respect to the absolute temperature, of the rate constant k_{ij} of the reaction between carbocation i and monomer j are given by the classical equation:

$$k_{ij} = A_{ij} \exp(-E_{ij}/RT)$$

or, the r_1 and r_2 definition being taken into account:

$$\log r_1 = \log |A_{11}/A_{12}| - (E_{11} - E_{12})/RT \quad (1)$$

and

$$\log r_2 = \log |A_{22}/A_{21}| - (E_{22} - E_{21})/RT \quad (2)$$

with

$$\log |A_{11}/A_{12}| = (S_{11} - S_{12})/R$$

and

$$\log |A_{22}/A_{21}| = (S_{22} - S_{21})/R$$

The $S_{ii} - S_{ij}$ and $E_{ij} - E_{ii}$ values obtained from $\log r_2$ with respect to $1/T$ are given in Table 3.

The variations of $r_1 r_2$ with respect to the polymerization temperature (θ °C) for 4-methylstyrene are given in Figure 1. A decrease of $r_1 r_2$ with increasing temperature is observed, which is in agreement with what is generally observed in radical copolymerization and with theory; since when θ increases the copolymer becomes more and more statistic. However, until now, the opposite result has always been observed in all the cases studied in cationic copolymerization. The curve in Figure 1 represents the variation of $r_1 r_2$ with respect to θ , obtained from relations (1) and (2) and from the values shown

Table 1 Variations of r_1 and r_2 with polymerization temperature for 3-methylstyrene

θ (°C)	r_1	r_2	$1/r_2$	$r_1 r_2$
-78	0.85 ± 0.10	1.3 ± 0.10	0.76	1.11
-55	1.20 ± 0.30	1.55 ± 0.40	0.64	1.86
-15	1.30 ± 0.10	2.30 ± 0.10	0.43	2.99

Table 2 Variations of r_1 and r_2 with polymerization temperature for 4-methylstyrene

θ (°C)	r_1	r_2	$1/r_2$	$r_1 r_2$
-75	2.0 ± 0.3	0.90 ± 0.06	1.42	1.80
-30	2.5 ± 0.3	0.65 ± 0.10	1.53	1.63
0	2.9 ± 0.3	0.48 ± 0.06	2.02	1.37
25	3.15 ± 0.20	0.36 ± 0.10	2.73	1.14

Table 3 $S_{ii} - S_{ij}$ and $E_{ij} - E_{ii}$ values obtained from $\log r_2$

Monomer 1	Monomer 2	$E_{12} - E_{11}$ (kcal/mol)	$E_{21} - E_{22}$ (kcal/mol)	$S_{11} - S_{12}$ (cal mol ⁻¹ °C ⁻¹)	$S_{22} - S_{21}$ (cal mol ⁻¹ °C ⁻¹)
4-Methylstyrene	styrene	-0.48	0.99	3.83	-5.15
3-Methylstyrene	styrene	-0.67	-1.01	3.10	5.15

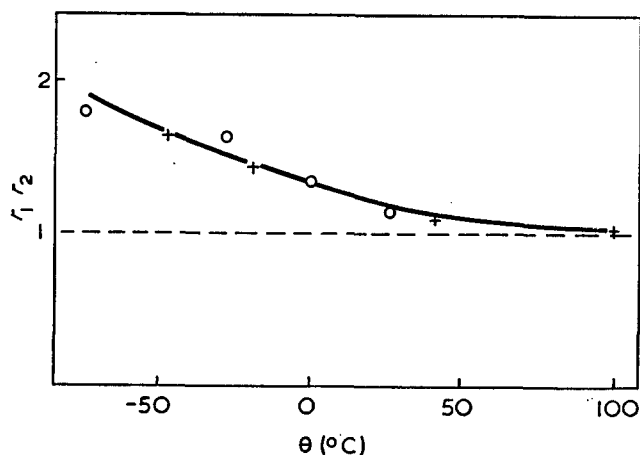


Figure 1 Variations of $r_1 r_2$ with polymerization temperature. Open circles are relative to experimental values

in Table 3, whose equation is:

$$r_1 r_2 = \exp \left[-0.66 + \frac{255}{\theta + 273} \right]$$

As it is impossible to work above 30°C with methylene chloride as a solvent, and difficult to compare the results obtained in various solvents, we have obtained the limit temperature θ_{lim} for which $r_1 r_2 = 1$ only by extrapolation of the curve. We found $\theta_{lim} = 113^\circ\text{C}$ and for this temperature: $r_1 = 3.65$, and $r_2 = 0.27$.

The value of $r_1 r_2$ has been determined at 5°C in various solvents for 4-methylstyrene: CCl_4 , 1.54; CH_2Cl_2 , 1.95; $\text{C}_6\text{H}_5\text{NO}_2$, 1.41. From the examination of these values it would appear that the polymer prepared in methylene chloride is the less statistic.

The index 1 relative to methylstyrenes (in a general

way) will now be changed to the index 3 for 3-methyl- and the index 4 for 4-methyl-styrene. As before, the index 2 is relative to styrene. The value given by Table 3 and the value E_{22}^5 being taken into account, we obtain $E_{23} \approx 7.50$ and $E_{24} \approx 9.50$ kcal/mol.

From these values it appears that when 3-methyl- and 4-methyl-styrenes react with the same cation, the rate of the reaction depends more on the temperature for 4-methyl- than for 3-methyl-styrene. This fact is in agreement with experimental results. It is worth noting that the average value of activation enthalpy relative to a reaction of styryl cation with *m*- and *p*-methylstyrenes is exactly the one obtained for the same reaction with styrene.

The relations $r_1 = \exp(1.91 - 240/T)$ and $r_2 = \exp(-2.57 + 495/T)$ for 4-methylstyrene, and $r_1 = \exp(1.55 - 335/T)$ and $r_2 = \exp(2.57 - 505/T)$ for 3-methylstyrene show that, in the range of temperature used the selection between the two monomers by the same cation is highly dependent on entropy, particularly in the case of 4-methylstyrene. From this fact, it appears that the propagation reaction is probably highly dependent upon the solvation and desolvation phenomena, themselves being greatly influenced by the superdelocalizability of the active centre and the nature of the solvent.

REFERENCES

- 1 Tobolsky, A. V., Kelley, D. J., O'Driscoll, K. F. and Rogers, C. E. *J. Polym. Sci.* 1958, **28**, 425
- 2 O'Driscoll, K. F. and Tobolsky, A. V. *J. Polym. Sci.* 1959, **37**, 363
- 3 Furukawa, J., Kobayashi, E. and Taniguchi, S. *Polymer* submitted (presented at Rouen Symp., 1973)
- 4 Ham, G. E. 'Copolymerization, High Polymers', Interscience, New York, 1964, p 18
- 5 Higashimura, T. 'Structure and Mechanism in Vinyl Polymerization', Marcel Dekker, New York, 1969, p 329

Heat capacity of polychlorotrifluoroethylene

W. K. Lee, P. C. Lau* and C. L. Choy

Department of Physics, The Chinese University of Hong Kong, Shatin, Hong Kong
(Received 18 December 1973)

The heat capacities of a slow-cooled (crystallinity=0.65) and a quenched (crystallinity=0.46) sample of polychlorotrifluoroethylene (PCTFE) have been measured between 80 and 340K and are found to be independent of crystallinity. The results can be understood as the sum of two terms: the optical contribution as calculated from the vibrational-band assignment given in the literature, and the acoustical contribution obtained from the Tarasov continuum model. By comparing the one-dimensional Debye temperature of PCTFE with that of polyethylene, it is concluded that the C-C bond has approximately the same force constants for all polymers with a carbon backbone.

INTRODUCTION

There have been quite a number of measurements on the heat capacity of linear polymers but comparatively few detailed analyses of the results¹, mainly because most polymers have side groups which may give rise to vibrations active in the Raman or infra-red. Because of the difficulty involved in the vibrational analysis of polymers almost all of the lattice dynamical calculations had been made using simplified models and applied only to the case of polyethylene, the organic polymer with the simplest structure²⁻⁴. Even when used to calculate the heat capacity of polyethylene⁵ these simplified lattice dynamical models did not give very satisfactory results. Instead, it was found that the continuum model proposed by Tarasov⁶ was in better agreement with experiments⁵. Although it was expected that the continuum model would not give an accurate representation of the vibrational spectrum, it should be generally valid for solids with chain structure. Hence it can be confidently used to describe the skeletal vibration of any polymer. Recently the Tarasov model was applied successfully to some linear polymers other than polyethylene and important information has been obtained¹.

At sufficiently low temperatures when low frequency vibrations become dominant, many chains interact with one another through the weak interchain interaction, so the vibrations become essentially three-dimensional. At higher temperatures more vibrations at higher frequencies are excited; these vibrations are essentially along the chain skeleton and therefore one-dimensional in nature. Tarasov⁶ assumes that the low frequency three-dimensional vibrations can be calculated according to the Debye model up to a cut-off frequency ω_3 . Higher frequency vibrations are treated as a one-dimensional continuum from ω_3 to ω_1 , the final cut-off frequency. If the number of repeating units is N , the frequency spectrum for each acoustical branch

is:

$$g(\omega) = \begin{cases} \frac{3N\omega^2}{\omega_1\omega_3^3} & 0 < \omega \leq \omega_3 \\ \frac{N}{\omega_1} & \omega_3 < \omega \leq \omega_1 \end{cases} \quad (1)$$

Here it is assumed that a fraction ω_3/ω_1 of the total number of vibrations is three-dimensional and the remainder one-dimensional. The heat capacity of one mole of repeating units for each acoustical branch is given by:

$$\frac{C}{R} = D_1(\theta_1/T) - \frac{\theta_3}{\theta_1} [D_1(\theta_3/T) - D_3(\theta_3/T)] \quad (2)$$

where $\theta_1 = \hbar\omega_1/k$, $\theta_3 = \hbar\omega_3/k$, D_1 and D_3 are, respectively, the one- and three-dimensional Debye functions.

The crystallinity of a polymer depends^{1,7} on its stereochemical structure and its thermal history. Polychlorotrifluoroethylene (PCTFE) is a typical polymer the crystallinity of which can be changed appreciably by quenching. In order to investigate the crystallinity effect we have measured the heat capacities of a quenched and a slow-cooled sample of PCTFE between 80 and 340K. Using the available assignment of optical modes the data have also been analysed in great detail so as to determine the general validity of the Tarasov model for organic polymers.

EXPERIMENTAL

Calorimetric measurements

Heat capacity of the sample was measured with an adiabatic calorimeter similar in design to that described in the literature⁸. The sample container was a thin-walled copper vessel of 2 in. (1 in. = 25.4 mm) diameter and 3 in. length. Along the central axis of the vessel was a re-entrant well in which a Leeds and Northrup type 8164 platinum resistance thermometer and a 300 Ω constantan heater were accommodated. Eight copper fins were soldered to the re-entrant well inside the

* Present address: Department of Physics, University of Akron, Akron, Ohio, USA.

vessel to promote distribution of heat throughout the sample. The outside surface of the vessel was rhodium-plated to reduce heat exchange by radiation. Helium gas was admitted into the vessel after it has been filled with a sample in order to promote heat exchange.

The vessel was suspended by three nylon strings within a copper adiabatic shield, which in turn was suspended within a copper radiation shield. The outer surfaces of both shields were covered with 700 Ω heaters and the inner surfaces were rhodium-plated to reduce radiation. The whole assembly was hung by a thin-walled stainless steel tubing within a brass chamber which could be evacuated to 10^{-6} mmHg.

One junction of a copper-constantan differential thermocouple was connected to the sample container with the other junction on the adiabatic shield. The thermocouple voltage was amplified with a Keithley Model 150-B microvoltmeter and recorded on a Leeds and Northrup Speedomax-H strip chart recorder. Any deviation from the control set point of the recorder drives a Series 80 CAT current control unit. The 0 to 5 mA output of the CAT unit was amplified and fed into the shield heater. With this arrangement the temperature difference between the sample container and the adiabatic shield could normally be controlled to within 0.001K except at the beginning and end of the heating period when the temperature difference momentarily increased to 0.01K.

The radiation shield was maintained at a temperature a few Kelvins below that of the adiabatic shield. The voltage from a copper-constantan differential thermocouple between these two shields was sensed by a Keithley model 149 microvoltmeter, the reading of which was adjusted to zero with the zero suppress dial. Any deviation from zero was then amplified and fed to the radiation shield heater. The temperature difference was controlled to 0.1K.

The temperature of the sample container was determined with a platinum-resistance thermometer which had been calibrated against another platinum-resistance thermometer certified by NBS. The resistance was measured with a Leeds and Northrup G-2 Mueller Bridge and a Keithley Model 147 nanovoltmeter. The accuracy was better than 0.001K.

Heat capacity measurements were taken by the discontinuous heating method. Current was supplied by a Hewlett-Packard 6181-B constant current source to the sample heater. The power supplied was determined by the voltage drop across the heater and across a standard resistor in series with the heater. These voltage drops were measured with a Fluke 8300-A digital voltmeter. The time duration of the heat application was measured by an electronic timer coupled to the heat switch. The heat supplied could thus be determined with an accuracy of 0.1%.

In a typical run the brass chamber was evacuated to 10^{-6} mmHg and then immersed in liquid nitrogen. Helium gas was admitted to increase the cooling rate. After the whole assembly had reached liquid nitrogen temperature the brass assembly was again evacuated to 10^{-6} mmHg when measurements could be started. Heat was applied for a period of about 1000 sec and the subsequent temperature rise, which varied from 3 to 10K, was measured. The accuracy of this set-up was tested by making measurements on a standard sample of benzoic acid. The data were found to agree

with those in the literature⁹ to within 0.3% which is taken as our overall accuracy.

Sample

The two samples were made with Kel-F PCTFE kindly supplied by 3M Co in the form of pellets about 3 mm in diameter. The quenched sample was prepared by pressing the Kel-F pellets at 250°C into sheets of 1 mm thickness and then quenching them in ice water. The slow-cooled sample was prepared by pressing the pellets into 1 mm sheets at 250°C and then cooling them slowly at a rate of 5°C/min to room temperature. The quenched sample was rather transparent and the slow-cooled sample had a cloudy appearance. Both samples were cut into small strips 1 mm thick and about 100 g was used in each experiment. Densities of both samples were measured by hydrostatic weighing in water at 20°C and their crystallinities were determined from these densities using the following values¹⁰: $\rho_a = 2.077$ g/cm³; $\rho_c = 2.187$ g/cm³ where ρ_a and ρ_c are the densities for amorphous and crystalline PCTFE. The crystallinities χ of the quenched and slow-cooled samples were found to be 0.46 and 0.65, respectively.

RESULTS AND DISCUSSION

Effect of crystallinity

Between 80 and 325K (glass temperature) the slow-cooled and quenched samples are found to have the same heat capacity within experimental error (0.3%). Because PCTFE is a partly crystalline polymer, no sharp increase in heat capacity at the glass temperature is observed. Above 325K the quenched sample shows a heat capacity slightly higher than that of the slow-cooled sample, the difference reaching 0.8% at 340K. The heat capacity curve for the slow-cooled sample ($\chi = 0.65$) is shown in *Figure 1* and the smoothed values at 10K intervals are given in *Table 1*.

The fact that slow-cooled and quenched samples show the same heat capacity below glass temperature is in agreement with results obtained for other polymers^{1, 11, 12}. For instance, Furukawa *et al.*¹¹ obtained the same heat capacity for slow-cooled and quenched polytetrafluoroethylene (PTFE) between 120 and 270K. Karasz *et al.*¹² also obtained the same heat capacity for a slow-cooled ($\chi = 0.37$) and a quenched ($\chi = 0$) sample of isotactic polystyrene between 300K and the glass temperature at 360K. The same effect was also thoroughly demonstrated¹ for many samples of polyethylene (PE) having different numbers of branches. So it seems the difference in crystallinity produced by quenching or branching has very little effect on the heat capacity of polymers between 80K and the glass temperature.

The only other heat capacity measurements on PCTFE was made by Hoffman¹³ between 280 and 510K. It was found that between 280 and 330K the heat capacity of a quenched sample exceeded that of a slow-cooled one by 6%. This, in fact, provided the impetus for our present investigation at lower temperatures. The few data points in the temperature region of overlap with our data are plotted in *Figure 1*. At 280K Hoffman's data for quenched and slow-cooled sample are 12% and 6% higher than ours, but because of the steeper slope of our curve, all the data points are within $\pm 1.5\%$

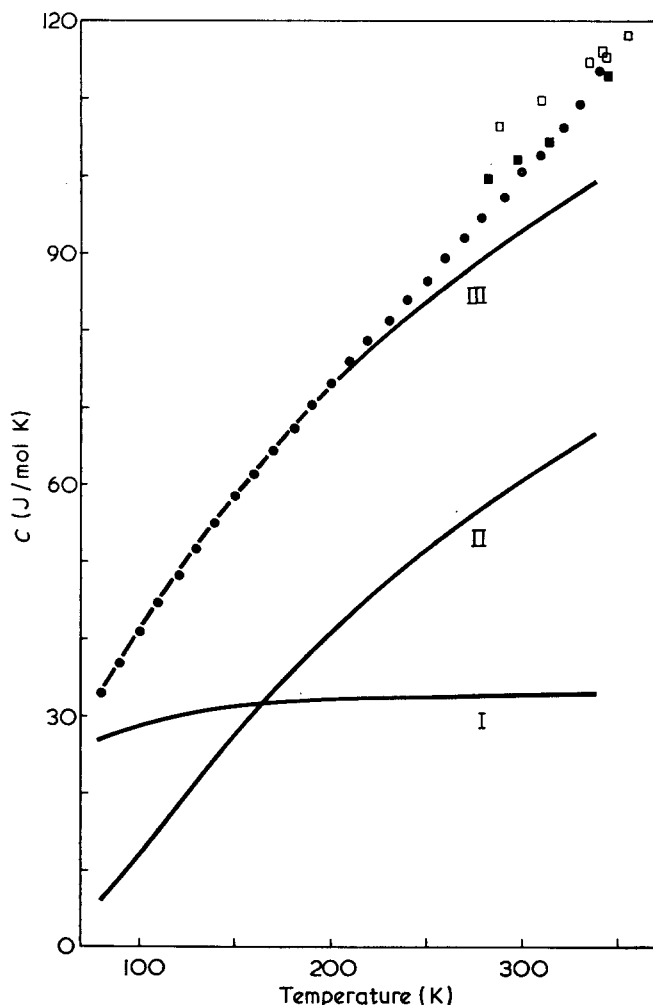


Figure 1 Heat capacity of PCTFE vs. temperature. I, Calculated acoustical contribution according to the Tarasov model using $\theta_1=235\text{K}$; II, calculated optical contribution of 14 modes; III, calculated total heat capacity; ●, measured heat capacity on slow-cooled sample; ■, Hoffman's data on slow-cooled sample; □, Hoffman's data on quenched sample

when the temperature reaches 340K. No reason can be found to account for this discrepancy. It is noted that the estimated accuracy of 0.8% in ref 13 is not as good as ours (0.3%), and by comparison with the heat capacity of PTFE¹¹, it seems that the steeper slope obtained by us is more reasonable.

Comparison with the Tarasov model

In order to interpret our results in the light of the Tarasov model the optical contribution has to be subtracted from the measured heat capacity first. Although detailed vibrational analysis of PCTFE has not been performed it is fortunate that for PTFE the dispersion curves have been calculated¹⁴ and found to be in excellent agreement with its infra-red (i.r.) and Raman spectra^{15, 16}. With the help of this calculation and the i.r.¹⁷ and Raman¹⁸ spectra of PCTFE, we assign the frequency bands of the optical modes as shown in Table 2. The C-C stretching modes are also included in the 14 optical modes of the chemical repeat unit $\text{CF}_2\text{-CFCl}$. Thus there are only four acoustical modes per repeat unit, corresponding to the bending and torsional motions of the C-C bonds. The contribution of each optical mode is represented by an Einstein function corresponding to the average frequency shown in Table 2. Even for this polymer of

comparatively simple structure and without bulky side groups the optical modes already contribute 20% to the total heat capacity at 80K. At 260K the optical contribution reaches 60%.

After subtraction of the optical contributions the remaining heat capacity can be fitted with a one-dimensional Debye function $D_1(\theta_1/T)$ using four acoustical modes per repeat unit, resulting in a θ_1 value of 235K. As shown in Figure 1 and Table 1, the agreement between experiment and theory is quite good, being within 1% below 200K and 4% between 200 and 260K, indicating that the frequency assignment of the optical modes is essentially correct. Above 260K the discrepancy becomes larger and at 340K the calculated values are lower by 12%. This is because the measured values are in fact the heat capacity at constant pressure C_p while the calculated ones are the heat capacity at constant volume C_v . The thermodynamic relation between C_p and C_v is:

$$C_p - C_v = \frac{\beta^2 VT}{K} \quad (3)$$

where β = expansion coefficient, K = isothermal compressibility, V = molar volume and T = temperature. Insufficient data are available for us to evaluate this correction term throughout our temperature range. However, for PE at 300K, Wunderlich^{5, 19} estimated this to be 9% which is large enough to account for our present discrepancy.

The θ_1 value for PE¹ being 540K, we obtain the ratio:

$$\frac{\theta_1(\text{PCTFE})}{\theta_1(\text{PE})} = 0.44$$

Table 1 Heat capacity of slow-cooled PCTFE. See text for detail of calculation

Temperature (K)	Observed heat capacity (J/mol K)	Calculated heat capacity (J/mol K)	Deviation* (%)
80	32.6	32.8	+0.61
90	36.7	36.6	-0.27
100	40.6	40.5	-0.24
110	44.6	44.2	-0.89
120	48.2	48.0	-0.40
130	51.7	51.6	-0.19
140	55.1	55.1	0.00
150	58.2	58.3	+0.17
160	61.2	61.4	+0.33
170	64.4	64.4	0.00
180	67.3	67.1	-0.30
190	70.2	69.8	-0.57
200	73.0	72.3	-0.95
210	75.8	74.7	-1.4
220	78.4	77.1	-1.7
230	81.0	79.3	-2.1
240	83.7	81.4	-2.7
250	86.3	83.5	-3.3
260	89.1	85.6	-3.9
270	91.8	87.5	-4.7
280	94.6	89.3	-5.6
290	97.4	91.2	-6.4
300	100.6	92.9	-7.7
310	102.7	94.7	-7.8
320	106.4	96.3	-9.5
330	109.4	97.9	-10.5
340	113.4	99.4	-12.3

* Deviation =

$$\frac{\text{calculated heat capacity} - \text{observed heat capacity}}{\text{observed heat capacity}} \times 100\%$$

Table 2 Optical vibrations in PCTFE

Vibrational mode	CF ₂ group			CFCl group		
	Frequency range (cm ⁻¹)	Average frequency (cm ⁻¹)	Einstein temperature (K)	Frequency range (cm ⁻¹)	Average frequency (cm ⁻¹)	Einstein temperature (K)
Twisting	235-357	296	426	185-281	233	335
Bending	297-411	354	509	335	335	482
Rocking	305-490	398	572	272-438	355	511
Wagging	506-580	543	781	422-483	453	651
Symmetric stretching	729-1152	941	1354	608-960	784	1128
Asymmetric stretching	1130-1290	1210	1741	942-1075	1008	1451
C-C stretching	1065-1277	1171	1685	1065-1277	1171	1685

The average mass per chain atom for PCTFE and PE is 58 and 14, respectively, so that

$$\left[\frac{M(\text{PE})}{M(\text{PCTFE})} \right]^{1/2} = 0.49$$

Thus the difference in θ_1 value can be accounted for by the mass difference in the chain atoms, showing that the force constants for the C-C bond are nearly the same for all polymers with a carbon backbone.

At sufficiently low temperatures equation (2) becomes:

$$\frac{C}{R} = \frac{4\pi^4}{5} \frac{T^3}{\theta_1 \theta_3^2} \quad (4)$$

which is the Debye T^3 law. Using the heat capacity data²⁰ of PCTFE below 4K, θ_3 is calculated to be 38K. Thus $\theta_3 \ll \theta_1$ and in our temperature range the second term is negligible compared to the first term in equation (2). The θ_3 value for PCTFE is smaller than the corresponding values for PTFE¹ at 46K and for PE¹ at 147K, indicating correspondingly smaller force constants between chains.

CONCLUSIONS

Crystallinity has little effect on the heat capacity of PCTFE between 80 and 325K (glass temperature). It would be interesting to extend the measurements to lower temperatures because heat capacity will be more sensitive to structural changes by quenching. Near 1K it should be possible to determine the frequency and number of the non-acoustical modes associated with the amorphous portion of the polymer^{7, 21}. We calculate the optical contribution to heat capacity by making vibrational-band assignments on the basis of available i.r. and Raman spectra. After subtraction of this contribution from the measured heat capacity, the remainder is found to agree well with the Tarasov model. By comparing the θ_1 value for PE and PCTFE it is concluded that the force constants of the C-C bonds for these two polymers are the same, in agreement with analysis¹ on other polymers with a carbon backbone.

ACKNOWLEDGEMENTS

The authors are indebted to Mr P. D. Detomaso and W. B. Isaacson of the Minnesota Mining and Manufacturing Company for supplying us with Kel-F pellets and Dr E. J. Prosen of the National Bureau of Standards for supplying benzoic acid. Thanks are also due to Dr E. J. Boerio of the Department of Material Science and Metallurgical Engineering, University of Cincinnati for sending us unpublished Raman spectra of PCTFE and Dr F. C. Chen of the Physics Department of the Chinese University for reading the manuscript and making valuable suggestions. We are also grateful for the financial support of the Institute of Science and Technology of The Chinese University of Hong Kong.

REFERENCES

- 1 Wunderlich, B. and Baur, H. *Adv. Polym. Sci.* 1970, **7**, 151
- 2 Stockmayer, W. H. and Hecht, C. E. *J. Chem. Phys.* 1953, **21**, 1954
- 3 Genensky, S. M. and Newell, G. F. *J. Chem. Phys.* 1957, **26**, 486
- 4 Kitagawa, T. and Miyazawa, T. *Rep. Progr. Polymer Phys. Japan* 1965, **8**, 53
- 5 Wunderlich, B. *J. Chem. Phys.* 1962, **37**, 1203, 1207
- 6 Tarasov, V. V. *Zh. Fiz. Khim.* 1950, **24**, 111
- 7 Tucker, J. E. and Reese, W. *J. Chem. Phys.* 1967, **46**, 1388
- 8 Karasz, F. E. and O'Reilly, J. M. *Rev. Sci. Instrum.* 1966, **37**, 255
- 9 Ginnings, D. C. and Furukawa, G. T. *J. Am. Chem. Soc.* 1953, **75**, 522
- 10 Hoffman, J. D. and Weeks, J. C. *J. Res. Nat. Bur. Stand.* 1958, **60**, 465
- 11 Furukawa, G. T., McCoskey, R. E. and King, G. L. *ibid.* 1952, **49**, 273
- 12 Karasz, F. E., Bair, H. E. and O'Reilly, J. M. *J. Phys. Chem.* 1965, **69**, 2657
- 13 Hoffman, J. D. *J. Am. Chem. Soc.* 1952, **74**, 1969
- 14 Hannon, M. J., Boerio, F. J. and Koenig, J. L. *J. Chem. Phys.* 1969, **50**, 2829
- 15 Krimm, S. *Adv. Polym. Sci.* 1960, **2**, 51
- 16 Koenig, J. L. and Boerio, F. J. *J. Chem. Phys.* 1969, **50**, 2823
- 17 Liang, C. Y. and Krimm, S. *J. Chem. Phys.* 1956, **25**, 563
- 18 Boerio, F. J. personal communication
- 19 Bares, V. and Wunderlich, B. *J. Polym. Sci. (A-2)* 1973, **11**, 197
- 20 Reese, W. and Tucker, J. E. *J. Chem. Phys.* 1965, **43**, 105
- 21 Choy, C. L., Hunt, R. G. and Salinger, G. L. *J. Chem. Phys.* 1970, **52**, 3629

A technique for the detailed investigation of polymer crystallization at high pressures

B. C. Edwards and P. J. Phillips

Department of Materials, Queen Mary College, London E1 4NS, UK
(Received 7 December 1973; revised 21 January 1974)

A technique based on an intensified argon high pressure system has been developed for the experimental determination of lamellar growth rates and the concurrent observation of developments in crystalline morphology. The technique is applicable, at the present time, to polymers such as polydienes which contain double bonds in the backbone. *In situ* electron staining of the crystallizing film, by osmium tetroxide vapour, has been made possible by the incorporation of an additional chamber to contain the stainant which is separated from the main chamber by means of a solenoid valve. Three apparently different modes of crystallization have been observed in *cis*-polyisoprene in different regions of the pressure-temperature plane. The effect of increasing pressure on the kinetics of spherulitic lamellar growth is to increase the maximum rate of crystallization and to shift the crystallization curve to higher temperatures.

INTRODUCTION

Over the last decade, a considerable literature has been established on the effect of high pressures (up to 7 kbar) on the crystallization of polymers. This has been mainly due to the pioneering work of Wunderlich¹ and co-workers on polyethylene, a polymer which has since been studied by several other investigators²⁻⁵. In addition, the high pressure crystallization of polychlorotrifluoroethylene (PCTFE)⁶ and nylon-6⁷ has been studied. The investigations have concentrated mainly on the structure of the fracture surface of the bulk material, using a replication technique for transmission electron microscopy. Differential thermal analysis^{5, 8, 9} has been performed, as well as some direct observations of the crystallization process using optical microscopy¹⁰. The growth^{11, 12} and annealing¹³ of solution grown single crystals at high pressures have also been studied.

The most obvious and generally accepted conclusion is that the lamellae produced at high pressures in bulk samples are much thicker than those produced at atmospheric pressure, the lamellar thickness often approaching the value of the molecular length¹. It has been demonstrated³ that full molecular extension is not normally attained for high molecular weight material and suggested¹⁴ that chain-folded and chain-extended crystallization are distinct processes. It is important to emphasize that chain-extended crystals of polyethylene¹⁵ can be grown at atmospheric pressure, the effect of increasing pressure being to increase the thickness of the lamellae. In addition, chain-extended crystals of polytetrafluoroethylene (PTFE)¹⁶ and selenium¹⁷ have been grown at atmospheric pressure by slow crystallization from the melt. The solution crystallization studies at high pressure have shown that folded chain single crystals, similar to those obtained at atmospheric pressure, are formed with no evidence of extended chain formation.

In view of these developments, it has become all the more necessary for direct investigations to be made into the crystallization processes of polymers at high pressures as they occur, especially in relation to the kinetics of crystallization. This is only possible for polymers which have measurable rates of crystallization. Additionally, polymers other than polyethylene need to be investigated in order to ascertain how generally applicable are the reported phenomena.

cis-Polyisoprene (natural rubber) was chosen for this study because of its relatively low rate of crystallization and its well documented thin film crystallization kinetics and morphology at atmospheric pressure^{18, 19}. A note has already been published²⁰ on the high pressure crystallization of *cis*-polyisoprene using an extension of the thin film technique of Andrews²¹. In this paper we wish to report the details of a more definitive technique for the direct investigation of the crystallization kinetics and the development of crystalline morphology.

EXPERIMENTAL

High pressure system

A line diagram of the high pressure generating system is shown in *Figure 1*. High pressure was generated by a two stage intensification of the cylinder pressure of high purity argon gas and was a variant of that described by Crawford²². The cylinder gas pressure was first compressed using a gas pump (Haskel Gas Booster; Olin Energy Systems Ltd, Sunderland, Co Durham) which operated via a standard compressed air line of 5.5-7.0 bar. This first stage is capable of generating pressures up to 1.4 kbar (1 kbar = 100 MN/m²). Higher pressures were obtained by the introduction of a high pressure intensifier (Harwood Engineering Co, Walpole, Mass, USA) which was operated by means of a compressed air-driven oil pump (Olin Energy Systems Ltd),

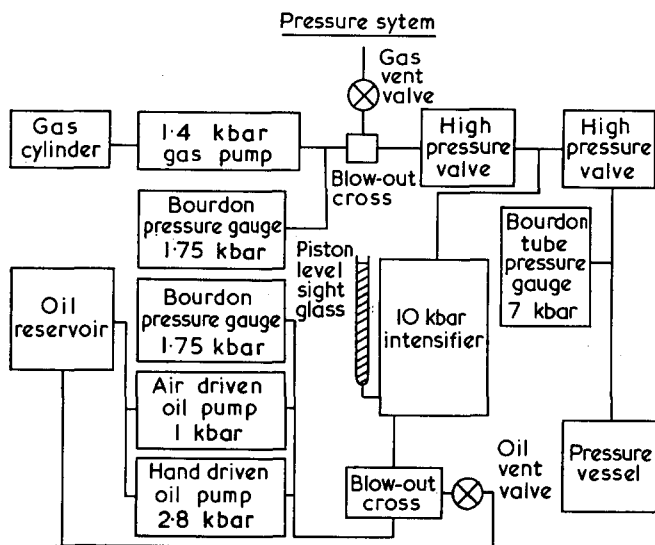


Figure 1 Line diagram of pressure generating system

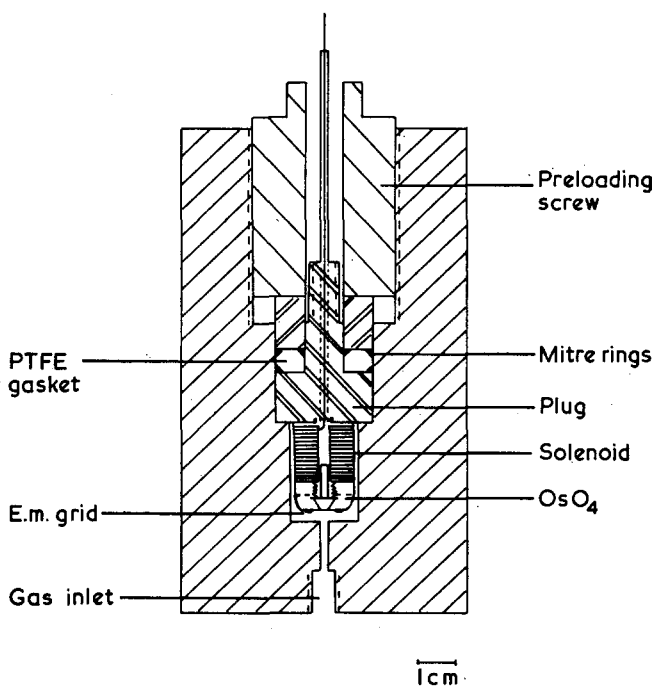


Figure 2 High pressure crystallization bomb

which compressed the initial 1.4 kbar enabling pressures of up to 10 kbar to be achieved. The pressures were measured using Bourdon pressure gauges (Budenberg and Co., Altrincham, Cheshire) to an accuracy of ± 0.01 kbar. The tubing used was 0.25 in (1 in = 25.4 mm) o.d., 0.080 in wall thickness (maximum sustainable pressure 7 kbar) (Tube Sales, Southampton); relevant connections and couplings were supplied by Olin Energy Systems Ltd (for Nova Swiss) and Harwood Engineering.

Crystallization bomb

The specially constructed bomb allows the crystallization of the thin film electron microscope specimens to be terminated at any time by 'fixing' the polymer using electron staining at elevated pressure.

The bomb (Figure 2) was constructed of EN 58B stainless steel and was sealed using a Bridgeman unsupported area type seal. The seal consisted of a mushroom-shaped plug made from EN 57 stainless steel, a PTFE

gasket and three mitred brass anti-extrusion rings. The plug was positioned using the preloading screw and could be withdrawn using the screw thread on the plug. The electron microscope grids were loaded onto the outside of the sample holder, which was attached to the plug. The holder comprised a solenoid valve and an inner chamber containing osmium tetroxide crystals and their vapour. The high pressure electrical connection of the solenoid was made by silver soldering mineral insulated wire along the axis of the plug, and sealing the exit of the wire into the staining assembly with epoxy resin.

The temperature of crystallization was controlled by placing the bomb in a thermostatically controlled bath and pressure was applied in less than 3 min to the samples using the above system. The staining was performed by electrically activating the solenoid valve after the required crystallization time, thus releasing the stainant to the grids in the outer chamber, a 5 min staining period being normally employed. Using this technique the crystalline morphology can be 'fixed' at any stage of the crystallization process, and the films can be studied using transmission electron microscopy^{19, 20}.

Preparation of thin films

The thin films were prepared in the same manner as described for atmospheric crystallization²¹. Natural rubber (*cis*-polyisoprene) was dissolved in benzene to form a 2% solution by weight and allowed to homogenize. Thin films, 80–100 nm thick, were cast from the solution onto a grease-free distilled water surface, the thickness being judged by the interference colours. The samples were placed under vacuum for 30 min prior to loading in order to dry and remove any excess solvent.

RESULTS

Morphology

In contrast to crystallization at atmospheric pressure, where only spherulites are normally observed, three distinct types of morphological species have been observed within the pressure-temperature range so far investigated.

Single crystals. At low pressures (e.g. below 1.5 kbar at 0°C and below 2 kbar at 21°C) large tapered crystals were observed concurrently with normal spherulitic growth (Figure 3). These tapered crystals grown at 0°C for pressures corresponding to low supercoolings, developed a corrugated structure along the long axis if crystallized for times in excess of 4 h. The development of the corrugations would seem to be an annealing effect since they appear in a definitive form after maximum crystal size has been achieved. The size and perfection of these crystals are related inversely to both supercooling and pressure. They become smaller and less specific in shape as supercooling is increased by the application of pressure at 0°C. These misshapen crystals take on the form of dendritic sheafs if grown at the same pressure but at a higher temperature.

At low supercoolings the crystals appear with a growth rate 25–30 times larger than that for concurrent spherulitic growth. There would appear to be competition for growth between these crystals and the concurrent

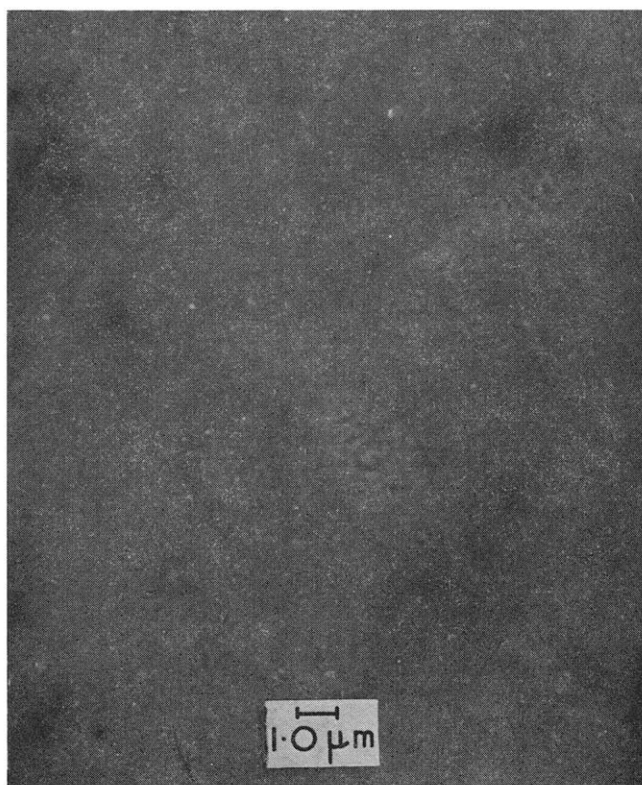


Figure 3 Tapered crystals observed after 21 h at 0.5 kbar and 0°C, showing the development of the corrugated structure along the crystal

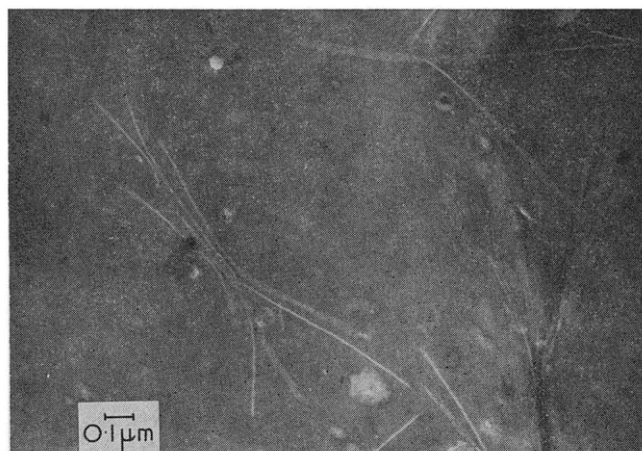


Figure 4 Spherulitic lamellar crystals present after crystallizing for 21 h at 0.5 kbar and 0°C, displaying 'twisting' of the lamellae, growth in the 'side-on' position and the spawning of new lamellar crystals

spherulitic growth since on increasing pressure at a given temperature the spherulitic growth rate is increased (see below) and the growth of the crystals is decreased. Indeed their growth is totally suppressed by the time the pressure is reached which corresponds to the maximum spherulitic growth rate at a given temperature. These crystals have not been observed in the sector of the pressure-temperature diagram which corresponds to diffusion control of spherulitic growth.

The nature of these crystals is not known at the present time and is the subject of further investigations.

Spherulitic growth. The mode of spherulitic growth is essentially the same as that observed at atmospheric pressure. In Figures 4 and 5 the twisting of the lamellar crystals can be seen, in addition to the spawning^{18, 23}

of new lamellar crystals. With increasing pressure, at a given temperature, the lamellar crystals grow increasingly in the 'side-on' position²³ in the plane of the film (Figure 5) and appear more like hedrites²⁴ than the usual ribbon-like lamellae (Figure 4). The growth is in general as a sheaf rather than as a spherulite, the nucleation of lamellae in the equatorial region being somewhat suppressed. On allowing the film to crystallize to completion it takes on the usual appearance of an impinged spherulitic film (Figure 6). The equatorial regions of spherulites have been filled in by both lamellae which have curved in to continue propagation and by the slower growing equatorial lamellae themselves. The regions of different tone in the central regions of the spherulites correspond to the initial highly aligned sheaf-like growth.

Lamellar growth in the region of the pressure-temperature plane corresponding to diffusion control of the secondary nucleation process has a mottled appearance (see Figure 7). The lamellae, whether edge-on or side-on, have an apparently discontinuous structure, the growth seeming to have been diverted around obstacles.

Oblate spheroids. Crystallization at 3 kbar and 21°C produced a morphology which has not yet been detected at 0°C under the pressure conditions so far investigated (up to 5.5 kbar). This structure is shown in Figure 8 and can be interpreted as oblate spheroidal crystals (53.0 nm



Figure 5 Spherulitic morphology obtained by crystallizing at 1 kbar and 0°C, for 2 h. Note the growth of the lamellae in the 'side-on' position

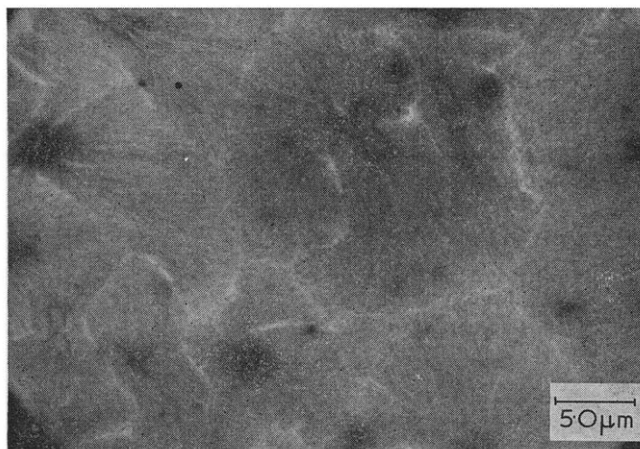


Figure 6 Completely spherulitic thin film obtained by crystallizing for 5.5 h at 1.5 kbar and 0°C

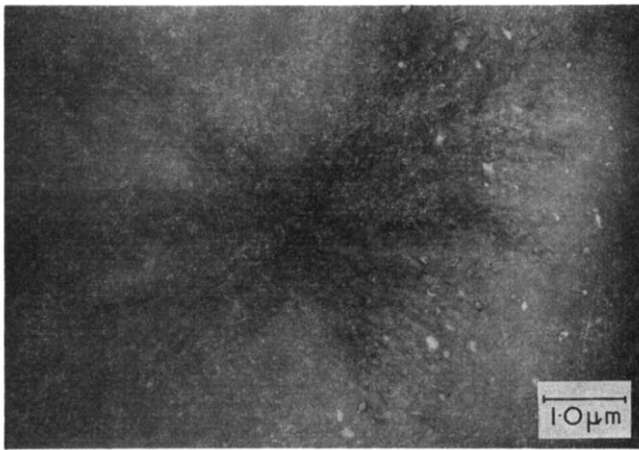


Figure 7 Spherulitic morphology produced by crystallizing for 19h at 2kbar and 0°C. Note mottled appearance of spherulitic growth in 'side-on' orientation

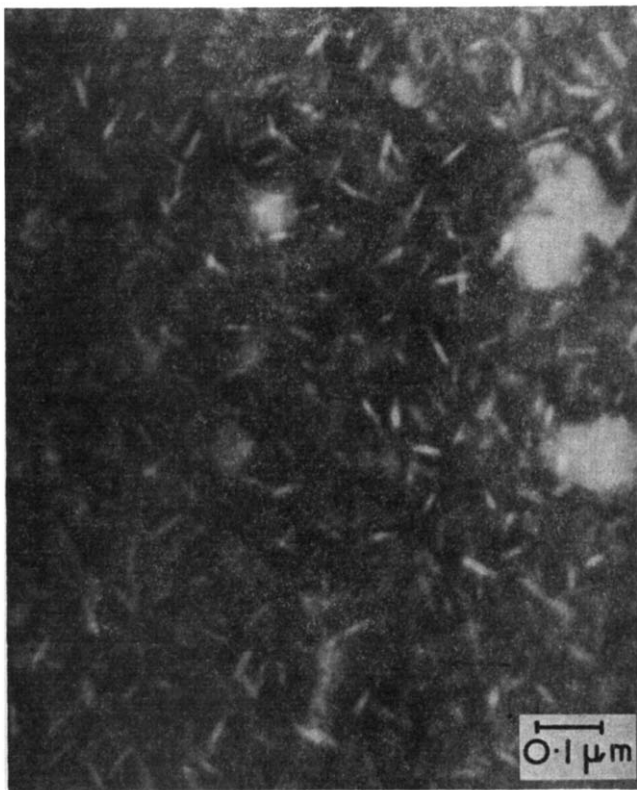


Figure 8 Oblate spheroidal crystals obtained by crystallizing for 1h at 3kbar and 21°C

in diameter, 11.5 nm in thickness) present with a very high nucleation density ($\sim 10^{22} \text{ m}^{-3}$). There is no preferred crystal orientation. This structure is similar to that observed at the same temperature and 4 kbar which was reported earlier²⁰ but with a higher nucleation density and smaller crystal dimensions. It appears to be a totally new phase, the conditions under which it appears not being completely specified at the present time. On crystallizing for 20 h over the same pressure range at a temperature just 3°C higher (24°C) spherulitic growth is observed concurrently. There is some evidence for the transformation of the rapidly formed spheroids into slowly formed spherulitic lamellar crystals at long times.

Kinetics of lamellar growth

In the determination of lamellar growth rates at atmospheric pressure^{18, 19} it has been usual to measure the length of a row-nucleated lamella, produced in a strained film, as a function of time of crystallization. The reason for this has been that the complication due

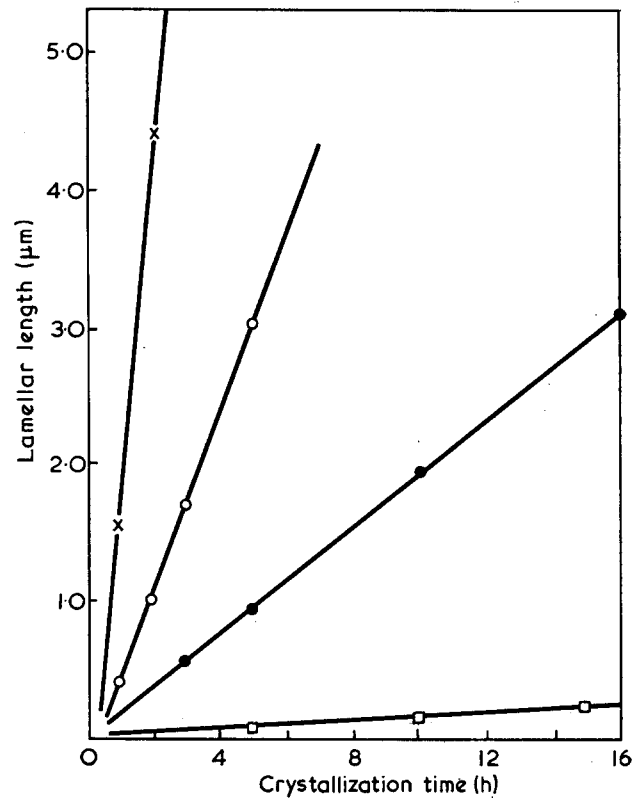


Figure 9 Graph of lamellar length versus crystallization time at 0°C. □, 1 bar; ●, 0.75 kbar; ○, 1.00 kbar; ×, 1.50 kbar

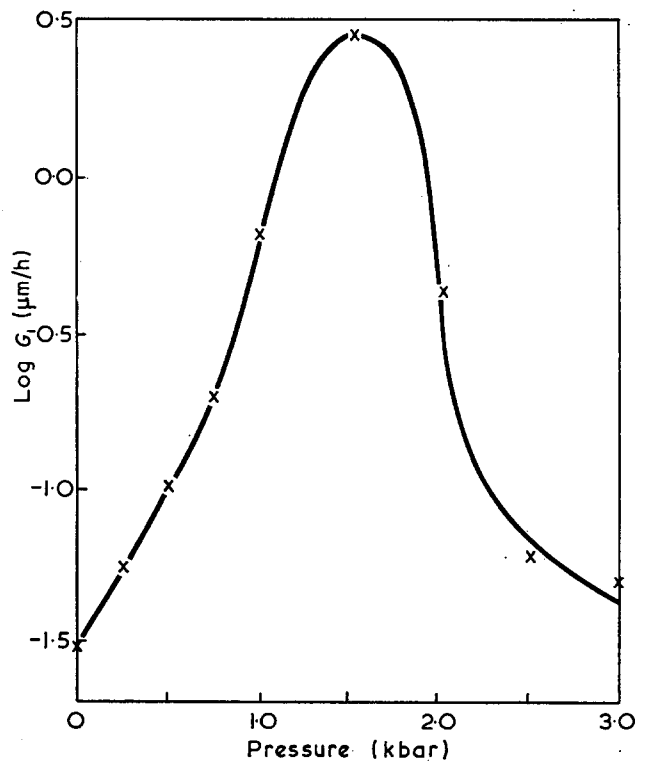


Figure 10 Logarithm of lamellar growth rate, G , as a function of pressure at 0°C

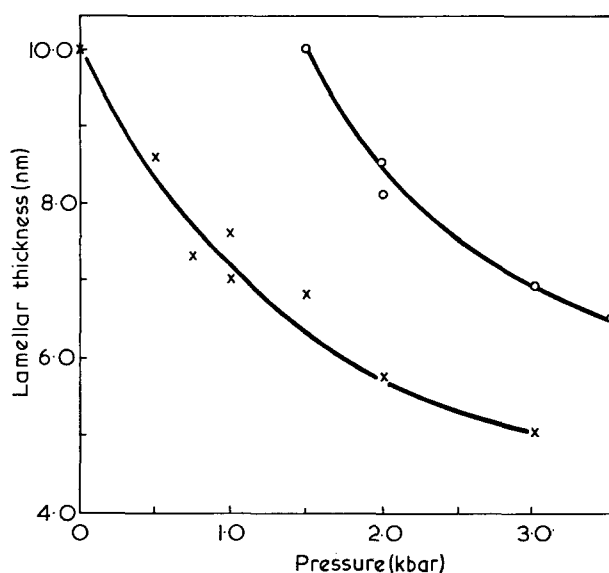


Figure 11 Lamellar thickness as a function of pressure at 0°C (x) and 24°C (o)

to the rate of spherulitic nucleation is eliminated and it can be assumed that the backbone filaments which serve as nuclei are present at zero time. We have attempted to use this procedure for crystallization under pressure but found it difficult to pressurize strained films without causing their collapse. The growth rates have therefore been obtained by determining the maximum length attained by a lamellar crystal in each specimen, the measurement being made from the centre of the spherulite to the growth front of the lamella concerned.

The maximum lamellar length (L) was plotted as a function of time of crystallization at a given pressure and temperature, as shown in Figure 9. A linear dependence of L on time was found in all cases, indicating a constant growth rate from the initial secondary nucleation event.

The logarithm of growth rate (G) as a function of pressure at 0°C is plotted in Figure 10. A bell-shaped curve is obtained with a maximum lamellar growth rate of $2.85 \mu\text{m/h}$ at 1.5 kbar. This maximum growth rate is six times greater than the maximum growth rate obtained at atmospheric pressure (i.e. at -26°C). The behaviour may be explained by the pressure influencing the melting point to a greater degree than the glass transition temperature (i.e. $dT_m/dP > dT_g/dP$) or to an effect on the pre-exponential factor G_0 , or to both. A detailed analysis of the data cannot be made until measurements of the melting points and glass transition temperatures under pressure have been made.

Lamellar thickness

The variation of lamellar thickness as a function of pressure is given in Figure 11, and is similar to that

found at atmospheric pressure as a function of supercooling. Hence it may be deduced that the effect of pressure at a constant temperature is simply to influence the degree of supercooling for this polymer. The data would suggest that an increase in T_m of 16°C/kbar would be appropriate. This compares with 18°C/kbar for polyethylene, 65°C/kbar for PCTFE⁶ and 140°C/kbar for PTFE⁶. Under the limited conditions so far investigated the lamellar thickness appears to be constant for a constant degree of supercooling, but this cannot be stated categorically until melting points at pressure have been determined.

ACKNOWLEDGEMENTS

We wish to thank Professor E. H. Andrews for continuing encouragement, to SRC for a grant and Dr D. N. Batchelder of the Physics Department, QMC, for use of his high pressure line in the early stages of this work.

REFERENCES

- 1 Wunderlich, B. *Pure Appl. Chem.* 1972, **31**, 49
- 2 Rees, D. V. and Bassett, D. C. *J. Polym. Sci. (A-2)* 1971, **9**, 385
- 3 Kardos, J. K., Li, H. M. and Huckshold, K. A. *J. Polym. Sci. (A-2)* 1971, **9**, 2061
- 4 Calvert, P. D. and Uhlmann, D. R. *J. Polym. Sci. (A-2)* 1972, **10**, 1811
- 5 Yasuniwa, M., Nakafuka, C. and Takemura, T. *Polym. J.* 1973, **4**, 526
- 6 Miyamoto, Y., Nakafuka, C. and Takemura, T. *Polym. J.* 1972, **3**, 122
- 7 Gogolewski, S. and Pennings, A. J. *Polymer* 1973, **14**, 463
- 8 Davidson, T. and Wunderlich, B. *J. Polym. Sci. (A-2)* 1969, **3**, 377
- 9 Bassett, D. C. and Carder, D. R. *Phil. Mag.* 1973, **28**, 513
- 10 Jackson, J. F., Hsu, T. S. and Brasch, J. W. *J. Polym. Sci. (B)* 1972, **10**, 207
- 11 Wunderlich, B. *J. Polym. Sci. (A)* 1963, **1**, 1245
- 12 Bassett, D. C. and Khalifa, B. A. *Polymer* 1973, **14**, 390
- 13 Roe, R. J., Gieniewski, C. and Vadimsky, R. G. *J. Polym. Sci. (Polym. Phys. Edn.)* 1973, **11**, 1653
- 14 Bassett, D. C., Khalifa, B. A. and Turner, B. *Nature (Phys. Sci.)* 1972, **239**, 106
- 15 Anderson, F. R. *J. Appl. Phys.* 1964, **35**, 64
- 16 Bunn, C. W., Cobbold, A. J. and Palmer, R. P. *J. Polym. Sci.* 1958, **28**, 365
- 17 Fritton, B. and Griffiths, C. H. *J. Appl. Phys.* 1968, **39**, 3663
- 18 Owen, P. J. *PhD Thesis* University of London, 1970
- 19 Andrews, E. H., Owen, P. J. and Singh, A. *Proc. R. Soc. (A)* 1971, **324**, 79
- 20 Phillips, P. J. and Andrews, E. H. *J. Polym. Sci. (B)* 1972, **10**, 321
- 21 Andrews, E. H. *Proc. R. Soc. (A)* 1964, **277**, 562
- 22 Crawford, R. K. *PhD Thesis* Princeton University, NJ, 1968
- 23 Edwards, B. C. and Phillips, P. J. *Polymer* 1974, **15**, 351
- 24 Geil, P. H. 'Polymer Single Crystals', Interscience, New York, 1963

Polarization effect in an epoxy resin at elevated temperatures

V. Adamec*

Cables and Insulating Materials Research Institute, Bratislava, Czechoslovakia

(Received 1 November 1973; revised 17 January 1974)

The elucidation of a polarization process at elevated temperatures in an epoxy–novolac resin cured by BF_3 complex is made. Measurements of permittivity and dissipation factor with various types of electrodes as well as measurements of potential distribution inside the specimen are described.

INTRODUCTION

During the investigation of a commercial epoxy–novolac resin (DEN 438, Dow Chemical) cured by 3 phr BF_3 /ethylamine complex (BF_3 -400, Harshaw), comparatively high permittivities have been observed under certain conditions¹. At the early stage of the isothermal cure, the permittivity reaches values above 10 000 and then, according to the cure temperature, it falls more or less quickly. The permittivity can also attain comparatively high values in the cured state as can be seen in *Figure 1*.

The corresponding polarization process cannot be due to dipole orientation, because, even at a high concentration 10^{22}cm^{-3} of great dipole moments $\mu=2\text{D}$ with complete establishing of the polarization at 200°C , the permittivity increment would be only about 7. Higher permittivities may be explained by restricted ion transport along microdistances but larger than atomic dimensions or by the pile-up of charge in a layer adjacent to the electrode. Measurements carried out on specimens with different thickness support the latter concept¹.

In the following, further experiments are described which ought to aid the decision, as to whether it is a volume effect or an electrode blocking effect.

EXPERIMENTAL AND DISCUSSION

The first experiment tested the effect of electrode material on the polarization. For this purpose, a series of disc shaped specimens of 20 mm diameter and 0.6 mm thickness was prepared from the epoxy resin by curing for 6 h at 160°C . These specimens were provided with electrodes and guard rings of conductive silver paint,

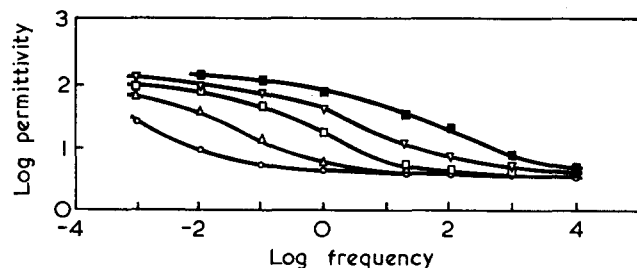


Figure 1 Frequency dependence of permittivity of the specimen cured for 8 h at 160°C and post-cured for 6 h at 240°C at various temperatures: \circ , 120°C ; \triangle , 150°C ; \square , 180°C ; ∇ , 209°C ; \blacksquare , 240°C

* Present address: Department of Electrical Engineering, University of Salford, Salford M5 4WT, UK.

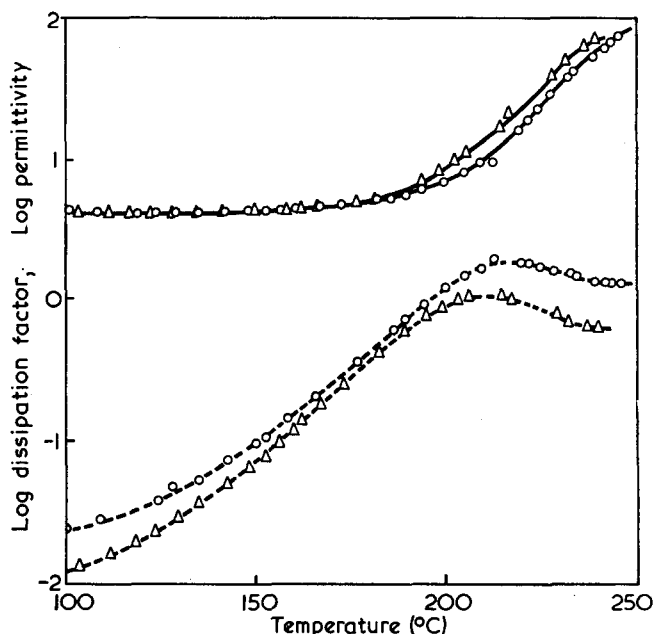


Figure 2 Temperature dependence of ϵ' (—) and $\tan \delta$ (---) of the cured (\circ) and post-cured specimen (3h, \triangle) with silver paint electrodes

and of vacuum evaporated gold, silver, and aluminium. The capacitance and conductance were measured at 50 Hz with an a.c. bridge during a linear temperature rise at the rate of $0.8^\circ\text{C}/\text{min}$ from room temperature up to 240°C . Then, the last temperature was maintained constant for 3 h (post-curing) and, afterwards, the heating was turned off.

Figures 2–5 show temperature dependences of permittivity and dissipation factor of cured and successively post-cured specimens at 240°C , determined by using different types of electrodes. In *Figures 3–5*, the properties determined on post-cured specimens with paint electrodes are also included, shown with broken lines.

The large effect of the post-cure, which results in a lowering of the dissipation factor peak as well as in its shift towards the lower temperatures, is striking. The measured properties depend also on the type of electrodes used. The differences are pronounced particularly before post-curing; after it, the effect of electrode material is much smaller. It may be inferred that, as the post-curing proceeds, the blocking effect of the electrodes becomes more significant probably owing to the interaction of epoxy resin with metal at elevated temperatures.

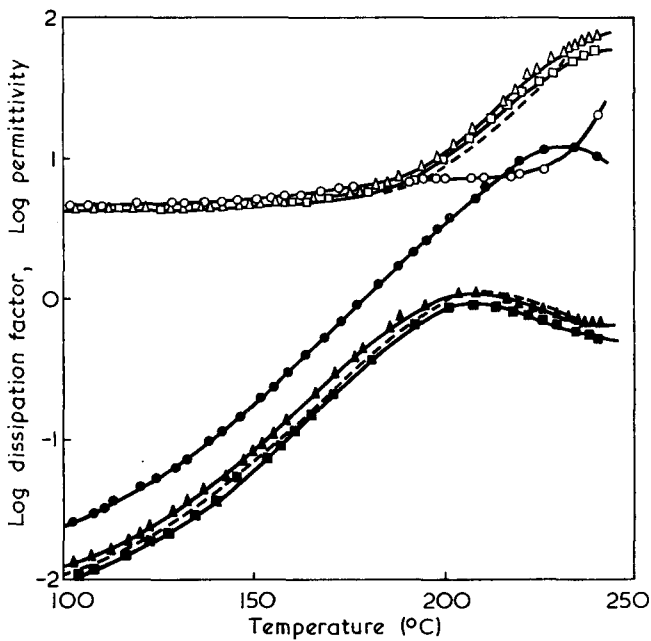


Figure 3 Temperature dependence of ϵ' (open symbols) and $\tan \delta$ (solid symbols) of the cured (\circ) and post-cured (3h, Δ ; 6h, \square) specimen with gold electrodes; ----, from Figure 2

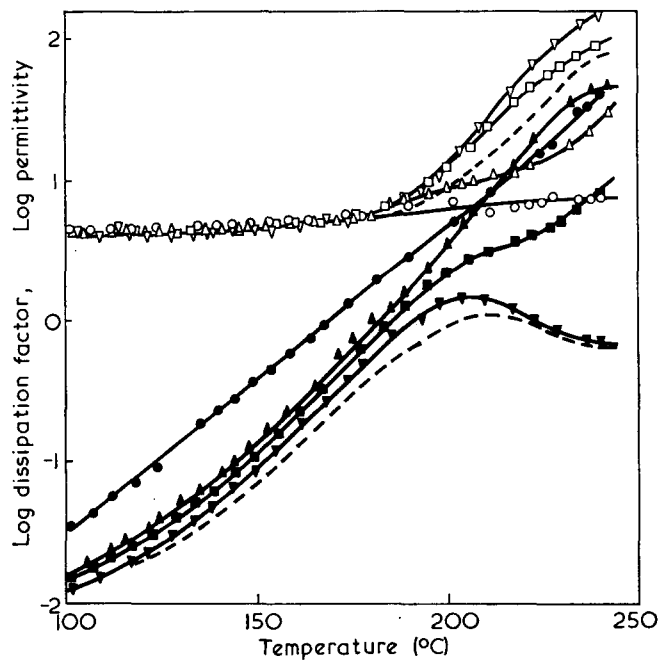


Figure 5 Temperature dependence of ϵ' (open symbols) and $\tan \delta$ (solid symbols) of the cured (\circ) and post-cured (3h, Δ ; 6h, \square , 9h, ∇) specimen with aluminium electrodes; ---- from Figure 2

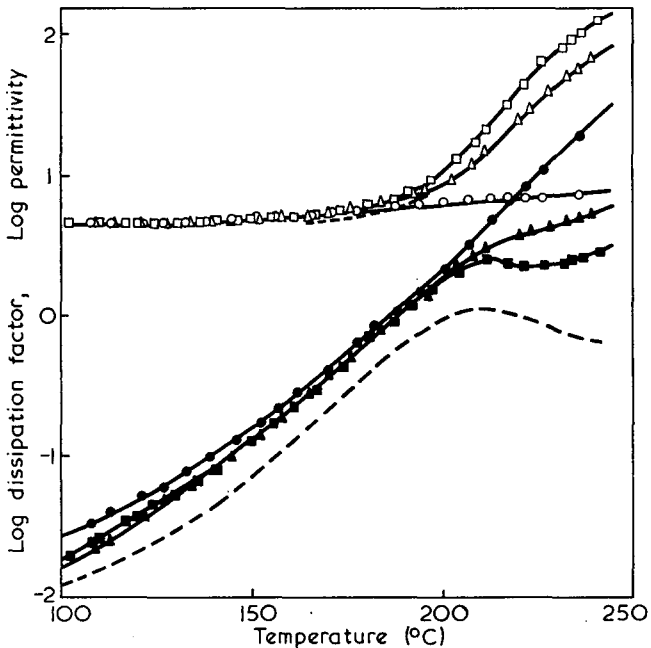


Figure 4 Temperature dependence of ϵ' (open symbols) and $\tan \delta$ (solid symbols) of the cured (\circ) and post-cured (3h, Δ ; 6h, \square) specimen with silver electrodes; ----, from Figure 2

After the last a.c. measurement on the post-cured samples, the current flowing after d.c. voltage application has been measured at linearly rising temperature. The temperature dependences of conductivity obtained using different electrodes are given in Figure 6. The differences in conductivity are large but, on repeating the measurement, they diminish. This effect is very pronounced with aluminium electrodes as shown in Figure 6.

The observations described support the concept of accumulation of charges near the electrodes; in case of a volume effect, the measured properties should not depend on the electrode material used.

Another experiment consisted in the measurement of potential distribution between the electrodes. With high permittivities, caused by the pile-up of charges

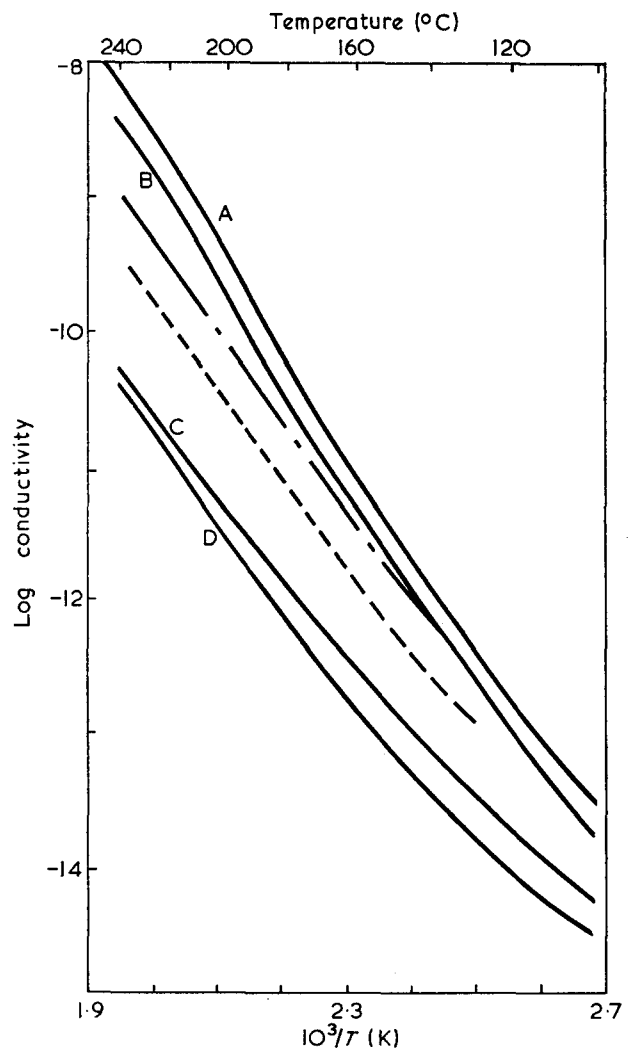


Figure 6 Temperature dependences of conductivity of post-cured specimens with various types of electrodes used. A, Al; B, Ag; C, Au; D, paint; ----, Al'; ----, Al''

in a layer adjacent to electrodes, the field distribution has to be very inhomogeneous.

A disc specimen of the epoxy resin, 54 mm in diameter and 13.5 mm in thickness with three embedded potential probes and with silver paint electrodes on both surfaces, was prepared. The specimen was fixed between two metal frames with insulating spacers inserted and then put in a screening cover. A sketch of this arrangement is given in Figure 7. The potential of the probes was measured using a compensation circuit shown in Figure 8 with a Wulf fibre electrometer.

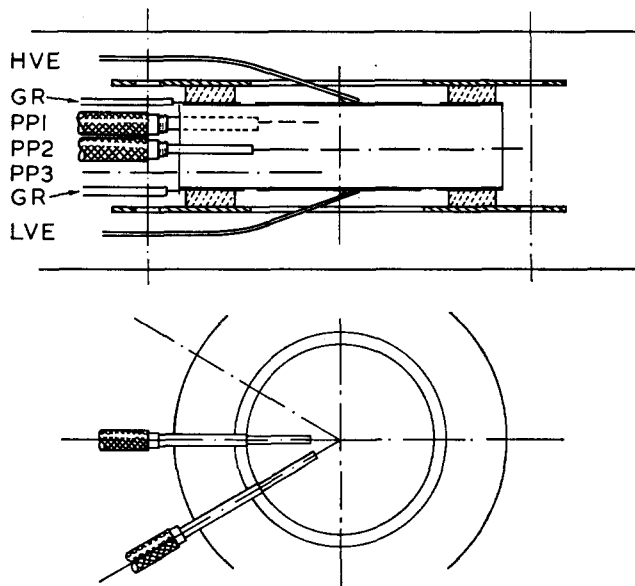


Figure 7 Sketch of the specimen with potential probes

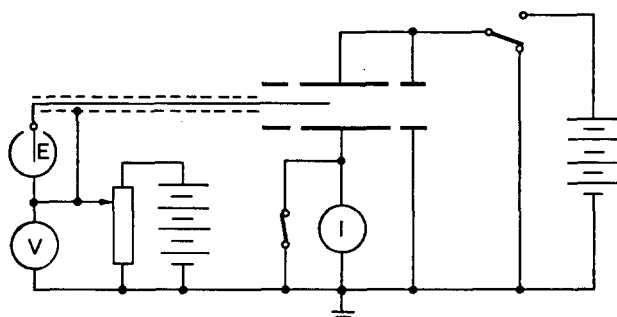


Figure 8 Diagram of the measuring circuit

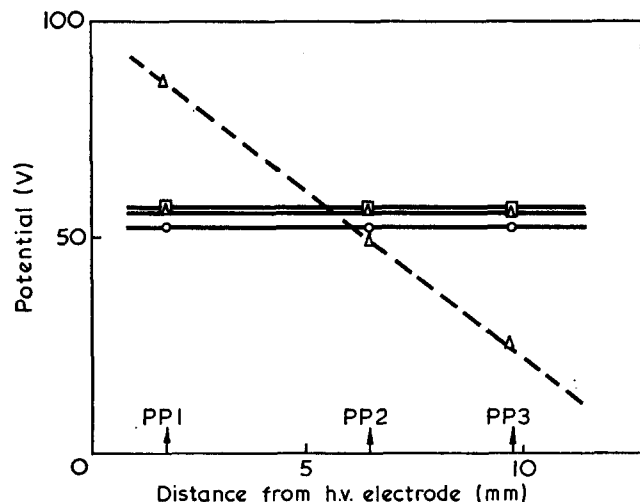


Figure 9 Potential distribution inside the cured (---) and the post-cured (—) specimen at various temperatures: ○, 150°C; △, 180°C; □, 210°C

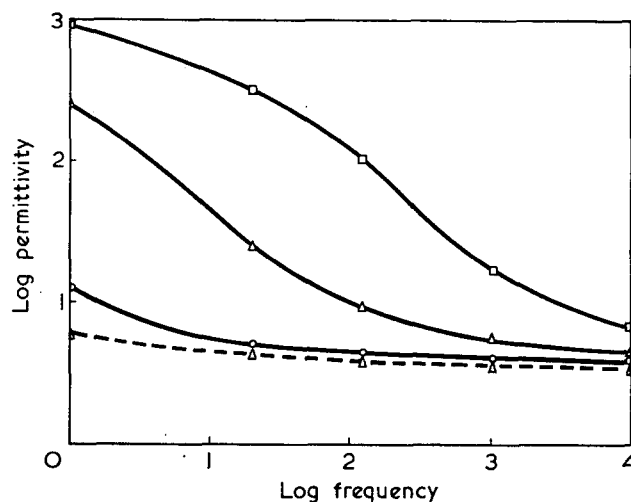


Figure 10 Frequency dependence of permittivity of the cured (---) and post-cured (—) specimen at various temperatures: ○, 150°C; △, 180°C; □, 210°C

In order that the material of the specimen between the probe and electrodes should act as a resistance divider with an adequate time constant, the conductivity of the specimen had to be higher than 10^{-12} mho/cm. This condition was checked by measurement of the current flowing between the electrodes. Further, the permittivity was measured at frequencies in the range from 1 to 10 000 Hz by means of a VLF bridge and a transformer bridge¹.

The potential distribution at 150, 180, and 210°C in the cured specimen differed only slightly from a linear one. In Figure 9 such a distribution at 180°C is shown with a broken line. In this case, a small change in frequency dependence of permittivity was also found (Figure 10). After the post-cure for 6 h at 240°C, the permittivity rose considerably at low frequencies. The measurement of the potential distribution revealed (Figure 9) that the potential inside the specimen was almost constant and thus the whole potential drop took place in the layers adjacent to electrodes. The thickness of these layers has been estimated to be approximately 0.1 mm¹. The comparatively good symmetry of the potential distribution between the electrodes is very interesting; it means that the charge accumulated in the vicinity of both electrodes is approximately the same.

CONCLUSION

Experiments carried out on epoxide resin specimens using different electrode materials as well as determinations of potential distribution inside the specimen confirm the concept of charge pile-up at the electrodes which results in a polarization effect at elevated temperatures. This process probably occurs also in insulating polymers around T_g , when the conductivity of these materials becomes pronounced.

ACKNOWLEDGEMENTS

The author's thanks are due to Mr V. Krchňák for his assistance in carrying out the experiments and Ing A. de Reyová for help with the preparation of the manuscript.

REFERENCE

- 1 Adamec, V. *J. Polym. Sci. (A-1)* 1972, 10, 1277

Solid solutions and precipitation in flame retardant polystyrene-tetrabromoxylene systems

A. Siegmann, M. Narkis* and A. Dagan

*Plastics Institute, Center for Industrial Research (CIR) Ltd, POB 311, Haifa, Israel
(Received 7 December 1973)*

Flammability and certain mechanical properties of high impact and general purpose polystyrene-tetrabromoxylene (TBX) systems were studied. TBX was found to be an efficient fire retardant and did not affect significantly basic mechanical properties of the polymer in proportions up to 10phr. It has been shown that polystyrene-TBX mixtures can form solid solutions. On annealing above the T_g , supersaturated solid solutions precipitate crystalline TBX from the amorphous matrix, affecting the optical properties and softening temperatures of the system.

INTRODUCTION

Tetrabromoxylene (TBX), a new product developed by Bromine Compounds Ltd in Israel, has been evaluated as a fire retardant for polystyrene (PS). TBX contains a high percentage (76%) of bromine, melts at 250°C and crystallizes in the form of needles. It is soluble only in a small selective group of solvents and can be compounded homogeneously with molten thermoplastic materials. The high thermal stability of TBX permits easy processing with thermoplastics. Halogenated compounds are well known as fire retardants¹ in plastic materials; however, their addition very often results in a decrease in mechanical properties². The mode of dispersion, interaction, compatibility, etc. play an important role in the mechanical behaviour. The common practice is to choose a system where a balance between mechanical properties and flammability is achieved.

This work concentrates on the system PS-TBX, which has been found intriguing from aspects other than mere fire retardancy. For example, transparent compatible amorphous PS-TBX systems can be obtained from which TBX can be precipitated.

EXPERIMENTAL

Polystyrene pellets (high impact, Lustrex HT88, Monsanto or general purpose Hostyrene A1301, Hoechst) were mixed with various amounts of TBX in a Sigma blade kneader (Werner and Pfliederer, Germany) at 220°C. TBX was added into the molten polymer and mixed for 10 min. After cooling to room temperature the solid mixture was granulated (Dreher granulator, Germany). ASTM specimens for testing of mechanical and physical properties and flammability were injection moulded with an Esco laboratory scale injection moulding machine at 220°C (mould at room temperature). A

few specimens were injection moulded at 270°C, i.e. above the melting temperature of TBX (250°C). In addition sheets were compression moulded at 220°C. Samples were annealed, below and slightly above the T_g of the polymer in an air oven.

The following properties were measured: tensile and flexural (Instron machine), Izod impact (Zwick pendulum Impact Tester 5102), Vicat softening point (Zwick Model 4204), burning (burning test—ASTM D 635-68 and oxygen index test—ASTM E 4-64) and flow (melt flow indexer, Tinius Olsen Thermosyne).

RESULTS AND DISCUSSION

The flammability of high impact polystyrene (HIPS) containing various concentrations of TBX was studied. As shown in *Table 1*, TBX changes significantly the flammability of HIPS. At a loading of 3 phr, the polymer is rated as a burning material, at 6 phr it is a self-extinguishing material, and a non-burning material is obtained at 10 phr TBX. As a bromine carrier compound TBX is similar to other bromine compounds as far as the effect of the bromine content on the flammability of the polymer is concerned^{1,3}. Antimony oxide, a well known synergistic additive to halogenated compounds, does not improve the burning resistance of HIPS containing 6 phr TBX, in agreement with other literature data⁴. Polymers characterized by oxygen indices of 21 and below and 27 and above are considered⁵ as burning and non-burning polymers respectively, in agreement with the results shown in *Table 1*.

The effect of TBX on some mechanical properties of HIPS can be summarized as follows: both the modulus and ultimate tensile strength are practically unchanged and average values found are 3.5×10^5 lbf/in² and 3500 lbf/in² (1 lbf/in² = 6874.76 N/m²) respectively for the concentration range of 0 to 10 phr TBX. *Figure 1* shows that the ultimate tensile elongation and flexural

* Also with the Department of Chemical Engineering, Technion—Israel Institute of Technology, Haifa, Israel.

Table 1 Flammability evaluation of polystyrene containing TBX and antimony oxide

Sample	Burning characteristics			Oxygen index, n (ASTM E4-64)
	ASTM D635-68 classification	Extent of burning (cm)	Burning rate (cm/min)	
HIPS	Burning	—	3.1	17.5
HIPS + 3phr TBX	Burning	—	2.14	25
HIPS + 6phr TBX	Self-extinguishing	2	—	26
HIPS + 10phr TBX	Non-burning	0	0	29
HIPS + 2phr Sb ₄ O ₆ + 6 phr TBX	Self-extinguishing	1.8	—	25
HIPS + 4phr Sb ₄ O ₆ + 6phr TBX	Self-extinguishing	1.8	—	25
HIPS + 6phr Sb ₄ O ₆ + 6phr TBX	Self-extinguishing	1.8	—	26

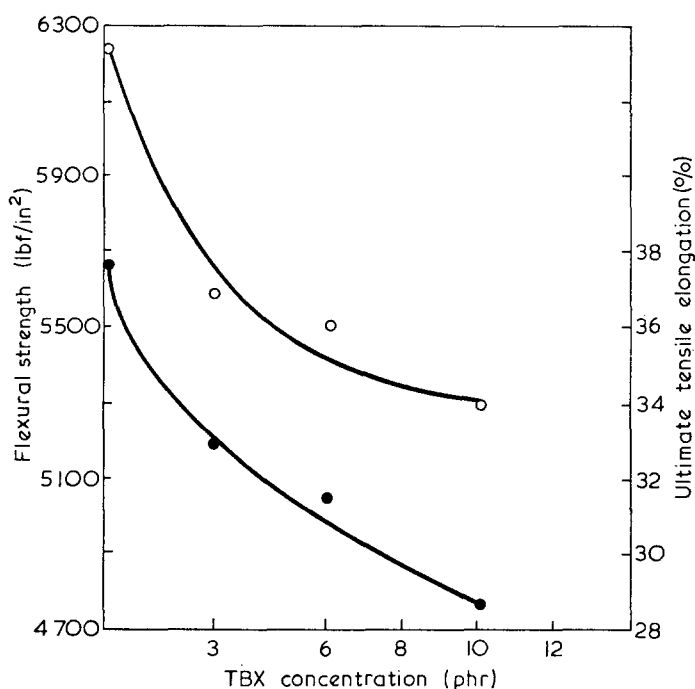


Figure 1 Flexural strength (○) and ultimate tensile elongation (●) of high impact polystyrene containing various amounts of TBX

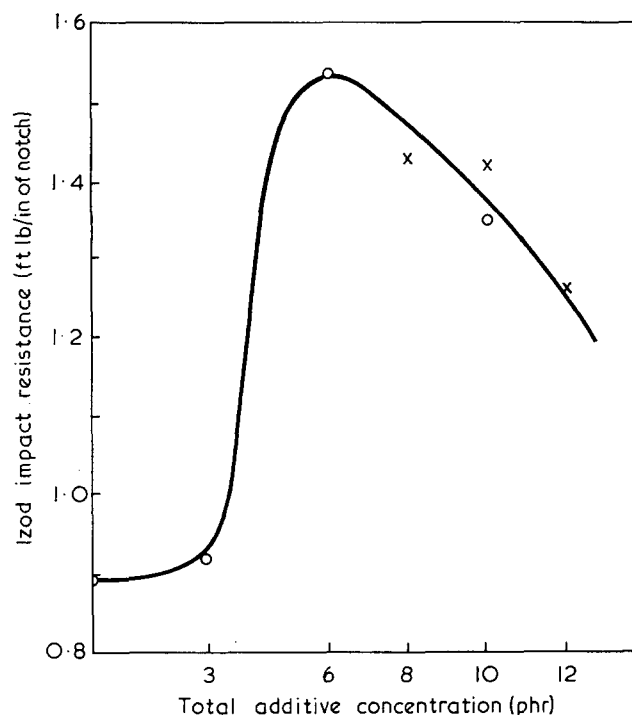


Figure 2 Izod impact resistance of high impact polystyrene containing TBX (○) and 6phr TBX and various amounts of antimony oxide (×)

strength decrease monotonically by increasing the TBX content in the studied range of up to 10 phr TBX. A different behaviour is shown in Figure 2 where the Izod impact resistance initially increases up to about 6 phr TBX and then decreases. Figure 2 also shows that the addition of antimony oxide to HIPS containing 6 phr TBX reduces the impact resistance in the same manner as would further addition of TBX (beyond 6 phr) change the impact resistance.

The effect of TBX on Vicat softening point (VSP) of general purpose polystyrene (GPPS) is shown in Figure 3. The softening temperature decreases with TBX content, attains a minimum at about 20 phr and then increases gradually. The addition of antimony oxide in the concentration range studied does not affect the VSP or T_g (the latter was measured with a DuPont 990 Thermal Analyzer). All the samples prepared for the VSP test by injection moulding were visually transparent up to a content of 17.5 phr TBX, while samples containing 20 phr and above were opaque (HIPS could not be used

for transparency studies owing to its opacity). Upon annealing of GPPS-TBX samples below their T_g , no changes in VSP and impact resistance have been found. However, upon annealing at 100°C (i.e. above T_g) the samples containing more than 10 phr TBX became opaque and their softening temperature increased as shown in Figure 3.

The observed mechanical behaviour of HIPS containing TBX indicates that TBX can be considered in these systems as a high melting solid plasticizer. High melting solid plasticizers such as tri(*p*-*t*-butylphenyl)-phosphate (m.p. 99.5°C), dicyclohexylphthalate (m.p. 65°C) and triphenyl phosphate (m.p. 49°C) have been reported previously⁶. For example, tri(*p*-*t*-butylphenyl)-phosphate gives compositions with ethylcellulose that are tougher and harder than corresponding ones made with conventional liquid plasticizers. The systems studied in this work behave similarly to the systems described above as far as toughness (impact resistance),

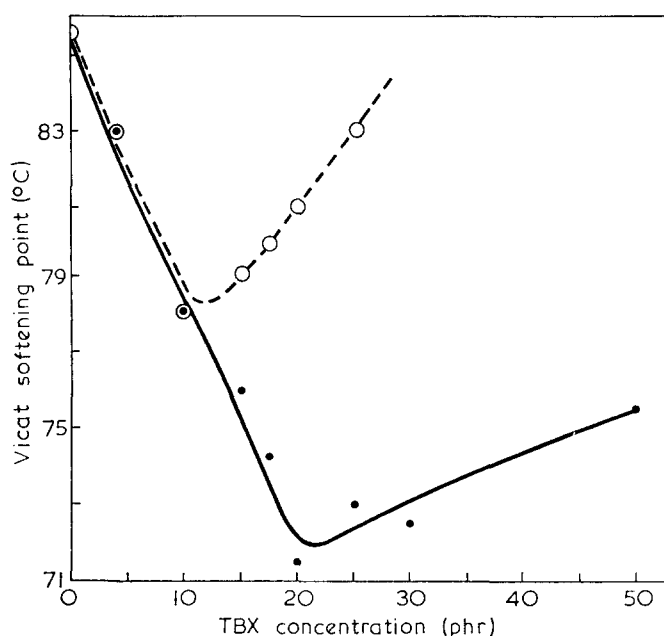


Figure 3 Vicat softening point of general purpose polystyrene containing various amounts of TBX before (●) and after (○) annealing

modulus and yield strength, are concerned. TBX, being a solid plasticizer reduces the elongation to break (Figure 1) of ductile HIPS whereas liquid compatible plasticizers usually result in greater elongations. Experimental data on the effect of solid plasticizers on the mechanical behaviour of brittle polymers, such as GPPS, are not available.

The Vicat softening temperature behaviour shown in Figure 3 suggests that up to about 20 phr TBX, the system, as prepared, is a solid solution whereas at higher TBX loadings it forms a second discrete solid phase. The solute decreases the *VSP* while the excess, forming the second dispersed rigid phase, increases the *VSP*. The 20 phr minimum in *VSP* corresponds approximately to the transition concentration from visually transparent to opaque systems. The behaviour of the PS-TBX system is similar to the well known nitrocellulose-camphor (m.p. 176°C) system which is characterized by a discontinuity in the elongation-camphor content curve⁷ at 35% camphor. It has been suggested that a nitrocellulose-camphor complex is formed up to a saturation concentration of 35% camphor and all excess camphor is unbound. The discontinuity at 35% results from the transition between two different dispersion modes which affect the mechanical response of the system.

The 20 phr minimum shown in Figure 3 and the transition in the optical properties were initially surprising, since the room temperature saturation solubility of TBX in styrene monomer is only about 6%. It is clearly difficult to assume a higher solubility in the polymer than in the monomer. It is suggested that under the sample preparation conditions, injection moulding of a hot molten mixture into a cold mould (actually a quenching process), a solid solution or a supersaturated solid solution is formed. At the processing temperature (220°C), which is well below the melting temperature of TBX (250°C), TBX (in the concentration range studied) is completely dissolved and upon quench-

ing a glassy solid solution is obtained. The solid solution is considered here as supersaturated for TBX contents higher than about 5 phr (the exact saturation solubility is not known). The opaque samples containing more than 20 phr TBX were further studied under an optical microscope (magnification of 240×) and dispersed needle shaped crystallites were observed, as shown in Figure 4. Pure TBX crystallizes also in the form of needles about 100 times larger. Samples containing more than 20 phr TBX and injection moulded at 270°C (20°C above the m.p. of TBX) also exhibit needle shaped crystals. Rheological measurements at a constant shear stress, $\tau = 7 \times 10^4$ dyne/cm², at 220°C have shown that the addition of 25 phr TBX reduces the melt viscosity of the polymer by a factor of 3.5. In another experiment an opaque sample containing 20 phr TBX turned transparent upon heating to 150°C, showing that the needles are redissolved, and became opaque upon cooling to room temperature, showing reprecipitation.

These observations support the view that TBX is dissolved in the polymer at processing conditions used in this work. Thus the needle shaped crystallites found in the polymer were crystallized during the quenching process and are not residuals of the original TBX crystals.

Joseph *et al.*⁸ studied the *in situ* crystallization of acetanilide (m.p. 113°C), or anthracene (m.p. 216°C) from amorphous styrene-acrylonitrile copolymer. They have reported the effect of the dissolved low-molecular weight materials on the polymer glass transition, using this effect to determine phase diagrams and crystallization kinetics.

Supersaturated solutions are thermodynamically unstable and tend to approach their equilibrium compositions⁹. This can be accomplished by thermal treatment which is a time dependent process. In our studies samples were annealed at 100°C, i.e. above T_g , for 1 h.

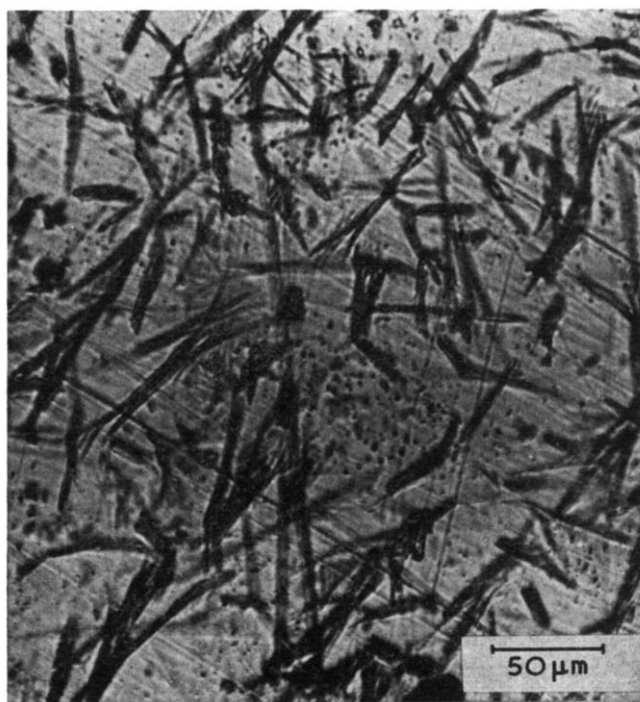


Figure 4 Transmission optical micrograph of polystyrene film containing 25 phr TBX

All the transparent samples containing 10 to 20 phr TBX became opaque and their *VSP* shifted to higher values as shown in *Figure 3*. The shifted values reflect the amount of TBX which is rejected from the solution and forms a second crystalline phase upon annealing. This process has a multiple effect on the *VSP*, namely stiffening by reducing the plasticizer concentration and simultaneously adding rigid particles into the system. A different behaviour is observed for samples containing up to 10 phr TBX since their transparency and *VSP* were not affected by annealing at the same conditions (see *Figure 3*). The shape of the *VSP* curve for annealed samples is as qualitatively expected based on the observed phenomenon of precipitation. It should be noticed that the minimum in this curve occurs at 10 phr TBX which is somewhat above saturation. This result stems from the different precipitation conditions in these supersaturated solutions compared to simple supersaturated liquid solutions. In the former, approach to equilibrium composition is much slower, thus the composition at the minimum is controlled by the specific precipitation conditions, and is expected to vary with annealing temperature and period. In addition, by cooling from 100°C the amorphous sample will rapidly pass through T_g which is accompanied by a dramatic viscosity increase; thus the approach to room temperature equilibrium solubility is hindered. It is important to emphasize that an enhanced precipitation will occur from crystalline polymers owing to rejection of solute from the lattice.

One can conclude that annealing at 100°C for 1 h of GPPS containing more than 10 phr TBX results in the formation of a two phase system with about 10 phr TBX in solid solution with all excess TBX as a discrete crystalline phase.

The solubility of TBX in the softening temperature range (70–90°C, see *Figure 3*) is higher than at room temperature. Hence, the 10 phr minimum in the annealing curve of *Figure 3* does not necessarily coincide with the minimum (or maximum) in a room temperature property such as impact resistance, elastic modulus etc. As shown previously in *Figure 2*, the impact resistance reaches a maximum at the lower concentration of 6 phr TBX which is a decrease as expected. It is important to point out that one would expect a better solubility of TBX in GPPS than in HIPS. The impact data are for HIPS while the *VSP* data are for GPPS—a fact which also supports the results.

An interesting result relevant to our system is mentioned by Doolittle⁶. It is concerned with triphenyl

phosphate, a crystalline solid plasticizer (m.p. 50°C) which has flame retarding properties. This material tends to crystallize when used in high proportions enough to exude from films of cellulose ester plastics.

In summary, it has been shown that polystyrene-TBX mixtures can form solid solutions, a physical system which is known in metal alloys⁹. Such solid solutions are not limited to the pair polystyrene-TBX⁸ and may be expected to occur also in other polymeric systems where chemical affinity between the components exists. Precipitation of the non-polymeric solid component will occur in systems of limited solubility under proper conditions.

By mixing polystyrene and TBX at elevated temperatures and quenching to room temperature a supersaturated solid solution can be formed. At a temperature below the solvus curve the solid solution is no longer structurally stable and tends to reject solute molecules from itself. It is assumed that during annealing, clusters which had been previously formed grow to form stable nuclei, followed by growth into precipitate particles from the addition of solute molecules from the matrix.

The practical consequences of these phenomena are not yet exploited in polymers and call for further studies.

ACKNOWLEDGEMENTS

The authors extend their thanks to Drs I. Saxe and E. Wurman of Bromine Compounds Ltd for supplying the materials and for permission to publish this work, and to Professor A. T. DiBenedetto for helpful discussions during his stay at the Center for Industrial Research.

REFERENCES

- 1 Lyons, J. W. 'The Chemistry and Uses of Fire Retardants', Wiley, New York, 1970
- 2 Nametz, R. C. *Ind. Eng. Chem.* 1967, **59**, 99
- 3 Narkis, M., Grill, M. and Leeser, G. *J. Appl. Polym. Sci.* 1969, **13**, 535
- 4 Cooper, A. US Pat. 3 039 991
- 5 Fenimore, C. P. and Martin, F. J. *Mod. Plast.* 1966, **43** (11), 141
- 6 Doolittle, A. K. 'The Technology of Solvents and Plasticizers', Wiley, New York, 1954
- 7 McNally, J. G. and Sheppard, S. E. *J. Phys. Chem.* 1931, **35**, 2498
- 8 Joseph, J. R., Kardos, J. L. and Nielsen, L. E. *J. Appl. Polym. Sci.* 1968, **12**, 1151
- 9 'Precipitation from Solid Solution', ASM, Cleveland, 1959

N.m.r. of solid polymers: a review

Vincent J. McBrierty

Physical Laboratory, Trinity College, University of Dublin, Dublin 2, Eire
(Received 4 January 1974)

INTRODUCTION

The application of nuclear magnetic resonance (n.m.r.) to the study of solid polymers has developed significantly in recent years. The emergence of more refined mathematical procedures for data interpretation, improvements in spectrometer design, the availability of well characterized samples and, most important, the introduction of the rotating frame experiment have been largely responsible. The rotating frame relaxation time, $T_{1\rho}$, is sensitive to motions with correlation frequencies, ν_c , in the kHz range whereas spin-lattice relaxation times, T_1 , respond to much more rapid motions in the MHz region. As a result, $T_{1\rho}$ measurements extend the dynamic range of molecular motions, sensitive to n.m.r., to the ultraslow region.

The use of fibre materials for n.m.r. investigation has enhanced the value of the technique considerably because of the additional information contained in the anisotropy of the n.m.r. data, recorded as a function of fibre orientation in the laboratory magnetic field. Theoretical predictions, based upon plausible molecular models, are tested more stringently when compared with anisotropic fibre data. These magnitude comparisons have been most successful for spin-spin relaxation time, T_2 , measurements. Second, M_2 , and fourth, M_4 , moment measurements of the resonance absorption envelope have been comparably informative. Comparison with T_1 and $T_{1\rho}$ data, on the other hand, is often severely hampered by spin diffusion and correlation frequency distribution effects; theories are usually based upon the description of molecular motion in terms of a single correlation frequency which results in predicted magnitudes which are low compared with experimental values.

The translation of raw n.m.r. data into molecular information is not, as yet, totally unambiguous. Complications principally arise from the non-exponential character of the various magnetization decays which are often observed. For example, at low temperatures, the decays are more Gaussian than Lorentzian. Two and sometimes three discrete components may be observed which are usually ascribed to morphological inhomogeneities in the polymer in which the resonant nuclei experience appreciably different molecular environments. Typically, nuclei in the amorphous regions of a semi-crystalline polymer which is above its glass transition temperature, T_g , are undergoing rapid motions, evidenced by a long T_2 value (or narrow line in the absorption spectrum) while the crystalline regions may still be well below their melting point for which a much shorter T_2 (or broad line) is appropriate. Non-exponential

decays interpreted in this way have been used to determine the crystallinity of several polymers by measuring the relative intensities of the T_2 or second moment components¹⁻⁵. Such measurements in fact provide the 'mobile fraction' which has obvious temperature dependence. To equate this measurement, in a general way, with crystallinity is clearly inappropriate. Rather, the mobile fraction must be viewed as complementing the wider range of experimental estimates available⁶.

There has been the suggestion that the intensities of component $T_{1\rho}$ decays may be used as a measure of crystallinity⁷. As discussed in detail in a subsequent section, both the magnitudes and intensities of $T_{1\rho}$ components, attributed to different regions in the polymer, may be affected appreciably by spin diffusion⁸. In such cases the relative intensities in no way reflect the amounts of material contributing to each component and therefore may not be used as an estimate of either mobile fraction or crystallinity.

Less obvious composite spectra have been analysed rigorously in an attempt to separate out the overlapping components⁹⁻¹¹. Theoretical lineshapes have been synthesized from up to four components for comparison with experimental traces from drawn polyethylene (PE)¹¹. Similar studies have been undertaken on the spectra from polymers rotated at the magic angle^{12, 13}.

It is important to realize that other reasons may be responsible for non-exponential behaviour. Molecular weight distributions may be responsible or indeed relaxations which are dominated by defect diffusive mechanisms will lead to T_1 and $T_{1\rho}$ decays which are non-exponential.

While specific motions in polymers such as side group or main chain re-orientations, main chain translations or motions of a more general nature (glass transition phenomena) may be readily detected and identified by n.m.r. methods, precise information about the motional mechanism is generally not forthcoming. T_2 , for example, is insensitive to motions below $\sim 10^4$ Hz, while changes in T_2 due to the onset of rotation about an axis at frequencies in excess of 10^4 Hz cannot distinguish between classical rotation and rotation over a threefold or higher potential. In some cases combined T_1 , $T_{1\rho}$, and T_2 measurements can be helpful as, for example, for methyl group motion in poly(vinyl acetate) (PVAc) where quantum mechanical tunnelling is indicated¹⁴.

The fact that the three relaxation times sample widely different frequency ranges in the spectrum of molecular motions allows activation energies, ΔE , to be determined. T_1 and $T_{1\rho}$ minima and T_2 transitions are translated

into correlation frequencies by means of established formulae¹⁵. The temperature dependence usually obeys the relation $\nu_c = \nu_0 \exp(-\Delta E/RT)$. If the plot of $\log \nu_c$ vs. reciprocal temperature is curved, indicating a temperature dependent activation energy, then the treatment of Williams *et al.*¹⁶ is appropriate. The effects of a distribution of correlation frequencies on the magnitude of ΔE has been examined¹⁷.

General trends are emerging from the large body of n.m.r. data now accumulated for a wide variety of polymers. Overall similarities in the results from different polymers are in evidence while the correlation of n.m.r. data with dielectric and dynamic mechanical measurements would imply that the same molecular process is responsible for a variety of different experimental observations¹⁵. Indeed, this cross-correlation of experimental data for a given polymer often provides a deeper understanding of the molecular processes which underlie the macroscopic responses of the polymer. The overall consistency between the various results is gratifying and indicates a measure of confidence in the existing procedures for the analysis and interpretation of n.m.r. data.

In this review, an exhaustive survey of the literature is not contemplated. Rather, our principal concern will be to highlight the recent important developments in the application of n.m.r. to solid polymers. Anisotropic materials will be emphasized to illustrate the distinct advantages to be gained in their use. Spin diffusion, which is responsible for many apparently anomalous features of n.m.r. behaviour will be examined along with other aspects of data interpretation. A major area of endeavour over the past few years has been the acquisition of high resolution spectra from polymers in the solid state. Examples of the type of detailed information which can be derived from such spectra will be included.

THEORETICAL CONSIDERATIONS

The theory of nuclear magnetic relaxation, appropriate to polymers, is well established both for isotropic and oriented materials¹⁸⁻³¹. Here we will attempt no more than a brief review of the more important results since the details of their derivation are clearly presented in the original references.

Relaxation in polymers may be described by three equations²⁸:

$$1/T_1 = 3\gamma^4 \hbar^2 I(I+1)/2 \left\{ 2\tau_c / (1 + \omega_0^2 \tau_c^2) \sum_k \langle |f_{k1}|^2 \rangle + 2\tau_c / (1 + 4\omega_0^2 \tau_c^2) \sum_k \langle |f_{k2}|^2 \rangle \right\} \quad (1)$$

$$1/T_{1\rho} = 3\gamma^4 \hbar^2 I(I+1)/8 \left\{ 2\tau_c / (1 + 4\omega_e^2 \tau_c^2) \sum_k \langle |f_{k0}|^2 \rangle \right\} \quad (2)$$

$$1/T_2^2 = 3\gamma^4 \hbar^2 I(I+1)/8 \sum_k \langle |f'_{k0}|^2 \rangle = \gamma^2 M_2^2 / 2 \quad (3)$$

γ , \hbar and I have their usual significance. ω_0 and ω_e are, respectively, the resonance frequency and the effective precession frequency in the rotating frame. τ_c is the correlation time, $1/2\pi\nu_c$, which governs the assumed exponential decay of the correlation function for the molecular motion. The nuclear position functions have

the form:

$$\langle |f'_{k0}|^2 \rangle = 16\pi/5 \langle \llbracket Y_{2,0}(\Theta_k, \Phi_k) / r_k^3 \rrbracket^2 \rangle \quad (4)$$

$$\langle |f_{kn}|^2 \rangle = C_n \{ \langle \llbracket Y_{2,n}(\Theta_k, \Phi_k) / r_k^3 \rrbracket_{lt}^2 \rangle - \langle \llbracket Y_{2,n}(\Theta_k, \Phi_k) / r_k^3 \rrbracket_{ht}^2 \rangle \} \quad (5)$$

The subscript $n=0, 1, 2$ and $C_0=16\pi/5$, $C_1=8\pi/15$, $C_2=32\pi/15$. Θ_k, Φ_k are the polar angles of the internuclear vector, r_k , relative to the laboratory field direction. The internuclear vector extends from a reference nucleus and the sum over k takes all other nuclei into account. The brackets $\llbracket \rrbracket$ denote the motional average over rapid molecular motions and the subscripts lt and ht indicate averages over motions operative at temperatures below and above the transition, respectively. We note that the T_2 formula derives from the static part of the local field at the reference nucleus ($T_2 \ll T_1$ for solid polymers). T_1 and $T_{1\rho}$, on the other hand, depend on the time-dependent fluctuating part of the local field. The derivation of the T_2 expression follows Bloembergen's treatment for correlation times $\tau_c \geq T_2$ ¹⁹; molecular motions become apparent when this condition is satisfied. Equation (3) is used to compute T_2 and M_2 plateaux on either side of a transition. This equation is analogous to the Van Vleck expression for the second moment²³.

The expressions for T_1 and $T_{1\rho}$ are based upon the Bloembergen, Purcell and Pound (BPP) treatment of relaxation²⁰, for which $\tau_c \ll T_{2RL}$, where T_{2RL} denotes the rigid lattice value of T_2 . Equation (2) is a valid expression for $T_{1\rho}$ if $H_1^2 \gg H_L^2$ ²¹. H_L^2 is the square of the local field which equals one-third of the powder second moment³² H_1 is the amplitude of the r.f. field which may be easily adjusted to a value which satisfies the required condition.

At low temperatures, the conditions $\tau_c > T_2$ and $H_1 \approx H_L$ may prevail in which case the BPP analysis is no longer valid. This is the Slichter-Ailion region²² for which:

$$1/T_{1\rho} = 2(1-p)/\tau_c \{ H_L^2 / (H_1^2 + H_L^2) \} \sim 1/\tau_c \quad (6)$$

If $H_1 \gg H_L$ the expression for $T_{1\rho}$ is:

$$1/T_{1\rho} = 2(1-p)/\tau_c \{ 3H_L^2 / 4H_1^2 \} \quad (7)$$

The parameter p is normally set equal to zero through lack of precise information (in any event p can never exceed unity). The Slichter-Ailion conditions are infrequently met, the main problem arising from the interference from overlapping motions. A notable exception is the analysis of the α relaxation process in PE³⁴.

Magnitudes of T_1 and $T_{1\rho}$ minima, for which $\omega_e \tau_c$ and $\omega_0 \tau_c \approx 0.5$, may be conveniently expressed in terms of T_2 by the simplified approximate formulae³⁵:

$$T_{1 \text{ min}} \approx (2)^{1/2} \pi \nu_0 T_{2LT}^2 \quad (8)$$

$$T_{1\rho \text{ min}} \approx 4\gamma H_1 T_{2LT}^2 \quad (9)$$

where

$$1/T_{2LT}^2 = 1/T_{2lt}^2 - 1/T_{2ht}^2 \quad (10)$$

The subscripts lt and ht again refer, respectively, to the low and high temperature sides of the transition. Note that $T_{2LT} \approx T_{2lt}$ if the change in T_2 across the transition is large.

Thus one may either use measured T_2 data to estimate the corresponding T_1 and $T_{1\rho}$ minima or, alternatively, these relaxation times may be computed directly from

the appropriate lattice sums and equations (1) and (2).

It is appropriate to include the expression for the fourth moment of the absorption envelope. Although fourth moment computations are difficult, recent studies have demonstrated the advantages to be gained from their quantitative interpretation^{36, 37}. The Van Vleck²³ expression for M_4 may be written:

$$M_4 = \gamma^4 \hbar^4 / 144N \sum_{i,j,k \neq} \left\{ 27B_{ij}^2 B_{ik}^2 - 4B_{ij}^2 (B_{ik} - B_{jk}) + 2B_{ij} B_{jk} (B_{ik} - B_{ij})(B_{ik} - B_{jk}) \right\} + \gamma^4 \hbar^4 / 8N \sum_{i>j} B_{ij}^4 \quad (11)$$

The dipolar interaction coefficients have the form:

$$B_{ik} = -3(4\pi/5)^{1/2} Y_{2,0}(\Theta_{ik}, \Phi_{ik}) / r_{ik}^3 \quad (12)$$

N is the number of reference nuclei over which the summations are taken. Lattice sums of the type

$$\sum_{i,j,k \neq} B_{ij}^2 B_{ik} B_{jk}$$

only contribute a few percent to the total fourth moment and are usually neglected in view of the lengthy computational time involved in their evaluation³⁶. The B coefficients are suitably averaged when the nuclei are in rapid motion³⁷.

Table 1 lists the various expressions required to translate n.m.r. data into the corresponding correlation frequencies³⁵. The range of ν_c and τ_c monitored by the various measurements are also included. It may be noted that the range in ν_c covers some seven decades, the lower limit being set by the applicability, or otherwise, of the Slichter-Ailion conditions²².

The anisotropy in relaxation times and moment values which results from preferred orientations of polymer chains in drawn materials has not been discussed in this general outline. Nor indeed have the effects of spin diffusion been treated. Specific attention will be given to these considerations in subsequent sections of the review.

THE ROLE OF SPIN DIFFUSION

An understanding of the phenomenon of spin diffusion is fundamental to the interpretation of many otherwise puzzling features of n.m.r. relaxation data. Since $T_1 \gg T_2$ in polymers, excess energy can remain in the spin system for a time long compared with T_2 before being transferred to the lattice³. This energy transfer is particularly efficient near paramagnetic impurities, lattice imperfections or indeed near molecular segments which are in rapid motion^{18, 20, 38, 39}. Even minute concentrations of such relaxation sites can produce noticeable effects

Table 1 Correlation frequency relationships and the ranges of ν_c and τ_c appropriate to each measurement

N.m.r. feature	Expression for ν_c	Range of ν_c (Hz)	Range of τ_c (sec)
T_1 minimum	$\nu_c = (2)^{1/2} \nu_0$	$4 \times 10^6 - 4 \times 10^8$	$4 \times 10^{-8} - 4 \times 10^{-10}$
$T_{1\rho}$ minimum	$\nu_c = \gamma H_1 / 2\pi$	$10^4 - 5 \times 10^5$	$2 \times 10^{-5} - 3 \times 10^{-7}$
S-A region of $T_{1\rho}$	$\nu_c = 1/2\pi T_1 \rho$	$10 - 10^3$	$2 \times 10^{-2} - 2 \times 10^{-4}$
T_2 transition	$\nu = 1/2\pi T_2 L T$	$10^4 - 10^5$	$2 \times 10^{-5} - 2 \times 10^{-6}$
Linewidth transition	$\nu = \gamma \delta H L T / 2\pi$	$10^4 - 10^5$	$2 \times 10^{-5} - 2 \times 10^{-6}$

in the overall relaxation behaviour^{39, 40}. The term 'spin diffusion' relates to the transfer of excess spin energy to these preferred relaxation sites. The coefficient of spin diffusion is typically of the order of 10^{-12} cm²/sec.

The definitive paper by Douglass and Jones³² on the effects of spin diffusion in n-alkanes contains most of the essential results of interest in polymers. A one-dimensional diffusion model is treated, in which relaxation takes place via the rotating methyl end groups. There are two limiting situations.

Fast diffusion limit:

$$T_1 \propto L \cdot T_1^r \propto X_M^{-1} \cdot T_1^r \quad (13)$$

Slow diffusion limit:

$$T_1 \propto L^2 / \pi^2 D \quad (14)$$

L is the length of the molecular chain and T_1^r is the characteristic relaxation time of the methyl end group. X_M is the fraction of methyl protons. Analogous expressions may be written for $T_{1\rho}$. In the fast diffusion limit, the end groups act as a bottleneck to the transfer of excess spin energy into thermal motions of the lattice. In the slow diffusion limit, the diffusion rate is slow compared with the rate of relaxation of the end groups.

The role of spin diffusion in PE is interesting^{3, 41-43}. Branched PE, which contains a few percent of methyl groups, exhibits a well defined low temperature T_1 minimum with no corresponding T_2 transition⁴¹. The small number of rotating methyl groups are relaxing the rigid protons by the mechanism of spin diffusion. Yet there are insufficient methyl groups to produce any noticeable change in the rigid lattice T_2 . In linear PE, motions in the amorphous regions are responsible for the T_1 minimum observed at -20°C ⁴². Spins in the crystalline regions are coupled by spin diffusion to the spins in the amorphous regions which are sufficiently mobile as to constitute an ensemble of relaxation centres⁴². The magnitude of the T_1 minimum is given by equation (13) in the form of:

$$1/T_{1\text{min}} = (1 - X) / T_1^a \quad (15)$$

where X is the crystallinity and T_1^a is the relaxation time appropriate to the amorphous regions⁴².

The low temperature T_1 minimum (-130°C), observed in a series of atactic polystyrenes (PS) has been examined in detail, in terms of spin diffusion to end groups by Connor⁴⁴ and later re-evaluated by Crist⁴⁵. It was observed that both the intensity and the low temperature slope of the minimum decreased with increasing molecular weight. These observations have been analysed in terms of a temperature-independent relaxation process and a molecular weight-dependent process. Separation of the two relaxations shows that the intensity of the minimum for the molecular weight-dependent process is linearly proportional to \bar{M}_n^{-1} , the reciprocal of the number-average molecular weight. As a result, the proposal has been made to use such measurements for molecular weight determinations.

It has been the established procedure to analyse non-exponential magnetization decays, displaying two or more components, in terms of discrete non-interacting regions in the polymer. The coefficients of these component decays are taken to be a measure of the number of nuclei represented by the individual decay terms. In Figure 1, the $T_{1\rho}$ component intensities for fibre

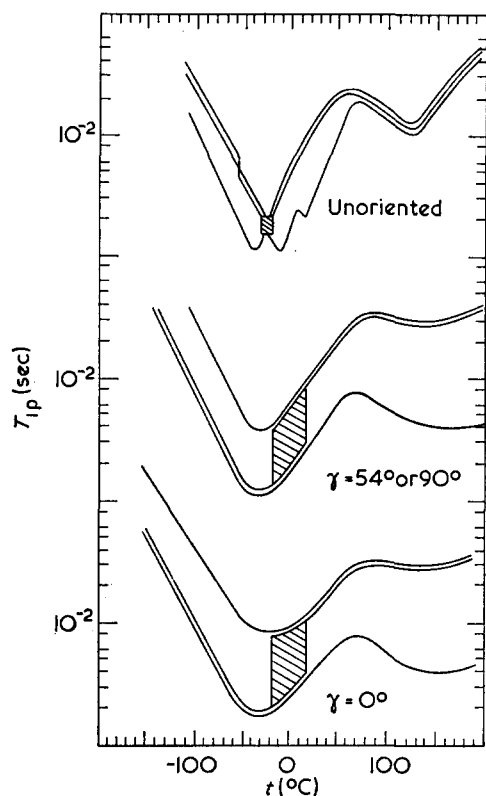


Figure 1 N.m.r. rotating frame relaxation time, $T_{1\rho}$ for FEP. γ is the angle between the fibre axis and the magnetic field direction. Each solid line represents about one-third of the total intensity. [Reproduced from Douglass, D. C. and McBrierty, V. J. *J. Chem. Phys.* 1971, 54, 4085 by permission of the American Institute of Physics, New York]

and bulk FEP (a tetrafluoroethylene-hexafluoropropylene copolymer) are presented⁴⁶. γ is the angle between the fibre axis and the laboratory field H_0 (see also Figure 19). The long $T_{1\rho}$ component in the bulk material has twice the intensity of the short $T_{1\rho}$ over the complete temperature range. For fibres, at low temperatures, the short $T_{1\rho}$ is twice as intense as the long $T_{1\rho}$, but, around room temperature, the greater intensity switches to the long $T_{1\rho}$. The explanation of this anomalous intensity behaviour necessitates the inclusion of spin diffusion effects between the discrete regions: they can no longer be viewed as non-interacting⁸.

In this case the flow of energy associated with the magnetization between the two regions in the polymer, denoted respectively by the subscripts 1 and 2, and also to the lattice may be described by the differential equations:

$$\begin{aligned} dM_1/dt &= -M_1/T_{1\rho}(1) - K_1M_1 + K_2M_2 \\ dM_2/dt &= -M_2/T_{1\rho}(2) - K_2M_2 + K_1M_1 \end{aligned} \quad (16)$$

K_1 and K_2 are parameters which control the strength of the diffusion coupling between the crystalline and amorphous regions. When assigned a value zero, the two regions relax independently and a simple superposition of magnetization decays results. The solution of these equations provides an adequate explanation of the intensity behaviour observed in FEP. The detailed analysis which has been carried out may be explained schematically in Figure 2. The first point to note is

that the assignment of the long and the short $T_{1\rho}$ components to the crystalline and amorphous regions is no longer appropriate. The short $T_{1\rho}$ now reflects the internal establishment of an approximately steady state for energy flow between the two spin systems. The long $T_{1\rho}$ is associated with energy flow to the lattice through the phase which is dominant, that is, relaxing more efficiently. Spatial considerations have been neglected in the interpretation of the bulk data. In order to explain the fibre results, an idealized model has been used in which the amorphous regions form a layer over a crystalline interior. At low temperatures, the amorphous layer acts as a sink which relaxes the crystalline interior. At higher temperatures the concept of a sink is no longer valid and the situation reverts to the simplified analysis for the bulk material.

This model has also been used to explain the T_1 behaviour of PS in a styrene-butadiene-styrene (SBS) block copolymer⁴⁷. In the region of the first order transition minimum of the butadiene component, the T_1 values for PS are much lower than for the comparable homopolymer. Spin diffusion is operative between the styrene and butadiene regions. The PS is partly relaxed by the butadiene regions which are in rapid motion which results in lower observed T_1 values for PS.

EXPERIMENTAL CONSIDERATIONS

In recent years, pulse techniques, which provide rapid and precise determinations of T_1 , T_2 and $T_{1\rho}$, have augmented the more traditional steady state methods for recording n.m.r. data (quoted in terms of the line-width, δH , second moment, M_2 and fourth moment, M_4 of the resonance absorption envelope). Pulse equipment has the further advantage in that self diffusion coefficients, greater than $\sim 10^{-8}$ cm²/sec, may be measured⁴⁸⁻⁵⁰. The details of the steady state experiment are abundantly documented⁵¹ and as such our attention will focus principally upon the measurement and interpretation of T_1 , T_2 and $T_{1\rho}$ in solid polymers by pulse methods. The effects of sample purity on the recorded n.m.r. values will be included.

It is not proposed to dwell upon the details of spectrometer design since commercially available spectrometers are now in an advanced stage of sophistication. However, it is relevant to note some of their more important

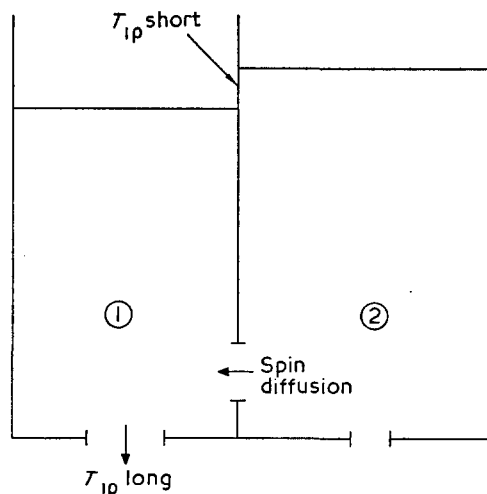


Figure 2 Schematic explanation of the spin diffusion effects in FEP

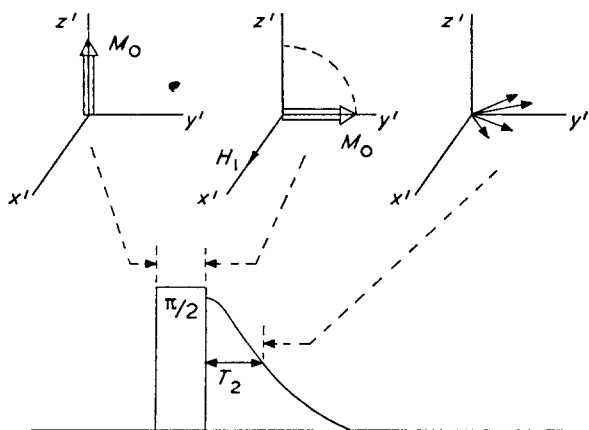


Figure 3 Pulse sequence used to measure the spin-spin relaxation time, T_2

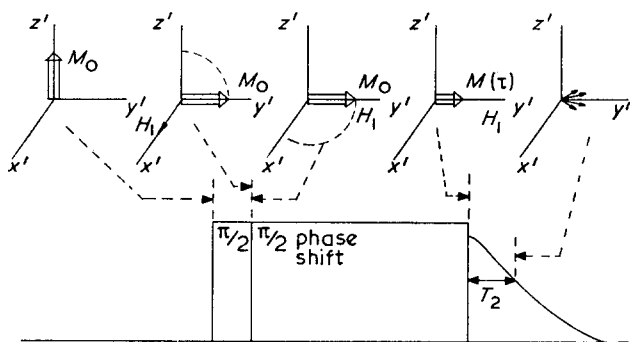


Figure 4 Pulse sequence used to measure the rotating frame relaxation time, $T_{1\rho}$

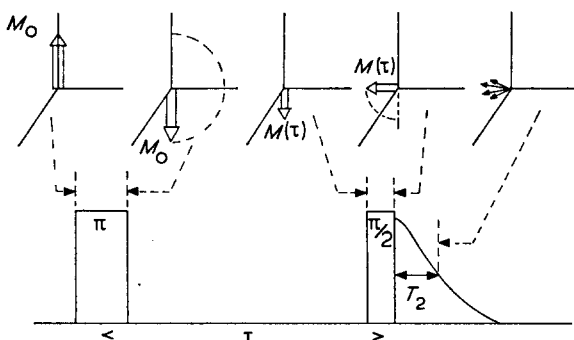


Figure 5 Pulse sequence used to measure the spin-lattice relaxation time, T_1

characteristics. Fully coherent fixed and variable frequency spectrometers are available with a range of operational frequencies between 3 and 300 MHz. Good signal to noise ratios have been achieved in addition to short pulse widths and short recovery times. For an operating frequency of 60 MHz and a cylindrical sample of 0.6 cm in diameter, a recovery time $\tau_r = 2.5 \mu\text{sec}$ and a 90° pulse width $\tau_{90} = 1.3 \mu\text{sec}$ are reported⁵². These values are optimal and it is more usual to find $\tau_r = 5-10 \mu\text{sec}$ and $\tau_{90} = 2 \mu\text{sec}$. We recall that τ_{90} is the time required for H_1 to turn the magnetization M_0 through 90° . H_1 fields for the rotating frame experiment are available within the range $\sim 2-60$ G.

Figures 3-5 illustrate a series of pulse sequences which may be used to measure the three relaxation

times. The diagrams refer to the behaviour of M_0 in the rotating frame. The pulse sequences described are by no means exclusive; others may be used not only to measure the three relaxation times but also to perform more detailed examinations of solid polymers⁵³. Multiple pulse cycles have been devised which severely attenuate the dipolar coupling and therefore permit high resolution studies to be carried out⁵⁴⁻⁵⁹. This aspect will be discussed more fully in a later section.

T_2 measurement

T_2 values range from about 10^{-5} sec for the rigid lattice to values greater than 10^{-3} sec for the viscous or rubbery state. Measurements are taken in the majority of cases from the free induction decay which follows a 90° pulse (Figure 3)³. When inhomogeneities in the laboratory field become important, at higher temperatures, the Carr-Purcell pulse sequence may be employed⁵⁰ ($T_2 \geq 1$ msec for a good magnet).

The free induction decay is the Fourier transform of the absorption lineshape⁶⁰. If the lineshape is Lorentzian, the decay is exponential and T_2 is defined as $t_{1/2}/\ln 2$, where $t_{1/2}$ is the time required for the signal to fall to half its initially observed value. However, the lineshapes which are encountered in polymers are temperature dependent and cannot be defined precisely over a wide temperature range. In an attempt to overcome this difficulty, the decay has been sometimes described in terms of the Weibull function, $\exp(-t/T_2)^E$ where E is the Weibull coefficient⁶¹. The function may take on either exponential ($E=1$), Gaussian ($E=2$) or intermediate character.

Instrumental difficulties add to the problem. As we have already mentioned, the recovery time of the spectrometer is typically of the order of $5 \mu\text{sec}$. This means that the first $5 \mu\text{sec}$ of the decay is lost and, in addition, that component signals from composite traces have decayed by different amounts in that time. The 'solid echo' sequence may be used to alleviate this problem somewhat⁵⁴.

In view of the difficulties outlined above, the arbitrary procedure has usually been adopted where T_2 is defined as $t_{1/2}/\ln 2$, irrespective of lineshape³. Furthermore, in the case of composite traces in which two components are clearly resolved, the procedure illustrated in Figure 6 has been used to extract the magnitudes and intensities of the individual T_2 components. Composite T_2 decays do not suffer from the instrumental difficulties encountered with complex wide-line spectra. The modulation

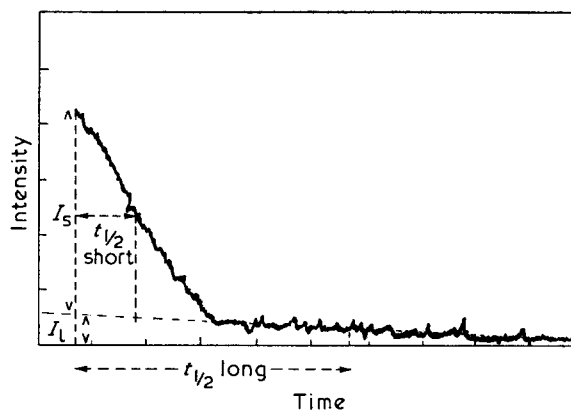


Figure 6 Typical composite, $T_2 (=t_{1/2}/\ln 2)$ signal from a semi-crystalline polymer

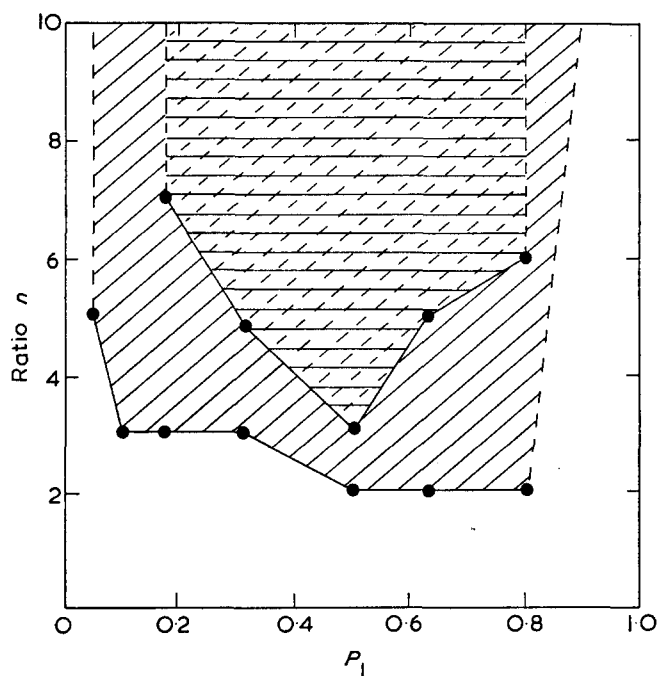


Figure 7 Experimentally derived confidence limits for extracting the two T_2 component relaxation times and their intensities as a function of the ratio of the relaxation times, n , and the intensity of the long component P_1 . Within the area defined by the oblique hatching the component relaxation times can be determined to an accuracy better than 10%. Within the smaller area defined by the horizontal hatching the component intensities can be determined to an accuracy better than ± 0.05 . [Reproduced from Wardell, G. E. and McBrierty, V. J. *Proc. R. Irish Acad.* 1973, 73, 63 by permission of the Royal Irish Academy, Dublin]

amplitude which is optimal for the broad line produces saturation in the narrow line and, as a result, a compromise has to be made.

An experimental assessment has been made of the accuracy of the component T_2 magnitude and intensity values derived in this way. Confidence limits have been established for the decomposition of proton resonance signals which derive from physical mixtures of two polymers each of which displays a single relaxation time⁶². Curves synthesized in this way closely resemble the decay traces observed for semi-crystalline polymers. The results are summarized in Figure 7. Within the area defined by the oblique hatching, the component relaxation times may be determined to an accuracy better than 10%. Within the smaller area defined by the horizontal hatching, the component intensities may be estimated to an accuracy better than ± 0.05 .

The analysis has been extended to three component systems. The confidence limits in Figure 7 hold for any two of the three components; however, the results for the short component are consistently better than for the intermediate or long component.

$T_{1\rho}$ measurement

$T_{1\rho}$ is the characteristic time for M_0 to decay along the r.f. field H_1 and falls within the approximate range 10^{-4} – 10^{-1} sec. The magnetization is spin-locked along H_1 by the pulse sequence of Figure 4, a 90° pulse followed by a 90° phase shift. If the decay is exponential then:

$$M(\tau) = M_0 \exp(-\tau/T_{1\rho}) \quad (17)$$

where $M(\tau)$ is the initial height of the free induction decay when H_1 is switched off. Non-exponential behaviour is frequently encountered especially for semi-crystalline polymers where two component $T_{1\rho}$'s may be resolved: the long $T_{1\rho}$ is identified with the crystalline part and the short $T_{1\rho}$ with the amorphous part as a general rule⁴. A typical non-exponential decay is illustrated in Figure 8.

Connor³³ has theoretically assessed the decomposition procedure for extracting two component $T_{1\rho}$ magnitudes and intensities. His results are presented in Figure 9 in

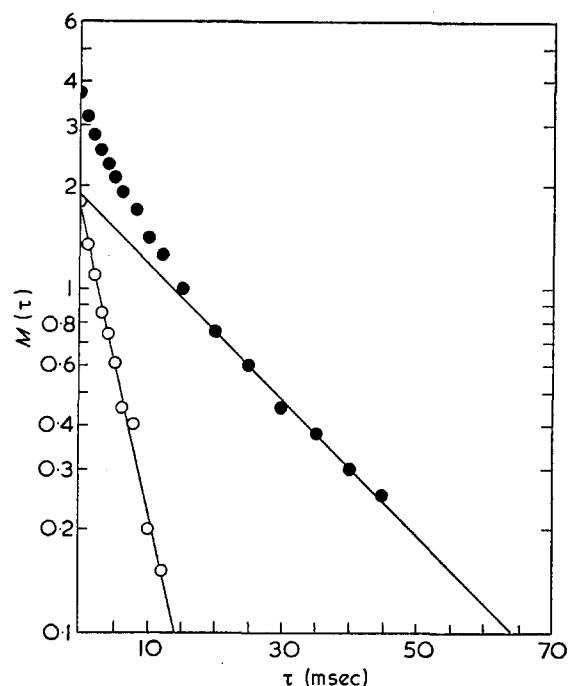


Figure 8 $T_{1\rho}$ decay observed in fibres of PP at $+98^\circ\text{C}$ indicating the presence of two components. \circ , $T_{1\rho}$ (short) = 5 msec; \bullet , total decay, $T_{1\rho}$ (long) = 21 msec

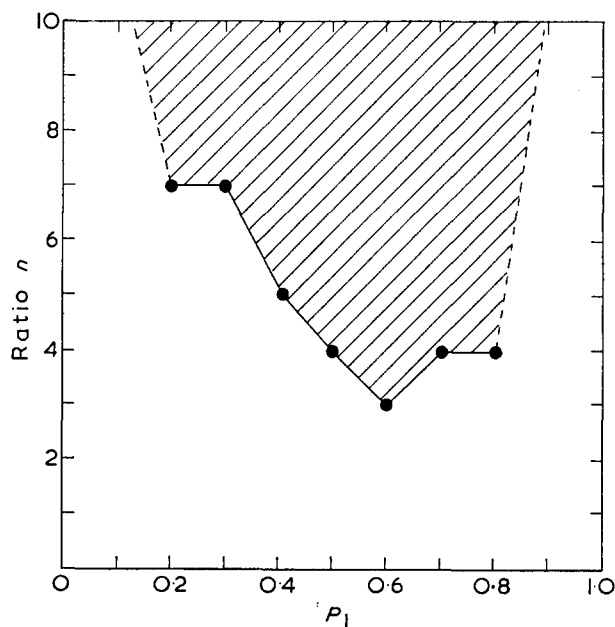


Figure 9 Theoretical confidence limits of Connor for the separation of two $T_{1\rho}$ components in terms of the ratio, n , of the two relaxation times and the intensity of the long component, P_1 . A reasonable decomposition may be achieved within the shaded area. [Reproduced by permission of Connor, T. M. (personal communication)]

which the shaded area defines the limits within which a reasonably accurate decomposition may be achieved.

T_1 measurement

A $180^\circ\text{-}\tau\text{-}90^\circ$ pulse sequence provides the T_1 relaxation time (Figure 5). T_1 values for polymers lie within the range $\sim 10^{-2}$ –10 sec. The inverted magnetization, following the 180° pulse, decays through zero to return to its equilibrium state along H_0 with a characteristic time T_1 . Periodically the magnetization $M(\tau)$ is monitored by applying a 90° pulse to bring the magnetization into the xy plane; the detector only responds to magnetization with a component in this plane. The initial height of the free induction decay, following the 90° pulse, is described by:

$$M(\tau) = M_0[1 - 2\exp(-\tau/T_1)] \quad (18)$$

$M(\tau) = 0$ when $\tau = T_1 \ln 2$ from which a value of T_1 may be obtained. This is referred to as the null method. Alternatively, T_1 may be derived from the slope of the graph of $\ln [M_0 - M(\tau)]$ vs. τ . The effect of a non-uniform H_1 field over the sample volume on the measured T_1 value has been examined by Farrar and Becker⁵³.

Non-linearity in the graph of $\ln [M_0 - M(\tau)]$ vs. τ is a manifestation of non-exponential decay in which case component T_1 values may be extracted in a manner similar to that illustrated in Figure 8. If the null method is used, the presence of more than one component is indicated by a change in the initial amplitude and the shape of the decay as τ is altered. Two-component T_1 magnetization decays, measured by a $180^\circ\text{-}\tau\text{-}90^\circ$ sequence, may be described by:

$$M(\tau) = M'_0[1 - 2\exp(-\tau/T'_1)] + M''_0[1 - 2\exp(-\tau/T''_1)] \quad (19)$$

Trappeniers and coworkers³⁹ have discussed ways in which component T_1 relaxation times and their intensities

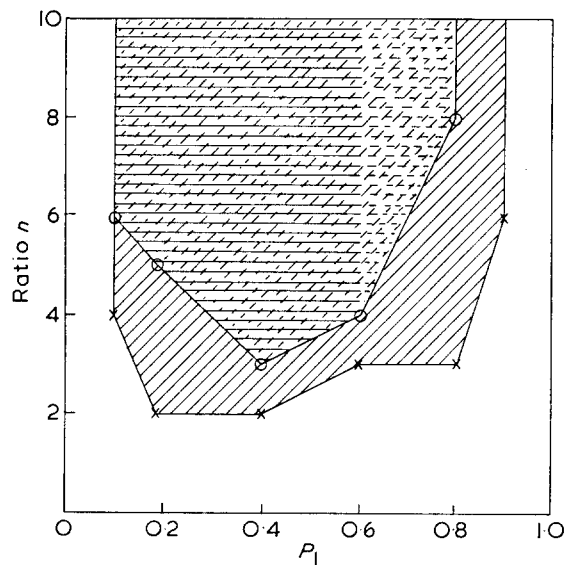


Figure 10 Experimentally derived confidence limits for extracting the two T_1 component relaxation times and their intensities as a function of the ratio of the relaxation times, n , and the intensity of the long component, P_1 . Within the area defined by the oblique hatching the long T_1 and the short T_1 have accuracies of 5% and 10%, respectively. For intensities of the long component less than 60%, the measured intensities are good to 10%; above 60% the accuracy is of the order of 20%. Intensity measurements refer to the horizontal hatching.

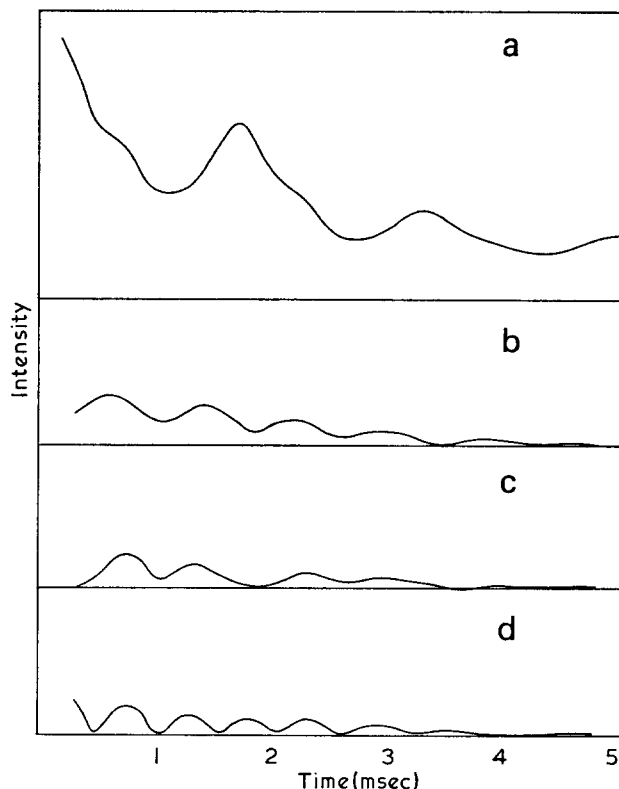


Figure 11 Free induction decay (a) observed in a low molecular weight PCTFE wax under a $180^\circ\text{-}\tau\text{-}90^\circ$ pulse sequence at $+90^\circ\text{C}$. (b) $\tau = 77$ msec; (c) $\tau = 90$ msec; (d) $\tau = 115$ msec

may be extracted from this equation. Accuracies of 5% for the longer relaxation time and 10% for the shorter are quoted when the relaxation times differ by at least a factor of 4; the two T_1 values are unresolved when they differ by a factor of less than 2.

An experimental assessment has been carried out for the decomposition of T_1 decays which result from physical mixtures of two polymers, in a manner similar to the analysis of composite T_2 traces described earlier⁴⁷. Within the area defined by the oblique hatching of Figure 10, the long and short T_1 components have accuracies of 5% and 10%, respectively. The horizontal hatching defines the area in which the intensities may be determined within the following accuracies: for intensities of the long component less than 60%, the measured intensities are good to 10%. For higher values of the long component the accuracy is of the order of 20% or worse.

An interesting example of the analysis of multiple T_1 decays is illustrated in Figure 11 which describes the behaviour of the magnetization in a low molecular weight polychlorotrifluoroethylene (PCTFE) wax at $+100^\circ\text{C}$ under a $180^\circ\text{-}\tau\text{-}90^\circ$ sequence⁶³. Three relaxation processes are operative for which:

$$M(\tau) = M_a[1 - 2\exp(-\tau/T_{1a})] + M_b[1 - 2\exp(-\tau/T_{1b})] + M_c[1 - 2\exp(-\tau/T_{1c})] \quad (20)$$

At $\tau = 77$ msec, the shortest T_1 is nulled out and the remaining two relaxations display the symmetrical beat pattern of 11b. At $\tau = 90$ msec, $M(\tau) = 0$. The long T_1 is nulled out at 115 msec, again providing the symmetrical beat pattern of 11d (diode detection was employed in recording these traces with the result that the negative parts of the cycle are inverted in 11d). Only

two of the three relaxation times could be determined directly in this way from τ_{null} ; a third null could not be resolved in these measurements. However, the third T_1 along with the component intensities may be calculated from the experimental data of Figure 11, used in conjunction with equation (20). Intensity determinations by this procedure are not very accurate but T_1 values, accurate to a few percent, may be derived. The problem would appear to be ideally suited to an analysis by Fourier transform spectroscopy.

Sample impurity effects

The relaxation behaviour of a polymer sample may be profoundly altered by the presence of impurities, especially at low temperatures^{39, 64}. Particularly troublesome is the presence of oxygen which, as a paramagnetic impurity, is an efficient relaxation agent in the polymer. Sorbed O_2 in polytetrafluoroethylene (PTFE), for example, can lead to low temperature T_1 values which are an order of magnitude smaller than those observed in a degassed sample³⁹.

The nature of the sample is important in this context. The effect is greatly enhanced if the material is in fine powder form in contrast to the solid form. The T_1 results of Slichter⁶⁵ for poly(methyl methacrylate) (PMMA), shown in Figure 12, clearly demonstrate the type of behaviour which can result. The open circles denote the T_1 response as the sample, in powder form, is heated above the softening point. A subsequent rerun leads to the upper T_1 curve denoted by the triangles. In the first set of measurements adsorbed air was progressively driven off. In addition, the surface area of the sample decreased through sintering which greatly reduced the possibility of re-adsorption.

Anomalous behaviour can arise from entrapped monomer or oligomer which can behave as a plasticizer in the polymer. Perhaps this is responsible for the large differences in relaxation behaviour observed in PS at low temperatures^{64, 66}.

Of course, the introduction of paramagnetic impurities may be turned to advantage to obtain manageable T_1 values which would otherwise be much too long.

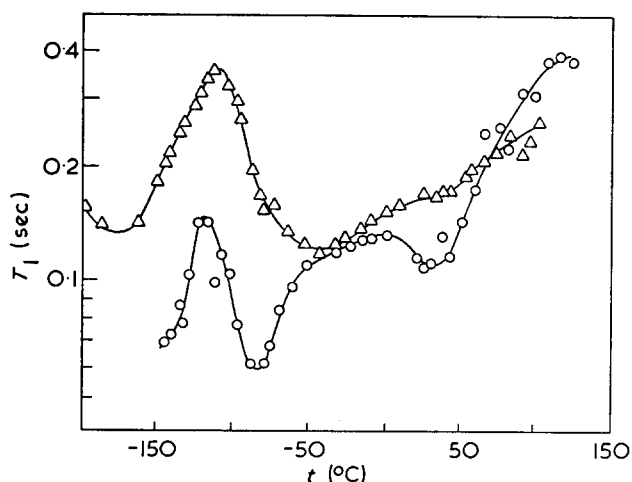


Figure 12 Data of Slichter for PMMA ($\bar{M}_v = 100 \times 10^6$) at 50 MHz. \circ and \triangle denote T_1 measurements on an initial temperature run and then a rerun, respectively. [Reproduced from Slichter, W. P. J. Polym. Sci. (C) 1966, 14, 33 by permission of John Wiley, New York]

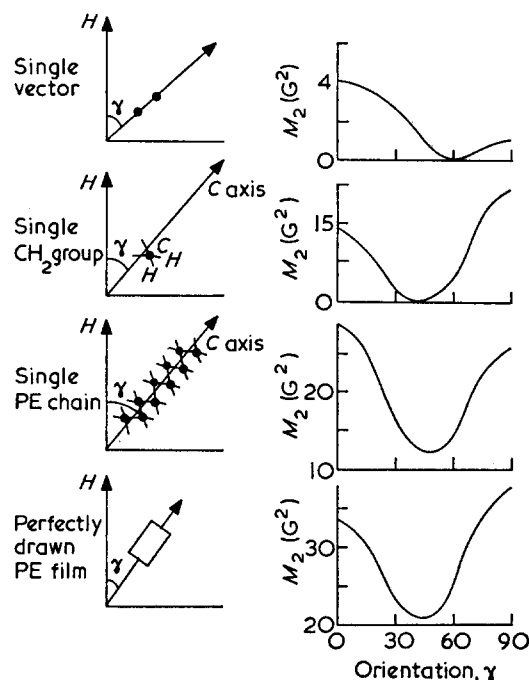


Figure 13 Diagram which illustrates the development of anisotropy in M_2 for a highly drawn crystalline PE sample

ORIENTATION DISTRIBUTION ANALYSIS

In bulk polymers, the angular terms in the relaxation expressions (1)–(3) which define the orientation of internuclear vectors with respect to H_0 are averaged uniformly over all space with a consequent loss of molecular information. For these materials the n.m.r. response is characterized by a relaxation time or moment value which is independent of sample orientation in the laboratory field H_0 . This loss of information is avoided if the sample is in the form of a single crystal. Unfortunately, polymer single crystals, suitable for study by n.m.r., are generally not available. On the other hand, angular dependence can arise in drawn films and fibres in which the molecular chains tend to align along the fibre axis or draw direction^{25–30, 36, 37, 67–85}. As a result, n.m.r. fibre data are often anisotropic when recorded as a function of fibre axis orientation in H_0 .

Figure 13 illustrates the way in which the anisotropy in M_2 is developed in a highly drawn crystalline sample of PE. The M_2 dependence upon the angle γ between the draw axis and the direction of H_0 is portrayed for a single internuclear vector, an isolated $-\text{CH}_2-$ group, a single PE chain and, finally, for the case where all contributions to the local field at the reference nucleus are taken into account. It is interesting to note that the essential features of the anisotropy are already well developed for the $-\text{CH}_2-$ group, which demonstrates the dominant effect of nearest neighbours in the lattice sum computations.

In recent years, several studies have been reported for partly drawn polymers in which the constituent chains are preferentially, but not fully, oriented by the drawing process^{25, 30, 36, 37, 73, 86, 87}. The distributions of molecular chain orientations which are present in these partly ordered systems are of primary importance in the description of the overall macroscopic properties of the polymer.

The detailed application of n.m.r. to the study of

these distributions requires a precise physical description of the polymer which is generally unavailable. Rather, idealized models are used which are, as far as possible, consistent with the available morphological information. One such model describes the basic structural features of a drawn semi-crystalline polymer in terms of discrete crystalline and amorphous regions. The crystalline component is viewed as an aggregate of units, each of which has the properties of the fully drawn structure. The units become oriented upon drawing and thereby give rise to the observed anisotropy⁸⁸.

Often, the amorphous regions may be regarded as isotropic from an n.m.r. viewpoint^{25, 46, 76, 83}. This assumption, however, does not preclude a degree of preferred orientation which is undoubtedly present in the amorphous regions of the drawn material. For example, in the case of PE it is known that the amorphous regions contain a variety of rotational isomers. *Trans* and *gauche* conformations are present with the result that the molecular chains do not adopt the usual planar zig-zag form. Thus the local orientation of pairs of protons in the $-\text{CH}_2-$ groups, which we have shown to be mainly responsible for the observed anisotropy in M_2 , may be random to a much better approximation than the orientation of the chain as a whole. While the concept of an isotropic amorphous component or indeed of a two-phase model is a useful one which has been applied successfully to a number of polymers, such approximations are not always valid. Distinct anisotropy is observed in the amorphous T_2 signal from fibres of PCTFE⁸⁹ and also in the amorphous M_2 component in doubly oriented nylon-6,⁶²⁷.

As our remarks in the introductory section have indicated, quantitative analysis is best suited to M_2 , M_4 and T_2 data. Anisotropy considerations favour M_2 and M_4 . To understand this, we recall the expression $M_2 \approx 2/\gamma^2 T_2^2$, from which it is evident that the anisotropy in T_2 is scaled down in relation to M_2 because of the square root relationship. It is for this reason that the marked anisotropy in M_2 for PE²⁵ and polypropylene (PP)⁷⁰ is not observed in the corresponding T_2 measurements⁸⁴. In the study of orientation distributions in polymers, measurements are made at low temperatures to avoid the complications associated with the presence of molecular motion. The moment expression appropriate to the two-phase model described above may be written:

$$\langle M_n \rangle = x \langle M_n \rangle_{\text{cryst}} + (1-x) \langle M_n \rangle_{\text{amorph}} \quad (21)$$

where x is the crystalline mass fraction and $n=2,4$, respectively.

Following upon these preliminary considerations, we are now in a position to focus upon the nature of the orientation distribution of chains in the drawn polymer. The most general orientation of a typical structural unit, referred to a macroscopic set of axes, requires three Euler angles to be specified (*Figure 14*). The distribution of units may be described mathematically by $f(\alpha_1, \Delta, \alpha_2)$, the functional form of which may be expressed in a series of generalized spherical harmonics^{29, 30, 90, 91}:

$$f(\alpha_1, \Delta, \alpha_2) = \sum_{l=0}^{\infty} \sum_{n, m=-l}^{+l} P_{lmn} \mathcal{D}_m^{(l)}, n(\alpha_1, \Delta, \alpha_2) \quad (22)$$

The coefficients, P_{lmn} , of the summation are referred to as 'moments' of the distribution. The significance

of f may be realized by noting that the average of any function, F , over the distribution, denoted by angled brackets, has the form:

$$\langle F \rangle = \int_0^{2\pi} \int_0^{\pi} \int_0^{2\pi} f(\alpha_1, \Delta, \alpha_2) \cdot F d\alpha_1 \sin\Delta d\Delta d\alpha_2 \quad (23)$$

A general expression has been derived for the crystalline contribution to M_2 in terms of the distribution moments, P_{lmn} , which may be written²⁹⁻³¹:

$$\langle M_2 \rangle_{\text{cryst}} = \sum_{l=0,2,4} \sum_{m,n=-l}^{+l} D_l P_{lmn} Y_{l,m}^*(\gamma, \phi_\gamma) S_{ln} \quad (24)$$

where the coefficients $D_l = 192\gamma^2 \hbar^2 I(I+1)\pi^3 a_l / (2l+1)^2$ in which $a_0=1/5$, $a_2=2/7$ and $a_4=18/35$. Values of D_l for ^1H and ^{19}F nuclei are listed in *Table 2*. S_{ln} are lattice sums defined as:

$$S_{ln} = 1/N \sum_k Y_{l,n}(\theta_k, \phi_k) / r_k^6 \quad (25)$$

The lattice sums are computed in pairs to avoid the complex terms. θ_k , ϕ_k and γ , ϕ_γ are, respectively, the polar and azimuthal angles of r_k with respect to the symmetry axis of the structural unit and of H_0 with respect to the draw axis in the polymer. Equation (24) expresses the crystalline second moment in terms of: (i) fundamental constants; (ii) lattice sums appropriate to the particular polymer; (iii) the direction of H_0 ; and (iv) the even moments of the distribution up to order 4.

Equations (22) and (24) simplify considerably when there are symmetry elements in the polymer⁹¹. For example, if S in *Figure 14* is identified as the draw axis and there is fibre symmetry, then f becomes independent of the angle α_1 ($m=0$). If, in addition, the structural unit is transversely isotropic, that is, rotations of the unit about its symmetry axis C leaves the value of $\langle M_2 \rangle_{\text{cryst}}$

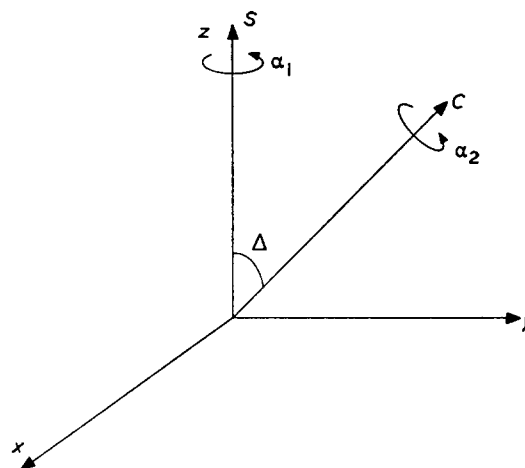


Figure 14 Diagram which illustrates the most general orientation of a typical structural unit, referred to a sample coordinate frame, in terms of the three Euler angles $\alpha_1, \Delta, \alpha_2$

Table 2 Values of the coefficients D_l and D'_l for ^1H and ^{19}F nuclei

	$D_l \times 10^{-4} (\text{G}^2 \text{A}^6)$		$D'_l \times 10^{-2} (\text{G}^2 \text{A}^6)$	
	^1H	^{19}F	^1H	^{19}F
0	71.081	63.069	7.164	6.357
2	4.062	3.604	10.234	9.081
4	2.257	2.002	18.422	16.345

unchanged, then the dependence on the angle α_2 also vanishes ($n=0$). Equations (22) and (24) then become^{25, 36}:

$$\rho(\Delta) = \sum_{l=0}^{\infty} (l + \frac{1}{2}) \overline{P_l(\cos\Delta)} P_l(\cos\Delta) \quad (26)$$

and

$$\begin{aligned} \langle M_2 \rangle_{\text{cryst}} &= \sum_{l=0, 2, 4} D_l \overline{P_l(\cos\Delta)} P_l(\cos\gamma) S_l \\ &= \sum_{l=0, 2, 4} C'(\gamma, l) \overline{P_l(\cos\Delta)} \end{aligned} \quad (27)$$

The lattice sums in this expression, S_l , have the form

$$1/N \sum_k P_l(\cos\theta_k) / r_k^6$$

The moments P_{l00} have been expressed in their explicit form in terms of Legendre polynomials, $\overline{P_l(\cos\Delta)}$. The coefficient $D'_l = 6\gamma^2 \hbar^2 I(I+1) a_l$.

There is a fourth moment analog to equation (27)³⁶:

$$\langle M_4 \rangle_{\text{cryst}} = \sum_{l=0, 2, \dots, 8} C(\gamma, l) \overline{P_l(\cos\Delta)} + \langle M_4 \rangle_c \quad (28)$$

$\langle M_4 \rangle_c$ is a small correction term due to lattice sums of the type

$$\sum_{i, j, k \neq} B_{ij}^2 B_{ik} B_{jk}$$

in the fourth moment calculation. We note in this case that the first five terms of the distribution to order 8 are required in this expression. Only three terms are required for $\langle M_2 \rangle_{\text{cryst}}$.

McCall and Hamming⁹², and later Roe²⁹, have shown that the second moment may be described fully by 15 parameters for the most general type of crystal, that is, there are 15 independent lattice sums. When there is crystallographic or statistical symmetry in the material, not all the lattice sums are mutually independent and, as a result, the number of independent moments of the distribution measurable by n.m.r. is greatly reduced^{25, 29, 30}. To quote the example of a fibre material, consisting of orthorhombic crystal units, there are six non-zero independent P_{lmn} coefficients, namely, P_{000} , P_{200} , P_{202} , P_{400} , P_{402} and P_{404} .

The orientation distribution theory outlined above has been applied to a variety of polymers, both semi-crystalline and amorphous. Results have been reported for poly(vinyl chloride) (PVC)⁸⁷, PMMA⁸⁶, poly(ethylene terephthalate) (PET)³⁰, polyoxymethylene (POM)³⁷ and PE^{25, 36}. With the exception of PET, the simplified theory contained in equations (26)–(28), has been used to analyse the experimental data. The results of Kashiwagi *et al.*³⁰ for oriented PET have been interpreted in terms of orthorhombic statistical symmetry (the subscript m is restricted to values which are positive and even) and transversely isotropic units ($n=0$). Fourth moment measurements have been confined to PE³⁶. Figures 15 and 16 illustrate the agreement between theoretical predictions, based upon equations (21), and (26)–(28), and the experimental M_2 and M_4 measurements for PE as a function of draw ratio. Moments of the distribution have been derived from a least squares fit of the experimental data, and subsequently used to construct polar representations of $\rho(\Delta)$ for the three draw ratios examined (Figure 17). The moments of the distribution obtained from the n.m.r. analysis have been complemented in this study by higher order

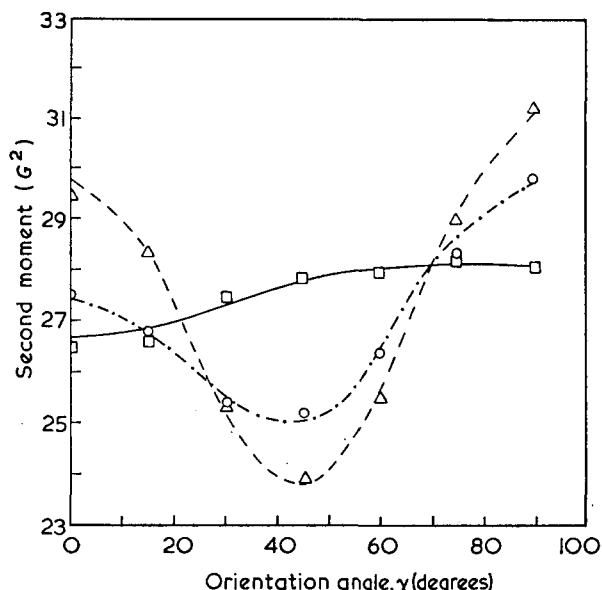


Figure 15 Comparison of the experimental and theoretical variation of M_2 plotted against the orientation angle, γ , in the magnetic field for low-density PE. The lines are theoretical and the points experimental data. Draw ratios: Δ , 3.7; \circ , 2.3; \square , 1.3. [Reproduced from McBrierty, V. J. and Ward, I. M. *J. Phys. (D)* 1968, 1, 1529 by permission of the Institute of Physics, Bristol ©]

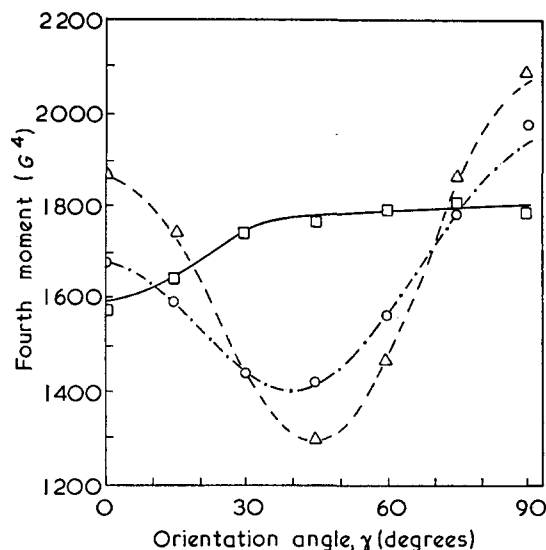


Figure 16 Comparison of experimental and theoretical variation of M_4 plotted against orientation angle, γ , in the magnetic field for low-density PE. The lines are theoretical and the points experimental data. Draw ratios: Δ , 3.7; \circ , 2.3; \square , 1.3. [Reproduced from McBrierty, V. J., McDonald, I. R. and Ward, I. M. *J. Phys. (D)* 1971, 4, 88 by permission of the Institute of Physics, Bristol ©]

moments estimated on the basis of a smoothing procedure which suggested itself from X-ray diffraction measurements. The polar plots of Figure 17 are consistent with those derived from X-ray data and are indicative of a very non-affine deformation process⁹³. The P_{lmn} values derived in this study have been used to reasonably predict the mechanical anisotropy exhibited by the drawn polymer.

The values of the coefficients $C'(\gamma, l)$ and $C(\gamma, l)$ for drawn POM are listed in Tables 3 and 4 in order to illustrate an important aspect of orientation distribution analysis by n.m.r.³⁷. We note that terms for $l=2$ make

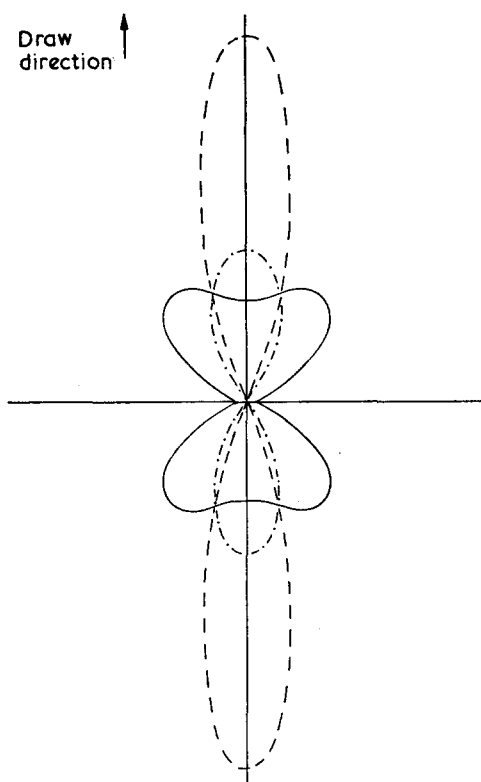


Figure 17 Polar representations of the distribution functions $\mu(\Delta)$ derived from data of Figures 15 and 16. Draw ratios: -----, 3.7; - · - · - ·, 2.3; ———, 1.3. [Reproduced from McBrierty, V. J., McDonald, I. R. and Ward, I. M. *J. Phys. (D)* 1971, 4, 88 by permission of the Institute of Physics, Bristol ©]

Table 3 Values of the coefficients $C'(\gamma, l)$ in G^2 for oriented POM. [Reproduced from McBrierty, V. J. and McDonald, I. R. *J. Phys. (D)* 1973, 6, 131 by permission of the Institute of Physics, Bristol ©]

l	γ (degrees)						
	0	15	30	45	60	75	90
0	19.54	19.54	19.54	19.54	19.54	19.54	19.54
2	-0.01	-0.01	-0.06	0.00	0.00	0.00	0.01
4	-13.93	-9.53	-0.32	5.66	4.03	-2.00	-5.22

Table 4 Values of the coefficients $C(\gamma, l)$ in G^4 for oriented POM. [Reproduced from McBrierty, V. J. and McDonald, I. R. *J. Phys. (D)* 1973, 6, 131 by permission of the Institute of Physics, Bristol ©]

l	γ (degrees)						
	0	15	30	45	60	75	90
0	837	837	837	837	837	837	837
2	-9	-9	-6	-2	1	4	5
4	-963	-659	-23	391	278	-138	-361
6	75	30	-28	-11	24	3	-23
8	130	12	-44	39	-10	-22	36

insignificant contributions to the calculated moments. This results from the fact that the angle between the internuclear vector in the methylene group and the helical axis of the POM chain is almost exactly equal to $\cos^{-1} [1/(3)^{1/2}]$ and therefore $P_2(\cos\theta_k)$ for this pair, which is the major contributor to the lattice sum, is almost zero⁷⁵. Thus, n.m.r. is totally insensitive to the second moment of the distribution in this case.

In conclusion, the application of n.m.r. to the study of statistical distributions in partly oriented polymers has been successful up to a point in providing some, but not all, of the even moments of the distribution up to order 4 for M_2 and order 8 for M_4 measurements. The method is sensitive to the crystallographic details of molecular structure and as such does not have universal application. A further drawback relates to the direct dependence of $\mu(\Delta)$ on l in equation (26); the coefficients in the summation become increasingly important as l increases and it is these higher order moments which are the least accurately assessed (see Table 4). Nevertheless, for low draw ratios, the first few terms provide a reasonable approximation to the distribution. Finally, it may be noted that these procedures are a necessary prerequisite if motional studies in partly oriented polymers are contemplated³⁷.

MOLECULAR MOTIONAL STUDIES

The motions of molecules which are responsible for relaxation phenomena in polymers have been investigated extensively and, in this section, specific examples will be cited to illustrate the ways in which the theoretical considerations, presented earlier, have been exploited in the examination of polymeric systems^{33, 35, 94}. Fibre materials will be emphasized.

For semi-crystalline polymers, there is characteristic motional behaviour in the crystalline and amorphous regions for which discrete components may be resolved in the recorded data, at least over a range of temperature. Long T_1 and $T_{1\rho}$ and short T_2 (or broad component of the absorption envelope) signals are manifestations of crystalline behaviour³⁵.

In those cases where the interpretation of n.m.r. data from individual polymers is uncertain, it is often advantageous to examine related polymers in which chemical modifications have been introduced⁶⁵. The correlation of the combined results can be more revealing than the data from the individual polymers, considered separately. The effects of isomerism may be similarly studied. Slichter and Davis have recorded T_1 data for polybutadiene as a function of *cis-trans* content⁹⁵. They observed a shift of the T_1 minimum to higher temperatures as the *trans* content was increased, indicating increasing restrictions to motion.

The effects of a variety of agents which alter the molecular motional behaviour, often profoundly, have been examined by n.m.r. either to clarify, further, the motional mechanisms or to elucidate information on the combined polymer-agent system. The use of irradiation to produce crosslinks⁹⁶ or swelling agents to enhance motion⁹⁷⁻¹⁰¹ are examples. The incorporation of filler particles such as carbon black into elastomers can lead to systems which are of great practical importance. Recent n.m.r. studies have examined the reinforcing effects of filler particles in terms of the suppression of molecular motion which is produced in the polymer^{61, 102}. The molecular details of the curing process in epoxy resins is under current examination¹⁰³.

The types of molecular motion to which n.m.r. is sensitive fall into three broad categories: motions which involve side groups, main chain or segmental effects and motions of a general character which are typical of glass transition phenomena. Vibrations are essentially

undetected. Examples of these three types of motion will now be considered in turn.

Side group motions

Probably the most documented side group motion pertains to the rotation of methyl groups about their threefold axis of symmetry^{41, 84, 104}. Such motions are observed at low temperatures, down to a few Kelvin¹⁴. In some polymers the motion is not fully activated until relatively higher temperatures as, for example, in the polycarbonate (PC)⁴¹ or the diglycidyl ether of bisphenol A (DGEBA)¹⁰³. The higher temperatures and the accompanying high values of the activation energy for the motion, ~ 5 kcal/mol, reflect the steric hindrance associated with two methyl groups attached to the one carbon atom. In PVAc, quantum mechanical tunnelling is probably operative and, in this case, it is misleading to use the concept of an activation energy across a barrier¹⁴.

The n.m.r. relaxation data for fibres of PP are presented in Figure 18⁸⁴. The small T_2 transition and $T_{1\rho}$ minimum around -180°C and the T_1 minimum at -110°C are manifestations of methyl group rotations. An explicit expression for $T_{1\rho}$ has been derived for this motion in terms of the angle, β , between the symmetry axis of a typical group and the laboratory field direction. The expression for $T_{1\rho\text{min}}$ has the form:

$$T_{1\rho\text{min}} = 50/\sin^4\beta \mu\text{sec} \quad (29)$$

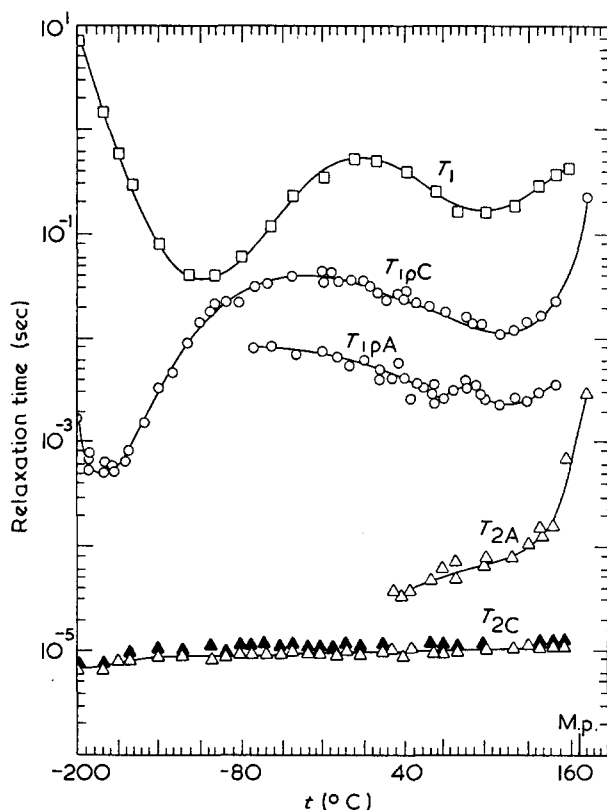


Figure 18 Temperature dependence of the relaxation times T_1 , T_2 and $T_{1\rho}$ for fibres of PP. The triangles denote T_2 measurements; Δ , relate to orientations $\gamma=0^\circ$ and 90° and \blacktriangle to the 54° orientation to the magnetic field. The T_1 and $T_{1\rho}$ data are denoted respectively by \square and \circ . The amorphous and crystalline assignments are subscripted A and C, respectively. [Reproduced from McBrierty, V. J., Douglass, D. C. and Falcone, D. R. *JCS Faraday Trans. II* 1972, **68**, 1051 by permission of the Chemical Society, London]

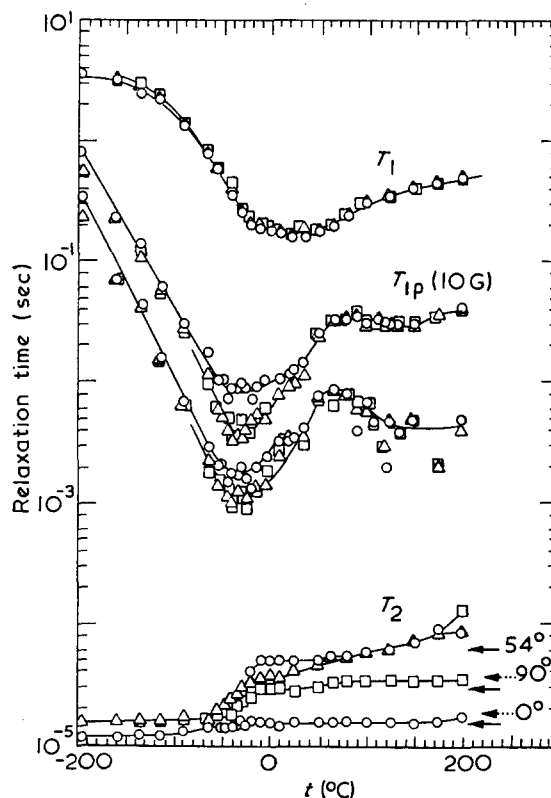


Figure 19 N.m.r. relaxation times T_1 , T_2 and $T_{1\rho}$ for FEP fibres. γ is the angle between the fibre axis and the magnetic field direction. The arrows indicate calculated T_2 values: \rightarrow , chains rotating about their helical axis; $\dots\rightarrow$, chains rotating and translating. \circ , $\gamma=0^\circ$; Δ , $\gamma=54^\circ$; \square , $\gamma=90^\circ$. [Reproduced from McBrierty, V. J. et al. *J. Chem. Phys.* 1970, **52**, 512 by permission of the American Institute of Physics, New York]

The approximation of isolated methyl groups has been made. The introduction of a distribution of relaxation times, considered to result from a random distribution of CH_3 groups in the polymer, leads to an average value of ~ 0.25 for $\sin^4\beta$. This raises the $T_{1\rho\text{min}}$ to $200 \mu\text{sec}$. If, in addition, spin diffusion is operative, which allows the rotating methyl groups to relax the remaining 50% of protons in PP, the predicted minimum is $400 \mu\text{sec}$, which is in reasonable agreement with the observed value of $550 \mu\text{sec}$. This example illustrates the use of a physically meaningful distribution of relaxation times as opposed to the purely mathematical procedures which are commonly employed¹⁷.

In several polymers, the small T_2 transition is absent. Such is the case with PVAc¹⁴ (a feature of quantum mechanical tunnelling), with DGEBA¹⁰³ and with PE⁴¹. As we have already explained, spin diffusion is responsible for the observations in PE. In any event, the predicted size of the T_2 transition is small. Substitution of the value for the $T_{1\rho\text{min}}$ derived above into equation (9) shows that an increase of about a few μsec is all that is ideally expected.

The effects of bulky side groups have been examined in substituted polysiloxanes⁹⁸. Replacement of half of the methyls in polydimethylsiloxane (PDMS) with phenyl groups leads to a significant increase in the corresponding T_1 minimum, of the order of a factor of 2. This is interpreted in terms of rigid phenyl groups and steric hindrance to motion of the remaining methyls. The effects are less pronounced when trifluoropropyl groups are used instead of phenyl groups.

An interesting, if not unusual result emerges from the data on FEP shown in Figure 19. There is no indication of $-\text{CF}_3$ group motion which one might expect. The groups are locked in and do not rotate.

It is possible for n.m.r. to detect and resolve more than one type of side group motion as in PMMA⁶⁵. On the other hand, known side group motions can remain undetected by n.m.r. as in the case of ester side groups in PVAc¹⁴. The vexed question of phenyl side group behaviour in PS remains unanswered^{44, 47, 64} although the likely candidate would appear to be small amplitude oscillations.

Main chain motions

An emerging feature of the current work on the application of n.m.r. to polymers has been the exploita-

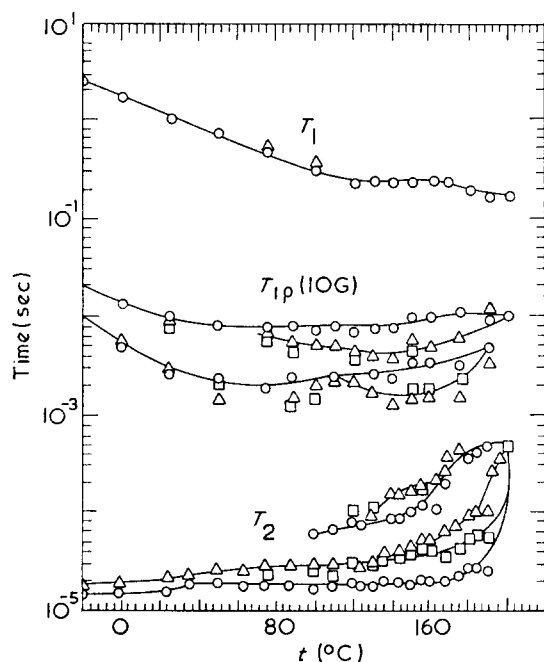


Figure 20 N.m.r. relaxation times for PCTFE fibres: \circ , $\gamma=0^\circ$; Δ , $\gamma=54^\circ$; \square , $\gamma=90^\circ$ where γ is the angle between the fibre axis and the magnetic field. [Reproduced from McBrierty, V. J., McCall, D. W. and Douglass, D. C. *Bull. Am. Phys. Soc.* 1970, 15, 307 by permission of the authors]

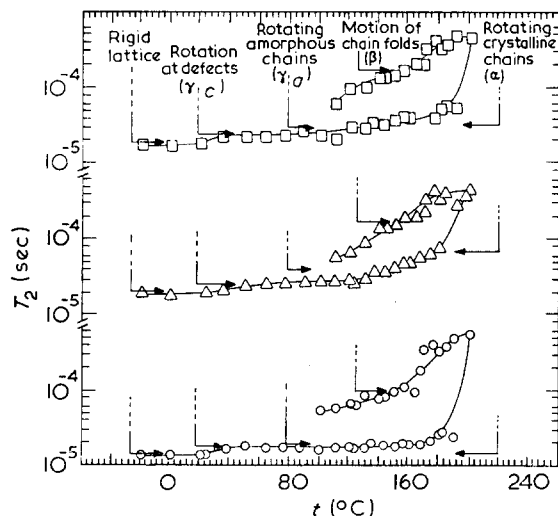


Figure 21 T_2 data of Figure 20 expanded for clarity. The arrows indicate the theoretical predictions for the various relaxation processes in the polymer (see text)

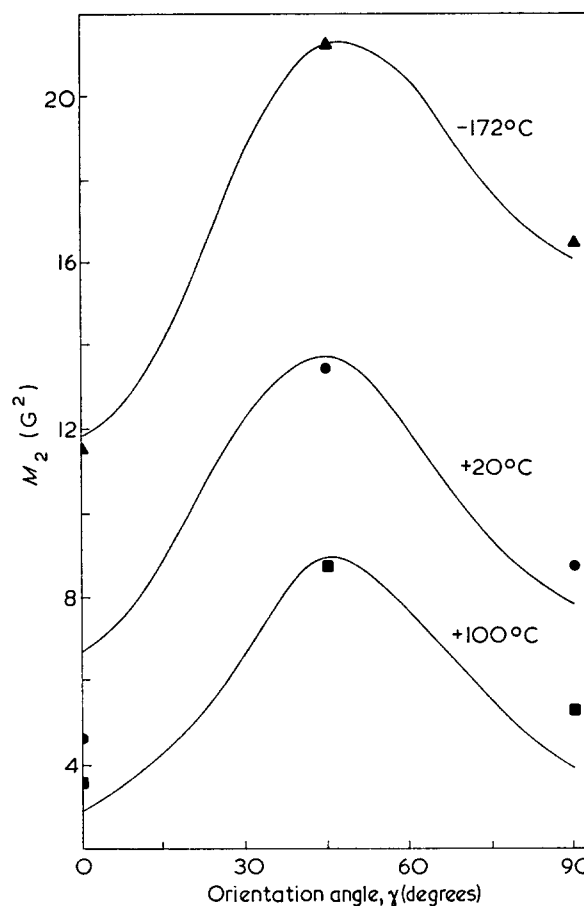


Figure 22 Second moment of partly oriented POM. Points represent the experimental data; the curves are calculated values for the rigid lattice (-172°C), for crystalline chains oscillating with amplitude 42° ($+20^\circ\text{C}$) and for chains which are both oscillating and translating ($+100^\circ\text{C}$). [Reproduced from McBrierty, V. J. and McDonald, I. R. *J. Phys. (D)* 1973, 6, 131 by permission of the Institute of Physics, Bristol \odot]

tion of improved theories and the availability of more refined materials to identify rather than merely detect the characteristic main chain motions which prevail. Specialized motions have been proposed to interpret successfully various experimental data: these include main chain oscillations, rotations, discrete jumps between sites, and main chain translations. These effects of chain flexibility, which becomes important for long chains, have also been examined quantitatively²⁶.

The onset of rotation about the main chain axis may be abrupt or gradual. For example, the first order transition in PTFE is abrupt with $\nu_c \approx 10\text{ Hz}$ below the transition rising to $\sim 10^7\text{ Hz}$ some 10°C higher in temperature⁴. In FEP the transition is more gradual⁴⁶ (Figure 19) while in PCTFE main chain rotation is not fully activated in the n.m.r. sense until just below the melting point (Figures 20 and 21)¹⁰⁶.

Chain rotations can occur in either all or part of the crystalline or amorphous regions. The γ_c relaxation process in PCTFE has been interpreted in terms of rotations of crystalline chains only in the vicinity of row vacancies or defects^{89, 105}.

The broadline results for a number of aromatic polyamides¹⁰⁷ indicate that part of a chain may undergo preferred motion, probably rotation, depending upon the details of molecular structure. Alternatively, small

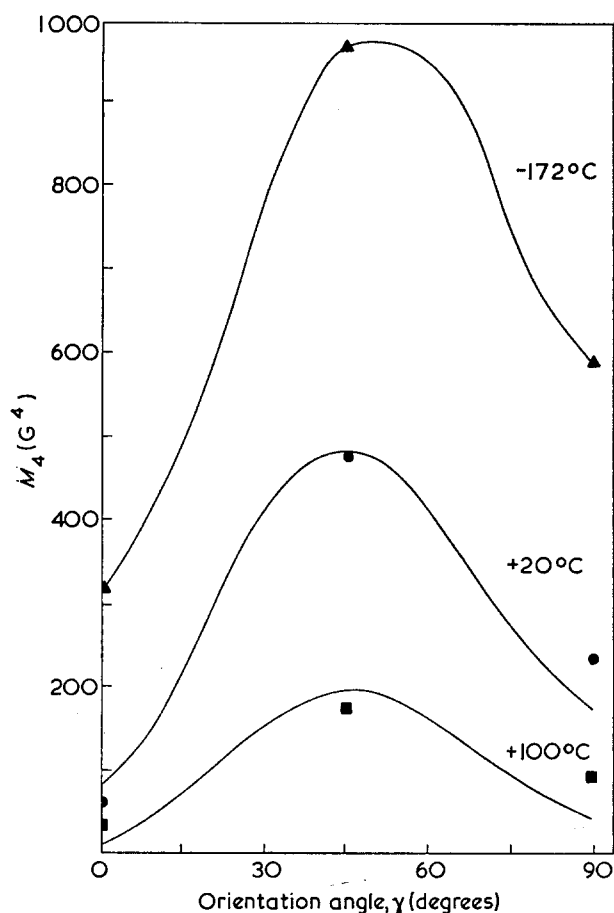


Figure 23 Fourth moment of partly oriented POM. Points represent the experimental data; the curves are calculated values for the rigid lattice (-172°C), for crystalline chains oscillating with amplitude 42° ($+20^{\circ}\text{C}$) and for chains which are both oscillating and translating ($+100^{\circ}\text{C}$). [Reproduced from McBrierty, V. J. and McDonald, I. R. *J. Phys. (D)* 1973, 6, 131 by permission of the Institute of Physics, Bristol ©]

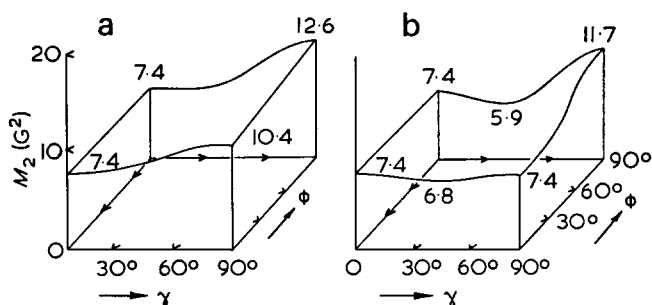


Figure 24 Experimental decrease in the second moment of doubly oriented nylon-6,6 over (a) the temperature interval -196°C to $+20^{\circ}\text{C}$ and (b) $+20^{\circ}\text{C}$ to $+180^{\circ}\text{C}$ as a function of the angles γ and ϕ (see text). [Reproduced from Olf, H. G. *J. Polym. Sci. (A-2)* 1971, 9, 1851 by permission of John Wiley, New York]

segments of a chain may dictate its overall behaviour. The symmetrical incorporation of terphenylene or terdiphenylene units into the chain leads to low barriers to chain motion. This is contrasted with the situation in poly(1,3-phenylene isophthalamide) where the units are not symmetrically incorporated with consequently higher barriers.

Main chain translations in PTFE and FEP, suggested earlier from X-ray diffraction data¹⁰⁸, have been quantitatively confirmed by n.m.r. (Figure 19)^{4, 46}.

The use of fourth moment measurements in the study of molecular motions has been neglected in the past.

This is not surprising in view of the inherent difficulties in their measurement and the long computer times required to perform the lattice sums. Figures 22 and 23 contain the experimental and theoretical results of a recent study on fibres of POM³⁷. The low temperature data provide the distribution functions which describe the statistical orientation of chains in the polymer. These are then used in the subsequent molecular motional calculations. The room temperature data are analysed in terms of main chain oscillations of amplitude 42° , while at 100°C the chains are considered to be both oscillating and translating.

The examples quoted thus far clearly demonstrate the inherent benefits in the use of fibre materials. The method has been extended in a recent study to a sample of nylon-6,6 which had been rolled to produce double orientation²⁷. Fibre symmetry no longer applies since the crystallographic 010 planes lie predominantly parallel to the plane of the polymer film. The direction of H_0 now requires two angles, γ , ϕ , to be uniquely specified. The decrease in M_2 , recorded as a function of γ and ϕ between the temperature intervals -196°C to $+20^{\circ}\text{C}$ and $+20^{\circ}\text{C}$ to $+180^{\circ}\text{C}$, is presented in Figure 24. The decrease in the low temperature interval is explained in terms of segmental motion in the amorphous regions. The strong dependence of this decrease on both γ and ϕ implies double orientation in these regions. The decrease at the higher temperatures is consistent with the onset of large amplitude rotational oscillation which is essentially indistinguishable from full segmental rotation²⁶.

Motions of a general character

The onset of general motions in a polymer is usually associated with the glass transition, that is, the passage from a rigid glass to a rubbery or viscous liquid¹⁵. For semi-crystalline polymers below their melting point, such motions occur in the amorphous regions. Existing theories of the glass transition have been evaluated in terms of the n.m.r. of *o*-terphenyl¹⁰⁹, a material which may be prepared in either the glass or crystalline state. The central feature of the glass transition, as discussed by McCall^{15, 35}, is the cessation of long range order in the regions which are passing through their T_g .

The change in the amorphous T_2 associated with the glass transition is an increase of about two orders of magnitude from $\sim 10^{-5}$ sec to $\sim 10^{-3}$ sec. This increase implies that motions of a very general nature have been attained since virtually all directions are available to the internuclear vectors above T_g ¹¹⁰. The degree of motional vigor attained is not the same in every case. The high temperature T_2 in FEP (Figure 19), for example, is only $\sim 10^{-4}$ sec, which indicates that liquid-like motion is not reached.

The increase in the amorphous T_2 can display an intermediate plateau as observed in branched PE⁴¹ and PCTFE (Figure 21)^{89, 106}. This feature of n.m.r. data requires an explanation in terms of specialized motions, especially in view of the anisotropic nature of the PCTFE fibre results. Preliminary calculations on the preferred motions of loose folds or chain ends at the surface of crystal lamellae, which are of essentially amorphous character, would appear to provide an adequate description of the observed data⁸⁹.

When polymers form the components of a copolymer

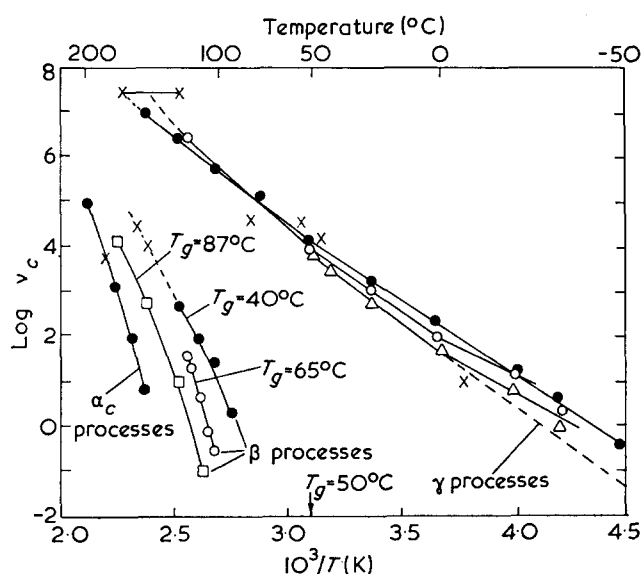


Figure 25 Transition map for PCTFE. \times , n.m.r. correlation frequencies determined from the n.m.r. data of Figure 20. The remaining points are the dielectric and dynamic mechanical data of Hoffman *et al.*¹⁰⁵. Crystallinity: \bullet , 0.80; \circ , 0.44; Δ , 0.12; \square , 0.73

there are often significant differences in their general motional behaviour. Anderson and Liu¹¹¹ have reported T_1 results for a series of diblock copolymers of PS and polybutadiene (PB) as a function of the relative content of each. As the PS content increases beyond 50%, the PB T_1 minimum shifts to higher temperatures, indicating increasing restrictions to motion in the PB. In this case the PB domains are held at constant volume in the glassy PS matrix: PS is well below its T_g and therefore its thermal expansion is much less than for the PB component which is above its T_g . The restrictions to motion are therefore not surprising.

A feature of the T_1 and T_2 results for a SBS block copolymer, which contains 30% PS, is the onset of general motion in PS at a lower temperature in SBS (lower T_g) than in the comparable homopolymer. This is because the PS domains are located in a PB matrix which is in a state of vigorous motion at the temperatures in question⁴⁷. Conversely, the presence of the PS domains leads to a more hindered motion in the PB component of SBS as compared with the homopolymer, as a result of the crosslinking effects of the PS domains.

Transition maps

The correlation of n.m.r. relaxation data with dielectric and dynamic mechanical measurements has been carried out for a large number of polymers¹⁵. The combined results are presented in terms of transition maps which are plots of $\log \nu_c$ vs. reciprocal temperature. The transition map for PCTFE is presented in Figure 25 in which the correlation frequencies, obtained by application of the expressions listed in Table 1 to the n.m.r. data of Figure 20, are compared with the dielectric and mechanical results of Hoffman *et al.*¹⁰⁵. The satisfactory agreement between the various measurements is typical of most polymers.

HIGH RESOLUTION STUDIES IN SOLID POLYMERS

The relaxation theory outlined in the earlier part of this review derives solely from the dipolar mechanism:

chemical shift, σ , and scalar spin-spin J coupling interactions have been neglected because of their relative insignificant contributions. This is reflected in the type of spectra observed for solids which are generally structureless and lack the fine detail associated with σ and J type interactions. The high resolution spectra of liquids in which the dipolar interactions are randomized to zero may be contrasted with typical spectra from solids.

The observation of high resolution spectra from solids has been a compelling goal which has been achieved with a reasonable measure of success. The aim of the high resolution experiment is to remove or severely attenuate the dipolar contribution. In one approach the sample is rotated rapidly at 54.7° , the 'magic angle', to the laboratory field H_0 ^{112, 113}. The angular dependence introduced into the dipolar Hamiltonian by such macroscopic rotations has the form of the second Legendre polynomial which is zero at the magic angle. An alternative method is to leave the sample fixed and to rotate the magnetic field electrically^{114, 116}. A third approach involves the use of multiple pulses^{54-59, 117-122}. High resolution spectra of rare species, ^{13}C ($\sim 1.1\%$ abundance), have recently been achieved by double resonance methods^{121, 122}.

Multiple pulse methods

When a solid is subjected to a sequence of suitable identical pulse cycles, a time dependence is imposed upon the nuclear spin vectors in such a way as to cause severe attenuation of the dipolar Hamiltonian when averaged over a cycle. The scalar coupling and chemical shift effects do not vanish and a liquid-like situation prevails in the solid. In addition, the anisotropy in the chemical shift is preserved, in contrast to liquids. Several pulse sequences, of differing degrees of refinement and complexity, have been devised to achieve this result. The free induction decay is prolonged to much longer times, of the order of $T_{1\rho}$ as opposed to the normal T_2 ⁵⁹. This is equivalent to line narrowing of the absorption spectrum. The closer the values of these two relaxation times the less chance there will be of achieving line narrowing. In a polymer at low temperatures $T_{1\rho}$ and T_2 tend to be widely different while the vigorous general motions above T_g can yield values of $T_{1\rho}$ and T_2 which are not very different. In viscous liquids it may well be that no line narrowing is possible by artificial means⁵⁹. It follows then that the presence of internal motion places a limit on the ultimate degree of line narrowing which can be achieved. Limiting linewidths of 1-2 kHz have been observed in several fluorocarbons at room temperature^{59, 123}.

Consider now the results of Ellett *et al.*¹²³ for the copolymer tetrafluoroethylene-perfluoromethylvinylether (TFE/PFMVE). The sample was subjected to the following pulse cycle:

$$(P_x, 2\tau, P_{-x}, \tau, P_y, 2\tau, P_{-y}, \tau)$$

where P_x denotes a pulse which rotates the nuclear magnetization through 90° about the x axis etc. The nuclear signal is sampled once every cycle. About 100 cycles are required to construct the free induction decay of Figure 26. This decay may be compared with the normal block decay which is structureless and which is characterized by a $T_2 \approx 50 \mu\text{sec}$ at room temperature. The narrow line of the absorption spectrum

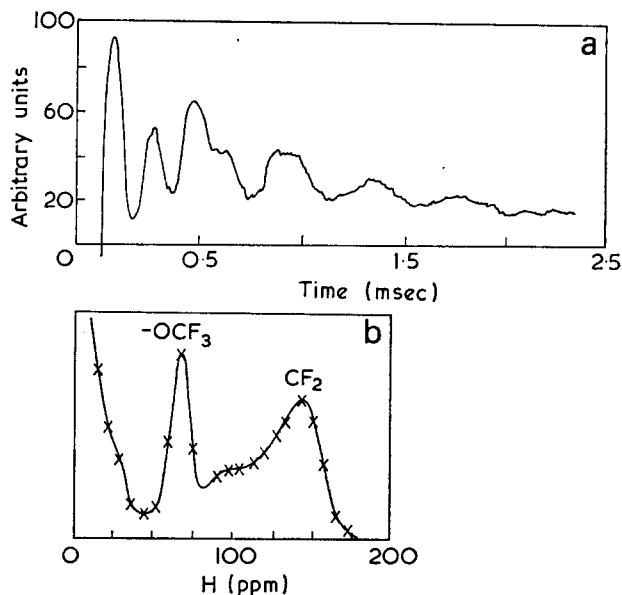


Figure 26 (a) High resolution free induction decay observed in TFE/PFMVE and (b) its Fourier transform, the ^{19}F absorption spectrum. [Reproduced from Ellett, D., Haeberlen, U. and Waugh, J. S. *J. Polym. Sci. (B)* 1969, 7, 71 by permission of John Wiley, New York]

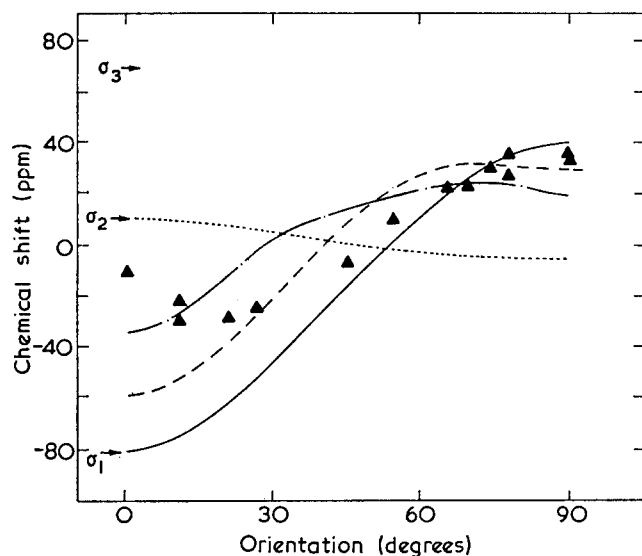


Figure 27 Chemical shift pattern in PTFE fibres as a function of fibre orientation, θ , in the magnetic field H_0 . \blacktriangle , experimental; theoretical: —, $\psi=0^\circ$; ---, $\psi=30^\circ$; - · - ·, $\psi=45^\circ$; ····, $\psi=90^\circ$

Table 5 Principal values of the ^{19}F shielding tensor for PTFE with C_6F_6 as reference (ppm)

σ_{11}	σ_{22}	σ_{33}	$\bar{\sigma}$	Temperature (K)	Sample form	Reference
-71	+20	+51	-41	153	Bulk	126
-80	+21	+59	-40	81	Bulk	126
-100	+22	+78	-39	77	Bulk	56
-80	+10	+70	-30	77	Fibres	125

on the low field side is assigned to the $-\text{OCF}_3$ and the high field peak to $-\text{CF}_2-$ groups. The areas under the peaks agree reasonably with the relative amounts of material present in the polymer. The separation of the peaks is 73 ± 4 ppm compared with 65 ± 0.3 ppm determined from the high resolution spectrum of the polymer

in solution. The asymmetry of the $-\text{CF}_2-$ peak is consistent with anisotropy in the chemical shift tensor¹²⁴.

Mansfield and coworkers have measured the principal values of the ^{19}F shielding tensor in PTFE, both in bulk and fibre form^{56, 125}, using symmetrized pulse sequences¹¹⁹. Their fibre results are summarized in Figure 27 as a function of fibre orientation in the laboratory field H_0 . Their data indicate that the most screened component lies along the CF bond while the least screened component is aligned at $\psi=30-45^\circ$ to the helical axis of the polymer chain. Their chemical shift results are compared with those of Mehring *et al.*¹²⁶ in Table 5.

In a double resonance experiment they have observed chemical shift anisotropy of ^{13}C in bulk PTFE¹²². They assign the values -130 ± 25 ppm to the isotropic chemical shift, $\bar{\sigma}$, -30 ppm to σ_{\perp} and $+60$ ppm to σ_{\parallel} , respectively.

Macroscopic rotation method

Several polymers have been studied by the macroscopic rotation technique, which include PTFE, PMMA, PS, PE and polyisobutylene (PIB)^{12, 13, 127-129}. Line narrowing at room temperature was achieved in all but the last polymer. Ideally one would expect line narrowing to occur when the frequency of macroscopic rotation, Ω_r , becomes comparable with the static line width, $\delta\omega$, expressed in frequency units. The maximum spinning frequencies which can be attained at present, 12.5 kHz ¹³⁰, fall short of the typical rigid lattice linewidths which are of the order of 50 kHz in polymers. It emerges that internal motions within the polymer play a fundamental role in the experiment. Andrew and Jasinski¹³¹ have examined the problem in detail and have found that rotation at the magic angle reduces the linewidth to a limiting value $\delta\omega_l$ given by the expression:

$$\delta\omega_l = \omega_a \tau_a + \left(\frac{\omega_{1b}}{\Omega_r} \right)^2 \tau^{-1} \quad (30)$$

The internal restricted motion reduces the rigid lattice second moment by the amount ω_{1a}^2 to a residual value of ω_{1b}^2 , expressed in angular frequency units. The motion responsible for the internal narrowing is characterized by the correlation time τ_a ($\omega_{1a}\tau_a < 1$). Any other motions which may be present and which are too slow to produce line narrowing are characterized by the correlation time τ_b ($\omega_{1b}\tau_b > 1$). Thus we see that the limiting linewidth depends upon the τ values for the internal microscopic motions. The linewidth will be narrowest under microscopic rotation when τ_a is very short and τ_b is very long¹¹². For viscous fluids $\omega_{1b} \approx 0$ and therefore $\delta\omega_l = \omega_{1a}^2 \tau_a$ whether at rest or rotated. Generally speaking, there is no further narrowing possible when there is extensive internal isotropic motion. It is therefore not surprising that narrowing could not be achieved in PIB which is well above its T_g at room temperature¹⁵.

The expression for the limiting linewidth, equation (30), in rotated specimens is also applicable to the multiple pulse method which suffers from the same limitations; in that case Ω_r is identified as the cycle frequency instead of the specimen rotation frequency.

Schneider *et al.*¹³ have applied the results of Andrew and Jasinski to a series of PE samples. The broad crystalline peak is unaffected by sample rotation. The amorphous peak narrows considerably and side bands are developed. Their experimental spectra cannot be

Table 6 Results of analysis of n.m.r. spectra of PE samples measured at magic angle rotation. [Reproduced from Schneider, B., Pivcova, H. and Dosekocilova, D. *Macromolecules* 1972, 5, 120 by permission of the American Chemical Society, Washington, D.C. ©]

Sample density (g/cm ³)	Composition (%)				Static linewidth (G)		Residual linewidth (G)	
	Crystal	Amorphous		$\delta\omega_{1b}$		$\delta\omega_f$		
		I	II	I	II	I	II	
0.962	89.8	3.4	6.8	1.6	4.4	0.35	0.8	
0.960	81.4	6.2	12.4	1.6	4.4	0.35	0.8	
0.953	81.4	6.2	12.4	1.6	4.4	0.35	0.8	
0.930	68.0	16.8	15.2	0.8	2.4	0.2	0.4	
0.929	68.0	16.2	15.2	0.8	2.4	0.2	0.4	
0.919		47.5	52.5	0.2	1.5	0.1	0.3	

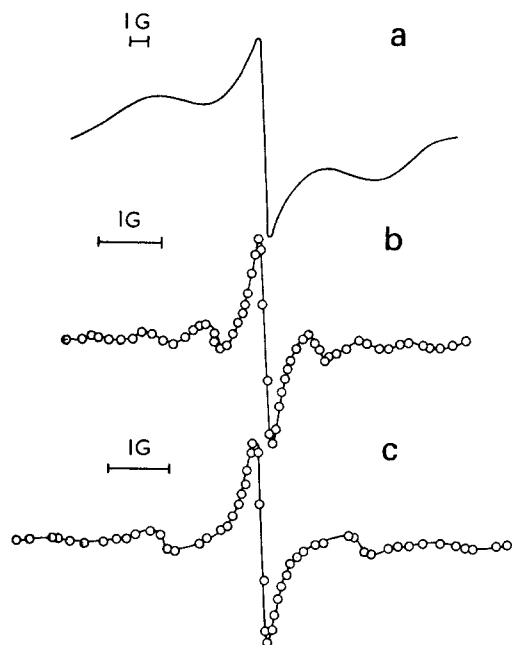


Figure 28 High resolution spectra of PE derived from macroscopic rotation of the sample. The lines are experimental traces and the points theoretical. (a) $\Omega_r=0$; (b) $\Omega_r=3650$; (c) $\Omega_r=6800$ Hz. [Reproduced from Schneider, B., Pivcova, H. and Dosekocilova, D. *Macromolecules* 1972, 5, 120 by permission of the American Chemical Society, Washington, D.C. ©]

interpreted in terms of a single amorphous component; at least two are required. The results of their analysis are presented in Table 6 and their calculated line shapes are compared with the experimental spectra in Figure 28. It is appropriate to note that the term rigid or crystalline is here attached to those regions for which the residual linewidth is larger than the spinning frequency Ω_r . The estimated correlation time τ_a for the internal motion in the amorphous regions varies between 10^{-6} sec for component II in the most highly crystalline sample to 10^{-7} sec for component I in the sample of lowest crystallinity.

High resolution studies by the rotation method are finding increasing application in the study of biopolymers. While it is not intended to digress into the area of biopolymers in this review, a particularly interesting example may be quoted in which the internal motions in lecithin and other biopolymers of interest in relation to membranes have been examined¹³².

In summary, the application of these techniques to polymers has yet to be fully developed and exploited.

The profound effects of internal motion on the observation, or otherwise, of narrowed spectra may be examined further as a function of temperature. The implications of correlation frequency distributions which are undoubtedly present in polymers¹⁷ have yet to be fully assessed.

ACKNOWLEDGEMENTS

The author is indebted to Professors E. R. Andrew, C. F. G. Delaney and D. C. Pepper and Drs P. Mansfield, D. C. Douglass, T. M. Connor, I. R. McDonald and T. Morton-Blake who critically read the manuscript. Professor Andrew and Dr Mansfield kindly provided results prior to publication. Valuable technical assistance was provided by Mr V. Weldon.

REFERENCES

- Wilson, C. W. and Pake, G. E. *J. Polym. Sci.* 1953, 10, 503
- Slichter, W. P. and McCall, D. W. *J. Polym. Sci.* 1957, 25, 230
- McCall, D. W. and Douglass, D. C. *Polymer* 1963, 4, 433
- McCall, D. W., Douglass, D. C. and Falcone, D. R. *J. Phys. Chem.* 1967, 71, 998
- McCall, D. W. and Anderson, E. W. *J. Chem. Phys.* 1962, 32, 237
- Richardson, M. J. *Br. Polym. J.* 1969, 1, 132
- Connor, T. M. *Br. Polym. J.* 1969, 1, 116
- Douglass, D. C. and McBrierty, V. J. *J. Chem. Phys.* 1971, 54, 4085
- Bergmann, K. and Nawotki, K. *Kolloid-Z. Z. Polym.* 1967, 219, 132
- Loboda-Cackovic, J., Hosemann, R. and Wilke, W. *Kolloid-Z. Z. Polym.* 1969, 235, 1253
- Piesczek, W. and Fischer, E. W. *IUPAC Macromol. Symp. Prepr., Leiden* 1970, 13, 873
- Schneider, B., Dosekocilova, D. and Pivcova, H. *IUPAC Macromol. Symp. Prepr.* 1970, 12, 869
- Schneider, B., Pivcova, H. and Dosekocilova, D. *Macromolecules* 1972, 5, 120
- Hoch, M. J. R., Bovey, F. A., Davis, D. D., Douglass, D. C., Falcone, D. R., McCall, D. W. and Slichter, W. P. *Macromolecules* 1971, 4, 712
- McCall, D. W. *Nat. Bur. Stand. Spec. Pub.* 310 1969, p 475
- Williams, M. L., Landel, R. F. and Ferry, J. D. *J. Am. Chem. Soc.* 1955, 77, 3701
- Connor, T. M. *Trans. Faraday Soc.* 1963, 60, 1574
- Abragam, A. 'The Principles of Nuclear Magnetism', Clarendon Press, Oxford, 1961
- Bloembergen, N. 'Nuclear Magnetic Relaxation', Benjamin, New York, 1961
- Bloembergen, N., Purcell, E. M. and Pound, R. V. *Phys. Rev.* 1948, 73, 679
- Jones, G. P. *Phys. Rev.* 1966, 148, 332
- Slichter, C. P. and Ailion, D. *Phys. Rev. (A)* 1964, 135, 1099
- Van Vleck, J. H. *Phys. Rev.* 1948, 74, 1168
- Yamagata, K. and Hirota, S. *Rep. Progr. Polym. Phys. Japan* 1962, 5, 236
- McBrierty, V. J. and Ward, I. M. *J. Phys. (D)* 1968, 1, 1529
- Olf, H. G. and Peterlin, A. *J. Polym. Sci. (A-2)* 1970, 8, 753
- Olf, H. G. *J. Polym. Sci. (A-2)* 1971, 9, 1851
- McBrierty, V. J. and Douglass, D. C. *J. Magnet. Reson.* 1972, 2, 352
- Roe, R.-J. *J. Polym. Sci. (A-2)* 1970, 8, 1187
- Kashiwagi, M., Cunningham, A., Manuel, A. J. and Ward, I. M. *Polymer* 1973, 14, 111
- McBrierty, V. J. *J. Chem. Phys.* in press
- Douglass, D. C. and Jones, G. P. *J. Chem. Phys.* 1966, 45, 956
- Connor, T. M. 'NMR Basic Principles and Progress', Springer-Verlag, Berlin, 1971, Vol 4, p 247
- McCall, D. W. and Douglass, D. C. *Appl. Phys. Lett.* 1965, 7, 12
- McCall, D. W. *Acc. Chem. Res.* 1971, 4, 223
- McBrierty, V. J., McDonald, I. R. and Ward, I. M. *J. Phys. (D)* 1971, 4, 88

- 37 McBrierty, V. J. and McDonald, I. R. *J. Phys. (D)* 1973, **6**, 131
- 38 Bloembergen, N. *Physica* 1949, **15**, 386
- 39 Trappeniers, N. J., Gerritsma, C. J. and Oosting, P. H. *Physica* 1964, **30**, 997
- 40 Powles, J. G. and Hunt, B. I. *Phys. Lett.* 1965, **14**, 202
- 41 McCall, D. W. and Falcone, D. R. *Trans. Faraday Soc.* 1970, **66**, 262
- 42 Crist, B. and Peterlin, A. *J. Polym. Sci. (A-2)* 1969, **7**, 1165
- 43 Crist, B. and Peterlin, A. *J. Macromol. Sci. (B)* 1970, **4**, 791
- 44 Connor, T. M. *J. Polym. Sci. (A-2)* 1970, **8**, 191
- 45 Crist, B. *J. Polym. Sci. (A-2)* 1971, **9**, 1719
- 46 McBrierty, V. J., McCall, D. W., Douglass, D. C. and Falcone, D. R. *J. Chem. Phys.* 1970, **52**, 512
- 47 Wardell, G. E., McBrierty, V. J. and Douglass, D. C. to be published
- 48 Douglass, D. C. and McCall, D. W. *J. Phys. Chem.* 1958, **62**, 1102
- 49 Stejskal, E. O. and Tanner, J. E. *J. Chem. Phys.* 1965, **42**, 288
- 50 Carr, H. Y. and Purcell, E. M. *Phys. Rev.* 1954, **94**, 630
- 51 e.g. Ingram, D. J. E. 'Spectroscopy at Radio and Microwave Frequencies', Butterworths, London, 1967
- 52 Technical specifications of the Bruker spectrometer, Type 321-3
- 53 Farrar, T. C. and Becker, E. D. 'Pulse and Fourier Transform NMR', Academic Press, New York, 1971
- 54 Mansfield, P. and Ware, D. *Phys. Lett.* 1966, **22**, 133
- 55 Ostroff, E. D. and Waugh, J. S. *Phys. Rev. Lett.* 1966, **16**, 1097
- 56 Mansfield, P., Orchard, M. J., Stalker, D. C. and Richards, K. H. B. *Phys. Rev. (B)* 1973, **7**, 90
- 57 Waugh, J. S., Huber, L. M. and Haeberlen, U. *Phys. Rev. Lett.* 1968, **20**, 180
- 58 Waugh, J. S., Wang, C. H., Huber, L. M. and Vold, R. L. *J. Chem. Phys.* 1968, **48**, 662
- 59 Haeberlen, U. and Waugh, J. S. *Phys. Rev.* 1968, **175**, 453; 1969, **185**, 420
- 60 Lowe, I. J. and Norberg, R. E. *Phys. Rev.* 1957, **107**, 46
- 61 Kaufman, S., Slichter, W. P. and Davis, D. D. *J. Polym. Sci. (A-2)* 1971, **9**, 829
- 62 Wardell, G. E. and McBrierty, V. J. *Proc. R. Irish Acad.* 1973, **73**, 63
- 63 Douglass, D. C. and McBrierty, V. J. to be published
- 64 Shevelev, V. A. *Polym. Sci. USSR* 1972, **13**, 2601
- 65 Slichter, W. P. *J. Polym. Sci. (C)* 1966, **14**, 33
- 66 Hunt, B. I., Powles, J. G. and Woodward, A. E. *Polymer* 1964, **5**, 339
- 67 Meyer, L. H. *Thesis Univ. of Illinois* (1963)
- 68 Slichter, W. P. *J. Polym. Sci.* 1957, **24**, 173
- 69 McCall, D. W. and Slichter, W. P. *J. Polym. Sci.* 1957, **26**, 171
- 70 Hyndman, D. and Origlio, G. F. *J. Polym. Sci.* 1959, **39**, 556
- 71 Hyndman, D. and Origlio, G. F. *J. Appl. Phys.* 1960, **31**, 1849
- 72 Hyndman, D. and Origlio, G. F. *J. Polym. Sci.* 1960, **46**, 259
- 73 Yamagata, K. and Hirota, S. *Rep. Progr. Polym. Sci. Japan* 1962, **5**, 236
- 74 Peterlin, A. and Olf, H. G. *J. Polym. Sci. (B)* 1964, **2**, 409
- 75 Peterlin, A. and Olf, H. G. *J. Polym. Sci. (B)* 1964, **2**, 769
- 76 Olf, H. G. and Peterlin, A. *J. Appl. Phys.* 1964, **35**, 3108
- 77 Koltzov, A. I. and Volkenstein, M. W. *Vysokomol. Soedin.* 1965, **7**, 250
- 78 McMahan, P. E. *J. Polym. Sci. (A-2)* 1966, **4**, 639
- 79 Lando, J. B., Olf, H. G. and Peterlin, A. *J. Polym. Sci. (A-1)* 1966, **4**, 941
- 80 Peterlin, A. and Olf, H. G. *J. Polym. Sci. (A-2)* 1966, **4**, 587
- 81 Olf, H. G. and Peterlin, A. *Makromol. Chem.* 1967, **104**, 135
- 82 Olf, H. G. and Peterlin, A. *J. Polym. Sci. (A-2)* 1970, **8**, 771, 791
- 83 McBrierty, V. J., McCall, D. W., Douglass, D. C. and Falcone, D. R. *Macromolecules* 1971, **4**, 584
- 84 McBrierty, V. J., Douglass, D. C. and Falcone, D. R. *JCS Faraday Trans. II* 1972, **68**, 1051
- 85 Slonim, I. Ya. and Lyubimov, A. N. 'The NMR of Polymers', Plenum Press, New York, 1970
- 86 Kashiwagi, M., Folkers, M. J. and Ward, I. M. *Polymer* 1971, **12**, 697
- 87 Kashiwagi, M. and Ward, I. M. *Polymer* 1972, **13**, 145
- 88 Ward, I. M. *Proc. Phys. Soc.* 1962, **80**, 1176
- 89 McBrierty, V. J. and Douglass, D. C. to be published
- 90 McBrierty, V. J. *J. Chem. Phys.* in press
- 91 Roe, R.-J. *J. Appl. Phys.* 1963, **36**, 2024
- 92 McCall, D. W. and Hamming, R. W. *Acta Crystallog.* 1959, **12**, 81
- 93 Gupta, V. B. and Ward, I. M. *J. Macromol. Sci. (B)* 1970, **4**, 453
- 94 Slichter, W. P. 'NMR Basic Principles and Progress', Springer-Verlag, Berlin, 1971, Vol 4, p 209
- 95 Slichter, W. P. and Davis, D. D. *J. Appl. Phys.* 1964, **35**, 3013
- 96 Fuschillo, N. and Sauer, J. A. *J. Appl. Phys.* 1957, **28**, 1073
- 97 McCall, D. W., Douglass, D. C. and Anderson, E. W. *J. Polym. Sci. (A)* 1963, **1**, 1709
- 98 Barrier, J. A., Fredrickson, M. J. and Sheppard, R. *Polymer* 1972, **13**, 431
- 99 July, H. R., Miller, W. G. and Bryant, R. G. *Macromolecules* 1973, **6**, 262
- 100 Bezrukov, O. F., Budtov, V. P., Kilolayev, B. A. and Fokanov, V. P. *Vysokomol. Soedin. (A)* 1971, **13**, 876; *Polym. Sci. USSR* 1971, **13**, 988
- 101 Blundell, D. J., Keller, A. and Connor, T. M. *J. Polym. Sci. (A-2)* 1967, **5**, 991
- 102 Droste, D. H., DiBenedetto, A. T. and Stejslal, E. O. *J. Polym. Sci. (A-2)* 1971, **9**, 187
- 103 Larsen, D. W. and Strange, J. H. *J. Polym. Sci. (Polym. Phys.)* 1973, **11**, 65; 1973, **11**, 449
- 104 McCall, D. W., Douglass, D. C., McBrierty, V. J. and Hoch, M. J. R. *Discuss. Faraday Soc.* 1969, **48**, 205
- 105 Hoffman, J. D., Williams, G. and Passaglia, E. *J. Polym. Sci. (C)* 1966, **14**, 173
- 106 McBrierty, V. J., McCall, D. W. and Douglass, D. C. *Bull. Am. Phys. Soc.* 1970, **15**, 307
- 107 Woodward, A. E., Landis, J. and Frosini, V. *J. Polym. Sci. (A-2)* 1972, **10**, 2051
- 108 Bunn, C. W. and Howells, E. R. *Nature* 1962, **174**, 119
- 109 McCall, D. W., Douglass, D. C. and Falcone, D. R. *J. Chem. Phys.* 1969, **50**, 3839
- 110 McCall, D. W. and Anderson, E. W. *J. Polym. Sci. (A)* 1963, **1**, 1175
- 111 Anderson, J. E. and Liu, K.-J. *Macromolecules* 1971, **4**, 260
- 112 e.g., Andrew, E. R. *Pure Appl. Chem.* 1972, **32**, 41
- 113 Lowe, I. J. *Phys. Rev. Lett.* 1959, **2**, 285
- 114 Andrew, E. R. and Eades, R. G. *Discuss. Faraday Soc.* 1962, **34**, 38
- 115 Andrew, E. R., Apaydin, Y. and Moore, W. S. *Phys. Lett. (A)* 1967, **25**, 44
- 116 Bradbury, A., Eades, R. G. and McCarten, J. G. *Phys. Lett. (A)* 1968, **26**, 405
- 117 Mansfield, P., Richards, K. H. B. and Ware, D. *Phys. Rev. (B)* 1970, **1**, 2048
- 118 Mansfield, P. in 'Progress in Nuclear Magnetic Resonance Spectroscopy' (Eds J. W. Emsley, J. Feeney and L. H. Sutcliffe), Pergamon, Oxford, 1971, Vol 8, p 41
- 119 Mansfield, P. *J. Phys. (C)* 1971, **4**, 1444
- 120 Mansfield, P. and Haeberlen, U. *Z. Naturforsch. (A)* 1973, **28**, 1081
- 121 Grannell, P. K. and Mansfield, P. *Phys. Rev.* in press
- 122 Grannell, P. K. and Mansfield, P. *Ist Spec. Colloq. Ampere, Cracow (Poland)* 1973
- 123 Ellett, D., Haeberlen, U. and Waugh, J. S. *J. Polym. Sci. (B)* 1969, **7**, 71
- 124 Andrew, E. R. and Tunstall, D. P. *Proc. Phys. Soc.* 1963, **81**, 986
- 125 Garroway, A. N., Stalker, D. C. and Mansfield, P. *Ist Spec. Colloq. Ampere, Cracow (Poland)* 1973
- 126 Mehring, M., Griffin, R. G. and Waugh, J. S. *J. Chem. Phys.* 1971, **55**, 746
- 127 Schnabel, B. and Taplick, T. *Phys. Lett. (A)* 1968, **27**, 310
- 128 Moritz, P. and Schnabel, B. *Plaste Kautsch.* 1972, **19**, 281
- 129 Benoit, H. and Rabii, M. C. R. *16th Ampere Congr., Bucharest* 1970, p 1060
- 130 Andrew, E. R., Farnell, L. F., Firth, M., Gledhill, T. D. and Roberts, I. *J. Magnet. Reson.* 1969, **1**, 27
- 131 Andrew, E. R. and Jasinski, A. *J. Phys. (C)* 1971, **4**, 391
- 132 Chapman, D., Oldfield, E., Doskocilova, D. and Schneider, B. *FEBS Lett.* 1972, **25**, 261

Liquid rubbers and the problems involved in their application*

J. P. Berry and S. H. Morrell

*Rubber and Plastics Research Association, Shawbury, Shrewsbury SY4 4NR, UK
(Received 17 December 1973)*

INTRODUCTION

The techniques used in conventional rubber technology are based on and related to the properties of the first available raw material, natural rubber, which in the most commonly used form of baled smoked sheet is a high molecular weight polymer ($\sim 6 \times 10^6$) of such high viscosity as to be effectively solid. When synthetic rubbers became available, they were produced in the same base form as natural rubber, so as to be compatible with the available processing machinery and technological practices. To convert the solid mass into useful products requires that it be transformed into the desired shape and that this shape be rendered dimensionally stable by vulcanization. The chemical ingredients required for vulcanization, and the other agents such as fillers which are used to modify the final properties, are finely divided powders, and there is consequently a basic problem of homogeneously dispersing these ingredients into the solid rubber. In order to do so it is necessary to break down the structure of the rubber and reduce its molecular weight by mechanical action (mastication). Because of the high viscosity of the raw rubber the mastication process requires heavy duty machinery and it consumes large amounts of energy. The reduction in viscosity which permits the incorporation of powders also facilitates the shaping process. However, the high abrasion and fatigue resistance of vulcanisates as well as their good tensile strength and tear resistance are a direct consequence of the network structure produced by the crosslinking of long molecules. Thus in all current processes of the manufacture of rubber products there is a continual compromise between the need to maintain the final properties of the vulcanisate by maintaining the high molecular weight of the polymer and the need to reduce the viscosity to enable the powder ingredients to be incorporated and to allow moulding to be carried out under reasonably convenient conditions.

One way of overcoming the difficulty of mixing-in the powder ingredients is to start with a lower molecular weight and hence less viscous material. Accordingly, natural rubber can be degraded chemically and the polymerization of synthetic rubbers terminated at an earlier stage, but unfortunately the final products made from such liquid rubbers have poor mechanical properties because of the high proportion of elastically inactive free chain ends. A way out of this difficulty is

indicated by the polyurethane elastomers. In these systems the basic material is a relatively low molecular weight polyether or polyester with the important distinction that the polymer chains are terminated by chemically reactive hydroxyl groups. These groups are reacted with di-isocyanates to give chain extension and crosslinking. The free end fraction of the resultant network is thereby reduced and the mechanical properties correspondingly increased.

This principle has been applied to the synthesis of reactively terminated low molecular weight rubbers, based on butadiene homo- and co-polymers. These materials have found extensive use as binders for solid rocket propellants, an application which does not make severe demands on their physical properties and where dispersion of the filler poses no significant problems, because of its relative coarseness. There has, however, been increasing interest in the possibility of using these materials more generally for the manufacture of mechanical rubber goods and to fulfil the requirements of these applications poses significant problems, chemical, physical, mechanical and technological as well as economic.

CHEMICAL PROBLEMS

In principle the reactively terminated liquid rubbers offer the opportunity to produce networks of known structure and topology by starting with a strictly linear polymer of known molecular weight distribution and with a reactive group at each end of each molecule, and reacting this polymer with crosslinking agents of known and consistent functionality. The present level of understanding of the relation between structure and properties indicates that the reduction or elimination of network defects by the use of such systems would result in greatly improved physical properties. However, the structure of the available liquid rubbers (*Table 1*) is not closely controlled or even well defined¹. Thus although average molecular weights are quoted, little is known about the molecular weight distribution. Of perhaps greater import is the uncertainty associated with the functionality of the polymer, i.e. the average number of reactive groups per molecule. As indicated in *Table 1* this is, in most cases, greater than 2, and may be as high as 2.8. Furthermore, it must be recognized that this is only an average figure and the distribution of the functionality of the molecules is not known. Consequently there may be present in the system molecules which do not possess any reactive groups and

* Presented as a Symposium Lecture at the IUPAC International Symposium on Macromolecules, Aberdeen, September 1973.

Table 1 Liquid rubbers

Name	Chemical type	Mol Wt	Functionality
A. Not reactively terminated			
Flosbrene MV	Low SBR	5000	0
B. Reactively terminated			
ARCO R45M	OH-terminated polybutadiene	2400-3200	2·2-2·4
R45HT	OH-terminated polybutadiene	3100-3500	2·2-2·4
R15M	OH-terminated polybutadiene	3500-4000	2·5-2·8
ARCO CS15	OH-terminated SBR	3800-4300	2·5-2·8
CN15	OH-terminated nitrile (15%)	4200-4700	1·5-2·8
Polymer Corp. Ltd. XPRD-B241	Br-terminated polybutadiene		
Thiokol HC434	COOH-terminated polybutadiene	3800	1·9-2·25
Hycar CTB	COOH-terminated polybutadiene	5000	~2·0

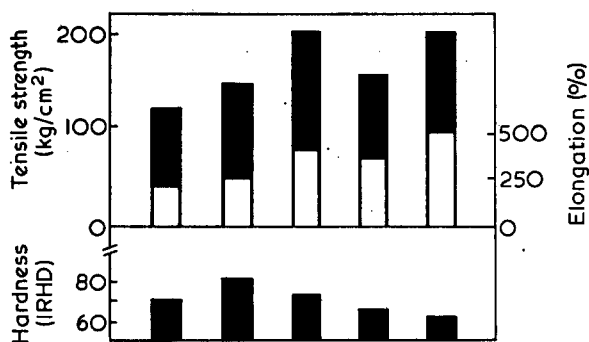


Figure 1 Comparison of physical properties of black-loaded liquid rubbers². From left to right: liquid SBR polymer; hydroxyl-terminated polybutadiene; bromine-terminated polybutadiene; carboxyl-terminated polybutadiene; solid polybutadiene. ■, Tensile strength or hardness; □, elongation

which therefore will not be incorporated into the network, but will remain as a plasticizer or sol fraction. Similarly, molecules containing only one reactive group will severely limit the capacity of the system to increase in molecular weight by chain extension. Significant proportions of molecules of functionality 3 or more will cause chain-branching and ultimately gelation.

The hydroxyl-terminated polymers can be chain-extended and crosslinked with di-isocyanates, in the same way as the polyether and polyester precursors of the polyurethanes, and, as in these latter systems, traces of water can cause undesirable side reactions. Carboxyl-terminated liquid rubbers can be chain-extended with di-epoxides such as the diglycidyl ether of bisphenol A (4,4'-dihydroxydiphenyl-2,2-propane), while a mixture of difunctional and trifunctional epoxides will yield a crosslinked product. The third commercially available type of liquid rubber is terminated with bromine and this can be treated with a mixture of di- and polyamines to give a solid vulcanisate. The physical properties of the simple (gum) elastomers prepared in the various ways are inadequate for most practical applications and reinforcement with carbon black is necessary. At a filler loading of 50 parts by weight of HAF black to 100 parts by weight of rubber (i.e. 50 phr) typical mechanical properties are as shown in Figure 1.

PHYSICAL AND MECHANICAL PROBLEMS

It is well known that the full reinforcing effect of carbon black in rubber is only obtained if the filler is adequately dispersed, a result which is difficult to achieve because of the tendency of the particles to form large agglomerates. Deaggregation requires high local shear forces that have to be transmitted through the intervening liquid medium. Thus two levels of mixing of filler into rubber can be distinguished: (a) distribution; and (b) dispersion. In the first the filler is incorporated into and distributed through the rubber to give a macroscopically homogeneous mass and this can best be effected by a folding or kneading action. Here the low viscosity of the liquid rubbers is a distinct advantage.

As indicated in Table 1, the molecular weights of the commercially available liquid rubbers are in the region of 3000-5000, values which correspond to viscosities of between 100 and 500 P at 30°C. They can therefore be poured, albeit slowly, at room temperature and powders, including carbon black, can be readily incorporated by simple paddle stirrers or Z-blade mixers, little power being required for this operation. However, this mild treatment is quite inadequate to achieve the dispersion of the filler to the level needed to confer reinforcement. The relatively low viscosity is, in fact, a disadvantage in this respect since it is correspondingly more difficult to transmit the required level of shear forces through the liquid; high shear rates are required, such as are obtainable for instance on a laboratory three-roll paint mill. Such a technique is not suitable for continuous production and a novel high-shear mixing device has been developed by RAPRA for this purpose² (Figure 2). This machine employs an arrangement of roller bearings to provide the necessary intensive shear and is capable of a throughput of about 25 kg/h. It is perhaps surprising that a 7·5 kW motor is required for this machine since this is about the size required

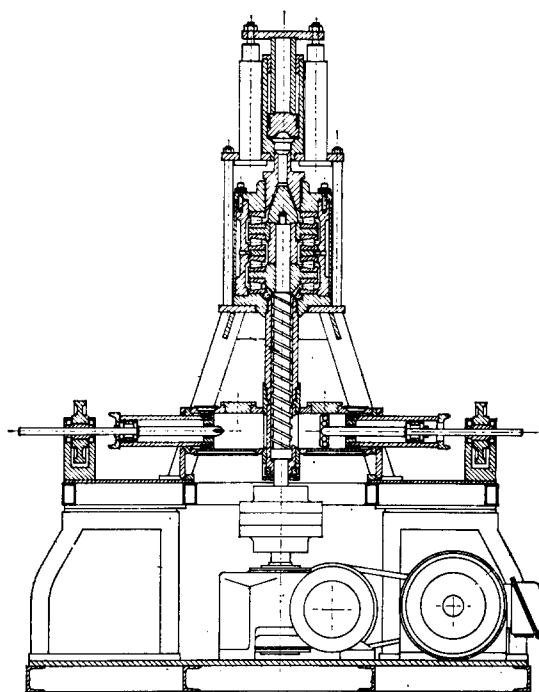


Figure 2 General view of RAPRA intensive mixer for liquid rubbers²

Table 2 Dispersion of carbon black²

	Comment	Best dispersion (Cabot scale)
Tweedy dough mixer	Inadequate; lengthy; large aggregates	G5
Winkworth Z-blade	Lengthy unless fluffy black used	C4-G6
Acheson triple cone mixer	Inadequate; lengthy	B3-D5
Vickers Transfermix	Longer screw required; no back pressure; difficult to feed	F6-G6
3-Roll paint mill	Excellent dispersion; unsuitable for continuous mixing	A1
RAPRA mixer	Continuously produces excellent dispersion	A1

to drive a conventional internal mixer to produce the same output of compound from solid rubber. It seems probable that the limiting factor is the amount of power required to break down the carbon black agglomerates and that this is independent of the viscosity of the rubber matrix. The nature of the dispersion on the Cabot scale obtained by different mixing techniques is indicated in *Table 2*, and micrographs of some of those dispersions are shown in *Figure 3*, together with that of a dispersion obtained with a conventional solid rubber using traditional mixing techniques.

The viscosity of the liquid rubbers is essentially independent of shear rate over the two decades at which measurements have been made (*Figure 4*). However, incorporation and dispersion of carbon black causes a dramatic change in properties. Not only is the viscosity increased but it shows a very marked dependence on

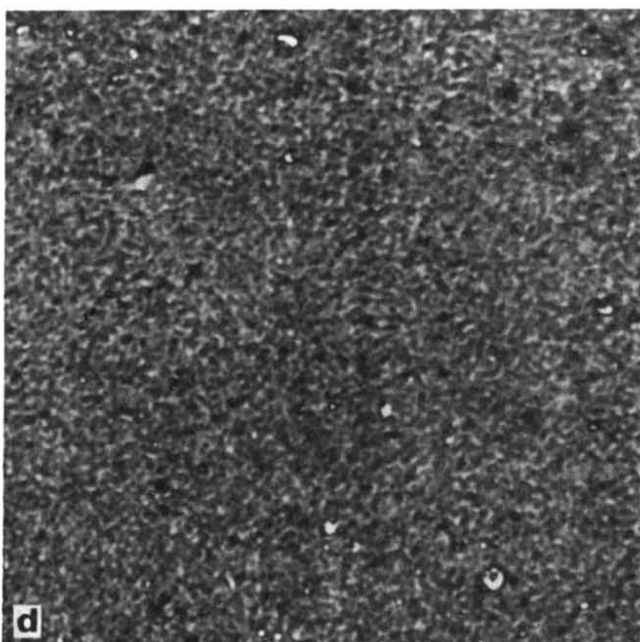
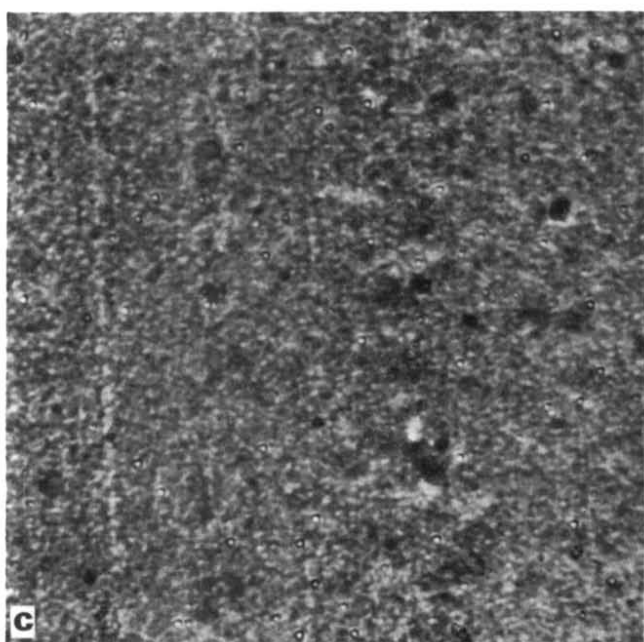
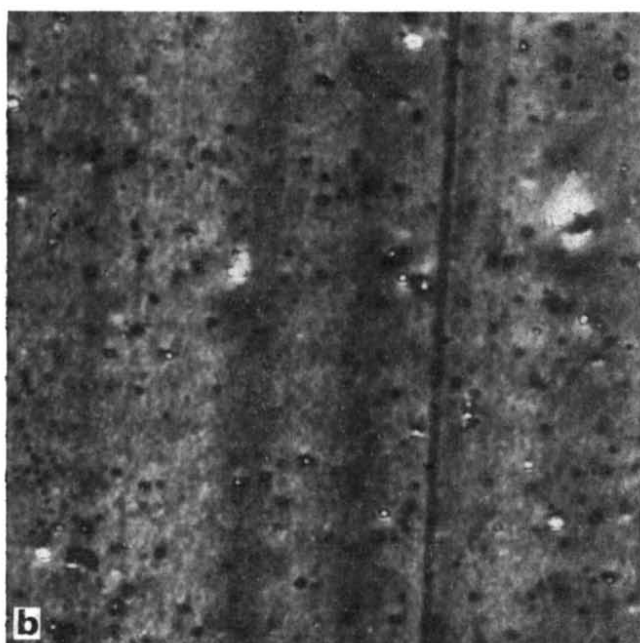
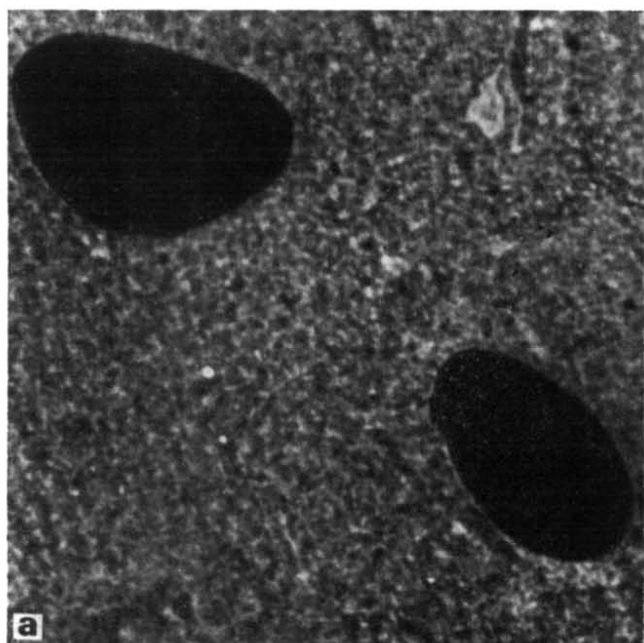


Figure 3 Dispersion of black in liquid rubber². (a) Dough mixer; (b) 3-roll paint mill; (c) RAPRA mixer; (d) solid rubber mixed in internal mixer

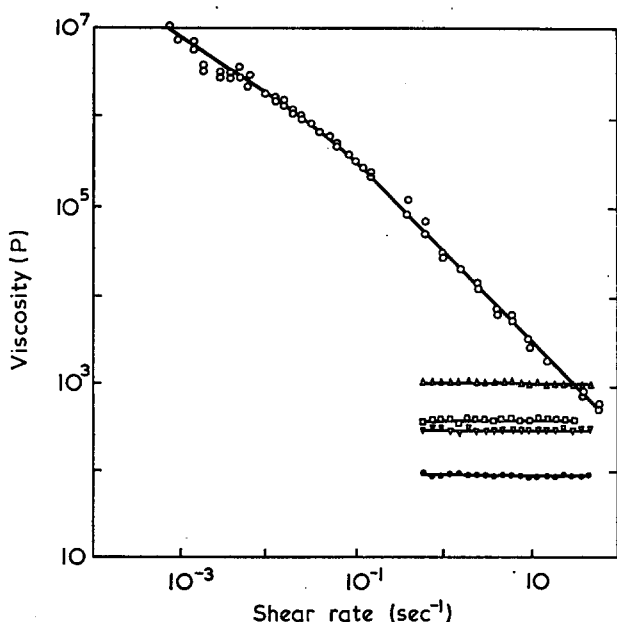


Figure 4 Plots of viscosity against shear rate for rubbers mentioned in Table 1. ○, R45M+50phr HAF black; △, CN15; □, CS15; ▽, HC434; ●, R45M

shear rate, increasing with decreasing shear rate and attaining a value of 10^7 P at the lowest rate at which measurement was possible. The trend of the data is such that even higher viscosities would be expected at lower rates of shear. These results account for the observation that the filled material shows no tendency to flow under its own weight when stored for long periods of time, i.e. it appears to have the consistency of a paste or grease. Once it is caused to flow, however, the resistance to flow decreases rapidly with increasing rate and at sufficiently high rates the viscosity approaches that of the unfilled liquid rubber. Thus the materials have the capacity to retain their shape at rest, but to be readily transported and transformed under the action of relatively small forces; properties which are clearly of importance in developing the appropriate processing technology.

TECHNOLOGICAL PROBLEMS

Processing

Because of their fluid character the unfilled liquid rubbers can be pumped and metered relatively easily. Powdered ingredients can also be metered, using conventional techniques, and the components of a formulation can therefore be fed continuously and in the correct proportions to a mixing unit. The prepared compound can also be transported through pipes to the lightweight equipment required for shaping and vulcanization. These operations can therefore be carried out in a completely closed system without any of the raw materials entering the atmosphere. Such a development is desirable, not only because of the toxic (di-isocyanate) or unpleasant (carbon black) ingredients, but also because of the possibility of greater consistency of the compound and hence of the product. This system also lends itself to the use of injection moulding as a fabrication technique, since full advantage can be taken of the easy flow properties of the compounded liquid rubbers. The working pressures of most injection moulding machines for

conventional rubbers is of the order of 150 MN/m^2 , but it is possible to injection mould liquid rubber compounds at pressures at only 5 MN/m^2 . On an experimental injection moulding machine, discs of 15 cm diameter and 2 mm thickness have been produced and a simple hand toggle lever is sufficient to hold the mould closed under the injection pressure required to fill it.

Liquid rubber compounds are particularly suited to the manufacture of complex mouldings and those involving inserts, where the good flow properties at low pressures ensure that the most complicated mould can be readily filled without disturbing any inserts that might be present. A particular case in point is the injection moulding of a liquid rubber tyre tread compound onto a conventional carcass, where the pressures needed for the injection moulding of conventional rubber compounds would so distort the carcass as to make the process unacceptable to tyre retreaders. The feasibility of the process has been established by the use of a modified retreading mould (Figure 5), with which a tyre retreaded with a liquid rubber compound has been produced (Figure 6).

Many rubber products are composite structures, relying on the relative inextensibility of textile cord to confer directional mechanical properties; the most important examples are tyres and braided hose. The fabrication of such products is labour intensive and hand building is often required. Considerable saving in cost could therefore be realized by exploiting the possibility of automation that arises when liquid rubbers are used. Thus the injection moulding of complete tyres from liquid rubbers has been claimed³ although no details of the process or the material have been divulged. However, the tyres are said to contain no

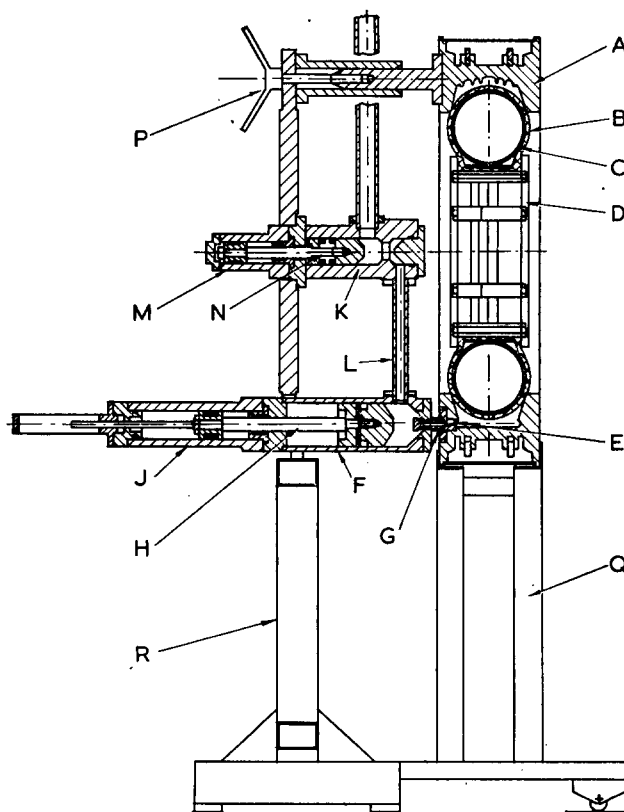


Figure 5 Diagram of injection moulding machine for retreading tyres with liquid rubber²

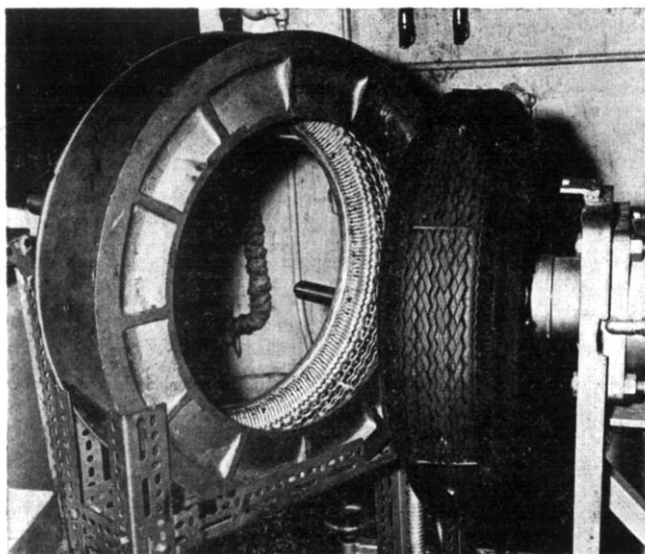


Figure 6 Tyre retreaded with liquid rubber

Table 3 Physical properties of tyre tread compounds

	Solid SBR	Liquid rubbers	
		-COOH	-OH
Tensile strength (MN/m ²)	24	15	15.5
Elongation (%)	540	340	270
200% modulus (MN/m ²)	5.2	5.3	7.2
Hardness (IRHD)	61	63	85
Resilience (%) at 20°C	45	41	50
Resilience (%) at 70°C	55	40	51
Akron abrasion loss (cm ³ /1000 rev)	0.21	1.21	0.43
De Mattia (kcycles to grade J)	> 250	52	44
Heat build-up (°C in 25 min)	49	74	100

'conventional fabric reinforcement' and should this be the case, the prospect of the elimination of hand building that it implies would be of major significance.

There is also the possibility that the use of woven fabrics or braided reinforcement could be avoided by the use of liquid rubber compounds containing short textile fibres as reinforcement⁴. The low viscosity of the compound is again an asset since it ensures good wetting and hence good bonding of the fibre, and even with the fibrous filler incorporated, the mixture can still be moulded easily. Furthermore, the flow processes involved in moulding can cause orientation of the fibres and hence the development of directional mechanical properties.

Compounding

The physical properties of hydroxyl- and carboxyl-terminated liquid rubbers, compounded as for tyre treads, are given in Table 3, together with those of a standard SBR tyre tread compound for comparison. It is evident that the tensile strengths and ultimate elongations of both the liquid rubber compounds are relatively low, while the hardness of the hydroxyl-terminated rubber is unacceptably high. The carboxyl-terminated rubber shows a particularly high abrasion loss while both rubbers have poor flex cracking resistance and high heat build-up properties. It is believed that the deficiency in these properties is due primarily

to the unsatisfactory network structure of the vulcanized elastomers, which, as already discussed, arise from a lack of control of the structure and constitution of the basic liquid rubbers themselves. For this reason the available liquid rubbers are unsuitable for the most demanding applications, even though the processing technology is essentially fully developed. However, they can be used, even now, in general mouldings which are not subject to abrasion or rapid flexing in service.

The incorporation of fibres into liquid rubber compounds has not progressed beyond the laboratory stage and even there the problems arising from the curing systems have restricted the experimental work to the non-reactively terminated liquid rubbers such as the Flosbrene SBR materials. The textile fibres are introduced into the liquid rubber compound on a two-roll mill or internal mixer to give a product which can be extruded by means of a ram extruder, or calendered to give a sheet in which some alignment of the fibres occurs. The physical properties can be considerably improved by the use of the hexamine-resorcinol-silica (HRS) system. The values quoted in Table 4 are for compounds containing randomly oriented fibres.

The reinforcing effect of fibres depends on the staple length, although long fibres tend to be broken during the mixing operation. However, 6 mm fibres are unaffected by this process and tend to give superior properties (Table 5). Alignment of the fibres also has a significant effect on mechanical properties (Table 6).

Table 4 Properties of sulphur-cured Flosbrene containing 6mm staple nylon

Nylon (pphr)	Additive system	Tensile strength (MN/m ²)	Elongation at break (%)
20	None	3.0	75
20	Coumarone/indene resin	3.5	70
10	HRS	8.0	30
20	HRS	9.0	25
30	HRS	17.5	20
40	HRS	19.0	20
50	HRS	17.5	20
70	HRS	15.0	20
Tyre carcass across cord		6.1	180
Tyre carcass with cord		26.5	10

Table 5 Effect of fibre length on tensile properties

		Tensile strength (MN/m ²)	Elongation at break (%)
6mm	crimpless nylon	17	20
12.5mm	crimpless nylon	10	25
32mm	crimpless nylon	9	30
100-150mm	super-crimpled nylon	9	20

Table 6 Effect of alignment of fibres on mechanical properties

	With fibres		Across fibres	
Tensile strength (MN/m ²)	11.4,	13.4	5.2,	4.4
Elongation (%)	44,	27 (?)	41,	41
Permanent set at break (%)	0,	5	5,	5

ECONOMIC FACTORS

The economic analysis of the potential of liquid rubbers carried out about two years ago is still generally valid today¹. The hydroxyl-terminated liquid polybutadienes are currently available in the USA at a price about twice that of conventional (solid) polybutadiene, while that of other liquid rubbers is even higher. This price differential is likely to persist until increased demand, actual or projected, justifies the investment necessary for larger scale production. The overall economics of manufacture of rubber products are heavily dependent on labour costs, which over the last five years have increased from about 27% to some 40% of the total, in the non-tyre section of the industry. Thus one of the principle attractions of liquid rubbers lies in the possibility of reduced labour content in production by increasing automation and the feasibility of this has been amply demonstrated. However, the shortcomings in performance of the present materials is a serious deterrent to their wider application; they cannot yet be used in tyres, the most important volume application.

There is, therefore, a cyclic situation in which the materials producers are unwilling to invest the resources necessary to develop the raw materials with improved structure and properties or to scale up production and hence reduce prices, without some assurance of increased demand. So far as the consumer is concerned, the increased demand is dependent upon the improvement in properties and reduction in price. The future of these potentially revolutionary materials is critically dependent on the resolution of this problem.

REFERENCES

- 1 Daniel, T. J., Needham, A. and Pyne, J. R. *J. Inst. Rubber Ind.* 1972, **6**, 253
- 2 Humpidge, R. T. and Morrell, S. H. *Proc. Inst. Rubber Conf. Brighton* 1972, Paper E4
- 3 Alliger, G., Smith, W. A. and Smith, F. M. *Rubber World* 1971 (June), p 52
- 4 Humpidge, R. T., Matthews, D., Morrell, S. H. and Pyne, J. R. *Rubber Chem. Technol.* 1973, **46**, 148

Polyarylates (polyesters from aromatic dicarboxylic acids and bisphenols)*

G. Bier

*Dynamit Nobel AG, 521 Troisdorf Bez. Köln, West Germany
(Received 7 November 1973)*

After a short review on the literature of aromatic polyarylates synthesis the following aspects are described: preparation of some monomers; preparation of the polymers by different chemical processing routes; physical properties; moulding behaviour. Amorphous polymers are especially considered. Figures on continuous melt condensation via the diphenylester route are given. Some polyarylates have attractive mechanical and electrical properties. Injection moulding is only possible if the glass temperature is not too high ($\leq 200^\circ\text{C}$), and even with these polymers thermal decomposition during injection moulding is a limiting factor for their technical use. The weak point is the ester group. Extrusion, pressing, and solution casting are technically feasible.

INTRODUCTION

The high volume synthetic polymers of the 1930s and 1940s [e.g. polyethylene, poly(vinyl chloride), polystyrene, polymethacrylates, nylon] and polypropylene and polyacetal of the 1950s all have aliphatic structures in the chains of the molecules. 20–30 years ago commercially produced polycarbonates, terephthalic polyesters and the bisphenol A based epoxides were developed having an aromatic or partial aromatic character in the chains of the molecules. The success of these products and the development of theories on the relation between structure and properties of polymers activated the search for further aromatic members. Nomex[®] and Kevlar[®] were developed as aromatic polyamide fibres by Du Pont; these basic materials are not suitable for thermoplastic use. The polyimide thermosetting resins were also developed, again by Du Pont. Different aromatic polysulphones came on the market as products of UCC, 3M and ICI; also an aromatic polythioether from Phillips USA. A mixed aromatic polyamide of Dynamit Nobel (Trogamid[®] T) should also be mentioned.

The first synthetic commercialized polymer, resins based on phenol and formaldehyde, also has a partial aromatic structure. The cellulose, the cellulose nitrate and cellulose acetate, have structurewise a closer relation to the aromatic than to the aliphatic polymers.

Theory and experience show that aromatic groups and other ring groups in the main chain have a stiffening effect on the chains. Compared with aliphatic structures the aromatic groups increase the glass temperature.

According to one definition, the polyarylates are polyesters from diphenols and dicarboxylic acids. They are aromatic or partial aromatic polyesters. When the

carboxylic acid is replaced by aliphatic dicarboxylic acids such as succinic acid or adipic acid mixed aromatic aliphatic polyesters are obtained with T_g 's (glass temperature) lower than the T_g of polycarbonate. If terephthalic, isophthalic acid or a similar acid is used full aromatic polyesters with higher glass temperatures than the corresponding polycarbonates are obtained. This paper is mainly concerned with this type of polyarylates—highly aromatic polyesters.

The literature on polyarylates based on aromatic dicarboxylic acids is extensive. In a book by Korshak and Vinogradova¹ on polyesters about 80 pages have been devoted to polyarylates. In a later book by Korshak² 140 different formulae of polyarylates are listed and described and 279 references are given, 110 of them originating from Korshak's laboratory.

Besides these publications, papers by Conix³, Levine and Temin⁴, Morgan⁵, Eareckson⁶ and Weyland *et al.*⁷ should also be mentioned.

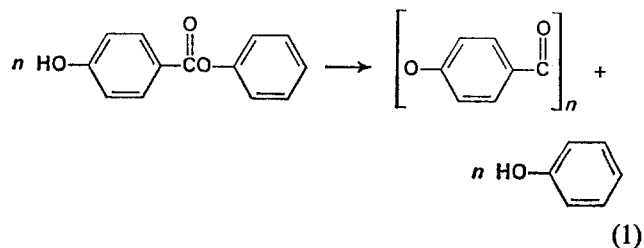
In Korshak and Vinogradova's book it is stated¹: 'there is every reason to assume that they (polyesters of diphenols and aromatic dicarboxylic acids) will find wide practical application in the near future'. Where do we stand with these polyarylates?

From the patent literature it can be seen that in the western world many companies have been actively engaged in polyarylates research.

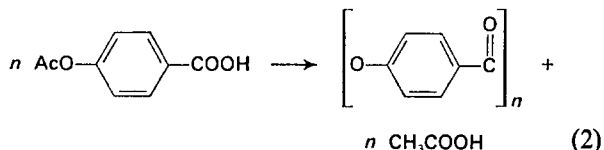
In 1970 Carborundum marketed a poly(*p*-hydroxybenzoate) under the name Ekonol[®]. The polyhydroxybenzoate is not a polyarylate according to the original definition of Korshak. However, no doubt, this polymer should be mentioned here briefly. This type of polyester is highly crystalline. Korshak reports a melting point of 420°C . With thermogravimetric analysis we found 5% weight loss at 480°C . Judging from the Carborundum patents⁸ it must be assumed that the synthesis proceeds

* Presented as a Symposium Lecture at the IUPAC International Symposium on Macromolecules, Aberdeen, September 1973.

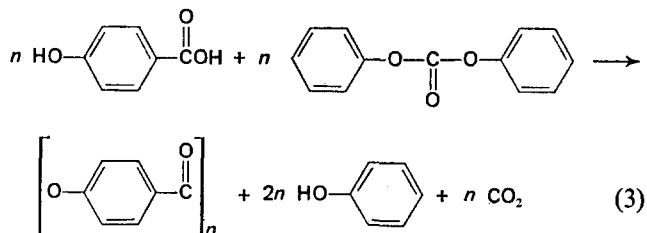
according to the following route (equation 1):



In earlier literature on this polyester⁹, the acetate of the *p*-hydroxybenzoic acid is the starting material:



Wolfes (personal communication) studied the condensation of aromatic hydroxyacids, and he found that polycondensation is very easy according to the equation¹⁰:



In inert organic solvents hydroxybenzoic acid reacts with equimolar amounts of diphenyl carbonate under addition of a catalyst such as tetrabutyltitanate.

Because the polyester is insoluble, its molecular weight could not be determined. Ekonol can only be thermofomed by sintering in hot presses or by mixing with other types of polymers, such as polysulphone.

The final products are brittle, they are stable against pressure, but not against bending and impacting. The product has a high thermal stability probably as a consequence of its high crystallinity, which prevents the thermal oscillation of the molecules and the penetration of oxygen.

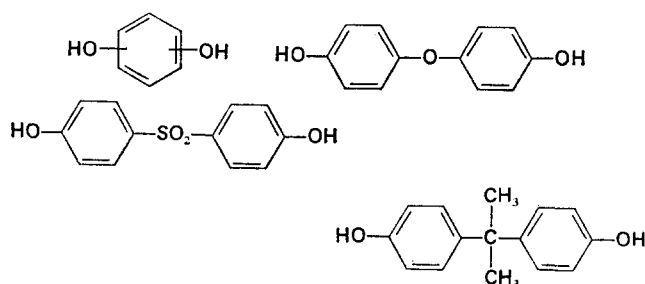
Recently Carborundum announced a new range of polymers—Ekkzel® C 1000. This material is said to be mouldable in extruders and injection machines. We do not have any experience with this material. On a small press-moulded sample we analysed the composition: a polyarylate based on 4,4'-dihydroxydiphenyl and isophthalic acid.

From the different publications on polyarylates one can learn that the crystalline polymers have low solubilities and are not easily thermomouldable and that only some of the various amorphous polymers are thermomouldable. The information from the scientific literature and the patents is not extensive enough for the evaluation of industrial use. This paper gives details of some of these production aspects, the monomers, the polycondensation and the properties of the polymers. Our main interests were the amorphous thermomouldable polymers.

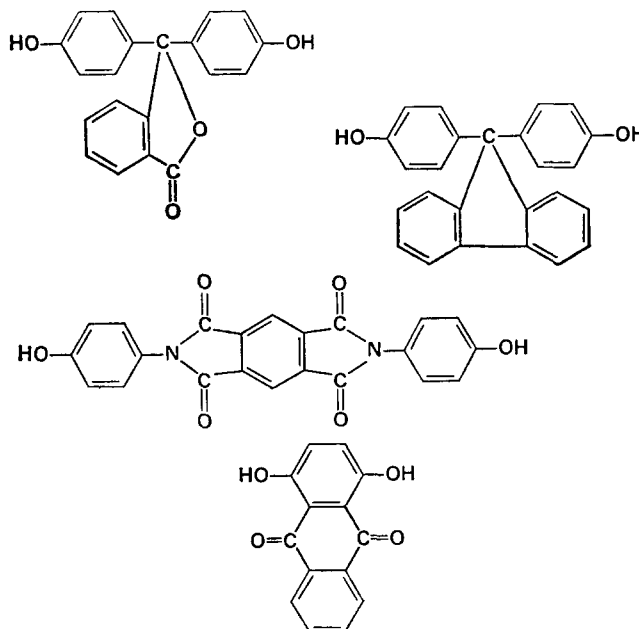
SYNTHESIS

Some types of diphenols

Some simple structured diphenols are:

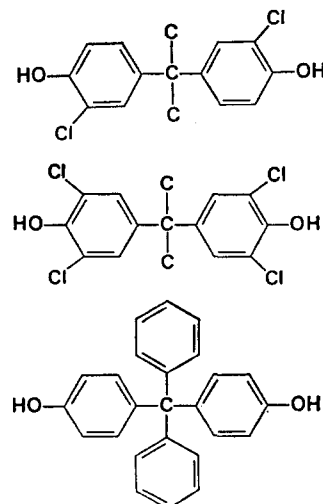


Some of the numerous diphenols with a more complicated structure, particularly studied by Korshak and coworkers are:



Morgan⁵ has also tested diphenols with large crossplanar substituents in the synthesis of poly(aryl esters).

In this company we mostly worked with diphenols of simple structure such as 2,2-bis(4-hydroxyphenyl)propane (bisphenol A, dian) which is produced in large quantities by several companies, and its chlorination products dichloro-dian and the tetrachloro-dian and with the dihydroxytetraphenylmethane:



Synthesis of these diphenols has been worked out in our laboratories up to the pilot plant level. The results will be summarized briefly. Richtzenhain and Zoche developed the synthesis of dichloro- and tetrachloro-dian by the chlorination of dian. They found in cooperation with E. Bessler* that the hydrogens of the phenyls show different activities against chlorination. First, a monochlorination in one *ortho* position for each of the two OH groups occurs. Only then does substitution at the second *ortho* positions of the two rings take place. This is more exactly illustrated in Figure 1 where the concentrations of the compounds during the chlorination (gas chromatography method) are plotted. A side reaction product, 2,4-dichlorophenol, is not given.

The main product originating from the reaction with 2 or 4 mol Cl₂ is relatively pure. The purity, however, is not yet sufficient for the production of high molecular weight poly(aryl esters). An additional purification step by recrystallization is necessary. Here it was found¹¹ that the dichloro- and tetrachloro-derivatives form adducts with water, the adducts having low solubility in certain organic solvents such as ethylene dichloride, methylene chloride, ethylene dibromide, dichlorobutane. The 1-chloro, 3-chloro and 5-chloro compounds do not form such adducts of low solubility. A separation and purification is possible via these adducts. The simplest procedure is to chlorinate the dian with the necessary amount of chlorine in one of these solvents and separate the dichloro- or tetrachloro-product by adding water. Yield is over 90%.

Behr and Gresser have been working on the synthesis of the dihydroxytetraphenylmethane. After testing various possible routes the following method of synthesis seemed to be acceptable (see also Morgan⁵).

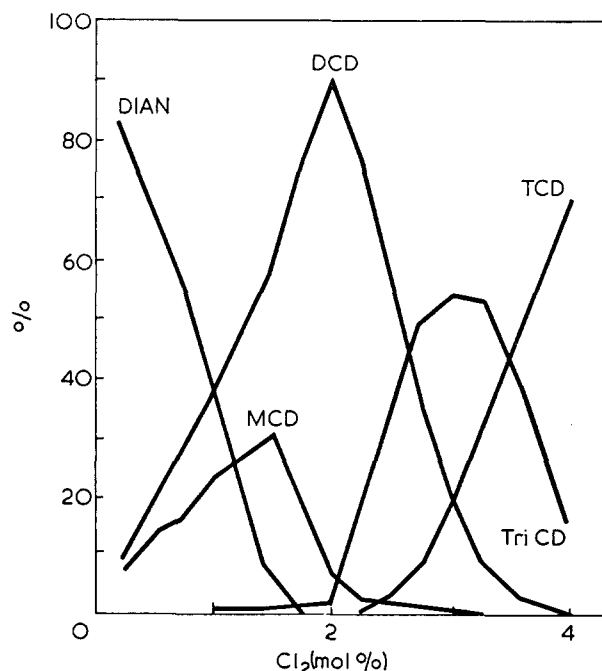
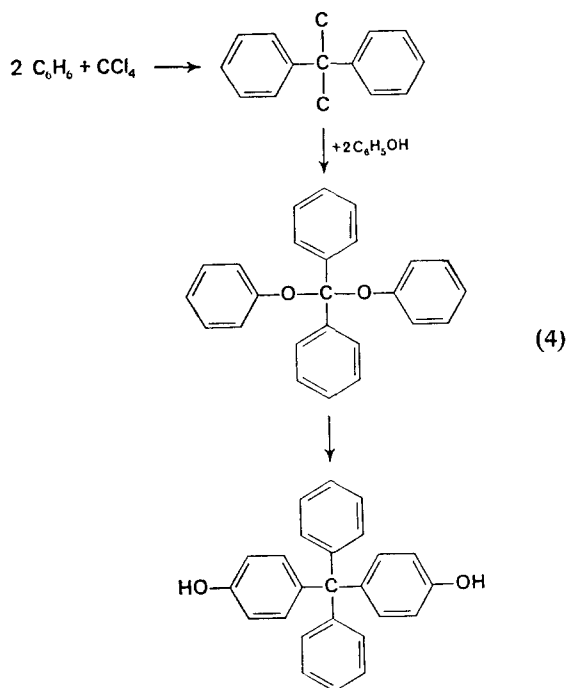


Figure 1 Chlorination of bisphenol A (dian). MCD= monochloro-dian; DCD=dichloro-dian; TriCD=trichloro-dian; TCD=tetrachloro-dian

* Bessler, E. Pontificia Universidad Católica del Peru, Departamento de Ciencias, Apartado 1761, Lima, Peru.

Carbon tetrachloride is reacted with 2 mol benzene to give dichlorobenzophenone:



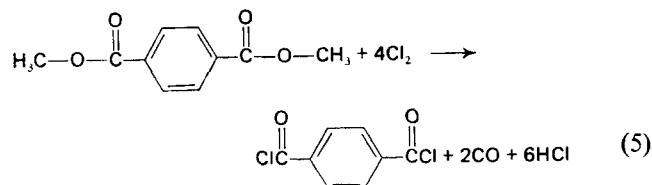
The purified dichlorobenzophenone is reacted with 2 mol phenol to give the ether which immediately rearranges into the dihydroxy compound. For the first step a 72% yield of pure product is obtained, for the second step 53%. This yield, however, does not include the reaction products dissolved in the mother liquors. The yield can, no doubt, be increased.

Aromatic dicarboxylic acids and their derivatives

For preparing linear aromatic polyesters from dicarboxylic acids, terephthalic acid and isophthalic acid are most important, especially their derivatives. They are produced by oxidizing the corresponding xylenes. There are various large scale processes, such as the Witten DMT (terephthalic acid dimethylester) process of Dynamit Nobel or the TPA (terephthalic acid) process of Amoco.

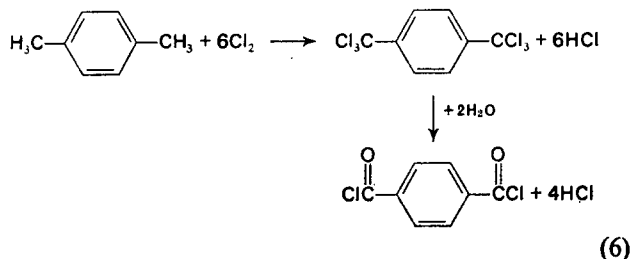
For the synthesis of poly(aryl esters), terephthalic acid dimethylester and terephthalic acid cannot usually be used. A more reactive derivative of the acids such as the acid chloride or the diphenylester of the acids is needed.

Acid chlorides. The classical way of synthesis is the reaction of the acid with thionyl chloride or other inorganic acid chlorides. Some other methods of synthesis have been worked out in our laboratories: Katzschmann and Burkhardt¹² found that by chlorination of terephthalic acid dimethylester or isophthalic acid dimethylester according to:



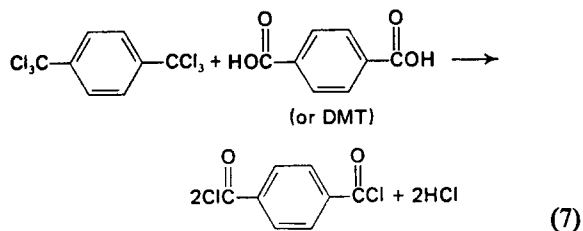
tere(iso)phthalic dichloride can be obtained in good yields. The methoxyl group is converted to carbon monoxide.

Another way of making the dichlorides, first mentioned in an old IG-Farben patent¹³ starts from xylene:



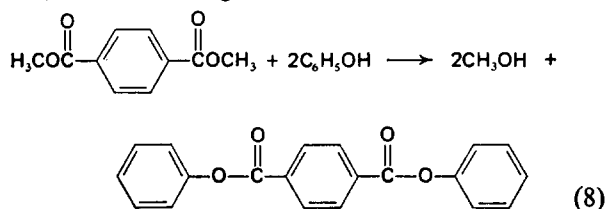
The methyl groups of xylene are perchlorinated. With stoichiometric amounts of water the hexachloroxylene is hydrolysed to the acid dichloride.

It is also possible to react the hexachloroxylene with terephthalic acid dimethylester or terephthalic acid for producing the dichloride:

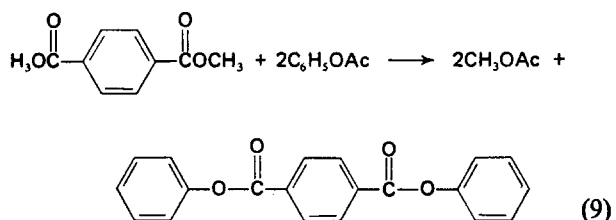


The last 2 processes have been worked out by Richtzenhain and Riegger. In our opinion all processes mentioned here are technically feasible.

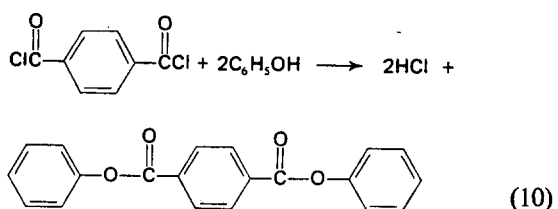
Diphenylester. Another monomer for the production of poly(aryl esters) is the diphenylester of the dicarboxylic acid, which can be obtained from terephthalic acid dimethylester according to:



However, the reaction rate, particularly of the second ester group, is extremely low. The reaction runs much better if the acetate of the phenol is used:



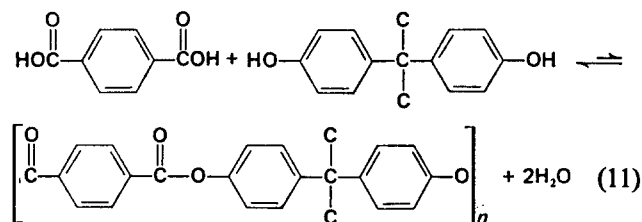
The reaction also works if acetic anhydride is added to the two components phenol and terephthalic acid dimethylester. These processes were developed by Hülsmann and Renckhoff¹⁴. Another way to obtain diphenylesters is the well-known reaction of acid chloride and phenol:



The routes for making the diphenylesters according to equations (9) and (10) are technically feasible.

METHODS FOR PRODUCING POLYARYLATES

In the synthesis of poly(glycol terephthalate), terephthalic acid dimethylester or terephthalic acid reacts with glycol. In the synthesis of polyarylates this method does not work, because the equilibrium is strongly on the side of the starting material:



We have two chemical routes for making the polymers. One route goes through the reactive acid chlorides, the other route goes through special re-esterification reactions. There are also different processing routes, a two-phase process (interfacial condensation) and single phase processes (solution and melt condensation).

Acid chloride route

Generally applicable and mostly used for the synthesis of polyarylates is the reaction of the chlorides of the dicarboxylic acids with the diphenols. Most of the numerous polyarylates of Korshak have been prepared by the acid chloride route. The reaction can be performed by three different processes.

Interfacial condensation. This is normally performed at room temperatures. The technique has been described by Morgan¹⁵. The interfacial condensation method has been realized on a commercial scale by Bayer AG in the production of polycarbonate.

In Table 1 a series of polyarylates is shown, where the ratio of iso- and tere-phthalic dichloride is systematically changed⁶. In the middle of the series there is low crystallinity, at the ends higher crystallinity. The values for crystallinity are only qualitative.

Solution condensation. (a) At normal temperature. With this process it is necessary to have stoichiometric or superstoichiometric amounts of HCl acceptors such as pyridine or triethylamine. The advantage of this process is, that low boiling solvents and normal pressure can be applied. High molecular weights are easily obtained. However, in our experience it is difficult to obtain products with good colour after processing.

Table 1 Properties of a series of polyarylates of bisphenol A/iso- or tere-phthalic dichloride copolymers

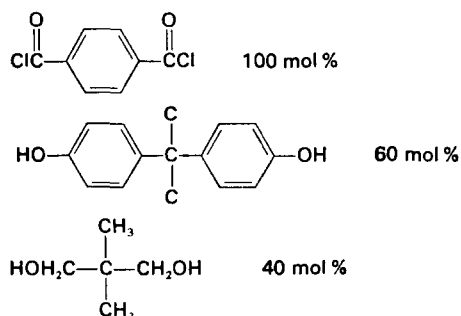
Iso-/tere-phthalic dichloride ratio	η_{inh}	Crystallinity	Polymer melt temp. (°C)	T_g (°C)	Film toughness
100:0	0.52	3.0	235	—	Brittle
90:10	0.67	2.7	255	181	Tough
80:20	1.08	1.5	250	188	Very tough
70:30	1.33	0.3	255	188	Very tough
60:40	1.53	0.3	255	188	Very tough
50:50	1.38	0.3	260	194	Very tough
40:60	0.94	1.3	250	191	Tough
30:70	0.79	1.8	260	192	Tough
20:80	0.74	2.0	245	203	Brittle
10:90	0.68	2.1	290	—	Very brittle
0:100	0.51	2.4	315	—	Very brittle

As far as it is known, an analogous process for polycarbonate is performed by General Electric on a large production scale. The General Electric polycarbonate is water white, which means the colour problems with polyarylates can probably be solved.

(b) At high temperatures. Here one works in the presence of catalysts. Hydrogen chloride is continuously removed from the reaction. Because reaction temperatures of 150°C and higher are preferable, it is necessary either to use solvents having high boiling points or to work under pressure with solvents having low boiling points. Catalysts such as amines or metallic magnesium play a significant role.

Melt condensation. With higher degree of condensation one has the problem of high viscosity and the demand for thin layers to remove the hydrogen chloride.

A suitable apparatus for moving polymers of high viscosity and producing new surfaces is a Banbury mixer or an extruder. There is the additional problem of having a reactor surface stable against the combined attack of hydrogen chloride and phenolic (alcoholic) groups at high temperatures. Gouinlock *et al.*¹⁶ did some comparative trials by the interfacial method in a batch equipment and by the melt method in an extruder. They condensed the following products:



The neopentene glycol has the main task of reducing the melt viscosity. In the melt process these authors made first a prepolymer in a batch reactor and then they fed the prepolymer to an extruder for finishing the condensation. They found that there are differences of properties between the interfacial and melt polymers.

At the same intrinsic viscosity the melt polymers had higher melt viscosities and lower notched impact values as shown in Figures 2 and 3. The authors conclude that branching of the melt condensate occurs by Friedel-Crafts reaction between the acid chloride and the bisphenol ring. For comparison they prepared a polymer

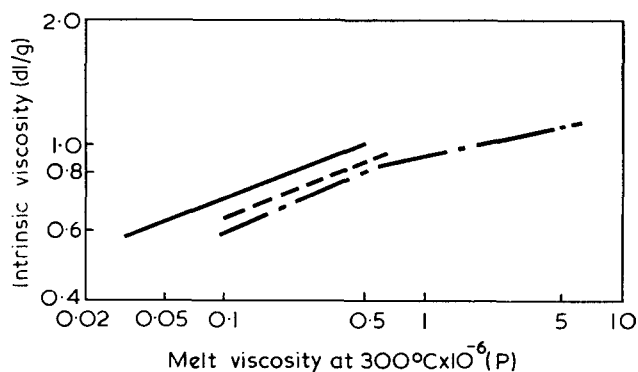


Figure 2 Copolyesters in a vented extruder. —, Interfacial polymerization; ---, melt (extrusion) polymerization; - · - ·, branched interfacial polymerization

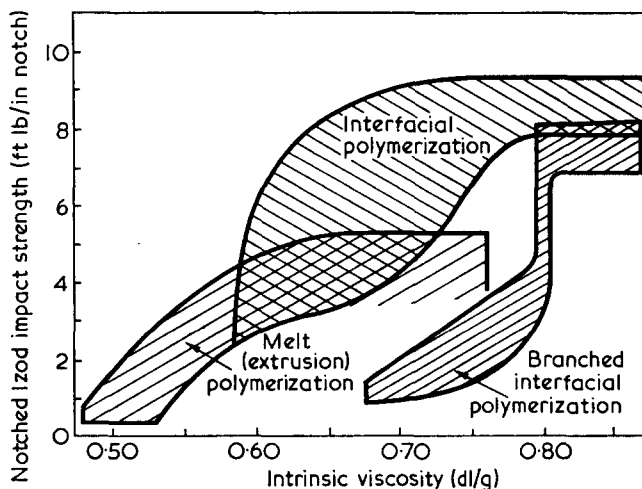


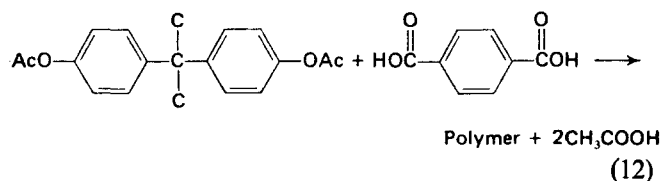
Figure 3 Copolyesters in a vented extruder

with a low degree of branching with the interfacial method by adding a small amount of a trifunctional phenol. The intentionally branched polymers had even higher melt viscosities and lower impacts than the melt polymers without addition of a trifunctional phenol. The results seem to support the idea of branching.

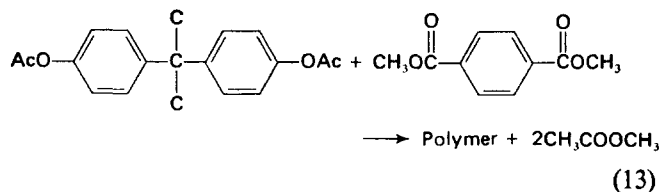
Re-esterification routes

The following routes are described in the literature:

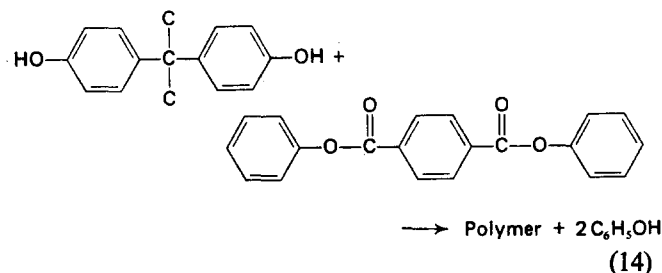
(a) ester of diphenol + acid



(b) ester of diphenol + ester of dicarboxylic acid



(c) diphenol + diphenylester of dicarboxylic acid



Equation (12) has been described repeatedly, for instance by Levine and Temin⁴. Usually the acetates of the diphenols are used. According to our experience considerable colour problems arise in this process.

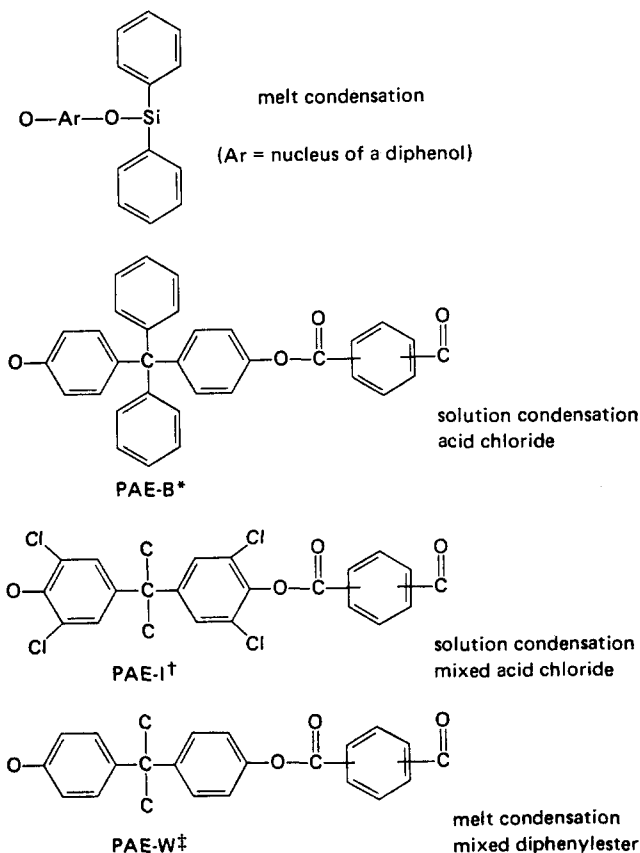
Only a little is known about equation (13) for producing poly(aryl esters). Clearly, it runs insufficiently, as in our trials only oligomers resulted. This was not expected because there was a high yield in the synthesis of the monomer diphenylterephthalate from terephthalic acid dimethylester and phenyl acetate.

The ester exchange via the diphenyl ester of the aromatic dicarboxylic acid can be performed easily (equation 14). This process is known from the polycarbonate synthesis¹⁷ on the basis of bisphenol A. It works economically in the melt. A remarkable aspect of this process is that approximately the same weight quantity of phenol has to split off, as bisphenol A is needed. The phenol has to be removed from the equilibrium. The poly(aryl esters) with molecular weight above 10 000 have a high viscosity. The diffusion rate determines the rate of polymerization. One needs thin layers of the polymer melt to get a reasonable diffusion rate of the phenol. The technical process will be described later.

The reaction of the ester exchange via diphenyl ester cannot be applied to all diphenols, e.g. not to the tetrachloro-dian. It is likely that in this case the hydroxy groups are sterically blocked so that a reaction with the phenyl-ester cannot take place.

POLY(ARYL ESTERS) PRODUCED BY DYNAMIT NOBEL

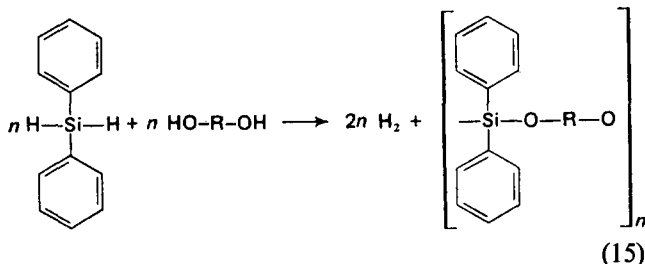
Some examples of the polyarylates prepared by this company are listed below as well as their preferred condensation methods:



Only the first is a really new one. This polyester on the basis of diphenyl-Si-acid was made only on a laboratory scale by Steffen¹⁸. This is not a classic poly(aryl ester), it is an outsider. The polycondensation

* B=Behr, E. Dynamit Nobel.
 † I=Ismail, R. Organ.-Chem. Institut der Universität Bonn, 53 Bonn, Meckenheimer Allee 168.
 ‡ W=Wolfes, W. Dynamit Nobel.

has been carried out according to:



This reaction is non-reversible. One hydrogen reacts as cation and another hydrogen as anion; these ions form 1 mol hydrogen which does not interfere with the equilibrium. The synthesis works in solution and in the melt.

The products PAE-B and PAE-I above have been prepared by the high temperature solution method via the acid chloride route. The reaction in the reverse direction is only carried out with difficulty; however, one can obtain high molecular weight polymers only when the hydrogen chloride is removed from the solution. The reaction was performed on a laboratory scale and in pilot plant scale, where a glasslined reactor was used.

Figure 4 gives some information on the kinetics of the hydrogen chloride removal (PAE-I). The nature of the catalyst has a considerable influence on the rate of hydrogen chloride formation. Dichlorobenzene was usually used as solvent at atmospheric pressure.

For the melt condensation of the bisphenol A (PAE-W) the diphenylester of the aromatic dicarboxylic acid was used. Since we were only interested in amorphous polymers, mixtures of the acid derivatives (e.g. 50% diphenylterephthalate + 50% diphenylisophthalate) were used. The polymers are completely amorphous contrary to polymers of the same composition prepared by the interfacial route⁵.

On a laboratory scale the reaction was made batchwise in two steps within 1.3-2 h: a pre-condensation with stirring (possible in any scale) and a polycondensation in small quantities of 5 g *in vacuo*. During the polycondensation the polymer foams and the viscosity increases up to 10⁵ P, i.e. stirring is not possible using standard equipment.

In the pilot plant (Figure 5) an extruder type of reactor was used. No corrosion problems as with the acid chlorides are expected. Again a two-step procedure was applied. At first a prepolymer was performed batchwise

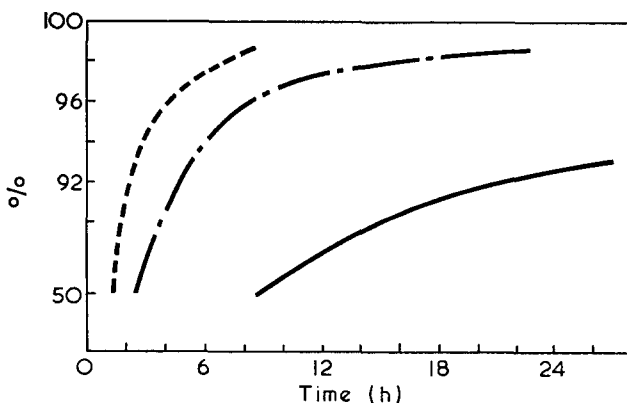


Figure 4 Production of a poly(aryl ester) in solution. —, Without catalysis; ----, quinoline; - · - ·, HMPA

in a normal reactor which took 3 h. About 96% of the phenol was removed. The prepolymer with a molecular weight of 2000–3000 was drained off, cooled, crushed and then was subjected to a continuous reaction in a Werner and Pfeiderer extruder with vacuum nozzles. After the prepolymerization we needed the intermediate cooling and disintegration step because the two condensation plants were installed at different locations.

With the extruder type ZSK 53 used Ruff and Wolfes obtained an output of 10–30 kg/h, depending on the polymer item. In the work of Gouinlock¹⁶ a small extruder from Welding Engineers with an output of 60 g/min was used. A residence time of 15–30 min was needed. The residence time in our experiments was 2–3.5 min. Our longest condensation run was 50 h; this run was stopped because of a lack of material. We do not see any objection to continuous production with this type of reactor.

For commercial production, however, a bigger type of extruder would be required, e.g. type ZDSK 83 with a calculated output of about 25–75 kg/h or type ZDSK 120 with a calculated output of 70–150 kg/h. The colour of our polymers was yellowish.

PROPERTIES OF THE POLYMERS

The glass temperatures of some Si-polyesters are listed in Table 2¹⁸. It is well-known of silicones that the O–Si–O group in the chain brings high flexibility and low T_g . However, as the Table shows, it is possible to get polymers containing OSiO groups with high T_g . Clearly, here the flexibility of the O–Si–O groups is restricted by the voluminous substituents and chain groups. Also the OSiO group content of the polymers is low. The above mentioned Si-containing poly(aryl esters) are all sensitive to hydrolysis. The lower the pH value of the diphenol the more unstable is the Si–O–R

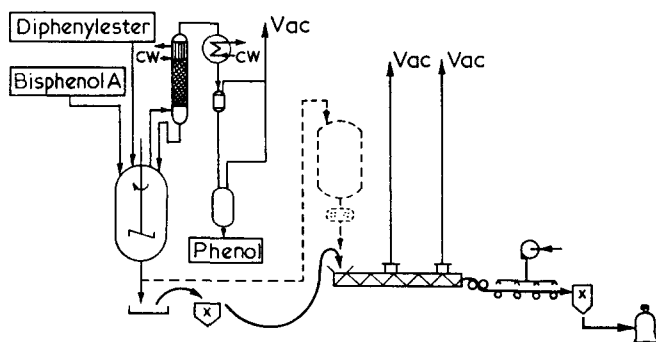


Figure 5 Manufacture of polyarylates

Table 2 Glass temperatures of Si-polyesters

Diols	T_g (d.t.a.) (°C)
Resorcinol	51–53
Hydroquinone	70
2,2-Bis(4-hydroxyphenyl) propane (bisphenol A)	94–96
4,4'-Dihydroxytetraphenyl-methane	124–125
2,5-Bis(4-hydroxyphenyl)-1,3,4-oxadiazole	147
Phenolphthalein	162–166
2,2-Bis(3,5-dichloro-4-hydroxyphenyl) propane	159–160
3,3',5,5'-Tetrachloro-4,4'-biphenol	209
2,2,4,4-Tetramethyl cyclobutane-diol-(1,3):	
<i>cis-trans</i> ratio=57: 43	107
=52: 48	106
= 0:100	107

Table 3 Physical properties of some polyarylates and polysulphone

	PAE-B	PAE-I	PAE-W	UCC poly- sulphone
Tensile strength at 20°C (kg/cm ²)	700–750	900	700	550
Elongation (%)	3–5	10	10–15	10–15
E modulus (kg/cm ²)	28 000– 30 000	27 000– 29 000	20 000	27 000
T_g (by torsion pendulum method) (°C)	270	230	190	180

Table 4 Physical properties of polyarylates, polycarbonate and polysulphone

	Testing pre- scribed in DIN standard	PAE PAE-W (60:40)	Poly- carbon- ate	UCC Poly- sulphone	
Yield strength (kg/cm ²)	53455	130	690	675	800
Elongation (%)	53455	30	23	90	55
E modulus (kg/cm ²)	53457	21 000	21 200	24 000	27 000
Impact strength (cm kg/cm ²)	53453	ng	ng	ng	ng
Notched impact strength (cm kg/cm ²)	53453	15	15	20	65
Heat distortion at 18 kg/cm ² (°C)	53461	165	155	125–130	175
Heat distortion at 4.6 kg/cm ² (°C)	53461	160	165	140–145	

linkage against hydrolysis. In this case the SiOR group evidently has the character of a mixed acid anhydride.

The polyester on the basis of diphenylsilane and 2,2,4,4-tetramethylcyclobutane-diol-(1,3) has proved to be stable to hydrolysis. Perhaps the Si–O–R group has the character more of an ester; maybe for steric reasons the stability against saponification is strongly improved.

In Table 3 some physical properties of various poly(aryl esters) determined from solution casted thin films are listed. The properties are of interest if compared with UCC polysulphone. The glass transition temperatures are quite high; indeed, in some cases too high for injection moulding. In Table 4 the properties of the following two injection moulded samples are summarized. PAE-W: tere-/iso-phthalic acid 50:50, bisphenol A; PAE 60/40: 60 diphenylterephthalate: 40 diphenylcarbonate, bisphenol A. One can see that the heat distortion of the two polyarylates is higher than the heat distortion of polycarbonate.

The electrical properties of the polyarylates are generally good as is known from the literature and by Tables 5 and 6, where the influence of temperature and frequency on dielectric properties can be seen. The dissipation factor of the different polyarylates is higher than that of polysulphone or in the same range.

It seems, that there are differences of polarity between the different products of Tables 5 and 6. Temperature dependence of PAE-I is very low.

In order to gauge the thermal stability for long times, films have been stored for many weeks at higher temperatures and the loss of weight during that time was determined. From the results one can construct curves for the weight losses of 2%, 5%, 10% etc (see Figure 6).

Table 5 Variation of dielectric properties, ϵ , of polyarylates with frequency at 20°C

Frequency (Hz)	PAE-B	PAE-I	PAE-W	Polysulphone
60	—	64/2.9	30/3.4	21/3.0
10 ³	35/3.0	42/2.8	50/3.4	17/3.0
10 ⁴	65/3.0	37/2.8	100/3.3	26/3.0
10 ⁵	100/3.0	42/2.8	190/3.3	—
10 ⁶	110/3.0	40/2.7	200/3.3	65/2.9
10 ⁷	110/3.0	38/2.7	200/3.3	62/3.0
10 ⁸	120/3.0	42/3.7	200/3.1	64/3.1

Table 6 Variation of dielectric properties, ϵ , of polyarylates with temperature at 16Hz

Temperature (°C)	PAE-B	PAE-I	PAE-W	Polysulphone
20	110/3.0	40/2.8	200/3.2	65/2.9
100	50/—	38/2.8	150/3.3	16/2.8
150	~40	70/2.9	115/3.4	17/2.9
180	~30	100/2.8	150/3.4	31/2.9

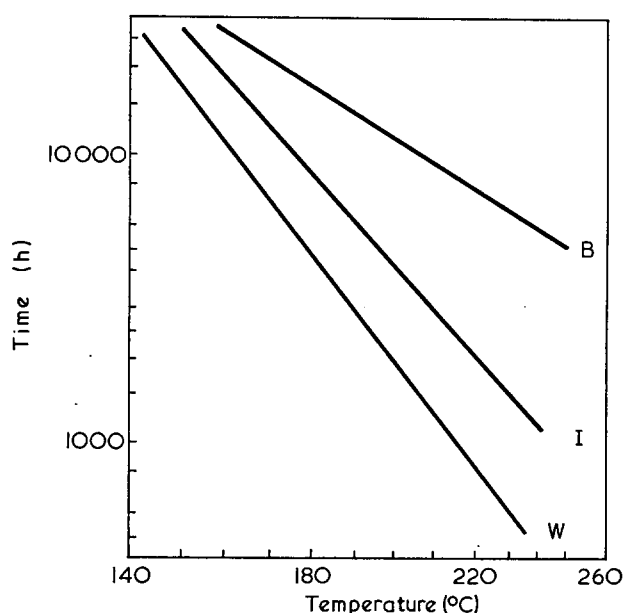


Figure 6 30% weight loss of PAE-B (B), PAE-W (W) and PAE-I (I)

This test has information of value for the long time behaviour at higher temperatures. A polyarylate based on dioxytetraphenylmethane has a higher stability than the polyarylate based on tetrachlorobisphenol A and the polyarylate based on bisphenol A.

A frequently used standard test for heat stability consists of determining the weight loss while heating at constant rate (t.g.a.). Some figures are given in Table 7. The stability of our polyarylates is between that of polycarbonate and polysulphone.

British, American and Russian workers have determined the nature of volatile products from heated bisphenol A polyarylates. The British¹⁹ and American²⁰ authors suggest that first one obtains carbon monoxide and carbon dioxide from the ester group and then methane from the isopropylidene group. The Russians²¹ found a remarkable stability of the ester group. They found that at first the isopropylidene group develops methane. The conditions of testing were different for each group.

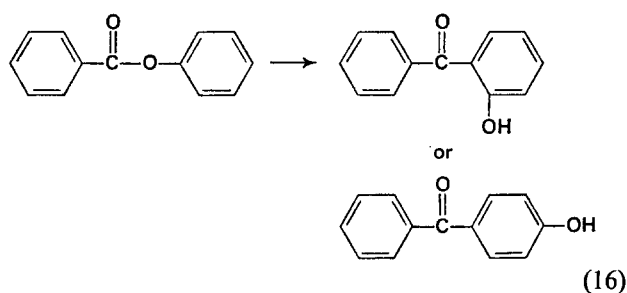
The result, that in the t.g.a. test first carbon monoxide and carbon dioxide are developed, is in agreement with

Table 7 Weight loss on heating under nitrogen (8°C/min) in °C

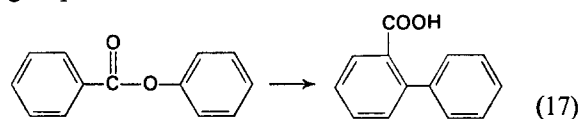
	1%	5%	10%	20%
PAE-B	430	475	490	515
PAE-I	410	440	455	470
PAE-W	420	465	480	500
Polysulphone (UCC)	475	500	515	525
PC	410	430	440	455

our studies. The PAE-I has in this test the highest weight loss (the lowest thermal stability) in spite of the lowest weight content of ester groups; PAE-I is better in the test of Figure 6. When heating model compounds such as phenylbenzoate it is known that there are two types of reactions at higher temperatures:

- (1) Fries rearrangement. Ketone and phenolic hydroxy groups are given. Catalysts for this reaction are cationic compounds such as aluminium chloride.



- (2) Thermal rearrangement with a resulting carboxylic group.



During storage at higher temperatures several authors have observed crosslinking reactions of the polyarylates. These are understandable, if new phenolic or carboxylic groups are formed at the side of the molecules.

In the case of the Gouinlock polymers (Figures 2 and 3) made from acid chlorides with a mixture of bisphenol and glycol by melt condensation in a metallic equipment (extruder) a Fries reaction and branching could have occurred.

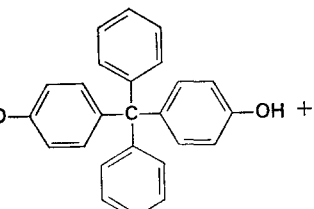
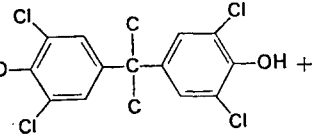
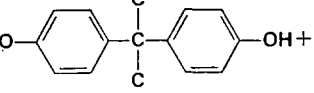
In our melt polymers made by the route of diphenylester of carboxylic acids, we could not detect any irregular structure; the chains are not branched.

In some Russian publications²² some hints are given that the method of preparation and the temperature of synthesis is influencing the conformation of the macromolecules, the viscosity-molecular weight relation, properties etc.

Moulding properties

Our three typical polyarylates have the mouldabilities given in Table 8. All three polymers are amorphous. Only the bisphenol A-polyarylate is injection mouldable. However, processability of this polymer is difficult as is shown in the spiral test (Figure 7). High temperatures are needed for injection moulding of the polyarylates and even under hard conditions one cannot reach the mouldability of UCC polysulphone. Also, one is very near to the decomposition temperature. In an injection

Table 8 Mouldability of amorphous polyarylate

Bisphenol	Press	Extrusion	Injection
 PAE-B HO-C ₆ H ₄ -C(C ₆ H ₅) ₂ -C ₆ H ₄ -OH	-	-	-
 PAE-I HO-C ₆ H ₃ (Cl) ₂ -C(C ₆ H ₃ (Cl) ₂)-C ₆ H ₃ (Cl) ₂ -OH	+	+	-
 PAE-W HO-C ₆ H ₄ -C(C ₆ H ₅) ₂ -C ₆ H ₄ -OH	+	+	+

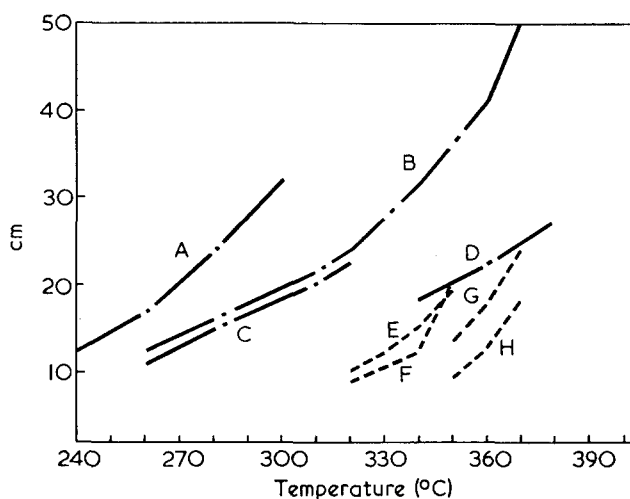


Figure 7 Spiral test of aromatic polymers. A, Lexan® 121; B, Makrolon® 3000W; C, Makrolon® 3100; D, Polysulfon® P1700; E, PAE 60:40 ($\eta=0.54$); F, PAE 60:40 ($\eta=0.65$); G, PAE-W ($\eta=0.68$); H, PAE-W ($\eta=0.97$)

run in a commercial machine under the conditions of manufacture, Brüning and Pohl observed a degradation of the molecular weight after several attempts and a short time later the formation of gas bubbles. If the residence time of the material in the injection cylinder is too long moulded articles with defects are produced. Larger articles form less problems than small ones. The polysulphone does not show this critical processing attitude, as the decomposition temperature is considerably higher than the processing temperature.

The extrusion process is much safer. Thin films, sheets and monofilaments have been produced without any difficulty. Solution casting also works very well.

In principle we consider it possible that the thermal behaviour of the polyarylates which causes such difficulties at the injection moulding, can be improved by stabilization, end group capping, and maybe by other methods of preparation, i.e. by solution polymerization at low temperature, etc. One can look forward with certain optimism when considering the development of the polycarbonates. The polycarbonates produced in 1973 are considerably more stable than the first market products of 20 years ago.

Chemical stability

The amorphous polyarylates are slightly more stable on hydrolysis than the amorphous polycarbonates. It seems that there is a certain relation to the glass temperature. This may be accidental. On hydrolysis the stability of the crystalline polyarylates is much better than that of the amorphous polyarylates. However, the crystalline materials cannot be thermomoulded. The amorphous polyarylates are more or less soluble or capable of swelling in a series of solvents, halogenated hydrocarbons, esters, ketones, epoxides. In contact with some solvents they show stress crazing as also shown by the commercial polycarbonates.

CONCLUSIONS

On the positive side, the raw materials are easily available. Polymerization on a technical scale is feasible. Mechanical and electrical properties are attractive. Extrusion and solvent casting work well. On the negative side, the mouldability by injection is poor. The stability against hydrolysis is not good. The market for extruded or solution casted articles of the polyarylate class seems small. Hence there are several drawbacks restraining us from building a plant for amorphous polyarylates at present.

ACKNOWLEDGEMENTS

The author would like to thank W. Wolfes, H. Richtzenhain, G. Zoche, E. Behr, W. Gresser, P. Riegger, H. L. Hülsmann, G. Renckhoff, K. Ruff, G. Tappe, R. Minke, K. Brüning and W. Pohl of Dynamit Nobel for carrying out most of the work reported in this paper.

REFERENCES

- 1 Korshak, V. V. and Vinogradova, S. V. 'Polyesters', Pergamon Press, Oxford, 1965
- 2 Korshak, V. V. 'The Chemical Structure and Thermal Characteristics of Polymers', Israel Program for Scientific Translations, (Keter, London), 1971
- 3 Conix, A. *Ind. Eng. Chem.* 1959, **57**, 147
- 4 Levin, M. and Temin, S. S. *J. Polym. Sci.* 1958, **28**, 179
- 5 Morgan, P. W. *J. Polym. Sci. (A)* 1964, **2**, 437; *Macromolecules* 1970, **3**, 536
- 6 Eareckson, W. M. *J. Polym. Sci.* 1959, **40**, 399
- 7 Weyland, H. G., Hoefs, C. A., Yutema, K. and Mip, W. I. *Eur. Polym. J.* 1970, **6**, 1339
- 8 Carborundum, DOS 1 720 440
- 9 Gilkey, R. and Caldwell, J. R. *J. Polym. Sci.* 1959, **40**, 198
- 10 Bayer AG, DAS 1 495 626
- 11 Dynamit Nobel AG, DOS 1 946 610; 1 956 235
- 12 Dynamit Nobel AG, DP 1 064 495; 1 152 400
- 13 IG Farben, Fr. P. 820 698
- 14 Dynamit Nobel AG, DP 1 244 797; 1 493 509; 1 267 224; 1 283 849; DOS 2 109 102
- 15 Morgan, P. W. 'Condensation Polymers by Interfacial and Solution Method', Interscience, New York, 1965
- 16 Gouinlock, E. V., Quinn, E. I., Murciniak, H. W. and Hinder-sinn, R. R. *J. Appl. Polym. Sci.* 1968, **12**, 2403
- 17 Schnell, H. *Angew. Chem.* 1956, **68**, 633
- 18 Steffen, Kl. D. *Angew. Macromol. Chem.* 1972, **24**, 21
- 19 Davis, A. and Golden, J. H. *Eur. Polym. J.* 1968, **4**, 581
- 20 Ehlers, G. F. L., Fisch, K. R. and Powell, W. R. *J. Polym. Sci. (A-1)* 1969, **7**, 2969
- 21 Rodivilova, L. A., Akutin, M. S., Morosova, S. A. and Pshenitsina, V. P. *USSR Chem. Eng.* 1965 (24 May)
- 22 Slonimskii, G. L. *et al. Polym. Sci. USSR* 1967, **9**, 453; Slonimskii, G. L., Askadskii, A. A. and Pavlov, V. I. *Polym. Sci. USSR* 1967, **9**, 408; Korshak, V. V. *et al. Izv. Akad. Nauk SSSR (Ser. Khim.)* 1972, **6**, 1409

Note to the Editor

Homogeneity of annular extrusion of polystyrene

Toshikazu Fujimura and Takashi Kawamura

*Department of Polymer Chemistry, Faculty of Engineering, Yamagata University, Yonezawa-shi 992, Japan
(Received 14 May 1973; revised 2 January 1974)*

INTRODUCTION

The blown film process with a circular die has the advantages of a simple apparatus, low operating costs, easy biaxial orientation, and less trimming loss compared to the flat film process with a slot die, but is said to show poorer gauge tolerance and troublesome control by means of decentring of the die lip-ring. The rotation of die or the take-up is not only a superficial solution of these problems, but also requires complex and expensive machinery.

In order to mitigate these disadvantages, many designs of circular die have been suggested^{1, 2}. Concerning the design variables, the slot die^{3, 4} and the spiral mandrel die were recently analysed⁵, but operation variables were studied only partly in an article on the behaviour of sheet extrusion⁶.

The purpose of this investigation was to show experimentally the effects of operating conditions on the homogeneity of the annular extrusion of especially polystyrene, which has a melt viscosity highly sensitive to shear and temperature. For this purpose, the variance of melt flow rate between quadrants of the circular die was determined, changing the output rate with the rotational screw speed, and the specified temperature at various positions of the apparatus, i.e. its longitudinal and circumferential distribution. To facilitate the discussion of various factors, we have devised a special spider-type die, which can control the pressure distribution between quadrants of the die lip, and a differential thermometer, which can measure accurately the melt temperature distribution in the die channels.

EXPERIMENTAL

The material used was high-impact polystyrene made by Dainippon Ink and Chemicals, Inc.: density, 1045 kg/m³; melt index, 0.10 g/10 min; and, as power law fluid, a flow behaviour index, 2.3.

The melt was fed from a 30 mm diameter extruder (L/D 20) through the adapter to a vertical inlet at the bottom of the circular die. As shown in *Figure 1*, the die had a construction, which conveyed the melt into four crosswise located manifolds with valves at the upward turnings, then through horizontal spreading channels followed by a vertical annular channel, up to the die lip. The total channel length was designed to be the same around the annular channel by adjusting the inclination of the spreading channel. The profile of the land was corrected by means of trial-and-error, to ensure a uniform flow rate around the die lip at the constant gap.

Die constants of each of the parts were calculated on the assumption of infinite parallel plate or circular pipe, and the observed pressure drops through the die are given in *Table 1*.

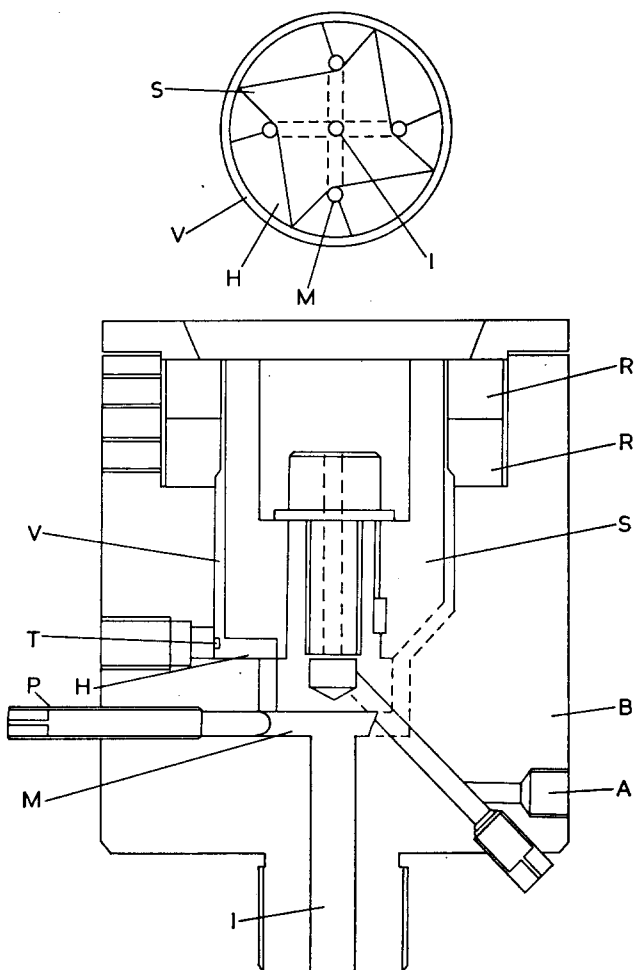


Figure 1 Design configuration of a spider-type die. I, inlet; M, manifold; P, pressure control valves; H, horizontal spreading channels; V, vertical annular channel; R, R', die lip rings; S, spider mandrel; B, body; T, thermometers; A, blowing air inlet (R' is omitted in this experiment)

Table 1 Calculated die constant and pressure drop distribution

Parts	Die constant $\times 10^{-10}$ (m ³)	Pressure drop (% to total)	
Manifolds	0.244	26.1	
Spreading and annular channel	4.655	11.3	flow behaviour index of 2.00
Die lip	0.053	62.6	

The ratio of back pressure flow to drag flow was estimated from the difference between the extrusion rates with and without die.

With pressure control by means of valves at each of the manifolds, the variance of flow rate between the quadrants could be reduced to within 1%. The extrusion pressure was measured at the inlet of the adapter with a Bourdon-type gauge.

The temperature at the barrel was controlled automatically. The circumferential temperature in the die was controlled manually by band heaters sectioned in quadrants. The temperature of melt in the die was estimated with a differential thermometer made by Toa Electronic Co. It has two pairs of thermistors, which can detect the differences in the protecting sheath due to the conduction to the die wall, following the suggestion by Van Leeuwen⁷. The temperature of the tip was read up to $\pm 0.1^\circ\text{C}$, controlling the root temperature within $\pm 0.02^\circ\text{C}$.

The uniformity of flow rate around the die lip was estimated from the weights of the film portions, which were extruded without blowing and divided in quadrants. It is expressed as the coefficient of variance, $VC(Q)$, or the deviation from mean value.

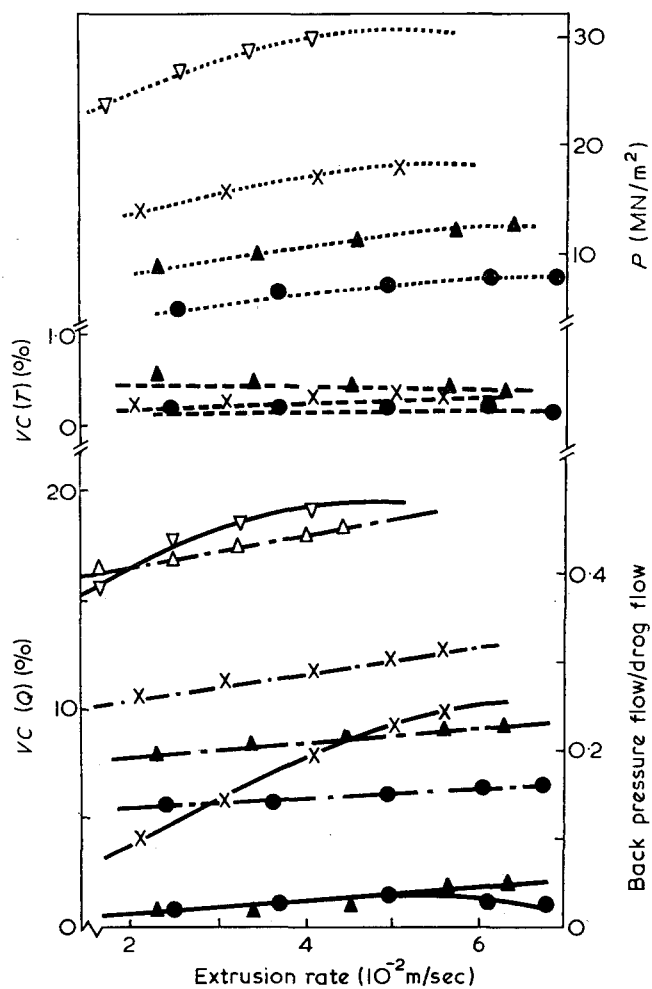


Figure 2 Effects of linear extrusion rate and stock temperature on the variance of extrusion rate (—), the variance of temperature at die (---), the pressure drop (.....), and the back pressure flow ratio (-.-.-). ∇ , 170°C; \times , 190°C; \blacktriangle , 210°C; \bullet , 230°C

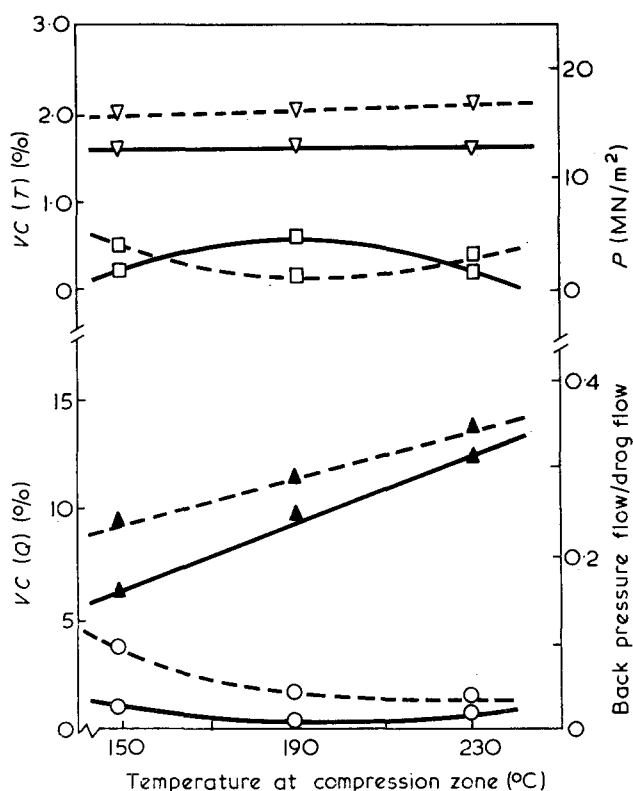


Figure 3 Effect of temperature at compression zone with other fixed temperatures on the variance of extrusion rate (\square), the variance of temperature (∇), the pressure drop (∇), and the back pressure flow ratio (\blacktriangle), for various rotational speeds of screw. —, 20 rev/min; ---, 50 rev/min. Temperatures at other controlled points are kept at 190°C

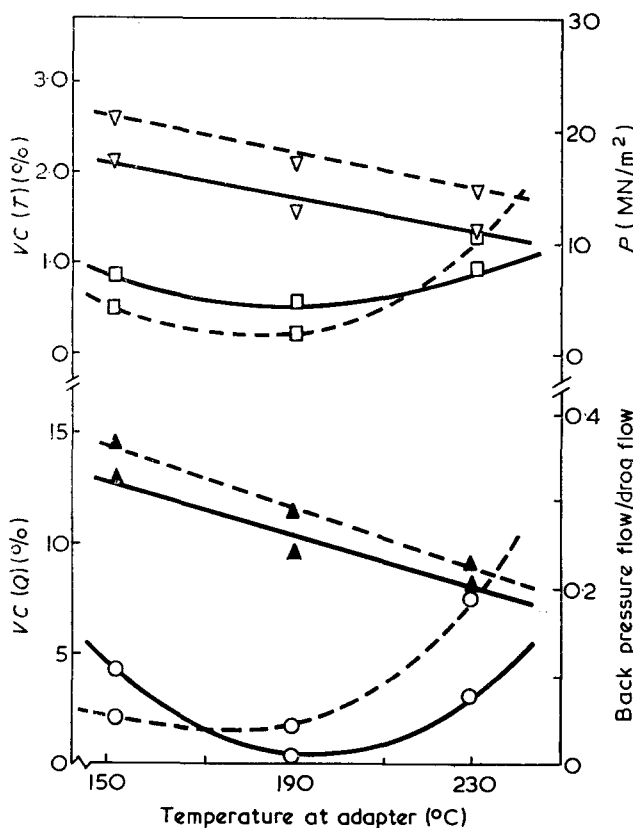


Figure 4 Effect of temperature at adapter with other fixed temperatures on the variance of extrusion rate, the variance of temperature at die, the pressure drop, and the back pressure flow ratio, for various speeds of screw. Temperatures at other controlled points are fixed at 190°C. (Same notations as Figure 3)

RESULTS

As shown in Figure 2, increase in the rotational speed of the screw, i.e. output rate, increased the pressure drop through the die and the fraction of back pressure flow. The $VC(Q)$ increased with output rate at lower temperature, but less significant at higher temperature. The coefficient of variance in temperature, $VC(T)$, was held within experimental error.

Higher specified temperature reduced the heterogeneity of flow rate and pressure drop.

As shown in Figures 3 and 4, the heterogeneous temperature profile in the longitudinal direction increased $VC(Q)$. The temperature change at the adapter seemed to have a more marked effect on $VC(Q)$ and $VC(T)$. In these cases, more back pressure flow showed a tendency of less $VC(T)$, which suggests more homogeneous mixing, but it did not always have a correlation with $VC(Q)$.

The distribution of extrusion rate around the die lip, shown in Figure 5, became more heterogeneous by varying the temperature from other specified temperatures.

The effects of circumferential temperature distribution are given in Figure 6. The flow rate increased at the locally more heated quadrants and decreased at the

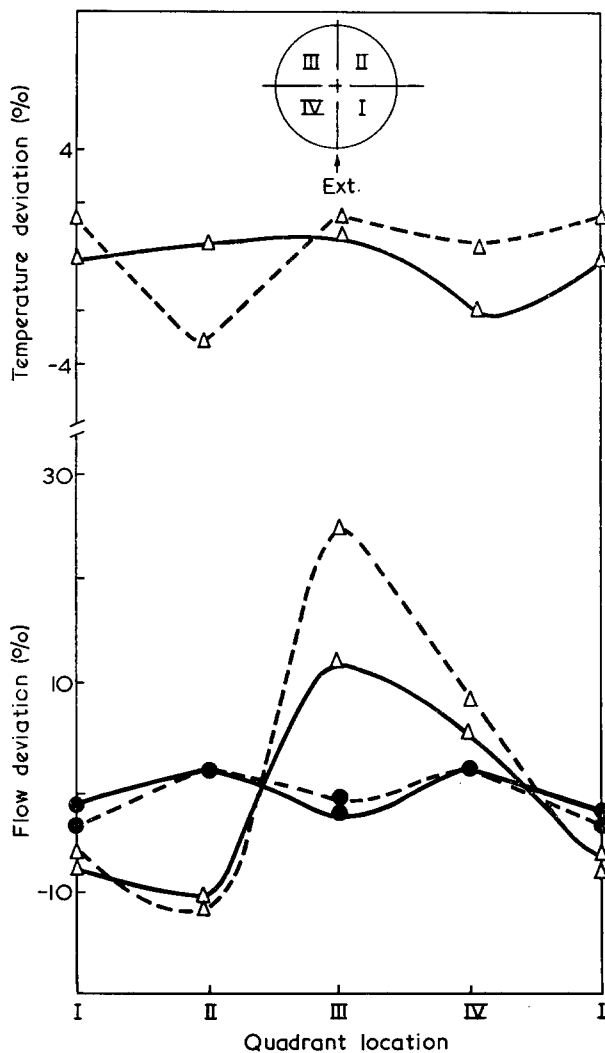


Figure 5 Effect of temperature at die on the extrusion flow rate distribution and the temperature distribution of melt in die, for various rotational speeds of screw. —, 20rev/min; ---, 50rev/min. ●, 210°C; △, 170°C. Temperatures at other controlled points are fixed at 210°C

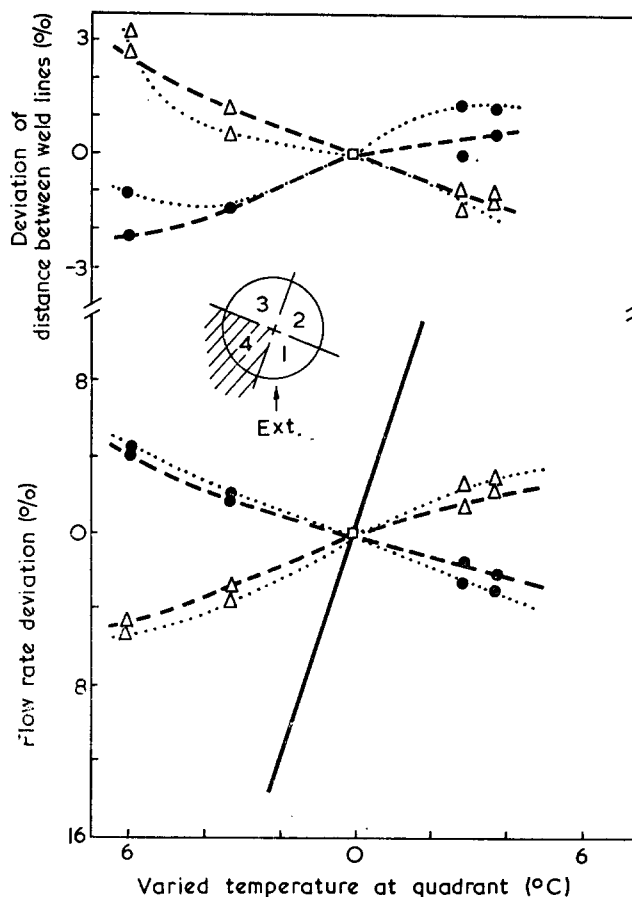


Figure 6 Effect of local temperature variation at die on the extrusion flow deviation, and the distance between weld lines, for various rotational speeds of screw. ·····, 20rev/min; ---, 50rev/min; △, at the varied quadrant; ●, at the opposite quadrant. Reference temperature at die is 210°C. — represents the calculated flow rate deviation

opposite quadrant. The distance between weld lines decreased or increased, respectively, at the more heated quadrant or at the opposite quadrant. Therefore, the linear velocity at the more heated quadrant was higher.

DISCUSSION

The homogeneity of extrusion rate from the die is dependent on many variables. As estimated in Table 1, the pressure dropped mostly across the die lip in our experiment. Therefore, the problem was simplified and the discussion of flow rate was confined at the die lip, which was approximated as infinite parallel plates. The flow rate deviation in non-dimensional terms as a fraction of mean flow can be expressed as follows:

$$\Delta Q/Q = (2+n)(\Delta H/H) - n(\Delta L/L) - n(\Delta\eta^0/\eta^0) + n(\Delta P/P) \quad (1)$$

where Q is the flow rate per unit of circumference, L is the die land length, H is the gap width of lip, P is the pressure applied to die lip, η^0 is the viscosity at reference shear, and n is the flow behaviour index expressed in the equation, $\log\eta = \log\eta^0 - (n-1)\log(P/P_0)$. This equation indicates that the temperature of melt, at the die lip, affects the flow rate significantly through the considerable change of viscosity. Although the longitudinal temperature profile is specific to the extruder and die combination, the non-uniform controlling

condition would result in the higher variance of extrusion rate, probably due to insufficient heat transfer. However, the more mixing with reduced output or more back pressure flow could compensate the difference.

In the experiment with more uniform temperature profile, shown in *Figure 2*, $VC(Q)$ increased with pressure drop, despite higher mixing degree by back pressure flow. Hence, the pressure distribution at the die lip could have an important effect. The calculated value plotted in *Figure 6*, which corresponds to a higher flow rate due to reduced viscosity at higher temperature was steeper than the observed lines and opposite to the width between weld lines. Therefore, the flow pattern in the annular channel of the die might change and compensate for the heterogeneous pressure drop.

Warmuth⁶ observed the similar effect of the rotational screw speed on polystyrene and polypropylene, but different results were obtained on polybutene and polyethylene. Since the rotational screw speed changes the flow pattern, depending on design, material parameters, and operational conditions, this phenomenon would be no definite effect.

From the above discussion, it is important to devise a die which can compensate the heterogeneity of resistance around the lip, in addition to precise manufacturing, as suggested by Proctor⁴. In our design, the gross balancing can be obtained with valves at manifolds and the small difference can be corrected by the profile of land length at constant gap width because, based on equation (1), the land length is less critical and more easily adjustable than the gap width. Since the flow behaviour index affects the effect of die design,

our lip-ring can be replaced corresponding to various types of material.

Because the flow behaviour index n exhibits serious effects on the homogeneity of annular extrusion, according to equation (1), uniform gauge might be difficult in the case of polystyrene, which has higher flow behaviour index and higher activation energy of flow.

CONCLUSIONS

(1) Temperature distribution, particularly near the die, and pressure drop distribution, which are dependent on operation variables, i.e. rotational screw speed, back pressure or stock temperature, appear to have serious effects on the homogeneity of annular extrusion. But some gauge heterogeneity could be scattered in transit through the annular channel of die, probably owing to the change of flow pattern, and compensations for temperature and pressure drop.

(2) The die design, which can adjust the resistance around the lip, would be useful particularly in the case of material with high shear-sensitivity.

REFERENCES

- 1 Kock, K. *Ind. Anz.* 1968, **90**, (80), 26
- 2 Caton, J. A. *Br. Plast.* 1971, **44**, (4), 140
- 3 Mckelvey, J. M. and Ito, K. *Polym. Eng. Sci.* 1971, **11**, 258
- 4 Knappe, W. and Schönewald, H. *Kunststoffe* 1970, **60**, 657; 1971, **61**, 497
- 5 Proctor, B. *SPE J.* 1972, **28**, (2) 34
- 6 Warmuth, J. *Plastverarbeiter* 1972, **23**, (2), 95
- 7 Van Leeuwen, J. *Kunststoffe* 1965, **55**, 491; *Polym. Eng. Sci.* 1967, **7**, 98

Letters

¹³C n.m.r. spectra of styrene-butadiene copolymers on solid samples

Many papers have been published on the determination of polymer microstructure in solution by n.m.r. In the last few years ¹³C n.m.r. has proved to be a powerful tool in this field. However, very few experiments have been reported on solid samples of polymers.

The attainment of a good resolution in solid samples depends on the structural state of macromolecular chains; but more strictly on the relaxation times relative to the different nuclei, which are dependent on the mobility of the chain. As a consequence for a random polymer with sufficient segmental motion, we might expect a ¹³C n.m.r. spectrum which is sufficiently satisfactory and not very different from the analogous one in solution.

On the other hand, a very poor spectrum should be obtained in the case of crystalline polymers or in the case of restricted segmental motions. In fact during a previous study¹ characterizing ethylene-vinyl acetate copolymers we were able to obtain spectra on solid samples, showing a sufficient degree of resolution. This result prompted us to try a similar approach on different copolymers. The present communication concerns some preliminary results on the ¹³C n.m.r. spectra of solid samples of styrene-butadiene copolymers.

¹³C n.m.r. spectra of these copolymers in solution will be discussed in a later paper².

The spectrum of a random copolymer is shown in *Figure 1*, in solution (a) as well as in the solid state (b). The high field portion of the spectrum (25–47 ppm from TMS) is due to the CH and CH₂ backbone resonances and the low field portion (110–147 ppm) portion is due to the aromatic, vinyl and vinylenic ¹³C atoms.

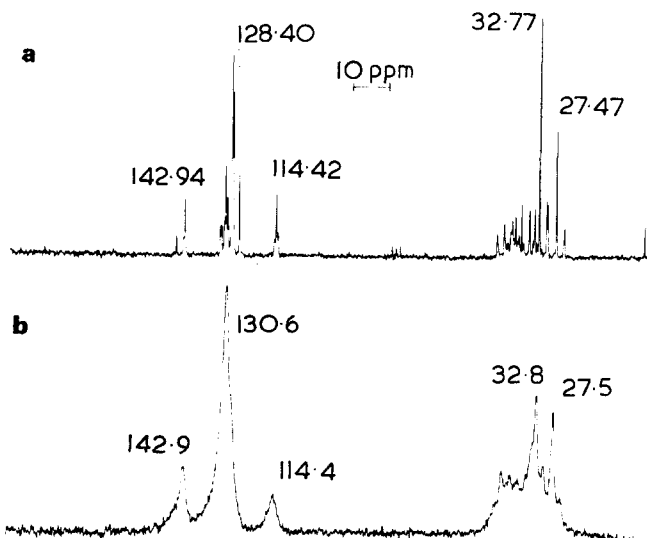


Figure 1 ¹³C n.m.r. spectrum of a random butadiene-styrene copolymer. (a) In solution; (b) in the solid state

condition would result in the higher variance of extrusion rate, probably due to insufficient heat transfer. However, the more mixing with reduced output or more back pressure flow could compensate the difference.

In the experiment with more uniform temperature profile, shown in *Figure 2*, $VC(Q)$ increased with pressure drop, despite higher mixing degree by back pressure flow. Hence, the pressure distribution at the die lip could have an important effect. The calculated value plotted in *Figure 6*, which corresponds to a higher flow rate due to reduced viscosity at higher temperature was steeper than the observed lines and opposite to the width between weld lines. Therefore, the flow pattern in the annular channel of the die might change and compensate for the heterogeneous pressure drop.

Warmuth⁶ observed the similar effect of the rotational screw speed on polystyrene and polypropylene, but different results were obtained on polybutene and polyethylene. Since the rotational screw speed changes the flow pattern, depending on design, material parameters, and operational conditions, this phenomenon would be no definite effect.

From the above discussion, it is important to devise a die which can compensate the heterogeneity of resistance around the lip, in addition to precise manufacturing, as suggested by Proctor⁴. In our design, the gross balancing can be obtained with valves at manifolds and the small difference can be corrected by the profile of land length at constant gap width because, based on equation (1), the land length is less critical and more easily adjustable than the gap width. Since the flow behaviour index affects the effect of die design,

our lip-ring can be replaced corresponding to various types of material.

Because the flow behaviour index n exhibits serious effects on the homogeneity of annular extrusion, according to equation (1), uniform gauge might be difficult in the case of polystyrene, which has higher flow behaviour index and higher activation energy of flow.

CONCLUSIONS

(1) Temperature distribution, particularly near the die, and pressure drop distribution, which are dependent on operation variables, i.e. rotational screw speed, back pressure or stock temperature, appear to have serious effects on the homogeneity of annular extrusion. But some gauge heterogeneity could be scattered in transit through the annular channel of die, probably owing to the change of flow pattern, and compensations for temperature and pressure drop.

(2) The die design, which can adjust the resistance around the lip, would be useful particularly in the case of material with high shear-sensitivity.

REFERENCES

- 1 Kock, K. *Ind. Anz.* 1968, **90**, (80), 26
- 2 Caton, J. A. *Br. Plast.* 1971, **44**, (4), 140
- 3 Mckelvey, J. M. and Ito, K. *Polym. Eng. Sci.* 1971, **11**, 258
- 4 Knappe, W. and Schönwald, H. *Kunststoffe* 1970, **60**, 657; 1971, **61**, 497
- 5 Proctor, B. *SPE J.* 1972, **28**, (2) 34
- 6 Warmuth, J. *Plastverarbeiter* 1972, **23**, (2), 95
- 7 Van Leeuwen, J. *Kunststoffe* 1965, **55**, 491; *Polym. Eng. Sci.* 1967, **7**, 98

Letters

¹³C n.m.r. spectra of styrene-butadiene copolymers on solid samples

Many papers have been published on the determination of polymer microstructure in solution by n.m.r. In the last few years ¹³C n.m.r. has proved to be a powerful tool in this field. However, very few experiments have been reported on solid samples of polymers.

The attainment of a good resolution in solid samples depends on the structural state of macromolecular chains; but more strictly on the relaxation times relative to the different nuclei, which are dependent on the mobility of the chain. As a consequence for a random polymer with sufficient segmental motion, we might expect a ¹³C n.m.r. spectrum which is sufficiently satisfactory and not very different from the analogous one in solution.

On the other hand, a very poor spectrum should be obtained in the case of crystalline polymers or in the case of restricted segmental motions. In fact during a previous study¹ characterizing ethylene-vinyl acetate copolymers we were able to obtain spectra on solid samples, showing a sufficient degree of resolution. This result prompted us to try a similar approach on different copolymers. The present communication concerns some preliminary results on the ¹³C n.m.r. spectra of solid samples of styrene-butadiene copolymers.

¹³C n.m.r. spectra of these copolymers in solution will be discussed in a later paper².

The spectrum of a random copolymer is shown in *Figure 1*, in solution (a) as well as in the solid state (b). The high field portion of the spectrum (25–47 ppm from TMS) is due to the CH and CH₂ backbone resonances and the low field portion (110–147 ppm) portion is due to the aromatic, vinyl and vinylenic ¹³C atoms.

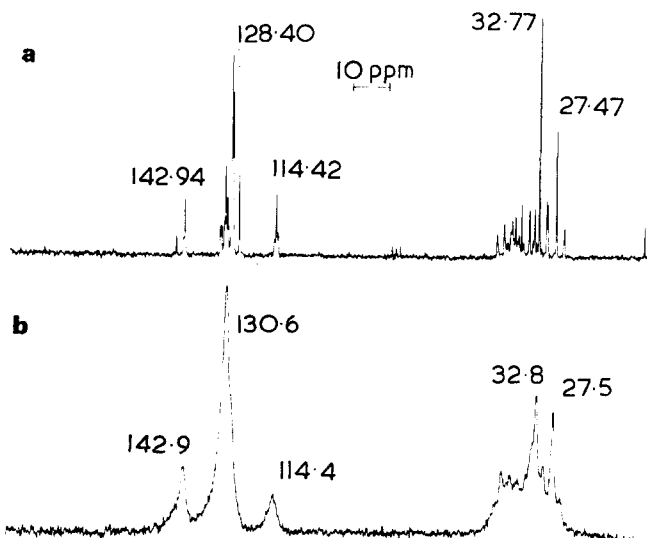


Figure 1 ¹³C n.m.r. spectrum of a random butadiene-styrene copolymer. (a) In solution; (b) in the solid state

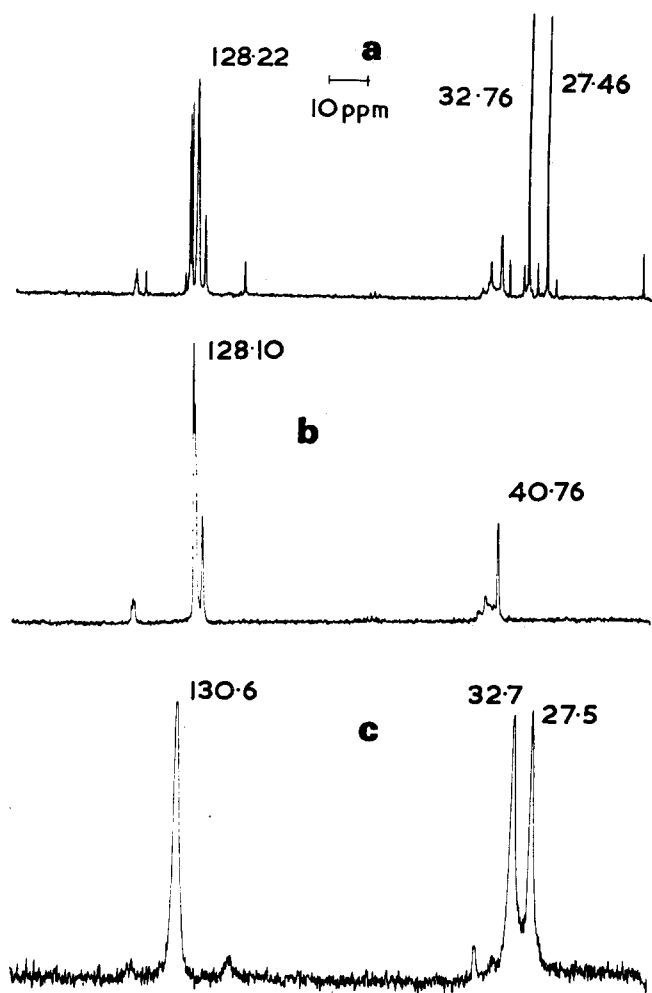


Figure 2 ^{13}C n.m.r. spectrum of (a) a block butadiene-styrene copolymer in solution, (b) atactic polystyrene and (c) a block butadiene-styrene copolymer in the solid state

In both regions of the spectrum the high number of resonances is due to the presence of different sequences of monomeric units and all experimental lines have been assigned² on the basis of correlation with homopolymers and on the basis of additivity rules.

Regardless of their attribution it can be seen that all bands present in the spectrum of the solution are also observed in the spectrum of the solid copolymer, in which obviously the resolution is partly lost.

The spectrum of a block copolymer of the S-B type is shown in Figure 2, in solution (a), as well as in the solid state (c); the spectrum of an atactic polystyrene sample in solution is also shown (b). The spectrum of Figure 2a is identical to the superimposition of a polybutadiene spectrum³ plus the spectrum of atactic polystyrene (see Figure 2b).

The high field portion of the spectrum (25–47 ppm) is due to the backbone methine and methylene carbon atoms, while the low field portion (110–147 ppm) is due to aromatic, vinyl and vinylenic carbon atoms². It can be easily seen by comparison of Figures 2a, 2b and 2c that all the peaks of the atactic polystyrene, which are observed in the spectrum in solution, are missing in the solid state spectrum. We must also note that lack of sensitivity is out of the question in this experiment, owing to the fact that in the second sample the styrene content is almost twice as much than in the first polymer.

A coarse structure proposed by Kraus and Railsback⁴ for S-B copolymers, consists of domains of polystyrene, held together by weak interactions, connected by long threads of polybutadiene.

A structure of this type might be the origin of the observed spectra. In fact, if we suppose the polybutadiene to be in a state in which it has a large segmental mobility, as in a glassy type structure suggested by Bishop *et al.*⁵ and the polystyrene is confined into compressed domains, the experimental results are meaningful.

The above explanation is obviously a tentative one and more detailed studies at variable temperature are in progress.

Experimental

The copolymers studied were prepared as follows. Random copolymer: sample I; catalyst: n-butyl-Li/tetrahydrofuran; adiabatic reaction between 50°C and 110°C. Block copolymer: sample II; S-B type; catalyst: n-butyl-Li/tetrahydrofuran; adiabatic reaction between 50°C and 95°C.

The analysis in terms of percentages of composition of units in the copolymer is (by ^1H and ^{13}C n.m.r.)

	Sample I	Sample II
styrene	16%	28%
1,2-butadiene	26%	9%
cis-1,4-butadiene	19%	25%
trans-1,4-butadiene	39%	38%

The butadiene-styrene ratio has been verified by elemental analysis. ^{13}C n.m.r. spectra have been run on 10% solutions (by weight) in CDCl_3 , with tetramethylsilane as an internal reference.

Spectral conditions:

Spectral width (Hz)	5000
Acquisition time (sec)	0.8
Pulse width (μsec)	10
Signal enhancement (sec)	0.4
K transients	4

The ^{13}C n.m.r. spectra of the solid samples have been run under the following conditions:

Spectral width (Hz)	5000
Acquisition time (sec)	0.4
Pulse width (μsec)	14
Signal enhancement (sec)	0.2
K transients	1

The spectrometer used was a Varian XL-100.

Acknowledgement

The authors are grateful to Dr F. N. Wehrly of Varian AG Zug for recording the spectra.

F. Conti, M. Delfini and A. L. Segre

Istituto Chimica,
Università di Roma,
00185 Rome, Italy

(Received 3 May 1974; revised 13 June 1974)

References

- 1 Delfini, M., Segre, A. L. and Conti, F. *Macromolecules* 1973, **6**, 456
- 2 Segre, A. L., Delfini, M., Boicelli, A. and Conti, F. *Polymer* in press
- 3 Conti, F., Segre, A. L., Pini, D. and Porri, L. *Polymer* 1974, **15**, 5; Mochel, V. D. *J. Polym. Sci. (A-1)* 1972, **10**, 1009; Elgert, K. F., Stutzel, B., Frenzel, P., Cantow, H. J. and Streck, R. *Makromol. Chem.* 1973, **170**, 257
- 4 Kraus, G. and Railsback, H. R. *Polym. Prepr.* 1973, **14**, 1051
- 5 Bishop, E. T. and Davison, S. J. *Polym. Sci. (C)* 1969, **26**, 59

Microphase separation in an ABC block terpolymer

Introduction

An important feature of many block and graft polymers is the ability of the components to undergo microphase separation. For block copolymers having a well defined primary structure (e.g. AB and ABA type systems) it has been found that microphase separation can lead to ordered arrays of regular domains; the type of domain involved (spheres, cylinders and lamellae) is dependent on such factors as the structural nature of the monomeric repeat units, block lengths and overall composition, and the thermal and mechanical history of the sample^{1, 2}.

Recently there have been several reports of work on ABC type block terpolymers. Cooper *et al.*³ discussed the properties of triblock polymers formed from styrene, isoprene (or butadiene) and ethylene sulphide. Electron micrographs of cast films and ultramicrotomed sections gave clear evidence of microphase separation. Contrast in the polyisoprene phase was enhanced by staining with osmium tetroxide, but it was not possible to distinguish between domains of polystyrene and poly(ethylene sulphide). Fielding-Russell and Pillai⁴ reported a study of the phase structure of benzene cast films of terpolymers of the type poly(α -methylstyrene)/polybutadiene/polystyrene. Electron microscopy showed microphase separation occurred, but again it was not possible to distinguish directly between two of the blocks (in this case between poly(α -methylstyrene) and polystyrene). On the basis of dynamic mechanical and differential scanning calorimetry (d.s.c.) measurements, however, it was concluded that the polymer formed a two-phase microstructure consisting of a composite glassy phase of poly(α -methylstyrene) and polystyrene randomly dispersed in a rubbery matrix of polybutadiene.

In this communication we report some results of an electron microscopical study of a polystyrene/polyisoprene/poly(2-vinylpyridine) three-block terpolymer. The system is of particular interest because we have found it possible to selectively stain two of the polymer components separately.

Experimental and Results

Polymer sample. Details of the method of synthesis, fractionation and structural characterization of the sample (designated 1L1) will be reported later. Briefly, the terpolymer was synthesized by stepwise anionic polymerization of styrene, isoprene and 2-vinylpyridine using butyl lithium as the primary initiator for styrene. The number-average molecular weights of the polystyrene,

polyisoprene, and poly(2-vinylpyridine) blocks were 23 000, 102 000 and 23 000 respectively. The apparent weight-average molecular weight of the overall copolymer, determined by light scattering in 1,2-dimethoxyethane, was 172 000. The polymerization conditions gave polyisoprene blocks having 91% *cis*-1,4 structure.

Electron microscopy. Electron micrographs of specimens were obtained using an AEI EM6G electron microscope operated at an accelerating voltage of 100 kV. Ultrathin polymer films were obtained by solvent casting from methylcyclohexane and benzene. The method employed was to allow a drop of a dilute solution of the polymer (~0.2% by wt. polymer) to evaporate on an ultrathin carbon film mounted on an electron microscope grid. This approach was somewhat different from that used in our earlier studies on ABA block copolymers⁵ in which casting was carried out on a mercury surface and then the polymer film was freely supported by the electron microscope grid. The advantage of the new method was that the carbon film gave additional support to the specimen and permitted a variety of exploratory staining experiments to be carried out without breakage of the film.

An electron micrograph of the ABC terpolymer cast from methylcyclohexane is shown in *Figure 1*. The specimen was stained by suspending it in the vapour of a 1% solution of osmium tetroxide in *n*-heptane. Since osmium tetroxide reacts selectively with olefinic bonds of the polyisoprene, dark regions in the micrograph indicate the presence of polyisoprene, whilst light regions (mainly 'circular' domains in the micrograph) indicate the presence of either polystyrene or poly(2-vinylpyridine).

Figure 2 also shows an electron micrograph of the ABC terpolymer cast from methylcyclohexane. In this case, however, the specimen was stained by dipping it in a 0.1% aqueous solution of silver nitrate. Residual solution was removed by rinsing with water. We believe that that reagent selectively stains regions containing poly(2-vinylpyridine). When subjected to a similar staining procedure, a polystyrene/polyisoprene/polystyrene copolymer showed no enhancement of contrast. Comparison

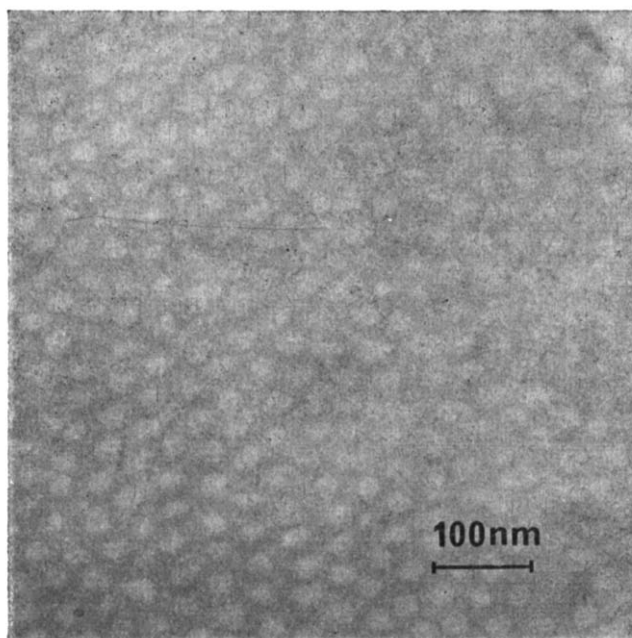


Figure 1 Electron micrograph of a film of block terpolymer 1L1 cast from methylcyclohexane and stained with osmium tetroxide

References

- 1 Delfini, M., Segre, A. L. and Conti, F. *Macromolecules* 1973, **6**, 456
- 2 Segre, A. L., Delfini, M., Boicelli, A. and Conti, F. *Polymer* in press
- 3 Conti, F., Segre, A. L., Pini, D. and Porri, L. *Polymer* 1974, **15**, 5; Mochel, V. D. *J. Polym. Sci. (A-1)* 1972, **10**, 1009; Elgert, K. F., Stutzel, B., Frenzel, P., Cantow, H. J. and Streck, R. *Makromol. Chem.* 1973, **170**, 257
- 4 Kraus, G. and Railsback, H. R. *Polym. Prepr.* 1973, **14**, 1051
- 5 Bishop, E. T. and Davison, S. J. *Polym. Sci. (C)* 1969, **26**, 59

Microphase separation in an ABC block terpolymer

Introduction

An important feature of many block and graft polymers is the ability of the components to undergo microphase separation. For block copolymers having a well defined primary structure (e.g. AB and ABA type systems) it has been found that microphase separation can lead to ordered arrays of regular domains; the type of domain involved (spheres, cylinders and lamellae) is dependent on such factors as the structural nature of the monomeric repeat units, block lengths and overall composition, and the thermal and mechanical history of the sample^{1, 2}.

Recently there have been several reports of work on ABC type block terpolymers. Cooper *et al.*³ discussed the properties of triblock polymers formed from styrene, isoprene (or butadiene) and ethylene sulphide. Electron micrographs of cast films and ultramicrotomed sections gave clear evidence of microphase separation. Contrast in the polyisoprene phase was enhanced by staining with osmium tetroxide, but it was not possible to distinguish between domains of polystyrene and poly(ethylene sulphide). Fielding-Russell and Pillai⁴ reported a study of the phase structure of benzene cast films of terpolymers of the type poly(α -methylstyrene)/polybutadiene/polystyrene. Electron microscopy showed microphase separation occurred, but again it was not possible to distinguish directly between two of the blocks (in this case between poly(α -methylstyrene) and polystyrene). On the basis of dynamic mechanical and differential scanning calorimetry (d.s.c.) measurements, however, it was concluded that the polymer formed a two-phase microstructure consisting of a composite glassy phase of poly(α -methylstyrene) and polystyrene randomly dispersed in a rubbery matrix of polybutadiene.

In this communication we report some results of an electron microscopical study of a polystyrene/polyisoprene/poly(2-vinylpyridine) three-block terpolymer. The system is of particular interest because we have found it possible to selectively stain two of the polymer components separately.

Experimental and Results

Polymer sample. Details of the method of synthesis, fractionation and structural characterization of the sample (designated 1L1) will be reported later. Briefly, the terpolymer was synthesized by stepwise anionic polymerization of styrene, isoprene and 2-vinylpyridine using butyl lithium as the primary initiator for styrene. The number-average molecular weights of the polystyrene,

polyisoprene, and poly(2-vinylpyridine) blocks were 23 000, 102 000 and 23 000 respectively. The apparent weight-average molecular weight of the overall copolymer, determined by light scattering in 1,2-dimethoxyethane, was 172 000. The polymerization conditions gave polyisoprene blocks having 91% *cis*-1,4 structure.

Electron microscopy. Electron micrographs of specimens were obtained using an AEI EM6G electron microscope operated at an accelerating voltage of 100 kV. Ultrathin polymer films were obtained by solvent casting from methylcyclohexane and benzene. The method employed was to allow a drop of a dilute solution of the polymer (~0.2% by wt. polymer) to evaporate on an ultrathin carbon film mounted on an electron microscope grid. This approach was somewhat different from that used in our earlier studies on ABA block copolymers⁵ in which casting was carried out on a mercury surface and then the polymer film was freely supported by the electron microscope grid. The advantage of the new method was that the carbon film gave additional support to the specimen and permitted a variety of exploratory staining experiments to be carried out without breakage of the film.

An electron micrograph of the ABC terpolymer cast from methylcyclohexane is shown in *Figure 1*. The specimen was stained by suspending it in the vapour of a 1% solution of osmium tetroxide in *n*-heptane. Since osmium tetroxide reacts selectively with olefinic bonds of the polyisoprene, dark regions in the micrograph indicate the presence of polyisoprene, whilst light regions (mainly 'circular' domains in the micrograph) indicate the presence of either polystyrene or poly(2-vinylpyridine).

Figure 2 also shows an electron micrograph of the ABC terpolymer cast from methylcyclohexane. In this case, however, the specimen was stained by dipping it in a 0.1% aqueous solution of silver nitrate. Residual solution was removed by rinsing with water. We believe that that reagent selectively stains regions containing poly(2-vinylpyridine). When subjected to a similar staining procedure, a polystyrene/polyisoprene/polystyrene copolymer showed no enhancement of contrast. Comparison

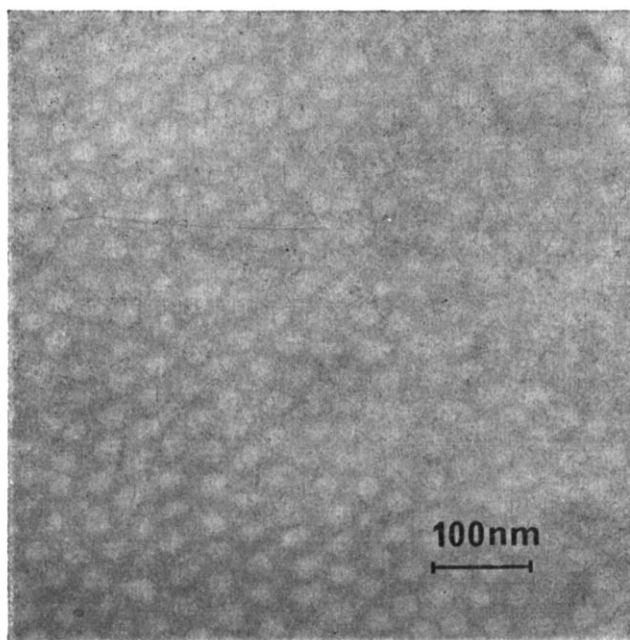


Figure 1 Electron micrograph of a film of block terpolymer 1L1 cast from methylcyclohexane and stained with osmium tetroxide

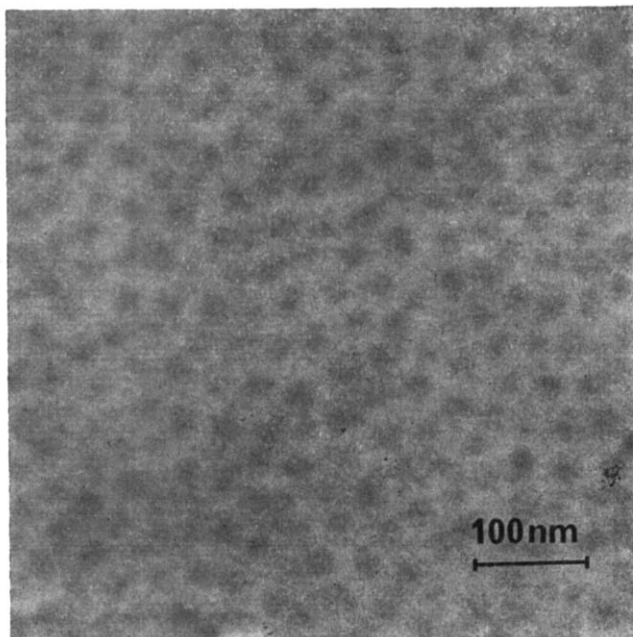


Figure 2 Electron micrograph of a film of block terpolymer 1L1 cast from methylcyclohexane and stained with silver nitrate

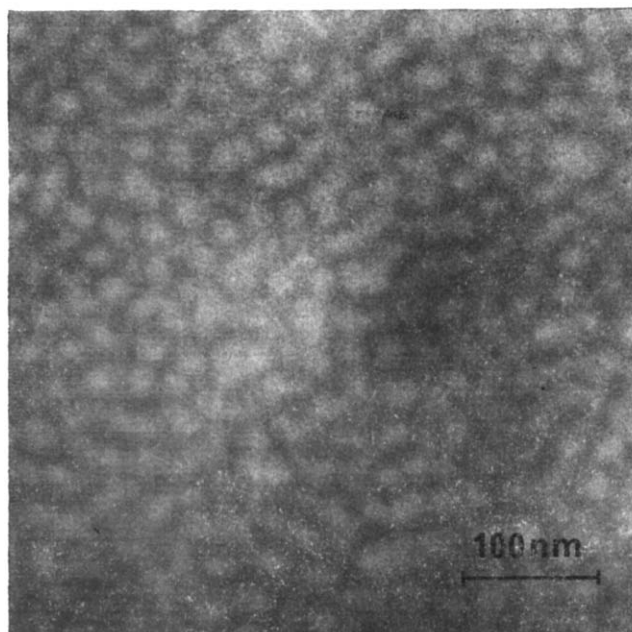


Figure 3 Electron micrograph of an ultramicrotomed section of block terpolymer 1L1 cast from methylcyclohexane and stained with osmium tetroxide

of Figures 1 and 2 indicates that all the domains are stained by $\text{AgNO}_3(\text{aq.})$. This result suggests that when cast from methylcyclohexane the polystyrene and poly(2-vinylpyridine) blocks form a mixed microphase. The elastomeric properties of strips of polymer cast from methylcyclohexane provide evidence for the presence in the bulk polymer of a physically crosslinked network. This behaviour is understandable since both polystyrene and poly(2-vinylpyridine) are glassy polymers at room temperature (having very similar glass transition temperatures), whilst polyisoprene is a rubber. The elastomeric properties serve to rule out the slight possibility that the polystyrene might be located in the polyisoprene matrix rather than with the poly(2-vinylpyridine). The

solubility parameters (δ) of methylcyclohexane, polyisoprene, polystyrene and poly(2-vinylpyridine) are respectively 16.0, 16.6, 18.6 and $21.7 \text{ J}^{1/2} \text{ cm}^{-3/2}$. Thus on evaporation of the solvent from the solution, the polystyrene and poly(2-vinylpyridine) blocks probably separate at an early stage from the polyisoprene blocks to form a mixed microgel phase.

In order to establish the three-dimensional shape of the domains, electron micrographs were taken of ultrathin sections of the ABC terpolymer cast from methylcyclohexane. Relatively thick sections were first cut away from the specimen and soaked in a solution of osmium tetroxide in *n*-heptane. The osmium tetroxide served to both stain and harden the rubbery polyisoprene. The impregnated specimens were then set in an embedding medium and ultrathin sections were cut away at several orientations using an LKB model 3 ultramicrotome. Figure 3 shows an electron micrograph of a section; similar features were observed for other orientations studied. The distorted 'circles' suggest that the morphology consists of an array of particles roughly spherical in shape [composed of a mixture of polystyrene and poly(2-vinylpyridine) blocks] embedded in a polyisoprene matrix. Ultramicrotomy of the samples was found to be particularly difficult, and some slight deformation of the domains probably occurred during this procedure.

Studies have also been made of specimens cast from benzene ($\delta = 18.8 \text{ J}^{1/2} \text{ cm}^{-3/2}$). Similar features were observed to those discussed above, although in general the morphology was more irregular and many of the domains were worm-like in shape rather than spherical. An electron micrograph of a film cast from benzene and stained with osmium tetroxide is shown in Figure 4. Staining with $\text{AgNO}_3(\text{aq.})$ again suggested that the glassy domains consisted of a blend of polystyrene and poly(2-vinylpyridine).

At the present time in our laboratory, investigations are being made of the mechanical properties of polystyrene/polyisoprene/poly(2-vinylpyridine) block terpolymers and we hope to present a detailed account of structure-property relationships for the system at a later time.

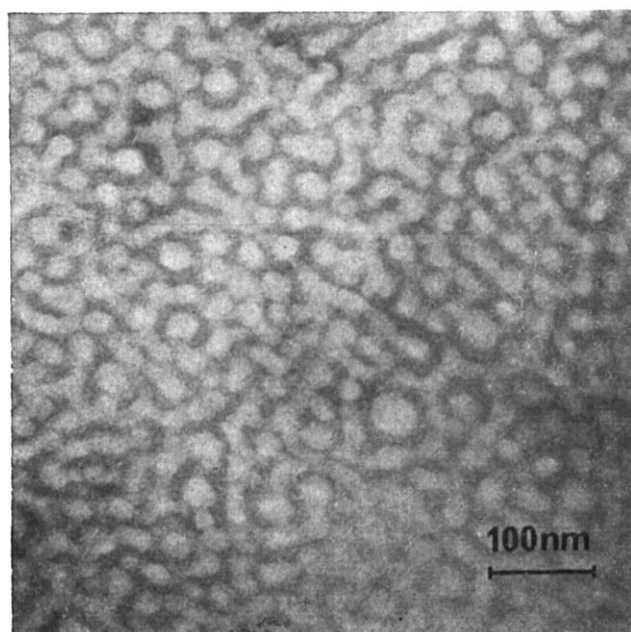


Figure 4 Electron micrograph of a film of block terpolymer 1L1 cast from benzene and stained with osmium tetroxide

Acknowledgement

We are indebted to SRC for providing general support for our programme of research on block polymers.

C. Price, T. P. Lally and R. Stubbersfield

Department of Chemistry,
University of Manchester,
Manchester M13 9PL, UK

(Received 14 June 1974)

References

- 1 Matsuo, M., Sagal, S. and Asai, H. *Polymer* 1969, **10**, 79
- 2 Lewis, P. R. and Price, C. *Nature* 1969, **223**, 494
- 3 Cooper, W., Hale, P. T. and Walker, J. S. *Polymer* 1974, **15**, 175
- 4 Fielding-Russell, G. S. and Pillai, P. S. *Polymer* 1974, **15**, 97
- 5 Lewis, P. R. and Price, C. *Polymer* 1972, **13**, 20

More efficient stabilizers for PVC

Stabilizers to inhibit the thermal degradation of PVC have been developed by empirical means and various dialkyltin compounds have been found to be particularly effective. Recently many of the beneficial reactions occurring between the stabilizer and the polymer have been identified^{1, 2}. A stabilizer R_2SnX_2 (R =alkyl; X =various groups, e.g. alkyl thioglycollate or alkyl maleate) by exchange reactions with labile chlorine atoms in the polymer and by absorption of hydrochloric acid becomes converted to the dichloride R_2SnCl_2 ^{2, 3}. The latter compound has a deleterious effect since it functions as a Lewis acid catalyst for the dehydrochlorination reaction.

The aim in the work now described was to produce an organotin compound in which the stabilization reactions (exchange with labile chlorine and absorption of HCl) would be unimpaired but the undesirable catalytic function of the ensuing organotin dichloride would be suppressed. A compound containing weak to moderate strength donor groups in the alkyl chains would be suitable since in a stabilizer such as $R Sn(SCH_2COOC_8H_{17-i})_2$ (R^D =alkyl chain containing a donor group) the Lewis acidity at tin is unlikely^{2, 4} to be sufficiently high to allow internal coordination from the donor groups R^D and consequently the stabilizing function should be unaltered. The increased Lewis acidity of the corresponding dichloride $R_2^D SnCl_2$ would ensure coordination by the R^D groups and the prodegradant catalytic activity would be suppressed.

Di(4-ketopentyl)tin dichloride and dibromide were prepared⁵ and treatment of either dihalide with the sodium derivative of iso-octylthioglycollate or sodium laurate gave $(CH_3COCH_2CH_2CH_2)_2Sn(SCH_2COOC_8H_{17-i})_2$ (I) and $(CH_3COCH_2CH_2CH_2)_2Sn(OCOC_{11}H_{23})_2$ (II). N.m.r. measurements (Table 1) show that the carbonyl moieties in the ketopentyl groups are free in compounds I and II but are complexed in the corresponding dihalides where increased deshielding causes the protons to be displaced downfield. Treatment of the dihalides with the more powerful donor 2,2'-bipyridyl frees the carbonyl groups and the resonance signals revert to positions characteristic of the uncomplexed ketopentyl group.

Table 1 N.m.r. measurements of compounds containing the 4-ketopentyl group ($=R$) in deuteriochloroform

Compound	τ values	
	a	b
$R_2Sn(SCH_2COOC_8H_{17-i})_2$ (I)	7.93	7.50
$R_2Sn(OCOC_{11}H_{23})_2$ (II)	7.92	7.52
R_2SnCl_2	7.74	7.23
$R_2SnCl_2 \cdot 2,2'$ -bipyridyl	7.89	7.42
R_2SnBr_2	7.76	7.27
$R_2SnBr_2 \cdot 2,2'$ -bipyridyl	7.95	7.55

Compounds I and II and standard stabilizers were then milled at 155°C into PVC (Corvic D55/09) at a concentration of 1% for 5 min. The testpieces were aged at 190°C and specimens were removed at intervals of 3 min.

The stabilizing effect of the dilaurate (II) was very similar to that of the corresponding butyl compound. However, di(4-ketopentyl)tin di(iso-octylthioglycollate) (I) showed a remarkable improvement when compared with the corresponding butyl compound $Bu_2Sn(SCH_2COOC_8H_{17-i})_2$ (III). Immediately after milling in the stabilizers the specimens containing I were noticeably clearer and more transparent than those containing the dibutyl compound (III). The latter specimens showed the first sign of discoloration after 6 min at 190°C while those stabilized with the diketopentyltin compound (I) did not produce a comparable colour until they had been aged for 15 min though the first slight signs of discoloration could be discerned after 12 min. Introduction of the carbonyl groups into the alkyl chains therefore improved the effectiveness of the thioglycollate stabilizer by a factor of 2 to 2.5.

The observation that I shows enhanced effectiveness in stabilization whereas II does not is explained by the fact that organotin di(iso-octylthioglycollates) rapidly exchange with allylic chlorines generating organotin dichloride whereas dilaurates react slowly to give the chloride laurate³. Although the latter would eventually be converted to the dichloride it appears that it is the reactions which occur in the earliest stages of stabilization which are most important.

Acknowledgement

We thank Albright and Wilson Ltd for technical assistance with the testing of the stabilizers.

S. Z. Abbas and R. C. Poller

Department of Chemistry,
Queen Elizabeth College,
Campden Hill, London W8 7AH, UK

(Received 24 May 1974)

References

- 1 Poller, R. C. 'The Chemistry of Organotin Compounds', Logos, London; Academic Press, New York, 1970, p 293
- 2 Ayrey, G., Head, B. and Poller, R. C. *Macromol. Rev.* in press
- 3 Ayrey, G., Poller, R. C. and Siddiqui, I. H. *J. Polym. Sci. (A-1)* 1970, **10**, 725
- 4 Ref 1, p 186
- 5 Abbas, S. Z. and Poller, R. C. *JCS Dalton Trans.* in press

Acknowledgement

We are indebted to SRC for providing general support for our programme of research on block polymers.

C. Price, T. P. Lally and R. Stubbersfield

Department of Chemistry,
University of Manchester,
Manchester M13 9PL, UK

(Received 14 June 1974)

References

- 1 Matsuo, M., Sagal, S. and Asai, H. *Polymer* 1969, **10**, 79
- 2 Lewis, P. R. and Price, C. *Nature* 1969, **223**, 494
- 3 Cooper, W., Hale, P. T. and Walker, J. S. *Polymer* 1974, **15**, 175
- 4 Fielding-Russell, G. S. and Pillai, P. S. *Polymer* 1974, **15**, 97
- 5 Lewis, P. R. and Price, C. *Polymer* 1972, **13**, 20

More efficient stabilizers for PVC

Stabilizers to inhibit the thermal degradation of PVC have been developed by empirical means and various dialkyltin compounds have been found to be particularly effective. Recently many of the beneficial reactions occurring between the stabilizer and the polymer have been identified^{1, 2}. A stabilizer R_2SnX_2 (R =alkyl; X =various groups, e.g. alkyl thioglycollate or alkyl maleate) by exchange reactions with labile chlorine atoms in the polymer and by absorption of hydrochloric acid becomes converted to the dichloride R_2SnCl_2 ^{2, 3}. The latter compound has a deleterious effect since it functions as a Lewis acid catalyst for the dehydrochlorination reaction.

The aim in the work now described was to produce an organotin compound in which the stabilization reactions (exchange with labile chlorine and absorption of HCl) would be unimpaired but the undesirable catalytic function of the ensuing organotin dichloride would be suppressed. A compound containing weak to moderate strength donor groups in the alkyl chains would be suitable since in a stabilizer such as $R Sn(SCH_2COOC_8H_{17-i})_2$ (R^D =alkyl chain containing a donor group) the Lewis acidity at tin is unlikely^{2, 4} to be sufficiently high to allow internal coordination from the donor groups R^D and consequently the stabilizing function should be unaltered. The increased Lewis acidity of the corresponding dichloride $R_2^D SnCl_2$ would ensure coordination by the R^D groups and the prodegradant catalytic activity would be suppressed.

Di(4-ketopentyl)tin dichloride and dibromide were prepared⁵ and treatment of either dihalide with the sodium derivative of iso-octylthioglycollate or sodium laurate gave $(CH_3COCH_2CH_2CH_2)_2Sn(SCH_2COOC_8H_{17-i})_2$ (I) and $(CH_3COCH_2CH_2CH_2)_2Sn(OCOC_{11}H_{23})_2$ (II). N.m.r. measurements (Table 1) show that the carbonyl moieties in the ketopentyl groups are free in compounds I and II but are complexed in the corresponding dihalides where increased deshielding causes the protons to be displaced downfield. Treatment of the dihalides with the more powerful donor 2,2'-bipyridyl frees the carbonyl groups and the resonance signals revert to positions characteristic of the uncomplexed ketopentyl group.

Table 1 N.m.r. measurements of compounds containing the 4-ketopentyl group ($=R$) in deuteriochloroform

Compound	τ values	
	a	b
$R_2Sn(SCH_2COOC_8H_{17-i})_2$ (I)	7.93	7.50
$R_2Sn(OCOC_{11}H_{23})_2$ (II)	7.92	7.52
R_2SnCl_2	7.74	7.23
$R_2SnCl_2 \cdot 2,2'$ -bipyridyl	7.89	7.42
R_2SnBr_2	7.76	7.27
$R_2SnBr_2 \cdot 2,2'$ -bipyridyl	7.95	7.55

Compounds I and II and standard stabilizers were then milled at 155°C into PVC (Corvic D55/09) at a concentration of 1% for 5 min. The testpieces were aged at 190°C and specimens were removed at intervals of 3 min.

The stabilizing effect of the dilaurate (II) was very similar to that of the corresponding butyl compound. However, di(4-ketopentyl)tin di(iso-octylthioglycollate) (I) showed a remarkable improvement when compared with the corresponding butyl compound $Bu_2Sn(SCH_2COOC_8H_{17-i})_2$ (III). Immediately after milling in the stabilizers the specimens containing I were noticeably clearer and more transparent than those containing the dibutyl compound (III). The latter specimens showed the first sign of discoloration after 6 min at 190°C while those stabilized with the diketopentyltin compound (I) did not produce a comparable colour until they had been aged for 15 min though the first slight signs of discoloration could be discerned after 12 min. Introduction of the carbonyl groups into the alkyl chains therefore improved the effectiveness of the thioglycollate stabilizer by a factor of 2 to 2.5.

The observation that I shows enhanced effectiveness in stabilization whereas II does not is explained by the fact that organotin di(iso-octylthioglycollates) rapidly exchange with allylic chlorines generating organotin dichloride whereas dilaurates react slowly to give the chloride laurate³. Although the latter would eventually be converted to the dichloride it appears that it is the reactions which occur in the earliest stages of stabilization which are most important.

Acknowledgement

We thank Albright and Wilson Ltd for technical assistance with the testing of the stabilizers.

S. Z. Abbas and R. C. Poller

Department of Chemistry,
Queen Elizabeth College,
Campden Hill, London W8 7AH, UK

(Received 24 May 1974)

References

- 1 Poller, R. C. 'The Chemistry of Organotin Compounds', Logos, London; Academic Press, New York, 1970, p 293
- 2 Ayrey, G., Head, B. and Poller, R. C. *Macromol. Rev.* in press
- 3 Ayrey, G., Poller, R. C. and Siddiqui, I. H. *J. Polym. Sci. (A-1)* 1970, **10**, 725
- 4 Ref 1, p 186
- 5 Abbas, S. Z. and Poller, R. C. *JCS Dalton Trans.* in press

Book Reviews

Flame retardancy of polymeric materials

Edited by W. C. Kuryla and A. J. Papa

Marcel Dekker, New York, 1973, Vol 1: 317 pp; Vol 2: 242 pp. \$24.50

'These volumes are designed to fill the existing need for a comprehensive review of the basic aspects of the field of flame retardancy. Both synthetic and naturally occurring polymers are examined, and particular emphasis is placed on polymers of commercial significance. The contributing authors (who are active workers in the field) present factual information along with their own theories and interpretations in order to provide diversified viewpoints on this complex subject.'

This description on the fly leaf adequately describes these volumes. They provide an excellent review by chemists for chemists in the textiles, fibres, plastics and coating industries. A feature of each chapter is the large number of supporting references provided. In some chapters nearly three hundred references are cited.

The first chapter lists the available flame retardants which are classified into inorganic, phosphorus, halogen, nitrogen and composite compounds. Chemical formulae, reactive functionality, analysis of active components, product name and supplier are tabulated for each compound. No indication is given at this stage of the polymers in which the compounds are most effective.

Inorganic flame retardants and their mode of action are then considered in some detail. The remaining chapters describe in detail the actions to improve the fire retardancy of poly(vinyl chloride) and related polymers; wool, nylon and other natural and synthetic polyamides. Volume 2 contains the chapters dealing with polystyrene and related polymers; polyethylene and polypropylene; natural and synthetic rubbers; phenolic resins and urea- and melamine-formaldehyde resins.

Each chapter is complete in itself and contains a description of the range of polymers available, together with an indication of applications. Pyrolysis studies and the mechanism of flame retardancy are then described and the behaviour of a substantial range of flame retardants is analysed. Usually too, attention is given to future developments. Some reference is made to the smoke problem but this is not a major consideration in this work.

The chapters were obviously written before the US Federal Trade Commission's complaint regarding misleading test results described as self-extinguishing and non-burning. However, bearing in mind that the book is intended for workers in the flame retardancy field, the use of ASTM D635, D2843, D2863, etc. in no way invalidates the value of the book. Indeed many of the authors go to great pains to emphasize that many of the small scale laboratory

tests are excellent for evaluating new formulations in the laboratory, but may not always reflect behaviour in the product's application.

The book reflects the extensive skills and ingenuity shown by chemists in their efforts to contribute to a 'safer' fire situation through minimizing the ease of ignition and reducing the flammability of combustible polymeric materials.

These volumes are strongly recommended but one critical note must be made. It is that unsaturated polyester resins have not been included. This is surprising since a considerable amount of work has been done not only with additives for GRP products but also in modifying the polyester chain, monomers etc. to reduce flammability. The resins are also used extensively in aircraft transport.

K. A. Scott

Peptides 1972

Edited by H. Hanson and H.-D. Jakubke

North-Holland, Amsterdam, 1973, 470 pp. Dfl. 90.00

This account of the proceedings of the Twelfth European Peptide Symposium, held in East Germany in September 1972, has been produced with commendable speed, for which the editors are to be congratulated. As with its predecessors, it deals mainly with peptide synthesis (both methods and achievements) and there is little in it of direct interest to readers of *Polymer*, apart perhaps from the three papers on insulin and pre-insulin, by Professors Hodgkin and Zahn and Dr Markussen.

One whole section (13 contributions) is devoted to problems of peptide synthesis using polymeric supports. There is no doubt that this, the Merrifield solid-phase method, is the one method which offers the promise of eventual successful synthesis of enzymes and other biologically active proteins. It has at present, however, many deficiencies some, at least, of which might be overcome by using something better than the chloromethylated, or otherwise chemically modified, divinylbenzene crosslinked polystyrenes at present used in the procedure. If this review leads any reader of *Polymer* to address himself to this problem and come up with something better it will have more than achieved its purpose.

H. N. Rydon

Developments in PVC technology

Edited by J. H. L. Henson and A. Whelan

Applied Science, Barking, 1973, 161 pp. £4.50

This book is based on a symposium at the Polytechnic of North London in February 1973, and although interference of the editors with the individual authors' contributions appears to be minimal most of the ten chapters do present reasonably balanced statements of the subject matter with which they are concerned. While appropriate in its original context the opening chapter on the pattern of usage of PVC is perhaps out of place here, as readers will either be aware of its contents or can readily find them elsewhere. Important aspects of the rapidly growing technology of processing of unplasticized PVC receive appropriate treatment in chapters devoted to lubricants, impact modifiers, and dry blends, although the second of these is remarkable for its scant reference to acrylic impact modifiers. A similar criticism of possible bias might be levelled at the chapter on mass PVC, which seems to overplay possible deficiencies of suspension polymers. Bottle production and injection moulding are treated mainly with respect to machine and processing characteristics, while guidance on formulation for these processes is almost absent apart from what can be gleaned from the chapters concerned with additives.

The book is well produced and clearly printed with generally clear diagrams, tables and photographs, apart perhaps from Figure 2 on p 80 which is a little obscure, and Figure 11 on p 27 which is reproduced upside down. At 161 pages this is a relatively small book, but its price is reasonable by today's standards. It should be read by all concerned with the technology of PVC in industry, whether the main interest is with materials, machinery or processing. The subject matter is too specific to be very relevant to undergraduate courses, but will be of interest to postgraduate academics working in appropriate fields.

G. A. R. Matthews

Conference Announcement

ACS Division of Polymer Chemistry, Inc.

7th Biennial Polymer Symposium

Florida, 9-12 December 1974

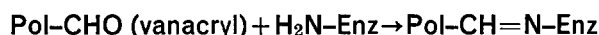
The ACS Division of Polymer Chemistry, Inc. will hold its Seventh Biennial Polymer Symposium at the Tides Hotel and Bath Club of North Redington Beach, Florida, from 9 to 12 December 1974. The conference is being arranged so that lectures will be given in the mornings and evenings with the afternoons free for the many recreational activities in the area. Further information and registration forms may be obtained from Dr J. C. Salamone, Publicity Chairman, c/o Department of Chemistry, Lowell Technological Institute, Lowell, Mass. 01854, USA.

Immobilized enzymes: 7. Use of vanacrils in the preparation of immobilized arginase and alkaline phosphatase

Eric Brown and Roger Joyeau

Laboratoire de Synthèse Organique, Centre Universitaire du Mans,
BP 535, 72017 Le Mans-Cedex, France
(Received 8 October 1973; revised 11 March 1974)

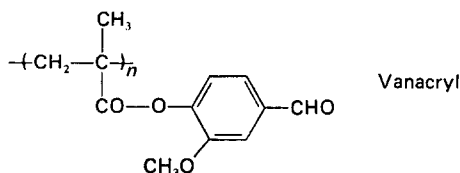
The vanacrils (vanillin polymethacrylates) were successfully used for immobilizing arginase and alkaline phosphatase, according to the probable scheme:



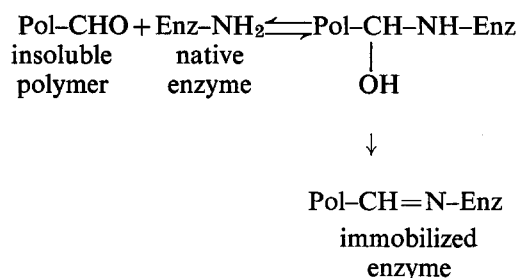
The properties of both these immobilized enzymes are described.

ARGINASE

To our knowledge, only one combination of immobilized arginase has been described in the literature¹. Our object was to immobilize this enzyme with the help of new linear macromolecular carriers insoluble in water which we have described recently². These polymers are vanillin polymethacrylates (*vanacrils*) or copolymers of allylic alcohol and vanillin methacrylate (*covanacryl-P*, P indicating the number of moles of vanillin methacrylate used per mole of allylic alcohol in the polymerization).



The free amine functions of the enzyme are likely to react with the aldehyde groups of the carrier as follows³:



Fixation rate and residual activity of immobilized arginase

Arginase was reacted with vanacryl and various covanacrils in a maleate buffer solution for varying periods, in the presence of MnCl_2 to activate the enzyme. At the end of the reaction, the insoluble derivatives

were filtered and washed. The immobilized arginase was then kept in suspension in buffered medium.

The fixation rate was determined by measuring the protein concentration of the washing filtrates of the insoluble derivatives. These measurements were carried out using the Folin-Ciocalteu reagent⁴.

The mass (μg) of protein fixed per mg of carrier and the enzymatic activity (m_1) of 1 mg of insoluble derivative expressed in μg of native arginase which, in identical measuring conditions, transformed the same quantity of substrate as 1 mg of immobilized arginase were then determined. Next, the rate of residual activity (*REA* %) for each of the resulting combinations was settled.

The results show that the mass (m_2) of immobilized protein per mass unit of carrier is almost constant for the various carriers used, yet at the same time the residual enzymatic activity seems to be closely connected with the value of the ratio between the number of alcohol functions and the number of aldehyde functions on the polymer. The relative increase of the number of alcohol functions with respect to the aldehyde functions involves a sharp rise of the residual activity of the corresponding insoluble derivatives. This phenomenon can be interpreted in various ways: either the alcohol function makes up a more favourable microenvironment than the aldehyde function, to the activity of arginase, or an excess of aldehyde functions react with a greater number of amine functions of the enzyme, which would be more or less connected with the arginase activity.

Reactions of fixation at 4°C for 6 h and then at 20°C for 3 h and 6 h were successively carried out. The results obtained show that within the given variation limits, neither temperature nor fixation time seem to have a measurable effect on the activity of the insoluble derivatives.

Judging from what was observed (*Figure 1*), one can assume that the grafting of arginase on the carrier is relatively fast.

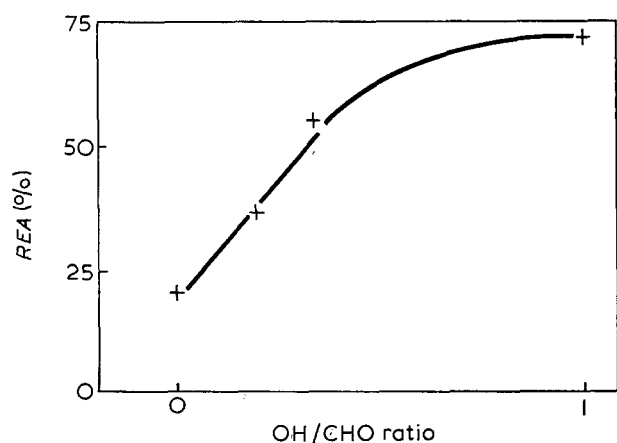


Figure 1 Fixation, expressed as ratio of residual activity of the derivatives (REA), as a function of the OH:CHO ratio in various carriers

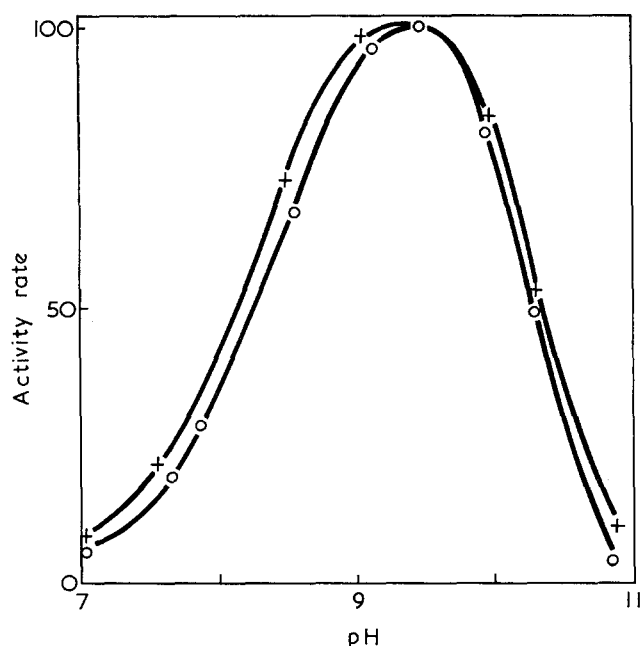


Figure 2 Activity curve of arginase as a function of pH. +, Native; o, immobilized arginase

Activity as a function of pH

The pH of optimum activity is one of the characteristics of an enzyme, whose chemical alteration and immobilization can entail a change in the activity profile of the enzyme as a function of the pH⁵. The results show (Figure 2) that the immobilization of arginase did not alter in a conspicuous way either the value of the pH of optimum activity, or the profile of the activity curve.

Study of an immobilized arginase column

After making an enzyme column, a solution of arginine hydrochloride was made to percolate through it. The insoluble derivatives were obtained in a form which did not lend itself to filling the column and consequently they had to be mixed with an inert carrier. Celite was selected, it being a hydrophilic silicate denser than the immobilized enzyme.

In the course of time, both the output of the column and the quantity of urea present in the eluate collected, were measured; a slow variation of the output made it necessary to take into account the latter in order to

find out the activity of the column which is defined as the mass of urea formed per unit time.

It is supposed that in the conditions of the experiment, the quantity of urea present in the eluate per volume unit was inversely proportional to the output, which means that the quantity of urea formed per unit time was independent of the output.

The column activity can then be represented by the product of the output by the urea concentration in the corresponding eluate.

The results (Figure 3) show a sudden loss of activity of the column, about 50% for the first 24 h, followed by a relative stabilization. This variation could be neither avoided nor explained. This loss of activity does not seem to be due to a solubilization of the enzyme since no measurable arginase activity could be observed in the first eluates. The activity curves of the various columns all showed the same profile.

Stability of immobilized arginase

The derivatives of immobilized arginase were kept in suspension in maleate buffer (pH 7 at 4°C).

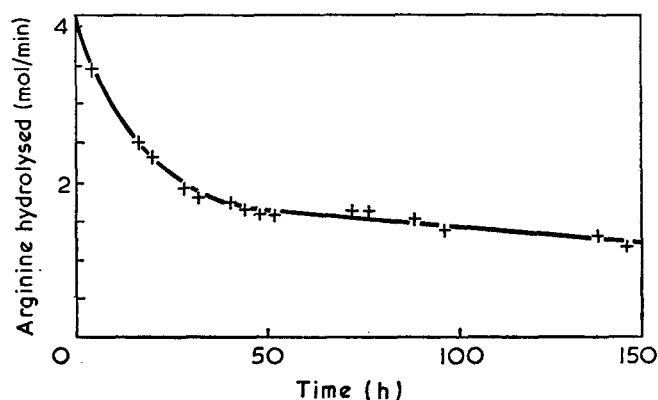


Figure 3 Activity of a column of immobilized arginase

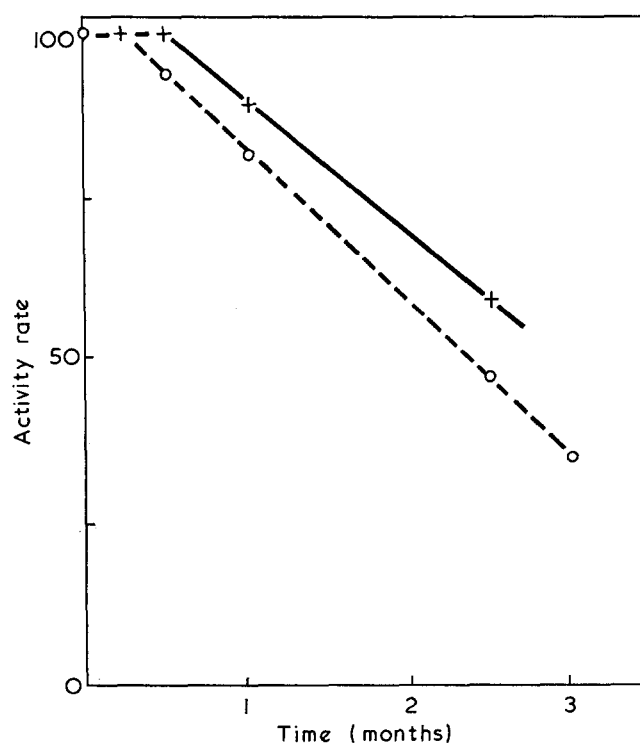


Figure 4 Activity of immobilized (o) and native (+) arginase over a period of time

The variations in activity of the native and immobilized forms of arginase were compared over a period of time. The values obtained are expressed in percentage of initial activity for each of the two forms of the enzyme.

Activity of immobilized arginase and native arginase in the course of time

Immobilized arginase kept all its activity during the first week following its preparation; the activity rate still reached 50% after more than two months, in the conditions of conservation described herewith. After two and a half months, the enzymatic activity of the suspension of immobilized arginase proved to be only that of the solid phase, no arginase activity being detected in the filtrates (Figure 4).

ALKALINE PHOSPHATASE

A few preparations of water-insoluble derivatives of alkaline phosphatase have been described in the literature.

Alkaline phosphatase has been immobilized by covalent linkage onto derivatives of cellulose, either on carboxymethyl (CM) cellulose having azide groups⁶, or on cellulose activated by 2,4-dichloro-6-(carboxymethyl-amino)-s-triazine⁷.

Other preparations of immobilized alkaline phosphatase were obtained by means of ethylene/maleic anhydride or methyl vinyl ether/maleic anhydride copolymers, or copolymers of methacrylic acid and *m*-fluoronitromethacrylanilide⁸. These various combinations were prepared in order to be used in the sequential analysis of polynucleotides. Alkaline phosphatase was also immobilized on glass preactivated by γ -aminopropyltriethoxy silane: the derivatives thus obtained contained 0.74 mg of enzyme/g of glass⁹. Last of all, a preparation of immobilized alkaline phosphatase was obtained by adsorption of the enzyme on CM cellulose, starch and poly(vinyl pyrrolidone)¹⁰. Our purpose then was to prepare new insoluble derivatives of alkaline phosphatase, using the vanacryl and the various covanacryls-P described above.

The activity of alkaline phosphatase was measured by following the hydrolysis of disodium *p*-nitrophenyl phosphate on a spectrophotometer.

Fixation rate and residual activity of alkaline phosphatase

The alkaline phosphatase was made to react with vanacryl and various covanacryls in buffered solution. At the end of the reaction, the insoluble derivative was washed with a solution of 1 M NaCl (pH 9) and distilled water until the filtrate no longer showed measurable enzymatic activity. The mass m_2 of enzyme fixed per mass unit of carrier was then defined by measuring the enzymatic activity of the filtrates and not by estimating the proteins directly as was the case with arginase; a standard curve gave the mass of enzyme left in solution after each reaction of fixation and m_2 was obtained by subtraction from the mass of enzyme involved (m_2 was expressed in μ g of enzyme per mg of carrier).

The residual activity (REA %) of the immobilized enzyme, proportional to the native enzyme, is given by the ratio $100 (m_1/m_2)$, wherein m_1 is the mass of soluble

enzyme releasing the same quantity of product (*p*-nitrophenol) as 1 mg of insoluble derivative in similar conditions.

A series of fixations performed with the various carriers has shown that neither the fixation rate nor the residual enzymatic activity of the derivatives vary in an important way according to the number of aldehyde functions present on the carrier: m_2 remained between 7 and 8 μ g of alkaline phosphatase per mg of polymer. On the other hand, the residual activity of the derivatives varied from 56 to 69% of the activity of the free enzyme.

A series of fixations performed with covanacryl-5, operating from pH 5 to pH 9 has shown that the mass of immobilized enzyme was maximum and constant for a pH inferior or equal to 7 (Figure 5), whereas the residual activity of the derivatives obtained was independent of the fixation pH and remained approximately equal to 60%.

A series of grafting reactions was carried out, using various quantities of carrier (25, 50, 75 and 100 mg) for a same mass of alkaline phosphatase (1 mg).

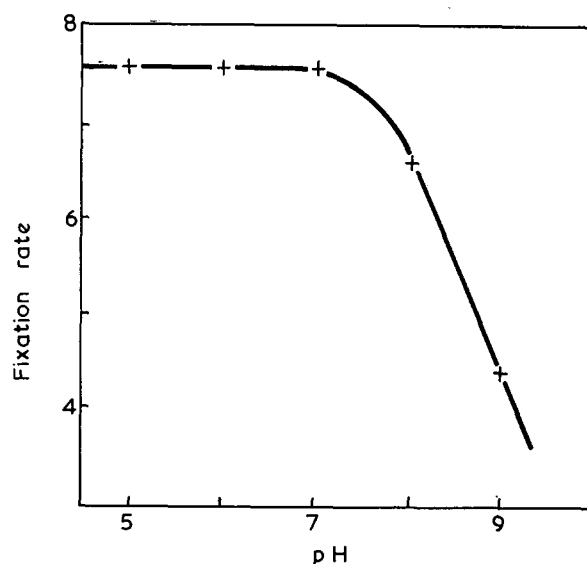


Figure 5 Fixations at various pH values

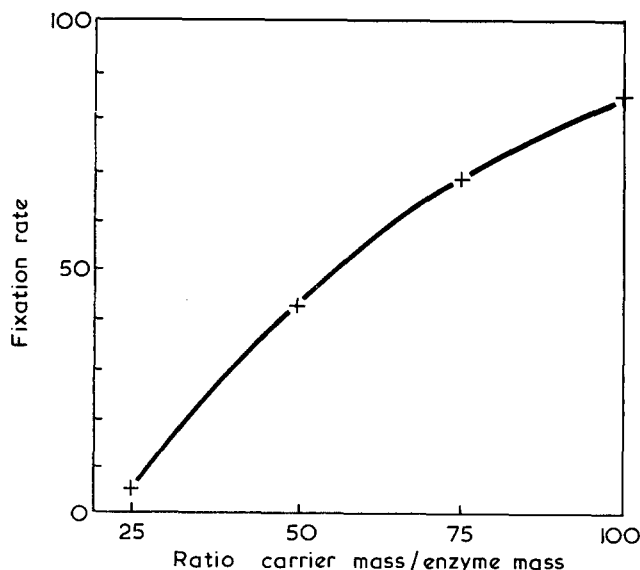


Figure 6 Fixation rate (ratio of immobilized enzyme to mass of enzyme $\times 100$) as a function of the ratio of mass of carrier to mass of enzyme involved

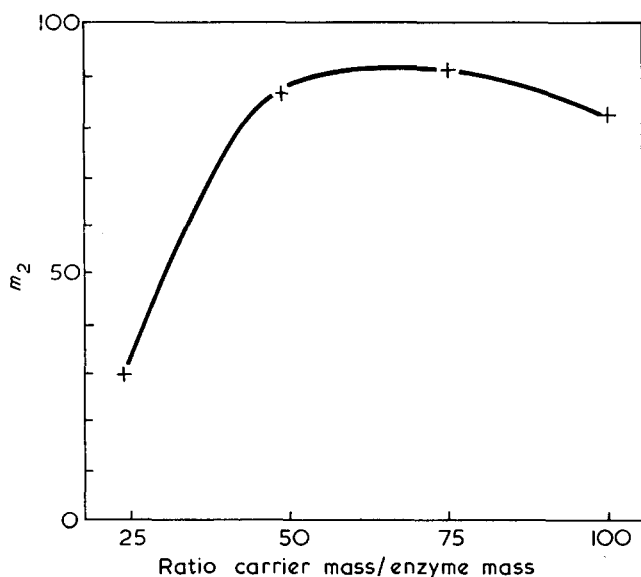


Figure 7 m_2 as a function of the ratio of carrier mass to enzyme mass involved

It was observed that the fixation rate is a growing function of the mass of carrier used (Figure 6). On the other hand, the mass m_2 of enzyme fixed per mass unit of carrier remained approximately constant in the cases when 50, 75 and 100 mg of carrier were used, but was found to decrease slightly when only 25 mg of polymer were used (Figure 7).

This phenomenon could be interpreted as resulting from a selective fixation on the carrier of protein deprived of enzymatic activity. It should be remembered, actually, that m_2 was obtained by the difference between the mass of enzyme initially involved and the enzyme mass not fixed and present in the filtrates after the grafting reaction. Now the latter mass was defined by measuring its enzymatic activity. Under these conditions, it is clear that the values given for m_2 could be exact only if the enzyme was pure or at least deprived of extraneous proteins.

On the other hand, we tried to immobilize alkaline phosphatase on 4-iodo-n-butyl polymethacrylate (Poliodal-4) which had already been used to immobilize various enzymes (urease, trypsin and chymotrypsin). By making a series of fixations at various pH values, insoluble preparations were obtained, which contained only $2 \mu\text{g}$ of enzyme per mg of carrier and whose residual enzymatic activity was less than 10%.

Activity as a function of pH

When comparing the curves of activity obtained for each of the two forms of the enzyme, one can notice (Figure 8) that the pH of optimum activity is not altered (pH 9.5). On the contrary, immobilization altered the profile of the activity curve as it contracted the area next to the optimum pH; the immobilized enzyme was therefore more pH-dependent than the free enzyme. This phenomenon has already been observed when immobilizing some enzymes⁵.

Since all the activity measurements of the native and immobilized forms of alkaline phosphatase were taken at pH 8.8, the values of residual activity of the various derivatives prepared are inferior to the values which would have been obtained if the measures had been taken at the pH of optimum activity. Indeed, at pH 8.8,

the activity rate of native alkaline phosphatase is 62% whereas the activity rate of immobilized enzyme is only 47% at the same pH.

Determination of Michaelis constants

The K_m (Michaelis constant) of the free and immobilized forms of alkaline phosphatase were determined, in order to judge whether the enzymatic activity had been altered during immobilization and in order to ensure also that the activity measurements of the immobilized form of the enzyme had been taken in conditions of saturation of the substrate. These measures were taken at pH 8.8, using concentrations of *p*-nitrophenyl phosphate (NPP) included between 10^{-4} M and 25×10^{-4} M. A rate of hydrolysis of the NPP was then defined for each substrate concentration used. Hence using the Lineweaver-Burk equation, the K_m corresponding to the soluble and insoluble forms of alkaline phosphatase could be defined graphically. These following values were obtained: 8.6×10^{-5} M and 16.2×10^{-5} M for the native enzyme and for the insoluble derivative, respectively.

Repeated use of a suspension of immobilized alkaline phosphatase

An attempt was made to hydrolyse a solution of NPP using a stirred suspension of alkaline phosphatase in varying conditions of pH and Mg^{2+} concentration. Every 24 h the substrate solution was renewed and the concentration of product formed during the preceding 24 h was measured to find the hydrolysis rate of the NPP solution. Analysis of the results has shown that the rate of NPP hydrolysed/24 h period was about 66% during the first days of utilization and remained so in whatever ionic conditions. This was no longer

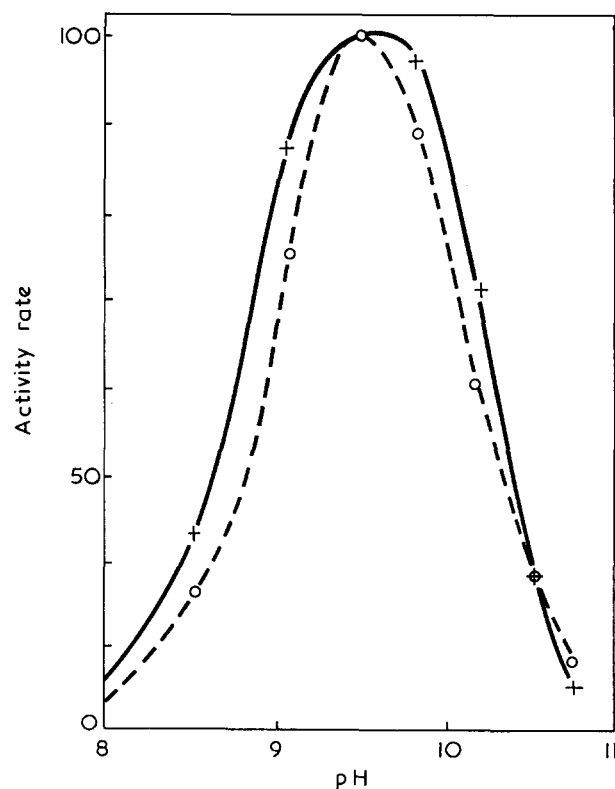


Figure 8 Activity curve of alkaline phosphatase as a function of pH. +, Native; o, immobilized alkaline phosphatase

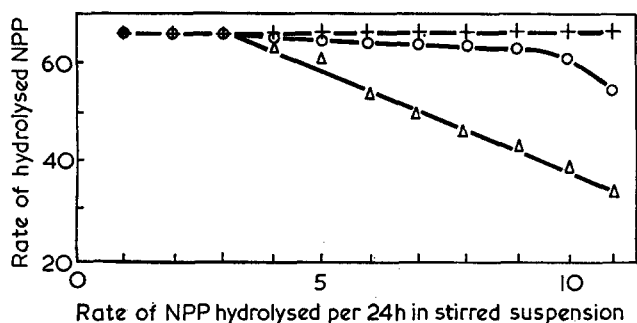


Figure 9 Rate of NPP hydrolysed per 24h in stirred suspension. Δ , pH 8.8, 0.01 MMg^{2+} ; \circ , pH 8.8, 0.1 MMg^{2+} ; +, pH 9.4, 0.1 MMg^{2+}

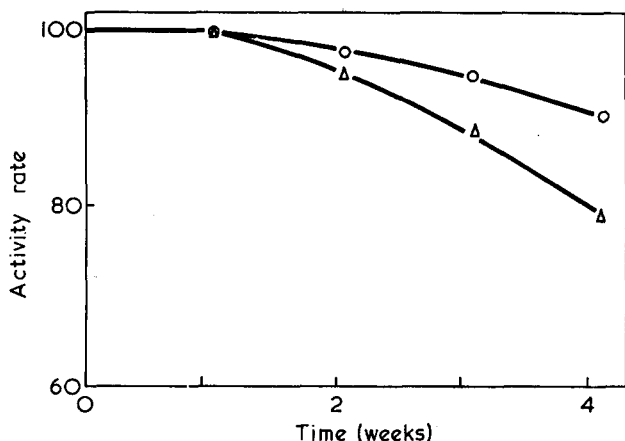


Figure 10 Activity of alkaline phosphatase as a function of time. Δ , Native alkaline phosphatase in solution; \circ , immobilized alkaline phosphatase kept in suspension

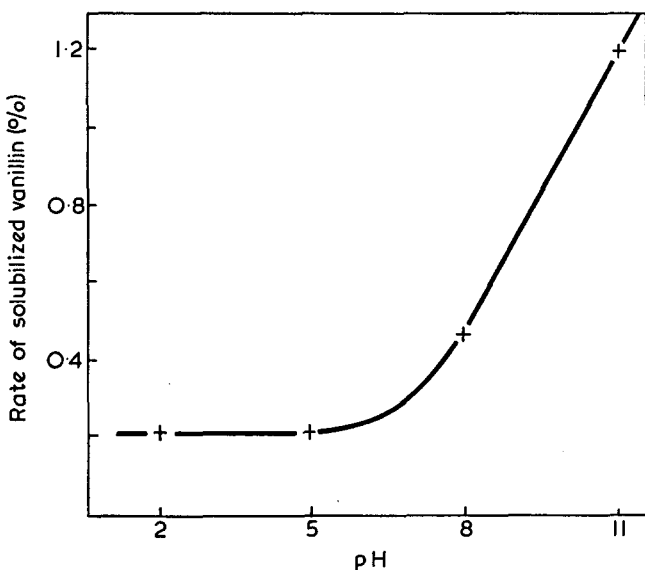


Figure 11 Hydrolysis of covanacryl-5 in stirred suspension at various pH values. Ordinate=rate of vanillin hydrolysed per 24h at 20°C, reckoned from the total mass of vanillin contained per mass unit of copolymer

true afterwards: a pH equal to 9.4 seemed better to the keeping of enzymatic activity than a pH of 8.8. In the same way, a concentration of 0.1 M Mg^{2+} was better than a concentration 0.01 M of the same ion (Figure 9).

Activity as a function of time

The preparations of immobilized alkaline phosphatase were kept in suspension in pH 8.8 buffer (0.1 M Mg^{2+}). Under such conditions the immobilized phosphatase retained more than 95% of its initial activity three weeks after it had been prepared (Figure 10).

By measuring the activity of the filtrate of a suspension of the insoluble derivative after this period, the filtrate was found to contain 6-9% of the enzymatic activity of the original suspension.

This solubilization of the enzyme could be accounted for by a slow hydrolysis of the ester functions of the polymer. Incidentally, a basic hydrolysis of the ester functions of covanacryl was revealed (Figure 11) and proved to be responsible for some vanillin passing into solution. The presence of vanillin in the solution could be established by studying the u.v. spectra of aqueous solutions previously brought into contact with covanacryl-5.

CONCLUSIONS

Insoluble derivatives of arginase have been prepared by reaction of the enzyme with the aldehyde groups of vanacryl and various covanacryls-P. The mass, m_2 , of protein fixed during the reaction varied from 35 to 45 μg per mg of carrier according to the cases considered.

The residual arginase activity of the various enzyme-carrier combinations progressively increased from 20 to 72% as more alcohol functions were introduced into the polymer and results tend to show that the grafting reaction is relatively fast. On the other hand, the curves of activity as functions of pH for the two forms of arginase have shown that immobilization caused no obvious modifications of the ionic micro-environment of the enzyme.

At last, it can be said that fixed arginase does not pass into solution while being kept in aqueous suspension.

Preparations of alkaline phosphatase insoluble in water were obtained by reaction of the enzyme on vanacryl and various covanacryls.

The enzyme-carrier derivatives obtained contained only 7 to 8 μg of phosphatase per mg of polymer but their residual enzymatic activity (REA) was relatively high: the values of the REA in the various preparations obtained varied from 56 to 72%.

Immobilization of alkaline phosphatase made the enzyme more pH-dependent and entailed a considerable increase in the value of its apparent K_m .

The insoluble derivatives obtained lend themselves readily to an intermittent use in stirred suspension. Besides, when kept in stock, the immobilized enzyme appeared to be markedly more stable than the native form. However, in the course of time, the enzyme went partly into solution, which could be explained either by the hydrolysis of the ester functions of the polymer, or by the hydrolysis of the imine functions resulting from the reaction of the enzyme on the aldehyde groupings of the carrier.

EXPERIMENTAL

Arginase

Immobilization of arginase on vanacryl and various covanacryls. A suspension of 5 mg of arginase (Koch-Light) and 50 mg of polymer (vanacryls) was stirred in

4 cm³ of 5 × 10⁻² M maleate MnCl₂ buffer, pH 7, for 20 h at 4°C. At the end of the reaction, the derivatives obtained were recovered on Millipore filters, then washed first with a solution of 1 M NaCl (3 × 4 cm³) and successively with distilled water up to a total volume of 20 cm³.

The derivatives were put in 2.5 cm³ of 5 × 10⁻² M maleate MnCl₂ buffer solution, pH 7 and activated for 4 h at 37°C with stirring, before beginning the activity measurements¹². Such an activation indeed causes an increase of about 15 to 25% in the activity of the derivatives with respect to that which could be observed without previous activation. Immobilized arginase was then kept under suspension at 4°C in the activation buffer.

Measures taken on each filtrate using the Folin-Ciocalteu reagent made it possible to find out the quantity of proteins remaining in solution and m_2 (expressed in μg of protein per mg of carrier) was then obtained by subtraction from the mass of protein involved in the fixation reaction.

Arginase activity was defined by colorimetry using the Ehrlich reagent and arginine hydrochloride as a substrate¹³.

A standard curve of the optical density at 450 nm as a function of the mass of soluble arginase (used per test sample when measuring the enzymatic activity) made it possible to express the arginase activity of 1 mg of derivative in μg of soluble enzyme (m_1) and to define the residual activity rate of the corresponding derivatives [$100(m_1/m_2) = \text{REA} \%$] (see Figure 1).

Influence of temperature and fixation time with covanacryl-1. Attempts at fixing arginase on covanacryl-1 were made at various temperatures and for various periods of time, the other conditions being the same as those described previously. The following table gives the activities (m_1) of the insoluble derivatives of arginase obtained (fixation rate not defined).

Fixations conditions	m_1 (μg)
6 h at 20°C	28.5
3 h at 20°C	30
6 h at 4°C	32

Activity of immobilized arginase as a function of pH

The activity was measured at 37°C in the presence of 0.1 M arginine hydrochloride using 0.1 M phosphate buffer for the values of pH ranging from 6 to 8 and 0.1 M glycine buffer for the upper values (see Figure 2).

Column of immobilized arginase. In a chromatography column thermostated at 37°C, a mixture was introduced, composed of 6 g of Celite and 20 mg of immobilized arginase and moistened by a 5 × 10⁻³ M maleate MnCl₂ buffer, pH 7, solution.

The column thus prepared was 1 cm wide and 18 cm high; it was topped with a separating funnel containing a 10 g/l solution of arginine hydrochloride (pH 9.05).

The quantity of urea present in the eluate was determined in the course of time (see Figure 3).

Stability of the insoluble derivatives. The derivatives of immobilized arginase were kept at 4°C in a 5 × 10⁻² M maleate MnCl₂ buffer, pH 7. The activity values obtained

in the course of time for immobilized arginase were expressed as percentage of the initial activity of the insoluble derivative considered (see Figure 4).

Alkaline phosphatase

Immobilization of alkaline phosphatase on vanacryl and various covanacryls. 1 mg of alkaline phosphatase (alkaline phosphatase from calf bowels as supplied by Koch-Light) and 100 mg of polymer (vanacryl or covanacryls) were stirred in 4 cm³ of 0.05 M phosphate buffer, pH 7, for 20 h at 4°C. At the end of the reaction, the derivatives obtained were recovered by filtration on a sintered glass funnel, then washed first with a solution of 1 M NaCl, pH 9 (5 × 6 cm³) and subsequently with distilled water up to a total volume of all the filtrates equal to 40 cm³.

The immobilized alkaline phosphatase was then suspended in 10 cm³ of 0.1 M Tris/HCl, 0.1 M Mg²⁺ buffer, pH 8.8, and kept at 4°C.

The fixation rate and the mass m_2 of enzyme fixed per mg of carrier were determined by measuring the enzymatic activities of the washing filtrates which were compared to a sample solution of enzyme. The activity of the alkaline phosphatase in the filtrates was determined by following the hydrolysis of nitrophenyl phosphate (NPP) at 410 nm¹⁴.

Measuring the activity of the insoluble derivatives of alkaline phosphatase was carried out on aliquots taken from a suspension of immobilized enzyme stirred in the presence of substrate and by determining the absorbance of these aliquots after filtration.

The activity of 1 mg of immobilized enzyme was expressed by the quantity m_1 (μg) of native enzyme producing the same variation of absorbance (at 410 nm) in identical conditions.

The results obtained by making fixations on various carriers are given below:

Carrier	m_1 (μg)	m_2 ($\mu\text{g}/\text{mg}$)	100 $\frac{m_1}{m_2}$
Vanacryl	5.5	8	68.5
Covanacryl-5	4.85	7.7	63
Covanacryl-3	4.5	7.2	62.5
Covanacryl-2	4.95	7.6	65
Covanacryl-1	3.9	6.95	56

Immobilization of alkaline phosphatase on covanacryl-5 at various pH values. A series of graftings of alkaline phosphatase on covanacryl-5 at various pH values, was performed, using 0.05 M phosphate buffer for pH 5, 6 and 7 and Tris/HCl for pH 8 and 9. All the other experimental conditions remained the same as before (see Figure 5).

Study of the derivatives as a function of the ratio enzyme mass to polymer mass involved in the fixation reaction. Several fixations were made on various quantities of carrier (25, 50, 75 and 100 mg) but using the same mass (1 mg) of alkaline phosphatase, the other conditions remaining the same as those described previously. Once they have been filtered and thoroughly washed, the various derivatives obtained were put respectively into 2.5, 5, 7.5 and 10 cm³ of 0.1 M Tris/HCl, 0.1 M Mg²⁺ buffer, pH 8.8, and their activity was then defined as

has been described previously. The results obtained are collected below:

Mass of carrier used (mg)	Fixation rate	m_2 ($\mu\text{g}/\text{mg}$)	REA (%)
25	7.8	3.1	61.5
50	43.5	8.7	72.5
75	69	9.2	66
100	84	8.4	59

Fixation rate is defined as being the ratio of mass of fixed enzyme to mass of enzyme involved in the reaction $\times 100$ (see Figures 6 and 7).

Activity as a function of pH. The activities of the native and immobilized forms of the enzyme (alkaline phosphatase/covanacryl-5) were measured at 25°C, from pH 7.9 to 10.75.

A 0.1 M Tris/HCl buffer was used from pH 7.9 to 9.1 and a 0.1 M $\text{NaHCO}_3/\text{Na}_2\text{CO}_3$ buffer from pH 9.5 to 10.75. For both forms of the enzyme, measurements were taken according to the process previously described except that the final concentration of Mg^{2+} was equal to 3.3 mM (see Figure 8).

Determination of Michaelis constants. The activity of alkaline phosphatase and of its insoluble derivative (with covanacryl-5) was measured at various concentrations of NPP (10^{-4} to 25×10^{-4} M) by following the hydrolysis of NPP over a period of time according to the process previously described.

In order to determine the value of K_m , $1/V$ is set graphically as a function of $1/S$ according to Lineweaver and Burk¹¹ (see Figure 12). The results were $K_m = 8.6 \times 10^{-5}$ M for the native enzyme and $K_m = 16.2 \times 10^{-5}$ M for its insoluble derivative.

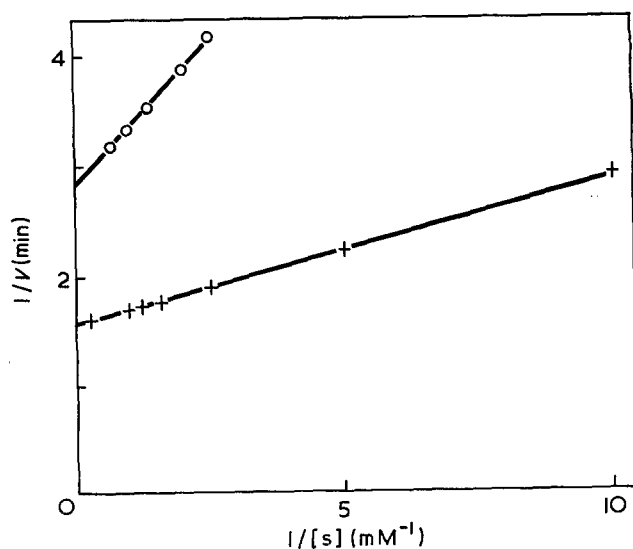


Figure 12 Determination of Michaelis constants, K_m for active (+) and immobilized (O) alkaline phosphatase with NPP as substrate

Intermittent use of a suspension of immobilized alkaline phosphatase. In a series of centrifuging tubes placed in a bath thermostated at 25°C, 20 mg of immobilized alkaline phosphatase were added, followed by 5 cm³ of a solution of 10^{-2} M NPP in 0.1 M Tris/HCl buffer with pH and Mg^{2+} concentration differing for each tube. A solution of NPP was thus used at pH 8.8 and 0.01 M Mg^{2+} , then at pH 8.8 and 0.1 M Mg^{2+} and last at pH 9.4 and 0.1 M Mg^{2+} .

After stirring for 24 h, each suspension was filtered on Millipore filters, the various filtrates were collected and their concentrations in *p*-nitrophenol were determined.

Each derivative was washed with an aqueous solution of 10^{-1} M or 10^{-2} M Mg^{2+} according to the cases, until a colourless filtrate was obtained.

Each derivative was then put in 5 cm³ of the same solution of NPP as before, and stirred again for 24 h. This operation was thus repeated daily; the filtrates corresponding to each hydrolysis were collected and the optical density at 410 nm developed by each filtrate previously diluted with distilled water, was determined.

A standard curve of the absorbance as a function of the concentration in *p*-nitrophenol was plotted in order to determine the rate of NPP hydrolysed every 24 h (see Figure 9).

Stability of immobilized alkaline phosphatase. The derivatives of immobilized alkaline phosphatase were kept at 4°C in suspension, with a concentration of 10 mg of derivative per cm³ of 0.1 M Tris/HCl, pH 8.8, 0.1 M Mg^{2+} buffer. In the course of time, measurements were taken of the activities of native enzyme and immobilized enzyme kept in the same conditions (see Figure 10).

ACKNOWLEDGEMENT

This work has been financed by a contract from the DGRST.

REFERENCES

- 1 Broun, G. *Actualité chim.* 1973 (5), 30
- 2 Brown, E. and Racois, A. *Tetrahedron Lett.* 1972, p 5077
- 3 Brown, E. and Joyeau, R. *Makromol. Chem.* in press
- 4 Lowry, O. H., Rosebrough, N. J., Lewis Farr, A. and Randall, R. J. *J. Biol. Chem.* 1951, 193, 265
- 5 Thomas, D. *Thèse d'Etat* Rouen, 1971
- 6 Weliky, N. and Weetall, H. H. *Immunochem.* 1965, 2, 293
- 7 Crook, E. M. and Kay, G. *Brev. S. Afr.* 68 04 010; *Chem. Abstr.* 1969, 71, 14363y
- 8 Zingaro, R. A. and Uziel, M. *Biochim. Biophys. Acta* 1970, 213, 371
- 9 Weetall, H. H. *Nature* 1969, 223, 959
- 10 Roozen, J. P. and Pilnik, W. *Lebensn. Wiss. Technol.* 1971, 4, 196
- 11 Lineweaver, H. and Burk, D. *J. Am. Chem. Soc.* 1934, 56, 658
- 12 Mohamed, M. S. and Greenberg, D. M. *Arch. Biochem. Biophys.* 1945, 8, 349
- 13 Hagan, J. J. and Dallam R. D. *Analyt. Biochem.* 1968, 22, 518
- 14 Garen, A. and Levinthal, C. *Biochim. Biophys. Acta* 1960, 38, 470

Effect of ethylamine pretreatment on the oxidation of cellulose by periodate

T. P. Nevell and I. S. Shaw*

*Department of Polymer and Fibre Science, University of Manchester Institute of Science and Technology, Manchester M60 1QD, UK
(Received 18 December 1973)*

The effect of ethylamine pretreatment on the rate and uniformity of the periodate oxidation of cotton has been studied. Although water is essential to the oxidation its presence has been kept to a minimum by using 40% aqueous dimethylformamide as the oxidation medium. This both retarded the rate of oxidation sufficiently to eliminate its dependence on diffusion and reduced the extent to which the swollen structure produced by ethylamine collapsed when the amine was replaced by periodate solution. The best way that has been found of maintaining the open structure consists in partial acetylation of the ethylamine-treated material. This resulted in a much more nearly random attack on the 1,2-diol groups by periodate than occurred with untreated cotton.

INTRODUCTION

Most previous work on the oxidation of cotton cellulose by periodates has been done with material that has received no pretreatment other than purification by scouring. It is now widely believed that native cotton consists of highly crystalline elementary fibrils which form the basic building units of larger fibrillar aggregates¹. The larger fibrils contain voids and dislocations where the packing of the elementary fibrils is less than perfect and these voids account for the accessibility of the material to chemical reagents. For this reason oxidation cannot take place uniformly throughout the fibre, but must occur first in the accessible regions, and then more slowly in the rest of the material as its crystalline structure gradually breaks down.

The object of the present work was to study the periodate oxidation of cellulose that had been rendered as nearly as possible uniformly accessible to the reagent, under conditions in which diffusion was not the rate-controlling process in the reaction. The method chosen to increase the accessibility consisted in swelling with anhydrous ethylamine. The originators of this process called it 'decrystallization'², but it will be shown that this is not a very appropriate term to describe the effects reported in this paper. The more open structure of the ethylamine-treated cellulose survives removal of the amine to a greater or lesser extent according to the method of removal used^{2b, 3}. Solvent exchange with pyridine has proved particularly suitable for maintaining a high accessibility^{4, 5}, and *N,N*-dimethylformamide (DMF) has now been found to be equally effective. Periodate oxidations have been carried out in 40% aqueous DMF. Although it was not possible to prevent some loss of accessibility due to the presence of water, this was reduced to a minimum consistent

with a reasonable rate of reaction. The rate was sufficiently low to be independent of the rate of diffusion of periodate into the fibres. The effect on periodate oxidation of preventing the collapse of the cellulose structure by partial acetylation has also been investigated.

EXPERIMENTAL

Materials

Most of the work was done with a softly twisted two-fold yarn (count, 10/2) spun from Sudan Sakel cotton. Before use it was steeped overnight in 0.2 N sulphuric acid at 60–70°C, boiled twice for 3 h at an excess pressure of 35 lbf/in² with 1% sodium hydroxide, steeped for 1 h in cold 0.2 N hydrochloric acid, and washed with water until free from acid. Some work was also done with regenerated cellulose. A continuous-filament bright viscose yarn (denier, 150/27), supplied by Courtaulds Ltd, was purified by boiling with a 1% solution of the Shell non-ionic detergent RD 107 for 15 min and washing well with water; cellulose sheet, 0.387 mm thick and supplied by the Transparent Paper Co. Ltd, was soaked in cold water for 24 h, the water being changed several times.

Ethylamine (BDH) was distilled from solid potassium hydroxide as previously described⁴. Pyridine (BDH, Analar) was dried over solid potassium hydroxide and fractionated, the portion boiling from 115 to 116°C being collected. Dimethylformamide (DMF) was dried over phosphorus pentoxide and fractionated, the portion boiling from 150 to 152°C being collected.

'Cadoxen', in which the intrinsic viscosities of the treated cellulose samples were determined, was prepared as described by Henley⁶. An excess of cadmium oxide was stirred rapidly for 24 h with a 28% w/w aqueous solution of redistilled ethylene diamine at 3°C. The cadmium content of the resulting solution was determined by titration with EDTA. The solution was centrifuged

* Present address: Science Department, Stockport College of Technology, Stockport, Cheshire, UK.

and diluted with sufficient of a solution of sodium hydroxide in 28% ethylene diamine to bring the final cadmium concentration to 5% w/w and the sodium hydroxide concentration to 0.35 M.

Treatment with ethylamine

Cotton (10 g) was placed in a flanged reaction vessel and dried by evacuation through a tube containing phosphorus pentoxide. Ethylamine (500 ml) was cooled to 0°C in a separating funnel which was fitted into the lid of the reaction vessel by means of a ground-glass joint. The taps of the funnel and of the inlet tube of the vessel were then opened so that the ethylamine was drawn into the vessel; care was taken to see that no air was drawn in with it. The cotton was kept immersed in ethylamine for 4 h at 0°C, after which it was removed and thoroughly washed with several portions of either pyridine, DMF, or water, over a period of 24 h. It was stored in the solvent until required for acetylation or oxidation. Some of the pyridine-washed samples were solvent-exchanged with water, and some of the DMF-washed samples with 40% aqueous DMF and with water, before being acetylated or oxidized.

Acetylation

Ethylamine-treated cotton (2 g) was solvent exchanged with pyridine, if it was not already wet with this solvent, and treated with a mixture of pyridine (50 ml) and acetic anhydride (50 ml) at 25°C for 15 min in the case of the material to be oxidized with periodate, and for 45 min in the case of materials to be used for accessibility measurements. The products were washed with cold water until free from acid and dried by exposure to air. A sample of cotton that had received no pretreatment other than soaking in pyridine was also acetylated for 45 min.

Oxidation by periodate

The experiments were conducted with 0.1 M solutions of sodium metaperiodate in 40% aqueous DMF at $25 \pm 0.01^\circ\text{C}$, the ratio of cotton to solution being 1 g to 50 ml; some comparative experiments in water were also carried out.

Samples of treated cotton, of known weight, were solvent-exchanged with DMF unless they were already wet with that solvent or with water. They were then freed from as much DMF as possible by squeezing, weighed, and added to a solution containing such quantities of periodate, DMF, and water that the final mixture had the desired composition. After the required period, the oxycelluloses were removed from the solution, washed with water, and dried in air. The periodate consumptions were determined by running 10 ml portions of solution into a mixture of 0.1 N sodium arsenite (25 ml), saturated sodium bicarbonate solution (10 ml), and 10% potassium iodide solution (10 ml), and titrating the excess of arsenite with 0.05 N iodine⁷. It was shown that, under the prevailing conditions, free iodine did not react to a measurable extent with DMF, and that the method gave accurate and precise results. Oxidations were carried out for a series of times so that rate curves could be obtained under each set of conditions.

The oxidation of samples that were wet with water after being treated with ethylamine was done in an

analogous way to that described above, the only difference being that water, instead of DMF, was added with the sample to the reaction mixture. Untreated cotton and cotton that had been partly acetylated (6% acetyl, degree of substitution = 0.24) and dried after ethylamine treatment were added to the reagent in the air-dry state.

Characterization of products

For the intrinsic viscosity measurements a suitable weight of material (0.05 to 0.2 g, according to the extent of oxidation) was moistened with a few drops of water and shaken with 25 ml of cadoxen until it had dissolved. The solution was then diluted to 50 ml with water, allowed to stand for four days, filtered through sintered glass (No. 3), and transferred to an Ubbelohde viscometer. The flow time was measured at 25°C at the original concentration and at several others obtained by adding known volumes of 1:1 mixture of cadoxen and water to the viscometer. The intrinsic viscosity was determined by extrapolating the plots of η_{sp}/c and $\ln \eta_r/c$ against c to $c=0$ and taking a mean of the two values. The viscosity-average degree of polymerization (DP) was calculated from the relation⁸:

$$[\eta] = 0.018(\overline{DP})_v^{0.77}$$

The reason for waiting for four days before measuring the flow time of the solution was to allow all the alkali-sensitive chain-linkages in the material to be broken⁹. Figure 1, which illustrates the rate of fall of relative viscosity for a slightly oxidized oxycellulose, shows that

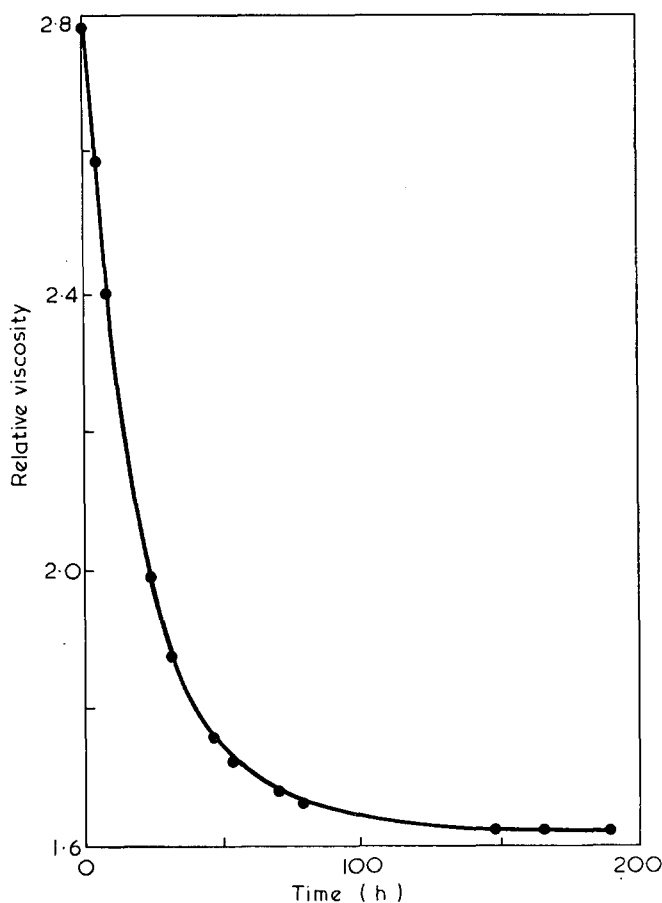


Figure 1 Rate of fall of relative viscosity of a 0.1% solution of a periodate oxycellulose in cadoxen at 25°C

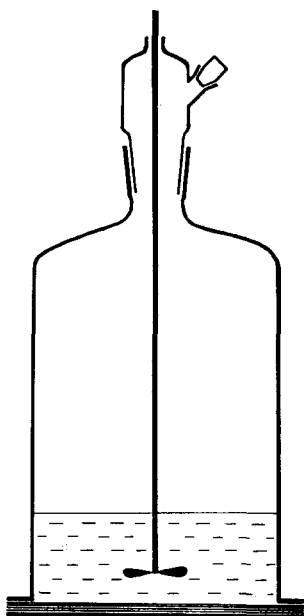


Figure 2 Apparatus for oxidation of multiple sandwich of cellulose sheets

four days are required for the attainment of a constant value.

Copper numbers were measured by Braidy's method¹⁰ and acetyl contents were measured as previously described⁴.

Moisture regains were measured as previously described⁴ at 59% r.h., which was obtained by means of a saturated solution of sodium bromide.

Diffusion studies

Sheets of regenerated cellulose were soaked in either water or 40% DMF and were rolled tightly together to expel as much liquid as possible from between them. A sandwich of ten sheets was placed on a glass plate and a bell-jar reaction vessel was clamped firmly on top of them (Figure 2). Periodate solution (0.1 M) was admitted to the vessel and stirred continuously for the required length of time, during which the apparatus was kept in the dark at 25°C. The sheets were then separated, washed with water, and dried. Their copper numbers were determined and served as a measure of the degree of oxidation reached in each layer of the sandwich. The overall degree of oxidation was determined from the fall in concentration of the periodate solution.

RESULTS AND DISCUSSION

Choice of oxidation medium

Although pyridine was known to be an excellent solvent for maintaining the accessibility of ethylamine-treated cellulose^{4, 5}, it could not be used for the study of periodate oxidation because pyridinium periodate is insoluble in it. DMF appeared to be an alternative, since its hydrogen bonding properties were thought to be similar to those of pyridine and it is a solvent for sodium metaperiodate. Work on accessibility to be described below justified the choice of DMF. However, periodate in pure DMF has no action on cellulose¹¹. The presence of water is necessary for oxidation and the choice of 40% aqueous DMF as a reaction medium

represents an attempt to strike a balance between loss of accessibility owing to the presence of water² and the attainment of a reasonably convenient rate of oxidation.

The rate of oxidation of cellulose by periodate in aqueous solution is diffusion-controlled. This is evident from the results of multiple-sandwich diffusion studies shown in Figure 3; for a given reaction time the extent of oxidation falls in going from sheet to sheet away from the periodate solution. On the other hand, the reaction in 40% DMF is much slower and proceeds at a practically constant rate throughout each sandwich (Figure 4). It may therefore be concluded that diffusion no longer plays a part in determining the reaction rate. This conclusion will also apply to any sample of cellulose with an accessibility similar to that of viscose sheet.

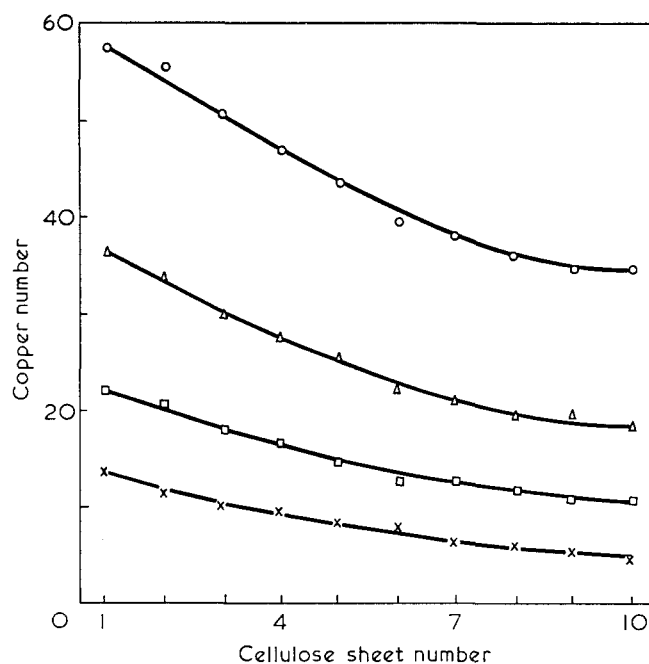


Figure 3 Copper numbers of cellulose sheets oxidized at 25°C by 0.1 M periodate in water by the multiple sandwich method. Oxidation time (h)/overall periodate consumption (mol/glucose unit): ×, 0.25, 0.041; □, 0.50, 0.066; Δ, 1.00, 0.108; ○, 2.00, 0.171

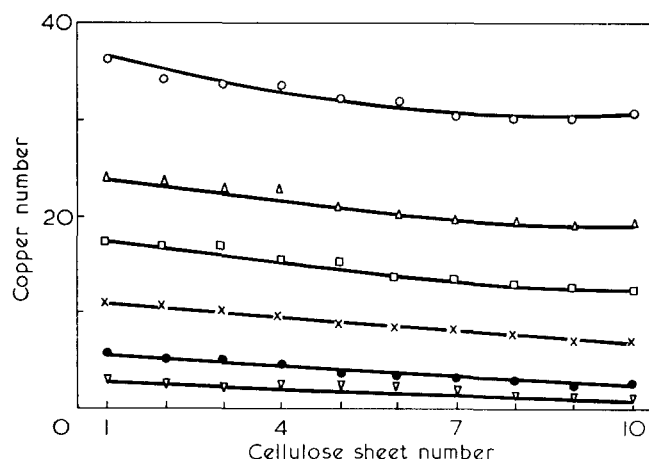


Figure 4 Copper numbers of cellulose sheets oxidized at 25°C by 0.1 M periodate in 40% DMF by the multiple sandwich method. Oxidation time (h)/overall periodate consumption (mol/glucose unit): ▽, 0.25, 0.022; ●, 0.50, 0.029; ×, 1.50, 0.051; □, 3.00, 0.073; Δ, 5.00, 0.093; ○, 10.00, 0.136

Effect of ethylamine on the accessibility of cellulose

In order to obtain some estimate of the effect of ethylamine treatment and of various solvents used to remove it on the accessibility of cellulose to water vapour (subsequently abbreviated to 'accessibility') it was necessary to take into account the loss of accessibility that inevitably accompanies the production of a dry fibre. This was done by inhibiting the collapse of the cellulose structure by partial acetylation before measuring its moisture regain. The moisture regain at zero acetyl content was calculated from the relation representing Zeronian's results⁵, viz., $c = y + 0.225x$, where x is the acetyl content, y the actual moisture regain, and c the moisture regain at $x \rightarrow 0$, all expressed as percentages by weight. The value of c was then substituted in Jeffries' equation¹² $A = 0.05795 + 0.05416c$, where A was called by Jeffries the amorphous fraction but is here called the accessibility. Table 1 gives the results for six ethylamine-treated samples of cotton solvent-exchanged as indicated in column 2, pyridine-treated cotton, and three untreated samples of cellulose (for which c and y are identical). It will be noted that the final treatment of each sample before acetylation was a solvent exchange with pyridine; this was because pyridine was to be used as an acetylating medium. It was, however, to determine the effects of the treatments prior to pyridine exchange that these experiments were done. The last three materials were included for purposes of comparison.

Table 1 shows that DMF and pyridine are equally effective in preserving the increase in the accessibility of cellulose produced by ethylamine treatment. However, if water is included in the washing treatment, either before or after pyridine, or after DMF, some (but by no means all) of the increase in accessibility is lost.

Effect of ethylamine pretreatment on the rate of oxidation of cellulose

Rate curves for the early stages of the reaction of periodate with cellulose that has received various pretreatments are illustrated in Figures 5 and 6. In general, the rates of oxidation rank the treatments in the same order as the accessibility measurements. Thus cellulose that has been treated with ethylamine and washed with water ($A = 0.64$) consumes periodate more rapidly than untreated cotton ($A = 0.40$) both from aqueous solution (Figure 5, both curves) and from 40% DMF (Figure 6,

Table 1 Accessibility of various samples of cellulose

Material	Treatment	Moisture content (%)	Acetyl content (%)	A
Cotton	EtNH ₂ /pyridine	8.80	16.1	0.73
Cotton	EtNH ₂ /DMF/pyridine	8.82	16.3	0.73
Cotton	EtNH ₂ /water/pyridine	8.31	11.9	0.64
Cotton	EtNH ₂ /pyridine/water/pyridine	8.38	11.4	0.65
Cotton	EtNH ₂ /DMF/water/pyridine	8.47	11.7	0.67
Cotton	EtNH ₂ /DMF/40% DMF aq./pyridine	8.52	12.2	0.68
Cotton	pyridine	6.63	3.6	0.46
Cotton	none	6.37	—	0.40
Viscose rayon	none	13.01	—	0.76
Viscose sheet	none	12.81	—	0.75

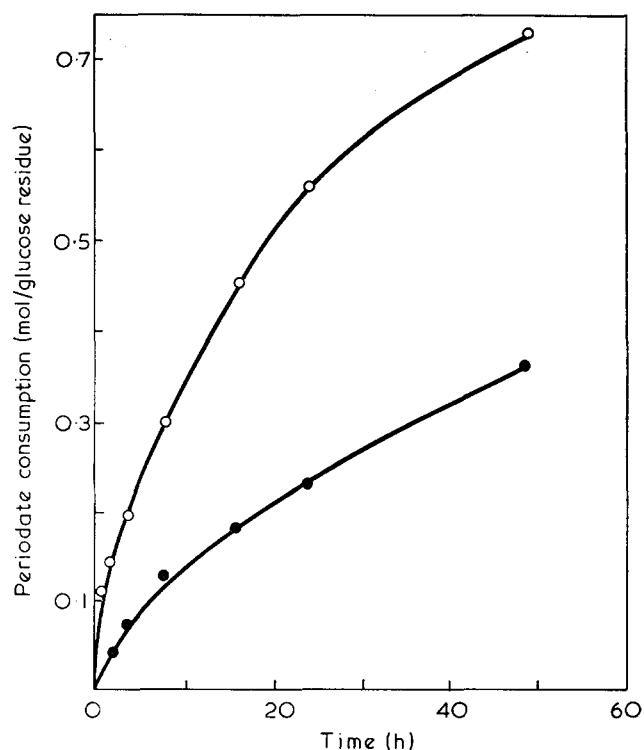


Figure 5 Rate of oxidation of cotton (●) and of water-washed ethylamine-treated cotton (○) by aqueous 0.1M periodate at 25°C

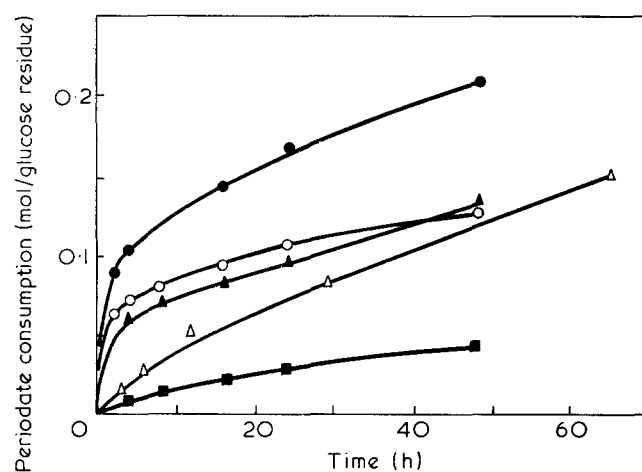


Figure 6 Effect of pretreatment on the rate of oxidation of cotton by 0.1M periodate in 40% DMF at 25°C. Pretreatments: ●, ethylamine/DMF and ethylamine/pyridine/DMF; ○, DMF and pyridine/DMF; △, ethylamine/pyridine/part. acetylated; ▲, ethylamine/water; ■, none

solid triangles and squares). On the other hand, it consumes periodate from 40% DMF less rapidly than ethylamine-treated cellulose that has been washed with DMF, or with pyridine followed by DMF ($A = 0.73$; Figure 6, solid circles). Washing cellulose with pyridine increases its accessibility slightly (from 0.40 to 0.46) and causes an increase in the initial rate of consumption of periodate which, though appreciable, is much less (Figure 6, open circles) than when the material is first treated with ethylamine; washing with pyridine followed by DMF and with DMF alone have the same effect on the rate of periodate consumption.

The curves for oxidation in 40% DMF shown in Figure 6 fall into two groups: those for material that was wet with either DMF or water when introduced

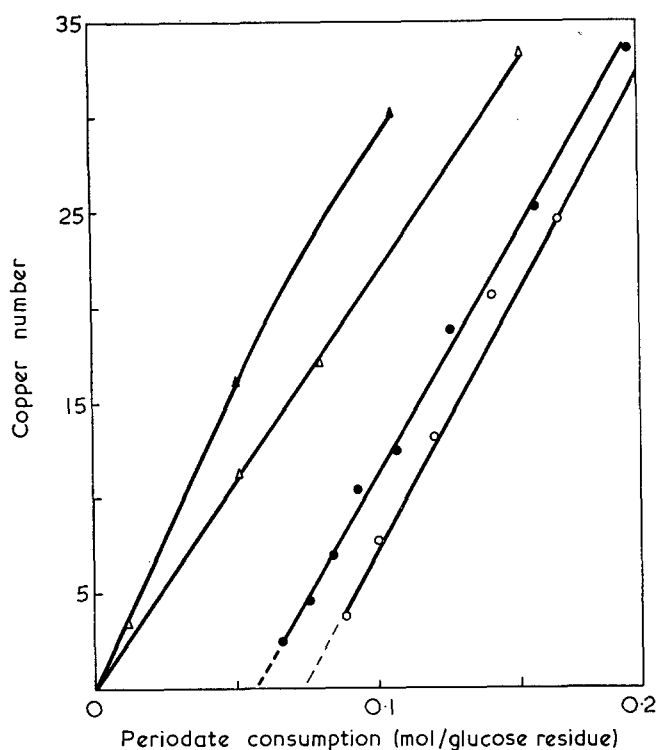


Figure 7 Effect of pretreatment on relation between copper number and periodate consumption of oxycelluloses. Pretreatments before oxidation in 40% DMF: O, ethylamine/DMF; ●, DMF; △, ethylamine/pyridine/part. acetylated; ▲, untreated cotton oxidized in water

into the periodate solution (solid and open circles and solid triangles), and those for material that had been dried in the air before being introduced (open triangles and solid squares). Curves of the first group are clearly composite, a very rapid initial consumption of periodate being followed by consumption at a much slower, practically constant, rate. Curves of the second group show little or no sign of a break. The initial rapid consumption of periodate by materials that have not been dried is not accompanied by oxidation of the cellulose. This is shown in Figure 7, where the copper numbers of the treated samples are plotted against periodate consumption. The curves with open and solid circles, which correspond to the curves with solid and open circles in Figure 6, are straight lines that cut the periodate consumption axis at values not very different from those obtained by extrapolating the linear portions of the curves in Figure 6 to zero time. Non-oxidative periodate consumption has been ascribed to the formation of a moderately stable intermediate periodate ester of cellulose¹³, but the amounts observed previously have been much smaller than in the present instance. When untreated cotton and partly acetylated ethylamine-treated cotton are oxidized respectively in water and in 40% aqueous DMF the amounts are so small that the lines relating copper number to periodate consumption appear to pass through the origin (Figure 7, open and solid triangles).

The main, nearly linear, portions of the curves in Figure 6 show that the rates of actual oxidation of cellulose samples that have been treated with ethylamine do not differ greatly but all are appreciably higher than those of samples that have not been so treated. This applies equally to material that has been partly acetylated

and dried in the air after treatment and to material that has been solvent-exchanged and never dried. The explanation of these curves depends upon several factors. Hydrogen bonding reagents such as pyridine, DMF, and ethylamine, all increase the susceptibility of cellulose to attack by periodate by causing interfibrillar swelling. Ethylamine, in addition, causes intrafibrillar swelling; it distends the unit cell of crystalline cellulose by about 0.75 nm in the direction perpendicular to the 101 planes whilst leaving the distance between the 101 planes unchanged¹⁴. It thus renders the whole of the fibre accessible to periodate ions (H_4IO_6^-), which have a diameter of between 0.5 and 0.55 nm, and this increased accessibility may be stabilized by partial acetylation. The large non-oxidative periodate consumptions are clearly associated with the imbibed DMF in the samples when they were introduced into the periodate solutions. It is unlikely that more than a small proportion of these consumptions is attributable to intermediate ester formation. However, although the imbibed DMF facilitates the passage of periodate from the aqueous to the cellulose phase, it inhibits actual oxidation until enough of it has been exchanged with water to allow the reaction to proceed at an appreciable rate. It has already been pointed out¹¹ that at concentrations of DMF greater than about 50% periodate oxidation is extremely slow. The role of DMF in bringing periodate into the cellulose phase is illustrated by the fact that ethylamine-treated cotton imbibes about 37% more DMF, and consumes non-oxidatively about 40% more periodate, than does untreated cotton. Thus, although the presence of DMF may increase the extent of non-oxidative periodate consumption by cotton cellulose, the actual rate of oxidation only shows an increase when intrafibrillar swelling by ethylamine has been employed at some stage in the pretreatment.

Effect of ethylamine on the randomness of attack of periodate on cellulose

If the intrafibrillar swelling of cotton cellulose by ethylamine were complete it might be expected that the sites of periodate attack would be randomly distributed along the chain molecules. This possibility has been tested by calculating stoichiometrically the fraction of glycosidic bonds broken by periodate oxidation followed by treatment with alkali⁹ and comparing it with the fraction calculated from the viscosity measurements in cadoxen assuming random attack. Periodate consumptions by ethylamine-treated cotton in aqueous DMF were corrected for the amount consumed but not reduced (derived from the intercept of the curve with open circles in Figure 7 with the axis of abscissae). It was then assumed that each molecule of periodate reduced resulted in one 2,3-dialdehyde chain unit, which in turn gave rise to the scission of the adjacent glycosidic bond when the material was allowed to come to equilibrium in the alkaline cadoxen solvent. In calculating the proportion of bonds broken from the viscosity measurements it had to be assumed that the number-average DP was equal to half the viscosity-average DP over the range covered by the experiments ($\overline{DP}_v = 2450$ for the original cotton and about 150 for the most highly oxidized alkali-degraded samples). Figure 8 illustrates the results of these calculations.

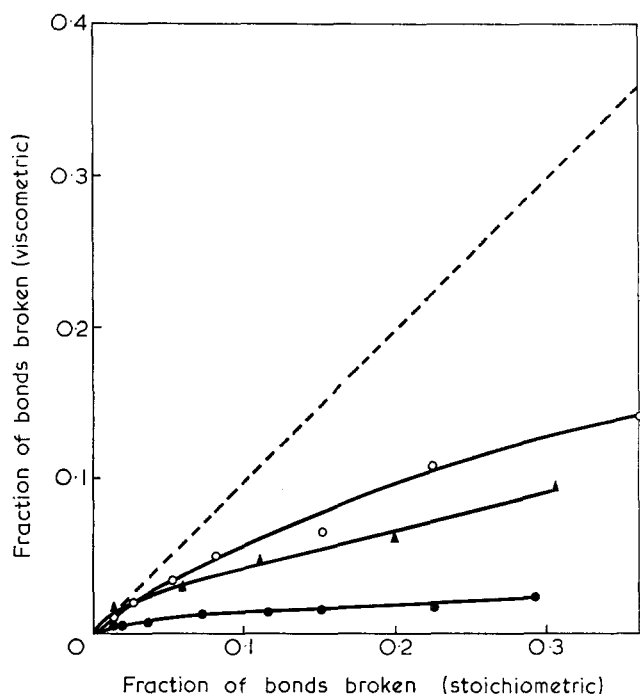


Figure 8 Relation between the stoichiometrically and viscometrically calculated fractions of bonds broken in cotton (●), ethylamine/DMF-treated cotton (▲), and ethylamine/DMF-treated part. acetylated cotton (○), oxidized by 0.1M periodate in 40% DMF at 25°C and dissolved in cadoxen

The broken straight line of unit slope represents the ideal situation where all the pairs of 2,3 alcohol groups in a portion of fibre are equally accessible to periodate. The curve with solid circles shows that untreated cotton is far removed from this situation, the material clearly being highly heterogeneous towards periodate attack. The curve with solid triangles shows that ethylamine treatment goes a long way towards permitting random

attack to occur and the curve with open circles that an even better result can be achieved by a small amount of acetylation after ethylamine treatment. Even this last curve, however, diverges considerably from the ideal line at high degrees of oxidation, possibly owing to the formation of hemi-acetal crosslinks as discussed in the next paper¹⁵. Thus no way has been found for rendering all possible reaction sites in cotton equally available to periodate ions. The most effective treatment studied has been swelling with ethylamine followed by the introduction of a few bulky acetyl groups to inhibit the collapse of the swollen structure when the ethylamine is removed. It is to be noted that, when this is done, the material does not lose its enhanced reactivity towards periodate by being dried in air.

REFERENCES

- 1 Warwicker, J. O. *et al.* 'A Review of the Literature on the Effect of Caustic Soda and Other Swelling Agents on the Fine Structure of Cotton', Pamphlet No. 93, Shirley Institute, Manchester, 1966
- 2 (a) Segal, L., Nelson, M. L. and Conrad, C. M. *J. Phys. Colloid Chem.* 1951, **55**, 325; *Text. Res. J.* 1953, **23**, 428
(b) Segal, L. 'Decrystallised Cotton', Mellow, Watford, 1971
- 3 Zeronian, S. H. *Rep. Prog. Appl. Chem.* 1965, **50**, 523
- 4 Nevell, T. P. and Zeronian, S. H. *Polymer* 1962, **3**, 187
- 5 Zeronian, S. H. *J. Appl. Polym. Sci.* 1965, **9**, 313
- 6 Henley, D. *Svensk. Papperstidn.* 1960, **63**, 143
- 7 Fleury, P. and Lange, J. *J. Pharm. Chim.* 1933, **17**, 107
- 8 Henley, D. *Arkiv Kemi* 1961, **18**, 327
- 9 Corbett, W. M. in 'Recent Advances in the Chemistry of Cellulose and Starch', (Ed. J. Honeyman), Heywood, London, 1959, p 129
- 10 Nevell, T. P. in 'Methods in Carbohydrate Chemistry', (Eds R. L. Whistler and J. W. Green), Academic Press, New York, 1963, Vol III, p 44
- 11 Nevell, T. P. and Shaw, I. S. *Chem. and Ind.* 1968, p 772
- 12 Jeffries, R. *J. Appl. Polym. Sci.* 1964, **8**, 1213
- 13 Nevell, T. P. *J. Text. Inst.* 1957, **48**, T484
- 14 Davis, W. E. *et al. J. Am. Chem. Soc.* 1943, **65**, 1294
- 15 Nevell, T. P. and Shaw, I. S. *Polymer* 1974, **15**, 559

Effect of ethylamine pretreatment on the tensile strength of periodate oxycelluloses

T. P. Nevell and I. S. Shaw*

*Department of Polymer and Fibre Science, University of Manchester Institute of Science and Technology, Manchester M60 1QD, UK
(Received 18 December 1973)*

A study has been made of the effect of ethylamine pretreatment on the changes in strength suffered by cotton fibres and viscose rayon filaments on oxidation with periodate and on subsequent reduction with borohydride. The extent of chain scission during periodate oxidation has been estimated roughly from intrinsic viscosity measurements in cadoxen on the borohydride-reduced materials and has proved to be small. The variation of strength with the degree of oxidation of the oxycelluloses themselves has been interpreted in terms of Bueche's model for rubbery polymers. It appears to be a combination of the effects of chain scission, chain flexibility, swelling and the formation of hemi-acetal crosslinks. By assuming that the first two are the same in both the original and the reduced oxycelluloses, the effects on the strength of the oxycelluloses of the destruction of intermolecular hydrogen bonds by swelling and the formation of intermolecular hemi-acetals have been estimated. In the early stages of the oxidation of cotton, hemi-acetal formation causes a fall in strength, which is much smaller in ethylamine-treated than in untreated cotton. This is because of the more uniform distribution of reactive sites in the former material. As oxidation proceeds the destruction of hydrogen bonds through swelling more than offsets the number of hemi-acetals formed, and an increase in strength occurs. In viscose rayon, no initial fall of strength occurs because this material is far less effectively crosslinked than cotton.

INTRODUCTION

The changes in the tensile strength of cotton yarn brought about by periodate oxidation, and by subsequent reduction with potassium borohydride, are complex, but they are believed to reflect similar changes in the strength of the fibres of which the yarns are composed. In the oxycelluloses they have been attributed to a combination of the effects of the formation of hemi-acetal crosslinks and of chain scission resulting from non-Malaprade side reactions^{1, 2}. In the reduced materials they have been thought to arise solely from chain scission since reduction destroys the hemi-acetal crosslinks. The present work has been undertaken to determine the effect on these changes of the more uniform attack by periodate that can be achieved by pretreating the cellulose with ethylamine³. In order to eliminate any possible interference from changes of yarn structure the tensile strength measurements have been made on individual fibres, and this has incidentally justified the earlier assumption that changes of fibre strength and yarn strength follow the same course. The effect of ethylamine pretreatment has proved smaller than was expected, but the results have demonstrated the importance of taking intermolecular hydrogen bonds as well as hemi-acetal crosslinks into account when interpreting the tensile behaviour of the chemically modified fibres.

* Present address: Science Department, Stockport College of Technology, Stockport, Cheshire, UK.

EXPERIMENTAL

Materials and chemical methods

The materials, methods of chemical treatment, and the method of determining intrinsic viscosities in cadoxen, have been described in the previous paper³. Oxycelluloses were reduced by shaking 1 g samples with 0.01 *x* M potassium borohydride (50 cm³) for 24 h at room temperature, where *x* is the periodate consumption of the material in mol/glucose unit⁴. The products were washed with 10% acetic acid and numerous portions of distilled water before being dried by exposure to air.

Tensile strength measurements

Single cotton fibres and viscose rayon filaments were carefully mounted on rectangular paper mounts (4.5 × 2.5 cm) having a hole 1 cm in diameter in the centre with the help of adhesive tape. The mounts were fixed in clips (1 cm apart) attached to the jaws of the A cell of an Instron tester (Model TM-M) in an atmosphere controlled at 65% r.h. and 20°C. The sides of the mounts were then cut away and the load-extension curve recorded at a constant rate of extension of 1 mm/min until the specimen broke. The full-scale pen deflection was set at 10 g for fibres and 20 g for filaments. Fifty measurements were made with each cotton sample, and twenty with each rayon. The results were expressed as relative breaking loads, that of the original material

being taken as unity. Extensions at break were expressed as fractions of the original sample length.

RESULTS AND DISCUSSION

Chain scission during periodate oxidation

Since chain scission has been considered to be part of the cause of the loss of strength suffered by cotton on oxidation by periodate and almost the whole cause of the loss of strength in borohydride-reduced oxycelluloses, an attempt has been made to assess, at least qualitatively, the importance of this reaction. It is clear from Head's measurements⁴ of the cuprammonium fluidity of borohydride-reduced periodate oxycelluloses that very little scission occurs during the early stages of oxidation. In the present work the relationship has been determined between the intrinsic viscosity of the reduced oxycelluloses in cadoxen and periodate consumption (corrected for non-oxidative consumption); Figure 1 shows the results for the original cotton, ethylamine-treated cotton, and partly acetylated ethylamine-treated cotton (6% acetyl). Since the borohydride-reduced materials are stable to alkali, the fall of intrinsic viscosity can be due either to chain scission during periodate oxidation, or to increased flexibility of the polymer chains arising from the breaking of the C₍₂₎-C₍₃₎ bond in the glucose rings, or to a combination

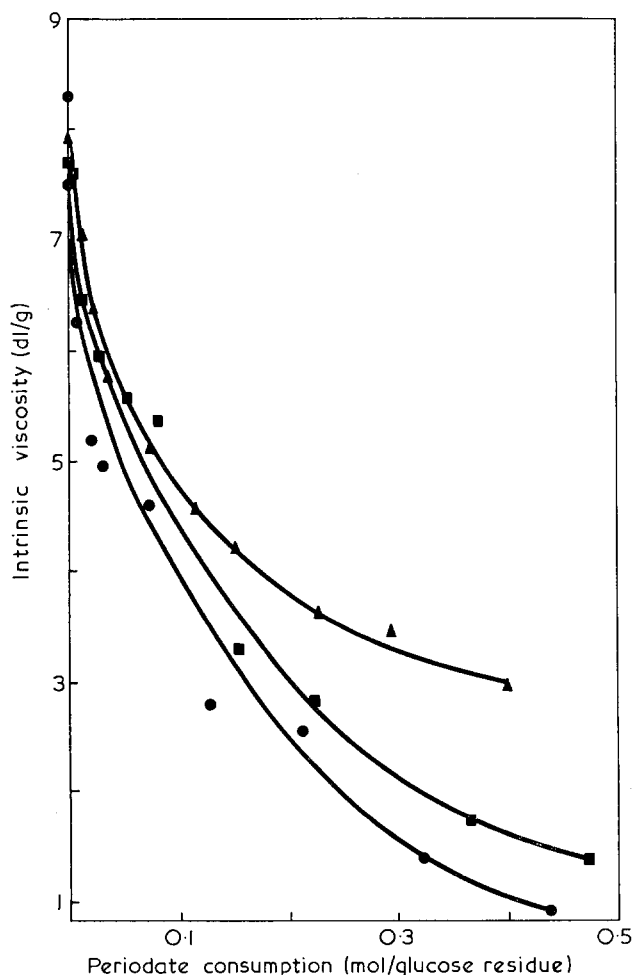


Figure 1 Intrinsic viscosity in cadoxen at 25°C of reduced periodate oxycelluloses from: ▲, untreated cotton; ●, DMF-washed ethylamine-treated cotton; ■, partly acetylated ethylamine-treated cotton

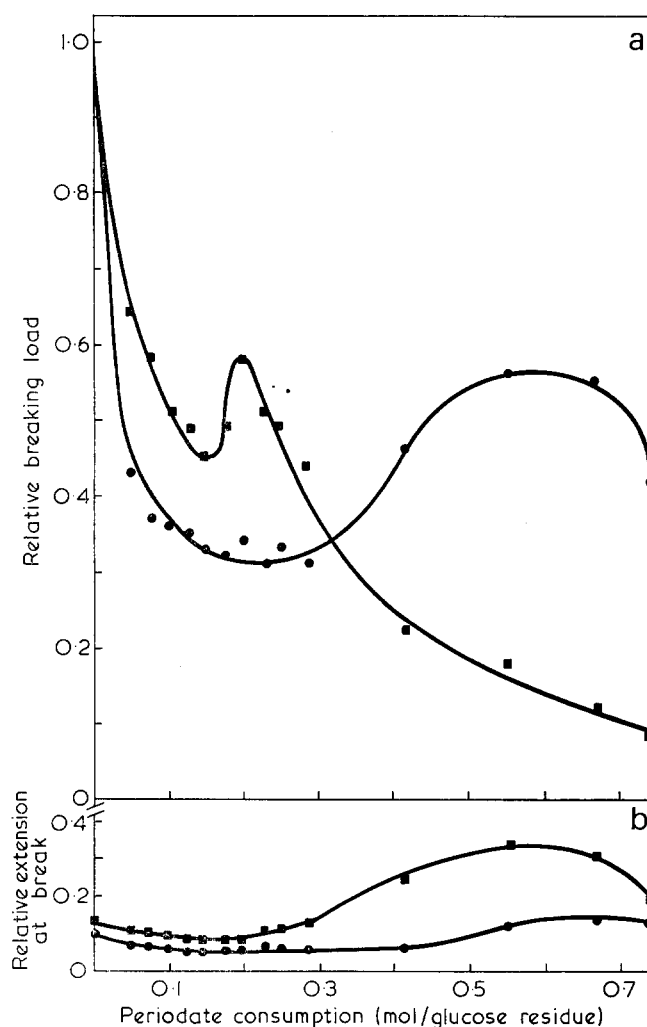


Figure 2 Relative breaking load (a) and extension at break (b) of untreated cotton: ●, oxidized by periodate; ■, oxidized by periodate and reduced with borohydride

of both. If it were due solely to random chain scission, halving the degree of polymerization (*DP*) (originally³ $\overline{DP}_v=2450$) would reduce the intrinsic viscosity from about 6.7 to 4.5, which corresponds to a periodate consumption between 0.1 and 0.2 molecules per glucose unit, or 120 and 240 molecules per cellulose chain molecule. Thus the maximum number of glycosidic bonds broken is less than 1% of the number of dialdehyde groups formed and would probably turn out to be still smaller if chain flexibility could be allowed for. The fact that intrinsic viscosity falls more rapidly with increasing periodate consumption with ethylamine-treated cotton than with the original material is due to the more uniform susceptibility of the former to chemical attack.

Breaking load and extensibility of the fibres

The effect of periodate oxidation and of subsequent borohydride reduction on the relative breaking load and extension at break of cotton fibres is shown in Figure 2. The curves are very similar to those previously reported for cotton yarns¹ except that the maximum in the breaking-load curve of the reduced materials at a periodate consumption of about 0.2 mol/glucose unit was not then observed. Figures 3 and 4 show the results of similar experiments with DMF-washed ethylamine-

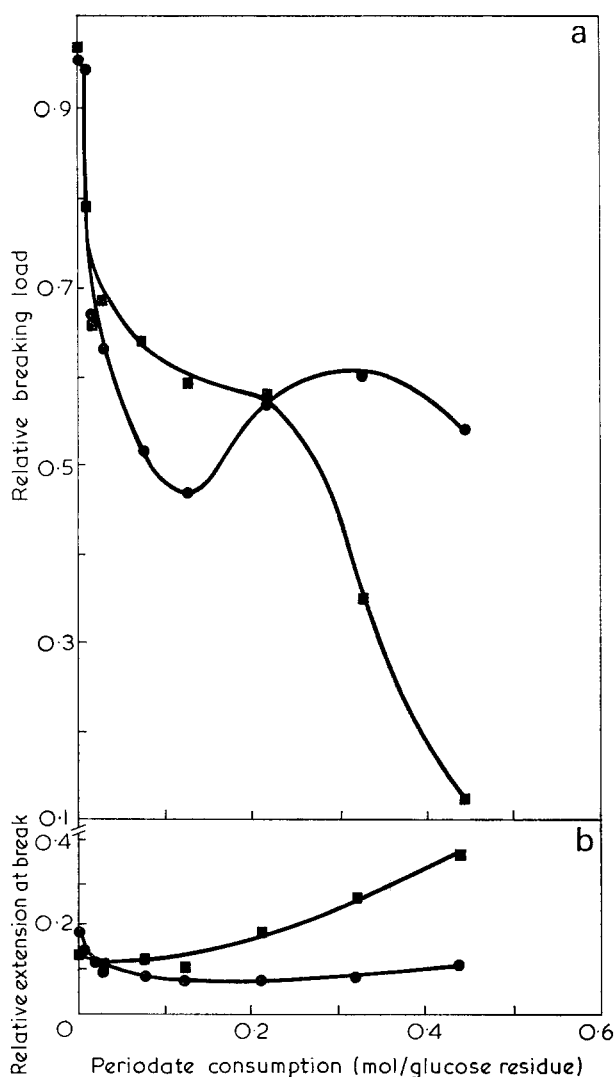


Figure 3 Relative breaking load (a) and extension at break (b) of DMF-washed ethylamine-treated cotton: ●, oxidized by periodate; ■, oxidized by periodate and reduced with borohydride

treated fibres and partly acetylated ethylamine-treated fibres respectively. The curves are similar in form to those in Figure 2; but the minima in the breaking-load curves of the oxycelluloses themselves have become sharper and represent considerably smaller losses of strength. Furthermore the minima in the curves for the reduced materials have become mere points of inflection, and the initial losses of strength are also smaller.

Reduced oxycelluloses. If the initial strength loss in the reduced oxycelluloses is due entirely to chain scission during the periodate oxidation, the diminution of this loss brought about by pretreatment with ethylamine may be attributed to the more uniform susceptibility to chemical attack already referred to. This explanation is consistent with the well-known fact that the *DP* of commercial yarns of regenerated cellulose is lower than the *DP* of cotton that has been sufficiently degraded by acid hydrolysis to make it useless for textile purposes. It is also borne out by the results shown in Figure 5 for the periodate oxidation and borohydride reduction of viscose rayon. The rate of loss of strength of the reduced oxyrayon is much lower than that of the corresponding cotton products because of the greater accessibility of the rayon.

Although it is reasonable to assume that chain scission is the only cause of strength changes in the reduced materials with low periodate consumptions, it is clear that other factors need to be taken into account at higher degrees of chemical modification. The diminution in the rate of fall of the relative breaking load (Figures 3, 4 and 5), or its temporary reversal (Figure 2), occurs at a stage when swelling of the fibre during treatment is appreciable and when the cellulose chain molecules have been rendered significantly more flexible than they were originally by scission of the $C_{(2)}-C_{(3)}$ bonds. This enables the chain molecules to rearrange themselves in such a way that a higher proportion of them can be fully extended before they break under stress, and so the fibres lose less strength than they otherwise would have done. When further molecular rearrangement is impossible, the fibres continue to lose strength through chain scission as chemical modification proceeds. Swelling continues to increase simultaneously, as is shown by the increasing extension at break of the fibres, but it no longer exerts an overriding effect on the fibre strength.

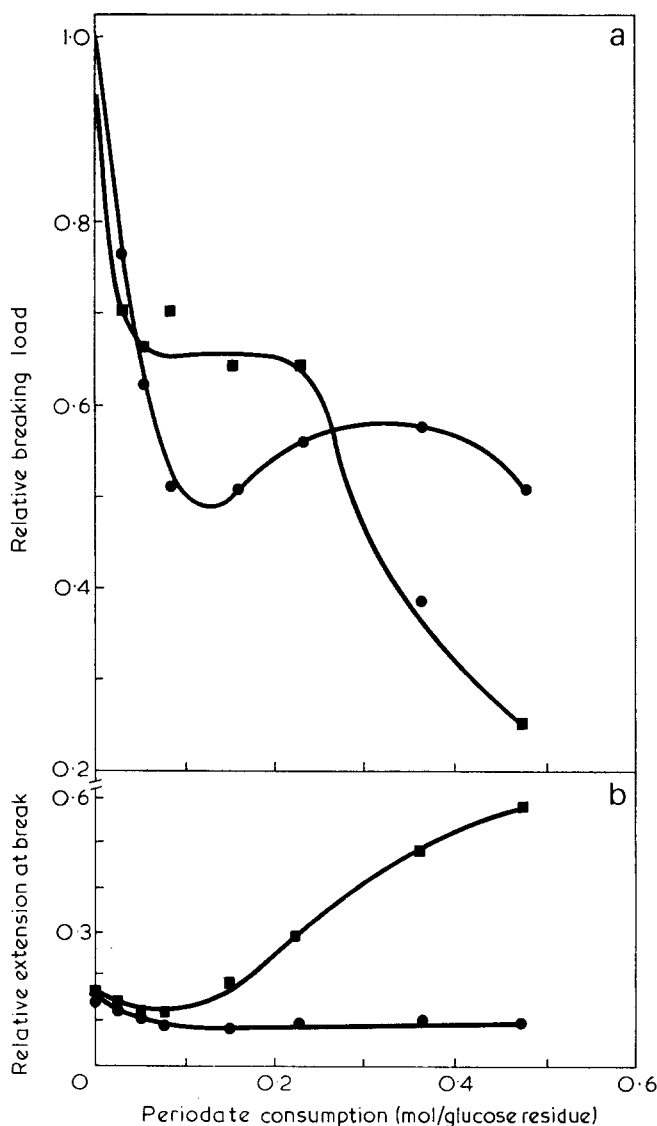


Figure 4 Relative breaking load (a) and extension at break (b) of partly acetylated ethylamine-treated cotton: ●, oxidized by periodate; ■, oxidized by periodate and reduced with borohydride

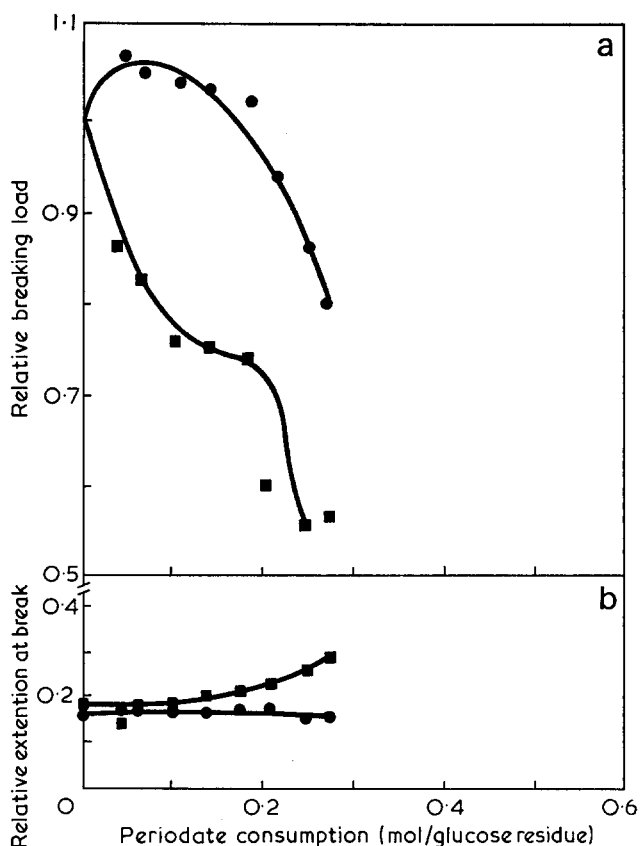


Figure 5 Relative breaking load (a) and extension at break (b) of viscose rayon: ●, oxidized by periodate; ■, oxidized by periodate and reduced with borohydride

Original oxycelluloses. In the early stages of the oxidation of cotton fibres (up to about 0.25 mol/gluucose unit) the loss of strength due to oxidation alone is greater than that due to oxidation followed by reduction. This has already been attributed to the presence in the oxycelluloses of hemi-acetal crosslinks, which do not withstand reduction with borohydride¹. These crosslinks also account for the fact that the oxycelluloses are less extensible before borohydride reduction than after it.

The effect of crosslinking on the tensile strength of a rubber-like polymer was examined theoretically by Bueche⁵ and his model was applied to cellulose materials by Gardon and Steele⁶. Bueche showed that the introduction of crosslinks progressively increases the tensile strength of a fibrous material up to a maximum. Beyond this further crosslinking causes a fall in strength, basically because it reduces the proportion of chain molecules that can be fully extended simultaneously before they break under stress. In terms of this model, cotton is a cross-linked polymer (the crosslinks being intermolecular hydrogen bonds) with a crosslink density well beyond that at which maximum strength occurs. Thus the formation of still more crosslinks, by whatever means, causes a loss of strength. This application of Bueche's theory not only accounts for the loss of strength during the early stages of periodate oxidation but also gives a more satisfactory explanation than that given previously¹ of the subsequent increase in strength that supervenes between periodate consumptions of about 0.15 and 0.4 molecules per glucose unit. The point at which the strength begins to rise is precisely the point at which fibre swelling becomes appreciable⁷. Progressive

swelling causes a progressive reduction in the number of intermolecular hydrogen bonds larger than the increase of newly formed hemi-acetal links. Thus the strength continues to rise until eventually further swelling has little effect, and hemi-acetal formation again becomes the predominant influence.

The variation of the tensile strength of viscose rayon oxidized with periodate (Figure 5) confirms the above picture. The density of intermolecular hydrogen bonds in this material is well below that at which maximum strength occurs, and so oxidation brings about an increase in strength until that point is reached. Thereafter the continued formation of hemi-acetals causes the strength to fall. The curve for borohydride-reduced oxidized rayon shows the same evidence of progressive but slow concomitant chain scission as did the corresponding curves for cotton.

It may be wondered why ethylamine-treated cotton, which has an accessibility similar to that of viscose rayon³, does not behave like this material, rather than like untreated cotton, on oxidation. The reason must lie in the impreciseness of accessibility as a characteristic of fibre structure. The high accessibility of rayon is due to its low degree of crystallinity and high crystallite surface area. That of ethylamine-treated cotton is due to the enlargement, but not the destruction, of the cellulose crystal lattice^{3, 8, 9}.

The effects of crosslinking resins on the tensile properties of cellulosic materials have been broadly understood for some time¹⁰, but it has never been possible to exclude with certainty the effects of embedded resin not chemically combined with the material. In the present work, however, a system has been used in which the covalently bound crosslinks are part of the cellulose chain molecules themselves.

Attempted isolation of the effect of crosslinking on the strength of oxycelluloses

It has been suggested that the overall effect of oxidizing cellulose with periodate on its fibre strength is a combination of the effects of crosslinking, chain scission, and increased chain flexibility, the net extent of crosslinking being the difference between the number of intermolecular hemi-acetal groups formed and the number of intermolecular hydrogen bonds broken through swelling. If the assumption is made that the changes of relative breaking load due to chain scission and increased chain flexibility are the same for each oxycellulose and its reduced derivative (an assumption which at best can be only approximate), the changes in relative breaking load due to crosslinking alone can be calculated by adding to the experimental results the difference between 1.00 and the relative breaking loads of corresponding reduced materials. The results of calculations of this type for untreated cotton, ethylamine-treated cotton, and viscose rayon are shown in Figure 6. The loss of strength suffered by the two cotton samples during the early stages of oxidation clearly distinguishes them from rayon, which gains in strength, thus illustrating the structural difference between the two types of material. At periodate consumptions greater than about 0.2 mol/gluucose unit rayon develops sufficient crosslinks to cause a diminution of strength, whereas cotton gains strength rapidly through the destruction of intermolecular hydrogen bonds. Ethylamine-treated cotton

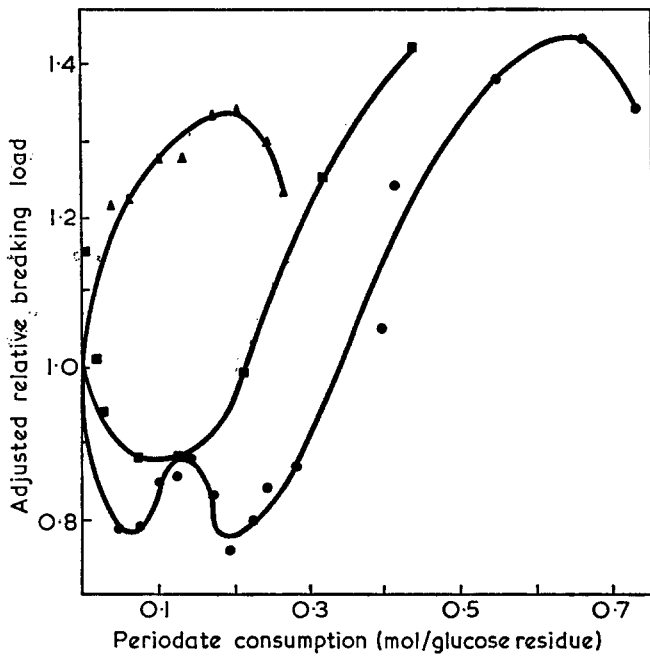


Figure 6 Relative breaking load (adjusted to allow for chain scission and increased chain flexibility) of periodate oxycelluloses from: ●, untreated cotton; ■, ethylamine-treated cotton; ▲, viscose rayon

reaches a minimum strength at a degree of oxidation of about 0.15 mol/glucose unit. The loss of strength is approximately half that suffered by untreated cotton, which again illustrates the more uniform distribution of hemi-acetal crosslinks in the former material.

The curve for untreated cotton in Figure 6 has a small subsidiary maximum at about 0.15 mol of periodate/glucose unit. It is probable that this is a real effect, but it is not considered worthwhile to offer speculative explanations of it.

REFERENCES

- 1 Nevell, T. P. and Zeronian, S. H. *J. Text. Inst.* 1962, **53**, T90
- 2 Colbran, R. L., Nevell, T. P. and Zeronian, S. H. *J. Text. Inst.* 1963, **54**, T192
- 3 Nevell, T. P. and Shaw, I. S. *Polymer* 1974, **15**, 553
- 4 Head, F. S. H. *J. Text. Inst.* 1955, **46**, T400
- 5 Bueche, F. J. *Polym. Sci.* 1957, **24**, 189
- 6 Gardon, J. L. and Steele, R. *Text. Res. J.* 1961, **31**, 160
- 7 Nevell, T. P. *J. Text. Inst.* 1956, **47**, T287
- 8 Davis, W. E. *et al. J. Am. Chem. Soc.* 1943, **65**, 1294
- 9 Segal, L., Loeb, L. and Creely, J. I. *J. Polym. Sci.* 1954, **13**, 193
- 10 see e.g. Heap, S. A. *et al.* in 'Chemical Aftertreatment of Textiles' (Eds H. Mark, N. S. Wooding and S. M. Atlas), Wiley-Interscience, New York, 1971, p 283

Crosslinked poly(acryloylaminoacetaldehyde dimethylacetal) and derived urease conjugates

R. Epton and J. V. McLaren

*Department of Physical Sciences, Wolverhampton Polytechnic,
Wolverhampton WV1 1LY, UK*

and T. H. Thomas

*Department of Chemical Pathology, Leeds General Infirmary,
Leeds LS1 3EX, UK*

(Received 20 February 1974; revised 28 March 1974)

The synthesis of crosslinked poly(acryloylaminoacetaldehyde dimethylacetal) is described. Controlled hydrolysis of this material with aqueous acid, led to polyaldehydrol gels, two of which were used to immobilize urease. With the more expanded urease derivative a modified substrate concentration-activity profile was observed in which saturation kinetics were evident between 50mM and 500mM urea concentration. This conjugate exhibited greater stability during continuous use in perfused columns, on storage in aqueous buffer suspension, to removal of substrate and to temperature change. The strategy of synthesizing reactive polyaldehydrol gels, their mode of binding enzymes and the mechanism of substrate inhibition in polyaldehydrol-urease conjugates are discussed.

INTRODUCTION

A variety of methods have been described for the immobilization of enzymes by covalent binding to water-insoluble support matrices¹⁻³. To date, the most popular semi-synthetic supports have been those derived from agarose⁴, cellulose⁵⁻⁷, crosslinked dextran⁸ and porous glass⁹. Totally synthetic carriers have included poly(amino acids)¹⁰, crosslinked polyacrylamides^{11, 12}, copolymers of methacrylic acid¹³ and a copolymer of ethylene and maleic anhydride¹⁴.

A number of these enzyme carriers are non-ideal. In order to ensure the stability of the bound enzyme, it is essential that support matrices should be hydrophilic overall and devoid of prominent hydrophobic features¹. Non-ionic carriers are preferable because charged groups can lead to enzyme instability. Of the supports listed only neutral, hydrophilic derivatives of polysaccharides, porous glass and crosslinked polyacrylamide enjoy regular use. Since it is of interest to study the properties of a given enzyme when it is constrained within a variety of different micro-environments there is some need for alternative supports.

In this laboratory, we have devised a new type of support matrix for enzyme immobilization, namely, crosslinked poly(acryloylaminoacetaldehyde dimethylacetal) (Enzacryl Polyacetal). Treatment of this polymer with dilute mineral acid leads to polyaldehydrol gels. We have shown these to be effective in immobilizing glycoside and protein hydrolases and have reported on the biological properties of the resulting conjugates^{15, 16}. Although these enzyme derivatives were found to undergo slight

dissociation in contact with their natural, macromolecular substrates they were found to be quite stable during continuous use against small, synthetic ones.

The present paper describes the synthesis of crosslinked poly(acryloylaminoacetaldehyde dimethylacetal) together with the preparation and properties of some derived polyaldehydrol-urease conjugates. Urease was selected because its natural substrate, urea, is a small molecule. Polyaldehydrol gels are unusual support matrices in that the functional groups active in enzyme binding also confer the characteristic hydrophilicity of the polymer. Consequently, these groups are present in large excess. This leads to the possibility of several enzyme to carrier linkages for each bound enzyme molecule. This could have an important effect on allosteric processes.

EXPERIMENTAL

Synthesis of N-acryloylaminoacetaldehyde dimethylacetal

Aminoacetaldehyde dimethylacetal (31.5 g, 300 mmol) (Aldrich Ltd, USA) was dissolved in peroxide free, dry ether (150 cm³) and the solution was maintained at 0°C. A mixture of acryloyl chloride (13.6 g, 150 mmol) (Koch-Light Ltd, UK) and peroxide free, dry ether (50 cm³) was added slowly during 1 h with efficient mechanical stirring. A few minutes after the addition was complete the precipitate of aminoacetaldehyde dimethylacetal hydrochloride was removed by filtration. Evaporation of the ether under reduced pressure gave *N-acryloylaminoacetaldehyde dimethylacetal* (21.3 g, 90%), b.p. 104-105°C at 0.1 mmHg, η_D^{25} 1.4665, ν_{\max} (liquid film) 3280 (amide

N—H str.), 1655 (amide C=O str.), 1620 (C=C str.) and 1126 cm⁻¹ (acetal C—O str.), δ (CDCl₃; 60 MHz) 3.40–3.52 [8H, CH(OCH₃)₂ and NHCH₂CH], 4.42 [1H, t, $J \sim 5$ Hz, CH₂CH(OCH₃)₂], 5.61 (1H, dd, $J \sim 8$ and 5 Hz, CH₂=CHCO), 6.25 (2H, m, CH₂=CHCO), and 7.04 ppm (1H, br s, CONH). (Found: m/e 128.0711 (M—OCH₃)⁺; C₇H₁₃NO₃—OCH₃ requires m/e 128.0712.

2,4-Dinitrophenylhydrazone, m.p. 186–187°C (from chloroform). (Found: C, 44.90%; H, 3.75%; N, 23.88%. C₁₁H₁₁N₅O₅ requires: C, 45.05%; H, 3.78%; N, 23.88%); *syn* oxime m.p. 145–147°C (from ethanol/petroleum ether, b.p. 40–60°C). (Found: C, 46.84%; H, 6.26%; N, 21.81%. C₅H₈N₂O₂ requires: C, 46.87%; H, 6.29%; N, 21.86%.)

Synthesis of crosslinked poly(acryloylaminoacetaldehyde dimethylacetal)

To a solution of *N*-acryloylaminoacetaldehyde dimethylacetal (7.95 g, 50 mmol) and *N,N'*-methylene-diacrylamide (0.96 g, 6.25 mmol) in peroxide free tetrahydrofuran (25 cm³) was added a solution of potassium persulphate (10 mg) and riboflavin (2 mg) in distilled water (25 cm³). Nitrogen was bubbled through the mixture until an increase in viscosity occurred (~ 30 min) when it was irradiated for 15 min with a photoflood lamp (500 W) placed 8 cm above the surface of the liquid. Polymerization was allowed to proceed to completion overnight. The gel was broken up by grinding in a mortar and equilibrated with distilled water. Particles of <300 μ m wet mesh were retained and stored in aqueous suspension. The weight of the crosslinked poly(acryloylaminoacetaldehyde dimethylacetal) matrix was 8.3 g (93%) (estimated by drying out a sample of the hydrated gel).

Preparation of polyaldehydrol gels

Crosslinked poly(acryloylaminoacetaldehyde dimethylacetal) was activated for enzyme coupling by shaking with aqueous 0.25 M HCl at 30°C for 48 h. After exhaustive washing with distilled water, the neutral polyaldehydrol gel (PG 1) was stored wet at 0–2°C. Dry samples were obtained, as required, by equilibration of aliquots of the aqueous suspension with ethanol, washing with ether, and evaporation of the solvent *in vacuo*. Re-hydration of the dried material led to a less expanded polyaldehydrol gel (PG 2). The aldehydrol content of the gels, determined by the method of Bryant and Smith¹⁷ was 5.4 mequiv./g (71% theoretical). The water content of the gel particles was calculated from the extinction change (615 nm) observed on equilibration of aliquots of the aqueous suspension with a 0.2% w/v aqueous solution of blue dextran (Pharmacia Ltd). Polyaldehydrol gels PG 1 and PG 2 had water contents of 10.9 and 5.0 cm³/g respectively.

Preparation of polyaldehydrol-urease conjugates

Prior to enzyme coupling, samples of the polyaldehydrol gels PG 1 and PG 2 (each equivalent to 100 mg of dry copolymer) were equilibrated with 25 mM phosphate buffer (pH 7.5). After centrifuging, excess buffer was discarded and aliquots (0.25 cm³) of a 2% w/v solution of purified urease, 210 Sumner units/mg (P-L Biochemicals Inc.), in 25 mM phosphate buffer, added. The resulting polyaldehydrol-urease conjugates, PU 1 and PU 2 respectively, were washed six times at 0–2°C

with aliquots (10 cm³) of 25 mM phosphate buffer (pH 7.5) containing 5 mM EDTA. Washings were of 30 min duration and were carried out with vigorous magnetic stirring. Finally, each conjugate was suspended in buffered EDTA solution (10 cm³) and stored at 0–2°C.

Determination of immobilized protein

Samples of each conjugate were hydrolysed by treatment with 6 M HCl at 110°C for 18 h. The resultant amino acids were separated into groups¹⁸ by paper chromatography and subjected to quantitative ninhydrin estimation¹⁹. The bound protein originally present in the conjugates was calculated with the aid of a standard graph obtained on chromatographic assay of known amounts of a hydrolysate of the free enzyme.

Determination of urease activity

A substrate solution of 150 mM urea in 100 mM phosphate buffer (pH 7.5) containing 5 mM EDTA was used²⁰. In the case of magnetically stirred reactors, aliquots (0.2 cm³) of the suspensions of the polyaldehydrol-urease conjugates were incubated with aliquots (10 cm³) of the urea solution at 30°C. At intervals, aliquots of the reaction mixture were withdrawn, centrifuged and the ammonia concentration in the supernatant was estimated with Nessler's reagent. For continuous use in packed columns, samples (estimated dry weight 5 mg) of each conjugate were dispersed in a large excess (dry weight 200 mg) of hydrated Bio-Gel P-30 (Bio-Rad Laboratories Ltd). The columns (5.0 \times 0.7 cm) were thermostated at 30°C and perfused with urea solution at a flow rate of 5 cm³/h. The ammonia concentration in the effluent was determined periodically.

Substrate concentration-activity measurements

The activities of both the water-insoluble conjugates and the free enzyme in solution were determined at a series of urea concentrations between 0.001 M and 1.0 M in stirred reactors at 30°C. Buffer and EDTA concentrations were as described above.

RESULTS AND DISCUSSION

In order to synthesize polyaldehydrol gels in which the identity of each aldehydrol group is preserved, it is necessary to design the polymer matrix with some care. Otherwise suitably placed aldehydrol groups may undergo undesirable condensation reactions within the gel. For example, in the case of polyacraldehyde, aldehyde or aldehydrol groups condense spontaneously with their nearest neighbours to give an extended polyacetal structure²¹. This results in conversion of the polymer to a crosslinked system of fused pyran rings.

One approach to the synthesis of stable, polyaldehydrol gels of the polyacrylate type is to situate the aldehydrol groups at the end of short molecular chains pendant on the hydrocarbon backbone. This has been achieved in the present studies by preparing gels derived from crosslinked poly(acryloylaminoacetaldehyde dimethylacetal) and subjecting them to controlled acid hydrolysis. Hemiacetal formation in the resulting polyaldehydrol gels, by condensation of neighbouring aldehydrol groups, is unlikely because this would necessitate the formation of twelve membered rings. Moreover, by constructing molecular models, it has been possible to demonstrate that sequences of fused acetal rings are not feasible.

Another reaction which might occur within a polyaldehydrol gel and result in loss of aldehydrol groups is acid or base catalysed aldol condensation. This is also unlikely in the case of the polyaldehydrol gels of the present studies because the methylene residues next to the aldehydrol (aldehyde) groups in the acylaminoacetaldehyde side chains are deactivated by the adjacent nitrogen function. The high aldehydrol content (71% theoretical) of the polyaldehydrol gels, which were necessarily exposed to mineral acid during generation of the aldehydrol groups, together with the fact that the gels could be stored hydrated for several weeks without deterioration or diminution of water content, reflect their excellent stability.

The water content of a given polyaldehydrol gel could be diminished by carrying out a cycle of drying and re-hydration. It is possible that this change in swelling property was caused by the formation of intercatenate hemi-acetal linkages in the solid state. When the freshly generated polyaldehydrol gel, PG 1, was subject to a single drying and re-hydration cycle, the water content of the resultant gel, PG 2, was approximately half that of the original. Both gels were used for the immobilization of urease.

The protein bound in polyaldehydrol-urease conjugate PU 1, 19.8 mg/g and polyaldehydrol-urease conjugate PU 2, 8.5 mg/g reflects the respective swelling of the polyaldehydrol gels, PG 1 and PG 2, from which they were derived. The bound urease retained 29.6% and 19.9% respectively of the free solution activity. It is usual for the most expanded matrix to be the more effective, both from the point of view of enzyme binding and activity retention². Values of K_m determined for conjugates PU 1 and PU 2, 7 mM and 10 mM respectively, and for the free enzyme in solution, 8 mM, did not differ significantly.

For each polyaldehydrol-urease conjugate, an incubation mixture consisting of the conjugate and a buffered solution of urea was centrifuged and the supernatant was tested rigorously for re-solubilized urease activity. These tests proved negative. Although not unexpected, this is an important result which has some implications on the nature of the binding reaction.

Simple reaction between aldehydrol groups on the aqueous gel and primary amino groups on the enzyme might be expected to result in the formation of primary aminol and azomethine linkages (*Figure 1a*). An objection to this hypothesis is that, in the case of most monomeric aldehydes and amines, the binding equilibrium favours extensive dissociation. However, Falb *et al.*²² have predicted that the high concentration of aldehydrol groups within a polyaldehydrol gel will provide a micro-environment within which the binding equilibrium is displaced to favour the formation of the polyaldehydrol-amine conjugate.

If the binding process is reversible it should be possible to bring about dissociation. In previous studies we have observed that repeatedly washing a polyaldehydrol-dextranase conjugate⁸ with an aqueous solution of its macromolecular substrate, dextran, brought about slight re-solubilization of the enzyme. Probably affinity of the bound enzyme for its macromolecular substrate in solution is sufficient to displace the binding equilibrium and cause significant partitioning of the enzyme between the gel and aqueous phase. It was not possible to bring about total dissociation in the case of the dextranase.

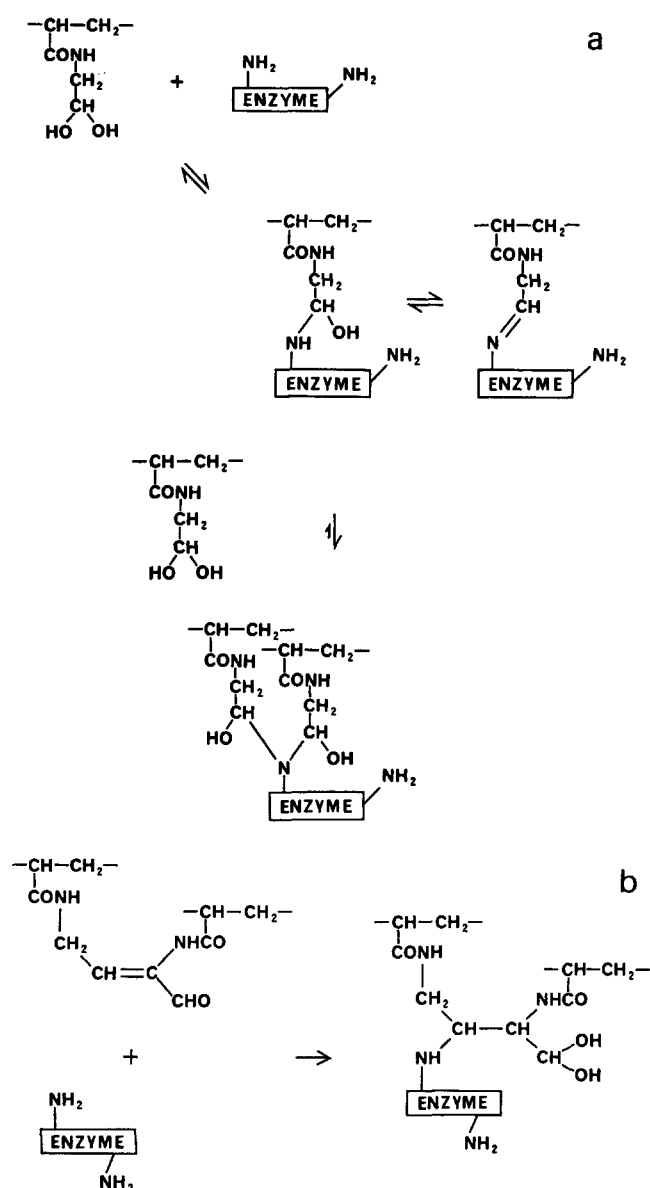


Figure 1 Possible modes of aldehydrol-enzyme coupling. (a) Reversible binding via primary aminol and azomethine linkages and possible irreversible binding via the secondary aminol linkage; (b) Michael type coupling

Rather, re-solubilized activity fell exponentially until it became very difficult to detect. The fact that substantial activity remained on the gel at this stage was indicative of a second, irreversible, binding mechanism.

It is known that reaction of enzymes with glutaraldehyde, either alone^{23, 24} or in the presence of carriers such as aminoethyl cellulose^{25, 26} or partly hydrolysed nylon-6²⁷ is a useful method of achieving irreversible immobilization. During the binding process, glutaraldehyde undergoes random aldol condensation which is followed by β -elimination²⁸. This results in a mixture of oligomeric unsaturated dialdehydes. Primary amino groups on the enzyme then undergo irreversible Michael addition across the conjugated double bonds (*Figure 1b*). In view of the structures of the polyaldehydrol gels derived from crosslinked poly(acryloylaminoacetaldehyde dimethylacetal), enzyme binding via Michael addition was thought unlikely. However, it was deemed prudent to consider the possibility. With this in mind it is relevant to examine the infra-red (i.r.) spectra of

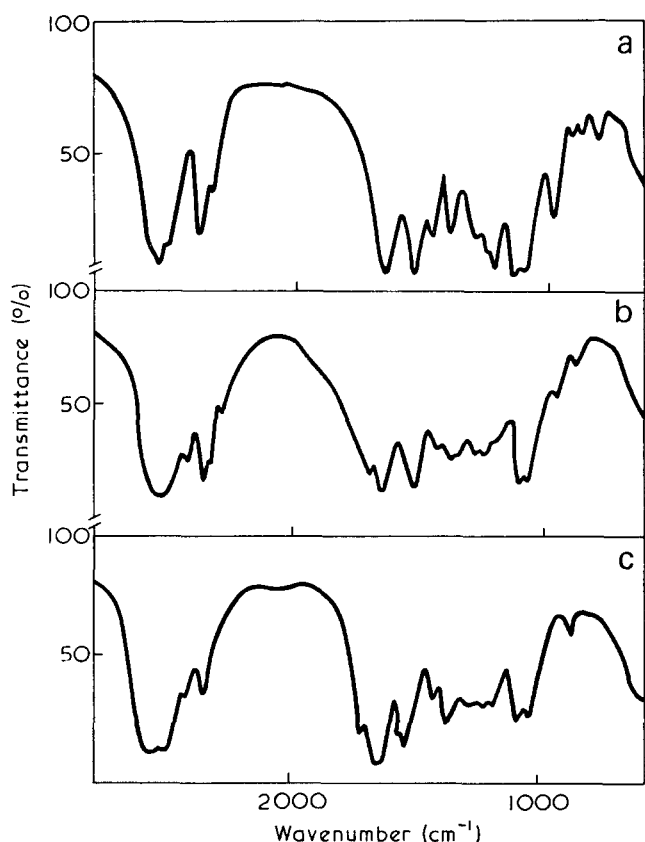


Figure 2 Infra-red spectra. (a) Crosslinked poly(acryloylaminoacetaldehyde dimethylacetal); (b) polyaldehyde gel (PG 1) derived by treatment of crosslinked poly(acryloylaminoacetaldehyde dimethylacetal) with 0.25 M HCl for 24 h at 20–25°C; (c) polyaldehyde gel derived by treatment of crosslinked poly(acryloylaminoacetaldehyde dimethylacetal) with 2 M HCl for 7 days at 20–25°C

exhaustively dried samples of crosslinked poly(acryloylaminoacetaldehyde dimethylacetal), and the polyaldehyde gel (Figure 2).

Drying the polyaldehyde gels should lead to conversion of aldehydrol groups to aldehyde residues. This is apparent from the absorption at 1710 cm^{-1} in the i.r. spectrum. In simple compounds, the stretching absorption of an alkene in conjugation with an aldehyde carbonyl group should be apparent at 1620 cm^{-1} . Unfortunately, in the case of the dried polyaldehyde gels, this region of the spectrum is obscured by a broad band arising from the carbonyl of the amide group. However, unambiguous evidence against unsaturation is provided by the absence of any absorption between 790 and 840 cm^{-1} (Figure 2b and 2c). If alkenyl C—H were present in the dried polymer there would be a strong, highly characteristic absorption in this region owing to the alkenyl C—H out-of-plane bending deformation²⁹. This absorption was not apparent even in the spectrum of a dried sample of polyaldehyde gel which had been generated by treatment of the polyacetal with 2 M HCl for 7 days at room temperature. Absence of unsaturation must preclude any binding process involving Michael addition.

Our own tentative hypothesis for the binding reaction is that the high concentration of aldehydrol groups in the polyaldehyde gel not only displaces the binding equilibrium to facilitate primary aminol formation, but permits further reaction to form secondary aminol

linkages (Figure 1a). In the case of suitably placed aldehydrol groups, secondary aminol formation could be irreversible. A similar reaction scheme may be involved in the facile immobilization of enzymes by polymeric dialdehydes derived by periodate oxidation of cellulose^{30, 31} and dextran³⁰.

It is well known that saturation kinetics are not obtained for native urease owing to substrate inhibition^{20, 32}. A similar situation is apparent in the case of conjugate PU 2 (Figure 3). However, in the case of conjugate PU 1, saturation kinetics were evident between 50 mM and 500 mM urea concentration. This phenomenon has not been reported in the case of covalent urease conjugates derived from such materials as poly(amino acids)³³, porous glass⁹ or linear polymers and copolymers of 4-methacryloxy-3-methoxy benzaldehyde³⁴. The last two materials are of interest because, in contrast to the xerogel polymers of the present studies, they provide a simple, solid polyaldehyde matrix for binding urease.

Conjugate PU 1 was superior to conjugate PU 2 in its activity retention during continuous use in packed columns (Figure 4). Furthermore, on storage for 6 months in buffer suspension, conjugate PU 1 retained 48% of its original activity whereas conjugate PU 2

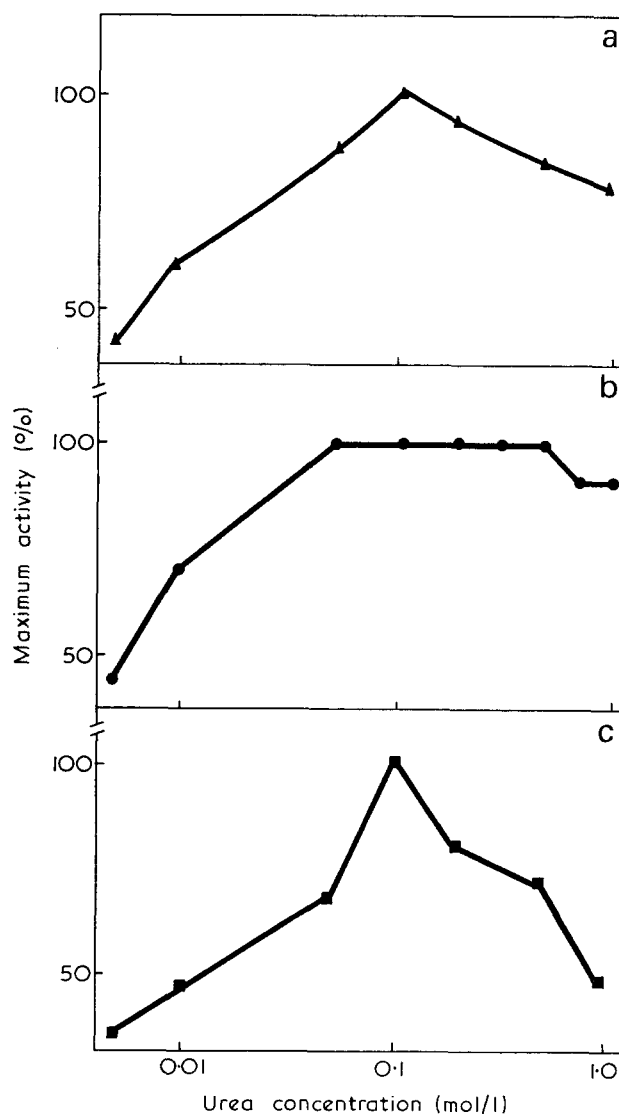


Figure 3 Substrate concentration-activity profiles. (a) Native urease; (b) conjugate PU 1; (c) conjugate PU 2

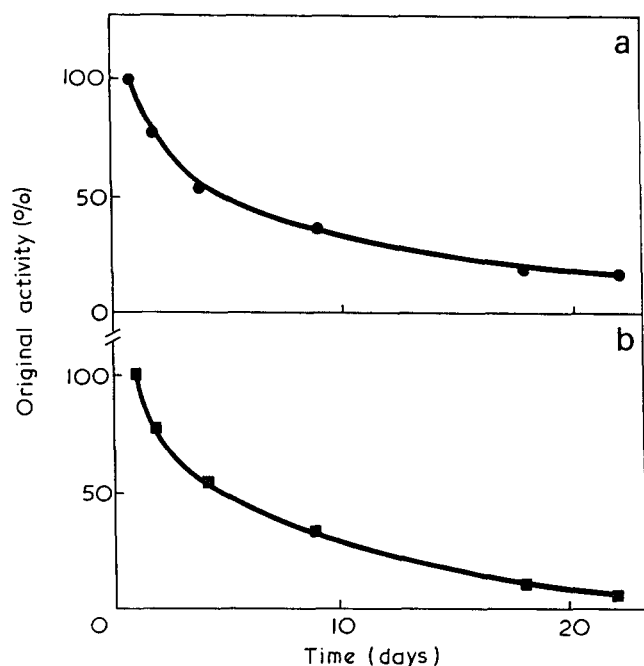


Figure 4 Continuous use of polyaldehyde-urease conjugates in packed columns at 30°C. (a) Conjugate PU 1; (b) conjugate PU 2

Table 1 Heat denaturation of native and polyaldehyde bound urease at 60°C

Heating time (h)	Percentage of original activity remaining		
	Conjugate PU 1	Conjugate PU 2	Native urease
0	100	100	100
2	48	56	63
4	39	46	54
8	32	33	45
24	15	14	24

retained only 17%. Both conjugates were slightly less stable to heat denaturation than the native enzyme in solution (Table 1). On recovery from stirred reactors followed by washing with 25 mM EDTA conjugates PU 1 and PU 2 lost 17% and 18% respectively of their activity. This loss in activity was shown to be caused by the removal of urea. However, whereas urease bound in conjugate PU 2 could be inactivated merely by diminution of substrate concentration, the enzyme bound in conjugate PU 1 was relatively insensitive to such changes. Consequently conjugate PU 1 could be repeatedly transferred between stirred reactors with full activity retention.

It is pertinent to consider the binding environment of the enzyme in the two conjugates. With the more expanded gel the proportionately larger cavities between the solvated polymer chains should favour penetration by the enzyme molecules and thereby facilitate multiple contact. It is reasonable to suppose that this leads to greater numbers of carrier to enzyme linkages as well as providing more general support for the enzyme molecule. This should help to preserve tertiary structure¹⁸ and is consistent with the superiority of conjugate PU 1 both in storage and in continuous use. On the other hand the external constraint imposed by multiple linkage

might prevent or severely impede allosteric effects. In connection with the insensitivity of conjugate PU 1 to substrate inhibition it is interesting to note that Laidler and Hoare²⁰, in describing their classical investigation of urease kinetics, suggested that allosteric substrate inhibition of urease was just as acceptable an interpretation of their results as their more widely accepted hypothesis of urea molecules competing directly for a 'water site' in the active centre of the enzyme. The relative insensitivity of conjugate PU 1 to variation in substrate concentration may also be consistent with the mode of binding impeding an allosteric process.

ACKNOWLEDGEMENTS

The authors wish to thank Koch-Light Laboratories Ltd for general support and a studentship (T.H.T.).

REFERENCES

- Silman, I. H. and Katchalski, E. *A. Rev. Biochem.* 1966, **35**, 873
- Melrose, G. J. H. *Rev. Pure Appl. Chem.* 1971, **21**, 83
- Gryszkiewicz, J. *Folia Biologica* 1971, **19**, 119
- Porath, J., Axen, R. and Ernback, S. *Nature* 1967, **215**, 1491
- Mitz, M. A. and Summaria, L. J. *Nature* 1961, **189**, 576
- Barker, S. A., Somers, P. J. and Epton, R. *Carbohydr. Res.* 1968, **8**, 491
- Kay, G. and Crook, E. M. *Nature* 1967, **216**, 514
- Axen, R. and Porath, J. *Nature* 1966, **210**, 367
- Weetall, H. H. and Hersh, L. S. *Biochim. Biophys. Acta* 1969, **185**, 464
- Cebra, J. J., Givol, D., Silman, I. H. and Katchalski, E. *J. Biol. Chem.* 1961, **236**, 1720
- Epton, R. Br. Patent 1 265 818 (1972)
- Inman, J. K. and Dintzis, H. M. *Biochemistry* 1969, **8**, 4074
- Manecke, G. *Pure Appl. Chem.* 1962, **4**, 507
- Levin, Y., Pecht, M., Goldstein, L. and Katchalski, E. *Biochemistry* 1964, **3**, 1905
- Epton, R., McLaren, J. V. and Thomas, T. H. *Biochem. J.* 1971, **123**, 21P
- Epton, R., McLaren, J. V. and Thomas, T. H. *Carbohydr. Res.* 1972, **22**, 301
- Bryant, W. M. D. and Smith, D. M. *J. Am. Chem. Soc.* 1935, **57**, 57
- Barker, S. A., Somers, P. J., Epton, R. and McLaren, J. V. *Carbohydr. Res.* 1970, **14**, 287
- Kay, R. E., Harris, D. C. and Entenman, C. *Arch. Biochem. Biophys.* 1956, **63**, 14
- Laidler, K. J. and Hoare, J. P. *J. Am. Chem. Soc.* 1949, **71**, 2599
- Maher, G. G., Douglas, J. A., Russell, C. R. and Rist, C. E. *J. Polym. Sci. (A-1)* 1970, **8**, 1537
- Falb, R. D., Arapakos, P. G., Nack, H. and Kim, B. C. 'Annual Report on Microcapsule System for Artificial Kidney Applications', Battelle Memorial Institute, Columbus, 1968
- Quijcho, F. A. and Richards, F. M. *Proc. Nat. Acad. Sci. US* 1964, **52**, 833
- Ogata, K., Ottensen, M. and Svendsen, I. *Biochim. Biophys. Acta* 1968, **159**, 403
- Green, M. L. and Crutchfield, G. *Biochem. J.* 1969, **115**, 183
- Habeeb, A. F. S. A. *Arch. Biochem. Biophys.* 1956, **63**, 14
- Sundaram, P. V. and Hornby, W. E. *FEBS Lett.* 1970, **10**, 325
- Richards, F. M. and Knowles, J. R. *J. Mol. Biol.* 1966, **37**, 231
- Sheppard, N. and Sutherland, G. B. B. M. *Proc. R. Soc.* 1949, **196**, 195
- Flemming, C., Gabert, A., Roth, P. and Rudd, M. DDR Pat. 83 154 (1973)
- Flemming, C., Gabert, A. and Roth, P. *Acta Biol. Med.* 1973, **30**, 177
- Kistiakowsky, G. B. and Rosenberg, A. J. *J. Am. Chem. Soc.* 1952, **74**, 5020
- Riesel, E. and Katchalski, E. *J. Biol. Chem.* 1964, **239**, 1521
- Brown, E. and Racois, A. *Tetrahedron Lett.* 1972, **50**, 5077

Exact and approximate eigenvalues and intrinsic functions for the Gaussian chain theory

G. B. Thurston

Department of Mechanical Engineering, University of Texas at Austin, Austin, Texas 78712, USA
(Received 21 December 1973)

Eigenvalues for the Gaussian chain theory for dilute solutions of linear polymers have been determined in an exact manner for chain segments up to 100 and for a wide range of hydrodynamic interaction. It is found that these exact results may be closely approximated by a simple equation. The intrinsic functions of the eigenvalues which describe the molecular weight dependence of the intrinsic viscosity and terminal relaxation time of the chain are presented using both the exact and the approximate eigenvalues. It is shown that by using the simple approximate calculation good results are easily determined. The approximate equation is available for manipulation and analysis of complex eigenvalue functions.

INTRODUCTION

The Gaussian chain theory for the behaviour of linear polymer molecules in solution¹⁻⁶ has greatly expanded our insight into the phenomena underlying intrinsic viscosity⁷, viscoelasticity⁸, flow birefringence⁸ and configurational relaxation⁹. However, the quantitative applicability of the theory has been impeded by lack of precise eigenvalues. A set of exact eigenvalues were first given by Thurston and Morrison¹⁰ for short Gaussian chains and have been extended to longer chains by Lodge and Wu¹¹. Apart from the 'free draining' case, all other published values have been approximations of unspecified accuracy. Even when exact eigenvalues in tabular form are available, the labour of handling the large number of values is of major concern. Thus, it would be highly desirable to have a simple function which will generate the eigenvalues on demand, thus avoiding laborious tabulations. In the present work, such a function is presented and its accuracy is evaluated.

The eigenvalues are used in this paper to show the dependence of theoretical functions determining intrinsic viscosity, intrinsic birefringence, and terminal relaxation time on the number, N , of sub-chain segments making up the chain and the hydrodynamic interaction parameter h^* measuring the intrachain coupling through hydrodynamic forces. It was first emphasized by Thurston and Schrag¹² that N should be retained in the theory as being proportional to the molecular weight of the polymer. The parameter h^* was introduced by Thurston and Peterlin⁸ as a segmental property. Exact eigenvalues are presented in the following as a function N from 1 to 100 and h^* from 0.0 to 0.3. These are compared with values generated by a simple empirical relationship. Intrinsic functions of these eigenvalues are also compared.

EIGENVALUE DETERMINATIONS

The generation of the product matrix (HA) having eigenvalues λ_p and a method for determining their

values has been previously described¹⁰. The solution was carried out using a Control Data Corporation 6600 computer. Determinations were made using a program designated EISPKL for obtaining eigenvalues for a real, general (non-symmetric) matrix, the values then being ordered using a TSORT routine. For the case $h^*=0.0$, the 'free draining' case, eigenvalues are given by the exact relation:

$$\lambda_{p, \text{free}} = 4 \sin^2 [p \pi / 2(N + 1)] \quad (1)$$

where the integer p takes on all values from 1 to N .

The exact λ_p are given in Figure 1 where logarithmic scales are used and λ_p are plotted against $[p/(N+1)]$. Values plotted are for $N=1, 2, 3, 5, 7, 10, 20, 30, 100$

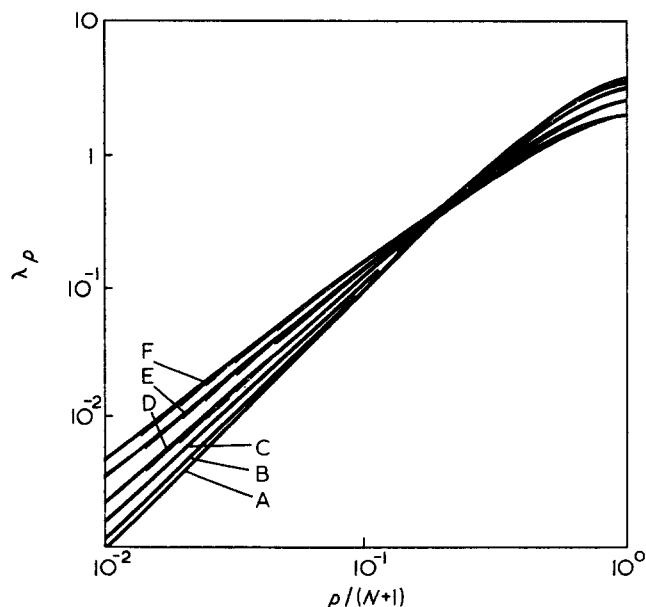


Figure 1 Exact eigenvalues $\lambda_p(N, h^*)$ versus $p/(N+1)$. Plotted are values for $p=1$ to N for $N=1, 2, 3, 5, 7, 10, 20, 30, 50, 70, 100$ and for $h^*=0.0$ (A), 0.01 (B), 0.05 (C), 0.1 (D), 0.2 (E), 0.3 (F)

and for $h^* = 0.0, 0.01, 0.05, 0.1, 0.2$ and 0.3 . By plotting the λ_p in this manner, a wide range of eigenvalues may be graphed compactly.

The form of the graphs of the exact eigenvalues in Figure 1, suggests that an equation which will approximate these values is:

$$\tilde{\lambda}_p = \lambda_{p, \text{free}} k [p/(N+1)]^\sigma \quad (2)$$

where k and σ are functions of h^* and $\tilde{\lambda}_p$ indicates an approximate value. Using the exact values for λ_1 for

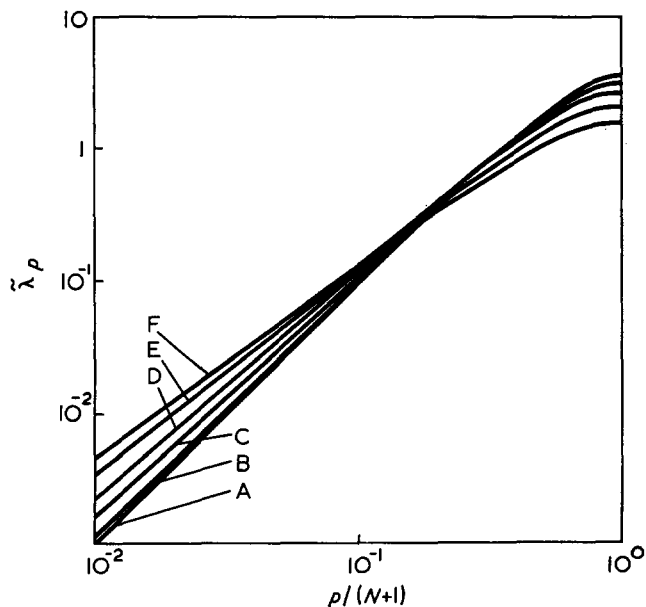


Figure 2 Approximate eigenvalues $\tilde{\lambda}_p(N, h^*)$ versus $p/(N+1)$ from equation (2)

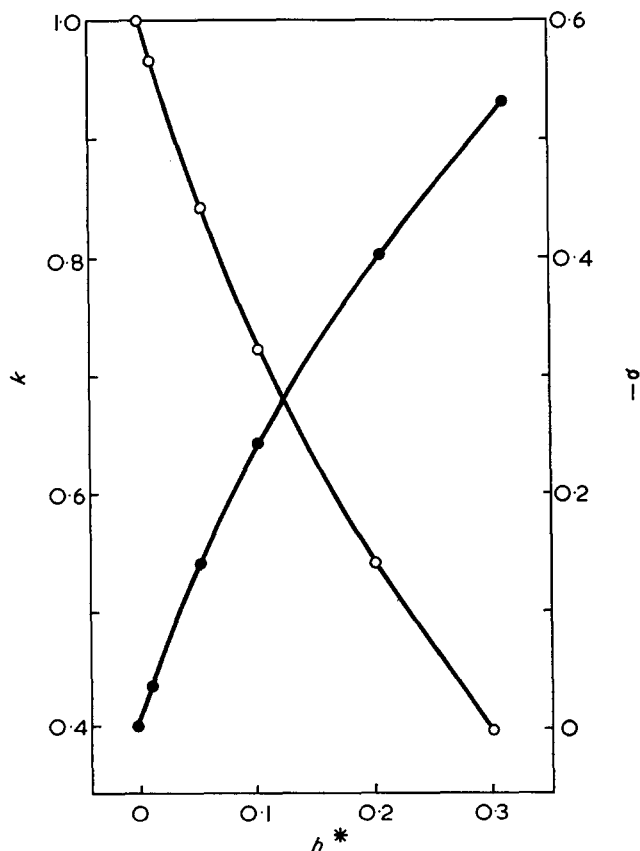


Figure 3 Factors k (○) and σ (●) versus hydrodynamic interaction parameter h^* as needed for equation (2) for $\tilde{\lambda}_p$ calculation

Table 1 Numerical factors for approximate eigenvalue equation

h^*	k	σ
0.0	1	0
0.01	0.96330	-0.0334
0.05	0.84225	-0.1419
0.10	0.72496	-0.2441
0.20	0.54333	-0.4006
0.30	0.39804	-0.5327

$N=1$ and $N=100$, values of k and σ are determined to give $\tilde{\lambda}_1$ this same value. This was done for each of the h^* values. Then, using the k and σ thus determined, the $\tilde{\lambda}_p$ are calculated using equation (2) for all values of p .

The results of these calculations of $\tilde{\lambda}_p$ are shown in Figure 2. These curves are to be compared with their exact λ_p counterparts in Figure 1. The values of k and σ used are graphed in Figure 3 and are well approximated by:

$$k \approx 1 - 1.66h^{*(0.78)} \quad (3)$$

$$\sigma \approx -1.40h^{*(0.78)} \quad (4)$$

Numerical values are given in Table 1. While these tabulated values do give exact λ_p for $p=1$ and $N=1$ and 100 , a comparison of Figures 1 and 2 shows some differences at intermediate values. However, they are generally in agreement to within 10% or better. Despite the approximate character of the $\tilde{\lambda}_p$ the values given by equation (2) are much more accurate than those given by the frequently used equation of Pyun and Fixman¹³ in this range.

INTRINSIC FUNCTIONS OF THE EIGENVALUES

The terminal, or longest of the N relaxation times of the chain is an important factor for polymer characterization. It may be determined experimentally from steady flow birefringence measurements⁹, from the frequency dependence of viscosity and oscillatory flow birefringence⁸ and with auxiliary information may be determined using the intrinsic viscosity in steady flow¹⁰. The two principal relations which give the terminal relaxation time, τ_1 in terms of the eigenvalues are:

$$\tau_1 = b^2 f / 6kT \lambda_1(N, h^*) \quad (5)$$

and

$$\tau_1 = C(N, h^*) [\eta] M \eta_s / N_a kT \quad (6)$$

where

$$C(N, h^*) = \left[\sum_p \lambda_1 / \lambda_p \right]^{-1} \quad (7)$$

In these equations b is the segment length, f is the friction factor, k is Boltzmann's constant, T is the absolute temperature, $\lambda_1(N, h^*)$ is the first eigenvalue, $[\eta]$ is the intrinsic viscosity in steady flow, M is the molecular weight, η_s is the solvent viscosity and N_a is Avogadro's number. Equations (5) and (6) have been used to determine τ_1 for polystyrene solutions^{10, 14} but the functions $\lambda_1(N, h^*)$ and $C(N, h^*)$ have only been given previously using the approximate eigenvalues of Pyun and Fixman and for exact eigenvalues for N up to 15. Figures 4 and 5 show more extensive determinations of these functions of the eigenvalues. In Figure 4, the function $[1/\lambda_1(N, h^*)]$ is plotted against N on logarithmic scales with h^* as parameter. The circles

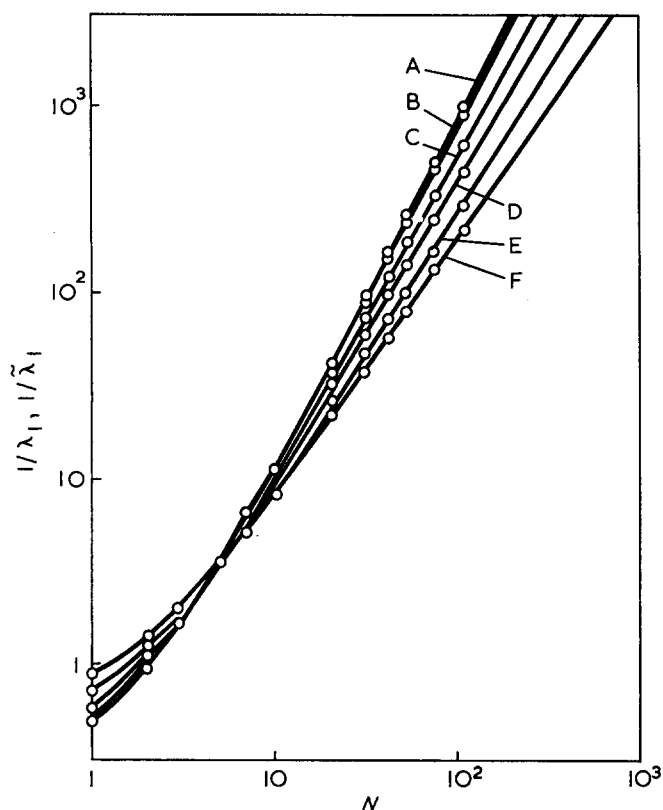


Figure 4 Reciprocal of the eigenvalues $1/\lambda_1, 1/\tilde{\lambda}_1$ versus the number of chain segments N . This function relation is proportional to the molecular weight dependence of the terminal relaxation time, according to equation (5). The circles are exact while the solid lines are approximate values from equation (2)

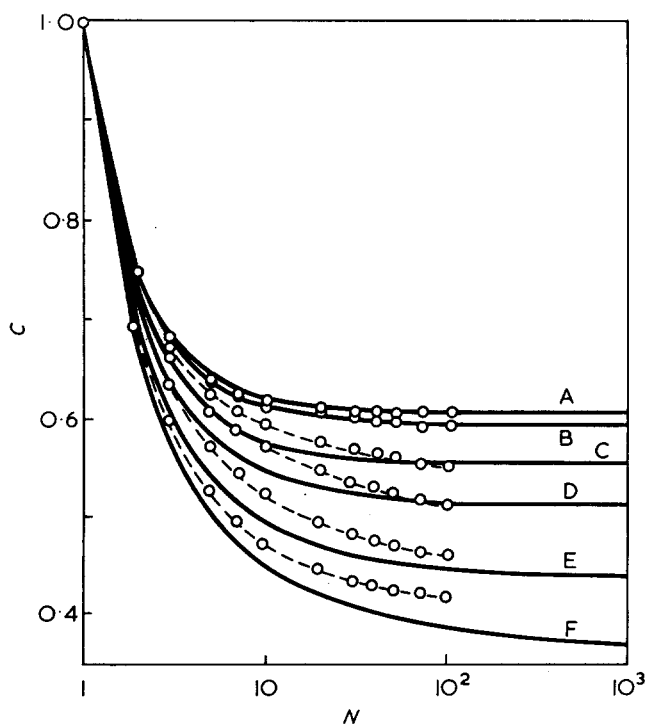


Figure 5 Parameter $C(N, h^*)$ versus N of equations (6) and (7). The circles are exact while the solid lines are approximate

are exact and the solid line is determined using the approximate eigenvalues of equation (2). It has been shown that for polystyrene, the molecular weight is directly proportional to the number of segments $N^{14, 15}$ and thus the curves of Figure 4 are to within a multiplicative constant of a plot of τ_1 versus M . In Figure 5,

$C(N, h^*)$ is plotted against N on a logarithmic scale, the circles being exact values while the solid line is obtained using the approximate equation (2).

The molecular weight dependence of the intrinsic viscosity in steady flow is dependent upon the eigenvalues

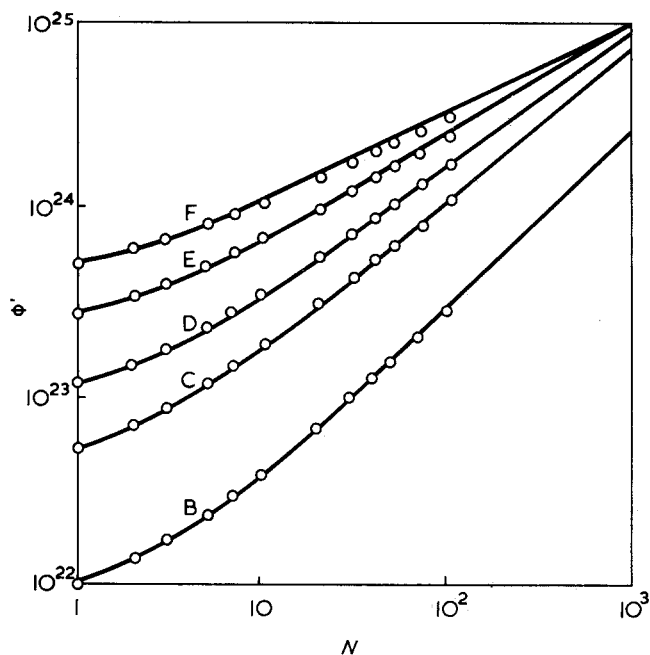


Figure 6 Function $\phi'(N, h^*)$ versus N of equations (8) and (9). This functional relation is proportional to the molecular weight dependence of the intrinsic viscosity. The circles are exact while the solid lines are approximate

Table 2 Exact values of eigenvalue functions

h^*	N	ϕ'	C	$1/\lambda_1$
0.0	1	—	1.00000	5.00000 E-01
	3	—	0.68284	1.70711 E+00
	10	—	0.61718	1.23435 E+01
	30	—	0.60908	9.74530 E+01
	100	—	0.60804	1.03366 E+03
0.01	1	9.81976 E+21	1.00000	5.07171 E-01
	3	1.62762 E+22	0.68108	1.71761 E+00
	10	3.84507 E+22	0.61262	1.21660 E+01
	30	9.95727 E+22	0.60076	9.26858 E+01
	100	2.99717 E+23	0.59330	9.18409 E+02
0.05	1	5.20871 E+22	1.00000	5.38039 E-01
	3	8.43653 E+22	0.67356	1.76095 E+00
	10	1.87416 E+23	0.59442	1.15076 E+01
	30	4.38679 E+23	0.57082	7.75984 E+01
	100	1.12247 E+24	0.54916	6.36738 E+02
0.10	1	1.12752 E+23	1.00000	5.82343 E-01
	3	1.77002 E+23	0.66304	1.81842 E+00
	10	3.65327 E+23	0.57164	1.07859 E+01
	30	7.73578 E+23	0.53893	6.45973 E+01
	100	1.74597 E+24	0.51198	4.61685 E+02
0.20	1	2.69964 E+23	1.00000	6.97156 E-01
	3	3.94280 E+23	0.63706	1.94594 E+00
	10	7.08577 E+23	0.52508	9.60808 E+00
	30	1.29165 E+24	0.48562	4.85938 E+01
	100	2.50845 E+24	0.46189	2.99206 E+02
0.30	1	5.04389 E+23	1.00000	8.68357 E-01
	3	6.74383 E+23	0.60133	2.09446 E+00
	10	1.06370 E+24	0.47497	8.69803 E+00
	30	1.72955 E+24	0.43800	3.91254 E+01
	100	3.04376 E+24	0.42370	2.22026 E+02

through a function $\phi'(N, h^*)$ by:

$$[\eta] = \phi'(N, h^*) [b^3/N_a m_s] \quad (8)$$

where m_s is the mass of the segment and

$$\phi'(N, h^*) = (N_a \pi^{3/2} / 3^{1/2}) (h^*/N) \sum_p 1/\lambda_p \quad (9)$$

Since $[b^3/N_a m_s]$ is expected to be constant for a given polymer and solvent, a logarithmic plot of $\phi'(N, h^*)$ versus N has the form of the molecular weight dependence of $[\eta]$. Figure 6 shows such a series of plots with h^* as parameter. Again, the circles are exact and the solid lines are approximate. Exact values of this eigenvalue function together with (N, h^*) and $1/\lambda_1(N, h^*)$ are given in Table 2 for selected N and h^* values. The functional form for intrinsic birefringence¹² is similar to that of equation (9).

CONCLUSIONS

A comparison of the functions plotted in Figures 4, 5 and 6 using both exact and approximate eigenvalues gives a ready indication of the accuracy of the approximation. The values of $1/\lambda_1(N, h^*)$ are in good agreement while some differences of up to 10% are seen for $C(N, h^*)$. The exact and approximate values of function $\phi'(N, h^*)$ differ by as much as 10% for larger values of h^* and N . The accuracy in the range of N from 100 to 1000 is not specified since the exact values are not determined.

The empirical equation giving approximate eigenvalues is more accurate than theoretically derived approximations that have been used in the past. The

equation is of sufficiently simple form as to speed calculations and thus is useful in cases where the labour of the exact determination is not practical.

ACKNOWLEDGEMENTS

The author wishes to acknowledge the support of the US National Science Foundation during the course of this work. The assistance of Mr Mohammed Osman in performing the numerical computations is gratefully acknowledged.

REFERENCES

- 1 Kuhn, W. and Kuhn, H. *J. Colloid Sci.* 1948, 3, 11
- 2 Rouse, Jr, P. E. *J. Chem. Phys.* 1953, 21, 1272
- 3 Bueche, F. *J. Chem. Phys.* 1954, 22, 603
- 4 Zimm, B. H. *J. Chem. Phys.* 1956, 24, 269
- 5 Kirkwood, J. G. and Riseman, T. *J. Chem. Phys.* 1948, 16, 565
- 6 Cerf, R. *J. Polym. Sci.* 1957, 22, 125; *J. Phys. Radium* 1958, 19, 122
- 7 Thurston, G. B. *Polymer* 1967, 8, 561
- 8 Thurston, G. B. and Peterlin, A. *J. Chem. Phys.* 1967, 46, 4881
- 9 Thurston, G. B. *Kolloid-Z.* 1968, 222, 34
- 10 Thurston, G. B. and Morrison, J. D. *Polymer* 1969, 10, 421
- 11 Lodge, A. S. and Wu, Y.-J. Mathematics Research Center Technical Summary Report No. 1250, University of Wisconsin, 1972
- 12 Thurston, G. B. and Schrag, J. L. *J. Chem. Phys.* 1966, 45, 3373
- 13 Pyun, C. W. and Fixman, M. *J. Chem. Phys.* 1965, 42, 3838
- 14 Thurston, G. B. and Schrag, J. L. *J. Polym. Sci. (A-2)* 1968, 6, 1331
- 15 Thurston, G. B. *J. Chem. Phys.* 1967, 47, 3582

A model study on the ionic polymerization in a flow reactor

P. I. Penchev

Centre of Research and Development of Heavy Chemical Industry, Sofia 74, Bulgaria

V. V. Ivanov and V. A. Minin

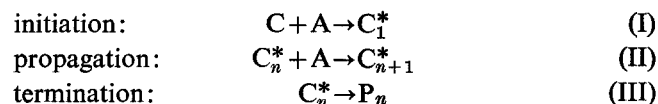
Institute of Chemical Physics, Academy of Sciences of the USSR, Moscow V-334, USSR
(Received 9 July 1973; revised 18 February 1974)

A general theoretical study of heterogeneous ionic polymerization in a continuous stationary reactor is presented. Equations have been calculated that describe the dependence of the substances' concentration in the reaction vessel, of the polymer yield and molecular weight on the initial concentration of the monomer, catalyst and chain-transfer agent. The problem is solved with assumptions based on actual anion processes. The obtained functional dependences have been analysed for different values of their parameters. The characteristic features of the reaction are also emphasized.

There exists quite a considerable interest towards carrying out polymerization processes in a flow reactor with ideal mixing. The reaction takes place under stationary conditions and can be conveniently investigated. It is also possible in practice to use a continuous technology. In this connection already there have been suggested mathematical descriptions of the homogeneous radical polymerization¹⁻⁴ and the copolymerization⁵. As far as the ionic polymerization is concerned, similar studies do not exist. A more general approach to the problem is extremely difficult because of the great variety of complex mechanisms and the incomplete data available for most of them. For this reason it is necessary to consider certain principal cases.

The purpose of the present examination is to analyse theoretically some aspects of the continuous ionic polymerization, carried out under heterogeneous conditions. A kinetic model is used with the following basic characteristics: the principal steps are initiation, propagation, and unimolecular termination; initiation is rapid; the average residence time is much longer than the average life of the growing macromolecules, i.e. active centres do not escape from the reactor; the average length of the material chain is great; a stationary state is established in the system; the polymer is obtained in the form of a solid disperse phase distributed in the dispersion medium; the reaction takes place under kinetic conditions and is first order with respect to the elementary particles. The model so described is based on experimental data obtained from the anionic polymerization of formaldehyde in the presence of triethylamine⁶⁻¹⁰. The model is comparatively simple and makes it possible to get an idea of the fundamental laws of the process, without leading to rather complicated equations, rendering the discussion difficult.

The basic kinetic scheme of polymerization may be written as follows.



where A is the monomer, C is catalyst, C* is the active centre, P is the polymer, *n* is the number of units.

We will now consider the capacity flow polymerization of a gaseous monomer in a gaseous phase. In general, the monomer concentration may vary by mixing with inert gas. (For instance, in this way it is possible to adjust the average molecular weight, while maintaining the molecular weight distribution.) Under the above-mentioned kinetic conditions the following equations hold:

$$\frac{dA}{dt} = \frac{v_1 A_0}{V} - k_A C^* A - \frac{v_2 A}{V} = 0 \quad (1)$$

$$\frac{dG}{dt} = \frac{v_1 G_0}{V} - \frac{v_2 G}{V} = 0 \quad (2)$$

Substituting the rate of catalyst consumption for the rate of formation of active centres (rapid initiation), and neglecting the escape of the active centres (small):

$$\frac{dC^*}{dt} = \frac{v_1 C_0}{V} - k C^* = 0 \quad (3)$$

Neglecting the small amounts of catalyst we may write the following concentration quantities:

$$A_0 + G_0 = A + G = s = \frac{p}{RT} \quad (4)$$

where *A*₀, *G*₀ and *A*, *G* are the concentrations of monomer and diluent at the inlet and in the reactor (at the outlet); *C*₀ and *C** are the concentrations of catalyst at the inlet and of the active centres in the reactor; *v*₁ and *v*₂ are the volume rates of the incoming and outgoing flow; *V* is the volume of the reactor; *k*_A and *k* are rate constants of the propagation and unimolecular termination of kinetic chains; *s* is total concentration of the gaseous substances; *p* is the atmospheric pressure; *T* is the absolute temperature; *R* is the gas constant. Dimensionless monomer concentration *A/s* in the reactor may be obtained from equations (1)–(4), as

follows:

$$\left(\frac{A}{s}\right)^2 - \left(1 + \frac{1}{\alpha}\right)\frac{A}{s} + \frac{1}{\alpha}\frac{A_0}{s} = 0 \quad (5)$$

where
$$\alpha = \frac{k_A C_0}{k} \quad (6)$$

The monomer conversion degree (relative polymer yield) q is determined from:

$$q = \frac{k_A C^* A}{(v_1/V)A_0}$$

and having applied equations (3) and (6), we obtain:

$$q = \frac{k_A C_0}{k} \cdot \frac{A}{A_0} = \alpha \frac{A}{A_0} \quad (7)$$

Figure 1 shows that A/s decreases while q increases with the growth of α . The possible values of the considered functions A/s and q are closed between the boundary curves:

$$\frac{A}{s} = 1 \text{ for } \alpha \leq 1 \text{ and } \frac{A}{s} = \frac{1}{\alpha} \text{ for } \alpha > 1, \text{ and for } \frac{A_0}{s} = 1$$

$$\frac{A}{s} = 0 \text{ for } \frac{A_0}{s} \rightarrow 0$$

$$q = \alpha \text{ for } \alpha \leq 1 \text{ and } q = 1 \text{ for } \alpha > 1, \text{ and for } \frac{A_0}{s} = 1$$

$$q = \frac{\alpha}{1 + \alpha} \text{ for } \frac{A_0}{s} \rightarrow 0$$

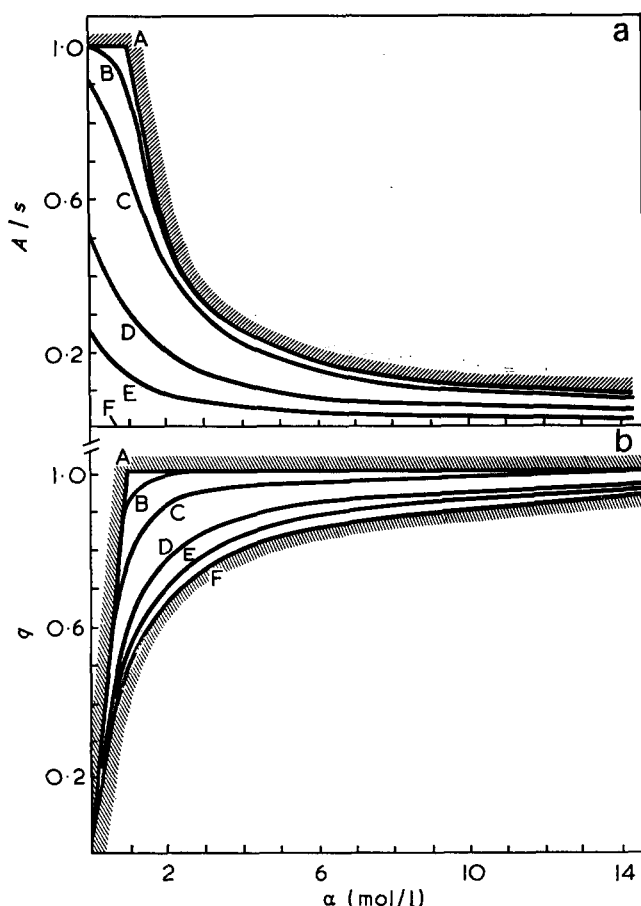


Figure 1 Dependence of (a) monomer concentration in the reactor and (b) the monomer conversion degree on catalyst concentration at the inlet with various A_0/s : A, 1; B, 0.99; C, 0.9; D, 0.5; E, 0.25; F, $A_0/s \rightarrow 0$

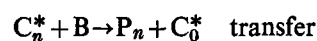
Catalyst concentration $C_0 = k/k_A$ corresponding to $\alpha = 1$ appears particular in the sense that, for $\alpha < 1$, always $q < 1$, while for all $\alpha > 1$, $A/s < 1$. The physical meaning of $A/s < 1$ for $A_0/s = 1$ (when diluent is absent) is that pressure in the reactor remains equal to atmospheric pressure, i.e. s does not change as a result of the inert gas coming back through the outlet. For $\alpha = 1$, the ratio $q(A/s=1)/q(A/s \rightarrow 0)$ is maximal and equals 2.

Since the average sizes of polymer molecules are determined by the unimolecular death of the active centre the number-average degree of polymerization \bar{r} is expressed by:

$$\bar{r} = \frac{k_A A}{k}$$

i.e. it behaves as A , namely, it is reduced by increasing α and by decreasing A_0/s . q and \bar{r} have simultaneously maximum values only for $\alpha = 1$. This result is quite essential for the synthesis of polymers from a gaseous monomer.

Let a kinetic chain-transfer agent B take part further in the process, i.e. there occurs, apart from reactions (I)–(III), a



where C_0^* is the newly formed active centre which does not contain monomer units. Besides, poly-, oligo- and telo-merization are possible. The complex reaction is described in equations (1)–(3), by the relation for the chain-transfer agent:

$$\frac{dB}{dt} = \frac{v_1 B_0}{V} - k_B C^* B - \frac{v_2 B}{V} = 0 \quad (8)$$

and by the new concentration balance:

$$A_0 + G_0 + B_0 = A + G + B = s = \frac{P}{RT} \quad (9)$$

where B_0 and B are the concentrations of the chain-transfer agent at the inlet and in the reactor; k_B is the rate constant of the chain-transfer to B. Using equations (1)–(3), (8) and (9), we obtain the following system of two square equations with variables A and B , represented for convenience in our further analysis, as follows:

$$A = \frac{A_0 - \alpha A}{1 - \alpha A/s - \beta B/s} \quad (10)$$

$$B = \frac{B_0 - \beta B}{1 - \alpha A/s - \beta B/s} \quad (11)$$

where

$$\beta = \frac{k_B}{k} C_0$$

The following two cubic equations are equivalent to this system:

$$\begin{aligned} (\alpha^2 - \alpha\beta) \left(\frac{A}{s}\right)^3 + \left(\beta - \alpha - \frac{\alpha A_0}{s} - \frac{\beta B_0}{s} + \alpha\beta - \alpha^2\right) \left(\frac{A}{s}\right)^2 + \\ \left(\frac{A_0}{s} + \frac{2\alpha A_0}{s} - \frac{\beta A_0}{s}\right) \frac{A}{s} - \left(\frac{A_0}{s}\right)^2 = 0 \quad (12) \end{aligned}$$

$$\begin{aligned} (\beta^2 - \alpha\beta) \left(\frac{B}{s}\right)^3 + \left(\alpha - \beta - \frac{\alpha A_0}{s} - \frac{\beta B_0}{s} + \alpha\beta - \beta^2\right) \left(\frac{B}{s}\right)^2 + \\ \left(\frac{B_0}{s} + \frac{2\beta B_0}{s} - \frac{\alpha B_0}{s}\right) \frac{B}{s} - \left(\frac{B_0}{s}\right)^2 = 0 \quad (13) \end{aligned}$$

A particular case of practical importance is the condition where the chain-transfer agent reacts much more slowly than the monomer, i.e. $B_0 \ll A_0$ or $k_B \ll k_A$ (for instance, chain-transfer occurs owing to the impurity or to the molecular weight regulator). Then the terms $\beta B/s$ in equations (10) and (11) may be neglected. Besides, simplification of the relation for A coincides with equation (5), and for B takes the form:

$$B = \frac{B_0}{1 - \alpha A/s + \beta} \quad (14)$$

As far as q is concerned, equation (4) holds, i.e. the magnitude depends only on the inflow of A and C . When the molecular weight is controlled by the chain-transfer reaction, \bar{r} is expressed by:

$$\bar{r} = \frac{k_A A}{k_B B}$$

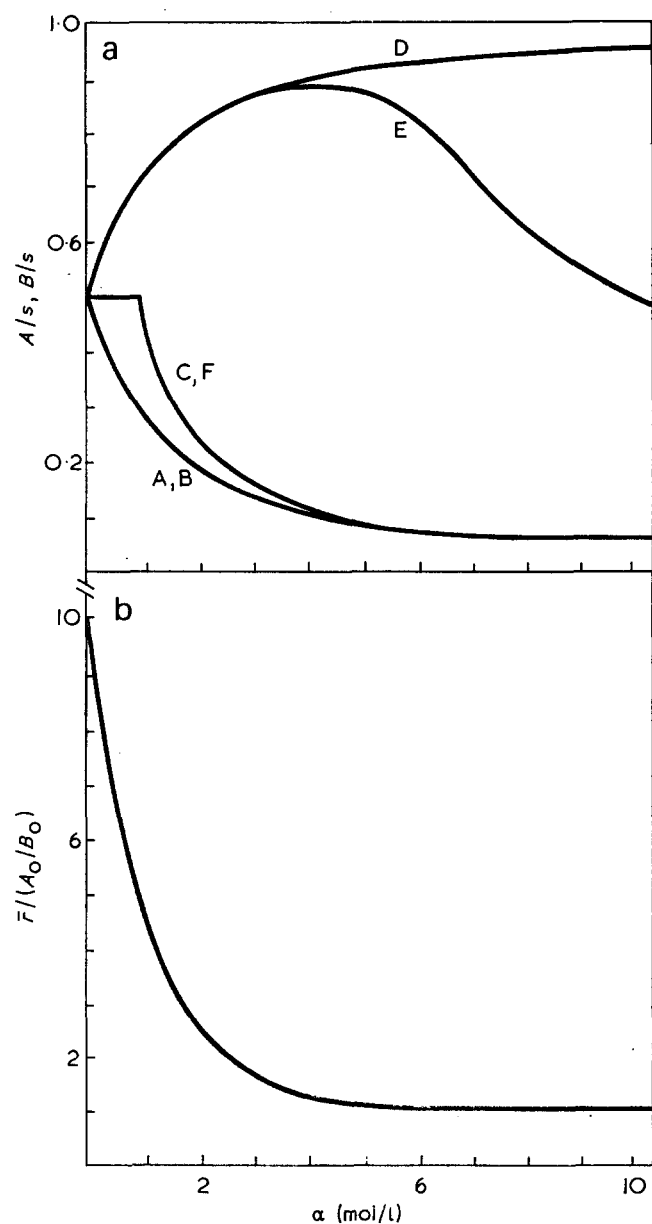


Figure 2 Dependence of (a) monomer (A-C) and the chain-transfer agent (D-F) concentration in the reactor and of (b) the polymer number-average degree of polymerization on catalyst concentration at the inlet with $A_0/s = B_0/s = 0.5$ and various k_B/k_A : A, D, 0; B, E, 0.1; C, F, 1 and (b) 0.1; the curves A, B and C, F coincide

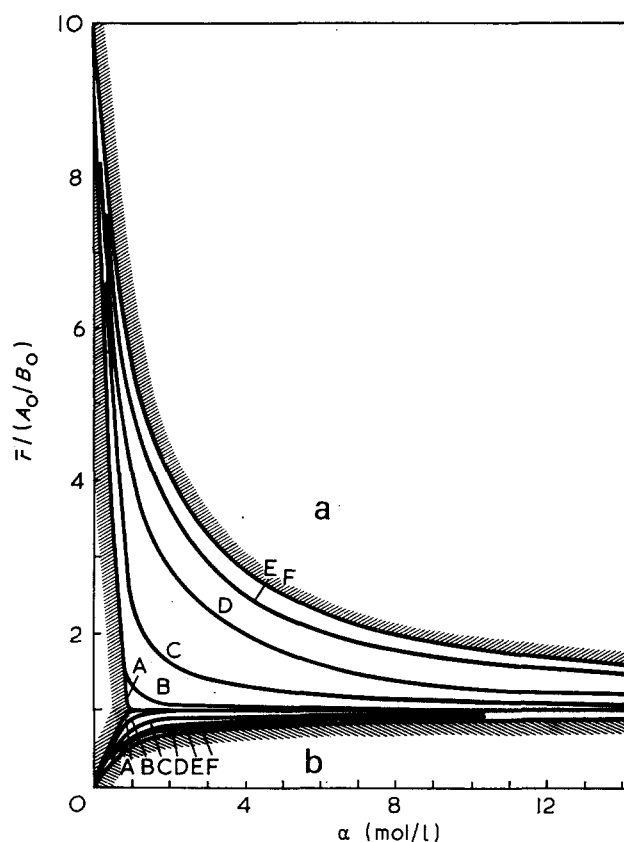


Figure 3 Dependence of the polymer number-average degree of polymerization on catalyst concentration at the inlet with small expenditure of the chain-transfer agent and various k_B/k_A : (a) 0.1; (b) 10. A_0/s : A, 1; B, 0.99; C, 0.9; D, 0.5; E, 0.25; F, $A_0/s \rightarrow 0$

and varies in the range $\bar{r} \rightarrow k_A A_0/k_B B_0$ for $\alpha \rightarrow 0$, and $\bar{r} \rightarrow A_0/B_0$ for $\alpha \rightarrow \infty$.

Figure 2 shows the change of A/s , B/s and of the relative magnitude $\bar{r}/\bar{r}(\alpha \rightarrow \infty) = \bar{r}/(A_0/B_0)$ (more convenient for analysis than \bar{r}) with respect to α , calculated according to the exact equations (12) and (13) in the example of equal concentrations of the monomer and of the chain-transfer agent. When $\beta/\alpha = k_B/k_A < 1$, with the growth of α , B/s assumes a maximum, while \bar{r} decreases. Figure 3 gives the graphs $\bar{r}/(A_0/B_0)$ against α which are constructed with the help of the simplified equations (5) and (14). We can see that when α increases \bar{r} decreases for $k_B/k_A < 1$ (the monomer has a higher reactivity than the chain-transfer agent), or increases for $k_B/k_A > 1$ (impurity is more active than A). The boundary curves are given by the expressions:

$$\frac{\bar{r}}{A_0/B_0} = \frac{\beta/\alpha}{1 + \beta - \alpha} \quad \text{for } \frac{A_0}{s} = 1$$

$$\frac{\bar{r}}{A_0/B_0} = \frac{\beta}{\alpha} \cdot \frac{\alpha + 1}{\beta + 1} \quad \text{for } \frac{A_0}{s} \rightarrow 0$$

If the monomer, being fed to the flow reactor with ideal mixing, is liquid, and the heterogeneous polymerization takes place in a liquid phase, then the kinetic equations for the elementary particles are analogous to equations (1)-(3). The quantities for balancing are different from equation (4). For the liquid phase of the polymer system it is possible to write, neglecting the

insignificant contraction or dilatation:

$$aA_0 + lL_0 = aA + lL = 1 \quad (15)$$

where a and l are the molar volumes of the monomer and diluent, L_0 and L are the concentrations of diluent at the inlet and in the reactor. On the basis of equations (1)–(3), and (15) we arrive finally at:

$$A^2 - \left(1 + \frac{1}{\alpha}\right) \frac{A}{a} + \frac{A}{\alpha a} = 0 \quad (16)$$

This equation (16) for A is of the same type (with coefficients depending on α), as is equation (5), obtained for the gaseous monomer. Here, in fact, with the increase of α processes up to such values of q take place, that the fluidity of the reaction mass is kept sufficiently great

and it becomes possible for the reaction mass to be mixed and moved.

REFERENCES

- 1 Jenkins, A. D. *Polymer* 1960, **1**, 79
- 2 Lui, S. and Amundson, N. R. *Z. Elektrochem.* 1961, **65**, 276
- 3 Bero, M. and Laszkowski, M. *Faserforsch. Textiltech.* 1966, **17**, 8
- 4 Bero, M. *Kinet. Katal.* 1970, **11**, 1123
- 5 Litmanovich, A. D. and Agasandjan, V. A. *Kinet. Katal.* 1966, **7**, 2
- 6 Penchev, P. I., Ivanov, V. V. and Enikolopyan, N. S. *Dokl. Akad. Nauk SSSR* 1969, **188**, 145
- 7 Penchev, P. I., Ivanov, V. V. and Enikolopyan, N. S. *Dokl. Akad. Nauk SSSR*, 1969, **188**, 395
- 8 Penchev, P. I., Ivanov, V. V. and Enikolopyan, N. S. *Vysokomol. Soedin. (A)* 1970, **12**, 329
- 9 Fr. Pat. 1 291 999
- 10 Bulg. Pat. 939 369

Preparation, thermal characterization and tribological evaluation of some polyquinazolinediones and polyquinazolones

A. Ghafoor, J. M. Senior, R. H. Still and G. H. West

*Department of Polymer and Fibre Science, University of Manchester Institute of Science and Technology, Manchester M60 1QD, UK
(Received 21 December 1973)*

The preparation of a series of pre-polymers by solution polycondensation of 4,4'-diaminodiphenyl-3,3'-dicarboxylic acid (BDC) and di-isocyanates, and the melt polycondensation of BDC and diacetyl derivatives of aromatic diamines is described. These pre-polymers have been characterized and cyclized to yield polyquinazolinediones and polyquinazolones whose structures and thermal stabilities have been investigated. The physical characteristics of films made from these materials were determined after cyclization, and friction and wear characteristics of composite films containing polytetrafluoroethylene, lead oxide and graphite were evaluated in a journal bearing bush configuration. The relationship between wear behaviour and polymer structure, thermal stability and physical properties is discussed.

INTRODUCTION

The work described stems from the desire to prepare polymers of greater temperature stability than those in current use for low wear coating compositions. Epoxy polymers are examples of materials in commercial use and the compositions frequently contain polytetrafluoroethylene (PTFE), graphite and/or lead oxide. It has been found¹ that the limited stability of the epoxy at temperatures greater than 130°C contributes to the poor wear properties at high *PV* ratings or elevated temperatures and in order to improve the wear under these conditions it is necessary to employ a polymer of greater temperature stability than an epoxy. In these formulations the polymer can be considered as a binder material for the other components which are thought to function as transfer film-forming materials and hence in addition to tempera-

ture stability the polymer-additive adhesive bond may be important. The influence of additive composition on wear is the subject of another paper and in the work described the influence of the polymer binder or matrix is determined at a fixed optimum additive composition².

The choice of polyquinazolinediones and polyquinazolones as the matrix material was based on their reported temperature stability^{3,4}, ease of preparation, and their ability to be fabricated in a pre-polymer stage. The latter is important as it enables coatings to be formed by spraying or casting methods on metal substrates relatively easily and these can be converted to the more thermally stable cyclized form by heating. This is a much more simple operation than plasma spraying or high pressure sintering techniques which are the only methods available for the fabrication of some high temperature polymers.

PREPARATION AND CHARACTERIZATION

EXPERIMENTAL

Reaction of BDC with di-isocyanates

BDC (4,4'-diaminodiphenyl-3,3'-dicarboxylic acid) was prepared as the dihydrochloride from *o*-nitrobenzoic acid by the method of Kurihara and Yoda⁵. Free BDC was obtained by suspending the hydrochloride in excess distilled water. The suspension was centrifuged and the BDC so obtained was resuspended several times in distilled water. BDC was finally obtained by filtration at the pump. It was further purified by washing with hot distilled water until the filtrate was free from chloride ion. Finally, the yellow BDC was washed with methanol

and dried under vacuum at 70°C and 3 mmHg (m.p. 299°C).

Commercially available hexamethylene di-isocyanate was dried over anhydrous sodium sulphate and stored over molecular sieves but was used without further purification. Methylene di-*p*-phenylene di-isocyanate was purified by recrystallization from *n*-hexane (m.p. 41–42°C). Triethylamine was purified by distillation. Solution polymerization of BDC and methylene di-*p*-phenylene di-isocyanate was effected by the method previously described by Yoda⁶ yielding the pre-polymer, poly(urea acid)_A, $[\eta]_0 = 0.33$ in *N*-methylpyrrolidone at 25°C. Calculated for poly(urea acid), $[I_A, (C_{29}H_{22}N_4O_6)_n]$:

C, 66.66%; H, 4.23%; N, 10.73%; O, 18.37%. Found: C, 62.80%; H, 4.80%; N, 10.00%.

Yoda's method was also used for hexamethylene di-isocyanate. BDC (5.46 g) and triethylamine (4.02 g) were dissolved in *N*-methylpyrrolidone (100 ml) and hexamethylene di-isocyanate (3.36 g) was added dropwise with stirring over a period of 2 h at room temperature. The clear solution so obtained was dropped into an excess of aqueous hydrochloric acid with vigorous stirring. The white powder obtained was filtered, washed with water and methanol and finally dried at 78°C and 0.5 mmHg. The pre-polymer, poly(urea acid)II_A so obtained was soluble in *N*-methylpyrrolidone, dimethyl sulphoxide, and dimethylacetamide. The pre-polymer solution in *N*-methylpyrrolidone gave a tough transparent film when dried at 100–120°C for 1 h. Calculated for poly(urea acid) [II_A, (C₂₂H₂₄N₄O₆)_n]: C, 59.99%; H, 5.49%; N, 12.72%; O, 21.80%. Found: C, 58.50%; H, 6.20%; N, 12.60%. It had $[\eta]_0 = 0.19$ in *N*-methylpyrrolidone at 25°C.

Reaction of BDC with diacetamide compounds

Diacetamido derivatives of 4,4'-diaminodiphenyl methane (m.p. 226–227°C), 4,4'-diaminodiphenyl ether (m.p. 220°C) [calculated for (C₁₆H₁₆N₂O₃): C, 68.10%; H, 5.80%; N, 10.03%; O, 16.07%. Found: C, 69.01%; H, 5.63%; N, 9.86%], 4,4'-diaminodiphenyl sulphone (m.p. 285°C) and 4,4'-diaminodiphenyl disulphide (m.p. 208°C) were prepared by acetylation with acetic anhydride in aqueous suspension.

Polymerization of equimolecular quantities of powdered BDC and the diacetamido compound was effected under nitrogen in the melt phase at 230–240°C for 1 h. The polymer was cooled to room temperature in dynamic nitrogen and then the solid glass was freed from the polymerization tube by cooling in liquid nitrogen. This method yielded: (a) Pre-polymer I_B from BDC and 4,4'-diacetamidodiphenyl methane as a pale yellow glass, $[\eta]_0 = 0.045$ in *N*-methylpyrrolidone at 25°C. Calculated for I_B, (C₃₁H₂₆N₄O₄)_n: C, 71.80%; H, 5.05%; N, 10.81%; O, 12.34%. Found: C, 70.60%; H, 5.40%; N, 11.50%. (b) Pre-polymer II_B from BDC and 4,4'-diacetamidodiphenyl ether as a pale yellow glass, $[\eta]_0 = 0.040$ in *N*-methylpyrrolidone at 25°C. Calculated for II_B, (C₃₀H₂₄N₄O₅)_n: C, 69.22%; H, 4.65%; N, 10.76%; O, 15.37%. Found: C, 67.30%; H, 5.70%; N, 10.40%. (c) Pre-polymer III_B from BDC and 4,4'-diacetamidodiphenyl sulphone as a greenish yellow glass, $[\eta]_0 = 0.038$ in *N*-methylpyrrolidone at 25°C. Calculated for III_B, (C₃₀H₂₄N₄O₄S)_n: C, 63.37%; H, 4.25%; N, 9.85%; O, 16.88%; S, 5.64%. Found: C, 63.30%; H, 5.10%; N, 10.00%; S, 5.40%. (d) Pre-polymer IV_B from BDC and 4,4'-diacetamidodiphenyl disulphide as a dark amber glass, $[\eta]_0 = 0.034$ in *N*-methylpyrrolidone at 25°C. Calculated for IV_B, (C₃₀H₂₄N₄O₄S₂)_n: C, 63.36%; H, 4.25%; N, 9.85%; O, 11.25%; S, 11.28%. Found: C, 62.20%; H, 5.10%; N, 10.10%; S, 10.90%.

Cyclization of the pre-polymers

Pre-polymers I_A and II_A were cast as films on to glass plates and heated from room temperature to 180°C in 10 min and maintained at this temperature for 1 h in a nitrogen atmosphere. The temperature was then raised to 250°C in 10 min and then maintained at this tempera-

ture for a further hour. The resulting hard black films were insoluble in *N*-methylpyrrolidone and gave the following elemental analyses. Calculated for the polyquinazolinedione I_A, (C₂₉H₁₈N₄O₄)_n: C, 71.80%; H, 3.73%; N, 11.52%; O, 13.16%. Found: C, 71.40%; H, 4.70%; N, 11.90%. Calculated for the polyquinazolinedione II_A, (C₂₂H₂₀N₄O₄)_n: C, 65.33%; H, 4.99%; N, 13.86%; O, 15.83%. Found: C, 62.30%; H, 5.00%; N, 12.10%.

Pre-polymer films from polymers I_B–IV_B were heated from room temperature to 280°C in 10 min and maintained at this temperature for 2 h in a nitrogen atmosphere. The resulting polyquinazolones were obtained as hard black films which gave the following elemental analyses. Calculated for polyquinazolone I_B, (C₃₁H₂₂N₄O₄)_n: C, 77.16%; H, 4.60%; N, 11.61%; O, 6.63%. Found: C, 78.10%; H, 4.30%; N, 11.90%. Calculated for polyquinazolone II_B, (C₃₀H₂₀N₄O₃)_n: C, 74.37%; H, 4.16%; N, 11.57%; O, 9.91%. Found: C, 75.40%; H, 4.70%; N, 11.30%. Calculated for polyquinazolone III_B, (C₃₀H₂₀N₄O₄S)_n: C, 67.65%; H, 3.79%; N, 10.52%; O, 12.02%; S, 6.02%. Found: C, 67.80%; H, 4.50%; N, 10.80%; S, 5.80%. Calculated for polyquinazolone IV_B, (C₃₀H₂₀N₄O₂S₂)_n: C, 67.65%; H, 3.79%; N, 10.52%; O, 6.01%; S, 12.04%. Found: C, 64.80%; H, 4.20%; N, 10.40%; S, 10.70%.

Preparation of model compounds

2-Methylbenzoxazone was prepared by the method of Zentmyer and Wagner⁷ and recrystallized from benzene (m.p. 80–81°C). Acetamidobenzanilide was prepared by heating 2-methylbenzoxazone (3.04 g) with redistilled aniline (1.06 g) for 3 h on a steam bath. The product was recrystallized from a 3:1 v/v mixture of ethyl acetate and *n*-hexane (m.p. 115°C). Calculated for C₁₅H₁₄N₂O₂: C, 70.80%; H, 5.47%; N, 11.00%; O, 12.93%. Found: C, 71.20%; H, 5.40%; N, 10.90%. 3-Phenyl-2-methyl-4-ketoquinazoline(3-phenyl-2-methylquinazolone) was prepared from acetamidobenzanilide by heating it at 240–250°C for 30 min. The cooled melt was dissolved in hot ethylacetate and *n*-hexane was added until precipitation occurred. The suspension was chilled and the product was obtained by filtration. The crystals were washed with 10% aqueous ammonia and recrystallized from ethyl acetate (m.p. 137°C). Calculated for C₁₅H₁₂N₂O: C, 76.60%; H, 5.20%; N, 11.40%; O, 6.80%. Found: C, 75.90%; H, 5.10%; N, 11.20%.

Thermal analysis

Studies were made using thermogravimetry (t.g.) and differential scanning calorimetry (d.s.c.).

Dynamic t.g. was carried out in a convected air atmosphere using a Stanton decimilligramme thermobalance (Model TRO1) with the furnace programmed for a heating rate of 6°C/min (nominal). Samples (10 mg) were contained in a platinum crucible (12 mm o.d. × 8 mm high).

Isothermal t.g. studies were made on the polymers by the following method. The furnace was pre-heated to the required temperature without the crucible in place on the rise rod. The furnace was then raised, the sample was placed in position, the furnace was lowered and the weight loss was recorded. A convected air atmosphere was used and sample weights and the crucible were those previously described above. All temperatures quoted are

furnace wall temperatures. D.s.c. studies were made on a Dupont 900 Thermal analyser with a d.s.c. attachment. Samples were contained in open aluminium pans and an open pan acted as the reference. A heating rate of 20°C/min and a sample size of ≈ 6 mg was employed for studies in a convected air atmosphere.

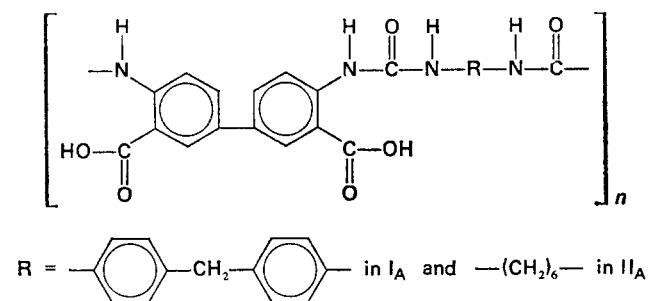
Infra-red spectroscopy

Spectra of the model compounds, the pre-polymers and cyclized polymers were obtained from 2% suspensions in potassium bromide using a Unicam SP200 spectrophotometer.

DISCUSSION

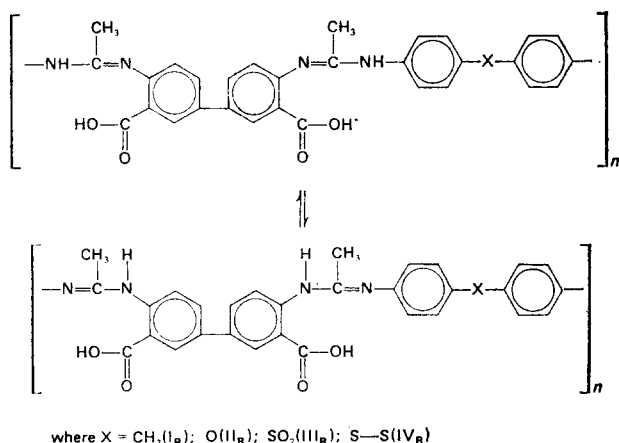
Preparation of the pre-polymers

Poly(urea acid) I_A was prepared by the method previously reported by Yoda⁶ and gave essentially the same spectra and elemental analysis. Poly(urea acid)II_A had not been previously reported but its spectrum (Figure 1 (A)) and elemental analysis are in accord with the structure:



Pre-polymers I_B-IV_B are new compounds and the spectra [Figure 2 (A)] show absorptions at 3300, 1540 and 1640 cm⁻¹ for the $-NH-C=N-$ grouping, 1680 cm⁻¹ for the carbonyl group of the aromatic acid and 3100 cm⁻¹ ($-OH$ of acid). In addition absorptions at 1190, 1285 and 1340 cm⁻¹ indicated the presence of C-N stretching in the $-C_6H_4-N-$ unit.

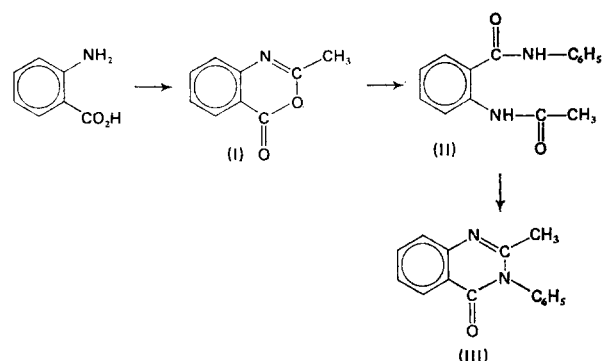
This information together with the elemental analysis data is consistent with the tautomeric structure for the pre-polymers shown below:



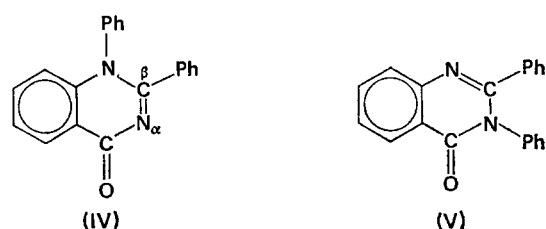
No attempts were made to determine absolute molecular weights for the pre-polymers because of the exotic nature of solvents in which they could be dissolved.

Preparation and spectra of model compounds

3-Phenyl-2-methyl-quinazolone (III) was prepared from anthranilic acid by the route:



The elemental analysis and the i.r. spectrum (Figure 3 (A)) are in accord with the proposed structure. Hagiwara and coworkers⁸ have found that the position of the carbonyl absorption for the isomeric diphenyl quinazolones depends on whether the carbonyl group is conjugated with the C=N grouping as in compound IV or in a $\beta\gamma$ position as in compound V:

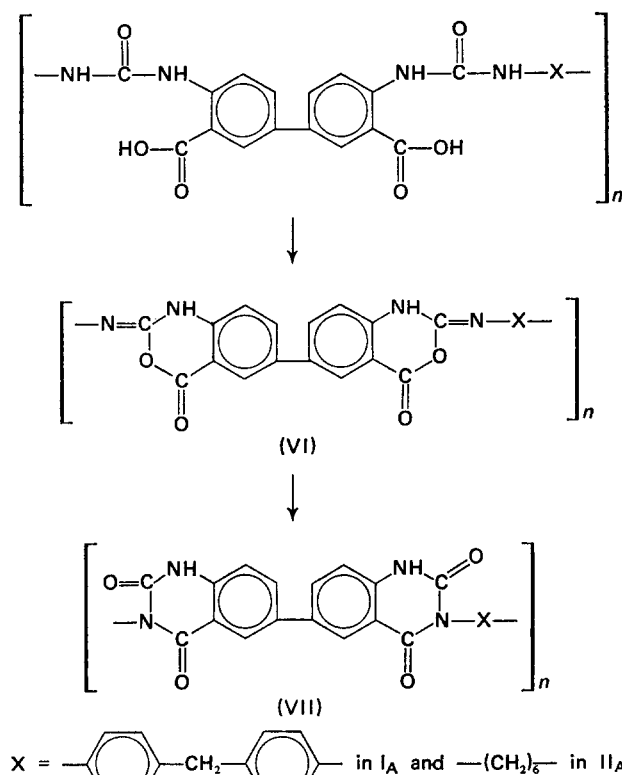


Carbonyl absorption in IV occurred at 1649 cm⁻¹ and in V at 1679 cm⁻¹. In the model compound III the C=O absorption occurs at 1680 cm⁻¹ confirming the proposed structure III. This spectra was used to establish the nature of the cyclized polymers I_B-IV_B. The spectra of 2-methylbenzoxazinone (I) [Figure 3 (B)] was used to evaluate the course of cyclization of pre-polymers I_A and II_A.

Cyclization of pre-polymers

D.s.c. and t.g. studies showed that the pre-polymers were stable to 300°C and that cyclodehydration was best effected in nitrogen or *in vacuo*. D.s.c. studies on pre-polymers I_A and II_A showed baseline shifts ascribable to the glass transition followed by three endothermic processes which have been ascribed as shown in Table 1 by complementary studies using hot-stage microscopy and i.r. spectroscopy. Kurihara and coworkers⁹ have shown that cyclization for I_A occurs in two distinct stages via the intermediate formation of the polyiminobenzoxazinone (VI).

This has been confirmed by heating II_A at 180°C which yielded a compound having the i.r. spectrum shown in Figure 1(B) where it is compared to that of the pre-polymer [Figure 1(A)]. It can be seen that the C=O absorption at 1670 cm⁻¹ is lost and a new lactone C=O is formed at 1770 cm⁻¹ together with absorptions for C-N at 1644 cm⁻¹, $-N=C-O-C-$ at 1250 cm⁻¹ and $-C-O-C-$ at 1060 cm⁻¹ similar to those observed for the model compound 2-methylbenzoxazinone [Figure



3(B). After heating to 250°C the i.r. spectrum [Figure 1(C)] was obtained which indicates the formation of the quinazolinedione structure⁶ by absorption at 1730 and 1650 cm⁻¹ due to 4-carbonyl and 2-carbonyl groups of quinazolinedione.

Pre-polymer I_A was shown to behave in a similar manner.

However, the elemental analyses and the spectra indicate that cyclization is not complete in these polymers. Pre-polymers I_B-IV_B behaved similarly on d.s.c. showing 3 endothermic peaks but cyclodehydration occurred above the *T_m* and was not followed by a subsequent structural rearrangement as with polymers of the A series. The basic features of the thermograms are shown in Table 1. In Figure 2 the spectra of a representative polymer of the B series (I_B) is shown as pre-polymer (A); cyclized polymer (B) which may be compared with the model compound 3-phenyl-2-methyl-4-ketoquinazoline [Figure 3(A)]. From these spectra it can be seen that the conversion to the quinazolone is not quantitative as is evidenced by the incomplete removal of -NH absorption. In addition the different extents to which cyclization occurs under the stated conditions is reflected in the elemental analysis data.

Thermal stability studies

T.g. studies were made in air to simulate the bearing running condition. Preliminary studies were made on the pre-polymers to establish the temperature range for cyclodehydration and for degradation. All the pre-polymers studies gave thermograms showing a three process weight loss curve. There was a primary weight loss process whose onset temperature was defined as procedural decomposition temperature 1 (*PDT* 1) which was followed by a region of zero or very low weight loss. This 'stable' region was then followed by catastrophic degradation whose onset temperature was defined as *PDT* 2. The *PDT* data obtained are shown in Table 2.

The weight loss which occurred during the primary weight loss process was always higher than that required for quantitative cyclodehydration. This indicates that there is loss of some monomeric or oligomeric species, or that oxidative degradation occurs during cyclization. That the former explanation is correct is shown by the observation that cyclization on the thermobalance in dynamic nitrogen atmosphere affords an equivalent % weight loss in this temperature range. The *PDT* 2 values observed are always higher than the *PDT* values observed for the cyclized polymers (Table 3). This is due to the difference in sample size and form of the cyclized materials. The polymer cyclized in bulk in the crucible will have a lower surface area than that cyclized as a film and subsequently run on the thermobalance as a powder. This will significantly influence the rate of oxidative degradation leading to volatile products and hence alter the *PDT* observed. The *PDT* 1 and *PDT* 2

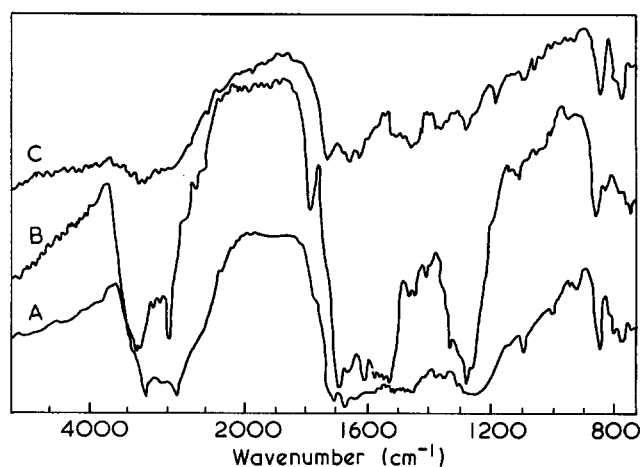
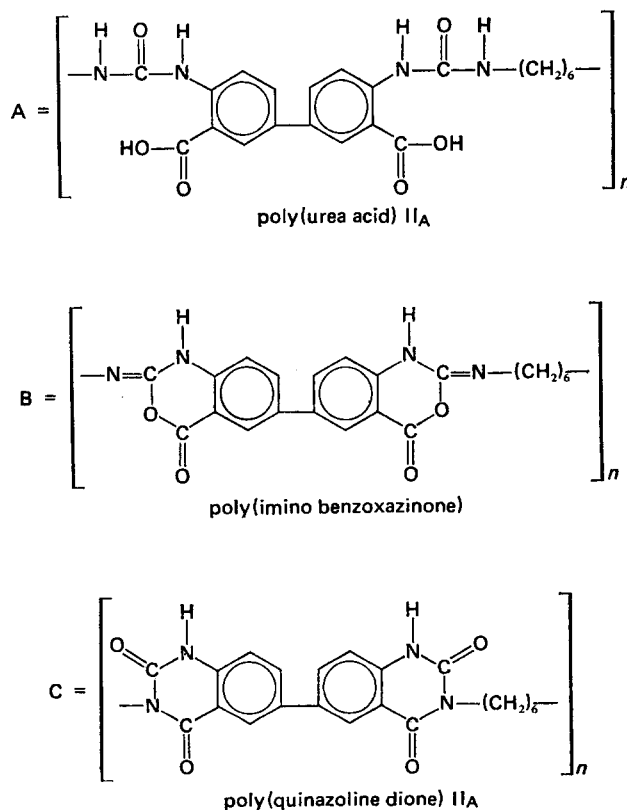


Figure 1 Infra-red spectra of polyquinazolinedione II_A and its pre-polymers



values obtained suggested that cyclization was best affected at temperatures below 300°C in either an inert atmosphere or *in vacuo*. For ease of preparation, the bearings studied later in this paper were cyclized in a nitrogen atmosphere after spin-casting. Thus, in order that thermal stabilities could be measured on comparable materials laboratory cyclizations were also made in a nitrogen atmosphere.

The thermal stabilities of the polymers have been assessed in terms of the following parameters. The PDT and the 50% decomposition temperature (50% DT) have been obtained from dynamic t.g. experiments (Table 3). Isothermal t.g. experiments have yielded the time for 50% decomposition (50% D) at various temperatures and the weight loss in 30 min (W30) at 400°C (Tables 4 and 5). The t.g. behaviour of representative samples of polymers from the A and B series are shown in Figure 4 where they are compared to poly(phenylene sulphide) and Ekonol [poly(*p*-hydroxybenzoic acid), Carborundum]. The cyclized polymers were found to have similar stabilities to the commercially available materials as assessed by dynamic thermogravimetry. However, these commercial polymers, with the exception of poly(phenylene sulphide) had other features which prevented their

Table 1 Thermal characterization of pre-polymers

Polymer	T_g (°C)	T_m (°C)	CD (°C)	DT (°C)
IA	52	180*	180-250†	425
IIA	50	170*	170-250†	350
IB	30	64	250-300	450
IIIB	23	46	250-325	350
IIIIB	30	72	250-300	400
IVB	30	72	260-320	400

CD=Cyclodehydration; DT=decomposition temperature

* Melting accompanied by dehydration

† Rearrangement of structure

Table 2 Procedural decomposition temperatures for pre-polymers

Pre-polymer	PDT 1 (°C)	PDT 2 (°C)
IA	120	325
IIA	140	340
IB	220	350
IIIB	220	360
IIIIB	140	300
IVB	220	360

Table 3 PDT and 50% DT values for polymers in air

Commercially available high temperature polymer	Source	PDT (°C)	50% DT (°C)	Cyclized polymer	PDT (°C)	50% DT (°C)
Polybenzimidazole* (Imidite 2801)	Whittaker Corporation (USA)	310	550	IA	320	520
Polybenzoxazole* (PBO3)	Yorkshire Chemicals	360	550	IIA	300	494
				IB	305	525
Polyimide* (QX-13)	RAE Farnborough	380	580	IIIB	280	520
Polyimide (Keramid 601)	Societe des Usine Chimique	380	550	IVB	290	525
Poly(phenylene sulphide) (Ryton)	Phillips Petroleum (UK)	410	580			
Ekonol	Carborundum	340	524			
Ekonol (plasma sprayed)	Carborundum	340	487			

* Cured samples

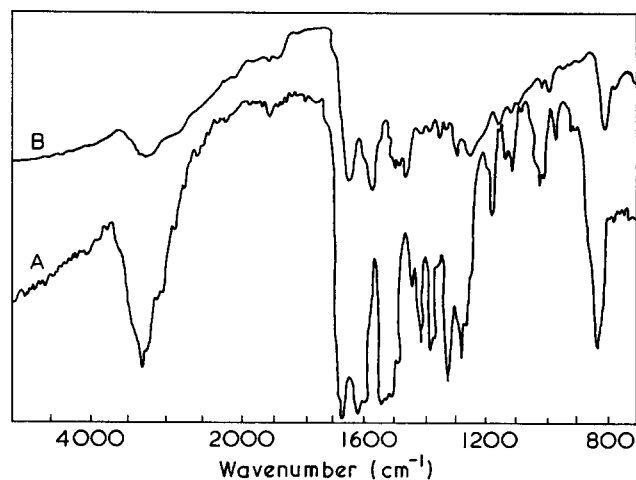


Figure 2 I.r. spectra of polyquinazolone IB and its prepolymer

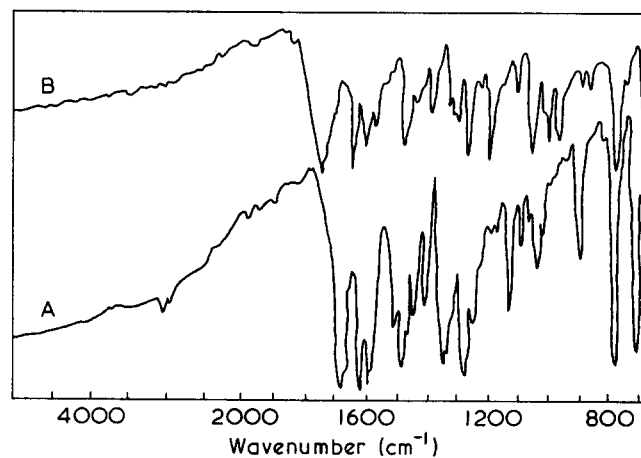
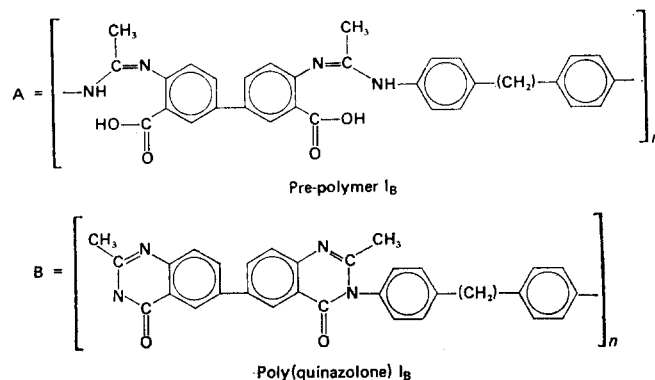


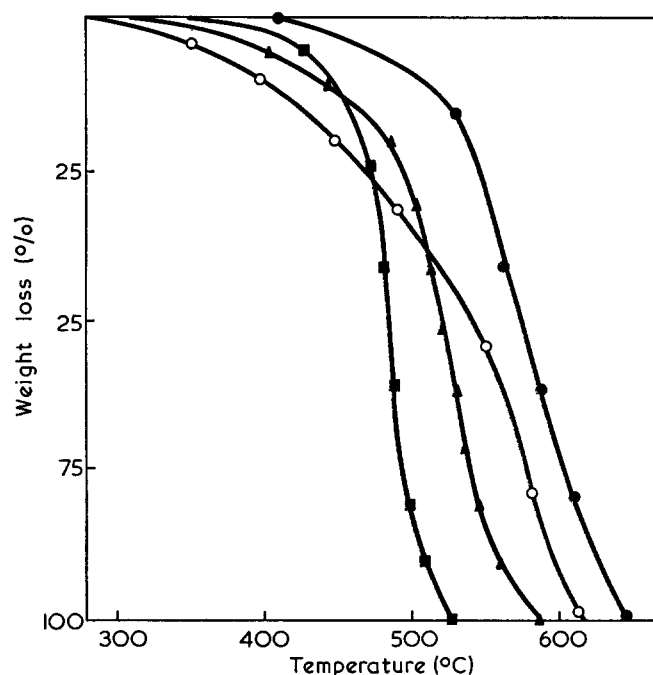
Figure 3 Infra-red spectra of model compounds: A, 3-phenyl-2-methyl-4-ketoquinazolone; B, 2-methylbenzoxazone

Table 4 % Weight loss of cyclized polymers in 30 min at 400°C in air

Polymer	I _A	II _A	I _B	II _B	III _B	IV _B
W30	31	61	28	31	42	30

Table 5 Time for 50% decomposition in air for cyclized polymers

Cyclized polymer	50% decomposition time (min) at stated isothermal temperature			
	375°C	400°C	425°C	450°C
I _A	240	55	46	17
II _A	200	20	18	12
I _B	235	89	40	30
II _B	150	61	33	25
III _B	130	55	35	29
IV _B	230	81	56	45

Figure 4 Thermograms in static air. ●, Poly(phenylene sulphide); ■, Ekonol; ▲, polyquinazolinedione I_A; ○, polyquinazolone I_B

use as bearing materials. These features include the difficulty in fabrication of Ekonol which could be plasma sprayed on a flat surface but proved impossible to coat on the inside of a bearing bush. In addition as can be seen from Table 3 plasma spraying reduces the thermal stability of the polymer. Polymers 1-4 yielded poor bearings by the spray casting technique employed in this study which were not amenable to testing.

In order to attempt to further thermally characterize polymers of the A and B series, isothermal weight loss studies were made and the data are presented in Tables 4 and 5. The results shown in Table 5 for 50% D, W30, PDT and 50% DT indicate that polymer I_A is more thermo-oxidatively stable than polymer II_A. This is to be expected since in I_A the heterocyclic unit of the quinazolinedione is linked by *p*-phenylene units separated by a methylene grouping, whereas in polymer II_A the linking unit is a fully aliphatic $-(CH_2)_6-$ chain which is more susceptible to thermo-oxidative attack.

Polymers I_B-IV_B differ only in the nature of the 'hinge grouping' ($-X-$) in the structure (see above), and the following order of stability of the 'hinge group' in air is apparent from the above results: $-CH_2->-O->-S_2->-SO_2-$. This result may be compared with those from other workers on polyimides whose only structural differences are similar 'hinge groupings' to those studied above. The following orders of stability have been reported in air: $-O->-S->-CH_2-$ (Bower and Frost¹⁰); $-O->-CH_2-$ (Sroog *et al.*¹¹); $-O->-CH_2->-SO_2-$ (Nishizaki¹²); and $-S->-SO_2->-CH_2->-O-$ (Dine-Hart and Wright¹³). Dine-Hart and Wright¹³ have reviewed the above work and have ascribed the apparent lack of correlation between workers to differences in preparative conditions which may have resulted in the presence of low molecular weight species; differences in environmental conditions during degradation, and differences in the mode of assessment. Thus, it is not surprising that the results in this study do not correlate exactly with previous workers, since no attempts were made to remove low molecular weight materials. The polymers studied contain different heterocyclic units and the percentage cyclization in the B series of polymers differs from polymer to polymer.

PHYSICAL PROPERTIES OF CURED POLYMER FILMS

EXPERIMENTAL

The hardness, ductility and thermal diffusivity of the cured polymer films were measured as these properties assume major significance when the material is employed as a bearing surface. In addition, hardness measurements were employed to determine the thermal mechanical ageing of the polymers.

Hardness measurements were conducted at room temperature using an ICI Pneumatic Micro-indentation Apparatus¹⁴. The penetration of a 1.6 mm diameter needle into a 0.18 mm thick cyclized polymer layer deposited on a stainless-steel disc was measured under a load of 8 g. After 72 sec the load was removed and the viscoelastic recovery of the film was observed. Total

penetration (h), elastic recovery (E) and permanent deformation (η) were recorded. For the six polymers tested values of h are shown in Table 6 and h , E and η are plotted in Figure 5. Also shown in Figure 5 are the values obtained after ageing the films at various temperatures for 100 h in an air-circulating oven.

Ductility measurements designed to complement the hardness tests were conducted with a 0.15 mm thick polymer film deposited on the 4 mm wide neck of a dumbbell-shaped brass sheet and subsequently cured. The composite specimens were clamped on the neck portion at a separation of 20 mm and extended at 0.017 mm sec⁻¹ (corresponding to about 0.1% sec⁻¹) and the percentage elongation at which edge cracking of the polymer film first appeared was recorded (Table 6).

Table 6 Physical properties and wear behaviour of cured films and filled compositions

Polymer	Penetration, h (μm)	Elongation to break (%)	Thermal diffusivity $\times 10^{-6}$ ($\text{m}^2\text{sec}^{-1}$)	Wear factor, k , $\times 10^{-15}$ (m^2N^{-1})	Friction coefficient, μ
IA	5.0	1.8	0.0075	1.28	0.28
IIA	5.5	1.7	1.22	1.36	0.23
IB	5.8	3.4	0.076	4.80	0.23
IIB	5.7	2.7	0.47	4.20	0.31
IIIB	5.8	2.9	0.58	7.80	0.33
IVB	6.0	3.8	0.51	7.20	0.21
PPS	—	—	0.177	0.74	0.18

These values are related, amongst other properties, to the ductility of the films.

Thermal diffusivity for the composite specimen was measured at 200°C by the heat pulse method using the HABEA computer programme (UKAEA, Risley)^{15,16}. The specimens consisted of 0.72 mm thick stainless-steel discs coated with a 0.1 mm film of cyclized polymer. The results are shown in Table 6.

DISCUSSION

An examination of the values of total hardness (h) and elongation to break reveals similar trends for the various samples suggesting that related properties are being determined. The ageing results shown in Figure 5 reveal that while it is possible to distinguish between the samples as far as total penetration is concerned this is not the case for elastic and permanent deformation which are similar for all polymers. It is seen that on ageing the polymer becomes much more ductile suggesting that intermolecular attractions have been reduced due possibly to molecular weight or cyclization changes.

As far as the thermal diffusivity measurements are concerned a possible source of error lies in the partial transparency of the films at the wavelength of the detector and this might contribute to the unexpectedly high value recorded for sample IIA. The significance of these results to the tribological behaviour is discussed below.

WEAR CHARACTERISTICS OF FILLED COMPOSITIONS

EXPERIMENTAL

One of the immediate objectives of this work lay in the development of polymeric matrix materials for composite plastic bearing which would possess greater temperature stability than the epoxy-based compositions in current use¹⁷. A constant additive composition was accordingly selected and journal bearings manufactured with varying matrix materials by a spin casting technique. The composition chosen corresponded to 55% polymer, 25% PTFE, 10% graphite and 10% lithage (by weight). The pre-polymer and additives were blended with *N*-methylpyrrolidone in a Potter homogenizer and the resulting dispersion was spun cast at 2000 rev/min on the inside of a brass bush of length 19.05 mm, i.d. 19.43 mm and wall thickness 6.05 mm. The inside of the bush had previously been prepared by grit blasting with 100 mesh alumina to assist adhesion. In order to cure the polymer the bush was heated to 280°C from ambient over a period of 3 h. After casting the bushes were

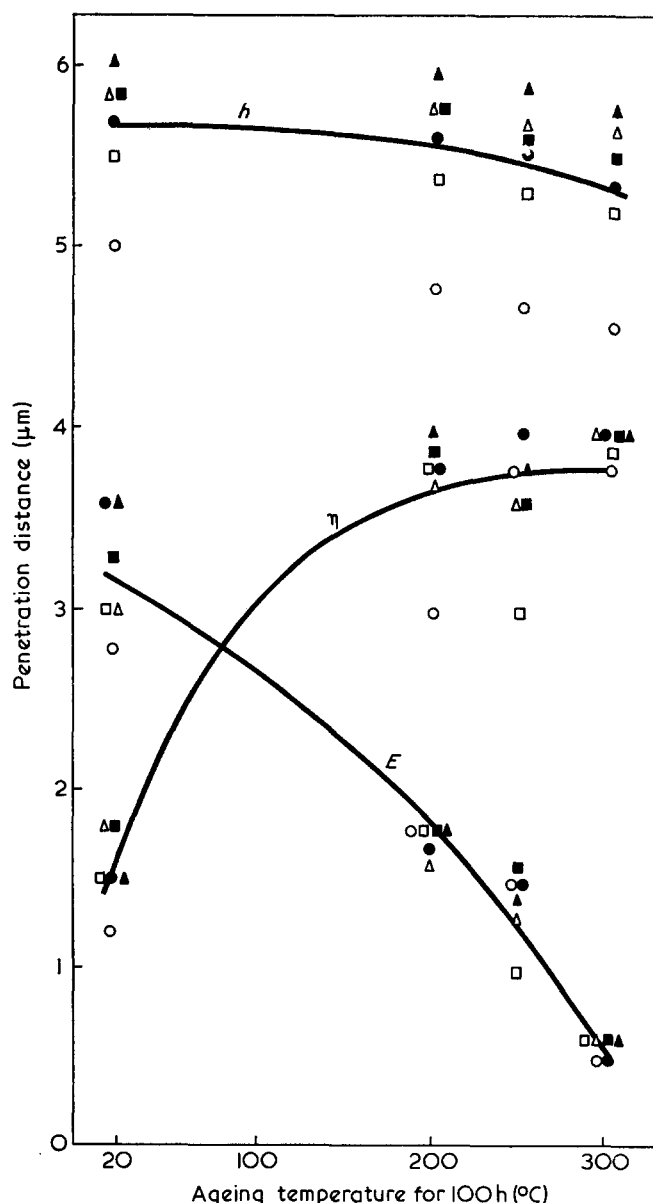


Figure 5 Penetration characteristics of cured films. h is the total penetration, E the elastic recovery and η the permanent deformation. \circ , IA; \square , IIA; \triangle , IB; \bullet , IIB; \blacksquare , IIIB; \blacktriangle , IVB

machined to an internal diameter of 19.15 mm corresponding to a 0.14 mm thick plastic lining.

The bearings were tested on a modified Dow-Corning LFW-5 bearing test machine against 700 VHN steel shaft of 19.05 mm diameter and 100–250 nm c.l.a., at a load of 133 N and a shaft speed of 1610 rev/min corresponding to a PV value of $0.6 \times 10^6 \text{ N m}^{-1} \text{ sec}^{-1}$. The results are expressed in terms of wear factor K (radial wear rate/ PV) in Table 6. The validity of this technique in the case of non-metallic bearings is discussed by Lancaster¹⁸. It is seen that the polymers tested display a wide variation of wear factor which is in every case significantly higher than poly(phenylene sulphide) (PPS) based compositions². Simultaneous measurements of coefficient of friction were also made (Table 6).

DISCUSSION

In discussing possible wear mechanisms for composite bearings it is necessary to consider first the effect of

operating temperature. During the wear testing equilibrium temperatures of 110–130°C for the bearing housing was observed. The rubbing surface will, however, be at a higher temperature and the value of this can be determined by experiments in which the shaft was replaced by a stationary dummy shaft containing a cartridge heater. The energy input to the heater was varied until similar housing temperatures resulted and it was found, using this technique, that a temperature difference of about 20°C existed between the rubbing surface and the housing. This is relatively small when considering the effects on physical properties and hence variations in polymer thermal diffusivity will in this case produce only minor changes in bearing operating conditions.

An examination of the results shown in Table 6 reveals that a definite relation exists between wear factor and hardness. A similar type of relation has been noted previously¹⁸ and this and the results given in Table 6 are shown plotted in Figure 6. It has been suggested that polymers wear by an adhesive mechanism and this is confirmed with the present materials by the relations between wear on the one hand and hardness, contact area and adhesion on the other. The mechanism of action of the filler components in composite bearings is the subject of a previous paper² but from the present results it can be concluded that compositions of increased wear resistance result from matrix polymers possessing higher hardness values. Although the wear factors of compositions manufactured from the polyquinazolinediones and polyquinazolones are higher than those based

on epoxy polymers the operating temperatures which those materials can withstand are likely to be of the order of 80°C higher than existing commercial materials and hence they could find uses under certain conditions where moderate wear life at temperatures greater than 120°C is desired.

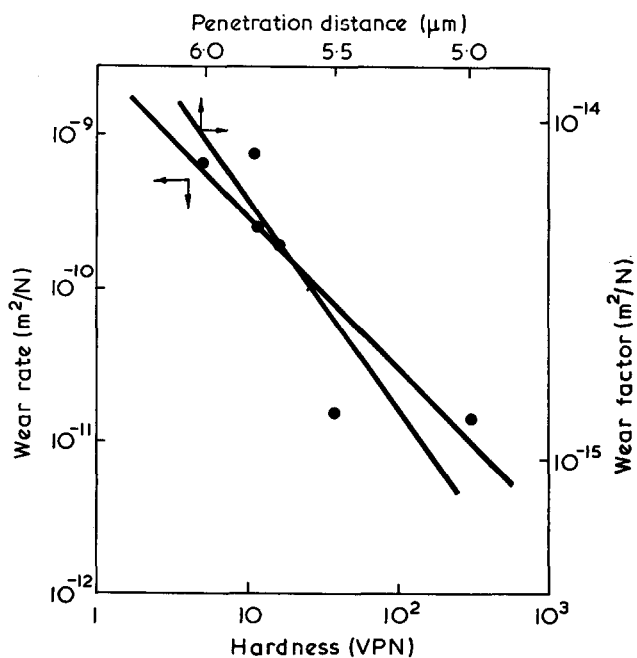


Figure 6 Wear rate/hardness relations (after Lancaster¹⁸). ●, Data from Table 6. Lines represent least squared data analysis

CONCLUSIONS

In the first section the preparation of novel polyquinazolinedione and polyquinazolone polymers has been described. The precursors to these polymers have been characterized and cyclization has been described in a nitrogen atmosphere; this is not, however, quantitative and may be improved by cyclization *in vacuo*. Thermal stability studies have revealed a stability order consistent with the structural differences of the polyquinazolinediones but the order obtained for the polyquinazolones is complicated by the presence of low molecular weight fragments, and the differences in percentage cyclization achieved for each system.

In the second section the variation in hardness or ductility of the cyclized polymers was discussed. A comparison with structural considerations reveals that the ductility of the polymers is increased and the hardness decreased as the groupings between the heterocyclic units allow more flexibility. This is particularly marked in the case of IV_B which has a —S—S— linking unit, and in the case of I_A and II_A where aromatic and aliphatic linking groupings are involved.

The comparatively small increase in hardness that occurs on ageing as the ageing temperature is raised is accompanied, as noted previously, by a large reduction in the ratio of elasticity/permanent deformation. This could possibly be due to thermal oxidative degradation/thermal rearrangement resulting in the scission of the polymer into smaller units and possibly the formation of a 'graphite-like' structure. The improvement of wear resistance as hardness increases suggests that polymers possessing the quinazolinedione structural features offer promise for use in high temperature journal bearing compositions when the bearings are operated under

certain conditions. Polyquinazolones similarly might prove useful in this application as would other polymers having the combination of high hardness and thermo-oxidative stability such as poly(phenylene sulphide)².

ACKNOWLEDGEMENTS

Thanks are due to Dr R. Taylor and Dr A. R. Thompson of UMIST for assistance with parts of the experimental programme, to the National Centre of Tribology for the loan of testing facilities and to the Science Research Council for financial support.

REFERENCES

- West, G. H. and Senior, J. M. Conf. 'Plastics in Bearings' (Plastics Institute, Solihull) 1973 (Feb), Paper 3
- West, G. H. and Senior, J. M. *Tribology* 1973, **6**, 269
- Kurihara, M. and Hagiwara, Y. *Polym. J.* 1970, **1**, 425
- Kurihara, M. and Yoda, N. *J. Polym. Sci. (B)* 1966, **4**, 11
- Kurihara, M. and Yoda, N. *Bull. Chem. Soc. Japan* 1967, **40**, 2429
- Kurihara, M. and Yoda, N. *J. Polym. Sci. (A-1)* 1967, **5**, 1765
- Zentmyer, D. T. and Wagner, E. C. *J. Org. Chem.* 1949, **14**, 967
- Hagiwara, Y., Kurihara, M. and Yoda, N. *Tetrahedron* 1968, **25**, 783
- Kurihara, M. *Makromol. Chem.* 1967, **105**, 84
- Bower, G. M. and Frost, L. W. *J. Polym. Sci. (A)* 1963, **1**, 3135
- Sroog, C. E. *et al. J. Polym. Sci. (A)* 1965, **3**, 1373
- Nishizaki, S. *Kogyo Kagaku Zasshi* 1965, **68**, 1756
- Dine-Hart, R. A. and Wright, W. W. *Makromol. Chem.* 1972, **153**, 237
- Monk, J. H. and Wright, T. A. *J. Oil Colour Chem. Assoc.* 1965, **48**, 520
- Parker, W. J. *et al. J. Appl. Phys.* 1961, **32**, 1679
- Larson, K. B. and Koyama, K. *J. Appl. Phys.* 1967, **38**, 465
- Design Eng.* 1972, p 131
- Lancaster, J. K. Conf. 'Plastics in Bearings' (Plastics Institute, Solihull), 1973 (Feb), Paper 1

Electric permittivity of polyelectrolytes: 2. Effect of the concentration and ionic specificity

G. Muller

Laboratoire de Chimie Macromoléculaire, Université de Rouen,
76130 Mont-Saint-Aignan, France
(Received 29 January 1974; revised 11 March 1974)

The dielectric behaviour of a polycondensate between L-lysine and 1,3-benzenedisulphonyl chloride (PLL) was studied at different concentrations and the effect of the nature of counterions was investigated. The effect of concentration on the dielectric increments and relaxation times are explained by the influence of polyion-polyion interactions on the dielectric parameters. In the presence of a bulky quaternary ammonium counterion (tetrabutylammonium), larger dielectric increments are found together with an increase in the high-frequency relaxation time.

INTRODUCTION

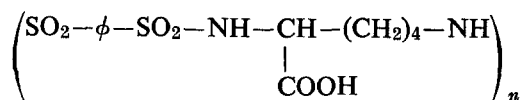
In a previous paper¹, the effect of ionization on the dielectric properties of PLL (polycondensate between L-lysine and 1,3-benzenedisulphonyl chloride) neutralized with sodium hydroxide has been reported. A pH-induced conformational change, from a compact to an extended mean conformation, was clearly shown from potentiometric and viscosity data². In the ionization range where the transition occurs a marked change in the dielectric moment, $\Delta\epsilon_s$, was observed which can be directly related to an increase in the molecular dimensions of PLL. Over the ionization range corresponding to the hypercoiled state of PLL (degree of ionization, α below 0.2), the dielectric dispersion of PLL could be described with one mean relaxation time whereas two separated dispersion regions are found for the extended conformation as is usual for solutions of flexible polyelectrolytes. From potentiometric and viscosity data, it has been reported that the transition is shifted to higher values of the degree of ionization when PLL is neutralized in the presence of quaternary ammonium cations. In the peculiar case where PLL is neutralized with tetrabutylammonium hydroxide (TBA) the hypercoiled state of PLL is maintained in a large range of ionization ($0 < \alpha < 0.7$) and it can be deduced that TBA has a stabilizing effect on the compact conformation of PLL.

Here we wish to present results on the effect of the concentration and the nature of counterions on the dielectric behaviour of PLL.

EXPERIMENTAL

Materials and preparation of polymer solutions

PLL was prepared as described previously³ by polycondensation between L-lysine and 1,3-benzenedisulphonyl chloride. Its structural unit is:



A stock solution of PLL ($C_p = 0.01$ mol/l) was prepared by dissolving PLL in an excess of sodium hydroxide. The solution was then de-ionized with an ion-exchange column. The different concentrations were obtained by dilution from the stock solution and adjusted to the desired degree of ionization by adding differing amounts of hydroxide.

Dielectric measurements

The dielectric permittivity was measured in the frequency range 2.5 kHz–100 MHz. In the low frequency part (2.5–600 kHz) a specially designed bridge was employed⁴. The high frequency measurements (1–100 MHz) were performed with an RX Meter type 250 Schering impedance bridge and a coaxial cell with variable electrode length. Only the value of the real part of the frequency-dependent complex permittivity could be determined. The experimental values of ϵ were fitted by a least-squares procedure according to the following analytical expression with two separated dispersion regions, each one being described by the dispersion relation proposed by Cole⁵:

$$\epsilon = \epsilon_\infty + \frac{1}{2} \Delta\epsilon_1 \left(1 - \frac{\sinh \beta x_1}{\cosh \beta x_1 + \cos \beta \pi / 2} \right) + \frac{1}{2} \Delta\epsilon_2 \left(1 - \frac{\sinh \beta x_2}{\cosh \beta x_2 + \cos \beta \pi / 2} \right) \quad (1)$$

where $x_1 = \ln(2\pi f \tau_1)$, $x_2 = \ln(2\pi f \tau_2)$ and β is the Cole-Cole parameter ($0 < \beta < 1$).

The two dispersion regions are characterized by mean relaxation times τ_1 and τ_2 and dielectric increments $\Delta\epsilon_1 = \epsilon_s - \epsilon_2$ and $\Delta\epsilon_2 = \epsilon_2 - \epsilon_\infty$ where ϵ_s and ϵ_∞ are the extrapolated values of the electric permittivity at the low and the high frequency end of the dispersion curve. The total dielectric increment is given by $\Delta\epsilon_s = \epsilon_s - \epsilon_\infty$. It has been found that all curves could be fitted by a superposition of two Cole-Cole functions with the same value for β . We have tried this for β values between 0.5 and 1 and it has been found that the best standard

Table 1 Effect of the concentration on the dielectric dispersion of PLL-Na

Degree of ionization, α	C_p (g/l)	$\Delta\epsilon_s$	$\Delta\epsilon_2$	$\Delta\epsilon_s/C_p$ (l/g)	$\Delta\epsilon_2/C_p$ (l/g)	$\tau_1 \times 10^6$ (sec)	$\tau_2 \times 10^6$ (sec)
0.20	1.74	6.3±1.2	4.5±0.7	3.6	2.6	2.5±0.5	1.0±0.6
0.20	1.04	5.5±1.4	3.6±0.5	5.2	3.4	3.9±0.7	1.9±0.8
0.20	0.69	5.3±0.4	2.9±0.2	7.6	4.0	2.5±0.5	3.0±0.8
0.20	0.35*	3.6±0.8	1.2±0.4	10.2	3.5	2.0±1.0	10.0±6.0
0.40	1.40	14.0±0.5	6.8±0.3	10.1	4.9	1.8±0.3	3.5±0.5
0.40	1.04	13.4±0.6	6.2±0.2	12.8	5.9	2.2±0.2	3.6±0.8
0.40	0.69	12.6±0.6	5.6±0.3	18.1	8.1	2.8±0.4	7.2±1.1
0.40	0.28	12.8±0.9	5.3±0.5	46.0	19.0	8.0±2.0	17.4±5.0

* For this concentration the two dispersion regions are not well separated and the whole dispersion can be described with a mean relaxation time $\tau=8.9(\pm 3.0) \times 10^{-7}$ sec and a dielectric increment $\Delta\epsilon_s=3.1 \pm 0.2$

 Table 2 Effect of the nature of counterion on dielectric dispersion of PLL solutions (polymer concentration $C_p=0.096$ g/l)

Counter-ion	Degree of ionization	$\Delta\epsilon_s$	$\Delta\epsilon_2$	$\tau_1 \times 10^6$ (sec)	$\tau_2 \times 10^8$ (sec)
Li	0.5	16.0±0.6	7.4±0.3	2.5±0.3	4.0±0.6
Na	0.5	13.7±0.6	6.7±0.3	2.0±0.35	5.3±0.9
TMA	0.5	11.4±0.7	5.2±0.3	2.2±0.5	3.3±0.5
TEA	0.5	12.2±1.3	6.4±0.7	2.0±0.9	7.2±1.5
Li	1.0	21.5±1.0	8.1±0.3	2.8±0.4	3.5±0.5
Na	1.0	19.6±1.3	8.3±0.5	3.1±1	2.6±0.6
TMA	1.0	20.6±1.3	8.8±0.3	4.0±0.9	2.9±0.4
TEA	1.0	19.8±1.0	10.1±0.4	2.5±0.7	3.8±0.6
TPA	1.0	23.4±0.8	12.1±0.3	2.8±0.4	4.8±0.5
TBA	1.0	24.0±1.4	13.2±0.8	3.2±0.7	13.2±2
Ba	0.3	1.5±0.2		$\tau=3.9(\pm 1.4) \times 10^{-7}$ sec	

deviations of the fitting procedure were obtained for $\beta=0.75-0.80$. Therefore all results were fitted by a curve with $\beta=0.80$.

RESULTS

The effect of the polymer concentration has been investigated for two values of the degree of ionization of PLL ($\alpha=0.2$ and 0.4). The experimental results are reported in Table 1.

The dependence of dielectric dispersion on the counterion type has been investigated for solutions of X-PLL where X is: Li⁺, Na⁺, (CH₃)₄N⁺ (TMA), (C₂H₅)₄N⁺ (TEA), (C₃H₇)₄N⁺ (TPA), (C₄H₉)₄N⁺ (TBA) and Ba²⁺. The experimental results are collected in Table 2.

DISCUSSION

The dielectric behaviour of polyelectrolytes is usually ascribed to the polarization of the ionic atmosphere⁶⁻⁹. In the theoretical interpretation the molecule is generally considered as a rigid rod. Clearly, the rigid rod model is rather crude as most synthetic polyelectrolytes are more or less flexible and thus a quantitative explanation of experimental results is difficult. van der Touw and Mandel¹⁰ have proposed a new model taking into account the flexibility of the molecule. It has been found that the dielectric properties of poly(L-glutamic acid) could be interpreted in terms of this theory¹¹. The polyion is considered as a collection of rigid rodlike parts (of length b) along which bound counterions can move. This theory predicts two separated dispersion regions if

the rigid parts of the molecule are separated by energy barriers higher than kT .

The total dielectric increment due to the perturbation of the bound counterions distribution along the whole chain is given by:

$$\Delta\epsilon_s = \frac{1}{3\epsilon_0} C_p \sigma \frac{n(ze)^2(L^2)}{12kT} \quad (2)$$

where C_p is the polymer concentration (expressed in number of polyions per unit volume), ϵ_0 is the electric permittivity of vacuum, σ is a field correction factor, n is the number of counterions of charge ze associated per polyion and L^2 is the average square length of the polyion.

The corresponding relaxation time τ_1 can be determined by fluctuations in the bound counterions distribution over the whole molecule, the orientational motion of the polyion or the exchange mechanism between bound and free counterions. The amplitude of the high-frequency dispersion region $\Delta\epsilon_2$ is given by an expression similar to equation (2) in which L^2 is replaced by the square of the length b of each rigid part. The relaxation time τ_2 belonging to this high-frequency dispersion region, which is determined by the diffusion process of bound counterions along each part b , is given by:

$$\tau_2 = b^2/\pi^2 ukT \quad (3)$$

where u is the mobility of counterions along the part b . Values for b can be calculated from equation (3) assuming that u does not differ from the mobility u_0 of ions free in solution.

Concentration dependence

Figure 1 illustrates the dielectric behaviour of PLL-Na at $\alpha=0.4$. It can be seen that the reduced increments and the relaxation times are dependent on the polymer concentration C_p . As shown in Figure 2 for both degrees of ionization investigated ($\alpha=0.2$ and 0.4) the reduced increments $\Delta\epsilon_s/C_p$ increase with increasing dilution as already reported by many authors on other kinds of polyelectrolytes. The reduced increment for $\alpha=0.4$ is found to be more dependent on C_p than for $\alpha=0.2$. From relation (2) such a behaviour is consistent with an extension of the polyion upon dilution as is also evidenced by viscosity measurements (Figure 2). The dielectric behaviour can be described by the empirical relation:

$$\Delta\epsilon_s/C_p = \frac{(\Delta\epsilon_s/C_p)_{C_p \rightarrow 0}}{1 + B_s C_p} \quad (4)$$

where $(\Delta\epsilon_s/C_p)_{C_p \rightarrow 0}$ is the limiting value of the reduced increment at infinite dilution (intrinsic increment) and

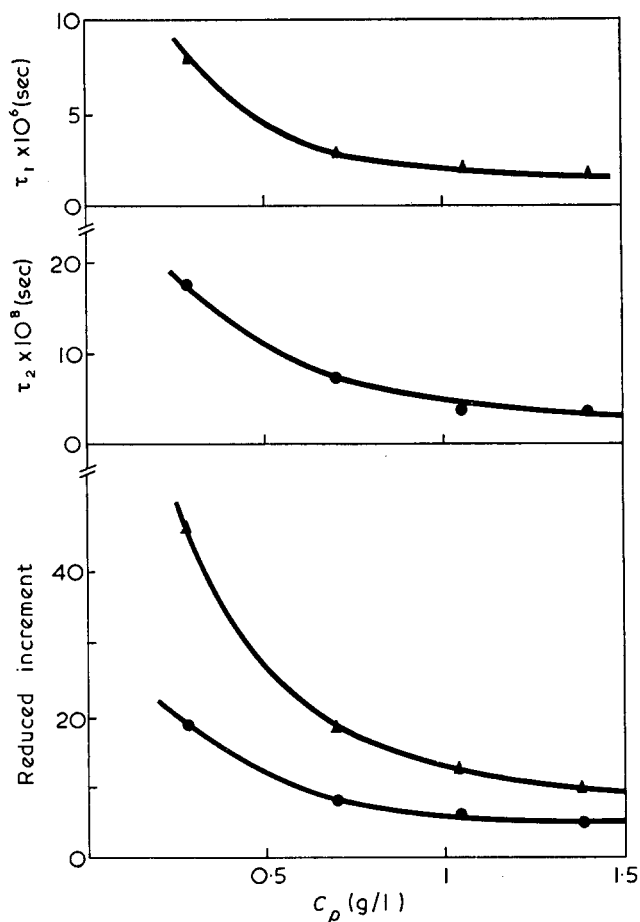


Figure 1 Dielectric behaviour of PLL-Na ($\alpha=0.4$). Dependence of the relaxation times τ_1 (\blacktriangle) and τ_2 (\bullet) and the reduced increments $\Delta\epsilon_s/C_p$ (\blacktriangle) and $\Delta\epsilon_2/C_p$ (\bullet) on the concentration C_p

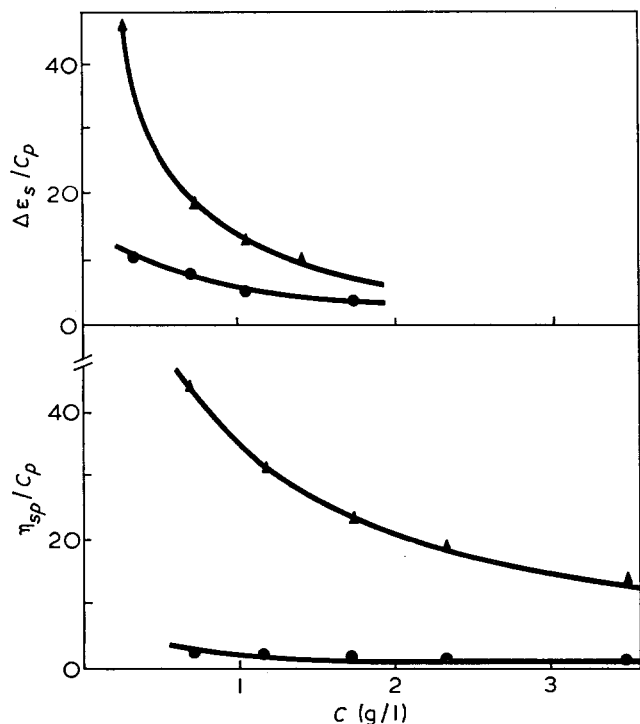


Figure 2 Variation of the reduced increment ($\Delta\epsilon_s/C_p$) and of the reduced viscosity η_{sp}/C_p as function of the concentration for PLL-Na: \bullet , $\alpha=0.2$; \blacktriangle , $\alpha=0.4$

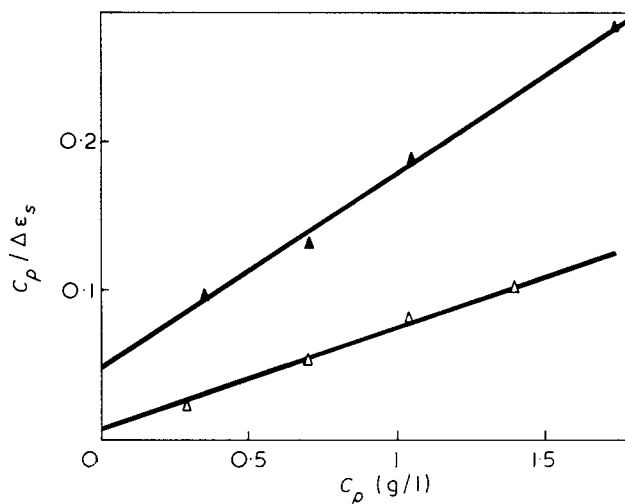


Figure 3 Dependence of the reciprocal reduced increment $C_p/\Delta\epsilon_s$ on the polymer concentration C_p for PLL-Na; \blacktriangle , $\alpha=0.2$; \triangle , $\alpha=0.4$

B_s is a parameter related to intermolecular interactions. Experimentally $(\Delta\epsilon_s/C_p)_{C_p \rightarrow 0}$ and B_s can be determined by plotting the reciprocal values of the specific increment ($C_p/\Delta\epsilon_s$) against the concentration C_p . As shown in Figure 3, the reciprocal values of the reduced increments depend linearly on the concentration. The same behaviour is also observed for the concentration dependence on $(\Delta\epsilon_2/C_p)$ and thus $(\Delta\epsilon_2/C_p)_{C_p \rightarrow 0}$ and B_2 can be determined in the same way. Extrapolation to infinite dilution yields the following values for the intrinsic increments and for parameters B_s and B_2 :

α	$(\Delta\epsilon_s/C_p)_{C_p \rightarrow 0}$ (l/g)	B_s	$(\Delta\epsilon_2/C_p)_{C_p \rightarrow 0}$ (l/g)	B_2
0.20	21	2.7	7	1.0
0.40	250	17.5	25	3.0

It is observed that B_s is strongly dependent on the degree of ionization. The change in B_s from $\alpha=0.2$ to 0.4 is not only due to the change in the ionization and seems consistent with the conformational transition of PLL already reported as also viscosity measurements have pointed out a marked change of the parameter B_v around $\alpha=0.2$ (B_v , being defined in the same way as B_s , is also characteristic of intermolecular interactions).

The observed increase in τ_2 with decreasing concentration can be interpreted by the increase in the thickness of the ionic atmosphere with decreasing concentration. The low frequency relaxation time τ_1 seems to be independent on C_p for PLL-Na: $\alpha=0.2$, which is in agreement with the fact that the average conformation of PLL is less dependent on the concentration at low α .

Ionic specificity

As was already reported there is a marked difference in the viscosimetric and potentiometric properties of PLL in the presence of Li, Na and the quaternary ammonium ions. From the apparent pK values determined from the potentiometric titration curves, it could be concluded that the following sequence for association holds: Li > Na > K > TMA > TBA. On the other hand,

the reduced viscosity of the system PLL-TBA has been found to be much smaller than for PLL-Na (at $\alpha=1$) and TBA was found to have a marked effect on the stabilization of the compact structure of PLL in a large range of ionization ($0 < \alpha < 0.7$). These facts suggest that TBA may interact with PLL by non-electrostatic interactions.

It has been found that the transition between a very compact form to a more extended one which is initiated at $\alpha \approx 0.2$ in the presence of Na^+ is shifted to higher values of α in the presence of TBA as evidenced by the sharp increase in viscosity observed near $\alpha = 0.7$. Owing to the hydrophobic nature of the PLL chain, the effect of a hydrophobic ion such as TBA leads to a situation in which non-electrostatic hydrophobic interactions are favoured. We have shown that the effect of TBA on the observed transition is quite similar to that of Acridine Orange and leads to a stabilization of the compact form.

The $\Delta\epsilon_s$ values, reported in Table 2, for Li, Na and TMA are consistent with the potentiometric and viscosimetric behaviour. In the presence of the bulky quaternary ammonium ion TBA, larger dielectric increments and an increase in the high-frequency relaxation time are observed. Primarily this is due to the field effect of the counterion and its dependence on the ability of the counterion to approach the polyion. Unfortunately, the dielectric behaviour of PLL in the presence of different counterions has been studied for only one fixed concentration and it has been shown, in the preceding paragraph, that the dielectric parameters are strongly dependent on the polymer concentration. It is not to be excluded that the effect of the concentration for the system PLL-TBA might be different from that for the system PLL-Na, as indicated from the concentration dependence on the viscosity behaviour in the presence of Na and TBA (Figure 4). Extrapolation of dielectric parameters to

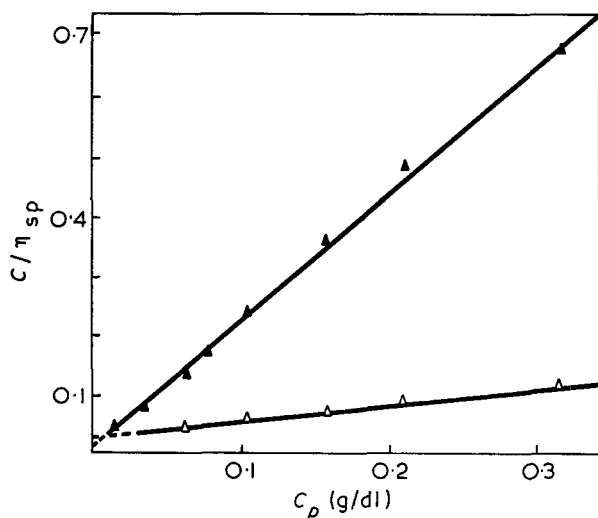


Figure 4 Effect of the concentration on the reduced viscosity of PLL-Na (Δ) and PLL-TBA (\blacktriangle) solutions fully neutralized ($\alpha=1$)

infinite dilution should allow a more detailed interpretation as in more dilute solution a larger fraction of counterions is separated from the chain thus decreasing the specific effects.

In the case of divalent ion (Ba^{2+}), only one dispersion can be found with a very small dielectric increment which can be attributed to the fact that Ba^{2+} is so strongly bound to PLL that it does not contribute to the polarizability.

CONCLUSION

As generally observed for solutions of flexible polyelectrolytes the dielectric parameters are found to be dependent on the concentration. For both degrees of ionization investigated, the reduced increments and the high-frequency relaxation time τ_2 , increase with decreasing concentration which is consistent with an extension of the macromolecule upon dilution as is also observed from viscosity measurements. The effect of polymer concentration can be explained in terms of polyion-polyion interactions which reduce extension of the polyion and its ionic atmosphere. The $\Delta\epsilon_s$ values for PLL in the presence of Li, Na and TMA are consistent with the potentiometric and viscosimetric behaviour. In the presence of a bulky quaternary ammonium ion (TBA), larger dielectric increments and an increase in τ_2 are observed. A detailed interpretation of the effect of counterion size is difficult insofar as the measurements were performed at one single concentration; extrapolation of all experimental results to infinite dilution might allow a more quantitative explanation as it is not to be excluded that the concentration dependence on the dielectric properties should be different for the systems PLL-Na and PLL-TBA.

ACKNOWLEDGEMENTS

This work was carried out during a stay in University of Leiden. The author wishes to express his sincere thanks to Professor Mandel and Dr van der Touw for their welcome and their helpful discussions.

REFERENCES

- 1 Muller, G. *J. Polym. Sci.* to be published
- 2 Fenyó, J. C. *Eur. Polym. J.* 1974, **10**, 233
- 3 Beaumais, J., Fenyó, J. C. and Selegny, E. *Eur. Polym. J.* 1973, **9**, 15
- 4 van der Touw, F. and Mandel, M. *Trans. Faraday Soc.* 1971, **67**, 1336
- 5 Cole, K. S. and Cole, R. H. *J. Chem. Phys.* 1941, **9**, 341
- 6 Mandel, M. *Mol. Phys.* 1961, **4**, 489
- 7 McTague, J. P. and Gibbs, J. H. *J. Chem. Phys.* 1966, **44**, 4245
- 8 Schwarz, G. *Z. Phys.* 1956, **145**, 563; 1959, **19**, 286; *J. Phys. Chem.* 1962, **66**, 2636
- 9 Oosawa, F. *Biopolymers* 1970, **9**, 677
- 10 van der Touw, F. and Mandel, M. *Biophys. Chem.* in press
- 11 Muller, G., van der Touw, F., Zwolle, S. and Mandel, M. *Biophys. Chem.* in press

Filler effect on the relaxation time of fibre suspensions in polymeric solutions

L. Nicodemo and L. Nicolais

Istituto di Principi di Ingegneria Chimica, Università di Napoli, 80125 Naples, Italy
(Received 28 January 1974; revised 9 May 1974)

Viscosity measurements on suspensions of short glass fibres in aqueous solutions of poly(ethylene oxide) are presented. The volumetric filler fraction ranges between 0.01 and 0.07 and the shear rate from 0.1 to 1000 sec⁻¹. The results indicate that the filler enhances the non-Newtonian pseudoplastic behaviour of the suspending solution increasing its relaxation time. Furthermore, at low shear rate, in the region of Newtonian behaviour of the unfilled solutions, most of the suspensions show a viscosity increase with decreasing shear rate owing to fibre aggregate formation. These effects are compared with previously published results on glass bead suspensions in polymeric liquids.

INTRODUCTION

In previous papers^{1,2} the viscosity of glass bead suspensions in polymeric liquids as a function of the shear rate and filler content has been studied. The present work deals with suspensions of short glass fibres in polymeric solutions with the purpose of modelling the behaviour of fibre composites based on polymeric matrices. The relevance of this study is connected with such operations as moulding, extrusion, etc., which are encountered in the processing of these materials. Moreover, in the literature much more work has been presented for bead suspension than for fibre filled materials in spite of the major applications of short fibre composites.

EXPERIMENTAL

Viscosity measurements were made on suspensions of glass fibres in aqueous solutions of poly(ethylene oxide) (PEO) of $M_w \approx 4 \times 10^5$ at concentrations, c , of 3.8, 5.8 and 7.6 g/dl (PEO-4, PEO-6 and PEO-8 respectively).

With each solution, suspensions of filler volumetric loading ϕ of 0.01, 0.03, 0.05 and 0.07 were prepared. Suspensions with ϕ larger than 0.07 were difficult to prepare because at these concentrations the fibres were forming aggregates of finite dimensions with entrapped liquid and air.

The short fibres were prepared by cutting long glass fibres embedded in paraffin wax and removing the wax after melting. The fibres were then repeatedly washed with benzene and dried in an oven under vacuum. The length of the fibres was in the range 0.4–0.7 mm with an average value of 0.53 mm while the values of the diameter, d , comprised a narrow range around the average value of 0.014 mm. The aspect ratio l/d was then 37.8.

The suspensions were prepared by stirring the polymeric solutions and the fibres in the desired amount under a pressure low enough to remove the entrapped

air without water evaporation. Viscosities in shear flow were measured with a Weissenberg rheogoniometer (Model R 18 manufactured by Sangamo Controls Ltd) of 5 cm diameter and 2° angle cone. Data were taken at steadily decreasing shear rates in the range between 1000 and 0.1 sec⁻¹, but check measurements at higher shear rates were made at the completion of a run. To prevent heating of the sample, the readings were made as quickly as possible. The temperature was 22°C.

RESULTS AND DISCUSSION

In Figure 1 results obtained with the polymeric solutions and their relative suspensions are reported as viscosity η vs. shear rate $\dot{\gamma}$. The general appearance of these diagrams is typical of non-Newtonian pseudoplastic materials. However, the filler enhances the viscosity of the suspending medium by an amount which depends on shear rate

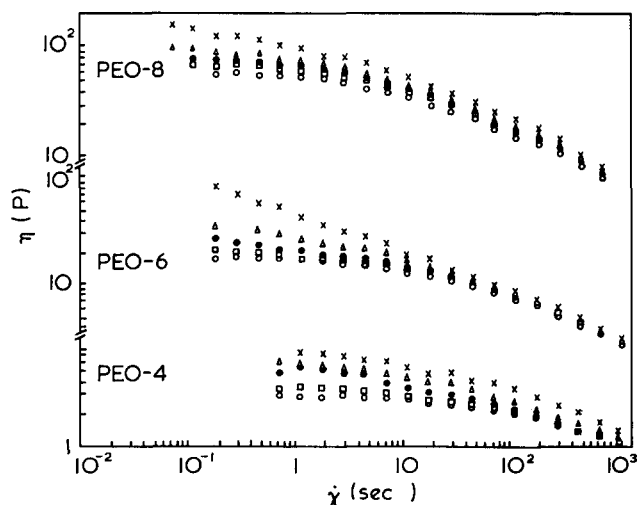


Figure 1 Viscosity vs. shear rate for PEO-4, PEO-6 and PEO-8 slurries at different volumetric filler loadings, ϕ : \circ , 0; \square , 0.01; \bullet , 0.03; \triangle , 0.05; \times , 0.07

and, for a fixed PEO concentration, while the curves relative to different ϕ are generally well distinguishable in the range of low $\dot{\gamma}$ values, they crowd together at increasing $\dot{\gamma}$.

Furthermore at low $\dot{\gamma}$ values, while the unfilled solutions show the well known Newtonian plateau, there is, for most suspensions at higher filler contents, a tendency towards an increase of viscosity at decreasing shear rate. This behaviour has been previously observed also for glass bead suspensions in polymeric solutions¹⁻³ and for particulate filled melt polymers^{4, 5}.

The behaviour of suspensions at low $\dot{\gamma}$ can be interpreted² as due to filler aggregate destruction with increasing shear rate while the subsequent drawing together of the $\eta-\dot{\gamma}$ curves can be attributed to a change of the relaxation time of the macromolecules owing to the presence of the filler.

Extending the procedure outlined previously² for the case of glass bead slurries to the fibre suspensions it is possible to show this change in relaxation time by means of a superposition of the $\eta-\dot{\gamma}$ curves.

In Figure 2 a master curve of reduced viscosity η' vs. reduced shear rate $\dot{\gamma}'$ for the unfilled solutions obtained with a double shift procedure⁶⁻⁸ assuming as reference curve that $c=7.6$ g/dl (PEO-8), is reported. In this plot the reduced variables are defined as:

$$\eta' = a_\eta \cdot \eta; \quad \dot{\gamma}' = a_{\dot{\gamma}} \cdot \dot{\gamma} \quad (1)$$

where a_η and $a_{\dot{\gamma}}$ are the vertical and horizontal shift factors respectively. a_η is defined as:

$$a_\eta = \frac{\eta_{0,8}}{\eta_0} \quad (2)$$

where η_0 is the zero shear viscosity of the solutions used and $\eta_{0,8}$ is that of PEO-8.

These η_0 values are reported in Table 1 and logarithmically plotted vs. the polymer concentration c in Figure 3, where also the $a_{\dot{\gamma}}$ values are plotted vs. η_0 . The straight line which fits the $a_{\dot{\gamma}}$ data has the equation:

$$a_{\dot{\gamma}} = 0.022 \eta_0^{0.95} \quad (3)$$

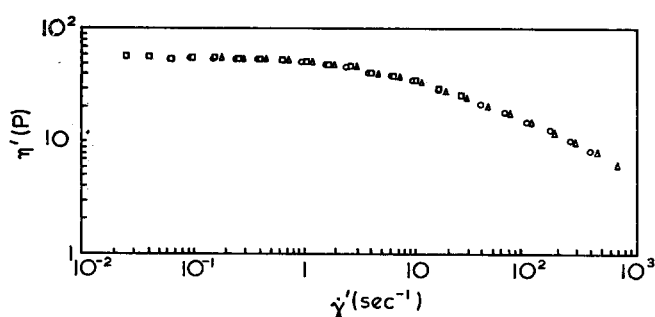


Figure 2 Master curve of reduced viscosity vs. reduced shear rate for unfilled PEO solutions at reference concentration of 7.6 g/dl. □, PEO-4; △, PEO-6; ○, PEO-8

In Figure 4 the master curves for the four filler loadings tested are reported. The master curve at a fixed ϕ is obtained with the superposition of the part of the $\eta-\dot{\gamma}$ plots corresponding to the non-Newtonian zone of the relative unfilled solution assuming as reference curve that $c=7.6$ g/dl. As can be seen from Table 1 the vertical

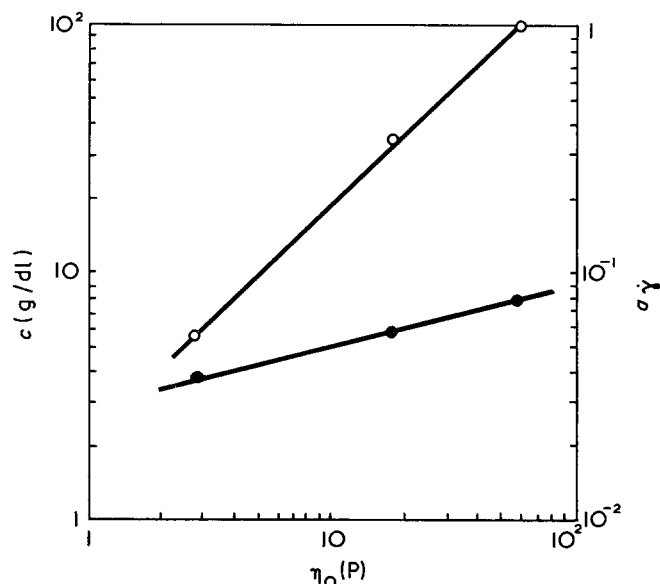


Figure 3 Horizontal shift factor (○) and polymer concentration (●) vs. zero shear viscosity of unfilled PEO solutions

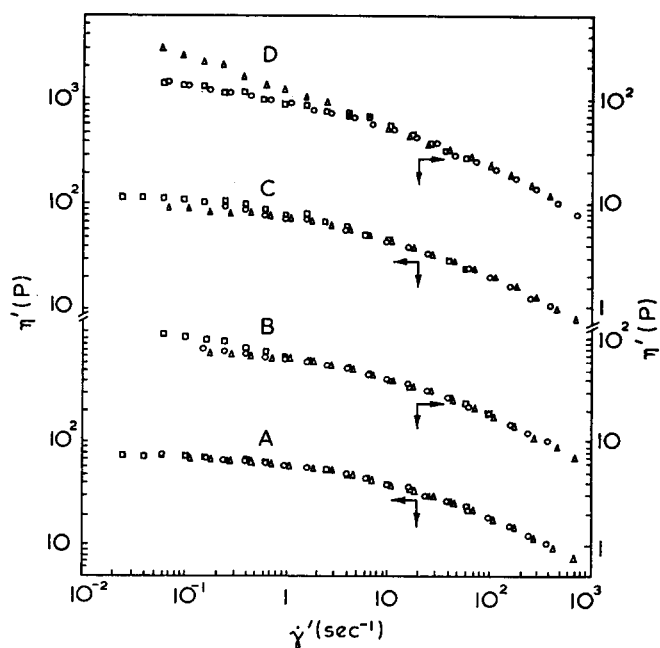


Figure 4 Master curves of reduced viscosity vs. reduced shear rate for slurries at volumetric filler fraction of 0.01 (A), 0.03 (B), 0.05 (C) and 0.07 (D), at a reference polymer concentration of 7.6 g/dl. □, PEO-4; △, PEO-6; ○, PEO-8

Table 1 Shift factors for the master curves at fixed ϕ and zero shear viscosity of PEO solutions

c (g/dl)	ϕ										
	$\eta_0(P)$	0		0.01		0.03		0.05		0.07	
		a_η	$a_{\dot{\gamma}}$	a_η	$a_{\dot{\gamma}}$	a_η	$a_{\dot{\gamma}}$	a_η	$a_{\dot{\gamma}}$	a_η	$a_{\dot{\gamma}}$
3.8	2.8	20	0.056	22	0.056	22	0.056	20.6	0.056	20	0.056
5.8	17.5	3.2	0.35	2.7	0.35	2.7	0.35	2.9	0.35	3.9	0.35
7.6	56	1	1	1	1	1	1	1	1	1	1

shift factors a_η at a fixed ϕ are within the 15% of the value for $\phi=0$ and the a_γ (the horizontal shift factors) are equal to those for $\phi=0$. The scattering of the a_η values is mainly due to experimental errors and to the usual uncertainty connected with the superposition procedure.

The a_γ values reported in Table 1 indicate that, if τ is the relaxation time of the polymeric solution, one can write⁶⁻⁸:

$$a_\gamma = \frac{\tau_{c,\phi}}{\tau_{8,\phi}} \quad (4)$$

where the subscripts c and ϕ refer to polymer concentration and filler loading (including $\phi=0$) respectively, while the subscript 8 indicates the reference solution PEO-8. From equation (4) it can be deduced that:

$$\tau_{c,\phi} = A_\gamma \tau_{c,0} \quad (5)$$

where the proportionality factor A_γ depends on filler content and is independent of polymer concentration. The values of A_γ are obtained by means of a superposition of the master curves at different ϕ on that relative to the unfilled solutions.

This general master curve is plotted in Figure 5 as reduced viscosity η^* vs. reduced shear rate $\dot{\gamma}^*$, defined by:

$$\begin{aligned} \eta^* &= A_\eta \eta' = A_\eta a_\eta \eta \\ \dot{\gamma}^* &= A_\gamma \dot{\gamma} = A_\gamma a_\gamma \dot{\gamma} \end{aligned} \quad (6)$$

where A_η and A_γ are the horizontal and vertical shift factors respectively. In Table 2 the A_γ values obtained at different filler contents are reported; they are larger than unity, which corresponds to a non-Newtonian behaviour of the suspension stronger than that of the relative suspending medium. In Table 2 also the $\bar{\eta}_r$ values defined as $(A_\eta)^{-1}$ are listed. $\bar{\eta}_r$ represents the ratio between the viscosity of the suspension and that of the suspending solution at the same $\dot{\gamma}^*$ and therefore it should be the relative viscosity of the suspension when there is no

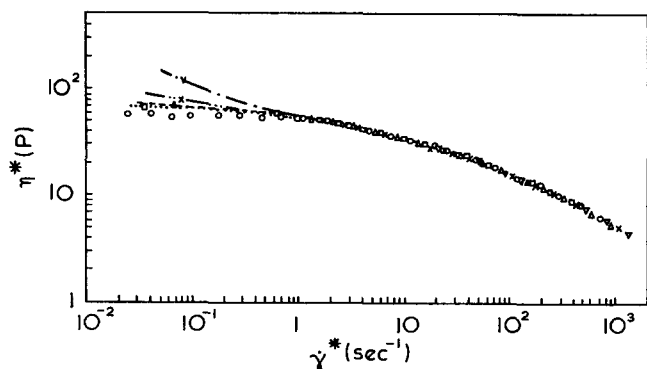


Figure 5 General master curve of reduced viscosity vs. reduced shear rate for slurries of glass fibre in PEO solutions assuming the reference curve is that of unfilled PEO-8. Filler content: ○, 0; □, 0.01; △, 0.03; ×, 0.05; ▽, 0.07

Table 2 Shift factors for the general master curve

	ϕ				
	0	0.01	0.03	0.05	0.07
η_r	1	1.12	1.3	1.5	1.85
A_γ	1	1.04	1.3	1.53	1.9

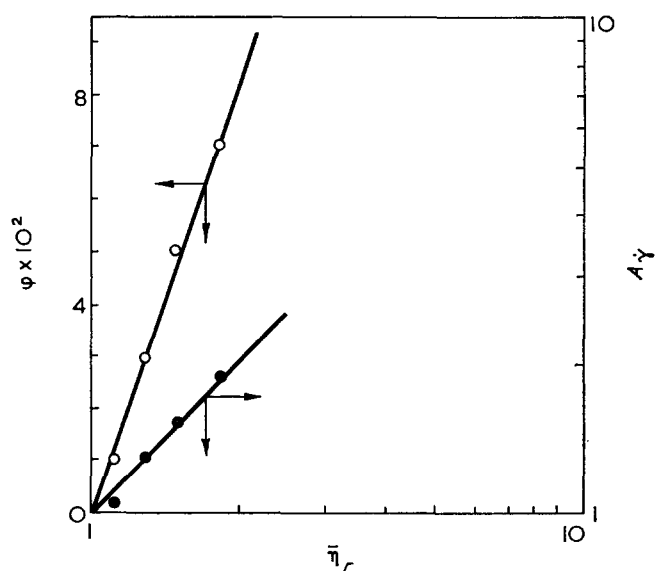


Figure 6 Horizontal shift factor A_γ (●) and filler content ϕ (○) vs. relative viscosity $\bar{\eta}_r$

change in the relaxation time and the mechanism of aggregate destruction is exhausted.

In Figure 6, $\bar{\eta}_r$ values are plotted vs. ϕ . The full line, which fits the experimental data well, is the plot of the equation:

$$\bar{\eta}_r = e^{8.52\phi} \quad (7)$$

which has been proposed elsewhere⁹ for the relative viscosity of suspensions obtained with the same glass fibres used here, in Newtonian liquids. This relation has been derived from the Mooney equation¹⁰ extending the Brodnyan approach¹¹ relative to prolate ellipsoids with Brownian motions to the case of short rigid fibres where these motions are absent.

In Figure 6 are also reported the A_γ values vs. $\bar{\eta}_r$. The best fit is obtained with the straight line of equation:

$$A_\gamma = \bar{\eta}_r \quad (8)$$

From equations (5) and (8) it can be seen that the filler enhances the relaxation time of the solution by an amount which depends on the increase in viscosity. This effect is analogous to that obtained with increasing polymer concentration (equation 3) although in this latter case the viscosity and then the relaxation time are more strongly affected owing to entanglement formation between molecules.

The presence of entanglements can be inferred from the fact that η_0 is proportional to $c^{4.35}$ as can be derived from the slope of the straight line which fits the data of polymer concentration vs. η_0 , reported in Figure 3.

In conclusion, the results of this work confirm the presence of two different mechanisms active in the region of low and high shear rate of the flow curves relative to suspensions in polymeric liquids. The enhanced viscosity increases the relaxation time of the suspending solution and then the shear rate dependence of these already non-Newtonian fluids. This effect is stronger for fibre suspensions than for microbead slurries because the dependence of $\bar{\eta}_r$ on the filler content is higher for the former. In fact, for example, while for the glass bead suspensions $\bar{\eta}_r = 1.5$ is reached for $\phi = 0.14^2$, $\phi = 0.05$ is sufficient for the suspension of the fibres with $l/d = 37.8$ used in this work.

Qualitatively also the appearance of the $\eta-\dot{\gamma}$ curves in the low shear rate range is similar to that of microbead suspensions, i.e. the viscosity increases with decreasing shear rate as shown in *Figure 5* where average curves for each ϕ are reported. This effect appears to be less relevant with respect to microbead suspensions².

ACKNOWLEDGEMENTS

This work was supported by CNR Grant No. 73.0046.03/115.1729. Thanks are due to Drs M. Gasparroni and R. Riviera for their help in the experimental work.

REFERENCES

- 1 Nicodemo, L., Nicolais, L. and Landel, R. F. *Chem. Eng. Sci.* 1974, **29**, 729
- 2 Nicodemo, L. and Nicolais, L. *J. Appl. Polym. Sci.* in press
- 3 Highgate, D. J. and Whorlow, R. W. *Rheol. Acta* 1970, **9**, 569
- 4 Mills, N. J. *J. Appl. Polym. Sci.* 1971, **15**, 2791
- 5 Zosel, A. *Rheol. Acta* 1972, **11**, 229
- 6 Graessley, W. W., Hazleton, R. L. and Lindeman, L. R. *Trans. Soc. Rheol.* 1967, **11**, 267
- 7 Graessley, W. W. and Segal, L. *Am. Inst. Chem. Eng. J.* 1970, **16**, 261
- 8 Bruce, C. and Schwarz, W. H. *J. Polym. Sci. (A-2)* 1969, **7**, 909
- 9 Nicodemo, L. and Nicolais, L. *Chem. Eng. J.* in press
- 10 Mooney, M. J. *Colloid Sci.* 1951, **6**, 162
- 11 Brodnyan, J. G. *Trans. Soc. Rheol.* 1959, **3**, 61

Characterization of styrene-butadiene copolymers by light scattering

T. C. Chau and Alfred Rudin

Department of Chemistry, University of Waterloo, Waterloo, Ontario, Canada
(Received 4 December 1973)

The general theory of Stockmayer and Benoit and their coworkers yields the weight average molecular weight of a binary copolymer and parameters which reflect the heterogeneity of chemical composition of the copolymer, using light scattering data from solutions in at least three solvents with different refractive indices. Although this theory has been applied successfully to block and graft copolymers and to mixtures of homopolymers, it has not seemed to be valid for random copolymers.

In this report, molecular weight and heterogeneity parameters of a number of gel-free styrene-butadiene emulsion copolymers were estimated from results of light scattering measurements in toluene, cyclohexane and 1,2-dichloroethane. The calculated heterogeneity parameters contradict expectations from copolymerization theory and appear to be in error. It is suggested that the particular difficulties with statistical copolymers result from a dependence of specific refractive index increment on polymer molecular weight. This dependence varies with different solvents. The effect is illustrated by experimental results for polystyrenes in toluene, cyclohexane and 1,2-dichloroethane. Accurate study of copolymer characteristics requires selection of solvents such that the differences between specific refractive indices of the appropriate homopolymer solutions do not depend strongly on polymer molecular weight in the molecular weight range which corresponds to the sum of homopolymer sequences in the particular copolymers. The apparent inapplicability of the theory to random copolymers appears to be an artifact of the particular systems which were studied.

INTRODUCTION

Treatment of the results of light scattering experiments on solutions of homopolymers relies on the assumption that all polymer molecules have the same refractive index. This practical rule does not hold for copolymers, since the intensity of light scattered at given viewing angle from a particular concentration depends not only on the mean molecular weight of the solute, but also on the heterogeneity of its chemical composition. The correct molecular weight of a binary copolymer can be determined, in principle, by measuring the scattering of light from its solutions in at least three solvents with different refractive indices. The general equations which have been developed in this context yield the weight average molecular weight, \bar{M}_w , of the copolymer along with parameters which characterize the heterogeneity of the chemical composition of the solute species^{1, 2}.

The theory mentioned has been applied with some success to block and graft copolymers³, but studies of random copolymers have usually yielded estimates of heterogeneity parameters which are not consistent with those from copolymerization theory^{2, 4-6}.

This paper reports results of a light scattering study of butadiene-styrene copolymers. Such materials are of considerable technical importance as SBR rubber and in various toughened polystyrene formulations.

The possibility of using light scattering data for characterization of such materials is discussed. Reasons are suggested for the apparent contradiction between light scattering and copolymerization theory assessments of the heterogeneity of these copolymers.

THEORY

The specific refractive index increment, ν , of a solution is defined at fixed wavelength and temperature by:

$$\nu = \lim_{c \rightarrow 0} \left(\frac{\Delta n}{c} \right) \quad (1)$$

where Δn is the difference between the refractive index, n , of the solution with concentration c and n_0 , the solvent refractive index. For scattered light intensity extrapolated to zero viewing angle and zero concentration, the excess (of solution over solvent) Rayleigh ratio, R , is given by:

$$R = K' c M \nu^2 \quad (2)$$

Here the optical constant K' is given by:

$$K' = \frac{2\pi n_0^2}{N_0 \lambda_0^4} \quad (3)$$

with N_0 being Avogadro's number and λ_0 the wavelength of the light *in vacuo*.

A solute which is polydisperse in molecular weight but uniform in refractive index may be considered to be composed of a mixture of monodisperse species, each with molecular weight M_i and concentration c_i . Since the intensity of scattered light is ideally additive, then:

$$R = K' \nu^2 \sum c_i M_i = K' c \bar{M}_w \nu^2 \quad (4)$$

Here, $\sum c_i = c$ and by definition:

$$\bar{M}_w = \frac{\sum c_i M_i}{\sum c_i} = \frac{\sum c_i M_i}{c} \quad (5)$$

If the solute is polydisperse with respect to composition as well as molecular weight, contributions to scattered light intensity are still additive under conditions of zero viewing angle and sufficiently low concentration. The Rayleigh ratio is then:

$$R = K' \sum c_i M_i \nu_i^2 \quad (6)$$

where species i has concentration c_i , molecular weight M_i , refractive index increment ν_i and composition x_i . In the present context consideration is restricted to binary (AB) copolymers and x_i is the weight fraction of component A in species i . As with homopolymer solutions, an apparent average molecular weight \bar{M}_{app} , can be deduced such that:

$$R = K' c \nu^2 \bar{M}_{app} \quad (7)$$

where ν is the specific refractive index of the copolymer solution, as determined experimentally.

Stockmayer *et al.*¹ and Benoit and coworkers²⁻⁴ have approximated ν for binary copolymer mixtures as a linear function of average composition taken as independent of molecular weight:

$$\nu_i = x_i \nu_A + (1 - x_i) \nu_B \quad (8)$$

where the subscripts A and B denote the refractive index increments characteristic of the respective homopolymers, poly(A) and poly(B). This equation is applicable to a mixture of homopolymers as well as to a copolymer. It is based on the premise that the specific refractive index ν_i of a species depends only on its composition and not on its molecular weight.

\bar{M}_{app} is not independent of the solvent used in its measurement since it depends on the specific refractive index increment of each hypothetical monodisperse species. If the dependence of ν on x is as shown in equation (8) then^{1, 2}:

$$\bar{M}_{app} = \bar{M}_w + 2bP + Qb^2 \quad (9)$$

where:

$$b = \frac{\nu_A - \nu_B}{\nu} \quad (10)$$

and P and Q are parameters which characterize the compositional heterogeneity of the polymer. In detail²:

$$P = \sum \gamma_i M_i (x_i - x) \quad (11)$$

$$Q = \sum \gamma_i M_i (x_i - x)^2 \quad (12)$$

Here γ_i is the weight fraction ($\gamma_i = c_i/c$) of component i , with molecular weight M_i , composition x_i and specific refractive index ν_i . The mean weight fraction of constituent monomer A is denoted by x .

The correct weight average molecular weight of a binary copolymer which is heterogeneous as to chemical composition can be obtained in principle by measuring

scattered light intensity in at least three solvents which differ in refractive index. These measurements also yield the parameters P and Q , from equation (9). The parameter Q characterizes the average compositional heterogeneity. It may have a value between zero ($x_i = x$, the copolymer composition is uniform) and $Q_{max} = \bar{M}_w x(1-x)$. The latter is the value for a mixture of homopolymers, each with molecular weight \bar{M}_w , in the same proportion as indicated by the mean composition, x . That is:

$$0 \leq Q \leq x(1-x)\bar{M}_w = Q_{max} \quad (13)$$

and parameter P reflects the influence of polymer molecular weight on the chemical heterogeneity. Its limits are given by:

$$-x\bar{M}_w \leq P \leq (1-x)\bar{M}_w \quad (14)$$

and P may be positive or negative.

For a statistical copolymer formed from an invariant monomer feed composition the general copolymerization formulae of Stockmayer⁷ lead to the expectation^{2, 4} that:

$$P = 0 \quad (15)$$

$$Q = x(1-x)M_0[1 - 4x(1-x)(1 - r_A r_B)]^{1/2} \quad (16)$$

where M_0 is the weight of a copolymer repeating unit and the reactivity ratios, r_A and r_B , have their usual meaning⁸.

EXPERIMENTAL

The styrene-butadiene polymer samples were gel-free, purified emulsion copolymers prepared and characterized as described elsewhere⁹. Samples were available with 19.6, 43.5 and 70.3 weight % styrene. The specific refractive index increments of these polymers were measured at 25°C in various solvents and at two wavelengths, as noted below. An emulsion polystyrene (sample B of ref 10) was also studied. Refractive index increments were measured at 25°C with a thermostated Brice-Phoenix differential refractometer.

The particular copolymers were intended for a study of the effects of ⁶⁰Co γ -radiation on styrene-butadiene elastomers. Details and conclusions of that study are given elsewhere⁹. It suffices for present purposes to record that the \bar{M}_w of sol portions of irradiated polymers were determined by light scattering in toluene, 1,2-dichloroethane and cyclohexane.

Solvents and polymer solutions were filtered under nitrogen pressure through 0.22, 0.88 or 1.20 μ m steel filters before use. The larger apertures were needed for the more intensely irradiated polymers. Dry copolymer samples which were obtained as described elsewhere⁹ were dissolved in the appropriate solvent by mechanical shaking at room temperature for about 12 h. Light scattering of most samples was measured shortly after this solution procedure. Otherwise, the solutions were stored cold until used. No antioxidant was added to the mixtures for light scattering or specific refractive index increment measurements.

Scattered light intensity was measured with a Brice-Phoenix light scattering photometer modified essentially as described by Roche and Tanner¹¹. The outer vat in this apparatus was filled with a thermostated, circulating

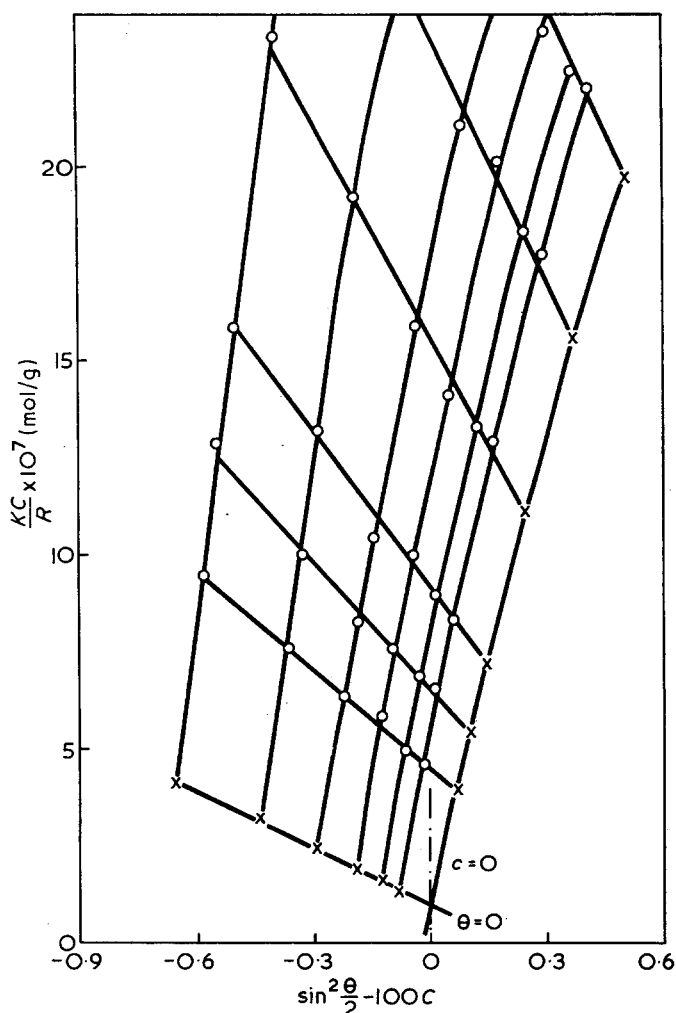


Figure 1 Zimm plot for copolymer (80.4/19.6). Sample taken after 2.61 Mrad irradiation. Toluene solution at 25°C

low viscosity (45 cP) polydimethylsiloxane fluid. Scattered intensities were measured at nine viewing angles between 30° and 145° with unpolarized 546 nm light. The Rayleigh scattering of benzene at 90° was used as a calibration standard and this value was taken to be $1.62 \times 10^{-5} \text{ cm}^{-1}$.¹² Two anionic polystyrene standard samples with nominal molecular weights 5.55×10^5 and 1.85×10^6 yielded respective \bar{M}_w values of 4.98×10^5 and 1.80×10^6 in toluene solution, with this apparatus and calibration standard.

The light scattering data were treated by Zimm's procedure¹³, with a negative concentration multiplier to spread the low angle data points¹⁴. A typical Zimm plot is shown in Figure 1, for the 19.6 weight % styrene copolymer.

RESULTS

Specific refractive index measurements were made with 546 and 436 nm wavelength light in benzene, toluene, 1,2-dichloroethane, cyclohexane, carbon tetrachloride and cyclohexanone. The data are listed in Table 1, along with comparative values from the literature.

The results in Table 1 are plotted in Figure 2 according to equation (8). The results are seen to be linear in weight fraction of styrene, as expected, and to extrapolate to the available literature values for specific refractive index increments of homopolymers in the particular solvents. The extrapolated homopolymer ν values for the various solvents are listed in Table 1. The extrapolated homopolymer figures are all very close to literature results except for polystyrene/dichloroethane at 546 nm and polybutadiene/benzene at 546 nm. The good agreement of all the other values with those of a variety of sources lends support to the reliability of the present data.

Table 1 Specific refractive index increment (cm^3/g) data of styrene-butadiene polymers in various solvents at 25°C

Sample ^a	Styrene content (wt. %)	ν at 546 nm						ν at 436 nm					
		Benzene	Toluene	1,2-Di-chloro-ethane	Cyclo-hexane	Carbon tetra-chloride	Cyclo-hex-anone	Benzene	Toluene	1,2-Di-chloro-ethane	Cyclo-hexane	Carbon tetra-chloride	Cyclo-hex-anone
Polybutadiene	0	0.011 ¹⁵	—	—	0.118 ¹⁶	—	—	—	—	—	0.126 ¹⁶	—	—
Polybutadiene extrapolated values (Figure 2)	—	0.021	0.031	0.088	0.118	—	0.081	0.022	0.034	0.092	0.127	—	—
Copolymer (80.4/19.6)	19.6	0.037	0.046	0.099	0.127	(0.0995 ²²)	0.091	0.038	0.048	0.104	0.134	—	0.106
Copolymer (56.5/43.5)	43.5	0.058	0.063	0.112	0.138	0.112	0.103	0.059	0.069	0.123	0.149	0.122	0.121
Copolymer (29.7/70.3)	70.3	0.083	0.084	0.131	0.155	—	—	0.084	0.088	0.146	0.167	—	—
Polystyrene B10	100	0.107	—	—	—	—	—	0.109	—	—	—	—	—
		0.106 ²	0.109 ¹⁷	0.155 ¹⁸	0.170 ²¹	(0.148 ²³)	—	0.109 ²⁴	0.113 ²⁶	0.168 ¹⁸	0.181 ²⁵	0.159 ²⁷	0.151 ²⁸
		0.108 ¹⁵	—	0.161 ¹⁹	—	—	—	0.112 ²⁵	—	—	—	—	—
		—	—	0.168 ²⁰	—	—	—	—	—	—	—	—	—
Polystyrene extrapolated values (Figure 2)		0.106	0.108	0.149	0.170	—	0.132	0.109	0.113	0.168	0.182	—	—

^a Copolymer compositions are given in terms of weight % of butadiene and styrene, respectively

Table 2 lists experimental values for \bar{M}_{app} of irradiated copolymers in the various solvents. All the results in toluene exhibit minima with increasing radiation dose, whereas \bar{M}_{app} values in the other solvents increase monotonically with radiation dose in the pre-gel region. Figure 3 illustrates these tendencies, for the 80.4/19.6 copolymer in the three solvents studied here. The steady increase in molecular weight is as expected from the radiation chemistry of this system⁹.

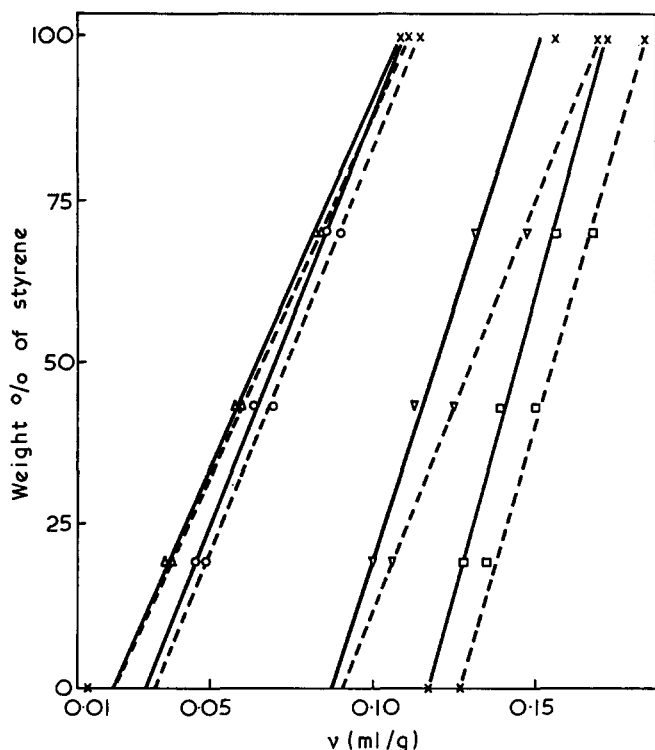


Figure 2 Specific refractive index increments of styrene-butadiene copolymers vs. styrene content. —, 546 nm; ---, 436 nm. Δ , Benzene; \circ , toluene; ∇ , 1,2-dichloroethane; \square , cyclohexane. Homopolymer values (x) from literature sources cited in Table 1

\bar{M}_{app} of the unirradiated 80.4/19.6 and 56.5/43.5 copolymers were also measured in carbon tetrachloride and cyclohexanone. These results, shown in Table 2, are consistent with \bar{M}_{app} values obtained in other solvents in which ν was about 0.1 ml/g. There would thus seem to be no anomalous effects which could be ascribed to incomplete dissolution of the polymer. The data appear to reflect refractive index difference influences as expected^{1, 2}.

The heterogeneity parameters calculated by fitting experimental \bar{M}_{app} values to equation (9) are given in

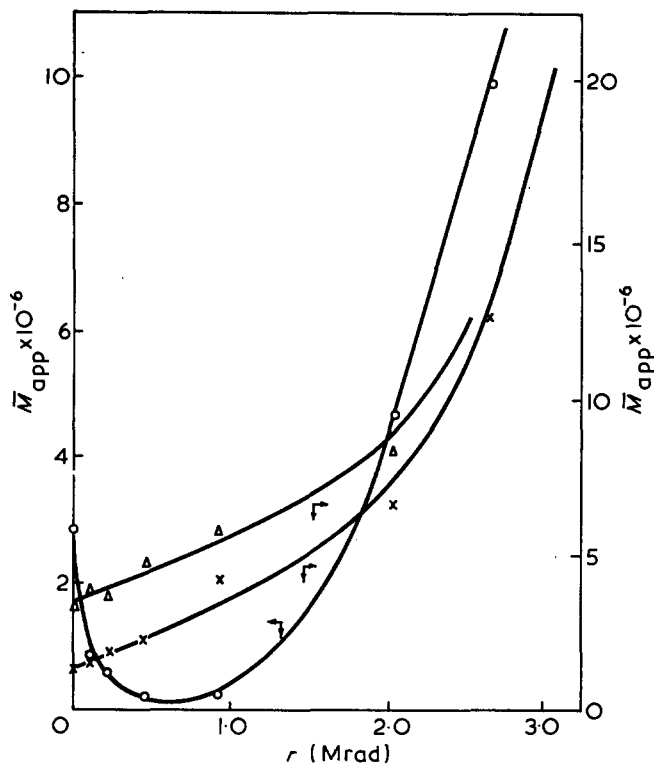


Figure 3 Apparent \bar{M}_w as a function of radiation dose in various solvents. Copolymers with 19.6 weight % styrene. \circ , Toluene; \times , 1,2-dichloroethane; Δ , cyclohexane

Table 2 Light scattering molecular weights ($\times 10^{-3}$) of irradiated copolymers in the pre-gel region

Sample	Dose (Mrad)	\bar{M}_{app}					\bar{M}_w (eqn 21)
		Toluene	Dichloroethane	Cyclohexane	Carbon tetrachloride	Cyclohexanone	
(80.4/19.6) polymer	0	2 860	122	330	150	175	1 419
	0.12	850	159	389	—	—	1 151
	0.23	650	171	366	—	—	992
	0.46	230	223	465	—	—	1 130
	0.92	200	435	478	—	—	935
	2.07	4 760	667	833	—	—	1 252
	2.61	10 000	1 220	—	—	—	—
(56.5/43.5) copolymer	0	1 620	126	160	167	155	818
	0.12	130	200	206	—	—	201
	0.23	182	227	222	—	—	189
	0.35	290	250	229	—	—	173
	0.46	401	278	340	—	—	611
	0.92	740	345	451	—	—	951
	1.59	1 230	590	700	—	—	1 302
	2.30	4 350	2 000	16 700	—	—	66 900
(29.7/70.3) copolymer	0	2 500	105	286	—	—	2 258
	0.02	1 640	208	1 000	—	—	5 179
	0.04	710	228	1 280	—	—	5 968
	0.08	390	910	1 700	—	—	4 943
	0.12	10 000	1 390	67 000	—	—	346 000
	0.23	∞	—	—	—	—	—

Table 3 Composition heterogeneity parameters of the irradiated polymers

Sample	Dose (Mrad)	P/\bar{M}_w	Q/\bar{M}_w	$Q_{\max} \times 10^{-5}$	Q/Q_{\max}
(80.4/19.6) copolymer	0	-1.33	1.92	2.24	12.2
	0.12	-1.04	1.13	1.82	7.20
	0.23	-0.98	1.04	1.57	6.57
	0.46	-0.87	0.75	1.79	4.75
	0.92	-0.55	0.39	1.48	2.46
	2.07	-0.48	0.35	1.98	2.23
	2.61	—	—	—	—
(56.5/43.5) copolymer	0	-1.71	3.40	2.01	13.8
	0.12	0.11	-0.41	0.54	-1.53
	0.23	0.34	-0.58	0.47	-2.33
	0.35	0.50	-0.36	0.43	-1.47
	0.46	-0.80	1.12	1.50	4.57
	0.92	-0.96	1.41	2.34	5.73
	1.59	-0.87	1.37	3.20	5.59
	2.30	-1.27	1.44	165.0	5.82
(29.7/70.3) copolymer	0	-2.07	4.58	4.72	21.9
	0.02	-1.68	2.82	10.8	13.5
	0.04	-1.56	2.35	12.5	11.2
	0.08	-1.23	1.57	10.3	7.55
	0.12	-1.59	2.29	724.0	10.9

Table 3. These parameters are expressed in the forms P/\bar{M}_w , Q/\bar{M}_w and Q/Q_{\max} , which are most useful for comparative purposes.

The P parameter is a measure of the drift in composition of the copolymer with molecular weight. In the present case, the negative sign reflects a predominance of butadiene in the high molecular weight fractions. The values of (P/\bar{M}_w) are numerically much greater than the theoretical limits indicated in equation (14).

The (Q/Q_{\max}) values obtained are obviously impossible since they exceed the theoretical limit of unity. Some of the Q values for the 56.5/43.5 copolymer are negative, and this also is physically impossible. The negative Q/\bar{M}_w values are a consequence of the low \bar{M}_{app} figures obtained in toluene solutions.

The failure of the heterogeneity analysis in this case parallels examples recorded in previous studies of statistical copolymers^{2, 4-6}.

Heterogeneity parameters were estimated from toluene, dichloroethane and cyclohexane data. The \bar{M}_{app} values from carbon tetrachloride and cyclohexanone solutions were not used since these solvents provided ν and \bar{M}_{app} data close to values which were already available from the other three solutions.

DISCUSSION

Application of the light scattering method to random copolymers has generally yielded disappointing results, as noted above. Benoit and Froelich³ have suggested some possible explanations for the disagreement between heterogeneity measurements and copolymerization theory, but none of these reasons seems to be very satisfactory.

The equations developed by Stockmayer¹ and Benoit² and their coworkers depend explicitly on use of molecular weight-independent homopolymer ν values in equation (8). The specific refractive index increment of a polymer in a given solvent will be essentially constant and independent of degree of polymerization provided the degree of polymerization exceeds a certain minimum value. This minimum may be a function of the solvent as well as the polymer.

This possibility is illustrated by results of measurements of ν of four anionic polystyrenes with molecular weights of 2.0×10^3 , 4.0×10^3 , 1.0×10^4 and 2.04×10^4 . The specific refractive index increments obtained with 546 nm light are shown in Figure 4, from which we see that the dichloroethane solutions are most sensitive to molecular weight while the toluene solutions tend to be least affected by molecular weight changes. The curves recorded here for toluene and cyclohexane mixtures agree well with those given by Barrall and coworkers²⁹ and Kratochvil³⁰.

In this particular case, \bar{M}_n of the initial styrene-butadiene copolymers was in the 30 000–50 000 range and was essentially unchanged by irradiation in the pre-gel dose region⁹. We may assume reasonably that the homopolymer ν value applicable to a given copolymer molecule is that of a homopolymer with degree of polymerization equal to the sum of the sequence lengths of the particular monomer in the copolymer. From equation (9), \bar{M}_{app} is strongly dependent on the parameter b which is defined in turn by equation (10). The sums of the polystyrene sequence lengths in the present copolymers are within the molecular weight ranges encompassed by the data points in Figure 4 and b is not a constant quantity for these samples, except in dichloroethane solutions.

The parameter b may vary slightly in cyclohexane and apparently changes strongly in toluene mixtures.

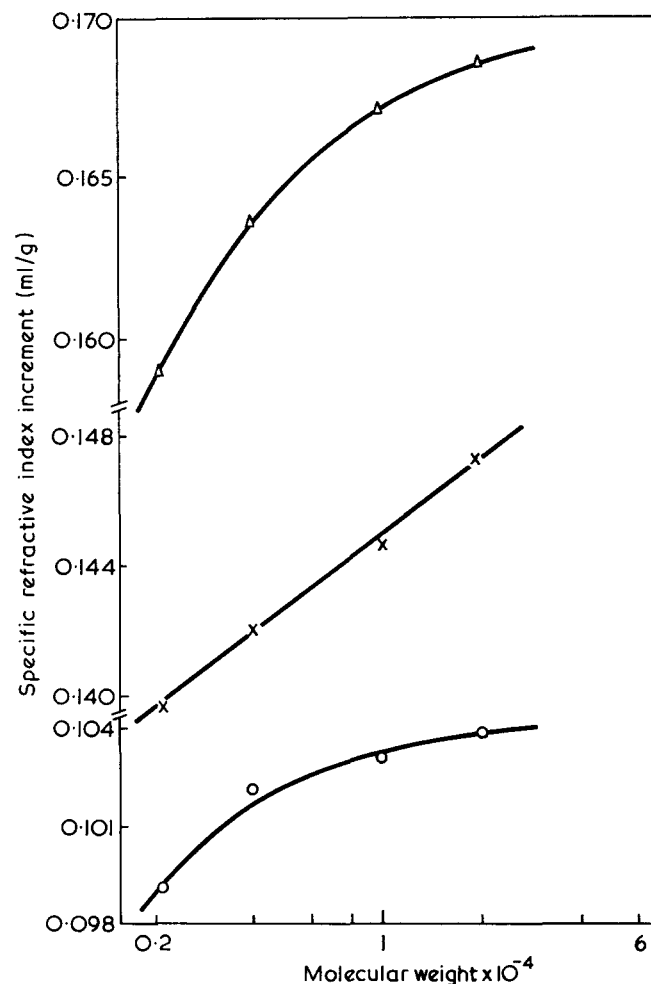


Figure 4 Specific refractive index increment as a function of molecular weight of anionic polystyrenes. Δ , Cyclohexane; \times , 1,2-dichloroethane; \circ , toluene

This explains the anomalous variation of toluene \bar{M}_{app} values with radiation dose shown in Figure 3, since progressive crosslinking increases the effective molecular weight of polystyrene in the larger molecules which are thus formed. The concurrent decrease in b at low radiation doses results in a decrease in \bar{M}_{app} in accordance with the expected parabolic dependence of \bar{M}_{app}/\bar{M}_w on $(\nu_A - \nu_B)/\nu^5$.

The theory of light scattering of copolymers is a direct extension of the fundamental equations which apply to homopolymers, except for the assumption of additivity of refractive indices. It is tempting to ascribe the apparent inapplicability of the theory to random copolymers to failure of the additivity rule for short monomer sequences. This explanation is not consistent, however, with the established fact that the refractive index of a copolymer agrees with the value estimated from additivity rules³ and with the general coincidence of extrapolated and measured specific refractive indices of homopolymers recorded in Table 1. The solvent dependence of the molecular weight- b parameter relation suggested here seems to be in better accord with all the experimental facts. It suggests also that the reported differences between block and random copolymers are more likely artifacts of the particular solvents and polymer molecular weights used than reflections of basic differences between the two kinds of copolymer.

Tuzar and coworkers^{31, 32} have summarized the requirements of the specific refractive indices of homopolymer solutions for the accurate study of copolymer characteristics. It seems necessary to add to their list the requirement that the solvents be such that $(\nu_A - \nu_B)/\nu$ is not strongly dependent on molecular weight in the molecular weight range which corresponds to the sum of homopolymer sequences in the particular copolymers.

ACKNOWLEDGEMENT

This work was supported in part by the National Research Council of Canada.

REFERENCES

1 Stockmayer, W. H., Moore, Jr, L. D., Fixman, M. and Epstein, B. N. *J. Polym. Sci.* 1955, **16**, 517

2 Bushuk, W. and Benoit, H. *Can. J. Chem.* 1958, **36**, 1616
 3 Benoit, H. and Froelich, D. in 'Light Scattering from Polymer Solutions' (Ed. M. B. Huglin), Academic Press, New York, 1972
 4 Leng, M. and Benoit, H. *J. Chim. Phys.* 1961, **58**, 480
 5 Eskin, V. E., Baranskovskaya, I. A., Litmanovich, A. D. and Topchiev, A. V. *Vysokomol. Soedin.* 1964, **6**, 896
 6 Jordan, J. R. *J. Polym. Sci. (A-1)* 1968, **6**, 2209
 7 Stockmayer, W. H. *J. Chem. Phys.* 1945, **13**, 199
 8 Alfrey, Jr, T., Bohrer, J. J. and Mark, H. 'Copolymerization', Interscience, New York, 1952
 9 Chau, T. C. and Rudin, A. *Can. J. Chem. Eng.* 1974, **52**, 79
 10 Rudin, A. and Chau, T. C. *J. Polym. Sci. (Polym. Chem. Edn)* 1973, **10**, 3589
 11 Roche, R. S. and Tanner, A. G. *Angew. Makromol. Chem.* 1970, **13**, 183
 12 Claesson, S. and Ohman, J. *Ark. Kemi* 1964, **23**, 69
 13 Zimm, B. H. *J. Chem. Phys.* 1948, **16**, 1093, 1099
 14 van Wijk, R. and Staverman, A. J. *J. Polym. Sci. (A)* 1964, **2**, 1011
 15 Angelo, R. J., Ikeda, R. M. and Wallach, M. L. *Polymer* 1965, **6**, 377
 16 Ribeyrollis, Ph., Guyot, A. and Benoit, H. *J. Chim. Phys.* 1959, **56**, 377
 17 Norberg, P. N. and Sundelof, L. O. *Makromol. Chem.* 1964, **77**, 77
 18 Krause, S. *J. Phys. Chem.* 1961, **65**, 1618
 19 Outer, P., Carr, C. I. and Zimm, B. H. *J. Chem. Phys.* 1950, **18**, 830
 20 Kotaka, T., Donka, N., Ohnuma, H. and Inagaki, H. *J. Polym. Sci. (A-2)* 1968, **6**, 1803
 21 Cantow, H. J. Z. *Phys. Chem.* 1956, **7**, 58
 22 Bahary, W. S. and Bsharah, L. *J. Polym. Sci. (A-1)* 1968, **6**, 2819
 23 Smith, T. E. and Carpenter, D. K. *Macromolecules* 1968, **1**, 204
 24 Bodmann, O. *Makromol. Chem.* 1969, **122**, 210
 25 Cowie, J. M. G. and Bywater, S. *J. Macromol. Chem.* 1966, **1**, 581
 26 Ohnuma, H., Kotaka, T. and Inagaki, H. *Rep. Progr. Polym. Phys. Japan* 1968, **11**, 29
 27 Eskin, V. E., Izyumnikov, A. L., Royozhkina, E. D. and Vyrski, Yu. P. *Polym. Sci. USSR* 1965, **7**, 1310
 28 Guthrie, J. T., Huglin, M. B. and Phillips, G. O. *J. Appl. Polym. Sci.* 1972, **16**, 1017
 29 Barrall, E. M., Cantow, M. J. R. and Johnson, J. F. *J. Appl. Polym. Sci.* 1968, **12**, 1373
 30 Kratochvil, J. P. in 'Characterization of Macromolecular Structure' (Ed. D. McIntyre), Nat. Acad. Sci. Publication 1573, Washington, D.C., 1968
 31 Tuzar, Z. and Bohdanecky, M. *Coll. Czech. Chem. Commun.* 1969, **34**, 289
 32 Tuzar, Z. and Kratochvil, P. *J. Polym. Sci. (B)* 1969, **7**, 825

Solvent stress crazing in PMMA:

1. Geometrical effects

E. H. Andrews and G. M. Levy

*Department of Materials, Queen Mary College, London E1 4NS, UK
(Received 27 November 1973; revised 19 March 1974)*

Single crazes were propagated in poly(methyl methacrylate) (PMMA) by loading sheet specimens containing 'starter' cracks and immersed in various alcohols. Craze lengths and propagation velocities were measured (as functions of the applied load) using an ultrasonic scanning technique, for three types of behaviour. These were: (I) where craze arrest occurs after some growth; (II) where the craze grows at a constant velocity for an unlimited distance; and (III) where constant velocity growth continues after removal of the original 'starter' crack and re-application of the load. The results are analysed using the concept of an 'equivalent crack', whose length l turns out to be related to the length c_0 of the starter crack. At temperatures above a previously identified 'characteristic temperature', l is commensurate with c_0 , but at lower temperatures, $l \ll c_0$. These results are discussed in terms of the strain hardening properties of the craze matter which fills the craze.

INTRODUCTION

The application of fracture mechanics to the growth of solvent induced cracks and crazes in a glassy polymer has been discussed in a number of papers¹⁻⁴. The work reported here extends these studies with particular reference to geometrical effects associated with the 'starter' crack used to localize and initiate craze formation.

Marshall *et al.*³ observed that craze propagation velocities in poly(methyl methacrylate) (PMMA) immersed in methanol were governed not by the applied stress σ_0 , but by the stress intensity factor K_0 given (for tensile loading of wide sheets containing an edge crack) by:

$$K_0 = Z\sigma_0 c_0^{1/2} \quad (1)$$

where Z is a constant (related to the ratio of c_0 to the specimen width, b) and c_0 is the length of the starter crack inserted in the edge of the sheet before immersion. This applied even when the craze length c so far exceeded c_0 that the stress field of the starter crack could exert no significant influence at the propagating craze tip.

In the original work of Marshall *et al.*, the stress was applied by a 'dead-load' which remained constant throughout any given test. Thus σ_0 and c_0 were not independently variable in a given test. In a subsequent paper, Marshall and Williams⁵ showed that fatigue-type loading could be treated as an extension of the constant load situation. In the present study also, variations of σ_0 could be made without interruption of craze propagation, throwing light on the nature of the K_0 dependence of craze velocity.

The predominance of K_0 as the rate-determining factor causes obvious difficulties in applying the results of the investigations cited above to the crazing of virgin specimens. In the absence of a starter crack, c_0 is either zero or, at least, of microscopical dimensions, giving equally small K_0 values. Nevertheless crazes do initiate and grow

at reasonable velocities under these conditions, in apparent contradiction to equation (1). In order to elucidate this point, crazes were initiated and grown from starter cracks under three sets of conditions.

(1) First, under relatively low applied stress, crazes grow for a short distance from the starter crack and then arrest. The craze length at arrest increases with the stress until a 'breakaway' point is reached at which the craze continues to grow indefinitely at constant stress. These effects were described by Marshall *et al.*³. Crazes which arrest will be described as exhibiting 'type I' behaviour.

(2) Craze growth subsequent to 'breakaway' occurs at constant velocity under a steady applied stress, and will be described as type II behaviour.

(3) Type III behaviour is obtained by establishing type II growth, removing the specimen from the solvent, machining away the edge containing the starter crack, and recommencing the experiment. This has the result of entirely removing any instantaneous effects of the starter-crack stress field on craze growth. This is particularly relevant since Marshall *et al.* explained the K_0 dependence of craze velocity in terms of the instantaneous crack opening displacement at the tip of the starter crack. It also throws light on the behaviour of crazes initiated and grown in virgin material.

The results of these experiments are described in this paper.

EXPERIMENTAL

Materials and specimen preparation

The polymer used was poly(methyl methacrylate) (Perspex, ICI Ltd) supplied as 1 mm cast sheets. All experiments were carried out on a single batch of material. The polymer was characterized in terms of molecular

weight, intrinsic viscosity, density and glass transition temperature. Details are given in the Appendix.

Ethyl and n-butyl alcohols (general purpose grades) were chosen as solvents.

Specimens were cut from the polymer sheet with dimensions $0.16 \times 0.07 \times 0.001$ m, the tensile load being applied in the direction of their long axis. In order to localize craze growth, and thus ensure that only a single craze develops, it is necessary to insert a starter crack in the edge of the specimen. This was done by the method described by Andrews and Bevan² which involved cooling the specimen edge in liquid nitrogen and propagating a brittle crack which arrested when it ran into the uncooled region of the sheet. The specimen edge was then milled away to give a starter crack of any desired length, c_0 . Milling was also used to remove the starter crack when type III growth was to be studied.

These steps in specimen preparation are shown schematically in Figure 1. To avoid unwanted crazes growing from other points on the specimen edge, the milled edges of the sheet were polished to a glass-like finish.

Measurements of craze growth

All craze velocity measurements were made automatically using the ultrasonic scanning equipment described previously by Andrews and Levy⁶ and developed specially for this work. It was established that ultrasonic irradiation did not affect the rate of craze propagation in any way.

The specimen was subjected to uniform tensile loading applied, and measured, by deflection of a simply supported steel beam. The specimen grips had been specially designed to produce an evenly-spread tensile stress field, whose uniformity was checked photoelastically.

The specimen was totally immersed in solvent in a thermostatically controlled, heated chamber containing observation windows. Temperature control was better than ± 0.2 K.

The lengths c_0 of the starter crack, and c of arrested crazes were measured with a travelling microscope.

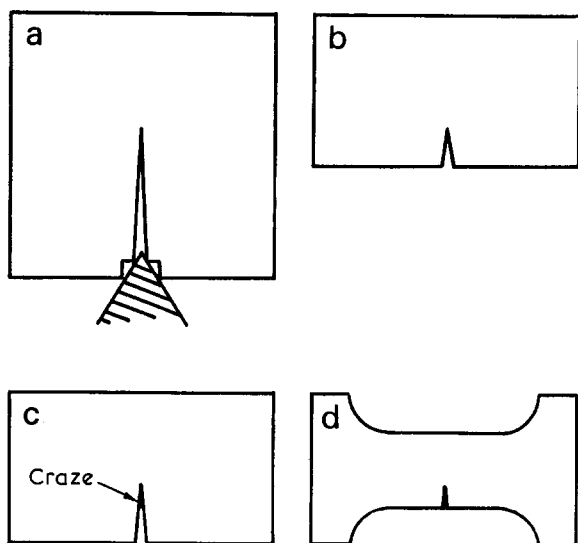


Figure 1 Specimens preparation. (a) Crack produced in cooled edge of sheet; (b) excess crack length cut away; (c) craze growth from crack; (d) starter crack milled away for type III experiments

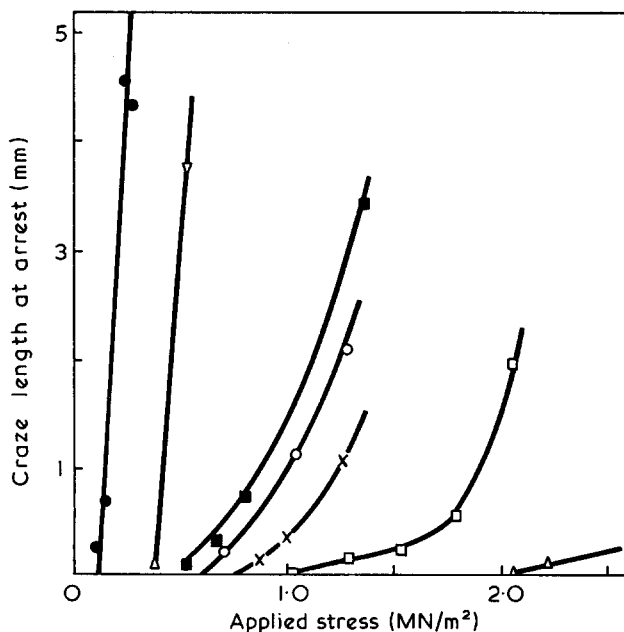


Figure 2 Type I growth, ethyl alcohol at 293K. c_0/b ratios: Δ , 0.01; \square , 0.03; \times , 0.05; \circ , 0.11; \blacksquare , 0.10; ∇ , 0.24; \bullet , 0.45

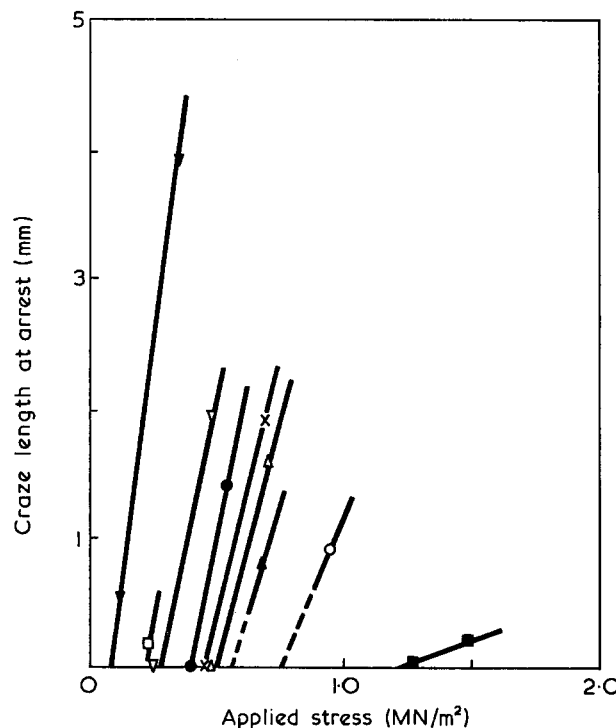


Figure 3 As Figure 2 but for ethyl alcohol at 303K. c_0/b ratios: \blacksquare , 0.02; \circ , 0.03; \blacktriangle , 0.03; \triangle , 0.08; \times , 0.07; \bullet , 0.10; ∇ , 0.18; \square , 0.19; \blacktriangledown , 0.31

RESULTS AND DISCUSSION

Type I behaviour

Type I (craze arrest) behaviour clearly occurs whilst the craze tip lies within the stress-field of the starter crack, and can be largely understood in these terms. The collected experimental data are shown in Figures 2 to 4, where the craze length at arrest (c_a) is plotted as a function of applied stress σ_0 for different values of the ratio c_0/b where b , the specimen width, is a fairly constant quantity. The quantity c_a is measured from the starter crack tip, i.e. the total discontinuity length (crack plus craze) at arrest is $(c_0 + c_a)$.

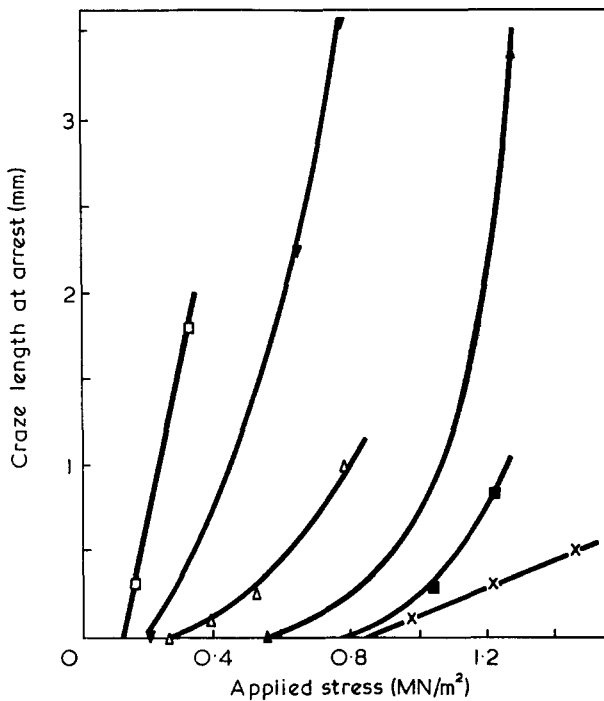


Figure 4 As Figure 2 but for butyl alcohol at 298K. c_0/b ratios: \times , 0.01; \blacksquare , 0.02; \blacktriangle , 0.06; \triangle , 0.14; \blacktriangledown , 0.15; \square , 0.40

The most numerous data are for immersion in ethyl alcohol at 293K (Figure 2), but the results for ethyl alcohol at 303K and n-butanol at 298K follow a similar pattern.

The craze length at arrest increases with the applied stress in all cases, eventually tending to infinity as the 'breakaway' point is reached for transition from type I to type II behaviour. If the curves are extrapolated to $c_a=0$, they intersect the applied stress axis at a stress σ_{I1} which is the threshold applied stress necessary to form a craze at the tip of the starter crack (the 'critical' applied stress for type I growth). This threshold stress is clearly dependent upon c_0/b , increasing as c_0 decreases. The slope of the curve of c_a vs. σ_0 also changes with c_0 , being smaller for small c_0 .

These data are wholly consistent with the idea that the craze propagates as long as the major principal stress at its tip is above some critical local value, p . This would be expected from the experiments of Sternstein *et al.*⁷ who found the pattern of crazing around a hole in a stressed sheet of PMMA could be explained precisely in terms of just such a critical stress for craze growth.

If it be assumed that growth of the craze does not significantly modify the stress field of the starter crack, the idea can be tested quantitatively. This assumption is not unreasonable, since the craze (unlike a crack) is a load-bearing entity though, clearly, it cannot be wholly valid.

Consider first the behaviour of the threshold stress σ_{I1} . According to linear mechanics, the major principal stress at the crack tip is⁸:

$$\sigma_{yy} = \sigma_0 [1 + 2(c_0/\rho)^{1/2}] \quad (2)$$

where ρ is the crack tip radius. If $c_0 \gg \rho$, and σ_{yy} has some critical value, p , for craze formation,

$$\sigma_0^2 \equiv \sigma_I^2 = \sigma_{yy}^2 / 4c_0 = p^2 \rho / 4c_0 \quad (3)$$

A plot of σ_I^2 against c_0^{-1} should therefore be a straight line through the origin. A finite width correction must

first be applied⁹ by multiplying c_0 by the quantity Z^2 where:

$$Z = 1.99 - 0.41(c_0/b) + 18.70(c_0/b)^2 - 38.48(c_0/b)^3 + 53.85(c_0/b)^4 \quad (4)$$

Figure 5 is a plot of σ_I^2 against $(Z^2 c_0)^{-1}$ and shows good linearity within the limitations of experimental error, both for ethyl alcohol at 303K and n-butanol at 298K. The slope of these plots:

$$s \equiv p^2 \rho / 4 \quad (5)$$

is also equal to the product of $2E$ (where E is the Young's modulus) and the surface work \mathcal{F} for formation of unit area of fresh interface¹, which gives the following values for \mathcal{F} :

Environment	Temperature (K)	\mathcal{F} (J/m ²)
Ethyl alcohol	293	1.2
Ethyl alcohol	303	1.1
n-Butanol	298	0.6

It appears, then, that the idea of a critical local stress for craze formation accounts for the dependence of the threshold applied stress σ_{I1} upon c_0 .

Consider secondly the craze arrest length c_a . A convenient approximation for the major principal stress in the vicinity of the crack tip is given¹⁰ by:

$$\sigma_{yy}(x) = \sigma_0 \left\{ 1 - \left[\frac{\sin \frac{\pi c_0}{2b}}{\sin \frac{\pi(c_0+x)}{2b}} \right]^2 \right\}^{-1/2} \quad (6)$$

where x is the distance ahead of the crack tip along the crack (or x) axis. For $c_0/b \ll 1$, equation (6) can be simplified to:

$$\sigma_{yy}(x) = \sigma_0 \left\{ 1 - \left[\frac{c_0}{c_0+x} \right]^2 \right\}^{-1/2} \quad (7)$$

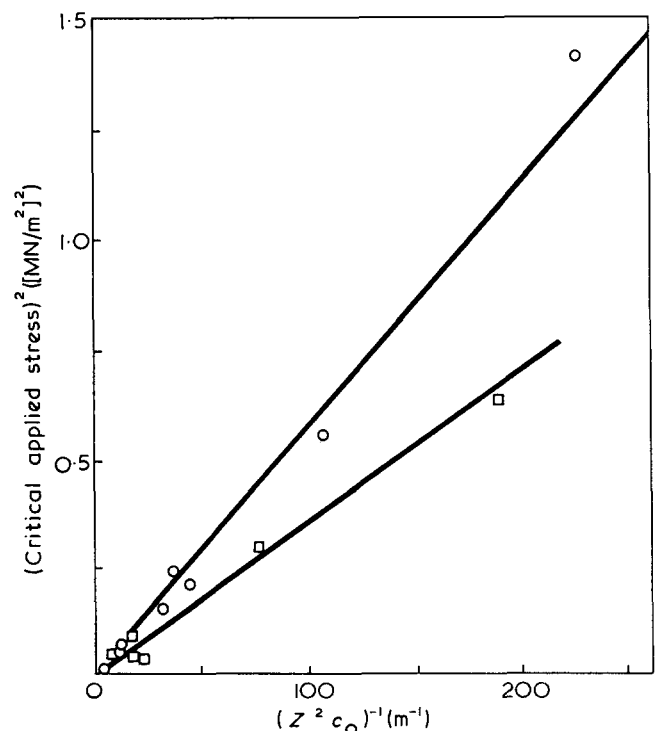


Figure 5 (Critical applied stress)² for type I growth, as a function of reciprocal crack length. \circ , Ethyl alcohol at 303K; \square , butyl alcohol at 298K

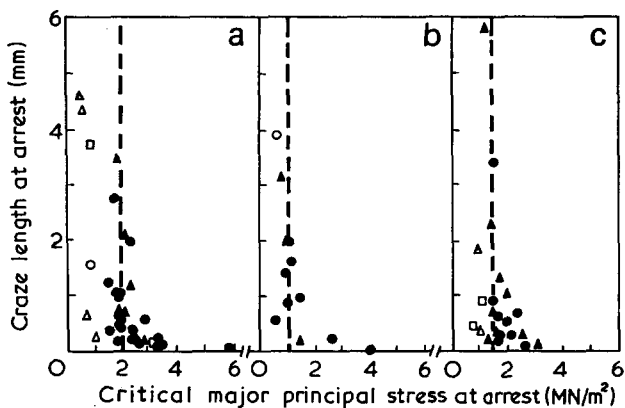


Figure 6 Constancy of the critical local stress required at the craze tip for propagation. Different symbols refer to various c_0/b ratios; open symbols refer to $c_0/b > 0.2$. (a) Ethyl alcohol at 293K; (b) ethyl alcohol at 303K; (c) butyl alcohol at 298K

The major principal stress at the craze tip is obtained simply by replacing x by the craze length c (again assuming that craze growth does not perturb the starter-crack stress field). At arrest we expect $c = c_a$, and $\sigma_{yy} = p$, giving:

$$p = \sigma_0 \left\{ 1 - \left[\frac{c_0}{c_0 + c_a} \right]^2 \right\}^{-1/2} \quad (8)$$

i.e. the right-hand side of equation (8), involving the applied stress σ_0 and the arrest length of the craze, should be constant.

The data of Figures 2-4 have been replotted with the right hand side of equation (8) as abscissa and c_a as ordinate, and the results are shown in Figure 6. Apart from data for large c_0/b (> 0.3), most of the points are reasonably well represented by equation (8), i.e. by a constant value of p . For large c_0/b the formulae used for σ_{yy} are not accurate.

Departures from $p = \text{constant}$ are also found at craze lengths $c_a < 0.2$ mm, under which conditions p is predicted to be unusually large. This is to be expected if, as suggested elsewhere², the important factor in craze formation is the local hydrostatic component of stress, rather than the major principal stress. In a narrow craze consisting of rigid boundaries either side of a compliant layer, a stress σ_{yy} normal to the craze plane in the rigid continuum will produce a hydrostatic stress σ_{yy} in the compliant zone^{11,12} (see Figure 7a). This situation will exist at the tip of a craze whose length is more than, say, ten times its thickness.

$$p(\text{hydrostatic}) = \sigma_{yy}(\text{tensile})$$

When the craze is very short, however, the 'sandwich' configuration discussed above does not exist and the compliant craze material is more nearly subject to simple tension (Figure 7b). In simple tension, however,

$$p(\text{hydrostatic}) = \frac{\sigma_{yy}(\text{tensile})}{3}$$

so that, to obtain the same hydrostatic tension in very short crazes as in 'sandwich' crazes requires a tensile stress three times as large for the former than for the latter.

We would thus expect p to tend to a constant value for 'long' crazes which is one-third the value for very short crazes. The limited data for very small c_a , shown in Figure 6, are consistent with this expectation.

Type II and type III behaviour

Type II behaviour is characterized by constant velocity propagation under a steady applied load, suggesting that the stress conditions at the craze tip do not change as the craze grows. The alternative explanation is that craze velocity is not sensitive to the local stress level, but this is contradicted by the immediate change in craze velocity which occurs if the external load is altered.

Figure 8 shows typical type II data as plots of craze tip velocity against applied stress for various c_0/b ratios. The extreme sensitivity of craze velocity to applied stress is evident, as is the influence of c_0 . Extrapolation of the curves to zero velocity allows us to define a critical stress

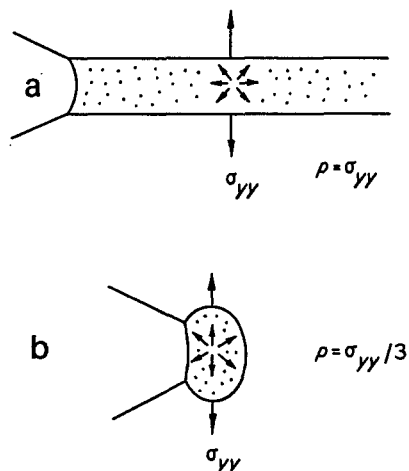


Figure 7 Possible relationship between hydrostatic and tensile stress components for (a) long craze and (b) short craze

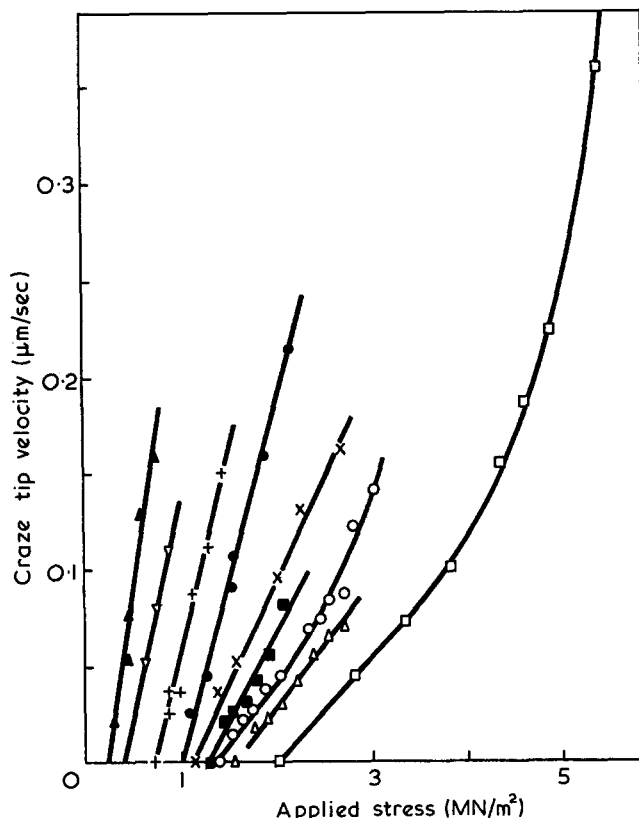


Figure 8 Type II growth, ethyl alcohol at 293K. c_0/b ratios: \square , 0.03; \triangle , 0.06; \circ , 0.11; \blacksquare , 0.10; \times , 0.18; \bullet , 0.23; $+$, 0.32; ∇ , 0.47; \blacktriangle , 0.42

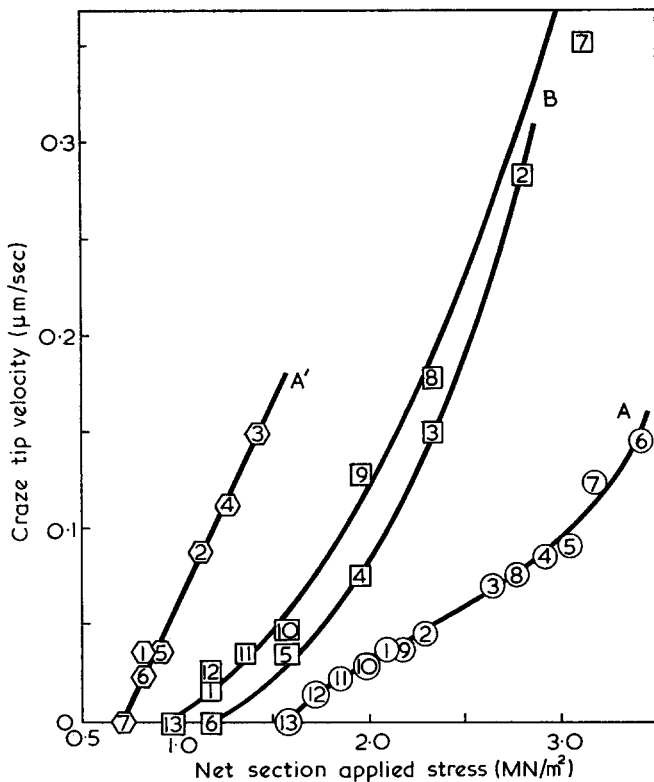


Figure 9 Effect of load cycling on craze tip velocity. c_0/b ratios: A, 0.12; B, 0.23; A', 0.32. Numbers enclosed by experimental points denote loading sequence. The centre pair of curves (B) show hysteresis arising from large load-change steps. The two outer curves (A, A') show absence of hysteresis when load steps are small

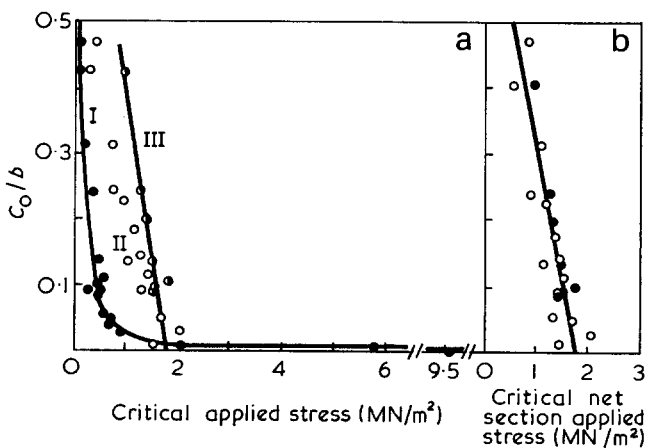


Figure 10 (a) Critical stresses for types I (●), II (○) and III (○) growth as functions of c_0/b . (b) Critical stresses for types II (○) and III (●) showing reconciliation achieved by use of net section stresses

σ_{II} for type II growth, analogous to σ_I , the threshold applied stress for type I growth. In either case no new craze is formed if the applied stress is less than the critical value.

Figure 9 shows the effect of cycling the applied stress. Provided the changes of stress are not too rapid, the curve of craze velocity against stress for a given c_0 is reversible, and the critical stress σ_{II} is not affected by the loading history (A in Figure 9). Significant shifts of σ_{II} can be obtained, however, with sudden load changes (B in Figure 9).

Entirely parallel results were obtained in type III experiments in which the starter crack was removed

after the establishment of type II propagation. Again curves of craze velocity against applied stress are obtained which can be extrapolated to zero velocity to give a threshold stress σ_{III} for propagation. Like σ_{II} , σ_{III} is clearly a function of c_0/b .

In Figure 10a are shown the values of σ_{II} and σ_{III} obtained for PMMA in ethanol at 293K as functions of c_0/b . The differences between σ_{II} and σ_{III} can be entirely eliminated by calculating σ_{II} as a net-section stress, i.e. by dividing the applied load by the unsevered cross-section of the specimen rather than the total cross-section (see Figure 10b). Thus

$$\sigma_{II} (\text{nominal}) = \text{load} / (\text{sheet thickness} \times \text{breadth})$$

$$\sigma_{II} (\text{net section}) = \text{load} / (\text{sheet thickness} \times [b - c_0])$$

Since σ_{III} relates to the situation after the removal of the non load-bearing region of the specimen, it seems reasonable to work in terms of σ_{II} (net section) and σ_{III} will hereafter bear this meaning.

To summarize, then, craze velocity in both type II and type III growth is controlled by the instantaneous value of the net-section applied stress regardless of the presence or absence of a starter crack. This clarifies two important points. First, it demonstrates that the initial stress intensity factor K_0 exerts its subsequent influence on craze growth via the starter crack length c_0 rather than the initial applied stress under which craze growth was established. This was not clear from the previous work of Marshall *et al.* since in their work any one craze was initiated and grown under the *same* steady load. Secondly, the correspondence of type II and type III behaviour shows that the effect of c_0 on subsequent craze growth is a 'memory' effect not requiring the continued physical presence of the starter crack. In particular the effect is not due to the instantaneous crack opening displacement under load of the starter crack.

Comparison of type I and type II/III behaviours

In Figures 11a-11c the threshold applied stresses σ_I , σ_{II} and σ_{III} are plotted against c_0/b for the various solvents and temperatures employed. As previously discussed, σ_{II} and σ_{III} define the same curve, but σ_I is significantly smaller for ethanol at 293K and for n-butanol. For ethanol at 303K, however, σ_I and σ_{II} , σ_{III} values are nearly indistinguishable.

The relationship between σ_I and σ_{II} , σ_{III} can be clarified by use of the 'equivalent crack' concept introduced by Andrews and Bevan². These authors accounted for the unknown stress concentration at the tip of a craze by defining a parameter l , the equivalent crack length. This parameter is the length of a true crack which would give rise at its tip to a stress concentration equal to that actually existing at the tip of the craze. The 'equivalence' relates to the magnitude of the maximum stress and does not necessarily imply that the stress distributions at a craze and a crack are qualitatively similar.

It is now proposed that a certain minimum amount of work, \mathcal{F}_0 per area, is required to effect the local transformation of polymer to craze matter, whether at the tip of the starter crack or at the tip of a craze. Thus:

$$\mathcal{F}_0 = \frac{\pi \sigma_I^2 c_0}{2E} = \frac{\pi \sigma_{II}^2 l}{2E} \quad (9)$$

adopting the linear equations (Griffith equation) and assuming that $c_0 \ll b$. The use of the net section stress

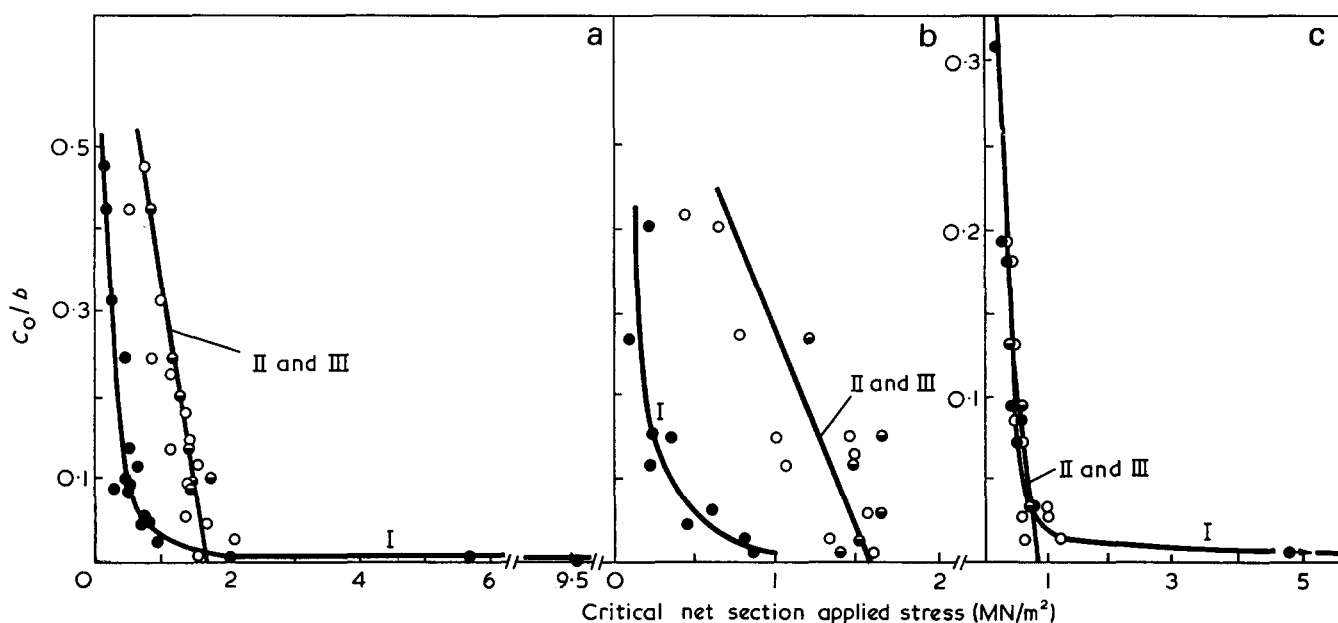


Figure 11 Critical net section stresses as functions of c_0/b for types I, II and III growth for (a) ethyl alcohol at 293K, (b) n-butyl alcohol at 298K and (c) ethyl alcohol at 303K

σ_{II} in equation (9) is appropriate since we are here comparing a real edge crack with a long craze having a notional crack l at its tip, in the absence of complications arising from a residual starter crack. From equation (9) immediately,

$$l = \sigma^2 c_0 / \sigma_{II}^2 \quad (10)$$

and l can be evaluated numerically. The parameter l can also be expressed in terms of the 'threshold' parameters K_N and K_m of Marshall *et al.*³ as:

$$l = (K_m / K_N)^2 c_0 \quad (10a)$$

The results for l are given in Figure 12, and assume the form:

$$l = \alpha + \beta c_0 \equiv \beta(c_0 + \alpha/\beta) \quad (11)$$

where α is a constant which may be independent of temperature but certainly depends on the solvent, and β is both solvent and temperature dependent. The values of α , β are, for the conditions studied, as follows:

	Ethanol (293K)	Ethanol (303K)	Butanol (298K)
α (mm)	0.3	0.0.3	0.15
β	0.05	0.85	0.03
α/β (mm)	6.0	0.0.4	3.0

At the lower temperatures (which are below the 'characteristic temperature'² for the solvents concerned), the equivalent crack length l is governed largely by the term α , though its dependence on c_0 cannot be ignored. The term α is, of course, the 'natural' equivalent crack length which would apply to a craze initiated spontaneously at a surface. The effect of initiating crazes at starter cracks is to increase the stress concentrating power of the craze tip over and above that of the 'natural' craze. It is interesting to note that the equivalent crack length for a natural solvent craze is of the order of 0.1–0.3 mm even when the craze itself may be several cm in length. This bears quantitative testimony to the load-bearing capacity of the craze matter.

At the higher temperature of 303K for ethanol, a dramatic increase in β has occurred so that l is now dominated by (and only slightly smaller than) c_0 . This enormous c_0 dependence at this temperature is relevant to the findings of Marshall *et al.*³ that craze velocity is controlled by K_0 , i.e. the stress intensity factor calculated for the starter crack.

It is significant that β becomes large as the temperature rises from below to above the characteristic temperature T_c identified by Andrews and Bevan² and proven in a later paper⁴ to correspond to the glass transition temperature of an equilibrium-swollen zone at the tip of the craze. It is suggested that the strain-hardening propensities of craze matter decrease rapidly across this range to give a much higher effective l at temperatures above T_c .

Physical significance of the equivalent crack

So far the equivalent crack length l has been used as a parameter to characterize the craze for the purposes of a fracture mechanics analysis. Even this is valuable because it provides, for the first time, a characteristic parameter for crazing mechanics and allows crack and craze propagation phenomena to be reconciled. A value of l which does not change with growth of the craze further explains the observation that crazes propagate at constant velocity under steady load, in spite of their increasing length, yet respond immediately to changes in applied load.

The fact that l remains constant during craze propagation points to a self-stabilizing mechanism at the growth tip and there can be little doubt that this stabilization arises from the ability of the craze matter to strain-harden at some point behind the advancing tip. This idea, in turn, points to a possible physical model of the equivalent crack.

In this model it is suggested that the craze tip region can be represented by a 'bullet-shaped' crack of length l , with a sharp advancing tip and a blunt rear end coinciding with the point at which the craze matter strain hardens strongly as it is progressively extended. This is sketched in Figure 13a.

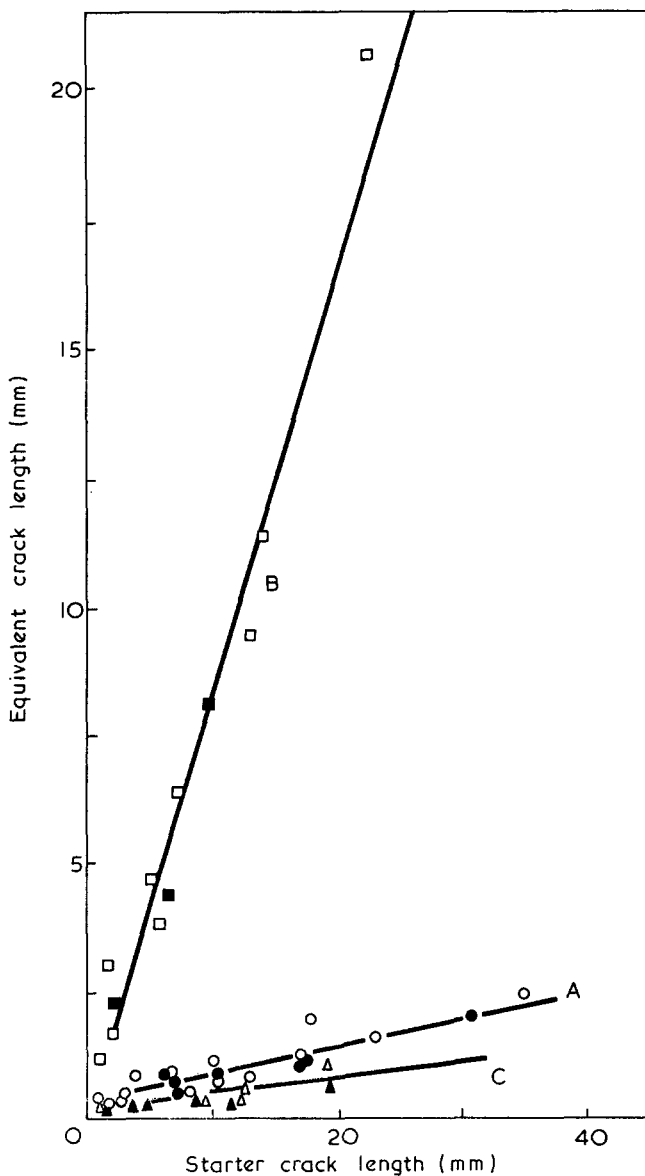


Figure 12 Equivalent crack length as function of starter crack length for (A) ethyl alcohol at 293K, (B) ethyl alcohol at 303K and (C) n-butyl alcohol at 298K. Solid symbols refer to type III and open symbols to type II growth data

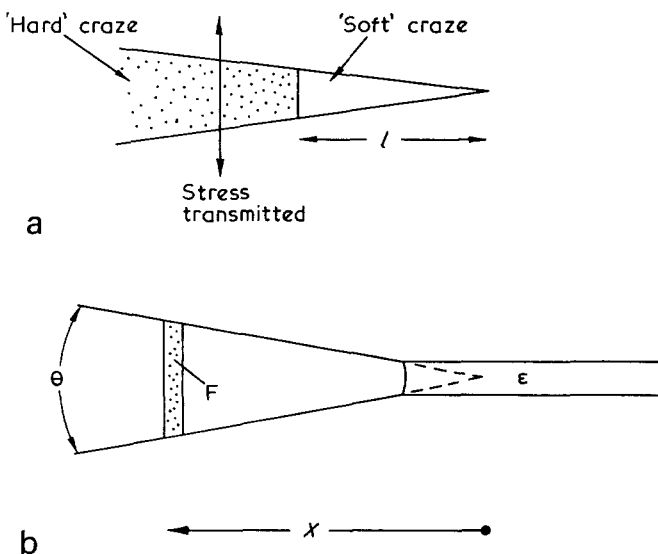


Figure 13 Model for craze growth in terms of the equivalent crack l

Suppose that a layer of polymer of thickness, ξ , is being transformed into craze matter at the propagating tip and that the craze assumes a wedge-like geometry with a wedge-angle, θ (this geometry is strongly supported by electron micrographs¹³).

This is all shown in Figure 13b, where a filament of craze matter F at a distance x behind the tip is seen to have undergone a tensile strain:

$$\epsilon(x) = x\theta/\xi \quad (12)$$

providing θ is small.

It is now supposed that an element of material originating in the layer ξ undergoes a stress-strain history such as shown in Figure 14, where the stress σ_{yy} normal to the craze plane is represented as falling abruptly on cavitation, remaining fairly level during initial flow and then strain hardening strongly at a tensile strain denoted by ϵ^* . If this behaviour is considered reasonable, it can be maintained that the normal stress σ_{yy} over some length x^* measured from the tip of the craze is low and can be approximated to zero, as it would be for a crack. At $x \geq x^*$, the strain $\epsilon \geq \epsilon^*$ and σ_{yy} rises steeply thus terminating the crack-like region. Finally, then, we equate x^* to the equivalent crack length, obtaining:

$$l \simeq x^* = \xi \epsilon^* / \theta \quad (13)$$

It is now necessary to investigate the parameters θ and ξ .

The wedge angle θ . Figure 15 shows experimental data obtained for a craze propagating under steady load in PMMA immersed in ethanol at 293K. The craze shape profiles were obtained by microscopical measurement at different times. These results show that the craze propagated at an almost constant wedge angle of about 10^{-3} , varying by no more than a factor of two over a propagation distance of 3 cm. Figure 16 shows the effect of varying load, and surprisingly shows that the gross wedge angle defined by the major part of the craze is very little affected by the applied stress. The effect of raising the stress appears to be to blunt the craze rather than to increase the wedge angle, i.e. to increase ξ rather than θ . The effect of increased temperature (Figure 17) is similar to that of increased stress.

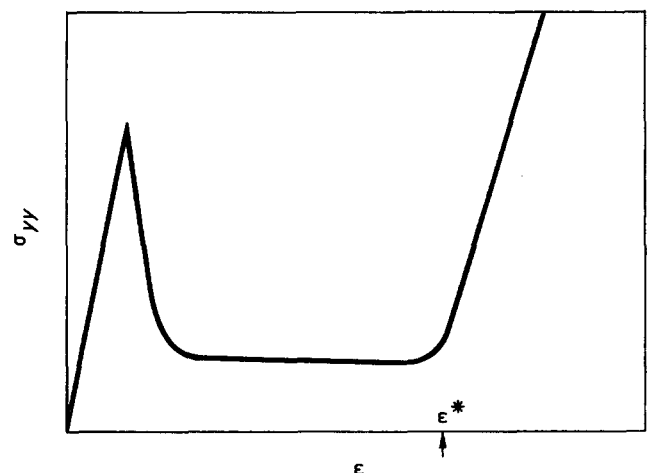


Figure 14 Speculated stress-strain history of an element of material transforming from solid polymer to craze. The initial peak coincides with the cavitation event and ϵ^* is the point of rapid strain hardening

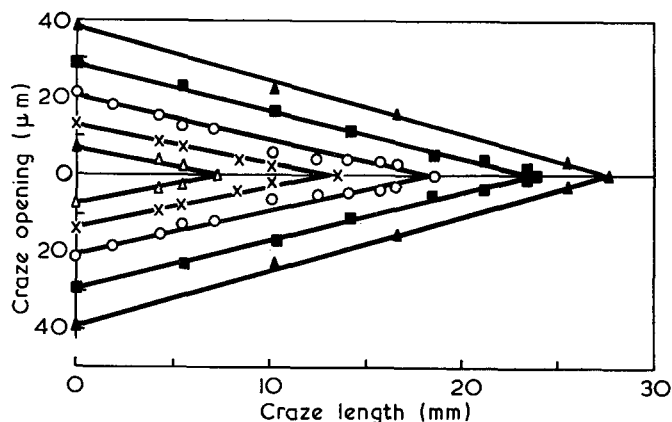


Figure 15 Experimental craze profiles at successive times, t , after load application. Reading from smaller to greater craze lengths, $t=1516$ (Δ), 3202 (\times), 4427 (\circ), 5810 (\blacksquare) and 7336 (\blacktriangle) min. Ethyl alcohol at 293K

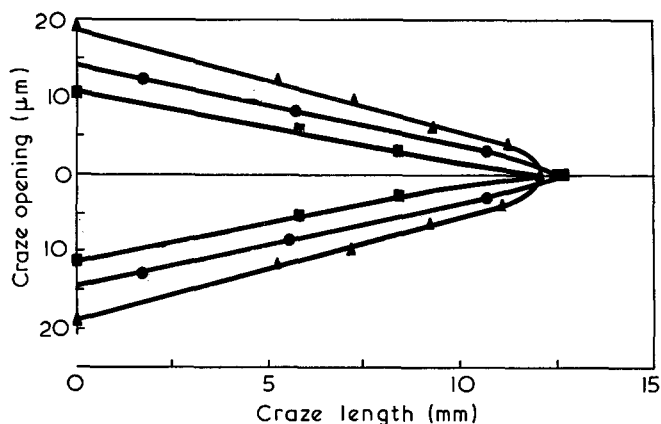


Figure 16 As Figure 15 but for various K_0 values obtained by varying load and c_0 values. K_0 : \blacksquare , 6.59 ; \bullet , 6.77 ; \blacktriangle , 7.30 N/mm²/2

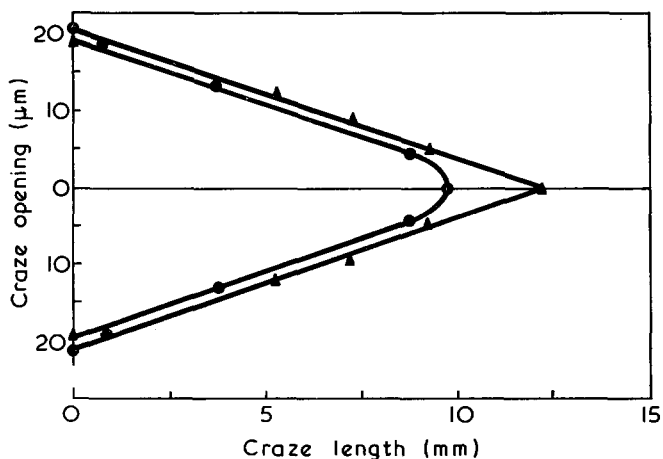


Figure 17 As Figure 15 but for two temperatures: \blacktriangle , 293K; \bullet , 303K

Of course, some caution must be exercised in identifying the gross wedge angle of Figures 16 and 17 with the angle appropriate to the extreme tip and used in equation (13). On the other hand, the values of l given in Figure 12 show that our model is on the scale of 1 mm, a scale comprehended by the results on craze shape, and this gives some confidence in the use of the 'gross' wedge angle in equation (13).

It is concluded, therefore, on the grounds of empirical observation that θ is a nearly constant quantity for a

given alcohol-polymer system, independent of time, craze length, applied stress and temperature.

The parameter ξ . The quantity ξ is the thickness of the layer of polymer which is transformed into craze matter. Since it represents merely a dimension in the bulk polymer it is not, like θ , accessible to direct measurement. It is nevertheless a dimension fixed by physical processes since it defines the region within which cavitation occurs. We are forced to conclude that ξ is determined by the stress distribution at the craze tip. This in turn is determined by the stress intensity factor K .

Since ξ in equation (13) is an independent variable, with l a consequent parameter, it is necessary to ask what fixes ξ in the first place? To answer this question we must go back to the initiation of the craze at the starter crack tip.

Let ξ_i be the initial value of ξ within the stress field of the starter crack. Then if ξ_i is determined solely by this stress field we have:

$$\xi_i = f(K_i) = f(\sigma_i, c_0) \quad (14)$$

where σ_i is the initial applied stress and f is a function. This assumes the tip radius to be zero and the specimen to be infinite so that c_0 is the only linear dimension to be considered. Then, by dimensional analysis:

$$\xi_i = c_0 g(\sigma_i) \quad (15)$$

where g is another, non-dimensional function.

At any subsequent point in the craze growth history, when the applied stress is σ :

$$\begin{aligned} \xi &= \xi_i + \int_{\sigma_i}^{\sigma} \frac{\partial \xi}{\partial \sigma} d\sigma \\ &= c_0 \left\{ g(\sigma_i) + \int_{\sigma_i}^{\sigma} \frac{\partial g}{\partial \sigma} d\sigma \right\} \\ &= c_0 h(\sigma_i, \sigma) \end{aligned} \quad (16)$$

where h is another function. Being dimensionless, h can also be written $h(\sigma_i/\sigma)$.

Substituting in equation (13):

$$l \approx c_0 h(\sigma_i/\sigma_{II}) \epsilon^* / \theta \quad (17)$$

remembering that l is defined under 'threshold' conditions i.e. when $\sigma = \sigma_{II}$. Further σ_i must of necessity equal our previously defined σ_I , since this is by definition the applied stress at which craze begins to form at the starter crack tip. Thus,

$$h = h(\sigma_I/\sigma_{II})$$

and from equation (10):

$$h = j(c_0/l) \quad (18)$$

where j is another function. Since ϵ^* , θ are constants for a given system at a given temperature, the relation:

$$l \approx c_0 j(c_0/l) \epsilon^* / \theta \quad (19)$$

can only be satisfied by the solution:

$$l = \gamma c_0 \quad (20)$$

where γ is a constant of proportionality given by:

$$\gamma = j(\gamma^{-1}) \epsilon^* / \theta$$

Equation (20) is in complete harmony with the experimental data for l shown in Figure 12, allowing that, in

the absence of a deliberate starter crack, there exist intrinsic flaws of effective length α/β (equation 11); values of α/β are given in the table. Then γ becomes equivalent to β . It does not immediately explain the dependence of l upon sheet thickness implicit in the results of Marshall *et al.*³. Possibly the wedge angle, θ , is thickness dependent, but we have no data bearing on this point.

Equation (19) provides a plausible explanation of the large increase in β which occurs for the ethanol/PMMA system as the temperature is raised through the characteristic temperature T_c defined by Andrews and Bevan. Since this temperature (26°C for ethanol) is the glass transition temperature of the swollen zone at the craze tip, it would be expected that the critical strain-hardening strain ϵ^* to which β is proportional, would increase dramatically across this range. Indeed, one might expect ϵ^* to become indefinitely large above T_c were it not for the possibility of solvent being squeezed out of the straining filaments, restoring them to a glassy condition.

The derivation of equation (20) can be criticized in that it relies upon dimensional arguments and lacks physical interpretation. The analysis does, however, provide a foundation for future work on the physical mechanisms involved in the dependence of l upon c_0 .

CONCLUSION

The conditions for craze propagation can be treated by a fracture mechanics analysis by the introduction of a new concept, that of the 'equivalent crack' which allows equations normally valid only for cracks (i.e. discontinuities having traction-free surfaces) to be applied to crazes. The dependence of the equivalent crack length l upon starter crack length c_0 and upon temperature can be explained by use of a plausible physical model, namely a bullet-shaped crack located at the tip of the growing craze. The treatment explains the nature of the K_0 (or c_0) effect discovered by Marshall *et al.* and indicates how this effect can be subtracted to predict the behaviour of crazes grown in virgin specimens ($c_0 \rightarrow 0$). The present work also focuses attention on the importance of strain-hardening in the filaments of craze matter

as a factor determining l and thus the critical stresses necessary to propagate environmental crazes.

ACKNOWLEDGEMENTS

Thanks are due to the Science Research Council for a research grant and for a research studentship (G.M.L.).

REFERENCES

- 1 Andrews, E. H. and Bevan, L. in 'Physical Basis of Yield and Fracture', Institute of Physics, London, 1966, p 209
- 2 Andrews, E. H. and Bevan, L. *Polymer* 1972, **13**, 337
- 3 Marshall, G. P., Culver, L. E. and Williams, J. G. *Proc. R. Soc. (A)* 1970, **319**, 165
- 4 Andrews, E. H., Levy, G. M. and Willis, J. J. *Mater. Sci.* 1973, **8**, 1000
- 5 Marshall, G. P. and Williams, J. G. *J. Appl. Polym. Sci.* 1973, **17**, 987
- 6 Andrews, E. H., and Levy, G. M. *J. Mater. Sci.* 1971, **6**, 1093
- 7 Sternstein, S. S., Ongchin, L. and Silverman, A. *Appl. Polym. Symp.* 1968, **7**, 175
- 8 Inglis, C. E. *Trans. Inst. Nav. Arch.* 1913, **60**, 219
- 9 Gross, B., Srawley, J. E. and Brown, W. F. Tech. Note D-2396, NASA, Washington, D.C., 1964
- 10 Report of a Special ASTM Committee *ASTM Bull.* 1960
- 11 Gent, A. N. and Lindley, P. *Proc. R. Soc. (A)* 1959, **249**, 195
- 12 Andrews, E. H. in 'Physics of Glassy Plastics' (Ed. R. N. Haward) Applied Science, Barking, 1973, p 440
- 13 Beahan, P., Bevis, M. and Hull, D. *Phil. Mag.* 1971, **24**, 1267

APPENDIX

PMMA characterization data

Source: ICI Perspex batch No. 943/170

Molecular weights: $M_n = 2.22 \times 10^5$

$M_w = 1.84 \times 10^6$

$M_z = 4.92 \times 10^6$

$M_n : M_w : M_z = 1 : 8.30 : 22.1$

Intrinsic viscosity: 2.54 dl/g (toluene)

4.72 dl/g (chloroform)

Density: 1.88 g/ml

Glass transition temperature: 381K by d.t.a., heating rate 10K/min.

Dielectric relaxation in polymethyltrifluoropropylsiloxane

M. E. Baird and C. R. Sengupta

*Department of Applied Physics, University of Wales Institute of Science and Technology, Cardiff CF1 3NU, UK
(Received 27 February 1974)*

Previous studies^{1,2} at low temperatures with amorphous polyphenylmethylsiloxane and crystalline polydimethylsiloxane have revealed the presence of an α relaxation in the audio frequency region for each polymer.

In polyphenylmethylsiloxane² the normalized plot of ϵ''/ϵ_m'' against $\log_{10}(f/f_m)$ (where ϵ_m'' is the maximum loss factor occurring at a frequency f_m) was reasonably broad and asymmetric (broader on the high frequency side) consistent with the empirical decay function^{3,4} for charge $\phi(t) = \exp-(t/\tau_0)^\beta$ as often found with amorphous polymers^{3,4}. With polydimethylsiloxane the normalized plots were also asymmetric but broader on the low frequency side. This behaviour was consistent with that usually found for crystalline polymers⁵. Measurements² in the glassy region below T_g have revealed no β relaxation in either polymer. However, a β relaxation in the glassy region has been observed with many amorphous polymers with or without side groups⁶⁻⁸. In order to elucidate more clearly what molecular motions may occur in the glassy region with siloxane polymers, measurements have been made with polymethyltrifluoropropylsiloxane [repeat unit $(CF_3CH_2CH_2Si(CH_3)O)$] containing a dipolar side group. The polymer had a number-average molecular weight of about 2000, as supplied by Dow Corning Ltd. The glass transition T_g was about $-71^\circ C$ (referred to a scan rate of $1^\circ C/min$) as determined by RAPRA from d.s.c. measurements. The polymer did not crystallize. The dielectric behaviour of this polymer was evaluated using a laboratory constructed 3 terminal dielectric cell as described previously² and a G.R.1615A Capacitance Bridge over the frequency range 10^2-10^5 Hz and temperature range $-190^\circ C$ to $0^\circ C$. The polymer samples were stored over P_2O_5 *in vacuo* for at least 3 h before use in order to minimize air and water absorption.

The plots of loss factor against temperature for polymethyltrifluoropropylsiloxane are shown in Figure 1 and indicate two relaxations, the α occurring in the temperature region -80 to $-30^\circ C$ and the β occurring in the glassy region over the range -190 to $-130^\circ C$. For the α relaxation the shape of the plots of loss factor ϵ'' against \log frequency f were independent of temperature, since for the normalized plots of ϵ''/ϵ_m'' against $\log_{10}(f/f_m)$ all the points fell on a smooth asymmetric master curve. This had a total half width Δ (for $\epsilon'' = \epsilon_m''/2$) of about 1.75. The decay function $\phi(t)$ for charge was evaluated from the normalized plot as described previously² using Romberg (numerical) integration and conformed to the empirical decay function $\phi(t) = \exp-(t/\tau_0)^\beta$ with $\beta = 0.67$. This is similar to the value of 0.62 found for polyphenylmethylsiloxane². The plot of $\log_{10} f_m$ against $1000/T$ was linear (Figure 2) and from the slope the experimental activation energy ΔH (equal to $2.303R |d \log_{10} f_m / d(1/T)|$) was calculated as 112 kJ/mol (compared to 320 kJ/mol for polyphenylmethylsiloxane). The magnitude $\epsilon_s - \epsilon_\infty$

of the α relaxation was calculated from the equation⁴:

$$(\epsilon_s - \epsilon_\infty)_\alpha = k \epsilon_m'' \Delta \log_{10} f \quad (1)$$

with $k = 1.66$ and was found to be in the range 5.5-6.0 over the range of temperature used. This is over ten times larger than the values² found for the α relaxation in polydimethylsiloxane and polyphenylmethylsiloxane.

The β relaxation is of much smaller magnitude than the α relaxation as shown in Figure 1. The half-width of the plots against \log frequency was about 4-5 decades with peak heights in the region 0.026-0.030 in the range

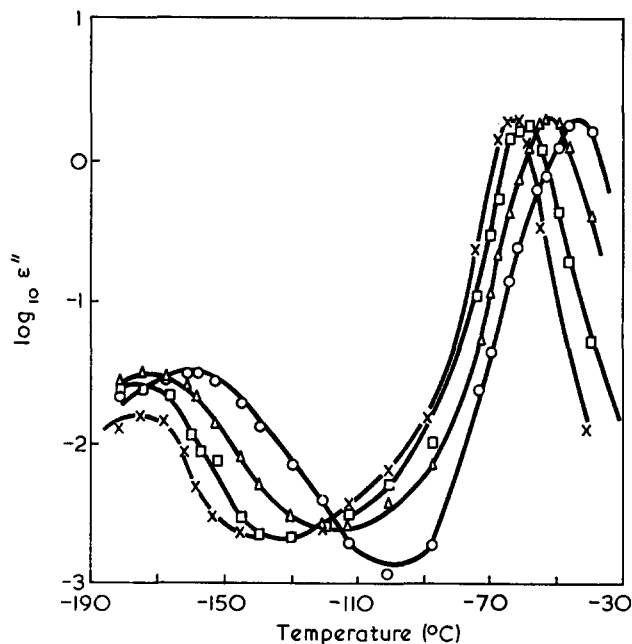


Figure 1 Plots of \log_{10} loss factor ϵ'' against temperature for polymethyltrifluoropropylsiloxane at different frequencies: \circ , 100 kHz; Δ , 10 kHz; \square , 1 kHz; \times , 200 Hz

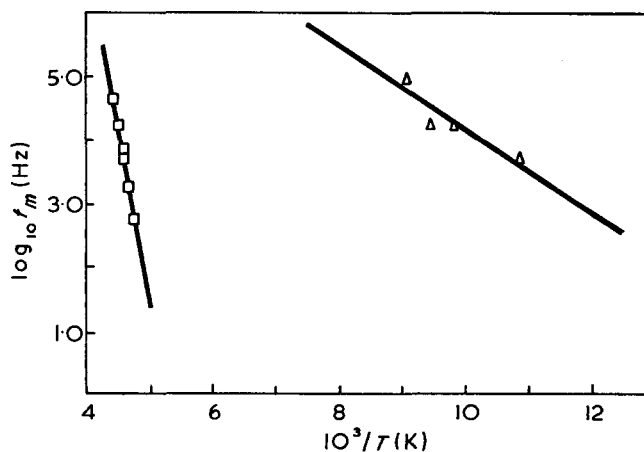


Figure 2 Plots of $\log_{10} f_m$ against $1000/T$ for the α (\square) and β (Δ) relaxations in polymethyltrifluoropropylsiloxane

of temperature used (-160 to -180°C). This gives an average magnitude $(\epsilon_s - \epsilon_\infty)_\beta$ of about 0.22 in the temperature range studied, using equation (1) with $k = 1.75$ (i.e. assuming that the loss peaks may be expressed in terms of a Fuoss-Kirkwood distribution, k being independent of the breadth of the distribution^{6, 9}). Thus $(\epsilon_s - \epsilon_\infty)_\beta$ is considerably less than $(\epsilon_s - \epsilon_\infty)_\alpha$.

The plots of $\log_{10} f_m$ against $1000/T$ for the β relaxation was approximately linear (Figure 2) and from the slope the experimental activation energy was about 13 kJ/mol. This low value is somewhat lower than that usually found for the β relaxation in amorphous polymers. Assuming that the most probable relaxation time τ is of the form $\tau = A^{-1}[\exp(-\Delta S/R)\exp(\Delta H/RT)]$ for a 2 site model¹⁰, where A is of the order of a frequency of oscillation of the entity in its equilibrium position (10^{12} Hz) and ΔS is the entropy of activation, ΔS was calculated from the locus as near zero, certainly much lower than that quoted for local motion in poly(ethylene terephthalate)¹¹, or that suggested for local motion in the amorphous regions of polychlorotrifluoroethylene¹⁰.

In polymers containing rotatable side groups⁶⁻⁸ (e.g. the poly(alkyl methacrylates)] the β relaxation has been attributed to side group motions whilst in polymers with dipoles rigidly attached to the main chain [e.g. poly(ethylene terephthalate) or poly(vinyl chloride)] it has been assigned to local mode motions⁶⁻⁸. However, there is evidence that the side group motion is not independent of the main chain motion^{7, 12, 13} and a more satisfactory model has recently been proposed^{12, 13}. A dipole may exist in a variety of different local environments and in a given environment, r , may be partly relaxed by local motions. In polymers with flexible side groups the local motion may involve the re-orientation of side groups whilst in the absence of side groups the local motion involves only short segments of the dipolar chain molecule. The dipole moment (auto) correlation function¹⁴ averaged over all possible environments is given by:

$$\Gamma(t) = \frac{\langle \mu(0) \cdot \mu(t) \rangle}{\mu^2} = \phi_\alpha(t) \sum_r^0 p_r q_{\alpha r} + \phi_\alpha(t) \sum_r^0 p_r q_{\beta r} \phi_{\beta r}(t) \quad (2)$$

$\phi_\alpha(t)$ is the decay function for microbrownian motions (α process) and $\phi_{\beta r}(t)$ is the decay function for the β process in environment r . $^0 p_r$ is the probability of obtaining the environment r and $q_{\alpha r} = [\langle \mu \rangle_r]^2 / \mu^2$ where $\langle \mu \rangle_r$ is the mean dipole moment residing in environment r , observed over a time scale long compared with that for the β_r process but short compared with that for the α process. $q_{\alpha r} + q_{\beta r} = 1$.

The complex relative permittivity is then given by:

$$\frac{\epsilon(\omega) - \epsilon_\infty}{\epsilon_s - \epsilon_\infty} = \sum_r^0 p_r q_{\alpha r} \mathcal{L} \left[-\frac{d\phi_\alpha(t)}{dt} \right] + \sum_r^0 p_r q_{\beta r} \mathcal{L} \left[-\frac{d\phi_\alpha(t)\phi_{\beta r}(t)}{dt} \right] \quad (3)$$

At low temperatures $\phi_{\beta r}(t)$ decays far faster than $\phi_\alpha(t)$ and equation (3) predicts two relaxation regions, α and β .

Although $(\epsilon_s - \epsilon_\infty)_\beta \ll (\epsilon_s - \epsilon_\infty)_\alpha$ in polymers^{6, 7} containing dipolar groups rigidly attached to the main chain, for several polymers containing flexible dipolar side groups $(\epsilon_s - \epsilon_\infty)_\beta > (\epsilon_s - \epsilon_\infty)_\alpha$ ^{6, 13} (e.g. PMMA). In polymethyltrifluoropropylsiloxane with a strongly dipolar side group, ΔH and ΔS for the β relaxations are very small, and $(\epsilon_s - \epsilon_\infty)_\beta \ll (\epsilon_s - \epsilon_\infty)_\alpha$, whilst in polydimethylsiloxane and polyphenylmethylsiloxane no β relaxation was detected at all. This suggests that the local motion in siloxane polymers may be quite limited and that in polymethyltrifluoropropylsiloxane the β relaxation may arise virtually entirely by motion within the side group.

ACKNOWLEDGEMENTS

The authors are grateful to Dow Corning Ltd for supplying the polymer sample and to RAPRA for carrying out d.s.c. measurements.

REFERENCES

- Baird, M. E. and Sengupta, C. R. *Polymer* 1971, **12**, 802
- Baird, M. E. and Sengupta, C. R. *JCS Faraday Trans. II* 1972, **68**, 1795
- Williams, G. and Watts, D. C. *Trans. Faraday Soc.* 1970, **66**, 80
- Williams, G., Watts, D. C., Dev, S. B. and North, A. M. *Trans. Faraday Soc.* 1971, **67**, 1323
- Ishida, Y., Yamafuji, K., Ito, H. and Takayanagi, M. *Kolloid-Z. Z. Polym.* 1962, **184**, 97
- McCrum, N. G., Read, B. E. and Williams, G. 'Anelastic and Dielectric Effects in Polymeric Solids', John Wiley, New York, 1967
- Ishida, Y. *J. Polym. Sci. (A-2)* 1969, **7**, 1835
- Baird, M. E., 'Electrical Properties of Polymeric Materials', Plastics Institute, London, 1973
- Fuoss, R. M. and Kirkwood, J. G. *J. Am. Chem. Soc.* 1941, **63**, 385
- Hoffman, J. D., Williams, G. and Passaglia, E. *J. Polym. Sci. (C)* 1966, **14**, 173
- Reddish, W. *Trans. Faraday Soc.* 1950, **46**, 459
- Williams, G. and Watts, D. C. 'N.M.R.—Basic Principles and Progress', Springer-Verlag, Berlin, 1971, p 271
- Williams, G. and Watts, D. C. *Trans. Faraday Soc.* 1971, **67**, 1971
- Cook, M., Watts, D. C. and Williams, G. *Trans. Faraday Soc.* 1970, **66**, 2503

Effect of swelling agent on the determination of the crosslinking density in ethylene-propylene copolymer

A. Romanov, V. Pollák and K. Marcinčin

Polymer Institute of the Slovak Academy of Sciences, Dúbravská cesta, 809 34 Bratislava, Czechoslovakia
(Received 13 November 1973; revised 8 March 1974)

INTRODUCTION

The Gaussian elasticity theory of rubberlike networks gives the following expression for the stress at uniaxial strain by extension¹:

$$f = \phi \nu RT (\lambda - \lambda^{-2}) \nu_r^{-1/3} \quad (1)$$

where f is the equilibrium force per unit cross-section of non-strained dry sample, ν is the effective crosslinking density per volume unit, λ is the relative elonga-

of temperature used (-160 to -180°C). This gives an average magnitude $(\epsilon_s - \epsilon_\infty)_\beta$ of about 0.22 in the temperature range studied, using equation (1) with $k = 1.75$ (i.e. assuming that the loss peaks may be expressed in terms of a Fuoss-Kirkwood distribution, k being independent of the breadth of the distribution^{6, 9}). Thus $(\epsilon_s - \epsilon_\infty)_\beta$ is considerably less than $(\epsilon_s - \epsilon_\infty)_\alpha$.

The plots of $\log_{10} f_m$ against $1000/T$ for the β relaxation was approximately linear (Figure 2) and from the slope the experimental activation energy was about 13 kJ/mol. This low value is somewhat lower than that usually found for the β relaxation in amorphous polymers. Assuming that the most probable relaxation time τ is of the form $\tau = A^{-1}[\exp(-\Delta S/R)\exp(\Delta H/RT)]$ for a 2 site model¹⁰, where A is of the order of a frequency of oscillation of the entity in its equilibrium position (10^{12} Hz) and ΔS is the entropy of activation, ΔS was calculated from the locus as near zero, certainly much lower than that quoted for local motion in poly(ethylene terephthalate)¹¹, or that suggested for local motion in the amorphous regions of polychlorotrifluoroethylene¹⁰.

In polymers containing rotatable side groups⁶⁻⁸ (e.g. the poly(alkyl methacrylates)] the β relaxation has been attributed to side group motions whilst in polymers with dipoles rigidly attached to the main chain [e.g. poly(ethylene terephthalate) or poly(vinyl chloride)] it has been assigned to local mode motions⁶⁻⁸. However, there is evidence that the side group motion is not independent of the main chain motion^{7, 12, 13} and a more satisfactory model has recently been proposed^{12, 13}. A dipole may exist in a variety of different local environments and in a given environment, r , may be partly relaxed by local motions. In polymers with flexible side groups the local motion may involve the re-orientation of side groups whilst in the absence of side groups the local motion involves only short segments of the dipolar chain molecule. The dipole moment (auto) correlation function¹⁴ averaged over all possible environments is given by:

$$\Gamma(t) = \frac{\langle \mu(0) \cdot \mu(t) \rangle}{\mu^2} = \phi_\alpha(t) \sum_r^0 p_r q_{\alpha r} + \phi_\alpha(t) \sum_r^0 p_r q_{\beta r} \phi_{\beta r}(t) \quad (2)$$

$\phi_\alpha(t)$ is the decay function for microbrownian motions (α process) and $\phi_{\beta r}(t)$ is the decay function for the β process in environment r . $^0 p_r$ is the probability of obtaining the environment r and $q_{\alpha r} = [\langle \mu \rangle_r]^2 / \mu^2$ where $\langle \mu \rangle_r$ is the mean dipole moment residing in environment r , observed over a time scale long compared with that for the β_r process but short compared with that for the α process. $q_{\alpha r} + q_{\beta r} = 1$.

The complex relative permittivity is then given by:

$$\frac{\epsilon(\omega) - \epsilon_\infty}{\epsilon_s - \epsilon_\infty} = \sum_r^0 p_r q_{\alpha r} \mathcal{L} \left[-\frac{d\phi_\alpha(t)}{dt} \right] + \sum_r^0 p_r q_{\beta r} \mathcal{L} \left[-\frac{d\phi_\alpha(t)\phi_{\beta r}(t)}{dt} \right] \quad (3)$$

At low temperatures $\phi_{\beta r}(t)$ decays far faster than $\phi_\alpha(t)$ and equation (3) predicts two relaxation regions, α and β .

Although $(\epsilon_s - \epsilon_\infty)_\beta \ll (\epsilon_s - \epsilon_\infty)_\alpha$ in polymers^{6, 7} containing dipolar groups rigidly attached to the main chain, for several polymers containing flexible dipolar side groups $(\epsilon_s - \epsilon_\infty)_\beta > (\epsilon_s - \epsilon_\infty)_\alpha$ ^{6, 13} (e.g. PMMA). In polymethyltrifluoropropylsiloxane with a strongly dipolar side group, ΔH and ΔS for the β relaxations are very small, and $(\epsilon_s - \epsilon_\infty)_\beta \ll (\epsilon_s - \epsilon_\infty)_\alpha$, whilst in polydimethylsiloxane and polyphenylmethylsiloxane no β relaxation was detected at all. This suggests that the local motion in siloxane polymers may be quite limited and that in polymethyltrifluoropropylsiloxane the β relaxation may arise virtually entirely by motion within the side group.

ACKNOWLEDGEMENTS

The authors are grateful to Dow Corning Ltd for supplying the polymer sample and to RAPRA for carrying out d.s.c. measurements.

REFERENCES

- Baird, M. E. and Sengupta, C. R. *Polymer* 1971, **12**, 802
- Baird, M. E. and Sengupta, C. R. *JCS Faraday Trans. II* 1972, **68**, 1795
- Williams, G. and Watts, D. C. *Trans. Faraday Soc.* 1970, **66**, 80
- Williams, G., Watts, D. C., Dev, S. B. and North, A. M. *Trans. Faraday Soc.* 1971, **67**, 1323
- Ishida, Y., Yamafuji, K., Ito, H. and Takayanagi, M. *Kolloid-Z. Z. Polym.* 1962, **184**, 97
- McCrum, N. G., Read, B. E. and Williams, G. 'Anelastic and Dielectric Effects in Polymeric Solids', John Wiley, New York, 1967
- Ishida, Y. *J. Polym. Sci. (A-2)* 1969, **7**, 1835
- Baird, M. E., 'Electrical Properties of Polymeric Materials', Plastics Institute, London, 1973
- Fuoss, R. M. and Kirkwood, J. G. *J. Am. Chem. Soc.* 1941, **63**, 385
- Hoffman, J. D., Williams, G. and Passaglia, E. *J. Polym. Sci. (C)* 1966, **14**, 173
- Reddish, W. *Trans. Faraday Soc.* 1950, **46**, 459
- Williams, G. and Watts, D. C. 'N.M.R.—Basic Principles and Progress', Springer-Verlag, Berlin, 1971, p 271
- Williams, G. and Watts, D. C. *Trans. Faraday Soc.* 1971, **67**, 1971
- Cook, M., Watts, D. C. and Williams, G. *Trans. Faraday Soc.* 1970, **66**, 2503

Effect of swelling agent on the determination of the crosslinking density in ethylene-propylene copolymer

A. Romanov, V. Pollák and K. Marcinčin

Polymer Institute of the Slovak Academy of Sciences, Dúbravská cesta, 809 34 Bratislava, Czechoslovakia
(Received 13 November 1973; revised 8 March 1974)

INTRODUCTION

The Gaussian elasticity theory of rubberlike networks gives the following expression for the stress at uniaxial strain by extension¹:

$$f = \phi \nu RT (\lambda - \lambda^{-2}) \nu_r^{-1/3} \quad (1)$$

where f is the equilibrium force per unit cross-section of non-strained dry sample, ν is the effective crosslinking density per volume unit, λ is the relative elonga-

Notes to the Editor

tion, ν_r is the degree of swelling of the network and ϕ is the so-called front factor.

For small strains by compression in swollen state it is possible to simplify equation (1) which thus assumes the following form²:

$$f = \phi 3 \nu RT \frac{\Delta h}{h_0} \quad (2)$$

where h_0 is the original height of unswollen sample and Δh is the change in height of the swollen sample due to the compressive stress, f .

As the determination of equilibrium stress for the strain of unswollen (dry) samples is rather tedious, it is frequently necessary to use swollen samples. There are, however, only sporadic papers in the literature which are concerned with the effect of solvent on the determination of ν from stress-strain relations³⁻⁵. In this paper the effect of solvent on the determination of crosslinking density according to equation (2) is discussed.

EXPERIMENTAL

Materials

The ethylene-propylene copolymer (EP) (Dutral; ethylene content 45 mol%; $M_n = 7 \times 10^4$) was used for experiments. Dicumyl peroxide (DCP), precipitated three times from ethanol, was used as crosslinking agent.

Methods

The vulcanization mixtures of EP with DCP were prepared in a laboratory calender. For 100 parts by weight of copolymer 2.0, 3.0, 4.0, or 5.0 parts by weight of DCP were used. The samples were vulcanized in a laboratory press at 160°C for 45 min in the form of foils of about 1 mm or 6 mm thickness.

The samples with the dimensions according to ASTM-D 1708-5 ST were cut from the foils 1 mm thick. These samples were used for the determination of the relationship between equilibrium stress and elongation in dry state. The measurements were performed with a Cambridge Textile Extensometer adapted to the thermostating of samples. Quasi-equilibrium stress was attained at 70°C after about 5-7 h relaxation. The measurements themselves were carried out at 30°C.

The samples, of approximate dimensions 6 × 7 × 7 mm, were cut from the foils of 6 mm thickness. These samples, after precise measurement of their dimensions, were swollen in the solvents recorded in Table 1 up to the equilibrium swelling (about 6 days). The relations between the change in height of the swollen sample and compressing load were measured on a similar instrument and by a similar method as described in the literature².

Table 1 Solvents used and their solubility parameters^{9,10}

Solvent	δ
n-hexane	7.3
n-heptane	7.45
n-octane	7.55
cyclohexane	8.2
CCl ₄	8.6
toluene	8.9
benzene	9.2

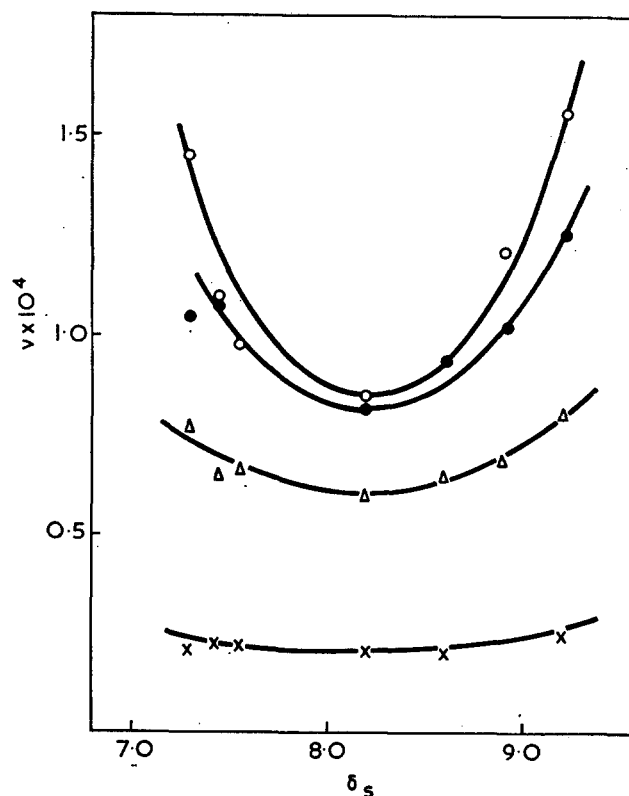


Figure 1 Relationship between the effective crosslinking density ν and the solubility parameter of the solvent used δ_s for the ethylene-propylene copolymer (100 parts by weight) crosslinked with dicumyl peroxide. \times , 2; Δ , 3; \bullet , 4; \circ , 5 parts by weight DCP

RESULTS AND DISCUSSION

The crosslinking density, ν , of individual samples swollen in different swelling agents was calculated from equation (2) assuming that $\phi = 1$. The values of ν found are, however, different according to the solvent used. Provided the difference between the solubility parameters of polymer, δ_{EP} , and swelling agent, δ_s , is taken for the measure of the quality of swelling agent, this method gives higher values of ν in a poorer swelling agent (Figure 1). For the samples crosslinked to a higher degree the differences between the values found for ν are higher. It is worth noticing that the error introduced by simplifying equation (1) is negligible because of the use of low strains (to 5%).

The fact that different values of ν are obtained by using different swelling agents is likely because of the assumption that ϕ in equation (2) is a constant (~ 1). According to some workers^{7,8} $\phi = r_0^2/r_f^2$ holds where r_0^2 is the mean square end-to-end distance of the network chains in the unstretched, unswollen state and r_f^2 is the mean square end-to-end distance that the network chains would assume in the stretched (swollen) state if the crosslinks were removed. From the paper by Tobolsky and Goebel⁸ it follows that ϕ is not a constant. Parameter r_f^2 increases with the improving quality of solvent. This fact suggests that the calculated values of ν (provided $\phi = 1$) decrease with the improving quality of swelling agent.

Assuming that the ratio of r_f^2 in the two different solvents is proportional to the swelling ratio of the sample in these swelling agents according to:

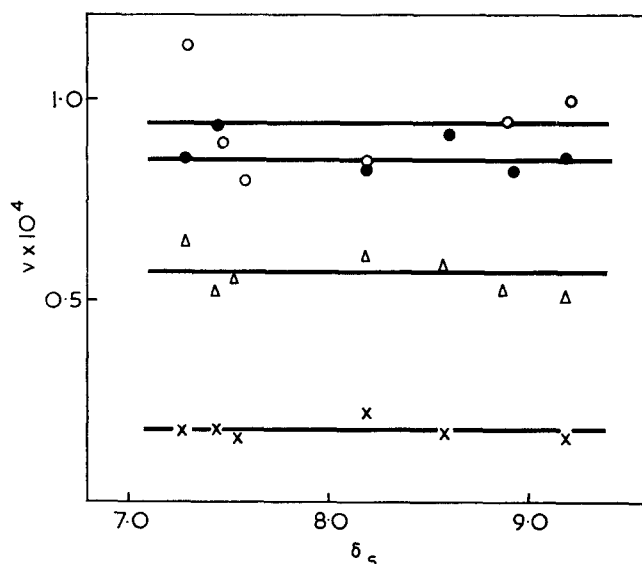


Figure 2 Variation of the modified values of crosslinking density with the solubility parameter of the swelling agents used for the ethylene-propylene copolymer (100 parts by weight) cross-linked with dicumyl peroxide. x, 2; Δ , 3; \bullet , 4; \circ , 5 parts by weight DCP

$$\frac{r_{fx}^2}{r_{fy}^2} = \frac{v_{rx}^{2/3}}{v_{ry}^{2/3}} \quad (3)$$

(indices x and y denote different swelling agents), equation (2) assumes the form:

$$f = 3\nu RT \frac{\Delta h}{h_0} \frac{v_{rx}^{2/3}}{v_{ry}^{2/3}} \quad (4)$$

The use of equation (4) allows the determined values to be recalculated so that they are independent of the solvent used. In Figure 2 the values of ν adjusted according to equation (4) are presented while the values ν (or respectively ν_r) measured in cyclohexane are taken for the reference values.

For comparison, the values of ν for the dry samples

Table 2 Properties of the EP vulcanizates obtained by different methods

DCP (parts by wt)	$\nu \times 10^4$ (mol/cm ³)	
	Mooney-Rivlin	Cluff*
2	0.20	0.21
3	0.52	0.61
4	0.86	0.83
5	0.84	0.85

* Samples swollen in cyclohexane

subjected to strain by extension were also determined by using the well-known Mooney-Rivlin equation³:

$$f = 2A_0(\lambda - \lambda^{-2})(C_1 + C_2\lambda^{-1}) \quad (5)$$

in which the following identity is generally supposed:

$$2C_1 = \nu RT \quad (6)$$

As evident from Table 2 the values calculated according to equation (5) for dry samples are approximately equal to the values of ν determined from equation (2) for the samples swollen in cyclohexane.

REFERENCES

- 1 Flory, P. J. *J. Am. Chem. Soc.* 1956, **78**, 5222
- 2 Cluff, E. F., Gladding, E. K. and Pariser, R. *J. Polym. Sci.* 1960, **45**, 341
- 3 Mullins, L. J. *J. Appl. Polym. Sci.* 1959, **2**, 1
- 4 Seeley, R. D. and Dyckes, G. W. *J. Appl. Polym. Sci.* 1965, **9**, 151
- 5 Smith, D. A. *J. Polym. Sci. (C)* 1967, **16**, 525
- 6 Treloar, L. R. G. 'The Physics of Rubber Elasticity', 2nd edn, Oxford University Press, 1958
- 7 Ilavský, M. and Prins, W. *Macromolecules* 1970, **3**, 415
- 8 Tobolsky, A. V. and Goebel, J. C. *Macromolecules* 1970, **3**, 556
- 9 Baranwal, K. C. *Makromol. Chem.* 1967, **100**, 242
- 10 Holzmüller, W. and Altenburg, K. 'Physics of Polymers', State Publishing House of Technical Literature, Prague, 1966, p 149

ERRATA

'Conversion of work of deformation to heat in polymers' by P. Zoller and H. Bont, *Polymer* 1974, **15**, 239-242.

Equation (16) on page 241 should read:

$$K(t_0) = 100 \left[1 - \frac{\int_{-\infty}^{+\infty} H(\tau)(\tau/t_0)f_1(\tau/t_0)d\log(\tau/t_0)}{\int_{-\infty}^{+\infty} H(\tau)(\tau/t_0)f_2(\tau/t_0)d\log(\tau/t_0)} \right]$$

This equation, with f_1 and f_2 as previously given (Table 2) permits the calculation of the conversion factor for a given distribution of relaxation times $H(\tau)$.

The last paragraph of the paper was based on the wrong expression for equation (16) and should be ignored.

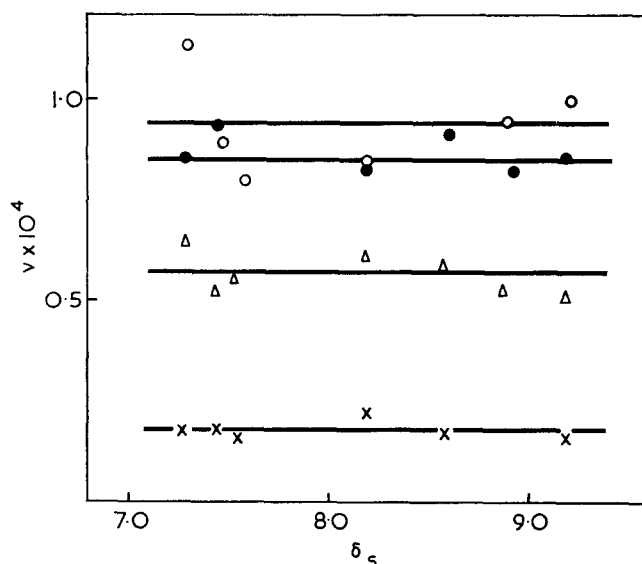


Figure 2 Variation of the modified values of crosslinking density with the solubility parameter of the swelling agents used for the ethylene-propylene copolymer (100 parts by weight) cross-linked with dicumyl peroxide. x, 2; Δ , 3; \bullet , 4; \circ , 5 parts by weight DCP

$$\frac{r_{fx}^2}{r_{fy}^2} = \frac{v_{rx}^{2/3}}{v_{ry}^{2/3}} \quad (3)$$

(indices x and y denote different swelling agents), equation (2) assumes the form:

$$f = 3\nu RT \frac{\Delta h}{h_0} \frac{v_{rx}^{2/3}}{v_{ry}^{2/3}} \quad (4)$$

The use of equation (4) allows the determined values to be recalculated so that they are independent of the solvent used. In Figure 2 the values of ν adjusted according to equation (4) are presented while the values ν (or respectively ν_r) measured in cyclohexane are taken for the reference values.

For comparison, the values of ν for the dry samples

Table 2 Properties of the EP vulcanizates obtained by different methods

DCP (parts by wt)	$\nu \times 10^4$ (mol/cm ³)	
	Mooney-Rivlin	Cluff*
2	0.20	0.21
3	0.52	0.61
4	0.86	0.83
5	0.84	0.85

* Samples swollen in cyclohexane

subjected to strain by extension were also determined by using the well-known Mooney-Rivlin equation³:

$$f = 2A_0(\lambda - \lambda^{-2})(C_1 + C_2\lambda^{-1}) \quad (5)$$

in which the following identity is generally supposed:

$$2C_1 = \nu RT \quad (6)$$

As evident from Table 2 the values calculated according to equation (5) for dry samples are approximately equal to the values of ν determined from equation (2) for the samples swollen in cyclohexane.

REFERENCES

- 1 Flory, P. J. *J. Am. Chem. Soc.* 1956, **78**, 5222
- 2 Cluff, E. F., Gladding, E. K. and Pariser, R. *J. Polym. Sci.* 1960, **45**, 341
- 3 Mullins, L. J. *J. Appl. Polym. Sci.* 1959, **2**, 1
- 4 Seeley, R. D. and Dyckes, G. W. *J. Appl. Polym. Sci.* 1965, **9**, 151
- 5 Smith, D. A. *J. Polym. Sci. (C)* 1967, **16**, 525
- 6 Treloar, L. R. G. 'The Physics of Rubber Elasticity', 2nd edn, Oxford University Press, 1958
- 7 Ilavský, M. and Prins, W. *Macromolecules* 1970, **3**, 415
- 8 Tobolsky, A. V. and Goebel, J. C. *Macromolecules* 1970, **3**, 556
- 9 Baranwal, K. C. *Makromol. Chem.* 1967, **100**, 242
- 10 Holzmüller, W. and Altenburg, K. 'Physics of Polymers', State Publishing House of Technical Literature, Prague, 1966, p 149

ERRATA

'Conversion of work of deformation to heat in polymers' by P. Zoller and H. Bont, *Polymer* 1974, **15**, 239-242.

Equation (16) on page 241 should read:

$$K(t_0) = 100 \left[1 - \frac{\int_{-\infty}^{+\infty} H(\tau)(\tau/t_0)f_1(\tau/t_0)d\log(\tau/t_0)}{\int_{-\infty}^{+\infty} H(\tau)(\tau/t_0)f_2(\tau/t_0)d\log(\tau/t_0)} \right]$$

This equation, with f_1 and f_2 as previously given (Table 2) permits the calculation of the conversion factor for a given distribution of relaxation times $H(\tau)$.

The last paragraph of the paper was based on the wrong expression for equation (16) and should be ignored.

On the structure of equibinary *cis*-1,4-/*trans*-1,2-polybutadiene by ^{13}C n.m.r.

^{13}C n.m.r. spectroscopy has been recognized as a powerful tool for studying the structure of polybutadienes¹⁻⁵. As reported in previous papers^{6,7} the resonance region of the carbon double bond is very sensitive to small differences in the sequence distribution of *cis* and *trans* units in the polymer chain.

The purpose of this communication is to report the first results observed in the ^{13}C n.m.r. spectrum of polybutadiene containing *cis*-1,4- and -1,2-units in the backbone chain. The polymer sample under study contains 46% *cis*-, 3% *trans*- and 51% 1,2-units in random-like enchainment.

Figure 1 shows the expanded spectrum of the olefinic carbon atoms. Within the resolution of the spectrometer

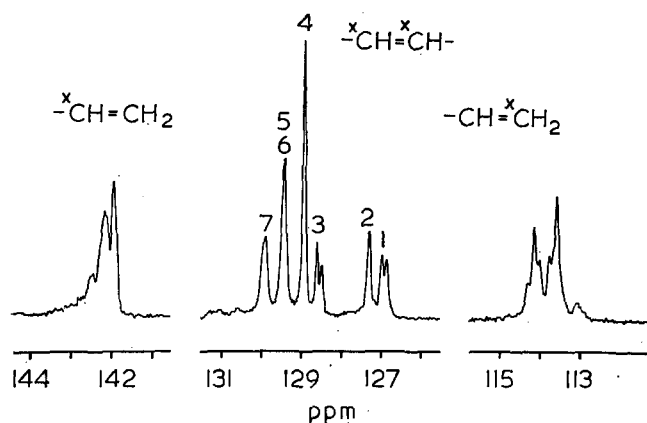
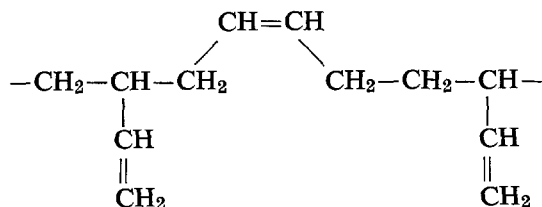


Figure 1 Expanded ^{13}C n.m.r. spectrum of equibinary *cis*-1,4-/*trans*-1,2-polybutadiene in the resonance region of the carbon double bond (OMTS=0ppm)

8 signals are resolved clearly in the region of the *cis*-1,4 double bond atoms. These resonance signals result from neighbouring influences of 1,2-units. In a sequence of three monomer units, e.g. vinyl(*v*)/*cis*-1,4(*c*)/vinyl(*v*), (*-v/c/-v*):



the resonance signals of the two carbon atoms of the *cis*-1,4 double bond have different chemical shifts owing to their different distances to the vinyl side group. In analogy to low molecular weight alkanes⁸ and alkanes⁹ we determined an empirical set of parameters which take into account whether the double bond of the vinyl

group is three (γ) or four (δ) carbon bonds away from that carbon atom of the *cis*-1,4 double bond under consideration. The parameters (γ') and (δ') refer to the influence of the vinyl double bond on the opposite side of the *cis*-1,4 double bond. Head-to-tail addition is highly probable because no other signals for other linkages could be verified. Consequently four parameters describe the influence of the vinyl group on the resonance signals of the *cis*-1,4 double bond atoms relatively to the *cis*-1,4 block signals at 128.91 ppm.

$$\begin{array}{ll}
 \gamma = -1.60 \text{ ppm} & \gamma' = +0.48 \text{ ppm} \\
 \delta = +0.48 \text{ ppm} & \delta' = -0.36_5 \text{ ppm}
 \end{array}$$

Assignment of the signals of the *cis*-1,4 double bond atoms and relative intensities are listed in Table 1. The

Table 1 Chemical shift data and relative intensities in *cis*-1,4-/*trans*-1,2-polybutadiene. Resonance region of the *cis*-1,4 carbon double bond

Signal	Carbon atom	Sequence	Chem. shift (ppm)	Relative intensities	
				Exp.	Calc.*
1	- $\overset{\bullet}{\text{C}}=\overset{\bullet}{\text{C}}-$	<i>-v/c/-v</i>	126.89	0.05	0.14
			127.00	0.08	
2		<i>-v/c/c</i>	127.31	0.13	0.12
			128.49	0.04	0.12
3		<i>c/c/-v</i>	128.60	0.08	
			128.91	0.25	0.23
4	- $\overset{\bullet}{\text{C}}=\overset{\bullet}{\text{C}}-$	<i>c/c/c</i>	128.91	0.25	0.23
			129.39	0.22	0.25
5	- $\overset{\bullet}{\text{C}}=\overset{\bullet}{\text{C}}-$	<i>c/c/-v</i>	129.39	0.22	0.25
			129.88	0.14	0.14
6		<i>-v/c/c</i>	129.39	0.22	0.25
			129.88	0.14	0.14
7		<i>-v/c/-v</i>	129.39	0.22	0.25
			129.88	0.14	0.14

* Calculated from a Bernoullian distribution

assignment has been proved by the ^{13}C n.m.r. spectra of pure *cis*-1,4 and isomerized polybutadienes⁶ and by comparison of experimental peak intensities with those calculated from a Bernoullian distribution of the monomer units in the polymer chain.

Signals 1 and 3, however, are split up by $\pm 0.05_5$ ppm into two single resonances. These additional signals may result from the asymmetric carbon atom of the 1,2-unit on the opposite side of the *cis*-1,4 double bond. Additionally the next following monomer unit may have influence. Signals 6 and 7 were expected to split also into two signals. This is not detectable, however, within the given resolution.

On the other hand, the influence of neighbouring *cis*-1,4-units on the chemical shift of the vinyl carbon atoms has been detected in the resonance region of the configurational triads and pentads of 1,2-polybutadienes⁵. Unfortunately, as shown in Figure 1, the difference in chemical shifts of configuration 1,2- and of compositional 1,2-/*cis*-1,4- sequences are too small to be resolved by the spectrometer.

Experimental

The equibinary *cis*-1,4-/*trans*-1,2-polybutadiene was poly-

merized with Co(III) triacetylacetonate/ $\text{AlEt}_3/\text{H}_2\text{O}$ catalyst according to the method of Furukawa *et al.*¹⁰. The proton decoupled ^{13}C n.m.r. spectra were obtained in CDCl_3 at 35°C with a HX 270 (Spectrospin AG, Zürich) at 67.88 MHz. Internal standard was octamethyltetrasiloxane (OMTS)=0 ppm.

Acknowledgement

The financial support of the Arbeitsgemeinschaft Industrieller Forschungsvereinigungen is gratefully acknowledged.

K.-F. Elgert, G. Quack and B. Stützel

Institut für Makromolekulare Chemie,
Universität Freiburg,
D-78 Freiburg i. Br., West Germany

(Received 24 May 1974)

References

- 1 Duch, M. W. and Grant, D. M. *Macromolecules* 1970, **3**, 165
- 2 Mochel, V. D. *J. Polym. Sci. (A-1)* 1972, **10**, 1009
- 3 Alaki, Y., Yoshimoto, T., Imanari, S. and Takeuchi, M. *Kobunshi Kagaku* 1972, **29**, 397
- 4 Furukawa, J., Kobayashi, E., Katshuki, N. and Kawagoe, T. *Makromol. Chem.* 1974, **175**, 237
- 5 Elgert, K.-F., Quack, G. and Stützel, B. *Makromol. Chem.* 1974, **176**, in press
- 6 Elgert, K.-F., Stützel, B., Frenzel, P., Cantow, H.-J. and Streck, R. *Makromol. Chem.* 1973, **170**, 257
- 7 Elgert, K.-F., Stützel, B., Cantow, H.-J., Seiler, E. and Frenzel, P. *IV Symp. Polymere 73, Varna* 1973, **4**, 11
- 8 Lindeman, L. P. and Adams, J. Q. *Analyt. Chem.* 1971, **43**, 1245
- 9 Dorman, D. E., Jautelat, M. and Roberts, J. D. *J. Org. Chem.* 1971, **36**, 2757
- 10 Furukawa, J., Haga, K., Kobayashi, E., Iseda, J., Joshimoto, T. and Sakamoto, K. *Polym. J.* 1971, **2**, 371

Polypropylene stability adversely affected by volatile oxidation products

In one of frequently used tests for measuring antioxidant effectiveness, the polymer compositions are oven-aged at selected temperatures¹. The results obtained from such tests and those from individual cell ageing units are often difficult to reconcile². It seems that in the case where many samples of different stability are exposed simultaneously the tendency of equalization of results is observed whereas the testing arrangements where individual samples are examined seem to discriminate better between two unlike samples. We wish to present results that could offer a possible explanation to this phenomenon.

Since all the samples being oven tested are more or less subjected to the influence of volatile products evolved from those samples which are already decomposing, it was of interest to examine the role of these volatiles in polypropylene thermo-oxidation.

Two polypropylene strips (each 0.2 g), one of which was fully stabilized and the other was either unstabilized or only partly stabilized (see Table 1), were placed into an open test-tube in such a manner that the direct contact of samples was avoided, the strips being 8 mm apart. The tube was then heated to 150°C until the deterioration of both samples occurred. The time required

for the appearance of first surface cracks was considered as the induction period, I_p . The value of I_p was noted for each strip. The results in Table 1 show that the induction period of a fully stabilized sample is strongly influenced by the second sample of the pair and it may

Table 1 Induction periods of various polypropylene sample pairs

Samples	I_p (days)
Fully stabilized pair	58 60
Unstabilized	1
Fully stabilized	4
Irganox 1076 (Ciba-Geigy) (0.1% w/w)	20
Fully stabilized	20
Dilauryl thiodipropionate (0.3% w/w)	28
Fully stabilized	31
Tinuvin 327 (Ciba-Geigy) (0.6% w/w)	1
Fully stabilized	3

Fully stabilized samples contained 0.1% w/w Irganox 1076, 0.25% w/w dilauryl thiodipropionate, 0.5% w/w Tinuvin 327 and 0.15% w/w calcium stearate

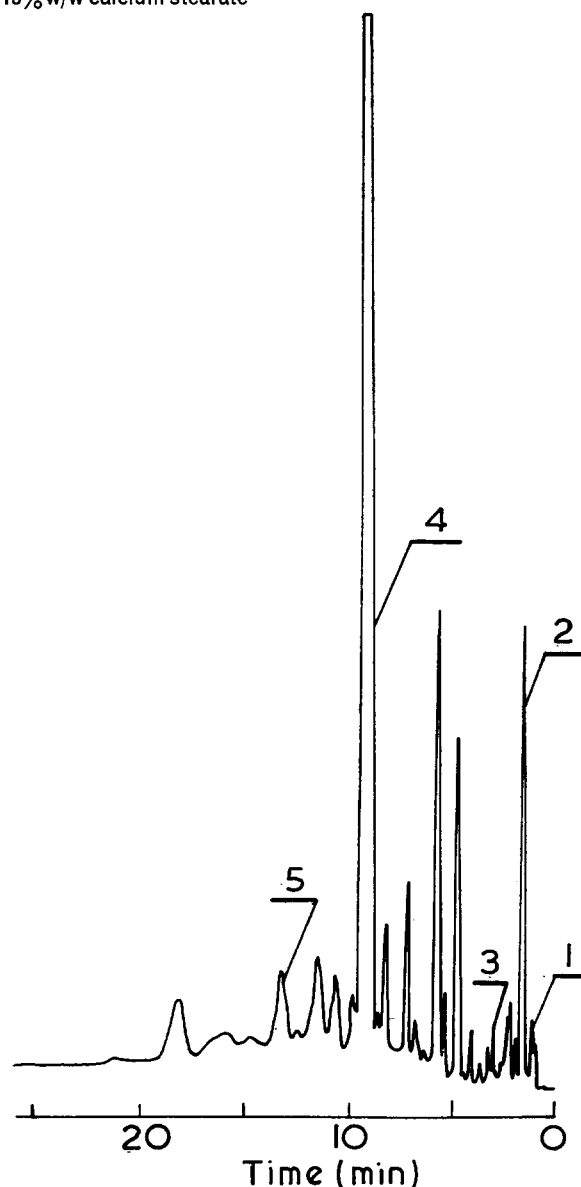


Figure 1 Fractogram of polypropylene thermo-oxidation products. Sample size, $0.6\ \mu\text{l}$; column, 6ft Carbowax 1540 on Chromosorb; temperature, $50\text{--}130^\circ\text{C}$; carrier gas, argon; flow, $30\ \text{ml}/\text{min}$. 1, Acetaldehyde; 2, acetone; 3, biacetyl; 4, acetic acid; 5, pyruvic acid

merized with Co(III) triacetylacetonate/ $\text{AlEt}_3/\text{H}_2\text{O}$ catalyst according to the method of Furukawa *et al.*¹⁰. The proton decoupled ^{13}C n.m.r. spectra were obtained in CDCl_3 at 35°C with a HX 270 (Spectrospin AG, Zürich) at 67.88 MHz. Internal standard was octamethyltetrasiloxane (OMTS)=0 ppm.

Acknowledgement

The financial support of the Arbeitsgemeinschaft Industrieller Forschungsvereinigungen is gratefully acknowledged.

K.-F. Elgert, G. Quack and B. Stützel

Institut für Makromolekulare Chemie,
Universität Freiburg,
D-78 Freiburg i. Br., West Germany

(Received 24 May 1974)

References

- 1 Duch, M. W. and Grant, D. M. *Macromolecules* 1970, 3, 165
- 2 Mochel, V. D. *J. Polym. Sci. (A-1)* 1972, 10, 1009
- 3 Alaki, Y., Yoshimoto, T., Imanari, S. and Takeuchi, M. *Kobunshi Kagaku* 1972, 29, 397
- 4 Furukawa, J., Kobayashi, E., Katshuki, N. and Kawagoe, T. *Makromol. Chem.* 1974, 175, 237
- 5 Elgert, K.-F., Quack, G. and Stützel, B. *Makromol. Chem.* 1974, 176, in press
- 6 Elgert, K.-F., Stützel, B., Frenzel, P., Cantow, H.-J. and Streck, R. *Makromol. Chem.* 1973, 170, 257
- 7 Elgert, K.-F., Stützel, B., Cantow, H.-J., Seiler, E. and Frenzel, P. *IV Symp. Polymere 73, Varna* 1973, 4, 11
- 8 Lindeman, L. P. and Adams, J. Q. *Analyt. Chem.* 1971, 43, 1245
- 9 Dorman, D. E., Jautelat, M. and Roberts, J. D. *J. Org. Chem.* 1971, 36, 2757
- 10 Furukawa, J., Haga, K., Kobayashi, E., Iseda, J., Joshimoto, T. and Sakamoto, K. *Polym. J.* 1971, 2, 371

Polypropylene stability adversely affected by volatile oxidation products

In one of frequently used tests for measuring antioxidant effectiveness, the polymer compositions are oven-aged at selected temperatures¹. The results obtained from such tests and those from individual cell ageing units are often difficult to reconcile². It seems that in the case where many samples of different stability are exposed simultaneously the tendency of equalization of results is observed whereas the testing arrangements where individual samples are examined seem to discriminate better between two unlike samples. We wish to present results that could offer a possible explanation to this phenomenon.

Since all the samples being oven tested are more or less subjected to the influence of volatile products evolved from those samples which are already decomposing, it was of interest to examine the role of these volatiles in polypropylene thermo-oxidation.

Two polypropylene strips (each 0.2 g), one of which was fully stabilized and the other was either unstabilized or only partly stabilized (see Table 1), were placed into an open test-tube in such a manner that the direct contact of samples was avoided, the strips being 8 mm apart. The tube was then heated to 150°C until the deterioration of both samples occurred. The time required

for the appearance of first surface cracks was considered as the induction period, I_p . The value of I_p was noted for each strip. The results in Table 1 show that the induction period of a fully stabilized sample is strongly influenced by the second sample of the pair and it may

Table 1 Induction periods of various polypropylene sample pairs

Samples	I_p (days)
Fully stabilized pair	58 60
Unstabilized	1
Fully stabilized	4
Irganox 1076 (Ciba-Geigy) (0.1% w/w)	20
Fully stabilized	20
Dilauryl thiodipropionate (0.3% w/w)	28
Fully stabilized	31
Tinuvin 327 (Ciba-Geigy) (0.6% w/w)	1
Fully stabilized	3

Fully stabilized samples contained 0.1% w/w Irganox 1076, 0.25% w/w dilauryl thiodipropionate, 0.5% w/w Tinuvin 327 and 0.15% w/w calcium stearate

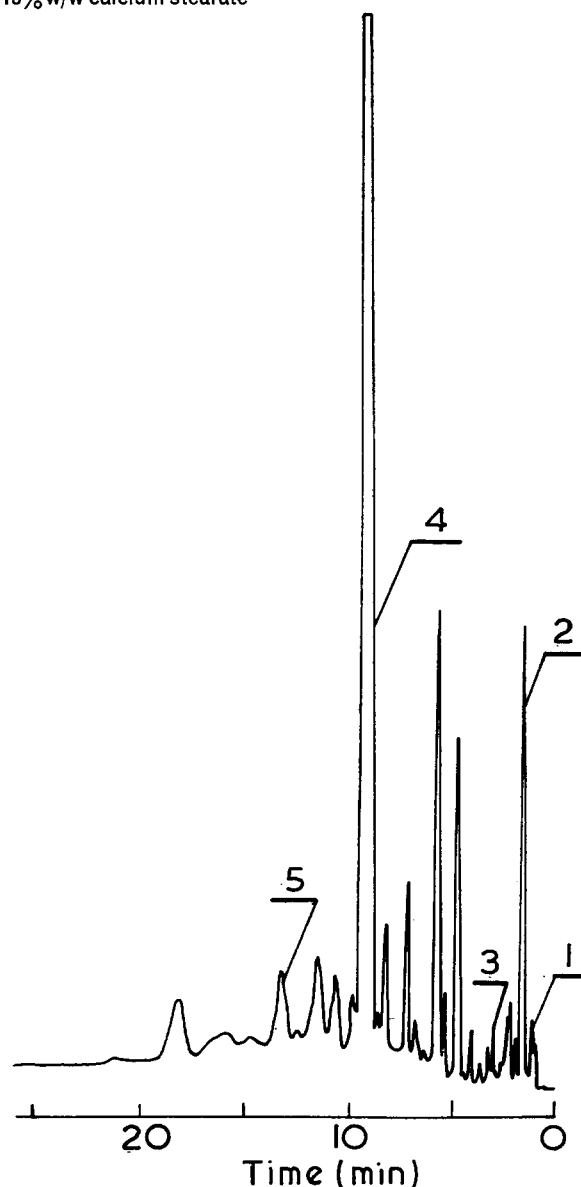


Figure 1 Fractogram of polypropylene thermo-oxidation products. Sample size, $0.6\ \mu\text{l}$; column, 6ft Carbowax 1540 on Chromosorb; temperature, $50\text{--}130^\circ\text{C}$; carrier gas, argon; flow, 30 ml/min . 1, Acetaldehyde; 2, acetone; 3, biacetyl; 4, acetic acid; 5, pyruvic acid

Letters

be reduced from 60 days down to even 3–4 days. Moreover, the fact that, under given conditions, the fully stabilized sample cannot survive the already degrading sample by more than three days indicates that volatiles formed due to degradation are involved. Table 1 also indicates that these volatiles are arising from the oxidation of polymer and not from the decomposition of additives.

We isolated the liquid mixture of products formed during polypropylene thermo-oxidation at 150°C in pure oxygen. The mixture was well resolved using gas-liquid chromatography (Figure 1). Some of the degradation products were identified by comparative gas chromatography using different column packings and are listed in Table 2.

These compounds, as well as the original liquid mixture of degradation products, were introduced into the system in which the polymer samples were degrading. With the exception of acetone all the compounds substantially accelerate the thermo-oxidation of fully

stabilized polypropylene samples placed in an oxygen filled, sealed glass tube (70 ml) heated at 140°C, the amount of added liquid being 5 μ l (see Table 2). In order to find out whether these additions influence also the degradation of unstabilized polypropylene, the experiment was repeated, degrading the latter at 80°C. At this temperature the process is sufficiently slowed down to see the differences in I_p values. No influence on the I_p values, however, was observed this time. This is in agreement with the observation of Miller *et al.*³ who examined the influence of acetaldehyde on the degradation of pure polypropylene.

It seems that the deleterious effects of degradation products formed through polypropylene thermo-oxidation consists of the attack on stabilizing additives and thus increasing the rate of their consumption.

The observed effect of volatiles should be taken into consideration when designing accelerated ageing tests.

J. Sedlář and J. Pác

Table 2 Degradation of fully stabilized polypropylene in the presence of various compounds

Compound	I_p (days)
Acetone	34
Acetic acid	3
Acetaldehyde	4
Biacetyl	3
Degradation products mixture	5

Research Institute of Macromolecular Chemistry,
656 49 Brno, Czechoslovakia

(Received 21 June 1974)

References

- 1 Hawkins, W. L. 'Polymer Stabilisation', John Wiley, New York, 1972
- 2 ICI Technical Information R 42, Dyestuffs Div., 1969
- 3 Miller, V. B., Neiman, M. B., Pudov, V. S. and Lafer, L. I. *Vysokomol. Soedin.* 1959, 1, 1696

Book Reviews

Plastic foams

Edited by K. C. Frisch and J. H. Saunders

Marcel Dekker, New York, 1973, Part II, 572 pp. \$47.50

This is Part II of a USA monograph series, Part I being published in 1972 (reviewed in *Polymer* 1973, 14, 175) and dealing with foams from flexible polymers. Rigid foams are described in this second volume covering both organic and inorganic polymeric structural materials. In this sense the book is unique, which is perhaps as well as the price of \$47.50 will surely put it firmly in the 'library only' price bracket. Despite this disadvantage, the authors have carried out an excellent job in bringing together a new team of industrially based authors whose contribution is valuable in presenting a current account of many new commercial foam systems with the latest developments in older cellular technologies.

Chapters are written on established foams from rigid polyurethanes, polystyrene and related thermoplastics, phenolics, urea-formaldehyde, epoxy resins. A special chapter has been compiled on new high temperature resistant plastic foams based on polyisocyanates, polybenzimidazoles, polyamides. This is most timely given the current pressing needs of fire retardancy and low smoke emission requirements in structural foams.

A wide range of cellular polymers not yet in large scale commercial production but possessing interesting potential is detailed. Thus covered are poly(vinyl carbazole), pyroxyl, polyester, cellulose acetate, poly(vinyl alcohol)-formaldehyde, polyamide, irradiated acrylic, fluorocarbon, polysulphone, ionomer, temperature-adaptable fabrics and temperature-reversible foams.

Unusually, inorganic foams are included based on glass, metals, refractories, concrete and sulphur. This area is little touched upon by most polymer publications but must now be regarded of much future importance with the increasingly stringent fire resistance performance now demanded. A further section on thermal decomposition and flammability emphasizes such present interest, it being supported by an account of cell geometry on foam performance.

Application areas are included in some detail. Usually the product and field use of foams is neglected in polymer technology books

despite their crucial importance and the fact that the majority of technical personnel earn their living in such areas. Uses covered over three chapters are transportation, agricultural, military and space applications.

No author or subject index is provided in Part I; Part II contains a rather meagre index supplemented by detailed chapter contents. Printing and paper quality are first-class and few typographical errors were noted. A minor criticism concerns the exclusive use of USA trade names and units perpetuating the need for most technical personnel to remain conversant with imperial, cgs and SI systems.

Undoubtedly this book provides much information which would be very useful for new entrants to the growing specialized foam field and serve as a balanced review for older established practitioners. As material costs increase and scarcity grows, so foamed structures offer many cost and weight economy advantages; hence this book and its companion volume are welcome and timely additions to the now rapidly growing volume of foam literature. Chemists and foam technologists will likely be the personnel most likely to require access to this book supplemented by marketing people interested in exploiting the various new application areas.

C. Hepburn

Conformational properties of macromolecules

A. J. Hopfinger

Academic Press, New York, 1974, 348 pp. £11.30

The need which this book sets out to fill is very real: to provide an up-to-date review of theoretical conformational analysis, including (to quote from the jacket) 'in-depth discussions of the forces that dictate molecular conformation'.

The reviewer found the stated objectives only imperfectly fulfilled. The mathematics is often expressed verbally at excessive length. On p 26, ' $x_i > x_j$ for $i > j$ ' is rendered, 'each successive skeletal atom has an associated x coordinate which has greater positive value than the x coordinate of any preceding atom (any atom whose

Letters

be reduced from 60 days down to even 3–4 days. Moreover, the fact that, under given conditions, the fully stabilized sample cannot survive the already degrading sample by more than three days indicates that volatiles formed due to degradation are involved. Table 1 also indicates that these volatiles are arising from the oxidation of polymer and not from the decomposition of additives.

We isolated the liquid mixture of products formed during polypropylene thermo-oxidation at 150°C in pure oxygen. The mixture was well resolved using gas-liquid chromatography (Figure 1). Some of the degradation products were identified by comparative gas chromatography using different column packings and are listed in Table 2.

These compounds, as well as the original liquid mixture of degradation products, were introduced into the system in which the polymer samples were degrading. With the exception of acetone all the compounds substantially accelerate the thermo-oxidation of fully

stabilized polypropylene samples placed in an oxygen filled, sealed glass tube (70 ml) heated at 140°C, the amount of added liquid being 5 μ l (see Table 2). In order to find out whether these additions influence also the degradation of unstabilized polypropylene, the experiment was repeated, degrading the latter at 80°C. At this temperature the process is sufficiently slowed down to see the differences in I_p values. No influence on the I_p values, however, was observed this time. This is in agreement with the observation of Miller *et al.*³ who examined the influence of acetaldehyde on the degradation of pure polypropylene.

It seems that the deleterious effects of degradation products formed through polypropylene thermo-oxidation consists of the attack on stabilizing additives and thus increasing the rate of their consumption.

The observed effect of volatiles should be taken into consideration when designing accelerated ageing tests.

J. Sedlář and J. Pác

Table 2 Degradation of fully stabilized polypropylene in the presence of various compounds

Compound	I_p (days)
Acetone	34
Acetic acid	3
Acetaldehyde	4
Biacetyl	3
Degradation products mixture	5

Research Institute of Macromolecular Chemistry,
656 49 Brno, Czechoslovakia

(Received 21 June 1974)

References

- 1 Hawkins, W. L. 'Polymer Stabilisation', John Wiley, New York, 1972
- 2 ICI Technical Information R 42, Dyestuffs Div., 1969
- 3 Miller, V. B., Neiman, M. B., Pudov, V. S. and Lafer, L. I. *Vysokomol. Soedin.* 1959, 1, 1696

Book Reviews

Plastic foams

Edited by K. C. Frisch and J. H. Saunders

Marcel Dekker, New York, 1973, Part II, 572 pp. \$47.50

This is Part II of a USA monograph series, Part I being published in 1972 (reviewed in *Polymer* 1973, 14, 175) and dealing with foams from flexible polymers. Rigid foams are described in this second volume covering both organic and inorganic polymeric structural materials. In this sense the book is unique, which is perhaps as well as the price of \$47.50 will surely put it firmly in the 'library only' price bracket. Despite this disadvantage, the authors have carried out an excellent job in bringing together a new team of industrially based authors whose contribution is valuable in presenting a current account of many new commercial foam systems with the latest developments in older cellular technologies.

Chapters are written on established foams from rigid polyurethanes, polystyrene and related thermoplastics, phenolics, urea-formaldehyde, epoxy resins. A special chapter has been compiled on new high temperature resistant plastic foams based on polyisocyanates, polybenzimidazoles, polyamides. This is most timely given the current pressing needs of fire retardancy and low smoke emission requirements in structural foams.

A wide range of cellular polymers not yet in large scale commercial production but possessing interesting potential is detailed. Thus covered are poly(vinyl carbazole), pyroxyl, polyester, cellulose acetate, poly(vinyl alcohol)-formaldehyde, polyamide, irradiated acrylic, fluorocarbon, polysulphone, ionomer, temperature-adaptable fabrics and temperature-reversible foams.

Unusually, inorganic foams are included based on glass, metals, refractories, concrete and sulphur. This area is little touched upon by most polymer publications but must now be regarded of much future importance with the increasingly stringent fire resistance performance now demanded. A further section on thermal decomposition and flammability emphasizes such present interest, it being supported by an account of cell geometry on foam performance.

Application areas are included in some detail. Usually the product and field use of foams is neglected in polymer technology books

despite their crucial importance and the fact that the majority of technical personnel earn their living in such areas. Uses covered over three chapters are transportation, agricultural, military and space applications.

No author or subject index is provided in Part I; Part II contains a rather meagre index supplemented by detailed chapter contents. Printing and paper quality are first-class and few typographical errors were noted. A minor criticism concerns the exclusive use of USA trade names and units perpetuating the need for most technical personnel to remain conversant with imperial, cgs and SI systems.

Undoubtedly this book provides much information which would be very useful for new entrants to the growing specialized foam field and serve as a balanced review for older established practitioners. As material costs increase and scarcity grows, so foamed structures offer many cost and weight economy advantages; hence this book and its companion volume are welcome and timely additions to the now rapidly growing volume of foam literature. Chemists and foam technologists will likely be the personnel most likely to require access to this book supplemented by marketing people interested in exploiting the various new application areas.

C. Hepburn

Conformational properties of macromolecules

A. J. Hopfinger

Academic Press, New York, 1974, 348 pp. £11.30

The need which this book sets out to fill is very real: to provide an up-to-date review of theoretical conformational analysis, including (to quote from the jacket) 'in-depth discussions of the forces that dictate molecular conformation'.

The reviewer found the stated objectives only imperfectly fulfilled. The mathematics is often expressed verbally at excessive length. On p 26, ' $x_i > x_j$ for $i > j$ ' is rendered, 'each successive skeletal atom has an associated x coordinate which has greater positive value than the x coordinate of any preceding atom (any atom whose

label number is a smaller integer)'. Besides, a few lines later, a definition is said to be rendered unique by a procedure which does not render it unique in all cases. The physical and chemical theory is occasionally marred by basic misstatements. On p 49 it is clearly implied that thermodynamic behaviour such as phase transition can in principle be explained in terms of interparticle potentials like that of Lennard-Jones, only if the parameters occurring therein are made temperature-dependent. In reality, such potentials are capable of modelling thermodynamic and transition behaviour without making them dependent on temperature; such dependence runs counter to the basic framework of statistical mechanics, although it is used as an empirical adjustment to compensate other faults in the model. On p 164, an equilibrium constant is wrongly defined without regard to stoichiometry since n units are made to disappear and $n+j$ to appear. But the book's worst fault is the lack of critical assessment of data, which are often presented in tables without clear indication of their sources or error limits. Table I-1, for instance, lists Lennard-Jones parameter A , for various contact pairs, all to 0.1 kcal-A⁶/mole, though individual values vary almost 20-fold. The text warns against numerous approximations in the underlying computations, without disclosing them adequately. On p 132, it 'is left to the reader to decide upon the reliability of the proposed potential functions for a specific type of structural calculation'. Thereafter, however, chapter three, at least, does give a helpfully critical evaluation of the accuracy and refinement of potential functions.

This book could in principle fill a much greater need than this first edition suggests. A thoroughly revised text, with fuller authentication of calculations and data, and less wordy exposition elsewhere, would make an early second edition worthwhile. In particular, those working on conformational computer calculations often have to rely on verbal instructions from programming experts for want of guidance in published form; Professor Hopfinger could help here by including more details of his programming procedures.

M. Gordon

Polymer chemistry

B. Vollmert (Translated by E. H. Immergut)
Springer Verlag, Berlin, 1973, 630 pp. \$27.80

This book takes on the formidable task of covering the whole field of polymer chemistry and physics in a single volume. Clearly any author of such a work must be prepared to tackle a very wide range of subjects indeed. On the other hand, most reviewers are likely to find their own knowledge rather limited in relation to certain parts of the book, and so tend to evaluate reliability in relation to those parts where their expertise is more well developed.

Generally the level is that of the advanced student. In the first chapters the chemistry of polymers and their preparation is systematically set out. Thus the first 250 pages cover the major polymerization processes, normally approaching the subject from the organic chemist's point of view, although a substantial amount of kinetic treatment is also included. The next 30-40 pages then give a short summary of recent work in the field of biopolymers including DNA, protein synthesis and biosynthesis. The strictly chemical part of the book then closes with sections covering graft and block copolymer and the chemical reactions of polymer chains (mainly degradation processes).

There follows a large section on the macromolecular coil, molecular weight distribution and the solution properties of polymers (about 130 pages). The properties of polymers in the rubbery and solid state are finally dealt with in some 60 pages. This part is, of course, rather short, as is perhaps appropriate in a book on polymer chemistry, but it nevertheless goes well beyond the requirements of a work dealing exclusively with chemical properties and reactions.

The main value of the book lies in a comprehensive presentation of the chemistry of polymerization processes. These are generally very good, though in the case of Ziegler polymerization the bimetallic mechanism of Patat and Sinn is rather exclusively presented and Cossee's monometallic mechanism is mentioned only in the section dealing with soluble Al-Ti complexes.

On the physical side the book is not quite up to date in discussing the structure of block copolymers, though crystalline polymers both natural and synthetic are well summarized. Further though strength and toughness are discussed, modern theories of yield and fracture are omitted, and crazing is not mentioned as having anything to do with the properties of impact polystyrene. On the other hand, the

structural information on the preparation of high impact polystyrene is very good. These limitations no doubt reflect the great difficulties which face any single author in providing a comprehensive work of this nature.

The general presentation of the work is very satisfactory, though the inclusion of some of the main references would have been helpful. Translation from the German is fully adequate, though not completely free from Germanic structures. The foreign origin is also apparent in the use of k_w as the propagation content in a radical polymerization (normally k_p) and by the description of poly(vinyl alcohol) monomer on p 14 as 'not bystander'. In spite, however, of these minor blemishes the reviewer can recommend the book as a good summary of modern polymer chemistry.

R. N. Haward

Allyl compounds and their polymers (including polyolefins)

C. E. Schildknecht

Wiley-Interscience, New York & London, 1973,
736 pp. £15.50

The books of Cal Schildknecht have been of considerable value to many of us concerned over the years with polymer science and technology. His *Vinyl and Related Polymers* published by Wiley in 1952 formed a major source of information and reference, as did his *Polymer Processes* which appeared a few years later as Vol X of the Interscience High Polymers series, and one therefore took up his latest book with considerable interest and expectation. It forms Vol XXVIII of this same series and has the uniform binding, but there was some dismay on seeing the lay-out and type which, although no doubt helping to keep down costs, hardly contribute to comfortable reading. However, a glance at the contents list showed how comprehensive and erudite one could expect his book to be and on reading it there was no disappointment.

As the title implies, the book deals with all aspects of compounds in which the CH₂:CHCH· or related groups occur and surveys the preparation, chemical reactions and properties of such compounds, their behaviour towards polymerization and copolymerization, and their applications in plastics, elastomers, fibres, and adhesives. Other aspects where allylic compounds enter into flavours, perfumes, bactericides, insecticides, pharmaceuticals, catalysts, are also included (and often make fascinating reading) so that in all the book forms a welcome and useful addition to the literature not only of polymer organic chemistry but also of organic synthesis in general. It is based on a carefully made and extensive collection of the scientific and patent literature and one cannot but be impressed by its wide coverage.

The thirty-one chapters deal with polymerization and copolymerization in vinyls and alkenes, discussing the effects of structure, and in a very comprehensive manner with the preparation and behaviour of allylic compounds—olefins, halides, alcohols, ethers, acids, amides, esters, etc.; included also are derivatives where phosphorus, silicon, boron and metal complexes are involved. For many of the compounds discussed preparative detail, often taken from patent examples, is given. Lists give some physical constants and primary references, while each chapter carries a list of references to the relevant scientific, patent and commercial literature, so bringing each survey very much up-to-date.

In this comprehensive, almost encyclopaedic, review, the author shows the wide applications of allyl compounds in many branches of polymer chemistry where they give rise to novel or modified materials like CR39 resins, diallyl phthalate, triallyl cyanurate, acrylic copolymers, starch ethers, and polyelectrolytes for flocculants, conducting and ion-exchange materials.

Despite covering such a wide field the contents of each chapter are well defined and it is easy to select portions relating to specific topics. A good index is provided but surprisingly this does not include the Alfin catalysts mentioned on p 712. The book appears to have been well edited and few errors appear (the formulae or nomenclature on page 274 and references 100 and 101 in Chapter 3 need attention).

This book fills a gap in the literature of polymer and organic chemistry and as such will be of value to a large number of academic and industrial workers and to students, useful both as a textbook and as a source of reference. On modern standards the price is not excessive and there is no doubt that it is worthy of its place as Vol XXVIII of the well-known High Polymers series.

R. J. W. Reynolds

Letters

be reduced from 60 days down to even 3–4 days. Moreover, the fact that, under given conditions, the fully stabilized sample cannot survive the already degrading sample by more than three days indicates that volatiles formed due to degradation are involved. Table 1 also indicates that these volatiles are arising from the oxidation of polymer and not from the decomposition of additives.

We isolated the liquid mixture of products formed during polypropylene thermo-oxidation at 150°C in pure oxygen. The mixture was well resolved using gas-liquid chromatography (Figure 1). Some of the degradation products were identified by comparative gas chromatography using different column packings and are listed in Table 2.

These compounds, as well as the original liquid mixture of degradation products, were introduced into the system in which the polymer samples were degrading. With the exception of acetone all the compounds substantially accelerate the thermo-oxidation of fully

stabilized polypropylene samples placed in an oxygen filled, sealed glass tube (70 ml) heated at 140°C, the amount of added liquid being 5 μ l (see Table 2). In order to find out whether these additions influence also the degradation of unstabilized polypropylene, the experiment was repeated, degrading the latter at 80°C. At this temperature the process is sufficiently slowed down to see the differences in I_p values. No influence on the I_p values, however, was observed this time. This is in agreement with the observation of Miller *et al.*³ who examined the influence of acetaldehyde on the degradation of pure polypropylene.

It seems that the deleterious effects of degradation products formed through polypropylene thermo-oxidation consists of the attack on stabilizing additives and thus increasing the rate of their consumption.

The observed effect of volatiles should be taken into consideration when designing accelerated ageing tests.

J. Sedlář and J. Pác

Table 2 Degradation of fully stabilized polypropylene in the presence of various compounds

Compound	I_p (days)
Acetone	34
Acetic acid	3
Acetaldehyde	4
Biacetyl	3
Degradation products mixture	5

Research Institute of Macromolecular Chemistry,
656 49 Brno, Czechoslovakia

(Received 21 June 1974)

References

- 1 Hawkins, W. L. 'Polymer Stabilisation', John Wiley, New York, 1972
- 2 ICI Technical Information R 42, Dyestuffs Div., 1969
- 3 Miller, V. B., Neiman, M. B., Pudov, V. S. and Lafer, L. I. *Vysokomol. Soedin.* 1959, 1, 1696

Book Reviews

Plastic foams

Edited by K. C. Frisch and J. H. Saunders

Marcel Dekker, New York, 1973, Part II, 572 pp. \$47.50

This is Part II of a USA monograph series, Part I being published in 1972 (reviewed in *Polymer* 1973, 14, 175) and dealing with foams from flexible polymers. Rigid foams are described in this second volume covering both organic and inorganic polymeric structural materials. In this sense the book is unique, which is perhaps as well as the price of \$47.50 will surely put it firmly in the 'library only' price bracket. Despite this disadvantage, the authors have carried out an excellent job in bringing together a new team of industrially based authors whose contribution is valuable in presenting a current account of many new commercial foam systems with the latest developments in older cellular technologies.

Chapters are written on established foams from rigid polyurethanes, polystyrene and related thermoplastics, phenolics, urea-formaldehyde, epoxy resins. A special chapter has been compiled on new high temperature resistant plastic foams based on polyisocyanates, polybenzimidazoles, polyamides. This is most timely given the current pressing needs of fire retardancy and low smoke emission requirements in structural foams.

A wide range of cellular polymers not yet in large scale commercial production but possessing interesting potential is detailed. Thus covered are poly(vinyl carbazole), pyroxyl, polyester, cellulose acetate, poly(vinyl alcohol)-formaldehyde, polyamide, irradiated acrylic, fluorocarbon, polysulphone, ionomer, temperature-adaptable fabrics and temperature-reversible foams.

Unusually, inorganic foams are included based on glass, metals, refractories, concrete and sulphur. This area is little touched upon by most polymer publications but must now be regarded of much future importance with the increasingly stringent fire resistance performance now demanded. A further section on thermal decomposition and flammability emphasizes such present interest, it being supported by an account of cell geometry on foam performance.

Application areas are included in some detail. Usually the product and field use of foams is neglected in polymer technology books

despite their crucial importance and the fact that the majority of technical personnel earn their living in such areas. Uses covered over three chapters are transportation, agricultural, military and space applications.

No author or subject index is provided in Part I; Part II contains a rather meagre index supplemented by detailed chapter contents. Printing and paper quality are first-class and few typographical errors were noted. A minor criticism concerns the exclusive use of USA trade names and units perpetuating the need for most technical personnel to remain conversant with imperial, cgs and SI systems.

Undoubtedly this book provides much information which would be very useful for new entrants to the growing specialized foam field and serve as a balanced review for older established practitioners. As material costs increase and scarcity grows, so foamed structures offer many cost and weight economy advantages; hence this book and its companion volume are welcome and timely additions to the now rapidly growing volume of foam literature. Chemists and foam technologists will likely be the personnel most likely to require access to this book supplemented by marketing people interested in exploiting the various new application areas.

C. Hepburn

Conformational properties of macromolecules

A. J. Hopfinger

Academic Press, New York, 1974, 348 pp. £11.30

The need which this book sets out to fill is very real: to provide an up-to-date review of theoretical conformational analysis, including (to quote from the jacket) 'in-depth discussions of the forces that dictate molecular conformation'.

The reviewer found the stated objectives only imperfectly fulfilled. The mathematics is often expressed verbally at excessive length. On p 26, ' $x_i > x_j$ for $i > j$ ' is rendered, 'each successive skeletal atom has an associated x coordinate which has greater positive value than the x coordinate of any preceding atom (any atom whose

label number is a smaller integer)'. Besides, a few lines later, a definition is said to be rendered unique by a procedure which does not render it unique in all cases. The physical and chemical theory is occasionally marred by basic misstatements. On p 49 it is clearly implied that thermodynamic behaviour such as phase transition can in principle be explained in terms of interparticle potentials like that of Lennard-Jones, only if the parameters occurring therein are made temperature-dependent. In reality, such potentials are capable of modelling thermodynamic and transition behaviour without making them dependent on temperature; such dependence runs counter to the basic framework of statistical mechanics, although it is used as an empirical adjustment to compensate other faults in the model. On p 164, an equilibrium constant is wrongly defined without regard to stoichiometry since n units are made to disappear and $n+j$ to appear. But the book's worst fault is the lack of critical assessment of data, which are often presented in tables without clear indication of their sources or error limits. Table I-1, for instance, lists Lennard-Jones parameter A , for various contact pairs, all to 0.1 kcal-A⁶/mole, though individual values vary almost 20-fold. The text warns against numerous approximations in the underlying computations, without disclosing them adequately. On p 132, it 'is left to the reader to decide upon the reliability of the proposed potential functions for a specific type of structural calculation'. Thereafter, however, chapter three, at least, does give a helpfully critical evaluation of the accuracy and refinement of potential functions.

This book could in principle fill a much greater need than this first edition suggests. A thoroughly revised text, with fuller authentication of calculations and data, and less wordy exposition elsewhere, would make an early second edition worthwhile. In particular, those working on conformational computer calculations often have to rely on verbal instructions from programming experts for want of guidance in published form; Professor Hopfinger could help here by including more details of his programming procedures.

M. Gordon

Polymer chemistry

B. Vollmert (Translated by E. H. Immergut)
Springer Verlag, Berlin, 1973, 630 pp. \$27.80

This book takes on the formidable task of covering the whole field of polymer chemistry and physics in a single volume. Clearly any author of such a work must be prepared to tackle a very wide range of subjects indeed. On the other hand, most reviewers are likely to find their own knowledge rather limited in relation to certain parts of the book, and so tend to evaluate reliability in relation to those parts where their expertise is more well developed.

Generally the level is that of the advanced student. In the first chapters the chemistry of polymers and their preparation is systematically set out. Thus the first 250 pages cover the major polymerization processes, normally approaching the subject from the organic chemist's point of view, although a substantial amount of kinetic treatment is also included. The next 30-40 pages then give a short summary of recent work in the field of biopolymers including DNA, protein synthesis and biosynthesis. The strictly chemical part of the book then closes with sections covering graft and block copolymer and the chemical reactions of polymer chains (mainly degradation processes).

There follows a large section on the macromolecular coil, molecular weight distribution and the solution properties of polymers (about 130 pages). The properties of polymers in the rubbery and solid state are finally dealt with in some 60 pages. This part is, of course, rather short, as is perhaps appropriate in a book on polymer chemistry, but it nevertheless goes well beyond the requirements of a work dealing exclusively with chemical properties and reactions.

The main value of the book lies in a comprehensive presentation of the chemistry of polymerization processes. These are generally very good, though in the case of Ziegler polymerization the bimetallic mechanism of Patat and Sinn is rather exclusively presented and Cossee's monometallic mechanism is mentioned only in the section dealing with soluble Al-Ti complexes.

On the physical side the book is not quite up to date in discussing the structure of block copolymers, though crystalline polymers both natural and synthetic are well summarized. Further though strength and toughness are discussed, modern theories of yield and fracture are omitted, and crazing is not mentioned as having anything to do with the properties of impact polystyrene. On the other hand, the

structural information on the preparation of high impact polystyrene is very good. These limitations no doubt reflect the great difficulties which face any single author in providing a comprehensive work of this nature.

The general presentation of the work is very satisfactory, though the inclusion of some of the main references would have been helpful. Translation from the German is fully adequate, though not completely free from Germanic structures. The foreign origin is also apparent in the use of k_w as the propagation content in a radical polymerization (normally k_p) and by the description of poly(vinyl alcohol) monomer on p 14 as 'not bystander'. In spite, however, of these minor blemishes the reviewer can recommend the book as a good summary of modern polymer chemistry.

R. N. Haward

Allyl compounds and their polymers (including polyolefins)

C. E. Schildknecht

Wiley-Interscience, New York & London, 1973,
736 pp. £15.50

The books of Cal Schildknecht have been of considerable value to many of us concerned over the years with polymer science and technology. His *Vinyl and Related Polymers* published by Wiley in 1952 formed a major source of information and reference, as did his *Polymer Processes* which appeared a few years later as Vol X of the Interscience High Polymers series, and one therefore took up his latest book with considerable interest and expectation. It forms Vol XXVIII of this same series and has the uniform binding, but there was some dismay on seeing the lay-out and type which, although no doubt helping to keep down costs, hardly contribute to comfortable reading. However, a glance at the contents list showed how comprehensive and erudite one could expect his book to be and on reading it there was no disappointment.

As the title implies, the book deals with all aspects of compounds in which the CH₂:CHCH· or related groups occur and surveys the preparation, chemical reactions and properties of such compounds, their behaviour towards polymerization and copolymerization, and their applications in plastics, elastomers, fibres, and adhesives. Other aspects where allylic compounds enter into flavours, perfumes, bactericides, insecticides, pharmaceuticals, catalysts, are also included (and often make fascinating reading) so that in all the book forms a welcome and useful addition to the literature not only of polymer organic chemistry but also of organic synthesis in general. It is based on a carefully made and extensive collection of the scientific and patent literature and one cannot but be impressed by its wide coverage.

The thirty-one chapters deal with polymerization and copolymerization in vinyls and alkenes, discussing the effects of structure, and in a very comprehensive manner with the preparation and behaviour of allylic compounds—olefins, halides, alcohols, ethers, acids, amides, esters, etc.; included also are derivatives where phosphorus, silicon, boron and metal complexes are involved. For many of the compounds discussed preparative detail, often taken from patent examples, is given. Lists give some physical constants and primary references, while each chapter carries a list of references to the relevant scientific, patent and commercial literature, so bringing each survey very much up-to-date.

In this comprehensive, almost encyclopaedic, review, the author shows the wide applications of allyl compounds in many branches of polymer chemistry where they give rise to novel or modified materials like CR39 resins, diallyl phthalate, triallyl cyanurate, acrylic copolymers, starch ethers, and polyelectrolytes for flocculants, conducting and ion-exchange materials.

Despite covering such a wide field the contents of each chapter are well defined and it is easy to select portions relating to specific topics. A good index is provided but surprisingly this does not include the Alfin catalysts mentioned on p 712. The book appears to have been well edited and few errors appear (the formulae or nomenclature on page 274 and references 100 and 101 in Chapter 3 need attention).

This book fills a gap in the literature of polymer and organic chemistry and as such will be of value to a large number of academic and industrial workers and to students, useful both as a textbook and as a source of reference. On modern standards the price is not excessive and there is no doubt that it is worthy of its place as Vol XXVIII of the well-known High Polymers series.

R. J. W. Reynolds

Treatise on adhesion and adhesives, Vol 3

Edited by R. L. Patrick

Marcel Dekker, New York, 1973. 240 pp. \$21.75

This third volume of Dr Patrick's treatise differs in several respects from the other two. According to the prefatory remarks this volume instead of dealing with the technology of adhesives as originally planned deals with four special topics and subsequent volumes, if any, will continue this type of treatment. These special topics are handled in a very different manner from the ordered textbook theory approach of the previous volumes and will appeal to and be used by a very different clientele. Unlike Volumes 1 and 2, this book is produced by offset litho from typewriter setting without line justification or changes in type face and with underlining replacing both italic and bold insertions in the text. This method of book production has also resulted in a non-uniform graph and figure production. There is also the annoying consequence that many tables take too much space and require rotation of the book in order to refer to them. Three of the four subjects treated in the text are cast in the form of reviews. The first deals with structural adhesives for metal bonding and is an easily read, valuable contribution with sufficient organic chemistry to make chemical aspects intelligible within the compass of the ordinary technologist. This section is particularly illuminating on epoxy adhesives. The second on the durability of adhesive bonded joints is rather too much like a report to a government agency with all data meticulously graphed when the results could be more succinctly subsumed. It also suffers from codification of the commercial adhesives to preserve anonymity. The discussion on surface treatment of aluminium is inadequate. The third review type paper discusses the increasingly popular field of polymers in the glassy state with some interesting analysis of thermal and mechanical data especially for polycarbonates clearing up the so-called glass transition at about 145°C and putting the true second order transition down to -120°C. The discussion of the brittle-ductile transition could have been much more extensive.

The last article in the book illustrates the use of stereo scanning electron microscopy in adhesion science but does so with a detailed

manner of experimental presentation more appropriate to a research journal. The message and results tend to get lost in the exposition but their importance repays close study.

A few mistakes were noticed; polyethylene for polyether on p 30; calandered for calendered; Aero Corporation for Aero Research Ltd, and Dr Salomon's name repeatedly anglicized to Solomon. A simple monomolecular layer does not suffice to give a weak boundary layer (p 207)—the layer must be duplex for cohesive failure. The Figure on p 132 is a waste and that on p 135 contains insufficient identification of what the three curves represent and this cannot be deduced easily from the text.

It is not a flawless book but it is a valuable one.

A. R. Payne

Polymerization kinetics and technology

(Advances in Chemistry Series 128)

Edited by N. A. J. Platzer

American Chemical Society, Washington, 1973, 288 pp. \$15.95

This is the publication of eighteen papers from a symposium and as such covers a wide field of polymerization kinetics with attention to radical and ionic mechanisms and stereocontrol. There is a clear direction to industrial interests with contributions on equipment and process design and to the modification of polymers by grafting, blocking, blending and crosslinking. The important formation of polyesters is not forgotten and mechanisms for the synthesis of these and other condensation polymers such as polyurethanes are discussed.

This is a well-produced and illustrated volume which presents modern growth points in the science and technology of polymerization in a condensed manner. For industrial chemists, this offers much of immediate interest and for the academic worker, an opportunity to see how fundamental studies are being applied.

As present prices go, this is good value for money.

J. C. Robb

RESOURCES POLICY

the economics, planning and use
of mineral resources

A NEW QUARTERLY JOURNAL

first issue · September 1974

Main articles

The concept and measurement of mineral reserves and resources
G.J.S. Govett and M.H. Govett

The use of by-products in concrete
W. Gutt

Non-renewable mineral resources
Sir Kingsley Dunham

Analysis of the life cycle of non-ferrous minerals
F. Roberts and I. Torrens

Other sections

- Current topics
- Conference reports
- Forthcoming meetings
- Book reviews and announcements
- Publications received

RESOURCES POLICY will present multi-disciplinary discussions at an upper management/academic level. The aim is to identify policy options for the future supply and demand of mineral resources. It will encompass the many disciplines and examine options as they affect industrial, commercial and social institutions at world and regional levels

Published quarterly in March, June, September, December, commencing September 1974

One-year subscription (four issues) £20.00 (\$50.00).

For full details apply to: IPC Science and Technology Press Limited (Dept. AD.RP)
IPC House, 32 High Street, Guildford, Surrey, England GU1 3EW
Telephone: Guildford (0483) 71661 Telex: Scitechpress Gd. 85556

Effect of molecular weight on the partial specific volume of polystyrenes in solution

Jeanne François, Françoise Candau and Henri Benoit

Centre de Recherches sur les Macromolécules, CNRS, 67083 Strasbourg, France
(Received 18 February 1974)

The partial specific volume \bar{v}_2 of linear and branched polystyrenes has been measured as a function of molecular weight ($1300 < M_w < 9 \times 10^6$). In the low molecular weight range, the effect of end-groups is predominant. In the high molecular weight range ($M_w >$ about 20 000), we have detected small but significant variations due to the intramolecular segment-segment contacts within the coil. We have proposed an empirical relation between \bar{v}_2 and the segment density of the macromolecule; this relation has been confirmed using highly branched polystyrenes. These results relative to dissolved polystyrenes are compared to experimental data obtained by different authors on pure liquid polystyrenes at different temperatures. Starting from simple additivity rules and from the known chemical composition of liquid polymers, we have shown that the variation of specific volume with high molecular weights is due to some phenomenon different from an effect of chain-ends.

INTRODUCTION

The partial specific volume, \bar{v}_2 , and the refractive increment dn/dc , of solutions of polymers have been extensively studied in the past few years. Apart from their intrinsic interest as physical properties, the knowledge of these quantities and their dependence on molecular weight have to be known without ambiguity for a correct interpretation of the measurements given by techniques such as ultracentrifugation, light scattering and gel permeation chromatography^{1, 2}.

It is generally assumed that \bar{v}_2 as well as dn/dc are linear functions of reciprocal molecular weight. This variation is attributed to the sole influence of the end groups attached to a polymer chain and is supposed to be negligible in systems of sufficiently high degree of polymerization^{3, 4}.

In a recent paper⁵, we have shown that a linear relationship of the type:

$$\bar{v}_2 = \bar{v}_{0m} + K/M_n \quad (1)$$

holds for polystyrenes with molecular weight below about 4×10^4 , whatever the end groups and the nature of the solvent. Moreover, we have been able through simple calculations, to relate the variation of the K coefficient to the nature and the partial specific volume of the end groups.

On the other hand, studying the case of large molecular weights, we have shown that the \bar{v}_{0m} quantity is not a constant, since we have observed a decrease of \bar{v}_2 for increasing M ($M > 4 \times 10^4$). Such a discrepancy does not appear in the literature data. As an example, let us mention the values 0.900 and 0.906 cm³/g we have obtained for two polystyrene samples of molecular weights respectively equal to 9×10^6 and 1.06×10^6 , in solution in benzene. These values differ significantly from the value 0.918 cm³/g which corresponds to the

intercept of the straight line $\bar{v}_2 = f(1/M)$. The fact that no systematic work has been carried out in the high molecular weight range may explain why this significant difference in partial specific volumes (about 2%) is so far unknown.

Since the behaviour of specific volume and refractive index increment are very similar^{2, 6}, we can expect for dn/dc the same variation as a function of molecular weight. Effectively, some authors have revealed a significant variation of dn/dc with molecular weight which is of the same order of magnitude as the effect we observed¹. Nevertheless, the limited amount of data available is not sufficient to consider this phenomenon as well established. It was then of great interest to study the dependence of \bar{v}_2 and dn/dc on molecular weight, by means of very accurate techniques and covering a large molecular weight region. The polystyrene samples we have used ranged in molecular weight from 1300 to 9×10^6 .

In this paper we shall deal with results concerning the variation of \bar{v}_2 with molecular weight, and in the next paper, those related to the refractive index increment.

EXPERIMENTAL

Partial specific volume measurements have been carried out with an automatic densimeter DMA 02 of the Kratky type⁷. After improvement of the cell⁸, we have been able to obtain an accuracy on the \bar{v}_2 values of $\pm 10^{-3}$ cm³/g, the precision being limited by the estimate for concentration⁵.

Our polystyrene samples, except the radically prepared polymer PS 22, have been synthesized by anionic polymerization and consequently have narrow molecular weight distributions. The preparation of the homologous series of linear polystyrenes with different end groups,

according to the nature of the initiator, has already been described^{5,9}. Comb-like polystyrene samples have been obtained by anionic deactivation of a living polystyrene with a chloromethylated polystyrene¹⁰; their thermodynamic properties in dilute solutions have been recently studied¹¹. Their structural characteristics are very well defined and are listed in Table 4.

RESULTS AND DISCUSSION

Dependence on molecular weight

According to recent results⁵, the partial specific volume \bar{v}_2 may be expressed by the following relationship:

$$\bar{v}_2 = \bar{v}_m(M) + \frac{M_e}{M_n}(\bar{v}_e - \bar{v}_{0m}) = \bar{v}_m(M) + K/M_n \quad (1')$$

In this expression, M_e and \bar{v}_e represent the molecular

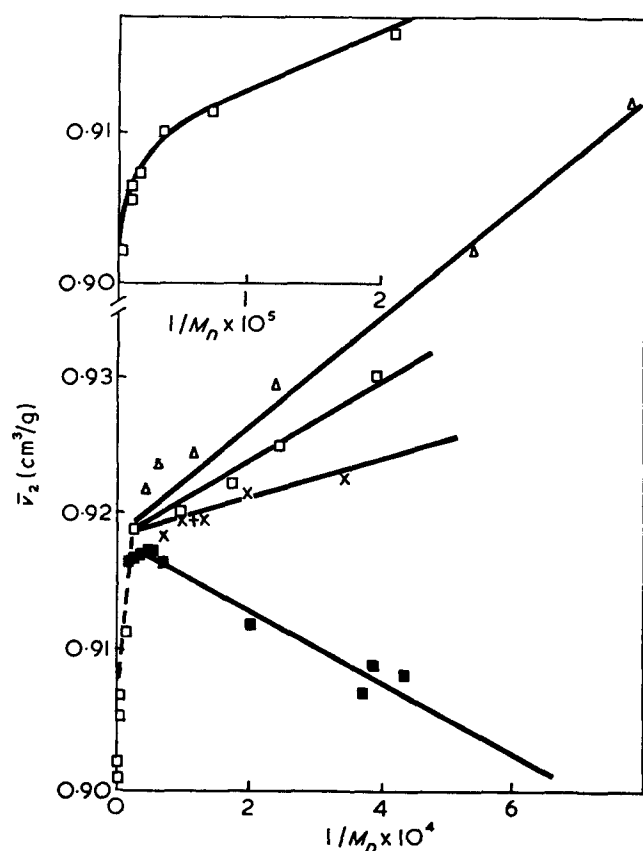


Figure 1 Variation in \bar{v}_2 of benzene-polystyrene solutions with reciprocal of M_n at 25°C. Samples initiated by butyl-lithium (series I, Δ), by cumyl-potassium (series II, \square), by α -methylstyrene tetramer (series III, \times), by naphthalene sodium (series IV, $+$). ■, Data of Schulz *et al.*³

weight and the partial specific volume of the end groups. M_n is the number-average molecular weight of the polymer, and the parameter $\bar{v}_m(M)$ stands for the partial specific volume of the monomeric unit, which varies with molecular weight.

Figure 1 shows the variation of the partial specific volume \bar{v}_2 as a function of $1/M_n$, for a few series of polystyrene samples, with different end groups in solution in benzene. The \bar{v}_{0m} and K values obtained from the intercepts and the slopes of the experimental straight lines, in a number of solvents are reported in Table 1.

Since we are not concerned in the present work, with the influence of the end groups, we have subtracted for each sample its contribution to the partial specific volume \bar{v}_2 . It may be noted that, for high molecular weight samples, the \bar{v}_m value thus obtained coincides with the experimental value \bar{v}_2 , since the end groups do not contribute significantly to the partial specific volume.

The resulting data are reported in Table 2, and the corresponding plot \bar{v}_m versus reciprocal molecular weight is given in Figure 2. It is apparent from this Figure that, as the polymer molecular weight decreases towards a value approximately equal to 4×10^4 , \bar{v}_m reaches a limiting value \bar{v}_{0m} , which remains constant even for molecular weights as low as 1300.

Dependence on the solvent

In Table 1 are listed, for various good solvents at 25°C, the $\Delta\bar{v}_2$ values representing the difference between the value \bar{v}_{0m} corresponding to the plateau and the partial specific volume of a high molecular weight polymer sample ($M_n = 1.05 \times 10^6$). These differences can be considered as a measure of the divergence arising from the linear law of variation $\bar{v}_2 = f(1/M_n)$. It appears, by inspection of the data, that the $\Delta\bar{v}_2$ values do not significantly differ with the solvent. The $\Delta\bar{v}_2$ value obtained in cyclohexane at 35°C is also reported in Table 1. At this temperature, which is the θ -temperature, the chain is Gaussian and unexpanded. This shows that, even in a θ -solvent, the effect is still apparent although less pronounced.

Dependence on the segment density within the coil

At first sight, these results are rather surprising since it is not clear why, after elimination of the influence of end-groups, there is still an effect of molecular weight on specific volume. These results may be connected to the conclusions of a recent study concerning macromolecular solutes in mixed solvents¹². Benoit and coworkers have shown the existence of a molecular weight dependence

Table 1 Values of \bar{v}_{0m} , K and $\Delta\bar{v}_2$ in various solvents

Solvent	T (°C)	Molar volume (cm ³)	\bar{v}_{0m} (cm ³ /g)	K (cm ³)			$\Delta\bar{v}_2$ (cm ³ /g)
				Butyl end-group	Cumyl end-group	Styryl end-group	
Acetone	25	73.70	0.906 ₅	36.0			
Benzene	25	89.43	0.918 ₀	41.0	29.5	14.5	0.013
Butanone	25	90.12	0.915 ₀	37.0			
Carbon tetrachloride	25	97.07	0.918 ₀	38.0			0.016
Toluene	25	107.14	0.926 ₀	35.0			0.015
Cyclohexane	25	108.48	0.930 ₅	35.0			
	35		0.930 ₇	35.2			0.010

Table 2 Parameters of linear polystyrenes in solution in benzene at 25°C

Polymer No.	Initiator	M_n	M_w^*	\bar{v}_2 (cm ³ /g)	\bar{v}_m (cm ³ /g)	$\rho_{\max} \times 10^4$ (g/cm ³) $\times 10^6$ (segments/Å ³)
1915	Butyl-lithium	1 300 (t)†	—	0.950 ₀	0.918 ₄	7488
1811		2 000 (o)	1 950	0.938 ₃	0.917 ₈	5337
		1 711 (t)	—	—	—	—
PS PE 3		4 100 (t)	4 500	0.929 ₃	0.919 ₃	3039
PS PE 1		8 500 (t)	9 500	0.924 ₂	0.919 ₃	1715
PS PE 2		15 600 (o)	16 000	0.923 ₅	0.920 ₀	1065
1753		23 900 (o)	25 000	0.921 ₇	0.919 ₉	802.3
1795	α -methylstyrene tetramer	2 800 (o)	3 600	0.922 ₄	0.917 ₂	4106
1903		4 150 (t)	4 990	0.920 ₄	0.916 ₉	3040
31		7 300 (o)	—	0.919 ₃	0.917 ₃	1940
1895		5 000 (t)	—	0.921 ₂	0.918 ₃	2602
1829		10 000 (t)	—	0.919 ₄	0.917 ₉	1509
1278		53 000 (g.p.c.)	74 000	0.917 ₂	0.916 ₉	317
3'		naphthalene sodium	8 500 (t)	—	0.919 ₀	0.917 ₂
PSTT 18	cumyl-potassium	2 500 (t)	4 000	0.930 ₅	0.918 ₇	4485
		3 450 (q)	—	—	—	—
1742		6 000 (g.p.c.)	6 300	0.921 ₈	0.916 ₈	2255
1764		8 400 (g.p.c.)	9 600	0.920 ₈	0.916 ₆	1557
A		33 000 (g.p.c.)	40 000	0.919 ₀	0.918 ₁	507.8
1		1.35×10^5 (g.p.c.)	1.4×10^5	0.911 ₅	0.911 ₂	190.0
3		6.6×10^5 (g.p.c.)	7×10^5	0.906 ₆	0.906 ₅	53.7
2		1.05×10^6 (g.p.c.)	1.1×10^6	0.905 ₂	0.905 ₂	37.60
11B		1.06×10^6 (g.p.c.)	1.6×10^6	0.906 ₀	0.906 ₀	28.10
6951 F _{1B}		—	4.1×10^6	0.901 ₂	0.901 ₂	13.70
PS 22		—	9×10^6	0.900 ₀	0.900 ₀	7.20
C		—	3.0×10^5	0.910 ₀	0.909 ₂	103.1

* Molecular weight determined from light scattering measurements

† Molecular weight determined from vapour pressure measurements (t), osmotic pressure measurements (o), gel permeation chromatography (g.p.c.)

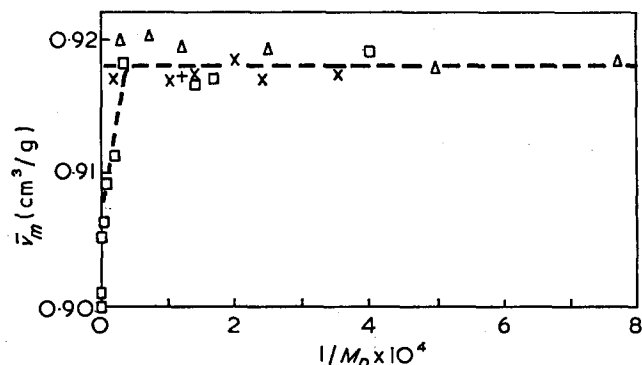


Figure 2 Variation of \bar{v}_m as a function of $1/M_n$, for linear polystyrenes in solution in benzene at 25°C. Δ , Series I; \square , series II; \times , series III; $+$, series IV

of the preferential adsorption not predicted by the classical lattice model theory of polymer solutions¹³. A qualitative explanation has been proposed where the segment density within the macromolecular coil appears as the fundamental parameter¹⁴, arising from the fact that the only difference between two solutions of the same concentration in the same solvent, differing only by molecular weight, lies in the repartition of the segments.

It was then of interest to see if, by analogy, a correlation between \bar{v}_2 and segment distribution can be established. In order to characterize this segment distribution, we shall use the maximum density within the coil as parameter, i.e. the density at the centre of mass assuming a Gaussian distribution of segments.

Table 3 Parameters of linear polystyrenes in cyclohexane at 35°C

Polymer No.	M_n	M_w	\bar{v}_2 (cm ³ /g)	\bar{v}_m (cm ³ /g)	$\rho_{\max} \times 10^4$ (g/cm ³)
1764	8 400	9 600	0.932 ₀	0.929 ₀	1550
A	33 000	40 000	0.929 ₀	0.928 ₀	759
1	1.35×10^5	1.4×10^5	0.926 ₅	0.926 ₀	406
2	1.05×10^6	1.1×10^6	0.920 ₀	0.920 ₀	144

The validity of this assumption can be checked using branched polymers since it is known that the density of segments can be changed in this kind of sample without changing the molecular weight. More precisely, the segment density can be evaluated, in a branched polymer, if its structure is known. One of us has shown earlier how to prepare and characterize comb-like polymers¹⁰. With these polymers, it is possible to increase the density of segments by a very important factor, increasing the number of the branches.

In a recent paper, we have revealed in a quantitative way the dependence of the number of end-groups and of the junction points of branches on the partial specific volumes of some comb-like polystyrenes¹⁵. To compare the results relative to linear and branched polymers, we have to get rid of the influence of chain ends and of junction points of branches; we have thus calculated the partial specific volume \bar{v}_m for each branched sample (see Appendix 1).

Tables 3 and 4 summarize the values of \bar{v}_m and of the segment densities measured at the centre of mass of the coils, for different linear and branched polystyrene

Table 4 Parameters of comb-like polystyrenes in solution in benzene at 25°C

Polymer No.	M_{wb}	M_{ws}	M_{wg}	ρ	\bar{v}_2 (cm ³ /g)	\bar{v}_m (cm ³ /g)	ρ_{max} $\times 10^4$ (g/cm ³)
1 A	0.9×10^6	7×10^5	4×10^4	5	0.908 ₂	0.908 ₂	60
2 A	1.5×10^6	7×10^5	4×10^4	20	0.912 ₆	0.912 ₆	80.5
4 A	8.5×10^6	7×10^5	4×10^4	195	0.917 ₇	0.917 ₇	240
1752 f ₁	4.8×10^5	7.5×10^4	4.5×10^3	86	0.917 ₇	0.917 ₉	904
1752 f ₂	2.58×10^5	4.0×10^4	4.5×10^3	46	0.917 ₆	0.918 ₃	1250
1752 f ₃	1.57×10^5	2.45×10^4	4.5×10^3	28	0.918 ₂	0.918 ₉	1503
1752 f ₄	9.8×10^4	1.53×10^4	4.5×10^3	17	0.917 ₂	0.917 ₈	1645

M_{wb} = molecular weight of the branched polymer
 M_{ws} = molecular weight of the backbone
 M_{wg} = molecular weight of the branch
 ρ = number of branches

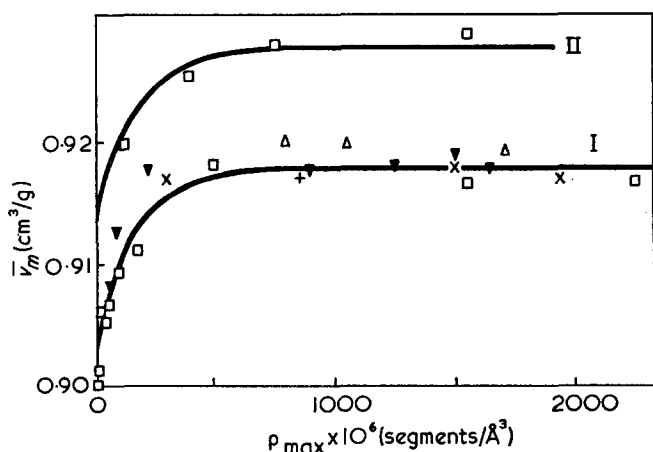


Figure 3 Plot of \bar{v}_m versus the segment density at the centre of mass of the polymer. Curve I: linear and branched polystyrenes in solution in benzene at 25°C; Δ , Series I; \square , series II; \times , series III; $+$, series IV; ∇ , branched polystyrenes. Curve II: linear polystyrenes in solution in cyclohexane at 35°C; \square , Series II.

samples. This density can be evaluated using the well known relation¹⁶:

$$\rho_{max} = N \left[\frac{3}{2\pi \bar{R}^2} \right]^{3/2} \quad (2)$$

where N is the total number of segments and \bar{R}^2 the mean square radius of gyration of the polymer.

Determinations of the mean square radii of gyration of linear samples were obtained from the following relations¹⁷:

$$\begin{aligned}
 R_A &= 0.145 M_w^{0.595} && \text{in benzene at } 25^\circ\text{C} \\
 R_A &= 0.347 M_w^{0.500} && \text{in cyclohexane at } 35^\circ\text{C}
 \end{aligned}$$

In the case of comb-like structures, we have calculated \bar{R}^2 using Stockmayer's formula¹⁸:

$$\bar{R}_b^2 = g \bar{R}_{linear}^2$$

where \bar{R}_{linear}^2 is given by the preceding formulae and g is a factor determined by Orofino *et al.*¹⁹.

Figure 3 represents the variation of \bar{v}_m versus ρ_{max} for polymers in solution in benzene and cyclohexane. It clearly appears that the experimental points relative to both linear and branched polystyrenes lie on a single curve. This justification of our crude hypothesis relating specific volume anomalies to the segment density is quite remarkable. If we had used $1/M^{1/2}$ as a parameter instead of ρ_{max} , the experimental points would have been scattered. For instance, the comb-like polystyrene sample

4A ($M_w = 8.5 \times 10^6$) possesses a segment density comparable to that of the linear polystyrene 1 of molecular weight 1.35×10^5 ; its partial specific volume \bar{v}_m is effectively equivalent to that of the polystyrene sample 1. On the contrary, sample 1A which possesses a backbone of molecular weight 7×10^5 with very few branches presents a behaviour similar to that of a high molecular weight linear polystyrene. It seems therefore clear that the segment density is the fundamental parameter of the \bar{v}_m dependence on molecular weight. In the high molecular weight range, \bar{v}_m varies almost linearly with ρ_{max} . When the segment density increases (M_w decreases) the \bar{v}_m values reach a plateau.

We have attempted empirically to find an analytical function which would represent the observed results. The following expression:

$$\bar{v}_m = \bar{v}_{0m} - B \exp(-C \rho_{max}) \quad (3)$$

seems to be in reasonable agreement with experimental data as shown in Figure 3. In this Figure, the solid lines represent the best least squares fits to the preceding equation. The B and C values are the same for both cyclohexane and benzene solvents and are equal to 1.4×10^{-2} and 5.7×10^3 respectively. When ρ_{max} is small enough (high molecular weights), equation (3) can be expanded in powers of ρ_{max} ; by limiting the development of $\exp(-C \rho_{max})$ to the first two terms:

$$\bar{v}_m = (\bar{v}_{0m} - B) + BC \rho_{max} \quad (4)$$

we find again a linear dependence of \bar{v}_m as a function of ρ_{max} .

The points corresponding to linear polystyrenes of molecular weights 4.1×10^6 and 9×10^6 are not taken into account by this empirical equation. Anyway, it seems very difficult to explain these values since at these high molecular weights the distribution of segments in the solution is uniform even at high dilution and therefore no effect of molecular weight should be observed.

Nevertheless, the empirical equation we have proposed accounts for most of our experimental data, but it would be important to understand, at least qualitatively, the reasons of such a behaviour.

We may relate the observed influence of the segment density to the inhomogeneity of a dilute solution which can be regarded as a dispersion of clouds of segments separated by regions of pure solvent. The partial specific volume, evaluated under the assumption that for solvent it remains constant in the solution, should thus reflect volume alterations undergone by both the macromolecule and the solvent molecules within the coil.

Qualitatively, one can think that for each intramolecular segment-segment contact, a 'free volume' is created which is inaccessible to solvent molecules, and should produce, as a consequence, an increase of \bar{v}_2 .

Assuming that the probability of occurrence of polymer-polymer contacts within the coil is directly proportional to the square of local segment density, it can be shown that the average number of intersegmental contacts per chain segment is proportional to ρ_{\max}^{20} . This gives:

$$\bar{v}_2 = \bar{v}_\infty + A\rho_{\max}$$

which corresponds to our empirical relation for low values of ρ_{\max} (\bar{v}_∞ is the limiting value at infinite molecular weight). If we try to evaluate the A factor from this relation, assuming that the total free volume created at each segment-segment contact corresponds to the volume of a few solvent molecules, we find a value which seems much lower than the experimental one. Besides, this relation does not account for the observed behaviour when the segment density increases; this can be explained taking into account the fact that in the high segment density region, a single contact approximation is no longer valid and the chains do not obey Gaussian statistics.

It seems therefore that the dependence of the partial specific volume on molecular weight is well explained, if one assumes the effect of the segment density. The only difficulty which is not yet resolved is a quantitative explanation of the parameter A and of the observed behaviour at very high values of ρ_{\max} .

As mentioned above, the idea of plotting the results as functions of ρ_{\max} was suggested by some previous work on branched polymers²¹ and on preferential adsorption¹⁴. It seems to be well established that as soon as deviations occur from the law valid for infinitely dilute solutions one can, as a first approximation, explain them by the effect of the local segment density or more precisely by the density ρ_{\max} at the centre of mass of the macromolecule. It is worth noting that the assumption of the proportionality of the deviation on ρ_{\max} is only valid for small values of ρ_{\max} , i.e. at high molecular weights. For instance, Hert *et al.*¹⁴ have shown that for linear polystyrenes in benzene-methanol (0.78:0.22 ml/ml), it is necessary to introduce higher terms in the expansion of the preferential adsorption coefficient as a function of ρ , i.e.:

$$\lambda = \lambda_\infty + a\rho + b\rho^2 \dots$$

The squared term $b\rho^2$ cannot be neglected for molecular weights lower than 20 000. In our case also, the linear relation (4) fails for the same limiting molecular weight.

This shows the close relation between preferential adsorption and specific volume. At first sight, these two phenomena seem to be quite different, but we believe we have been able to show their similarity. A modification of preferential adsorption is due to the replacement of a non-adsorbed molecule by an adsorbed molecule, when intramolecular contacts occur. A modification of specific volume is due to the replacement of a solvent molecule by a hole.

This similarity is, indeed, a hypothesis which should be checked on complementary experiments.

Concentration effects

Since the values of \bar{v}_2 depend on the intramolecular concentration, they should also depend on the total

concentration, i.e. on the intermolecular segment-segment interactions.

In order to check whether the progressive apparition of intermolecular contacts have an influence on the partial specific volume, we have measured \bar{v}_2 of sample 2 ($M_w = 1.05 \times 10^6$), at concentrations ranging from 0.5 to 10% g/g, when the polymer is dissolved in benzene and 0.05 to 3% g/g if dissolved in toluene. In both cases, there is no evidence of concentration effect⁵. This last result confirms those reported by Scholte relative to a polystyrene-toluene mixture²².

This first result is not very significant and in order to check the existence of such an effect in the high concentration range, more experiments should be carried out over a wide range of concentrations.

Effect of the molar volume of the solvent

Heller suggested that specific volumes in solution are insensitive to the thermodynamic quality of the solvents and depend on their molar volume⁶. Qualitatively speaking, it seems reasonable to assume that, when the size of solvent molecules increases, the number and the size of the holes should also increase and consequently the partial specific volume.

In Figure 4, we have plotted the \bar{v}_{0m} value obtained for each solvent against the molar volume V_s , of the corresponding solvent. It can be seen that \bar{v}_{0m} varies in a regular manner, practically linearly with this quantity, increasing with V_s as it was predicted. Studying a linear polystyrene of $M_w = 150\,000$, in bulk, we were able to determine its specific volume at the room temperature, by extrapolation of the Fox and Ueberreiter^{23, 24} data obtained at different temperatures; by this procedure, we obtain for this liquid polymer a value of the specific volume equal to 0.926 cm³/g at 25°C. This value which corresponds also to the value of a polystyrene solution in polystyrene can be plotted in Figure 4 and gives for

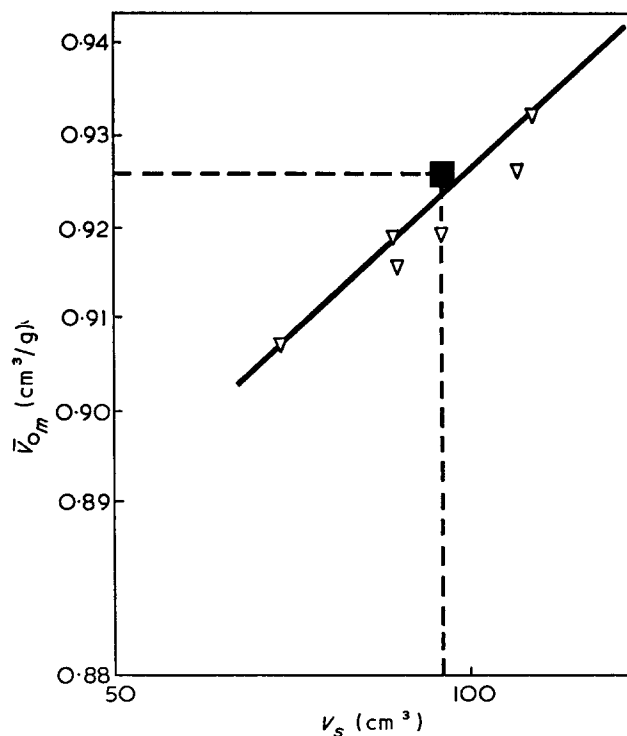


Figure 4 Plot of \bar{v}_{0m} against the molar volume of the solvent. ■, Pure polystyrene^{23, 24}

the molar volume of the solvent a value of the order of 95 cm^3 . This corresponds approximately to the molar volume of the monomeric unit at this temperature, regardless of the nature of the solvent. It seems therefore that a polymeric solvent has, at least with regard to the specific volume, the same properties as a low molecular weight solvent possessing a volume identical to that of the monomeric unit. Each chain therefore can be considered as dissolved in monomeric units.

Consequently, it was interesting to see whether the law we have established for solutions, can be extrapolated to pure polymers.

Specific volumes of pure liquid polystyrenes

The specific volumes of pure liquid polystyrenes have been widely investigated in the two last decades²³⁻²⁵, in order to determine their glass temperature and its dependence on molecular weight. The most extensive data have been obtained by Fox *et al.* and Ueberreiter *et al.* who have performed their measurements in the temperature range ($T_g < T < 237^\circ\text{C}$) for thermally initiated polystyrenes with molecular weights ranging respectively from 2970 to 85 000 and 100 to 94 000.

Both authors have observed at a given temperature, a linear variation of v_2 with $1/M$ which they attribute to the influence of the chain ends, as we did for solutions of low molecular weight polystyrenes. In Figure 5, we have plotted for molecular weights higher than 10^3 , the specific volume values, as measured by these authors at 140°C versus $1/M$. The good agreement between the results obtained by these different authors shows the precision of their measurements. If we consider carefully

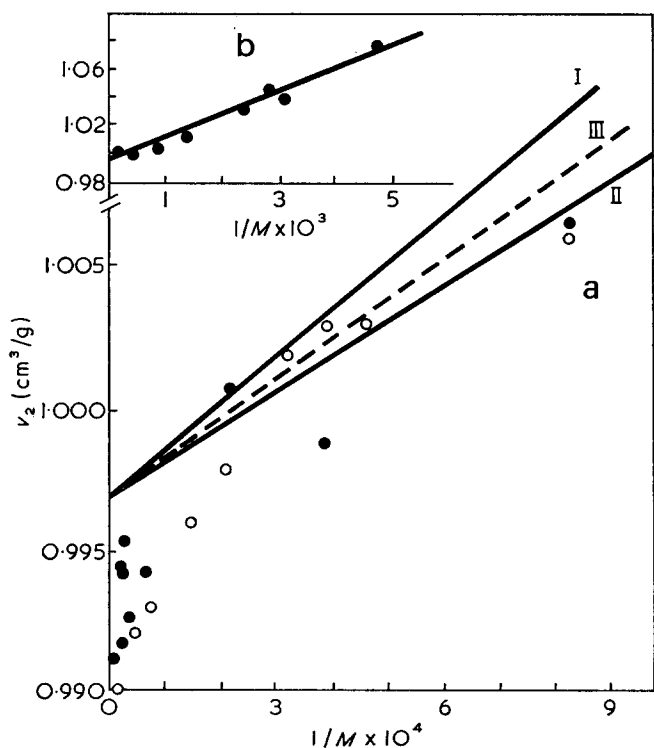


Figure 5 Variation of specific volume for liquid polystyrenes with $1/M$. (a) \circ , experimental data of Fox *et al.*²³; \bullet , Ueberreiter *et al.*²⁴; curves I and II, calculated for samples of Ueberreiter *et al.*; curve III, calculated for samples of Fox *et al.*; (b) experimental data of Ueberreiter *et al.* for low molecular weight polystyrenes (200)

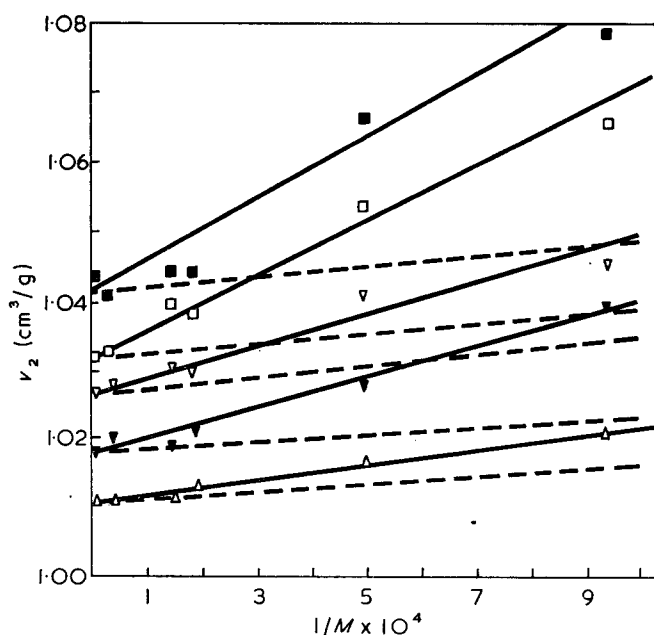


Figure 6 Data of Chee and Rudin²⁵ relative to the variation of \bar{v}_2 as a function of $1/M$, at different temperatures. \blacksquare , 237° ; \square , 217° ; ∇ , 204° ; \blacktriangledown , 186° ; \triangle , 170.1°C . —, experimental results; ---, calculated curves

the behaviour for large values of M , the first approximation of \bar{v}_2 as a linear function of $1/M$ does not completely explain the experimental results. These results seem very similar to those we have obtained in solution. Since we have been able to explain them by two different effects, chain ends and segment density, it is interesting to see whether such an explanation could not give a better fit. Therefore, we assume that in the low molecular weight range ($< 10\,000$) the end effects are predominant, which yields a straight line of equation: $v_2 = v_{0m} + A/M$. The A value can be estimated from the known values of specific volumes of the end groups, following a method which has been described elsewhere (see Appendix 2). The theoretical value ($14 < A < 17$) is in good agreement with the experimental slope equal to 15. This shows clearly that it is impossible to explain the value of v_2 at high molecular weights by the influence of the end groups. More precisely, (i) it is impossible to draw a straight line going through all the points taking into account the precision of the data, (ii) if we do so the obtained slope is incompatible with our knowledge about specific volume of the end groups, being much too large.

That statement is confirmed by recent results of Chee and Rudin²⁵ who have measured the specific volumes of anionically prepared polystyrenes initiated by butyllithium, with molecular weights between 9×10^3 and 7×10^5 at 170 – 237°C . These authors have studied the temperature dependence of the slope corresponding to $v_2 = f(1/M)$ and Figure 6 illustrates their data. They remark that the slope varies considerably with temperature and is much higher than the average slopes obtained by Fox *et al.* and Ueberreiter *et al.* They conclude then, by assessing this anomalous behaviour to the nature of the end groups. We have calculated, as we did previously, the theoretical slopes of $v_2 = f(1/M)$ from the specific volume values of the end groups (see Appendix 2) and compared them to the experimental data. We observe a considerable discrepancy, which increases greatly with temperature. Moreover, the same authors have found

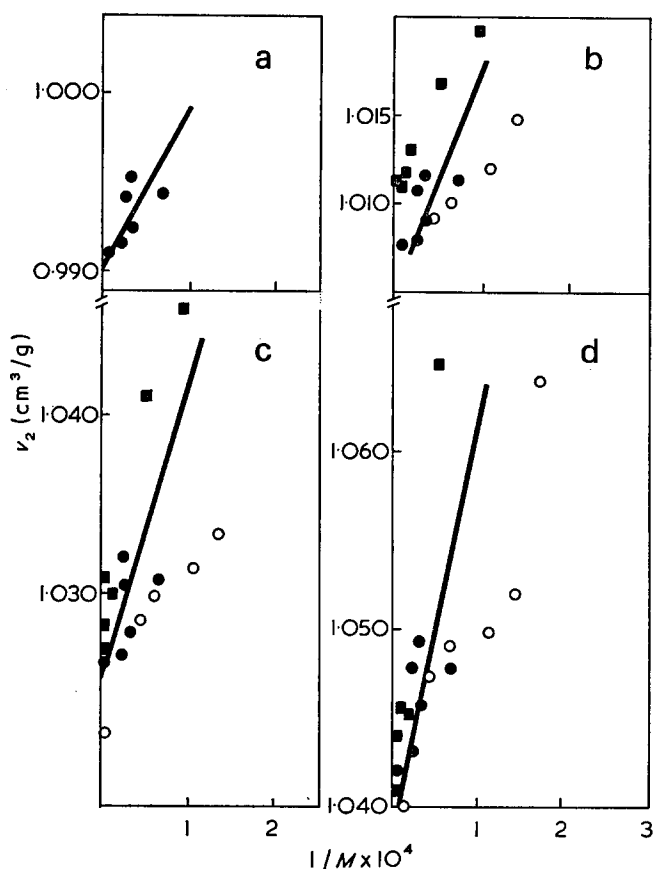


Figure 7 Plots of specific volumes of liquid polystyrenes versus $1/M$ at different temperatures: (a) 140° ; (b) 170° ; (c) 204° ; (d) 237°C . \circ , Data of Fox *et al.*; \bullet , data of Ueberreiter *et al.*; \blacksquare , data of Chee and Rudin

for a liquid polystyrene of molecular weight 3000 a specific volume value consistently below the general lines $v_2 = f(1/M)$, the deviations from the lines increasing with temperature. Presumably, the shape of the curves $v_2 = f(1/M)$ over the entire molecular weight range should be similar to that obtained by Fox *et al.* and Ueberreiter *et al.*; it is only in the low molecular weight range that the influence of end groups can affect the specific volume.

If we focus our attention on the high molecular weight range, we can plot on the same diagrams all the available results at different temperatures (140° , 170° , 204° and 237°C) for polymers with different end-groups. If the variation of v_2 as a function of M would depend on these end-groups, we should have had a larger scattering of the experimental data (Figure 7).

It seems therefore quite probable that the origin of the high molecular weight dependence of v_2 is not due to an end-groups effect, as it was assumed previously, but to some different physical phenomena. It is, of course, tempting to extrapolate our explanation for dilute solutions to liquid polymers, since the shape of the curves is practically the same. Formally, this can be done, for we have seen that, with regard to a given molecule, the bulk material is equivalent to a solvent having the same molar volume as the monomeric unit. But, even assuming that in bulk state the chain has a Gaussian character²⁶, it is difficult to understand such a difference between intramolecular and intermolecular contacts.

APPENDIX 1

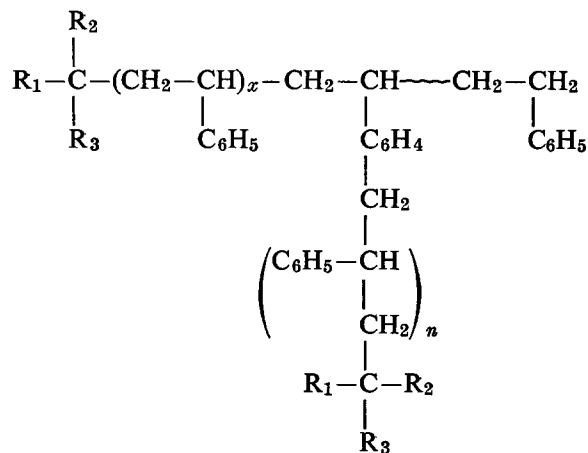
In a recent paper¹⁵, we have shown that the partial specific volume of a comb-like polystyrene may be expressed by the following relation:

$$\bar{v}_2 = \bar{v}_m + \frac{1}{M} [(1+p)M_{e1}(\bar{v}_{e1} + \bar{v}_m) + pM_{e3}(\bar{v}_{e3} - \bar{v}_m) + M_{e2}(\bar{v}_{e2} - \bar{v}_m)] \quad (\text{A1})$$

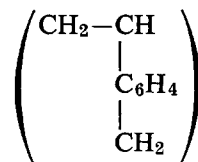
where \bar{v}_m represents the partial specific volume of the monomeric unit, p the total number of branches and M the molecular weight of the branched polymer. M_{e1} and \bar{v}_{e1} are respectively the molecular weight and the partial specific volume of the cumyl radical attached to the end of each branch and to one side of the backbone; M_{e2} and \bar{v}_{e2} the molecular weight and the partial specific volume of the styryl group attached to the other end of the backbone. As for M_{e3} and \bar{v}_{e3} , they represent the molecular weight and the partial specific volume of the monomeric units bound to the grafts.

The present study requires the knowledge of \bar{v}_m and consequently that of the quantities \bar{v}_{e1} , \bar{v}_{e2} , \bar{v}_{e3} . The partial specific volumes \bar{v}_{e1} and \bar{v}_{e2} have already been calculated⁵ and are respectively equal to 1.166 and $0.997 \text{ cm}^3/\text{g}$.

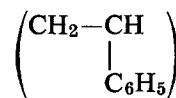
As for the \bar{v}_{e3} estimate, it may be useful to represent roughly the formula of a comb-like polystyrene, as prepared from our method:



Thus, the monomeric unit bound to a graft may be represented by



instead of the classical unit



The substitution of the hydrogen atom by the CH_2 group should produce as a consequence a change in the partial specific volume of these units. We can estimate that difference comparable to that existing in a compound like toluene and the radical $(\text{CH}_3 - \text{C}_6\text{H}_4 - \text{CH}_2)$ included in the 4-heptyl toluene. The values of the partial specific volume of toluene and 4-heptyl toluene are respectively equal to 1.155 and $1.168 \text{ cm}^3/\text{g}$ ²⁷. Accounting for the

specific volume of the hexyl radical which is easily estimated from homologous paraffin series²⁷ we obtain for the (CH₃-C₆H₄-CH₂) group a value equal to 0.873 cm³/g, which gives a difference of 0.282 with toluene specific volume.

If we assume that this last difference represents, in the same manner, the difference between the classical monomeric unit and the junction monomeric unit, we can substitute in equation (A1) \bar{v}_{e3} by the quantity ($\bar{v}_m - 0.282$) and then calculate \bar{v}_m for each comb-like polystyrene sample (see Table 4).

APPENDIX 2

Estimates of the slopes of the lines $\bar{v}_2 = f(1/M)$ for low molecular weight polystyrenes at 140°C.

Polystyrenes prepared by Ueberreiter and Kanig²⁴

These polymers are polymerized thermally without any catalyst and possess a styryl radical at each end of the chain. The slope of the straight line evaluated from equation (1') is then equal to $M_e(\bar{v}_e - \bar{v}_{0m})$ if M_e is the total molecular weight of the two styryl end groups. The quantity \bar{v}_e has already been calculated in a preceding paper from alkyl phenyl compounds and is equal to 0.997 at 25°C. Assuming that the specific volume expansion coefficient $d\bar{v}/dT$ is similar to that of a low molecular weight polystyrene sample, i.e. 0.000581 cm³/gK, we obtain $\bar{v}_e(140^\circ) = 1.063$ to which corresponds a slope of 13.86 cm³. If now we use the value 1.080 given by Ueberreiter and Kanig for the dimer of polystyrene, we find a slope of 17.43 cm³.

Polymer samples used by Fox and Flory²³

These samples have been prepared by thermal polymerization in diethylbenzene in the absence of added catalyst. Most of the molecules possess, at one end, a (C₂H₅-C₆H₄-(CH₃)CH-) group and a styryl radical at the other. We will evaluate, at 140°C, the slope of the line resulting from equation (1'). The specific volume at 25°C of diethylbenzene is equal to 1.156 cm³/g. From considerations similar to that mentioned above for branched polystyrenes, we have evaluated, at 25°C, the specific volume of the corresponding end group which is equal to 0.964 cm³/g. Assuming that the volume temperature coefficient is equivalent to that of the styryl radical, the latter becomes equal to 1.045 cm³/g at value 140°C. From this value and the one corresponding to the styryl end-group as calculated above, we have obtained for the slope a value of 14.52 cm³.

Polymers used by Chee and Rudin²⁵

These anionically prepared polystyrenes are initiated by butyllithium. We have evaluated the slopes at different temperatures. For that purpose, we have used the specific volume values of octane and styryl radical at different temperatures, as reported below. The \bar{v}_m values have been given by Chee and Rudin.

Temperature (°C)	170	186	204	217	237
\bar{v}_{0m} (cm ³ /g)	1.001	1.018	1.027	1.033	1.042
\bar{v}_{e1} (styryl) (cm ³ /g)	1.088	1.092	1.105	1.114	1.128
\bar{v}_{e2} (butyl) (cm ³ /g)					
Calculated slope (cm ³)	51.0	53.7	58.0	61.7	68.7
Experimental slope (cm ³)	98.9	161.9	232.9	284.1	362.9

REFERENCES

- Barrall, E. M., Cantow, M. J. R. and Johnson, J. F. *J. Appl. Polym. Sci.* 1968, **12**, 1373
- Lorimer, J. W. and Jones, D. E. G. *Polymer* 1972, **13**, 52
- Schulz, G. V. and Hoffmann, M. *Makromol. Chem.* 1957, **23**, 220
- Fox, G. and Loshaek, S. *J. Polym. Sci.* 1955, **15**, 371
- François, J. and Candau, F. *Eur. Polym. J.* 1973, **9**, 1355
- Heller, W. *J. Polym. Sci. (A-2)* 1966, **4**, 209
- Stabinger, H., Leopold, H. and Kratky, O. 'Digital Densimeter for Liquids and Gases', (Ed. Anton Paar), Graz, Austria, 1966
- François, J., Clément, R. and Franta, E. *C.R. Hebd. Séanc. Acad. Sci., Paris (C)* 1971, **273**, 1577
- Szwarc, M. 'Carbanions, Living Polymers and Electron Transfer Processes', Interscience, New York, 1968, p 151
- Candau, F. and Franta, E. *Makromol. Chem.* 1971, **149**, 41
- Candau, F. and Rempp, P. *Eur. Polym. J.* 1972, **8**, 757
- Dondos, A. and Benoit, H. *Makromol. Chem.* 1970, **133**, 119
- Read, B. E. *Trans. Faraday Soc.* 1960, **56**, 382
- Hert, M., Strazielle, C. and Benoit, H. *Makromol. Chem.* 1973, **172**, 169, 185
- Candau, F. and François, J. *C.R. Hebd. Séanc. Acad. Sci., Paris* 1973, **276**, 571
- Flory, P. J. 'Principles of Polymer Chemistry', Cornell University Press, Ithaca, 1953
- Decker, D. *Thesis* Strasbourg (1968)
- Zimm, B. H. and Stockmayer, W. H. *J. Chem. Phys.* 1949, **17**, 1301
- Berry, G. C. and Orofino, T. A. *J. Chem. Phys.* 1964, **40**, 1614
- Casassa, F. F. *Polym. J.* 1972, **3**, 517
- Candau, F., Rempp, P. and Benoit, H. *Macromolecules* 1972, **5**, 627
- Scholte, Th. G. *J. Polym. Sci. (A-2)* 1972, **10**, 519
- Fox, T. G. and Flory, P. J. *J. Appl. Phys.* 1950, **2**, 581
- Ueberreiter, K. and Kanig, G. *Z. Naturforsch. (A)* 1951, **6**, 551
- Chee, K. K. and Rudin, A. *J. Macromol. Sci. (B)* 1973, **7**, 503
- Benoit, H. *et al. Nature (Phys. Sci.)* 1973, **245**, 13
- Doolittle, A. K. *J. Appl. Phys.* 1951, **22**, 1471

Effect of molecular weight on the refractive index increment of polystyrenes in solution

Françoise Candau, Jeanne François and Henri Benoit

Centre de Recherches sur les Macromolécules, CNRS, 67083 Strasbourg, France
(Received 18 February 1974)

The variation of refractive index increment dn/dc with molecular weight has been studied using solutions of monodisperse polystyrenes ($2000 < M_w < 4 \times 10^6$) in benzene. The results are in good agreement with those obtained by several authors using other systems.

We have shown that the linear relationship:

$$\frac{dn}{dc} = \left(\frac{dn}{dc}\right)_m + \frac{K''}{M_n}$$

where $(dn/dc)_m$ is the refractive index increment of the repeating unit and K'' a constant, holds only for low molecular weights. With the assumption of volume additivity, we have estimated quantitatively the linear portion of the curve, $dn/dc = f(1/M)$, observed for molecular weights below 20 000 as a function of polymer composition. Beyond this limit, the increase of dn/dc with molecular weight may be probably related to segment-segment interactions within the coil.

INTRODUCTION

It has been shown in a number of recent papers that partial specific volume and refractive index increment are two quantities which are closely related¹⁻⁶. We have seen, in the preceding paper, that the partial specific volume of a polymer is a function of its molecular weight. More precisely, we have shown that end-groups affect the specific volume only in the low molecular weight range (less than 20 000 in our experiments). In the high molecular weight range, we have detected small but significant variations which have been explained by a decrease in segment density within the coil when the molecular weight increases. We could expect the same behaviour and the same interpretation for refractive index increment dn/dc . Some authors have effectively found such a variation for molecular weights up to 300 000 and higher but they did not give any general explanation for their results⁷. Moreover, the refractive index increment dependence on molecular weight has to be known without any ambiguity, because small changes in dn/dc would affect absolute values of molecular weights calculated from light scattering or from gel permeation chromatography (g.p.c.) data.

The present paper confirms from an experimental point of view, the systematic molecular weight-refractive index dependence. The results, in connection with those obtained for partial specific volumes, should provide additional information for a better interpretation of this phenomenon.

EXPERIMENTAL

Differential refractometer

A Waters Associates differential refractometer R400 was used to measure the refractive index difference

between solution and solvent. This apparatus which is highly sensitive is generally used in g.p.c. to determine the weight of polymer eluting at any time.

The operating principle of the R400 is the conventional differential technique which measures the deflection of a light beam, as it passes through a partition at an angle to the beam, and therefore detects small changes in refractive index.

We have employed a Schneider digital millivoltmeter as a detector.

With this technique, the refractive index increment measurements are accurate to $\pm 10^{-3}\%$ ml/g. Such an accuracy is not usually obtained with a Brice-Phoenix refractometer which generally requires solutions of higher concentrations (0.05 to 5% g/g) than those necessary with the Waters refractometer (0.03 to 0.07% g/g); the measurements performed on the latter instrument should then give more valuable information.

The instrument was thermostated using a circulating water thermostat. The temperature was controlled with a Hewlett-Packard quartz thermometer and remained constant at $25 \pm 0.01^\circ\text{C}$.

Samples

The anionic polystyrene samples were synthesized in our laboratory using cumyl-potassium as initiator⁸. They range in molecular weight from 2500 to 4×10^6 and have narrow molecular weight distributions as can be seen in Table 1.

The solvent used for dn/dc measurements was benzene obtained from Merck Company and graded for ultra-violet spectroscopy.

Calibration of the instrument

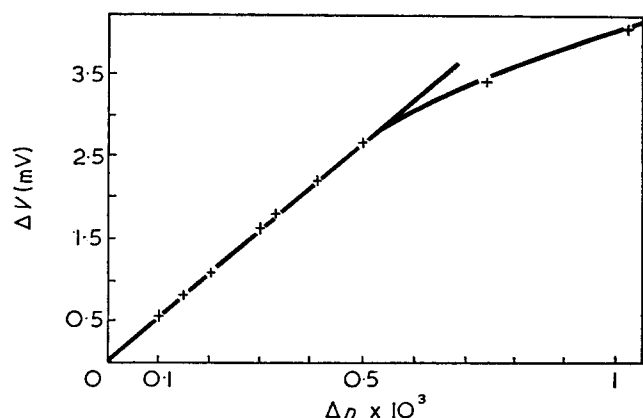
The calibration experiments have been performed with solutions of carbon tetrachloride in benzene; these

Table 1 Characteristics of polystyrene samples and values of their refractive index increment in solution in benzene

Polymer No.	M_n	M_w^*	M_w/M_n	dn/dc (ml/g)
PSTT 18	2500 (t)† 3450 (o)	4000	—	0.097 ₇
1764	8400 (g.p.c.)	9600	1.14	0.101 ₄
A	3.3×10^4 (g.p.c.)	4×10^4	1.20	0.104 ₄
1	1.35×10^5 (g.p.c.)	1.4×10^5	1.04	0.106 ₀
2	1.05×10^6 (g.p.c.)	1.1×10^6	1.05	0.108 ₀
6951 F _{1B}	—	4.1×10^6	—	0.108 ₅

* Weight-average molecular weight determined from light scattering measurements

† Number-average molecular weights determined from vapour pressure (t), osmotic pressure (o), gel permeation chromatography (g.p.c.) measurements


Figure 1 Potential difference plotted against refractive index difference between benzene and solutions of carbon tetrachloride in benzene employed in the calibration experiments

two solvents of similar boiling points but different refractive index do not have a significant degree of association when they dissolve. Thus the relationship of the refractive index of the mixture with concentration is a linear relationship between the two pure refractive index values when mixtures are made on a volume basis.

Figure 1 demonstrates the variation of the potential difference Δv versus Δn , which represents the refractive index difference between the pure solvent and the solution of CCl_4 in benzene. This variation is linear as long as Δn remains below a limiting value approximately equal to 0.5×10^{-3} , which corresponds to a Δv value of 2.75 mV. Beyond this limit, a deviation from the straight line is observed, arising from the very response of the instrument.

The instrumental constant C was calculated as the slope of the linear part of the curve Δv versus Δn and was found to be equal to 5.45 V; this constant does not, at least in our experimental conditions, change with time.

We have studied solutions of polystyrene in benzene having refractive index increments lower than 0.5×10^{-3} ml/g. Several sets of measurement were made on each sample.

This instrument is equipped with white light. We have compared the dn/dc values obtained with this instrument to the classical dn/dc values determined with monochromatic light (usually = 546 nm). For instance, for a polystyrene in benzene of molecular weight equal to 140 000, we have found, using our calibration constant,

the value of $dn/dc = 0.106$ ml/g which is in good agreement with many others experiments⁹; we can thus assume that our absolute values are correct.

Even if it was not the case, it would only change the absolute values by a constant factor and not the dn/dc variation as a function of M .

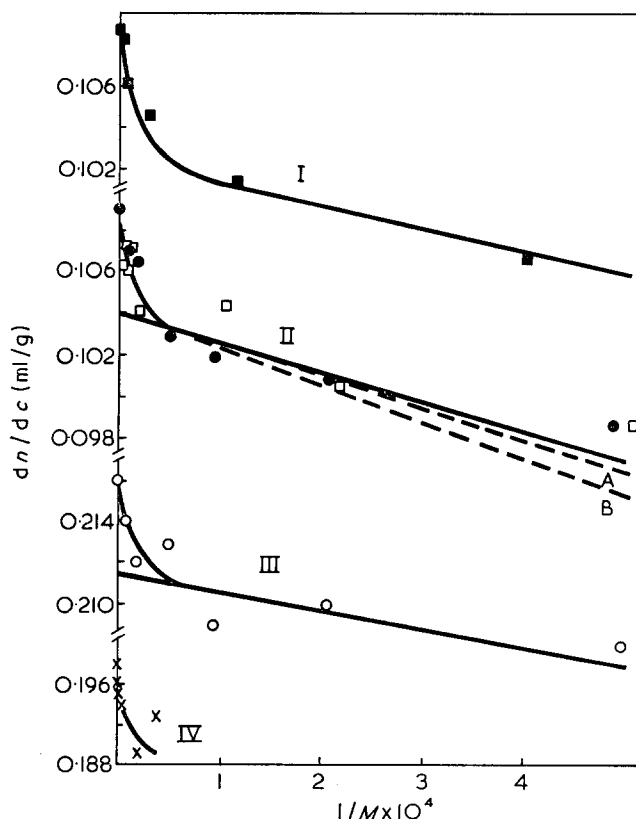
RESULTS AND DISCUSSION

Variation of refractive index increment with molecular weight

In **Figure 2** several dn/dc values as obtained by different authors, are plotted against the reciprocal molecular weight, in order to see if the linear relationship⁴:

$$dn/dc = (dn/dc)_m + K''/M_n \quad (1)$$

holds for the entire range of molecular weights studied. In this equation $(dn/dc)_m$ stands for the refractive index increment of the repeating unit, and K'' is a constant characteristic of the nature of the end-groups. M_n is the number-average molecular weight of the polymer. In **Figure 2** curve I represents our data which correspond to a series of anionic polystyrene samples in solution in benzene with a cumyl radical at one end of the chain (**Table 1**). We may note that equation (1) holds only for molecular weights lower than about 20 000. Beyond this limit, an abrupt change in the slope is observed which compares well to that obtained from densitometric


Figure 2 Variation in dn/dc of polystyrenes with reciprocal molecular weight. I, Polystyrene in benzene at 25°C; ■, our results. II, Polystyrenes in toluene at 25°C; ●, data of Barrall et al.⁷; □, data of Margerison et al.¹⁰. — represents the best fit to the complete data from these authors; ----, calculated curves. III, Polystyrenes in butanone at 25°C; ○, data of Barrall et al. IV, Polystyrenes in tetrahydrofuran at 25°C; ×, data of Schulz et al.¹¹

measurements, occurring at the same value of molecular weight. We have also reported (curve II) the results obtained in toluene by Barrall *et al.*⁷ relative to commercial polystyrene samples initiated by butyllithium. Their results are in very good agreement with ours and exhibit the same change in slope which takes place again for about 20 000 molecular weight. Margerison *et al.*¹⁰ repeated their experiments in the same conditions. Their results are reported in the same Figure. They seem to be much more scattered and do not allow the conclusion, as do these authors, that the variation of dn/dc with $1/M_n$ is consistently linear in the whole molecular weight range. The single curve we have drawn for both results of Barrall *et al.* and Margerison *et al.* clearly demonstrates there are no significant differences between their data.

The same behaviour has been observed for polystyrenes in butanone⁷ (curve III) and for polystyrenes in tetrahydrofuran¹¹ (curve IV). Unfortunately, in the last case, low molecular weight polystyrenes have not been studied.

All these results suggest that these curves consist of two parts. The first relative to the low molecular weight region, is correctly represented by equation (1); the second corresponds to the high molecular weight range.

The best confirmation of these two different behaviours may be given by a quantitative estimate of the linear portion of the curves as a function of polymer composition.

Influence of the end-groups on the refractive index increment of polymers

It is well known that the Lorenz-Lorentz and Dale-Glstone mixture rules¹² may be respectively expressed in the limiting case of $c \rightarrow 0$ by:

$$(dn/dc)_{c \rightarrow 0} = \frac{(n_1^2 + 2)^2}{6n_1} \left(\bar{R}_2 - \frac{n_1^2 - 1}{n_1^2 + 2} \cdot \bar{v}_2 \right) \quad (2)$$

$$(dn/dc)_{c \rightarrow 0} = \bar{R}_2 - (n_1 - 1)\bar{v}_2 \quad (3)$$

where n_1 represents the refractive index of the solvent and \bar{v}_2 and \bar{R}_2 the partial specific volume and partial specific refractivity of the polymer, respectively. We have evaluated, from our partial specific volume measurements¹³, the partial specific refractivity of each sample in solution in benzene, toluene and butanone, according to the Lorenz-Lorentz expression:

$$\bar{R}_2 = \bar{v}_2 \left(\frac{n_2^{*2} - 1}{n_2^{*2} + 2} \right) \quad (4)$$

and to the less accurate Dale-Glstone version:

$$\bar{R}_2 = \bar{v}_2(n_2^* - 1) \quad (5)$$

The quantity n_2^* represents the refractive index of the dissolved polymer which is not supposed to be equal to the refractive index n_2 of the pure polymer; it has been calculated following a procedure suggested by Heller².

The dn/dc values needed for this calculation have been deduced from interpolation of the curves $dn/dc = f(1/M)$ corresponding either to the results of Barrall *et al.*⁷ or to ours, depending on the solvent used. The n_2^* and \bar{R}_2 values thus calculated are listed in Table 2.

The partial specific refractivity of some polystyrene samples in benzene, as calculated from the Lorenz-Lorentz equations is plotted against $1/M$ in Figure 3.

Table 2 Variation of \bar{v}_2 , dn/dc , \bar{R}_2 and n_2^* of polystyrene samples with molecular weight in various solvents

M_n	\bar{v}_2 (ml/g)	dn/dc (ml/g)	\bar{R}_2^a	n_2^*a	\bar{R}_2^b	n_2^*b
Benzene ($n_1=1.5016$)						
1 300	0.950 ₀	0.093 ₀	0.326 ₄	1.603 ₂	0.569 ₅	1.599 ₄
2 000	0.938 ₃	0.097 ₀	0.325 ₀	1.609 ₃	0.567 ₆	1.604 ₉
4 100	0.929 ₃	0.099 ₇	0.323 ₇	1.613 ₄	0.565 ₈	1.608 ₈
8 500	0.924 ₂	0.101 ₀	0.322 ₈	1.615 ₆	0.564 ₅	1.610 ₈
15 600	0.923 ₅	0.102 ₀	0.323 ₁	1.616 ₉	0.565 ₂	1.612 ₀
23 900	0.921 ₇	0.102 ₅	0.322 ₈	1.617 ₆	0.564 ₈	1.612 ₇
53 000	0.917 ₂	0.104 ₅	0.322 ₄	1.620 ₇	0.564 ₄	1.615 ₃
1.35×10^5	0.911 ₅	0.106 ₂	0.321 ₇	1.623 ₅	0.563 ₄	1.618 ₁
6.6×10^5	0.906 ₈	0.107 ₂	0.320 ₆	1.625 ₃	0.561 ₉	1.619 ₇
1.05×10^6	0.905 ₂	0.108 ₀	0.320 ₇	1.626 ₇	0.562 ₀	1.620 ₉
4.1×10^6	0.901 ₂	0.109 ₀	0.320 ₀	1.628 ₅	0.561 ₀	1.622 ₅
Toluene ($n_1=1.4962$)						
1 300	0.949 ₀	0.093 ₀	0.323 ₇	1.597 ₈	0.563 ₈	1.593 ₄
2 000	0.940 ₀	0.097 ₀	0.323 ₁	1.603 ₄	0.563 ₄	1.599 ₃
4 100	0.932 ₀	0.100 ₅	0.322 ₅	1.608 ₀	0.562 ₉	1.603 ₉
8 500	0.927 ₆	0.102 ₂	0.322 ₁	1.611 ₀	0.562 ₄	1.606 ₀
15 600	0.926 ₀	0.103 ₀	0.322 ₀	1.612 ₁	0.562 ₄	1.607 ₀
23 900	0.924 ₀	0.103 ₅	0.321 ₇	1.613 ₁	0.562 ₀	1.608 ₂
53 000	0.921 ₅	0.104 ₅	0.321 ₅	1.614 ₆	0.561 ₇	1.609 ₅
1.35×10^5	0.918 ₅	0.106 ₃	0.321 ₄	1.617 ₂	0.562 ₀	1.612 ₀
6.6×10^5	0.914 ₀	0.108 ₆	0.321 ₃	1.620 ₀	0.562 ₁	1.614 ₉
1.05×10^6	0.920 ₀	0.108 ₇	0.320 ₂	1.621 ₁	0.560 ₂	1.615 ₆
Butanone ($n_1=1.3778$)						
2 000	0.920 ₁	0.207 ₀	0.324 ₆	1.623 ₃	0.554 ₈	1.602 ₇
4 100	0.915 ₃	0.209 ₄	0.324 ₄	1.627 ₈	0.554 ₈	1.601 ₁
15 600	0.914 ₇	0.211 ₀	0.325 ₄	1.630 ₀	0.555 ₈	1.607 ₆

a Determined from the Lorenz-Lorentz mixture rule¹²

b Determined from the Dale-Glstone mixture rule¹²

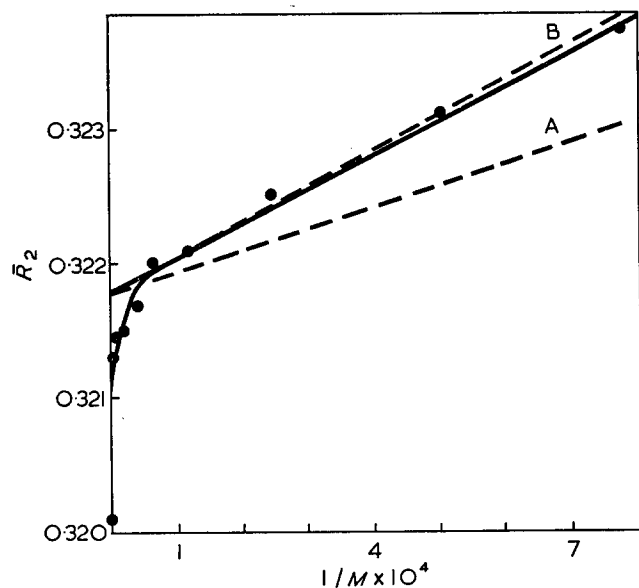


Figure 3 Partial specific refractivity of polystyrenes in toluene plotted against the reciprocal of the molecular weight. —, Experimental data; ----, calculated curves

It is necessary to emphasize here that, as for dn/dc and \bar{v}_2 measurements, we observe a linear variation for molecular weights below 20 000 and the same departure from linearity beyond that limit.

The linear variation which arises at low molecular weights has already been shown by Bodmann¹⁴ and corresponds (according to his assumptions and that of Lorimer and Jones⁴) to the additivities of the specific

refractivities of the end-groups \bar{R}_e and of the repeating units \bar{R}_m :

$$\bar{R}_2 = (1 - w_e)\bar{R}_m + w_e\bar{R}_e \quad (6)$$

where w_e represents the mass concentration of the end-groups with respect to the total weight of the macromolecule, then:

$$\bar{R}_2 = \bar{R}_m + \frac{M_e(\bar{R}_e - \bar{R}_m)}{M_n} = \bar{R}_m + K'/M_n \quad (7)$$

In this relationship, M_e is the molecular weight of the end-groups. Since \bar{v}_2 may be replaced by:

$$\bar{v}_m + K/M_n = \bar{v}_m + \frac{M_e(\bar{v}_e - \bar{v}_m)}{M_n} \quad (8)$$

it is easy to calculate from the Lorenz-Lorentz equation (2) and from equations (7) and (8), the relation between dn/dc and M . One finally obtains, if A stands for the quantity $(n_1^2 - 1)/(n_1^2 + 2)$:

$$\begin{aligned} dn/dc &= \frac{3(\bar{R}_m - A\bar{v}_m)}{2n_1(1 - A)^2} + \frac{1}{M_n} \left(\frac{3(K' - AK)}{2n_1(1 - A)^2} \right) \\ &= (dn/dc)_m + K''/M_n \end{aligned} \quad (9)$$

Provided that the refractive index n_e and the partial specific volume \bar{v}_e of the end-groups are known, it is then possible to calculate, starting from this simple hypothesis, the theoretical slopes of the lines $dn/dc = f(1/M)$. For this purpose, we have assumed for \bar{R}_m and \bar{v}_m the extrapolated values of the experimental straight lines obtained in the low molecular weight range.

For instance, in the case of polystyrene samples terminated by a butyl group, we have evaluated the theoretical slope, assuming for this end group the properties of the octane compound dissolved in the same solvent (at 25°C, $n_e(\text{butyl}) = 1.3975$ and $\bar{v}_e(\text{butyl}) = 1.459 \text{ cm}^3/\text{g}$). Assuming a value for \bar{R}_m of $0.3218 \text{ cm}^3/\text{g}$ which corresponds to $(dn/dc)_m = 0.104 \text{ cm}^3/\text{g}$, when polystyrene is dissolved in toluene, we obtain values for K' and K'' of 1.69 cm^3 (Figure 3, curve A) and -14.6 cm^3 (Figure 2, curve IIA) respectively.

A more elaborate calculation consists of assuming¹³ that the refractive index [$n_e(\text{styryl}) = 1.584$] and the partial specific volume [$\bar{v}_e(\text{styryl}) = 0.989 \text{ cm}^3/\text{g}$] of the last monomeric unit differ from that of the central repeating units. The resulting K' and K'' values are found to be equal to 2.65 cm^3 (Figure 3, curve B) and -17.06 cm^3 (Figure 2, curve IIB) respectively.

These calculated values are in good agreement with the experimental ones $K'_{\text{exp}} = 2.5 \text{ cm}^3$ and $K''_{\text{exp}} = 14 \text{ cm}^3$ determined in the range of molecular weights below 20 000 and are anyhow much lower than the average experimental slope corresponding to molecular weight data over 20 000.

All these results show it is possible to explain quantitatively the linear portion of the curve corresponding to the low molecular weight range. They suggest also that there exists always, at least for polystyrenes in the three considered solvents, an increase of dn/dc with molecular weight, which is definitively outside the limit of errors.

We believe that the explanation we gave for the behaviour of specific volume in this range of molecular weight is also valid, but we do not have enough experimental data to verify that dn/dc , as a function of $M^{-1/2}$ gives a straight line.

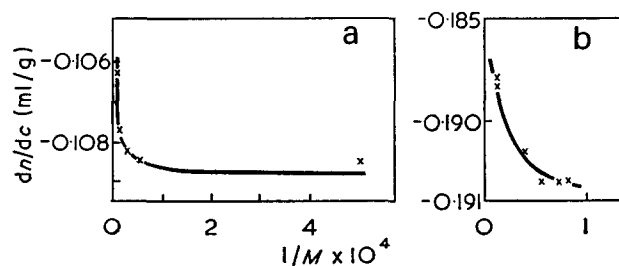


Figure 4 Variation in dn/dc of polyethylenes with reciprocal molecular weight (data of Wagner and Hoeve¹⁵). (a) Polyethylenes in trichlorobenzene at 135°C; (b) polyethylenes in 1-chloronaphthalene at 135°C

The effect just described seems also to exist for other systems, as shown by the few data available in the literature. Wagner and Hoeve¹⁵ performed tests on n-alkanes and polyethylenes in solutions of 1,2,4-trichlorobenzene and chloronaphthalene at 135°C (Figure 4). They determined the $(dn/dc)_m$ and K'' factors included in equation (1) for n-alkanes dissolved in 1,2,4-trichlorobenzene and have shown that the variation of dn/dc with molecular weight in this case was less than half the one observed for polyethylenes above 20 000 in the same solvent. If we use our representation $dn/dc = f(1/M)$, we find curves which are very similar to ours, presenting a linear part in the low molecular weight region (below 10 000) and an anomalous increase at high molecular weights.

CONCLUSIONS

From the results of this paper and the preceding one, it appears that the variation of the partial specific volume, as well as the refractive index increment, depend on molecular weight in a much more complicated way than it is generally assumed.

Two domains have to be considered separately: (a) in the low molecular weight range (below 20 000 for polystyrenes) the effect of end-groups is predominant. If one knows the exact chemical composition of the polymer, it is possible, applying simple additivity rules, to predict and evaluate quantitatively the variations of these two parameters with molecular weight; (b) in the high molecular weight range, these calculations predict a constant value for these quantities. We have shown that this is not the case: a small variation of both \bar{v}_2 and dn/dc does exist. We suggested that this variation is due to intramolecular contacts; this gives a linear relation between \bar{v}_2 and dn/dc as functions of $M^{-1/2}$ which has been confirmed for \bar{v}_2 using highly branched polymers.

However, some remarks can be made concerning these tentative explanations. Molar refractivity usually does not depend on temperature. If we assume that the change in free volume introduced by intramolecular contacts is similar to that which could be created by a temperature change, we should expect an effect of molecular weight on \bar{v}_2 and dn/dc but not on \bar{R}_2 . This is not the case, showing that intramolecular contacts do affect also the internal field probably by mutual orientation of segments.

We may also note that the partial specific refractivity of the polymer depends on the nature of the solvent

(Table 2). Likewise, the proper refractive index n_2^* of the dissolved polymer, as defined by Heller² is different from the refractive index of the pure polymer, usually assumed to be equal to 1.602. Relating to this, it is interesting to point out that, according to the results obtained by Heller, the refractive index of polystyrenes in butanone is much higher than in the other solvents considered. As suggested in the preceding paper, the penetration of the polymer coil by the solvent molecules should depend on their size and on their conformation.

The results presented here may have some incidence in all fields where dn/dc and \bar{v}_2 appear as working parameters, e.g. molecular weight determinations by light scattering and by g.p.c., studies relative to macromolecular solutes in mixed solvents¹⁶ etc.

The numerous applications of dn/dc and \bar{v}_2 in macromolecular science and their particular importance on the characterization of polymers would require a generalization of these results to other systems.

REFERENCES

- 1 Heller, W. *J. Phys. Chem.* 1965, **69**, 1123
- 2 Heller, W. *J. Polym. Sci. (A-2)* 1966, **4**, 209
- 3 Lorimer, J. W. *Polymer* 1972, **13**, 46
- 4 Lorimer, J. W. and Jones, D. E. G. *Polymer* 1972, **13**, 52
- 5 Looyenga, H. *J. Polym. Sci. (Polym. Phys. Edn)* 1973, **11**, 1331
- 6 Scholte, Th. G. *J. Polym. Sci. (A-2)* 1972, **10**, 519
- 7 Barrall, E. M., Cantow, M. J. R. and Johnson, J. F. *J. Appl. Polym. Sci.* 1968, **12**, 1373
- 8 Szwarc, M. 'Carbanions, Living Polymers and Electron Transfer Process', Interscience, New York, 1968, p 151
- 9 Bodmann, O. *Thesis* University of Mainz
- 10 Margerison, D., Bain, D. R. and Kiely, B. *Polymer* 1973, **14**, 133
- 11 Schulz, G. V. and Baumann, H. *Makromol. Chem.* 1968, **114**, 122
- 12 Bottcher, G. J. F. 'Theory of Electric Polarization', Elsevier, Amsterdam, 1952, Sections 40, 44, 48, 49
- 13 François, J. and Candau, F. *Eur. Polym. J.* 1973, **9**, 1355
- 14 Bodmann, O. *Makromol. Chem.* 1969, **122**, 210
- 15 Wagner, H. L. and Hoeve, C. A. J. *J. Polym. Sci. (A-2)* 1971, **9**, 1763
- 16 Dondos, A. and Benoit, H. *Makromol. Chem.* 1970, **133**, 119

Anionic polymerization of styrene in triglyme-benzene mixtures

K. Takaya, H. Tatsuta and N. Ise

*Department of Polymer Chemistry, Kyoto University, Kyoto, Japan
(Received 22 October 1973; revised 1 April 1974)*

Living anionic polymerization of styrene was kinetically investigated in triglyme-benzene mixtures. At low concentrations of triglyme the overall propagation rate constant, k_p , was much larger than at the same concentration of monoglyme (DME) in DME-benzene mixtures. The Szwarc-Schulz plot did not have negative slopes for lithium and sodium salts at triglyme contents of 5~20vol%, and no contribution of free anions to the propagation was observed for the sodium salt. The sodium ion pair was more highly reactive than the lithium ion pair; thus at 25°C, the ion pair rate constant, k_p' , for the lithium salt was 43, 102, 135 and 165 M⁻¹sec⁻¹ at triglyme concentrations of 5, 10, 15, and 20%, respectively, while that for the sodium salt was 410, 920, and 1460 M⁻¹sec⁻¹ in 5, 10, and 15% triglyme, respectively. The dissociation constant, K , for the lithium salt was 2.4×10^{-11} , 1.9×10^{-10} and 1.3×10^{-9} M in 10, 15, and 20% triglyme, respectively and the free ion rate constant, k_p'' , was $2 \sim 2.5 \times 10^4$ M⁻¹sec⁻¹ for the lithium salt.

INTRODUCTION

In general, ion pairs, free ions, triple ions, quadrupole ions, etc., contribute to the propagation step of ionic polymerizations¹⁻⁴. Ion pairs and triple ions exist in different types such as 'contact' ion pairs or 'solvent-separated' ion pairs (or 'tight' or 'loose' ion pairs). The latter have higher reactivities than the former. The fraction of the ionic species and their reactivity depend on solvents, gegenions and temperature, etc.

For example, lithium and sodium salts of living polystyrene are present in large amounts of the dimeric ion pairs (less reactive) and in small amounts of reactive (monomeric) ion pairs in benzene⁵, and in contact ion pairs in dioxane⁶. In the latter case, the ion pairs with large alkali metal gegenions, such as caesium, form loose ion pairs to give higher reactivities than those for smaller gegenions^{5, 6} (Na⁺ and Li⁺) owing to the lack of solvation; Coulombic forces between the electric charges affect the reactivity of ion pairs in such a poor-solvating medium. On the contrary, lithium ion pairs are highly solvated and very reactive in tetrahydrofuran (THF)^{7, 8}, even more so in the case of 1,2-dimethoxyethane (DME)^{9, 10}. This is because the fraction of highly reactive solvent-separated ion pairs is larger in DME than in THF. Though the polarity of THF and DME is nearly the same, the latter has a higher solvation power than the former. This is due to the structure of the DME molecules. The strong solvation power of DME was made clear in previous studies¹¹ of living anionic polymerizations of styrene in DME-benzene mixtures, in which the formation of highly reactive intermolecular solvent-separated triple ions was noted. The physical properties of the DME-benzene mixture and the THF-benzene mixture are about the same, but triple ions were observed only in the former mixtures¹². Thus the role of solvent is

determined not only by the macroscopic properties such as dielectric constant, but also by factors such as structure and fitness of solvent molecules and ions.

It is well known in the spectroscopic studies of fluorenyl salts¹³ that polyethers such as diglyme, triglyme, tetraglyme, and pentaglyme have much larger solvation power than monoglyme owing to the specific solvation. In the present paper we studied living anionic polymerizations of styrene in triglyme-benzene mixtures in which lithium and sodium ions were used as gegenions, in order to discuss interactions of growing ends with gegenions and solvating agents (triglyme and monoglyme).

EXPERIMENTAL

Commercial triglyme CH₃O-(CH₂CH₂O)₃-CH₃ was preliminarily dehydrated by contact with metal sodium plates, refluxed over calcium hydride for a few days and distilled over sodium-potassium alloy under 7 mmHg pressure at 81.5°C. Triglyme was set on a vacuum line, vigorously stirred with a magnetic stirrer at room temperature, frozen and de-aerated. The stirring and freeze-de-aeration cycles was repeated several times until degassing became steady and relatively weak. Then the glyme was distilled into thoroughly flamed ampoules with a break-seal. The dark blue colour of a charge transfer complex was observed during the purification process. On heating the solution, the colour disappeared instantly.

Ethyllithium and α -methylstyrene tetramer dianions were used as the initiators for lithium and sodium salts of living polystyrene, respectively. Ethyllithium was recrystallized in benzene, and then styrene was seeded. α -Methylstyrene tetramer dianions were prepared by a reaction of pre-purified α -methylstyrene with metal sodium (mirror) in THF.

All the experiments were carried out using a high vacuum line with break-seal. The apparatus and its operating procedure have been described elsewhere¹¹. Polymerization rate was determined spectrophotometrically at 25°C and 0°C. The observed absorption maxima were at 335 and 337 nm for lithium and sodium salts, and at 291.5 nm for styrene. A Hitachi EPS-3T spectrophotometer was used. The molecular absorption coefficient, ϵ , was assumed to be 1.2×10^4 for both polystyryl salts.

The conductance of the 'living' polymer solutions was measured by a Wayne-Kerr B331 MkII autobalance precision bridge method (a.c.). The absorption of polystyryl salts was measured just before and after the conductance measurement. The conductance measurement was carried out also by applying a high voltage to the solution (d.c. method).

RESULTS

In Figure 1, the dielectric constant and viscosity of triglyme-benzene mixtures at 25°C are given.

According to the two-state mechanism, the apparent propagation rate constant, k_p , is given as:

$$k_p = k'_p + k''_p K^{1/2} / [LE]^{1/2} \quad (1)$$

where k'_p and k''_p are the ion pair and free ion rate constants, K is the dissociation constant of the ion pair, and $[LE]$ is the living end concentration. The Szwarc-Schulz plot (viz. k_p vs. $[LE]^{-1/2}$) for the lithium salt of living polystyrene in triglyme-benzene system is given in Figure 2. The slopes for the triglyme concentration of 5 and 10% were practically zero, but they became positive at the higher triglyme concentrations of 15 and 20%. A negative slope was not observed. The intercept k'_p increased as the triglyme content increased, being 43, 102, 135 and 165 $M^{-1}sec^{-1}$ for 5, 10, 15 and 20% triglyme at 25°C respectively.

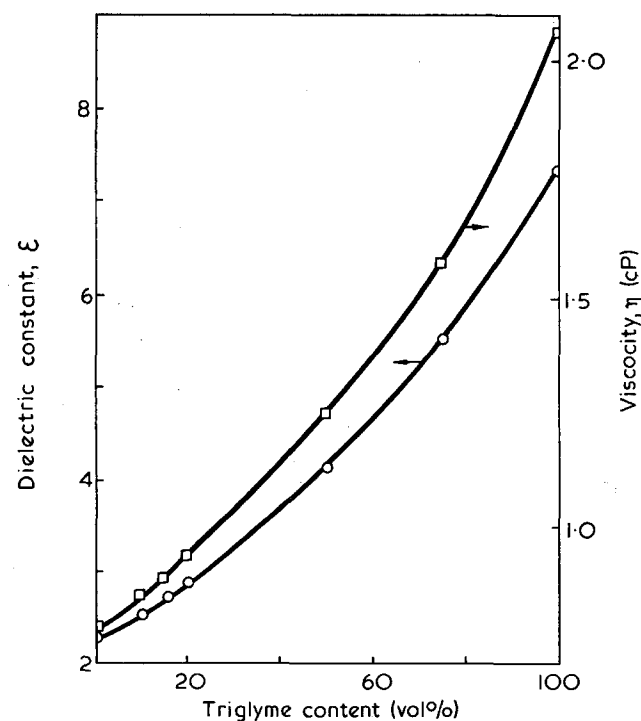


Figure 1 Dielectric constant (○) and viscosity (□) of triglyme-benzene mixtures at 25°C

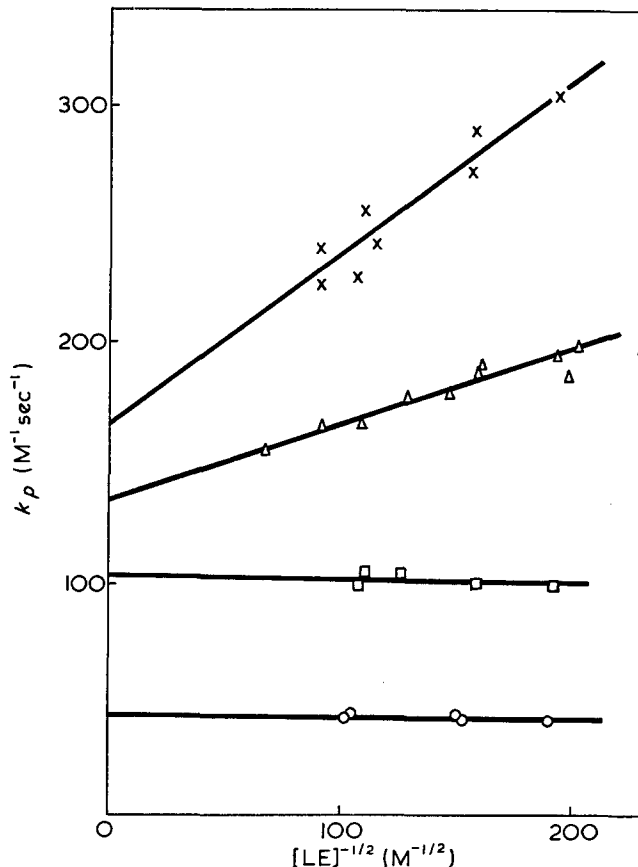


Figure 2 Linear dependence of the apparent propagation rate constants, k_p , on the living end concentration $[LE]$ in 20% (x), 15 (Δ), 10 (□) and 5% (○) triglyme-benzene mixtures at 25°C

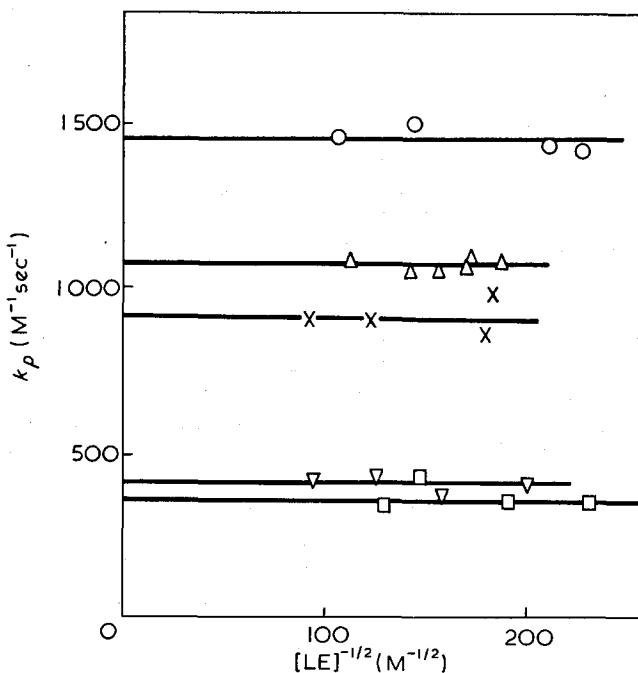


Figure 3 Linear dependence of the apparent propagation rate constants, k_p , on the living end concentration $[LE]$ in 15 (○), 10 (x), and 5% (▽) triglyme-benzene mixtures at 25°C, and 10 (Δ) and 5% (□) triglyme-benzene mixtures at 0°C

In Figure 3 the Szwarc-Schulz plot for polystyryl sodium in triglyme-benzene systems is given. This Figure suggests that the contribution of the free ions is negligible for 5, 10 and 15% triglyme at 25°C. Experimental difficulties prevented us from carrying out the rate

measurements at higher glyme contents, because the contribution of free anions makes the reaction too fast. The ion pair rate constant k_p' for the sodium salts was 410, 920 and 1460 $M^{-1}sec^{-1}$ for 5, 10 and 15% triglyme at 25°C.

Kinetically, the propagation of polystyryl sodium was studied also at 0°C and the slope of the Szwarc-Schulz plot was also zero as shown in Figure 3. The intercept (k_p) was 380 and 1080 $M^{-1}sec^{-1}$ for 5 and 10% triglyme, respectively.

In weak electrolyte solutions containing ion pairs and free ions, a logarithmic plot of equivalent conductance, Λ vs. [LE] gives a linear relation with a slope of -0.5 , as shown in Figure 4. Even at 10% triglyme, this Figure indicates the presence of free ions, although the slope of the Szwarc-Schulz plot was zero (Figure 2).

The dissociation constant, K , was evaluated by the Kraus-Bray plot¹⁴, as shown in Figure 5. The intercept

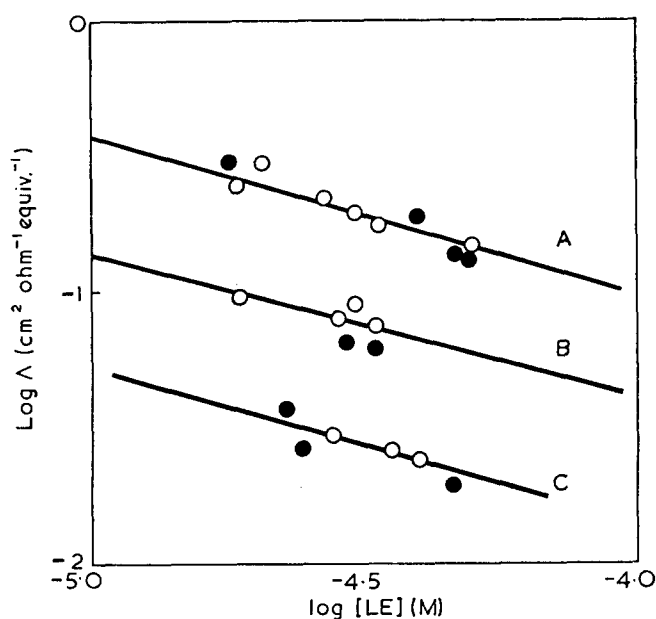


Figure 4 Dependence of the equivalent conductance Λ on living end concentration [LE] in, 20 (A), 15 (B), and 10% (C) triglyme-benzene mixtures at 25°C

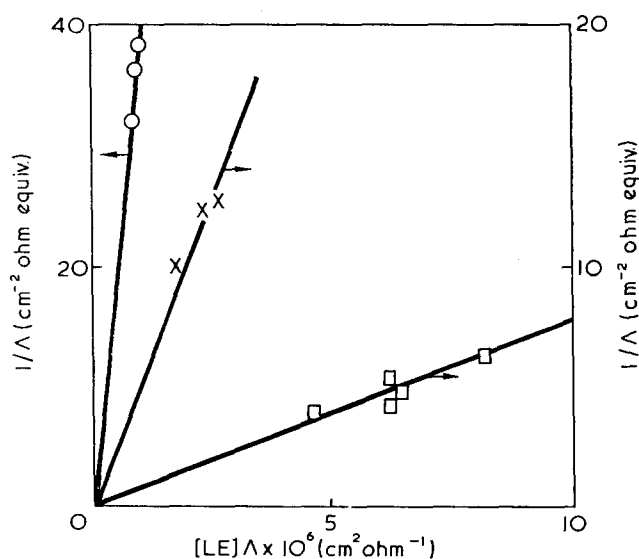


Figure 5 Kraus-Bray plot for polystyryllithium in 10 (O), 15 (x) and 20% (O) triglyme-benzene mixtures at 25°C

Table 1 Kinetic and conductivity results in triglyme-benzene system

	Triglyme (vol%)			
	5	10	15	20
Li ⁺ salt at 25°C				
ϵ	2.40	2.54	2.72	2.90
k_p ($M^{-1}sec^{-1}$)	43	102	135	165
Λ_0 ($cm^2 ohm^{-1} equiv^{-1}$)	—	33.8	32.4	31.0
K (M)	—	2.4×10^{-11}	1.9×10^{-10}	1.3×10^{-9}
k_p'' ($M^{-1}sec^{-1}$)	—	—	2.5×10^4	2.0×10^4
Na ⁺ salt at 25°C				
k_p'' ($M^{-1}sec^{-1}$)	410	920	1460	—
Na ⁺ salt at 0°C				
k_p'' ($M^{-1}sec^{-1}$)	380	1080	—	—

$1/\Lambda_0$ is nearly zero, so that the limiting equivalent conductance Λ_0 was assumed by the Walden rule. The product $\Lambda_0 \eta$ ($=0.291 cm^2 P ohm^{-1} equiv^{-1}$) in DME¹⁵ was used assuming that $\Lambda_0^+(Na^+) = \Lambda_0^+(Li^+)$ ¹⁶. Thus the dissociation constants of polystyryl ion pairs were determined to be 2.4×10^{-11} , 1.9×10^{-10} and 1.3×10^{-9} M at 10, 15, and 20% triglyme, respectively. Consequently, the free ion rate constant k_p'' was evaluated to be 2.5×10^4 and $2.0 \times 10^4 M^{-1}sec^{-1}$ at 15 and 20% triglyme, respectively. All results of kinetic and conductometric measurements are summarized in Table 1.

DISCUSSION

Dissociation constant, K

The dissociation constant, K , of the lithium salt in the triglyme-benzene systems was much smaller than that in THF⁸ or in pure DME (monoglyme)¹⁵, and close to that in THP¹⁶⁻¹⁸, i.e. the K values in the triglyme-benzene systems are in the order of $10^{-11} \sim 10^{-9}$ M for 10~20% triglyme, which is close to the values in mixtures of DME-benzene containing 40~50% DME. The K value of the sodium salt in the triglyme-benzene was too small to be evaluated by the conductivity measurement. If the dissociation constant reflects the electrostatic energy with which an ion pair is separated to infinity, then K would become larger in more polar solvents. Because free anions contribute to the propagation in the present system as seen from the conductivity data for the lithium case, in which dielectric constant, ϵ (2.54, 2.72, and 2.90 at 10, 15, and 20% triglyme, respectively) is much smaller than that in DME-benzene system¹¹ (3.81 and 4.33 at 40 and 50% DME respectively) and in THP (5.61)¹⁶⁻¹⁸ the lithium ions seem to be stabilized by solvation of triglyme molecules. The larger sodium ion is solvated by triglyme molecules to a lesser extent; in fact no free ion contribution was observed in triglyme-benzene system (see Figure 3).

The intercharge distance a in the lithium ion pair was calculated to be 7.1 Å from the $(\log K - 1/\epsilon)$ plot based on the Fuoss equation¹⁹ for the sphere-in-continuum model:

$$K = \frac{3000}{4\pi Na^3} \exp\left(-\frac{e^2}{a\epsilon kT}\right) \quad (2)$$

The fact that the a value is larger than in other solvent systems (e.g. $a=4.5$ Å in THF⁷) means that the solvation power of triglyme molecules is strong.

Reactivity of ion pairs

In triglyme-benzene systems, k_p' for the lithium salt of living polystyrene was much larger than that in DME-benzene systems (7, 30, 57, and $135 \text{ M}^{-1} \text{ sec}^{-1}$ for 10, 30, 40, and 50% DME respectively). Also for the sodium salt the k_p' values at low triglyme concentrations were much higher than those in DME-benzene ($k_p' = 30, 140, 220, 360$ and $700 \text{ M}^{-1} \text{ sec}^{-1}$ for 10, 30, 40, 50 and 60%²⁰).

The log k_p' vs. $(\epsilon - 1)/(2\epsilon + 1)$ plots¹¹ show deviation from linearity (convex). This is in contrast with previous observations for other binary systems^{11, 12, 21}, and would imply that specific solvation by glyme molecules is important in the present system.

The differences in physical properties (such as polarity) between the triglyme-benzene system and the DME-benzene system are small. Thus, the difference in k_p' of the lithium and sodium salts is due to the difference in the solvation power of the glymes to the alkali cation. This means that highly reactive solvent-separated ion pairs are more abundant in the triglyme system than in the DME system. In the study of the ion pairs of fluorenyl salts¹³, it was also clear that triglyme molecules had much higher solvating ability towards cations than DME molecules.

We discuss next the effect of ionic size. Sodium ion pairs are more reactive by one order of magnitude than lithium ion pairs both in the triglyme-benzene system and in the DME-benzene system. It is well known that, in polar ethereal solvents such as THF or DME, ion pairs with a smaller cation can easily be solvated and have a high reactivity. Consequently, the inversion of the reactivity should be attributed not to the fraction of glyme-separated ion pairs, but to the structure of glyme-separated ion pairs.

Shinohara et al.^{22, 23} reported the reactivity (k_s) of tetraglyme-separated sodium ion pair in the system THP-tetraglyme-polystyrylsodium, which was much smaller ($3900 \text{ M}^{-1} \text{ sec}^{-1}$) than that of THF-separated ion pair ($3 \times 10^4 \text{ M}^{-1} \text{ sec}^{-1}$) or monoglyme-separated ion pair ($2 \times 10^4 \text{ M}^{-1} \text{ sec}^{-1}$). They interpreted the difference by the tightness of tetraglyme-separated sodium ion pair. It is clear from the spectroscopic studies of fluorenyl salts in the presence of glymes that triglyme 'fits' just the lithium ion pairs and tetraglyme the sodium ion pairs. This would account for the reactivity of the solvent-separated ion pairs. The triglyme-separated lithium ion pair is much tighter than the sodium one.

The temperature dependence of the ion-pair rate constant, k_p , of the sodium salt (see Table I) suggests that, as the activation energy is either negative (at 10% glyme content) or very small (at 5% glyme content), the contribution of solvent-separated ion pair $\text{---S}^-/\text{triglyme}/\text{Na}^+$ should become larger at 0°C and even more so at higher triglyme contents.

Reactivity of free ions and formation of triple ions

The k_p'' values of the lithium salts in the triglyme-benzene system were 2×10^4 and $2.5 \times 10^4 \text{ M}^{-1} \text{ sec}^{-1}$ for 20 and 15% triglyme respectively. These are close to $3 \times 10^4 \text{ M}^{-1} \text{ sec}^{-1}$ for the DME-benzene system¹¹ (lithium

salt), but smaller than $9 \sim 10 \times 10^4 \text{ M}^{-1} \text{ sec}^{-1}$ for the DME-benzene system²⁰ (sodium, potassium and caesium salts), $4 \sim 13 \times 10^4 \text{ M}^{-1} \text{ sec}^{-1}$ in DME^{9, 10}, $6.5 \sim 15 \times 10^4 \text{ M}^{-1} \text{ sec}^{-1}$ in THF^{7, 8}, $6 \sim 7 \times 10^4 \text{ M}^{-1} \text{ sec}^{-1}$ in THP^{17, 18} and $4 \sim 7 \times 10^4 \text{ M}^{-1} \text{ sec}^{-1}$ in MeTHF²⁴. The reason why the free carbanions in the present case are less reactive in the case of the lithium salts than other salts is not clear: the presence of impurity or isomerization reaction was not observed. It may be due to the neglect of the contribution of intermolecular triple ions which are more reactive than the free anions, as was the case for triple ions $\text{---S}^-//\text{Li}^+//\text{S}^-$ in the DME-benzene system¹¹. If the intermolecular triple ion is more reactive than the free ions, the slope of the Szwarc-Schulz plot will be made apparently smaller, i.e. k_p'' may be underestimated. Accordingly, zero slope of the k_p vs. $[\text{LE}]^{-1/2}$ plot for the 10% triglyme system in Figure 2 might be attributed to the contribution of not so highly reactive triple ions as those found earlier in DME-benzene systems¹¹.

REFERENCES

- 1 Bywater, S. *Adv. Polym. Sci.* 1965, **4**, 66
- 2 Szwarc, M. 'Carbanions, Living Polymers, and Electron Transfer Processes', Interscience, New York, 1968; Szwarc, M. *Acc. Chem. Res.* 1969, **2**, 87
- 3 Ise, N. *Adv. Polym. Sci.* 1969, **6**, 347; Hirohara, H. and Ise, N. *Macromol. Rev.* 1972, **6**, 295
- 4 Böhm, L. L., Chmelir, M., Löhr, G., Schmitt, B. J. and Schulz, G. V. *Adv. Polym. Sci.* 1972, **9**, 1
- 5 Roovers, J. E. and Bywater, S. *Trans. Faraday Soc.* 1966, **62**, 701
- 6 Bhattacharyya, D. N., Smid, J. and Szwarc, M. *J. Phys. Chem.* 1965, **69**, 624
- 7 Bhattacharyya, D. N., Lee, C. L., Smid, J. and Szwarc, M. *J. Phys. Chem.* 1965, **69**, 612
- 8 Shimomura, T., Tölle, K. J., Smid, J. and Szwarc, M. *J. Am. Chem. Soc.* 1967, **89**, 796; Schmitt, B. J. and Schulz, G. V. *Makromol. Chem.* 1971, **142**, 325
- 9 Shimomura, T., Smid, J. and Szwarc, M. *J. Am. Chem. Soc.* 1967, **89**, 5743
- 10 Löhr, G. and Schulz, G. V. *Makromol. Chem.* 1968, **117**, 283
- 11 Ise, N., Hirohara, H., Makino, T., Takaya, K. and Nakayama, M. *J. Phys. Chem.* 1970, **74**, 606
- 12 Ise, N., Hirohara, H., Makino, T. and Sakurada, I. *J. Phys. Chem.* 1968, **72**, 4543
- 13 Chan, L. L., Wong, K. H. and Smid, J. *J. Am. Chem. Soc.* 1970, **92**, 1955
- 14 Kraus, C. A. and Bray, W. C. *J. Am. Chem. Soc.* 1913, **35**, 1315
- 15 Carvajal, C., Tölle, K. J., Smid, J. and Szwarc, M. *J. Am. Chem. Soc.* 1965, **87**, 5548
- 16 Nicholls, D., Sutphen, C. and Szwarc, M. *J. Phys. Chem.* 1968, **72**, 1021
- 17 Hirohara, H., Nakayama, M., Takaya, K. and Ise, N. *Trans. Faraday Soc.* 1970, **66**, 1165
- 18 Beylen, M. van, Fisher, M., Smid, J. and Szwarc, M. *Macromolecules* 1969, **2**, 575
- 19 Fuoss, R. M. and Accascina, F. 'Electrolytic Conductance', Interscience, New York, 1959
- 20 Ise, N. et al. to be published
- 21 Beylen, M. van, Bhattacharyya, D. N., Smid, J. and Szwarc, M. *J. Phys. Chem.* 1966, **70**, 157
- 22 Shinohara, M., Smid, J. and Szwarc, M. *J. Am. Chem. Soc.* 1968, **90**, 2175
- 23 Shinohara, M., Smid, J. and Szwarc, M. *Chem. Commun.* 1969, p 1232
- 24 Hirohara, H., Takaya, K., Nakayama, M. and Ise, N. *Trans. Faraday Soc.* 1970, **66**, 3163

Anionic polymerization of styrene in 2-methyltetrahydrofuran: temperature dependence of the field effect

K. Takaya and N. Ise

Department of Polymer Chemistry, Kyoto University, Kyoto, Japan
(Received 22 October 1973; revised 1 April 1974)

Kinetics of living anionic polymerizations of styrene was investigated for lithium, sodium, and potassium salts in 2-methyltetrahydrofuran at 35, 25, 0, and -70°C in the presence and absence of a high intensity electric field. At 35 and 25°C , a field acceleration effect was observed whereas no effect was found at 0 and -70°C . The propagation rate constant of ion pairs was almost independent of gegen ions and their temperature dependence was smaller than that of free anions. The free ions seem to be more strongly solvated as the temperature decreases.

INTRODUCTION

The influence of an electric field on the propagation step of living anionic polymerizations of styrene has been studied in this laboratory¹. When a high intensity electric field was applied, the propagation was generally accelerated. The acceleration was neither due to increase of the ion pair rate constant nor to increase of the fraction of free ions, but to the increase in the reactivity of the free anion itself¹. The increase in the free-ion rate constant was suggested to be due to desolvation of the free anion by the electric field, although without direct evidence.

Previously, it was believed that the carbanions such as the styryl anions were not solvated by ethereal solvents². There, however, are a few solvents such as monoglyme(DME) which can coordinate the anions, though weakly³. The temperature dependence of living anionic polymerizations in the presence and absence of the field seems to be of interest. As the field effect was not observed in the DME-benzene system because the solvation was strong towards anions, we chose 2-methyltetrahydrofuran (MeTHF) as a solvent, which is a weaker solvating agent than DME. We studied the kinetic and electrolytic behaviour of lithium, sodium and potassium salts of living polystyrene in MeTHF between 35°C and -70°C .

EXPERIMENTAL

The preparation of the living polymers and the purification of reagents were carried out using a high vacuum line. The details were described elsewhere^{4, 5}.

The initiator for the lithium salt of the living polystyrene was ethyllithium (Mitsuwa Chemicals, Osaka, Japan), which was recrystallized in benzene, and seeded to give styryllithium (degree of polymerization ~ 10) in benzene. The solvent was replaced by MeTHF according to the method described in previous papers^{4, 5}. For sodium and potassium salts, α -methylstyrene oligomer dianions were used as initiators; they were prepared by

the reaction of α -methylstyrene with the corresponding metal film.

The determination of the propagation rate was spectrophotometrically carried out using a Hitachi EPS-3T spectrophotometer. The absorption maxima were at 291.5 nm for styrene, and at 338, 343 and 344 nm for polystyryllithium, sodium, and potassium, respectively. The apparent propagation rate constant, k_p , was calculated at conversions below 85%.

The electric conductivity was measured by using an a.c. autobalance precision bridge Wayne Kerr B331 MkII and a d.c. method with high voltage.

Temperature control was carried out as follows. The measurements near room temperature were carried out by circulation of water from a thermostat whose temperature was regulated at $25 \pm 0.01^{\circ}\text{C}$ or $35 \pm 0.01^{\circ}\text{C}$. A quartz Dewar with optical windows was used for the measurements at 0°C and -70°C . As a cooling medium, ice-water or methanol was used for studies at $0 \pm 1.5^{\circ}\text{C}$ and $-70 \pm 2^{\circ}\text{C}$, respectively. The polymerization cell was pre-cooled in another large Dewar set at the experimental temperature. Just before and after the kinetic measurements, the temperature of the quartz Dewar was checked.

RESULTS

In a polar ethereal solvent such as MeTHF, the propagation proceeds by a two-state mechanism, in which a small amount of free ions and a large amount of ion pairs contribute, and the apparent propagation rate constant, k_p , is proportional to the reciprocal square root of living end concentration $[\text{LE}]^2$:

$$k_p = k_p' + k_p'' K^{1/2} / [\text{LE}]^{1/2} \quad (1)$$

The k_p vs. $[\text{LE}]^{-1/2}$ plot is given in *Figure 1* for the sodium salt in the presence and absence of an electric field at 35, 25, 0 and -70°C . In the presence and absence of the electric field, the higher the temperature, the higher

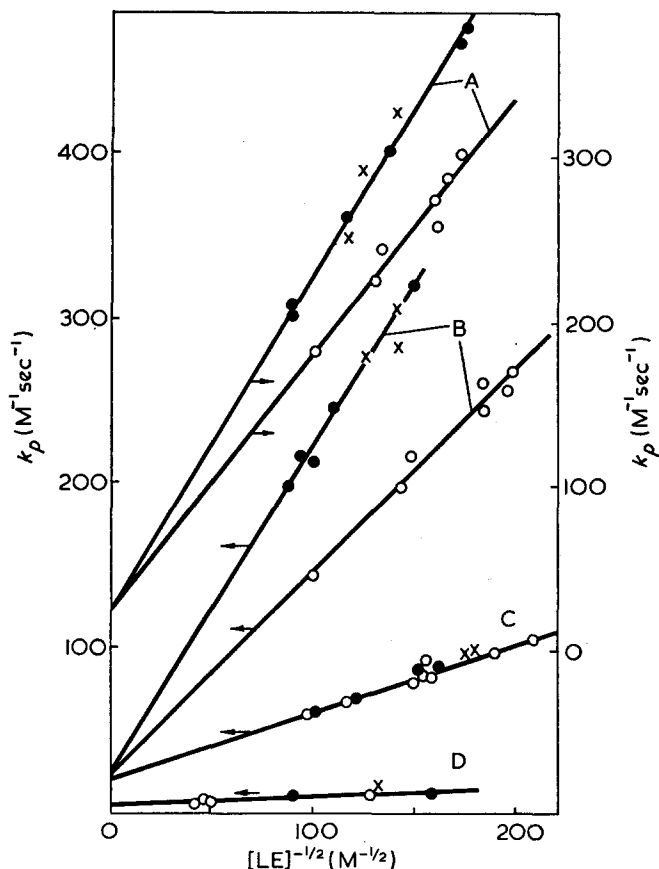


Figure 1 Linear dependence of the observed propagation rate constant, k_p , on living end concentration [LE] for sodium salt in MeTHF. A, 35°; B, 25°; C, 0°; D, -70°C. ○, 0; ●, 3.0; ×, 4.5 kV/cm

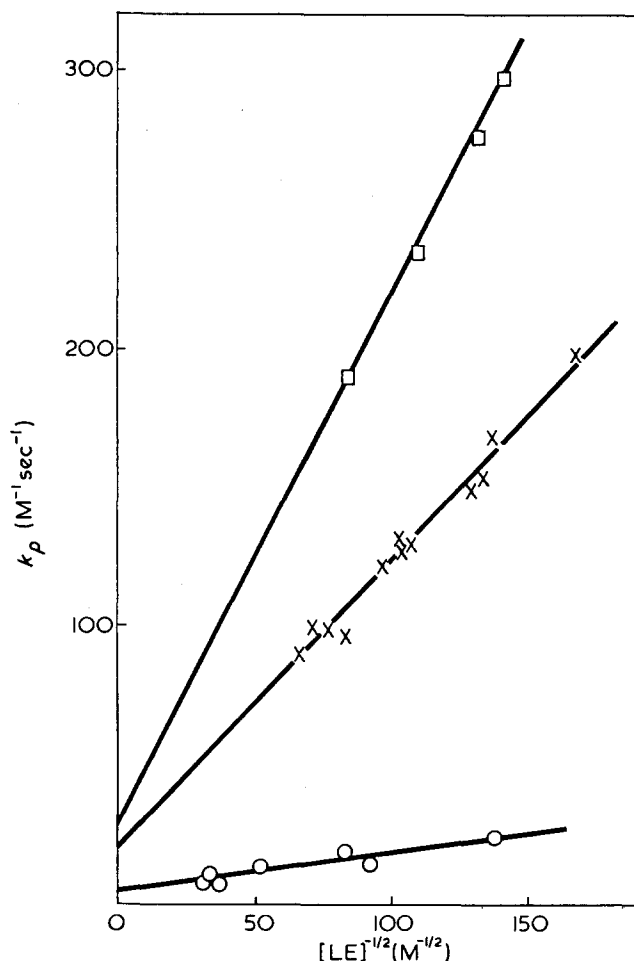


Figure 3 Linear dependence of the observed propagation rate constant, k_p , on living end concentration [LE] for lithium salt in MeTHF. □, 25°; ×, 0°; ○, -70°C

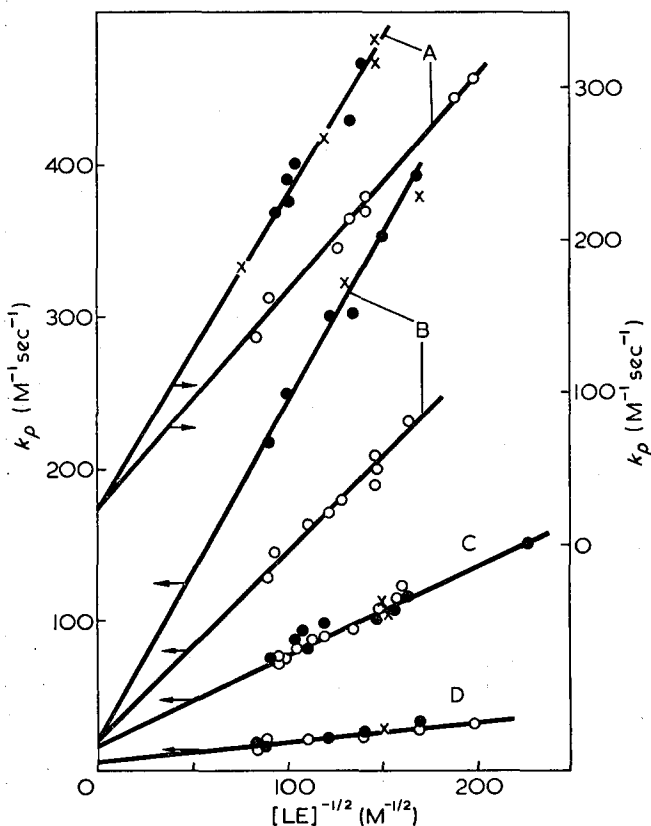


Figure 2 Linear dependence of the observed propagation rate constant k_p on living end concentration [LE] for potassium salt in MeTHF. A, 35°; B, 25°; C, 0°; D, -70°C. ○, 0; ●, 3.0; ×, 4.5 kV/cm

the reactivity. In Figure 2, the k_p values for the potassium salt are given. For both cases, field acceleration effect was observed at 25°C and 35°C, but not at 0°C and -70°C.

As was observed for many other systems¹, the electric field did not increase the intercept k'_p , but the slope $k''_p K^{1/2}$. The ion-pair rate constant k'_p was 25, 23, 20 and 5.5 M⁻¹ sec⁻¹ for the sodium salt at 35, 25, 0 and -70°C, respectively. The k'_p value of the potassium salt was 25, 20, 18 and 6.5 M⁻¹ sec⁻¹ at 35, 25, 0 and -70°C, respectively. The k'_p value of the lithium salt was 25, 20 and 6.0 M⁻¹ sec⁻¹ at 25, 0 and -70°C, respectively, as is seen from Figure 3.

In Figure 4, the dependence of the equivalent conductance Λ on the living end concentration [LE] is given for the potassium salt at 35, 25, 0 and -70°C, where the slope of the straight line was -0.5. This value implies that the propagation proceeds via the two-state mechanism. For the lithium and sodium salts, we note that quite similar results were obtained.

Assuming the limiting equivalent conductance Λ_0 from the Walden product to be 67, 58, 42 and 12 cm² ohm⁻¹ equiv.⁻¹ for the lithium, sodium and potassium salts at 35, 25, 0 and -70°C, respectively, the dissociation constant, K , of the ion pair was estimated by the Kraus-Bray plot⁶ as 1.5 × 10⁻¹⁰, 2.4 × 10⁻¹⁰, 4.1 × 10⁻¹⁰ and 1.6 × 10⁻⁹ M for the sodium salt, 1.5 × 10⁻¹⁰, 3.4 × 10⁻¹⁰, 5.7 × 10⁻¹⁰ and 1.6 × 10⁻⁹ M for the potassium salt, and 7.8 × 10⁻¹⁰, 1.3 × 10⁻⁹, and 1.32 × 10⁻⁸ M for the lithium salt.

Based on these K values, we obtained the free anion rate constant k_p' for polystyryl salts in the presence and absence of an electric field, which is summarized in Table 1. For the sodium and potassium salts, field acceleration was observed at higher temperatures.

DISCUSSION

Ion-pair rate constant k_p'

The activation energy of the propagation by the ion pairs was 1.0~1.5 kcal/mol for lithium, sodium, and potassium salts from the Arrhenius plot. The low value might be attributed to increase of the contribution of solvent-separated ion pairs at low temperatures.

The k_p' values were practically independent of the ionic size in the present solvent. When we compare the reactivity of the lithium and potassium ion pairs in other solvents, the order of reactivity in MeTHF is different from both that in THF⁷ and that in THP^{8,9}. Thus MeTHF seems to have a weaker solvation power than THF, but a stronger solvating power than THP as far as the lithium ion-pair is concerned. The reactivity was in the order: THF \gg MeTHF > THP. On the other hand,

the reactivity of the potassium ion-pair in THP is larger than in MeTHF: THP \sim THF > MeTHF.

Dissociation constant, K

The K value of the lithium salt was larger than those of sodium and potassium salts, but that of the potassium salt was not less than that of sodium salt. The K values were between that in THF ($2.0 \times 10^{-9} \sim 2.2 \times 10^{-7}$ M at 25°C)⁷ and that in THP ($3.7 \times 10^{-11} \sim 1.3 \times 10^{-10}$ M at 25°C)⁸.

The heat of dissociation ($-\Delta H$) became larger with increasing temperature as shown in Figure 5. The $-\Delta H$ values were 2.9, 2.1, and 1.6 kcal/mol for lithium, sodium and potassium salts at lower temperature (between 0°C and -70°C), respectively; it, however, became larger (4.8, \sim 6, and \sim 9 kcal/mol for lithium, sodium and potassium salts, respectively) above 0°C. This temperature dependence is closely related to the fraction of solvent-separated ion pairs.

Free-ion rate constant k_p'' and field effect

From the kinetic results in Table 1, we obtained the free energy of activation ΔG^\ddagger for the propagation by

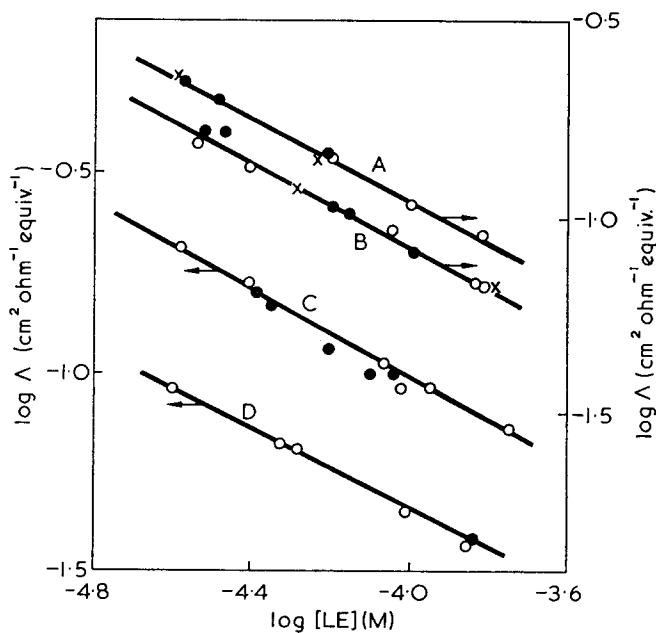


Figure 4 Dependence of the equivalent conductance Δ on living end concentration for polystyryl potassium in MeTHF. A, 35°C; B, 25°C; C, 0°C; D, -70°C. \circ , 0 kV/cm (a.c. value); \bullet , 3.0 kV/cm (d.c. value); \times , 4.5 kV/cm (d.c. value)

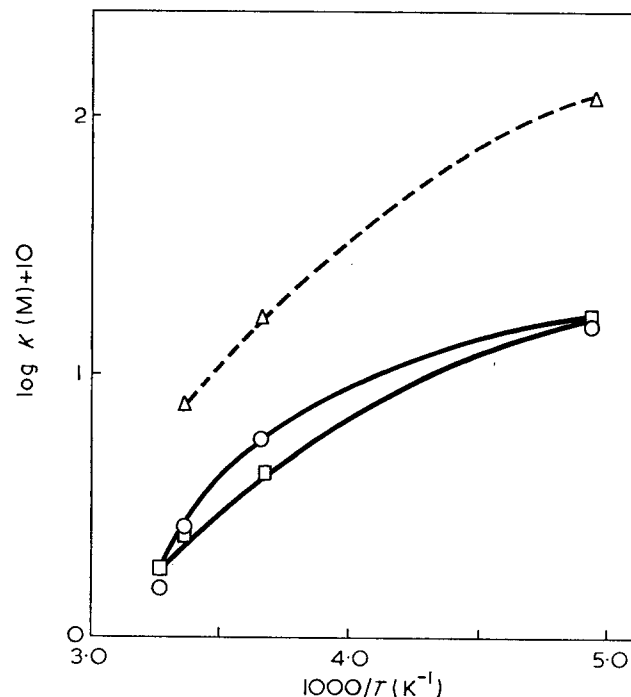


Figure 5 Temperature dependence of dissociation constant, K . Δ , Li⁺ salt; \circ , Na⁺ salt; \square , K⁺ salt

Table 1 Kinetic results for polystyryl salts in MeTHF

Gegen ion	Temperature (°C)	k_p' (M ⁻¹ sec ⁻¹)	Δ_0^* (cm ² ohm ⁻¹ equiv ⁻¹)	$K \times 10^{10}$ (M)	$k_{p0}'' \times 10^{-4}$ (M ⁻¹ sec ⁻¹)	$k_{pE}'' \times 10^{-4}$ (M ⁻¹ sec ⁻¹)
Li ⁺	25	25	58	7.8	7.0	—
	0	20	42	16	2.9	—
	-70	6.0	12	130	0.13	—
Na ⁺	35	25	67	1.5	12	16
	25	23	58	2.4	7.4	12
	0	20	42	4.1	2.7	2.7
K ⁺	-70	5.5	12	16	0.14	0.14
	35	25	67	1.5	13	16
	25	20	58	3.4	7.1	12
K ⁺	0	18	42	5.7	2.3	2.3
	-70	6.5	12	16	0.17	0.17

* Assumed from the Walden product

the free anions as 11.8 ± 0.05 kcal/mol and 12.2 ± 0.05 kcal/mol in the presence and absence of the field at 25°C , respectively. The activation energy of propagation by the free anions in the presence of the field seems to be smaller than in its absence (7.0 ± 1.2 kcal/mol), although the large experimental errors prevent us from detailed discussion.

The field acceleration has been accounted for in terms of desolvation and has been fairly small, as found in other systems.¹ This seems to be related to the very weak solvation of carbanions. In a polar ethereal solvent such as THF, it is clear from the n.m.r. spectra of living oligomers¹⁰⁻¹² that a styryl anion has a highly delocalized π -electron cloud. The delocalization is distinct for a large alkali cation; the larger portion of negative charge of styryl anions or α -methylstyryl anions scatters over the phenyl ring.

The lower electron density of the carbanion due to the delocalization would cause very weak interactions between the styryl anion and solvent molecules. There are no solvents capable of coordinating strongly with anions except glymes among ethereal solvents, while a number of solvents can coordinate towards cations, which contain lone electron pairs such as $\ddot{\text{O}}$, $\ddot{\text{N}}$ and $\ddot{\text{S}}$.

The larger the sp^2 character (hybridization) of the α -carbon in the free ion type growing end, the more strongly the π -electron delocalizes over the phenyl ring. The styryl or α -methylstyryl anions have an intermediate structure between the sp^2 - and sp^3 -hybrid orbitals, so

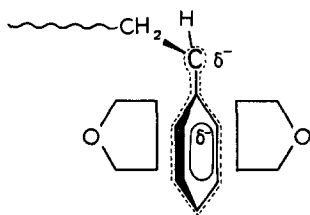


Figure 6 Solvated free styryl anion

that the solvation takes place toward the phenyl ring. If we imagine a collision complex between THF and styrene molecules in the manner as suggested by Ledaal¹³, the coordination of MeTHF towards styryl anions should be such as shown in Figure 6. The sp^2 character of the α -carbon of a free styryl anion would facilitate the formation of the collision complex shown in this Figure. As the interaction with the phenyl rings seems to give a rather smaller steric effect on the propagating step, desolvation, which has been suggested to be caused by field application, would not lead to a large acceleration. Actually the field effect (k_{pE}/k_{p0}) is only $1.2 \sim 1.8$ for various alkali salts of living polystyrene and its derivatives in several solvents.

REFERENCES

- 1 Ise, N. *Adv. Polym. Sci.* 1969, **6**, 347; Hirohara, H. and Ise, N. *Macromol. Rev.* 1972, p 295
- 2 Szwarc, M. 'Carbanions, Living Polymers and Electron Transfer Processes', Interscience New York, 1968; Böhm, L. L. *et al.* *Adv. Polym. Sci.* 1972, **9**, 1; Bywater, S. *Adv. Polym. Sci.* 1965, **4**, 66
- 3 Shimomura, T., Smid, J. and Szwarc, M. *J. Am. Chem. Soc.* 1967, **89**, 5743
- 4 Hirohara, H., Takaya, K., Nakayama, M. and Ise, N. *Trans. Faraday Soc.* 1970, **66**, 3163
- 5 Hirohara, H., Takaya, K. and Ise, N. *Macromolecules* 1971, **4**, 288
- 6 Kraus, C. A. and Bray, W. C. *J. Am. Chem. Soc.* 1913, **35**, 1315
- 7 Bhattacharyya, D. N., Lee, C. L., Smid, J. and Szwarc, M. *J. Phys. Chem.* 1965, **69**, 612
- 8 Hirohara, H., Nakayama, M., Takaya, K. and Ise, N. *Trans. Faraday Soc.* 1970, **66**, 1165
- 9 Beylen, M. van, Fisher, M., Smid, J. and Szwarc, M. *Macromolecules* 1969, **2**, 575
- 10 Takahashi, K., Takaki, M. and Asami, R. *J. Phys. Chem.* 1972, **75**, 1062
- 11 Bywater, S. and Worsfold, D. J. *J. Organometall. Chem.* 1971, **33**, 273
- 12 Brownstein, S. and Worsfold, D. J. *Can. J. Chem.* 1972, **50**, 1246
- 13 Ledaal, T. *Tetrahedron Lett.* 1968, **14**, 1683

Low temperature dielectric relaxation in polymers containing an aromatic group in the main chain

S. J. Rigby* and D. Dew-Hughes

Department of Physics, University of Lancaster, Lancaster, LA1 4YB, UK
(Received 1 November 1973; revised 27 March 1974)

Dielectric measurements of samples of polymers containing phenylene rings in the backbone chain have been obtained in the frequency range 62 Hz to 100 kHz and at temperatures between 4.2 K and 330 K. Most of the polymers with a phenylene ring in the main chain exhibit a dielectric relaxation in the temperature range 120 to 185 K (62 Hz). In poly(2,6-dimethyl-*p*-phenylene oxide) a single relaxation region occurs, ranging from 125 K (62 Hz) to 170 K (100 kHz). In poly(phenylene sulphide) a very broad relaxation region occurs over the temperature range ~ 70 K to 190 K. Poly(*p*-xylylene) exhibits a well defined relaxation centred at 185 K (62 Hz) moving to 250 K (100 kHz). In poly(dichloro-*p*-xylylene) the relaxation region is in the same temperature range as for poly(*p*-xylylene), although less sharp; in poly(monochloro-*p*-xylylene) the beginnings of relaxation region are visible at 330 K (62 Hz). In all these polymers the low temperature relaxation region is believed to be caused by a local re-orientation of the phenylene ring, or substituted phenylene ring. The substitution of a single chlorine atom on the phenylene ring causes the relaxation to appear at higher temperatures, whereas the disubstitution causes the relaxation region to re-appear at a similar temperature to that for the unsubstituted polymer. The activation energies of these processes lie in the range 30–45 MJ/kg mol (7–11 kcal/mol). The temperatures and activation energies of this process appear to depend on the units adjacent to the phenylene ring, and on steric and polar effects caused by substituents on the ring.

INTRODUCTION

Linear high polymers frequently exhibit relaxation processes in the region of 180 K^{1–4}. This relaxation is usually referred to as the γ -relaxation process, and ascribed to local twisting or re-orientational motions, in the amorphous phase, of a small number of $-\text{CH}_2-$ sequences^{5–7}. Relaxations at lower temperatures have also been found in polymers with pendant phenyl groups, and are usually attributed to motions of the pendant phenyl side group^{8–10}. The temperature at which this relaxation process, usually termed the δ -relaxation, occurs can be raised by an amount which depends upon the nature of any side substituent on the phenyl group^{8,9}.

Dynamic mechanical^{11,12} and dielectric¹³ relaxations have been found to occur in polymers containing the phenylene group in the main chain. The present work was carried out in order to determine the origin of these relaxations and to obtain their activation energies. The polymers studied were poly(*p*-xylylene) (PPX), poly(monochloro-*p*-xylylene) (PMCPX), poly(dichloro-*p*-xylylene) (PDCPX), poly(2,6-dimethyl-*p*-phenylene oxide) (PDMPO) and poly(phenylene sulphide) (PPS), all being commercial samples unpurified in any way. Their structures are shown in Figure 1.

Chung and Sauer^{11,12} in their mechanical studies of PPX, PDCPX, PMCPX and PDMPO, found relaxa-

tion regions centred around 159 K (0.54 Hz) for PPX, 254 K (0.4 Hz) for PMCPX, 156 K (0.34 Hz) for PDCPX and two peaks, one at 125 K (1.4 Hz) and at 277 K (1325 Hz) for PDMPO. They also studied poly(4,4'-isopropylidene-diphenylene-co-4,4'-sulphonylidiphenylene dioxide) (PSF) and poly(dian carbonate) (PDC), obtaining peaks at 162 K (0.67 Hz) for PSF and 165 K

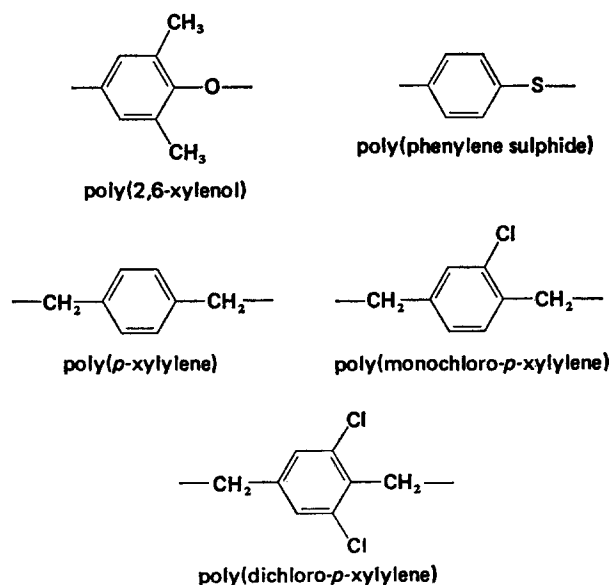


Figure 1 Chemical structure of the polymers studied

* Present address: Department of Electrical Engineering, University of Southampton, Southampton, UK.

(1.24 Hz) for PDC. PDMPO has been studied both mechanically and electrically by workers other than Chung and Sauer. Karasz *et al.*¹³ found two relaxation regions, one centred at 173 K (0.1 kHz) and the other centred at 513 K (0.1 kHz). De Petris *et al.*¹⁴ reported a shoulder at 150 K in their mechanical data (7 kHz). Stoelting *et al.*¹⁵ also found this low temperature relaxation in their mechanical data.

EXPERIMENTAL

Preparation of specimens

The PDMPO was obtained in the form of grey moulding pellets from Engineering Polymers Ltd, Wilmslow, marketed under the trade name of Noryl 731. PPS (Ryton PPS) was obtained from Phillips Petroleum Co., London, in the form of a creamy-grey free flowing powder. All samples of the poly(*p*-xylylenes) were obtained from Union Carbide Corporation in the form of thin films.

Specimens, in the form of 35.8 mm diameter discs, were either cut from sheet [poly(*p*-xylylenes)] or moulded (PDMPO and PPS). The free-flowing PPS powder was first converted to block form by heating to 583K for 2 hours. The resulting brittle chocolate-brown mass was broken into pieces prior to moulding. Sample preparation is summarized in Table 1. Moulded samples had aluminium electrodes evaporated onto their face to ensure good electrical contact; this was not necessary for samples cut from sheet.

Apparatus and method

The dielectric loss tangent, $\tan \delta$, of each specimen was measured by means of a dielectric cell similar in type to that designed by McCammon and Work¹⁶. The only modifications were the addition of heating coils directly on the cell, and the insertion of thermocouples into the two electrodes. The dielectric cell was held in a vacuum-tight can, which was inserted into a single-vacuum jacketed helium cryostat. Loss tangent measurements were made by means of a General Radio 1615-A transformer ratio arm bridge, at frequencies of 62 Hz and then (1.0, 1.6, 2.55, 4.0, 6.2, 10) $\times 10^n$ Hz where $n=2, 3, 4$. Starting at a temperature of 330K the dielectric cell was cooled down to 4.2K in 10K steps, the temperature being held at its required value until thermal equilibrium had been achieved. Measurements were then made over the frequency range of interest, the temperature being held constant by means of a temperature controller. This was attached to one of the thermocouples, whilst the temperature was monitored by the other thermocouple. In this way, loss

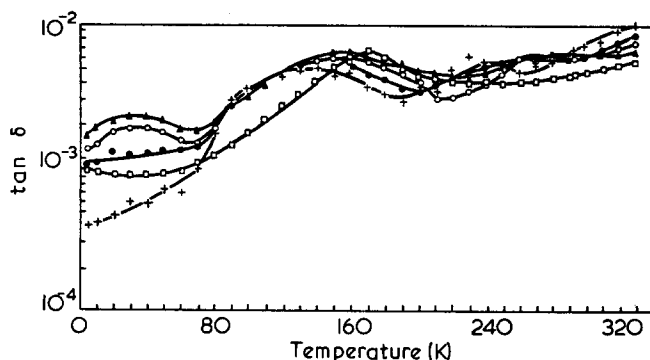


Figure 2 Dielectric loss tangent versus temperature at different frequencies for PDMPO. +, 100Hz; ●, 1kHz; ○, 4kHz; Δ, 10kHz; □, 100kHz

tangent could be measured to an accuracy of better than $\pm 3 \times 10^{-6}$ whilst temperature could be held to ± 0.2 K at worst. A more detailed description of the experimental apparatus and techniques is given elsewhere¹⁷.

RESULTS AND DISCUSSION

Poly(2,6-dimethyl-*p*-phenylene oxide) (PDMPO)

Figure 2 shows the temperature dependence of loss tangent at frequencies from 10^2 to 10^5 Hz. Two distinct relaxation regions are visible; a broad region, termed the γ -relaxation region, in the range 120 to 200K, and a frequency dependent region from 4.2 to 60K. The γ region has been found before in the dielectric studies of Karasz *et al.*¹³, in the dynamic mechanical data of Chung and Sauer¹², de Petris *et al.*^{14, 18} and Heijboer¹⁹. The low temperature region, tentatively termed the δ region appears not to have been observed before. No evidence was seen in agreement with Karasz, of the very broad loss peak, termed the β peak, found by Chung and Sauer and de Petris.

Baccaredda *et al.*¹⁸ have also studied several other poly(*p*-phenylene oxides), including poly(2-monomethyl-*p*-phenylene oxide), the disubstituted polymer and the unsubstituted polymer. All of these exhibit the β -relaxation near 370K and a γ -relaxation shoulder in the region 140 to 170K at 7kHz. Thus it is clear that the methyl groups themselves cannot be the cause of the relaxations, and n.m.r. experiments and calculations confirm this. From comparison of observed second moments with values calculated on the basis of a rigid lattice, and from the gradual reduction in linewidth from 80K to room temperature, Mathes and Rochow²⁰ conclude that both methyls rapidly re-orient at a temperature of 80K.

The γ -relaxation found in this present work can be interpreted, using the results of Chung and Sauer¹² and of Karasz *et al.*¹³, as a result of re-orientations of the phenylene group about colinear C-O bonds. If this is so, it would appear that the steric hindrance is somewhat less for PDMPO, where the oscillations can occur about colinear C-O bonds, than for other polymers studied, such as PPX or PPS, where the colinear bonds are C-C or C-S. Barrales-Rienda and Pepper²¹ calculated the unperturbed dimensions and gyration radius of PDMPO in solution, and showed that the steric factor for the C-O bond is much lower than the usual values found for the simple C-C bond. The continued high level of dielectric loss, as well as the gradual n.m.r. drop, over the temperature range from 160 to 330K,

Table 1 Sample preparation

Sample	Moulding data				Glass temp.* (K)
	Temp. (K)	Pressure (MN/m ²)	Thickness (mm)	Crystallinity (%)	
PDMPO	548	23	0.297 ± 0.029	Amorphous	483
PPS	583	31	0.563 ± 0.007	Amorphous	365
PPX	As received	—	0.020 ± 0.001	50-70	330-340
PMCPX	As received	—	0.022 ± 0.002	50-70	350-370
PDCPX	As received	—	0.062 ± 0.002	50-70	383

* Manufacturer's data

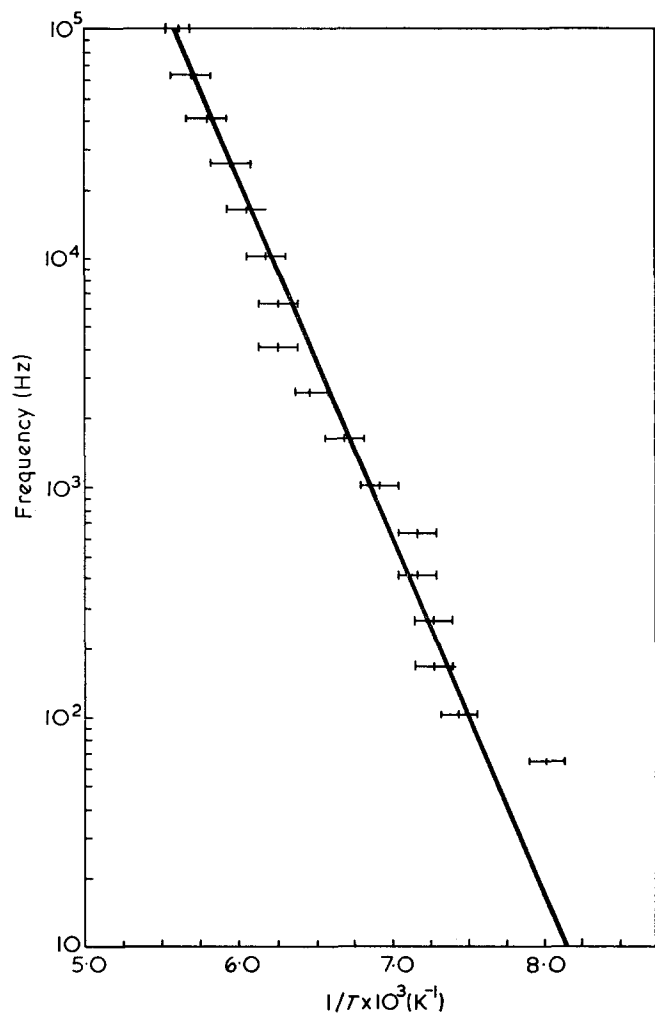


Figure 3 Arrhenius plot of the γ -maximum in PDMPO

may indicate an increasing amplitude of phenyl group oscillation.

The magnitude of the δ -relaxation process is frequency dependent with a maximum at 10 kHz, and remains in the same place with respect to temperature. The effect is similar to that found by Carter *et al.*²² for carbon black loaded rubbers, and could be due to additives in the commercial sample.

Figure 3 shows a plot of log frequency for the loss maximum (γ peak) against the reciprocal of the temperature at which the maximum occurs. The activation energy is 30.05 ± 6.95 MJ/kg mol (7.18 ± 1.66 kcal/mol), which is low when compared to that of Karasz *et al.*¹³ (8.7 kcal/mol) and Chung and Sauer¹² (9.6 kcal/mol). This low result could be attributed to the effect of plasticizer in the sample, acting as a swelling agent and thus reducing the hindrance to motion.

Poly(phenylene sulphide) (PPS)

Figure 4 shows the temperature dependence of loss tangent at frequencies from 62 Hz to 10^5 Hz. Two relaxation regions are visible, a very broad plateau from 80 K to 190 K which gradually resolves into a slight peak at 150 K (10^5 Hz); and a region rising up from about 260 K. There is also slight evidence of a low temperature region as found for PDMPO. Since the glass transition temperature of this polymer is 365 K the marked rise in loss tangent from 260 K is probably the beginning of the α -transition region. The relaxation region from 80 to 190 K is termed the γ -relaxation, and

since it covers approximately the same range as that for both PDMPO and the unsubstituted poly(phenylene oxide)¹⁸ it is assumed to be due to the same relaxation.

If this relaxation is considered to be re-orientation of a phenylene ring around a C-S bond, the magnitude of the relaxation process would be expected to be smaller than that for PDMPO, since: (i) there is a larger steric hindrance for rotation about a C-S bond than a C-O bond (see above); (ii) this sample was moulded at 575 K in air, so crosslinking will have taken place²³.

Calculating the activation energy for this γ -relaxation by estimating the shift in temperature with increase in frequency of the centre of the relaxation gives (from Figure 5) a value of 36.8 ± 8.3 MJ/kg mol (8.76 ± 2.06 kcal/mol). This value compares reasonably favourably with that for PDMPO and the hypothesis of a phenylene group rotation appears reasonable.

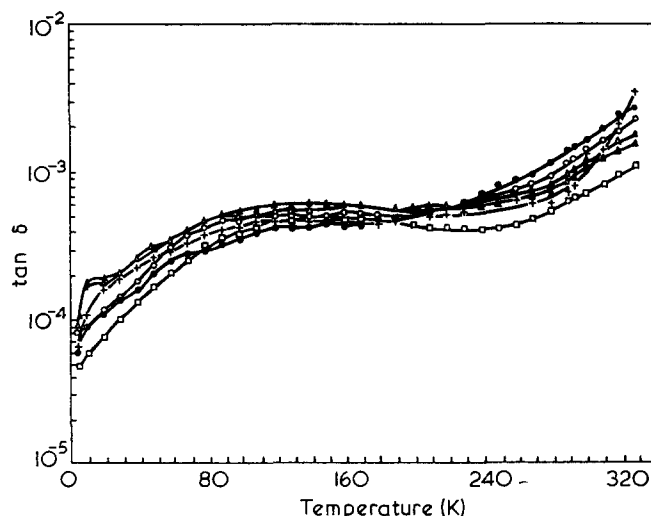


Figure 4 Dielectric loss tangent versus temperature at different frequencies for PPS. +, 62 Hz; O, 255 Hz; O, 1 kHz; Δ, 4 kHz; ▲, 10 kHz; □, 100 kHz

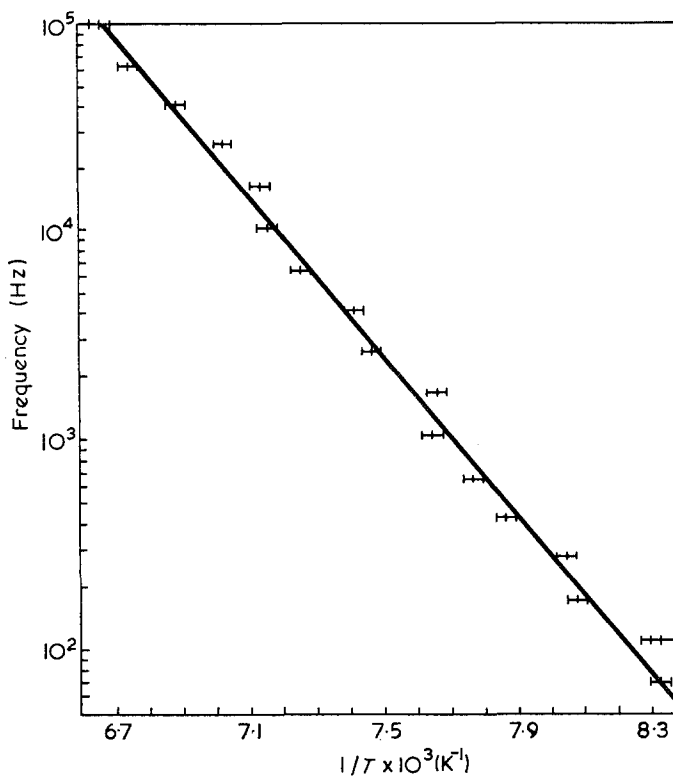


Figure 5 Arrhenius plot of the γ -maximum in PPS

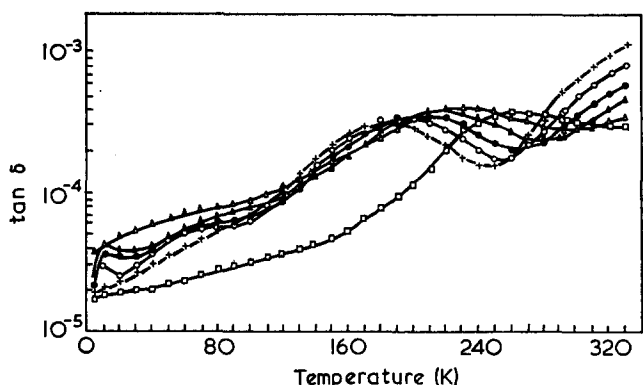


Figure 6 Dielectric loss tangent versus temperature at different frequencies for PPX. +, 62Hz; O, 255Hz; ●, 1kHz; ▲, 4kHz; △, 16kHz; □, 100kHz

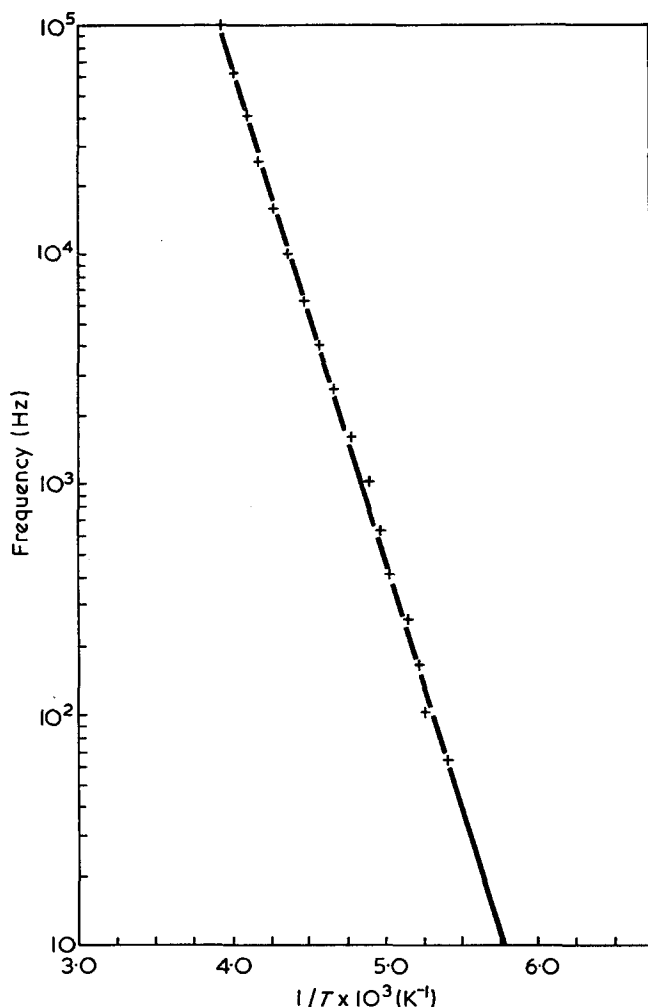


Figure 7 Arrhenius plot of the γ -maximum in PPX

Poly-p-xylylene (PPX)

The temperature dependence of the loss tangent for PPX is shown in Figure 6. There are two relaxation regions visible, the γ -relaxation in the range 140K to 240K (62Hz), which moves to 220 to 320K (10^5 Hz), and a very small loss peak at 10K, which disappears at frequencies above 4.0kHz. The γ -relaxation is better defined in magnitude compared with other samples studied. Chung and Sauer^{11, 12} have reported a γ -relaxation in their mechanical measurements. Their peak was situated at 154 K (0.5 Hz) whilst the maximum in the present work was situated at 185K (62 Hz), which

allowing for the frequency difference can be considered as good agreement.

Chung and Sauer¹² attribute this relaxation region to the local re-orientation of the phenylene ring and not re-orientation of the CH₂ units. The activation energy for this process, expected to be of the same order as that for the similar process in PPS and PDMPO, is from Figure 7 40.8 ± 1.2 MJ/kg mol (9.74 ± 0.30 kcal/mol). This is in reasonable agreement with the previous results, considering the greater steric hindrance for re-orientation around a C-C bond than a C-O bond. This value also suggests that the steric hindrance for C-C rotation is greater than for C-S rotation. No independent confirmation for this is available.

The cause of the low temperature loss peak is very difficult to assign, since the sample was in the form of a thin film which had been polymerized directly from the dimer *in vacuo*²⁴. The only impurities likely to be present are small amounts of unpolymerized dimer which could well give rise to a relaxation in this region.

Poly(monochloro-p-xylylene) (PMCPX)

This polymer with one chlorine atom substituted on the phenylene ring should be highly polar. That this is so can be seen by the fact that the dielectric constant for the PMCPX is the order of 3.3 at 1 kHz and 293K whilst that for PPX is 2.7. This difference is fairly constant throughout the temperature range. The values for dielectric constant are not absolute, but being obtained under the same conditions for each sample should give an indication of the difference involved. The fact that PMCPX is polar explains why the overall value of loss tangent is greater than that for previous samples by a factor of ten.

The plot of loss tangent versus temperature (Figure 8) shows no relaxation region in the range 100 to 200K. There is a very frequency dependent (in magnitude) region below 80K, which is probably due to unpolymerized dimer. The relaxation region associated with the re-orientation of the phenylene ring would now appear to occur at higher temperatures. Careful study of the 62 Hz curve in Figure 8 shows that this curve is levelling off at 330K, implying that this is now the γ -relaxation region. This shift in position of the relaxation process to higher temperatures is in agreement

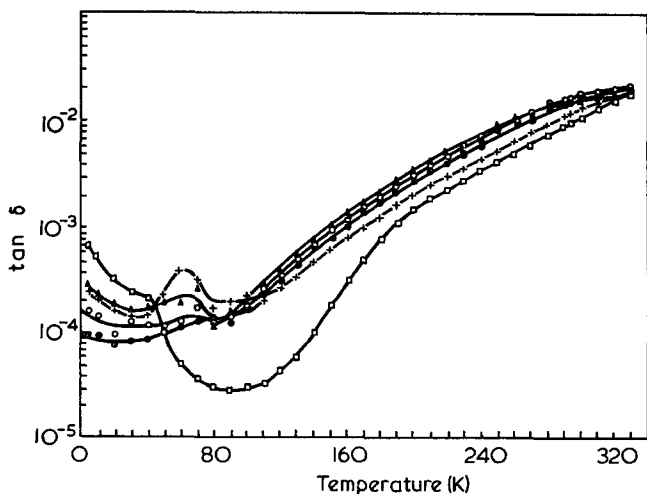


Figure 8 Dielectric loss tangent versus temperature at different frequencies for PMCPX. ▲, 62Hz; O, 255Hz; ●, 1 kHz; +, 16kHz; □, 100kHz

with Chung and Sauer^{11, 12} who found that the γ -relaxation region moved from 159K (0.5 Hz) for PPX to 254K (0.4 Hz) for PMCPX. Using the one result of Chung and Sauer and the point at 330K (62 Hz) in the present work to obtain a tentative value of the activation energy of the γ -relaxation gives $\Delta H = 44.8$ MJ/kg mol (10.7 kcal/mol). This, if correct, is in good agreement with previous values, considering that the chlorine atom on the phenylene ring will further hinder the re-orientation of the phenylene ring.

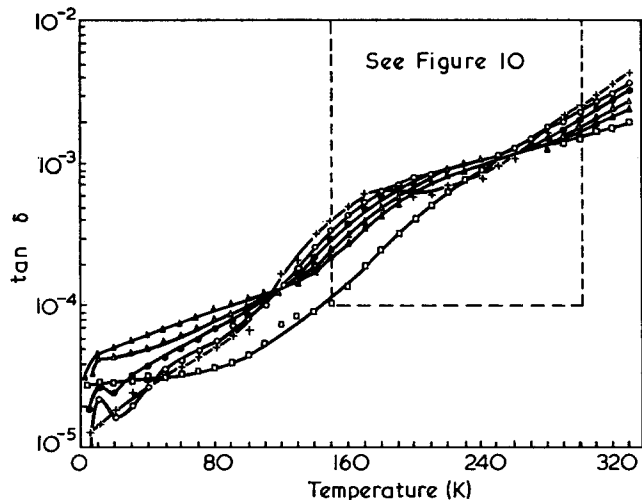


Figure 9 Dielectric loss tangent versus temperature at different frequencies for PDCPX. +, 62 Hz; O, 255 Hz (A); ●, 1 kHz (B); Δ, 6.2 kHz (C); ▲, 16.6 kHz (D); □, 100 kHz (E)

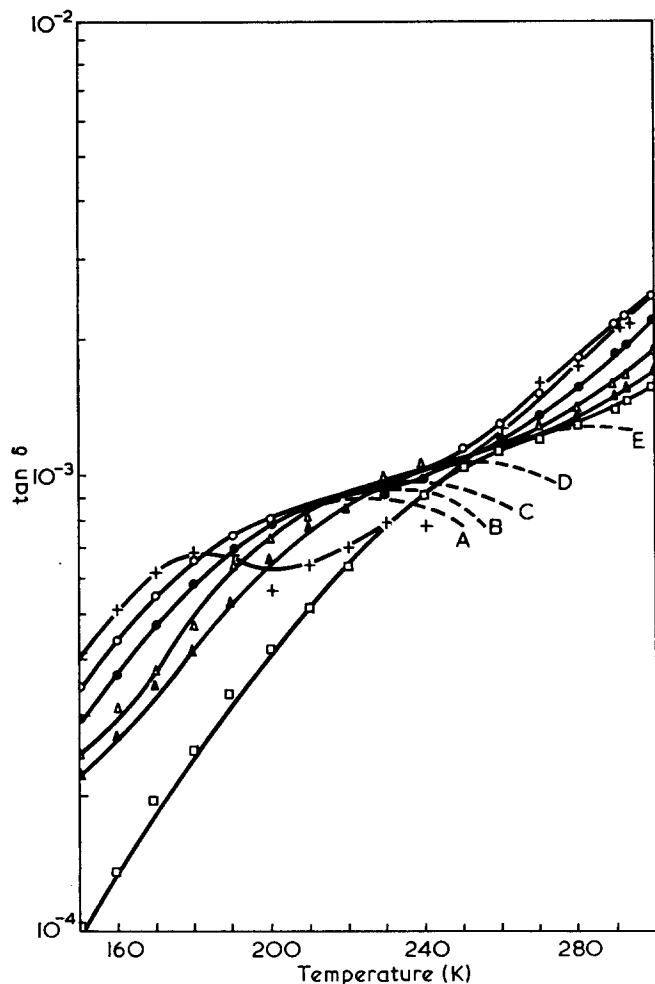


Figure 10 Enlargement of a portion of Figure 9, showing the γ -loss peak extrapolated to higher temperatures. Symbols as in Figure 9

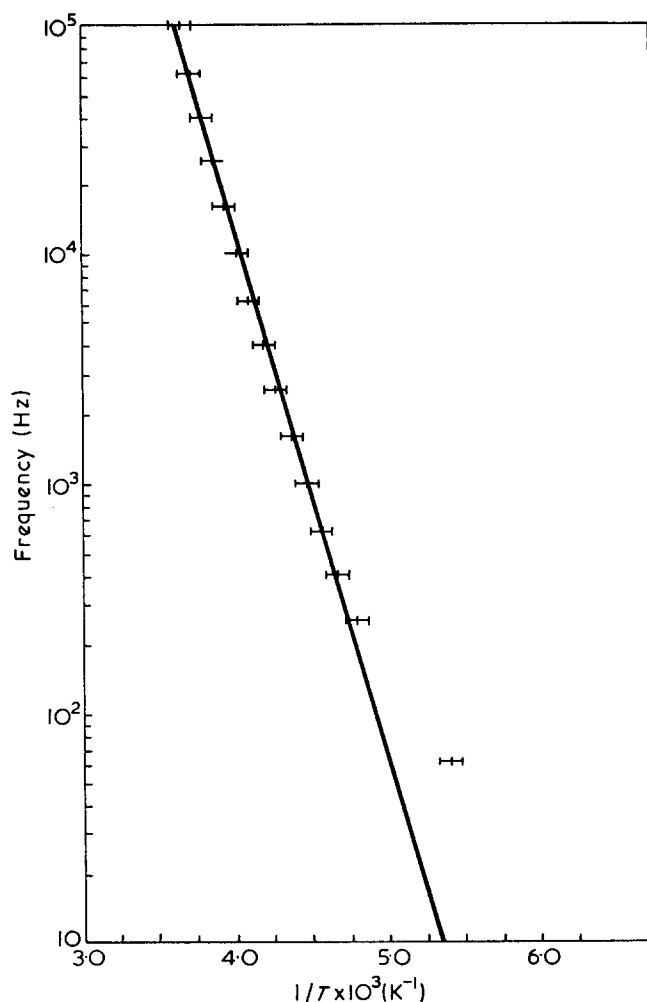


Figure 11 Arrhenius plot of the γ -maximum in PDCPX

Poly(dichloro-p-xylylene) (PDCPX)

The loss tangent versus temperature plot (Figure 9) shows that the γ -relaxation process again occurs in the region of 180K and there is, as previously seen, a small frequency dependent relaxation process taking place at 10K. The γ -relaxation is, however, less well defined than that in PPX (Figure 10). The substitution of chlorine atoms has moved the γ -relaxation process down in temperature, compared with the singly substituted polymer, since PDCPX is less polar than PMCPX. The dielectric constant is reduced to 2.9, as compared to 3.3 for PMCPX. The location of the second chlorine atom on the phenylene group is not precisely known²⁵ and some polarity is expected. This polarity accounts for both the larger loss tangent and dielectric constant of PDCPX compared with PPX. Chung and Sauer¹² show that in order that the phenylene ring should have a small dipole moment (which from Figure 9 appears to be correct), the substitution must be in either the 2,5 or 2,6 positions, the former having the greater dipole moment. However, it has been shown by gas chromatography¹¹ that 85% of the phenylene groups have two chlorine atoms per ring, 10% have three chlorine atoms per two phenylene rings and 5% have five chlorine atoms per two phenylene rings, and these excess chlorine atoms could account for the observed polarity.

The activation energy of this γ -relaxation was calculated from Figure 11 and found to be 43.9 ± 1.7 MJ/kg mol (10.5 ± 0.4 kcal/mol). Again there is good

agreement with the activation energies of the γ -relaxation for the other polyxylylenes.

CONCLUSIONS

The results obtained show that for the polymers studied, even though they do not possess three or more adjacent $-\text{CH}_2-$ groups in the structure, there is a low temperature relaxation region. The common feature of all these polymers is that they contain phenylene groups in the main chain. Comparing the results with previous dielectric¹³ and mechanical^{11,12} studies leads to an interpretation in terms of re-orientation of the phenylene ring, probably coupled with torsional rotational motions of nearby chain units. The location of this relaxation region is a function of the units adjacent to the phenylene ring, as well as the nature of the ring substituents.

The results are outlined in Table 2, from which it appears that when the phenylene ring is adjacent to two oxygen atoms there is less hindrance to motion than when the neighbours are sulphur or carbon atoms, and PDMPO exhibits a relaxation region at lower temperatures than the other polymers studied, in keeping with theoretical considerations²¹. Crosslinking, as in PPS, does not substantially change the position of the relaxation, but decreases the magnitude of the process. The ring motion is affected considerably by a polar substitution on the phenylene ring, as in the case of PMCPX, where the relaxation is moved up in temperature by 150K. If the substitution is symmetric, the relaxation occurs at roughly the same temperature as for the unsubstituted polymers, implying that the motion responsible for the relaxation is the same. A further confirmation of this hypothesis is the fact that all the activation energies for these processes are of the same order of magnitude. Since the only common structural factor in all the polymers studied is the phenylene ring, the implication is that the γ -relaxation is associated with re-orientation of the ring.

If this assumption is correct, then it would be expected that other polymers containing aromatic rings in the main chain should show the same relaxation. Chung and Sauer¹² found in their dynamic mechanical experiments a relaxation region occurring at 162K (0.67 Hz) for Polysulfone and at 165K (1.24 Hz) for poly(dian carbonate), interpreted as re-orientation of the aromatic groups in the main chain. Illers and Breuer's study²⁶ of poly(ethylene terephthalate) showed that the β -relaxation could be composed of three overlapping processes, one of which occurs at 168K. This could be assigned to re-orientation of the phenylene ring, and not, as they postulate, due to the motions of the $-\text{COO}-$ groups associated with the *gauche* conformation of the polymer chain. Also as the number of methylene sequences is

increased in the poly(methylene terephthalates) the loss peak experiences a shift to lower temperatures, which implies less steric hindrance for phenylene ring re-orientation. Bernier and Kline²⁷ have studied polyimide, and in a dried sample found an internal friction peak at 130K (700 Hz), which has been associated with the addition of water^{26, 28}. However, Butta *et al.*²⁹ studied the effect of water on polyimide at a frequency of 15 kHz, and found for a sample dried at 200°C a broad asymmetric low temperature tail in the loss peak. The addition of water caused a new peak to arise at 230K (700 Hz). They draw attention to the similarity between dried polyimide, which has an unsubstituted phenylene ring between a nitrogen atom and an oxygen atom, and PDMPO. Since the phenylene ring in the polyimide is situated between a nitrogen and an oxygen atom it would be expected that the barrier to re-orientation for the phenylene ring should be similar to that for the phenylene ring in PDMPO.

ACKNOWLEDGEMENTS

This work was supported by a research grant from the Science Research Council, which is gratefully acknowledged. One of us (S. J. R.) also acknowledges the award of an SRC Research Studentship.

Thanks are due to the Union Carbide Corporation, USA, for the gift of the poly(*p*-xylylenes), to Engineering Polymers for the PDMPO and Phillips International Petroleum Company for the PPS.

The authors would also like to thank the members of the Materials Science Group of the Physics Department for assistance in sample preparation and to members of the Physics Department who offered expert advice on various aspects of the work.

REFERENCES

- 1 Krum, F. and Müller, F. H. *Kolloid-Z.* 1959, **164**, 8
- 2 Mikhailov, G. P. *et al. J. Tech. Phys. (USSR)* 1957, **27**, 2050
- 3 Ishida, Y. *Kolloid-Z.* 1960, **171**, 149
- 4 Curtis, A. J. *J. Res. Nat. Bur. Stand.* 1961, **65A**, 185
- 5 McCrum, N. G. *et al.* 'Anelastic and Dielectric Effects in Polymeric Solids', Wiley, London, 1967
- 6 Willbourn, A. H. *Trans. Faraday Soc.* 1958, **54**, 717
- 7 Lawson, K. D. *et al. J. Appl. Phys.* 1963, **34**, 2492
- 8 McCammon, R. D. *et al. J. Polym. Sci. (A-2)* 1969, **7**, 1721
- 9 Armeniades, C. D. *et al. J. Appl. Polym. Sci.* 1970, **14**, 2635
- 10 Yano, O. and Wada, Y. *J. Polym. Sci. (A-2)* 1971, **9**, 669
- 11 Chung, C. I. and Sauer, J. A. *Polymer* 1970, **11**, 454
- 12 Chung, C. I. and Sauer, J. A. *J. Polym. Sci. (A-2)* 1971, **9**, 1097
- 13 Karasz, F. E. *et al. J. Appl. Phys.* 1970, **41**, 4357
- 14 Petris, S. de, *et al. Makromol. Chem.* 1967, **109**, 54
- 15 Stoelting, J. *et al. Polym. Eng. Sci.* 1970, **10**, 133
- 16 McCammon, R. D. and Work, R. N. *Rev. Sci. Instrum.* 1965, **36**, 1169
- 17 Rigby, S. J. *PhD Thesis* University of Lancaster (1972)
- 18 Baccaredda, M. *et al. Mat. Sci. Eng.* 1968, **3**, 157
- 19 Heijboer, J. J. *Polym. Sci. (A-1)* 1968, **6**, 3755
- 20 Mathes, R. and Rochow, E. G. *J. Polym. Sci. (A-2)* 1966, **4**, 375
- 21 Barrales-Rienda, J. M. and Pepper, D. C. *J. Polym. Sci. (B)* 1966, **4**, 939
- 22 Carter, W. C. *et al. Trans. Faraday Soc.* 1946, **42A**, 213
- 23 'Ryton Polyphenylene Sulfide Resins', Phillips Petr. Int. Tech. Centre, 1971
- 24 Gorman, W. F. *J. Polym. Sci. (A-1)* 1966, **4**, 3027
- 25 Gorman, W. F. 'Encyclopaedia of Polymer Science and Technology', John Wiley, New York, 1971
- 26 Illers, K. H. and Breuer, H. *J. Colloid Sci.* 1963, **18**, 1
- 27 Bernier, G. A. and Kline, D. E. *J. Appl. Polym. Sci.* 1968, **12**, 593
- 28 Reddish, W. *Trans. Faraday Soc.* 1950, **46**, 459
- 29 Butta, E. *et al. J. Appl. Polym. Sci.* 1969, **13**, 1073

Table 2 Summary of experimental results

Polymer	Temp. of γ -relaxation maximum at 62Hz (K)	ΔH		Dielectric constant at 293K and 1kHz
		MJ/kg mol	kcal/mol	
PDMPO	125	30.05 ± 6.95	7.18 ± 1.66	3.1
PPS	120	36.8 ± 8.3	8.76 ± 2.06	3.0
PPX	185	40.8 ± 1.2	9.74 ± 0.30	2.7
PMCPX	330	44.8	10.7	3.3
PDCPX	185	43.9 ± 1.7	10.5 ± 0.4	2.9

A study of molecular orientation in poly(methyl methacrylate) by means of laser-Raman spectroscopy

J. Purvis* and D. I. Bower

Department of Physics, University of Leeds, Leeds LS2 9JT, UK
(Received 11 February 1974; revised 14 March 1974)

Measurements have been made of the polarization dependence of the intensity of the Raman scattering from uniaxially oriented samples of poly(methyl methacrylate). Lines at wavenumber shifts 486, 562, 604 and 1732 cm^{-1} were studied. With the right-angle scattering geometry used, four combinations of polarization directions of incident and observed scattered light could be chosen and the angle between the draw direction and the direction of the incident laser beam could be varied. The observed intensities were found to fit equations derived in an earlier publication. Five parameters which would determine the scattered intensity for any scattering geometry and combination of polarization vectors were derived. They were shown to contain information about the distribution of orientations of the structural units of the polymer despite the fact that their values also suggest that either the nature of the structural units or the interactions between them are modified by drawing. Values of $\overline{\cos^2\theta}$ and $\overline{\cos^4\theta}$ deduced for the structural units, where θ is the angle between a unique axis in a typical unit and the draw direction, are in good agreement with those obtained by other authors from broadline n.m.r. measurements. For the sample with the highest birefringence, -1.8×10^{-4} , the values of $\overline{\cos^2\theta}$ and $\overline{\cos^4\theta}$ were 0.52 ± 0.03 and 0.43 ± 0.04 respectively.

INTRODUCTION

It has recently been shown¹⁻³ that it should be possible to obtain fairly detailed information about the distribution of orientations of the structural units in an oriented solid polymer from suitable measurements of the intensity of the Raman scattering of polarized light. In this paper the results of some measurements of this kind that have been made on uniaxially oriented specimens of poly(methyl methacrylate) (PMMA) are reported.

PMMA has certain advantages as a material on which to test some of the predictions of the theoretical treatment. It forms a clear glassy solid which produces very little Tyndall scattering, so that polarized light can pass through a considerable thickness of sample without appreciable polarization scrambling, and it can be worked to a reasonable optical finish so that surface scattering and deviation of the incident and Raman-scattered light are small. The birefringence of oriented PMMA is quite low, which enables the predicted effect of the birefringence on the observed intensities to be tested and permits all the potentially available independent data containing information about the distribution of molecular orientations to be obtained in practice. In order to test a fairly simple form of the theory it is convenient to deal with samples of uniaxial symmetry, and for PMMA these can be easily prepared in the form

of quite thick sheets, which simplifies the experimental arrangements for obtaining all the independent intensities and makes it easier to study the effects of birefringence on them. An additional incentive to use PMMA was that suitable drawn samples were available for which information about the distribution of molecular orientations had already been obtained from measurements of broadline nuclear magnetic resonance (n.m.r.) by Kashiwagi *et al.*⁴ A comparison of the results of two independent methods of studying molecular orientation could thus be made.

A disadvantage of PMMA is that the ordinary commercial material, such as that used in preparing these samples, does not have a very well-defined molecular structure⁵. The success of the n.m.r. work, in which certain simple assumptions about the structure were made, suggested that this disadvantage might not outweigh the advantages.

THEORY

Although this paper is concerned with uniaxially oriented samples we shall begin by considering briefly the theory for samples of the more general orthotropic symmetry. Such samples have, statistically, three mutually perpendicular two-fold axes of rotational symmetry and we shall choose a right-handed set of axes $O-x_1x_2x_3$ fixed in the sample so that each axis is parallel to one of the two-fold axes. When the simpler uniaxial symmetry is considered, Ox_3 will be chosen parallel to the unique axis.

* Present address: CEGB Scientific Services Department, Otley Road, Harrogate HG3 1PR, UK.

It will be assumed that the vibrational Raman scattering from the structural units making up the polymer solid is incoherent. Since PMMA is non-crystalline the simplest assumption would be that these structural units are individual chain segments. It was shown earlier¹ that the intensity of Raman scattering for any combination of polarization vectors of the incident and observed scattered light can be expressed in terms of nine quantities, $\Sigma\alpha_{ij}\alpha_{pq}$, where α_{ij} is the ij th component (with respect to $O-x_1x_2x_3$) of the Raman tensor of a typical structural unit. The summation is over all structural units contributing to the observed intensity and $ijpq$ is of the form $ijij$ or $ijij$. Any component α_{ij} can be expressed in terms of the principal components, $\alpha_1, \alpha_2, \alpha_3$, of the Raman tensor and the Euler angles which define the orientation of its principal axes with respect to the axes $O-x_1x_2x_3$. The quantities $\Sigma\alpha_{ij}\alpha_{pq}$ thus contain information about the distribution of orientations of the structural units. For uniaxial symmetry, the number of independent $\Sigma\alpha_{ij}\alpha_{pq}$ is reduced to five.

We choose right-handed sets of axes $O-x'_1x'_2x'_3$ oriented identically within each structural unit, with Ox'_3 parallel to the long axis of the unit. If we assume that the units have no preferred orientation around the Ox'_3 axes and consider a vibration for which the principal axes of the Raman tensor coincide with $O-x'_1x'_2x'_3$, equation (20) of ref 1 shows that for a uniaxial sample:

$$\Sigma\alpha_{ij}\alpha_{pq} = 4\pi^2 N_0 \sum_{l=0,2,4} M_{l00} A_{l00}^{ijpq} \quad (1)$$

In this equation N_0 is the number of structural units contributing to the observed intensity and A_{l00}^{ijpq} is a sum of quadratic terms in $\alpha_1, \alpha_2, \alpha_3$ (see Table I of ref 1). M_{l00} is (apart from a factor $4\pi^2$) a coefficient in the expansion of the distribution function for the structural units in terms of a series of (normalized) Legendre polynomials $P_l(\cos\theta)$, where θ is the angle between Ox_3 and Ox'_3 for a typical structural unit. $M_{000} = 1/(2^{1/2} \cdot 4\pi^2)$ and M_{200} and M_{400} are linearly related to $C_2 = \overline{\cos^2\theta}$ and $C_4 = \overline{\cos^4\theta}$, where the bars denote that the quantities are averaged over the distribution.

As already stated, for uniaxial symmetry, only five $\Sigma\alpha_{ij}\alpha_{pq}$ are independent. If these are determined experimentally (as they can be apart from an unknown scaling factor, I_0) equation (1) represents, after multiplying both sides by I_0 , five independent equations in five unknowns, $M_{200}, M_{400}, (N_0I_0)^{1/2}\alpha_1, (N_0I_0)^{1/2}\alpha_2$ and $(N_0I_0)^{1/2}\alpha_3$, which can thus, in principle, be determined. The equations are linear in M_{200} and M_{400} but quadratic in the tensor components and it is thus not straightforward to solve them and the solution is not unique. Since α_1 and α_2 occur in the quantities A_{l00}^{ijpq} only in the combinations $(\alpha_1^2 + \alpha_2^2), (\alpha_1 + \alpha_2)\alpha_3$ and $\alpha_1\alpha_2$, it is possible to obtain an approximate solution for M_{200} and M_{400} (or C_2 and C_4) for any vibration for which α_1 and α_2 have the same sign and are not too different in magnitude by substituting $\alpha_1 = \alpha_2 (= \alpha_t)$ in equation (1).

The explicit forms of the equations then become:

$$I_0 \Sigma\alpha_{11}^2 = I_0 \Sigma\alpha_{22}^2 = \frac{1}{8} N_0 I_0 [8\alpha_t^2 + 8\alpha_t\alpha_L + 3\alpha_L^2 - (8\alpha_t\alpha_L + 6\alpha_L^2)C_2 + 3\alpha_L^2 C_4] \quad (2a)$$

$$I_0 \Sigma\alpha_{33}^2 = N_0 I_0 [\alpha_t^2 + 2\alpha_t\alpha_L C_2 + \alpha_L^2 C_4] \quad (2b)$$

$$I_0 \Sigma\alpha_{12}^2 = \frac{1}{8} N_0 I_0 \alpha_L^2 [1 - 2C_2 + C_4] \quad (2c)$$

$$I_0 \Sigma\alpha_{23}^2 = I_0 \Sigma\alpha_{13}^2 = \frac{1}{2} N_0 I_0 \alpha_t^2 [C_2 - C_4] \quad (2d)$$

$$I_0 \Sigma\alpha_{22}\alpha_{33} = \frac{1}{2} N_0 I_0 [2\alpha_t^2 + \alpha_t\alpha_L + (\alpha_L^2 + \alpha_t\alpha_L)C_2 - \alpha_L^2 C_4] \quad (2e)$$

$$\Sigma\alpha_{11}\alpha_{22} = \Sigma\alpha_{11}^2 - 2\Sigma\alpha_{12}^2, \quad \Sigma\alpha_{33}\alpha_{11} = \Sigma\alpha_{22}\alpha_{33} \quad (3)$$

where

$$\alpha_L = \alpha_3 - \alpha_t \quad (4)$$

From equations (2a), (2b) and (2e) it follows that:

$$I_0 \Sigma\alpha_{22}^2 - 2I_0 \Sigma\alpha_{22}\alpha_{33} + I_0 \Sigma\alpha_{33}^2 = \frac{1}{8} N_0 I_0 \alpha_L^2 (3 - 14C_2 + 19C_4) \quad (5)$$

and approximate values of C_2 and C_4 may thus be obtained directly by using equations (2c), (2d) and (5). In addition, by using equations (2a) and (2b), suitable approximate values for $(N_0I_0)^{1/2}\alpha_1, (N_0I_0)^{1/2}\alpha_2$ and $(N_0I_0)^{1/2}\alpha_3$ may be obtained for substitution as starting values in an iterative least squares computer program to solve equations (1).

It has been shown¹ that it should be possible to determine the values of the five independent quantities $I_0 \Sigma\alpha_{ij}\alpha_{pq}$ for a material of uniaxial symmetry by arranging that the incident light travels along a diameter of a disc cut so that the unique axis (Ox_3) lies in its plane and determining the intensity of the Raman light scattered along the normal (Ox_1) to that plane as a function of the angle of rotation of the disc about the normal. This arrangement is used in the experiments reported here. We choose axes $O-X_1X_2X_3$ in the laboratory and assume that the disc is placed so that OX_1 and Ox_1 coincide (see Figure 1). Let the incident light travel along OX_3 with polarization vector parallel to OX_1 or OX_2 and let the light scattered along OX_1 be observed using an analyser with polarization vector parallel to OX_3 or OX_2 . Four observed intensities $I_{ij}(\beta)$ can be defined, where i and j refer to the polarization vectors of the scattered and incident radiations, respectively, and Ox_3 makes a variable angle β with OX_3 . These intensities are given by:

$$I_{ij}(\beta) = I_0(I_{ij0} + I_{ij2} \cos 2\beta + I_{ij4} \cos 4\beta) \quad (6)$$

where

$$I_{214} = I_{314} = I_{322} = 0 \quad (7)$$

The five independent non-zero values of I_{ijk} are linear functions of the five independent quantities $\Sigma\alpha_{ij}\alpha_{pq}$ and are given by setting $\Sigma\alpha_{13}^2$ equal to $\Sigma\alpha_{23}^2$ in equations (23) of ref 1. This equality implies that:

$$I_{21}(\pi/2) = I_{32}(0) \quad (8)$$

or

$$I_{210} - I_{212} = I_{320} - I_{224} \quad (9)$$

For a sample of the more general orthotropic symmetry equations (8) and (9) do not hold. The five independent $I_0 \Sigma\alpha_{ij}\alpha_{pq}$ for uniaxial symmetry can be determined by fitting equations (6) to experimental intensity data.

So far the effects of the birefringence of the polymer have been neglected. If these are taken into account I_{220} and I_{324} are modified by the subtraction, and I_{224} and I_{320} by the addition, of a term

$$I_b = \frac{1}{4} (\Sigma\alpha_{22}\alpha_{33} + \Sigma\alpha_{23}^2)(1 - \overline{\cos\eta}) \quad (10)$$

where η is the relative phase shift that occurs between two scattered light waves polarized parallel to Ox_3 or Ox_2 as they travel a distance d parallel to Ox_1 . The average of $\cos\eta$ is to be taken over the volume of the sample illuminated by the incident light. For a material of low birefringence, this average can be made very close to 1 or -1, as explained in the experimental section.

The possible conformations of the molecular chains in PMMA will be discussed in a later section and it is

concluded that helical structures may be present. Bower and Purvis² have shown that for those vibrations of a helix for which it is not possible to resolve the A , E_1 and E_2 modes corresponding to what would be the same mode of vibration of side groups attached to the helix backbone if there were no coupling between the groups, equation (1) holds with a modification to the significance of the quantities A_{100}^{ijpq} . These now become functions of four quantities P , Q , R and S which depend on the components of the Raman tensors for the A , E_1 and E_2 modes.

EXPERIMENTAL

Sample preparation

The material used was a commercial type of isotropic Perspex, originally in sheet form of approximately 3 mm thickness, which was drawn in a tensometer, at a number of temperatures, to a fixed draw ratio. Discs of diameter 1 cm were cut with the draw direction of the material in the plane of the disc. The surfaces of the discs were polished to an optical finish using diamond dust. Each of the specimens was examined under a polarizing microscope for any serious inhomogeneities which might have been produced during its preparation, but none were observed. This examination was repeated after the samples had been exposed to the laser beam. The drawing temperatures and birefringences of the specimens are given in *Table 1*.

Apparatus

The Raman spectra were excited by light of wavelength 488 nm from a CRL model 52A Ar⁺ laser. The power in the laser beam was approximately 1 W continuous. The Raman light collected at right angles to the direction of the incident beam was focused on the entrance slit of a Coderg PHO double monochromator and the light from the exit slit was detected by an EMI S-20 photomultiplier tube. This tube was cooled to -30°C and a magnetic field was applied to it by means of a pancake solenoid in order to improve the signal-to-noise ratio. The signal from the photomultiplier was amplified by a low-noise d.c. amplifier and recorded both on a chart recorder and digitally on paper tape using a Solartron Data Transfer Unit coupled to a Facit tape punch.

The vertically polarized laser beam was first incident upon a beam splitter so that the power of the laser light could be monitored continuously. The beam reflected from the beam-splitter travelled parallel to the optical transfer plate of the spectrometer on which were mounted a half-wave plate, which permitted rotation of the plane of polarization of the incident light through a right angle, and a narrow band-pass dielectric filter which removed unwanted plasma lines from the exciting light. The width of the beam striking the specimen was limited by means of a variable-width slit placed immediately in front of it.

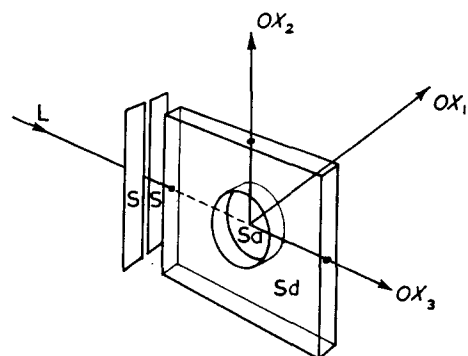


Figure 1 Detail of sample mount. L, laser beam; S, slit jaws; Sa, sample; Sd, Perspex surround. Sample can be rotated around OX_1 and scattered light is collected in this direction. Sample and surround can be moved together parallel to OX_1 , the slit remaining stationary

The specimen disc was attached by one face (using double-sided tape) to a holder which permitted it to be rotated about an axis perpendicular to its faces and which also incorporated a movement parallel to this axis. The specimen was placed so that the exciting beam passed along a diameter of the disc, which was surrounded by a close-fitting fixed rectangle of ordinary PMMA, so that the incident laser light passed through the specimen as a parallel beam (see *Figure 1*). Tests were carried out to ensure that no measurable scattered light was collected from this surround. In order to reduce scatter and deviation of the laser beam the very small gap between the specimen and the surround was filled with water. An analyser and quarter-wave plate were placed between the collecting lens and the spectrometer entrance slit. The purpose of the quarter-wave plate was to reduce the differential sensitivity of the spectrometer to light polarized parallel or perpendicular to the slit length.

Procedure for determining relative intensities

The Raman lines studied were at 486, 562, 604 and 1732 cm^{-1} from the exciting line. The first three of the lines were obtained by scanning the spectrum over a range from 430 to 690 cm^{-1} . The slit width and specimen position were adjusted so that a slice of the sample 0.1 mm thick was illuminated at a depth corresponding to an integral or half-integral wave plate below the surface from which the observed Raman light emerged. This made it possible to correct quite accurately for the effects of the birefringence of the specimen on the observed intensities.

If the incident light illuminates a slice of specimen at depth d below the surface, equations (6) and (10) show that the maximum variation of intensity with d is obtained for $\beta = \pi/4$ and that the intensity should vary as $\cos[2\pi d(n_3 - n_2)/\lambda]$. Whether the intensity for $d=0$ should be a maximum or a minimum depends on the sign of $(\Sigma\alpha_{33}^2 + \Sigma\alpha_{22}\alpha_{33})$ and cannot be predicted. *Figure 2* shows the observed intensity variation in a particular case. It is in reasonable agreement with a cosine variation and clearly indicates a maximum at the surface. Using the measured values of $(n_3 - n_2)$ we can calculate the spatial period of this variation and in *Table 2* the measured and calculated periods are compared for the three specimens for the 604 and 1732 cm^{-1} lines. For these

Table 1 Drawing temperatures and birefringences of samples

Sample	Draw temp. ($^\circ\text{C}$)	Birefringence $(n_3 - n_2) \times 10^4$
MF 5	155	-3.72
AG	130	-8.80
MF 12	115	-14.78

two lines the appropriate values of $\overline{\cos^2\eta}$ could be determined directly. Since the slice of specimen illuminated was very much smaller than the period of the variation of scattered intensity with d , $\overline{\cos^2\eta}$ could be made very close to 1 or -1 , depending on whether the sample was positioned for $d=m\lambda/(n_3-n_2)$ or $d=(m+\frac{1}{2})\lambda/(n_3-n_2)$, where m is an integer. It was not possible to measure the variation of the intensity of the 486 and 562 cm^{-1} lines with d because these lines were relatively weak and the variation was very small. The specimen was therefore

positioned for a maximum in the variation of intensity with d for the 604 cm^{-1} line.

The Raman spectra were recorded for a number of angles, β , between the draw direction (Ox_3) of the sample and the horizontal axis (Ox_3) for the four combinations of incident light polarized parallel to Ox_1 or Ox_2 and analyser polarization direction parallel to Ox_2 or Ox_3 .

The spectra obtained in the region 430–690 cm^{-1} were analysed by a computer program into five overlapping Lorentzians plus a linear background (Figure 3). No corrections for slit function were made, since the slit width corresponded to only about 5 cm^{-1} compared with linewidths of $\sim 25 \text{ cm}^{-1}$ or greater. The line at 1732 cm^{-1} did not appear to overlap any other line, thus making computer fitting unnecessary.

In fitting the spectra of specimen MF12, for which the intensities were measured by hand at intervals of 2 cm^{-1} before the digital equipment was available, a completely free fit was performed to every spectrum taken and the average value of the half-intensity width and centre of each line was subsequently calculated. The spectra were then all refitted with the half-intensity widths and centres fixed at these average values. For the other two specimens, the spectra were recorded digitally on paper tape at intervals of 0.5 cm^{-1} and these data were then treated in a similar manner. In this way good fits were obtained for all the spectra and the intensities of the lines could be specified by the fitted peak heights, since no comparison of the intensities of different lines was to be made. The intensities obtained in this manner were corrected for changes in laser power and for the remaining differential polarization sensitivity of the spectrometer. The maximum values of these corrections were 5% and 18% respectively.

The theoretical treatment assumes that scattered light of only one polarization is observed, whereas this is impossible with a finite collection angle. To check directly the effect of aperture, the semi-angle of the collection cone was reduced by a factor of about $\sqrt{2}$ and the spectra were run again for the specimen MF12. Analysis of the data for the 604 cm^{-1} line for both apertures by the first of the methods discussed in a later

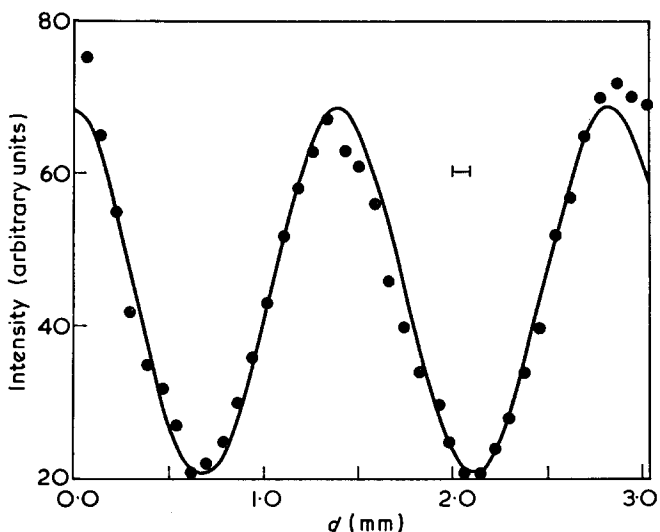


Figure 2 Variation of intensity $I_{22}(\pi/4)$ with distance, d , of incident laser beam below surface from which scattered light emerges. ●, Experimental points; —, cosine curve; I—, slit width. Data for 604 cm^{-1} line of sample MF5

Table 2 Calculated and measured spatial periods

Line (cm^{-1})	MF 5 period (mm)		AG period (mm)		MF 12 period (mm)	
	Meas.	Calc.	Meas.	Calc.	Meas.	Calc.
604	1.40	1.35	0.81	0.57	0.36	0.34
1732	1.50	1.43	0.78	0.61	0.38	0.36

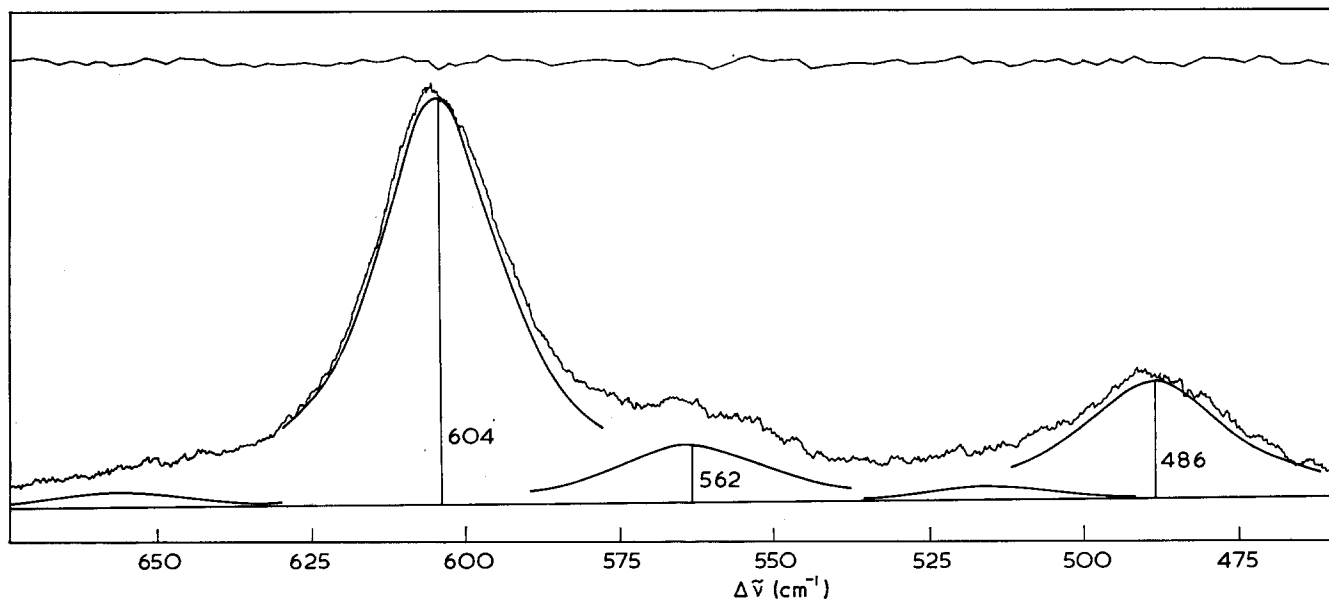


Figure 3 Raman spectrum of sample MF12 in range $\Delta\tilde{\nu}=460\text{--}670 \text{ cm}^{-1}$ showing the five Lorentzian peaks and linear background fitted to it. Upper line shows deviation from sum of Lorentzians and background (with arbitrary zero shift)

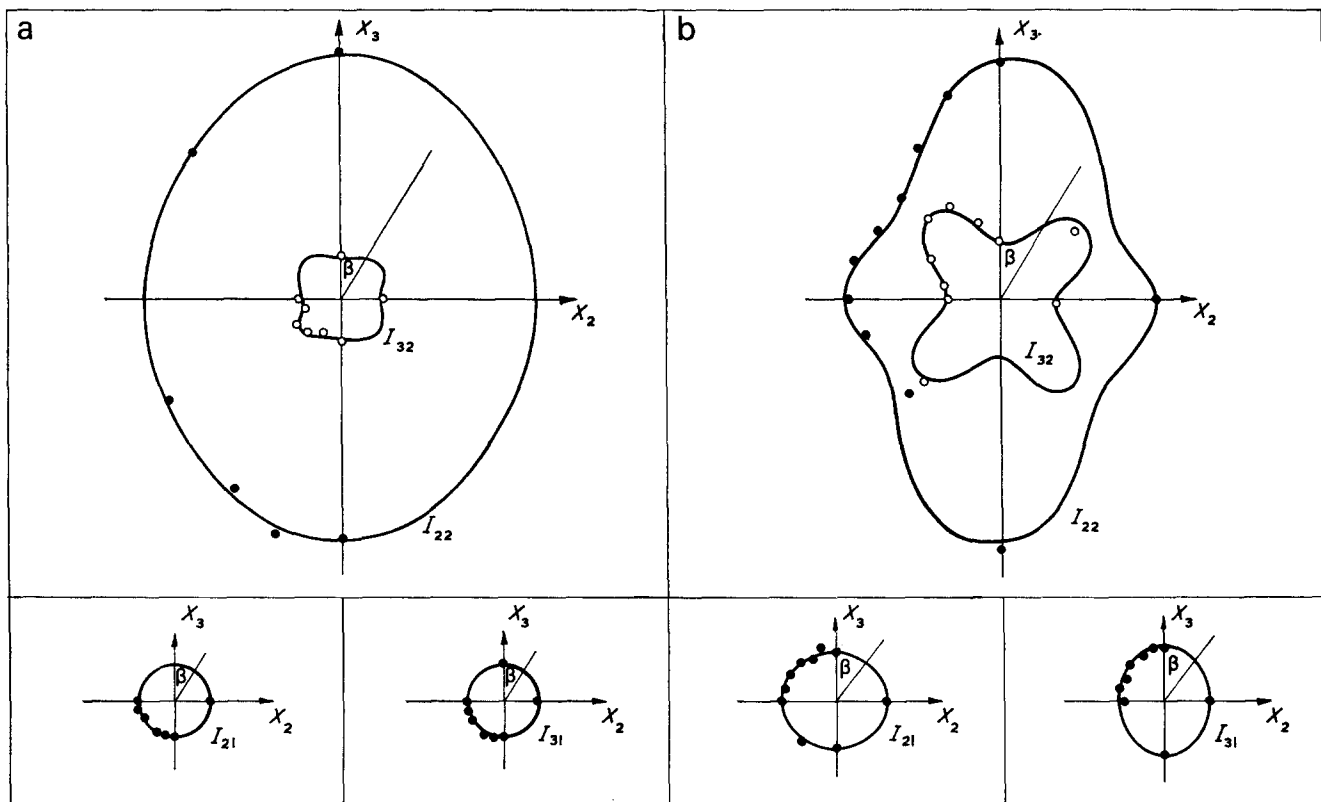


Figure 4 Polar plots of the four intensities $I_{ij}(\beta)$ for the 604 cm^{-1} line. (a) Sample MF5; (b) sample MF12. All intensities to same arbitrary scale within each set of four plots. \circ , \bullet Experimental points; —, least squares fits

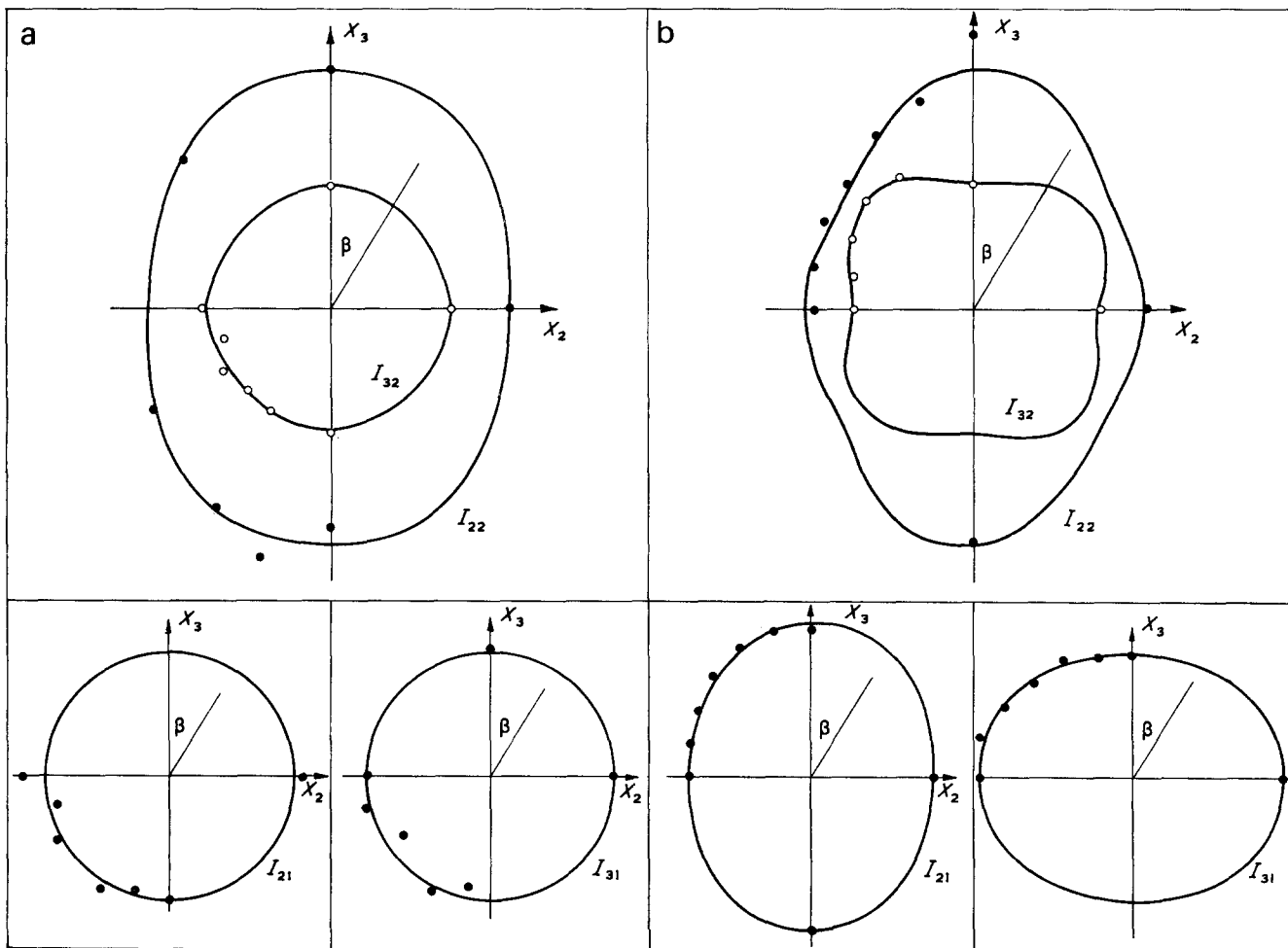


Figure 5 Polar plots of the four intensities $I_{ij}(\beta)$ for the 486 cm^{-1} line. (a) Sample MF5; (b) sample MF12. All intensities to same arbitrary scale within each set of four plots. \circ , \bullet Experimental points; —, least squares fits

section showed no significant difference in the parameters obtained.

The linearity of response of the system to intensity was checked by recording the same spectrum for two different laser powers (differing by a factor of approximately two) and analysing both spectra. The results showed that, within experimental uncertainties, the positions and widths of the lines remained constant and the peak heights scaled by a common factor. The linearity was also checked directly using neutral density filters.

RESULTS AND DISCUSSION

Values of $I_0 \sum \alpha_{ij} \alpha_{pq}$

The corrected intensities yield the values of the quantities $I_0 \sum \alpha_{ij} \alpha_{pq}$ via equations (6) and (10). Figures 4 and 5 show the polar diagrams for the observed intensities $I_{ij}(\beta)$, together with the best fits to equations (6), for the 604 cm⁻¹ and 486 cm⁻¹ lines of specimens MF5 and MF12. For each specimen and line the four diagrams are on the same intensity scale, and although the condition of uniaxial symmetry, equation (9), has not been imposed in the fits it is seen to be well satisfied, i.e. $I_{21}(\pi/2) = I_{32}(0)$. The polar plots also serve to confirm the correction factors applied for the differential polarization sensitivity of the spectrometer, since $I_{21}(\beta)$ is seen to be equal to $I_{31}(\beta + \pi/2)$ within experimental error for all β . The fits were made using a computer program in which a least squares criterion of fit was imposed and values of the five independent $I_0 \sum \alpha_{ij} \alpha_{pq}$ were obtained from them. An extra parameter, β_0 , was included in the fits to allow for experimental error in determining the orientation of the specimen corresponding to $\beta = 0$.

There are two independent invariants of second order in the α_{ij} which are usually chosen as the squares of the spherical part of the Raman tensor, $\bar{\alpha}$, and the anisotropy, β , defined by⁶:

$$9\bar{\alpha}^2 = (\alpha_{11} + \alpha_{22} + \alpha_{33})^2 = (\alpha_1 + \alpha_2 + \alpha_3)^2 \tag{11}$$

$$2\beta^2 = (\alpha_{11} - \alpha_{22})^2 + (\alpha_{22} - \alpha_{33})^2 + (\alpha_{33} - \alpha_{11})^2 + 6(\alpha_{12}^2 + \alpha_{23}^2 + \alpha_{31}^2) = (\alpha_1 - \alpha_2)^2 + (\alpha_2 - \alpha_3)^2 + (\alpha_3 - \alpha_1)^2 \tag{12}$$

Summing over the N_0 structural units contributing to the observed intensity and taking account of the restrictions of uniaxial symmetry we obtain:

$$9N_0\bar{\alpha}^2 = 4\sum\alpha_{22}^2 + \sum\alpha_{33}^2 - 4\sum\alpha^2 + 4\sum\alpha_{22}\alpha_{33} \tag{13}$$

$$N_0\beta^2 = \sum\alpha_{22}^2 + \sum\alpha_{33}^2 + 5\sum\alpha_{12}^2 + 6\sum\alpha_{31}^2 - 2\sum\alpha_{22}\alpha_{33} \tag{14}$$

Since only values of $I_0 \sum \alpha_{ij} \alpha_{pq}$ are available and N_0 and I_0 are unknown it is not possible to evaluate $\bar{\alpha}^2$ or β^2 directly. It is, however, possible to evaluate the ratio $\beta^2/\bar{\alpha}^2$ and to check whether this is the same, for a given Raman line, for the three specimens. The values obtained, together with those for an isotropic sample, are shown in Table 3, which also shows the values of the more familiar depolarization ratio, ρ_i , given by⁷:

$$\rho_i = \frac{3\beta^2}{45\bar{\alpha}^2 + 4\beta^2} \tag{15}$$

For each line, except that at 562 cm⁻¹ for which the scatter in the data is large, the anisotropy of the Raman

Table 3 Tensor invariants and depolarization ratios

Line (cm ⁻¹)		Sample			
		ISO	MF5	AG	MF12
486	$\beta^2/\bar{\alpha}^2$	6.7	32	131	157
	ρ_i	0.48	0.55	0.69	0.70
562	$\beta^2/\bar{\alpha}^2$	1.6	5.5	18.9	8.6
	ρ_i	0.13	0.25	0.47	0.33
604	$\beta^2/\bar{\alpha}^2$	1.7	3.6	5.2	10.1
	ρ_i	0.13	0.18	0.24	0.35
1732	$\beta^2/\bar{\alpha}^2$	1.7	6.3	27.5	30.4
	ρ_i	0.14	0.27	0.53	0.55

Table 4 Values of $(\sum \alpha_{ij} \alpha_{pq}) / (N_0 \bar{\alpha}^2)$

Line (cm ⁻¹)	$\alpha_{ij} \alpha_{pq}$	ISO	MF5	AG	MF12
486	α_{22}^2	1.3	4.0	15.7	17.6
	α_{33}^2		3.1	12.3	12.6
	α_{23}^2	0.6	2.1	8.1	9.4
	α_{12}^2		2.1	8.2	11.5
	$\alpha_{22}\alpha_{33}$	(0.1) ^a	-0.4	-8.3	-6.9
562	α_{22}^2	1.06	1.64	3.51	2.24
	α_{33}^2		1.01	2.95	1.78
	α_{23}^2	0.14	0.38	2.09	0.53
	α_{12}^2		0.29	0.86	0.36
	$\alpha_{22}\alpha_{33}$	(0.78)	0.68	-1.12	-0.73
604	α_{22}^2	1.07	1.45	1.83	2.51
	α_{33}^2		1.18	1.37	1.63
	α_{23}^2	0.15	0.23	0.31	0.55
	α_{12}^2		0.21	0.22	0.48
	$\alpha_{22}\alpha_{33}$	(0.77)	0.72	0.29	-0.18
1732	α_{22}^2	1.07	1.84	4.21	5.74
	α_{33}^2		1.65	3.67	4.96
	α_{23}^2	0.15	0.29	1.59	0.87
	α_{12}^2		0.32	1.55	1.41
	$\alpha_{22}\alpha_{33}$	(0.77)	0.28	-1.37	-3.34

^a Values in parentheses obtained by using equation (16c)

tensors appears to increase with increasing birefringence of the specimen.

Table 4 shows the values of $(\sum \alpha_{ij} \alpha_{pq}) / (N_0 \bar{\alpha}^2)$ for each line and each specimen and those for the 604 cm⁻¹ and 1732 cm⁻¹ lines are plotted against the birefringence in Figures 6 and 7. The straight lines in these Figures have been drawn mainly as a guide to the eye in following the trends in the values, although for constant Raman tensors approximately straight lines might be expected in the low orientation region. The lines have been drawn so that the values extrapolated to zero birefringence are consistent with random orientation of the structural units. For random orientation the following equations apply:

$$\sum \alpha_{11}^2 = \sum \alpha_{22}^2 = \sum \alpha_{33}^2 = \sum \alpha_{ii}^2 \tag{16a}$$

$$\sum \alpha_{12}^2 = \sum \alpha_{23}^2 = \sum \alpha_{31}^2 = \sum \alpha_{ij}^2 \quad (i \neq j) \tag{16b}$$

$$\sum \alpha_{ii} \alpha_{jj} = \sum \alpha_{ii}^2 - 2 \sum \alpha_{ij}^2 \tag{16c}$$

Values obtained from a randomly oriented specimen of PMMA are also shown in the Figures. The less precise data for the 486 and 562 cm⁻¹ lines show much greater scatter but follow similar general trends. The data deviate systematically from agreement with equations (16) as the birefringence increases, and this shows that despite the changes in the tensors from one specimen to another, some information about the orientation of the structural units is certainly preserved.

Before attempting to obtain the orientation parameters M_{200} and M_{400} , or C_2 and C_4 , for the structural units

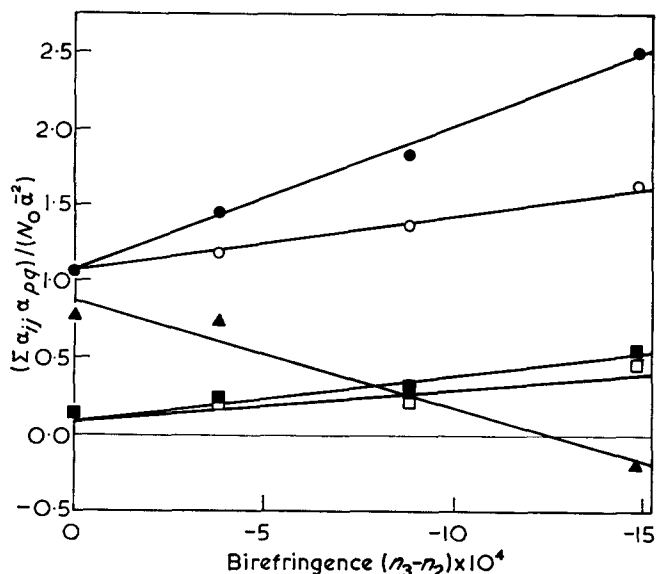


Figure 6 $(\sum \alpha_{ij} \alpha_{pq}) / (N_0 \alpha^2)$ for 604 cm^{-1} line plotted against birefringence, $(n_3 - n_2)$. $ijpq$: ●, 2222; ○, 3333; ■, 3232; □, 1212; ▲, 2233

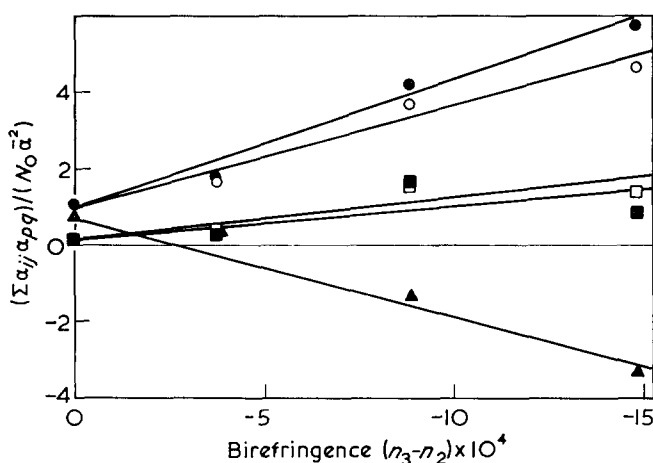


Figure 7 $(\sum \alpha_{ij} \alpha_{pq}) / (N_0 \alpha^2)$ for 1732 cm^{-1} line plotted against birefringence, $(n_3 - n_2)$. $ijpq$: ●, 2222; ○, 3333; ■, 3232; □, 1212; ▲, 2233

it is necessary to ask whether the assumptions leading to equation (1) are likely to be satisfied. The assumption of uniaxial symmetry has been confirmed both by measurements of refractive index and by the Raman scattering results. The validity of the assumptions that the structural units have no preferred orientation around the Ox'_3 axes and that the principal axes of the Raman tensor coincide with $O-x'_1x'_2x'_3$, depends on the nature of the structural units and on the mode of vibration involved.

Nature of structural units

We shall for the moment assume that the structural units are individual molecular chain segments. The validity of the remaining assumptions will then depend on the configurations and conformations of these chain segments and on the assignments of the Raman lines.

A 5_1 helix conformation has been assigned to the pure crystalline isotactic species⁸⁻¹⁰ and Kashiwagi *et al.*⁴ used this structure in their interpretation of the broadband n.m.r. spectra of the ordinary amorphous material. This material is, however, predominantly syndiotactic¹¹ and a planar zig-zag conformation has been suggested^{12, 13}

for the syndiotactic species. Some form of helix cannot, however, be ruled out, particularly in view of the apparently successful application of a helix model in the n.m.r. study. Because of the uncertainty about the conformation or conformations of the molecules, we shall consider both helical and planar zig-zag structures. We shall further assume that in either conformation the ester group is planar and that in the planar zig-zag molecule the plane of the ester group is normal to the chain axis, while in any possible helical structure the normal to the plane of the ester group makes a fairly small angle with the helix axis. These assumptions about the ester group have been shown to be reasonable by other authors^{8, 10, 12}.

If the molecules are helical the assumption of no preferred orientation around the Ox'_3 axes is not required, but no attempt will be made to justify the assumption for the planar zig-zag conformation. The assumption that the observed scattering from any molecular segment for the lines studied may be regarded as essentially due to a single Raman tensor with one axis parallel to Ox'_3 will now be considered. An attempt will also be made to predict whether α_1 and α_2 are likely to be of the same sign and similar magnitude so that the applicability of equations (2) can be assessed.

Vibrational assignments and theoretical Raman tensors

Willis *et al.*¹⁴ have attempted a complete assignment of the Raman spectrum of predominantly syndiotactic PMMA. They assigned lines at 487 , 604 and 1732 cm^{-1} to vibrations of the $-C_a-(C_b=O_a)-O_b-$ part of the ester group, and they consider, following Hummel⁵, that this group of atoms vibrates essentially as if it had C_{2v} symmetry. The three lines are then assigned, respectively, to the vibrations ν_6 , ν_1 and ν_2 in Herzberg's notation⁶ for the XYZ_2 molecule. The nearest line which they observed to that observed in the present work at 562 cm^{-1} was at 537 cm^{-1} and it was assigned to a $\delta(C-C-C)$ skeletal mode. Manley and Martin¹³ have assigned a line at 552 cm^{-1} to a B_1 species of skeletal vibration, considering the factor group of the chain to be isomorphous with the point group C_{2v} . Since the line at 562 cm^{-1} overlaps the much stronger line at 604 cm^{-1} , and since the 562 cm^{-1} line is quite broad ($\sim 45 \text{ cm}^{-1}$), a difference of 10 cm^{-1} in reported position is not improbable, particularly as other authors have not attempted curve fitting.

In considering the modes of vibration of the syndiotactic molecule it is necessary to note that there are two ester groups per repeat unit. Havriliak and Roman¹² consider that the splitting of the ester lines in the region $1100-1300 \text{ cm}^{-1}$ is primarily due to the in-phase and out-of-phase vibrations of the two ester groups. No such splitting seems to be observed for the lines under consideration here. This may be either because the splitting is too small to be resolved or because one component is inactive or of very low intensity. Havriliak and Roman considered as a source of secondary splitting of the lines the two possible orientations of the ester group obtained by rotation through 180° about the C_a-C_b bond. It will be assumed here that these two orientations occur randomly and that the effective Raman tensor for the group may be obtained by averaging the tensors for the two orientations. The assumption of approximate C_{2v} symmetry for the important part of the ester group will be extended to assuming that the Raman tensors for the C_a-C_b and C_b-O_b bonds are not very different.

In the following paragraphs, as already implied, we shall make use of the assumption of the additivity of Raman tensors for individual bonds^{15,16}, although the discussion is intended to be only semi-quantitative. Each line will be considered in turn, and in considering the forms of the Raman tensors use will be made of a set of axes $O-xyz$ defined with Ox parallel to $C_b=O_a$ and Oz perpendicular to the plane of the ester group.

604 cm^{-1} line. The vibration ν_1 is essentially the symmetric stretch of the C_a-C_b and C_b-O_b bonds. It follows from the assumption of similar Raman tensors for these symmetrically stretching bonds that unless the ratio of the transverse to longitudinal component of the Raman tensor for the bond is of order -1 the averaging over the two orientations around the C_a-C_b bonds leads to a tensor for which the principal components perpendicular to Oz are of the same sign and of similar magnitude. For the planar zig-zag molecular conformation the Oz axis is parallel to the chain axis. It follows that the mode of vibration of the repeat unit in which the two ester groups vibrate out of phase will give rise to much lower intensity of Raman scattering than the mode in which they vibrate in phase, and that the in-phase mode will have a tensor which is approximately axially symmetric about the chain axis ($\alpha_1 \simeq \alpha_2$). For helical molecules, the argument would be similar if the Oz axis were parallel to the axis of the helix, and provided that the angle between them is small enough the assumption of a single Raman tensor with axial symmetry about the helix axis should be a reasonable first approximation.

1732 cm^{-1} line. The vibration ν_2 is essentially the $C_b=O_a$ stretching vibration. If we assume that the Raman tensor for this vibration has principal components $\alpha_x, \alpha_y, \alpha_z$, with α_x and α_y of the same sign, similar conclusions can be drawn to those for the 604 cm^{-1} line. If, however, α_x and α_y are of opposite sign, serious deviations from the simple axially symmetric tensor model could occur.

486 cm^{-1} line. The ν_6 vibration for C_{2v} symmetry is an out-of-plane bending vibration and would have α_{zx} ($=\alpha_{xz}$) non-zero and all other components zero. Averaging over the two orientations around the C_a-C_b bond gives a new tensor of similar form, but with the reference axes rotated around Oz so that the new Ox axis lies parallel to C_a-C_b . The in-phase and out-of-phase combinations for the syndiotactic planar zig-zag are then also of the same form, with axes again rotated about Oz so that in one case the new Ox axis is parallel, and in the other perpendicular, to the plane of the zig-zag. It is possible to show from results in ref 2 that superposition of lines due to two such tensors would give:

$$\begin{aligned} & \Sigma\alpha_{22}^2: \Sigma\alpha_{33}^2: \Sigma\alpha_{12}^2: \Sigma\alpha_{22}\alpha_{33}: \Sigma\alpha_{23}^2 \\ & = (1+2C_2-3C_4): 8(C_2-C_4): (1-C_4): \\ & \quad -4(C_2-C_4): (1-3C_2+4C_4) \quad (17) \end{aligned}$$

These ratios are quite different from those given by equations (2). If helical molecules are considered, there seems to be no reason to expect that the approximation of a single tensor with axial symmetry about the helix axis would be a good one.

It should be noted that any combination of tensors of the type appropriate to the pure ν_6 vibration for C_{2v}

symmetry would have $\bar{\alpha}=0$. The experimental ratios $\beta^2/\bar{\alpha}^2$ for this line are quite high (see Table 3) and the observations are thus consistent with the assignment to this extent at least.

562 cm^{-1} line. The B_1 species skeletal vibration would have a tensor with principal components $\alpha, -\alpha, 0$. The principal axes corresponding to the first two components would be normal to the chain axis. The observed ratios $\beta^2/\bar{\alpha}^2$ are rather low for this line and do not support the assignment very convincingly.

Orientation parameters and experimental Raman tensors

The above discussions are only expected to give, at best, some indication of the possible forms of the Raman scattering tensors. They do, however, suggest that the scattering for the 604 cm^{-1} line, and possibly that for the 1732 cm^{-1} line, might be reasonably well described in terms of an axially symmetric tensor model, which is one of the forms of tensor for which unambiguous values of C_2 and C_4 can be determined directly. The 486 and 562 cm^{-1} lines would not be expected to give good fits to this model, if their assignments are correct. It was found in practice that for each specimen the data for the 604, 1732 and 562 cm^{-1} lines gave similar values for C_2 and C_4 when analysed using equations (2), whereas, the data for the 486 cm^{-1} line gave quite different values and the fit was poorer. The data for this line did not fit equation (17).

In the absence of any definite assumptions about the Raman tensors, the most general model for which a fit can be made using data from only one line and one specimen is that to which equations (1) apply, a general tensor with one principal axis parallel to the Ox'_3 axis of the structural unit. Values of $C_2, C_4, I_0N_0\alpha_x^2$, and α_t/α_L obtained from the axially symmetric tensor model were used to provide starting values for an iterative least squares computer program to solve equations (1) for the 604, 1732 and 562 cm^{-1} lines. The unknowns were taken to be C_2, C_4 and the principal Raman components $\alpha_1, \alpha_2, \alpha_3$ [or strictly, $(I_0N_0)^{1/2}\alpha_1, (I_0N_0)^{1/2}\alpha_2, (I_0N_0)^{1/2}\alpha_3$]. The starting values of C_2 and C_4 for a similar fit to the data for the 486 cm^{-1} line were chosen as those obtained for the 604 cm^{-1} line, while the initial values of $(I_0N_0)^{1/2}\alpha_1, (I_0N_0)^{1/2}\alpha_2, (I_0N_0)^{1/2}\alpha_3$ were somewhat arbitrarily set at values suggested by the attempted fit to the axially symmetric tensor model. The results of these fits are shown in Table 5 and the values of C_2 and C_4 are plotted in Figure 8. The values obtained confirm the good fit of the data for the 604 cm^{-1} line to the axially symmetric

Table 5 General tensor model

Sample	Line (cm^{-1})	α_1/α_3	α_2/α_3	C_2	C_4
MF5	486	-3.6	0.3	0.40	0.25
	562	-5.9	-2.8	0.44	0.27
	604	-6.2	-6.2	0.40	0.27
	1732	-3.4	-3.1	0.41	0.32
AG	486	-3.0	0.7	0.43	0.32
	562	-2.4	-1.3	0.47	0.37
	604	-3.0	-3.0	0.46	0.37
	1732	-1.5	-0.9	0.43	0.32
MF12	486	-2.5	0.4	0.53	0.39
	562	-2.0	-2.0	0.46	0.37
	604	-2.0	-1.7	0.52	0.41
	1732	-1.5	-0.9	0.57	0.50

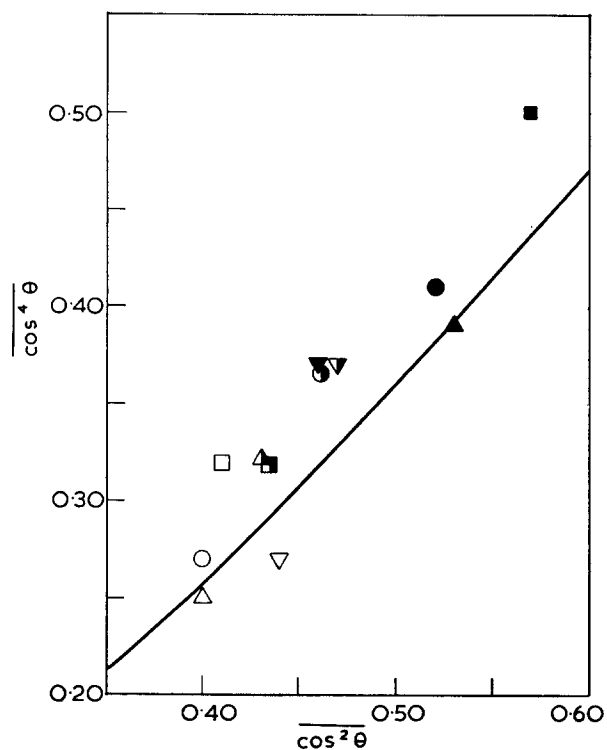


Figure 8 $\overline{C_2}$ plotted against $\overline{C_4}$ for general tensor model. Δ , 486 cm^{-1} line; ∇ , 562 cm^{-1} line; \circ , 604 cm^{-1} line; \square , 1732 cm^{-1} line. Open symbols, sample MF5; half-filled symbols, sample AG; filled symbols, sample MF12; —, pseudo-affine deformation scheme

Raman tensor model and the somewhat less good fit of the data for the 562 and 1732 cm^{-1} lines to that model. The 486 cm^{-1} line is seen to yield values of C_2 and C_4 which are reasonably consistent with those obtained from the other lines but α_1 and α_2 are always of opposite sign.

As has already been pointed out, a good fit to the axially symmetric model for some lines may simply be an indication that the molecule is helical. It is not possible, however, to fit the helix model to data for a single line and a single specimen, since this model requires an extra parameter to describe the tensor components and thus has one more unknown than there are independent equations. We therefore made the arbitrary assumption that $R=S$ in the equations for the helix model. If R and S are small this may be a reasonable approximation, since they are necessarily both positive². The results obtained using the helix model are shown in Table 6 and the values of C_2 and C_4 are plotted in Figure 9. For the 562, 604 and 1732 cm^{-1} lines the values of R/Q are small compared with P/Q , as expected from the reasonable fit of these lines to the axially symmetric tensor model. The values of R/Q for the 486 cm^{-1} line are not small. The values of C_2 and C_4 for this line are in poor agreement with those for the other lines and in one case an impossible value is obtained for C_4 . These results suggest that the approximation $R=S$ is not reasonable for the 486 cm^{-1} line and that the values of C_2 and C_4 obtained using the helix model should therefore be rejected.

There is good grouping of the remaining values of C_2 and C_4 derived from the data for different lines for the same specimen, and there is little difference between the closeness of the grouping for the two models. It is thus not possible to decide, on the basis of the present

results alone, whether the molecular conformation is helical or not. In Table 7 the average values of C_2 and C_4 obtained from the two methods of interpretation are compared with the values obtained by broadline n.m.r.⁴.

Figures 8 and 9 show, in addition to the experimental values of C_2 and C_4 , the relationship between them predicted by the pseudo-affine aggregate deformation scheme¹⁷. The experimental values lie reasonably close to the line and thus correspond to distributions of orientations that are reasonable on physical grounds. The results are, however, not sufficiently accurate to permit the conclusion that the orientation process is really of the aggregate, rigid-rod-rotation type, since the theoretical curve for the affine rubber deformation model¹⁸ is shifted from the pseudo-affine curve by less than the scatter in the experimental values. It should be possible to discriminate between the two models by making measurements on a series of samples drawn to different draw ratios at the same temperature, since the theoretical curves for C_2 and C_4 as functions of draw ratio are quite different for the two models.

Table 6 Helix model

Sample	Line (cm^{-1})	P/Q	R/Q	C_2	C_4
MF5	486	-1.6	0.9	0.43	0.27
	562	-2.1	0.0	0.44	0.30
	604	-6.3	0.0	0.40	0.27
	1732	-3.3	0.0	0.41	0.33
AG	486	-1.0	0.7	0.70	0.65
	562	-1.5	0.0	0.48	0.37
	604	-3.0	0.0	0.46	0.37
	1732	-1.3	0.5	0.48	0.40
MF12	486	-1.3	1.8	0.74	8.29
	562	-2.0	0.0	0.46	0.37
	604	-1.9	0.1	0.52	0.41
	1732	-1.2	0.1	0.56	0.50

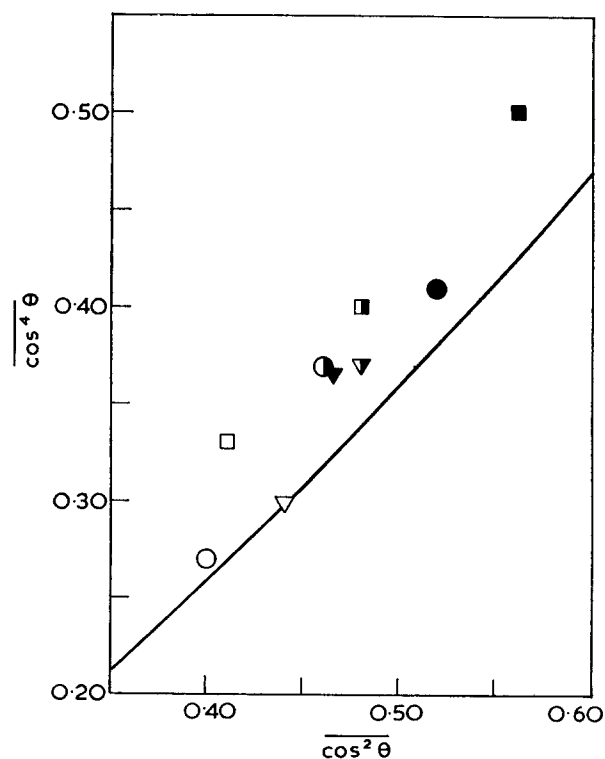


Figure 9 $\overline{C_2}$ plotted against $\overline{C_4}$ for helix model. ∇ , 562 cm^{-1} line; \circ , 604 cm^{-1} line; \square , 1732 cm^{-1} line. Open symbols, sample MF5; half-filled symbols, sample AG; filled symbols, sample MF12; —, pseudo-affine deformation scheme

Table 7 Comparison of orientation parameters with those obtained by means of broadline n.m.r.⁴

Sample	Raman				N.m.r.	
	General tensor		Helix ^a		C ₂	C ₄
	C ₂	C ₄	C ₂	C ₄		
MF5	0.41 ±0.01	0.29 ±0.03	0.42 ±0.02	0.30 ±0.02	0.37 ^b	0.22 ^b
AG	0.45 ±0.02	0.35 ±0.03	0.47 ±0.01	0.38 ±0.01	0.49 ^c	0.33 ^c
MF12	0.52 ±0.03	0.42 ±0.04	0.52 ±0.04	0.43 ±0.05	0.55 ^d	0.39 ^d

a Excluding data for 486 cm⁻¹ line

b No n.m.r. data available for this specimen. Those given are for a specimen prepared in a similar manner which had birefringence $n_3 - n_2 = 3.5 \times 10^{-4}$

c Values from ref 4

d Unpublished values obtained by the authors of ref 4

CONCLUSIONS

The results of the present experiments on uniaxially oriented specimens of PMMA show that, for the scattering geometry used, the dependence of the intensity of the polarized Raman scattering on the angle between the unique axis of the specimen and the direction of the incident laser beam is adequately described, for the four possible combinations of polarization directions of the incident and scattered radiations, by equations (6) with the appropriate restrictions on the coefficients I_{ijk} . Provided that the effects of the birefringence of the samples are correctly allowed for, the coefficients I_{ijk} can be interpreted in terms of five quantities $I_0 \Sigma \alpha_{ij} \alpha_{pq}$ which could be used to predict the intensity of the Raman scattering for other geometries.

The quantities $I_0 \Sigma \alpha_{ij} \alpha_{pq}$ are expected to contain information about the distribution of orientations of the structural units and they can be combined to provide values of $I_0 N_0 \bar{\alpha}^2$ and $I_0 N_0 \beta^2$, where $\bar{\alpha}$ and β are certain tensor invariants. The values of $(\Sigma \alpha_{ij} \alpha_{pq}) / (N_0 \bar{\alpha}^2)$ can thus be calculated and they are found to change systematically with the degree of orientation of the samples (as indicated by the birefringence), showing that they do contain information about the degree of orientation. The values of $\beta^2 / \bar{\alpha}^2$ also change with the degree of orientation, however, and this indicates either that the nature of the structural units changes on drawing or that there are significant interactions between them which affect the values of their Raman tensors and which depend on their degree of orientation.

If it is assumed that whatever the nature of the structural units, or of the interactions between them, the Raman tensor for each of the modes of vibration studied has one principal axis parallel to a unique axis of the unit which is preferentially oriented parallel to the draw direction, values of $\overline{\cos^2 \theta}$ and $\overline{\cos^4 \theta}$ can be deduced, where θ is the angle between the unique axis and the draw direction. Values of $\overline{\cos^2 \theta}$ and $\overline{\cos^4 \theta}$ can also be derived using the more specialized assumption that the structural units are helices. The results obtained using either model are in quite good agreement with those deduced from measurements of broadline n.m.r. using a helix model for the structural unit. The good agreement is somewhat surprising for, as already pointed out, it is not certain that the molecules are helical and it is possible

that the n.m.r. data would give different values of $\overline{\cos^2 \theta}$ and $\overline{\cos^4 \theta}$ for a different model, even if this were only another helix different from the isotactic one assumed. Re-analysis of the n.m.r. data for a different model is thus desirable.

In order to progress further with the understanding of the Raman scattering from oriented PMMA it will be necessary to make measurements on a variety of samples oriented by means of different procedures. For instance, a study of samples having the same birefringence but produced by orienting at different temperatures might help to establish the origin of the changes taking place in the Raman tensors. Results obtained on another polymer, poly(ethylene terephthalate), by Purvis *et al.*³ suggest that the Raman tensors for the modes of vibration studied do not change with the degree of orientation of the sample. The vibrations studied for this polymer were not expected to be sensitive to the precise conformation of the molecules and it is thus possible that the changes of the Raman tensors observed for PMMA may be due to conformational changes. Orienting at different temperatures may produce samples with a different distribution of conformers for a given birefringence. Studies on other polymers are also desirable so that a general understanding can be obtained of the conditions under which the Raman tensors can be regarded as at least approximately independent of the degree of orientation of the structural units.

ACKNOWLEDGEMENTS

The drawn PMMA samples were prepared by the Department of Polymer and Fibre Science, UMIST and were made available to us by courtesy of Professor L. R. G. Treloar and Professor I. M. Ward. We should like to thank Professor Ward for his interest and suggestions during the progress of the work. One of us (J.P.) is indebted to the Science Research Council for the award of a maintenance grant.

REFERENCES

- 1 Bower, D. I. *J. Polym. Sci. (Polym. Phys.)* 1972, **10**, 2135
- 2 Bower, D. I. and Purvis, J. to be published
- 3 Purvis, J., Bower, D. I. and Ward, I. M. *Polymer* 1973, **14**, 398 and work to be published
- 4 Kashiwagi, M., Folkes, M. J. and Ward, I. M. *Polymer* 1971, **12**, 697
- 5 Hummel, D. O. 'Infrared Spectra of Polymers' (*Polym. Rev.* 14) Interscience, New York, 1966, pp 52 and 41
- 6 Herzberg, G. 'Molecular Spectra and Molecular Structure', Vol. II, van Nostrand-Reinhold, New York, 1945, pp 247 and 65
- 7 Wilson, E. B., Decius, J. C. and Cross, P. C. 'Molecular Vibrations', McGraw-Hill, New York, 1955, p 47
- 8 D'Alagni, M., De Santis, P., Liquori, A. M. and Savino, M. *J. Polym. Sci. (B)* 1964, **2**, 925
- 9 Liquori, A. M., Anzuino, G., Coiro, V. M., D'Alagni, M., de Santis, P. and Savino, M. *Nature* 1965, **206**, 358
- 10 Tadokoro, H., Chatani, Y., Kusanagi, H. and Yokoyama, M. *Rep. Prog. Polym. Phys. Japan* 1969, **12**, 173
- 11 Bovey, F. A. and Tiers, G. V. D. *J. Polym. Sci.* 1960, **44**, 173
- 12 Havriliak, S. and Roman, N. *Polymer* 1966, **7**, 387
- 13 Manley, T. R. and Martin, C. G. *Polymer* 1971, **12**, 524
- 14 Willis, H. A., Zichy, V. I. J. and Hendra, P. J. *Polymer* 1969, **10**, 737
- 15 Wokenstein, M. *C.R. Acad. Sci. URSS* 1941, **32**, 185
- 16 Chantry, G. W. in 'The Raman Effect', Vol. 1 (Ed. A. Anderson) Marcel Dekker, New York, 1971, p 74
- 17 Ward, I. M. 'Mechanical Properties of Solid Polymers', Wiley, London, 1971, p 258
- 18 Roe, R.-J. and Krigbaum, W. R. *J. Appl. Phys.* 1964, **35**, 2215

Time lag in mechanical and optical response of polymers

P. S. Theocaris

Department of Theoretical and Applied Mechanics, The National Technical University, Athens (147), Greece

(Received 15 October 1973; revised 12 February 1974)

The time dependent transient values of the stress, strain and dielectric susceptibility tensors were measured in a circular disc made of a rheo-optically simple material and subjected to two equal pairs of diametric loads oriented at right angles. The loading programme was suddenly transferred from a rheologic equilibrium of the four-load situation to a transition state with only one pair of diametric loads. In this way the isotropic point (stress, strain or birefringent), existing at the centre of the disc for the four equal-load configuration, split into a pair of isotropic points moving along a diameter of the disc and tending to its circular boundary. The velocities of isotropic points along the diameter of the disc with time allowed the study of the phase lag between the stress, strain, and optical principal axes. The material chosen for the experiments was a strongly plasticized epoxy polymer. The study extended along the whole viscoelastic spectrum of the material. Important results were revealed for the mechanical and optical viscoelastic behaviour of rheo-optically simple materials.

INTRODUCTION

High polymers at their transition region do not have, in general, an instantaneous coincidence of their stress, strain and dielectric susceptibility tensors, when subjected to any type of loading and displacement, as it is the case with purely elastic materials.

At the glassy and rubbery regions of the viscoelastic spectrum the mechanical and optical behaviour of polymers is quasi-elastic with an immediate response between applied stresses and created strains and birefringence. At the transition region, however, this response is not instantaneous, and there is a time lag between the mechanical and optical viscoelastic response of the polymer.

The optical properties of high polymers used in photoelasticity have been the subject of correlated studies with their mechanical properties. The stress-optical and the strain-optical coefficient functions, which relate the birefringence with the applied stress and strain on the specimen, proved to be monotonically varying with time, temperature or frequency for crosslinked polymers. It has been shown that the principle of reduced variables was also valid for the optical viscoelastic properties of a substance, provided that this principle is valid for its mechanical properties¹⁻⁴. Furthermore, it has been proved experimentally that approximately the same time factors are valid for optical and mechanical properties, and the WLF equation for optical characteristic properties is similar to the corresponding equation for mechanical properties of the high polymer. Williams and Arenz⁵ and Dill^{6,7}, among others, have given expressions in integral form, interrelating birefringence or better the dielectric susceptibility with time-varying stresses and strains.

All these studies are based on the main assumption that the relation between stress and birefringence (i.e. the stress-optic law) is of the same form as the stress-strain law for the material. This is not precisely true, especially at the transition region. The most extensive study for the proof of the non-coincidence of the stress, strain, and dielectric susceptibility tensors was made by van Geen⁸, who showed that the stress, strain, and birefringence isotropic points in a two-dimensional viscoelastic stress field are in general non-coincident and only under certain and specified conditions may coincide. In spite of the relatively large number of papers dealing with this phenomenon, van Geen did not consider any quantitative evaluation of these discrepancies between the appropriate tensors and he restricted his studies to the proof of the various aspects of this non-coincidence.

In this paper an extensive experimental study was undertaken to measure the non-coincidence of the stress, strain, and dielectric susceptibility tensors in a plane stress specimen made of a typical high polymer, where the orientation of the molecular chains determines both the mechanical behaviour and the dielectric susceptibility of the material.

THEORETICAL CONSIDERATIONS

For an elastic material submitted to any type of loading conditions the principal stress directions, the principal strain directions and the principal directions of the refractive index or the dielectric susceptibility are always aligned. Therefore the isoclinics observed in photoelasticity, which are the loci of points for which the principal stress directions are parallel, are indiscriminately defining stress isoclinics, strain isoclinics and birefring-

ence isoclinics. However, for a viscoelastic birefringent material we must distinguish between stress isoclinics, strain isoclinics and birefringence isoclinics, since the three tensors defining stress, strain and birefringence are not always coincident, when pronounced viscoelastic behaviour is apparent.

In order to investigate the eventual coincidence of the three types of isoclinics in a typical viscoelastic material, a specimen geometry and load configuration were selected which yield an exact theoretical solution for the instantaneous principal stress and principal strain directions. The specimen was a thin circular disc, which was loaded equally by concentrated forces, applied along two orthogonally oriented diameters of the disc. While the side (horizontal) loads were applied permanently, the vertical loads could be applied or removed rapidly. Under conditions of viscoelastic equilibrium the birefringence isoclinics almost coincided with the stress and strain isoclinics derived from the corresponding elastic solution.

The material used for the specimens was a cold-setting epoxy polymer (Shell Epon 628), plasticized by adding 60% by weight of Thiokol LP3 polysulphide plasticizer. The mixture was hardened by adding 8% TET hardener in a glass mould, after it has been thoroughly mixed and properly degassed. The cast plate was cured and annealed, so that the polymer was stable and without any residual fringes during the period of the experiments.

It has been shown¹⁻⁴ that epoxy polymers (pure or plasticized) behave admirably as linear viscoelastic substances up to a certain limit of loading (different for each region of the viscoelastic spectrum) obeying Boltzmann's superposition principle and the principle of reduced variables. Furthermore, the WLF equation is applicable in the transition region of these polymers and the same molecular mechanism determines the mechanical and optical properties of the material, so that composite curves expressing mechanical and optical characteristic functions are similar⁴. Therefore, this type of material is ideal for the study of the eventual non-coincidence of stress, strain and dielectric susceptibility tensors at the transition region, because if this non-coincidence exists for this rheologically simple material, the same behaviour may be expected for any other viscoelastic substance presenting a more complicated rheologic behaviour.

Since addition of plasticizer in the epoxy polymer merely shifts the composite curves of the material towards lower temperature levels, while it does not appreciably alter its characteristic viscoelastic properties⁹, the plasticized epoxy polymer was selected because it presents a rubbery plateau at a temperature of 80°C and a glassy state at -10°C which are convenient temperatures. The material selected presents compliances and moduli at the glassy and rubbery states which are essentially constant.

For the study of the relative position of the three types of isoclinics in the transition region, where the principal directions of stresses, strains and birefringence change rapidly and drastically, we make use of the fact that, when the four-load configuration abruptly changes to a two-load configuration, the isoclinic pattern changes from Figure 1a to Figure 1b. These two patterns correspond to two-load and four-load isoclinic ensembles for the corresponding elastic case. The same appearance of isoclinics is valid for the glassy and rubbery states of

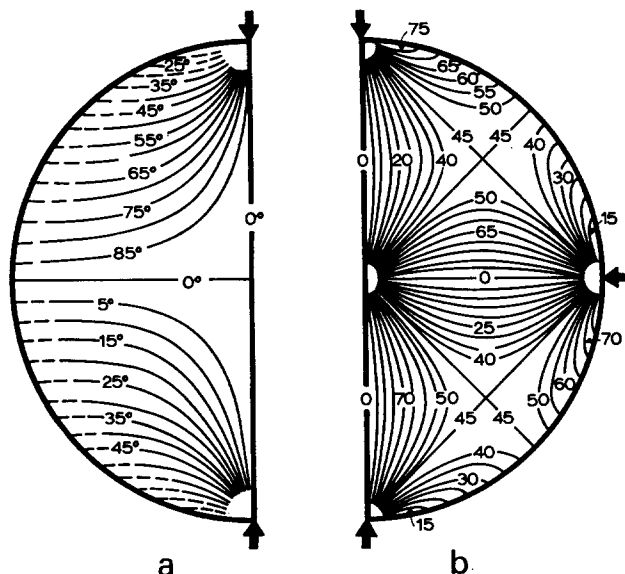


Figure 1 Isoclinics for a disc subjected either to (a) a diametral compression or (b) four equal-load compression

the material, where in a very short period of time the one configuration changes to the other, as the one pair of loads is suddenly removed or applied after some time interval had elapsed from the first application of the four-load pattern (for the removal) or the two-load pattern (for the application of additional loads).

The testing programme for the unloading test adopted in our experiments consisted of a sudden application of the four compressive and equal loads $\pm P_x$ and $\pm P_y$ along the coordinate axes O_x and O_y of the circular disc ($P_x = P_y$) at time $t = 0$ and under isothermal conditions. The loads were kept constant (creep test) until $t = t_c$, where t_c corresponded to the equilibrium time for the temperature of the test. At time $t = t_c$ the vertical pair of loads $\pm P_y$ was relieved and the disc was left to recover for another interval from $t = t_c$ until $t = (t_c + t_e)$, where $t_e = 16'$. The first time interval from $t = 0$ until $t = t_c$ is called the *creep interval*, and the second time interval from $t = t_c$ until $t = (t_c + t_e)$ the *recovery interval*.

The circular disc subjected to compressive loads P_x and P_y along two perpendicular diameters is convenient to create a variable two-dimensional stress field at the centre of the disc, which depends on the ratio $k = P_y/P_x$ of the externally applied loads. The creation of isotropic points (singularities) at the interior of the stress field, which are movable, depending on the ratio k , is most convenient for the detailed and accurate study of the eventual coincidence of the principal axes of stresses, strains and birefringence. The corresponding isotropic points define the points where the stress, strain, and dielectric susceptibility tensors are spherical, that is where $\sigma_1 = \sigma_2$, $\epsilon_1 = \epsilon_2$ and $n_1 = n_2$.

For the case when the two pairs of loads are equal ($k = 1$) it is well known that a single isotropic point S_0 appears at the centre of the disc. If $P_y < P_x$, a pair of isotropic points S_1 and S_2 appears along the y -axis symmetrically placed to the centre O of the disc. Quantity δ^* , which expresses the distance δ between S_1 and S_2 normalized to the diameter D of the disc, is expressed by the simple relation⁸:

$$\delta^* = \left[\frac{1 - k^{1/2}}{1 + k^{1/2}} \right]^{1/2} \quad (1)$$

Figure 2 presents the variation of the distance δ^* between the singularities S_1 and S_2 , as the ratio k varies between zero and unity.

In order to find the position of the strain-isotropic points along the y -axis for $P_x = P_y$ and their relative position to the corresponding birefringence isotropic points, which are defined experimentally from the photoelastic test in creep and subsequent recovery of the disc, it is necessary to equate the two components of strain at each time instant. Since the applied loads to the disc are step functions with time and the polymer is linear, it is possible to apply the correspondence principle and derive the viscoelastic solution from the respective elastic solution by introducing, instead of a constant modulus and Poisson's ratio, the corresponding creep compliance in extension and the lateral contraction ratio function at each time. In this case it can be shown that¹⁰:

$$\frac{P_x}{P_y} \left[\frac{1 - \delta^{*2}}{1 + \delta^{*2}} \right]^2 = \left[1 - \frac{D_c(t - t_c)}{D_c(t)} \cdot \frac{[1 + \nu_c(t - t_c)]}{[1 + \nu_c(t)]} \right] \quad (2)$$

In the case when the two loads are equal ($P_x = P_y$) and the LCR function does not change drastically, that is when $\nu_c(t) \approx \nu_c(t_c - t)$, relation (2) becomes:

$$\left[\frac{1 - \delta^{*2}}{1 + \delta^{*2}} \right]^2 = \left[1 - \frac{D_c(t - t_c)}{D_c(t)} \right] \quad (3)$$

Solving relations (2) or (3) with respect to δ^* , we define the distances δ^* along the y -axis in both sides of the origin O , where the isotropic points are lying for each time interval during recovery. These are compared with the corresponding birefringence-isotropic points found experimentally by photoelasticity. Figure 3 presents typical photoelastic patterns for a disc made of cold-setting plasticized epoxy resin C-100-60-8 at temperatures $T = 70^\circ, 50^\circ, 20^\circ$, and 0°C , where the times t_c were

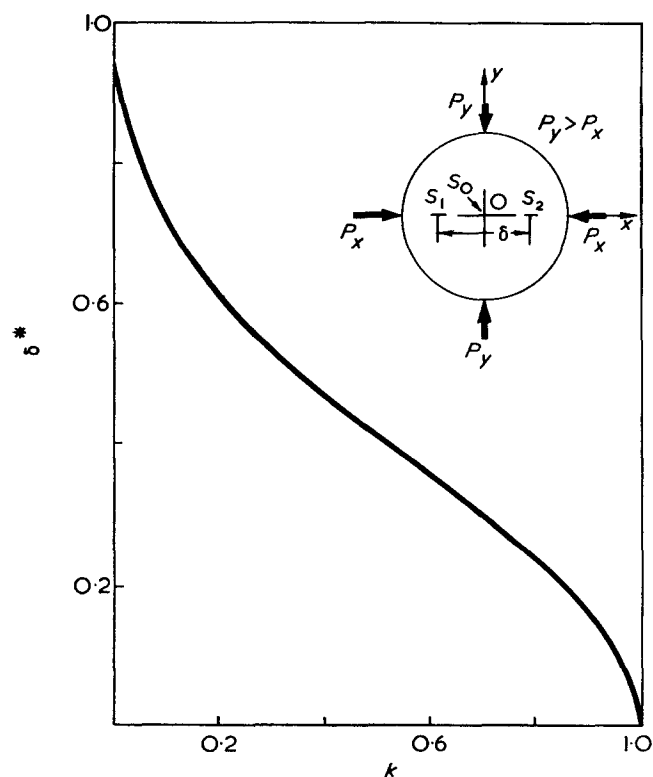


Figure 2 Variation of distance δ^* between isotropic points normalized to the diameter of the disc versus the ratio k of the applied compressive loads P_x and P_y

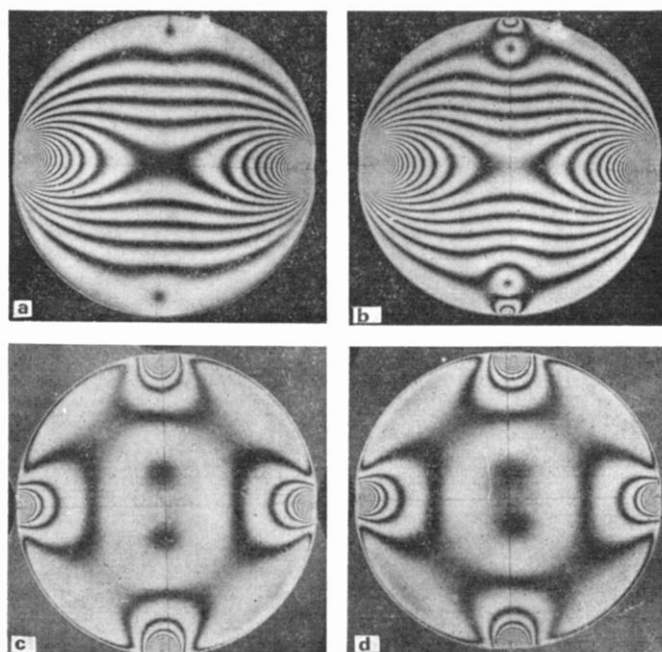


Figure 3 Typical isochromatic patterns for a disc made of a plasticized epoxy polymer, subjected to a four-equal load configuration until viscoelastic equilibrium is reached and then submitted to a recovery period by releasing the one pair of loads. The patterns correspond to recovery times: (a) 30 min; (b) 16 min; (c) 4 min; (d) 4 min; and the corresponding temperatures of the tests: (a) 70° ; (b) 50° ; (c) 20° ; (d) 0°C

taken equal to the equilibrium times of the material at the corresponding temperatures and $(t - t_c) = 30, 16, 4$ and 4 min respectively.

For the stress-isotropic points, the components of stresses expressed by relations which are independent of the viscoelastic functions $D(t)$ and $\nu_c(t)$, there is an abrupt transposition of the stress-isotropic points from the centre of the disc to the circular boundary at time $t = t_c$. Therefore, the principal directions of the stress tensor for $t > t_c$ do not coincide with the principal directions of the two other tensors at the transition region.

VISCOELASTIC CHARACTERIZATION OF THE MATERIAL

For the study of the relative lag between characteristic functions of mechanical and optical viscoelastic behaviour of the high polymer tested it is necessary to define the creep compliance function of the material along the whole viscoelastic spectrum. This function is sufficient for the determination of the strain-isotropic points in the disc, as it can be derived from relation (3). For this purpose tensile specimens were cut from a plate of the material 2 mm thick. These specimens have a standard 'dogbone' shape, convenient for viscoelastic tests, of a width of $w = 12.10$ mm and a length $l = 48.00$ mm along the reduced section, which was considered as uniformly loaded. The test equipment used in the experiments has been previously described³. Measurements of the longitudinal component of strain, as well as of the applied constant stress, were taken at equal intervals in a logarithmic scale from 0.25 min up to 16 min for each isothermal test. The creep tests were carried out at various steps of temperature from the glassy up to the rubbery state of material, in order to obtain the extension creep compliance composite curve along the whole viscoelastic

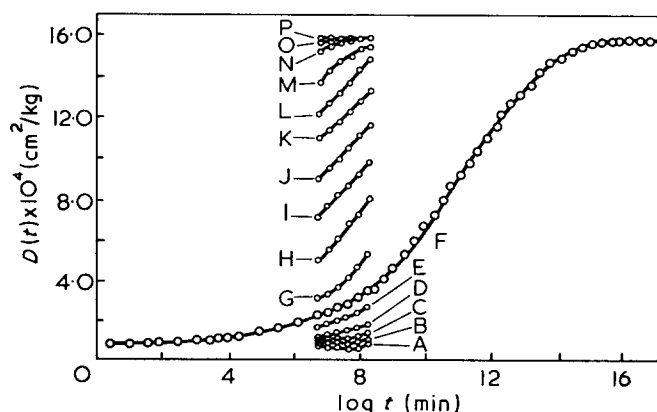


Figure 4 Individual isothermal creep curves for the extension creep compliance at various steps of temperature and the composite $D(t)$ curve derived by applying the principle of reduced variables versus log time. A, -10° ; B, 0° ; C, 10° ; D, 20° ; E, 25° ; F, 30° ; G, 35° ; H, 40° ; I, 45° ; J, 50° ; K, 55° ; L, 60° ; M, 65° ; N, 70° ; O, 75° ; P, 80° C

range of the substance. For this purpose the method of reduced variables was applied for the formation of the composite $D(t)$ curve.

Since the material did not present any kind of flow for the range of deformations applied during the experiments, the technique of using a single sample for all steps of temperature was practised. This presents the advantage of reducing errors, owing to variability of samples from different batches. The specimen was allowed to recover completely after each loading cycle, and the next loading step started only when the specimen has been returned to its initial condition.

Figure 4 presents the individual creep curves for the extension creep compliance at various steps of temperature, as well as the composite curve formed by applying the method of reduced variables. The glass transition temperature T_g was experimentally determined and found to be 30° C.

EXPERIMENTAL

The experimental set-up for the determination of the birefringence-isotropic points on the disc consisted of a temperature chamber, which was equipped with transparent windows in two opposite sides, so that the specimen could be observed during tests. The loading frame consisted of two pairs of cylindrical steel protrusions, orthogonally placed to each other, which could be adjusted by screws, and the applied pressure by each of these protrusions could be measured separately by pressure meters. The whole loading set-up, which was attached to an alignment frame, was placed at the interior of the temperature chamber. The application of loads could be adjusted electrically by a console outside the chamber. The chamber was interposed in a circular polariscope, illuminated by a monochromatic sodium light, and the fringe pattern at each instant was recorded in a 36 mm camera.

Vertical loads were always applied first and then the side loads were adjusted until symmetrical patterns were produced with the single isotropic point at the centre of the disc. Since the loading and unloading times lasted only fractions of a second, the difference between the beginning time for both pairs of loads did not influence the results. The duration of the loading and unloading

times were very small and the first measurement of strains and birefringence was taken at 30 sec after the sudden application of load, so that the loading cycle could be considered as a step function. Furthermore, vibration of the specimen during the sudden unloading was not observed at any test. The loading cycle in our experiments consisted in submitting the specimen to the four-load configuration and leaving it with constant loads, until a state of equilibrium was reached in the specimen. This was indicated by the constancy of the fringe patterns with time and the constancy of the applied pairs of loads, without operating at the electric regulators.

The experiment started at a temperature very close to the rubbery state, where viscoelastic equilibrium was reached very quickly. The creep period for this and subsequent tests was limited. As soon as viscoelastic equilibrium was achieved the recovery period was started by the instantaneous release of one pair of loads (the horizontal loads). The position of the birefringence-isotropic points was recorded for each time interval in the log time scale. Furthermore, the position of the strain-isotropic points was determined by substituting in relations (2) or (3) $D_c(t) = D_{\infty}$ and $v_c(t) = v_{\infty}$ (i.e. the values of these functions at the rubbery state) and $D_c(t-t_c)$ and $v_c(t-t_c)$ the corresponding values from the isothermal individual creep curve at the corresponding recovery time interval. The recovery experiments lasted always 16 min and measurements were taken at 1/2, 1, 2, 4, 8 and 16 min in a logarithmic scale.

As soon as the experimental cycle was terminated, the temperature was lowered by 5° C, and the four-load configuration was started again. This constant loading lasted until again equilibrium was reached, which for the lower temperature level necessitated a longer time period. When viscoelastic equilibrium was established, the recovery cycle started, which again lasted for 16 min, and measurements of the position of the birefringence-isotropic points were executed in the same time intervals.

Figure 5 presents the individual isothermal curves of the relative positions of isotropic points $\delta^* = \delta/D$ corresponding to birefringence and strains. Since the relative position of the individual curves suggests the application of the method of reduced variables, this method was

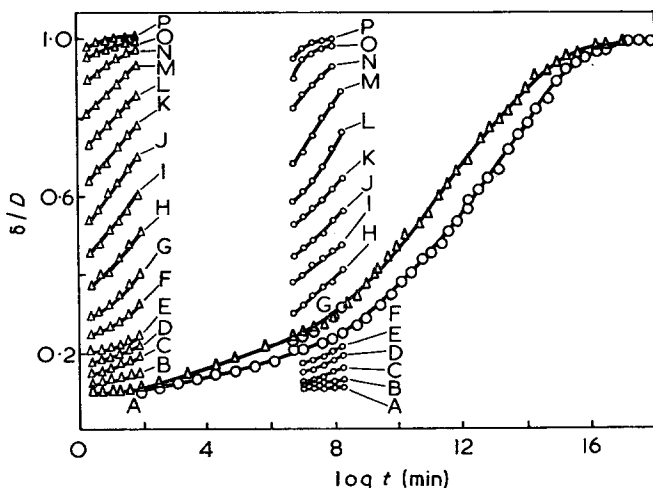


Figure 5 Individual isothermal curves for the relative positions of isotropic points expressed by the distance $\delta^* = \delta/D$ corresponding to birefringence (Δ) and strain (\circ). A, -10° ; B, 0° ; C, 10° ; D, 20° ; E, 25° ; F, 30° ; G, 35° ; H, 40° ; I, 45° ; J, 50° ; K, 55° ; L, 60° ; M, 65° ; N, 70° ; O, 75° ; P, 80° C

applied to the experimental and analytical curves for the distance between birefringence- and strain-isotropic points.

RESULTS

Application of the method of reduced variables to the individual isothermal curves for $\delta^* = f(\log t)$ gave the composite curves shown in Figure 5. It is clear from the relative position of these two composite curves that in the glassy and rubbery states of the polymers there is a satisfactory coincidence of the birefringence- and strain-isotropic points. Since the response of the material at these extreme states was almost instantaneous, it is reasonable to accept that, in these regions, all three tensors are coincident.

However, as soon as we withdraw from these two limiting states, there is an increasing discrepancy between the δ^* composite curve for birefringence-isotropic points and the corresponding curve for strain-isotropic points. This discrepancy becomes maximum for the distinctive creep time, K_a , as defined by Tobolsky¹¹. Since the stress-isotropic points always move instantaneously, as the lateral loads are removed, at this distinctive time the discrepancy between stress, strain and birefringence tensors becomes maximum.

It has been found from previous tests that the glass transition temperature of this plasticized polymer was 30°C³. This limit was confirmed by the present tests. The values of shift factors a_T for the birefringence- and strain-isotropic points were determined and the curves $\log a_T = f(T)$ for both composite curves were plotted as shown in Figure 6. It is clear from this Figure that above T_g both $\log a_T = f(T)$ curves for birefringence- and strain-isotropic points coincide. Below T_g , i.e. in the glassy region, the birefringence-isotropic points values of a_T lie in a different curve than the strain-isotropic points values of a_T . Both curves $\log a_T = f(T)$ along a large part of their transition region coincide with the corresponding curve traced by using the WLF equation for $T_g = 30^\circ\text{C}$ and $C_1 = -16.14$ and $C_2 = 56$ ¹¹. However, the unique

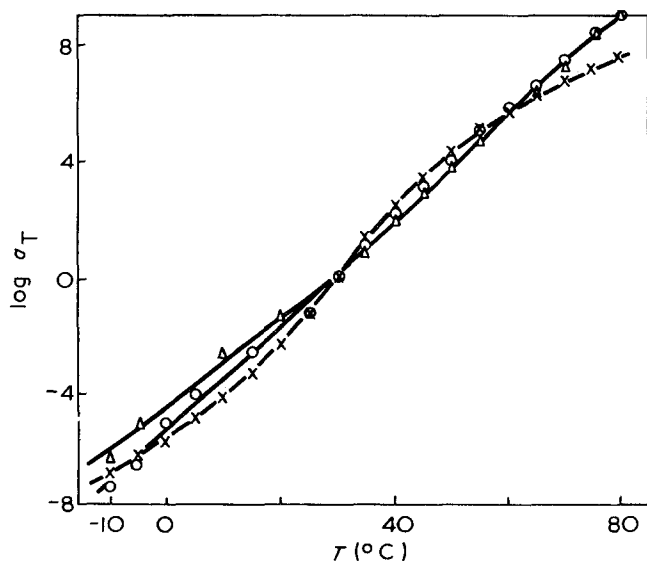


Figure 6 Logarithm of the shift factor a_T versus temperature for composite curves $\delta^* = f(\log t)$ corresponding to birefringence (Δ)- and strain (\circ)-isotropic points. The corresponding WLF equation for $T_g = 30^\circ\text{C}$ (\times) was also plotted for comparison

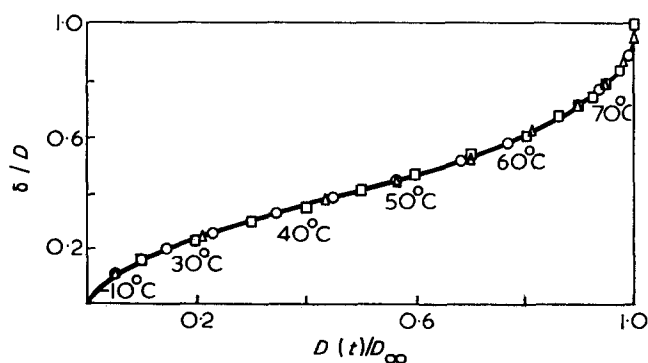


Figure 7 Variation of distance δ^* of birefringence (Δ)- and strain (\circ)-isotropic points versus the ratio of the instantaneous values of the creep compliance, normalized to its rubbery plateau value. The positions of δ^* for different values of $D(t)/D_\infty$ were plotted, as they have been derived from relation (3) (\square)

curve expressing both curves $\log a_T = f(T)$ in the transition zone is almost a straight line and the discrepancies from the WLF curve become more important at the vicinity of the rubbery region. Furthermore, the WLF curve at the glassy region lies closer to the $\log a_T = f(T)$ curve for strain-isotropic points than the corresponding curve for the birefringence-isotropic points.

Finally, as a check of the whole procedure, the variation of the quantity δ^* versus the ratio of the instantaneous value of the extension creep compliance $D(t)$ and its limiting value at the rubbery plateau D_∞ was plotted in Figure 7 by applying the simplified relation (3). In the same Figure the positions of different values for δ^* , as they have been either measured (birefringence-isotropic points) or calculated (strain-isotropic points) for different temperature levels, were plotted. It is again clear from this Figure that all values of δ^* for birefringence- and strain-isotropic points lie on the theoretical curve. This proves the validity of the testing procedure.

It is worthwhile mentioning here that the use of the simplifying relation (3), instead of the accurate form of equation (2), where the values of LCR function along the viscoelastic range were taken as constant, does not influence the results more than a maximum of 3%, for values of lateral contraction ratio between 0.5 (rubbery state of polymer) and 0.365 (glassy state). It is therefore indifferent which one of these two relations was used for our calculations.

DISCUSSION

It has been shown in this paper that even for a rheo-optically simple polymer, such as the plasticized epoxy polymer used in our tests, where the optical viscoelastic behaviour presumably follows the mechanical behaviour of the substance, there is always in the transition zone a time lag of the mechanical viscoelastic phenomena relatively to the corresponding optical phenomena.

For non rheo-optically simple polymers, where the mechanism defining the optical viscoelastic behaviour is of a different form than the mechanism determining the mechanical behaviour, it is expected that this difference in optical and mechanical viscoelastic behaviour will be much stronger in the transition zone.

However, although it is stated that for linear viscoelastic substances the same values of the shift factor a_T must superpose all viscoelastic functions¹², this principle is only approximately true. Previous experimental evidence

shows that, if one runs simultaneous creep or relaxation tests under isothermal conditions and in simple tension, up to a certain limit of loading, which may or may not be the viscoelastic equilibrium limit, and then leave the specimen to recover under continuing isothermal environment, one can find that birefringence relaxes much earlier than the strain applied to the specimen and this difference is much higher deep in the transition zone¹³.

Furthermore, experimental results obtained by extension and compressibility tests on the same polymeric substance corroborate the above theory and prove that, while the transition regions appear in the following order: lateral contraction ratio, bulk, extension and shear compliances, they end in the reverse order except the lateral contraction ratio function, which enters first in the rubbery region. The broadest transition region appears for the lateral contraction ratio function and the shortest for the shear compliance. Moreover, the inflection points of these curves, that is the maxima of the corresponding retardation spectra, appear in the same order of the appearance of transition regions^{3,4}.

An analogous phenomenon has already been indicated for the relaxation spectra¹⁴. The first approximations of the shear, extension, bulk and lateral contraction ratio relaxation spectra for the National Bureau of Standards polyisobutylene were calculated from the transient extension relaxation modulus data given by Tobolsky and Catsiff¹⁵ and the dynamic shear and bulk moduli data given by Ferry *et al.*¹⁶ and Marvin *et al.*¹⁷ respectively. The dynamic data were converted into transient values by applying Tobolsky's conversion method¹⁸. It is again clear that the rate of relaxation is decreasing from the shear modulus, to the extension modulus, to the bulk modulus and to the lateral contraction ratio relaxation function. The maxima of the relaxation spectra are following the inverse order.

Thus, although the viscoelastic behaviour of the polymer in shear and bulk is qualitatively the same, and it is governed by the same molecular mechanisms, there are certain quantitative differences of the behaviour of the material, which differentiate the two deformation modes.

Indeed, it could be reasoned that at the glassy region, where a complete absence of any configurational rearrangements of the chain backbones of the molecule is accepted, the scission and interchange mechanisms create the same results in bulk as in shear deformation. The distribution of retardation times for both types of deformation is therefore similar. Optical phenomena, which are

related to side group movements and scission, follow closely the shear and bulk deformation mechanisms.

Above the glass transition temperature, long-range configurational changes in the chain backbones result in a considerable increase of the shear compliance. The bulk compliance and optical phenomena depend only on the scission and interchange between crosslinks in the network. Therefore, they do not present a very strong dispersion, like the shear compliance, and their mechanisms deviate from the mechanisms of shear deformation, which is the main contributor to the mechanical characteristic properties of high polymers.

ACKNOWLEDGEMENTS

The research work contained in this paper was partly sponsored by the Scientific Affairs Committee of NATO under grant No 577. The author is indebted to this agency for its financial help. He also gratefully acknowledges the assistance of his collaborator, Miss Catherine Blontzou, for her contribution in the experimental work contained in this paper.

REFERENCES

- 1 Theocaris, P. S. *Rheol. Acta* 1961, **2**, 92
- 2 Theocaris, P. S. *J. Appl. Polym. Sci.* 1964, **8**, 399
- 3 Theocaris, P. S. and Hadjijoseph, C. *Proc. 4th Int. Congr. Rheology* 1965, **3**, 485
- 4 Theocaris, P. S. and Hadjijoseph, C. *Kolloid-Z. Z. Polym.* 1965, **202**, 133
- 5 Williams, M. L. and Arenz, R. J. *Exp. Mech.* 1964, **4**, 249
- 6 Dill, E. H. *Dep. Aeron. & Astron. Univ. Wash. Rep. 63-1* 1963
- 7 Dill, E. H. *J. Polym. Sci. (C)* 1964, **5**, 67
- 8 Van Geen, R. *C. R. Acad. Sci., Paris* 1964, **258**, 5164. *Sci. Tech. Armement, Mém. Artill. Fr.* 1971, **45**, 381
- 9 Theocaris, P. S. and Hadjijoseph, C. *Rev. Roum. Sci. Tech. Méc. Appl.* 1970, **15**, 875
- 10 Theocaris, P. S. *Proc. IUTAM Symp. Photoelasticity, Brussels*
- 11 Tobolsky, A. V. 'Properties and Structure of Polymers', John Wiley, New York, 1962
- 12 Ferry, J. D. 'Viscoelastic Properties of Polymers', John Wiley, New York, 1st Edn, 1961
- 13 Theocaris, P. S. *Rheol. Acta* 1967, **6**, 246
- 14 Theocaris, P. S. *Kolloid Z. Z. Polym.* 1970, **236**, 59
- 15 Tobolsky, A. V. and Catsiff, E. *J. Polym. Sci.* 1956, **19**, 111
- 16 Ferry, J. D., Grandine, L. D. and Fitzgerald, E. R. *J. Appl. Phys.* 1953, **24**, 911
- 17 Marvin, R. S., Aldrich, R. and Sack, H. S. *J. Appl. Phys.* 1954, **25**, 1213
- 18 Catsiff, E. and Tobolsky, A. V. *J. Colloid Sci.* 1955, **10**, 375

Microscopic observations of the crystallization processes of polyethylene under high pressure

Munehisa Yasuniwa* and Tetuo Takemura

Department of Applied Science, Faculty of Engineering, Kyushu University, Fukuoka, Japan
(Received 21 December 1973; revised 4 March 1974)

Microscopic observations of the three-stage crystallization processes of polyethylene at 5000 kg/cm² reported previously as those of 'unknown structure', 'extended-chain crystal' and 'folded-chain crystal' have been performed precisely using a diamond-anvil cell. At first, a lens-like and structureless crystal grows at the crystallization temperature of unknown structure. This lens-like crystal develops into the form of 10 μm diameter and 3 μm width with time. Secondly, the lens-like and structureless crystal forms a band-like structure (band width 1 μm) rapidly at the crystallization temperature of extended-chain crystal. Thirdly, a slight gap between band structures is filled up rapidly by many fine spherulites at the crystallization temperature of folded-chain crystal.

INTRODUCTION

Recently, many authors have studied the melting and crystallization processes of polyethylene under high pressure¹⁻⁵. The results are summarized in Table 1. The unknown structure¹, the large extended-chain crystal (ECC)^{2,3} and the intermediate phase⁴ are the same ones which appear above the temperature range of extended-chain crystal phase. The crystallization

* Present address: Kurume Technical College, Kurume, Fukuoka, Japan.

Table 1 Summary of melting and crystallization processes

Methods	Results	Ref.
Micro d.t.a. under high pressure. Electron microscopy	A. 3 stages: unknown, ECC, FCC B. Direct and rapid formation of ECC at T_{Ec} . FCC grows for the first time at T_{Fc} and gradually thickens into ECC. That referred to as 'unknown structure' has no clear structure	1
Dilatometry under high pressure. Electron microscopy	A. 2 stages: large ECC, FCC B. Formation of large ECC	2 3
D.t.a. under high pressure. Dilatometry. Optical microscopy	A. 2 stages: intermediate phase, ECC B. ECC has a texture of spherulite with only embryonic sheaving	4
Optical observation under high pressure (diamond anvils)	B. Direct observation of acicular or bladed crystals of polyethylene under high pressure	5

A. Melting and crystallization processes: ECC, FCC mean extended-chain crystal and folded-chain crystal respectively
B. Observation by electron microscopy, optical microscopy and other methods. T_{Ec} and T_{Fc} mean the crystallization temperatures of extended-chain and folded-chain crystals respectively

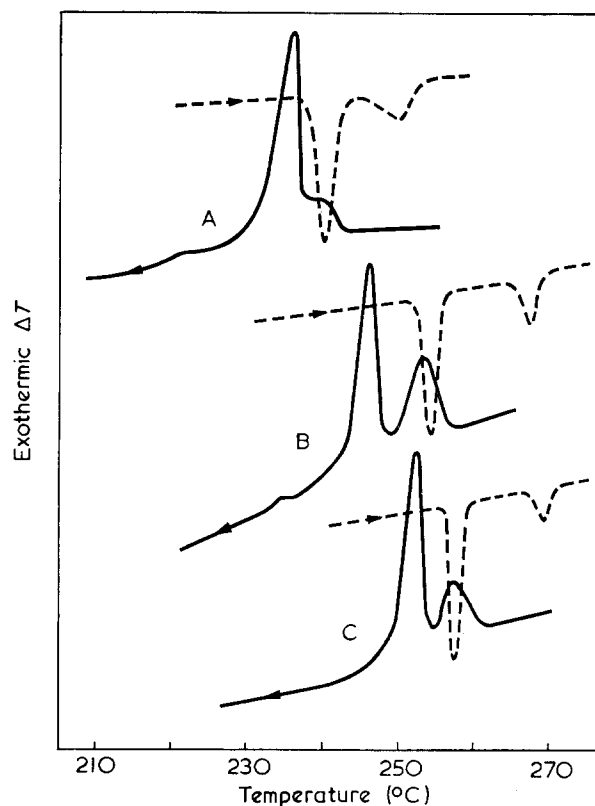


Figure 1 D.t.a. curves of melting (---) and crystallization (—) of polyethylene ($M_w=130\,000$) under high pressure. A, 5000; B, 6000; C, 6300 kg/cm²

condition of acicular or bladed crystal⁵ observed under high pressure at the initial stage of the crystallization process is not clear owing to the absence of detailed

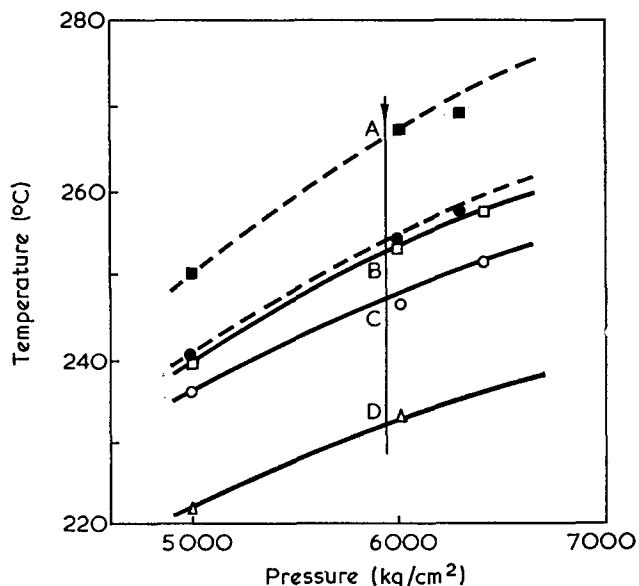


Figure 2 Melting (----) and crystallization (—) curves. ■, □, Unknown structure; ●, ○, extended-chain crystal; △, folded-chain crystal

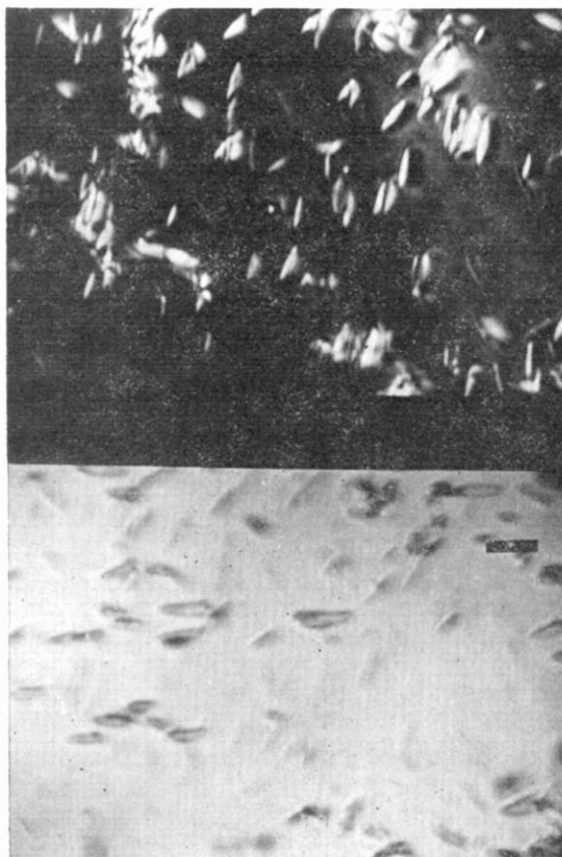


Figure 3 Photomicrograph of the growth (2.3min after the start of nucleation) of lens-like crystal at 5900 kg/cm² and 254°C (crystallization temperature of unknown structure). Upper and lower photographs show cases of crossed and paralleled Nicols, respectively. The scale bar on this and subsequent micrographs represents 10 μm

data, but will correspond to the crystallization of the unknown structure.

To clarify these complicated melting and crystallization processes, it is necessary to develop many precise measurements under high pressure. As the first step of this project, a more precise microscopic observation under high pressure is desirable.

EXPERIMENTAL

A most important imperfection of the diamond-anvil cell is the unreliability of applied pressure. Recently, an optical fluorescence system for quantitative rapid pressure measurement⁶ has been developed and used fairly successfully. But in this study, a simple method to estimate the applied pressure from its melting temperature employed a fractionated linear polyethylene ($M_w = 130\,000$). The melting and crystallization micro d.t.a. signals of this sample obtained with our equipment¹ are shown in Figure 1. The melting and crystallization curves of unknown structure, extended-chain crystal and folded-chain crystal (crystallization curve only) are shown in Figure 2.

A soft nickel-chromel alloy (Ni 93%, Cr 7%) plate (0.2mm thickness) was used as a gasket material of the diamond-anvil cell (High Pressure Diamond Optic Inc.). This plate was drilled (0.2mm diameter hole) at high speed (20 000 rev/min), so that no burrs were evident. A square plate (3mm × 3mm) with a hole in the centre was cut from this and used as a gasket. The use of this soft gasket prevented completely pressure leakage during the melting state of the sample. (The final thickness of gasket under high pressure was about 40 μm.)

The diamond faces were polished by abrasive paper and cleaned by the blank replicating method using cellulose acetate sheet and acetone.

Gasket setting on the diamond faces was carried out by the following new method. Under the visual field of a microscope, the piston of the diamond-anvil was

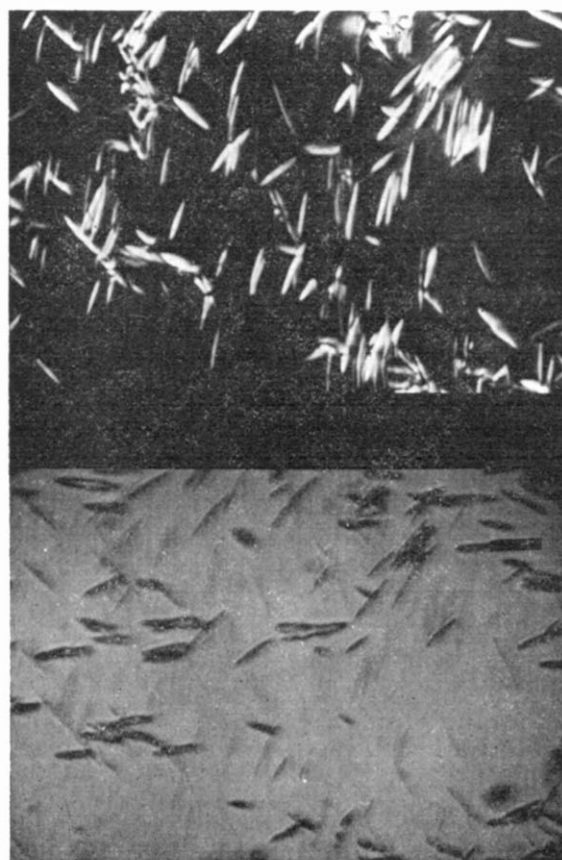


Figure 4 Photomicrograph of the growth (4.8min after the start of nucleation) of lens-like crystal at the same condition

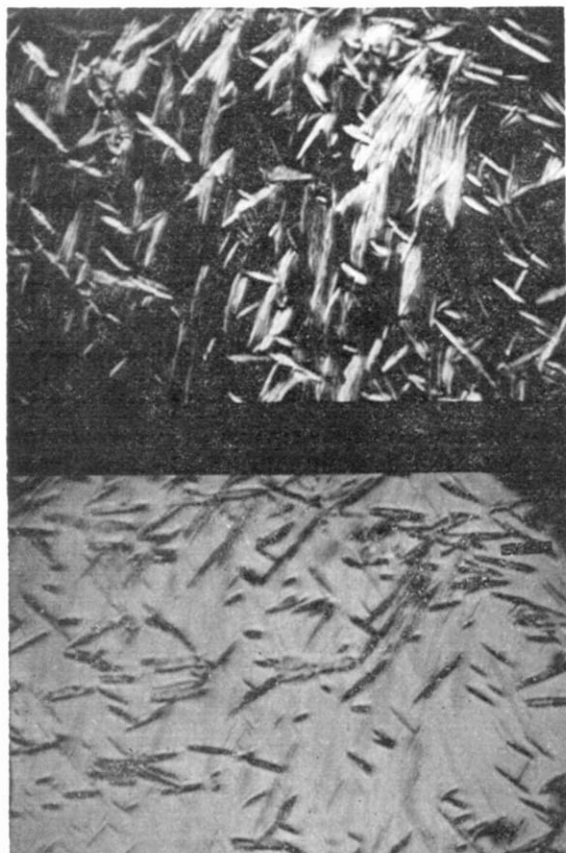


Figure 5 Photomicrograph of the growth of extended-chain crystal at 5900 kg/cm² and 245°C (crystallization temperature of extended-chain crystal). A rapid generation of striations in the lens-like crystal can be seen. The distance between striations is about 1 μm and it corresponds to the band width of extended-chain crystal

254°C), lens-like and structureless crystals formed gradually (Figure 3). These developed in the direction of its lens diameter, and reached the diamond surface, seeming to be cigarlike (Figure 4). The growth rate of this diameter (l in μm) of lens-like crystal at this temperature is expressed as:

$$l(t) = (25t)^{1/2}$$

where t is time in minutes. This feature is similar to the growth feature of liquid crystal droplet of *p*-azoxyanisole. When the temperature decreased and reached the crystallization temperature of extended-chain crystal (C in Figure 2, 245°C), the lens-like and structureless crystals are divided by striations and turn into band structures (Figure 5). The width of striations is about 1 μm and this corresponds to the band width observed at the fracture surface of the sample under the electron microscopic field. The growth of this band structure is very rapid at this temperature, and the visual field of the microscope is filled by these bands in a few minutes as shown in Figure 6. When the temperature decreased and reached the crystallization temperature of folded-chain crystal (D in Figure 2, 232°C), a slight gap between band structure is filled up rapidly by many fine spherulites as shown in Figure 7. The quantity of the fraction of these spherulites is very small as shown in the d.t.a. curve (Figure 1), but the surface effect of this thin sample strongly emphasizes this phenomenon.

From these observations we can conclude that the crystallization process of polyethylene under high

set and fixed on the stage of the microscope so that the centre of the anvil face was consistent with the crosspiece of the microscope, the gasket was then set and the edge was bonded with epoxy resin so that the centre of the gasket was also consistent with the crosspiece of the microscope. After this preparation, the powder sample was mounted between the diamond faces in the gasket by usual powder mounting method⁷. This procedure prevents a miss-setting of the gasket and any contamination of the sample, and we can obtain a complete setting easily.

The temperature of the sample was measured by a copper-constantan thermocouple set on the surface of the gasket.

RESULTS AND DISCUSSION

Above 5000 kg/cm², the crystallization processes had the features of a three-stage crystallization. For example, we show crystallization behaviour under 5900 kg/cm² in Figures 3–7. The melting temperature of this sample was 266°C under high pressure. This melting temperature was kept constant during cycles of melting and crystallization processes, and corresponds to that under 5900 kg/cm² from the melting curve (A in Figure 2). When the temperature decreased and reached the crystallization temperature of unknown structure (B in Figure 2,



Figure 6 Photomicrograph of the growth of extended-chain crystal at the same condition a few minutes after that of Figure 5. The striations change colour with time and perfect extended-chain crystals are formed rapidly

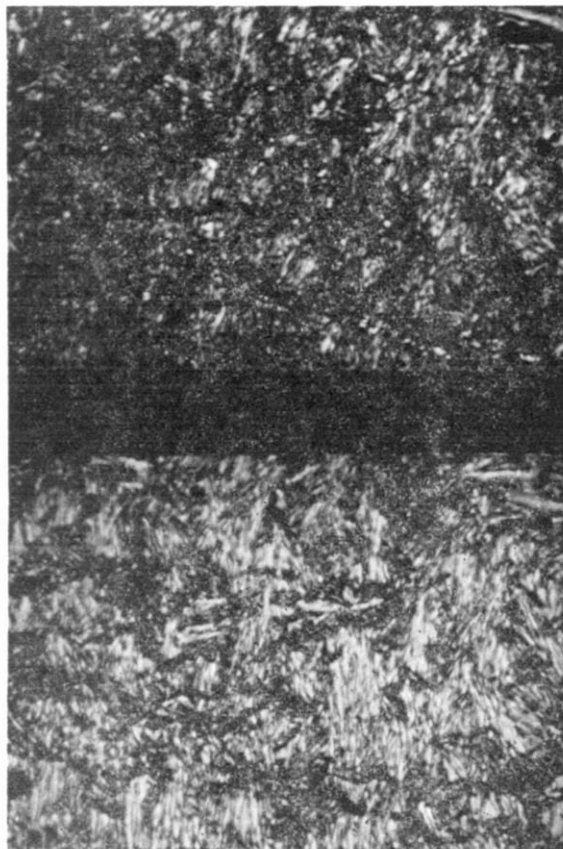


Figure 7 Photomicrograph of the growth of folded-chain crystal at 5900 kg/cm² and 232°C (crystallization temperature of folded-chain crystal). A slight gap between band structure is filled up with many fine spherulites, rapidly. The observer feels as if he was looking at a firecracker

pressure has three stages. At first, a lens-like and structureless crystal grows at the crystallization temperature of unknown structure. This structure may be a nematic liquid crystal having the *c*-axis parallel to the lens-axis from this optical observation and the d.t.a. curve. Secondly, the lens-like crystal forms a band-like structure (band width 1 μm) rapidly at the crystallization temperature of extended-chain crystal. This shows the rapid direct formation of extended-chain crystal at this temperature. This temperature may be the nematic-solid phase transition of this sample. Thirdly, a slight gap between bands is filled up rapidly by many fine spherulites at the crystallization temperature of folded-chain crystal.

ACKNOWLEDGEMENT

This work was supported in part by the Scientific Research Fund of the Ministry of Education.

REFERENCES

- 1 Yasuniwa, M., Nakafuku, C. and Takemura, T. *Polym. J.* 1973, **4**, 526
- 2 Maeda, Y. and Kanetsuna, H. *22nd A. Meet. Discuss. Polym. Sci., Tokyo* 1973
- 3 Hatakeyama, T. and Kanetsuna, H. *J. Macromol. Sci. (B)* 1973, **7**, 411
- 4 Bassett, D. C. and Turner, B. *Nature (Phys. Sci.)* 1972, **240**, 146; Bassett, D. C., Khalifa, B. A. and Turner, B. *Nature (Phys. Sci.)* 1972, **239**, 106
- 5 Jackson, J. F., Hsu, T. S. and Brasch, J. W. *J. Polym. Sci.(B)* 1972, **10**, 207
- 6 Barnett, J. D., Block, S. and Piermarini, G. *J. Rev. Sci. Instrum.* 1973, **44**, 1
- 7 Wier, C. E., Lippincott, E. R., Van Valkenburg, A. and Bunting, E. N. *J. Res. Nat. Bur. Stand.* 1959, **63A**, 55

Poly(ether sulphone) as an engineering material*

K. V. Gotham and S. Turner

Imperial Chemical Industries Ltd, Plastics Division, Welwyn Garden City, Herts AL7 1HD, UK
(Received 21 March 1974)

The polysulphones exhibit a unique blend of toughness at low temperatures and deformation resistance at high temperatures which makes them invaluable as engineering plastics. At room temperature, poly(ether sulphone) can withstand a stress of 50 MN/m² for many months without crazing or excessive creep. In this respect it is superior to all other commercial unreinforced thermoplastics. The deformation resistance at 150°C is still such that the working lifetime is at least three years at a tensile stress of 10 MN/m²; at lower stresses the lifetime is much longer. The experimental techniques and results on which these conclusions are based are reported. Complex changes occur in the mechanical properties of polymers stored at high temperatures, and poly(ether sulphone) is no exception; some of the phenomena are discussed.

INTRODUCTION

The primary requirement of an engineering plastic is that it should be able to withstand an applied stress without breaking and without excessive deformation. As a general rule, a polymer that has a high modulus and low sensitivity to elapsed time is not particularly tough under impact conditions, but members of the polysulphone family are an exception displaying an attractive combination of toughness and stiffness. This paper discusses in particular the creep and creep rupture properties of poly(ether sulphone) (ICI Ltd, Plastics Division)†, which is tough under impact at temperatures as low as -80°C and has good resistance to creep at +150°C.

The investigations reported here were in direct support of the development of commercially acceptable grades of poly(ether sulphone), rather than independent background studies. Thus their course was influenced by fluctuations in the state of the overall programme and its changing priorities, so that some of the features that emerge have not been pursued to their logical limit.

The creep experiments were carried out in accordance with test classification A of BS 4618¹ using apparatus developed by Mills and Turner². The creep rupture experiments were carried out in the manner described by Gotham³, on waisted specimens with no parallel-sided section and on parallel-sided specimens notched on both edges.

CREEP AND CREEP RUPTURE AT 20°C

Because of their high glass-rubber transition temperatures, the polysulphones are naturally of particular interest for high temperature applications and the room

temperature properties might be regarded to some degree as of secondary importance. Good creep resistance at high temperatures combined with impact toughness at sub-zero temperatures virtually guarantees good load-bearing capability at room temperature but it transpires that poly(ether sulphone) is outstandingly good in this respect.

The data in *Table 1* demonstrate that the moduli at short times and small strains are similar to, rather than superior to, those for many common plastics in their glassy state.

The superiority arises rather from a very low sensitivity to elapsed time, coupled with a high yield stress as exemplified by *Table 2*. Thus a creep specimen of poly(ether sulphone) at a stress of 50 MN/m² has endured for more than two years, developed only slight crazing

Table 1 100sec tensile creep modulus at 20°C, 0.002 strain

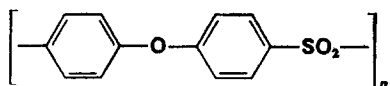
Polymer	Modulus (GN/m ²)
Poly(ether sulphone)	3.00
Udel Polysulfone (Union Carbide)	2.55
Nylon-6,6 (dry)	3.00
PMMA	3.05
Unplasticized PVC	3.10
Polystyrene	3.20
Styrene-acrylonitrile copolymer (high styrene)	3.50
Styrene-acrylonitrile copolymer (low styrene)	4.50
Polycarbonate	2.30

Table 2 Yield stresses of some common plastics

Polymer	σ_Y (MN/m ²)
Poly(ether sulphone)	100
Nylon-6,6 (dry)	85
PMMA (slightly drawn)	106
Unplasticized PVC	59
Styrene-acrylonitrile copolymer (low styrene)	104
Polycarbonate	64

* Presented at 31st SPE ANTEC Conference, Montreal, 7-10 May 1973.

† Structural formula:



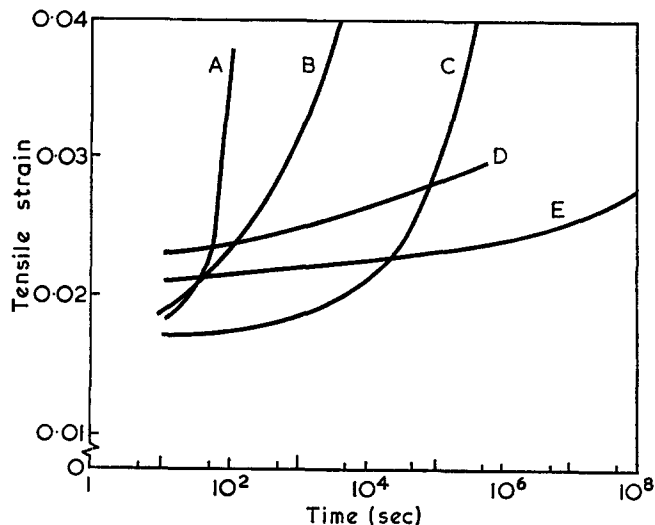


Figure 1 Tensile creep at 20°C, 50 MN/m². A, Unplasticized PVC; B, PMMA; C, nylon-6,6; D, Polysulfone; E, poly(ether sulphone). Poly(ether sulphone) has superior properties at high stress and long times

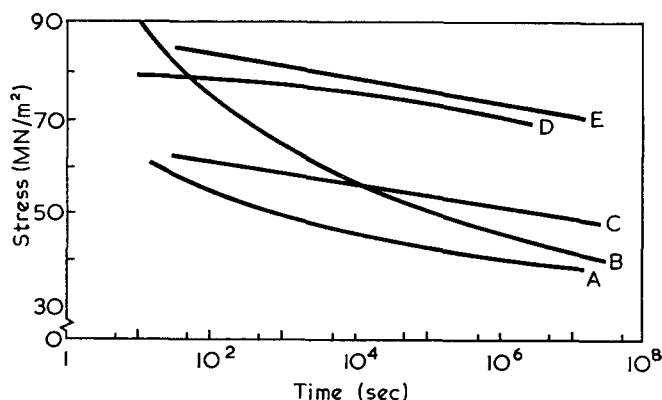


Figure 2 Onset of necking in glassy plastics at 20°C. Stress applied across the nominal direction of flow. A, Unplasticized PVC; B, PMMA; C, polycarbonate; D, nylon-6,6; E, poly(ether sulphone)

and showed no inclination towards runaway creep. Although PVC, PMMA and dry nylon can withstand such a stress for short periods, excessive creep, the precursor to ductile failure, quickly ensues, as is shown by Figure 1.

The creep rupture behaviour of poly(ether sulphone) is correspondingly good. Figure 2 compares its stress vs. time to the onset of necking with that of several plastics in their glassy state. Poly(ether sulphone) is the best, by this criterion, but such curves illustrate only part of the long-term strength behaviour, of course. The effect of notches of different severities and of fluctuations in the applied stress is important information. This has not yet been assessed at 20°C in any comprehensive fashion because of the main preoccupation with properties at elevated temperatures but it has been ascertained that poly(ether sulphone) remains strong, withstanding stresses of about 30 MN/m² even when the specimen has been sharply notched (notch tip radius $\approx 10 \mu\text{m}$) in an unfavourable direction with respect to molecular orientation (see later). In comparison with the non-crystalline plastics detailed in Figure 2, poly(ether sulphone) is stronger under these conditions than poly(methyl methacrylate) (PMMA) and poly(vinyl chloride) (PVC) but is not so strong as polycarbonate. Its performance compares

favourably with that of nylon-6,6 the only crystalline plastic included in the Figure.

CREEP AND CREEP RUPTURE AT ELEVATED TEMPERATURES

Creep at 150°C

A family of creep curves for poly(ether sulphone) at 150°C is shown in Figure 3. The solid lines were derived by numerical interpolation between the experimental data (extrapolated where necessary). The experiments were carried out on two different batches, differently processed (Batch 13 compression moulded, Batch 204 injection moulded). The implicit agreement between the results from the two batches is better than that observed for most polymers, particularly when different moulding techniques are compared, but this is a feature of the deformation behaviour of polysulphones that has been borne out by many results. In particular, modulus anisotropy due to molecular orientation in the injection moulded sample might have been expected to cause some difference between the results for the two batches, but measurements of the 100 sec Poisson's ratio at 20°C are consistent with little anisotropy. Specimens cut from compression moulded and/or injection moulded samples of several poly(ether sulphones) and polysulfones with different molecular weights gave values of Poisson's ratio all within the range 0.39-0.41.

It is now generally accepted that a family of creep curves, or a family of related cross-sections, is an efficient means of presenting the data necessary for deformation calculations in the course of engineering design, and the curves can be derived with high accuracy almost as a matter of simple routine using well established experimental procedures. However, in the one case of glassy

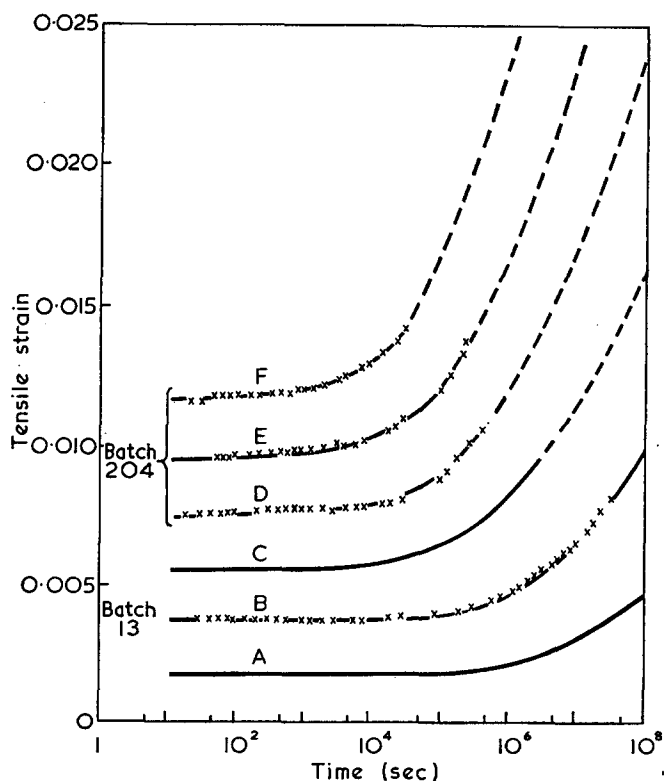


Figure 3 Tensile creep curves for poly(ether sulphone) at 150°C. Specimens conditioned at test temperature for 12 days prior to creep. —, Computed curves; x, experimental data; ----, notional creep curves. A, 5; B, 10; C, 15; D, 20; E, 25; F, 30 MN/m²

amorphous plastics at a temperature not far below the glass-rubber transition the regularity and apparent simplicity hides a degree of experimental complexity. Most of the mechanical properties of glassy amorphous plastics, including the creep resistance, are affected by the thermal history of the sample and particularly by prolonged heating at temperatures just below the glass-rubber transition temperature. Thus the strain developing during a prolonged creep test in that temperature region is not merely a straightforward viscoelastic response to the applied stress, and the data are correspondingly difficult to interpret unless appropriate control measures are introduced. The problem is largely overcome by the imposition of a conditioning period at the test temperature prior to the start of any creep experiment. The general effects of a conditioning period are the same as those found for PVC⁴; the resistance to creep at 60°C, particularly that at long times, was increased if the specimen was held for some time at that temperature prior to the test. The effect was progressive and seemingly endless; it was completely reversed by a period at a higher temperature followed by rapid cooling. There is now evidence that long storage at room temperature also produces the same effect and the picture that emerges is of some molecular rearrangement process that is achieved more rapidly and more completely as the temperature rises up to some limiting temperature associated with the glass-rubber transition. The phenomenon is common to many different glassy amorphous polymers, and apparently also in crystalline ones, so that it is probably a general property of polymer networks rather than the consequence of some specific molecular feature.

During our experiments on poly(ether sulphone), these effects have been regarded as a minor inconvenience rather than as a topic for deep study, and hence a conditioning period of about 12 days was chosen arbitrarily for most of the experiments, e.g. those leading to Figure 3. Ideally, this period should be longer than the intended duration of the creep experiment, because a genuine equilibrium state seems to be unattainable. As a practical compromise 12 days seems to be very suitable. At 150°C, for instance, the short-term modulus increases by about 20% during that time, but a significant proportion of the increase occurs within the first 24 hours and it might be argued, therefore, that a shorter period would suffice for many purposes. However, this would not be a sound procedure because the trend towards apparent equilibrium as indicated by a short term test is an inadequate index of the changes that occur in the creep response under a stress maintained for long times. There is also the strictly practical objection that the adoption of short conditioning periods would entail adherence to a strict timetable for conditioning and testing, which is difficult to attain in a busy laboratory with high utilization of machines. A twelve day period, on the other hand, allows some latitude in the starting times for the experiments.

The advocates of a short conditioning period can justifiably say that a long one introduces an element of artificiality into the results. The counter-argument is that the observed creep or creep rupture response of an unconditioned specimen is difficult to interpret, as was mentioned above and as may be inferred from a few results presented in Figure 4. The specimens were cut from injection moulded ASTM Type I tensile bars of Batch 204, conditioned for one hour only, just to ensure temperature equilibrium, and subjected to a range of

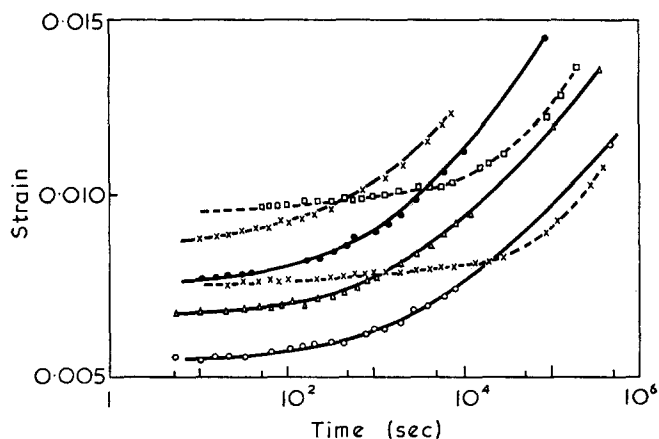


Figure 4 Effect of thermal conditioning on tensile creep of poly(ether sulphone) at 150°C. —, Unconditioned; ----, conditioned at 150°C for 12 days prior to creep. ○, 12.5; △, 15; ●, 17.5; ×, 20; □, 25 MN/m²

stresses at 150°C. The creep curves are significantly different from those for conditioned specimens, two of which have been transposed from Figure 3, and the difference would have been even greater but for the fact that the unconditioned specimens were tested at a much later date than the others. The prolonged delay constituted a storage period at 20°C which was equivalent to some short period at 150°C. Apart from the complicated interaction between the creep response and the changes induced by thermal conditioning, the behaviour is interesting in that crazes in unconditioned specimens do not develop rapidly into serious defects as they do in conditioned ones; thus a simple summary of the effect of a conditioning period is that it increases the modulus and lowers the ductility.

Recovery after creep

Under a wide range of conditions, the strain arising in a thermoplastic from a period under stress is very largely recoverable if the stress is reduced to zero. In this respect thermoplastics are very different from metals, for which the creep strain is irrecoverable. This characteristic of plastics is rightly regarded as an advantage in some practical situations and recovery experiments are an important feature of any comprehensive evaluation of load bearing capability. However, there is some uncoordinated evidence from several sources that the recovery after creep of glassy amorphous plastics at high temperatures is significantly poorer than that after creep at 20°C, and the results for unconditioned poly(ether sulphone) at 150°C, plotted as fractional recovery vs. log (reduced time) in Figure 5, suggest the same, though the actual comparisons with data for 20°C are not given. When recovery data are presented against such axes the curves assume similar shapes but are shifted downwards and to the right as either the duration of the preceding creep period or the maximum creep strain increases, that is the recovery is retarded after creep for long times and/or to large strains. In these experiments the effect of creep duration is particularly pronounced, the transposition being mainly vertical, which strongly suggests that part of the creep strain is truly irreversible. Thermoplastics of reasonable molecular weight are not normally regarded as undergoing a 'viscous flow' creep process at small strains such as those involved in these experiments but a tentative explanation is that substantial molecular

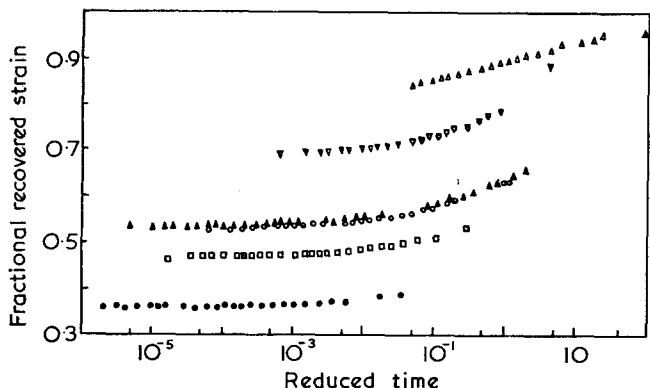


Figure 5 Recovery after creep of poly(ether sulphone) at 150°C. Open symbols: unconditioned; solid symbols; conditioned. Glassy amorphous plastics near their glass-rubber transition recover less readily than thermoplastics in general

Symbol	Creep duration (sec)	Final creep strain
△	7.2×10^2	0.01515
▽	7.2×10^3	0.01225
○	8.1×10^4	0.01452
□	3.29×10^5	0.01312
▲	1.037×10^6	0.01478
●	5.4×10^6	0.00970

re-ordering, associated with the approach to equilibrium free volume, occurs in the unconditioned specimens during the creep period and that this essentially creates a new zero state when it occurs under the bias of an applied stress, analogously to the more spectacular thermoforming processes that exploit the enormous change in molecular mobilities in the vicinity of the glass-rubber transition temperature.

Two recovery curves for conditioned specimens are included in Figure 5. When due consideration is given to the relevant parameters, which could not be properly matched for this comparison because of other restraints on the experiments, it is clear that the recovery of conditioned specimens is superior to that of unconditioned specimens, which supports the contention that an irreversible component of strain is generated when molecular re-ordering occurs during creep. However, the recovery at 150°C of the so-called 'conditioned' specimens was not impressive either, the probable reason being that a similar re-ordering, though to a lesser degree, must have occurred during the creep stage because there is no evidence that a true equilibrium can be achieved within the arbitrarily chosen 12 days. A further complication is that the phenomenon is not simply a matter of slow equilibration. An isotropic glassy amorphous polymer has a Poisson's ratio of about 1/3 (but see reference to the Poisson's ratio of polysulphones in the previous section) and hence tensile creep is accompanied by a volumetric strain of the order: $\Delta V/V = \text{tensile strain}/3$. Under typical creep conditions, therefore, a specimen will increase in overall volume by between 0.1% and 0.3%; this will constitute a significant increase in the free volume, that will augment whatever non-equilibrium state exists as a consequence of the thermal history.

Creep rupture

The excellent creep rupture resistance at 20°C is maintained at elevated temperatures at least up to, and

probably well beyond, 100°C. At 150°C, however, the behaviour is inferior, both in the magnitude of the stress that can be endured and in the brittle nature of the failures occurring at the longer times. At that temperature, crazing occurs at a tensile strain of about 0.008 and brittle failure ensues fairly rapidly, whereas at 20°C crazing occurs, if at all, at a strain of 0.040 or more and does not induce brittle failure.

The typical stress vs. log (lifetime) curves for poly(ether sulphone) in Figure 6 demonstrate the general response to elapsed time and the change in failure characteristics as the temperature rises. There is nothing particularly untoward in the deterioration of performance at high temperatures and the results must be seen in proper perspective. The data indicate a lifetime of at least 9 months at 150°C under a stress of 10 MN/m² applied in an unfavourable direction with respect to the molecular orientation, i.e. to a specimen cut with its axis transverse to the nominal flow direction in an edge-gated injection moulded disc, and the results of the creep experiments strongly suggest that this is an underestimate of the lifetime in practice. In addition to this, the time at which the lifetime curve at 150°C sweeps downwards

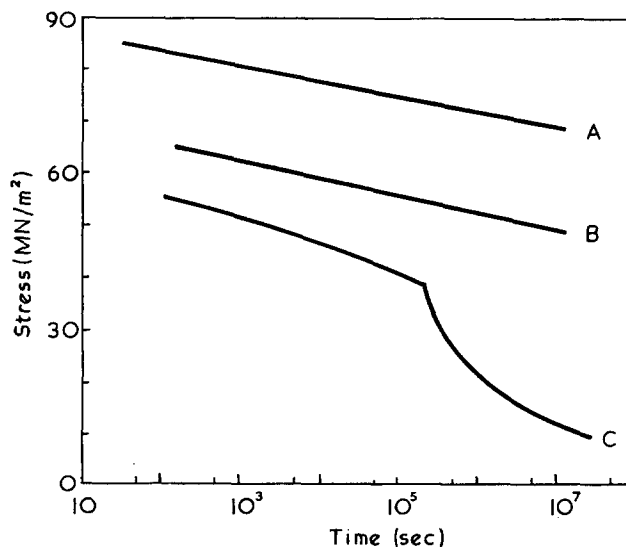


Figure 6 Static fatigue in unnotched specimens of poly(ether sulphone). Stress applied across the nominal direction of flow. A, Batch 99D at 20°C; B, Batch 204 at 100°C; C, Batch 204 at 150°C

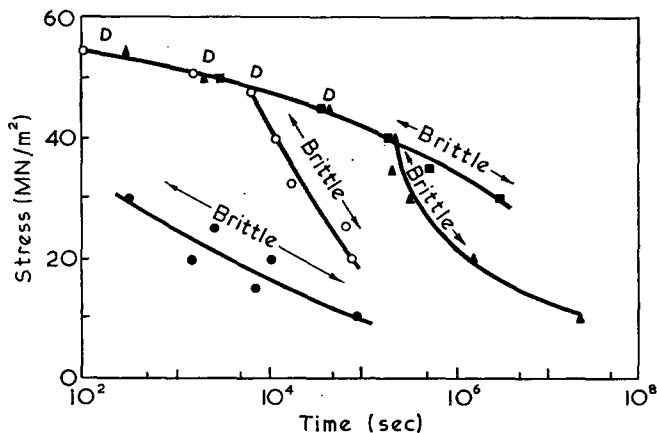


Figure 7 Effect of molecular weight on the failure characteristics of poly(ether sulphone) at 150°C (see reference to RV in text footnote). ●, RV=0.37; ○, RV=0.42; ▲, RV=0.46; ■, RV=0.54. D=ductile failure

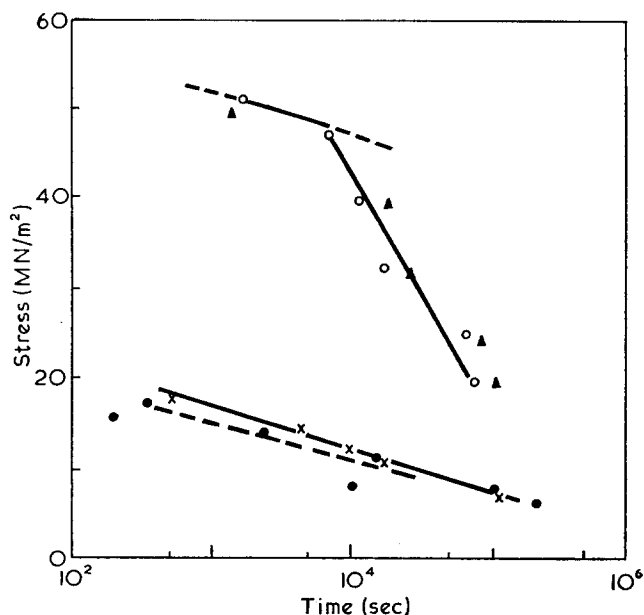


Figure 8 Effect of thermal conditioning on the lifetime of poly(ether sulphone) at 150°C. Notched (tip radius 10 μm); \times , heat treated at 150°C for 12 days; \bullet , no heat treatment. Unnotched: \circ , heat treated at 150°C for 12 days (data from Figure 7); \blacktriangle , no heat treatment

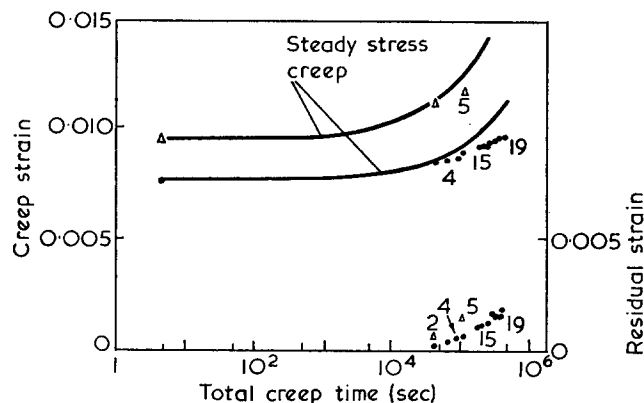


Figure 9 Creep under intermittent stress of poly(ether sulphone) at 150°C. The datum points show the maximum strain reached during, or the residual strain immediately prior to, the n th creep cycle. Some values of n are given. \circ , 20; \times , 25 MN/m²

dramatically—the tough brittle transition—is strongly dependent on the molecular weight* (see Figure 7). The lowest molecular weight sample ($RV=0.37$) always failed in a brittle manner, apparently without crazing, presumably because any craze that did form was so weak that failure ensued rapidly. The transition from ductile to brittle behaviour was less abrupt for the polymer with the highest molecular weight.

Reference has already been made in a previous section to the effect of a conditioning period on the creep rupture behaviour. The combined effect of decreased ductility and increased creep modulus is that the overall time to fail remains insensitive to the thermal history. This was first ascertained with sharply notched specimens of poly(ether sulphone) (notch tip radius 10 μm), and then later on unnotched specimens (Figure 8).

* There has been no quantitative assessment of molecular weight, but for this purpose the reduced viscosity (RV) is an adequate guide. It was measured at 25°C using a 1% w/v (1 g/100 cm³ total volume) solution in dimethylformamide.

Creep and creep rupture under intermittent stress

The stress to which a component may be subjected in service will seldom be constant, and it has been shown that a very useful subsidiary experiment is one in which the stress is applied intermittently. Our original experiments on polypropylene and polyacetal showed that the creep under intermittent stress is significantly less than that under continuous stress because of the retraction that occurs during the unstressed periods, and that such behaviour can be predicted on the basis of an elementary model⁵. Glassy amorphous plastics behave similarly in a viscoelastic sense, but work on PVC at 20°C reported recently⁶ and experiments on poly(ether sulphone) at 150°C show that such polymers are prone to early failure under fluctuating stress.

Batch 204 of poly(ether sulphone), which has good load bearing characteristics under steady stress (Figure 3), was subjected to a diurnal cycle of 6 h creep and 18 h recovery, in tension at 20 MN/m² and 25 MN/m². The results are shown in Figure 9; the maximum creep strain in successive creep periods conformed to the expected pattern, i.e. it increased in successive cycles but lay always below the curve for steady stress, but the specimen broke after a few cycles due to the growth of crazes which, under steady stress would have remained innocuous for a very much longer period, as seen in the steady creep experiments.

The probable explanation is that during the unloaded periods a large proportion of the creep strain disappears and the size of the plastic zone at the craze tip also decreases. Successive loadings do little more than re-establish the strain state that existed during earlier creep periods and the conditions in which the craze grows are nearly constant during successive cycles. During steady stress creep this retraction mechanism is absent and, in fact, the plastic zone size, and hence the fracture toughness, increases.

The residual strains observed during the recovery periods in these experiments, and plotted in Figure 9, are very similar in magnitude to those that arose in the PVC experiments⁶ and in no sense atypical of glassy amorphous thermoplastics. This is not in conflict with the poor recovery exemplified in Figure 5 because the latter mainly involved unconditioned specimens or very much longer creep times. No feature of the intermittent stress results could be used as a counter argument to the proposition that molecular re-ordering occurs during creep.

DISCUSSION

The load-bearing properties at 20°C have been studied rather cursorily because they are self-evidently satisfactory. At 150°C some influence of the nearby glass-rubber transition is evident and more comprehensive experiments were clearly necessary. At this temperature the deformation resistance remains very adequate. For instance, a strain of only 0.01 develops in three years under a continually applied stress of 10 MN/m², which is far better resistance to creep than is shown by propylene homopolymer at 20°C and only slightly worse resistance than that of a rigid PVC pipe formulation at 20°C. Since these two polymers are widely accepted as 'engineering plastics' at 20°C, poly(ether sulphone) should be similarly acceptable at 150°C. Furthermore, this temperature is not the upper limit for load-bearing service; limited

creep tests at 170°C have indicated that 0.010 strain is reached after about 1 week at 10 MN/m², but at 5 MN/m², which is still a substantial stress, the time would probably be much more than a year. The material is form stable under lower stresses at even higher temperatures, of course.

The choice of 0.01 strain, rather than some other value, was deliberate. It was governed by the well authenticated crazing threshold of 0.008. If the molecular weight is reasonable, crazes do not progress immediately to failure, and hence there is no urgent necessity to adopt 0.008 rather than 0.010 as a limit for service strains. Creep rupture specimens cut with their axis perpendicular to the nominal flow direction, i.e. specimens likely to give a reasonable approximation to worst case conditions, survived for about 9 months at 10 MN/m².

A low strain limit for components in service is uneconomic because load-bearing sections have to be correspondingly robust, whereas a high strain limit is often, though by no means always, unacceptable on aesthetic or functional grounds. Crystalline polymers are often inherently satisfactory at strains up to 0.03, but glassy amorphous polymers are not widely used above about 0.01. In this respect, therefore, poly(ether sulphone) is particularly satisfactory at 20°C since there is no evidence of either runaway creep or premature creep rupture due to cracking after long times in the strain region 0.02 to

0.03 (see *Figures 1 and 2*). It is also satisfactory at 150°C by the criteria that have hitherto proved to be meaningful and practical for a wide range of polymers at lower temperatures.

The use of a strain limit for service is a simplifying concept that circumvents some of the complexities inherent in the assessment of durability. It is not very satisfactory where the material is likely to be brittle, which means, in the case of poly(ether sulphone), at long elapsed times at high temperatures, where there is a significant stress concentration such as a notch or an inhomogeneity, and where the stress fluctuates sharply. The reduced durability of poly(ether sulphone) in these particular conditions is typical of glassy amorphous polymers and is in no way peculiar to the polysulphones.

REFERENCES

- 1 'Creep in uniaxial tension and compression (with particular reference to solid plastics)', BS 4618: 1970, Subsection 1.1.1, BSI, London
- 2 Mills, W. H. and Turner, S. *Symp. Mat. Test. Machine Design, Manchester* 1965, Paper 23
- 3 Gotham, K. V. *Plastics and Polymers* 1969, 37, 309
- 4 Turner, S. *Br. Plast.* 1964, 37, 682
- 5 Turner, S. *Appl. Polym. Symp.* 1971, No 17
- 6 Gotham, K. V. and Turner, S. *Polym. Eng. Sci.* 1973, 13, 113

An interpretation of ductile fracture process of uncrosslinked polymers in the rubbery state

Yo Takano

Department of Physics, Faculty of General Study, Gunma University, Maebashi 371, Japan

and Shingo Kondo

Research Institute of Composite Materials, Faculty of Technology, Gunma University, Kiryu 376, Japan

(Received 30 November 1973)

The weak network theory previously developed is applied to explain the failure envelope for the ductile fracture of uncrosslinked amorphous polymers in a constant rate of elongation, with the assumption that the reformed chain requires a lapse of time after its reformation to contribute to maintenance of the network structure. The chain that contributes to maintain the structure is called the 'structure chain'. The criterion is used that the fracture occurs provided the apparent average force per one 'structure chain' reaches a certain critical value. The result agrees well with the failure envelope obtained experimentally.

INTRODUCTION

The ultimate tensile properties of crosslinked amorphous polymers such as elastomers can often be characterized by a failure envelope¹⁻¹⁰, which is represented schematically^{1, 2} in Figure 1. The failure envelope is constructed from the values of the tensile stress at break σ_b and the associated ultimate strain γ_b by applying the well

known time-temperature superposition principle to the ultimate properties data obtained at different temperatures and strain rates. The lines emanating from the origin of the diagram represent stress-strain curves determined at various rates and temperatures. The rupture point moves anticlockwise around the envelope either as the strain rate is increased or as the test temperature is decreased. Such a failure envelope is independent of time (or strain rate) and temperature and thus it depends only on basic characteristics of the polymeric network. Several models^{5, 8, 11, 12} have been proposed to explain these phenomena. Some^{5, 11} of them are based on the view that the fracture of the sample results from a certain accumulation of scission of molecular chains, and the others^{8, 12} are phenomenological ones.

On the other hand, it is found that in the ductile fracture of uncrosslinked amorphous polymers, e.g. polystyrene, the ultimate tensile properties show the same tendencies^{13, 14} as elastomers. Uncrosslinked polymers, unlike crosslinked polymers, have no permanent junctions. Therefore there would be little possibility of scission of molecular chains under the action of mechanical force above the glass transition temperature and it is not correct to treat the ductile fracture of uncrosslinked amorphous polymer only on the basis of the concept of this chain scission.

One of us previously has given¹⁵ a good explanation to non-linear viscoelasticities of concentrated polymer solutions and melts by adding a few assumptions to Yamamoto's network theory¹⁶. In this paper we shall attempt to interpret on the same basis as the previous one¹⁵ the failure envelope for uncrosslinked amorphous polymers in the rubbery state from the point of view of the breakage (in the weak network theory the term

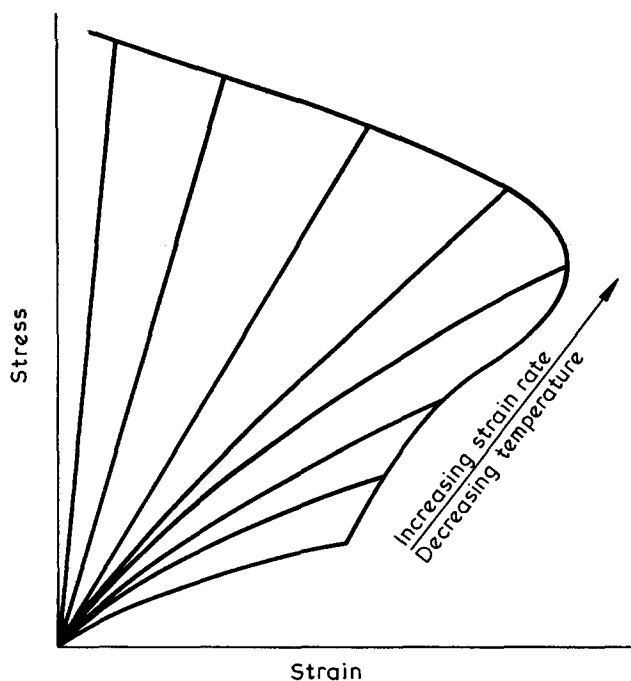


Figure 1 Schematic representation of the dependence of stress-strain curves on strain rate and temperature¹

'breakage' means not 'scission' but 'disappearance') and the reformation of the network chain.

THEORETICAL

Our basic picture is as follows. Uncrosslinked amorphous polymers with no permanent junctions should have the weak network structure. The weak network chains repeat breakage and reformation processes under the action of an external force. According to Yamamoto's weak network theory¹⁶, a mechanical quantity such as stress is calculated from the chain distribution function $F(h, N, t)$. The distribution function is proportional to the number of chains which have the end-to-end distance vector $h(\xi, \eta, \zeta)$ and the number of segments N at time t . Suppose a 'structure chain', which contributes to maintain the network structure, is chosen out of all the weak network chains. It is assumed that the reformed chain does not become the structure chain until a characteristic time τ_c elapses. This is our essential assumption which is more precisely discussed later. The degree of instability of the network structure would be expressed by the intensity of apparent average force $f(t)$ per one structure chain. The $f(t)$ is obtained by dividing the network normal stress parallel to the tensile direction by the number of structure chains per unit area perpendicular to the tensile direction. We employ as the criterion for the fracture that the network chain cannot possibly maintain the network structure when $f(t)$ reaches a certain critical value f_c .

Then, to find out the average force $f(t)$ and the number of the structure chains, we can use the Yamamoto network theory¹⁶ as in the previous paper¹⁵. It tells us that the stress tensor of network σ_n and the number of chains $F(h, N, t)$ per unit volume are given in terms of the chain reformation function $G(h, N, t)$, the chain-breakage coefficient $\beta(h, N)$ and the free energy of a chain $\phi(|h|, N, T)$ by:

$$\sigma_n = e(t)S(t)e^+(t) \tag{1}$$

$$S(t) = S_0(t) + \int_0^t e^{-1}(t')T(t, t')e^{-1}(t')dt' \tag{2}$$

$$S_0(t) = \sum_N \int_{-\infty}^{\infty} \int_{-\infty}^{\infty} \int_{-\infty}^{\infty} (hh) \left(\frac{1}{r} \frac{d\phi}{dr} \right)_{r=|e(t)h|} \times F(h, N, 0) \exp \left[- \int_0^t \beta\{e(t')h, N\} dt' \right] dh \tag{3}$$

$$T(t, t') = \sum_N \int_{-\infty}^{\infty} \int_{-\infty}^{\infty} \int_{-\infty}^{\infty} (hh) \left(\frac{1}{r} \frac{d\phi}{dr} \right)_{r=|e(t)e^{-1}(t')h|} \times G(h, N, t') \exp \left[- \int_{t'}^t \beta\{e(t'')e^{-1}(t')h, N\} dt'' \right] dh \tag{4}$$

$$F(h, N, t) = F_R(h, N, t) + \int_0^t f_s(h, N, t') dt' \tag{5}$$

$$F_R(h, N, t) = \frac{1}{|e(t)|} F\{e^{-1}(t)h, N, 0\} \times \exp \left[- \int_0^t \beta\{e(t'')e^{-1}(t)h, N\} dt'' \right] \tag{6}$$

$$f_s(h, N, t') = \frac{1}{|e(t')|} G\{e(t')e^{-1}(t)h, N, t'\} \times \exp \left[- \int_{t'}^t \beta\{e(t'')e^{-1}(t)h, N\} dt'' \right] \tag{7}$$

where T is the absolute temperature, and $e(t)$ and (hh) are the deformation tensor and a tensor defined by:

$$(hh) = \begin{bmatrix} \xi^2 & \xi\eta & \xi\zeta \\ \eta\xi & \eta^2 & \eta\zeta \\ \zeta\xi & \zeta\eta & \zeta^2 \end{bmatrix} \tag{8}$$

respectively.

The first term, called 'relax term', of equation (5) is the contribution from the chains which initially constructed the network, and the second term, called 'steady term', is that from the newly formed chains during the course of the deformation.

Following the previous treatment, we assume $G(h, N, t)$, $\beta(h, N)$ and $\phi(|h|, N, T)$ as:

$$G(h, N, t) = G_0 \exp \left(- \frac{3h^2}{2Na^2} \right) \tag{9}$$

$$\beta(h, N) = \left(\frac{\beta_0}{Na^2} \right) h^2 \tag{10}$$

$$\phi(|h|, N, T) = \left(\frac{3kT}{2} \right) \left(\frac{h^2}{a^2N} \right) \tag{11}$$

where k and a are the Boltzmann constant and the effective length of a segment respectively. Moreover it is assumed that the distribution of N is neglected.

Consider an incompressible sample being stretched in the x direction by a constant rate of elongation, the deformation tensor $e(t)$ is given by:

$$e(t) = \begin{bmatrix} \alpha & 0 & 0 \\ 0 & \frac{1}{(\alpha)^{1/2}} & 0 \\ 0 & 0 & \frac{1}{(\alpha)^{1/2}} \end{bmatrix} \tag{12}$$

$$\alpha = 1 + \gamma = 1 + ct \tag{13}$$

where c and γ are the rate of elongation and the tensile strain in the x direction respectively. Using equations (1)-(4) and (8)-(13), and also assuming $F(h, N, 0) = \beta(h, N)G(h, N, 0)$ in the natural state, we obtain the stress tensor of network:

$$\sigma_{n11} = \alpha^2 \left[S_{011} + \int_0^t \frac{1}{\alpha'^2} T_{11} dt' \right] \tag{14}$$

$$\sigma_{n22} = \sigma_{n33} = \frac{1}{\alpha} \left[S_{022} + \int_0^t \alpha' T_{22} dt' \right] \tag{15}$$

$$\sigma_{n12} = \sigma_{n23} = \sigma_{n31} = 0 \tag{16}$$

$$S_{011} = \frac{3kT}{\beta_0} (p' - q')^{-3/2} \times \left[\ln \left(\frac{(p' - q')^{1/2} + p'^{1/2}}{q'^{1/2}} \right) - \left(\frac{p' - q'}{p'} \right)^{1/2} \right] \tag{17}$$

$$S_{022} = S_{033} = \frac{3kT}{2\beta_0 q' p'^{1/2}} - \frac{1}{2} S_{011} \tag{18}$$

$$T_{11} = \frac{kT}{p^{3/2} q} \tag{19}$$

$$T_{22} = T_{33} = \frac{kT}{p^{1/2} q^2} \tag{20}$$

where:

$$p' = 1 + \frac{2\beta_0}{3} \left(t + ct^2 + \frac{c^2}{3} t^3 \right) \quad (21)$$

$$q' = 1 + \frac{2\beta_0}{3c} \ln \alpha \quad (22)$$

$$p = 1 + \frac{2\beta_0}{3\alpha'^2} \left[(t-t') + c(t^2-t'^2) + \frac{c^2}{3}(t^3-t'^3) \right] \quad (23)$$

$$q = 1 + \frac{2\beta_0\alpha'}{3c} \ln \left(\frac{\alpha}{\alpha'} \right) \quad (24)$$

$$\alpha' = 1 + ct' \quad (25)$$

The normal stress difference σ is given by:

$$\sigma = \sigma_{n11} - \sigma_{n22} \quad (26)$$

Next, let us find the number of structure chains per unit area perpendicular to the tensile direction. From the definition of the structure chain and equation (5), the number of structure chains $F_{st}(h, N, t)$ per unit volume is given by:

$$F_{st}(h, N, t) = F_R(h, N, t) + \int_0^{t-\tau_c} f_s(h, N, t') dt' \quad (27)$$

where $\tau_c(h, N)$ is the characteristic time of reformed chain with h and N . The probability that a chain with h in unit volume passes across a unit area perpendicular to the tensile direction is proportional to the tensile direction component ξ of the chain length. Accordingly, multiplying the chain number in unit volume by ξ , we can get the number of the structure chains having h and N per unit area perpendicular to the tensile direction as:

$$F_{st}(h, N, t) \xi \quad (28)$$

Considering that the chain effectively supports an external force by a factor $\cos\theta (= \xi/|h|)$, where θ is the angle between the chain vector and the tensile direction, the total effective number of the structure chains having N segments in unit area perpendicular to the tensile direction $n_{st}(N, t)$ is expressed by:

$$n_{st}(N, t) = \int_{-\infty}^{\infty} \int_{-\infty}^{\infty} \int_{-\infty}^{\infty} \frac{\xi^2}{|h|} F_{st}(h, N, t) dh \quad (29)$$

and, accordingly, the apparent average force $\bar{f}(N, t)$ is given by:

$$\bar{f}(N, t) = \sigma_{n11}/n_{st}(N, t) \quad (30)$$

Then, we assume $\tau_c(h, N)$ to be equal to the relaxation time of chains which consists of N segments, that is:

$$\tau_c(h, N) = \frac{Na^2}{\beta_0 h^2} \quad (31)$$

Finally, the effective number of structure chains is obtained by:

$$n_{st}(N, t) = F_R(N, t) + F_S(N, t) \quad (32)$$

where:

$$F_R(N, t) = \frac{1}{\beta_0} \left(\frac{3Na^2}{2\pi} \right)^{1/2} \frac{1}{\alpha p'_N - \alpha^{-2} q'_N} \times \left[\left(\frac{\alpha^3}{\alpha^3 - 1} \right)^{1/2} \ln \frac{\alpha^{3/2} + (\alpha^3 - 1)^{1/2}}{\alpha^{3/2} - (\alpha^3 - 1)^{1/2}} - 2 \left(\frac{q'_N}{p'_N - q'_N} \right) \tan^{-1} \left(\frac{p'_N - q'_N}{q'_N} \right)^{1/2} \right] \quad (33)$$

$(p'_N > q'_N)$

$$F_R(N, t) = \frac{1}{\beta_0} \left(\frac{3Na^2}{2\pi} \right)^{1/2} \frac{1}{\alpha p'_N - \alpha^{-2} q'_N} \times \left[\left(\frac{\alpha^3}{\alpha^3 - 1} \right)^{1/2} \ln \frac{\alpha^{3/2} + (\alpha^3 - 1)^{1/2}}{\alpha^{3/2} - (\alpha^3 - 1)^{1/2}} - \left(\frac{q'_N}{q'_N - p'_N} \right)^{1/2} \ln \frac{q'_N^{1/2} + (q'_N - p'_N)^{1/2}}{q'_N^{1/2} - (q'_N - p'_N)^{1/2}} \right] \quad (34)$$

$(p'_N < q'_N)$

$$F_S(N, t) = \frac{3}{2} \left(\frac{3Na^2}{2\pi} \right)^{1/2} \int_0^t \int_0^\pi \cos^2\theta \sin\theta \frac{1}{Q} \times \left[\frac{1}{Q} + \frac{1}{(t-t')\beta_0} \right] \exp \left[-\frac{Q}{(t-t')\beta_0} \right] dt' d\theta \quad (35)$$

where:

$$p'_N = p'/\alpha^2 \text{ and } q'_N = q' \alpha \quad (36)$$

$$Q = \frac{3}{2} [p(\alpha'/\alpha)^2 \cos^2\theta + q(\alpha/\alpha') \sin^2\theta] \quad (37)$$

The tensile strength σ_b and the ultimate tensile strain γ_b are obtained from the criteria for the fracture, that is:

$$f_c = \bar{f}(N, t_b) = \sigma_{n11}(t_b)/n_{st}(N, t_b) \quad (38)$$

$$\gamma_b = ct_b \quad (39)$$

$$\sigma_b = \sigma_{n11}(t_b) - \sigma_{n22}(t_b) \quad (40)$$

RESULT AND DISCUSSIONS

Figure 2 shows the stress-strain curves calculated from equations (12)–(15) and (17)–(25). The symbols indicate

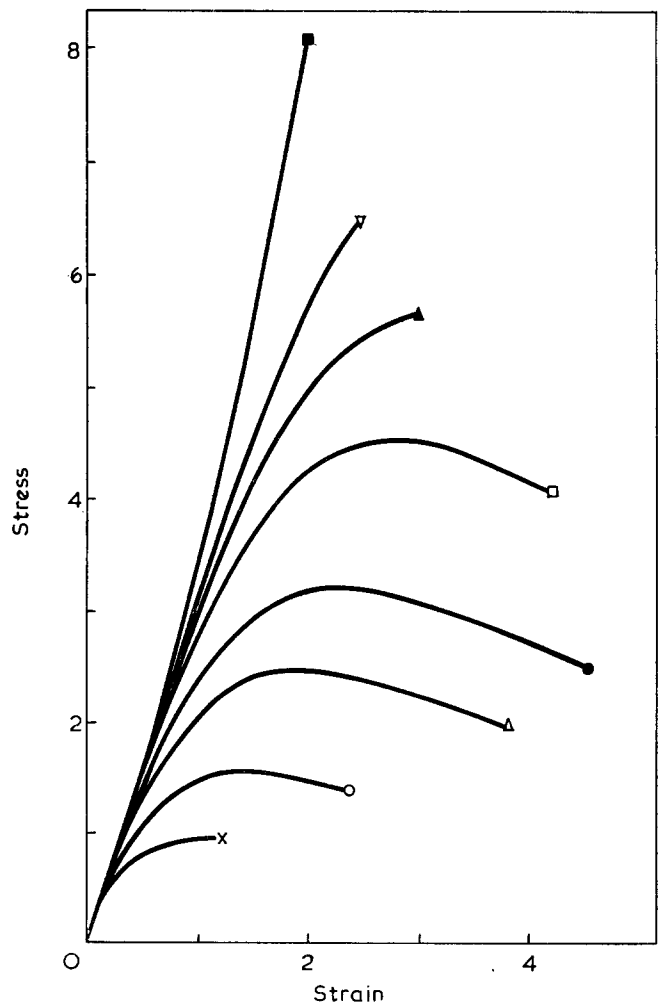


Figure 2 Dependence of stress-strain curves on strain rate: x, 0.5; O, 1; Δ, 2; ●, 3; □, 5; ▲, 7; ▽, 10; ■, 100

the fracture point defined by equations (38)–(40) and the envelope of them agrees well with the tendencies of the schematic diagram shown in *Figure 1*.

In the present paper, we have attempted to interpret the tensile failure envelope for uncrosslinked amorphous polymers. Here, we shall refer to the assumptions that the reformed chain requires the lapse of the characteristic time τ_c after its reformation to contribute to the maintenance of network structure and, moreover, τ_c is equal to the relaxation time of chains.

In general the major part of the intermolecular interaction between polymer molecules in amorphous polymers is interpreted by the concept of entanglement. As for entanglement, unfortunately, a definite picture has not yet been established, although many authors have treated its effect on the mechanical properties. In the present network theory, complicated breakdown and formation process of entanglement of real polymeric chains is simply idealized in the breakage and reformation of the network chain and both kinds of relaxation time for formation and breakdown are not explicitly taken into account, especially the time for formation. On the other hand, Graessley¹⁷ and Tanaka *et al.*¹⁸ have successfully treated this relaxation time for its formation in their semi-molecular models to explain non-linear viscoelastic properties of concentrated polymer systems. As behaviour of entanglement of the rubbery state essentially differs from that of concentrated systems only in time scale, the concept of entanglement in the above treatments will be useful in the present investigation also. In this treatment it is uncertain whether the time when the chain is reformed in the network model corresponds to the time when the formation of entanglement begins or to the time when it has finished in real polymeric systems. If the time corresponds to the former, we can consider that the chain becomes a 'structure chain' when the time required for formation of entanglement elapses after the chain reformation. The chain is called a weak chain until a state of entanglement reaches its equilibrium state, although, strictly speaking, the weak chain partly belongs to the structure chain a little, but it is assumed not to belong to the structure chain in equation (27). Since the formation time of entanglement may be of the same order as relaxation time for its breakdown, we assumed that the characteristic time is equal to the relaxation time of the

chain. The result of the evaluation shows that the 'steady term' makes little contribution to the structure chain.

Although some problems remain to be solved about relationship between real entanglement and the present network chain, we shall propose the present network fracture model as an interpretation of the tensile failure envelope for uncrosslinked amorphous polymers.

ACKNOWLEDGEMENTS

The authors wish to express their thanks to Professor M. Yamamoto of Tokyo Metropolitan University for his instructive discussions and encouragement. One of the authors (Y. T.) gratefully acknowledges the valuable assistance of Miss F. Seki of Kirigaoka Gakuen.

The numerical calculations were performed on HITAC 8700 of University of Tokyo. One of the authors (Y. T.) was indebted for the Grant-in-Aid for Scientific Research from the Ministry of Education.

REFERENCES

- 1 Smith, T. L. *J. Polym. Sci.* 1958, **32**, 99
- 2 Smith, T. L. and Stedry, P. J. *J. Appl. Phys.* 1960, **31**, 1892
- 3 Smith, T. L. *J. Polym. Sci. (A)* 1963, **1**, 3597
- 4 Smith, T. L. *J. Appl. Phys.* 1964, **35**, 27
- 5 Bueche, F. and Halpin, J. C. *J. Appl. Phys.* 1964, **35**, 36
- 6 Halpin, J. C. *J. Appl. Phys.* 1964, **35**, 3133
- 7 Halpin, J. C. and Bueche, F. *J. Appl. Phys.* 1964, **35**, 3142
- 8 Landel, R. F. and Fedors, R. F. 'Fracture Processes in Polymeric Solids,' (Ed. B. Rosen), Interscience, New York, 1964, Ch 3B, pp 361–485
- 9 Smith, T. L. and Frederick, J. E. *J. Appl. Phys.* 1965, **36**, 2996
- 10 Smith, T. L. and Dickie, R. A. *J. Polym. Sci. (A-2)* 1969, **7**, 635
- 11 Knauss, W. G. *PhD Thesis* California Institute of Technology, California, 1963
- 12 Hata, T. *J. Soc. Mater. Sci. Japan* 1968, **17**, 322
- 13 Fujimoto, T., Kondo, Y., Kimura, T. and Nagasawa, M. *Toyoda Kenkyu Hokoku* 1972, **25**, 34
- 14 Onogi, S., Matsumoto, T. and Kamei, E. *Polym. J.* 1972, **3**, 531
- 15 Takano, Y. *Polym. J.* 1974, **6**, 61
- 16 Yamamoto, M. *J. Phys. Soc. Japan* 1956, **11**, 413
- 17 Graessley, W. W. *J. Chem. Phys.* 1965, **43**, 2696
- 18 Tanaka, T., Yamamoto, M. and Takano, Y. *J. Macromol. Sci. (B)* 1970, **4**, 931

Fracture and mechanical properties of epoxy resins and rubber-modified epoxy resins

Alan C. Meeks

Shell Research Ltd, Egham Research Laboratories, PO Box 11, Egham, Surrey TW20 9NJ, UK
(Received 13 November 1973; revised 16 April 1974)

Fracture and mechanical property data on a wide range of epoxy resin systems are presented. The extent to which toughening can be induced by heterophase rubber inclusions depends more on the curing agent used than on the resin component. The greatest improvements in toughness were obtained by rubber modification of epoxy resins cured with an anhydride. A preformed ABS polymer can be used to toughen many epoxy resin systems. With one major exception (where a large improvement was found) only small changes in tensile properties occur when small amounts of rubber are present.

INTRODUCTION

It has long been known that the resistance of polystyrene to cracking is improved considerably if many small rubber particles are dispersed in the polymer. The principle of toughening by heterophase rubber dispersions has been applied to other thermoplastic polymers, e.g. ABS, and recent work has shown that a similar method is applicable to some thermosetting polymers.

McGarry and coworkers¹⁻³ showed that a low molecular weight, carboxyl terminated, butadiene-acrylonitrile copolymer (Hycar CTBN*) is soluble in a conventional epoxy resin but during cure with amine curing agents, micron sized rubber particles are precipitated. All McGarry's reported work is based on a diglycidyl ether of bisphenol A (DGEBA) type epoxy resin (Epikote 828) cured with amines [tris(dimethylaminomethyl)phenol (DMP-30) or curing agent D]. He evaluated toughness using a double cantilever cleavage test in which a crack was propagated along the grooved median of a parallel sided strip of the test material.

Temperature of cure, curing agent concentration and rubber molecular weight were shown by McGarry to influence the heterophase particle size and concentration and these in turn influenced the fracture energy. For example 10 parts of Hycar CTBN per 100 parts of resin raised fracture energy from 165 Nm/m² to between 1690 and 2720 Nm/m² depending upon the molecular weight of the rubber. The mechanism of toughening was said to be an increase in the extent of crazing and cold drawing but no strong evidence for this was presented. Indeed, evidence which might support the existence of crazing in crosslinked materials has only recently been obtained⁴.

Rowe and coworkers⁵ used a wide range of acrylonitrile-butadiene rubbers as modifiers for amine-cured epoxy resins. Their results showed considerable scatter but confirmed that large increases in fracture energy could be obtained.

Soldatos and Burhans⁶ reported that CTBN raised the tensile strength and the 'ball impact strength' of a cycloaliphatic resin cured with an anhydride. The same resin cured with a boron trifluoride-monoethylamine complex was not significantly toughened by the heterophase so the authors concluded that the nature of the crosslinking agent greatly influences the ability of the rubber to toughen the cured resin system.

The object of the work reported here was to determine the fracture and mechanical properties of crosslinked resins prepared from a wider range of resin and curing agent types than reported hitherto. The results give further information on the factors which control the toughness potential of cured epoxy resins. Hycar CTBN liquid rubber and Blendex 311, a preformed ABS powder, were chosen as the modifiers. The latter emerged as a promising candidate from the screening of several rubbery materials.

EXPERIMENTAL

Preparation of cast resin

Since the materials used differ widely in properties (viscosity, melting point etc.) identical techniques could not be used in the preparation of all the castings. The following general method was used for most systems: (1) resin and rubber were heated to lower the viscosity, if necessary, then blended together using a high shear stirrer. In order to obtain a fine dispersion, Blendex 311 had to be mixed with the resin at about 95°C for 30 min; (2) dissolved and trapped air which would have caused bubbles in the final castings was removed by vacuum degassing the hot blend; (3) curing agent, melted if normally a solid, was stirred into the rubber/resin blend taking care not to entrain more air bubbles; (4) metal moulds treated with silicone release agent and preheated to the required gel temperature were filled with the liquid resin system; (5) curing was carried out in air-circulating ovens for the required gel and cure cycles. These times and temperatures as well as formulation details are given in *Table 1*. On completion of the cure cycle the ovens were switched off and the moulds were

* For sources of commercial materials see Appendix.

allowed to cool slowly to minimize stresses in the resin castings. Step (1) was omitted for the unmodified materials.

Preparation of anhydride-cured resins differed slightly in that the molten anhydride was added to the resin/rubber blend before it was degassed. Accelerator was added after the degassing process.

Fracture testing

The parallel sided double cantilever cleavage test⁷ was used in early work. All resins studied fractured in a 'stick-slip' mode, i.e. crack jumping occurred, so several cracks could be initiated successively on each testpiece. The number of jumps varied between 3 for the toughest material and 50 or 60 for resins with low fracture energy.

Our studies of alternative fracture tests showed that the tapered cleavage test⁸ gave improvements in reproducibility and crack direction control, and so it was used for most of the fracture work reported here. The testpiece shown in *Figure 1* was loaded in tension until crack jumping followed by crack arrest occurred.

Beam theory relates sample geometry and compliance⁸:

$$\frac{dc}{da} = \frac{8}{ET} \left[\frac{3a^2}{H^3} + \frac{1}{H} \right] \quad (1)$$

where c = compliance, a = crack length, E = Young's Modulus, T = sample thickness, H = sample height above tip of the crack.

For the geometry used:

$$H = ka + kb \quad (2)$$

where $k = 0.21$, $b = 3.65$. Substitution of H from equation (2) into equation (1) and integration gives:

$$c = \frac{8}{ET} \left(\frac{1}{k^3} \left[\frac{6b}{(a+b)} - \frac{3b^2}{2(a+b)^2} + (3+k^2) \log_e(a+b) \right] \right) + \text{constant of integration} \quad (3)$$

The term in the outer parentheses of equation (3) and compliance c , were calculated for each crack length and the term $8/ET$ was determined by least squares regression. This value was then substituted in equation (1) to obtain values of dc/da for later use.

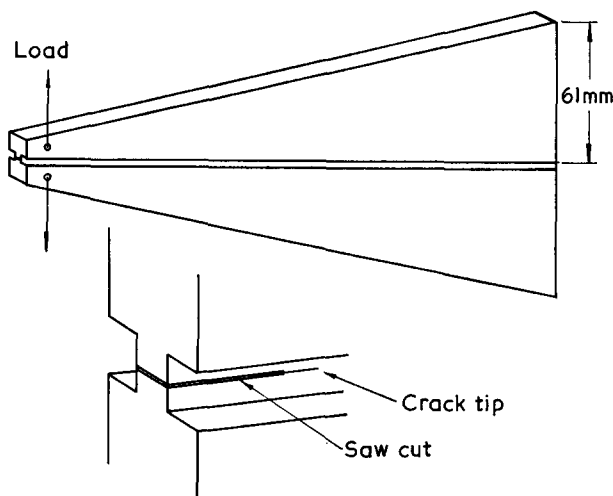


Figure 1 Tapered cleavage testpiece. Sample length, 260mm; thickness, 6mm

The stress intensity factor Kc , is related to fracture load P , crack width W , etc. by the Irwin-Kies relation⁹:

$$Kc^2 = \frac{P^2 E}{2W} \cdot \frac{dc}{da} \quad (4)$$

For generalized plane stress, fracture energy γ , is given by:

$$Kc^2 = 2E\gamma \quad (5)$$

Combining equations (4) and (5)

$$\gamma = \frac{P^2}{4W} \cdot \frac{dc}{da} \quad (6)$$

Thus fracture energy γ was calculated from equation (6) using the value of dc/da obtained previously.

Impact tests were carried out in accordance with ASTM D256-56. Tensile properties were measured using an Instron Model TT-D testing machine and Instron strain gauge extensometers. Samples similar to those described in ASTM D1708-66 were cut from 3 mm thick resin plates.

RESULTS AND DISCUSSION

Formulations and cure conditions of all systems studied are listed in *Table 1*. The effects of cure time and temperature on the glass transition temperatures (T_g) of the cured compositions were determined in separate experiments. Conditions used for the preparation of test samples were chosen as a balance between achieving maximum T_g and using convenient cure times. Higher T_g values could have been achieved under more severe conditions but thermal degradation might then have occurred.

Because of the wide range of curing agents and resin types which we have studied it is convenient to divide the results and discussion into sections. In this way one or more of the variables can be held constant to simplify the interpretation of effects.

Effect of curing agent on resin toughness

The limited literature information on toughening of epoxy resins indicates that the degree of toughening by rubbery modifiers depends on which curing agent is used to crosslink the resin. To check and amplify this finding we have determined the effect of a wide range of curing agents on fracture and tensile properties of a conventional resin (a diglycidylether of bisphenol A) of low polydispersity (Epon 825). A liquid rubber which was compatible with the uncured resin and a preformed ABS powder were used as the modifiers.

Results given in *Table 2* show that Hycar CTBN reduces the tensile modulus, in proportion to the rubber concentration. As a rough approximation a given percentage of Hycar in the final resin reduces the tensile modulus by twice that percentage. The effect on tensile strength is less clear cut however, changes varying from a 35% reduction to a 30% increase. Changes in elongation at break are usually not statistically significant because of the large scatter in this measurement. With two major exceptions glass transition temperatures (determined by torsion pendulum at about 0.7 Hz) are unaffected by the presence of the rubber. The 30°C reduction in T_g of the catalytically cured and NMA-cured resins is probably due to incomplete cure not caused by the presence of Hycar.

Table 1 Formulations and curing conditions

Resin	Curing agent (parts)*	Accelerator (parts)*	Gel		Cure	
			Time (h)	Temp. (°C)	Time (h)	Temp. (°C)
Epon 825	ED (8.6)	—	48	23	3	120
			2	80		
			0.5	60		
Epon 825	HMD (16.7)	—	2	100	24	150
			2	100		
Epon 825	DDM (28.4)	—	1	100	1	200
Epon 825	MPD (15.5)	—	24	23	18	150
			2	120		
			2	100		
Epon 825	DMP-30 (4.0)	—	2	100	12	175
Epon 825	HHPA (88.5)	BDMA (1.0)	2	100	6	140
Epon 825	NMA (102.3)	BDMA (3.0)	—	—	12	200
Epon 825	Epikure BF ₃ 400 (3.0)	—	0.5	60	12	175
			2	100		
			1	120		
Epikote 171	HHPA (100)	BDMA (1.0)†	2	120	4	160
Epikote 190	HHPA (97)	BDMA (0.3)	2	100	6	140
Epikote 191	HHPA (100)	Epikure 110 (6.0)	—	—	8	140
Epikote 828	HHPA (80)	BDMA (1.0)	2	100	6	140
Epikote 828	DDM (27)	—	1	100	2	125
			1	100	1	200
Epikote 828	MPD (14.6)	—	2	80	4	160
Epikote 828	DMP-30 (4.0)	—	2	100	4	125
Epikote 154	Epikure BF ₃ 400 (3.0)	—	4	105	4	200

* Parts by weight per 100 parts of resin

† Plus 1.5 parts of ethylene glycol

BDMA=benzylidimethylamine; DDM=diaminodiphenylmethane; ED=ethylenediamine; HMD=hexamethylene diamine; MPD=*m*-phenylene diamine; NMA=Nadic methyl anhydride

Table 2 Fracture and mechanical properties of Epon 825 cured resin systems at 23°C

Tensile data based on mean values for 8 tests

Fracture energy data based on minimum of 2 testpieces (data at each arrest point); standard deviation of fracture energy was usually about 10%

Type of curing agent	Curing agent	Hycar CTBN (% wt in cured product)	Tensile properties			Cleavage fracture energy (J/m ²)	Glass transition temperature (°C)
			Strength (MN/m ²)	Modulus (GN/m ²)	Elongation at break (%)		
Aliphatic amines	ED	—	70.4 ± 10.6	2.76 ± 0.02	6.48 ± 0.31	60	—
	ED	8.43	58.9 ± 1.5	2.22 ± 0.09	7.77 ± 0.98	136	—
	HMD	—	58.0 ± 3.9	2.28 ± 0.13	5.75 ± 0.78	104	127
Aromatic amines	HMD	7.89	49.4 ± 3.6	1.92 ± 0.16	7.83 ± 0.94	175	117
	DDM	—	75.7 ± 3.4	2.67 ± 0.05	6.12 ± 0.60	66	180
	DDM	7.23	60.0 ± 5.0	2.30 ± 0.12	5.05 ± 0.80	87	179
Other amines	MPD	—	78.4 ± 6.5	2.97 ± 0.14	6.20 ± 0.84	58	181
	MPD	7.97	50.7 ± 7.7	2.43 ± 0.13	3.26 ± 0.80	74	189
	Piperidine	—	51.4 ± 11.4	3.00 ± 0.05	7.60 ± 2.26	—	89
Anhydrides	Piperidine	8.70	58.0 ± 1.9	2.72 ± 0.07	8.10 ± 0.48	—	93
	DMP-30	—	74.2 ± 1.4	2.73 ± 0.02	5.45 ± 0.47	126	124
	DMP-30	8.77	60.5 ± 3.7	2.24 ± 0.21	6.43 ± 1.04	127	125
Catalyst	HHPA	—	83.8 ± 5.9	2.92 ± 0.13	6.22 ± 2.02	27	143
	HHPA	5.01	79.8 ± 3.6	2.66 ± 0.13	5.48 ± 0.32	140	140
	NMA	—	60.2 ± 1.7	3.62 ± 0.07	2.09 ± 0.26	24	136
Catalyst	NMA	4.64	78.2 ± 1.2	3.25 ± 0.38	5.06 ± 0.41	162	106
	Epikure	—	47.3 ± 3.8	2.79 ± 0.15	2.04 ± 0.46	—	200
	BF ₃ 400	8.85	49.7 ± 3.6	2.44 ± 0.09	3.18 ± 0.63	42	170

± Values represent standard deviations of one result

Fracture toughness of the resin with the highest degree of crosslinking (the BF₃400-cured material) is reduced by Hycar but in every other case studied, fracture energy and critical stress intensity factor are increased. The magnitude of the increases depend upon the type of curing agent used. There is little difference between the effects of curing agents of a particular class but this may be due to similarity of chain lengths. Unmodified resins which had relatively high fracture energies were less readily toughened than the more brittle materials. The ability of CTBN to toughen the resin matrix increases in the curing agent series: aromatic amines, aliphatic amines, anhydrides. Both anhydrides raised fracture energy of Epon 825 by a factor of about 5 and similar improvements are described later for other epoxy resins cured with anhydride.

We were unable to measure fracture energies of piperidine-cured resins using the cleavage test because of the difficulty in introducing the initial crack into test-pieces. The use of blunt initial cracks gave high apparent fracture energies. However, more recent work has shown that when sharp cracks are produced in SEN testpieces of this system the material is not as tough as anticipated. In conflict with McGarry's work¹ we found no toughening effect of Hycar on DMP-30 cured resin but this may be due to differences in cure conditions producing different heterophase particle size and extent of cure of the resin matrix. Fracture surfaces of this system showed 0.5 μm diameter irregular markings which appeared to be holes and there was little evidence for protruding heterophase particles (Figure 2).

The effects of the curing agent on ease of toughening of resins may be due to differences in compatibility between the rubber and the resin/curing agent system. In the case of a compatible rubber/resin blend the addition of curing agent will alter the solubility of the rubber in the total system and influence phase separation.

The anhydrides which are reacted with the epoxy in nearly equal proportions will change the compatibility markedly. Catalytic curing agents (DMP-30, BF₃400 etc.) are used in small amounts so compatibility will

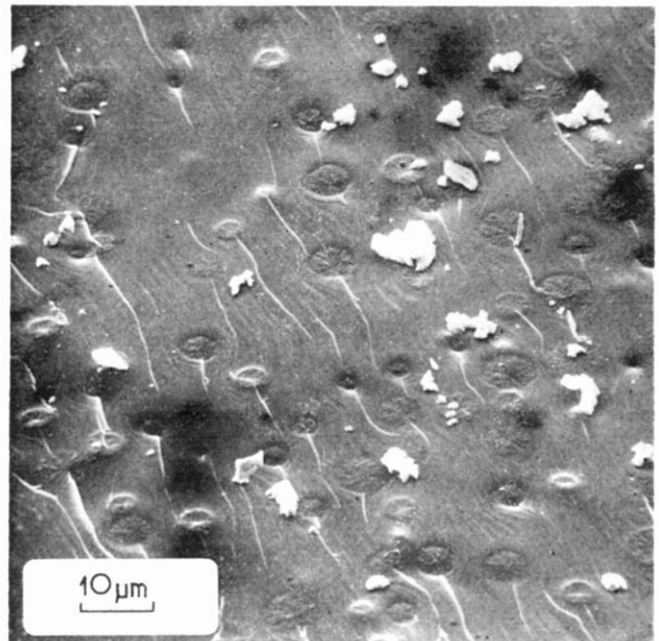


Figure 3 Fracture surface of Epon 825/BF₃400/Hycar CTBN

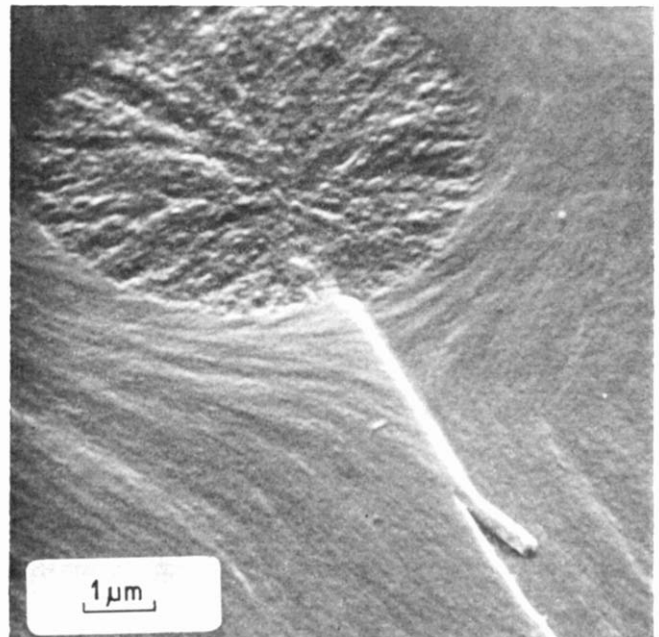


Figure 4 Fracture surface of Epon 825/BF₃400/Hycar CTBN

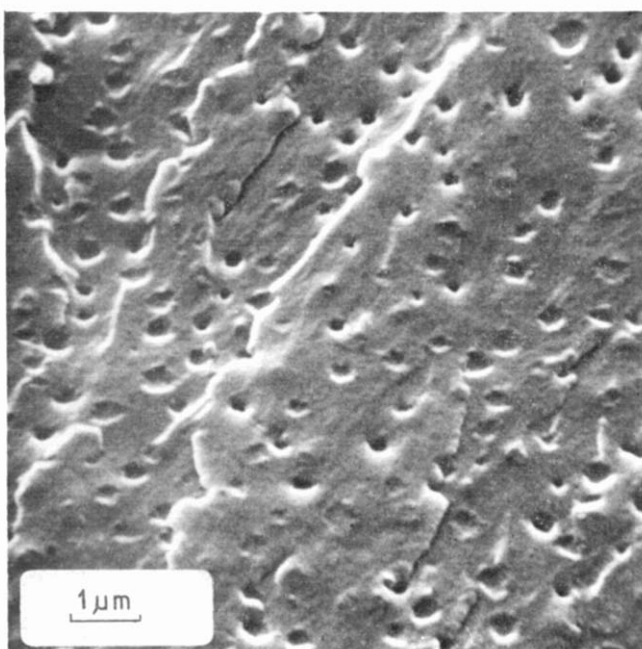


Figure 2 Fracture surface of Epon 825/DMP-30/Hycar CTBN

be governed more by the epoxy/rubber solubility. Thus the extent to which phase separation occurs during polymerization will depend upon the curing agent type and amount. Since the reactions which occur during cure are complex (chain extension of the epoxy, polymerization of the CTBN etc.) phase separation will be further affected. If preformed rubber particles are used as the modifier, particle size will not change significantly during cure but matrix-particle bonding will influence any toughening effect.

These comments are qualitatively in accord with our findings that Hycar CTBN is highly compatible with anhydride-containing resins (1:1 resin/curing agent) and no heterophase is produced during cure. The system which contained the smallest amount of curing agent, BF₃400 (100:3 resin/curing agent), contained

the largest heterophase particles. These particles (see *Figure 3*) were between about 4 and 8 μm in diameter and steps on the fracture surfaces intersected or originated from most of the particles (*Figures 3* and *4*). Aliphatic diamine-cured resins (100:10 to 30 resin/curing agent) containing Hycar CTBN were opaque and contained intermediate sized particles between about 0.5 and 2 μm in diameter (*Figure 5*).

Anhydride-cured resins

In the previous section it was demonstrated that Hycar CTBN greatly improves the fracture toughness of Epon 825 cured with hexahydrophthalic anhydride (HHPA). Results given in *Table 3* show this to be a more general effect for a range of resins, which includes both aromatics and cycloaliphatics, cured with HHPA.

The cycloaliphatic resin Epikote 171 is toughened in proportion to the Hycar concentration. The unmodified system has a rather low tensile strength but this is doubled when 4.7% of Hycar or Blendex is present. A

similar strengthening effect has previously been reported⁶ and is probably due to the reduction of flaw sensitivity of the system by raising the ductility of the material. Where comparisons are available Blendex 311 has the same effect on fracture properties as the same proportion of Hycar CTBN. Impact strengths are raised to a lesser extent than the lower strain rate fracture energy. Blendex is less effective than Hycar in raising impact strength probably because of the higher T_g components, polyacrylonitrile and polystyrene, in Blendex.

There are obvious morphological differences between the Hycar and Blendex-containing materials. Hycar modified resins (anhydride cured) are transparent or show only slight cloudiness and scanning electron microscopy (s.e.m.) examination shows no well developed heterophase. However, the resins which contain Blendex are translucent or opaque and s.e.m. shows the presence of irregular heterophase particles (*Figure 6*) of the same form as the Blendex powder. The mechanism of toughening in this case may be similar to the craze mechanism

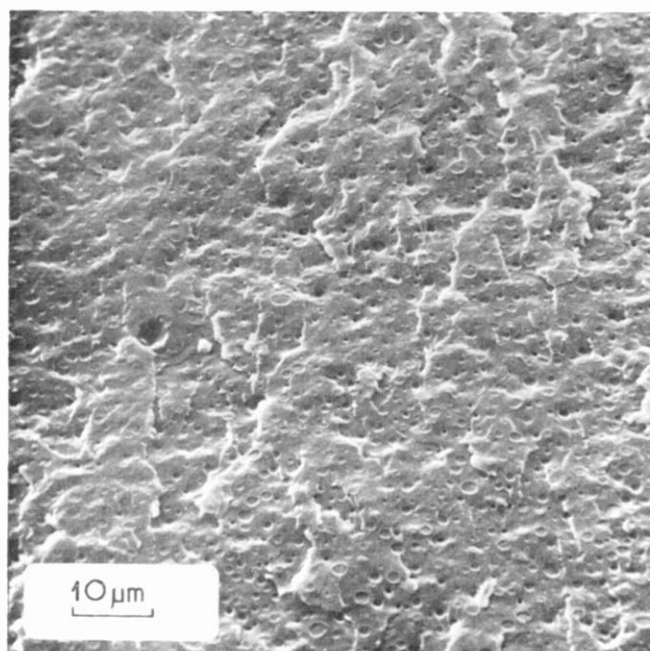


Figure 5 Fracture surface of Epon 825/ethylene diamine/Hycar CTBN

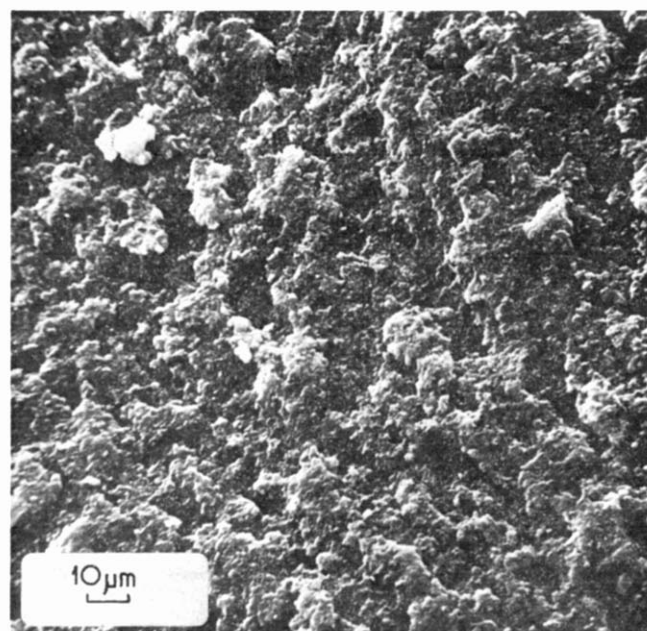


Figure 6 Fracture surface of Epikote 828/Epikure MPD/Blendex 311

Table 3 Fracture and mechanical properties of HHPA cured resins at 23°C

Resin	Rubber modifier	Rubber (% wt in cured resin)	Tensile properties			Cleavage fracture energy (J/m ²)	Impact strength (kJ/m ²)
			Strength (MN/m ²)	Modulus (GN/m ²)	Elongation at break (%)		
Epikote 171	—	—	34.0	2.95	1.15	24	1.05
	Hycar CTBN	4.7	67.9	2.74	3.45	42	1.16
	Hycar CTBN	11.0	60.3	2.29	3.75	68	1.31
	Hycar CTBN	16.5	56.1	1.92	4.80	90	1.42
	Blendex 311	4.7	71.7	2.74	3.95	37	1.00
Epikote 190	—	—	89.7	3.35	—	18	1.21
	Hycar CTBN	4.8	78.2	3.39	6.8	165	1.79
Epikote 191	—	—	—	—	—	—	—
	Blendex 311	2.4	—	—	—	—	—
	Blendex 311	4.6	—	—	—	—	—
Epikote 828	—	—	—	—	—	37	1.23
	Hycar CTBN	10.0	—	—	—	240	1.85
	Blendex 311	10.0	—	—	—	258	1.36

Table 4 Fracture and mechanical properties of various resin systems at 23°C

Resin	Curing agent	Rubber (% wt in cured resin)	Tensile properties				
			Strength (MN/m ²)	Modulus (GN/m ²)	Elongation at break (%)	Fracture energy (J/m ²)	Impact strength (kJ/m ²)
Epikote 154	Epikure BF ₃ 400	—	33.2	3.43	1.20	16	
		Hycar CTBN (8.8)	33.3	2.66	1.75	27	
Epikote 828	Epikure DDM	—	79.3	2.94	6.7	170	
		Hycar CTBN (7.3)	67.4	2.43	6.3	230	
Epikote 828	MPD	Hycar CTBNX (7.3)	67.1	2.39	5.5	200	
		Blendex 311 (15)	87.1	3.25	7.5	55	3.1
Epikote 828	Epikure DDM	—	63.2	2.49	9.6	250	4.1
		Herclor H (7.3)	—	—	—	85	3.0
Epikote 828	DMP-30	—	—	—	—	140	2.6
		Hycar CTBN (8.8)	—	—	—	90	
						140	

operative in some thermoplastics. The extent to which crazing could occur in thermosets will be hindered by the crosslinks¹⁰. Holloway⁴ has found evidence for crazing in thermosets but there is no other evidence in the literature.

The mechanism of toughening of anhydride-cured epoxies by Hycar is also in doubt since no heterophase appears to be present. If it acted solely as a flexibilizer (i.e. a compatible long chain material which raises the molecular weight between crosslinks) a reduction in T_g would be expected even at low concentrations of the modifier. In these systems, T_g is usually not significantly altered so a flexibilization process is not supported.

Failure in tension of the Hycar-containing diglycidyl ester Epikote 191, cured with HHPA, is accompanied by extensive shear deformation and fracture surfaces are extremely irregular under s.e.m. Blendex modified diglycidyl esters and cycloaliphatics usually undergo marked stress whitening, the whole of the gauge section of the tensile dumbbell becoming whitened, at stresses close to the ultimate. Whitening could have been caused by failure of the resin/heterophase bond or by microcavitation as in crazing, but we do not know which mechanism occurred here. Fracture surfaces are irregular with both modifiers and this is consistent with the similarity in toughening effect. Fracture surfaces of Hycar-containing resins cured with amines are completely different and show spherical particles or voids due to pull-out of poorly bonded particles. A deeper insight into the mechanism of failure could be gained using Bucknall's technique¹¹ of determining the lateral and longitudinal creep at high strains. This would indicate the relative importance of crazing and shear deformation.

Other resin systems

Toughness improvements produced by Hycar and Blendex have been observed in other types of resin/curing agent systems (see Table 4) but the increases are usually smaller than those observed in anhydride cured resins. The Hycar-containing resins were opaque, and spherical markings up to about 10 μ m in diameter were present on fracture surfaces. These markings were usually in the form of craters which may originally have contained poorly bonded heterophase particles. Few well defined particles were identified except in the case of Epikote 154/BF₃400/Hycar CTBN where the fracture plane cut through the particles themselves and steps on the fracture

surface intersected most of the particles. The particles appear to have a resolvable fine structure (Figures 3 and 4).

The Epikote 828/MPD system is exceptional among amine-cured resins in that it may be toughened by rubber modifier. Blendex 311 (15%) raises fracture energy by a factor of 5 and impact strength is improved by 30%. Fracture surfaces were extremely rugged.

CONCLUSIONS

The results reported here confirm that the curing agent has an important effect on the ability of certain rubbers to toughen cured epoxy resins. Anhydrides have been shown to be the most useful in this respect with only modest toughening being observed with most of the other curing agents used. Scanning electron microscopy has shown that the compatibility between the resin and the rubber is greatest with anhydrides; indeed no heterophase was visible in resin/anhydride materials containing added Hycar. The presence of a distinct heterophase is not essential for toughening even when flexibilization does not occur.

The mechanism of toughening remains obscure but toughening is favoured when the resin system and the rubber are compatible.

In general the tensile properties and glass transition temperature are little affected by the small rubber loadings necessary to raise fracture toughness.

Generally Blendex 311 (itself a toughened polymer) is at least as good a toughening agent as Hycar CTBN and it will also toughen some systems which are unaffected by Hycar. We have yet to find a resin system whose fracture toughness cannot be improved by Blendex 311.

REFERENCES

- McGarry, F. J. and Willner, A. M. *MIT Dept. Civil Eng. Rep. R68-8* 1968 (March)
- McGarry, F. J. and Sultan, J. N. *24th A. Tech. Conf. SPI* 1969, Section 11-B
- McGarry, F. J. and Willner, A. M. *ACS Div. Org. Coat. Plast. Chem. Prepr.* 1968, 28, paper 55
- Holloway, D. G. personal communication
- Rowe, E. H., Siebert, A. R. and Drake, R. S. *Mod. Plast.* 1972, p 110
- Soldatos, A. C. and Burhans, A. S. *25th A. Tech. Conf. SPI* 1970, Section 3-C
- Berry, J. P. *J. Appl. Phys.* 1963, 34, 62

- 8 Marshall, G. P., Culver, L. E. and Williams, J. G. *Plastics and Polymers* 1969, **37**, 75
 9 Irwin, G. R. and Kies, J. A. *Weld. J. Res. Suppl.* 1954, **33**, 1935
 10 Kambour, R. P. *Macromol. Rev.* 1973, **7**, 1
 11 Bucknall, C. B., Clayton, D. and Keast, W. E. *J. Mat. Sci.* 1972, **7**, 1443

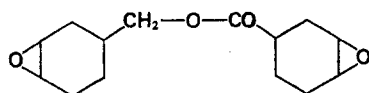
APPENDIX

Commercial materials and suppliers

Epikure BF₃400 Boron trifluoride-monoethylamine complex
 Shell Chemicals UK Ltd

Epikote 154 An epoxy-novolac resin
 Shell Chemicals UK Ltd

Epikote 171 Epoxy resin of the type



Shell Chemicals UK Ltd

Epikote 190 Diglycidyl ester of tetrahydrophthalic acid
 Shell Chemicals UK Ltd

Epikote 191 Diglycidyl ester of hexahydrophthalic acid
 Shell Chemicals UK Ltd

Epikote 828 Diglycidyl ether of bisphenol A and homologues
 Shell Chemicals UK Ltd

Epon 825 Similar to Epikote 828 but with a narrower molecular weight range
 Shell Chemical Co.

Blendex 311 An acrylonitrile-butadiene-styrene (ABS) copolymer with high butadiene content
 Marbon (UK) Ltd

Hycar CTBN A carboxyl-terminated acrylonitrile-butadiene copolymer
 B. F. Goodrich Chemical Company

Herclor H Epichlorohydrin elastomer
 Hercules Powder Co. Ltd

Chain conformation in molten polyethylene by low angle neutron scattering

The technique of low angle neutron scattering from solid solutions of isotopically labelled chains has recently been developed to measure molecular dimensions in bulk amorphous polymers. We have now applied this technique to the study of a crystallizable polymer (polyethylene). The principles of the method have already been described in detail¹⁻⁴. A small number of isotopically labelled chains (tagged molecules) are dispersed in a matrix of polymer molecules to form the sample and the scattering from the tagged molecules is obtained by subtracting the scattering of an equivalent blank (without tagged molecules) from the sample scattering.

For these measurements two series of samples were prepared. Series 1 consisted of five samples with a protonated polyethylene (PEH) matrix with 5, 4, 2, 1 and 0.5% (by wt) of linear deuterated polyethylene (PED) as tagged molecules. Series 2 consisted of two samples with a PED matrix and 5 and 0.75% PEH as tagged molecules. For all samples equivalent blanks with no tagged molecules were prepared. Thermal analysis of both PEH and PED with a Perkin-Elmer DSC 2 instrument gave peak melting points of $135 \pm 1^\circ\text{C}$ and $128 \pm 1^\circ\text{C}$ respectively after slow cooling from the melt. These melting points are consistent with linear PEH and PED molecules⁵. For all samples the tagged and matrix molecules were matched in molecular weight.

All samples were prepared by dissolving PED and PEH in the required proportions in boiling xylene (boiling range $137-142^\circ\text{C}$) and precipitating into excess methanol. Samples were then pressed into bubble free films approximately 1 mm thick. During the course of the experiments it was discovered that prolonged boiling in xylene can apparently cause exchange of H and D atoms, and it was therefore necessary to measure X , the degree of deuteration of the PED chains after the mixing process. This was accomplished by standard n.m.r. techniques.

The experimental procedures for scattering measurements, temperature control etc. are identical to those described earlier⁴. Measurements of the differential scattering cross-section per unit solid angle $(d\Sigma/d\Omega)(k)$ were performed as a function of $k = (4\pi/\lambda)\sin\theta$ (where $\lambda = 8 \text{ \AA}$ is the incident wavelength and 2θ is the scatter angle), in the range $0.005 < k < 0.04 \text{ \AA}^{-1}$. Data were taken initially at 25°C and then at 150°C for all samples. Figure 1 shows a 25°C plot of $(d\Sigma/d\Omega)(k)/K_N C$ vs. k for the 0.5% sample of series 1 (K_N is a calibration constant⁴ and $C = 0.005$ is the concentration of tagged molecules).

Also shown is the scattering from the equivalent blank, and the general (flat) background level of incoherent scattering originating almost completely from ^1H nuclei. From this Figure we conclude that the difference scattering is due to the tagged molecules.

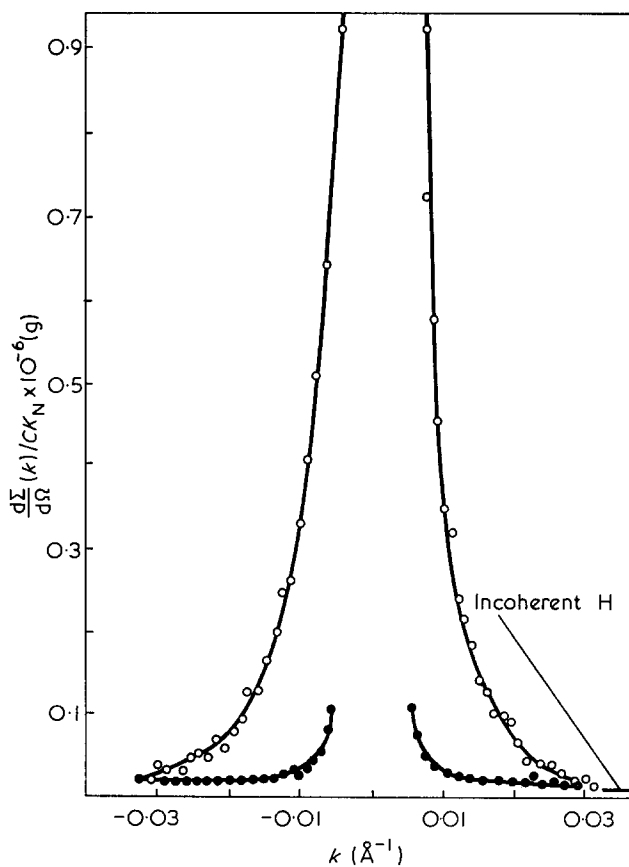


Figure 1 Scattering patterns from PEH matrix with 0.5% PED molecules (O) and from blank with PEH matrix (●)

The upturn in the blank scattering at low k is due to void scattering from the matrix. Normally void scattering dominates low angle X-ray scattering patterns from polyethylene, but in the case of neutron scattering from PEH, cancellation between the positive scattering length of ^{12}C ($b_c = +0.66 \times 10^{-12} \text{ cm}$) and the negative scattering from ^1H ($b_H = -0.37 \times 10^{-12} \text{ cm}$) means that the coherent neutron scattering is almost completely eliminated. The scattering is proportional to the mean square density of coherent scattering amplitudes ρ_{COH}^2 which is 0.11 for PEH (in 10^{20} cm^{-4} units). In PED, on the other hand, there is no such cancellation (as $b_D = +0.62 \times 10^{-12} \text{ cm}$ for ^2D) and $\rho_{\text{COH}}^2 = 64.0$ in the same units. This means that the low angle data are dominated by background (void) scattering as in the case of low angle X-ray scatter patterns. Measurements of molecular dimensions in a solid PED matrix are therefore virtually impossible and were not attempted.

In the melt, however, measurements on samples with both PEH and PED matrices are possible as voids can be eliminated from the matrix owing to the expansion on melting. Provided the amount of dissolved air in the system is sufficiently low the voids are eliminated and the background scattering drops by several orders of magnitude when the samples are melted, to the point where the blank scattering again represents only a small correction to the sample scattering at low k . Figure 2 shows the scattering from the tagged molecules from the 5% sample of series 2 (i.e. after subtraction

of the blank) showing that measurements are quite feasible in the melt with a PED matrix. Figure 3 shows the equivalent Guinier plot which is linear as required. Table 1 shows the values of radius of gyration, $\langle S^2 \rangle^{1/2}$, for series 1 samples in the melt. The measured data represent the Z average which is then converted to a weight average⁶. Also shown is $(1/K_N C)(d\Sigma/d\Omega)(k)$ extrapolated to $k=0$. The extrapolated values give the molecular weight when themselves extrapolated to $C=0^4$. However, these values may be taken as good estimates of (weight averaged) molecular weight assuming a zero virial coefficient for the solution as found in deuterio- and proto-polystyrene^{3, 4} and PMMA solutions².

Comparison of these estimates with those determined by a combination of g.p.c. and intrinsic viscosity measurements, also shown in Table 1, reveals a marked discrepancy for some samples (4% and 1%).

This discrepancy is definitely outside the experimental error, and any error in the absolute calibration procedures is ruled out by the correct prediction of the background incoherent scattering level (Figure 1). Also measurements on polystyrene which were performed simultaneously with PEH/PED measurements gave exact agreement between neutron and osmometry methods for molecular weight⁴. The same tagged molecules were used in all samples and it may be seen that as the apparent molecular weight increases so does the apparent radius of gyration. Table 2 shows the equivalent results for series 2 and again the same pattern is evident with one sample showing an apparent molecular weight higher than the true molecular weight and a correlation between high apparent molecular weight and a higher value of radius of gyration.

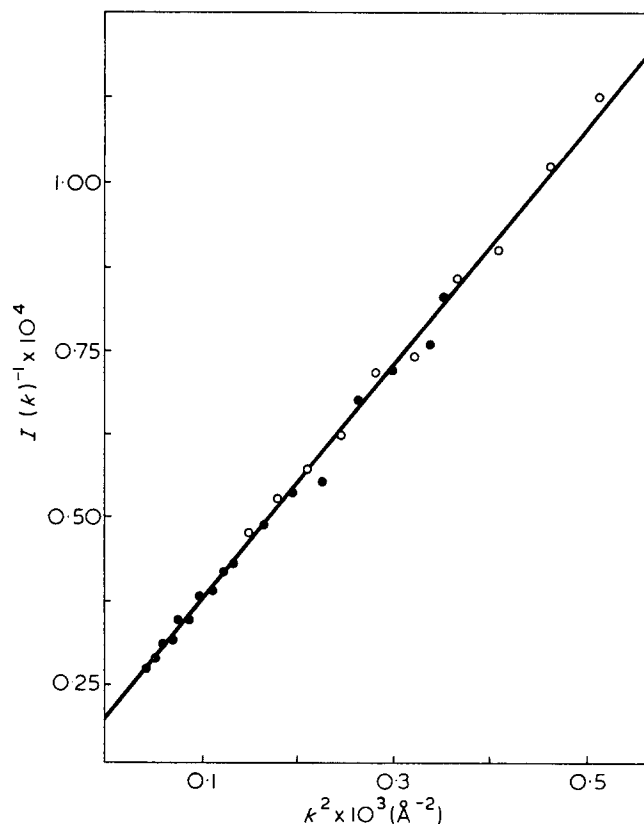


Figure 3 Guinier plot for 5% PEN molecules in PEH matrix. O and ● represent scattering on both sides of the $k=0$ position

Table 1 Molecular dimensions of series 1 samples (with PEG matrix) at $T=150^\circ\text{C}$

Concentration PED (%)	$\langle S^2 \rangle_Z^{1/2}$	$\langle S^2 \rangle_W^{1/2}$	$\frac{1}{K_N C} \frac{d\Sigma}{d\Omega}(k)$ at $k=0 \times 10^5(\text{g})$
5.0	250	207	1
4.0	365	300	6
2.0	230	190	2
1.0	350	287	10

Tagged molecules (PED): $M_w=150\ 000$; $M_w/M_n=2.2$

Table 2 Molecular dimensions of series 2 samples (with PED matrix) at $T=150^\circ\text{C}$

Concentration PEH (%)	$\langle S^2 \rangle_Z^{1/2}$	$\langle S^2 \rangle_W^{1/2}$	$\frac{1}{K_N C} \frac{d\Sigma}{d\Omega}(k)$ at $k=0 \times 10^5(\text{g})$
5.0	185	167	1.0
	190	171	0.6
	172	155	0.66
0.75	200	180	2.5

Tagged molecules (PEH): $M_w=61\ 000$; $M_w/M_n=1.3$

If we consider first samples with molecular weights close to the true value (5, 2% in series 1 and 5% in series 2) we find a value of $K = \langle S^2 \rangle_W^{1/2} / M_w^{1/2}$ of 0.52 for series 1 and 0.74 for series 2. Comparing these values with the values in θ solvents⁷ we find estimates of K_θ in the range $K_\theta = 0.45 \pm 0.08$. Thus the chain dimensions in the melt appear to be close to those found in θ solvents.

We believe that the results giving significantly higher molecular weights and radius of gyration can be best explained as follows.

The expected value of molecular weight is based on the assumption that the tagged molecules scatter inco-

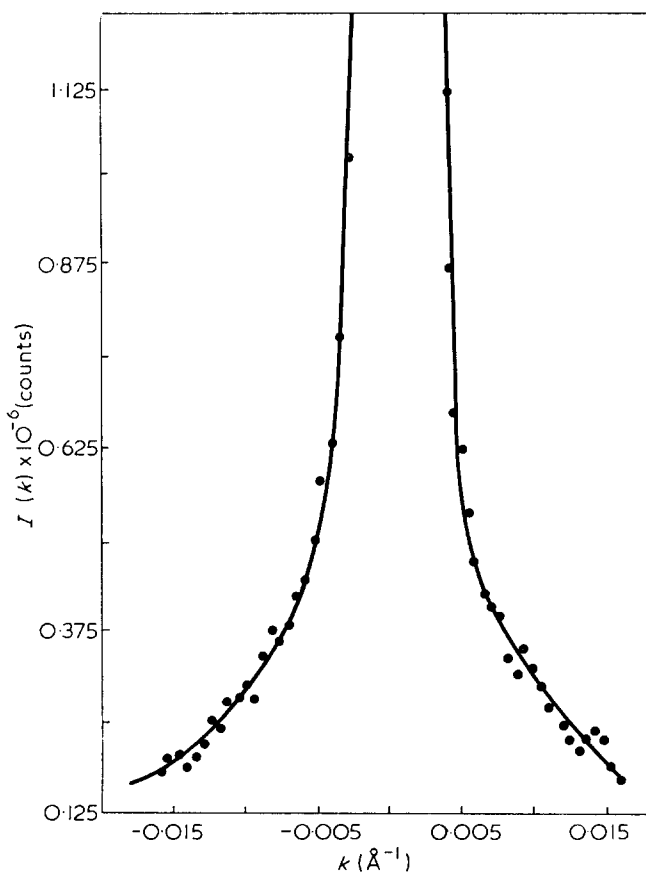


Figure 2 Scattering pattern from 5% PEH molecules in PED matrix after correction for the blank scattering

herently with respect to each other, in order that the scattering is described by:

$$\frac{d\Sigma^{\text{inc}}(k)}{d\Omega} = M \cdot CK_N \langle [f(k)]^2 \rangle \quad (1)$$

$$K_N = \rho \left[2X \cdot \frac{1}{M_{\text{CD}_2\text{xH}_2(1-x)}} (b_D - b_H)^2 \right] A_0 \quad (2)$$

where $\rho = 0.92 \text{ g/cm}^3$ is the density, $X = 0.88$ is the degree of deuteration of the PED chains, $M_{\text{CD}_2\text{xH}_2(1-x)} = 15.78$ is the same mass of a (partly deuterated) chain segment, A_0 is Avogadro's number and b_D and b_H are the scattering lengths of ^2D and ^1H .

The small angle scattering from a sample which consists of two types of molecules A and B with concentrations C_A and C_B can be derived from first principles and the cross-section $d\Sigma/d\Omega(k)$ is given by:

$$\frac{d\Sigma}{d\Omega}(k) = MK_N C \left\{ \langle [f(k)]^2 \rangle + \int d_3r p_a(r) \alpha(r) \langle f_x(k) f_{x+r}^*(k) \rangle \exp(i\mathbf{k}r) \right\}$$

where $f_x(k)$ is the form of a molecule, whose centre of mass is at a position x , $f_x(k)$ is unity for $k=0$. $p_a(r)$ is the mean probability of finding a molecular centre of mass at a distance r from the origin, which is also the centre of mass of another molecule. $\alpha(r)$ is the short range order parameter defined by $\alpha(r) = -n_{AB}(r)/C_B$, where $n_{AB}(r)$ is the probability of finding a B (tagged) molecule B at a distance r from the origin, which is the centre of an A (protonated) molecule ($C_B = C$). The first term in equation (3) is the incoherent part of the scattering cross-section, which is already described in equation (1).

Two conditions have to be fulfilled in order to achieve accordance with the experimental result $(d\Sigma/d\Omega)(k)$ much larger than $d\Sigma^{\text{inc}}/d\Omega$:

$$(1) \quad \langle f_x(k) \cdot f_{x+r}^*(k) \rangle \neq 0$$

$$(2) \quad \alpha(k) \neq 0$$

Not only the configurations of two different molecules must be correlated but also a correlation in space between the centres of the tagged molecules must be assumed. It is understandable, that for polystyrene with its Gaussian configuration, the first condition does not hold and therefore only $d\Sigma^{\text{inc}}/d\Omega$ has been measured independent of a possible heterogeneity of the sample. However, if one assumes correlations of the configuration of neighbouring molecules in a sample of polyethylene, the tagged molecules have to be statistically distributed in the sample in order to measure only $d\Sigma^{\text{inc}}/d\Omega$. Conversely one reason why some experimental values are greater than $d\Sigma^{\text{inc}}/d\Omega$ would be a non-statistical distribution, i.e. clusters of tagged molecules. This possibility would also explain that as $d\Sigma/d\Omega$ exceeds $d\Sigma^{\text{inc}}/d\Omega$ then the apparent radius of gyration grows, as the size of the cluster is convoluted with the molecular conformation to give a higher radius of gyration. The reason why molecules might cluster is the small thermodynamic differences between PED and PEH molecules⁵.

The tendency to clustering appears to be much marked in the solid state as may be seen from Table 3, where the tagged molecules appear to form clusters of 15–30 molecules. It appears that on melting the correlations

Table 3 Molecular dimensions of series 1 samples (with PEH matrix) at $T = 25^\circ\text{C}$

Concentration PED (%)	$\langle S^2 \rangle_z^{1/2}$	$\langle S^2 \rangle_w^{1/2}$	$\frac{1}{K_N C} \frac{d\Sigma}{d\Omega}(k)$ at $k=0 \times 10^5$ (g)
5.0	550	442	24
4.0	480	386	14
2.0	500	402	14
1.0	470	378	28
0.5	470	378	29

Tagged molecules (PED): $M_w = 150\,000$; $M_w/M_n = 2.2$

(clusters) of the configurations partly disappear and therefore $d\Sigma/d\Omega$ comes closer to $d\Sigma^{\text{inc}}/d\Omega$ and correspondingly the measured radius of gyration approaches that for a single molecule.

We may remark in passing that relative measurements of intensity which are not calibrated in absolute units and hence cannot yield an absolute estimate of $(1/K_N C)(d\Sigma/d\Omega)(k) = k=0$ are very misleading. There is no way of checking whether the molecular weight is correct and of estimating the degree of clustering if any. Where absolute measurements are performed conclusions can be restricted to specimens exhibiting the correct molecular weight for which the radius of gyration corresponds to that of a single molecule (5, 2% of series 1 and 5% of series 2 in the melt). Conversely samples exhibiting anomalously high molecular weights which very probably contain clusters (all samples at $T = 25^\circ\text{C}$) can be recognized. This cross-checking procedure is not possible with relative measurements performed with arbitrary intensity units.

Our findings and their interpretation in terms of clustering could have important implications for recent studies of chain re-entry in polyethylene crystals^{8,9}. Bank and Krimm (BK)⁹ used experimental infra-red studies of mixed crystals of PEH and PED to distinguish between chain folding with adjacent re-entry and random re-entry. Basing their interpretation on the earlier work of Tasumi and Krimm they concluded that folding occurred with adjacent re-entry for both dilute solution grown crystals and melt crystallized polymer. This interpretation was subsequently challenged by Stehling *et al.*⁵ (SEM) whom claimed that while adjacent re-entry could account for the observed infra-red splittings, these splittings could also arise from compositional heterogeneity of crystals formed at different stages of crystallization in the samples. Subsequently Krimm and Ching¹⁰ replied that compositional heterogeneities had been recognized in the infra-red analysis and that a detailed analysis of the results of SEM provided additional support for the interpretation of BK. While we do not wish to comment on this discussion we would like to make the point that even if there is no appreciable overall heterogeneity between crystals formed at different stages of crystallization, our results indicate the possibility of heterogeneity at the molecular level, i.e. clustering of like molecules within crystals of the same overall composition. BK used sample preparation methods similar to ours in making mixed crystals of polyethylene, mixing the components in *p*-xylene and cooling from the melt. If clustering were present in their samples then part or all of the infra-red splitting might arise from this source.

Clearly more work is needed to establish whether clustering occurs under the conditions used by BK,

and to use different methods of sample preparation to avoid this problem. Only in samples where clustering has been shown to be absent can unequivocal conclusions be drawn concerning the conformation from infra-red or neutron data in solid polyethylene.

Acknowledgements

The authors wish to acknowledge the help and advice of Dr J. C. Padget (ICI Corporate Laboratory) and Dr R. W. Hendricks (Oak Ridge National Laboratory) in sample preparation and data evaluation respectively.

J. Schelten

Institut für Festkörperforschung,
KFA Jülich 1, West Germany
Present address: Metals and Ceramics Division,
Oak Ridge National Laboratory,
Oak Ridge, Tenn. 37830, USA

G. D. Wignall

ICI Europa Research and Development Ltd,
B-3078 Everberg, Belgium

and D. G. H. Ballard

ICI Corporate Laboratory,
The Heath, Runcorn,
Cheshire WA7 4QE, UK
(Received 1 July 1974)

References

- 1 Kirste, R. G., Kruse, W. A. and Schelten, J. *Makromol. Chem.* 1973, **162**, 299
- 2 Ballard, D. G. H., Schelten, J. and Wignall, G. D. *Eur. Polym. J.* 1973, **9**, 965
- 3 Benoit, H. *et al. Nature* 1973, **245**, 13
- 4 Wignall, G. D., Ballard, D. G. H. and Schelten, J. *J. Appl. Crystallog.* 1974, **7**, 190; *Eur. Polym. J.* 1974, **10**, in press
- 5 Stehling, F. S., Ergos, E. and Mandelkern, L. *Macromolecules* 1971, **4**, 672
- 6 Altgelt, K. and Schutz, G. V. *Makromol. Chem.* 1960, **36**, 209
- 7 Brandrup, J. and Immergut, E. H. 'Polymer Handbook', Interscience, New York, 1969
- 8 Tasumi, M. and Krimm, S. *J. Polym. Sci. (A-2)* 1968, **6**, 995
- 9 Bank, M. I. and Krimm, S. *J. Polym. Sci. (A-2)* 1969, **7**, 1785
- 10 Krimm, S. and Ching, J. H. C. *Macromolecules* 1972, **5**, 209

Temperature effects on some solution properties of poly(n-alkyl isocyanates)

It has been suggested, on the basis of very different experiments that poly(n-alkyl isocyanates) have a rod-like conformation in solution and the hydrodynamic properties of these polymers have been studied extensively¹.

Nevertheless, there is still a lack of agreement between the chain dimensions calculated by different authors and the exact cause of the high rigidity of these macromolecules is still uncertain. The hypothesis has been advanced that this rigidity is due to a resonance interaction in the nitrogen-carbonyl system² which gives a partial double bond character to the carbon-nitrogen bond. However, Troxell and Scheraga³ concluded from electric dichroism measurements that the delocalization is very weak along the polymer backbone.

Shmueli and coworkers⁴ have suggested, from X-ray diffraction data that the polymer in the solid state has a

helical structure with a translation of 1.94 Å and a rotation of 135° per monomeric unit; however, there is no definite proof that such a helical conformation is partly maintained in solution. Recently, Fetters⁵ identified a conformational change in carbon tetrachloride solutions of poly(n-alkyl isocyanates) which was induced by the addition of pentafluorophenol. The transition observed is apparently non-cooperative and reversible; Berger and Tidswell⁶ have also studied the effects of trifluoroacetic acid and a temperature increase on the viscosity of poly(n-hexyl isocyanate).

In order to try to clarify the origin of the chain stiffness of the alkyl polyisocyanates, we have studied systematically the effect of temperature on different solution properties of these polymers. We report here the results obtained by viscosity and light scattering measurements.

The polymers were prepared by the method described by Shashova and fractionated by precipitation using the carbon tetrachloride-methanol system. The fractions have been analysed by gel permeation chromatography (THF solutions at 25°C) and have a polydispersity of around 1.2.

The viscosity measurements were performed in a new type of sealed capillary viscosimeter⁷ between 0° and 55°C; the rate of shear was between 300 and 500 sec⁻¹; the concentration of the poly(n-hexyl isocyanate) (PHIC) solutions was in the range of 10⁻³ g/ml and was corrected for the change of density with temperature.

Figures 1 and 2 illustrate the variation of η_{sp}/c with increasing temperature for PHIC samples of different molecular weight, dissolved in carbon tetrachloride, in chloroform and toluene. There are two definite discontinuities in the curves around 20° and 40°C when

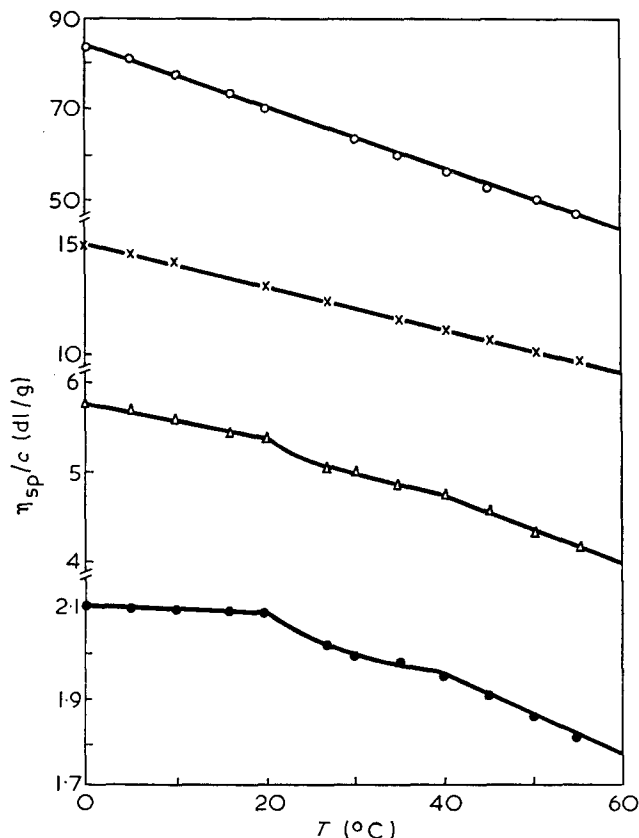


Figure 1 Variation of η_{sp}/c with temperature for PHIC of different molecular weights in carbon tetrachloride: ○, 6×10^5 ; ×, 2×10^5 ; △, 10^5 ; ●, 5×10^4 . Concentration $\sim 10^{-3}$ g/ml

and to use different methods of sample preparation to avoid this problem. Only in samples where clustering has been shown to be absent can unequivocal conclusions be drawn concerning the conformation from infra-red or neutron data in solid polyethylene.

Acknowledgements

The authors wish to acknowledge the help and advice of Dr J. C. Padget (ICI Corporate Laboratory) and Dr R. W. Hendricks (Oak Ridge National Laboratory) in sample preparation and data evaluation respectively.

J. Schelten

Institut für Festkörperforschung,
KFA Jülich 1, West Germany
Present address: Metals and Ceramics Division,
Oak Ridge National Laboratory,
Oak Ridge, Tenn. 37830, USA

G. D. Wignall

ICI Europa Research and Development Ltd,
B-3078 Everberg, Belgium

and D. G. H. Ballard

ICI Corporate Laboratory,
The Heath, Runcorn,
Cheshire WA7 4QE, UK
(Received 1 July 1974)

References

- 1 Kirste, R. G., Kruse, W. A. and Schelten, J. *Makromol. Chem.* 1973, **162**, 299
- 2 Ballard, D. G. H., Schelten, J. and Wignall, G. D. *Eur. Polym. J.* 1973, **9**, 965
- 3 Benoit, H. *et al. Nature* 1973, **245**, 13
- 4 Wignall, G. D., Ballard, D. G. H. and Schelten, J. *J. Appl. Crystallog.* 1974, **7**, 190; *Eur. Polym. J.* 1974, **10**, in press
- 5 Stehling, F. S., Ergos, E. and Mandelkern, L. *Macromolecules* 1971, **4**, 672
- 6 Altgelt, K. and Schutz, G. V. *Makromol. Chem.* 1960, **36**, 209
- 7 Brandrup, J. and Immergut, E. H. 'Polymer Handbook', Interscience, New York, 1969
- 8 Tasumi, M. and Krimm, S. *J. Polym. Sci. (A-2)* 1968, **6**, 995
- 9 Bank, M. I. and Krimm, S. *J. Polym. Sci. (A-2)* 1969, **7**, 1785
- 10 Krimm, S. and Ching, J. H. C. *Macromolecules* 1972, **5**, 209

Temperature effects on some solution properties of poly(n-alkyl isocyanates)

It has been suggested, on the basis of very different experiments that poly(n-alkyl isocyanates) have a rod-like conformation in solution and the hydrodynamic properties of these polymers have been studied extensively¹.

Nevertheless, there is still a lack of agreement between the chain dimensions calculated by different authors and the exact cause of the high rigidity of these macromolecules is still uncertain. The hypothesis has been advanced that this rigidity is due to a resonance interaction in the nitrogen-carbonyl system² which gives a partial double bond character to the carbon-nitrogen bond. However, Troxell and Scheraga³ concluded from electric dichroism measurements that the delocalization is very weak along the polymer backbone.

Shmueli and coworkers⁴ have suggested, from X-ray diffraction data that the polymer in the solid state has a

helical structure with a translation of 1.94 Å and a rotation of 135° per monomeric unit; however, there is no definite proof that such a helical conformation is partly maintained in solution. Recently, Fetters⁵ identified a conformational change in carbon tetrachloride solutions of poly(n-alkyl isocyanates) which was induced by the addition of pentafluorophenol. The transition observed is apparently non-cooperative and reversible; Berger and Tidswell⁶ have also studied the effects of trifluoroacetic acid and a temperature increase on the viscosity of poly(n-hexyl isocyanate).

In order to try to clarify the origin of the chain stiffness of the alkyl polyisocyanates, we have studied systematically the effect of temperature on different solution properties of these polymers. We report here the results obtained by viscosity and light scattering measurements.

The polymers were prepared by the method described by Shashova and fractionated by precipitation using the carbon tetrachloride-methanol system. The fractions have been analysed by gel permeation chromatography (THF solutions at 25°C) and have a polydispersity of around 1.2.

The viscosity measurements were performed in a new type of sealed capillary viscosimeter⁷ between 0° and 55°C; the rate of shear was between 300 and 500 sec⁻¹; the concentration of the poly(n-hexyl isocyanate) (PHIC) solutions was in the range of 10⁻³ g/ml and was corrected for the change of density with temperature.

Figures 1 and 2 illustrate the variation of η_{sp}/c with increasing temperature for PHIC samples of different molecular weight, dissolved in carbon tetrachloride, in chloroform and toluene. There are two definite discontinuities in the curves around 20° and 40°C when

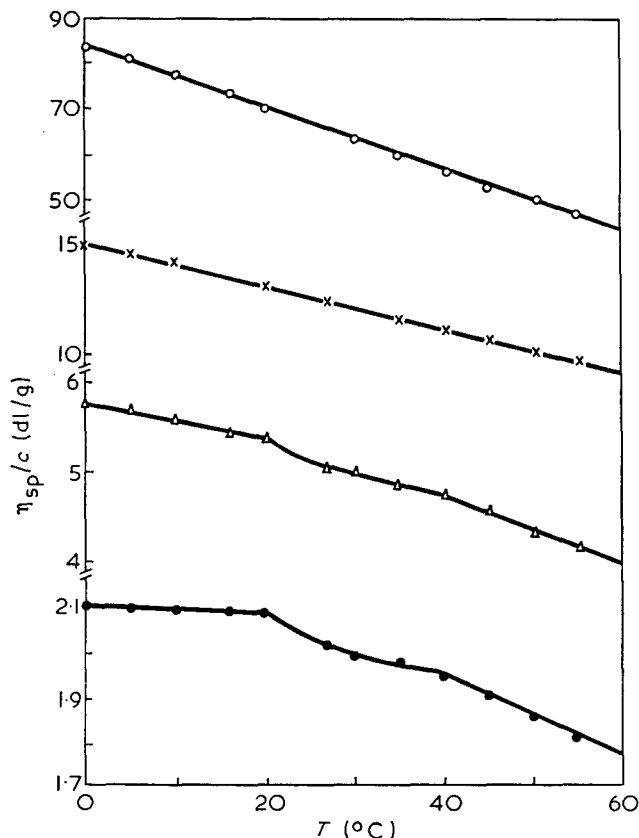


Figure 1 Variation of η_{sp}/c with temperature for PHIC of different molecular weights in carbon tetrachloride: ○, 6×10^5 ; ×, 2×10^5 ; △, 10^5 ; ●, 5×10^4 . Concentration $\sim 10^{-3}$ g/ml

the molecular weight is below 2×10^5 ; the slopes of the curves above 40°C and below 20°C are considerably different for the low molecular weight fractions; the decrease of η_{sp}/c between 20° and 40°C is much smaller than the one observed at constant temperature by Fetters by addition of pentafluorophenol and by Berger *et al.* by addition of a small quantity of trifluoroacetic acid. The observed anomaly is more pronounced at low concentration and is entirely reversible.

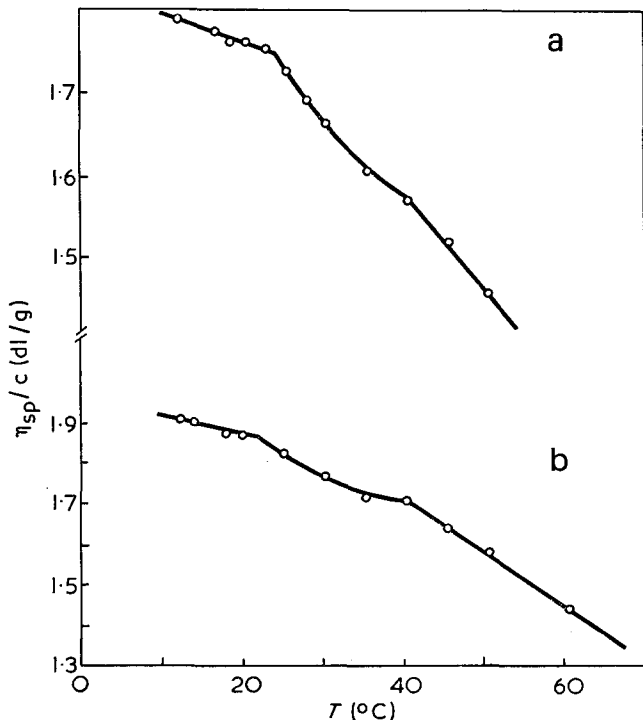


Figure 2 Variation of η_{sp}/c with temperature of samples of PHIC in (a) chloroform and (b) toluene. (a) $\bar{M}_w = 5 \times 10^4$; (b) $\bar{M}_w = 3 \times 10^4$

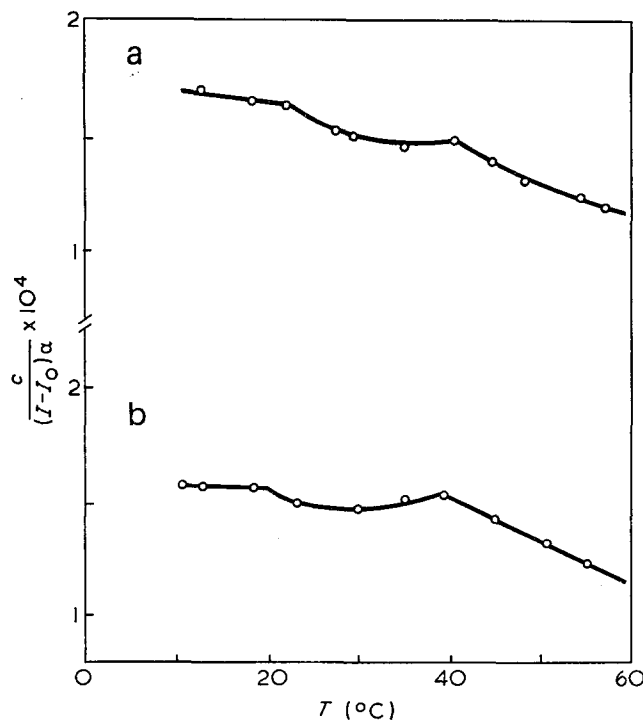


Figure 3 Variation of $[c/(I-I_0)\alpha]$ with temperature for a sample of (a) PHIC and (b) PBIC in chloroform. $\theta = 135^\circ$. (a) $\bar{M}_w = 6.3 \times 10^4$; (b) $\bar{M}_w = 7.3 \times 10^4$

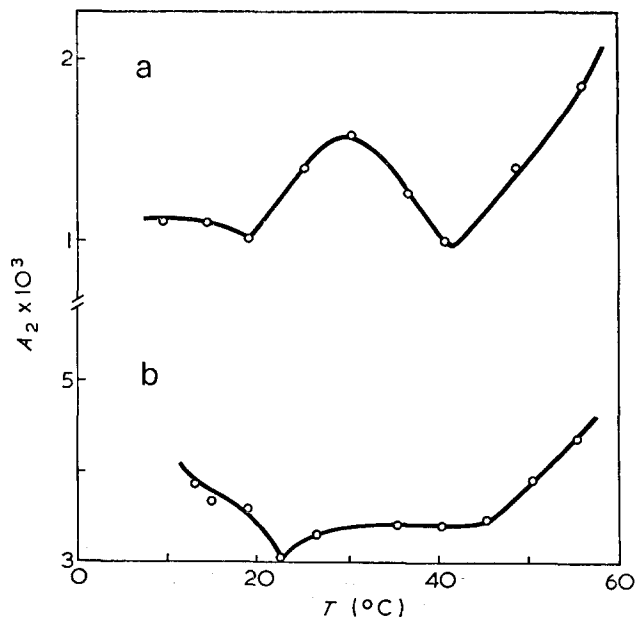


Figure 4 Variation of A_2 with temperature for a sample of (a) PHIC and (b) PBIC in chloroform. (a) $\bar{M}_w = 5 \times 10^4$; (b) $\bar{M}_w = 10^5$

We have observed the same kind of abnormal viscosity curve in the same temperature range with solutions of poly(*n*-butyl isocyanate) (PBIC) and poly(*n*-nonyl isocyanate) (PNIC) in chloroform and carbon tetrachloride.

Light scattering data on chloroform solutions were obtained at different temperatures with a Sofica photometer (polarized light; 5460 Å; tight cells). We have observed again an anomaly between 20° and 40°C as illustrated in Figure 3; the values of $[c/(I-I_0)\alpha]$ at an angle of 135° and at a concentration of around $0.6\text{--}0.7 \times 10^{-2}\text{ g/ml}$ are plotted against the temperature for two samples of PBIC and PHIC.

The proportional decrease of $[c/(I-I_0)\alpha]$ with temperature is of the same order of magnitude for solutions of different concentrations. The dissymmetry values below 20° and above 40°C are nearly the same.

The values of the second virial coefficient A_2 are abnormal in the same temperature range (Figure 4). The observed phenomena are again entirely reversible and no time effect has been observed.

In conclusion, the poly(*n*-alkyl isocyanates) dissolved in different solvents undergo, between 20° and 40°C , a reversible transformation as illustrated by the anomalies in the viscosity and light scattering curves. The length of the aliphatic side chain does not seem to have a great influence on the transition which, consequently occurs probably in the main chain; however, no change in the infra-red spectrum with temperature has been observed. The rod-like conformation of the chains is preserved after the transition which must be different from the one observed by Fetters. The same anomaly in the same temperature range has been displayed by other methods, namely by dielectric absorption measurements⁸.

Further investigations on the nature of the transition are in progress.

J. Pierre and V. Desreux

Laboratoire de Chimie Physique,
Université de Liège,
B 4000 Liège, Belgium
(Received 31 July 1974)

References

- Berger, M. N. *J. Macromol. Sci. (C)* 1973, 9(2), 269
- Tsvetkov, V. N. *et al. Eur. Polym. J.* 1971, 7, 767
- Troxell, T. C. and Scheraga, H. A. *Macromolecules* 1971, 4, 528
- Schmueli U., *et al. J. Polym. Sci. (A-2)* 1969, 7, 515
- Fetters, L. J. *J. Polym. Sci. (B)* 1972, 10, 577
- Berger, M. N. and Tidswell, B. M. *J. Polym. Sci. (C)* 1973, 42(3), 1063
- to be published
- Pierre, J. and Marchal, E. to be published

Influence of particle diameter on chromatogram broadening in g.p.c. with porous silica columns

Introduction

Theoretical treatments of solute dispersion in gel permeation chromatography (g.p.c.) predict that chromatogram broadening decreases as the particle diameter of the column packing falls¹. Polymer separations with porous oxide packings have mainly been confined to particles with mean diameters in the range 40–250 μm . These experimental studies have differed on the influence of particle diameter and its distribution on column efficiency^{1–5}. Here, initial g.p.c. results are reported for the column efficiency of Spherisorb silica (mean particle diameter = 20 μm) which has been prepared recently at AERE (Harwell, Berks, UK). This packing consists of almost perfectly spherical particles which have a narrow particle size distribution with 90% of the spheres lying within $\pm 20\%$ of the mean particle diameter⁶. Spherisorb is compared with Porasil silica which has been studied extensively by other workers^{1–3}.

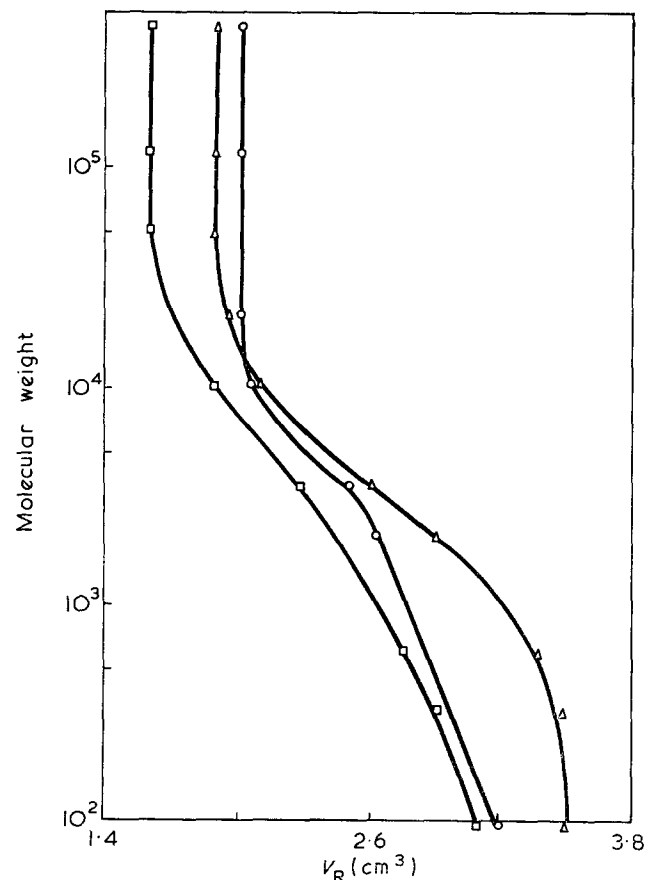


Figure 1 Calibration curves. Δ , Porasil A (37–75 μm); \square , sieved Porasil A (37–50 μm); \circ , Spherisorb silica S.20.W (20 μm)

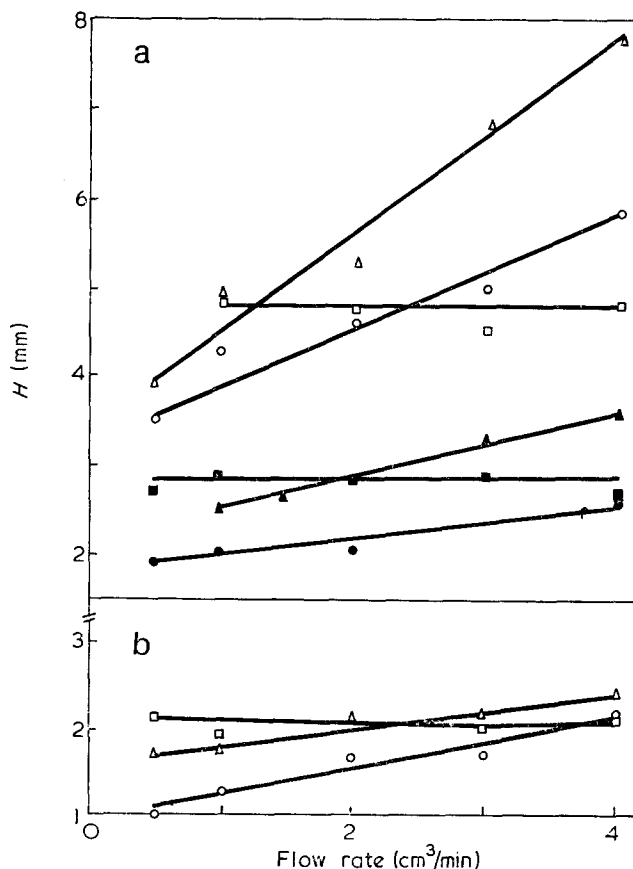


Figure 2 Dependence of column efficiency on eluent flow rate. \circ , Toluene; Δ , tetraphenylethylene; \square , polystyrene standard (molecular weight = 111 000). (a) Open symbols, Porasil A(60) (37–75 μm); solid symbols, sieved Porasil A(60) (37–50 μm); (b) Spherisorb silica S.20.W (20 μm)

Experimental

Spherisorb silica S.20.W was supplied by Phase Separations Limited and Porasil A(60) (particle size range = 37 to 75 μm) by Waters Associates Inc. Sieving showed that the particle size distribution of Porasil A is skewed to high particle diameters; $\sim 70\%$ of the packing was retained on a 60 μm sieve. The sieved Porasil A (particle size = 37–50 μm) was the fraction passing through a 50 μm sieve. The silica particles were dry-packed into individual stainless-steel columns (0.47 m long \times 3.0 mm i.d.). With the addition of each increment of packing, the column was tapped and tamped with a close-fitting Teflon-ended rod. Separations were performed with an Applied Research Laboratories Limited modular liquid chromatograph LC 750 having a constant pressure pump [$\leq 1350 \text{ lbf/in}^2$ ($1 \text{ lbf/in}^2 \equiv 6894.8 \text{ N/m}^2$), 60 cm^3 capacity] and an ultra-violet detector (254 nm, cell volume = 8 μl)². Valve/loop ($\sim 0.5 \text{ cm}^3$) injection (20.0 to 2.5 sec injection time) at pressures $\leq 1000 \text{ lbf/in}^2$ was used for flow rates between 0.5 and 4.0 cm^3/min . Solute concentrations were 0.05% (w/v) for toluene (Analar) and polystyrene standards (Waters Associates) and 0.005% (w/v) for tetraphenylethylene (Aldrich Chem. Co.). The eluent was tetrahydrofuran (Maybridge Chem. Co.) which was destabilized and distilled before use. The packings settled very little ($\leq 2 \text{ mm}$) after flushing the columns at 1000 lbf/in^2 .

Results and Discussion

Plots of log molecular weight versus retention volume V_R are shown in Figure 1, illustrating that Porasil A

References

- Berger, M. N. *J. Macromol. Sci. (C)* 1973, 9(2), 269
- Tsvetkov, V. N. *et al. Eur. Polym. J.* 1971, 7, 767
- Troxell, T. C. and Scheraga, H. A. *Macromolecules* 1971, 4, 528
- Schmueli U., *et al. J. Polym. Sci. (A-2)* 1969, 7, 515
- Fetters, L. J. *J. Polym. Sci. (B)* 1972, 10, 577
- Berger, M. N. and Tidswell, B. M. *J. Polym. Sci. (C)* 1973, 42(3), 1063
- to be published
- Pierre, J. and Marchal, E. to be published

Influence of particle diameter on chromatogram broadening in g.p.c. with porous silica columns

Introduction

Theoretical treatments of solute dispersion in gel permeation chromatography (g.p.c.) predict that chromatogram broadening decreases as the particle diameter of the column packing falls¹. Polymer separations with porous oxide packings have mainly been confined to particles with mean diameters in the range 40–250 μm . These experimental studies have differed on the influence of particle diameter and its distribution on column efficiency^{1–5}. Here, initial g.p.c. results are reported for the column efficiency of Spherisorb silica (mean particle diameter = 20 μm) which has been prepared recently at AERE (Harwell, Berks, UK). This packing consists of almost perfectly spherical particles which have a narrow particle size distribution with 90% of the spheres lying within $\pm 20\%$ of the mean particle diameter⁶. Spherisorb is compared with Porasil silica which has been studied extensively by other workers^{1–3}.

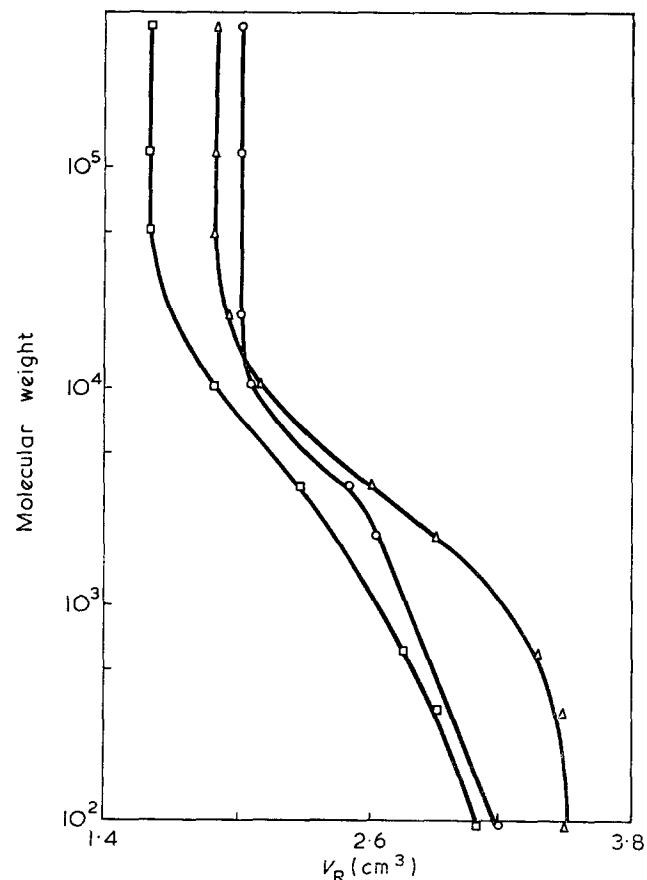


Figure 1 Calibration curves. Δ , Porasil A (37–75 μm); \square , sieved Porasil A (37–50 μm); \circ , Spherisorb silica S.20.W (20 μm)

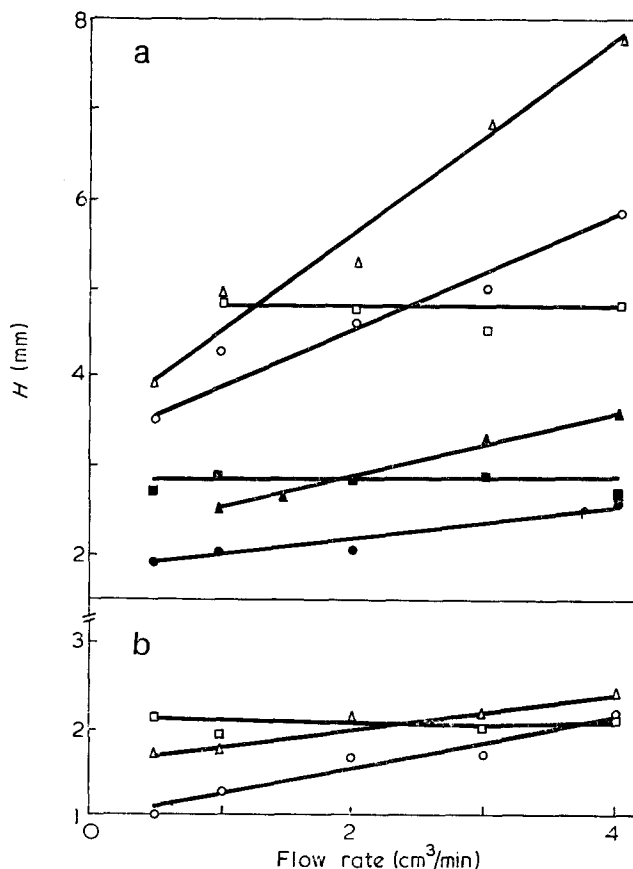


Figure 2 Dependence of column efficiency on eluent flow rate. \circ , Toluene; Δ , tetraphenylethylene; \square , polystyrene standard (molecular weight = 111 000). (a) Open symbols, Porasil A(60) (37–75 μm); solid symbols, sieved Porasil A(60) (37–50 μm); (b) Spherisorb silica S.20.W (20 μm)

Experimental

Spherisorb silica S.20.W was supplied by Phase Separations Limited and Porasil A(60) (particle size range = 37 to 75 μm) by Waters Associates Inc. Sieving showed that the particle size distribution of Porasil A is skewed to high particle diameters; $\sim 70\%$ of the packing was retained on a 60 μm sieve. The sieved Porasil A (particle size = 37–50 μm) was the fraction passing through a 50 μm sieve. The silica particles were dry-packed into individual stainless-steel columns (0.47 m long \times 3.0 mm i.d.). With the addition of each increment of packing, the column was tapped and tamped with a close-fitting Teflon-ended rod. Separations were performed with an Applied Research Laboratories Limited modular liquid chromatograph LC 750 having a constant pressure pump [$\leq 1350 \text{ lbf/in}^2$ ($1 \text{ lbf/in}^2 \equiv 6894.8 \text{ N/m}^2$), 60 cm^3 capacity] and an ultra-violet detector (254 nm, cell volume = 8 μl)². Valve/loop ($\sim 0.5 \text{ cm}^3$) injection (20.0 to 2.5 sec injection time) at pressures $\leq 1000 \text{ lbf/in}^2$ was used for flow rates between 0.5 and 4.0 cm^3/min . Solute concentrations were 0.05% (w/v) for toluene (Analar) and polystyrene standards (Waters Associates) and 0.005% (w/v) for tetraphenylethylene (Aldrich Chem. Co.). The eluent was tetrahydrofuran (Maybridge Chem. Co.) which was destabilized and distilled before use. The packings settled very little ($\leq 2 \text{ mm}$) after flushing the columns at 1000 lbf/in^2 .

Results and Discussion

Plots of log molecular weight versus retention volume V_R are shown in Figure 1, illustrating that Porasil A

and Spherisorb S.20.W have a somewhat different internal pore volume although they separate a similar range of solute sizes. The suppliers quote mean pore diameters of <10 and 8 nm for Porasil and Spherisorb respectively.

Column efficiency was expressed in terms of the height equivalent to a theoretical plate H defined by¹:

$$H = L \left(\frac{W}{4V_R} \right)^2$$

where W is the distance between the baseline intercepts of lines drawn tangent to the points of inflection of the chromatogram and L is the column length. Possible contributions to W from extra-column dispersion are included in the H value. From *Figure 1*, the polystyrene standard having a molecular weight of 111 000, and above, is a non-permeating solute. The dispersion behaviour of this solute, tetraphenylethylene (molecular weight=332) and toluene (molecular weight=92) is shown in *Figure 2*. It is clear that H decreases as the particle size falls, taking mean particle diameters of $\sim 65 \mu\text{m}$, $\sim 45 \mu\text{m}$ and $20 \mu\text{m}$ for Porasil A, sieved Porasil A and Spherisorb silica respectively. In *Figure 2*, H for polystyrene remains almost constant as flow rate increases, as observed by Kelley and Billmeyer¹ for a non-permeating solute having a low diffusivity. H for the permeating solutes rises as flow rate increases, and for Porasil A the curves diverge possibly because of a dependence of permeation dispersion on solute diffusivity as proposed by Kelley and Billmeyer¹. For Spherisorb silica, this divergence is much less marked, suggesting

that solute mass transfer between the mobile and stationary phases is facilitated with the smaller Spherisorb particles.

These results suggest that a significant decrease in chromatogram broadening in g.p.c. may be possible with small porous particles. Polymer dispersion for smaller Spherisorb particles is being investigated, using high-pressure liquid chromatography instrumentation.

Acknowledgement

The authors thank Mr R. E. Buxton, Department of Chemical Engineering, for helpful discussions on sieving.

J. V. Dawkins and G. Taylor

*Department of Chemistry,
Loughborough University of Technology,
Loughborough, Leics. LE11 3TU, UK
(Received 1 August 1974)*

References

- 1 Kelley, R. N. and Billmeyer, F. W. *Separation Sci.* 1970, **5**, 291
- 2 Le Page, M., Beau, R. and de Vries, A. J. *J. Polym. Sci. (C)* 1968, **21**, 119
- 3 Sliemers, F. A., Boni, K. A., Nemzer, D. E. and Nance, G. P. *Proc. 6th Int. Semin. Gel Permeation Chromatography, Miami Beach* 1968, p 463
- 4 Otocka, E. P. *J. Chromatog.* 1973, **76**, 149
- 5 Cooper, A. R. and Kiss, I. *Br. Polym. J.* 1973, **5**, 433
- 6 Spherisorb L. C. Column Supports, Data Sheet No. 1 (1974), Phase Separations Ltd, Queensferry
- 7 Leaflet 023/1, Applied Research Laboratories Ltd, Luton

RESOURCES POLICY

the economics, planning and use
of mineral resources

A NEW QUARTERLY JOURNAL
first issue · September 1974

Main articles

The concept and measurement of mineral reserves and resources
G.J.S. Govett and M.H. Govett

The use of by-products in concrete
W. Gutt

Non-renewable mineral resources
Sir Kingsley Dunham

Analysis of the life cycle of non-ferrous minerals
F. Roberts and I. Torrens

Other sections

- Current topics
- Conference reports
- Forthcoming meetings
- Book reviews and announcements
- Publications received

RESOURCES POLICY will present multi-disciplinary discussions at an upper management/academic level. The aim is to identify policy options for the future supply and demand of mineral resources. It will encompass the many disciplines and examine options as they affect industrial, commercial and social institutions at world and regional levels

Published quarterly in
March, June, September, December,
commencing September 1974

One-year subscription (four issues) £20.00 (\$50.00).

For full details apply to: IPC Science and Technology Press Limited (Dept. AD.RP)
IPC House, 32 High Street, Guildford, Surrey, England GU1 3EW
Telephone: Guildford (0483) 71661 Telex: Scitechpress Gd. 85556

Conformations of macromolecular sequential polypeptides in solution: 2. Sequential polypeptides containing both D- and L-residues

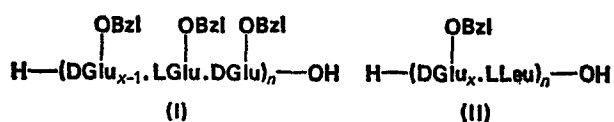
H. T. Storey, R. C. Thompson, P. M. Hardy and H. N. Rydon*

Department of Chemistry, University of Exeter, Exeter EX4 4QD, UK
(Received 4 January 1974; revised 9 April 1974)

The conformations adopted in solution by two series of macromolecular sequential polypeptides containing up to four γ -benzyl-D-glutamyl and one γ -benzyl-L-glutamyl or L-leucyl residue in the repeating unit have been studied by spectroscopic methods (i.r., o.r.d., n.m.r.). The nature of the ordered conformations encountered is discussed; it is suggested that they are a distorted form of the α -helix and special types of cross β -structure.

INTRODUCTION

In an earlier paper¹, we described spectroscopic studies of the conformations adopted in solution by 'alternating' sequential polypeptides of the type H-(A.B)_n-OH in which A and B were residues of amino acids which give rise to poly(amino acids) of opposite helical sense. The present paper describes the extension of these studies to cases in which the repeating unit contains more than one residue of type A. As in the earlier work, A was γ -benzyl-D-glutamyl; B was either γ -benzyl-L-glutamyl or L-leucyl, the polypeptides having the structures (I) and (II), where $x=2, 3$ and 4.



The size of the polypeptides was such as to make the differences at the ends of (I) and (II) insignificant and both series can be regarded as examples of the same general type, H-(A_x.B)_n-OH. Much of the experimental data on the cases where $x=1$ were given in the earlier paper¹ but some additional data are given below.

EXPERIMENTAL AND RESULTS

The preparation of the polypeptides, by polymerization of the appropriate oligopeptide succinimidyl esters, and their characterization has been described elsewhere^{2, 3}. The molecular weights of the polypeptides, as determined by gel filtration of their debenzoylation products, are given in Table 1. The degree of racemization of the C-terminal residues in the polymerization process was estimated to be about 2% for series (I)² and about 1% for series (II)³.

The infra-red (i.r.) spectra, in chloroform solution at room temperature, were recorded with a Hilger and Watts Infrascan H900 Recording Spectrometer. The

positions of the principal absorption bands are given in Table 2; in all but one instance (I; $x=2$) neither the positions nor the relative areas of the bands changed when the concentration was varied from 2 to 40 g/dm³.

Optical rotatory dispersion (o.r.d.) measurements were made at $\sim 25^\circ\text{C}$ in 3 to 5% solutions in mixtures of deuteriochloroform and trifluoroacetic acid (TFA)

Table 1 Molecular weights of sequential polypeptides (I) and (II)

Polypeptide	M_w	M_n	M_w/M_n	n^*
I ($x=1$)	28 300	23 400	1.21	53
I ($x=2$)	37 200	28 300	1.32	43
I ($x=3$)	18 400	15 500	1.19	18
I ($x=4$)	22 900	18 400	1.25	17
II ($x=1$); fraction 2†	18 400	12 200	1.51	36
II ($x=2$); fraction 2	22 900	15 900	1.44	28
II ($x=2$); fraction 3	12 800	10 400	1.23	19
II ($x=3$); fraction 1	20 800	12 600	1.65	16
II ($x=3$); fraction 2	25 500	13 800	1.85	18
II ($x=3$); fraction 3	21 000	13 100	1.60	17
II ($x=4$)	34 000	22 400	1.52	22

* Based on M_n

† Fraction numbers as in ref 3

Table 2 Principal infra-red absorptions of sequential polypeptides (I) and (II)

Polypeptide	Ester		Amide I	Amide II	Amide II'
	N-H	C=O			
I ($x=1$)	3300	1738	1650, 1665	1549	1457
I ($x=2$)	3300	1736	1624, 1663, 1693	1554	1456
I ($x=3$)	3300	1737	1625, 1662, 1695	1550	1456
I ($x=4$)	3300	1735	1627, 1659	1552	1455
II ($x=1$); fraction 2*	3290	1736	1641, 1663	1549	1454
II ($x=2$); fraction 2	3300	1735	1625, 1657, 1695	1550	1455
II ($x=2$); fraction 3	3300	1735	1627, 1660, 1695	1550	1455
II ($x=3$); fraction 1	3300	1737	1628, 1659, 1695	1548	1457
II ($x=3$); fraction 2	3300	1735	1628, 1659, 1695	1548	1457
II ($x=3$); fraction 3	3300	1735	1659	1548	1457
II ($x=4$)	3300	1738	1628, 1660	1548	1456

* Fraction numbers as in ref 3

* To whom enquiries should be addressed.

Table 3. O.r.d. parameters for sequential polypeptides (I) and (II)

Polypeptide	TFA (%)	a_0	b_0	Polypeptide	TFA (%)	a_0	b_0	
I ($x=1$)	0	+106	-115	II ($x=2$); fraction 2	0	-508	+464	
	1	+70	-83		2	-437	+419	
	2	+55	-71		5	-294	+272	
	3	+32	-56		7	+42	+15	
	4	+16	-32		10	+53	+4	
	5	-1	-18		20	+60	-8	
	100	-27	+1		50	+61	-4	
					100	+36	-1	
I ($x=2$)	0	-455	+374		II ($x=2$); fraction 3	0	-289	+246
	5	-362	+320			1	-276	+252
	6	-83	+73	2		-162	+181	
	7	-22	+22	3	-44	+99		
	10	+13	-11					
I ($x=3$)	0	-307	+123	II ($x=3$); fraction 1	0	-526	+30	
	2	-286	+239		1	-403	+234	
	4	-209	+198		2	-331	+203	
	6	-106	+105		5	+4	+76	
	8	+6	+4		10	+74	+6	
	100	+135	-28		50	+98	-3	
				100	+168	-4		
I ($x=4$)	0	-318	+390	II ($x=3$); fraction 2	0	-410	+457	
	6	-235	+299		2	-409	+441	
	7.5	-166	+229		3	-376	+404	
	9	-64	+118		6	-111	+147	
	12	+65	-10					
	100	+226	-27					
II ($x=1$); fraction 2	0	+191	+225	II ($x=3$); fraction 3	0	-376	+418	
	2	+281	+34		1	-325	+394	
	3	+241	-54		3	-223	+278	
	4	+165	-88		3.5	-167	+226	
	5	+43	-73		4	-110	+173	
	100	-40	-2	5	-7	+58		
				II ($x=4$)	0	-369	+416	
				1	-340	+460		
				3	-286	+383		
				5	-9	+99		
				7	+78	+17		
				10	+109	-12		
				100	+238	-25		

with a Bendix-Ericsson Polarmatic 62 Recording Spectropolarimeter, using a pathlength of 1 mm. [We are indebted to Professor L. C. Crombie for access to this instrument.] The results can be adequately described, within experimental error, in terms of the Moffitt equation; the parameters a_0 and b_0 given in Table 3 relate to reduced mean residue rotations, $[m']_\lambda$, with $\lambda_0=212$ nm.

^1H nuclear magnetic resonance (n.m.r.) spectra for 3 to 4% solutions in CDCl_3/TFA mixtures were recorded at 33°C on a Perkin-Elmer R10 60 MHz NMR Spectrometer fitted with a Digico Digiacc computer for averaging accumulated spectra. The spectra were similar to those illustrated in the earlier paper¹; the chemical shifts (τ) for the various types of proton were as follows: NH , 1-2; C_6H_5 , 2.7(s); Ph.CH_2 , 4.9(s); $\alpha\text{-CH}$, 5-6; $\text{Glu C}_2\text{H}_4$, 7.3-8.0(m); Leu CH_2 and $\gamma\text{-CH}$, 8.3(m); $\text{Leu (CH}_3)_2$, 9.1(m). The multiplet nature of the leucine methyl signal indicates magnetic non-equivalence of the two methyl groups, although at the resolution of our instrument this band often approximated to a broad singlet; the doublet expected for an isopropyl group with magnetically equivalent methyls (AB_6 system) was never seen. The broad multiplet for the glutamate side-chain methylene groups showed a maximum at

about 7.6τ ; a second maximum, at 7.9τ , often developed at higher TFA concentrations.

In general, as with poly(amino acids)⁴, the n.m.r. spectra in CDCl_3 were almost featureless, single scans showing a distinct peak only for the C_6H_5 protons; the other peaks were very broad, often so broad as to be quite undetectable, but could be revealed by accumulation of spectra and expansion of the amplitude scale. Addition of TFA caused 'unfreezing', the peaks for the various types of proton sharpening successively, from the periphery of the molecule inwards, as more TFA was added until, in 100% TFA, all the peaks were easily observable in single scans. Separate NH and $\alpha\text{-CH}$ peaks for ordered and random-coil conformations were observable in expanded accumulated spectra⁵; the controversy regarding the significance of such 'double peaks' now appears to have been resolved⁶ and it seems that, although separate peaks for ordered and random-coil forms are only observable with polydisperse specimens, they nevertheless do correspond to different conformations, albeit in molecules of different molecular weights. Quantitative interpretation was, however, not possible, except for the polydipeptide (I; $x=1$), owing to the complicating effect of the different types of side-chain, especially in the leucine series (II).

DISCUSSION

Polydipeptides (I and II; $x=1$)

The spectroscopic data for the polydipeptide (I; $x=1$) were fully discussed in the earlier paper¹ and little need be added, save that all the evidence points to the mid-point of the 'perfect' \rightleftharpoons random coil transition being at about 1% TFA and that for the right-handed α' -helix \rightleftharpoons random coil transition at about 2.5%.

Less was said about the leucyl polydipeptide (II; $x=1$) and further comment is needed. As with its simpler analogue (I; $x=1$), the presence in chloroform solution of molecules with the 'perfect' conformation* is indicated by the presence of a low-field α -CH n.m.r. band at $\sim 5.2\tau$, and an anomalous amide I band, at 1641 cm^{-1} . Both of these disappear on adding 1 to 2% of TFA, the mid-point of the 'perfect' \rightleftharpoons random coil transition being at about 1.5% TFA. The n.m.r. spectrum contains a second, weaker, α -CH band, due to the α' -helix, at $\sim 6.2\tau$. This, like that at 5.2τ , is replaced by a random coil band at 5.5τ on adding TFA; the mid-point of this α' -helix \rightleftharpoons random coil transition occurs at about 4% TFA. The optical titration data (Figure 1) are consistent with these two transitions. The shapes of the curves are such that the 'perfect' conformation must have a positive b_0 , while the more stable α' -helical conformation must have a negative b_0 and a positive a_0 . The negative b_0 so inferred for the α' -helix indicates that this is right-handed; this is surprising, since any racemization of the C-terminal residues during the polymerization processes would give rise to an excess, albeit slight, of D-residues and a left-handed helix might be expected. The explanation of this apparent anomaly probably lies in the greater inherent strength of polyleucine as compared with poly(γ -benzyl-glutamyl α -helices)⁷.

In Part I, the findings for these polypeptides were interpreted as showing the presence in chloroform solution of two ordered conformations, the weaker of

* By 'perfect' molecules we mean those in which the specified regular sequence of configurations is wholly uninterrupted by racemization.

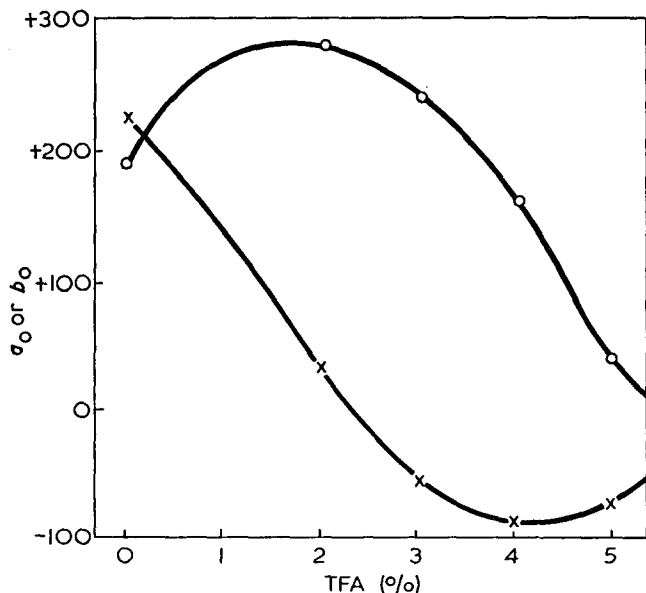


Figure 1 Optical titration of poly(γ -benzyl-D-glutamyl-L-leucine) (II; $x=1$). O, α_0 ; X, β_0

these, ascribed to 'perfect' molecules, being the α_{II} , ribbon-like, structure of Huggins⁸, and the other the distorted α -helical conformation of Némethy *et al.*⁹ (called α_{II} by these authors but α' by us to avoid confusion with Huggins' structure).

Recent theoretical work on the conformations of polypeptide chains with alternating D- and L-residues calls for re-appraisal. Ramachandran and Chandrasekaran¹⁰ conclude that the most stable conformation for poly(L-alanyl-D-alanine) is that termed by them LD_{3P}, which they find to be very nearly as stable as is the right-handed helix for poly(L-alanine). It is of interest to point out that the intra-chain hydrogen-bonding pattern in the LD_{3P} helix is the same as the inter-chain hydrogen-bonding pattern in the parallel β -pleated sheet; the helix can in fact be generated from the sheet by suitably rolling this up and joining chain ends together, a relationship not previously noted in the literature. On the other hand, Hesselink and Scheraga¹¹ find, surprisingly, that alternate D- and L-residues can be readily incorporated into either left or right handed α -helices, without appreciable effect on stability and with only slight modification of the torsion angles. These authors also find the LD helix of Ramachandran and Chandrasekaran to be much less stable, illustrating, perhaps, the limitations of such calculations. Further, the seven-membered hydrogen-bonded ring (γ -turn) present in Huggins' α_{II} structure is no longer regarded as inherently unstable^{12,13} and evidence has been presented for its presence in thermolysin¹⁴; it has been shown¹² to be capable of accommodating alternating L- and D-residues.

There is clearly no lack of theoretically acceptable conformations for the polydipeptides (I and II; $x=1$). We see no reason to change our previous assignment of an α' -helical structure to the more stable ordered conformation, emphasizing, as pointed out before¹, that the actual conformation may lie somewhere between this and the α -helix. The LD_{3P} helix of Ramachandran and Chandrasekaran¹⁰ is, however, an attractive alternative to the Huggins α_{II} -structure for the conformation adopted by the 'perfect' molecules; it has the advantage that it appears to be incapable of accommodating any exchange of an L- for a D-residue or *vice versa*. On the other hand the α_{II} -ribbon fits well into the series of cross- β -structures suggested below for the 'perfect' components of the other sequential polypeptides and the question must remain open.

Polytripeptides (I and II; $x=2$)

The i.r. spectrum of the polytripeptide (I; $x=2$) showed two principal amide I bands, at 1663 and 1624 cm^{-1} , with a shoulder at 1693 cm^{-1} ; these indicate the presence of α' -helix and β -structure[†]. The ratio of the areas of the 1663 and 1624 cm^{-1} bands is concentration dependent and corresponds to 23% of the β -form at 2 g/dm^3 , 37% at 9 g/dm^3 and 42% at 18 g/dm^3 . Taking there to be 35% of the β -form at the concentration (6.4 g/dm^3) at which the o.r.d. measurements were made and $b_0 = +630$ for the left-handed α' -helix, the observed

† The expression ' α' -helix' is used to denote a distorted form of the α -helix, with torsion angles, ϕ and ψ , intermediate between those for the undistorted α -helix and those for the helix of Némethy *et al.*⁹. By the term ' β -structure' is to be understood one or other of the special types of cross- β -structure described later (III-VI).

value of +374 for b_0 leads to the reasonable value of -100 for the β -structure. Addition of 1% of TFA leads to the disappearance of the 1624 cm^{-1} (β -structure amide I) band from the i.r. spectrum. In 100% CDCl_3 the n.m.r. spectrum is very poorly developed. Addition of 1% of TFA results in the appearance of broad bands, assigned to the α' -helix, at 1.5 (NH) and 6.1 (α -CH) τ . Addition of more TFA leads to the progressive replacement of these by bands at 2.1 and 5.5 τ , characteristic of the random coil; in the early stages of the transition there is some indication of an NH band, presumably for the β -structure, with a chemical shift between 1.5 and 2.1 τ . The mid-point for the overall order \rightleftharpoons disorder transition, based on the n.m.r. spectra, is at about 3% TFA. The plot of b_0 against TFA concentration shows a sharp transition (α' -helix \rightleftharpoons random coil) at 5.5% TFA.

Spectroscopic studies were carried out with two specimens of the leucyl polytripeptide (II; $x=2$), one of which (fraction 2) was less soluble in chloroform-methanol (1:2) than the other (fraction 3) and had almost double the molecular weight. The i.r. spectrum of fraction 2 showed amide I bands at 1657 and 1625 cm^{-1} , with a shoulder at 1695 cm^{-1} , indicating the presence of α' -helix and β -structure; the relative areas of the principal bands were 0.75 and 0.25, suggesting 25% of β -structure; the 1625 cm^{-1} band disappeared on adding 2% of TFA. The value of b_0 was +464; assuming that b_0 is +630 for the left-handed α' -helix, this leads to $b_0 = -35$ for the β -structure. The n.m.r. spectrum in 100% CDCl_3 was poorly developed. Addition of 1% TFA resulted in the appearance of a broad NH band, centred at about 1.7 τ , and a sharper α -CH band at 6.0 τ ; addition of more TFA brought about the progressive replacement of these α' -helical bands by random coil bands at 2.0 and 5.5 τ . Both the plot of b_0 against TFA concentration and inspection of the n.m.r. spectra indicate a midpoint for the helix \rightleftharpoons random coil transition at about 4.5% TFA.

The i.r. spectrum of fraction 3 of II ($x=2$) is very similar to that of fraction 2 and the ratio of the areas of the 1660 and 1627 cm^{-1} bands is again 0.75:0.25; the 1627 cm^{-1} band disappears on adding 1 to 2% of TFA. However, the o.r.d. is very different, b_0 , although still positive, being much smaller (+246). The n.m.r. spectrum in 100% CDCl_3 is much more fully developed than that of fraction 2, all the side-chain proton signals being discernible in a single scan. Addition of 1% TFA sharpens the spectrum further; in the NH region there are peaks at 1.4 τ (α' -helix), 1.85 τ (β -structure) and 2.0 τ (random coil), and in the α -CH region peaks, almost equal in area, at 5.55 τ (random coil) and 5.95 τ (ordered structures). The i.r. spectrum suggests the presence of 25% of β -structure, the remaining 75% being distributed between α' -helix and random coil. Taking b_0 to be +630 for the α' -helix and -35 for the β -structure, as for fraction 2, the proportion of α' -helix comes to 40%, the remaining 35% being random coil. The data indicate that the TFA concentrations for the midpoints of the β -structure \rightleftharpoons random coil and α' -helix \rightleftharpoons random coil transitions are 1% and 3% respectively.

Polytetrapeptides (I and II; $x=3$)

The i.r. spectrum of the polytetrapeptide (I; $x=3$) is similar to that of the corresponding polytripeptide,

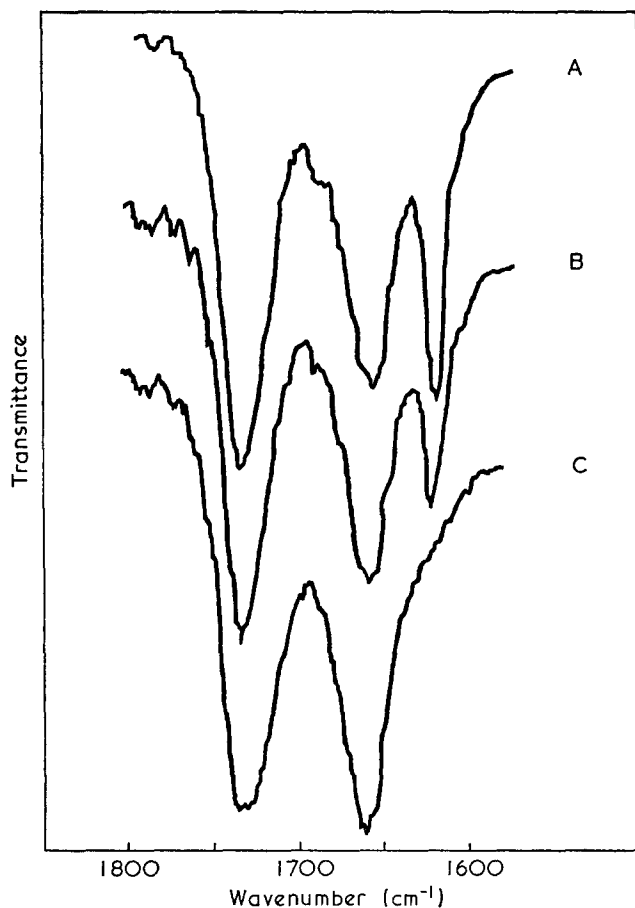


Figure 2 Infra-red spectrum of I ($x=3$) in CHCl_3/TFA mixtures. A, 0%; B, 1%; C, 2% TFA

showing amide I bands at 1662 and 1625 cm^{-1} and a shoulder at 1695 cm^{-1} . The two bands have approximately equal areas in 1% solution, suggesting the presence of 50% each of α' -helix and β -structure. The o.r.d. is very different, however, the value of b_0 rising from +123 in 100% chloroform to a maximum (+239) with 2% TFA and then falling again. Calculation on the basis of equal amounts of the two conformations and taking b_0 as +630 for the α' -helix, leads to a value of b_0 (-380) for the β -structure, which is well outside the normal range. In 100% CDCl_3 the n.m.r. spectrum is poorly developed. In accumulated spectra a very broad NH band extending from 1 to 2 τ and a sharper α -CH band centred at 6.0 τ (ordered structure) can be seen; there are no observable signals attributable to the random coil. These appear, at 2.1 and 5.5 τ , on addition of 1% of TFA, together with an α' -helix peak at 1.7 τ , and progressively replace the other bands as more TFA is added. The disappearance of the 1623 cm^{-1} amide I band from the i.r. spectrum on addition of 1 to 2% of TFA (see Figure 2) shows that the TFA concentration for the midpoint of the β \rightleftharpoons random coil transition is about 1.5%; optical titration indicates that the midpoint of the α' -helix \rightleftharpoons random coil transition occurs at about 5% TFA.

Three specimens of the leucyl polytetrapeptide (II; $x=3$) were studied. All were obtained from the crude polypeptide by precipitation from chloroform with methanol. Fraction 1 was precipitated by addition of one volume of methanol and fraction 2 by addition of another; fraction 3 separated slowly from the mother liquor of fraction 2. Although not greatly different in

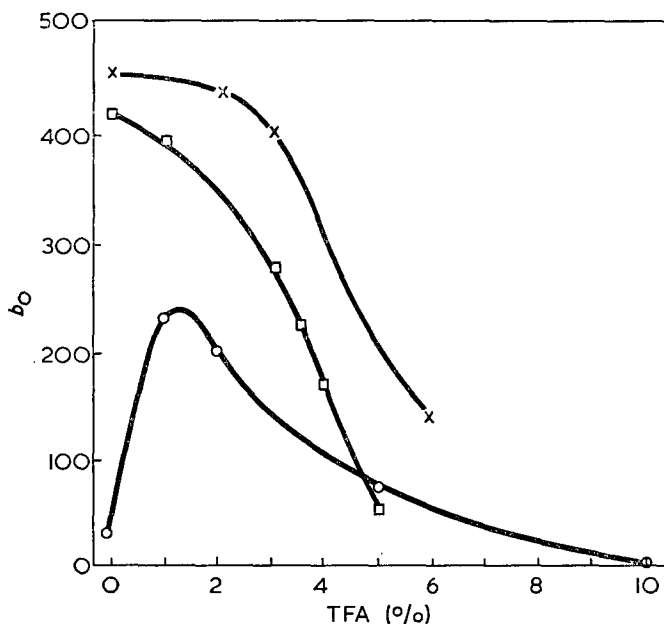


Figure 3 Optical titration of poly(tri- γ -benzyl-D-glutamyl-L-leucine) (II, $x=3$). \circ , Fraction 1; \times , fraction 2; \square , fraction 3

molecular weight, these three specimens were the most polydisperse of any studied in the present work; in particular, gel filtration showed fraction 1 to have a bimodal molecular weight distribution (M_n 9300 and 35 300; 0.8:0.2 by wt).

The i.r. spectrum of fraction 1 shows amide I bands at 1659 and 1628 cm^{-1} , with a weak band at 1695 cm^{-1} ; the relative areas of the major bands suggest a mixture of 30% of α' -helix and 70% of β -structure; the 1628 and 1695 cm^{-1} bands disappear on addition of 2% of TFA. The o.r.d. (Figure 3) is similar to that of the analogous polyglutamate (I; $x=3$), b_0 rising from +30 in 100% chloroform to +234 on addition of 2% TFA and falling again with more TFA. Calculation, taking $b_0 = +630$ for the α' -helix, leads to a value of -230 for b_0 for the β -structure. The n.m.r. spectrum in 100% CDCl_3 is very poorly developed; addition of 1 to 2% of TFA sharpens the spectrum and both NH and α -CH bands can be observed in accumulated spectra. In the α -CH region there are bands at 5.5 and 5.9 τ (random coil and ordered structure); addition of more TFA leads to disappearance of the ordered band, the midpoint of the transition occurring at about 2% TFA. The NH region is much more complex and ill resolved, but again there is clear evidence of an overall transition, with a midpoint at about 2% TFA, involving replacement of a broad band stretching from 1 to 2 τ by a sharper band at 2.1 τ (random coil).

The i.r. spectrum of fraction 2 indicates that it, too, is a mixture of α' -helix and β -structure (amide I bands at 1628 and 1659 cm^{-1} , with a much weaker band at 1695 cm^{-1}); the β -structure bands at 1628 and 1695 cm^{-1} disappear on adding 2% of TFA. The ratio of the areas of the major bands suggests 80% of α' -helix and 20% of β -structure. This is supported by the o.r.d. measurements. The value of b_0 in 100% chloroform is +457; taking the proportions of the conformations suggested by the i.r. spectrum and $b_0 = +630$ for the α' -helix, calculation leads to -235 for b_0 for the β -structure, in good agreement with the value found for fraction 1. The optical titration curve (Figure 3) shows a mid-point for the α' -helix \rightleftharpoons random coil transition at about 5%

TFA. The n.m.r. spectrum in 100% CDCl_3 is very ill developed; the main transition observed on adding TFA involves replacement of bands at 1.5 and 6.0 τ (α' -helix) by bands at 1.9 and 5.5 τ (random coil).

The i.r. spectrum of fraction 3 shows only one amide I band, at 1659 cm^{-1} ; the absence of absorption at 1628 cm^{-1} shows the absence of β -structure. The value of b_0 (+418) in 100% chloroform indicates a mixture of 65% of α' -helix and 35% of random coil; optical titration (Figure 3) gives 3.5% as the TFA concentration for the midpoint of the transition. The n.m.r. spectrum in 100% CDCl_3 shows sharper bands than those seen with similar solutions of the other two fractions; the main transition observed on adding TFA, again with the midpoint at about 3% TFA, involved the progressive replacement of bands at 1.5 and 6.1 τ (α' -helix) by bands at 1.9 and 5.5 τ (random coil).

Polypentapeptides (I and II; $x=4$)

The i.r. spectrum of the polypentapeptide (I; $x=4$) showed a single amide I band at 1659 cm^{-1} , with a shoulder at 1627 cm^{-1} , corresponding to only a small amount of β -structure. The n.m.r. spectrum of a chloroform solution was consistent with the view that this polypeptide was almost entirely helical; accumulation revealed a broad α -CH band at 6.0 τ , with no trace of a random coil peak at 5.5 τ . Addition of 1% of TFA caused the appearance, in accumulated spectra, of an NH band at 1.7 τ . Addition of more TFA led to the progressive replacement of these α' -helix bands by random coil bands at 2.1 and 5.4 τ , the transition being half complete at about 4% TFA. It is, however, not easy to reconcile this interpretation with the o.r.d. findings. In 100% chloroform, b_0 was +390, corresponding to only about 60% of left-handed helix, if b_0 for the α' -helix has the value (+630) which it appears to have in the other cases (above); however, 40% of random coil would surely have been evident in the n.m.r. spectrum. An alternative explanation is that b_0 for the α' -helix in this particular case is about +400, which is possible but not very probable. The optical titration indicated that the midpoint for the helix \rightleftharpoons random coil transition was at 8% TFA.

The i.r. spectrum of the leucyl polypentapeptide, (II; $x=4$), showed amide I bands at 1660 and 1628 cm^{-1} ; the relative areas pointed to a mixture of 75% of α' -helix and 25% of β -structure. The β -structure band at 1628 cm^{-1} disappeared on adding 2% of TFA. For a solution in 100% chloroform, b_0 was +416; on the usual assumptions, calculation leads to a value of -225 for b_0 for the β -structure. Optical titration indicated a midpoint for the α' -helix \rightleftharpoons random coil transition at about 4% TFA. The n.m.r. spectrum in 100% CDCl_3 was very poorly developed. Addition of 1% of TFA led to the appearance, in accumulated spectra, of a broad NH band at 1.7 τ and a broad α -CH band at 6.0 τ , both corresponding to the α' -helix; further addition of TFA resulted in the progressive replacement of these by bands, at 2.1 and 5.5 τ , due to the random coil conformation; the transition was half complete at about 5% TFA.

General

Our suggestions regarding the conformations adopted in chloroform solution by the eight sequential polypeptides we have studied are collected together in

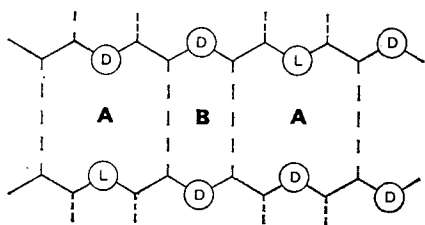
Table 4 Conformations of sequential polypeptides (I) and (II) in chloroform

Polypeptide	Mass fraction of				TFA (%) at midpoint of		
	α' -helix	β -structure	α or LD ₃ P	Random coil	$\alpha' \rightleftharpoons RC$	$\beta \rightleftharpoons RC$	$\alpha \rightleftharpoons RC$
I (x=1)	0.60	0	0.40	0	2.5	—	1.0
II (x=1)	0.35	0	0.65	0	4.0	—	1.5
I (x=2)	0.65	0.35	0	0	5.5	1.0	—
II (x=2); fraction 2*	0.75	0.25	0	0	4.5	1.0	—
II (x=2); fraction 3	0.40	0.25	0	0.35	3.0	1.0	—
I (x=3)	0.50	0.50	0	0	5.0	1.5	—
II (x=3); fraction 1	0.30	0.70	0	0	4.0	1.0	—
II (x=3); fraction 2	0.80	0.20	0	0	5.0	1.0	—
II (x=3); fraction 3	0.65	0	0	0.35	3.5	—	—
I (x=4)	0.95	0.05	0	0	4.0 or 8.0†	—	—
II (x=4)	0.75	0.25	0	0	4.0	1.5	—

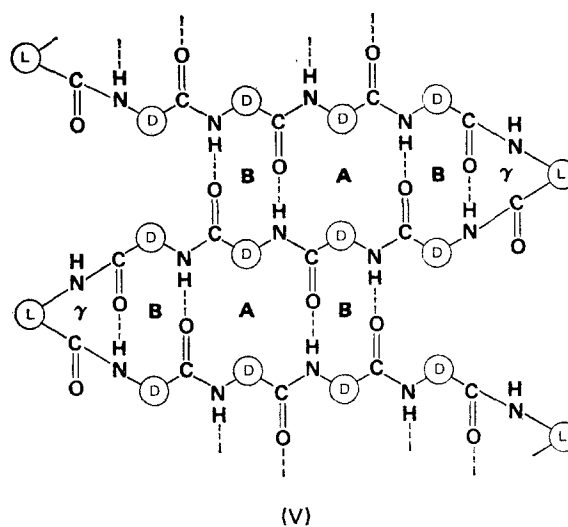
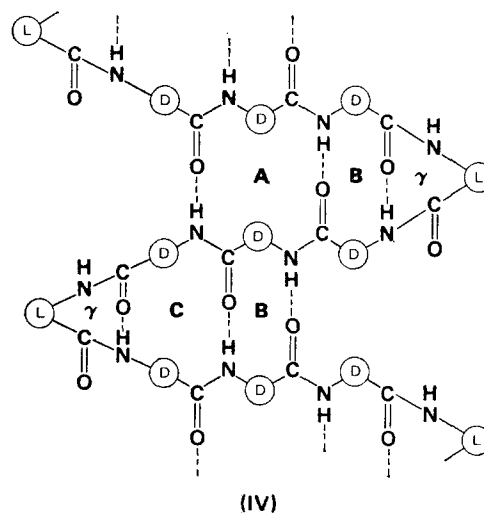
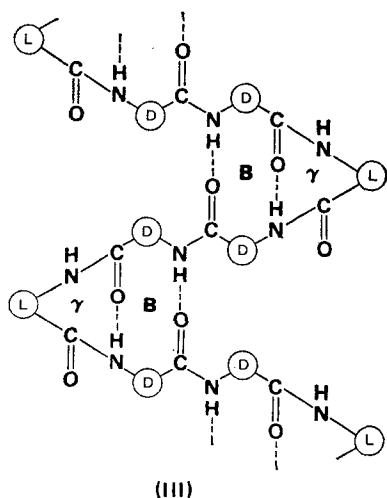
* Fraction numbers as in ref 3

† N.m.r. and o.r.d. respectively

Table 4. The most striking feature of these results is the occurrence of substantial amounts of β -structure, especially since it is difficult to accommodate both D- and L-residues in the normal cross- β -structure, owing to the unfavourable contacts which models show to occur when such residues are at the apices of type A rings, e.g.:

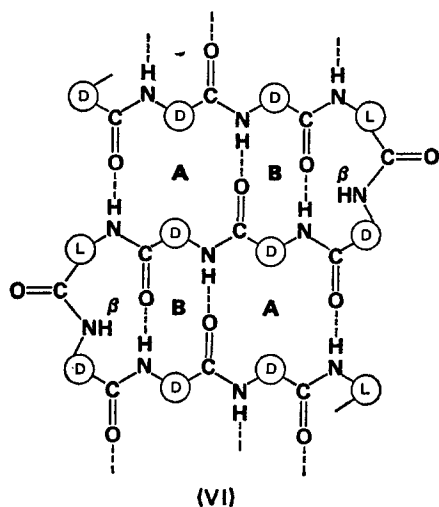


However, special structures (III, IV and V) of the cross- β -type can be written for DDL, DDDL and DDDDL sequential polypeptides which avoid this difficulty, involving only pairs of D-residues at the apices of type A rings, and it is suggested that it is these types of structure which we have encountered in our work. These structures all contain γ -turns^{12, 13} adjacent to B-type rings, as in the arrangement around Thr₂₆ in thermolysin¹⁴. In all of them the NH and CO groups of the L-residues situated at the apices of the γ -turns are not involved in hydrogen bonds and this may account for some of the anomalies (e.g. anomalous values of b_0) encountered in our work. Replacement of any of the



D-residues in these structures by an L-residue leads to unfavourable DL interactions and it is tempting to conclude that they are, for this reason, assumed only by the 'perfect' sequential molecules present in our polypeptides. As pointed out in Part 1¹, the low degree of racemization in our polymerization reactions would result in the presence of very substantial amounts of such 'perfect' molecules.

An alternative cross- β -structure (VI) may be written for the DDDL polypeptides. It differs from (IV) in having β - instead of γ -turns and may for this reason be more



stable¹²; the unusual 12-membered hydrogen-bonded rings, C, present in (IV) is absent from (VI). Similar structures cannot be constructed for the DDL and DDDL polypeptides and it is noteworthy that the two polypeptides containing the largest amount of cross- β -structure (I; $x=3$, and II; $x=3$, fraction 1) both belong to the DDDL series. It is also perhaps significant that one of these, (I; $x=3$), contained a β -structure with the very anomalous b_0 of -380 .

The nature of the helical conformations assumed by the polytri-, tetra- and penta-peptides is less clear than it was in the earlier work¹ on the alternating polydipeptides. The position of the amide I bands attributed to the helical structure (Table 2) varied from 1657 to 1663 cm^{-1} , the mean being 1660 cm^{-1} ; although substantially higher than the mean value (1653 cm^{-1}) for undoubted α -helices, this is not as high as the mean value (1663 cm^{-1}) found for α' -helices in the earlier work¹. In the n.m.r. spectra the low field NH band at 1.5 τ and the high field α -CH band at 6.3 τ were seen only rarely, the chemical shifts for these protons being generally much closer to those observed for undistorted α -helices. However, it still seems probable to us that the introduction of L-residues into a left-handed α -helix must lead to some distortion and to the adoption of a helical conformation somewhat different from that in the strict α -helix, lying somewhere in the low potential energy trough between the α - and α' -helices in the conformational map. In this connection the ease with which the helical structures we have encountered are

split by TFA is noteworthy. In general (Table 4) the midpoint for the helix \rightleftharpoons random coil transition in our sequential polypeptides comes at about 4 to 5% TFA. This is markedly lower than the midpoint TFA concentrations for the corresponding poly(amino acids)⁷ [25% TFA for poly(γ -benzyl-L-glutamate) and 60% for poly(L-leucine)] and is again indicative of a modified, strained, helical conformation.

ACKNOWLEDGEMENT

We thank the Science Research Council for Research Studentships awarded to H. T. S. and R. C. T.

REFERENCES

- Hardy, P. M., Haylock, J. C., Marlborough, D. I., Rydon, H. N., Storey, H. T. and Thompson, R. C. *Macromolecules* 1971, **4**, 435
- Hardy, P. M., Rydon, H. N. and Storey, H. T. *JCS Perkin Trans. I* 1972, p 1523
- Hardy, P. M., Rydon, H. N. and Thompson, R. C. *JCS Perkin Trans. I* 1972, p 5
- Bovey, F. A., Tiers, G. V. D. and Filipovich, G. J. *Polym. Sci.* 1959, **38**, 73; Goodman, M. and Masuda, Y. *Biopolymers* 1964, **2**, 107; Marlborough, D. I., Orrell, D. G. and Rydon, H. N. *Chem. Commun.* 1965, p 518
- Ferretti, J. A. *Chem. Commun.* 1967, p 1030; Markley, J. L., Meadows, D. H. and Jardetzky, O. *J. Mol. Biol.* 1967, **27**, 25; Haylock, J. C. and Rydon, H. N. in 'Peptides 1968', North-Holland, Amsterdam, 1970, p 19; Bradbury, E. M., Crane-Robinson, C., Goldman, H. and Rattle, H. W. E. *Nature* 1968, **217**, 812
- Nagayama, K. and Wada, A. *Chem. Phys. Lett.* 1972, **16**, 50; *Biopolymers* 1973, **12**, 2443; Bradbury, E. M., Crane-Robinson, C. and Hartman, P. G. *Polymer* 1973, **14**, 543
- Fasman, G. D. in 'Poly- α -Amino Acids', (Ed. G. D. Fasman), Arnold, London 1967, p 499
- Huggins, M. L. *Chem. Rev.* 1943, **32**, 195; Bamford, C. H., Hanby, W. E. and Happey, F. *Proc. R. Soc. (A)* 1951, **205**, 30
- Némethy, G., Phillips, D. C., Leach, S. J. and Scheraga, H. A. *Nature* 1967, **214**, 363
- Ramachandran, G. and Chandrasekaran, R. *Indian J. Biochem. Biophys.* 1972, **9**, 1
- Hesselink, F. T. and Scheraga, H. A. *Macromolecules* 1972, **5**, 455
- Némethy, G. and Printz, M. P. *Macromolecules* 1972, **5**, 755
- Bystrov, V. F., Portnova, S. L., Tsetlin, V. I., Ivanov, V. T. and Ovchinnikov, Yu. A. *Tetrahedron* 1969, **25**, 493; Crippen, G. M. and Scheraga, H. A. *Proc. Nat. Acad. Sci. USA* 1969, **64**, 42; Maigret, B., Pullman, B. and Perahia, D. *J. Theor. Biol.* 1971, **31**, 269
- Matthews, B. W. *Macromolecules* 1972, **5**, 818

Crystallinity and crystallite size measurement in cellulose fibres: 2. Viscose rayon*

A. M. Hindeleh

Department of Physics, University of Jordan, Amman, Jordan

and D. J. Johnson

Textile Physics Laboratory, Department of Textile Industries, University of Leeds, Leeds LS2 9JT, UK

(Received 10 December 1973; revised 17 May 1974)

A new X-ray diffraction procedure is established for the determination of crystallinity, crystallite size, and the relative proportions of cellulose II and cellulose IV in viscose rayons. The method involves resolution of the diffraction traces into peaks which are described by combined Gaussian-Cauchy functions, $fG+(1-f)C$. The profile-function parameter f is considered to be a useful new measure of order. Samples were heat treated in dry nitrogen gas and in glycerol for the preparation of the cellulose IV modification which is produced by a real lattice transformation from cellulose II.

INTRODUCTION

It is now generally accepted that the characteristic molecular order and aggregation in a material determines its physical properties. Estimates of structural parameters such as X-ray crystallinity, crystallite size, orientation, birefringence, and degree of polymerization (DP), may be related to physical properties such as elastic modulus, tensile strength, yield point, abrasion resistance, degree of swelling and moisture content¹⁻⁴.

The characterization of normal textile viscose rayons by X-ray diffraction methods has been hindered by the lack of adequate quantitative methods for measuring crystallinity and crystallite size in a material essentially cellulose II, which is normally considered to have relatively low crystallinity when compared to most native celluloses or synthetic polymers such as nylon-6 or nylon-6,6. Indeed even though crystallinity is expected to improve with heat treatment in water or steam, changes found by the usual methods of X-ray analysis are relatively small⁵⁻¹⁶. A contributory problem is the occurrence of the cellulose IV configuration in addition to cellulose II. In normal textile viscose rayons cellulose IV is found after heat treatment in steam or water, after stretching in cold or hot water, and particularly after heat treatment in glycerol. There are also traces of cellulose IV in high-tenacity viscose rayons which can again be enhanced by various heat treatments¹³⁻¹⁶. The presence of cellulose IV in the viscose rayon structure complicates the traditional X-ray methods for evaluating crystallinity; although a drop in DP and reduction in degree of swelling are amongst the modifications observed^{13, 14}, there is no possibility of relating the effect of cellulose IV to the physical properties of viscose

rayons since there is no adequate procedure for estimating the amount of cellulose II and IV in fibres after different treatments.

METHODS OF ASSESSMENT OF CELLULOSE IV

Hermans and Weidinger¹⁶ have made an attempt to analyse the equatorial X-ray diffraction traces of various viscose rayons into peaks and background by a method which assumes identical Gaussian distributions for the overlapping $[10\bar{1}, 002]$ interferences. This procedure is an improvement on their earlier method which fits the background to minima in the diffraction trace and disregards peak overlap, but it does not allow a precise determination of the cellulose II and cellulose IV components. Okajima and Inoue¹⁴ assessed various rayons in terms of the increase in the X-ray equatorial intensities at 15.5° $[(101)_{IV}$ and $(10\bar{1})_{IV}]$, and 22° $[(002)_{II}$ and $(002)_{IV}]$ as the heat treatment temperature increases. Philipp *et al.*¹³ carried out a semi-quantitative determination of cellulose IV by a comparison of the 101 intensity of cellulose IV to the 101 intensity of cellulose II and IV together. Manjunath and Peacock¹⁵ carried out a comprehensive study of the conditions under which cellulose IV occurred in viscose rayons and judged its content by qualitative assessment of the equatorial X-ray diffraction traces.

Because of the absence of a reliable method or analysing the X-ray diffraction patterns of viscose rayons, the question remains open whether cellulose IV increases at the expense of disordered material or by a real lattice transformation from cellulose II^{13, 14}.

It is our aim in the present paper to discuss a new X-ray procedure for the quantitative evaluation of cellulose II and cellulose IV in equatorial X-ray diffraction traces from viscose rayon fibres. At the same time we will illustrate our new method for the determination

* A project supported in part by the Jordan Science Research Council, Amman, and the British Council.

of crystallinity and crystallite size, deduce a measure of lattice order and suggest a mechanism for the transformation of cellulose II to cellulose IV.

EXPERIMENTAL

Material

The material used for this investigation was normal textile viscose rayon yarn, 120 denier, 36 filaments, spun on a Dobson and Barlow continuous-filament spinning machine which includes a drying section where the yarn is heated to around 100°C. Prior to heat treatment the rayon was cleaned in a Soxhlet apparatus using petroleum ether to dissolve the surface oil.

Heat treatment

Heat treatment was carried out in (a) dry nitrogen gas within the temperature range 110° to 260°C at intervals of 10°C, and (b) in glycerol within the temperature range 220° to 270°C. In the case of dry nitrogen, the yarn was wound around a wire frame in order to avoid shrinkage. Heat treatment was carried out in a tubular oven in which a stream of dry nitrogen gas was allowed to pass continuously. The temperature of the oven was raised at a rate of about 3°C/min, starting at 50°C, until the designated temperature had been attained; the sample was then annealed for 30 min and finally cooled to room temperature in a desiccator. The temperature was measured to an accuracy of ±1°C by a thermocouple mounted over the sample. For heat treatment in glycerol the sample was immersed in the liquid at room temperature, then the temperature was raised gradually to the desired level where it was held for 2 h; the sample was then washed with water and air-dried.

X-ray diffraction

X-ray diffraction photographs of the various rayon samples were taken in a camera using Ni-filtered CuK α radiation, a lead-glass collimator with a capillary 0.3 mm in diameter, and a flat-film cassette. The specimen was made in the form of a bundle of parallel filaments held between the jaws of a special frame.

Equatorial X-ray diffraction traces were recorded with a modified Hilger and Watts Y115 diffractometer and a Y90 constant-output generator; the diffractometer employs a scintillation counter whose output can be fed through a single-channel pulse-height analyser to a counter or, via a ratemeter, to a chart recorder. Corrections to the diffraction traces were made for air scatter, polarization, Lorentz factor and Compton scatter; they were then normalized to a convenient standard area²² and analysed in the range 3° to 50° (2 θ) by a resolution program¹⁸ which resolves multi-peak data into individual peaks and a background. The program incorporates an iterative procedure based on Powell's method of conjugate directions which ensures efficient convergence of the function S where:

$$S = \sum_{i=1}^n [Y_{(\text{obs})i} - Y_{(\text{calc})i}]^2$$

for n values of $Y_{(\text{obs})}$ obtained from the corrected diffraction traces, and n values of $Y_{(\text{calc})}$ evaluated from the expression:

$$Y_{(\text{calc})} = \sum_{t=1}^B Q_t + R$$

where B is the number of diffraction peaks, and $Q_t = fG_t + (1-f)C_t$. Here f is called the profile-function parameter of the resolved peak; its value is 1 when the profile is Gaussian and 0 when the profile is Cauchy. G_t is the Gaussian function:

$$G_t = A_t \exp \left[-\ln 2 \left(\frac{2(X - P_t)}{W_t} \right)^2 \right]$$

and C_t is the Cauchy function:

$$C_t = A_t / [1 + [2(X - P_t)/W_t]^2]$$

where X represents the angle 2θ . Each peak is defined in terms of A_t the peak height, P_t the peak position, and W_t the peak width at half height.

The background scatter R is defined in terms of the parameters a' , b' , c' , and d' in a polynomial expression of the form:

$$R = a' + b'x + c'x^2 + d'x^3$$

We have already reported¹⁹ a rigorous analysis of the highly crystalline forms of cellulose I and cellulose II, Ramie and Fortisan, and showed that the resolved reflections are well fitted by combined Gaussian/Cauchy profiles. We also demonstrated how crystallinity, defined as the percentage X-ray scatter under the resolved peaks, and crystallite size, must be considered as parameters which have their optimum values when the best profile-function parameter has been fitted. In the earlier programs we evaluated S and the crystallinity C corresponding to different f values ranging from 1, a Gaussian profile, to 0, a Cauchy profile. S and C were then plotted against f and hence the optimum value of f and C were determined at minimum S .

In the present work we have developed our programs so that the profile-function parameter f becomes a variable parameter for each peak and the best-fit values can be computed directly. In effect Q_t is now:

$$Q_t = f_t G_t + (1 - f_t) C_t$$

To calculate the crystallite size from the width W_t or integral breadth IB_t of the interference profiles, the line broadening due to the experimental conditions was corrected by the approximation for the deconvolution procedure discussed by Jones²⁰. We have used the form:

$$\beta = f(B^2 - b^2)^{1/2} + (1 - f)(B - b)$$

to include the profile-function parameter f . The corrected breadth is β , the uncorrected breadth is B , and b is the instrumental breadth obtained for the diffraction trace of hexamethylenetetramine crystals compacted at 85°C¹⁹.

RESULTS

X-ray photographs

Qualitative examination of the high-angle X-ray diffraction photographs showed a very gradual sharpening of the diffraction arcs in the heat-treated samples with increasing annealing temperature. In the range 210°C to 260°C the photographs show the development of a cellulose IV reflection around 16° between the

101 and $10\bar{1}$, 002] reflections of cellulose II. After treatment in glycerol this additional reflection becomes more pronounced. Accordingly for detailed quantitative analysis we have chosen an untreated specimen, samples annealed at 120°, 180°, 210°, and 260°C in nitrogen, and a sample heated in glycerol at 270°C.

X-ray diffraction traces

Normalized equatorial diffraction traces for the above samples are given in Figure 1. The untreated specimen and the sample annealed at 120°C show no evidence of cellulose IV and the computational analysis was carried out in terms of cellulose II peaks only. It was suspected that the specimens annealed at 180°C and 210°C contained small amounts of cellulose IV, consequently tests were made for the presence of cellulose IV reflections in the region (2θ) 15° to 15°. Since evidence for cellulose IV can be seen clearly in the traces for the 260°C nitrogen and 270°C glycerol-treated specimens, analysis of these materials necessitated the inclusion of both lattices in all resolution work. Published values for lattice spacings in cellulose II and cellulose IV are given in Table 1^{15, 17}.

We have used 79 data points in these experiments with an error in the fit of $Y_{(calc)}$ to $Y_{(obs)}$ of around 3.5%. Diffraction traces resolved into the three main equatorial reflections of the cellulose II lattice are given in Figures 2a–2d, for the untreated viscose rayon and for examples heat-treated at 120°, 180°, and 210°C in nitrogen. In the case of samples annealed at 180°C

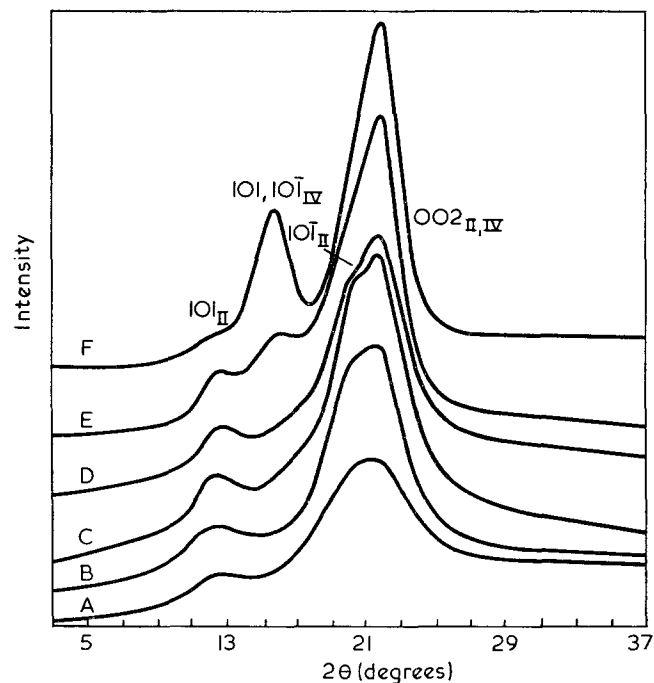


Figure 1 Corrected and normalized X-ray diffraction traces from viscose rayon, untreated (A), heated to 120° (B), 180° (C), 210° (D) and 260°C (E) in nitrogen, and heated to 270°C in glycerol (F). Each trace has a different base level

Table 1 Equatorial spacings of cellulose lattices in Å

	101	$10\bar{1}$	002
Cellulose II	7.19	4.40	4.04
Cellulose IV	5.68	5.68	4.02

and 210°C, the additional peak for cellulose IV was included at 16°; after resolution this peak was found to be very small, consequently it has not been included in the illustrations. Figures 3 and 4 show resolution of the diffraction traces for samples annealed at 260°C in nitrogen and at 270°C in glycerol. Figures 3a and 4a illustrate the resolution of the diffraction traces into 4 peaks only; the cellulose IV peak at 15.6° is clearly resolved in both Figures. However, the peak at 21.75° is a composite of both the 002 reflection of cellulose II and 002 reflection of cellulose IV. In order to estimate the relative quantities of cellulose II and IV present in each specimen it is necessary to resolve the complete trace into 6 peaks corresponding to the spacings indicated in Table 1. The results of this analysis are illustrated in Figures 3b and 4b, and full details of all the parameters are given in Tables 2 and 3. It can be seen that the 101 and $10\bar{1}$ peaks of cellulose II are unchanged in Figures 3a and b as well as in Figures 4a and b; but the composite reflection of cellulose IV at 15.6° is resolved into two separate peaks for the 101 and $10\bar{1}$ reflections. However, since there is no change in position of these resolved peaks and the total area remains unchanged, this resolution may be considered redundant. At the same time the composite peak at 21.75° has been resolved into the 002 peak of cellulose II and the 002 peak of cellulose IV, hence we are now able to add together the respective crystallinities due to cellulose II and IV.

Crystallinity

The parameters obtained after the resolution procedures which relate to the illustrations in Figures 2, 3b and 4b are given in Tables 2 and 3. The untreated specimen, essentially cellulose II, has a crystallinity of 45% as evaluated in the diffraction range 3° to 50°. After annealing at 120°C and 180°C the crystallinity increases to 60% and 67% respectively; however, at 210°C it has fallen to 57%. When the suspected reflections of cellulose IV were included in the resolution procedure, a small peak at 16° (2θ) was found corresponding to a cellulose IV content of 1.6% in the 180°C sample and 2.4% in the 210°C sample. The fact that the detected cellulose IV content is small, while the decrease in crystallinity between 180°C and 210°C samples is about 10%, suggests that a part of the cellulose II has been transformed into an intermediate disordered structure prior to complete transformation into cellulose IV. Thus we can deduce from the table of results that this difference (10%) appeared as an increase in the background scatter at 210°C. At the higher annealing temperature (260°C) the total crystallinity increased to 65%, of which 45% is cellulose II and 20% is cellulose IV. Thus one-third of the ordered cellulose II at 180°C was transformed into ordered cellulose IV at 260°C.

When annealed in glycerol at 270°C the cellulose IV content increased to 40% while the cellulose II content decreased to 21% giving a total crystallinity of 61%. In this case, two-thirds of the cellulose II has been transformed to cellulose IV.

Crystallite size

From the analysis of the peak breadths in the untreated specimens we find that the calculated crystallite sizes are small, only three or four times the d spacing for the appropriate lattice, as indicated by the values of L_{ij} in Table 2 obtained from the integral breadths.

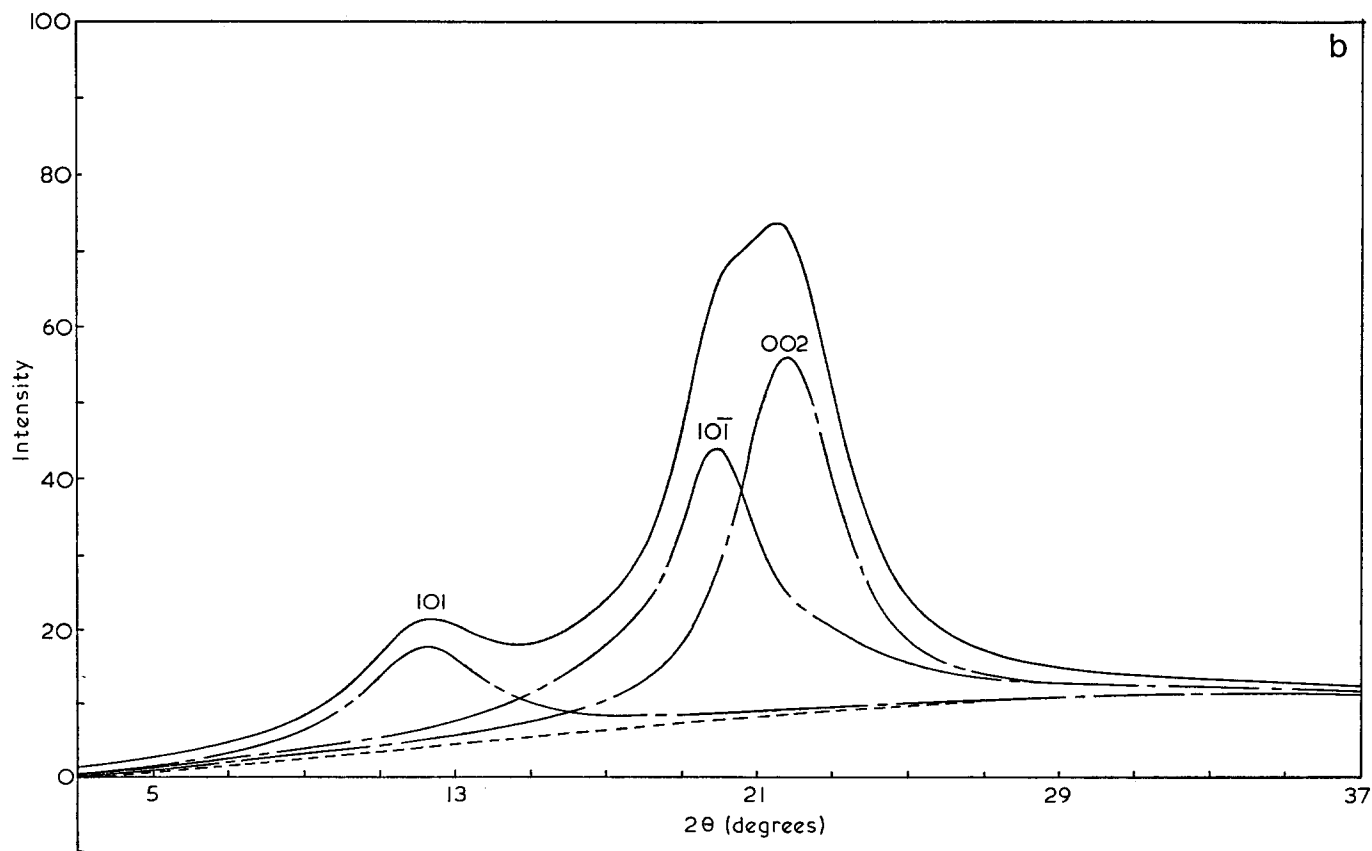
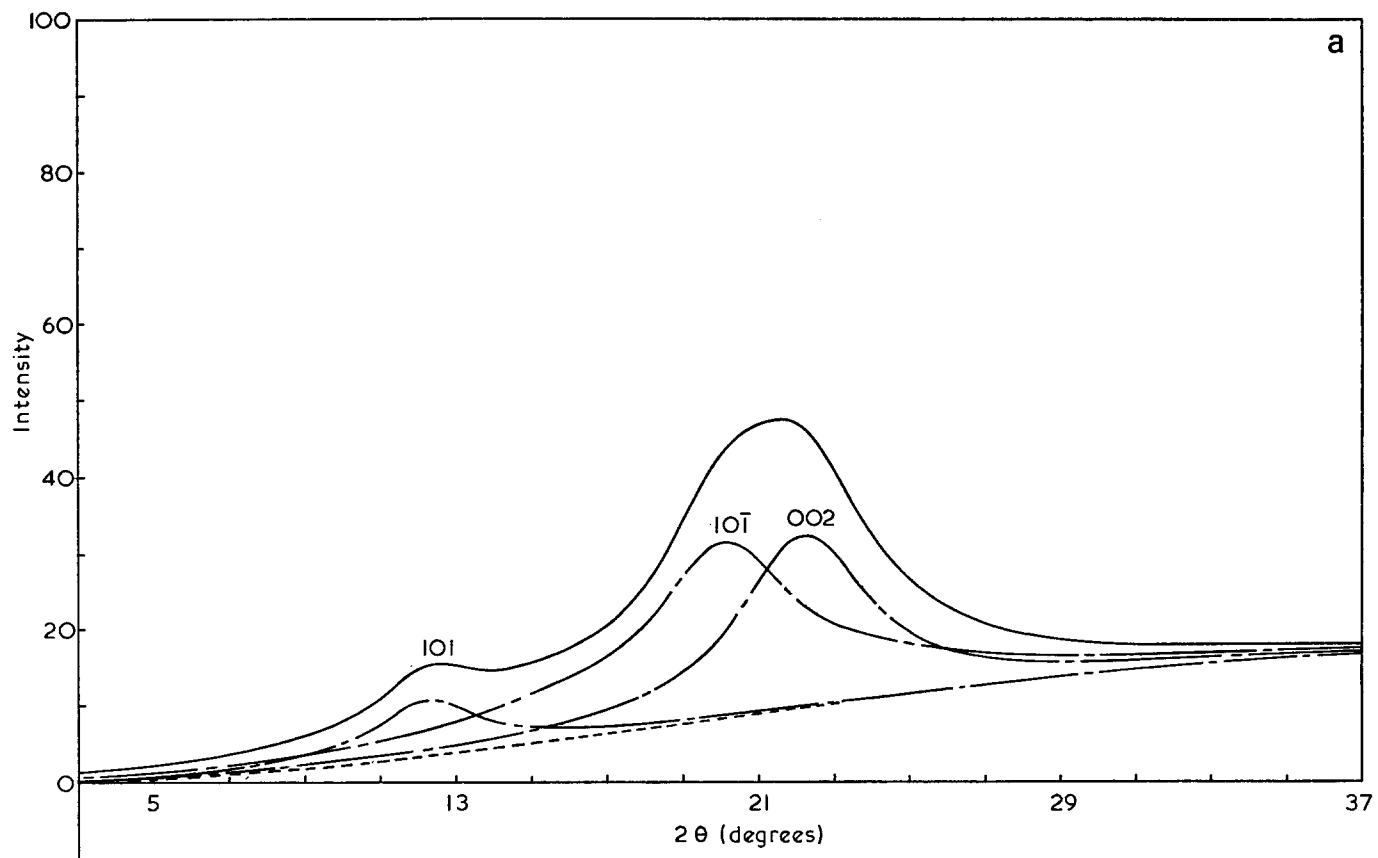


Figure 2 Peak resolution for viscose rayon: (a) untreated, (b, c, d) heat treated at 120, 180, and 210°C respectively. —, Corrected and normalized X-ray diffraction trace; ----, computed background; - - - -, best-fit resolved peak profiles

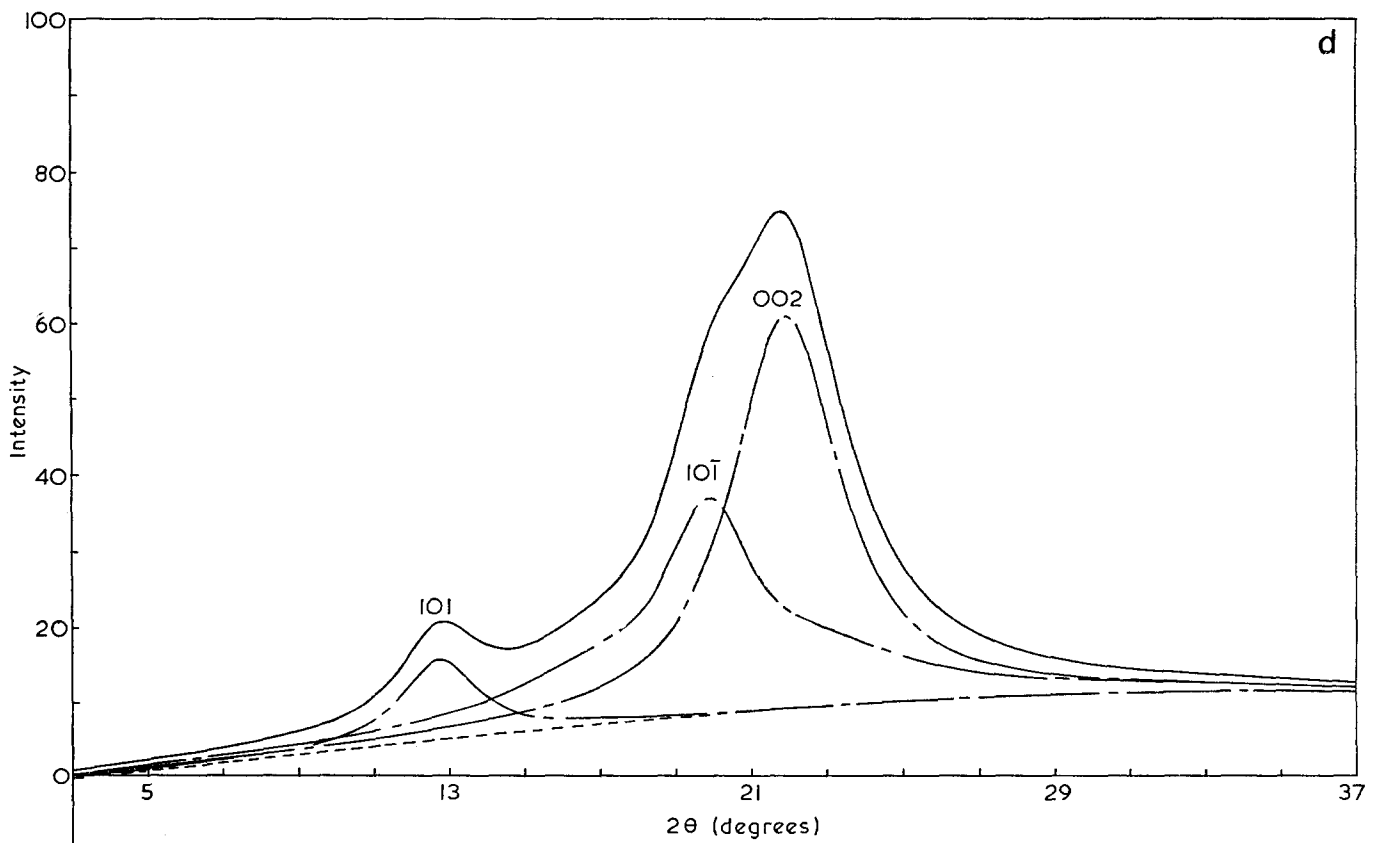
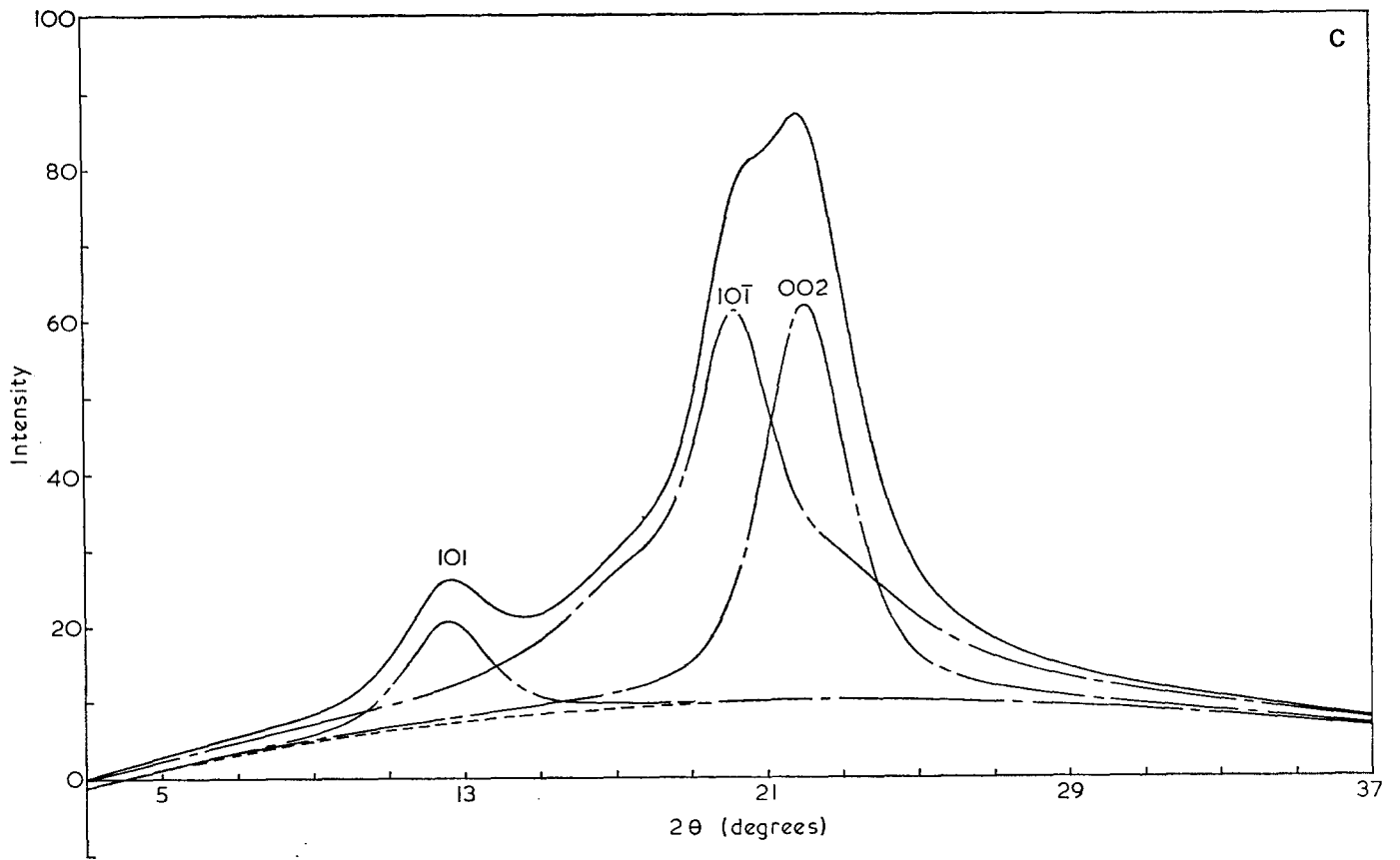


Figure 2 (c) and (d)

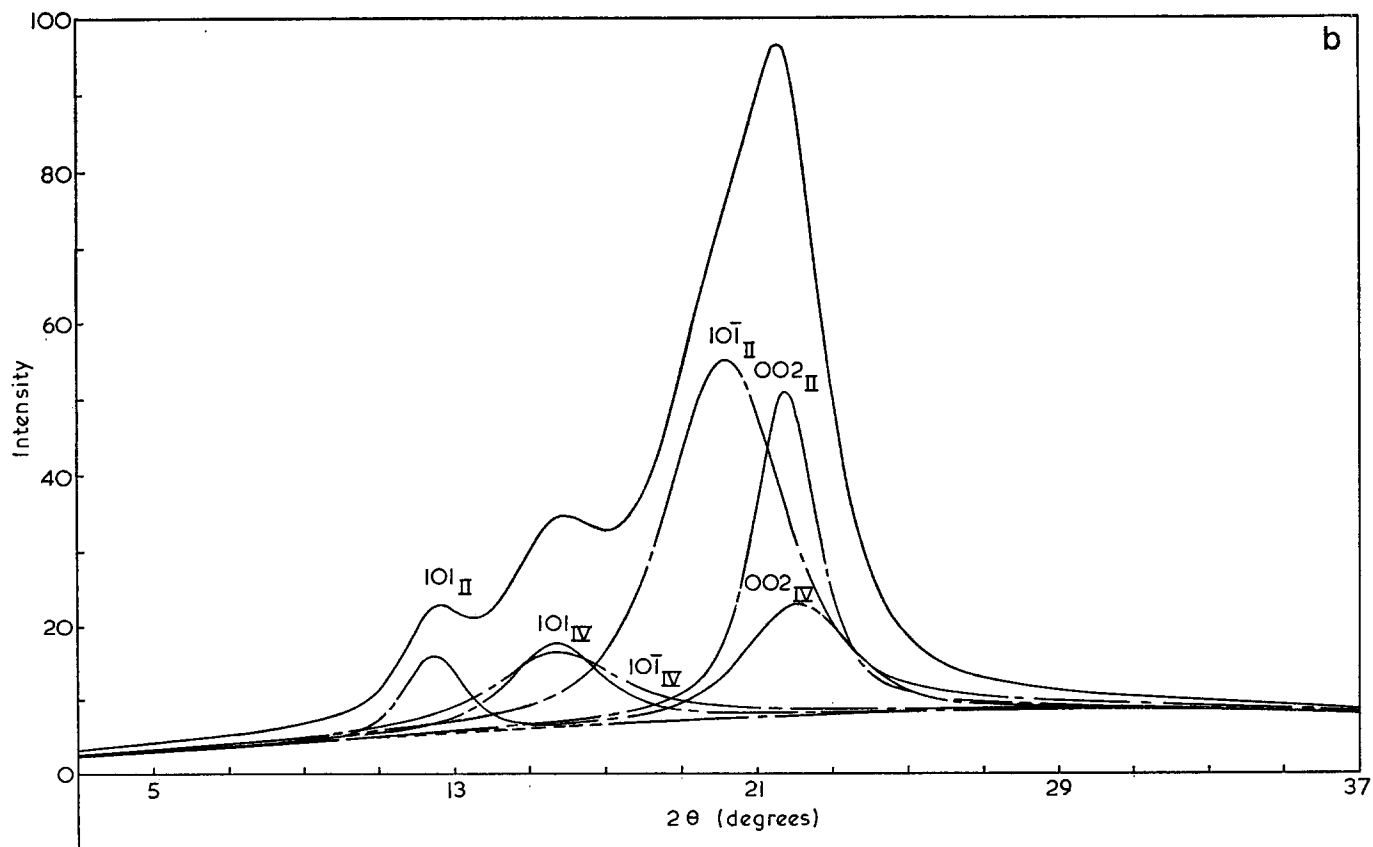
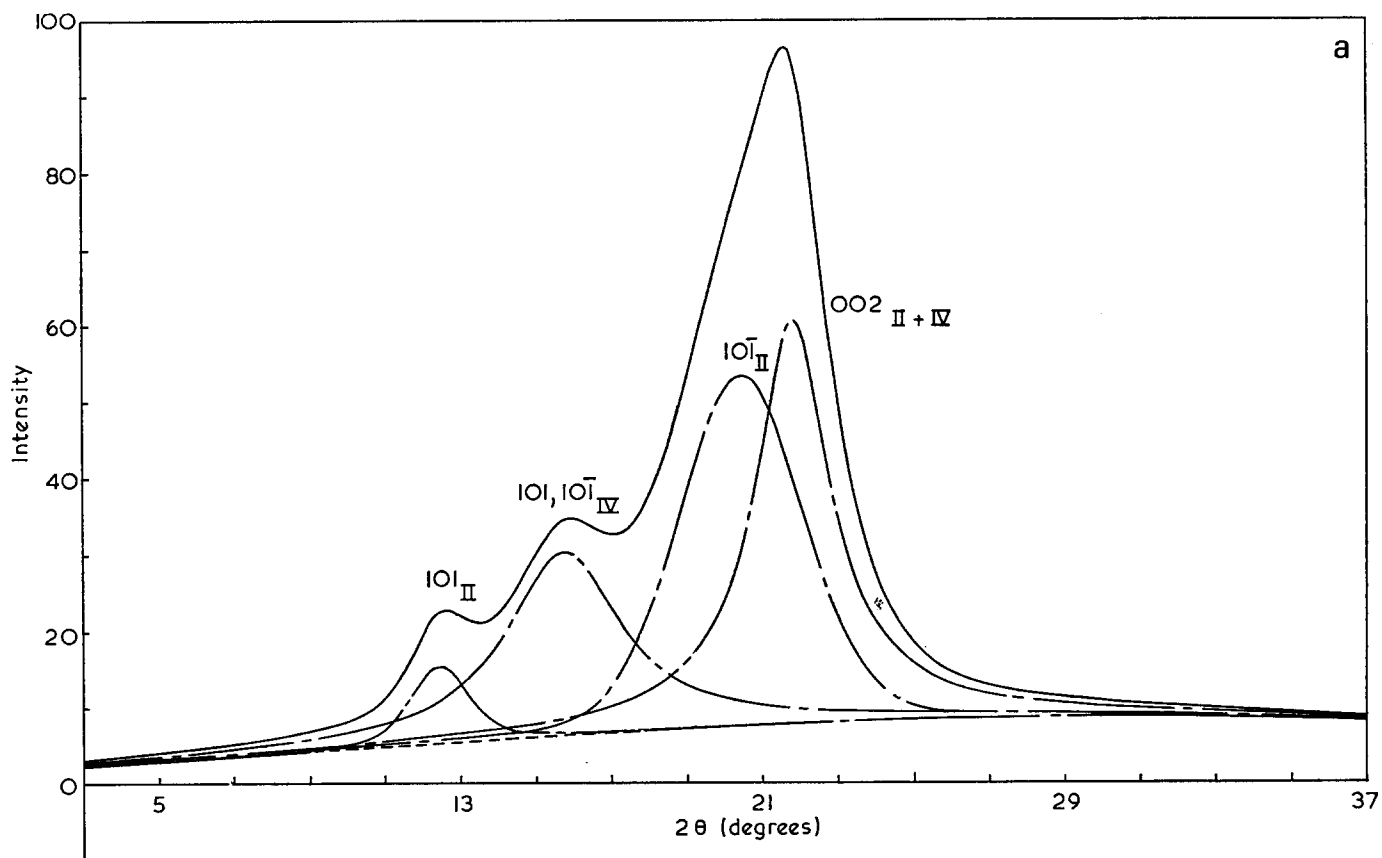


Figure 3 Peak resolution for viscose rayon heat treated at 260°C: (a) four peak resolution; (b) six peak resolution. —, Corrected and normalized X-ray diffraction trace; ----, computed background; - · - · -, best-fit resolved peak profiles; hk/l_{II} , cellulose II peaks; hk/l_{IV} , cellulose IV peaks

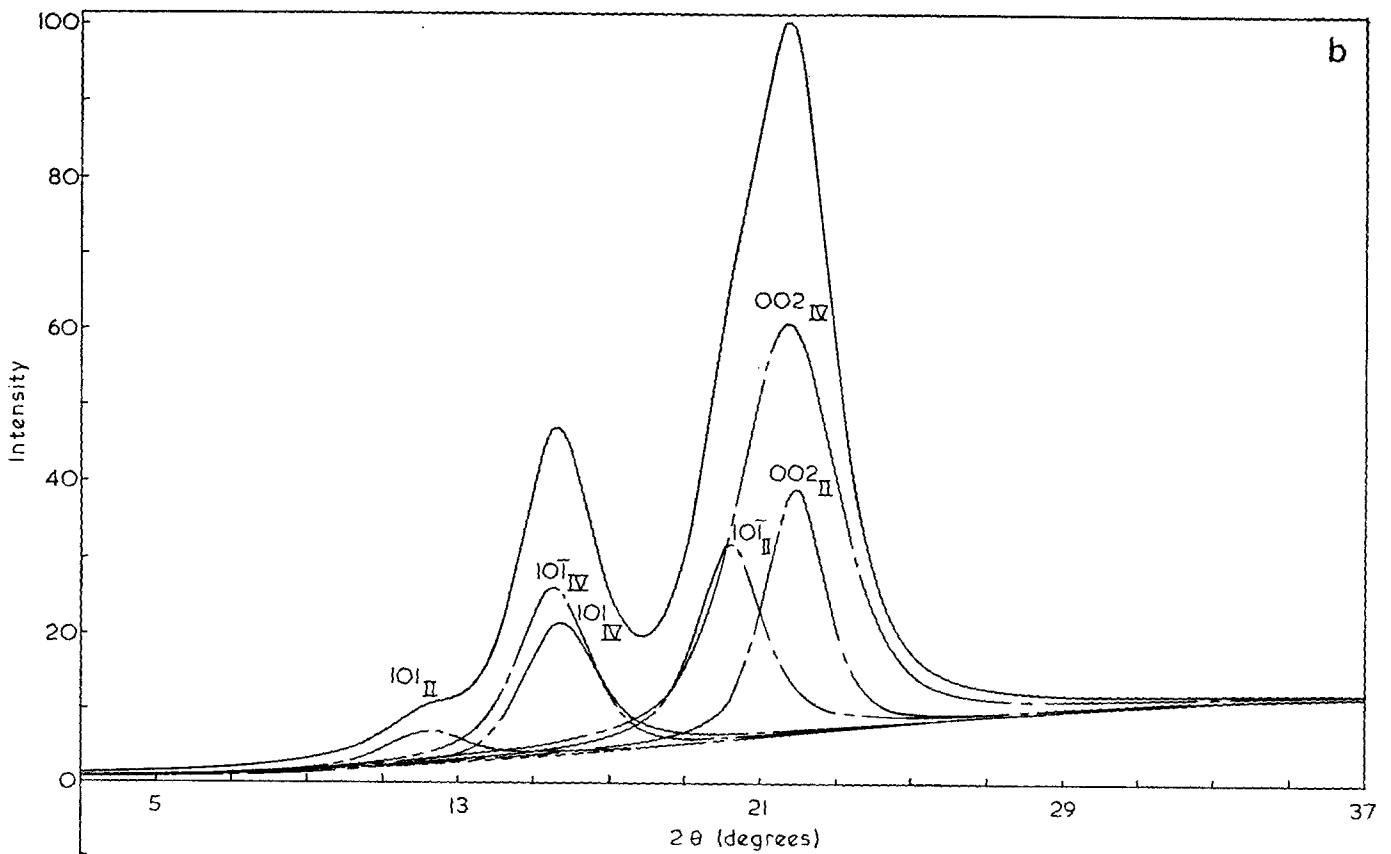
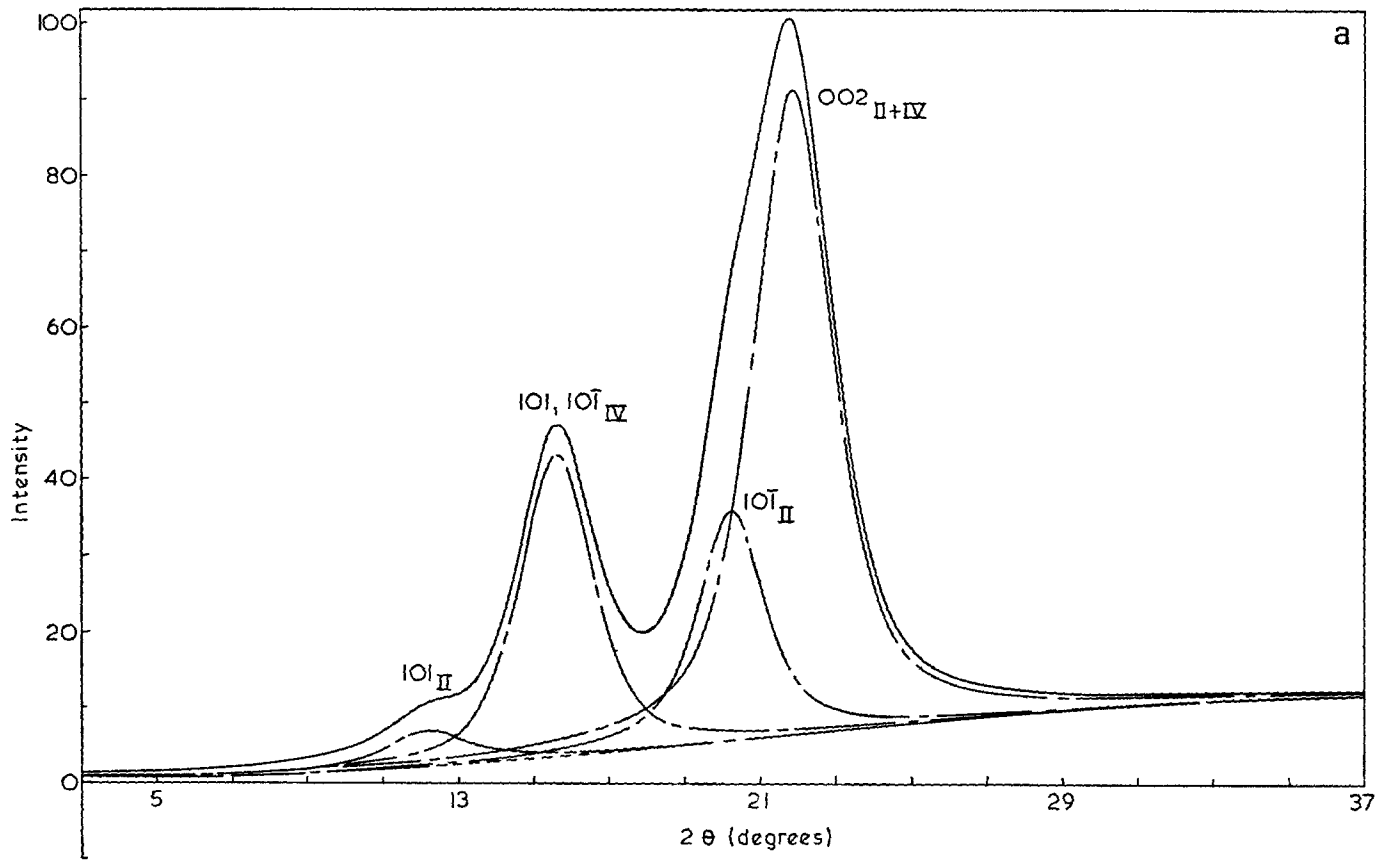


Figure 4 Peak resolution for viscose rayon heat treated in glycerol at 270°C: (a) four peak resolution; (b) six peak resolution. —, Corrected and normalized X-ray diffraction trace; ---, computed background; — — —, best-fit resolved peak profiles; hk/l_{II} , cellulose II peaks; hk/l_{IV} , cellulose IV peaks

Table 2 Parameters of the resolved peaks for specimens annealed in nitrogen

Specimen	Peak	f	A	P	W	C	Lwj	Lij	II	IV
Untreated	101	-0.24	7.18	12.19	3.41	44.8	30.5	18.5		
	10 $\bar{1}$	-0.53	23.24	20.03	5.17		19.7	11.3		
	002	0.03	22.66	22.14	4.23		23.5	15.5		
120°C	101	0.07	13.48	12.13	4.08	60.2	24.0	16.6		
	10 $\bar{1}$	-0.62	35.93	19.88	3.33		33.4	17.2		
	002	0.17	47.24	21.77	3.28		30.6	20.8		
180°C	101	0.44	13.29	12.51	2.65	66.7	36.9	27.7		1.6
	10 $\bar{1}$	-0.94	51.10	20.15	3.45		33.4	15.6		
	002	0.36	51.65	22.01	2.63		38.2	27.4		
210°C	101	0.11	10.83	12.69	2.46	57.4	42.3	28.4		2.4
	10 $\bar{1}$	-0.87	28.64	19.82	3.68		30.5	15.1		
	002	0.08	51.57	21.87	3.43		29.5	19.7		
260°C	101 _{II}	0.49	10.78	12.41	1.88	65.5	53.7	40.3	45	20
	101 _{IV}	0.29	11.46	15.64	2.95		33.6	23.8		
	10 $\bar{1}$ _{IV}	0.07	10.30	15.65	4.05		24.3	16.3		
	10 $\bar{1}$ _{II}	0.41	47.62	20.12	3.72		25.9	19.3		
	002 _{II}	0.28	43.01	21.70	2.01		52.8	35.9		
	002 _{IV}	0.49	15.30	22.04	3.36		28.7	22.0		

f =profile-function parameter; A =peak height (arbitrary units); P =peak position ($2\theta^\circ$); W =peak width ($2\theta^\circ$); C =area under peaks (%), i.e. crystallinity; Lwj =crystallite size from peak width corrected by the Jones approximation; Lij =crystallite size from integral breadth corrected by the Jones approximation; II=percentage of cellulose II; IV=percentage of cellulose IV

Table 3 Parameters of the resolved peaks for the specimen annealed in glycerol at 270°C

Peak	f	A	P	W	C	Lwj	Lij	II	IV
101 _{II}	0.25	4.57	12.15	2.61	60.9	38.6	26.9	20.5	40.4
101 _{IV}	0.63	17.70	15.66	2.33		41.3	33.1		
10 $\bar{1}$ _{IV}	0.30	22.26	15.47	2.32		44.0	30.7		
10 $\bar{1}$ _{II}	0.28	25.95	20.15	2.08		50.5	33.7		
002 _{II}	0.50	32.15	21.68	1.91		53.5	39.8		
002 _{IV}	0.46	54.24	21.87	3.10		31.4	23.6		

f =profile-function parameter; A =peak height (arbitrary units); P =peak position ($2\theta^\circ$); W =peak width ($2\theta^\circ$); C =area under peaks (%), i.e. crystallinity; Lwj =crystallite size from peak width corrected by the Jones approximation; Lij =crystallite size from integral breadth corrected by the Jones approximation; II=percentage of cellulose II; IV=percentage of cellulose IV

The high values of peak breadth may be due not only to small crystallite size but also to a high disorder in the lattice; essentially the crystal structure may be regarded as paracrystalline.

After annealing at 120°C and 180°C the peak breadths decrease. At 210°C there is a slight increase in peak breadth (002) a change which has accompanied the drop in crystallinity and the appearance of a large background scatter; consequently this increase may well be attributed to the transitional state of the cellulose and the onset of crystallization into the cellulose IV configuration. At the higher annealing temperatures, 260°C in nitrogen and 270°C in glycerol, the crystallites of cellulose IV and the remaining crystallites of cellulose II have increased in size.

The profile-function parameter, f

For the untreated viscose rayon specimen we obtained very low values of the profile-function parameter f in comparison with earlier work on the highly crystalline cellulose fibres, Ramie and Fortisan¹⁹ where best-fit f values of 0.7 and 0.4 were obtained. In particular we note that f may take negative values when it is allowed to become a variable parameter unconstrained by the limits $1 > f > 0$. The concept of a negative f value is

illustrated in Figure 5 where four test peaks with amplitudes of 10, half-height widths of 2, and f ranging from 1 to -0.5 are drawn. It is evident that as f decreases the tails become longer and the area under the peak increases. Since an increase in the tails of a reflection is generally attributed to increased disorder in the paracrystalline lattice, we believe, to a first approximation, that the profile-function parameter f of the resolved peaks can be considered as a measure of lattice order. At the higher annealing temperatures (260°C in nitrogen and 270°C in glycerol) f becomes more Gaussian, i.e. it increases for all peaks (see Table 4). Since it is well known that annealing paracrystalline polymers at high temperatures causes an increase in both crystallite size and order²¹, we may deduce that the lattices of cellulose II and IV have an increased order as f increases. We can now examine the variation of f at the lower annealing temperatures; here for the 101 and 002 peaks of cellulose II we found an increase when cellulose II is the only polymorphic form, this is followed by a decrease at 210°C when cellulose IV is first detected; finally, at 260°C, there is an increase in f as cellulose IV becomes

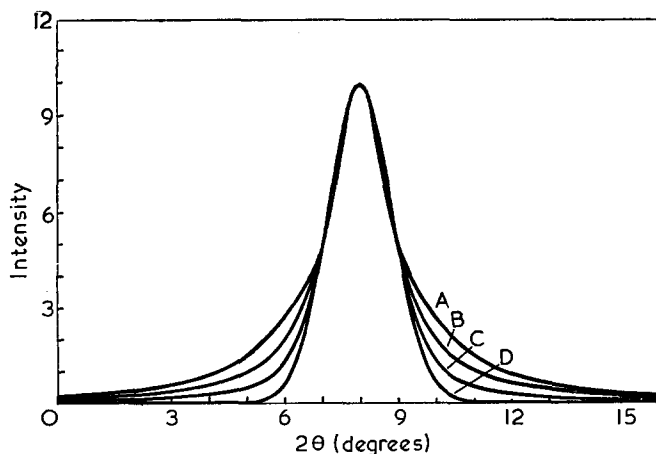


Figure 5 Test peaks with amplitudes=10, half-height widths=2, positions=8, and profile-function parameters f =-0.5 (A), 0 (B), 0.5 (C) and 1.0 (D)

Table 4 The profile-function parameter f of the resolved peaks

	101	10 $\bar{1}$	002
Untreated	-0.24	-0.53	0.03
120°C in nitrogen	0.07	-0.62	0.17
180°C in nitrogen	0.44	-0.94	0.36
210°C in nitrogen	0.11	-0.87	0.08
260°C in nitrogen			
Cellulose II	0.49	0.41	0.28
Cellulose IV	0.29	0.07	0.49
270°C in glycerol			
Cellulose II	0.25	0.30	0.46
Cellulose IV	0.63	0.28	0.50

more prominent. Since we have observed a general loss of order in the 210°C sample, we have additional proof that f may be regarded as a measure of lattice order.

An important observation regarding the transformation of cellulose II to cellulose IV can be made in terms of the 10 $\bar{1}$ reflection of cellulose II. This reflection has a decreasing f value (-0.53 to -0.94) in the temperature range up to 210°C, and it would seem that this indicates increasing disorder of the chain molecules normal to the (10 $\bar{1}$) planes. Since infra-red evidence²³ suggests that intramolecular hydrogen bonds are predominantly in the (10 $\bar{1}$) planes, this disorder may be due to breakdown of the less dominant hydrogen bonds in the (002) planes. Recrystallization into the cellulose IV lattice will occur at higher temperatures after rotation of the pyranose rings into positions approximately parallel to the (002) planes and reformation of intramolecular hydrogen bonds.

CONCLUSION

We have established a quantitative method for the determination of crystallinity, crystallite size, and relative content of cellulose II and cellulose IV in viscose rayons. After an initial increase in crystallinity after annealing at temperatures up to 180°C, where only cellulose II is present, there is a significant decrease around 210°C; annealing at higher temperatures causes recrystallization of cellulose IV with a total crystallinity which remains around 60 to 65%. This constancy of

total crystallinity and the onset of molecular disorder perpendicular to the (10 $\bar{1}$) planes at the intermediate temperatures, suggests that there is a real lattice transformation from cellulose II to cellulose IV. Although crystallite size in cellulose IV is always lower than in cellulose II, even after heat treatment in glycerol, both types of crystallite increase in size and lattice order as annealing temperature increases. We have also found that the profile-function parameter f can be considered as a measure of lattice order.

ACKNOWLEDGEMENTS

One of us (A. M. H.) thanks the Jordan Research Council and the British Council for financial support.

REFERENCES

- Hindeleh, A. M. and Johnson, D. J. *Polymer* 1970, **11**, 666
- Barakat, N. and Hindeleh, A. M. *Text Res. J.* 1964, **34**, 581
- Kraessig, H. and Kitchen, W. *J. Polym. Sci.* 1961, **51**, 123
- 'Encyclopaedia of Polymer Science and Technology', Interscience, New York, 1969, Vol 10, p 534
- Ingersoll, H. G. *J. Appl. Phys.* 1946, **47**, 924
- Preston, J. M., Nimkar, N. M. and Gundarda, S. P. *J. Soc. Dyers Colour.* 1951, **67**, 169
- Preston, J. M. and Gundarda, S. P. *J. Soc. Dyers Colour.* 1952, **68**, 511
- Yazawa, M. and Okajima, S. *Kogyo Kagaku Zasshi* 1954, **57**, 512
- Mukoyama, S. and Tsuda, T. *Kogyo Kagaku Zasshi* 1957, **60**, 934
- Okajima, S. and Kikuchi, T. *Kogyo Kagaku Zasshi* 1961, **64**, 1665
- Yurugi, T. and Ogihara, T. *Kogyo Kagaku Zasshi* 1960, **63**, 1457
- Yazawa, M. and Okajima, S. U.S. Pat. Appl. 155 324 (1961); U.S. Pat. Appl. 177 382 (1962)
- Phillip, B., Baudisch, J. and Ruscher, Ch. *Tappi* 1969, **52**, 693
- Okajima, S. and Inoue, K. *J. Polym. Sci. (A)* 1964, **2**, 461
- Manjunath, B. R. and Peacock, N. *Text. Res. J.* 1969, **39**, 70
- Hermans, P. H. and Weidinger, A. *Text. Res. J.* 1961, **31**, 558
- Wellard, H. J. *J. Polym. Sci.* 1954, **13**, 471
- Hindeleh, A. M. and Johnson, D. J. *J. Phys. (D: Appl. Phys.)* 1971, **4**, 259
- Hindeleh, A. M. and Johnson, D. J. *Polymer* 1972, **13**, 423
- Jones, F. W. *Proc. R. Soc. (A)* 1938, **166**, 16
- Buchanan, D. R. and Miller, R. L. *J. Appl. Phys.* 1966, **37**, 4003
- Hindeleh, A. M. and Johnson, D. J. *Polymer* 1972, **13**, 27
- Marrinan, H. J. and Mann, J. *J. Polym. Sci.* 1956, **21**, 301

A review of statistical structures in synthetic polypeptides and biological macromolecules

A. Miller

*Laboratory of Molecular Biophysics, Department of Zoology, University of Oxford,
South Parks Road, Oxford, UK*

and D. A. D. Parry

*Department of Chemistry, Biochemistry and Biophysics, Massey University, Palmerston North,
New Zealand*

(Received 26 February 1974)

INTRODUCTION

The relationship between the structure and function of biological macromolecules is fundamental to our understanding of molecular biology. It is generally true that those proteins which are rich in charged residues have a high axial ratio (fibrous proteins) and those which are low in charged residues tend to have a small axial ratio (globular proteins). Rod-shaped proteins have a larger surface area and smaller internal volume per unit volume than do the globular proteins. The surface charge per unit area is reduced by the protein adopting a cylindrical shape. Also, a larger percentage of apolar residues can be accommodated in the centre of a globular unit than in a cylindrical unit. This review is primarily concerned with attempting to understand how the long, rod-shaped molecules found in fibrous proteins pack together in three dimensions in a regular or quasi-regular manner to produce functionally useful filaments or fibrils such as are present in muscle, tendon, cartilage, skin etc. Since it is often possible to produce synthetic filaments by self-assembly of the long molecules from solution, the structure of the molecular aggregate must be specifically related to the packing of the individual molecules. Electron microscopy has allowed the visualization of orderly arrays of filaments in muscle and hair but technical limitations still prevent easy recognition of regular packing of the molecules themselves. X-ray diffraction, however, conclusively shows the existence of such regular assemblies of molecules in the native state of many biological fibres. Long rod-shaped macromolecules are specifically designed by nature to aggregate. The kind of molecular interactions in the aggregate are normally dictated by thermodynamic considerations of free energy. In the event of the possible formation of several structures of similar free energy, that which is biologically useful must be preferred.

The purpose of a structural investigation of a fibrous protein is to see how the molecular structure can lead to specific interactions which produce regular aggregates and also how these interactions bestow properties appropriate to the biological role on the resulting aggregate. In this review we draw attention to a particular

aspect of regular arrays of fibrous proteins, their synthetic analogues and also the nucleic acids, viz. statisticality. We first describe the various possible categories of statisticality and show how the X-ray diffraction patterns from such structures may be calculated. Then follows a review of the known occurrences of statisticality in assemblies of biopolymers and their analogues and a discussion of the biological implications. We also point out the characteristic features of X-ray diffraction patterns from structures which exhibit statistical ordering.

TYPES OF STATISTICALITY

Statistical structures are arrangements of molecules (or molecular aggregates) which exhibit a limited and highly specific form of disorder. Whilst in a crystal lattice the contents of the unit cells are identical, in many statistical structures there are two or more unit cells of differing contents which occur throughout the lattice. The differences between these unit cells is brought about in the cases we shall consider, by the molecules or the molecular aggregates packing together in two or more different ways. The crystal lattice parameters remain closely similar in different unit cells, but the unit cell contents may be one of a finite number of kinds.

Two general types of statisticality are geometrically possible. In the first type we imagine each unit cell can be one of t different kinds, each of which may be unrelated to the kind of their neighbours. For example, suppose a unit cell contains a molecule which can either point 'up' or 'down' (i.e. $t = 2$). In the first type of statisticality the occurrence of molecules in 'up' and 'down' directions will be randomly distributed throughout the crystal lattice, i.e. a molecule found in the 'up' direction will not be determined by the direction of the neighbouring molecules. The unit cell of the statistical structure will be the same as that of a perfect lattice with all the molecules pointing in the same direction. However, in the former case each unit cell can be thought of as containing a statistical molecule which comprises a half weighted 'up' and 'down' molecule at the same lattice site. In the second type of statisticality, the particular kind of one unit cell

may affect that of neighbouring cells. The kinds of unit cells are 'coupled' in some manner. This usually results in the unit cell of the statistical structure being larger than that of the perfect lattice with all unit cells of one type.

EFFECT OF STATISTICAL ORDERING ON THE FOURIER TRANSFORM

If a 'unit' is a molecule or molecular aggregate, then in order to define that unit fully, its position and nature must be specified. If both of these parameters are statistically distributed in an independent manner (as will be the usual case in the types of system which we will discuss), then the scattering power of a set of N units which have scattering factors $f_j (j = 1, \dots, N)$ will be¹:

$$I_N(\mathbf{s}) = \sum_1^N f_j^2 + \sum_{j \neq j'} \sum f_j f_{j'} \cos(2\pi \mathbf{s} \cdot \mathbf{r}_{jj'}) \quad (1)$$

where \mathbf{s} and \mathbf{r} are the vectors in reciprocal and real space respectively and $\mathbf{r}_{jj'} = \mathbf{r}_{j'} - \mathbf{r}_j$. It follows directly from equation (1) that the observed intensity will be the average value of equation (1) determined over all possible states, i.e.

$$\begin{aligned} \overline{I_N(\mathbf{s})} &= \overline{Nf_j^2} + \overline{\sum \sum f_j f_{j'} \cos(2\pi \mathbf{s} \cdot \mathbf{r}_{jj'})} \\ &= N\overline{f_j^2} + \overline{\sum \sum f_j f_{j'} \cos(2\pi \mathbf{s} \cdot \mathbf{r}_{jj'})} \\ &= N[\overline{f_j^2} - (\overline{f_j})^2] + (\overline{f_j})^2 [N + \overline{\sum \sum \cos(2\pi \mathbf{s} \cdot \mathbf{r}_{jj'})}] \quad (2) \end{aligned}$$

Now $[\overline{f_j^2} - (\overline{f_j})^2]$ may be expressed as:

$$\frac{1}{N^2} \sum_1^{i=N} \sum_i^{j=N} (f_i - f_j)^2$$

and $(\overline{f_j})^2$ as:

$$\frac{1}{N^2} \left(\sum_1^{j=N} f_j \right)^2$$

The second term in equation (2) is instantly recognizable as the diffracted intensity for a group of N identical units with scattering factor $\overline{f_j}$ and will therefore give rise to discrete Bragg reflections. However, the first term arises from the differences in the scattering units. As such, its magnitude will in general be small and it will not be confined to discrete points in reciprocal space but will vary relatively smoothly along the layer lines. This feature in a diffraction pattern is often called 'a layer line streak'. Particularly clear examples may be seen in patterns obtained from nylon-6 (γ -form)² and α -poly(L-alanine)^{3, 4}. If a structure exhibits 'pure' randomness, then the intensity of the Bragg reflections will be zero (as $\sum f_i = 0$). The corresponding intensity of the layer line streaks will be proportional to:

$$\frac{1}{N^2} \sum_1^{i=N} \sum_i^{j=N} (f_i - f_j)^2 = F^2 \neq 0$$

In the case where the molecules are coaxial but not otherwise ordered with respect to one another, only continuous layer line streaks (i.e. no discrete Bragg reflections) will be present in the X-ray diagram.

EXAMPLES OF STATISTICAL ORDERING

Polarity disorder

Using X-ray diffraction methods, Brown and Trotter⁵ investigated the structure of highly crystalline fibres

of α -poly(L-alanine). The equatorial reflections were readily accounted for by a hexagonal cell of side 8.55 Å, which can contain only one molecule on density considerations. Brown and Trotter also measured a meridional reflection of spacing 1.495 Å which is characteristic of an α -helical structure. However, they were unable to obtain quantitative agreement between an α -helical model and the observed data. Three years later, Elliott and Malcolm³ recognized the source of the problem and suggested that an incorrect choice of crystal structure had been made. Polypeptide chains exhibit chain sense $-\text{NH} \cdot \text{CHR} \cdot \text{CO}-$ and if α -helical molecules point 'up' or 'down' on a random basis, then the molecular site in the unit cell may be considered a half weighted 'up' and 'down' molecule, i.e. the unit cell still contains only 'one' molecule. This arrangement was investigated by Elliott and Malcolm using optical diffraction and consequently better agreement between the observed data and the model was achieved. This synthetic polypeptide therefore exhibits polarity statisticality at the molecular level. The structure was finally refined by Arnott and Wonacott⁴ using the method devised⁶⁻⁸ by them. Furthermore, they were able to show that if methyl groups were assumed to be spherical, the packing energy of two 'up' α -helices of poly(L-alanine) would be very similar to that of an 'up' and 'down' pair. Even though some energy differences were noted when the approximation to the methyl group was replaced by the individual hydrogen atoms, it would seem likely that in this case the statistical structure arises as a consequence of the energy balance between the alternative modes of packing.

The transition from an 'up' to a 'down' molecule or aggregate of molecules is not unique. The change is made by a rotation about some axis perpendicular to the long axis of the molecule or molecular aggregate. The molecule or molecular aggregate may then be translated in the direction of the fibre axis and rotated about that axis by amounts consistent with optimum packing and interactions. These two parameters were refined by Arnott and Wonacott who eventually reduced the R factor for their structure determination of α -poly(L-alanine) to the satisfactory value of 0.206. As we have previously mentioned, statistical structures often give rise to continuous layer line streaks (in addition to discrete Bragg reflections) in the X-ray diffraction patterns. α -Poly(L-alanine) shows two such streaks on the 13th and 21st layer lines (axis repeat = 70.4 Å, see Figure 1a). Arnott and Wonacott calculated both the positions and intensities of streaks expected from their statistical model and found an extremely satisfactory correlation with the data, thus removing any doubt as to the validity of their conclusions.

One point should be emphasized. The introduction of statisticality into a structure determination implies that as more parameters are used in the refinement procedure, the 'fit' between model and data is likely to be improved. This is certainly not necessarily the case and is well illustrated in the case of poly(L-proline)II. This system was investigated by Cowan and McGavin⁹ who showed that the polypeptide formed left-handed three fold helices. Furthermore, they postulated that all the helices were similarly directed with respect to one another. Arnott⁸ studied a statistical structure where the axes of the helices were parallel but randomly directed. Despite the fact that the statistical structure

had more degrees of freedom, the resulting refinement showed that the non-statistical structure not only fitted the X-ray data more satisfactorily but also led to the undefined parameters refining to physically more reasonable values. Consequently, we may conclude that the introduction of statisticality to a structure determination does not imply a reduction in the difficulty of fitting a structure to the observed data.

Hamilton¹⁰ has discussed the problem of whether the incorporation of extra parameters in a structure refinement leads to a meaningful improvement of the fit of the model to the data. He has shown that the arbitrary definition of 'fit' as a function of the number of refinable parameters can be put on a firm mathematical basis thus illustrating the point that the most satisfactory structure may not be the one with the lowest *R* factor.

It is worth noting that nylon-6(γ form)(polycapromide) exhibits a polarity statisticality of a different sort. In this case, it is not the individual chains which show randomness of direction but rather the sheets of parallel similarly directed molecules. With this arrangement, good agreement (*R* factor=0.15) between the model and the observed X-ray diffraction data was obtained by Bradbury *et al.*². The strong seventh layer line streak observed in the X-ray pattern (Figure 1*b*) was the only streak predicted from this statistical structure and therefore served to confirm the findings of Bradbury *et al.*

Screw disorder

Considerable effort has been put into structural studies on tobacco mosaic virus (TMV). Early work by Bernal and Frankuchen¹¹ indicated that the TMV particles were rod-shaped with a diameter of about 150 Å. Caspar¹² showed that the TMV is built up of units which are packed in a helical manner and that the surface of the TMV may be thought of as a series of grooves and protuberances. The maximum diameter of the particle has now been determined as about 185 Å¹³. As adjacent TMV units are able to pack closer to one another than might be expected, some sort of interlocking of the grooves and protuberances must occur. X-ray patterns from oriented gels of TMV show a continuous distribution of layer line intensity which means that the individual particles are scattering X-rays in an independent manner^{14, 15}. The results of Bernal and Frankuchen¹¹ imply that TMV particles are rotating or oscillating about their long axes over a complete range of concentration. When the gels are gradually dried, the particles oscillate less and less, become more closely packed and eventually form a hexagonal array. This type of statistical structure, commonly known as screw disorder, is therefore one in which the relative translation and rotation of one molecule (or molecular aggregate) with respect to its neighbour is precisely determined by the grooves on the outer surface of the molecule (or molecular aggregate) and is not dependent on the actual structure of the grooves. Franklin and Klug were the first to observe the presence of a screw disorder in TMV¹⁵.

Although it is not the intention of this review to discuss statistical structures found in polymers, we have included that found in polytetrafluoroethylene (PTFE) because of its unusual character. Bunn and Howells¹⁶ showed that the X-ray pattern of PTFE changed when

the temperature was raised above 25°C. The reflections on the equator and on the 6th and 7th layer lines ($c = 16.8$ Å) remain discrete whilst those on the remaining layer lines become diffuse. Klug and Franklin¹⁴ disagreed with Bunn and Howells' interpretation that the change in order was due to either a random displacement of the molecules about their long axis or a random rotation about the axis and they suggested that the combination, i.e. a screw disorder was more likely. This case was particularly interesting as two screw disorders must be present which would have similar pitch length but opposite hands. PTFE, like TMV, packs in a hexagonal array.

In order to be able to understand the effect of screw disorders on an X-ray diffraction pattern, part of the theory of diffraction from helical molecules put forward by Cochran *et al.*¹⁷ must be stated. They showed that the structure factor per asymmetric unit of helix can be expressed as:

$$F(R, \psi, 1/c) = \sum_n G_{n,1}(R) \exp i n (\psi + \pi/2)$$

where

$$G_{n,1}(R) = \sum_j f_j J_n(2\pi R r_j) \exp i \left(-n\Phi_j + 2\pi \frac{1}{c} z_j \right),$$

f_j = scattering factor of atom j ,

$r_j \Phi_j, z_j$ = cylindrical coordinates of atom j ,

$R, \psi, 1/c$ = reciprocal space cylindrical coordinates,

J_n = Bessel function of the first kind of order n .

Furthermore, if P is the pitch length of the helix and h is the axial rise per subunit on that helix, then the diffraction is confined to those axial regions in reciprocal space which are satisfied by:

$$\frac{l}{c} = \frac{n}{P} + \frac{m}{h}$$

where l is the layer line index, c is the axial repeat and n and m are integers. A continuous helix is one in which $m=0$. The layer line maxima fall approximately on the axes of a cross originating from the centre of the diffraction pattern. The angle that the arms of the cross make with the R axis depends on the pitch angle of the helical molecule, where the pitch angle is given by $\arctan(2\pi r/P)$, r being the radius of the continuous helix measured from its long axis. A discontinuous helix may produce a diffraction pattern in which there are a series of these 'crosses' originating not only from the centre of the pattern ($m=0$) but also from points at $(1/h)$ intervals along the $1/c$ axis.

Klug *et al.*¹⁸ have shown that screw disorders lead to a characteristic X-ray diffraction pattern in which the inner part remains crystalline and consists of discrete reflections (on layer lines where $m=0$) whilst the outer part (where $m \neq 0$) comprises only diffuse layer line streaks. Klug and Franklin¹⁴ postulated that this type of statistical ordering may also be found in the structures of the nucleic acids. The X-ray patterns from C-DNA¹⁹, A'-RNA²⁰ and the triple stranded polynucleotide poly(U).poly(A).poly(U)²¹ (see Figure 1*c*) have been shown to have the features expected of a system with screw disorder. In each case, the macromolecules pack in a hexagonal array.

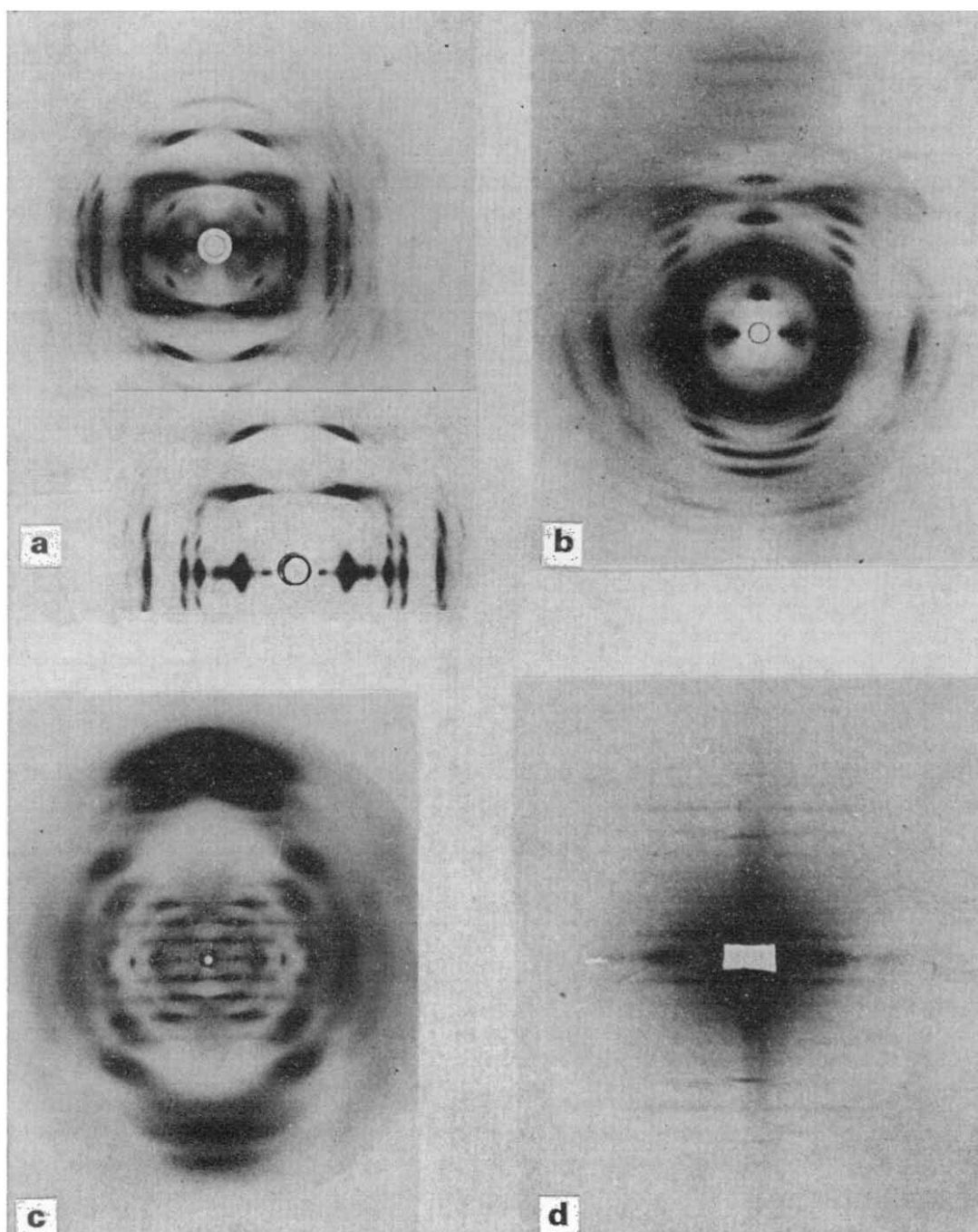


Figure 1 (a) X-ray diffraction pattern from an oriented α -poly(L-alanine) fibre showing a strong layer line streak on the 13th layer line (c axis repeat 70.4 \AA) and a weaker streak on the 21st layer line. This plate has been photographically modified to reduce the intensity of the inner part of the pattern in order to show the 13th and 21st layer line with their Bragg maxima and continuous layer line streaks on the same print. The inset is a weaker exposure of the 13th layer line and clearly shows the arced Bragg reflection superimposed on the continuous layer line streak. (We are indebted to Dr A. Elliott for providing this plate.) (b) X-ray diffraction pattern from nylon-6(γ -form) (polycapraamide) taken at room temperature after heating to 195°C *in vacuo*. The specimen was tilted by 18° from the normal in order to show the strong 7th layer line streak ($c=16.7 \text{ \AA}$). (c) X-ray diffraction pattern from oriented fibres of the sodium salt of poly(U).poly(A).poly(U) at 75%r.h. The pattern shows discrete maxima near the centre but continuous layer line diffraction elsewhere. (We are indebted to Professor S. Arnott for providing this plate.) (d) X-ray diffraction pattern from glycerinated water-bug flight muscle in rigor. This shows sampling on the $m=0$ set of layer lines but not clearly on layer lines for which $m \neq 0$. Rodger²³ has observed sampling on layer lines where $m \neq 0$ (see text)

It is clear that screw disorders may be found in molecules or molecular aggregates of vastly different structure and function. In all cases, the molecules or molecular aggregates have an outermost surface showing pronounced helical ridges and troughs. In general, the stability of any system will be enhanced when the assemblies are packed closest together and it is therefore

likely that there will always be the maximum interlocking of the ridges and grooves of neighbouring molecules or molecular aggregates. This type of statistical ordering implies that the molecules or molecular aggregates do not take up a specific azimuthal orientation (or axial translation) with respect to one another, possibly as a consequence of the number of units (or residues) per

pitch length being non-integral. In other words, when the pattern of contacts does not repeat between particles at pitch length intervals then screw disorders are more likely to occur. This is undoubtedly an over simplification and it is certainly not true in the case of poly(U).poly(A).poly(U) which has an eleven fold axis. In all the cases discussed, the molecules or molecular aggregates pack in a hexagonal array which corresponds to the closest packing of cylindrical rods.

The angle the grooves make with the long fibre axis direction of the molecules or molecular aggregates varies considerably in different species. It is small in the case of TMV and large for the nucleic acids. Also the nature of the grooves and protuberances greatly varies between that for the nucleic acids, where the protuberances are continuous phosphate ester chains and that for PTFE, where the protuberances are discontinuous and comprise discrete fluorine atoms. In the former structure, the pitch length and hand of the screw disorder are unique but in the latter arrangement, several possible screw dislocations are possible though it would appear that the screw disorders of shortest pitch length are more likely.

Lateral, axial or azimuthal disorder

An example of azimuthal statisticality occurs in insect flight muscle. The thick filaments of muscle are arranged on the 6_1 axes of a hexagonal lattice of plane group P6. This plane group has diad axes midway between the 6_1 axes and three-fold axes at the trigonal points. In muscles of different types the thin filaments are arranged in different ways in the P6 lattice. In vertebrate striated muscles the thin filaments lie on the trigonal points and in insect flight muscle they lie on the diads. The thin filament consists of actin, tropomyosin and troponin. The actin helix may be regarded as a two stranded rope of pitch 770 Å. The axial separation between globular actin molecules in one strand is 54 Å and the two strands are related to each other by an axial shift of 27 Å and an azimuthal rotation of almost 180°. There is therefore, no way in which the symmetry of thin filaments centred on the trigonal points can conform to the symmetry of the P6 lattice, and X-ray diffraction patterns from vertebrate striated muscle in rigor show no sampling of any of the layer lines originating from thin filaments marked by myosin heads. However, thin filaments placed on the diads can conform to the symmetry of the P6 lattice but only partly. If the thin filament is considered as a two strand rope where the strands are continuous, then it has a 2-fold axis and can sit on the diad axis of the P6 lattice. However, when the globular actin molecules are considered in the two strand rope, the thin filament no longer has a two-fold axis and so can no longer conform to the symmetry of the P6 lattice. These geometrical considerations may be followed in the X-ray diffraction pattern from water-bug flight muscle²² (Figure 1d).

It may be observed that the layer lines $m=0$ are sampled by the hexagonal reciprocal lattice indicating that, considered as continuous helices, the thin filaments conform to the P6 lattice. Layer lines with $m \neq 0$ are not clearly sampled and show diffuse layer line streaks. Miller and Tregear²² pointed out that a lattice could be constructed in which the thin filaments were statistically distributed between two azimuthal orientations separated by π . Various types of distribution are possible and

were mentioned by Miller and Tregear²², some of which require a super lattice to index all the observed reflections. In order to define the type of statisticality which exists in water-bug flight muscle it is necessary to have detailed knowledge of the intensity distribution along the layer lines from the thin filaments with $m \neq 0$. Improved X-ray diffraction patterns have recently been obtained by Rodger²³ which show discrete reflections on the 59 and 70 Å layer lines in addition to diffuse scatter. These reflections may be indexed on the simple hexagonal reciprocal lattice. This suggests that there is no super-lattice in water-bug flight muscle but that in the small cell the thin filaments are equally distributed between the two azimuthal orientations. We note that this is a special type of screw disorder; it is screw disorder where only one of two defined azimuthal orientations are possible as distinct from all azimuthal orientations which occur in complete screw disorder.

β -Poly(L-alanine) is another example of this type of statistical organization. There had been considerable doubt for many years as to whether the polypeptide chains in the β -pleated sheet were arranged in a parallel or anti-parallel manner. Infra-red (i.r.) evidence favoured an anti-parallel arrangement²⁴⁻²⁶ whilst the X-ray data showed evidence of a one molecule unit cell which was taken at the time as indicating parallel chains. Brown and Trotter⁵ studied the X-ray pattern but were unable to suggest a model in agreement with all the X-ray results. The problem was neatly solved by Arnott *et al.*²⁷ who suggested that the β -sheets consisted of anti-parallel chains and that adjacent sheets were randomly displaced from the orthogonal packing position by $\pm a/2$ in a direction perpendicular to the chain axes and in the plane of the pleated sheet (where a is the distance between chains in this direction). In this model, each molecular site in the unit cell can be considered as a half 'up' and a half 'down' chain. By finding the way in which sheets pack together, Arnott *et al.* were able to refine the molecular structure of β -poly(L-alanine) to a satisfactory level (R factor = 0.136). Although β -poly(L-alanine) is a statistical structure, there do not appear to be any strong layer line streaks in addition to the usual Bragg maxima. We may generalize this point by stating that whilst the presence of layer line streaks and discrete reflections infer some type of statistical structure, the absence of layer line streaks cannot be taken as evidence for the absence of 'statisticality'.

The intensity distribution in the X-ray pattern from Tussah silk is the same as that from β -poly(L-alanine)^{5, 27, 28}. This type of statistical ordering must therefore be found in at least one protein and is not confined to synthetic polypeptides.

β -Keratin has a similar history to that of β -poly(L-alanine) in that there had been no general agreement on whether the β -chains were parallel, anti-parallel or randomly directed with respect to each other. Fraser *et al.*^{29, 30} re-investigated the entire problem using quantitative X-ray and i.r. data. They considered two particular models. In the first the β -sheets were assumed to contain a perfect arrangement of anti-parallel chains. These sheets were then displaced randomly from the orthogonal packing position by $\pm \frac{1}{2}(4.7)$ Å in a direction perpendicular to the chain axes and parallel to the plane of the sheet directly analogous to that proposed by Arnott *et al.* for β -poly(L-alanine). In the second model, the

β -sheets were considered to comprise extended chains which were either 'up' or 'down' on a random basis. Fraser *et al.* showed that both models could be refined to a high level of significance as regards the X-ray diffraction data alone (R factors of 0.133 and 0.129 respectively) but the inter sheet disorder model was more likely in terms of the minimum energy calculations and the i.r. data. In two appendixes to their paper, Fraser *et al.* determined explicitly the effect on the X-ray patterns of both of these types of ordering. For the inter sheet disorder model, reflections whose Miller indices h were even would be unaffected whilst those with odd values of h would be reduced in magnitude by a factor \bar{M} , where \bar{M} was defined as the average number of sheets per crystallite. It is now apparent why the β -poly(L-alanine) pattern showed no evidence of a two molecule unit cell, i.e. the intensities of all reflections with odd values of h (those that would indicate a unit cell of twice the measured size) were multiplied by $1/\bar{M}$ where \bar{M} was extremely large. Layer line streaks characteristic of a statistical structure of this type will have no intensity at lattice points where h is even. For the intra sheet disorder model, reflections with both even and odd h indices would be affected by factors which are dependent on the probability (P) that a particular chain is 'correctly' directed with respect to the preceding chain ($P=0$ and $P=1$ correspond to parallel and antiparallel chain pleated sheets respectively).

With both β -poly(L-alanine) and β -keratin, the pleated sheet is a perfect arrangement of anti-parallel chains. Shifting the β -sheets laterally by $\pm a/2$ with respect to each other implies that each position is energetically favourable and is equally likely to occur on a statistical basis. In the case of β -poly(L-alanine), \bar{M} is large and the side chain methyl group is small (and approximately spherical). For β -keratin, the side chains are not all the same and \bar{M} is only 2 or 3. This may imply that there is some relationship between the size and type of side chains involved in the energy stabilization of a structure exhibiting this type of statisticality and the mean number of sheets in a crystallite. Even so, the two positions of minimum energy appear to be sufficiently pronounced to dominate the overall stability of the aggregate.

Because of the existence of this type of statistical ordering, Fraser *et al.* were able to conclude that there seemed no compelling reason for believing in the existence of parallel (or random) chain β -pleated sheets in any fibrous protein or synthetic polypeptide that has yet been investigated. It would appear that the anti-parallel β -sheet is a more stable entity than its 'parallel' or random analogue.

The X-ray pattern from the lithium salt of DNA (hexagonal C-form) shows streaks on the 1st and 3rd layer lines ($c=30.8 \text{ \AA}$) and discrete reflections on adjacent layer lines. This is consistent with the DNA molecules being randomly displaced by $\pm c/2$ in the fibre axis direction with respect to one another^{14, 31, 32}. In general, therefore, if adjacent molecules are axially staggered with respect to one another on a random basis by $\pm c/q$, (where c is the fibre axis repeat length and q is an integer) then the X-ray diffraction pattern will show discrete reflections on layer lines which are multiples of q and diffuse layer line streaks elsewhere. The extreme case of axial disorder is one in which molecules or molecular aggregates remain on lattice

sites but are completely free to move axially. This has the effect of maintaining the lateral sharpness of the equatorial reflections and producing layer line streaks elsewhere. Such a situation often occurs for synthetic polypeptides in solution as for example in the case of poly(γ -benzyl-L-glutamate) in *m*-cresol³³. However, this situation should not be confused with statistical ordering in which only a finite number of discrete axial displacements are allowed.

DISCUSSION

We can analyse the structures of these various biological macromolecules and synthetic polypeptides and attempt to determine the type of interactions that may be important. What are the properties of a biological molecule or aggregate that enable it to function optimally and why does statisticality play such an important part? There appears to be two main reasons.

The ideal arrangement of molecules or molecular aggregates will be one in which the greatest number of satisfactory interactions between molecules or molecular aggregates can arise. This will occur in general when the individual units are related by symmetry elements. However, such an arrangement may be one which cannot be physically satisfied by all members of the group in the same way. If only a few of these molecules or molecular aggregates cannot satisfy (say) a space group symmetry requirement, it appears that these exceptions may adopt an alternative position in keeping with as many symmetry elements as possible. It should be noted that it is not usually steric hindrance which prevents the attainment of full symmetry but rather the difficulty (or even impossibility) of being able to position all the molecules or molecular aggregates in equivalent environments. In other words, statisticality may arise as an attempt by the molecules or molecular aggregates to arrange themselves with a higher degree of order than is physically possible. Possibly the best example is given by the actin filaments in water-bug flight muscle. At low resolution, these have a diad axis but at high resolution the globular units along each strand are resolved and the true symmetry is no longer 2-fold, i.e. at high resolution, the space group symmetry no longer holds strictly.

When the energy differences between specific but alternative modes of packing or organization are small, then statistically any mode is equally likely. Anisotropy will consequently be reduced at this level at least.

The importance in biological systems of a self-assembly mechanism³⁴ has now been well established. Such a mechanism implied that the molecules have a single set of primary aggregating interactions which can organize the molecules into some three-dimensional aggregate. Having reached this level the various protein assemblies will then (in general) interact with one another in a specific manner. In most cases, the symmetry of an aggregate is such that the surrounding assemblies will not all interact in the same way. What must the molecular aggregate do in this case? Presumably, an equilibrium must be set up where the optimum number of ideal relationships are made and it is at this level that 'statisticality' is most often encountered. For instance, a molecular aggregate might have to be in two different axial positions simultaneously

in order to satisfy the necessary symmetry conditions inherent in the system. The problem may be partly overcome if it is assumed that a statistical relationship exists where either position is equally favoured. It should be emphasized that the biological entity may be equally satisfied irrespective of which of the statistical possibilities arises in practice. The energies of the alternative structures will be the same or very similar unless the function of the assembly so demands a difference to exist.

The invariant set of *in vivo* primary aggregating interactions enable the myosin molecules to build a thick filament, the actins to form a thin filament, the tropocollagens to form a microfibril, the extended chains to produce an ordered pleated sheet and so on. Once this degree of organization has been achieved and the molecules are in regular three-dimensional form, a second set of aggregating interactions can be made. It is equally important to realize that whilst biological systems may have one type of statisticality, other types are functionally unallowable. For instance, the thick and thin filaments in muscle exhibit polarity and no directional variability can be introduced without the mechanism of muscle contraction being lost. The collagen fibre also exhibits strict polarity as may be seen in the electron microscope using, for example, positively stained sections from rat tail tendon collagen.

In summary we have shown that statisticality is becoming an increasingly more evident and important facet of structure determination. We believe that the concept of statisticality helps to explain how flexible and dynamic protein assemblies may be able to interact in a more highly symmetrical manner than the symmetry of the molecule or molecular aggregate theoretically allows.

ACKNOWLEDGEMENTS

This project is part of the programme of the MRC Research Group in Molecular Biophysics. One of us (D. A. D. P.) acknowledges the support of the Science Research Council during the initial part of this work.

REFERENCES

- 1 Guinier, A. 'X-ray Diffraction', W. H. Freeman, San Francisco, 1963
- 2 Bradbury, E. M., Brown, L., Elliott, A. and Parry, D. A. D. *Polymer* 1965, 6, 465
- 3 Elliott, A. and Malcolm, B. R. *Proc. R. Soc. (A)* 1959, 249, 30
- 4 Arnott, S. and Wonacott, A. *J. J. Mol. Biol.* 1966, 21, 371
- 5 Brown, L. and Trotter, I. F. *Trans. Faraday Soc.* 1956, 52, 537
- 6 Arnott, S. and Wonacott, A. *J. Polymer* 1966, 7, 157
- 7 Wonacott, A. J. *PhD Thesis* Univ. of London (1966)
- 8 Arnott, S. 'Symp. on Fibrous Proteins', (Ed. W. G. Crewther), Butterworths, London, 1968, p 26
- 9 Cowan, P. M. and McGavin, S. *Nature* 1955, 176, 501
- 10 Hamilton, W. C. *Acta Crystallog.* 1965, 18, 502
- 11 Bernal, J. D. and Fankuchen, I. *J. Gen. Physiol.* 1941, 125, 111
- 12 Caspar, D. L. D. *Nature* 1956, 177, 475
- 13 Franklin, R. E., Klug, A. and Holmes, K. C. 'The Nature of Viruses' (CIBA Foundation Symposium) J. and A. Churchill, London, 1956, p 39
- 14 Klug, A. and Franklin, R. E. *Discuss. Faraday Soc.* 1958, 25, 104
- 15 Franklin, R. E. and Klug, A. *Biochim. Biophys. Acta* 1956, 19, 403
- 16 Bunn, C. W. and Howells, E. R. *Nature* 1954, 174, 549
- 17 Cochran, W., Crick, F. H. C. and Vand, V. *Acta Crystallog.* 1952, 5, 581
- 18 Klug, A., Crick, F. H. C. and Wyckoff, H. W. *Acta Crystallog.* 1958, 11, 199
- 19 Marvin, D. A., Spencer, M., Wilkins, M. H. F. and Hamilton, L. D. *J. Mol. Biol.* 1961, 3, 547
- 20 Arnott, S., Fuller, W., Hodgson, A. and Prutton, I. *Nature* 1968, 220, 561
- 21 Arnott, S. and Bond, P. J. *Nature (New Biol.)* 1973, 244, 99
- 22 Miller, A. and Tregear, R. T. *J. Mol. Biol.* 1972, 70, 85
- 23 Rodger, C. D. *DPhil Thesis* Univ. of Oxford (1973)
- 24 Miyazawa, T. *J. Chem. Phys.* 1960, 32, 1647
- 25 Miyazawa, T. and Blout, E. R. *J. Am. Chem. Soc.* 1961, 83, 712
- 26 Bradbury, E. M. and Elliott, A. *Polymer* 1963, 4, 47
- 27 Arnott, S., Dover, S. D. and Elliott, A. *J. Mol. Biol.* 1967, 30, 201
- 28 Bamford, C. H., Brown, L., Elliott, A., Hanby, W. E. and Trotter, I. F. *Nature* 1954, 173, 27
- 29 Fraser, R. D. B., MacRae, T. P., Parry, D. A. D. and Suzuki, E. 'Symp. on Fibrous Proteins', (Ed. W. G. Crewther), Butterworths, London, 1968, p 42
- 30 Fraser, R. D. B., MacRae, T. P., Parry, D. A. D. and Suzuki, E. *Polymer* 1969, 10, 810
- 31 Feughelman, M. *et al. Nature* 1955, 175, 834
- 32 Wyckoff, H. W. *Thesis* Mass. Institute of Technology (1955)
- 33 Parry, D. A. D. *PhD Thesis* Univ. of London (1966)
- 34 Caspar, D. L. D. and Klug, A. *Cold Spring Harbor Symp. Quant. Biol.* 1962, 27, 1

N.m.r. studies on the effect of water on the glass transition of polystyrene

Edward G. Smith and Ian D. Robb

*Unilever Research, Port Sunlight Laboratory, Port Sunlight, Wirral, Cheshire L62 4XN, UK
(Received 2 January 1974; revised 15 March 1974)*

These investigations are concerned with water-polymer interactions in polymer latices. It is known that water can act as a plasticizer for many solid polymers and cause a reduction in the glass transition temperature, T_g , of the amorphous regions. Experiments were carried out to determine whether pulsed n.m.r. techniques could be used to study the T_g of a polymer suspension and hence the influence of water and electrolyte on it. From T_1 and T_2 proton relaxation measurements as a function of temperature on polystyrene latex systems it was shown that the presence of water lowers the T_g of the polymer particles (by about 10°C), the effect being slightly greater in the presence of concentrated electrolyte. The extent of electrolyte penetration into the particles was deduced by studying relaxation as a function of particle diameter in latices containing paramagnetic Mn^{2+} ions. Using simple theories of relaxation and spin diffusion it was concluded that for all but the smallest particles electrolyte penetration is restricted to a very thin shell of the order of 1 nm. These conclusions were supported by the results of similar measurements on PTFE particles.

INTRODUCTION

The effect of temperature on the molecular behaviour of solid polymers has been studied over many years and is the subject of several reviews¹⁻³. The glass transition temperature, T_g , has been measured by a number of techniques and the results, though largely in agreement, depend on the method of measurement. Both broad line⁴ and pulsed n.m.r.⁵ were used to investigate not only T_g , but also other transitions, such as occur in crystalline phases of polymers⁶, and side chain motions. Small molecules incorporated into solid polymers normally lower T_g ⁷, and theories based mainly on the concept of additivity of free volume have been outlined⁸.

In this work, the influence of water on the T_g of polystyrene was investigated by pulsed n.m.r. The polymer was in two different physical forms, namely normal solid and dispersed as latex particles in water. N.m.r. techniques have been used to study water structure^{9,10} in latex systems, though no investigation appears to have been made of the polymer. In the latex suspension, the high solid/liquid surface area allowed rapid equilibration of the polymer and water. The effect of paramagnetic manganese ions on the polymer's nuclear relaxation times was measured for different latex particle sizes, and the results interpreted in terms of electrolyte and water penetration of the polymer.

EXPERIMENTAL

Three of the polystyrene latices were prepared in this laboratory by the usual emulsion polymerization technique using hydrogen peroxide initiator and sodium laurate as the emulsifying agent¹¹. Particle diameters

produced were: 210 nm, 89 nm and 30 nm (seed). Surfactant and unreacted monomer were removed by dialysis for 6-8 weeks. A latex of larger diameter, 1.3 μ m, was obtained from the Dow Chemical Company Ltd. For n.m.r. purposes, H_2O was exchanged for D_2O by repeated processes of centrifugation, D_2O exchange and redispersion and the samples were finally concentrated to about 10-20% solid. Electrolyte was introduced before the last stage of centrifugation (in these experiments, 1M sodium chloride and 0.1M manganous sulphate solutions were employed). Atmospheric oxygen was removed from dry samples by maintaining under vacuum for several days. Pellets of polystyrene were used, as supplied by BDH.

A PTFE (Fluon) latex (diameter 200 nm) and a granular PTFE sample were supplied by ICI Ltd (Plastics Division); the latex sample was concentrated as above.

Relaxation times, T_1 and T_2 were measured using a Bruker (BKR 322S) pulsed spectrometer operating at a frequency of 20 MHz.

T_1 (spin-lattice relaxation time) was measured by monitoring the growth of longitudinal magnetization using either a 180°-90° or 90°-90° pulse programme.

For solids, such as polystyrene at normal temperatures, the free induction decay is governed by the direct spin-spin interaction between nuclei. T_2 , which characterizes the rate of this decay was taken as the time for the signal to drop to e^{-1} of the maximum value. The temperature was controlled to within $\pm 1^\circ C$ by means of a gas-flow thermostat system.

Errors in the relaxation time values are probably in the region of 5-10% as judged by the reproducibility of the data, these being influenced by sample preparations and variations in signal-to-noise ratio. The effect

of dissolved oxygen on T_1 is difficult to estimate but would be significant only for T_1 values higher than about 1 sec.

RESULTS

Both the spin-lattice (T_1) and spin-spin (T_2) relaxation times were measured as a function of temperature for the latex (44.5 nm radius) (a) in D_2O , (b) in 1 M NaCl and (c) dried. In all cases, single component relaxations were observed for 90-95% of the relaxation, and the results are presented in Figure 1. The relaxation behaviour of the dried latex was similar to that of the high molecular weight commercial polystyrene pellets. Below about 100°C the curves are typically those for relaxation in an amorphous solid, T_2 exhibiting a value normally found for solids and T_1 a relatively high limiting value characteristic of low mobility. The marked change of T_1 and T_2 with increasing temperature at about 100°C reflects the onset of significant segmental motion associated with the glass transition temperature of polystyrene. In the presence of D_2O , this transition took place at a lower temperature. It is unlikely that oxygen was responsible for this effect, since T_2 in this system would be insensitive to small quantities of paramagnetic materials, but is probably due to inclusion of water molecules within the polymer. Addition

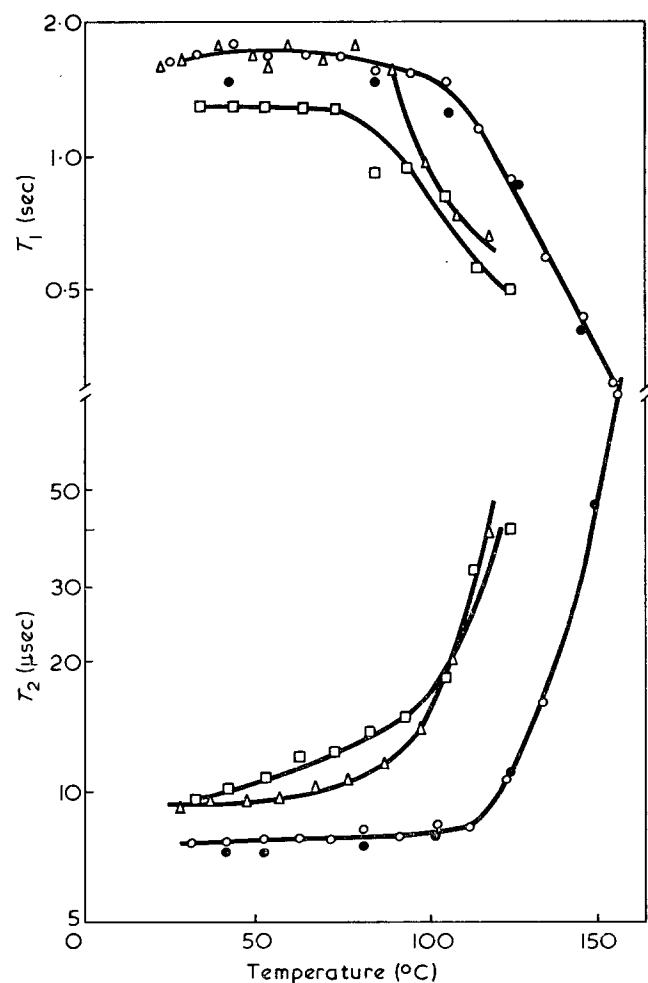


Figure 1 Dependence of relaxation times, T_1 and T_2 , on temperature for protons in polystyrene particles (89nm diameter latex). Δ , Latex (in D_2O); \circ , dried latex; \square , latex+electrolyte; \bullet , polystyrene pellets

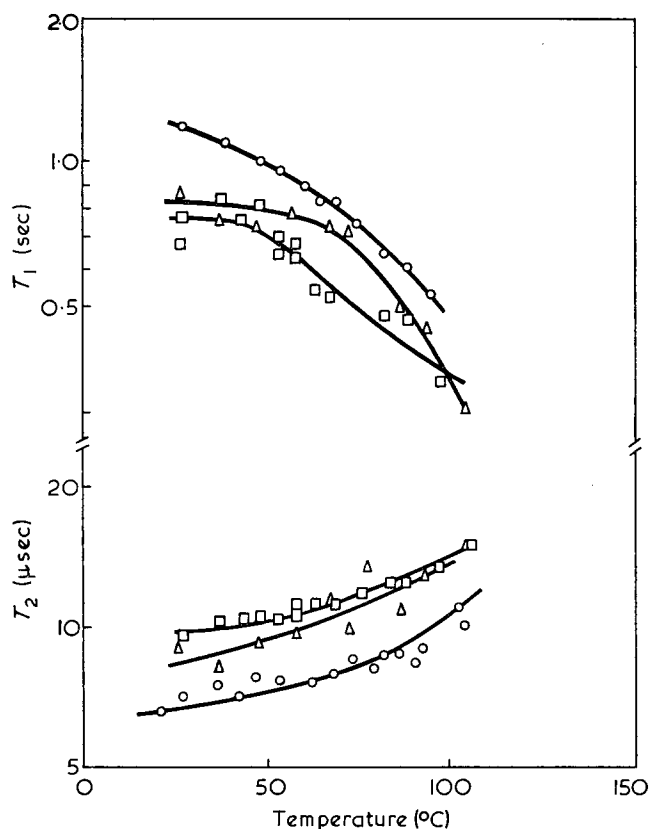


Figure 2 Variation of T_1 and T_2 with temperature for polystyrene protons in seed latex (diameter 15-35nm). Δ , Latex (in D_2O); \circ , dried latex; \square , latex+electrolyte

Table 1 Relaxation times for polystyrene particles of different diameter in the presence of paramagnetic ions (Mn^{2+})

Particle radius r (nm)	$T_{1(obs)}$ (sec)	T_{1D}^{-1} (sec $^{-1}$)
650	1.43	0.10
104	0.83	0.61
44.5	0.48	1.49
17.5 } seed	0.21	3.44
7.5 }	0.05	17.20

of electrolyte modified the relaxation-temperature behaviour further and indicated a slight lowering of T_g , although at higher temperatures ($T > T_g$), the degree of motion represented by the absolute values of T_1 and T_2 coincides with that exhibited by the polymer in the absence of electrolyte. The temperature dependence of the relaxation behaviour of the seed latex is shown in Figure 2. The glass transition, as indicated particularly by T_1 results, took place over a wider and lower temperature range, even in the absence of water.

In order to estimate the degree of penetration, if any, of electrolyte into particles, polymer proton T_1^{-1} values were measured in the presence of Mn^{2+} . Again, except for the seed latex, the relaxation process could be represented by a single exponential decay and the results are shown in Table 1. Experiments were performed at 25°C. $T_{1(obs)}^{-1}$ is the relaxation rate in the presence of Mn^{2+} and T_{1D}^{-1} is the corresponding result in the absence of Mn^{2+} , the difference between these being T_{1D}^{-1} .

Electron micrographs showed that the seed latex

had a bimodal size distribution, and the relaxation was best described by two relaxation times.

DISCUSSION

The results in *Figure 1* show that water lowers the T_g of polystyrene. The T_1 results below 100°C for the pellets are slightly lower than for the dried latex, but as the corresponding T_2 results are equal, the difference is probably due to the presence of oxygen in the pellets. Water has been shown to lower the T_g of more hydrophilic polymers, such as nylon⁷, whereas it is considered that water absorption by hydrophobic polymers such as Terylene is mainly a surface effect¹². Since the T_g , as indicated by both T_1 and T_2 results is lowered by water its uptake by the polymer must include some bulk absorption. The solubility of water in benzene¹³ is about 0.2 mol% at 25°C and hence it is not unreasonable that polystyrene latex particles contain small quantities of water, which act as plasticizer for the polymer. The results with sodium chloride have no obvious explanation at present, since as indicated below, electrolyte penetration of the polymer is probably small and confined to a thin shell around the particle.

The results with the seed latex (*Figure 2*) are possibly explained by the greater influence of surface groups on the average relaxation times. T_1 is more affected than T_2 , suggesting that dissolved oxygen or spin diffusion averaging of the groups on the surface with those in the bulk of the particle is causing the unusual relaxation behaviour. Since T_1 is not constant below about 90°C, the latter possibility seems more likely. The molecular weight of the polystyrene in the seed latex was found by viscometry to be 9×10^5 , this value being too high to allow molecular weight to account for the T_1 results.

To evaluate the data obtained with added Mn^{2+} , the following model was used. Manganese ions were assumed to penetrate the latex particle by a distance dr and produce a polymer proton relaxation rate T_{IP}^{-1} within this shell. In the absence of spin diffusion, the remaining core of radius $(r-dr)$ would have a rate T_{IN}^{-1} . In this system spin diffusion would lead to an average value for the relaxation rate and the observed value would be:

$$T_{I(obs)}^{-1} = X_c T_{IN}^{-1} + X_s T_{IP}^{-1} \quad (1)$$

where X_c and X_s are the mole fractions of protons in the core and shell respectively. Although there is some debate¹⁴ about the morphology of the latex particles, the implicit assumption in equation (1) of uniform density across the particle seems justified. Using equation (1) the model leads to the following expression:

$$T_{ID}^{-1} = \left(\frac{3dr}{r} - \frac{3dr^2}{r^2} + \frac{dr^3}{r^3} \right) [T_{IP}^{-1} - T_{IN}^{-1}] \quad (2)$$

This expression predicts that, when $r \gg dr$, the product rT_{ID}^{-1} should be a constant as r varies. Within experimental error this appears to be the case for all but the seed particle (radius 7.5 nm) as shown in *Table 2*. This indicates that for the larger particles the model is consistent with the experimental data and that uniform penetration of the particle by Mn^{2+} ions did not occur. When r becomes small, i.e. as r

Table 2 Dependence of rT_{ID}^{-1} on r

r	T_{ID}^{-1}	rT_{ID}^{-1}
650	0.10	65.0
104	0.61	63.5
44.5	1.49	66.4
17.5	3.44	60.3
7.5	17.20	129

approaches dr , it is expected that the product rT_{ID}^{-1} would decrease below the average value of 65.0 nm/sec. The value of rT_{ID}^{-1} obtained for the seed particle ($r=7.5$ nm) is too high to be accounted for by errors in particle size determination or relaxation time measurements. The data can be explained by assuming either a larger value of dr or a greater surface concentration of Mn^{2+} ions for the seed latex, although there are no obvious reasons for this.

The value of dr depends on that of T_{IP}^{-1} which in turn is influenced by the concentration of ions in the polymer and at the surface of the particle. The relationship governing proton nuclear relaxation (T_{INE}) by unpaired electrons is¹⁵:

$$T_{INE}^{-1} = (4/30)g^2\beta^2\gamma^2s(s+1)[3\tau_c + 7\tau_c/(1 + \omega_s^2\tau_c^2)]r^{-6} \quad (3)$$

where g is the Lande factor, β is the Bohr magneton, γ is the magnetogyric ratio, s is the spin quantum number for the ion, ω_s is the electron spin frequency and τ_c is the correlation time for the interaction.

For the ions at the surface, the correlation time was taken to be about 10^{-11} sec, since relaxation is probably dominated by translational diffusion of the ions and hence fluctuations in the value of r . Protons, 1 nm from the Mn^{2+} , have a T_{IP}^{-1} of 28 sec^{-1} , a rate which as equation (3) shows, decreases rapidly with increasing r . A shell of about 1 nm with an average relaxation rate of 50 sec^{-1} is sufficient to account for the relaxation rates in *Table 1*, for particles greater than 7.5 nm radius. The actual value of this average relaxation rate will depend on the concentration of Mn^{2+} at the latex surface, a quantity which is not known exactly.

A further contribution would come from Mn^{2+} which have penetrated the polymer, and expressions have been calculated for solids containing low concentrations of paramagnetic centres. In this case, the correlation time for the proton relaxation would probably be the relaxation time of the free electrons¹⁶ of the manganese, 10^{-8} to 10^{-9} sec⁻¹. A concentration of 0.1 mol/dm³ of Mn^{2+} in a shell of 1 nm would be sufficient to account for the results in *Table 1*. Relaxation is produced by Mn^{2+} both at the surface of, and inside the polymer. The relative contributions from these two sites cannot be estimated although penetration by the Mn^{2+} is probably limited to a thin surface layer.

PTFE particles

Relaxation times obtained for PTFE particles, both wet and dry are shown in *Figure 3*, and agree with literature values where comparison is possible¹⁷. They indicate that water has no influence on polymer molecular motion. Both X-ray¹⁸ and n.m.r. data showed that the sample was highly crystalline although any penetration of water into the polymer would still alter both T_1 and T_2 . Manganese ions were added to the

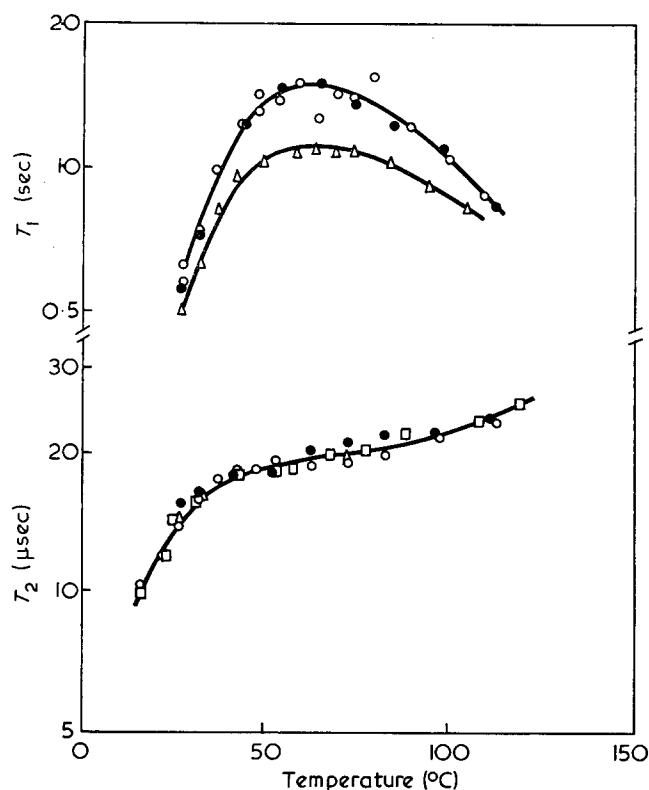


Figure 3 Temperature dependence of T_1 and T_2 for fluorine nuclei in PTFE latex particles. \circ , Latex (in H_2O); \bullet , dried latex; \square , granular PTFE; \triangle , latex + Mn^{2+} ions

PTFE latex in the same way as for polystyrene, and the resulting temperature dependence of T_1 and T_2 plotted in Figure 3. Though a direct comparison with the polystyrene system is difficult, as the PTFE particles were not spherical, the results could be explained by a model in which there was no penetration of the surface by Mn^{2+} .

CONCLUSIONS

The relaxation time/temperature results have indicated that the presence of water in polystyrene latex system has some plasticization effect on the bulk of the polymer, penetration of water molecules into the particles causing

a decrease in T_g (of about $10^\circ C$). It has been shown that this effect is slightly greater in the presence of concentrated electrolyte. Although the differences in T_g are quite distinct, the increase in mobility due to the penetration of water indicates that swelling of the particles does not occur to any major extent (probably less than 1% by vol).

From the results of relaxation by paramagnetic ions in the polystyrene latex samples it was concluded that for all but the smallest seed particle penetration by electrolyte is restricted to a very thin shell of the order of 1 nm. The results obtained on PTFE latices support this conclusion.

ACKNOWLEDGEMENT

The authors wish to thank Dr W. Derbyshire for helpful discussions.

REFERENCES

- 1 Boyer, R. F. *Rubber Chem. Technol.* 1963, **36**, 1303
- 2 McCrum, N. G., Read, B. E. and Williams, G. 'Anelastic and Dielectric Effects in Polymeric Solids', Wiley, London, 1967
- 3 Woodward, A. E. *Rev. Pure Appl. Chem.* 1966, **12**, 341
- 4 Smith, J. A. S. *Discuss. Faraday Soc.* 1955, **19**, 207
- 5 McCall, D. W. and Falcone, D. R. *Trans. Faraday Soc.* 1970, **66**, 262
- 6 Olf, H. G. and Peterlin, A. *J. Polym. Sci. (A-2)* 1971, **9**, 1449
- 7 Olf, H. G. and Peterlin, A. *J. Polym. Sci. (A-2)* 1971, **9**, 2033
- 8 Bueche, F. 'Physical Properties of Polymers', Interscience, New York, 1962
- 9 Johnson, G. A., Lecchini, S. M. A., Smith, E. G., Clifford, J. and Pethica, B. A. *Discuss. Faraday Soc.* 1966, **42**, 120
- 10 Clifford, J., Oakes, J. and Tiddy, G. J. T. *Discuss. Faraday Soc.* 1970, No 1, 175
- 11 Ottewill, R. H. and Shaw, J. M. *Kolloid-Z. Z. Polym.* 1967, **218**, 34
- 12 Morton, W. E. and Hearle, J. W. S. 'Physical Properties of Textile Fibres', Butterworths, London, 1962, p 261
- 13 Black, C., Joris, G. C. and Taylor, H. S. *J. Chem. Phys.* 1948, **16**, 537
- 14 Napper, D. H. *J. Polym. Sci. (A-1)* 1971, **9**, 2089
- 15 Blumberg, W. E. *Phys. Rev.* 1960, **119**, 79
- 16 Tinkman, M., Weinstein, R. and Kip, A. F. *Phys. Rev.* 1951, **84**, 848
- 17 McCall, D. W., Douglass, D. C. and Falcone, D. R. *J. Phys. Chem.* 1967, **71**, 998
- 18 Clark, A. T. personal communication, 1973

Mechanism of vinyl chloride polymerization initiated by the AlEt_3 /diethylenetriamine/ CCl_4 catalyst system

Akira Akimoto

Central Research Laboratory, Toyo Soda Manufacturing Co. Ltd, Yamaguchi-ken, Japan
(Received 15 January 1974; revised 14 May 1974)

The mechanism of vinyl chloride polymerization initiated by the catalyst system AlEt_3 /diethylenetriamine/ CCl_4 has been investigated. The kinetic equations for the vinyl chloride polymerization and the catalyst components interaction reaction support the radical mechanism of the process. A possible mechanism of the initiation is suggested.

INTRODUCTION

It is well known that organo-aluminium compounds are among the most reactive metal alkyls. They enter into the most varied reactions, particularly with chlorine, alkyl halides and metal halides. Extensive work has been carried out on the polymerization of vinyl chloride catalysed by the reaction of alkyl aluminiums with certain halide-containing organic compounds¹⁻⁴. In a previous paper⁵, the author reported that a system of AlEt_3 and CCl_4 could initiate the polymerization of vinyl chloride at a moderate temperature in the presence of various Lewis bases, especially diethylenetriamine (DETA).

The role of DETA in the initiating system was also pointed out. Recently the polymerization of vinyl monomer was investigated in the presence of oligo (n) ethylene ($n+1$) amine, a trace amount of Cu^{2+} ion and CCl_4 ^{6,7}. In connection with the problem of free-radical formation in the system of oligo (n) ethylene ($n+1$) amine, a transfer metal ion and CCl_4 , the results of the vinyl chloride polymerization with AlEt_3 , DETA and CCl_4 prompted the author to elucidate the reaction mechanism.

The mechanism of the polymerization of vinyl chloride with Ziegler-Natta type catalysts has already been elucidated by means of a kinetic study^{8,9}. Bearing in mind that kinetic methods could be useful in the elucidation of the mechanism of this process the author has undertaken a kinetic study of vinyl chloride polymerization in fine detail. This paper reports the results of the kinetic study of the vinyl chloride polymerization initiated by AlEt_3 , DETA and CCl_4 as well as some data about the initiation reaction in such a system.

EXPERIMENTAL

Reagents

Vinyl chloride (VC) (supplied by Toyo Soda Manufacturing Co. Ltd) was dried over phosphorus pentoxide, purified by means of trap-to-trap distillation into traps cooled with solid carbon dioxide in methanol

(-78°C). The purity of the monomer was checked by chromatography. Others were purified in the usual manner.

Benzene was dried by refluxing over calcium hydride for 6 h. The middle fraction was then stored over sodium wire in a dry box. Tetrahydrofuran was dried by refluxing over calcium hydride and was then fractionated just before use.

Triethyl aluminium was purified by distillation under reduced pressure and was stored as a normal solution in benzene.

DETA was purified by distillation under reduced pressure.

Carbon tetrachloride was purified in the conventional way.

Polymerization procedure

All experiments were carried out in either glass tubes or dilatometers. Both tubes and dilatometers contained glass-enclosed iron stirrers which could be operated magnetically. The dilatometers had a capacity of about 15 ml with a capillary calibrated to 0.01 ml. The catalyst components were introduced into the reaction vessel in a dry box. Solutions of the catalyst components were prepared in benzene in a dry box. Benzene was added to the reaction vessel (the tube or the dilatometer) by means of a syringe and then the solutions of the catalyst components were added in the following order: DETA, CCl_4 and AlEt_3 . The reaction vessel (the tube or the dilatometer) was removed from the dry box and attached to a high vacuum line. The contents were frozen down at -78°C and then degassed, when a known amount of monomer was distilled into the dilatometer or the tube.

After all the monomer had been distilled into the vessel, the vessel neck was sealed. The vessel was then attached to the stirrer and placed in the thermostat bath. In the kinetic experiments the polymerization rate was calculated for a 3-9% conversion, this being estimated from contraction.

The contraction coefficient was found as a mean

value from several experiments on the basis of gravimetric measurements of the polymer yield.

Isolation of polymer and measurement of the degree of polymerization

The polymer mixture was sucked out of the dilatometer (or the tube) and poured into methanol containing hydrochloric acid (or, for polymerization of vinyl acetate, into n-hexane). The polymer was filtered, washed and dried under high vacuum. The intrinsic viscosity of the poly(vinyl chloride) was determined by measurements on their dilute nitrobenzene solutions at 30°C. The degree of polymerization (\bar{p}) was calculated from the following equation¹⁰:

$$\bar{p} = 500 (\text{anti log } [\eta]/0.168 - 1)$$

N.m.r. spectrum of the $AlEt_3$ and DETA

The n.m.r. spectrum of an equimolar mixture of $AlEt_3$ and DETA in benzene was measured at 30°C on a 100 MHz n.m.r. spectrometer using benzene as internal standard.

RESULTS AND DISCUSSION

Table 1 shows that polymerization initiated by the $AlEt_3/DETA/CCl_4$ system is selective for the type of vinyl monomer. Vinyl monomers such as vinyl acetate and methyl acrylate, which polymerize readily by free-radical catalyst showed very little tendency to polymerize. The results seem to suggest that DETA plays a greater part, and that the participation of a polar monomer in the initiating system is essential for the initiation, and this behaviour will be more fully discussed in a later publication. From these results vinyl chloride was used as monomer in the kinetic investigation.

Figure 1 shows a typical plot of percentage conversion against time. It can be seen that there is a fall off in rate, and that there is no induction period. This decreasing overall rate of polymerization as a function of time is characteristic of many Ziegler-Natta type catalysts^{8, 9}.

However, the kinetic curves are nearly linear in the initial stage of the polymerization (Figure 2).

Therefore the main kinetic characteristics were determined at 40°C continuing the polymerization to not more than 3–9% conversion. The dependence of the initial overall rate of polymerization on the concentrations of the components of the catalyst system was investigated systematically.

Table 1 Vinyl polymerization with $AlEt_3/DETA/CCl_4$ catalyst system

No.	Vinyl monomer	Concentration (mol/l)	Yield (%)
1	Vinyl chloride	7.87	33.5
2	Methyl methacrylate	4.70	10.6
3	Styrene	4.33	7.4
4	Vinyl acetate	5.43	1.5
5	Acrylonitrile	7.59	7.0
6	Methyl acrylate	5.54	trace

^a $[AlEt_3] = 7.87 \times 10^{-2}$ mol/l; $[DETA] = 7.87 \times 10^{-2}$ mol/l; $[CCl_4] = 7.87 \times 10^{-2}$ mol/l; solvent = benzene; polymerization at 40°C for 20 h

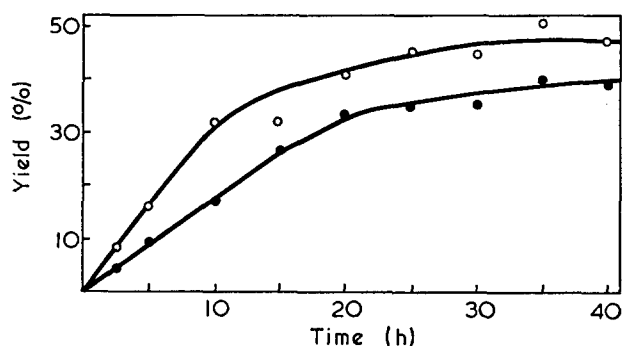


Figure 1 Plot of % yield versus time at 40°C. ●: $[VC] = 7.87$ mol/l; $[AlEt_3] = 7.87 \times 10^{-2}$ mol/l; $[DETA] = 7.87 \times 10^{-2}$ mol/l; $[CCl_4] = 7.87 \times 10^{-2}$ mol/l; solvent = benzene. ○: $[VC] = 7.87$ mol/l; $[AlEt_3] = 15.7 \times 10^{-2}$ mol/l; $[DETA] = 15.7 \times 10^{-2}$ mol/l; $[CCl_4] = 15.7 \times 10^{-2}$ mol/l; solvent = benzene

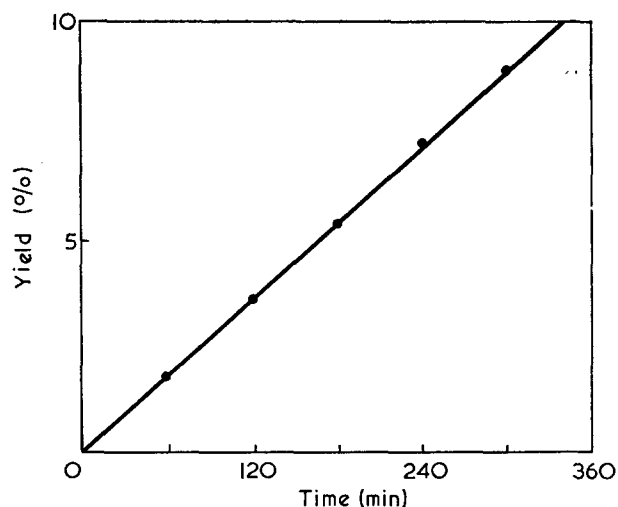


Figure 2 Plot of % yield versus time at 40°C. $[VC] = 7.87$ mol/l; $[AlEt_3] = 7.87 \times 10^{-2}$ mol/l; $[DETA] = 7.87 \times 10^{-2}$ mol/l; $[CCl_4] = 7.87 \times 10^{-2}$ mol/l; solvent = benzene

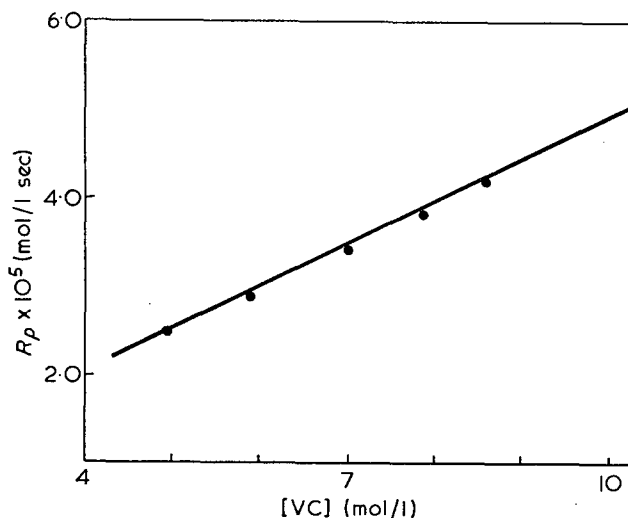


Figure 3 Variation in rate of polymerization with $[VC]$ at 40°C. $[AlEt_3] = 7.87 \times 10^{-2}$ mol/l; $AlEt_3:DETA:CCl_4 = 1:1:1$ (mol); solvent = benzene

The effect of increasing the monomer concentration on the rate of polymerization was investigated at 40°C. A series of polymerizations in dilatometers were carried out in which the concentration of monomer was varied from 4.95 to 8.60 mol/l whilst the catalyst concentration remained constant. Experimental details of these experiments are given in Figure 3. It can be seen that the

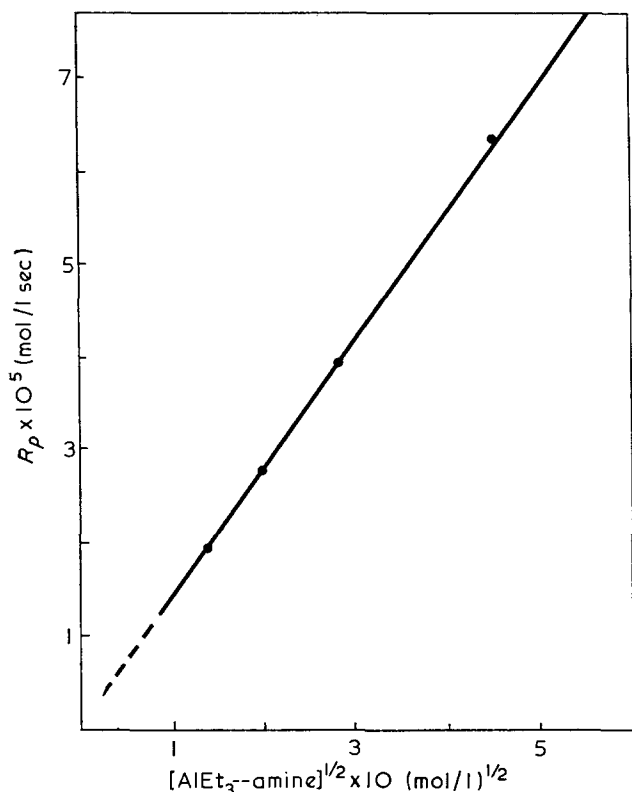


Figure 4 Variation in rate of polymerization with $[\text{AlEt}_3\text{-amine}]$ at 40°C . $[\text{VC}] = 7.87 \text{ mol/l}$; $[\text{CCl}_4] = 7.87 \times 10^{-2} \text{ mol/l}$; solvent = benzene

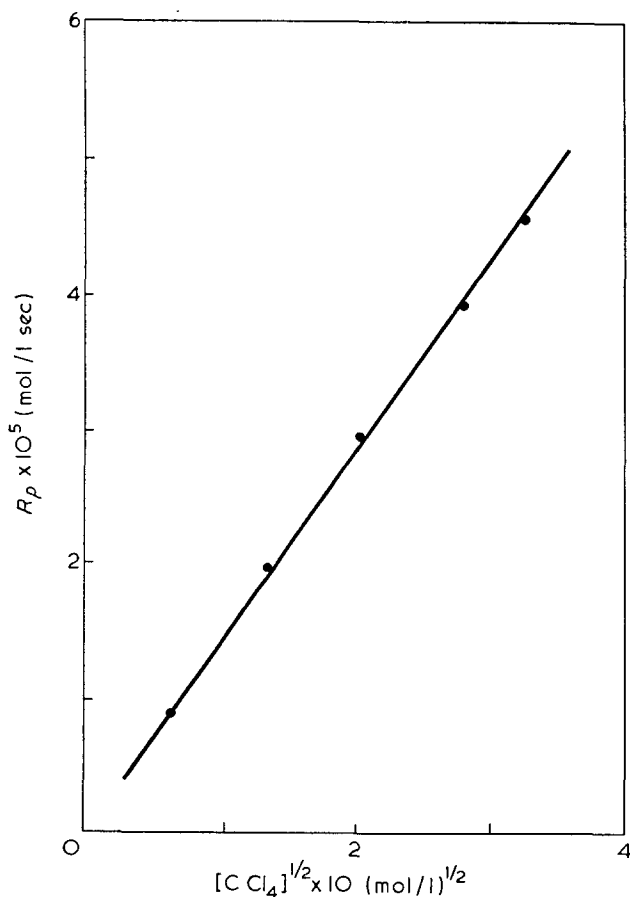


Figure 5 Variation in rate of polymerization with $[\text{CCl}_4]$ at 40°C . $[\text{VC}] = 7.87 \text{ mol/l}$; $[\text{AlEt}_3] = 7.87 \times 10^{-2} \text{ mol/l}$; $[\text{DETA}] = 7.87 \times 10^{-2} \text{ mol/l}$; solvent = benzene

initial rate of polymerization is first order with respect to the monomer concentration.

The results of experiments in which the concentrations of monomer and CCl_4 remained constant, whilst the concentration of AlEt_3 and DETA (1:1 molar ratio) was varied from 1.96×10^{-2} to $20.25 \times 10^{-2} \text{ mol/l}$ are shown in Figure 4. Similarly, Figure 5 shows the relationship between the initial rate of polymerization and CCl_4 concentration when the concentration of AlEt_3 and DETA were kept constant. From these Figures it can be seen that the initial rate of polymerization is square root order with respect to the concentration of initiator components.

These kinetic results show that the reaction order for the components of the initiating system corresponds to that found for radical polymerization¹¹.

The results of experiments in which the concentrations of monomer and CCl_4 remained constant, whilst DETA to AlEt_3 ratio was varied from 0.1:1.0 to 2.0:1.0 are shown in Figure 6. It can be seen that the initial rate rapidly increases as the ratio of DETA to AlEt_3 is increased, and then flattens out as the ratio is equal to or greater than unity. From Figure 6 one can conclude that under the experimental conditions the formation of the complex resulting from the reaction between AlEt_3 and DETA greatly influences the polymerization of vinyl chloride. It is likely that the free-radical formation under given conditions is a result of the interaction between CCl_4 and the AlEt_3 -DETA complex.

Figure 7 gives the dependence of the overall rate constant of the process on the inverse temperature

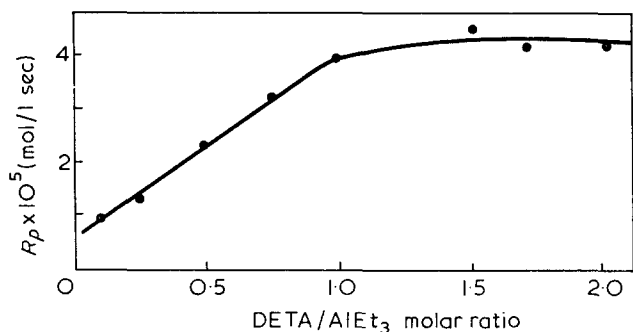


Figure 6 Plot of rate of polymerization versus DETA/ AlEt_3 molar ratio at 40°C . $[\text{VC}] = 7.87 \text{ mol/l}$; $[\text{AlEt}_3] = 7.87 \times 10^{-2} \text{ mol/l}$; $[\text{CCl}_4] = 7.87 \times 10^{-2} \text{ mol/l}$; solvent = benzene

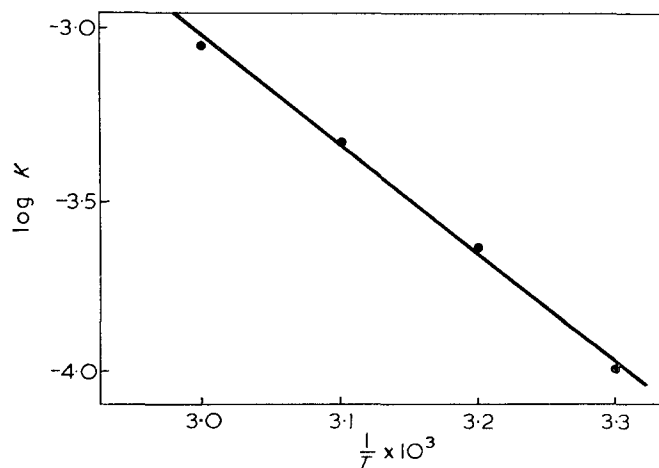


Figure 7 Dependence of the rate constant on the inverse temperature

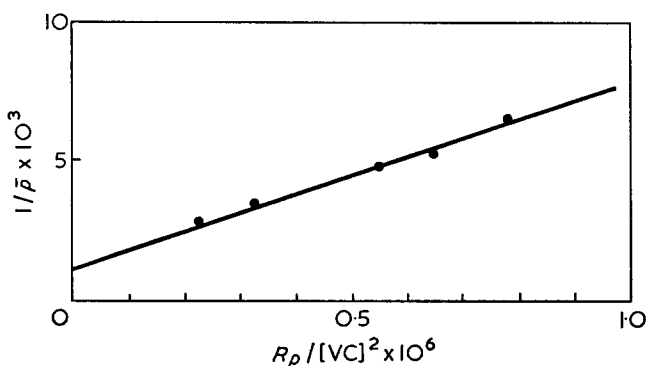


Figure 8 $1/\bar{p}$ versus $R_p/[\text{VC}]^2$. [Vinyl chloride]= 7.87 mol/l ; $[\text{AlEt}_3]=1 \times 10^{-2}$ to $12.3 \times 10^{-2} \text{ mol/l}$; $\text{AlEt}_3:\text{DETA}:\text{CCl}_4=1:1:1$ (molar ratio); solvent=benzene; polymerization at 40°C

Table 2 Polymerization of vinyl chloride by $\text{AlEt}_n\text{Cl}_{3-n}/\text{diethylenetriamine}/\text{CCl}_4$ catalyst system^a

No.	$\text{AlEt}_n\text{Cl}_{3-n}$	Yield (%)
1	AlEt_3	35.0
7	AlEt_2Cl	15.0
8	$\text{AlEt}_{1.5}\text{Cl}_{1.5}$	3.8
9	AlEtCl_2	2.3
10	AlCl_3	0.0

^a [Vinyl chloride]= 7.87 mol/l ;
 $[\text{AlEt}_n\text{Cl}_{3-n}]=7.87 \times 10^{-2} \text{ mol/l}$;
 $[\text{DETA}]=7.87 \times 10^{-2} \text{ mol/l}$; $[\text{CCl}_4]=$
 $7.87 \times 10^{-2} \text{ mol/l}$; solvent=benzene;
 polymerization at 40°C for 20 h

from which E_0 is estimated to be 14.4 kcal/mol . This value is somewhat higher than that in the $\text{AlEt}_3/\text{benzoyl peroxide}/\text{ethyl acetate}$ catalyst system¹².

As the value of $(E_p - \frac{1}{2}E_t)$ was reported to be 1.5 kcal/mol for vinyl chloride, E_{in} is 25.8 kcal/mol .

Plots of $1/\bar{p}$ vs. $R_p/[\text{M}]^2$ (where \bar{p} is the degree of polymerization, and R_p is the polymerization rate) make a straight line making an intercept on the ordinate axis (Figure 8).

This dependence corresponds to the well-known equation for radical polymerization:

$$\frac{1}{\bar{p}} = \frac{1+\lambda}{2} \frac{k_t R_p}{k_p^2 [\text{M}]^2} + C_m + C_s \frac{[\text{S}]}{[\text{M}]} + C_i \frac{[\text{I}]}{[\text{M}]}$$

where k_p and k_t are the rate constants of propagation and termination respectively; C_m , C_s and C_i are the constants for chain transfer through monomer, solvent and initiator; λ is the part of the termination reaction caused by disproportionation.

Taking $\lambda=1$ the author obtained 6150 mol sec/l for k_t/k_p^2 ; this value is very high compared with that found for the vinyl chloride polymerization with Ziegler-Natta type catalyst⁸. According to the above equation an intercept on the ordinate axis equal to 1.1×10^{-3} represents $C_m + C_s[\text{S}]/[\text{M}] + C_i[\text{I}]/[\text{M}]$. C_m was reported to be 4×10^{-4} at 25°C ¹⁴.

The difference between 1.1×10^{-3} and 4×10^{-4} is due to the chain transfer reaction through initiator, particularly AlEt_3 , CCl_4 and DETA ^{6, 15}.

Table 2 summarizes the results of the vinyl chloride polymerization by the $\text{AlEt}_n\text{Cl}_{3-n}$, DETA and CCl_4 catalyst system. It is obvious that the use of AlEt_2Cl , AlEtCl_2 and $\text{AlEt}_{1.5}\text{Cl}_{1.5}$ instead of AlEt_3 decreased

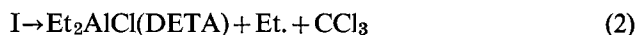
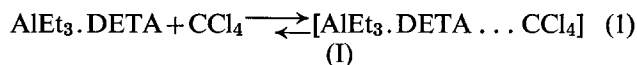
the yield of polymer, and polymerization did not occur with the use of AlCl_3 .

The difference seems likely to be attributable to both the stability of the polar complex between aluminium alkyl and DETA and the reactivity of this complex towards CCl_4 .

The kinetic studies show that AlEt_3 , DETA and CCl_4 catalyst system can initiate the free-radical polymerization of vinyl chloride and the formation of the AlEt_3 - DETA complex plays an important role.

The formation of the AlEt_3 - DETA complex was determined by n.m.r. spectroscopy. The chemical shifts of the amino protons of DETA are increased in the presence of AlEt_3 from an initial absorption band. The reaction of DETA with AlEt_3 produces 1:1 molecular addition compound. In the n.m.r. spectrum of this compound, there is a single NH_2 peak, indicating that both amine groups are equivalent. The amine groups are symmetrically located with respect to the aluminium atom, and therefore the aluminium atom is penta-coordinate.

On the basis of the n.m.r. spectrum obtained during the reaction of AlEt_3 with DETA and also the information of the experimentally established function of the total process, the reaction sequence leading to free-radical formation can be visualized as follows,



Equation (1) is the complex formation reaction between $\text{AlEt}_3 \cdot \text{DETA}$ and CCl_4 . Equation (2) is the special redox reaction.

The fact that Et_2AlCl is also an initiator indicates that it can undergo the same reaction to give EtAlCl_2 , but that AlEtCl_2 and $\text{AlEt}_{1.5}\text{Cl}_{1.5}$ do not react with CCl_4 to form radicals.

ACKNOWLEDGEMENTS

The author is grateful to Dr Y. Kosaka and Mr S. Imura for valuable discussions.

REFERENCES

- Minsker, K. S., Sangalov, Yu. A. and Razuwayev, G. A. *J. Polym. Sci. (C)* 1967, **16**, 1489
- Razuwayev, G. A., Sangalov, Yu. A., Minsker, K. S. and Kovaleva, N. V. *Polym. Sci. USSR* 1965, **7**, 597
- Breslow, D. S., Christman, D. L., Espy, H. N. and Lukach, C. A. *J. Appl. Polym. Sci.* 1967, **11**, 73
- Kawai, W., Ogawa, M. and Ichihashi, T. *J. Polym. Sci. (A-1)* 1970, **8**, 3033
- Akimoto, A. *Polymer* 1974, **15**, 216
- Inaki, Y., Ishiyama, M. and Takemoto, K. *Makromol. Chem.* 1972, **160**, 127
- Inaki, Y., Ishiyama, M. and Takemoto, K. *Angew. Makromol. Chem.* 1971, **19**, 1
- Mazurek, V. V., Nesterchuk, G. T. and Merkuréva, A. V. *Polym. Sci. USSR* 1969, **11**, 693
- Hazeldine, R. N., Hyde, T. G. and Tait, P. J. T. *Polymer* 1973, **14**, 215
- Sakurada, I., Matsuda, J., Shiotani, S. and Kawasaki, A. *Kogyo Kagaku Zasshi* 1958, **61**, 1362
- Milovskaya, E. B., Zamoyskaya, L. V. and Vinogradova, S. I. *Eur. Polym. J.* 1970, **6**, 1589
- Kopp, Ye. L. and Milovskaya, Ye. B. *Vysokomol. Soedin. (A)* 1969, **11**, 750
- Burnett, G. and Wright, W. *Proc. R. Soc. (A)* 1954, **231**, 28
- Danusso, F. and Sianesi, D. *Chim. Ind.* 1955, **37**, 965
- Huff, T. and Perry, E. *J. Polym. Sci. (A-1)* 1963, **1**, 1553

On crystallization phenomena in polytetrafluoroethylene

D. C. Bassett and R. Davitt

*J. J. Thomson Physical Laboratory, University of Reading, Reading RG6 2AF, UK
(Received 21 January 1974; revised 3 May 1974)*

The crystal thickness of PTFE has been measured for a variety of crystallization conditions. It increases with the temperature and time of crystallization as well as molecular weight, and also with the temperature and time of annealing. The data are fitted by the kinetic theory of chain folding as well as are those for chain-folded polyethylene. On this basis PTFE may be regarded as a chain-folded polymer whose large thickness derives essentially from its low entropy of fusion. It is also suggested that a single theory of polymeric crystallization may be able to predict the crystal thicknesses not only of PTFE and chain-folded polyethylene but also of chain-extended polyethylene, but it would have to be a theory in which account were taken of lamellar thickening behind the narrowed growing edge of a lamella.

INTRODUCTION

The microstructure of melt-crystallized polytetrafluoroethylene (PTFE) is unusual in that although it consists of lamellae these have a much greater thickness than is observed in nearly all other crystalline polymers¹. For comparison, polyethylene (PE) crystallized from the melt under vacuum would normally have average lamellar thicknesses of 300–400 Å, a figure which under extreme conditions might increase to perhaps 1500 Å. In contrast, measurements on PTFE reported in this paper give typical average lamellar thicknesses of 1000 to 2500 Å and maximum values approaching 10⁵ Å. The explanation of this disparity and its relation to underlying crystallization mechanisms are the main concern of this paper.

Nowadays PTFE is generally regarded as one of a small class of chain-extended polymers² whose other members include polytrichlorofluoroethylene and polyethylene which has been recrystallized at high pressures (CEPE). The basis of this classification is empirical and rests upon firstly the large layer thicknesses and secondly similar morphologies, notably the narrowing of lamellae at their edges. The purpose of this research, starting from a background of work on CEPE, was to investigate whether there is also a fundamental basis for this classification. We shall conclude that there is not and that PTFE conforms to the general pattern of chain-folded crystallization behaviour found in other polymers with its large thickness stemming essentially from its low entropy of fusion.

EXPERIMENTAL AND RESULTS

Temperature dependence of lamellar thickness

Notwithstanding the description 'chain-extended', molecules in PTFE are not generally fully extended. On the contrary, they fold into lamellae whose thickness

increases with crystallization temperature³. We have measured this variation for the coagulated dispersion polymer Fluon CDI* which is estimated to have a molecular weight of $\sim 10^6$.

The standard crystallization procedure adopted used samples in the form of 5 mm discs, prepared by cold-pressing the original powder, which fitted in the sample pan of a Perkin-Elmer DSCIB differential scanning calorimeter (d.s.c.). They were held for 5 min at 400°C in a nitrogen atmosphere—a procedure which from the reproducibility of subsequent crystallization behaviour produced negligible thermal degradation—before being lowered in about 12 sec to a crystallization temperature in the range 312 to 322°C and then, after a further 20 min, quenched to ambient temperature. Afterwards specimens were fractured in liquid nitrogen, exposing surfaces whose two-stage replicas were photographed in the electron microscope. These were similar in appearance to those published by other workers^{1–3}.

The determination of lamellar thickness from such micrographs followed the procedure used in earlier work on CEPE^{4, 5} which has since been justified as an objective method for that polymer by comparison with molecular lengths left after degradation with nitric acid⁶. Briefly, the technique consists of drawing arbitrary lines on the micrograph and for each line measuring the thickness parallel to *c* at the region of intersection for every layer crossing that line. In practice the coordinates of two points, lying at opposite ends of the characteristic fracture-induced striation for each layer are recorded on punched tape. After computation the output data are presented in a normalized frequency histogram as shown in *Figure 1* together with the value of the mean lamellar thickness and its standard error. Re-measurements of the same replica gave a repeatability within

* This and all other samples of PTFE used in this work were kindly supplied by A. J. Cobbold of ICI Ltd (Plastics Division).

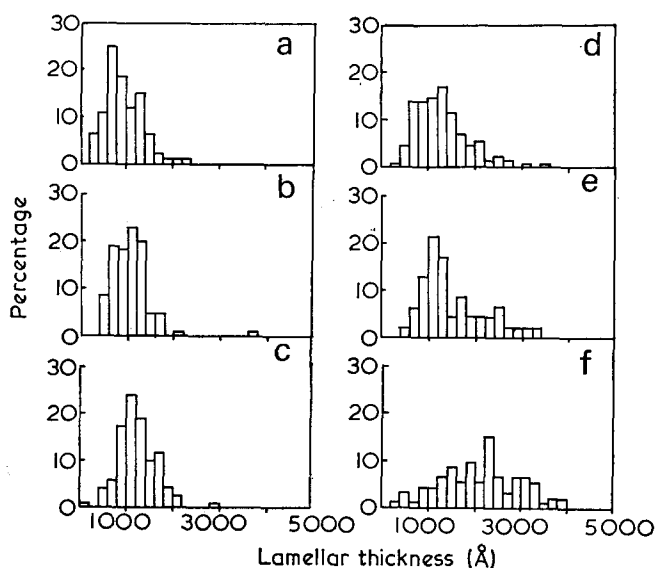


Figure 1 Normalized histograms of crystal thicknesses for samples crystallized for 20 min at various temperatures. (a) $T_c=312^\circ\text{C}$, $N=92$, $\bar{L}_N=946\pm 42\text{ \AA}$; (b) $T_c=314^\circ\text{C}$, $N=105$, $\bar{L}_N=1074\pm 42\text{ \AA}$; (c) $T_c=316^\circ\text{C}$, $N=121$, $\bar{L}_N=1243\pm 37\text{ \AA}$; (d) $T_c=318^\circ\text{C}$, $N=130$, $\bar{L}_N=1302\pm 49\text{ \AA}$; (e) $T_c=320^\circ\text{C}$, $N=97$, $\bar{L}_N=1527\pm 68\text{ \AA}$; (f) $T_c=322^\circ\text{C}$, $N=91$, $\bar{L}_N=2129\pm 87\text{ \AA}$

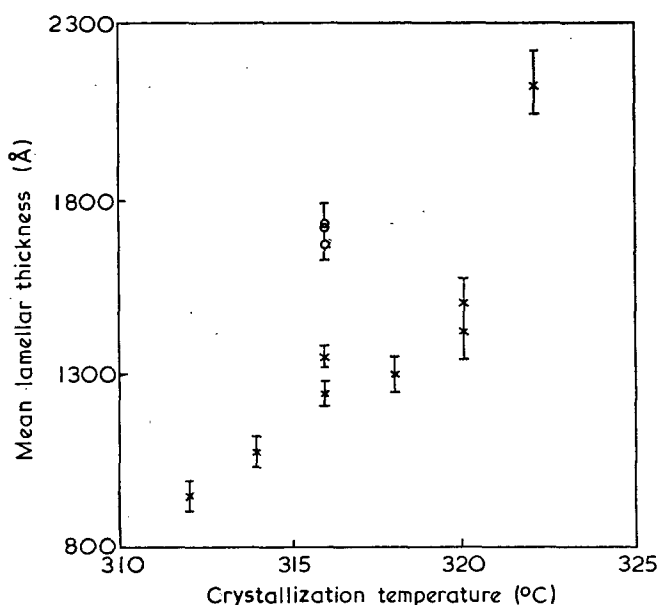


Figure 2 Mean crystal thickness along c as a function of crystallization temperature for 20 min crystallization. \times , Fluon CD1; \circ , Fluon G163

$\pm 7\%$ and repeatability of the same order was also obtained between different samples crystallized at the lower temperatures in the range. For crystallization at 320 and 322°C, however, problems of nucleation arose which will be described in connection with measurements of time dependence.

The collected data are assembled in Figure 2 which has the familiar upward curving shape found for crystallization of other polymers from solution⁷, from the melt under chain-folded conditions and for chain-extended growth of polyethylene^{4, 8}.

Also in Figure 2 are three points recording the average lamellar thickness found in three different samples of the higher molecular weight (estimated at $\sim 10^7$) PTFE Fluon G163, a granular polymer, after crystallization at 316°C. These are significantly higher than measured

for Fluon CD1 under identical crystallization conditions indicating that the higher molecular weight polymer formed thicker lamellae.

Lamellar thickening

Among explanations advanced for the formation of chain-extended lamellae, enhanced lamellar thickening has attracted especial attention, not least because it has been demonstrated that chain-folded PE can be converted by high pressure annealing into CEPE^{5, 9} and because morphological studies suggest that growing lamellae thicken behind a narrowed growing edge^{4, 10}. For PTFE we have attempted to measure the longer term thickening during both crystallization and annealing treatments of Fluon CD1.

The first experiments were of prolonging the crystallization time of specimens held at 316°C from 20 min to 18 h. This did not produce any significant change in mean crystal thickness. At 322°C, however, there is clear evidence of substantial lamellar thickening. Figure 3 illustrates six specimens which after the standard 5 min at 400°C were held at 322°C for times varying from 20 min to 51.5 h, then kept at 316°C for a further 20 min and finally quenched. This procedure gave a more repeatable product than did direct quenching. After the longest times some lamellae which were very large indeed were produced, with thicknesses as high as 6 μm . The numerical data of the increase in mean thickness with time are shown in Figure 4, but have to be treated with some caution, because of the very considerable variation found in the onset of crystallization at this temperature. This was discovered by interrupting the crystallization procedure described immediately after the end of the period at 322°C, then heating a sample up again in the DSCIB and checking for the occurrence of a melting endotherm. Sometimes samples had crystallized within 20 min—and it seems from the smoothly rising data that the point in Figure 2 represented such a sample—while others remained molten after many hours. This behaviour was unchanged by the addition of talc in an attempt to induce more regular nucleation. Nevertheless as the error in crystallization time will diminish for long periods, an order of magnitude estimate of the rate of isothermal thickening at 322°C may be obtained by dividing the overall range of thicknesses observed by the maximum crystallization time. This gives a figure of order 1000 $\text{\AA}/\text{decade}$ of minutes.

Figure 5 shows specimens of Fluon CD1, which have a fibre orientation around c . These were prepared in connection with mechanical studies by annealing samples at 325°C without constraint after previous cold drawing to a draw ratio of 3 but also demonstrate that molecular orientation is maintained during annealing, in a similar way to the known behaviour of both chain-folded PE and CEPE^{5, 9}. The average lamellar thickness increases with annealing time from an initial value of nearly 1000 \AA to 2000 \AA after 54 h at 325°C and maximum thicknesses of order 1 μm . The rate of thickening increases rather faster than the logarithm of time (Figure 6), and whereas the first three points fall on a line having a slope of 245 $\text{\AA}/\text{decade}$ of minutes, the last two give a line of slope 688 $\text{\AA}/\text{decade}$. On annealing without constraint at 326°C, all orientation was lost within 2 h. However, if specimens were clamped at both ends, they could be annealed to 340°C and still remain oriented.

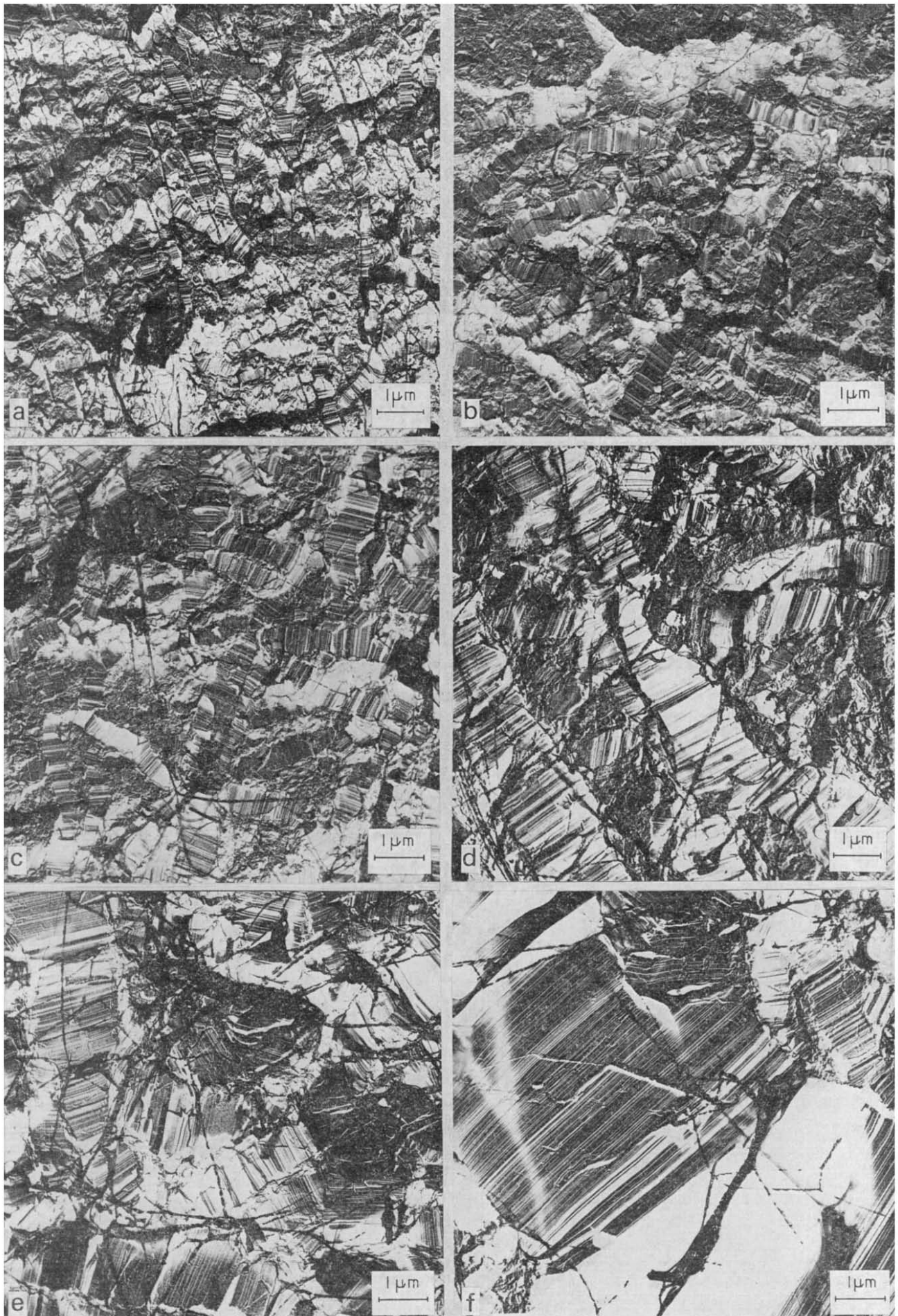


Figure 3 Fracture surface replicas of Fluon CD1 crystallized at 322°C for the following times: (a) 20 min; (b) 2 h; (c) 9·3 h; (d) 18·25 h; (e) and (f) 51·5 h

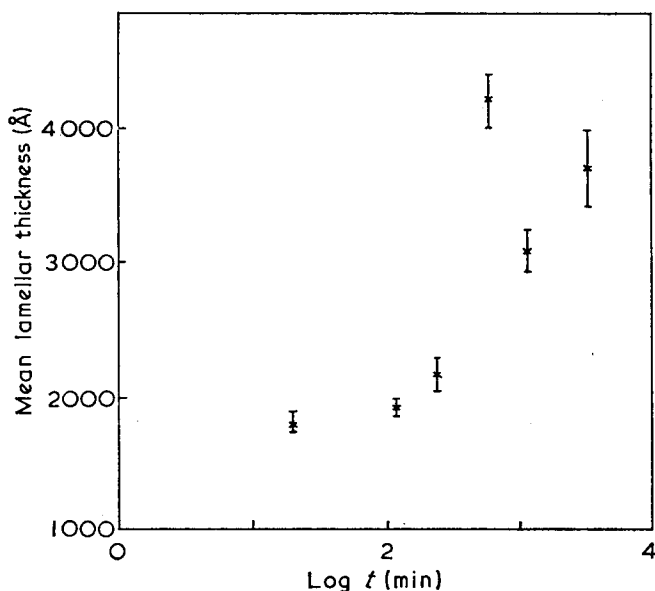


Figure 4 Mean crystal thickness as a function of crystallization time for the samples illustrated in Figure 3

Lamellar thickness and melting point

The melting point T_m of a crystalline polymer containing lamellae of thickness l should, according to basic thermodynamics, be:

$$T_m = T_m^0 \left(1 - \frac{2\sigma_e l}{\Delta h_f l} \right) \quad (1)$$

where T_m^0 is the melting point of infinitely thick crystals, σ_e the end surface free energy and Δh_f the enthalpy of fusion per unit volume of crystal. The melting points of all our samples of PTFE have been measured as a matter of course using the DSCIB at a scanning rate of 8 K/min (the recommended compromise between thickening at slow rates and superheating at fast ones¹¹) and calibrated against the melting point of 1 mg high purity lead at 327°C by a comparison of peak temperatures. This gave a repeatability on the same sample within ± 0.5 K. Data obtained on crystallized samples are plotted against $1/l$ in Figure 7 and fit adequately to a straight line as required by equation (1). The slope of the least squares line has a magnitude of 8.45×10^3 K Å which taking the values of T_m^0 as 334.1°C (the intercept on Figure 7) and Δh_f as 14.6 cal/g¹² multiplied by a density of 2.2 g/cm³ gives σ_e as 94 erg/cm².

There is, however, a problem with the melting points of PTFE which we must now consider. It is that the virgin, as-polymerized material may show two melting peaks. For Fluon G163 these are well-resolved and occur at 336 and 339.5°C. For Fluon CD1 there is only a broad plateau which we choose to regard as two unresolved peaks falling at 333.8°C and 338.1°C. We now note that the lower peak for Fluon CD1 is consistent with the best straight line drawn in Figure 7. Similarly for Fluon G163 the lower original melting point and the data in Figure 8 for recrystallized polymer are consistent with a line of similar slope to that drawn in for the dispersion polymer but displaced by some 2 K to higher temperatures. Evidently, therefore, it is the higher of the two melting peaks of the virgin polymer which requires explanation.

Two possible reasons for this have been considered. The first, for which X-ray diffraction provided no

evidence, is that a different crystalline phase is present. The other is the possibility of superheating, i.e. of crystals being unable to melt sufficiently quickly to avoid being heated above their thermodynamic melting point. If this is occurring then melting at a slower rate should reduce the effect. There was indeed only one melting peak, at 331.5°C when virgin Fluon CD1 was melted at a scan rate of 1 K/min in the DSCIB. Melting points of recrystallized samples are also moved to lower temperatures by consistent amounts of ~ 2 K so that the slope of the line in Figure 7 would not be altered. A shift in this sense would be expected from thermal lags in the apparatus.

Additional evidence bearing on this point comes from the melting points of a dispersion based PTFE which had been subjected to varying amounts of radiation in air from a ⁶⁰Co source. The initial molecular weight was estimated to be slightly higher than for Fluon CD1 but still to be of order 10⁶. Figure 8 shows that at doses less than 0.1 Mrad two endothermic peaks are resolved during melting but that as the radiation dose increases, both melting peaks move to lower values, the higher doing so more quickly; the two have merged by 0.1 Mrad.

The factor responsible for the double melting peak in as-polymerized PTFE is clearly very sensitive to radiation. It is highly unlikely that the crystalline texture of such a high-melting material could be sufficiently affected by irradiation at room temperature to give the effect and we must look rather to molecular behaviour. As is well known the chief effect of radiation on PTFE is to cause main chain scission. The combined evidence suggests, therefore, that the higher melting peak of virgin PTFE is due to superheating associated with the longer molecules. As the molecular weight is reduced, presumably it is easier for shorter molecules to nucleate the molten phase during heating and so remove the cause of superheating. There is also the implication that molecular constraints are different after recrystallization than when the polymer is first formed.

An estimate of the molecular lengths associated with superheating may be made by noting that in 1 g of polymer there will initially be N/M_0 and finally N/M molecules where N is Avogadro's number and M_0 , M are the number-average molecular weights before and after irradiation. The difference $[(N/M) - (N/M_0)]$ must be equal to the number of breaks in the main chain D/E_a for a dose D in which E_a is absorbed per scission¹³. If we take the G value for scission as ~ 3 ¹³ and take 1 rad = 6.25×10^{13} eV absorbed energy/g then we reach the relation:

$$\frac{1}{M} - \frac{1}{M_0} \sim \frac{10^{-6}}{3}$$

for a dose of 0.1 Mrad. Setting $M_0 = 10^6$, 2×10^6 and 10^7 in turn gives M as 7.5×10^5 , 1.2×10^6 and 2×10^6 respectively and lastly, dividing by 38.5 converts to corresponding chain lengths of 2×10^4 , 3.3×10^4 and 5×10^4 Å. According to this crude calculation therefore, it would be molecules longer than these lengths which would be involved in superheating.

Finally, we consider the case of two melting peaks produced by crystallizing in two stages so that a sample contains a double population of lamellae. Figure 9 is the melting trace of such a sample produced in this case by growth partly at 322°C and partly during

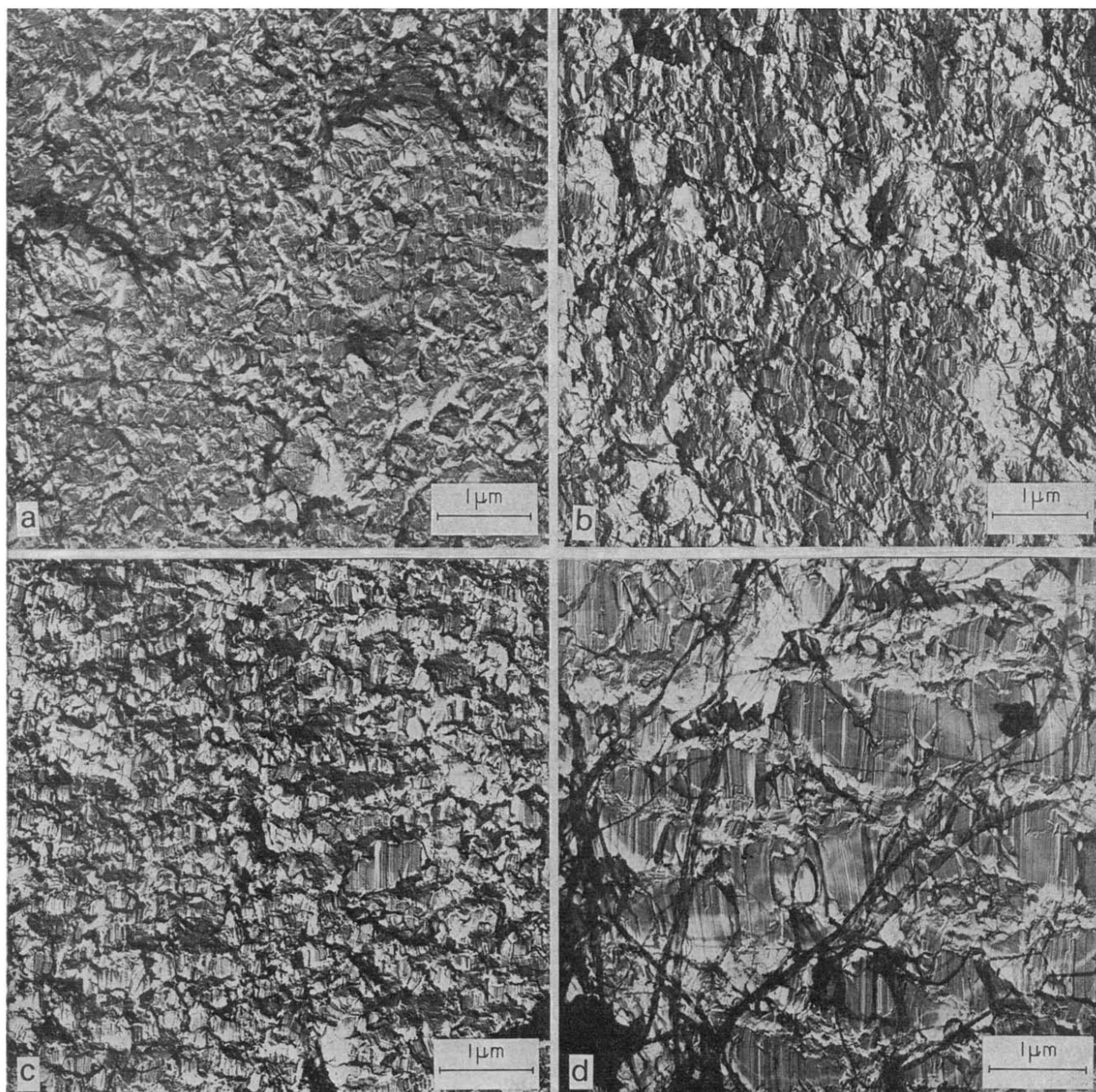


Figure 5 Fracture surface replicas of oriented Fluon CD1 annealed at 325°C for the following times: (a) 1 h; (b) 9-3 h; (c) and (d) 54 h

cooling. The histogram of crystal lengths in fracture surfaces, in which each lamella is counted once, for this specimen is *Figure 10a*. It is instructive to compare *Figures 9* and *10a* which are in principle related by equation (1). To do this we first convert *Figure 10a* into *Figure 10b*, a distribution in $1/l$. This shows two peaks (as does *Figure 9*) but with the ratio of the lower to the higher as 3:4 whereas in the d.s.c. trace they are as 4:3 on an apparently reasonable baseline. Using *Figure 7*, *Figure 10b* leads to expectations of peak melting temperatures of about 325 and $\sim 333^\circ\text{C}$ respectively in comparison with those observed of 326.9 and $\sim 333^\circ\text{C}$ respectively (with the latter peak drawn out by superheating). This is not unreasonable agreement, and the interesting point is that exact agreement would only be expected (ignoring instrumental factors) if *Figure 10b* is in fact the weight average distribution in $1/l$. Whether this is so depends on the relationship between average thicknesses measured on a surface and

the true value in the sample. This interesting question is discussed elsewhere⁶ in connection with measurements on CEPE which have shown the same correspondence of the surface number-average figure with the volume weight-average value as reported here. Other simple distributions notably that of $\ln(1/l)$ do not show two clear peaks from which we conclude that for PTFE, $n(1/l)$ measured on a surface is a fair approximation to the true weight average distribution in $1/l$.

DISCUSSION

We wish to consider whether the phenomena observed in PTFE constitute a case for regarding it as an exception to the pattern of chain-folded crystallization from the melt. Current kinetic theories of chain folding are strictly applicable only to crystallization from dilute solution, but are normally carried over to the melt case because no more complete theory is available. In doing

so the time dependence of lamellar thickness, which is absent during growth from solution, is ignored. If we make this translation then we have to consider observed thicknesses in relation to the equation:

$$l = \frac{2\sigma_{\text{eff}}}{\Delta s_f \Delta T} + \delta l \quad (2)$$

in which δl is usually assumed to be small and σ_{eff} is increased beyond σ_e measured using equation (1) from melting experiments (because of supposed surface roughness during growth) in order to fit the data. It is shown in Table 1 that the product $l\Delta T$ is approximately constant. This indicates that equation (2) does represent the PTFE data reasonably well and that δl is indeed small. The plot of l against $1/\Delta T$ is not shown but it is similar to that reported previously for chain-folded and chain-extended PE⁸.

An equivalent statement is that $\sigma_{\text{eff}}/\sigma_e$ should be constant. Values of this ratio calculated from the data

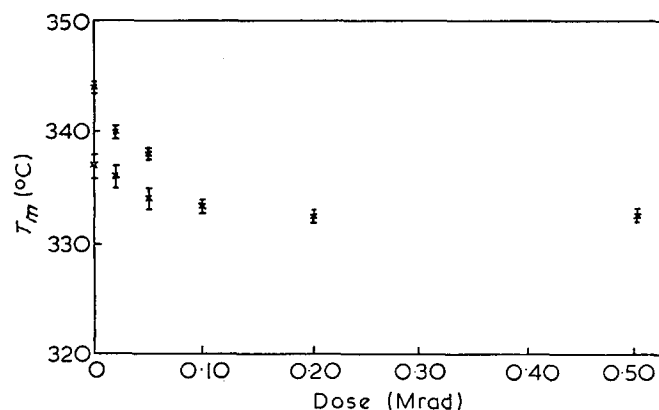


Figure 8 Melting point as a function of radiation dose for a dispersion PTFE

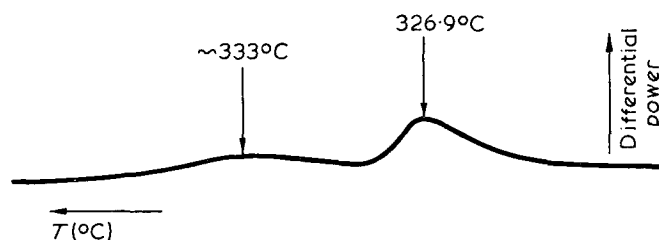


Figure 9 Melting endotherm of a sample of Fluon CD1 crystallized in two stages

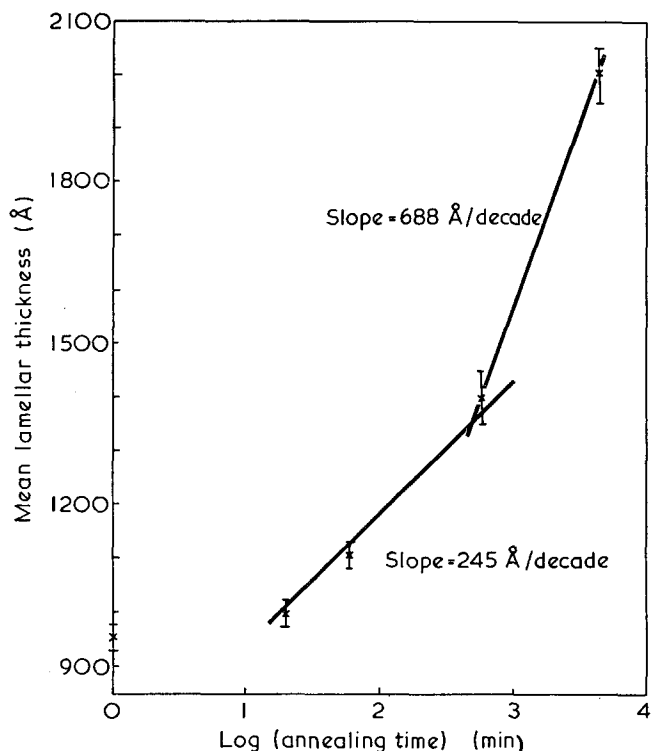


Figure 6 Mean crystal thickness as a function of annealing time for the samples illustrated in Figure 5

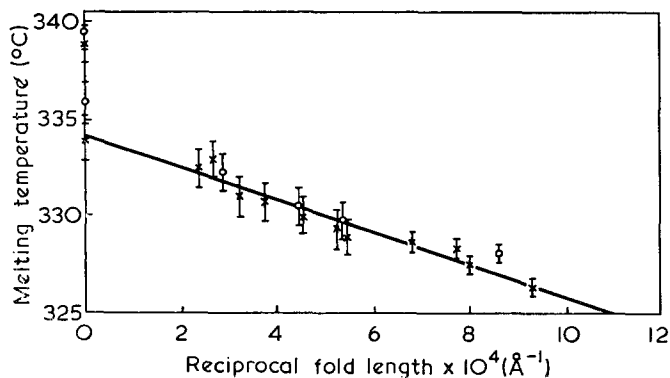


Figure 7 Melting point as a function of the reciprocal of crystal thickness for PTFE. x, Fluon CD1; o, Fluon G163. $\sigma_e = 94$ erg/cm²

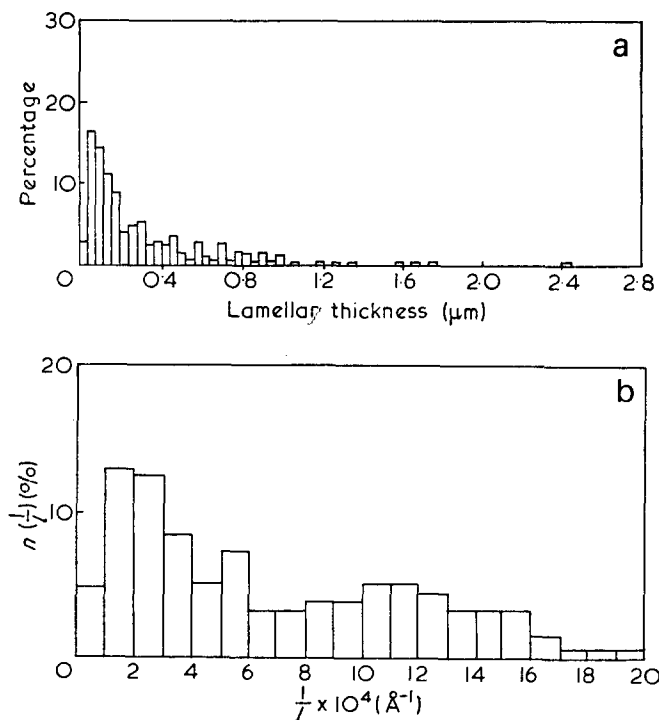


Figure 10. (a) Normalized histogram of lamellar thicknesses along c for the sample of Figure 9. (b) The distribution in reciprocal crystal thickness corresponding to (a)

of Figure 2 are also listed in Table 1. They give an average value of 2.6, which interestingly enough is very much the same figure as applies to chain-folded crystallization of polyethylene at 1 bar. For example, an average lamellar thickness of 360 Å resulting from the crystallization of PE at 1 bar and 15K supercooling gives $\sigma_{\text{eff}} = 2.4\sigma_e$ when Δh_f is taken as 280 J/cm³ and $\sigma_e = 77$ erg/cm²¹⁴.

On the basis of the above data there is no reason to regard the large lamellar thickness of PTFE as anomalous. It can be fitted as well as can the measurements for chain-folded PE to existing kinetic theories of chain folding. The increase in thickness for PTFE in comparison with chain-folded PE is, as equation (2)

Table 1 Crystallization data for PTFE

Crystallization temperature (°C)	Supercooling, ΔT (K)	Mean lamellar thickness, l (Å)	$l/\Delta T$ ($\mu\text{m K}$)	σ_{eff} (erg/cm ²)	$\sigma_{\text{eff}}/\sigma_e$
312	22.1	946	2.09	233	2.48
314	20.1	1074	2.16	238	2.54
316	18.1	1243	2.25	249	2.68
318	16.1	1302	2.10	231	2.47
320	14.1	1527	2.15	237	2.53
322	12.1	2129	2.58	284	3.03

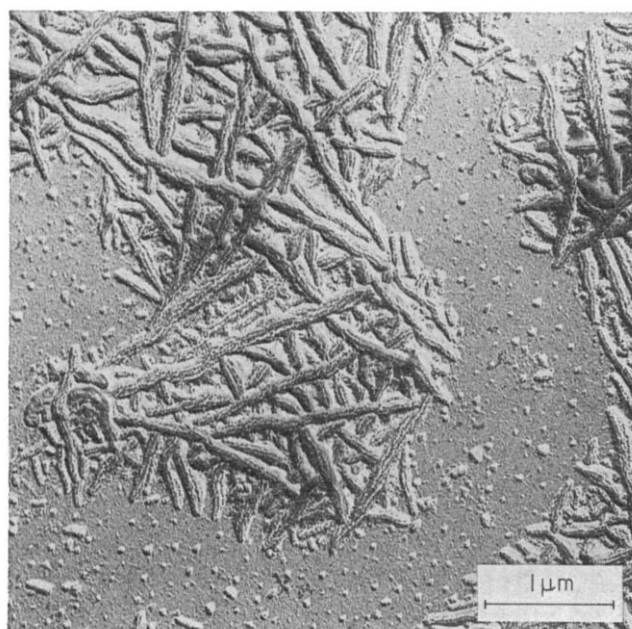


Figure 12 Appearance of particles of a dispersion PTFE after recrystallization from the melt

requires, in the same proportion as the reduction in the entropy of fusion per unit volume of crystal. From this point of view, therefore, PTFE may be regarded as a chain-folded polymer with a large lamellar thickness.

Similar considerations can also be applied to the case of CEPE. This is now known to form as a consequence of the melt solidifying first into the recently identified hexagonal phase¹⁵ instead of directly into the orthorhombic structure^{16, 17}. As at 5 kbar the hexagonal form has an entropy of fusion only some 20% of that of the orthorhombic¹⁷, i.e. $\sim 0.1 \text{ J cm}^{-3} \text{ K}^{-1}$ one expects that, other things being equal, CEPE lamellae should be five times thicker than chain-folded. This is essentially true¹⁸. One notes also that lamellae of PTFE formed at 1 bar are half as thick as those of CEPE formed at 5 kbar⁴ and the same supercooling. This is in agreement with the inverse ratio of their entropies of fusion per unit volume (the values are 0.11 and $0.22 \text{ J cm}^{-3} \text{ K}^{-1}$ for CEPE and PTFE respectively) which, because equation (2) fits both cases reasonably well, implies that σ_{eff} is more or less the same at $\sim 250 \text{ erg/cm}^2$ in both cases.

On the basis of the above considerations, there is a *prima facie* case for bringing the crystallization of PTFE, chain-folded PE and also CEPE into a unified scheme. This is strengthened by the morphological similarities between CEPE and PTFE¹⁹. If this be so, however, there are important implications for the premises of a suitable theory. Current theories of chain folding, which are formulated for solution, consider the layer thickness as established, except for relatively minor readjustments, when molecules are laid down on the growing crystal face. This concept has to be correlated with the appearance of growing lamellae which for the PTFE studied here and high molecular weight ($> 10^5$) CEPE⁴ have narrowed edges. In some cases this appearance is undoubtedly due to impingement or interference of separate lamellae but it has also been argued⁴ and recently confirmed by direct observation¹⁵ that this is also the normal contour of a growing lamella. Supporting evidence for this view is shown in Figures 11

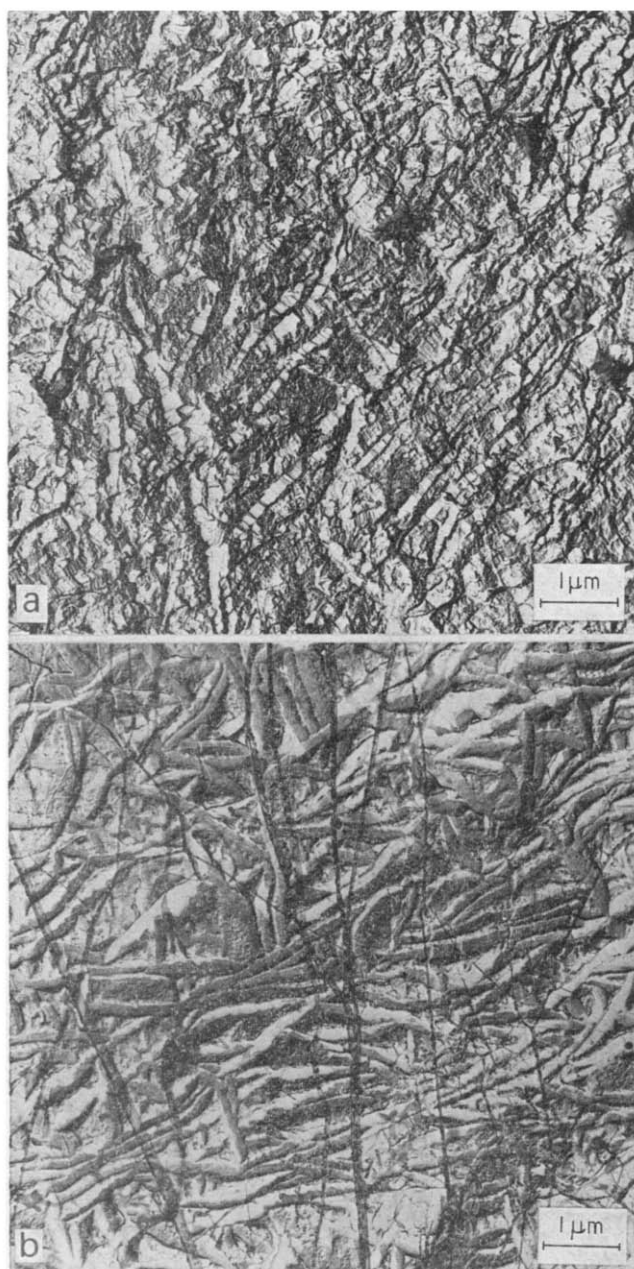


Figure 11 (a) Internal fracture surfaces and (b) external surface of a thin film of recrystallized dispersion PTFE

and 12. Figure 11 shows the internal fracture surface and external surface of a thin film of recrystallized dispersion polymer. These show that the *c* axis lies transverse to the lamellar units. Figure 12, on the other hand, is another dispersion PTFE polymer which was sprayed from aqueous suspension and then recrystallized on a glass substrate. Here the lamellar units, which appear similar to those examined by Symons²⁰, are not restricted and yet still have tapered edges. Exactly the same phenomenon occurs in thin films of CEPE, provided the polymer is $>10^5$ in molecular weight, with the *c* axis still transverse to the lamellar units²¹. If we are to have a single theory of polymeric growth from the melt then this thickening behind the growth edge would have to be regarded as the normal mode of growth but one which, perhaps, may not be readily observed either in thin crystals or where thickening is more rapid (as in CEPE of lower molecular weight, $\sim 2 \times 10^4$)⁴. Thus in producing data which appear to remove PTFE from the anomalous position it has seemed to hold in polymeric crystallization, we are questioning the basis on which theories of crystallization must be established.

ACKNOWLEDGEMENT

R. D. is indebted to the Science Research Council for a postgraduate studentship.

REFERENCES

- 1 Bunn, C. W., Cobbold, A. J. and Palmer, R. P. *J. Polym. Sci.* 1958, **9**, 385
- 2 Wunderlich, B. *Pure Appl. Chem.* 1972, **31**, 49
- 3 Speerschnieder, C. J. and Li, C. H. *J. Appl. Phys.* 1962, **33**, 1871
- 4 Rees, D. V. and Bassett, D. C. *J. Polym. Sci. (A-2)* 1971, **9**, 385
- 5 Bassett, D. C. and Carder, D. R. *Phil. Mag.* 1973, **28**, 513
- 6 Bassett, D. C., Khalifa, B. A. and Olley, R. G. in preparation
- 7 Keller, A. and O'Connor, A. *Discuss. Faraday Soc.* 1958, **25**, 114
- 8 Bassett, D. C. and Phillips, J. M. *Polymer* 1971, **12**, 730
- 9 Rees, D. V. and Bassett, D. C. *Nature* 1968, **219**, 368
- 10 Wunderlich, B. and Melillo, L. *Makromol. Chem.* 1968, **118**, 250
- 11 Hellmuth, E., Wunderlich, B. and Rankin, J. M. *J. Appl. Polym. Symp.* 1966, **2**, 101
- 12 Mandelkern, L. 'Crystallisation of Polymers', McGraw-Hill, New York, 1964, p 120
- 13 Chapiro, A. 'Radiation Chemistry of Polymeric Systems', Wiley-Interscience, New York, 1962, pp 379, 531
- 14 Hoffman, J. D., Lauritzen, J. I., Passaglia, E., Ross, G. S., Frolen, L. J. and Weeks, J. J. *Kolloid-Z.* 1969, **231**, 564
- 15 Bassett, D. C., Block, S. and Piermarini, G. J. *J. Appl. Phys.* in press
- 16 Bassett, D. C. and Turner, B. *Nature (Phys. Sci.)* 1972, **240**, 146
- 17 Bassett, D. C. and Turner, B. *Phil. Mag.* 1974, **29**, 925
- 18 Bassett, D. C. and Turner, B. *Phil. Mag.* 1974, **29**, 285
- 19 Melillo, L. and Wunderlich, B. *Kolloid-Z.* 1972, **250**, 417
- 20 Symons, N. K. *J. Polym. Sci. (A)* 1963, **1**, 2843
- 21 Bassett, D. C. and Khalifa, B. A. unpublished

High temperature vulcanization of elastomers:

3. Network structure of efficiently vulcanized natural rubber mixes

C. T. Loo*

Institute of Polymer Technology, Loughborough University of Technology, Loughborough, Leics LE11 3TU, UK

(Received 25 January 1974; revised 18 March 1974)

The effect of vulcanization temperature (140–200°C) and time on the structures of pure gum natural rubber vulcanizates with two different *N*-cyclohexyl-2-benzothiazylsulphenamide (CBS): sulphur ratios (A, 3.5:1.5; B, 6.0:0.4 CBS/S) has been determined. Analyses of vulcanizates were carried out as reported in Part 2. Results show that both mixes are efficient in crosslinking, resulting in mainly monosulphidic crosslinks and relatively few modifications of the rubber chains. Raising the cure temperature from 140°C reduces the density of chemical crosslinks, particularly those of monosulphidic crosslinks, obtainable in the vulcanizates. This decrease in crosslink density has been shown to be irreversible with respect to cure temperature. The formation of intramolecular sulphidic groups and zinc sulphide increases with rising cure temperature, but this increase is small compared with that reported for the conventional CBS-accelerated system. The main difference between mixes A and B is that mix A yields a higher level of crosslinks and a major proportion of cyclic sulphides as main-chain modification. Negligible chain scission occurs during vulcanization at 140–200°C. These network results are interpreted mechanistically, and essential network features for obtaining good physical properties in high temperature vulcanizates are deduced.

INTRODUCTION

Efficient vulcanization (*EV*) systems, which utilize sulphur efficiently in crosslinking, have been advocated to eliminate reversion during high temperature vulcanization, as usually encountered in injection moulding and continuous extrusion^{1–3}. Several methods have been developed to achieve this efficient vulcanization^{4–6}. They include the use of sulphurless vulcanization, the use of a synergistic combination of accelerators and the use of an increased ratio of accelerator to elemental sulphur. Although many vulcanizate networks of these *EV* systems, prepared at a conventional temperature of 140°C have been characterized, those obtained at temperatures higher than 140°C are seldom studied. In this paper, the vulcanizate structures of natural rubber (NR) with one of these *EV* systems, namely, 6.0 phr *N*-cyclohexyl-2-benzothiazylsulphenamide (CBS): 0.4 phr sulphur, cured at temperatures in the range 140–200°C have been determined.

In Part 1⁷, the effect of cure temperature (140–220°C) on the physical properties of NR tread type mixes vulcanized with various sulphur and CBS proportions was reported. A mix with 3.5 phr CBS: 1.5 phr sulphur was found to be more suitable for high temperature vulcanization than the conventional cure system (0.5 phr CBS: 2.5 phr sulphur) in that better technological properties were obtained. Part 2⁸ described the network

structures accounting for the inferior physical properties of the conventional cure system vulcanized at high temperatures. The present paper additionally reports the influence of cure temperature (140–200°C) on the vulcanizate structures of a NR gum mix with the 3.5 phr CBS: 1.5 phr sulphur system. This work aims to establish the network features essential for providing good physical properties in high temperature vulcanizates.

Bi-thermal vulcanization

In Part 2⁸, elevated cure temperatures were shown to reduce the chemical crosslink densities obtainable in conventional CBS-accelerated natural rubber vulcanizates. T. Moore reached the same conclusion in the case of the 2-mercaptobenzothiazole (MBT) accelerated natural rubber vulcanizates⁹. Using a technique based on bi-thermal vulcanization, he further showed that this loss in chemical crosslink density is a reversible effect depending on cure temperature. The MBT-accelerated mix was initially cured at 180°C until the crosslink density reached a maximum value (for 180°C), and the vulcanizate was quenched. The cure temperature was then lowered to 100°C, and the curing of the sample was continued, when the crosslink density was found to increase and to reach the level achieved at the lower temperature of 100°C. Part of this paper examines whether such a reversible effect, in the relationship between cure temperature and crosslink density, occurs in the present efficient CBS-accelerated vulcanization.

* Present address: Rubber Research Institute of Malaysia.

The results from bi-thermal vulcanization can throw light on the mechanisms occurring during high temperature curing.

EXPERIMENTAL

Mixes A and B (Table 1) were prepared and vulcanized in a manner similar to that described in Part 2⁸.

Bi-thermal vulcanization

The selected rubber mix (mix B, Table 1) was first cured in a steam-heated press at 180°C for 6 min, and then immediately transferred to an electric press, thermostated at 140°C, where the curing was continued for various times. The cure time of 6 min corresponds to the maximum value of chemical crosslink density at 180°C (Figure 2). 140°C was chosen as the lower temperature for the bi-thermal vulcanization because it is the lowest used in this investigation. To record the heat input during the bi-thermal vulcanization, the time-temperature data at the centre of the moulding were measured by the thermocouple procedure described in Part 1⁷.

Characterization of vulcanizates

The vulcanizate networks were characterized to ascertain: (a) the density of chemical crosslink, (b) the proportions of mono-, di-, and poly-sulphidic crosslinks, (c) the crosslinking efficiencies, namely, E and E' (atoms of sulphur combined in the network per chemical crosslink before and after treatment with triphenylphosphine, Ph_3P), (d) the content of zinc sulphide present, and (e) the extent of main-chain scission during vulcanization. The methods for these determinations were described in Part 2⁸.

RESULTS

Chemical crosslink density

Figures 1 and 2 show how vulcanization temperature (140–200°C) and time affect the chemical crosslink densities of vulcanizates of mix A and mix B (Table 1) respectively. They reveal clearly that, for both mixes, the maximum degree of crosslinking decreases as the cure temperature is raised from 140°C. This conclusion is similar to that found for the conventional cure system

Table 1 Mix formulations and molecular weights (\bar{M}_n)

	Parts by wt	
	A	B
Natural rubber (SMR 5)	100	100
Zinc oxide	5	5
Stearic acid	1	1
Antioxidant ^a	2	2
CBS ^b	3.5	6.0
Sulphur	1.5	0.4
Wallace Rapid plasticity	20	20.5
$[\eta]$ toluene of rubber hydrocarbon component of mix at 25°C (dl/g)	2.97	3.29
$\bar{M}_n \times 10^{-5}$ of rubber hydrocarbon component of mix	2.16	2.30

a Polymerized 1,2,-dihydro-2,2,4-trimethylquinoline (Flectol H)
 b *N*-cyclohexyl-2-benzothiazylsulphenamide (Santocure)

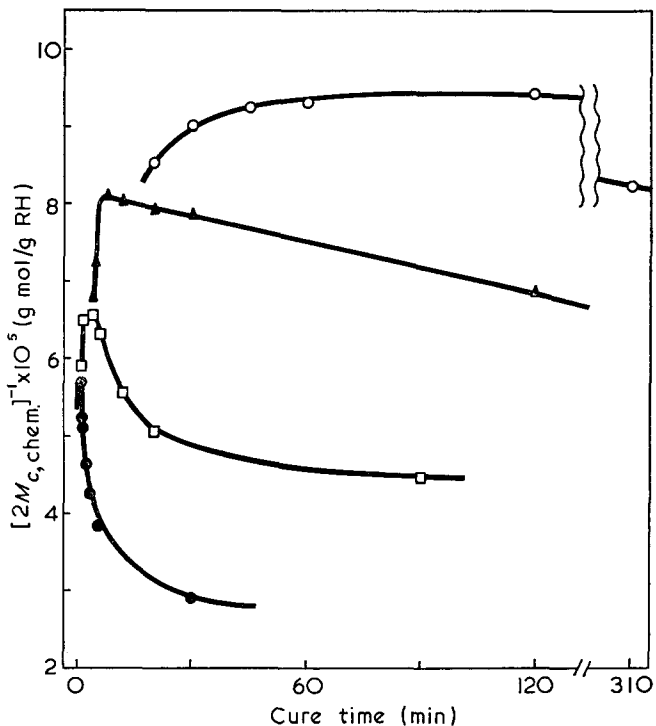


Figure 1 Influence of vulcanization temperature and time on the chemical crosslink density of mix A. ○, 140°C; ▲, 160°C; □, 180°C; ●, 200°C

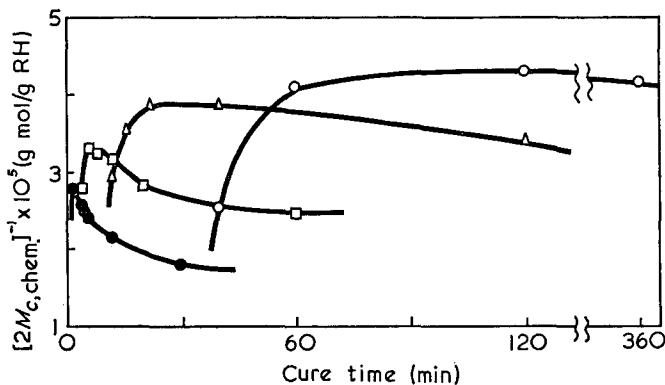


Figure 2 Influence of vulcanization temperature and time on the chemical crosslink density of mix B. ○, 140°C; △, 160°C; □, 180°C; ●, 200°C

(0.5 phr CBS:2.5 phr sulphur)⁸. There are some differences, however, between mix A and mix B. First, as cure temperature increases, the drop in the maximum degree of crosslinking and the rate of subsequent reduction in crosslink density are greater in the case of mix A. Secondly, at any cure temperature in the range of 140–200°C, the degree of crosslinking of mix A is higher than that of mix B. The high crosslink density of mix A can be accounted for by the presence of a high content of CBS accelerator with a moderate amount of sulphur (3.5 phr CBS:1.5 phr sulphur). This is consistent with the observations of Morita and Young¹⁰.

Distribution of crosslink types with cure time

Mix A. The density of each type of crosslink (mono-sulphidic, S_1 ; disulphidic, S_2 ; and polysulphidic, S_x) is plotted against cure time in Figures 3 and 4 for mix A vulcanized at 140°C and 200°C respectively. At 140°C the polysulphidic crosslinks disappear in the early stages of vulcanization, the concentration of disulphidic

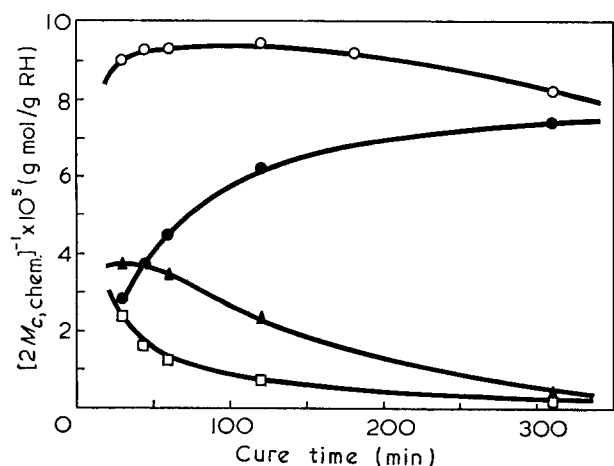


Figure 3 Distribution of crosslink types as a function of vulcanization time at 140°C for mix A. ○, Total crosslinks; ●, monosulphidic crosslinks; ▲, disulphidic crosslinks; □, polysulphidic crosslinks

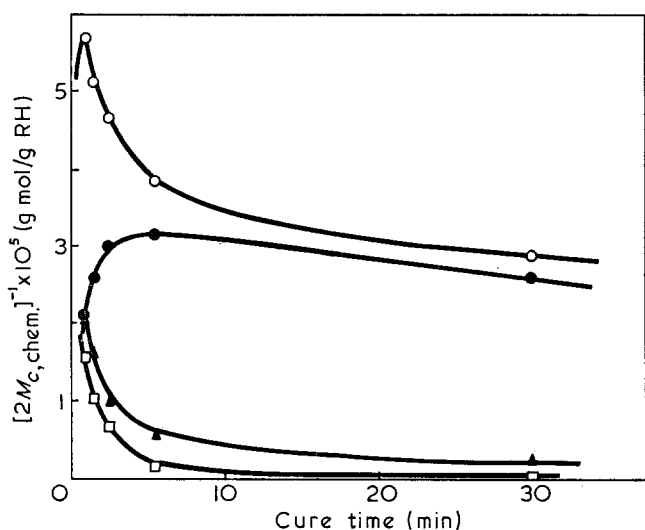


Figure 4 Distribution of crosslink types as a function of cure time at 200°C for mix A. ○, Total crosslinks; ●, monosulphidic crosslinks; ▲, disulphidic crosslinks; □, polysulphidic crosslinks

crosslinks is a maximum at the optimum crosslink density (~ 45 min, Figure 3), and the concentration of monosulphidic crosslinks builds up rapidly with cure time and continues to increase. At a cure temperature of 200°C, the concentration of polysulphidic crosslinks falls much faster than at 140°C. This result is in accord with the thermal instability of polysulphidic crosslinks. The concentration of disulphidic crosslinks at the optimum crosslink density (2.05×10^5 mol/g RH for 1 min at 200°C, Figure 4) is lower than that obtained at 140°C (3.80×10^5 mol/g RH for 45 min at 140°C, Figure 3). The concentration of monosulphidic crosslinks increases very rapidly with cure time, reaches a maximum value of 3.15×10^5 mol/g RH at 6 min, and then declines very slowly on prolonged vulcanization. Compared with the 7.45×10^5 mol/g RH recorded at 310 min at 140°C, the maximum level of monosulphidic crosslinks has been considerably reduced by raising the cure temperature from 140°C to 200°C.

Mix B. The densities of each crosslink type for mix B at 140°C and at 180°C are shown in Figures 5 and 6 respectively. As in the case of mix A, the majority of the crosslinks present in the network are monosulphidic. The rate of desulphuration of polysulphidic crosslinks

into monosulphidic crosslinks is higher than that occurring in mix A. For example, at a cure time of 60 min at 140°C, the concentration of monosulphidic crosslinks in mix B is 74% of the total, compared with 48% in the case of mix A. The results at 140°C (Figure 5) agree reasonably well with those reported by Campbell¹¹ and Moore¹² for a similar cure system. At a cure temperature of 180°C, the number of monosulphidic crosslinks builds up very rapidly to a value of 2.85×10^5 mol/g RH in 20 min (Figure 6), but this value is considerably lower than that observed at 140°C (3.90×10^5 mol/g RH for 360 min, Figure 5).

Therefore, the reduction in the concentration of monosulphidic crosslinks accounts for the major portion of the fall in the total crosslink density with increasing cure temperature for both mixes A and B. The decrease in the concentration of monosulphidic crosslinks at long cure times at 200°C and at 180°C, which is shown in both Figures 4 and 6, is real and not due to experimental error. It is not unexpected in view of the severity of the curing conditions, namely 30 min at 200°C or 60 min at 180°C. In the case of mix B, the conclusion is supported by measurements of relaxed stress at

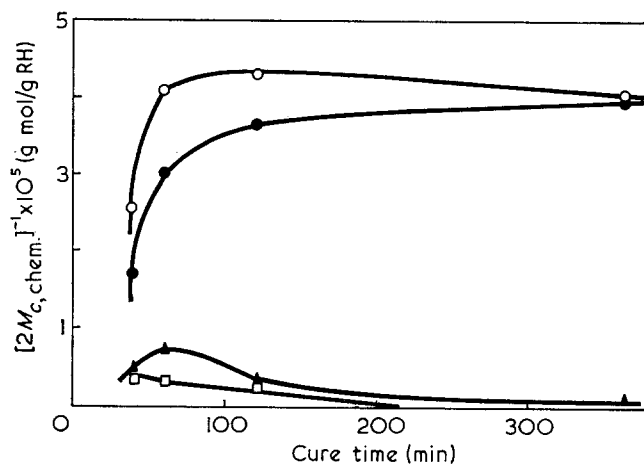


Figure 5 Distribution of crosslink types as a function of cure time at 140°C for mix B. ○, Total crosslinks; ●, monosulphidic crosslinks; ▲, disulphidic crosslinks; □, polysulphidic crosslinks

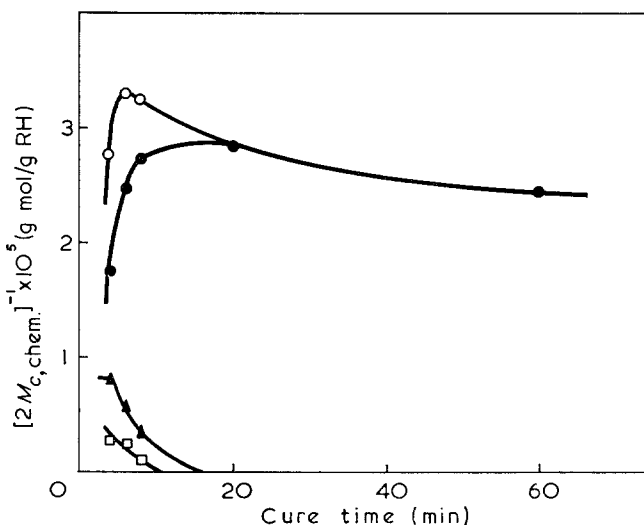


Figure 6 Distribution of crosslink types as a function of cure time at 180°C for mix B. ○, Total crosslinks; ●, monosulphidic crosslinks; ▲, disulphidic crosslinks; □, polysulphidic crosslinks

Table 2 Chemical characterization of vulcanizates derived from mixes A and B

Cure time (min)	$[2M_{c,chem.}]^{-1} \times 10^5$ (g mol/gRH)	Network combined sulphur $\times 10^4$ (gatom/gRH)		Sulphur efficiencies (atoms/chemical crosslink)		Sulphide sulphur, $[S^{2-}] \times 10^4$ (g ion/gRH)	F (sulphide ions/chemical crosslink)
		$[S_c]$, before Ph ₃ P treatment	$[S_c]$, after Ph ₃ P treatment	E, before Ph ₃ P treatment	E', after Ph ₃ P treatment		
Mix A							
At 140°C:							
30	9.03	3.57	2.33	4.0	2.6	1.06	1.2
60	9.30	3.39	2.51	3.7	2.7	1.38	1.5
120	9.42	3.35	2.61	3.6	2.8	1.71	1.8
180	9.25	3.28	2.48	3.5	2.7	1.93	2.1
310	8.25	3.20	2.55	3.9	3.1	2.22	2.7
At 160°C:							
4	6.80	3.31	1.57	4.9	2.3	0.73	1.1
6	8.10	3.28	2.44	4.1	3.0	0.98	1.2
12	8.04	3.20	2.48	4.0	3.1	1.35	1.7
30	7.85	3.02	2.44	3.9	3.1	1.78	2.3
120	6.85	2.95	2.44	4.3	3.6	2.37	3.5
At 180°C:							
1	5.90	3.90	1.64	6.6	2.8	0.57	1.0
3	6.55	3.79	2.73	5.8	4.2	1.06	1.6
6	6.10	3.31	2.58	5.4	4.2	1.67	2.7
12	5.55	3.13	2.69	5.6	4.8	2.00	3.6
90	4.47	2.66	2.66	6.0	5.9	2.51	5.6
At 200°C:							
0.5	5.80	4.00	2.37	6.9	4.1	0.80	1.4
1	5.70	3.79	2.69	6.7	4.7	1.13	2.0
2	5.15	3.57	2.88	6.9	5.6	1.46	2.8
5.5	3.85	3.31	3.09	8.6	8.0	1.97	5.1
30	2.90	3.09	2.88	10.7	9.9	2.29	7.9
Mix B							
At 140°C:							
40	2.57	1.73	1.22	6.7	4.7	0.07	0.3
60	4.10	1.58	1.25	3.9	3.1	0.02	0.5
120	4.30	1.40	1.25	3.3	2.9	0.33	0.8
360	4.05	1.22	1.22	3.0	3.0	0.52	1.3
At 160°C:							
12	2.45	1.77	1.07	7.2	4.4	0.11	0.5
16	3.55	1.47	1.36	4.1	3.8	0.18	0.5
22	3.85	1.44	1.36	3.7	3.5	0.26	0.7
120	3.40	1.22	1.18	3.6	3.5	0.63	1.9
At 180°C:							
4	2.77	1.77	1.36	6.4	4.9	0.11	0.4
6	3.30	1.77	1.40	5.4	4.2	0.26	0.8
8	3.25	1.73	1.40	5.3	4.3	0.37	1.1
20	2.82	1.62	1.36	5.7	4.8	0.59	2.1
60	2.45	1.29	1.29	5.3	5.3	0.74	3.0
At 200°C:							
2	2.80	1.70	1.44	6.1	5.2	0.33	1.2
4	2.60	1.58	1.55	6.1	6.0	0.48	1.8
6	2.40	1.55	1.51	6.5	6.3	0.63	2.6
12	2.17	1.51	1.47	7.0	6.8	0.70	3.2
30	1.80	1.40	1.40	7.8	7.8	0.77	4.3

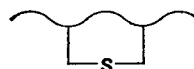
100% elongation which show a marked decrease at these long cure times at 200°C, and at equivalent cure times at 140°C¹³.

Crosslinking efficiencies of sulphur

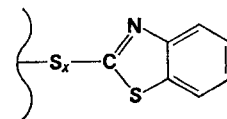
Table 2 summarizes the E and E' values of the networks of mix A and mix B vulcanized for various times at 140–200°C. The following conclusions can be drawn from these results.

First, the E and E' values for both cure systems (mixes A and B, Table 2) are relatively low, compared with those reported for the conventional CBS-accelerated

system⁸. This reflects the efficient utilization of sulphur in crosslinking and the relatively few modifications of the rubber chain by cyclic sulphides (I) and pendent sulphidic groups terminated with accelerator residues (II):



(I)



where $x \geq 1$

(II)

Secondly, raising the cure temperature from 140°C to 200°C increases the values of E and E' (Table 2, mixes A and B). The increase is, however, small in contrast with the considerable increase in E and E' values in the case of the conventional system^{8, 14}. This suggests that the elevated cure temperature results in a relatively small increase of sulphidic chain modification.

Thirdly, some appreciation of the amount of sulphur in the network as cyclic sulphides (I) and pendent groups (II) can be deduced from an examination of the sulphur analysis values (Table 2). By assuming that (a) the sulphur present in the chemical crosslinks, cyclic sulphides, and zinc sulphide is derived only from the available elemental sulphur and not from the sulphur in the CBS accelerator, and (b) the concentration of free sulphur and the amount of elemental sulphur combined in the polysulphidic sulphurating complexes^{15, 16} present in the vulcanizates are negligible, a calculated value, E^* , can be obtained:

$$E^* = \frac{[\text{elemental S}] - [\text{S}^{2-}]}{[2M_{e, \text{chem.}}]^{-1}}$$

where [elemental S] is the concentration of the elemental sulphur used in the mix formulation, and is expressed as g atoms of sulphur per g RH. Since assumption (b) can only be true when the degree of crosslinking has reached its maximum level¹⁵, the E^* values were obtained for cure times at optimum and above. The correctness of this assumption is proved by the values of free sulphur (Table 3) determined on the vulcanizates by the copper spiral method (BS 903: Part B7). The difference between the found and calculated efficiency values (i.e. $E - E^*$) gives the amount of network-combined sulphur present in the pendent groups (II). It is apparent from the ($E - E^*$) values (Table 3) that, in the case of mix B, the proportion of pendent sulphidic

Table 3 Atoms of sulphur per chemical crosslink present as pendent and cyclic sulphidic groups in vulcanizates of mixes A and B

Cure time (min)	'Pendent' sulphur ($E - E^*$)	'Cyclic' sulphur [$(E' - 1) - (E - E^*)$]	Free sulphur (% w/w)
Mix A			
At 140°C:			
60	—	1.7	< 0.005
120	0.3	1.5	< 0.005
180	0.4	1.4	< 0.005
310	0.7	1.4	< 0.005
At 200°C:			
1	0.2	3.6	—
2	0.3	4.3	0.04
5.5	1.1	5.9	0.03
30	1.9	7.0	< 0.005
Mix B			
At 140°C:			
40	1.9	1.8	< 0.005
60	1.3	0.8	< 0.005
120	1.1	0.8	< 0.005
360	1.1	0.9	< 0.005
At 200°C:			
2	2.7	1.5	0.01
6	3.7	1.6	< 0.005
12	4.3	1.5	< 0.005
30	4.9	1.9	< 0.005

Experimental errors were well within $\pm 6\%$ of the reported values for ($E - E^*$); $\pm 10\%$ of the reported values for [$(E' - 1) - (E - E^*)$] and $\pm 0.003\%$ w/w for free sulphur

groups increases as the cure temperature is raised from 140°C to 200°C. For mix A, the values of ($E - E^*$) are relatively small, suggesting a smaller proportion of pendent sulphidic groups. Alternatively, this result means that, in mix A, the intramolecular sulphidic groups are predominantly cyclic sulphides.

Since ($E' - 1$) is a quantitative measure of the amount of sulphur combined in the network as cyclic sulphides and as pendent accelerator groups¹⁷, the quantity [$(E' - 1) - (E - E^*)$] gives a measure of sulphur combined in the network as cyclic sulphides. The calculated values of [$(E' - 1) - (E - E^*)$] in Table 3 show that, as the cure temperature is raised from 140°C to 200°C, the proportion of cyclic sulphides increases substantially for mix A while it increases only moderately for mix B.

The relative abundance of the pendent accelerator groups for mix B at 140°C is consistent with the radio-tracer findings of Campbell¹¹ and Park *et al.*¹⁸, in that the number of pendent groups relative to crosslink density increases as the ratio of accelerator to sulphur increases. Skinner and Watson⁴ reached a similar conclusion for a similar cure system (mix B) on the basis of sulphur analysis values. Furthermore, the numerical results given in Table 3 for mix B at 140°C agree with the observation of Campbell¹¹, also for a similar cure system, that cyclic sulphides and pendent groups make approximately equal contributions to the network features. Calculations show that, for mix B at a cure time of 60 min at 140°C, the amount of sulphur per g RH in pendent groups is 11.4% of the total sulphur in the CBS accelerator initially present in the mix. This agrees well with Campbell's finding that 11% of the accelerator was combined in the network as the pendent groups¹¹.

Zinc sulphide formation

The formation of zinc sulphide during vulcanization at 140–200°C for various times is recorded in Table 2 as values of $[\text{S}^{2-}]$, g ions of sulphide per g RH and as F values (ratios of $[\text{S}^{2-}]/[2M_{e, \text{chem.}}]^{-1}$). At 140°C, the F values for both mixes A and B (Table 2) are low, reflecting the efficiency of the crosslinking¹⁹. With increasing cure temperatures, F values increase, particularly in the case of mix A. This could be accounted for by the greater extent of thermal decomposition of the chemical crosslinks (Figure 3). The sulphur released from the destroyed crosslinks may further react to form zinc sulphide and cyclic sulphides simultaneously.

Main-chain scission during vulcanization

Table 4 gives the sol-gel data of the vulcanizates prepared at 140–200°C for various times. These sol-gel data were analysed using the Charlesby and Pinner equation²⁰:

$$S + S^{1/2} = pq^{-1} + (q\bar{y}_n)^{-1}$$

where S is the sol fraction, p and q are the fractions of sites at which random scission and crosslinking have occurred respectively, and \bar{y}_n is the number-average chain length of an uncured polymer having a random chain length distribution^{8, 21}.

Figures 7 and 8 show the plots of ($S + S^{1/2}$) versus q^{-1} for mix A and mix B using the sol-gel data given in Table 4. Both plots show a linear fit to all the data obtained from four different cure temperatures. Therefore, there is no significant dependence of chain scission

Table 4 Sol-gel data for vulcanizates of mixes A and B

Cure time (min)	Sol		Gel	
	Wt%	(S+S ^{1/2})	[2M _{c, chem.}] ⁻¹ × 10 ⁵ (g mol/g RH)	q ⁻¹ × 10 ⁻²
Mix A				
At 140°C:				
30	0.050	0.0229	9.03	0.81
60	0.041	0.0207	9.30	0.79
120	0.042	0.0208	9.42	0.78
310	0.061	0.0252	8.25	0.89
At 160°C:				
5	0.070	0.0272	7.50	0.98
8	0.063	0.0257	8.10	0.91
120	0.094	0.0315	6.85	1.07
At 180°C:				
3	0.102	0.0329	6.55	1.12
8	0.113	0.0348	6.10	1.20
20	0.146	0.0397	5.05	1.45
90	0.225	0.0497	4.47	1.64
At 200°C:				
0.5	0.114	0.0349	5.80	1.27
1.5	0.147	0.0398	5.26	1.40
2.5	0.167	0.0425	4.67	1.57
5.5	0.285	0.0563	3.85	1.91
Mix B				
At 140°C:				
40	0.344	0.0621	2.57	2.86
60	0.165	0.0423	4.10	1.79
120	0.140	0.0404	4.30	1.71
360	0.183	0.0446	4.05	1.81
At 160°C:				
16	0.253	0.0528	3.55	2.07
22	0.208	0.0477	3.85	1.91
120	0.290	0.0568	3.40	2.16
At 180°C:				
6	0.305	0.0583	3.30	2.23
8	0.299	0.0577	3.25	2.26
12	0.307	0.0585	3.17	2.31
20	0.373	0.0648	2.82	2.60
60	0.522	0.0775	2.45	2.97
At 200°C:				
2	0.386	0.0660	2.80	2.62
4	0.474	0.0736	2.60	2.82
5	0.482	0.0743	2.50	2.94
6	0.551	0.0798	2.40	3.06
12	0.676	0.0890	2.17	3.38
30	1.024	0.114	1.80	4.08

on cure temperature in the range 140–200°C. The linear equations derived from the application of the least square principle are:

$$S + S^{1/2} = -0.0018 + 2.99 \times 10^{-4} q^{-1} \text{ for mix A}$$

$$S + S^{1/2} = -0.0071 + 2.82 \times 10^{-4} q^{-1} \text{ for mix B}$$

An additional statistical analysis of the plotted data shows that, at the confidence limit of 98%, p/q is less than 0.002 and 0.0015 for mix A and mix B respectively. These statistical results suggest that less than one random chain scission has occurred for every five hundred events of crosslinking. As a check on the accuracy of these plots (Figures 7 and 8), the \bar{M}_n values of 2.28 and 2.41×10^5 , calculated from the slopes of the linear equations, are in close agreement with the respective \bar{M}_n values of 2.16 and 2.30×10^5 (Table 1), determined using the solution viscosity method.

Bi-thermal vulcanization

Figure 9 records a typical heat history of the centre of a moulding during the bi-thermal vulcanization of

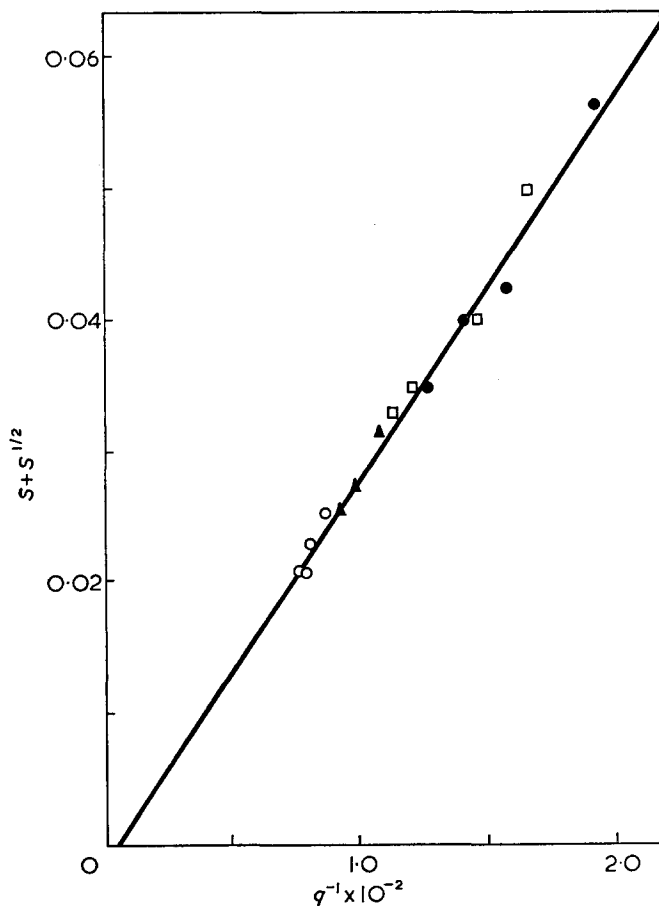


Figure 7 Plot of $S + S^{1/2}$ versus q^{-1} for natural rubber vulcanized with a 3.5:1.5phr CBS/sulphur system (mix A) at 140–200°C. ○, 140°; ▲, 160°; □, 180°; ●, 200°C

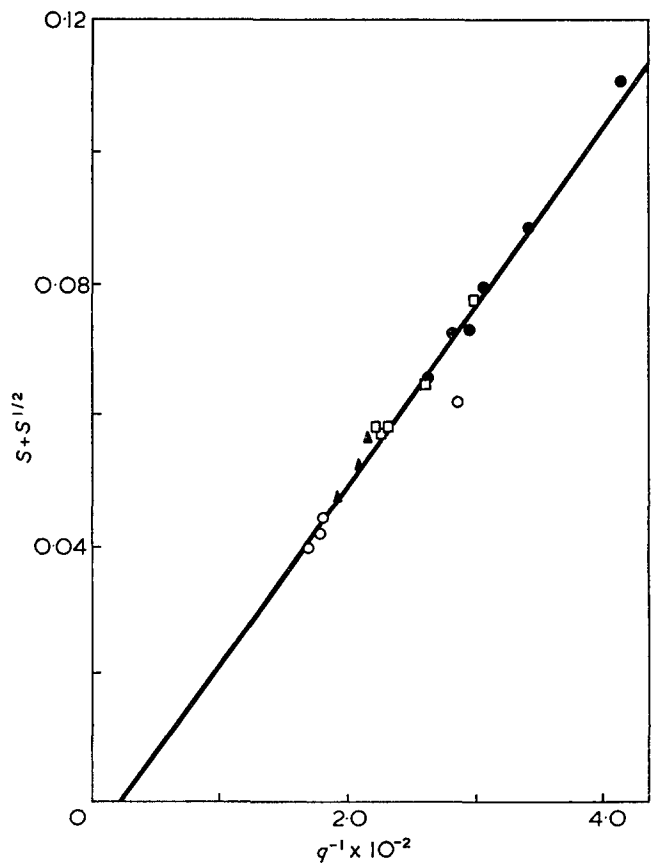


Figure 8 Plot of $S + S^{1/2}$ versus q^{-1} for natural rubber vulcanized with a 6.0:0.4phr CBS/sulphur system (mix B) at 140–200°C. ○, 140°; ▲, 160°; □, 180°; ●, 200°C

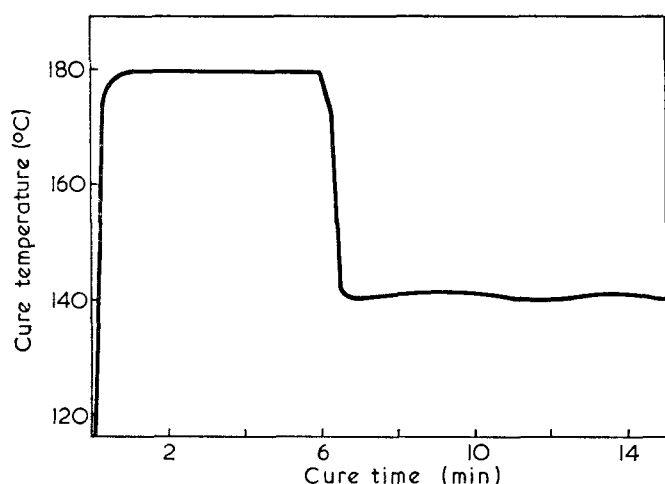


Figure 9 Time-temperature data at the centre of the moulding (mix B) during bi-thermal (180°C/140°C) vulcanization

Table 5 Crosslink density and distribution of crosslink types in mix B vulcanized isothermally and bithermally

Cure time (min)	$[2M_c, \text{chem.}]^{-1} \times 10^5$ (g mol/g RH)			
	Total	S ₁	S ₂	S _x
At 180°C, 6 min followed at 140°C:				
20	3.25	—	—	—
50	3.20	3.09	0.03	0.08
100	3.16	3.14	0.01	0.01
180	3.14	3.14	0	0
At 140°C:				
40	2.57	1.70	0.51	0.36
60	4.10	3.02	0.74	0.34
120	4.30	3.65	0.35	0.30
360	4.05	3.95	0.10	0
At 180°C:				
4	2.77	1.72	0.78	0.27
6	3.30	2.47	0.57	0.26
8	3.25	2.74	0.34	0.10
20	2.85	2.85	0	0

mix B. It shows clearly that the curing temperature was effectively stepped down from 180° to 140°C in less than 40 sec after the 6 min cure at 180°C.

Table 5 shows how the total crosslink density and proportion of each crosslink type of mix B vulcanizates vary with cure time during the bi-thermal curing. Some results of the isothermal cures at 140°C and at 180°C are included in Table 5 to provide numerical comparisons. They prove that when the cure temperature is stepped down from 180°C to 140°C, the crosslink densities, particularly the density of monosulphidic crosslinks recorded during subsequent vulcanization at 140°C, are intermediate between those for vulcanizates cured isothermally at 140°C and at 180°C. There is no evidence that the chemical crosslink density increases even at long cure times after the step-down in temperature is effected. There is also no evidence that more polysulphidic and disulphidic crosslinks are formed; neither is there any indication that the crosslink density of bi-thermal (180°C/140°C) vulcanizates would ever reach the level achieved by the isothermal vulcanizates at 140°C. Therefore, the loss of chemical crosslinks in the CBS-accelerated vulcanizates is an irreversible effect. This conclusion is to be compared with that

of T. Moore⁹ who found that the influence of cure temperature on the crosslink formation in the 2-mercaptobenzothiazole accelerated vulcanizates was reversible at cure times in the region of the peak degree of crosslinking.

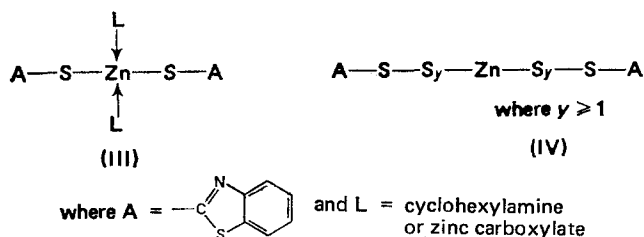
DISCUSSION

Mechanistic interpretations

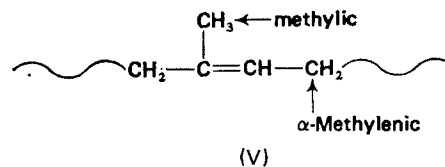
The network structure of an accelerated sulphur vulcanizate has been shown to depend significantly on the maturing reactions of the polysulphidic crosslinks formed in the early part of vulcanization. The relative rates of these maturing reactions, namely, desulphuration, decomposition and interchange of sulphur bonds, are governed by: (a) the chemical structure of crosslink termini, (b) the structure, concentration and reactivity of the sulphurating complexes formed from the accelerators and activators, and (c) the vulcanization temperature and time^{12, 22}.

Influence of cure temperature on crosslink maturation.

In the present vulcanization systems, the high ratios of accelerator : sulphur in mix A (2:3:1) and mix B (15:1) give a high concentration of chelated zinc mercaptide complexes (III)^{23, 24} which are believed to react with sulphur to form the active sulphurating complexes of zinc perthiomercaptides (IV)¹⁶:



The high concentration of sulphurating complexes may lead to the formation of polysulphidic crosslinks predominantly at the methyl groups (V) in the natural rubber hydrocarbon.



Such polysulphidic crosslinks desulphurate very rapidly to form thermally stable monosulphidic crosslinks, consequently suppressing the thermal decomposition of crosslinks. This accounts for the majority of the crosslinks being monosulphidic (Figures 3-6), and for the small extent of the chain modification (see E and E' values in Table 2). The higher rate of desulphuration observed for mix B may be due to the greater amount of active sulphurating complexes which catalyse the desulphuration of polysulphidic crosslinks.

One less expected feature of the present network results is that elevated cure temperature brings about a substantial drop in the monosulphidic crosslink density, although the desulphuration of polysulphidic crosslinks into thermally stable monosulphidic crosslinks is known to be very rapid for efficient vulcanization systems^{16, 22}. The dependence of crosslink density on cure temperature suggests that mechanisms other than crosslink maturation may be important. Fewer polysulphidic crosslinks

may be formed at higher cure temperatures because the concentration of the crosslinking intermediates available for crosslink formation is lower; at the same time, these intermediates may have a reduced reactivity.

Influence of cure temperature on sulphurating complexes. It is not clear from the present results how the cure temperature influences the structure and reactivity of sulphurating complexes (IV) and the zinc mercaptide complexes (III). It is possible that, at elevated cure temperatures, some amine complexes may be partly dissociated into free amine, and sparingly soluble zinc mercaptide. Alternatively, high cure temperatures may favour the dissociation products of the CBS accelerator to react directly with the rubber chain forming pendent accelerator residues (II, $x=1$) which are unreactive. In consequence, the intermediate complexes (III and IV) may have a reduced reactivity, leading to less effective crosslink formation. Another possible consequence is that some elemental sulphur may react directly with the rubber chain to form cyclic sulphides.

Influence of cure temperature on pendent accelerator groups. The pendent accelerator groups of polysulphidic character are believed to be the precursor of polysulphidic crosslinks^{11, 25, 26}. In the case of the high CBS : low sulphur cure system (mix B), it may be that the average number of sulphur atoms in the polysulphidic pendent groups is lower in mix B than in mix A. This would lead to the formation of polysulphidic crosslinks with a lower sulphur rank. Since polysulphidic species of fewer sulphur atoms are expected to be more thermally stable, the polysulphidic pendent groups and polysulphidic crosslinks formed in the case of mix B would be less susceptible to the thermal destruction at high cure temperature. This mechanism would account for the smaller drop in the peak level of crosslink density, the lower rate of crosslink decomposition (*Figure 2*), and the smaller increase in E , E' and F values (*Table 2*, mix B) as the cure temperature is raised from 140° to 200°C. One interesting result obtained for mix B is that, as cure temperature increases, the number of pendent sulphidic groups increases. This suggests that, at the higher cure temperatures, more polysulphidic pendent groups (II, $x > 1$) are desulphurated into thermally stable monosulphidic pendent groups (II, $x=1$) before they can be utilized in crosslinking; such undesirable reaction would account for the lower crosslink density. Calculations obtained from *Table 3* show evidently that the sulphur present in pendent groups increases from 4.7 g atoms per g RH at 120 min/140°C to 8.8 g atoms per g RH at 6 min/200°C while the chemical crosslink density decreases from 4.30 to 2.40 g mol/g RH.

The results of the bi-thermal vulcanization (*Table 5*) rationalize the above discussions in two respects. First, the irreversible relationship between the cure temperature and crosslink density is consistent with the mechanism that more sulphur is wasted in forming the intramolecular sulphidic groups irreversibly at high cure temperature. Secondly, once the polysulphidic crosslink is formed, the influence of cure temperature on the crosslink maturation becomes important in governing the vulcanizate structures. The results of the chain scission investigation (*Figures 7 and 8*) confirm that the loss of chemical crosslinks at high cure temperature cannot arise from a reduction in the rubber chain length. It is to be noted that the network features of a

conventional CBS-accelerated system have been interpreted by a similar mechanism⁸.

Network structures essential for good high temperature vulcanizates

The network structures, necessary for obtaining good technological properties from high temperature vulcanization, can be deduced from the vulcanizate structures established for mixes A and B.

(a) To reduce the crosslink destruction at elevated cure temperature, the polysulphidic crosslinks formed initially must be relatively short (i.e. with a lower sulphur rank) and capable of desulphurating very rapidly into thermally stable monosulphidic crosslinks. This requirement calls for a vulcanization system which favours sulphur crosslink formation at methyl group rather than at α -methylene group (V) in the natural rubber hydrocarbon¹². This has been achieved by the use of the *EV* formulations. Furthermore, the vulcanizates of the *EV* systems possess the superior resistance to thermal-oxidative ageing, and improved compression set^{5, 27}. In the case of the CBS-accelerated *EV* system, the zinc mercaptides formed during the vulcanization have been found to render the rubber network very responsive to antioxidant protection⁵. The abrasion resistance, strength, resilience and fatigue life (under relaxing conditions) of these *EV* systems are, however, inferior to those of the conventional vulcanization system. Considering the serious reversion associated with the conventional vulcanization system⁷, and the increasing demand for retention of physical properties at high service temperature, it is more desirable to use the *EV* systems for high temperature curing.

(b) As shown by the crosslink densities of mix A at 200°C (*Figure 1*), a sufficient number of crosslinks must be present in the network formed at high cure temperatures, in order to provide a good level of physical properties⁷. For example, the crosslink density of 5.70×10^5 mol/g RH for 1 min at 200°C is as high as that of the conventional vulcanizates cured at 140°C for 45 min⁸. The *EV* formulations currently recommended for vulcanization at 140–160°C may not be suitable for high temperature curing, owing to an insufficient number of crosslinks being formed. This is exemplified by the results of mix B at 200°C (*Figure 2*). The crosslink density of 2.80×10^5 mol/g RH for 2 min at 200°C may be inadequate to provide enough strength and may accelerate the failure process during the service life of the vulcanizates²⁸. The use of the increased CBS and sulphur contents (mix A, *Table 1*) is therefore advantageous for high temperature vulcanization. O'Mahoney recently reported a similar conclusion from studying the effect of high cure temperature (193–215°C) on the physical properties of accelerated vulcanizates of *cis*-polyisoprene with different low sulphur-sulphenamide accelerator combinations²⁹.

(c) The thermal stability and reactivity of the crosslinking intermediates may play an important role during vulcanization. Accelerators which are capable of producing active and stable sulphurating complexes would be more suitable for high temperature curing. It is of particular interest that the crosslink densities of the diphenylguanidine and tetramethylthiuram disulphide accelerated vulcanizates of NR have recently been reported to remain unchanged with rising cure tem-

peratures³⁰. This contrasts with the present results of the CBS-accelerated vulcanizates.

ACKNOWLEDGEMENTS

The author is grateful to Dr C. M. Blow of the Institute of Polymer Technology for his guidance and advice. His thanks are due to Drs D. Barnard, D. S. Campbell, M. Porter and B. K. Tidd of the MRPRA for their assistance and valuable discussions. Acknowledgement is also made to the Malaysian Rubber Research and Development Board for awarding a scholarship.

REFERENCES

- 1 Wheelans, M. A. *Rubber World* 1967, **156**, 71
- 2 Hammersley, D. A. 'Injection Moulding of Elastomers', (Ed. W. S. Penn), Maclaren, London, 1969, p 46
- 3 Lloyd, D. G. *Rubber World* 1968, **158**, 51
- 4 Skinner, T. D. and Watson, A. A. *Rubber Age* 1967, **99** (11), 76; *Rubber Chem. Technol.* 1969, **42**, 404
- 5 Russell, R. M., Skinner, T. D. and Watson, A. A. *Rubber Age* 1967, **99** (12), 69; *Rubber Chem. Technol.* 1969, **42**, 418
- 6 Dibbo, A. and Lloyd, D. G. *Proc. Int. Rubber Conf., Brighton 1967* p 83
- 7 Blow, C. M. and Loo, C. T. *J. Inst. Rubber Ind.* 1973, **7**, 205
- 8 Loo, C. T. *Polymer* 1974, **15**, 357
- 9 Moore, T. *PhD Thesis* National College of Rubber Technol., London (1971)
- 10 Morita, E. and Young, E. J. *Rubber Chem. Technol.* 1963, **36**, 844
- 11 Campbell, D. S. *J. Appl. Polym. Sci.* 1970, **14**, 1409
- 12 Moore, C. G. *Proc. NRPRA Jubilee Conf. 1964* (Ed. L. Mullins), Maclaren, London, 1965, p 167
- 13 Porter, M. personal communication (1970)
- 14 Porter, M., Skinner, T. D. and Wheelans, M. A. *J. Appl. Polym. Sci.* 1967, **11**, 2271
- 15 Campbell, R. H. and Wise, R. W. *Rubber Chem. Technol.* 1964, **37**, 650
- 16 Porter, M. 'The Chemistry of Sulfides', (Ed. A. V. Tobolsky), Interscience, New York, 1968, p 165
- 17 Saville, B. and Watson, A. A. *Rubber Chem. Technol.* 1967, **40**, 100
- 18 Parks, C. R., Parker, D. K., Chapman, D. A. and Cox, W. L. *Rubber Chem. Technol.* 1970, **43**, 572
- 19 Barton, B. C. *J. Polym. Sci.* 1955, **18**, 559
- 20 Charlesby, A. and Pinner, S. H. *Proc. R. Soc. (A)* 1959, **249**, 367
- 21 Bristow, G. M. *J. Appl. Polym. Sci.* 1965, **9**, 3255
- 22 Bateman, L., Moore, C. G., Porter, M. and Saville, B. 'The Chemistry and Physics of Rubber-like Substances', (Ed. L. Bateman), Maclaren, London, 1963, p 449
- 23 Milligan, B. *J. Chem. Soc. (A)* 1966, p 34
- 24 Milligan, B. *Rubber Chem. Technol.* 1966, **39**, 1115
- 25 Coran, A. Y. *Rubber Chem. Technol.* 1965, **38**, 1
- 26 Parks, C. R., Parker, D. K. and Chapman, D. A. *Rubber Chem. Technol.* 1972, **45**, 467
- 27 Blackman, E. J. and McCall, E. B. *Rubber Chem. Technol.* 1970, **43**, 651
- 28 Doyle, G. M., Humphreys, R. E. and Russell, R. M. *J. Appl. Polym. Sci.* 1971, **15**, 1855
- 29 O'Mahoney, Jr., J. F. *Rubber Chem. Technol.* 1972, **45**, 1403
- 30 Polyak, M. A., Cernyak, N. B., Zakharov, N. D. and Kostyukina, G. I. *Int. Symp. Isoprene Rubber, Moscow* 1972

Equilibrium ring concentrations and the statistical conformations of polymer chains: Part 13. Cyclics in two aliphatic polyesters

F. R. Jones, L. E. Scales and J. A. Semlyen

Department of Chemistry, University of York, Heslington, York YO1 5DD, UK
(Received 22 March 1974)

Methods have been developed for measuring the molar cyclization equilibrium constants K_x for cyclics $[O(CH_2)_{10}OCO(CH_2)_4CO]_x$ with $x=1-5$ in an undiluted ring-chain equilibrate of poly(decamethylene adipate) (PDA) at 423K, and for cyclics $[O(CH_2)_3OCO(CH_2)_2CO]_x$ with $x=1-7$ in an undiluted equilibrate of poly(trimethylene succinate) (PTS) at the same temperature. The experimental K_x values are compared with theoretical values calculated by the Jacobson and Stockmayer theory. The latter were obtained by assuming that chains in the undiluted melts adopt random-coil conformations obeying Gaussian statistics and have average dimensions predicted by the rotational isomeric state model of Flory and Williams. The agreement between experiment and theory is excellent for the cyclic oligomers containing 54, 72 and 90 skeletal bonds in the PDA equilibrate. By contrast, the experimental K_x values for cyclic oligomers of comparable size in the PTS equilibrate are approximately half the calculated values. These differences suggest that the statistical conformations of oligomeric aliphatic polyester chains depend on the relative numbers of methylene groups and ester linkages that they contain.

INTRODUCTION

Experimental and theoretical studies of the relationship between the concentrations of cyclics in polymeric ring-chain equilibrates and the statistical conformations of the corresponding open chain molecules have already been carried out for a number of systems including some polysiloxanes¹⁻⁶, a paraffin-siloxane⁷, a polyether⁸, a polyamide^{9,10} and an aromatic polyester¹¹. The primary aim of such studies has been to establish a new experimental method for probing the structures of polymeric melts, polymer solutions and solid polymers. They have also been directed at the investigation of the conformational statistics of real chain molecules containing only a few to as many as several hundred skeletal bonds.

This paper describes the first investigations of the concentrations of individual cyclics in ring-chain equilibrates of two aliphatic polyesters. The polyesters chosen for this study were poly(decamethylene adipate) (PDA) and poly(trimethylene succinate) (PTS), with the repeat units $-O(CH_2)_{10}OCO(CH_2)_4CO-$ and $-O(CH_2)_3OCO(CH_2)_2CO-$. They were selected because they contain pairs of cyclics which have the same number of skeletal bonds (viz. 18, 36, 54) but different numbers of ester groups. Hence a comparison of the experimental molar cyclization equilibrium constants for such cyclics with those predicted theoretically allows for an assessment of the relative effects of methylene groups and ester linkages on the conformational statistics of oligomeric polyester chains.

Up to the present time, the only reported experimental

study of the ring-chain equilibration reaction of a linear aliphatic polyester was that carried out in 1950 by Jacobson *et al.*¹² to test their new cyclization theory¹³. These authors used viscometry to estimate the total concentrations of cyclics in ring-chain equilibrates of PDA in chloroform solution, but made no attempt to measure the concentrations of individual cyclic oligomers. Experimental studies that are more closely allied to those described here include the classical investigations of Carothers^{14,15} and the extensive work of Billmeyer and his coworkers¹⁶⁻¹⁹.

EXPERIMENTAL

Ring-chain equilibration reaction of PDA

Dimethyl adipate was prepared from adipic acid and methanol in toluene solution using concentrated sulphuric acid as catalyst. A water/toluene/methanol azeotrope was removed from the reactants by distillation and the product that remained was fractionally distilled twice under vacuum.

Decamethylene glycol was obtained commercially and it was fractionally distilled under vacuum before use.

Equimolar portions of dimethyl adipate and decamethylene glycol were added to a four-necked glass reaction kettle. This was equipped with a thermometer, a stirrer, a distillation head and either a nitrogen or a vacuum connection. The contents of the kettle were purged with nitrogen, homogenized by stirring and heated to 373K. When 0.5% w/w of freshly distilled

tetraisopropyl titanate (Pfaltz and Bauer Inc.) was added to the reactants, transesterification began immediately. The reaction temperature was raised to 438K and maintained at that temperature for 4 h, within which time 85% w/w of the theoretical yield of methanol had distilled from the reactants. The temperature was then raised to 468K for 5 h to expel further methanol. The undiluted polymer containing the catalyst was maintained under vacuum at the equilibration temperature of 423K for 24 h. Nitrogen was then allowed into the vessel and a 25 ml sample was removed from the reaction mixture using a pipette. The polymeric melt was then maintained at 423K for a further 24 h and a second 25 ml sample was taken. After a further 24 h at 423K, the reaction mixture was cooled to room temperature and a third sample was removed for analysis.

The density of the PDA melt at 423K was measured separately. It was found to be 0.94 g/ml.

Ring-chain equilibration reaction of PTS

Dimethyl succinate was prepared from succinic acid and methanol in toluene solution using concentrated sulphuric acid as catalyst. The reactants were heated and the water/toluene/methanol azeotrope was removed by distillation. When the temperature of the vapour had reached 353K, the distillation was stopped and the distillate was dried with anhydrous magnesium sulphate. It was then filtered and returned to the reaction flask before being removed again by distillation at temperatures up to 353K. The dimethyl succinate remaining in the reaction flask was fractionally distilled under vacuum, a centre cut only being retained.

1,3-Propane diol was obtained commercially and purified by vacuum distillation before use.

The condensation polymerization reaction and ring-chain equilibration reaction of PTS were carried out in the manner described above for PDA. Particular care was taken to maintain the required concentration of the volatile reactant dimethyl succinate. 25 ml samples were removed for analysis after the polymeric product had been maintained at 423K for 24 h, and then for a further period of 24 h.

The density of the PTS melt at 423K was measured separately. It was found to be 1.10 g/ml.

Extraction of cyclics from the polymeric equilibrates

The following procedure was found to be satisfactory for the quantitative extraction of cyclics from the samples obtained from the ring-chain equilibration reactions. Each polyester sample was dissolved in about twice its weight of chloroform and the solution was poured into a 4:1 mixture of diethyl ether and low-boiling petroleum ether (b.p. 40–60K), which was maintained at 273K in an ice bath. The ratio of chloroform solution to ether mixture was adjusted to 1:6 v/v. Even relatively short chain molecules were found to precipitate, although the cyclics remained in solution. After filtering, the cyclic-free polymers were washed with the ether mixture and dried. The solvents were removed from the filtrates using a rotary evaporator. The solid cyclic extracts were dissolved separately in carbon tetrachloride, and this solvent was itself removed to yield samples suitable for analysis. Each polyester sample removed from the ring-chain equilibration reactions was subject to four such extractions, and each cyclic extract and polymeric residue was analysed separately.

Preparation of reference materials

The general pyrolytic method of Carothers^{14, 15} was used to prepare the cyclic monomer of PDA and a mixture containing mainly the cyclic monomer and dimer of PTS.

The following procedure was employed. Approximately 30 g of the polyester were mixed with 2.5% w/w magnesium chloride hexahydrate catalyst and placed in a molecular still at 543K under a pressure of 0.05 mmHg. A sublimate collected on the probe over a period of about 40 h. It was dissolved in chloroform and washed with water. The chloroform solution was then dried and the solvent was removed to give a residue which was dissolved in warm methanol. Concentration of this methanol solution gave samples of the low molecular weight cyclics.

Gel permeation chromatography (g.p.c.)

Cyclic extracts were analysed using a g.p.c. fitted with a Waters Model R4 differential refractometer detector. The instrument was fitted with four sample columns [each 1.22 m (4 ft) long and 6.35 mm (0.3 in) i.d.] packed with SX-1 Bio-beads (obtained from Biorad Laboratories, St Albans). Samples were analysed in chloroform solution at room temperature.

The molecular weights and molecular weight distributions of the cyclic-free polymers were measured using a Waters Associated g.p.c. This was fitted with four columns containing Styragel with nominal porosities in the range 10^2 \AA to $5 \times 10^6 \text{ \AA}$. Samples were analysed in solution in tetrahydrofuran at room temperature.

Spectroscopic methods

Proton nuclear magnetic resonance spectra were measured in deuteriochloroform or carbon tetrachloride using a Perkin-Elmer 60 MHz Model R10 spectrometer.

Infra-red spectra were obtained as thin films between sodium chloride plates using Unicam SP200 and SP200G instruments.

RESULTS AND DISCUSSION

Analysis of cyclics from PDA and PTS equilibrates

Both the specially prepared low molecular weight cyclic oligomers and the oligomeric extracts from the PDA and PTS samples were analysed by g.p.c. Their carbon and hydrogen contents were determined and their infra-red and nuclear magnetic resonance spectra were measured. These studies showed that the extracts from the polyester equilibrates consisted almost entirely of cyclic oligomers, although some of them contained small amounts of chain polymers*. A g.p.c. tracing of a mixture of cyclics $[\text{O}(\text{CH}_2)_3\text{OCO}(\text{CH}_2)_2\text{CO}]_x$ obtained from a PTS equilibrate is shown in *Figure 1*. Cyclics above the monomers were not completely resolved in chromatograms of cyclic extracts from PDA or PTS samples, and the areas under the curves were apportioned to their respective cyclic components by assuming that each cyclic produced a peak of Gaussian shape, and that the response of the differential

* G.p.c. tracings of the cyclic extracts from the PDA equilibrates showed the presence of small amounts of a side-product which eluted after the cyclic with 36 skeletal bonds. The identity of this compound was not established.

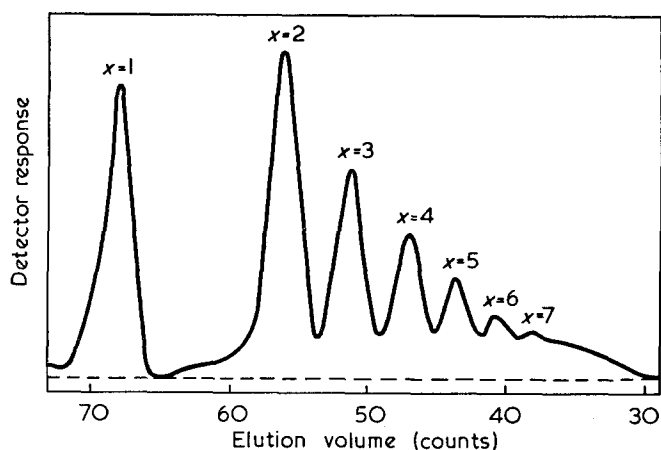


Figure 1 Gel permeation chromatogram of cyclics $[O(CH_2)_3O CO(CH_2)_2CO]_x$ with $x=1-7$ extracted from PTS equilibrated in the melt at 423K

refractometer detector was independent of the size of the cyclic oligomer. This latter assumption was tested using the specially prepared low molecular weight cyclics and different oligomeric extracts. It was found to apply well over the range of cyclic oligomers studied. As expected, pairs of cyclics in PDA and PTS extracts with the same number of skeletal bonds were found to have similar g.p.c. elution volumes.

Experimental molar cyclization equilibrium constants

Ring-chain equilibria were established in both the PDA and PTS melts within 24 h. Samples removed after a further 24 h were found to have similar molecular weights and molecular weight distributions, and to contain the same weight fractions of individual cyclic oligomers. These ring-chain equilibria may be represented as:



where M symbolizes a monomer unit and $-M_y-$ and $-M_{y-x}-$ represent linear species.

G.p.c. analysis showed that the cyclic-free polymers produced in the equilibration reactions had distributions of chain lengths close to their most probable distributions. Hence, the molar cyclization equilibrium constants K_x for cyclics in both polymers were calculated using the relation:

$$K_x = [M_x]/p^x \quad (2)$$

where p represents the extent of reaction of functional groups in the chain polymer. Values for p were determined by measuring the number average molecular weights \bar{M}_n of the cyclic-free polymers and applying Flory's relation²⁰:

$$\bar{M}_n = M_0/(1-p) \quad (3)$$

where M_0 represents the molecular weight of a monomeric unit.

Experimental K_x values for cyclics in PDA and PTS equilibrates at 423K are plotted as $\log K_x$ against $\log x$ in Figures 2 and 3. The degree of uncertainty associated with these values is believed to be less than $\pm 10\%$ for all but the largest cyclics.

Theoretical molar cyclization equilibrium constants

The Jacobson and Stockmayer¹³ cyclization theory relates the experimental molar cyclization equilibrium

constants for cyclics in ring-chain equilibrates to the statistical conformations of the corresponding open chain molecules. For present purposes, the experimental K_x values (plotted in Figures 2 and 3) will be compared with theoretical values calculated by assuming that

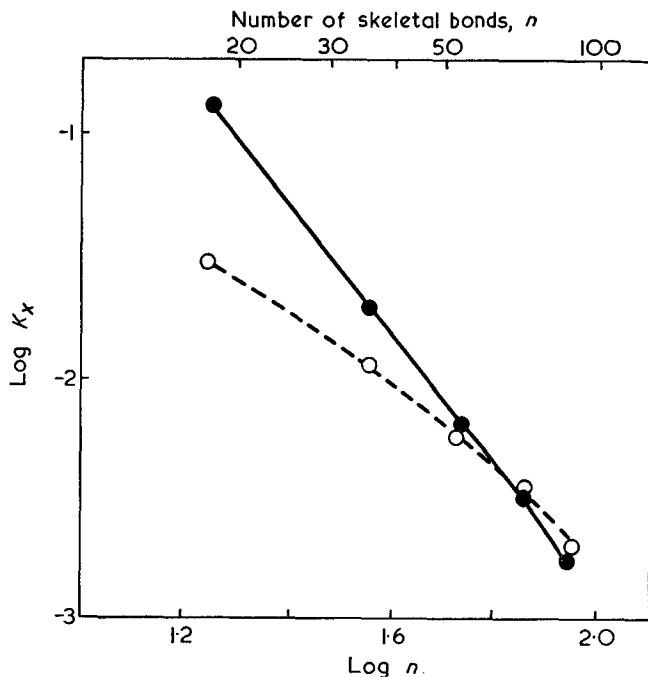


Figure 2 Experimental molar cyclization equilibrium constants K_x (in mol/l) for cyclics $[O(CH_2)_6OCO(CH_2)_4CO]_x$ in the PDA melt at 423K (O) are plotted as $\log K_x$ against $\log n$, where n represents the number of skeletal bonds in the ring. They are compared with theoretical values calculated by equation (4) (●)

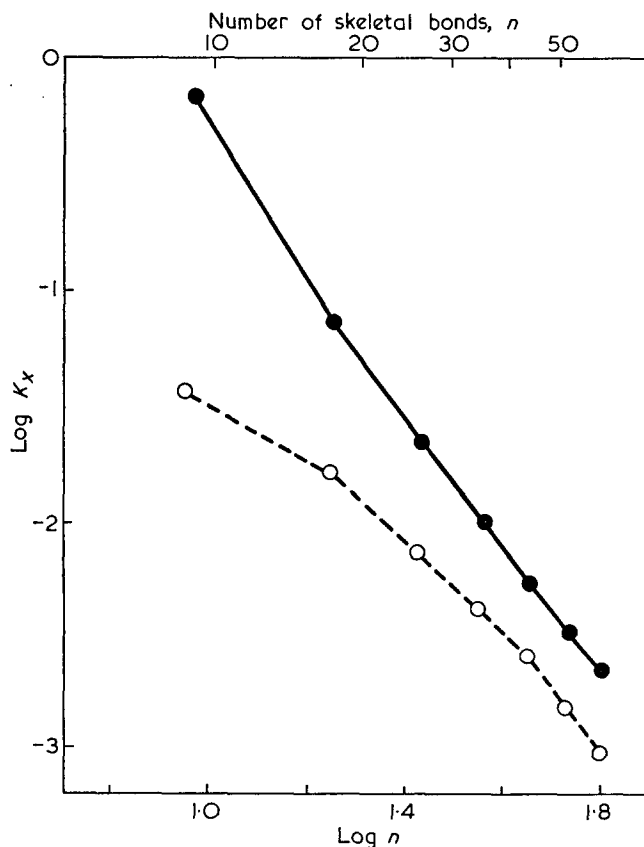


Figure 3 Experimental molar cyclization equilibrium constants K_x (in mol/l) for cyclics $[O(CH_2)_3OCO(CH_2)_2CO]_x$ in the PTS melt at 423K (O) are plotted as $\log K_x$ against $\log n$, where n represents the number of skeletal bonds in the ring. They are compared with theoretical values calculated by equation (4) (●)

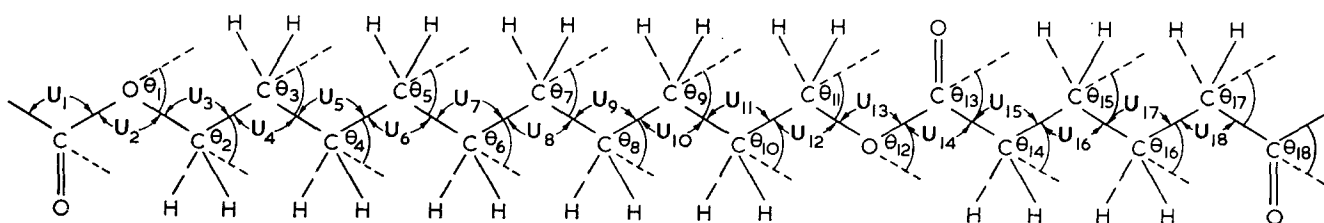


Figure 4 Section of the PDA chain in the all-*trans* conformation. Structural parameters were assigned to the chain by Flory²⁴ as follows. Bond angle supplements of 67° at CO-O-CH₂ (e.g. θ_1), 70° at O-CH₂-CH₂ (e.g. θ_2), 68° at CH₂-CH₂-CH₂ (e.g. θ_3), 68° at CH₂-CH₂-CO (e.g. θ_{17}) and 66° at CH₂-CO-O (e.g. θ_{18}). Bond lengths $l_{\text{CO-O}}=1.33 \text{ \AA}$, $l_{\text{O-CH}_2}=1.44 \text{ \AA}$, $l_{\text{CH}_2\text{-CH}_2}=1.53 \text{ \AA}$ and $l_{\text{CH}_2\text{-CO}}=1.51 \text{ \AA}$

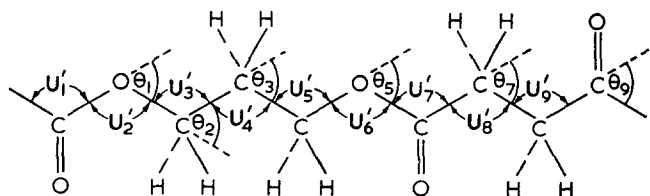


Figure 5 Section of the PTS chain in the all-*trans* conformation. Structural parameters assigned to the chain were similar to the corresponding values of the PDA chain (see caption to Figure 4)²⁴

chains in the aliphatic polyester melts adopt random-coil conformations and obey Gaussian statistics. If these conditions are fulfilled, the K_x values for the cyclics M_x are related to the mean-square end-to-end distances $\langle r_x^2 \rangle_0$ of the corresponding unperturbed x -meric chain molecules by^{3, 13}:

$$K_x = (3/2\pi \langle r_x^2 \rangle_0)^{3/2} (1/2N_A x) \quad (4)$$

where K_x is in mol/l and N_A is the Avogadro constant.

Theoretical values for $\langle r_x^2 \rangle_0$ were computed by the exact mathematical methods of Flory and Jernigan^{21, 22} using the rotational isomeric state models of the chains set up by Flory and Williams^{23, 24}. Sections of PDA and PTS chains in their all-*trans* conformations are shown in Figures 4 and 5. Structural parameters of the chains (assigned by Flory²⁴) are listed in the captions to these Figures. In the Flory-Williams model, ester groups are assumed to adopt the planar *trans* conformation only and all other skeletal bonds are assigned to rotational states in *trans* ($\phi=0^\circ$) and *gauche* ($\phi=\pm 120^\circ$) positions. Statistical weight matrices U_i are introduced to take account of the interdependences of rotations about adjacent pairs of skeletal bonds. The elements of these matrices are indexed on the rows and columns by the rotational states of pairs of skeletal bonds $i-1$ and i as shown in Figures 4 and 5, and they are defined by Boltzmann factors as follows:

$$E/u_{\zeta\eta; i} = \exp(-E/\zeta\eta; i/RT) \quad (5)$$

where R is the gas constant, T is the temperature and $E_{\zeta\eta; i}$ represents the difference between the conformational energy of a section of the chain when the skeletal bonds $i-1$ and i are in rotational states ζ and η (and all other bonds are *trans*) and the corresponding conformational energy when bonds $i-1$ and i are in *trans* states. At the temperature of 423K used for the ring-chain equilibration reactions, the elements of the statistical weight matrices U_1 - U_{18} for PDA and U'_1 - U'_9 for PTS are given as follows:

$$U_1 = U'_1 = [1 \ 0 \ 0] \quad (6)$$

$$U_2 = U'_2 = U'_7 = \begin{bmatrix} 1 & 1 & 1 \\ 0 & 0 & 0 \\ 0 & 0 & 0 \end{bmatrix} \quad (7)$$

$$U_3 = U_{12} = U_{15} = U_{17} = U_{18} = \begin{bmatrix} 1 & 1 & 1 \\ 1 & 1 & 0.20 \\ 1 & 0.20 & 1 \end{bmatrix} \quad (8)$$

$$U_4 = U_{11} = U_{16} = \begin{bmatrix} 1 & 0.55 & 0.55 \\ 1 & 0.55 & 0.11 \\ 1 & 0.11 & 0.55 \end{bmatrix} \quad (9)$$

$$U_5 = U_6 = U_7 = U_8 = U_9 = U_{10} = \begin{bmatrix} 1 & 0.55 & 0.55 \\ 1 & 0.55 & 0.05 \\ 1 & 0.05 & 0.55 \end{bmatrix} \quad (10)$$

$$U_{13} = U'_6 = \begin{bmatrix} 1 & 0 & 0 \\ 1 & 0 & 0 \\ 1 & 0 & 0 \end{bmatrix} \quad (11)$$

$$U_{14} = \begin{bmatrix} 1 & 1 & 1 \\ 0 & 0 & 0 \\ 0 & 0 & 0 \end{bmatrix} \quad (12)$$

The Flory-Williams rotational isomeric state model for aliphatic polyesters predicts values for the characteristic ratios $\langle r^2 \rangle_0/n\bar{l}^2$ taken in the limit $n \rightarrow \infty$ (where n represents the number of skeletal bonds of mean-square length \bar{l}) of 5.4 for PDA and 5.3 for PTS at 423K. These theoretical values may be compared with the experimental characteristic ratios of a number of aliphatic polyesters which were measured recently by Knecht and Elias²⁵. At temperatures from 291 to 308K the latter were found to lie in the range $5.5 < (\langle r^2 \rangle_0/n\bar{l}^2)_{n \rightarrow \infty} < 7.0$.

Comparison of experiment with theory

In Figures 2 and 3, the experimental K_x values for cyclics in undiluted PDA and PTS equilibrates are compared with theoretical values calculated by equation (4) using the Flory-Williams model (equations 5-12) to compute the required end-to-end distances $\langle r_x^2 \rangle_0$ of the corresponding x -meric open chain molecules. The experimental K_x values for the smallest cyclics fall well below the theoretical values predicted for rings corresponding to chains that obey the Gaussian relationship for the probability that they will intramolecularly cyclize. It is noted that the discrepancy between experiment and theory is similar for the cyclics in PDA and PTS which contain 18 skeletal bonds, even though they contain two and four ester groups respectively. The agreement between experiment and theory is excellent for the largest cyclics analysed in the PDA equilibrates. The K_3 , K_4 and K_5 values for the trimeric, tetrameric and pentameric cyclics (containing 54, 72 and 90 skeletal bonds respectively) are similar to the theoretical values calculated as described above. By contrast, the experimental K_4 , K_5 , K_6 and K_7 values for the tetrameric, pentameric, hexameric and heptameric cyclics (containing 36, 45, 54 and 63 skeletal bonds respectively)

in the PTS equilibrates are about half the corresponding theoretical values. Cyclics in this latter system contain twice as many ester groups as cyclics of similar size in PDA. The close agreement between experiment and theory in the PDA system, and lack of agreement in the PTS system, indicate that the conformational characteristics of oligomeric aliphatic polyester chains are considerably more sensitive to the relative numbers of methylene groups and ester linkages than is predicted by the Flory and Williams model.

ACKNOWLEDGEMENTS

We are indebted to the Science Research Council for a Research Fellowship (to F. R. J.) and for a Research Studentship (to L. E. S.). We are grateful to Dr D. R. Cooper, who carried out helpful preliminary studies of cyclic concentrations in aliphatic polyester systems in our laboratory at York, and to Mr J. D. Balfour for practical assistance with the PTS system. We thank the Computation Department of the University for providing computational facilities.

REFERENCES

- 1 Carmichael, J. B. and Winger, R. *J. Polym. Sci. (A)* 1965, **3**, 971
- 2 Brown, J. F. and Slusarczuk, G. M. *J. Am. Chem. Soc.* 1965, **87**, 931
- 3 Flory, P. J. and Semlyen, J. A. *J. Am. Chem. Soc.* 1966, **88**, 3209
- 4 Semlyen, J. A. and Wright, P. V. *Polymer* 1969, **10**, 543
- 5 Wright, P. V. and Semlyen, J. A. *Polymer* 1970, **11**, 462
- 6 Wright, P. V. *J. Polym. Sci. (Polym. Phys. Edn)* 1973, **11**, 51
- 7 Beevers, M. S. and Semlyen, J. A. *Polymer* 1972, **13**, 523
- 8 Andrews, J. M. and Semlyen, J. A. *Polymer* 1972, **13**, 142
- 9 Semlyen, J. A. and Walker, G. R. *Polymer* 1969, **10**, 597
- 10 Andrews, J. M., Jones, F. R. and Semlyen, J. A. *Polymer* 1974, **15**, 420
- 11 Cooper, D. R. and Semlyen, J. A. *Polymer* 1973, **14**, 185
- 12 Jacobson, H., Beckmann, C. O. and Stockmayer, W. H. *J. Chem. Phys.* 1950, **18**, 1607
- 13 Jacobson, H. and Stockmayer, W. H. *J. Chem. Phys.* 1950, **18**, 1600
- 14 Hill, J. W. and Carothers, W. H. *J. Am. Chem. Soc.* 1933, **55**, 5031
- 15 Spanagel, E. W. and Carothers, W. H. *J. Am. Chem. Soc.* 1935, **57**, 929
- 16 Zavaglia, E. A., Mosher, W. A. and Billmeyer, F. W. *Off. Dig. Fed. Soc. Paint Technol.* 1965, **33**, 229
- 17 Chang, P. S., Zavaglia, E. A. and Billmeyer, F. W. *Off. Dig. Fed. Soc. Paint Technol.* 1965, **33**, 235
- 18 Billmeyer, F. W. and Eckard, A. D. *Macromolecules* 1969, **2**, 103
- 19 Billmeyer, F. W. and Katz, I. *Macromolecules* 1969, **2**, 105
- 20 Flory, P. J. 'Principles of Polymer Chemistry', Cornell Univ. Press, Ithaca, 1953
- 21 Flory, P. J. *Proc. Nat. Acad. Sci., Wash.* 1964, **51**, 1060
- 22 Flory, P. J. and Jernigan, R. L. *J. Chem. Phys.* 1965, **42**, 3509
- 23 Flory, P. J. and Williams, A. D. *J. Polym. Sci. (A-2)* 1967, **5**, 399
- 24 Flory, P. J. 'Statistical Mechanics of Chain Molecules', Interscience, New York, 1969
- 25 Knecht, M. R. and Elias, H.-G. *Makromol. Chem.* 1972, **157**, 1

Determination of molecular orientation by polarized infra-red radiation in an oriented polymer of high polarizability

A. Cunningham*, G. R. Davies and I. M. Ward

Department of Physics, University of Leeds, Leeds LS2 9JT, UK
(Received 8 March 1974)

A quantitative treatment is presented for the absorption of polarized infra-red radiation at normal incidence by a transversely isotropic polymer film. In addition to the reflectivity correction, an approximate treatment of the internal field problem is also carried out. This is important where the polymer is of high polarizability. It is shown how the orientation and concentration of the absorbing species can be derived from experimental data.

INTRODUCTION

It is customary to consider the absorption of infra-red radiation by a polymer in terms of the non-interacting molecular gas approximation. The rate of absorption of energy is then given in terms of the absorbance or optical density A by:

$$A = \log_{10} \frac{I_0}{I} \propto (\boldsymbol{\mu} \cdot \mathbf{E})^2 \quad (1)$$

where I_0 , I are the incident and transmitted intensities at the absorbing wavelength respectively, $\boldsymbol{\mu}$ is the transition moment vector and \mathbf{E} the electric field vector. If the angle between $\boldsymbol{\mu}$ and \mathbf{E} is β , the absorbance is proportional to $\cos^2\beta$, and thus for an oriented sample, measurements with polarized radiation can in principle provide information regarding the orientation of the transition moment vectors and hence, hopefully, valuable structural information. Notable amongst studies of this nature, have been the early work of Elliott and co-workers on polypeptides¹, and that of Read and Stein on polyethylene².

We have recently been examining the use of polarized infra-red measurements on oriented poly(ethylene terephthalate) (PET). It appears that in this case the molecular gas approximation, although adequate for qualitative measurements, suffers from two important objections. First, the electric field \mathbf{E} in the sample is assumed to be identical with the incident electric field. Our studies of the anisotropic dielectric absorption of such materials, however, have clearly demonstrated the necessity of a local field correction³. Moreover, all previous studies of optical anisotropy in PET and other oriented polymers, implicitly assume a local field correction, in that the Lorentz-Lorenz relationship is used to relate refractive indices to molecular polarizabilities^{4,5}. It therefore appears mandatory to apply the local field correction to the infra-red data both on

the evidence of previous experimental work, and on grounds of consistency, so that orientation data so obtained can be comparable with those from measurements of optical anisotropy.

Secondly, in the simplest and most usual application of equation (1), I is considered to be the transmitted intensity at the peak of the infra-red absorption band and I_0 that at its base, assuming an empirically drawn base line. The reflection losses, however, will in principle vary with the amount of absorption and must therefore be treated quantitatively if the data are to be analysed correctly.

In this paper we therefore present a treatment for the infra-red absorption by an oriented polymer, dealing quantitatively with both the reflection correction and the internal field problem. These are considered for the case of uniaxial symmetry, and for the situations where the electric field vector is incident along a principal axis.

In the next paper⁶, results will be presented for oriented PET films and it will be shown that the theoretical treatments presented in this paper provide a satisfactory basis for the interpretation of these results.

THEORY

The reflectivity correction

Figure 1 shows the experimental arrangement in the double beam spectrometer for normal incidence of the infra-red (i.r.) radiation. To reduce reflection effects at the sample surface (which will normally produce interference fringes) the sample is sandwiched between potassium bromide (KBr) plates with a thin layer of Nujol between the sample surfaces and the KBr plates. An orthogonal coordinate frame is set-up within the sample with z parallel to the draw direction and x in the plane of the film. The i.r. radiation is incident along the y direction, with the electric vector along either z or x .

The reflectivities of the four interfaces are denoted

* Present address: ICI Corporate Laboratory, Runcorn, Cheshire, UK

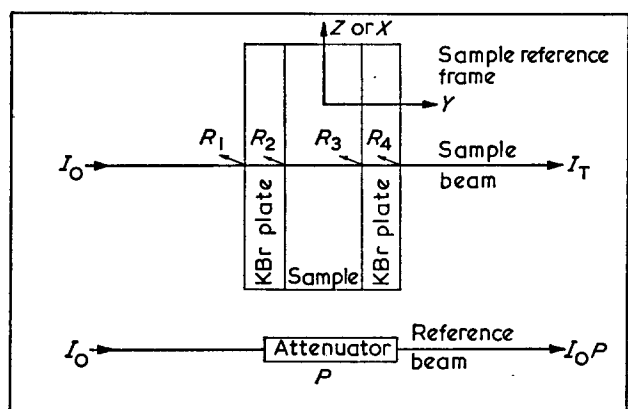


Figure 1 The experimental arrangement in the double-beam infra-red spectrometer

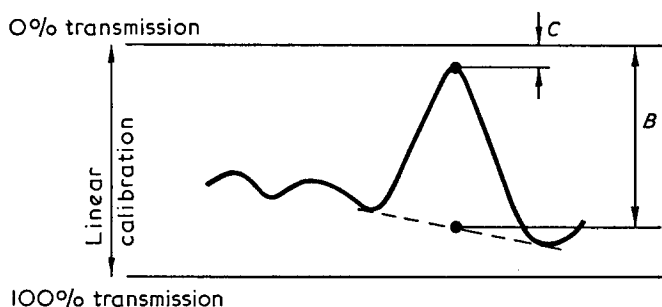


Figure 2 The definition of the experimentally measured quantities B and C

by R_1 , R_2 , R_3 and R_4 respectively (Figure 1). If the total attenuation within the sample is L , the final transmitted intensity I_T is related to the incident intensity I_0 by:

$$I_T = I_0(1 - R_1)(1 - R_2)L(1 - R_3)(1 - R_4) \quad (2)$$

Only the principal (first) reflection at each interface is considered, the correction due to multiple reflections being taken to be negligible.

Putting $R_1 = R_4 = R_{\text{KBr}}$ and $R_2 = R_3 = R$, we have:

$$I_T = I_0(1 - R_{\text{KBr}})^2(1 - R)^2L \quad (3)$$

The spectrometer compares the transmitted intensity I_T with the attenuated incident intensity I_0P , where P is the attenuation, and is calibrated to give a linear representation of the percentage transmission, so that:

$$\% \text{ transmission} = 100 \times \frac{I_T}{I_0P}$$

The attenuation is chosen so that the majority of the spectrum can be recorded within the range 20–80% transmission, where the instrument is most accurate.

Figure 2 shows a typical infra-red band, with $B = I_T/P I_0$, $C = I_T'/P I_0$, where I_T , I_T' are the transmitted intensities at the base and peak of the absorption band, respectively. We now have:

$$\frac{B}{C} = \frac{I_T}{I_T'} = \frac{I_0(1 - R_{\text{KBr}})^2(1 - R)^2L}{I_0(1 - R_{\text{KBr}})^2(1 - R')^2L'} \quad (4)$$

where the primes show that the quantities R' , R'_{KBr} and L' have to be evaluated at the peak of the absorption, as distinct from the unprimed quantities which are evaluated at the base.

Clearly as R_{KBr} only involves the air/KBr interface and KBr is non-absorbing $R'_{\text{KBr}} = R_{\text{KBr}}$ and we have

$$\frac{B}{C} = \frac{I_T}{I_T'} = \frac{(1 - R)^2L}{(1 - R')^2L'} \quad (5)$$

The quantities R and R' are readily evaluated by considering the equations of continuity at the KBr/polymer interface. For normal incidence we have:

$$E_1^* - E_2^* = E_3^*$$

and

$$H_1^* + H_2^* = H_3^*$$

where E_1^* , E_2^* , E_3^* are the incident, reflected and transmitted electric vectors at the interface, and H_1^* , H_2^* and H_3^* the corresponding magnetic field vectors. We have allowed for phase differences by allowing all these quantities to be complex. In each case H^* and E^* are related by the corresponding refractive index, so that in the polymer $H^* \propto n^* E^*$, where $n^* = n - ik$; and in the KBr $H^* \propto n_{\text{KBr}} E^*$. It can then be shown that the reflectivity, R , is:

$$R = \frac{|E_2^*|^2}{|E_1^*|^2} = \frac{(n - n_{\text{KBr}})^2 + k^2}{(n + n_{\text{KBr}})^2 + k^2} \quad (6)$$

Similarly it can be shown that

$$R' = \frac{(n' - n_{\text{KBr}})^2}{(n' + n_{\text{KBr}})^2} \quad (7)$$

Although in general the reflectivity will depend markedly on wavenumber, we need only consider its value at the peak of the absorption. Figures 3a and 3b show typical variations of n and k respectively in the region of an absorption band. Although n can vary between large limits its value at resonance $n(s_0)$ falls between the much narrower limits of the high and low

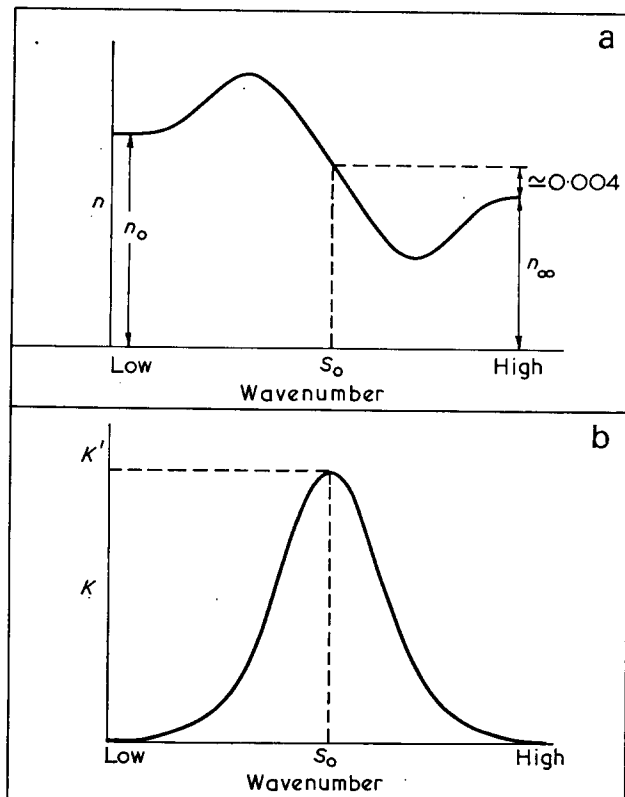


Figure 3 Idealized dispersion (a) and absorption (b) curves

Table 1 Comparison of refractive index values for oriented films measured at 551 nm (optical region) and at 3000 cm⁻¹

Optical refractive* index (551 nm)	Infra-red refractive index	
	P-E457 spectrometer	Grubb-Parsons spectromaster
1.584	1.646	1.670
1.592	—	1.602
1.593	1.584	1.569
1.604	—	1.670
1.614	1.673	1.654
1.619	1.670	1.655
1.620	1.795	1.683

* Average refractive index in the plane of the film

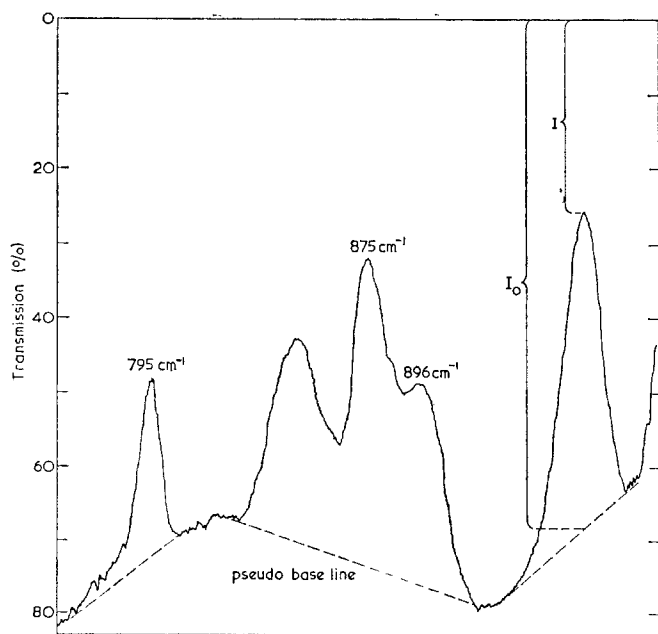


Figure 4 An infra-red spectrum in the region 700–1000 cm⁻¹ showing the pseudo base lines adopted

wavenumber refractive indices n_∞ and n_0 . Calculations using the Kramers–Krönig relationships showed that the difference $n_\infty - n_0 = \Delta n \approx 0.008$ for the i.r. absorption bands used in this study. The major contribution to the refractive index at the absorption peak therefore comes from the high electronic contribution n_∞ (~ 1.6). This was confirmed by an experimental determination of the refractive index at 3000 cm⁻¹ by measuring the spacing of interference bands in a film which was not sandwiched between KBr plates. The results, listed in *Table 1*, show a very small increase compared with the optical values determined at 18 000 cm⁻¹. Because the optical refractive indices can be determined more readily and to greater accuracy, we have therefore used these values in the reflectivity correction. We have also assumed that the value of k is zero at the base of the absorption peak, and that $n' \equiv n$.

Finally, the value of n_{KBr} varies less than 1% in this wavenumber range, and is taken to have a constant value of 1.524. In practice, the reflectivity correction changes the value of the final calculated absorbance by a maximum of about 10%. Thus very precise values of n , k and n_{KBr} are not required (even a 10% error in this correction will only affect the final absorbance value by 1%).

The experimental absorbance

It is customary in i.r. spectroscopy to use a base line method of determining the absorbances. In *Figure 4* a typical base line is shown for the absorption bands investigated in the companion experimental study. In a conventional analysis the absorption is given by $\log I_0/I$ in *Figure 4*. The equivalent assumptions in the present analysis are to assume that the attenuation L is unity and the value of k is zero at the base of an absorption peak. The orientation functions which we seek are primarily determined from the anisotropy in k and not by its absolute magnitude. A consistent error in the absolute magnitude of the peak value of k will not therefore proportionally affect the determination of the orientation functions.

Consider the situation for plane polarized radiation incident normally, as shown in *Figure 1*, with the electric vector along z and the direction of propagation along y .

The equation of propagation is given by:

$$\begin{aligned} E_z^*(y) &= E_z(0) \exp \left[i\omega \left(t - \frac{n_z^* y}{c} \right) \right] \\ &= E_z(0) \exp \left[\frac{-k_z y}{\lambda} \right] \exp \left[i\omega \left(t - \frac{n_z y}{c} \right) \right] \end{aligned} \quad (8)$$

where $E_z^*(y)$ is the electric vector at a distance y into the sample, $E_z(0)$ is the amplitude of the electric vector at ($y=0$), $n_z^* = n_z - ik_z$ is the relevant complex refractive index, ω is the angular frequency and c the velocity of light.

The corresponding intensity at y is given by:

$$I_z(y) = I_z(0) \exp \left(\frac{-2k_z y}{\lambda} \right) \quad (9)$$

For a sample thickness y_0 , the attenuation L is therefore

$$L = \exp \left(\frac{-2k_z y_0}{\lambda} \right) \quad (10)$$

Combining equations (5), (6), (7) and (10) we now evaluate the ratio of intensities at the peak and base of the absorption band

$$\frac{B}{C} = \frac{I_T}{I_T'} = \left\{ \frac{(n_z + n_{\text{KBr}})^2 + k^2}{(n_z + n_{\text{KBr}})^4} \right\} \exp \left(\frac{2k_z y_0}{\lambda} \right) \quad (11)$$

The experimentally determined absorbance is therefore given to a good approximation by:

$$\log_{10} \frac{I_T}{I_T'} = 0.4343 \left\{ \frac{2k_z y_0}{\lambda} + \frac{2k_z^2}{(n_z + n_{\text{KBr}})^2} \right\} \quad (12)$$

It can now be clearly seen how the experimental absorption depends on k and n . Both k and n are anisotropic, and in unfavourable cases where k is large, the reflectivity term can be appreciable for these thin films where $y_0 \sim \lambda$. We now wish to show how the values of k_x and k_z determined from these experiments can be used to determine first, orientation functions and secondly, the concentrations of particular molecular conformations.

The local field effect

We therefore wish to relate the macroscopic, experimentally determined parameters n and k to the orientation of molecular units at the microscopic level. This necessarily involves consideration of the local field.

We introduce a molecular polarizability tensor α_{ij}^m defined in such a way that the change in total dipole moment of the molecule $\Delta\mathbf{m}$ is related to the local electric field \mathbf{E}^L by

$$\Delta\mathbf{m} = \alpha_{ij}^m \mathbf{E}_j^L \quad (13)$$

In general, the tensor α_{ij}^m is complex and includes both infra-red and electronic processes. In order to study a particular i.r. absorption band we further define:

$$\Delta\mathbf{m} = \boldsymbol{\mu} + \mathbf{p}$$

where $\boldsymbol{\mu}$ is that part of $\Delta\mathbf{m}$ due to the i.r. process of interest (cf. the i.r. transition moment), and \mathbf{p} contains all the other effects. Since the contribution to \mathbf{p} from absorption bands away from resonance is small, \mathbf{p} is essentially an electronic polarization. α_{ij}^m is now decomposed into α_{ij}^e and α_{ij}^* such that:

$$\begin{aligned} p_i &= \alpha_{ij}^e E_j^L \\ \mu_i^* &= \alpha_{ij}^* E_j^L \end{aligned} \quad (14)$$

The tensor α_{ij}^e is considered totally real since the electronic polarization is in phase with the applied field at i.r. frequencies and the i.r. bands included in \mathbf{p} are not at resonance. α_{ij}^* must, however, be complex since we are detecting the i.r. band by its absorption properties. We therefore let:

$$\alpha_{ij}^* = \alpha'_{ij} - i\alpha''_{ij}$$

In general, each molecule is acted upon by a different local field and we do not have enough information about the microscopic structure of the polymer to compute the actual local field for any given molecule. We therefore consider a small volume V of the sample which contains sufficient molecules for its polarization \mathbf{P} (the dipole moment per unit volume) to be a sensible average value over the molecular orientations, independent of the size or position of V . We now introduce average polarizabilities $\langle\alpha^*\rangle$ and $\langle\alpha^e\rangle$ such that:

$$\mathbf{P} = \{N\langle\alpha^*\rangle + N^e\langle\alpha^e\rangle\}\langle\mathbf{E}^L\rangle \quad (15)$$

where $\langle\alpha^*\rangle$ and $\langle\alpha^e\rangle$ are to be evaluated, N and N^e are the concentrations of species/unit volume and $\langle\mathbf{E}^L\rangle$ indicates an average local field which we take to be that used in the Lorentz-Lorenz or Clausius-Mosotti equation. Thus:

$$\langle\mathbf{E}^L\rangle = \mathbf{E} \left(\frac{n^{*2} + 2}{3} \right)$$

The advantage of the Lorentz local field is that a real cavity is not excavated in a dielectric hence \mathbf{E} , $\langle\mathbf{E}^L\rangle$ and \mathbf{P} are all uniform and parallel. Any other local field theory requires the calculation of these quantities in a dielectric, perturbed by a real cavity. The Lorentz field is strictly only applicable provided that the polarization results from parallel, weakly interacting dipoles which are either randomly arranged or situated as a cubic lattice. This is not the case in our samples, but in the absence of a formal theoretical treatment of this very complex situation, the calculation will be continued, accepting that the Lorentz field is an approximation.

\mathbf{E} , $\langle\mathbf{E}^L\rangle$ and \mathbf{P} are only parallel in an anisotropic sample provided that \mathbf{E} lies along a principal axis. The average polarizabilities are therefore only readily evaluated for the situations where \mathbf{E} lies along the z

or x direction. In these cases, using the Lorentz-Lorenz equation as in much previous work, we have:

$$\frac{n_z^{*2} - 1}{n_z^{*2} + 2} = \frac{4\pi}{3} \{N\langle\alpha_z^*\rangle + N^e\langle\alpha_z^e\rangle\}$$

and

$$\frac{n_x^{*2} - 1}{n_x^{*2} + 2} = \frac{4\pi}{3} \{N\langle\alpha_x^*\rangle + N^e\langle\alpha_x^e\rangle\} \quad (16)$$

As before, $\langle\alpha_z^*\rangle$ and $\langle\alpha_x^*\rangle$ relate to the infra-red band and $\langle\alpha_z^e\rangle$ and $\langle\alpha_x^e\rangle$ to the electronic processes. We may remove $\langle\alpha_z^e\rangle$ and $\langle\alpha_x^e\rangle$ from direct consideration by taking the imaginary parts of these equations. This gives:

$$6n_z k_z \{n_z^4 + 2n_z^2 k_z^2 + 4n_z^2 - 4k_z^2 + k_z^4 + 4\}^{-1} = \frac{4\pi}{3} N \langle\alpha_z''\rangle$$

and

$$6n_x k_x \{n_x^4 + 2n_x^2 k_x^2 + 4n_x^2 - 4k_x^2 + k_x^4 + 4\}^{-1} = \frac{4\pi}{3} N \langle\alpha_x''\rangle \quad (17)$$

For convenience, we introduce the function ϕ_i , defined by:

$$\phi_i = 6n_i k_i \{n_i^4 + 2n_i^2 k_i^2 + 4n_i^2 - 4k_i^2 + k_i^4 + 4\}^{-1}$$

where

$$\phi_i = \frac{4\pi}{3} N \langle\alpha_i''\rangle$$

Then

$$\phi_z = \frac{4\pi}{3} N \langle\alpha_z''\rangle$$

and

$$\phi_x = \frac{4\pi}{3} N \langle\alpha_x''\rangle \quad (17a)$$

Equations (17) relate n_z , k_z and n_x , k_x to $\langle\alpha_z''\rangle$ and $\langle\alpha_x''\rangle$ and it remains to calculate $\langle\alpha_z''\rangle$ and $\langle\alpha_x''\rangle$ in terms of α_{ij}^* , the concentration of the absorbing species, and the molecular orientation functions.

The magnitude of the molecular polarizability associated with i.r. absorption is defined from the situation where the change in an individual dipole moment, i.e. the transition moment $\boldsymbol{\mu}$, is parallel to the local field. Here $\boldsymbol{\mu} = \alpha^* \mathbf{E}^L$. Since the electronic field is small the direction of $\boldsymbol{\mu}$ is not influenced by a change in the direction of \mathbf{E}^L . Hence α_{ij}^* is defined by the tensor

$$\begin{bmatrix} \alpha^* & 0 & 0 \\ 0 & 0 & 0 \\ 0 & 0 & 0 \end{bmatrix}$$

referred to axes where x is parallel to $\boldsymbol{\mu}$. For the case where the dipole moment vector makes an angle β with \mathbf{E}^L we have, therefore:

$$|\boldsymbol{\mu}| = \alpha^* |\mathbf{E}^L| \cos\beta \quad (18)$$

and the component of $\boldsymbol{\mu}$ parallel to \mathbf{E}^L is given by:

$$\mu_{\parallel} = \alpha^* E^L \cos^2\beta \quad (19)$$

We now wish to calculate the polarization \mathbf{P} for the situation where the applied field \mathbf{E} is parallel to a principal axis of the sample, i.e. for the situation where \mathbf{E} , $\langle\mathbf{E}^L\rangle$ and \mathbf{P} are parallel.

\mathbf{P} is obtained by summing over the molecular dipoles in the volume V .

$$\mathbf{P} = \frac{1}{V} \{\sum \boldsymbol{\mu}_i + \sum \mathbf{p}_i\} \quad (20)$$

where, as before, μ_i and \mathbf{p}_i represent individual contributions from the infra-red and electronic components respectively. The second term in this equation is used in standard calculations of polymer refractive indices (see Appendix).

If we assume that all the local fields are parallel to \mathbf{E} , the component of the infra-red contribution to the polarization along x or z is then given by:

$$P_{ir} = \frac{1}{V} \sum \alpha^* E_i^L \cos^2 \beta_i \quad (21)$$

which we may write in terms of average quantities as

$$P_{ir} = N \langle \alpha^* E^L \cos^2 \beta \rangle \quad (22)$$

The orientation on a microscopic level can be defined by the average polarizability $\langle \alpha^* \rangle$, defined by equation (15).

$$\langle \alpha^* \rangle = \frac{P_{ir}}{N \langle E^L \rangle} \quad (23)$$

Combining equations (22) and (23) we have:

$$\langle \alpha^* \rangle = \frac{\langle \alpha^* E^L \cos^2 \beta \rangle}{\langle E^L \rangle} \quad (24)$$

If β and E^L are independent variables we have: $\langle E^L \cos^2 \beta \rangle = \langle \cos^2 \beta \rangle \langle E^L \rangle$. Hence

$$\langle \alpha^* \rangle = \alpha^* \langle \cos^2 \beta \rangle \quad (25)$$

where β is the angle between μ and the electric field which lies along the z or x direction.

The same result is obtained at greater length if one does not require that the local field at each dipole is parallel to \mathbf{E} , provided that the directions of μ and the individual local fields are uncorrelated.

The required imaginary parts of the average polarizabilities are therefore given by:

$$\langle \alpha_z'' \rangle = \alpha'' \langle \cos^2 \beta \rangle_z$$

and

$$\langle \alpha_x'' \rangle = \alpha'' \langle \cos^2 \beta \rangle_x \quad (26)$$

where $\langle \cos^2 \beta \rangle_z$ and $\langle \cos^2 \beta \rangle_x$ are the average values of $\cos^2 \beta$ for the applied electric field lying along the z and x directions respectively.

The final expressions relating the measured quantities n_z , k_z and n_x , k_x to these orientation parameters are then:

$$\frac{4\pi}{3} N \alpha'' \langle \cos^2 \beta \rangle_z = \phi_z$$

and

$$\frac{4\pi}{3} N \alpha'' \langle \cos^2 \beta \rangle_x = \phi_x \quad (27)$$

The evaluation of the orientation functions for samples with fibre symmetry

We now wish to relate the quantities $\langle \cos^2 \beta \rangle_z$ and $\langle \cos^2 \beta \rangle_x$ to the molecular orientation in the sample. To do this, first consider a set of Cartesian axes $\{u, v, w\}$ fixed within a repeat unit of the polymer, the w axis being parallel to the chain axis (Figure 5a). The transition moment μ makes angles θ_m , ϕ_m with the w and u axes respectively. The electric field \mathbf{E} makes an angle β with μ and angles δ , ϕ_m with the w and u axes respectively.

Assuming that θ_m is a constant angle and that there

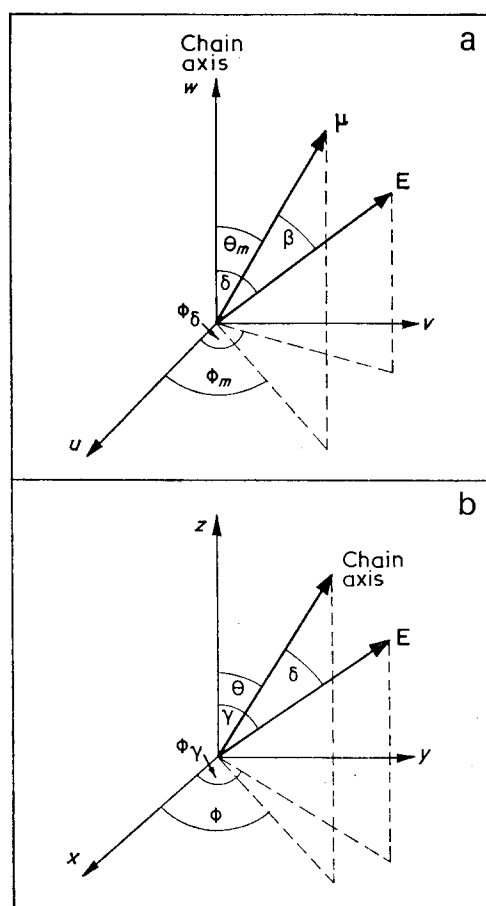


Figure 5 Diagrams showing orientation of the electric field \mathbf{E} and the transition moment μ with respect to unit axes u, v, w (a) and the orientation of the electric field \mathbf{E} and the chain axis with respect to coordinate axes x, y, z for the sample (b)

is no preferred orientation of the transition moment about the chain axis we can use the Legendre addition theorem to write:

$$\langle P_2(\beta) \rangle = P_2(\theta_m) \langle P_2(\delta) \rangle \quad (28)$$

(No preferred orientation implies that we must average over the angle ϕ_m with a uniform probability function. In the addition theorem ϕ_m and δ appear in a combination $(\phi_m - \delta)$ which is independent of the u axis from which they are defined. $P_2(\beta)$ is therefore a function of θ_m and δ only.)

We now wish to express this result in terms of a set of Cartesian axes conveniently situated with respect to the macroscopic shape of our drawn film sample. We therefore choose axes $\{xyz\}$ such that the xz plane is the film plane and the draw direction is parallel to z (Figure 5b). The electric field \mathbf{E} and the chain axis make angles γ , θ and ϕ , ϕ with the z and x axes respectively.

Because there is no preferred orientation of the chain axis about the draw direction (the sample is transversely isotropic, with z as its unique axis) the Legendre addition theorem can be used again to give the result:

$$\langle P_2(\delta) \rangle = \langle P_2(\theta) \rangle P_2(\gamma) \quad (29)$$

We wish to evaluate the two situations where the applied electric field \mathbf{E} is along z and x respectively.

For \mathbf{E} parallel to z , we have $\gamma=0$ and $P_2(\gamma)=1$ and for \mathbf{E} parallel to x , we have $\gamma=\pi/2$ and $P_2(\gamma)=-\frac{1}{2}$.

This gives:

$$\langle P_2(\beta) \rangle_z = P_2(\theta_m) \langle P_2(\theta) \rangle$$

and

$$\langle P_2(\beta) \rangle_x = -\frac{1}{2} P_2(\theta_m) \langle P_2(\theta) \rangle \quad (30)$$

Using the results of the previous section, we can now proceed to relate the orientation functions to ϕ_z and ϕ_x . Noting that:

$$\langle \cos^2 \beta \rangle_z + 2 \langle \cos^2 \beta \rangle_x = 1 \quad (31)$$

$$\phi_z + 2\phi_x = \frac{4\pi}{3} N \alpha'' = 3\phi_0 \quad (32)$$

where ϕ_0 is a convenient normalization factor. Combining equations (30) and (32) together with the definition of $P_2(\theta) = \frac{1}{2}(3\cos^2\theta - 1)$, we have:

$$\langle \cos^2 \beta \rangle_z - \langle \cos^2 \beta \rangle_x = P_2(\theta_m) \langle P_2(\theta) \rangle \quad (33)$$

Using equations (27) and (33) the final result is:

$$\frac{\phi_z - \phi_x}{\phi_z + 2\phi_x} = \frac{\phi_z - \phi_x}{3\phi_0} = P_2(\theta_m) \langle P_2(\theta) \rangle \quad (34)$$

The quantities ϕ_z and ϕ_x , which can be directly evaluated from experiment have therefore been related to the constant quantity $P_2(\theta_m)$ which depends only on the molecular structure of the polymer and the quantity $\langle P_2(\theta) \rangle$ which relates directly to the distribution of chain axis orientations. Finally we note that the quantity ϕ_0 is proportional to the concentration of the absorbing species, since α'' will be a constant for a given infra-red absorption band.

CONCLUSION

A theoretical treatment has been given for the infra-red absorption by an oriented polymer, which incorporates a reflectivity correction and attempts to deal with the internal field correction for the situations where the electric vector lies along a principal axis. The case of a transversely isotropic film with radiation incident normally has been analysed and it has been shown how the orientation and concentration of the absorbing species can be quantitatively related to the experimentally measured quantities.

REFERENCES

- 1 Ambrose, E. J. and Elliott, A. *Proc. R. Soc. (A)* 1951, **206**, 206
- 2 Read, B. E. and Stein, R. S. *Macromolecules* 1968, **1**, 116
- 3 Davies, G. R. and Ward, I. M. *J. Polym. Sci. (A-2)* 1972, **10**, 1153
- 4 Ward, I. M. *Proc. Phys. Soc.* 1962, **80**, 1176
- 5 Kashiwagi, M., Cunningham, A., Manuel, A. J. and Ward, I. M. *Polymer* 1973, **14**, 111
- 6 Cunningham, A., Ward, I. M., Willis, H. A. and Zichy, V. *Polymer* 1974, **15**, 749

APPENDIX

$P_2(\theta)$ from the optical refractive index of an oriented sample

We define the electronic polarizability of a polymer

repeat unit by the tensor α_{ij}^e referred to its principal axes.

$$\alpha_{ij}^e = \begin{bmatrix} \alpha_{11}^e & 0 & 0 \\ 0 & \alpha_{22}^e & 0 \\ 0 & 0 & \alpha_{33}^e \end{bmatrix}$$

We assume that one of these is the chain axis (α_{33}^e say). The other two are therefore perpendicular to the chain axis. If there is no preferred orientation of chains about the chain axis, we need only consider the average polarizability perpendicular to the chain axis (α_{\perp}^e):

$$\alpha^e = \frac{1}{2}(\alpha_{11}^e + \alpha_{22}^e)$$

In a similar fashion to the infra-red calculation, the component of the polarization parallel to E^L is given by:

$$P_i^e = \frac{1}{V} \sum E_i^L (\alpha_{33}^e \cos^2 \beta_i + \alpha_{\perp}^e \sin^2 \beta_i) \quad (A1)$$

where β is the angle between E^L and a chain axis. Thus

$$\begin{aligned} \langle \alpha_z^e \rangle &= \alpha_{33}^e \langle \cos^2 \beta \rangle_z + \alpha_{\perp}^e \langle \sin^2 \beta \rangle_z \\ \langle \alpha_x^e \rangle &= \alpha_{33}^e \langle \cos^2 \beta \rangle_x + \alpha_{\perp}^e \langle \sin^2 \beta \rangle_x \end{aligned} \quad (A2)$$

If θ is the angle between a chain axis and the z axis, $\beta = \theta$ for E along z hence:

$$\langle P_2(\beta) \rangle_z = \langle P_2(\theta) \rangle \quad (A3)$$

For E along X :

$$\langle P_2(\beta) \rangle_x = -\frac{1}{2} \langle P_2(\theta) \rangle \quad (A3')$$

Defining the isotropic polarizability by $3\alpha_0 = \alpha_{33}^e + 2\alpha_{\perp}^e$, and the difference $\Delta\alpha^e = \alpha_{33}^e - \alpha_{\perp}^e$, we have:

$$\langle \alpha_z^e \rangle = \alpha_0^e + \frac{2\Delta\alpha^e}{3} \langle P_2(\theta) \rangle \quad (A4)$$

$$\langle \alpha_x^e \rangle = \alpha_0^e - \frac{\Delta\alpha^e}{3} \langle P_2(\theta) \rangle \quad (A4')$$

These may be combined to give:

$$\frac{\langle \alpha_z^e \rangle - \langle \alpha_x^e \rangle}{\langle \alpha_z^e \rangle + 2\langle \alpha_x^e \rangle} = \frac{\Delta\alpha}{3\alpha_0} \langle P_2(\theta) \rangle \quad (A5)$$

The quantities $\langle \alpha_i^e \rangle$ are obtained by measurements of $\langle n_i \rangle$ and the Lorentz-Lorentz equation:

$$\frac{n_i^2 - 1}{n_i^2 + 2} = \frac{4\pi N^e}{3} \langle \alpha_i^e \rangle = \phi^e \quad (A6)$$

ϕ_i^e is convenient since it can be calculated, without a knowledge of N^e , directly from n_i . The final result then becomes:

$$\frac{\phi_z^e - \phi_x^e}{\phi_z^e + 2\phi_x^e} = \frac{\Delta\alpha}{3\alpha_0} \langle P_2(\theta) \rangle \quad (A7)$$

The quantity $\Delta\alpha/\alpha_0$ may be estimated from the maximum birefringence of a highly oriented sample where $P_2(\theta) \simeq 1^5$, thus allowing calculation of $P_2(\theta)$ for lower orientations.

An infra-red spectroscopic study of molecular orientation and conformational changes in poly(ethylene terephthalate)

A. Cunningham and I. M. Ward

Department of Physics, University of Leeds, Leeds LS2 9JT, UK

and H. A. Willis and Veronica Zichy

Research Department, Imperial Chemical Industries Ltd, Plastics Division, Welwyn Garden City, Herts AL7 1HD, UK

(Received 8 March 1974)

Polarized infra-red (i.r.) spectroscopy has been used to study the changes in molecular orientation and conformation which occur on drawing poly(ethylene terephthalate) sheets. The i.r. data provided orientation functions $\langle P_2(\theta) \rangle_{ir}$ where θ is the angle between the molecular chain axis and the draw direction for these uniaxially oriented sheets. Excellent agreement was obtained between the i.r. orientation functions for absorption bands associated with benzene ring mode vibrations, and orientation functions obtained from optical birefringence. Infra-red orientation functions for absorption bands associated with the *trans* and *gauche* conformations of the glycol residue, were then combined with i.r. estimates of the *trans/gauche* concentrations to examine the changes occurring in drawing. For drawing at 80°C up to a draw ratio of about 3.5, there was good agreement with expectations based on the deformation of a rubberlike network.

INTRODUCTION

Although the examination of polymers by infra-red (i.r.) spectroscopy with polarized radiation has been undertaken for many years, it is only comparatively recently that the measurements have been used to obtain an absolute measure of molecular orientation in terms of orientation functions similar to those employed in optical, X-ray diffraction and n.m.r. studies. Most of these quantitative i.r. studies have been carried out on polyethylene, notably by Read, Stein and their collaborators, and extensive measurements have been made on low density polyethylene¹, oxidized polyethylene¹, ethylene-carbon monoxide copolymers² and crosslinked amorphous polyethylene³.

The particular value of assessing the i.r. data in terms of orientation functions, rather than dichroic ratios, is that they can then be used to compare with other measures of orientation. In this paper we describe an i.r. spectroscopic study of poly(ethylene terephthalate) (PET) where the i.r. results are combined with measurements of refractive indices to provide quantitative information regarding both molecular orientation and conformational changes. The i.r. data will be analysed using the theoretical results derived in the previous paper⁴, which take into account both the reflectivity correction and the internal field effect.

There have been several previous i.r. structural studies of oriented PET fibres and films. Two aspects

have been given particular attention. First, there is the molecular orientation. In one way drawn films this is complicated by preferred orientation of the (100) planes of the crystalline regions^{5,6}. We have taken particular care to reduce this effect to a minimum in the films prepared for the present investigation. Secondly, there are the changes in rotational isomer content with changing degrees of deformation or draw ratio. It is now generally accepted that these are primarily associated with the *trans* and *gauche* isomerism of the ethylene glycol linkage⁷⁻⁹, and there have been a number of publications where it has been shown that the *trans* content increases and the *gauche* content decreases with increasing draw ratio or density¹⁰⁻¹². In the present paper, by combining quantitative measures of both molecular orientation and rotational isomer content, we are able to carry the analysis forward to a greater degree of sophistication than has hitherto been achieved.

THEORY

As the theory to be used has been described in detail in the previous paper⁴, only a brief summary will be given here.

The measurements are made with the electric vector of the polarized i.r. radiation along the draw direction (z) or perpendicular to the draw direction in the plane of the film (x). Absorption coefficients k_z and k_x are then calculated from equation (12) of the previous

paper, where the absorbance A is given by:

$$A = \log_{10} \frac{I_T}{I_T'} = 0.4343 \left\{ \frac{2ky_0}{\lambda} + \frac{2k^2}{(n + n_{\text{KBr}})^2} \right\} \quad (1)$$

where I_T , I_T' are the incident and transmitted intensities respectively at the peak of the absorption, n and k are the real and imaginary parts of the complex refractive index of the polymer at the free space wavelength λ , and n_{KBr} is the refractive index of the potassium bromide plates used to contain the sample (assumed constant and real). The thickness of the sample is y_0 , and the free space wavelength at the absorption peak is λ .

The value of k can be found directly from equation (1). This equation is a quadratic in k and has two solutions, one of which may be rejected by inspection, since an approximate value of k can be obtained in the absence of the reflectivity correction term $2k^2/(n + n_{\text{KBr}})^2$.

These values for k_z and k_x are then combined with the optical values of n_z and n_x , to obtain the imaginary parts of the corresponding average complex polarizabilities $\langle \alpha_z^* \rangle = \langle \alpha_z' \rangle - i \langle \alpha_z'' \rangle$ and $\langle \alpha_x^* \rangle = \langle \alpha_x' \rangle - i \langle \alpha_x'' \rangle$ (see ref 4), using the Lorentz-Lorenz equation. We have:

$$6n_z k_z \{ n_z^4 + 2n_z^2 k_z^2 + 4n_z^2 - 4k_z^2 + k_z^4 + 4 \}^{-1} = \frac{4\pi N}{3} \langle \alpha_z'' \rangle$$

$$= \phi_z$$

and

$$6n_x k_x \{ n_x^4 + 2n_x^2 k_x^2 + 4n_x^2 - 4k_x^2 + k_x^4 + 4 \}^{-1} = \frac{4\pi N}{3} \langle \alpha_x'' \rangle \quad (2)$$

$$= \phi_x$$

These polarizabilities, where N is the concentration of absorbing species/unit volume, relate to the distribution of molecular orientations as follows. It is assumed that an individual transition moment direction makes a fixed angle θ_m with the chain axis, and that the corresponding chain axis makes an angle θ with the draw direction.

It was shown in the previous paper that for a uniaxially oriented polymer:

$$\frac{\phi_z - \phi_x}{\phi_z + 2\phi_x} = P_2(\theta_m) \langle P_2(\theta) \rangle_{\text{ir}} \quad (3)$$

It is perhaps worth commenting that this equation is very closely related to the more familiar relationship in terms of the absorbances A_z and A_x , which follows directly from the molecular gas approximation without taking into account reflection losses and the internal field effect. In this case we have:

$$\frac{A_z - A_x}{A_z + 2A_x} = P_2(\theta_m) \langle P_2(\theta) \rangle_{\text{ir}}$$

In these equations $P_2(\theta_m) = \frac{1}{2}(3\cos^2\theta_m - 1)$ and is assumed to be a constant quantity depending only on the molecular structure of the polymer. It is, of course, quite possible that this assumption does not hold if there are changes in molecular conformation on drawing. $\langle P_2(\theta) \rangle_{\text{ir}} = \frac{1}{2}(3\langle \cos^2\theta \rangle_{\text{ir}} - 1)$, defines the mean value of $P_2(\theta)$, determined by the i.r. method for the molecular chain axes and is the orientation function which we will be primarily concerned with in this paper. The measurement thus provides a direct measure of the product of the constant quantity $P_2(\theta_m)$ and the orienta-

tion function $\langle P_2(\theta) \rangle_{\text{ir}}$. An absolute measure of the chain axis orientation can therefore be obtained either if θ_m is known or if the method can be calibrated by comparison with another method of measuring molecular orientation. In this investigation we have combined the i.r. measurements with refractive index measurements to examine the validity of the i.r. method and to provide a possible measure of absolute calibration.

For a transversely isotropic sample, the refractive indices n_z and n_x can also be used to calculate $\langle P_2(\theta) \rangle$. Since this is a different measure, we introduce the subscript 'opt'. Following the previous paper, letting

$$\frac{n_z^2 - 1}{n_x^2 + 2} = \phi_z^e \quad (4)$$

We then have:

$$\frac{\phi_z^e - \phi_x^e}{\phi_z^e + 2\phi_x^e} = \left\{ \frac{\Delta\alpha}{3\alpha_0} \right\} \langle P_2(\theta) \rangle_{\text{opt}} \quad (5)$$

$\Delta\alpha/3\alpha_0$ can be estimated from measurements on highly oriented samples where $\langle P_2(\theta) \rangle \rightarrow 1$. We have used the value 0.105 calculated from data in ref 6.

It can be appreciated that if the i.r. method provides an accurate measure of chain axis orientation then a plot of $P_2(\theta_m) \langle P_2(\theta) \rangle_{\text{ir}}$ against $\langle P_2(\theta) \rangle_{\text{opt}}$ will be linear. Moreover, the optical measurements can be regarded as providing a calibration of the i.r. technique, by allowing $P_2(\theta_m)$ to be calculated. Alternatively, if an independent estimate of θ_m can be obtained (say from crystallographic data) then the i.r. data can be directly converted to an absolute measure of chain axis orientation.

EXPERIMENTAL

Sample preparation

The starting material for all the samples investigated was isotropic amorphous PET film (intrinsic viscosity 0.61) of thickness 30 μm . This film was prepared by melt extrusion and quenching onto a chill roll. Two series of oriented films were studied. Series (i) was prepared by drawing strips of the isotropic film to a constant draw ratio of 4:1 at temperatures in the range 60°C to 100°C. Series (ii) was prepared by drawing at constant temperature (80°C) to different draw ratios in the range 1.5:1 to 5:1. Details of the sample dimensions, and the extensometer crosshead speeds used are listed in Table 1. For convenience a range of cross-head speeds was utilized in the sample preparation. Subsidiary experiments showed that this did not significantly affect the degree of molecular orientation achieved.

The sample thicknesses were measured with a precision dial indicator and were checked by near i.r. interference fringe measurements. These results are also shown in Table 1, together with density measurements obtained using a density column prepared from an aqueous solution of sodium bromide and water.

Refractive index measurements

The measurements of refractive index were undertaken using an image splitting interference microscope (Zeiss Zena Interphako) with accurately calibrated immersion liquids. All measurements were made at 551 nm. The results are shown in Table 2.

Table 1 Details of sample preparation

Temp. (°C)	Draw ratio	Crosshead speed (cm/min)	Gauge length (cm)	Width (cm)	Shape	Average thickness after drawing (μm)	Density
Series (i)							
60	4:1	5	8	3	Strip	11.5	1.362
65	4:1	5	8	3	Strip	12	1.362
70	4:1	5	8	3	Strip	14	1.362
75	4:1	5	8	3	Strip	14	1.358
80	4:1	5	8	3	Strip	16	1.358
87	4:1	5	4	3	Strip	16	1.355
94	4:1	5	4	3	Strip	11	1.356
100	4:1	5	4	3	Strip	12	1.356
Series (ii)							
80	1.5:1	Unknown (dead-loaded)	10	3	Taper	25	1.339
80	2.3:1	Unknown (dead-loaded)	10	2.5	Taper	20	1.340
80	2.7:1	Unknown (dead-loaded)	10	2	Taper	14	1.343
80	3.4:1	Unknown (dead-loaded)	10	1.5	Taper	16	1.354
80	3.7:1	Unknown (dead-loaded)	10	1	Taper	16.5	1.356
80	4.5:1	20	4	1	Dumbbell	12.5	1.365
80	5:2	20	4	1	Dumbbell	12.5	1.365
Isotropic	1:1	—	—	—	—	30	1.337

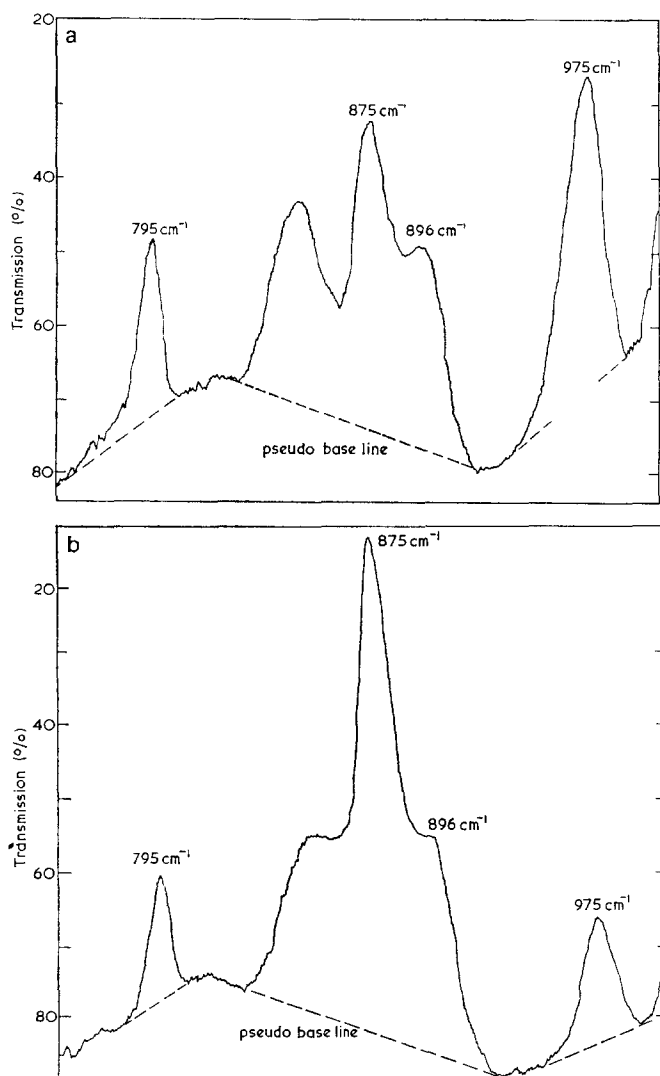


Figure 1 The infra-red spectrum of PET in the region 700–1000 cm⁻¹. Electric vector parallel to (a) z direction or (b) x direction

Infra-red measurements

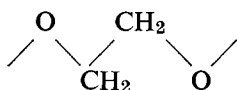
The i.r. measurements were carried out using a Hilger H800 double beam i.r. spectrometer, with a wire grid polarizer Cambridge Consultants Limited type 1CR 55. The measurements were made at normal incidence and the film sample was sandwiched between potassium bromide plates with a very thin film of Nujol between each surface. This reduces the reflection at the polymer surface, which for an isolated polymer film gives rise to interference fringes. The Nujol forms an approximate match for the refractive index of the polymer and has a low absorption in the region 750–1300 cm⁻¹. The wire grid polarizer was assumed to transmit radiation with the electric vector in one plane only, and the chart recorder was calibrated as a linear vertical scale so that the ratio I_T/I_T' could be determined directly from the curves, using a pseudo-base line as shown in *Figure 1*.

For each sample, two spectra were recorded in the normal incidence case, one with the electric vector parallel to the z direction and the other at right angles in the x direction. For each polarization the spectrometer was scanned through the range 750–1100 cm⁻¹ at a speed of 42.5 cm⁻¹/min and the slit width was gradually reduced from 0.9 mm at 750 cm⁻¹ to 0.5 mm at 1100 cm⁻¹. Typical examples of such spectra, obtained from a sample of intermediate draw ratio, are shown in *Figures 1a* and *1b*.

Absorption band assignments

The detailed assignment of the absorption bands in the i.r. spectrum of PET has been the subject of much attention and controversy. Some of this stems from the proposal originally made by one of us⁷⁻⁹, that the major differences between the i.r. spectra of amorphous and partly crystalline samples of PET are due to rotational

isomerism of the



group. Crystallographic studies¹³, showed that the conformation of this group in the crystalline regions is *trans*. It was proposed that in the amorphous regions the *gauche* conformation of this group is present as well as the *trans* conformation. Although this proposal was initially not generally accepted^{14, 15}, in most later papers^{12, 16-18} there is a general consensus that certain absorption bands can be identified with the *trans* and *gauche* conformations. In this paper we have chosen the 975 cm⁻¹ *trans* band and the 896 cm⁻¹ *gauche* band for quantitative analysis.

It is also valuable to analyse the behaviour of absorption bands associated with the terephthalate group, and more particularly the benzene ring. Here we have chosen the 795 cm⁻¹ and 875 cm⁻¹ bands. The 875 cm⁻¹ band has the added advantage that it can be assigned with some certainty to an out-of-plane C-H deformation vibration, in which the transition moment vector lies normal to the plane of the benzene ring. From the crystallographic data¹³, θ_m the angle which the transition moment vector makes with the chain axis would then be about 86°.

RESULTS AND DISCUSSION

The optical measurements of the refractive indices n_z and n_x were used to calculate the refractive index of the isotropic polymer n_{iso} , on the basis of averaging the polarizabilities and assuming that the samples were transversely isotropic. As before, the Lorentz-Lorenz equation is used to relate polarizabilities and refractive index. We have:

$$\frac{n_{iso}^2 - 1}{n_{iso}^2 - 2} = \frac{1}{3} \frac{\rho_t}{\rho_0} \left(\frac{n_z^2 - 1}{n_z^2 + 2} + \frac{2(n_x^2 - 1)}{n_x^2 + 2} \right)$$

Table 2 Refractive index measurements

Temp. (°C)	Draw ratio	n_z	n_x	n_i (predicted)	$\langle P_2(\theta) \rangle_{opt}$
Series (i)					
60	4:1	1.713†	1.540	1.582	0.729
65	4:1	1.709	1.540	1.590	0.715
70	4:1	1.703	1.542	1.580	0.682
75	4:1	1.695	1.540	1.579	0.663
80	4:1	1.679	1.549	1.580	0.557
87	4:1	1.660	1.555	1.580	0.453
94	4:1	1.620	1.570	1.576	0.219*
100	4:1	1.587	1.576	1.570	0.049*
Series (ii)					
80	1.5:1	1.592	1.576	1.580	0.071
80	2.3:1	1.621	1.563	1.580	0.256
80	2.7:1	1.623	1.563	1.580	0.264
80	3.4:1	1.658	1.553	1.578	0.455
80	3.7:1	1.684	1.547	1.581	0.586
80	4.5:1	1.704	1.540	1.578	0.696
80	5:1	1.705	1.540	0.578	0.700
Isotropic	—	1.582	1.582	1.582	0

* These samples were not used in the subsequent i.r. analysis because of the poor predicted value of n_i

† These values were obtained by extrapolation of the higher temperature n_z data

where ρ_t and ρ_0 are the densities of the isotropic polymer and the oriented film respectively. Table 2 shows that the predicted values of n_{iso} correspond very closely to the experimental value of 1.582, confirming that these samples are transversely isotropic to a very good approximation.

The optical data have also been used to calculate the overall molecular orientation function $\langle P_2(\theta)_{opt} \rangle$ on the basis of equations (4) and (5) above, and the results are shown in Table 2.

The i.r. measurements on the bands at 875, 795 and 896 cm⁻¹ were first used to calculate the absorbances A_z and A_x , corrected for reflection at the interfaces using equation (1). These absorbances were then used to calculate the quantities ϕ_z and ϕ_x , on the basis of equations (4). Finally values of the i.r. orientation function product $P_2(\theta_m)\langle P_2(\theta) \rangle_{ir}$ were calculated using equation (3).

It is also possible to calculate the orientation functions ignoring the local field correction, by assuming that $\langle \alpha^* \rangle \propto n^{*2} - 1$, i.e. $\langle \alpha'' \rangle \propto nk$. Values of $P_2(\theta_m)\langle P_2(\theta) \rangle_{ir}$ so calculated for the 875 cm⁻¹ band are shown in Figure 4.

Comparison of the i.r. and optical orientation functions

The 875 and 795 cm⁻¹ bands are both associated with vibrations of the benzene ring. They are therefore not directly affected by conformational changes in the same way as the 975 and 896 cm⁻¹ bands, and might be expected to give an indication of the overall chain orientation. The optical orientation functions are derived on the premise that they relate to the orientation of an extended repeat unit. Figures 2 and 3 show values

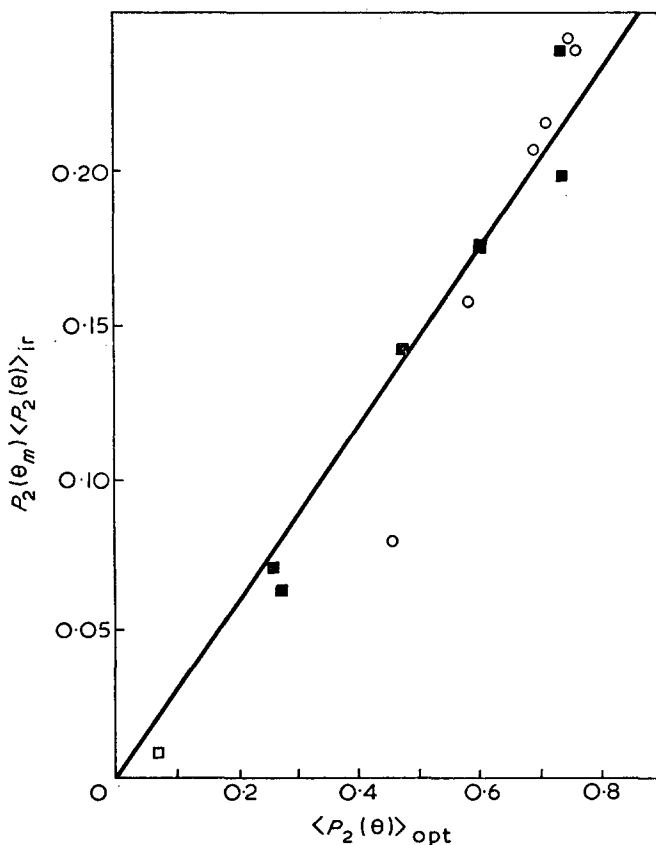


Figure 2 Values of $P_2(\theta_m)\langle P_2(\theta) \rangle_{ir}$ for the 875 cm⁻¹ band as a function of $\langle P_2(\theta) \rangle_{opt}$. ○, Series (i); ■, series (ii)

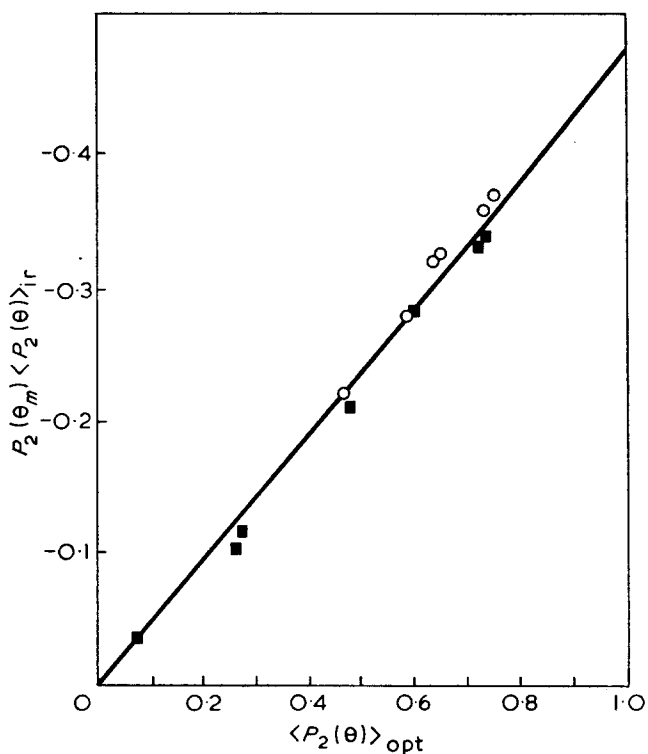


Figure 3 Values of $P_2(\theta_m) \langle P_2(\theta) \rangle_{\text{ir}}$ for the 795cm^{-1} band as a function of $\langle P_2(\theta) \rangle_{\text{opt}}$. ○, Series (i); ■, series (ii)

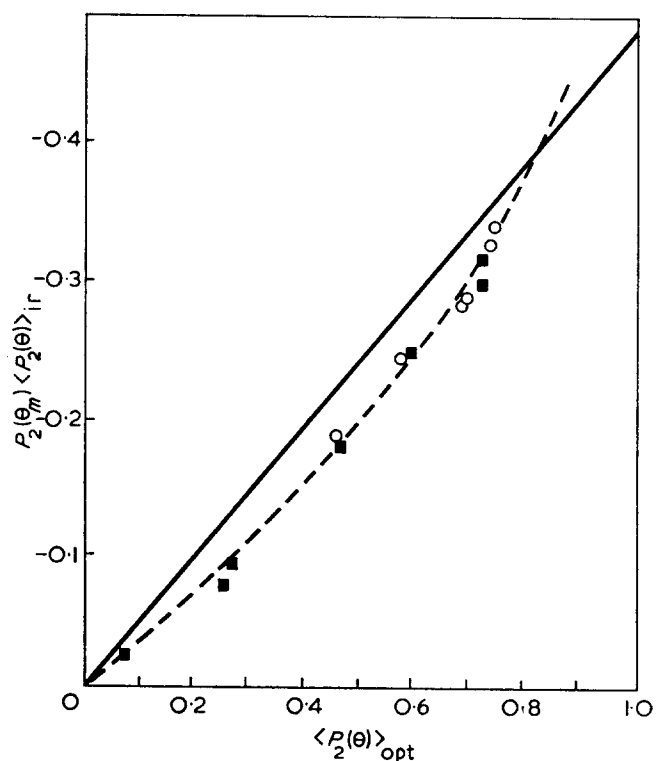


Figure 4 Values of $P_2(\theta_m) \langle P_2(\theta) \rangle_{\text{ir}}$ for the 875cm^{-1} band as a function of $\langle P_2(\theta) \rangle_{\text{opt}}$; results obtained ignoring the internal field correction. ○, Series (i); ■, series (ii)

of $P_2(\theta_m) \langle P_2(\theta) \rangle_{\text{ir}}$ plotted as a function of $\langle P_2(\theta) \rangle_{\text{opt}}$ for the 875 and 795cm^{-1} bands respectively, for the two series of oriented samples. There is an excellent linear relationship between these two parameters for both bands, confirming that both are measuring similar quantities. The greater consistency of the results for the 875cm^{-1} band can be attributed to its greater

degree of anisotropy in absorbance. In the case of the 875cm^{-1} band, if it is assumed that the optical measurements provide an absolute calibration, the value of θ_m is found to be 85° . This agrees well with the value expected on the basis of the band assignment*. Hence we can make the following identity, $\langle P_2(\theta) \rangle_{\text{ir}}^{875} \equiv \langle P_2(\theta) \rangle_{\text{opt}}$.

These results were obtained using the Lorentz-Lorenz internal field correction. Figure 4 shows a comparison of the optical orientation functions with those deduced from the i.r. data for the 875cm^{-1} band ignoring the local field correction. The solid line shows the expected correlation for $\theta_m = 85^\circ$. The experimental correlation is now less good, and it appears that the value of $\langle P_2(\theta) \rangle$ is an underestimate. These results give some support for the validity of our treatment.

The orientation behaviour of the 975 and 896cm^{-1} bands associated with the *trans* and *gauche* conformations respectively, is much more complicated than for the 875 and 795cm^{-1} bands. Figure 5 shows values of $P_2(\theta_m) \langle P_2(\theta) \rangle_{\text{ir}}$ for the 975cm^{-1} *trans* band as a function of $\langle P_2(\theta) \rangle_{\text{opt}}$. In this case there is not a linear relationship, but the *trans* orientation function increases rapidly for low optical orientation function values to achieve an almost constant value for $\langle P_2(\theta) \rangle_{\text{opt}} > 0.5$. This result shows that the orientation of the *trans* conformation is not representative of the overall chain axis orientation. Figure 6 shows the corresponding results for the 896cm^{-1}

* In view of the possible errors in $\Delta\alpha/3\alpha_0$ such close agreement may well be fortuitous.

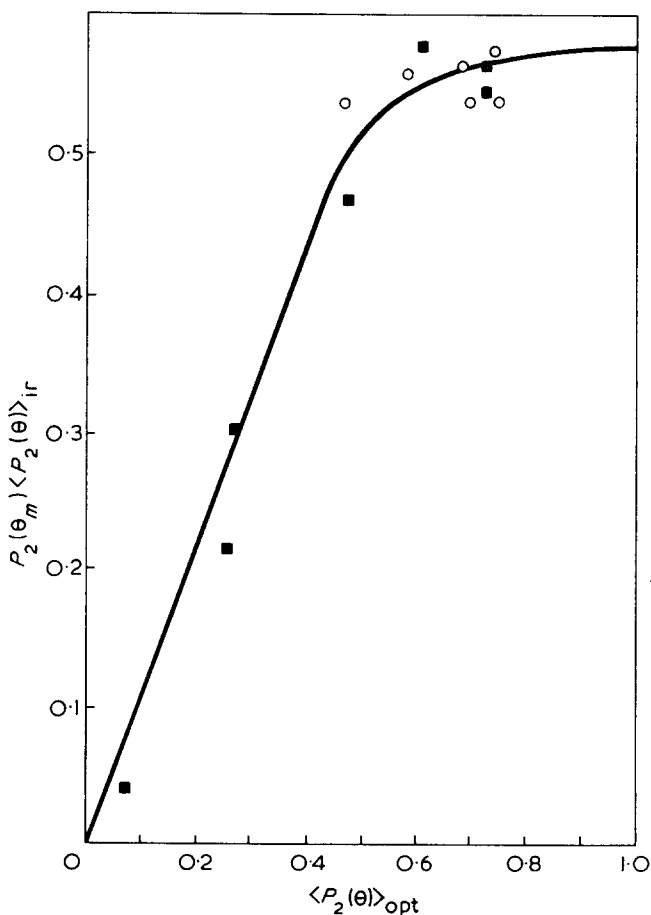


Figure 5 Values of $P_2(\theta_m) \langle P_2(\theta) \rangle_{\text{ir}}$ for the 975cm^{-1} *trans* band as a function of $\langle P_2(\theta) \rangle_{\text{opt}}$. ○, Series (i); ■, series (ii)

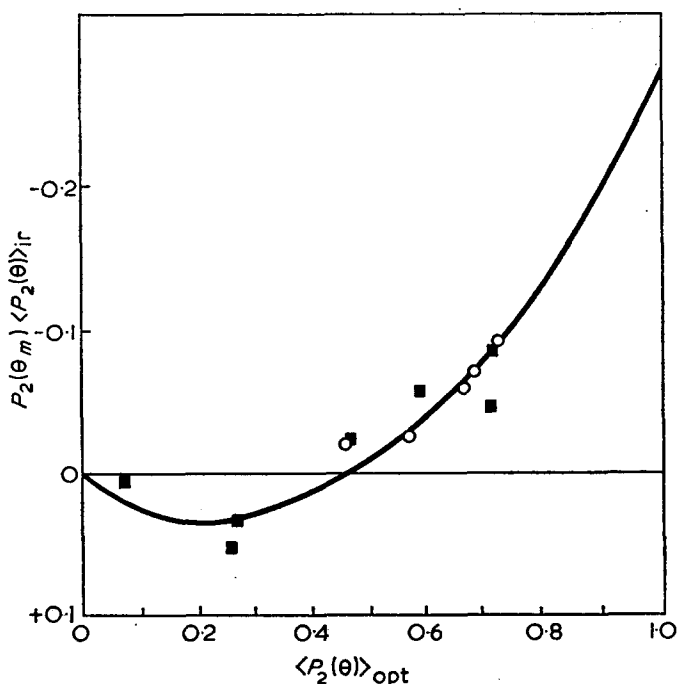


Figure 6 Values of $P_2(\theta_m) \langle P_2(\theta) \rangle_{ir}$ for the 896 cm^{-1} gauche band as a function of $\langle P_2(\theta) \rangle_{opt}$. \circ , Series (i); \blacksquare , series (ii)

gauche conformation band. In this case a completely different pattern is observed. The gauche orientation function is small and positive for $\langle P_2(\theta) \rangle_{opt} < 0.45$ and then becomes negative, the numerical value increasing rapidly in the highly oriented samples.

These results, taken together, suggest the following. First, that the molecular segments which contain the trans conformation possess at low overall orientation much higher orientation than those segments which contain the gauche conformation. Secondly, that up to $\langle P_2(\theta) \rangle_{opt} \sim 0.45$ the gauche orientation distribution is very close to isotropic. There is even an indication that the gauche segments for low orientation may be oriented transversely to the draw direction. However, it is difficult to study the 896 cm^{-1} band quantitatively in terms of orientation because it overlaps with the strong 875 cm^{-1} band. The i.r. data must therefore be regarded as inconclusive in this particular detail. Finally, it is clear that at high degrees of overall molecular orientation there is appreciable alignment of the gauche segments.

The concentration of the absorbing groups

The concentration of the absorbing groups can be estimated from a calculated value of ϕ_0 .

It was found that the calculated values of ϕ_0 for the 875 and 795 cm^{-1} bands are approximately constant for all degrees of molecular orientation. This result is an expected one, since these bands have been assigned to vibrational modes which are independent of the conformational state of the molecule.

On the other hand, the values of ϕ_0 for the 975 cm^{-1} trans band and 896 cm^{-1} gauche band show a strong dependence on the degree of overall molecular orientation. This can be seen in Figure 7 where ϕ_0 is shown as a function of $\langle P_2(\theta) \rangle_{opt}$, and we observe a smooth increase in trans content and a smooth decrease in gauche content with increasing overall molecular orientation. We have attempted to make the extrapolations of ϕ_0 to full overall molecular orientation (i.e.

$\langle P_2(\theta) \rangle_{opt} = 1$) for both the trans and gauche bands. If we combine these extrapolations (shown in Figure 7) with the assumption that there is 100% trans concentration at full overall orientation, we have a very simple picture. The extrapolation of the 975 cm^{-1} band then gives us the value of the polarizability for 100% trans concentration; hence we can find the trans concentration for an isotropic sample and thus the corresponding gauche concentration. We are then able to calculate the trans and gauche concentrations for each sample, which, of course, should total 100%. In fact, we chose the value of ϕ_0 for 100% trans concentration, which gave the best overall fit to the data so that the sum of the trans and gauche concentration totalled as close to 100% as a least squares fit would provide. Table 3 lists these intermediate concentration values and it can be seen that there is very good internal consistency. A remarkable result, which is not to be expected, is that absolute values obtained for the polarizabilities of the trans and gauche species by this fitting procedure are identical. It can readily be appreciated that this is so

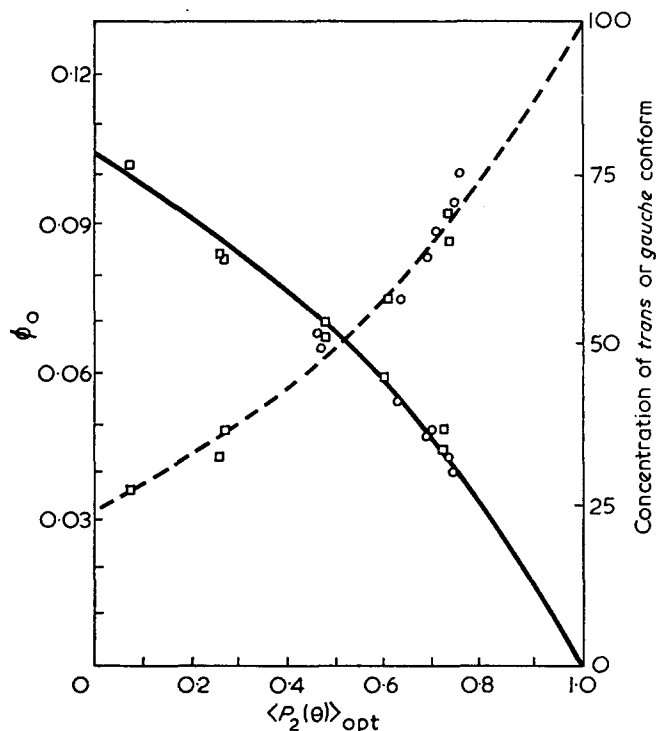


Figure 7 Values of ϕ_0 and concentration for the trans conformation (975 cm^{-1} band) and the gauche conformation (896 cm^{-1} band) as a function of $\langle P_2(\theta) \rangle_{opt}$. - - -, trans; —, gauche. \circ , Series (i); \square , series (ii)

Table 3 trans and gauche concentrations

$\langle P_2(\theta) \rangle_{opt}$	% trans (x_i)	% gauche (y_i)	($x_i + y_i$)
0.0	24	76	100
0.1	28	72	100
0.2	32	67	99
0.3	38	61	99
0.4	44	56	100
0.5	50	49	99
0.6	58	42	100
0.7	68	34	102
0.8	77	24	101
0.9	88	13	101
1.0	100	0	100

by noting that the ϕ_0 curves for the *trans* and *gauche* species (Figure 7) cross at a point corresponding to 50% *trans*. It should perhaps be pointed out that although the absolute values of the polarizabilities of the *trans* and *gauche* species are identical for the present series of samples this may not hold for other samples where high degrees of crystallinity are obtained. In the samples examined here the crystallinities were always very low, and usually less than 10%.

Relationship between molecular orientation and changes in molecular conformation

It has already been remarked that the *gauche* orientation is very low over most of the orientation range. This implies that the overall molecular orientation arises largely from those molecular chains possessing the *trans* conformation. Moreover, at high overall molecular orientation there is little further increase in the *trans* orientation. The values of the orientation function for the 975cm^{-1} *trans* band, $\langle P_2(\theta) \rangle_{\text{ir trans}} \times P_2(\theta_m^{\text{trans}})$ can be extrapolated to give a constant value for high overall molecular orientation. If it is assumed that this value corresponds to complete orientation of the *trans* conformers, this gives a value for θ_m^{trans} of 32° . With this result we can then calculate absolute values of $\langle P_2(\theta) \rangle_{\text{ir trans}}$ for intermediate degrees of overall molecular orientation. These results are shown in Table 4.

Furthermore, recalling that the orientation of the *gauche* conformers is very small, it can be suggested that to a good first approximation the optical orientation function $\langle P_2(\theta) \rangle_{\text{opt}}$ which reflects the overall orientation is given by:

$$\langle P_2(\theta) \rangle_{\text{opt}} = f_{\text{trans}} \langle P_2(\theta) \rangle_{\text{ir trans}}$$

where f_{trans} is the *trans* mass fraction. The results shown in Table 4 confirm that this is a reasonable approximation.

A more remarkable feature of all the results, however, is the exact similarity of the data for the two series of samples, and this suggests that there is a unique relationship between the concentration of *trans* and *gauche* conformers and the overall orientation as revealed by optical measurements or by the orientation of the 875 or 795cm^{-1} bands.

A possible explanation of this remarkable result is that both the conformational content and the molecular orientation relate only to the overall strain, irrespective of the temperature and conditions of draw. This explanation would certainly hold for a given temperature if the drawing process can be regarded as the extension

Table 4 Comparison of $\langle P_2(\theta) \rangle_{\text{opt}}$ with $f_{\text{trans}} \langle P_2(\theta) \rangle_{\text{ir trans}}$

$\langle P_2(\theta) \rangle_{\text{opt}}$	$\langle P_2(\theta) \rangle_{\text{ir trans}}$	$f_{\text{trans}} \langle P_2(\theta) \rangle_{\text{ir trans}}$
0.0	0.0	0.0
0.1	0.2	0.06
0.2	0.4	0.13
0.3	0.6	0.23
0.4	0.8	0.35
0.5	0.9	0.45
0.6	0.9(5)	0.55
0.7	1.0	0.68
0.8	1.0	0.77
0.9	1.0	0.88
1.0	1.0	1.00

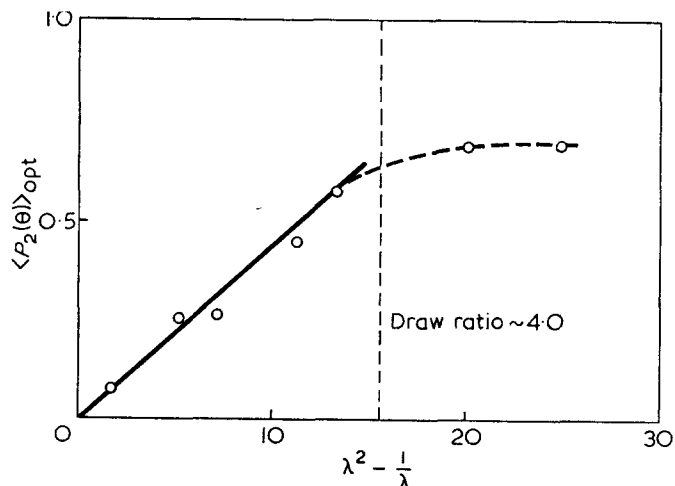


Figure 8 Plot of $\langle P_2(\theta) \rangle_{\text{opt}}$ against $[\lambda^2 - (1/\lambda)]$ for series (ii) (samples drawn to a series of draw ratios at 80°C)

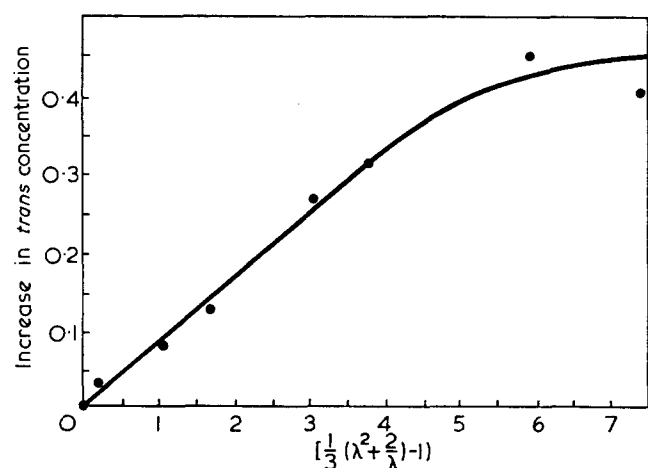


Figure 9 The change in *trans* concentration for series (ii) as a function of $[1/3(\lambda^2 + (2/\lambda)) - 1]$

of a rubberlike network, and we will discuss two pieces of evidence which support this view. First, there is the development of orientation in a rubberlike network. If it is assumed that the network can be considered as a network of freely jointed chains of identical links¹⁹ (the so-called random links), it can be shown²⁰ that the orientation function $\langle P_2(\theta) \rangle_{\text{random link}}$ for the random links is given by:

$$\langle P_2(\theta) \rangle_{\text{random link}} = \frac{1}{5N} \left(\lambda^2 - \frac{1}{\lambda} \right) + \text{terms in } \frac{1}{N^2}, \text{ etc.}$$

where N is the number of random links between the network junction points (the entanglements) and λ is the extension or draw ratio. Stress-optical data on PET in the temperature range 60 – 90°C showed²¹ that the behaviour fitted this model to a good approximation, and a value of about 6 was obtained for N . A plot of the present 80°C results for $\langle P_2(\theta) \rangle$, based on the values obtained for the overall molecular orientation, is shown in Figure 8. It can be seen that there is a good linear relationship between $\langle P_2(\theta) \rangle$ and $[\lambda^2 - (1/\lambda)]$ up to a draw ratio λ of 3.5, and this gives a value for N of about 5, in reasonable agreement with the previous stress-optical results.

A second piece of evidence comes from a consideration of the conformational content as a function of draw ratio. According to Abe and Flory²², the average

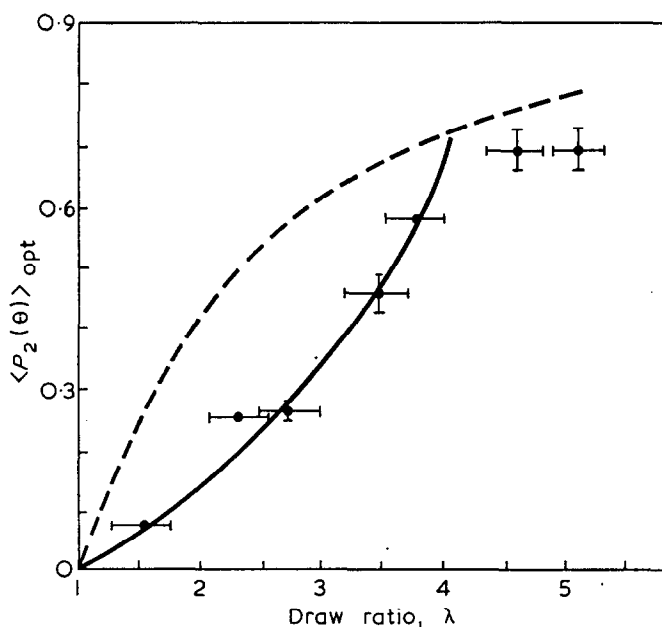


Figure 10 $\langle P_2(\theta) \rangle_{\text{opt}}$ as a function of draw ratio, showing fit to rubberlike (number of random links, $N=4.8$) network (—) at low draw ratios and turn over to pseudo-affine deformation scheme (---) at high draw ratios

change in the content of a particular conformer, Δm_{trans} , say, relates to the extensional strain λ , by an equation of the form:

$$\Delta m_{\text{trans}} = \nu D_2 \left[\frac{1}{3} \left(\lambda^2 + \frac{2}{\lambda} \right) - 1 \right]$$

where ν is the total number of chains in the network and D_2 is a constant of proportionality which can in theory be calculated provided that the internal energies of the different conformational states is defined.

In Figure 9 the change in the concentration of the *trans* conformer is plotted as a function of $[1/3 \times \{\lambda^2 + (2/\lambda)\} - 1]$ for series (ii). Again a reasonable straight line relationship is obtained up to a draw ratio of about 3.5.

These results suggest, therefore, that it is not unreasonable to obtain a good correlation between molecular orientation and conformer content in the low draw ratio range where the extension of the polymer is akin to that of a rubberlike network. It is perhaps more remarkable that the correlation holds to high draw ratios where the behaviour fits the pseudo-affine deformation scheme²³ more closely, as shown by the broken line in Figure 10. This aspect will be discussed in detail in a future paper, where measurements of

molecular orientation by polarized Raman spectroscopy and polarized fluorescence are also presented.

CONCLUSIONS

- (1) Polarized infra-red spectroscopy can provide accurate measures of overall molecular orientation in PET. There is confirmation that corrections for reflectivity and the internal field effect are required.
- (2) The combination of measurements of molecular orientation with concentration of conformers can throw light on the deformation mechanisms occurring during drawing.

ACKNOWLEDGEMENTS

During the period of this research A. C. held a Science Research Council CAPS studentship. We are indebted to Imperial Chemical Industries, Plastics Division as the industrial sponsor. We also wish to thank Mr P. I. Vincent for useful discussions and for assistance with sample preparation, and to Dr G. R. Davies for his advice on some of the theoretical aspects.

REFERENCES

- 1 Read, B. E. and Stein, R. S. *Macromolecules* 1968, **1**, 116
- 2 Phillips, P. J., Wilkes, G. L., Delf, B. W. and Stein, R. S. *J. Polym. Sci. (A-2)* 1971, **9**, 499
- 3 Read, B. E. and Hughes, D. A. *Polymer* 1972, **13**, 495
- 4 Cunningham A., Davies, G. R. and Ward, I. M. *Polymer* 1974, **15**, 743
- 5 Heffelfinger, C. J. and Burton, R. C. *J. Polym. Sci.* 1960, **47**, 289
- 6 Kashiwagi, M., Cunningham, A., Manuel, A. J. and Ward, I. M. *Polymer* 1973, **14**, 111
- 7 Ward, I. M. *Chem. Ind.* 1956, p 905
- 8 Ward, I. M. *Chem. Ind.* 1957, p 1102
- 9 Grime, D. and Ward, I. M. *Trans. Faraday Soc.* 1958, **54**, 959
- 10 Miller, R. G. J. and Willis, H. A. *J. Polym. Sci.* 1956, **19**, 485
- 11 Farrow, G. and Ward, I. M. *Polymer* 1960, **1**, 330
- 12 Schmidt, P. G. *J. Polym. Sci. (A)* 1963, **1**, 1271
- 13 Daubeny, R. de P., Bunn, C. W. and Brown, C. J. *Proc. R. Soc. (A)* 1954, **226**, 531
- 14 Liang, C. Y. and Krimm, S. *J. Mol. Spectros.* 1959, **3**, 554
- 15 Boye, C. A. *J. Polym. Sci.* 1961, **55**, 261
- 16 Krimm, S. *Adv. Polym. Sci.* 1960, **2**, 51
- 17 Daniel, W. W. and Kitson, R. E. *J. Polym. Sci.* 1958, **33**, 161
- 18 Miyake, A. *J. Polym. Sci.* 1959, **38**, 479
- 19 Kuhn, W. and Grün, W. *Kolloid-Z.* 1942, **101**, 248
- 20 Roe, R. J. and Krigbaum, W. R. *J. Appl. Phys.* 1964, **35**, 2215
- 21 Pinnock P. R. and Ward, I. M. *Trans. Faraday Soc.* 1966, **62**, 1308
- 22 Abe, Y. and Flory, P. J. *J. Chem. Phys.* 1970, **52**, 2814
- 23 Ward, I. M. 'Mechanical Properties of Solid Polymers', Wiley, London, 1971, p 258

Note to the Editor

Molecular weight dependence of the spherulitic growth rate of isotactic polystyrene

P. J. Lemstra, J. Postma and G. Challa

Laboratory of Polymer Chemistry, State University of Groningen, Groningen, The Netherlands
(Received 16 April 1974)

The influence of molecular weight on the crystallization rate of polymers has been the subject of various papers¹⁻⁵. However, no study on the molecular weight dependence of the spherulitic growth rate of isotactic polystyrene (i-PS) has been published before. Owing to the low crystallization rate we were able to study the spherulitic growth rate in a broad temperature between the melting temperature and the glass transition temperature.

Samples of different molecular weight were obtained by heating high molecular weight i-PS at 290°C under nitrogen atmosphere for various times. At this temperature the molecular weight rapidly decreases owing to random chain scission⁶. Hereafter each sample was dissolved into dichloromethane and the solution was added slowly to boiling methyl ethyl ketone. By evaporation of dichloromethane i-PS precipitated quantitatively from the ketone leaving the contaminating atactic polystyrene in solution. The purified samples were dissolved in toluene and pumped through a column filled with Merckogel GPC glass granules (type S1, 1000 Å) in order to fractionate the samples. The eluate was collected with a fractional collector (Baird and Tatlock). The low and high molecular weight tails were omitted and the remaining parts were used for further experiments. This roundabout method of sample preparation was necessary because normal Ziegler-Natta polymerization of styrene produces very high molecular weight i-PS.

¹³C n.m.r. (FT) spectra recorded on the Varian XL-100/15 at 25.2 MHz, showed that the degrees of isotacticity⁷ of the various samples were the same within experimental error (92% isotactic triads).

The number-average molecular weights of the samples were measured in toluene at 35°C with an automatic osmometer (Hallikainen) and the viscosity average molecular weights in toluene at 30°C with a Ubbelohde

viscometer. The glass transition temperatures (T_g) and melting temperatures (T_m) were measured with a differential scanning calorimeter (Perkin-Elmer DSC-1B). All sample data are compiled in *Table 1*. The melting temperature T_m^0 as found by extrapolation of the melting temperatures T_m versus the crystallization temperature T_c was the same for each sample, viz. 242°C as found before⁸.

The spherulitic growth rates G were measured using a Leitz hotstage microscope. Temperature control was within $\pm 0.2^\circ\text{C}$. The samples were heated on the microscope up to 250°C and after complete melting (for 15 min) cooled down to T_c . At this temperature the diameter of the spherulites was measured as a function of time by means of a Leitz ocular. *Figure 1* shows the temperature dependence of the spherulitic growth rate for the various samples. In comparing the growth rates G with those found by other authors^{9, 10} differences were found. In our opinion degradation is the cause of these differences. When i-PS is not thoroughly purified catalyst residues enhance the rate of degradation enormously during melting prior to crystallization.

To analyse the experimental data we used the following rate equation^{11, 12}:

$$G = G_0 \exp[-c_1 c_2 / (c_2 + T_c - T_g)] \exp(-4b_0 \sigma \sigma_e / \Delta F k T_c) \quad (1)$$

G_0 is a pre-exponential factor which is generally assumed to be constant or proportional to T_c . The first exponential term, the transport term, contains two constants c_1 and c_2 originating from the empirical relationship for viscous flow given by Williams *et al.*¹³. In the second exponential term b_0 is the thickness of a monomolecular layer on the crystal surface, σ and σ_e are interfacial free energies per unit area parallel and perpendicular respectively to the molecular chain direction of the growing crystal, and ΔF is the Gibbs free energy difference per unit

Table 1 Crystallization parameters for different samples of isotactic polystyrene

Sample	$\bar{M}_n \times 10^{-3}$	$\bar{M}_v \times 10^{-3}$ *	T_g (°C)	$\sigma \sigma_e$ (erg ² /cm ⁴)†	G_0 (μm/min)	$\sigma \sigma_e$ (erg ² /cm ⁴)‡	G_0^+ (μm/min K)
A	290	460	87	126	1730	117	5.0
B	220	390	87	121	1820	114	5.4
C	180	330	87	116	1970	111	5.7
D	85	125	86	114	2380	108	6.7
E	70	110	85	110	2508	105	7.0
F	30	58	84	107	3060	102	8.2

* From $[\eta] = K \cdot \bar{M}_v^a$ dl/g with $K = 9.3 \times 10^{-5}$ and $a = 0.72$ (data taken from Trossarelli, L. *et al.* *J. Polym. Sci.* 1959, 35, 205)

† Calculated from *Figure 2*

‡ Calculated from *Figure 3*

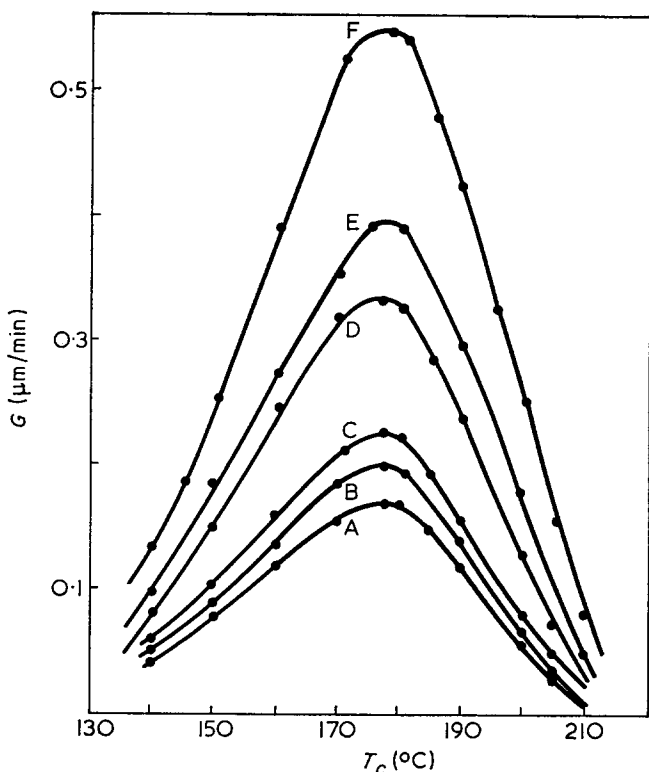


Figure 1 Spherulitic growth rate vs. crystallization temperature for various samples of isotactic polystyrene. Letters A-F refer to samples in Table 1

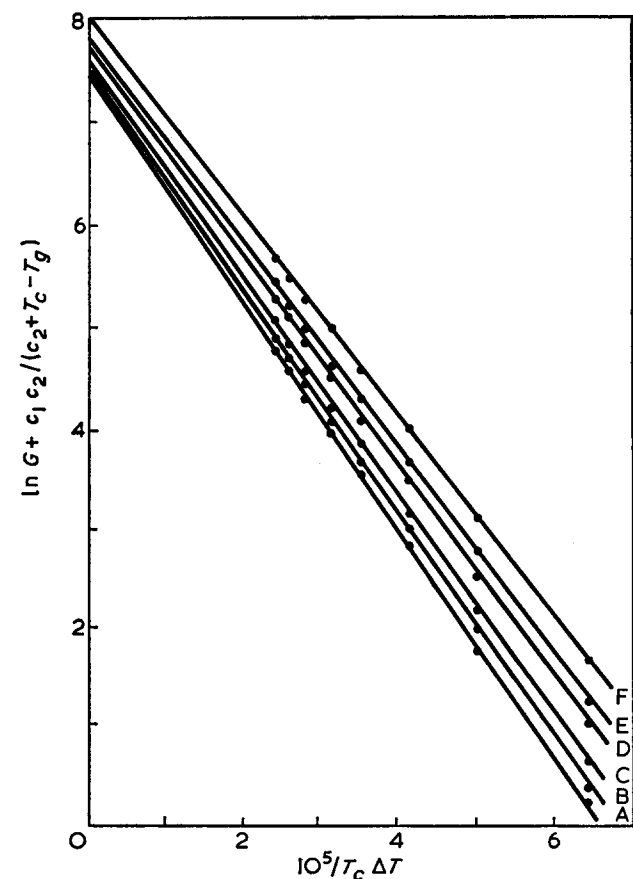


Figure 2 Plots of $\ln G + c_1c_2/(c_2 + T_c - T_g)$ vs. $1/T_c\Delta T$ for various samples of isotactic polystyrene. Letters A-F refer to samples in Table 1

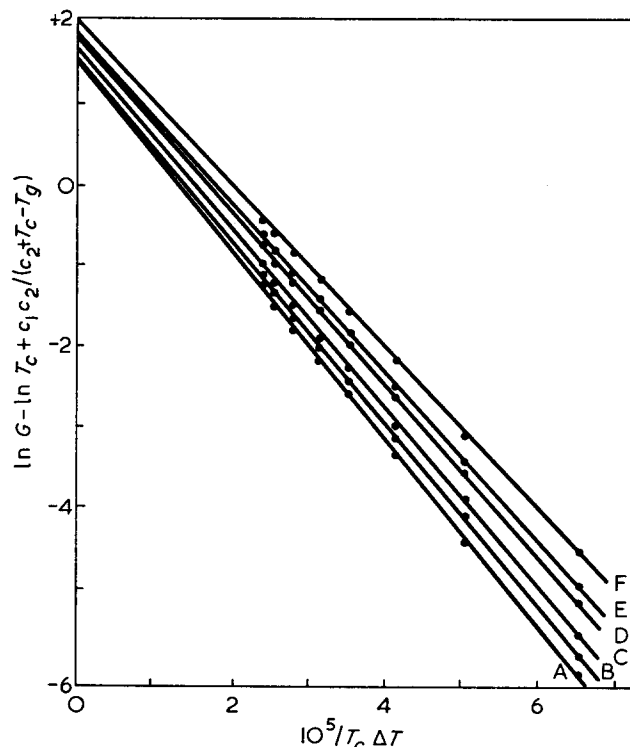


Figure 3 Plots of $\ln G - \ln T_c + c_1c_2/(c_2 + T_c - T_g)$ vs. $1/T_c\Delta T$ for various samples of isotactic polystyrene. Letters A-F refer to samples in Table 1

volume between the supercooled melt and the crystalline phase. ΔF can be approximated by¹²:

$$\Delta F = \Delta H \cdot \Delta T / T_m^0 \quad (2)$$

ΔH is the heat of fusion per unit volume and ΔT is the supercooling $T_m^0 - T_c$. In the case of i-PS this is a fairly good approximation as shown by Suzuki and Kovacs⁹ because the degree of supercooling is rather large and the transport term makes the more important contribution to G . Substitution of equation (2) into (1) yields:

$$G = G_0 \exp[-c_1c_2/(c_2 + T_c - T_g)] \times \exp(-4b_0\sigma\sigma_e T_m^0/k\Delta H T_c \Delta T) \quad (3)$$

When we plot $\ln G + c_1c_2/(c_2 + T_c - T_g)$ vs. $1/T_c\Delta T$ a straight line should be obtained provided that the correct values for c_1 and c_2 are substituted. In principle several combinations (c_1, c_2) are possible*. Taking $c_2 = 30K$, which seems a reasonable value⁹, straight lines are obtained for $c_1 = 22$ for all samples (see Figure 2). For different samples G_0 can be calculated from the intercepts in Figure 2. It appears that G_0 depends on molecular weight and is proportional to $\bar{M}_n^{-0.25}$ which can be calculated from the slope of the graph $\ln G_0$ vs. $\ln \bar{M}_n$ (see Figure 4). Taking $b_0 = 5.5 \times 10^{-8} \text{ cm}$, as introduced by Suzuki and Kovacs⁹, and $\Delta H = 86 \times 10^7 \text{ erg/cm}^3$ ¹⁵ the products $\sigma\sigma_e$ were calculated from the slopes in Figure 2 (see Table 1). The product $\sigma\sigma_e$ increases

* Some authors^{1, 9, 14} analysed their data of spherulitic growth rates in terms of a rate equation analogous to equation (3) but with a first exponential term $\exp[-C/R(c_2 + T_c - T_g)]$. With a computer program they optimized the parameters G_0, C_1, c_2 , and the nucleation parameter $4b_0\sigma\sigma_e T_m^0/k\Delta H$. In this way they found optimum values for C_1 and c_2 . However, this optimization procedure is not quite correct because C_1 and c_2 are mutually dependent: $C_1/R = c_1c_2$.

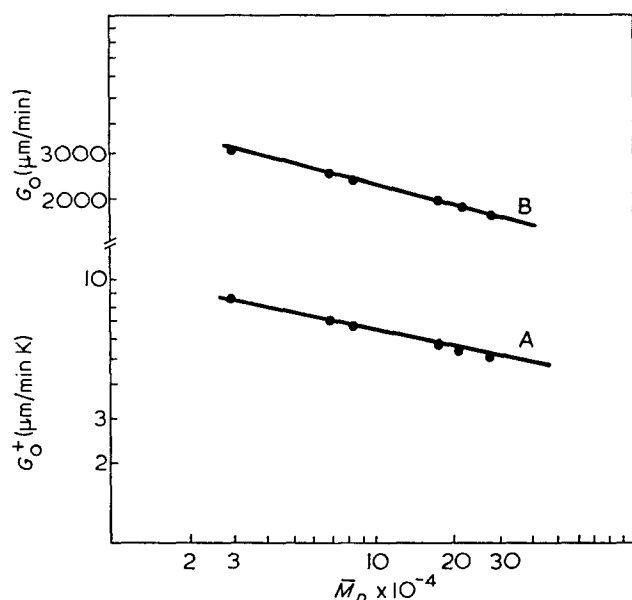


Figure 4 The pre-exponential factors G_0 (B) and G_0^+ (A) vs. \bar{M}_n on double logarithmic scale

with increasing molecular weight as usually found for other polymers too⁵.

When we analyse our data, taking into account that G_0 in equation (3) may be proportional to T_c , straight lines are obtained for the same combination $c_1=22$; $c_2=30\text{K}$ when plotting: $\ln G - \ln T_c + c_1 c_2 / (c_2 + T_c - T_g)$ vs. $1/T_c \Delta T$.

From the intercepts in Figure 3, $G_0^+ (= G_0/T_c)$ can be calculated (see Table 1). We see that G_0^+ also depends on molecular weight and that the values for the product $\sigma\sigma_e$ are in the same range as found above. The molecular weight dependence of G_0^+ is given by $\bar{M}_n^{-0.20}$ (see Figure 4).

The values for $\sigma\sigma_e$ which were calculated from Figures

2 and 3 are close* to those found by Suzuki and Kovacs⁹. In contrary to polyethylene¹¹ the values of G_0 and $G_0^+ \cdot T^+$ are much smaller than the theoretical limit of the Eyring theory $b_0 k T^+ / h = 3.1 \times 10^{11} \mu\text{m}/\text{min}$. (T^+ is the temperature at which G has its maximum value, h is Planck's constant.) This shows that other factors may play an important role in the crystallization of i-PS such as chain conformation and chain stiffness which give rise to a different crystallization mechanism¹⁶. The small dependence of G_0 and G_0^+ on molecular weight supports this view.

REFERENCES

- 1 van Antwerpen, F. and van Krevelen, D. W. *J. Polym. Sci. (A-2)* 1972, **10**, 2423
- 2 Lovering, E. G. *J. Polym. Sci. (A-2)* 1970, **8**, 747
- 3 Magill, J. H. *J. Polym. Sci. (A-2)* 1969, **7**, 1187
- 4 Ueberreiter, K. and Lucas, K. *J. Makromol. Chem.* 1970, **140**, 65
- 5 Devoy, C. and Mandelkern, L. *J. Polym. Sci. (A-2)* 1969, **7**, 1883
- 6 Boon, J. and Challa, G. *Makromol. Chem.* 1965, **84**, 25
- 7 Inoue, Y., Nishioka, A. and Riihioro, C. *Makromol. Chem.* 1972, **156**, 207
- 8 Lemstra, P. J., Kooistra, T. and Challa, G. *J. Polym. Sci. (A-2)* 1972, **10**, 823
- 9 Suzuki, T. and Kovacs, A. J. *Polym. J.* 1970, **1**, 82
- 10 Yeh, G. S. Y. and Lambert, S. L. *J. Polym. Sci. (A-2)* 1972, **10**, 1183
- 11 Hoffman, J. D. and Weeks, J. J. *J. Chem. Phys.* 1962, **37**, 1723
- 12 Hoffman, J. D. *SPE Trans.* 1964, **4**, 315
- 13 Williams, M. L., Landel, R. F. and Ferry, J. D. *J. Am. Chem. Soc.*, 1955, **77**, 370
- 14 Boon, J., Challa, G. and van Krevelen, D. W. *J. Polym. Sci. (A-2)* 1968, **6**, 1791
- 15 Dedeurwaerder, R. and Oth, J. F. M. *J. Chim. Phys.* 1959, **56**, 940
- 16 Lauritzen, J. I. and Hoffman, J. D. *J. Appl. Phys.* 1973, **44**, 4340

* In a recent paper Lauritzen and Hoffman give a new theory for polymer crystallization. Following this theory the values for $\sigma\sigma_e$ should be taken twice as large¹⁶.

Letter

Effect of temperature on the wettability of oxidized polyethylene films

In previous papers¹⁻³ it was shown that the wettability and the free energy of adhesion between a polyethylene film and reference liquids increase when a polyethylene film is oxidized by a mixture of sulphuric acid and potassium chlorate.

Under given conditions of potassium chlorate concentration in the mixture, temperature and immersion time of the films in the mixture, the oxidation produced a well determined amount of high energy, hydrophilic superficial sites, mainly carbonyls.

The effect of the oxidation is the increase of the critical surface tension, γ_c , of the polymer by several dynes/cm.

A linear relationship is obtained when the surface

density of the polar sites created is plotted against the free energy of adhesion of the films with a reference liquid. This is verified up to the saturation of the polyethylene surface by polar sites. The higher degree of oxidation of the films, achieved by increasing the potassium chlorate concentration in the mixture, does not modify the free energy of adhesion of the oxidized films. It follows from these observations that the strong chemical oxidation produces polar sites in the bulk of the polyethylene, below the surface. They do not modify the polymer wettability, which depends on the chemical composition of the outermost layer of the molecules.

The present work illustrates the effect of temperature on the wettability of the oxidized polyethylene films.

Neumann^{4, 5} has already demonstrated that the shifts in the temperature dependence of polymer-liquid adhesion may be related to the polymorphic transitions in the bulk of a polymer.

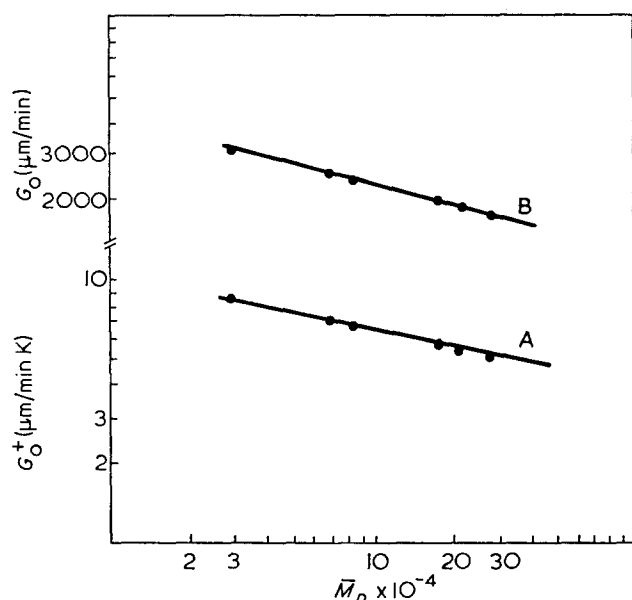


Figure 4 The pre-exponential factors G_0 (B) and G_0^+ (A) vs. \bar{M}_n on double logarithmic scale

with increasing molecular weight as usually found for other polymers too⁵.

When we analyse our data, taking into account that G_0 in equation (3) may be proportional to T_c , straight lines are obtained for the same combination $c_1=22$; $c_2=30\text{K}$ when plotting: $\ln G - \ln T_c + c_1 c_2 / (c_2 + T_c - T_g)$ vs. $1/T_c \Delta T$.

From the intercepts in Figure 3, $G_0^+ (= G_0/T_c)$ can be calculated (see Table 1). We see that G_0^+ also depends on molecular weight and that the values for the product $\sigma\sigma_e$ are in the same range as found above. The molecular weight dependence of G_0^+ is given by $\bar{M}_n^{-0.20}$ (see Figure 4).

The values for $\sigma\sigma_e$ which were calculated from Figures

2 and 3 are close* to those found by Suzuki and Kovacs⁹. In contrary to polyethylene¹¹ the values of G_0 and $G_0^+ \cdot T^+$ are much smaller than the theoretical limit of the Eyring theory $b_0 k T^+ / h = 3.1 \times 10^{11} \mu\text{m}/\text{min}$. (T^+ is the temperature at which G has its maximum value, h is Planck's constant.) This shows that other factors may play an important role in the crystallization of i-PS such as chain conformation and chain stiffness which give rise to a different crystallization mechanism¹⁶. The small dependence of G_0 and G_0^+ on molecular weight supports this view.

REFERENCES

- 1 van Antwerpen, F. and van Krevelen, D. W. *J. Polym. Sci. (A-2)* 1972, **10**, 2423
- 2 Lovering, E. G. *J. Polym. Sci. (A-2)* 1970, **8**, 747
- 3 Magill, J. H. *J. Polym. Sci. (A-2)* 1969, **7**, 1187
- 4 Ueberreiter, K. and Lucas, K. *J. Makromol. Chem.* 1970, **140**, 65
- 5 Devoy, C. and Mandelkern, L. *J. Polym. Sci. (A-2)* 1969, **7**, 1883
- 6 Boon, J. and Challa, G. *Makromol. Chem.* 1965, **84**, 25
- 7 Inoue, Y., Nishioka, A. and Riichirō, C. *Makromol. Chem.* 1972, **156**, 207
- 8 Lemstra, P. J., Kooistra, T. and Challa, G. *J. Polym. Sci. (A-2)* 1972, **10**, 823
- 9 Suzuki, T. and Kovacs, A. J. *Polym. J.* 1970, **1**, 82
- 10 Yeh, G. S. Y. and Lambert, S. L. *J. Polym. Sci. (A-2)* 1972, **10**, 1183
- 11 Hoffman, J. D. and Weeks, J. J. *J. Chem. Phys.* 1962, **37**, 1723
- 12 Hoffman, J. D. *SPE Trans.* 1964, **4**, 315
- 13 Williams, M. L., Landel, R. F. and Ferry, J. D. *J. Am. Chem. Soc.*, 1955, **77**, 370
- 14 Boon, J., Challa, G. and van Krevelen, D. W. *J. Polym. Sci. (A-2)* 1968, **6**, 1791
- 15 Dedeurwaerder, R. and Oth, J. F. M. *J. Chim. Phys.* 1959, **56**, 940
- 16 Lauritzen, J. I. and Hoffman, J. D. *J. Appl. Phys.* 1973, **44**, 4340

* In a recent paper Lauritzen and Hoffman give a new theory for polymer crystallization. Following this theory the values for $\sigma\sigma_e$ should be taken twice as large¹⁶.

Letter

Effect of temperature on the wettability of oxidized polyethylene films

In previous papers¹⁻³ it was shown that the wettability and the free energy of adhesion between a polyethylene film and reference liquids increase when a polyethylene film is oxidized by a mixture of sulphuric acid and potassium chlorate.

Under given conditions of potassium chlorate concentration in the mixture, temperature and immersion time of the films in the mixture, the oxidation produced a well determined amount of high energy, hydrophilic superficial sites, mainly carbonyls.

The effect of the oxidation is the increase of the critical surface tension, γ_c , of the polymer by several dynes/cm.

A linear relationship is obtained when the surface

density of the polar sites created is plotted against the free energy of adhesion of the films with a reference liquid. This is verified up to the saturation of the polyethylene surface by polar sites. The higher degree of oxidation of the films, achieved by increasing the potassium chlorate concentration in the mixture, does not modify the free energy of adhesion of the oxidized films. It follows from these observations that the strong chemical oxidation produces polar sites in the bulk of the polyethylene, below the surface. They do not modify the polymer wettability, which depends on the chemical composition of the outermost layer of the molecules.

The present work illustrates the effect of temperature on the wettability of the oxidized polyethylene films.

Neumann^{4, 5} has already demonstrated that the shifts in the temperature dependence of polymer-liquid adhesion may be related to the polymorphic transitions in the bulk of a polymer.

As in the previous work the low density polyethylene (0.929 g/cm^3 at 23°C) thin film ($25 \mu\text{m}$) Cryovac L Film (provided by Grace Society, France) was used. The reference liquids were formamide and ethylene glycol, both Merck analytical grades. Small volumes of these liquids were thoroughly degassed *in vacuo* with a series of freeze-thaw cycles and were then vacuum-distilled into reservoir flasks on the vacuum line. Their surface tensions measured by the Wilhelmy method were consistent with literature data (formamide, 58.2 dyne/cm ; ethylene glycol, 47.7 dyne/cm).

Contact angles were measured by a drop-on-plate method employing a device built for us by Société Bouty, Paris. The main part of the apparatus is the thermostatically heated contact angle cell. It operates in the temperature range $20\text{--}140^\circ\text{C}$. A thermocouple incorporated in the sample holder measures the temperature with an accuracy of $\pm 1^\circ\text{C}$. The cell allows saturation of the air phase with vapour of the reference liquid, thus avoiding drafts and contaminants. By means of a suitable syringe a liquid drop was placed on the polymer surface. The sample holder may be turned round by an exterior command enabling contact angle measurements to be made on various sites of the sample surface. A telescope equipped with a goniometer device enables direct readings of contact angle values.

For each system at each temperature 3–5 separate drops were examined and the average advancing contact angles were recorded.

The series of contact angle measurements performed on the oxidized and unoxidized polyethylene films are shown in Figure 1. Curve 1 of this Figure shows that for the untreated polyethylene the contact angle remains constant within the temperature range $20\text{--}98^\circ\text{C}$ and that neither during the heating nor during the cooling runs could any variation of its value be observed. The temperature dependence of the contact angle of the oxidized polyethylene measured with formamide and ethylene glycol are shown in Figure 1 by curves 2 and 3 respectively. For both liquids a remarkable shift of the contact angle value in the temperature region of $79\text{--}92^\circ\text{C}$ may be noticed. For ethylene glycol the contact angle value increased from an average of 52° to 64° and for formamide from 54° to 70° . Furthermore, these values remain almost constant during the cooling run of the sample to 20°C and during the second increase of the temperature to about 100°C .

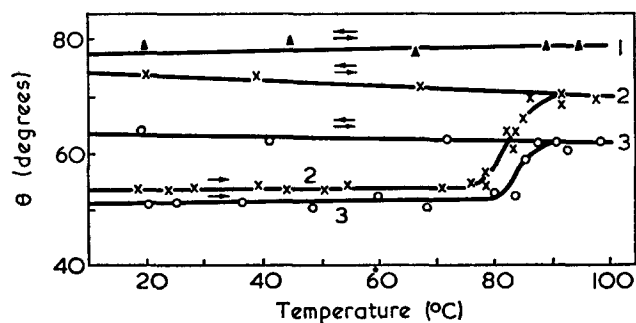


Figure 1 Temperature dependence of contact angle on polyethylene films oxidized in sulphuric acid and potassium chlorate mixture at 20°C . Potassium chlorate concentration in the mixture is 4.76%. Under these conditions oxidation yields a surface density of polar sites equal to 14.0×10^{14} molecules/cm 2 . 1, Formamide/unoxidized polyethylene; 2, formamide/oxidized polyethylene; 3, ethylene glycol/oxidized polyethylene

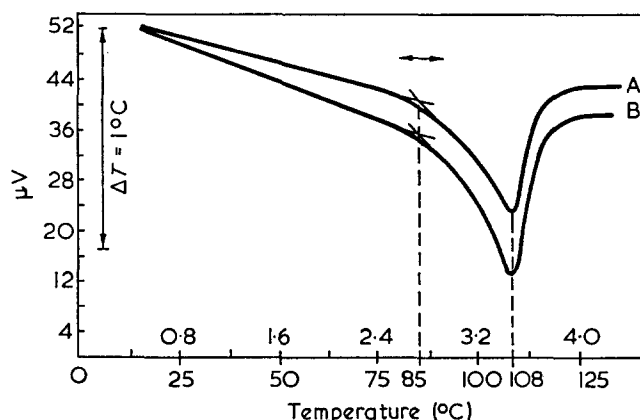


Figure 2 Thermograms of polyethylenes. A, Unoxidized polyethylene; B, oxidized polyethylene. \leftrightarrow . Temperature range where the shift of the contact angle takes place (see Figure 1)

The decrease of the wettability of the oxidized polyethylene at about 80°C and the irreversibility of this phenomenon suggests that some essential changes of the surface nature and composition occur in this temperature region.

These changes involve, most probably, the decrease of the surface free energy, γ_s , of the polymer.

Measurements of melting points and heats of melting for the untreated and oxidized polyethylenes were carried out using differential thermal analysis (d.t.a.). The thermograms represented in Figure 2 show that for both samples the beginning of the melting transition is at about 85°C .

The close agreement between the temperature of the beginning of the melting transition and the decrease of the wettability of the oxidized polyethylene seems to have an important significance.

The most probable interpretation of the observed phenomenon is the following. At the beginning of the melting transition the increase of the chain mobility leads to the redistribution of the external polar groups initially located at the solid-air interface. Thus some groups become immersed in the bulk of the polymer and a decrease of the surface density of these polar groups results. This is spectacularly demonstrated by the shift of the contact angle value. The new equilibrium value leads to a contact angle value close to that of the untreated polyethylene and remains constant during the cooling and successive heating of the polymer sample.

A. Baszkin and L. Ter-Minassian-Saraga

Equipe de Recherche du CNRS,
UER Biomédicale 81,
Université René Descartes,
75006 Paris, France
(Received 5 July 1974)

References

- Baszkin, A. and Ter-Minassian-Saraga, L. *C. R. Acad. Sci. Paris (C)* 1968, **258**, 315
- Baszkin, A. and Ter-Minassian-Saraga, L. *J. Polym. Sci. (C)* 1971, **34**, 243
- Baszkin, A. and Ter-Minassian-Saraga, L. *J. Colloid Interface Sci.* 1973, **43**, 190
- Neumann, A. W. and Tanner, W. *J. Colloid Interface Sci.* 1970, **34**, 1
- Neumann, A. W., Haage, G. and Renzow, D. *J. Colloid Interface Sci.* 1971, **35**, 379

Spherulitic crystallization in biopolymers

P. J. Barham, E. D. T. Atkins and I. A. Nieduszynski

*H. H. Wills Physics Laboratory, University of Bristol, Bristol BS8 1TL, UK
(Received 8 April 1974; revised 16 May 1974)*

Banded spherulites with diameters of the order of $150\mu\text{m}$ have been grown by evaporation from solutions of the branched polysaccharide, dextran, in DMSO, formamide and water. The average size of the spherulites depends on molecular weight, evaporation temperature, and the solvent used. Activation energies for spherulitic growth were measured as a function of molecular weight and solvent environment. Two distinct types of spherulite were obtained depending only on the molecular weight: negative, banded spherulites from the high molecular weight dextran; and positive, unbanded spherulites from the low molecular weight dextran.

INTRODUCTION

In the synthetic polymer field spherulitic growth patterns are an established facet of polymeric morphology, which has been investigated in some detail over the last two decades, especially by Keller¹⁻³. It is somewhat surprising therefore to find that spherulites, admittedly rather small, have only recently been reported⁴ for a biological polymer*. On general considerations no fundamental difference is expected between the crystallization behaviour of synthetic and biological polymers. Indeed recent work in this laboratory on the crystallization of the connective tissue polysaccharides⁶⁻⁹ in the form of oriented fibres and films bears out this philosophy. In order to demonstrate that banded spherulites may also be obtained from a biopolymer we have undertaken an investigation concerned with the crystallization of the polysaccharide dextran¹⁰, which is commonly used as a blood plasma filler. Our interest in this particular biopolymer was prompted by the reported observation by Pasika and West of the first laboratory produced biological spherulites⁴.

The spherulitic films of dextran reported by Pasika and West consisted of spherulites with diameters in the range $8-25\mu\text{m}$. In the present paper a somewhat different method of obtaining spherulitic dextran films, by evaporation of solutions at relatively high temperatures, is described. Using this method dextran films with spherulitic diameters in the range $10-150\mu\text{m}$ have been obtained. These spherulites, which are very similar to spherulites from synthetic polymers, may be able to give information about spherulitic morphology in general since in several cases they are of a better quality than those observed for synthetic polymers which exhibit similar properties. Dextran is an α -1,6-linked polysaccharide, the molecular shape of which is illustrated in *Figure 1* (for a review of dextran see ref 10) and as such the molecule is able to rotate, subject to steric hindrance, about three bonds at each monomer unit. The polysaccharide chain is branched and furthermore

* We wish to distinguish between these observations and the Maltese cross seen in starch granules between crossed polars⁵, which results from distinctly different morphological features.

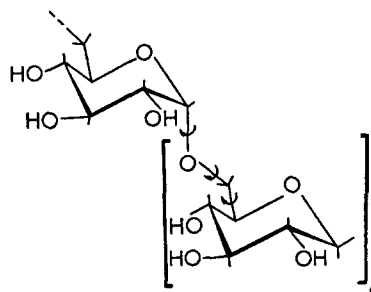


Figure 1 Schematic diagram of α -1,6-linked dextran. Note that rotation can occur about three successive bonds, subject to steric hindrance, which allows considerable flexibility

it is believed that in the longer molecules the branching is concentrated into long side chains. Dextran has also been crystallized by precipitation from aqueous solution¹¹. X-ray powder diagrams were obtained from such samples, and four different X-ray patterns were observed depending primarily on the temperature at which the precipitation was performed.

EXPERIMENTAL

The dextrans used in this work were kindly provided by Dr A. deBelder of Pharmacia AB, Uppsala, Sweden. The molecular weights and degrees of polymerization (*DP*) of the dextrans used were 2400 (*DP* ~15), 3200 (*DP* ~20), 40 000 (*DP* ~250) and $>10^7$ (*DP* ~63 000). Three different types of dextrans with molecular weight $>10^7$ were used, but no significant differences were observed. All the dextrans were branched with approximately 5% of the material in the branches.

Spherulitic films of dextran were prepared by evaporation of solutions of dextran in dimethylsulphoxide (DMSO), formamide or water, or mixtures of these solvents at temperatures between 70° and 180°C ¹². Growth rates, and hence activation energies were measured by evaporating solutions at fixed temperatures for fixed lengths of time and then measuring the mean diameter of the spherulites formed.

The birefringence of the spherulites was measured by cutting a series of successive thin ($\sim 10\ \mu\text{m}$) sections through a sample and selecting those sections which passed through the centre of a spherulite. When the spherulites were banded the birefringence was measured at the centre of a bright band. The magnitude of birefringence was measured using a Brace-Köhler rotating quartz compensator and the sign measured using a whole wave plate using standard techniques¹³.

RESULTS

Spherulitic size

The main factors which determined the size to which spherulites would grow were the molecular weight of the dextran, the evaporation temperature, and the solvent used. In addition the initial concentration of the solution appears to play some part in determining the size of spherulites. It was found that with initial concentrations greater than 10% (w/v) the size to which spherulites would grow steadily decreased with increasing initial concentration. The maximum initial concentration of solution that produced spherulites which could be resolved in the polarizing microscope was found to be 60% (w/v). The sizes to which spherulites grew as a function of evaporation temperature, molecular weight and solvent are shown in *Table 1* (the sizes of spherulites of molecular weight 3200 were similar to those from molecular weight 2400). All these results refer to the mean diameter of at least fifty spherulites grown from a 10% (w/v) solution.

When dextrans with different molecular weights were mixed, the sizes of spherulites obtained were generally those which would be expected from a weighted average of the sizes given in *Table 1*. There was, however, one notable exception to this empirical rule. A mixture of the 2400 and 40 000 molecular weight dextrans with 5–10% w/w of the 40 000 molecular weight dextran dissolved in DMSO produced spherulites smaller than those from either pure system, generally about 70% of the expected size.

Birefringence of spherulites

The most striking birefringence effects of spherulites are the dark Maltese cross and the concentric bands^{1, 2}. Both these effects were always observed in spherulites grown from the 40 000 and $>10^7$ molecular weight dextrans as illustrated in *Figure 2*. However, in spherulites from the 2400 molecular weight sample (see *Figure 3*) banding was rarely observed, and in any event was

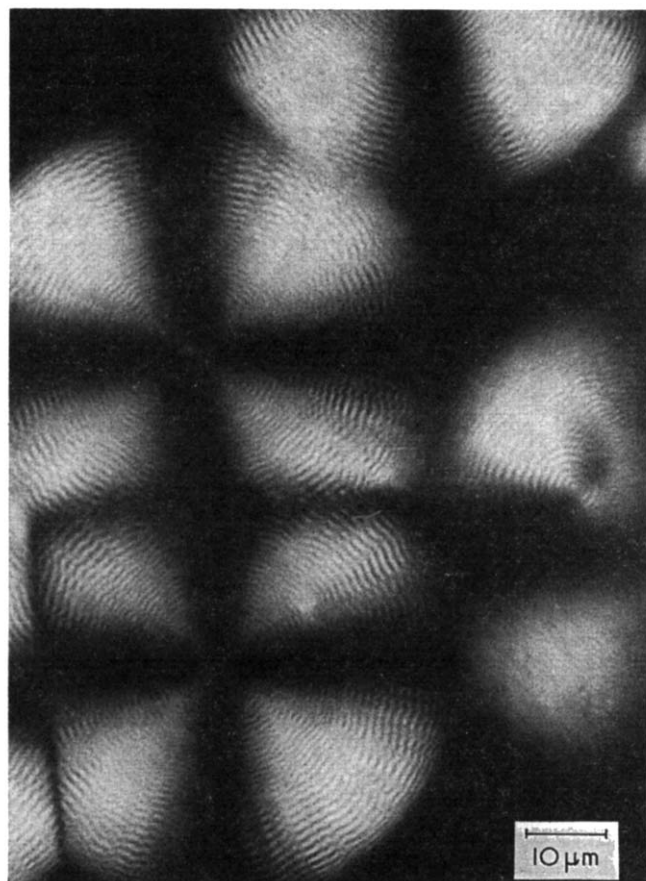


Figure 2 Banded dextran spherulites grown from an 8% (w/v) solution of 40 000 molecular weight dextran in DMSO at 180°C. The micrograph was taken between crossed polars

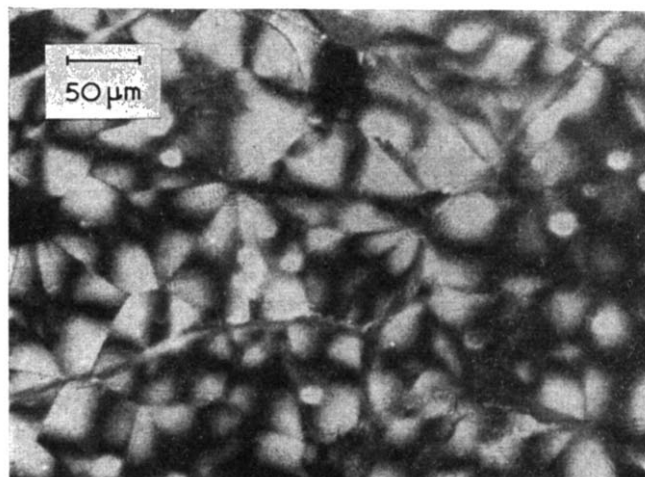


Figure 3 Spherulites of low molecular weight dextran grown by evaporation at 160°C from a 10% (w/v) solution of the 2400 molecular weight dextran sample in DMSO (micrograph between crossed polars)

Table 1 Mean diameter (in μm) of dextran spherulites grown from 10% (w/v) solutions

Solvent	Molecular weight	Evaporation temperature (°C)					
		80	100	120	140	160	180
DMSO	2 400	5	12	25	60	100	120
DMSO	40 000	5	15	30	70	120	150
DMSO	$>10^7$	0	2	5	10	15	30
Formamide	2 400	0	2.5	8	15	30	40
Formamide	40 000	3	5	10	20	35	45
Formamide	$>10^7$	0	0	2	5	8	10
Water	2 400	1.5	2	—	—	—	—
Water	40 000	2	4	—	—	—	—
Water	$>10^7$	0	0.5	—	—	—	—

irregular. In some of the 2400 molecular weight spherulites the Maltese cross was very distorted and in a few it was completely absent (interestingly these particular spherulites were banded).

The spacing between bands was observed to depend on the evaporation temperature only, the bands being further apart in those spherulites grown at higher temperatures. The spacing was approximately the same for spherulites grown from the 40 000 and the $>10^7$

molecular weight dextran samples, but the bands were closer together in spherulites of the 2400 molecular weight sample which were grown at the same temperature.

It was found that spherulites of 40 000 and $>10^7$ molecular weight dextrans were negatively birefringent, while those from the 2400 molecular weight dextran were positively birefringent. (A positive spherulite is one in which the radial refractive index is greater than the tangential refractive index and *vice versa* for a negative spherulite.) Positive and negative banded spherulites with very low birefringence, and also non-birefringent banded spherulites could all be grown from solutions of the 3200 molecular weight dextran fraction, depending on the evaporation temperature. Evaporation below 150°C provided positive spherulites, while evaporation above 160°C produced negative spherulites. At evaporation temperatures between 150°C and 160°C non-birefringent spherulites could be grown. It was found possible to grow complex spherulites with the sign of birefringence changing along a radius, by varying the evaporation temperature during crystallization. Such spherulites were banded in a continuous fashion. Mixing the 40 000 and 2400 molecular weight samples again gave unexpected results. When there was up to 3% w/w of the 40 000 molecular weight material present the proportion of negative spherulites was about 1%. With 3–7% of the longer molecules present the proportion of negative spherulites increased to 10%. When there was more than 10% of the 40 000 molecular weight dextran present very few (less than 1%) of the spherulites were positive. All the negative spherulites were banded but with the bands closer together than in spherulites of pure 40 000 molecular weight dextran.

The magnitude of the birefringence in the spherulites was measured for the 2400, 40 000 and $>10^7$ molecular

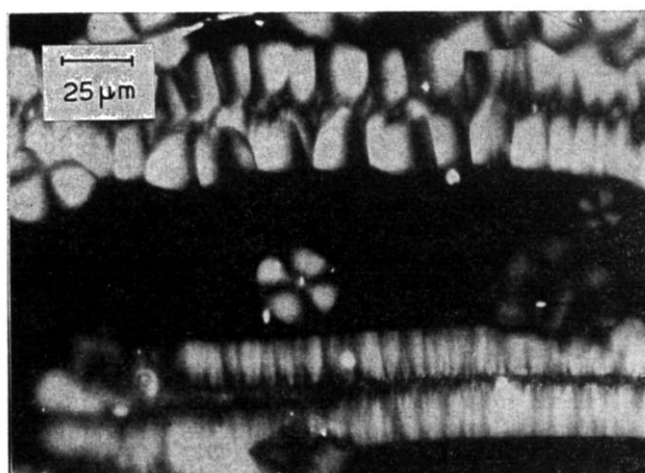


Figure 4 Row nucleated structures grown by evaporation at 160°C from a stirred 10% (w/v) solution of the 40 000 molecular weight dextran in DMSO (micrograph between crossed polars)

weight dextrans and these results are given in Table 2. The birefringence of the 3200 molecular weight dextran was too low to be measured accurately.

Activation energies

The activation energy for spherulitic growth^{14, 15} was measured as a function of solvent environment, initial concentration of the solution and the molecular weight of the particular dextran used. The results of these measurements are shown in Table 3. It should be noted that although several trends are detectable all the measured activation energies lie within the experimental error of each other. The principal trends are: (i) an increase in activation energy with increasing length of the molecular chains; and (ii) a variation with the solvent used. There also may be an increase in activation energy with increasing concentration of the initial solution.

Row nucleated structures

Row nucleated structure is the name given to a crystal morphology often occurring in synthetic polymers which have undergone a flowing process prior to crystallization². A row nucleated structure is a series of spherulites all of which have their origins nucleated on a common line. The spherulites grow out perpendicularly to this line without constraint but growth parallel to the line is restricted as the spherulites grow into one another.

Row nucleated structures were first observed in dextran films around the edges of the film where the solution had flowed inwards during evaporation. The few row nucleated structures which were thus observed were aligned roughly perpendicular to the edges of the film. Further investigation showed that these structures could be consistently grown if the solution was stirred with a needle during evaporation. This technique gave many row nucleated structures randomly arranged within the film (see Figure 4). These structures grew best in a mixture of 40 000 and about 5% w/w of the $>10^7$ molecular weight material, although they were observed in films of all the dextran fractions which were used. However, row nucleated structures were only observed to form from DMSO solutions.

The temperature range over which row nucleated structures were observed to form was the same as for spherulites. Their widths were also of the same order

Table 2 Birefringence of spherulites (the error in all measurements is $\pm 8\%$)

Molecular weight	Solvents		
	Water	DMSO	Formamide
2 400	+0.00071	+0.00075	+0.00068
40 000	-0.00079	-0.00073	-0.00074
$>10^7$	-0.00070	-0.00068	-0.00072

Results refer to difference between mean radial refractive index and mean tangential refractive index for light of wavelength 4861 Å

Table 3 Activation energies (in kcal/mol) for spherulitic growth in dextran

Solvent	Molecular weight	Initial concentration of solution (w/v) (%)			
		1	10	20	40
DMSO	2 400	26 ± 4	24 ± 5	28 ± 4	28 ± 7
DMSO	40 000	28 ± 3	30 ± 2	31 ± 3	33 ± 4
DMSO	$>10^7$	—	33 ± 6	—	—
Formamide	2 400	30 ± 5	29 ± 5	30 ± 5	34 ± 7
Formamide	40 000	31 ± 5	33 ± 5	36 ± 5	35 ± 5
Formamide	$>10^7$	—	35 ± 6	—	—
Water	2 400	—	38 ± 9	—	—
Water	40 000	38 ± 8	41 ± 8	39 ± 8	35 ± 8
50% DMSO/ 50% formamide	2 400	28 ± 5	30 ± 5	32 ± 6	32 ± 6
50% DMSO/ 50% formamide	40 000	30 ± 4	32 ± 5	33 ± 4	33 ± 5

of magnitude as the diameters of spherulites grown under similar conditions. Row nucleated structures were normally $\sim 300 \mu\text{m}$ long although several over 1 mm long were observed.

X-ray data

Spherulitic films of all types were subjected to X-ray diffraction and all gave powder diagrams with the same interplanar spacings. These patterns were similar to the L-2 patterns obtained by Jeanes *et al.*¹¹ (see Table 4). The only variation between the patterns obtained from the different films was the relative intensity of the amorphous halo, which enables the crystallinity to be estimated. The intensity of the amorphous halo was found to vary considerably with the evaporation temperature, solvent environment, and the molecular weight of the particular dextran used. It was greatest at low evaporation temperatures in all cases. At evaporation temperatures below 60°C for DMSO and 65°C for both formamide and water solutions no crystallinity was observed.

The 2400 and $>10^7$ molecular weight dextran spherulites showed a strong amorphous halo at all evaporation temperatures (although the relative intensity was observed to decrease slightly with increasing evaporation temperature). The 40 000 molecular weight dextran spherulites showed a distinct drop in amorphous content at evaporation temperatures above 120°C, especially from DMSO solutions, where the amorphous halo was very weak. In general there was least amorphous scattering from films grown from DMSO solution, and most from films grown from aqueous solutions.

DISCUSSION

Most of the effects observed in dextran spherulites have been observed in the past in spherulites of synthetic polymers. This adds further weight to the argument that there is no fundamental difference between the behaviour of natural and synthetic polymers.

The results concerning the sizes and activation energies of dextran spherulites are stated for the reader's information and require little discussion, except to mention that the lower activation energy for growth of spherulites in the 2400 molecular weight dextran may be easily understood. Since in spherulites grown from synthetic polymers it is well established that the molecular chains are in the chain-folded configuration, it is reasonable

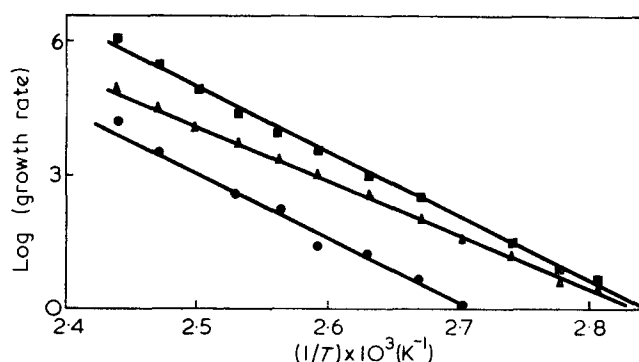


Figure 5 Graph showing the variation of spherulitic growth rate (plotted as the logarithm) with reciprocal temperature for 10% (w/v) solutions in DMSO. The experimental results for samples with molecular weights 40 000, 2400 and $>10^7$ are represented by the symbols \blacksquare , \blacktriangledown , \bullet respectively. Note that the growth rate of the 40 000 molecular weight material is greater than for the 2400 molecular weight material which in turn is greater than that of the $>10^7$ molecular weight material. The growth rates used to prepare this graph were measured in purely arbitrary units, since to obtain an activation energy only the gradient is needed

to expect a similar situation to occur in dextran spherulites. However, in the case of the 2400 molecular weight dextran the chains are short (~ 15 monomer units) and therefore are very unlikely to crystallize in the chain-folded configuration. Thus with no energy to fold the chains required, a lower activation energy is to be expected. The birefringence phenomena observed in dextran spherulites will be discussed in more detail and compared with observations of synthetic polymer spherulites. The effects on spherulitic morphology of mixing molecular weight fractions has not been examined in detail in the synthetic polymer field; however, the observed birefringence effects in dextran spherulites grown from such mixtures may be explained as follows.

Figure 5 shows that spherulites of the 40 000 molecular weight fraction always grow faster than those of the 2400 molecular weight fraction. Thus it would be expected that in the mixture the shorter molecular chains will be 'forced' to adopt the growth mechanism and morphology common to the 40 000 molecular weight dextran spherulites so that most spherulites grown from such a mixture would have negative birefringence.

The observation of positive and negative spherulites from the same polymeric material is not a common occurrence, although observations have been reported for polyamides¹⁶⁻²⁰ and polyesters^{16, 17}. A brief resumé of these reports will be given here, for the sake of comparison with dextran. In 1955 Keller^{16, 17} observed positive and negative spherulites in poly(ethylene terephthalate) (PET) and polyamides and in addition gave results of X-ray microbeam diffraction analysis to determine molecular orientation within these spherulites. The quality of the diffraction patterns was quite poor due to many practical difficulties; however, he was able to detect some differences in orientation phenomena in PET spherulites and concluded that the change in sign of birefringence was due to a change in crystal habit. In 1961 and 1962 Mann and Roldan-Gonzalez^{18, 19} reported that they were unable to detect any similar differences in orientation phenomena in polyamide spherulites, and concluded that there was no change in crystal habit in this case. This was taken up by Cannon *et al.*²⁰ who examined the temperature dependence of

Table 4 Interplanar spacings (in Å) as determined from X-ray powder diagrams

Spherulites grown at 140°C	Jeanes <i>et al.</i> ¹¹ 'L-2' type
5.93	
5.60	5.65
4.97	4.95
4.51	4.52
4.06	4.00
3.85	
3.57	3.57
3.20	3.24
	3.06
2.87	
2.56	2.55
2.33	2.36
2.16	

the birefringence of polyamide spherulites. They only found one model consistent both with their own studies and with those of Mann and Roldan-Gonzalez, in which in the positive spherulites the *c*-axis (i.e. the chain direction) was approximately tangential and the *b*-axis approximately radial; while in the negative spherulites the *c*-axis was tangential but otherwise the orientation was completely random.

In the case of PET the negative spherulites were obtained by degrading (heating the undried preparation) the polymer¹⁶ and the positive spherulites were obtained from the undegraded material. No quantitative results of the particular molecular weights are available for these results. In the case of nylons the spherulites obtained are negative if crystallized above some critical temperature and positive if crystallized below that temperature. Spherulites grown at the critical temperature have zero birefringence. No experiments growing spherulites from different molecular weight fractions have been reported for the polyamides. In both PET and polyamides all the spherulites were grown from the melt.

The phenomena which cause changes in sign of the birefringence of PET, nylon and dextran spherulites may be common to many polymers, but go unobserved in those polymers where there is no accompanying change in sign of birefringence. It should be noted in this context that only those polymers which have a comparatively large polarizability perpendicular to the molecular chain axis will be able to form both positive and negative spherulites.

Indeed it has been suggested²¹ that the sheaf-like structures of polyethylene grown from solution can have either the *a* or the *b* axis oriented radially depending on the crystallization conditions. If spherulites grew from both types of sheaf and retained their crystal habit then they could not be distinguished by birefringence measurements alone.

Spherulites grown from dextran solutions exhibit a variation in sign with molecular weight as do the PET spherulites; and the 3200 molecular weight dextran fraction exhibits a temperature dependence comparable with the polyamides. At present the reasons for these changes in birefringence of dextran spherulites are not

understood; however, dextran may prove to be a useful model material for further investigation into these phenomena, owing to the ease with which good quality spherulites may be grown from dextran solutions. However, it must be remembered that the positive spherulites are all grown from short molecules which are unlikely to adopt the chain-folded configuration, and so care must be taken in comparing dextran with the long chain synthetic polymers.

ACKNOWLEDGEMENTS

We thank Dr A. deBelder of Pharmacia AB, Uppsala, Sweden for his collaboration and Professor A. Keller for many valuable discussions. This investigation was supported by the Science Research Council.

REFERENCES

- 1 Keller, A. *Nature* 1952, **169**, 913
- 2 Keller, A. *J. Polym. Sci.* 1955, **15**, 31
- 3 Keller, A. *J. Polym. Sci.* 1959, **39**, 151
- 4 Pasika, W. M. and West, A. *Chem. Eng. News* 1972, **50**, (20), 13
- 5 Badenhuizen, N. P. and Dutton, R. W. *Biochem. J.* 1966, **62**, 13P
- 6 Atkins, E. D. T. and Mackie, W. *Biopolymers* 1972, **11**, 1685
- 7 Atkins, E. D. T. and Sheehan, J. K. *Nature (New Biol.)* 1972, **235**, 253
- 8 Atkins, E. D. T. and Laurent, T. C. *Biochem. J.* 1973, **133**, 605
- 9 Nieduszynski, I. A. and Atkins, E. D. T. *Biochem. J.* 1973, **135**, 729
- 10 Neely, W. B. *Adv. Carbohyd. Chem.* 1960, **15**, 341
- 11 Jeanes, A., Shieltz, N. C. and Wilham, C. A. *J. Biol. Chem.* 1948, **176**, 617
- 12 Barham, P. J. *MSc Thesis* University of Bristol (1973)
- 13 Hartshorne, N. H. and Stuart, A. 'Practical Optical Crystallography', 2nd edn, Arnold, London, 1969
- 14 Flory, P. J. and McIntyre, A. D. *J. Polym. Sci.* 1955, **18**, 592
- 15 Kahle, B. and Stuart, H. A. *J. Polym. Sci.* 1957, **25**, 485
- 16 Keller, A. *J. Polym. Sci.* 1955, **17**, 291
- 17 Keller, A. *J. Polym. Sci.* 1955, **17**, 351
- 18 Mann, J. and Roldan-Gonzalez, L. *Br. J. Appl. Phys.* 1961, **12**, 265
- 19 Mann, J. and Roldan-Gonzalez, L. *J. Polym. Sci.* 1962, **60**, 1
- 20 Cannon, C. G., Chappel, F. P. and Tidmarsh, J. I. *J. Textile Inst.* 1963, **54**, T210
- 21 Bassett, D. C., Keller, A. and Mitsuhashi, S. *J. Polym. Sci. (A)* 1963, **1**, 763

Synthesis, characterization, and conformational studies of *N*-*t*-butyloxycarbonyl-oligo-*L*-leucine methyl esters

G. M. Bonora, A. Maglione and C. Toniolo

Institute of Organic Chemistry, University of Padua, Padua, Italy
(Received 13 February 1974; revised 24 April 1974)

The conformational properties of *N*-*t*-butyloxycarbonyl-oligo-*L*-leucine methyl esters were examined in anhydrous and aqueous organic solvents. This study demonstrates that these oligomers may exist in predominantly β -associated or unordered conformations depending upon the solvent. The β -structure, which appears at the pentamer in ethylene glycol (EG) and trifluoroethanol (TFE)-water (20:80 v/v), could be disrupted by dilution or by increasing the temperature. The stability of the β -structures was found to be lower than those formed by oligopeptides derived from *L*-isoleucine and *L*-valine and comparable to those formed by oligo-*L*-methionines.

INTRODUCTION

Conformational energy calculations^{1, 2} have shown that the right-handed α -helix is a structure of great stability for poly(*L*-leucine). Also, recent experiments have demonstrated that poly(*L*-leucine) and various copolymers assume this structure in the solid state, in aqueous solution and in non-denaturing organic solvents³⁻¹⁴. Leucine was also found to be the amino acid residue with the highest propensity for forming ordered secondary structures (total helical and β -regions) in proteins¹⁴. In previous papers we reported evidence of β -associated structure formation in homo-oligopeptides derived from amino acids with saturated side chain, i.e. isoleucine¹⁵⁻¹⁷, valine¹⁸, and methionine^{19, 20}. In this paper we wish to discuss the synthesis and characterization of the homologous series BOC-(*L*-Leu)_{*n*}OMe (*n*=2-7) (BOC, *t*-butyloxycarbonyl; Leu, leucine; OMe, methyl ester), and its conformational properties in anhydrous and aqueous organic solvents. For this investigation we have used polarimetry, ultraviolet (u.v.) absorption and circular dichroism (c.d.). A brief account of some of this work has already been reported²¹. Leucine oligomers have been scarcely investigated, and no conclusive structural assignments have been made²²⁻²⁴.

EXPERIMENTAL

Preparation of compounds

t-Butyloxycarbonyl-*L*-leucine^{25, 26}. This compound was prepared following the procedure described by Schnabel²⁵, m.p. 81-83°C, $[\alpha]_{\text{D}}^{25} = -24.1^\circ$ (*c* = 1, acetic acid).

L-Leucine methyl ester hydrochloride²⁷. This compound was prepared following the procedure described by Boissonnas *et al.*²⁸, m.p. 149°C, after recrystallization

from anhydrous methanol-ethyl ether, $[\alpha]_{\text{D}}^{25} = +13.3^\circ$ (*c* = 4.9, H₂O).

t-Butyloxycarbonyl-*L*-leucyl-*L*-leucine hydrazide. This compound was synthesized according to the procedure previously described¹⁶, m.p. 115-116°C, after recrystallization from hot methanol-water, $[\alpha]_{\text{D}}^{25} = -57^\circ$ (*c* = 0.4, trifluoroethanol). Calculated for C₁₇H₃₄N₄O₄: C, 57.0%; H, 9.6%; N, 15.6%. Found: C, 56.7%; H, 9.6%; N, 15.5%.

The BOC-(*L*-Leu)_{*n*}OMe (*n*=2-7) oligomers were synthesized according to the procedures previously reported¹⁶. The elemental analytical data are summarized in *Table 1* and the physical properties in *Table 2*.

Methods

The optical rotation measurements were carried out on a Perkin-Elmer Model 141 polarimeter equipped with a thermostat. The values are expressed in terms of ϕ_{D} , total molar rotation at sodium D line. The u.v. absorption measurements were carried out using a Cary Model 15 spectrophotometer equipped with a hydrogen light source and a thermostat. The spectrophotometer was kept oxygen-free by continuous flushing with dry prepurified nitrogen. The values are expressed in terms of total molar absorption coefficients. C.d. spectra were recorded using a Cary 60 spectropolarimeter modified with a Model 6001 circular dichroism attachment, and 0.5 mm, 1 mm, and 1 cm path length cells. Dry prepurified nitrogen was employed to purge the instrument before and during the experiments. The values are expressed in terms of $[\theta]_{\text{M}}$, total molar ellipticity. The solvents used for the spectral measurements were trifluoroethanol (Fluka, Büchs), hexafluoroisopropanol and hexafluoroacetone sesquihydrate (Du Pont and Co., Wilmington, Delaware), ethylene glycol

Table 1 Summary of elemental analytical data of BOC-(*L*-Leu)_{*n*}OMe

<i>n</i>	Formula	Mol. wt	C (%)		H (%)		N (%)	
			Calc.	Found	Calc.	Found	Calc.	Found
2*	C ₁₈ H ₃₄ N ₂ O ₅	358.5	60.1	60.1	9.6	9.7	7.8	7.9
3*	C ₂₄ H ₄₅ N ₃ O ₆	471.6	61.1	61.0	9.6	9.6	8.9	8.8
4*	C ₃₀ H ₅₆ N ₄ O ₇	584.8	61.6	61.8	9.6	9.5	9.6	9.6
5	C ₃₆ H ₆₇ N ₅ O ₈	698.0	61.9	61.6	9.7	9.7	10.0	10.0
6	C ₄₂ H ₇₈ N ₆ O ₉	811.1	62.2	61.8	9.7	9.8	10.4	10.3
7	C ₄₈ H ₈₉ N ₇ O ₁₀	924.3	62.4	62.2	9.7	9.7	10.6	10.5

* For a previous synthesis and elemental analytical data of this compound, see ref 22

Table 2 Summary of physical properties of BOC-(*L*-Leu)_{*n*}OMe

<i>n</i>	Method	Yield (%)	M.p. (°C) (recryst.)	Solvents ^a	[α] _D ²⁵ (HFA) ^b	φ _D ²⁵ (HFA) ^b	R _{f1} ^c	R _{f2} ^c
2 ^d	DCCI	72	141–142	EA/pet. ether	–46.9	–1.68	0.90	0.90
3 ^d	DCCI	75	158–159	EA/pet. ether	–75.1	–3.54	0.90	0.90
4 ^d	Azide	88	208–209	DMF/water	–92.6	–5.42	0.90	0.70
5	Azide	87	>250	hot DMF/water	–101.0	–7.05	0.90	0.50
6	Azide	91	>250	hot DMF/water	–111.1	–9.01	0.20	0.10
7	Azide	71	>250	hot DMF/water	–120.0	–11.09	0.10	0.10

^a EA = ethyl acetate; DMF = dimethylformamide

^b φ_D²⁵ = [α]_D²⁵ × (molecular weight/10 000) × (degree.cm²/mol). The concentration used for the polarimetric measurements was 3 × 10^{–3} M

^c Thin-layer chromatography on SiO₂ (Merck); R_{f1}, methanol–benzene (1:6); R_{f2}, benzene–ethyl acetate (1:1). A single spot was observed in each case

^d For a previous synthesis and physical properties of this compound, see ref 22

(Erba RS, Milan) and double distilled water. All solvents were of the highest purity commercially available and were used without further purification.

RESULTS AND DISCUSSION

Synthesis and characterization of oligomers

The oligopeptide series BOC-(*L*-Leu)_{*n*}OMe (*n* = 2–7) has been synthesized following the scheme illustrated in ref 16. The DCCI coupling method²⁹ has been employed for preparing the dimer and trimer, and the Rudinger's acid azide route³⁰ has been used for producing the higher oligomers. These methods, as applied here, are known to give products of high chemical and optical purity^{16–20}. The chemical purity of the oligopeptides is demonstrated by the elemental analytical data (Table 1), thin-layer chromatography in a number of solvent systems (two representative examples are listed in Table 2), and comparison of melting points where available²². The linearity of the Goodman's plot³¹ (total molar rotations of oligomers vs. *n*) in hexafluoroacetone sesquihydrate (HFA), a denaturing solvent for the secondary structures of oligopeptides¹⁶, confirms the almost complete absence of racemization in the various synthetic steps (Table 2 and Figure 1).

Conformational analysis

At first, as a physico-chemical method sensitive to α-helical and β-conformations of oligopeptides, we employed u.v. absorption in the 190 nm π → π* amide region³². Hypochromism of the 190 nm band and the appearance of a shoulder at 205 nm indicate the presence of a helix, while hyperchromism and a 5 nm red shift indicate the presence of a β-conformation³². For these spectral studies we employed trifluoroethanol (TFE) as solvent since it is suitable for use in the far u.v.

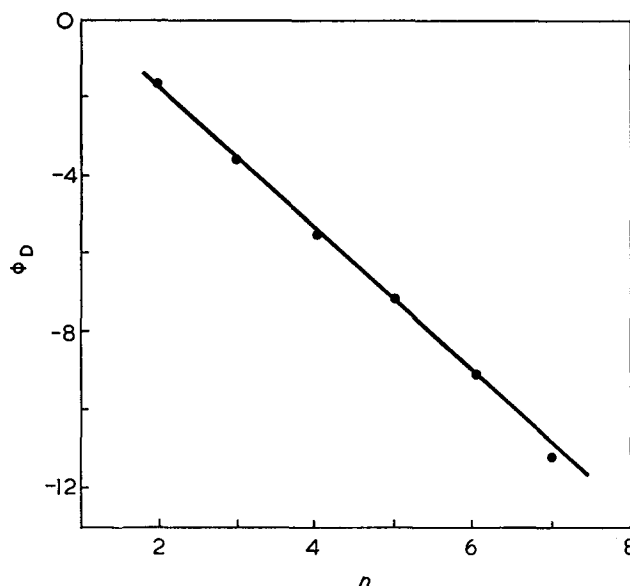


Figure 1 Plot of total molar rotation values of BOC-(*L*-Leu)_{*n*}OMe vs. *n* at the sodium D line in HFA at 25°C (conc. 3 × 10^{–3} M)

In the 3 × 10^{–4} to 1.5 × 10^{–5} M concentration range the wavelength absorption maxima of all oligo-*L*-leucines occur at 189–190 nm, in contrast to oligo-*L*-isoleucines¹⁶ and oligo-*L*-valines³³ which exhibit an abrupt bathochromic shift of ~4 nm from hexamer to heptamer, indicative of the onset of a β-structure at this stage. Furthermore, a negative deviation from linearity is apparent at the heptamer in the plot of total molar extinction coefficients at 195 nm vs. *n* in oligo-*L*-leucines. This hypochromic effect is concentration independent; however, it is too small to represent a convincing proof of α-helical formation.

C.d. in the region of the peptide chromophore is an extremely useful technique for assigning the secondary

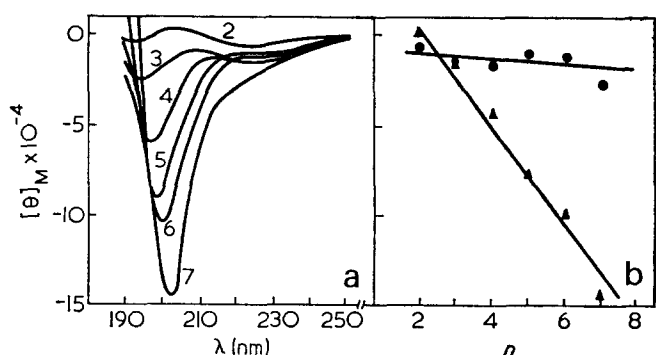


Figure 2 (a) Circular dichroism spectra of BOC-(L-Leu)_nOMe in TFE at 25°C (conc. 3 × 10⁻⁴M); (b) plot of total molar ellipticity values at 222 nm (●) and 202 nm (▲) vs. *n*

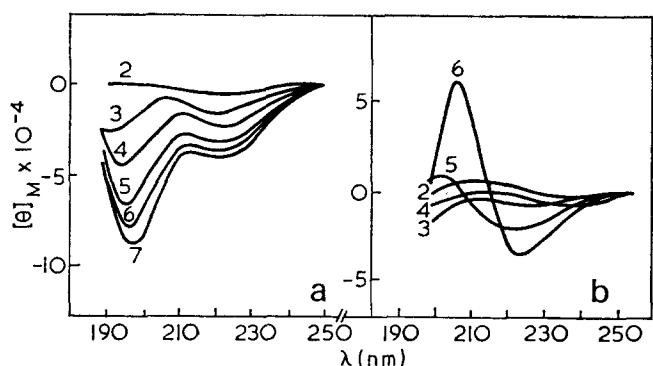


Figure 3 Circular dichroism spectra of BOC-(L-Leu)_nOMe at 25°C (conc. 3 × 10⁻⁴M) in (a) HFIP and (b) EG

structures of oligopeptides in solution^{15, 17-21, 33-39}. Thus, we undertook to investigate the conformational properties of the leucine oligomers using c.d. The c.d. spectra of BOC-(L-Leu)_nOMe in TFE (3 × 10⁻⁴M) are shown in Figure 2. In going from dimer to heptamer, the negative short wavelength band shifts gradually from 193 nm to 202 nm while increasing in intensity whereas the other two bands present in the dimer, the positive one at 204 nm and the negative one at 224 nm, disappear at the trimer and heptamer, respectively. In addition, a small deviation from a straight line dependence of total molar ellipticity values vs. *n* is present at the heptamer (Figure 2). However, there is no evidence of spectral patterns resembling those of ordered secondary structures⁴⁰. The c.d. curve of the heptamer does not vary either in the concentration range 3 × 10⁻³ to 3 × 10⁻⁴M or increasing the temperature to 65°C (only a 15% decrease of the intense negative Cotton effect has been observed at higher temperatures). Therefore, we conclude that the leucine oligopeptides up to hexamer are essentially unordered in TFE, whereas the heptamer exists predominantly in the random coil state in this solvent. In any case our results indicate that hepta-L-leucine does not form β-associated structures in TFE as opposed to the behaviour of hepta-L-isoleucine¹⁵⁻¹⁷ and hepta-L-valine^{18, 33}.

In hexafluoroisopropanol (HFIP) (Figure 3) and HFA, however, the c.d. curves do not change significantly from dimer to heptamer. Also, a gradual increase in the intensity of the two negative bands has been observed. This finding is not surprising since HFIP and HFA are considerably more acidic than TFE⁴¹ and thus require a longer chain length for the onset of secondary structures. In fact, the structure-disrupting properties

of these two fluoroalcohols have been shown in other oligopeptide series^{15-17, 20, 33, 35}. In addition, these c.d. results confirm our preliminary polarimetric conformational analysis (Figure 1).

The chiroptical properties of the oligo-L-leucines in ethylene glycol (EG) are also shown in Figure 3. This solvent dissolves the oligopeptide series to the hexamer. The c.d. spectrum of hexa-L-leucine is reminiscent of those typical of β-conformations⁴⁰, even if the Cotton effects are slightly red shifted and less intense than those of hepta-L-isoleucine^{15, 17} and hepta-L-valine^{18, 33} in TFE. The β-associated structure of hexa-L-leucine could be disrupted by dilution, addition of TFE and HFIP (Figure 4), or by increasing the temperature (Figure 4).

Since proteins function primarily in water, it is of interest to investigate peptide model compounds in aqueous solution. Unfortunately, these oligopeptides are insoluble in water. We were able, however, to examine their c.d. properties in TFE-water mixtures. The addition of 80% water (v/v) to a solution of hepta-L-leucine in TFE induces a dramatic variation in the c.d. pattern (Figure 5). Consequently, we have investigated all the peptide series in this solvent mixture. The spectral properties typical of the β-form⁴⁰ appear at the pentamer (Figure 5). Again, dilution or increasing temperature (*T*_m = 34°C for the heptamer) disrupts the β-aggregates. We have also compared the tendencies of water and EG in supporting the β-structure. The different c.d. curves of the heptamer in 20% TFE and

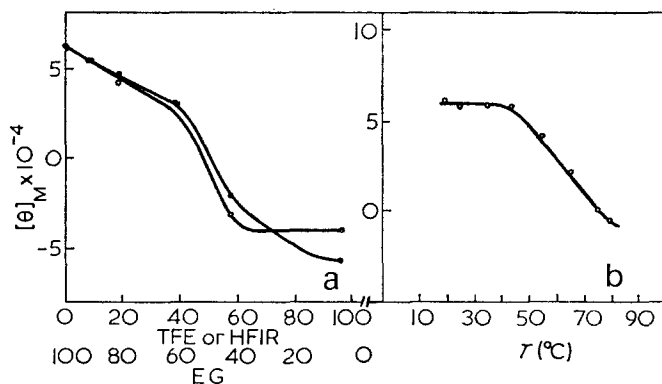


Figure 4 (a) Plot of total molar ellipticity values at 207.5 nm of BOC-(L-Leu)₆OMe in various TFE-EG (●) and HFIP-EG (○) mixtures at 25°C (conc. 3 × 10⁻⁴M); (b) plot of total molar ellipticity values at 207.5 nm of BOC-(L-Leu)₆OMe in EG vs. temperature

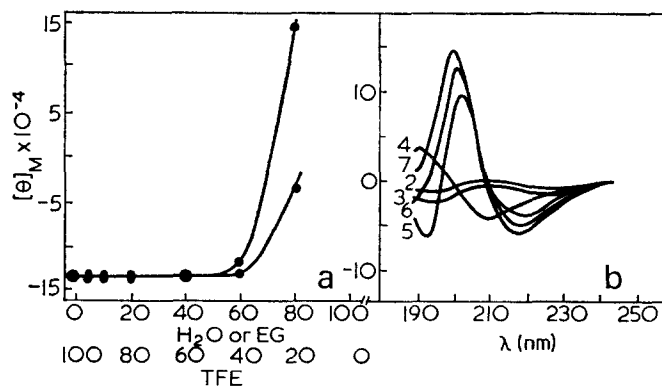


Figure 5 (a) Plot of total molar ellipticity values at 200 nm of BOC-(L-Leu)₇OMe in various TFE-water (○) and TFE-EG (●) mixtures at 25°C (conc. 3 × 10⁻⁴M); (b) circular dichroism spectra of BOC-(L-Leu)_nOMe in TFE-water (20:80, v/v) at 25°C (conc. 3 × 10⁻⁴M)

80% water or EG indicate that the stability of the β -structure of these oligomers is higher in water than in EG. The present c.d. analysis of L-leucine oligomers confirms that the β -structure has a solvent-dependent critical chain length^{15-21, 33-35}, in analogy to the critical size necessary for α -helix formation^{3, 37-39}. Also, the β -conformation is the preferred structure of oligo-L-leucines in water as of other homo-oligopeptides derived from other aliphatic and aromatic amino acid residues^{15-21, 33-35}. Our results additionally show the greater tendency of water, when compared to EG and TFE, in supporting the β -conformation of oligopeptides with saturated side chains^{15-21, 33-35, 42}. In this context, the higher tendency of isoleucine¹⁵⁻¹⁷ and valine^{18, 33} with respect to leucine (and methionine^{19, 20}) in assuming the β -structure points to the contribution of β -branching in directing peptide conformations³; finally, the comparable conformational behaviour of leucine and methionine oligopeptide series suggests similarity in structural role of $-\text{CH}_2-\text{CH}(\text{CH}_3)_2$ and $-\text{CH}_2-\text{CH}_2-\text{S}-\text{CH}_3$ groups¹⁴.

ACKNOWLEDGEMENT

The authors wish to thank Dr E. Celon of the Department of Chemistry, University of Padua, for carrying out the elemental analyses reported in *Table 1*.

REFERENCES

- 1 Maigret, B., Perahia, D. and Pullman, B. *Biopolymers* 1971, **10**, 491
- 2 Ponnuswamy, P. K. and Sasisekharan, V. *Biopolymers* 1971, **10**, 565
- 3 Fasman, G. D. 'Poly- α -Amino Acids', (Ed. G. D. Fasman), Marcel Dekker, New York, 1967, Vol 1, p 499
- 4 Ferretti, J. A. *Chem. Commun.* 1967, p 1030
- 5 Stewart, W. E., Mandelkern, L. and Glick, R. E. *Biochemistry* 1967, **6**, 143
- 6 Itoh, K., Shimanouchi, T. and Oya, M. *Biopolymers* 1969, **7**, 649
- 7 Warashina, A., Iio, T. and Isemura, T. *Biopolymers* 1970, **9**, 1445
- 8 Koenig, J. L. and Sutton, P. L. *Biopolymers* 1971, **10**, 89
- 9 Alter, J. E., Taylor, G. T. and Scheraga, H. A. *Macromolecules* 1972, **5**, 739
- 10 Ostroy, S. E., Lotan, N., Ingwall, R. T. and Scheraga, H. A. *Biopolymers* 1970, **9**, 749
- 11 Chou, P. Y., Wells, M. and Fasman, G. D. *Biochemistry* 1972, **11**, 3028
- 12 Snell, C. R. and Fasman, G. D. *Biochemistry* 1973, **12**, 1017
- 13 Snell, C. R. and Fasman, G. D. *Biopolymers* 1972, **11**, 1723
- 14 Chou, P. Y. and Fasman, G. D. *J. Mol. Biol.* 1973, **74**, 263
- 15 Toniolo, C. *Chim. Ind. (Milan)* 1970, **52**, 1039
- 16 Toniolo, C. *Biopolymers* 1971, **10**, 1707
- 17 Goodman, M., Naider, F. and Toniolo, C. *Biopolymers* 1971, **10**, 1719
- 18 Toniolo, C. and Bonora, G. M. *Makromol. Chem.* in press
- 19 Toniolo, C. and Bonora, G. M. *Int. J. Sulphur Chem.* in press
- 20 Bonora, G. M. and Toniolo, C. *Biopolymers* in press
- 21 Toniolo, C. and Bonora, G. M. *Makromol. Chem.* 1974, **175**, 1665
- 22 Shields, J. E., McDowell, S. T., Pavlos, J. and Gray, G. R. *J. Am. Chem. Soc.* 1968, **90**, 3549
- 23 Dunstan, D. R. and Scopes, P. M. *J. Chem. Soc. (C)* 1968, p 1585
- 24 Sluyterman, L. A. A. and Wijdenes, J. *Biochim. Biophys. Acta* 1972, **289**, 194
- 25 Schnabel, E. *Liebigs. Ann. Chem.* 1967, **702**, 188
- 26 Anderson, G. W. and McGregor, A. C. *J. Am. Chem. Soc.* 1957, **79**, 6180
- 27 Rachele, J. R. *J. Org. Chem.* 1963, **28**, 2898
- 28 Boissonnas, R. A., Guttman, St., Jaquenoud, P. A. and Waller, J. P. *Helv. Chim. Acta* 1956, **39**, 1421
- 29 Sheehan, J. C. and Hess, G. P. *J. Am. Chem. Soc.* 1955, **77**, 1067
- 30 Honzl, J. and Rudinger, J. *Colln Czech. Chem. Commun.* 1961, **26**, 2333
- 31 Goodman, M., Listowsky, I. and Schmitt, E. E. *J. Am. Chem. Soc.* 1962, **84**, 1296
- 32 Gratzer, W. B. 'Poly- α -Amino Acids', (Ed. G. D. Fasman), Marcel Dekker, New York, 1967, Vol 1, p 177
- 33 Toniolo, C., Bonora, G. M. and Fontana, A. *Int. J. Peptide Protein Res.* in press
- 34 Peggion, E., Palumbo, M., Bonora, G. M. and Toniolo, C. *Bioorg. Chem.* 1974, **3**, 125
- 35 Goodman, M., Naider, F. and Rupp, R. *Bioorg. Chem.* 1971, **1**, 310
- 36 Imae, T. and Ikeda, S. *Biopolymers* 1972, **11**, 509
- 37 Goodman, M., Verdini, A. S., Toniolo, C., Phillips, W. D. and Bovey, F. *Proc. Nat. Acad. Sci. US* 1969, **64**, 444
- 38 Goodman, M., Toniolo, C. and Verdini, A. S. 'Peptides 1969', (Ed. E. Scoffone) North-Holland, Amsterdam, 1971, p 207
- 39 Toniolo, C. 'Dynamic Aspects of Conformation Changes of Biological Macromolecules', (Ed. C. Sadron), Reidel, Dordrecht, 1973, p 87
- 40 Beychok, S. 'Poly- α -Amino Acids', (Ed. G. D. Fasman), Marcel Dekker, New York, 1967, Vol 1, p 293
- 41 Middleton, W. J. and Lindsey, R. V. Jr. *J. Am. Chem. Soc.* 1964, **86**, 4948
- 42 Toniolo, C., Bonora, G. M. and Fontana, A. *Int. J. Peptide Protein Res.* in press

Sorption, diffusion and conduction in polyamide-penetrant systems:

1. Sorption phenomena

G. Skirrow and K. R. Young*

*Department of Inorganic, Physical and Industrial Chemistry, University of Liverpool,
PO Box 147, Liverpool L69 3BX, UK
(Received 20 February 1974)*

Isotherms for the uptake of water, methanol, ethanol, propan-1-ol and propan-2-ol by nylon-6 have been determined by gravimetric methods (quartz spiral spring and electronic recording microbalance) over wide temperature and concentration ranges. The isotherm shapes and the partial molar free energy, enthalpy and entropy changes associated with the uptake are consistent with sorption at specific sites. The data have been used to explain the order of the equilibrium uptake: propan-1-ol > water > propan-2-ol > ethanol > methanol. Some isotherms showed an upward sweep at high penetrant concentrations, and examination by the Zimm-Lundberg method showed clustering to become apparent in this region.

INTRODUCTION

In recent years a number of authors¹⁻⁵ have reported sorption investigations of penetrant-polyamide systems during studies of penetrant-polymer interactions and the consequent change in polymer structure. Generally, results have been restricted to a limited number of penetrants, to a small temperature range or both. This paper outlines an investigation of the uptake of a series of penetrants (water and alcohols) by nylon-6 over a wide temperature range.

EXPERIMENTAL

Nylon-6 film (2.8×10^{-3} cm thick) was obtained in the form of tubular sheet from British Cellophane Ltd. Before use each sample cut from the sheet was soaked in distilled water for 48 h.

The penetrants used were distilled water and Analar grade alcohols. Most of the sorption isotherms were obtained using a calibrated quartz spiral spring⁶ (92.2 cm extension/g) which was mounted in a Pyrex jacket connected to a conventional high vacuum system, a penetrant storage system and a mercury manometer. The portion of the apparatus containing the sample was mounted in a thermostat, the temperature of which could be controlled to $\pm 0.2^\circ\text{C}$, and the upper portion of the spring (jacket) was maintained at a temperature close to that of the sample so as to minimize convection. The manometer used to measure the applied penetrant pressure and all connecting lines were heated so as to prevent condensation of vapour, and care was taken to prevent the distillation of mercury vapour onto the

spring or sample by isolating the manometer except when readings were taken. The extension of the spring was measured by means of a precision cathetometer to $\pm 10^{-3}$ cm.

A vacuum electronic recording microbalance (Combustion Instruments Microforce Balance, Mark 2 model B) was used to obtain absorption/desorption isotherms (and also to follow the kinetics of the vapour uptake by a semi-automatic method⁷) for a number of systems. When using this method, the sample was suspended in a jacket, the temperature of which was controlled to $\pm 0.2^\circ\text{C}$ by a forced-draught thermostat. Particular care was taken to minimize vibrations by isolating the jacket from mechanical contact with the thermostat by mounting it on a vibration-damping support. The entire microbalance system was mounted on vibration resisting support. The balance was calibrated against the spring by comparison of equivalent isotherms. Samples were degassed for 6 h until a stable zero was attained, a pre-determined pressure of penetrant (measured using a wide-bore mercury manometer and cathetometer) introduced from a reservoir and the weight change to equilibrium followed.

RESULTS AND DISCUSSION

Isotherms were obtained using as penetrants water (36, 40, 43.9, 48.0, 52.0, 55.0, 59.0, 70.0, 80.0 and 90.0°C), methanol (32.0, 36.0, 40.1, 44.1, 47.9, 52.0, 59.0, 70.0, 80.0 and 90.0°C), ethanol (48.0, 59.0, 70.0, 80.0 and 90.0°C), propan-1-ol (70.0, 80.0 and 90.0°C) and propan-2-ol (80.0, 90.0 and 100.0°C). Those for water and methanol penetrants are shown in *Figures 1* and *2*, the concentration being expressed in cm^3 penetrant vapour (at STP) taken up by 1 cm^3 of the dry polymer. Occasionally, slight hysteresis was observed, particularly

* Present address: The Queen's School, City Walls Road, Chester, CHI 2NN, UK.

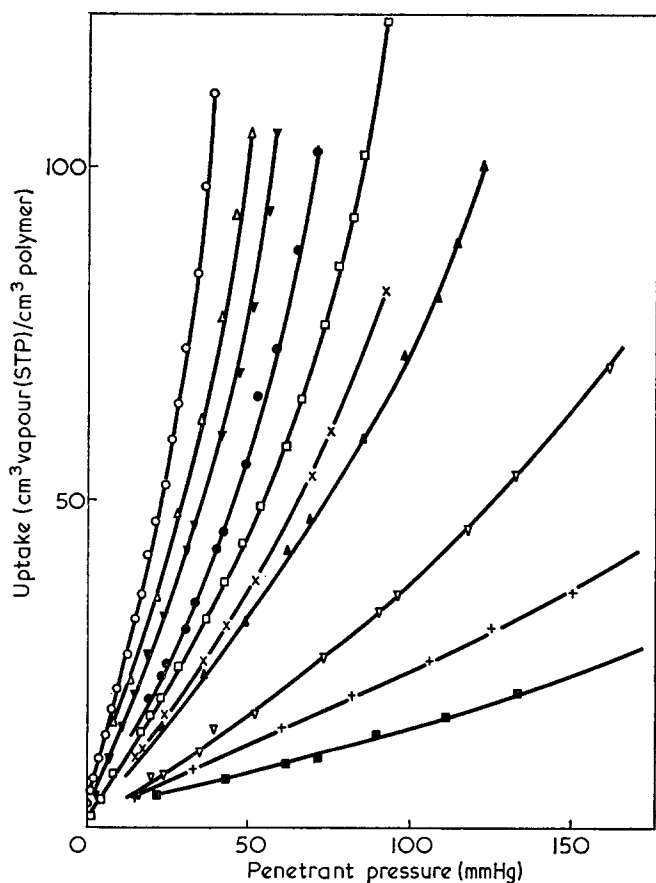


Figure 1 Isotherms: nylon-6/water system. ○, 36.0; △, 40.0; ▼, 43.9; ●, 48.0; □, 52.0; ×, 55.0; ▲, 59.0; ▽, 70.0; +, 80.0; ■, 90.0°C

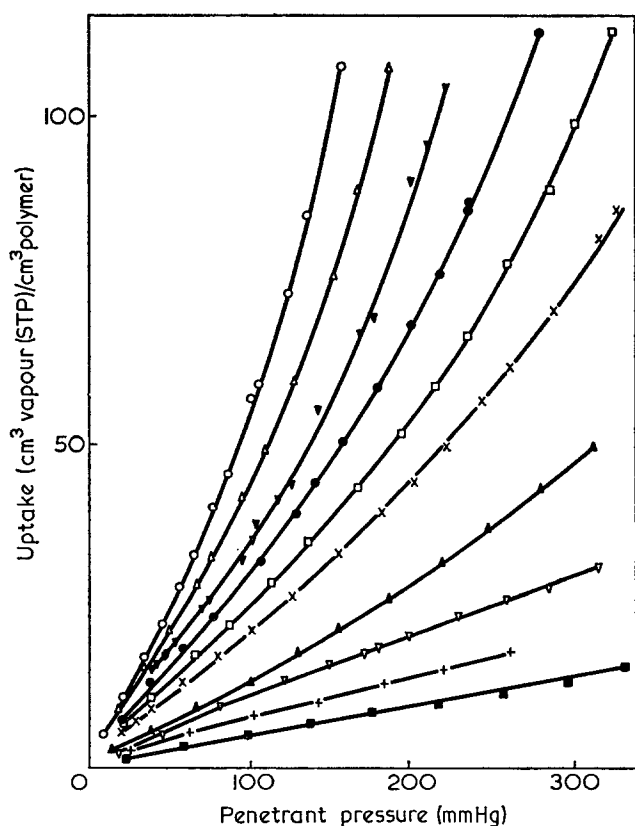


Figure 2 Isotherms: nylon-6/methanol systems. ○, 32.0; △, 36.0; ▼, 40.1; ●, 44.1; □, 47.9; ×, 52.0; ▲, 59.0; ▽, 70.0; +, 80.0; ■, 90.0°C

for large uptake changes. The magnitude of this hysteresis was similar to that observed previously in a number of other polyamide-water systems¹. Absorption isotherms are considered in this paper.

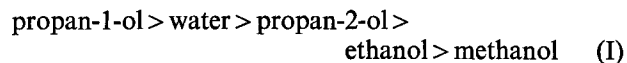
Isotherm shape

For small amounts of penetrant uptake, most of the isotherms were convex to the pressure axis; at high applied penetrant vapour pressure an upward sweep was apparent. The general shape of the isotherms is characteristic of nylon-water systems and has often been noted for various polyamide-penetrant systems^{2, 3, 8-12}. The initial Langmuir-type behaviour suggests the presence of a limited number of sorption sites which are immediately available to the penetrant molecules, and the eventual upward sweep is probably indicative of clustering or multi-layer formation⁹ at the higher penetrant concentrations.

Although the sorption process in nylons is complex, it is generally considered that the penetrant molecules do not readily enter the crystalline regions but that they are confined to the amorphous portions or to the crystalline surfaces (see, however, Campbell¹³). Since in the unperturbed polymer a small fraction (~6%) of the imide groups in the amorphous regions are not hydrogen bonded to other chains¹⁴, the initial uptake of water probably occurs on these 'free' sites. This primary monolayer formation is likely to be complete at about 2 wt% (~20 cm³ (STP)/cm³) uptake, a value consistent with the position of the inflection of the isotherms for water shown in Figure 1. Studies of the effect of water on the narrow line n.m.r. intensity for the nylon-6/water system at 25°C by Kawasaki and Sekita³ indicated a further region of low water content over which the penetrant molecules are relatively immobile. In this region the uptake is accompanied by the breaking of intramolecular hydrogen bonds. Above about 4 wt% the water molecules are much more mobile, and it is in this region (~40 cm³ (STP)/cm³) that clustering in nylon-6 is apparent (see below). For these higher uptakes when there are no longer available singly occupied primary sites, penetrant molecules must attach to secondary sites or, where suitable voids in the polymer matrix exist or can be created, associate with other water molecules in clusters.

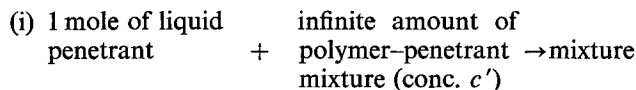
Comparison of isotherms

For a particular penetrant pressure, the equilibrium uptake sequence by nylon-6 is:



although at low pressures the uptake for ethanol is closely similar to that for methanol. Clearly, neither polarity nor molecular size can be used as simple criteria for predicting the relative uptakes. Thus, steric effects, which might be expected to restrict access of propan-2-ol to sites do not appear to be critical.

The partial molar free energy, enthalpy and entropy changes for uptake at a concentration c' of penetrant can be defined on the basis of one or other of the three processes:



- (ii) 1 mole of penetrant infinite amount of vapour at saturated + polymer-penetrant → mixture vapour pressure (p_s) mixture (conc. c')
- (iii) 1 mole of penetrant infinite amount of vapour at reference + polymer-penetrant → mixture pressure p_r mixture (conc. c')

For each polymer/penetrant system at a given temperature, provided that the vapour can be regarded as a perfect gas, the partial molar enthalpy changes in these three processes are inter-related by:

$$\Delta\bar{H}_{ii} = \Delta\bar{H}_{iii} = \Delta\bar{H}_i - \Delta H_c \quad (1)$$

where ΔH_c is the molar enthalpy of condensation of the penetrant. Also:

$$\Delta\bar{G}_i = \Delta\bar{G}_{ii} = \Delta\bar{G}_{iii} - RT \ln(p_s/p_r) \quad (2)$$

where R and T have their usual meanings. The appropriate quantities can be obtained by making use of standard relationships¹⁵. For example:

$$\left(\frac{\partial \ln p}{\partial T}\right)_c = \frac{\Delta\bar{H}_{ii}}{RT^2} \quad (3)$$

where p and c are the penetrant pressure and concentration respectively, and if $\Delta\bar{H}_{ii}$ is temperature independent:

$$\ln p = \frac{\Delta\bar{H}_{ii}}{RT} + \text{constant} \quad (4)$$

Typical isosteres are shown in Figure 3, and values for $\Delta\bar{H}_{ii}$ and $\Delta\bar{H}_i$ (derived from the isostere slopes) are given in Table 1. Mean values¹⁶ for ΔH_c for the relevant temperature range were used to evaluate $\Delta\bar{H}_i$.

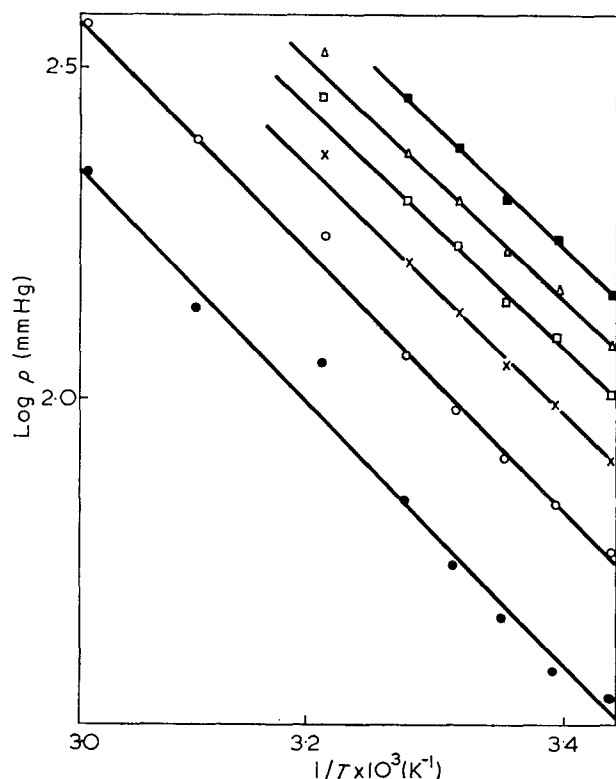


Figure 3 Isosteres: nylon-6/methanol systems. ●, 15; ○, 25; ×, 35; □, 45; △, 55; ■, 70 cm³ (STP)/cm³

Table 1 Enthalpy changes for polyamide-penetrant systems

System	Concentration (cm ³ vapour (STP)/cm ³ polymer)	$-\Delta\bar{H}_{ii}$ (kJ/mol)	$-\Delta\bar{H}_i$ (kJ/mol)
nylon-6/water ($\Delta H_c = -42.05$ kJ/mol)	20	46.61	4.56
	30	44.85	2.80
	40	44.02	1.97
	70	44.22	2.18
	100	42.43	0.38
nylon-6/methanol ($\Delta H_c = -34.84$ kJ/mol)	15	38.65	3.80
	25	37.97	3.12
	35	36.19	1.35
	45	35.62	0.77
	55	33.32	0.47
	70	35.47	0.63
nylon-6/ethanol ($\Delta H_c = -39.91$ kJ/mol)	15	38.20	-1.71
	25	37.50	-2.41
	35	38.05	-1.87
	45	36.22	-3.69
	55	36.07	-3.85
nylon-6/propan-1-ol ($\Delta H_c = -43.30$ kJ/mol)	15	28.62	-16.78
	25	33.51	-11.88
	35	35.86	-9.54
nylon-6/propan-2-ol ($\Delta H_c = -40.08$ kJ/mol)	15	35.56	-4.51
	20	32.76	-7.32
	25	30.59	-9.49

With the exception of the nylon-6/propan-1-ol system (for which the data were not sufficiently precise to allow a trend to be detected), both $\Delta\bar{H}_{ii}$ and $\Delta\bar{H}_i$ became less exothermic with increasing concentration of penetrant. Process (ii) is exothermic, but as the concentration increased, the exothermicity decreased. Process (i) incorporating as it does penetrant vaporization, is sometimes endothermic (see e.g. the values for the uptakes of ethanol and propanol).

For the nylon-6/water systems, $\Delta\bar{H}_{ii}$ (and $\Delta\bar{H}_i$) become progressively less exothermic by about 4.2 kJ/mol over the concentration range 20–100 cm³ (STP)/cm³ (Figure 4a). Calorimetrically determined values for $\Delta\bar{H}_i$ for this system show a similar fall at least over part of the range¹. Thus, Nekryach and Samchenko¹⁷ found the heat of wetting ($-\Delta\bar{H}_i$) for the nylon-6/water system at 20°C to be constant (~ 9.2 kJ/mol, exothermic) up to 5 wt%, but beyond this uptake it became progressively less exothermic until at 9 wt% it was almost zero and constant. The first region of constant $\Delta\bar{H}_i$ was attributed to sorption on sites, and the second to clustering or multi-layer formation. Similar behaviour was noted by Muller and Hellmuth¹⁰ (using the data obtained by Bull¹⁸) for the nylon-6,6/water system. For the nylon-6/water system they found $\Delta\bar{H}_i$ to be -12.9 kJ/mol at a concentration of 9.66 cm³ (STP)/cm³; this value should be compared with that of -4.56 kJ/mol found in this work for a concentration of 20 cm³ (STP)/cm³ (Table 1).

Isosteric determinations of $\Delta\bar{H}_i$ (and possibly also of $\Delta\bar{H}_{ii}$) are generally regarded as not being sufficiently precise compared with calorimetrically determined values to allow computation of meaningful $\Delta\bar{S}_i$ values (cf. Puffr and Sebenda¹). Both $\Delta\bar{H}_i$ and $\Delta\bar{S}_i$ are very sensitive to isostere slope. This limitation on the accuracy of $\Delta\bar{S}_i$ must be borne in mind when examining the estimates for it given in Table 2 and Figure 4b.

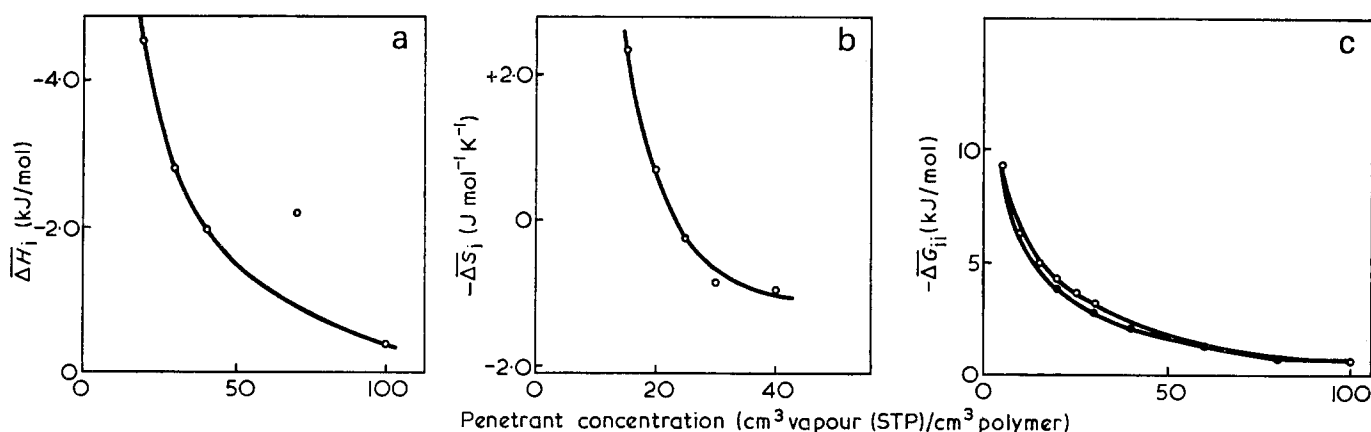

 Figure 4 $\Delta\bar{H}_i$, $\Delta\bar{S}_i$, $\Delta\bar{G}_{ii}$ for nylon-6/water systems. (c): ●, 40; ○, 90°C

 Table 2 Thermodynamic data, nylon-6/water system at 80°C: $\Delta\bar{G}_i$; $\Delta\bar{H}_i$ (kJ/mol); $\Delta\bar{S}_i$ (J mol⁻¹K⁻¹)

	cm ³ vapour (STP)/cm ³ polymer				
	15	20	25	30	40
$-\Delta\bar{G}_i$	5.19	4.31	3.64	3.10	2.30
$-\Delta\bar{H}_i$	6.02	4.56	3.56	2.80	1.97
$-\Delta\bar{S}_i$	2.38	0.71	-0.25	-0.84	-0.96

 Table 3 Thermodynamic data (kJ/mol), nylon-6/penetrant systems at 80°C; $p_r=100$ mmHg; $c=10$ cm³ vapour (STP)/cm³ polymer

	H ₂ O	methanol	ethanol	propan-1-ol	propan-2-ol
$\Delta\bar{G}_d$	3.72	7.66	6.15	3.81	5.65
$-\Delta\bar{G}_{ii}$	6.53	6.74	5.44	6.99	6.02
$-\Delta\bar{G}_{iii}$	2.81	-0.92	-0.71	3.18	0.37
$-\Delta\bar{H}_{ii}$	46.41	38.66	38.20	28.62	35.56
$-T\Delta\bar{S}_{iii}$	43.80	39.58	38.91	25.44	35.19

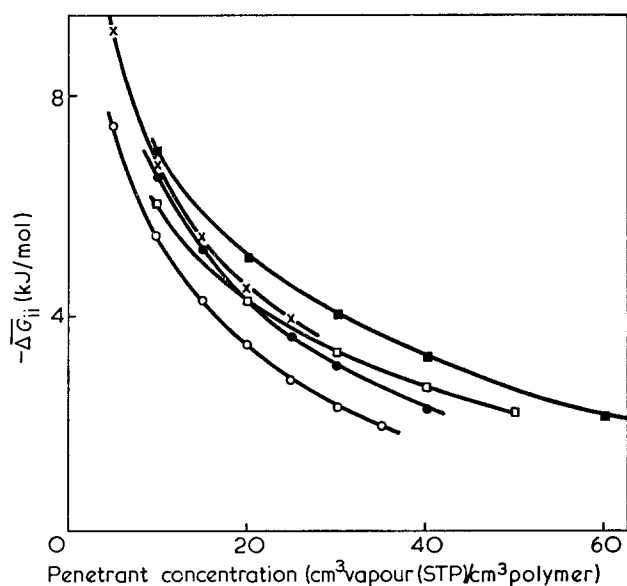
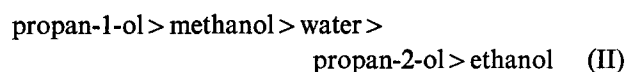


Figure 5 Free energy changes for nylon-6/penetrant systems at 80°C. ●, water; ×, methanol; ○, ethanol; ■, propan-1-ol; □, propan-2-ol

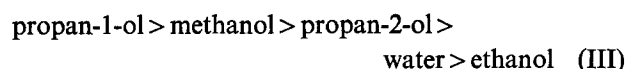
Thus, the apparent tendency for $\Delta\bar{S}_i$ to become more positive with increasing water concentration is surprising if with increasing concentration the likelihood of a water molecule taking part in more than one hydrogen bond simultaneously increases. $\Delta\bar{G}_{ii}$ ($=\Delta\bar{G}_i$)-concentration curves (based on p_s values taken from the literature¹⁹⁻²¹) for a number of systems are shown in Figures 4c and 5. For all the systems examined, $\Delta\bar{G}_{ii}$ is negative, the numerical value decreasing with increasing penetrant concentration. The effect of temperature on $\Delta\bar{G}_{ii}$ for water uptake is small, but there is a tendency for it to become more negative at higher temperatures. Muller and Hellmuth¹¹ found $\Delta\bar{G}_{ii}$ for the nylon-6/water system to fall from -6.3 kJ/mol at 14°C to -5.4 kJ/mol at 59°C. In the present work the mean value for $\Delta\bar{G}_{ii}$

over the range 36–59°C was -6.3 kJ/mol for a similar concentration to that used by previous workers (~ 10 cm³ (STP)/cm³).

For the nylon-6/alcohol systems at 80°C (Figure 5), $-\Delta\bar{G}_{ii}$ ($=-\Delta\bar{G}_i$) for processes (i) and (ii) is in the order:



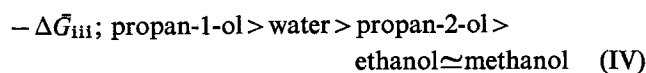
for low uptakes, and



for higher uptakes. These orders are, of course, immediately evident if the isotherms obtained (e.g. Figures 1 and 2) are replotted showing the uptakes as a function of p/p_s .

In the above discussion of the partial molar quantities, $\Delta\bar{G}_{ii}$ corresponds to the uptake of one mole of penetrant (either as a liquid or as the vapour at the saturated vapour pressure) by an infinite amount of the penetrant-polymer mixture at the reference concentration. However, $\Delta\bar{G}_{iii}$ (see above) and the corresponding value of $\Delta\bar{S}_{iii}$ are, unlike $\Delta\bar{G}_i$ ($=\Delta\bar{G}_{ii}$), $\Delta\bar{S}_i$ and $\Delta\bar{S}_{ii}$, uncomplicated by the process of vaporization of the penetrant, and the acceptance of a common reference pressure (p_r) as the standard state for the pure penetrant means that direct comparison of the changes of the thermodynamic parameters for the different systems is more realistic.

The quantities $\Delta\bar{G}_d$ [$=RT\ln(p_s/p_r)$], $\Delta\bar{G}_{ii}$, $\Delta\bar{G}_{iii}$, $\Delta\bar{H}_{ii}$ and $T\Delta\bar{S}_{iii}$ for the various nylon-6/penetrant systems at 80°C and a penetrant concentration of 10 cm³ (STP)/cm³ are given in Table 3. The following sequences are evident:



$$-\Delta\bar{H}_{ii}; \text{ water} > \text{ methanol} > \text{ ethanol} > \\ \text{propan-2-ol} > \text{ propan-1-ol} \quad (\text{V})$$

$$-T\Delta\bar{S}_{iii}; \text{ water} > \text{ methanol} > \text{ ethanol} > \\ \text{propan-2-ol} > \text{ propan-1-ol} \quad (\text{VI})$$

The equilibrium uptake sequence (I) is, of course, the same as that for $\Delta\bar{G}_{iii}$ (sequence IV). Thus, although water uptake shows the highest exothermicity (as expected because of its high polarity), the effect of this on $\Delta\bar{G}_{iii}$ is offset by the large value for $-T\Delta\bar{S}_{iii}$ and consequently the uptake of water is, relative to the other penetrants, lower than might otherwise have been expected.

The $-T\Delta\bar{S}_{iii}$ values indicate that the nylon-6/water system is more ordered than the corresponding nylon/alcohol systems. This is understandable if the water molecules are more tightly bound and are capable of multiple hydrogen bonding in a comparatively ordered structure. It is known that each oxygen atom in liquid water may cooperatively form four hydrogen bonds with its neighbours and thereby give an ordered structure whereas the evidence available suggests that for alcohols the maximum number of hydrogen bonds which can normally be formed is two²². It seems likely that the relative facilities of water and alcohols for hydrogen bond formation may be preserved to some extent when they enter the polymer system.

Clustering

When the polymer and penetrant differ in polarity, a tendency for penetrant clustering might be expected, particularly at high concentrations. This tendency is usually examined by the method proposed by Zimm and Lundberg^{23, 24}. These authors defined a cluster integral G_{AA} , viz.:

$$\frac{G_{AA}}{\bar{V}_A} = -v_B \left[\frac{d(a_A/v_A)}{da_A} \right]_{p, T} - 1$$

where v_A and v_B are the volume fractions of penetrant and polymer respectively, a_A is the penetrant activity and \bar{V}_A is the partial molar volume of the penetrant. According to this treatment, when $G_{AA}/\bar{V}_A > -1$, clustering occurs whereas when $G_{AA}/\bar{V}_A < -1$ sorption occurs on sites with little tendency for clustering.

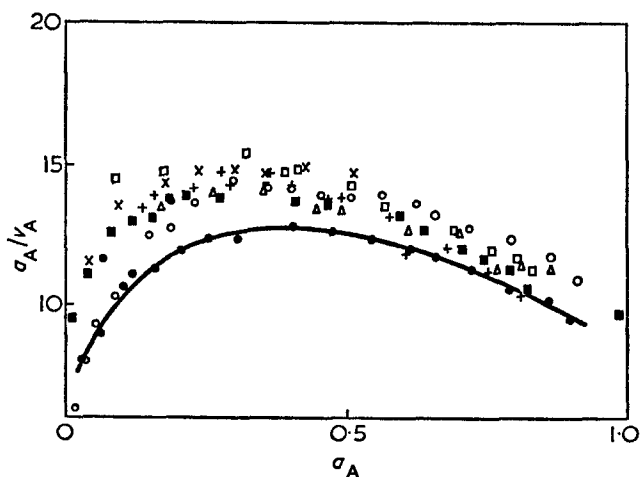


Figure 6 Clustering in the nylon-6/water system. ○, 36.0; ●, 40.0; +, 48.0; ■, 52.0; △, 59.0; □, 70.0; ×, 80.0°C

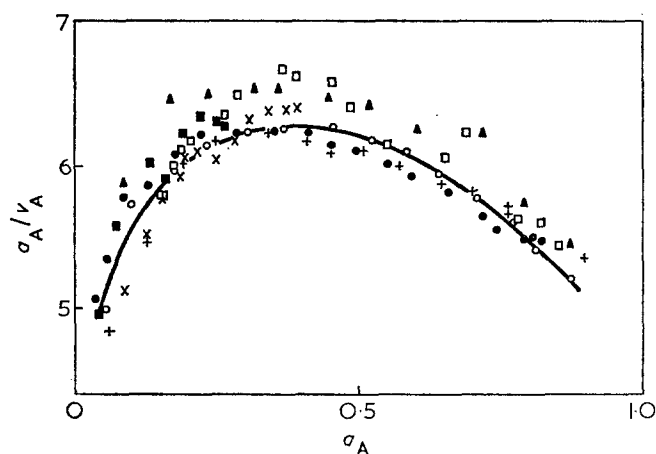


Figure 7 Clustering in the nylon-6/methanol system. ▲, 36.0; □, 40.1; +, 44.1; ○, 47.9; ●, 52.0; ×, 70.0; ■, 80.0°C

When using this approach, it is customary to take the activity of the penetrant to be p/p_s and to plot a_A/v_A against a_A . Typically, for a system in which clustering develops as the concentration increases a curve with a maximum is obtained; the concentration corresponding to the activity at which the maximum occurs is that for the onset of clustering. Plots of this sort derived from the basic data for nylon-6/water and nylon-6/methanol isotherms are shown in Figures 6 and 7. There is some scatter, particularly for the points corresponding to low uptakes where the measurement precision is low, but it is apparent that clustering is evident in both the methanol and water systems.

Within the precision of the measurements there is no detectable shift with temperature of the position for the onset of clustering, and for both systems this position falls within the range 26 to 40 cm³ (STP)/cm³, the majority being in the range 28 to 32 cm³ (STP)/cm³.

Evidence for clustering during the uptakes of ethanol and the propanols is less conclusive, partly because of some scatter in the basic data. However, it is possible that the greater bulk of these molecules in relation to their polarity may make their localized aggregation in a relatively inflexible polymer network more difficult. This is not inconsistent with the smaller decrease in $\Delta\bar{S}_{iii}$ for uptake of these molecules compared with that of water. Further examination of the uptakes of these penetrants is desirable.

The agreement between the amounts of water and methanol taken up at the onset of clustering implies that at this point there is one penetrant molecule per accessible sorption site. If it is assumed that in the polymer network there is one polar site per polymer unit, then for a polymer of density 1.16 g/cm³ the potential molar concentration of sites is 9.4×10^{-3} mol/cm³. A penetrant uptake of 30 cm³ (STP)/cm³ is equivalent to a concentration of 1.35×10^{-3} mol/cm³. Evidently only some 15% or so of the polar sites are accessible. Of the remaining 85%, a large proportion will constitute the crystalline regions and for this reason will be unavailable.

ACKNOWLEDGEMENTS

The authors wish to thank British Cellophane for the provision of samples and D. L. Dare for technical assistance. One of us (K. R. Y.) would also like to

thank the Science Research Council for the provision of a Research Studentship.

REFERENCES

- 1 Puffr, R. and Sebenda, J. *J. Polym. Sci. (C)* 1966, **16**, 79
- 2 Puffr, R. *Kolloid-Z.* 1968, **222**, 130
- 3 Kawasaki, K. and Sekita, Y. *J. Polym. Sci. (A)* 1964, **2**, 2437
- 4 Ash, R., Barrer, R. M. and Palmer, D. G. *Polymer* 1970, **11**, 421
- 5 Dodding, R. A. and Skirrow, G. to be published
- 6 McBain, J. W. and Bakr, A. M. *J. Am. Chem. Soc.* 1926, **48**, 690
- 7 Skirrow, G. and Young, K. R. to be published
- 8 Sebenda, J. and Puffr, R. *Colln. Czech. Chem. Commun.* 1964, **29**, 60
- 9 Kawasaki, K., Sekita, Y. and Kanou, K. *J. Colloid Sci.* 1962, **17**, 865
- 10 Muller, F. H. and Hellmuth, E. *Kolloid-Z.* 1961, **177**, 1
- 11 Ramsden, D. K., Wood, F. and King, G. *J. Appl. Polym. Sci.* 1966, **10**, 1191
- 12 Rogers, C. E. in 'Engineering Design of Plastics', (Ed. E. Baer), Reinhold, New York, 1964
- 13 Campbell, G. A. *J. Polym. Sci. (B)* 1969, **7**, 629
- 14 Pauling, L. *J. Am. Chem. Soc.* 1945, **67**, 555
- 15 Young, K. R. *PhD Thesis* University of Liverpool (1970)
- 16 Washburn, E. H. (Ed.) 'International Critical Tables', Nat. Res. Council, Washington, D.C., 1926, Vol 5, p 138
- 17 Nekryach, E. F. and Samchenko, Z. A., *Zolloidn Zh.* 1960, **22**, 288
- 18 Bull, H. B. *J. Am. Chem. Soc.* 1944, **66**, 1499
- 19 Stall, D. R. *Ind. Eng. Chem.* 1947, **39**, 517
- 20 Young, S. *Sci. Proc. R. Dublin Soc.* 1910, **12**, 374
- 21 Weast, R. C. (Ed.) 'Handbook of Chemistry and Physics', 49th edn, Chemical Rubber Co., Cleveland, 1968
- 22 Franks, F. and Ives, D. J. G. *Q. Rev. Chem. Soc.* 1966, **20**, 1
- 23 Zimm, B. H. and Lundberg, J. L. *J. Phys. Chem.* 1956, **60**, 425
- 24 Lundberg, J. L. *J. Macromol. Sci. (B)* 1969, **3**, 393

Upper and lower critical solution temperatures in polyethylene solutions

N. Kuwahara, S. Saeki, T. Chiba and M. Kaneko

Department of Polymer Science, Hokkaido University, Sapporo, Japan
(Received 15 January 1974; revised 8 April 1974)

Upper and lower critical solution temperatures have been determined for solutions of polyethylene in n-butyl acetate and n-amyl acetate over the molecular weight range of $M_w=1.36 \times 10^4$ to 17.5×10^4 . Polyethylene solution in n-butyl acetate displays a smaller miscibility region than that of the polyethylene/n-amyl acetate system, as indicated by the relative positions of their upper and lower critical solution temperatures. Contributions of the energy and the equation of state terms to the χ_1 parameter have been examined by an application of the Patterson-Delmas corresponding state theory to the experimental results of the polyethylene solutions.

INTRODUCTION

Phase diagrams of non-crystalline polymer solutions show two regions of limited miscibility in the temperature-composition plot. One of limited miscibility is found below the upper critical solution temperature (*UCST*), the other above the lower critical solution temperature (*LCST*). The *UCST* and *LCST* are predicted by the Patterson-Delmas¹⁻⁴ and Flory theories⁵⁻⁷ of polymer solution thermodynamics. The pairs of the *UCST* and *LCST* have been given for a number of systems, e.g., polyisobutylene solutions^{8,9}, polystyrene solutions¹⁰⁻¹⁵. The *UCST* is raised and the *LCST* lowered as the molecular weight of polymer is increased. If a solvent of poor quality is chosen, the temperature region of complete polymer-solvent miscibility is reduced giving coalescence of two regions of limited miscibility with an increase of the molecular weight of polymer. The featured studies have been done by Cowie *et al.* for cellulose acetate-acetone systems¹⁶ and Siow *et al.* for polystyrene solutions¹⁷. Appearance of both the *UCST* and *LCST* is very general in polymer solutions.

Richards¹⁸ first studied the solubility and swelling of low-density polyethylene in various solvents. The *UCST* for solutions of polyethylene in a number of solvent has been extensively examined by Nakajima *et al.*^{19,20}. For solutions of polyethylene, a typical crystalline polymer, the *UCST* appearing in low polymer concentrations is followed by the solubility curve at high polymer concentrations representing the depression of the melting point of polyethylene by the solvent. If a solvent of good quality is used, the *UCST* is lowered and thus is merged below the solubility curve giving liquid/solid phase equilibrium. The *LCST* of the polyethylene/n-alkane system has been extensively studied²¹⁻²⁴ from the view point of applications of the Patterson-Delmas and Flory theories of polymer solution thermodynamics.

It is very interesting to study the occurrence of a pair of the *UCST* and *LCST* in polyethylene solutions. There is, however, little work showing appearance

of a pair of the *UCST* and *LCST* for solutions of polyethylene in a solvent. The present work was done to give phase diagrams for polyethylene solutions in n-butyl and n-amyl acetate. Except for the solubility curve representing liquid/solid phase equilibrium the phase diagram of polyethylene solutions is essentially the same as that of polystyrene solutions. Thus molecular parameters characterizing thermodynamic properties of polyethylene solutions can be derived by applications of the recent theories of polymer solution thermodynamics to the *UCST* and *LCST*.

EXPERIMENTAL

Polyethylenes (Japan Olefin Chem. Co. Products Sholex 6050: $M_w=4.3 \times 10^4$ and Sholex 4002: $M_w=7.2 \times 10^4$, M_w being the viscosity-average molecular weight) were fractionated into eleven and seven fractions, respectively. Fractionation was carried out through the solution fractionation technique called the coacervation method. After adding poly(ethylene glycol) 200 to the polyethylene-xylene solution more dilute than 0.15 g/dl under constant temperature of 125°C, the solution was kept for a day at 115°C in a poly(ethylene glycol) bath controlled to $\pm 0.05^\circ\text{C}$. After a complete attainment of the liquid/liquid phase equilibrium the dilute solution phase, in which lower molecular weight polyethylene is richer, was carefully separated from the other concentrated solution phase. A fractionated polyethylene was obtained from the dilute phase and the concentrated phase was redissolved by a mixture of xylene and ethylene glycol 200 for further fractionation. The fractions were precipitated and collected in methanol and dried to constant weight at 60°C for 7 days under vacuum.

The molecular weights of polyethylene samples were determined from the limiting viscosity numbers for solutions of polyethylene in tetralin at 120°C, according to the equation²⁵:

$$[\eta] = 32.6 \times 10^{-5} M^{0.77}$$

Viscosity measurements were made in a modified Ubbelohde-type viscometer having negligible kinetic energy corrections with the aid of a silicone oil bath controlled within $\pm 0.02^\circ\text{C}$. Preparation of solutions of polyethylene in tetralin was carried out inside the viscometer and the solutions were filtered through a medium sintered-glass filter fixed within the viscometer.

Chromatographic grade tetralin and reagent grade n-butyl acetate and n-amyl acetate were further purified before use. Tetralin was dried over anhydrous potassium carbonate and n-butyl acetate and n-amyl acetate over anhydrous magnesium sulphate. The dried solvents were fractionally distilled by use of a column of 100 cm length and 10 mm diameter packed with stainless-steel helices.

Several solutions in n-butyl acetate and n-amyl acetate were prepared from each sample in the concentration range of 0.4 to ~ 12 wt% and flame sealed under dry nitrogen gas in 7 mm i.d. cylindrical cells. Preparation of solutions of polyethylene in n-butyl acetate and n-amyl acetate was carried out by keeping the solution cells and frequently turning them upside down at a temperature between the UCST and the LCST by use of a silicone oil bath controlled to $\pm 0.2^\circ\text{C}$.

Cloud-point temperatures for the UCST and LCST were optically determined with an accuracy of $\pm 0.2^\circ\text{C}$ in the silicone oil bath,¹ as described elsewhere^{1,2}. After measurements of the precipitation temperature for the LCST, thermal degradation of polyethylene was examined by the reproducibility of the precipitation temperature for the UCST. No thermal degradation of polyethylene in n-butyl acetate and n-amyl acetate was observed.

RESULTS

The cloud-point curves for solutions of polyethylene in n-butyl acetate are shown in Figure 1, in which w_2 is the weight fraction of the polymer. The cloud-point

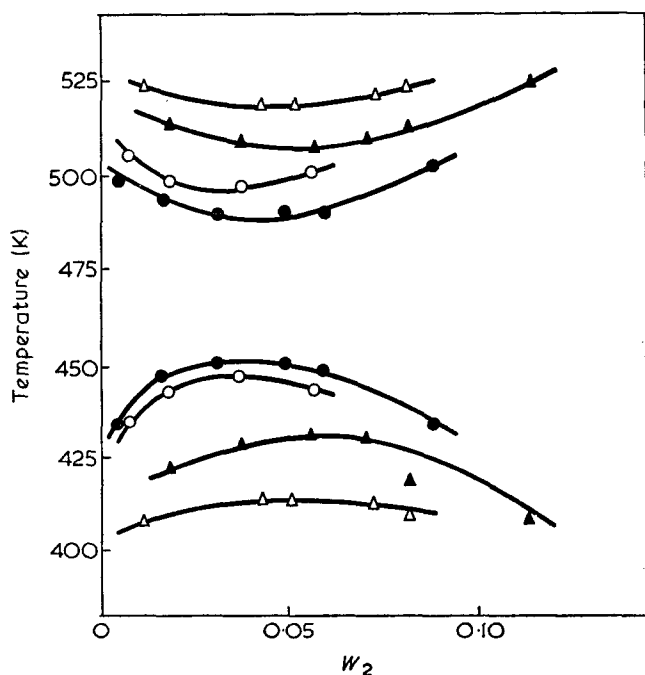


Figure 1 Phase diagrams for the polyethylene samples in n-butyl acetate: Δ , A-2; \blacktriangle , A-4; \circ , B-3; \bullet , A-8

Table 1 Reduced critical temperatures for polyethylene/n-butyl acetate system

Sample	$M_n \times 10^{-4}$	$r^{-1/2} \times 10^2$	UCST		LCST	
			(K)	$\tilde{T}_{1,u} \times 10$	(K)	$\tilde{T}_{1,l} \times 10$
A-2	1.36	9.87	415	0.870	518	1.085
A-4	2.00	8.14	431	0.903	507	1.062
B-3	6.11	4.66	448	0.939	497	1.041
A-8	6.40	4.55	451	0.945	490	1.027

Table 2 Reduced critical temperatures for polyethylene/n-amyl acetate system

Sample	$M_n \times 10^{-4}$	$r^{-1/2} \times 10^2$	UCST		LCST	
			(K)	$\tilde{T}_{1,u} \times 10$	(K)	$\tilde{T}_{1,l} \times 10$
A-2	1.36	10.5	389	0.766	553	1.089
A-4	2.00	8.65	396	0.780	547	1.077
B-3	6.11	4.95	410	0.807	535	1.053
A-8	6.40	4.83	415	0.817	533	1.049
B-7	17.5	2.92	421	0.829	528	1.039

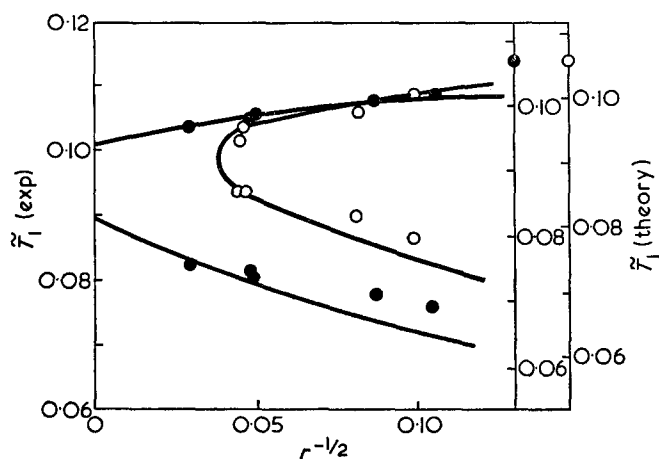


Figure 2 Comparison of experimental reduced temperature \tilde{T}_1 with theoretical curves of equation (4) for solutions of polyethylene in n-butyl acetate (\circ) and n-amyl acetate (\bullet)

curves obtained in n-amyl acetate were similar to those in Figure 1 except for the somewhat wider temperature region of complete miscibility. The UCST is raised and the LCST lowered as the molecular weight of the polymer is increased. If the polymer were completely monodisperse, the critical point would be given by the maximum or minimum points of the cloud-point curves. Polydispersity tends to displace the critical point to lower temperature and higher concentration for the UCST and higher temperature and higher concentration for the LCST depending on the polydispersity of the polymer sample²⁶⁻²⁸. The differences of the maximum and minimum temperatures from their critical temperatures should be small because of polymer samples obtained by fractionation by the solution fractionation technique. Since we are mainly interested in semi-quantitative features of miscibility, the maximum and the minimum temperatures are assumed as the critical solution temperatures for the UCST and the LCST, respectively. Values of the UCST and LCST for the systems are compiled in Tables 1 and 2.

Experimental reduced temperatures \tilde{T}_1 for the systems of polyethylene in n-butyl acetate and n-amyl acetate are plotted against $r^{-1/2}$ in Figure 2, in which r is defined by the ratio of the molar volumes of the polymer and

solvent. The reduced critical temperature \tilde{T}_1 is calculated from⁵:

$$\tilde{T}_1 = \tilde{V}_1^{-1}(1 - \tilde{V}_1^{-1/3}) = T/T_1^* \quad (1)$$

and

$$\tilde{V}_1 = \{\alpha_1 T/3(1 + \alpha_1 T) + 1\}^3 \quad (2)$$

where T_1^* , \tilde{V}_1 , and α_1 are the characteristic temperature reduction parameter, the reduced volume, and the thermal expansion coefficient of the solvent. Values of the experimental \tilde{T}_1 are given in *Tables 1* and *2*, in which the subscript u is for the *UCST* and the subscript l for the *LCST*. The values of T_1^* were obtained from \tilde{V}_1 by use of α_1 for solvents taken from the literature²⁹.

DISCUSSION

The value of the *LCST* is markedly increased with an increase of pressure³⁰⁻³² bringing out a corresponding enhancement of polymer solubility. A small dependence on pressure for the *UCST* of the polystyrene-cyclohexane system has been observed³³. Pressure dependence of the *UCST* and *LCST* should be generally expected in the polymer-solvent systems and displacements of the *UCST* and *LCST* by pressure are related to the reduced volume of the solvent². The cloud-point curves of the n-butyl acetate system were obtained under the solution vapour pressure of 1 to ~4 atm. [1 atm. \equiv 101.33 N/m²] for the *UCST* and 8 to ~14 atm. for the *LCST* depending on the molecular weight of the samples. The critical solution temperatures corrected to the zero pressure condition would be negligible small for the *UCST* and lower than the observed ones by 4 to ~7°C for the *LCST*. The pressure condition of determinations of the *LCST* for the n-amyl acetate solutions is estimated as 10 to ~16 atm., which lowers the observed critical solution temperatures by 5 to ~8°C in correcting to the zero pressure condition. On the other hand, the observed critical temperatures for the *LCST* obtained from the minimum points of the cloud-point curves should be a little lower than their critical temperatures depending on the molecular weight polydispersity of the sample²⁶⁻²⁸. The somewhat compensating displacements of the critical temperatures by pressure and molecular weight polydispersity should be practically of minor importance in determinations of main features of miscibility.

Two types of cloud-point curves for solutions of polyethylene in n-butyl acetate and n-amyl acetate behave like mirror images across the temperature axis of the intermediate region of the *UCST* and *LCST*. The usual type of liquid/liquid immiscibility is found in the n-amyl acetate system except for the solubility curve at high polymer concentrations representing the depression of the melting-point of polyethylene by the solvents, which is first discussed by Richards¹⁸. Complete miscibility occurs above the *UCST* and below the *LCST* in the n-amyl acetate system. The two regions of miscibility for the n-butyl acetate system approach each other suggesting cloud-point curves of an 'hourglass' shape as the molecular weight of the polymer is increased. No complete miscibility was observed for the sample B-7 of $M_\eta = 17.5 \times 10^4$ over w_2 of 0.004 to 0.082 suggesting the limits of miscibility at concentrations lower than $w_2 = 0.004$ and higher than $w_2 = 0.082$. If

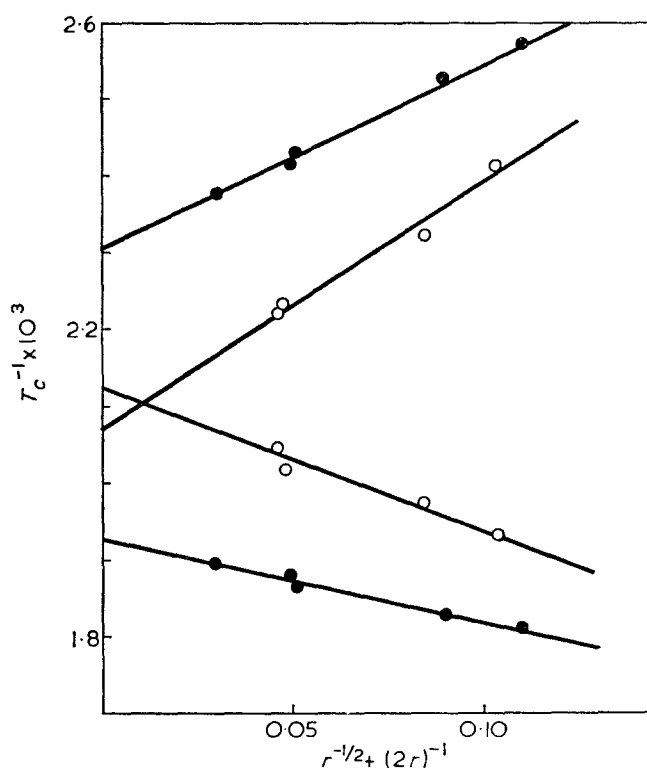


Figure 3 Reciprocal critical solution temperature vs. $r^{-1/2} + (2r)^{-1}$ plots for solutions of polyethylene in n-butyl acetate (O) and n-amyl acetate (●)

n-propyl acetate of poorer quality than n-butyl acetate is chosen as a solvent, the two regions of limited miscibility coalesce to give an 'hourglass' shape even for a solution of polyethylene of the low molecular weight of $M_\eta = 1.36 \times 10^4$. The *UCST* of polymer solutions has been usually found at temperatures lower than the boiling point of the solvent. It should be noted, however, that the *UCST* for the n-butyl solutions lies above the boiling point of n-butyl acetate.

The dependence of the *UCST* and *LCST* on molecular weight is usually described by a relation¹⁰, which is given by:

$$1/T_c = (1/\theta)\{1 + (1/\psi_1)(1/r^{1/2} + 1/2r)\} \quad (3)$$

where ψ_1 is the entropy parameter and θ is the Flory temperature. The molecular weight dependence of the *UCST* and *LCST* is shown in *Figure 3* representing the Shultz-Flory plot. The complete miscibility region of the n-amyl acetate system is given by the intermediate region between a pair of lines in *Figure 3* or a pair of curves in *Figure 2*. However, coalescence of the *UCST* and *LCST* in the n-butyl acetate system would occur in the neighbourhood of $r^{-1/2} = 0.037$ corresponding to $M_\eta = 9.7 \times 10^4$, in *Figure 2*, which is much larger than $r^{-1/2} = 0.01$ to $M_\eta = 146 \times 10^4$ in *Figure 3*. Deviation from linearity in the Shultz-Flory plot has been usually observed to the *UCST* and *LCST* for solutions of polystyrene in expanded solvents^{13, 15, 17}. Values of empirical parameters ψ_1 and θ determined by assumption of linearity of the Shultz-Flory plot are given in *Table 3*, in which the subscripts u and l are for the *UCST* and *LCST*, respectively. The θ_u of both the n-butyl and n-amyl acetate systems lies above their boiling point temperatures. It is recognized that the values of ψ_{1u} and ψ_{1l} in *Table 3* would be different if the dependence

Table 3 Parameters of systems

System	Flory's parameters				Relative values of ν^2 and τ^2 terms in equation (4)			
	θ_u (K)	θ_l (K)	$\psi_{1,u}$	$\psi_{1,l}$	At θ_u		At θ_l	
					ν^2	τ^2	ν^2	τ^2
Polyethylene/n-butyl acetate	483	471	0.65	-1.12				
Polyethylene/n-amyl acetate	434	519	0.98	-1.77	0.320	0.180	0.250	0.250

Table 4 Parameters of systems

System	T_1^* (K)	c_1	$\tau^2 \times 10$	$\nu^2 \times 10$	$c_1 \tau^2$	$c_1 \nu^2$
Polyethylene/n-butyl acetate	4770	1.26	0.477	0.374	0.060	0.047
Polyethylene/n-amyl acetate	5080	0.850	0.706	0.471	0.060	0.040

of the χ parameter on concentration is taken into account^{17, 27, 28}.

The Patterson-Delmas¹⁻⁴ and Flory theories⁵⁻⁷ of polymer solution thermodynamics give essentially the same expressions for χ_1 as a function of temperature⁴. Using a van der Waals model χ_1 at a critical point under zero pressure is given as a function of the reduced volume \tilde{V}_1 of the solvent by^{4, 17}:

$$\chi_1(\text{crit}) = c_1 \nu^2 / (1 - \tilde{V}_1^{-1/3}) + c_1 \tau^2 / 2 \{ (4/3) \tilde{V}_1^{-1/3} - 1 \} \\ = (1/2)(1 + r^{-1/2})^2 \quad (4)$$

where $3c_1$ is the number of external degrees of freedom of the solvent molecules and the ν^2 parameter is related to the differences of the cohesive energy and segment size of the solution components. The τ parameter is a measure of the difference of free volumes of the solution components and is defined by:

$$\tau = 1 - T_1^* / T_2^* = 1 - \tilde{T}_2 / \tilde{T}_1 \quad (5)$$

where T_1^* is the characteristic temperature reduction parameter and \tilde{T}_1 is the reduced temperature of the solvent (1) and polymer (2).

Theoretical curves of \tilde{T}_1 against $r^{-1/2}$ for the two systems derived by equations (1) and (4) using suitable pairs of the molecular parameters $c_1 \nu^2$ and $c_1 \tau^2$ are given in Figure 2. The procedure of the analysis for \tilde{T}_1 was described in detail elsewhere¹². Values of pairs of $c_1 \nu^2$ and $c_1 \tau^2$ adopted for fitting of the theoretical curves to the experimental points are given in Table 4. The τ^2 value was calculated from T_1^* and $T_2^* = 6500\text{K}$. The temperature shifts required for fitting of the calculated curves to the experimental critical temperatures are 38°C for the n-butyl acetate system and 33°C for the n-amyl acetate system.

Equation (4) predicts the temperature dependence of χ_1 at zero pressure. Values of χ_1 are calculated by the aid of equation (4) with the suitable molecular parameters such as $c_1 \nu^2$ and $c_1 \tau^2$ given in Table 4. The temperature dependence of χ_1 for the systems is given in Figure 4, in which the dependences of the $c_1 \nu^2$ and $c_1 \tau^2$ terms on temperature are also included. Comparison of the relative values of the $c_1 \nu^2$ and $c_1 \tau^2$ terms at θ_u and θ_l for the n-amyl acetate system is given in Table 3. In the polyethylene solutions the first $c_1 \nu^2$ term contributes more to χ_1 as compared with the second $c_1 \tau^2$ term, although the two terms equally contribute to χ_1 at θ_l . This feature is a contrast to polystyrene solutions, in which the two terms equally contribute to

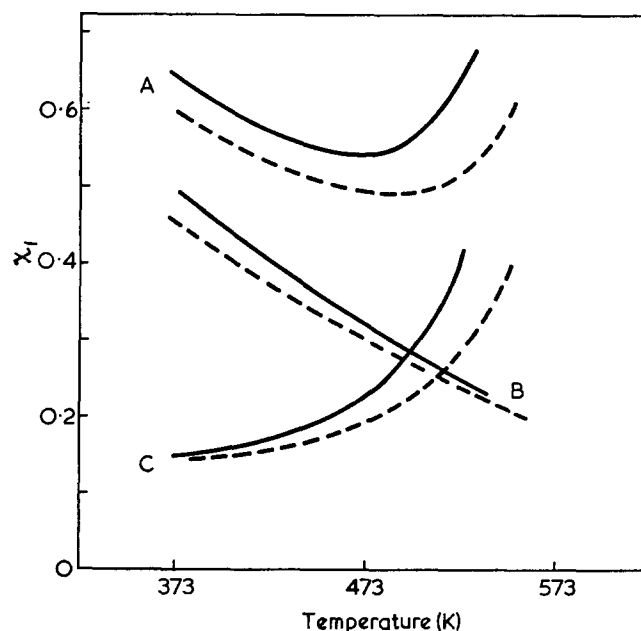


Figure 4 Interaction parameter χ_1 (A), $c_1 \nu^2$ (B) and $c_1 \tau^2$ (C) vs. temperature plots. —, Polyethylene/n-butyl acetate system; ----, polyethylene/n-amyl acetate system

χ_1 at θ_u and the second $c_1 \tau^2$ term dominates over the first $c_1 \nu^2$ term at temperatures above θ_u ¹²⁻¹⁵. The less contribution of the $c_1 \tau^2$ term to χ_1 in polyethylene solutions as compared with that in polystyrene solutions would be qualitatively explained by the Patterson-Delmas¹⁻⁴ and Flory theories⁵⁻⁷ by taking account of T_2^* of polyethylene lower than T_2^* of polystyrene.

It should be also noted that χ_1 for the n-butyl acetate solution in Figure 4 is larger than 0.5 suggesting immiscibility for the solution of polyethylene with the infinite molecular weight in n-butyl acetate. Equation (4) suggests that $\chi_1(\text{crit})$ for polymer solutions increases as the molecular weight of polymer decreases. As a result complete miscibility occurs for the solutions of the polyethylene samples of the molecular weight less than $M_w = 9.7 \times 10^4$ in n-butyl acetate.

In this work appearance of both the UCST and LCST is shown to be found even for solutions of polyethylene, a typical crystalline polymer. It should be recognized that the contributions of the two terms to χ_1 for the polyethylene solutions are in a different way from the polystyrene solutions and miscibility of the polyethylene solutions in a series of n-alkyl acetates

is mainly dominated by the differences of the cohesive energy and segment size between the components.

ACKNOWLEDGEMENTS

The authors thank Dr K. Kamide and Mr K. Sugamiya of Asahi Chemical Industry Company Ltd for supplying polyethylene studied. Also they thank the Ministry of Education in Japan for supporting them.

REFERENCES

- 1 Delmas, G., Patterson, D. and Somcynsky, T. *J. Polym. Sci.* 1962, **57**, 79
- 2 Patterson, D. and Delmas, G. *Trans. Faraday Soc.* 1969, **65**, 708
- 3 Patterson, D. and Delmas, G. *Discuss. Faraday Soc.* 1970, **49**, 98
- 4 Biros, J., Zeman, L. and Patterson, D. *Macromolecules* 1971, **4**, 30
- 5 Flory, P. J., Orwoll, R. A. and Vrij, A. *J. Am. Chem. Soc.* 1964, **86**, 3507
- 6 Flory, P. J., Orwoll, R. A. and Vrij, A. *J. Am. Chem. Soc.* 1964, **86**, 3515
- 7 Flory, P. J. *J. Am. Chem. Soc.* 1965, **87**, 1833
- 8 Fox, T. G. and Flory, P. J. *J. Am. Chem. Soc.* 1951, **73**, 1909
- 9 Liddell, A. H. and Swinton, F. L. *Discuss. Faraday Soc.* 1970, **49**, 115
- 10 Shultz, A. R. and Flory, P. J. *J. Am. Chem. Soc.* 1952, **74**, 4760
- 11 Delmas, G. and Patterson, D. *Polymer* 1966, **7**, 513
- 12 Saeki, S., Kuwahara, N., Konno, S. and Kaneko, M. *Macromolecules* 1973, **6**, 246
- 13 Saeki, S., Kuwahara, N., Konno, S. and Kaneko, M. *Macromolecules* 1973, **6**, 589
- 14 Kuwahara, N., Saeki, S., Konno, S. and Kaneko, M. *Polymer* 1974, **15**, 66
- 15 Saeki, S., Konno, S., Kuwahara, N., Nakata, M. and Kaneko, M. *Macromolecules* 1974, **7**, 521
- 16 Cowie, J. M. G., Maconnachie, A. and Ranson, R. J. *Macromolecules* 1971, **4**, 57
- 17 Siow, K. S., Delmas, G. and Patterson, D. *Macromolecules* 1972, **5**, 29
- 18 Richards, R. B. *Trans. Faraday Soc.* 1945, **41**, 10, 20
- 19 Nakajima, A., Fujiwara, H. and Hamada, F. *J. Polym. Sci. (A-2)* 1966, **4**, 507
- 20 Nakajima, A., Hamada, F. and Hayashi, S. *J. Polym. Sci. (C)* 1966, **15**, 285
- 21 Freeman, P. I. and Rowlinson, J. S. *Polymer* 1960, **1**, 20
- 22 Orwoll, R. A. and Flory, P. J. *J. Am. Chem. Soc.* 1967, **89**, 6814
- 23 Patterson, D., Delmas, G. and Somcynsky, T. *Polymer* 1967, **8**, 503
- 24 Hamada, F., Fujisawa, K. and Nakajima, A. *Polym. J.* 1973, **4**, 316
- 25 Wesslau, H. *Makromol. Chem.* 1958, **26**, 96
- 26 Koningsveld, R. and Staverman, A. J. *J. Polym. Sci. (C)* 1967, **16**, 1775
- 27 Koningsveld, R., Kleintjens, L. A. and Shultz, A. R. *J. Polym. Sci. (A-2)* 1970, **8**, 1261
- 28 Kuwahara, N., Nakata, M. and Kaneko, M. *Polymer* 1973, **14**, 415
- 29 Weissberger, A., Proskauer, E. S., Riddick, J. A. and Toops, Jr. E. E. 'Organic Solvents', Interscience, New York, 1955
- 30 Allen, G. and Baker, C. H. *Polymer* 1965, **6**, 181
- 31 Myrat, C. D. and Rowlinson, J. S. *Polymer* 1965, **6**, 645
- 32 Ehrlich, P. and Kurpen, J. J. *J. Polym. Sci. (A)* 1963, **1**, 3217
- 33 Ham, J. S., Bolen, M. C. and Hughes, J. K. *J. Polym. Sci.* 1962, **57**, 25

220 MHz proton magnetic resonance analysis of some methyl methacrylate–chloroprene copolymers

J. R. Ebdon

*Department of Chemistry, University of Lancaster, Bailrigg, Lancaster LA1 4YA, UK
(Received 19 March 1974)*

220MHz proton magnetic resonance (p.m.r.) spectra of some free-radically prepared methyl methacrylate–chloroprene copolymers have been recorded. The intensities of the α -methyl signals are related to the relative proportions of various methyl methacrylate (MMA) centred triads. Triad fractions obtained from the α -methyl signals indicate that the Mayo–Lewis copolymerization scheme is not strictly applicable to this system, and are in good agreement with those calculated from the penultimate reactivity ratios $r_{11}=0.107 \pm 0.008$, $r_{21}=0.057 \pm 0.004$ and $r_2=6.7 \pm 0.5$ where MMA=monomer 1. However, although a small penultimate group effect is indicated, some deviation from the Mayo–Lewis scheme may be due to the occurrence of anomalous head–head and tail–tail methyl methacrylate–chloroprene linkages.

INTRODUCTION

It has long been recognized that measurements of copolymer sequence distributions can give valuable information about the kinetics of copolymerizations, and that as a rule measurements of sequence distributions can be expected to be a more sensitive indicator of kinetic anomalies than measurements of copolymer compositions¹. With the advent of proton magnetic resonance (p.m.r.) spectrometers capable of operating at a frequency of 220MHz, a powerful technique for the measurement of copolymer sequence distributions has become available. Over the last few years, many copolymer systems have been studied by p.m.r. spectroscopy including a number involving dienes^{2–9}. Recently it has been shown that the α -methyl proton resonances of the methyl methacrylate (MMA) units in methyl methacrylate–butadiene copolymers provide a measure of the various methacrylate centred triads and pentads in the copolymers¹⁰. Triad and pentad fractions calculated from the areas of these resonances were in good agreement with those obtained from the measured reactivity ratios ($r_1=0.17$ and $r_2=0.60$ where MMA is monomer 1). This paper describes a similar analysis of some methyl methacrylate–chloroprene copolymers.

EXPERIMENTAL

Methyl methacrylate (BDH Ltd) was freed from stabilizer and purified by the usual techniques. Chloroprene (BP Chemicals Ltd) was supplied as a 50% solution in xylene containing 2000 ppm each of *t*-butyl catechol and phenothiazine as stabilizers. It was purified by fractionation under a reduced pressure of nitrogen followed by distillation on a vacuum line just prior to use.

Mixtures of chloroprene and methyl methacrylate

were prepared under vacuum with benzene as solvent and benzoyl peroxide (1g/l) as initiator. An overall monomer concentration of 5.0mol/l was used in all experiments. Polymerizations were carried out at 60°C and stopped at 2 wt% conversion or less. The copolymers were recovered by precipitation in excess methanol, were purified by reprecipitation from benzene/methanol and finally were freeze-dried from benzene solutions.

Proton magnetic resonance spectra of the copolymers were recorded at ambient temperatures on Varian A60A and HR 220 spectrometers using CDCl₃ and C₆D₆ as solvents and tetramethylsilane (TMS) as internal reference. Infra-red spectra of copolymer films cast on rock-salt plates from ~2% CHCl₃ solutions were recorded on a Perkin–Elmer 237 grating infra-red spectrometer.

RESULTS AND DISCUSSION

Copolymer compositions and reactivity ratios

Mole fractions of methyl methacrylate, x , in the copolymers were calculated from 60MHz proton magnetic resonance spectra recorded with CDCl₃ as solvent using the equation:

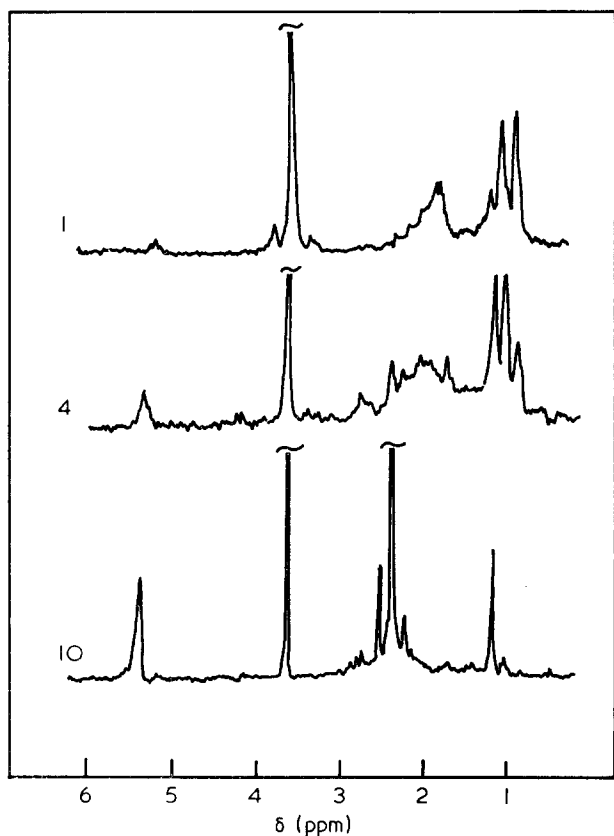
$$x = 5A_{\text{OMe}} / (3A_{\text{total}} - 3A_{\text{OMe}}) \quad (1)$$

where A_{OMe} is the area of the peak due to the methoxy protons of the methacrylate units and A_{total} is the total proton peak area. The compositions of the copolymers together with those of the monomer feeds from which they were prepared are given in *Table 1*.

Attempts to obtain a unique pair of reactivity ratios for this system by application of the Fineman and Ross¹¹ equation proved unsatisfactory; the Fineman and Ross plot has a pronounced curvature which cannot

Table 1 Compositions of copolymers and monomer feeds

No.	Mole fraction MMA in feed	Mole fraction MMA in copolymer
1	0.98	0.86 ± 0.02
2	0.97	0.77 ± 0.02
3	0.96	0.71 ± 0.02
4	0.95	0.64 ± 0.02
5	0.93	0.56 ± 0.02
6	0.90	0.48 ± 0.02
7	0.85	0.40 ± 0.02
8	0.80	0.34 ± 0.02
9	0.70	0.22 ± 0.02
10	0.60	0.18 ± 0.02
11	0.50	0.13 ± 0.02
12	0.40	0.11 ± 0.01
13	0.30	0.08 ± 0.01

Figure 1 Complete p.m.r. spectra in CDCl_3 at 220 MHz for copolymers 1, 4 and 10

be accounted for solely in terms of experimental errors. Thus it would seem that the Mayo and Lewis copolymerization scheme¹² is not strictly applicable to the methyl methacrylate-chloroprene system. However, a pair of reactivity ratios which give the closest fit to the experimental data have been obtained by the curve-fitting procedure of Braun *et al.*¹³ This method gives $r_1=0.08$ and $r_2=5.1$ where MMA is monomer 1. These values are close to those previously published¹⁴ for this system at 60°C (0.080 and 6.12 respectively).

220 MHz p.m.r. spectra

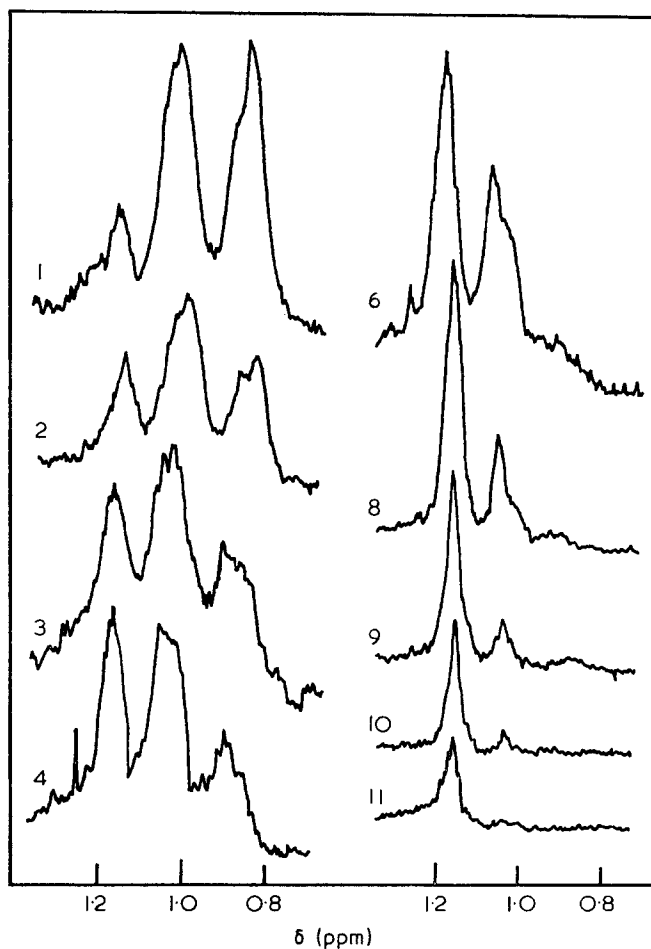
The complete 220 MHz p.m.r. spectra recorded in CDCl_3 for three of the copolymers (1, 4 and 10) are shown in Figure 1. Features to note are: (a) the peaks

due to the olefinic protons of the chloroprene units (5.2–5.5 δ , ppm relative to TMS); (b) the peaks due to the methoxy protons of the MMA units ($\sim 3.6 \delta$); (c) the peaks due to the backbone methylene groups (1.3–3.0 δ) which include a peak at 2.4 δ arising from the adjacent methylene groups in chloroprene-chloroprene diads; and (d) the peaks due to the α -methyl groups of the MMA units (0.7–1.3 δ).

It is apparent from the p.m.r. spectra that the chloroprene units of the copolymers are almost entirely in the 1,4-configuration. There is no evidence in the spectrum of any of the samples of a peak at $\sim 5 \delta$ arising from the $\text{CH}_2=$ protons of pendant vinyl groups in 1,2- or 3,4-units. Thus, these types of unit must constitute less than 2% of the chloroprene units.

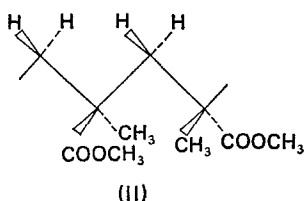
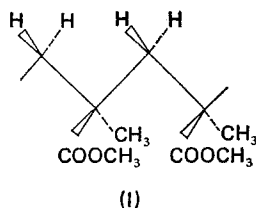
Of particular interest in the p.m.r. spectra are the peaks arising from the α -methyl groups of the MMA units which are clearly grouped in three main regions: A (1.3–1.1 δ), B (1.1–0.95 δ) and C (0.95–0.7 δ). The methyl peaks for copolymers 1–4, 6 and 8–11 are shown in Figure 2. This grouping of the methyl signals is similar to that observed for methyl methacrylate-butadiene copolymers¹⁰ and the following assignments are made (MMA=M, chloroprene=C):

- (1) Group A is assigned to MMA units at the centre of isotactic MMM triads, CMC triads and MMC and CMM triads in which the constituent MM diad is in the *meso* configuration (I).
- (2) Group B is assigned to MMA units at the centre of heterotactic MMM triads and MMC and

Figure 2 α -Methyl peaks for copolymers 1–4, 6 and 8–11

CMM triads in which the constituent MM diad is in the racemic configuration (II).

- (3) Group C is assigned to MMA units at the centre of syndiotactic triads.



M-centred triad fractions

The relative areas of groups A, B and C have been measured for nine of the copolymers using a Du Pont 310 curve resolver to assist in the deconvolution of the overlapped areas and assuming a Lorentzian peak shape for the overlapping portions of the three groups. From these areas, relative proportions of CMC, CMM + MMC, and MMM triads have been calculated. It has been assumed that the tacticity of the MMM triads is the same in the copolymers as it is in a sample of poly(methyl methacrylate) prepared under identical conditions (6% isotactic, 38% heterotactic and 56% syndiotactic). The results are presented in Table 2. Also included in this Table are M-centred triad fractions calculated from the reactivity ratios $r_1=0.08$ and $r_2=5.1$ using a version of the computer program devised by Harwood *et al.*¹⁵. The computed triad fractions are corrected for the effects of finite conversion.

It can be seen from Table 2 that whilst the measured fractions of MMM triads are in reasonable agreement with those calculated from the reactivity ratios, there are considerable discrepancies between the measured and calculated fractions of CMC and CMM + MMC triads, especially for the copolymers richest in methyl methacrylate. These discrepancies cannot be accounted for in terms of experimental errors and are a further

indication that the Mayo-Lewis scheme cannot be properly applied to this system.

Penultimate group effect

Deviations from the Mayo and Lewis scheme¹² have been observed before in a number of copolymerizations and have been interpreted usually in terms either of the influence of penultimate units on the reactivities of polymer radicals¹⁶⁻²⁴ or of an effect arising from monomer-monomer complexes²⁵⁻²⁹.

If it is assumed that a penultimate group effect is responsible for the deviations observed here, two new penultimate reactivity ratios (r_{11} and r_{21}) can be calculated from the measured M-centred triad fractions using the equations first proposed by Chûjô *et al.*³⁰. The relevant equations for the methyl methacrylate-chloroprene system are:

$$r_{11} = \frac{[C]_0}{[M]_0} \cdot \frac{2(MMM)}{(MMC + CMM)} \quad (2)$$

and

$$r_{21} = \frac{[C]_0}{[M]_0} \cdot \frac{(MMC + CMM)}{2(CMC)} \quad (3)$$

where $[M]_0$ and $[C]_0$ are the initial concentrations of methyl methacrylate and chloroprene in the feed, and (MMM), (MMC + CMM) and (CMC) are the fractions of the three different types of M-centred triad. r_{11} represents the reactivity of a methyl methacrylate ended radical bearing a penultimate methyl methacrylate unit and r_{21} represents the reactivity of a methyl methacrylate ended radical bearing a penultimate chloroprene unit. The reactivity ratios obtained from the triad fractions given in Table 2 with the aid of equations (2) and (3) are: $r_{11}=0.107 \pm 0.008$; and $r_{21}=0.057 \pm 0.004$.

A new value of r_2 (reactivity ratio for a chloroprene ended radical) can be calculated from r_{11} and r_{21} together with the measured copolymer compositions using the equation:

$$r_2 = \frac{F(1-f)}{f} + \frac{r_{21}F^2(1+r_{11}F)}{f(1+r_{21}F)} \quad (4)$$

where f is the ratio of methyl methacrylate units to chloroprene units in the copolymer and F is the ratio of methyl methacrylate to chloroprene in the monomer feed, $[M]_0/[C]_0$. The average value of r_2 obtained from the composition data given in Table 1 for copolymers 1-4, 6 and 8-11 is 6.7 ± 0.5 . Subdivision of r_2 into two

Table 2 Methyl peak areas and M-centred triad fractions

No.	Relative peak areas* (%)			M-centred triad fractions (%)					
				Obtained from A, B and C*			Calculated using $r_1=0.08, r_2=5.1$		
	A	B	C	CMC	MMC+CMM	MMM	CMC	MMC+CMM	MMM
1	15	45	40	6	22	72	3	28	69
2	22	48	30	10	37	53	6	36	58
3	31	42	27	20	32	48	9	42	49
4	32	47	21	20	43	37	13	46	41
6	49	39	12	37	42	21	31	49	20
8	71	26	3	62	32	6	55	38	7
9	76	20	4	70	23	7	71	27	2
10	87	12	1	83	15	2	79	20	1
11	91	9	0	88	12	0	85	14	1

* Areas and triad fractions accurate to within $\pm 2\%$

Table 3 Copolymer compositions and M-centred triad fractions based on $r_{11}=0.107$, $r_{21}=0.057$ and $r_2=6.7$

No.	Mole fraction MMA in copolymer	M-centred triad fractions (%)		
		CMC	MMC+CMM	MMM
1	0.84	4	25	71
2	0.78	8	32	60
3	0.72	12	37	51
4	0.67	17	40	43
6	0.50	38	41	21
8	0.33	64	30	6
9	0.23	76	21	3
10	0.17	84	15	1
11	0.12	89	10	1

Table 4 Comparison of measured and calculated pentad fractions having central syndiotactic MMM triad

No.	CMMC+CMMM+MMMMC (%)		MMMMM (%)	
	Measured (peak C1)	Calculated	Measured (peak C2)	Calculated
1	13±1	11	27±1	29
2	13±1	13	17±1	21
3	14±1	13	13±1	15
4	14±1	11	7±1	6

penultimate reactivity ratios r_{22} and r_{21} is not possible since the p.m.r. spectra do not give any information about the fractions of the various possible chloroprene-centred triads.

Theoretical copolymer compositions and M-centred triad fractions based on the new reactivity ratios r_{11} , r_{21} and r_2 are given in Table 3. It can be seen by comparing the data in Tables 2 and 3 that the new reactivity ratios give a substantially better agreement between measured and calculated M-centred fractions than that given by the reactivity ratios obtained by the curve-fitting procedure.

M-centred pentads

For copolymers 1, 2, 3 and 4, it is apparent that group C of the α -methyl peaks is composed of two overlapping signals (C1 and C2) centred at 0.87 and 0.84 δ respectively. Following the procedure adopted with the methyl methacrylate-butadiene copolymers¹⁰, peak C1 is assigned to syndiotactic MMM triads at the centre of CMMC, CMMM and MMMMC pentads, whilst C2 is assigned to syndiotactic MMM triads at the centre of MMMMM pentads. The relative areas of these two peaks have been obtained with the aid of the Du Pont curve resolver using generated peaks of Lorentzian shape. The relative areas of these two peaks are compared with the relevant pentad fractions calculated from r_{11} , r_{21} and r_2 in Table 4.

Configuration of the chloroprene units

In the p.m.r. spectra of methyl methacrylate-butadiene copolymers¹⁰ containing 42 mol% or more of butadiene (B), group A of the α -methyl peaks was found to consist largely of two overlapping peaks the ratio of which was independent of the copolymer composition. Since in these methyl methacrylate-butadiene copolymers,

group A largely arises from BMB triads, this splitting was considered to reflect the configuration of one of the diene units in the triad, i.e. that the position of the BMB methyl resonance depended on whether one of the constituent butadiene units was in a *cis*-1,4- or a *trans*-1,4-configuration. However, for the methyl methacrylate-chloroprene copolymers, no such splitting of group A can be discerned even at the highest chloroprene contents. Thus, it seems likely that the chloroprene units are predominantly of a single configuration. The most probable configuration is *trans*-1,4- since polychloroprene prepared free radically is predominantly of this configuration³¹.

The infra-red spectra of the copolymers are not particularly helpful since they show that the chloroprene =CH- out-of-plane deformation occurs between 825 and 835 cm^{-1} depending on the chloroprene content (*trans*-polychloroprene, 822 cm^{-1} ; *cis*-polychloroprene, 847 cm^{-1} ³¹) and that the C=C stretch occurs between 1655 and 1660 cm^{-1} (*trans*-polychloroprene, 1660 cm^{-1} ; *cis*-polychloroprene, 1653 cm^{-1} ³¹).

Methoxy signals

When C_6D_6 is used as solvent, the methoxy signals of the methacrylate units in the 220 MHz p.m.r. spectra of copolymers 1 and 2 are partly resolved into three peaks (D, E and F) centred at 3.50, 3.42 and 3.35 δ respectively (Figure 3). A similar partial resolution of the methoxy signals in methyl methacrylate-butadiene copolymers is observed when $\text{C}_5\text{D}_5\text{N}$ is used as a solvent¹⁰. Since the ratio D:E:F for each of the copolymers is close to that of A:B:C, it can be assumed that the three methoxy peaks represent, in a similar way to the methyl signals, the various M-centred triads.

Head-head and tail-tail linkages

Whilst it is clear that the occurrence of a small penultimate group effect could account for the deviations of the methyl methacrylate-chloroprene system from the ideal Mayo and Lewis scheme, other reasons for these deviations can be envisaged. For example, an unsymmetrically substituted diene like chloroprene can add to a growing polymer radical in two distinct orientations to form either a head-tail linkage or a head-head

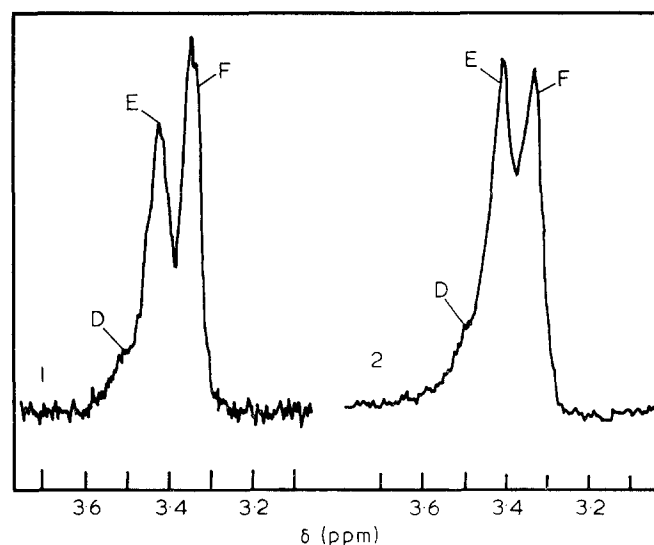


Figure 3 Methoxy peaks for copolymers 1 and 2

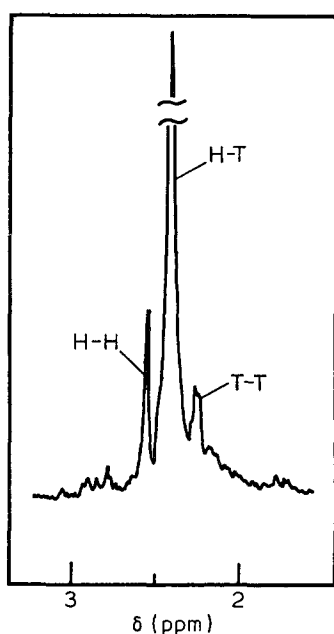


Figure 4 Methylene peaks of head-head (H-H), head-tail (H-T), and tail-tail (T-T) chloroprene-chloroprene linkages in copolymer 11

linkage with the preceding monomer unit. In the p.m.r. spectrum of *trans*-polychloroprene in CS₂, head-head and tail-tail linkages give rise to characteristic methylene peaks at 2.50 and 2.18 δ, whilst head-tail linkages give a methylene peak centred around 2.35 δ³¹. Head-head and tail-tail linkages are found to constitute between 20 and 30% of the linkages in polychloroprene depending on the exact conditions of preparation. Recently, Guyot *et al.*³² have demonstrated that the occurrence of head-head linkages in copolymerizations can lead to kinetic anomalies akin to those more usually attributed to penultimate group effects; the system they studied was vinyl chloride-vinylidene chloride. The occurrence of anomalous methyl methacrylate-chloroprene linkages could be an important factor in the present system, but unfortunately 220 MHz p.m.r. spectroscopy does not appear to provide a way of measuring the proportions of such linkages. However, methylene peaks from head-head and tail-tail chloroprene-chloroprene linkages are evident in the spectra of copolymers comparatively rich in chloroprene (Figure 4). Relative amounts of head-head and tail-tail linkages estimated from the areas of these methylene peaks (2.54 δ and 2.25 δ in CDCl₃) average 19 ± 2% for copolymers 8, 9, 10 and 11; the corresponding amount for a sample of polychloroprene prepared under similar conditions is 23 ± 2%.

At present, ¹³C magnetic resonance and ozonolysis studies of the copolymers are in progress. It is hoped that these will provide further information about the microstructure of the copolymers and in particular allow quantitative measurements of the various possible methyl methacrylate-chloroprene linkages.

ACKNOWLEDGEMENTS

The author thanks BP Chemicals Ltd for the gift of chloroprene and the Physico-Chemical Measurements Unit at Harwell for obtaining the 220 MHz p.m.r. spectra.

REFERENCES

- Berger, M. and Kuntz, I. *J. Polym. Sci. (A)* 1964, **2**, 1687
- Oikawa, E. and Yamamoto, K. *Polym. J.* 1970, **1**, 669
- Schmolke, R., Kimmer, W., Kuzay, P. and Hufenreuter, W. *Plast. Kautsch.* 1971, **18**, 95
- Kuzay, P. and Kimmer, W. *Plast. Kautsch.* 1971, **18**, 743
- Bevington, J. C. and Ebdon, J. R. *Makromol. Chem.* 1972, **153**, 173
- Masaki, A. and Yamashita, I. *J. Macromol. Sci. (A)* 1972, **6**, 439
- Masaki, A. *J. Macromol. Sci. (A)* 1972, **6**, 1267
- Elgert, K. F., Seiler, E., Puschendorf, G. and Cantow, H.-J. *Makromol. Chem.* 1973, **165**, 245, 261
- Suzuki, T., Takegami, Y., Furukawa, J., Kobayashi, E. and Arai, Y., *Polym. J.* 1973, **4**, 657
- Ebdon, J. R. *J. Macromol. Sci. (A)* 1974, **8**, 417
- Fineman, M. and Ross, S. D. *J. Polym. Sci.* 1950, **5**, 259
- Mayo, F. R. and Lewis, F. M. *J. Am. Chem. Soc.* 1944, **66**, 1594
- Braun, D., Brendlein, W. and Mott, G. *Eur. Polym. J.* 1973, **9**, 1007
- Doak, K. W. and Dineen, D. L. *J. Am. Chem. Soc.* 1951, **73**, 1084
- Harwood, H. J., Johnston, N. W. and Piotrowski, H. *J. Polym. Sci. (C)* 1968, **25**, 23
- Mertz, E. T., Alfrey, T. and Goldfinger, G. *J. Polym. Sci.* 1946, **1**, 75
- Barb, W. G. *J. Polym. Sci.* 1953, **11**, 117
- Ham, G. E. *J. Polym. Sci.* 1961, **54**, 1
- Ham, G. E. *J. Polym. Sci.* 1962, **61**, 9
- Kinsinger, J. B. and Fischer, T. *J. Polym. Sci. (B)* 1967, **5**, 285
- Guyot, A. and Guillot, J. *J. Macromol. Sci. (A)* 1968, **2**, 889
- Guillot, J., Guyot, A. and Tho, P. Q. *J. Macromol. Sci. (A)* 1968, **2**, 1303
- Inaki, Y., Hirose, S., Yasufuku, K., Nozakura, S. and Murahashi, S. *Polym. J.* 1971, **2**, 481
- Guillot, J., Vialle, J. and Guyot, A. *J. Macromol. Sci. (A)* 1971, **5**, 735
- Bartlett, P. D. and Nozaki, K. *J. Am. Chem. Soc.* 1946, **68**, 1495
- Gaylord, N. G. and Antropiusova, H. *Macromolecules* 1969, **2**, 442
- Seiner, J. A. and Litt, M. *Macromolecules* 1971, **4**, 308
- Shirota, Y., Matsumoto, A. and Mikawa, H. *Polym. J.* 1972, **3**, 643
- Caze, C. and Loucheux, C. *J. Macromol. Sci. (A)* 1973, **7**, 991
- Chûjô, R., Ubara, H. and Nishioka, A. *Polym. J.* 1972, **3**, 670
- Ferguson, R. C. *J. Polym. Sci. (A)* 1964, **2**, 4735
- Guyot, A., Pichot, C., Guillot, J. and Tho, P. Q. *J. Macromol. Sci. (A)* 1972, **6**, 1681

E.s.r. study of u.v.-irradiated polypropylene: effect of the stereoregularity on the behaviour of free radicals produced by u.v. irradiation

Y. Hama, T. Ooi*, M. Shiotsubo and K. Shinohara

Science and Engineering Research Laboratory, Waseda University, Tokyo, Japan
(Received 2 January 1974; revised 8 April 1974)

The effect of stereoregularity on the behaviour of free radicals produced in polypropylene by ultra-violet light at low temperature was investigated by an electron spin resonance method. Ultra-violet (u.v.) light is absorbed mainly by carbonyl groups produced in polypropylene by oxidation. The radicals produced at low temperature are identified as $-\text{CH}_2-\dot{\text{C}}(\text{H})-\text{CH}_2-$ and methyl. A large yield of radicals is obtained in samples of poor tacticity. Some of the $-\text{CH}_2-\dot{\text{C}}(\text{H})-\text{CH}_2-$ radicals convert to acyl and some to $-\text{CH}_2-\dot{\text{C}}(\text{CH}_3)-\text{CH}_2-$ on warming the sample. The conversion to acyl is remarkable in atactic and stereoblock polypropylene, and that to $-\text{CH}_2-\dot{\text{C}}(\text{CH}_3)-\text{CH}_2-$ in isotactic polypropylene. These acyl and $-\text{CH}_2-\dot{\text{C}}(\text{CH}_3)-\text{CH}_2-$ radicals return to $-\text{CH}_2-\dot{\text{C}}(\text{H})-\text{CH}_2-$ by illumination, respectively, by visible and u.v. light at 77K. The decay of radicals is attributed to the local motion or microbrownian motion of molecules.

INTRODUCTION

Electron spin resonance (e.s.r.) studies of free radicals produced in irradiated high polymers have hitherto been reported by many authors. Free radicals were produced, in most cases, by ionizing radiation such as electron beams, γ -rays or X-rays, but in some cases by ultra-violet (u.v.) light¹⁻⁸. Some of these studies were carried out also on polypropylene^{2, 3, 6}. A methyl radical has been detected in the case of u.v. irradiation but not in ionizing radiations. Blowning *et al.*² noted that u.v. light tends to be selectively absorbed by impurities and chain imperfection.

In our recent e.s.r. study⁵ of u.v.-irradiated polyethylene, it was found that major absorption of light occurs at oxidized segments in the sample and also that the resulting acyl radicals $-\text{CH}_2-\text{CH}_2-\dot{\text{C}}\text{O}$ are converted by absorption of visible light to $-\text{CH}_2-\dot{\text{C}}\text{H}-\text{CHO}$.

In a polymer such as polypropylene with high stereoregularity, the structure and number of chain imperfections may be strongly dependent on the stereoregularity. Moreover, it was expected that the characteristics of free radicals produced by u.v. irradiation may be strongly affected by the stereoregularity and that they are different from those in the case of ionizing radiation.

In the present paper, the effect of stereoregularity on the behaviour of free radicals produced in u.v.-irradiated polypropylene has been investigated.

EXPERIMENTAL

Preparation of samples

Polypropylene (PP) used in the present work was manufactured by Mitsui Toatsu Chemicals, Inc. Four

* Research Center, Mitsui Toatsu Chemicals Inc., Totsuka-ku, Yokohama-city, Japan.

samples having different stereoregularity were prepared by extracting from the original polymer with ether and/or n-heptane. The characteristics of the samples thus obtained are listed in Table 1. They were dried sufficiently before use. Three samples except sample A were then formed in a film of 2 mm thickness by hot pressing in vacuum. Each sample was placed in a quartz tube which was evacuated to about 10^{-3} mmHg at room temperature and then sealed.

Irradiation

Irradiation was carried out with u.v. light from a low pressure mercury lamp (UL2-1HQ) manufactured by Ushio Electric Co. Ltd and in some cases with γ -rays from a ⁶⁰Co source. Predominant wavelengths from this u.v. lamp are 2537 Å and 1849 Å. In all cases of u.v. irradiation the sample was kept in liquid nitrogen.

E.s.r. measurement

E.s.r. measurements were carried out by using an X-band spectrometer, manufactured by Japan Electron Optics Laboratory Co. Ltd. The frequency of field modulation used was 100 kHz. Measurements at 77K were carried out by inserting a Dewar flask with a transparent cylindrical tip into the cavity. The sample was held in the Dewar flask filled with liquid nitrogen.

Table 1 Characteristics of samples used

Sample	Solvents		Stereo-regularity	Content in original polymer (%)
	Ether	n-Heptane		
A	soluble	soluble	atactic	3
B	insoluble	soluble	stereoblock	3
I	insoluble	insoluble	isotactic	94

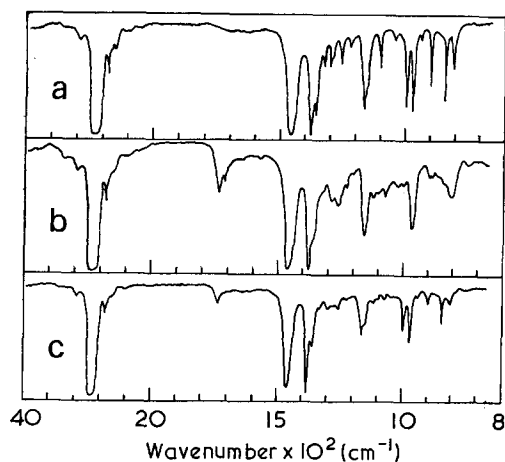


Figure 1 Infra-red absorption spectra of (a) sample I, (b) sample A and (c) sample B

Heat treatment of sample was carried out by keeping the sealed sample in a bath of isopentane at the desired temperature for 3 min and then returning it quickly into liquid nitrogen.

RESULTS

Infra-red absorption spectra of samples A, B and I

The infra-red (i.r.) absorption spectra of the samples used are shown in Figure 1. In these spectra, differences due to the difference of the tacticity are found at 995 cm^{-1} and 975 cm^{-1} . It is also seen that an absorption appears at 1750 cm^{-1} in the spectrum of samples A and B, which could not be observed for samples I and M. It is well known that the absorption appearing at a wavenumber between 1600 and 1800 cm^{-1} can be attributed to carbonyl groups bound in the form of ketone or acid. This absorption at 1750 cm^{-1} , therefore, may also be attributed to such groups bound to the polymer chain. The carbonyl groups probably were introduced into the polymer by oxidation. The i.r. spectrum suggests that PP of low tacticity is oxidized more easily than one of high tacticity.

E.s.r. spectrum at 77K

The first derivative e.s.r. spectrum of each sample, except sample M, irradiated by u.v. light at 77K and measured immediately after irradiation at 77K is shown in Figure 2. Samples I and A, and also sample M, though not shown in Figure 2, gave a similar spectrum. This spectrum is also similar to that observed by previous investigators^{2, 3, 6}. The spectrum of sample B, however, was different from that of the other samples in the centre, although in other sections it was similar. Each of these spectra consist of a sharp quartet (spectrum I) and a broad quartet (spectrum II). These spectra also seem to include a weak singlet although it is manifested rather prominently only in the spectrum of sample B. The average hyperfine splitting of these quartet spectra were 21.5 and 25G, respectively. The sharp quartet was unstable at 77K and its intensity decreased very gradually even at 77K. This was attributed to methyl radical, as was already noted in previous papers^{2, 3, 6}. The broad quartet was stable at 77K.

If the u.v. irradiation was carried out on samples M and I which were prepared shortly after synthesis,

only a weak e.s.r. spectrum, but of the same shape, was obtained. When these samples were kept in air for several months and irradiated, larger e.s.r. signals were obtained, the intensity of which increased with the time of storage.

When samples A and B which have lower tacticities than that of sample I, were kept in air for the same period of time as sample I, they gave a far larger e.s.r. signal than that of sample I.

Change of the e.s.r. spectrum by heat treatment

Sample I. When sample I stored in air for several months was irradiated by u.v. light at 77K and the e.s.r. measurement was carried out at 77K after heat treating at various temperatures, the spectra shown in Figure 3 were obtained. The methyl radical (spectrum I), which was observed at 77K immediately after u.v. irradiation and the e.s.r. spectrum which showed a sharp quartet (spectrum I), had already disappeared after heat treatment at 123K and the remaining spectrum was composed of the broad quartet having an average hyperfine splitting of 25G and a weak singlet.

As the temperature of heat treatment was raised further, a gradual change was observed in the spectrum. On heat treatment at 173K, spectrum II decayed slightly and the weak broad singlet (spectrum III) made its appearance more clearly at the centre (Figure 3b). On heat treatment above 173K, the central broad singlet

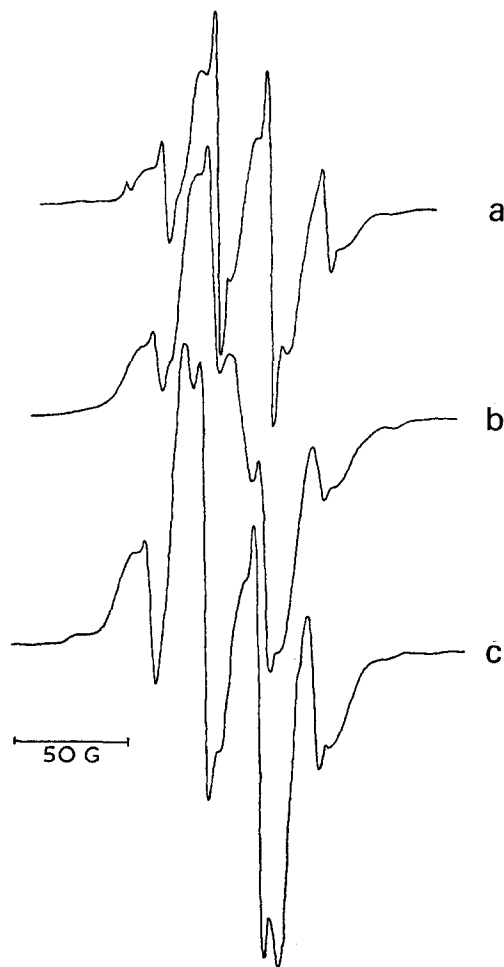


Figure 2 First derivative e.s.r. spectra of samples irradiated by u.v. light at 77K and measured immediately at 77K after irradiation. (a) Sample I; (b) sample B; (c) sample A

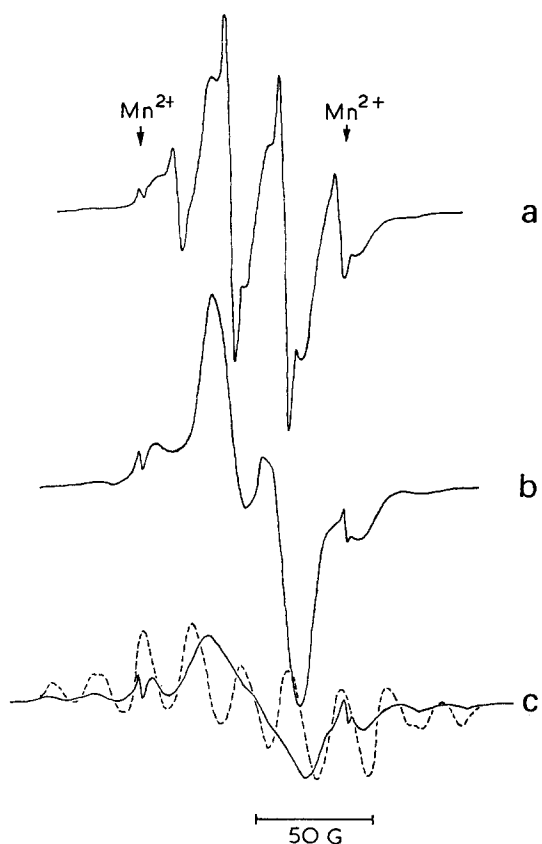


Figure 3 E.s.r. spectra of sample I irradiated by u.v. light at 77K: (a) observed immediately at 77K after irradiation; (b), (c) observed at 77K after heat treatment of (a) at 173K (b) and 283K (c); ----, 9 line spectrum of isotactic PP irradiated by γ -rays at room temperature and measured at 77K

disappeared gradually and spectrum II converted gradually to a spectrum (spectrum IV) which seems to be composed of 9 lines. The solid curve of Figure 3c shows this 9 line spectrum converted from spectrum II. The average hyperfine splitting of the 9 line spectrum was 21.5 G. This value agrees with that of the spectrum obtained in sample I γ -irradiated at room temperature and measured at 77K, which is shown as a broken curve in Figure 3c.

When sample I was kept at room temperature for a sufficiently long time, or heated above room temperature, the 9 line spectrum disappeared very gradually and a weak broad singlet which was broader than the singlet appearing at low temperatures, appeared. These experiments seem to indicate that the spectrum shown by the solid line of Figure 3c consists of superposition of the 9 line spectrum (spectrum IV) and a rather weak, broad singlet (spectrum V). This singlet may make poor resolution in the centre of the 9 line spectrum. It seems that this broad singlet is not due to the acyl radical which gives the broad singlet appearing at low temperatures as described below, but its origin is not yet known.

Sample B. Change due to heat treatment of the e.s.r. spectrum obtained by u.v. irradiation at 77K on sample B is shown in Figure 4. On heat treatment at 163K, spectrum II became very weak and the same broad singlet (spectrum III), observed in sample I, appeared with a far larger intensity. This broad singlet decayed gradually by heat treatment above 183K and a weak spectrum which looks as it is was composed of 7 or

9 lines was observed after heat treatment at 243K (Figure 4c).

Sample A. The e.s.r. spectrum of sample A obtained by u.v. irradiation showed a similar change as sample B on heat treatment. The change is shown in Figure 5. The broad singlet which appeared after heat treatment above 143K was larger in intensity than that of the other samples. The e.s.r. spectrum observed after heat treatment above 243K appears more clearly and it seems to be a composite spectrum made up of a 6 line spectrum and a singlet rather than a 7 line spectrum.

Dependence of the intensity of e.s.r. spectrum on temperature of heat treatment

The decrease of the relative intensity of the e.s.r. spectra of samples I, B and A by heat treatment is shown in Figure 6. There exist three decay regions in the decay curve for sample I, i.e. 113–133K (D-I), 163–193K (D-II) and a region above 243K (D-III). Two decay regions, one at a temperature of 113–133K (D-I) and the other above 183K (D-IV), are found in the decay curve for samples B and A.

Figure 6 shows that the decrease of the intensity in the decay regions D-I and D-II is fairly small compared with that in D-III and D-IV. In the case of samples B and A, free radicals decay almost completely in the decay region D-IV and only several per cent of those produced at 77K remain after heat treatment at room temperature. For sample I, the decrease of about 35% of free radicals produced at 77K was observed in the decay region D-III of 243 to 293K and 35% of free radicals remained even after heat treatment at 293K.

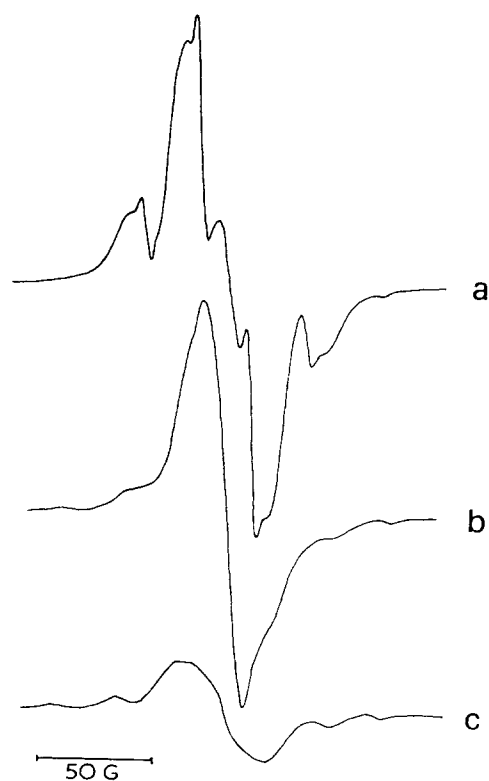


Figure 4 E.s.r. spectra of sample B irradiated by u.v. light at 77K: (a) observed immediately at 77K after irradiation; (b), (c) observed at 77K after heat treatment of (a) at 163K (b) and 243K (c)

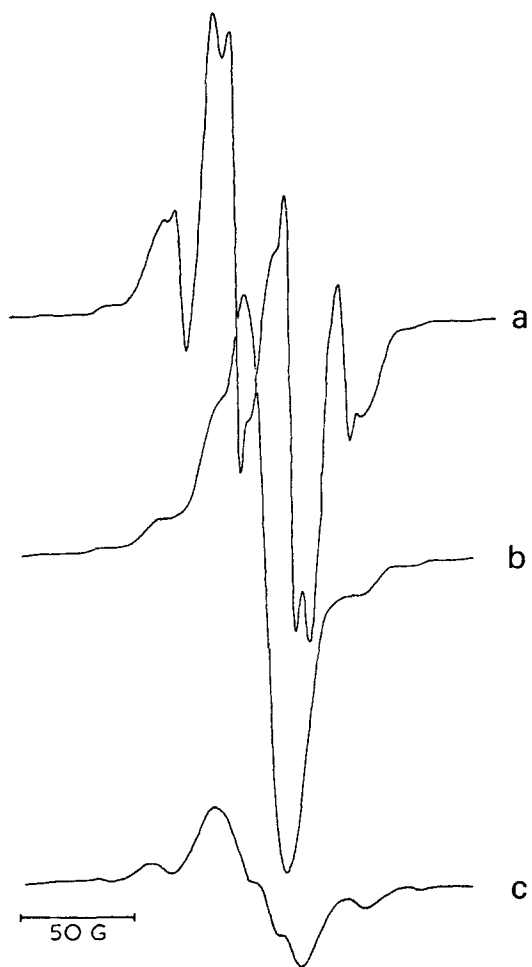


Figure 5 E.s.r. spectra of sample A irradiated by u.v. light at 77K: (a) observed immediately at 77K after irradiation; (b), (c) observed at 77K after heat-treatment of (a) at 183K (b) and 249K (c)

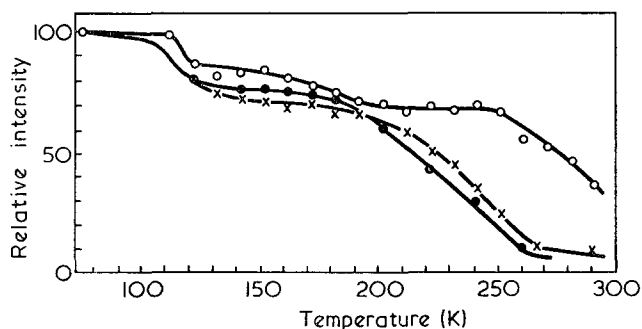


Figure 6 Relationship between relative intensity and temperature of heat treatment for each sample: ○, sample I; ×, sample B; ●, sample A

Thus residual free radicals decayed gradually by storing the sample at room temperature.

Photoinduced conversion between the broad singlet (spectrum III) and the 9 line spectrum (spectrum IV)

Most of the broad singlet (spectrum III) appearing prominently after heat treatment at a temperature of around 158K was converted into the broad quartet (spectrum II) by illumination with light from a tungsten lamp at 77K. The result of heat treatment and illumination with light, carried out on sample A, is shown in Figure 7.

When sample A was irradiated by u.v. at 77K and observed at 77K, a spectrum composed mainly of the broad quartet (spectrum II) shown by Figure 7a is obtained. This spectrum includes a weak broad singlet, but the singlet cannot be seen distinctly in the spectrum because it is masked by the stronger broad quartet. If this sample is heat-treated at 138K and observed at 77K, the intensity of the broad quartet (spectrum II) decreases slightly and a weak broad singlet (spectrum III) appears distinctly (Figure 7b). If this sample is again heat-treated, this time at 158K, intensity of the broad quartet (spectrum II) decreases further and the spectrum showing a prominent broad singlet (spectrum III) is obtained (Figure 7c). On illuminating this sample with light from a tungsten lamp for 15 min, spectrum III converts into the spectrum shown by Figure 7d. This spectrum is quite similar to that shown by Figure 7b (composite spectra of spectra II and III). This spectrum, i.e. the spectrum shown by Figure 7b or 7d, is converted into spectrum III by heat-treating the sample again at 158K. Further illumination and heat treatment causes the conversion of the spectrum between those two. Moreover, there is no change in the total spectral intensity during this conversion.

A similar reversible conversion was observed between the broad quartet (spectrum II) and the 9 line spectrum

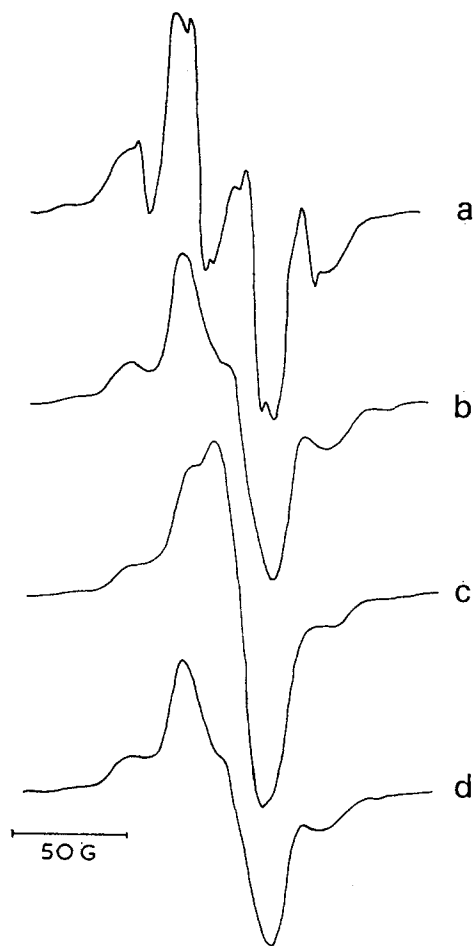


Figure 7 Change of e.s.r. spectrum by heat treatment and illumination by light from W lamp: (a) observed immediately after irradiation at 77K; (b), (c) observed at 77K after heat treatment of (a) at 138K (b) and 158K (c); (d) observed at 77K after illuminating (c) by light from tungsten lamp at 77K

and also in the semi-crystalline region such as the folding part or loose loop of the lamella of PP, those 40% of radicals will probably be located in the semi-crystalline region. This interpretation also explains the fact that their decay is not so slow as the radicals of the same kind produced in isotactic PP by γ -irradiation, most of which probably exist in the crystalline region.

Decay region D-IV, observed for samples A and B begins at about 183K, and most of the radicals disappear at 273K. The fact that radicals hardly remain at room temperature suggests that most of the radicals are produced in the amorphous region, especially in sample A which has only amorphous structure. The glass transition temperature of sample A or B is lower than that of isotactic PP of about 253K because of its lower regularity in structure¹³. Moreover, it was reported that a local mode relaxation has been observed at $\sim 193\text{K}$ ¹³. The disappearance of radicals in region D-IV may be attributed to the motions of such origin.

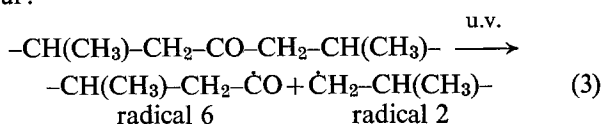
Formation of free radicals by u.v. irradiation on PP and their behaviour

Formation of free radicals by low temperature irradiation. It is fairly certain that most of the absorption of u.v. light occurs at carbonyl groups in the main chain of PP produced by oxidation while the sample is stored in air, since a larger yield of free radicals is obtained in a sample which showed an existence of a larger number of carbonyl groups in i.r. absorption measurement and also since the quantum energy of the u.v. light used to produce radicals are distributed in the same range of light in which absorption by ketones occur.

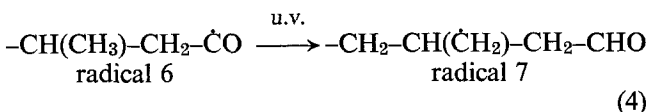
In the neighbourhood of carbonyl groups, the molecules probably have the following structure:



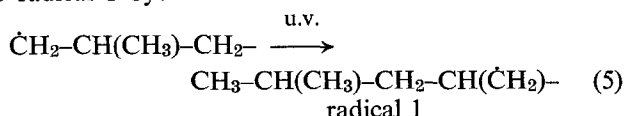
When a carbonyl group absorbs u.v. light at liquid nitrogen temperature, scission of the main chain will occur:



Most of radical 6 may absorb u.v. light during the irradiation and change over to radical 7 by:



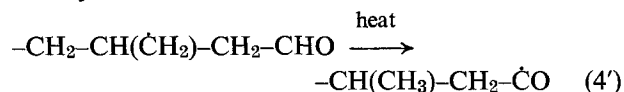
Radical 2 may also absorb u.v. light and change over to radical 1 by:



but it may also undergo hydrogen abstraction, even at low temperature, to produce another radical, probably radical 1. There is, thus, the possibility of the existence of four kinds of radicals after irradiation at 77K, i.e. methyl radical, radical 7, radical 1 and radical 6.

Sample A. When sample A which contains these radicals is heat-treated at a temperature above 143K,

radical 7 will change over to acyl radical in the manner shown by:



Equation (4') together with equation (4) explains the mutual conversion, observed by e.s.r. measurement, between the broad singlet given by acyl radical and the broad quartet given by radical 7.

By heat treatment at a still higher temperature above 243K, an e.s.r. signal composed of a fairly weak singlet and a 6 line spectrum due to radical 4 appears.

Sample I. In the case of sample I, similar a e.s.r. spectrum is obtained by irradiation with u.v. light at 77K, but the behaviour is different.

By heat treatment at 173K a weak broad singlet due to the acyl radical appears but it disappears by further heat treatment at temperatures above 173K and the broad quartet converts gradually into the 9 line spectrum. In the case of sample I, free radicals will be produced in the semi-crystalline part and also in the part having a more irregular structure. Radical 7 produced in a poor tacticity which exists even in sample I and forming part of the amorphous region, may behave similarly as radical 7 produced in sample A.

It was shown above that in sample A a prominent broad singlet due to acyl radical which is converted from the broad quartet is observed. In sample I, however, the broad quartet converts into the 9 line spectrum and only a very weak spectrum due to acyl radical is observed. This fact can be explained if it is assumed that the activation energy for the conversion to the acyl radical of radical 7 which are produced in the isotactic PP is much higher than that of the same radical produced in the atactic PP. Such radical 7 will disappear by recombination or by some other process before converting into acyl radical when the heat treatment is carried out at a higher temperature. On the other hand, radical 1 produced in the semi-crystalline region converts into radical 4 giving the 9 line spectrum.

REFERENCES

- 1 Charlesby, A. and Thomas, D. K. *Proc. R. Soc. (A)* 1962, **269**, 104
- 2 Browning, Jr., H. L., Ackermann, H. D. and Patton, H. W. *J. Polym. Sci. (A-1)* 1966, **4**, 1433
- 3 Rånby, B. and Yoshida, H. *J. Polym. Sci. (C)* 1966, **12**, 263
- 4 Hama, Y. and Shinohara, K. *J. Polym. Sci. (A-1)* 1970, **8**, 651
- 5 Hama, Y., Hosono, K., Furui, Y. and Shinohara, K. *J. Polym. Sci. (A-1)* 1971, **9**, 1411
- 6 Tsuji, K. and Seiki, T. *Polym. J.* 1970, **1**, 133
- 7 Tsuji, K. and Seiki, T. *Polym. J.* 1971, **2**, 606
- 8 Takeshita, T., Tsuji, K. and Seiki, T. *J. Polym. Sci. (A-1)* 1972, **10**, 2315
- 9 Loungo, J. P. *J. Appl. Polym. Sci.* 1960, **3**, 302
- 10 Loy, B. R. *J. Polym. Sci. (A)* 1963, **1**, 2251
- 11 Iwasaki, M., Ichikawa, T. and Toriyama, K. *J. Polym. Sci. (B)* 1967, **5**, 423
- 12 Ayscough, P. B. and Munari, S. *J. Polym. Sci. (B)* 1966, **4**, 503
- 13 Sauer, J. A., Wall, R. A., Fuschillo, N. and Woodward, A. E. *J. Appl. Phys.* 1958, **29**, 1385
- 14 Willbourn, A. H. *Trans. Faraday Soc.* 1958, **54**, 717
- 15 Muus, L. T., McCrum, N. G. and McGrew, F. C. *Soc. Plast. Eng. J.* 1959, **15**, 368

Studies on the surface of as-grown and annealed polyethylene single crystals by the spin-probe method

N. Kusumoto, M. Yonezawa* and Y. Motozato

*Department of Synthetic Chemistry, Faculty of Engineering, Kumamoto University,
Kumamoto, Japan*

(Received 12 February 1974; revised 14 May 1974)

Studies on molecular motions at the surface of as-grown and annealed polyethylene single crystals in relation to the surface structure have been made by dispersing electron paramagnetic probes on the surface of the crystals and detecting them by the electron spin resonance method. A relatively large scale molecular motion supposedly associated with the glass transition was detected as a change in hyperfine patterns at around -50°C . Rotational correlation frequency of the paramagnetic probe was found to rapidly increase above the crystallization temperature suggesting that the new mode of molecular motion takes place by thickening of crystals. For the annealed crystals the frequency was much depressed compared with that of the as-grown crystals indicating the decrease in mobility of the surface by annealing. Extensive study revealed that the mobility of the surface of annealed crystals is uniquely determined by the increased portion of the lamellar thickness by annealing.

INTRODUCTION

The surface structure of polymer single crystals has interested many investigators. It has been widely recognized that almost all molecules have the folding structure at the surface of the single crystal. However, opinions vary as to whether sharp folding¹, long loop² or switch board structure³ is present, leaving an ambiguity to the folding structure. In addition to the problem of the structure of individual molecules, the state of aggregation of molecules has not been clarified yet, although it characterizes the properties of the surface.

We describe here the molecular motion and related structure of the surface of as-grown and annealed polyethylene single crystals using the spin-probe method. This method was first applied to synthetic polymers by Strukov⁴ and demonstrated to be useful in characterizing polymers by Rabold⁵. In this method stable free radicals are used as electron paramagnetic probes surveying a polymer matrix in which the probes have been embedded. They are detected by the electron spin resonance (e.s.r.) method to give information about their motions. Further, since the motions of the probes are controlled by the motion of their surroundings^{4,5} one can obtain information about a polymer matrix through motion of the probe.

Meanwhile, since the size of the probe does not exceed that of the crystal lattice of common synthetic polymers, this method gives selective information about a non-crystalline phase. In the present case, the probes were dispersed in polyethylene single crystal mats and

attempts were made to reveal the surface properties of the single crystals in relation to the molecular motions.

EXPERIMENTAL

Sample preparation

Linear polyethylene (Hizex 1200 J, Mitsui Petrochemical Co.) was used as the material. Isothermal crystallization was conducted by the method used in the previous work⁶. The polyethylene pellets were dissolved in xylene at a concentration of 1.5 g/l. This solution was then added dropwise to xylene, which had been kept at a regulated temperature to within $\pm 0.1^{\circ}\text{C}$, to reach a final concentration of 0.06%. Crystals differing in lamellar thickness were prepared by varying the crystallization temperature of the solution from 46.6 to 84.2°C. The suspensions of the single crystals were filtered to form single crystal mats and then dried under reduced pressure for more than 6 days. *Table 1* gives the crystallization conditions and the lamellar thickness estimated by the small angle X-ray scattering.

Annealing of single crystal mats was conducted by keeping them at regulated temperatures in reduced pressure for 30 min. The annealing temperature and the lamellar thickness are shown in *Table 2*.

Nitroxide radical, 2,2,6,6-tetramethyl-4-piperidinol-1-oxyl, was used as the paramagnetic probe. This was obtained by oxidizing 2,2,6,6-tetramethyl-4-piperidinol using the method of Briere⁷. The structure and the principal values of the hyperfine coupling tensor are shown in *Figure 1a*. The probe was dispersed in the

* Present address: Toshiba Silicone Co., Kawasaki 210, Japan.

Table 1 Crystallization conditions and lamellar thickness

No.	Crystallization temperature (°C)	Crystallization time (h)	Lamellar thickness (Å)
1	46.6	24	96
2	60.0	24	103
3	70.2	24	120
4	76.5	24	129
5	81.0	72	139
6	84.2	120	147

Table 2 Annealing temperature and lamellar thickness

Annealing temp. (°C)	Lamellar thickness (Å)					
	1	2	3	4	5	6
50	97					
60	99					
70	101	105				
80	105	109	123	130		
90	110	113	128	135	143	151
100	118	120	135	141	150	158
110	132	133	147	153	161	169
120	160	159	172	177	184	192

single crystal mats by immersing them in the 0.2% xylene solution of the probe for 24 h at room temperature, and then the mats were dried at a reduced pressure for more than 3 days. Attention was paid to using a dilute solution to avoid spin-spin interactions among the probes which result in the exchange narrowing of e.s.r. spectra when the probes are closely located to each other in the specimen.

E.s.r. measurements

E.s.r. spectra were recorded on a Nihon Denshi JES-3BSX ESR spectrometer using X-band and 100 kHz field modulation. Measuring temperature was varied from -160 to 100°C using the JES-VT-3A temperature controller and the JES-UCT-2A gas flow cryostat. Since the temperature measurement was very important in this experiment, the sample temperature was confirmed by a thermocouple inserted into a sample tube with the sample during e.s.r. measurements as well as the temperature indicator of the instrument. For exact estimation of the rotational correlation frequency of the probe from the e.s.r. spectra, the field modulation width and the microwave power level were carefully controlled to decrease the line broadening and the power saturation, respectively, while maintaining necessary sensitivity of the spectrometer.

Analysis of e.s.r. spectra

The probe of nitroxide radical shows fundamentally a three line spectrum as shown in Figures 1b and 1c. These patterns are caused mainly by the hyperfine interaction of an unpaired electron with the nitrogen atom in the probe. When the probe is in a frozen state, in view of the e.s.r. frequency, the pattern is broad as shown in Figure 1b, but it becomes well resolved as the motion of the probe is fully increased at elevated temperature as shown in Figure 1c, because of the time averaging of the anisotropy of the hyperfine interaction and the *g*-value.

We can conveniently obtain two parameters from these spectra concerning the motion of the probe: (1) isotropic rotational correlation time of the probe, τ_c , which is derived from the linewidth of the spectrum using the theory of Kivelson⁸; (2) separation of outermost peaks of a derivative e.s.r. spectrum, denoted by W in Figure 1b⁵.

The correlation time, τ_c , is related to the line shape parameters by:

$$\tau_c = W_0[(h_0/h_1)^{1/2} - (h_0/h_{-1})^{1/2}]C \quad (1)$$

$$\tau_c = W_0[(h_0/h_1)^{1/2} + (h_0/h_{-1})^{1/2} - 2]C' \quad (2)$$

where W_0 is the maximum slope linewidth of the central peak of the three line spectrum, h is the peak height whose subscript represents the nuclear magnetic quantum number of nitrogen atom, C and C' are constants determined by experimental conditions such as the hyperfine interaction characteristic of the probe and the magnitude of a static magnetic field. These two equations are mathematically equal, but accuracy in employment has been discussed by Strukov⁴. In this theory the rate conditions must be fulfilled, namely, $(\pi a \tau_c)^2 \ll 1$, $(b \tau_c)^2 \ll 1$ and $(2\pi \nu \tau_c)^2 \gg 1$, where a and b are related to the principal values of the hyperfine tensor and ν is the microwave frequency used.

These equations are applicable only to a well resolved spectrum such as shown in Figure 1c, because of the restriction by the rate conditions. The separation of the outermost peaks is found to be a conventional measure showing the motion of the probe when the time range larger than that derived from the above equations is required, since the separation begins to change by the time averaging of anisotropic hyperfine interaction and the anisotropy of the *g* factor. Although some efforts have been made to expand the estimation of correlation time into a larger time range corresponding to the larger separation of outermost peaks⁹⁻¹¹, these methods are not convenient to use here.

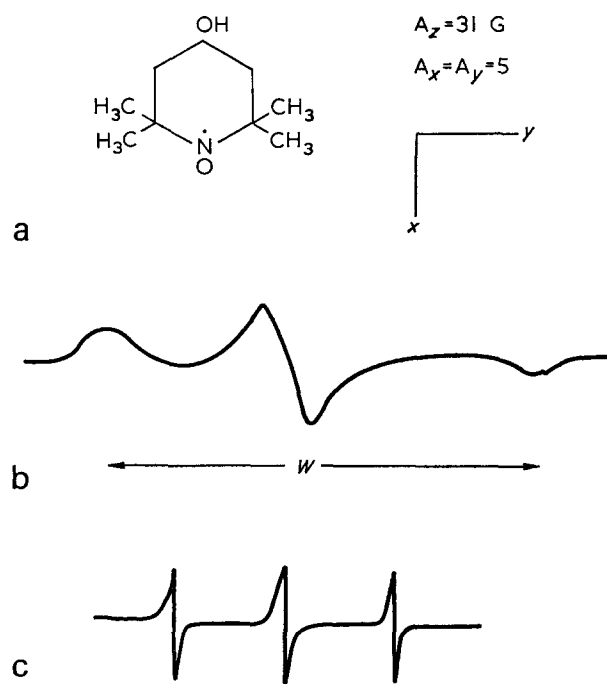


Figure 1 (a) Structure of nitroxide radical; (b) e.s.r. spectrum when probes are in a rigid state; and (c) e.s.r. spectrum when probes are fully in motion

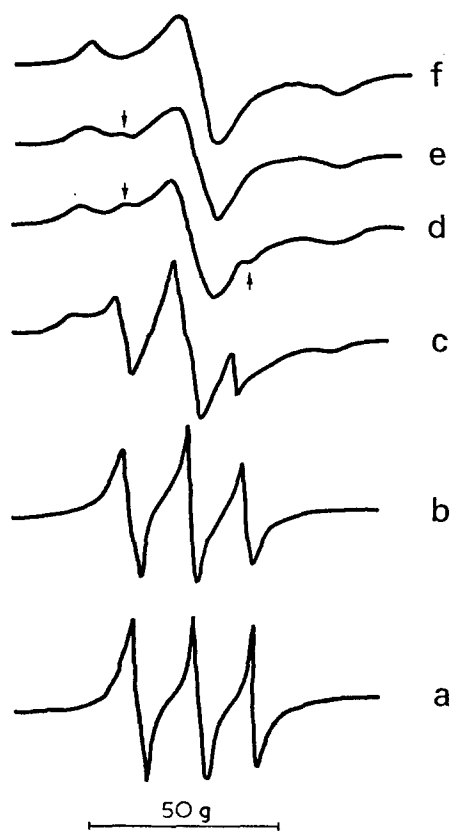


Figure 2 Change of e.s.r. spectrum with temperature for as-grown crystals formed at 76.5°C. (a), 60°; (b), -20°; (c), -50°; (d) -100°; (e), -110°; (f) -130°C

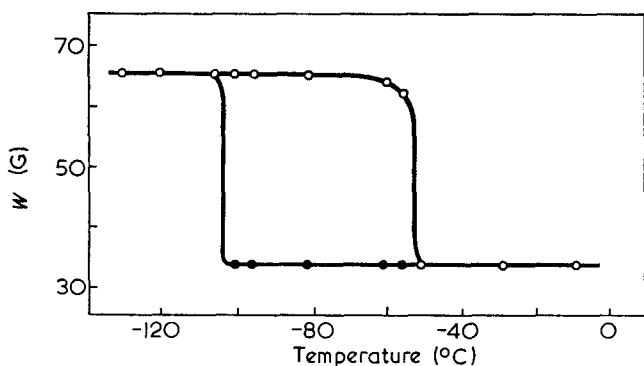


Figure 3 Plots of W vs. temperature for as-grown crystals formed at 76.5°C. \circ , W_m ; \bullet , W_s

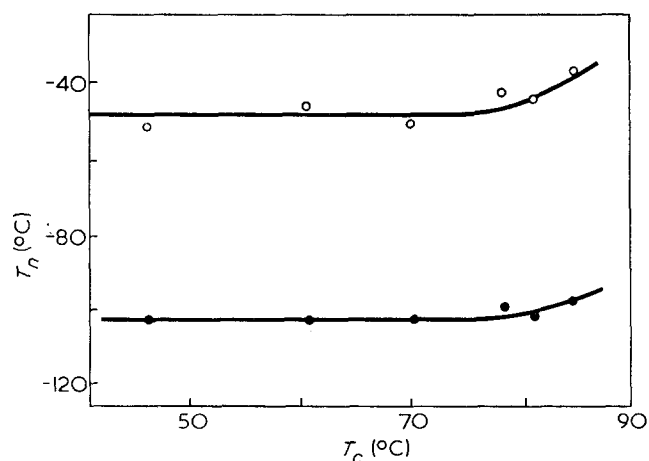


Figure 4 Plots of T_n vs. crystallization temperature for as-grown crystals. \circ , W_m ; \bullet , W_s

RESULTS AND DISCUSSION

As-grown crystals

Figure 2 shows e.s.r. spectra at different temperatures for the crystals crystallized at 76.5°C. Quite similar spectra were obtained for all samples. At low temperatures the spectra have a broad line shape suggesting that the polymer matrix is in a rigid state. With increasing temperature a small subsplitting appears as indicated by the arrow at about -110°C. This subsplitting shifts inwards and increases its intensity as the temperature is increased. As to the development of this subsplitting two mechanisms can be considered: (i) part of the probe begins to rotate sufficiently to cause change of hyperfine pattern as the temperature is increased, and a spectrum with a sharp hyperfine pattern overlaps on the broad one as suggested by Rabold⁵; (ii) a subsplitting similar to ours appears essentially in a certain rotational correlation time range of the probe as a result of the partial averaging of the anisotropy of the hyperfine interaction and the g value. Case (i) seems likely when the complexity of the structure of polymer matrix is considered. If the supposition proposed by Rabold⁵ is permitted, it is likely that this appearance of the subsplitting is caused by a certain heterogeneity of the surface structure of single crystals such as chain ends and long loops at the surface. However, the spectra which have the subsplitting have been simulated by Itokowitz¹⁰ and it may be beneficial to clarify the cause of this subsplitting in future.

At about -40 to -50°C a marked narrowing of the peak separation occurs. When the separation is plotted against temperature a drastic change is seen as shown in Figure 3. In this Figure both narrowing of the subsplitting W_s and the main splitting W_m are shown. The narrowing temperature of W_m , T_n , may be related to the molecular motion associated with the glass transition because the linear relation between this temperature and the glass transition temperature T_g has been found for several polymers⁵. Additionally, the agreement of T_n and T_g was found for poly(vinyl alcohol) and poly(vinyl acetate) by the authors.

Further study of the narrowing temperature for all samples revealed that T_n was slightly increased above the crystallization temperature of 75°C, at which a lamellar thickness of 100 Å was achieved as shown in Figure 4. This result indicates that the surface structure is not largely affected by the crystallization temperature, and agrees with the result of the nitric acid etching experiment that the thickness of the non-crystalline surface layer was independent of the crystallization temperature¹², and supports our previous work of irradiation effects on single crystals of linear polyethylene⁶.

Above room temperature spectral patterns became sufficiently resolved to calculate the correlation time of tumbling motion of the probe by equations (1) or (2). Figure 5 shows an example of plots of the logarithmic correlation frequency τ_c^{-1} versus the reciprocal of observation temperature for the crystals formed at 76.5°C. The frequency below 10⁹ Hz may be somewhat inaccurate because of the limitation of the rate conditions mentioned earlier. However, it is useful to know the tendency of the change in frequency with variation in temperature. It should be noticed that the frequency increases linearly with increasing temperature up to the

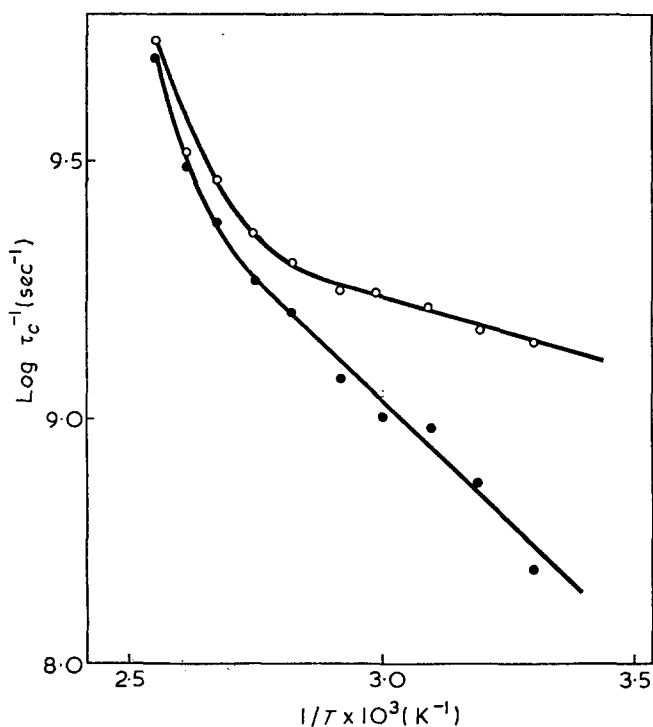


Figure 5 Plots of correlation frequency vs. reciprocal temperature for as-grown crystals formed at 76.5°C. ○, Increasing temperature; ●, decreasing temperature

crystallization temperature, satisfying the Arrhenius relation, and then it increases more rapidly beyond this temperature as shown in the Figure by the open circles. It is well known that as-grown polyethylene single crystals cause thickening above the crystallization temperature. The abrupt increase in the increasing rate of frequency suggests that the new mode of molecular motion is initiated along the whole surface of the crystals to cause thickening of the crystals. When the temperature is decreased from above the crystallization temperature, the irreversible decrease in the frequency is seen as shown by the solid circles of Figure 5. This decrease in the frequency indicates that the crystal surface was changed into some immobilized state by annealing, and the progressive increase of the slope of the curve with increasing temperature implies that the surface structure changes as the temperature increases.

One may feel some fear for the supposition that the probes were located at the surface of crystals even after the thickening of crystals had occurred since molecular motions in the thickening process may possibly confine the probes within the thickened crystal core. This fear, however, was dispelled by the fact that the correlation frequency observed at room temperature was considerably decreased even for the annealed crystals in which the probes were dispersed after annealing as shown below.

As to the change in slope at elevated temperatures, the desaturation effect on e.s.r. spectra, from which the correlation frequency is derived, might be considered. Rabold⁵ has reported that the e.s.r. spectra of the nitroxide radical were very sensitive to the incident microwave power level. Increasing temperature increases the saturation factor, and then the correlation frequency may possibly increase. However, this phenomenon has not been found for the completely amorphous materials such as natural rubber and nitrile-butadiene rubbers

(NBR)¹³; accordingly this may be due to change of unstable structures in polycrystalline materials such as partial melting. Similar results have been found for the behaviour of trapped radicals in γ -irradiated polyethylene⁶.

The Arrhenius relation below the crystalline temperature in Figure 5 gives about 1.5 kcal/mol of activation energy to the tumbling motion of the probe. This relatively small value implies that the rotational oscillation of the probe occurs in this temperature range. Strukov⁴ and Rabold⁵ obtained about 10 kcal/mol for the bulk crystallized linear polyethylene, corresponding to the higher temperature region where the slope in Figure 5 is continuously changing. In this region, jumping of the probes into adjacent holes may possibly occur as well as the polymer segments jump above T_g with increasing free volume. It is interesting to note that the value of 1.5 kcal/mol is comparable to that of the wideline n.m.r. data obtained for the bulk polyethylene by McCall¹⁴ although the temperature region is somewhat different. He found two temperature regions where the correlation frequency of the motion of molecules obeys the Arrhenius law giving 6.1 and 1.5 kcal/mol for the high and the low temperature region, respectively. Such a coincidence between e.s.r. and n.m.r. data has been pointed out by Wasserman¹⁵ for several polymers, except polyethylene.

Annealed crystals

Figure 6 shows the change of W with temperature for the annealed crystals in which the probes were dispersed after annealing. It should be noticed that the narrowing temperature T_n is shifted to higher temperatures by about 50°C compared with that of as-grown crystals indicating the fact that the surface structure is immobilized by annealing. This fact is further confirmed by plotting logarithmic correlation frequencies at room temperature versus annealing temperature as shown in Figure 7. The frequency is found to decrease above the crystallization temperature (arrow) suggesting that the thickening of the crystals by annealing changes the surface structure into immobilized state. The arrangement of the folding molecules in the annealed crystals is believed to have the highest regularity compared with that of the melt crystallized sample ($T_n = -50^\circ\text{C}$) and as-grown crystals. As far as these e.s.r. data are concerned, the arrangement of the

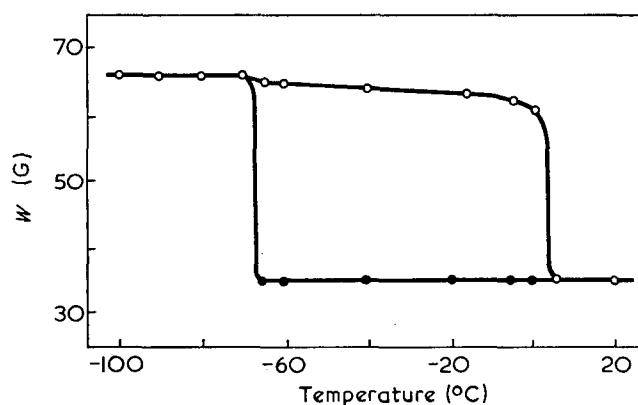


Figure 6 Plots of W vs. temperature for crystals annealed at 90°C. Crystallization temperature, 76.5°C; lamellar thickness, 135 Å. ○, W_m ; ●, W_s

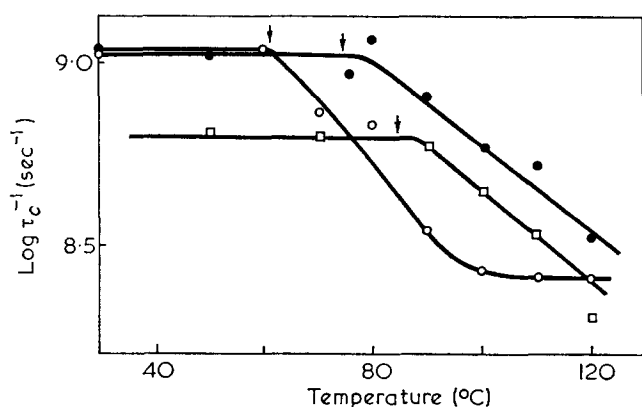


Figure 7 Plots of logarithmic correlation frequency vs. annealing temperature for annealed crystals crystallized at: ○, 60.6°; ●, 76.5°; □, 84.2°C

surface molecules of the as-grown crystals may have some irregularity. This irregularity can be introduced by loose loops and chain ends at the surface, but they are tightened by being taken into the crystal core during the thickening process. In the melt crystallized state, tie molecules and the irregularity of crystallographic folding direction may disturb the increase of regularity of chain arrangement at the surface.

The activation energy of the tumbling motion of the probe was found to be about 3 kcal/mol for the crystals annealed at 90°C, suggesting that the polymer matrix changed to hinder the motion of the probe. According to the cavity model of Strukov⁴, the probe will be trapped in a cavity formed as a micro-void among polymer molecules, and rotates with a certain steric hindrance. The degree of hindrance can be evaluated by the activation energy. Further, it can be said that the hindrance is mainly controlled by the thermal motion of polymer molecules since the activation energy of molecular motions detected by n.m.r. agrees with that of the paramagnetic probe^{4, 15}. In the present study, therefore, it is deduced that the cavity wall, namely molecular arrangement around the probe, was changed to immobilized state by annealing decreasing microvoids also in view of the activation energy.

It has been found that the mobile fraction of wideline n.m.r. spectra increased when polyethylene single crystals were annealed above the crystallization temperature¹⁶. This phenomenon has been interpreted by two conflicting situations: (1) the increased mobile fraction is originated from a disordered phase increased by annealing at the surface of crystals^{17, 18}; and (2) mobile segments are introduced within crystals to form crystal defects^{6, 19, 20}. The data and the discussion mentioned above lead us to the conclusion that molecular arrangement at the surface of as-grown crystals have some irregularity and it becomes more regular and immobilized by annealing above the crystallization temperature, as represented by the model shown in Figure 8. This was originally proposed to explain the results of our previous work^{6, 21}, slightly modified as to the state of chain ends. The broken lines in the annealed model show the defects within the crystal and the wriggling folding stems represent the distortion of planar zig-zag chains in the vicinity of the defects.

Figure 9a shows the plots of logarithmic correlation frequency versus lamellar thickness L for the annealed crystals. The frequency is found to increase above the

crystallization temperature and becomes constant at higher temperatures for each sample. These plots were reduced to one curve when the logarithmic frequency was replotted against the increased portion of the lamellar thickness as shown in Figure 9b. This means that the surface structure of the annealed crystals was determined uniquely by the increased portion of lamellar thickness, and the structure of the annealed crystals was almost settled when the increased portion reaches about 0.3 during the thickening process.

ACKNOWLEDGEMENT

The authors thank Professor Takayanagi of Kyushu University for giving facilities for small angle X-ray measurements.

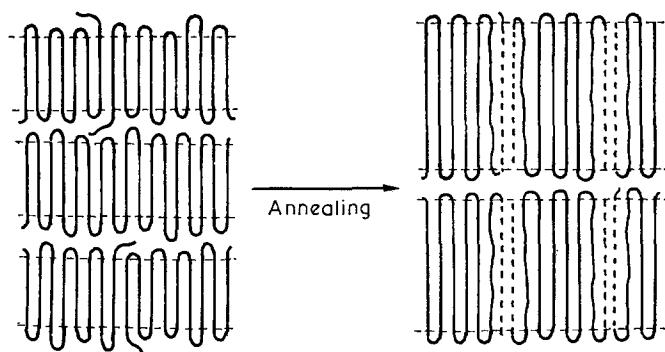


Figure 8 Schematic representation of change in surface structure of as-grown crystals by annealing

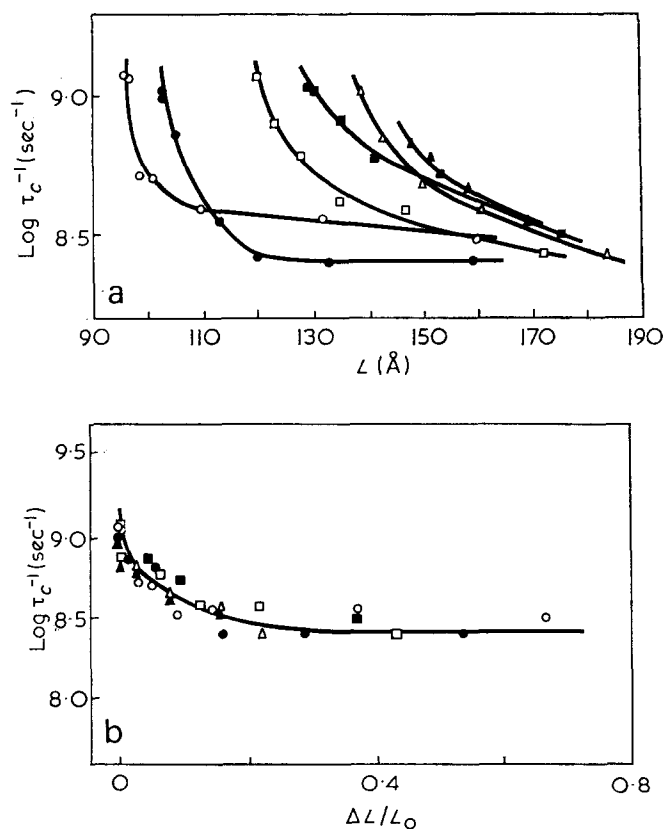


Figure 9 (a) Plots of logarithmic correlation frequencies vs. lamellar thickness of annealed crystals crystallized at: ○, 46.6°; ●, 60.6°; □, 70.2°; ■, 76.5°; △, 81.0°; ▲, 84.2°C. (b) Plots of logarithmic correlation frequencies vs. increased portion of lamellar thickness for annealed crystals. L_0 , lamellar thickness before annealing. $\Delta L = L - L_0$

REFERENCES

- 1 Keller, A. *Kolloid-Z. Z. Polym.* 1964, **197**, 98
- 2 Fischer, E. W. and Lorentz, R. *Kolloid-Z. Z. Polym.* 1963, **189**, 97
- 3 Flory, P. J. *J. Am. Chem. Soc.* 1962, **84**, 2857
- 4 Strukov, V. B. and Rozantzev, E. G. *Vysokomol. Soedin. (A)* 1968, **10**, 626
- 5 Rabold, G. P. *J. Polym. Sci. (A-1)* 1969, **7**, 1203
- 6 Kusumoto, N., Yamamoto, T. and Takayanagi, M. *J. Polym. Sci. (A-2)* 1971, **9**, 1173
- 7 Briere, B., Lemaire, H. and Ressay, A. *Bull. Soc. Chim. France* 1965, p 3273
- 8 Kivelson, D. *J. Chem. Phys.* 1960, **33**, 1904
- 9 Stryer, L. and Greffth, O. H. *Biochemistry* 1965, **54**, 1789
- 10 Itokowitz, M. S. *J. Chem. Phys.* 1967, **46**, 3048
- 11 Shioya, M. and Sohma, J. *12th ESR Meeting, Matsuyama, Japan* 1973
- 12 Brundell, D. J., Keller, A. and Connor, T. M. *J. Polym. Sci. (A-2)* 1967, **5**, 991
- 13 Kusumoto, N., Zaitzu, Y. and Sano, S. unpublished work
- 14 McCall, D. W. and Slichter, W. P. *J. Polym. Sci.* 1957, **26**, 171
- 15 Wasserman, A. M., Buchachenko, A. L., Kovarskii, A. L. and Neiman, M. B. *Eur. Polym. J. (Suppl.)* 1969, p 473
- 16 Slichter, W. P. *J. Appl. Phys.* 1961, **31**, 1865
- 17 Fischer, E. W. and Peterlin, A. *Makromol. Chem.* 1964, **74**, 1
- 18 Olf, H. G. and Peterlin, A. *J. Polym. Sci. (A-2)* 1970, **8**, 771
- 19 Kedzie, W. R. cited in 'Polymer Single Crystals' (by Geil, P. H.), Wiley, New York, 1963, p 338
- 20 Takayanagi, M. and Matsuo, T. *J. Macromol. Sci. (B)* 1967, **3**, 407
- 21 Takayanagi, M. *Kogyo Kagaku Zasshi* 1970, **73**, 1278

Dielectric properties of standard and modified electrical grade phenol-formaldehyde resin-paper laminates*

J. T. Jux and A. M. North

Department of Pure and Applied Chemistry, University of Strathclyde, Glasgow G1 1XL, UK

and R. Kay

*The De La Rue Research Centre, 68 Lower Cookham Road, Maidenhead, Berks, UK
(Received 6 February 1974; revised 7 March 1974)*

The dielectric properties of phenol-formaldehyde cellulose laminates show four loss processes. There is a very low frequency polarization, the amplitude of which varies as an inverse function of charging voltage and which requires long charging times. This is ascribed to the formation of space charge at the resin-electrode interface. A low frequency internal process which is very dependent on absorbed moisture is ascribed to Maxwell-Wagner-Sillars interfacial polarization of the resin/wet cellulose boundary. A.c. conduction (again dependent on water absorption) is evident below about 1 MHz, and at the highest frequencies a further relaxation exists which is ascribed to dipole orientation of hydroxyl groups.

The dielectric properties are much improved by addition of small (less than 10^{-3} mol/kg) quantities of agents capable of oxidizing hydroxyl groups. In the case of the high frequency process this arises directly by reduction of hydroxyl content. However, the effect on a.c. conduction and the low frequency processes arises through a primary reduction of moisture absorption as the hydrophilic character of the resin and cellulose surface is diminished.

INTRODUCTION

Crosslinked phenol-formaldehyde resins, reinforced with either paper, cotton or glass, are used as insulating materials in the construction of an electrical insulating sheet which, when clad with copper, forms printed circuit boards for use in electronic equipment. These materials must often operate in adverse environmental conditions (such as high temperatures and humidities), when it is found that, unless the materials are specifically selected, the electrical properties may deteriorate.

Few studies of the dielectric properties of phenol-formaldehyde resins and laminates have been reported in which deductions are made in relation to molecular structure or in which measurements have been carried out over an extended frequency range. The early work of Hartshorn *et al.*^{1, 2} showed well-defined loss processes which are dependent on the amount of impurities present, of which water was extremely important. It was concluded that water passed easily through the resin layers to be absorbed by the paper. However, these studies were conducted over an extended temperature, rather than frequency, range and the molecular origins of the loss processes remained unclear. Modifications to the resin by changes in the phenol derivative³ or catalyst² have also been shown to reduce the loss factor

of dried materials, but the improvement was lost on the absorption of a few percent of water.

Formica International Limited has discovered⁴ that the electrical properties of laminates are altered by the addition of metal cations during the resin synthesis. For example, when Fe(III) salts were added to the liquid resol before paper impregnation and curing, improvements were noted in moisture resistance, with a corresponding decrease in electrical conductivity and dielectric loss at 1 MHz.

There are a number of possible explanations of this behaviour. The hydrophilic character of the resin could be reduced by formation of a metal complex or by oxidation of phenolic hydroxyl groups. Alternatively the surface of the cellulose filler might be rendered less hydrophilic by oxidative or complexing reactions.

A number of metal salts have been shown⁵⁻⁸ to form complexes with phenol-formaldehyde resins, and a very large amount of work has been done on phenol oxidation. Of particular relevance are oxidations using potassium ferricyanide^{9, 10}, cerium(IV) compounds¹¹, and sodium periodate¹². In addition oxidative modification of cellulose can be achieved using cerium salts^{13, 14} or periodates¹⁵.

In this paper measurements are reported over ten decades of frequency of the dielectric properties of phenol-formaldehyde resins and resin-paper laminates. These show the effect of water absorption, and the consequences of modification by oxidizing additives.

* Patent applications embodying subject matter disclosed in this paper are or will be pending in one or more countries.

EXPERIMENTAL

Materials

Formica electrical grade laminates and the A-stage resol from which these had been prepared were supplied by Formica Int. Ltd. The initial resol was formed by ammonia catalysed polymerization, and laminates were prepared by pressing on a standard cycle seven sheets of impregnated bleached Kraft paper prepared by treating the paper in the resin. The final resite, or C-stage, laminates had a thickness of 1.5 mm and conformed to BSS 2782 tests: (a) relative permittivity less than 5.8, power factor less than $0.045 \text{ ohms}^{-1} \text{ F}^{-1}$; (b) water content less than 0.8%; (c) electrical strength greater than 25 kV edgewise, 18 kV flat; (d) surface resistivity greater than $10^{14} \Omega$, volume resistivity greater than $10^{14} \Omega \text{ cm}$.

Samples of resin without filler were prepared as follows. The resol (A-stage) resins were heated at 120°C to remove volatile impurity and bring the degree of cure to the resitol (B-stage). They were then ground in a ball-mill to a fine powder and moulded between Melinex release film.

Samples for electrical measurement were cut to discs 45 mm in diameter. Contact with test electrodes was obtained either by flash deposition of aluminium on the sample, by pressing aluminium foil on to a greased surface, or by coating the sample surfaces with graphite. The following additives were studied: iron(III) sulphate, iron(II) sulphate, iron(III) malonate, iron(III) naphthenate, potassium ferricyanide, cerium(IV) ammonium sulphate, cerium(IV) ammonium nitrate and sodium periodate. These were added, as solutions in 60 ml of distilled water, to 3 kg of the liquid resol prior to impregnation of the wet sized paper or to resin formation. The additive concentrations studied ranged from 10^{-5} to 10^{-3} mol/kg of resin.

Apparatus

Dielectric measurements between 10^{-5} and 10^{-1} Hz were made using the d.c. transient technique. The measurement circuit¹⁶ included a Keithley 610C electrometer with the output displayed on a Servoscribe recorder. Current-time curves were converted to the appropriate permittivity-frequency data using standard computational procedures¹⁷. Charging times were always several times longer than the discharge times of interest, and were usually 18 h.

The frequency range 10^{-1} to $3 \times 10^2 \text{ Hz}$ was covered using a Scheiber bridge¹⁸ fitted with a frequency selective detector amplifier. Between 10^2 and 10^6 Hz measurements were made using Wayne Kerr B221 and 3601 transformer ratio arm bridges. Between 5×10^5 and 10^2 Hz measurements were made (at room temperature only) using a Hartshorn-Ward resonant circuit technique¹⁹.

Samples were measured in a three-terminal parallel plate test cell, the container for which could be placed in any convenient thermostat bath.

RESULTS

Unmodified resin and laminate

The a.c. and short-time d.c. transient behaviour of samples coated with graphite was found to be the same as that of samples vacuum-coated with aluminium. Since the former technique was both rapid and repro-

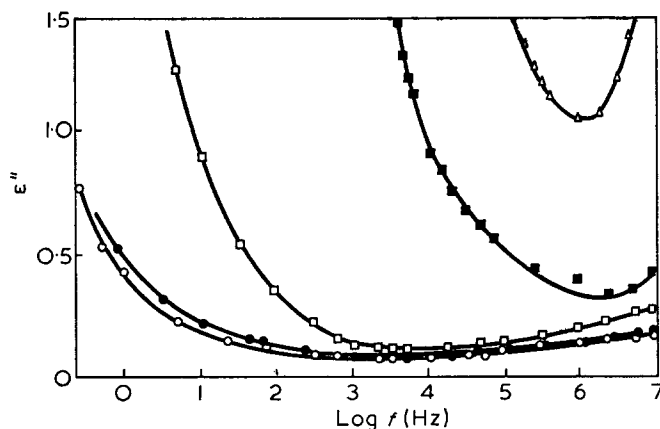


Figure 1 A.c. dielectric loss, ϵ'' , at 25°C . \circ , Unmodified resin at room humidity (0.2% w/w water); \bullet , unmodified resin after 30 days at 100% r.h. (0.3% w/w water); \square , unmodified laminate at room humidity (0.6% w/w water); \blacksquare , unmodified laminate after 30 days at 100% r.h. (0.8% w/w water); \triangle , unmodified laminate (4% w/w water)

ducible, and could be applied to samples with a large water content (which vacuum procedures could not) all measurements reported refer to this technique unless otherwise stated.

The a.c. dielectric losses of the standard resin and laminate at laboratory humidity (40–50%) and after 30 days in an atmosphere of 100% relative humidity are illustrated in Figure 1. The pronounced effect of absorbed water on the laminate, is apparent, as is the existence of loss processes at high and low frequencies.

The low frequency values of dielectric loss measured as a transient discharge current depend on both the charging voltage (Figure 2) and charging time (Figure 3). The log-log plots of discharge currents against time for a relaxation obeying the Cole-Cole empirical function:

$$\frac{\epsilon^* - \epsilon_\infty}{\epsilon_0 - \epsilon_\infty} = [1 + (i\omega\tau_0)^n]^{-1}$$

should exhibit²⁰ a slope of $-(1-n)$ at times shorter than τ_0 and $-(1+n)$ at times longer than τ_0 . Such graphs for laminate samples charged for 18 h showed at least two changes of slope. As well as an increase in negative slope between about 10^1 and 10^2 sec , a decrease in negative slope occurred above 10^2 sec . Such a phenomenon is normally ascribed to a second relaxation process of long relaxation time. On the assumption that the discharge currents from the two processes are independent and additive²¹, extrapolation of the 'long-time' current and subtraction allows evaluation of the discharge current due to the 'short-time' process. This can be transformed in the normal way, as illustrated in Figure 4. The process was found to be independent of electrode nature and of charging field and time so long as these exceeded $6.7 \times 10^3 \text{ V/m}$ and 10^3 sec respectively. However, the loss was very dependent on water content and temperature (Figures 4 and 5). The apparent activation energy obtained from the frequency of maximum loss was $140 \pm 20 \text{ kJ/mol}$ compared with $120 \pm 20 \text{ kJ/mol}$ for d.c. conduction over the same temperature range (below 41°C). A similar loss process (though requiring a higher water content for comparable magnitude) was observed in the cured resin (Figure 6).

The 'long-time' process was found to have similar characteristics in both resin and laminate samples and

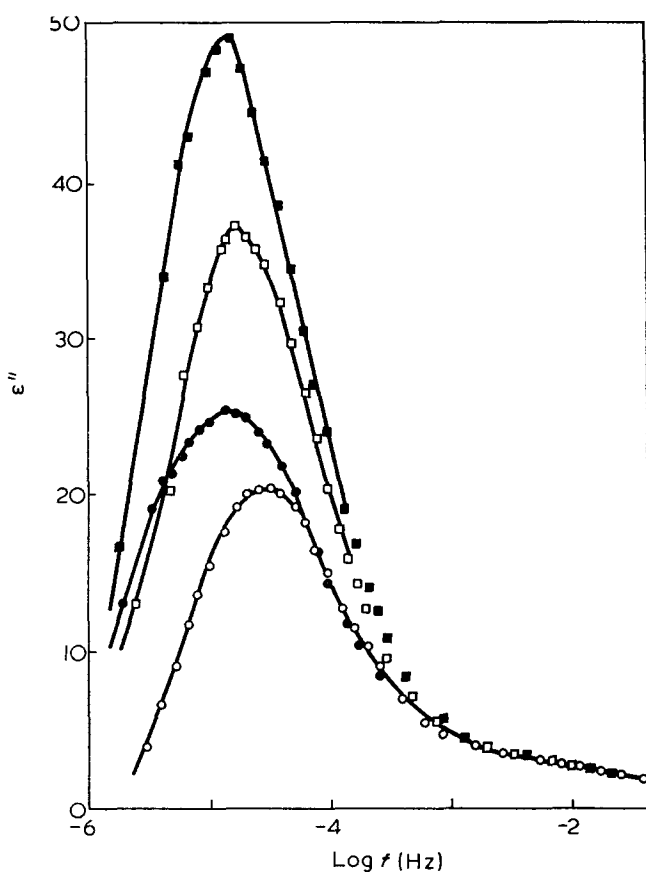


Figure 2 Resin d.c. transient dielectric loss, ϵ'' , at 25°C at various charging fields; charging time 18h. \circ , 2.4×10^4 ; \bullet , 1.7×10^4 ; \square , 9.3×10^3 ; \blacksquare , 3.1×10^3 V/m

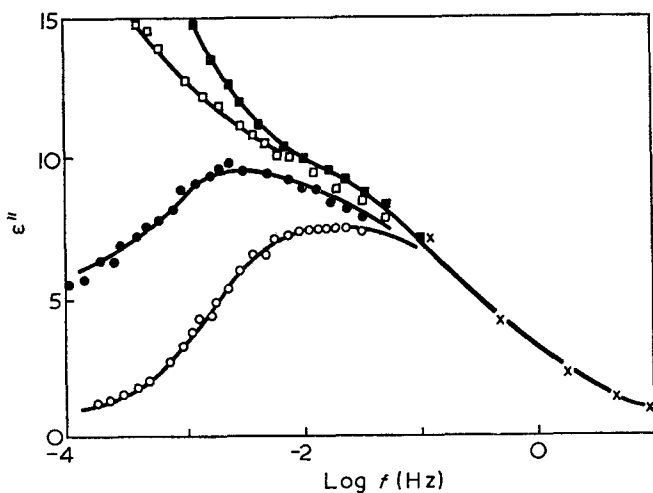


Figure 3 Laminate low frequency dielectric loss, ϵ'' , at 25°C at various charging times; charging field 6.1×10^3 V/m. \times , A.c. data; \circ , 100 sec; \bullet , 300 sec; \square , 35 min; \blacksquare , 18 h

so did not involve the cellulose filler. The process depended on charging time up to 18 h, but was independent of it above this value. The height of the loss maximum was found to vary as $E^{-0.2}$ where E was the charging field. By comparison the steady d.c. leakage current (measured during the charging cycle) was found to vary as $E^{+0.2}$. An interesting feature of the temperature dependence of the d.c. conductivity is that a decrease in the apparent activation energy (120 ± 20 kJ/mol to 60 ± 20 kJ/mol) is observed at 41°C. A similar change in slope occurs in an Arrhenius plot of the thermally stimulated depolarization current obtained when a

sample is heated after being quenched from 100°C to 20°C under the influence of a 1.7×10^4 V/m polarizing field.

Modified resin and laminate

Effect on water absorption. Since the dielectric loss processes of interest were profoundly affected by water content, the effect of additive on water uptake was studied first. The water absorption of dried laminate and resin samples placed in an atmosphere of 100% relative humidity at 25°C is illustrated in Figure 7, where it can be seen that the addition of iron(III) or cerium(IV) compounds lowers the rate of water absorption, having little effect on cured resin. It was found that the additives exhibited the maximum beneficial

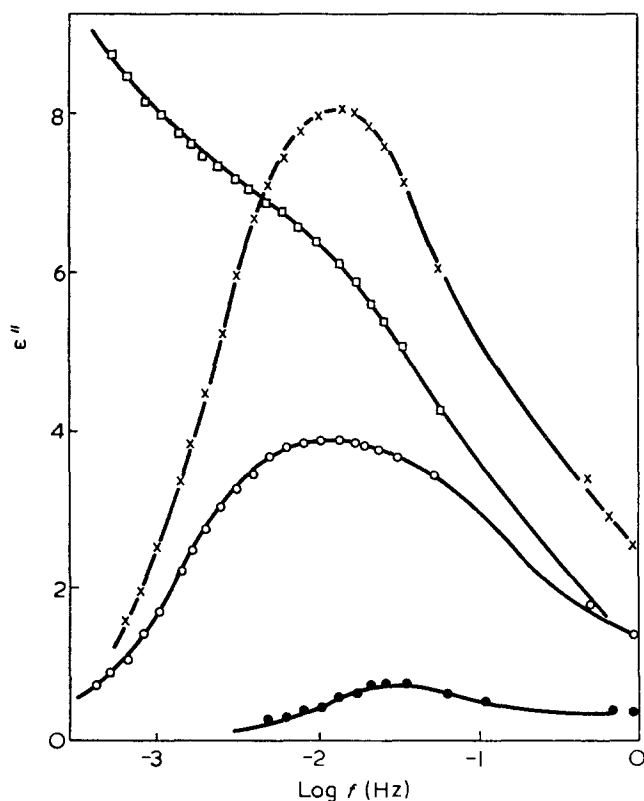


Figure 4 Resolved 'short-time' process in laminate. Charged at 1.7×10^4 V/m for 18h at 25°C. \square , Total loss at room humidity (0.6% w/w water); \circ , 'short-time' loss process at room humidity after subtraction of 'long-time' discharge current; \bullet , 'short-time' loss after drying *in vacuo* for 5 days; \times , 'short-time' loss after 5h at 100% r.h. (0.8% w/w water)

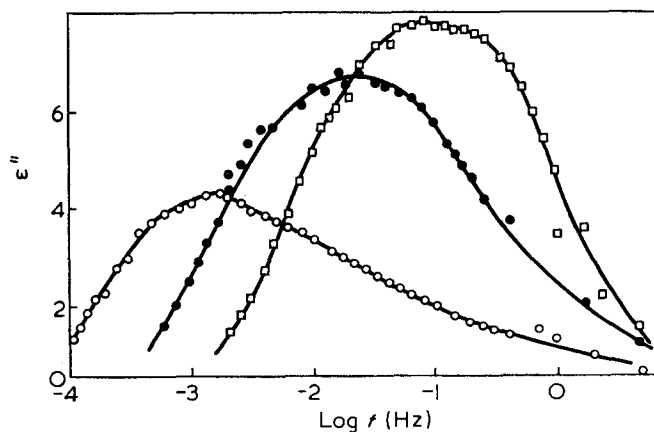


Figure 5 Resolved 'short-time' process in laminate. Charged at 1.7×10^4 V/m for 18h; 0.6% w/w water. \circ , 12°C; \bullet , 25.5°C; \square , 34.6°C

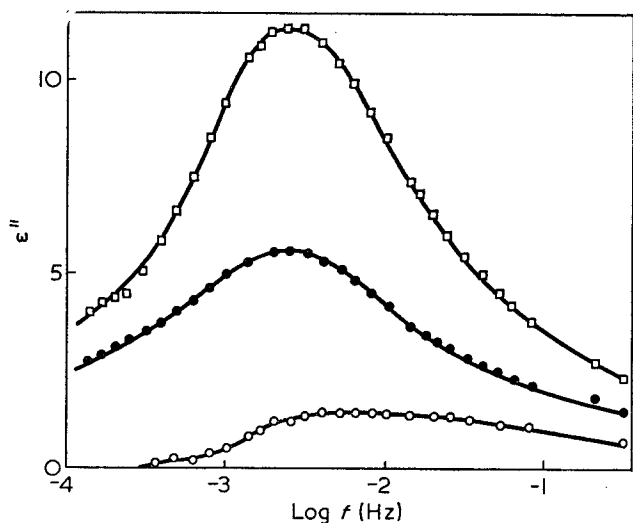


Figure 6 Resolved 'short-time' process in cured resin. Charged at 1.7×10^4 V/m for 18h at 25°C. Water content (w/w): ○, 0.3%; ●, 1.25%; □, 2.5%

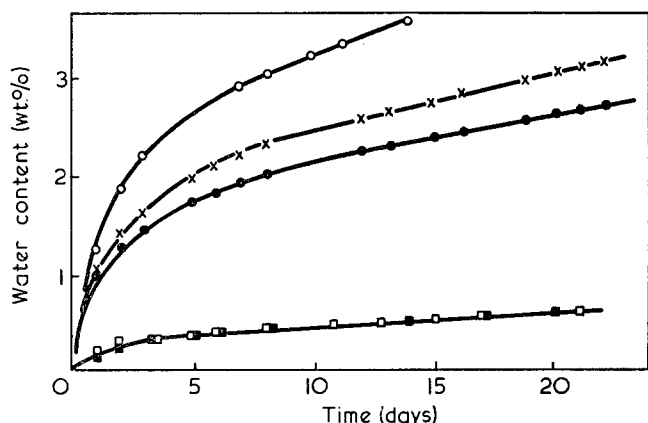


Figure 7 Water absorption by laminate and resin. ○, Standard laminate; ×, laminate with 1.8×10^{-3} mol/kg iron(III) sulphate; ●, laminate with 1.6×10^{-4} mol/kg cerium(IV) ammonium sulphate; □, standard cured resin; ■, resin with 1.8×10^{-3} mol/kg iron(III) sulphate

effect only when present in concentrations less than 10^{-3} mol/kg. Samples prepared in this way with higher additive concentrations were often more susceptible to moisture absorption than standard materials.

Effect on high frequency dielectric loss. the general effect of oxidizing cations on the a.c. dielectric loss of laminates at room humidity is illustrated in Figure 8. The high frequency loss process can be more easily studied at low temperatures, where the influence of the oxidizing power of the cation is evident (Figure 9). Although this Figure illustrates iron(II) sulphate as an additive, it must be pointed out that some oxidation of iron(II) to iron(III) occurred during the curing process, so that the effect must be considered as due to a mixture of Fe^{2+} and Fe^{3+} ions of greater total iron ion content than when iron(III) sulphate was added initially.

These low temperature-high frequency losses have a rather low temperature coefficient. From the variation with temperature of the frequencies of maximum loss (Figure 9 and two other temperatures) an Arrhenius activation energy for this process can be estimated as 45 ± 5 kJ/mol.

Effect on low frequency a.c. loss. The effect of a range of iron(III) salts, and of cerium(IV) ammonium sulphate on the low frequency (a.c. conduction) can be seen in

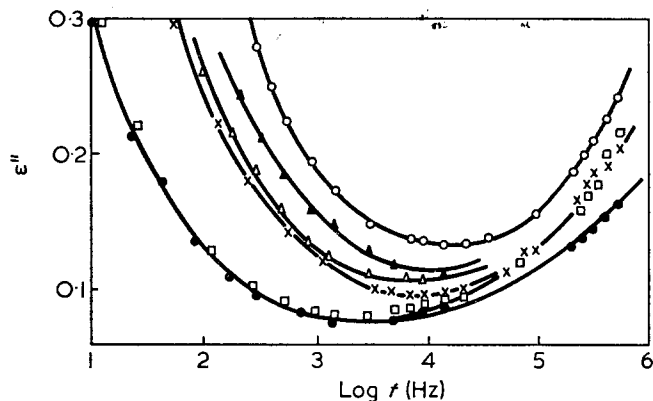


Figure 8 A.c. loss of modified laminate at 25°C, room humidity. ○, Standard laminate; ×, 1.8×10^{-4} mol/kg iron(III) sulphate; ●, 1.8×10^{-3} mol/kg iron(III) sulphate; □, 1.6×10^{-4} mol/kg cerium(IV) ammonium sulphate; △, 1×10^{-4} mol/kg iron(III) naphthenate; ▲, 3×10^{-4} mol/kg iron(III) malonate]

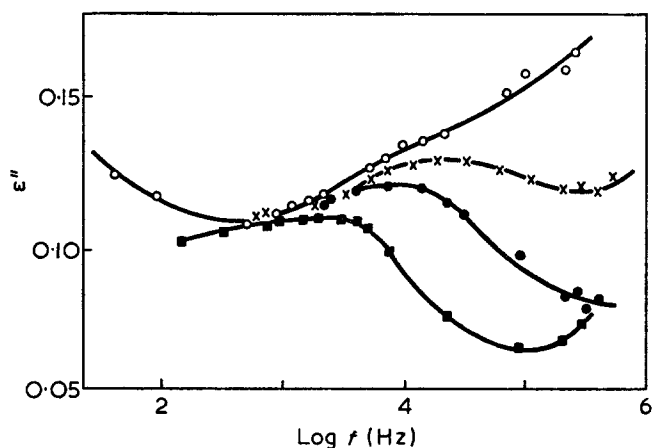


Figure 9 High frequency loss process in modified laminates. ○, Standard laminate at -45°C; ×, laminate with 3.6×10^{-3} mol/kg iron(II) sulphate at -48°C; ●, laminate with 1.8×10^{-3} mol/kg iron(III) sulphate at -48°C; ■, laminate with 1.8×10^{-3} mol/kg iron(III) sulphate at -58°C

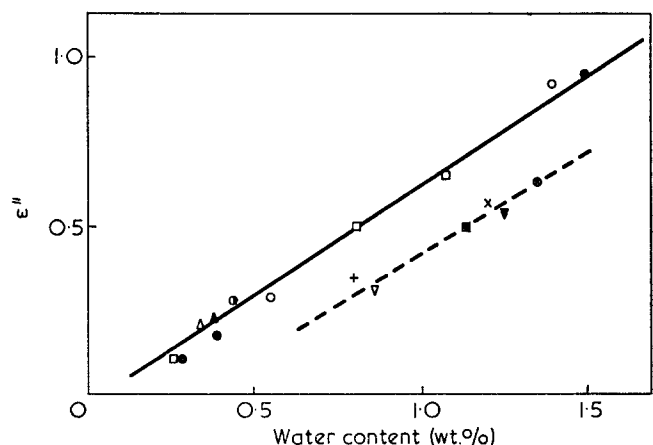


Figure 10 A.c. loss at 200Hz, 25°C. ○, Standard laminate; ●, 1.8×10^{-4} mol/kg iron(III) sulphate; ●, 1.8×10^{-3} mol/kg iron(III) sulphate; △, 1×10^{-4} mol/kg iron(III) naphthenate; ▲, 3×10^{-4} mol/kg iron(III) malonate; +, 1×10^{-5} mol/kg sodium periodate; ×, 1×10^{-2} mol/kg sodium periodate; ⊗, 1×10^{-3} mol/kg cerium(IV) ammonium sulphate; ■, 1×10^{-2} mol/kg cerium(IV) ammonium nitrate; ▼, 5×10^{-5} mol/kg cerium(IV) ammonium nitrate; ▽, 1×10^{-4} mol/kg potassium ferricyanide. —, factory batch 1; - - -, factory batch 2

Figure 8. In general the cerium(IV) salts are more effective in reducing losses than the iron (III), with the salts of organic acids being least effective.

It was observed that the dielectric loss in this frequency range correlated with the water content of the sample rather than with the concentration of additive. This is illustrated for the loss at 200 Hz at 25°C for samples measured after exposure to atmospheres of different relative humidity (Figure 10). Small variations in the dependence of ϵ'' at 200 Hz on water content were found for laminates prepared in different batches. This was ascribed to differences in water and hydroxyl content of the different papers and resins used, and to differences in the relative humidity in the factory at the time of fabrication. Consequently the intercept illustrated in Figure 10 for each batch is dependent on the variables of fabrication.

Measurements of the temperature dependence of the amplitude of loss at 200 Hz above 55°C yielded an apparent activation energy of 40 ± 10 kJ/mol, in comparison with 60 ± 20 kJ/mol observed for d.c. conduction in the same temperature range. The large uncertainty in the d.c. measurement arises because of the difficulty in obtaining a constant leakage current after very long-time polarization effects. As remarked earlier, the presence of large amounts of additive caused a deterioration in dielectric performance resulting from the enhanced susceptibility to water absorption.

Effect on 'short-time' transient process. The additives affect the 'short-time' relaxation observed in the d.c. transient experiment simply by affecting the water content, which in turn controls the amplitude of the loss (Figure 4).

DISCUSSION

Low frequency processes observed in transient discharge currents

The d.c. transient technique allows, by observation of discharge currents, the examination of relaxation processes which in an a.c. measurement might be swamped by conduction. In this work two distinct processes are apparent.

The lowest frequency process, requiring very long charging times for the establishment of polarization (Figure 3) and varying as an inverse function of charging voltage (Figure 2) is similar to the electrode polarization reported²¹⁻²⁴ for a number of other polymer systems. The exponents of field strength found for this process and for d.c. conduction (-0.2 and $+0.2$ respectively) are in line with the generalized form²⁵ of the Schottky law of space charge limited conduction currents. Under these circumstances the observed relaxation and polarization characterize the formation of space charge at the electrode-resin interface. The long relaxation times and the influence of water suggests that these arise by ionic rather than electronic charge carriers.

Beyond noting that this phenomenon appears to be general, and depends on the conductivity of the polymer (and so on water content) it is not possible to draw further conclusions relating the relaxation to chemical structure of the resin.

The 'short-time' process, being profoundly affected by the presence of the paper filler but not by the resin-electrode interface can be described as an 'internal polarization'. The relationship to the conduction process

(evidenced in both the activation energy and the amplitude dependence on water content) indicates that the polarization may have its origins in the localization of charge carriers. Under these circumstances the process is probably some kind of Maxwell-Wagner-Sillars interfacial polarization²⁶. The importance of this process, too, in a variety of polymer systems has been emphasized recently²¹⁻²³.

The apparent independence of the loss frequency upon water content could arise from uncertainties in the resolution of the two low frequency loss processes, or from comparable increases in both the conductivity and the permittivity in the region of charge localization. It should be noted that these low frequency interfacial polarizations in polymer systems do not always obey^{20-22, 26} (either in frequency or amplitude) the idealized Maxwell-Wagner-Sillars equations.

It is not immediately apparent whether the resin or the cellulose constitutes the phase of higher conductivity. The existence of a similar (albeit much reduced) phenomenon in very wet resin in which clustering of water may occur in regions of low crosslink density suggests that the phase difference of importance is between resin and a predominantly aqueous system. Under these circumstances charge carriers could arise by dissociation of water molecules when the observed activation energy (for both d.c. conduction and interfacial polarization) would be made up of dissociation and diffusion terms. On this basis the experimental value of about 130 kJ/mol would be made up of approximately 60 kJ/mol for dissociation to give charge carriers leaving 70 kJ/mol for diffusion in wet resin, which compares well with literature values^{27, 28}. The cellulose filler, presenting a hydrophilic surface of hydroxyl groups, would then function as a favourable location for the formation of a water-resin interface. The oxidation of the cellulose hydroxyl groups by the additives would render the surface less hydrophilic and so decrease both water absorption and interfacial polarization as observed.

The change in temperature coefficient at 41°C indicates that a transition comparable to a glass transition occurs in the cured resin at this temperature.

Processes contributing to a.c. permittivity and loss

The low frequency (10^0 - 10^4 Hz) process observed in the a.c. measurements is a.c. conduction. This is dependent on water content, and consequently is always higher in laminates than in unfilled resins. Again the mode of action of the additives seems to be by reduction of hydrophilic character in the resin and cellulose. The general similarity of the a.c. and d.c. conduction processes suggests that both have their origin in the migration of ionic species through the wet resin.

The loss process observed above 10^4 Hz exhibits the characteristics of dipole orientation polarization. The amplitude, frequency and activation energy of this process lead us to suggest that it arises in rotational movement of the many (and chemically varied) hydroxyl groups present in the resin and cellulose. As there will be many different molecular environments for these groups, a broad absorption reaching to very high frequencies would be expected, and is observed. Again the magnitude of the loss is much greater in the laminate than in the resin, as would be expected on a simple consideration of hydroxyl group concentration.

The oxidizing additives reduce, but do not totally remove this process. This is in line with a mode of action in which the oxidation occurs predominantly at susceptible groups in the resin and at the resin-cellulose interface. Other studies^{13, 14} have shown that methylol units are unaffected in such oxidations. Thus it appears that the observed reduction in water uptake and dielectric loss arises by oxidation of phenolic hydroxyl in the resin and some 1,2-diol units on the cellulose surface. The methylol units would then be responsible for the highest frequency loss which is just becoming apparent at 10⁶ Hz in *Figure 9*, and which is not greatly affected by an oxidizing additive, an important point for certain technical processes.

CONCLUSIONS

The dielectric properties of phenol-formaldehyde cellulose laminates show evidence of four loss processes. These are a very low frequency polarization ascribed to formation of a space charge at the resin electrode interface, a low frequency internal polarization ascribed to Maxwell-Wagner-Sillars interfacial polarization of a wet resin/cellulose boundary, a.c. conduction, and a high frequency polarization ascribed to dipole orientation of hydroxyl groups.

The addition of small quantities of oxidizing agents reduces the losses arising from all these processes. The highest frequency process is diminished by oxidation of certain hydroxyl groups (although others remain unaffected) and the processes associated with movement of charge carriers are affected indirectly by reduction of water absorption.

ACKNOWLEDGEMENTS

The authors acknowledge with thanks the provision of a maintenance grant (J. T. J.) by Formica International Limited, and the assistance of the Science Research Council with the provision of measuring equipment.

REFERENCES

- 1 Hartshorn, L., Megson, N. J. L. and Rushton, E. *J. Inst. Elect. Eng.* 1938, **83**, 474
- 2 Hartshorn, L., Megson, N. J. L. and Rushton, E. *J. Soc. Chem. Ind.* 1940, **59**, 129
- 3 Lilley, A. C. and McDowell, J. R. *J. Appl. Phys.* 1968, **39**, 141
- 4 Formica Int. Ltd, Br. Pat. Appln 18458/73
- 5 Hultzsich, K. *ACS Div. Org. Coat. Plast. Chem. Prepr.* 1966, **26**, 121
- 6 Ackroyd, E. T. and Broughton, G. T. *J. Phys. Chem.* 1938, **42**, 343
- 7 Tolmacher, V. N., Orlova, N. N. and Maksutina, L. I. *Vysokomol. Soedin (A)*, 1970, **12**, 1379
- 8 Adams, P. A. and Holmes, E. J. *J. Soc. Chem. Ind.* 1935, **54**, 1
- 9 Taylor, W. and Battersby, A. R. 'Oxidative Coupling of Phenols', Arnold, London, 1967, p 52
- 10 Hintz, H. L. and Johnston, D. C. *J. Org. Chem.* 1967, **32**, 556
- 11 Barton, D. H. R. *Chem. Brit.* 1967, **3**, 330
- 12 Hecker, E. and Lattrell, R. *Annalen* 1963, **662**, 48
- 13 Ogiwara, Y. and Kubota, H. *J. Polym. Sci. (A-1)* 1969, **7**, 2087
- 14 Gugliemelli, L. A. and Russell, C. R. *J. Polym. Sci. (B)* 1969, **7**, 2087
- 15 Duke, F. R. *J. Am. Chem. Soc.* 1947, **69**, 3054
- 16 Reddish, W. *J. Polym. Sci. (C)* 1966, **14**, 123
- 17 Dev, S. B., North, A. M. and Pethrick, R. A. *Adv. Mol. Relax. Processes* 1972, **4**, 159
- 18 Scheiber, D. J. *J. Res. Nat. Bur. Stand.* 1961, **65C**, 23
- 19 Hartshorn, L. and Ward, W. H. *J. Inst. Elect. Eng.* 1936, **79**, 597
- 20 Baird, M. E. *Rev. Mod. Phys.* 1968, **40**, 219
- 21 Baird, M. E., Goldsworthy, G. T. and Creasey, C. J. *Polymer* 1971, **12**, 159
- 22 North, A. M. and Reid, J. C. *Eur. Polym. J.* 1972, **8**, 1129
- 23 Dev, S. B., North, A. M. and Reid, J. C. 'Dielectric Properties of Polymers', (Ed. F. E. Karasz), Plenum Press, New York, 1972, p 217
- 24 Hirota, S., Saito, S. and Nakajima, T. *Kolloid Z.* 1966, **213**, 109
- 25 Taylor, D. M. and Lewis, T. J. *J. Phys. (D: Appl. Phys.)* 1971, **4**, 1346
- 26 Sillars, R. W. *J. Inst. Elect. Eng.* 1937, **80**, 378
- 27 Seanor, D. A. in 'Polymer Science', (Ed. A. D. Jenkins), North-Holland, Amsterdam, 1972, Vol 2, p 1187
- 28 Barrie, J. A. in 'Diffusion in Polymers', (Eds J. Crank and G. S. Park), Academic Press, London, 1968, p 259

Mechanical properties of polymers at cryogenic temperatures: relationships between relaxation, yield and fracture processes*

Anne Hiltner and Eric Baer

*Department of Macromolecular Science, Case Western Reserve University,
Cleveland, Ohio 44106, USA*

(Received 29 April 1974)

Semi-crystalline as well as amorphous polymers generally develop some measure of molecular mobility at temperatures well below their melting temperature, T_m , or their glass transition temperature, T_g . In these polymers, one or more damping or internal friction peaks are usually found to occur in the low temperature region from 4K to 300K. The magnitude and temperature position of these maxima are dependent upon the structure of the polymer, its mode of preparation and past history, and the local environment of the moving units. Various examples are given of polymers that show significant low temperature relaxation processes, and the influence of chemical structure, structural substitution, crystallinity and low molecular weight diluents is illustrated. The extent to which relaxation behaviour can be correlated to macroscopic ductility and fracture toughness is also discussed.

INTRODUCTION

It is now well recognized that semi-crystalline as well as amorphous polymers develop considerable molecular mobility in the solid state at temperatures well below their melting or glass transition temperature. These motions frequently manifest themselves as one or more mechanical loss or dispersion peaks in the temperature region 4·2 to 300K. There is also growing evidence that the molecular and defect motions that give rise to secondary relaxations are intimately related to transitions in bulk deformation and fracture behaviour. This paper is not intended as a review of the literature since this has been done elsewhere¹⁻³. Rather, with the use of specific examples, some of the problems in the area of low temperature relaxation and mechanical properties which have been of particular interest to the authors will be discussed. These include: (i) very low temperature relaxations in polymers with and without pendant side groups; (ii) relationship of secondary relaxation processes to yield and fracture; (iii) variation in chemical structure as a tool in understanding relaxation processes; and (iv) the effect of small molecular weight additives on relaxation behaviour with particular reference to the study of water in biologically relevant materials.

CRYOGENIC RELAXATION PROCESSES

In recent years an increasing number of studies have been concerned with extending relaxation measurements to very low temperatures, usually down to 4·2K. The

rationale for this approach is important. Molecular motions which occur at very low temperatures will be the most primitive, i.e., the mobile unit will be small and the re-orientation modes will be relatively simple. It is reasonable to assume that processes which become active at higher temperatures do not occur independently, but are built up on the lower temperature modes by involvement of larger units of the molecule in more complex motion. An understanding of the lowest temperature relaxation processes is thus of fundamental importance to the interpretation of higher temperature relaxations. Moreover, the relative simplicity of the low temperature modes facilitates the formulation and theoretical analysis of meaningful models.

Many of the polymers exhibiting cryogenic relaxation peaks have pendant side groups, and re-orientation of all or part of the side group is often the proposed mechanism³. For example, there is evidence that the δ peak in polystyrene (PS) at about 40K can be described by the simple barrier model for re-orientation of the phenyl side group.

Dielectric measurements on copolymers of 4-methylstyrene and 4-chlorostyrene have been made by Irvine and Work⁴. It was found that the strength of the δ peak varied linearly with composition (4-chlorostyrene being the dielectrically active moiety) while both the activation energy and peak shape were independent of composition. The authors conclude that the phenyl groups relax independently of each other, and propose that a simple barrier model is adequate for discussion of the roles of inter- and intra-molecular forces in the δ relaxation.

Dielectric and mechanical measurements have been made on chloro-substituted polystyrenes^{5,6}, and mechan-

* Presented as a Symposium Lecture at the IUPAC International Symposium on Macromolecules, Aberdeen, September 1973.

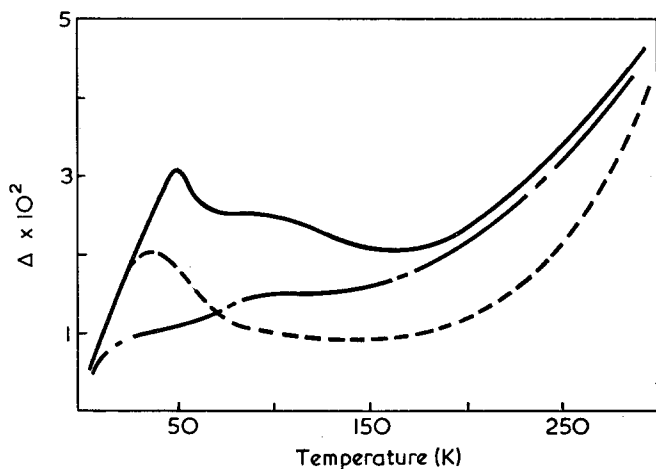


Figure 1 Internal friction of fluorinated polystyrenes: poly(2,3,4,4,6-pentafluorostyrene) (—); poly(α,β,β' -trifluorostyrene) (---); and polystyrene (-·-·-). [Reproduced from Hiltner, A. and Baer, E. *Crit. Rev. Macromol. Sci.* 1972, 1, 215 by permission of The Chemical Rubber Company, Cleveland, Ohio ©]

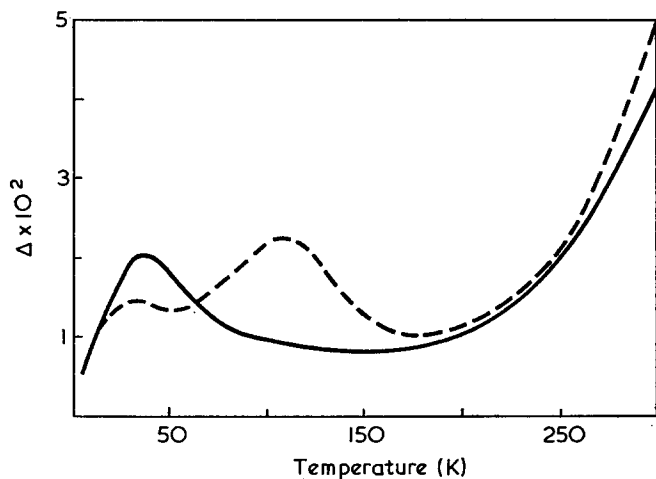


Figure 2 Effect of mineral oil on the internal friction of atactic polystyrene. —, polystyrene; ---, polystyrene+2% mineral oil. [Reproduced from Hiltner, A. and Baer, E. *Crit. Rev. Macromol. Sci.* 1972, 1, 215 by permission of The Chemical Rubber Company, Cleveland, Ohio ©]

ical measurements on bromo-, fluoro- and methylpolystyrenes⁶⁻⁸. It is found, in part, that backbone substitution, which causes a stiffening of the chain, has a greater effect on the relaxation curve than ring substitution (Figure 1). The effect of substitution on the δ peak is consistent with a spectrum of vibration and torsional modes for which the distribution of barrier heights is determined by intramolecular forces.

While the activation energy and shape of the δ peak are determined primarily by intramolecular forces, the relaxation strength is thought to depend on intermolecular or 'free volume' considerations. This is an on-off effect where the cavity size and shape determine whether or not a phenyl group can re-orient between equilibrium positions. The effect of the density of the glass on the δ peak has not been investigated, although mechanical data for amorphous and semi-crystalline isotactic polystyrene have been reported⁷. The relaxation strength is lower in the semi-crystalline specimen but the shape and temperature of the peak do not change.

Low molecular weight additives can potentially modify both intra- and inter-molecular forces. For example, the addition of 2% mineral oil alters both the

temperature and strength of the δ peak (Figure 2). Many other small molecules have also been found to change the δ peak, the precise effect appears to depend on the aromatic nature of the additive and its size and shape⁹. The presence of a low molecular weight additive is often accompanied by the appearance of a second peak at higher temperatures (γ peak), which in some cases corresponds to the glass transition of the additive⁵.

Dynamic mechanical loss peaks have also been observed below 77K in polymers without pendant side groups. Peaks at 26 and 46K have been observed in heat treated and drawn specimens respectively of poly(ethylene terephthalate) (PET)¹⁰. Linear polyethylene (LPE) and polyoxymethylene (POM) also have a loss peak in the 45–50K range, the intensity of which is very dependent on specimen history^{11,12}. The dramatic effect of deformation and thermal history on the intensity of these processes precludes a mechanism involving either specific group motions in the amorphous regions or motions at fold surfaces. Rather the data suggest that the relaxation arises from the crystalline or ordered regions of the polymer, and a mechanism involving limited segmental motion at dislocations within the crystalline regions has been proposed¹³.

This δ relaxation has many experimental features in common with the Bordoni peaks observed at cryogenic temperatures in FCC metals. The principal features of the Bordoni and δ peaks are compared in Table 1.

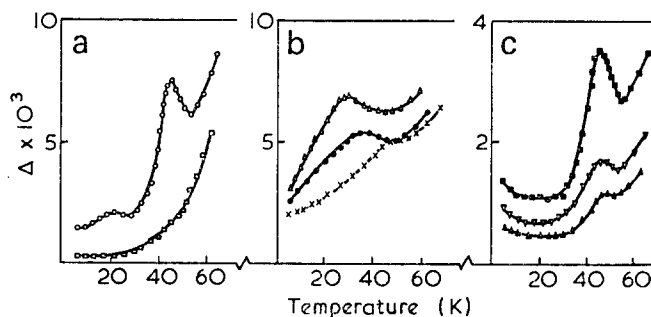


Figure 3 Effect of annealing on the δ_c relaxation; the samples of lowest density refer to the quenched material, PE(a) and PET(b) were subsequently annealed with fixed ends at 129° and 240°C, respectively, the POM(c) samples were prepared using different cooling rates. ρ : ○, 0.970; □, 0.954; △, 1.406; ●, 1.337; ×, 1.331; ■, 1.440; ▽, 1.425; ▲, 1.403. [Reproduced from Hiltner, A. and Baer, E. *Crit. Rev. Macromol. Sci.* 1972, 1, 215 by permission of The Chemical Rubber Company, Cleveland, Ohio ©]

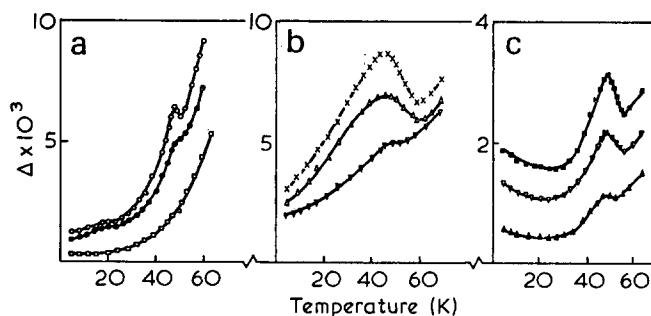


Figure 4 Effect of deformation of δ_c relaxation; the PE samples (a) were drawn at room temperature, PET(b) was drawn at 40°C, and POM(c) was rolled at room temperature. ρ : ○, 0.970 (8.5×); ●, 0.963 (5.5×); □, 0.954; ×, 1.368 (5.0×); △, 1.360 (3.5×); ▽, 1.331; ■, 1.434 (7×); ▽, 1.430 (5×); ▲, 1.403. [Reproduced from Hiltner, A. and Baer, E. *Crit. Rev. Macromol. Sci.* 1972, 1, 215 by permission of The Chemical Rubber Company, Cleveland, Ohio ©]

Table 1 The δ and Bordoni peaks—comparison of experimental features

Bordoni peak in copper ¹⁴	δ peak in linear polymers
Appears in both single crystals and polycrystalline specimens	Observed in crystalline or ordered polymers, is weak or absent in specimens quenched from the melt
Generally not observed in fully annealed specimens	Strongly dependent on thermal history, is weak or absent in specimens annealed without constraint but is present in specimens annealed constrained (Figure 3)
Height of the peak increases rapidly with increasing amount of cold work for deformations up to about 2%, but for greater deformations there is little change	Observed in rolled or drawn specimens and increases in intensity with increasing amount of deformation and decreasing deformation temperature (Figure 4)
Height of the peak and the temperature at which it occurs are almost independent of the amplitude of the vibrations	Dependence on amplitude is not known
In addition to the main peak, a smaller subsidiary peak is generally observed at a lower temperature	In addition to the primary peak at 45–50K, POM has a subsidiary peak below 4.2K (1 Hz). LPE also has a smaller peak at 20K and a dielectric peak has been reported between 1.2 and 4.2K ^{15,16} . Intensity of the subsidiary peaks shows the same dependence on deformation and heat treatment as the primary peak
Impurities reduce the heights of the peaks	Comonomer units which are accommodated in the crystal lattice reduce the intensity of the peak ¹⁷
Temperature at which the peak maximum occurs is lower if the internal friction is measured at a lower frequency	Frequency dependence of the δ peak temperature is not known. The dielectric peak below 4.2K is observed at a lower frequency when measurements are made at a lower temperature
For a given frequency the temperatures at which the peaks occur are only slightly affected by either the amount of cold work or the impurity content of the material	For any polymer, the temperature of the peak does not change with the amount of deformation or the presence of a comonomer

The similarity in experimental characteristics suggests that the δ peak may arise from a polymeric analogue of the Bordoni mechanism. The Bordoni peaks are believed to arise from motion of kinks in the dislocation segments between pinning points. Kinks in metallic dislocations are thought to be best represented by a smooth curve extending over many atomic distances rather than as an abrupt or discontinuous step. In crystalline polymers, interatomic forces are highly anisotropic compared to metals, with covalent bonds in the chain direction and non-bonded van der Waals interactions between chains. The geometry of a kink, whether abrupt or smooth, will be determined by the relative contributions of the intra- and inter-molecular forces. The abrupt kink model may be better suited for polymeric systems, than metallic ones, where the number of possible chain conformations is limited by restrictions on bond lengths and angles.

The abrupt kink model of the δ mechanism is similar to that proposed by Brailsford for the Bordoni peaks^{13, 18}.

It is based on the assumption that dislocations are present in crystalline polymers as a result of lattice deformation in the vicinity of local stresses. Non-uniform stresses may produce a dislocation with a Burgers vector having a component in the chain direction. In this case it is proposed that discontinuities or kinks are formed where sections of the dislocation are displaced in the chain direction (Figure 5). The kinks have an equilibrium distribution along the dislocation which corresponds to a minimum in the free energy. When an external stress is applied, the distribution changes and since the process is thermally activated, it gives rise to a relaxation.

The size and density of dislocations required to produce an observable relaxation can be calculated. Motion of a kink is approximated by a two state model for the re-orientation of the jogged chain segment at the edge of the kink. The jog is translated by the distance of one lattice spacing along the chain axis thus moving the kink one chain diameter along the dislocation. For a dislocation in PE with a Burgers vector in the *ac* plane, the logarithmic decrement is given by:

$$\Delta_{\max} \approx 50N_0^3 |\tan \theta|$$

The intensity is a function of three parameters: N , the dislocation density; l_0 , the mean dislocation length between pinning points; and θ which reflects the kink density in the dislocation (Figure 5). Since $|\tan \theta|$ changes by less than an order of magnitude for $10 \leq \theta \leq 40^\circ$, θ is arbitrarily chosen and the values of N and l_0 which give rise to an observable maximum in the logarithmic decrement calculated (Figure 6). If for example $l_0 = 40 \text{ \AA}$, a dislocation density of 10^{14} dislocations/cm³ would not be detectable while a density of 10^{15} would produce an observable relaxation.

The δ process may be a precursor to higher energy dislocation processes. The γ peak in both PE and POM contains a contribution from the crystalline phase which is attributed to molecules located near defects in the crystal¹⁹. Defect models for the crystalline γ component have been suggested for PE²⁰ and POM¹². The models are similar in that both propose motion of a dislocation over a Peierls barrier as the thermally activated process.

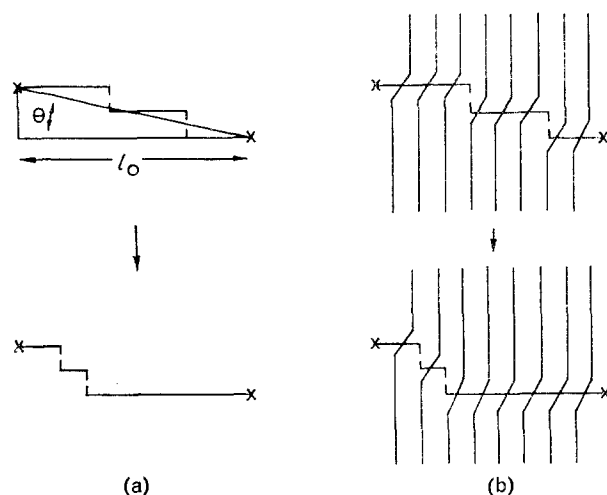


Figure 5 Redistribuition of kinks along a dislocation; (a) schematic representation, and (b) schematic including jogged chain segments. [Reproduced from Hiltner, A. and Baer, E. *Crit. Rev. Macromol. Sci.* 1972, 1, 215 by permission of The Chemical Rubber Company, Cleveland, Ohio ©]

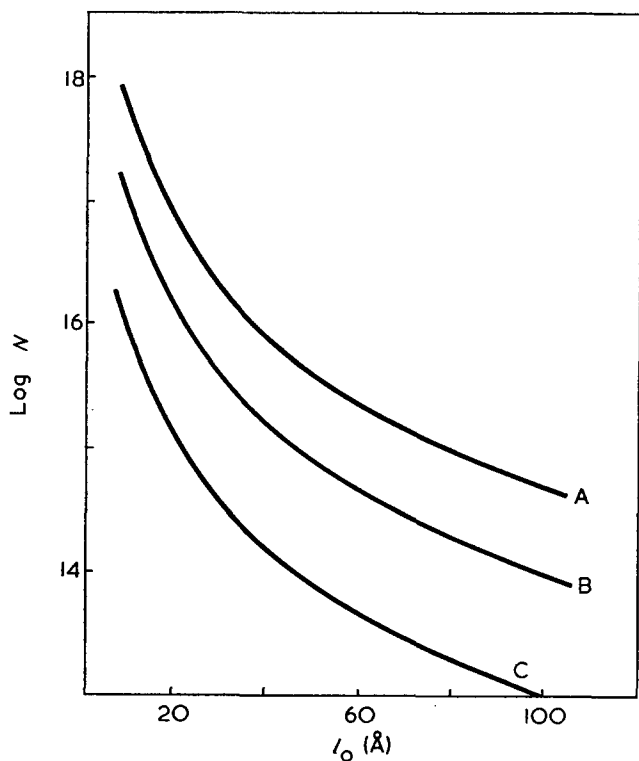


Figure 6 Relationship between l_0 the mean dislocation length and N the dislocation density: A, $\Delta_{\max}=5 \times 10^{-3}$; B, $\Delta_{\max}=10^{-3}$; C, $\Delta_{\max}=10^{-4}$. [Reproduced from Hiltner, A. and Baer, E. *Polym. J.* 1972, 3, 378 by permission of the Society of Polymer Science, Tokyo ©]

DEFORMATION AND FRACTURE AT LOW TEMPERATURES

It is well known that the high strain mechanical response of a polymeric material is strongly affected by both temperature and rate and, depending upon these parameters, may range from ductile yielding to brittle fracture. Deformation may also be accompanied by crazing or other morphological changes, again depending upon the temperature, rate and environment. The extent to which mechanical behaviour is influenced by secondary relaxation processes, which of course are also rate and temperature dependent, is not well understood. A simple correlation may not exist between relaxation measurements made at very low strains, in the region of linear viscoelastic response, and large deformation, yield and fracture studies which may be dominated by non-linear effects. Nevertheless there is growing evidence that the molecular and defect motions that give rise to secondary relaxations are also intimately related to transitions in solid state properties. Changes in impact strength, thermal expansion coefficients and tensile and compressive behaviour have been correlated with secondary relaxations. Such correlations are improved when differences in experimental time scales are compensated by means of temperature shift factors.

The high strength engineering polymers polycarbonate (PC) and poly(ethylene terephthalate) (PET), are distinctive in that they are ductile at temperatures considerably below the glass transition. These polymers both exhibit two secondary relaxation regions (γ and δ), and these relaxation regions have been found to coincide with transitions in tensile properties^{21, 22}. The vacuum stress strain curves of PET show considerable departure from

linearity above about 40K, which is the temperature region of the δ relaxation. Below this temperature the curves are very close to linear. Ductile behaviour is observed at temperatures considerably below room temperature, the onset of yielding occurs at about 200K or roughly the temperature of the γ relaxation.

Contact with nitrogen significantly alters the tensile behaviour in the region between 45 and 80K. Specimens tested under these conditions are heavily crazed, and the abrupt yielding is thought to be a consequence of craze nucleation and growth.

The transitions in tensile behaviour are most clearly seen when the maximum stress is plotted *versus* temperature (Figure 7). Several regimes of behaviour can be distinguished on the basis of the temperature dependence of the maximum stress and on failure type. The two commonly encountered regimes of 'brittle' and 'ductile' are apparent in the vacuum data. The brittle-ductile transition is indicated at about 160K by the intersection of the yield-stress and fracture-stress curves. Within the brittle regime (50 to 160K) the strain at fracture decreases with decreasing temperature but the fracture stress is approximately temperature independent. Such behaviour has been observed in other polymers and may be a general phenomenon.

There is a marked change in the temperature dependence of the brittle fracture stress at the δ relaxation. Below, the fracture stress decreases rapidly with decreasing temperature indicative that stress concentration effects are activated. This suggests that the molecular motions giving rise to the δ relaxation are also involved in the lowest temperature stress relief mechanism. Whether or not this mechanism also plays a role in nitrogen stress-crazing remains unresolved since the temperature region in which nitrogen is a liquid, and hence an effective stress crazing agent, is above the δ temperature.

Polycarbonate behaves in a manner similar to PET, with the difference that ductile behaviour extends down

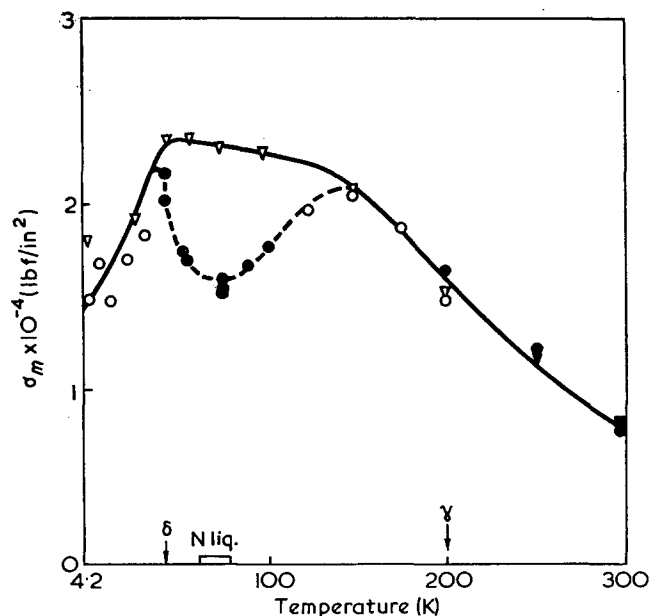


Figure 7 Temperature dependence of the poly(ethylene terephthalate) failure stress (maximum stress) in vacuum (∇) and in the presence of nitrogen (\circ). \bullet , indicates yield. [Reproduced from Kastelic, J. R. and Baer, E. *J. Macromol. Sci. (B)* 1973, 7, 679 by permission of Marcel Dekker, New York ©]

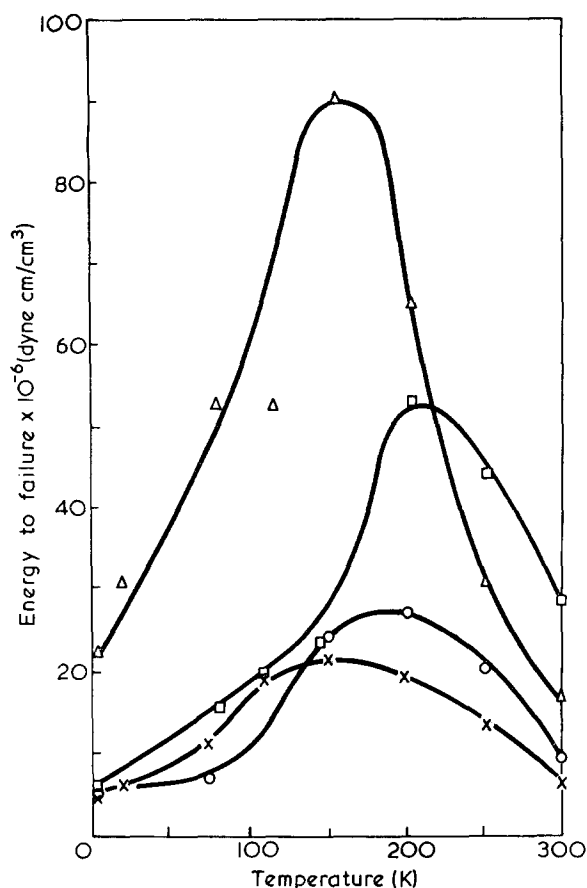


Figure 8 Energy to failure for amorphous polymers which yield below T_g showing correlation between toughness and damping: Δ , PCA; \square , CHDMT; \times , PET; \circ , PPO (solvent cast). [Reproduced from Roe, J. M. and Baer, E. *Int. J. Polym. Mat.* 1972, 1, 133 by permission of Gordon & Breach, New York ©]

to 78K, below the γ relaxation and close to the temperature of the δ relaxation. In this regard it would be noted that the δ relaxation region is broader and much more intense in PC than PET.

A low temperature brittle-ductile transition has been observed in other 'tough' amorphous polymers. These include poly(1,4-cyclohexylene dimethylene terephthalate) (CHDMT), a polyimide and poly(2,6-dimethyl phenylene oxide) (PPO)²³. In this case the energy to failure (area under stress strain curve at yield or fracture) has been plotted as a function of temperature (Figure 8). The transition from brittle fracture to ductile yielding coincides with the maximum in the energy curve. For each of these polymers, this transition is also in the temperature region of a major secondary relaxation (γ peak)²⁴. The conclusion is that backbone motions, which give rise to the γ peaks in these polymers, are also important in the macroscopic yielding process.

EFFECT OF CHAIN STRUCTURE

A γ peak in the region 100–200K is frequently observed in linear polymers with in-chain phenyl rings and no large pendant side groups. Examples include the 'tough' amorphous polymers discussed in the preceding section. The mechanisms involved in the γ process are not understood although it is generally agreed that restricted motion of small chain segments including the phenyl group is involved. Both amorphous and crystalline phases are believed to contribute to the overall magni-

tude of the γ process. In PET, the dynamic loss modulus and the dielectric decrement decrease linearly with decreasing amorphous content but do not extrapolate to zero at 100% crystallinity^{25, 26}.

Dynamic mechanical and dielectric studies of the γ process in PET have shown it to be composed of at least two peaks at 160 and 205K (1 Hz)^{10, 27–29}. These have been associated with *gauche* and *trans* glycol conformations respectively. Orientation of PET induces the *gauche* to *trans* conversion, where the amount of conversion depends on the conditions of the process rather than only the amount of orientation. A shift in the mechanical peak to higher temperature with orientation has been attributed to this increase in relative amount of *trans* isomer¹⁰. In a dielectric study of biaxially oriented PET the areas of the two component peaks were found to be in approximately the same ratio as the amount of *gauche* and *trans* isomers²⁹.

Further evidence that the two components of the γ peak are associated with the *gauche* and *trans* isomers is inferred from a dynamic mechanical study of a series of poly(methylene terephthalates), C_2 to C_{10} . With increasing number of carbon atoms in the glycol the temperature of the γ peak decreased and the asymmetry was reversed with the low temperature component becoming more intense³⁰. This has been attributed to the increased probability of *gauche* isomers as the number of methylene groups increases.

Direct evidence that the γ temperature of terephthalate polyesters depends on the geometry of the glycol is obtained from poly(1,4-cyclohexylene dimethylene terephthalate)³¹. In this case, non-interconvertible *cis* and *trans* isomers of the glycol are possible (Figure 9). Mechanical loss curves for the homopolymers show the γ peak at 175 and 210K for *trans* and *cis* respectively (Figure 10). The peaks are essentially symmetrical, which suggests a single dominant mechanism involving in part the glycol. The motion also appears to be very localized since the discrete contributions of *cis* and *trans* modes can be resolved in the asymmetric γ peak of a random copolymer (Figure 11).

The effect of crystallinity on the loss curves of the homopolymers is to decrease the intensity of the γ peak without changing the shape. Resolution of the composite γ peak of a crystalline specimen of the copolymer shows that only the *trans* component (175K) decreases in intensity. The blocks of *cis* or *trans* in the

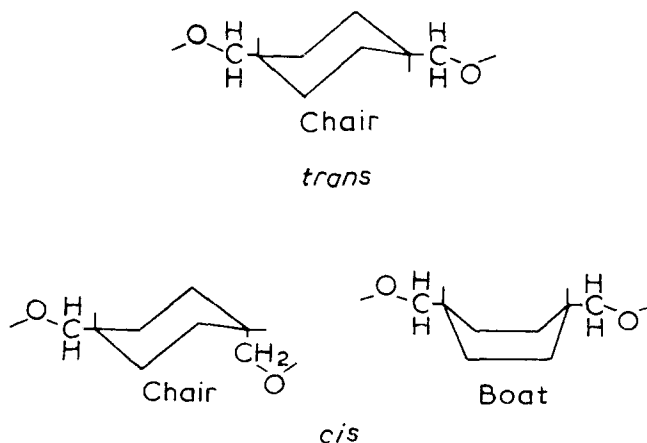


Figure 9 Possible conformations of the cyclohexane ring in PCT. [Reproduced from Hiltner, A. and Baer, E. *J. Macromol. Sci. (B)* 1972, 6, 545 by permission of Marcel Dekker, New York ©]

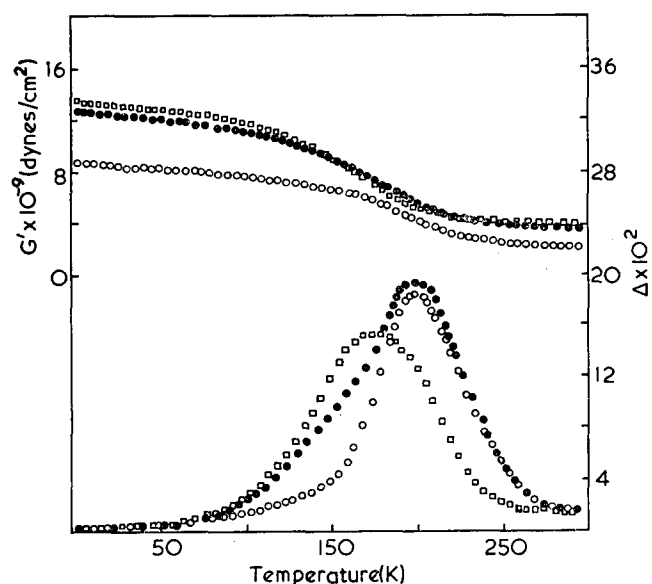


Figure 10 Effect of glycol configuration on the γ relaxation of PCT. \square , *trans*; \bullet , *trans/cis* 68:32; \circ , *cis*. [Reproduced from Hiltner, A. and Baer, E. *J. Macromol. Sci. (B)* 1972, 6, 545 by permission of Marcel Dekker, New York ©]

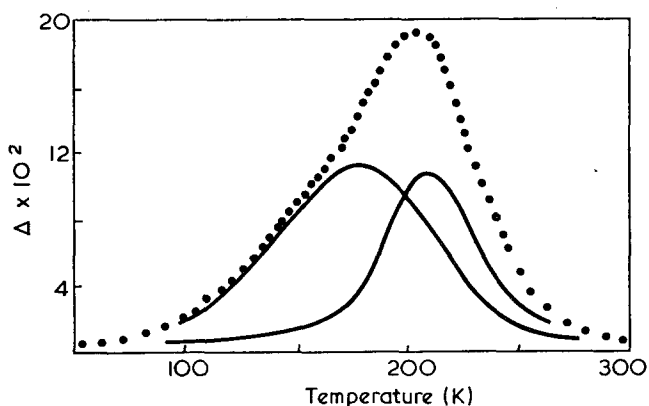


Figure 11 The γ relaxation of PCT (*trans/cis* 68:32) resolved into its components. [Reproduced from Hiltner, A. and Baer, E. *J. Macromol. Sci. (B)* 1972, 6, 545 by permission of Marcel Dekker, New York ©]

normal random distribution are not large enough to crystallize separately and it is assumed that the *cis* and *trans* units co-crystallize. Also, copolymers with as little as 15% *trans* isomer crystallize in a deformed *trans* crystal structure, the extent of deformation depending on the composition³². Taken together with the loss measurements, it appears that the *cis* units are present in the lattice as defects where their mobility is not greatly different from that in the amorphous state.

A similar approach, utilizing specific modification of molecular geometry, was employed in a study of vinyl-type polymers. The polymers of interest were two series of amorphous polyolefins, $-(\text{CH}_2)_m\text{C}(\text{CH}_3)_2-$ and $-(\text{CH}_2)_m\text{C}(\text{CH}_3)(\text{CH}_2\text{CH}_3)-$ where $m=1, 2, 3$ ³³. The intramolecular flexibility of the polymers in each series is varied by increasing the number of *in-chain* methylene units between substituted carbon atoms. Because of the absence of other structural variables such as polar forces, tacticity and crystallinity, the relaxation behaviour can be interpreted solely in terms of the molecular flexibility in the bulk state. The decrement

curves for the temperature region below the glass transition are shown in Figures 12 and 13. Two relaxation regions (γ and β) have been identified.

γ Region

Each member of the second series has one more secondary peak (γ) than the corresponding member of the first series. Polymers in the second series have an

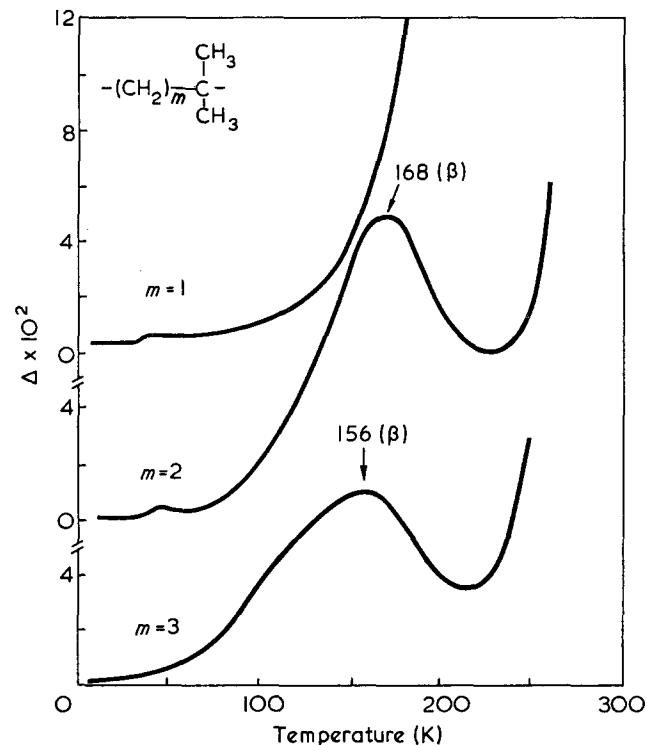


Figure 12 Relaxation behaviour of amorphous polyolefins, series 1. [Reproduced from Hiltner, A. *et al. J. Macromol. Sci. (B)* 1974, 9, 255 by permission of Marcel Dekker, New York ©]

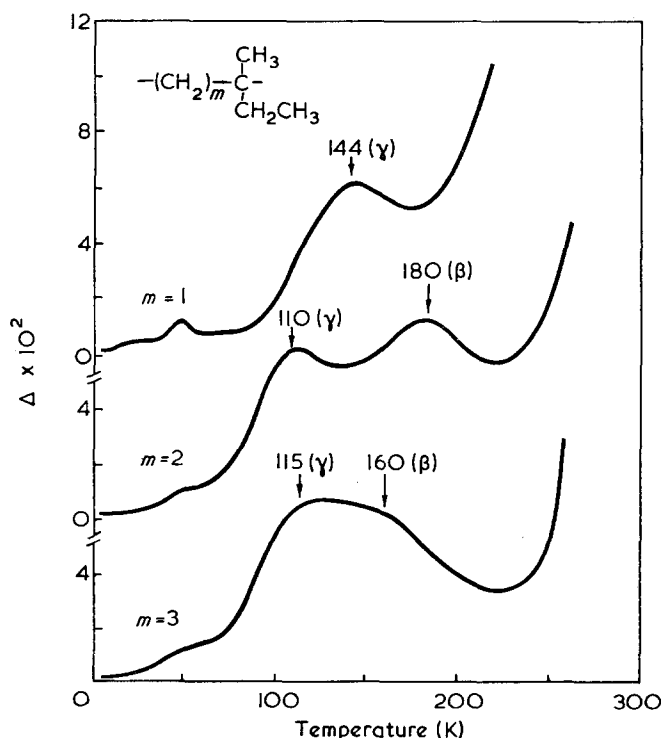


Figure 13 Relaxation behaviour of amorphous polyolefins, series 2. [Reproduced from Hiltner, A. *et al. J. Macromol. Sci. (B)* 1974, 9, 255 by permission of Marcel Dekker, New York ©]

ethyl side group, and the γ peak is attributed to re-orientation of this ethyl group. Members of the first series do not exhibit an analogous peak associated with the methyl side group. Extrapolation of wide-line n.m.r. data for the first member of the first series (polyisobutylene) predicts such a relaxation should be at about 95K at 1 Hz³⁴, but this is not observed. Other polyolefins with methyl side groups such as polypropylene and hydrogenated hevea also show no mechanical side group relaxation. The reason a methyl side group process is absent in mechanical measurements is not understood, although the symmetry of methyl group rotation may be important.

β Region

The second and third members of each series have one more secondary peak (β) than the first member. It is proposed that the β process is associated with restricted backbone motion. Although the formal crankshaft motion is forbidden in these polymers, certain minimum chain flexibility requirements must be necessary since the process is not observed in the first members of the series. The constant ratio T_β/T_g for all four polymers (Table 2) is further evidence that backbone motion is involved and suggests that the β process is a precursor to the glass transition. For example, the glass transition can be considered as a freeing of the localized β motions permitting the entire chain to move cooperatively. The existence of a β process where $T_\beta < T_g$ has been predicted on theoretical grounds³⁶, and it has been found empirically that for many polymers T_β/T_g is a constant³⁷. This relationship strongly supports the idea of a common glass transition mechanism.

The first members are exceptions to this generality in that no β process is observed. These polymers also exhibit anomalous glass transition temperatures. From considerations of intramolecular steric hindrance the first members would be expected to have the highest glass temperature. However, in both series the glass temperature of the first member is lower than that of the second and third members. This observation, together with the absence of the β process, suggests that a different glass mechanism is operative. For example, the molecular motion associated with the glass process may be very restricted, as indicated by the unusually low glass temperature and activation energy (Table 2). In this case, the barriers to motion over long chain

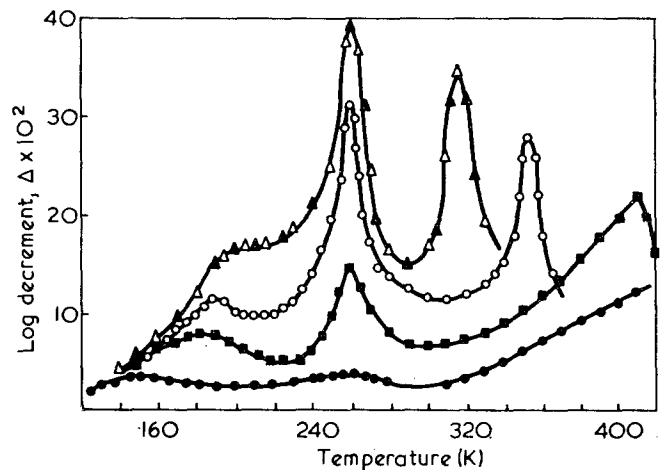


Figure 14 Effect of water content on the relaxation spectrum of human diaphragm tendon collagen (age, 30 years). ●, Dehydrated; ■, 10% H₂O; ○, 26% H₂O; ▲, native 35% H₂O; △, rehydrated 35% H₂O. [Reproduced from Baer, E. *et al. J. Macromol. Sci. (B)* 1972, 6, 761 by permission of Marcel Dekker, New York ©]

segments may not differ greatly from the barriers to local motion, and therefore the local processes would be observed at temperatures very close to the glass temperature. Similar considerations may also apply to other sterically hindered polymers with unusually low glass temperatures such as poly(vinylidene chloride) and poly(vinylidene fluoride).

It is of interest to extend these ideas to a discussion of the glass temperature in some highly crystalline polymers. Polyethylene does not have the steric hindrance of the first members of the polyolefin series and hence would be expected to exhibit a secondary relaxation. The lowest temperature *amorphous* relaxation in PE is the higher temperature component of the γ peak at 160K (1 Hz). If this is taken as T_β a glass transition would be predicted in the vicinity of 240K ($T_\beta/T_g=0.67$, 1 Hz) for amorphous PE. This coincides with the temperature of the so-called β peak observed in low density, branched PE. Also, if extrapolation of the constant T_β/T_g ratio to $m=\infty$ is valid, it indicates that T_g decreases only slightly with increasing values of m .

Like PE, polyoxymethylene has a complex γ relaxation with the higher temperature component (205K, 1 Hz) associated with the amorphous regions. Admittedly some modification of the empirical relationship between T_β and T_g may be appropriate for polymers without the C-C backbone. However, as described above, the relationship predicts the glass transition of POM to be around room temperature, possibly corresponding to the so-called β process at about 270K (1 Hz).

EFFECT OF WATER

The role of water in influencing the mechanical and physicochemical properties of fibrous proteins and related materials is clearly recognized but not well understood. Figure 14 illustrates the astounding effect that water has on the mechanical relaxation behaviour of tendon. Loss processes occur above (α) and below (β) the devitrification of water which are affected both in temperature position and intensity by the water content³⁸. These cannot be attributed independently to either the protein or water phase but may be a result of specific interactions which produce unique structures

Table 2 Relaxation temperatures (K) for amorphous polyolefins

Polymer	M_v^*	T_g^*	T_β	T_γ	T_β/T_g	
CH ₃	$m=1$	200 000	208	—	—	
-(CH ₂) _m -C-	$m=2$	30 000	22 kcal/mol	168	—	0.63
			48 kcal/mol	258	—	0.60
CH ₃	$m=3$	460 000	253	—	144	
-(CH ₂) _m -C-	$m=1$	18 500	28 kcal/mol	180	110	0.65
			44 kcal/mol	278	110	0.65
-(CH ₂) _m -C-	$m=2$	25 100	28 kcal/mol	160	115	0.62
			44 kcal/mol	258	115	0.62
CH ₂ CH ₃	$m=3$	268 000	258	160	115	0.62
-(CH ₂ CH ₂) _n	Poly-ethylene	—	240†	160†	—	0.67

* Ref 35

† Refer to text

with characteristic loss processes. Data obtained directly from protein-water systems are useful, but the chemical and organizational complexity of tendon-water³⁸⁻⁴⁰ and stratum corneum-water⁴¹ shows the need to investigate the interactions of water with less complex macromolecular systems.

It is well known that the relaxation spectra of many polar polymers exhibit features which can be associated with the presence of water. Polymers with the amide linkage are of particular interest in a discussion of the proteins. Two types of sorbed water have been postulated for nylon-6⁴². The 'tightly bound' water, about 2% by weight, is associated with a large decrease in the temperature of the α process, 362 to 317K, and the appearance of a β process at about 200K (Figure 15). Sorbed water in excess of 2%, up to about 8%, is termed 'loosely bound' water and has little additional effect on the relaxation behaviour.

Other model systems which have a closer structural resemblance to the proteins are the synthetic poly(α -amino acids). Below physiological temperature the low frequency relaxation spectra of dry poly(α -amino acids) are dominated by side group processes. Those with aliphatic side chains (alanine, valine, leucine) have a peak in the 120K region^{43, 44}, and derivatives of lysine (ϵ -carbobenzoxy) and glutamic acid (methyl and benzyl esters) have a side chain peak near room temperature⁴³. The local mode process which is observed at about 150K in almost all polymers with sequences of 3 or more methylene groups in the backbone, including nylon-4 and higher members of the nylon series, is absent or very weak in nylon-2 (polyglycine)^{38, 44}. This suggests that side groups, especially those with hydrophilic groups, may play an important role in determining the relaxation behaviour of proteins below physiological temperature.

Copolymers of L-leucine and L-glutamic acid show relaxation peaks which can be identified with specific side groups: the isobutyl group of leucine at 120K (1 Hz) and the glutamic acid side group at 278K⁴⁵. Water suppresses the side group processes while giving rise to a relaxation at about 175°K (β). In a 50% glutamic acid copolymer, the β peak increases in intensity up to about 1% water (approximately 1 water molecule to 15 peptide residues) (Figure 16). At higher water content

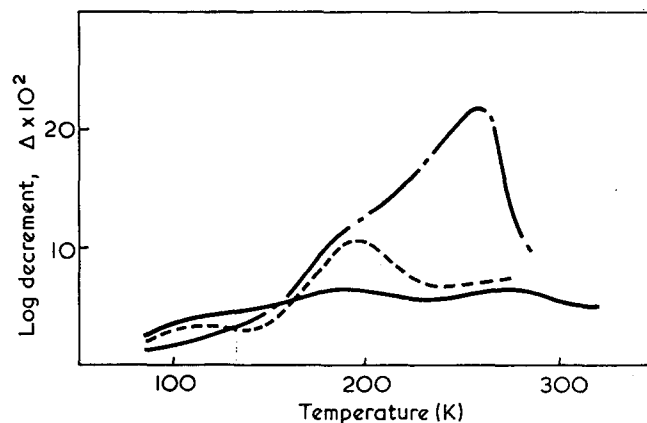


Figure 16 Effect of water content on the relaxation spectrum of a 50:50 glutamic acid/leucine copolymer. —, Dry; ----, 0.9% water; - · - ·, 27.8% water

Table 3 Relaxation temperatures (K) (1 Hz) for poly(α -amino acids), collagen and nylon-6

		T_γ	T_β	T_{H_2O}	T_α	Ref
Collagen	dry	—	—	—	450	38
	wet	—	200	260	315	
50:50 L-glutamic acid/L-leucine	dry	120, 278	—	—	—	45
	wet	—	180	260	—	
20:80 L-glutamic acid/L-leucine	dry	120, 278	—	—	—	45
	wet	120, 278	175	—	—	
Poly(L-leucine)	dry	120, (220)	—	—	—	45
	wet	120	175	—	—	
Nylon-6	dry	145	—	—	362	2, 47
	wet	125	190	—	317	

the intensity of the β remains constant and a broad devitrification peak is observed at about 260K.

Relaxation temperatures for the poly(α -amino acids) are compared with those of collagen and nylon-6 in Table 3. Experimentally, the β process appears initially with water sorption, is difficult to remove completely, and the intensity remains constant above a certain water content. This implies that water molecules occupying a specific number of high energy sites are involved, and the β process has been associated with 'tightly bound' water. The β process observed in wet nylon-6 at about the same temperature is also associated with 'tightly bound' water. In nylon-6 the 'tightly bound' water is thought to form interchain hydrogen bonded bridges between two amide groups⁴⁶. The diffusion of the 'tightly bound' water molecules, accompanied by the breaking and reforming of 2 hydrogen bonds, is a suggested mechanism for the β process⁴⁷. A similar mechanism has been suggested to explain the ability of water to catalyse structural re-arrangements of glycine peptides in the solid state⁴⁸.

In the α -helical conformation the peptide is intramolecularly hydrogen bonded, and formation of peptide-water hydrogen bonds would necessitate that the peptide carbonyl be doubly hydrogen bonded. Polarized infra-red measurements have been interpreted to indicate at least partial hydrogen bond character to the water-peptide interaction in several α -helical poly(α -amino acids)^{49, 50}. However, the 'tightly bound' water sites which have been postulated with regard to the β relaxation in the copolymers may also involve peptide groups in non-helical regions, the carboxyl side groups, or other

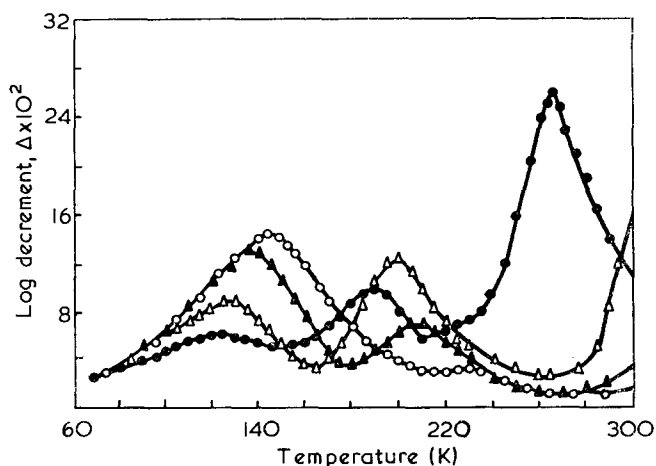


Figure 15 Differences in the magnitude of the α , β , and γ relaxations of rolled specimens of nylon-6 due to different amounts of adsorbed water: ○, 0%; ▲, 0.5%; △, 1.4%; ●, 8% water by wt. [Reproduced from Papir, Y. S. et al. *J. Polym. Sci. (A-2)* 1972, 10, 1305 by permission of John Wiley, New York ©]

water-peptide interactions such as dipolar interactions between water and α -helical peptide groups. The width of both the β and devitrification peaks also indicates that there is a spectrum of water-polymer interactions with the two predominate states represented by the 'tightly bound' and 'vitreous' water models.

REFERENCES

- 1 McCrum, N. G., Read, B. E. and Williams, G. 'Anelastic and Dielectric Effects in Polymeric Solids', Wiley, New York, 1967
- 2 Sauer, J. A. *J. Polym. Sci. (C)* 1971, **32**, 69
- 3 Hiltner, A. and Baer, E. *Crit. Rev. Macromol. Sci.* 1972, **1** 215
- 4 Irvine, J. D. and Work, R. N. *J. Polym. Sci. (Polym. Phys. Edn)* 1973, **11**, 175
- 5 McCammon, R. D., Saba, R. G. and Work, R. N. *J. Polym. Sci. (A-2)* 1969, **7**, 1721
- 6 Morgan, R. J., Nielsen, L. E. and Buchdahl, R. *J. Polym. Sci. (A-2)* 1971, **9**, 1915
- 7 Armeniades, C. D., Baer, E. and Rieke, J. K. *J. Appl. Polym. Sci.* 1970, **14**, 2635
- 8 Crissman, J. M., Woodward, A. E. and Sauer, J. A. *J. Polym. Sci. (A)* 1965, **3** 2693
- 9 Morgan, R. J., Nielsen, L. E. and Buchdahl, R. *Polym. Prepr.* 1971, **12**(2), 687
- 10 Armeniades, C. D. and Baer, E. *J. Polym. Sci. (A-2)* 1971, **9**, 1345
- 11 Papir, Y. S. and Baer, E. *J. Appl. Phys.* 1971, **42**, 4667
- 12 Papir, Y. S. and Baer, E. *Mat. Sci. Eng.* 1971, **8**, 310
- 13 Hiltner, A. and Baer, E. *Polym. J.* 1972, **3**, 378
- 14 Niblett, D. H. and Wilks, J. *Adv. Phys.* 1960, **9**, 1
- 15 Heybey, von O. and Muller, F. H. *Kolloid-Z. Z. Polym.* 1973, **251**, 383
- 16 Phillips, W. A. *Proc. R. Soc. (A)* 1970, **319**, 565
- 17 Hojfors, R. J. V., Baer, E. and Geil, P. H. *J. Macromol. Sci. (B)* 1974, in press
- 18 Brailsford, A. D. *Phys. Rev.* 1961, **122**, 778
- 19 Sauer, J. A., Richardson, G. C. and Morrow, D. R. *J. Macromol. Sci. (C)* 1973, **9**, 149
- 20 Matsui, M., Masui, R. and Wada, Y. *Polym. J.* 1971, **2**, 134
- 21 Kastelic, J. R. and Baer, E. *J. Macromol. Sci. (B)* 1973, **7** 679
- 22 Hiltner, A., Kastelic, J. R. and Baer, E. 'Advances in Polymer Science and Engineering', (Ed. K. D. Pae), Plenum Press, New York, 1972, p 335
- 23 Roe, J. M. and Baer, E. *Int. J. Polym. Mat.* 1972, **1**, 133
- 24 Roe, J. M. and Baer, E. *Int. J. Polym. Mat.* 1972, **1**, 111
- 25 Takayanagi, M., Yoshino, M. and Minami, S. *J. Polym. Sci.* 1962, **61**, 57
- 26 Ishida, Y., Yamafuji, K., Ito, H. and Takayanagi, M. *Kolloid-Z.* 1962, **184**, 97
- 27 Frosini, V. and Woodward, A. E. *J. Macromol. Sci. (B)* 1969, **3**, 91
- 28 Illers, K. H. and Breuer, H. *J. Colloid. Sci.* 1963, **18**, 1
- 29 Sacher, E. *J. Polym. Sci. (A-2)* 1968, **6**, 1935
- 30 Farrow, G., McIntosh, J. and Ward, I. M. *Makromol. Chem.* 1960, **38**, 147
- 31 Hiltner, A. and Baer, E. *J. Macromol. Sci. (B)* 1972, **6**, 545
- 32 Boye, C. A. *J. Polym. Sci.* 1961, **55**, 275
- 33 Hiltner, A., Baer, E., Martin, J. R. and Gillham, J. K. *J. Macromol. Sci. (B)* 1974, **9**, 255
- 34 Slichter, W. P. *J. Chem. Educ.* 1970, **47**, 193
- 35 Martin, J. R. and Gillham, J. K. *J. Appl. Polym. Sci.* 1972, **16**, 2091
- 36 Goldstein, M. *J. Chem. Phys.* 1969, **51**, 3728
- 37 Matsuoka, S. and Ishida, Y. *J. Polym. Sci. (C)* 1966, **14**, 247
- 38 Baer, E., Kohn, R. and Papir, Y. S. *J. Macromol. Sci. (B)* 1972, **6**, 761
- 39 Chien, J. C. W. and Chang, E. P. *Biopolymers* 1972, **11**, 2015
- 40 Stefanou, H., Woodward, A. E. and Morrow, D. *Biophys. J.* 1973, **13**, 772
- 41 Wilkes, G. L. and Wildnauer, R. *Biochim. Biophys. Acta* 1973, **304**, 276
- 42 Papir, Y. S., Kapur, S., Rogers, C. E. and Baer, E. *J. Polym. Sci. (A-2)* 1972, **10**, 1305
- 43 Hiltner, A., Anderson, J. M. and Borkowski, E. *Macromolecules* 1972, **5**, 446
- 44 Krug, R. R. and Gillham, J. K. *J. Appl. Polym. Sci.* 1973, **17**, 2089
- 45 Hiltner, A., Anderson, J. M. and Baer, E. *J. Macromol. Sci. (B)* 1973, **8**, 449
- 46 Puffr, R. and Sebenda, J. *J. Polym. Sci. (C)* 1967, **16**, 79
- 47 Kapur, S., Rogers, C. E. and Baer, E. *J. Polym. Sci. (Polym. Phys. Edn)* 1972, **10**, 2297
- 48 Chirgadze, Yu. N. and Ovsepyan, A. M. *Biopolymers* 1972, **11**, 2179
- 49 Baddiel, C. B., Breuer, M. M. and Stephens, R. *J. Colloid Interface Sci.* 1972, **40**, 429
- 50 Malcolm, B. R. *Nature* 1970, **227**, 1358

Note to the Editor

Bound rubber and vulcanizate properties

C. M. Blow

Institute of Polymer Technology, Loughborough University, Loughborough, Leics LE11 3TU, UK

(Received 14 August 1974)

In a recent review of the bound rubber phenomena¹, discussion of the contribution of bound rubber to the vulcanizate properties was omitted. Recently Brennan and Lambert² postulated that the curing ingredients in a mix containing fine particle black will have a higher concentration in the unbound rubber than in the bound rubber and developed this to account for the lower swelling of reinforced vulcanizates. Whereas these authors allowed for an increase in bound rubber during the induction period of vulcanization, they did not refer to the increase that takes place during the storage in the unvulcanized state of many mixes. By inference, owing to this storage effect, the vulcanizing ingredients must migrate from the bound rubber as it is formed. The investigation reported in this note follows up this suggestion.

Because the bound rubber content of some mixes increases on storage, it is possible to prepare a series of vulcanizates differing only in the amount of bound rubber present immediately before vulcanization. The uncertainty remains, however, that the bound rubber content will change during the heating which is applied to bring about the crosslinking. This can be taken care of, at least partly, by having a control mix, containing no vulcanizing ingredients, subjected to storage and heat treatment identical to that given to the vulcanizable mix.

Two mixes were prepared using the blended pre-masticated natural rubber batches 2 and 3 referred to in Table 8 of the previous publication¹. Twenty parts, by weight, of HAF-HS black per hundred of rubber were added (mix U); to half the batch vulcanizing ingredients were added: zinc oxide 5, stearic acid 1, sulphur 2.5, CBS 1 phr (mix V). Within 20 min of the completion of the mixing, samples were immersed in

toluene in which they were completely soluble. At the same time, 20 g blanks of each mix, measuring approximately 40 × 40 × 12 mm were pressed out to sheets 135 × 135 × 1 mm between Melinex in a mould between steam heated platens for 10 min at 150°C. Mix V gave a well-cured product. This moulding procedure was repeated on samples of mixes U and V which had been stored in the dark for three periods of time. In addition, one sheet of mix U was reheated (still encased in its Melinex sheets) in the press for 10 min at 150°C, 14 days after the original heating.

Bound rubber determinations of mix U after storage and/or heating and of mix V after storage were made by immersing small samples in toluene (1:25 by vol) for 72 h; equilibrium was substantially reached in this time with no change of solvent; the result is expressed as the percentage of the original rubber retained in the jelly. Swelling tests on the four vulcanizates of mix V were carried out in toluene to equilibrium (also reached in 72 h), approximately 2% of solubles being extracted; the results are expressed as v_r , the volume fraction of polymer in the jelly (polymer and toluene), i.e. correcting for the presence of black and zinc oxide.

To reduce the extent of flow that occurred during the moulding procedure, one sheet of mix V was produced from six blanks approximately 23 × 23 × 6 mm spaced over the cavity area. Furthermore, replicate samples for bound rubber and swelling determinations were taken from various positions in the sheets.

The increase in bound rubber on storage of both mixes is similar (*Table 1*). Heating of the fresh batch of mix U led to the development of some bound rubber not detectable in the unheated mix, but flowing and heating of the stored mix reduced the bound rubber content, and, indeed, the value did not increase to that

Table 1 Bound rubber contents (%) and (gel rigidity/solution colour)

Time lapse between mixing/heating and testing (days)	Vulcanizing mix V original batch	Non-vulcanizing mix U				
		1 Original batch	2 Heated on same day	3 Heated 14 days after mixing	4 Sheet 3 reheated 14 days later	5 Heated 28 days after mixing
<2h	0	0	11.8 (2/4)	23.2 (6/2)	21.1 (6/2)	17.8 (6/2)
7	—	—	—	—	22.4 (5/1)	—
14	*	*	22.8 (5/2)	21.2 (5/1)	—	25.2 (6/2)
28	—	29.0 (5/2)	—	—	—	—
35	44.2 (7/1)	46.9 (6/1)	23.2 (7/1)	—	—	—
42	56.0 (7/1)	54.5 (7/1)	—	—	—	—
70	—	—	—	—	24.2 (7/1)	25.2 (7/1)
98	—	—	23.0 (7/1)	—	—	26.8 (7/2)†

* Jelly not satisfactorily separable from the solution

† Mean of five testpieces from different positions in sheet; all results within ±1.3 of this value

Table 2 Swelling values of vulcanizates of mix V (v_r =volume fraction of polymer in swollen jelly)

Time lapse between moulding and testing (days)	Days storage between mixing and moulding			
	0	14	28	49
0	214	—	234	—
7	—	—	—	230*
21	—	234	—	—
28	—	—	236	—
35	233	—	—	—
42	—	238	—	—
56	237	—	—	—
77	—	—	—	234†

* Result from sheet moulded from one blank identical with that from sheet moulded from six blanks

† Mean of 10 testpieces from different positions in the sheets moulded from one and six blanks; all results within ± 2 of this value

between cold platens failed, not unexpectedly, to produce thin sheets; the rubber retracted to nearly its original shape on removal of the pressure. Bound rubber determinations carried out immediately on the pressed and unpressed mixes showed no significant difference.

The swelling results show remarkable consistency (Table 2) with any differences in the v_r values being barely significant, with the exception of the value on the vulcanizate made from the freshly mixed rubber. Furthermore no marked lack of uniformity was shown in the v_r results from different parts of the sheet, and no difference between the sheets from one and six blanks.

As a further check, stress-strain data were obtained for the four vulcanizates using the relaxed modulus tester, described by Loo³. It is to be noted, from the results given in Table 3, that the stored mixes give lower modulus vulcanizates, the % difference decreasing as the strain is increased; it can be expected that swelling—corresponding to a linear strain of 160%—would show less effect on storage.

It is concluded from the results presented here that there is no correlation between the amount of bound rubber present immediately before vulcanization (varying from less than 10% to, perhaps, 50%) and the extent of swelling of the vulcanizate in toluene. This conclusion, moreover, casts doubt on the hypothesis of Brennan and Lambert and emphasizes their neglect of the storage effects associated with bound rubber. It does not rule out the reasonable conclusion that both phenomena are manifestations of a similar polymer/filler interaction.

Table 3 'Modulus' values of vulcanizates (MPa)

	Storage between mixing and moulding (days)				% Difference (1-4)/4
	0	14	28	49	
	Storage between moulding and testing (days)				
	140 (1)	126 (2)	112 (3)	92 (4)	
Stress at 10%	0.36	0.33	0.31	0.29	23
50%	1.05	1.00	0.98	0.97	8.5
100%	1.75	1.69	1.69	1.64	7.0

found in the untouched mix. Assessment of gel rigidity and the black content of the solution are given in the Table, using the same coding as before¹. Pressing blanks of the two mixes which had been stored for some weeks

REFERENCES

- 1 Blow, C. M. *Polymer* 1973, 14, 309
- 2 Brennan, J. J. and Lambert, D. H. *Rubber Chem. Technol.* 1972, 45, 94
- 3 Loo, C. T. *Polymer* 1974, 15, 357

Letter

¹³C n.m.r. spectra of polybutadienes : 2

Introduction

In the past twenty years much attention has been devoted to the spectroscopic characterization of polybutadienes, both by i.r.¹, ¹H n.m.r.^{2,3} and ¹³C n.m.r. spectroscopy⁴⁻⁷.

The problem of a quantitative analysis of *cis*, *trans* and 1,2-content was first resolved¹, but there are only few results^{2,3} with regard to the distribution of the various units characterizing the polymer microstructure.

A quantitative analysis of the *cis*-1,4- and *trans*-1,4-monomeric unit distribution was made on the basis of the ¹³C spectra of equibinary polybutadienes⁷, and of isomerized *cis*-1,4-polybutadiene⁶.

Owing to the usefulness of this approach to these polymers we decided to extend this type of analysis to polybutadienes prepared with different catalysts, resulting in mixed 1,2/1,4-microstructures.

Experimental

The experimental conditions for the ¹³C n.m.r. spectra were as previously reported⁷.

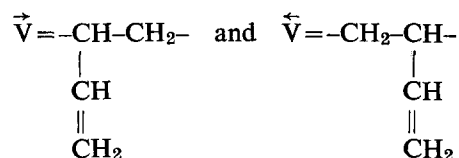
The polybutadiene, composed of 1,2- and *cis*-1,4-units, was prepared using the catalyst system AlEt₃-V(acac)₃¹³.

Experimental conditions: AlEt₃, 0.023 ml; V(acac)₃, 0.72 × 10⁻³ mol; benzene, 40 ml; butadiene, 15 g; polymerization temperature, 20°C; polymerization time, 24 h. The catalyst was aged for 2 min before the introduction of the monomer. The crude polymer was extracted with boiling diethyl ether and then with boiling benzene. ¹³C n.m.r. examination was performed on the fraction extracted with benzene. I.r. analysis: 85% 1,2- the remaining units being *cis*-1,4-. The fraction exhibited crystallinity typical of syndiotactic 1,2-polybutadiene.

The atactic 1,2-polybutadiene was prepared using n-BuLi in THF. Experimental conditions: n-BuLi, 0.42 ml; THF, 42 ml; butadiene, 6 g. ¹³C n.m.r. examination was carried out on the crude polymer, whose i.r. analysis was as follows: 94% 1,2-; 6% *trans*-1,4-.

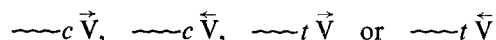
Possible triads in polybutadienes

The addition of a butadiene monomeric unit to a polymeric chain in growth can give rise to a 1,4- or a 1,2-unit. In the case of 1,4-addition the butadiene unit can be in a *cis* or *trans* configuration. If the growing polymer chain ends with a 1,4-unit the addition of a 1,2-unit can result in two different ways. Using the notation:

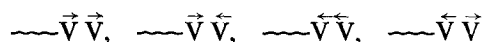


and *c* and *t*, for the 1,4-units respectively in a *cis* or

trans configuration, the addition can take place in the following ways:



If the chain ends with a 1,2-unit, the addition of another 1,2-unit can take place, in principle, in the following ways:



The great sequential multiplicity which can result from the different possible combinations in terms of triads is therefore evident. The number of possible triads is 4³=64, i.e. 4 units *c*, *t*, \vec{V} and \overleftarrow{V} , 3 at a time, in all possible dispositions, each of which will give rise to two resonances in the aliphatic portion of the spectrum.

Clearly these two resonances might or might not be different depending on the symmetry.

The number of possible triads is, however, reduced to 50 if we exclude the presence of diads $\vec{V}\overleftarrow{V}$ and $\overleftarrow{V}\vec{V}$, which seems reasonable in view of the fact that head-to-head and tail-to-tail placements are practically non-existent in regular polybutadienes prepared by transition metal catalysts⁸.

Calculation of the backbone ¹³C chemical shifts

All the central units of possible triads gave rise to two n.m.r. signals, corresponding to the saturated carbon atoms of the backbone.

The assignment of different resonance signals to the

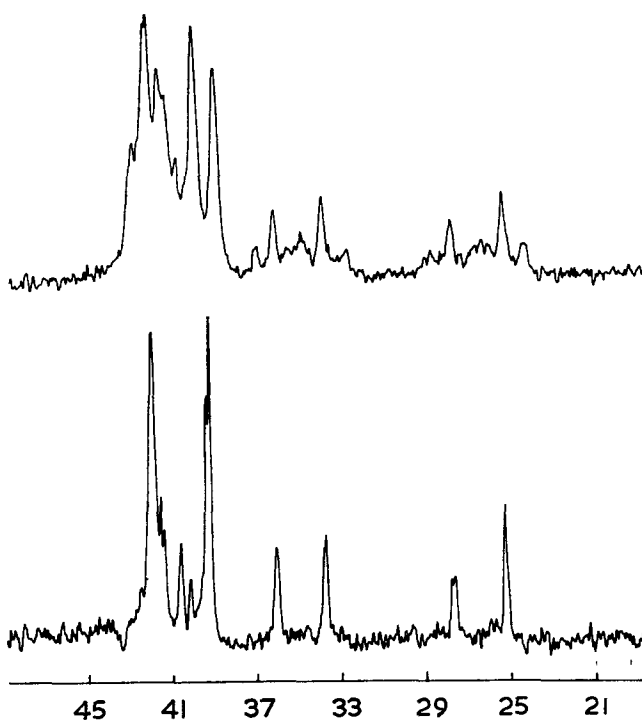


Figure 1 Aliphatic portion of the spectrum of polybutadiene containing 85% 1,2-units and 15% *cis*-1,4-units. Upper, off resonance decoupled; lower, noise decoupled

possible sequences has been done either by direct comparison with regular polymer, or by calculating the chemical shifts relative to various groups according to additivity rules⁹, i.e. adding the contribution relative to α , β and γ positions.

Contributions relative to position δ , ϵ ... have been neglected¹⁰. Clearly no steric effect can be kept in consideration with this type of approach. Values for α , β and γ contributions to the *cis* and *trans* double bonds in the backbone were obtained by Roberts *et al.*¹¹ and are consistent with the spectra of regular 1,4-polymers⁴, as well as with the spectrum of 'equibinary' polybutadienes⁷. Thus, these values can be accepted without any criticism. In order to get the vinyl group contribution, if model compounds with a vinyl, such as 1-octene, 1-heptene etc. are used, the calculated values for the spectra relative to 1,2-polybutadiene show a very poor fit. Thus it was necessary to get the vinyl contribution from the polymer spectra themselves. For this purpose a polymer containing 85% 1,2-units and 15% 1,4-*cis* units was used. The aliphatic portion of the spectrum (noise decoupled from protons as well as decoupled in off resonance condition) is shown in Figure 1. The peak at 27.4 ppm is attributed to *cis*-1,4- sequences by comparison with the *cis*-1,4-regular polymer⁴. If we admit that the γ contribution of a vinyl is negative, and the α and β contributions are positive¹¹, we can attribute the peak at ~25 ppm as due to the γ effect of a vinyl on the CH₂ of a *cis*-1,4-unit. In this way it is easy to get the γ vinyl contribution. The α and β contribution can be obtained from the spectrum of atactic 1,2-polybutadiene. As a check on the obtained values, all the other peaks of the 85% 1,2-/15% *cis*-1,4 sample can be used; more-

over a reasonable agreement with all the observed peaks in a n-BuLi 1,2-polybutadiene (Figure 2) has been observed.

Branching corrections, as indicated by Grant and Paul⁹ were added; the polyethylene chemical shift,

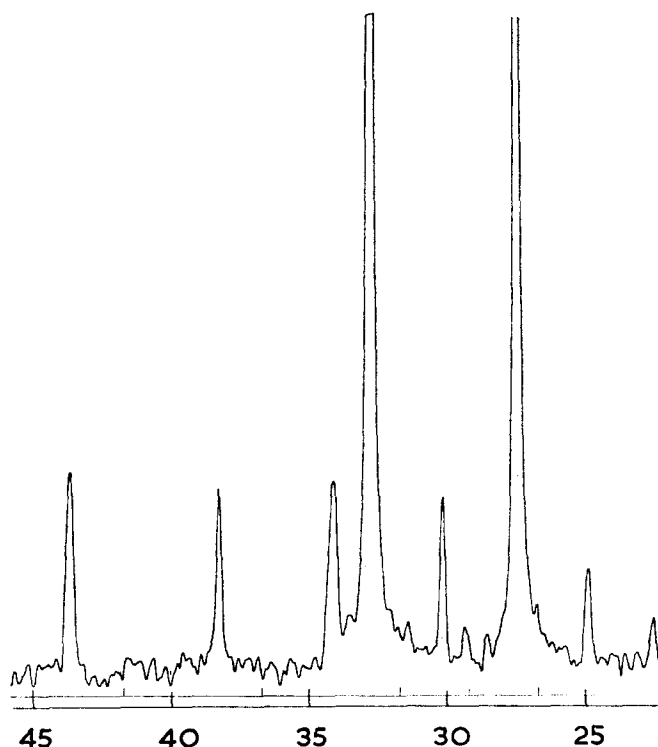


Figure 2 Aliphatic portion of the spectrum of n-BuLi catalysed polybutadiene

Table 1 Experimental and calculated ¹³C chemical shifts of some polybutadienes

Line number	Calculated frequency	Sequence attribution (C ₁ is on the left, C ₂ is on the right side of central unit, tertiary carbon atoms with *)	Exp. frequencies (ppm) from TMS		
			Polybutadiene n-BuLi	Polybutadiene <i>cis</i> -1,4-/1,2- (syndiotactic) in C ₆ D ₆	Polybutadiene as in ref 12
1	25.0	$\vec{V}cc(C_1), \vec{V}ct(C_1), \vec{V}c\vec{V}(C_1), \vec{V}c\vec{V}(C_2), \vec{V}c\vec{V}(C_1, C_2), cc\vec{V}(C_2), tc\vec{V}(C_2)$	24.94	25.21	~25.0
2	27.4	$ccc(C_1, C_2), tcc(C_1, C_2), tct(C_1, C_2) cct(C_1, C_2), \vec{V}cc(C_2), \vec{V}cc(C_2), \vec{V}ct(C_2), \vec{V}ct(C_2), cc\vec{V}(C_1), cc\vec{V}(C_1), tc\vec{V}(C_1), tc\vec{V}(C_1)$	27.44	27.58	~27.4
3	30.5	$\vec{V}tt(C_1), \vec{V}tc(C_1), \vec{V}t\vec{V}(C_2), \vec{V}t\vec{V}(C_1), \vec{V}t\vec{V}(C_1, C_2), tt\vec{V}(C_2), ct\vec{V}(C_2)$	30.15		~30.3
4	32.9/33.3	$ttt(C_1, C_2), ttc(C_1, C_2), ctt(C_1, C_2), ctc(C_1, C_2), \vec{V}tc(C_2), \vec{V}tc(C_2), \vec{V}tt(C_2), \vec{V}tt(C_2), tt\vec{V}(C_1), tt\vec{V}(C_1), ct\vec{V}(C_1), ct\vec{V}(C_1)/\vec{V}cc(C_1), \vec{V}ct(C_1) \vec{V}c\vec{V}(C_1), \vec{V}c\vec{V}(C_2), \vec{V}c\vec{V}(C_1, C_2), cc\vec{V}(C_2), tc\vec{V}(C_2)$	32.73	33.59	~32.6/~33.2
5	35.3	$c\vec{V}c, c\vec{V}c, c\vec{V}t, c\vec{V}t, t\vec{V}c, t\vec{V}c, t\vec{V}t, t\vec{V}t$	34.13	33.67	~34.0
6	35.8	$c\vec{V}\vec{V}, t\vec{V}\vec{V}, \vec{V}\vec{V}c, \vec{V}\vec{V}t$		35.93	~35.5
7	38.6	$\vec{V}\vec{V}\vec{V}^*, \vec{V}\vec{V}\vec{V}^*$		39.02	~38.6
8	38.8	$\vec{V}tt(C_1), \vec{V}tc(C_1), \vec{V}t\vec{V}(C_1), \vec{V}t\vec{V}(C_2), \vec{V}t\vec{V}(C_1, C_2), tt\vec{V}(C_2), ct\vec{V}(C_2)$	38.23	39.16	~39.5
9	40.5	$c\vec{V}\vec{V}^*, t\vec{V}\vec{V}^*, \vec{V}\vec{V}c^*, \vec{V}\vec{V}t^*$		40.41	~39.9
10	41.0	$c\vec{V}\vec{V}^*, t\vec{V}\vec{V}^*, \vec{V}\vec{V}c^*, \vec{V}\vec{V}t^*$		41.19	
11	41.2	$c\vec{V}\vec{V}, t\vec{V}\vec{V}, \vec{V}\vec{V}c, \vec{V}\vec{V}t$		41.34	~40.8
12	41.7	$\vec{V}\vec{V}\vec{V}, \vec{V}\vec{V}\vec{V}$		41.71	~41.1
13	42.9	$c\vec{V}c^*, c\vec{V}c^*, c\vec{V}t^*, c\vec{V}t^*, t\vec{V}c^*, t\vec{V}c^*, t\vec{V}t^*, t\vec{V}t^*$	43.62	43.00	~43.2

Letter

29.9 ppm from TMS was chosen as a reference, in which all CH₂ contributions must be considered nil.

The values for the contributions (all in ppm) are:

Polyethylene chemical shift	29.9 ppm
Correction for CH (tertiary saturated)	$\alpha = -2.5$ $\beta = 0$ $\gamma = 0$
Contribution for <i>cis</i> double bond	$\alpha = -2.5$ $\beta = 0$ $\gamma = -0.5$
Contribution for <i>trans</i> double bond	$\alpha = 3.0$ $\beta = 0$ $\gamma = -0.5$
Contribution for a vinyl	$\alpha = 13.5$ $\beta = 8.4$ $\gamma = -2.4$

Hence it is possible to calculate the values of chemical shifts relative to different carbon atoms in the different triads, and these values can be compared with the peaks experimentally observed (see *Table 1*).

In *Table 1* are reported the values obtained for a sample containing only 1,2- and *cis*-1,4-units. It can be observed that the experimental frequencies and the calculated ones correspond very well.

A recent paper by Furukawa *et al.*¹² reports the ¹³C n.m.r. spectrum of a so-called 'equibinary' 1,2/*cis*-1,4-polybutadiene. It is noticeable that none of the experimental peaks have the same chemical shift of previously reported spectra of polybutadienes in the same solvent^{4, 5, 7}; however, it is remarkable that this apparent disagreement disappears by shifting 1.2 ppm upfield all the reported peaks. In this way the spectrum of this polymer shows a perfect agreement both with our observations and with other spectra in the literature. Moreover, the peak labelled 'd' in ref 12 has exactly the chemical shift of *trans*-1,4-polybutadiene, as can be seen in *Table 1*; according to this observation and also

the calculated values, an assignment of all the resonance peaks is reported for the experimental spectrum of ref 12.

Finally, the spectrum of a n-BuLi polybutadiene is also reported in *Table 1*. The spectrum does not differ substantially from previously reported data⁵, except for the better resolution (*Figure 2*). The assignment of all the experimental peaks is also shown.

F. Conti, M. Delfini and A. L. Segre

*Istituto Chimico,
Università di Roma,
00185 Roma, Italy*

D. Pini

*Istituto di Chimica Organica Industriale,
Università di Pisa, Pisa, Italy*

and L. Porri

*Istituto Chimica Industriale del Politecnico,
20133 Milano, Italy
(Received 2 July 1974; revised 2 October 1974)*

References

- 1 Morero, D., Santambrogio, A., Porri, L. and Ciampelli, F. *Chim. Ind.* 1959, **41**, 758
- 2 Santee, E. R., Chang, R. and Morton, M. *J. Polym. Sci. (Polym. Lett. Edn)* 1973, **11**, 449
- 3 Santee, E. R., Mochel, V. D. and Morton, M. *ibid.* 1973, **11**, 453
- 4 Duch, M. W. and Grant, D. M. *Macromolecules* 1970, **3**, 165
- 5 Mochel, V. D. *J. Polym. Sci. (A-1)* 1972, **10**, 1009
- 6 Elgert, K. F., Stützel, B., Frenzel, P., Cantow, H. J. and Streck, R. *Makromol. Chem.* 1973, **170**, 257
- 7 Conti, F., Segre, A. L., Pini, D. and Porri, L. *Polymer* 1974, **15**, 5
- 8 Natta, G. and Corradini, P. *Nuovo Cimento* 1960, **15**, Suppl. 1, 9
- 9 Grant, D. M. and Paul, E. G. *J. Am. Chem. Soc.* 1964, **86**, 2984
- 10 Lindeman, L. P. and Adams, J. C. *Analyt. Chem.* 1971, **43**, 1245
- 11 Dorman, D. E., Jautelat, M. and Roberts, J. D. *J. Org. Chem.* 1971, **36**, 2557
- 12 Furukawa, J., Kobayashi, E., Katsuki, N. and Kawagoe, T. *Makromol. Chem.* 1974, **175**, 237

ERRATA

'Chain conformation in molten polyethylene by low angle neutron scattering' by J. Schelten, G. D. Wignall and D. G. H. Ballard, *Polymer* 1974, **15**, 682-685.

Page 683, *Figure 3*, caption:
for PEN read PED

Page 683, *Table 1*, caption:
for PEG read PEH

Page 684, right hand column, 8 lines below *Table 3* should read:

$$(1/K_N C) d\Sigma/d\Omega(k) \text{ at } k=0 \text{ etc.}$$

We apologize for these errors.

Letter

29.9 ppm from TMS was chosen as a reference, in which all CH₂ contributions must be considered nil.

The values for the contributions (all in ppm) are:

Polyethylene chemical shift	29.9 ppm
Correction for CH (tertiary saturated)	$\alpha = -2.5$ $\beta = 0$ $\gamma = 0$
Contribution for <i>cis</i> double bond	$\alpha = -2.5$ $\beta = 0$ $\gamma = -0.5$
Contribution for <i>trans</i> double bond	$\alpha = 3.0$ $\beta = 0$ $\gamma = -0.5$
Contribution for a vinyl	$\alpha = 13.5$ $\beta = 8.4$ $\gamma = -2.4$

Hence it is possible to calculate the values of chemical shifts relative to different carbon atoms in the different triads, and these values can be compared with the peaks experimentally observed (see *Table 1*).

In *Table 1* are reported the values obtained for a sample containing only 1,2- and *cis*-1,4-units. It can be observed that the experimental frequencies and the calculated ones correspond very well.

A recent paper by Furukawa *et al.*¹² reports the ¹³C n.m.r. spectrum of a so-called 'equibinary' 1,2/*cis*-1,4-polybutadiene. It is noticeable that none of the experimental peaks have the same chemical shift of previously reported spectra of polybutadienes in the same solvent^{4, 5, 7}; however, it is remarkable that this apparent disagreement disappears by shifting 1.2 ppm upfield all the reported peaks. In this way the spectrum of this polymer shows a perfect agreement both with our observations and with other spectra in the literature. Moreover, the peak labelled 'd' in ref 12 has exactly the chemical shift of *trans*-1,4-polybutadiene, as can be seen in *Table 1*; according to this observation and also

the calculated values, an assignment of all the resonance peaks is reported for the experimental spectrum of ref 12.

Finally, the spectrum of a n-BuLi polybutadiene is also reported in *Table 1*. The spectrum does not differ substantially from previously reported data⁵, except for the better resolution (*Figure 2*). The assignment of all the experimental peaks is also shown.

F. Conti, M. Delfini and A. L. Segre

*Istituto Chimico,
Università di Roma,
00185 Roma, Italy*

D. Pini

*Istituto di Chimica Organica Industriale,
Università di Pisa, Pisa, Italy*

and L. Porri

*Istituto Chimica Industriale del Politecnico,
20133 Milano, Italy
(Received 2 July 1974; revised 2 October 1974)*

References

- 1 Morero, D., Santambrogio, A., Porri, L. and Ciampelli, F. *Chim. Ind.* 1959, **41**, 758
- 2 Santee, E. R., Chang, R. and Morton, M. *J. Polym. Sci. (Polym. Lett. Edn)* 1973, **11**, 449
- 3 Santee, E. R., Mochel, V. D. and Morton, M. *ibid.* 1973, **11**, 453
- 4 Duch, M. W. and Grant, D. M. *Macromolecules* 1970, **3**, 165
- 5 Mochel, V. D. *J. Polym. Sci. (A-1)* 1972, **10**, 1009
- 6 Elgert, K. F., Stützel, B., Frenzel, P., Cantow, H. J. and Streck, R. *Makromol. Chem.* 1973, **170**, 257
- 7 Conti, F., Segre, A. L., Pini, D. and Porri, L. *Polymer* 1974, **15**, 5
- 8 Natta, G. and Corradini, P. *Nuovo Cimento* 1960, **15**, Suppl. 1, 9
- 9 Grant, D. M. and Paul, E. G. *J. Am. Chem. Soc.* 1964, **86**, 2984
- 10 Lindeman, L. P. and Adams, J. C. *Analyt. Chem.* 1971, **43**, 1245
- 11 Dorman, D. E., Jautelat, M. and Roberts, J. D. *J. Org. Chem.* 1971, **36**, 2557
- 12 Furukawa, J., Kobayashi, E., Katsuki, N. and Kawagoe, T. *Makromol. Chem.* 1974, **175**, 237

ERRATA

'Chain conformation in molten polyethylene by low angle neutron scattering' by J. Schelten, G. D. Wignall and D. G. H. Ballard, *Polymer* 1974, **15**, 682-685.

Page 683, *Figure 3*, caption:
for PEN read PED

Page 683, *Table 1*, caption:
for PEG read PEH

Page 684, right hand column, 8 lines below *Table 3* should read:

$$(1/K_N C) d\Sigma/d\Omega(k) \text{ at } k=0 \text{ etc.}$$

We apologize for these errors.

Book Reviews

Polymerization reactions and new polymers

(*Advances in Chemistry Series 129*)

Edited by N. A. J. Platzer

American Chemical Society, Washington, 1973,
287 pp. \$15.95

This volume comprises those papers presented at a symposium on polymerization and polymerization processes to the Division of Polymer Chemistry during the American Chemical Society meeting in Boston, April 1972, which relate to new polymers and novel polymerization processes.

The demand for a wider range and variety of plastics to meet the future demands of polymer science and technology is growing constantly and eighteen papers survey some of the newer materials in terms of their synthesis, properties and uses. New elastomers and polymers include polycyanoprene, a new rubber with mechanical properties similar to commercial polychloroprene but with better oil resistance; terpolymers of tetrafluoroethylene, perfluoro(methyl vinyl ether) and certain cure site monomers; polymers obtained by the hydrogenation of styrene-butadiene block copolymers; segmented copolymers of polyethers and polyesters.

New heat resistant polymers described include: (a) the use of perfluoroethylene ether intermediates and their amine and isocyanatophenoxy derivatives in the synthesis of polyimides and polyisocyanurates; (b) poly(ethylene sulphides) made by the reaction of *p*-dichlorobenzene and sodium sulphide in a polar solvent (Rytex) and a separate paper describes the properties of the coating grade of this material; (c) the polymerization of cyclic bis(arylene tetrasulphides) and their use as tyre cord adhesives and metal-to-metal binders; (d) the synthesis and properties of a range of poly(thiol esters), and finally (e) a practical route to a heat resistant poly(aryl sulphone) showing improved flow during processing.

The group of papers on novel polymerization reactions covers the subjects of ring opening and simultaneous polymerization of small cyclic hydrocarbons; the polymerization of pivalolactone; radiation-induced copolymerization of hexafluoroacetone with α -olefins; alternating copolymer graft copolymers; new block copolymers from macroradicals; cationic block copolymerization of styrene with cyclic ethers. The final two chapters deal with photopolymerization, viz. photopolymerization in the solid state and photopolymerization of urethane-modified methacrylates. The chapters as a whole provide an overall cross-section of improved products and new candidates for the future.

C. E. H. Bawn

Natural chelating polymers

R. A. A. Muzzarelli

Pergamon Press, Oxford, 1974, 254 pp. £4.95

Professor Muzzarelli's book examines in detail the three polymers, viz. alginic acid, chitin [poly(*N*-acetylglucosamine)] and chitosan. The latter is apparently produced by fusing chitin with potassium hydroxide at 180°C to give a product with considerably diminished acetyl content. Roughly a quarter of the text is devoted to each one of the three polymeric species in turn, accounting for the major part of the book. This whole section is sandwiched between an initial chapter on 'Recent applications of modified celluloses in inorganic chemistry' and a short final chapter on 'Other chelating polymers'. The main part of the book turns out to be a generalized review of the structure and characteristics of these polymeric substances.

The tone of the molecular interpretation of possible chelating mechanisms is set by statements such as, 'alginic acid has the same backbone and functional groups as carboxymethylcellulose . . .' (preface), together with covalent repeats of alginic acid showing a tetrasaccharide containing three D-mannuronic acid and one L-guluronic acid unit. The three-dimensional shapes of the polymers are not considered except insofar as projections of crystalline chitin are presented.

The chapter on alginic acid misses out many of the important points regarding the block type distribution of L-guluronic acid and D-mannuronic acid units, and takes no account of the molecular shape of the L-guluronic acid segments which strongly chelate such divalent ions as calcium. The next chapter (chapter 3) entitled 'Chitin' covers occurrence, availability, detection, isolation bio-synthesis, properties, degradation, a large section on macrostructure, association with protein and derivatives. Quite a good review of chitin but the reader is left still wondering how all this information is relevant to chelation. Similarly the following chapter on chitosan—which is not polyglucose, but somewhat close one would guess—is in the main, a review of its preparation and characteristics. Sections in the last chapter concerned with other chelating polymers will raise a few eyebrows, for example the covalent repeat of heparin is shown as alternating 1→4 and 1→3 glycosidically linked and containing galactose derivatives!

The book is rather superficial and is in general a catalogue of information concerning these three polysaccharide species. The text is one of the international series of monographs in analytical chemistry and the data may well be useful to the analytical chemist wishing to separate minute quantities of metal ions from other metal ion types. However, there is little attempt to offer explanations for the molecular mechanisms involved in such chelating processes. The diagrams and tables are clearly presented; the layout of the text is good and commensurate with a price of £4.95.

E. D. T. Atkins

Conference Announcement

5th Polymer Meeting Point

University of Essex, 10 January 1975

Phase equilibria and phase separation in polymer systems is the subject of the 5th Polymer Meeting Point being organized as a one day symposium by the Polymer Physics Group of the Institute of Physics on 10 January 1975 at the Institute of Polymer Science, University of Essex. Invited papers will be given by: R. Koningsveld (DSM, Holland); J. M. G. Cowie (University of Stirling); F. L. Swinton (New University of Ulster); A. J. Pennings (University of Groningen, Holland); and M. Gordon (University of Essex).

Further details and registration forms are available from the Meetings Officer, Institute of Physics, 47 Belgrave Square, London SW1X 8QX, UK.

Classified Contents

- ABS polymers, improved etch method for electron microscopy, 254
- AlEt₃/diethylenetriamine/CCl₄ catalyst system, mechanism of vinyl chloride polymerization initiated by, 717
- Adhesion analysis, (for) diagnosis of graft copolymers, 189
- ω -Amino acid polyamides, transition and relaxation processes, 42
- Biopolymers, spherulitic crystallization, 762
- Birefringence, flow and magnetic, (for) conformation of polycarbonate, 301
- Birefringence, magneto-optic, evidence for aggregation of polystyrene in solution, 187
- Bisphenol A, poly(2-chlorocyanurate) of, preparation and properties, 56
- Block copolymer, determination of the molecular weight and hydrodynamic dimensions of micelles formed from, 228
- Block copolymers, amorphous styrene/*cis*-1,4-isoprene, organized structures in: low angle X-ray scattering and electron microscopy, 137
- Block copolymers, phase structure of solution cast films of α -methylstyrene/butadiene/styrene, 97
- Block copolymers, segmental orientation studies: 2. Non-hydrogen bonded polyurethanes, 433
- Block polymers, elastomeric, from ethylene sulphide, 175
- Block polymers, some observations on colloidal behaviour, 325
- Block terpolymer, ABC, microphase separation, 541
- N*-t-Butyloxycarbonyl - oligo - L - leucine methyl esters, synthesis, characterization and conformational studies, 767
- Cellulose fibres, viscose rayon, crystallinity and crystallite size measurement, 697
- Cellulose, oxidation, effect of ethylamine pretreatment by periodate, 553
- Chain conformation in molten polyethylene by low angle neutron scattering, 682
- Chain defects, effects on thermal behaviour of polyethylene, 306
- Chain folding, and shrinkage, in drawn poly(ethylene terephthalate) fibres, 277
- Chain theory, Gaussian, exact and approximate eigenvalues and intrinsic functions, 569
- Circular dichroism and magnetic circular dichroism of the haemin-poly(L-lysine) complex system, 330
- Composites formed by interstitial polymerization of vinyl monomers in polyurethane elastomers: 3. The role of graft copolymerization, 13. 4. Preparation, properties and structure of acrylonitrile and styrene based composites, 19. 5. Variation of modulus with composition, 28. 6. Low angle X-ray scattering and turbidity, 33
- Conformation of polycarbonate by flow and magnetic birefringence, 301
- Conformations of macromolecular sequential polypeptides in solution: 2. Sequential polypeptides containing both D- and L-residues, 690
- Copolymerization and oligomerization by transition metal catalysts, 162
- Copolymers, methyl methacrylate-chloroprene, 220 MHz p.m.r. analysis, 782
- Crack stability in PMMA, 251
- Crazing phenomena, thermal, in epoxy resins, 441
- Crazing, solvent stress, in PMMA: 1. Geometrical effects, 599
- Creep deflection processes, non-isothermal: characterization of the thermomechanical behaviour of polymers, 243
- Crosslinking density in ethylene-propylene copolymer, effect of swelling agent on determination, 609
- Crosslinks (defects), intramolecular, introduced into a rubbery network, effects of crosslink density and length on, 194
- Crystallinity and crystallite size measurement in cellulose fibres: 2. Viscose rayon, 697
- Crystallization, eutectic, of pseudo binary systems of polyethylene and high melting diluents, 413
- Crystallization kinetics of polyacrylonitrile: single crystal growth rate and thermodynamic considerations, 402
- Crystallization phenomena in polytetrafluoroethylene, 721
- Crystallization, polymer, a technique for the detailed investigation at high pressures, 491
- Crystallization processes of polyethylene under high pressure, 661
- Crystallization rates, effect of chemical structure and melting of polymers: 2. Aliphatic polyesters, 407
- Crystallization, row-nucleated, effect of molecular weight on, and the morphology of melt-crystallized PTFE, 272
- Crystallization, spherulitic, in biopolymers, 762
- Crystallization studies of isotactic polystyrene, 351
- DNA, sonicated, reversal of birefringence sign at low fields, 396
- Deformation, conversion of work, to heat in polymers, 239
- Degradation, thermal, of phosphorylated poly(vinyl alcohol), 335
- Dielectric properties of standard and modified electrical grade phenol-formaldehyde resin-paper laminates, 799
- Dielectric relaxation in polymethyltrifluoropropylsiloxane, 608
- Dielectric relaxation, low temperature, in polymers containing an aromatic group in the main chain, 639
- Dilute solution behaviour of polymers near the phase separation temperature, 346
- E.s.r. studies of spin-labelled polymers: Part 6. End-labelled poly(methyl methacrylate), 74
- E.s.r. study of u.v.-irradiated polypropylene: effect of the stereoregularity on the behaviour of free radicals produced by u.v. irradiation, 787
- Eigenvalues, exact and approximate, and intrinsic functions for the Gaussian chain theory, 569
- Elastomeric block polymers from ethylene sulphide, 175
- Elastomers, high temperature vulcanization: 2. Network structures in conventional sulphenamide-sulphur natural rubber vulcanizates, 357. 3. Network structures of efficiently vulcanized natural rubber mixes, 729
- Electron microscopy of ABS polymers, an improved etch method, 254
- Enzymes, immobilized: 7. Use of vanacryls in preparation of immobilized arginase and alkaline phosphatase, 546
- Epoxy resin, polarization effect at elevated temperatures, 496
- Epoxy resins and rubber modified epoxy resins, fracture and mechanical properties, 675
- Epoxy resins, thermal crazing phenomena, 441
- Equilibrium ring concentrations and the statistical conformations of polymer chains: Part 12. Cyclics in molten and solid nylon-6, 420. Part 13. Cyclics in two aliphatic polyesters, 738
- Ethylene-propylene copolymer, effect of swelling agent on determination of crosslinking density, 609
- Extrusion, annular, of polystyrene, homogeneity, 536
- Extrusion, solid-state, of isotactic polypropylene through a tapered die: 2. Structure and some properties of extrudates, 446
- Filler effect on relaxation time of fibre suspensions in polymeric solutions, 589
- Films, thin polymer, formation of supermolecular structure, 211
- Flame retardant polystyrene-tetrabromoxylene systems, solid solutions and precipitation, 499
- Fracture and mechanical properties of epoxy resins and rubber-modified epoxy resins, 675
- Fracture, ductile, of rigid poly(vinyl chloride), 149
- Fracture process, ductile, of uncrosslinked polymers in the rubbery state, an interpretation, 671
- Fracture properties of thermosets, 101
- Fracture surface energy of PMMA, dependence of molecular weight, 394
- G.p.c., influence of particle diameter on chromatogram broadening, with porous silica columns, 687
- G.p.c.: rapid thin-layer characterization of aqueous gel networks using dyed protein standards, 466
- Gelation in the reactions of aliphatic diisocyanates with triols, 315
- Glass transition, polystyrene, n.m.r. studies on the effect of water, 713
- Graft copolymer, effect of addition on the microstructure and impact strength of PS/LDPE blends, 119
- Graft copolymer, microphase separation, 117
- Graft copolymers, cellulosic, synthesis and analysis by ultra-violet and infra-red spectroscopy, 133
- Graft copolymers, diagnosis by adhesion analysis, 189
- Graft copolymers, light scattering study of micelle formation by poly(styrene-g-polyisoprene), 389

- Haemin-poly(L-lysine) complex system, circular dichroism and magnetic circular dichroism, 330
- Heparin, macromolecular properties in dilute solution: 1. Application of various hydrodynamic models in 0.5 M NaCl, pH 2.5, 197. 2. Dimensional parameters as a function of pH, ionic strength and desulphation, 204
- 'Hydroxymethyl groups, introduction into polystyrene and styrene' [Comments on paper by C. H. Bamford and H. Lindsay (*Polymer* 1973, **14**, 330-332)], 323
- I.r. spectroscopic study of molecular orientation and conformational changes in poly(ethylene terephthalate), 749
- Infra-red, far, spectrum of crystalline polytetrafluoroethylene, 69
- Interfacial and aqueous solution synthesis of titanium polymers, tentative identification of reactive species, 9
- Laminates, resin-paper, dielectric properties of standard and modified electrical grade phenol-formaldehyde, 799
- Laser-Raman spectroscopy, a study of molecular orientation in poly(methyl methacrylate), 645
- Light scattering, anisotropic, measurements; application to the determination of the difference $H_h - H_v$ for $\theta = \pi/2$, 77
- Light scattering, characterization of styrene-butadiene copolymers, 593
- Light scattering study of micelle formation by polystyrene-g-polyisoprene graft copolymers, 389
- Liquid rubbers and the problems involved in their application, 521
- Mechanical and optical response of polymers, time lag in, 655
- Mechanical losses, and impact strength in thermoplastics, 111
- Mechanical properties, and fracture, of epoxy resins and rubber-modified epoxy resins, 675
- Mechanical properties, and thermal history, 451
- Mechanical properties, effect of molecular weight and molecular weight distribution on drawing behaviour, of ultra-high modulus linear polyethylenes, 233
- Mechanical properties of oriented polymers, 379
- Mechanical properties of polymers at cryogenic temperatures: relationships between relaxation, yield and fracture processes, 805
- Membranes, solvent resistant, 127
- α -Methylstyrene/butadiene/styrene block copolymers, phase structure of solution cast films, 97
- Moduli, and preparation, of model polymer networks, 366
- Modulus, variation with composition (of vinyl monomers in polyurethane elastomer composites), 28
- Molecular orientation and conformational changes in poly(ethylene terephthalate), i.r. spectroscopic study, 749
- Molecular orientation by polarized infra-red radiation in an oriented polymer of high polarizability, 743
- Molecular orientation in poly(methyl methacrylate) by means of laser-Raman spectroscopy, 645
- Molecular weight and hydrodynamic dimensions of micelles formed from a block copolymer, 228
- Molecular weight averages, variation during polycondensation, 326
- Molecular weight dependence of the spherulitic growth rate of isotactic polystyrene, 757
- Molecular weight, effect of, on the morphology of melt-crystallized PTFE and the occurrence of row-nucleated crystallization, 272
- Molecular weight, effect of, on partial specific volume of polystyrenes in solution, 618
- Molecular weight, effect of, on refractive index increment of polystyrenes in solution, 626
- Morphology, polymer, solvent uptake as a tool for, 2
- Motions of free nitroxyl radicals in poly(ethylene glycol), effect of end-groups, 248
- Motions of nitroxyl radicals in polymers, mechanisms, 124
- N.m.r., ^{13}C , spectra of polybutadienes: 2, 816
- N.m.r., ^{13}C , spectra of styrene-butadiene copolymers on solid samples, 539
- N.m.r. of random copolymers of benzyl-L-aspartate with *o*- and *p*-nitrobenzyl-L-aspartate, 474
- N.m.r. of solid polymers: a review, 503
- N.m.r. studies of polydienes: 1. ^{13}C n.m.r. of 1,4-polybutadiene obtained by π -allyl nickel trifluoroacetate catalysts, 5
- N.m.r. studies on the effect of water on the glass transition of polystyrene, 713
- Neutron scattering, low angle, chain conformation in molten polyethylene, 682
- Nucleic acids and nucleoproteins, electro-optical properties: 6. Reversal of the birefringence sign for sonicated DNA at low fields, 396
- Nylon-6, molten and solid, cyclics in, 420
- Nylon-6, studies of crystalline forms by X-ray and i.r. spectrophotometry, 130
- Orientations of fluorescent molecules incorporated in uniaxially oriented poly(ethylene terephthalate) tapes, 287
- Oxycelluloses, periodate, effect of ethylamine pretreatment on tensile strength, 559
- P.m.r., 220 MHz, of some methyl methacrylate-chloroprene copolymers, 782
- Partial specific volume of polystyrenes in solution, effect of molecular weight, 618
- Permeability of a series of alcohols through poly(γ -methyl-D-glutamate), 517
- Phase separation temperature, dilute solution behaviour of polymers near, 346
- Phase transition in a polymer chain in dilute solution, 259
- Physics of polymers—*Editorial*, 258
- Polyacrylonitrile, crystallization kinetics: single crystal growth rate and thermodynamic considerations, 402
- Poly(acryloylaminoacetaldehyde dimethylacetal), crosslinked, and derived urease conjugates, 564
- Poly(*n*-alkyl isocyanates), temperature effects on some solution properties, 685
- Polyamides, ω -amino acid, transition and relaxation processes, 42
- Polyamide-penetrant systems, sorption, diffusion and conduction. 1. Sorption phenomena, 771
- Poly[(\pm)- β -aminobutyric acid], investigation of orientation phenomena in drawn films, 146
- Polyarylates (polyesters from aromatic dicarboxylic acids and bisphenols), 257
- Poly(arylene ether sulphones) preparation, and properties, 456
- 1,4-Polybutadiene obtained by π -allyl nickel trifluoroacetate catalysts, ^{13}C n.m.r., 5
- cis*-1,4-/1,2-Polybutadiene, structure of, 612
- Polybutadienes, ^{13}C n.m.r. spectra: 2, 816
- Polycarbonate, conformation by flow and magnetic birefringence, 301
- Polychlorotrifluoroethylene, heat capacity, 487
- Poly(*trans*-2,5-dimethylpiperazine-3,4-thiofurazan amide), some solution properties, 393
- Polyelectrolytes, electric permittivity: 2. Effect of the concentration and ionic specificity, 585
- Poly(ether sulphone) as an engineering material, 665
- Polyethylene and high diluents, eutectic crystallization of pseudo binary systems, 413
- 'Polyethylene, branched, steady flow and dynamic viscoelastic properties' (Comments on paper in *Polymer* 1973, **14**, 384-386), 123
- Polyethylene, crystallization phenomena, 721
- Polyethylene, dose kinetics of u.v. excited thermoluminescence, 425
- Polyethylene, effects of chain defects on the thermal behaviour, 306
- Polyethylene fibres, high density, morphology of cold-drawn, 81
- Polyethylene films, oxidized, effect of temperature on wettability, 759
- Polyethylene, microscopic observations of crystallization processes under high pressure, 661
- Polyethylene, molten, chain conformation by low angle neutron scattering, 682
- Polyethylene single crystals, as grown and annealed, surface studies by the spin-probe method, 793
- Polyethylene solutions, upper and lower critical solution temperatures, 777
- Polyethylenes, chlorinated, viscometric studies in dilute solution, 219
- Polyethylenes, preparation of ultra-high modulus; effect of molecular weight and molecular weight distribution on drawing behaviour and mechanical properties, 233
- Poly(ethylene glycol), effect of end-groups on the motions of free nitroxyl radicals, 248
- PET, semi-crystalline, quantitative morphological characterization, 61
- Poly(ethylene terephthalate) fibres, shrinkage and chain folding, 277
- Poly(ethylene terephthalate), i.r. spectroscopic study of molecular orientation and conformational changes, 749
- Poly(ethylene terephthalate), oriented, crystallization of, 283
- Poly(ethylene terephthalate) tapes, uniaxially oriented, orientations of fluorescent molecules in, 287
- Polymerizability, and synthesis, of 5-methyl-2-vinyliminobibenzyl and 10-ethyl-2-vinylphenothiazine, 387
- Polymerization, anionic, of styrene in triglyme-benzene mixtures, 631

Classified Contents

- Polymerization catalysts, highly active, of long life derived from σ - and π -bonded transition metal alkyl compounds, 169
- Polymerization, cationic, influence of polymerization temperature on reactivity of 3-methyl- and 4-methyl-styrenes, 485
- Polymerization, ionic, in a flow reactor, a model study, 573
- Polymerization of vinylferrocene in chloroform, 397
- Polymerization, oxidative, of 1-naphthol using Cu^{I} -pyridine initiator system, 392
- Polymerization, vinyl chloride, initiated by the $\text{AlEt}_3/\text{diethylenetriamine}/\text{CCl}_4$ catalyst system, mechanism, 717
- Polymethacrylate, dilatometric study of monovalent counter-ion association, 468
- Poly(γ -methyl-D-glutamate), permeability of a series of alcohols through, 157
- PMMA, crack stability, 251
- PMMA, fracture surface energy, dependence of molecular weight, 394
- PMMA, illuminated, energy transfer, 60
- PMMA, solvent stress crazing: 1. Geometrical effects, 599
- Poly(methyl methacrylate), a study of molecular orientation, by means of laser-Raman spectroscopy, 645
- Poly(methyl methacrylate); e.s.r. studies of spin-labelled polymers (Part 6), 74
- Polymethyltrifluoropropylsiloxane, dielectric relaxation, 608
- Polypeptides, macromolecular sequential, conformations in solution: 2. Sequential polypeptides containing both D- and L-residues, 690
- Polypeptides, synthetic, and biological macromolecules, review of statistical structures, 706
- Polypivalolactone, structure and properties, 49
- Polypropylene, isotactic, solid-state extrusion through a tapered die, 446
- Polypropylene stability adversely affected by volatile oxidation products, 613
- Polypropylene, u.v. irradiated, e.s.r. study: effect of the stereoregularity on the behaviour of free radicals produced by u.v. irradiation, 787
- Polyquinazolinediones and polyquinazolones, preparation, thermal characterization and tribological evaluation, 577
- Poly(squaryl amides), 339
- PS/LDPE blends, effect of addition of graft copolymer on the microstructure and impact strength, 119
- 'Polystyrene and styrene, introduction of hydroxymethyl groups into' [Comments on paper by C. H. Bamford and H. Lindsay (*Polymer* 1973, 14, 330-332)], 323
- Polystyrene-cyclopentane system, temperature dependence of polymer chain dimensions, 66
- Polystyrene, homogeneity of annular extrusion, 536
- Polystyrene in solution, evidence for aggregation from magneto-optic birefringence, 187
- Polystyrene, isotactic, crystallization studies, 351
- Polystyrene, isotactic, molecular weight dependence of spherulitic growth rate, 757
- Polystyrene, n.m.r. studies on the effect of water on the glass transition, 713
- Polystyrene-tetrabromoxylene systems, flame retardant, solid solutions and precipitation, 499
- Polystyrenes in solution, effect of molecular weight on partial specific volume, 618
- Polystyrenes in solution, effect of molecular weight on refractive index increment, 626
- PTFE, melt-crystallized, effect of molecular weight on the morphology, and occurrence of row-nucleated crystallization, 272
- Polytetrafluoroethylene, crystalline, the far infra-red spectrum, 69
- Polyurethane elastomers, composites formed by interstitial polymerization of vinyl monomers in: 3. The role of graft copolymerization, 13. 4. Preparation, properties and structure of acrylonitrile and styrene based composites, 19. 5. Variation of modulus with composition, 28. 6. Low angle X-ray scattering and turbidity, 33
- Polyurethanes, non-hydrogen bonded: Segmental orientation studies, Part 2, 433
- Polyuronides: their molecular architecture, 263
- Poly(vinyl alcohol), phosphorylated, thermal degradation, 335
- PVC, more efficient stabilizers, 543
- Poly(vinyl chloride), oriented, a correlation of Young's modulus with yield stress, 107
- Poly(vinylidene fluoride), solution properties and unperturbed dimensions, 429
- Radiation sensitive polymers, image intensification and electron microscopy, 37
- Random copolymers, n.m.r. of benzyl-L-aspartate with *o*- and *p*-nitrobenzyl-L-aspartate, 474
- Reactivities towards the benzoyloxy radical of some conjugated dienes, 467
- Refractive index increment of polystyrenes in solution, effect of molecular weight, 626
- Relaxation time of fibre suspensions in polymeric solutions, filler effect on, 589
- Resonance, externally shifted and restored, (for) measurement of dynamic rheological properties, 253
- Review: n.m.r. of solid polymers, 503
- Rubber, bound, and vulcanizate properties, 814
- Rubbers, liquid, and the problems involved in their application, 521
- Rubber, natural, network structure of efficiently vulcanized mixes, 729
- Rubber, natural, network structures in conventional sulphenamide-sulphur vulcanizates, 357
- Soda-cellulose II, structural aspects, 125
- Solvent uptake as a tool for investigating polymer morphology, 2
- Sorption, diffusion and conduction in polyamide-penetrant systems. 1. Sorption phenomena, 771
- Stability, polypropylene, adversely affected by volatile oxidation products, 613
- Stabilizers for PVC, 543
- Statistical structures in synthetic polypeptides and biological macromolecules, a review, 706
- Styrene-butadiene copolymers, ^{13}C n.m.r. spectra of solid samples, 539
- Styrene-butadiene copolymers, characterization by light scattering, 593
- Styrene/butyl methacrylate/methacrylic acid system, simulation of kinetic analysis on terpolymerization, 479
- Styrene in 2-methyltetrahydrofuran, anionic polymerization: temperature dependence of the field effect, 635
- Styrene in triglyme-benzene mixtures, anionic polymerization, 631
- Styrenes, 3-methyl- and 4-methyl-, influence of polymerization temperature on the reactivity, in cationic polymerization, 485
- Sulphenamide-sulphur natural rubber vulcanizates, network structures, 357
- Temperature effects on some solution properties of poly(n-alkyl isocyanates), 685
- Tensile strength of periodate oxycelluloses effect of ethylamine pretreatment on, 559
- Tentative identification of reactive species in the interfacial and aqueous solution synthesis of titanium polymers, 9
- Terpolymerization of styrene/butyl methacrylate/methacrylic acid system, simulation of kinetic analysis, 479
- Thermoluminescence, u.v. excited, dose kinetics in polyethylene, 425
- Thermoplastics, impact strength and mechanical losses, 111
- Thermosets, fracture properties, 101
- Transition metal alkyl compounds, σ - and π -bonded, highly active polymerization catalysts of long life, 169
- Transition metal catalysts, copolymerization and oligomerization, 162
- U.v.-irradiated polypropylene, e.s.r. study: effect of the stereoregularity on the behaviour of free radicals produced by u.v. irradiation, 787
- Ultra-high modulus linear polyethylenes, preparation; effect of molecular weight and molecular weight distribution on drawing behaviour and mechanical properties, 233
- Vanacrils, use in preparation of immobilized arginase and alkaline phosphatase, 546
- Vibrations, torsional, effect of polymer microstructure on methyl group, 319
- Vinyl chloride polymerization initiated by the $\text{AlEt}_3/\text{diethylenetriamine}/\text{CCl}_4$ catalyst system, mechanism, 717
- Vinyl chloride polymerization with $\text{Al}(\text{C}_2\text{H}_5)_3/\text{CCl}_4$, catalyst system participation of Lewis base, 216
- Vinylferrocene, polymerization in chloroform, 397
- Vulcanizates reinforced by fibrillar fillers, solvent swelling, 373
- Vulcanization, high temperature, of elastomers: 2. Network structures in conventional sulphenamide-sulphur natural rubber vulcanizates, 357. 3. Network structures of efficiently vulcanized natural rubber mixes, 729
- Wettability of oxidized polyethylene films, effect of temperature, 759
- X-ray scattering, low angle, and electron microscopy of organized structures in amorphous styrene/*cis*-1,4-isoprene block copolymers, 137
- X-ray scattering, low angle (of vinyl monomers in polyurethane elastomer composites), 33
- Young's modulus, correlation with yield stress in oriented poly(vinyl chloride), 107
- Ziegler-Natta catalysis: 6. Effect of electron donors on the course of polymerization, 87

Author Index

- Abbas, S. Z. and Poller, R. C.: More efficient stabilizers for PVC, 543
- Adamec, V.: Polarization effect in an epoxy resin at elevated temperatures, 496
- Akimoto, Akira: Mechanism of vinyl chloride polymerization initiated by the $AlEt_3$ /diethylenetriamine/ CCl_4 catalyst system, 717. Participation of Lewis base on vinyl chloride polymerization with $Al(C_2H_5)_3/CCl_4$ catalyst system, 216
- Allegrezza, A. E. Jr, Seymour, R. W., Ng, H. N. and Cooper, S. L.: Segmental orientation studies of block copolymers: 2. Non-hydrogen bonded polyurethanes, 433
- Allen, G.: *see* Walsh, D. J., Allen, G. and Ballard, G.
- Allen, G., Bowden, M. J., Lewis, G., Blundell, D. J. and Jeffs, G. M.: Composites formed by interstitial polymerization of vinyl monomers in polyurethane elastomers: 3. The role of graft polymerization, 13
- Allen, G., Bowden, M. J., Lewis, G., Blundell, D. J., Jeffs, G. M. and Vyvoda, J.: Composites formed by interstitial polymerization of vinyl monomers in polyurethane elastomers: 4. Preparation, properties and structure of acrylonitrile and styrene based composites, 19
- Allen, G., Bowden, M. J., Todd, S. M., Blundell, D. J., Jeffs, G. M. and Davies, W. E. A.: Composites formed by interstitial polymerization of vinyl monomers in polyurethane elastomers: 5. Variation of modulus with composition, 28
- Allen, G. and De Boos, A. G.: Preparation and properties of the poly(2-chlorocyanurate) of bisphenol A, 56
- Allen, G., Wright, C. J. and Higgins, J. S.: Effect of polymer microstructure on methyl group torsional vibrations, 319
- Ando, M.: *see* Komiyama, J., Takeda, Y., Ando, M. and Iijima, T.
- Andrews, E. H. and Levy, G. M.: Solvent stress crazing in PMMA: 1. Geometrical effects, 599
- Andrews, J. M., Jones, F. R. and Semlyen, J. A.: Equilibrium ring concentrations and the statistical conformations of polymer chains: Part 12. Cyclics in molten and solid nylon-6, 420
- Aoyagi, J.: *see* Tsuchida, E., Aoyagi, J., Shinzo, K. and Shinohara, I.
- Ast, D. G.: *see* Thomas, E. L. and Ast, D. G.
- Atkins, E. D. T.: *see* Barham, P. J., Atkins, E. D. T. and Nieduszynski, I. A.
- Atkins, E. D. T.: *see* Whitaker, P. M., Nieduszynski, I. A. and Atkins, E. D. T.
- Atkins, E. D. T., Isaac, D. H., Nieduszynski, I. A., Phelps, C. F. and Sheehan, J. K.: The polyuronides: their molecular architecture, 263
- Baer, E.: *see* Hiltner, Anne and Baer, E.
- Baird, M. E. and Sengupta, C. R.: Dielectric relaxation in polymethyltrifluoropropylsiloxane, 608
- Bajah, S. T.: *see* Carraher, C. E. Jr
- Ballard, D. G. H.: *see* Schelten, J., Wignall, G. D. and Ballard, D. G. H.
- Ballard, D. G. H., Jones, E., Wyatt, R. J., Murray, R. T. and Robinson, P. A.: Highly active polymerization catalysts of long life derived from σ - and π -bonded transition metal alkyl compounds, 169
- Ballard, G.: *see* Walsh, D. J., Allen, G. and Ballard, G.
- Bandyopadhyay, A. K.: *see* Mukherjee, R. N. and Bandyopadhyay, A. K.
- Barentsen, W. M., Heikens, D. and Piet, P.: Effect of addition of graft copolymer on the microstructure and impact strength of PS/LDPE blends, 119
- Barham, P. J., Atkins, E. D. T. and Nieduszynski, I. A.: Spherulitic crystallization in biopolymers, 762
- Bassett, D. C. and Davitt, R.: On crystallization phenomena in polytetrafluoroethylene, 721
- Baszkin, A. and Ter-Minassian-Saraga, L.: Effect of the temperature on the wettability of oxidized polyethylene films, 759
- Batty, N. S. and Guthrie, J. T.: Solvent resistant membranes, 127
- Benoit, Henri: *see* Candau, Françoise; François, Jeanne; and Benoit, Henri
- Benoit, Henri: *see* François, Jeanne; Candau, Françoise; and Benoit, Henri
- Berghmans, H.: *see* Groeninckx, G., Reynaers, H. and Berghmans, H.
- Berry, J. P. and Morrell, S. H.: Liquid rubbers and the problems involved in their application, 521
- Bertolotto, J. A.: *see* Colson, P., Houssier, C., Fredericq, E. and Bertolotto, J. A.
- Bevington, J. C. and SenGupta, P. K.: Reactivities towards the benzoyloxy radical of some conjugated dienes, 467
- Bianchi, U.: *see* Cuniberti, C. and Bianchi, U.
- Bier, G.: Polyarylates (polyesters from aromatic dicarboxylic acids and bisphenols), 527
- Blackadder, D. A. and Vincent, P. I.: Solvent uptake as a tool for investigating polymer morphology, 2
- Blow, C. M.: Bound rubber and vulcanizate properties, 814
- Blundell, D. J.: *see* Allen, G., Bowden, M. J., Lewis, G., Blundell, D. J. and Jeffs, G. M.
- Blundell, D. J.: *see* Allen, G., Bowden, M. J., Lewis, G., Blundell, D. J., Jeffs, G. M. and Vyvoda, J.
- Blundell, D. J.: *see* Allen, G., Bowden, M. J., Todd, S. M., Blundell, D. J., Jeffs, G. M. and Davies, W. E. A.
- Blundell, D. J., Longman, G. W., Wignall, G. D. and Bowden, M. J.: Composites formed by interstitial polymerization of vinyl monomers in polyurethane elastomers: 6. Low angle X-ray scattering and turbidity, 33
- Blundo, D.: *see* Pavan, A., Rink, M., Blundo, D. and Danusso, F.
- Boerio, F. J.: *see* Chantry, G. W., Fleming, J. W., Nicol, Elisabeth A., Willis, H. A., Cudby, M. E. A. and Boerio, F. J.
- Bonora, G. M., Maglione, A., and Toniolo, C.: Synthesis, characterization, and conformational studies of *N*-*t*-butyl-oxycarbonyl-oligo-L-leucine methyl esters, 767
- Bont, H.: *see* Zoller, P. and Bont, H.
- Bowden, M. J.: *see* Allen, G., Bowden, M. J., Lewis, G., Blundell, D. J. and Jeffs, G. M.
- Bowden, M. J.: *see* Allen, G., Bowden, M. J., Lewis, G., Blundell, D. J., Jeffs, G. M. and Vyvoda, J.
- Bowden, M. J.: *see* Allen, G., Bowden, M. J., Todd, S. M., Blundell, D. J., Jeffs, G. M. and Davies, W. E. A.
- Bowden, M. J.: *see* Blundell, D. J., Longman, G. W., Wignall, G. D. and Bowden, M. J.
- Bower, D. I.: *see* Nobbs, J. H., Bower, D. I., Ward, I. M. and Patterson, D.
- Bower, D. I.: *see* Purvis, J. and Bower, D. I.
- Brown, E. and Joyeau, R.: Immobilized enzymes: 7. Use of vanacyrls in the preparation of immobilized arginase and alkaline phosphatase, 546
- Bucknall, C. B. and Drinkwater, I. C.: An improved etch method for electron microscopy of ABS polymers, 254
- Bullock, A. T., Cameron, G. G. and Elsom, J. M.: Electron spin resonance studies and spin-labelled polymers: Part 6. End-labelled poly(methyl methacrylate), 74
- Burfield, D. R. and Tait, P. J. T.: Ziegler-Natta catalysis: 6. Effect of electron donors on the course of polymerization, 87
- Cameron, G. G.: *see* Bullock, A. T., Cameron, G. G. and Elsom, J. M.
- Candau, Françoise: *see* François, Jeanne; Candau, Françoise; and Benoit, Henri
- Candau, Françoise; François, Jeanne; and Benoit, Henri: Effect of molecular weight on the refractive index increment of polystyrenes in solution, 626
- Cappacio, G. and Ward, I. M.: Preparation of ultra-high modulus linear polyethylenes; effect of molecular weight and molecular weight distribution on drawing behaviour and mechanical properties, 233
- Carraher, C. E. Jr and Bajah, S. T.: Tentative identification of reactive species in the interfacial and aqueous solution synthesis of titanium polymers, 9
- Challa, G.: *see* Lemstra, P. J., Postma, J. and Challa, G.
- Champion, J. V., Desson, R. A. and Meeten, G. H.: Conformation of polycarbonate by flow and magnetic birefringence, 301
- Chantry, G. W., Fleming, J. W., Nicol, Elisabeth A., Willis, H. A., Cudby, M. E. A. and Boerio, F. J.: The far infra-red spectrum of crystalline polytetrafluoroethylene, 69
- Chau, T. C. and Rudin, A.: Characterization of styrene-butadiene copolymers by light scattering, 593
- Chiba, T.: *see* Kuwahara, N., Saeki, S., Chiba, T. and Kaneko, M.
- Choy, C. L.: *see* Lee, W. K., Lau, P. C. and Choy, C. L.
- Colson, P., Houssier, C., Fredericq, E. and Bertolotto, J. A.: Electro-optical properties of nucleic acids and nucleoproteins: 6. Reversal of the birefringence sign for sonicated DNA at low fields, 396

Author Index

- Conti, F., Delfini, M. and Segre, A. L.: ^{13}C n.m.r. spectra of styrene-butadiene copolymers on solid samples, 539
- Conti, F., Delfini, M., Segre, A. L., Pini, D. and Porri, L.: ^{13}C n.m.r. spectra of polybutadienes: 2, 816
- Conti, F., Segre, A. L., Pini, D. and Porri, L.: Nuclear magnetic resonance studies of polydienes: 1. ^{13}C n.m.r. of 1,4-polybutadiene obtained by π -allyl nickel trifluoroacetate catalysts, 5
- Cooper, D. R.: Variation of molecular weight averages during polycondensation, 326
- Cooper, S. L.: *see* Allegranza, A. E., Jr, Seymour, R. W., Ng, H. N. and Cooper, S. L.
- Cooper, W., Hale, P. T. and Walker, J. S.: Elastomeric block polymers from ethylene sulphide, 175
- Coppola, G.: *see* D'Alo, B., Coppola, G. and Pallesi, B.
- Cornes, P. L. and Haward, R. N.: Ductile fracture of rigid poly(vinyl chloride), 149
- Cudby, M. E. A.: *see* Chantry, G. W., Fleming, J. W., Nicol, Elisabeth A., Willis, H. A., Cudby, M. E. A. and Boerio, F. J.
- Cuniberti, C. and Bianchi, U.: Dilute solution behaviour of polymers near the phase separation temperature, 346
- Cunningham, A., Davies, G. R. and Ward, I. M.: Determination of molecular orientation by infra-red radiation in an oriented polymer of high polarizability, 743
- Cunningham, A., Ward, I. M., Willis, H. A. and Zichy, V.: An infra-red spectroscopic study of molecular orientation and conformational changes in poly(ethylene terephthalate), 749
- Dagan, A.: *see* Siegmann, A., Narkis, M. and Dagan, A.
- D'Alo, B., Coppola, G. and Pallesi, B.: Studies of crystalline forms of nylon-6 by X-ray and i.r. spectrophotometry, 130
- Danusso, F.: *see* Pavan, A., Rink, M., Blundo, D. and Danusso, F.
- Davies, G. R.: *see* Cunningham, A., Davies, G. R. and Ward, I. M.
- Davies, W. E. A.: *see* Allen, G., Bowden, M. J., Todd, S. M., Blundell, D. J., Jeffs, G. M. and Davies, W. E. A.
- Davitt, R.: *see* Bassett, D. C. and Davitt, R.
- Dawkins, J. V. and Taylor, G.: Influence of particle diameter on chromatogram broadening in g.p.c. with porous silica columns, 687
- De Boos, A. G.: *see* Allen, G. and De Boos, A. G.
- Delfini, M.: *see* Conti, F., Delfini, M. and Segre, A. L.
- Delfini, M.: *see* Conti, F., Delfini, M., Segre, A. L., Pini, D. and Porri, L.
- Desreux, V.: *see* Pierre, J. and Desreux, V.
- Desson, R. A.: *see* Champion, J. V., Desson, R. A. and Meeten, G. H.
- Dew-Hughes, D.: *see* Rigby, S. J. and Dew-Hughes, D.
- Diggwa, A. D. S.: Fracture properties of thermosets, 101
- Domb, C.: Phase transition in a polymer chain in dilute solution, 259
- Doskočilova, D.: *see* Štamberg, J., Wichterle, O. and Doskočilova, D.
- Drinkwater, I. C.: *see* Bucknall, C. B. and Drinkwater, I. C.
- Duflot, Catherine: *see* Loucheux-Lefebvre, Marie-H, Forchioni, A. and Duflot, Catherine
- Dunn, C. M. R. and Turner, S.: Thermal history and mechanical properties, 451
- Ebdon, J. R.: 220 MHz proton magnetic resonance analysis of some methyl methacrylate-chloroprene copolymers, 782
- Edwards, B. C. and Phillips, P. J.: A technique for the detailed investigation of polymer crystallization at high pressures, 491. Crystallization studies of isotactic polystyrene, 351
- Ehrlich, J.: *see* Stivala, S. S. and Ehrlich, J.
- Ehrlich, J. and Stivala, S. S.: Macromolecular properties of heparin in dilute solution: 2. Dimensional parameters as a function of pH, ionic strength and desulphation, 204
- Elgert, K.-F., Quack, G., and Stützel, B.: On the structure of equibinary *cis*-1,4-/1,2-polybutadiene, 612
- Elsom, J. M.: *see* Bullock, A. T., Cameron, G. G. and Elsom, J. M.
- Epton, R., Holding, S. R. and McLaren, J. V.: G.p.c.: rapid thin layer characterization of aqueous gel networks using dyed protein standards, 466
- Epton, R., McLaren, J. V. and Thomas, T. H.: Crosslinked poly(acryloylaminoacetaldehyde dimethylacetal) and derived urease conjugates, 564
- Fielding-Russell, G. S. and Pillai, P. S.: Phase structure of solution cast films of α -methylstyrene / butadiene / styrene block copolymers, 97
- Fleming, J. W.: *see* Chantry, G. W., Fleming, J. W., Nicol, Elisabeth A., Willis, H. A., Cudby, M. E. A. and Boerio, F. J.
- Forchioni, A.: *see* Loucheux-Lefebvre, Marie-H, Forchioni, A. and Duflot, Catherine
- Fortunato, B.: *see* Manaresi, P., Pilati, F. and Fortunato, B.
- François, Jeanne: *see* Candau, Françoise; François, Jeanne; and Benoit, Henri
- François, Jeanne; Candau, Françoise; and Benoit, Henri: Effect of molecular weight on the partial specific volume of polystyrenes in solution, 618
- Fredericq, E.: *see* Colson, P., Houssier, C., Fredericq, E. and Bertolotto, J. A.
- Fujimura, Toshikazu; and Kawamura, Takashi: Homogeneity of annular extrusion of polystyrene, 536
- Furukawa, Junji: Copolymerization and oligomerization by transition metal catalysts, 162
- Gałęski, A.: *see* Kryszewski, M., Gałęski, A., Jabłoński, W. and Sapięha, S.
- Gall, M. J.: Effect of molecular weight on the morphology of melt-crystallized PTFE and the occurrence of row-nucleated crystallization, 272
- George, M. H. and Hayes, G. F.: Polymerization of vinylferrocene in chloroform, 397
- Ghafoor, A., Senior, J. M., Still, R. H. and West, G. H.: Preparation, thermal characterization and tribological evaluation of some polyquinazolinediones and polyquinazolones, 577
- Gilbert, Marianne and Hybart, F. J.: Effect of chemical structure on crystallization rates and melting of polymers: 2. Aliphatic polyesters, 407
- Gohill, R. M., Patel, K. C. and Patel, R. D.: Crystallization kinetics of polyacrylonitrile: single crystal growth rate and thermodynamic considerations, 402
- Gotham, K. V. and Turner, S.: Poly(ether sulphone) as an engineering material, 665
- Green, B. R.: *see* Neuse, E. W. and Green, B. R.
- Groeninckx, G., Reynaers, H. and Berghmans, H.: Quantitative morphological characterization of semi-crystalline PET, 61
- Guthrie, J. T.: *see* Batty, N. S. and Guthrie, J. T.
- Guthrie, J. T. and Haq, Z.: Synthesis of cellulosic graft copolymers and their analysis by ultra-violet and infra-red spectroscopy, 133
- Hale, P. T.: *see* Cooper, W., Hale, P. T. and Walker, J. S.
- Hama, Y., Ooi, T., Shiotsubo, M. and Shinohara, K.: E.s.r. study of u.v.-irradiated polypropylene: effect of the stereoregularity on the behaviour of free radicals produced by u.v. irradiation, 787
- Hamada, T.: *see* Takizawa, A., Hamada, T., Okada, H., Imai, S. and Kadota, S.
- Haq, Z.: *see* Guthrie, J. T. and Haq, Z.
- Hardy, P. M.: *see* Storey, H. T., Thompson, R. C., Hardy, P. M. and Rydon, H. N.
- Harland, W. G., Khadr, M. M. and Peters, R. H.: Morphology of cold-drawn high-density polyethylene fibres, 81
- Hatano, Masahiro: *see* Yamamoto, Seigo; Nozawa, Tsunenori; and Hatano, Masahiro.
- Haward, R. N.: *see* Cornes, P. L. and Haward, R. N.
- Hayes, G. F.: *see* George, M. H. and Hayes, G. F.
- Heikens, D.: *see* Barentsen, W. M., Heikens, D. and Piet, P.
- Hepburn, C.: *see* Mendis, L. P. and Hepburn, C.
- Higgins, J. S.: *see* Allen, G., Wright, C. J. and Higgins, J. S.
- Hiltner, Anne and Baer, E.: Mechanical properties of polymers at cryogenic temperatures: relationships between relaxation, yield and fracture processes, 805
- Hindeleh, A. M. and Johnson, D. J.: Crystallinity and crystallite size measurement in cellulose fibres. 2. Viscose rayon, 697
- Holding, S. R.: *see* Epton, R., Holding, S. R. and McLaren, J. V.
- Hopkins, W., Peters, R. H. and Stepto, R. F. T.: Gelation in the reactions of aliphatic di-isocyanates with triols, 315
- Houssier, C.: *see* Colson, P., Houssier, C., Fredericq, E. and Bertolotto, J. A.
- Hybart, F. J.: *see* Gilbert, Marianne and Hybart, F. J.
- Hyde, P., Kricka, L. J., Ledwith, A. and Smith, K. C.: Synthesis and polymerizability of 5-methyl-2-vinyliminobenzyl and 10-ethyl-2-vinylphenothiazine, 387
- Iijima, T.: *see* Komiyama, J., Takeda, Y., Ando, M. and Iijima, T.

- Imada, K.: *see* Nakamura, K., Imada, K. and Takayanagi, M.
- Imai, S.: *see* Takizawa, A., Hamada, T., Okada, H., Imai, S. and Kadota, S.
- Inagaki, Norihiro; Tomiha, Kiyoshi; and Katsuura, Kakuji: Studies on the thermal degradation of phosphorus containing polymers: 7. Thermal degradation of phosphorylated poly(vinyl alcohol), 335
- Isaac, D. H.: *see* Atkins, E. D. T., Isaac, D. H., Nieduszynski, I. A., Phelps, C. F. and Sheehan, J. K.
- Ise, N.: *see* Takaya, K. and Ise, N.
- Ise, N.: *see* Takaya, K., Tatsuta, H. and Ise, N.
- Ivanov, V. V.: *see* Penchev, P. I., Ivanov, V. V. and Minin, V. A.
- Jabłoński, W.: *see* Kryszewski, M., Gałęski, A., Jabłoński, W. and Sapieha, S.
- Jeffs, G. M.: *see* Allen, G., Bowden, M. J., Lewis, G., Blundell, D. J. and Jeffs, G. M.
- Jeffs, G. M.: *see* Allen, G., Bowden, M. J., Lewis, G., Blundell, D. J., Jeffs, G. M. and Vyvoda, J.
- Jeffs, G. M.: *see* Allen, G., Bowden, M. J., Todd, S. M., Blundell, D. J., Jeffs, G. M. and Davies, W. E. A.
- Johnson, D. J.: *see* Hindeleh, A. M. and Johnson, D. J.
- Jones, E.: *see* Ballard, D. G. H., Jones, E., Wyatt, R. J., Murray, R. T. and Robinson, P. A.
- Jones, F. R.: *see* Andrews, J. M., Jones, F. R. and Semlyen, J. A.
- Jones, F. R., Scales, L. E. and Semlyen, J. A.: Equilibrium ring concentrations and the statistical conformations of polymer chains: Part 13. Cyclics in two aliphatic polyesters, 738
- Joyeau, R.: *see* Brown, E. and Joyeau, R.
- Jux, J. T., North, A. M. and Kay, R.: Dielectric properties of standard and modified electrical grade phenol-formaldehyde resin-paper laminates, 799
- Kadota, S.: *see* Takizawa, A., Hamada, T., Okada, H., Imai, S. and Kadota, S.
- Kaneko, M.: *see* Kuwahara, N., Saeki, S., Chiba, T. and Kaneko, M.
- Kaneko, M.: *see* Kuwahara, N., Saeki, S., Konno, S. and Kaneko, M.
- Katsurra, Kakuji: *see* Inagaki, Norihiro; Tomiha, Kiyoshi; and Katsurra, Kakuji
- Kawamura, Takashi: *see* Fujimura, Toshikazu; and Kawamura, Takashi
- Kay, R.: *see* Jux, J. T., North, A. M. and Kay, R.
- Khadr, M. M.: *see* Harland, W. G., Khadr, M. M. and Peters, R. H.
- Kim, Min Gon: Comments on paper: 'Steady flow and dynamic viscoelastic properties of branched polyethylene' (*Polymer* 1973, 14, 384-386), 123
- Komiyama, J., Takeda, Y., Ando, M. and Iijima, T.: Dilatometric study of monovalent counter-ion association with polymethacrylate, 468
- Kondo, Shingo: *see* Takano, Yo; and Kondo, Shingo
- Konno, S.: *see* Kuwahara, N., Saeki, S., Konno, S. and Kaneko, M.
- Kricka, L. J.: *see* Hyde, P., Kricka, L. J., Ledwith, A. and Smith, K. C.
- Kryszewski, M., Gałęski, A., Jabłoński, W. and Sapieha, S.: Formation of supermolecular structure in thin polymer films, 211
- Kusumoto, N., Yonezawa, M. and Motozato, Y.: Studies on surface of as-grown and annealed polyethylene single crystals by the spin-probe method, 793
- Kusy, R. P. and Turner, D. T.: Dependence of fracture surface energy of PMMA on molecular weight, 394
- Kuwahara, N., Saeki, S., Chiba, T. and Kaneko, M.: Upper and lower critical solution temperatures in polyethylene solutions, 777
- Kuwahara, N., Saeki, S., Konno, S. and Kaneko, M.: Temperature dependence of polymer chain dimensions in the polystyrene-cyclopentane system, 66
- Lally, T. P.: *see* Price, C., McAdam, J. D. G., Lally, T. P. and Woods, D.
- Lally, T. P.: *see* Price, C., Lally, T. P. and Stubbersfield, R.
- Lally, T. P. and Price, C.: Some observations on the colloidal behaviour of block polymers, 325
- Lau, P. C.: *see* Lee, W. K., Lau, P. C. and Choy, C. L.
- Ledwith, A.: *see* Hyde, P., Kricka, L. J., Ledwith, A. and Smith, K. C.
- Lee, W. K., Lau, P. C. and Choy, C. L.: Heat capacity of polychlorotrifluoroethylene, 487
- Lemstra, P. J., Postma, J. and Challa, G.: Molecular weight dependence of the spherulitic growth rate of isotactic polystyrene, 757
- Levy, G. M.: *see* Andrews, E. H. and Levy, G. M.
- Lewis, G.: *see* Allen, G., Bowden, M. J., Lewis, G., Blundell, D. J. and Jeffs, G. M.
- Lewis, G.: *see* Allen, G., Bowden, M. J., Lewis, G., Blundell, D. J., Jeffs, G. M. and Vyvoda, J.
- Longman, G. W.: *see* Blundell, D. J., Longman, G. W., Wignall, G. D. and Bowden, M. J.
- Loo, C. T.: High temperature vulcanization of elastomers: 2. Network structures in conventional sulphenamide-sulphur natural rubber vulcanizates, 357. 3. Network structure of efficiently vulcanized natural rubber mixes, 729
- Lord, F. W.: Transition and relaxation processes in ω -amino acid polyamides, 42
- Loucheux-Lefebvre, Marie-H., Forchioni, A. and Duffot, Catherine: N.m.r. of random copolymers of benzyl-L-aspartate with *o*- and *p*-nitrobenzyl-L-aspartate, 474
- McAdam, J. D. G.: *see* Price, C., McAdam, J. D. G., Lally, T. P. and Woods, D.
- McBrierty, V. J.: N.m.r. of solid polymers: a review, 503
- McLaren, J. V.: *see* Epton, R., Holding, S. R. and McLaren, J. V.
- McLaren, J. V.: *see* Epton, R., McLaren, J. V. and Thomas, T. H.
- Maglione, A.: *see* Bonora, G. M., Maglione, A. and Toniolo, C.
- Manaresi, P., Pilati, F. and Fortunato, B.: Some solution properties of poly(trans-2,5-dimethyl-piperazine-3, 4-thiofuran amide), 393
- Marcinčin, K.: *see* Romanov, A., Pollák, V. and Marcinčin, K.
- Marechal, E.: *see* Visse, F. and Marechal, E.
- Marshall, G. P.: *see* Williams, J. G. and Marshall, G. P.
- Martuscelli, E. and Pracella, M.: Effects of chain defects on the thermal behaviour of polyethylene, 306
- Mayer, R.: Organized structures in amorphous styrene/*cis*-1,4-isoprene block copolymers: low angle X-ray scattering and electron microscopy, 137
- Mazeron, P.: *see* Ravey, J.-C., Mazeron, P. and Sere, Y.
- Meeks, A. C.: Fracture and mechanical properties of epoxy resins and rubber-modified epoxy resins, 675
- Meeten, G. H.: Evidence for aggregation of polystyrene in solution from magneto-optic birefringence, 187
- Meeten, G. H.: *see* Campion, J. V., Desson, R. A. and Meeten, G. H.
- Mendis, L. P. and Hepburn, C.: Diagnosis of graft copolymers by adhesion analysis, 189
- Miller, A. and Parry, D. A. D.: A review of statistical structures in synthetic polypeptides and biological macromolecules, 706
- Minin, V. A.: *see* Penchev, P. I., Ivanov, V. V. and Minin, V. A.
- Morrell, S. H.: *see* Berry, J. P. and Morell, S. H.
- Motozato, Y.: *see* Kusumoto, N., Yonezawa, M. and Motozato, Y.
- Mukherjee, R. N. and Bandyopadhyay, A. K.: Investigations on oxidative polymerization of 1-naphthol using Cu^I-pyridine initiator system, 392
- Muller, G.: Electric permittivity of polyelectrolytes: 2. Effect of the concentration and ionic specificity, 585
- Murray, R. T.: *see* Ballard, D. G. H., Jones, E., Wyatt, R. J., Murray, R. T. and Robinson, P. A.
- Nakamura, K., Imada, K. and Takayanagi, M.: Solid-state extrusion of isotactic polypropylene through a tapered die: 2. Structure and some properties of extrudates, 446
- Narkis, M.: *see* Siegmann, A., Narkis, M. and Dagan, A.
- Neuse, E. W. and Green, B. R.: Poly(squarylamides), 339
- Nevell, T. P. and Shaw, I. S.: Effect of ethylamine pretreatment on the oxidation of cellulose by periodate, 553. Effect of ethylamine pretreatment on the tensile strength of periodate oxycelluloses, 559
- Ng, H. N.: *see* Allegranza, A. E., Jr, Seymour, R. W., Ng, H. N. and Cooper, S. L.
- Nicodemo, L. and Nicolais, L.: Filler effect on the relaxation time of fibre suspensions in polymeric solution, 589
- Nicol, Elisabeth A.: *see* Chantry, G. W., Fleming, J. W., Nicol, Elisabeth A., Willis, H. A., Cudby, M. E. A. and Boerio, F. J.
- Nicolais, L.: *see* Nicodemo, L. and Nicolais, L.
- Nieduszynski, I. A.: *see* Atkins, E. D. T., Isaac, D. H., Nieduszynski, I. A., Phelps, C. F. and Sheehan, J. K.
- Nieduszynski, I. A.: *see* Barham, P. J., Atkins, E. D. T. and Nieduszynski, I. A.
- Nieduszynski, I. A.: *see* Whitaker, P. M., Nieduszynski, I. A. and Atkins, E. D. T.

Author Index

- Nobbs, J. H., Bower, D. I., Ward, I. M. and Patterson, D.: A study of the orientations of fluorescent molecules incorporated in uniaxially oriented poly(ethylene terephthalate) tapes, 287
- North, A. M.: *see* Jux, J. T., North, A. M. and Kay, R.
- Nozawa, Tsunenori: *see* Yamamoto, Seigo; Nozawa, Tsunenori; and Hatano, Masahiro
- Okada, H.: *see* Takizawa, A., Hamada, T., Okada, H., Imai, S. and Kadota, S.
- Ooi, T.: *see* Hama, Y., Ooi, T., Shiotsubo, M. and Shinohara, K.
- Oosterhof, H. A.: Structure and properties of poly(pivalolactone), 49
- Pác, J.: *see* Sedlář, J. and Pác, J.
- Paipetis, S. A.: *see* Theocaris, P. S., Paipetis, S. A. and Tsangaris, J. M.
- Pallesi, B.: *see* D'Alo, B., Coppola, G. and Pallesi, B.
- Parry, D. A. D.: *see* Miller, A. and Parry, D. A. D.
- Patel, K. C.: *see* Gohil, R. M., Patel, K. C. and Patel, R. D.
- Patel, R. D.: *see* Gohil, R. M., Patel, K. C. and Patel, R. D.
- Patterson, D.: *see* Nobbs, J. H., Bower, D. I., Ward, I. M. and Patterson, D.
- Pavan, A., Rink, M., Blundo, G. and Danusso, F.: Characterization of the thermomechanical behaviour of polymers: non-isothermal creep deflection processes, 243
- Penchev, P. I., Ivanov, V. V. and Minin, V. A.: A model study on the ionic polymerization in a flow reactor, 573
- Pennings, A. J.: *see* Smith, P. and Pennings, A. J.
- Peters, R. H.: *see* Harland, W. G., Khadr, M. M. and Peters, R. H.
- Peters, R. H.: *see* Hopkins, W., Peters, R. H. and Stepto, R. F. T.
- Phelps, C. F.: *see* Atkins, E. D. T., Isaac, D. H., Nieduszynski, I. A., Phelps, C. F. and Sheehan, J. K.
- Phillips, P. J.: *see* Edwards, B. C. and Phillips, P. J.
- Pierre, J. and Desreux, V.: Temperature effects on some solution properties of poly(n-alkyl isocyanates), 685
- Piet, P.: *see* Barentsen, W. M., Heikens, D. and Piet, P.
- Pilati, F.: *see* Manaresi, P., Pilati, F. and Fortunato, B.
- Pillai, P. S.: *see* Fielding-Russell, G. S. and Pillai, P. S.
- Pini, D.: *see* Conti, F., Delfini, M., Segre, A. L., Pini, D. and Porri, L.
- Pini, D.: *see* Conti, F., Segre, A. L., Pini, D. and Porri, L.
- Pollák, V.: *see* Romanov, A., Pollák, V. and Marcinčin, K.
- Poller, R. C.: *see* Abbas, S. Z. and Poller, R. C.
- Porri, L.: *see* Conti, F., Delfini, M., Segre, A. L., Pini, D. and Porri, L.
- Porri, L.: *see* Conti, F., Segre, A. L., Pini, D. and Porri, L.
- Postma, J.: *see* Lemstra, P. J., Postma, J. and Challa, G.
- Pracella, M.: *see* Martuscelli, E. and Pracella, M.
- Price, C.: *see* Lally, T. P. and Price, C.
- Price, C., Lally, T. P. and Stubbersfield, R.: Microphase separation in an ABC block terpolymer, 541
- Price, C., McAdam, J. D. G., Lally, T. P., Woods, D.: Determination of the molecular weight and hydrodynamic dimensions of micelles formed from a block copolymer, 228
- Price, C., Singleton, R. and Woods, D.: Microphase separation in a graft copolymer, 117
- Price, C. and Woods, D.: Light-scattering study of micelle formation by polystyrene-*g*-polyisoprene graft copolymers, 389
- Purvis, J. and Bower, D. I.: A study of molecular orientation in poly(methyl methacrylate) by means of laser-Raman spectroscopy, 645
- Quack, G.: *see* Elgert, K.-F., Quack, G. and Stützel, E.
- Ravey, J.-C., Mazon, P. and Sere, Y.: Measurements of anisotropic light scattering: application to the determination of the difference $H_h \times H_v$ for $\theta = \pi/2$, 77
- Rawson, F. F. and Rider, J. G.: A correlation of Young's modulus with yield stress in oriented poly(vinyl chloride), 107
- Reynaers, H.: *see* Groeninckx, G., Reynaers, H. and Berghmans, H.
- Rider, J. G.: *see* Rawson, F. F. and Rider, J. G.
- Rigbi, Z. and Sabatov, N.: Solvent-swelling of vulcanizates reinforced by fibrillar fillers, 373
- Rigby, S. J. and Dew-Hughes, D.: Low temperature dielectric relaxation in polymers containing an aromatic group in the main chain, 639
- Rink, M.: *see* Pavan, A., Rink, M., Blundo, G. and Danusso, F.
- Robb, I. D.: *see* Smith, E. G. and Robb, I. D.
- Robinson, P. A.: *see* Ballard, D. G. H., Jones, E., Wyatt, R. J., Murray, R. T. and Robinson, P. A.
- Romanov, A., Pollák, V. and Marcinčin, K.: Effect of swelling agent on the determination of the crosslinking density in ethylene-propylene copolymer, 609
- Rose, J. B.: Preparation and properties of poly(arylene ether sulphones), 456
- Rudin, A.: *see* Chau, T. C. and Rudin, A.
- Rydon, H. N.: *see* Storey, H. T., Thompson, R. C., Hardy, P. M. and Rydon, H. N.
- Sabatov, N.: *see* Rigbi, Z. and Sabatov, N.
- Saeki, S.: *see* Kuwahara, N., Saeki, S., Chiba, T. and Kaneko, M.
- Saeki, S.: *see* Kuwahara, N., Saeki, S., Konno, S. and Kaneko, M.
- Saito, Takanori and Yamaguchi, Kinya: Viscometric studies on chlorinated polyethylenes in dilute solution, 219
- Sapieha, S.: *see* Kryszewski, M., Gałęski, A., Jabłoński, W. and Sapieha, S.
- Scales, L. E.: *see* Jones, F. R., Scales, L. E. and Semlyen, J. A.
- Schelten, J., Wignall, G. D. and Ballard, D. G. H.: Chain conformation in molten polyethylene by low angle neutron scattering, 682
- Sedlář, J. and Pác, J.: Polypropylene stability adversely affected by volatile oxidation products, 613
- Segre, A. L.: *see* Conti, F., Delfini, M. and Segre, A. L.
- Segre, A. L.: *see* Conti, F., Delfini, M., Segre, A. L., Pini, D. and Porri, L.
- Segre, A. L.: *see* Conti, F., Segre, A. L., Pini, D. and Porri, L.
- Semlyen, J. A.: *see* Andrews, J. M., Jones, F. R. and Semlyen, J. A.
- Semlyen, J. A.: *see* Jones, F. R., Scales, L. E. and Semlyen, J. A.
- Sengupta, C. R.: *see* Baird, M. E. and Sengupta, C. R.
- SenGupta, P. K.: *see* Bevington, J. C. and SenGupta, P. K.
- Senior, J. M.: *see* Ghafoor, A., Senior, J. M., Still, R. H. and West, G. H.
- Sere, Y.: *see* Ravey, J.-C., Mazon, P. and Sere, Y.
- Seymour, R. W.: *see* Allegranza, A. E., Jr, Seymour, R. W., Ng, H. N. and Cooper, S. L.
- Shaw, I. S.: *see* Nevell, T. P. and Shaw, I. S.
- Sheehan, J. K.: *see* Atkins, E. D. T., Isaac, D. H., Nieduszynski, I. A., Phelps, C. F. and Sheehan, J. K.
- Sherriff, M. and Warburton, B.: Measurement of dynamic rheological properties using the principle of externally shifted and restored resonance, 253
- Shinohara, I.: *see* Tsuchida, E., Aoyagi, J., Shinzo, K. and Shinohara, I.
- Shinohara, K.: *see* Hama, Y., Ooi, T., Shiotsubo, M. and Shinohara, K.
- Shinzo, K.: *see* Tsuchida, E., Aoyagi, J., Shinzo, K. and Shinohara, I.
- Shiotsubo, M.: *see* Hama, Y., Ooi, T., Shiotsubo, M. and Shinohara, K.
- Siegmann, A., Narkis, M. and Dagan, A.: Solid solutions and precipitation in flame retardant polystyrene-tetrabromoxylene systems, 499
- Siesler, H. W.: Investigation of orientation phenomena in drawn films of poly([±]-β-aminobutyric acid), 146
- Singleton, R.: *see* Price, C., Singleton, R. and Woods, D.
- Skirrow, G. and Young, K. R.: Sorption, diffusion and conduction in polyamide-penetrant systems. 1. Sorption phenomena, 771
- Smith, E. G. and Robb, I. D.: N.m.r. studies on the effect of water on the glass transition of polystyrene, 713
- Smith, F. S. and Steward, R. D.: The crystallization of oriented poly(ethylene terephthalate), 283
- Smith, K. C.: *see* Hyde, P., Kricka, L. J., Ledwith, A. and Smith, K. C.
- Smith, P. and Pennings, A. J.: Eutectic crystallization of pseudo binary systems of polyethylene and high melting diluents, 413
- Štamberg, J., Wichterle, O. and Doskočilová, D.: Comment on the paper: 'Introduction of hydroxymethyl groups into polystyrene and styrene' by C. H. Bamford and H. Lindsay (*Polymer* 1973, 14, 330-332), 323
- Stepto, R. F. T.: *see* Hopkins, W., Peters, R. H. and Stepto, R. F. T.
- Steward, R. D.: *see* Smith, F. S. and Steward, R. D.
- Still, R. H.: *see* Ghafoor, A., Senior, J. M., Still, R. H. and West, G. H.
- Stivala, S. S.: *see* Ehrlich, J. and Stivala, S. S.
- Stivala, S. S. and Ehrlich, J.: Macromolecular properties of heparin in dilute solution: 1. Application of various hydrodynamic models in 0.5 M NaCl, pH 2.5, 197

- Storey, H. T., Thompson, R. C., Hardy, P. M. and Rydon, H. N.: Conformations of macromolecular sequential polypeptides in solution: 2. Sequential polypeptides containing both D- and L-residues, 690
- Stubbersfield, R.: *see* Price, C., Lally, T. P. and Stubbersfield, R.
- Stützel, E.: *see* Elgert, K.-F., Quack, G. and Stützel, E.
- Tait, P. J. T.: *see* Burfield, D. R. and Tait, P. J. T.
- Takano, Yo; and Kondo, Shingo: An interpretation of ductile fracture process of uncrosslinked polymers in the rubbery state, 671
- Takaya, K. and Ise, N.: Anionic polymerization of styrene in 2-methyl-tetrahydrofuran: temperature dependence of the field effect, 635
- Takaya, K., Tatsuta, H. and Ise, N.: Anionic polymerization of styrene in triglyme-benzene mixtures, 631
- Takayanagi, M.: *see* Nakamura, K., Imada, K. and Takayanagi, M.
- Takeda, Y.: *see* Komiya, J., Takeda, Y., Ando, M. and Iijima, T.
- Takemura, Tetuo: *see* Yasuniwa, Munehisa; and Takemura, Tetuo
- Takizawa, A., Hamada, T., Odada, H., Imai, S. and Kadota, S.: Permeability of a series of alcohols through poly-(γ -methyl-D-glutamate), 157
- Tatsuta, H.: *see* Takaya, K., Tatsuta, H. and Ise, N.
- Taylor, G.: *see* Dawkins, J. V. and Taylor, G.
- Ter-Minassian-Saraga, L.: *see* Baszkin, A. and Ter-Minassian-Saraga, L.
- Theocaris, P. S.: Time lag in mechanical and optical response of polymers, 655
- Theocaris, P. S., Paipetis, S. A. and Tsangaris, J. M.: Thermal crazing phenomena in epoxy resins, 441
- Thomas, E. L. and Ast, D. G.: Image intensification and the electron microscopy of radiation sensitive polymers, 37
- Thomas, T. H.: *see* Epton, R., McLaren, J. V. and Thomas, T. H.
- Thompson, R. C.: *see* Storey, H. T., Thompson, R. C., Hardy, P. M. and Rydon, H. N.
- Thurston, G. B.: Exact and approximate eigenvalues and intrinsic functions for the Gaussian chain theory, 569
- Todd, S. M.: *see* Allen, G., Bowden, M. J., Todd, S. M., Blundell, D. J., Jeffs, G. M. and Davies, W. E. A.
- Tomiha, Kiyoshi: *see* Inagaki, Norihiro; Tomiha, Kiyoshi; and Katsura, Kak-
uji
- Tonelli, A. E.: Effects of crosslink density and length on the number of intramolecular crosslinks (defects) introduced into a rubbery network, 194
- Toniolo, C.: *see* Bonora, G. M., Maglione, A. and Tonilo, C.
- Törmälä, P.: On the mechanism of motions of nitroxyl radicals in polymers, 124
- Törmälä, P., Tulikoura, J.: Effect of end-groups on the motions of free nitroxyl radicals in poly(ethylene glycol), 248
- Tsangaris, J. M.: *see* Theocaris, P. S., Paipetis, S. A. and Tsangaris, J. M.
- Tsuchida, E., Aoyagi, J., Shinzo, K. and Shinohara, I.: Simulation of kinetic analysis on terpolymerization of styrene/butyl methacrylate/methacrylic acid system, 479
- Tulikoura, J.: *see* Törmälä, P. and Tulikoura, J.
- Turner, D. T.: *see* Kusy, R. P. and Turner, D. T.
- Turner, S.: *see* Dunn, C. M. R. and Turner, S.
- Turner, S.: *see* Gotham, K. V. and Turner S.
- Vincent, P. I.: *see* Blackadder, D. A. and Vincent, P. I.
- Vincent, P. I.: Impact strength and mechanical losses in thermoplastics, 111
- Visse, F. and Marechal, E.: Influence of the polymerization temperature on the reactivity of 3-methyl- and 4-methylstyrenes in cationic polymerization, 485
- Vyvoda, J.: *see* Allen, G., Bowden, M. J., Lewis, G., Blundell, D. J., Jeffs, G. M. and Vyvoda, J.
- Walker, J. S.: *see* Cooper, W., Hale, P. T. and Walker, J. S.
- Walsh, D. J., Allen, G. and Ballard, G.: Preparation and moduli of model polymer networks, 366
- Warburton, B.: *see* Sherriff, M. and Warburton, B.
- Ward, I. M.: *see* Cappacio, G. and Ward, I. M.
- Ward, I. M.: *see* Cunningham, A., Davies, G. R. and Ward, I. M.
- Ward, I. M.: *see* Cunningham, A., Ward, I. M., Willis, H. A. and Zichy, V.
- Ward, I. M.: *Editorial*—The Physics of Polymers, 258
- Ward, I. M.: *see* Nobbs, J. H., Bower, D. I., Ward, I. M. and Patterson, D.
- Ward, I. M.: Mechanical properties of oriented polymers, 379
- Welch, G. J.: Solution properties and unperturbed dimensions of poly(vinylidene fluoride), 429
- West, G. H.: *see* Ghafoor, A., Senior, J. M., Still, R. H. and West, G. H.
- Whitaker, P. M., Nieduszynski, I. A. and Atkins, E. D. T.: Structural aspects of soda-cellulose II, 125
- Wichterle, O.: *see* Štamberg, J., Wichterle, O. and Doskočilova, D.
- Wignall, G. D.: *see* Blundell, D. J., Longman, G. W., Wignall, G. D. and Bowden, M. J.
- Wignall, G. D.: *see* Schelten, J., Wignall, G. D. and Ballard, D. G. H.
- Williams, J. G. and Marshall, G. P.: Crack stability in PMMA, 251
- Willis, H. A.: *see* Chantry, G. W., Fleming, J. W., Nicol, Elisabeth A., Willis, H. A., Cudby, M. E. A. and Boerio, F. J.
- Willis, H. A.: *see* Cunningham, A., Ward, I. M., Willis, H. A. and Zichy, V.
- Wilson, M. P. W.: Shrinkage and chain folding in drawn poly(ethylene terephthalate) fibres, 277
- Wintle, P. K.: Dose kinetics of u.v. excited thermoluminescence in polyethylene, 425
- Wong, P. K.: Energy transfer in illuminated PMMA, 60
- Woods, D.: *see* Price, C., McAdam, J. D. G., Lally, T. P. and Woods, D.
- Woods, D.: *see* Price, C., Singleton, R. and Woods, D.
- Woods, D.: *see* Price, C. and Woods, D.
- Wright, C. J.: *see* Allen, G., Wright, C. J. and Higgins, J. S.
- Wyatt, R. J.: *see* Ballard, D. G. H., Jones, E., Wyatt, R. J., Murray, R. T. and Robinson, P. A.
- Yamaguchi, Kinya: *see* Saito, Takanori and Yamaguchi, Kinya
- Yamamoto, Seigo; Nozawa, Tsunenori; and Hatano, Masahiro: Circular dichroism and magnetic circular dichroism of the haemin-poly(L-lysine) complex system, 330
- Yasuniwa, Munehisa; and Takemura, Tetuo: Microscopic observations of the crystallization processes of polyethylene under high pressure, 661
- Yonezawa, M.: *see* Kusumoto, N., Yonezawa, M. and Motozato, Y.
- Young, K. R.: *see* Skirrow, G. and Young, K. R.
- Zichy, Veronica: *see* Cunningham, A., Ward, I. M., Willis, H. A. and Zichy, Veronica
- Zoller, P. and Bont, H.: Conversion of work of deformation to heat in polymers, 239

UK EDITORS

C. H. Bamford PhD, ScD, FRS
Campbell Brown Professor of Industrial
Chemistry, University of Liverpool,
PO Box 147, Liverpool L69 3BX

C. E. H. Bawn CBE, FRS
Grant Brunner Professor of Inorganic and
Physical Chemistry, University of Liverpool,
PO Box 147, Liverpool L69 3BX

E. M. Bradbury PhD
Head of Biophysics Section,
Portsmouth Polytechnic,
Portsmouth PO1 2QG

Geoffrey Gee CBE, FRS
Sir Samuel Hall Professor of Chemistry,
University of Manchester,
Manchester M13 9PL

R. J. W. Reynolds PhD, FPI
Institute of Polymer Technology,
Loughborough University of Technology,
Loughborough LE11 3TU

J. G. Williams PhD, CEng
Reader in Polymer Engineering,
Department of Mechanical Engineering,
Imperial College of Science and Technology,
London SW7 2BX

Annual subscription including postage
£30; USA \$78.00 (surface mail)
Airmail USA \$130; Japan £50
Rates for other countries available on request

Published monthly by IPC Science and Technology
Press Ltd, IPC House, 32 High Street,
Guildford, Surrey, GU1 3EW, England
Telephone: Guildford (0483) 71661
Telegrams and Telex: Scitechpress Gd. 85556

Reprints (minimum quantity usually 100) of papers
may be ordered from the publishers. Write to the
Reprints Dept, IPC Science and Technology Press
Ltd, at the above address

Reprinted volumes of Vols 1-10 (1960-1969) are available
from Wm Dawson and Sons Ltd, Cannon House,
Folkestone, Kent UK at £15.00 (\$39.00) per volume
ISSN 0032-3861

American Representatives: IPC (America) Ltd,
205 East 42nd Street, New York, NY 10017, USA

© IPC Business Press Ltd, 1974

OVERSEAS EDITORS

H. C. Benoit PhD
Professor, University of Strasbourg
Director, Centre de Recherches
sur les Macromolécules,
6, Rue Boussingault,
67 Strasbourg, France

S. Bywater PhD
Head, Polymer Section,
National Research Council,
Ottawa KIA OR9, Canada

F. Danusso PhD
Professor of Macromolecular Chemistry,
Istituto Chimica Industriale del Politecnico,
Piazza Leonardo da Vinci 32,
20133 Milano, Italy

Hirotaro Kambe DSc
Professor, Polymer Research Division,
Institute of Space and Aeronautical Science,
University of Tokyo, Tokyo, Japan

Maurice Morton PhD
Director, Institute of Polymer Science,
University of Akron,
Akron, Ohio 44325, USA

M. Szwarc PhD, FRS
Director, Polymer Research Center,
State University of New York,
College of Environmental Science and
Forestry, Syracuse, NY 13210, USA

MANAGING EDITOR

J. A. G. Thomas PhD

ASSISTANT EDITOR

C. J. Rawlins BSc

EDITORIAL ARTIST

Ann Heat